NIST NCSTAR 1-6

Federal Building and Fire Safety Investigation of the World Trade Center Disaster

Structural Fire Response and Probable Collapse Sequence of the World Trade Center Towers

John L. Gross
Therese P. McAllister

NIST National Institute of Standards and Technology • Technology Administration • U.S. Department of Commerce

NIST NCSTAR 1-6

ABSTRACT

One of the four main objectives of the National

This page intentionally left blank.

TABLE OF CONTENTS

Abstract iii
List of Figures xi
List of Tables xxi
List of Acronyms and Abbreviations xxiii
Preface xxv
Acknowledgments xxxv
Executive Summary xxxvii

Chapter 1
Introduction 1
1.1 Project Objectives 1
1.2 Technical Approach and Tasks 2
1.2.1 Task A – Finite Element Reference Models 4
1.2.2 Task B – Material Properties 5
1.2.3 Task C – Passive Fire Protection 5
1.2.4 Task D – Standard Fire Resistance Tests 5
1.2.5 Task E – Aircraft Impact Damage 6
1.2.6 Task F – Observations and Timeline 6
1.2.7 Task G – Temperatures of Structural Components 6
1.2.8 Task H – Component and Subsystem Analyses 7
1.2.9 Task I – Major Subsystem Analyses 7
1.2.10 Task J – Global Structural Analyses 7
1.2.11 Task K – Probable Collapse Sequence 8
1.3 Challenges 9
1.4 Report Organization 10

Chapter 2
Passive Fire Protection 13
2.1 Fire Resistance of Structural Elements 13
2.2 Historical Review Related To Passive Fire Protection 14
2.2.1 Building Code Requirements for the Design of the WTC Towers 14
2.2.2 New York City Building Code Requirements 14
2.2.3 Classification of WTC Towers 15

2.2.4 Response to Local Law 5/1973 ... 16
2.2.5 Selection of Fire Resistive Materials ... 16
2.2.6 Specified Thickness of Fire Resistive Material ... 18
2.2.7 Upgrading SFRM on Floor Trusses ... 20
2.2.8 Need for Fire Resistance Tests ... 21
2.2.9 Maintenance of SFRM in Elevator Shafts ... 22
2.3 As-Applied Thickness of SFRM ... 22
2.3.1 1994 Measurements from WTC 1 Floors 23 and 24 ... 22
2.3.2 Analysis of Photographs ... 23
2.3.3 Port Authority Data on Upgraded SFRM on Trusses ... 25
2.4 Effect of the Variability of SFRM Thickness on Thermal Response ... 25
2.4.1 Effects of Thickness Variability and Gaps in SFRM ... 25
2.4.2 Thermally equivalent thickness of SFRM ... 27
2.4.3 Thickness of SFRM Used for Thermal Analyses ... 28
2.5 Summary of SFRM Thickness ... 29
2.6 Thermophysical Properties ... 30
2.6.1 Thermal Conductivity ... 31
2.6.2 Specific Heat Capacity ... 31
2.6.3 Density ... 32
2.6.4 Thermophysical Properties of Gypsum Panels ... 32
2.7 Estimation of SFRM Dislodged By to Aircraft Impact ... 33
2.7.1 In-place Density and Bond Strength ... 33
2.7.2 Specimen Preparation and Test Procedures ... 34
2.7.3 Test Results ... 35
2.8 References ... 36

Chapter 3
Fire Resistance Tests ... 37
3.1 Background ... 37
3.1.1 Motivation for Conducting Standard Fire Tests ... 37
3.1.2 Purpose of the Standard Fire Tests ... 37
3.2 Description of WTC Floor System ... 38
3.2.1 Structural System ... 38
3.2.2 Fireproofing Thickness ... 39
3.3 Fire Resistance Testing ... 39

3.3.1 General Description ... 39
3.3.2 Test Restraint Conditions and Ratings ... 39
3.3.3 Scale of Tests ... 40
3.3.4 Test Variables ... 40
3.4 Preparation of Test Assemblies ... 41
3.5 Description of Tests and Loading ... 43
3.5.1 Full-scale Tests (35 ft span) ... 43
3.5.2 Reduced-scale Tests (17 ft span) ... 44
3.6 Test Results ... 44
3.6.1 General Discussion of Tests ... 44
3.6.2 Fire Resistance Ratings ... 48
3.6.3 General Observations ... 49
3.6.4 Floor Deflections and Temperatures ... 51
3.6.5 Observations and Comparisons ... 54
3.7 Summary ... 55

Chapter 4
Structural Response of Components, Connections and Subsystems ... 57
4.1 Mechanical Properties of Concrete and Steel ... 57
4.1.1 Concrete Properties and Failure Criteria ... 58
4.1.2 Steel Properties and Failure Criteria ... 60
4.2 Floor Subsystem Analysis ... 65
4.2.1 Description of Floor Subsystem ... 66
4.2.2 Truss Seats ... 69
4.2.3 Knuckles ... 79
4.2.4 Single Truss and Concrete Slab Section ... 84
4.2.5 Floor Subsystem Analysis ... 89
4.3 Exterior Wall Subsystem ... 96
4.3.1 Exterior Wall Subsystem Description ... 97
4.3.2 One, Two, and Three-Story High Columns ... 100
4.3.3 Exterior Wall Section Analysis ... 103
4.3.4 Summary ... 119
4.4 References ... 119

Chapter 5
Aircraft Impact Damage 121

5.1 Introduction 121
5.2 Methodology and Criteria for Developing Input Data From Aircraft Impact Analysis Results .. 122
5.2.1 Core Column Damage 123
5.2.2 Structural Damage to Floor Slabs, Core Beams, and Floor Trusses 126
5.2.3 Fireproofing Damage 129
5.2.4 Summary of Aircraft Impact Damage 133
5.3 Structural and Fireproofing Damage to WTC 1 134
5.4 Structural and Fireproofing Damage to WTC 2 141
5.5 Observations of Aircraft Impact Damage to the Pentagon 147
5.6 Summary 150
5.7 References 151

Chapter 6
Observations and Timeline of Structural Events 153

6.1 Introduction 153
6.2 Observations of Structural Events 154
6.2.1 WTC 1 Structural Response Observations 155
6.2.2 WTC 2 Structural Response Observations 167

Chapter 7
Structural Response of Major Tower Subsystems to Aircraft Impact Damage and Fire . 185

7.1 Introduction 185
7.2 Core Subsystem 185
7.2.1 Model and Method of Analysis 186
7.2.2 WTC 1 Core Analysis Results 188
7.2.3 WTC 2 Analysis Results 192
7.3 Full Floor Subsystem 194
7.3.1 Model and Method of Analysis 194
7.3.2 WTC 1 Analysis Results 200
7.3.3 WTC 2 Analysis Results 205
7.4 Exterior Wall Subsystem 212
7.4.1 Finite Element Model and Methods of Analysis 213
7.4.2 WTC 1 Analysis Results 215
7.5 Summary of Subsystem Analyses 224

Chapter 8
Structural Response of the WTC Towers to Aircraft Impact Damage and Fire 229

8.1 Introduction 229
8.2 Global Model of Towers 230
8.2.1 Model Description 230
8.2.2 Model Modifications 233
8.3 Analysis Methodology 235
8.4 Results of WTC 1 Analysis 237
8.4.1 WTC 1 Structural Response to Aircraft Impact Damage 237
8.4.2 WTC 1 Structural Response to Elevated Temperatures 243
8.4.3 WTC 1 Hat Truss Members and Connections 251
8.5 Results of WTC 2 Analysis 253
8.5.1 WTC 2 Structural Response to Aircraft Impact Damage 254
8.5.2 WTC 2 Structural Response to Elevated Temperatures 260
8.5.3 WTC 2 Hat Truss Members and Connections 273
8.6 Structural Response of the WTC Towers Without Impact Damage and Subjected to the Same Fires 279
8.7 Summary of Structural Response of the WTC Towers 281

Chapter 9
Probable Collapse Sequences 285

9.1 Introduction 285
9.2 Methodology 285
9.2.1 Key Observed Events and Conditions 286
9.2.2 Collapse Hypotheses 286
9.2.3 Mathematical Modeling – Analysis Interdependencies 288
9.2.4 Sensitivity Studies to Identify Influential Variables 290
9.2.5 Evaluation of Collapse Hypotheses 294
9.3 Probable Collapse Sequences 296
9.3.1 Probable Collapse Sequence of WTC 1 297
9.3.2 Probable Collapse Sequence of WTC 2 306
9.4 Discussion and Summary 319
9.4.1 Structural Response to Impact Damage and Fire 320
9.4.2 Structural Response to Fire Without Impact Damage 321
9.4.3 Time to Collapse 322
9.4.4 Factors that Affected Performance 322

Chapter 10
Findings 329
10.1 Passive Fire Protection 329
10.2 Building Code Requirements for Structural Fire Resistance 329
10.2.1 Selection of Fire Resistive Materials 330
10.2.2 Equivalent Thickness of SFRM 330
10.3 Fire Resistance Tests 330
10.3.1 Structural Performance 331
10.3.2 Fire Resistance Ratings 331
10.4 Structural Response of Components 332
10.4.1 Floor System 332
10.4.2 Exterior Wall System 332
10.5 Fireproofing and Partition Damage Due to Aircraft Impact 332
10.6 Observations and Timeline 333
10.6.1 WTC 1 333
10.6.2 WTC 2 334
10.7 Structural Response of Major Tower Subsystems 335
10.7.1 Isolated Core Subsystem 335
10.7.2 Full Floor Subsystem 335
10.7.3 Isolated Exterior Wall Subsystem 335
10.8 Structural Response to Aircraft Impact Damage and Fire 336
10.8.1 General Findings 336
10.8.2 Performance with Intact fireproofing 337
10.9 Probable Collapse Sequences 337
10.9.1 Role of the Building Core 337
10.9.2 Role of the Building Floors 337
10.9.3 Role of Exterior Frame-Tube 338
10.9.4 Probable Collapse Sequences 338

LIST OF FIGURES

Figure P–1. The eight projects in the federal building and fire safety investigation of the WTC disaster. .....**Error! Bookmark not defined.**

Figure 1–1. Structural Analysis Sequence..... 4

Figure 2–1. Mock up of floor truss system..... 17

Figure 2–2. Demonstration of application of Monokote sprayed fire-resistive material to floor trusses..... 18

Figure 2–3. Example of measurement procedure used to estimate SFRM thickness from photographs..... 24

Figure 2–4. Example of "gap" in fire-resistive material on diagonal member of a bridging floor truss..... 26

Figure 2–5. Thermo-mechanical response of 1 in. bar compared with uniform thickness SFRM..... 28

Figure 3–1. Floor system of the WTC towers..... 38

Figure 3–2. Schematic of floor system viewed along the main steel trusses. (not to scale)..... 39

Figure 3–3. Drawing of 35 ft truss and end detail..... 42

Figure 3–4. Trusses being fit-up in test frame of 35 ft test assembly..... 43

Figure 3–5. 35 ft span test assembly loaded with concrete blocks and water-filled containers..... 43

Figure 3–6. 17 ft span test assembly loaded with concrete blocks, water-filled containers and hydraulic actuators..... 44

Figure 3–7. Unexposed surface of Assembly No. 1 after loading equipment was removed..... 45

Figure 3–8. Unexposed surface of Assembly No. 2 after loading equipment was removed..... 46

Figure 3–9. Unexposed surface of Assembly No. 3 after loading equipment was removed..... 47

Figure 3–10. Unexposed surface of Assembly No. 4 after loading equipment was removed..... 48

Figure 3–11. Fire exposure side of the 35 ft restrained test assembly after almost 2 hours of fire exposure 49

Figure 3–12. Sections cut through concrete slab to confirm extent and depth of spalling..... 50

Figure 3–13. Measurement of remaining slab thickness after spalling..... 50

Figure 3–14. Detail of spalling concrete at east end of Assembly No. 1. 51

Figure 3–15. Deflection measured at the center of each assembly. 52

Figure 3–16. Deflection measured at the center of each assembly divided by the span. 52

Figure 3–17. Average temperature of the unexposed surface for all four tests..... 53

Figure 3–18. Average temperatures of the bottom chord for Test Nos. 1, 2 and 3 (3/4 in. thick SFRM) ... 54

Figure 4–1. Temperature–dependent concrete properties. ... 59
Figure 4–2. Concrete stress-strain curves. ... 60
Figure 4–3. Temperature-dependent properties for all steels. ... 63
Figure 4–4. Stress-strain relationships for Material ID 1 steel. ... 64
Figure 4–5. Strain behaviors at elevated temperatures for Material ID 1 steel. ... 65
Figure 4–6. Maximum plastic strain from the finite element analysis and limiting plastic strain ... 65
Figure 4–7. Floor structural subsystem (WTC 1, Floor 96). ... 67
Figure 4–8. Primary truss components. ... 68
Figure 4–9. Plan view of truss seat connection, straps, and horizontal studs. ... 69
Figure 4–10. Truss seat detail location on northeast quadrant of Floor 96 of WTC 1. Reproduced with permission of The Port Authority of New York and New Jersey. ... 70
Figure 4–11. Finite element model of exterior seat. ... 71
Figure 4–12. Failure sequence of the exterior seats against tensile force. ... 72
Figure 4–13. Capacity of exterior seat against tensile force (Detail 1411 in Fig. 4–10). ... 73
Figure 4–14. Capacity of interior seat against vertical and horizontal force (Detail 22 in Fig. 4–10). ... 73
Figure 4–15. Truss seat capacity against vertical force. Reproduced with permission of The Port Authority of New York and New Jersey. Enhancements by NIST. ... 77
Figure 4–16. Truss seat capacity against horizontal force. Reproduced with permission of The Port Authority of New York and New Jersey. Enhancements by NIST. ... 78
Figure 4–17. Results of interior truss seat model at 500 ˚C. ... 80
Figure 4–18. Laclede Steel Company shear tests of a knuckle. ... 81
Figure 4–19. Compressive stresses in longitudinal shear finite element model (4,100 psi concrete). ... 82
Figure 4–20. Shear force versus displacement from finite element model for longitudinal shear of two knuckles (4,100 psi concrete). ... 82
Figure 4–21. Compressive stresses in transverse shear finite element model (2,500 psi concrete). ... 83
Figure 4–22. Shear force versus displacement from finite element model for transverse shear of two knuckles (2,500 psi concrete). ... 83
Figure 4–23. Composite truss and concrete slab model. ... 85
Figure 4–24. Vertical displacement at 700 ^{o}C. ... 87
Figure 4–25. Displacement versus temperature. ... 87
Figure 4–26. Comparison of detailed and reduced truss models. ... 88
Figure 4–27. Converted ANSYS model for Floor 96 of WTC 1. ... 90
Figure 4–28. Long span trusses of converted ANSYS model for Floor 96 of WTC 1. ... 91

Figure 4–29. Core floor beams and columns of converted ANSYS model for Floor 96 of WTC 1. 91
Figure 4–30. Full floor model before impact damage is included (without concrete floor slab). 94
Figure 4–31. Break element locations in the floor model (Floor 96, WTC1). 96
Figure 4–32. Exterior wall section model. 98
Figure 4–33. Schematic of exterior column cross-section. 98
Figure 4–34. One-story exterior column model. 101
Figure 4–35. Load-deflection of column at room temperature (RT) and 700 °C. 101
Figure 4–36. Local buckling of column at room temperature. 102
Figure 4–37. Plastic hinge in column at room temperature. 102
Figure 4–38. Deformed shape of column at maximum axial load at 700 °C. 103
Figure 4–39. SAP2000 shell model of prefabricated panel. 105
Figure 4–40. ANSYS model of prefabricated panel showing finite element mesh. 106
Figure 4–41. ANSYS model of prefabricated panel showing boundary conditions and loading. 106
Figure 4–42. Deflection of prefabricated panel under 100 kip lateral load. 107
Figure 4–43. Typical spandrel splice layout for exterior wall section model. 108
Figure 4–44. Modeling of a typical interior spandrel splice in the exterior wall section model. 108
Figure 4–45. Column Splice Model used in Exterior Wall Model. 109
Figure 4–46. Exterior wall subsystem model with boundary conditions. 110
Figure 4–47. Typical meshing of exterior wall model components. 110
Figure 4–48. Exterior wall model temperature time-histories. 112
Figure 4–49. Spandrel plate deformations. 114
Figure 4–50. Lateral deflections for Case 6 and Case 7. 114
Figure 4–51. Structural response (out-of-plane deformations) for temperature time history DBARE and pulled-in at three disconnected floors for Case 8. (10X displacement magnification). 115
Figure 4–52. Column splice contact element status for temperature time history and DBARE and pulled at three disconnected floors for Case 8. 116
Figure 4–53. Column splice bolt stresses for temperature time history and DBARE and pulled at three disconnected floors for Case 8. 116
Figure 4–54. Structural response (out-of-plane deformations) for temperature time history DBARE and pushdown with three disconnected floors for Case 9 (10X displacement magnification). 117
Figure 4–55. Out-of-plane deformation as a function of pushdown displacement after application of temperature DBARE with three disconnected floors for Case 9. 117
Figure 4–56. Total reaction at column base resulting from pushdown with temperature DBARE and three disconnected floors for Case 9. 118

Figure 4–57. Individual column reaction during pushdown with temperature DBARE and three disconnected floors for Case 9. 118

Figure 5–1. Validation of Aircraft Impact Analysis Prediction With Observations for WTC 1 North Exterior Wall Damage. 122

Figure 5–2. Validation of Aircraft Impact Analysis Prediction With Observations for WTC 2 South Exterior Wall Damage. 123

Figure 5–3. Core column damage levels. 124

Figure 5–4. Impact damage to WTC 1 Floor 95 for Case A (plan view). 127

Figure 5–5. Damage to WTC 1 Floor 95 framing and slab for Case A. 128

Figure 5–6. Debris and fuel field in WTC 1 Case B analysis of aircraft impact. 131

Figure 5–7. WTC 1 Case B aircraft impact damage to framing, partitions, and furnishings on Floor 95. 131

Figure 5–8. WTC 1 Case B Floor 95 partitions and furnishings layout prior to impact (layout provided in model only where interaction with aircraft was expected). 132

Figure 5–9. WTC 1 Case B Floor 95 partitions and furnishings layout after impact with overlay showing extent of dislodged insulation from direct debris impact. 132

Figure 5–10. Definition of structural floor and occupancy floor. 133

Figure 5-11. Plan view of WTC 1 Case B insulation and column damage for Occupancy Floor 95. 133

Figure 5-12. Plan view of WTC 1 Case B damage to Structural Floors 95. 134

Figure 5–13. Plan view of WTC 1 Case A cumulative damage for Floors 93 to 98. 135

Figure 5–14. Plan view of WTC 1 Case A insulation and column damage to Occupancy Floors 93 to 98. 136

Figure 5–15. Plan view of WTC 1 Case A damage to Structural Floors 93 to 98. 137

Figure 5–16. Plan view of WTC 1 Case B cumulative damage from Floors 93 to 98. 138

Figure 5–17. Plan view of WTC 1 Case B insulation and column damage to Occupancy Floors 93 to 98. 139

Figure 5–18. Plan view of WTC 1 Case B damage to Structural Floors 93 to 98. 140

Figure 5–19. Plan view of WTC 2 Case C cumulative damage from Floors 78 to 83. 141

Figure 5–20. Plan view of WTC 2 Case C insulation and column damage to Occupancy Floors 78 to 83. 142

Figure 5–21. Plan view of WTC 2 Case C damage to Structural Floors 78 to 83. 143

Figure 5–22. Plan view of WTC 2 Case D cumulative damage from Floors 78 to 83. 144

Figure 5–23. Plan view of WTC 2 Case D insulation and column damage to Occupancy Floors 78 to 83. 145

Figure 5–24. Plan view of WTC 2 Case D damage to Structural Floors 78 to 83. 146

Figure 5–25. Overlay of WTC Footprint on Pentagon damage area from aircraft impact (original figure from ASCE, 2003). 148

Figure 5–26. Typical damage to spirally reinforced columns in the Pentagon impacted and bent by large debris (ASCE, 2003). 149

Figure 5–27. Typical damage to spirally reinforced columns in the Pentagon not impacted or bent by large debris (ASCE, 2003). 150

Figure 6–1. Initial aircraft impact damage on WTC 1 north face. 157

Figure 6–2. Initial aircraft impact damage on WTC 1 west and south faces minutes after impact (exact time of image is unknown). 158

Figure 6–3. SFRM knocked off north exterior columns. Arrows show where fireproofing was damaged or missing. 159

Figure 6–4. South face of WTC 1 with fire visible only on the west side at 9:25. Arrow shows region where debris pile under missing panel was observed. 159

Figure 6–5. Fires on WTC 1 south face at 9:40 a.m. Note lack of inward bowing. 160

Figure 6–6. WTC 1 exterior columns bowing inward across most of the south face between Floors 95 to 97 (or 98) at 10:23 a.m. Note buckled panel at SW corner. 161

Figure 6–7. Expulsion of smoke and debris at WTC 1 Floor 98 on the east, north, and west faces. 162

Figure 6–8. Smoke expulsion at Floor 98 from north and west faces as collapse initiates. 163

Figure 6–9. Smoke expulsion at Floor 98 from north and east faces at collapse initiation. 164

Figure 6–10. Rotation of WTC 1 building section above the aircraft impact zone toward the south as viewed from due north. Note that there is no tilt in the east or west directions. 165

Figure 6–11. WTC 1 tilt to the south of approximately 8 degrees was measured before smoke and debris obscured view. Note view is from west and tilt is directly south. 166

Figure 6–12. Aircraft impact into WTC 2 and fireball, view from the east. 171

Figure 6–13. Hanging object (noted by arrows) in east windows of Floor 82 appears to be edge of Floor 83. 172

Figure 6–14. Debris piles at windows where fire are burning at the northeast corner. 172

Figure 6–15. Hanging object (noted by arrows) in north windows of Floor 79 appears to be edge of Floor 80. 173

Figure 6–16. Image showing damage to fireproofing on east face of WTC 2 due to internal impact. Red arrows highlight areas where fireproofing has been damaged. The blowup to the right shows a column where red Tnemec primer paint is visible. 174

Figure 6–17. WTC 2 exterior columns bowing inward across north side of the east face between Floors 77 to 83 at 9:21 a.m. 175

Figure 6–18. Inward Bowing of east Face of WTC 2 at 9:21 a.m. 175

Figure 6–19. Inward Bowing of east Face of WTC 2 at 9:53 a.m. 176

Figure 6–20. Inward Bowing of east Face of WTC 2 at 9:53 a.m. 177

Figure 6–21. WTC 2 exterior columns bowing inward across the east face between Floors 77 to 83 at 9:59 a.m. 178

Figure 6–22. View of WTC 2 buckling of east wall near northeast corner as collapse initiates from northeast. 179
Figure 6–23. View of east wall buckling and WTC 2 collapse from southeast. 180
Figure 6–24. View of upper building section of WTC 2 tilting to the east. 181
Figure 6–25. View of upper building section of WTC 2 tilting to the east from the northeast. 182
Figure 6–26. Kink on southeast corner near Floor 106 formed after collapse initiation. 183

Figure 7–1. Isolated core models. 188
Figure 7–2. Vertical displacement of WTC 1 isolated core model with impact damage and gravity loads. 189
Figure 7–3. North side vertical displacement of the WTC 1 core model at 100 min for Case A temperatures. 190
Figure 7–4. South side vertical displacement of the WTC 1 core model at 100 min for Case B temperatures. 191
Figure 7–5. Vertical displacement of the WTC 2 isolated core model with impact damage and gravity loads (south and east faces). 192
Figure 7–6. Vertical displacement of the WTC 2 core model at 60 min for Case C temperatures (south and east faces). 193
Figure 7–7. South and east side vertical displacement of the WTC 2 core model at 60 min for Case D temperatures. 194
Figure 7–8. Full floor model. 195
Figure 7–9. Fireproofing damage to WTC 1 Floor 97 for Case A i and Case A. 198
Figure 7–10. WTC 1 Floor 97 comparison of truss temperatures for Case A i and Case A. 199
Figure 7–11. Vertical deflection of WTC 1 Floor 95 for Case Bi at 10 min. 202
Figure 7–12. Vertical deflection of WTC 1 Floor 96 for Case Bi at 10 min. 202
Figure 7–13. Vertical deflection of WTC 1 Floor 97 for Case Bi at 100 min. 203
Figure 7–14. Vertical deflection of WTC 1 Floor 98 for Case Bi at 100 min. 203
Figure 7–15. Vertical deflection of WTC 1 Floor 99 for Case Bi at 100 min. 204
Figure 7–16. Loss of vertical supports in WTC 1 Floor 97 and Floor 98 for Case Bi. 204
Figure 7–17. Vertical deflection of WTC 2 Floor 79 for Case Ci at 60 min. 206
Figure 7–18. Vertical deflection of WTC 2 Floor 80 for Case Ci at 60 min. 206
Figure 7–19. Vertical deflection of WTC 2 Floor 81 for Case Ci at 60 min. 207
Figure 7–20. Vertical deflection of WTC 2 Floor 82 for Case Ci at 60 min. 207
Figure 7–21. Vertical deflection of WTC 2 Floor 83 for Case Ci at 60 min. 208
Figure 7–22. Loss of vertical supports in WTC 2 Floor 82 and Floor 83 for Case Ci. 208
Figure 7–23. Vertical deflection of WTC 2 Floor 79 for Case Di. 210
Figure 7–24. Vertical deflection of WTC 2 Floor 80 for Case Di. 210

Figure 7–25. Vertical deflection of WTC 2 Floor 81 for Case Di. 211
Figure 7–26. Vertical deflection of WTC 2 Floor 82 for Case Di. 211
Figure 7–27. Vertical deflection of WTC 2 Floor 83 for Case Di. 212
Figure 7–28. Isolated exterior wall segments from WTC 1 and WTC 2. 214
Figure 7–29. Boundary conditions applied on the isolated exterior wall segment. 214
Figure 7–30. Locations of WTC 1 disconnections and pull-in forces over five floors for Case B. 216
Figure 7–31. Inward displacement of the WTC 1 south wall at 80 min of the Case B temperatures with floor disconnections and 6 kip pull-in forces over five floors. 217
Figure 7–32. Inward displacement of the WTC 1 south wall at 100 min of the Case B temperatures with floor disconnections and 6 kip pull-in forces over five floors. 218
Figure 7–33. Out-of-plane displacements of the WTC 2 east wall calculated with 0.5 kip pull-in force with uniform magnitude distribution at 32 min. 220
Figure 7–34. Out-of-plane displacements of the WTC 2 east wall calculated with 5.0 kip pull-in force with uniform magnitude distribution at 18 min. 221
Figure 7–35. Out-of-plane displacements of east wall calculated with pull-in force of 1.0 kip on the south half and 4.0 kip on the north half of the WTC 2 east wall. 222
Figure 7–36. Out-of-plane displacements of east wall of WTC 2 calculated with pull-in forces of 1.5 kip on the south half and 5.0 kip on the north half. 223

Figure 8–1. Displaced shape of WTC 1 and WTC 2 at the end of gravity load analysis. 232
Figure 8–2. Office area and core floors and core beams. 233
Figure 8–3. Hat truss with labeled outriggers. 233
Figure 8–4. Vertical displacement at Floor 99 of WTC 1. Total displacements are shown before aircraft impact and incremental displacements, with total displacements in parentheses, are shown after impact. 238
Figure 8–5. Vertical displacement of WTC 1 east and north exterior walls before aircraft impact. 238
Figure 8–6. Vertical displacement of east and north exterior walls of WTC 1 after aircraft impact for Case B. 239
Figure 8–7. Vertical displacement of the east and north side of the WTC 1 core before aircraft impact. 239
Figure 8–8. Vertical displacement of the east and north side of the WTC 1 core after aircraft impact for Case B. 240
Figure 8–9. Maximum demand-to-capacity ratio for axial force in core columns between Floor 93 and Floor 99 of WTC 1 before aircraft impact. 241
Figure 8–10. Maximum demand-to-capacity ratio for axial force in core columns between Floor 93 and Floor 99 of WTC 1 after aircraft impact for Case B. 241
Figure 8–11. Out-of-plane displacement of south wall of WTC 1 at 80 min for Case B. 243
Figure 8–12. Out-of-plane displacement of south wall of WTC 1 at 100 min for Case B conditions with 5 kip pull-in forces. 244

Figure 8–13. Time history of maximum out-of-plane displacement of WTC 1 south wall for Case B with 5 kip pull-in forces. 244

Figure 8–14. Distribution of axial force in exterior columns at Floor 98 of WTC 1 south wall for Case B with 5 kip pull-in forces. 245

Figure 8–15. Distribution of axial force in exterior columns at Floor 98 of WTC 1 east wall for Case B with 5 kip pull-in forces. 246

Figure 8–16. Vertical displacement of west and south exterior walls of WTC 1 at 80 min for Case B. 246

Figure 8–17. Vertical displacement of west and south exterior walls of WTC 1 at 100 min for Case B. 247

Figure 8–18. Change in vertical displacement at Floor 99 of WTC 1 from the state before impact to 100 min for Case B. 247

Figure 8–19. Maximum elastic-plus-plastic-plus-creep strain for columns between Floor 93 and Floor 99 of WTC 1 at 10 min for Case B (strain values are in percent). 248

Figure 8–20. Maximum elastic-plus-plastic-plus-creep strain for columns between Floor 93 and Floor 99 of WTC 1 at 40 min for Case B (strain values are in percent). 249

Figure 8–21. Maximum elastic-plus-plastic-plus-creep strain for columns between Floor 93 and Floor 99 of WTC 1 at 100 min for Case B with 5 kip pull-in forces (strain value are in percent). 249

Figure 8–22. Maximum demand-to-capacity ratio for axial force in core columns between Floor 93 and Floor 99 of WTC 1 at 80 min for Case B conditions. 250

Figure 8–23. Maximum demand-to-capacity ratio for axial force in core columns between Floor 93 and Floor 99 of WTC 1 at 100 min for Case B with 5 kip pull-in forces. 251

Figure 8–24. Tension demand-to-capacity ratio for core column splices at WTC 1 Floor 106 at 100 min for Case B with 5 kip pull-in forces. 252

Figure 8–25. Location and label of outriggers and supporting columns for WTC 1. 253

Figure 8–26. Vertical displacement before impact of WTC 2 exterior wall for Case D. 255

Figure 8–27. Vertical displacement after impact of WTC 2 exterior wall for Case D. 256

Figure 8–28. Vertical displacement before impact of WTC 2 core for Case D. 256

Figure 8–29. Vertical displacement after impact of WTC 2 core for Case D. 257

Figure 8–30. Lateral displacements after impact above WTC 2 Floor 86 in the x-direction (north-south) for Case D. 257

Figure 8–31. Lateral displacements after impact above WTC 2 Floor 86 in the y-direction (east-west) for Case D. 258

Figure 8–32. Core column loads (kip) before impact at WTC 2 Floor 83 for Case D (compression is positive). 259

Figure 8–33. Core column loads (kip) after impact at WTC 2 Floor 83 for Case D (compression is positive). 260

Figure 8–34. Vertical displacement of exterior wall of WTC 2 at 20 min for Case D. 262

Figure 8–35. Vertical displacement at Floor 83 of WTC 2 at 20 min for Case D (note the tilt toward east and south) ... 262
Figure 8–36. Vertical displacement of exterior wall of WTC 2 at 43 min for Case D. ... 263
Figure 8–37. Vertical displacement at Floor 83 of WTC 2 at 43 min for Case D (note the tilt toward east and south) ... 263
Figure 8–38. Out-of-plane displacement of the east wall of WTC 2 at 20 min for Case D. ... 264
Figure 8–39. Out-of-plane displacement of the east wall of WTC 2 at 43 min for Case D. ... 266
Figure 8–40. Variation of maximum out-of-plane displacement on the east wall of WTC 2 over the time for Case D. ... 266
Figure 8–41. Vertical displacement of core of WTC 2 at 20 min for Case D. ... 267
Figure 8–42. Vertical displacement of core of WTC 2 at 43 min for Case D. ... 267
Figure 8–43. Core column loads (kip) at Floor 83 of WTC 2 at 20 min for Case D (compression is positive) ... 268
Figure 8–44. Core column loads (kip) at Floor 83 of WTC 2 at 43 min for Case D (compression is positive) ... 268
Figure 8–45. Total displacements of WTC 2 above Floor 86 at 43 min of Case D (deformed shape magnified 20 times). Note the tilt toward east and south. ... 269
Figure 8–46. Axial force in the east wall columns at Floor 83 of WTC 2 for Case D (compression is positive). ... 269
Figure 8–47. Axial force in the west wall columns at Floor 83 of WTC 2 for Case D (compression is positive). ... 270
Figure 8–48. Axial force in the south wall columns at Floor 83 of WTC 2 for Case D (compression is positive). ... 270
Figure 8–49. Axial force in the north wall columns at Floor 83 of WTC 2 for Case D (compression is positive). ... 271
Figure 8–50. Axial force in Floor 83 columns of WTC 2 before impact for Case D (compression is positive) ... 271
Figure 8–51. Axial force in Floor 83 columns of WTC 2 at 43 min for Case D (compression is positive) ... 272
Figure 8–52. Maximum elastic-plus-plastic-plus-creep strains at 20 min for columns between Floor 78 and Floor 83 of WTC 2 for Case D (strain values are in percent). ... 272
Figure 8–53. Maximum elastic-plus-plastic-plus-creep strains at 43 min for columns between Floor 78 and Floor 83 of WTC 2 for Case D (strain values are in percent). ... 273
Figure 8–54. Axial force in core columns (kip) at WTC 2 Floor 105 (at hat-truss level) before impact for Case D (compression is positive). ... 274
Figure 8–55. Axial force in core columns (kip) at WTC 2 Floor 105 (at hat-truss level) after impact for Case D (compression is positive). ... 275
Figure 8–56. Axial force in core columns (kip) at Floor 105 (at hat-truss level) of WTC 2 for Case D conditions (compression is positive). ... 276
Figure 8–57. State of core column splices at Floor 105 of WTC 2. ... 277

Figure 8–58. Location and IDs of outriggers and supporting columns 278

Figure 8–59. Temperatures of two adjacent trusses (left) and two adjacent perimeter columns (right) exposed to simulated fires in WTC 1. Data plotted in blue are for structural steel components with fireproofing; data in red are for steel components without fireproofing (from NIST NCSTAR 1-5). 281

Figure 9–1. Critical analysis inter-dependencies 289

Figure 9–2. Full analysis tree for influential parameter effects. 291

Figure 9–3. Pruned analysis tree for influential parameter effects. 292

Figure 9–4. Data used for validating probable collapse sequences. 295

Figure 9–5. Variability in global reserve capacity using model predictions and observables for sequential analyses with imperfect information. 296

Figure 9–6. Vertical displacement contour of the detailed truss model under thermal loading. 297

Figure 9–7. Combined flexural and catenary action in the floor system. 297

Figure 9–8. WTC 1 probable collapse sequence. 299

Figure 9–9. Vertical displacement of Floors of WTC 1 for Case B′ at 100 min. 302

Figure 9–10. Loss of vertical supports observed in Floor 97 and Floor 98 of WTC 1 for Case B′ (1x displacement magnification). 302

Figure 9–11. Inward bowing of the WTC 1 south wall of WTC 1 at 10:23 a.m. 303

Figure 9–12. Inward bowing of south wall of WTC 1 global model with creep at 100 min for Case B with 5 kip pull-in forces (5x displacement magnification). 304

Figure 9–13. Expulsion of smoke and debris at WTC 1 Floor 98 on the east, north, and west faces. 305

Figure 9–14. WTC 2 probable collapse sequence. 307

Figure 9–15. Vertical displacements of Floors 79 through Floor 88 of WTC 2 at 40 min (Case D). 311

Figure 9–16. Floor sagging observed on the east wall of WTC 2 at different stages. 312

Figure 9–17. Out-of-plane displacements on the east wall of WTC 2 (Case D). 313

Figure 9–18. Out-of-plane displacement estimates of the east wall of WTC 2 from photographs. 314

Figure 9–19. Variation of maximum out-of-plane displacement on the east wall of WTC 2 (Case D). 315

Figure 9–20. Total column loads at Floor 83 of the east wall of WTC 2 at different stages (Case D). 315

Figure 9–21. Maximum elastic + plastic + creep strains for columns between Floor 78 and Floor 83 of WTC 2 at different stages (Case D) (strain values are in percent). 316

Figure 9–22. Inward bowing of the east wall of WTC 2 when buckled at 43 min for Case D (4x displacement magnification). 317

Figure 9–23. Inward bending of exterior columns of the west wall of WTC 2 just before collapse. 318

Figure 9–24. Total displacements of WTC 2 above Floor 86 at 43 min for Case D. Note tilt toward east and south (20x displacement magnification). 319

LIST OF TABLES

Table P–1. Federal building and fire safety investigation of the WTC disaster.**Error! Bookmark not defined.**

Table P–2. Public meetings and briefings of the WTC Investigation. ....**Error! Bookmark not defined.**

Table 2–1. Average SFRM thickness from six measurements taken in 1994 on each of 16 random floor trusses on floors 23 and 24 of WTC 1 23

Table 2–2. Summary of specified, in-place and thermally equivalent thickness of SFRM 29

Table 2–3. Measured thermal conductivity as a function of temperature. 31

Table 2–4. Summary of physical characteristics of BLAZE-SHIELD DC/F specimens tested at NIST 35

Table 3–1. Results of ASTM E119 Standard Fire Tests. 49

Table 4–1. Steel types used in WTC 1 and WTC 2. 61

Table 4–2. Interior seat capacity against vertical force. 74

Table 4–3. Exterior seat capacity against vertical force. 75

Table 4–4. Interior seat capacity against horizontal tensile force. 75

Table 4–5. Exterior seat capacity against horizontal tensile force. 76

Table 4–6. Knuckle shear capacity reduction for elevated temperatures. 84

Table 4-7. Comparison of SAP2000 and ANSYS results for gravity load case. 92

Table 4-8. Comparison of SAP2000 and ANSYS Modal Analysis Results. 92

Table 4-9. Types of break elements. 95

Table 4-10. Column section properties. 99

Table 4-11. Spandrel Splice Details. 99

Table 4-12. Column Splice Details. 99

Table 4-13. Prefabricated panel validation results. 107

Table 4-14. Thermal loading conditions used in the exterior wall model. 111

Table 4-15. Analysis cases for exterior wall section model. 113

Table 5–1. WTC 1 Case A core column damage. 124

Table 5–2. WTC 1 Case B core column damage. 125

Table 5–3. WTC 2 Case C core column damage. 125

Table 5–4. WTC 2 Case D core column damage. 126

Table 6–1. WTC1 Timeline of Observed Structural and Fire Events. 154
Table 6–2. WTC2 Timeline of Observed Structural and Fire Events 167
Table 6–3. Possible floor damage observed in photos of WTC 2 windows. 168

Table 7–1. Maximum vertical displacement of WTC 1 floors for Case Ai. 199
Table 7–2. Maximum vertical displacement of WTC 1 floors for Case Bi. 199
Table 7–3. Maximum vertical displacement of WTC 2 floors for Case Ci. 203
Table 7–4. Maximum vertical displacement of WTC 2 floors for Case Di. 207

Table 8–1. Total column loads at Floor 98 of WTC 1 for Case B conditions. 240
Table 8–2. Total column loads at Floor 105 of WTC 1 for Case B conditions. 240
Table 8–3. Demand-to-capacity ratio for axial force in outriggers of WTC 1 for Case B. 251
Table 8–4. Total column loads at WTC 2 Floor 83 for Case D (Compression is positive). 256
Table 8–5. Total column loads at WTC 2 Floor 105 for Case D (Compression is positive). 257
Table 8–6. Change in total column loads before and after aircraft impact. (Loads After Impact) – (Loads Before Impact) (Compression is positive). 262
Table 8–7. Change in total column loads between 40 min and 43 min. (Loads at 43 min) – (Loads at 40 min) (Compression is positive). 262
Table 8–8. Demand-to-capacity ratios for outriggers of WTC 2 for Case D conditions (outrigger IDs are shown in Fig. 8–3). 276

Table 9–1. Aircraft impact analysis parameters. 290
Table 9–2. Fire dynamics analysis parameters. 291
Table 9–3. Thermal analysis parameters. 291
Table 9–4. Structural response analysis parameters. 292
Table 9–5. Observations for WTC 1. 296
Table 9–6. Total column loads at Floor 98 and Floor 105 of WTC 1 for Case B. 299
Table 9–7. Key observations on WTC 2. 304
Table 9–8. Total column loads at Floor 83 of WTC 2 for Case D. Compression is positive. 308
Table 9–9. Total column loads at Floor 105 of WTC 2 for Case D. Compression is positive. 308
Table 9–10. Change in total column loads when the east wall of WTC 2 buckles (Case D, compression is positive). 317

LIST OF ACRONYMS AND ABBREVIATIONS

Acronyms

ASTM	ASTM International
BPS	Building Performance Study
FEMA	Federal Emergency Management Agency
MIG	Metal Inert Gas (welding)
NIST	National Institute of Standards and Technology
PANYNJ	Port Authority of New York and New Jersey
SEAoNY	Structural Engineers Association of New York
USC	United States Code
ULI	Underwriters Laboratories Inc.
WTC	World Trade Center
WTC 1	World Trade Center 1 (North Tower)
WTC 2	World Trade Center 2 (South Tower)
WTC 7	World Trade Center 7

Abbreviations

°C	degrees Celsius
°F	degrees Fahrenheit
ft	feet
in.	inch
L	liter
m	meter
μm	micrometer
min	minute
s	second

This page intentionally left blank.

PREFACE

Genesis of This Investigation

Immediately following the terrorist attack on the World Trade Center (WTC) on September 11, 2001, the Federal Emergency Management Agency (FEMA) and the American Society of Civil Engineers began planning a building performance study of the disaster. The week of October 7, as soon as the rescue and search efforts ceased, the Building Performance Study Team went to the site and began its assessment. This was to be a brief effort, as the study team consisted of experts who largely volunteered their time away from their other professional commitments. The Building Performance Study Team issued its report in May 2002, fulfilling its goal "to determine probable failure mechanisms and to identify areas of future investigation that could lead to practical measures for improving the damage resistance of buildings against such unforeseen events."

On August 21, 2002, with funding from the U.S. Congress through FEMA, the National Institute of Standards and Technology (NIST) announced its building and fire safety investigation of the WTC disaster. On October 1, 2002, the National Construction Safety Team Act (Public Law 107-231), was signed into law. The NIST WTC Investigation was conducted under the authority of the National Construction Safety Team Act.

The goals of the investigation of the WTC disaster were:

- To investigate the building construction, the materials used, and the technical conditions that contributed to the outcome of the WTC disaster.
- To serve as the basis for:
  - Improvements in the way buildings are designed, constructed, maintained, and used;
  - Improved tools and guidance for industry and safety officials;
  - Recommended revisions to current codes, standards, and practices; and
  - Improved public safety.

The specific objectives were:

1. Determine why and how WTC 1 and WTC 2 collapsed following the initial impacts of the aircraft and why and how WTC 7 collapsed;
2. Determine why the injuries and fatalities were so high or low depending on location, including all technical aspects of fire protection, occupant behavior, evacuation, and emergency response;
3. Determine what procedures and practices were used in the design, construction, operation, and maintenance of WTC 1, 2, and 7; and
4. Identify, as specifically as possible, areas in current building and fire codes, standards, and practices that warrant revision.

NIST is a nonregulatory agency of the U.S. Department of Commerce's Technology Administration. The purpose of NIST investigations is to improve the safety and structural integrity of buildings in the United States, and the focus is on fact finding. NIST investigative teams are authorized to assess building performance and emergency response and evacuation procedures in the wake of any building failure that has resulted in substantial loss of life or that posed significant potential of substantial loss of life. NIST does not have the statutory authority to make findings of fault nor negligence by individuals or organizations. Further, no part of any report resulting from a NIST investigation into a building failure or from an investigation under the National Construction Safety Team Act may be used in any suit or action for damages arising out of any matter mentioned in such report (15 USC 281a, as amended by Public Law 107-231).

Organization of the Investigation

The National Construction Safety Team for this Investigation, appointed by the then NIST Director, Dr. Arden L. Bement, Jr., was led by Dr. S. Shyam Sunder. Dr. William L. Grosshandler served as Associate Lead Investigator, Mr. Stephen A. Cauffman served as Program Manager for Administration, and Mr. Harold E. Nelson served on the team as a private sector expert. The Investigation included eight interdependent projects whose leaders comprised the remainder of the team. A detailed description of each of these eight projects is available at http://wtc.nist.gov. The purpose of each project is summarized in Table P–1, and the key interdependencies among the projects are illustrated in Fig. P–1.

Table P–1. Federal building and fire safety investigation of the WTC disaster.

Technical Area and Project Leader	Project Purpose
Analysis of Building and Fire Codes and Practices; Project Leaders: Dr. H. S. Lew and Mr. Richard W. Bukowski	Document and analyze the code provisions, procedures, and practices used in the design, construction, operation, and maintenance of the structural, passive fire protection, and emergency access and evacuation systems of WTC 1, 2, and 7.
Baseline Structural Performance and Aircraft Impact Damage Analysis; Project Leader: Dr. Fahim H. Sadek	Analyze the baseline performance of WTC 1 and WTC 2 under design, service, and abnormal loads, and aircraft impact damage on the structural, fire protection, and egress systems.
Mechanical and Metallurgical Analysis of Structural Steel; Project Leader: Dr. Frank W. Gayle	Determine and analyze the mechanical and metallurgical properties and quality of steel, weldments, and connections from steel recovered from WTC 1, 2, and 7.
Investigation of Active Fire Protection Systems; Project Leader: Dr. David D. Evans; Dr. William Grosshandler	Investigate the performance of the active fire protection systems in WTC 1, 2, and 7 and their role in fire control, emergency response, and fate of occupants and responders.
Reconstruction of Thermal and Tenability Environment; Project Leader: Dr. Richard G. Gann	Reconstruct the time-evolving temperature, thermal environment, and smoke movement in WTC 1, 2, and 7 for use in evaluating the structural performance of the buildings and behavior and fate of occupants and responders.
Structural Fire Response and Collapse Analysis; Project Leaders: Dr. John L. Gross and Dr. Therese P. McAllister	Analyze the response of the WTC towers to fires with and without aircraft damage, the response of WTC 7 in fires, the performance of composite steel-trussed floor systems, and determine the most probable structural collapse sequence for WTC 1, 2, and 7.
Occupant Behavior, Egress, and Emergency Communications; Project Leader: Mr. Jason D. Averill	Analyze the behavior and fate of occupants and responders, both those who survived and those who did not, and the performance of the evacuation system.
Emergency Response Technologies and Guidelines; Project Leader: Mr. J. Randall Lawson	Document the activities of the emergency responders from the time of the terrorist attacks on WTC 1 and WTC 2 until the collapse of WTC 7, including practices followed and technologies used.

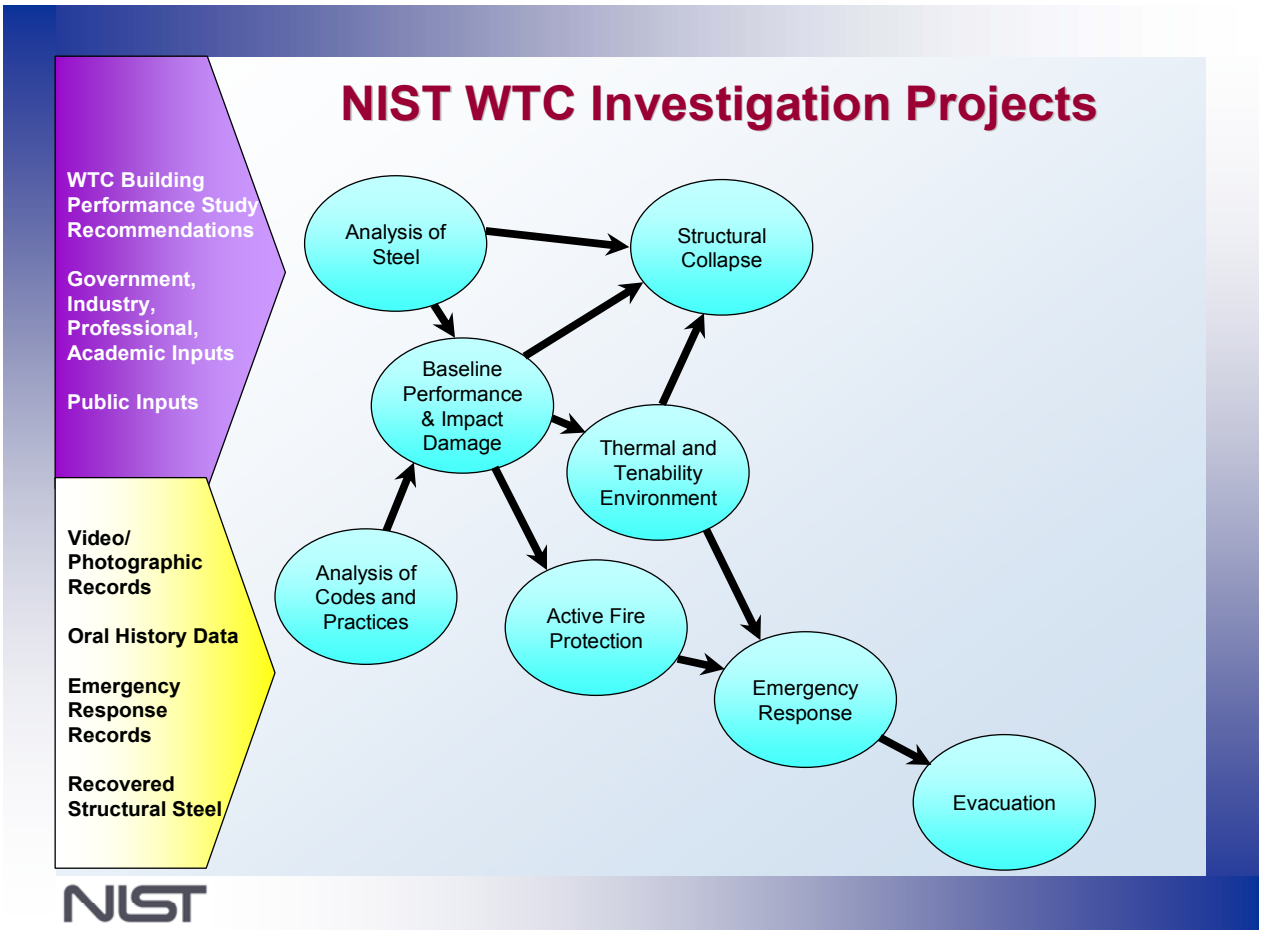

Figure P–1. The eight projects in the federal building and fire safety investigation of the WTC disaster.

National Construction Safety Team Advisory Committee

The NIST Director also established an advisory committee as mandated under the National Construction Safety Team Act. The initial members of the committee were appointed following a public solicitation. These were:

- Paul Fitzgerald, Executive Vice President (retired) FM Global, National Construction Safety Team Advisory Committee Chair
- John Barsom, President, Barsom Consulting, Ltd.
- John Bryan, Professor Emeritus, University of Maryland
- David Collins, President, The Preview Group, Inc.
- Glenn Corbett, Professor, John Jay College of Criminal Justice
- Philip DiNenno, President, Hughes Associates, Inc.

- Robert Hanson, Professor Emeritus, University of Michigan
- Charles Thornton, Co-Chairman and Managing Principal, The Thornton-Tomasetti Group, Inc.
- Kathleen Tierney, Director, Natural Hazards Research and Applications Information Center, University of Colorado at Boulder
- Forman Williams, Director, Center for Energy Research, University of California at San Diego

This National Construction Safety Team Advisory Committee provided technical advice during the Investigation and commentary on drafts of the Investigation reports prior to their public release. NIST has benefited from the work of many people in the preparation of these reports, including the National Construction Safety Team Advisory Committee. The content of the reports and recommendations, however, are solely the responsibility of NIST.

Public Outreach

During the course of this Investigation, NIST held public briefings and meetings (listed in Table P–2) to solicit input from the public, present preliminary findings, and obtain comments on the direction and progress of the Investigation from the public and the Advisory Committee.

NIST maintained a publicly accessible Web site during this Investigation at http://wtc.nist.gov. The site contained extensive information on the background and progress of the Investigation.

NIST's WTC Public-Private Response Plan

The collapse of the WTC buildings has led to broad reexamination of how tall buildings are designed, constructed, maintained, and used, especially with regard to major events such as fires, natural disasters, and terrorist attacks. Reflecting the enhanced interest in effecting necessary change, NIST, with support from Congress and the Administration, has put in place a program, the goal of which is to develop and implement the standards, technology, and practices needed for cost-effective improvements to the safety and security of buildings and building occupants, including evacuation, emergency response procedures, and threat mitigation.

The strategy to meet this goal is a three-part NIST-led public-private response program that includes:

- A federal building and fire safety investigation to study the most probable factors that contributed to post-aircraft impact collapse of the WTC towers and the 47-story WTC 7 building, and the associated evacuation and emergency response experience.
- A research and development (R&D) program to (a) facilitate the implementation of recommendations resulting from the WTC Investigation, and (b) provide the technical basis for cost-effective improvements to national building and fire codes, standards, and practices that enhance the safety of buildings, their occupants, and emergency responders.

Table P–2. Public meetings and briefings of the WTC Investigation.

Date	Location	Principal Agenda
June 24, 2002	New York City, NY	Public meeting: Public comments on the *Draft Plan* for the pending WTC Investigation.
August 21, 2002	Gaithersburg, MD	Media briefing announcing the formal start of the Investigation.
December 9, 2002	Washington, DC	Media briefing on release of the *Public Update* and NIST request for photographs and videos.
April 8, 2003	New York City, NY	Joint public forum with Columbia University on first-person interviews.
April 29–30, 2003	Gaithersburg, MD	NCST Advisory Committee meeting on plan for and progress on WTC Investigation with a public comment session.
May 7, 2003	New York City, NY	Media briefing on release of *May 2003 Progress Report.*
August 26–27, 2003	Gaithersburg, MD	NCST Advisory Committee meeting on status of the WTC investigation with a public comment session.
September 17, 2003	New York City, NY	Media and public briefing on initiation of first-person data collection projects.
December 2–3, 2003	Gaithersburg, MD	NCST Advisory Committee meeting on status and initial results and release of the *Public Update* with a public comment session.
February 12, 2004	New York City, NY	Public meeting on progress and preliminary findings with public comments on issues to be considered in formulating final recommendations.
June 18, 2004	New York City, NY	Media/public briefing on release of *June 2004 Progress Report.*
June 22–23, 2004	Gaithersburg, MD	NCST Advisory Committee meeting on the status of and preliminary findings from the WTC Investigation with a public comment session.
August 24, 2004	Northbrook, IL	Public viewing of standard fire resistance test of WTC floor system at Underwriters Laboratories, Inc.
October 19–20, 2004	Gaithersburg, MD	NCST Advisory Committee meeting on status and near complete set of preliminary findings with a public comment session.
November 22, 2004	Gaithersburg, MD	NCST Advisory Committee discussion on draft annual report to Congress, a public comment session, and a closed session to discuss pre-draft recommendations for WTC Investigation.
April 5, 2005	New York City, NY	Media and public briefing on release of the probable collapse sequence for the WTC towers and draft reports for the projects on codes and practices, evacuation, and emergency response.
June 23, 2005	New York City, NY	Media and public briefing on release of all draft reports for the WTC towers and draft recommendations for public comment.
September 12–13, 2005	Gaithersburg, MD	NCST Advisory Committee meeting on disposition of public comments and update to draft reports for the WTC towers.
September 13–15, 2005	Gaithersburg, MD	WTC Technical Conference for stakeholders and technical community for dissemination of findings and recommendations and opportunity for public to make technical comments.

- A dissemination and technical assistance program (DTAP) to (a) engage leaders of the construction and building community in ensuring timely adoption and widespread use of proposed changes to practices, standards, and codes resulting from the WTC Investigation and the R&D program, and (b) provide practical guidance and tools to better prepare facility owners, contractors, architects, engineers, emergency responders, and regulatory authorities to respond to future disasters.

The desired outcomes are to make buildings, occupants, and first responders safer in future disaster events.

National Construction Safety Team Reports on the WTC Investigation

A final report on the collapse of the WTC towers is being issued as NIST NCSTAR 1. A companion report on the collapse of WTC 7 is being issued as NIST NCSTAR 1A. The present report is one of a set that provides more detailed documentation of the Investigation findings and the means by which these technical results were achieved. As such, it is part of the archival record of this Investigation. The titles of the full set of Investigation publications are:

NIST (National Institute of Standards and Technology). 2005. *Federal Building and Fire Safety Investigation of the World Trade Center Disaster: Final Report on the Collapse of the World Trade Center Towers.* NIST NCSTAR 1. Gaithersburg, MD, September.

NIST (National Institute of Standards and Technology). 2008. *Federal Building and Fire Safety Investigation of the World Trade Center Disaster: Final Report on the Collapse of World Trade Center 7.* NIST NCSTAR 1A. Gaithersburg, MD, November.

Lew, H. S., R. W. Bukowski, and N. J. Carino. 2005. *Federal Building and Fire Safety Investigation of the World Trade Center Disaster: Design, Construction, and Maintenance of Structural and Life Safety Systems.* NIST NCSTAR 1-1. National Institute of Standards and Technology. Gaithersburg, MD, September.

Fanella, D. A., A. T. Derecho, and S. K. Ghosh. 2005. *Federal Building and Fire Safety Investigation of the World Trade Center Disaster: Design and Construction of Structural Systems.* NIST NCSTAR 1-1A. National Institute of Standards and Technology. Gaithersburg, MD, September.

Ghosh, S. K., and X. Liang. 2005. *Federal Building and Fire Safety Investigation of the World Trade Center Disaster: Comparison of Building Code Structural Requirements.* NIST NCSTAR 1-1B. National Institute of Standards and Technology. Gaithersburg, MD, September.

Fanella, D. A., A. T. Derecho, and S. K. Ghosh. 2005. *Federal Building and Fire Safety Investigation of the World Trade Center Disaster: Maintenance and Modifications to Structural Systems.* NIST NCSTAR 1-1C. National Institute of Standards and Technology. Gaithersburg, MD, September.

Grill, R. A., and D. A. Johnson. 2005. *Federal Building and Fire Safety Investigation of the World Trade Center Disaster: Fire Protection and Life Safety Provisions Applied to the Design and Construction of World Trade Center 1, 2, and 7 and Post-Construction Provisions Applied after Occupancy*. NIST NCSTAR 1-1D. National Institute of Standards and Technology. Gaithersburg, MD, September.

Razza, J. C., and R. A. Grill. 2005. *Federal Building and Fire Safety Investigation of the World Trade Center Disaster: Comparison of Codes, Standards, and Practices in Use at the Time of the Design and Construction of World Trade Center 1, 2, and 7.* NIST NCSTAR 1-1E. National Institute of Standards and Technology. Gaithersburg, MD, September.

Grill, R. A., D. A. Johnson, and D. A. Fanella. 2005. *Federal Building and Fire Safety Investigation of the World Trade Center Disaster: Comparison of the 1968 and Current (2003) New*

York City Building Code Provisions. NIST NCSTAR 1-1F. National Institute of Standards and Technology. Gaithersburg, MD, September.

Grill, R. A., and D. A. Johnson. 2005. *Federal Building and Fire Safety Investigation of the World Trade Center Disaster: Amendments to the Fire Protection and Life Safety Provisions of the New York City Building Code by Local Laws Adopted While World Trade Center 1, 2, and 7 Were in Use*. NIST NCSTAR 1-1G. National Institute of Standards and Technology. Gaithersburg, MD, September.

Grill, R. A., and D. A. Johnson. 2005. *Federal Building and Fire Safety Investigation of the World Trade Center Disaster: Post-Construction Modifications to Fire Protection and Life Safety Systems of World Trade Center 1 and 2*. NIST NCSTAR 1-1H. National Institute of Standards and Technology. Gaithersburg, MD, September.

Grill, R. A., D. A. Johnson, and D. A. Fanella. 2005. *Federal Building and Fire Safety Investigation of the World Trade Center Disaster: Post-Construction Modifications to Fire Protection, Life Safety, and Structural Systems of World Trade Center 7*. NIST NCSTAR 1-1I. National Institute of Standards and Technology. Gaithersburg, MD, September.

Grill, R. A., and D. A. Johnson. 2005. *Federal Building and Fire Safety Investigation of the World Trade Center Disaster: Design, Installation, and Operation of Fuel System for Emergency Power in World Trade Center 7*. NIST NCSTAR 1-1J. National Institute of Standards and Technology. Gaithersburg, MD, September.

Sadek, F. 2005. *Federal Building and Fire Safety Investigation of the World Trade Center Disaster: Baseline Structural Performance and Aircraft Impact Damage Analysis of the World Trade Center Towers.* NIST NCSTAR 1-2. National Institute of Standards and Technology. Gaithersburg, MD, September.

Faschan, W. J., and R. B. Garlock. 2005. *Federal Building and Fire Safety Investigation of the World Trade Center Disaster: Reference Structural Models and Baseline Performance Analysis of the World Trade Center Towers.* NIST NCSTAR 1-2A. National Institute of Standards and Technology. Gaithersburg, MD, September.

Kirkpatrick, S. W., R. T. Bocchieri, F. Sadek, R. A. MacNeill, S. Holmes, B. D. Peterson, R. W. Cilke, C. Navarro. 2005. *Federal Building and Fire Safety Investigation of the World Trade Center Disaster: Analysis of Aircraft Impacts into the World Trade Center Towers*, NIST NCSTAR 1-2B. National Institute of Standards and Technology. Gaithersburg, MD, September.

Gayle, F. W., R. J. Fields, W. E. Luecke, S. W. Banovic, T. Foecke, C. N. McCowan, T. A. Siewert, and J. D. McColskey. 2005. *Federal Building and Fire Safety Investigation of the World Trade Center Disaster: Mechanical and Metallurgical Analysis of Structural Steel.* NIST NCSTAR 1-3. National Institute of Standards and Technology. Gaithersburg, MD, September.

Luecke, W. E., T. A. Siewert, and F. W. Gayle. 2005. *Federal Building and Fire Safety Investigation of the World Trade Center Disaster: Contemporaneous Structural Steel Specifications.* NIST Special Publication 1-3A. National Institute of Standards and Technology. Gaithersburg, MD, September.

Banovic, S. W. 2005. *Federal Building and Fire Safety Investigation of the World Trade Center Disaster: Steel Inventory and Identification.* NIST NCSTAR 1-3B. National Institute of Standards and Technology. Gaithersburg, MD, September.

Banovic, S. W., and T. Foecke. 2005. *Federal Building and Fire Safety Investigation of the World Trade Center Disaster: Damage and Failure Modes of Structural Steel Components.* NIST NCSTAR 1-3C. National Institute of Standards and Technology. Gaithersburg, MD, September.

Luecke, W. E., J. D. McColskey, C. N. McCowan, S. W. Banovic, R. J. Fields, T. Foecke, T. A. Siewert, and F. W. Gayle. 2005. *Federal Building and Fire Safety Investigation of the World Trade Center Disaster: Mechanical Properties of Structural Steels.* NIST NCSTAR 1-3D. National Institute of Standards and Technology. Gaithersburg, MD, September.

Banovic, S. W., C. N. McCowan, and W. E. Luecke. 2005. *Federal Building and Fire Safety Investigation of the World Trade Center Disaster: Physical Properties of Structural Steels.* NIST NCSTAR 1-3E. National Institute of Standards and Technology. Gaithersburg, MD, September.

Evans, D. D., R. D. Peacock, E. D. Kuligowski, W. S. Dols, and W. L. Grosshandler. 2005. *Federal Building and Fire Safety Investigation of the World Trade Center Disaster: Active Fire Protection Systems.* NIST NCSTAR 1-4. National Institute of Standards and Technology. Gaithersburg, MD, September.

Kuligowski, E. D., D. D. Evans, and R. D. Peacock. 2005. *Federal Building and Fire Safety Investigation of the World Trade Center Disaster: Post-Construction Fires Prior to September 11, 2001.* NIST NCSTAR 1-4A. National Institute of Standards and Technology. Gaithersburg, MD, September.

Hopkins, M., J. Schoenrock, and E. Budnick. 2005. *Federal Building and Fire Safety Investigation of the World Trade Center Disaster: Fire Suppression Systems.* NIST NCSTAR 1-4B. National Institute of Standards and Technology. Gaithersburg, MD, September.

Keough, R. J., and R. A. Grill. 2005. *Federal Building and Fire Safety Investigation of the World Trade Center Disaster: Fire Alarm Systems.* NIST NCSTAR 1-4C. National Institute of Standards and Technology. Gaithersburg, MD, September.

Ferreira, M. J., and S. M. Strege. 2005. *Federal Building and Fire Safety Investigation of the World Trade Center Disaster: Smoke Management Systems.* NIST NCSTAR 1-4D. National Institute of Standards and Technology. Gaithersburg, MD, September.

Gann, R. G., A. Hamins, K. B. McGrattan, G. W. Mulholland, H. E. Nelson, T. J. Ohlemiller, W. M. Pitts, and K. R. Prasad. 2005. *Federal Building and Fire Safety Investigation of the World Trade Center Disaster: Reconstruction of the Fires in the World Trade Center Towers.* NIST NCSTAR 1-5. National Institute of Standards and Technology. Gaithersburg, MD, September.

Pitts, W. M., K. M. Butler, and V. Junker. 2005. *Federal Building and Fire Safety Investigation of the World Trade Center Disaster: Visual Evidence, Damage Estimates, and Timeline Analysis.* NIST NCSTAR 1-5A. National Institute of Standards and Technology. Gaithersburg, MD, September.

Hamins, A., A. Maranghides, K. B. McGrattan, E. Johnsson, T. J. Ohlemiller, M. Donnelly, J. Yang, G. Mulholland, K. R. Prasad, S. Kukuck, R. Anleitner and T. McAllister. 2005. *Federal Building and Fire Safety Investigation of the World Trade Center Disaster: Experiments and Modeling of Structural Steel Elements Exposed to Fire.* NIST NCSTAR 1-5B. National Institute of Standards and Technology. Gaithersburg, MD, September.

Ohlemiller, T. J., G. W. Mulholland, A. Maranghides, J. J. Filliben, and R. G. Gann. 2005. *Federal Building and Fire Safety Investigation of the World Trade Center Disaster: Fire Tests of Single Office Workstations.* NIST NCSTAR 1-5C. National Institute of Standards and Technology. Gaithersburg, MD, September.

Gann, R. G., M. A. Riley, J. M. Repp, A. S. Whittaker, A. M. Reinhorn, and P. A. Hough. 2005. *Federal Building and Fire Safety Investigation of the World Trade Center Disaster: Reaction of Ceiling Tile Systems to Shocks.* NIST NCSTAR 1-5D. National Institute of Standards and Technology. Gaithersburg, MD, September.

Hamins, A., A. Maranghides, K. B. McGrattan, T. J. Ohlemiller, and R. Anleitner. 2005. *Federal Building and Fire Safety Investigation of the World Trade Center Disaster: Experiments and Modeling of Multiple Workstations Burning in a Compartment.* NIST NCSTAR 1-5E. National Institute of Standards and Technology. Gaithersburg, MD, September.

McGrattan, K. B., C. Bouldin, and G. Forney. 2005. *Federal Building and Fire Safety Investigation of the World Trade Center Disaster: Computer Simulation of the Fires in the World Trade Center Towers.* NIST NCSTAR 1-5F. National Institute of Standards and Technology. Gaithersburg, MD, September.

Prasad, K. R., and H. R. Baum. 2005. *Federal Building and Fire Safety Investigation of the World Trade Center Disaster: Fire Structure Interface and Thermal Response of the World Trade Center Towers.* NIST NCSTAR 1-5G. National Institute of Standards and Technology. Gaithersburg, MD, September.

Gross, J. L., and T. McAllister. 2005. *Federal Building and Fire Safety Investigation of the World Trade Center Disaster: Structural Fire Response and Probable Collapse Sequence of the World Trade Center Towers.* NIST NCSTAR 1-6. National Institute of Standards and Technology. Gaithersburg, MD, September.

Carino, N. J., M. A. Starnes, J. L. Gross, J. C. Yang, S. Kukuck, K. R. Prasad, and R. W. Bukowski. 2005. *Federal Building and Fire Safety Investigation of the World Trade Center Disaster: Passive Fire Protection.* NIST NCSTAR 1-6A. National Institute of Standards and Technology. Gaithersburg, MD, September.

Gross, J., F. Hervey, M. Izydorek, J. Mammoser, and J. Treadway. 2005. *Federal Building and Fire Safety Investigation of the World Trade Center Disaster: Fire Resistance Tests of Floor Truss Systems.* NIST NCSTAR 1-6B. National Institute of Standards and Technology. Gaithersburg, MD, September.

Zarghamee, M. S., S. Bolourchi, D. W. Eggers, Ö. O. Erbay, F. W. Kan, Y. Kitane, A. A. Liepins, M. Mudlock, W. I. Naguib, R. P. Ojdrovic, A. T. Sarawit, P. R Barrett, J. L. Gross, and

T. P. McAllister. 2005. *Federal Building and Fire Safety Investigation of the World Trade Center Disaster: Component, Connection, and Subsystem Structural Analysis.* NIST NCSTAR 1-6C. National Institute of Standards and Technology. Gaithersburg, MD, September.

Zarghamee, M. S., Y. Kitane, Ö. O. Erbay, T. P. McAllister, and J. L. Gross. 2005. *Federal Building and Fire Safety Investigation of the World Trade Center Disaster: Global Structural Analysis of the Response of the World Trade Center Towers to Impact Damage and Fire.* NIST NCSTAR 1-6D. National Institute of Standards and Technology. Gaithersburg, MD, September.

Averill, J. D., D. S. Mileti, R. D. Peacock, E. D. Kuligowski, N. Groner, G. Proulx, P. A. Reneke, and H. E. Nelson. 2005. *Federal Building and Fire Safety Investigation of the World Trade Center Disaster: Occupant Behavior, Egress, and Emergency Communication.* NIST NCSTAR 1-7. National Institute of Standards and Technology. Gaithersburg, MD, September.

Fahy, R., and G. Proulx. 2005. *Federal Building and Fire Safety Investigation of the World Trade Center Disaster: Analysis of Published Accounts of the World Trade Center Evacuation.* NIST NCSTAR 1-7A. National Institute of Standards and Technology. Gaithersburg, MD, September.

Zmud, J. 2005. *Federal Building and Fire Safety Investigation of the World Trade Center Disaster: Technical Documentation for Survey Administration.* NIST NCSTAR 1-7B. National Institute of Standards and Technology. Gaithersburg, MD, September.

Lawson, J. R., and R. L. Vettori. 2005. *Federal Building and Fire Safety Investigation of the World Trade Center Disaster: The Emergency Response Operations.* NIST NCSTAR 1-8. National Institute of Standards and Technology. Gaithersburg, MD, September.

McAllister, T., R. G. Gann, J. D. Averill, J. L. Gross, W. L. Grosshandler, J. R. Lawson, K. B. McGrattan, H. E. Nelson, W. M. Pitts, K. R. Prasad, F. H. Sadek. 2008. *Federal Building and Fire Safety Investigation of the World Trade Center Disaster: Structural Fire Response and Probable Collapse Sequence of World Trade Center Building 7.* NIST NCSTAR 1-9. National Institute of Standards and Technology. Gaithersburg, MD, November.

MacNeill, R., S. Kirkpatrick, B. Peterson, and R. Bocchieri. 2008. *Federal Building and Fire Safety Investigation of the World Trade Center Disaster: Global Structural Analysis of the Response of World Trade Center Building 7 to Fires and Debris Impact Damage.* NIST NCSTAR 1-9A. National Institute of Standards and Technology. Gaithersburg, MD, November.

ACKNOWLEDGMENTS

The work reported herein was conducted with the assistance of several contractors and, in addition, many companies and individuals contributed in a substantial way.

The structural analyses presented in this report were conducted in collaboration with:

- Simpson Gumpertz & Heger Inc. (SGH), of Waltham, Massachusetts; Dr. Mehdi Zarghamee, Project Leader, whose work included the development of structural models and the conduct of the temperature-dependent analyses for the prediction of the structural performance of components and subsystems of the WTC towers and for the determination of collapse of each tower .

- Computer Aided Engineering Associates Inc. (CAEA), Woodbury, Connecticut; Dr. Peter Barrett, Project Leader, who provided technical assistance to SGH and to NIST on the complex computer analyses.

- Dr. R. Shankar Nair of Teng Associates, Prof. Daniele Veneziano of MIT, and Prof. Kaspar Willam of the University of Colorado, who provided expertise in the areas of computational mechanics, structural behavior of tall buildings and reliability.

The work in determining the fireproofing of the WTC towers during their construction and the upgrading of fireproofing on the steel trusses that took place in the 1990's involved many companies and individuals. Their cooperation and assistance in providing the needed information is gratefully acknowledged. The companies and key individuals included:

- Isolatek International, Paulette Kaminski

- Laclede Steel Co, David McGee

- Morse Zehnter Associates, Roger Morse

- Leslie E. Robertson Assoc. (LERA), William Faschen and Richard Garlock

In addition to providing information on the fireproofing, the Port Authority of New York and New Jersey (PANYNJ), and in particular Saroj Bohl, Joe Englot, and Frank Lombardi, researched and provided answers to specific questions at the request of NIST.

Investigative work into the fireproofing of the WTC was led by Dr. Monica Starnes. Data analysis and determination of fireproofing for the finite element calculations was made by Dr. Nicholas Carino. Concrete properties at elevated temperatures were established by Dr. Long Phan for component and subsystem finite element analyses.

Large-scale furnace tests of floor assemblies were conducted by Underwriters Laboratories Inc. (UL), Northbrook, Illinois, and the contribution of the many individuals who contributed to this effort, led by Joe Treadway and Frederick Hervey, is gratefully acknowledged. The cooperation and dedication of the project team are greatly appreciated.

In addition, the following WTC Investigation projects made significant contributions:

- Project 2: Baseline Structural Performance and Aircraft Impact Damage Prediction, led by Dr. Fahim Sadek, provided reference models and the aircraft impact simulations allowing the estimation of structural and fireproofing damage.

- Project 3: Mechanical and Metallurgical Analysis of Structural Steel, led by Dr. Frank W. Gayle, provided the mechanical characteristics of the tower steels that were used in the constitutive models for the finite element analyses. In addition, Dr. Tim Foecke conducted the photographic interpretation and estimation of bowing of the exterior walls of both towers.

- Project 5: Reconstruction of Thermal and Tenability Environment, led by Dr. Richard Gann, provided temperature histories for the structural components for use in the finite element analyses of components, subsystems and global systems. In addition, Dr. William M. Pitts provided assistance in the collection, cataloging and interpretation of the many videos and photographs relevant to this project.

NIST acknowledges the parties to the insurance litigation for voluntarily making their findings available to NIST.

EXECUTIVE SUMMARY

E.1 PURPOSE AND SCOPE

One of the four objectives of the National Institute of Standards and Technology (NIST) investigation of the collapse of the World Trade Center (WTC) towers was to determine why and how the two towers (WTC 1 and WTC 2) collapsed following the initial impacts of the aircraft. Both the north and south towers of the World Trade Center were severely damaged by the impact of Boeing 767 aircraft, yet they remained standing for some time. The ensuing fires were observed to move through both buildings and eventually, both buildings collapsed. The probable collapse sequence for each of the WTC towers as well as the extent and relative importance of the damage caused by the aircraft impact and subsequent weakening by fires were investigated under this project, *Structural Response and Collapse Analysis of WTC Towers to Aircraft Impact Damage and Fire Conditions.*

Events that played a significant role in the structural performance of the towers were the aircraft impact, rapid ignition of fire on multiple floors, and the growth and spread of fire in each tower. Detailed information was required on the condition of the structural system and its passive fire protection system (also referred to as fireproofing or thermal insulation), both before and after the aircraft impact, and during the ensuing fires that elevated temperatures in the structural members. The purpose of this project, then, was to analyze the response of the WTC towers to fires—both with and without aircraft damage—and to determine the probable sequence of structural collapse for each tower. Specifically, the *Structural Response and Collapse Analysis* project intended to:

- Determine the pre- and post-aircraft impact condition of the passive fire protection used to thermally insulate the structural members and provide resistance to fire damage,
- Conduct tests of structural components and systems under fire conditions to quantify their behavior,
- Evaluate the response of floor and column systems under impact and fire conditions to understand their response,
- Evaluate the response of the WTC towers under impact and fire conditions, with and without aircraft impact damage, and
- Develop and evaluate failure hypotheses, resulting in the probable sequence of structural events leading to collapse for each WTC tower.

The unprecedented complexity and sophistication of these analyses required the use of various strategies for managing the computational demands while adequately capturing the essential physics. The overall approach—from impact analysis to collapse initiation—combined mathematical modeling, statistical and probability-based analysis, laboratory testing, and analysis of photographic and videographic records.

Data were collected from a number of sources and included structural plans and specifications, thermal and mechanical (adhesion/cohesion) properties of sprayed fire-resistive material (SFRM), SFRM

thickness and condition in the towers, and recorded observations of structural events subsequent to aircraft impact and prior to collapse. Information about tower construction was obtained from original drawings, design and construction specifications, project documents including correspondence and reports, and records provided by The Port Authority of New York and New Jersey (PANYNJ or Port Authority), Leslie E. Robertson Associates (LERA), Silverstein Properties, and a number of contractors that had worked on the design, construction, or modifications of the towers. Information about the events that occurred in each tower on September 11, 2001, was obtained from analysis of available photographic and videographic records, eyewitness accounts, and mechanical and metallurgical analysis of recovered structural steel.

Computer simulations were used to model the complete sequence of events leading to the initiation of collapse of the WTC towers. The analyses simulated the damage to the towers resulting from aircraft impact, the spread of multi-floor fires, the heating and thermal weakening of structural components, and the progression of local structural failures that led to the collapse of the buildings. The structural response analyses relied upon the following information:

- Reference global structural models of the WTC 1 and WTC 2 towers, and typical floor and exterior wall subsystem models (NIST NCSTAR 1-2)
- Extent of damage to the structural systems and interior contents of the WTC 1 and WTC 2 towers resulting from aircraft impact (NIST NCSTAR 1-2)
- Temperature-dependent mechanical properties of the steels, welds, and bolts used in the construction of the towers, including elastic, plastic, and creep properties from 20 ºC to 700 ºC (NIST NCSTAR 1-3)
- Time-temperature histories for structural components and connections for standard fires (e.g., ASTM E 119) and actual fires based on fire dynamics simulations (NIST NCSTAR 1-5).
- Photographic and videographic records with time stamps that documented the observed sequence of events (NIST NCSTAR 1-5).

E.2 METHODOLOGY AND ANALYSIS RESULTS

E.2.1 Overview and Approach

The interdependence of the analyses of significant events is illustrated in Fig. E–1. Reference structural models were first developed and used to determine the baseline performance of each tower prior to September 11, 2001. The reference models were then used as a basis for the aircraft impact damage models and the structural response models to ensure consistency between structural models. The aircraft impact analysis determined damage to the interior of the building, including the structural system, passive fire protection, partition walls, and furnishings for each tower. The analysis also provided an estimate of the fuel dispersion in the towers. These results provided initial conditions to the fire dynamics analysis, thermal analysis, and structural analysis. The fire dynamics analysis simulated the growth and spread of fires and produced gas temperature histories for each floor involved in fire. The fire dynamics model accounted for window breakage and damage to interior partition walls and floors (both affecting ventilation conditions), and the distribution of debris and fuel. The thermal analysis used the heat transfer

model to determine temperature histories for the various structural components. The thermal analysis required input from the structural analysis model, fire dynamics analysis results, damage to fire protection, and temperature-dependent thermal material properties. The structural temperature histories, also referred to as thermal loads, were input to the structural analysis, along with the structural impact damage and temperature-dependent material properties, to determine the structural response of each tower.

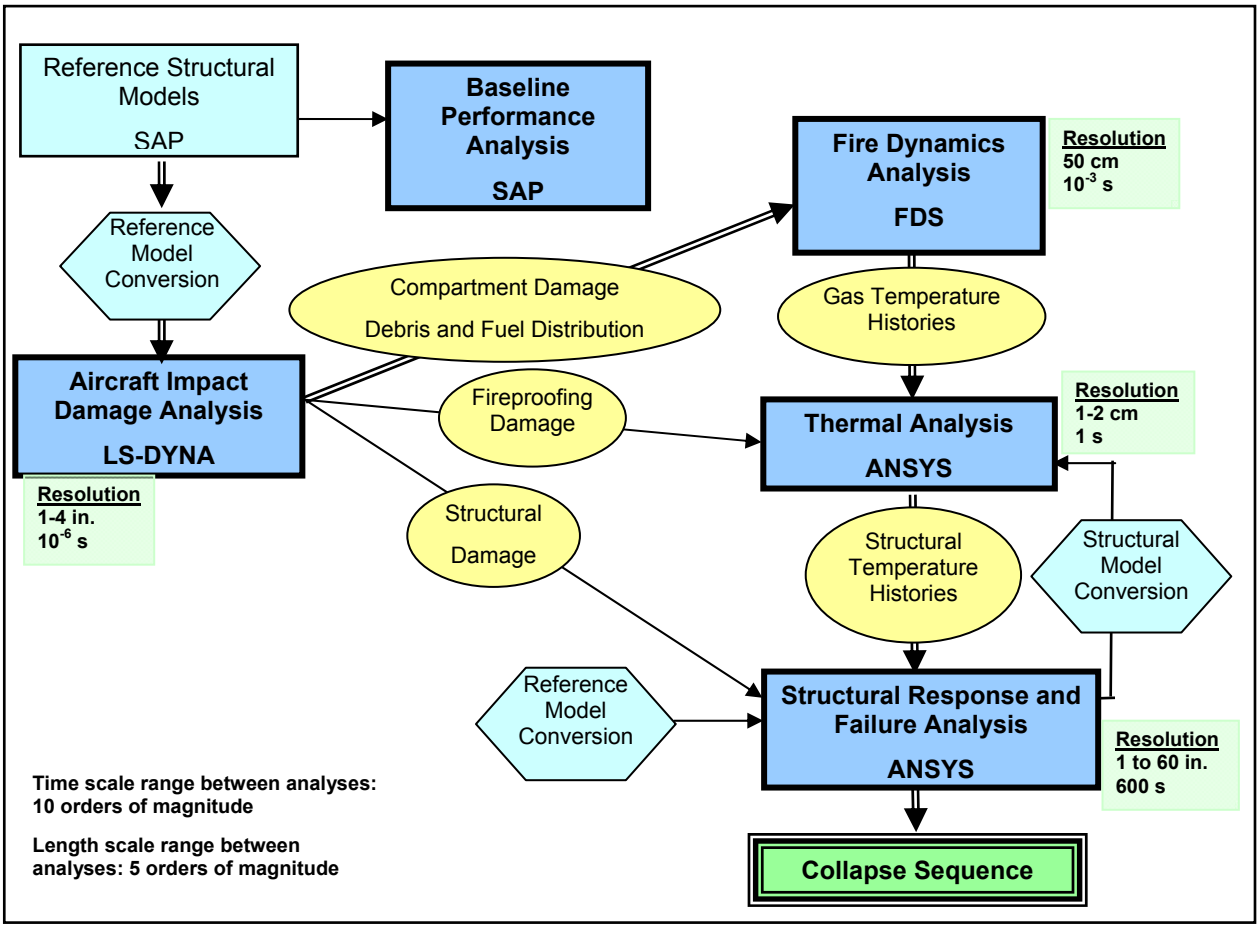

Figure E–1. Critical analysis inter-dependencies.

The WTC towers were large, complex structural systems. To include all of the structural components and connections and their associated behavior and failure mechanisms using refined finite element meshes would have been prohibitive. The analysis approach used was a variant of the well-established sub-structuring approach, adapted for the analysis of structures with highly nonlinear behavior that progressed from individual components to major subsystems to global systems, as shown in Fig. E–2. The component analyses were conducted to identify critical behavior and failure mechanisms that contributed to the global structural response of each tower. The subsystem analyses incorporated the behavior and failure mechanisms identified in the component studies, with modifications to reduce the model size and complexity, thereby enhancing computational performance, without adversely affecting the quality of the results. Whenever modeling modifications were used, they were validated against the detailed component model results. The global analyses incorporated critical behavior and failure mechanisms, determined from subsystem analyses, while making necessary modifications in the level of modeling detail.

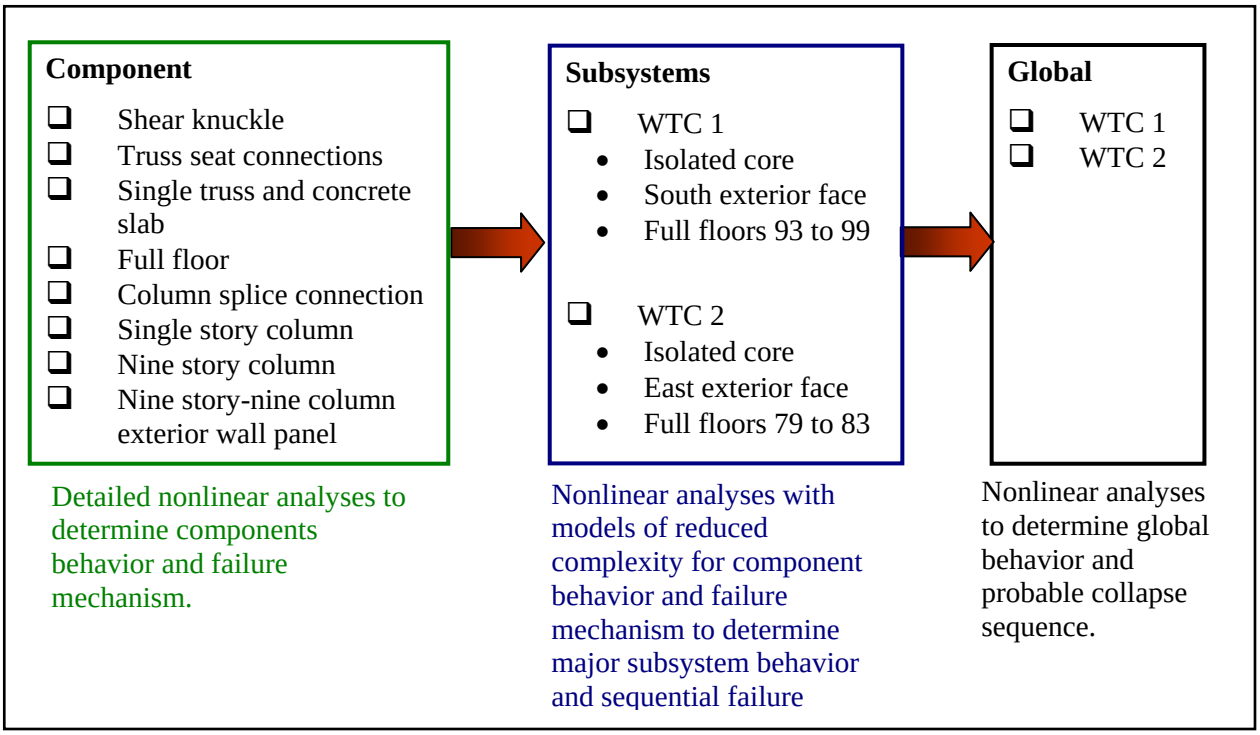

Figure E–2. Structural Analysis Sequence.

Analysis of the global behavior and determination of probable collapse sequences for both WTC 1 and WTC 2, which included work performed by other projects, was divided into the following tasks:

A. Develop finite element models based on reference models. Reference models faithfully represented the actual structures. These reference models became the basis for all subsequent finite element analyses.

B. Develop the constitutive relationships for the materials used in the construction of the towers. Mechanical and chemical properties were determined for steel specimens recovered from the WTC site to assure that the materials used were in conformance with properties specified in the original design. The mechanical properties at high loading rates for the aircraft impact analyses and at elevated temperatures (from room temperature to 800 °C) for the thermal and structural analyses were also determined from the steel specimens.

C. Characterize the passive passive fire protection applied to the structural steel. Neither the type of materials nor the required thicknesses of SFRM were identified in the contract documents or specifications. Estimates of the characteristics and condition of SFRM were needed for the thermal and structural modeling of the towers.

D. Conduct standard fire resistance tests of composite truss floor system. Tests were conducted to: (1) establish the baseline fire resistance rating of the composite truss floor system used in the WTC towers, (2) understand the influence of thermal restraint by testing the floor system under both thermally unrestrained and restrained conditions, and (3) provide experimental data to validate and provide guidance to the development of the floor models and to interpret the analyses results.

E. Establish the damage to the structure, passive fire protection, and partition walls as a result of aircraft impact. The aircraft impact resulted in significant damage to the exterior, floor, and core structures of the buildings. The jet fuel dispersed inside the towers ignited the building contents and furnishings as well as influenced the amount of oxygen reaching the fires. The fire protection of steel components was dislodged in areas of direct debris impact.

F. Document observations and data related to structural events. NIST validated analysis results with key observations obtained from its extensive collection of over 7,000 photographs and over 150 hours of videotape documenting the events at the World Trade Center on September 11, 2001. Key observations were used in the analyses in three ways: (1) to determine input parameters, (2) to impose time-related constraints upon an analysis, or (3) to validate analysis results.

G. Compute temperature histories for structural components subjected to fires. To determine how the towers were affected by the fires, estimates of the growth and spread of fires over time were developed using fire dynamics simulations. Temperature histories of the steel structural components and concrete floor slabs were predicted in thermal analyses.

H. Conduct component and subsystem analyses. These analyses provided understanding of the nonlinear behavior of structural components and subsystems under gravity and thermal loading and were used to develop reduced models for the global analyses. The components and subsystems considered included: (1) typical floor subsystem with (a) the shear knuckles, (b) truss seats, and (c) a single truss and concrete slab section; and (2) a nine-story by nine-column exterior wall subsystem with (a) bolted connection between exterior columns, (b) bolted connection between spandrels, (c) single exterior columns with spandrel sections, and (d) single exterior wall panel with three columns and three spandrels.

I. Conduct analyses of major subsystems. Analyses of three major subsystems - the isolated core framing subsystem, an exterior wall subsystem, and the composite floor subsystems - were analyzed to determine their ability to resist and redistribute loads after impact damage and response to elevated temperatures. The subsystem models used reduced models from the component analyses, which kept the analysis tractable while including nonlinear features and failure modes. These analyses were crucial for determining critical structural behaviors, including floor sagging under thermal loading, the resulting pull-in forces, and the inward bowing of the exterior walls.

J. Conduct a separate global analysis for each tower. These analyses determined the relative roles of impact damage and fires with respect to structural stability, sequential failures of components and subsystems, and probable collapse initiation sequences. Each global model was first evaluated for stability under gravity loads with structural impact damage. Temperature histories were applied in 10 min intervals and linearly ramped to the next temperature state. Pull-in forces from sagging floors were also applied during the appropriate 10 min intervals. The question of how the WTC towers would have responded to the same fires without the aircraft impact damage was considered to determine the vulnerability of the towers to collapse initiated by conventional large fires.

K. Determine the probable collapse sequence for each tower. A probable collapse sequence for each tower was determined. The collapse sequences were evaluated against key observables.

E.2.2 Structural Response

To conduct the global analysis of each tower, input data were collected from numerous sources, including fire dynamics, thermal, and impact analyses, as already described.

Thermal analyses to simulate the elevated temperatures of the structural components and consequent weakening required an assessment of the condition of the passive fire protection, including thermal properties and SFRM thicknesses. Additionally, tests of the WTC floor system under standard fire conditions provided insights into the dominant behavior of the floors at elevated temperatures and allowed validation of analytical results. Interpretation of the aircraft impact study results led to a determination of likely damage to load bearing structural elements and an estimation of damage to, and consequent loss of, passive fire protection of the floor trusses, core columns and beams, and exterior columns and spandrels. Properties of the materials of construction, including mechanical properties at room and elevated temperatures as well as thermal characteristics, were needed. The structural analyses of components, subsystems and, ultimately, the global systems could be accomplished with this information.

Passive Fire Protection for Structural Components

Passive fire protection delays the transfer of heat to structural components by providing an insulation barrier. Increasing thickness of passive fire protection materials, commonly referred to as fireproofing, correspondingly increases the time delay before the structural component temperature begins to rise. The amount of time delay for a given fire protection method, such as SFRM, is not predicted for design purposes because the actual fire conditions vary; instead, the relative performance is defined by comparative testing with the ASTM Standard Fire Test.

The structural steel in the WTC towers was sprayed with SFRM or protected with rigid fire-rated gypsum panels. SFRM is supplied as dry ingredients, and water is added at the time of application. The water mixes with the cementitious materials and allows the SFRM to adhere weakly to the steel. With time, the cementitious materials harden, and excess water evaporates resulting in a covering of insulation with some cohesive strength.

Three SFRM products that were used in the towers include:

- BLAZE-SHIELD DC/F for floor trusses, core columns, and the exterior surfaces of the exterior columns and spandrels
- BLAZE-SHIELD II for upgrades to floor trusses, which started in the 1990's
- W.R. Grace and Co., Monokote (sprayed cementitious vermiculite) for the interior surfaces of the exterior columns and spandrels

The gypsum panels were used to form fire resistant enclosures around steel core columns, stairwells, mechanical shafts, and the core area in the towers. The core column thermal insulation varied according to the column location and exposure to occupied spaces. Column surfaces in public access areas were protected with gypsum enclosures, while the remaining surfaces were protected with SFRM.

The following information was required to determine the in-place condition of the passive fire protection before and after aircraft impact and to conduct thermal analysis of structural components:

- Thermophysical properties of the passive fire protection materials,
- Effect of gaps in thermal insulation and variability of insulation thickness,
- Effective thickness of thermal insulation for use in thermal-structural analyses that accounts for thickness variability effects,
- Adhesive and cohesive strengths of BLAZE-SHIELD SFRM products (vermiculite product is no longer available).

Thermophysical properties were determined with ASTM standard tests for BLAZE-SHIELD DC/F, BLAZE-SHIELD II, and Monokote MK-5 SFRM products and for gypsum board. The specific heat, thermal conductivity, and density of each material were determined for temperatures ranging from 25 °C to 1200 °C. The standard tests used for SFRM products were ASTM C 1113 (1999), ASTM E 1269 (2001), ASTM E 1131 (1998), and ASTM E 228 (1995). The standard tests used for the gypsum board products were ASTM D 5334 (2000b) and ASTM E 1269 (2001). Densities were calculated from the thermogravimetric analysis and linear thermal expansion measurements.

Analyses showed that when the SFRM thickness is variable, the isotherms in the steel depend upon the shape of the SFRM surface contour. Thus, the temperature history at any point in the steel depends on the local thickness of the insulation. It was shown that an increase in thickness variability reduced the time to reach a certain temperature. In addition to the effect of variation in thickness, the effect of gaps in the SFRM coating was studied. As expected, thermal analysis results indicated that the exposed steel heated quickly and transmitted heat to the adjacent interior steel. However, the temperature rise quickly dissipated as the distance from the gap increased. Review of available photographs showed that gaps were a relatively infrequent occurrence in most floor truss areas. Because there was insufficient information to determine the frequency of occurrence of these gaps or their typical locations, insulation gaps were not considered in the thermal modeling.

SFRM thickness measurements were determined from analysis and interpretation of photographs showing the condition of the originally applied material. Finite element simulations were used to determine a thermally equivalent uniform thickness of SFRM for the original variable-thickness applied to the floor trusses. These values were used in the thermal analyses for determining temperature histories of structural components.

No information was available about the condition of thermal insulation for the exterior columns and spandrel beams, and little information was available for the core beams and columns. For thermal analyses of the towers, the SFRM on these elements was taken to have uniform thicknesses equal to the specified thickness.

The adhesive strength of BLAZE-SHIELD DC/F to steel coated with primer paint (average value of 171 psf to 185 psf) was found to be a third to a half of the adhesive strength to steel that had not been primed (average values of 450 psf to 666 psf). The SFRM products used in the WTC towers were applied

to steel components with primer paint. Cohesive strengths varied from average values of 367 psf to 610 psf.

Tests of Truss Floor Components and Subsystem

Review of available documents indicated that the fire performance of the composite floor system of the WTC towers was an issue of concern to the Port Authority and its contractors during the original design and throughout the service life of the buildings. NIST conducted a series of four standard fire tests to establish the baseline performance of the floor system of the WTC towers as they were originally built, to differentiate the factors that most influenced the response of the floors, and to study the procedures and practices used to accept an innovative structural and fire protection system. The ASTM E 119 furnace tests were performed on representative floor sections with SFRM for the as-specified thickness of 0.5 in. given in the design documents and the average as-built thickness of 0.75 in. that was applied before a program was established in the 1990's to upgrade the truss SFRM thickness to 1.5 in. The conditions in the standard test specified a prescribed temperature rise and duration until failure criteria were met; the estimated fire conditions in the WTC towers imposed varied heating and cooling conditions as the fires grew and spread.

The tested floor assemblies were similar, though not identical, to steel-joist-supported concrete floors that are widely used in low rise construction. The test results provided valuable insight into the behavior of these widely used assemblies and also identified issues that require further study for other types of structural components such as beams, girders, columns, trusses, etc.

The tests showed that the floors were capable of considerable sagging without collapse. The tests also showed thermal damage to the bridging trusses and buckling of compression diagonals and the vertical strut near the supports. No evidence of knuckle failures was seen in the tests.

The NIST tests have identified areas where further study related to the standard test method is warranted. Among the issues related to the test method that NIST identified as requiring further study are:

- the scale of the test for prototype assemblies that are larger than the tested assemblies,
- the effect of restraint conditions on test results,
- the repeatability of test results (e.g., do multiple fire resistance tests conducted under the same conditions yield the same results?),
- effects of test scale, end restraint, and test repeatability on other types of structural components (beams, girders, columns, trusses, etc.), and
- the acceptance criteria to evaluate the load carrying capacity of the tested assemblies (currently tests are stopped before the load carrying capacity of the assembly is reached because other acceptance criteria are met or if the deflection becomes excessive and assembly failure could damage the furnace).

Structural Response of Components and Detailed Subsystems to Assumed Damage and Fire

Material Properties and Failure Criteria

The WTC towers were designed and constructed using 14 grades of steel and two types of concrete. Nominal properties for these materials were provided in the design documents. Additional information was required about the mechanical properties at room and elevated temperature for analysis of the towers' response to the impact and elevated temperature conditions.

The collapse analyses of the WTC towers concentrated on modeling failure mechanisms in steel rather than concrete components, since the WTC towers were essentially steel structures; concrete was used only for the floor slabs.

The two general types of steel that were used in the towers are typically described as carbon steels and high strength steels. Carbon steels generally have lower strengths but are more ductile. The core columns, floor trusses, and beams and spandrel plates in the exterior wall were constructed with carbon steels, ranging from 36 ksi to 50 ksi specified yield strengths. The exterior columns were designed with various grades of high strength steels, ranging from 55 ksi to 100 ksi yield strength.

Normal weight concrete (150 pcf) was used in the core and mechanical floors, and lightweight concrete (110 pcf) was used in the floor system for the tenant spaces between the building core and exterior.

The mechanical properties of both steel and concrete are significantly affected by elevated temperatures. Steel and concrete properties that are temperature sensitive include modulus of elasticity, instantaneous coefficient of thermal expansion, tensile strength, and compressive strength. Additionally, creep strain rates for steel are also temperature dependent.

Mechanical properties of the various grades of steel used and normal and lightweight concrete, both at room temperature and throughout the expected temperature range, were determined. This information provided the bases for describing the material models used in the finite element analyses. In addition to material models, failure criteria were also developed for concrete and steel components. Failure criteria defined the necessary conditions to characterize and quantify the expected failure modes or mechanisms, including elastic or plastic buckling, yielding, or fracture. The state of component loads, material properties, and temperature also affected the mode of failure.

In addition, the following observations can be made:

- Modulus of elasticity is reduced by 25 percent at 600 °C for steel and by 50 percent to 75 percent for concrete.

- Steel yield strength reduces to 20 percent of its initial (room temperature) value and ultimate tensile strength is reduced to 40 percent of its initial value at 600 °C. Concrete compressive strength is reduced to between 30 percent and 50 percent of its initial value. Concrete tensile strength, which is already low, is also reduced to 30 percent.

- The instantaneous coefficient of thermal expansion for steel lies between that of lightweight and normal weight concrete for a given temperature. If steel truss and lightweight concrete

components are at the same temperature, the steel components will thermally expand more than the lightweight concrete. For steel beams and normal weight concrete in the core area, the normal weight concrete will expand more than the steel beams.

Floor Subsystem Analysis

The floors supported the occupants and furnishings and transferred these loads to the columns, acted as diaphragms to transfer loads between exterior faces when under wind loads, and provided lateral stability for columns. With damage to the SFRM on the floor trusses, fires caused thermal expansion and sagging of the floors in the impact damage areas.

The analysis of floors progressed from individual components to major subsystems to global systems. Three truss components were studied with detailed models using ANSYS, a general purpose finite element software package, before developing a model of a full floor subsystem:

- Shear connector between the truss and concrete slab,
- Truss seat connection to the columns,
- Composite section of a single floor truss and concrete slab that included the truss seats, knuckles, and section of the supporting exterior and core channel beam.

Shear connector tests conducted by the truss manufacturer, Laclede Steel, in the early 1960s were reviewed and modeled. The shear connector between the truss and the concrete slab was referred to as a knuckle, due to the bent bar configuration that extended past the top chord of the truss, instead of the studs that are typically welded to the top chord. Detailed ANSYS models of the knuckle and concrete slab were analyzed and compared to the measured transverse and longitudinal shear capacities of a knuckle. A reduced model of the knuckle for use in the single truss and full floor models was developed that captured the dominant temperature-dependent behavior and failure modes.

Truss seats connected the trusses to the core and exterior columns. Truss seats were constructed with standoff plates, seat angles, bolts, and welded gusset plates; details varied for each truss seat depending upon its location within the floor plan. Truss seats were designed to carry floor gravity loads and small horizontal loads, typically a few percent of the column capacity to which it was attached. Typical truss seats were analyzed to determine their failure modes and associated loading and thermal conditions. A series of analyses were conducted to determine the truss seat response to thermal expansion of the floor slab, floor sagging or deformation, and heating of the truss seat. A model of reduced complexity was developed that captured the behavior and failure modes of the truss seats for use in the single truss and full floor models.

With reduced models of the knuckle and truss seat, a composite section of a full single truss and concrete slab was modeled to determine its behavior and failure modes for elevated temperatures and additional debris loads. Steel components with damaged fire resistant coatings heated and softened within 10 to 15 minutes. The bottom surface of the concrete slab heated quickly, but the rate of heating through the slab depth was slower, so that the slab response to fire lagged behind the steel response. Concrete spalling was not included in the model. Analysis was conducted using uniform temperatures across the truss and an imposed linear thermal gradient across the slab depth to study the floor section response.

These conditions were assumed prior to completion of the fire and heat transfer analyses used for the full floor subsystem analysis. Two failure modes of interest were (1) floor component failures leading to sagging (i.e. buckling of truss components or knuckle separation from the concrete slab) and the truss pulling inward on the columns and (2) failure of the truss seats. Analysis results were used to develop a model of reduced complexity with break elements that captured the behavior and failure modes of the floor section for use in the full floor model.

The full floor model included core columns and floor beams, exterior columns and spandrel beams, floor trusses and bridging trusses, and normal and lightweight concrete in the core and floor truss areas, respectively. The columns were extended one floor level above and below the floor subsystem and were required to include the interaction between the floor subsystem and the core and exterior columns. The full floor model contained a number of modifications from the model developed using the SAP2000 software of Floor 96 (NIST NSTAR 1-2) that reduced the number of finite elements and incorporated the features for analyzing the structural response to thermal conditions.

Results of the floor system analyses showed that:

- Knuckle failures did not occur under gravity loading and elevated temperatures anticipated.
- Truss web diagonals buckled at loads and temperatures expected and, as a consequence, the floor system sagged.
- Sagging of the floor system resulted in possible inward pull on the exterior columns, although the magnitude of the force depended on fire conditions on surrounding floors.
- Truss seat connections could fail under elevated temperature conditions, and their behavior was included to accurately capture the overall performance of the floor system to impact and fire conditions.
- Essential floor behavior, including buckling of web diagonals and connection failures, could be achieved with reduced models.

Core Column and Exterior Column and Panel Analysis

The primary function of the core columns was to carry the building gravity loads. The exterior columns resisted wind loads and, in addition, carried approximately half of the gravity loads.

Preliminary analysis of the core and exterior columns considered their individual buckling behavior and how it varied for uniform elevated temperatures. The columns were found to have sufficient capacity for tower gravity loads even under elevated temperatures and a loss of lateral support at several floors. This was also found in more detailed finite element models of the columns.

The core columns were studied to determine the most efficient way to reduce the complexity of the model while still capturing buckling behavior at room and elevated temperatures.

Four exterior wall components were studied with detailed ANSYS models before developing a model of a nine-story by nine-column wall area:

- Bolted connection for exterior columns
- Bolted connections for spandrels
- Single exterior columns with spandrel sections
- Single exterior wall panel, fabricated as a single unit for construction purposes with three columns and three spandrels

The column and spandrel connections were analyzed to determine their failure modes and associated loading and thermal conditions. A reduced model was developed that captured the connector behavior and failure modes for use in exterior wall models.

The single column model with spandrel sections was loaded axially to determine its buckling load and post-buckling behavior at room and elevated temperatures for one, two, three, and nine story column heights.

The computer model of a single wall panel was validated against the reference structural models for the towers. The models were subjected to vertical and horizontal forces in the plane of the wall, representing intended design behavior, and a horizontal force transverse to the wall, representing a possible floor load.

The exterior wall had three connections: the column splice, the spandrel splice, and the truss seat (for the floors). The column splice had four bolts that connected columns through their end plates. The spandrel connection had a splice plate to connect the two spandrel plates using high strength bolts. The spandrel and column splices were represented in the nine by nine wall subsystem model and captured the spandrel failure modes of bolt shear, tearing of the spandrel plate, and tearout of the spandrel plate at the bolt holes.

The nine by nine wall model had a coarser mesh that used beam elements for the columns, shell elements for the spandrels, and break elements for the connections. The wall model was subjected to axial loads from above, lateral out-of-plane loads at the floor levels, and elevated temperature representative of fire conditions. The effect of missing floor supports was also evaluated.

Several analyses were run for a variety of temperature load cases and for various combinations of axial load, disconnected floors simulating floor failure and loss of lateral column support, and inward pull applied at one or more floor levels modeling floor sag due to elevated temperatures. Results showed that:

- Although spandrel plates experienced large distortions and high strains, column buckling did not occur under the various temperature loadings applied when floors remained in place and able to provide lateral support to the columns.
- Column buckling did not occur when lateral support was lost at three floors under the expected gravity load that included dead plus service live loads.
- Column buckling did occur when lateral support was lost at three floors and the gravity load was increased to 150 percent of the expected gravity load simulating redistribution of load to the exterior wall.

- Column buckling was found to occur when an inward lateral load (pull-in) of approximately 12 kips was applied to three adjacent floor levels. The inward deflection of the exterior wall when it could no longer support the gravity load (i.e., at the buckling load) was approximately 10 in.

Aircraft Impact Damage

The aircraft impact of the WTC towers caused extensive damage to the buildings' exterior, penetrated into the interior causing further damage to the structural system, dislodged thermal insulation, and ignited multi-floor fires. The structural damage to each tower resulting from the aircraft impact was estimated using a transient finite element analysis. Results of this analysis were used to predict damage to the structure, insulation, and partition walls in the path of the debris field.

The fire dynamics, thermal, and structural analyses all required input data derived from the aircraft impact analyses. The fire dynamics analyses used estimates of damage to the floors and partition walls to describe ventilation paths and to identify the distribution of fuel and debris immediately following impact. The thermal analysis required estimation of the areas that had dislodged insulation on the structural components of the towers. For the structural analyses, elements that represented severed or heavily damaged floors and columns were removed from the structural models of the towers.

The aircraft impact analyses considered three cases for each tower, where each case had a different set of input parameter values, based upon sensitivity studies and detailed component analyses. The results for the three cases were compared to observations from photographs and videos. Damage to the exterior walls predicted by the impact simulations matched reasonably well the exterior damage in photographic and video records. The observed exterior damage was used in the structural analyses. The analysis results from two cases for each tower were found to match observations reasonably well and were selected for continued analysis by the fire dynamics, thermal, and structural analyses. The cases for each tower were referred to as Case A and Case B for WTC 1 and Case C and Case D for WTC 2. However, prior to determining the final aircraft impact analysis results, earlier aircraft impact analyses produced an initial set of aircraft impact cases for each tower. These initial cases, referred to as Case A_i and Case B_i for WTC 1 and Case C_i and Case D_i for WTC 2, were used to develop experience and gain understanding of the fire spread and growth, the rate of structural component heating, and the structural response to damage and elevated temperatures.

The final set of impact damage data for fire dynamics, thermal, and structural analyses was Cases A, B, C, and D, with the exception of the full floor subsystem analyses which used initial damage Cases A_i to D_i. The use of the aircraft impact data in the sequence of structural analyses was as follows:

1. Full floor subsystem models were analyzed for all initial damage Cases A_i to D_i before the final damage cases were available.

2. Full floor subsystem models were evaluated for changes in damage between final Cases A to D and initial Cases A_i to D_i. Changes in impact damage to the structural components and insulation reflected in the two sets of Cases (i.e., initial and final) were found to have little effect on the floor subsystem structural response. The full floor subsystem structural response for Cases A_i to D_i and Cases A to D were found to be equivalent.

3. Isolated core and exterior wall subsystem models were analyzed for Cases A, B, C, and D.

4. The global model of WTC 1 and WTC 2 were analyzed for Case B and D, respectively, based upon the results of the subsystem analyses.

Four classifications of core column structural damage were established: severed, heavy damage, moderate damage, and light damage. Classification criteria included plastic strain levels and lateral deformation from the column centerline. Columns that were severed or heavily damaged were removed to simulate impact damage in the global analysis of each tower. Two types of floor structural damage were identified from the impact analysis results: (1) missing floor areas and (2) severely damaged floor areas incapable of supporting loads.

Thermal insulation was assumed to be dislodged from core columns only if the columns were subject to direct debris impact that failed wall partitions in the immediate vicinity of the column[1]. For exterior columns, the debris impact was required to be strong enough to damage or destroy room furnishings (modular office workstations) adjacent to the columns. For floor trusses, the debris impact was required to be strong enough to damage or destroy room furnishings (modular office workstations) in the same area of the affected floor.

The structural damage in WTC 1 extended from the north exterior wall into the north side of the core. An exterior panel was knocked out of the south wall by aircraft debris. Damage to the insulation from direct debris impact extended over a larger region and extended to central regions of the south floor areas. Case B predicted more damage to core columns and a larger extent of insulation damage to the south floor area than Case A, including damage to the south exterior wall insulation on the inside face, as shown in Fig. E–3.

The structural damage in WTC 2 extended from the south exterior wall to southeast region of the core. Exterior columns were severed by debris near the northeast corner. Damage to the insulation from direct debris impact extended over a larger region and extended over most of the east floor area to the north face. Case D predicted more damage to core columns than Case C, but the extent of the insulation damage was similar, as shown in Fig. E–4.

[1] The Pentagon was impacted by an aircraft of similar size and at a similar speed as the WTC towers. The observed stripping of the concrete cover from columns in similar circumstances provides an independent set of data that supports the criteria established for the removal of fireproofing materials subject to direct debris impact in the WTC towers.

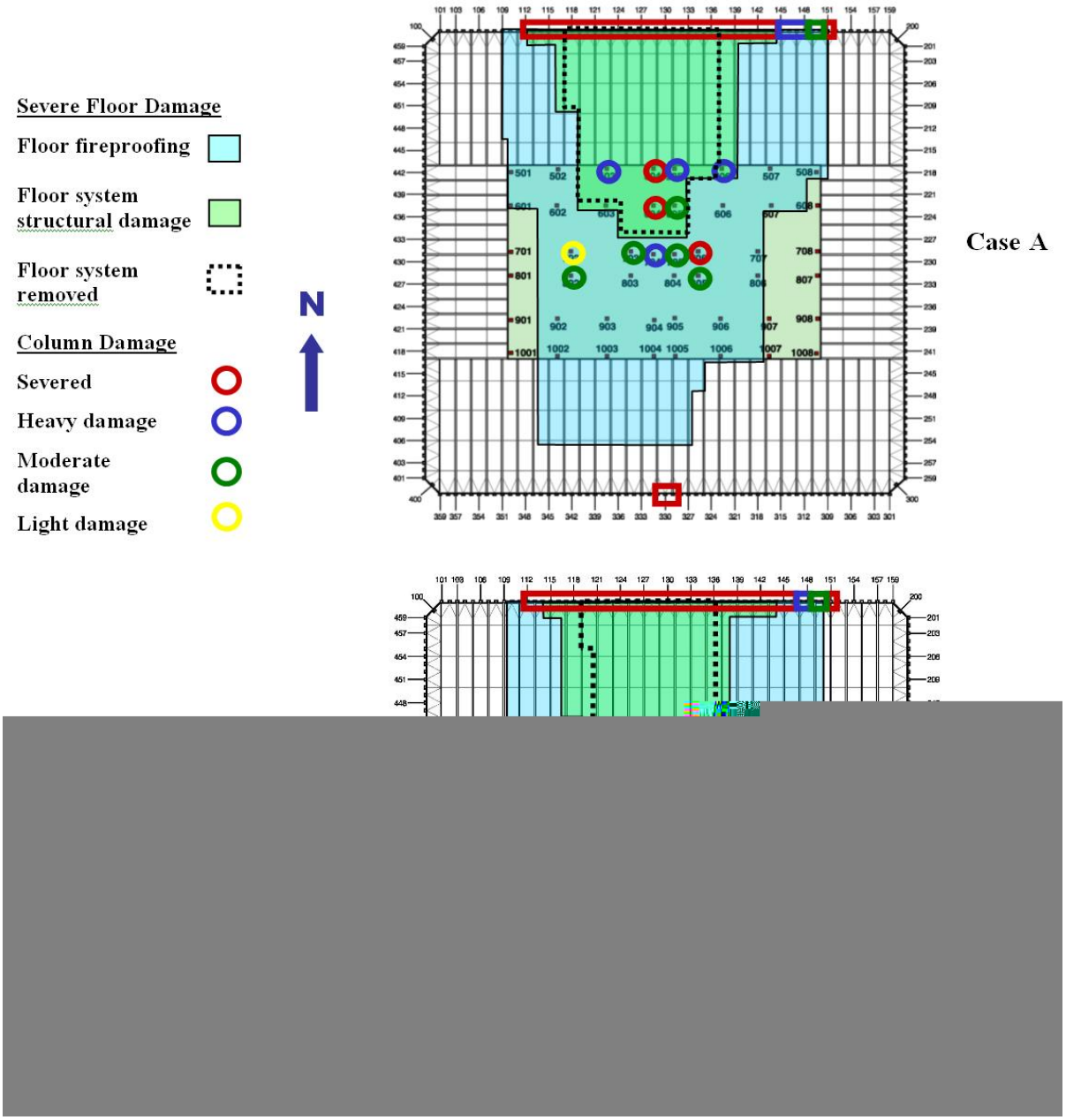

Figure E–3. Plan view of WTC 1 cumulative damage for Floors 93 to 99.

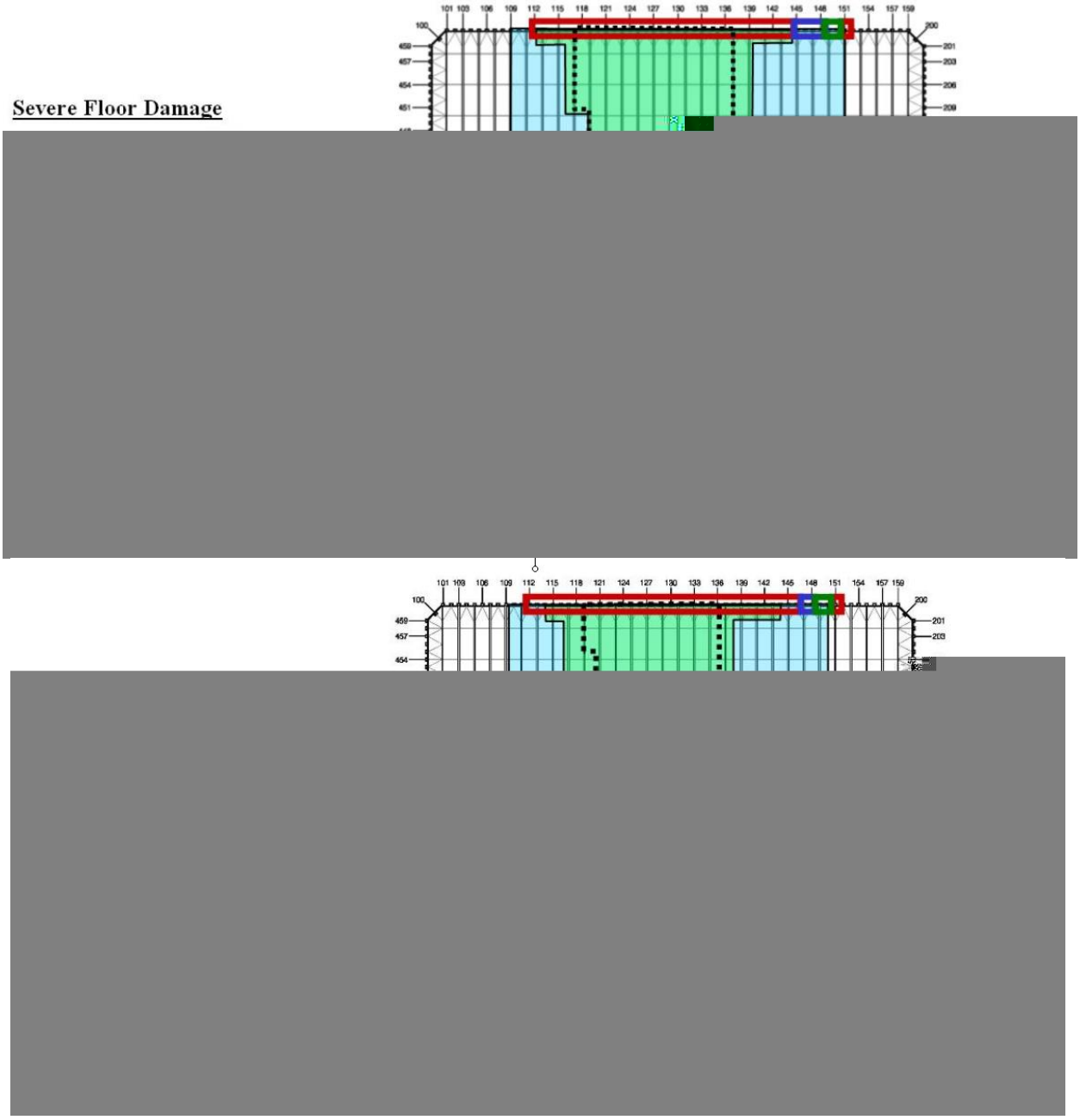

Figure E–4. Plan view of WTC 2 cumulative damage for Floors 78 to 84.

Observations and Timeline of Structural Events

NIST assembled a collection of nearly 150 hours of video footage and over 7,000 photographs, which were reviewed for insights into the structural performance of the towers. A timeline of significant events that characterized the weakening and eventual collapse of the WTC towers was developed with the photographs and videos that were time stamped. Quantitative information, such as the amount of inward bowing observed on the exterior walls of the buildings, was extracted from key photographs through image enhancement and scaled measurements. Key observations and the timelines were used to guide the global collapse analyses.

Development of the probable collapse sequence for each tower was shaped by evidence gathered in the investigation. Data about the events following the aircraft impact were primarily obtained from three sources:

- Photographic and videographic records that had been catalogued and time stamped for the NIST Investigation (NIST NCSTAR 1-5A)
- Interviews of individuals in the towers who survived and those who received telephone calls from individuals in the tower (NIST NCSTAR 1-7)
- Interviews of emergency response personnel and emergency communication records (NIST NCSTAR 1-8)

Photographs and videos provided knowledge about aircraft impact damage to the exterior walls, fire growth and spread at the building exterior, inward bowing of an exterior wall in each tower, and the direction of tilt for the building section above the impact and fire zone as the towers collapsed.

Changes in structural performance are generally difficult, if not impossible, to perceive until significant deformation has taken place relative to the dimensions of the structure and depend on the detail and resolution of the image being examined and the vantage point of the photographer. Observations of structural performance for the WTC towers included severed components, local deflections or buckling, possible sagging of floors, and relative alignment of columns or building sections.

Evidence was used in the analyses in three ways: (1) to determine input parameters, such as the aircraft speed and direction upon impact, (2) to impose time-related constraints upon an analysis, such as imposing observed broken windows over time to constrain the spread of fire, or (3) to validate analysis results, such as global stability after impact and during thermal loading.

Observations of structural behavior were broken into two groups: *key observations* and *noted observations*. Key observations were significant structural events that were explicitly addressed in or used to validate the structural analyses. Noted observations were events that may have been a structural response, but could not be conclusively identified as a structural response.

Key observations were used to develop a timeline of structural events for each tower. Structural analyses were used to support development of the collapse hypothesis for each tower and to develop and refine understanding of the probable sequence of events.

WTC 1 key observations were:

- Inward bowing of the south exterior wall was first observed at 10:23 a.m., as shown in Fig. E–5.
- The time to collapse initiation was 102 minutes from the aircraft impact (9:46:30 a.m. until 10:28:22 a.m.).
- From exterior observations, tilting of the building section appeared to take place near Floor 98. Column buckling was then observed to progress rapidly across the east and west faces.
- The WTC 1 building section above the impact and fire area tilted to the south as the structural collapse initiated, as shown in Fig. E–6. A tilt to the south of at least 8 degrees occurred before dust clouds obscured the view and the building section began to fall downward.

WTC 2 key observations were:

- Following the aircraft impact and fireballs, hanging objects were observed through the windows of the east and north faces. The hanging objects suggest that there was structural damage to WTC 2 Floor 83 along the east face and to Floors 81 to 83 of the north face near the northeast corner.
- Inward bowing of the east wall was first observed at 9:21 a.m. The inward bowing was approximately 10 in. at Floor 80.
- An increase of the inward bowing of the east wall was observed at 9:53 a.m. The greatest bowing was approximately 20 in.±1.0 in. at Floor 80 on the east face of WTC 1.
- Collapse initiated 56 minutes after the aircraft impact (9:02:59 a.m. to 9:58:59 a.m.).
- From a northeast viewpoint, initial downward motion was observed as columns moved inward on the north side of the east face, as shown in Fig. E–7. Tilt of the building section above the impact and fire area appeared to take place near Floor 82. Column buckling was then seen to progress across the north face.
- The building section above the impact and fire area tilted to the east and south as the structural collapse initiated as shown in Fig. E–8. There was approximately a 3 to 4 degree tilt to the south and a 7 to 8 degree tilt to the east prior to significant downward movement of the upper building section.

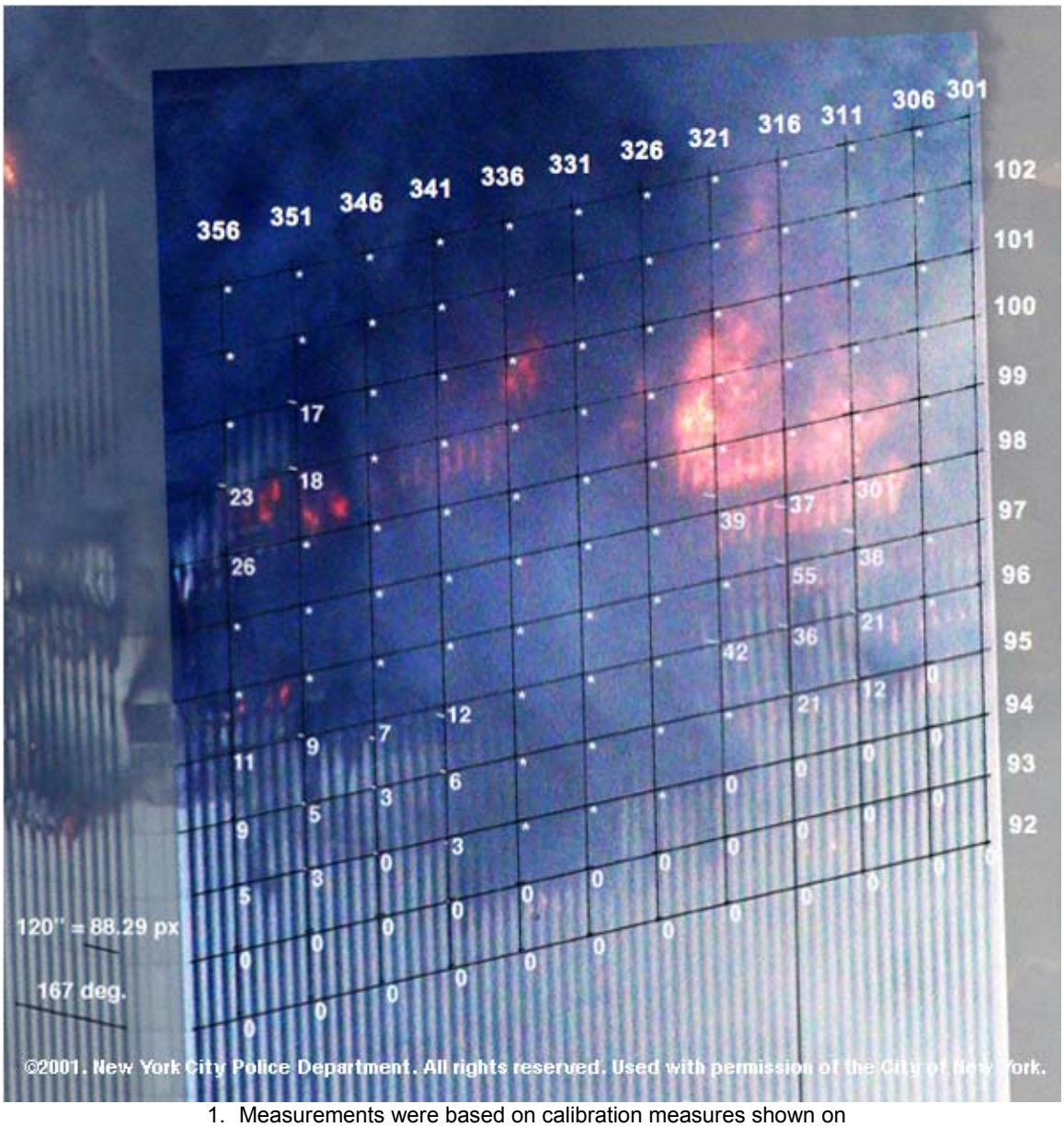

1. Measurements were based on calibration measures shown on the west face
2. Foreshortening into depth of field across the south face of 17% was included in the measurements
3. Measurement error was at least ± 6 inches

Figure E–5. WTC 1 exterior columns bowing inward across most of the south face between Floors 95 to 98 at 10:23 a.m.

Figure E–6. WTC 1 building section above impact damage zone tilts to the south.

Figure E–7. View of WTC 2 buckling of east wall near northeast corner as collapse initiates from southeast.

Figure E–8. View of upper building section of WTC 2 tilting to the east.

Structural Response of Major Tower Subsystems

Prior to conducting the analysis of the global structural response of each tower, major structural subsystems were analyzed to provide insight into their behavior within the WTC global system. The three major structural subsystems, the core framing, a single exterior wall, and full tenant floors, were analyzed separately for their response to impact damage and fire. The hat truss was not analyzed separately as its structural behavior did not require significant reduction in the global analysis. The component analyses provided a foundation for these large, nonlinear analyses with highly redundant load paths by determining component behavior and failure modes and enabling a significant reduction in finite element model complexity and size. The major subsystem models used final estimates of impact damage and elevated temperatures determined from the airplane impact analysis and the fire dynamics and thermal analyses.

The capacity of each subsystem to sustain loads from imposed damage and elevated temperatures was evaluated. The isolated subsystem models lacked the restraint and load paths to other subsystems found in the global analysis. Even so, the isolated subsystem response was useful for refining the global models and interpreting subsystem behavior in the global system. For instance, when the column connections to the hat truss in WTC 2 failed at the southeast corner of the core, the only load path available to carry those column loads was the floor system within the core structure. However, in the global structure, the hat truss at the top of the core would transfer loads to other core columns or the exterior walls, assuming the connections between the core columns and hat truss remained intact.

The subsystem models used model reductions from the component analyses, which kept the analysis tractable while maintaining required nonlinear effects. As previously noted, such the comwere

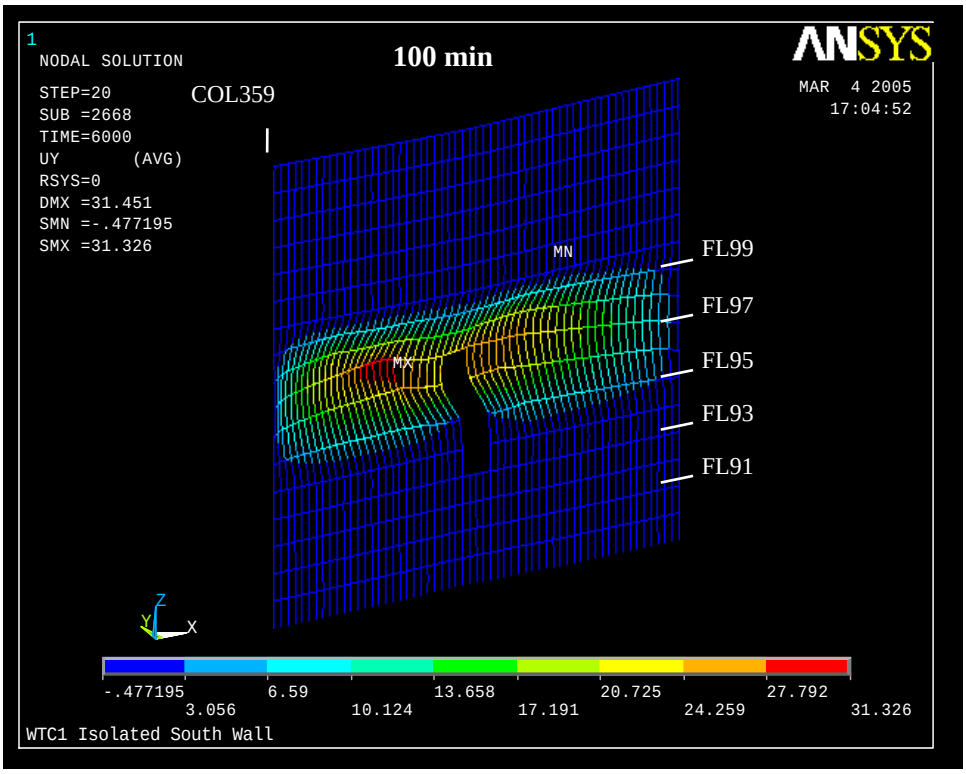

Figure E–9. Inward displacement of the WTC 1 south wall at 100 min of the Case B temperatures with floor disconnections and 6 kip pull-in forces over five floors.

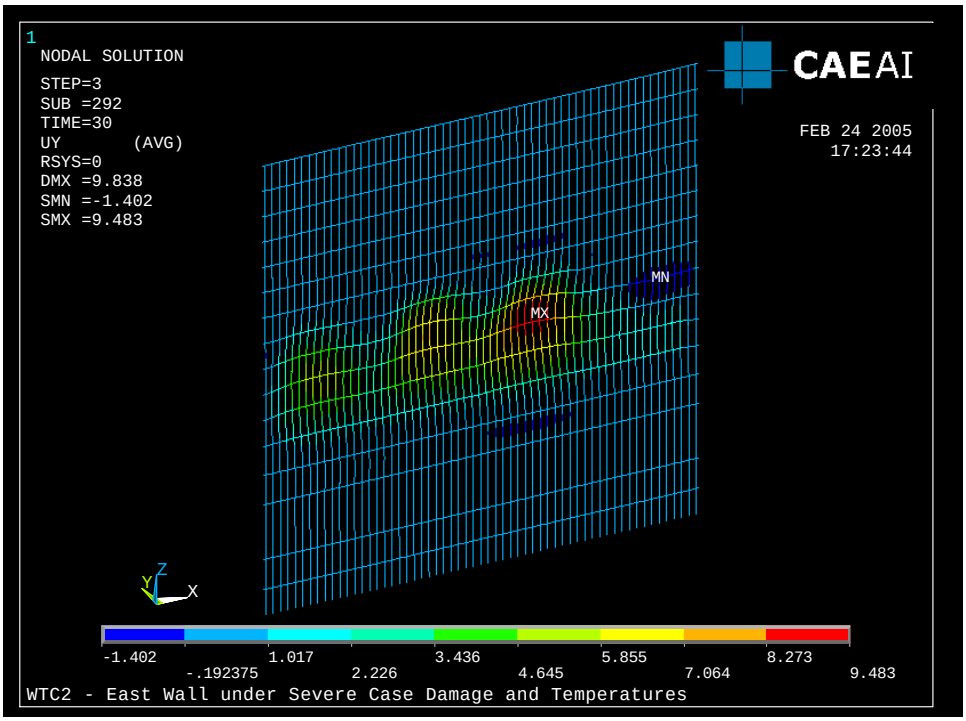

At 20 min

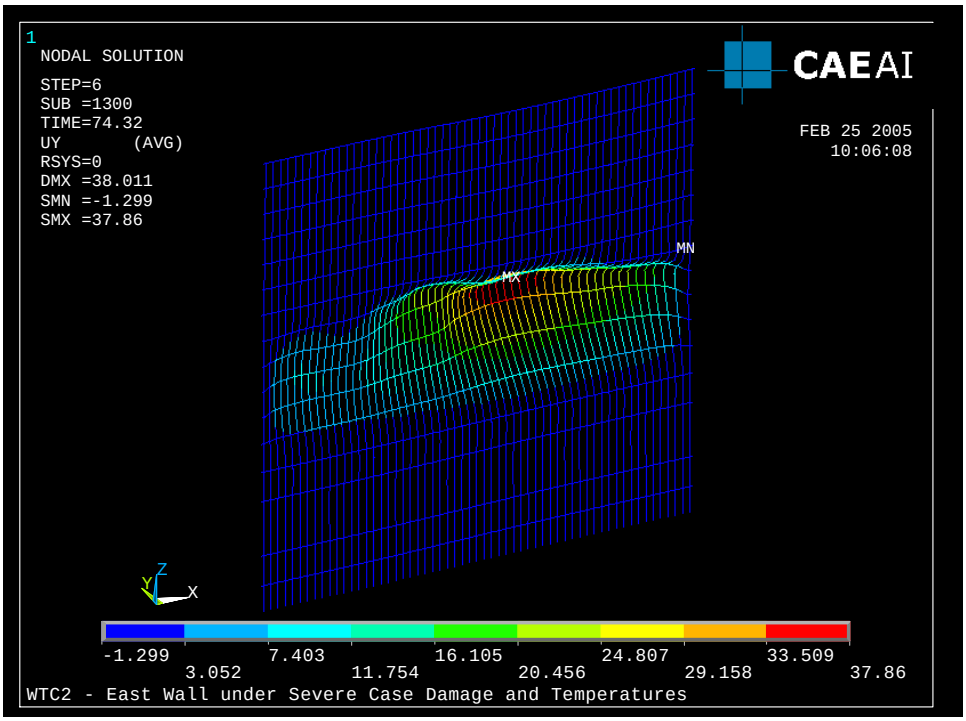

At 50 min

Figure E–10. Out-of-plane displacements of east wall of WTC 2 calculated with pull-in forces of 1.5 kip on the south half and 5.0 kip on the north half.

Structural Response of the WTC Towers

A separate global analysis of each tower helped determine the relative roles of impact damage and fires with respect to structural stability and sequential failures of components and subsystems and was used to determine the probable collapse initiation sequence.

Results of the major subsystem analyses were incorporated into the global models, reducing the complexity of the modeling approach and/or level of detail where possible, while retaining sufficient detail for nonlinear structural responses. The global models of the towers extended from several stories below the impact area to the top of the structure. WTC 1 was truncated at Floor 91 and WTC 2 was truncated from Floor 77. The global models included the core subsystem, the exterior wall subsystem, the hat truss, and an equivalent plate representation of the floor system. The core columns and exterior columns and spandrels were modeled with elements and features similar to those used in the isolated core and exterior wall analyses. Column analysis features included the effects of thermal expansion, plastic, and creep strains on column behavior within the global structural system. The full floor model was not included in the global models, as it would have made the models computationally too large. Instead, office area and core floors were modeled with an equivalent floor slab thickness and modulus calculated to match the in-plane stiffness of the composite floor system, including the concrete slab, floor trusses, and the floor seats. Floor loads applied as concentrated loads at the column connections. These modeling simplifications of the floor system were able to capture the floor behaviors observed in the full floor subsystem analyses while keeping the analysis tractable.

Each global model was first evaluated for stability under gravity loads, with structural impact damage modeled by removing severed and heavily damaged columns and floor areas. Temperature histories were applied in 10 min intervals and linearly ramped to the next temperature state. Pull-in forces from sagging floors were also applied during the appropriate 10 min intervals. The global analysis results provided a sequence of component and subsystem failures that led to the onset of global instability and collapse initiation.

WTC 1 Global Analysis Results

After the aircraft impact, gravity loads that were previously carried by severed columns were redistributed to other columns. The north wall lost about 7 percent of its loads after impact. Most of the load was transferred by the hat truss, and the rest was redistributed to the adjacent exterior walls by spandrels. Due to the impact damage and the tilting of the building to the north after impact, the south wall also lost gravity loads, and about 7 percent was transferred by the hat truss. As a result, the east and west walls and the core gained the redistributed loads through the hat truss.

In the early stages of the fire, structural temperatures in the core rose, and the thermal expansion of the core was greater than the thermal expansion of the exterior walls. The difference in the thermal expansion increased the loads in the core columns at about 20 min. Thereafter, the core lost gravity loads due to its thermal weakening and shortening until the south wall started to bow inward. At about 100 min, approximately 20 percent of the core loads were transferred by the hat truss to the exterior walls due to thermal weakening of the core; the north and south walls each gained about 10 percent more loads, and the east and west walls each gained about 25 percent more loads. Since the hat truss outriggers to the east and west walls were stiffer then the outriggers to the north and south walls, they transferred more loads to the east and west exterior walls.

The inward bowing of the south wall caused failure of exterior column splices and spandrels, and induced column instability. The instability progressed horizontally across the entire south face. The south wall unloaded and redistributed its gravity loads to the thermally weakened core through the hat truss and to the east and west walls through the spandrels. The building section above the impact zone began tilting to the south as column instability progressed rapidly from the south wall along the adjacent east and west walls, and increased the gravity load on the core columns. The change in potential energy due to downward movement of building mass above the buckled columns exceeded the strain energy that could have been absorbed by the structure. Global collapse then ensued.

WTC 2 Global Analysis Results

Before aircraft impact, the load distribution across the exterior walls and core was symmetric with respect to the centerline of each exterior wall. After aircraft impact, the exterior column loads on the south side of the east and west walls and on the east side of south wall increased. This was due to the leaning of the building toward the southeast. After aircraft impact, the core carried 6 percent less loads. The north wall loads reduced by 6 percent, and the east face loads increased by 24 percent. The south and west walls carried 2 percent to 3 percent more load.

In contrast to the fires in WTC 1, which generally progressed from the north side to the south side over approximately an hour, the fires in WTC 2 were located on the east side of the core and floors for the entire duration, with the fires spreading from south to north. With insulation dislodged over much of the same area, the structural temperatures became elevated in the core, floors, and exterior walls at similar times. During early stages of the fires, columns with dislodged insulation elongated due to thermal expansion. As the structural temperatures continued to rise, the thermal expansion was overcome by plastic and creep deformations under compressive loads.

Vertical displacements of the south and east exterior columns were essentially constant after impact and remained around 7.5 in. (over the severed columns) on the south face and about 3.5 in. on the east face until the east wall became unstable at 43 min. The east wall, which had bowed inward to a total of approximately 62 in., suddenly unloaded. The west wall also unloaded. Loads increased on the core and on the north and south walls. The core had weakened on the east side and shortened by 3.0 in. at the southeast corner. At the same time, the northwest corner of the exterior wall displaced upward about 2.0 in., as the tower was tilting to the southeast around an axis passing through the southwest and northeast corners.

The inward bowing of the east wall caused failure of exterior column splices and spandrels, and induced column instability. The instability progressed horizontally across the entire east face. The east wall unloaded and redistributed its gravity loads to the thermally weakened core through the hat truss and to the north and south walls through the spandrels. The building section above the impact zone began tilting to the east as column instability progressed rapidly from the east wall along the adjacent north and south walls, and increased the gravity load on the weakened east core columns. The change in potential energy due to downward movement of building mass above the buckled columns exceeded the strain energy that could have been absorbed by the structure. Global collapse then ensued.

Structural Response of the WTC Towers to Fire Without Impact Damage

Whether the towers would have collapsed if subjected to the same fires with no aircraft impact damage was considered as part of understanding the relative roles of the impact damage and fires. It was found from the global analyses that both WTC 1 and WTC 2 were stable after the aircraft impact and that they had considerable reserve capacity with structural impact damage. The global analyses also found that the combined effect of structural and insulation impact damage with the ensuing fires caused both towers to collapse. The effect of the fires on the towers without structural or insulation damage was considered by examining the subsystem and global analysis results for portions of the structures with intact insulation that were subject to the fires.

The towers would likely not have collapsed under the combined effects of aircraft impact and the subsequent multi-floor fires if the insulation had not been dislodged or had been only minimally dislodged by aircraft impact. The existing condition of the insulation prior to aircraft impact and the SFRM thickness on the WTC floor system did not play a significant role in initiating collapse of the towers.

Probable Collapse Sequences

To determine the probable collapse sequence for each tower, NIST adopted an approach that combined mathematical modeling, statistical and probability based analysis methods, laboratory experiments, and analysis of photographs and videos. The approach accounted for variations in models, input parameters, analyses, and observed events. It included the evaluation and comparison of possible collapse hypotheses based on different damage states, fire paths, and structural responses to determine the following:

- The probable sequence of events from the moment of aircraft impact until the initiation of global building collapse;
- How and why WTC 1 stood nearly twice as long as WTC 2 before collapsing (102 min for WTC 1 versus 56 min for WTC 2), though they were hit by virtually identical aircraft (Boeing 767-200ER);
- What factors, if any, could have delayed or prevented the collapse of the WTC towers.

Collapse hypotheses were developed over the course of the NIST Investigation. The first hypotheses were published in the May 2003 NIST Progress Report, and were updated in the June 2004 NIST Progress Report and October 2004 Public Meeting at NIST. The Probable Collapse Sequence for each tower was presented at the April 2005 Public Meeting in New York City. The stages of hypothesis development are summarized as follows:

- **Possible Collapse Hypotheses** (May 2003) – not building specific; key events not identified
- **Working Collapse Hypothesis** (June 2004) – single hypothesis for both WTC towers; identified chronological sequence of major events

- **Leading Collapse Hypotheses** (October 2004) – separate hypothesis for each WTC tower; identified building-specific load redistribution paths and damage scenarios in addition to chronological sequence of major events

- **Probable Collapse Sequences** (April 2005) – refined building specific collapse sequences with chronological sequence of major events, load redistribution paths, and damage scenarios.

To determine the probable collapse sequence for each tower, the following steps were required:

- identification of key observables, primarily from photographs and videos

- development of collapse hypotheses, which were updated periodically through the course of the investigation with the acquisition of new data and analysis results

- sensitivity studies to identify influential parameters, through the application of a formal statistical approach, orthogonal factorial design (OFD)

- development and refinement of mathematical modeling –fire dynamics simulation with computational fluid dynamics and structural response to aircraft impact and fire with finite element analyses

- evaluation of analysis results against observed and expected structural behavior, with adoption of the event tree concept, and pruning and updating branches based upon comparisons with observed data

These steps were applied to the degree needed for the sequence of analyses, from aircraft impact to structural response.

E.3 Probable Collapse Sequence of WTC 1 and WTC 2

The specific factors in the collapse sequences relevant to both towers (the sequences vary in detail for WTC 1 and WTC 2) are:

- Each aircraft severed exterior columns, damaged interior core columns, and knocked off insulation from steel as the planes penetrated the buildings. The weight carried by the severed columns was distributed to other columns.

- Subsequently, fires began that were initiated by the aircraft's jet fuel but were fed for the most part by the building contents and the air supply resulting from breached walls and fire-induced window breakage.

- These fires, in combination with the dislodged insulation, were responsible for a chain of events in which the building core weakened and began losing its ability to carry loads.
- The floors weakened and sagged from the fires, pulling inward on the exterior columns.
- Floor sagging and exposure to high temperatures caused the exterior columns to bow inward and buckle—a process that spread across the faces of the buildings.
- Collapse then ensued.

The sequences are supported by extensive computer modeling and the evidence held by NIST. The probable collapse sequences for WTC 1 and WTC 2 are presented in Figs. E–11 and E–12, respectively.

1. Aircraft Impact Damage

- Aircraft impact severed a number of exterior columns on the north wall from Floors 93 to 98, and the wall section above the impact zone moved downward.
- After breaching the building's exterior, the aircraft continued to penetrate into the building, severing floor framing and core columns at the north side of the core. Core columns were also damaged toward the center of the core and, to a limited extent, on the south side of the core. Fireproofing was damaged from the impact area to the south exterior wall, primarily through the center of WTC 1 and at least over a third to a half of the core width.
- Aircraft impact severed a single exterior panel at the center of the south wall between Floors 94 and 96.
- The impact damage to the exterior walls and to the core resulted in redistribution of severed column loads, mostly to the columns adjacent to the impact zones. The hat truss resisted the downward movement of the north wall, and rotated about the east-west axis.
- As a result of the aircraft impact damage, the north and south walls each carried about 7 percent less gravity loads after impact, and the east and west walls each carried about 7 percent more loads. The core carried about 1 percent more gravity loads after impact.

2. Effects of Subsequent Fires and Impact Damaged Fireproofing

A. Thermal Weakening of the Core:

- The undamaged core columns developed high plastic and creep strains over the duration the building stood, since both temperatures and stresses were high in the core area. The plastic and creep strains exceeded thermal expansion in the core columns.
- The shortening of the core columns (due to plasticity and creep) was resisted by the hat truss, which unloaded the core over time and redistributed loads to exterior walls.
- As a result of the thermal weakening (subsequent to impact and prior to inward bowing of the south wall), the north and south walls each carried about 10 percent more gravity loads, and the east and west walls each carried about 25 percent more loads. The core carried about 20 percent less gravity loads after thermal weakening.

B. Thermal Weakening of the Floors:

- Floors 95 to 99 weakened, with increasing temperatures over time on the long-span floors, and sagged. The floors sagged first and then contracted due to cooling on the north side; fires reached the south side later, the floors sagged, and the seat connections weakened.
- Floor sagging induced inward pull forces on the south wall columns.
- About 20 percent of the connections to the south exterior wall on Floors 97 and 98 failed due to thermal weakening of the vertical supports.

C. Thermal Weakening of the South Wall:

- South wall columns bowed inward as they were subjected to high temperatures and inward pull forces in addition to axial loads.
- Inward bowing of the south wall columns increased with time.

Figure E–11. WTC 1 probable collapse sequence.

3. Collapse Initiation

- The inward bowing of the south wall induced column instability, which progressed rapidly horizontally across the entire south face.
- The south wall unloaded and tried to redistribute the loads via the hat truss to the thermally weakened core and via the spandrels to the adjacent east and west walls.
- The entire section of the building above the impact zone began tilting as a rigid block (all four faces, not only the bowed and buckled south face) to the south (at least about 8º) as column instability progressed rapidly from the south wall along the adjacent east and west walls.
- The change in potential energy due to downward movement of building mass above the buckled columns exceeded the strain energy that could be absorbed by the structure. Global collapse then ensued.

Figure E–11. WTC 1 probable collapse sequence (cont).

1. Aircraft Impact Damage

- Aircraft impact severed a number of exterior columns on the south wall from Floors 78 to 84, and the wall section above the impact zone moved downward.
- After breaching the building's exterior, the aircraft continued to penetrate into the building, severing floor framing and core columns at the southeast corner of the core. Fireproofing was damaged from the impact area through the east half of the core up to the north and east exterior walls. The floor truss seat connections over about one quarter to one half of the east side of the core were severed on Floors 80 and 81 and over about one third of the east exterior wall on Floor 83.
- Aircraft impact severed a few columns near the east corner of the north wall between Floors 80 and 82.
- The impact damage to the exterior walls resulted in redistribution of severed column loads, mostly to the columns adjacent to the impact zones. The impact damage to the core columns resulted in redistribution of severed column loads mostly to other intact core columns and the east exterior wall. The hat truss resisted the downward movement of the south wall, and rotated about the east-west axis.
- As a result of the aircraft impact damage, the core carried 6 percent less gravity loads after impact and the north face carried 10 percent less loads. The east face carried 24 percent more gravity load, while the west face and the south face carried 3 percent and 2 percent more gravity load, respectively.
- After impact, the core was leaning toward the east and south exterior walls. The exterior walls acted to restrain the core structure.

Figure E–12. WTC 2 probable collapse sequence.

2. Effects of Subsequent Fires and Impact Damaged Fireproofing

A. Thermal Weakening of the Core:

- Several of the undamaged core columns near the damaged and severed core columns developed high plastic and creep strains over the duration the building stood, since both temperatures and stresses were high in the core area. The plastic and creep strains exceeded thermal expansion in the core columns.
- The core continued to tilt toward the east and south due to the combination of column shortening (due to plasticity, creep, and buckling) and the failure of column splices at the hat truss in the southeast corner.
- As a result of thermal weakening (subsequent to impact), the east wall carried about 5 percent more gravity loads, and the core carried about 2 percent less loads. The other three walls carried between 0 and 3 percent less loads.

B. Thermal Weakening of the Floors:

- Floors 79 to 83 weakened, with increasing temperatures over time on the long-span floors on the east side, and sagged.
- Floor sagging induced inward pull forces on the east wall columns.
- About an additional one third of the connections to the east exterior wall on Floor 83 failed due to thermal weakening of the vertical supports.

C. Thermal weakening of the east wall:

- East wall columns bowed inward as they were subjected to high temperatures and inward pull forces in addition to axial loads.
- Inward bowing of the east wall columns increased with time.

3. Collapse Initiation

- The inward bowing of the east wall induced column instability, which progressed rapidly horizontally across the entire east face.
- The east wall unloaded and tried to redistribute the loads via the hat truss to the weakened core and via the spandrels to the adjacent north and south walls.
- The entire section of the building above the impact zone began tilting as a rigid block (all four faces, not only the bowed and buckled east face) to the east (about 7º to 8º) and south (about 3º to 4º) as column instability progressed rapidly from the east wall along the adjacent north and south walls. The building section above impact continued to rotate to the east as it began to fall downward, and rotated to at least 20 to 25 degrees.
- The change in potential energy due to downward movement of building mass above the buckled columns exceeded the strain energy that could be absorbed by the structure. Global collapse then ensued.

Figure E–12. WTC 2 probable collapse sequence (cont).

E.4 FACTORS THAT AFFECTED PERFORMANCE

- From the collective knowledge and insights gained through the Investigation of the collapse of the WTC towers, the following factors were identified that enhanced the performance of both towers on September 11, 2001: The closely spaced columns, along with deep short spandrels, allowed a redistribution of loads as a result of aircraft impact damage to the exterior wall.

- Because there was effectively no wind on the morning of September 11, 2001, the capacity of the exterior wall provided to accommodate design wind loads was available to carry redistributed gravity loads.

- The large dimensional size of the WTC towers helped the buildings withstand the aircraft impact.

- The composite floor system with primary and bridging trusses forming a 2-way grid, and the two layers of welded wire fabric in the slab, acted to bridge over damaged areas without propagation of collapse from areas of aircraft impact damage to other locations, thereby avoiding larger scale floor collapse upon impact.

- The hat truss played a major role in the post-impact performance of the building. This was accomplished through redistribution of the loads from the significant weakening of the core, due to aircraft impact damage and subsequent thermal effects, by redistributing loads from the damaged core columns to adjacent intact columns and, ultimately, by redistributing loads to the exterior walls from the thermally weakened core columns that lost their ability to support the buildings' weight.

- The buildings would likely not have collapsed under the combined effects of aircraft impact and the subsequent jet-fuel ignited multi-floor fires, if the insulation had not been dislodged or had been only minimally dislodged by aircraft impact. The existing condition of the insulation prior to aircraft impact and the SFRM thickness on the WTC floor system did not play a significant role in initiating collapse on September 11, 2001.

E.5 FINDINGS

E.5.1 PASSIVE FIRE PROTECTION

The passive fire protection applied to the steel structural components in the WTC towers was investigated to provide information on the in-place condition of the thermal insulation before and after aircraft impact. The specified and "as applied" thicknesses, the variability in thickness, the condition of the insulation over a 30-year service life, and the effects that the variability and condition have on the structural behavior of insulated steel members were studied. The rationale behind the selection of the effective thickness of thermal insulation for use in thermal analyses was presented. Additionally, the procedures and practices used to provide the passive fire protection for the floor system of the WTC tower structures was documented.

Building Code Requirements for Structural Fire Resistance

Finding 1: The WTC towers were classified as Class 1B, as defined by the 1968 New York City Building Code. This classification required a 3 h fire rating for columns and 2 h for floors. The towers could have been classified as Class 1A since both Class 1A and 1B permitted buildings of unlimited height. Class 1A required a 4 h fire resistance rating for columns and a 3 h rating for floors. In 1969, the Port Authority specified the 0.5 in. SFRM for all beams, spandrels, and trusses, to maintain the Class 1A Fire Rating of the New York City Building Code. A condition assessment conducted in 2000 reported that the WTC towers were classified as Class 1B—noncombustible, fire-protected, and retrofitted with sprinklers in accordance with Local Law 5/1973.

Selection of Fire-Resistive Materials

Finding 2: The passive fire protection for the floor trusses was specified to be 0.5 in. of BLAZE-SHIELD Type D, although the technical basis for the selection of this product and required thickness value is not known. After applying the Type D sprayed fire-resistive material to the lower 40 floors of WTC 1, the BLAZE-SHIELD insulating material was switched to Type D/CF (reported to meet or exceed the insulating properties of Type D), which did not contain asbestos. In 1995, the Port Authority conducted a study to establish the SFRM requirements for the floor trusses in areas undergoing major tenant renovation. The thickness required to achieve a 2 h fire rating was determined to be 1.5 in. using the BLAZE-SHIELD II product. At the time of the WTC disaster, SFRM had been upgraded on a number of floors in the WTC towers: 18 floors in WTC 1, including all of the floors affected by the aircraft impact and fires, and 13 floors in WTC 2, although none were directly affected by the aircraft impact and fires.

Equivalent thickness of SFRM

Finding 3: Based on analyses of SFRM thickness measurements and interpretation of photographs showing the condition of the originally applied material, the average thickness of the original thermal insulation on the floor trusses was estimated to be 0.75 in. with a standard deviation of 0.3 in. (coefficient of variation of 0.40). The average thickness of the upgraded thermal insulation was estimated to be 2.5 in. with a standard deviation of 0.6 in. (coefficient of variation of 0.24). Based on finite-element simulations, it was concluded that the original passive fire protection on the floor trusses was thermally equivalent to a uniform thickness of 0.6 in., and the upgraded insulation was thermally equivalent to a uniform thickness of 2.2 in. These values were used in the thermal analyses for determining temperature histories of structural components.

Finding 4: No information was available on in-place conditions of the thermal protection on the exterior columns and spandrel beams, and little information was available on the conditions of fire-resistive material on core beams and columns. For thermal analyses of the towers, the SFRM on these elements was taken to have uniform thicknesses equal to the specified thickness. This assumption was supported by the observation that measured average thickness tended to be *greater* than the specified thickness while, due to variability, the effective thickness tended to be *less* than the average uniform thickness. The specified thickness values were 0.5 in. for beams and spandrels, 2.06 in. (2 1/16 in.) for columns lighter than 14WF228, and 1.19 in. (1 3/16 in.) for columns equal to or heavier than 14WF228.

Finding 5: The adhesive strength of BLAZE-SHIELD DC/F to primed steel was found to be a third to a half of the adhesive strength to steel that had not been coated with primer paint. The SFRM products used in the WTC towers were applied to steel components with primer paint.

E.5.2 FIRE RESISTANCE TESTS

Four Standard Fire Tests (ASTM E 119) were conducted on floor assemblies constructed to duplicate, as closely as practical, the floor system used in the WTC towers. Full scale tests with a 35 ft span, and having ¾ in. thick SFRM were tested; one in the restrained test condition and the other in the unrestrained test condition. Tests of half-scale specimens, which spanned approximately 17 ft, were conducted using SFRM conditions simulating the "as specified" condition (0.5 in. thick) and the "as-applied" condition (0.75 in. thick). The following findings are based on this series of four tests and a comparison of their results.

Structural Performance

Finding 6: Test assemblies, representative of the WTC floor system, exposed to the Standard Fire Test (ASTM E 119) conditions resulted in extensive spalling on the underside of the floor slab, thermal damage to the bridging trusses, and buckling of compression diagonals and vertical struts of the main trusses.

Finding 7: All four tests demonstrated that the floor assemblies were capable of sagging without failure. The unrestrained test, which had two 0.875 in. bolts fastening the main truss to the truss seats, did not sag sufficiently to bear on the bolts. In the three restrained tests, the main truss ends were welded to the truss seats to provide the required restraint. The magnitude of the sagging observed in the tests was consistent with that computed from finite element structural analyses. No evidence of knuckle failures was seen in the tests.

Finding 8: All four test assemblies supported their full design load under standard fire conditions for two hours without collapse.

Fire Resistance Ratings

Finding 9: The 1968 New York City (NYC) Building Code—the code that the WTC towers were intended but not required to meet when they were built—required a 2 h fire rating for the floor system.

Finding 10: The restrained floor system obtained a fire resistance rating of 1.5 h while the unrestrained floor system achieved a 2 h rating. This finding was unexpected since the unrestrained rating is typically less than the restrained rating.

Finding 11: The test of the 17 ft specimen with as-applied SFRM did not produce the same rating as the 35 ft test specimen, giving 2 h and 1.5 h, respectively. In both cases, the rating was established on the basis of temperatures of the unexposed surface (top of concrete slab) and not on the ability of the specimen to support the load.

Finding 12: The 45 min rating for the standard 17 ft test with the specified 0.5 in. SFRM did not meet the 2 h requirement of the 1968 NYC Building Code. This test had no SFRM on the bridging trusses nor on the underside of the metal deck.

Finding 13: The 2 h rating for the standard 17 ft test with the as-applied average 0.75 in. SFRM met the 2 h requirement of the 1968 NYC Building Code. This test had half the SFRM thickness on the bridging trusses (0.375 in.) and overspray on the underside of the metal deck.

Finding 14: The difference in test results for the two 17 ft specimens is due primarily to the concrete slab performance (spalling and cracking) and the presence or lack of SFRM overspray on the metal deck and not due to the SFRM thickness on the trusses. Differences in the degree of concrete spalling were possibly due to differences in moisture content and the slab cracking.

E.5.3 RESPONSE OF STRUCTURAL COMPONENTS

The response of the structural components and their connections for the tenant floors and exterior walls was examined with detailed structural models. Results of the floor and exterior wall component and connection analyses identified structural behaviors and failure modes that were required for inclusion in the global analyses.

Floor System

Finding 15: The interior truss seats had a greater vertical shear capacity than the exterior truss seats. The controlling failure mode for vertical shear was weld fracture. However, the vertical load at the truss connection of approximately 16 kip had to increase by a factor of two to six to reach failure (weld fracture) for temperatures near 600 °C to 700 °C.

Finding 16: Detailed structural analysis of a single truss section of the composite floor system subjected to elevated uniform temperatures was found to initially push out on the exterior columns as a result of the concrete slab thermal expansion and then pull inward as the web diagonals buckled and the truss sag increased. The magnitude of the pull-in force was found to depend highly on the stiffness of the exterior box column which, in turn, depended on expansion of floors above and below.

Finding 17: Detailed analysis of the knuckles (shear connectors in the floor system for composite action) through test simulation and detailed truss analysis found that failure of the knuckles in the floor system was unlikely. This finding was also supported by the lack of any knuckle failures in the four standard fire resistance tests (ASTM E119) of the floor truss assemblies with twice the floor load that was on the WTC floors.

Exterior Wall System

Finding 18: Large inelastic deformations and buckling of the spandrels at elevated temperatures were predicted, but were found not to significantly affect the stability of the exterior columns. Partial separations of the spandrel splices were also predicted at elevated temperatures, but were found not to significantly affect the stability of the exterior columns.

Finding 19: Analyses of bolted splices in the exterior columns found that the splice may slide or open when the exterior columns are bowing and subject to large lateral deflections. No column splice bolts were predicted to have failed.

Finding 20: An exterior wall section (9 columns wide and 9 floors high) was found to bow inward when the floor connections applied an inward pull force. For the condition where three sequential floors were disconnected, there was no bowing of the columns for five different elevated temperature conditions. When the column section with three disconnected floors was subjected to increased axial column loads, the wall section bowed outward over the unsupported column length.

E.5.4 FIRE PROTECTION AND PARTITION DAMAGE DUE TO AIRCRAFT IMPACT

The aircraft impacts into the WTC towers caused extensive damage to the buildings' exterior, penetrated into the interior causing further damage to the structural system, dislodged insulation, and ignited multi-floor fires. The structural damage to each tower resulting from the aircraft impact was estimated using a transient finite element analysis. Results of this analysis were used to predict damage to the structure, insulation, and partition walls in the path of the debris field.

Finding 21: For WTC 1, partitions were damaged and insulation was dislodged by direct debris impact over five floors (Floors 94, 95, 96, 97, and 98) and included most of the north floor areas between the north face and the core, the core, and central regions of the south floor areas, and on some floors, extended to the south wall. For WTC 2, partitions were damaged and insulation was dislodged by direct debris impact over six floors (Floors 78, 79, 80, 81, 82, and 83) and included the south floor area between the north face and the core, the central and east regions of the core, and most of the east floor area, and extended to the north wall.

Finding 22: The insulation damage estimates were conservative as they ignored possibly damaged and dislodged insulation in a much larger region that was not in the direct path of the debris but was subject to strong vibrations during and after the aircraft impact. Robust criteria to generate a coherent pattern of vibration-induced dislodging could not be established to estimate the larger region of damaged insulation.

E.5.5 OBSERVATIONS AND TIMELINE

Thousands of photographs and hours of video records were reviewed for insights into the structural performance of the towers. A timeline of significant events that characterized the weakening and eventual collapse of the WTC towers was developed with the photographs and videos that were time-stamped. Quantitative information, such as the amount of inward bowing observed on the exterior walls of the buildings, was extracted from key photographs through image enhancement and scaled measurements. Key observations and the timelines were used to guide the global collapse analyses.

WTC 1

Finding 23: Inward bowing of the south exterior wall was first observed at 10:23 a.m. The bowing appeared to extend between Floors 94 and 100 and Columns 305 and 359. The maximum bowing was estimated from images to be 55 in.±6 in. at Floor 97 on the east side of the south face of WTC 1. The central area in available images was obscured by smoke. The extent of fires observed on all faces of

WTC 1 was similar, although somewhat more extensive on the east and west faces (where short span floors were located) and similarly extensive on the north and south faces (where long span floors were located). Inward bowing was observed only on the south face. The north face had extensive aircraft impact damage, and the damaged floors were not capable of imposing inward pull forces on the north face.

Finding 24: The time to collapse initiation was 102 minutes from the aircraft impact (8:46:30 a.m. until 10:28:22 a.m.).

Finding 25: From exterior observations, tilting of the building section appeared to take place near Floor 98. Column buckling was then observed to progress rapidly across the east and west faces.

Finding 26: The WTC 1 building section above the impact and fire area tilted to the south as the structural collapse initiated. The tilt was toward the side of the building that had long span floors. Video records taken from east and west viewpoints showed that the upper building section tilted to the south. Video records taken from a north viewpoint showed no discernable east or west component in the tilt. A tilt to the south of at least 8 degrees occurred before dust clouds obscured the view and the building section began to fall downward.

WTC 2

Finding 27: On the east face and north face of WTC 2, draped objects were observed through the windows of Floor 82 on the east face and Floors 81 to 83 on the north face near the northeast corner. The draped objects appeared to be hanging floors. The drape of these objects was observed to increase with time and extend across approximately half of the east face.

Finding 28: Inward bowing of the east wall was first observed at 9:21 a.m. The inward bowing was approximately 10 in.±1 in. at Floor 80 and extended between Floors 78 and 83 and Columns 304 and 344. The remaining portion of the face to the south of Column 344 was not included in the image. The bowing appeared to extend over a large fraction of the east face and to be greatest near the center of the face. Fires were more extensive along the east face (where long span floors were located) and at the east side of the north and south faces (where short span floors were located). Fires were not observed on the west face (where long span floors were located). Inward bowing was observed only on the east face. The south face had extensive aircraft impact damage, and the damaged floors were not capable of imposing inward pull forces on the south face. There was no impact damage or fire on the west floors to cause pull-in forces on the west face.

Finding 29: An increase of the inward bowing of the east wall was observed at 9:53 a.m. The inward bowing appeared to extend between Floors 78 and 84 and Columns 305 and 341. The remaining portion of the face to the south of Column 344 was not included in the image. The maximum bowing was estimated from images to be 20 in.±1 in. at Floor 80 on the east face of WTC 1.

Finding 30: The time to collapse initiation was 56 minutes after aircraft impact (9:02:59 a.m. to 9:58:59 a.m.).

Finding 31: From exterior observations, tilt of the building section above the impact and fire area appeared to take place near Floor 82. Column buckling was then seen to progress across the north face.

Finding 32: The building section above the impact and fire area tilted to the east and south at the onset of structural collapse. The tilt occurred toward the east side with the long span floors. Estimates made from photographs indicate that there was approximately a 3 degree to 4 degree tilt to the south and a 7 degree to 8 degree tilt to the east, prior to significant downward movement of the upper portion of the building. The tilt to the south did not increase any further as the upper building section began to fall, but the tilt to the east continued, reaching 20 degrees to 25 degrees before dust clouds obscured the view.

E.5.6 STRUCTURAL RESPONSE OF MAJOR TOWER SUBSYSTEMS

Prior to conducting the analysis of the global structural response of each tower, major structural subsystems were analyzed to provide insight into their behavior within the WTC global system. The three major structural subsystems, the core framing, a single exterior wall, and full tenant floors, were analyzed separately for their response to impact damage and fire. The hat truss was not analyzed separately as its structural behavior did not require significant simplification in the global analysis. The component analyses provided a foundation for these large, nonlinear analyses with highly redundant load paths, and they enabled a significant reduction in finite element model complexity and size. The major subsystem models used final estimates of impact damage and elevated temperatures determined from the aircraft impact analysis and the fire dynamics and thermal analyses.

Isolated Core Subsystem

Finding 33: The WTC 1 isolated core subsystem analysis found that the core structure was most weakened from impact and thermal effects at the center of the south side of the core. Smaller displacements occurred in the global model due to the constraints of the hat truss and floors.

Finding 34: The WTC 2 isolated core subsystem analysis found that the core structure was unstable for the estimated structural damage to core columns. The core was most weakened from impact and thermal effects at the southeast corner and along the east side of the core. Larger displacements occurred in the global model as the isolated core model had lateral restraints imposed that were somewhat stiffer than in the global model.

Full Floor Subsystem

Finding 35: Floor sagging was caused primarily by either buckling of truss web diagonals or disconnection of truss seats at the exterior wall or the core perimeter. Except for the truss seat failures near the southeast corner of the core in WTC 2 following the aircraft impact, web buckling or truss seat failure was caused primarily by elevated temperatures of the structural components.

Finding 36: Analysis results from both the detailed truss model and the full floor models found that the floors began to exert inward pull forces when floor sagging exceeded approximately 25 in. for the 60 ft floor span.

Finding 37: Sagging at the floor edge was due to loss of vertical support at the truss seats. The loss of vertical support was caused in most cases by the reduction in vertical shear capacity of the truss seats due to elevated steel temperatures.

Isolated Exterior Wall Subsystem

Finding 38: Inward pull forces were required to produce inward bowing that was consistent with displacements measured from photographs. The inward pull was caused by sagging of the floors. Heating of the inside face of the exterior columns also contributed to inward bowing.

Finding 39: The observed inward bowing of the exterior wall indicated that most of the floor connections were intact to cause the observed bowing.

Finding 40: The floors that were identified through analysis to be affected by the fires and the dislodged insulation matched well with the floors that were observed to have participated in the inward bowing of the exterior walls.

Finding 41: The extent of floor sagging required at each floor was greater than that predicted by the full floor models. The estimates of the extent of sagging at each floor were governed by the combined effects of insulation damage and fire; insulation damage estimates were limited to areas subject to direct debris impact. Other sources of floor and insulation damage from the aircraft impact and fires (e.g., insulation damage due to shock and subsequent vibrations as a result of aircraft impact or concrete slab cracking and spalling as a result of thermal effects) were not included in the floor models.

E.5.7 STRUCTURAL RESPONSE TO AIRCRAFT IMPACT DAMAGE AND FIRE

Global analysis of WTC 1 and WTC 2 used final estimates of impact damage and elevated temperatures to determine the structural response and sequence of component and subsystem failures that led to collapse initiation.

General Findings

Finding 42: The structural analyses of WTC 1 and WTC 2 found that the collapse of the towers was due to the combined effects of structural and insulation damage from aircraft impact and the subsequent fires on the core, floor systems and exterior walls. The towers collapsed when the weakened core and exterior columns could no longer redistribute or support the building loads with their reduced load carrying capacity.

Finding 43: Impact damage alone did not cause collapse of the towers, as they were stable after the aircraft impact. Global analyses showed that both towers had substantial reserve capacity after the aircraft impact.

Finding 44: The multi-floor fires alone did not cause collapse of the towers. Without impact damage to the insulation, the structural steel temperatures would have been generally less than 200 °C to 300 °C, with a few isolated locations of structural steel temperatures exceeding 400 ˚C in WTC 1 floors and 500 ˚C in WTC 2 floors. The core would not have weakened, the floor sag would have been insufficient to pull inward on the exterior columns, and the exterior walls would not have bowed inward.

Finding 45: The towers would likely not have collapsed under the combined effects of aircraft impact and the subsequent multi-floor fires if the insulation had not been dislodged or had been only minimally dislodged by aircraft impact. Had insulation not been dislodged by the debris field, temperature rise of

structural components would likely have been insufficient to induce global collapse. Structural components that became thermally weakened were generally determined by impact of the debris field. The existing condition of the insulation prior to aircraft impact and the insulation thickness on the WTC floor system did not play a role in initiating collapse of the towers.

Finding 46: Creep strain was significant in the core and exterior columns over the 56 min to 102 min period of fire exposure in columns with temperatures greater than 500 ˚C to 600 ˚C and high stress. Columns with creep strains of sufficient magnitude to cause column shortening played a significant role in the collapse initiation.

Finding 47: The faces of the buildings that exhibited inward bowing were associated with the long span direction of the floor system. The primary direction of tilting at collapse initiation for WTC 1 and WTC 2 was in the direction of the bowed faces.

Performance with Intact Fire Protection

Finding 48: A detailed thermal-structural analysis, which did not include slab delamination/spalling effects, showed that a full collapse of the WTC floor system would not occur even with a number of failed trusses or connections.

Finding 49: Most of the horizontal and vertical capacity of the floor connections to the exterior and core columns significantly exceeded the demand under design load conditions.

E.5.8 PROBABLE COLLAPSE SEQUENCES

The results of structural analyses conducted in this study on components, subsystems, isolated exterior walls, cores, and global models of WTC 1 and WTC 2 showed that the collapses of the towers were initiated due to the combined effects of the structural and insulation damage from aircraft impact and the subsequent intense fires. The probable collapse sequence for WTC 1 and WTC 2 are based upon the collective consideration of structural analyses, statistical based methods, observations, and laboratory testing.

Role of the Building Core

Finding 50: The core columns were weakened significantly by the aircraft impact damage and thermal effects. Thermal effects dominated the weakening of WTC 1. As the fires moved from the north to the south side of the core, following the debris damage path, the core was weakened over time by significant creep strains on the south side of the core. Aircraft impact damage dominated the weakening of WTC 2. Immediately after impact, the vertical displacement at the southeast corner of the core increased 6 in. (from 4 in. to 10 in.). With the impact damage, the core subsystem leaned to the southeast and was supported by the south and east floors and exterior walls.

Finding 51: As the core was weakened from aircraft impact and thermal effects, it redistributed loads to the exterior walls primarily through the hat truss. Additional axial loads redistributed to the exterior columns from the core were not significant (only about 20 percent to 25 percent on average) as the exterior columns were loaded to approximately 20 percent of their capacity before the aircraft impact.

Role of the Building Floors

Finding 52: The primary role of the floors in the collapse of the towers was to provide inward pull forces that induced inward bowing of exterior columns (south face of WTC 1; east face of WTC 2).

Finding 53: Sagging floors continued to support floor loads as they pulled inward on the exterior columns. There would have been no inward pull forces if many of the floor truss seats had failed and disconnected.

Role of Exterior Frame-Tube

Finding 54: Column instability over an extended region of the exterior face ultimately triggered the global system failure as the loads could not be redistributed through the hat truss to the already weakened building core. In the area of exterior column buckling, load transferred through the spandrels to adjacent columns and adjacent exterior walls. As the exterior wall buckled (south face for WTC 1 and east face for WTC 2), the column instability propagated to adjacent faces and caused the initiation of the building collapse.

Finding 55: The exterior wall instability was induced by a combination of thermal weakening of the columns, inward pull forces from sagging floors, and to a lesser degree, additional axial loads redistributed from the core.

Probable Collapse Sequences

Finding 56: Although the north face of WTC 1 had extensive impact damage, thermal weakening of the core columns on the south side of the core and inward bowing of the south face caused the building to tilt to the south at collapse initiation. The extent of fires observed on all faces of WTC 1 was similar, although somewhat more extensive on the east and west faces (where short span floors were located) and somewhat less extensive on the north and south faces (where long span floors were located). Thermal weakening of exterior columns with floor sagging (which induced inward pull and occurred on the south side) caused inward bowing of the south face and tilting in the south direction.

Finding 57: Although the south face of WTC 2 had extensive impact damage, thermal weakening of the core columns on the east side of the core and inward bowing of the east face caused the building to tilt more to the east and less to the south at collapse initiation. Fires were more extensive along the east face and at the east side of the north and south faces. Thermal weakening of exterior columns with floor sagging (which induced inward pull and occurred on the east side) caused inward bowing of the east face and primary tilting in that direction (with additional southward tilting due to the aircraft impact damage).

Finding 58: The time it took for each WTC tower to collapse was due primarily to the differences in structural damage, the time it took the fires to travel from the impact area across the floors and core to critical locations, and the time it took to weaken the core and exterior columns. WTC 2 had asymmetric structural damage to the core, including the severing of a corner core column, and WTC 1 had more symmetrical damage. The fires in WTC 2 reached the east side of the building more quickly, within 10 to 20 minutes, than the 50 min to 60 min it took the fires in WTC 1 to reach the south side.

Finding 59: NIST found no corroborating evidence for alternative hypotheses suggesting that the WTC towers were brought down by controlled demolition using explosives planted prior to September 11, 2001. NIST also did not find any evidence that missiles were fired at or hit the towers. Instead, photographs and videos from several angles clearly showed that the collapse initiated at the fire and impact floors and that the collapse progressed from the initiating floors downward, until the dust clouds obscured the view.

Chapter 1
INTRODUCTION

1.1 PROJECT OBJECTIVES

The National Institute of Standards and Technology (NIST) investigation into the collapse of the World Trade Center (WTC) towers had eight interdependent projects. The purpose of each project is summarized in Table P–1, and the key interdependencies among the projects are illustrated in Fig. P–1, found in the Preface to this report.

One of the four objectives of the technical investigation was to determine why and how the WTC towers (WTC 1 and WTC 2) collapsed following the initial impacts of the aircraft. This objective is addressed in this report. Both the north and south towers of the World Trade Center were severely damaged by the impact of Boeing 767 aircraft, yet they remained standing for some time. The ensuing fires were observed to move through both buildings and eventually, both buildings collapsed. The extent and relative importance of the damage caused by the aircraft impact and subsequent weakening by fires were investigated under this project, *Structural Fire Response and Collapse Analysis*. This report presents the technical approach, modeling and testing methodologies, summary of results, and findings of the structural response of the WTC towers to aircraft impact damage and ensuing fires.

In addition, this project contributes to another investigation objective by determining the procedures and practices that were used in establishing the fire resistance ratings and providing passive fire protection to the components that made up the WTC tower structures.

The purpose of the project was to analyze the response of the WTC towers to fires – both with and without aircraft damage – and to determine the probable sequence of structural collapse for each tower. Specifically, this project attempted to:

- Determine the pre- and post-aircraft impact condition of the passive fire protection used to thermally insulate the structural members and provide resistance to fire damage,
- Conduct tests of structural components and systems under fire conditions to quantify their behavior,
- Evaluate the response of floor and column components and subsystems under fire conditions to understand their response,
- Evaluate the response of the WTC towers under fire conditions, with and without aircraft impact damage, and
- Determine the probable sequence of structural collapse for each WTC tower.

The project relied primarily on a series of computer simulations to model the complete sequence of events leading to the initiation of collapse of the WTC towers. The analyses included the damage to the towers

resulting from aircraft impact, the spread of multi-floor fires ignited by jet-fuel, the heating and thermal weakening of structural components, and the progression of local structural failures that led to the collapse of the buildings. Each of these models advanced the current state of the art and tested the limits of computational capabilities. The unprecedented complexity and sophistication of these analyses required the use of various strategies for managing the computational demands while adequately capturing the essential physics. The overall approach -- from impact analysis to collapse initiation -- combined mathematical modeling, statistical and probability-based analysis, laboratory testing, and analysis of photographic and videographic records.

1.2 TECHNICAL APPROACH AND TASKS

Events that played a significant role in the structural performance of the towers on September 11, 2001, were the aircraft impact, the fireballs immediately following the aircraft impact, and the ensuing fires across multiple floors in each tower. To estimate the structural response, detailed information was required on the condition of the structural system and its passive fire protection system, both before and after the aircraft impact. During the ensuing fires that resulted in elevated structural temperatures, information on the degradation of the stiffness and strength of the structural system was also required.

Data was collected and reviewed from a number of sources. Such data included structural geometry, details, and connections; thermal and mechanical (adhesion/cohesion) properties of fire resistant materials; the thickness and condition of the passive fire protection in the towers; and recorded observations of structural events subsequent to aircraft impact and prior to collapse. Information about tower construction was obtained from original drawings and specifications, reports, and available records from The Port Authority of New York and New Jersey (PANYNJ or Port Authority), Leslie E. Robertson Associates (LERA), Silverstein Properties, and a number of contractors that had worked on the design, construction, or modifications to the towers. Information about the events that occurred in each tower on September 11, 2001, was obtained from analysis of available photographic and videographic records, eyewitness accounts, and metallurgical analysis of recovered structural steel.

The analyses performed to determine the probable collapse sequence for each tower considered the as-built structural systems and their response to aircraft impact damage, temperature-dependent properties of steel and concrete, growth and spread of the fires, and heating of structural components. The structural response analyses relied upon the following information:

- Reference global structural models of the WTC 1 and WTC 2 towers, and typical floor and exterior wall subsystem models (NIST NCSTAR 1-2)[2]

- Extent of damage to the structural systems and interior contents of the WTC 1 and WTC 2 towers resulting from aircraft impact (NIST NCSTAR 1-2)

- Temperature-dependent mechanical properties of the steels, welds, and bolts used in the construction of the towers, including elastic, plastic, and creep properties from 20 ºC to 700 ºC (NIST NCSTAR 1-3)

[2] This reference is to one of the companion documents from this Investigation. A list of these documents appears in the Preface to this report.

- Time-temperature histories for structural components and connections for both standard fires (e.g., ASTM E 119) and actual fires based on fire dynamics simulations (NIST NCSTAR 1-6B).

- Photographic and videographic records with time stamps that documented the observed sequence of events (NIST NCSTAR 1-5).

To simulate the effects of aircraft impact into the towers, the growth and spread of fires, and the subsequent weakening of the structural system that ultimately led to collapse, a series of sophisticated computer analyses was conducted. The results of any computer analysis depend on the fidelity of the input data and the ability of the computer software to capture the fundamental physics that produce the output response.

The WTC towers were large, complex structural systems. To include all of the structural components and connections and their associated behavior and failure mechanisms using refined finite element meshes would have been prohibitive. The analysis approach used was a variant of the well-established sub-structuring approach, adapted for the analysis of structures with highly nonlinear behavior, that progressed from individual components to major subsystems to global systems, as shown in Fig. 1–1. Extensive component analyses were conducted to identify critical behavior and failure mechanisms that contributed to the global structural response of each tower. Similarly, extensive subsystem analyses were then performed. These analyses incorporated the behavior and failure mechanisms identified in the component studies, with modifications to reduce the model size and complexity, thereby enhancing computational performance, without adversely affecting the quality of the results. Whenever modeling modifications were used, they were validated against the detailed component model results. The global analyses incorporated critical behavior and failure mechanisms, determined from subsystem analyses, while making necessary modifications in the level of modeling detail.

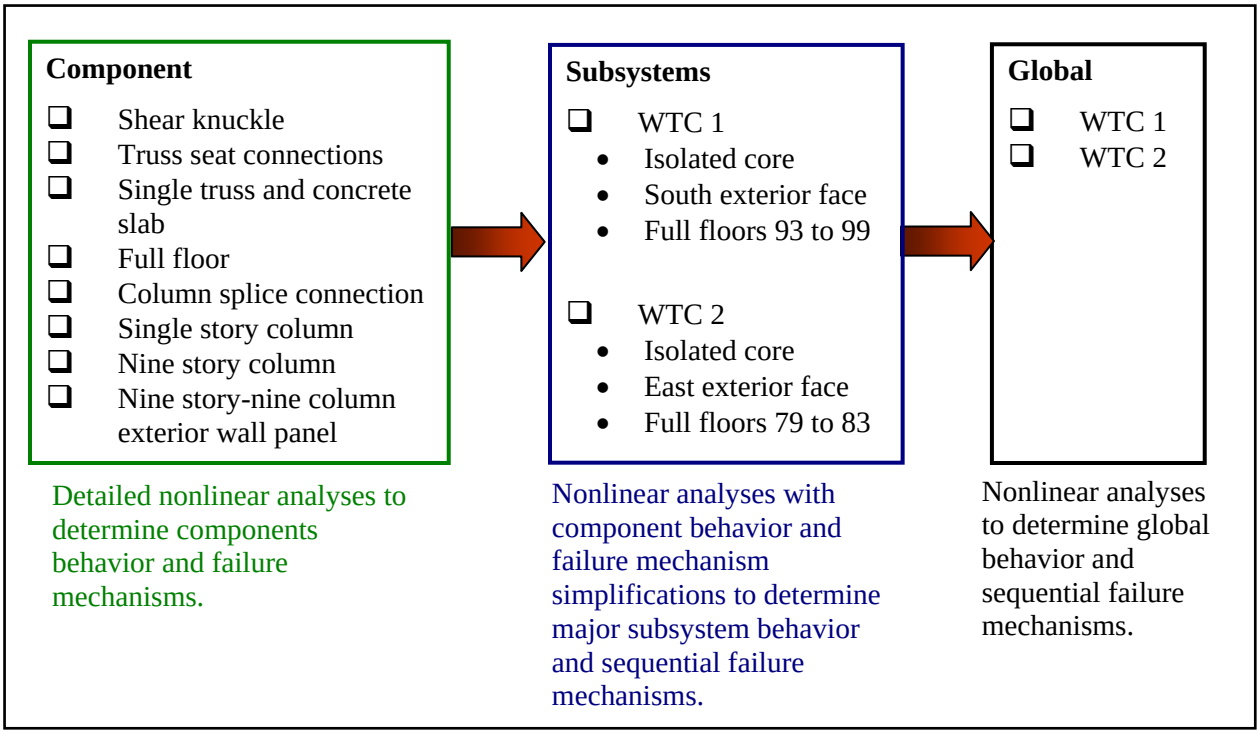

Figure 1–1. Structural Analysis Sequence.

As shown in Fig. 1–1, the structural response analyses began with the analysis of components, connections, and subsystems to develop an understanding of their structural behavior at elevated temperatures and associated failure mechanisms. Components, used herein, included single structural elements, such as a column or a truss web member. Subsystems were groups of components that had a major structural function, such as a floor system. Connections, such as a column splice or a floor truss seat, transfer loads between components or subsystems. Results of the component and subsystem analyses were used to develop the global models that were used to determine the global behavior and sequential failure mechanisms.

The response of WTC 1 and WTC 2 global systems was estimated by (1) evaluating the response of floor and column components, connections, and subsystems under thermal loading, (2) evaluating the response of the WTC towers with and without aircraft impact damage under actual fire conditions, (3) conducting tests of structural components and systems under fire conditions, and (4) developing and evaluating collapse hypotheses for the WTC towers. The effort, including work performed outside the scope of this project, was divided into the following tasks:

1.2.1 Task A – Finite Element Reference Models

Develop finite element models based on reference models: Modeling the structure of the towers, whether for the assessment of aircraft impact, the growth and spread of fires, or the structural response to those fires, necessitated that the geometry, cross-sectional properties, and the material properties of the structural components be a faithful representation of the actual structures. To that end, reference finite element models of both towers (since they were not identical) were developed. This was done under a contract to Leslie E. Robertson Associates (LERA), the designers of the WTC towers, within the

framework of Project 2 of the Investigation. The models underwent a thorough review process, including an in-house NIST review and a third-party review by the firm of Skidmore, Owings& Merrill LLP (SOM), also under contract to NIST, to test the accuracy of the models. The reviews included checking the consistency of the models with the original design documents, verification and validation of the models (including assumptions and level of detail), and testing the accuracy of the models under various loading conditions. The development of the reference models is described in NIST NCSTAR 1-2. These reference models became the basis for all subsequent finite element analyses.

1.2.2 Task B – Material Properties

Develop the constitutive relationships for the materials used in the construction of the towers: Properties of the structural steels used in the construction of the towers were part of the fundamental data needed for the development of models. Mechanical and chemical properties were determined for steel specimens recovered from the WTC site to assure that the materials used were in conformance with those specified in the original design. Further, the behavior of the structural steels used was characterized to determine the mechanical properties at high loading rates for the aircraft impact analyses and at elevated temperatures (from room temperature to 800 ºC) for the thermal-structural response analyses. Properties of structural materials are given in NIST NCSTAR 1-3 and summarized in Chapter 4 of this report.

1.2.3 Task C – Passive Fire Protection

Characterize the passive fire protection applied to the structural steel: The type of SFRM materials and required thickness were specified in correspondence between the Port Authority and SFRM contractor. Estimates of the characteristics of SFRM materials were deemed essential for the thermal-structural modeling of the towers. Of primary importance was the condition of the sprayed fire-resistive material (SFRM) used since the type of material (hence its thermal insulating properties), its average applied thickness, and variation in application thickness all had an effect on the temperatures developed in the structural elements as a result of exposure to fire. Since upgrading of the SFRM was begun in the 1990s, and the upgraded thickness was greater than that originally applied, it was important to determine: (1) the areas in the buildings where upgrading had been completed, and (2) the average thickness and its associated variability. Chapter 2 of this report addresses the passive fire protection and its application, the determination of thermal properties, and calculation of an equivalent uniform thickness of material used for the thermal and structural finite element analyses. Detailed information and a complete description of the procedures and practices used in the selection of fire protection for the WTC project is covered in NIST NCSTAR 1-6A.

1.2.4 Task D – Standard Fire Resistance Tests

Conduct standard fire resistance tests of composite truss floor system: Tests were conducted to: (1) establish the baseline fire resistance rating of the composite truss floor system used in the WTC towers, (2) understand the influence of thermal restraint by testing the floor system under both thermally unrestrained and fully restrained conditions, and (3) provide experimental data to validate and provide guidance to the development of the floor models and to the interpretation of analyses results. The standard ASTM E 119 fire test was selected since it represents a fairly severe condition both in the fire exposure and specimen loading and provides a frame of reference with respect to the historical performance of alternative floor systems. Four tests, representing both full-scale and reduced-scale

specimens, are covered in Chapter 3 of this report and are reported in more detail in NIST NCSTAR 1-6B.

1.2.5 Task E – Aircraft Impact Damage

Establish the damage to the structure, insulation, and partition walls as a result of aircraft impact: The damage induced by the impact of a Boeing 767 aircraft into each tower had significant influence on many facets of the analytical investigation into how and why the towers collapsed. First, the aircraft impact resulted in significant damage not only to the exterior of the buildings, but also to the floors and core structures inside the buildings and as a consequence, weakened the structures to some degree. Second, the jet fuel dispersed inside the towers ignited the building contents and furnishings, and the damage to the buildings' facades as well as damage to the interiors influenced the amount of oxygen reaching the fires and, therefore, the speed at which the fires grew and moved throughout the affected floors. Third, the impacts of the jet aircraft were of sufficient force to dislodge significant portions of the all-important SFRM in the impact and fire-affected regions. The finite element analyses required to predict the extent of damage due to aircraft impact are presented in NIST NCSTAR 1-2. This information was then used to estimate the extent of the SFRM damage based on the results of impact simulations, including the paths of the debris field and damage to interior partitions and furnishings. Chapter 5 summarizes the results of the impact damage and the approach used to estimate the extent of insulation damage.

1.2.6 Task F – Observations and Timeline

Document observations and data for structural events: NIST has made concerted efforts to validate analysis results with key observations obtained from its extensive collection of over 7,000 photographs and over 150 hours of videotape (NIST NCSTAR 1-5A) documenting the events at the World Trade Center on September 11, 2001. Development of the probable collapse sequence for each tower was shaped by evidence gathered from these photographs and videos, along with eyewitness accounts. The photographs and videos provided knowledge about aircraft impact damage to the exterior walls, fire growth and spread at the building exterior, inward bowing of an exterior wall in each tower, and the direction of tilt for the building section above the impact and fire zone as the towers collapsed. Evidence was used in the analyses in three ways: (1) to determine input parameters, such as the aircraft speed and trajectory upon impact, (2) to impose time-related constraints upon an analysis, such as imposing observed broken windows over time thereby affecting the spread of fire, or (3) to validate analysis results, such as global stability after impact and during thermal loading. A timeline of impact, fire, and structural events was developed for each tower, primarily from photographs and videos. Analyses were used to develop and refine the probable sequence of events between timeline observations. The quality of the results compared to the visual and physical evidence supports NIST's view that the significant phenomena relevant to the probable collapse sequence have been adequately captured. Details of this task are provided in Chapter 6 of this report.

1.2.7 Task G – Temperatures of Structural Components

Compute temperature histories for structural components subjected to fires: After the aircraft impacted each building, fires started on multiple floors, ignited by the rapid spread of burning jet fuel. To determine how the towers were affected by the high temperatures resulting from the fires, estimates of the growth and spread of fires over time were developed using fire dynamics simulations. These were based

on sophisticated computational fluid dynamics (CFD) modeling as described in NIST NCSTAR 1-5. These computations relied on: (1) the fire loads on each floor, (2) estimated ventilation as determined from the aircraft impact analyses (Task E), and (3) window breakage resulting from the fires as determined from photographic interpretation (Task F). Temperatures of the steel structural components and concrete floor slabs were predicted using accurate models of the structures (Task A), thermal properties of the steel and concrete (Task B), thermal properties of the insulation applied to protect the steel and its equivalent uniform thickness (Task C), and the time and spatially varying temperature fields predicted from the fire dynamics calculations as described above. The thermal analyses conducted to estimate realistic temperatures in the steel and concrete are covered in NIST NCSTAR 1-5.

1.2.8 Task H – Component and Subsystem Analyses

Conduct component and subsystem analyses: The purpose of these analyses was to provide a basic understanding of the behavior of the various structural components and subsystems of the towers under gravity and thermal loading and to develop reduced models that could be reliably used in the global models. The subsystems considered in this phase of the study included: (1) typical floor subsystem with its associated components: (a) the shear knuckles, (b) seats, and (c) a single truss and concrete slab; and (2) a nine-story by nine-column exterior wall subsystem with its associated components (a) bolted connection between exterior columns, (b) bolted connection between spandrels, (c) single exterior column with spandrel sections, and (d) single exterior wall panel with three columns and three spandrels. The floor and exterior wall subsystems included modeling reductions as developed from the component models. The models were based on the reference models developed in Task A, material properties estimated in Task B, and SFRM thickness and properties determined from Task C. The floor components and subsystem models were verified using the standard fire test results (Task D). Chapter 4 of this report describes the development of the component and subsystem models.

1.2.9 Task I – Major Subsystem Analyses

Conduct analyses of major subsystems: Analyses of three major subsystems - the isolated core framing subsystem, an exterior wall subsystem, and the core floor subsystems - were analyzed to determine their ability to resist and redistribute loads after impact damage and elevated temperatures. These major subsystem models used final estimates of impact damage and elevated temperatures determined from the aircraft impact analysis (Task E) and the fire dynamics and thermal analyses (Task G). The subsystem models used modifications from the component analyses, which kept the analysis solution times reasonable while maintaining required nonlinear features and failure modes. These analyses were crucial for determining critical structural behaviors of the

Chapter 5 summarizes the results of the analysis of aircraft impact damage to the WTC towers. The chapter describes how the structural damage due to impact was imposed on the subsystem and global models used in this study and outlines the methodology used to estimate the damage to insulation as a result of aircraft impact.

Chapter 6 describes the observations and timeline of structural events. The observations and timeline are based primarily on photographic and videographic records. Key observations were used to help validate the probable collapse sequence for each tower.

Chapter 7 describes the analyses conducted for three major tower subsystems to aircraft impact damage and fire. These analyses included full floors, core columns, and exterior walls of WTC 1 and WTC 2 in the impact and fire zones. These analyses were conducted prior to the global analysis for each tower. Each analysis description includes details of the model, applied loads, and structural results.

Chapter 8 describes the global structural response of each WTC tower to aircraft impact damage and fire conditions. The model for each tower is described, including aircraft impact damage and temperature-histories for the observed fires. Modeling simplifications based on the previous analyses are described, and the results of the analyses are presented. The chapter also evaluates the structural response of the WTC towers to fire conditions without aircraft impact damage. A separate global analysis was not conducted for this analysis. Instead, the results from the analyses conducted in previous chapters are used as the basis for evaluating this hypothetical condition.

Chapter 9 presents the probable collapse sequence for each tower, based on the analysis results presented in Chapter 8 and the key observations presented in Chapter 6.

Chapter 10 presents the findings of the study.

This page intentionally left blank.

Chapter 2
PASSIVE FIRE PROTECTION

Many structural materials are adversely affected by high temperatures resulting from an uncontrolled building fire where compartment temperatures can reach 1,100 ºC (2,000 ºF). Generally, some means of protecting, or insulating, the structural components is required to provide an acceptable level of performance in fire. Steel, for example, loses both its strength and stiffness at the elevated temperatures associated with building fires, and an insulating barrier is required to slow or prevent damage to structural steel components.

The structural steel in the World Trade Center (WTC) towers was protected with sprayed fire-resistive material (SFRM) or rigid fire-rated gypsum panels. SFRMs are a combination of fibrous material and cementitious binder that, when mixed with water, can be spray-applied to the steel (Gewain et al. 2003). With time, the cementitious materials harden and the excess water evaporates, and when dry, SFRMs provide an insulation barrier to limit excessive temperature rise in the steel during a fire. Similarly, fire-rated gypsum wallboard was used to enclose some structural steel core columns to provide the required level of fire protection.

The structural analysis of the WTC towers focused on the response of the two towers damaged by the aircraft impact and exposed to the subsequent fires. To reduce the uncertainties in the calculated temperature histories of various structural elements, the thermal properties and condition of the passive fire protection as it existed on September 11, 2001, was estimated as accurately as possible. In addition, reasonable estimates of the extent of SFRM dislodged by the aircraft impact and flying debris were made (see Chapter 5).

NIST NCSTAR 1-6A reports on many aspects of the passive fire protection in the WTC towers, beginning with an overview of U. S. building regulations that are intended to provide structural fire resistance. The report continues with a chronicle of the procedures and practices used in the selection and application of the SFRMs used in the construction of the WTC towers. The variability of SFRM application on the uncertainty in estimating the steel temperatures is covered. Finally, the thermal and mechanical properties of the SFRM materials are reported. This chapter summarizes the salient material covered in NIST NCSTAR 1-6A.

2.1 FIRE RESISTANCE OF STRUCTURAL ELEMENTS

Building codes require that elements that support loads are to be protected to achieve a specified fire resistance rating[3], expressed in hours. The fire rating of structural materials and assemblies is generally determined through testing, and in the United States, such testing is frequently conducted in accordance with the ASTM International standard, ASTM E 119, “Standard Test Methods for Fire Tests of Building Construction and Materials” (ASTM 2000).

[3] The term “fire resistance rating” (or simply “fire rating”) is variously called in the ASTM E 119 Standard, “period of resistance,” “performance,” “exposure” or classification.”

Building codes generally require the highest fire resistance rating for columns and other elements supporting multiple floors, and a somewhat lower resistance rating for columns and other elements supporting single floors, and for floors. The required fire resistance ratings have been reduced in recent years when fire sprinklers are installed in high-rise and other commercial buildings. In the past, high-rise buildings generally required a 4 h rating for columns; this has been reduced to 3 h in recent model codes, and can be as low as 2 h in current model codes, based on the additional mandatory requirement for sprinklers. Some codes allow a reduction in fire-resistance rating for high-rise buildings that have been retrofitted with sprinklers.

2.2 HISTORICAL REVIEW RELATED TO PASSIVE FIRE PROTECTION

2.2.1 Building Code Requirements for the Design of the WTC Towers

As an interstate compact, The Port Authority of New York and New Jersey (Port Authority or PANYNJ) was not required to comply with the New York City Building Code (NYCBC 1968), or any other building code, for the design and construction of the WTC towers. The Port Authority, however, made explicit statements that it would comply with the New York City Building Code. In a letter dated May 15, 1963[4], the Port Authority instructed its consulting engineers and architects to comply with the New York City Building Code. In areas where the Code was not explicit or where technological advances made portions of the Code obsolete, it directed that design could be based on acceptable engineering practice. At that time, the 1938 edition of the New York City Building Code was in effect, and a revised code was being drafted. In a directive dated September 29, 1965[5], the Port Authority instructed its consultants to revise the WTC design plans to comply with the second and third drafts of the Code revision. The revised New York City Building Code became effective in December 1968.

2.2.2 New York City Building Code Requirements

Application of the 1968 New York City Building Code (NYCBC) provisions affected the assigned building classification and, thus, the required fire rating of the WTC towers and their structural members. The WTC towers were classified as Occupancy Group E—Business. The 1968 NYCBC identified two construction groups: Noncombustible Construction (Group 1) and Combustible Construction (Group 2). The WTC towers were classified as Construction Group 1 because their walls, exit ways, shafts, structural members, floors, and roofs were constructed of noncombustible materials. At the time of design and construction, the towers were not sprinklered.

The 1968 New York City Building Code defined five Classes within Construction Group 1. For Business occupancy, each Class required a fire endurance rating as follows:

- Class 1A: 4-hour protected
- Class 1B: 3-hour protected

[4] Letter dated May 15, 1963 from Malcolm P. Levy (Chief, Planning Division, World Trade Department) to Minoru Yamasaki (Minoru Yamasaki & Associates) - see NIST NCSTAR 1-6A, Appendix Figure A-1.

[5] Letter dated September 29, 1965 from Malcolm P. Levy (Chief, Planning Division, World Trade Department) to Minoru Yamasaki (Minoru Yamasaki & Associates) – see NIST NCSTAR 1-6A, Appendix Figure A-2.

- Class 1C: 2-hour protected
- Class 1D: 1-hour protected
- Class 1E: unprotected

Construction Classes 1A and 1B permitted buildings of unlimited height. Thus, the WTC towers could have been designed to meet either Class 1A or Class 1B requirements.

2.2.3 Classification of WTC Towers

It was the practice at the time, and continues to be the practice, for the architect to establish the building classification, fire rating of members and systems, and thermal protection requirements. The review of documents uncovered during the investigation indicated a discrepancy in the classification, and therefore the fire ratings, to be used in the design of the towers. Documents issued in the early stages of the design appear to indicate that the towers were classified as Class 1A[6]. With the directive in 1965 to comply with the 1968 New York City Building Code, it appears that the towers were classified ultimately as Class 1B[7].

According to the 1968 New York City Building Code, construction classification 1B provided, in part, the following fire protection requirements:

- Columns, girders, trusses, other than roof trusses, and framing supporting more than one floor shall have 3-hour fire endurance;
- Columns, girders, trusses, other than roof trusses, and framing supporting one floor shall have 2-hour fire endurance
- Floor construction including beams shall have 2-hour fire endurance.
- Enclosure of vertical shafts, exits, passage-ways, and hoistways shall have 2-hour fire endurance; and
- Roof construction including beams, trusses, and framing including arches, domes, shells, cable supported roofs, and roof decks (for buildings over one story in height) shall have 2-hour fire endurance.

Thus, the columns were required to have a 3-hour fire endurance rating and the floor system was required to a have a 2-hour rating when tested in accordance with ASTM E 119 (ASTM 1961).

[6] Letter dated October 30, 1969 from Robert J. Linn (Manager, Project Planning, The World Trade Center) to Mr. Louis Di Bono, Mario & Di Bono Plastering Co., Inc. – see NIST NCSTAR 1-6A, Appendix Figure A-23.

[7] Memorandum dated January 15, 1987 from Lester S. Field (Chief Structural Engineer, World Trade Department) to Robert J. Linn (Deputy Director for Physical Facilities, World Trade Department) – see NIST NCSTAR 1-6A, Appendix Figure A-7.

2.2.4 Response to Local Law 5/1973

In 1973, New York City Local Law No. 5 amended the New York City Building Code (effective January 18, 1973). Local Law No. 5 required, in part, the retrofit of existing unsprinklered office buildings 100 ft or higher. The New York City Department of Buildings permitted either:

- Subdividing the floor area into compartments of specified square footage by fire separations (1-h or 2-h fire rated depending on the size of the compartment), or
- Providing sprinkler protection.

A code compliance evaluation of the towers, conducted in 1997, indicated that that all tenant floors in the two towers had been retrofitted with sprinklers (sprinklered) with the exception of four floors in WTC 1. In a 1999 update by the Port Authority, it was noted that all tenant floors had been sprinklered, and work was underway to complete sprinklering of the sky lobbies. In 2000, a property condition assessment report[8] stated that the WTC towers were classified as "Class 1B – noncombustible, fire-protected, retrofitted with sprinklers in accordance with New York City Local Law 5/1973."

2.2.5 Selection of Fire-Resistive Materials

Classification of a building leads to its overall fire endurance rating and ratings of the various structural components. The New York City Building Code, however, does not prescribe how the required fire resistance rating is to be achieved. The Port Authority chose to protect main structural components such as columns, spandrel beams, and floor trusses with sprayed fire-resistive material. This thermal protection technique was an established method for protecting columns, beams, and walls. In the 1960s, however, composite steel truss floor systems were usually protected using "lath and plaster" enclosures or fire-rated ceiling tiles. Figure 2–1 shows a mock-up of the steel truss system that supported the concrete floors in the World Trade Center towers, illustrating the thin steel rods that form the truss diagonals.

[8] Property Condition Assessment of World Trade Center Portfolio, prepared for the Port Authority by Merritt & Harris, Inc., December 2000 – see NIST NCSTAR 1-6A, Appendix Figure A-41.

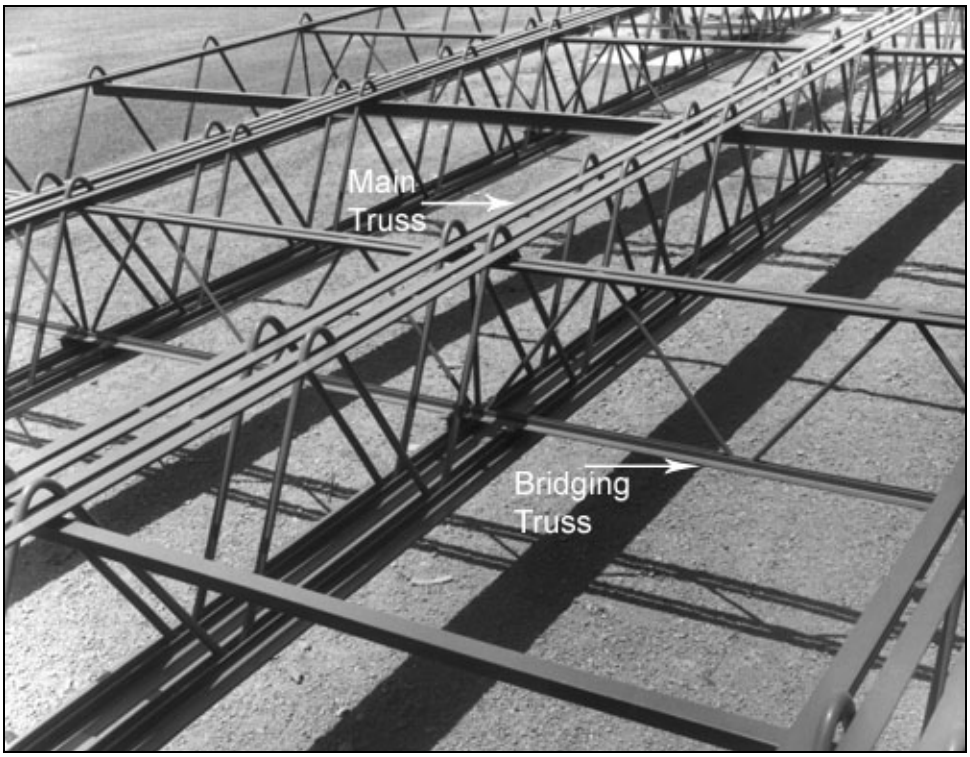

Source: (Photograph from about 1967) provided by Laclede Steel Co.

Figure 2–1. Mock up of floor truss system.

Since application of sprayed fire-resistive material to floor trusses was an innovative fire protection method, the Port Authority arranged for demonstrations to establish its feasibility for the World Trade Center (see Fig. 2–2). The demonstrations were successful, and in November 1968, the Port Authority awarded the contract for "spray fireproofing" of the interior portions (floor system and core) of the WTC towers to Mario & Di Bono Plastering Co., Inc. The fire protection of the exterior columns was included in the contract for the exterior aluminum cladding.

Source: Photograph provided by Laclede Steel Co.

Figure 2–2. Demonstration of application of Monokote sprayed fire-resistive material to floor trusses.

Several materials were considered for the sprayed thermal insulation. The exterior columns required insulation not only for fire protection but also to control column temperatures under service conditions. Alcoa recommended for the exterior columns the use of a sprayed material produced by U.S. Mineral Products, Co. known as BLAZE-SHIELD D. The same material was also selected for the floor trusses and core beams and columns. This product, however, contained asbestos fibers. On April 13, 1970, New York City issued restrictions on the application of sprayed thermal insulation containing asbestos. The use of BLAZE-SHIELD D was discontinued in 1970 at the 38th floor[9] of WTC 1. The asbestos-containing material was subsequently encapsulated with a sprayed material that provided a hard coating. A green dye was added to the encapsulating material so that the asbestos-containing SFRM could be identified. Thermal protection of the remaining floors of WTC 1 and all of WTC 2 was carried out using BLAZE-SHIELD DC/F, a product that contained mineral wool (glassy fibers) in place of the crystalline asbestos fibers. On the basis of tests, it was reported that the thermal properties of BLAZE-SHIELD DC/F were equal to or "slightly better" than those of BLAZE-SHIELD D[10].

2.2.6 Specified Thickness of Fire-Resistive Material

The thickness of fire-resistive material necessary to achieve the required fire endurance was being assessed in 1965, more than three years before the award of the thermal protection contract. At that time,

[9] Various floor levels at which the asbestos-containing SFRM was reported to have been discontinued have been found in the documents reviewed for the investigation. Floor 38 is reported here but the exact floor is of no consequence in the investigation into the response of the towers to impact and fire.

[10] Letter dated April 24, 1970 from S.W. Bell (Assistant Engineer, Fire Protection Department, Underwriters' Laboratories, Inc.) to R. Monti (Construction Manager, World Trade Center, Port of New York Authority) – see NIST NCSTAR 1-6A, Appendix Figure A-29.

Emory Roth & Sons (ER&S), the Architect-of-Record, recommended 1 in. of thermal protection for the top and bottom chords of the floor trusses and 2 in. for other members of the trusses[11]. WTC project specifications for sprayed fire-resistive material did not provide required material thickness or hourly ratings. In October 1969, the manager of project planning of WTC provided the following instructions to the contractor applying the sprayed insulation[12]:

> "…Tower 'A' columns that are less than 14WF228 will require 2 3/16″ thick of 'Cafco Glaze [sic]-Shield 'Type D'' spray-on fireproofing. All Tower columns equal to or greater than 14WF228 will require 1 3/16″ of fireproofing…
>
> All Tower beams, spandrels and bar joists requiring spray-on fireproofing are to have a 1/2″ covering of 'Cafco.'
>
> The above requirements must be adhered to in order to maintain the Class 1-A Fire Rating of the New York City Building Code"

NIST's review of available documents has not uncovered the reasons for selecting BLAZE-SHIELD fire-resistive material or the technical basis for specifying ½ in. thickness of thermal insulation for the floor trusses. The last sentence in the above excerpt indicates that, in October 1969, the towers were considered a Class 1A construction.

In February 1975, a fire broke out in WTC 1, spreading from the 9th to the 19th floor. After the fire, the Port Authority contracted Skilling, Helle, Christiansen, Robertson (SHCR), the Structural Engineer of Record for the design of the WTC towers, to assess the resulting structural damage and to report, in general, on the fire resistivity of the floor system. In its report to the Port Authority dated April 1, 1975[13], SHCR stated,

> "The fire of February, while reported in the press to have been very hot, did not damage a single primary, fireproofed element. Some top chord members (not needed for structural integrity [sic], some bridging members (used to reduce floor tremor and the like) and some deck support angles (used only as construction devices) were buckled an the fire – all were unfireproofed steel."

The 1975 post-fire report by SCHR stated further that thermal protection of the top chords of the floor trusses was not necessary, except for the corners of the buildings where the floor acted as a two-way system in bending. Additionally, it was stated that protection of the bridging trusses was not required because the bridging trusses were "not required as a part of the structural system." This information was used to guide the selection of the passive protection for the fire resistance tests conducted under Project 6 and discussed in Chapter 3.

---

[11] Letter dated December 23, 1965 from Julian Roth (ER&S) to Malcolm P. Levy (The Port of New York Authority) - see NIST NCSTAR 1-6A, Appendix Figure A-21.

[12] Letter dated October 30, 1969 from Robert J. Linn (Manager, Project Planning, The World Trade Center) to Mr. Louis DiBono (Mario & Di Bono Plastering Co., Inc.) - see NIST NCSTAR 1-6A, Appendix Figure A-23.

[13] Report on WTC Fire dated April 1, 1975 from Skilling Helle Christiansen Robertson (SHCR) to the Port Authority – see NIST NCSTAR 1-6A, Appendix Figure A-30.

2.2.7 Upgrading SFRM on Floor Trusses

In 1995, the Port Authority performed a study[14] to establish requirements for retrofit of SFRM to the floor trusses during major new construction or renovations when tenants vacated spaces in the towers. The study estimated the thermal protection requirements based on "the fireproofing requirements" for Design No. G805 contained in the Fire Resistance Directory published by Underwriters Laboratories (Underwriters Laboratories 2002). The study concluded that "a two hour fire rating for the steel floor joist trusses can be achieved by applying a 1 ½ inch thickness of spray-on mineral fiber fire protection material directly to the steel truss chords and webs." In the years between 1995 and 2001, thermal protection was upgraded on a number of floors and some of these were affected by the fires on September 11, 2001. In WTC 1, floors 92 through 100 and 102 had been upgraded, and in WTC 2, floors 77, 78, 88, 89, 92, 96 and 97 had been upgraded.

In 1999, the Port Authority established "guidelines regarding fireproofing repairs, replacement, and upgrades" for the towers[15]. The guidelines for tenant spaces may be summarized as follows:

- For full floors undergoing new construction or renovation, the floor trusses should be protected with 1 ½ in. of sprayed mineral fiber fire-resistive material. Retrofit of thermal protection requires removal of existing material and controlled inspection.

- For "tenant spaces less than a full floor undergoing either new construction or renovation," the floor trusses "need only meet the original construction standard. Fireproofing shall be inspected and patched as required to the greater of 3/4 in. or to match existing" if it has already been upgraded to 1 ½ in.

In July 2000, Buro Happold, an engineering consultant, commissioned by the Port Authority to conduct a fire-engineering assessment of the insulation of the floor trusses, issued a report on the requirements of the fire resistance of the floor system of the towers[16]. This report stated that BLAZE-SHIELD DC/F was used on the majority of the floor trusses. Based on calculations and a risk assessment, the consultant concluded that:

- "The structural design has sufficient inherent fire performance to ensure that the fire condition is never the critical condition with respect to loading allowances.

- A single coat application is possible.

- Significant savings are possible.

---

[14] White paper titled "Fireproofing Requirements for World Trade Center Tenant Floor Joist Construction that Requires Installation Due to Asbestos Removal or Local Removal to Facilitate Construction" transmitted by way of memorandum from Joseph Englot (Chief Structural Engineer, Port Authority) to Peter Sweeney (Engineering Program Manager, Port Authority) on August 18, 1995 – see NIST NCSTAR 1-6A, Appendix Figure A-34.

[15] Memorandum dated March 24, 1999 from Alan L. Reiss (Director, World Trade Department) to John Castaldo and Kent Piatt (Port Authority) – see NIST NCSTAR 1-6A,Appendix Fig. A-36.

[16] World Trade Center: Fire Engineering of Steelwork – Phase 1 Report, Buro Happold Consulting Engineers PC, February 2000 – see NIST NCSTAR Appendix Figure A-40.

- The target reduction of fiber content and increased long term durability can be achieved.
- Alternative materials should be considered."

As quoted, the report states that significant savings were possible by reducing the fiber content and considering alternative materials. The report suggested that the thickness of the SFRM could be reduced to ½ in. if the material properties at ambient temperature are applicable at higher temperature. The report recognized the lack of available temperature-dependent material data for BLAZE-SHIELD DC/F. Thus, considering the uncertainties in the material properties and having the understanding of material degradation with temperature and time, it was recommended that 1.3 in. of fire-resistive material be used for the floor trusses.

Later, in December 2000, the final draft of a report on *Property Condition Assessment of World Trade Center Portfolio*[17] stated that, based on existing conditions "The rating of the structural fireproofing in the Towers and subgrade has been judged to be an adequate 1-hour rating considering the fact that all Tower floors are now sprinklered." The report also noted the ongoing Port Authority program to upgrade the fire-resistive material thickness to 1 ½ in. in order to achieve a 2-hour fire rating.

2.2.8 Need for Fire Resistance Tests

The fire protection of a truss-supported floor system by directly applying sprayed fire-resistive material to the trusses was innovative at the time the WTC towers were designed and constructed. While the benefits of conducting fire endurance tests were realized by individuals involved in the 1967 demonstrations of the application of SFRM, apparently no tests were conducted on the floor system used in the WTC towers. The Architect-of-Record, in a letter to the Port Authority[18] addressing issues that "…might not conform to the New York City Building Code…", dated July 25, 1966, stated,

> "Obviously, with so many penetrations of the floor system the fire rating of the floor construction is of an indeterminate value unless tested. It is doubtful if it will meet a 3-hour test."

In the 1975 post-fire report to the Port Authority[19], the Structural Engineer-of-Record stated,

> "These special floor assemblies would best be fire tested—since actual testing is the only known, reliable method known [sic] to assure compliance with fire testing requirements."

Communication from the Port Authority in 2003[20] confirms that there is no record of fire endurance testing of assemblies representing the thermally protected floor system.

---

[17] Property Condition Assessment of World Trade Center Portfolio, prepared for the Port Authority by Merritt & Harris, Inc., December 2000 – see NIST NCSTAR 1-6A, Appendix Figure A-41.

[18] Letter dated July 25, 1966 from Harry J. Harman (ER&S) to Malcolm P. Levy (Port of New York Authority) - See NIST NCSTAR 1-6A, Appendix Figure A-26.

[19] Report on WTC Fire dated April 1, 1975 from Skilling Helle Christiansen Robertson (SHCR) to the Port Authority – see NIST NCSTAR 1-6A, Appendix Figure A-30 - see NIST NCSTAR 1-6A, Figure A-43.

[20] See NIST NCSTAR 1-6A, Appendix Figure A-31.

To address some of these open issues, standard fire resistance tests of the floor system used in the WTC towers were conducted as part of this investigation. Results of four tests and the fire resistance ratings determined from these tests are presented in Chapter 3 of this report and in NIST NCSTAR 1-6B.

2.2.9 Maintenance of SFRM in Elevator Shafts

Throughout the life of the WTC towers, the structural members that required the largest amount of inspection and maintenance within the core were the exposed columns and beams within the elevator shafts. Except for the floors, these columns and beams were the only accessible fire-protected elements in the buildings. Adhesion failures were common, likely because of the exposed conditions of the columns and the inherently low bond strength of the SFRM.

Inspections of the shafts and accessible columns were reported as early as 1971. Problems were noted in the form of fallen insulation or with the over-spray material used to provide a harder surface. In 1993, the Port Authority commissioned Leslie E. Robertson Associates (LERA) to carry out a continuing Structural Integrity Inspection Program to appraise the condition of the accessible columns located in the core of the towers (see NIST NCSTAR 1-1C). The columns were inspected visually for signs of rusting, cracking, bowing, and loss of thermal insulation. During the first inspection, carried out in 1993, particular shafts were chosen based on the quantity and types of accessible columns, and the convenience to the Port Authority. Subsequent inspections involved sampling of the structural components and assemblies, which were more important to the structural integrity of the towers, and at locations with a relatively higher potential for defects and problems. The Structural Integrity Inspection Report[21] stated that the accessible columns in selected elevator shafts in WTC 1 and WTC 2 were "generally in good condition, no structural deficiencies such as cracking or bowing were found, the most common irregularities observed were missing fireproofing and light surface rusting of the exposed steel." Based on the inspections, LERA recommended "that remedial action to be taken where spray fireproofing is damaged, deteriorated or missing and where there is corrosion of the column base due to water leaks at elevator pits."

2.3 AS-APPLIED THICKNESS OF SFRM

2.3.1 1994 Measurements from WTC 1 Floors 23 and 24

In its search of documents, NIST found no information related to measurements of the thickness of thermal insulation taken during construction. Reviewed documents, however, indicate that thickness appears to have been checked during construction. Recorded information on the in-place condition of the sprayed thermal insulation for the floor system first appeared in 1990 in the form of "Sample Area Data Sheets," which provided qualitative comments on the state of the in-place SFRM. Information regarding quantitative inspection of existing fire-resistive material appeared in documentation from 1994. That year, the Port Authority performed a series of thickness measurements of the existing SFRM on floors 23 and 24 of WTC 1 (see NIST NCSTAR Appendix A Figure A-58). Six measurements were taken from "both flanges and web" of each of 16 randomly chosen trusses on each floor (see Table 2–1). Measured average thickness varied between 0.52 in. and 1.17 in. For the 32 measurements (16 on each floor), the overall average was 0.74 in., and the standard deviation of these averages was 0.16 in. Four of

[21] Structural Integrity Inspection Report dated 14 April 1995 by LERA - see NIST NCSTAR 1-6A, Appendix Figure A-57.

the 32 floor trusses had average thicknesses between 0.52 in. and 0.56 in. These measurements suggest that the minimum average thickness exceeded ½ in. Analysis of the reported mean thicknesses data indicated that a lognormal distribution gave a better representation of the distribution than did a normal distribution.

Table 2–1. Average SFRM thickness from six measurements taken in 1994 on each of 16 random floor trusses on floors 23 and 24 of WTC 1.

SFRM Thickness (in.)	
Floor 23	**Floor 24**
0.60	0.76
0.53	0.60
0.70	0.90
0.76	0.72
0.88	0.64
0.89	0.80
0.83	0.68
1.17	0.65
0.88	0.67
0.71	0.77
0.82	0.96
0.52	0.66
0.69	0.65
0.52	1.11
0.64	0.95
0.52	0.56

Source: Data provided by The Port Authority of New York and New Jersey.

2.3.2 Analysis of Photographs

Additional SFRM thickness data were developed by evaluating photographs of floor trusses taken during inspections. Two groups of photographs were used. The first group included images of floor trusses from WTC 1 (floors 22, 23, and 27). These photographs were taken in the mid-1990s and illustrated conditions prior to the upgrade carried out by the Port Authority. Thus, SFRM thickness on the photographed trusses would be expected to be at least ½ in. The second group of photographs, taken in 1998, illustrated conditions after initiation of the upgrade program that began in 1995. These photographs were of trusses for floor 31 and below in WTC 1. Selection of the photographs to be used to estimate thickness of SFRM was based on clarity of SFRM edges and the presence of a feature of known dimension to provide a reference measurement. Figure 2–3 shows one such photograph used for the estimation of SFRM thickness. “Reference” points to a known dimension of the steel member which connects the damper to the bottom chord of the truss.

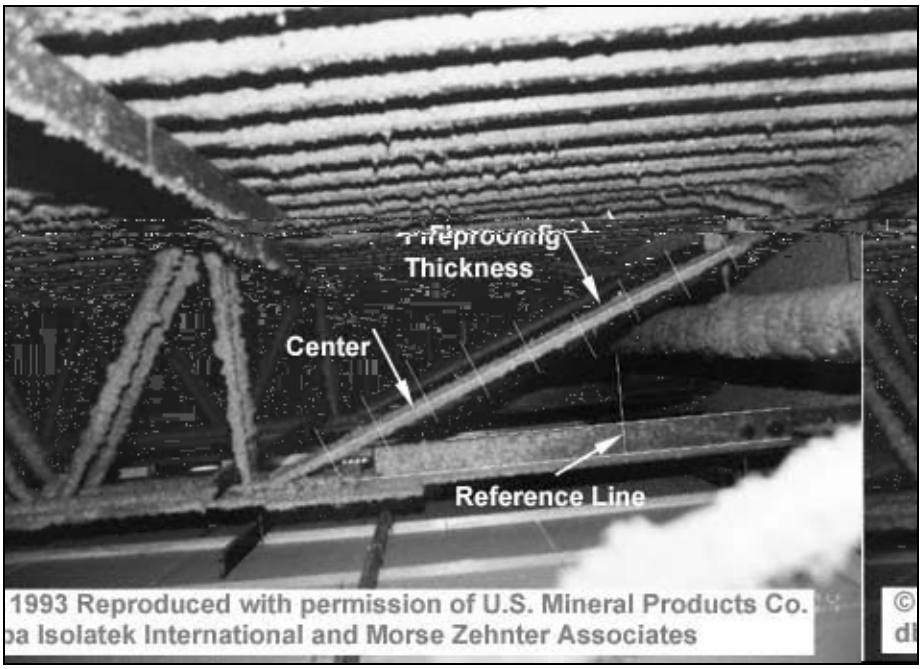

Figure 2–3. Example of measurement procedure used to estimate SFRM thickness from photographs.

For the floors that had not been upgraded, it was observed that the estimated thickness of SFRM on the webs of the main trusses tended to be greater than that on either the diagonal struts or on the webs of the bridging trusses. Hence, estimates of SFRM thickness for non-upgraded floors were divided into three groups: webs of main trusses, webs of bridging trusses, and diagonal struts at the exterior wall end of the truss.

It was not possible to estimate the thickness of the SFRM on any truss element except the round bars Consequently, for the upgraded floors in WTC 1 that were included in the second group of photographs, only estimates of the thickness on the webs of the main trusses were made. The average, standard deviation, and coefficient of variation were computed for the total number of measurements in each of these groups. The results are summarized as follows:

- Main trusses before upgrade (85 measurements): Average thickness 0.6 in., standard deviation = 0.3 in., and coefficient of variation = 0.5.

- Bridging trusses before upgrade (52 measurements): Average thickness 0.4 in., standard deviation = 0.25 in., and coefficient of variation = 0.6.

- Diagonal struts before upgrade (26 measurements): Average thickness 0.4 in., standard deviation = 0.2 in., and coefficient of variation = 0.5.

- Main trusses after upgrade (52 measurements): Average thickness 1.7 in., standard deviation = 0.4 in., and coefficient of variation = 0.2.

2.3.3 Port Authority Data on Upgraded SFRM on Trusses

In the 1990s, the thermal protection for some floor trusses was upgraded to a specified thickness of 1 ½ in. as tenants vacated their spaces. According to the Port Authority[22], 18 floors of WTC 1 and 13 floors of WTC 2 were upgraded. The Port Authority also stated that: "The entire impact zone for Tower 1 (92-99) was upgraded with 1 ½" spray-on fireproofing. Only the 78th floor was upgraded with the 1 ½" spray-on fireproofing within the impact zone in Tower 2 (78-84)." The Port Authority provided Construction Audit Reports to the NIST Investigation that included the density, average thickness, and strength characteristics of the upgraded SFRM (BLAZE-SHIELD II) as of 2000. In 2004, the Port Authority provided NIST reports of the individual measurements for many of the average thicknesses recorded in the Construction Audit Reports. These individual measurements permitted analysis of the variation of thickness at a cross section of a truss member and the variation in average thickness from truss to truss. A total of 18 data sets for WTC 1 (including floors 93, 95, 98, 99, and 100) and 14 data sets for WTC 2 (including floors 77, 78, 88, 89, and 92) were analyzed.

Data analysis indicated that the thickness measurements from the two towers represented similar distributions, and so the data were combined. It was also found that the distribution of thickness values could be approximated by a lognormal distribution.

The overall average thickness determined from the 256 individual measurements was found to be 2.5 in. with a standard deviation of 0.6 in. Thus, the average SFRM thickness on the upgraded upper floors appears to be greater than that estimated from photographs taken on the upgraded lower floors.

The overall standard deviation of 0.6 in. includes two contributions: (1) the variation of thickness at a cross section (within-truss variability), and (2) the variation of average thickness between trusses (between-truss variability). From analysis of variance, it was found that the within-truss standard deviation was 0.4 in., and the between-truss standard deviation was also 0.4 in. The within-truss standard deviation of 0.4 in. is similar to the standard deviation of the estimated individual thicknesses obtained from analysis of the photographs of upgraded main trusses.

2.4 EFFECT OF THE VARIABILITY OF SFRM THICKNESS ON THERMAL RESPONSE

As would be expected, and as confirmed by analyses of available data, the thickness of thermal insulation can have high variability. The effects of thickness variation on thermal response of a member are not well known. A sensitivity study using finite element analyses to simulate heat transfer was conducted to investigate the sensitivity of steel temperature rise to the variability in SFRM thickness.

2.4.1 Effects of Thickness Variability and Gaps in SFRM

A finite element model for thermal analysis was developed for a plate protected on both faces with SFRM of variable thickness. A random number generator was used to assign a lognormally distributed random thicknesses of insulation along the length of the plate, and the plate was subjected to a thermal flux representative of a 1,100 °C fire. A parametric study was conducted with average thickness of fire-

[22] Structural Integrity Inspection Report dated 14 April 1995 by LERA - see NIST NCSTAR 1-6A, Appendix Figure A-57.

resistive material varying from 0 in. to 2 in. in increments of 1/4 in. and a standard deviation varying from 0 in. to 1 in. Steel temperatures at five locations in the plate were recorded at 30 min, 60 min, 90 min, and 120 min of exposure to the thermal flux. For more details, refer to NIST NCSTAR 1-6A

The simulations showed that when the SFRM thickness is variable, the isotherms in the steel follow the shape of the SFRM surface contour. Thus, the temperature history at any point in the steel depends on the local thickness of the insulation. It was shown that an increase in thickness variability reduced the time to reach a critical temperature. Conversely, for a given time to reach a specific temperature, the required average thickness of thermal insulation increased with increasing variability in thickness of SFRM.

In addition to the effect of variation in thickness, the effect of missing SFRM over a portion of a member was studied. Figure 2–4 shows an example of a "gap" in fire-resistive material on a diagonal member of a bridging truss. As expected, thermal analysis results indicated that the bare steel where the insulation was missing reached the gas temperature quickly, which led to a transmission of heat into the interior steel.

The combined effects of variation in insulation thickness and extent of missing material were examined by a full factorial design study with the following factors:

- Average thickness of insulation varying from 0 in. to 2.0 in. in 1/4 in. increments;
- Standard deviation of insulation thickness of 0 in., 0.25 in., 0.5 in., 0.75 in., and 1.0 in.; and
- Length of missing insulation varying from 0 in. to 30 in., in 6 in. increments.

Figure 2–4. Example of "gap" in fire-resistive material on diagonal member of a bridging floor truss.

The results were summarized by a series of temperature-time plots representing the response for different combinations of the three factors (see NIST NCSTAR 1-6A). As expected, increasing the variability of insulation thickness or gap length reduced the time to reach a given critical temperature. Because there was not sufficient information to determine the frequency of occurrence of these gaps or their typical locations, gaps in insulation were not considered in the thermal modeling.

2.4.2 Thermally equivalent thickness of SFRM

A sensitivity study, reported in NIST NCSTAR 1-6A, indicated that increased variation in thickness reduced the "effective thickness" of the SFRM. It would be impractical to attempt to account for the variation in SFRM thickness in the thermal modeling of the WTC towers by introducing variable thickness insulation material in the finite-element models. As an alternative, a "thermally equivalent uniform thickness" was determined that would result in the same thermo-mechanical response of a member as the variable thickness thermal protection. In the analyses, an insulated 1 in. diameter by 60 in. long steel bar was subjected to the heat flux arising from a 1,100 °C fire. The temperature history along the length of the bar was computed and was used to calculate the length change of the unrestrained bar under a tensile stress of 12,500 psi. The bar was assumed to be similar to the steel used in the WTC floor trusses, and the temperature dependence of the coefficient of thermal expansion and the modulus of elasticity was based on NIST measurements.

The average SFRM thickness and variability in thickness used in the models were based on the measurements (summarized in NIST NCSTAR 1-6A) for the web bars of the main trusses with both the original insulation and the upgraded insulation. The following values were investigated:

- Original conditions: Average thickness = 0.75 in., standard deviation = 0.3 in., lognormal distribution.
- Upgraded conditions: Average thickness = 2.5 in., standard deviation = 0.6 in., lognormal distribution.

Three sets of random data were generated for each condition. When the randomly selected thicknesses of each element were applied to the bar, abrupt changes in insulation thickness along the length of the bar resulted. This "rough" surface texture was not representative of actual conditions. As an alternative, five-point averaging was used to reduce the roughness of the insulation profile and produce a profile that was consistent with photographic evidence. Care was taken to ensure the "smoothed" profiles maintained the required variability (i.e., mean and standard deviation).

The calculated temperature histories of the bar elements were used to calculate the unrestrained length changes of the bar due to thermal expansion and the applied stress. For comparison, elongations of the bar with different uniform thicknesses of thermal insulation were calculated. The "thermally equivalent thickness" was taken as the uniform thickness that resulted in approximately the same elongation of the bar as produced with the variable thickness insulation. Figure 2–5 shows a plot of the thermo-mechanical response of 1 in. diameter bar with both rough and smooth random thickness SFRM and thermally equivalent uniform thickness SFRM.

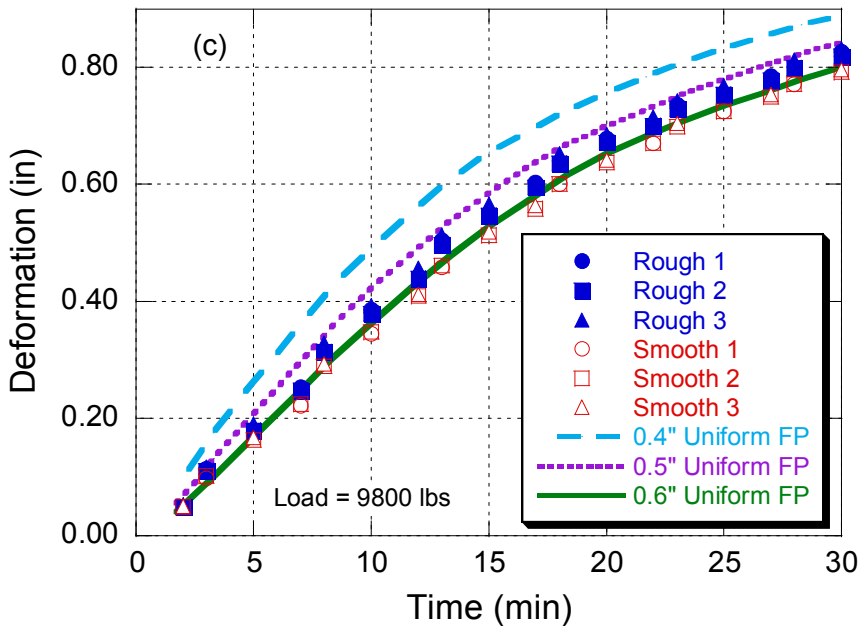

Figure 2–5. Thermo-mechanical response of 1 in. bar compared with uniform thickness SFRM.

On the basis of these analyses, it was concluded that SFRM with a uniform thickness of 0.6 in. provides thermally equivalent protection to an average thickness of 0.75 in. and a standard deviation of 0.3 in. (see the solid green line in Fig. 2–5). Similarly, 2.2 in. of uniform thickness insulation is thermally equivalent to an average SFRM thickness of 2.5 in. with a standard deviation of 0.6 in.

2.4.3 Thickness of SFRM Used for Thermal Analyses

Analyses of available data on SFRM thickness and thermal modeling revealed the following:

- From measurements of SFRM thickness, the average values exceeded the specified thickness.
- SFRM thickness was variable, and the distribution of thickness in the floor trusses was best described by a lognormal distribution.
- The standard deviation of SFRM thickness on the trusses varied between about 0.3 in. and 0.6 in.
- The standard deviation of SFRM thickness on columns and beams from the core tended to be lower, with a value of 0.2 in. obtained from the available data.
- No information was available on the SFRM thickness on the exterior columns and spandrel beams.
- Variation in thickness reduces the effectiveness of SFRM, and the thermally equivalent uniform thickness, based on thickness measurements, exceeded the specified thickness.

Based on the findings given above, the following uniform thicknesses for the undamaged SFRM were used in the thermal analyses to determine temperature histories of the WTC towers under various fire scenarios:

- Original SFRM thickness on all floor trusses (primary and bridging): 0.6 in.
- Upgraded SFRM thickness on all floor trusses (primary and bridging): 2.2 in.
- Thermal protection on other elements: the specified thickness.

The choice of specified thickness for those members lacking data is justified by the following offsetting factors: (1) measured average thicknesses were found to exceed specified values, and (2) variation in thickness reduces the effectiveness of the SFRM.

2.5 SUMMARY OF SFRM THICKNESS

Establishing the specified SFRM material and thickness for the protection of the steel trusses, columns and beams in the WTC towers required the review of documents, correspondence, photographs, and videos that chronicled the decisions made in selection of the passive fire protection in the towers. Since the towers were destroyed completely when they collapsed on September 11, 2001, establishing the in-place thicknesses and condition of the SFRM required analysis of available thickness measurement data and interpretation of available photographs. Lastly, the determination of appropriate thickness of the SRFM for use in thermal calculations required finite element thermal analyses to establish a thermally equivalent uniform thickness. Table 2–2 summarizes the specified thickness, in-place (or as-applied) thickness, and thermally equivalent thickness for the structural elements that were fire-protected using SFRM.

Table 2–2. Summary of specified, in-place and thermally equivalent thickness of SFRM

Building Component	Material	Thickness (in.)		
		Specified(1)	In-place	Thermally Equivalent
FLOOR SYSTEM				
Original				
Main trusses	BLAZE-SHIELD DC/F	1/2	0.75	0.6
Main truss diagonal Strut	BLAZE-SHIELD DC/F	1/2	0.75(2)	0.6
Bridging trusses – One-Way	BLAZE-SHIELD DC/F	1/2(3)	0.38(4)	(5)
Bridging trusses – Two-Way	BLAZE-SHIELD DC/F	1/2(3)	0.75(4)	0.6(6)
Metal deck		(7)	(8)	(9)
Upgraded				
Main trusses	BLAZE-SHIELD II	1 1/2	2.5	2.2
Main truss diagonal Strut	BLAZE-SHIELD II	1 1/2	2.5	2.2
Bridging trusses	BLAZE-SHIELD II	1 1/2	2.5	2.2
Metal deck		(7)	(8)	(9)

Building Component	Material	Thickness (in.)		
		Specified[1]	In-place	Thermally Equivalent
EXTERIOR WALL PANEL				
Box columns				
Exterior faces (plates 1 & 2)	BLAZE-SHIELD DC/F	1 3/16	(8)	1.2
Interior face (plate 3)	Vermiculite plaster	7/8	(8)	0.8
Spandrels (plate 4)				
Exterior face	BLAZE-SHIELD DC/F	1/2	(8)	0.5
Interior face	Vermiculite plaster	1/2	(8)	0.5
CORE COLUMNS				
Wide flange columns				
< WF14x228	BLAZE-SHIELD DC/F	2 3/16	(8)	2.2
≥ WF14x228	BLAZE-SHIELD DC/F	1 3/16	(8)	1.2
Box columns				
< 228 lb/ft	BLAZE-SHIELD DC/F	(6)	(8)	1.2[10]
≥ 228 lb/ft	BLAZE-SHIELD DC/F	(6)	(8)	2.2[10]
CORE BEAMS				
All	BLAZE-SHIELD DC/F	1/2	(8)	0.5

(1) In no case was a specified SFRM material or thickness found on contract documents. Rather, the term "specified" means material and thicknesses determined from correspondence among various parties.
(2) Anecdotal and photographic evidence suggests that there may have been, in general, less than 0.75 in. thick SFRM on the diagonal struts, but there is insufficient evidence to estimate what that value should be.
(3) Thickness of SFRM on bridging trusses was not expressly specified (only "trusses" were mentioned), and anecdotal and photographic evidence as well as written documentation, suggests that the one-way and two-way floor areas were treated differently; specifically SFRM was required for the two-way floor areas and, while not required, was also applied in the one-way areas.
(4) Analysis of photographs of originally applied SFRM indicates that the thickness on the bridging trusses was approximately one half that on the main trusses.
(5) A thermally equivalent thickness was not calculated for this condition and a value of 0.6 in. was used for the thermal analyses.
(6) 1975 report by LERA indicates bridging trusses in two-way areas were fire protected.
(7) Not specified.
(8) Unknown or not able to be determined.
(9) Not included in analyses.
(10) Since no information regarding specified thickness was found and installed thickness could not be determined, the same thickness specified for the wide flange columns (based on weight of section per foot) was used for thermal analyses.

2.6 THERMOPHYSICAL PROPERTIES

To provide thermophysical property data for modeling the fire-structure interaction of the towers, the thermal conductivity, specific heat capacity, and density of the SFRMs used in the WTC towers were determined as a function of temperature up to 1,200 °C (2,190 °F). Since there are no ASTM test methods for characterizing the thermophysical properties of SFRMs as a function of temperature, ASTM test methods developed for other materials were used. Samples were prepared by the manufacturers of the fire-resistive materials, which included BLAZE-SHIELD DC/F, which was originally applied, BLAZE-SHIELD II, used in the recent upgrade, and Monokote MK-5, assumed to be similar to the

vermiculite plaster applied to the inside surface of the exterior columns. Since Monokote MK-5 is no longer produced, the samples were manufactured specially for this study according to the original MK-5 formulation.

2.6.1 Thermal Conductivity

The thermal conductivity measurements were performed according to ASTM C 1113, Standard Test Method for Thermal Conductivity of Refractories by Hot Wire (Platinum Resistance Thermometer Technique) (ASTM 1999). The room temperature values were in general agreement with the manufacturer's published values for BLAZE-SHIELD DC/F and BLAZE-SHIELD II. No published values were available for Monokote MK-5. The thermal conductivities increased with temperature as shown in Table 2–3.

Table 2–3. Measured thermal conductivity as a function of temperature.

Temperature (°C)	Thermal Conductivity (W/(m · K))*		
	BLAZE-SHIELD DC/F	BLAZE-SHIELD II	Monokote MK-5
25	0.0460	0.0534	0.0954
50	0.0687	0.0745	0.0926
100	0.0628	0.0921	0.1252
200	0.0810	0.0895	0.0919
300	0.1106	0.1057	0.1214
400	0.1286	0.1362	0.1352
500	0.1651	0.1689	0.1504
600	0.2142	0.2156	0.1622
800	0.3380	0.2763	0.1895
1000	0.5010	0.3708	0.2618
1200	0.5329	0.4081	---------

* Results are presented in SI units because this system was used to make the measurements. To convert to BTU · in / (h · ft2 · °F) divide by 0.1442279.

2.6.2 Specific Heat Capacity

Specific heat capacity determinations were made with the same instrument as for thermal conductivity with a slight modification. A thermocouple was added to the system, which permitted determination of the thermal diffusivity of the material. Knowing the thermal conductivity, the thermal diffusivity, and the density obtained from other tests, the specific heat capacity was calculated. The inherently indirect nature of the technique used precluded the direct measurements of specific heat capacity peaks associated with chemical reactions.

To examine the chemical reactions associated with heating of SFRMs, differential scanning calorimetry (DSC) measurements were made in accordance with ASTM E 1269, Standard Test Method for Determining Specific Heat Capacity by Differential Scanning Calorimetry (ASTM 2001). Differential thermal analysis (DTA) which is a "fingerprinting" technique that provides information on the chemical reactions, phase transformations, and structural changes that occur in a specimen during a heating or

cooling cycle. These tests revealed large peaks in the specific heat capacities in the range of 125 °C to 140 °C, which were accounted for in the thermal analyses conducted in the course of this investigation.

2.6.3 Density

Bulk densities of the SFRMs were not measured directly (except at room temperature) but were calculated from thermal gravimetric analysis (TGA) and thermal expansion measurements. The TGA tests to measure mass loss were performed according to ASTM E 1131, Standard Test Method for Compositional Analysis by Thermogravimetry (ASTM 1998). Thermal expansion measurements were performed according to ASTM E 228, Standard Test Method for Linear Thermal Expansion of Solid Materials (ASTM 1995). Since the materials were not isotropic, separate measurements were performed in the plane of the SFRM sample and perpendicular to the free surface of the sample. Consequently, measurements were performed both in the plane of deposition and perpendicular to the plane of deposition. The density values were calculated from the results of the thermal gravimetric analysis and thermal expansion. The room temperature densities were found to be 15.7 pcf for BLAZE-SHIELD DC/F, 20.8 pcf for BLAZE-SHIELD II, and 19.4 pcf for Monokote MK-5.

2.6.4 Thermophysical Properties of Gypsum Panels

Thermophysical properties of four representative types of commercially available gypsum panels were examined. The materials were:

- 5/8 in. thick gypsum panel A,
- ½ in. thick gypsum panel,
- 5/8 in. thick gypsum panel B, and
- 1 in. thick gypsum liner panel.

Thermal conductivity was measured using the heated probe technique described in ASTM D 5334, Standard Test Method for Determination of Thermal Conductivity of Soil and Soft Rock by Thermal Needle Probe Procedure (ASTM 2000b). In general, the thermal conductivity initially decreased as the temperature increased to 200 °C and then increased with increasing temperature above 300 °C.

Specific heat capacities of the cores of the four gypsum panel samples were measured using a differential scanning calorimeter according to ASTM E 1269, Standard Test Method for Determining Specific Heat Capacity by Differential Scanning Calorimetry (ASTM 2001). The four panels had similar specific heat capacities as a function of temperature, with a high peak at about 150 °C and a smaller peak at about 250 °C.

Densities were calculated from the thermogravimetric analysis and linear thermal expansion measurements. All four materials showed the same trend as a function of temperature. The variation in density with temperature is associated with the mass loss and the change in volume of the gypsum material.

2.7 ESTIMATION OF SFRM DISLODGED BY AIRCRAFT IMPACT

To analyze the thermo-structural response of the WTC towers during the fires after the aircraft impacts, it was necessary to estimate the extent of dislodged thermal insulation on structural members. Dislodgement could occur as a result of direct impact by debris or due to inertial forces resulting from aircraft impact. The dislodgement due to flying debris was estimated from results of the aircraft impact analyses that predicted damage to the structure (columns, beams and floors), partitions, and furnishings. In addition, a study was conducted to estimate dislodgement due to inertial forces. NIST established conservative estimates for the extent of dislodged SFRM. However, since NIST was not able to establish robust criteria to predict the extent of vibration-induced dislodgement, insulation dislodged by inertial effects other than that dislodged by direct debris impact was ignored and not included in the analyses. The methodology and criteria for estimating the extent of damage and dislodgement of SFRM from results of the aircraft impact analysis are presented in Chapter 5.

2.7.1 In-place Density and Bond Strength

The magnitude of the inertial forces resulting from shock and vibration is dependent on the density and thickness of the thermal insulation. The insulation would dislodge if the stresses resulting from inertial forces exceed the bonding, or adhesive/cohesive strength of the insulation.

The Port Authority provided data on in-place density and bond strength characteristics of the thermal insulation (BLAZE-SHIELD II) applied to the floor trusses during tenant alterations. According to the manufacturer, BLAZE-SHIELD II is about 20 percent denser and has about 20 percent greater adhesive/cohesive strength than BLAZE-SHIELD DC/F. The Port Authority test reports indicate that bond strength was determined in accordance with ASTM E 736, Standard Test Method for Cohesion/Adhesion of Sprayed Fire-Resistive Materials Applied to Structural Members (ASTM 2000a). The method involves gluing a jar screw cap to the surface of the thermal insulation, and after the glue has cured, pulling on the cap until failure of the SFRM occurs. The force required to pull off the cap is divided by the area of the cap, and reported as the “cohesive/adhesive strength.” Failure is described as “cohesive” if it occurs within the insulation and is defined as “adhesive” if it occurs at the interface with the substrate.

Analysis of the reported density values indicated no statistically significant differences between the average SFRM densities in the two towers. The overall average density was 18.9 pcf with a standard deviation of 3.2 pcf, giving a coefficient of variation of 16 percent.

Analysis of the bond strength values indicated that there were statistically significant differences between the average bond strengths for the different floors, but there was no statistically significant difference between the average bond strengths for the two towers. The overall average bond strength was 302 psf, with a standard deviation of 91 psf, giving a coefficient of variation of 30 percent. This average value is less than the “tested performance” value of 360 psf indicated in the manufacturer’s catalogs, but this published value is for tests under controlled conditions and may not be representative of field strengths. The manfacturer’s product literature dated February 2002 refers to average bond strength of 150 psf as “standard performance,” and the same value is used in its guide specification for BLAZE-SHIELD II.

2.7.2 Specimen Preparation and Test Procedures

While the in-place bond strength data of BLAZE-SHIELD II reported by the Port Authority appear to indicate acceptable performance, ASTM E 736 tests do not provide sufficient information for predicting whether insulation would be dislodged from structural members under various impact conditions. The standard test does not provide unambiguous values of cohesive and adhesive strengths, and it does not provide tensile strength in a direction parallel to the surface, that is, the in-plane cohesive strength. Thus, tests were conducted by NIST to determine different tensile strength properties of sprayed thermal insulation. BLAZE-SHIELD DC/F was used because the Port Authority data did not include tests of this material.

Test specimens were made by applying the SFRM to ¼ in. steel plates measuring 8 in. by 16 in. One half of the plates were coated with primer paint. Nominal SFRM thicknesses of ¾ in. and 1 ½ in. were applied. Thickness was built up in several passes of the spray nozzle. Gentle hand rubbing was used to remove local high spots and produce reasonably uniform thicknesses. The plate specimens were allowed to dry for over five months in the laboratory before testing. Companion specimens were weighed periodically to determine loss of water, and it was found that the 1 ½ in. thick specimen reached equilibrium in about one month.

Tests were devised to determine adhesive strength, cohesive strength normal to the surface, and cohesive strength parallel to the surface of the SFRM. The first two properties were determined by adapting the pull-off test method described in ASTM C 1583, Standard Test Method for Tensile Strength of Concrete Surfaces and the Bond Strength or Tensile Strength of Concrete Repair and Overlay Materials by Direct Tension (Pull-off Method) (ASTM 2004). The SFRM layer was cut carefully in two orthogonal directions to create a prismatic test specimen, and a 3/8 in. by 2.7 in. by 2.7 in. aluminum plate was glued to the surface. The advantages of this approach over the ASTM 736 technique are that the resisting area is easily determined and it offers the ability to measure both adhesive and cohesive strengths.

From each plate, three specimens were prepared for measuring both density and in-plane cohesive strength, and two specimens were prepared for measuring adhesive strength and cohesive strength normal to the surface. Prismatic specimens were prepared by carefully removing strips of SFRM from the steel plates and sanding them to obtain uniform thickness. These specimens were weighed to determine their densities. Then the specimens were glued to a steel plate, and a small plate was glued to the other end for applying a tensile load.

The adhesive strength and cohesive strength normal to the surface were obtained using the modified pull-off procedure. An aluminum plate was bonded to the top surface of the SFRM using a fast curing, two-component urethane foam adhesive. After the adhesive had cured, the SFRM layer was cut to produce a prismatic test specimen. A hook was screwed into the aluminum plate, and a load was applied by hand using a 50-lb. digital force gauge. The average length and width of the failure area were measured and used to compute the adhesive or cohesive strength. After the first test, the specimen was repaired with the same polyurethane adhesive, and the test was repeated. If the first test resulted in an adhesive failure, the second test of the repaired specimen measured cohesive strength of the bulk SFRM. If the first test resulted in cohesive failure, specimens were repaired and retested until an adhesive failure was obtained.

2.7.3 Test Results

Table 2–4 summarizes the results of the test described in the previous section.

Table 2–4. Summary of physical characteristics of BLAZE-SHIELD DC/F specimens tested at NIST

Property	Bare Steel		Primed Steel	
	¾ in.	1 ½ in.	¾ in.	1 ½ in.
Density (pcf)			27.2 (0.8)*	29.7 (1.3)
In-plane cohesive strength (psf)			1120 (390)	1740 (540)
Adhesive strength (psf)	450 (63)	666 (151)	185 (96)	171+(196)
Cohesive strength normal to surface (psf)	433 (99)	610 (142)	367 (79)	595 (163)

* First number is the average and the number in parentheses is the standard deviation.
\+ Based on testing selected samples.

The densities of the BLAZE-SHIELD DC/F measured in this study were higher than published values in the manufacturer's catalogs and higher than the in-place average density of 18.9 pcf reported in Port Authority test reports for BLAZE-SHIELD II. The difference in average densities of the two thicknesses was statistically significant. The higher values in this study are attributed to the specimen preparation procedures, which tended to result in denser test specimens than would be representative of field application.

The difference in average adhesive strength for the two SFRM thicknesses is statistically significant. The relative strengths are consistent with the difference in density for the two thicknesses.

The presence of primer reduced the adhesive strength, especially for the 1 ½ in. thick specimens. Two-thirds of the specimens with the thicker SFRM had no adhesion to the coated steel plates.

Analysis of the cohesive strength normal to the surface indicated that there was no statistically significant effect due to the presence or absence of primer. This is logical because the condition of the steel surface is not expected to influence the properties of the bulk SFRM. There was a statistically significant difference in the average strengths for the two thicknesses, with the 1 ½ in. SFRM having higher strength.

For comparison with the measured cohesive strength normal to the surface, two tests were conducted in accordance with ASTM E 736. The results of the two tests were in agreement with those obtained by the pull-off technique. This suggests that the ASTM E 736 procedure probably provides a measure of cohesive strength.

A comparison was made of the adhesive strength and cohesive strength normal to the surface for the plates made with bare steel. An analysis of variance indicated that there is an 8 percent probability that the difference could be the result of randomness. Generally, if this probability is greater than 5 percent, it can be concluded that the difference is not statistically significant. Thus, for the case of good adhesion, the test results do not contradict the assumption that the adhesive strength and cohesive strength normal to the surface are equal. If this assumption is accepted, the average of the adhesive and cohesive strengths was found to be 409 psf for the ¾ in. SFRM, and the average is 622 psf for the 1 ½ in. SFRM. These values are considerably greater than the manufacturer's published strength of 295 psf, obtained using the ASTM E 736 method under laboratory conditions.

2.8 REFERENCES

ASTM 1961. Standard Test Methods for Fire Tests of Building Construction and Materials. ASTM E 119-61, ASTM International, West Conshohocken, PA.

ASTM 1995. Standard Test Method for Linear Thermal Expansion of Solid Materials With a Vitreous Silica Dilatometer, ASTM E 228-95, ASTM International, West Conshohocken, PA.

ASTM 1998. Standard Test Method for Compositional Analysis by Thermogravimetry, ASTM E 1131-98, ASTM International, West Conshohocken, PA.

ASTM 1999. Standard Test Method for Thermal Conductivity of Refractories by Hot Wire (Platinum Resistance Thermometer Technique), ASTM C 1113-99. ASTM International, West Conshohocken, PA.

ASTM 2000. Standard Test Methods for Fire Tests of Building Construction and Materials, ASTM E 119-00a. ASTM International, West Conshohocken, PA.

ASTM 2000a. Standard Test Method for Cohesion/Adhesion of Sprayed Fire-Resistive Materials Applied to Structural Members, ASTM E 736-00, ASTM International, West Conshohocken, PA.

ASTM 2000b. Standard Test Method for Determination of Thermal Conductivity of Soil and Soft Rock by Thermal Needle Probe Procedure, ASTM D 5334-00, ASTM International, West Conshohocken, PA.

ASTM 2001. Standard Test Method for Determining Specific Heat Capacity by Differential Scanning Calorimetry, ASTM E 1269-01, ASTM International, West Conshohocken, PA.

ASTM 2004. Standard Test Method for Tensile Strength of Concrete Surfaces and the Bond Strength or Tensile Strength of Concrete Repair and Overlay Materials by Direct Tension (Pull-off Method), ASTM C 1583-04. ASTM International, West Conshohocken, PA.

Gewain, R.G., Iwankiw, N.R. and Alfawakhiri, F. 2003. *Facts for Steel Buildings—Fire*, American Institute of Steel Construction, Chicago, IL, October 2003. 51 pp.

NYCBC 1968. Building Code—Local Law No. 76 of the City of New York. New York, NY.

Underwriters Laboratories Inc. (2002). Fire Resistance Directory – Volume 1, Northbrook, IL.

Chapter 3
FIRE RESISTANCE TESTS

3.1 BACKGROUND

3.1.1 Motivation for Conducting Standard Fire Tests

National Institute of Standards and Technology (NIST) review of available documents indicated that the fire performance of the composite floor system of the World Trade Center (WTC) towers was an issue of concern to the building owners and designers from the original design and throughout the service life of the buildings (NIST NCSTAR 1-6A). NIST found no evidence regarding the technical basis for the selection of the SFRM for the WTC floor trusses and for the SFRM thickness to achieve a 2 h rating. Further, NIST no evidence was found that fire resistance tests of the WTC floor system were conducted. Review of the documents did not identify a similar concern for other structural components of the WTC towers.

NIST NCSTAR 1-6B reports on the motivation for testing full- and reduced-scale assemblies representing the floor system used in the World Trade Center towers, and the purpose of the Standard Fire Test. The test variables are given and the construction of the floor test assemblies, test set-up, and loading are described. Results (fire resistance ratings) of the four tests are presented and discussed. This chapter summarizes the salient material covered in NIST NCSTAR 1-6B.

3.1.2 Purpose of the Standard Fire Tests

NIST conducted a series of four standard fire tests of the WTC floor system:

- to establish the baseline performance of the floor system of the WTC towers under thermal loading as they were originally designed,
- to differentiate the factors that most influenced the response of the WTC floors to fires as they may relate to normal building and fire safety considerations and those unique to the events of September 11, 2001,
- to determine whether there was an adequate technical basis for the original SFRM specification, and
- to study the procedures and practices used to accept an innovative structural and fire protection system.

3.2 DESCRIPTION OF WTC FLOOR SYSTEM

3.2.1 Structural System

The floor system design for the World Trade Center consisted of a lightweight concrete floor slab supported by steel trusses bridging between the core and exterior wall[23]. The main composite trusses, which were used in pairs, were spaced at 6 ft 8 in. on center (o.c.) and had a nominal clear span of either 60 ft or 35 ft. The trusses were fabricated using double-angles for the top and bottom chords and round bars for the webs. The web members protruded above the top chord in the form of a "knuckle," which was embedded in the concrete slab to develop composite action. Additionally, the floor system included bridging trusses (perpendicular to main trusses) spaced 13 ft 4 in o.c. In the corners of the towers, the bridging trusses acted with the main trusses to provide "two-way" slab action, i.e., bending moments existed in both principal directions. Figure 3–1 is a cut-away of the floor system showing the main trusses, bridging trusses, metal deck, and concrete floor slab. Figure 3–2 shows a cross-sectional view of the basic configuration of the floor system.

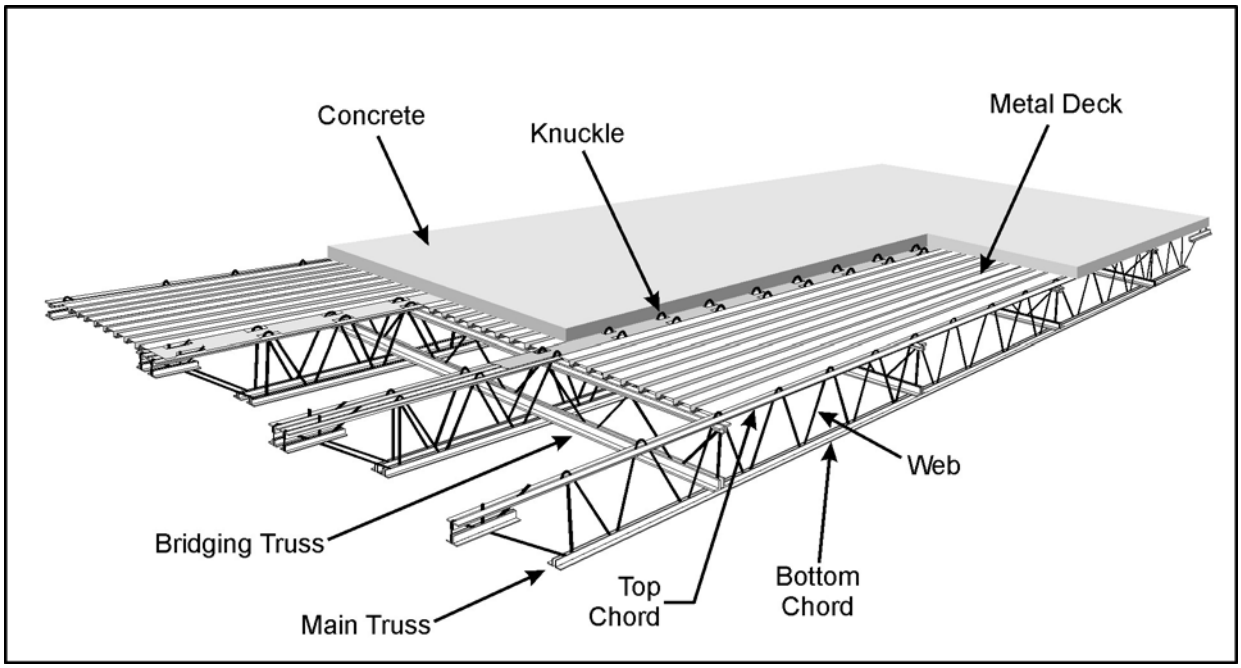

Figure 3–1. Floor system of the WTC towers.

[23] All information and data related to the design and construction of the WTC floor system were obtained from contract drawings provided to NIST by The Port Authority of New York and New Jersey. Refer to NIST NCSTAR 1-2A for a complete description of the WTC structural system and index of all structural drawings.

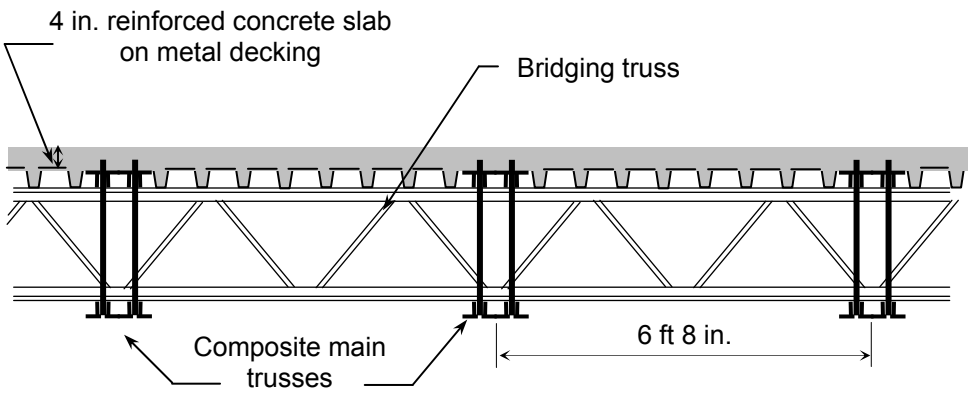

Figure 3–2. Schematic of floor system viewed along the main steel trusses. (not to scale)

3.2.2 Sprayed Fire-Resistive Material (SFRM) Thickness

As noted in Chapter 2, the average thickness of SFRM as originally installed was approximately ¾ in. The thicknesses of ½ in. representing the specified thickness, and ¾ in. representing average applied thickness, were used in the standard fire resistance tests described here.

3.3 FIRE RESISTANCE TESTING

3.3.1 General Description

The fire rating of structural materials and assemblies is generally determined through testing, and in the United States, such testing is frequently conducted in accordance with the ASTM International standard, ASTM E 119, "Standard Test Methods for Fire Tests of Building Construction and Materials." This standard was first published in 1917 as a tentative standard, ASTM C 19, and was first adopted as ASTM E 119 in 1933. Since its introduction, the test method has been modified and updated, although its essential character has remained unchanged. ASTM E 119 prescribes a standard fire exposure for comparing the test results of building construction assemblies. For the tests of floors and roofs, a test assembly is structurally loaded, and the standard fire exposure is applied to the underside of the specimen. The assembly is evaluated for its ability to contain a fire by limiting passage of flame or hot gases, and limiting heating of the unexposed surface, while maintaining the applied load. The assembly is given a rating, expressed in hours, based on these acceptance, or end-point, criteria.

3.3.2 Test Restraint Conditions and Ratings

ASTM E 119 Standard in 1971 introduced the concept of fire endurance classifications based on two conditions of support: restrained and unrestrained. A restrained condition[24] is "one in which expansion at the support of a load carrying element resulting from the effects of fire is resisted by forces external to the element." In an unrestrained condition, the element is free to expand and rotate at its supports.

[24] According to Appendix A4 of ASTM E 119-73.

The current standard describes a means to establish both restrained and unrestrained ratings from assemblies tested in the restrained condition. The conditions of acceptance are based on limiting passage of flame or hot gases, limiting temperatures on the unexposed surface of the slab, and failure to support the applied load. In addition, temperature limitations are placed on the main structural members. The location of temperature measurements on the structural members is specified in the Standard.

In addition, the Standard describes a means to establish unrestrained ratings from unrestrained test conditions. For tests of assemblies not restrained against thermal expansion, the fire resistance rating is based on limiting passage of flame and hot gases, exceeding temperatures on the unexposed surface of the slab, and failure to sustain the applied load; however, there are no limiting temperatures for the steel structural members.

Prior to 1970, restrained and unrestrained ratings were not defined in ASTM E 119. Ratings were determined based upon the requirements for restrained assemblies except that no temperature limitations were placed on the structural steel members.

In practice, a floor assembly such as that used in the WTC towers is neither restrained nor unrestrained against thermal expansion, but is likely somewhere in between. Testing under both restraint conditions bounds expected performance under standard fire exposure.

3.3.3 Scale of Tests

For floor and roof assemblies, ASTM E 119 requires that the area exposed to fire be a minimum of 180 ft^2 with neither dimension of the furnace less than 12 ft. Furnaces available in 2002 in the United States for conducting standardized fire resistance tests of floor and roof assemblies had a maximum span less than 18 ft (NIST GCR 02-843). Traditionally, relatively small scale assemblies have been tested, and results have been scaled to practical floor system spans.

The Underwriters Laboratories (UL) fire testing facility in Toronto, Canada has a furnace with nominal dimensions of 35 ft by 14 ft. Thus, full- or large-scale floor assemblies could be tested in this furnace. Availability of the 35 ft furnace in UL's Toronto facility, in addition to the 17 ft furnace at its Northbrook, Illinois, facility allowed NIST to conduct tests to compare the effect of scale.

3.3.4 Test Variables

To limit the number of tests and obtain information of greatest value to meet the investigation objectives discussed above, NIST studied three factors: SFRM thickness, scale of the test, and test restraint conditions. To this end, four tests were conducted as follows:

- Test #1: Full-scale (35 ft span), restrained test condition, ¾ in. thick SFRM.
- Test #2: Full-scale (35 ft span), unrestrained test condition, ¾ in. thick SFRM.
- Test #3: Reduced-scale (17 ft span), restrained conditions, ¾ in. thick SFRM.
- Test #4: Reduced-scale (17 ft span), restrained conditions, ½ in. thick SFRM.

The objective of the full-scale restrained test with ¾ in. thick SFRM, Test 1, was to determine the baseline fire resistance of the floor system with average as-applied SFRM thickness. This test also demonstrated whether the fire resistance of such a system was significantly different from that of a system with the specified SFRM thickness of ½ in.

The test conditions for Test 2, full-scale unrestrained test with ¾ in. thick SFRM, were the same as those for Test 1 except that the specimen was supported to allow thermal expansion and, therefore, represented the unrestrained test condition. Results of this test allowed a determination of the unrestrained rating by test and, by comparing with the results of Test 1, a comparison of unrestrained ratings from both a restrained and unrestrained assembly test.

Test 3 was a reduced-scale test which, other than scale, was the same as Test 1. Thus, a comparison of the results of these two tests allowed an examination of whether test results are independent of test assembly scale.

Test assemblies for Tests 1, 2 and 3 were fire protected in the same manner, with ¾ in. thick SFRM representing the average SFRM thickness in the impact and fire affected floors of WTC 2. Measurements taken from photographs of the originally applied SFRM indicated that, while the SFRM thickness on main the trusses was approximately ¾ in., the thickness on the bridging trusses was approximately half that value (see NIST NCSTAR 1-6A). Also, photographs indicated that the metal deck was sometimes sprayed and sometimes not. For these three tests (Tests 1, 2, and 3), then, the main trusses were protected with ¾ in. thick SFRM, the bridging trusses with ⅜ in. thick SFRM, and the metal deck was not intentionally sprayed but was also not masked from overspray and thereby had, in most instances, at least a light covering of SFRM. These conditions best represented the thickness of the SFRM as it was originally applied in the one-way slab areas.

The objective of the test with the ½ in. SFRM (Test 4) was to determine whether or not there was adequate technical basis for the original SFRM specification. As explained by the designer, it was not necessary to fire protect the bridging trusses in the one-way areas nor was it necessary to spray the metal deck (see NIST NCSTAR 1-6A). Consequently, the Test 4 specimen had ½ in. thick SFRM applied to the main trusses and no SFRM applied to either the bridging trusses or the underside of the metal deck. Both the bridging trusses and metal deck were masked to prevent overspray as well. These conditions best represented the SFRM that was necessary, in the opinion of the designer, to provide the required level of passive fire protection.

3.4 PREPARATION OF TEST ASSEMBLIES

Original shop drawings by Laclede Steel were used for the design of the 35 ft 0 in. span and 17 ft 5½ in. span test assemblies. Figure 3–3 shows a drawing for the trusses used in the 35 ft span assemblies. The steel trusses faithfully duplicated the geometry of the original design. Since equipment for making the resistance welds is not available in the United States, metal inert gas (MIG) welding was used, and the welds were designed per the American Institute of Steel Construction (AISC) weld criteria to develop the web capacities in tension or compression. This strength requirement was based on test data from Laclede's files indicating that weld capacities exceeded design loads by a factor of 2.

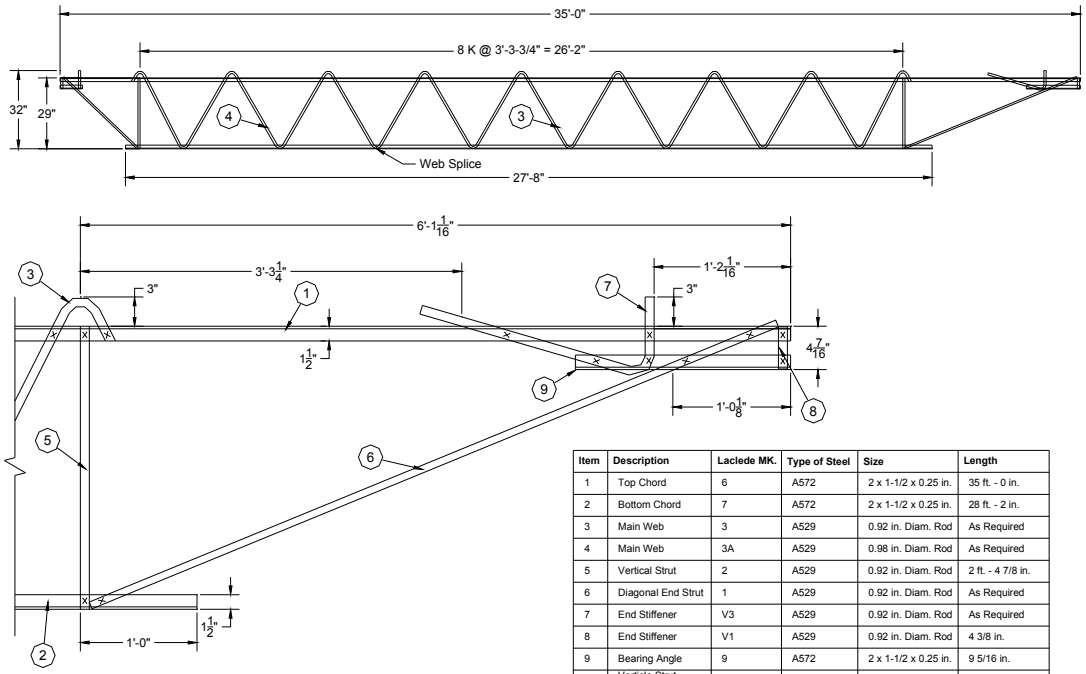

Item	Description	Laclede MK.	Type of Steel	Size	Length
1	Top Chord	6	A572	2 x 1-1/2 x 0.25 in.	35 ft. - 0 in.
2	Bottom Chord	7	A572	2 x 1-1/2 x 0.25 in.	28 ft. - 2 in.
3	Main Web	3	A529	0.92 in. Diam. Rod	As Required
4	Main Web	3A	A529	0.98 in. Diam. Rod	As Required
5	Vertical Strut	2	A529	0.92 in. Diam. Rod	2 ft. - 4 7/8 in.
6	Diagonal End Strut	1	A529	0.92 in. Diam. Rod	As Required
7	End Stiffener	V3	A529	0.92 in. Diam. Rod	As Required
8	End Stiffener	V1	A529	0.92 in. Diam. Rod	4 3/8 in.
9	Bearing Angle	9	A572	2 x 1-1/2 x 0.25 in.	9 5/16 in.
10	Verticle Strut Core Side	5	A529	0.98 in. Diam. Rod	As Required
11	Diagonal Strut	10	A529	0.98 in. Diam. Rod	As Required
12	End Stiffener	V2	A529	0.98 in. Diam. Rod	7 3/8 in.
13	End Stiffener	V1	A529	0.98 in. Diam. Rod	As Required

Figure 3–3. Drawing of 35 ft truss and end detail.

In addition, the steel angles, round bars, reinforcing steel, welded wire fabric (WWF), metal deck, lightweight concrete, and primer paint were all matched as closely as practical. Figure 3–4 shows the steel trusses being fit-up and welded in the test frame for one of the 35 ft span test assemblies. NIST NCSTAR 1-6B provides a complete description of the construction of the test assemblies, including materials used, sprayed fire-resistive material, and instrumentation.

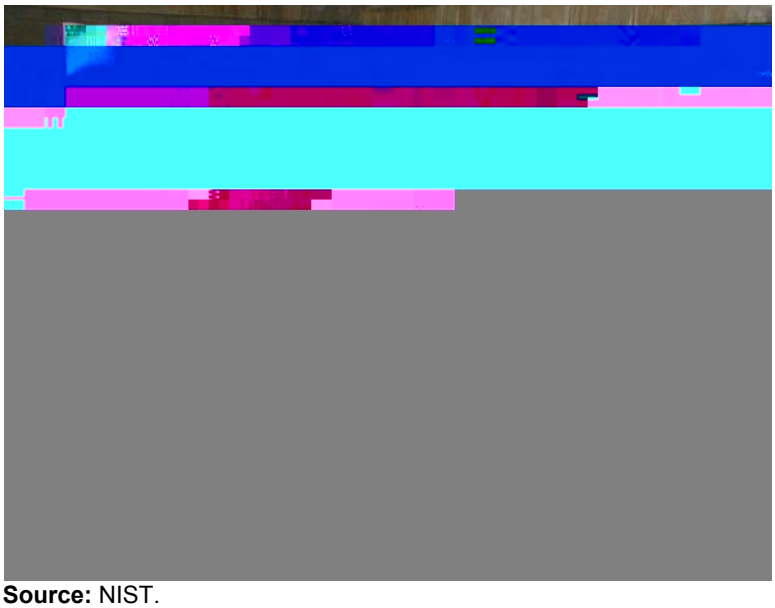

Source: NIST.

Figure 3–4. Trusses being fit-up in test frame of 35 ft test assembly.

3.5 DESCRIPTION OF TESTS AND LOADING

3.5.1 Full-scale Tests (35 ft span)

Full-scale (35 ft span) tests were conducted at the UL furnace facility in Toronto, Canada. Loading of the floor slab, to "simulate a maximum load condition" as required by ASTM E 119, was accomplished through a combination of concrete block and steel containers filled with water. The water containers were restrained using steel cables to prevent them from falling into the furnace and causing damage to the fire brick and instrumentation in the event of a catastrophic failure of the floor system. Figure 3–5 shows the water containers being placed on the concrete slab.

Source: NIST.

Figure 3–5. 35 ft span test assembly loaded with concrete blocks and water-filled containers.

3.5.2 Reduced-scale Tests (17 ft span)

The reduced-scale tests were designed to extract as much information as practicably possible considering that the purpose of the Standard Fire Resistance Test is to measure the ability of the test assembly to contain a fire and is, therefore, based on integrity (passage of hot gases), thermal insulation (heating of the unexposed surface) and load bearing capacity (support of the applied load). For the reduced-scale tests, the sizes of the steel members and the slab thickness were the same as in the full-scale tests. Otherwise, the length and depth of the trusses were scaled by one half. The spacing between the trusses was the same as in the full-scale test. The scaled length and depth, coupled with the original member sizes, slab thickness, and truss spacing, required an increase in the loading to produce the same stress levels as in the full-scale specimen. The loading represented the maximum calculated load condition as required by the ASTM E119 Standard.

The superimposed uniform load was applied through a combination of concrete blocks, water-filled containers, and hydraulic actuators located along the trusses. Figure 3–6 shows the assembly of blocks, water containers, and hydraulic actuators.

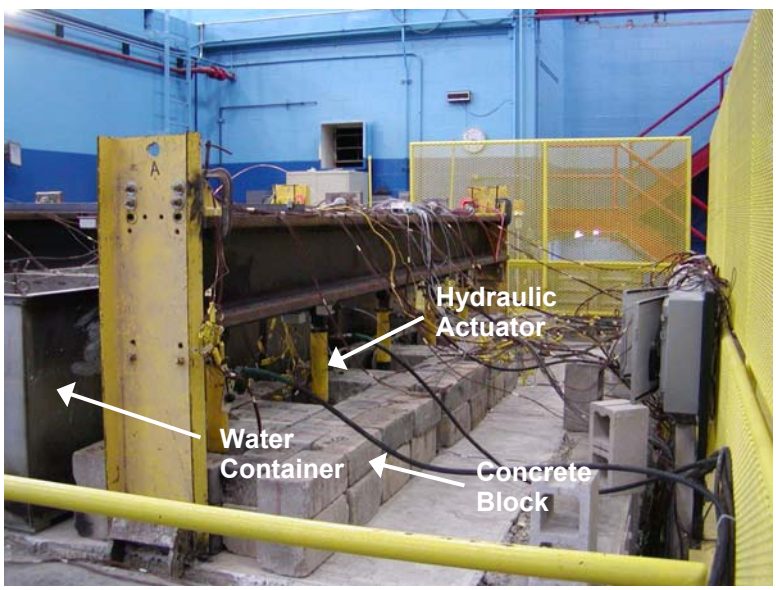

Source: NIST.

Figure 3–6. 17 ft span test assembly loaded with concrete blocks, water-filled containers and hydraulic actuators.

3.6 TEST RESULTS

3.6.1 General Discussion of Tests

Specimen No. 1: 35 ft span restrained specimen with 3/4in. SFRM

In the test of Specimen No. 1, loud noises (reports) were heard beginning roughly fifteen minutes after the start of the test. These loud, but somewhat muffled, reports continued and were often accompanied by noticeable bulging of the metal deck and the dislodging of deck SFRM. It is believed that these loud

noises were associated with spalling of the concrete on the underside of the slab. The slab was later sectioned to determine the depth of delamination resulting from the spalling.

At about 50 min, a very loud report was heard, associated with a noticeable sudden downward deflection of the specimen. When access to the top of the slab was possible after completion of the test, it was found that significant cracking and dislocation of the slab had occurred near the corners of the slab. Several of these events were recorded, and post-test inspection revealed that concrete failure had occurred in all four corners of the slab as shown in Fig. 3–7. It is believed that the very loud report and abrupt deflection was a result of the sudden concrete cracking. The test was stopped at 116 min when, after another sudden drop, the center span deflection reached about 15 in.

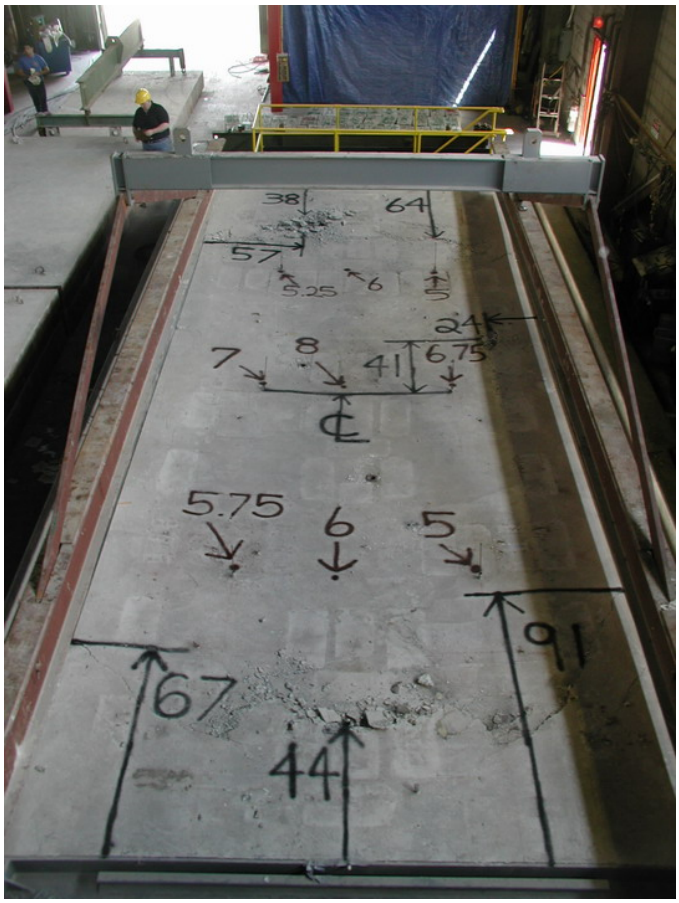

Source: NIST.

Figure 3–7. Unexposed surface of Assembly No. 1 after loading equipment was removed.

The specimen supported the applied load for the duration of the test. Post-test inspection showed that the corners of the slab had not deflected; rather, all of the slab deflection occurred beginning roughly 5 ft from the ends as seen in Fig. 3–7. It is believed that the thermal expansion of the concrete and the resistance provided by the test frame, put the slab in compression and “wedged” the slab so that no deflections could occur at the ends of the slab. The high compressive stresses that developed likely contributed to the failures noted above.

The test was conducted beyond the E119 end point criteria to obtain as much information as possible. This test, as well as the other three, were continued as long as practical. The tests were stopped, in general, when there was a risk of imminent failure or when deflections were so large as to affect instrumentation readings and, as a consequence, safe conduct of the test. The restrained and unrestrained ratings obtained from this test are given in Section 3.6.2.

Specimen No. 2: 35 ft span unrestrained specimen with 3/4in. SFRM

Reports were heard during the test of the 35 ft unrestrained Specimen No. 2 but were not as loud as those observed during the previous test. A significant difference was that no loud reports or attendant sudden increase in downward deflection were observed for the entire test period, which was 146 minutes, almost two and a half hours, and post-test inspection of the top of the concrete slab showed very little cracking as seen in Fig. 3–8. Since there was a gap between the concrete slab and test frame, thermal expansion of the slab did not produce a state of stress that resulted in significant and sudden cracking and crushing similar to that observed in Specimen No. 1. Additionally, the slab in this test was not wedged at the ends and, unlike Specimen No. 1, the slab deflected over its entire length.

Source: NIST.

Figure 3–8. Unexposed surface of Assembly No. 2 after loading equipment was removed.

The center-of-slab deflection at the end of the test was more than 13 in. The test had to be stopped when the slab deflections affected the instrumentation, and readings could not be obtained. The unrestrained rating for Specimen 2 obtained from this test is given in Section 3.6.1.

Specimen No. 3: 17 ft span restrained specimen with 3/4in. SFRM

As in the first two tests, the metal deck began bulging due to spalling of concrete on the underside of the slab within the first 15 min. At 82 min into the test, a very loud report was heard, and pieces of concrete flew in the air signifying explosive spalling at the north end of the slab as shown in Fig. 3–9. A slight increase in downward deflection at the center of the slab was recorded at 82 min. The test was continued for 210 min and was stopped when the deflections were so large as to affect instrumentation.

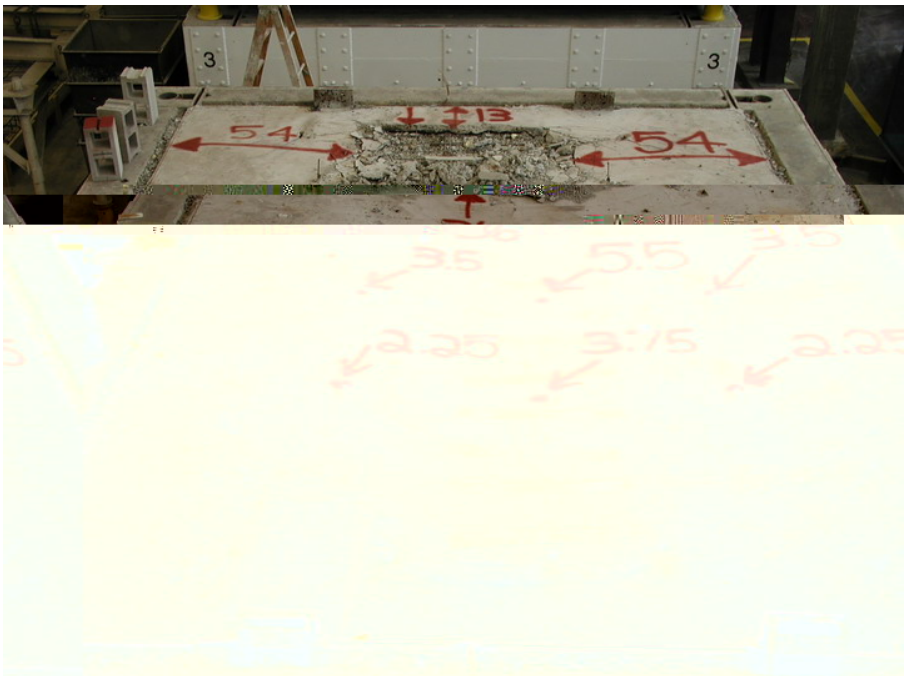

Source: NIST.

Figure 3–9. Unexposed surface of Assembly No. 3 after loading equipment was removed.

Specimen No. 4: 17 ft span restrained specimen with 1/2 in. SFRM

Specimen No. 4 behaved similarly to the other three specimens with regard to bulging of the metal deck on the underside of the slab beginning in the early stages of the test. At 55 minutes, a very loud report was heard, and a significant section of the slab spalled explosively, sending concrete fragments high in the air. As seen in Fig. 3–10, the resulting hole in the slab (left side of the photograph) measured over 2 ft in length and had to be covered with insulating material to safely continue the test as hot gases were coming through the hole.

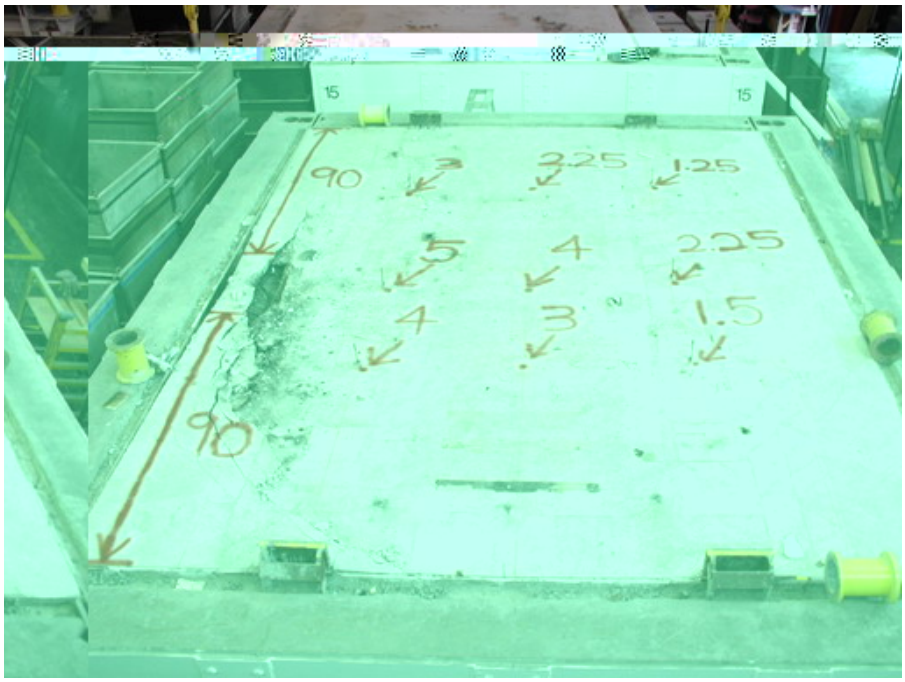

Source: NIST.

Figure 3–10. Unexposed surface of Assembly No. 4 after loading equipment was removed.

3.6.2 Fire Resistance Ratings

As noted above, prior to 1971, the ASTM E 119 Standard did not differentiate between testing and classifying thermally restrained and unrestrained floor assemblies. The 1961 revision of ASTM E 119, the revision referenced in the 1968 New York City Building Code, is used for reporting the Standard Fire Test rating (no distinction was made for an unrestrained rating). The year 2000 revision of the Standard is used for reporting restrained and unrestrained ratings.

Table 3–1 shows results for all four tests giving the times (in minutes) to reach the acceptance, or end-point, criteria and the Standard Fire Test rating (in hours) for both the 1961 and 2000 revisions of ASTM E 119. Note that in none of the tests did the floor assembly fail to support the superimposed load.

Table 3–1. Results of ASTM E119 Standard Fire Tests.

Test	Description	Times to Reach End-Point Criteria (min)					Test Termin-ated (min)	Standard Fire Test Rating (hr)		
		Temperature on Unexposed Surface		Steel Temperatures		Failure to Support Load		ASTM E 119-61	ASTM E119-00	
		Average (Ambient +250ºF)	Maximum (Ambient+ 325ºF)	Average (1100ºF)	Maximum (1300ºF)			Rating	Restrained Rating	Unrestrained Rating
1	35 ft, restrained, 3/4 in SFRM	---	111	66	62	(3)	116(1)	1 ½	1 ½	1
2	35 ft, unrestrained, 3/4 in SFRM	---	---	76	62	(3)	146(2)	2	---	2
3	17 ft, restrained, 3/4 in SFRM	180	157	86	76	(3)	210(2)	2	2	1
4	17 ft, restrained, 1/2 in SFRM	---	58	66	58	(3)	120(1)	¾	¾	¾

(1) Imminent collapse
(2) Vertical displacement exceeded capability to measure accurately
(3) Did not occur

3.6.3 General Observations

Buckling of Trusses

A photograph of the underside of the 35 ft, restrained test specimen after almost two hours of fire exposure is shown in Fig. 3–11. Buckling of the compression diagonals can be seen as well as sagging of the metal deck between supports. Note that, upon cooling, the test specimen recovered at least half of the deflection achieved during the test so deflections seen in Fig. 3–11 are considerably less than the deflections at the end of the test.

Source: NIST.

Figure 3–11. Fire exposure side of the 35 ft restrained test assembly after almost 2 hours of fire exposure

Spalling of Concrete

The sagging of the metal deck was asumed to be a result of spalling of the underside of the concrete slab. This was confirmed when, after the tests, concrete cores were removed and sections cut to determine the condition of the concrete as shown in Fig. 3–12. The depth of the delamination varied but the depth of the remaining slab was on the order of 2 in. to 3 in., essentially up to the double layer of welded wire fabric as seen in Fig. 3–13.

Source: NIST.

Figure 3–12. Sections cut through concrete slab to confirm extent and depth of spalling.

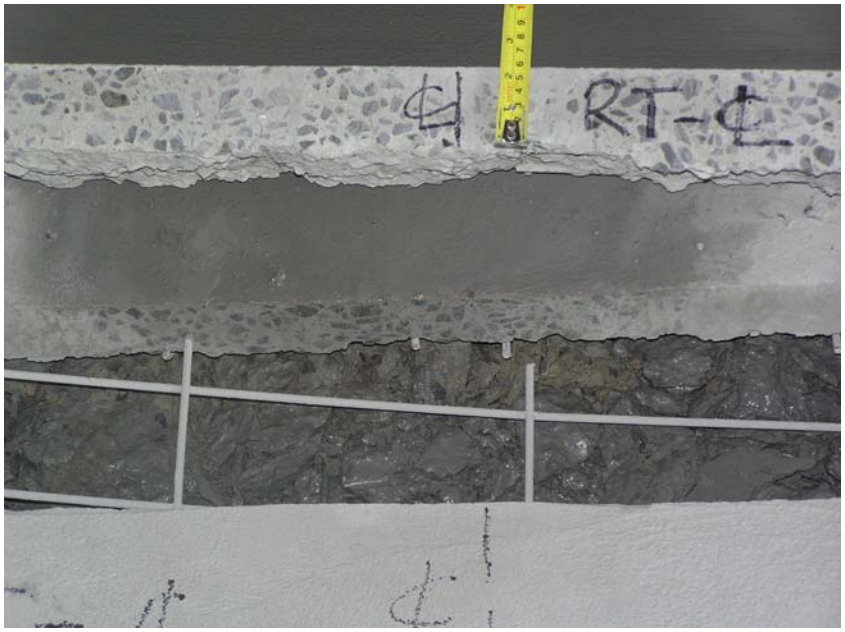

Source: NIST.

Figure 3–13. Measurement of remaining slab thickness after spalling.

Concrete Slab Failure

The three specimens that were restrained showed significant cracking and explosive spalling at the top surface of the concrete slab. The 35 ft restrained specimen had significant cracking and crushing of concrete near the ends and the corners as seen in Fig. 3–7 and Fig. 3–14. These major concrete failures were accompanied by sudden increases in deflection of the floor as seen in Fig. 3–15. The unrestrained 35 ft specimen showed little cracking and no crushing or explosive spalling at the top surface of the slab unlike the restrained specimen. The restrained 17 ft specimen with ½ in. of SFRM exhibited significant explosive spalling in which concrete fragments flew in the air and left a hole in the slab about 2 ft long through which hot gases escaped.

Source: NIST.

Figure 3–14. Detail of spalling concrete at east end of Assembly No. 1.

3.6.4 Floor Deflections and Temperatures

Deflections of floor assembly

The following plots show the vertical deflection measured at the center of each floor assembly. Figure 3–15 shows the deflection while Fig. 3–16 is a plot of the deflection normalized by the span length. It is seen that Specimen No.1 experienced a significant increase in vertical deflection at 49 min which corresponded directly to a loud report and visible increase in deflection noted during the test. A small increase in vertical deflection for Specimen No. 3 was seen to occur at 82 min, the time when the slab spalled explosively at one end.

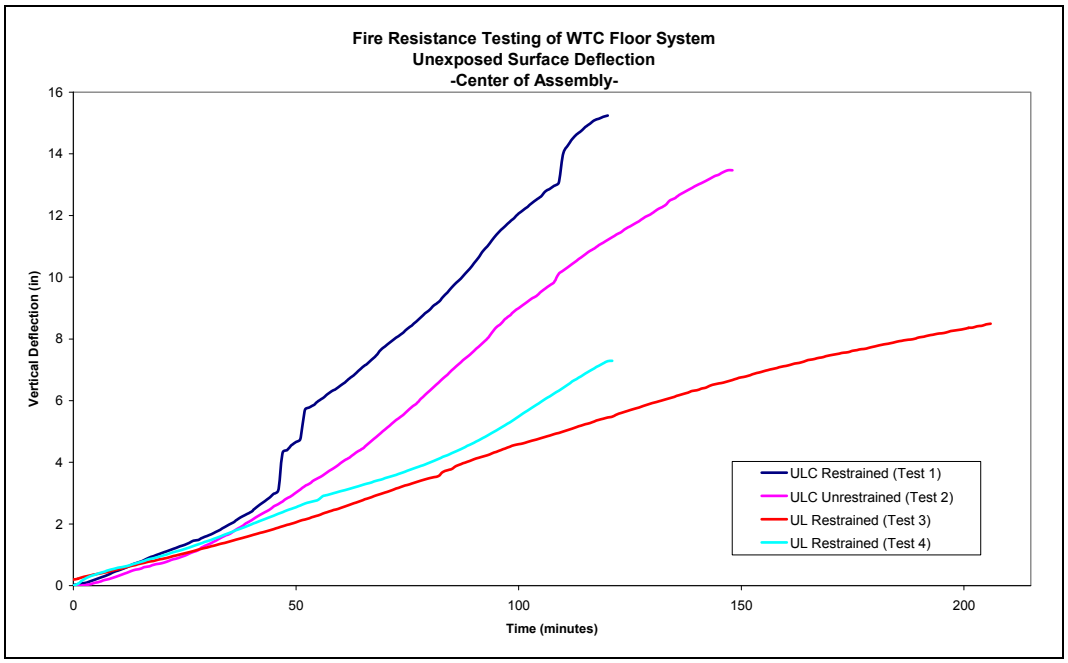

Figure 3–15. Deflection measured at the center of each assembly.

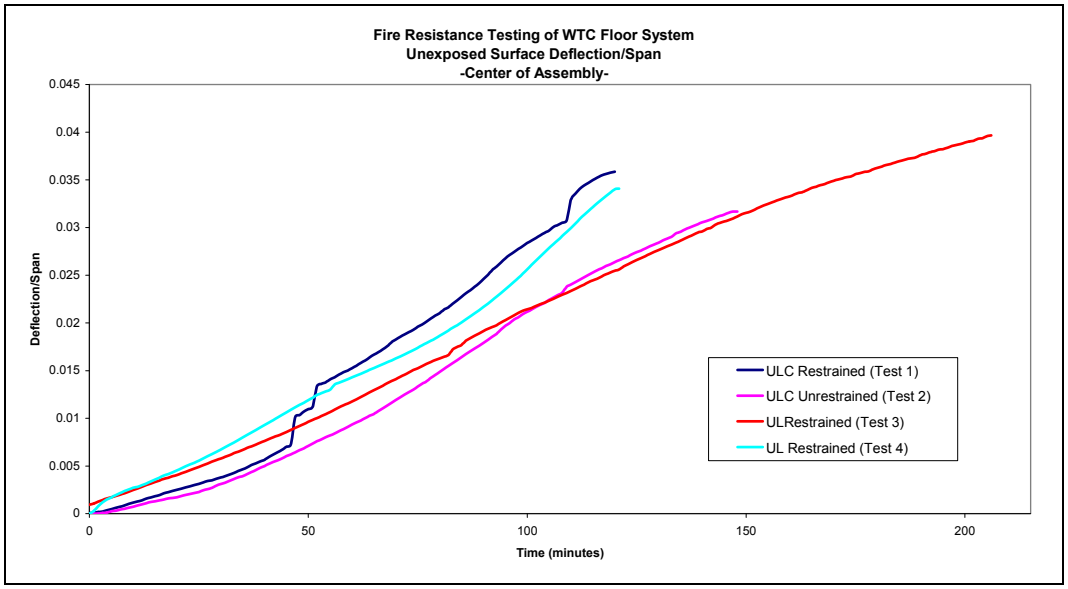

Figure 3–16. Deflection measured at the center of each assembly divided by the span.

Unexposed surface temperatures

The temperature of the top (unexposed) surface of the floor assemblies is plotted in Fig 3–17. It is observed that the unexposed surface temperatures of all four test assemblies were similar prior to the onset of significant concrete crushing and spalling at around 50 min. In Test 4, the surface-mounted thermocouple on the west edge near the center of the span was affected by the explosive failure of the slab and recorded hot gas temperatures.

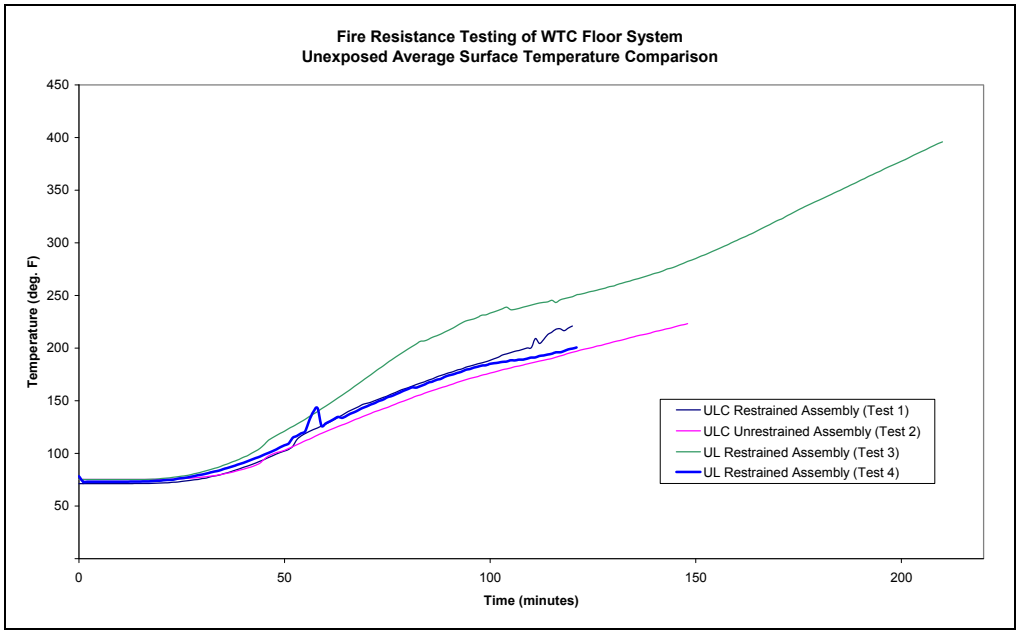

Figure 3–17. Average temperature of the unexposed surface for all four tests.

Steel temperatures

Steel temperatures were recorded at several locations on the main and bridging trusses. Figure 3–18 shows a comparison of the average temperature of the bottom chord for the three tests in which the thickness of the SFRM was ¾ in. Temperatures were seen to be very comparable up to about 75 min, which was around the time when SFRM began to dislodge. The location and extent of dislodged SFRM could not be ascertained through visual observation during the tests.

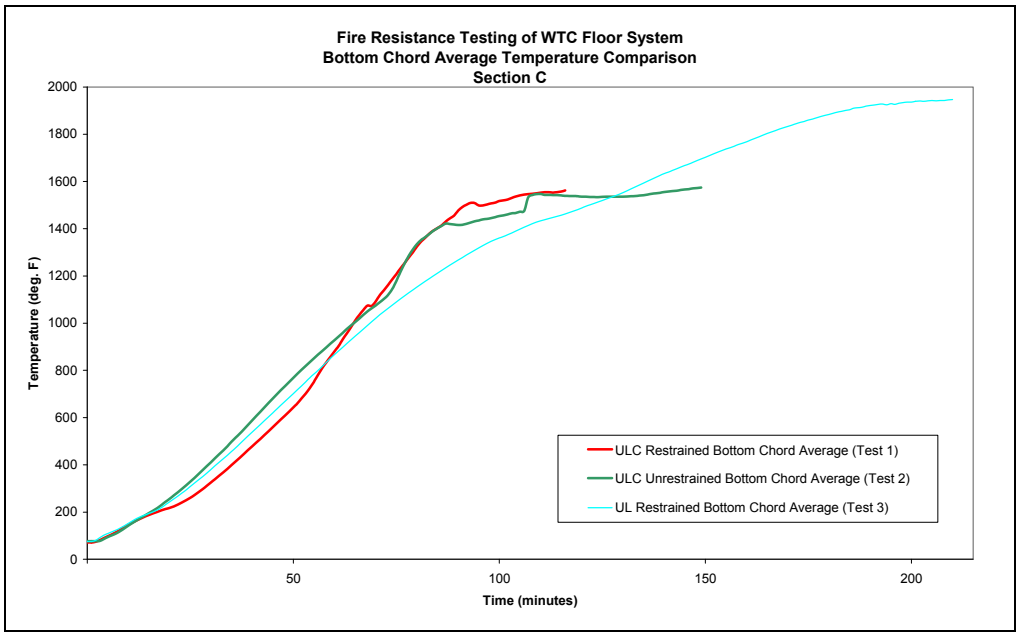

Figure 3–18. Average temperatures of the bottom chord for Test Nos. 1, 2 and 3 (3/4 in. thick SFRM).

3.6.5 Observations and Comparisons

Several observations can be made from the results presented and the summary table of hourly ratings (Table 3–1). The reader is referred to NIST NCSTAR 1-6B for a complete description of the fire resistance tests and the results obtained.

- The test assemblies were able to withstand standard fire conditions for between ¾ h and 2 h without exceeding the limits prescribed by ASTM E 119.

- Test specimens protected with ¾ in. thick spray applied fire-resistive material were able to sustain the maximum design load for approximately two hours (the minimum was 116 min) with no structural failure; in the 35 ft, unrestrained test, the load was maintained for 3½ h (210 min).

- The restrained 35 ft floor system obtained a fire resistance rating of 1½ h while the unrestrained 35 ft floor system achieved a 2 h rating. Past experience with the ASTM E 119 test method would lead investigators to expect that the unrestrained floor assembly would not perform as well as the restrained assembly, and therefore, would receive a lower fire rating.

- A fire rating of 2 h was determined from the 17 ft restrained test with the average applied SFRM thickness of ¾ in. while a fire rating of 1½ h was determined from the 35 ft restrained test with the same SFRM thickness.

- A fire rating of ¾ h was determined from the 17 ft restrained test with the specified SFRM thickness of ½ in.

3.7 SUMMARY

The tested floor assemblies were similar, though not identical, to steel-joist-supported concrete floors that are widely used in low rise construction. The test results provided valuable insight into the behavior of these widely used assemblies and also identified issues that require further study.

The fire resistance tests showed that the floors were capable of considerable sagging without collapse. The tests also showed fire damage to the bridging trusses and buckling of compression diagonals and the vertical strut near the supports. No evidence of knuckle failures was seen in the tests.

The standard test method has been used for many decades and has for the most part served its intended purpose well when taken together with the fire rating requirements. This is supported by historical fire loss data for more than half a century for different high-rise building occupancies. In addition, there is extensive data and experience that has been developed using the test method.

The NIST tests have identified areas where further study related to the standard test method may be warranted. Among the issues related to the test method that NIST identified as requiring further study are:

- Criteria for determining structural limit states, including failure, and means for measurement,
- Scale of test assembly versus prototype application,
- Effect of end restraint conditions (restrained and unrestrained) on test results, including the influence of stiffness,
- Structural connections (not currently addressed in ASTM E 119),
- Combination of loading and exposure (temperature profile) adequately represent expected conditions,
- Procedures to analyze and evaluate data from fire resistance tests of other building components and assemblies to qualify an untested building element,
- Repeatability of test results (single test currently defines rating for system),
- Reproducibility of heat flux environment between different furnaces and laboratories, and
- Relationships between prescriptive ratings and performance of the assembly in realistic building fires.

This page intentionally left blank.

Chapter 4
STRUCTURAL RESPONSE OF COMPONENTS, CONNECTIONS AND SUBSYSTEMS

In this chapter, the structural analysis of components, connections, and detailed analysis for the development of two subsystems -- a floor subsystem and an exterior wall subsystem -- are covered[25]. The subsystem response to impact damage and fire is addressed in Chapter 7. This work was conducted to provide guidance for the development of the global finite element models with respect to element types and sizes, appropriate constitutive models, and failure criteria for any given structural component. The subsystem models were also used to correlate the results of the fine mesh component analyses with the coarser mesh global analyses.

Work reported herein includes the following:

- Evaluation of the structural response of components, connections and subsystems to service loads due to gravity (dead and live loads) and elevated structural temperatures.
- Identification of the failure modes and failure sequences, the associated temperatures at failure, and where temperature histories were used, times to failure.
- Identification of the changes in mechanical properties or geometry at initiation of component and subsystems failure.
- Identification of modifications for the global structural models to reduce complexity and size while maintaining the quality of analysis results.

This chapter covers the mechanical properties of concrete and steel at elevated temperatures, analysis of components and connections for the floors and exterior wall, and the development of models for a full floor and portion of an exterior wall. The reader is referred to NIST NCSTAR 1-6C for a complete description of component, connection, and subsystem structural analyses.

4.1 MECHANICAL PROPERTIES OF CONCRETE AND STEEL

The mechanical properties of both steel and concrete are affected significantly by temperature. In the following sections, the material properties used in this study are specified as a function of temperature. For finite element analysis (FEA) of components, subsystems, and global models of the World Trade Center (WTC) towers, a material properties catalog was developed. Each material model was identified with a number in ANSYS[26]; steels were Material ID 1 through Material ID 29, and concretes were

[25] All information and data related to the design and construction of the WTC floors and exterior walls were obtained from contract drawings provided to NIST by The Port Authority or New York and New Jersey. Refer to NIST NCSTAR 1-2A for a complete description of the WTC structural system and an index of all structural drawings.

[26] ANSYS (ANSYS, Inc., Cannonsburg, PA) is the structural analysis software used for nonlinear finite element analyses.

Material ID 51 through Material ID 83. The details of concrete and steel materials are discussed separately in this section.

4.1.1 Concrete Properties and Failure Criteria

Two types of concrete were used for the floors of the World Trade Center towers: lightweight concrete in the tenant office areas and normal-weight concrete in the core area. Thermal properties of normal-weight concrete depend on the type of aggregate. Petrographic inspection of several samples of lightweight concrete taken from the debris showed siliceous sand in the lightweight concrete. Because coarse and fine aggregates are usually from the same source for a construction site, it was assumed that the normal-weight concrete had siliceous aggregate.

The specified design strength for lightweight concrete was 3,000 psi and either 3,000 psi or 4,000 psi for normal-weight concrete, depending upon the floor location within the buildings. The actual strength of concrete at room temperature is greater than that measured from cylinders poured for testing during construction, referred to as 28-day cylinder strength, as concrete continues to strengthen with age. Methods for estimating changes in concrete strength with age are specified by the American Concrete Institute (ACI) 209. The actual compressive strength of WTC concrete slabs was estimated to be 38 percent greater than the specified design strengths: 5,500 psi for 4,000 psi normal-weight concrete and 4,100 psi for 3,000 psi normal-weight and lightweight concretes (see NIST NCSTAR 1-6C).

Normal-weight and lightweight concrete had similar design strengths of 3,000 psi to 4,000 psi, but respond differently to elevated temperatures. Temperature dependent properties of concrete are modulus of elasticity, instantaneous coefficient of thermal expansion, compressive strength, and tensile strength.

The effects of elevated temperature on concrete mechanical properties, plotted in Fig. 4–1, are based upon Phan (1996) and Phan and Carino (2003). Lightweight concrete shows less degradation in modulus of elasticity and a constant instantaneous coefficient of thermal expansion as temperatures increase. Lightweight concrete heats more slowly than does normal weight concrete. Tensile strength is identical for lightweight and normal weight concretes with the same compressive strength, since tensile strength depends upon the formation of cracks. Compressive strength for lightweight concrete shows no degradation until 300 °C, whereas normal weight concretes begin degrading as temperatures exceed room temperature.

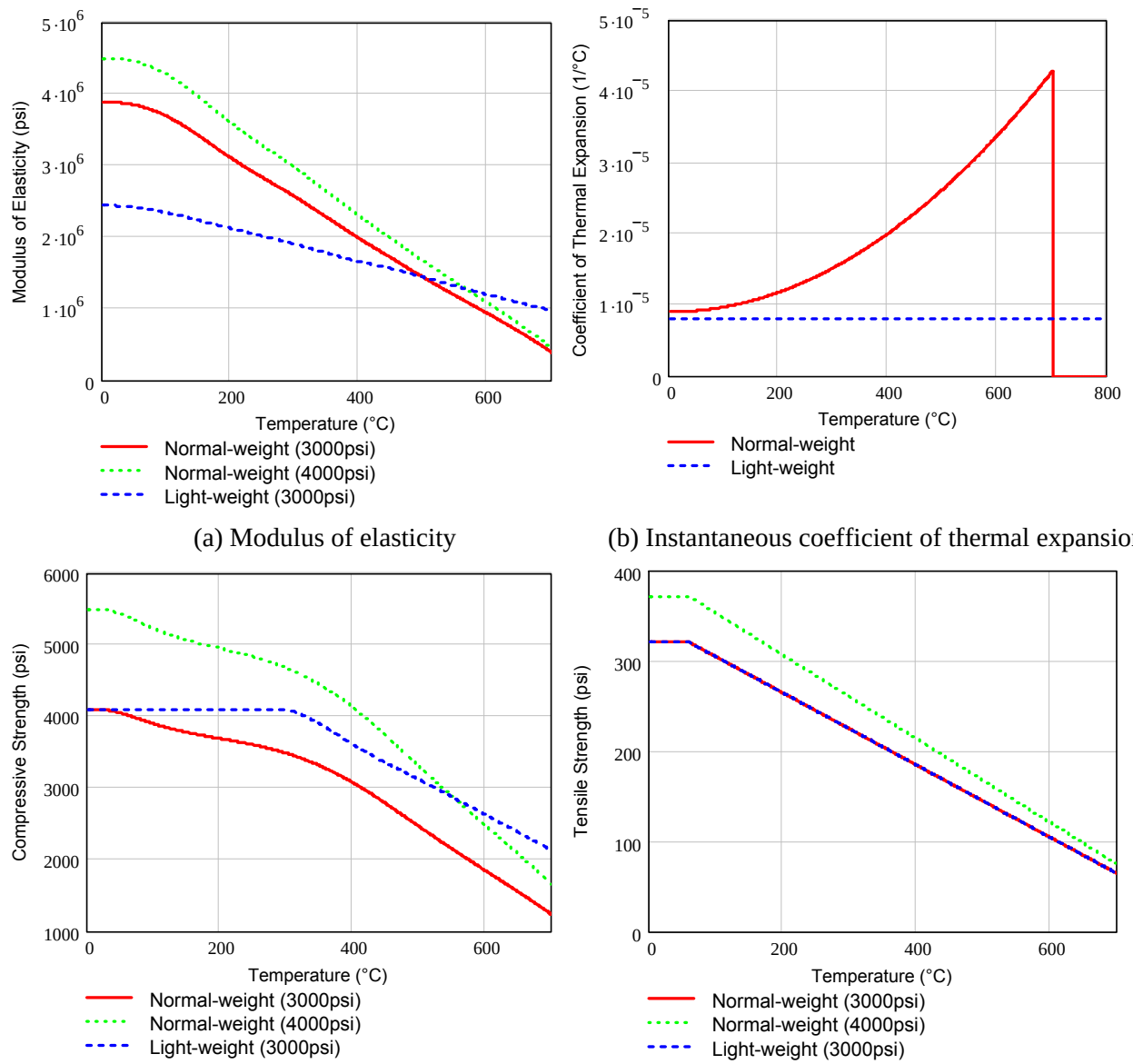

(a) Modulus of elasticity

(b) Instantaneous coefficient of thermal expansion

(c) Compressive strength

(d) Tensile strength

Figure 4–1. Temperature–dependent concrete properties.

Figure 4–2 shows concrete stress-strain curves at room and elevated temperatures, where compressive stresses and strains are negative and tensile stresses and strains are positive. Tensile stress in concrete increases linearly up to the tensile strength. When strained beyond this point, the concrete begins to crack and the stress across the section will drop. However, this drop in the stress-strain relationship caused significant numerical instability problems during structural analysis. Numerical instabilities were avoided by assuming that the reinforced concrete slab became plastic in tension as the reinforcement carried the tensile load.

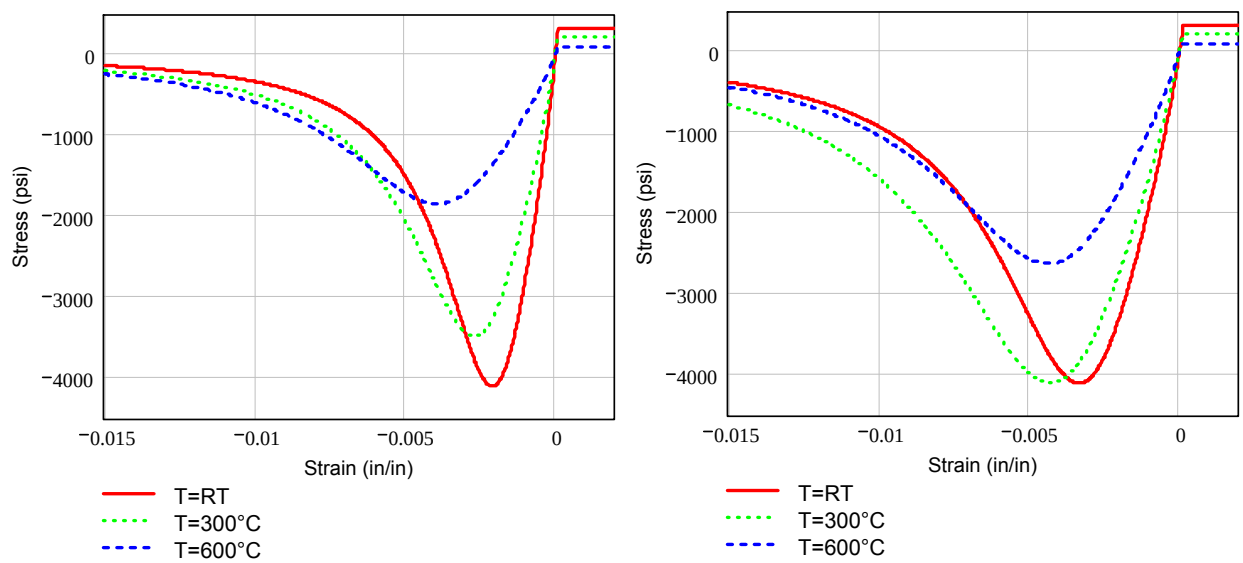

(a) Normal-weight concrete (3000psi) (b) Light-weight concrete

Figure 4–2. Concrete stress-strain curves.

The assumption of concrete plasticity after the onset of cracking is valid for balanced reinforcement in concrete. Although the reinforcement ratio in the WTC concrete slabs was smaller than the balanced reinforcement ratio, the inaccuracy was not significant.

Compressive failure of the concrete slabs was modeled with the von Mises yield criterion.

4.1.2 Steel Properties and Failure Criteria

Steels used in WTC 1 and WTC 2 are listed in Table 4–1. For each steel, described by its design strength, the table lists the estimated yield and ultimate strengths, σ_{yRT} and σ_{uRT} , respectively. Figure 4–3 shows the mechanical properties of steel that are affected by elevated temperatures: (a) modulus of elasticity; (b) Poisson's ratio; (c) yield strength reduction factor; (d) tensile strength reduction factor; and (e) instantaneous coefficient of thermal expansion. A single line is plotted for the properties of all steels in Table 4–1, since the reduction factors for elevated temperature effects on steel mechanical properties were assumed to be the same for all steels, except for the yield and tensile strength reduction factors for bolt steels. See NIST NSTAR 1-3C for a complete description of the development of the steel properties at elevated temperatures.

When compared to concrete properties, the following observations can be made:

- Modulus of elasticity is reduced by 25 percent at 600 °C for steel and by 50 percent to 75 percent for concrete.

- Poisson's ratio increases for steel but remains constant for concrete at 0.17. However, the values for steel up to 600 °C are close to the rounded value of 0.3 that is often assumed for design purposes at room temperature.

Table 4–1. Steel types used in WTC 1 and WTC 2.

Material ID	Description	σ_{yRT} (psi)	σ_{uRT} (psi)
1	All 36 ksi core box columns, plates, straps[a]	36,720	64,470
2	All 36 ksi core WF, channels, and tubes 36 ksi large area and large inertia "rigid" beams in SAP2000 model[a]	37,000	63,450
3	All 42 ksi box columns (1<=0.75 in.)	51,400	79,200
4	All 42 ksi box columns (0.75 in. < t <= 1.5 in.)	47,000	74,800
5	All 42 ksi box columns (t > 1.5 in.)	42,600	70,400
6	42 ksi or 45 ksi Group 3 WF core columns	53,800	74,400
7	42 ksi or 45 ksi Group 3 WF core columns	49,000	71,040
8	42 ksi Group 4&5 WF core columns	44,200	66,640
9	45 ksi Group 4&5 WF core columns	47,800	71,074
10	All 36 ksi Plates 1, 2, and 4 in perimeter columns	35,630	61,170
11	All (42, 45, or 46) ksi Plates 1, 2, and 4 in. perimeter columns	53,051	74,864
12	All 50 ksi Plates 1, 2, and 4 in. perimeter columns. All 50 ksi channels and plates[a]	53,991	75,618
13	All 55 ksi Plates 1, 2, and 4 with t<=1.5 in. in perimeter columns	60,817	82,558
14	All 60 ksi Plates 1, 2, and 4 with t<=1.25 in. in perimeter columns	62,027	87,250
15	All 65 ksi Plates 1, 2, and 4 with t<=0.5 in. in perimeter columns[b]	69,642	90,442
16	All 70 ksi Plates 1, 2, and 4 in. perimeter columns	76,735	91,951
17	All 75 ksi Plates 1, 2, and 4 in perimeter columns	82,469	96,821
18	All 80 ksi perimeter columns steels, regardless of plate	91,517	99,442
19	All (85, 90, 100) ksi perimeter column steels, regardless of plate	104,783	115,983
20	Laclede truss web bar rounds specified as A36	38,067	59,567
21	Laclede truss chord angels (regardless of ASTM Spec) and all rounds specified as A242	55,332	74,050
22	A325 bolts[c]	104,783	115,983
23	All 42 ksi Plate 3 in perimeter columns	42,600	67,216
24	All 45 ksi Plate 3 in perimeter columns	45,900	69,831
25	All 50 ksi Plate 3 in perimeter columns	51,400	74,188
26	All 55 ksi Plate 3 in perimeter columns	56,900	78,546
27	All 60 ksi Plate 3 in perimeter columns	62,400	83,903
28	All 65 ksi Plate 3 in perimeter columns	67,900	87,261
29	All 70 ksi and 75 ksi Plate 3 in perimeter columns	78,900	95,976

a. Steels in the following members are assumed to have the properties shown in the table:
36 ksi plates and straps (Material 1).
36 ksi channels, tubes, and "rigid" beams (Material 2).
50 ksi channels and plates (Material 12).
b. 65 ksi steels in perimeter columns with t>0.5 in. are assumed to have the same properties as those in Material 15.
c. In the column model, stress-strain relationships of bolts are used.
Note: Bolt properties are assumed to be the same as those in Material 19.

- Steel yield strength reduces to 20 percent of its initial value and its ultimate tensile strength is reduced to 40 percent at 600 °C. Concrete compressive strength is reduced to 30 percent to 50 percent of its initial value. Concrete tensile strength, which is already low, is also reduced to 30 percent.

- The instantaneous coefficient of thermal expansion for steel lies between the curves for lightweight and normal weight concrete. If steel truss and lightweight concrete components are at the same temperature, the steel components will thermally expand more than the lightweight concrete. For steel beams and normal weight concrete in the core area, the normal weight concrete will expand more than the steel beams.

To illustrate the effect of elevated temperature reduction factors on steel strength, Fig. 4–4 shows stress-strain curves for Material ID 1 (see Table 4–1) at room and elevated temperatures. Figure 4–4 (a) shows the low strain range and Fig. 4–4 (b) shows strain levels up to 0.3. These figures show elastic and plastic strains, but for temperatures above 350 °C, the stress-strain curve beyond the elastic limit may also include creep strains. The presence of significant creep strains relative to plastic strains depends upon the combination of three factors: temperature, stress level, and time duration at the temperature and stress level. Creep strain behavior for steel was based upon the creep model by Fields and Fields (1991). The creep model was validated against experimental data (NIST NCSTAR 1-3D). Figure 4–5 illustrates behavior of steel elastic, plastic, and creep strains at elevated temperatures for Material ID 1. Figure 4–5 (a) shows the effect of creep strain rate for various temperatures, and Fig. 4–5 (b) compares elastic, plastic, creep, elastic plus plastic, and total strains at T= 400 °C and constant loading for an 1,800 s duration.

The elastic-plastic behavior of steels was modeled with ANSYS “Multi-linear isotropic hardening von Mises plasticity” material model. Creep behavior was modeled using the ANSYS time hardening implicit creep model for nonlinear beam elements (BEAM 188 and BEAM 189) in the full floor model. For BEAM 24 in the global models, an explicit primary creep model was used. BEAM 188 and BEAM 189 elements include thermal expansion, creep, and temperature-dependent material properties. When the elements were used in the global model, numerical difficulties occurred for creep and post-buckling behaviors which were resolved by using BEAM 24 elements.

The failure criteria for steel were defined in terms of plastic strains. The multiaxial fracture strain criterion for true stress and true strain was evaluated under a uniaxial stress condition. For element sizes ranging from 0.025 in. to 0.75 in., a relationship between element size and equivalent uniaxial fracture plastic strain was established. The process was repeated for steel at temperatures 20 ºC, 100 ºC, 300 ºC, 500 ºC, and 700 ºC leading to a fracture criteria for various mesh sizes of components. Figure 4–6 (a) shows the ratio of the maximum plastic strain in the direction of applied displacement-to-uniaxial plastic strain vs. element size at various temperatures. The finite element analysis results were extrapolated to an element size of 50 in. based on the linear curve fit to the analysis results shown in Fig. 4–6 (a). Plastic strain shown in Fig. 4–6 (b) was used as the fracture criterion for the corresponding element size in subsequent finite element analyses.

Weld properties at all temperatures were assumed to have essentially the same material properties as the base metal of the same ultimate tensile strength (see NIST NCSTAR 1-3). High temperature properties of weld metals were not found in the literature, however, most observed fractures in the exterior columns were in the base metal and not the welds.

ASTM A325 bolts were used in the perimeter column, spandrel, and floor truss connections. In addition to accounting for shear strength, the analyses included load elongation curves developed for tensile loading of bolts.

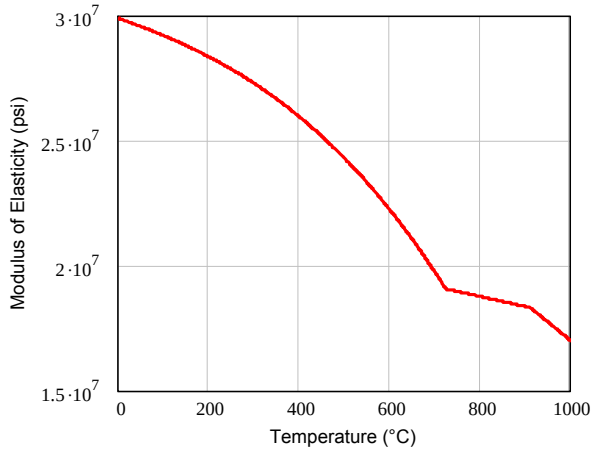

(a) Modulus of elasticity

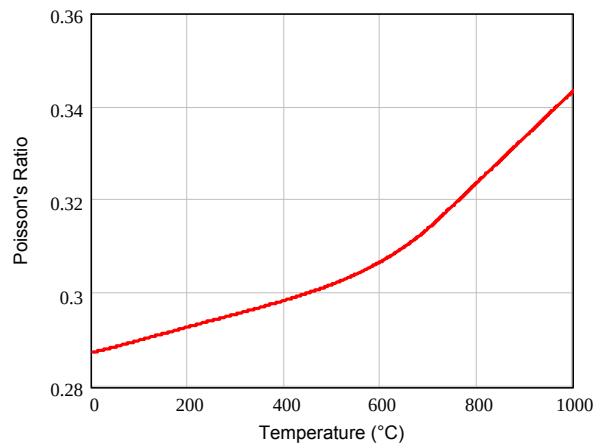

(b) Poisson's ratio

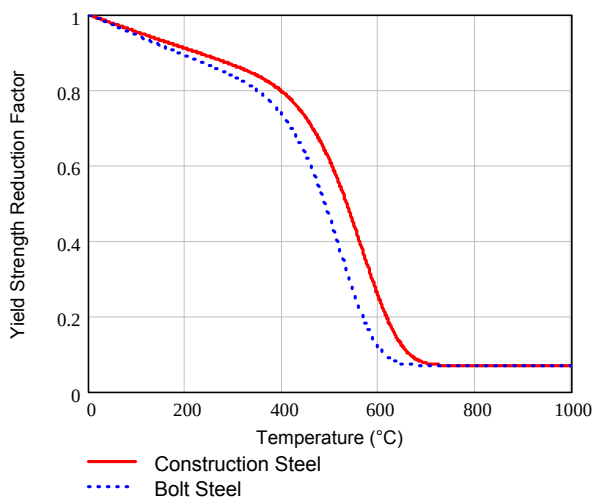

(c) Yield strength reduction factor

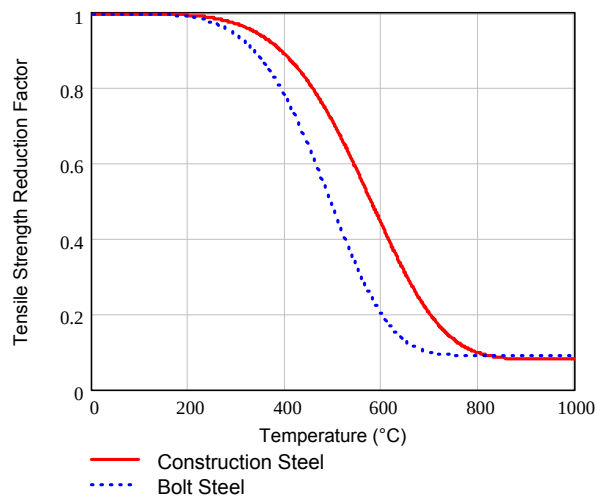

(d) Tensile strength reduction factor

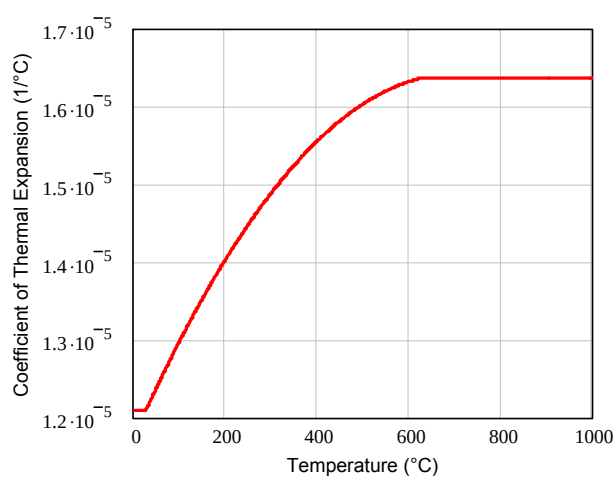

(e) Instantaneous coefficient of thermal expansion

Figure 4–3. Temperature-dependent properties for all steels.

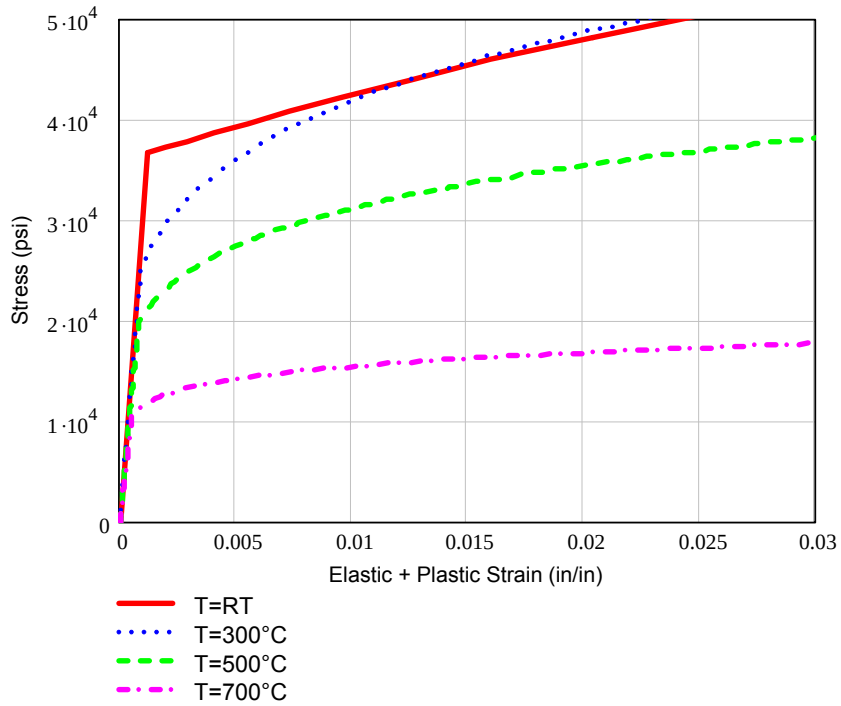

(a) Strain < 0.03

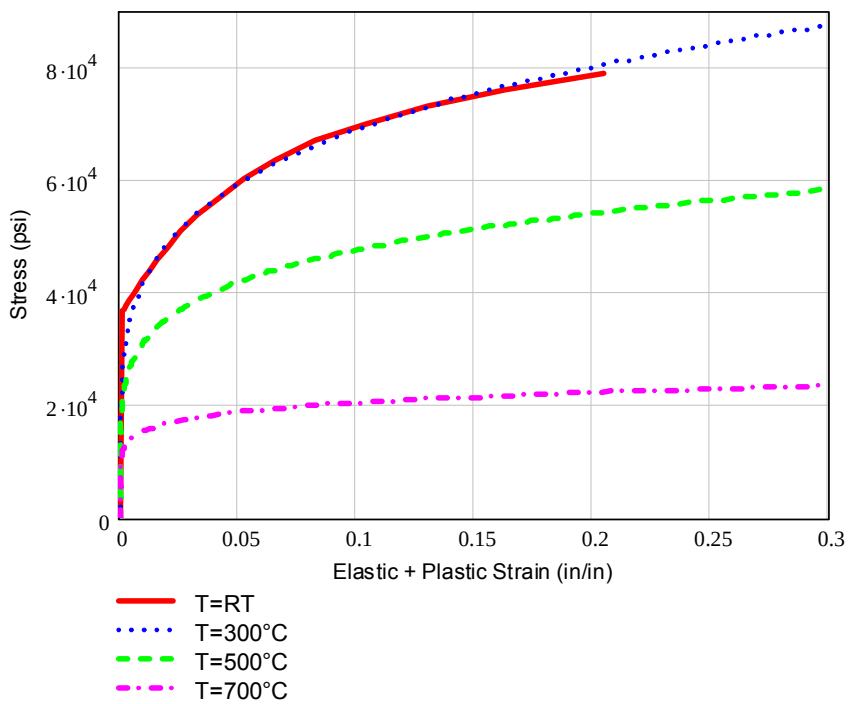

(b) Strain < 0.30

Figure 4–4. Stress-strain relationships for Material ID 1 steel.

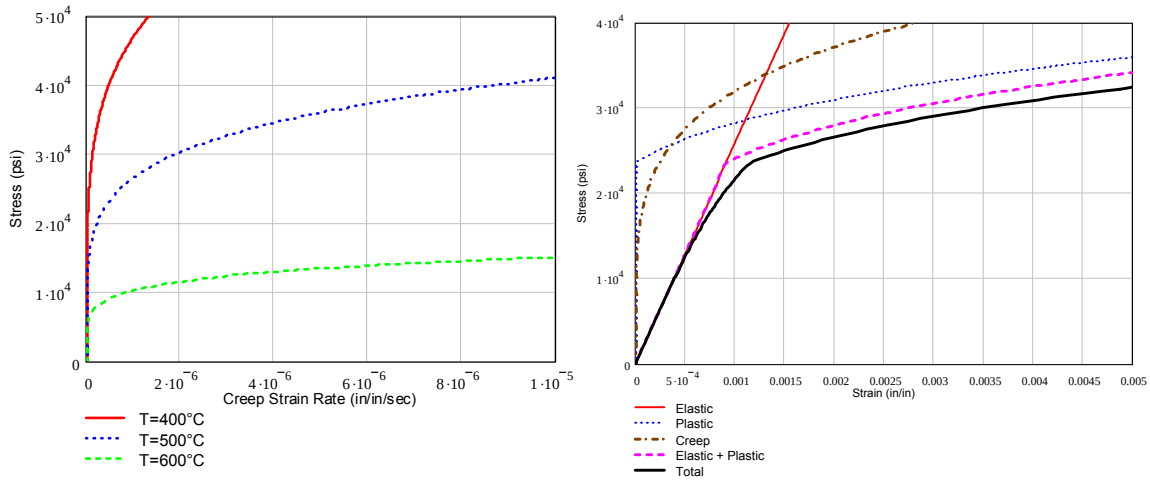

(a) Creep strain rate

(b) Components of strain at T=400 °C and t=1,800 s

Figure 4–5. Strain behaviors at elevated temperatures for Material ID 1 steel.

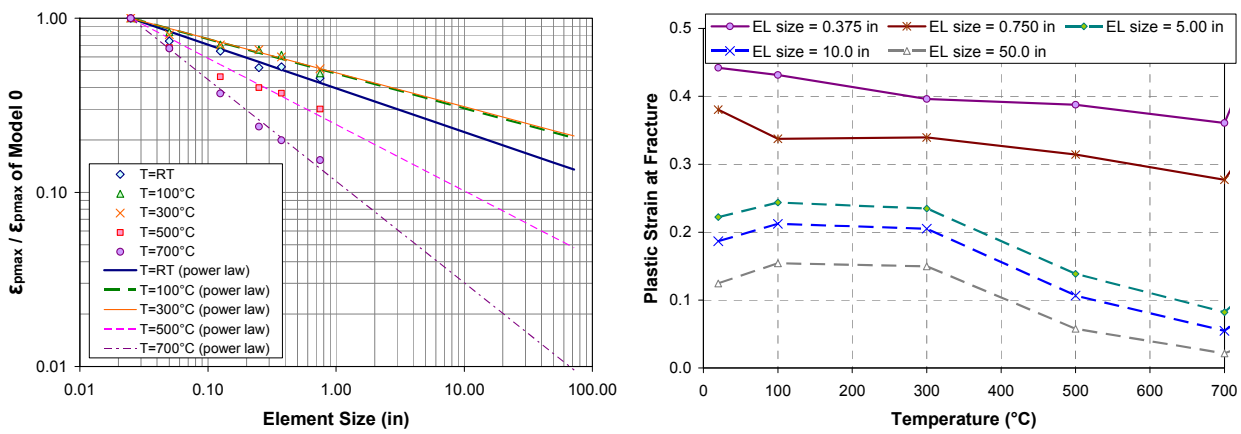

(a) FEA Results and Extrapolation

(b) Recommended Limiting Plastic Strain

Figure 4–6. Maximum plastic strain from the finite element analysis and limiting plastic strain.

4.2 FLOOR SUBSYSTEM ANALYSIS

The floors played an important role in the structural response of the World Trade Center towers to the aircraft impact and ensuing fires, and were identified as a critical subsystem requiring study prior to the development of global models for each tower. The floor system in the office area, outside the core, was a composite system consisting of a lightweight concrete slab supported by steel trusses. Within the core area, a composite steel beam and normal weight concrete slab floor system was used.

The floor subsystem analysis included: (1) the translation, validation, and modification of ANSYS models to incorporate nonlinear behavior, (2) evaluation of structural response under dead and live loads and elevated structural temperatures, (3) identification of failure modes and associated temperatures and times to failure, and (4) reduction in complexity of detailed component models for inclusion in the floor model.

Component analyses included the truss seat connections, shear connectors between the truss and lightweight concrete slab (referred to as knuckles), and a single truss and concrete slab section.

The failure modes and the failure loads for different components of the full floor subsystem were evaluated through analysis of detailed models of those components, using either hand calculations or finite element analyses. Models with a reduced size and/or complexity that captured the failure loads and failure modes were then developed for each component. These modified models of component behavior were incorporated in the full floor subsystem model.

4.2.1 Description of Floor Subsystem

The WTC towers had two types of floors above the plaza and mezzanine areas, tenant floors and mechanical floors. The structural layout and features of the tenant floors were similar throughout the towers, with minor differences in component dimensions and core framing layouts. Core framing changes were made to accommodate stairs, vents, and other features that varied in their locations between floors. Most of the floors in the towers were tenant floors. Mechanical floors were located at the skylobby levels and near the roof level of the towers (floors 7, 9, 41, 43, 75, 77, 107, 108, and 110). The aircraft impact and ensuing fires did not directly affect any mechanical floors.

Figures 4–7 (a) and (b) illustrate the structural layout and features of Floor 96 in WTC 1. The core area contained the elevators, stairways, mechanical shafts, restrooms, and storage areas. Office space was generally located outside the core where the floors were supported by truss framing. Above the 77th floor, a portion of the core was used for office space since there were fewer elevator shafts and the additional floor space could be used for tenant occupancy.

The floor system for WTC 1 and WTC 2 consisted of a lightweight concrete floor slab supported by steel trusses that spanned between the core and perimeter walls and a normal weight concrete floor slab supported by steel beams in the core area. There were three “types” of trusses comprising the floor system as illustrated in Fig. 4–7 (b). The trusses that spanned from the core to the exterior wall were referred to simply as “trusses” or were sometimes called “primary” or “main” trusses, or on some contract drawings, “C32” trusses. Trusses which ran perpendicular to the primary trusses were called “bridging trusses.” At the corners of the floor areas, special trusses referred to as “transfer trusses” supported the end reactions of several primary trusses. This section will focus on the load-carrying trusses which will be referred to as “primary trusses.”

Figures 4–8 and 4–9 illustrate a primary truss section and connection details. The primary trusses, which were installed in pairs, were spaced 6 ft-8 in. on center and had a nominal clear span of either 60 ft for the long span direction or 35 ft for the short span. The trusses, commonly referred to as steel bar joists, were fabricated using double-angles for the top and bottom chords, and round bars for the webs. The web members protruded above the top chord in the form of a “knuckle” which was embedded in the concrete slab and provided composite action between the trusses and the slab. Additionally, the floor system included bridging trusses (perpendicular to the primary trusses) spaced 13 ft-4 in. on center. In the corners of the towers, the bridging trusses acted with the primary trusses to provide two-way floor action, where loads were transferred to both perimeter walls near the corners and the transfer truss that ran between the core corner and the exterior wall.

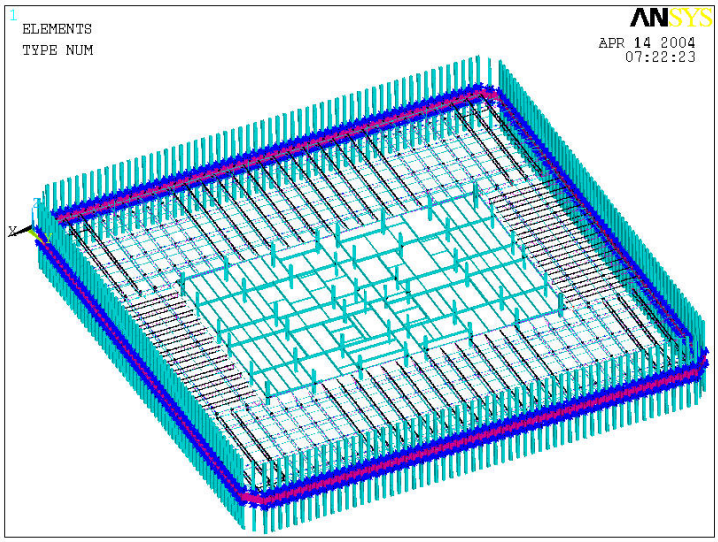

(a) Single floor structural system (without slab)

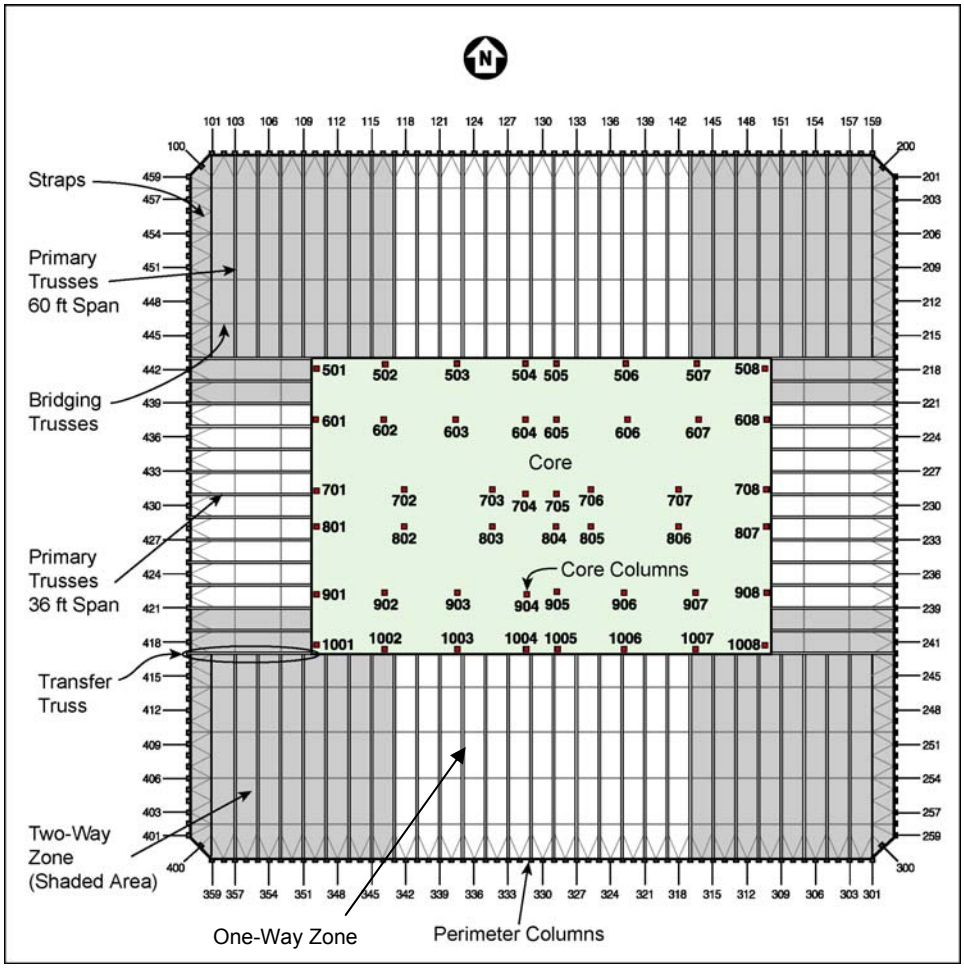

(b) Floor plan

Figure 4–7. Floor structural subsystem (WTC 1, Floor 96).

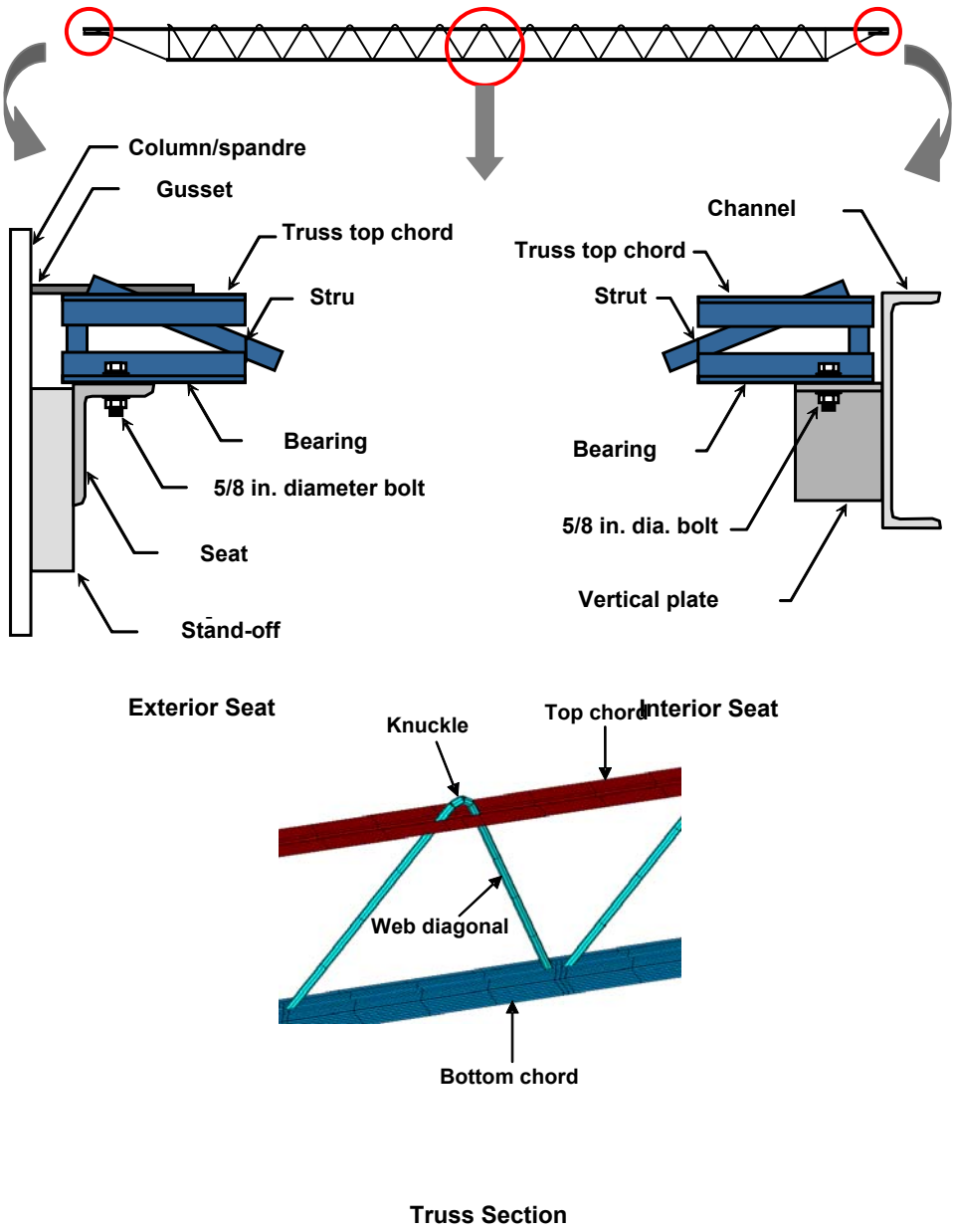

Figure 4–8. Primary truss components.

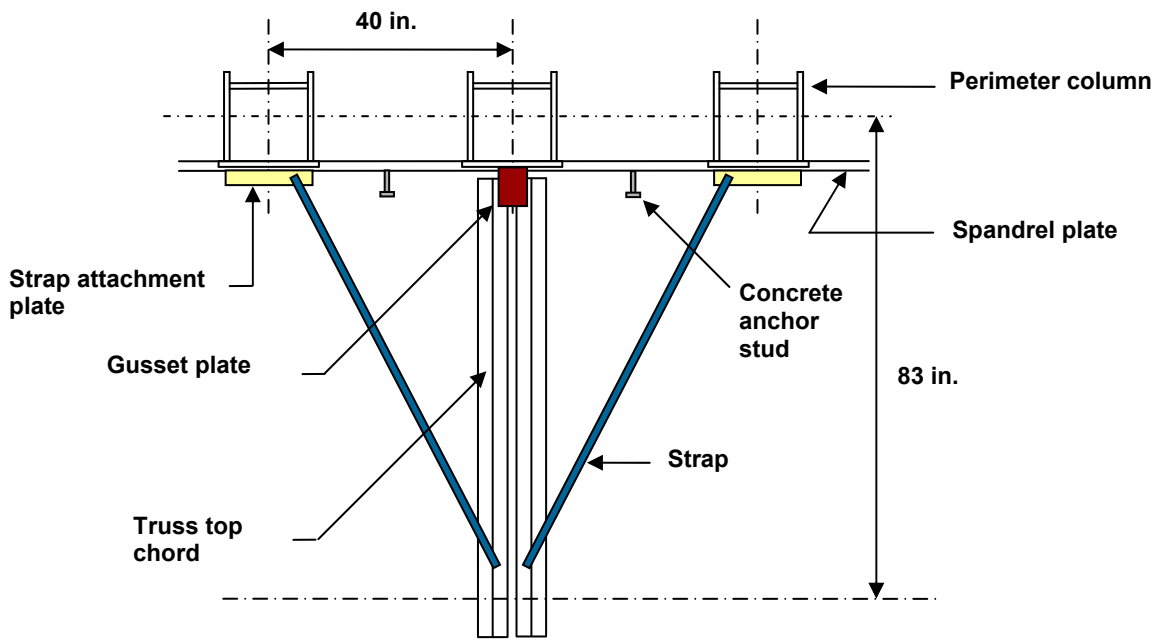

Figure 4–9. Plan view of truss seat connection, straps, and horizontal studs.

The primary trusses were supported by a seat angle at the exterior wall and a stiffened seat at the interior ends. The trusses framed into every other perimeter column (the odd numbered columns). The interior stiffened seat was welded to a steel channel that ran continuously around the core area. The steel channel was supported by the perimeter core columns through stub beam members. Each truss was attached to the seat with a 5/8 in. bolt through a truss bearing angle. The exterior seat angles and interior stiffened seat had 1 ¾ in. slotted holes. At the exterior wall connection, there were three additional components that tied the floor subsystem to the perimeter columns. A gusset plate was welded to the spandrel with a complete penetration groove weld and to the top chord of the two primary trusses with a fillet weld. Additionally, a pair of straps with shear studs tied the primary trusses to the intermediate columns and a shear stud, welded to the spandrels between each column, anchored the concrete slab.

The lightweight concrete slab was supported by a 22 gauge, 1 ½ in. deep "Type B" steel deck. The steel deck was supported by the top chord of the bridging trusses (which were 1 ½ in. below the primary truss top chord) and by deck support angles. The concrete slab had two layers of welded wire fabric reinforcement, and steel reinforcing bars at the perimeter of the floor, perpendicular to the primary trusses at the knuckles, over the trench headers (conduits for electrical wiring in the floor) and at the interface between the lightweight and normal weight concrete slabs to maintain slab continuity.

4.2.2 Truss Seats

The truss seat connections transferred floor gravity loads to the exterior and core columns and provided lateral bracing for the columns. All seat connections were similar in design, but varied in their dimensions and weld sizes. For Floor 96 of WTC 1, there were seven types of interior truss seats and eight types of exterior truss seats. The different types of interior truss seats were identified with Detail Numbers 15, 17, 20, 21, 22, 23, and 226A; and the exterior truss seats with Detail Numbers 1013, 1111, 1212, 1311, 1313, 1411, 1511, and 1611, as shown in Fig. 4–10.

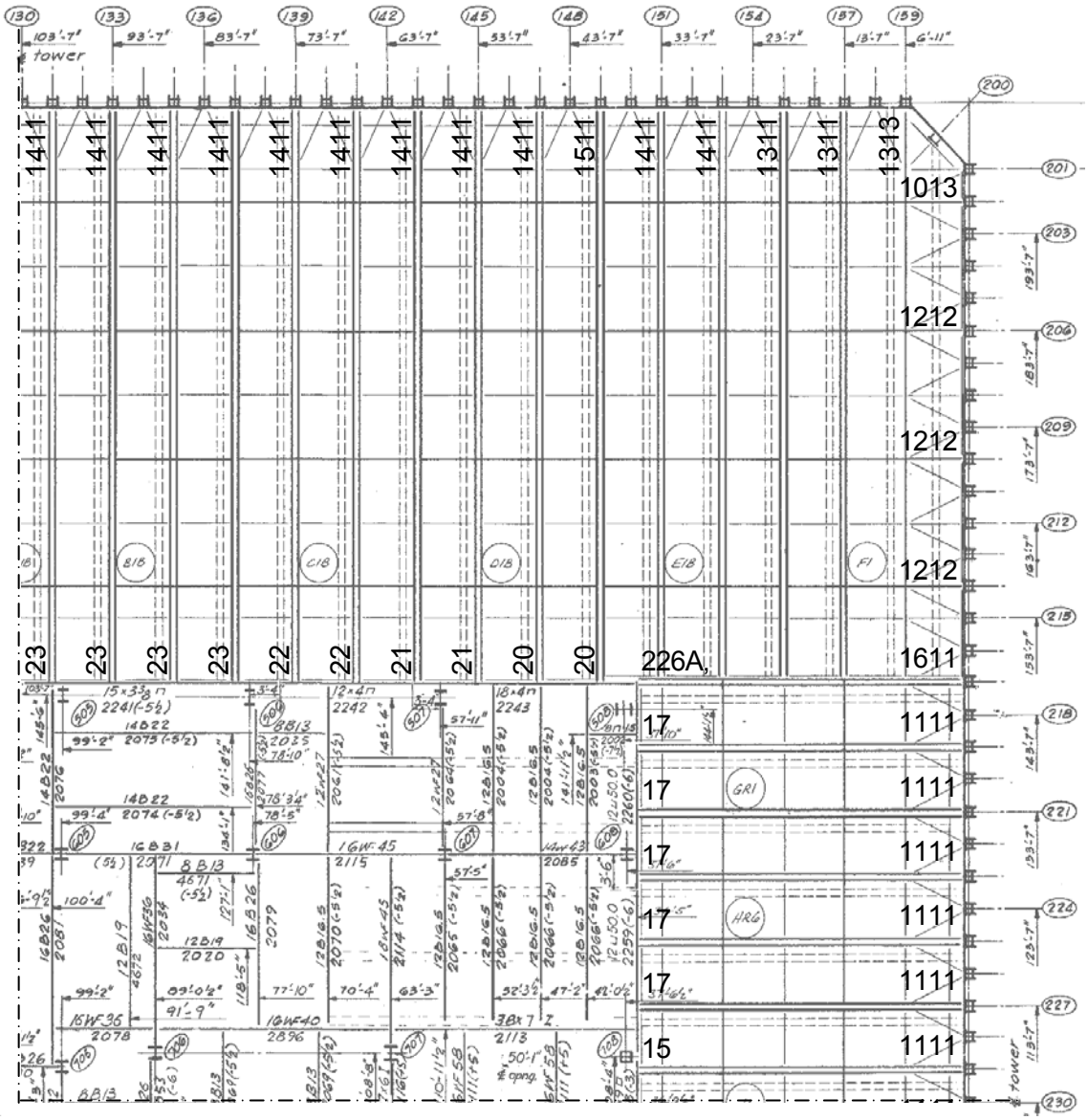

Figure 4–10. Truss seat detail location on northeast quadrant of Floor 96 of WTC 1. Reproduced with permission of The Port Authority of New York and New Jersey.

Failure Modes

The failure modes and associated load and temperature conditions were identified using a detailed finite element model. Each truss seat, strap, and spandrel stud was then represented by a submodel that captured failure of these components.

Figure 4–11 shows a finite element model of an exterior seat connection modeled using symmetry. The finite element analysis showed that vertical shear force was carried primarily by the stand-off plates, while the bending moment was resisted by tensile force in the gusset plate and compressive force in the

stand off plates (see Fig. 4–8). The seat restrained the moment until the horizontal force in the connection caused slip between the seat angle and bearing angle. Fillet welds, connecting the stand-off plates to the spandrel, resist shear, bending, and compression, and controlled the seat capacity. The controlling failure mode was fracture of the fillet welds at this connection, which resulted in loss of vertical support.

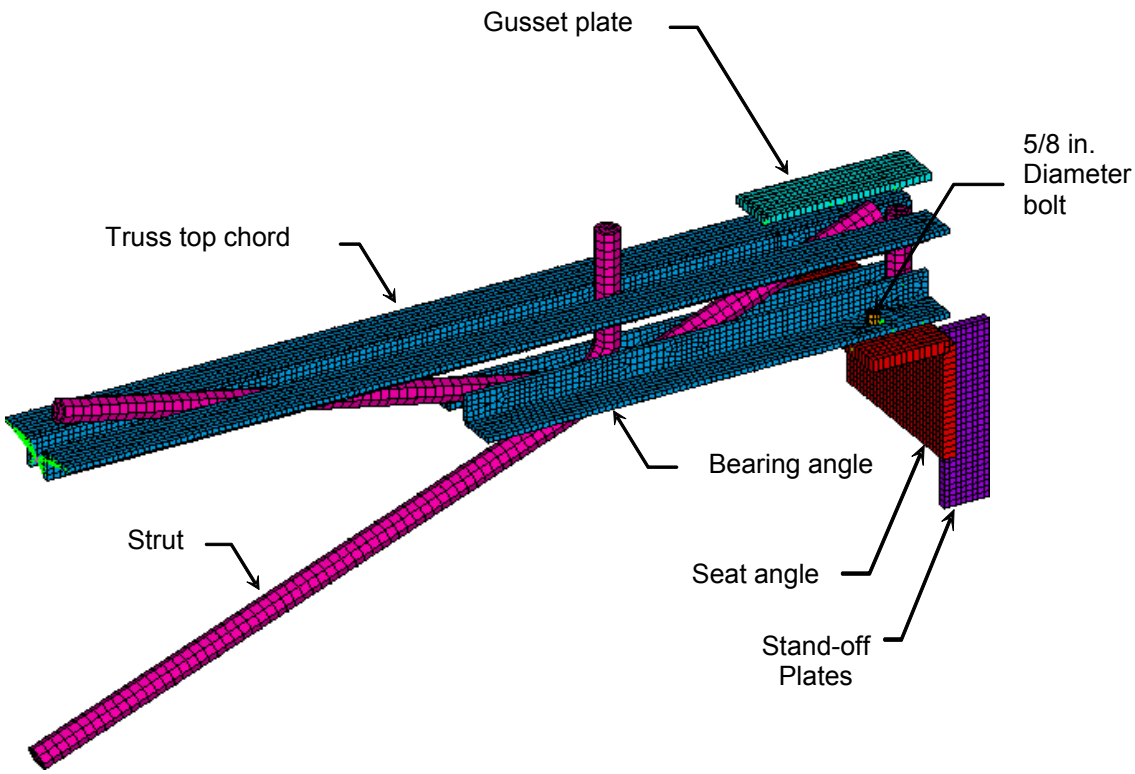

Figure 4–11. Finite element model of exterior seat.

The failure modes for the truss seats were identified for vertical force (shear), horizontal tensile force, horizontal compressive force, and combined vertical and horizontal force. Failure modes and sequences of failure were computed for each truss seat type. The capacity of, for example, an exterior seat due to horizontal tensile (pull-in) force was determined by considering: (1) fracture of the groove weld between the gusset plate and spandrel, (2) fracture of the fillet weld between the gusset plate and the truss top chord, (3) tensile fracture of the gusset plate, and (4) shear failure of the bolted connection by bolt shear, bolt bearing, tear-out, and block shear. For calculation purposes, the bolts were assumed to be centered in the slotted holes. The typical failure sequence of the truss seat was determined to be: yield failure of the gusset plate, yielding followed by fracture of the gusset plate groove weld, truss deformation leading to bolt bearing against the slotted hole, bolt shear failure, and finally the truss slipping or “walking off” the seat. The travel distance for the truss to walk off the seat was computed to be 4 5/8 in. This failure sequence is illustrated in Fig. 4–12 as path (A) and shown in Fig. 4–13, where the relationship between the tensile force resistance from the seat connection and the truss travel distance is plotted. In this plot, frictional resistance between the seat angle and bearing angle was not included.

Under combined vertical and horizontal forces, the failure modes were a combination of the individual failure modes for vertical and horizontal forces.

A typical interaction relationship for the capacity of an interior seat against combined vertical and horizontal tensile forces is shown in Fig. 4–14.

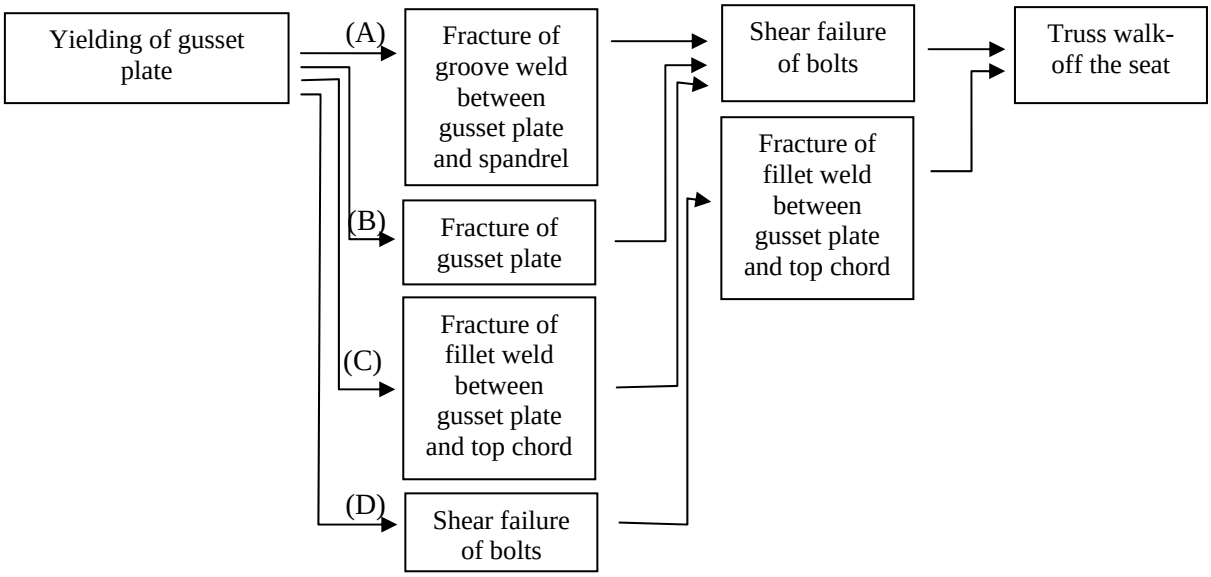

(A) Seat details 1311, 1411, 1511, and 1611 at all temperatures.

(B) Seat detail 1111 at all temperatures.

(C) Seat detail 1013 at temperatures below 100 °C.

(D) Seat details 1212 and 1313 at all temperatures, and detail 1013 at temperatures more than or equal to 100 °C.

Figure 4–12. Failure sequence of the exterior seats against tensile force.

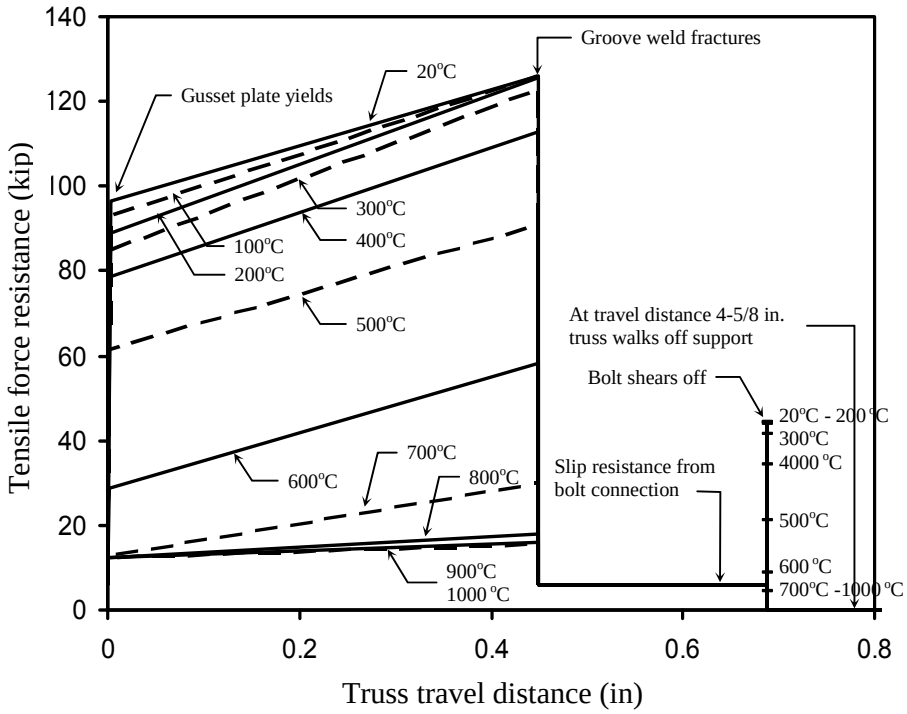

Figure 4–13. Capacity of exterior seat against tensile force (Detail 1411 in Fig. 4–10).

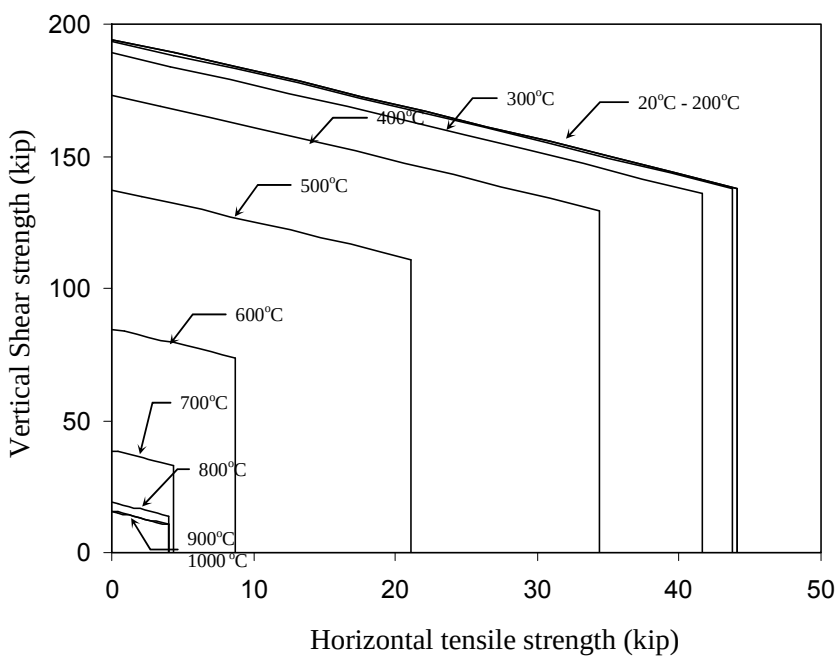

Figure 4–14. Capacity of interior seat against vertical and horizontal force (Detail 22 in Fig. 4–10).

Loads

Truss seat failures were analyzed for vertical and horizontal loads. The floor system gravity loads were approximately 80 psf for dead load and service live load. The dead load is the weight of the floor system and the service live loads are the loads due to occupancy that are supported by the floor, which are generally on the order of 25 percent of the design live loads. The load from the pair of trusses that each truss seat connection supported was approximately 16 kips for the 80 psf service gravity loads (where 16 kips = ½ x 60 ft span x 6.67 ft width x 80 psf).

Computation Results

Tables 4–2 through 4–5 show the computed capacity of each truss seat detail as a function of steel temperature and loading direction. Truss seat capacities against vertical and horizontal force are presented graphically in Figs. 4–15 and 4–16, respectively. In general, the exterior seat had a greater horizontal tensile capacity, and the interior seat had a greater vertical shear capacity. Even though the controlling failure mode for vertical shear was weld fracture, truss seat connection failure from vertical loads was less likely, given the capacities listed in Tables 4–2 and 4–3. The vertical load at the truss connection of approximately 16 kips would have had to increase by a factor of 2 to 6 to reach failure (weld fracture) for temperatures near 600 °C to 700 °C.

Table 4–2. Interior seat capacity against vertical force.

Temp. (°C)	Connection Capacity Against Vertical Force (kip)						
	#15	#17	#20	#21	#22	#23	#226A
20	233	233	274	229	194	194	395
100	233	233	274	229	194	194	395
200	232	232	273	228	194	194	393
300	226	226	267	223	189	189	384
400	207	207	244	204	173	173	352
500	164	164	194	162	137	137	279
600	101	101	119	100	85	85	172
700	46	46	54	45	39	39	78
800	23	23	27	22	19	19	38
900	19	19	22	18	16	16	32
1000	19	19	22	18	16	16	32

Table 4–3. Exterior seat capacity against vertical force.

Temp. (°C)	Connection Capacity against Vertical Force (kip)							
	#1013	#1111	#1212	#1311	#1313	#1411	#1511	#1611
20	94	94	111	94	94	140	193	207
100	94	94	111	94	94	140	193	207
200	93	93	110	93	93	139	192	206
300	91	91	108	91	91	136	187	201
400	84	84	100	84	84	126	172	184
500	69	69	81	69	69	102	136	146
600	45	58	53	60	45	78	84	90
700	29	26	34	27	29	35	38	41
800	14	13	17	13	14	17	19	20
900	12	11	14	11	12	14	16	17
1000	12	11	14	11	12	14	15	17

Table 4–4. Interior seat capacity against horizontal tensile force.

Temp. (˚C)	Capacity (kip)
	Shear Failure of Bolts
20	44
100	44
200	44
300	42
400	34
500	21
600	9
700	4
800	4
900	4
1000	4

Table 4–5. Exterior seat capacity against horizontal tensile force.

Temp (˚C)	Connection Detail Capacity for Horizontal Tensile Force (kip)							
	#1013	**#1111**	**#1212**	**#1311**	**#1313**	**#1411**	**#1511**	**#1611**
	Fracture of Fillet Weld/ Shear Failure of Bolts	Fracture of Gusset Plate	Shear Failure of Bolts	Fracture of Groove Weld	Shear Failure of Bolts	Fracture of Groove Weld	Fracture of Groove Weld	Fracture of Groove Weld
20	100	104	182	126	182	126	126	126
100	138	104	181	126	181	126	126	126
200	135	103	180	126	180	126	126	126
300	130	101	174	123	174	123	123	123
400	115	93	156	113	156	113	113	113
500	84	75	117	91	117	91	91	91
600	42	49	67	58	67	58	58	58
700	20	25	32	30	32	30	30	30
800	14	16	19	18	19	18	18	18
900	13	14	17	16	17	16	16	16
1000	13	14	17	16	17	16	16	16

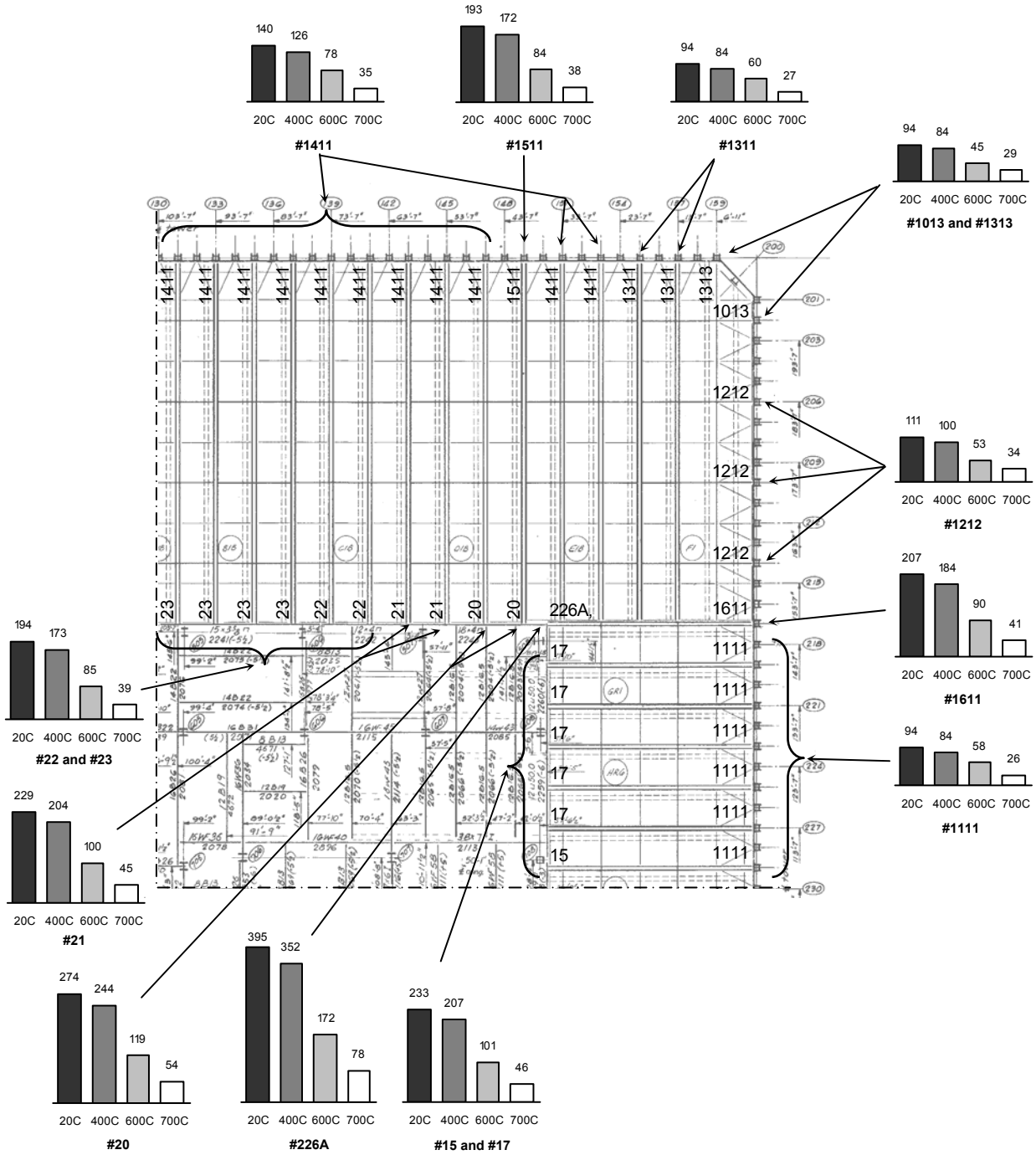

Figure 4–15. Truss seat capacity against vertical force. Reproduced with permission of The Port Authority of New York and New Jersey. Enhancements by NIST.

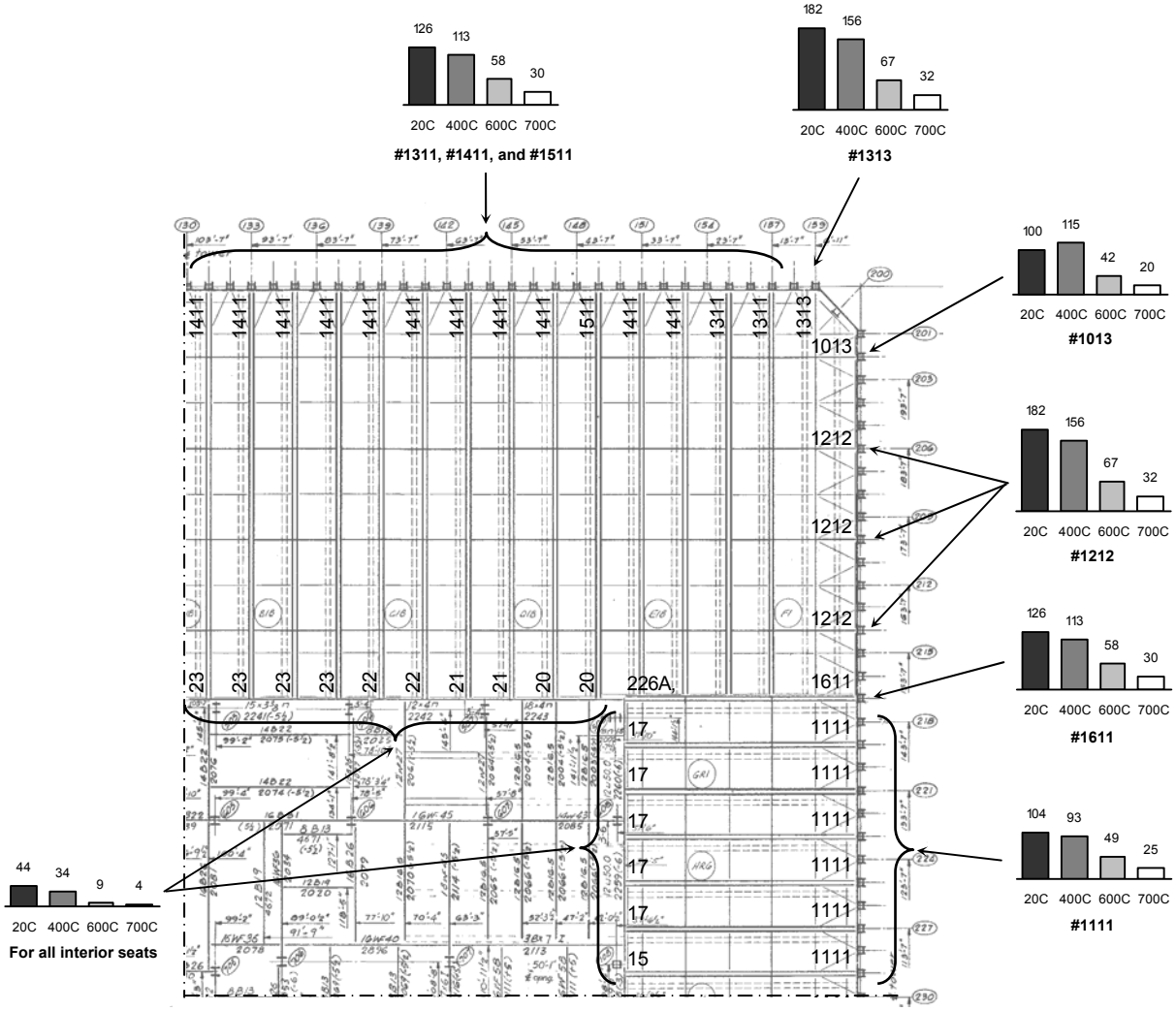

Figure 4–16. Truss seat capacity against horizontal force. Reproduced with permission of The Port Authority of New York and New Jersey. Enhancements by NIST.

Reduced Complexity Model

Break elements (ANSYS user-defined element) were developed for use in the full floor model that captured the temperature-dependent failure modes of the truss seat connections, strap anchors, and spandrel studs. These elements replaced the detailed 3-D solid finite element model used for the truss connection analysis, allowing a reduction in model size.

A break element is a unidirectional spring element that can simulate connection failure by disconnecting two “active nodes” when the relative displacement between two “control nodes” exceeds a specified threshold. Temperature dependence was achieved by coupling the active nodes to a beam element with specified thermal expansion characteristics. Failure modes that required multiple connection failures

were created with break elements using parallel and series constructs. For example, Fig. 4–17 illustrates the sequence of events that occurs for an interior truss seat under a) horizontal tensile loading and b) vertical shear loading.

Figure 4–17 a) shows the results from analysis where the interior truss seat was subjected to a constant vertical load and horizontal displacement increments at 500 ˚C. Failure of a truss seat subjected to a large horizontal tension and small vertical shear was by bolt shearing off followed by truss walking off the seat. The shear strength of the bolts controlled the truss seat horizontal tension capacity. The bolt shear by itself did not cause the truss to lose its vertical support, but was the prerequisite for truss walking off the seat. The travel distance for a truss to walk off a truss seat was 4 in. for an interior seat.

Figure 4–17 b) shows the results from analysis where the interior truss seat was subjected to a constant horizontal load and vertical displacement increments at 500 ˚C. In this case, seat failure was governed by fracture of the fillet welds between the vertical plate stiffeners and the channel beam resulting in loss of both vertical and horizontal support.

4.2.3 Knuckles

The “knuckle” is formed by the extension of the truss diagonals into the concrete slab and provides for composite action of the steel truss and concrete slab. The composite action is due to the shear transfer between the knuckle and the concrete slab both in the truss transverse and longitudinal directions. The purpose of this analysis was to predict the knuckle capacity when the truss and concrete slab act compositely and to develop a reduced model of the knuckle behavior for the full floor model.

Failure Modes

Failure modes for the knuckles included: (1) horizontal shear failure by crushing of concrete over a small region adjacent to the knuckle and (2) vertical tensile failure where the knuckle pulls a conical section of concrete out of the slab.

Experimental Data

As part of the original truss design, Laclede Steel Company in Saint Louis, Missouri, conducted experiments in 1967 to determine the transverse and longitudinal shear capacities of the knuckle. Knuckles were cast into two reinforced concrete blocks confined at the corners by angles, as shown in Figure 4–18, and loaded to determine the knuckle shear capacity in both the transverse and longitudinal directions.

The transverse tests were conducted when the lightweight concrete was 6 and 27 days old. The average shear capacity measured was 16.9 kips per knuckle when concrete shear failure occurred. A comparable value of 35 kips per knuckle for the WTC floor system was determined after adjusting for the strength of in-place, mature, lightweight concrete.

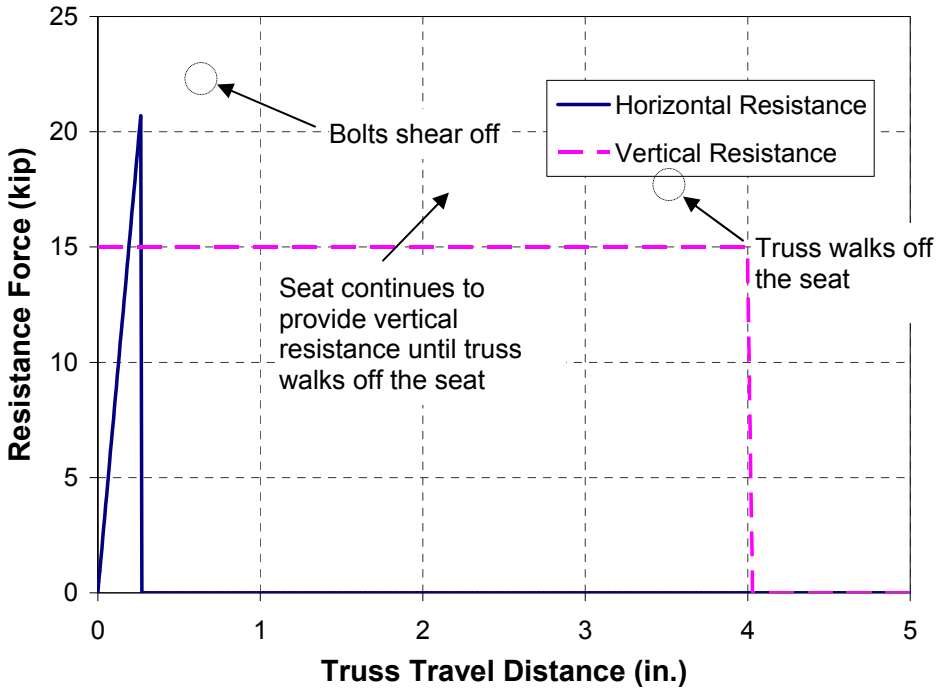

a) failure from horizontal force

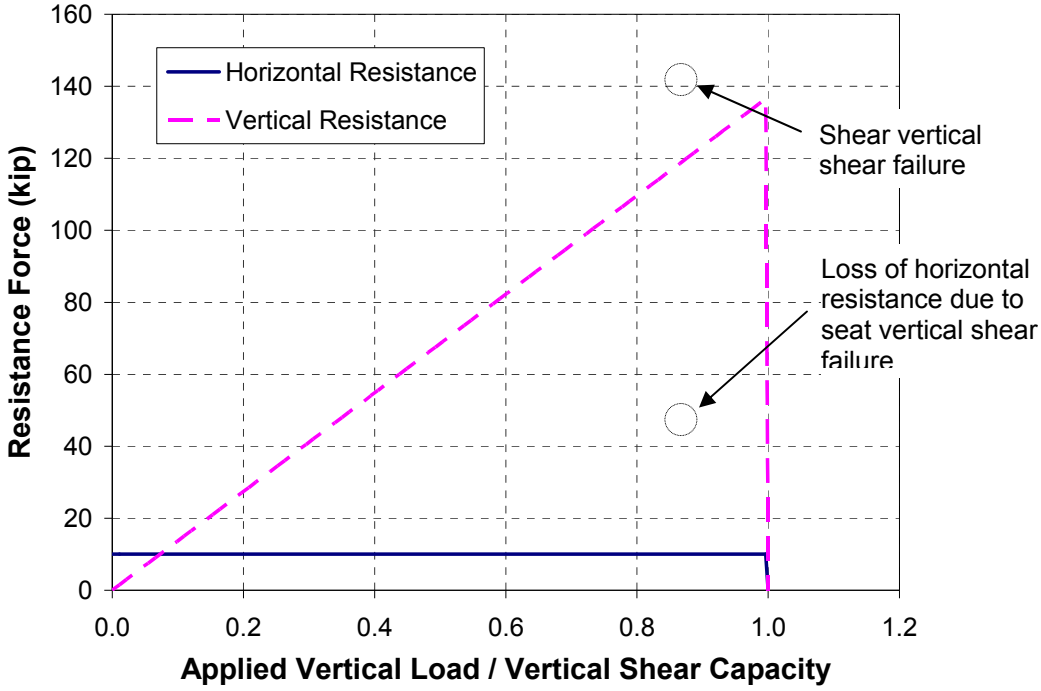

b) failure from vertical shear force

Figure 4–17. Results of interior truss seat model at 500 ˚C.

The longitudinal tests, which used normal weight concrete, were conducted when the concrete was 28 and 96 days old. Of the five tests conducted, three reported a weld failure in the rebar loading the knuckles, and two reported a failure in the concrete. The average shear capacity measured was 28.3 kips per knuckle. A value of 31 kips per knuckle for the WTC floor system was determined after adjusting for the strength of in-place, mature, lightweight concrete.

Analysis and Results

Finite element analyses of the Laclede knuckle test set-up were conducted to compare analysis results to the measured transverse and longitudinal shear capacities. The bond between the concrete and steel was varied in the analysis; the bars were assumed to be either full bonded or frictionless, which had a significant effect on the results.

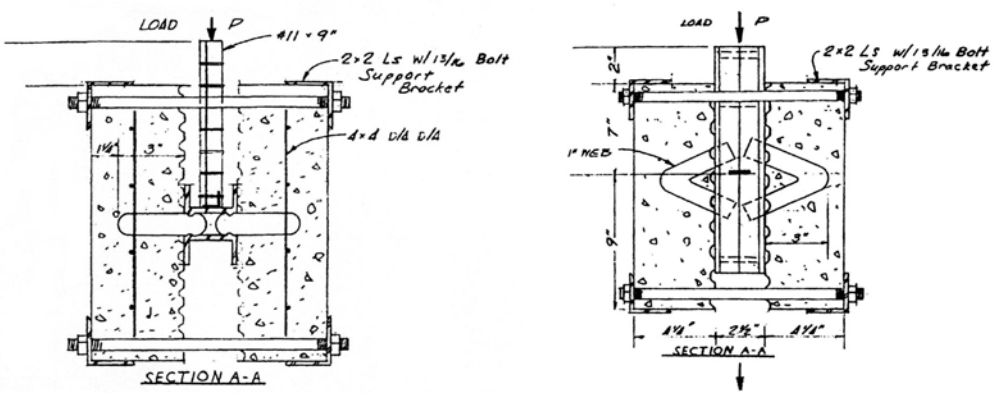

Reproduced with permission of Laclede Steel.
(a) Transverse shear test.

Reproduced with permission of Laclede Steel.
(b) Longitudinal shear test.

Figure 4–18. Laclede Steel Company shear tests of a knuckle.

Finite Element Analysis of Tests

The results of the finite element analyses modeling the Laclede tests are shown in Figs. 4–19 through 4–21. Analyses were conducted to establish both the longitudinal capacity and the transverse capacity of the knuckle. The results showed significant dependence on the interface characteristics between the steel and concrete. A plot of compressive stresses for the longitudinal shear model is shown in Fig. 4–19. Results of the analyses for longitudinal shear, with steel-to-concrete interface either fully bonded or completely unbonded (frictionless), are shown in Fig. 4–20. Results showed that each knuckle had strength in the range of 15 kip to 35 kip, depending on the interface condition. When the analysis results were compared to the test results, the fully bonded case showed better agreement.

Compressive stresses for the transverse shear model are plotted in Fig. 4–21. The small crushed regions indicate that a pair of knuckles can be expected to behave nearly independently of each other, and, therefore, have nearly double the capacity of a single knuckle. The transverse shear results (Fig. 4–22) showed that transverse knuckle strength was about 24 kip for the frictionless condition with 2,500 psi concrete, which corresponds to 39 kip for 4,100 psi concrete. For the full bonded case, the analysis was terminated at 20 kip per knuckle before reaching the ultimate strength.

Although the analysis showed the sensitivity of the results to the steel-concrete interface assumptions, it supported the shear capacities determined from test results.

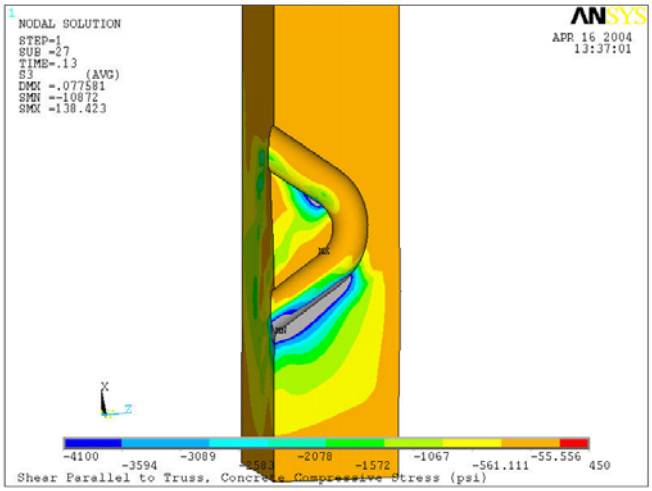

Figure 4–19. Compressive stresses in longitudinal shear finite element model (4,100 psi concrete).

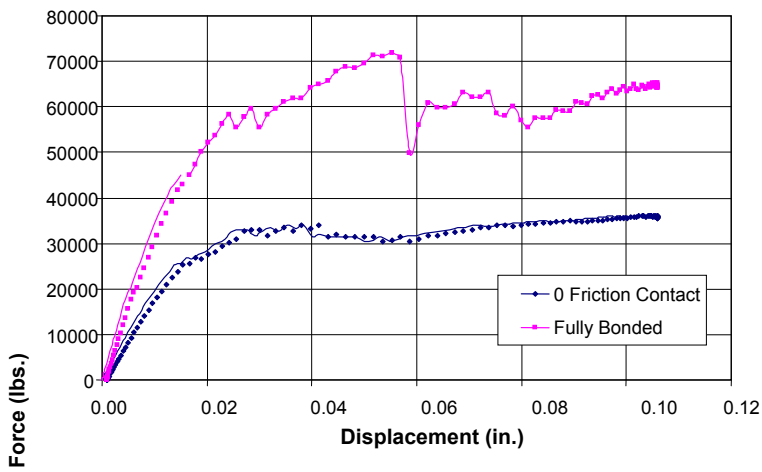

Figure 4–20. Shear force versus displacement from finite element model for longitudinal shear of two knuckles (4,100 psi concrete).

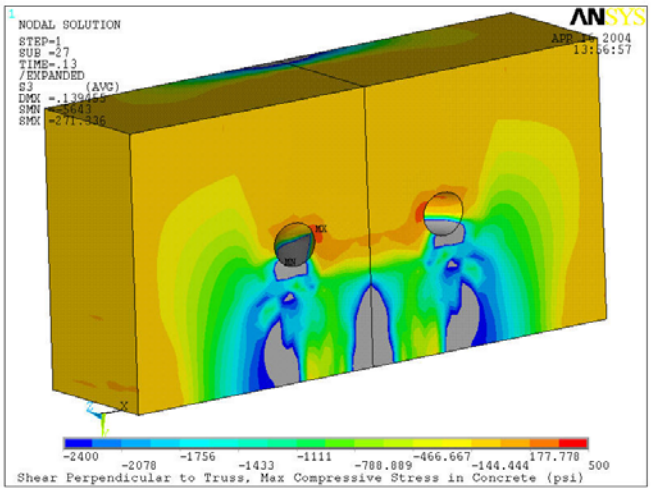

Figure 4–21. Compressive stresses in transverse shear finite element model (2,500 psi concrete).

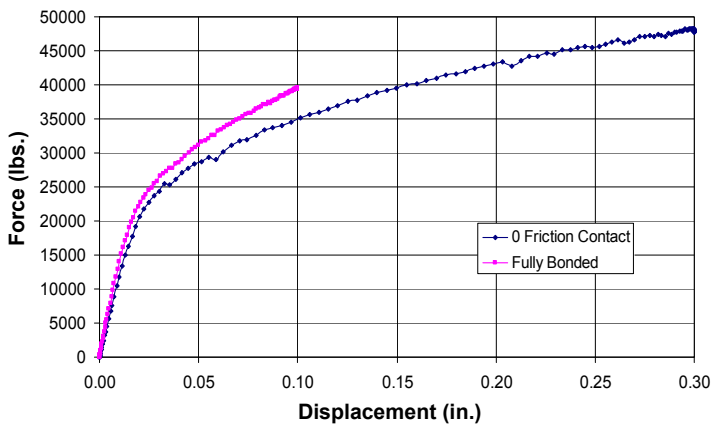

Figure 4–22. Shear force versus displacement from finite element model for transverse shear of two knuckles (2,500 psi concrete).

Reduced Model

Based upon the analysis results, a reduced model with beam and break elements was developed for the composite floor section with a single truss and the full floor models. The temperature-dependent knuckle behavior was represented with 15 break elements and five beam elements.

Based on the results of the Laclede tests and the finite element analyses, the knuckle capacity for the reduced model was estimated and is shown inTable 4–6. Steel temperatures in Table 4–6 were assumed with a corresponding reduction in concrete temperature immediately around the knuckle of 75 °C to 150 °C. Concrete has a lower coefficient of conductivity and does not respond as rapidly to rising temperatures as steel.

Table 4–6. Knuckle shear capacity reduction for elevated temperatures.

Steel temperature (˚C)	Concrete temperature (˚C)	Knuckle shear capacity (kip)
20 - 375	20 - 300	30
550	450	24
725	600	19
900	750	15

4.2.4 Single Truss and Concrete Slab Section

A single composite truss with concrete slab was modeled to study failure modes and sequences of failures under gravity and thermal loads. The thermal loading approximated a uniform heating condition, not a fire exposure from the WTC towers. The purpose of these analyses was to determine the relative importance of the truss and slab components and their failure modes. These results were used to develop a reduced truss model for the full floor model that captured essential behaviors while reducing the level of model complexity.

Failure Modes

Two possible deformation/failure modes were identified for the floor-truss section:

- Sagging of the floor section due to yielding or buckling of truss components or failures of the knuckle/concrete interface,
- Loss of truss seat support due to combinations of vertical and horizontal loads and thermal weakening that result in bolt shear and truss walk-off or stand-off plate weld failure at the spandrel.

Truss weld failures were not included as a failure mode. From data gathered from the truss manufacturer, the resistance welds between the web and chord members were found to have a greater capacity than the members they connected.

Finite Element Model

Figure 4–23 illustrates the composite truss and concrete slab model. Symmetry allowed modeling one of the two trusses and one half of the 80 in. composite concrete slab. The model included two perimeter columns, the spandrel, the truss seat, and strap attachments. Each column extended one floor above and one floor below the floor section to account for interaction between the exterior wall and the floor section. Each column was attributed with half of its area and bending properties to account for the symmetry reduction of the floor section. The interior and exterior truss seat connections were also included. The truss was restrained at bridging truss locations to simulate the lateral bracing that would be provided at the bottom chord.

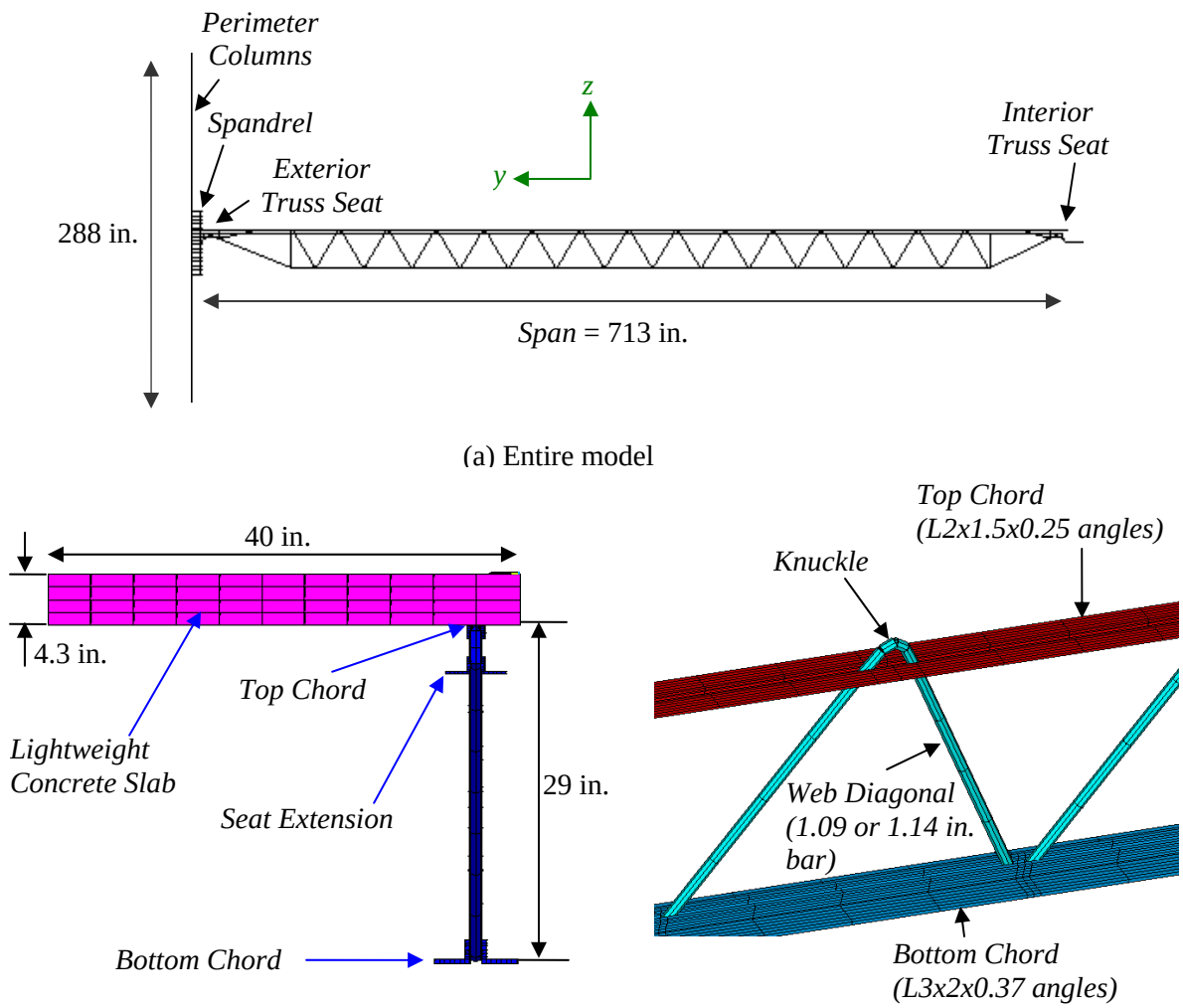

Figure 4–23. Composite truss and concrete slab model.

The concrete slab was modeled as an isotropic plate with a thickness of 4.3 in. (the average thickness of a 4 in. slab on 1 ½ in. metal deck) using eight-node solid elements. The Hjelm plasticity model was used with the solid elements to allow different yield strengths in tension and compression. Slab cracking was simulated by assuming tensile plasticity after the onset of cracking, where the reinforcement carried the tensile load.

The top and bottom chords of the truss were modeled with quadratic finite strain beam elements with temperature dependent elastic, plastic, and creep material properties. The chords had four elements between panel points (a panel point is the intersection of the web diagonal and chord).

Loading

Loading of the truss model consisted of gravity dead and live loads and temperature histories for the truss, truss seats, and concrete slab. The gravity loads included the weight of the structure, 8 psf superimposed dead load (including nonstructural dead loads due to architectural items and fixed service equipment), and 13.75 psf of live load equal to 25 percent of design live load of 55 psf. The temperature was ramped from 20 °C to 700 °C in the steel members; from 20 °C to 700 °C at the bottom surface of the slab and from 20 °C to 300 °C at the top surface of the slab over a period of 1,800 s. Thereafter, the truss and concrete temperatures were linearly increased by 200 °C at 2,400 s. A linear gradient through the thickness of the slab was assumed. Temperature loading was not applied to the columns.

Effects of construction sequence were included by applying the ANSYS "element birth and death" feature to the concrete slab. This feature allows elements to be treated as either acting or not acting, as defined by the user. In the first step, the self-weight of the truss members and concrete slab was applied to the truss without the concrete slab acting (i.e., fresh concrete has no strength). In the second step, the concrete slab was reactivated (i.e., cured concrete now able to carry load), and superimposed dead load and live load were applied.

To determine the effect of debris load on the truss behavior, the gravity load was increased until the analysis failed to converge, signaling collapse.

Analysis and Results

Under gravity load to simulate casting of the concrete slab, the maximum calculated vertical deflection was found to be 1.7 in. downward. Note that the design camber ranged from 1 in. to 2 in. to accommodate this deflection, resulting in a slab of uniform thickness. When the superimposed dead load and the live load were applied to the truss and concrete slab, the maximum calculated vertical deflection was 2.0 in. The maximum stress in the top chord, bottom chord, diagonal, and end diagonal strut were 14.8 ksi, 11.6 ksi, 6.7 ksi, and 15.7 ksi, respectively.

For gravity and thermal loading, the analysis was carried out statically until the solution failed to converge at which point the analysis was switched to dynamic mode with 5 percent Rayleigh damping to overcome convergence difficulties. The analysis proceeded to a temperature of 727 ºC. Figure 4–24 shows the vertical displacement contour at 700 ºC. Figure 4–25 presents plots of displacement versus temperature where Fig. 4–25 (a) is the horizontal displacement at Column 143, and Fig. 4–25 (b) is the vertical displacement at midspan after the self-weight is applied. A positive horizontal displacement indicates that the exterior columns were pushed out, and negative vertical displacement indicates that the truss deflected downward. For the assumed thermal loading, the analysis indicated that, at 445 ºC, the horizontal displacement at the exterior column started to decrease, and at 565 ºC, the exterior columns began to pull inward.

The plot of the deflected shape shown in Fig. 4–24, shows that compression diagonals at the core end of the truss have buckled, and the floor system has deflected approximately 42 in.

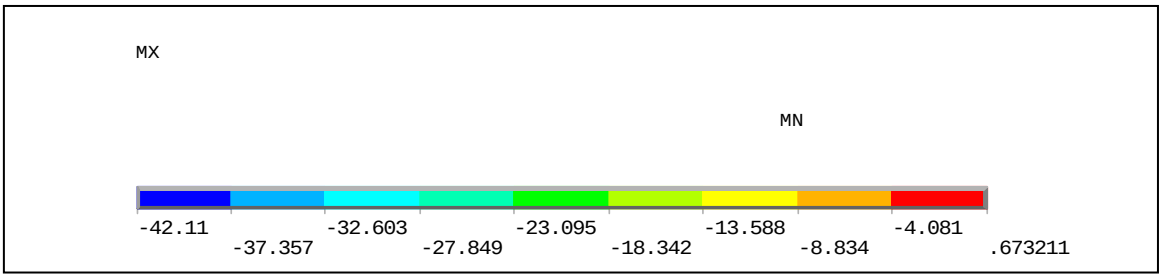

Figure 4–24. Vertical displacement at 700 °C.

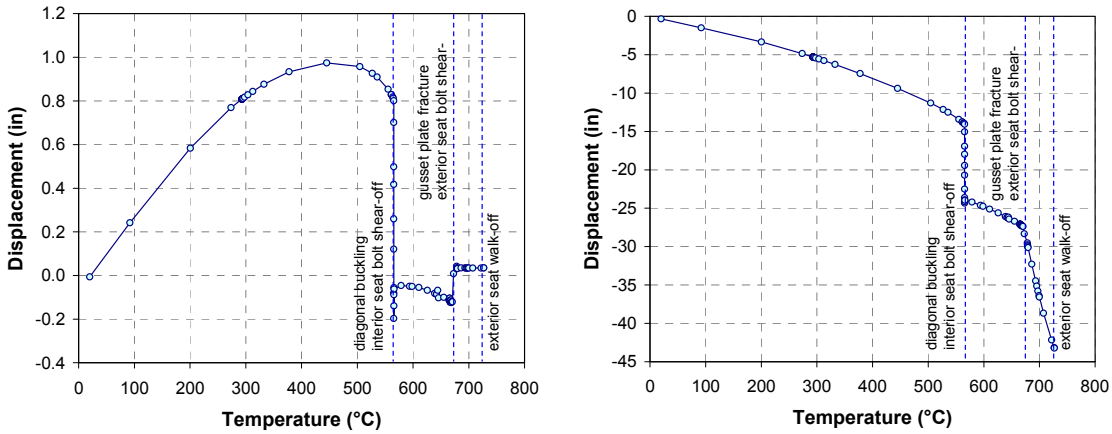

(a) Horizontal displacement at column 143 (b) Vertical displacement at midspan

Figure 4–25. Displacement versus temperature.

The truss behavior under the gravity and uniform thermal loading where the temperature was ramped up to 727 ºC can be summarized as follows:

- The stud on the spandrel and studs on the strap anchor failed in shear below 275 ˚C.
- The first knuckle from the interior end failed in vertical tension at around 100 ˚C, and the second and third knuckles from the interior end failed in the horizontal shear at 566 ˚C.
- Top chords yielded above 300 ˚C due to the difference in coefficients of thermal expansion of steel and lightweight concrete.
- Four compression web diagonals buckled due to high axial compressive force at 565 ˚C.
- The interior truss seat bolts sheared off at 566 ˚C.
- The gusset plate fractured and the exterior truss seat bolts sheared off at around 680 ˚C.
- The truss walked off the exterior truss seat at 730 ˚C.

Reduced Model

For the full floor subsystem model, the trusses were reduced in size. The reduced model captured essential behavior: (1) the same total horizontal reaction force under the thermal loading and (2) the same vertical deflection at midspan under the thermal loading. The reduced truss model had the following features:

- The geometry of the truss was preserved.
- A pair of trusses was merged into one truss. Areas of truss members were doubled.
- The top and bottom chords and diagonals were modeled by 3-D linear finite strain beam elements (BEAM 188). A member between two panel points was modeled by one element only.
- Break elements (ANSYS user-defined elements) were used to model the following failure modes: (a) seat bolt shear failure; (b) gusset plate fracture; (c) truss walk-off; (d) diagonal buckling/resistance weld failure; (e) failure of studs on the spandrel; and (f) weld failure between strap anchors and top chords.
- Steel had temperature-dependent elastic and plastic properties. Creep was not included.
- The concrete slab was modeled by SHELL 181 elements with temperature-dependent elastic properties.

Figure 4–26 shows the comparison between the detailed and reduced truss models. Figure 4–26 (a) compares the vertical deflection at midspan while Fig. 4–26 (b) compares the horizontal reaction at exterior columns. Although the reduced truss model predicted buckling of diagonals at roughly 530 ˚C, which is about 35 ˚C lower than the temperature at which diagonal buckling occurred in the detailed truss model, overall truss behavior under the uniform thermal loading was found to be in good agreement between the two models.

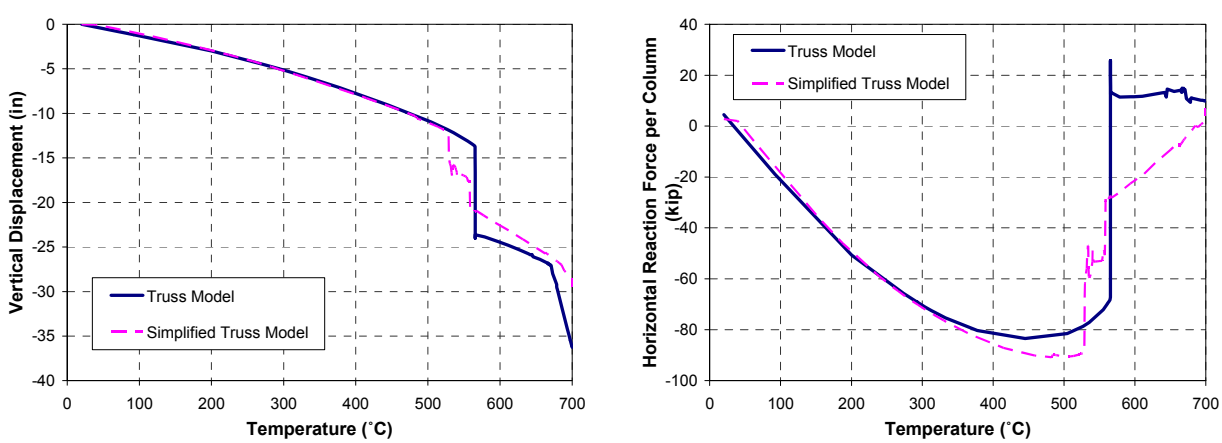

(a) Midspan vertical deflection (b) Horizontal reaction force at exterior columns

Figure 4–26. Comparison of detailed and reduced truss models.

4.2.5 Floor Subsystem Analysis

Analysis of a full floor of the World Trade Center towers involved:

- the translation, validation, and modification of finite element models in ANSYS to incorporate nonlinear behavior,
- evaluation of structural response under dead and live loads and elevated structural temperatures,
- identification of failure modes and associated temperatures and times to failure, and
- reduction of detailed component models for inclusion in the floor model.

Failure Modes

Possible deformation/failure modes of the floor subsystem that were investigated are as follows:

- Floor sagging *between edge supports* resulting from:
  - loss of stiffness and weakening of steel truss and/or concrete slab at high temperature,
  - change in floor behavior from flexure to catenary action due to yielding or buckling of diagonal web members required for truss action, or
  - loss of composite action from floor slab-knuckle failures.

  Note that floor sagging between supports may cause tensile failure of the truss seats, or development of tensile forces that pull columns inward.

- Floor sagging *at edge supports* resulting from failure of truss seat connections at either the interior or exterior supports.

  Floor sagging at the exterior edge was observed in photographs of the east exterior wall of WTC 2, near the impact zone. Floor sagging along one edge would have a tendency to reduce the buckling strength of columns supported by that floor and would increase demand on other components of the floor.

- Abrupt failure of the floor truss supports due to:
  - vertical shear failure resulting from debris and/or impact load of the dropping floor above,
  - vertical and/or horizontal shear failure resulting from slab expansion acting on truss support seats, or
  - tension failure of column truss seats from inward pull forces

Finite Element Model

A review of floors in the impact zones of WTC 1 and WTC 2 found that floor 96 in WTC 1 was representative of the floors of interest (see NIST NCSTAR 1-2A), and it was used for the floor analysis. Reference structural models of Floor 96 were developed in SAP2000 for traceability to a verified data set (see NIST NCSTAR 1-2) and translated into ANSYS models (see NIST NCSTAR 1-6C). The ANSYS floor model was used for the structural response analyses. Figure 4–27 shows an overall view of the converted ANSYS model of Floor 96. Figure 4–28 and Fig. 4–29 show a close-up of the truss floor and core framing, respectively.

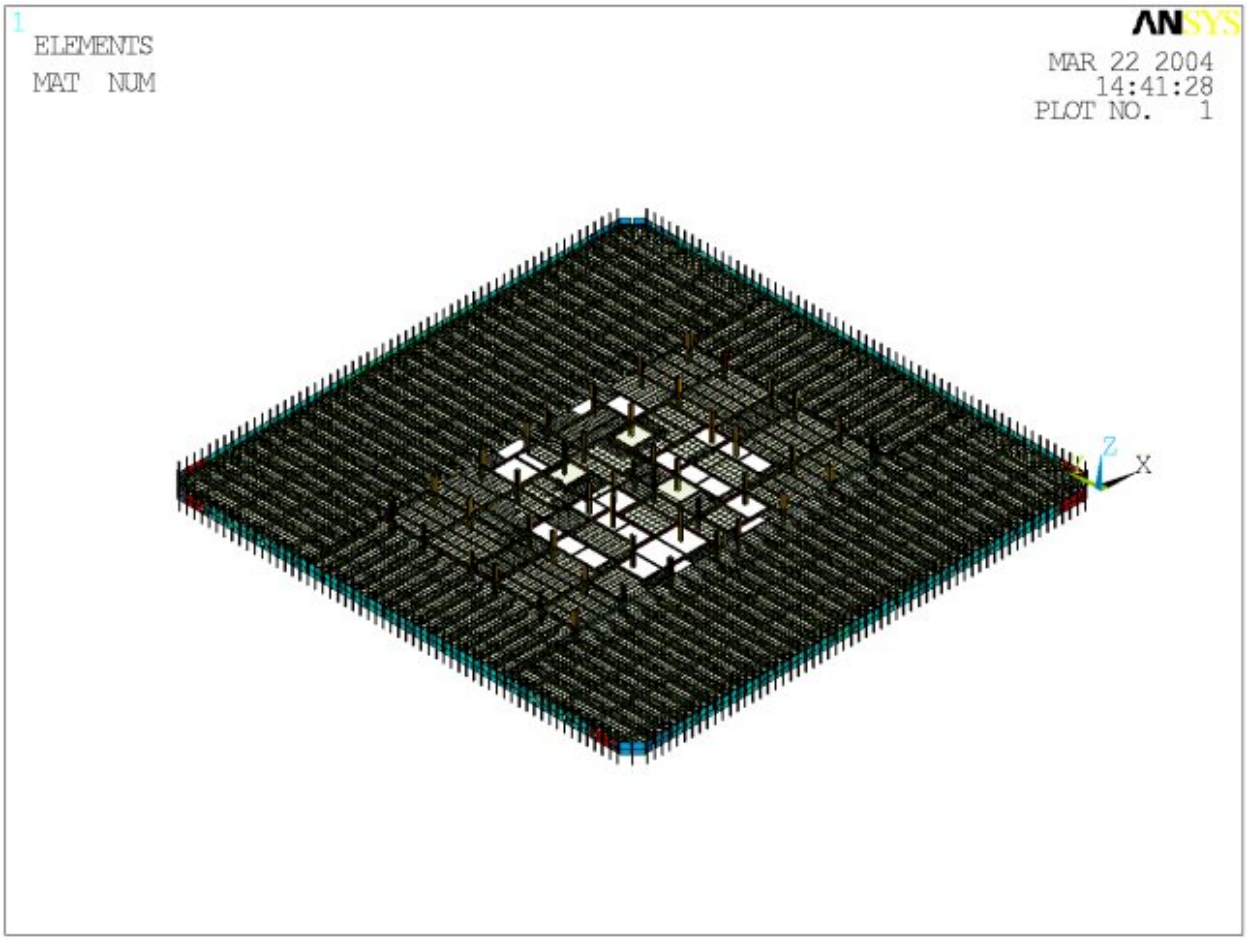

Figure 4–27. Converted ANSYS model for Floor 96 of WTC 1.

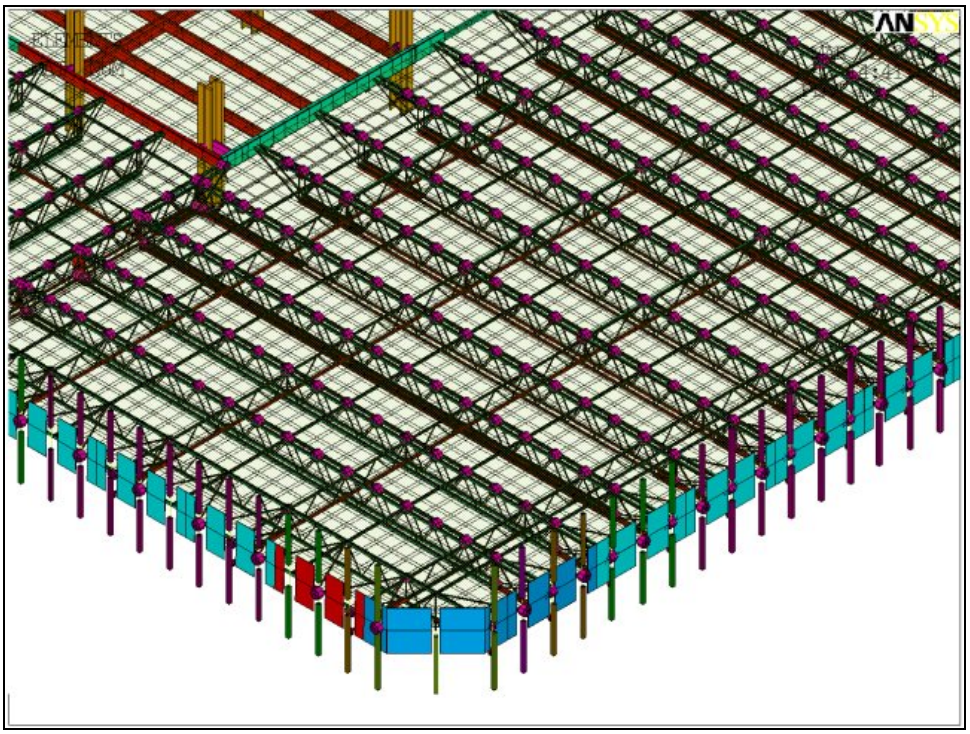

Figure 4–28. Long span trusses of converted ANSYS model for Floor 96 of WTC 1.

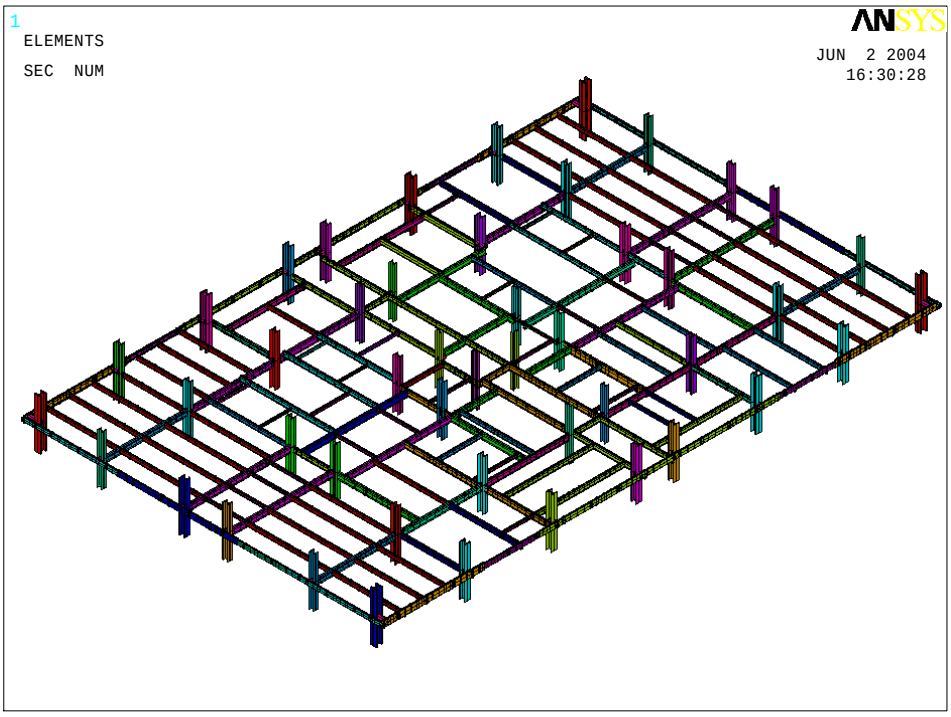

Figure 4–29. Core floor beams and columns of converted ANSYS model for Floor 96 of WTC 1.

Analyses were conducted to validate the converted ANSYS floor model against the verified SAP2000 model as follows:

- Static analysis with gravity loads.
- Modal analysis using structural mass only.

Comparisons of the SAP2000 and ANSYS results for the gravity load case are given in Table 4–7. The total reactions for the SAP2000 and ANSYS models were within 0.1 percent of each other. The maximum slab displacement predicted by the ANSYS model was 3.2 percent smaller than that obtained from the SAP2000 model.

Table 4-7. Comparison of SAP2000 and ANSYS results for gravity load case.

	SAP2000	ANSYS (BEAM 188)
Total reaction, kip	2,212.81	2,210.85 (-0.09 %)
Maximum slab displacement, in.	0.718	0.695 (-3.2 %)

Table 4–8 summarizes the comparison of the SAP2000 and ANSYS results for the modal analysis. The total masses of the SAP2000 and ANSYS models were within 0.02 percent of each other. The dominant natural frequency of the floor predicted by the ANSYS model was 2.5 percent higher than that obtained from the SAP2000 model, which is consistent with the discrepancy observed for gravity displacement.

Table 4-8. Comparison of SAP2000 and ANSYS Modal Analysis Results.

	SAP2000	ANSYS (BEAM 188)
Total mass, lb·sec^2/in.	5448.7	5447.7 (-0.018 %)
Dominant natural frequency of floor, Hz	4.32	4.43 (+2.5 %)

Reduced Model

The converted ANSYS model was modified to incorporate the nonlinear behaviors of the components and to reduce model complexity to achieve computation efficiency while retaining essential behaviors. The final model used for analyzing the floor response to gravity loads and elevated temperatures included the following modifications:

- Two adjacent trusses were combined into a single truss. The elements in the truss model had twice the areas and moments of inertia of elements in each single truss.
- Spandrels defined as beam sections in SAP2000 model were replaced with four-node finite strain shell (SHELL 181) elements (eight elements between two columns and four elements along the height). This modification eliminated the need for defining panel zone stiffness.
- Elastic column elements were changed to 3-D quadratic finite strain beam (BEAM 189) elements with user-defined composite sections and nonlinear material properties.

- Section offsets of exterior columns were removed, and nodes were placed at centroids of their cross sections.
- Spandrel plates were connected to exterior columns using rigid beam elements.
- The entire core was remeshed to produce a more uniform element size.
- Section offsets of core beams were removed to eliminate the end bending moment due to eccentricity. Core beams were placed at their centroids and connected to the slab by rigid beams.
- Beam elements of the top chord between panel points were merged into one element to prevent the top chord from buckling and penetrating the slab.
- Web diagonals were modeled by 3-D linear beam (BEAM 188) elements.
- Coincident nodes were provided for break elements.
- Break elements were incorporated into the model to represent:
  - buckling of diagonals;
  - truss seat failure;
  - failure of connections between primary and bridging trusses;
  - failure of connections between long-span and transfer trusses;
  - failure of studs connecting the slab and the spandrel;
  - failure of welds between strap anchors and top chords.

The full floor model as shown in Fig. 4–30 included the following structural members:

- Exterior and core columns extending from one floor below to one floor above
- Spandrels on the floor of interest
- Concrete floor slab
- Steel floor trusses including primary and bridging trusses
- Strap anchors
- Core beams
- Deck support angles

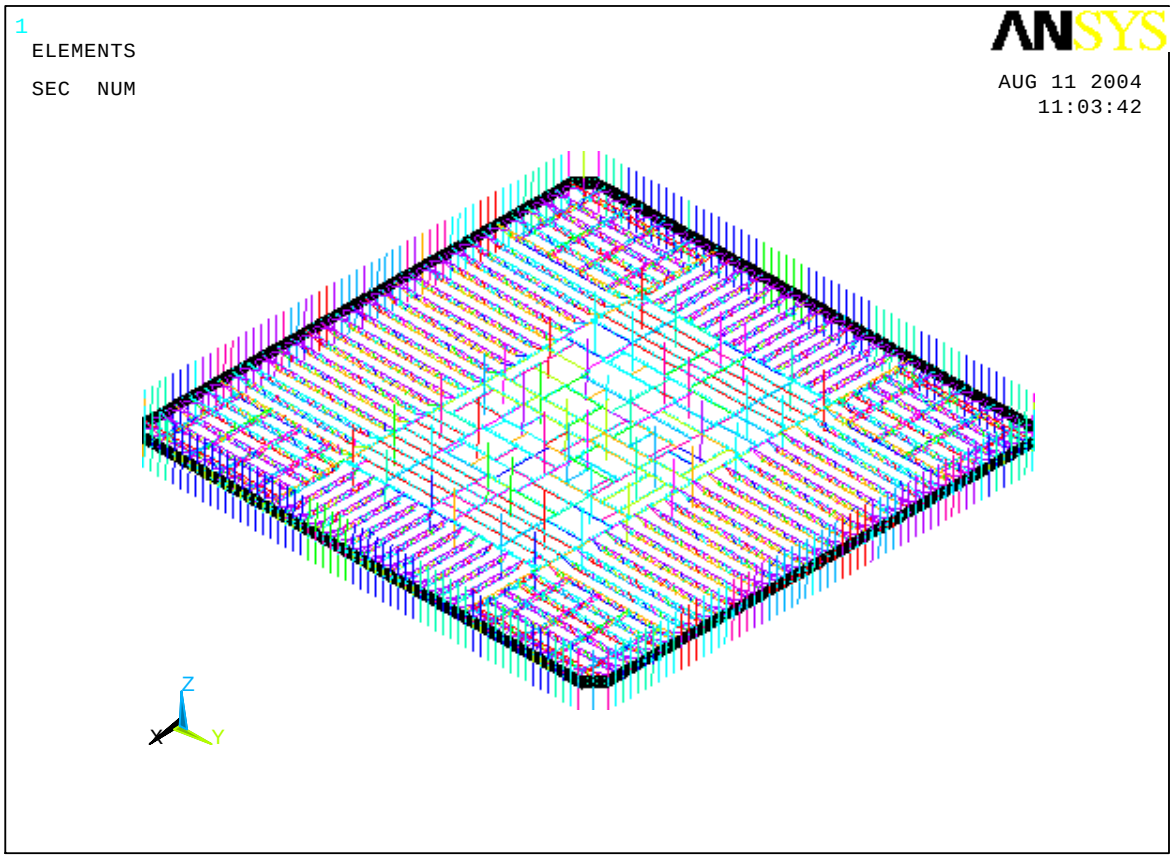

Figure 4–30. Full floor model before impact damage is included (without concrete floor slab).

Some components were found to fail in early stages of thermal loading, causing numerical solution difficulties, and were removed from the model. Removal of these components did not control the stability or failure mode of the full floor system under thermal loading. The removed members were:

- Deck support angles
- Shear studs on strap anchors and welds between strap anchors and truss top chords
- Bridging trusses in the one-way zone, and extending to the corner of the core
- Shear studs connecting the slab and the spandrel
- Strap anchors

The concrete slab was attached to the trusses at the knuckle nodes. Break elements were not used to represent knuckle failure as the detailed truss and slab analyses showed that web diagonal buckling, rather than knuckle failure, caused floors to sag. Concrete slab and trusses were always connected in the analysis.

Four different types of break elements were used in the full floor model. Their features are summarized in Table 4–9. There were a total of 2,028 break elements used to capture failure of the web diagonals, truss seats and truss-to-truss connections, welds, and studs. Figure 4–31 shows a summary of break element locations in the floor model.

Table 4-9. Types of break elements.

Type	D.O.F.	Capacities to be defined	Stiffness to be defined	Description	Usage in the floor model
102	UX UY UZ ROTX ROTY ROTZ	Positive FX Negative FX Positive FY Negative FY Positive FZ Negative FZ MX MY MZ	Initial and post-failure stiffness for UX, UY, and UZ Initial and post-failure stiffness for ROTX, ROTY, and ROTZ	All force and moment components are checked with corresponding capacities.	Failure of seats. Fracture of gusset plates. Failure of connections between primary and bridging trusses. Failure of connections between long-span and transfer trusses.
103	UX UY UZ	Positive F Negative F	Initial and post-failure stiffness for UX, UY, and UZ	SRSS* of three force components is checked with the capacity. The sign of force is determined by the direction specified by the user.	Failure of strap anchor welds.
104	UX UY UZ	Positive FX Negative FX Positive FY Negative FY Positive FZ Negative FZ	Initial and post-failure stiffness for UX, UY, and UZ	All force components are checked with corresponding capacities.	Failure of studs connecting the spandrel and the slab.
105	UX UY UZ ROTX ROTZ ROTZ	Positive F Negative F	Initial and post-failure stiffness for UX, UY, and UZ Initial and post-failure stiffness for ROTX, ROTY, and ROTZ	SRSS of three force components is checked with the capacity. The sign of force is determined by the direction specified by the user.	Buckling of web diagonals. Failure of resistance weld between web diagonals and chords.

*SRSS: square-root-of-sum-of-square

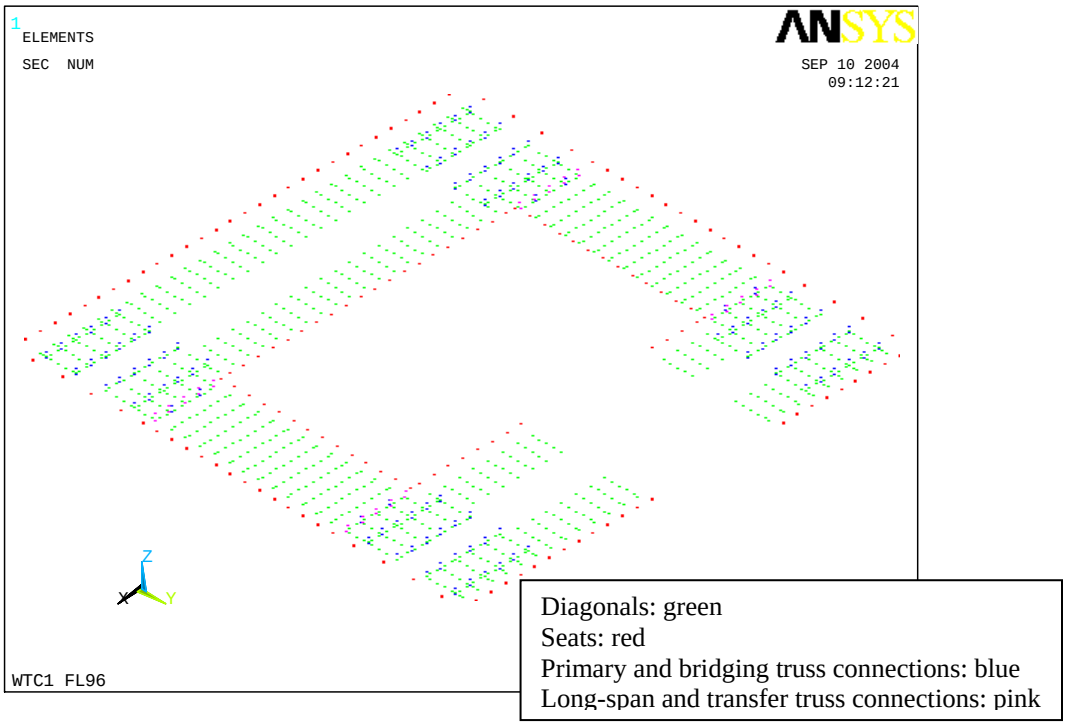

Figure 4–31. Break element locations in the floor model (Floor 96, WTC1).

Floor Analysis Results

The results of the full floor analyses are given in Chapter 7, Structural Response of Major Tower Subsystems. The floor models were analyzed for their response to impact damage and elevated temperatures from the fires for each floor in WTC 1 and WTC 2.

4.3 EXTERIOR WALL SUBSYSTEM

Just as the floors played an important role in the response of the World Trade Center towers to both aircraft impact and the ensuing fires, so did the exterior columns. Indeed, photographic and video evidence shows bowing of large sections and eventual buckling of an exterior wall of each tower at the time of collapse.

The exterior walls of the towers were made up of closely-spaced steel box columns and deep spandrel plates. For construction, three story high panels, consisting of three columns and three spandrels, were shop fabricated, lifted into position, and bolted together.

Component analyses were conducted to enable capturing all of the relevant failure modes for: (1) spandrel splices, (2) bolted column splices, and (3) a single column of one, two, or three stories.

A section of an exterior wall was analyzed that was three panels wide and three panels high and included the column and spandrel splices. Thus, the model had nine columns and nine spandrel plates. The objective of the exterior wall section model was to study the performance of the wall under the combined

effects of gravity and thermal loads for several conditions of lateral support. The wall section analyses included (1) the translation and validation of a single-panel ANSYS model, (2) development of the wall section model, and (3) evaluation of structural response under gravity loads and pull-in forces resulting from floor sag and elevated structural temperatures.

4.3.1 Exterior Wall Subsystem Description

The exterior wall of the towers was comprised of prefabricated wall panels, referred to hereafter as panels. Typical panels contained three-column segments spanning three stories with portions of the spandrels extending one half-span past the outer columns. The panels were typically arranged such that spandrel splices between panels aligned vertically and column splices between panels offset each other by one story.

The wall panel section selected for study was located on the north face of WTC 1 toward the east side and included nine columns, extending vertically from the column splice located below Floor 91 to the column splice above Floor 99, and nine spandrels, extending horizontally from the spandrel splice located at mid-span between Columns 149 and 150 to the spandrel splice at mid-span between Columns 158 and 159. This exterior wall subsystem model included seven full panels and portions of four other panels.

Figure 4–32 shows the exterior wall section, and Fig.4-33 is a schematic of an exterior box column showing the column plate notation. Tables 4–10 through 4–12 give the dimensions of the column and spandrel plates and their splice connections.

The odd-numbered columns supported floor trusses. Pairs of strap anchors extended diagonally from the top chords of truss pairs to the even-numbered columns. The trusses and the straps braced the exterior columns out-of-plane of the exterior wall.

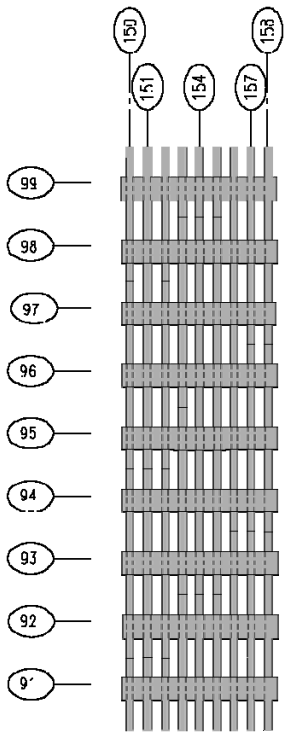

Figure 4–32. Exterior wall section model.

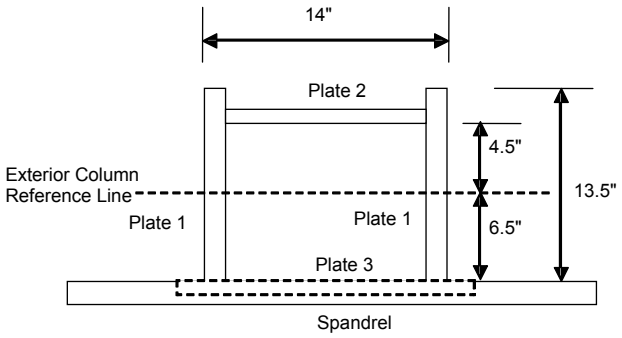

Figure 4–33. Schematic of exterior column cross-section.

Table 4-10. Column section properties.

Column Type	Plate 1 length by thickness (in. x in.)	Plate 2 length by thickness (in. x in.)	Plate 3 length by thickness (in. x in.)
120	13.5 x 0.25	13.5 x 0.25	15.75 x 0.25
121	13.5 x 0.3125	13.375 x 0.25	15.75 x 0.25
122	13.5 x 0.375	13.25 x 0.25	15.75 x 0.25
123	13.5 x 0.4375	13.125 x 0.25	15.75 x 0.25
124	13.5 x 0.5	13 x 0.25	15.75 x 0.25
125	13.5 x 0.5625	12.875 x 0.25	15.75 x 0.25

[1]All spandrels in exterior wall subsystem model are 52 in. deep x 3/8 in. thick.

Table 4-11. Spandrel Splice Details.

Spandrel Splice Type	Number of Bolts/Row	Total Number Of Rows	Bolt Spacing (No. of bolts@ spacing) (in.)	Gage (in.)	Overall Splice Plate Dimensions (in. x in. x in.)	Bolt to Centerline of Splice (in.)	Gap Between Spandrels (in.)	Spandrel Splice ID
101	6	2	5@9		49x6.75x.25	1.875	0.75	101
102	8	2	3,6,3@9,6,3		49x6.75x.25	1.875	0.75	102
111	6	4	5@9	3	49x12.75x.25	1.875	0.75	111
112	8	4	3,6,3@9,6,3	3	49x12.75x.25	1.875	0.75	112

[1]All spandrel splices use 7/8 in. A325 bolts; specified spandrel plate yield strength is 36 ksi.
[2]Holes in spandrel are 1/4 in. larger than bolts; holes in plates are bolt + 1/16 in. or option to match spandrel holes.

Table 4-12. Column Splice Details.

Column Splice Type	Butt Plate Thickness (in.)	Number of Bolts	Bolt Diameter (in.)	Gage (in.)	Bolt Spacing (in.)	Column Splice ID
411	1.375	4	0.875	3.5	6	411
421	1.625	4	0.875	3.5	6	421
431	1.875	4	1	3.5	6	431

[1]Butt plates have specified yield strength of 50 ksi.
[2]Bolts are A325.

4.3.2 One, Two, and Three-Story High Columns

Figure 4–34 shows the finite element model of a one-story high exterior column representing Column 151 (see Fig. 4–32). Shell elements were used to model the plates comprising the box column and the spandrels. Rigid elements connected the center of gravity of the column to its component plates and the spandrel at both the top and the bottom of the model. The column was simply supported in three directions at the bottom and simply supported in the horizontal directions at the top. Increments of axial displacement were applied at the top of the model.

Figure 4–35 shows the variation of axial load with imposed axial displacement and resulting lateral deflection for two assumed uniform temperature conditions, room temperature and 700 °C. Figure 4–35 also presents results of standard handbook calculations at room temperature and at 700 °C for (1) local buckling of plates 2 and 3, (2) uniform yielding of the column, and (3) gravity load demand.

Figure 4–36 shows the local buckling deformation of Plate 2 and Plate 3 at the maximum load level (approximately 1,050 kip) at room temperature. Figure 4–37 shows a plastic hinge at mid-height of the column for an axial displacement of 2 in. Figure 4–38 shows the presence of local buckling in Plate 2 and Plate 3 at 700 °C and the maximum load (approximately 250 kip).

It can be seen from Fig. 4–35 that, at room temperature, local buckling occurs at a load that is less than the maximum column load, but that at 700˚C the column yields before it buckles locally. This figure also shows that the column demand load of 175 kip is substantially lower than the local buckling load at room temperature and the column yield load at 700˚C. At room temperature, the post-buckling strength decreased rapidly; however, the reduction in the strength was much more gradual in the post-buckling regime at 700 ˚C.

Axial load-displacement behaviors of two- and three-story models are also examined, and the results are shown in Fig. 4–35. As can be seen, for longer unsupported lengths and higher temperatures, the slope of the axial load-deflection curve in the post-buckling regime became less steep.

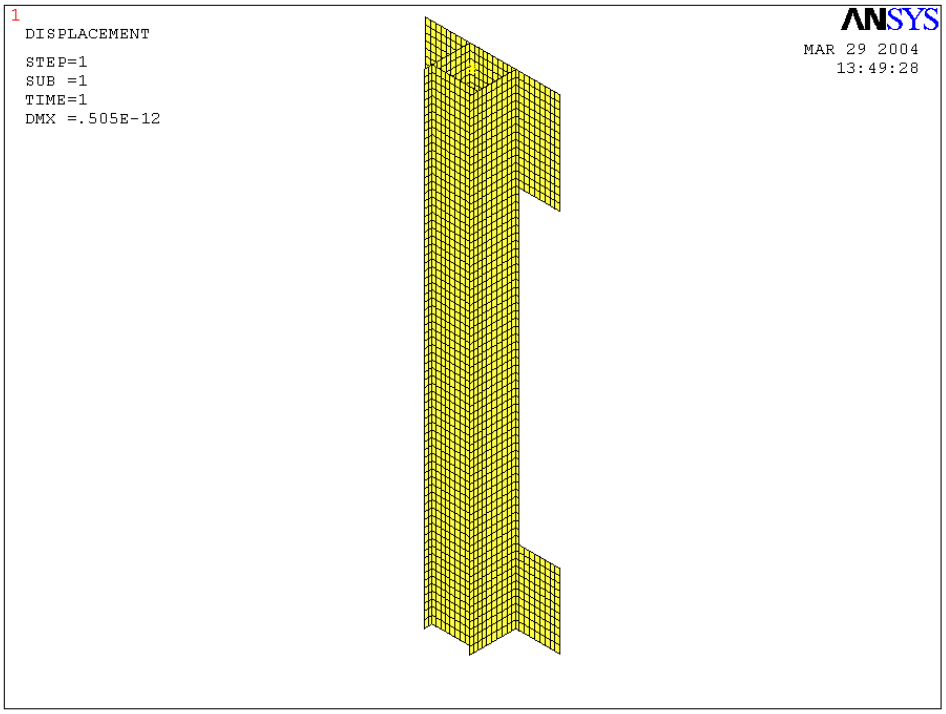

Figure 4–34. One-story exterior column model.

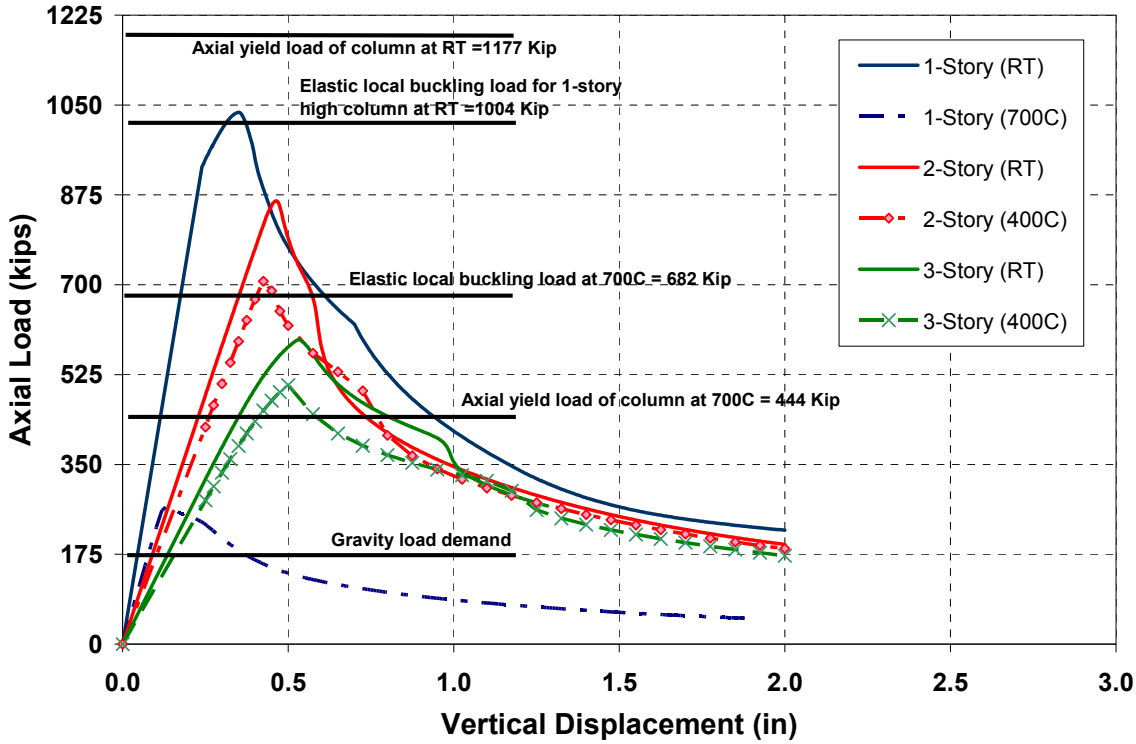

Figure 4–35. Load-deflection of column at room temperature (RT) and 700 °C.

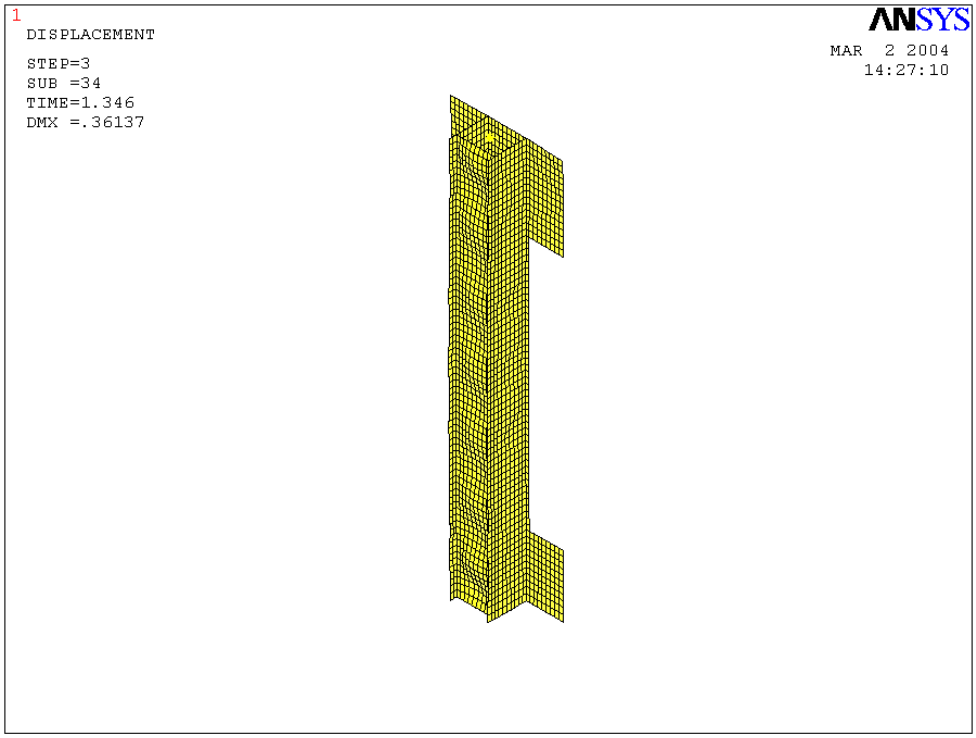

Figure 4–36. Local buckling of column at room temperature.

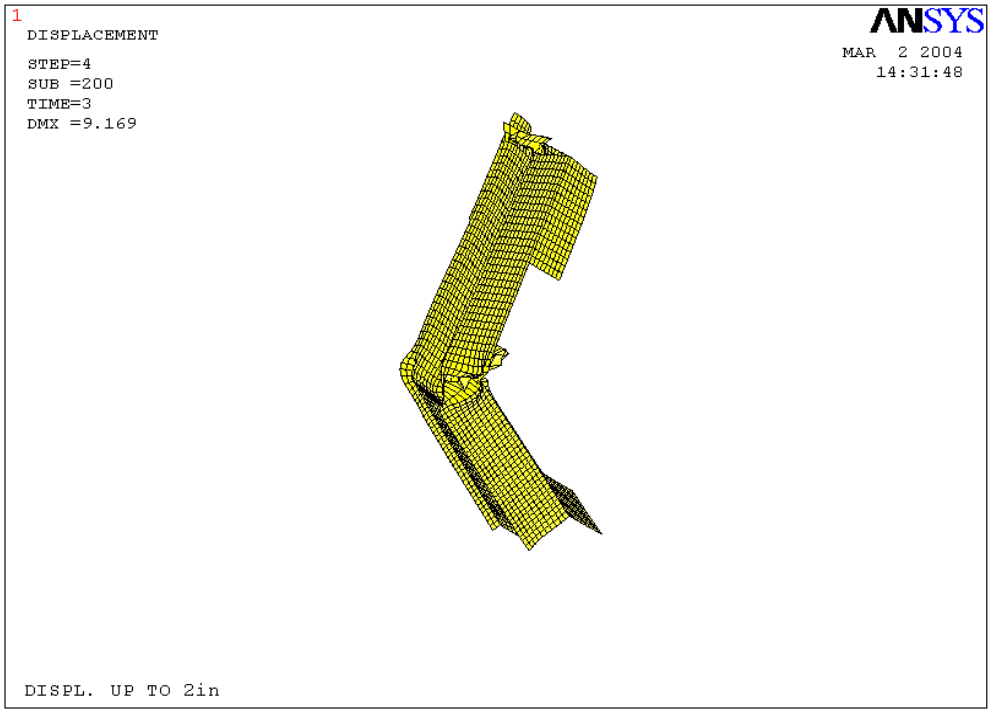

Figure 4–37. Plastic hinge in column at room temperature.

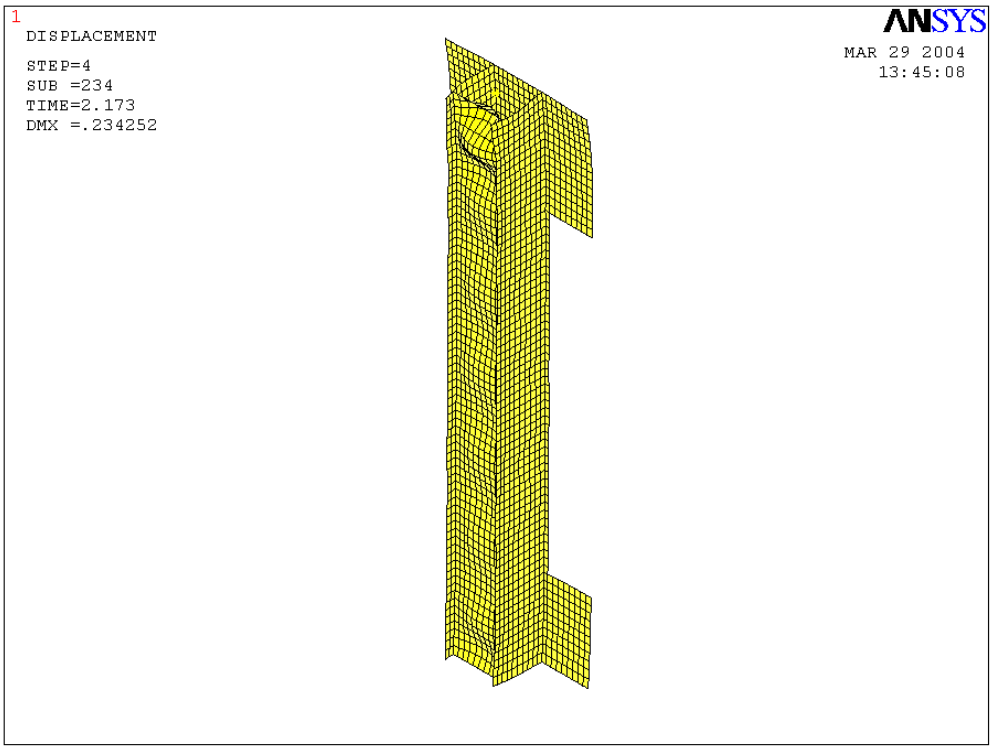

Figure 4–38. Deformed shape of column at maximum axial load at 700 °C.

4.3.3 Exterior Wall Section Analysis

Analysis of a section of the exterior wall of the World Trade Center towers involved:

- the translation and validation of a single panel finite element model to ANSYS and modification to include nonlinear behavior,
- development of the exterior wall section model,
- evaluation of structural response under dead and live loads and elevated structural temperatures, and
- determination of loads that cause buckling (instability).

Failure Modes

The exterior wall section model captured the following failure modes:

- Column buckling from large lateral deformations,
- Column buckling from loss of support at floor truss seats and diagonal straps,
- Failure of column splice bolts, and
- Failure of spandrel splice bolts or tearing of spandrel or splice plates at bolt holes.

Finite Element Model of Single Panel

A finite element model of a single exterior wall panel using both beam and shell elements was developed to reduce the model size. This model was validated against a finite element shell model of a single exterior wall panel developed by LERA (NIST NCSTAR 1-2A) by comparing the stiffnesses for a variety of loading conditions.

Figure 4–39 shows the SAP2000 shell model of a typical prefabricated panel at Floors 79 to 82, and Fig. 4–40 shows the reduced ANSYS model which had fewer degrees of freedom. In the ANSYS panel model, beam elements replaced shell elements to model the columns, while shell elements were used to model the spandrels, and beam elements attached the center of gravity of the columns to the mid-plane of its corresponding spandrel component at each shell element through the depth of the spandrel.

Each of the models was subjected to the following loads at room temperature as shown in Fig. 4–41:

- A vertical force (FZ) at the top of one of the outside columns.
- A horizontal force in the plane of the wall (FX) at the top of one of the outside columns. The stiff beam elements distributed this shear between the tops of all three columns.
- A transverse force (FY) on the middle column at Floor 81 (middle floor).

Figure 4–42 shows the deflected shape of the panel for both the SAP2000 and ANSYS models for the case of 100 kip lateral load at the top of the panel. Table 4–13 presents the results for this and the other two loading conditions.

Lateral and vertical displacements were found to be within 7 percent while the out-of-plane displacement for the ANSYS model was 13 percent less than that obtained from the SAP2000 model.

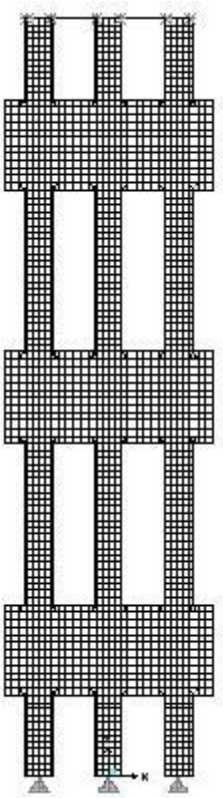

Figure 4–39. SAP2000 shell model of prefabricated panel.

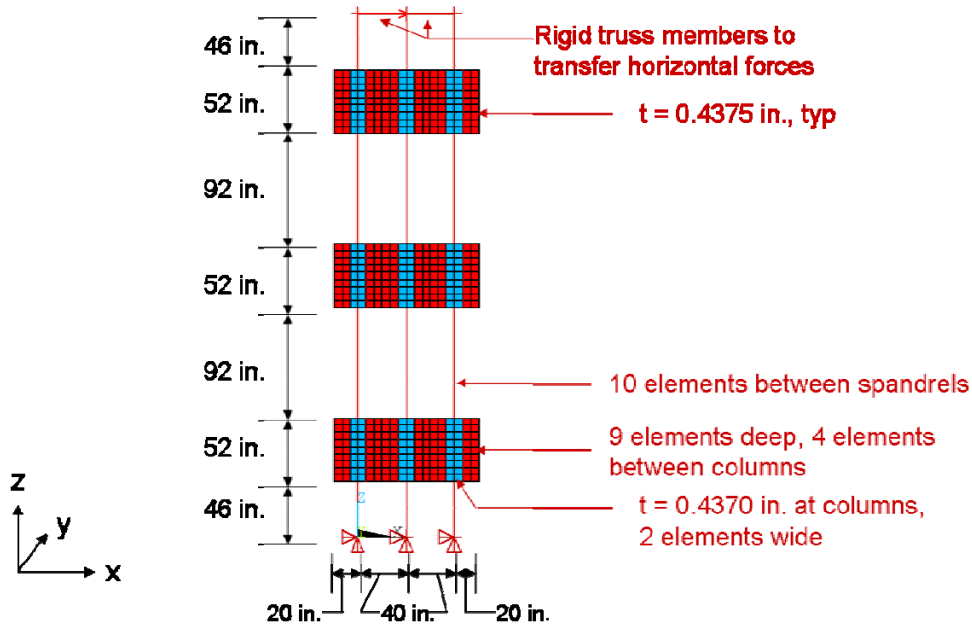

Figure 4–40. ANSYS model of prefabricated panel showing finite element mesh.

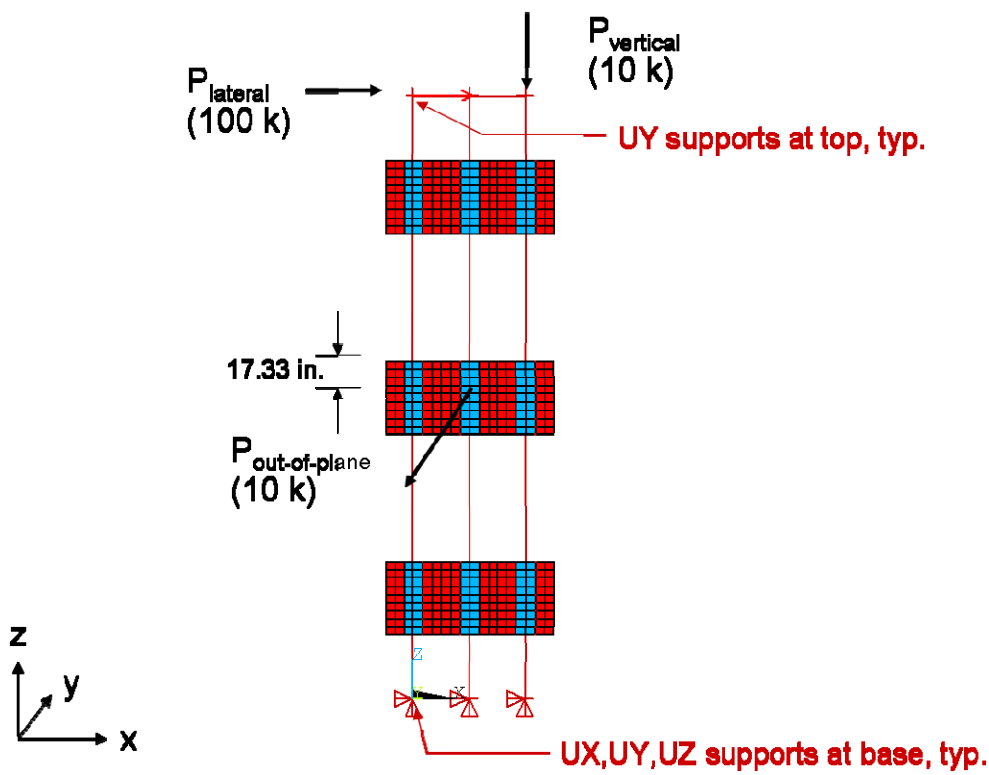

Figure 4–41. ANSYS model of prefabricated panel showing boundary conditions and loading.

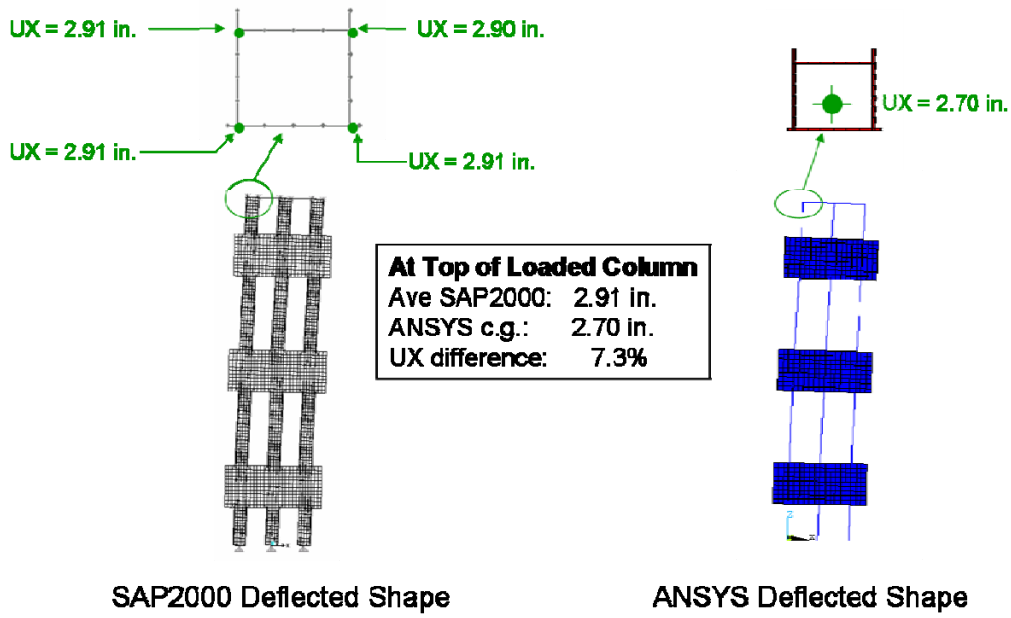

Figure 4–42. Deflection of prefabricated panel under 100 kip lateral load.

Table 4-13. Prefabricated panel validation results.

Loading Condition	SAP2000/ANSYS Difference Range	
	Reaction	Displacements[1]
Lateral FX	RX: -2% to +1%	UX: 7%
Transverse FY	RY: -6% to +7%	UY: -13%
Vertical FZ	RZ: -1% to +2%	UZ: -7%

1. Displacements considered at tops of columns for FX and FZ, and at points of load application for FY.

Spandrel Splice Model

Figure 4–43 shows a typical layout of the spandrel splices in the model. User-defined break elements model the interior spandrel splice connections, and nodal couples model the exterior spandrel splice connections. Figure 4–44 shows the modeling of an interior spandrel splice. User-defined break elements at each node through the depth of a spandrel allow the model to capture connection failure modes including (1) bolt shear, (2) tearing of the spandrel plate, and (3) tearing of the splice plates at the bolt holes. The break elements transfer forces and moments between nodes according to the initial stiffness values until the element reaches capacity in one direction. Upon reaching one of the capacities, the stiffness of the element in all directions changes to the corresponding failure stiffness, and the element sheds load through other load paths.

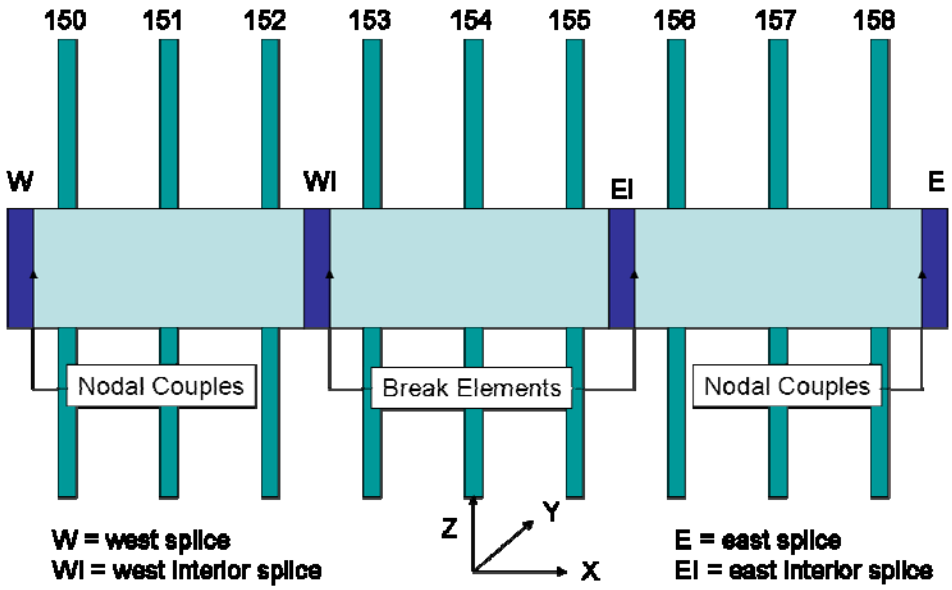

Figure 4–43. Typical spandrel splice layout for exterior wall section model.

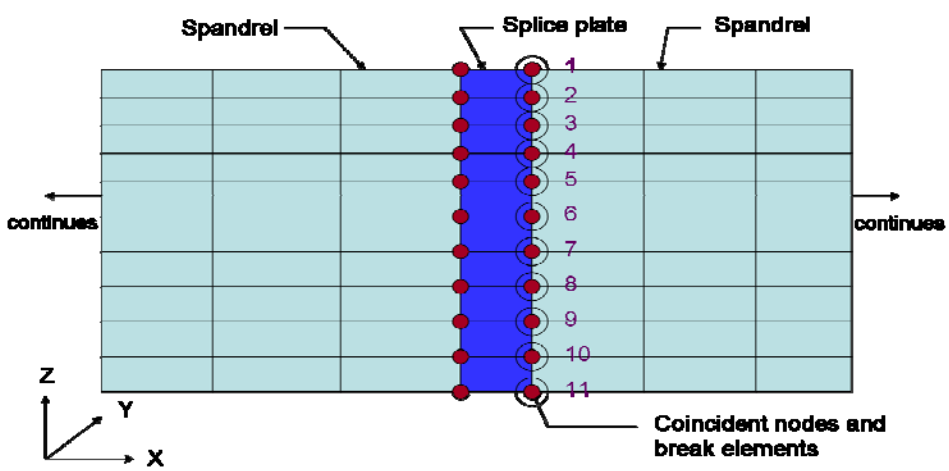

Figure 4–44. Modeling of a typical interior spandrel splice in the exterior wall section model.

Column Splice Model

Bolted column splices were modeled using beam elements for each of the four bolts, four pairs of contact elements at the faying (contact) surfaces between column ends (butt plates) and stiff beam elements connecting the tops of the bolts to the contact elements. Fracture of the column bolts was included and was based on test data (NIST NCSTAR 1-3). Figure 4–45 shows a schematic view of the column splice model. The contact elements use a coefficient of friction of 0.35. The 7/8 in. diameter column splice bolts are pretensioned to 36.05 kip at 20 ºC (AISC 1964).

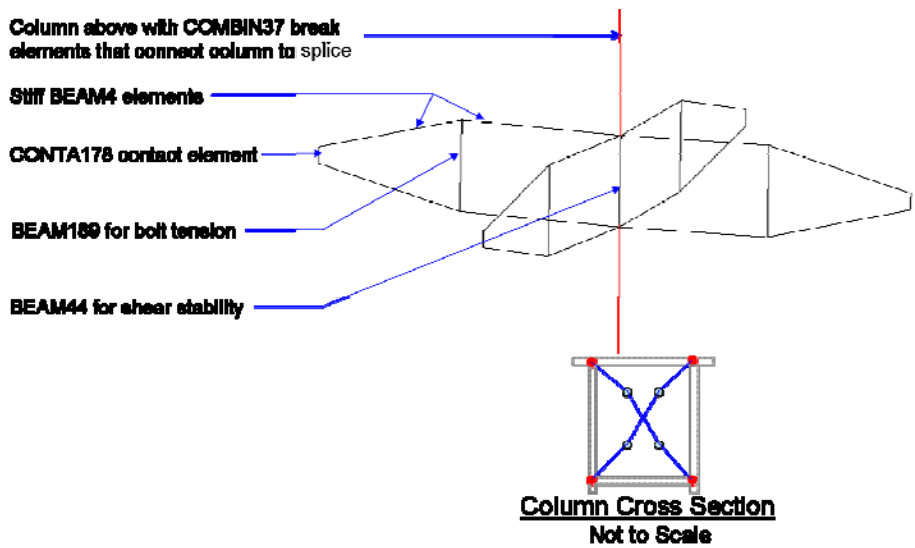

Figure 4–45. Column Splice Model used in Exterior Wall Model.

Finite Element Model of Exterior Wall Section

The single panel model was used to form a nine column by nine spandrel wall section model. Fig. 4–46 shows the model in elevation, and Fig. 4–47 shows a typical finite element mesh for a portion of the model. The colors of the elements illustrated in Fig. 4–47 represent the various element properties assigned. Element properties include large deflections, plastic deformation, and creep at elevated temperatures.

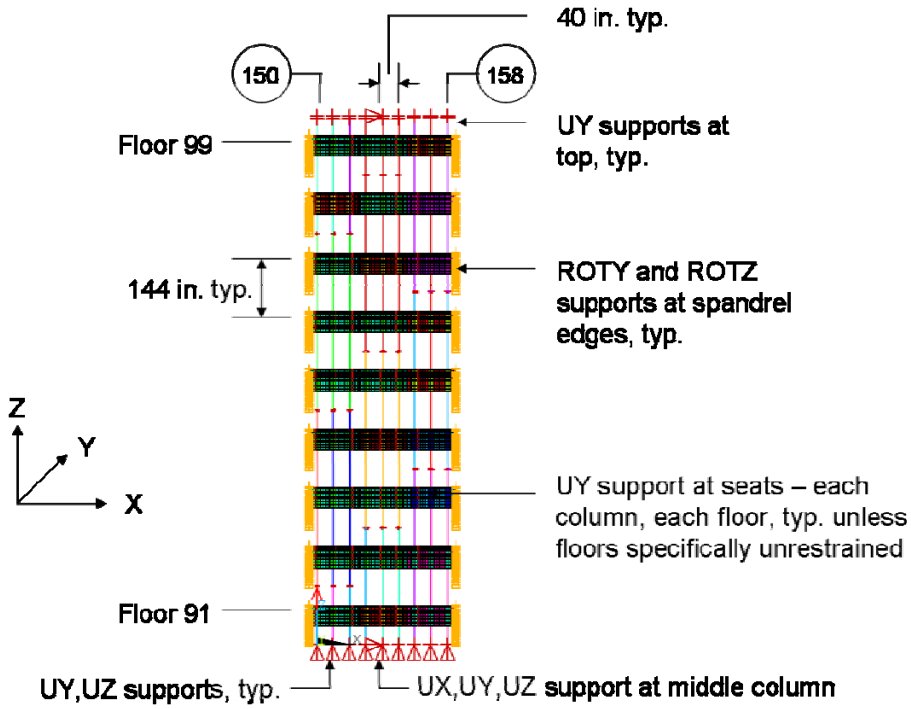

Figure 4–46. Exterior wall subsystem model with boundary conditions.

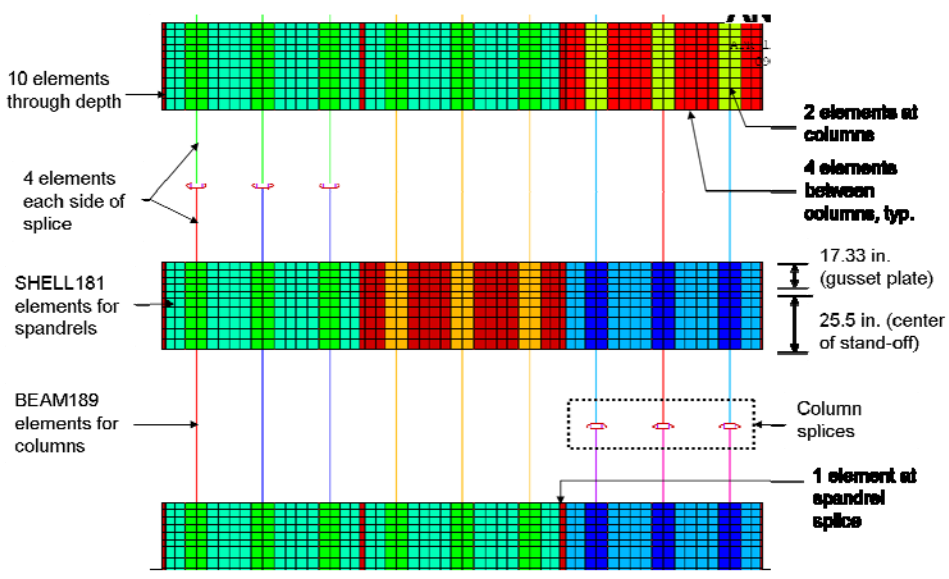

Figure 4–47. Typical meshing of exterior wall model components.

Loading

The exterior wall section was subjected to several loading conditions as described here. Gravity loads corresponding to dead load plus 25 percent of the design live load were applied to simulate the axial forces in the columns and floor loads applied to the truss seats. Five thermal load conditions were considered (see NIST NCSTAR 1-5G) that represented fire exposures and thermal insulation conditions at several locations in the towers. The most severe of these conditions was used for subsequent analyses. The five thermal loading conditions were labeled Cases D, E and F, DBARE (representing absence of insulation); and E119 (corresponding to the standard ASTM E 119 thermal loading). Table 4–14 presents the various thermal load conditions, and Fig. 4–48 shows how the maximum temperature anywhere in the model varied with time for each thermal loading condition. Thermal loading condition DBARE was selected as the most severe exposure from this group. (The designation of thermal load condition D used here should not be confused with Cases D introduced later on in this report.)

Table 4-14. Thermal loading conditions used in the exterior wall model.

Thermal Loading Condition	Building and Location	Columns	Floors	Insulation	Time Duration	Maximum Temperature °C
D	WTC1 South face towards West	340 – 348	91 – 99	as specified	5400 s	537 °C
DBARE	WTC1 Same as D	340 – 348	91 – 99	none	5400 s	598 °C
E	WTC1 East face towards North	221 – 229	91 – 99	as specified	5400 s	871 °C
E119	WTC1			as specified	5400 s	418 °C
F	WTC2 North face East corner	250 – 258	76 – 84	as specified	3600 s	382 °C

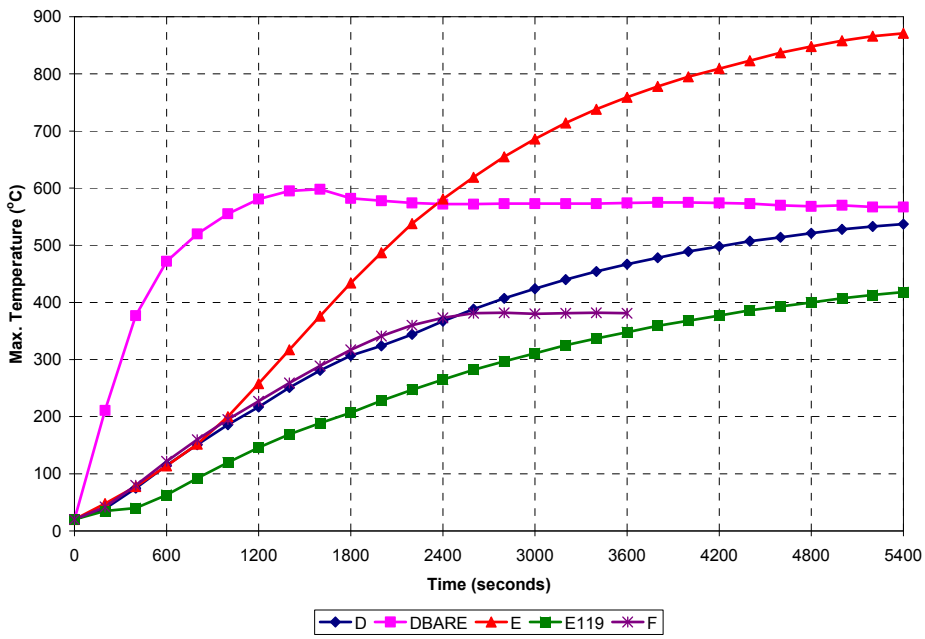

Figure 4–48. Exterior wall model temperature time-histories.

Table 4–15 shows the nine cases that were analyzed for the exterior wall model that included the thermal load cases, creep effects, and floor support conditions. Several combinations of disconnected floors were analyzed for the effects of loss of lateral support if a floor sagged or failed and the consequent increase in un-braced length of the columns.

Two cases were analyzed to investigate the stability of the exterior wall section. In one case, forces were applied to simulate pull-in from sagging floors to the point of instability. When trusses sag extensively, they pull the columns inward. Results of truss component analyses indicated approximately 14 kips of inward pull per truss. The strap anchors helped distribute this pull to the columns that did not support trusses. A 15 kip inward pull force was applied at each column that was laterally-unsupported, and in the second case, with three disconnected floors, a “push-down” analysis was conducted to simulate additional column loads being redistributed from the core. The top of the wall model was displaced downward until instability was reached.

The loads on the model were applied in stages in the following order:

- Self weight of the exterior wall components,
- Column splice bolt preload,
- Dead load of floor construction, including superimposed dead loads,
- 25 percent of floor design live loads,
- Temperatures of fire scenarios, and

- Transverse pull loading from sagging trusses, or
- Imposed vertical displacements at top of columns.

Table 4-15. Analysis cases for exterior wall section model.

Analysis Case	Thermal Load Condition	Bolt Temperatures	Creep Effects	Floor Supports	Pull-in Force	Push-Down Force
1	D	No	Yes	All		
2	DBARE	No	Yes	All		
3	E	Yes	Yes	All		
4	E119	No	Yes	All		
5	F	No	Yes	All		
6	DBARE	Yes	Yes	All but 95 and 96		
7	DBARE	Yes	No	All but 95, 96, and 97		
8	DBARE	Yes	No	All but 95, 96, and 97	X	
9	DBARE	Yes	No	All but 95, 96, and 97		X

Exterior Wall Analysis Results

Columns Laterally Supported at All Floors (Case 1 - Case 5)

The analysis results for the five thermal load conditions in Cases 1 to 5 indicated the following:

- Spandrels had the maximum stress (strains are plastic)
- Spandrels experienced large lateral distortions and separated partially; no spandrel splice separated completely in any of the five Cases.
- Lateral (out-of-plane) deflections of the columns were less than 1.0 in. and were due primarily to differential thermal expansion between the columns and spandrels.
- Column and spandrel thermal expansion was unrestrained. The columns elongated between 1 and 3 in.
- General instability (buckling) of exterior wall columns did not occur.

Deformations observed in the spandrel plates are illustrated in Fig. 4–49.

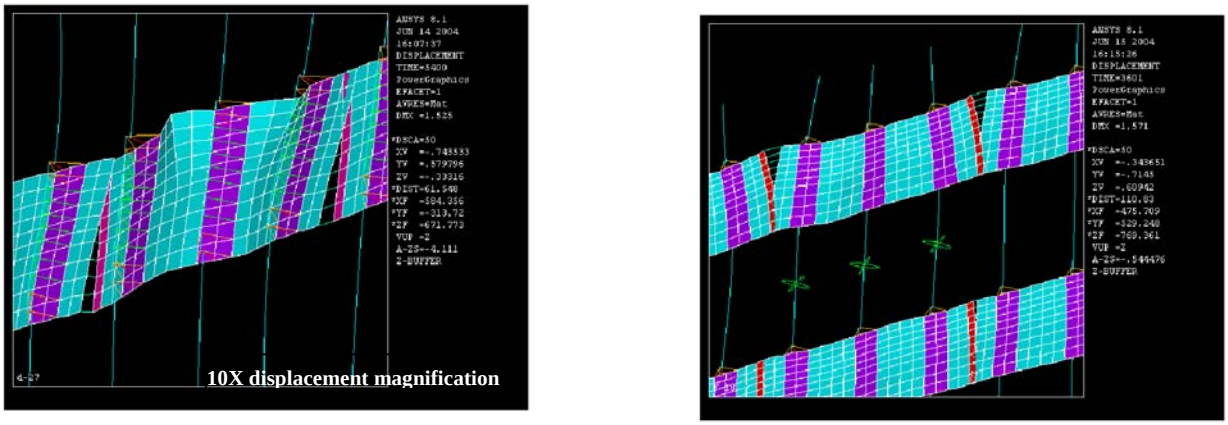

Fire Scenario D (Case 1) - Floor 94

Fire scenario F (Case 5) - Floor 99

Figure 4–49. Spandrel plate deformations.

Columns Not Laterally Supported at Two or Three Consecutive Floors (Cases 6 and 7)

The analysis results for Case 6 and Case 7 are similar and the following observations can be made for both conditions:

- Lateral deflections of the columns were less than 1.0 in. for the thermal loads.
- No plastic strain in the columns and spandrels.
- All column splices remained in contact.
- Spandrel splices separated partially on several floors; no spandrel splice separated completely
- The structures remained stable.

The out-of-plane deformations for the two cases are show in Fig. 4–50. Deformations for the case with three floors removed were somewhat greater than for the case with two floors removed, although the maximum deformations in both cases was less than 1.0 in.

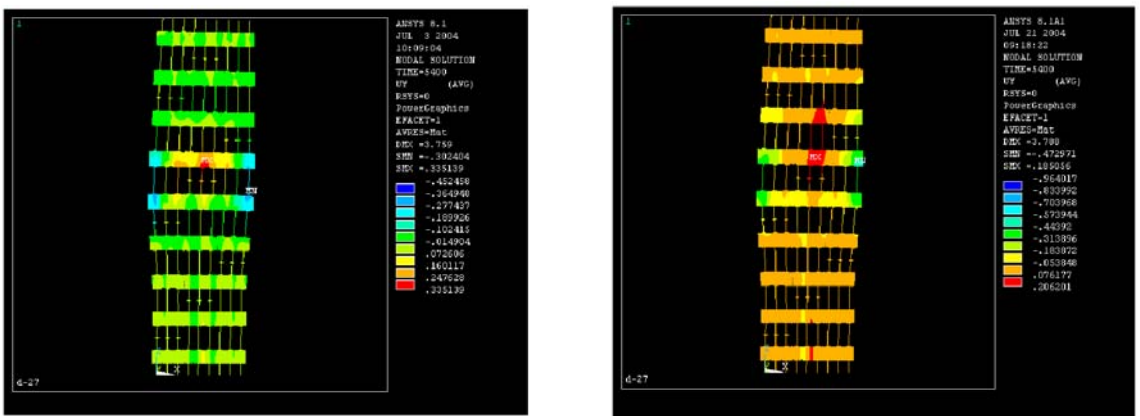

Two Floors Removed (Case 6)

Three Floors Removed (Case 7)

Figure 4–50. Lateral deflections for Case 6 and Case 7.

Columns Not Laterally Supported and Pulled-In at Three Floors (Case 8)

The analysis results for Case 8 indicated the following:

- Column instability (buckling) was reached with a transverse load of 12.6 kips per column
- For a lateral load of 12.6 kips, the inward deflection of the exterior wall section was 10.2 in.
- The maximum column tensile stress of 77.2 ksi was at Floor 94 where the lateral deflection was 10.2 in.
- Column splices experienced slip or opened up at several column locations; no column splice bolts fractured

Figure 4–51 shows the deflected shape of the exterior wall subsystem at the point of instability due to inward pull. The status of the column splice contact elements is shown in Fig. 4–52 and the column splice bolt stresses are shown in Fig. 4–53.

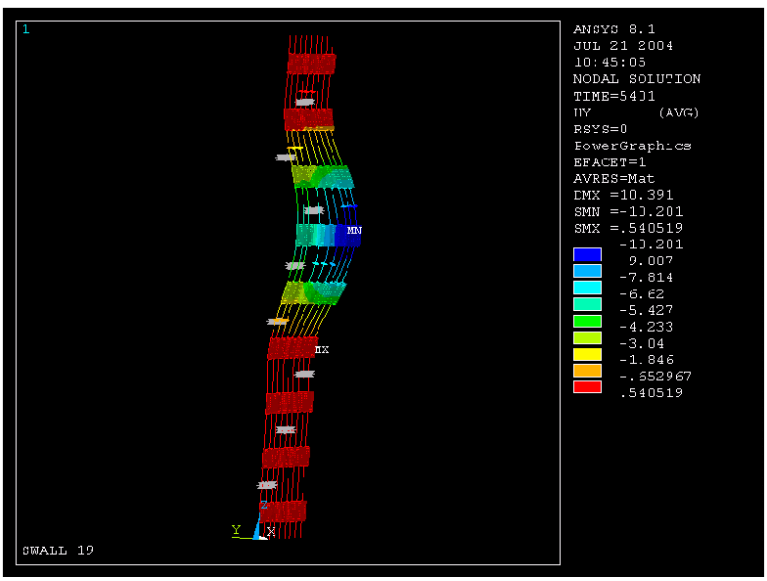

Figure 4–51. Structural response (out-of-plane deformations) for temperature time history DBARE and pulled-in at three disconnected floors for Case 8. (10X displacement magnification).

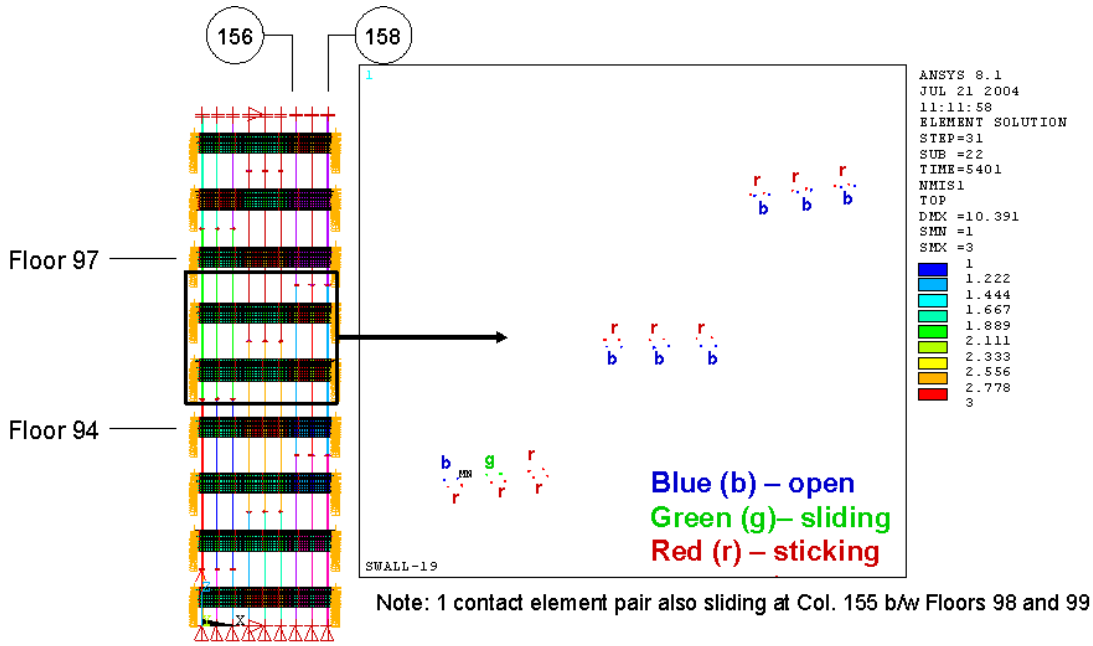

Figure 4–52. Column splice contact element status for temperature time history and DBARE and pulled at three disconnected floors for Case 8.

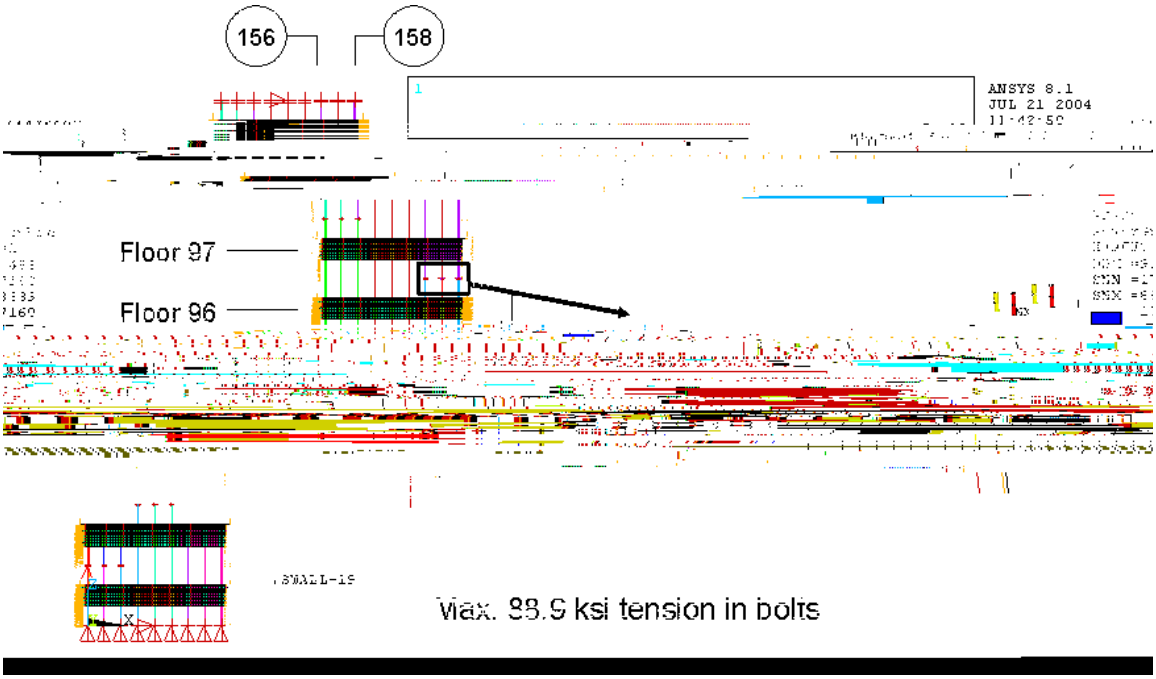

Figure 4–53. Column splice bolt stresses for temperature time history and DBARE and pulled at three disconnected floors for Case 8.

Columns Not Laterally Supported at Three Floors and Columns Pushed Down at Top (Case 9)

Figure 4–54 shows the deflected shape of the exterior wall subsystem due to push-down. The out-of-plane deformation as a function of push-down displacement is shown in Fig. 4–55.

The total vertical reaction (sum of the gravity and push-down loads) vs. imposed vertical displacement is plotted in Fig. 4-56. Plastic buckling was found to occur with a vertical applied displacement of approximately 1.2 in. which occurred, as can be seen in Fig. 4–56, at the point at which the total vertical reaction began to decrease. It is seen from Fig. 4–56 that, for the given thermal loading condition, the maximum total vertical reaction was approximately 2,700 kips, or an average of 300 kips on an individual column. Individual column forces are shown in Fig. 4–57 and are seen to range from approximately 250 kips to 350 kips. The gravity load on an individual column was approximately 200 kips.

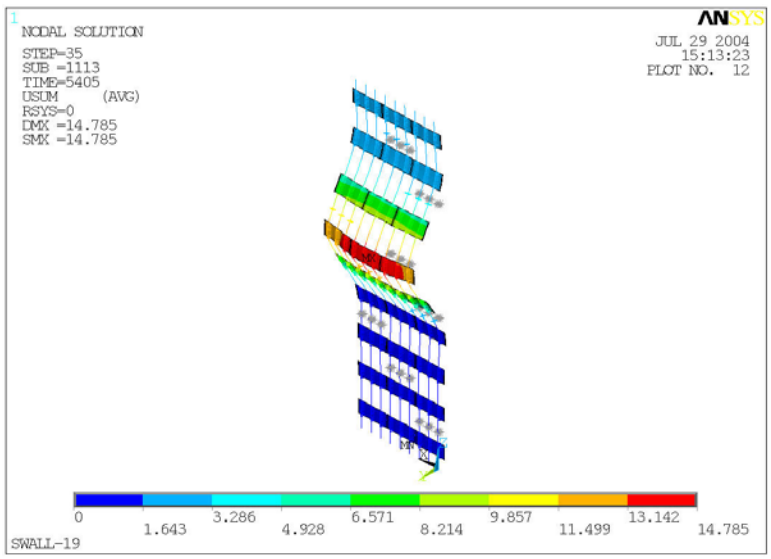

Figure 4–54. Structural response (out-of-plane deformations) for temperature time history DBARE and pushdown with three disconnected floors for Case 9 (10X displacement magnification).

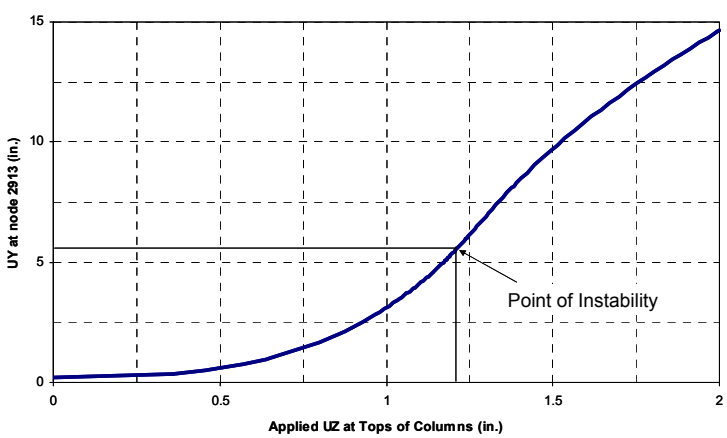

Figure 4–55. Out-of-plane deformation as a function of pushdown displacement after application of temperature DBARE with three disconnected floors for Case 9.

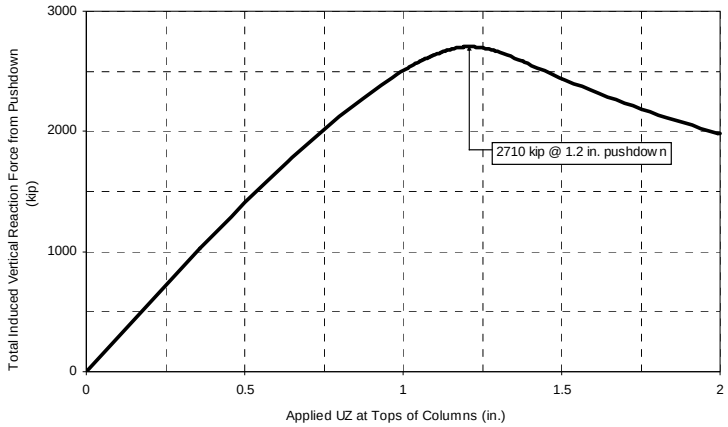

Figure 4–56. Total reaction at column base resulting from pushdown with temperature DBARE and three disconnected floors for Case 9.

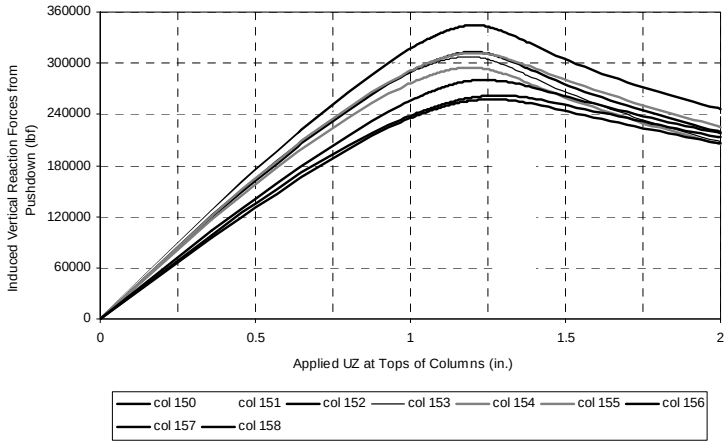

Chapter 5
AIRCRAFT IMPACT DAMAGE

5.1 INTRODUCTION

The structural damage to each tower resulting from th

This Chapter presents the methodology and criteria for developing input data from the aircraft impact analysis results for the fire dynamics, thermal, and structural analyses, and summarizes the aircraft impact damage data for Cases A, B, C, and D. A brief discussion of how aircraft impact affected the concrete columns in the Pentagon shows how direct debris impact dislodged the columns' concrete cover, which has a much higher bond strength than the SFRM and gypsum materials for thermal insulation of the structural steel. Data sets for structural analyses with Cases A_i, B_i, C_i, and D_i are presented in Appendix A and Cases A, B, C, and D are presented in Appendix B.

5.2 METHODOLOGY AND CRITERIA FOR DEVELOPING INPUT DATA FROM AIRCRAFT IMPACT ANALYSIS RESULTS

The fire dynamics, thermal, and structural analyses all required input data derived from the aircraft impact analyses. The fire dynamics analyses used estimates of damage to the floors and partition walls to describe ventilation paths and to identify the distribution of jet fuel and debris immediately following impact. The thermal analysis required estimation of the areas that had dislodged insulation on the structural components of the towers. For the structural analyses, elements that represented severed or heavily damaged floors and columns were removed from the structural models of the towers.

Damage to the exterior walls in the structural models was based on photographic and video records, which matched reasonably well the exterior damage predicted by the impact simulations (see NIST NCSTAR 1-2). Figures 5–1 and 5–2 show a comparison between the observed and predicted aircraft impact damage to the exterior walls for WTC 1 and WTC 2. The observed exterior damage was used in the structural analyses.

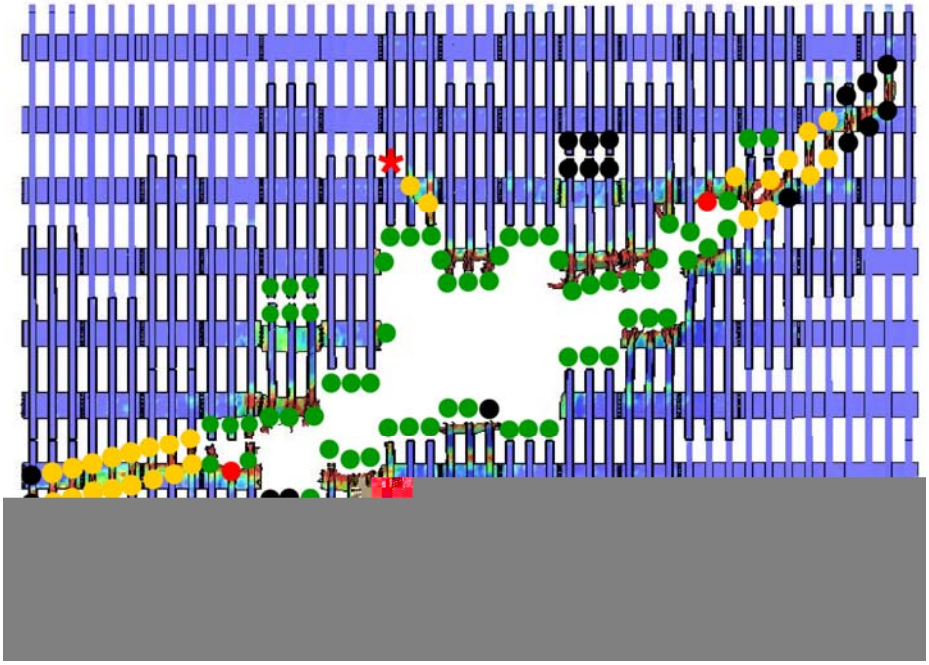

Figure 5–1. Validation of Aircraft Impact Analysis Prediction With Observations for WTC 1 North Exterior Wall Damage.

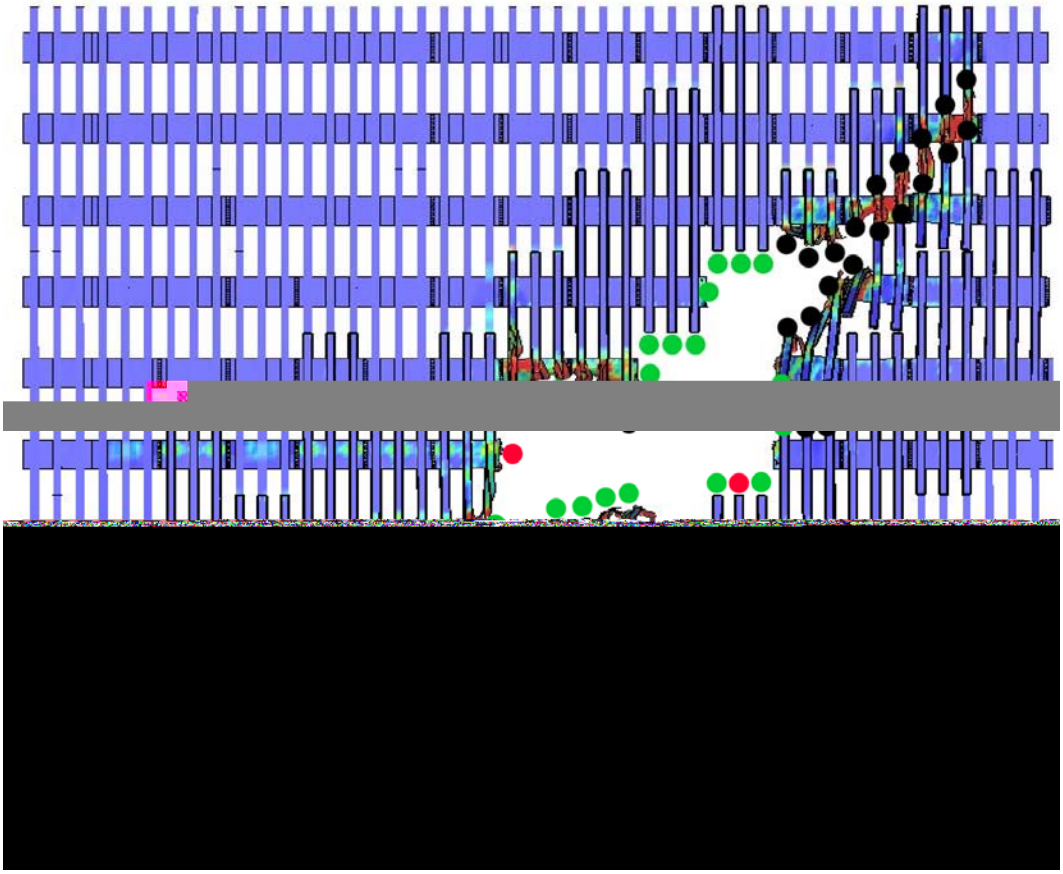

Figure 5–2. Validation of Aircraft Impact Analysis Prediction With Observations for WTC 2 South Exterior Wall Damage.

5.2.1 Core Column Damage

The damage predicted by the impact simulations was classified into four levels as shown graphically in Figure 5–3 (the colors represent plastic strain magnitude with undamaged sections in blue and strains at or above 5 percent shown in red). The classification levels were *light damage*, *moderate damage*, *heavy damage*, and *failed* (or severed). The light damage level had low level plastic strains but no significant structural deformations. The moderate damage level had visible local deformations of the column cross section (e.g. local flange bending) but without lateral displacements of the column centerline. The heavy damage level had significant global deformations that resulted in a permanent deflection of the column centerline. The failed columns were completely severed and could not carry any load. For details, refer to NIST NCSTAR 1-2.

The column damage criteria were applied to the aircraft impact analysis results. Tables 5–1 to 5–4 show the column damage classifications obtained from each analysis. Refer to Fig. 4–7 for core column numbering. Figure 4–7 shows the WTC 1 column layout with the 100 series exterior columns on the north side; WTC 2 column layout is the same except that the 200 series exterior columns face north. WTC 1 was estimated to have 3 severed core columns and 4 heavily damaged columns for Case A, and 6 severed core columns and 3 heavily damaged columns for Case B. The WTC 1 severed and heavily damaged columns were located at the center of the north side of the core. WTC 2 was estimated to have

5 severed core columns and 4 heavily damaged columns for Case C, and 10 severed core columns and a heavily damaged column for Case D. The WTC 2 severed and heavily damaged columns were located at the southeast corner of the core. The core column damage was used in the major subsystem and global analyses for each tower. The misalignment of the heavily damaged columns dramatically reduced their load carrying capacity. In the structural models described in this report, elements corresponding to the heavily damaged and severed columns were removed, while those corresponding to moderately or lightly damaged columns were retained without modifications.

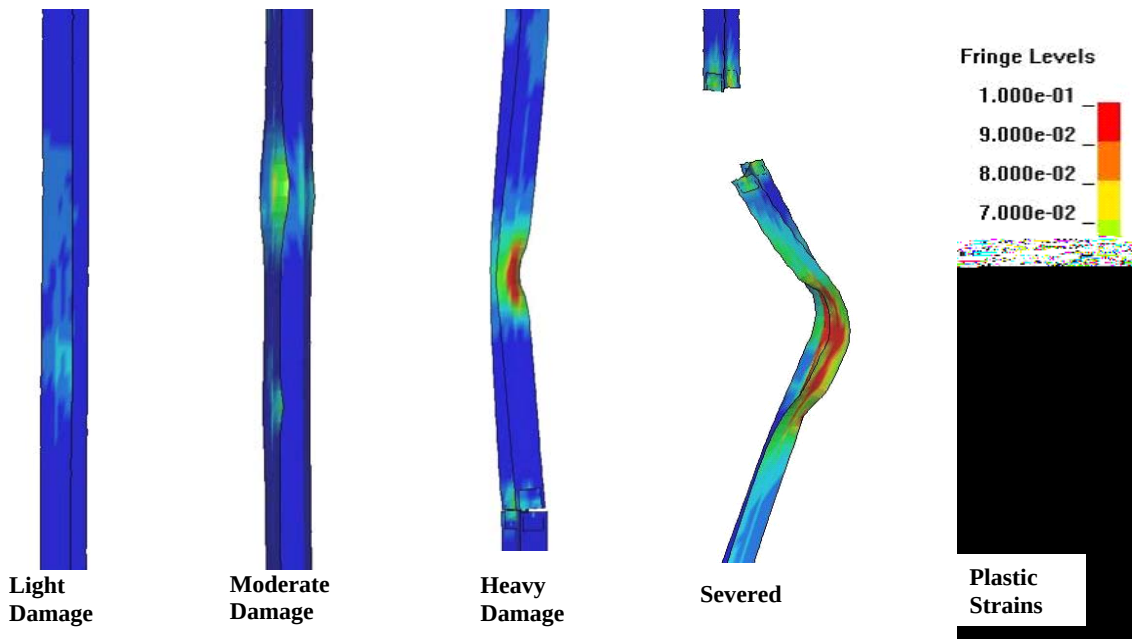

Figure 5–3. Core column damage levels.

Table 5–1. WTC 1 Case A core column damage.

Column	Location	Damage Level	Lateral Deflection of Column Centerline (in.)
Column 503	Floor 96	**Heavy**	18
Column 504	Floors 92-96	**Severed**	
Column 505	Floors 93-96	**Heavy**	20
Column 506	Floors 93-94	**Heavy**	10
Column 604	Floors 92-96	**Severed**	
Column 605	Floors 94-95	Moderate	
Column 702	Floor 96	Moderate	
Column 703	Floor 96	Moderate	
Column 704	Floor 94	**Heavy**	18
Column 705	Floor 95	Moderate	
Column 706	Floors 93-95	**Severed**	
Column 802	Floor 96	Moderate	
Column 805	Floor 94	Moderate	

Table 5–2. WTC 1 Case B core column damage.

Column	Location	Damage Level	Lateral Deflection of Column Centerline (in.)
Column 503	Floor 95-96	**Severed**	
Column 504	Floors 92-96	**Severed**	
Column 505	Floors 93-96	**Severed**	
Column 506	Floors 93-95	**Heavy**	24
Column 603	Floors 96-97	Moderate	
Column 604	Floors 92-96	**Severed**	
Column 605	Floors 94-95	Moderate	
Column 606	Floors 94	Light	
Column 702	Floor 97	Light	
Column 703	Floor 96	Moderate	
Column 704	Floors 92-96	**Severed**	
Column 705	Floor 95	Moderate	
Column 706	Floors 93-95	**Severed**	
Column 802	Floor 96	Light	
Column 803	Floors 96-97	Moderate	
Column 804	Floor 94-96	Moderate	
Column 805	Floors 93-95	**Heavy**	20
Column 903	Floor 96	Light	
Column 904	Floors 95-96	**Heavy**	19
Column 905	Floor 95	Light	

Table 5–3. WTC 2 Case C core column damage.

Column	Location	Damage Level	Lateral Deflection of Column Centerline (in.)
Column 801	Floor 79	**Heavy**	10
Column 901	Floors 79-82	**Severed**	
Column 902	Floor 79	**Heavy**	32
Column 903	Floors 77-83	**Severed**	
Column 904	Floor 79	Moderate	
Column 905	Floor 79	**Heavy**	18
Column 1001	Floors 77-83	**Severed**	
Column 1002	Floors 79-81	**Severed**	
Column 1003	Floor 80	**Severed**	
Column 1004	Floor 80	**Heavy**	18

Table 5–4. WTC 2 Case D core column damage.

Column	Location	Damage Level	Lateral Deflection of Column Centerline (in.)
Column 602	Floor 79	Moderate	
Column 605	Floor 79	Moderate	
Column 701	Floors 79-80	**Severed**	
Column 702	Floor 79	**Heavy**	16
Column 703	Floor 79	Moderate	
Column 704	Floor 79	Light	
Column 705	Floors 78-79	Light	
Column 705	Floor 78	Light	
Column 801	Floors 79-80	**Severed**	
Column 802	Floors 77-80	**Severed**	
Column 803	Floors 77-80	**Severed**	
Column 804	Floor 79	Light	
Column 901	Floors 80-81	**Severed**	
Column 902	Floor 79	Moderate	
Column 903	Floors 77-83	**Severed**	
Column 904	Floors 79-81	Moderate	
Column 905	Floors 79 & 81	Light	
Column 907	Floor 81	Light	
Column 1001	Floors 77-83	**Severed**	
Column 1002	Floors 79-83	**Severed**	
Column 1003	Floors 79-83	**Severed**	
Column 1004	Floors 79-83	**Severed**	
Column 1005	Floors 79-81	Moderate	

5.2.2 Structural Damage to Floor Slabs, Core Beams, and Floor Trusses

Two types of floor damage were identified from the impact analysis results: (1) missing floor areas and (2) severely damaged floor areas incapable of supporting loads. Figure 5–4 illustrates the floor damage computed by the aircraft impact analysis, with WTC 1 Structural Floor 95 Case A as an example. The damage to floor framing (i.e., trusses and beams) ranged from being severed and bent out of alignment to having localized damage to a component of the framing. Concrete slab damage ranged from crushed areas (failure of both concrete slab and metal decking) to permanent plastic strains (failure of concrete slab, but not metal decking). The concrete slab was failed in the red regions shown in Figure 5–4(c), which indicated a 2 percent plastic strain or greater. At these strain levels, the concrete slab was assumed to be severely damaged and likely exposed the supporting metal decking.

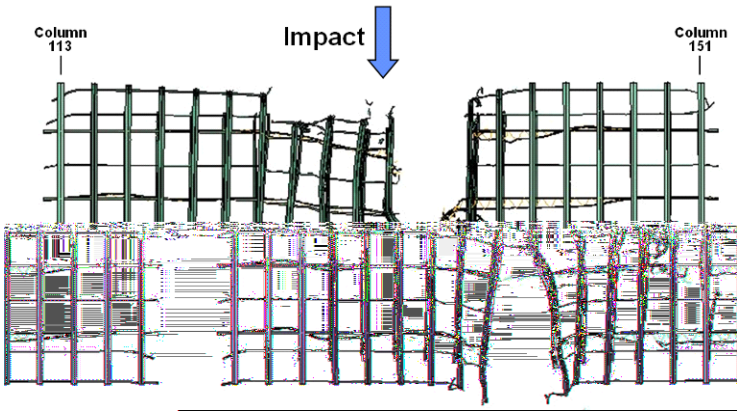

a. Floor trusses

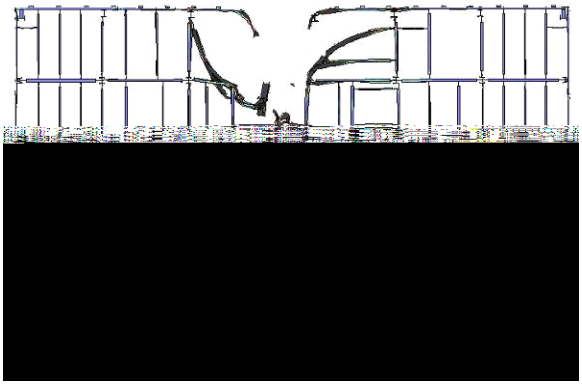

b. Core floor beams

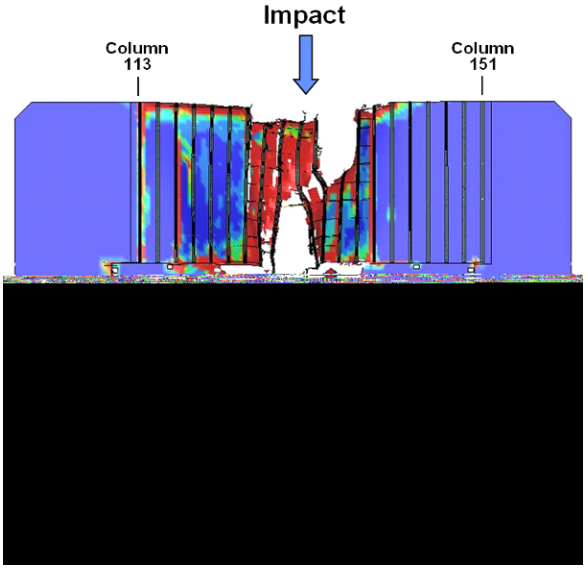

c. Floor slab

Figure 5–4. Impact damage to WTC 1 Floor 95 for Case A (plan view).

For the fire dynamics analysis, missing floor areas were important since they created new ventilation paths between floors. Ventilation is a critical parameter for fire growth and spread. For the structural analyses, floor areas were removed where the intended structural function of the floor was severely impaired or no longer available. For instance, if truss end connections were severed, the floor framing could not transfer its loads to the column at that point. The condition of the concrete slab was also important as the concrete slab and floor framing were designed to act compositely. Severe damage to the concrete over more than half of a truss or a beam length was considered to cause a severely impaired floor area.

Figure 5–5 shows an example of how the damage in Figure 5–4 was evaluated and summarized for the structural analysis. Areas with severed floor framing and crushed concrete (indicated by red zones) were outlined with a dashed line, indicating where floor areas were to be removed or considered missing. Areas with misaligned framing or loss of composite action with the slab (due to damaged concrete) over more than half the member length were marked with green shading as damaged floor areas. In this example, the dashed outline and green overlay cover nearly the same area, though this is not generally the case for all floors. For analysis purposes, only severe damage was considered; isolated member damage or small areas of concrete damage were ignored as they were considered localized damage. Damage ranges in Figure 5–5 were delineated by boxed areas as there was insufficient data to develop criteria for irregular boundaries.

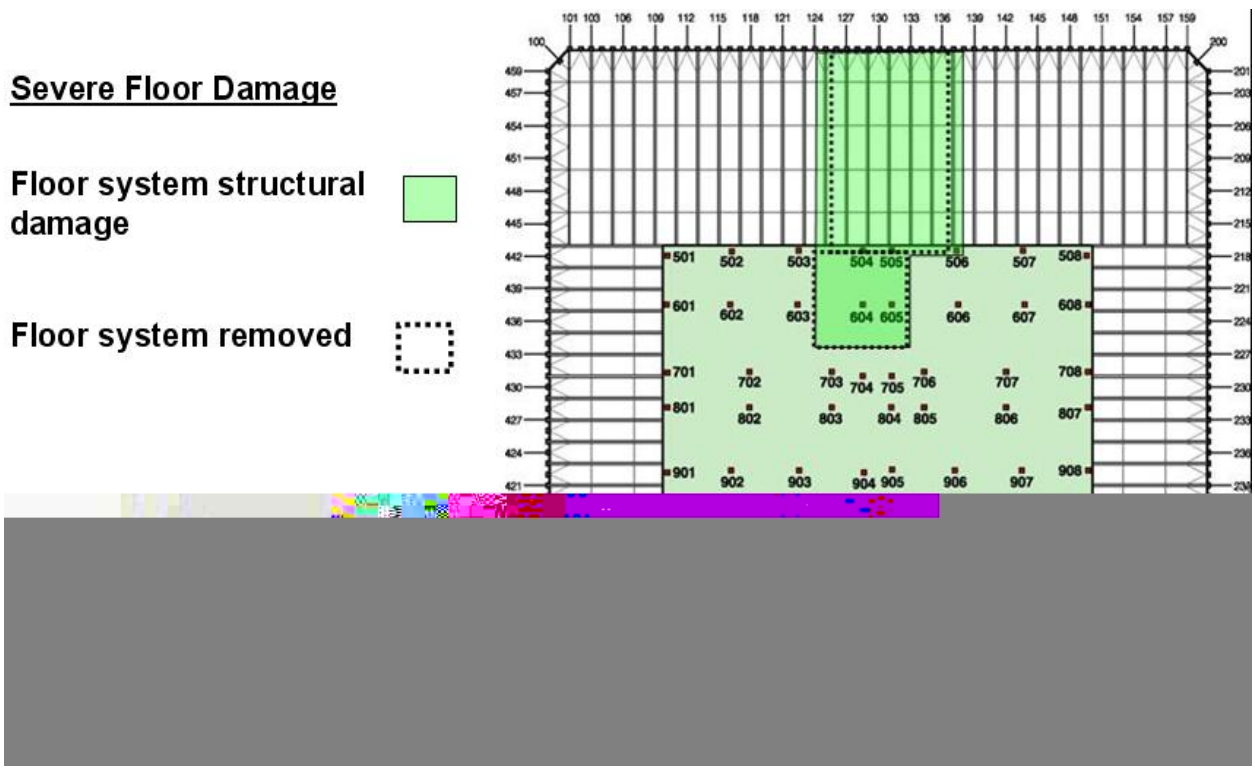

Figure 5–5. Damage to WTC 1 Floor 95 framing and slab for Case A.

5.2.3 Damage to Fire Protection for Structural Steel

The aircraft impact simulation models included not only the structural components of the towers and aircraft, but also representations of the partition walls and building contents and furnishings (modular office workstations). The results of the analyses included damage to the partition walls, workstations, and structural elements. Such damage estimates were crucial for the estimation of areas with dislodged insulation as explained in this section.

Estimates of the post-impact condition of the fire protection was based on criteria that considered damage to structural components, building partitions, and furnishings along with the debris field as calculated from the aircraft impact analyses. Estimates for the extent of dislodged insulation considered insulation damage to structural components only in the direct path of debris, as follows:

- Core columns had sprayed fire-resistant material (SFRM), gypsum wallboard enclosures, or a combination of both. Insulation was assumed to be dislodged from the columns if they were subject to direct debris impact that could fail wall partitions in the immediate vicinity. The representative bending strength of building partitions in the impact simulations was 500 psi (NIST NCSTAR 1-2), while the representative adhesive and cohesive strength of SFRM measured in the laboratory by NIST was generally less than 12 psi (NIST NCSTAR 1-6A). Gypsum column enclosures were also assumed to have a lesser representative strength than wall partitions.

  To consider that insulation on core columns was damaged, the predicted debris impact had to be sufficient to fail building partitions immediately in front of the columns. If the wall partitions remained intact in the core area after interaction with the debris field, then the insulation on core columns behind these partitions was assumed to remain intact. If wall partitions were damaged or destroyed by the debris field, then insulation on core columns behind these partitions was assumed to be dislodged over that floor height.

- To consider that insulation on exterior columns was damaged, the debris impact had to damage or destroy office furnishings (modular office workstations) adjacent to the columns. If the office furnishings remained intact after interaction with the debris field, then the insulation on the inside face of the exterior columns behind these furnishings was assumed to remain intact. If the room furnishings were damaged or destroyed after interaction with the debris field, then the insulation on the inside face of the exterior columns in the same vicinity was assumed to be dislodged over that floor height. The other three faces of the exterior columns were protected by the windows and/or aluminum cladding and were assumed to have no insulation damage.

- To consider that SFRM on floor trusses was damaged, the debris impact had to be sufficient to damage or destroy room furnishings (modular office workstations) in the same area of the affected floor. If the room furnishings remained intact, then the insulation on the steel trusses above these furnishings was assumed to remain intact. If the room furnishings were damaged or destroyed by the debris field, then the insulation on the steel trusses above these furnishings was assumed to be dislodged.

The insulation damage estimates were conservative as they ignored possibly damaged and dislodged insulation in a much larger region that was not in the direct path of the debris but was subject to strong

vibrations during and after the aircraft impact. A robust criteria to generate a coherent pattern of vibration-induced dislodging could not be established due to (1) the numerical noise inherent in the acceleration time-histories on structural components obtained from the aircraft impact analyses, and (2) lack of data on the strength of insulation materials under such a high rate of loading with sharp peaks in a very short duration. However, there were indications that insulation damage occurred over a larger region than that estimated. Photographic evidence showed insulation dislodged from exterior columns not directly impacted by debris (NIST NCSTAR 1-3C). The towers underwent a period of strong impact loading for about 0.6 to 0.7 s. Further, video analysis showed that WTC 2 vibrated for over 4 minutes after aircraft impact with amplitudes in excess of 20 inches at the roof top (NIST NCSTAR 1-5A). First-person interviews of building occupants indicated that building vibrations due to aircraft impact were strong enough to dislodge ceiling tiles and collapse walls throughout the height of both WTC towers and to cause nearly all elevators to stop functioning (NIST NCSTAR 1-7). Due to lack of experimental data, estimates of insulation damage ignored the possibility that the impact of jet fuel might also result in dislodging insulation. The global structural analyses used to determine the probable collapse sequence included some variation in the extent of dislodged insulation.

Figure 5–6 shows an elevation view of WTC 1 during the aircraft impact for Case B. As impact debris traveled across multiple floors, it tended to fill the space between the two floor slabs. Figure 5–7 shows more detail with specific damage to framing, partitions, and furnishings on Floor 95. The floor-to-floor dispersal pattern led to the assumption that when the insulation was dislodged from direct debris impact, it was dislodged over the full floor height. This assumption was consistent with the level of modeling detail (i.e. insulation was not included in the aircraft impact model) and with expected thermal behavior of a steel component if substantial portions of the insulation were removed.

As an example, Figs. 5–8 and 5–9 show plan views of WTC 1 Floor 95 for Case B impact damage. Figure 5–8 shows the location of floor furnishings and partitions prior to impact. The extent of furnishings and partitions in the impact models was limited to areas where interaction with the aircraft was expected due to computational limits on the number of nodes and elements in the model. Figure 5–9 shows the extent of damage to Floor 95. The area of dislodged insulation for columns and floor framing between floor slabs 95 and 96 is indicated by the shaded overlay. Where partition walls and furnishings remained intact, the insulation was also assumed to remain intact. Where the debris extended to the exterior wall, the insulation on the inside surface of the exterior columns and spandrels was assumed to be dislodged over the full floor height.

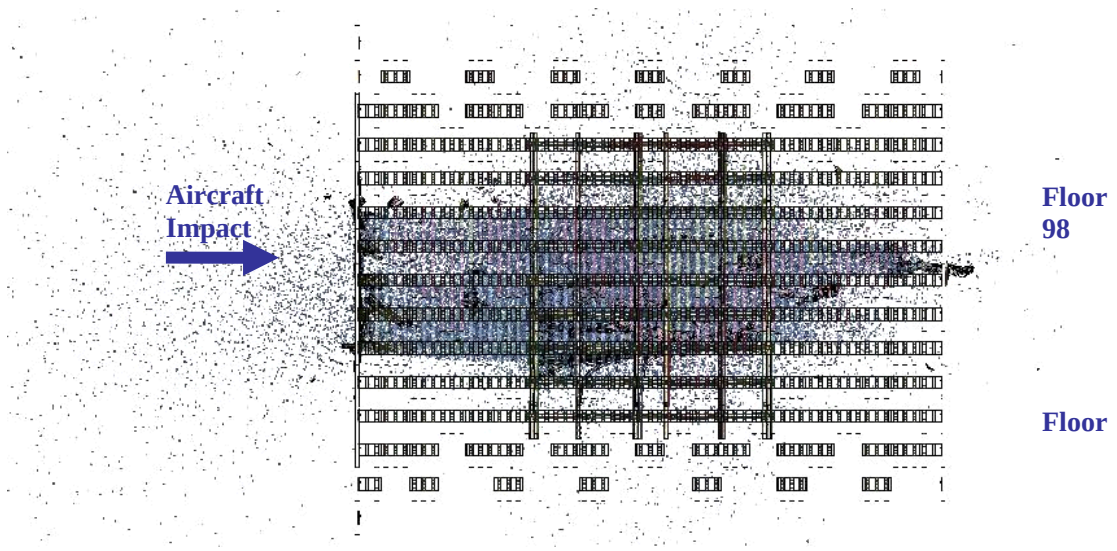

Figure 5–6. Debris and fuel field in WTC 1 Case B analysis of aircraft impact.

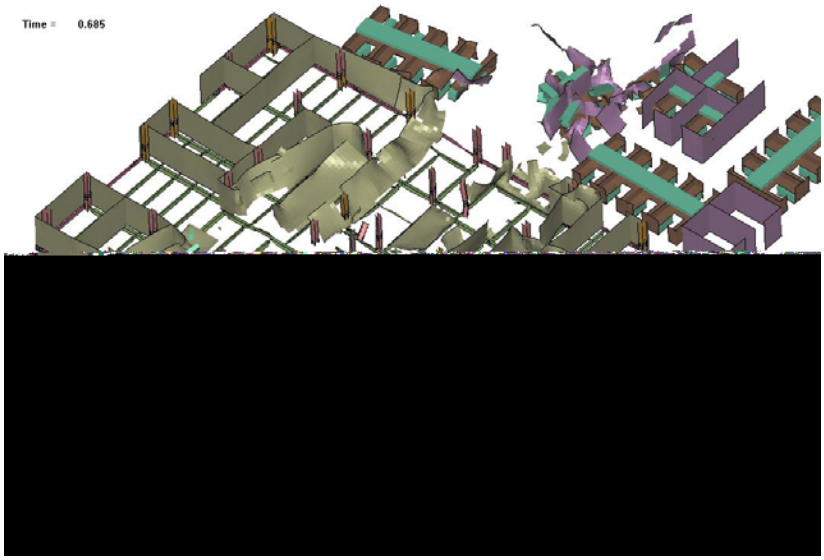

Figure 5–7. WTC 1 Case B aircraft impact damage to framing, partitions, and furnishings on Floor 95.

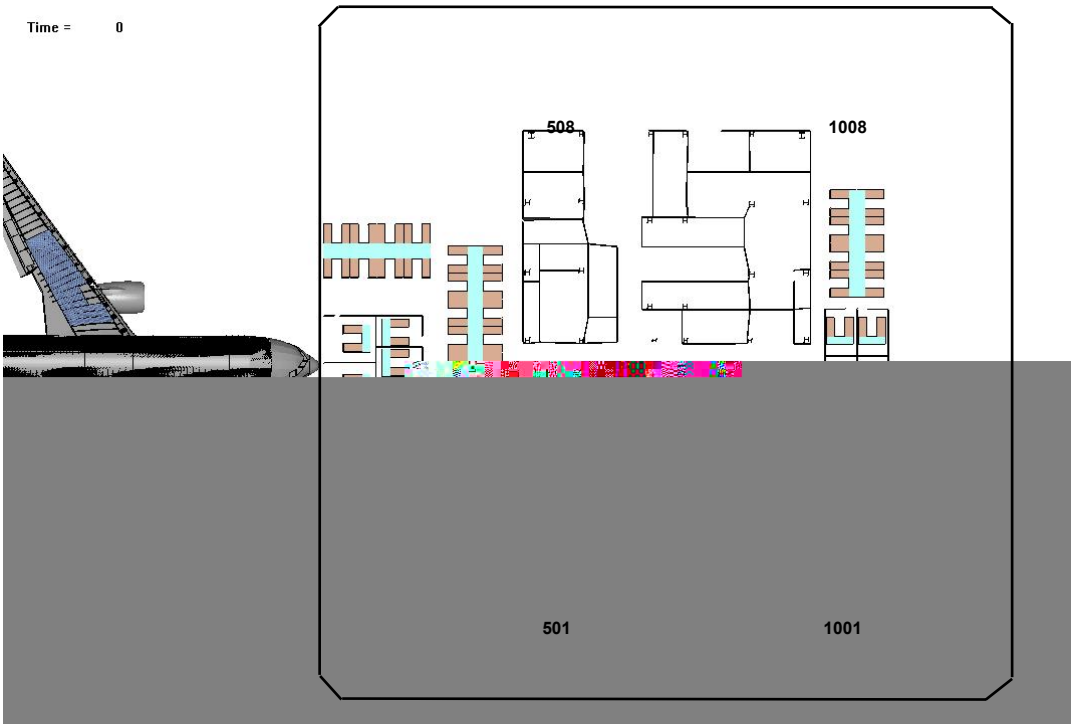

Figure 5–8. WTC 1 Case B Floor 95 partitions and furnishings layout prior to impact (layout provided in model only where interaction with aircraft was expected).

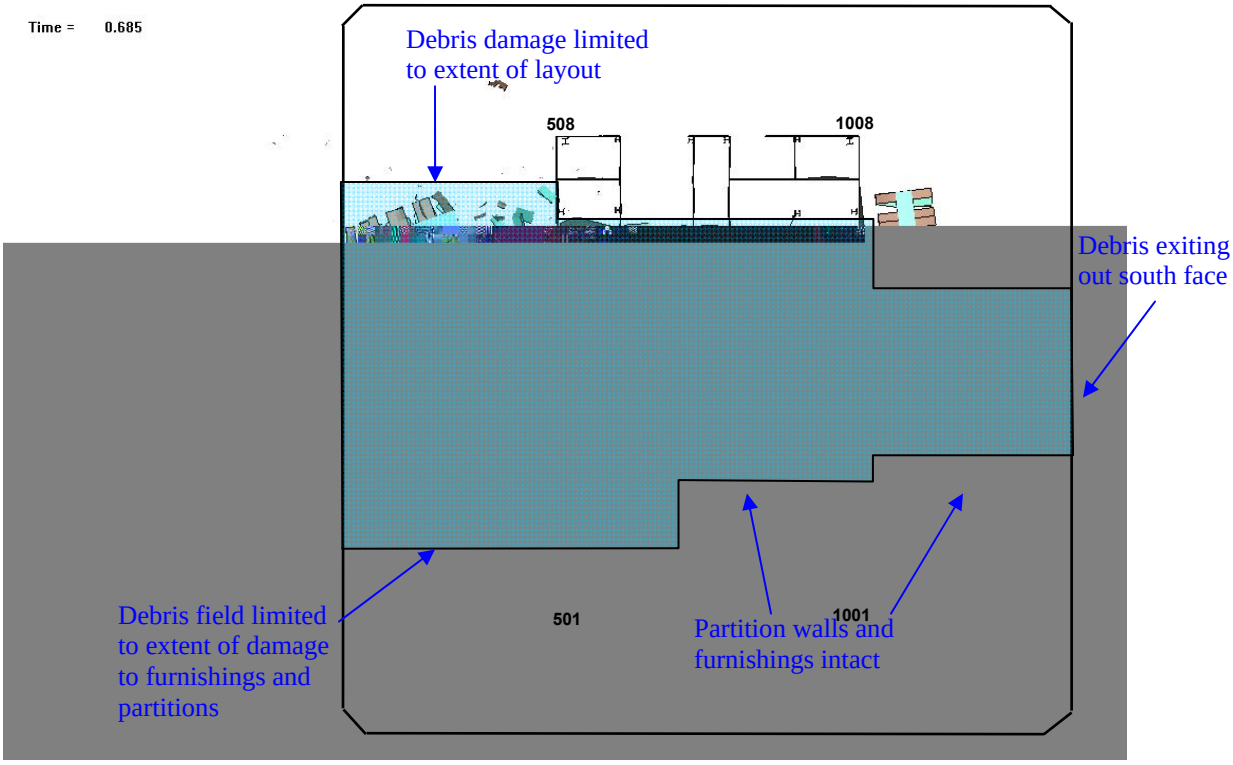

Figure 5–9. WTC 1 Case B Floor 95 partitions and furnishings layout after impact with overlay showing extent of dislodged insulation from direct debris impact.

5.2.4 Summary of Aircraft Impact Damage

The use of the aircraft impact results by the fire dynamics, thermal, and structural analyses required presentation of debris damage data in two formats, referred to here as 'occupancy floor' and 'structural floor' formats. Figure 5–10 illustrates the terms occupancy floor (e.g. the elevator floor number) and structural floor. Damage to columns, partitions, and insulation between floor slabs are presented in the occupancy floor format, as shown in Fig. 5–11. Structural damage to the composite floor (i.e. truss, beams, and floor slab) is presented in the structural floor format, as shown in Fig. 5–12. The aircraft impact, thermal, and structural analyses used both formats. The fire dynamics analyses used the occupancy floor format, as the floor slabs provided natural boundaries for fire.

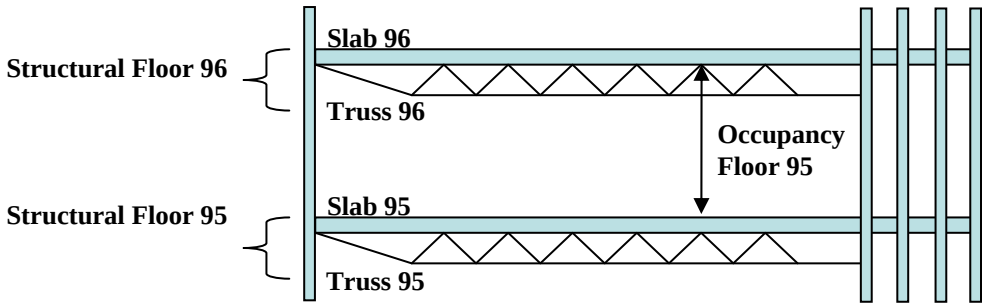

Figure 5–10. Definition of structural floor and occupancy floor.

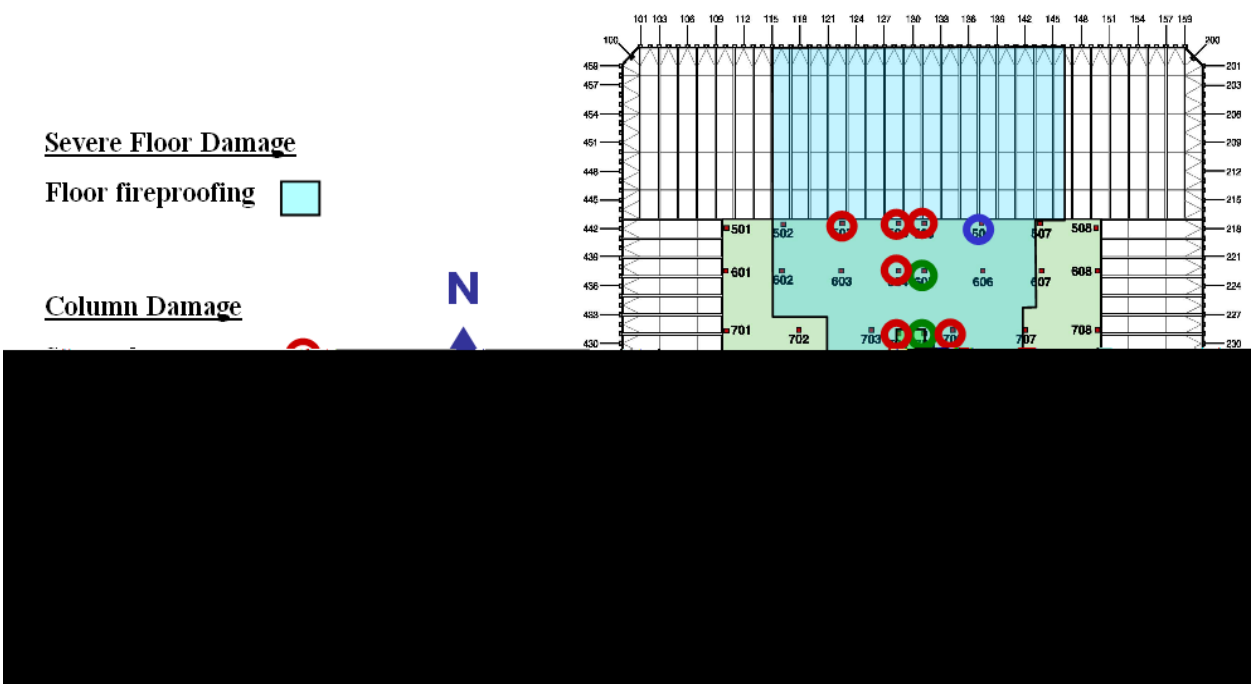

Figure 5-11. Plan view of WTC 1 Case B insulation and column damage for Occupancy Floor 95.

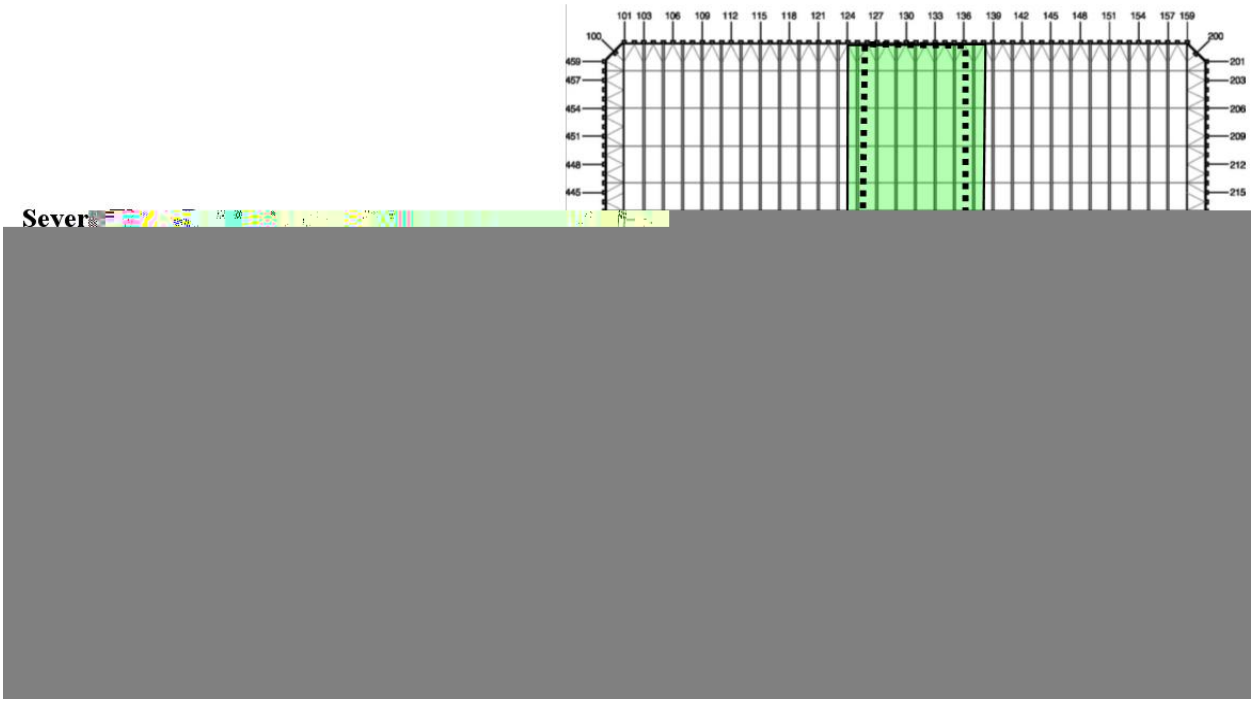

Figure 5-12. Plan view of WTC 1 Case B damage to Structural Floors 95.

5.3 STRUCTURAL AND FIRE PROTECTION DAMAGE TO WTC 1

This section presents summary graphics of structural and fire protection damage that were developed using results of the aircraft impact simulations. Figures 5–13 and 5–16 show plan views of the cumulative damage over Floors 93 to 99 for Case A and Case B, respectively. The impact damage at each floor level is shown in Figures 5–14 and 5–15 for Case A and 5–17 and 5–18 for Case B with occupancy and structural formats. The damage graphics for Cases A and B are also presented at a larger scale in Appendix B.

The structural damage in WTC 1 extended from the north exterior wall, through the central region of the north floor area and through to the south side of the core. An exterior panel was knocked out of the south wall by aircraft debris. Damage to the insulation from direct debris impact extended over a larger region and included most of the north floor areas, the core, and central regions of the south floor areas. Case B predicted more damage to core columns and a larger extent of insulation damage to the south floor area than Case A, including damage to the south exterior wall insulation on the inside face.

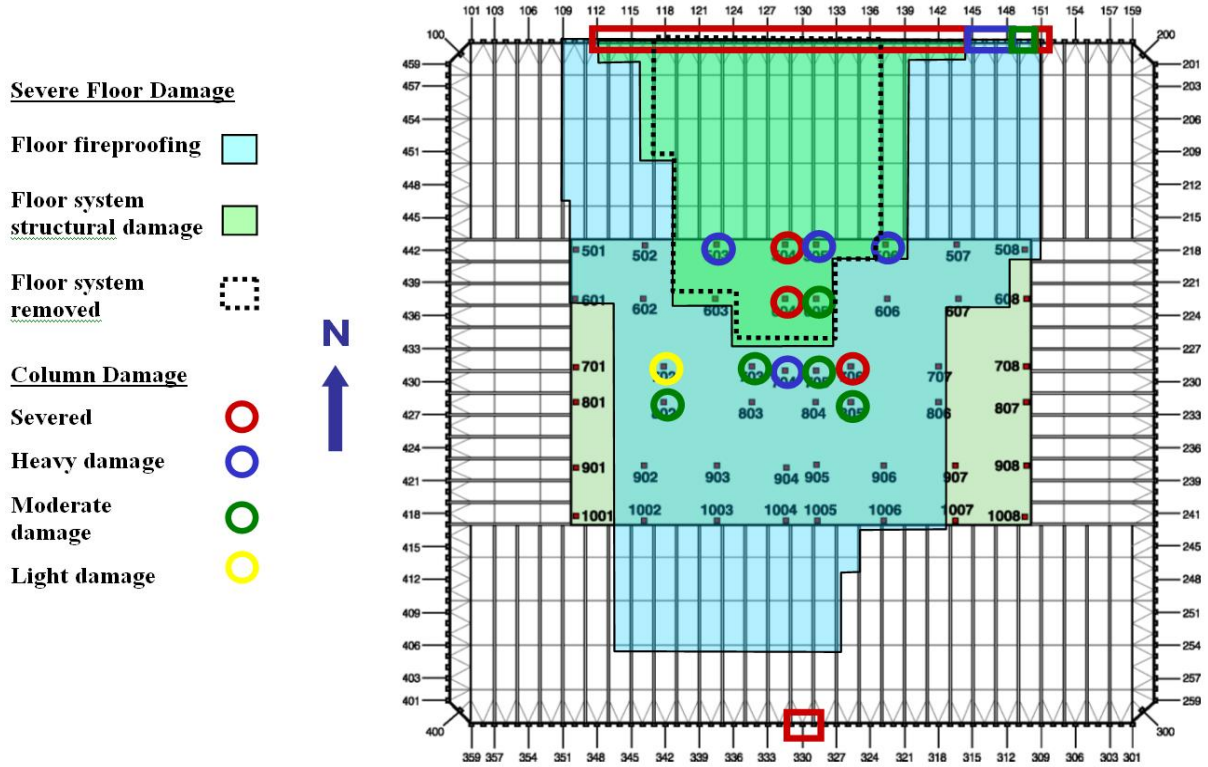

Figure 5–13. Plan view of WTC 1 Case A cumulative damage for Floors 93 to 98.

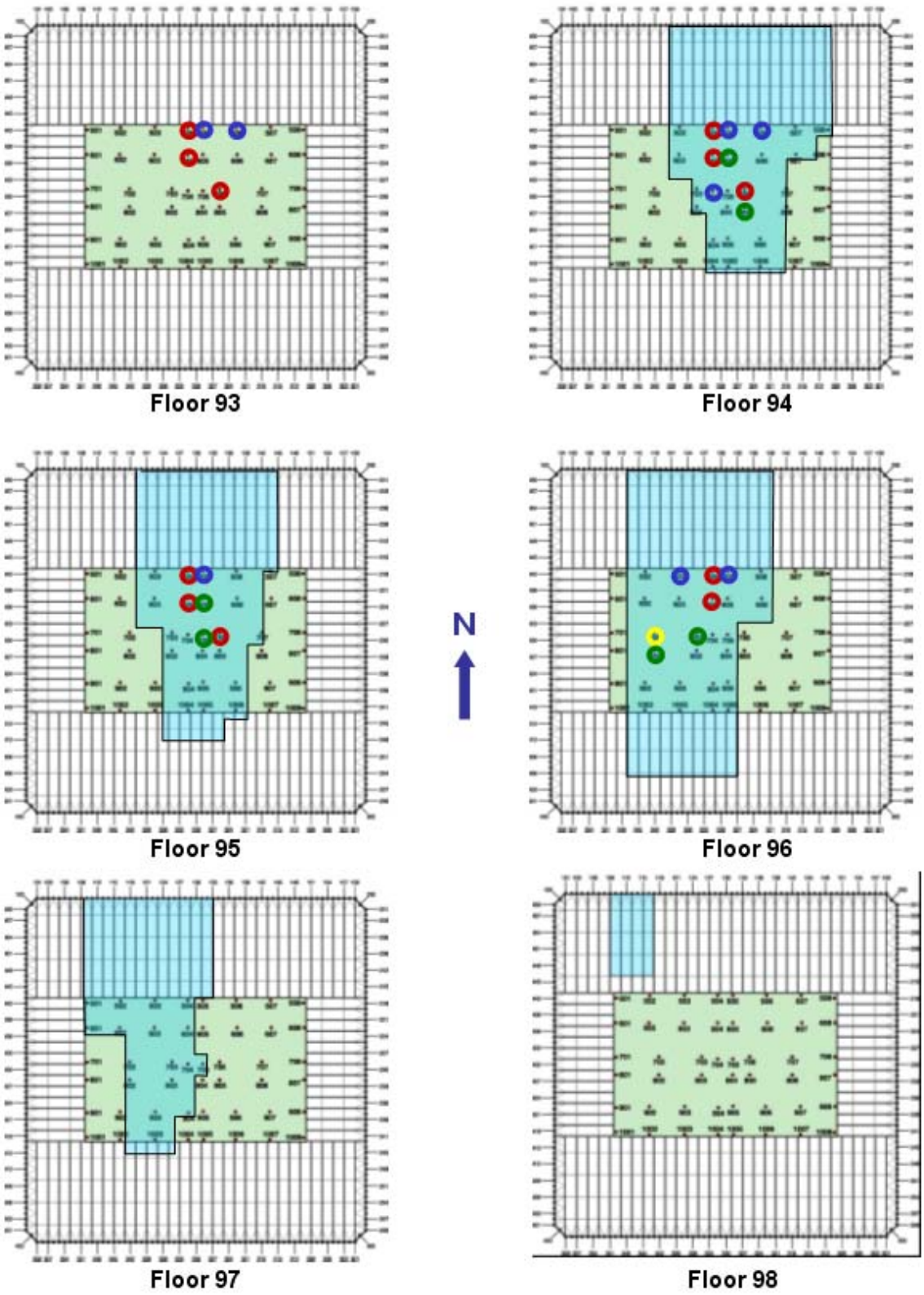

Figure 5–14. Plan view of WTC 1 Case A insulation and column damage to Occupancy Floors 93 to 98.

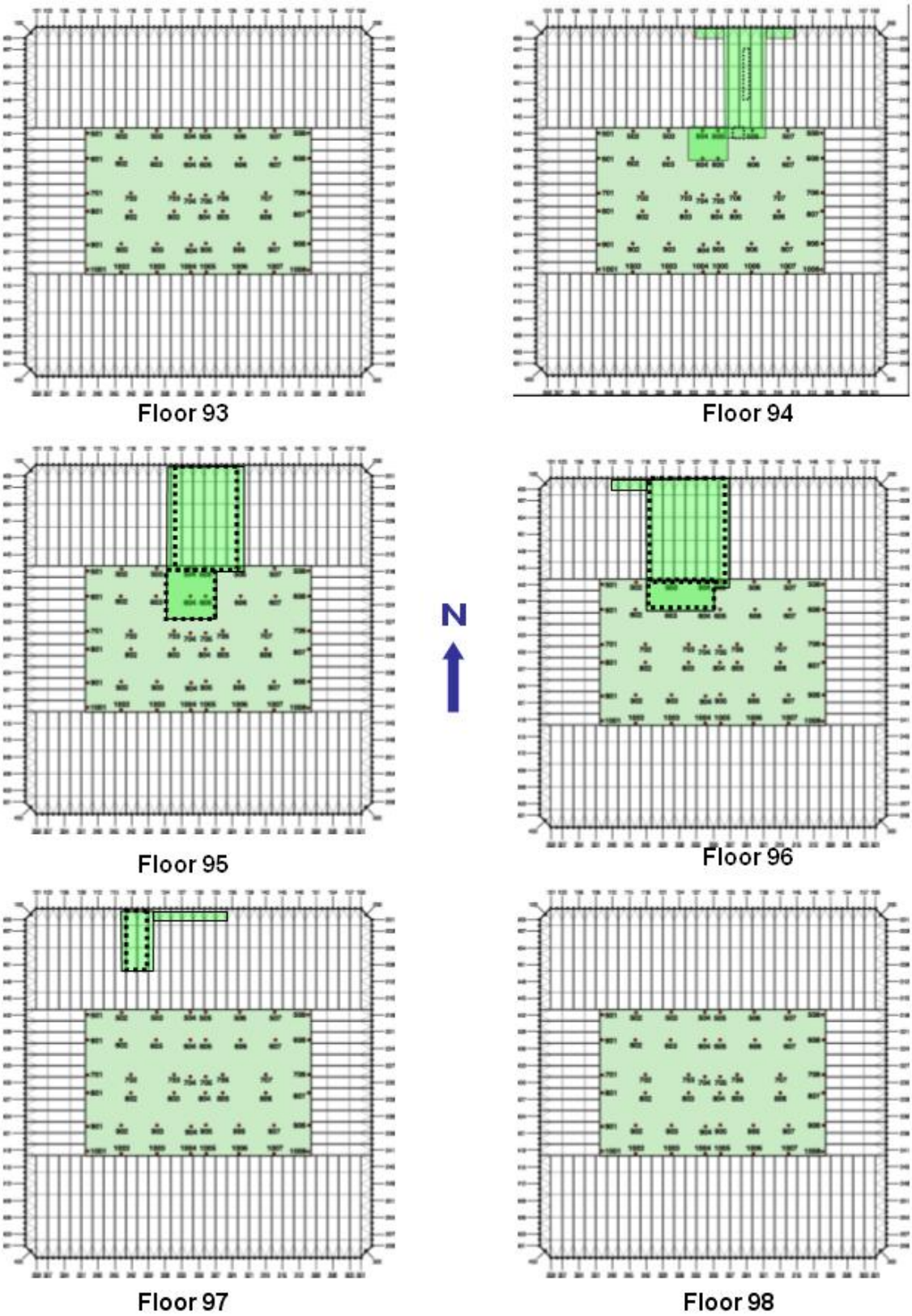

Figure 5–15. Plan view of WTC 1 Case A damage to Structural Floors 93 to 98.

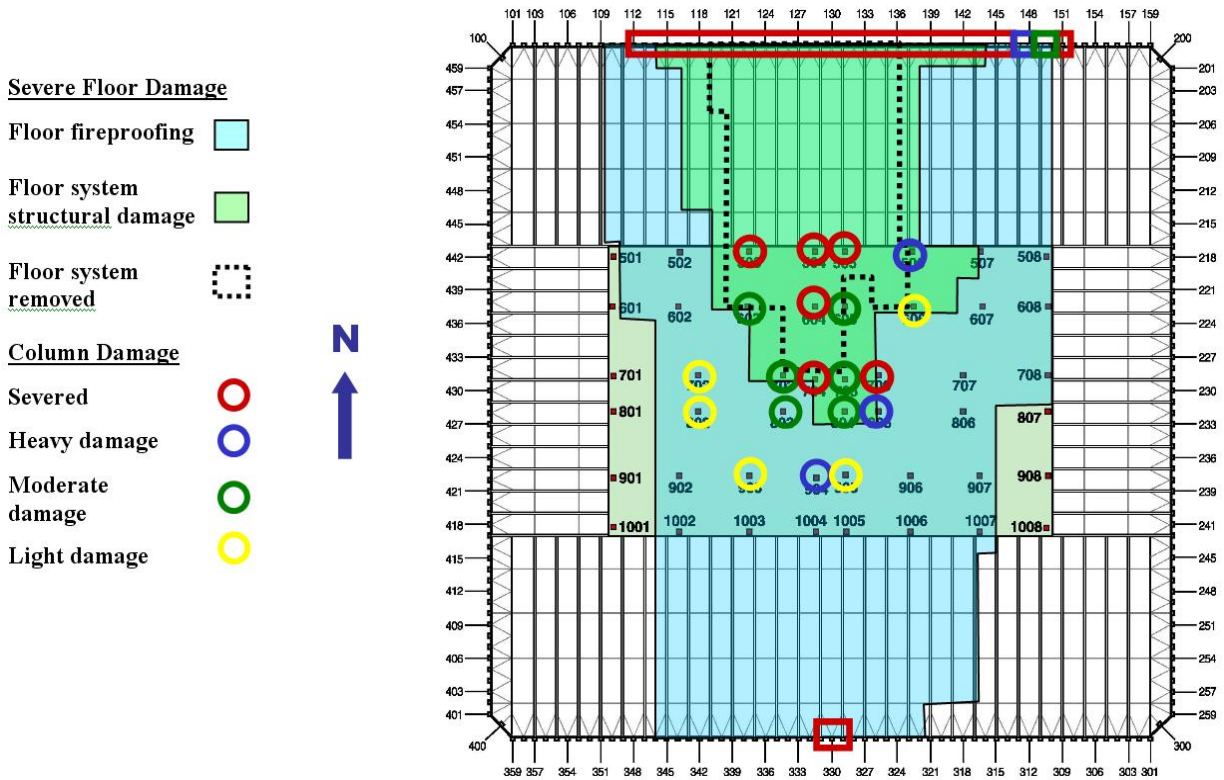

Figure 5–16. Plan view of WTC 1 Case B cumulative damage from Floors 93 to 98.

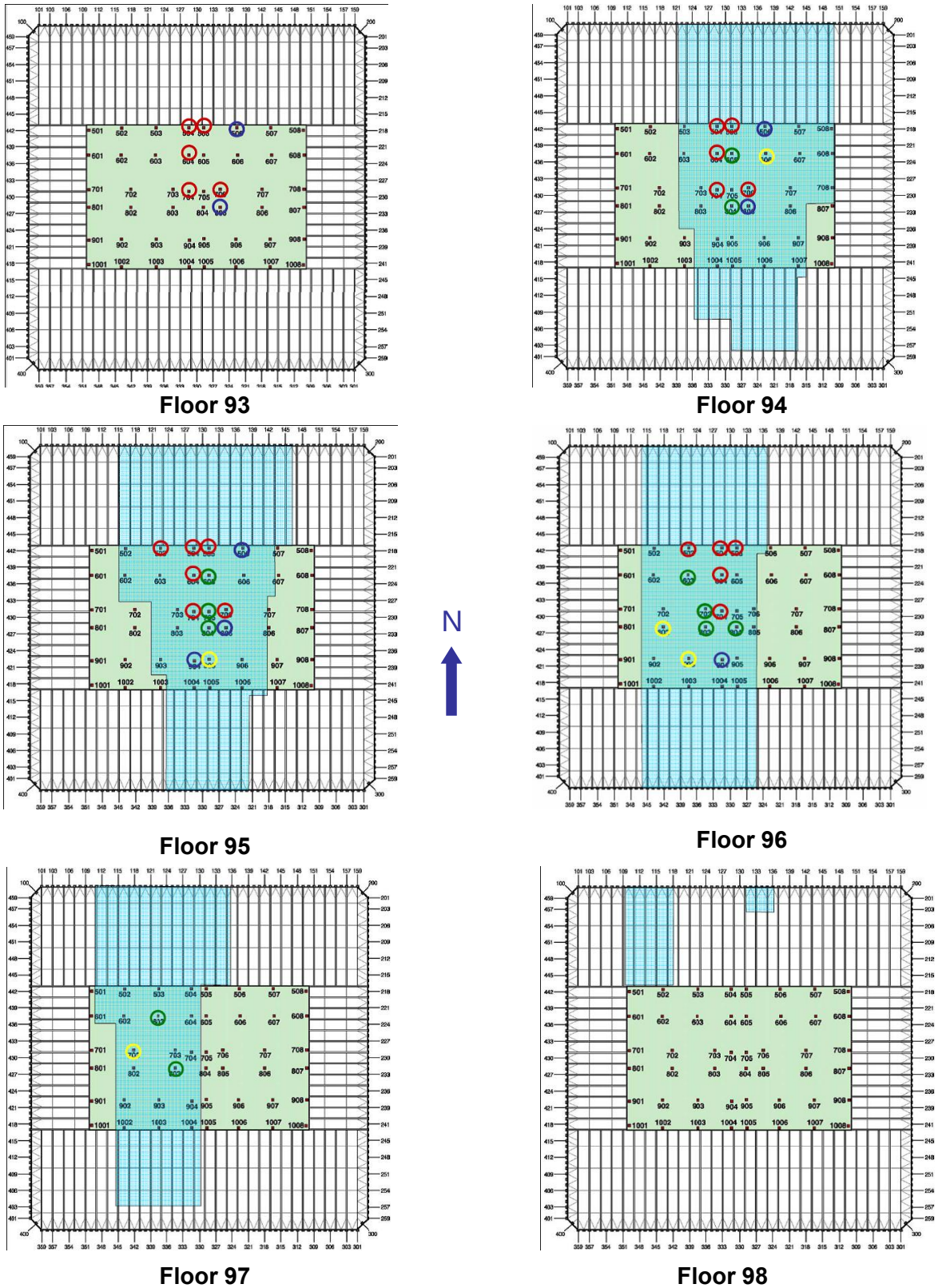

Figure 5–17. Plan view of WTC 1 Case B insulation and column damage to Occupancy Floors 93 to 98.

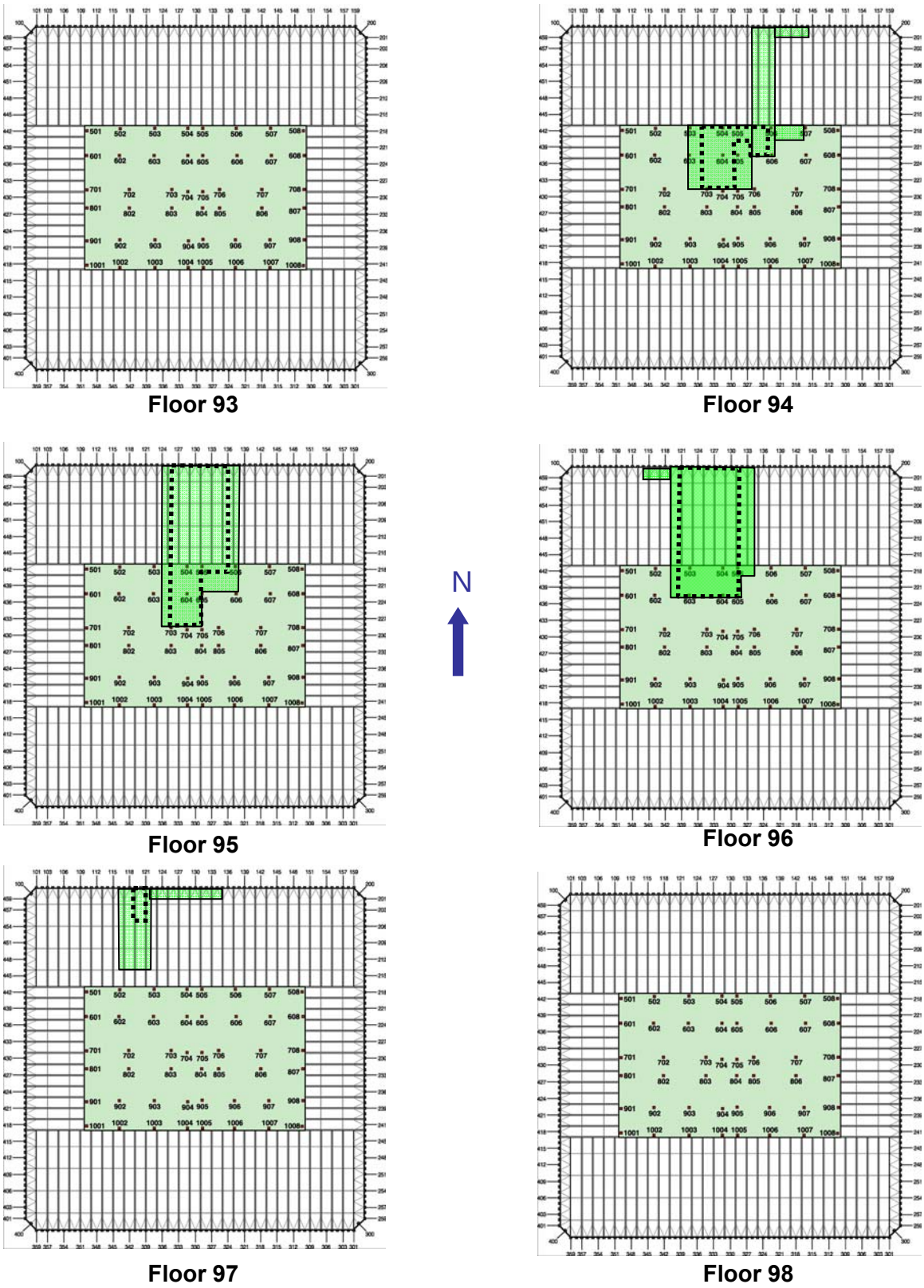

Figure 5–18. Plan view of WTC 1 Case B damage to Structural Floors 93 to 98.

5.4 STRUCTURAL AND FIRE PROTECTION DAMAGE TO WTC 2

This section presents summary graphics of structural and insulation damage that were developed using results of the aircraft impact simulations. Figures 5–19 and 5–22 show plan views of the cumulative damage over floors 78 to 84 for Case C and Case D, respectively. The impact damage at each floor level is shown in Figures 5–20 and 5–21 for Case C and 5–23 and 5–24 for Case D with occupancy and structural formats. The damage graphics for Cases C and D are also presented at a larger scale in Appendix B.

The structural damage in WTC 2 extended from the south exterior wall, through the south and east floor areas and the southeast region of the core, to the north side of the east floor area. Exterior columns were severed by debris near the northeast corner. Damage to the insulation from direct debris impact extended over a larger region, and included the south floor area, the central and east regions of the core, and most of the east floor area. Case D predicted more damage to core columns than Case A, but the extent of the insulation damage was similar.

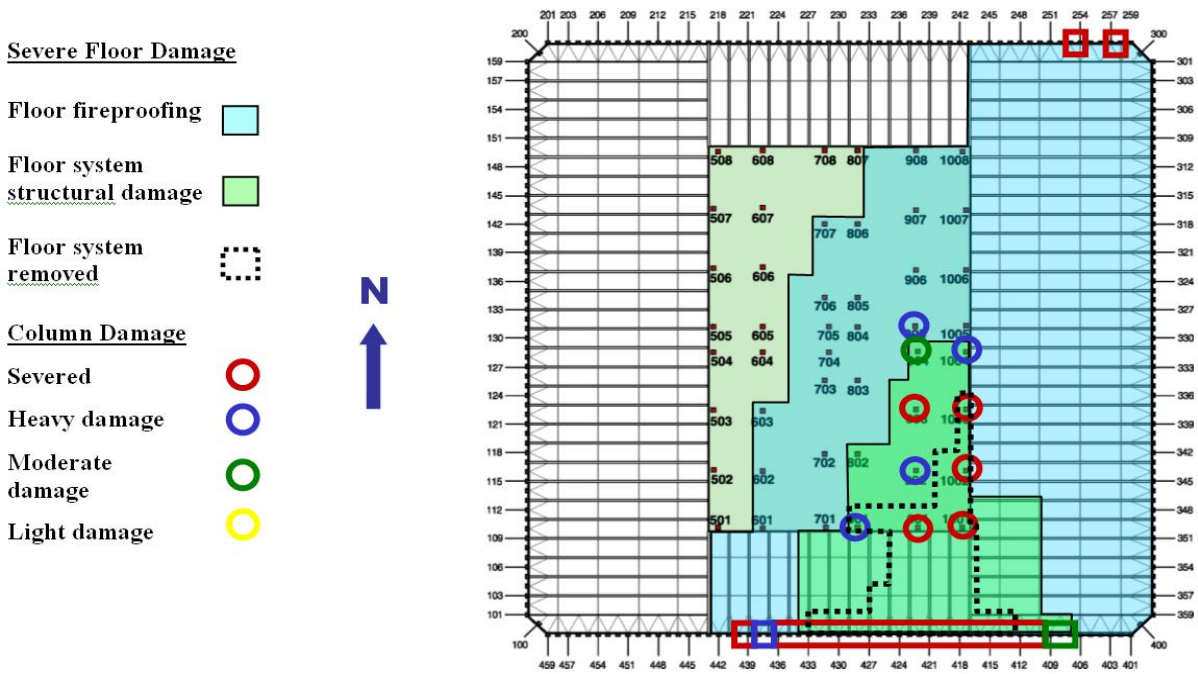

Figure 5–19. Plan view of WTC 2 Case C cumulative damage from Floors 78 to 83.

Figure 5–20. Plan view of WTC 2 Case C insulation and column damage to Occupancy Floors 78 to 83.

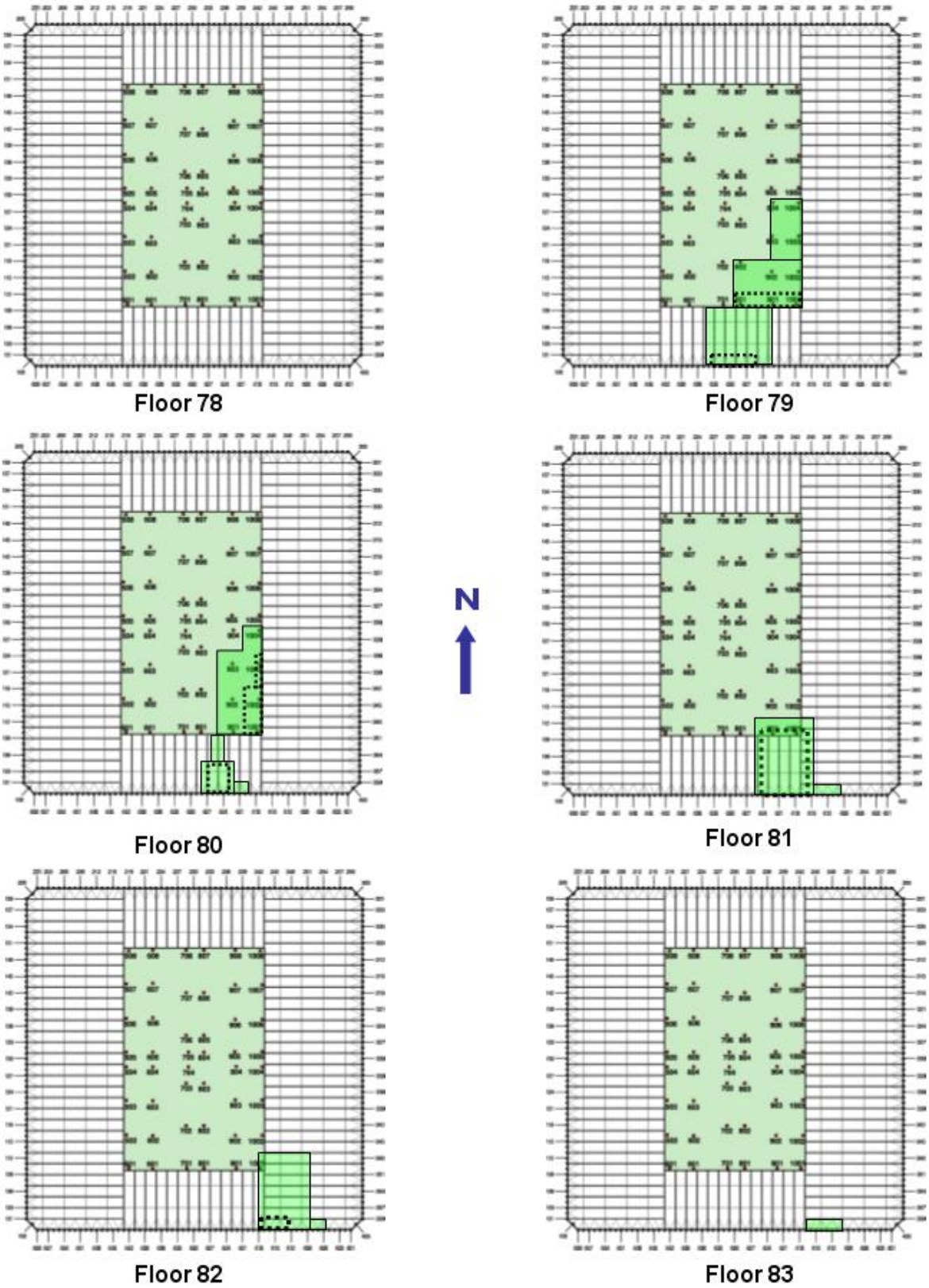

Figure 5–21. Plan view of WTC 2 Case C damage to Structural Floors 78 to 83.

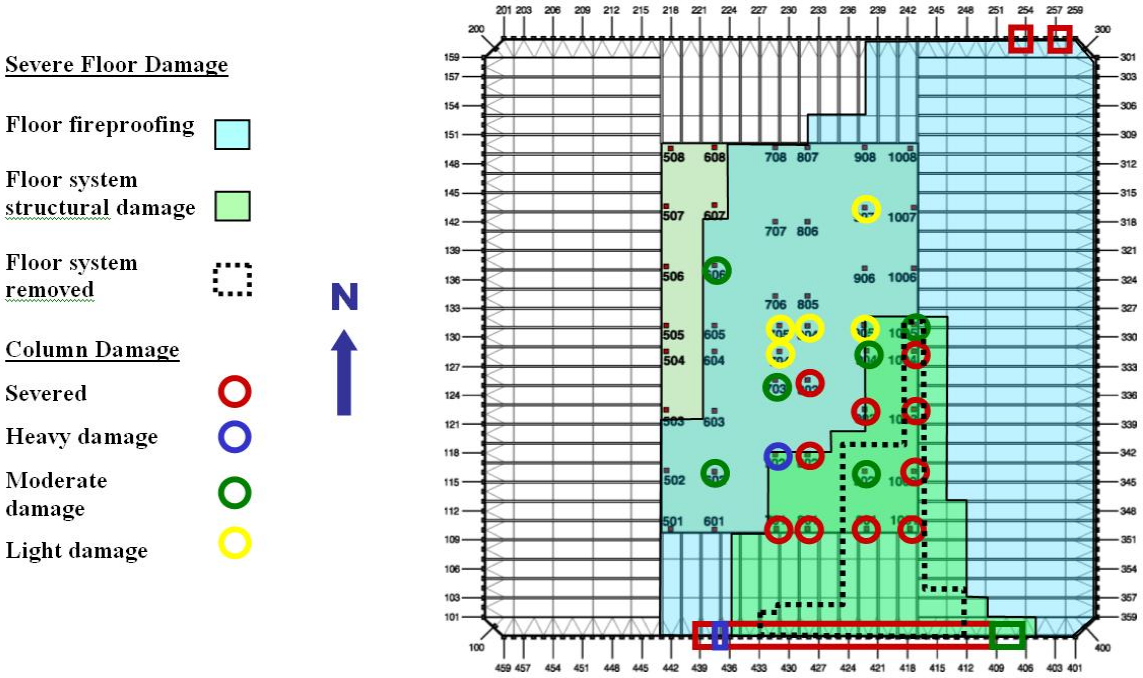

Figure 5–22. Plan view of WTC 2 Case D cumulative damage from Floors 78 to 83.

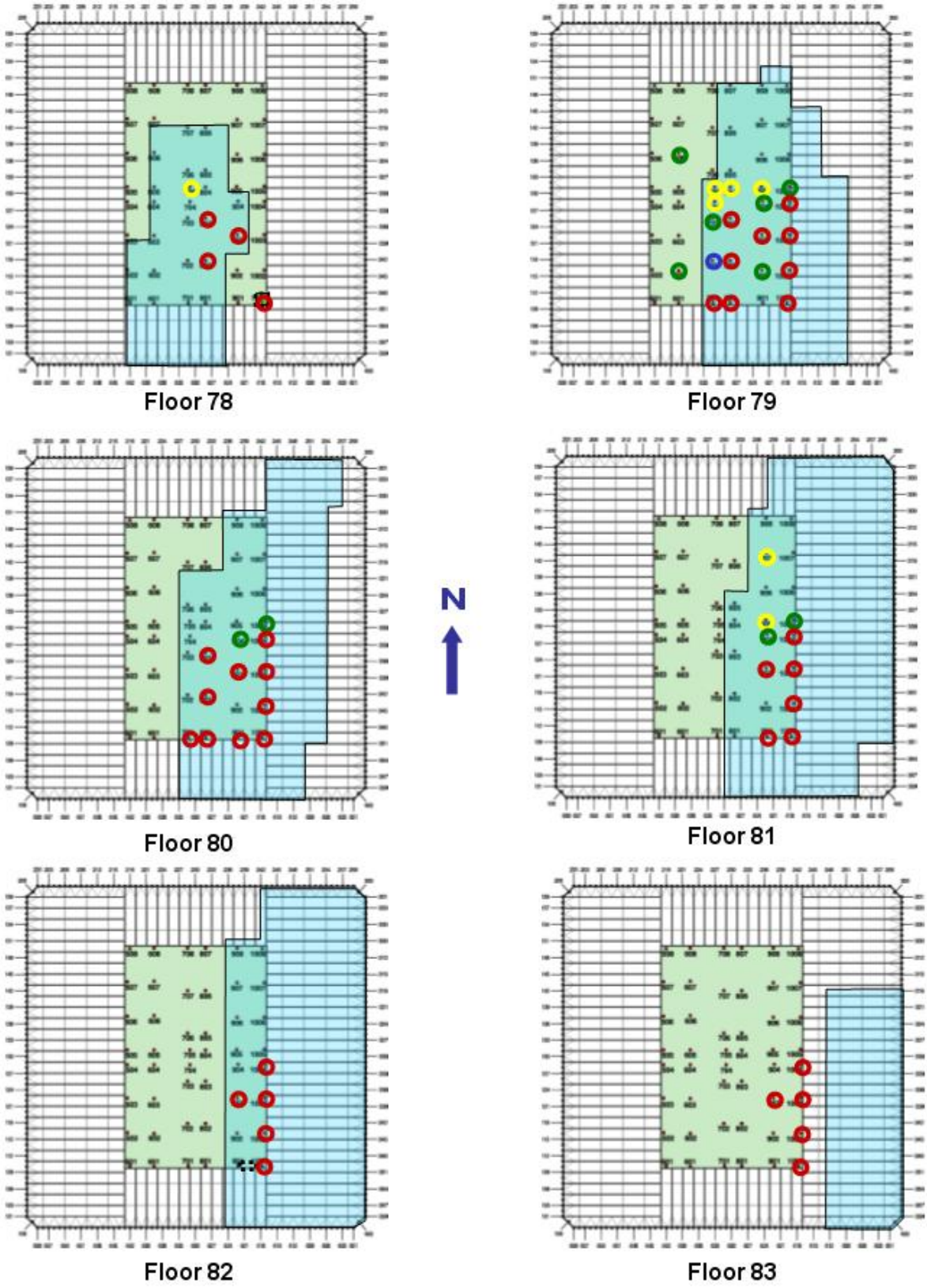

Figure 5–23. Plan view of WTC 2 Case D insulation and column damage to Occupancy Floors 78 to 83.

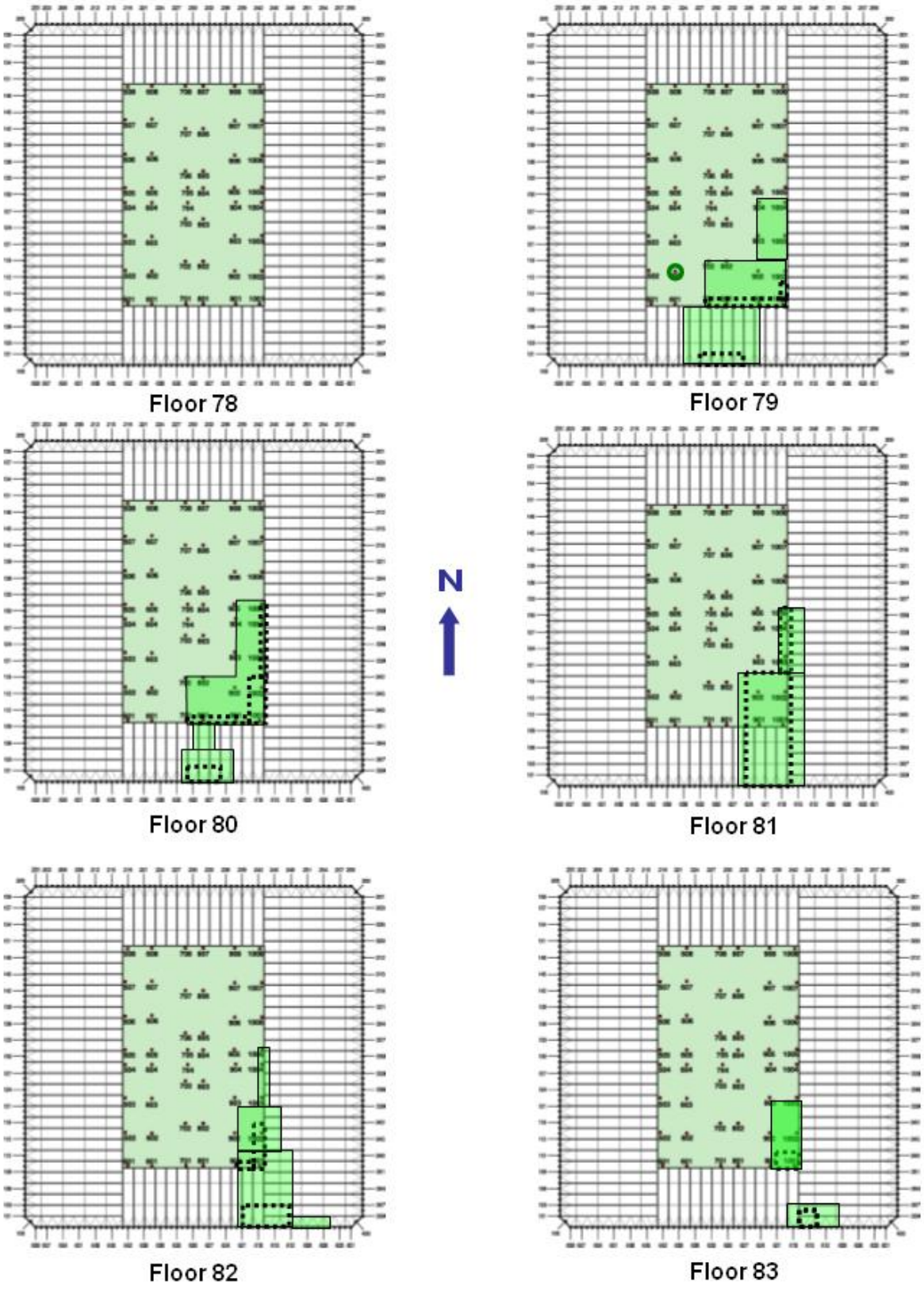

Figure 5–24. Plan view of WTC 2 Case D damage to Structural Floors 78 to 83.

5.5 OBSERVATIONS OF AIRCRAFT IMPACT DAMAGE TO THE PENTAGON

The Pentagon was impacted by an aircraft of similar size (Boeing 767) and at a speed similar to those of the WTC towers (ASCE 2003). The impact speed at the Pentagon was about 530 mph (460 knots or 780 fps), which is similar to the aircraft impact speeds of 443 mph and 542 mph for WTC 1 and WTC 2, respectively. The aircraft completely entered the lower floors of the Pentagon and traveled along a diagonal path for approximately 230 ft. The Pentagon was constructed with a reinforced concrete frame with columns spaced at regular intervals. Figure 5–25 shows a graphic depiction of the damage that was documented after the impact and subsequent fire. An overlay of the WTC tower footprint was added to the original graphic to provide a sense of scale between the two building footprints. Figure 5–25 shows column damage classifications similar to those described in Section 5.2.1—severed, heavy damage (permanently deformed laterally from the column centerline), moderate damage (some impairment of function), and light damage (concrete cracking and spalling but no impairment of function).

It is the light damage that is of interest relative to insulation damage from aircraft impact. Reinforced concrete columns have a concrete cover of at least one inch, and typically more, over the steel reinforcement. Figures 5–26 and 5–27 show two examples of columns with their concrete cover stripped by the debris field down to the spiral reinforcement over most of the column height. It was assumed that if the debris field could strip away concrete cover then a similar debris field would strip SFRM from steel components.

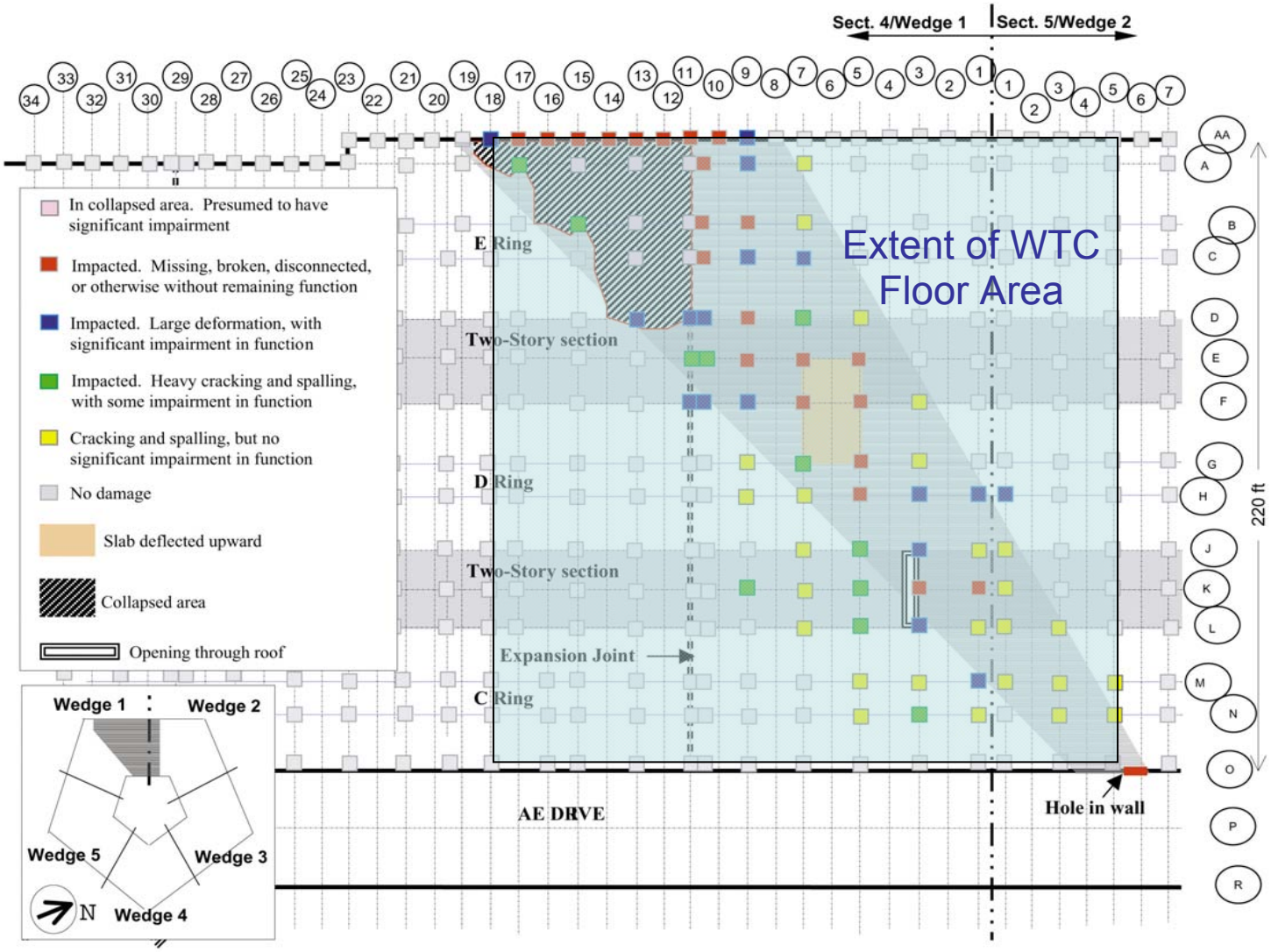

Source: Reproduced from "The Pentagon Building Performance Report" (2003) and use with permission of The American Society of Civil Engineers.

Figure 5–25. Overlay of WTC Footprint on Pentagon damage area from aircraft impact (original figure from ASCE, 2003).

Source: Reproduced from "The Pentagon Building Performance Report" (2003) and use with permission of The American Society of Civil Engineers.

Figure 5–26. Typical damage to spirally reinforced columns in the Pentagon impacted and bent by large debris (ASCE, 2003).

Source: Reproduced from "The Pentagon Building Performance Report" (2003) and use with permission of The American Society of Civil Engineers.

Figure 5–27. Typical damage to spirally reinforced columns in the Pentagon not impacted or bent by large debris (ASCE, 2003).

5.6 SUMMARY

The methodology and criteria for developing input data from the aircraft impact analysis results was summarized for Cases A, B, C, and D. The approach for identifying severe structural damage to columns and floors and insulation damage was described.

A four category classification of core column structural damage into four categories was established: severed, heavy damage, moderate damage, and light damage. Classification criteria included plastic strain levels and lateral deformation from the column centerline. Two types of floor structural damage were identified from the impact analysis results: (1) missing floor areas and (2) severely damaged floor areas incapable of supporting loads.

Insulation was assumed to be dislodged from core columns only if the columns were subject to direct debris impact that failed wall partitions in the immediate vicinity of the column. For exterior columns, the debris impact was required to be strong enough to damage or destroy room furnishings (modular office workstations) adjacent to the columns. For floor trusses, the debris impact was required to be strong enough to damage or destroy room furnishings (modular office workstations) in the same area of the affected floor.

The insulation damage estimates were conservative as they ignored possibly damaged and dislodged insulation in a much larger region that was not in the direct path of the debris but was subject to strong vibrations during and after the aircraft impact. A robust criteria to generate a coherent pattern of vibration-induced dislodging could not be established to estimate the larger region of damaged insulation.

The structural damage in WTC 1 extended from the north exterior wall, through the central region of the north floor area, into the north side of the core. An exterior panel was knocked out of the south wall by aircraft debris. Damage to the insulation from direct debris impact extended over a larger region, and included most of the north floor areas, the core, and central regions of the south floor areas. Case B predicted more damage to core columns and a larger extent of insulation damage to the south floor area than Case A, including damage to the south exterior wall insulation on the inside face.

The structural damage in WTC 2 extended from the south exterior wall, through the south and east floor areas and the southeast region of the core. Exterior columns were severed by debris near the northeast corner. Damage to the insulation from direct debris impact extended over a larger region and included the south floor area, the central and east regions of the core, and most of the east floor area. Case D predicted more damage to core columns than Case C, but the extent of the insulation damage was similar.

5.7 REFERENCES

ASCE (2003) “The Pentagon Building Performance Report”, American Society of Civil Engineers, Reston, VA, 20191.

This page intentionally left blank

Chapter 6
OBSERVATIONS AND TIMELINE OF STRUCTURAL EVENTS

6.1 INTRODUCTION

Development of the probable collapse sequence for each tower was shaped by evidence gathered in the investigation, from photographs and videos, design and maintenance documents, and eyewitness accounts. Data about the events following the aircraft impact were primarily obtained from three sources:

- Photographic and videographic records that had been catalogued and time stamped for the NIST Investigation (NIST NCSTAR 1-5A)
- Interviews of individuals in the towers who survived and individuals outside the towers who received telephone calls from individuals in the towers (NIST NCSTAR 1-7)
- Interviews of emergency response personnel and emergency communication records (NIST NCSTAR 1-8)

Changes in structural performance are generally difficult, if not impossible, to perceive until significant deformation has taken place relative to the dimensions of the structure. The ability to perceive structural changes depends on the detail and resolution of the image being examined and the vantage point of the photographer. Observations of structural performance for the WTC towers include severed components, local deflections or buckling, possible sagging of floors, and relative alignment of columns or building sections.

Photographic and videographic records were reviewed to identify structurally-related events. Where possible, all four faces of a building were examined for a given event or time period to provide complete understanding of the building response. Observations from a single vantage point can be misleading and may result in incorrect interpretation of events. For instance, photographic and videographic records taken from due north of the WTC 1 collapse appeared to indicate that the antenna was sinking into the roof (McAllister 2002). When records from east and west vantage points were viewed, it was apparent that the building section above the impact area tilted to the south as the building collapsed.

Photographs and videos provided information about events at or near the exterior walls of the towers. Events that occurred in the building interior were predicted through analytical simulations validated by exterior observations of aircraft impact, fire dynamics, and structural response.

Evidence was used in the analyses in three ways: (1) to determine input parameters, such as the aircraft speed and direction upon impact or floor sagging at exterior windows, (2) to impose time-related constraints upon an analysis, such as imposing observed broken windows over time to constrain the spread of fire or the extent of inward bowing of an exterior wall, or (3) to validate analysis results, such as global stability after impact and during thermal loading.

Observations of structural behavior were broken into two groups: *key observations* and *noted observations*. Key observations were significant structural events that were explicitly addressed in or used to validate the structural analyses. Noted observations were events that may have been a structural response but could not be conclusively identified as to their significance to the structural response.

Key observations were used to develop a timeline of structural events for each tower. Structural analyses were used to support development of the probable collapse sequence for each tower and to develop and refine understanding of the probable collapse sequence of events between observations.

6.2 OBSERVATIONS OF STRUCTURAL EVENTS

The following key observations were obtained primarily from photographic and videographic records and are shown in the structural events timeline developed for each tower. Some of the observations may not have directly reflected the structural condition of the towers, but they contributed to a determination of the extent of damage or the duration of fires in damaged areas. Other observations reported here were derived from testing of materials recovered from the collapse site.

Aircraft Impact:

- Aircraft impact conditions – aircraft velocity, location, orientation to building
- Structural damage to the exterior columns and spandrels
- Structural stability of each tower after the aircraft impact
- Areas of debris accumulation near the exterior walls
- Locations where debris exited the buildings
- Stairwell damage
- Damage to WTC 2 east and north face floor systems (observed as draped, hanging objects in windows)
- Damage to fireproofing on the exterior sides of the exterior columns

Fire and Thermal Analysis:

- Duration and location of fires and smoke near the perimeter of the floors
- Locations and times of window breakage

Structural Materials:

- Mechanical properties of all steel types from recovered steel
- Concrete composition from concrete samples

- Damage and fracture patterns in recovered steel

Structural Response:

- Additional damage to floor systems on the east and north sides of WTC 2 (observed as draped, hanging objects in windows)
- Inward bowing of an exterior wall on the south face of WTC 1 and the east face of WTC 2
- Tilting of the building section above the impact areas as the structural collapse initiated (WTC 1 tilted to the south, WTC 2 tilted primarily to the east and somewhat to the south)
- Time to collapse initiation
- Observed component and subsystem failures and building movements at collapse initiation

The specific events and timelines for each tower are given in the following sections.

6.2.1 WTC 1 Structural Response Observations

Table 6–1 summarizes the timeline of structural events for WTC 1. Column 6 of the table refers to the figure (Figs. 6–1 through 6–11) that illustrates the described event.

Key Observations

- Inward bowing of the south exterior wall was first observed at 10:23 a.m., as shown in Fig. 6–6. The bowing appeared to extend between Floors 94 to 100 and columns 305 to 359. The maximum bowing was estimated from images to be 55 in.±6 in. at Floor 97 on the east side of the south face of WTC 1. The central area in available images was obscured by smoke. The extent of fires observed on all faces of WTC 1 was similar, although somewhat more extensive on the east and west faces (where short span floors were located) and similar in extent on the north and south faces (where long span floors were located). Inward bowing was observed only on the south face.
- The time to collapse initiation was 102 minutes from the aircraft impact (9:46:30 a.m. until 10:28:22 a.m.)
- From exterior observations, tilting of the building section appeared to take place near Floor 98. Column buckling was then observed to progress rapidly across the east and west faces
- The WTC 1 building section above the impact and fire area tilted to the south as the structural collapse initiated, as shown in Fig. 6–7. The tilt was toward the side of the building that had long span floors. Video records taken from east and west viewpoints showed that the upper building section tilted to the south. Video records taken from a north viewpoint showed no discernable east or west component in the tilt. A tilt to the south of at least 8 degrees occurred before dust clouds obscured the view and the building section began to fall downwards.

Noted Observations

At 10:18 a.m., smoke was observed to be suddenly expelled on the north and west faces:

- North face - Floor 92, Floor 94 on the east side, and Floors 95 to 98 on west side
- West face - Floors 95 and 98 on north side; a lower floor on south side
- Smoke puffs were observed, but they occurred less frequently than in WTC 2.
- The first exterior sign of collapse (downward movement of building) was observed at Floor 98. From a northwest viewpoint (there were no useful south views), large amounts of smoke and dust were first expelled from Floor 98 across the north and west faces. Smoke and dust were also observed being expelled from the east face.

Table 6–1. WTC 1 Timeline of Observed Structural and Fire Events.

	Start Time	Floors	Face	Columns	Figures	Event Description
1	8:46:26	93-99	N	109-152	Fig. 6–1	WTC 1 was impacted by a Boeing 767 between Floors 93 to 99 and Columns 109 to 152. Fig. 6–1 (taken nearly an hour after impact) shows Columns 120 to 159.
2		94-96	S	329	Fig. 6–2	A perimeter wall panel face was knocked out by the aircraft nose or landing gear at the center of the south between Floors 94 to 96
3		92-95	N	130-151	Fig. 6–3	SFRM was knocked off the exterior sides of perimeter columns; the pattern of damage was irregular
4	9:25:28				Fig. 6–4	Fire was observed only on the west side of the south face (note debris under missing panel)
5	9:40		S	301-323	Fig. 6–5	No inward bowing of perimeter columns was visible
6	10:22:59	95-99	S	308-326+	Fig. 6–6	Inward bowing of the south perimeter wall was visible from Floor 95 to about Floor 99, with a maximum inward bowing of ~ 55 in. at Column 315 and Floor 97
7	10:28:18				Fig. 6–7 Fig. 6–8 Fig. 6–9	Pressure pulses of smoke were pushed out the west face at its north edge and center; Smoke and debris clouds were pushed out the north, east, west faces at Floor 98; Fire came out windows on the north, east, west, and south faces between Floors 92 to 98 and Floor 104
	10:28:20				Fig. 6–10 Fig. 6–11	WTC 1 began to collapse. The first exterior movement was at Floor 98. Rotation of the building section above the impact and fire zone to at least 8 degrees to the south occurred before the building section began to fall vertically.

Figure 6–1. Initial aircraft impact damage on WTC 1 north face.

Figure 6–2. Initial aircraft impact damage on WTC 1 west and south faces minutes after impact (exact time of image is unknown).

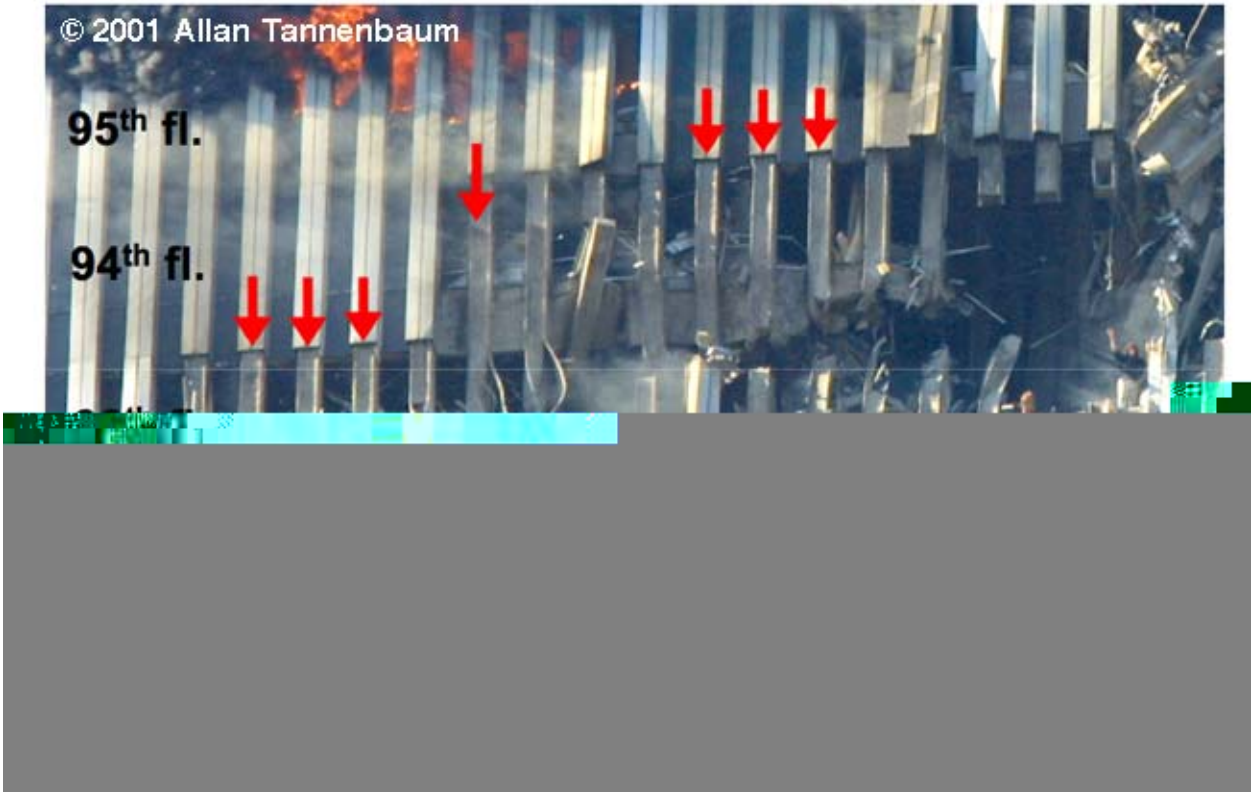

Figure 6–3. SFRM knocked off north exterior columns. Arrows show where fireproofing was damaged or missing.

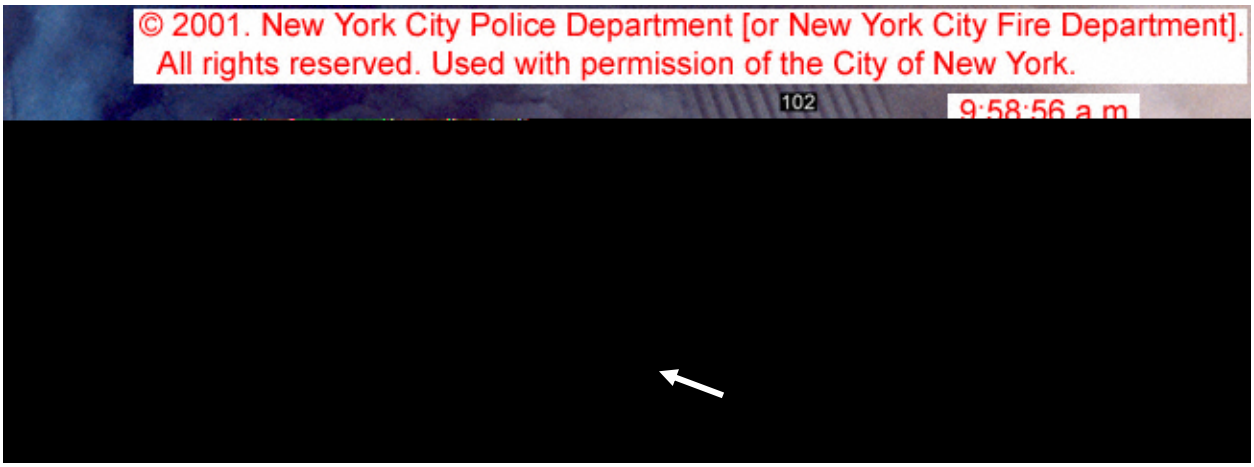

Figure 6–4. South face of WTC 1 with fire visible only on the west side at 9:25. Arrow shows region where debris pile under missing panel was observed.

Figure 6–5. Fires on WTC 1 south face at 9:40 a.m. Note lack of inward bowing.

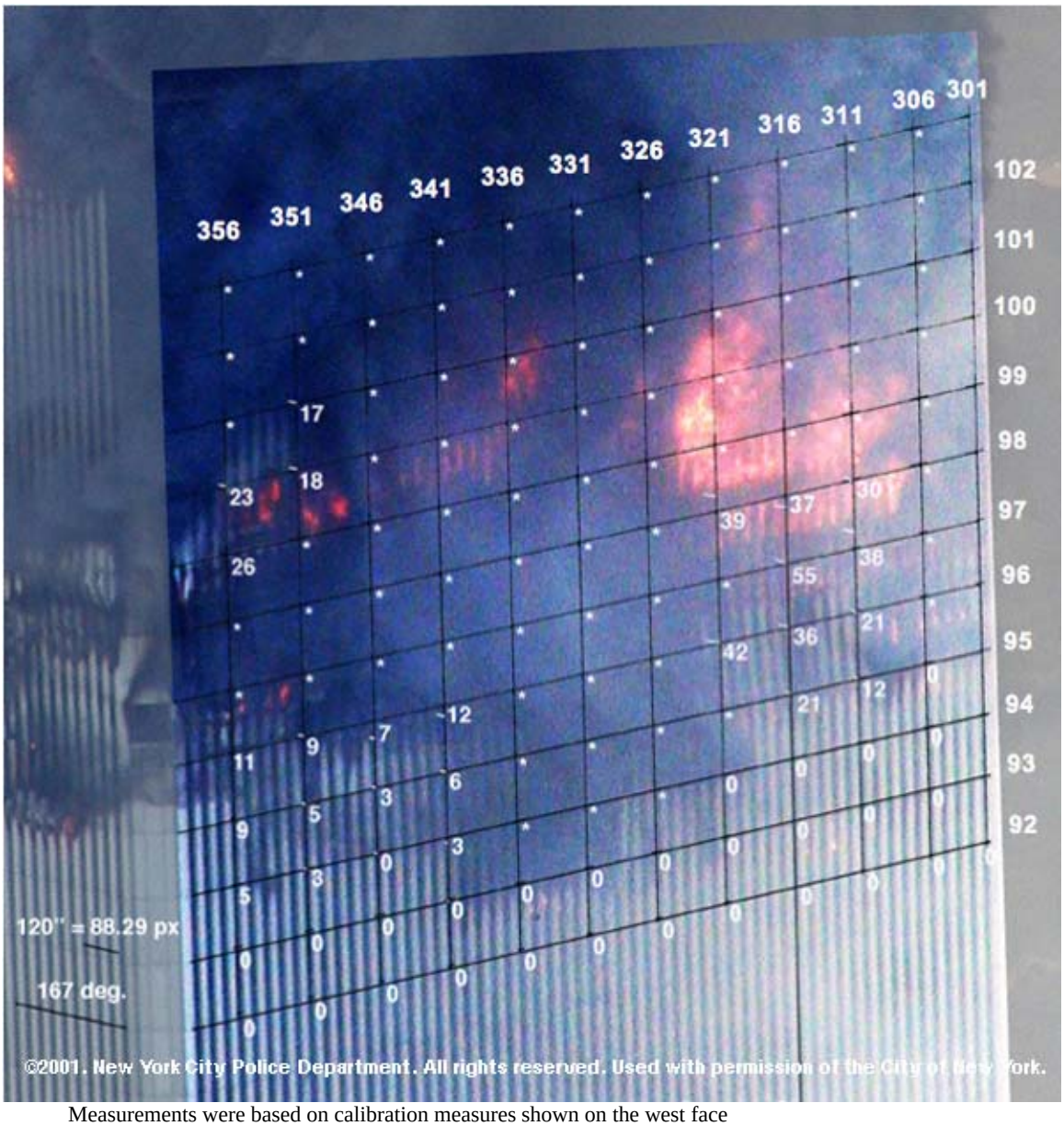

Measurements were based on calibration measures shown on the west face
Foreshortening into depth of field across the south face of 17% was included in the measurements
Measurement error was at least +/- 6 inches

Figure 6–6. WTC 1 exterior columns bowing inward across most of the south face between Floors 95 to 97 (or 98) at 10:22:59 a.m. Note buckled panel at SW corner.

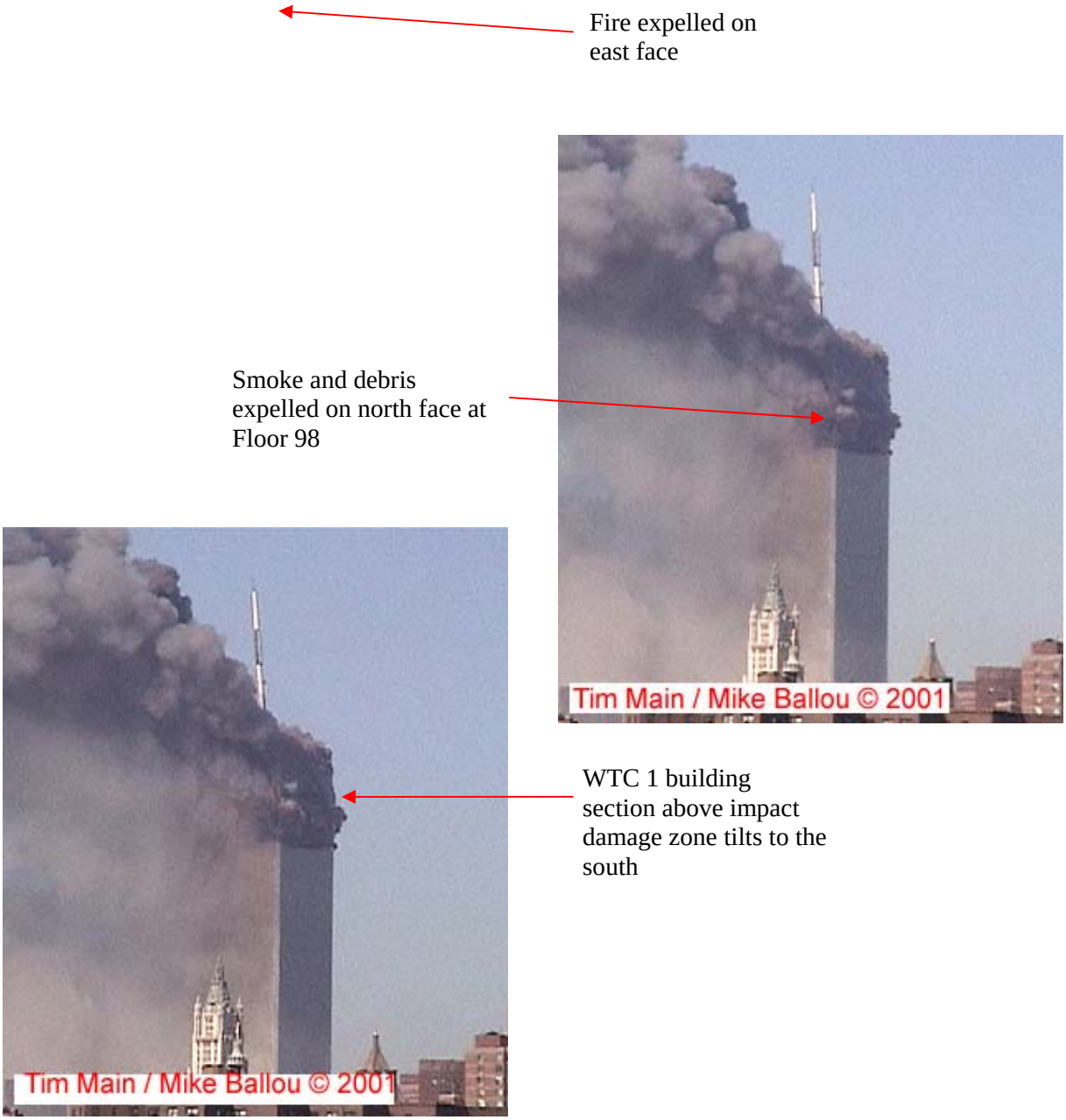

Figure 6–7. Expulsion of smoke and debris at WTC 1 Floor 98 on the east, north, and west faces.

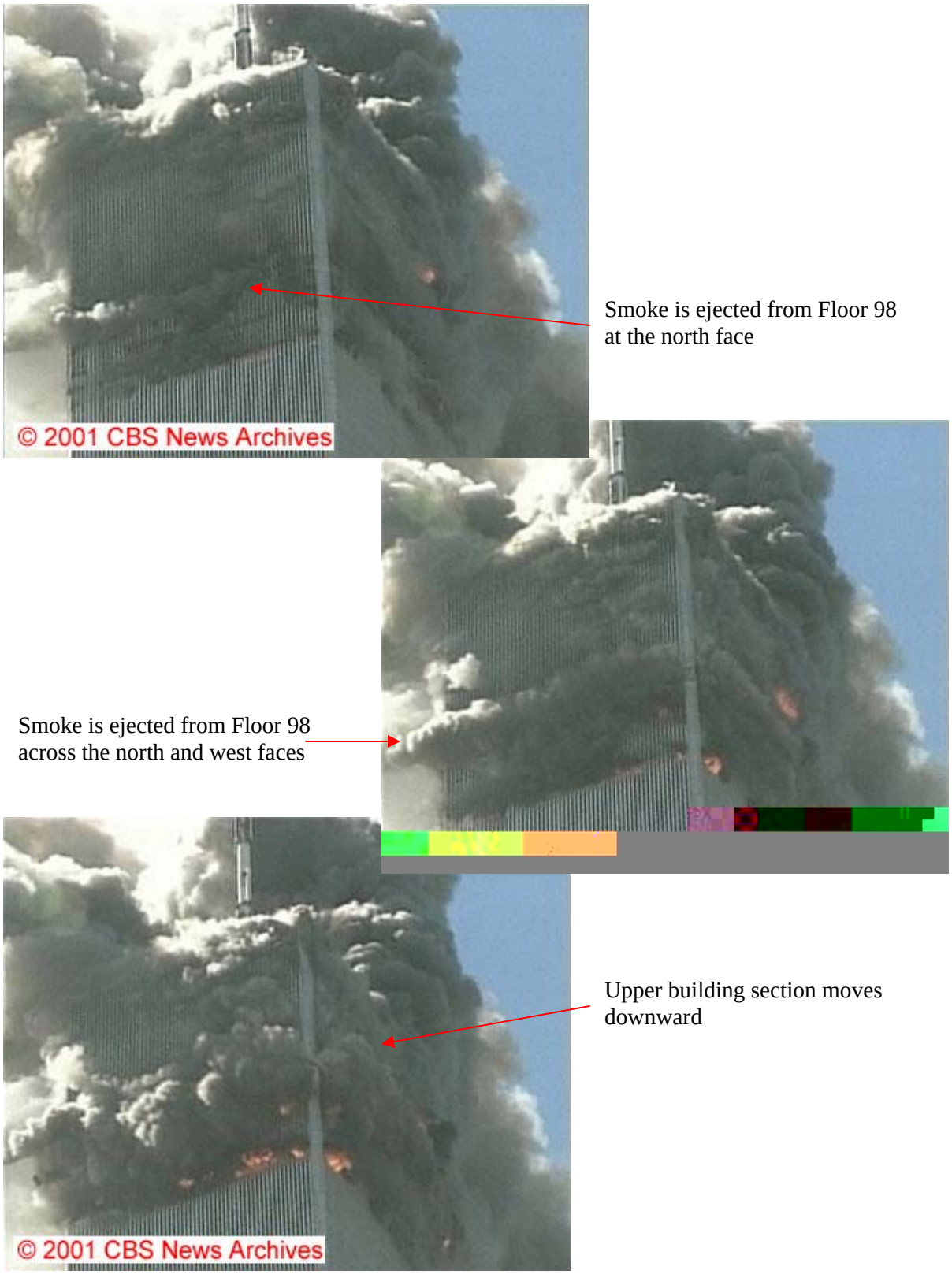

Figure 6–8. Smoke expulsion at Floor 98 from north and west faces as collapse initiates.

Figure 6–9. Smoke expulsion at Floor 98 from north and east faces at collapse initiation.

Figure 6–10. Rotation of WTC 1 building section above the aircraft impact zone toward the south as viewed from due north. Note that there is no tilt in the east or west directions.

Figure 6–11. WTC 1 tilt to the south of approximately 8 degrees was measured before smoke and debris obscured view. Note view is from west and tilt is directly south.

6.2.2 WTC 2 Structural Response Observations

Table 6–2 summarizes the timeline of structural events for WTC 1. Column 6 of the table refers to the figures and table (Figs. 6–12 through 6–26 and Table 6–3) that illustrate the described event.

Key Observations

- Following the aircraft impact and fireballs, hanging objects were observed through the windows of the east and north faces. These objects appeared to be floor slabs and were observed to change shape and/or length over time and extend across approximately half of the east face. The hanging objects suggest that there was structural damage to WTC 2 Floor 83 along the east face and to Floors 81 to 83 of the north face near the northeast corner.

- Inward bowing of the east wall was first observed at 9:21 a.m. The inward bowing was approximately 10 in. at Floor 80 and extended between Floors 78 and 83 and Columns 304 and 344. The remaining portion of the face to the south of Column 344 was not included in the image. The bowing appeared to extend over a large fraction of the east face and to be greatest near the center of the face. Fires were more extensive along the east face (where long span floors were located) and at the east side of the north and south faces (where short span floors were located). Fires were not observed on the west face (where long span floors were located). Inward bowing was observed only on the east face.

- An increase of the inward bowing of the east wall was observed at 9:53 a.m. The inward bowing appeared to extend between Floors 78 and 84 and Columns 305 and 341. The remaining portion of the face to the south of Column 344 was not included in the image. The greatest bowing was approximately 20 in.±1.0 in. at Floor 80 on the east face of WTC 1.

- Collapse initiated 56 minutes after the aircraft impact (9:02:59 a.m. to 9:58:59 a.m.).

- From a northeast viewpoint, initial downward motion was observed at several columns as they moved inward on the north side of the east face. From exterior observations, tilt of the building section above the impact and fire area appeared to take place near Floor 82. Column buckling was then seen to progress across the north face.

- The building section above the impact and fire area tilted to the east and south as the structural collapse initiated. Estimates from photographs indicated that there was approximately a 3 to 4 degree tilt to the south and a 7 to 8 degree tilt to the east prior to significant downward movement of the upper building section. The tilt to the south did not increase any further as the upper building section began to fall, but the tilt to the east continued up to 20 to 25 degrees before dust clouds obscured the view.

Noted Observations

- A fireball on the east face was observed coming from Floor 82. Fireballs on the north face were observed coming from Floors 79 to 82. The deflagration prior to the fireballs may have caused a pressure pulse to act on floors above and below.

- A ‘cold spot’ on the north face, where little or no fires were observed, may indicate that Floors 82 and 81 had disconnected and dropped over a 12 window span along the north face.
- Molten material pouring from the northeast corner indicated that Floor 81 on the east side of the north face may be shifting. If the substance was molten aluminum, that would have required temperatures on the order of 500 °C or higher.
- Numerous puffs of smoke may indicate internal changes in architectural or structural features.
- Outward bowing of the spandrel near the center of the north face on Floor 79 was observed near columns 237 and 238.
- As the portion of the building above the impact area tilted to the south and east:
    1. A kink formed at the southeast corner near Floor 106 as the upper building section tilted and collapse initiated.
    2. The southeast corner also kinked approximately midway between the impact and fire zone and the kink near Floor 106 as the upper building section tilted.

Hanging Objects

The hanging objects observed on the east face and north face of WTC 2 (listed in the Key Observations) appeared to be the exterior edges of the floor slabs.

The slab thickness was nominally 4 inches over a fluted deck with 1.5 in. ribbing. Scaling of the object in the windows found the depth to be approximately 4 in. to 6 in. The concrete slab was reinforced with two layers of welded wire fabric and had a flexural stiffness that was greater than other items that might have been draped in the windows, such as ductwork. The drape of the object was consistent with a floor flexural stiffness. There was ductwork between the damper at the lower chord of the truss and the floor slab at the exterior wall. However, for the ductwork to be draped in the windows, all the dampers would have had to fail while the floor slab would have had to remain in place. Such a sequence of events is unlikely. Also, such ductwork would be light and hang with a deeper drape. From these observations, it appears that the hanging objects were the exterior edges of floor slabs.

Table 6–2. WTC 2 Timeline of Observed Structural and Fire Events

	Start Time	Floors	Face	Columns	Figures and Tables	Event Description
1	9:02:59	77-85	S	404-443	Fig. 6–12	WTC 2 was impacted by a Boeing 767 between Floors 77 and 85 and Columns 404 and 443.
2	9:03:42	83	E	310-342	Fig. 6–13 Tbl. 6–3	The edge of Floor 83 appeared to be draped in Floor 82 windows between Columns 310 and 342.
3	910:01	79-83	N,E		Fig. 6–15	Hanging object in windows of Floor 79 that appears to be the edge of Floor 80.
4	9:11:14	79-82	N		Fig. 6–14 Tbl. 6–3	Debris piles were visible at windows where fires were burning at Floor 79, Columns 231 to 241, and Floors 81 to 82 at the northeast corner. Hanging objects noted with arrows.
5	9:14:03	79-82	N	237-254	Fig. 6–16	Missing SFRM on several columns.
6	9:21:29	78-82	E	302-342	Fig. 6–17 Fig. 6–18	Inward bowing of east face, maximum deflections of 10 in. at Floor 80.
7	9:53:04	~78-82	E	318-334+	Fig. 6–19 Fig. 6–20	Bowing in of columns, maximum deflections of 20 in. at Floor 80.
8	9:55:04	83	E	310-342	Tbl. 6–3	Floor edge is draped in Floor 82 windows between columns 310 and 342.
9	9:58:55		E		Fig. 6–21	Perimeter columns bowing inward on east face.
10	9:58:59					WTC2 begins to collapse.
11	9:58:59	78-83	E	324-359	Fig. 6–22 Fig. 6–23	Columns spring back from bowing as collapse initiates on east face near NE corner (every 3rd panel).
	9:58:59		E,N,W			Smoke and debris clouds are expelled from Floor 81 on E,N,W faces of the building.
	9:58:59		S		Fig. 6–24 Fig. 6–25	Building section above the impact area tilted to the east and south. Tilting appears to take place around Floor 82. Rotation of approximately 4 to 5 deg to the south and 20 to 25 deg to the east occurred before the building section begins to fall vertically.
	9:59:02	~ 106	SE + E		Fig. 6–26	Kink (and offset) about Floor 106 which propagates across the east face where degrades into a gentle curve on the northeast corner; indicates that the kink did not precede the initiation of the global collapse.

Table 6–3. Possible floor damage observed in photos of WTC 2 windows.

East Face				
Floor	***Estimated Left Intact Column Connection***	***Left Visible Floor Location***	***Right Visible Floor Location***	***Estimated Right Intact Column Connection***
9:03:42				
83	343	340	321	317
9:38:22				
83	317	317	311	308
9:55:04				
83	346	343	310	309
North Face				
Floor	***Estimated Left Intact Column Connection***	***Left Visible Floor Location***	***Right Visible Floor Location***	***Estimated Right Intact Column Connection***
9:10:01				
82				
81	251	248	241	241
80				
9:14				
83				
82	247	243	238	237
81	251 255	248 254	241 252	237 251
80				
9:58:37				
83	259	259	250	248
82	254	251	247	235
81	251	249	245	235
80	234 258	234 255	229 252	226 249

*Floor is not visible beyond this point, separation from wall was truncated at the closest intact point where there appeared to be no damage beyond the burning debris pile on Floor 79.

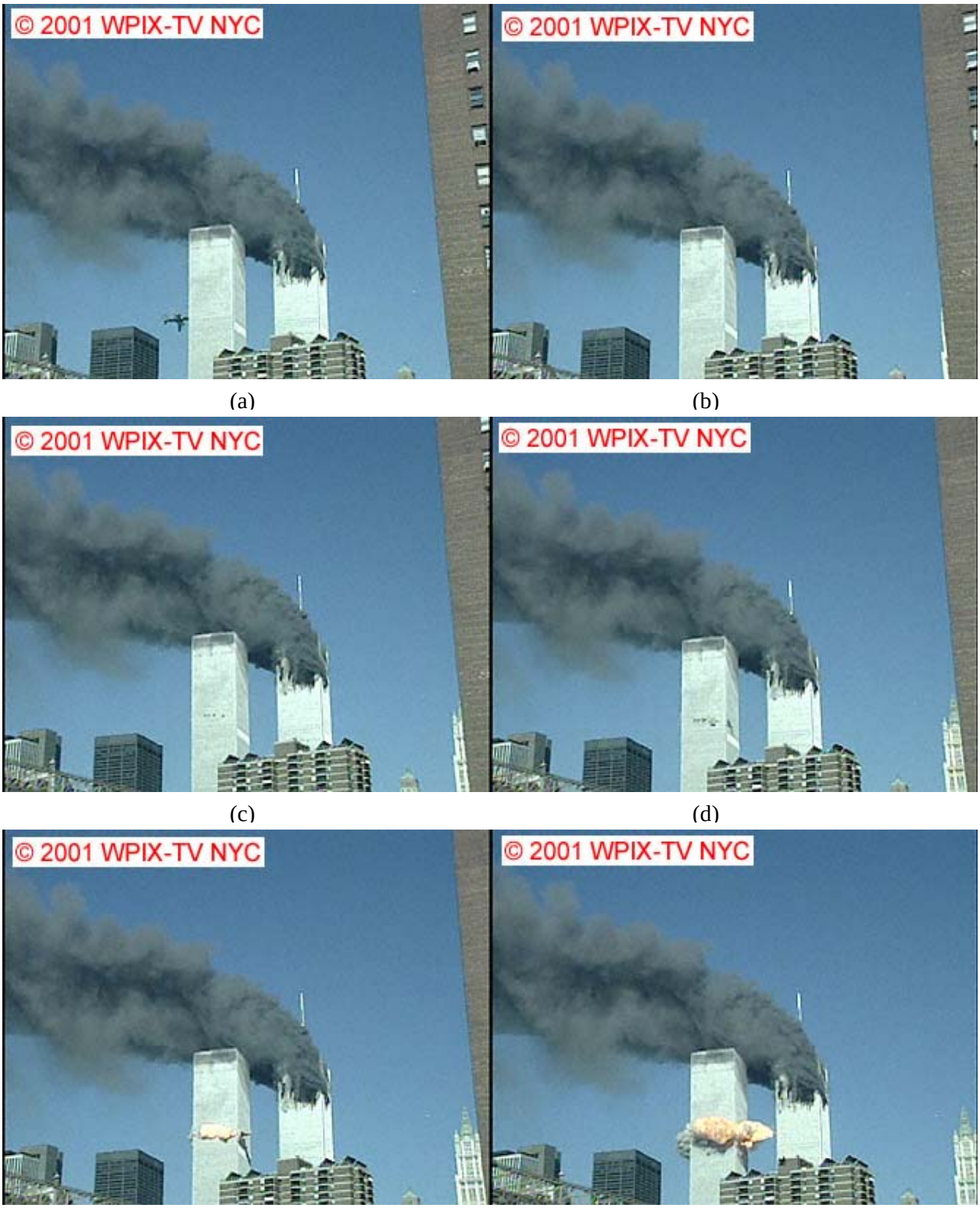

Figure 6–12. Aircraft impact into WTC 2 and fireball, view from the east.

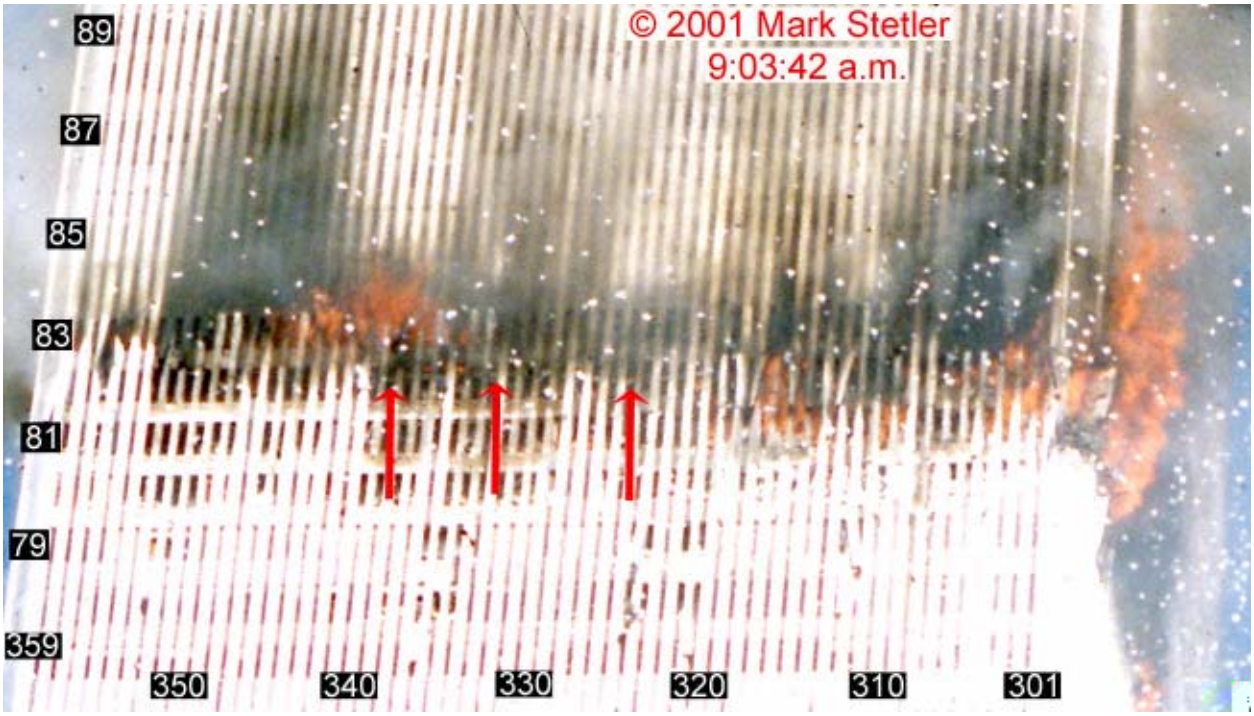

Figure 6–13. Hanging object (noted by arrows) in east windows of Floor 82 appears to be edge of Floor 83.

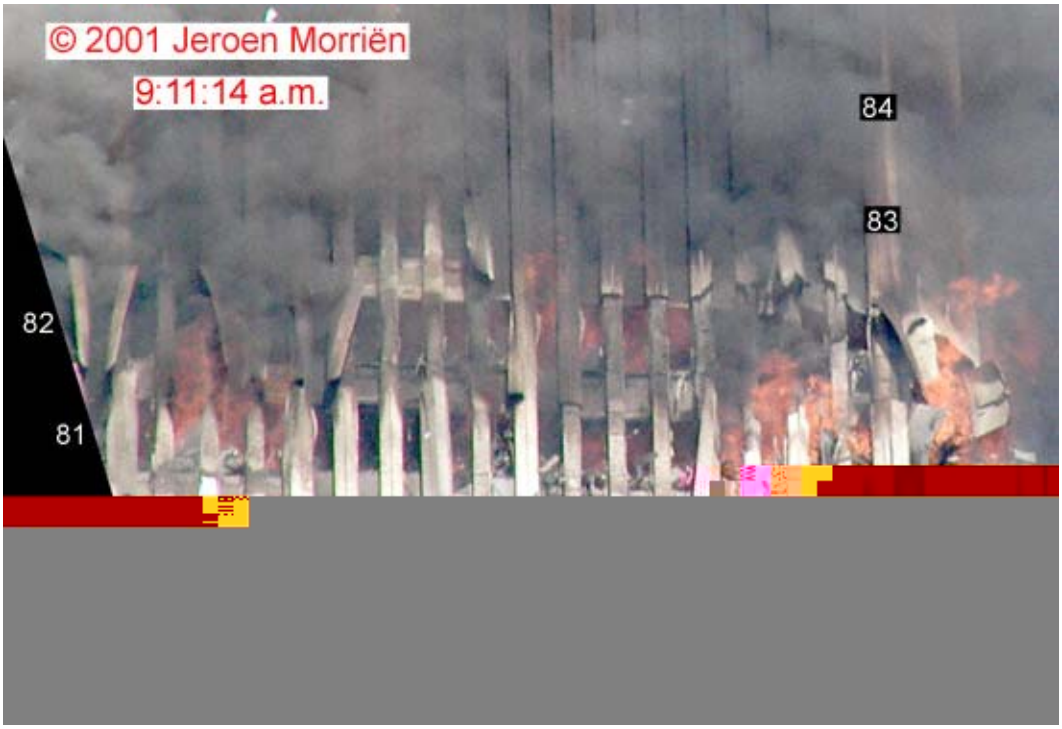

Figure 6–14. Debris piles at windows where fires are burning at the northeast corner.

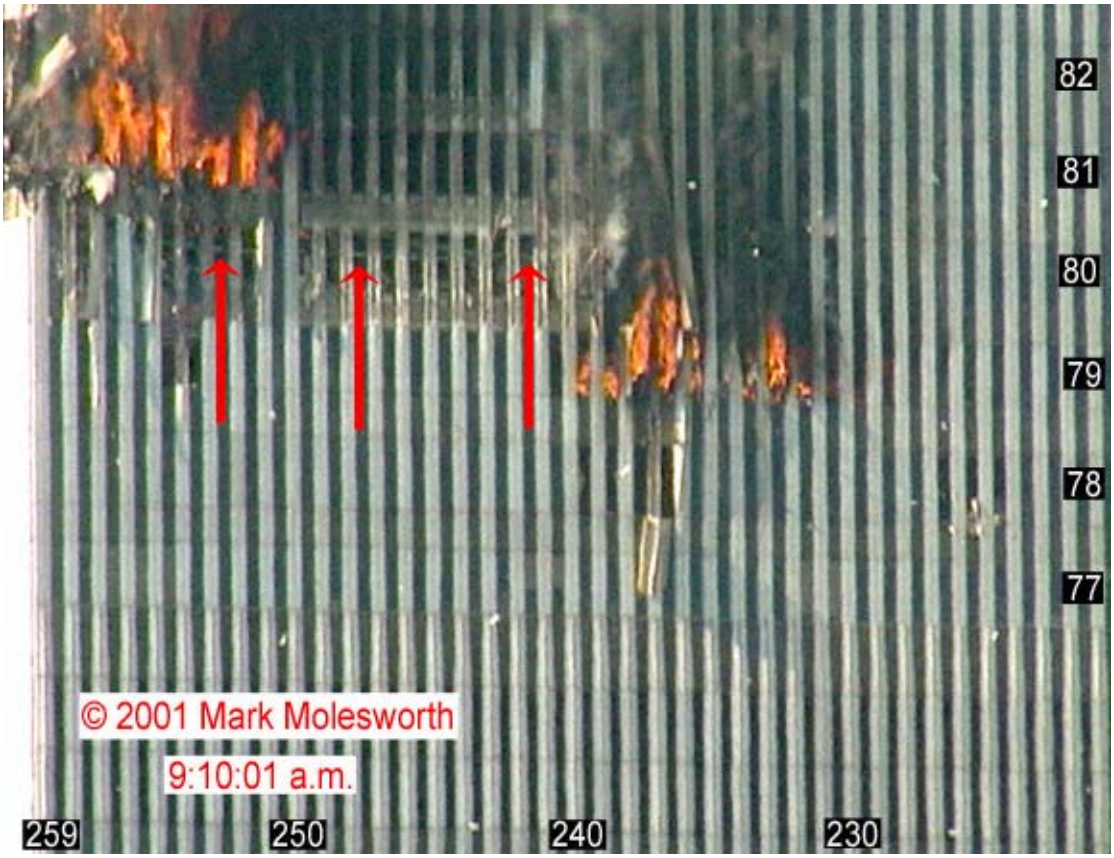

Figure 6–15. Hanging object (noted by arrows) in north windows of Floor 79 appears to be edge of Floor 80.

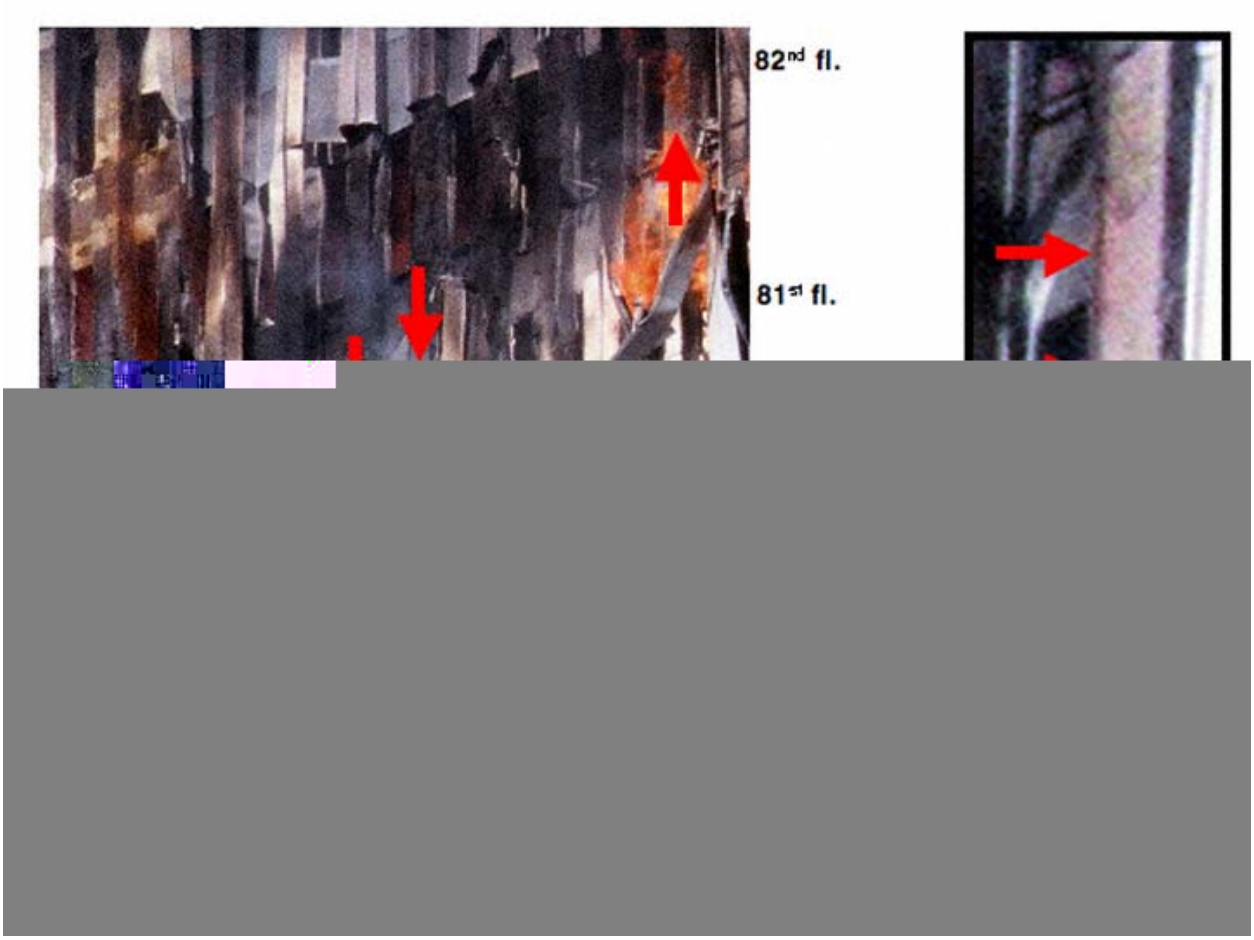

Figure 6–16. Image showing damage to fireproofing on east face of WTC 2 due to internal impact. Red arrows highlight areas where fireproofing has been damaged. The blowup to the right shows a column where red Tnemec primer paint is visible.

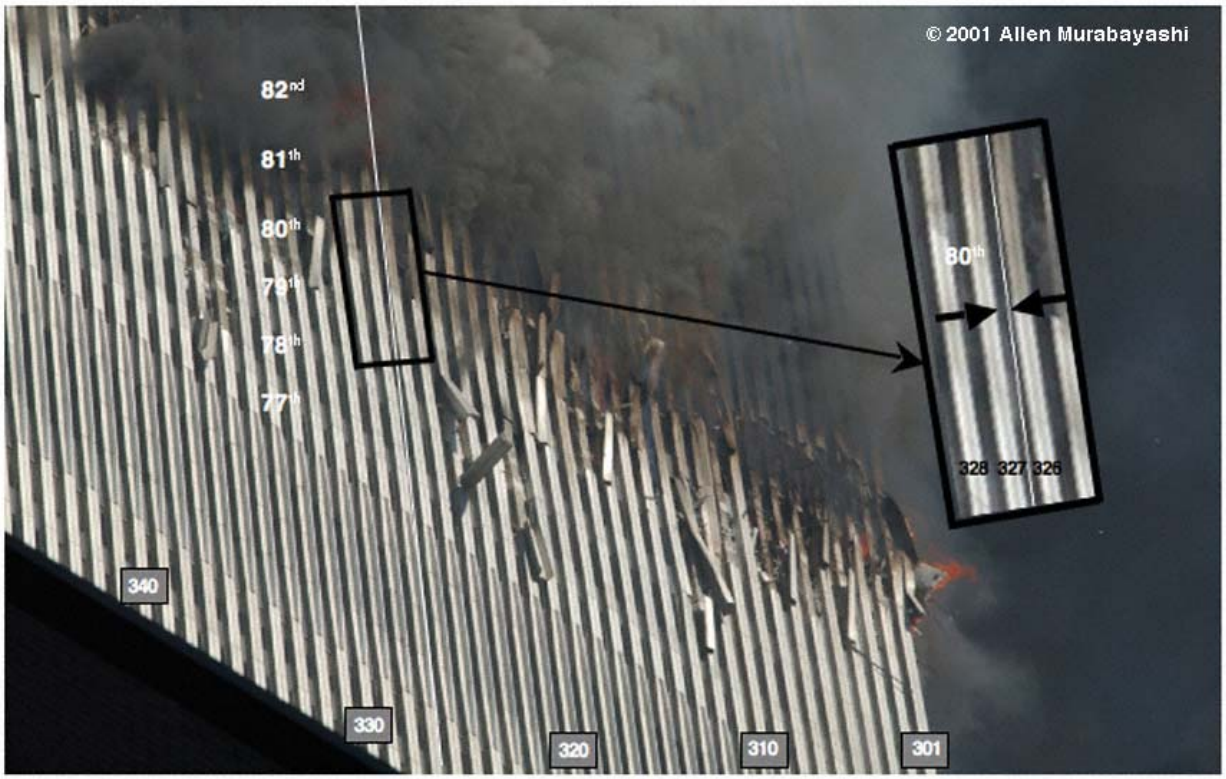

Figure 6–17. WTC 2 exterior columns bowing inward across north side of the east face between Floors 77 and 83 at 9:21 a.m.

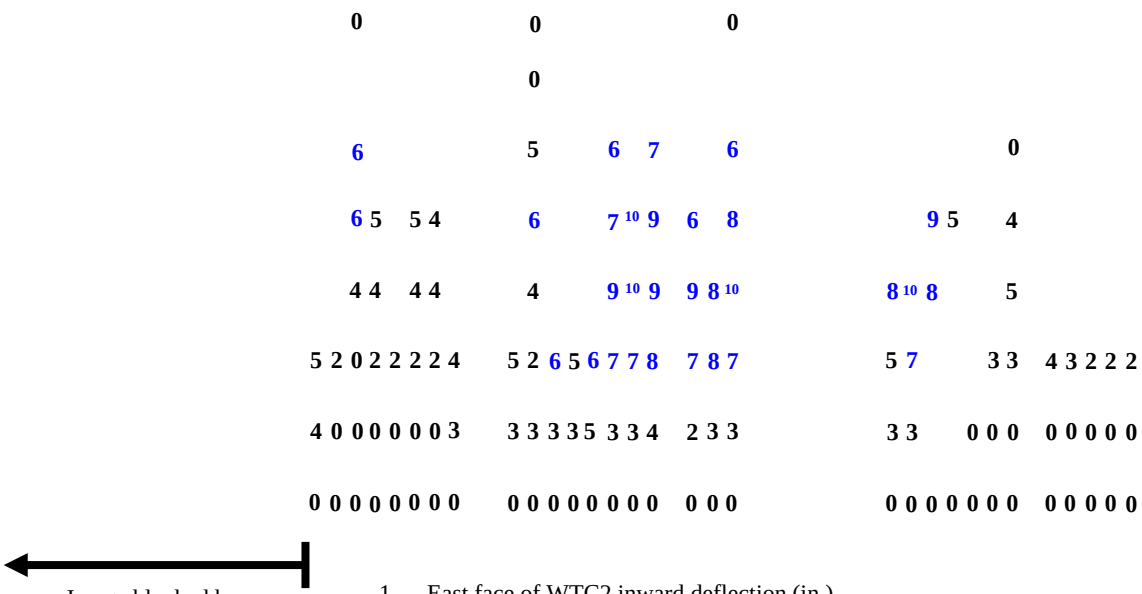

1. East face of WTC2 inward deflection (in.)
2. Estimated uncertainty: +/- 1 inch
3. Empty regions have no data (smoke, damaged aluminum, could not establish true vertical, etc.)

Figure 6–18. Inward Bowing of east Face of WTC 2 at 9:21 a.m.

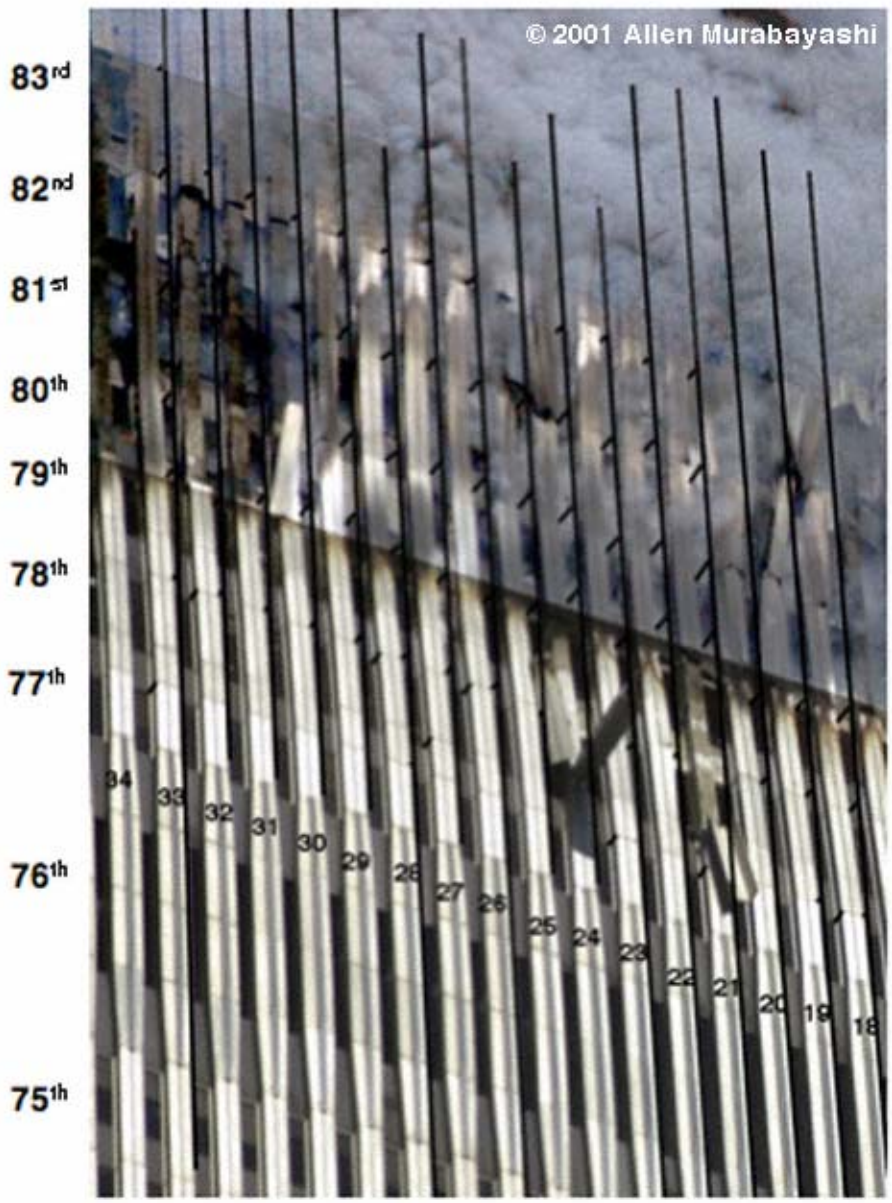

Figure 6–19. Inward Bowing of east Face of WTC 2 at 9:53 a.m.

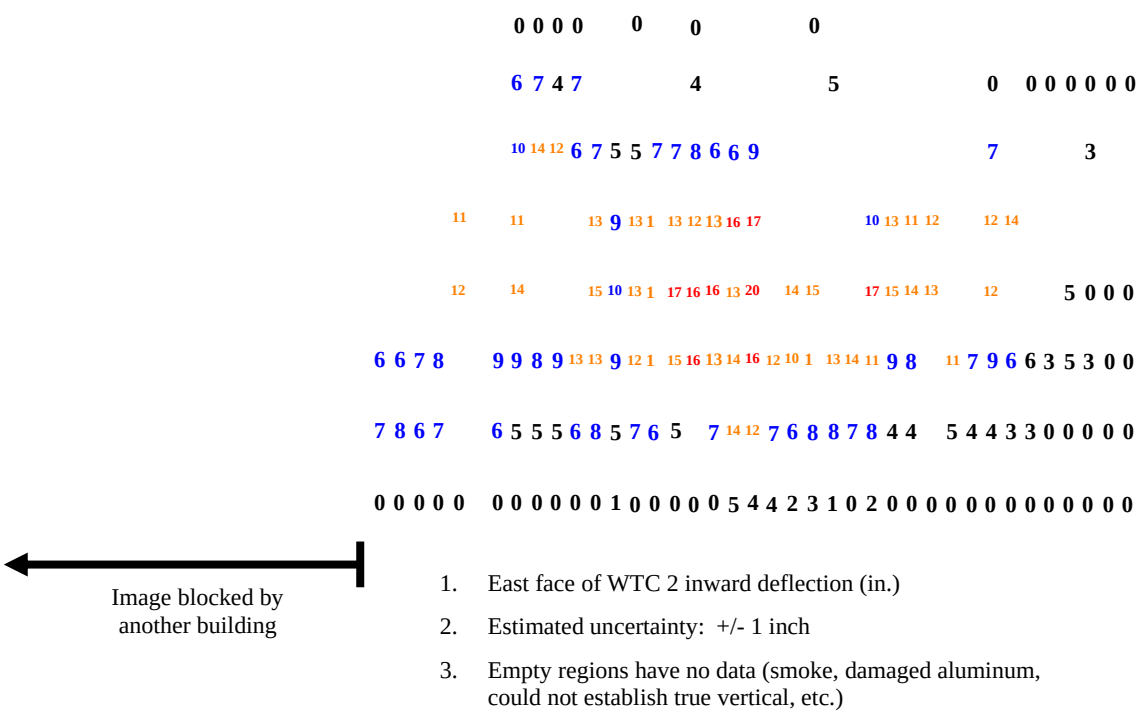

1. East face of WTC 2 inward deflection (in.)
2. Estimated uncertainty: +/- 1 inch
3. Empty regions have no data (smoke, damaged aluminum, could not establish true vertical, etc.)

Figure 6–20. Inward Bowing of east Face of WTC 2 at 9:53 a.m.

Figure 6–21. WTC 2 exterior columns bowing inward across the east face between Floors 77 and 83 at 9:58:55 a.m.

Figure 6–22. View of WTC 2 buckling of east wall near northeast corner as collapse initiates from northeast.

Figure 6–23. View of east wall buckling and WTC 2 collapse from southeast.

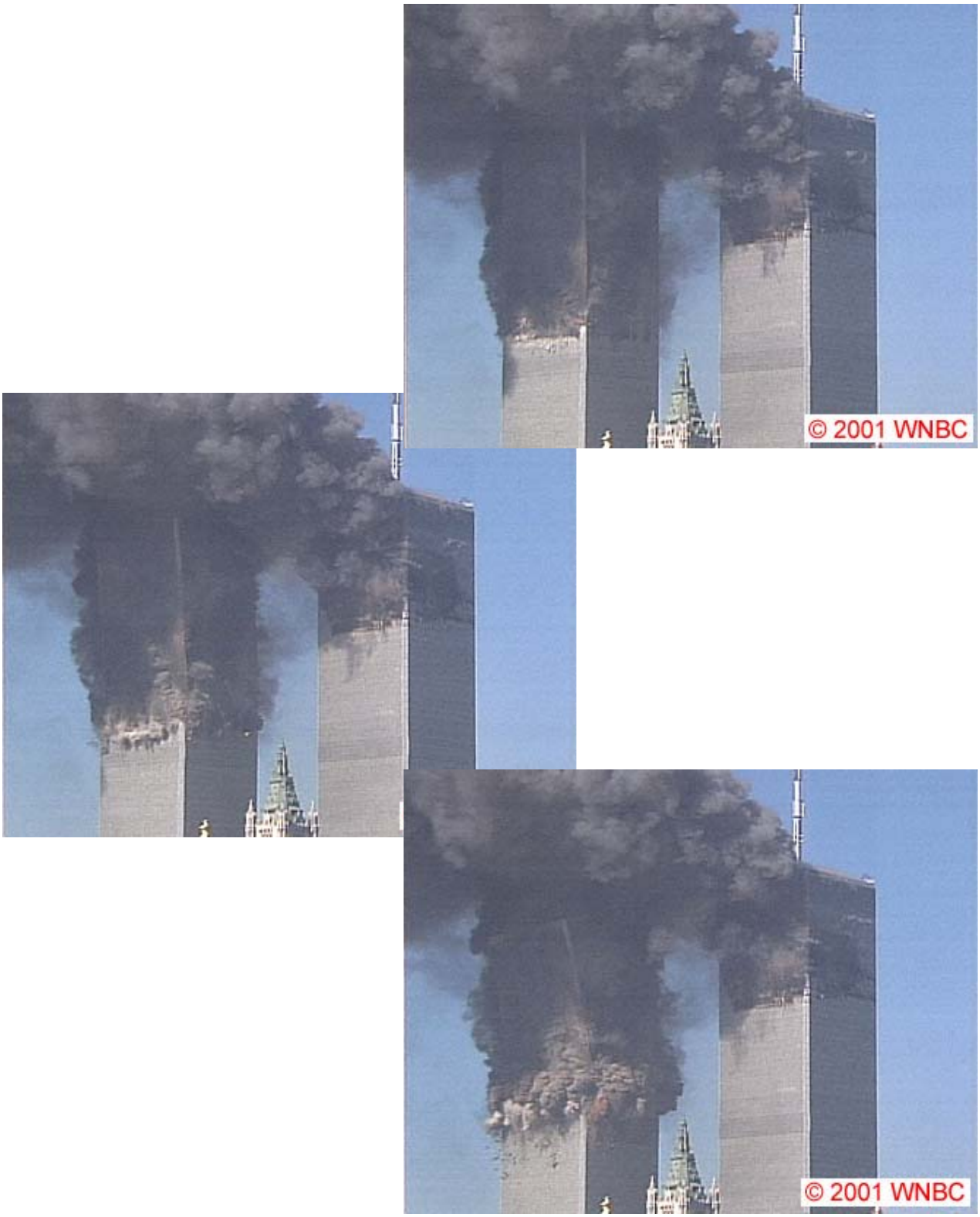

Figure 6–24. View of upper building section of WTC 2 tilting to the east.

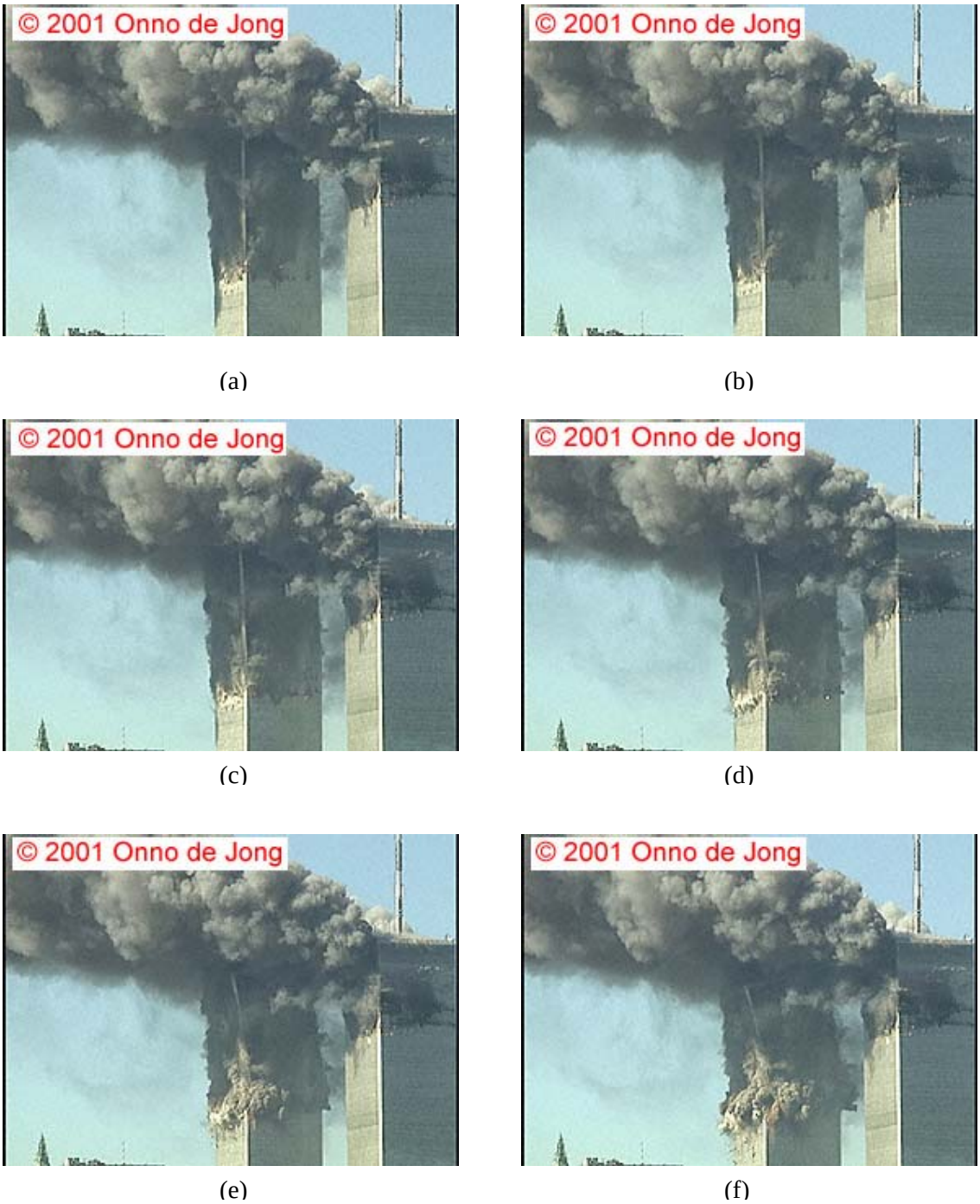

Figure 6–25. View of upper building section of WTC 2 tilting to the east from the northeast.

Figure 6–26. Kink on southeast corner near Floor 106 formed after collapse initiation.

This page intentionally left blank.

Chapter 7
STRUCTURAL RESPONSE OF MAJOR TOWER SUBSYSTEMS TO AIRCRAFT IMPACT DAMAGE AND FIRE

7.1 INTRODUCTION

Prior to conducting the analysis of the global structural response of each tower, major structural subsystems were analyzed to provide insight into their behavior within the WTC global system.[1] The three major structural subsystems, the core framing, a single exterior wall, and full tenant floors, were analyzed separately for their response to impact damage and fire. The hat truss was not analyzed separately as its structural behavior did not require significant reductions in model complexity for the global analysis. The component analyses provided a foundation for these large, nonlinear analyses with highly redundant load paths by determining component behavior and failure modes and enabling a significant reduction in finite element model complexity and size. While the component models used preliminary estimates of elevated temperatures, the major subsystem models used final estimates of impact damage and elevated temperatures determined from the aircraft impact analysis and the fire dynamics and thermal analyses.

The capacity of each subsystem to sustain loads from imposed damage and elevated temperatures was evaluated. The isolated subsystem models lacked the restraint and load paths to other subsystems found in the global analysis. Even so, the isolated subsystem response was useful for refining the global models and interpreting subsystem behavior in the global system. For instance, when a column buckled in the isolated core subsystem model, the only load path available to carry that column's load was the floor system within the core structure. However, in the global structure, the hat truss at the top of the core would transfer loads to other core columns or the exterior walls, assuming the connections between the core columns and hat truss remained intact.

7.2 CORE SUBSYSTEM

The core subsystem in the WTC towers was designed to carry gravity loads, which included the weight of the structure, equipment, furnishings, and occupants. The core system was not designed to carry lateral wind loads. The core comprised the structural steel [illegible] and floor [illegible] and was [illegible]

Case B and Case D impact damage could not be used for the isolated core models as no stable solution was obtained. Instead, for WTC 1, Case A impact damage was used for both Case A and Case B temperature histories and, for WTC 2, Case C impact damage was used for both Case C and Case D temperature histories. This approach allowed for comparison of the differences between Case thermal loads for the same impact damage for each tower.

Temperature histories were input as nodal temperatures at each node in the structural model that was subject to heating. The temperatures predicted in the structural members depended on the extent of insulation assumed to be in place and on the material properties and geometry of the structural members. In each tower, the temperature in the structural members varied through the length and cross section and changed with time. The temperature at every node in the global models was calculated by interpolation of temperatures from the thermal analysis, which had a much finer mesh than the global structural models. A linear temperature gradient was assumed across column cross sections and along the length of members. To reduce data handling, the continuous temperature time histories were replaced with piecewise linear time-histories without significant loss of accuracy. Elevated temperatures were applied to the damaged core structure in 10 min intervals, where a temperature state was given for all structural components at a given time and linearly ramped to the next temperature state. Examination of temperature histories indicated that no significant fluctuations between temperature states occurred for the 10 min intervals selected for analysis. Temperature data were provided at 10 min intervals up to 100 min for WTC 1 and up to 60 min for WTC 2 (see NIST NCSTAR 1-5G for more discussion of the 10 min intervals).

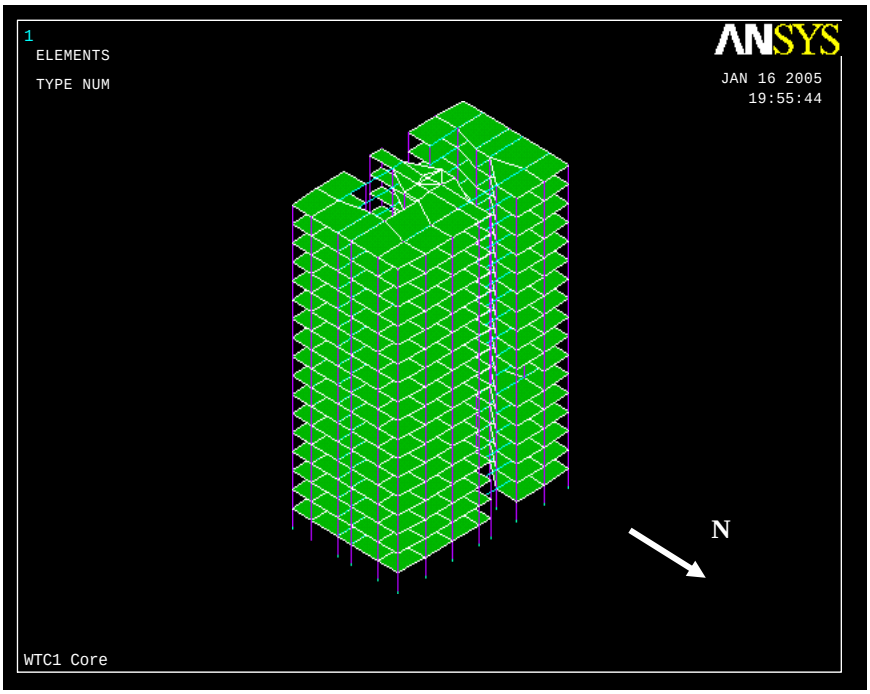

(a) WTC 1

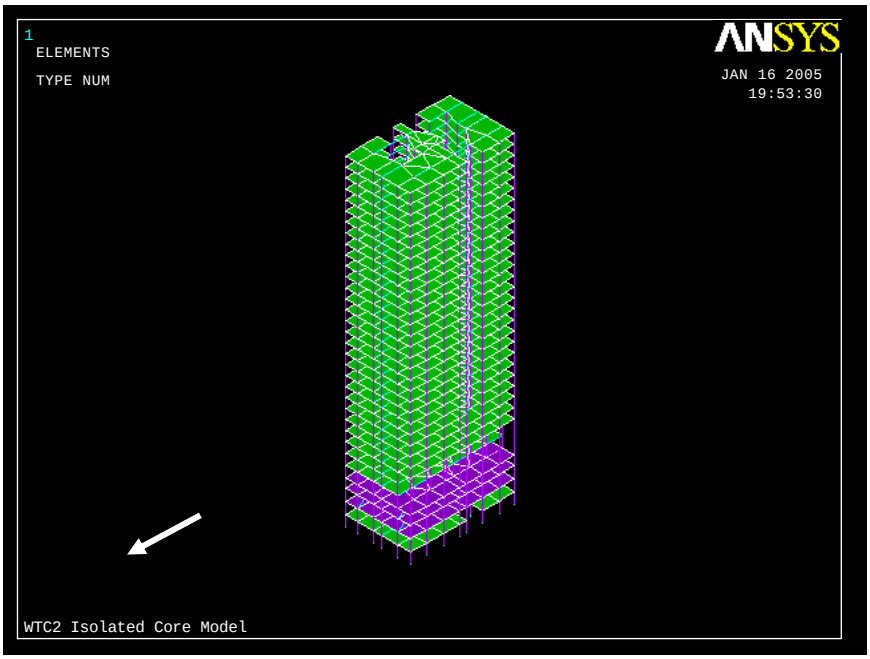

(b) WTC 2

Figure 7–1. Isolated core models.

7.2.2 WTC 1 Core Analysis Results

Figure 7–2 shows the vertical displacement of the WTC 1 isolated core model with impact damage (prior to applying thermal loading) for Case A, where the colors represent the magnitude of vertical displacement. The maximum vertical displacement was approximately 5 in. along the north side of the

core where core columns were severed. Figures 7–3 and 7–4 show the WTC 1 core structural response to Case A and Case B temperature histories, respectively. Case A resulted in column buckling at the northwest corner and the center of the south side between Floors 94 and 97. There was a 21 in. vertical displacement at the northwest corner and a 12 in. vertical displacement at the center of the south side of the core. Case B resulted in column buckling between Floors 94 and 98 and a 44 in. vertical displacement at the center of the south side of the core.

For Case A temperatures, the core structure was first weakened on the northeast side as fires started in that area after the aircraft impact and then on the south side as the fires spread. For Case B temperatures, the core structure weakened at the center of the north side and then the south side. The core structural responses to these two temperature conditions illustrate the slight difference in core areas that were weakened by the elevated temperatures (northeast versus center of north side). When the results of each isolated core model were compared to the observed behavior of WTC 1, the weakening on the south side of the core was best matched by Case A impact damage and Case B temperatures (Case A impact damage and Case A temperatures showed core weakening at the northwest corner of the core).

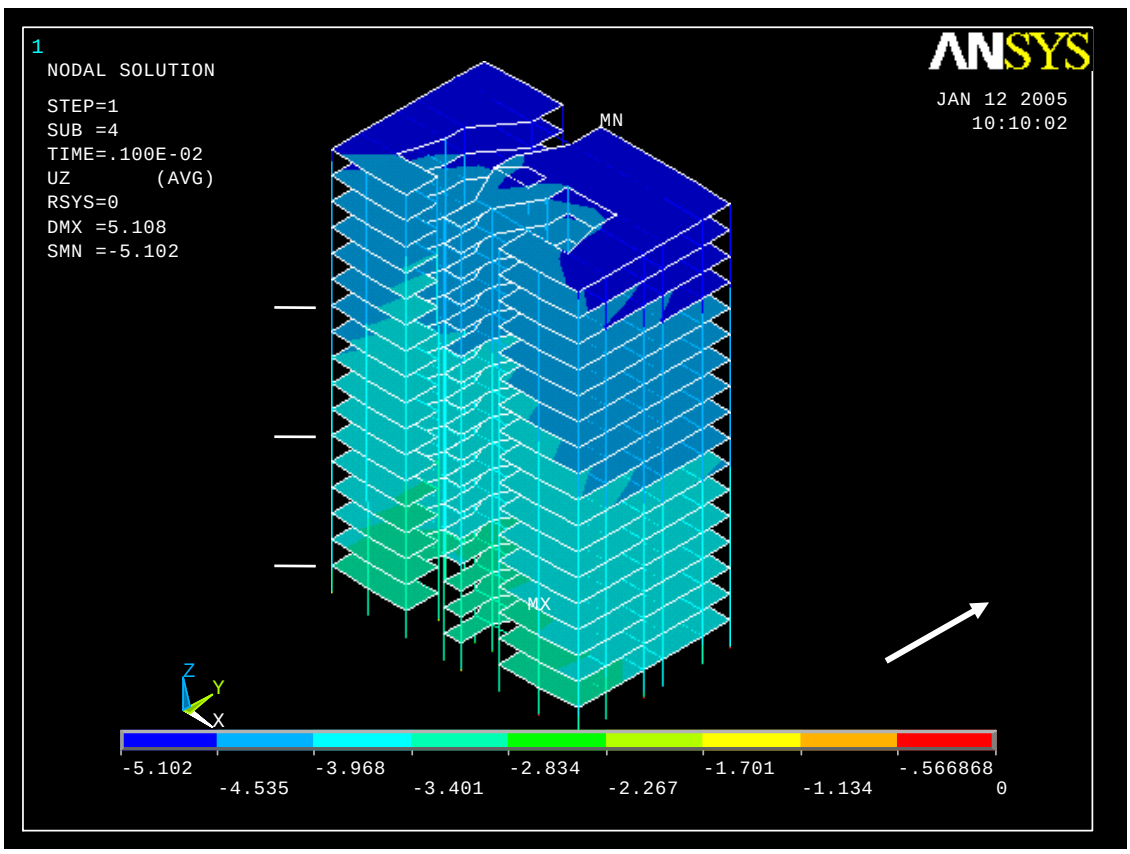

Figure 7–2. Vertical displacement of WTC 1 isolated core model with impact damage and gravity loads.

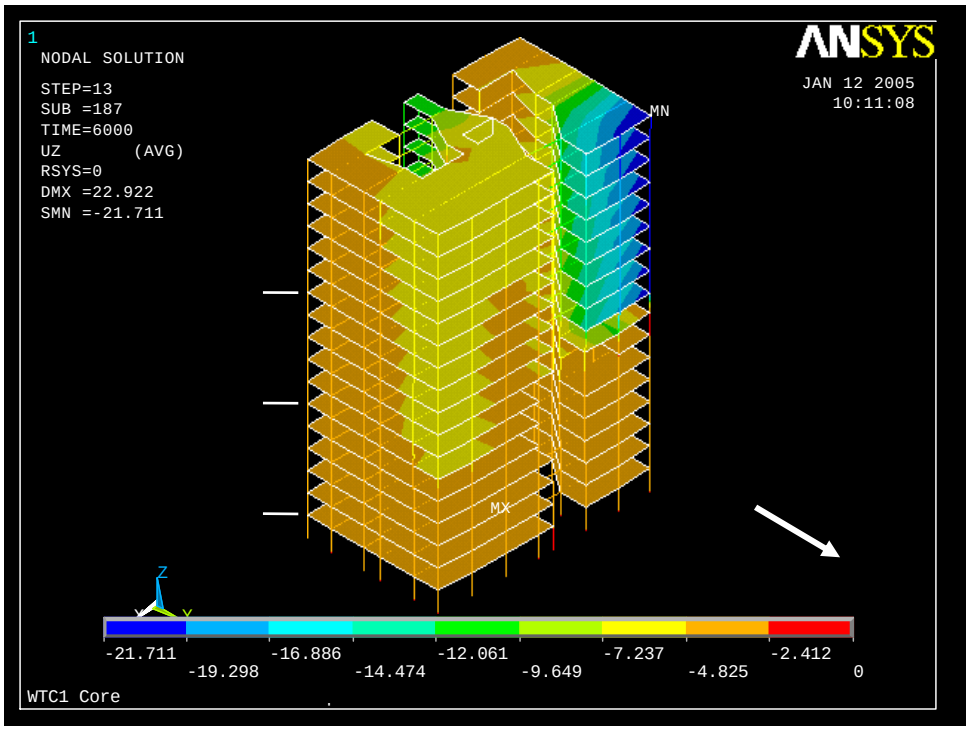

(a) North and east sides

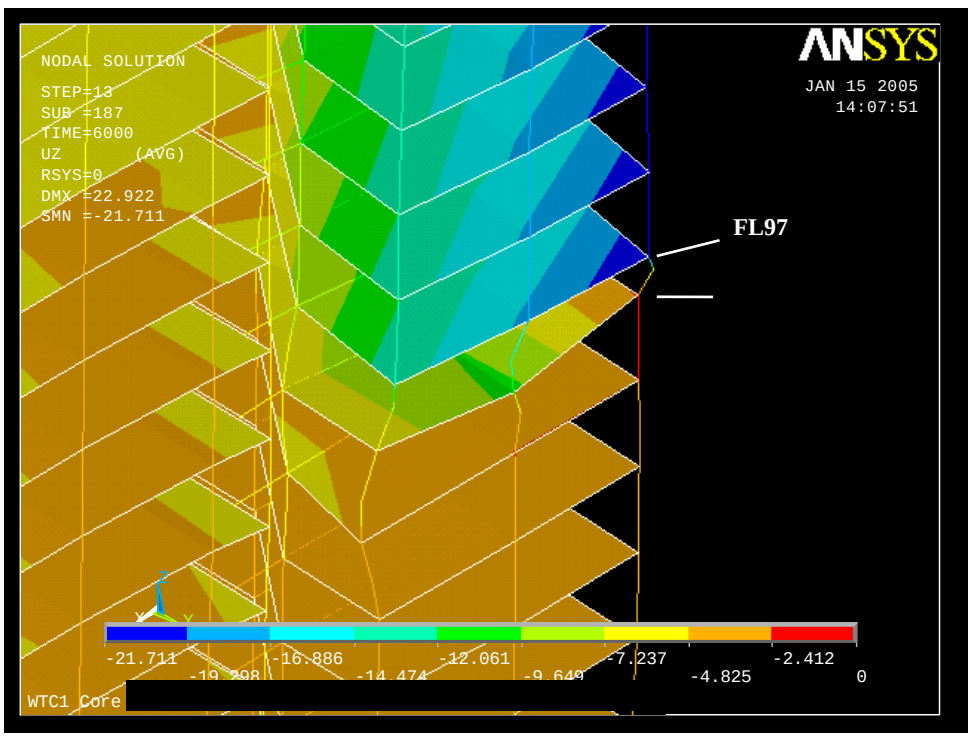

(b) Northwest corner (5X magnification)

Figure 7–3. North side vertical displacement of the WTC 1 core model at 100 min for Case A temperatures.

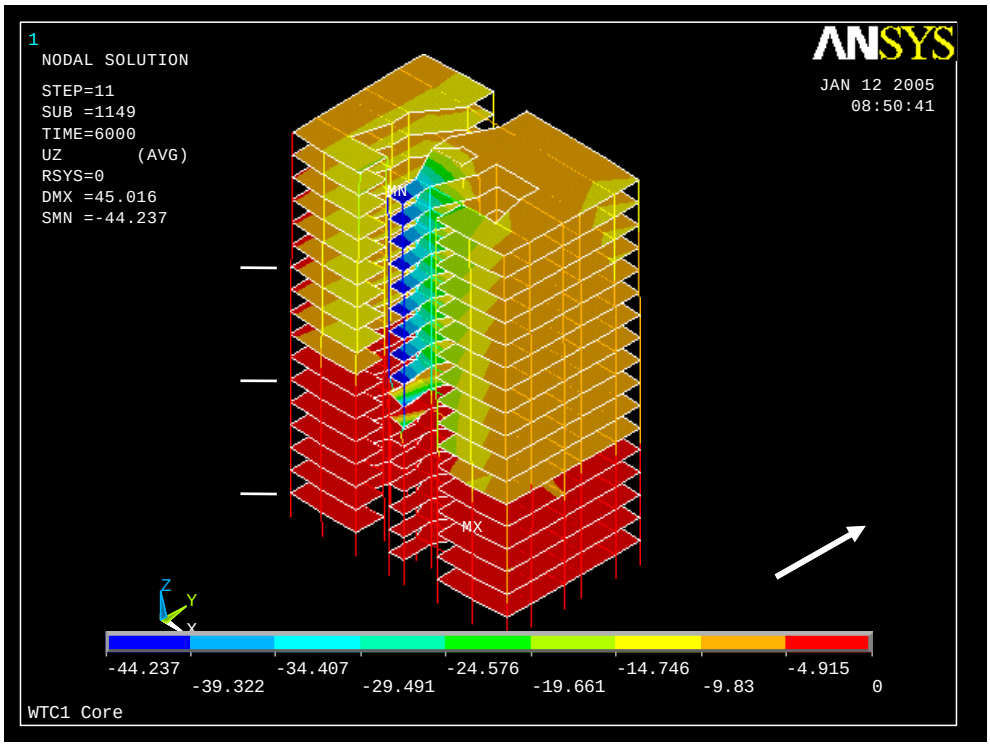

(a) South and east sides

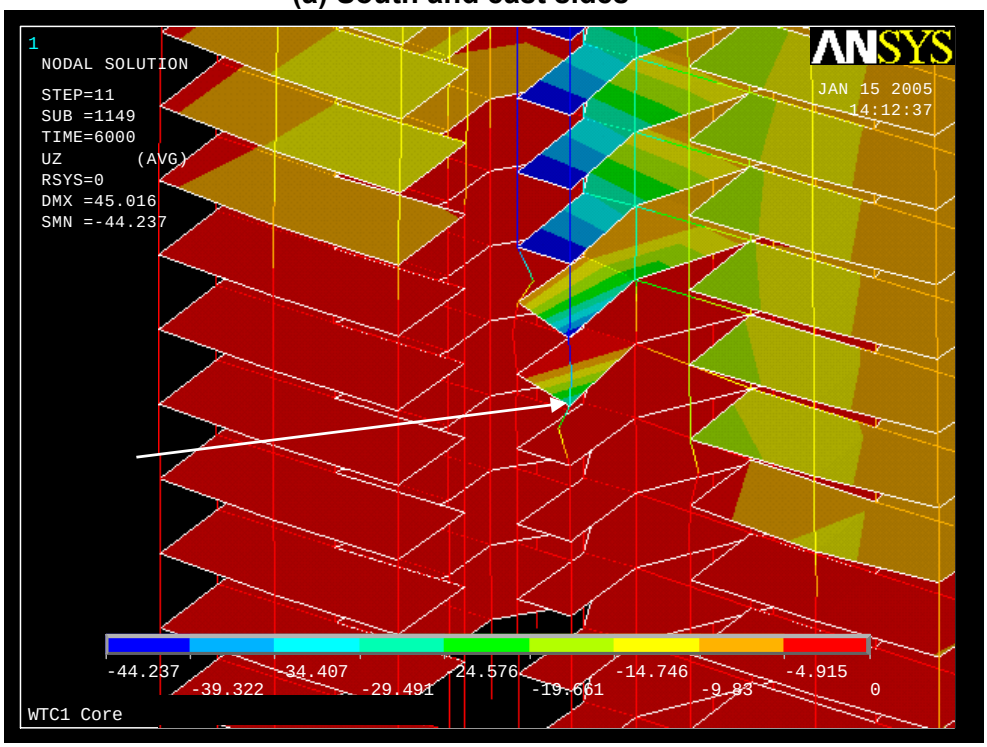

(b) South side (10X magnification)

Figure 7–4. South side vertical displacement of the WTC 1 core model at 100 min for Case B temperatures.

7.2.3 WTC 2 Analysis Results

Figure 7–5 shows the vertical displacement of the WTC 2 isolated core model with impact damage for Case C. The maximum vertical displacement was approximately 5.6 in. at the southeast corner of the core where core columns were severed. Figures 7–6 and 7–7 show the response (vertical displacement) of the WTC 2 core model to Case C and Case D temperature histories, respectively. Case C resulted in a 6.1 in. vertical displacement at the southeast corner. Case D resulted in an 8.1 in. vertical displacement at the southeast corner. Without horizontal restraints, the core would have tilted more toward the southeast corner, and the vertical displacement would have been larger. No columns buckled in either Case C or Case D.

For both Case C and Case D temperatures, the core structure was weakened at the southeast corner and along the east side of the core. The core structural responses to these two temperature conditions illustrate the slight difference in core weakening by the larger deflection in the southeast corner for Case D, which had more column damage. The WTC 2 response for Case C and Case D temperatures was similar, with a 2 in. increase for Case D. When the results of each isolated core model were compared to the observed behavior of WTC 2, both Cases provided a reasonable match.

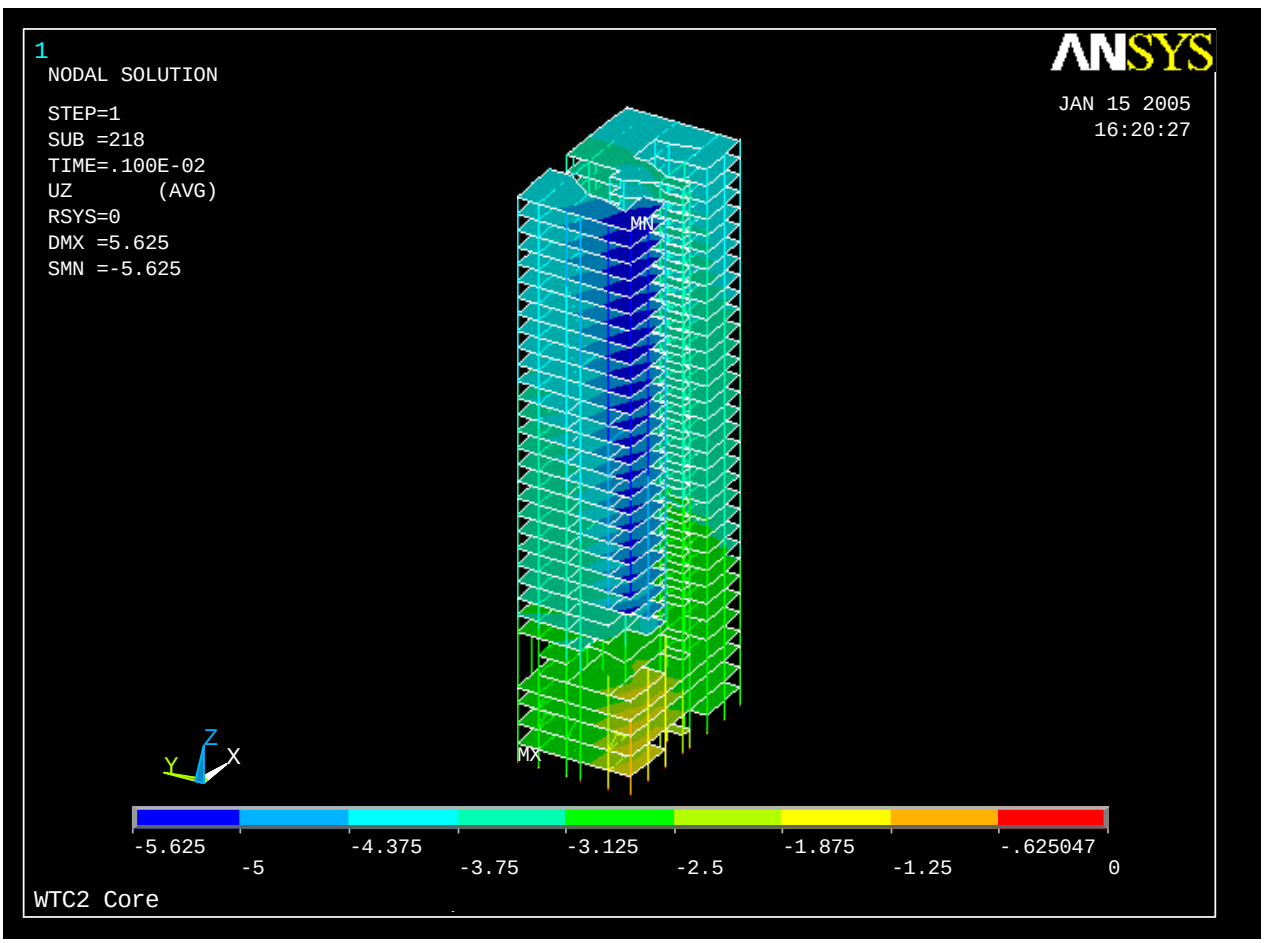

Figure 7–5. Vertical displacement of the WTC 2 isolated core model with impact damage and gravity loads (south and east faces).

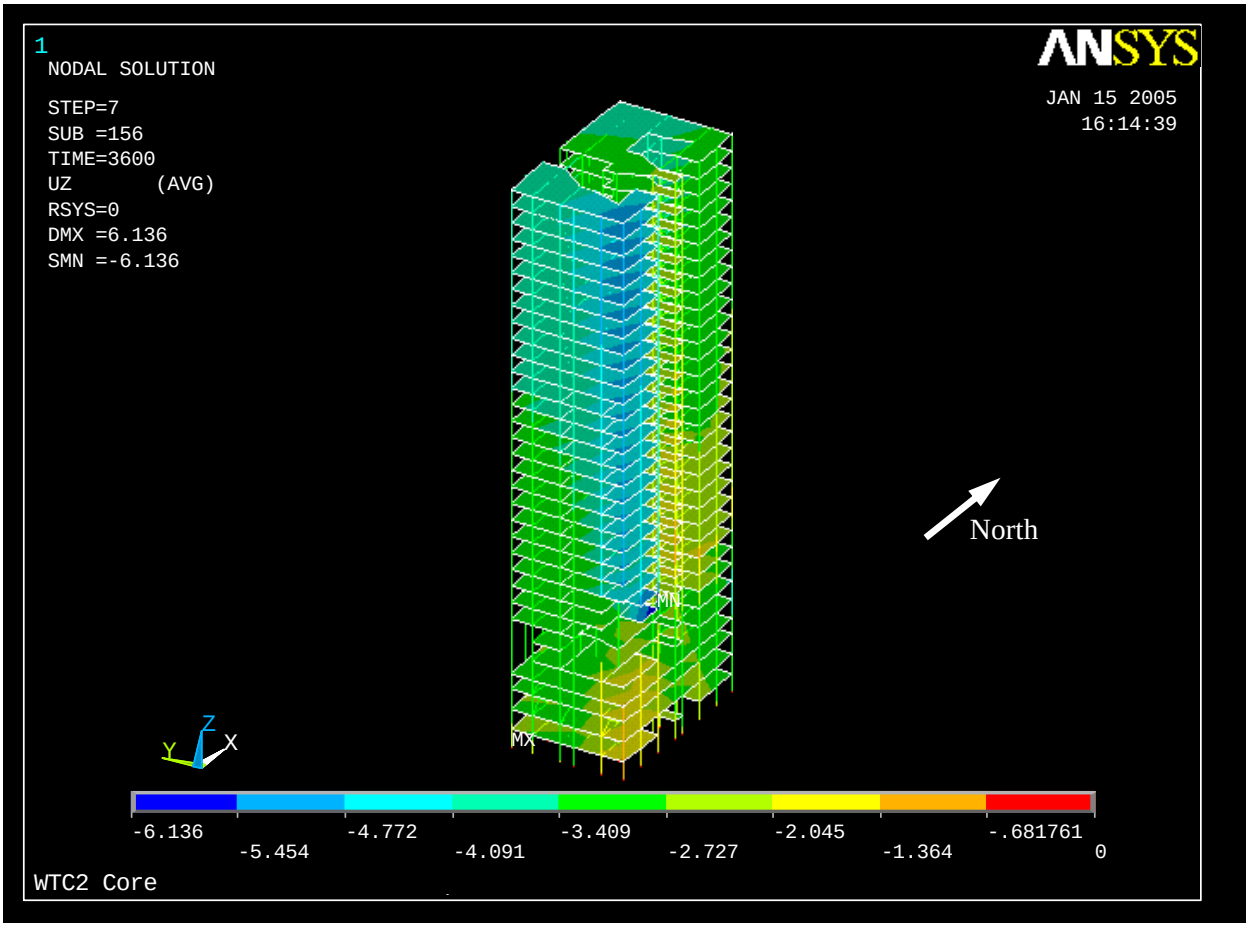

Figure 7–6. Vertical displacement of the WTC 2 core model at 60 min for Case C temperatures (south and east faces).

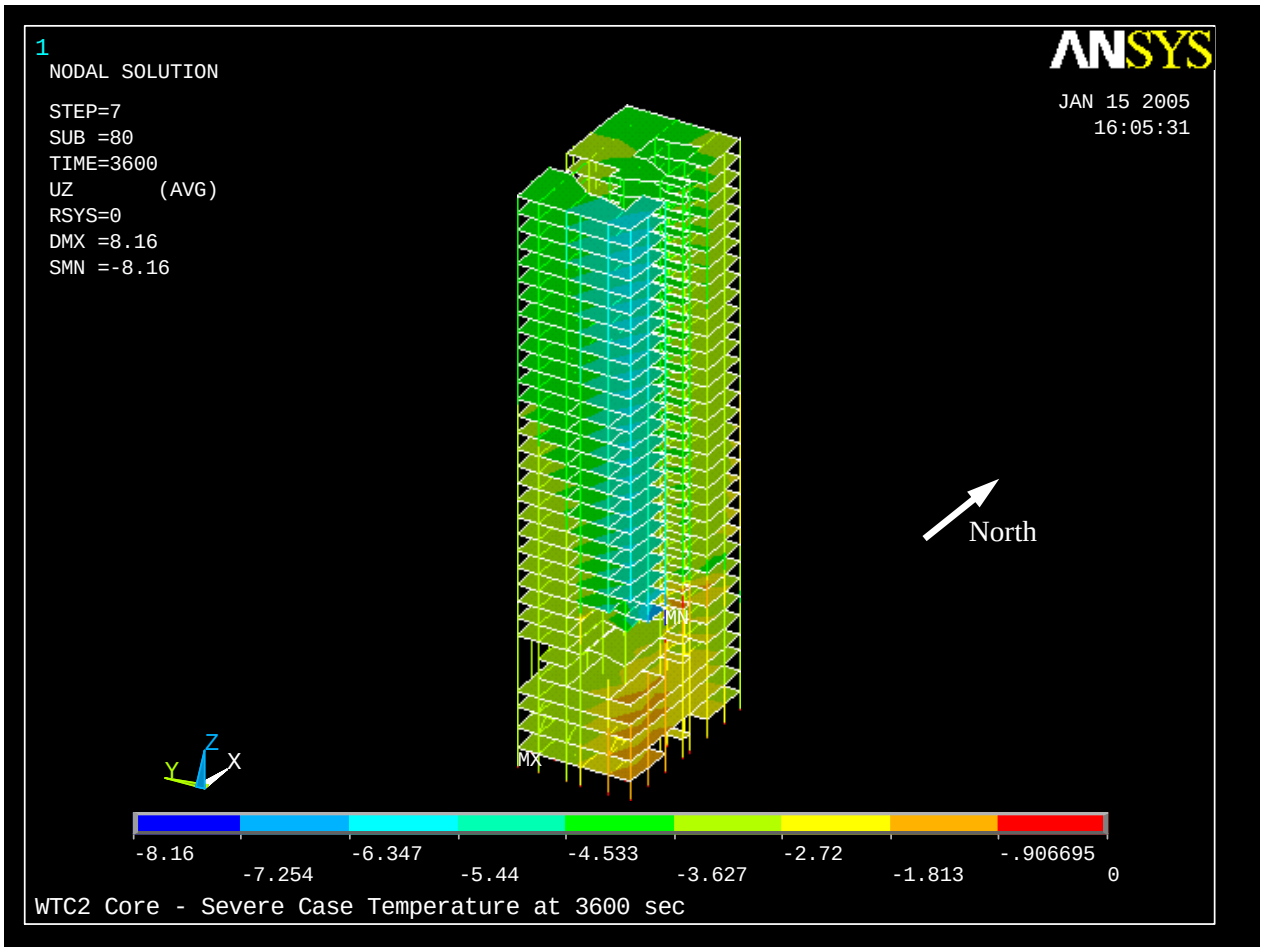

Figure 7–7. South and east side vertical displacement of the WTC 2 core model at 60 min for Case D temperatures.

7.3 FULL FLOOR SUBSYSTEM

7.3.1 Model and Method of Analysis

Figure 7–8 shows the full floor model (described in Chapter 4), which included 1) exterior and core columns extending one story below and one story above the floor model, 2) spandrels, 3) floor slab, 4) floor trusses (bridging trusses were retained only in the two-way floor areas), 5) strap anchors, 6) core beams, 7) deck support angles, and 8) break elements to capture failure modes. Both core and exterior columns were fixed against vertical movement at the lower ends and free to displace at the upper ends. Exterior columns were restrained from out of plane displacement and all three components of rotation at the both column ends. The core columns were free to displace horizontally. Note that the two-way zones shown in Fig. 7–8 extended only to the corners of the core rather than beyond the corners as shown in Fig. 4–7. The extent of two-way action shown in Fig. 7–8 was believed to better represent actual structural boundary conditions.

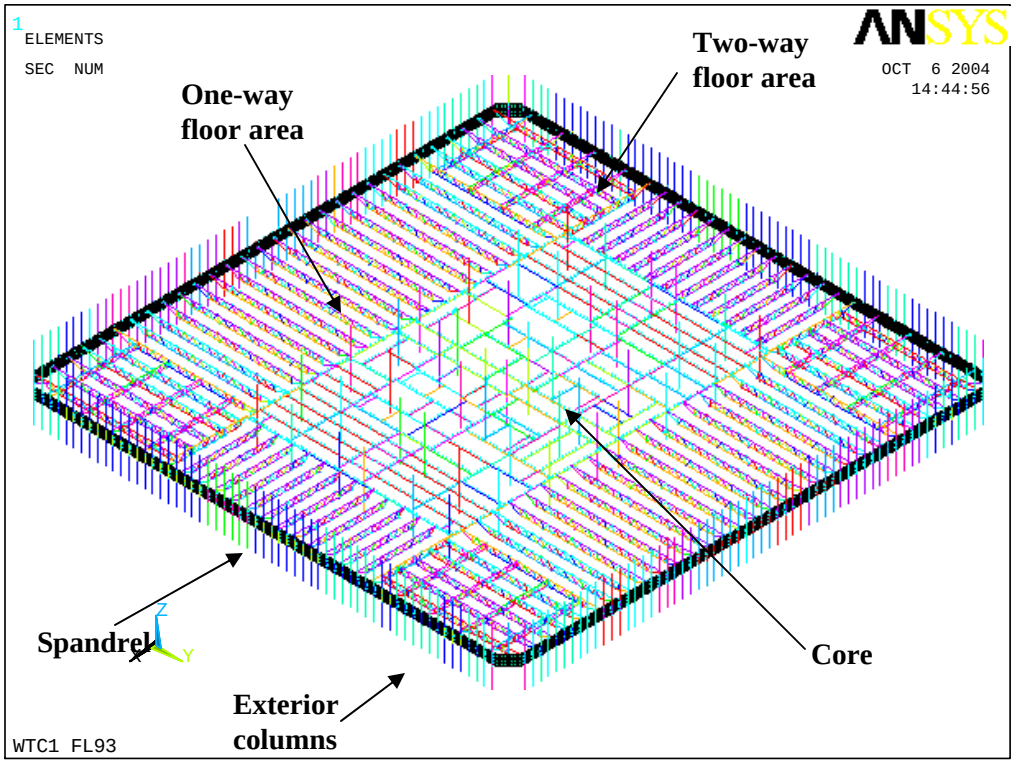

Figure 7–8. Full floor model.

The full floor subsystem models included large deflection and temperature-dependent material properties with plasticity for all steel components. The model was used to evaluate structural response under dead and live loads and elevated temperatures, identify failure modes and associated temperatures and times to failure, and identify reductions in modeling complexity for global models and analyses. The structural response included thermal expansion of steel and concrete members, temperature-dependent properties of steel and concrete that affected material stiffness and strength, and bowing or buckling of structural members. Creep was not included in the full floor models, as this analysis feature did not work with the BEAM 188/189 elements in version 8.0 of ANSYS (the detailed truss model had 3D finite strain elements that were changed to beam elements in the full floor model). Creep was included for beam elements in ANSYS 8.1, and subsequent analyses of the core and exterior wall subsystems included creep deformation.

The floor slab was modeled as lightweight concrete across the entire floor (tenant and core floor areas) with a bilinear stress-strain constitutive model that did not account for cracking or crushing. The concrete material model used the compressive strength as the yield point, with the same yield strength in both tension and compression (the reinforcing steel was assumed to provide the tensile capacity in the composite floor). With this material model, tensile strength of the concrete slab was not represented accurately, and the actual floor stiffness was overestimated. In the full floor models, bending stresses in the concrete slab that exceeded the actual tensile strength of concrete were found in few locations. This phenomenon was typically observed when the temperature of the top of the slab was higher than the temperature at the bottom of the slab, and the concrete slab still deflected down due to large thermal expansion of the truss. However, when the temperature is higher at the bottom, the simplified truss model

with this material model showed a very similar behavior to the detailed truss model, and the key failure modes of the floors were not significantly affected.

Failure modes of the full floor model included truss diagonal buckling and weld failure, exterior and interior truss seat failure, stud failure, strap anchor weld failure, connection failure between primary and bridging trusses, and connection failure between long-span and transfer trusses.

Separate floor models were created from the Floor 96 structural model by imposing the different damage and temperature conditions for WTC 1 Floors 93 to 99 and WTC 2 Floors 79 to 83. Structural components that were severed due to the aircraft impact were removed from each floor model, based upon four initial damage cases, WTC 1 Case A_i and Case B_i and WTC 2 Case C_i and Case D_i. Each full floor model was analyzed for stability under gravity loads consisting of dead load, superimposed dead load, and service live load (25 percent of design live load), which varied from 55 psf to 85 psf. No column loads were applied.

Each floor model was then subjected to the corresponding temperature conditions for each Case in 10 min intervals, as described previously. Temperatures were assigned at structural component nodes. A uniform distribution of temperatures through a cross section was assumed for truss members and spandrels. For columns, a linear gradient in two directions was assumed, and the slabs had temperatures defined at 5 nodes through the slab depth.

Some members were removed from the model to improve computational performance. They were found to fail in the early stages of thermal loading and caused convergence problems. Removal of the following members did not affect the stability and ultimate failure mode of the full floor system under fire:

- Deck support angles and bridging trusses, which buckled due to thermal expansion.
- Shear studs and welds between strap anchors and truss top chords, which failed due to shear force caused by differential thermal expansion between the floor and the exterior wall.

Final damage Cases A, B, C, and D were completed after the initial set of floor analyses were conducted, as described above. The fire simulations did not change between initial Cases A_i to D_i and final Cases A to D, which resulted in the same concrete slab temperatures for the initial and final Cases. The truss temperatures differed as a result of the different estimates of dislodged fireproofing. The full floor models were not rerun for Cases A through D as comparisons showed that the structural temperature histories of the floors were nearly identical for most floors and only slightly different for a few floors. The floor analysis results for Cases A_i to D_i were used for Cases A to D in the exterior wall subsystem (Section 7.4) and global analyses (Chapter 8).

For WTC 1, only Floor 97 showed a significant increase in damage to truss fireproofing on the south side between Case A_i and Case A, where the fireproofing damage over 11 trusses increased from just beyond the core to two thirds of the floor span, as shown in Fig. 7–9. Figure 7–10 shows the temperature distributions for WTC 1 Floor 97 trusses for Case A_i and Case A. Analysis of Floor 97 for Case A damage and temperature histories showed little difference in the floor behavior. Case B_i and Case B structural and fireproofing damage were similar for all floors.

A review of WTC 2 Cases showed that the differences in truss fireproofing damage between Cases C_i and C and Cases D_i and D (mostly on the east side) would cause little difference in the floor temperatures or in the structural behavior. The exception was Floor 83 for Cases C_i and C, where the fireproofing damage increased from half to three quarters of the floor area. However, observations from photographs suggested that the floor was disconnected immediately after the aircraft impact and fireball in this area. Since Floor 83 was assumed to be disconnected at the exterior wall over the area that would be heated in Case C, the analysis was not rerun for this case.

Case A$_i$

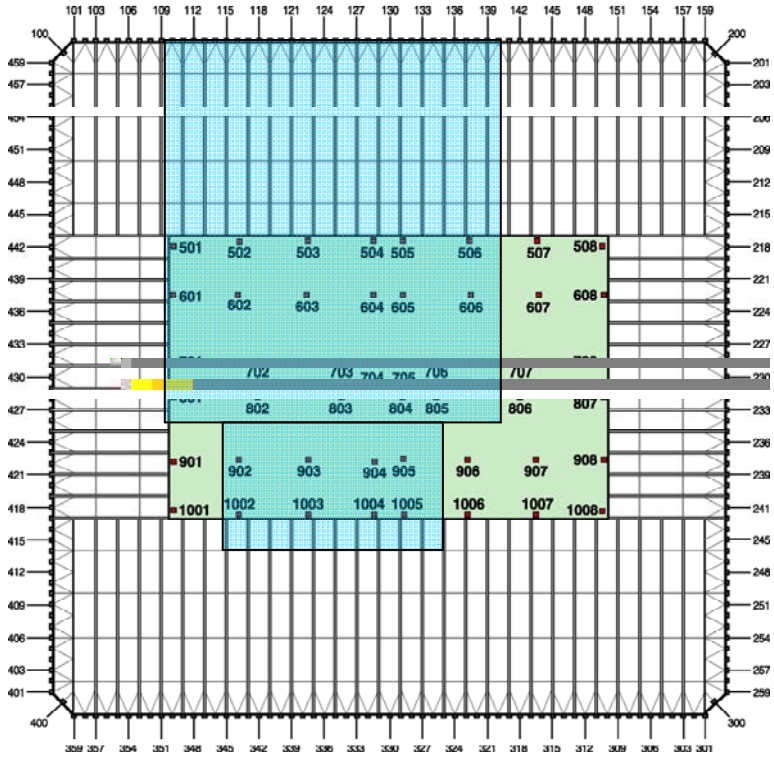

Case A

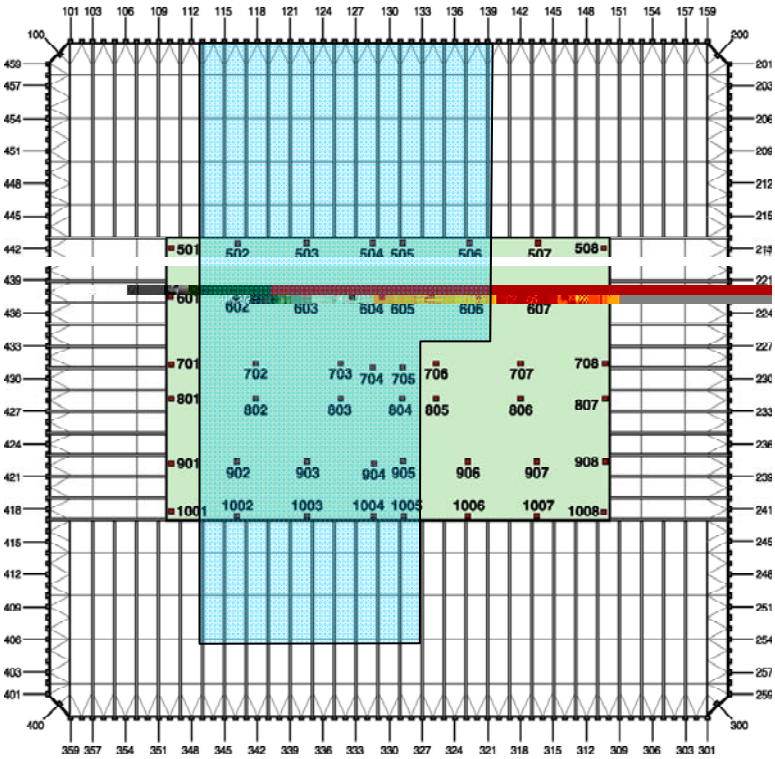

Figure 7–9. Fireproofing damage to WTC 1 Floor 97 for Case A$_i$ and Case A.

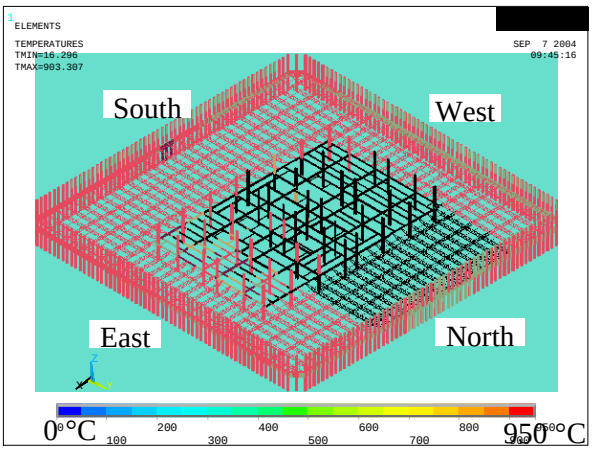

(a) Case A_i top view at 10 min

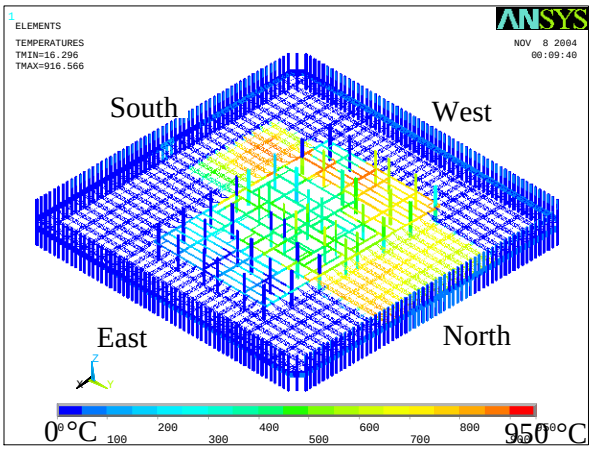

(b) Case A top view at 10 min

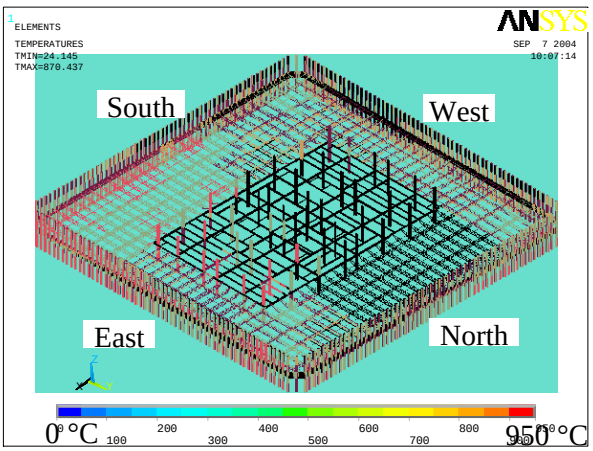

(c) Case A_i top view at 50 min

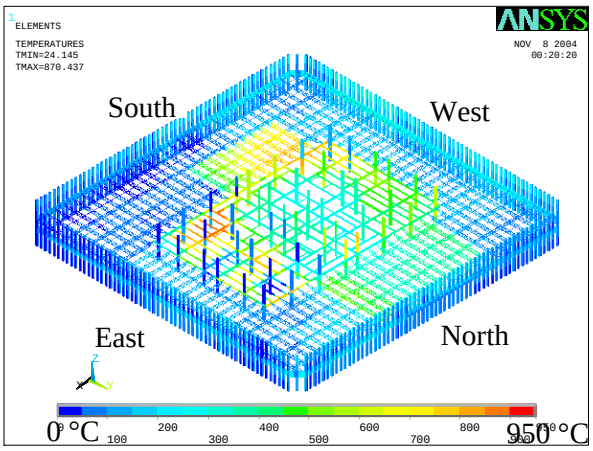

(d) Case A top view at 50 min

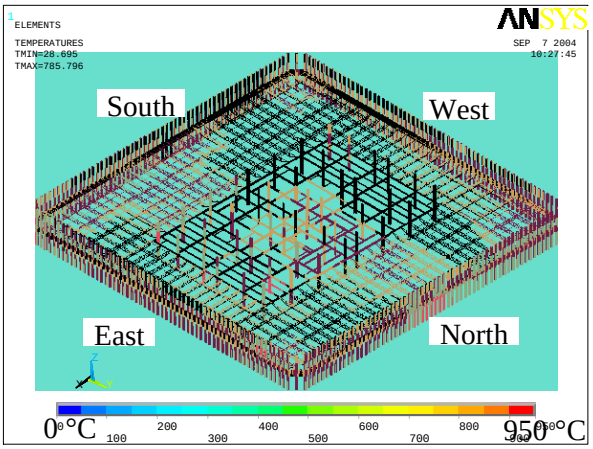

(e) Case A_i top view at 100 min

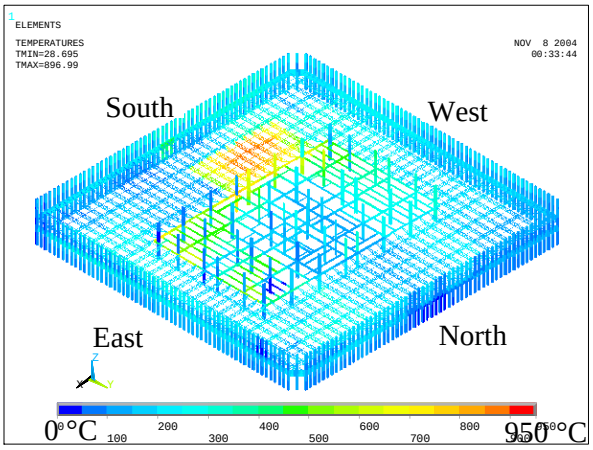

(f) Case A top view at 100 min

Figure 7–10. WTC 1 Floor 97 comparison of truss temperatures for Case A_i and Case A.

7.3.2 WTC 1 Analysis Results

Areas of the floors that were subject to the combined effects of dislodged fireproofing and exposure to fire were found to have two primary failure mechanisms: buckling of diagonal web members and associated sagging of the floor or disconnection of exterior truss seat connections. When the vertical support of truss seat connections failed, the floor would hang or sag between the remaining intact supports. The following descriptions of floor responses to structural impact damage and temperature histories for Cases A_i, B_i, C_i, and D_i present the time, locations, and maximum vertical displacements of the sagging predicted in the floors.

Case A_i

As shown in Fig. 7–9, the intact fireproofing on the south floor trusses resulted in delayed heating of the trusses. The WTC 1 floors in the impact zone had upgraded fireproofing thickness of 2.5 in. (modeled as a thermally equivalent 2.2 in. to account for variability in thickness, Chapter 2). The maximum temperatures shown for Floor 97 trusses on the south side ranged from 300 °C to 400 °C at 100 min. At these temperatures, the steel expanded thermally but had only a modest reduction in stiffness and strength (see Chapter 4).

The maximum vertical displacements of WTC 1 floors are listed in Table 7–1. Floor 95 to Floor 98 showed a significant vertical deflection (sag) in the north office area near the impact damage. The vertical deflection in the south office area was found to be insignificant for all floors. Many diagonals of Floor 95 to Floor 98 buckled in the hottest zones of the north office area. Although gusset plates fractured at several locations, a complete disconnection of the floor from the exterior wall was not predicted. Slab thermal expansion at 100 min (across the entire floor) ranged between 4 in. and 8 in. Since the floors did not sag except in areas adjacent to the impact zone on the north side, almost all the exterior columns were pushed out by the floors. The high level of restraint imposed on the slab expansion by the exterior columns, due to their fixed boundary conditions at column ends, resulted in compressive forces developing in the slab. These compressive forces would likely have been smaller in the towers, as the exterior columns would have expanded outward over the four to five floors subject to fires and provided minimal restraint against thermal expansion of the slab.

Case B_i

Table 7–2 gives the maximum vertical displacement of WTC 1 floors for Case B_i, and Figs. 7–11 through 7–15 show the vertical displacement contours at time of maximum displacement for Floors 95 to 99. Floors 93 and 94 had no fireproofing damage to the south floor trusses. The maximum deflection of Floors 95 and 96 occurred just after the aircraft impact on the north side next to the damage area. Floors 97 and 98 maximum deflection occurred at 100 min on the south side. The time and location of maximum floor deflections illustrate the movement of the fires from the north side just after impact to the south and the effect of the truss fireproofing. The large deflections on the south side of Floors 97 and 98 were caused by the exterior seat failures that began at 90 min, due to reduction of vertical shear strength under the elevated temperatures. Figure 7–16 shows the extent of truss seat failures for Floor 97 and Floor 98, which was a loss of 18 percent to 25 percent of exterior connections for the two floors on the south face. The average slab expansion across the entire floor ranged from 5 in. to 8.5 in. The interaction of the floor slab and exterior columns was the same as described for Case A_i.

Table 7–1. Maximum vertical displacement of WTC 1 floors for Case A_i.

Floor	Maximum Displacement (in.)	Location of Displacement on WTC 1 floor	Time after Aircraft Impact (min)
93	5.4	North side	30
94	13.5	North side	100
95	30.9	North side	10
96	23.3	North side	10
97	31.5	North side	60
98	26.4	North side	30
99	7.0	North side	50

Table 7–2. Maximum vertical displacement of WTC 1 floors for Case B_i.

Floor	Maximum Displacement (in.)	Location of Displacement on WTC 1 floor	Time after Aircraft Impact (min)
93	-5.8	South side	100
94	12.7	South side	100
95	29.2	North side	10
96	28.6	North side	10
97	37.4	South side	100
98	49.0	South side	100
99	6.8	North side	100

Note: Negative value represents upward displacement.

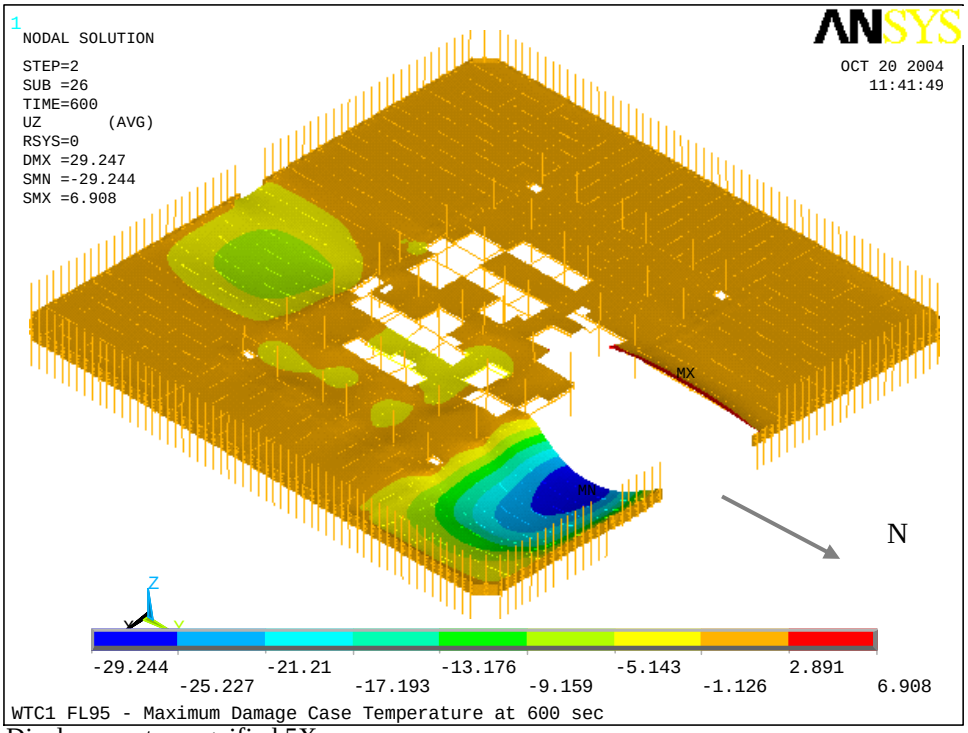

Displacements magnified 5Xs

Figure 7–11. Vertical deflection of WTC 1 Floor 95 for Case B_i at 10 min.

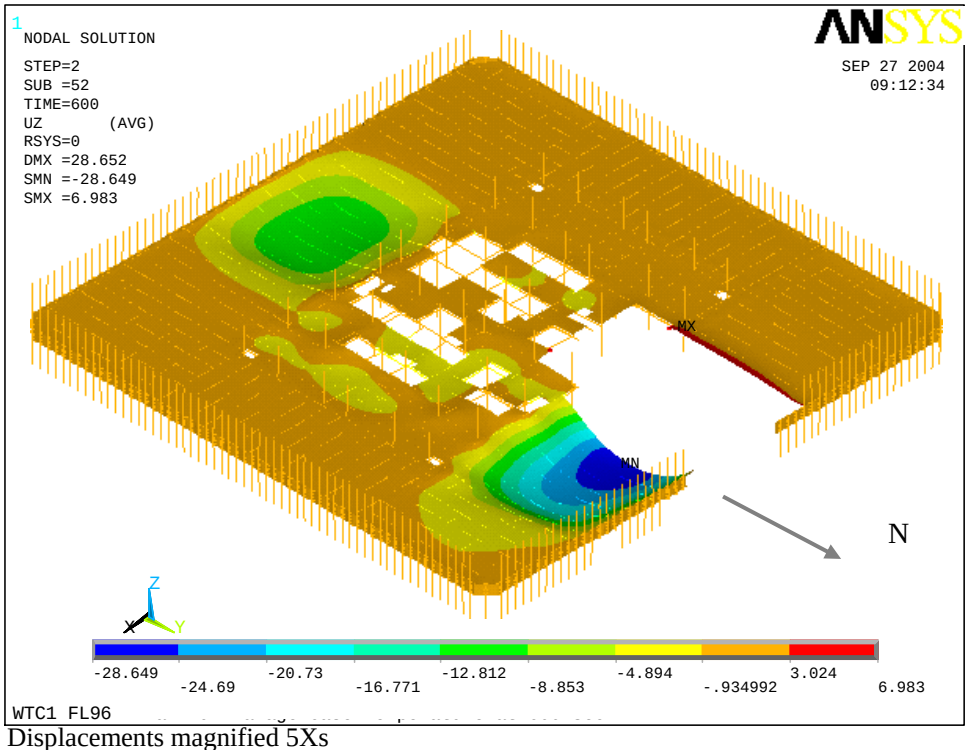

Displacements magnified 5Xs

Figure 7–12. Vertical deflection of WTC 1 Floor 96 for Case B_i at 10 min.

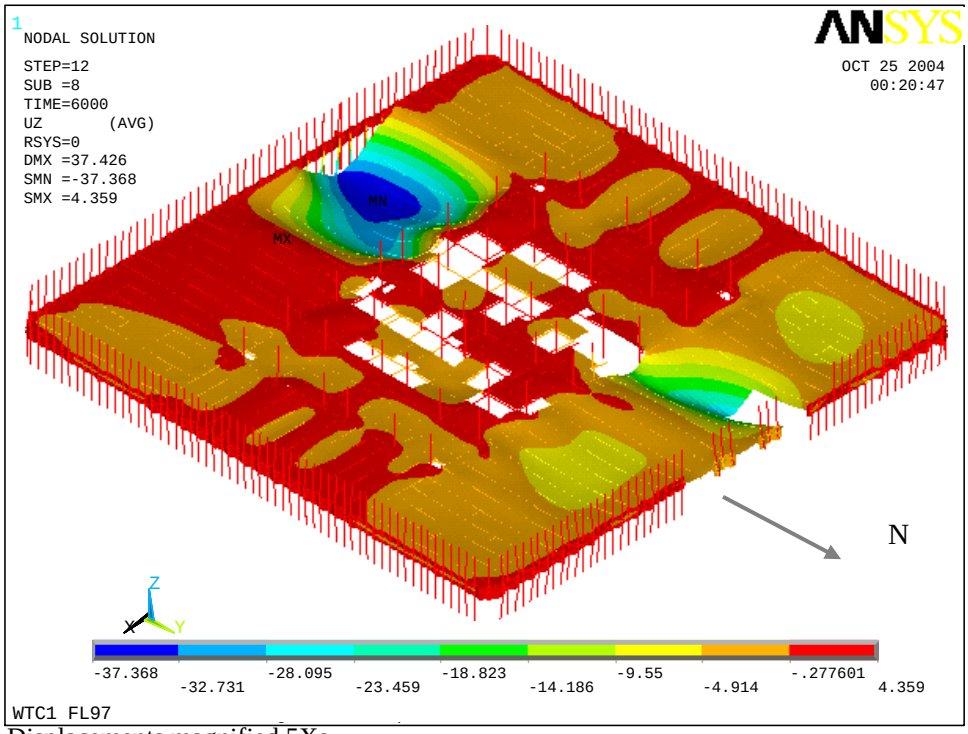

Displacements magnified 5Xs

Figure 7–13. Vertical deflection of WTC 1 Floor 97 for Case B_i at 100 min.

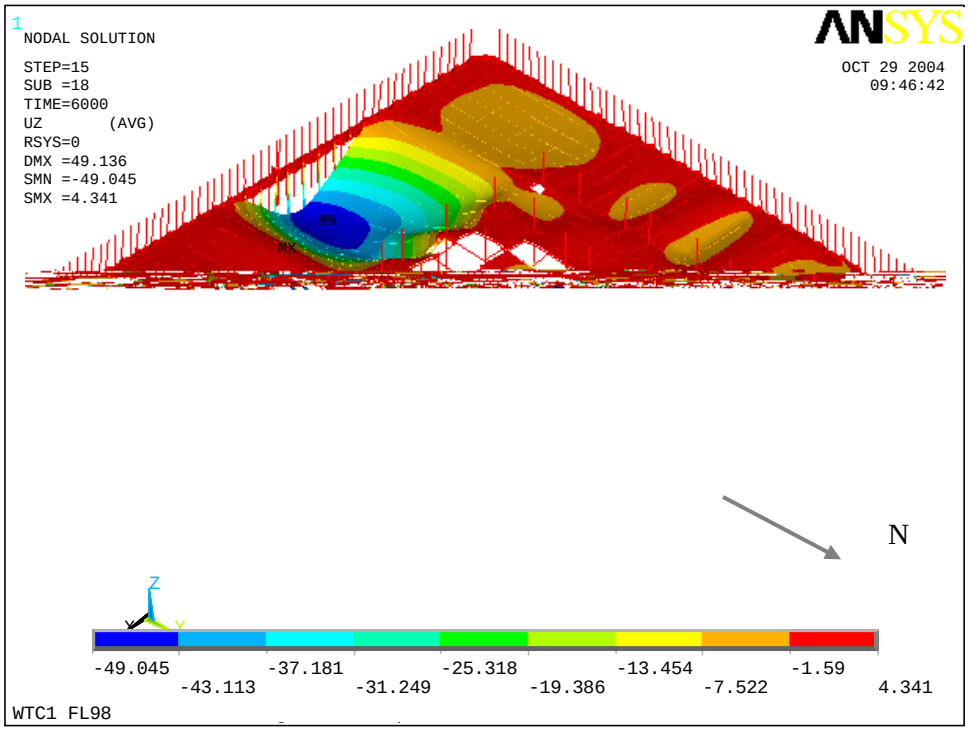

Displacements magnified 5Xs

Figure 7–14. Vertical deflection of WTC 1 Floor 98 for Case B_i at 100 min.

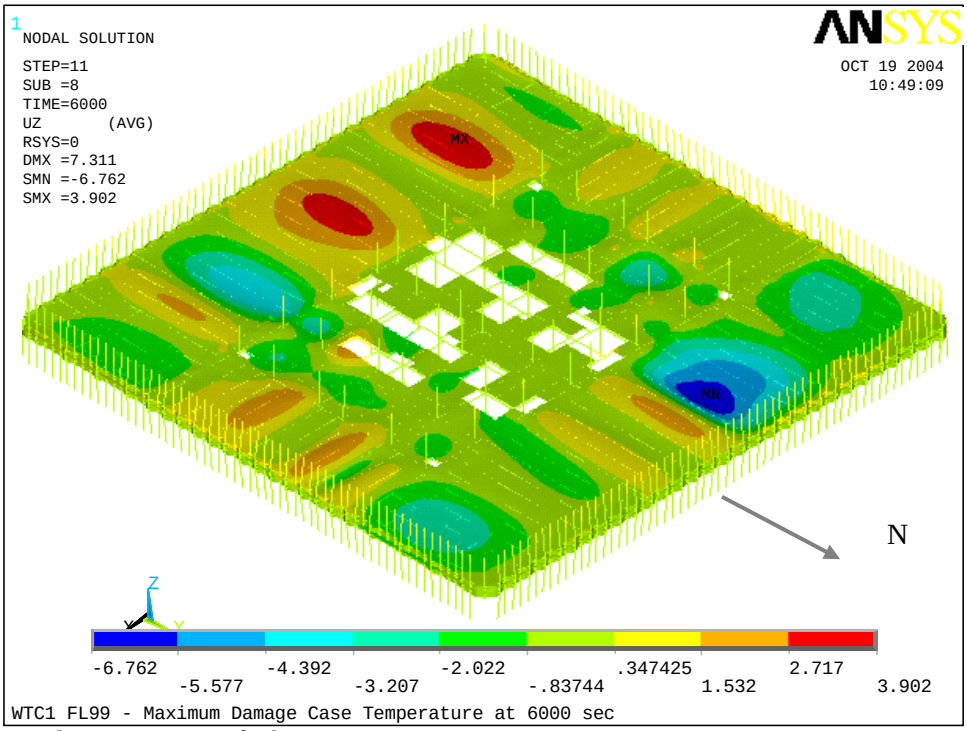

Displacements magnified 5Xs

Figure 7–15. Vertical deflection of WTC 1 Floor 99 for Case B_i at 100 min.

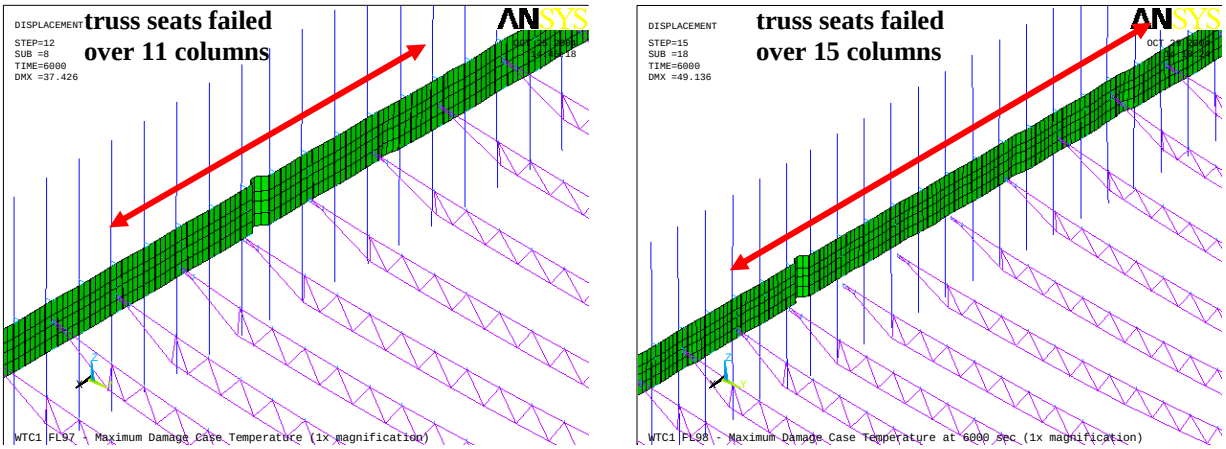

(a) Floor 97 **(b) Floor 98**

Figure 7–16. Loss of vertical supports in WTC 1 Floor 97 and Floor 98 for Case B_i.

7.3.3 WTC 2 Analysis Results

Case C_i

Table 7–3 lists the maximum vertical displacement of WTC 2 floors for Case C_i, and Figs. 7–17 through 7–21 show the vertical displacement contours at time of maximum displacement for Floors 79 to 83. Floors 79 to 83 had impact damage at the south side of the east floor area, but Floors 80 and 81 had many interior truss seats severed from the south exterior wall to the east side of the core perimeter. The maximum vertical deflection occurred in the southeast floor area near the impact damage for all floors, with the exception of Floor 82, which had a maximum deflection in the northeast floor area. The maximum deflection occurred at 60 min for all floors. The location of the maximum deflection was primarily due to the combined effects of impact damage and elevated temperatures. Floor 82 had a large span of unsupported floor along the exterior wall resulting from heat-induced truss seat failures, which led to floor sagging in the northeast corner (see Fig. 7–20).

The west office area of Floors 79 to 83 had vertical deflections ranging from 12 in. to 18 in. at 60 min, due to the combined effect of hot gases that spread throughout the floors and the 0.75 in. fireproofing on the trusses. The average thermal expansion of slabs across the entire floor ranged from 2.5 in. to 5.5 in. at 60 min.

A significant number of truss web diagonals buckled in the east floor area of Floor 81 to Floor 83. Truss seat failures were not observed on Floor 79 to Floor 81. Figure 7–22 shows the truss seat failures for Floor 82 and Floor 83, which extended over 15 percent to 30 percent of the exterior wall width.

Table 7–3. Maximum vertical displacement of WTC 2 floors for Case C_i.

Floor	Max. Displacement (in)	Location of Displacement On East Floor	Time After Aircraft Impact (min)
79	19.0	South side	60
80	30.1	South side	60
81	31.0	South side	60
82	45.2	North side	60
83	38.9	South side	60

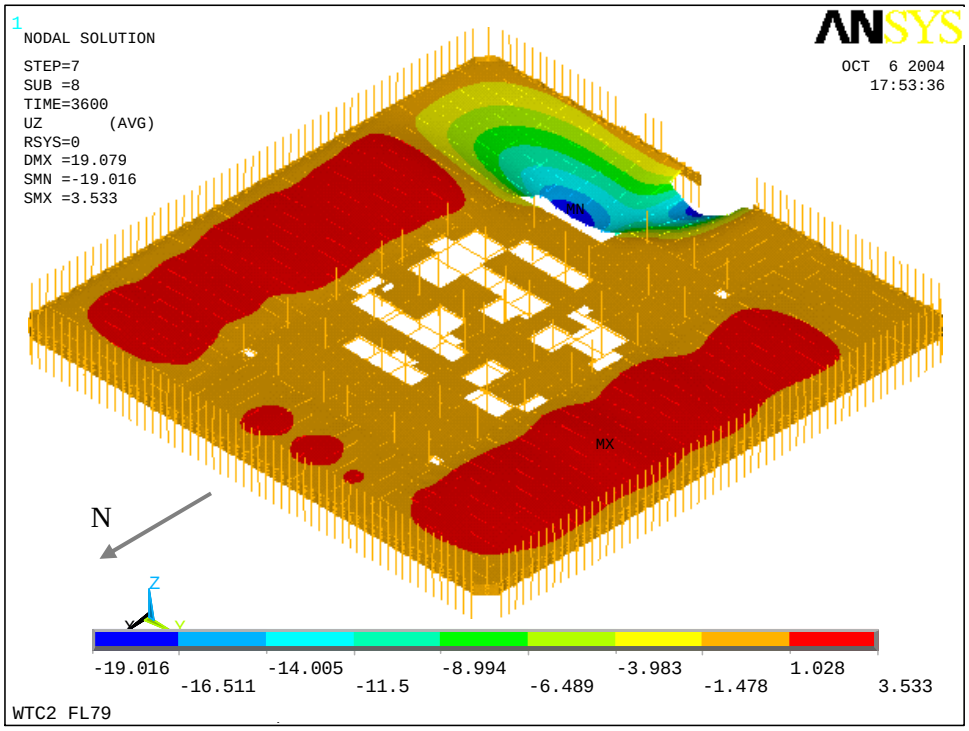

Displacements magnified 5Xs

Figure 7–17. Vertical deflection of WTC 2 Floor 79 for Case C_i at 60 min.

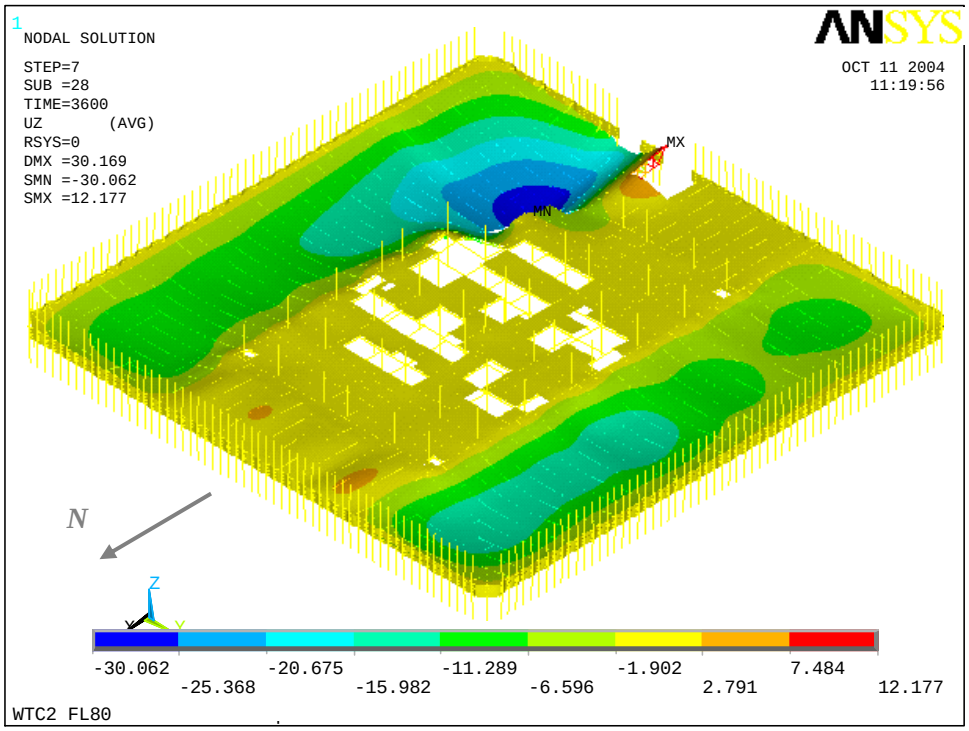

Displacements magnified 5Xs

Figure 7–18. Vertical deflection of WTC 2 Floor 80 for Case C_i at 60 min.

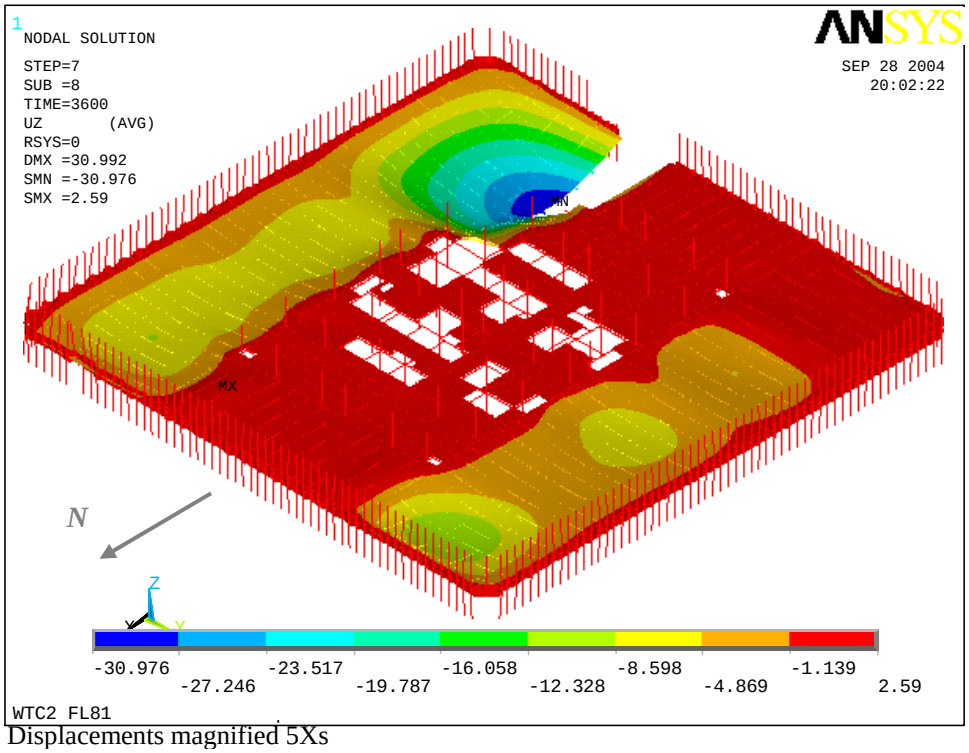

Displacements magnified 5Xs

Figure 7–19. Vertical deflection of WTC 2 Floor 81 for Case C_i at 60 min.

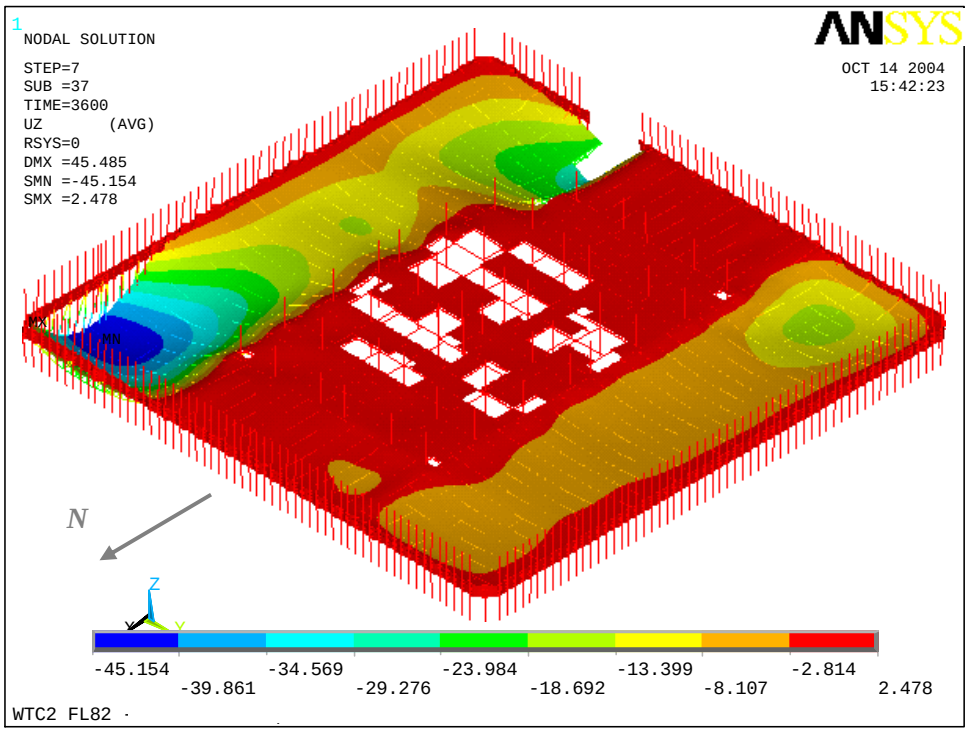

Displacements magnified 5Xs

Figure 7–20. Vertical deflection of WTC 2 Floor 82 for Case C_i at 60 min.

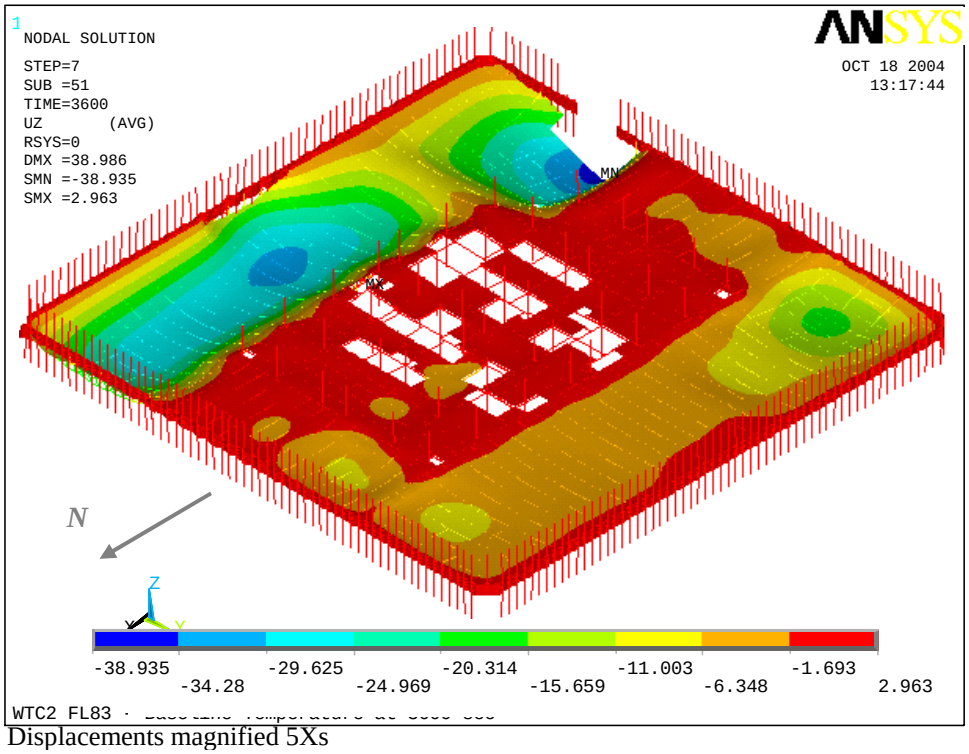

Displacements magnified 5Xs

Figure 7–21. Vertical deflection of WTC 2 Floor 83 for Case C_i at 60 min.

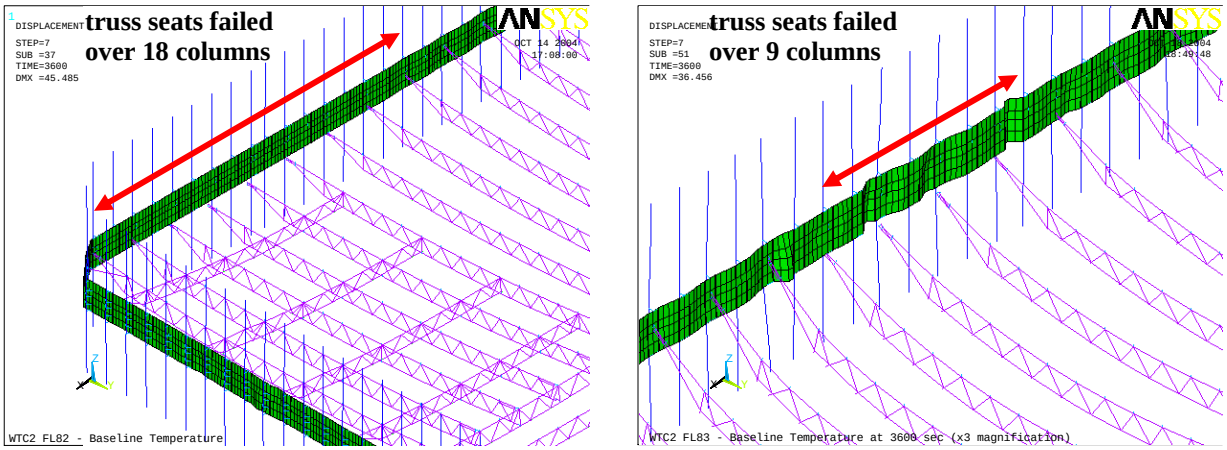

(a) Floor 82

(b) Floor 83
(3X displacement magnification)

Figure 7–22. Loss of vertical supports in WTC 2 Floor 82 and Floor 83 for Case C_i.

Case D_i

Table 7–4 lists the maximum vertical displacement of WTC 2 floors for Case D_i, and Figs. 7–23 through 7–27 show the vertical displacement contours at time of maximum displacement for Floors 79 to 83. Floors 79 to 83 had impact damage at the southeast floor area, but Floors 80 and 81 had many interior truss seats severed from the south exterior wall to the east side of the core perimeter. As Case D_i had more impact damage near the southeast corner of the core than did Case C_i, Floors 80 and 81 had much greater vertical deflections. At 50 min they were 66 in. and 97 in., respectively, in the southeast floor area. The maximum temperatures were similar for Case C_i and Case D_i, but differences in times and locations of maximum temperatures led to differences in locations of maximum vertical displacements. Bridging trusses that had been removed in Case C_i were replaced in Floors 80 and 81 to provide support to the primary trusses in the single-span (one-way) floor area during greater vertical deflections.

The slab expansion across the entire floor ranged from 1 in. to 5 in. Gusset plates and bolts at more than 75 percent of all the exterior seats along the east face of Floors 82 and 83 failed. These connection failures were due to horizontal shear, parallel to the exterior wall, which was caused by differential thermal expansion between the floor framing, the floor slab, and the exterior wall. The truss at Column 357 of Floor 81 was the only one that lost its vertical support at the exterior seat among all the floors. This truss walked off the truss seat.

Several columns along the east and west sides of Floor 80 were pulled inward by the floor sagging in the southeast area. (The inward pull on the west face was due to the lack of horizontal restraint for the core columns in the floor model; in the global model, the inward pull would be resisted by the core. The west face inward pull was not applied in the global model). Floor 79 and Floor 81 showed similar behaviors to Floor 80 in terms of column horizontal reaction forces. Many columns of the west face of Floor 82 were pulled inward, while reaction forces at many columns of the east face were close to zero. As described above, gusset plates and seat bolts failed at a number trusses on the east face of Floor 82. Because columns at these locations were not supported in the horizontal direction by the floor, the reaction force became zero at these columns.

Table 7–4. Maximum vertical displacement of WTC 2 floors for Case D_i.

Floor	Maximum Displacement (in)	Location of Displacement on East Floor	Time After Aircraft Impact (min)
79	35.8	South side	60
80	65.6	South side	40
81	96.7	South side	50
82	49.4	South side	60
83	44.6	South side	60

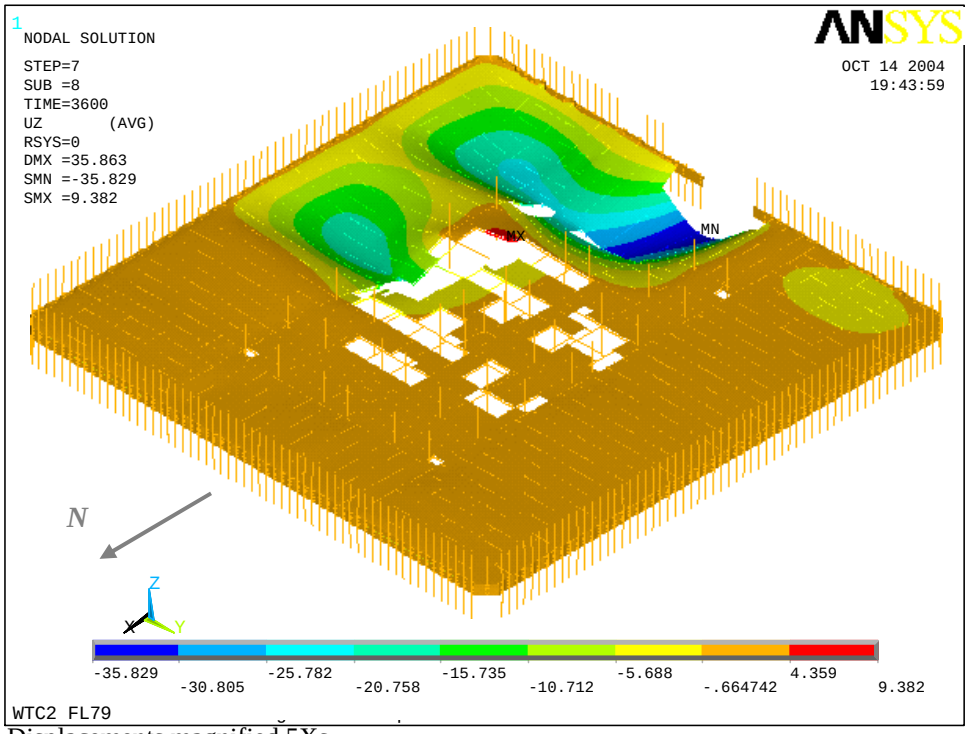

Displacements magnified 5Xs

Figure 7–23. Vertical deflection of WTC 2 Floor 79 for Case D_i.

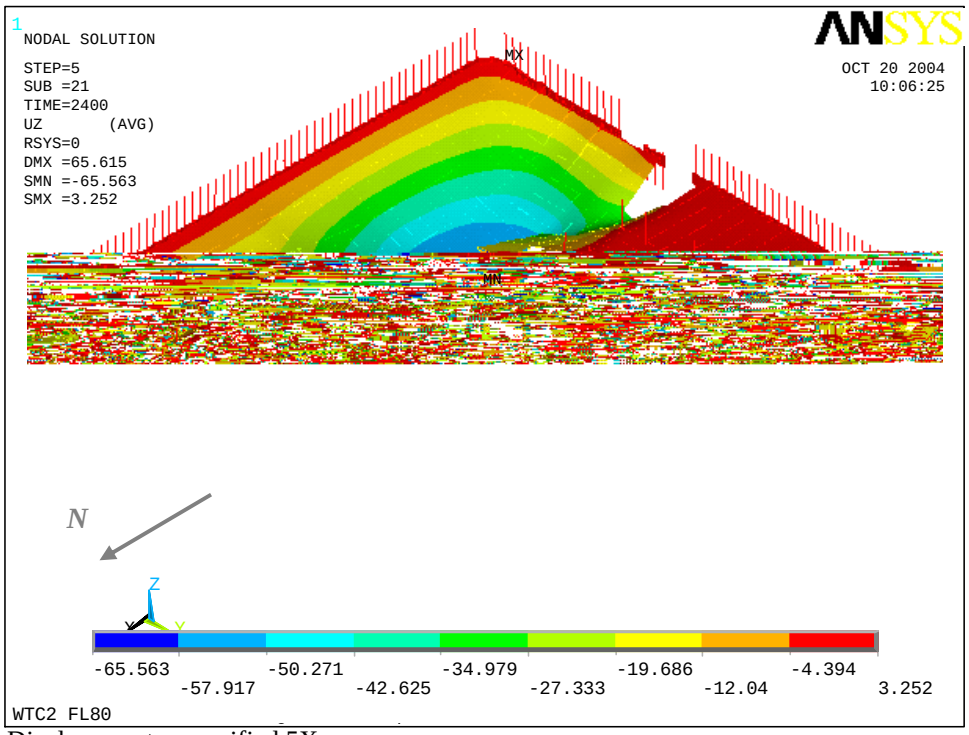

Displacements magnified 5Xs

Figure 7–24. Vertical deflection of WTC 2 Floor 80 for Case D_i.

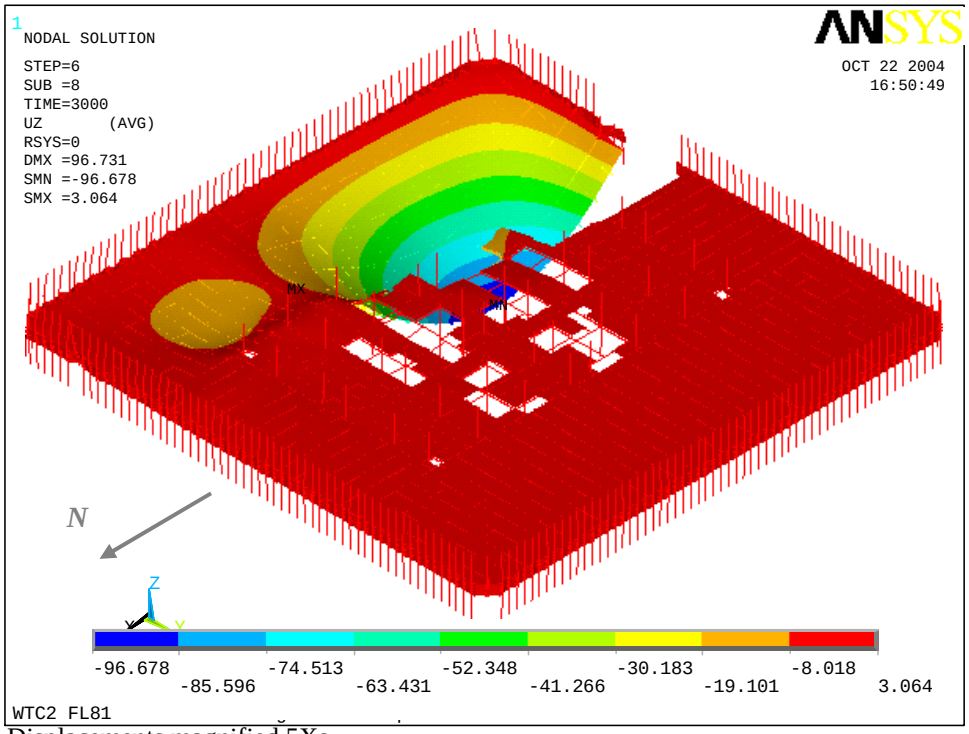

Displacements magnified 5Xs

Figure 7–25. Vertical deflection of WTC 2 Floor 81 for Case D_i.

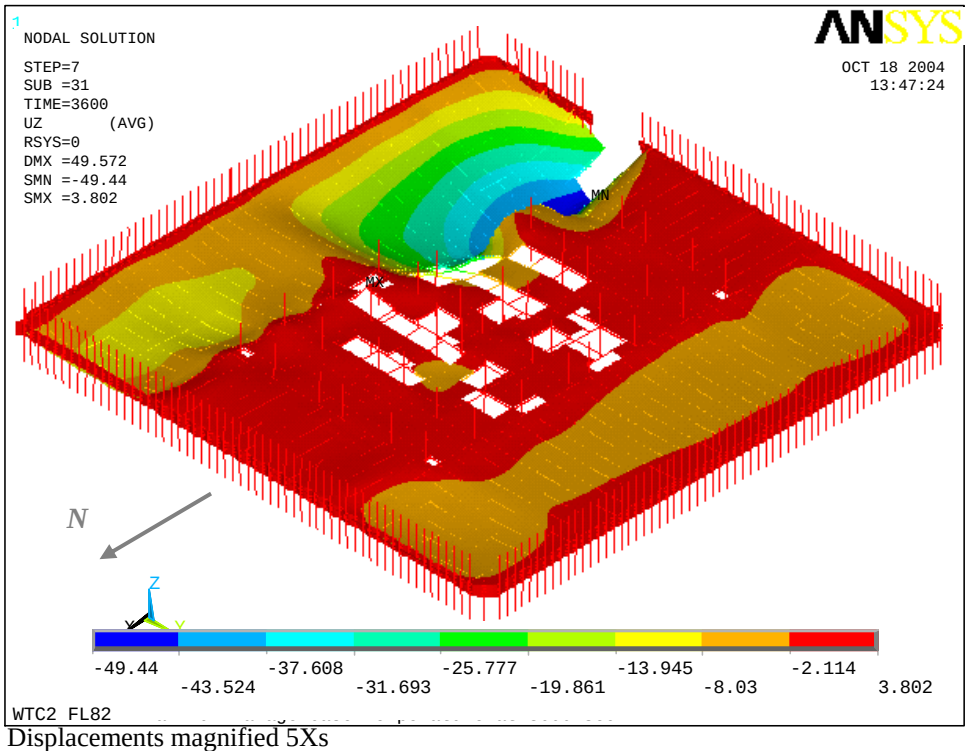

Displacements magnified 5Xs

Figure 7–26. Vertical deflection of WTC 2 Floor 82 for Case D_i.

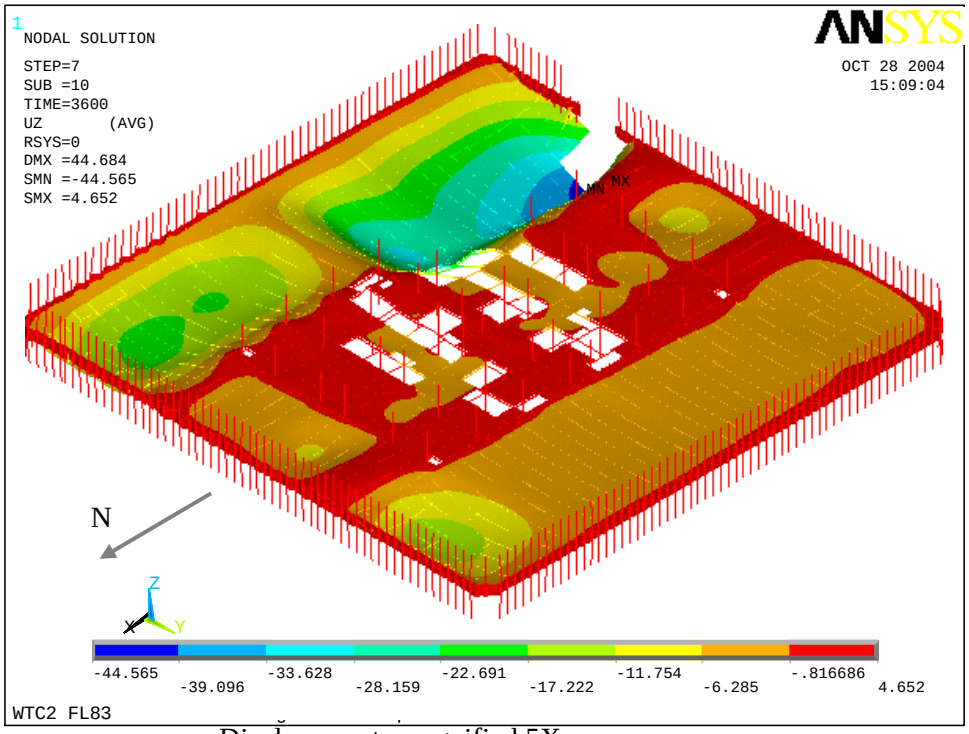

Displacements magnified 5Xs

Figure 7–27. Vertical deflection of WTC 2 Floor 83 for Case D_i.

7.4 EXTERIOR WALL SUBSYSTEM

The primary function of the exterior walls of the WTC towers was to resist wind loads, but they also carried approximately 50 percent of the building gravity loads. For the WTC tower response to impact damage and ensuing fires, the performance of the exterior wall under gravity loads was of interest and is addressed in this section. NIST NCSTAR 1-2 addresses the performance of the exterior wall under gravity and wind loads.

The exterior wall was assembled with panels that were 3 stories high and 3 columns wide with spandrel beams at each floor level. Adjacent panels were staggered by one floor to avoid alignment of the bolted panel connections across a given floor level. Panel geometry was generally uniform at the upper stories of the towers, but the steel grade and plate thickness varied within and between panels, depending upon a panel's location in the tower face. Examination of structural drawings showed that the plates at the impact floors had the same yield strength. Therefore, in the translation process, all plates in the same column cross section were considered to be of the same material. Panel connections were designed for compressive and tensile loads.

Floor trusses were attached to every other column, with the same set of columns loaded at every floor. The exterior columns and deep spandrel beams resulted in a rigid frame that was efficient at redistributing loads in the plane of the wall. The columns redistributed their loads within three to four floors. The floors and spandrels provided lateral support to the exterior columns. Loss of lateral support through failed floor connections increases the possibility of column instability (buckling), depending upon a column's load and temperatures. The hat truss was connected to each exterior wall at Floor 108 with four

truss members extending from the core perimeter. The hat truss provided a load path between the core and exterior walls. As discussed previously, the hat truss was the primary load path between the core and exterior walls, and the floors provided a secondary load path.

The analysis of a single exterior face provided insight into the conditions that would result in the inward bowing of the south wall of WTC 1 and the east wall of WTC 2 observed in photographs (see Chapter 6). Conditions examined included pull-in forces resulting from sagging floors, disconnected floors resulting from truss seat failure, additional vertical loads simulating load transfer to the exterior wall, and elevated temperatures.

7.4.1 Finite Element Model and Methods of Analysis

The exterior wall models extended over 18 floors for the full width of a single face and were centered around the areas of impact and fire damage. The south face of WTC 1 extended from Floor 89 to Floor 106, and the east face of WTC 2 extended from Floor 73 to Floor 90, as shown in Fig. 7–28. The exterior panel that was severed during the aircraft impact and found south of the tower was removed from the south face of WTC 1. No structural damage to the panels was observed on the east wall of WTC 2. The same boundary conditions were applied for both exterior wall models, shown in Fig. 7–29. Springs were included at the base of the global models to represent the response of the exterior wall below the model. The exterior wall models included temperature-dependent plasticity, creep, and plastic buckling behavior.

The exterior wall models were first analyzed for gravity loads with aircraft impact damage. The loads in the columns right after aircraft impact included a set of axial forces at the top of the isolated wall model that accounted for the columns above the top of the model. These loads were taken from an initial global model that did not include creep or column buckling. This global model is further described in NIST NCSTAR 1-6C. Floor gravity loads were also applied at each column with a floor connection.

The exterior wall models were then subjected to two temperature conditions for each tower: Case A and Case B for WTC 1 and Case C and Case D for WTC 2. Elevated temperatures were applied to the wall structure in 10 min intervals, as described previously. At the beginning of each 10 min interval, floor connections were either (1) disconnected where observed in photographs and videos or computed in the full floor analyses, or (2) loaded with an inward force where inward bowing was observed during that time interval. At later stages of the WTC 2 analysis, where additional floor disconnection occurred, the inward pull at that connection was removed.

Temperatures of structural components were based upon the combined effects of member size, fireproofing damage, and fire size and duration. For the exterior columns and spandrels, the interior face was heated directly by fires through radiation and convection and the adjacent faces were heated through conduction and cooled by convection. Elevated temperatures caused thermal expansion of heated columns and modified the stresses in affected and adjacent structural members. Elevated temperatures above 400 °C to 500 °C resulted in a reduction of load-carrying capacity and an increase in plastic and creep deformations.

Inward pulling forces were estimated through a trial and error procedure. In each trial, a magnitude of inward pull force was assumed and the model results were checked. The magnitude was kept constant until the end of the analyses unless a floor connection became disconnected (see Section 7.3), at which point the inward pulling force was set to zero. The inward bowing displacements were compared to the

displacements measured from photographs at the same time points. The wall response was significantly affected by accumulated plastic and creep strains, which were themselves functions of temperature and inward pull over time.

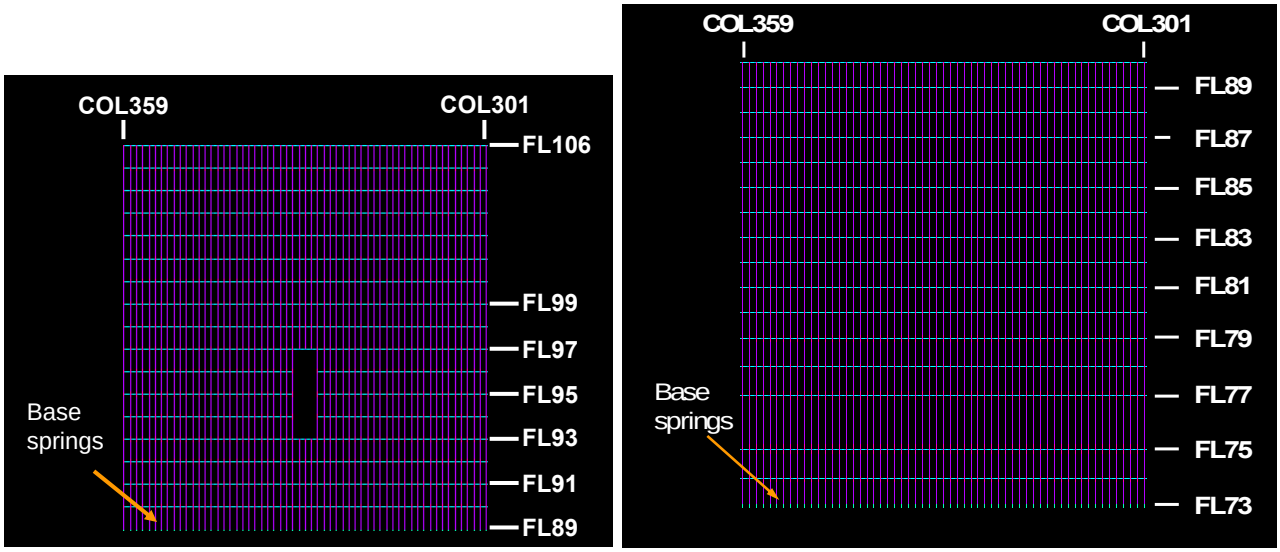

Model of WTC 1 south wall **Model of WTC 2 east wall**

Figure 7–28. Isolated exterior wall segments from WTC 1 and WTC 2.

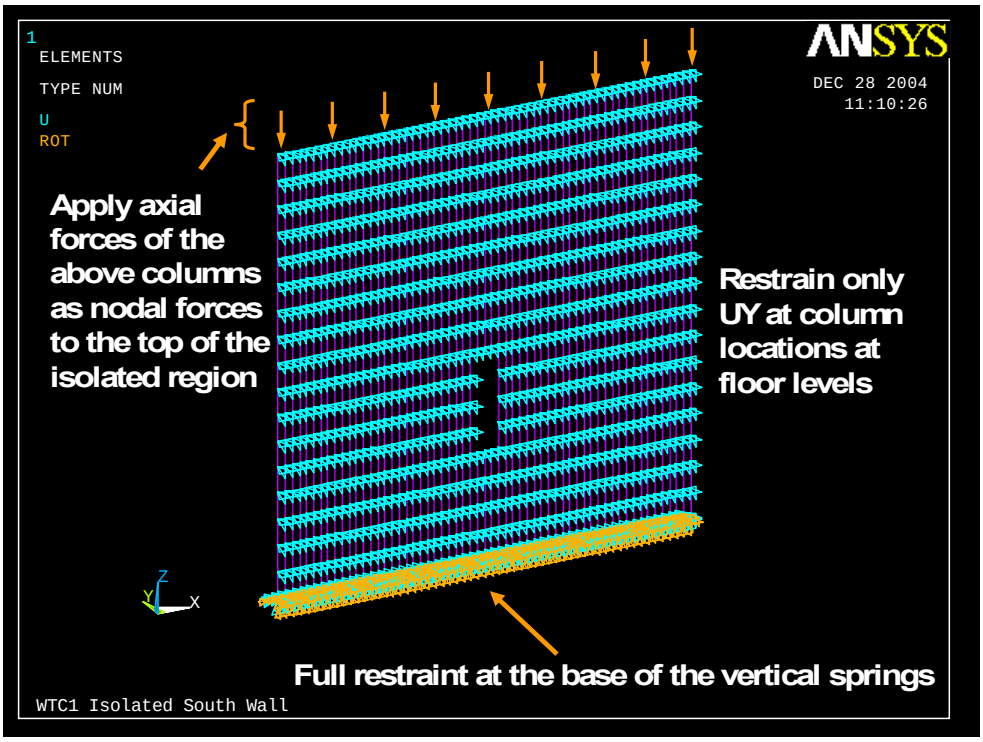

Figure 7–29. Boundary conditions applied on the isolated exterior wall segment.

7.4.2 WTC 1 Analysis Results

The magnitude and distribution of inward pull forces on the south wall, which resulted in inward bowing similar to that observed in photographs, were estimated from the WTC 1 exterior wall subsystem analyses. The final magnitude thus obtained was used in the WTC 1 global analysis.

Initial trials with Case A and Case B damage and temperatures limited pull-in forces to areas with floor sagging sufficient in the full floor models to cause pull-in forces. However, such limited areas of pull-in forces did not produce results that were consistent with the observed inward bowing. This was primarily due to the lack of fireproofing damage to the south exterior wall and floor truss on the south side in Case A impact damage estimates. With the thermally equivalent 2.2 in. of fireproofing intact on the south trusses, these trusses did not heat appreciably, and the floors did not sag.

Case B had elevated temperatures for the south floor trusses and exterior columns where fireproofing was damaged between Floors 94 and 98. A second set of trials applied a pull-in force uniformly across Floors 95 to 99, except where the floor connections had failed. This extent of pull-in forces from floor sagging was greater than that shown by the full floor analyses, but produced a better estimate of the inward bowing as evidenced from the photographs. The smaller extent of floor sagging in Floors 95 to 99 that was predicted by the full floor analyses was likely due to the conservative estimates of fireproofing damage. This assumption produced a lower bound on the bare steel surface area, thereby making it more difficult to heat the steel to the point of failure. Greater fireproofing damage from structural accelerations caused by the aircraft impact and subsequent vibrations as well as possible damage to the concrete slab from high thermal gradients near the slab surface may have contributed to the more extensive inward bowing of the exterior wall that was observed.

In one trial, the magnitude of the pull-in force was increased over time until the the wall became unstable at 90 min. When the magnitude of the pull-in force reached 9.37 kip per column, the analysis stopped due to non-convergence. At the end of analysis, the maximum inward bowing was 24.7 in.

In another trial, the effect of thermal loading in combination with pull-in forces was examined. Pull-in forces were applied at 80 min, since temperatures on the south side began to increase around that time, and the thermal loading was continued to 100 min. In this analysis, the magnitude of the pull-in force was set to 6 kip per column so that the wall would not become unstable as a result of pull-in forces alone.

Figure 7–30 shows the locations of floor disconnections and pull-in forces. After applying a 6 kip pull-in force per column from 80 min to 100 min, the maximum inward bowing increased from 12.2 in. to 31.3 in., as shown in Figs. 7–31 and 7–32. This analysis demonstrated that the thermal softening increased existing inward bowing. Analysis results also showed that, at 100 min, Columns 320 to 346 had reached their load capacity for their plastically buckled shape and steel temperatures and were shedding their loads to adjacent columns.

The maximum inward bowing of 31 in. was smaller than the observed maximum bowing of 55 in., and the bowed wall was still stable in the analysis at 100 min. The magnitude of pull-in forces was expected to be less than 6 kip in the global analysis with the addition of gravity loads from the core subsystem as it also weakened; therefore, pull-in forces of 4 kip to 5 kip were used in the global model analyses.

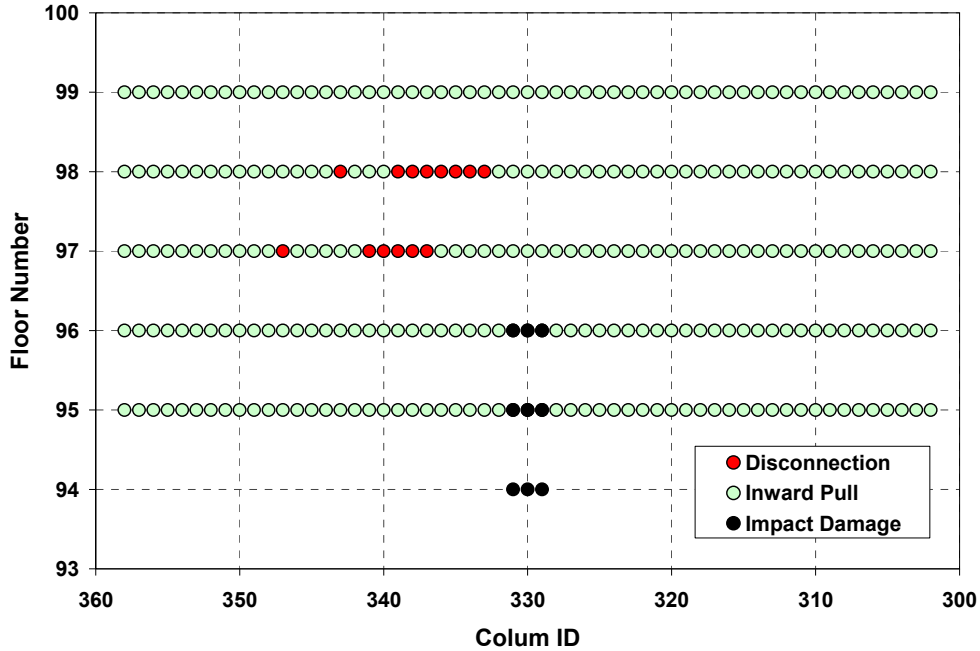

(a) Between 80 min and 90 min

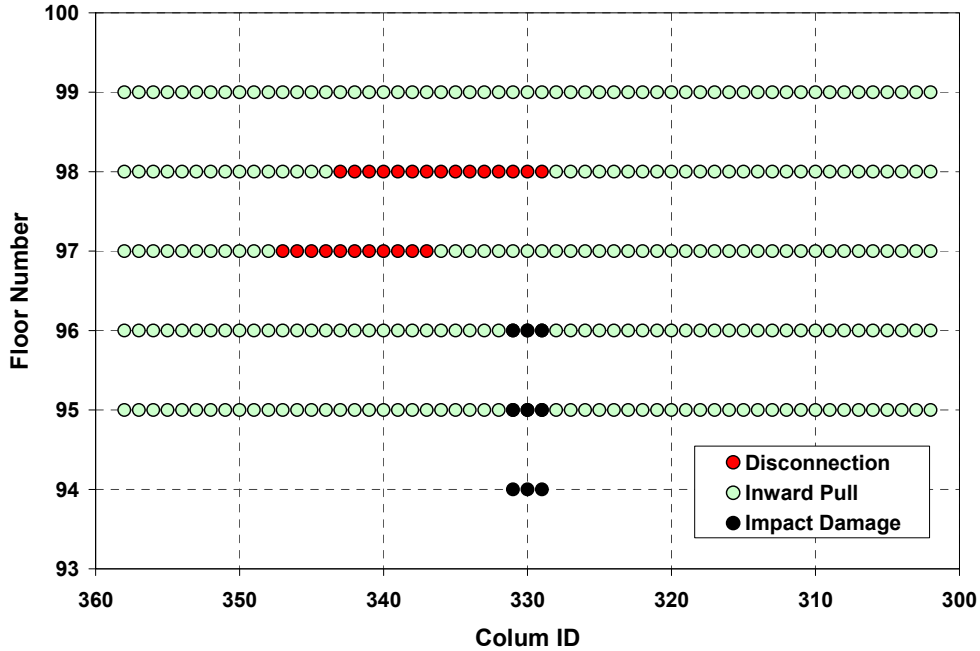

(b) Between 90 min and 100 min

Figure 7–30. Locations of WTC 1 disconnections and pull-in forces over five floors for Case B.

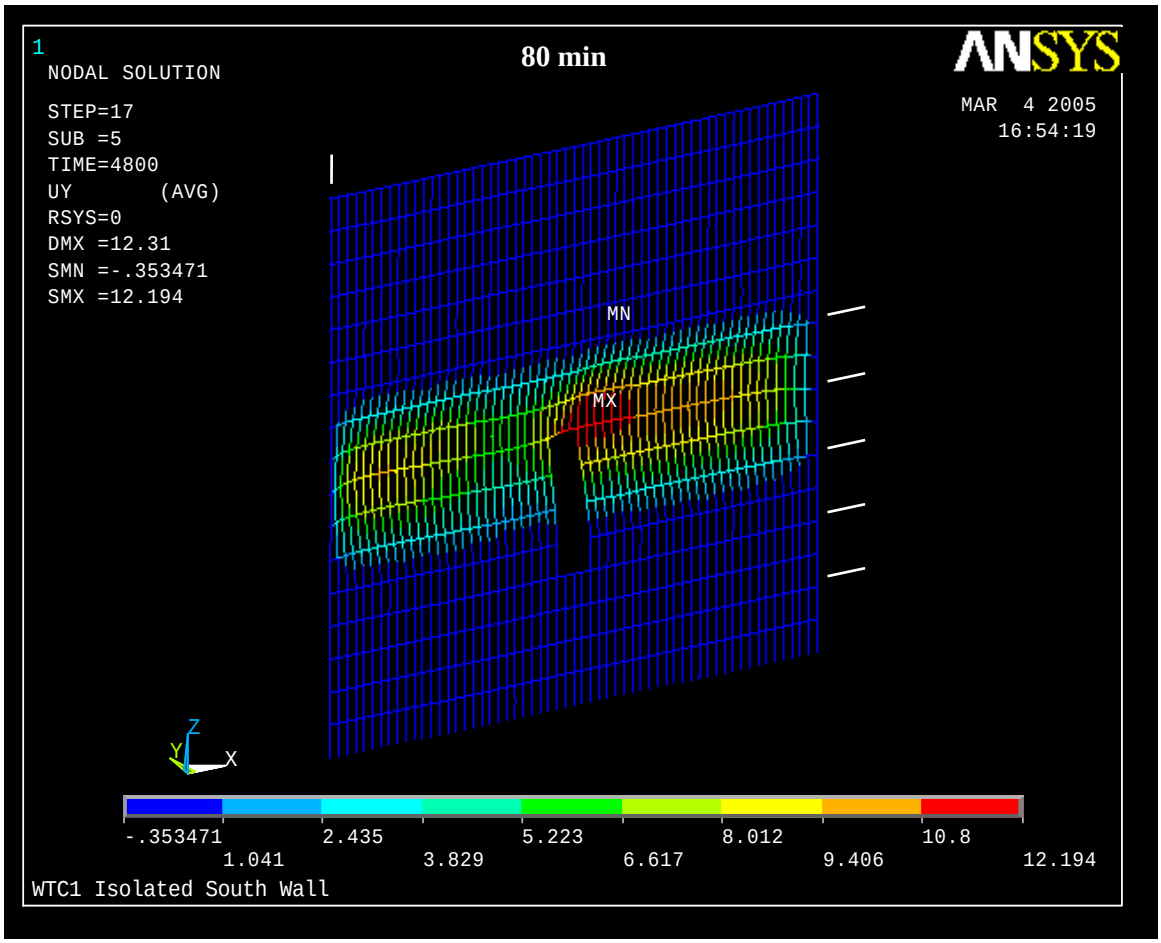

Figure 7–31. Inward displacement of the WTC 1 south wall at 80 min of the Case B temperatures with floor disconnections and 6 kip pull-in forces over five floors.

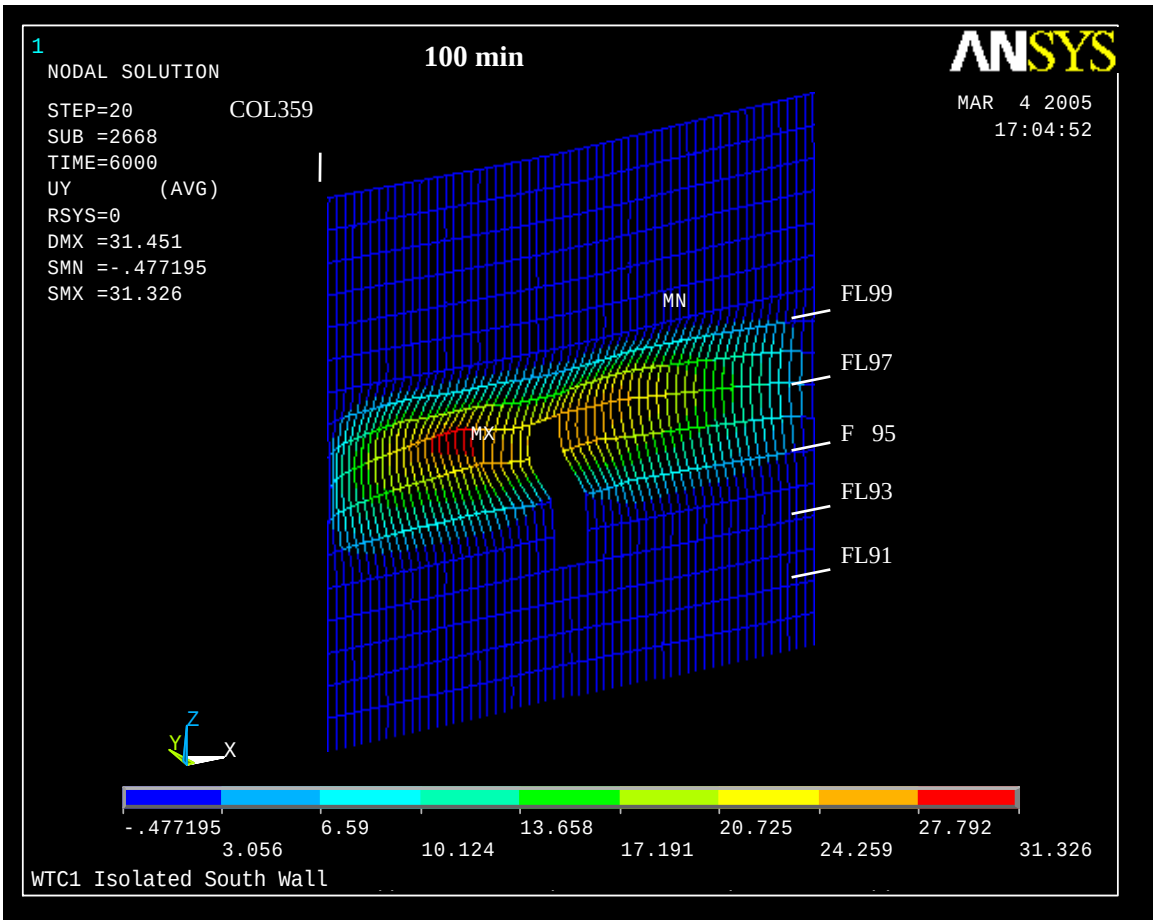

Figure 7–32. Inward displacement of the WTC 1 south wall at 100 min of the Case B temperatures with floor disconnections and 6 kip pull-in forces over five floors.

7.4.3 WTC 2 Analysis Results

The magnitude and distribution of inward pull forces on the east wall, which resulted in inward bowing similar to that observed in photographs at approximately 20 min and 50 min after the aircraft impact, were estimated with these analyses. The final estimated magnitude and distribution was used in the WTC 2 global analysis.

Initial trials with Case C and Case D damage and elevated temperatures limited pull-in forces to areas with floor sagging sufficient in the full floor models to cause pull-in forces. However, such limited areas of pull-in forces did not produce results that were compatible with the observed inward bowing. While damage to truss and exterior column fireproofing was similar for Cases C and D, the fire spread and growth was not the same and produced different temperature histories for structural elements. Case C full floor models sagged and had pull-in forces at the north side of the east wall, whereas Case D had floor sagging and pull-in forces at the south side of the east wall. Review of full floor model results showed that Case D temperature histories more closely matched the observed inward bowing of the east face. Case D was used for the global analyses.

A second set of trials with Case D elevated temperatures applied a pull-in force uniformly across Floors 79 to 83 of the east wall, except where the floor connections had failed. In two separate analyses, pull-in forces of 0.5 kip and 5 kip were held constant as the temperature histories were applied until the analysis failed to converge. The analysis with the 0.5 kip pull-in force failed to converge at 32 min. As shown in Fig. 7–33, the wall bowed primarily outward (positive displacement direction is inward) as the pull-in force was insufficient to cause inward bowing. The analysis with the 5.0 kip pull-in force failed to converge at 18 min. The inward bowing of the exterior wall had reached 31 in., as shown in Fig. 7–34. This value is about three times larger than the 10 in. displacement measured in photographs at this time, indicating that the assumed value of pull-in force was too large. Based on these two analyses, it was concluded that the magnitude of the pull-in force for a uniform distribution was bounded by 0.5 kip and 5.0 kip. This range for the pull-in force is of the same order of magnitude as the tension calculated from the detailed truss model (see Chapter 4).

The out-of-plane displacements shown in Fig. 7–33 at 20 min were inward on the south side and outward in the middle and north section of the wall. This difference in behavior was due to the combined effects of column temperatures and column loads across the east wall. Temperatures were higher at the middle and north half of the wall compared to the area near the southeast corner. The primary reasons for the outward bowing on the north side of the east wall are as follows: (1) the higher temperatures in the north side of the wall resulted in restrained thermal expansion and larger column loads; (2) the higher temperatures of the inside face of the columns, relative to the outside, caused higher plastic and creep strains and resulted in differential shortening of the inside relative to the outside; and (3) the plastic softening and creep of the inside caused an outward shift in the neutral axis, and a resulting outward bow of the columns.

This observation formed the basis for the next set of trials, where a step function was used to represent the distribution of pull-in forces along the east wall. In each trial, the magnitude of pull-in force for each half of the wall was assigned independently, with a higher magnitude on the north half of the east wall.

Two additional trials were analyzed. In the first trial, the magnitude of the pull-in forces was set to 1.0 kip and 4.0 kip for the south and north halves of the east wall, respectively. Figure 7–35 shows the out-of-plane displacements at 20 min and 50 min. As can be seen, the maximum inward bow calculated at 20 min was 7.5 in. and located near the middle of Floor 81. This agreed well with the measured displacements, which showed a maximum inward displacement of 10 in. near the middle of Floor 81.

The inward bowing started to decrease with time after 20 min and at around 40 min changed to outward bowing. The bowing at 50 min was mostly outward and did not agree with the measured displacements at this time. This indicated that the assumed magnitudes of the applied pull-in force were smaller than the actual pull-in force on the east wall.

In the second trial, the magnitude of the pull-in force was increased to 1.5 kip and 5.0 kip on the south and north portions of the east wall, respectively. Temperature histories were applied up to 50 min, at which point the analysis failed to converge. Figure 7–36 shows the magnitude of inward bowing at 20 min and at 50 min. The maximum inward bowing calculated at 20 min was 9.5 in. near the middle of Floor 81. This observation agreed well with the 10 in. measured displacements at that time. The inward bowing continued to increase with increasing time and reached a maximum of 37 in. at 50 min. As seen in Fig. 7–30, the location of the maximum displacements agreed well with the observations, but the calculated magnitude of 37 in. was twice as large as the measured inward displacement of 20 in.

This indicated that the magnitude of the applied pull-in force was close to the two sets of values assumed for the step function distribution, 1.0 kip to 1.5 kip and 4.0 kip to 5.0 kip on the south and north portions of the east wall, respectively. Considering the possible increase in column loads after impact for Case D conditions, a pull-in force of 1.0 kip on the south half and 4.0 kip on the north half of the east wall was selected as the initial estimate for the WTC 2 global model analysis.

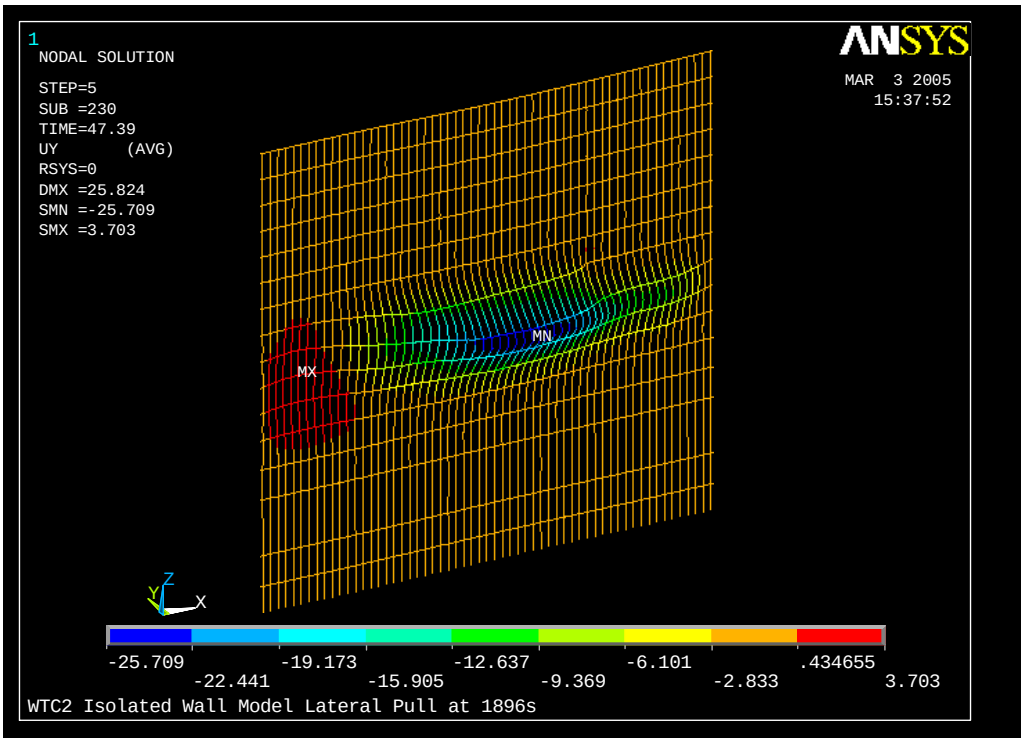

Figure 7–33. Out-of-plane displacements of the WTC 2 east wall calculated with 0.5 kip pull-in force with uniform magnitude distribution at 32 min.

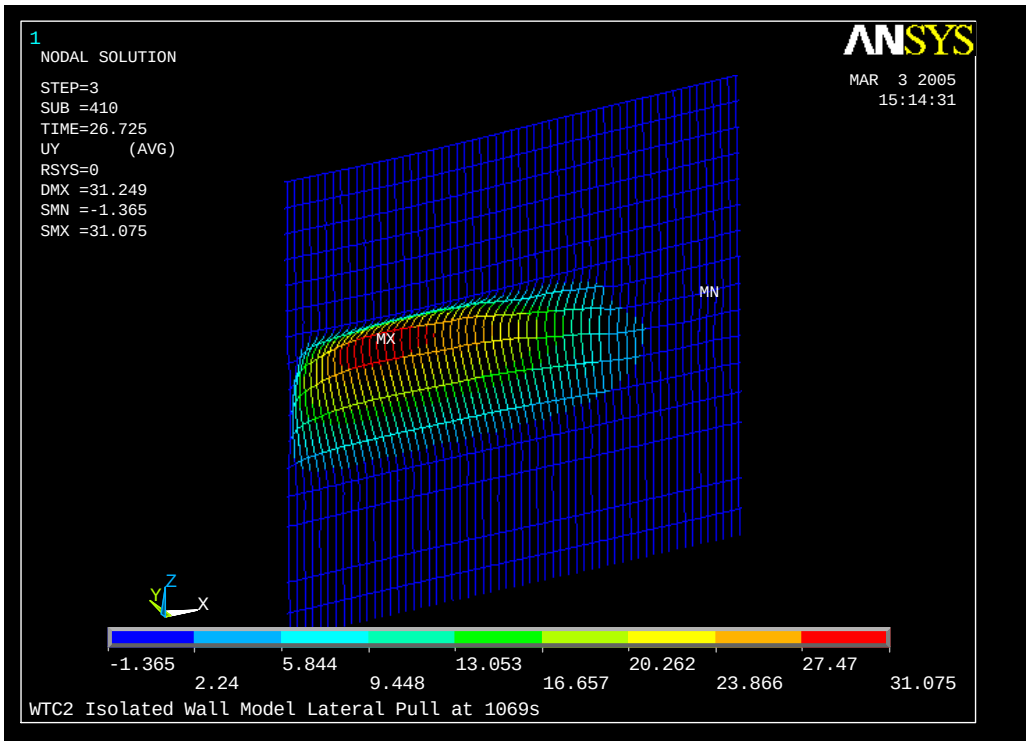

Figure 7–34. Out-of-plane displacements of the WTC 2 east wall calculated with 5.0 kip pull-in force with uniform magnitude distribution at 18 min.

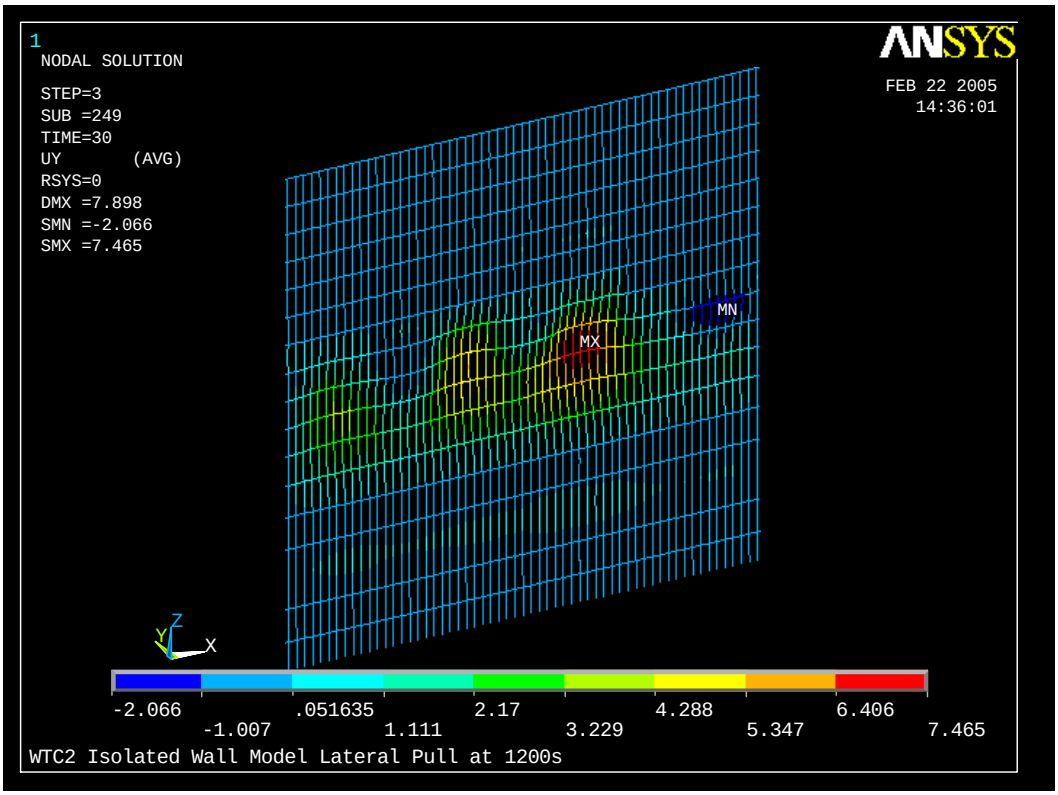

At 20 min

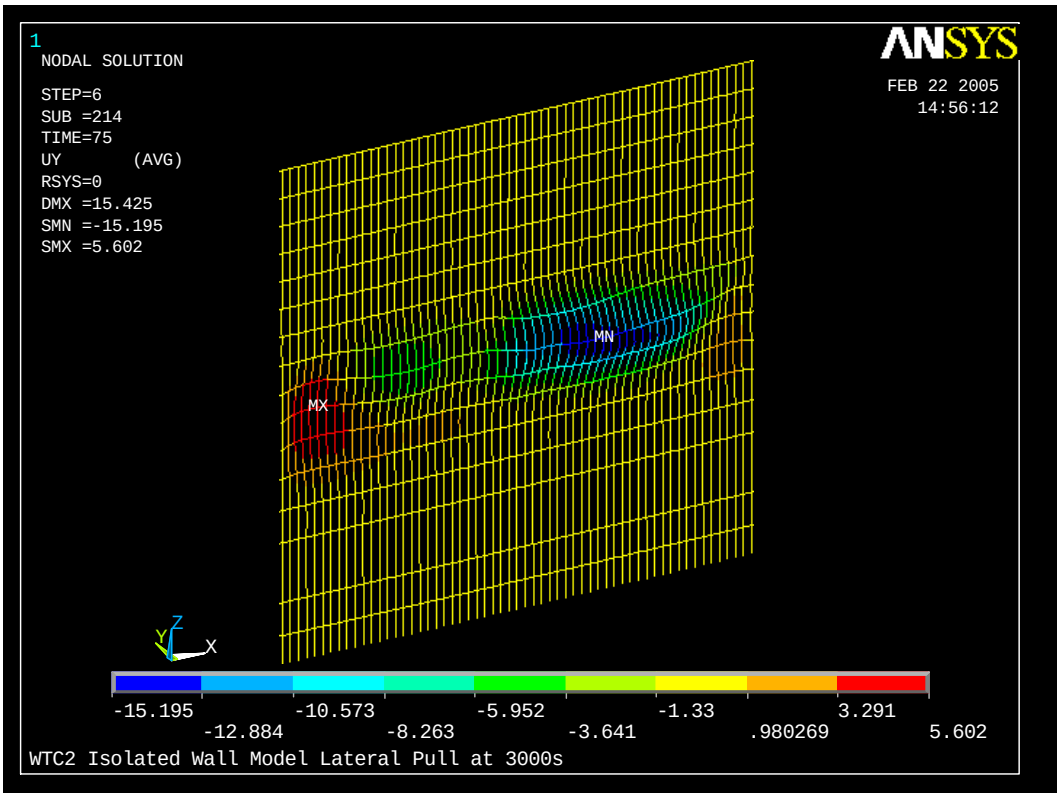

At 50 min

Figure 7–35. Out-of-plane displacements of east wall calculated with pull-in force of 1.0 kip on the south half and 4.0 kip on the north half of the WTC 2 east wall.

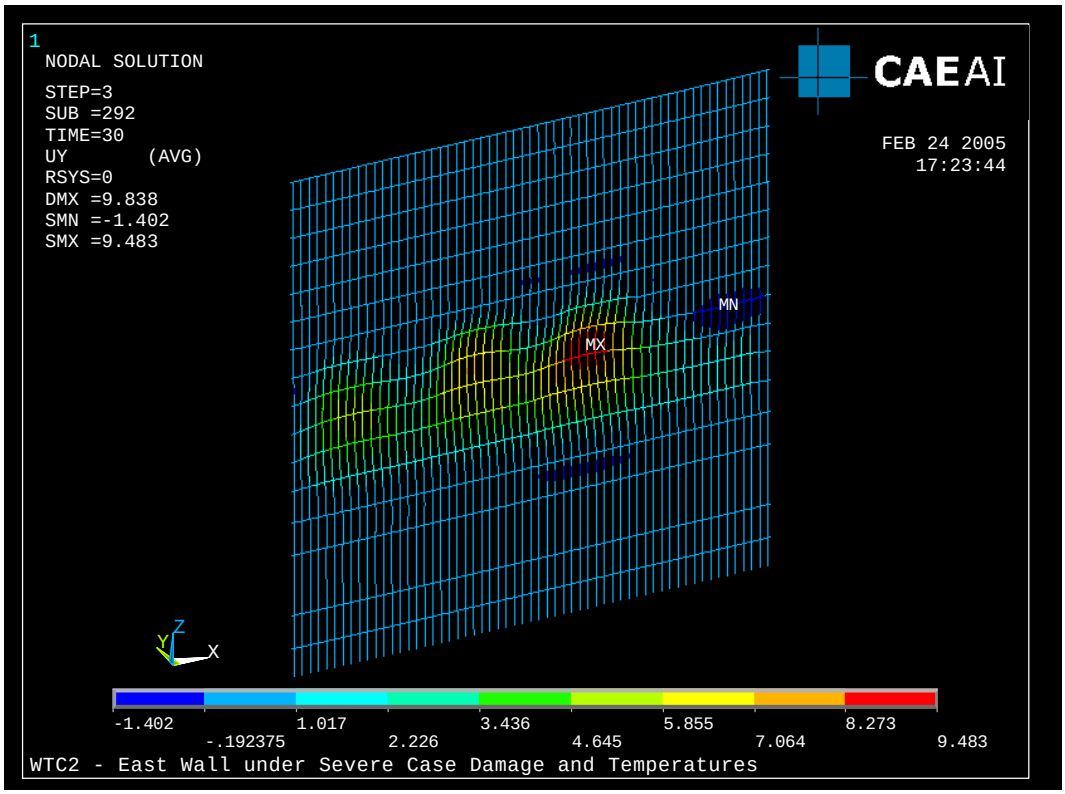

At 20 min

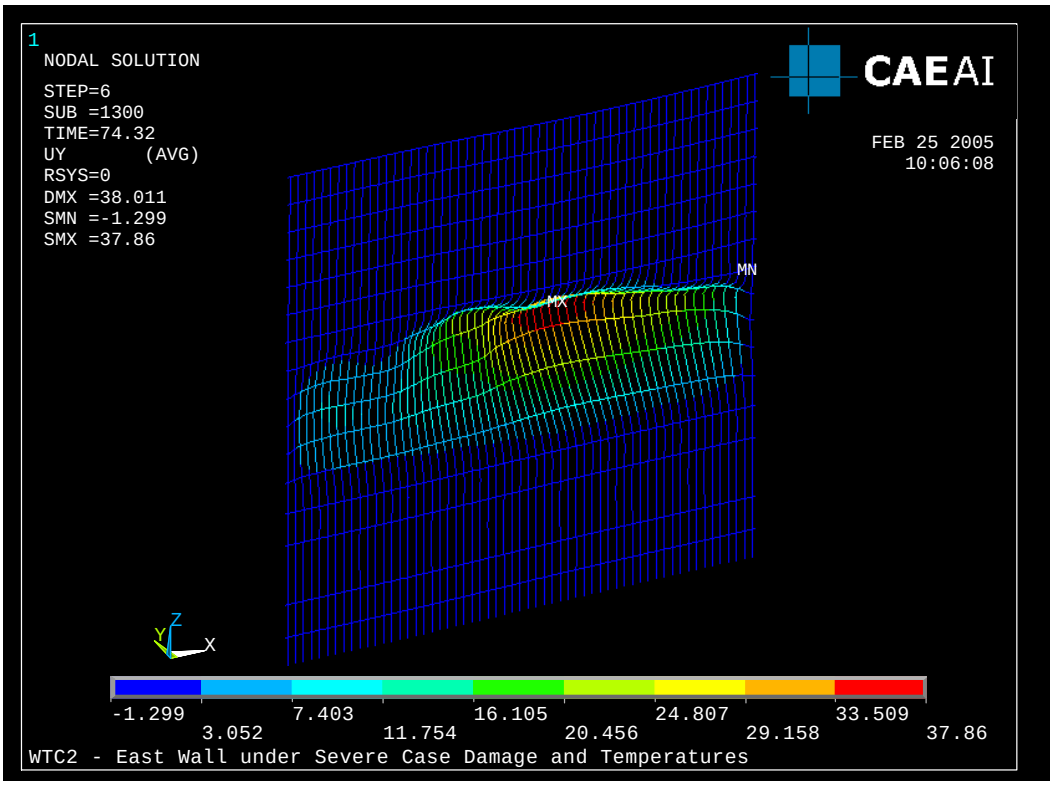

At 50 min

Figure 7–36. Out-of-plane displacements of east wall of WTC 2 calculated with pull-in forces of 1.5 kip on the south half and 5.0 kip on the north half.

7.5 SUMMARY OF SUBSYSTEM ANALYSES

The structural response of the isolated major subsystems (core, full floor, and exterior wall) to aircraft impact damage and fire are summarized here. These responses provided insight for the global model and results analysis.

Core Subsystem

- If core column connections to the hat truss failed, the core subsystem may have experienced large vertical deflections in the local area of the connection failure due to loss of the primary load path for the redistribution of loads and subsequent column plastic buckling and/or plastic and creep deformations.

- The WTC 1 isolated core subsystem was stable with Case A aircraft impact damage and gravity loads.

- To reach a stable solution for Case C structural damage and gravity loads, the WTC 2 isolated core model required horizontal restraints to be added in the east and south directions at each floor representing the lateral restraint provided by the office area floors. Without the horizontal restraints, the WTC 2 core model tilted significantly due to the severed columns in the southeast corner of the core.

- The isolated core models did not converge for WTC 1 Case B and WTC 2 Case D structural impact damage, which had more severed columns than Case A and Case C, respectively. The core needed to redistribute loads to other areas in the global system for a stable solution with Case B and Case D damage.

- The WTC 1 isolated core subsystem with Case A impact damage and Case B temperature histories resulted in column buckling between Floors 94 and 98 and a 44 in. vertical displacement at the center of the south side of the core. The core structure was most weakened from impact and thermal effects at the center of the south side of the core. Smaller displacements occurred in the global model due to the constraints of the hat truss and floors.

- The WTC 2 isolated core subsystem with Case C impact damage and Case D temperature histories resulted in an 8.1 in. vertical displacement at the southeast corner. Without the horizontal restraints, the core would have tilted more toward the southeast corner, and the vertical displacement would have been larger. No columns buckled. The core structure was weakened from impact and thermal effects at the southeast corner and along the east side of the core.

Full Floor Subsystem

- Final damage Cases A, B, C, and D were completed after the initial set of floor analyses were conducted with Cases A_i, B_i, C_i, and D_i. The fires did not change between initial Cases A_i to D_i and final Cases A to D. The concrete slab temperatures were the same for the initial and final Cases. The truss temperatures changed where the fireproofing damage changed. The full floor models were not rerun for Cases A through D as comparisons showed that the

structural temperature histories of the floors were nearly identical for most floors and only slightly different for a few floors. The floor analysis results for Cases A_i to D_i were used for Cases A to D in the exterior wall subsystem and global analyses.

- The full floor model boundary conditions for the exterior columns constrained thermal expansion of the concrete slab, which led to high compressive forces in the slabs, even with sagging of floors.

- At lower elevated temperatures (approximately 100 °C to 400 °C), the floors thermally expanded and displaced the exterior columns outward by a few inches; horizontal displacement of the core columns was insignificant. None of the floors buckled as they thermally expanded, even with the exterior columns restrained so that no horizontal movement was allowed at the floors above and below the heated floor, which maximized column resistance to floor expansion. Even with level of column restraint, the exterior columns did not develop a sufficient reaction force (push inward to resist the expansion outward) to buckle any of the floors.

- At higher elevated temperatures (above 400 °C), the floors began to sag as the floors' stiffness and strength were reduced with increasing temperature and the difference in thermal expansion between the trusses and the concrete slab became larger. As the floor sagging increased, the outward displacement of the exterior columns was overcome, and the floors exerted an inward pull force on the exterior columns.

- The floors began to exert inward pull forces when floor sagging exceeded approximately 25 in. for the 60 ft floor span. This is based upon analysis results of both the detailed truss model and the full floor models (which showed a reduction in compression instead of tension at the truss connections).

- Floor sagging was primarily caused by either buckling of truss web diagonals or disconnection of truss seats at the exterior wall or the core perimeter. Except for the truss seat failures near the southeast corner of the core in WTC 2 following the aircraft impact, web buckling or truss seat failure was caused primarily by elevated temperatures of the structural components.

- Sagging at the floor edge was due to loss of vertical support at the truss seats. The loss of vertical support was caused by the reduction in vertical shear capacity of the truss seats due to elevated steel temperatures in most cases.

- When the gusset plates and bolts of the truss seat failed in the floor models due to horizontal loads, it was rare that the truss also walked-off of the seats because the thermal expansion of the floor was restrained by the exterior columns. The straps and studs at the exterior wall had been removed from the floor models, which provided additional resistance to horizontal loads; if the floor slab expansion had not been restrained by the exterior columns, the horizontal loads between the slab and gusset plate and bolt would have been reduced.

- The high surface temperatures in the concrete slabs of fire affected floors could have resulted in delamination by spalling of the slab. This would possibly compromise knuckle strength,

crack the slab, or cause loss of integrity of the floor system, contributing to greater floor sagging.

- Case B impact damage and thermal loads for WTC 1 floors resulted in floor sagging on the south side of the tower over floors that reasonably matched the location of inward bowing observed on the south face. Case A impact damage and thermal loads did not result in sagging on the south side of the floors.

- Case C and Case D impact damage and thermal loads for WTC 2 both resulted in floor sagging on the east side of the tower over floors that reasonably matched the location of inward bowing observed on the east face. However, Case D provided a better match.

Exterior Wall Subsystem

- Inward forces were required to produce inward bowing that was consistent with displacements measured from photographs. The inward pull was caused by sagging of the floors. Heating of the inside face of the perimeter columns also contributed to inward bowing. Thermal expansion occurred as soon as steel temperatures began to rise; column shortening occurred when creep and plastic strains overcame thermal expansion strains, typically at temperatures greater than 500 °C to 600 °C with accompanying high stresses and duration of temperatures and stress levels.

- Models of exterior wall sections bowed outward in a pushdown analysis when several consecutive floors were disconnected, the interior face of the columns was heated, and column gravity loads increased (e.g., due to load redistribution from the core and hat truss). At lower temperatures, thermal expansion of the inside face was insufficient to result in inward bowing of the entire exterior column. At higher temperatures, outward bowing resulted from the combined effects of reduced steel strength on the heated inside face, which shortened first under column gravity loads, and the lack of lateral restraint from the floors.

- The observed inward bowing of the exterior wall indicated that most of the floor connections must be intact to cause the observed bowing.

- The floor levels predicted to have damaged fireproofing in the aircraft impact analysis matched well with the floors that were identified from photographic and video analysis to have participated in the inward bowing of the exterior walls.

- The extent of floor sagging required at each floor was greater than that predicted by the full floor models. The estimates of the extent of sagging at each floor were governed by the combined effects of fireproofing damage and fire; fireproofing damage was limited to areas subject to direct debris impact. Other sources of floor damage from the aircraft impact and fires (e.g., fireproofing damage from structural accelerations at impact and subsequent strong vibrations or floor damage from concrete cracking and spalling from thermal effects) were not included in the floor models.

- The exterior wall models were used to estimate the pull-in force magnitude and locations for each tower that would produce the observed bowing of the exterior wall.

- The WTC 1 isolated exterior wall analysis found that an inward pull force of 6 kip at each column at Floors 95 to 99, starting 80 min after the aircraft impact, caused a maximum inward bowing of 31 in. This inward deflection was smaller than the observed maximum bowing of 55 in., and the bowed wall was stable at 100 min. The magnitude of pull-in forces was expected to be less than 6 kip in the global analysis with the addition of gravity loads from the core subsystem as it also weakened; therefore, pull-in forces of 4 kip to 5 kip were used in the global model analyses.

- The WTC 2 isolated exterior wall analysis found that an inward pull force of 1.0 kip to 1.5 kip and 4.0 kip to 5.0 kip on the south and north portions of the east wall, respectively, over Floors 79 to 83, caused a maximum inward bowing of 9.5 in. at 20 min and 37 in. at 50 min. The observed deflections were 10 in. and 20 in., respectively. Considering the possible increase in column loads after impact for Case D conditions, a pull-in force of 1.0 kip on the south half and 4.0 kip on the north half of the east wall was selected for the initial estimate for the WTC 2 global model analysis.

This page intentionally left blank.

Chapter 8
STRUCTURAL RESPONSE OF THE WTC TOWERS TO AIRCRAFT IMPACT DAMAGE AND FIRE

8.1 INTRODUCTION

Prior to conducting global analysis of the structural response of each World Trade Center (WTC) tower, a tremendous amount of input data was obtained[2] and developed. Input data required for the structural response models included:

- Reference model of each WTC tower before the aircraft impact, based upon design and construction documents (NIST NCSTAR 1-2)
- Steel and concrete material properties for room and elevated temperatures (NIST NCSTAR 1-3 and Chapter 4)
- Structural damage to columns and floors from the aircraft impact (NIST NCSTAR 1-2 and Chapter 5)
- Passive fire protection conditions before and after impact (NIST NCSTAR 1-6A and Chapter 5)
- Temperature histories for all structural elements in the impact zone (NIST NCSTAR 1-5)
- Observed structural conditions and events from photographic and videographic records (NIST NCSTAR 1-5A and Chapter 6)

Input data was based on available records. For data that were not directly available, analytical and experimental results were used to develop the required information. The tower design and construction and the supplied structural materials were well documented. The passive fire protection conditions before impact were less well documented, but review of Port Authority of New York and New Jersey (PANYNJ) records and interpretation of photographs (from several sources throughout the life of the structure) provided a documented basis for determining the likely conditions that existed in both towers before September 11, 2001. Steel and concrete temperature-dependent properties were developed from available technical literature and from tests of samples recovered from the collapse site (steel tests were conducted at National Institute of Standards and Technology (NIST) and concrete tests were conducted at Simpson Gumpertz & Heger, Inc. (SGH) under contract to NIST) to assess conformance with specified properties. Temperature histories were developed from fire dynamics simulations and thermal analyses conducted at NIST. The observed structural conditions and events defined the known events that occurred that day. The structural response analyses helped determine the probable collapse sequence for each tower. These sequences were validated using the observed structural events.

[2] All information and data related to the design and construction of the WTC towers were obtained from contract drawings provided to NIST by The Port Authority or New York and New Jersey. Refer to NIST NCSTAR 1-2A for a complete description of the WTC structural system and an index of all structural drawings.

The global analyses of WTC 1 and WTC 2 used final estimates of impact damage and elevated temperatures to determine the structural response and sequence of component and subsystem failures that led to collapse initiation. Case B was used for WTC 1 and Case D was used for WTC 2 used, as described in previous chapters.

The global models and required input data are discussed in Section 8.2. The analysis methodology is presented in Section 8.3, and the results of the global analyses for WTC 1 and WTC 2 are presented in Sections 8.4 and 8.5, respectively. To better understand the relative contributions of impact damage and fire to each tower collapse initiation, the hypothetical condition of the towers subjected to the same fires without aircraft impact damage is discussed in Section 8.6.

8.2 GLOBAL MODEL OF TOWERS

8.2.1 Model Description

The global model of each tower, which was used to determine the structural collapse sequence, was based on the reference structural models developed for baseline structural analyses of the towers (NIST NCSTAR 1-2). The reference models were developed with SAP2000 and were used as a common basis for the aircraft impact analysis, using LS-DYNA, and the structural response analysis, using ANSYS.

The SAP2000 global models were more detailed than models typically used for structural design purposes. The models included exterior and core columns, the hat truss, and mechanical floors, but did not explicitly model the tenant floors due to model size limitations. The tenant floors were accounted for with constraint equations and concentrated floor loads at floor-to-column connection nodes.

The reference global models for WTC 1 and WTC 2 were translated into ANSYS models using an automated translator developed specifically for this effort by Computer Aided Engineering Associates, Inc. (CAEA), as a subcontractor under the NIST contract to SGH. The coordinates of the nodes, cross-sectional properties of members including orientation and offset of the cross-section, nodal loads, material properties, and member end releases were automatically converted from the SAP2000 format to the ANSYS format as described in
NIST NCSTAR 1-6C.

The ANSYS models were truncated several floors below the impact floors, as previous analyses showed that the structural response below the impact area remained elastic. WTC 1 was truncated at Floor 91, and WTC 2 was truncated at Floor 77. The axial stiffness of the remaining structure below the line of truncation was replaced with equivalent elastic springs. The global models of the two towers are shown in Fig. 8–1.

The truncated ANSYS global models were validated against the SAP2000 baseline global analyses for gravity loads. The results from the translated ANSYS global models showed good agreement with the baseline analyses: displacements were within 1.4 percent for WTC 1 and 0.7 percent for WTC 2, and base reactions were within 1.2 percent for WTC 1 and 0.3 percent for WTC 2. Based on these comparisons, it was concluded that the translation of the global models from SAP2000 to ANSYS was correct, and the ANSYS models and their derivatives were used for the global analyses. Details of the translation and validation are found in NIST NCSTAR 1-6C.

The core columns and exterior columns and spandrels were modeled with elements and features similar to those used in the isolated core and exterior wall analyses. Column analysis features included the effects of thermal expansion, plastic, and creep strains on column behavior within the global structural system. When thermally-induced strains were sufficiently large, column loads increased if they were restrained. Columns shortened and shed loads if either plastic or creep strains were large enough or if they buckled plastically. Plastic (or inelastic) buckling describes the condition where a column becomes bowed (displaced laterally between its ends) by plastic or creep strains, but continues to support a reduced axial load. As the bowing becomes larger, the column's capacity to carry load diminishes further (see Fig. 435) until the column no longer participates in carrying load in the global structure.

Floors in the global model were modeled by shell elements, which have their membrane stiffness equal to that of the full floor system. Floors in the global model functioned as diaphragms and transferred loads between the exterior wall system and the core. Office area and core floors were modeled with an equivalent floor slab thickness and modulus calculated to match the in-plane stiffness of the composite floor system, including the concrete slab, floor trusses, and the floor seats. Bending stiffness of the floor system was not matched because the floor loads were applied at the columns. Both core and office area floor slabs were modeled with linear-elastic material properties for lightweight concrete.

Figure 8–2 shows the model of the core and tenant floors and the core beams that had moment connections. Beams without moment connections cannot effectively transfer shear between columns without significant relative displacement and, thus, were not modeled individually. The stiffness of simply connected beams was smeared into that of the slab to capture the in-plane stiffness of the floor in the core. Inclusion of the core and office area floors was necessary for modeling force redistribution within the core and between the core and the exterior columns. The core was effective in redistributing loads from damaged core columns to adjacent core columns when the load path through the hat truss could not be developed due to either severed columns or column splices.

Floors in the global models were not intended to capture floor response and failure modes during fires. It was not practical, or in some cases not possible, to create computationally efficient global models that included all details of the floor system. The BEAM188/189 elements used in the full floor model caused severe convergence problems when creep was included and those elements experience thermally-induced buckling. Also, the extent of pull-in forces from sagging floors in the full floor models was less than estimated from the observed bowing of the exterior walls in photographs and videos because the aircraft impact damage to thermal insulation of the floors was conservatively estimated by limiting the dislodged thermal insulation to regions of direct debris impact.

Important failure modes were identified in the truss and full floor analyses and incorporated into the global models as floor/wall disconnections and pull-in forces at appropriate time intervals. Since the full floor models did not accurately estimate the pull-in forces at floor/wall connections, the fire-induced damage obtained from the full floor model analyses were modified by observations obtained from the examination of photographs and videos performed by NIST (NIST NCSTAR 1-5A). See Chapter 7 in NIST NCSTAR 1-6C and Chapter 2 in NIST NCSTAR 1-6D for more details.

The global model included the hat truss at the top of each tower. The hat truss was designed to support an antenna on top of the towers and transmitted loads to both the core and exterior columns. The loads were distributed primarily to the core columns. There were four outriggers to each exterior wall that provided rotational restraint for the antenna under wind loads. In addition, the outriggers provided a secondary

load path between the core and exterior walls as determined from the structural response of the towers to impact damage and fires. Figure 8–3 shows the hat truss, with the outriggers labeled A through P. During the global structural response to impact and fire, the hat truss provided a primary path for transferring loads between the core columns and between the core and exterior walls.

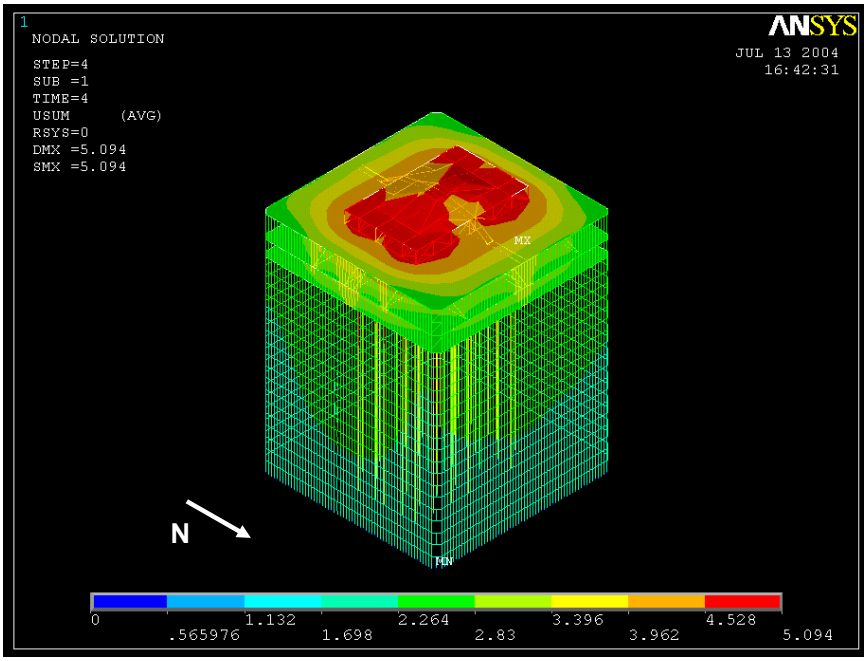

(a) WTC 1 ANSYS Model Vertical Displacements

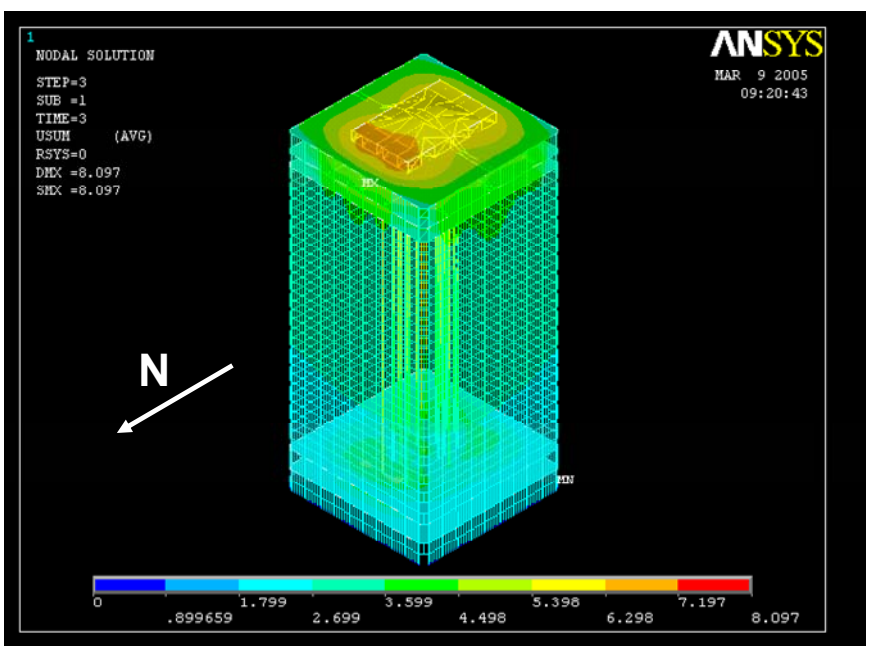

(b) WTC 2 ANSYS Model Vertical Displacements

Figure 8–1. Displaced shape of WTC 1 and WTC 2 at the end of gravity load analysis.

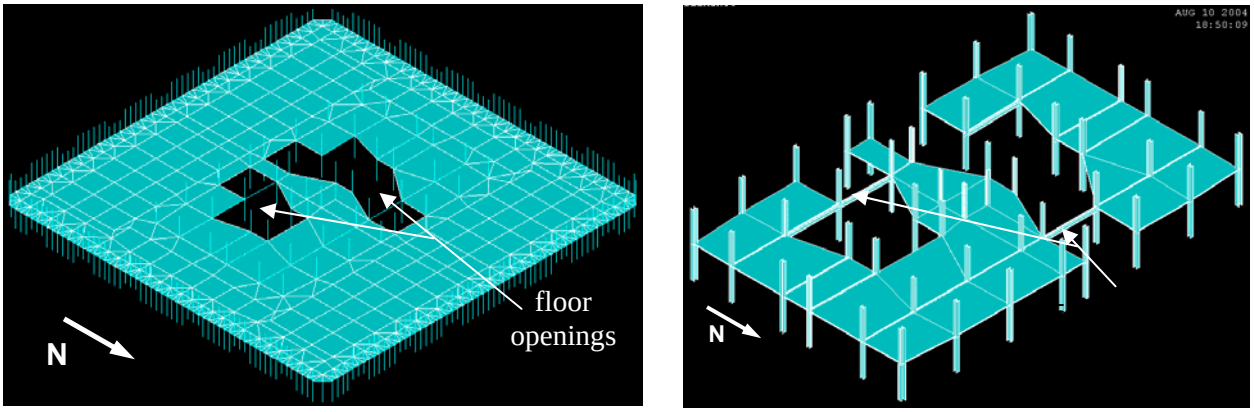

Figure 8–2. Office area and core floors and core beams.

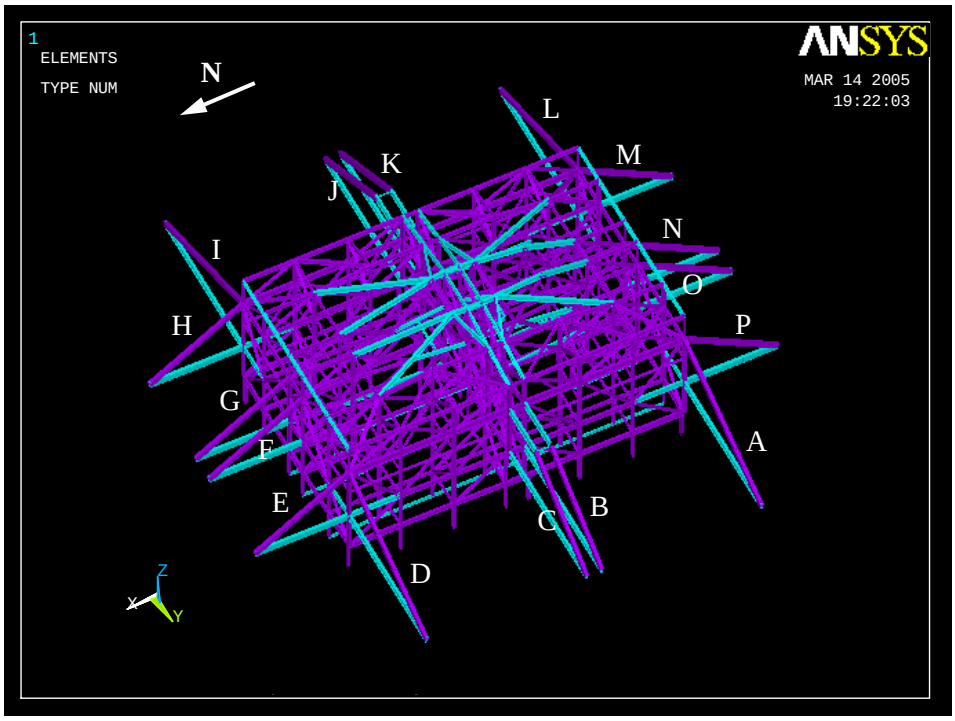

Figure 8–3. Hat truss with labeled outriggers.

8.2.2 Model Modifications

The validated ANSYS models were modified to incorporate nonlinear material and geometric behaviors required in areas subject to impact and fire. Modifications incorporated modeling enhancements and refined input data based on numerous component and subsystem analyses. Temperature-dependent modifications included material properties, coefficients of thermal expansion, plastic and creep strains. Nonlinear geometric behavior modifications included large displacements, plastic buckling and post-buckling of columns. Break elements were not included, based on the behaviors shown in the major subsystem analyses of the isolated core, exterior wall, and full floors. Break elements for knuckles, exterior wall bolted connections, and spandrel connections did not fail in the full floor and exterior wall

analyses. Truss seat connection failures were imposed during analyses according to the time they were calculated or observed to have occurred, rather than through use of break elements.

Preliminary global analyses had unacceptably slow rates of computation, due to the size of the models and the computational effects of temperature-dependent material properties, especially creep. To reduce the size of the global models and to increase the speed of the solution without adversely affecting the analysis results, modifications were made to the models to improve computational efficiency.

The spandrels were modeled with BEAM 188 elements which experienced convergence problems when thermal expansion caused them to buckle since there were not enough elements between two columns to capture the buckling detail. The buckling of spandrels did not compromise their ability to transfer shear and bending moment. Based on visual evidence, buckling of spandrels did not play an important role in the collapse sequence, and increasing the number of spandrel elements would have unnecessarily increased the model size. Therefore, the coefficient of thermal expansion for spandrels was set to zero, and the axial degree of freedom was released.

Since trusses were not modeled individually, the equivalent floor slab buckled easily when thermal expansion was restrained by the exterior wall. Buckling of the equivalent floor slab often caused convergence problems in the global analysis. The coefficient of thermal expansion of the floor in the office area was set to zero to eliminate the unrealistic buckling problem. Neglecting the thermal expansion of the office area floors introduced errors in bending of exterior columns between a heated floor and a cool floor. The effect of this modeling assumption was small for columns extending between two heated floors.

Neglecting the thermal expansion of the office area slabs did introduce small errors in the out-of-plane bending of columns extending between a hot floor and a cool floor, but such errors were small for columns extending between two hot floors. The error introduced by this modification was not expected to change failure modes or collapse sequence in the global analysis, because thermal expansion of floors was limited to less than a few inches (see Appendix A). The full floor models thermally expanded and pushed outward on the columns until the thermal expansion was overcome by the floor sagging and the floors pulled inward on the exterior columns.

Construction sequence was not included in the global models with creep. The effect of neglecting construction sequence was examined for both buildings. When construction sequence was not included in the analysis, the total axial loads in columns along the exterior walls increased by 7 percent to 15 percent. Similarly, the total column loads supported by the core columns decreased by about 10 percent.

The calculations showed that the outriggers in the WTC 1 simulations were more highly stressed when the construction sequence was not considered. Since it was believed that the hat truss played an important role in transferring loads in WTC 1, the yield strengths of the materials for these outriggers in WTC 1 were artificially increased to account for the incorrect increase in compressive stresses when construction sequence was not considered.

The term “super-element” in ANSYS is used for sub-structuring in an analysis, where a portion of the model with elastic behavior is condensed into a single element with a representative stiffness, damping and mass matrix. The WTC 2 model was suitable for such a simplification as the section of the building

above Floor 86 was expected to remain elastic, based on the results of the isolated core analyses and preliminary global analyses without creep strains or plastic buckling (see NIST NCTAR 1-6D).

The use of super-elements reduced the time to complete a single iteration by a factor of three. However, if at later stages of the analysis the hat truss members became inelastic, the nonlinearities associated with such inelastic behavior were not captured. A super-element cannot determine individual component behavior as the group of components is represented by a single 'super' element. Moreover, the effects of construction sequence on the load distribution between the core and wall elements could not be represented, since the birth and death option could not be used in a super-element. (Birth and death refer to the addition or removal, respectively, of an element during an analysis.) The effect of not including construction sequence was evaluated and found to introduce an error of less than 12 percent for vertical displacement. To evaluate whether the hat truss exceeded elastic limits, a separate model that included the components at and above Floor 86 in the super-element was created. The stresses in all the components were calculated at the end of each 10 min time interval and compared with their capacities.

As the use of a super-element in the WTC 2 global model precluded the application of construction sequence, construction sequence was not included in either the WTC 1 or WTC 2 global analysis. Construction sequence refers to an analysis method where the self-weight loads are applied to the structural model in steps to simulate the sequential loading that takes place as a building is constructed. When construction sequence was not included, the total column loads in each exterior wall increased by 7 percent to 15 percent, and the total core columns loads decreased by about 10 percent for both models. It was also found that the outriggers of the hat truss were more highly stressed in the WTC 1 model without construction sequence than in the translated ANSYS model which included construction sequence (see Section 8.2.1). Since the hat truss played an important role in transferring loads, the yield strengths of these outriggers in WTC 1 were increased to account for the artificially higher compressive stresses that resulted without consideration of construction sequence. The difference in the maximum displacement between the models with and without construction sequence was within 12 percent for both WTC 1 and WTC 2.

8.3 ANALYSIS METHODOLOGY

WTC 1 and WTC 2 global models were subjected to Case B and Case D aircraft damage and fires, respectively. The results of the isolated wall, core, and full floor analyses indicated that structural responses to Case B and Case D more closely matched observed structural behavior in photographs and videos than did Case A or Case C, respectively. Thus, Case B and Case D were chosen for the global analysis of WTC 1 and WTC 2, respectively.

The global analysis was conducted in steps. Severed and heavily damaged core columns, floors, and exterior columns and spandrels were removed from the model, and gravity loads were applied as concentrated loads at each column-floor node. Then, dead load and 25 percent of the design live loads were applied to the model without considering construction sequence. The solution for the first step, which determined the structural condition of the tower after aircraft impact, provided the initial condition for the application of temperature histories and thermally-induced structural damage.

Wind forces were not included in the global analysis of the WTC towers. Wind speeds were recorded at three nearby airports, and are shown in Table 8–1. The average wind speed on September 11, 2001,

ranged from 7 knots to 11 knots (10 mph to 13 mph). In comparison, the design wind speed was 98 mph averaged over 20 minutes at a height of 1,500 ft above ground (see Chapter 3 of NIST NCSTAR 1-2). This speed is equivalent to a 3 s peak gust wind speed of about 81 mph to 90 mph at 33 ft above ground in open terrain. Wind force is proportional to the wind velocity squared, therefore, the wind force on the towers from the 13 mph winds on September 11, 2001, were approximately two percent of the average design wind speed of 86 mph, which were negligible.

Table 8–1: Wind speeds recorded at airports near the WTC towers on September 11, 2001.

Airport	Time (a.m.)	Direction	Speed[1] (knots)	Speed[2] (mph)
LaGuardia (NOAA 2001a)	8:51	320	9	13
	9:51	340	9	13
John F. Kennedy (NOAA 2001b)	8:51	310	11	16
	9:51	350	7	10
Newark, NJ (NOAA 2001c)	8:51	330	8	12
	9:51	No data	No data	No data
Average Wind Speed			9	13

1. Wind speed recorded as a 20 min average at a 33 ft elevation.
2. Wind speed converted to a 3 s peak gust at 33 ft (knots (20min) * 1.4375 = mph (3 s))

Temperature data were provided for heated structural components at 10 min intervals up to 100 min for WTC 1 and up to 60 min for WTC 2. The temperature histories were based on the combined effects of impact damage to fireproofing and fire spread and growth. The structural analysis used time steps significantly less than 10 min, as a result the temperatures were linearly interpolated between the temperatures at 10 min intervals.

Column-floor disconnections and pull-in forces that occurred during a time step were imposed at the start of the time step. In the global models, nodal couplings tied the exterior columns to the floors. The nodal couplings were removed at locations of floor/wall disconnections. If disconnections were projected to occur or were observed in visual evidence at a time intermediate to the 10 min intervals used in the analyses, for example, between 10 min and 20 min, they were imposed starting at the earlier time point, in this example, at 10 min. Once a portion of a floor was disconnected from the exterior wall, it remained disconnected for the remainder of the analysis. Similarly, pull-in forces were also applied to the global models at the beginning of the 10 min time intervals in which they were predicted to occur or were observed, and they were maintained at a constant level for the 10 min time interval.

Thermal expansion of the floors was not included in the global models. Floor analyses showed that the floors initially pushed exterior column outward by a few inches. However, significant outward bowing was not observed and several inches of outward deflection of exterior columns would not affect the global stability of the towers.

8.4 RESULTS OF WTC 1 ANALYSIS

The global model of WTC 1 with creep, plastic buckling of columns, plasticity, and nonlinear geometry was analyzed with Case B structural damage and temperature histories.

8.4.1 WTC 1 Structural Response to Aircraft Impact Damage

Case B structural and passive fire protection damage after the aircraft impact was as follows:

- WTC 1 had 41 north exterior columns (Columns 112 to 151) severed, 9 core columns on the north central side of the core (Columns 503, 504, 505, 506, 604, 704, 706, 805, and 904), and one exterior panel of the south face (Columns 329 to 331 between Floors 93 and 96) severed or heavily damaged between Floors 93 and 98

- Floor slabs and framing were severed or heavily damaged in the north office floor area through to the central north region of the core on Floors 94 to 97

- WTC 1 fireproofing damage was centered primarily through the north face and floor area, the core, and into the south floor area between Floors 94 to 99.

Figure 8–4 shows the vertical displacements at Floor 99, just above the impact area, with total displacements before aircraft impact and incremental displacements after impact. Figures 8–5 through 8–8 show the vertical displacement contours of the exterior walls and the core area before and after the aircraft impact. Before the aircraft impact, the maximum vertical displacements of the exterior wall and the core at Floor 99 were 2.5 in. and 3.6 in., respectively. Due to severe impact damage on the north face and the north side of the core, WTC 1 tilted slightly to the north after the aircraft impact as can be seen in Fig. 8–4. The maximum displacement of the north wall increased from 2.5 in. to 5.7 in., and the maximum displacement of the south wall decreased from 2.5 in. to 2.4 in. The vertical displacement of the east and west wall slightly increased due to load redistribution.

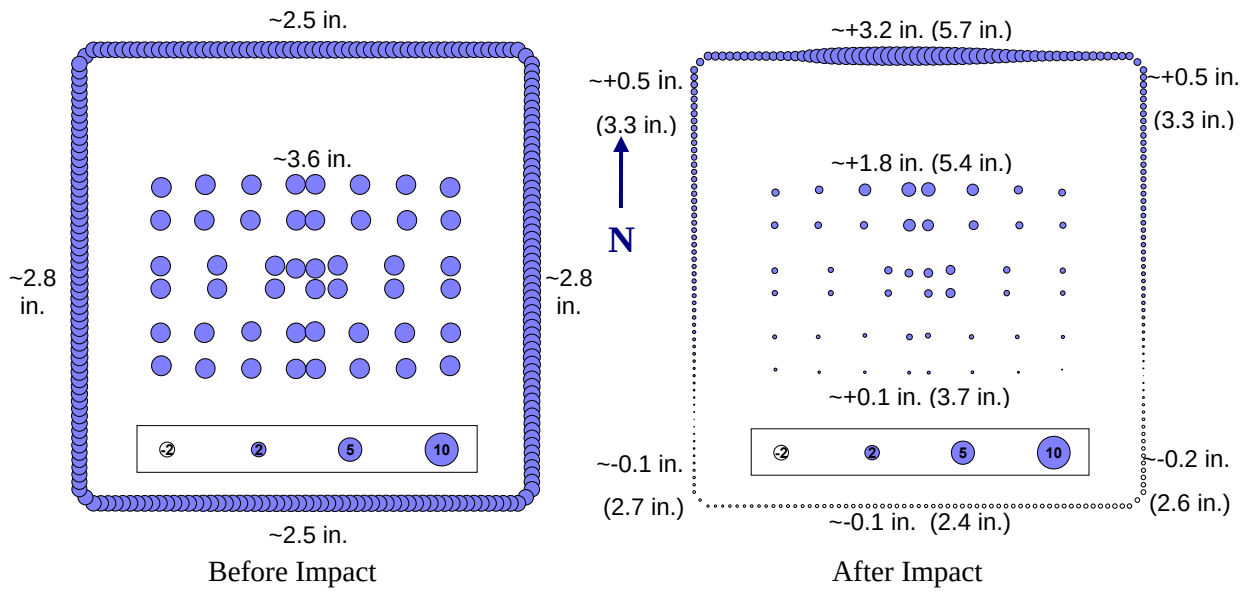

Note: displacements are shown as positive downward

Figure 8–4. Vertical displacement at Floor 99 of WTC 1. Total displacements are shown before aircraft impact and incremental displacements, with total displacements in parentheses, are shown after impact.

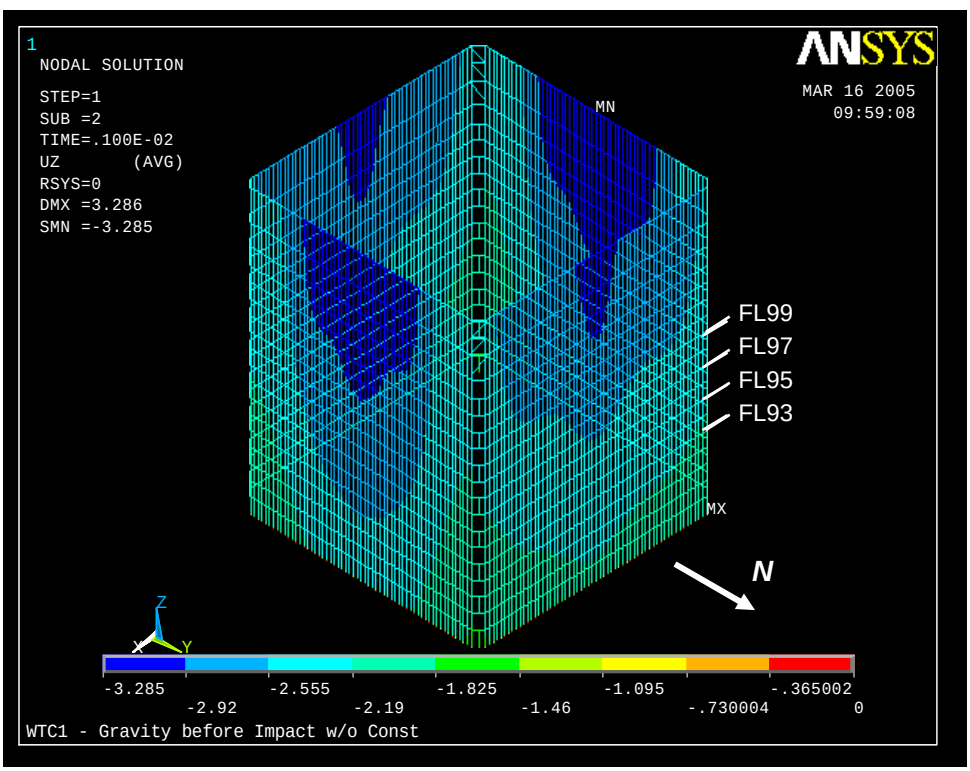

Figure 8–5. Vertical displacement of WTC 1 east and north exterior walls before aircraft impact.

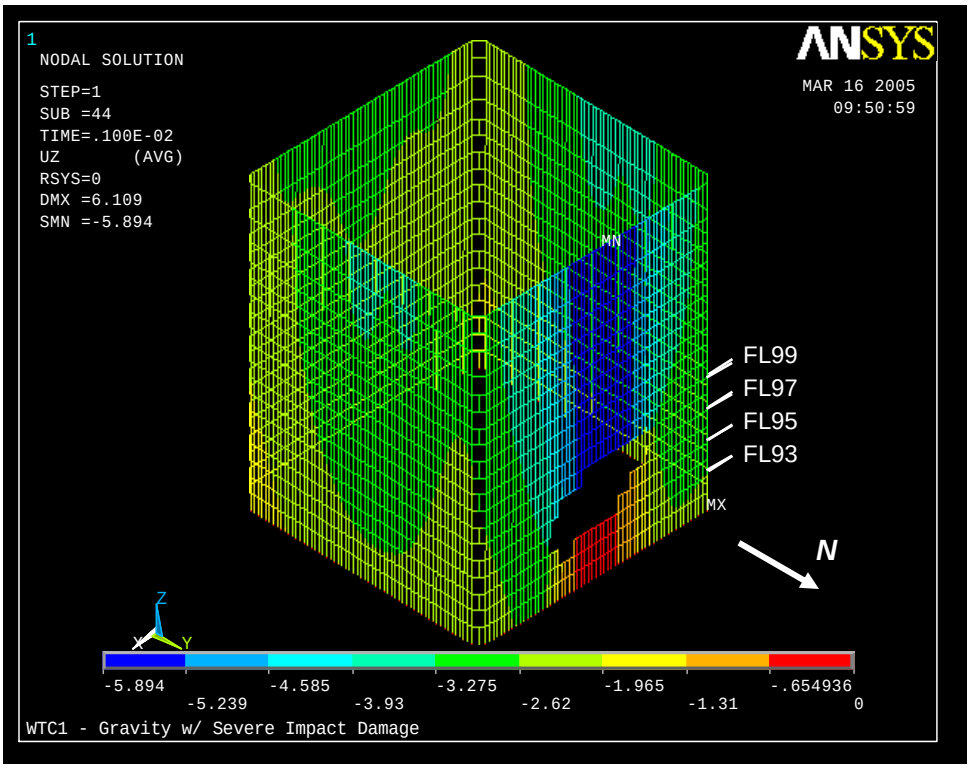

Figure 8–6. Vertical displacement of east and north exterior walls of WTC 1 after aircraft impact for Case B.

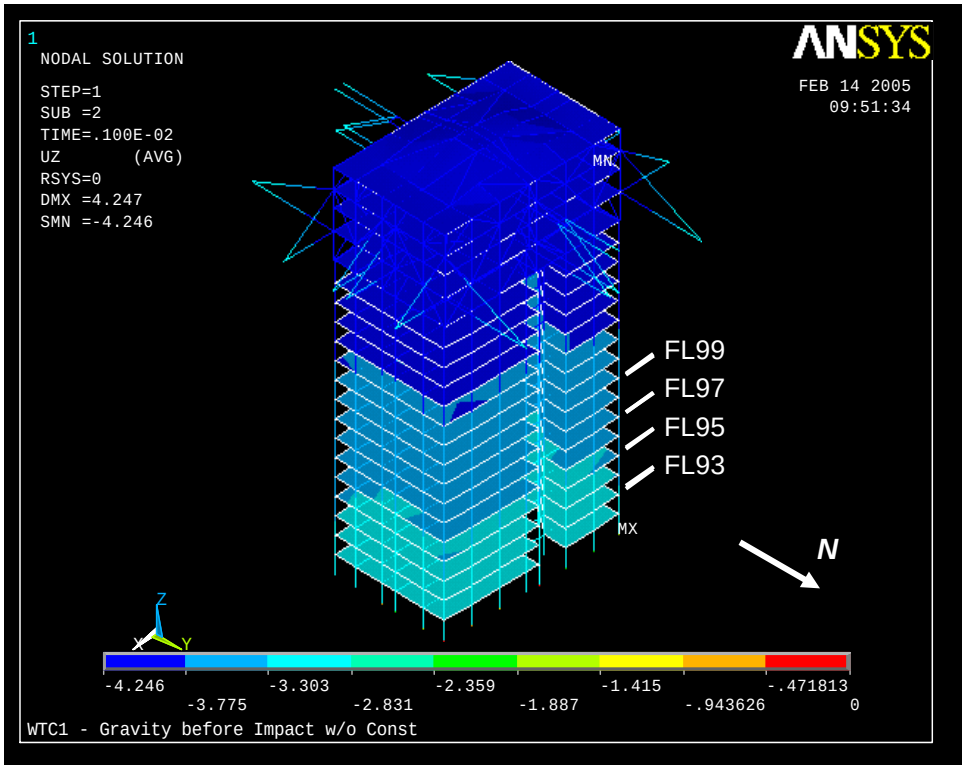

Figure 8–7. Vertical displacement of the east and north side of the WTC 1 core before aircraft impact.

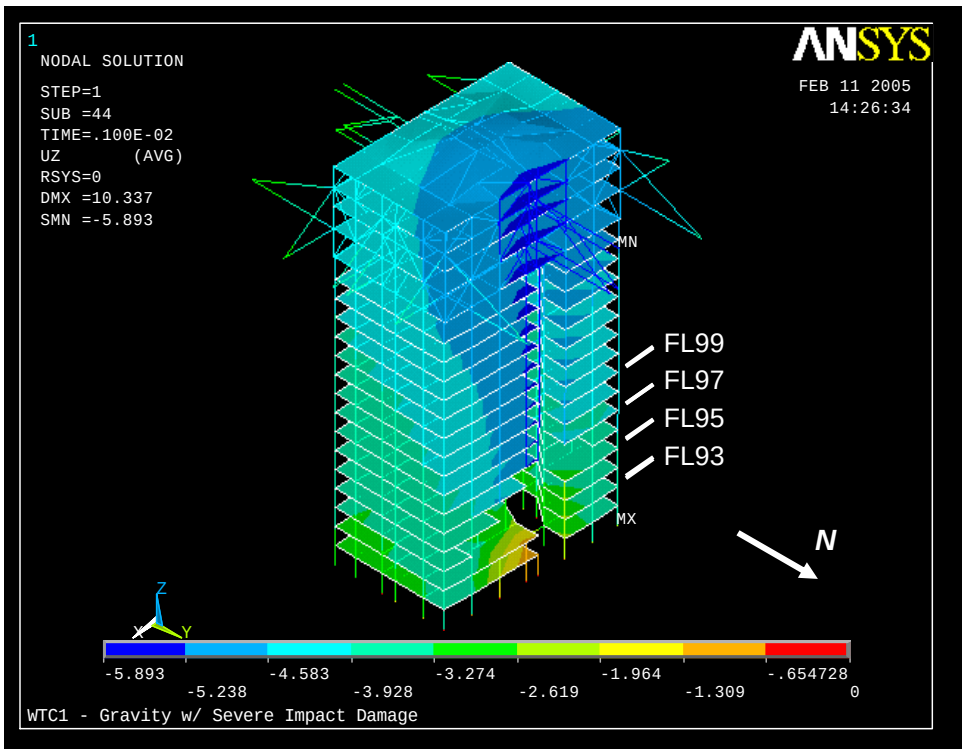

Figure 8–8. Vertical displacement of the east and north side of the WTC 1 core after aircraft impact for Case B.

The global analysis results showed that WTC 1 did not collapse following aircraft impact, as was observed, and had considerable reserve capacity. The core columns were loaded to approximately 50 percent of their capacity prior to impact, and the exterior columns were loaded to approximately 20 percent of their capacity. The exterior columns were capable of large load transfers from the core columns.

Gravity loads were redistributed to adjacent core columns and the exterior walls, primarily through the hat truss. Figures 8–9 and 8–10 show the demand-to-capacity ratios for the core columns before and after impact. The capacity of core and exterior columns was computed as the plastic (or inelastic) buckling load according the American Institute of Steel Construction (AISC) Load and Resistance Factor Design (LRFD) Specification procedures. Ratios less than 1.0 indicate that the column can carry additional gravity loads, where as ratios greater than 1.0 indicate that the column is carrying more than its computed capacity and, therefore, has plastic strains. Figure 8–10 shows that only two columns had a demand-to-capacity ratio greater than 1.0, and they were adjacent to severed or heavily damaged core columns.

After the aircraft impact, gravity loads that were previously carried by severed columns were redistributed to other columns. Table 8–2 shows that the north wall at Floor 98 carried a total load of 10,974 kip before aircraft impact, and 10,137 kip after the impact. The total load lost due to aircraft impact was 837 kip, or about 7 percent of the total load. Table 8–3 shows that the north wall at Floor 105 lost 732 kip of axial force after impact. Therefore, most of the core loads (732 kip out of 837 kip) were transferred by the hat truss, and the rest were redistributed to the adjacent exterior walls by the spandrels. Due to the impact damage and the tilting of the building to the north after impact, the south wall also lost gravity loads, and about 7 percent (604 kip) was transferred by the hat truss. As a result, the east and west walls

each gained about 7 percent (466 kip and 472 kip, respectively) and the core gained about 1 percent (400 kip) through the hat truss.

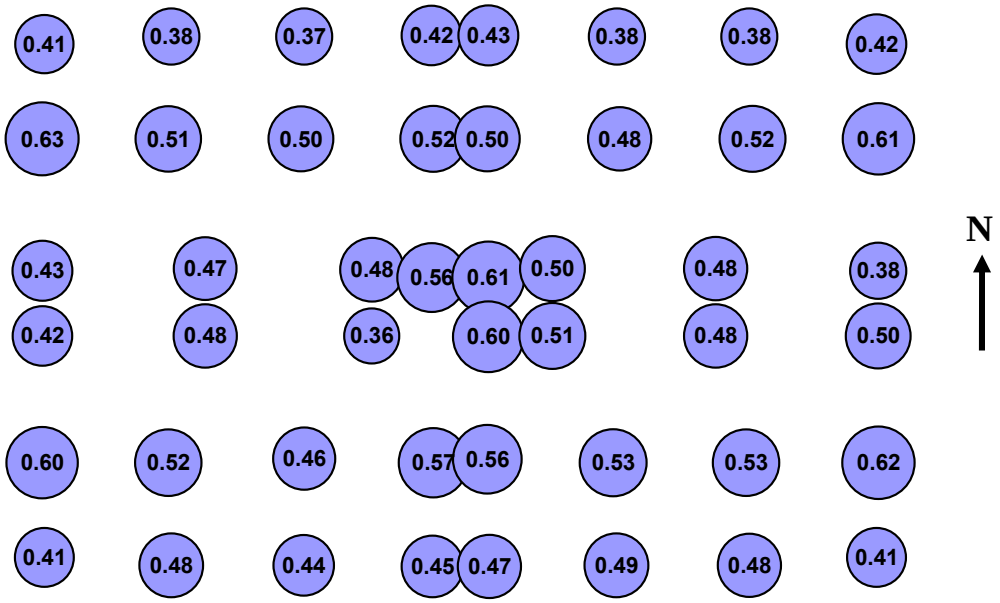

Figure 8–9. Maximum demand-to-capacity ratio for axial force in core columns between Floor 93 and Floor 99 of WTC 1 before aircraft impact.

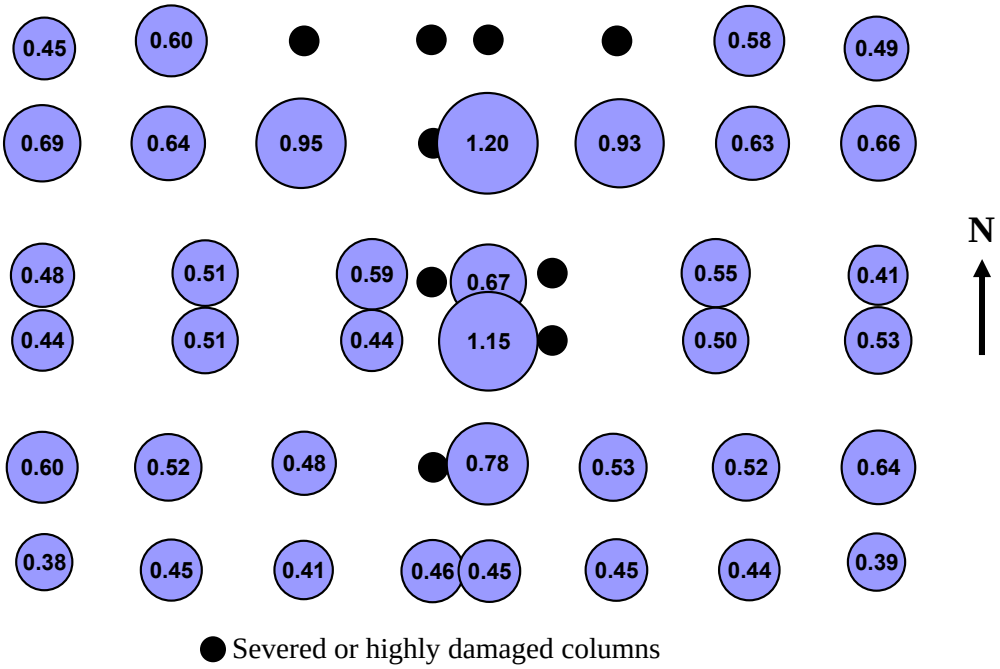

Figure 8–10. Maximum demand-to-capacity ratio for axial force in core columns between Floor 93 and Floor 99 of WTC 1 after aircraft impact for Case B.

Table 8–2. Total column loads at Floor 98 of WTC 1 for Case B conditions.

		North	East	South	West	Core	Total
(1)	Before Impact	10,974	8,545	11,025	8,572	34,029	73,144
(2)	After Impact	10,137	9,071	10,356	9,146	34,429	73,139
(3)	10 min	9,796	8,490	9,848	8,536	36,473	73,143
(4)	20 min	10,437	9,108	9,900	9,202	34,495	73,143
(5)	30 min	10,913	10,034	10,420	9,715	32,060	73,142
(6)	40 min	11,068	10,599	11,004	10,178	30,294	73,142
(7)	50 min	11,149	10,908	11,192	10,458	29,435	73,141
(8)	60 min	11,205	11,168	11,285	10,716	28,766	73,141
(9)	70 min	11,286	11,366	11,343	10,939	28,205	73,138
(10)	80 min	11,376	11,555	11,409	11,119	27,681	73,140
(11)	90 min	10,916	11,991	9,949	11,657	28,587	73,099
(12)	100 min	10,828	12,249	9,638	11,905	28,478	73,098
(13)	(2) - (1)	-837	526	-668	574	400	-5
(14)	(10) - (2)	1,239	2,484	1,052	1,973	-6,748	1
(15)	(12) - (2)	692	3,178	-719	2,759	-5,951	-41
(16)	(12) - (10)	-548	694	-1,771	786	797	-42

Note: Compression is positive. Units are in kip.

Table 8–3. Total column loads at Floor 105 of WTC 1 for Case B conditions.

		North	East	South	West	Core	Total
(1)	Before Impact	8,026	6,562	8,092	6,604	20,361	49,645
(2)	After Impact	7,294	7,028	7,488	7,076	20,761	49,646
(3)	10 min	6,944	6,461	6,981	6,469	22,790	49,646
(4)	20 min	7,551	7,075	7,057	7,158	20,806	49,647
(5)	30 min	8,020	7,998	7,569	7,685	18,377	49,648
(6)	40 min	8,193	8,571	8,129	8,147	16,608	49,649
(7)	50 min	8,285	8,878	8,315	8,428	15,743	49,650
(8)	60 min	8,351	9,130	8,414	8,687	15,069	49,650
(9)	70 min	8,435	9,319	8,481	8,914	14,502	49,651
(10)	80 min	8,528	9,497	8,551	9,097	13,978	49,651
(11)	90 min	8,096	9,847	7,327	9,506	14,876	49,652
(12)	100 min	8,023	10,076	7,066	9,720	14,767	49,653
(13)	(2) - (1)	-732	466	-604	472	400	1
(14)	(10) - (2)	1,234	2,470	1,063	2,021	-6,783	5
(15)	(12) - (2)	730	3,048	-422	2,644	-5,993	7
(16)	(12) - (10)	-504	579	-1,485	623	790	2

Note: Compression is positive. Units are in kip.

8.4.2 WTC 1 Structural Response to Elevated Temperatures

In the early stages of the fire, temperatures of structural components in the core rose between 500 °C and 700 °C over a 10 min to 20 min time interval (where fireproofing was damaged), and the thermal expansion of the core was greater than the thermal expansion of the exterior walls. The difference in the thermal expansion between the core and the exterior walls increased the loads in the core columns at 20 min. After 20 min, the core continued to lose gravity loads due to thermal weakening and shortening until the south wall started to bow inward. By 50 min, the core had displaced downward by 1.6 in on average at Floor 99 due to creep and buckling of core columns. About 20 percent (6,748 kip) of the gravity load was transferred by the hat truss to the exterior walls due to thermal weakening of the core at 80 min, as shown in Table 8–2; the north and south walls each carried about 10 percent more loads (1,239 kip and 1,052 kip, respectively)and the east and west walls each carried about 25 percent more loads (2,484 kip and 1,973 kip, respectively). Since the hat truss outriggers to the east and west walls were stiffer than the outriggers to the north and south walls, they transferred greater loads to the east and west exterior walls. At 100 min, the core displaced downward at Floor 99 by 2.0 in. on the south side of the core. As the core was weakened by creep and plastic buckling, gravity loads in the core were transferred to the exterior walls.

The full floor analyses for WTC 1 Case B showed that the floors on the south side in the impact zone did not begin to sag and apply a pull-in force at the column connections until approximately 80 min after impact. Based upon the full floor and isolated south wall subsystem analyses, 5 kip of pull-in force was applied to all columns across Floors 95 to 99 beginning at 80 min, as shown in Fig. 7–30. Figures 8–11 and 8–12 show the out-of-plane displacement contours of the south wall at 80 min and 100 min, respectively. Figure 8–13 shows the time history of the inward bowing of the south wall. Until the 5 kip pull-in forces were applied, no inward bowing had occurred. With the application of the 5 kip pull-in force, the maximum inward bow increased to 15.5 in.

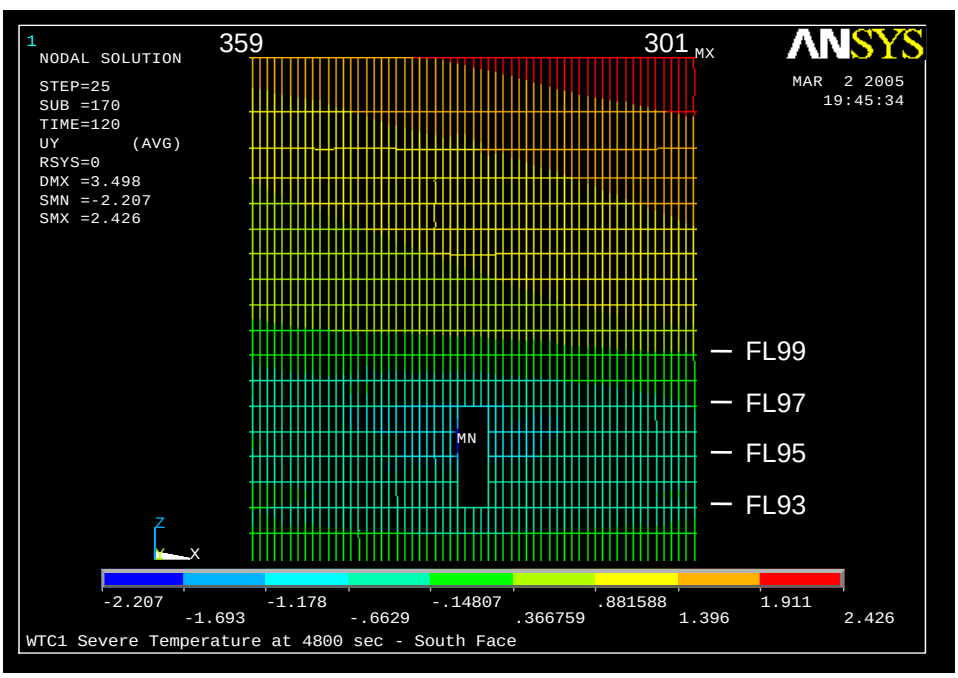

Figure 8–11. Out-of-plane displacement of south wall of WTC 1 at 80 min for Case B.

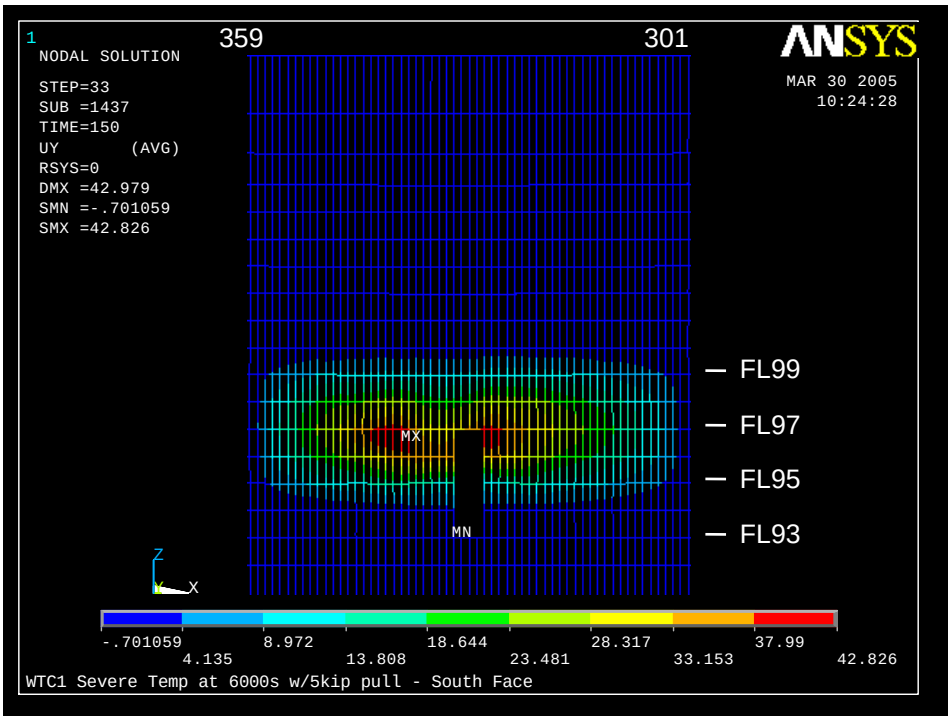

Figure 8–12. Out-of-plane displacement of south wall of WTC 1 at 100 min for Case B conditions with 5 kip pull-in forces.

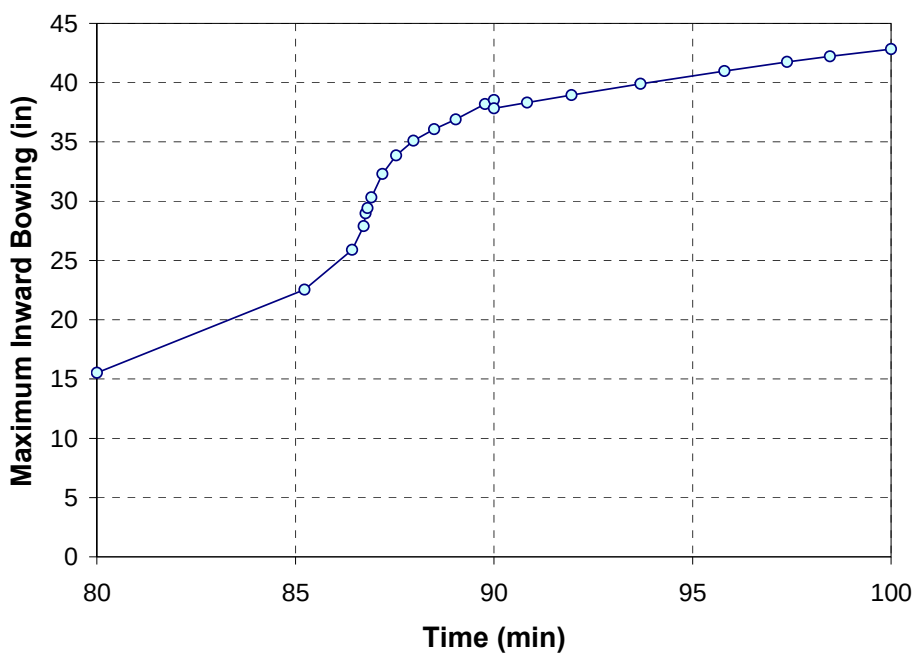

Figure 8–13. Time history of maximum out-of-plane displacement of WTC 1 south wall for Case B with 5 kip pull-in forces.

Figure 8–14 shows that Columns 318 to 346 on the south wall unloaded due to inward bowing after 80 min. The loads increased on the east and west walls. Figure 8–15 shows the load increase for the east

wall. Due to bowing of the south wall, the vertical displacement of the south wall increased as shown in Figs. 8–16 and 8–17, and the south wall lost about an additional 5 percent (1,771 kip) of load between 80 min and 100 min (see Table 8–2). As a result, the east and west walls and the core gained gravity loads.

By approximately 87 min, the inward bowing increased significantly. As the bowing of the south wall increased, a section of the south wall above the bowed-in area moved downward as can be seen in Fig. 8–18. By 90 min, the rate of increase in the inward bowing slowed down as the south wall redistributed the gravity loads to the east and west walls and to the core. The inward bowing increased to 42.8 in. at 100 min. However, the south wall remained stable (had not buckled) at 100 min.

Isolated exterior wall and global analyses showed that varying the inward pull force by a small amount caused a large difference in the amount of inward bowing. For a comparison, the inward bowing of the south wall at 100 min from the analysis with a 4 kip pull-in force was only 14.5 in. at 100 min. Given that the inward bowing increased from 14.5 in. to 42.8 in. when the inward pull force was increased from 4 kip to 5 kip, a slight increase in the pull-in force over 5 kip would have resulted in instability of the south wall.

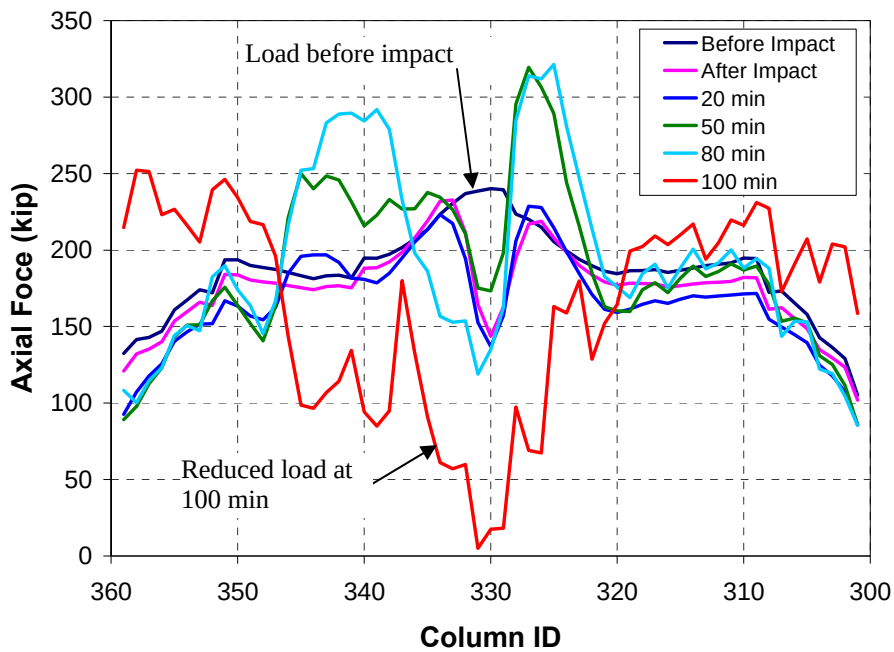

Figure 8–14. Distribution of axial force in exterior columns at Floor 98 of WTC 1 south wall for Case B with 5 kip pull-in forces.

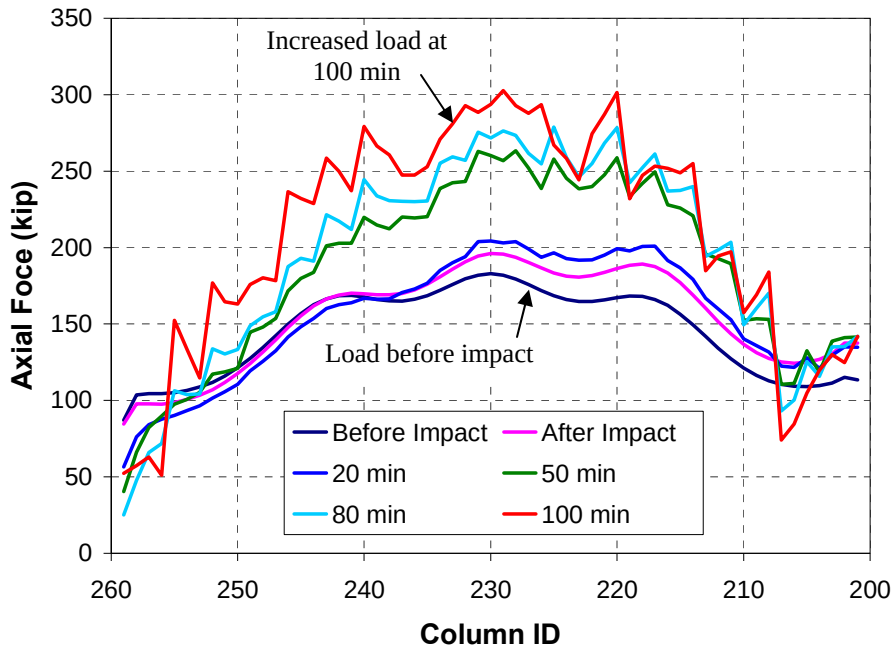

Figure 8–15. Distribution of axial force in exterior columns at Floor 98 of WTC 1 east wall for Case B with 5 kip pull-in forces.

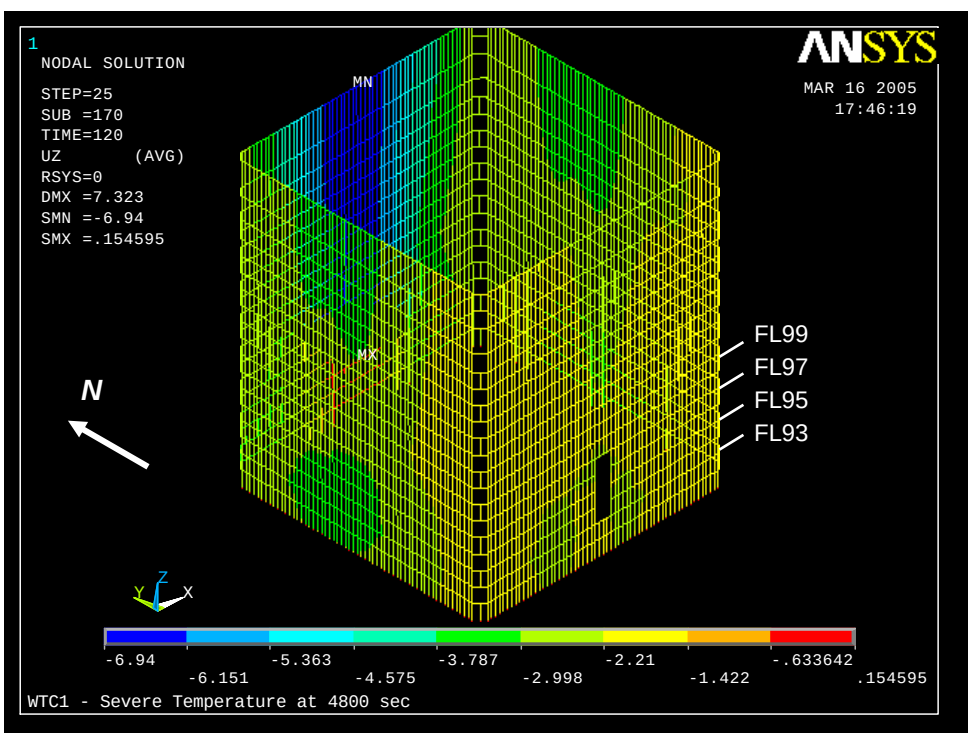

Figure 8–16. Vertical displacement of west and south exterior walls of WTC 1 at 80 min for Case B.

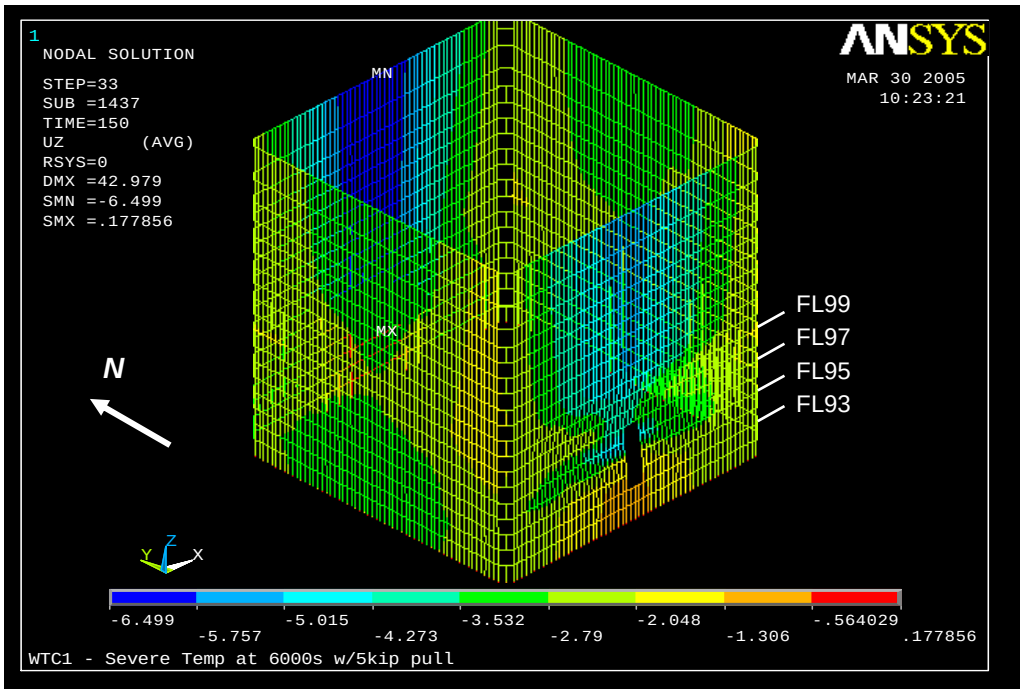

Figure 8–17. Vertical displacement of west and south exterior walls of WTC 1 at 100 min for Case B.

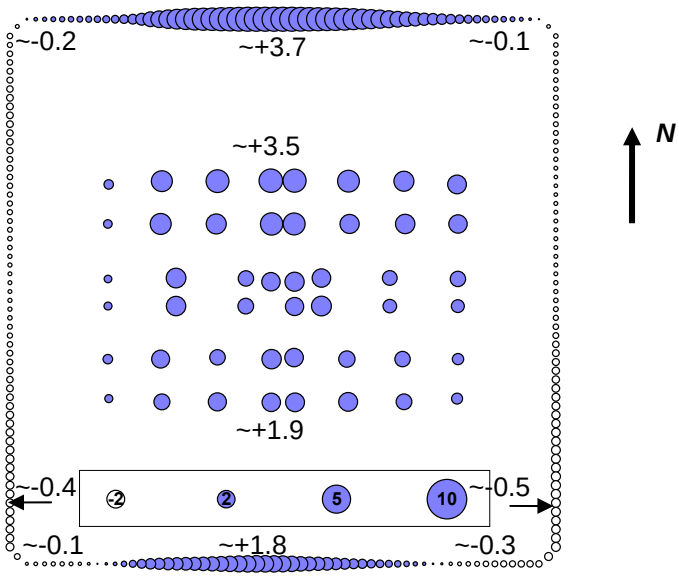

Note: downward displacement is shown as positive displacement

Figure 8–18. Change in vertical displacement at Floor 99 of WTC 1 from the state before impact to 100 min for Case B.

Plastic and creep strains played a significant role in the structural response of WTC 1 to the fires. Figures 8–19 to 8–21 show the maximum elastic-plus-plastic-plus-creep strain in each column between Floor 93 and Floor 99 at 10 min, 40 min, and 100 min, respectively. Before the aircraft impact, the columns had no plastic strain. After the aircraft impact, several columns that were close to severed and

highly damaged columns experienced plastic strains. Plastic strain of the core increased for the first 40 min, and then remained almost constant to 100 min. Plastic strain of the south exterior columns increased in almost all the bowed columns from 40 min to 100 min. However, creep strain was found to be far greater than plastic strain, especially in the core. At 40 min, 22 of 47 core columns had creep strain larger than 1.0 percent. After 40 min, creep strain in core columns on the south side had increased. The maximum elastic-plus-plastic-plus-creep strain at 100 min was 7.3 percent in Column 1006. As temperature increased on the south exterior wall in the later stages of the fire, creep strain also increased in about 20 columns on the south face. The maximum elastic-plus-plastic-plus-creep strain in the south exterior columns reached 2.9 percent.

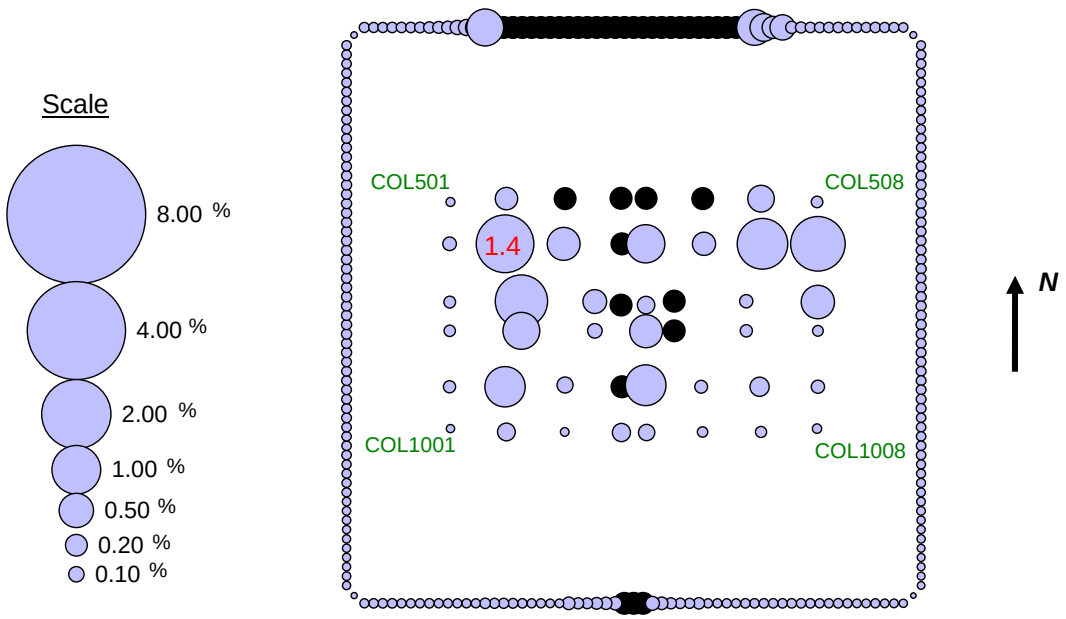

Figure 8–19. Maximum elastic-plus-plastic-plus-creep strain for columns between Floor 93 and Floor 99 of WTC 1 at 10 min for Case B (strain values are in percent).

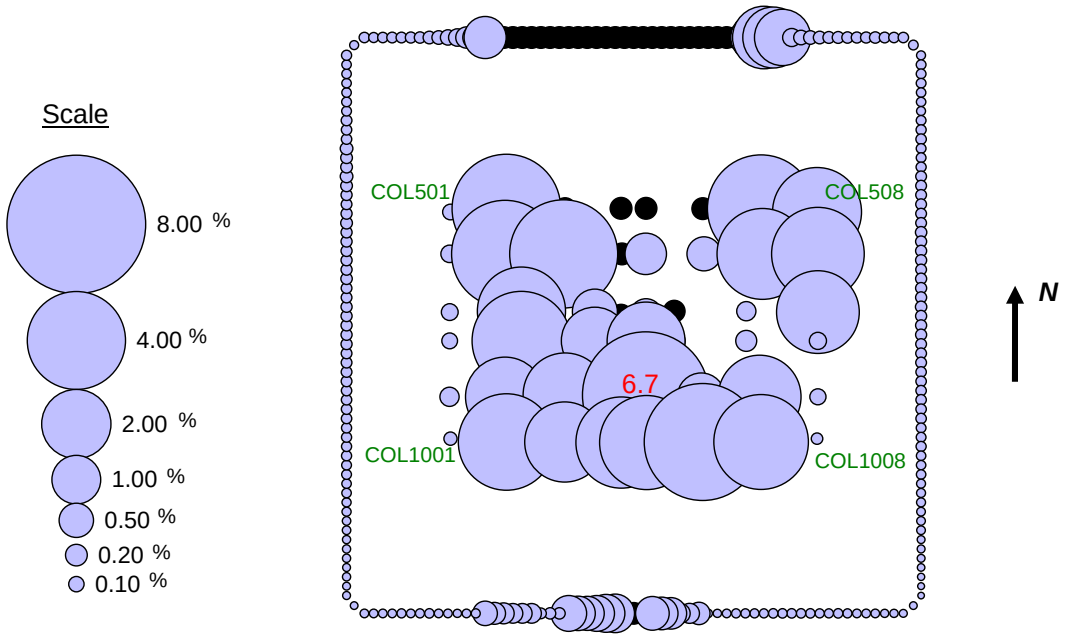

Figure 8–20. Maximum elastic-plus-plastic-plus-creep strain for columns between Floor 93 and Floor 99 of WTC 1 at 40 min for Case B (strain values are in percent).

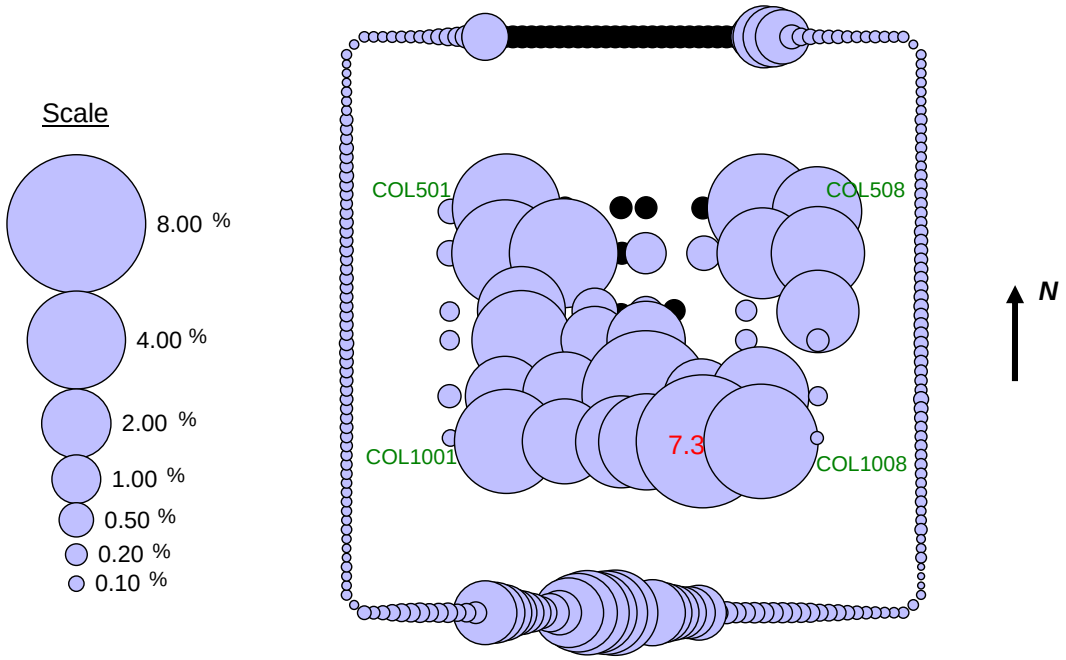

Figure 8–21. Maximum elastic-plus-plastic-plus-creep strain for columns between Floor 93 and Floor 99 of WTC 1 at 100 min for Case B with 5 kip pull-in forces (strain value are in percent).

Figures 8–22 and 8–23 show the axial force demand-to-capacity ratio for each core column at 80 min and 100 min, respectively. Compressive capacities of the core columns were calculated by AISC LRFD Eq. E2-1 for plastic buckling with effective length factor of K equal to 1.0 and a resistance factor of 1.0. Comparison of Figs. 8–10 and 8–23 shows that the demand-to-capacity ratio increased for core columns with relatively small elastic-plus-plastic-plus-creep strains and decreased for columns with high strains. Figure 8–21 shows that core columns with high creep strains had lower demand-to-capacity ratios. Columns with high compressive loads and large creep strains shortened and unloaded to stiffer columns with less creep.

At 100 min, the core had weakened on the south side and shortened by 1.6 in. The south wall had bowed inward approximately 43 in. and was unloading to the core and the adjacent east and west walls. As discussed previously, a small change in the magnitude of the inward pull force changed the rate at which the exterior wall bowed inward and reached a point of instability. Based upon observations and similar results for WTC 2 at collapse initiation (described in the next Section), the following sequence of events likely occurred as soon as the south wall reached instability and buckled.

The inward bowing of the south wall caused failure of exterior column splices and spandrels, and induced column instability. The instability progressed horizontally across the entire south face. The south wall unloaded and redistributed its gravity loads to the thermally weakened core through the hat truss and to the east and west walls through the spandrels. The beginning of this load redistribution is illustrated in Tables 8–1 and 8–2. The building section above the impact zone began tilting to the south as column instability progressed rapidly from the south wall along the adjacent east and west walls and increased the gravity load on the core columns. The change in potential energy due to downward movement of the building mass above the buckled columns exceeded the strain energy that could have been absorbed by the structure. Global collapse then ensued.

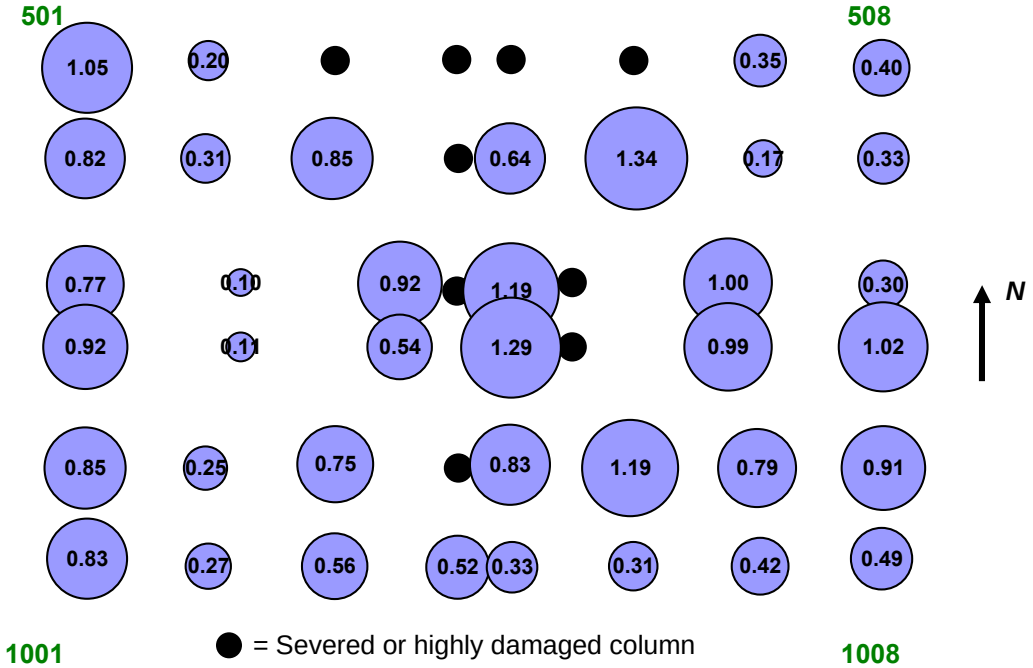

Figure 8–22. Maximum demand-to-capacity ratio for axial force in core columns between Floor 93 and Floor 99 of WTC 1 at 80 min for Case B conditions.

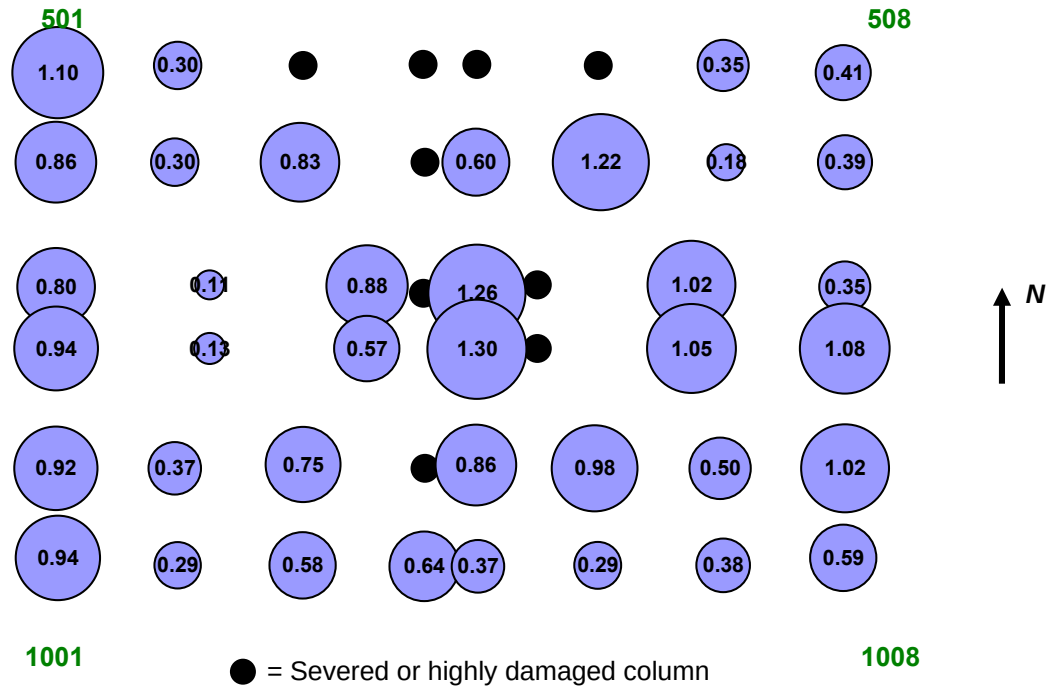

Figure 8–23. Maximum demand-to-capacity ratio for axial force in core columns between Floor 93 and Floor 99 of WTC 1 at 100 min for Case B with 5 kip pull-in forces.

8.4.3 WTC 1 Hat Truss Members and Connections

The state of the hat truss members and the connections were checked since the global model did not include break elements to capture column and hat truss splice failures or sufficient beam elements to capture buckling of the hat truss outriggers. The condition of the connections and the members in the primary load path of the hat truss was evaluated at various time intervals. The evaluation included the core column splices for tension, outriggers and supporting columns for compression, and the hat truss connections that were in the primary load path for tension.

Core column splices had compressive forces before the aircraft impact. With the aircraft impact damage and increasing plastic and creep strains, the core weakened and shortened, and some core columns were supported from the hat truss. At 100 min, nine core columns (503, 504, 505, 602, 603, 604, 605, 702, and 802) were in tension at Floor 105 as shown in Fig. 8–24. To evaluate the condition of the core column splices at Floor 106, the tension capacity of these splices was compared to the tensile forces developed during each 10 min time interval. To calculate the connection tensile capacity, AISC-LRFD procedures were used. It was found that tensile forces in the core columns were less than the capacities of the splices.

There were sixteen outriggers (four on each face), as shown in Fig. 8–25, that transferred gravity loads between the core and the exterior walls. In the global model, each of these outriggers was modeled by only one BEAM 24 element; therefore, buckling of the member was not captured although material nonlinearity was included. Table 8–4 lists demand-to-capacity ratios for the outrigger members over time. Capacities of the outriggers were calculated using AISC LRFD procedures for plastic (inelastic) buckling with effective length factor K equal to 0.75 (the outrigger end connections were different from those used for the core columns) and a resistance factor of 1.0. As the outrigger members were not

modeled with sufficient elements to capture plastic buckling, they yielded when the outrigger reached its compressive capacity; therefore, force redistribution to other outriggers was underestimated.

The hat truss connections within the hat truss itself were also checked. The hat truss connections in the primary load path were identified, and their capacities were compared to their forces. The primary load path was identified by selecting hat truss members with an absolute axial stress of 25 ksi or more at 80 min, as this was when maximum forces occurred. Only the connections that were transferring tensile forces were evaluated. In calculating the capacity of the connections, the AISC-LRFD procedures were used. None of the hat truss connection capacities were exceeded. It was concluded that the hat truss redistributed loads between the core and the exterior wall columns as modeled in the global analysis.

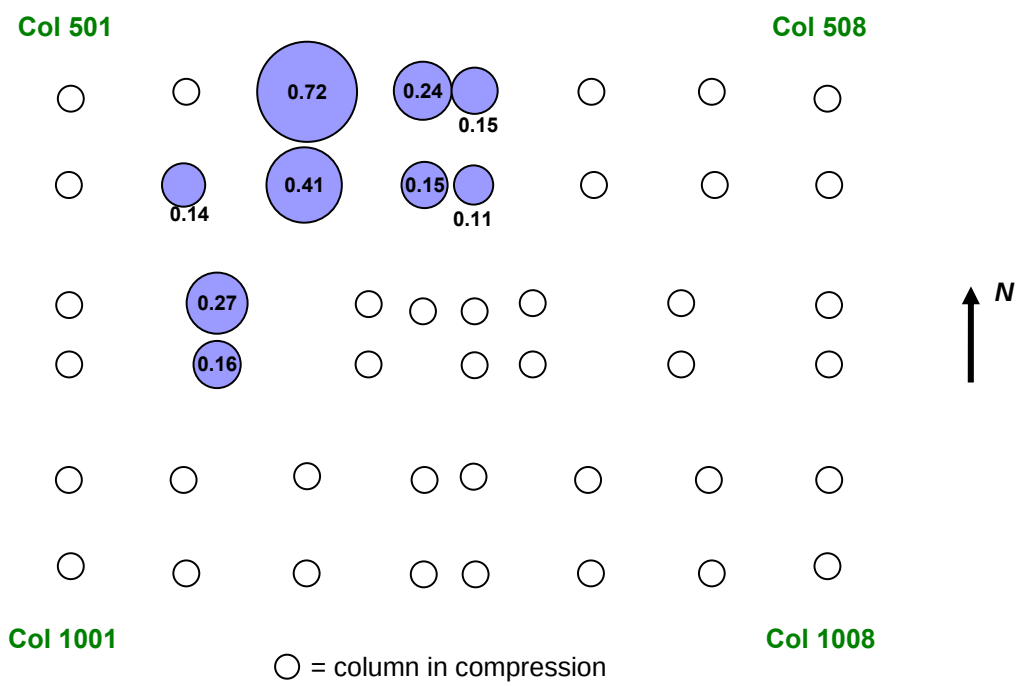

Figure 8–24. Tension demand-to-capacity ratio for core column splices at WTC 1 Floor 106 at 100 min for Case B with 5 kip pull-in forces.

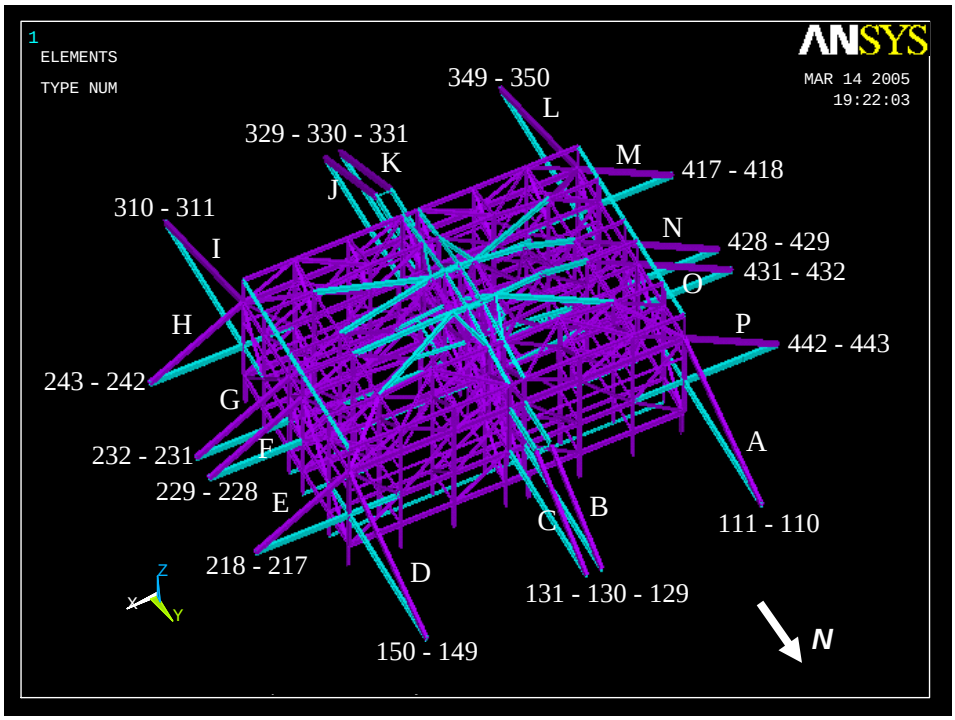

Figure 8–25. Location and label of outriggers and supporting columns for WTC 1.

Table 8–4. Demand-to-capacity ratio for axial force in outriggers of WTC 1 for Case B.

Outrigger ID	Bfr Imp	Aftr Imp	10 min	20 min	30 min	40 min	50 min	60 min	70 min	80 min	90 min	100 min
North												
A	0.26	0.35	0.26	0.40	0.49	0.53	0.56	0.59	0.62	0.65	0.54	0.52
B	0.22	-0.07	-0.13	-0.04	0.02	0.04	0.06	0.07	0.08	0.09	0.03	0.03
C	0.21	-0.05	-0.11	-0.02	0.04	0.06	0.08	0.08	0.09	0.11	0.05	0.04
D	0.25	0.35	0.29	0.45	0.61	0.67	0.70	0.72	0.73	0.75	0.65	0.63
East												
E	0.32	0.48	0.38	0.56	0.75	0.83	0.88	0.92	0.94	0.97	0.95	0.96
F	0.23	0.28	0.21	0.30	0.41	0.48	0.52	0.55	0.57	0.59	0.62	0.64
G	0.23	0.26	0.20	0.26	0.35	0.42	0.46	0.49	0.51	0.54	0.58	0.61
H	0.33	0.31	0.23	0.25	0.36	0.46	0.51	0.55	0.58	0.60	0.72	0.77
South												
I	0.25	0.12	0.04	0.03	0.12	0.20	0.23	0.26	0.27	0.28	0.28	0.28
J	0.21	0.10	0.01	0.03	0.13	0.24	0.28	0.29	0.30	0.31	0.04	-0.02
K	0.21	0.10	0.01	0.03	0.13	0.24	0.27	0.28	0.30	0.31	0.02	-0.04
L	0.26	0.12	0.02	0.05	0.11	0.20	0.24	0.27	0.29	0.31	0.19	0.18
West												
M	0.33	0.33	0.22	0.29	0.36	0.44	0.49	0.53	0.56	0.58	0.69	0.73
N	0.24	0.27	0.20	0.28	0.34	0.40	0.44	0.47	0.50	0.52	0.56	0.58
O	0.24	0.29	0.22	0.31	0.38	0.43	0.47	0.50	0.53	0.55	0.59	0.61
P	0.33	0.48	0.39	0.54	0.64	0.71	0.75	0.79	0.83	0.87	0.88	0.90

8.5 RESULTS OF WTC 2 ANALYSIS

The global model of WTC 2 with creep, plastic buckling of columns, plasticity, and nonlinear geometry was analyzed with Case D structural damage and temperature histories.

8.5.1 WTC 2 Structural Response to Aircraft Impact Damage

Case D structural and passive fire protection damage after the aircraft impact was as follows:

- WTC 2 had 34 severed columns on the south wall (Columns 407 to 440) and 11 core columns on the south side of the core (Columns 701, 702, 801, 802, 803, 901, 903, 1001, 1002, 1003, and 1004) and 4 exterior columns on the north wall (Columns 253, 254, 257, and 258) that were severed or heavily damaged between Floors 78 to 84.

- Floor slabs and framing were severed or heavily damaged in the south office floor area through the east side of the core between Floors 78 and 84.

- WTC 2 fireproofing damage extended from the south exterior wall, through the east side of the core, to the east and north exterior walls between Floors 78 and 84.

The vertical displacements of the exterior wall before the aircraft impact were about 2.0 in. to 3.0 in. (Fig. 8–26). After aircraft impact, the vertical displacements increased to 7.4 in. on the south wall (Fig. 8–27). There was no horizontal (out-of-plane) displacement on the east wall before the aircraft impact. After aircraft impact, the south side of the east wall at Floor 86 displaced outward about 2.0 in.; whereas, the north side at the same floor did not displace.

In the core, the vertical displacements were about 3.5 in. to 4.2 in. before the aircraft impact, as shown in Fig. 8-28. After aircraft impact, the vertical displacements increased to 10 in. at the southeast corner of the core where the aircraft impact had severed columns, as shown in Fig. 8–29.

Figures 8–30 and 8-31 show the north-south and east-west lateral displacements of the exterior wall above Floor 86 after aircraft impact. Floor 110 moved toward the south about 5.1 in. and toward the east about 5.0 in. There was also a slight twist around the z-axis of the tower of about 0.07 percent at Floor 110. The twist around the z-axis was calculated by taking the difference between the average in-plane displacement of the two opposing exterior walls (such as the east and the west walls) at Floor 110 and dividing the result by the distance between these walls (~200 ft).

The global analysis showed that WTC 2 was stable following aircraft impact, as was observed, and had considerable reserve capacity. Similar to WTC 1, the core columns were loaded to approximately 50 percent of their capacity prior to impact, and the exterior columns were loaded to approximately 20 percent of their capacity. The exterior columns were capable of large load transfers from the core columns after impact.

The loads in the severed exterior columns were transferred to adjacent exterior columns through the spandrels and to the core through the hat truss. Several of the severed core columns at the southeast corner of the core were computed to have failed splice connections to the hat truss (discussed in Section 8.5.3). The loads from these columns were transferred through the core floors to adjacent core columns and then to the east and south exterior walls through the hat truss. Additionally, the severed core columns at the southeast corner resulted in the core leaning to the southeast. While the isolated WTC 2 core model was not stable with the structural impact damage, within the global system the core was supported by the floors and exterior walls.

The leaning of the core to the southeast contributed to the load redistribution in WTC 2, with a general pattern of increased loads on the south and east columns (core and exterior) and decreased loads on the north and west columns. Tables 8–5 and 8–6 show the total columns loads at Floors 83 and 105, respectively, for the analysis stages from before impact to collapse initiation at 43 min. After impact, as shown in Table 8–5, the core carried 6 percent less loads (4,007 kip), and the east wall carried 24 percent more gravity loads (4,368 kip). The north wall loads decreased by 10 percent (1,374 kip), and the south and west walls loads increased by 2 percent (227 kip) and 3 percent (604 kip), respectively.

The loads on the core columns before aircraft impact were distributed essentially symmetrically with respect to the center of the core. There was a slight difference between corner columns on the south side (501 and 1001) and north side (508 and 1008) due to slightly higher dead and live loads in the north side columns. Columns 506, 507, 508, and 1008 at the northeast and northwest corners unloaded; the other intact core columns increased in load (Figs. 8–32 and 8–33). The loads in Columns 904 and 1005, which were adjacent to the severed and heavily damaged columns, increased substantially at Floor 83 after impact. Column 904 increased from 660 kip to 1,506 kip and Column 1005 increased from 1,287 kip to 2,794 kip.

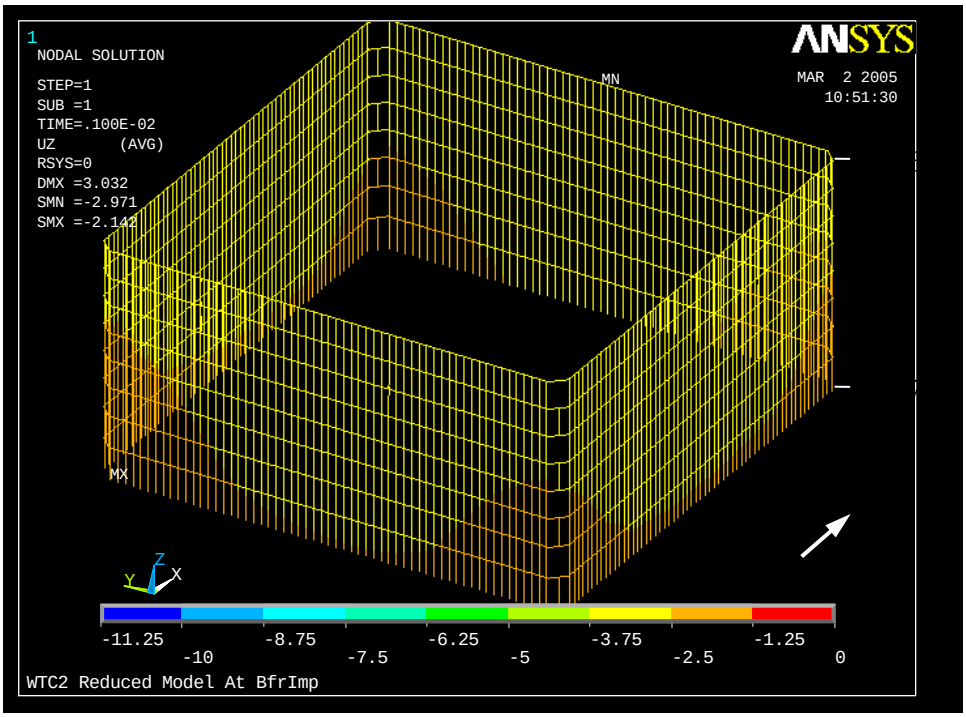

Figure 8–26. Vertical displacement before impact of WTC 2 exterior wall for Case D.

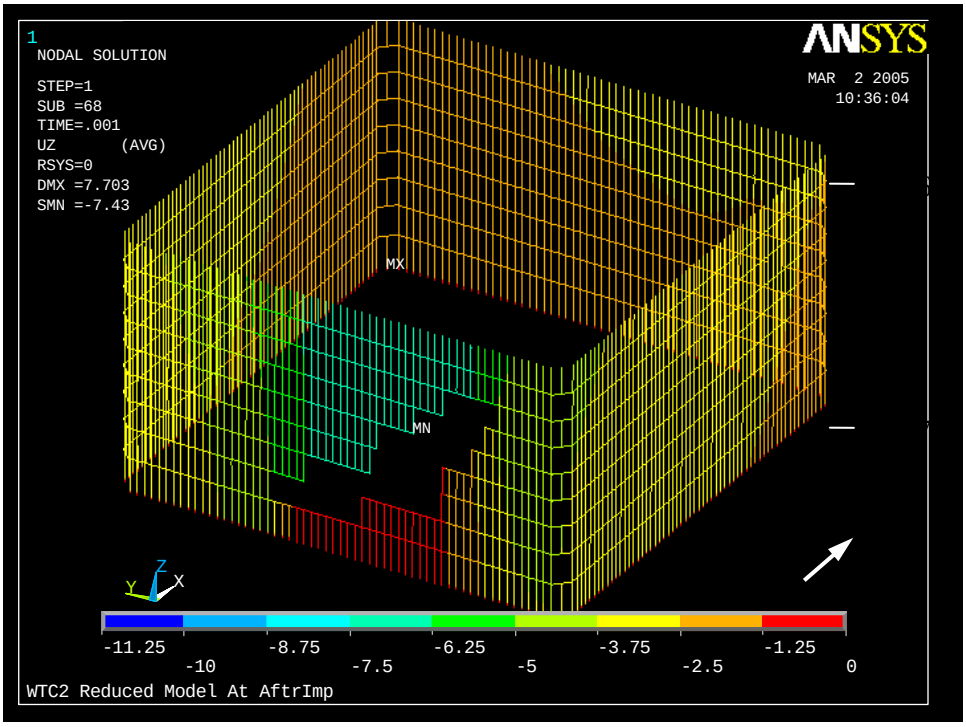

Figure 8–27. Vertical displacement after impact of WTC 2 exterior wall for Case D.

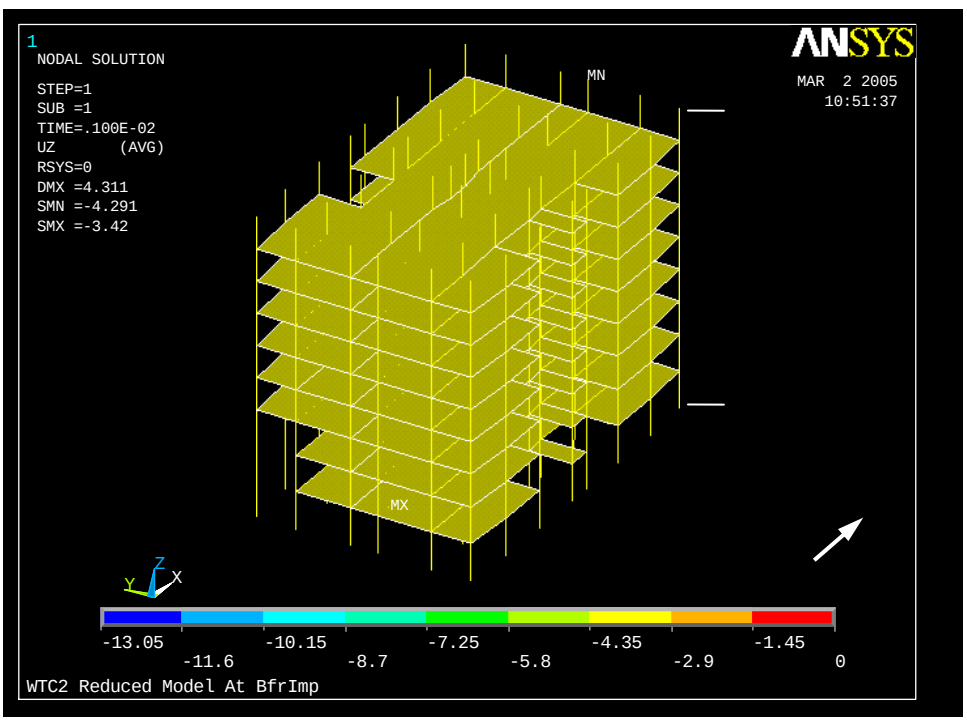

Figure 8–28. Vertical displacement before impact of WTC 2 core for Case D.

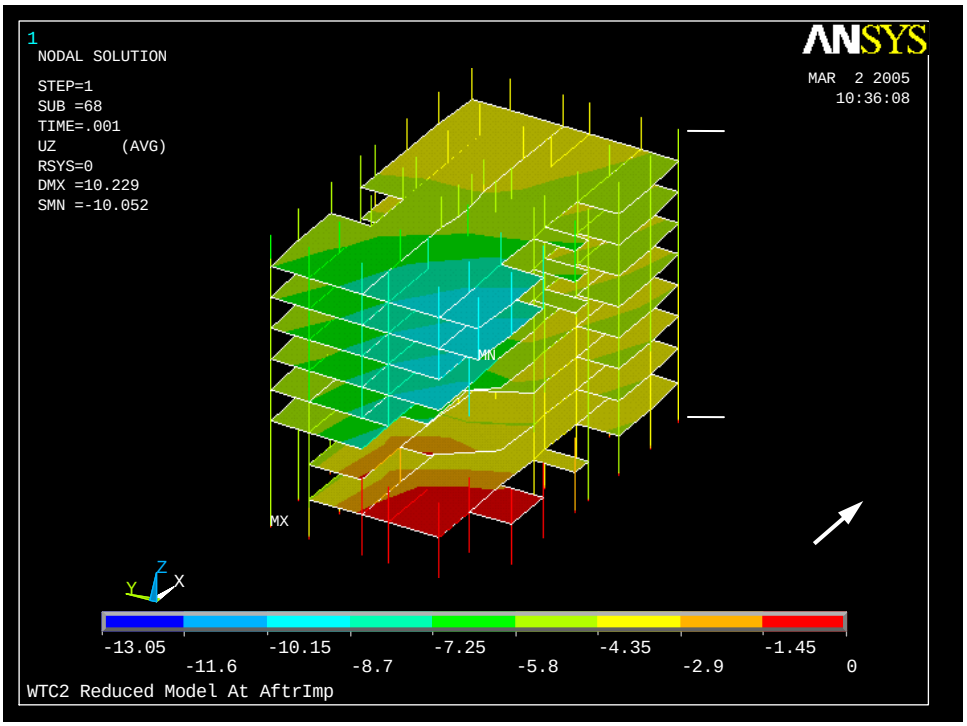

Figure 8–29. Vertical displacement after impact of WTC 2 core for Case D.

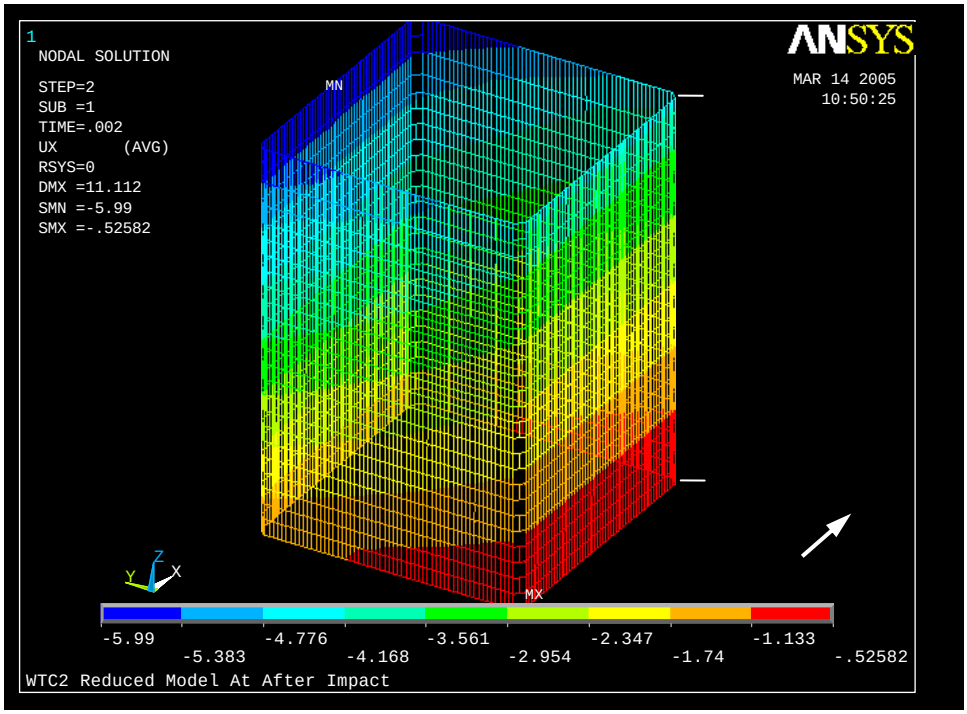

Figure 8–30. Lateral displacements after impact above WTC 2 Floor 86 in the x-direction (north-south) for Case D.

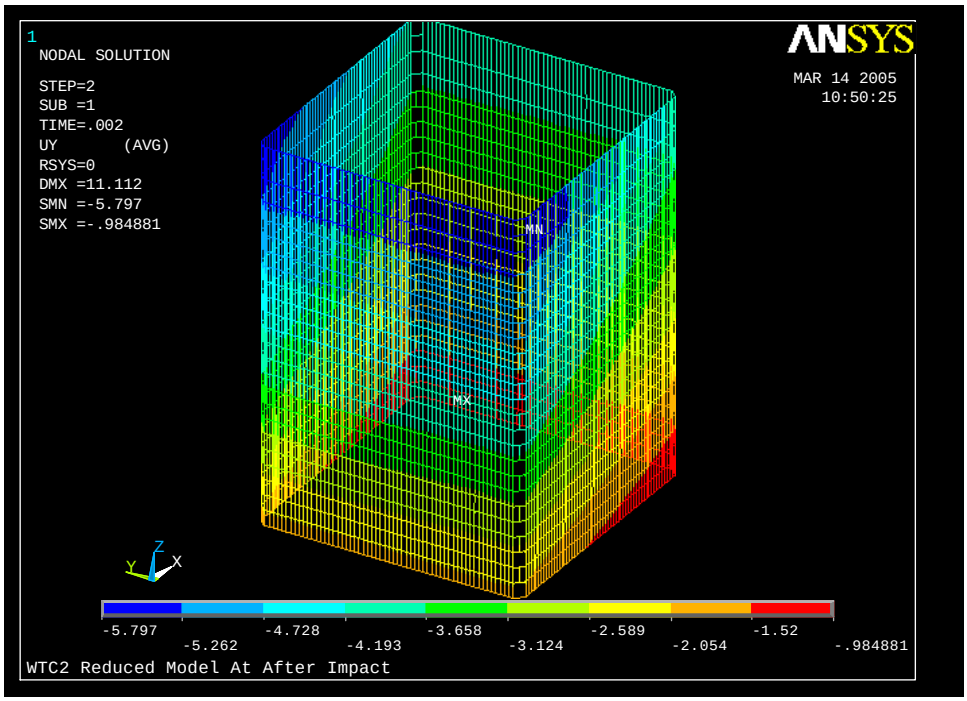

Figure 8–31. Lateral displacements after impact above WTC 2 Floor 86 in the y-direction (east-west) for Case D.

Table 8–5. Total column loads at WTC 2 Floor 83 for Case D (Compression is positive).

Row	Analysis Stage	West	East	North	South	Core	Sum
(1)	Before Impact	18065	18114	13567	13284	61828	124857
(2)	After Impact	18670	22481	12193	13511	57821	124676
(3)	10 min	18728	22226	11896	13358	58413	124621
(4)	20 min	18914	22208	12052	13318	58124	124616
(5)	30 min	18876	23681	11770	13365	56967	124659
(6)	40 min	18531	23682	11906	13473	56825	124418
(7)	43 min	15667	15143	14215	16292	62422	123738
(8)	(2)-(1)	604	4368	-1374	227	-4007	-181
(9)	(3)-(1)	662	4112	-1670	74	-3415	-236
(10)	(4)-(1)	849	4094	-1515	35	-3704	-241
(11)	(5)-(1)	811	5567	-1797	81	-4861	-199
(12)	(6)-(1)	466	5568	-1661	190	-5003	-439
(13)	(7)-(1)	-2398	-2971	648	3009	594	-1119

Table 8–6. Total column loads at WTC 2 Floor 105 for Case D (Compression is positive).

Row	Analysis Stage	West	East	North	South	Core	Sum
(1)	Before Impact	8497	8572	7382	7169	17123	48742
(2)	After Impact	9170	11272	6487	8432	13382	48742
(3)	10 min	9182	11061	6250	8275	13975	48742
(4)	20 min	9279	11120	6311	8351	13682	48742
(5)	30 min	9370	11859	6416	8553	12544	48742
(6)	40 min	9198	11927	6524	8691	12402	48742
(7)	43 min	7086	8026	6546	9169	17915	48742
(8)	(2)-(1)	674	2699	-895	1263	-3741	0
(9)	(3)-(1)	685	2489	-1132	1106	-3148	0
(10)	(4)-(1)	783	2547	-1071	1182	-3441	0
(11)	(5)-(1)	873	3287	-965	1384	-4579	0
(12)	(6)-(1)	702	3355	-858	1522	-4721	0
(13)	(7)-(1)	-1411	-547	-835	2000	792	0

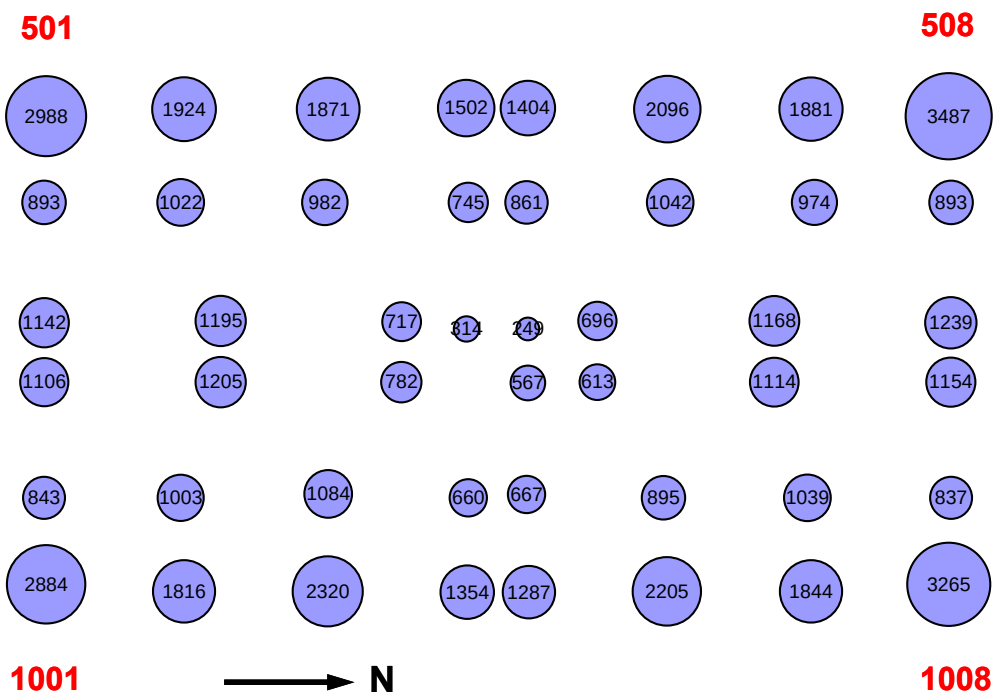

Figure 8–32. Core column loads (kip) before impact at WTC 2 Floor 83 for Case D (compression is positive).

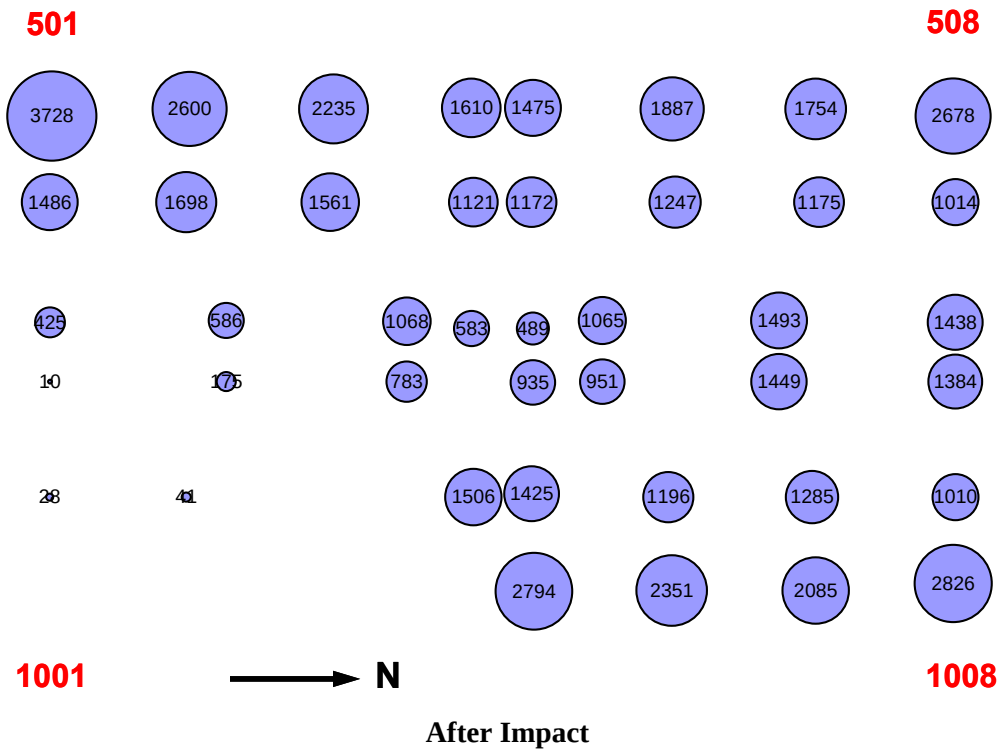

Figure 8–33. Core column loads (kip) after impact at WTC 2 Floor 83 for Case D (compression is positive).

8.5.2 WTC 2 Structural Response to Elevated Temperatures

In contrast to the fires in WTC 1, which generally progressed from the north side to the south side over approximately one hour, the fires in WTC 2 started and remained on the east side of the building until it collapsed, with the fires spreading from south to north. With fireproofing dislodged over much of the same area, the structural temperatures increased in the core, floors, and exterior walls at similar times. During the early stages of the fires, columns with dislodged fireproofing elongated due to thermal expansion. As the structural temperatures continued to rise beyond 500 °C, the thermal expansion was overcome by plastic and creep deformations under compressive loads.

Vertical displacement of the exterior walls before impact were 2.0 in. to 3.0 in. Vertical displacements of the south and east walls after impact were around 7.3 in. on the south face (over the severed columns) and about 3.5 in. on the east face, as shown in Figs. 8–34 and 8–35. These vertical displacements remained essentially constant after impact until the east wall became unstable at 43 min (Figs. 8–36 and 8–37).

After impact, the core and the north wall unloaded, and their load was redistributed to the south, west, and east walls. Table 8–7 shows that about 94 percent (3,740 kip/4,000 kip) of the load from the core was redistributed through the hat truss to the east, south, and west walls and 6 percent was redistributed through the floors to the east wall. A similar calculation for the east wall indicates that about 62 percent (2,699 kip/4,368 kip) of the load increase came through the hat truss and 38 percent was transferred through the spandrels to the north and south walls. Comparison of loads shown in Rows 8, 9, 10, and 11

in Tables 8–5and 8–6 show that the column loads did not significantly change until the core unloaded at 30 min. Prior to this point, the thermal expansion of the core columns caused loads to increase. When the plastic and creep strains exceeded the thermal strains, the core columns shortened and unloaded. Loads in weakened core columns were redistributed to adjacent columns primarily through the hat truss.

Shortly after impact, Floors 79 to 83 began to sag and pull inward on the east wall (except where truss seat connections had failed). At 20 min, the east wall had bowed inward 9.5 in. near the center of the east wall, as shown in Fig. 8–38. The computed inward displacement agrees well with the observed inward displacement (~10 in.) that was measured from photographs at 9:21 a.m. (approximately 20 minutes after the aircraft impact). Inward displacements of the east wall steadily increased until collapse initiation.

At 30 min, the core unloaded about 850 kip (from 4,861 kip to 4,007 kip), the east wall increased about 1,200 kip (from 5,567 kip to 4,368 kip), and the north wall unloaded about 420 kip (from 1,797 kip to 1,374 kip) at Floor 83. Floor 105 column loads remained almost constant after aircraft impact until the east wall became unstable at 43 min. From 40 min to 43 min, the east wall suddenly unloaded about 8,540 kip, the west wall unloaded about 2,860 kip, the core load increased by about 5,600 kip, the north wall load increased by about 2,310 kip, and the south wall load increased about 2,820 kip at Floor 83 (Table 8–8). Comparison of the load redistribution that took place at Floor 105 with that at Floor 83 indicates that essentially all the additional core load from the east and west walls was transferred through the hat truss. For the east wall, about 46 percent (3,901 kip/8,539 kip) of the load shed was redistributed through the hat truss to the core and 54 percent was redistributed primarily through the spandrels to the south and north walls. After the load redistribution, the total load in the core columns increased to the same level as before the aircraft impact.

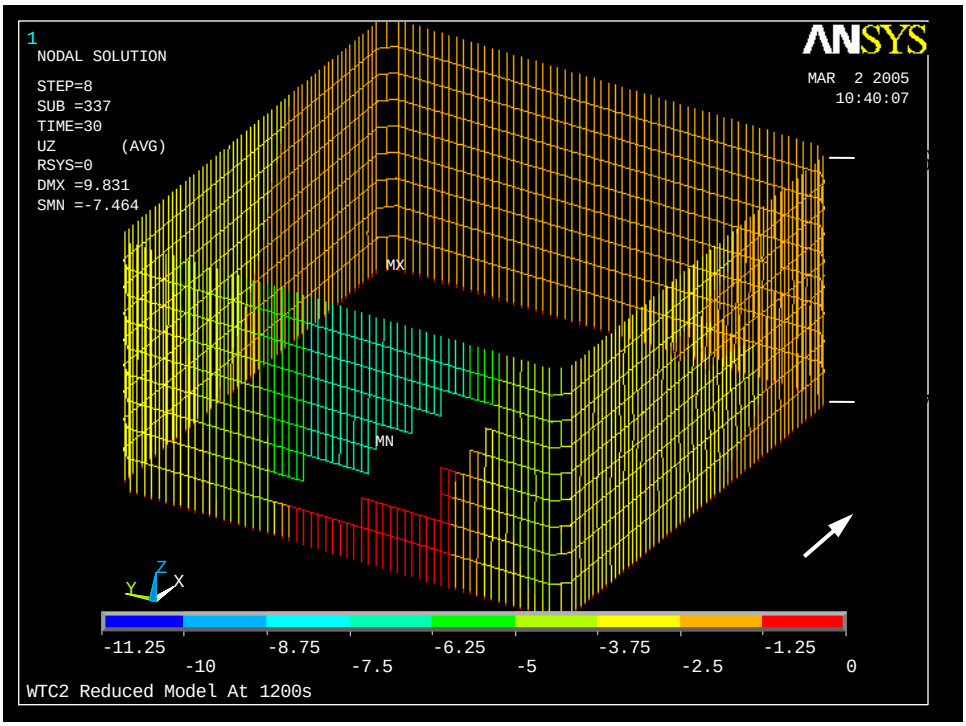

Figure 8–34. Vertical displacement of exterior wall of WTC 2 at 20 min for Case D.

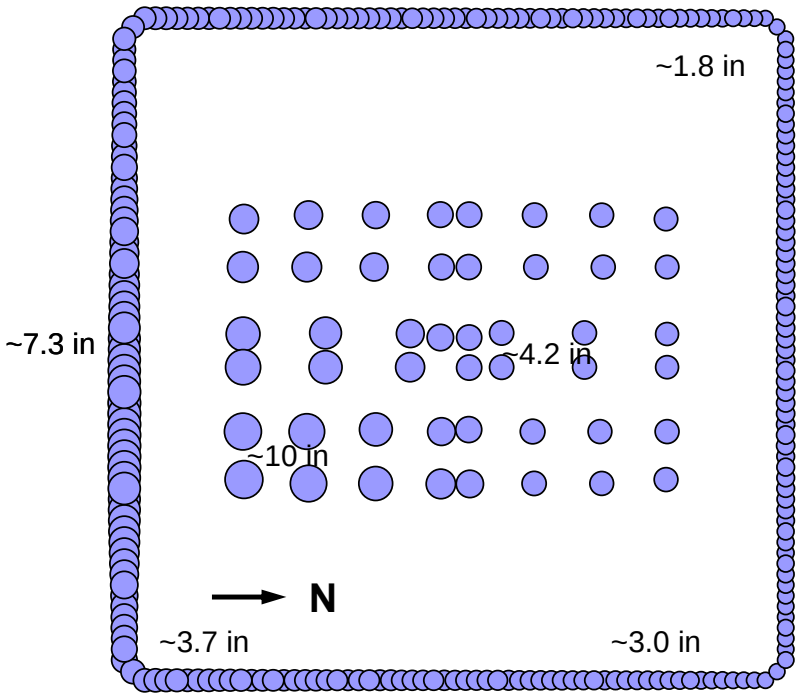

Figure 8–35. Vertical displacement at Floor 83 of WTC 2 at 20 min for Case D (note the tilt toward east and south).

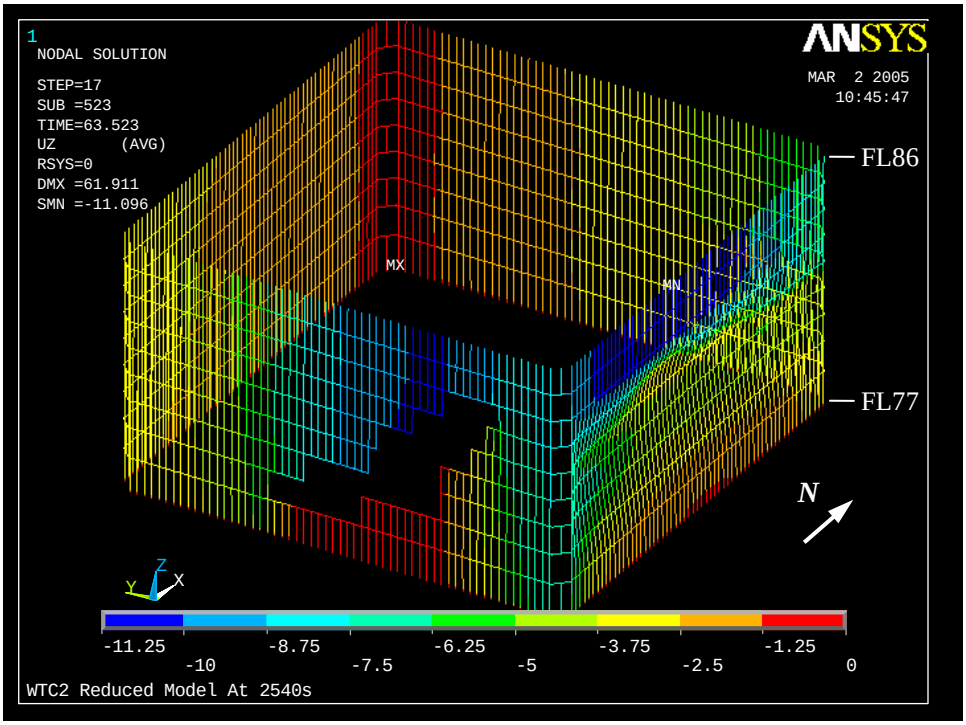

Figure 8–36. Vertical displacement of exterior wall of WTC 2 at 43 min for Case D.

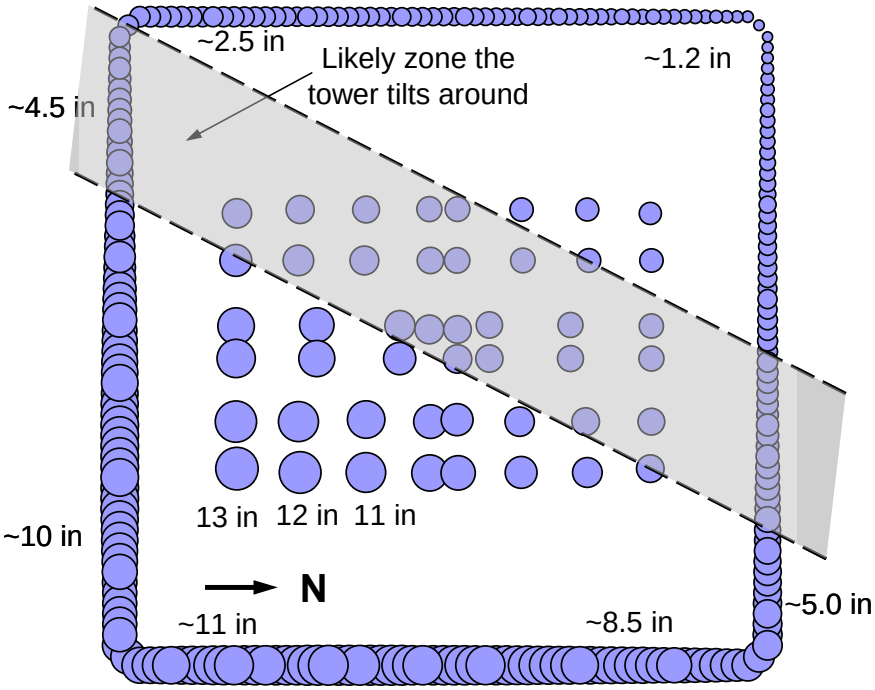

Figure 8–37. Vertical displacement at Floor 83 of WTC 2 at 43 min for Case D (note the tilt toward east and south).

Table 8–7. Change in total column loads before and after aircraft impact. (Loads After Impact) – (Loads Before Impact) (Compression is positive).

Row	Floor	West	East	North	South	Core
(1)	83	604	4368	-1374	227	-4007
(2)	105	674	2699	-895	1263	-3741
(3)	(2) - (1)	69	-1668	479	1035	266

Table 8–8. Change in total column loads between 40 min and 43 min. (Loads at 43 min) – (Loads at 40 min) (Compression is positive).

Row	Floor	West	East	North	South	Core
(1)	83	-2864	-8539	2309	2819	5596
(2)	105	-2112	-3901	23	479	5513
(3)	(2) - (1)	752	4637	-2286	-2340	-84

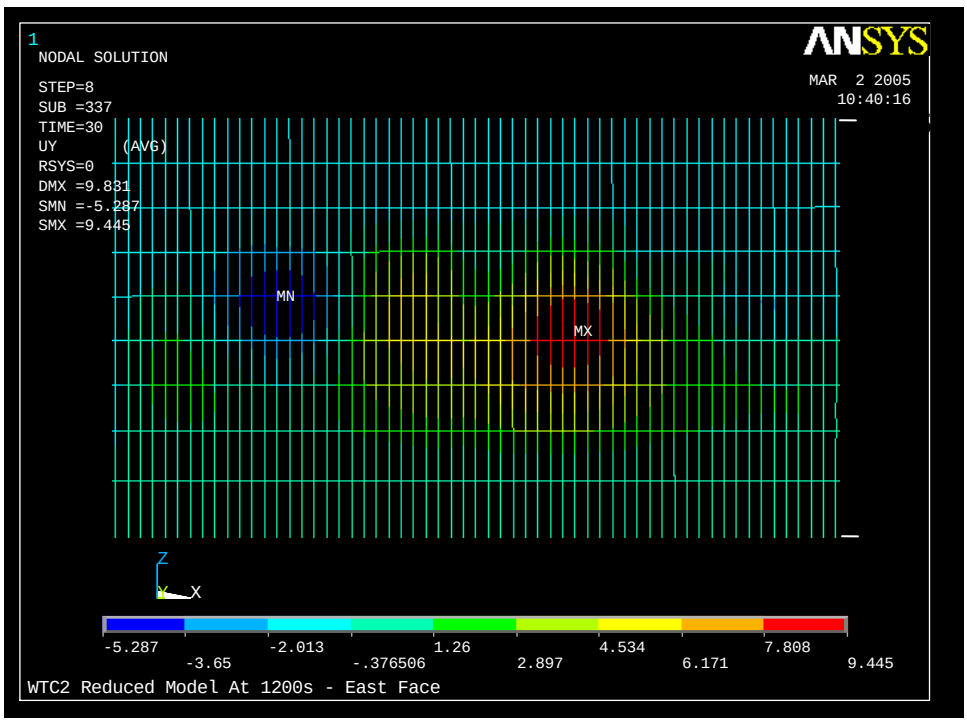

Figure 8–38. Out-of-plane displacement of the east wall of WTC 2 at 20 min for Case D.

At 43 min, the east wall became unstable and the inward displacement increased to 62 in., as shown in Figs. 8–39 and 8–40. The south and east wall vertical displacements increased to 11.3 in. The northwest corner of the exterior wall displaced upward about 1.0 in. to 2.0 in., as the tower tilted to the southeast around an axis passing through the southwest and northeast corners, as indicated in Fig. 8–37. The north exterior wall displaced laterally by an additional 15.2 in. to the east, and the south exterior wall displacement increased 6.7 in. to the south. The building section above the impact damage rotated about the tower axis an additional 0.10 percent at Floor 110.

The core displacements suddenly increased to 13 in. at the southeast corner of the core, as shown in Figs. 8–41 and 8–42. Loads on the core columns increased significantly, especially at the northeast corner. For instance, at Floor 83 the load in core column 1008 increased from 2,826 kip after aircraft impact (Figs. 8–33 and 8–43) to 5,317 kip at 43 min (Fig. 8–44), the load in core column 907 increased from 1,290 kip to 2,328 kip, the load in core column 805 increased from 950 kip to 1,483 kip.

Figure 8–45 shows the total displacements (deformed shape scaled by a factor of 20) above Floor 86 when the east wall buckled. The building section above the impact damage tilted to the southeast, and collapse initiated. For reference, the original undeformed tower is also shown.

When the east wall buckled, the load distribution changed significantly, due to the increased tilting of the building section above the impact damage towards the east. Figures 8–46 to 8–49 show how exterior columns loads changed in the exterior walls from before impact to when the east wall became unstable at 43 min. The exterior columns of the east wall unloaded about 200 kip on average at Floor 83. Similarly, the columns on the west face unloaded about 65 kip on average. Part of the load from the east and the west walls was redistributed to the east side of the south and the north walls. The column loads on the east side of the south wall increased from about 500 kip to 800 kip. The column loads on the east side of the north wall increased from about 250 kip to 400 kip.

Figures 8–50 and 8–51 illustrate the load redistribution among the exterior wall and core columns at Floor 83 before aircraft impact and at 43 min, respectively. The tilting of the building about an axis through the shaded area in Fig. 8–51 followed the buckling of the east wall and weakening of the core. Comparison of column loads before aircraft impact and when the east wall became unstable shows the columns unloading over the width of the east face and increasing at the east side of the south and north walls.

Figures 8–52 and 8–53 show the maximum elastic-plus-plastic-plus-creep strains in the columns between Floor 78 and Floor 83 at 20 min and 43 min, respectively. The elastic-plus-plastic strains, which were less than 0.05 percent before the aircraft impact, reached 0.60 percent in some exterior columns and 0.35 percent in some core columns after the aircraft impact, typically those adjacent to severed or heavily damaged columns. With increasing temperatures the plastic and creep strains increased, especially on the east wall and the east side of the core. When the east wall buckled, the elastic-plus-plastic strains reached their maximum of 2.2 percent in the east wall and 0.9 percent in the east side core columns. Creep strains were 1.0 percent to 2.0 percent in the east wall, about 2.0 percent to 6.0 percent in the core columns, and about 4.0 percent to 5.0 percent in the east side of the north wall.

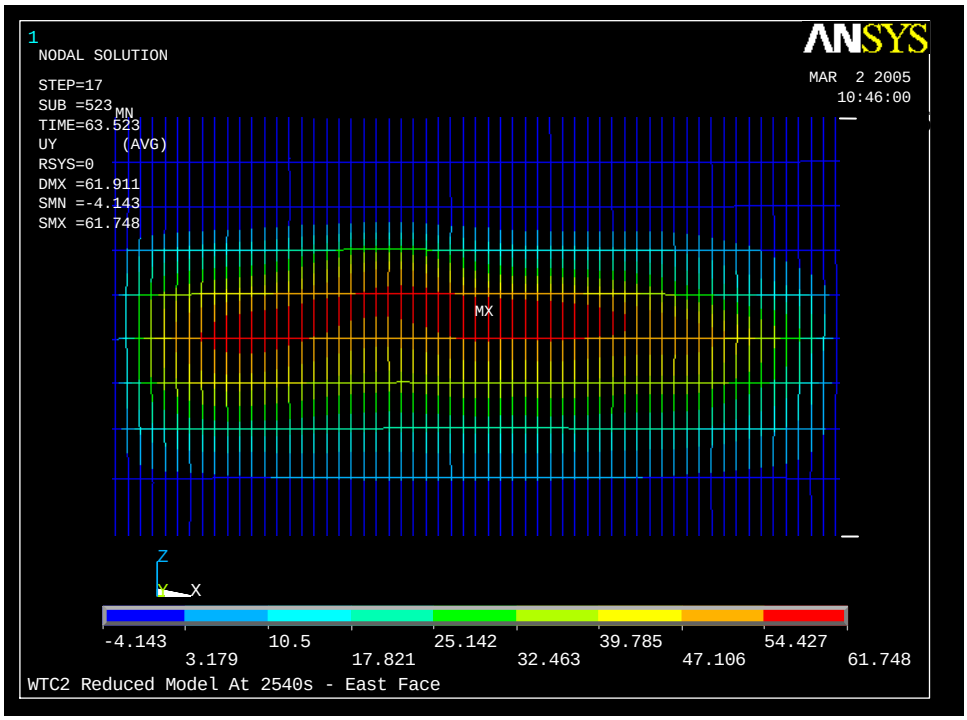

Figure 8–39. Out-of-plane displacement of the east wall of WTC 2 at 43 min for Case D.

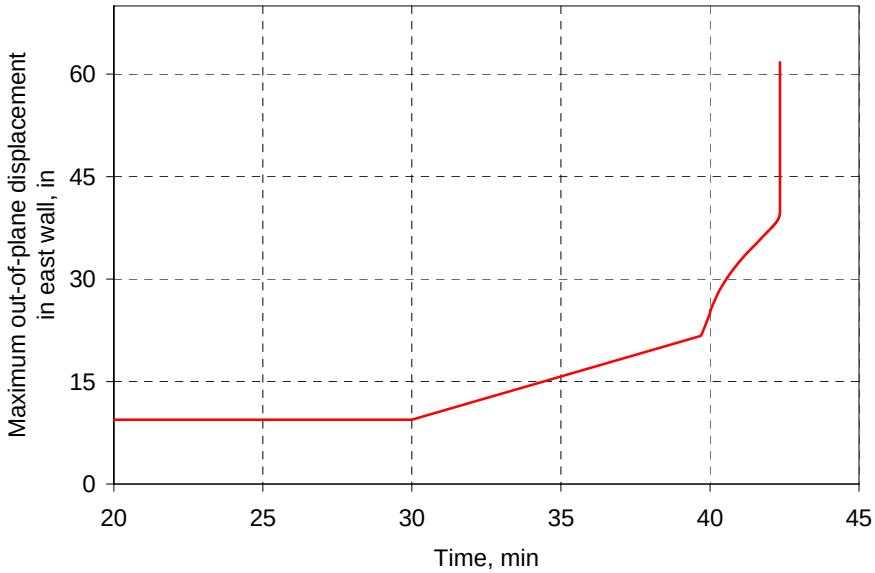

Figure 8–40. Variation of maximum out-of-plane displacement on the east wall of WTC 2 over time for Case D.

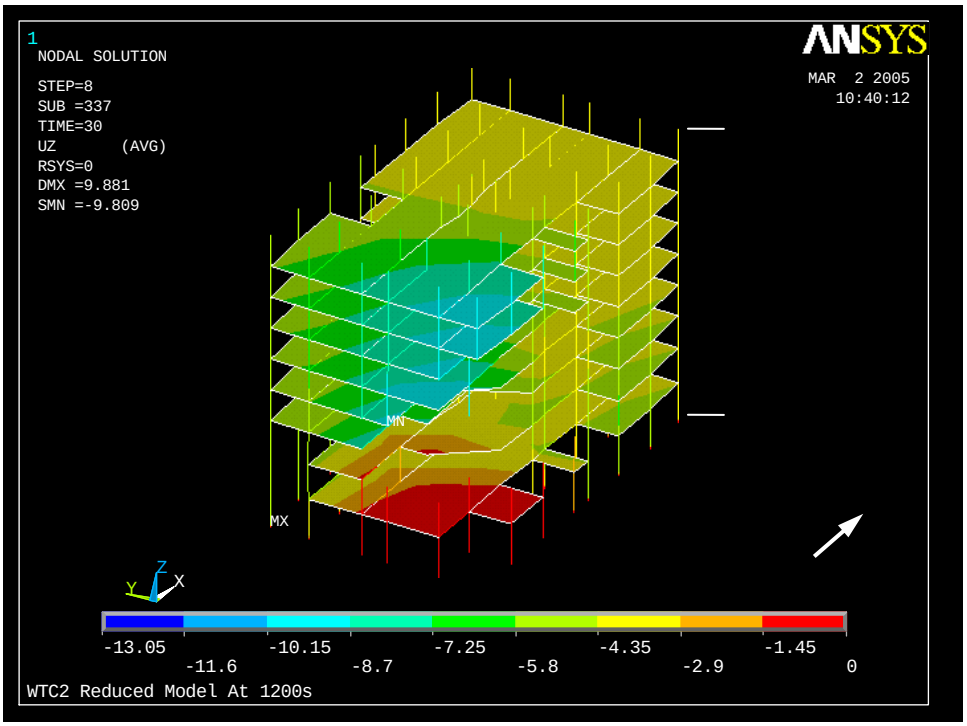

Figure 8–41. Vertical displacement of core of WTC 2 at 20 min for Case D.

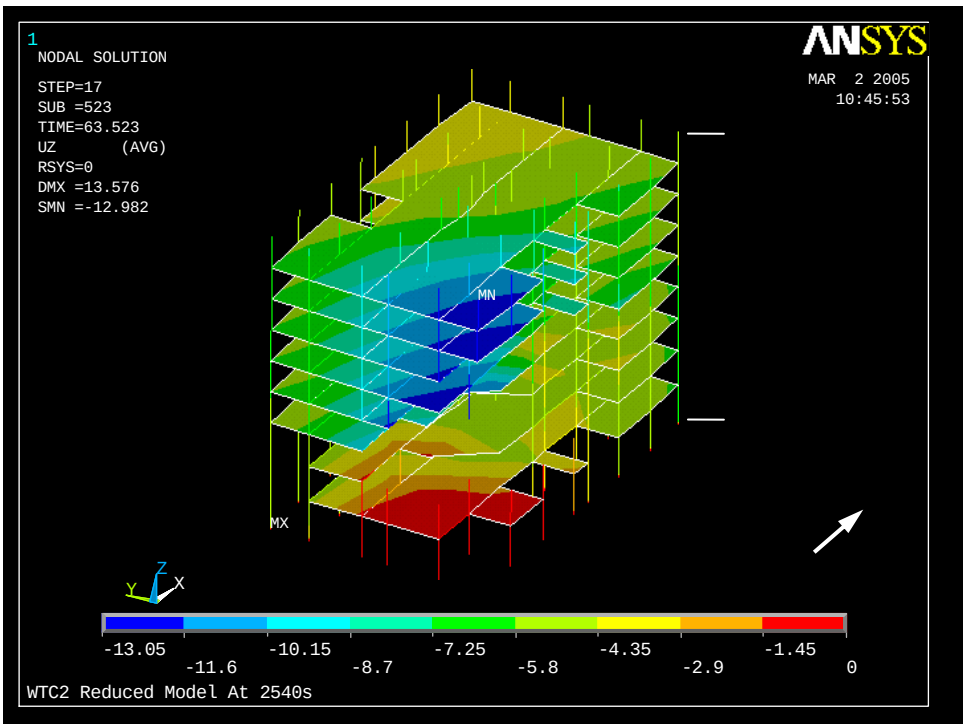

Figure 8–42. Vertical displacement of core of WTC 2 at 43 min for Case D.

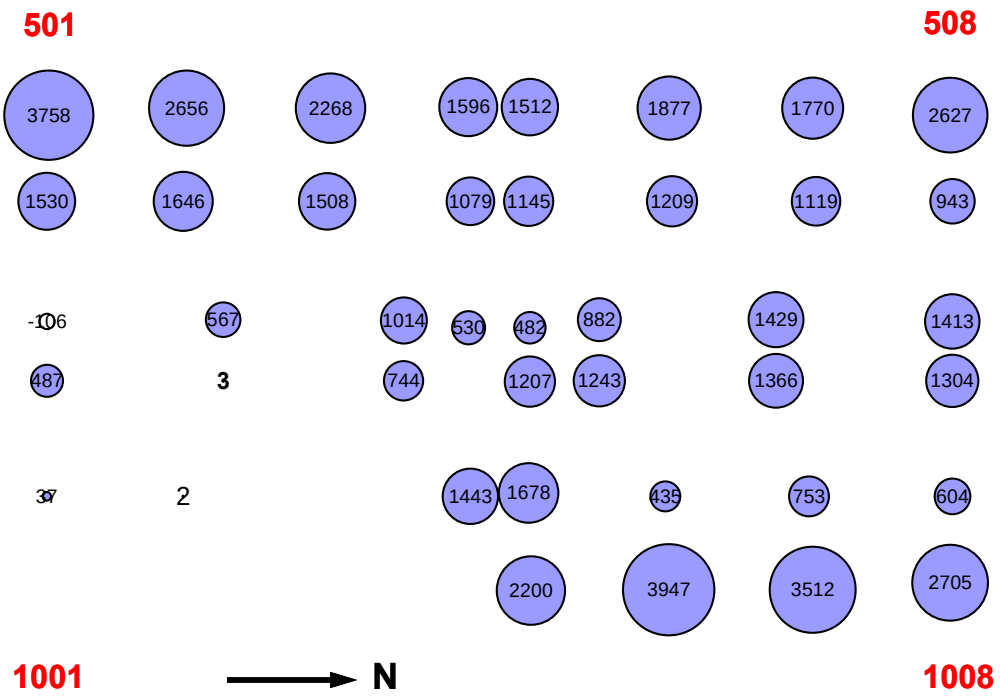

Figure 8–43. Core column loads (kip) at Floor 83 of WTC 2 at 20 min for Case D (compression is positive).

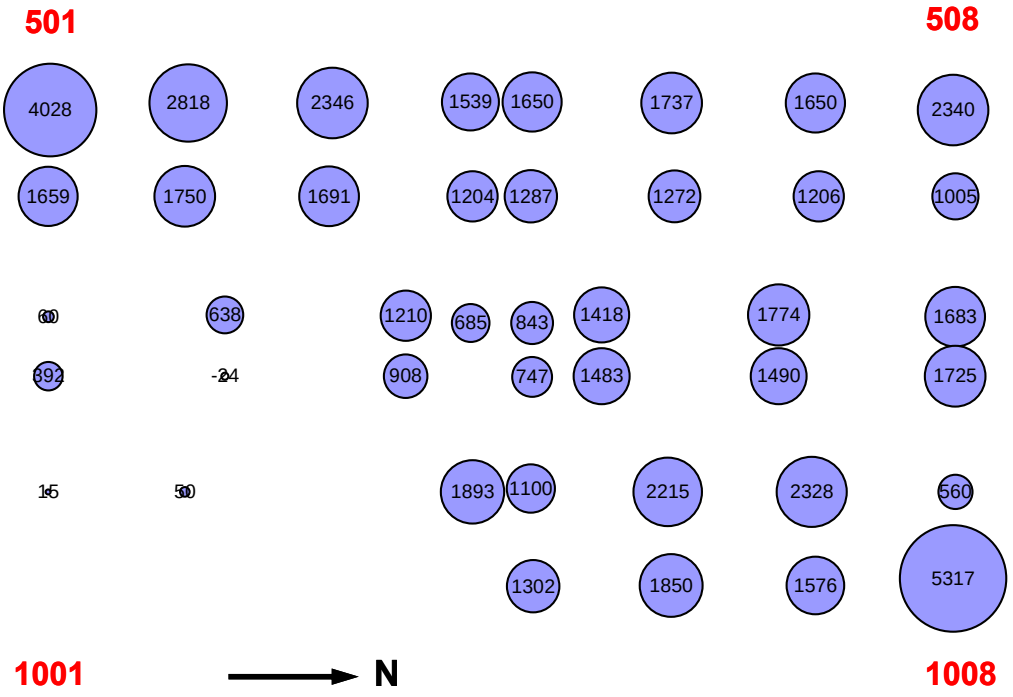

Figure 8–44. Core column loads (kip) at Floor 83 of WTC 2 at 43 min for Case D (compression is positive).

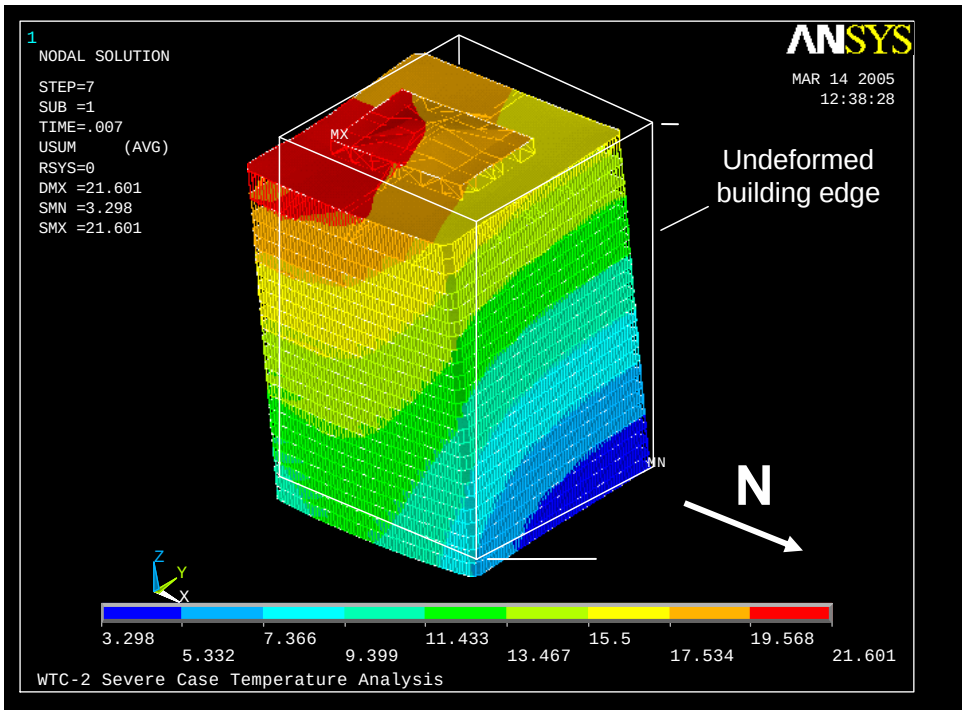

Figure 8–45. Total displacements of WTC 2 above Floor 86 at 43 min of Case D (deformed shape magnified 20 times). Note the tilt toward east and south.

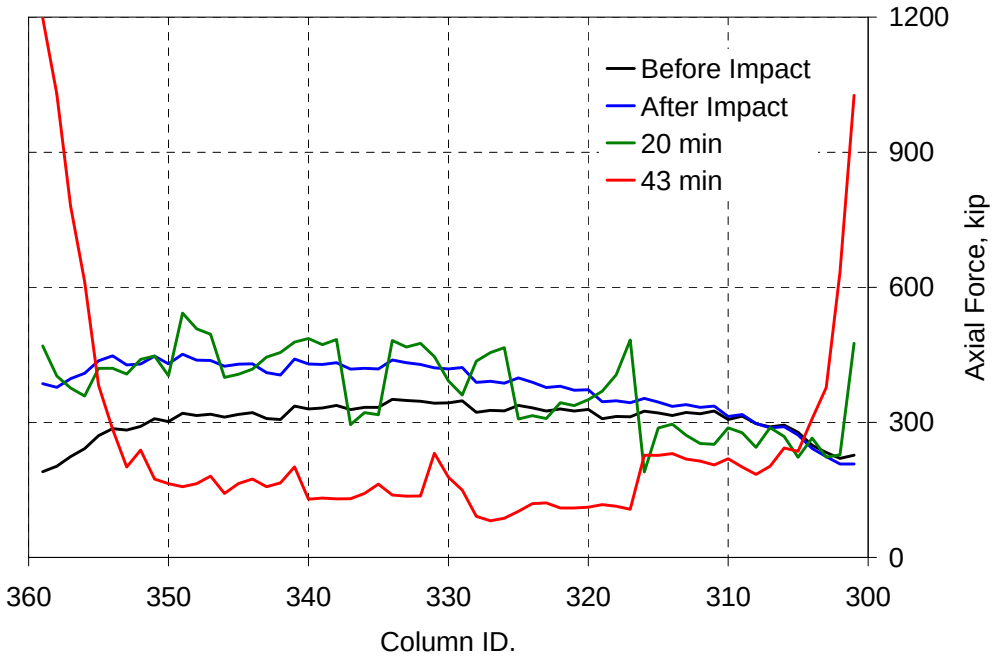

Figure 8–46. Axial force in the east wall columns at Floor 83 of WTC 2 for Case D (compression is positive).

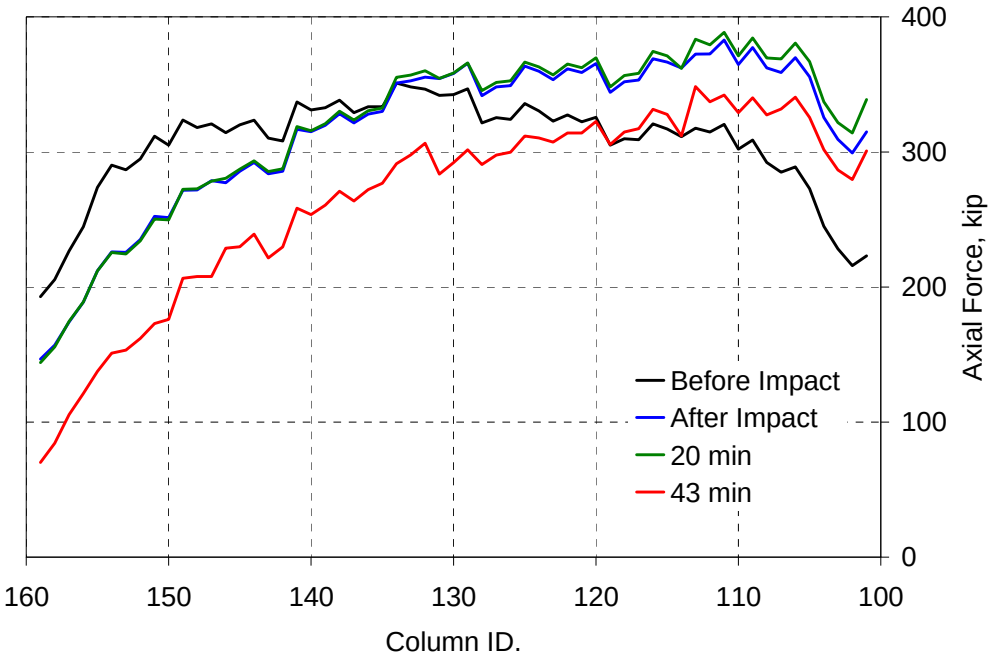

Figure 8–47. Axial force in the west wall columns at Floor 83 of WTC 2 for Case D (compression is positive).

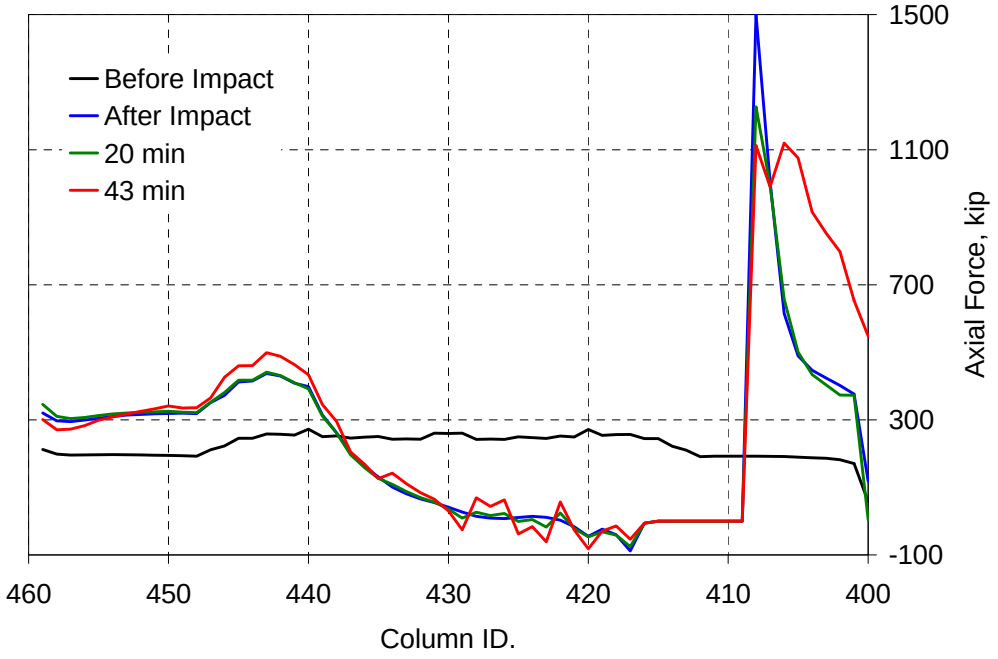

Figure 8–48. Axial force in the south wall columns at Floor 83 of WTC 2 for Case D (compression is positive).

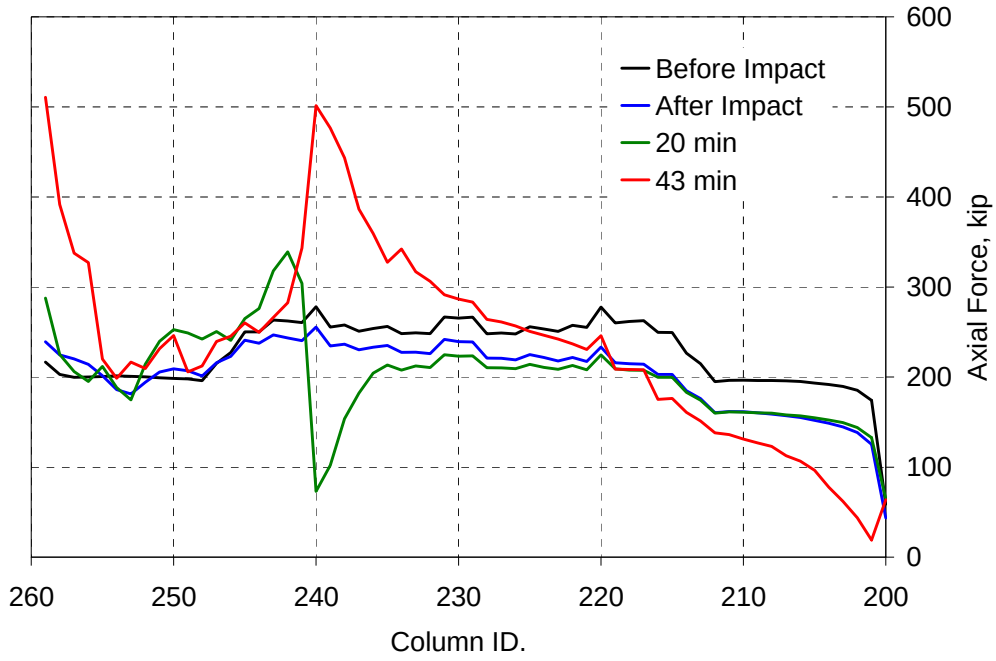

Figure 8–49. Axial force in the north wall columns at Floor 83 of WTC 2 for Case D (compression is positive).

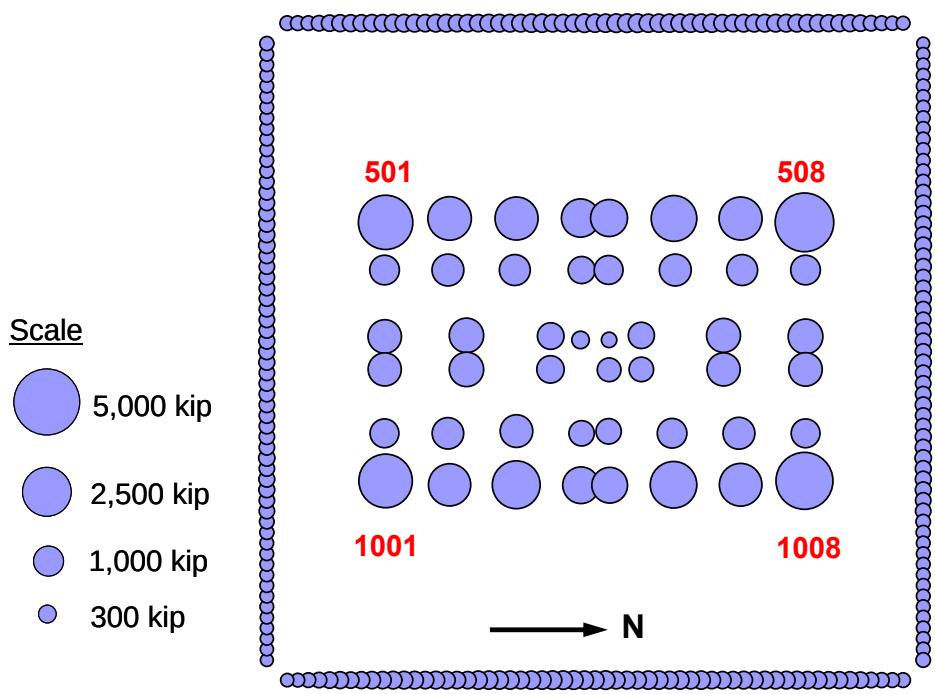

Figure 8–50. Axial force in Floor 83 columns of WTC 2 before impact for Case D (compression is positive).

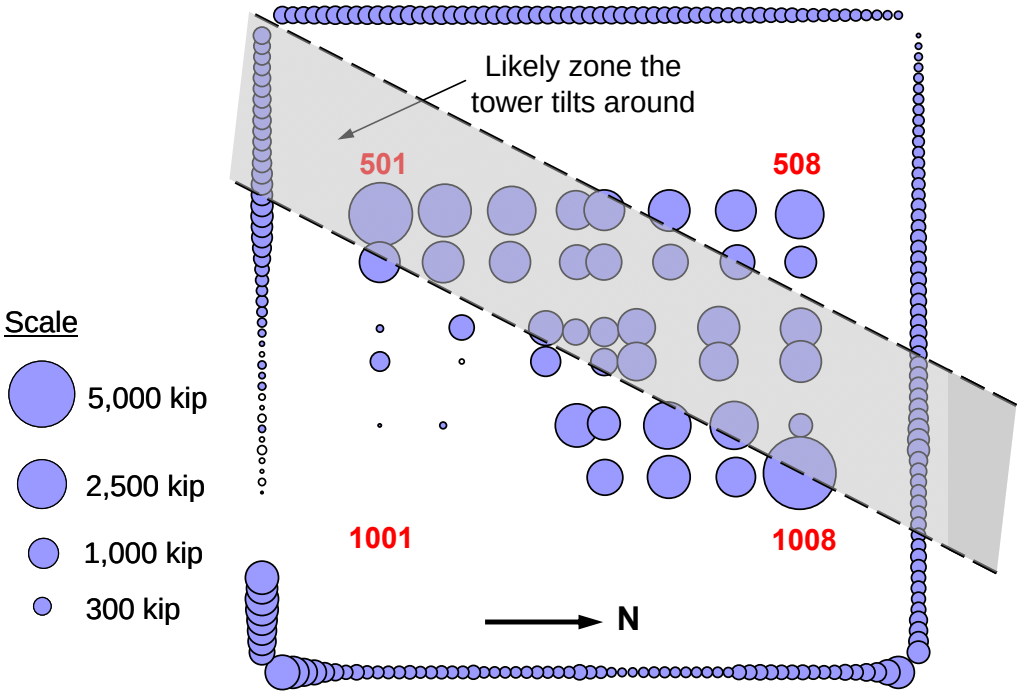

Figure 8–51. Axial force in Floor 83 columns of WTC 2 at 43 min for Case D (compression is positive).

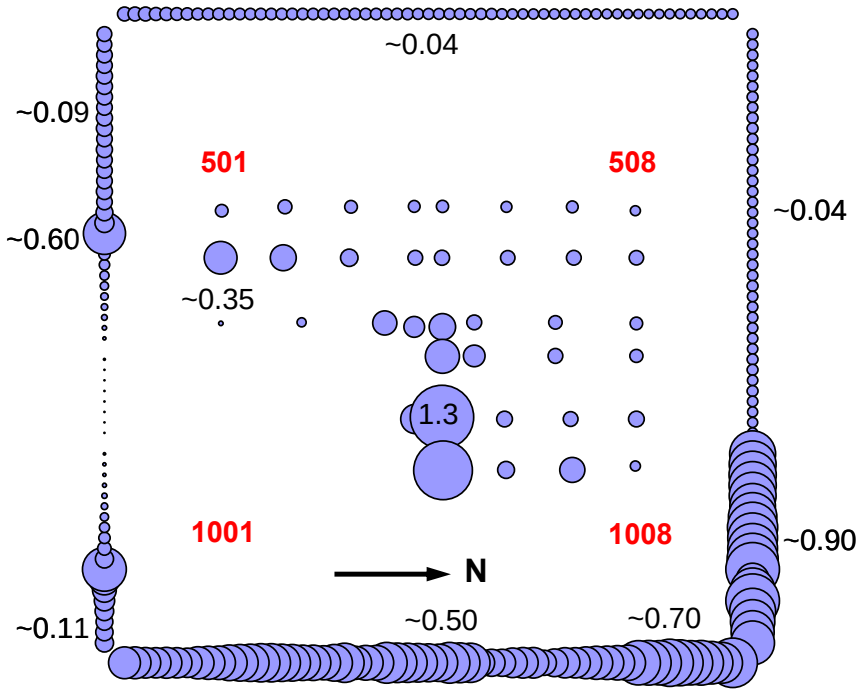

Figure 8–52. Maximum elastic-plus-plastic-plus-creep strains at 20 min for columns between Floor 78 and Floor 83 of WTC 2 for Case D (strain values are in percent).

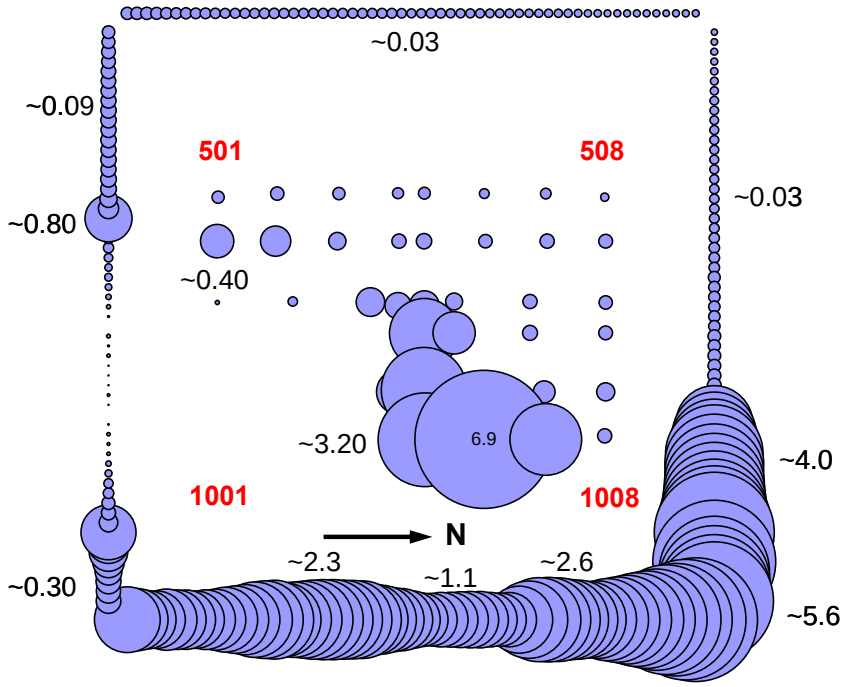

Figure 8–53. Maximum elastic-plus-plastic-plus-creep strains at 43 min for columns between Floor 78 and Floor 83 of WTC 2 for Case D (strain values are in percent).

At 43 min, the core had weakened on the east side and shortened by 3.0 in. at the southeast corner. The east wall had bowed inward approximately 62 in. and unloaded to the core and the adjacent north and south walls. The inward bowing of the east wall caused failure of exterior column splices and spandrels, and induced column instability. The instability progressed horizontally across the entire east face. The east wall unloaded and redistributed its loads to the thermally weakened core through the hat truss and to the east and west walls through the spandrels. This load redistribution is shown in Tables 8–5 and 8–6. The building section above the impact zone began tilting to the east (and to the south, although to a lesser extent) as column instability progressed rapidly from the east wall along the adjacent north and south walls, and increased the gravity load on the weakened east core columns. The change in potential energy due to downward movement of building mass above the buckled columns exceeded the strain energy that could have been absorbed by the structure. Global collapse then ensued.

8.5.3 WTC 2 Hat Truss Members and Connections

The state of the hat truss members and the connections were checked as the global model did not include break elements to capture column and hat truss splice failures or sufficient beam elements to capture buckling of hat truss outriggers. The condition of the connections and the members in the primary load path of the hat truss was evaluated at different time intervals. The evaluation included the core column splices for tension, outriggers and supporting columns for compression, and the hat truss connections that were in the primary load path for tension.

In the WTC 2 global model, the hat truss was part of the super-element above Floor 86. The elastic model that generated the stiffness matrix for the super-element, referred to as the “top model” hereinafter, was used to determine component forces. The displacements obtained at the interface nodes between the

super-element and the nonlinear portion of the building (Floor 86) were applied to the base of the top model for each analysis step.

Figures 8–54, 8–55, and 8–56 show the loads on the core column splices at the hat truss level at different steps of the analysis. Each splice was under compressive load before the aircraft impact. After the aircraft impact, the splices at severed core column lines started to carry tensile loads. The tensile capacity of the splices was compared to tensile forces at 40 min, which was when the maximum tensile forces occurred. In calculating the tensile capacity of the connections, AISC-LRFD procedures were used.

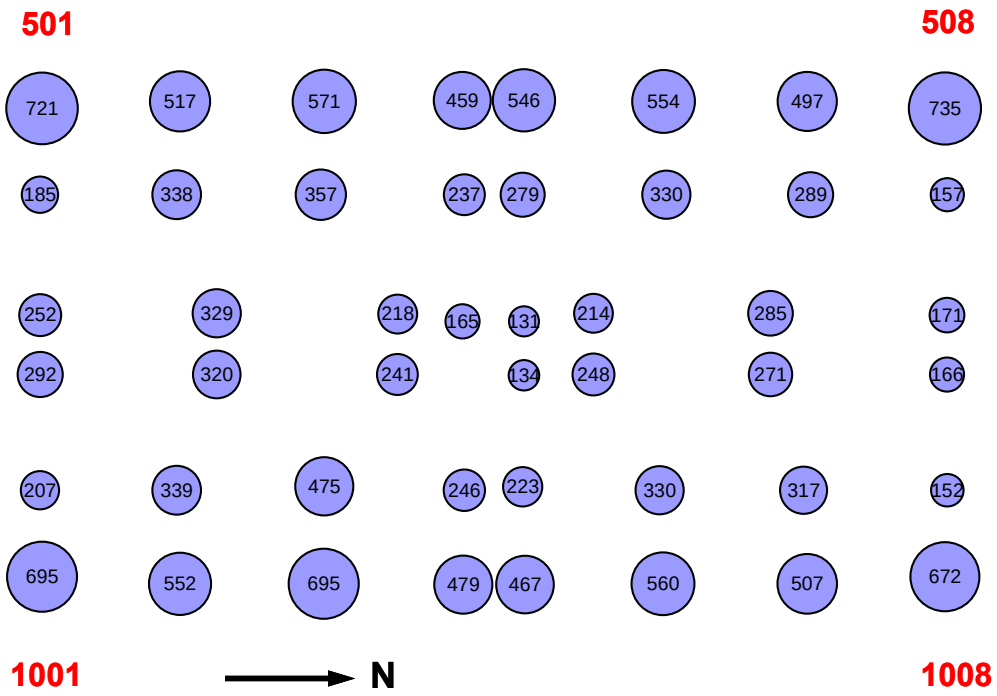

Figure 8–54. Axial force in core columns (kip) at WTC 2 Floor 105 (at hat truss level) before impact for Case D (compression is positive).

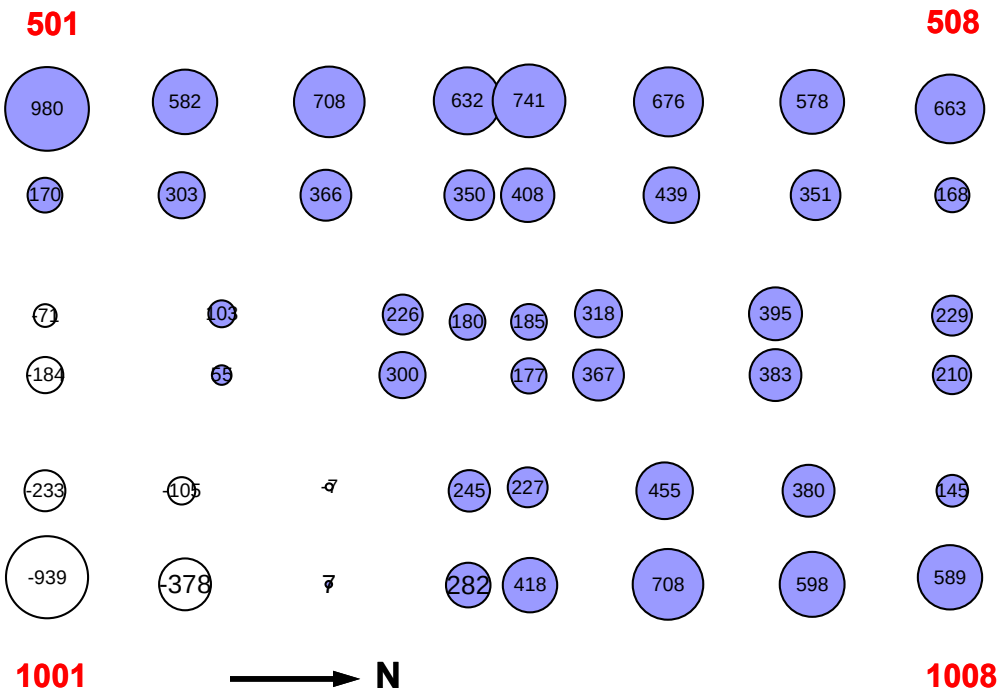

Figure 8–55. Axial force in core columns (kip) at WTC 2 Floor 105 (at hat truss level) after impact for Case D (compression is positive).

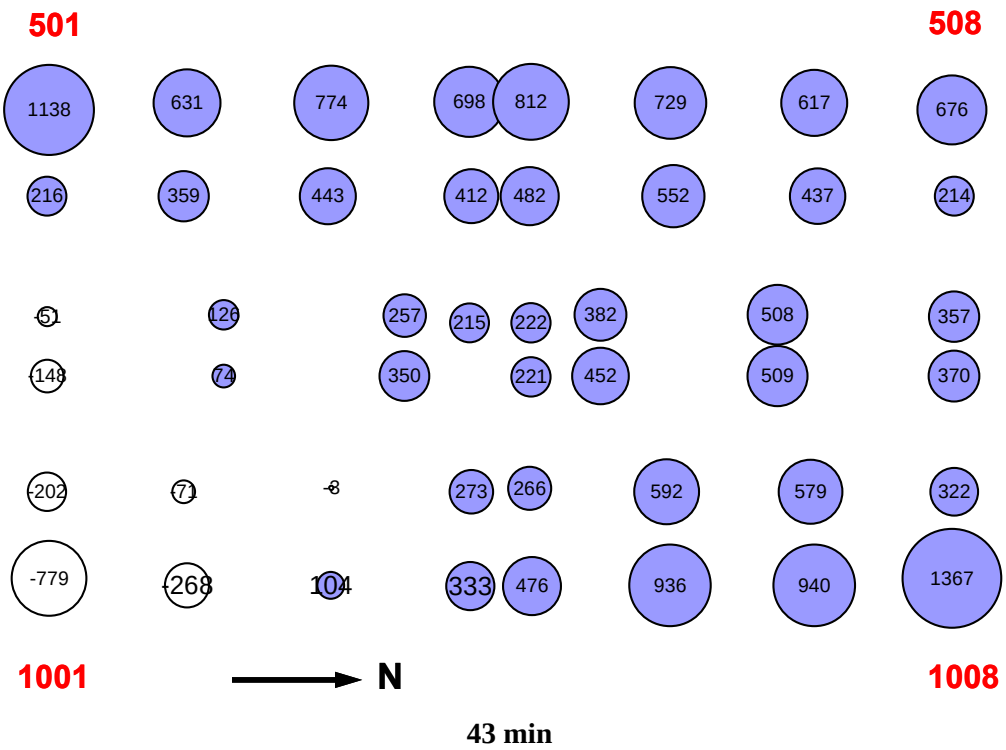

Figure 8–56. Axial force in core columns (kip) at Floor 105 (at hat truss level) of WTC 2 for Case D conditions (compression is positive).

The evaluation of core column splices required an iterative procedure as splice failures were not modeled in the top model. In the first iteration, the top model reached equilibrium using the interface node displacements at 40 min. Once equilibrium was reached, the columns exceeding their splice capacity were identified (in the first iteration columns 1001 and 1002 were identified) and removed from the top model. Before removing the columns, the displacement boundary conditions applied at the bottom of these column lines (at Floor 86) were replaced with the reaction forces that were obtained at the end of the first iteration. This conversion from displacement to force boundary condition allowed the remaining portion of the column lines to displace in the vertical direction when the columns were removed at Floor 105 to simulate splice failure. This iterative procedure was repeated until none of the remaining splices exceeded their tension capacity. A stable state was reached at the end of the fourth iteration. Fig. 8–57 shows the state of the core column splices at the end of the fourth iteration. Splices for columns 1001 and 1002 failed after impact, and splices for columns 701, 801, 901, 902, and 1003 failed either after impact or as the core responded to the fires.

In the global analyses, splice failures were not included in the super-element, which remained elastic throughout the analysis. However, based upon the analyses discussed below, it was concluded that the inclusion of splice failures would not have significantly affected the load redistribution in the global analysis. The core floors would have redistributed the loads in the failed columns to adjacent core columns, as occurred for columns with failed splice connections in the impact area. The adjacent columns would have then transferred the loads to the hat truss.

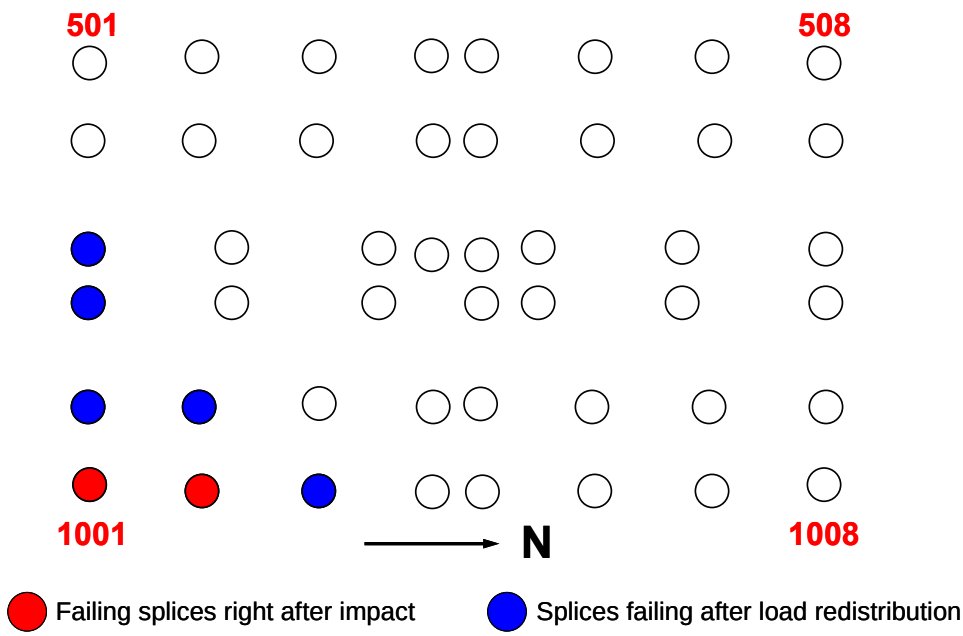

Figure 8–57. State of core column splices at Floor 105 of WTC 2.

To quantify the amount of load that was redistributed through the hat truss to the adjacent core columns, the total column loads on each face and at the core area were extracted at Floor 105. After several iterations, it was determined that about 73 percent of the released tension load was transferred through the hat truss, and 27 percent was transferred through the core floors. As a result of this redistribution, the loads on the southeast corner outriggers were reduced, but the loads on the adjacent outriggers were increased.

The axial stresses in the outriggers increased as a result of the aircraft impact damage. The maximum axial stress of 28.4 ksi before aircraft impact increased to 55.0 ksi after the buckling of the east wall. The specified grade of steel for the outriggers was 50 ksi. The NIST tests conducted on this grade of steel resulted in an average yield strength of about 54 ksi. Considering this yield strength and the 10 percent increase in the hat truss forces due to neglecting the construction sequence, it was concluded that the outriggers of the hat truss did not exceed their elastic limits.

To check the buckling capacities of the outriggers, the AISC LRFD procedures were used with an effective length factor K equal to 0.75 and a resistance factor of 1.0. The calculated capacities were compared with the axial compressive forces and corrected to account for the axial load increase due to construction sequence. The location of the outriggers and the supporting columns are shown in Fig. 8–58. Table 8–9 summarizes the demand-to-capacity ratios for the outriggers. Except for Outrigger L, none of the outriggers exceeded their buckling capacities. Outrigger L was located at the southeast corner of the core (the corner where the core columns were severed due to aircraft impact).

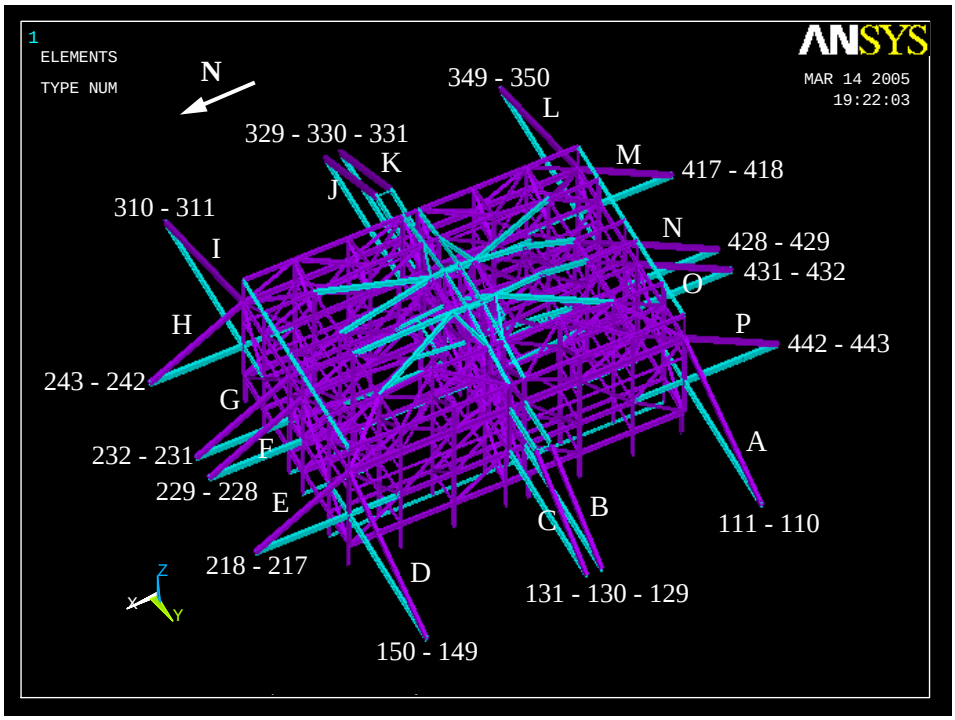

Figure 8–58. Location and IDs of outriggers and supporting columns

Table 8–9. Demand-to-capacity ratios for outriggers of WTC 2 for Case D conditions (outrigger IDs are shown in Fig. 8–3).

Outrigger ID	Bfr. Imp.	Aftr. Imp.	10 min	20 min	30 min	40 min	40* min	40** min	43 min
West									
A	0.23	0.61	0.61	0.64	0.66	0.63	0.63	0.38	0.25
B	0.19	0.30	0.30	0.32	0.33	0.31	0.31	0.25	-0.03***
C	0.19	0.27	0.27	0.28	0.30	0.27	0.28	0.22	-0.07
D	0.21	0.18	0.18	0.19	0.21	0.18	0.20	0.19	-0.29
North									
E	0.29	0.11	0.10	0.10	0.13	0.14	0.17	0.09	-0.01
F	0.21	0.10	0.08	0.08	0.10	0.12	0.13	0.11	0.08
G	0.20	0.11	0.08	0.08	0.11	0.13	0.14	0.13	0.10
H	0.30	0.21	0.16	0.18	0.19	0.18	0.19	0.24	0.24
East									
I	0.22	0.39	0.35	0.34	0.45	0.43	0.42	0.41	-0.18
J	0.18	0.56	0.52	0.53	0.66	0.65	0.61	0.71	0.02
K	0.18	0.62	0.58	0.59	0.72	0.72	0.66	0.79	0.09
L	0.22	1.12	1.09	1.12	1.24	1.30	1.11	0.00	0.72
South									
M	0.30	0.68	0.64	0.64	0.70	0.75	0.52	0.72	0.87
N	0.22	0.34	0.32	0.33	0.36	0.38	0.28	0.34	0.40
O	0.22	0.30	0.28	0.30	0.32	0.33	0.27	0.31	0.33
P	0.31	0.51	0.50	0.52	0.53	0.53	0.50	0.57	0.49

* After load redistribution due to core column splice failures.

** After Outrigger L was removed.

*** Negative value indicates tension

With the identified splice failures in Columns 1001 and 1002 and adjacent core columns, the load in this outrigger would have been redistributed to other outriggers. Based on the computed load redistribution after splice failures, the demand-to-capacity ratio on Outrigger L was estimated to be reduced from 1.3 to 1.1 (Column "40* min" in Table 8–9).

Outrigger L was removed from the top model after all the failed splices were removed to determine the effect on adjacent outriggers. Removal of the Outrigger L represented an upper bound solution as the load in the Outrigger would not have dropped down to zero. The adjacent outriggers increase in load; however, after the removal of the Outrigger L as presented in Column "40** min" of Table 8–9, none of the remaining outriggers exceeded their buckling or yield capacities.

The connections within the hat truss were also checked. The hat truss connections in the primary load path were identified, and their capacities were compared to their forces. The primary load path was identified by selecting hat truss members with an absolute axial stress of 25 ksi or more at 40 min, as this was when maximum forces occurred. Only the connections that transferred tensile forces were evaluated. In calculating the capacity of the connections, the AISC-LRFD procedures were used. None of the hat truss connection capacities were exceeded. Before redistribution of load due to the column-to-hat truss splice failure, none of the hat truss connections had exceeded their capacities except for the hat truss connections associated with the 1001 core column. After the load redistribution following the splice failure, the demand on the hat truss connections for the 1001 column was less than the yield capacities of all connections. It was concluded that the hat truss was capable of transferring loads from core columns to the outriggers.

Based on this discussion, it was concluded that the hat truss transferred the majority of the loads between core and exterior wall columns, even though some column splices may have failed and one outrigger may have buckled.

8.6 STRUCTURAL RESPONSE OF THE WTC TOWERS TO FIRE WITHOUT IMPACT DAMAGE

Whether the towers would have collapsed if subjected to an intense but conventional fire without aircraft impact was considered to better understand the relative roles of the impact damage and fires. This is not to imply that the fire growth and spread observed in the towers could be obtained without aircraft damage to the buildings and rapid ignition of multi-floor fires due to the dispersion of jet fuel. NIST used the observations, information, and analyses developed during the Investigation to enable the formulation of probable limits to the damage from such a fire. Since a complete analysis beyond the actual collapse times of the towers was not conducted, the findings in this section represent NIST's best technical judgment based upon the available observations, information, and analyses.

In making the comparison, the following points were considered.

- Both WTC 1 and WTC 2 were stable after the aircraft impact. The global analyses showed that both towers had considerable reserve capacity after structural impact damage. For example, Figs. 8–9 and 8–10 show the core column demand-to-capacity ratios remained nearly the same before and after impact, except for a few columns adjacent to the severed columns. Global analysis produced similar trend for the exterior columns. This was confirmed by analysis of video footage of the post-impact vibration of WTC 2, the more

severely damaged of the two towers, which showed that the period of vibration of the building before and after impact were nearly the same, thus showing that the building had significant reserve capacity. WTC 2 oscillated with a peak amplitude that was between 30 percent and 40 percent of the tower sway under design winds and at periods nearly equal to the first two translation and torsion mode periods calculated for the undamaged structure (see NIST NCSTAR 1-2).

- Results of both the multi-workstation experiments and the simulations of the WTC fires showed that the combustibles in a given location, if undisturbed by the aircraft impact, would have been almost fully burned out in about 20 min. Note that, for the occupancies in the World Trade Center, the fuel load was estimated—and supported by fire dynamics calculations and visual observations—to be approximately 4 psf (see NIST NCSTAR 1-5).

- The fires used in the Investigation (Cases A through D), estimated from fire dynamics simulations, represented fires that were far more severe than an intense conventional fire (see NIST NCSTAR 1-5).

- In WTC 1, if fires had been allowed to continue past the time of building collapse, complete burnout would likely have occurred within a short time since the fires had already traversed around the entire floor and most of the combustibles would already have been consumed (see NIST NCSTAR 1-5). During the extended period from collapse to burnout, the steel temperatures would likely not have increased very much. The installed insulation in the fire-affected floors of this building had been upgraded to an average thickness of 2.5 in.

- In a fire simulation of WTC 2, that extended Case D for 2 hours with all windows broken during this period, the temperatures in the truss steel on the west side of the building (where the insulation was undamaged) increased for about 40 minutes before falling off rapidly as the combustibles were consumed. Results for a typical floor (floor 81) showed that temperatures of 700 °C to 760 °C were reached over approximately 15 percent of the west floor area for less than 10 minutes. Approximately 60 percent of the floor steel had temperatures between 600 °C and 700 °C for about 15 minutes. Approximately 70 percent of the floor steel had temperatures that exceeded 500 °C for about 45 min. At these temperatures, the floors would be expected to sag and then recover a portion of the sag as the steel began to cool. Based on results for Cases C and D, the temperatures of the insulated exterior and core columns would not have increased to the point where significant loss of strength or stiffness would occur during these additional 2 hours. With intact, cool core columns, any inward bowing of the west exterior wall that might occur would be readily supported by the adjacent exterior walls and core columns.

- In the simulations of Cases A through D, none of the columns and trusses for which the insulation was intact reached temperatures at which significant loss of strength occurred for the duration analyzed. The relative effects of the presence or absence of insulation on structural components, subjected to the same fire conditions, are shown in Fig. 8–59 (see NIST NCSTAR 1-5) for both adjacent trusses and exterior columns. As the plots indicate, the rate of heating was found to differ significantly depending on whether the insulation was intact or not.

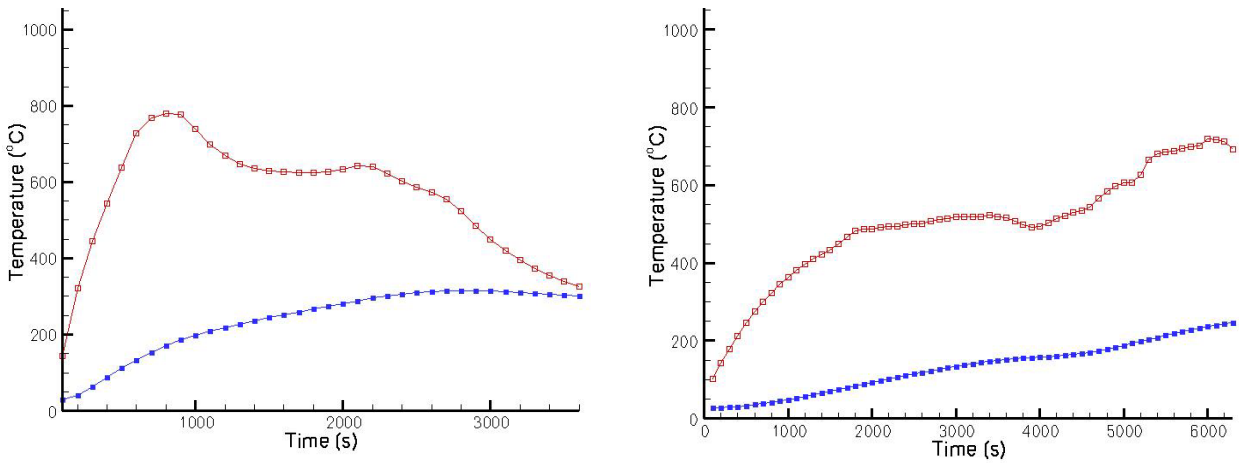

Figure 8–59. Temperatures of two adjacent trusses (left) and two adjacent perimeter columns (right) exposed to simulated fires in WTC 1. Data plotted in blue are for structural steel components with fireproofing; data in red are for steel components without fireproofing (from NIST NCSTAR 1-5).

- Structural computer simulations of the floor system (Chapter 7), supported by results of full-scale fire tests (NIST NCSTAR 1-5) and performance observed in standard fire tests (NIST NCSTAR 1-6B), showed that structural steel, insulated with ¾ in. thick fireproofing, would not have reached temperatures greater than 650 C prior to burnout of the combustibles (20 min as noted above). Simulations also showed that variations in thickness resulting from normal application, even with occasional gaps in coverage, would not have changed this result.

- The structural temperatures of core columns in WTC 1 and WTC 2 did not exceed 300 ˚C where the fireproofing was intact. Thermal analysis of the WTC 1 and WTC 2 floors and exterior columns indicated that the steel temperatures were generally lower than 300 ˚C, with a few isolated members that rarely exceeded temperatures of 400 ˚C for WTC 1 and 500 ˚C for WTC 2 (NIST NCSTAR 1-5). Under these temperatures, reductions of stiffness and strength were small and creep effects and buckling were found not to be significant (Chapters 4 and 7). Insulated floors thermally expanded and pushed outward on the exterior columns as well as sag in the full floor analyses, but the floor sag was insufficient to exert an inward pull on the exterior columns.

- Inward bowing of the exterior walls in both WTC 1 and WTC 2 was observed only on the face with the long-span floor system. In WTC 1, this was found to be the case even though equally extensive fires were observed on all faces. The impact damage to the north face reduced the area over which pull-in could occur. In WTC 2, fires were not observed on the long-span west face and were less intense on the short-span faces than on the east face.

- Inward bowing was a necessary but not sufficient condition to initiate collapse. In both WTC 1 and WTC 2, significant weakening of the core due to aircraft impact damage and thermal effects was also necessary to initiate building collapse.

- The tower structures had significant capacity to redistribute loads (a) from bowed walls to adjacent exterior walls with short-span floors via the arch action of spandrels, and (b) between the core and exterior walls via the hat truss and, to a lesser extent, the floors.

In evaluating how the undamaged towers would have performed in an intense, conventional fire, NIST considered the following factors individually and in combination:

- The temperatures that would be reached in structural steel components with intact insulation.

- The extent of the area over which high temperatures (e.g., greater than 600 °C where significant thermal weakening of the steel occurs) would be reached at any given time.

- The duration over which the high temperatures would be sustained concurrently in any given area.

- The length of the floor span (long or short) where high temperatures would be reached.

- The number of floors with areas where high temperatures would be sustained concurrently in the long-span direction.

- The potential for inward bowing of exterior walls (i.e., magnitude and extent of bowing over the width of the face and the number of floors involved) due to thermally-induced floor sagging of long-span floors and associated inward pull forces.

- The capacity of the structure to redistribute loads (e.g., via the spandrels, hat truss, and floors) if the thermal conditions were sufficiently intense to cause inward bowing of the exterior walls.

In addition, NIST considered the following known facts about the performance of the WTC tower structures in fires:

- Historical fires also provided evidence that the towers would not collapse if subjected to a major fire without accompanying impact damage. WTC 1 did not collapse during the major fire in 1975, which engulfed about 9,000 ft^2 on the southeast quadrant of Floor 11. The fire spread mostly via utility closets to ten floors. At the time, office spaces in the WTC towers were not sprinklered. The fire caused minimal damage to the floor system with the ½ in. specified insulation thickness applied on the trusses (four trusses were slightly distorted) and at no time was the load carrying capacity of the floor system compromised. The fire "did not damage a single primary, fireproofed element. Some top chord members (not needed for structural integrity), some bridging members (used to reduce floor tremor and the like) and some deck support angles (used only as construction elements) were buckled in the fire—all were unfireproofed steel." (SCHR Letter Report 1975).

- Additionally, the four Standard Fire Tests (ASTM E 119) of floor assemblies like those in the WTC towers showed that the load carrying capacity of the short span 35 ft floor system with a 0.75 in. insulation thickness was not compromised by heating for two hours at furnace temperatures with applied loads that exceeded those on September 11, 2001 by a factor of two. It took about 90 minutes of sustained heating in the furnace for temperatures to exceed 600 °C on steel truss members with either ½ in. or ¾ in. insulation thickness. The high temperature conditions in the furnace tests were at least as severe and lasting as long as the WTC fires, although the top of the slab was not heated. Although some web members buckled and the floor test assembly sagged up to 14 in. during the tests, the insulation remained intact during the tests.

From these points and observed performance, NIST concluded:

- In the absence of structural and insulation damage, a conventional fire substantially similar to or less intense than the fires encountered on September 11, 2001 likely would not have led to the collapse of a WTC tower.

- The condition of the insulation prior to aircraft impact, which was found to be mostly intact, and the insulation thickness on the WTC floor system contributed to, but did not play a governing role, in initiating collapse of the towers.

- The towers likely would not have collapsed under the combined effects of aircraft impact and the subsequent multi-floor fires encountered on September 11, 2001 if the insulation had not been widely dislodged or had been only minimally dislodged by aircraft impact.

These conclusions apply to fires that are substantially similar to or less intense than those encountered on September 11, 2001. They do not apply to a standard fire exposure or an assumed fire exposure which has (a) uniform high temperatures over an entire floor or most of a floor (note that the WTC floors were extremely large) and concurrently over multiple floors and (b) high temperatures that are sustained indefinitely or for long periods of time (greater than about 20 min at any location), and (c) combusted fire loads that are significantly greater than those considered in the analyses. They also do not apply if the capacity of the undamaged structure to redistribute loads via the spandrels, hat truss, and floors were not accounted for adequately in a full 3-dimensional simulation model of the structure.

8.7 SUMMARY OF STRUCTURAL RESPONSE OF THE WTC TOWERS

The structural analyses conducted of floors, isolated exterior walls and cores, and global models of WTC 1 and WTC 2 found that the collapse of the towers was due to the combined effects of structural and insulation damage from aircraft impact and the subsequent fires.

Impact damage alone did not cause collapse of the towers, as they were stable after the aircraft impact and analyses showed that they had substantial reserve capacity. The fires alone also would not have caused collapse of the towers. Without impact damage, there would not have been extensive dislodging of insulation, and the structural steel temperatures would have been generally less than 300 °C, with a few steel temperatures reaching 400 ˚C in WTC 1 floors and 500 ˚C in WTC 2 floors. The core would not have weakened, the floor sag would have been insufficient to pull inward on the exterior columns, and as a consequence the exterior walls would not have bowed inward.

Collapse occurred after the fires weakened areas of the core, floors, and exterior walls that had dislodged insulation, and the core and exterior columns were unable to support the gravity loads with their reduced capacity.

The towers would likely not have collapsed under the combined effects of aircraft impact and the subsequent multi-floor fires if the insulation had not been dislodged or had been only minimally dislodged by aircraft impact. The existing condition of the insulation prior to aircraft impact and the insulation thickness on the WTC floor system did not play a significant role in initiating collapse of the towers.

8.8 REFERENCES

National Oceanic and Atmospheric Administration (NOAA)/National Climatic Data Center (NCDC), (NOAA 2001a)"Automated Surface Observing System Data; Unedited Surface Weather Observations - Hourly Data, LaGuardia Airport, September 11, 2001"

National Oceanic and Atmospheric Administration (NOAA)/National Climatic Data Center (NCDC), (NOAA 2001b)"Automated Surface Observing System Data; Unedited Surface Weather Observations - Hourly Data, John F. Kennedy Airport, September 11, 2001"

National Oceanic and Atmospheric Administration (NOAA)/National Climatic Data Center (NCDC), (NOAA 2001c)"Automated Surface Observing System Data; Unedited Surface Weather Observations - Hourly Data, Newark, NJ Airport, September 11, 2001"

Chapter 9
PROBABLE COLLAPSE SEQUENCES

9.1 INTRODUCTION

World Trade Center (WTC) 1 and WTC 2 were subjected to aircraft impact and uncontrolled fires and experienced a series of events that required complex analyses to determine their probable collapse sequences. The analysis of these events required a formal approach to integrate multiple disciplines effectively, to discern which parameters significantly influenced the analysis methods and results, and to determine the probable sequence of events leading to the initiation of structural collapse. These methods were applied as appropriate to different scales of modeling—component, subsystem, and global scales—for the aircraft impact damage, fire dynamics, thermal, and structural response analyses.

To identify the probable collapse sequences, National Institute of Standards and Technology (NIST) adopted an approach that combined mathematical modeling, statistical-based analysis methods, laboratory experiments, and analysis of photographs and videos. The approach accounted for variations in models, input parameters, analyses, and observed events. It included the evaluation and comparison of possible collapse hypotheses based on various damage states, fire paths, and structural responses to determine the following:

- The probable sequence of events from the moment of aircraft impact until the initiation of global building collapse;
- How and why WTC 1 stood nearly twice as long as WTC 2 before collapsing (102 min for WTC 1 versus 56 min for WTC 2), although they were hit by virtually identical aircraft (Boeing 767-200ER);
- What factors, if any, could have delayed or prevented the collapse of the WTC towers.

Section 9.2 describes the methodology used to conduct the aircraft impact, fire dynamics, thermal, and structural response analyses for determining the probable collapse sequence of each tower, which is presented in Section 9.3. Section 9.4 presents a discussion and summary of the collapse sequences.

9.2 METHODOLOGY

To determine the probable collapse sequence for each tower, the following steps were required:

- identification of key observables, primarily from photographs and videos
- development of collapse hypotheses, which were updated periodically through the course of the investigation with the acquisition of new data and analysis results

- sensitivity studies to identify influential parameters through the application of a formal statistical approach, orthogonal factorial design (OFD)
- development and refinement of mathematical modeling—finite element analyses and computational fluid dynamics
- evaluation of analysis results against observed and expected structural behavior, with adoption of the event tree technique, and pruning and updating of the tree branches based upon comparisons with observed data

These steps were applied to the degree needed in each phase of the analyses, from aircraft impact to fire spread, thermal loads, and structural response.

9.2.1 Key Observed Events and Conditions

Observations and data about the events following the aircraft impact were primarily obtained from three sources:

- Photographic and video records that had been catalogued and time stamped for the NIST Investigation (NIST NCSTAR 1-5A)
- Interviews of individuals in the towers during the event and those contacted by individuals in the towers during the event (NIST NCSTAR 1-7)
- Interviews of emergency response personnel and emergency communication records (NIST NCSTAR 1-8)

Observations were used to develop timelines and refine collapse hypotheses for each tower. Key observations were used to guide the towers' structural analysis and are summarized in the structural timelines (Chapter 6). Structural analyses were used to develop and refine understanding of the sequences of events, particularly events near or in the core that could not be observed.

Observations were classified into two groups: key observations and noted observations. Key observations were significant structural events that were explicitly addressed in or used to validate the structural analyses. Noted observations were events that may have been linked to a structural response, but their significance could not be conclusively assessed.

Observables were used in all the analyses in three ways: (1) to determine input parameters, such as the aircraft speed and direction at impact, (2) to impose time-related constraints on the analysis, such as imposing observed broken windows over time to constrain the spread of fire, or (3) to validate analysis results, such as global stability after impact and during thermal loading.

9.2.2 Collapse Hypotheses

Collapse hypotheses were developed over the course of the NIST Investigation. The first hypotheses were published in the May 2003 NIST Progress Report, and were updated in the June 2004 Progress Report and October 2004 Public Meeting at NIST. The Probable Collapse Sequence for each tower was

presented at the April 2005 Public Meeting in New York City. The stages of hypothesis development are summarized as follows:

- **Possible Collapse Hypotheses** (May 2003) – not building specific; key events not identified
- **Working Collapse Hypothesis** (June 2004) – single hypothesis for both WTC towers; identified chronological sequence of major events
- **Leading Collapse Hypotheses** (October 2004) – separate hypothesis for each WTC tower; identified building-specific load redistribution paths and damage scenarios in addition to chronological sequence of major events
- **Probable Collapse Sequences** (April 2005) – refined building-specific collapse sequences with chronological sequence of major events, load redistribution paths, and damage scenarios.

Over the course of the investigation, NIST continued to investigate technical issues and modify or refine the collapse hypotheses for each tower as needed. Technical issues that were analyzed and refined during the investigation included:

- Aircraft impact damage to structural components, insulation, and partition walls.
- Dispersion of aircraft debris and damage to building contents.
- Thermal effects on core columns and floors, especially extent and movement of fires.
- Thermal effects on exterior columns, especially temperature gradients in columns.
- Extent of load redistribution within and between core columns and exterior wall columns and their reserve capacity to accommodate added gravity loads with thermal effects.
- Capacity of hat truss to accommodate load redistribution from severed columns.
- Capacity of bolted splices in the severed core columns to carry tensile loads to the hat truss.
- Relative magnitude of the load redistribution provided by the hat truss, local core floor, and the truss floor system for each tower.
- Axial/shear/bending capacity of floor connections to core and exterior columns.
- Mechanisms to propagate instability laterally in the exterior columns
- Capacity of spandrels, including splices, to transfer shear in the exterior walls.
- Role of bolted splices in the instability of exterior columns.
- Comparison and reconciliation of hypotheses with observed facts (photographs and videos, eyewitness accounts, emergency communication records).

The possible collapse hypotheses published in May 2003 were developed by NIST and considered several leading hypotheses that had been postulated publicly by experts. These are summarized in Appendix C, Table C-1. One hypothesis suggested that the load carrying core columns were weakened by the fires and failed, initiating overall building collapse without the need for any weakening or failure of the steel truss floor system. Another hypothesis suggested that significant portions of one or more floor truss systems sagged, as they were weakened by fires, pulling the exterior columns inward via the connections to initiate overall building collapse through combined compression and bending failure of the exterior columns. A variation of this hypothesis suggested that the sagging floor system failed in shear at its connections to the columns, leading to overall building collapse initiation through buckling failure of the exterior columns. Load eccentricities introduced by partially damaged floor systems could also have contributed to buckling failure of the columns.

The working collapse hypothesis published in June 2004 was developed to explain the collapse initiation of the WTC towers. The working hypothesis (summarized in Appendix C, Table C-2) identified the chronological sequence of major events as the WTC tower structures redistributed loads from one structural element to another to accommodate the aircraft impact and subsequent fire damage until no further load redistribution was possible, thus, leading to collapse. The working hypothesis was based on analysis of the available evidence and data, consideration of a range of hypotheses (including those postulated publicly by experts), and the understanding of structural and fire behavior at that time. It allowed for multiple load redistribution paths and damage scenarios for each building.

The leading collapse hypotheses for WTC 1 and WTC 2 that were presented in October 2004 are shown in Appendix C, Figs. C–3 and C–4. A separate collapse hypothesis was developed for each tower that identified load redistribution paths and damage scenarios for each major event. The leading hypotheses accounted for the WTC structural system, aircraft impact and subsequent fires, post-impact condition of insulation, the quality and properties of the structural steel and concrete, and the relative roles of the exterior and core columns and the composite floor system, including connections. The hypotheses were consistent with evidence held by NIST (at that time). They were based on the subsystem analysis described in Chapter 7.

The Probable Collapse Sequences for WTC 1 and WTC 2 were presented in April 2005 following completion of global structural response analyses and are shown in Section 9.3. The structural sequences of events were consistent with evidence held by NIST.

9.2.3 Mathematical Modeling – Analysis Interdependencies

Events that played a significant role in the structural performance of the towers were the aircraft impact, rapid ignition of fire on multiple floors, and the growth and spread of fire in each tower. To determine the structural response, detailed information was required on the condition of the structural system and its passive fire protection system both before and after the aircraft impact and during the ensuing fires that elevated temperatures in the structural members.

The interdependence of the various analyses is illustrated in Fig. 9–1. Reference structural models were developed before other structural models to determine the baseline performance of each tower prior to September 11, 2001. The reference models were used as a basis for the aircraft impact damage models and the structural response and failure models to ensure consistency between structural models. The

aircraft impact analysis determined damage to the exterior and the interior of the building and included the structural system, insulation, partition walls, and furnishings for each tower. The analysis also provided an estimate of the fuel dispersion in the towers. These results provided initial conditions for the fire dynamics analysis, thermal analysis, and structural analysis. The fire dynamics analysis simulated the growth and spread of fires and produced gas temperature histories for each floor subjected to fire. The fire dynamics model accounted for damage to interior partition walls and floors (which affected ventilation conditions) and the distribution of debris and fuel.

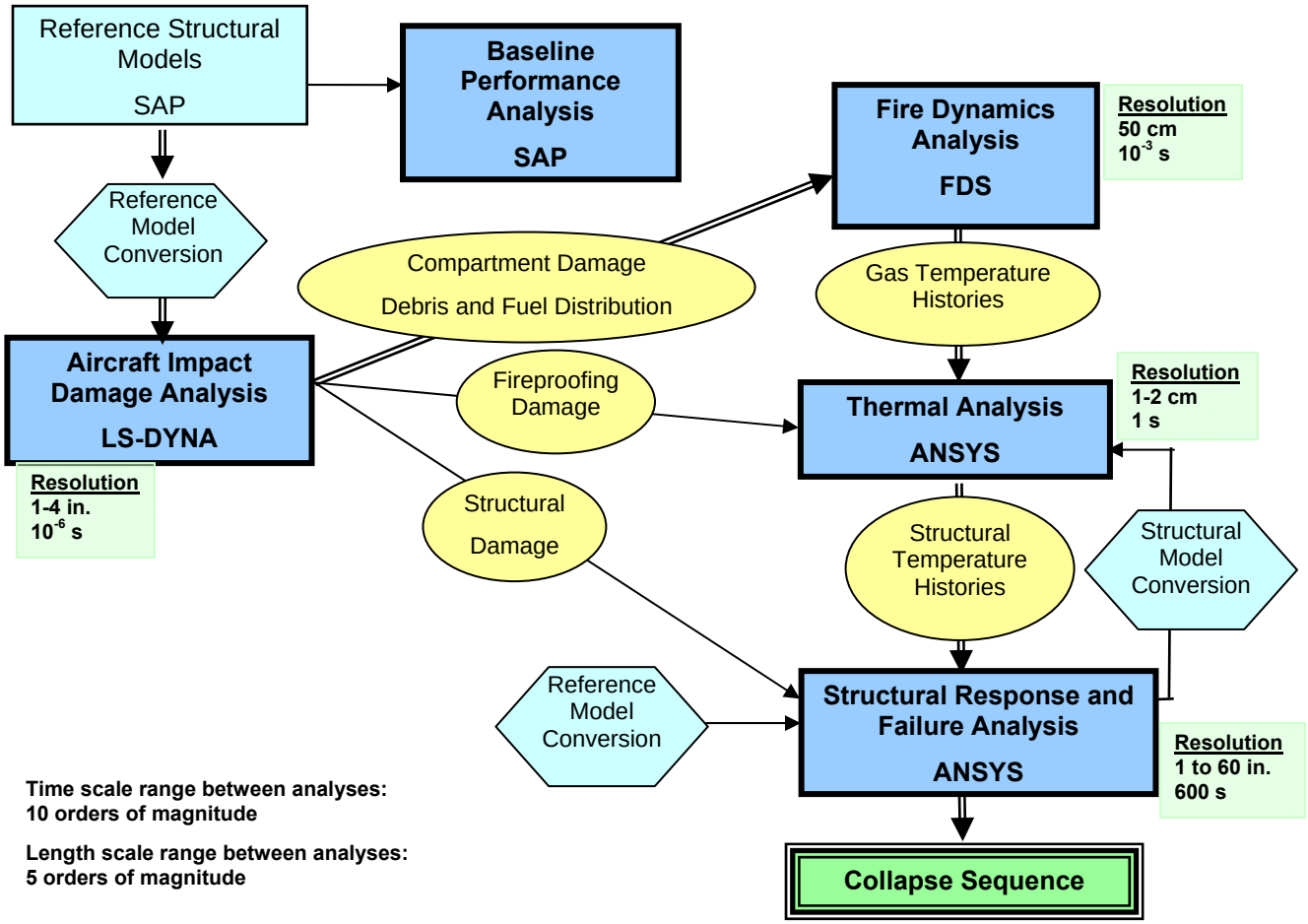

Figure 9–1. Critical analysis inter-dependencies.

The thermal analysis used a solid element heat transfer model to determine temperature histories for the various structural components accounting for the presence or dislodgement of insulation. The thermal analysis required input from the structural analysis model, fire dynamics analysis results, the analysis of damage to insulation, and temperature-dependent thermal material properties. The structural temperature histories, also referred to as thermal loads, were input to the structural analysis, along with the structural impact damage and temperature-dependent material properties, to determine the structural response of each tower.

9.2.4 Sensitivity Studies to Identify Influential Variables

Sensitivity studies were conducted for the aircraft impact, fire dynamics, and thermal analyses to identify the most influential parameters for component, connection, and subsystem behavior. To identify the most influential parameters, an orthogonal factorial design process was used to design analysis 'experiments' (Box, 1978). Numerical experiments with an orthogonal factorial design (OFD) method were conducted for detailed models of components and subsystems to identify parameters that strongly influenced the analysis results:

- Only parameters whose values were not accurately known were selected (parameters that were known with near certainty were set to the known values).
- Selected parameters were varied within a range of likely values, determined from available data and assigned three alternative values: lower value (-), central value (0), upper value (+).

The OFD approach allowed for identification of influential parameters that reduced the number of analysis runs at the global level. The influential parameters for the structural response analyses included the aircraft impact analyses through the impact damage and temperature histories that were part of the required input data. To determine structural response to damage and thermal loads, numerous component and subsystem studies were conducted that identified critical structural behavior and failure mechanisms and how they varied with temperature. Structural behaviors that were studied included restrained thermal expansion, thermal weakening of columns and floors, floor sagging and associated inward pull on exterior wall, and load redistribution through major structural subsystems. Failure mechanisms that were studied included, for example, tensile failure of core column splices and hat truss connections, column buckling, or loss of composite action in the floor system.

The influential parameters that were identified for each analysis, based on available information, were used to create three input data sets. Figure 9–2 illustrates the analysis tree with all influential parameter combinations resulting from this procedure for the three likely values, a lower value, a central value, and an upper value. It is apparent that analysis of all possible combinations required the number of analyses at each level to increase by a factor of three. The number of global structural response analyses was prohibitive with this approach.

However, computational analyses provided valuable insight into the relationship between input and output data for the aircraft impact, fire dynamics, thermal, and structural response analyses. These insights, along with the sensitivity studies, enabled significant reduction of the number of scenarios that were analyzed. Figure 9–3 shows the final pruned analysis tree, which was obtained as follows. After the aircraft impact analysis results were evaluated for the three sets of input parameters, the less severe damage case was discarded (pruned) as it did not reasonably match key observables. The base and more severe damage cases were each analyzed for fire growth and spread (FDS) and for the corresponding temperature histories of structural components (FSI). The linkage between the aircraft impact, fire dynamics, and thermal analyses for each damage case created highly correlated sets of input data and analysis results. For instance, the damage from the severe aircraft impact case provided input data for analysis of the fires corresponding to the severe impact damage, and both analyses provided input data for the thermal analysis of structural components subject to severe impact damage and the corresponding fires. The high level of correlation between the linked sets of aircraft impact, fire, and thermal analyses, as well as similar results for alternative fire conditions for the same impact damage, led to a single branch

at each successive analysis, as shown in Fig. 9–3. The temperature histories for the base and more severe cases (referred to as Case A and Case B for WTC 1 or Case C and Case D for WTC 2 elsewhere in this report) were used in the structural analysis of major subsystems—the isolated core, a full floor, and the exterior wall analyses. The results of the subsystem analyses showed that the more severe case impact damage results better matched key observables. The subsystem analysis results led to the pruning of the global structural analysis for the base case impact damage sub-tree, as shown in Fig. 9–3. Consequently, only the more severe cases (Cases B and D) were used in the global analysis of each tower.

Tables 9–1 to 9–4 list the observables used for the validation of analysis results, the significant input data, influential parameters, and significant output for each analysis.

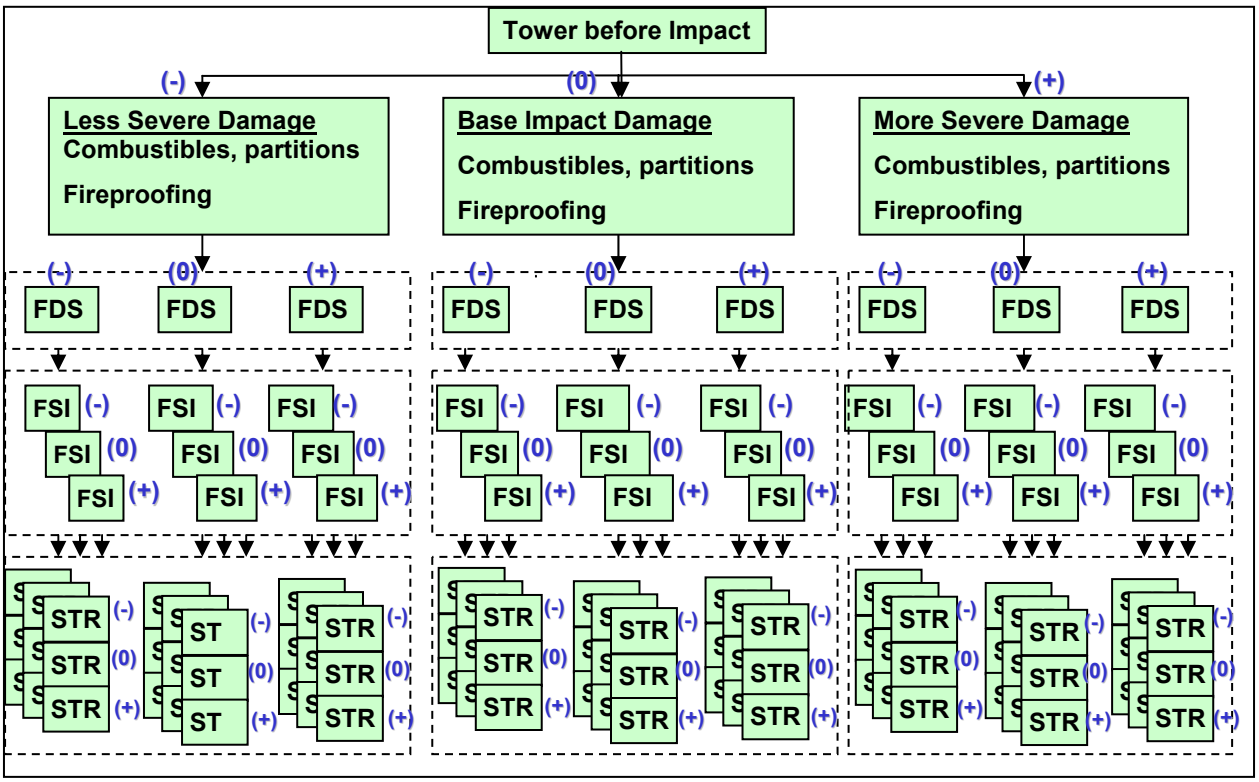

Figure 9–2. Full analysis tree for influential parameter effects.

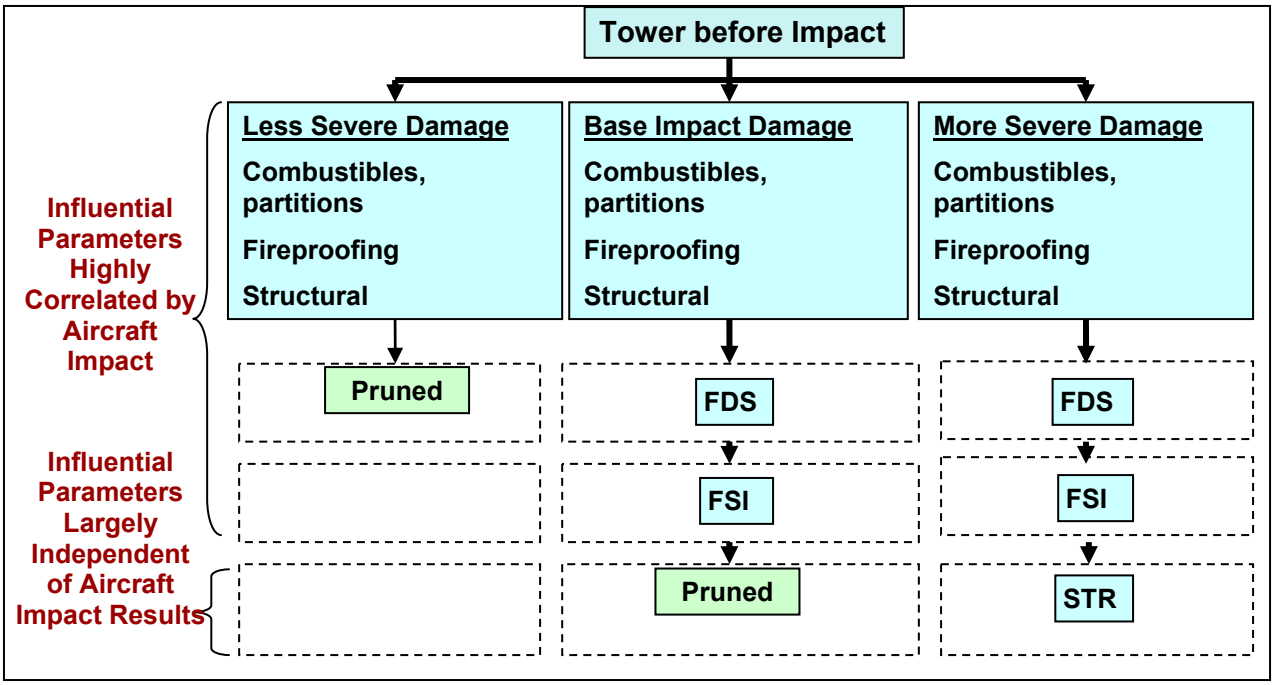

Figure 9–3. Pruned analysis tree for influential parameter effects.

Table 9–1. Aircraft impact analysis parameters.

Validation Data		*Model and Analysis*		
Observables from Photo/Video	**Observables from Interviews**	**Significant Input**	**Influential Parameters**	**Significant Output**
Impact damage to exterior wall Engine/landing gear exit location and speed Aircraft impact conditions for model input (velocity, location, orientation to building)	Stairwell damage	Structural model with service loads Aircraft model with proper contents and mass Floor content layout Material properties for high strain rates	Aircraft velocity Aircraft pitch Aircraft mass Aircraft material failure strain Tower steel failure strain Partition strength Live load weight	Structural damage Debris path (insulation and partition damage) Fuel path

Table 9–2. Fire dynamics analysis parameters.

Validation Data		*Model and Analysis*		
Observables from Photo/Video	**Observables from Interviews**	**Significant Input**	**Influential Parameters**	**Significant Output**
Fire near windows vs location and time Smoke out windows vs location and time Window breakage vs location and time	None	Ventilation sources from debris damage Added fuel from aircraft Fuel distribution after aircraft impact Window openings vs time Floor content layout	Average fuel density Distribution of intact contents vs rubble Shaft ventilation in core Partition damage	Gas temperature histories

Table 9–3. Thermal analysis parameters.

Validation Data		*Model and Analysis*		
Observables from Photo/Video	**Observables from Interviews**	**Significant Input**	**Influential Parameters**	**Significant Output**
None	None	Thermal models of structure Insulation initial condition Estimated insulation damage Gas temperatures	Insulation initial condition Estimated insulation damage	Structural temperature histories

Table 9–4. Structural response analysis parameters.

Evidence/ Data		*Model and Analysis*		
Observables from Photo/Video	**Observables from Interviews and Recordings**	**Significant Input**	**Influential Parameters**	**Significant Output**
Initial Stability Floors sagging at windows Exterior wall inward bowing and instability Tilt of building section above impact during collapse	NYPD Aviation Unit first responder communications	Initial structural condition after impact Structural temperature histories Pull-in force location and magnitude	Pull-in force location and magnitude Floor disconnections Creep strain	Probable collapse sequence Sequence of component and subsystem failures, including instability of exterior wall Global stability vs time

9.2.5 Evaluation of Collapse Hypotheses

Development and validation of the probable collapse sequence for each tower was shaped by evidence gathered in the investigation, including photographs and videos, design and maintenance documents, and eyewitness accounts. Photographs and videos provided knowledge about aircraft impact damage to the tower exterior walls, fire growth and spread at the building exterior, inward bowing of an exterior wall in each tower, and the direction of tilt for the building section above the impact zone as the towers collapsed. Eyewitness accounts provided some information about the interior conditions surrounding the impact areas, but the descriptions tended to be general in nature and often did not provide locations or specifics within a floor level. Figure 9–4 lists data (primarily based on photos and videos except for the metallurgical measurements) used to determine input data, impose time-related constraints, and validate analysis results for determining the probable collapse sequences.

The use of observables as a constraint had the important effect of reducing the uncertainty in the analysis results. The time and frequency of the applied constraints affected the degree to which the analysis uncertainty was reduced.

Figure 9–5 illustrates conceptually how the variance (or uncertainty) of the global stability of the towers (indicated here by the global reserve capacity RC) changed from the time of impact to the time of collapse. The shaded band qualitatively indicates the degree of uncertainty in RC at each time *t* after considering the analysis results and the observations made prior to *t*, except for collapse. The aircraft impact caused a reduction in the towers strength, but substantial reserve capacity remained afterward. The combined effect of the impact damage and fires caused a gradual reduction of the global capacity. The initial period of heating caused minimal changes in the structural capacity, but as time progressed,

various events occurred that caused a sudden or more rapid loss of global capacity. For instance, failure of critical columns from thermal weakening or inward bowing of an exterior wall may are events associated with a rapid loss of global capacity.

Based only on model predictions, the variance (or uncertainty) of the global reserve capacity grew with time. However, whenever an observable matched analysis results, it reduced the uncertainty in the analysis results. Alternatively, when the observables were used to constrain model parameters and adjust results to be consistent with observations, the variance of the global reserve capacity and the sequence of events that took place were reduced. As the structural analyses approached the time to collapse, the ability of the analyses to match the time to failure depended upon the variance in the analysis results. When considering the sequence of structural events and time to failure, it was more important to match the sequence of events as the time to collapse initiation was influenced by adjustments in influential parameters and imposition or matching of observables. As a result of using observables to constrain model parameters and analysis results, NIST believes that the probable collapse sequences that were determined are highly robust. The times to failure for the collapse sequences, however, are subject to considerable variability, particularly since they are sensitive to small changes in the magnitude of the pull-in forces.

Aircraft Impact

- Impact damage to exterior wall
- Engine exit location and speed
- Exit areas for debris
- Aircraft impact velocity, location, and orientation to building
- Stairwell damage

Fire/Thermal

- Fire in windows vs. location and time
- Smoke vs. location and time
- Window breakage vs. location and time

Material Properties

- Mechanical and metallurgical properties of recovered steel

Structural Response

- Global stability after impact and during thermal loading
- Floors draped in windows
- Inward bowing of exterior columns
- Tilting of building section above impact and fire zone
- Time to collapse

Figure 9–4. Data used for input, constraints, and validation of probable collapse sequences.

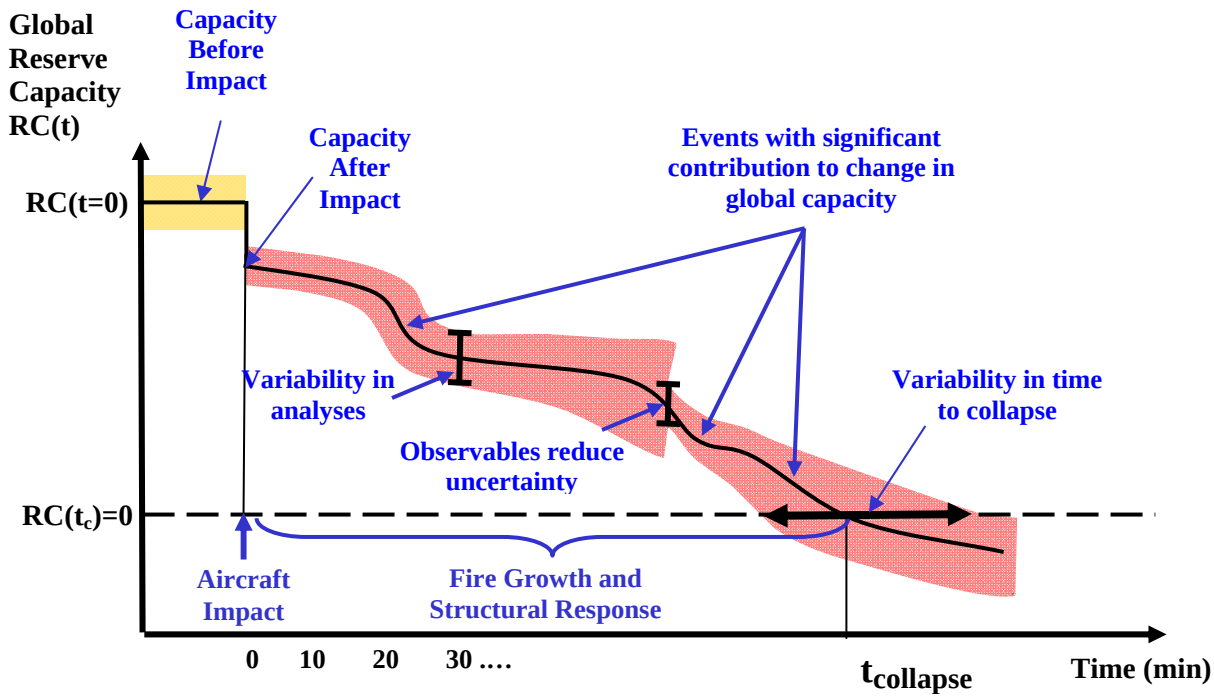

Figure 9–5. Variability in global reserve capacity using model predictions and observables for sequential analyses with imperfect information.

9.3 PROBABLE COLLAPSE SEQUENCES

The following four structural events that were common to both towers are part of the sequence of events described:

- **Floor sagging** was caused by elevated steel temperatures resulting from loss of insulation. Substantial sagging of the floor resulted in pull-in forces at column connections, and led to inward bowing of the exterior wall. Calculations, supported by the four Standard Fire Tests, showed that the most likely cause of floor sagging was buckling of the truss web diagonals, as shown in Fig. 9–6. In the figure, the left portion of the truss maintained flexural stiffness, but the right end lost some flexural stiffness as a result of extensive web buckling. The resultant sagging produced tensile forces in the floor system which was approximated by a combination of flexural and catenary behaviors as shown in Fig. 9–7. A floor system with tensile forces at its connections does not restrain the exterior wall from bowing inward.

- **Bowing and plastic buckling of an exterior wall** under the combined effects of elevated temperatures, redistributed gravity loads, pull-in forces from sagging floors, and loss of lateral support due to failure of truss seat connections.

- **Weakening of the core columns** (which was resisted by the hat truss) was caused by the combined effects of structural impact damage, redistributed gravity loads, elevated temperatures, plastic and creep strains, and plastic buckling of core columns.

- **Redistribution of gravity loads** resulted from impact damage, restrained thermal expansion, core weakening, leaning of the tower section above the impact damage, and bowing and buckling of exterior walls. Redistribution of gravity loads between the core to the exterior walls occurred primarily through the hat truss, while load redistribution between adjacent exterior walls occurred primarily through the spandrels. Restrained thermal expansion occurred in the exterior wall when heated columns were restrained by adjacent cooler columns. Restrained thermal expansion also occurred when the core columns were restrained by the hat truss connection to the exterior wall; elongation of the core columns transferred loads from the exterior wall to the core.

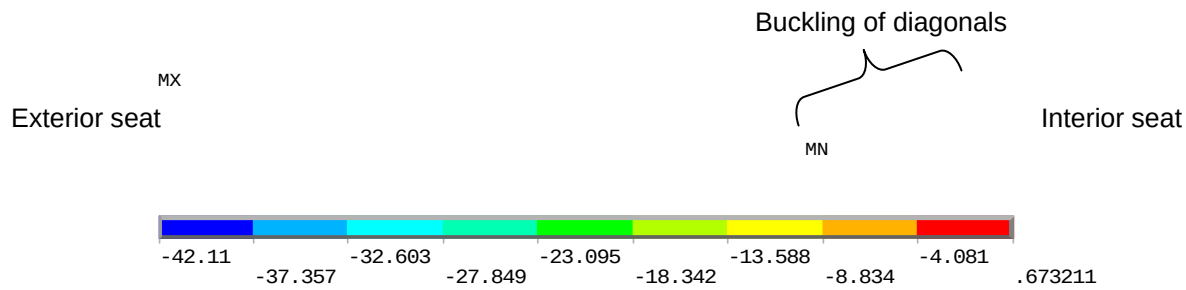

Figure 9–6. Vertical displacement contour of the detailed truss model under thermal loading.

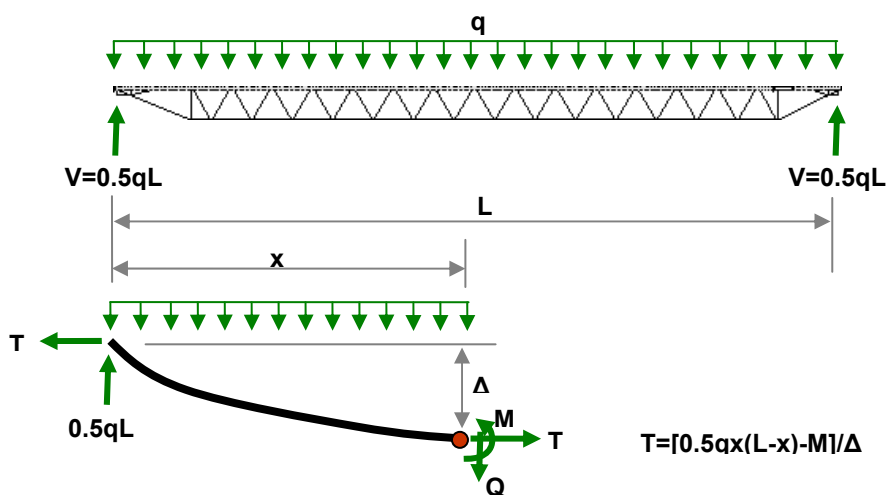

Figure 9–7. Combined flexural and catenary action in the floor system.

9.3.1 Probable Collapse Sequence of WTC 1

The aircraft impacted the north wall of WTC 1 at 8:46 a.m. The aircraft impact severed exterior columns and floors on the north side of the tower and into the core between Floors 93 and 98. The subsequent fires weakened structural subsystems, including the core, floors, and exterior walls. The core weakened, the floors sagged, and the south exterior wall bowed inward. At 10:28 a.m., about 102 min after the aircraft impact, WTC 1 began to collapse.

A sequence of main structural events that led to the collapse of WTC 1 starting from aircraft impact is discussed below. The WTC 1 collapse sequence consisted of five main events: aircraft impact, core weakening, floor sagging and disconnection, inward bowing of the south wall, and collapse initiation. Each event is discussed in terms of (1) the factors and sub-events that led to the event and (2) the consequential structural changes that were caused by the event. Observations for WTC 1 are presented again in Table 9–5. The probable collapse sequence is presented in Fig. 9–8.

Table 9–5. Observations for WTC 1.

Time	*Time from Impact*	*Observation*
8:46:26	0 min	WTC 1 was impacted by a Boeing 767 between Floors 93 and 99 and Columns 109 and 152. Fig 6–1 shows Columns 120 to 159.
9:25:28	39 min	Fire on west side of south wall.
9:40	69 min	No inward bowing of perimeter columns was visible
10:22:59	97 min	Inward bowing of the south perimeter wall was visible from Floor 95 to about Floor 99, with a maximum inward bowing of ~ 55 in. at Column 315 and Floor 97.
10:28:18	102 min	Smoke and debris clouds out of the north, east, and west walls on Floor 98. Fire out of windows on the north, east, west, and south walls between Floor 92 and Floor 98, and Floor 104.
10:28:20	102 min	Tower began to collapse – first exterior sign of collapse was at Floor 98. Rotation of at least 8 degrees to the south occurred before the building section began to fall vertically under gravity.
10:28:48	102 min	Remaining portion of core collapsed.

1. Aircraft Impact Damage:

- Aircraft impact severed a number of exterior columns on the north wall from Floor 93 and Floor 98, and the wall section above the impact zone moved downward.
- After breaching the building's exterior, the aircraft continued to penetrate into the building, severing floor framing and core columns at the north side of the core. Core columns were also damaged toward the center of the core and, to a limited extent on the south side of the core. Fireproofing was damaged from the impact area to the south exterior wall, primarily through the center of WTC 1 and at least over a third to a half of the core width.
- Aircraft impact severed a single exterior panel at the center of the south wall between floors 94 and 96.
- The impact damage to the exterior walls and to the core resulted in redistribution of severed column loads, mostly to the columns adjacent to the impact zones. The hat truss resisted the downward movement of the north wall, and rotated about the east-west axis.
- As a result of the aircraft impact damage, the north and south walls each carried about 7 percent less gravity loads after impact, and the east and west walls each carried about 7 percent more loads. The core carried about 1 percent more gravity loads after impact.

2. Effects of Subsequent Fires and Impact Damaged Fireproofing:

A. Thermal Weakening of the Core:

- The undamaged core columns developed high plastic and creep strains over the duration the building stood, since both temperatures and stresses were high in the core area. The plastic and creep strains exceeded thermal expansion in the core columns.
- The shortening of the core columns (due to plasticity and creep) was resisted by the hat truss, which unloaded the core over time and redistributed loads to exterior walls.
- As a result of the thermal weakening (and subsequent to impact and prior to inward bowing of the south wall), the north and south walls each carried about 10 percent more gravity loads, and the east and west walls each carried about 25 percent more loads. The core carried about 20 percent less gravity loads after thermal weakening.

B. Thermal Weakening of the Floors:

- Floors 95 to 99 weakened with increasing temperatures over time on the long-span floors and sagged. The floors sagged first and then contracted due to cooling on the north side; fires reached the south side later, the floors sagged, and the seat connections weakened.
- Floor sagging induced inward pull forces on the south wall columns.
- About 20 percent of the connections to the south exterior wall on floors 97 and 98 failed due to thermal weakening of the vertical supports.

C. Thermal Weakening of the South Wall:

- South wall columns bowed inward as they were subjected to high temperatures and inward pull forces in addition to axial loads.
- Inward bowing of the south wall columns increased with time.

Figure 9–8. WTC 1 probable collapse sequence.

3. Collapse Initiation

- The inward bowing of the south wall induced column instability, which progressed rapidly horizontally across the entire south face.
- The south wall unloaded and tried to redistribute the loads via the hat truss to the thermally weakened core and via the spandrels to the adjacent east and west walls.
- The entire section of the building above the impact zone began tilting as a rigid block (all four faces, not only the bowed and buckled south face) to the south (at least about 8º) as column instability progressed rapidly from the south wall along the adjacent east and west walls.
- The change in potential energy due to downward movement of building mass above the buckled columns exceeded the strain energy that could be absorbed by the structure. Global collapse then ensued.

Figure 9–8. WTC 1 probable collapse sequence (cont).

Aircraft Impact

WTC 1 was impacted by an aircraft on the north wall. Columns 112 to 151 between Floors 94 and 98 were severed or heavily damaged on the north wall. After breaching the building's perimeter, the aircraft continued to penetrate into the building. The north office area floor system sustained severe structural damage between Columns 112 and 145 at Floors 94 to 98. Core columns were severed or heavily damaged (nine were predicted) between Floor 92 and Floor 97. The aircraft impact also severed a single exterior panel at the center of the south wall from Columns 329 to 331 between Floor 93 and Floor 96. In addition, insulation on floor framings and columns were damaged from the impact area to the south perimeter wall, primarily through the center of WTC 1 and over one-third to one-half of the core width.

Gravity loads on severed columns were redistributed mostly to columns adjacent to the impact zone. Due to the severe impact damage to the north wall, the wall section above the impact zone moved downward. The hat truss resisted the downward movement of the north wall and rotated about its east-west axis, which reduced the load on the south wall. As a result, the north and south walls each carried about 7 percent less gravity loads at Floor 98 after impact, the east and west walls each carried about 7 percent more loads, and the core carried about 1 percent more gravity loads at Floor 98 after impact, as shown in Table 9–6.

Core Weakening

Temperatures in the core area rose quickly; therefore, the thermal expansion of the core was larger than the thermal expansion of the exterior walls in early stages of the fire, resulting in an increase in the gravity loads in the core columns until 10 min (8:56 a.m.), as shown in Table 9–6. The additional loads due to impact damage and high temperatures resulted in high plastic and creep strains in the core columns during early stages of the fire. Creep strain continued to increase until the collapse initiated. By 30 min (9:16 a.m.), the plastic-plus-creep strains exceeded thermal expansion strains. Due to high plastic and creep strains and plastic buckling of some core columns, at 100 min (10:26 a.m.), the core structure at Floor 99 had displaced downward 2.0 in. on average.

Table 9–6. Total column loads at Floor 98 and Floor 105 of WTC 1 for Case B.

		North		East		South		West		Core	
		Floor 98	Floor 105	Floor 98	Floor 105	Floor 98	Floor 105	Floor 98	Floor 105	Floor 98	Floor 105
(1)	Before Impact	10,974	8,026	8,545	6,562	11,025	8,092	8,572	6,604	34,029	20,361
(2)	After Impact	10,137	7,294	9,071	7,028	10,356	7,488	9,146	7,076	34,429	20,761
(3)	10 min	9,796	6,944	8,490	6,461	9,848	6,981	8,536	6,469	36,473	22,790
(4)	20 min	10,437	7,551	9,108	7,075	9,900	7,057	9,202	7,158	34,495	20,806
(5)	30 min	10,913	8,020	10,034	7,998	10,420	7,569	9,715	7,685	32,060	18,377
(6)	40 min	11,068	8,193	10,599	8,571	11,004	8,129	10,178	8,147	30,294	16,608
(7)	50 min	11,149	8,285	10,908	8,878	11,192	8,315	10,458	8,428	29,435	15,743
(8)	60 min	11,205	8,351	11,168	9,130	11,285	8,414	10,716	8,687	28,766	15,069
(9)	70 min	11,286	8,435	11,366	9,319	11,343	8,481	10,939	8,914	28,205	14,502
(10)	80 min	11,376	8,528	11,555	9,497	11,409	8,551	11,119	9,097	27,681	13,978
(11)	90 min	10,916	8,096	11,991	9,847	9,949	7,327	11,657	9,506	28,587	14,876
(12)	100 min	10,828	8,023	12,249	10,076	9,638	7,066	11,905	9,720	28,478	14,767
(13)	(2) - (1)	-837	-732	526	466	-668	-604	574	472	400	400
(14)	(10) - (2)	1,239	1,234	2,484	2,470	1,052	1,063	1,973	2,021	-6,748	-6,783
(15)	(12) - (2)	692	730	3,178	3,048	-719	-422	2,759	2,644	-5,951	-5,993
(16)	(12) - (10)	-548	-504	694	579	-1,771	-1,485	786	623	797	790

Note : Compression is positive. Units are in kip.

The shortening of core columns was resisted by the hat truss, which unloaded the core with time and redistributed the gravity loads from the core to the exterior walls, as can be seen in Table 9–6 at 80 min. As a result, the north, east, south, and west walls carried about 12 percent, 27 percent, 10 prcent, and 22 percent more gravity loads, respectively, for Floor 98 at 80 min than the state after impact, and the core carried about 20 percent less loads. At 80 min, the unloading of the core columns was at its maximum.

Sagging of Floors and Floor/Wall Disconnections

The floors thermally expanded in the early stages of the fires. However, the thermal expansion was overcome by the significant sagging of the floors, which then pulled inward on the exterior columns. Floor 95 to Floor 99 sagged due to elevated temperatures in the south floor areas with long-span trusses. While the north floors first sagged and then contracted due to cooling on the north side, the fires reached the south side later, and the south floors sagged. Figure 9–9 shows vertical displacement contours of Floor 95 to Floor 98 predicted by the full floor models at 100 min (10:26 a.m.). Floor sagging induced pull-in forces on the south wall columns over Floors 95 to 99. In addition, about 20 percent of the exterior seats of Floors 97 and 98 on the south wall failed due to their reduced vertical shear capacity, as shown in Fig. 9–10.

Bowing of South Wall

Exterior columns on the south wall bowed inward as they were subjected to high temperatures, pull-in forces from the floors (beginning at about 80 min), and additional loads redistributed from the core. The observed inward bowing of the south wall at 10:23 a.m. was 55 in. while the calculated inward bowing was 31 in., as shown in Figs. 9–11 and 9–12. Since no bowing was observed on the south wall at 9:55 a.m., the south wall was considered to begin bowing inward around 10:10 a.m. when the floors on the south side began to experience large sagging. The inward bowing of the south wall increased with time due to additional gravity loads caused by core weakening and increased temperatures on the south wall. As the floor applied inward pull to the south exterior wall at approximately 80 min, the south wall began to unload to adjacent walls and the core.

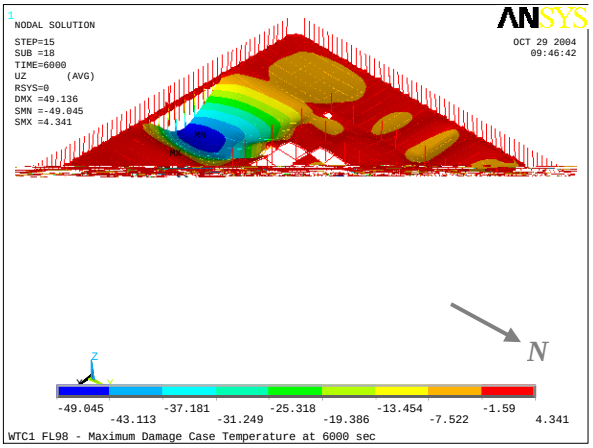

(a) Floor 98

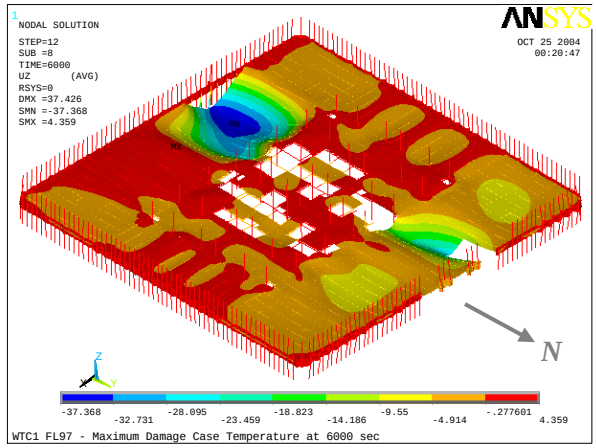

(b) Floor 97

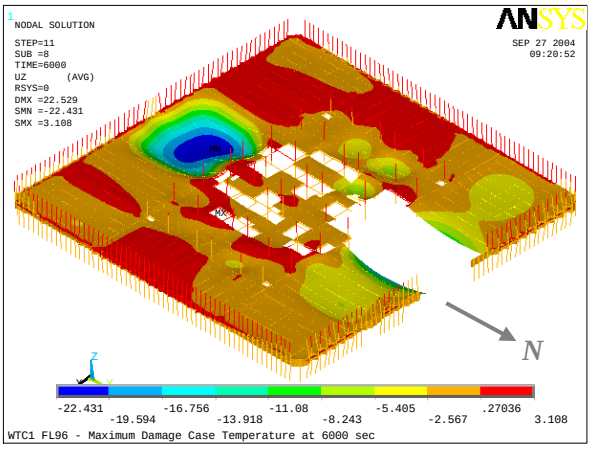

(c) Floor 96

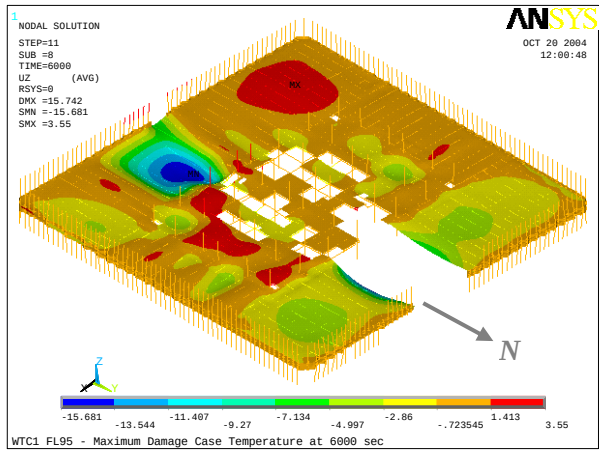

(d) Floor 95

Figure 9–9. Vertical displacement of Floors of WTC 1 for Case B′ at 100 min.

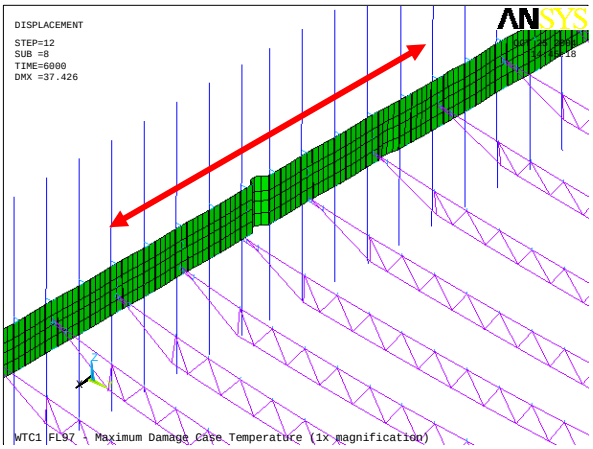

(a) Floor 97

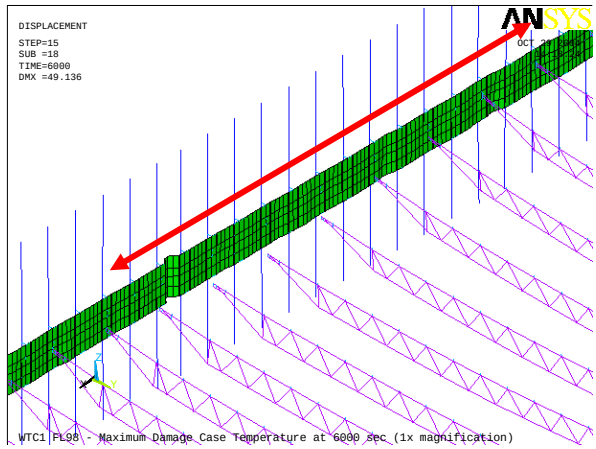

(b) Floor 98

Figure 9–10. Loss of vertical supports observed in Floor 97 and Floor 98 of WTC 1 for Case B′ (1x displacement magnification).

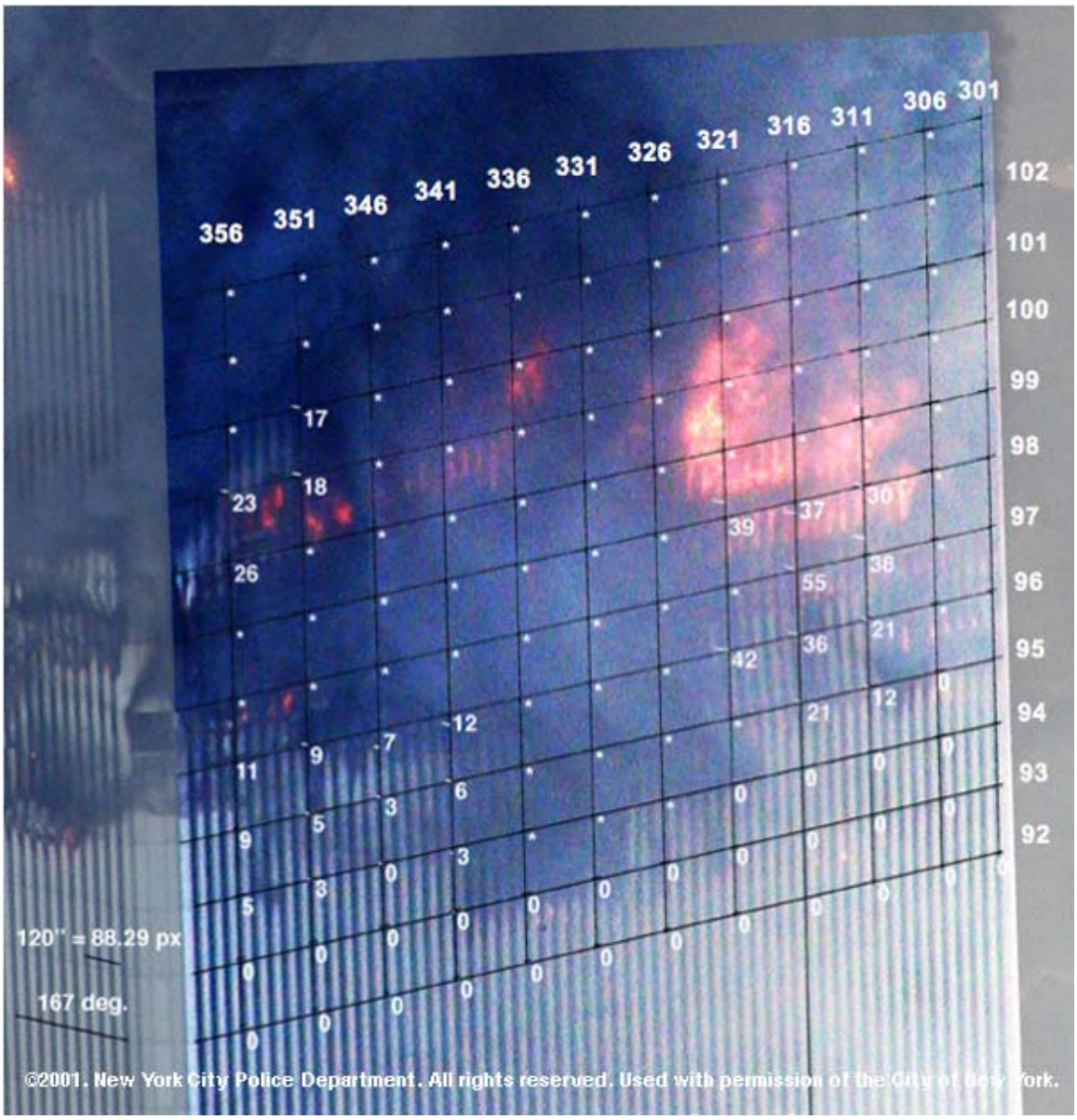

Figure 9–11. Inward bowing of the WTC 1 south wall of WTC 1 at 10:23 a.m.

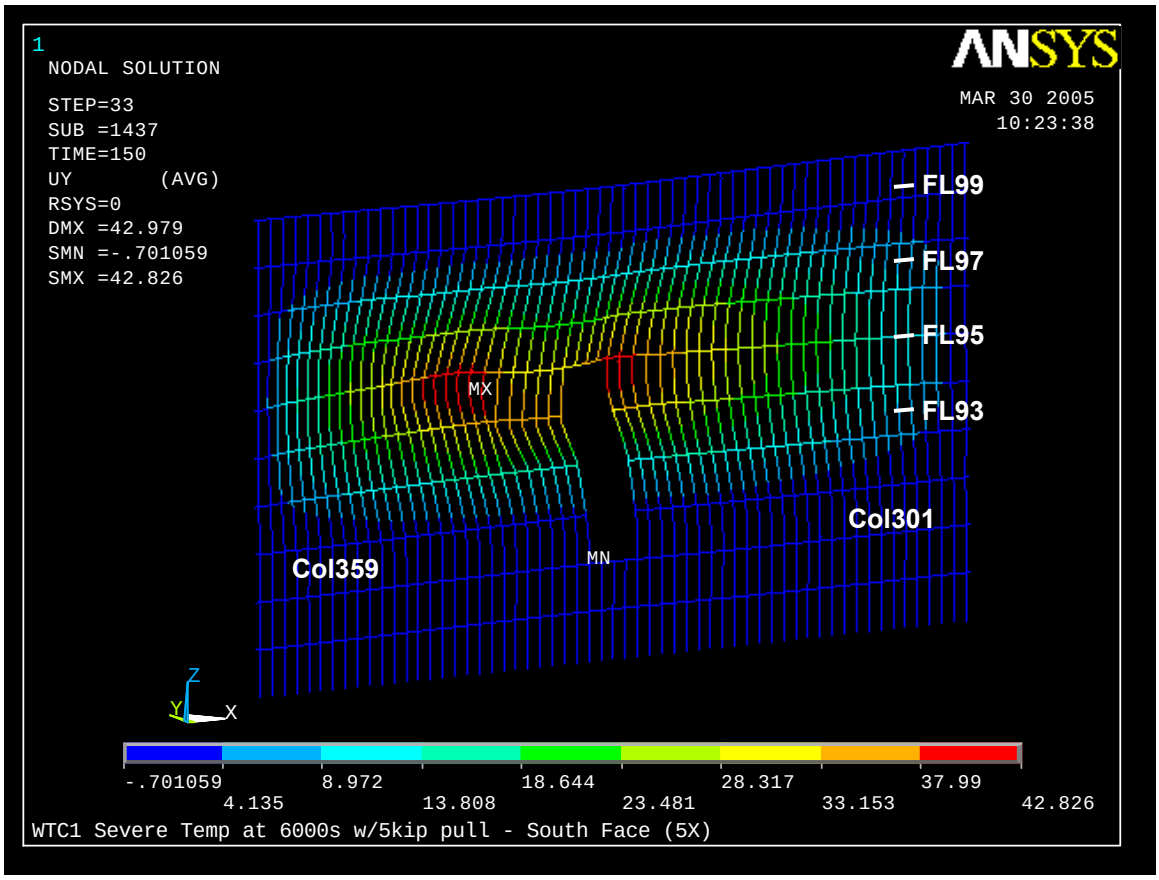

Figure 9–12. Inward bowing of south wall of WTC 1 global model with creep at 100 min for Case B with 5 kip pull-in forces (5x displacement magnification).

Buckling of South Wall and Collapse Initiation

The inward bowing of the south wall increased as the post-buckling strength of bowed columns continued to reduce. The bowed columns increased the loads on the unbuckled columns on the south wall by shear transfer through the spandrels. Consequently, instability progressed horizontally, and when it engulfed the entire south wall, it progressed along the east and west walls. Moreover, the unloading of the south wall resulted in further redistribution of gravity loads on the south wall to the east and west walls and to the thermally weakened core via the hat truss. At 100 min, the north, east, and west walls at Floor 98 carried about 7 percent, 35 percent, and 30 percent more gravity loads than the state after impact, and the south wall and the core carried about 7 percent and 20 percent less loads, respectively. The increased loads on the east and west walls were due to their relative higher stiffness compared to the impact damaged north wall and bowed south wall. The section of the building above the impact zone began tilting to the south at least about 8° as column instability progressed rapidly from the south wall along the adjacent east and west walls, as shown in Fig. 9–13. The gravity loads could no longer be redistributed, nor could the remaining core and perimeter columns support the gravity loads from the floors above. The change in potential energy due to downward movement of building mass above the buckled columns exceeded the strain energy that could have been absorbed by the structure. Global collapse ensued.

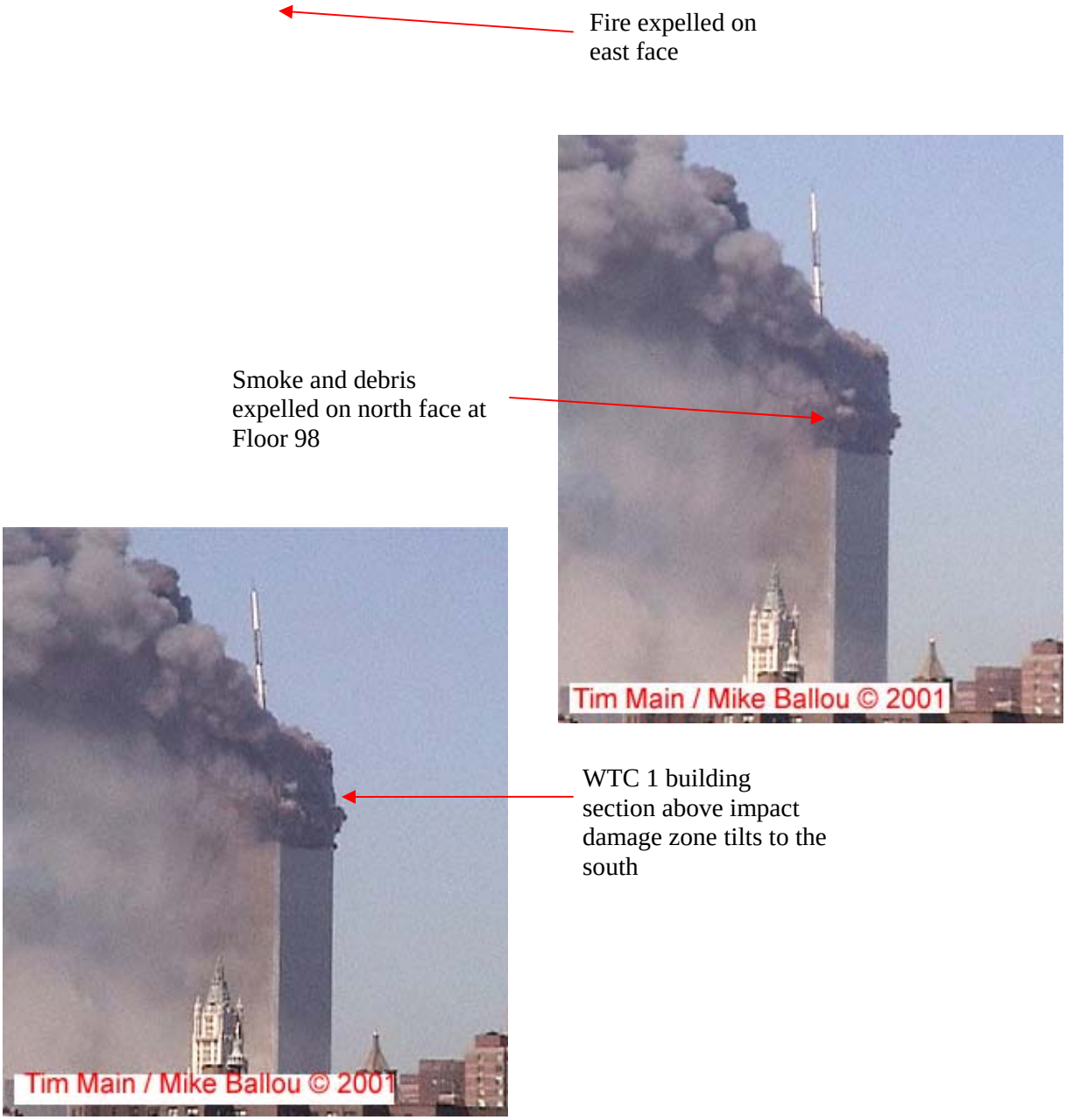

Figure 9–13. Expulsion of smoke and debris at WTC 1 Floor 98 on the east, north, and west faces.

9.3.2 Probable Collapse Sequence of WTC 2

The aircraft impacted the south wall of WTC 2 at 9:03 a.m. The impact mostly severed columns and floors that were toward the east side of the building between Floor 78 and Floor 84. The subsequent fires were also observed on the east side of the building. At 9:59 a.m., about 56 min after the aircraft impact, the building started to collapse, with the east wall buckling inward followed by tilting of the building portion above Floor 82 toward the east and south.

The section below discusses the sequence of main structural events that led to the collapse of WTC 2 starting from aircraft impact. Each event is discussed

1. Aircraft Impact Damage:

- Aircraft impact severed a number of exterior columns on the south wall from floors 78 to 84, and the wall section above the impact zone moved downward.
- After breaching the building's exterior, the aircraft continued to penetrate into the building, severing floor framing and core columns at the southeast corner of the core. Fireproofing was damaged from the impact area through the east half of the core up to the north and east exterior walls. The floor truss seat connections over about 1/4 to 1/2 of the east side of the core were severed on floors 80 and 81 and over about 1/3 of the east exterior wall on floor 83.
- Aircraft impact severed a few columns near the east corner of the north wall between floors 80 and 82.
- The impact damage to the exterior walls resulted in redistribution of severed column loads, mostly to the columns adjacent to the impact zones. The impact damage to the core columns resulted in redistribution of severed column loads mostly to other intact core columns and the east exterior wall. The hat truss resisted the downward movement of the south wall, and rotated about the east-west axis.
- As a result of the aircraft impact damage, the core carried 6 percent less gravity loads after impact and the north face carried 10 percent less loads. The east face carried 24 percent more gravity load, while the west face and the south face carried 3 percent and 2 percent more gravity load, respectively.
- After impact, the core was leaning toward the east and south exterior walls. The exterior walls acted to restrain the core structure.

2. Effects of Subsequent Fires and Impact Damaged Fireproofing:

A. Thermal Weakening of the Core:

- Several of the undamaged core columns near the damaged and severed core columns developed high plastic and creep strains over the duration the building stood, since both temperatures and stresses were high in the core area. The plastic and creep strains exceeded thermal expansion in the core columns.
- The core continued to tilt toward the east and south due to the combination of column shortening (due to plasticity, creep, and buckling) and the failure of column splices at the hat truss in the southeast corner.
- As a result of thermal weakening (and subsequent to impact), the east wall carried about 5 percent more gravity loads and the core carried about 2 percent less loads. The other three walls carried between 0 and 3 percent less loads.

B. Thermal Weakening of the Floors:

- Floors 79 to 83 weakened with increasing temperatures over time on the long-span floors on the east side and sagged.
- Floor sagging induced inward pull forces on the east wall columns.
- About an additional 1/3 of the connections to the east exterior wall on floor 83 failed due to thermal weakening of the vertical supports.

C. Thermal weakening of the east wall:

- East wall columns bowed inward as they were subjected to high temperatures and inward pull forces in addition to axial loads.
- Inward bowing of the east wall columns increased with time.

Figure 9–14. WTC 2 probable collapse sequence.

3. Collapse Initiation

- The inward bowing of the east wall induced column instability, which progressed rapidly horizontally across the entire east face.
- The east wall unloaded and tried to redistribute the loads via the hat truss to the weakened core and via the spandrels to the adjacent north and south walls.
- The entire section of the building above the impact zone began tilting as a rigid block (all four faces; not only the bowed and buckled east face) to the east (about 7º to 8º) and south (about 3º to 4º) as column instability progressed rapidly from the east wall along the adjacent north and south walls. The building section above impact continued to rotate to the east as it began to fall downward, and rotated to at least 20 to 25 degrees.
- The change in potential energy due to downward movement of building mass above the buckled columns exceeded the strain energy that could be absorbed by the structure. Global collapse then ensued.

Figure 9–14. WTC 2 probable collapse sequence (cont).

As a result of the impact damage, dead and live loads carried by severed columns on the south wall and in the southeast corner of the core were redistributed to adjacent intact columns and also to the columns on the east wall (see Table 9–8). After redistribution, the total axial load on the core columns reduced by 6 percent, and the total axial load on the north wall columns reduced by 10 percent. The total axial load on the east wall columns, however, increased by 24 percent, and the total axial load on the west and south wall columns slightly increased by 2 percent to 3 percent.

Just below the hat truss level (Floor 105), analyses predicted that about seven column splices failed for columns at the southeast corner of the core. This increased the core tilting toward the southeast and also increased the vertical downward displacement of the core at the impact zone. After the failure of the core column splices, the remaining core columns transferred 73 percent of the loads released in the failing core columns to the exterior walls through the hat truss and 27 percent of the loads were transferred through the core floors.

Even though some column loads on the south wall were reduced after impact, the total load did not change, as some of the loads from the core area were redistributed to that wall through the hat truss (see Table 9–9). At the end of the load redistribution after impact, the core was leaning toward the east and south. The perimeter walls acted to restrain the core structure in the lateral direction.

Sagging of Floors and Floor/Wall Disconnections

Thermal expansion of the floors also occurred early in the fires, but as floor temperatures increased, the floor sagged and began to pull inward on the exterior columns. As a result of the aircraft impact damage and increasing temperatures due to subsequent fires, Floor 79 through Floor 83 sagged over time. The amount of sagging was more significant at Floor 80 and Floor 81 where the truss seats on the east side of the core were failed due to aircraft impact (see Fig. 9–15). Increased temperatures also weakened the truss seats on the east exterior wall and caused additional disconnections at Floor 82 and Floor 83, which further increased the floor sag (see Fig. 9–16). Floor sagging induced pull-in forces on the east wall columns, and started shortly after impact and grew with time.

Bowing of East Wall

The east wall columns bowed inward as a result of increasing temperatures (reduced strength and stiffness) and pull-in forces induced by sagging floors (see Figs. 9–17 and 9–18). The amount of inward bowing in the east wall steadily increased with time due to the combined effects of pull-in forces from sagging floors, increased axial loads, and a continuous increase in thermally induced plastic and creep strains (see Fig. 9–19). The load in bowed columns decreased, with some load transferring to adjacent unbowed columns, but the total column load on the east wall remained more or less constant for the duration after aircraft impact (see Fig. 9–20).

Unloading and Tilting of Core

With increasing time and temperatures, the core columns developed high compressive plastic and creep strains, especially on the east side of the core. Plastic and creep strains started to exceed the thermal expansion strains approximately 30 min after the aircraft impact (see Fig. 9–21). High plastic and creep strains caused unloading on the east side core columns. This increased the core tilt toward the southeast and transferred more loads to the east wall. As a result, at Floor 83, the total axial load carried by the core columns were reduced by 8 percent, the east wall loads increased by 29 percent, and the north wall loads decreased by 12 percent, relative to the total loads before aircraft impact. The total loads on the south and west walls did not change significantly (see Tables 9–8 and 9–9).

Buckling of East Wall and Collapse Initiation

With continuously increased bowing and axial loads, the east wall became unstable. The instability started at the center portion of the wall and rapidly progressed horizontally on both sides. As a result of buckling, the east wall significantly unloaded, redistributing its loads to the weakened core through the hat truss and to the east side of the south and north walls through the spandrels (see Figs. 9–22 through 9–24 and Table 9–10). Furthermore, the portion of the building above the buckled columns suddenly moved downward, and the building tilt towards the east increased.

The section of the building above the impact zone began tilting to the east (about 7° to 8°) and south (about 3° to 4°) as column instability progressed from the east wall to the adjacent south and north walls. The building section above impact continued to rotate to the east as it began to fall downward, and rotated to at least 20 degrees to 25 degrees. The gravity loads could no longer be redistributed, nor could the remaining core and perimeter columns support the gravity loads from the floors above. The change in potential energy due to downward movement of the building mass above the buckled columns exceeded the strain energy that could be absorbed by the structure. The building portion above the impact zone became unstable, and building collapse ensued.

Table 9–8. Total column loads at Floor 83 of WTC 2 for Case D. Compression is positive.

Row	Analysis Stage	West	East	North	South	Core
(1)	Before Impact	18065	18114	13567	13284	61828
(2)	After Impact	18670	22481	12193	13511	57821
(3)	10 min	18728	22226	11896	13358	58413
(4)	20 min	18914	22208	12052	13318	58124
(5)	30 min	18876	23681	11770	13365	56967
(6)	40 min	18531	23682	11906	13473	56825
(7)	43 min	15667	15143	14215	16292	62422
(8)	(2)-(1)	604	4368	-1374	227	-4007
(9)	(6)-(2)	-138	1201	-287	-38	-996
(10)	(7)-(6)	-2864	-8539	2309	2819	5596

Table 9–9. Total column loads at Floor 105 of WTC 2 for Case D. Compression is positive.

Row	Analysis Stage	West	East	North	South	Core
(1)	Before Impact	8497	8572	7382	7169	17123
(2)	After Impact	9170	11272	6487	8432	13382
(3)	10 min	9182	11061	6250	8275	13975
(4)	20 min	9279	11120	6311	8351	13682
(5)	30 min	9370	11859	6416	8553	12544
(6)	40 min	9198	11927	6524	8691	12402
(7)	43 min	7086	8026	6546	9169	17915
(8)	(2)-(1)	674	2699	-895	1263	-3741
(9)	(6)-(2)	28	656	37	259	-980
(10)	(7)-(6)	-2112	-3901	23	479	5513

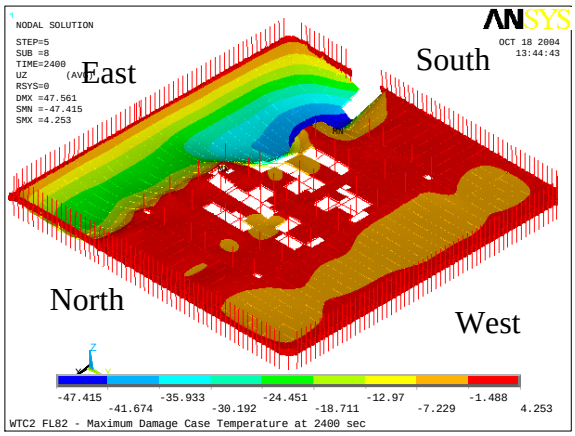

Floor 82

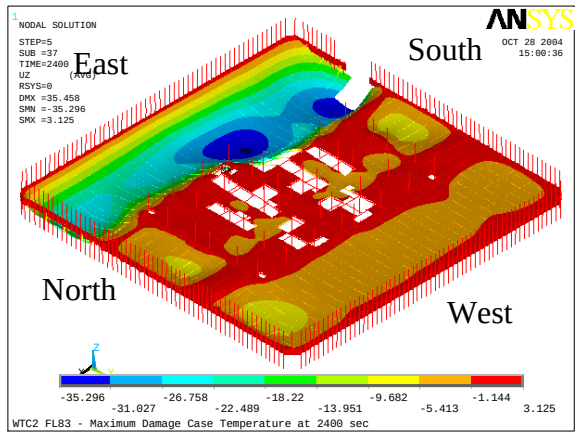

Floor 83

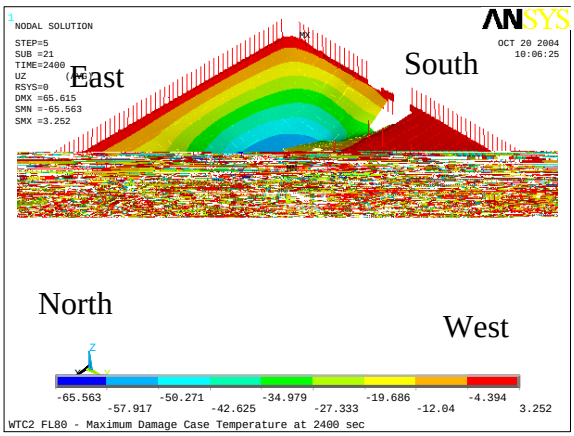

Floor 80

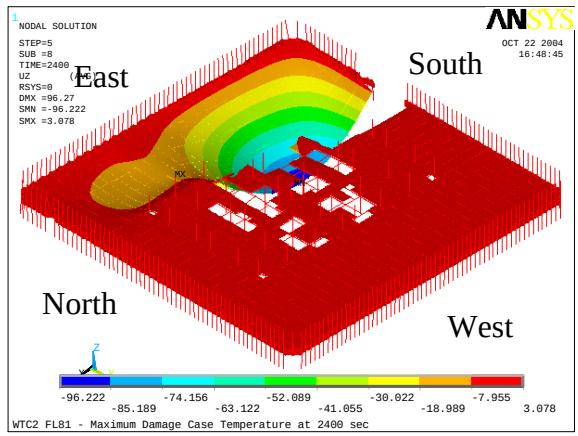

Floor 81

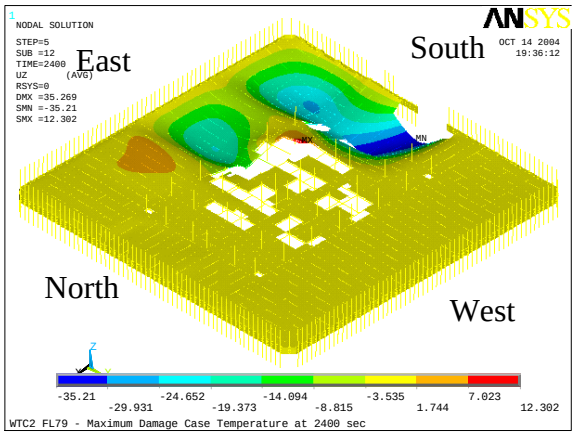

Floor 79

Figure 9–15. Vertical displacements of Floors 79 through Floor 88 of WTC 2 at 40 min (Case D).

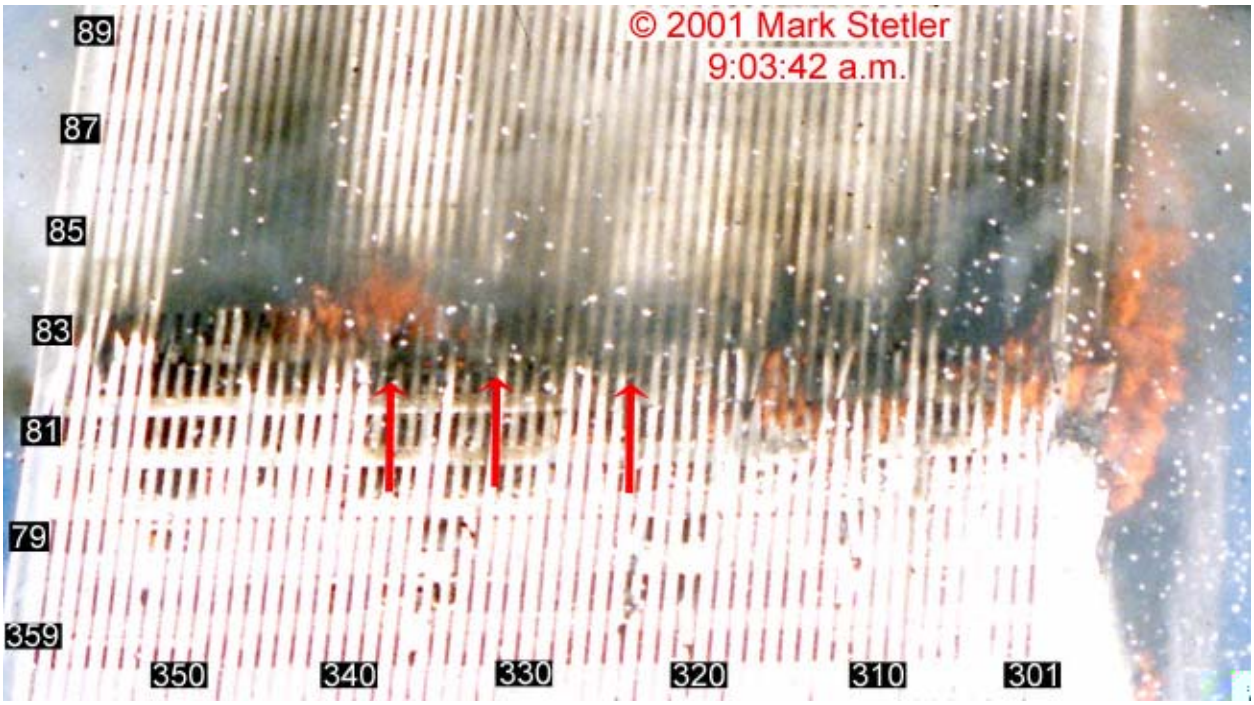

After impact damage

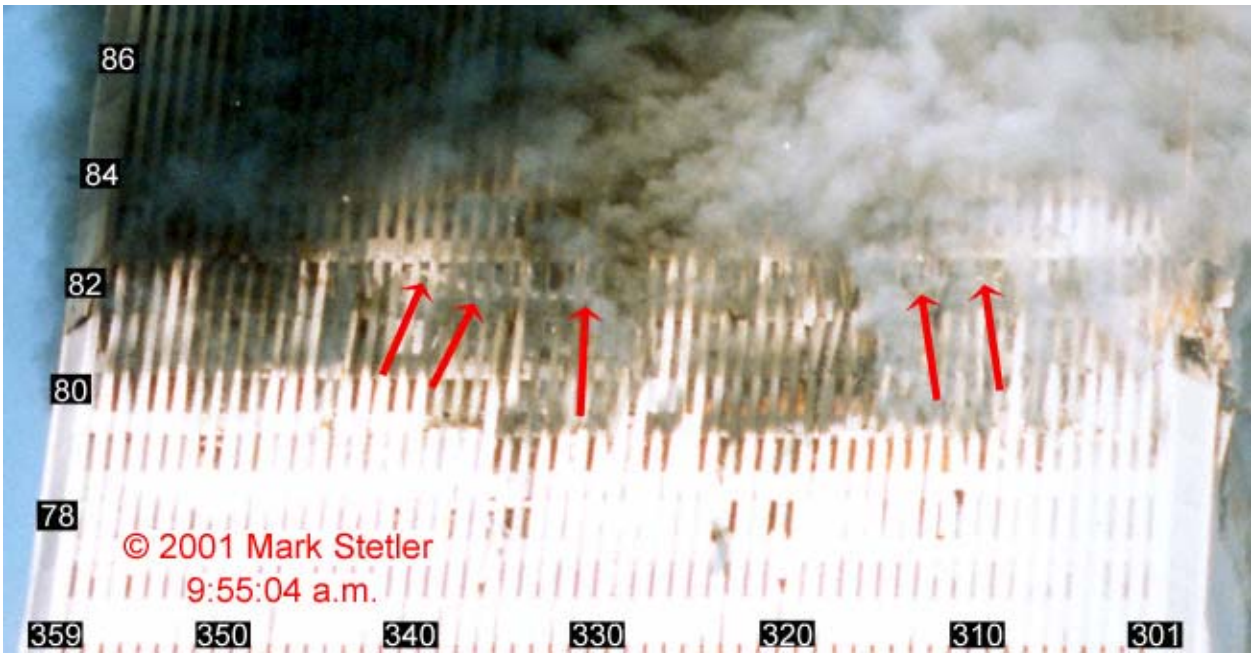

Damage a few minutes before collapse

Figure 9–16. Floor sagging observed on the east wall of WTC 2 at different stages.

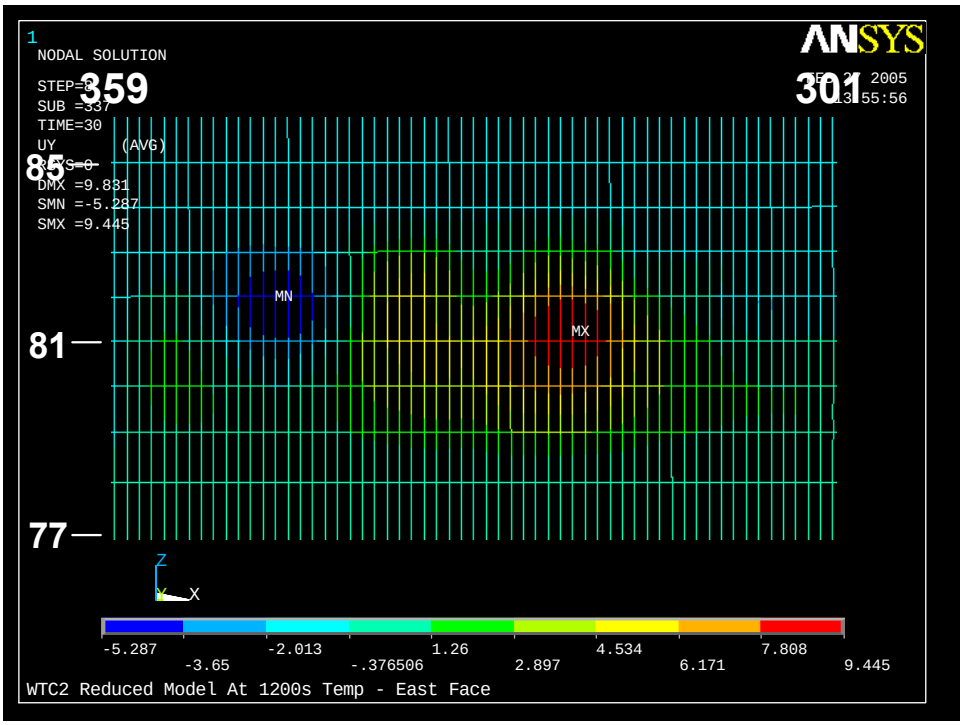

At 20 minutes

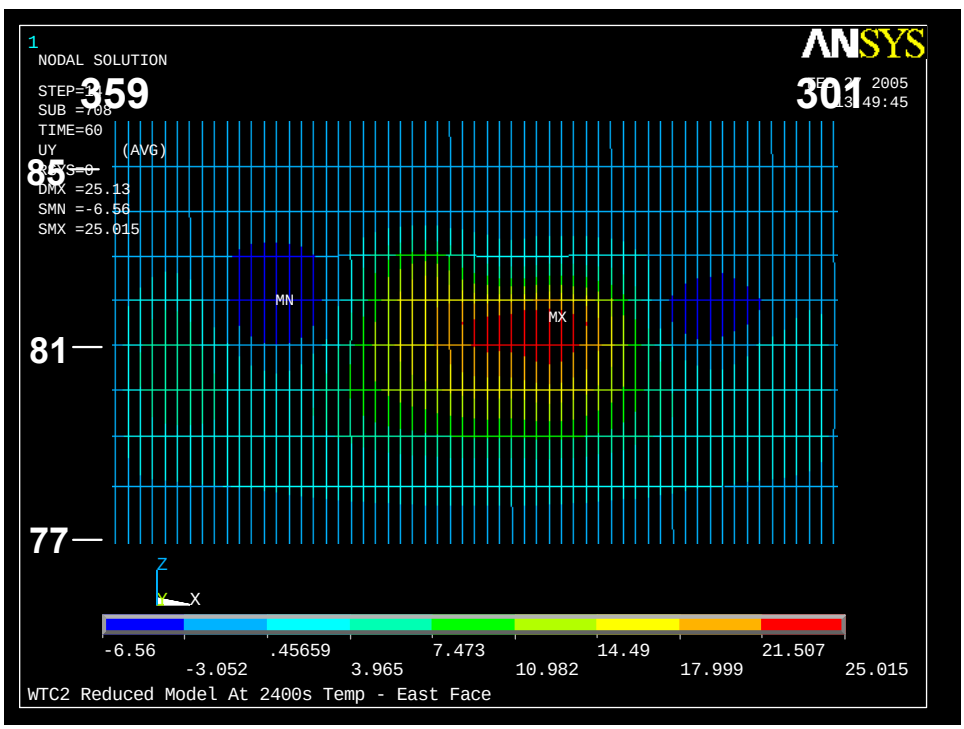

At 40 minutes

Figure 9–17. Out-of-plane displacements on the east wall of WTC 2 (Case D).

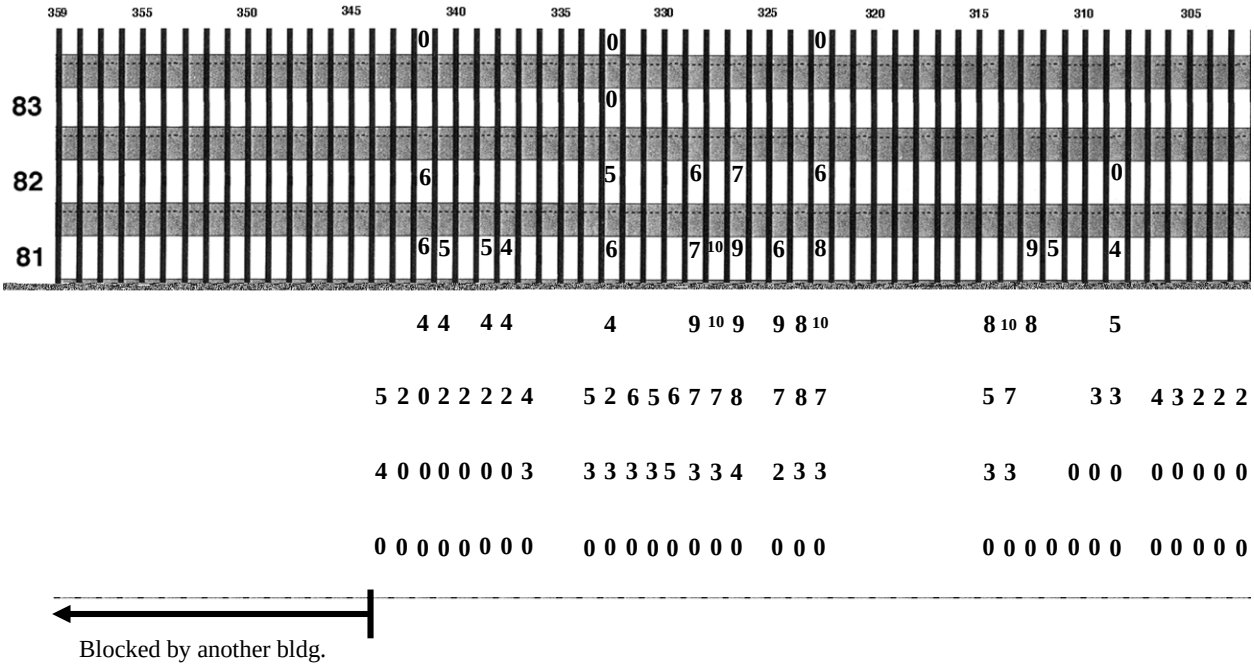

Displacement measurements at 9:21 a.m.

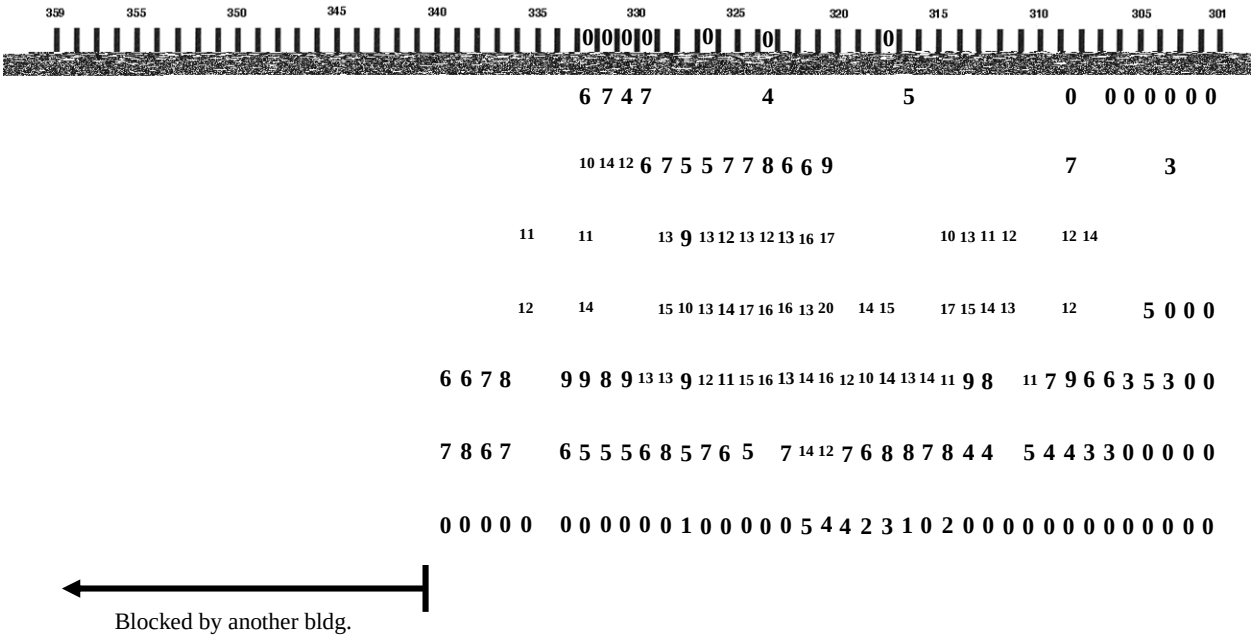

Displacement measurements at 9:53 a.m.

Figure 9–18. Out-of-plane displacement estimates of the east wall of WTC 2 from photographs.

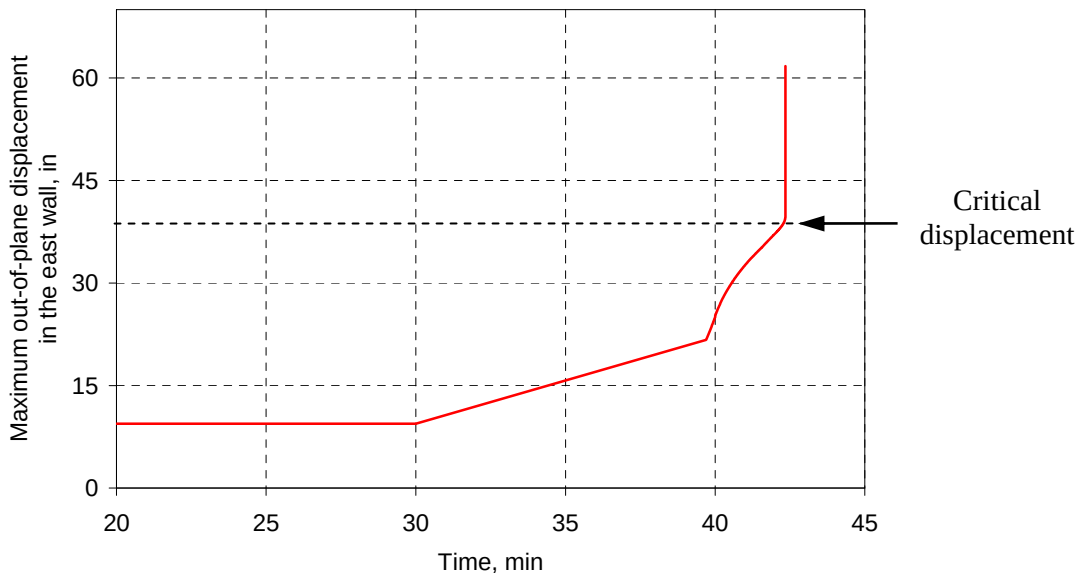

Figure 9–19. Variation of maximum out-of-plane displacement on the east wall of WTC 2 (Case D).

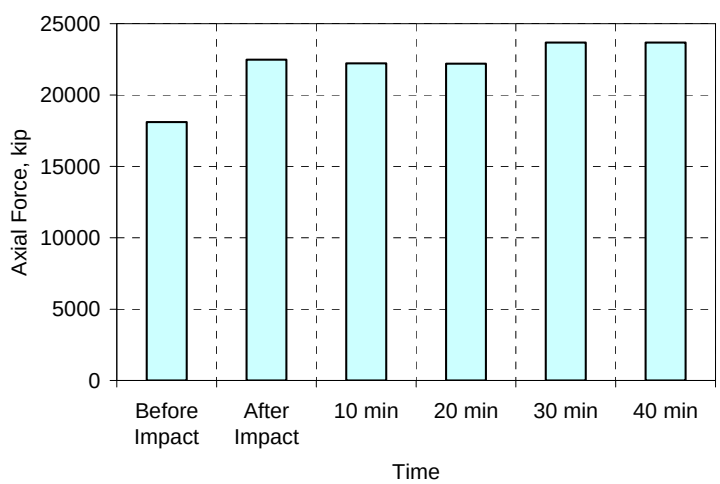

Figure 9–20. Total column loads at Floor 83 of the east wall of WTC 2 at different stages (Case D).

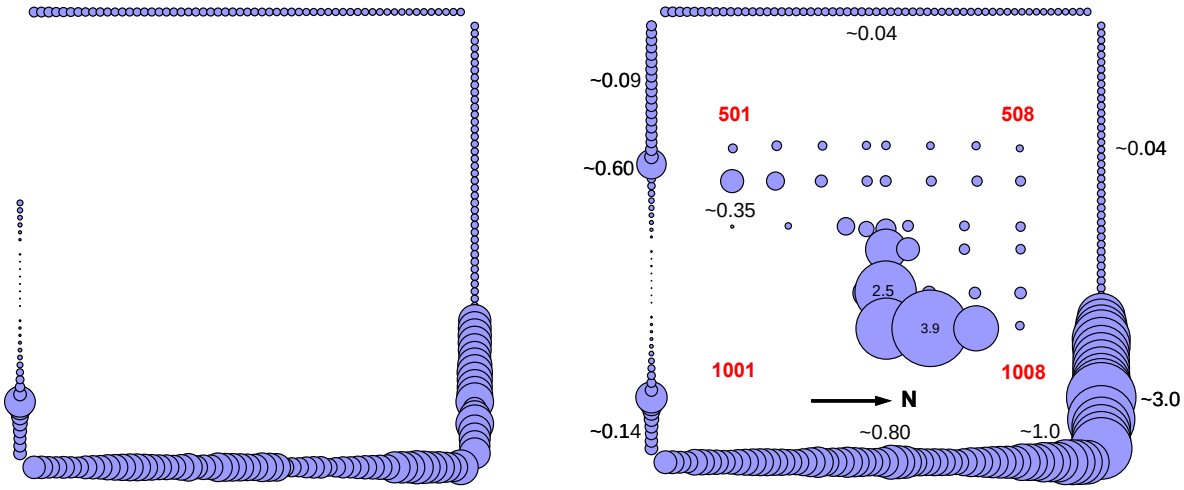

Figure 9–21. Maximum elastic + plastic + creep strains for columns between Floor 78 and Floor 83 of WTC 2 at different stages (Case D) (strain values are in percent).

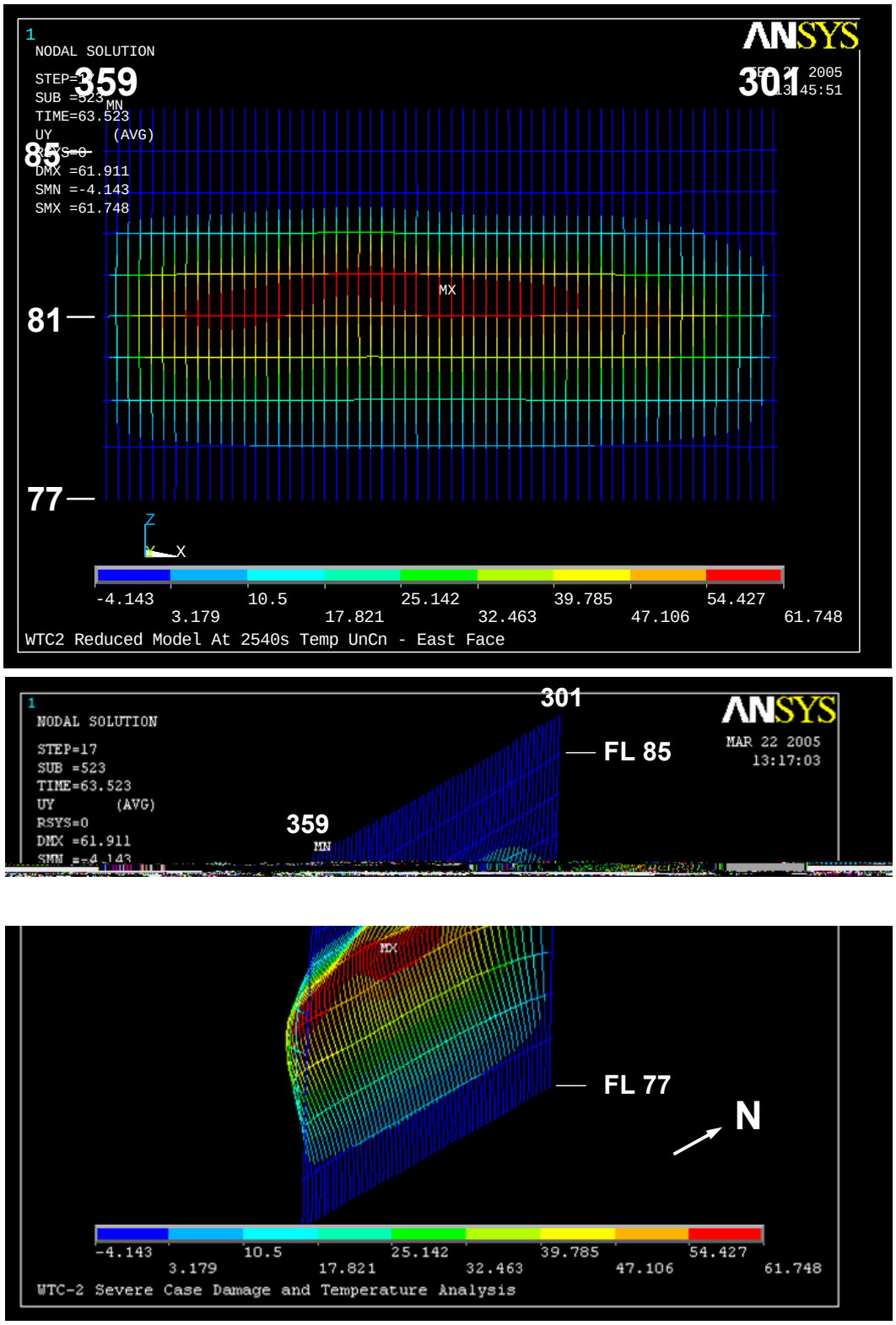

Figure 9–22. Inward bowing of the east wall of WTC 2 when buckled at 43 min for Case D (4x displacement magnification).

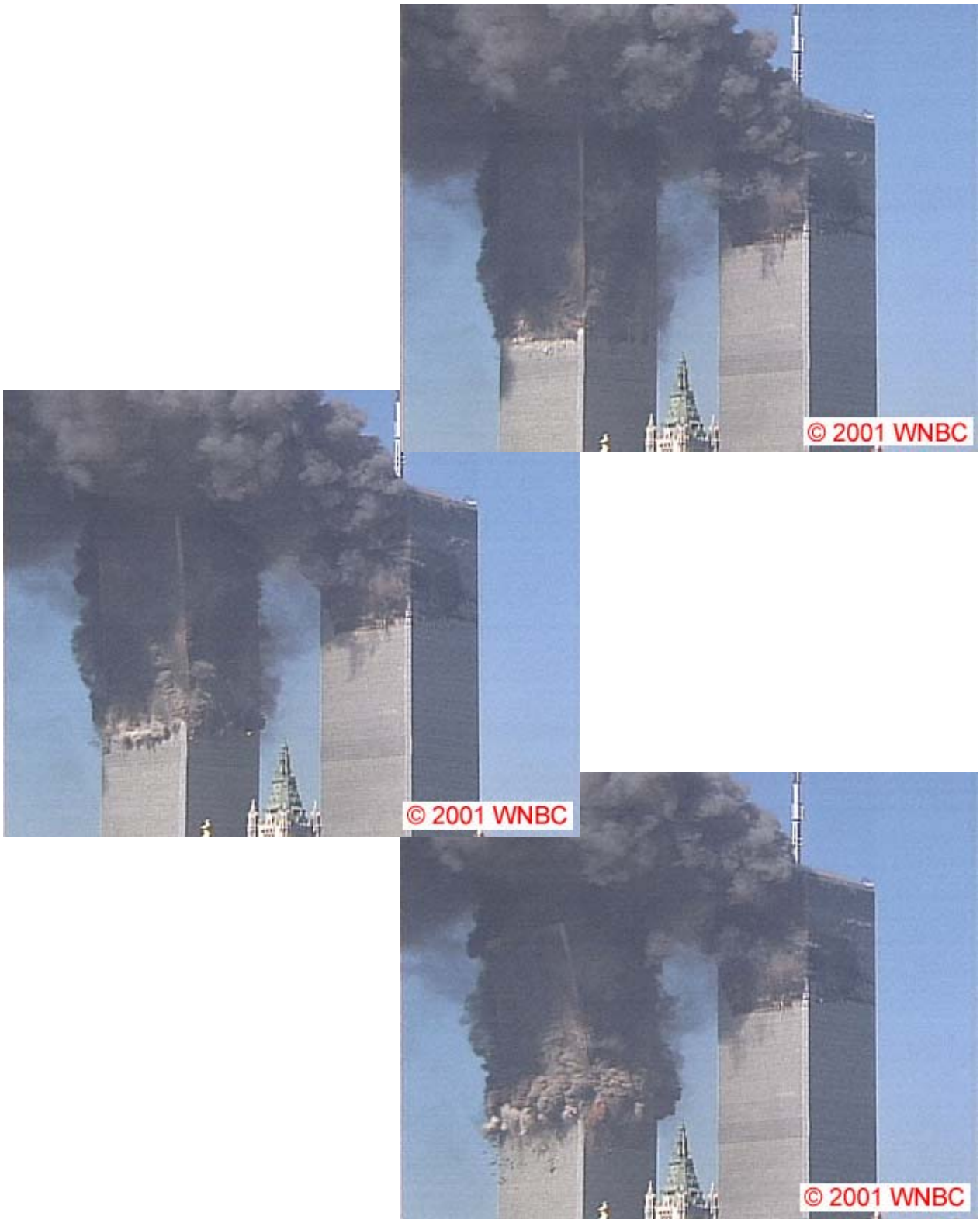

Figure 9–23. Inward bending of exterior columns of the west wall of WTC 2 just before collapse.

Table 9–10. Change in total column loads when the east wall of WTC 2 buckles (Case D, compression is positive).

Row	Floor	West	East	North	South	Core
(1)	83	-2864	-8539	2309	2819	5596
(2)	105	-2112	-3901	23	479	5513
(3)	(2) - (1)	752	4637	-2286	-2340	-84

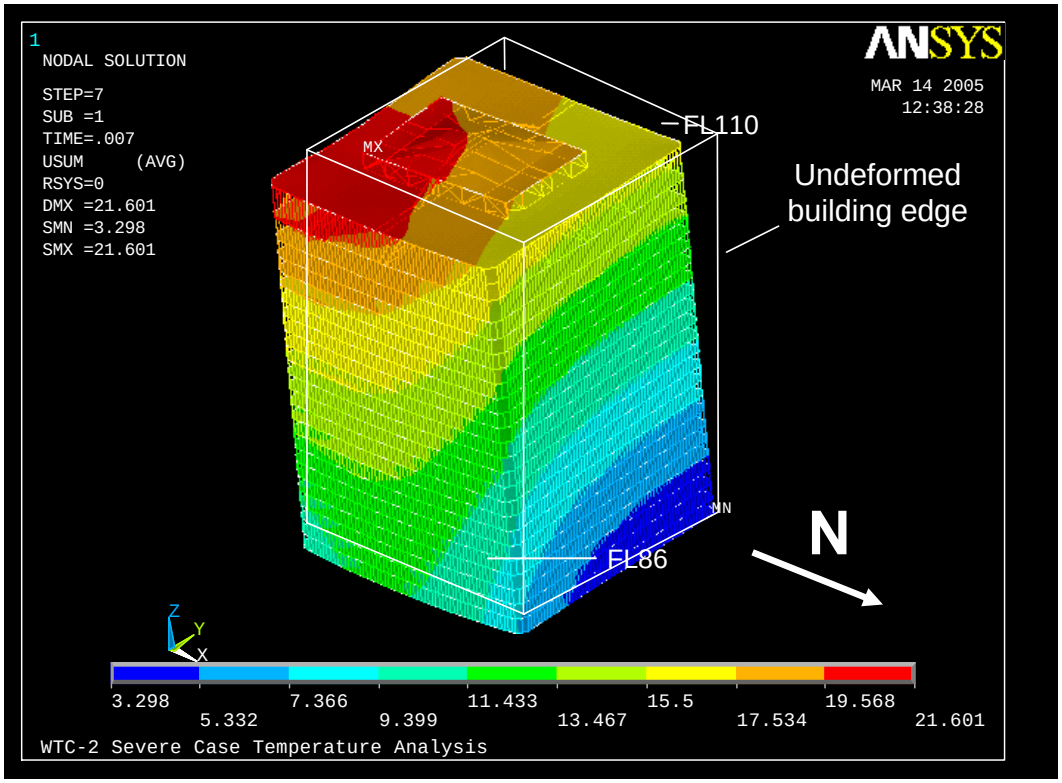

Figure 9–24. Total displacements of WTC 2 above Floor 86 at 43 min for Case D. Note tilt toward east and south (20x displacement magnification).

9.3.3 Events Following Collapse Initiation

Failure of the south wall in WTC 1 and east wall in WTC 2 caused the portion of the building above to tilt in the direction of the failed wall. The tilting was accompanied by a downward movement. The story immediately below the stories in which the columns failed was not able to arrest this initial movement as evidenced by videos from several vantage points.

The structure below the level of collapse initiation offered minimal resistance to the falling building mass at and above the impact zone. The potential energy released by the downward movement of the large building mass far exceeded the capacity of the intact structure below to absorb that through energy of deformation.

Since the stories below the level of collapse initiation provided little resistance to the tremendous energy released by the falling building mass, the building section above came down essentially in free fall, as seen in videos. As the stories below sequentially failed, the falling mass increased, further increasing the demand on the floors below, which were unable to arrest the moving mass.

The falling mass of the building compressed the air ahead of it, much like the action of a piston, forcing material, such as smoke and debris, out the windows as seen in several videos.

NIST found no corroborating evidence for alternative hypotheses suggesting that the WTC towers were brought down by controlled demolition using explosives planted prior to September 11, 2001. NIST also did not find any evidence that missiles were fired at or hit the towers. Instead, photographs and videos from several angles clearly showed that the collapse initiated at the fire and impact floors and that the collapse progressed from the initiating floors downward, until the dust clouds obscured the view.

9.4 DISCUSSION AND SUMMARY

The results of structural analyses conducted in this study on components, subsystems, isolated exterior walls and cores, and global models of WTC 1 and WTC 2 showed that the collapses of the towers were initiated by the combined effects of the structural and insulation damage from aircraft impact and the subsequent intense fires.

The impact damage alone did not cause collapse of the towers, as they stood for a period of time, and collapse occurred after the fire-induced weakening of core, floor systems and exterior walls. Global analyses showed that both towers had substantial reserve capacity after the aircraft impact.

Similarly, the fires alone did not cause the collapse of the towers. In the absence of insulation damage, the weakening of the core columns and sagging of the floors sufficient to pull in on the exterior walls would not have occurred.

9.4.1 Structural Response to Impact Damage and Fire

All three major subsystems played a role in the structural collapse sequence for WTC 1 and WTC 2 as described herein.

Role of the Building Core

The core columns were designed to carry the building gravity loads and were loaded to approximately 50 percent of their capacity before the aircraft impact.

The core columns were weakened significantly by the aircraft impact damage and thermal effects. Thermal effects dominated the weakening of WTC 1. As the fires moved from the north to the south side of the core, the core was weakened over time by significant creep strains on the south side of the core. Aircraft impact damage dominated the weakening of WTC 2. Immediately after impact, the vertical displacement at the southeast corner of the core increased 6 in. (from 4 in. to 10 in.). With the impact damage, the core subsystem leaned to the southeast and was supported by the south and east floors and exterior walls.

Gravity loads redistributed from the core to the exterior faces primarily through the hat truss due to aircraft impact and thermal effects. The WTC 1 core carried 1 percent less loads after impact but 20 percent less after thermal weakening. The WTC 2 core carried 6 percent less loads after impact and 2 percent less loads after thermal weakening.

Additional axial loads redistributed to the exterior columns from the core were not significant (only about 20 percent to 25 percent on average) as the exterior columns were loaded to approximately 20 percent of their capacity before the aircraft impact.

Role of the Building Floors

The floors were designed to support occupancy loads and transfer them to the core and perimeter columns. They were also designed to act as horizontal diaphragms when the buildings were subject to high winds. In the collapse of the towers, the primary role of the floors was to provide inward pull forces after sagging that induced inward bowing of exterior columns (South face of WTC 1; East face of WTC 2).

The floors provided inward pull forces as they sagged significantly under thermal loads. However, the sagging floors continued to support their floor loads despite the dislodged insulation and extensive fires. Some truss seat connections with dislodged insulation at the exterior columns did fail and disconnect from the exterior wall under thermal loads. Floor disconnections increased the unsupported length of the exterior columns and distributed floor loads to adjacent truss seats. There were no inward pull forces where the floors were disconnected.

Role of Exterior Walls

Column instability over an extended region of the exterior face ultimately triggered the global system collapse as the loads could not be redistributed through the hat truss to the already weakened building core. In the area of exterior column buckling, loads transferred through the spandrels to adjacent columns and adjacent exterior walls. As the exterior wall buckled (south face for WTC 1 and east face for WTC 2), the column instability propagated to adjacent faces and caused the initiation of the building collapse.

The exterior wall instability was induced by a combination of thermal weakening of the columns, inward pull forces from sagging floors, and to a much lesser degree, additional axial loads redistributed from the core.

9.4.2 Structural Response to Fire Without Impact Damage

Without insulation to delay the heating of steel components, steel temperatures began to rise upon exposure to fires. Thermal expansion occurred as temperatures increased; members restrained against thermal expansion increased in compressive load and may have caused a local or global load redistribution, depending upon the compressive load increase and extent of heating. Once steel temperatures exceeded 500 °C to 600 °C, the steel experienced significant reductions in stiffness and strength. The thermal analysis found that temperatures of floor trusses and columns with intact insulation rarely exceeded 400 ˚C during Case B fires (100 min long) for WTC 1 and 500 ˚C during Case D fires (60

min long) for WTC 2 . Insulated floors thermally expanded, pushed outward on the exterior columns, and sagged in the full floor analyses, but the floor sag was insufficient to exert an inward pull on the exterior columns.

Steel members with dislodged insulation were found to have temperatures greater than 600 ˚C and often higher than 800 ˚C within 10 min to 15 min after exposure to a nearby fire. Fire exposures considerably longer than the 60 to 100 min exposure in WTC 2 and WTC 1, respectively, were required for insulated members to reach these temperatures. Reductions in modulus of elasticity, yield strength, and ultimate tensile strength of steel in the WTC towers were predicted to be 13 percent, 20 percent, and 10 percent, respectively, at 400 ˚C, and 35 percent, 92 percent, and 80 percent, respectively, at 700 ˚C. Steel loses its strength significantly at 700 ˚C. At these temperatures, the long-span floors were found to sag sufficiently to exert and inward pull on the exterior walls, primarily due to buckling of truss web diagonal members. In addition, creep in steel columns becomes significant when the steel temperatures are greater than 500 ˚C and subject to high stresses for a period of time.

Inward bowing of an exterior wall was a necessary but not sufficient condition to initiate collapse. In both WTC 1 and WTC 2, significant weakening of the core due to aircraft impact damage and thermal effects was also necessary to initiate building collapse. The tower structures had significant capacity to redistribute loads (a) from bowed walls to adjacent exterior walls with short-span floors via the arch action of spandrels, and (b) between the core and exterior walls via the hat truss and, to a lesser extent, the floors. Without the impact damage, the towers' capacity to redistribute loads would have been even greater.

As shown in the analysis results, the temperatures in steel components without insulation damage were lower for the same fire. Lower temperatures resulted in reduced creep, plasticity, and buckling. Without insulation damage, floor sagging was insufficient to exert pull-in forces on the exterior wall; the core columns maintained their stiffness and strength; and the exterior wall did not bow inward. The lack of thermally induced damage would result in negligible load redistributions, and the towers would have remained stable.

9.4.3 Time to collapse

The difference in the time it took for each WTC tower to collapse was due primarily to the differences in structural damage, the time it took the fires to travel from the impact area across the floors and core to critical locations, and the time it took to weaken the core and exterior columns. WTC 2 had asymmetric structural damage to the core, including the severing of a corner core column, and WTC 1 had more symmetrical damage. The fires in WTC 2 reached the east side of the building more quickly, within 10 to 20 minutes, than the 50 to 60 minutes it took the fires in WTC 1 to reach the south side.

9.4.4 Comparison with Other Collapse Hypotheses

Alternate analyses and collapse hypotheses were performed and reported by other studies. A comparison of NIST and other hypotheses is presented to review assumptions, methodologies, and results. The comparison includes analyses performed by

- Northwestern University,

- Weidlinger Associates, Inc. with Hughes Associates and ArupFire,
- University of Maryland at College Park and the Israel Institute of Technology,
- Edinburgh University, and
- Arup.

The NIST structural response analyses included the effects of aircraft impact damage to the structure and thermal insulation, fire growth and spread, the resulting time-varying temperatures of the structural components, and the progression of local structural failure leading up to collapse initiation. The analyses included the effects of construction sequence, thermal expansion, plastic and creep strains, temperature-dependent material properties, and relevant failure modes for structural members and connections.

With the exception of the Weidlinger-led study, the analyses for the other collapse hypotheses presented here ignored impact damage, assumed time-temperature curves for structural subsystems (i.e. floor trusses and exterior columns), and conducted analyses of components or subsystems but did not conduct global analyses of the entire structure (i.e., core, floors, exterior walls, and hat truss) that considered all of the load redistribution paths as local members and subsystems were thermally weakened over time. The Weidlinger study included impact damage and assumed time-temperature curves for structural subsystems for their global analyses of each tower.

Northwestern University

The study performed by Northwestern University (Bazant 2002) was a simplified approximate analysis of the overall collapse of the WTC towers which addressed the question of why a total collapse occurred. The analysis addressed the results of prolonged heating which would have caused the columns of a single floor to lose their load carrying capacity and initiated the collapse of the building. The analysis assumed loss of thermal insulation during impact, uniform temperatures of 800 °C for a uniform column size and load across a single floor, and creep buckling and loss of load carrying capacity in over half of the columns. The analysis included evaluation of the dynamic amplification of the loads and the ability of the columns in the lower floors to dissipate the kinetic energy of the falling upper building mass through formation of plastic hinge mechanisms. The analysis found that the ratio of the kinetic energy of the upper building section dropping one floor to the deformation energy of plastic hinge rotation in the lower building columns was approximately a factor of eight.

The study by Northwestern did not address the details of impact damage, fire dynamics, or structural response of the towers. Rather, a generalized condition was assumed of heated columns, and the question of why there was total collapse was addressed. NIST agrees with the assessment of the tower's required structural capacity to absorb the released energy of the upper building section as it began to fall as an approximate lower bound. The likelihood of the falling building section aligning vertically with the columns below was small, given the observed tilting, so that the required capacity would be greater if interaction with the floors was also considered, as pointed out in the study.

Weidlinger Associates, Inc. with Hughes Associates and ArupFire

The study led by Weidlinger Associates, Inc. (Abboud 2003, Post 2002a, Post 2002b, Glanz 2002) used the SAP2000 and FLEX finite element code to calculate the aircraft impact damage to both towers and their structural response to damage and elevated temperatures. FLEX is an explicit, nonlinear, large deformation transient analysis finite element code for the analysis of structures subject to blast, impact, and shock loads. The fires were evaluated by Hughes Associates and ArupFire Inc. The fires were found to be less than fully developed office fires, with gas temperatures ranging from 400 °C to 700 °C in the impact regions and well ventilated regions near the exterior walls; exterior locations with persistent fires were assumed to have 1000 °C temperatures. Based upon study of smoke plumes and fire spread, it was concluded that the floors did not fail or have a significant role in the collapse of the towers. The structural response analysis found that the impact debris dislodged thermal insulation and that the hat truss played a significant role in transferring loads between the core and exterior walls. The analysis identified the specific cause of each towers' collapse to be the failure of core columns that either lost insulation or were destroyed during the aircraft impact. WTC 2 exterior columns on the east side began to fail first and redistributed loads to the core columns until the loads could no longer be supported, due to successive failures of core columns. WTC 1 core columns began to fail first due to damage and thermal weakening and attempted to redistribute loads to the exterior walls through the hat truss. WTC 2 was found to collapse first primarily because the damage was off-center and compromised the southeast corner of the core.

NIST agrees with many of the findings by the Weidlinger Associates, Inc. led study. However, there were some differences in the modeling approach and assessment of contributing factors. The most significant difference was that the floors were not analyzed for their response to fire, so that the collapse hypothesis did not account for floor sag and its contribution to inward bowing of the exterior columns. The reason for WTC 2 collapsing before WTC 1 was attributed to the off-center damage, particularly the damage to the southeast corner core column. NIST found that in addition to the differences in impact damage between the two towers, the time it took the fires to travel from the impact area across floors and the core to critical areas, and the time it took for the core and exterior columns to become thermally weakened, also contributed to the difference in times to collapse initiation.

University of Maryland and Israel Institute of Technology

The study performed by the University of Maryland and the Israel Institute of Technology (Quintiere 2002) was based upon a thermal conduction analysis of truss web members subjected to a uniform gas temperature and a structural failure analysis based on buckling of the truss web member due to a temperature-induced reduction in stiffness. Gas temperatures were estimated to be approximately 900 °C for the duration of the fires in each tower. A thermal conduction analysis of web members was conducted to estimate the temperature of the web member as a function of time and insulation thicknesses (0.75 in. and 1.5 in.). A web member with an assumed load was calculated to buckle when temperatures of about 630 °C to 770 °C were reached, due to a reduced modulus of elasticity. The time at which the insulated members reached temperatures that met the buckling criteria fell within the observed collapse time of each tower. It was noted that a bare steel web member would fail by this criteria in 10 min to 15 min, and that this time did not match the observed time to collapse initiation. Given the failure of truss web members, it was postulated (not supported by calculations) that the floors would sag and fail at their connections to the columns and that progressive collapse would ensue as the floors below also failed.

NIST findings differed from those given in this study. NIST also found that web members in the floor trusses buckled when heated sufficiently, which led to sagging of the floor, but did not find appreciable floor sagging when the truss insulation remained intact. The Maryland study suggested that the sagging floors resulted in failure of the floor to column connections; NIST analyses found that the sagging floors did not cause floor connections to fail, except at a few isolated locations, but rather produced an inward pull on the exterior walls. An inward pull of exterior columns would not occur if floor to column connections had failed. To produce the inward bowing of the exterior walls that was observed, the floors had to sag and exert an inward pull well before collapse initiated, not at the time of collapse as proposed in the Maryland study. Additionally, analysis of a floor collapsing onto a floor below, which was unlikely given the required event of all floor connections failing nearly at the same time, was not found to result in failure of the impacted floor.

University of Edinburgh

The University of Edinburgh study (Usmani 2003, Usmani 2005) performed a nonlinear, large displacement finite analysis of a typical 2D slice of the tower structure that encompassed twelve floors around the impact level of WTC 1 using ABAQUS. However, there were also some simplifying assumptions to reduce the model complexity, such as restraining lateral movement of the floor at the core end and a pinned connection to the external columns at the other end. The truss diagonals were modeled with a single axial element and connections were not explicitly modeled. It was assumed that the core columns were relatively cool and that the collapse would initiate at the exterior columns. A generalized exponential curve represented the time-temperature relationship, and assumed temperature profiles were applied to the floors for various fire scenarios. The exterior columns were linearly ramped from ambient temperatures. The analysis found that the heated floors expanded and pushed the exterior columns outward and that the outward movement was resisted by tension in the cool floors above and below the fire floors. The analysis also found that a floor buckled at 400 °C, causing the exterior column to ‘rebound’, resulting in large compressive loads on the floors above and below, which in turn buckled. It was stated that the same mechanism propagated to adjacent floors until it was arrested or caused collapse. Consideration of the hat truss, its capacity for redistribution of loads between the exterior walls and core, and its role in delaying the collapse mechanism until the structure’s redistribution capacity was exhausted was discussed, but no supporting analyses were presented. These results were cited as a possible fire-induced collapse mechanism for a tower without impact damage that was based on thermal expansion rather than fire-induced loss of strength and stiffness.

NIST findings also differed from the findings of the University of Edinburgh study. NIST included thermal expansion in its detailed analyses of full floor systems, and did not find that buckling of any floor system occurred. Rather, as truss web members began to buckle, the floors began to sag, which increased over time. The sudden buckling of the first floor in the Edinburgh analysis, followed by the sudden subsequent failure of floors above and below, does not match the observed inward bowing of the exterior walls which increased over time. Further, NIST found that failure of an exterior wall was necessary but not sufficient to initiate the collapse of either tower. In both WTC 1 and WTC 2, significant weakening of the core due to aircraft impact damage and thermal effects was also necessary to initiate building collapse.

Arup

The study by Arup (Lane 2005) was conducted to determine if the WTC towers had any collapse mechanisms specific to their structural system features. Based upon information available through presentations, studies included 2D analysis of a twelve-floor slice of the exterior column and floors to the core, a twelve-floor slice across the entire tower (from exterior column to exterior columns), and 3D quarter floor, half floor, and quarter-floor seven-story section models. None of the models included the hat truss; all of the models included individual floor trusses and the floor slabs. Temperatures from the fires for structural members were assumed, where the floor trusses reached 800 °C in a "very short time", the exterior columns and spandrels heated linearly to 400 °C by 3600 s. Slab temperatures were not reported. Three floors were heated to 800 °C, the floors sagged and the exterior wall section was pulled inward. The inward bowing of the exterior wall was considered to be a collapse mechanism for the towers. Arup stated that the behavior was calculated for the duration of the fire with no user intervention and without inclusion of any aircraft impact damage, including damage to thermal insulation.

The description of Arup analyses is based on presentations since no published reports by Arup were available prior to the release of this report. The study by Arup found that the composite truss floors sagged as they were heated and pulled inward on the exterior wall, similar to the findings by NIST. However, the NIST analyses did not find uniform temperatures across an entire floor nor simultaneously on multiple floors, as assumed in the Arup analyses. Further, NIST did not find any insulated truss members reaching temperatures of 800 °C prior to the collapse of either tower. NIST thermal analyses showed that steel temperatures in areas where the insulation remained intact rarely exceeded 400 °C in WTC 1 and 500 °C in WTC 2. The Arup 3D seven-floor model did not include load transfer mechanisms, including the hat truss, the core, and sufficient portions of the exterior wall to provide the arching action observed in the impact faces. NIST found that failure of an exterior wall was necessary but not sufficient to initiate the collapse of either tower. In both WTC 1 and WTC 2, significant weakening of the core due to aircraft impact damage and thermal effects and redistribution of loads between the core and exterior wall were found to be necessary to initiate building collapse.

9.4.5 Factors that Affected Performance

From the collective knowledge and insights gained through the Investigation of the collapse of the WTC towers, the following factors were identified that affected performance of both towers on September 11, 2001:

- The closely spaced columns, along with deep short spandrels, allowed a redistribution of loads as a result of aircraft impact damage to the exterior wall.
- Because there was effectively no wind on the morning of September 11, 2001, the capacity of the exterior wall provided to accommodate design wind loads was available to carry redistributed gravity loads.
- The large dimensional size of the WTC towers helped the buildings withstand the aircraft impact.
- The composite floor system with primary and bridging trusses forming a 2-way grid, and the two layers of welded wire fabric in the slab, acted to bridge over damaged areas without

propagation of collapse from areas of aircraft impact damage to other locations, thereby avoiding larger scale floor collapse upon impact.

- The hat truss played a major role in the post-impact performance of the building. This was accomplished through redistribution of the loads from the significant weakening of the core, due to aircraft impact damage and subsequent thermal effects, by redistributing loads from the damaged core columns to adjacent intact columns and, ultimately, by redistributing loads to the exterior walls from the thermally weakened core columns that lost their ability to support the buildings' weight.

- The buildings would likely not have collapsed under the combined effects of aircraft impact and the subsequent jet-fuel ignited multi-floor fires, if the insulation had not been dislodged or had been only minimally dislodged by aircraft impact. The existing condition of the insulation prior to aircraft impact and the insulation thickness on the WTC floor system did not play a significant role in initiating collapse on September 11, 2001.

9.5 REFERENCES

Zdenek Bazant and Yong Zhou (2002), *Why Did the World Trade Center Collapse?–Simple Analysis*, Journal of Engineering Mechanics, Vol. 128, No. 1

Abboud, Najib et.al., (2003), Anatomy of a disaster: A structural investigation of the World Trade Center collapses, Proceedings of the Third Congress Forensic Engineering, San Diego, CA, United States, Oct 19-21 2003, p 360-370

Nadine Post (2002a), Report Ties WTC Collapses to Column Failures, Engineering News Record, McGraw Hill Construction, 10/25/2002

Nadine Post (2002b), Study Absolves Twin Tower Trusses, Fireproofing, Engineering News Record, McGraw Hill Construction, 11/04/2002

James Glanz and Eric Lipton (2002), In Data Trove, A Graphic Look at Towers' Fall, The New York Times, October 29, 2002

J.G. Quintiere, M. di Marzio, and R. Becker (2002), A suggested cause of the fire-induced collapse of the World Trade Towers, Fire Safty Journal, Vol. 37, Issue 7, October 2002, p 707-716.

A.S. Usmani, Y.C. Chung, and J.L. Torero (2003), How did the WTC towers collapse: a new theory, Fire Safety Journal, vol 38, Isue 6, October 2003, p 501-533.

A.S. Usmani (2005), Stability of the World Trade Center Twin Towers Structural Frame in Multiple Floor Fires, Journal of Engineering Mechanics, Vol. 131, No. 6, Jun 2005, p 654-657.

B. Lane (2005), Comments on structural fire response and collapse analysis, Presentation given at the Technical Conference on the Federal Building and Fire Safety Investigation of the World Trade Center (WTC) Disaster, National Institute of Standards and Technology (NIST), Gaithersburg, Maryland, September 13-15, 2005, http://wtc.nist.gov

This page intentionally left blank.

Chapter 10
FINDINGS

There were many facets to the work reported herein. First, the thickness of the passive fire protection was established from recorded measurements and interpretation of photographs of the originally applied SFRM. This information was used, along with statistical analysis and thermal structural analyses, to establish the thickness of passive fire protection (insulation or fireproofing) to be used in finite element thermal analyses. Next, standard fire resistance tests were conducted to establish the appropriate classification (fire resistance rating) of the original design of the WTC floor system and structural performance of the floor system in standard fires for insight into performance in actual fires. Characterization of the temperatures of the structural components, determined from simulated WTC fires, allowed the calculation of the performance of major subsystems constituting the structural system of the towers. In turn, insights obtained from these analyses were used to formulate and execute global analyses to analyze the collapse sequence of each tower. The structural analyses results were guided, and where possible validated, by observations made from the review of thousands of photographs and video recordings. This chapter reports the findings resulting from these efforts to characterize the conditions of the WTC towers before the attacks, their weakening due to the aircraft impacts, their subsequent response to the growth and spread of fires, and the progression of local failure that ultimately led to the total collapse of both towers.

10.1 PASSIVE FIRE PROTECTION

The passive fire protection applied to the steel structural components in the WTC towers was investigated to provide information on the in-place condition of the thermal insulation before and after the aircraft impact. The specified and as applied thicknesses,

condition (0.75 in. thick SFRM). The following findings are based on this series of four tests and a comparison of their results.

10.3.1 Structural Performance

Finding 6: Test assemblies, representative of the WTC floor system, exposed to the Standard Fire Test (ASTM E 119) conditions resulted in extensive sagging on the underside of the floor slab, thermal

10.4 RESPONSE OF STRUCTURAL COMPONENTS

The response of the structural components and their connections for the tenant floors and exterior walls was examined with detailed structural models. Results of the floor and exterior wall component and connection analyses identified structural behaviors and failure modes that were required for inclusion in the global analyses.

10.4.1 Floor System

Finding 15: The interior truss seats had a greater vertical shear capacity than the exterior truss seats. The controlling failure mode for vertical shear was weld fracture. However, the vertical load at the truss connection of approximately 16 kip had to increase by a factor of two to six to reach failure (weld fracture) for temperatures near 600 °C to 700 °C.

Finding 16: Detailed structural analysis of a single truss section of the composite floor system subjected to elevated uniform temperatures was found to initially push out on the exterior columns as a result of the concrete slab thermal expansion and then pull inward as the web diagonals buckled and the truss sag increased. The magnitude of the pull-in force was found to depend highly on the stiffness of the exterior box column which, in turn, depended on expansion of floors above and below.

Finding 17: Detailed analysis of the knuckles (shear connectors in the floor system for composite action) through test simulation and detailed truss analysis found that failure of the knuckles in the floor system was unlikely. This finding was also supported by the lack of any knuckle failures in the four standard fire resistance tests (ASTM E 119) of the floor truss assemblies with twice the floor load that was on the WTC floors.

10.4.2 Exterior Wall System

Finding 18: Large inelastic deformations and buckling of the spandrels at elevated temperatures were predicted, but were found not to significantly affect the stability of the exterior columns. Partial separations of the spandrel splices were also predicted at elevated temperatures, but were found not to significantly affect the stability of the exterior columns.

Finding 19: Analyses of bolted splices in the exterior columns found that the splice may slide or open when the exterior columns are bowing and subject to large lateral deflections. No column splice bolts were predicted to have failed.

Finding 20: An exterior wall section (9 columns wide and 9 floors high) was found to bow inward when the floor connections applied an inward pull force. For the condition where three sequential floors were disconnected, there was no bowing of the columns for five different elevated temperature conditions. When the column section with three disconnected floors was subjected to increased axial column loads, the wall section bowed outward over the unsupported column length.

10.5 FIRE PROTECTION AND PARTITION DAMAGE DUE TO AIRCRAFT IMPACT

The aircraft impact of the WTC towers caused extensive damage to the buildings' exteriors, penetrated into the interiors causing further damage to the structural systems, dislodged insulation, and ignited multi-floor fires. The structural damage to each tower resulting from the aircraft impact was estimated using a transient finite element analysis. Results of this analysis were used to predict damage to the structure, fireproofing, and partition walls in the path of the debris field.

Finding 21: For WTC 1, partitions were damaged and fireproofing was dislodged by direct debris impact over five floors (Floors 94, 95, 96, 97, and 98) and included most of the north floor areas in front of the core, the core, and central regions of the south floor areas, and on some floors, extended to the south wall. For WTC 2, partitions were damaged and fireproofing was dislodged by direct debris impact over six floors (Floors 78, 79, 80, 81, 82, and 83) and included the south floor area in front of the core, the central and east regions of the core, and most of the east floor area, and extended to the north wall.

Finding 22: The fireproofing damage estimates were conservative as they ignored possibly damaged and dislodged fireproofing in a much larger region that was not in the direct path of the debris but was subject to strong vibrations during and after the aircraft impact. A robust criteria to generate a coherent pattern of vibration-induced dislodging could not be established to estimate the larger region of damaged fireproofing.

10.6 OBSERVATIONS AND TIMELINE

Thousands of photographs and hours of video records were reviewed for insights into the structural performance of the towers. A timeline of significant events that characterized the weakening and eventual collapse of the WTC towers was developed with the photographs and videos that were time-stamped. Quantitative information, such as the amount of inward bowing observed on the exterior walls of the buildings, was extracted from key photographs through image enhancement and scaled measurements. Key observations and the timelines were used to guide the global collapse analyses.

10.6.1 WTC 1

Finding 23: Inward bowing of the south exterior wall was first observed at 10:23 a.m. The bowing appeared to extend between Floors 94 and 100 and Columns 305 and 359. The maximum bowing was estimated from images to be 55 in.±6 in. at Floor 97 on the east side of the south face of WTC 1. The central area in available images was obscured by smoke. The extent of fires observed on all faces of WTC 1 was similar, although somewhat more extensive on the east and west faces (where short span floors were located) and similarly extensive on the north and south faces (where long span floors were located). Inward bowing was observed only on the south face. The north face had extensive aircraft impact damage, and the damaged floors were not capable of imposing inward pull forces on the north face.

Finding 24: The time to collapse initiation was 102 minutes from the aircraft impact (8:46:30 a.m. until 10:28:22 a.m.).

Finding 25: From exterior observations, tilting of the building section appeared to take place near Floor 98. Column buckling was then observed to progress rapidly across the east and west faces.

Finding 26: The WTC 1 building section above the impact and fire area tilted to the south as the structural collapse initiated. The tilt was toward the side of the building that had the long span floors. Video records taken from east and west viewpoints showed that the upper building section tilted to the south. Video records taken from a north viewpoint showed no discernable east or west component in the tilt. A tilt to the south of at least 8 degrees occurred before dust clouds obscured the view and the building section began to fall downward.

10.6.2 WTC 2

Finding 27: On the east face and north face of WTC 2, draped objects were observed through the windows of floor 82 on the east face and floors 81 to 83 on the north face near the northeast corner. The draped objects appeared to be hanging floors. The drape of these objects was observed to increase with time and extend across approximately half of the east face.

Finding 28: Inward bowing of the east wall was first observed at 9:21 a.m. The inward bowing was approximately 10 in.±1 in. at Floor 80 and extended between Floors 78 and 83 and Columns 304 and 344. The remaining portion of the face to the south of Column 344 was not included in the image. The bowing appeared to extend over a large fraction of the east face and to be greatest near the center of the face. Fires were more extensive along the east face (where long span floors were located) and at the east side of the north and south faces (where short span floors were located). Fires were not observed on the west face (where long span floors were located). Inward bowing was observed only on the east face. The south face had extensive aircraft impact damage, and the damaged floors were not capable of imposing inward pull forces on the south face. There was no impact damage or fire on the west floors to cause pull-in forces on the west face.

Finding 29: An increase of the inward bowing of the east wall was observed at 9:53 a.m. The inward bowing appeared to extend between Floors 78 and 84 and Columns 305 and 341. The remaining portion of the face to the south of Column 344 was not included in the image. The maximum bowing was estimated from images to be 20 in.±1 in. at Floor 80 on the east face of WTC 1.

Finding 30: The time to collapse initiation was 56 minutes after aircraft impact (9:02:59 a.m. to 9:58:59 a.m.).

Finding 31: From exterior observations, tilt of the building section above the impact and fire area appeared to take place near Floor 82. Column buckling was then seen to progress across the north face.

Finding 32: The building section above the impact and fire area tilted to the east and south at the onset of structural collapse. The tilt occurred toward the east side with the long span floors. Estimates made from photographs indicate that there was approximately a 3 degree to 4 degree tilt to the south and a 7 degree to 8 degree tilt to the east prior to significant downward movement of the upper portion of the building. The tilt to the south did not increase any further as the upper building section began to fall, but the tilt to the east continued, reaching 20 degrees to 25 degrees before dust clouds obscured the view.

10.7 STRUCTURAL RESPONSE OF MAJOR TOWER SUBSYSTEMS

Prior to conducting the analysis of the global structural response of each tower, major structural subsystems were analyzed to provide insight into their behavior within the WTC global system. The three major structural subsystems, the core framing, a single exterior wall, and full tenant floors, were analyzed separately for their response to impact damage and fire. The hat truss was not analyzed separately as its structural behavior did not require significant simplification in the global analysis. The component analyses provided a foundation for these large, nonlinear analyses with highly redundant load paths, and they enabled a significant reduction in finite element model complexity and size. The major subsystem models used final estimates of impact damage and elevated temperatures determined from the aircraft impact analysis and the fire dynamics and thermal analyses.

10.7.1 Isolated Core Subsystem

Finding 33: The WTC 1 isolated core subsystem analysis found that the core structure was most weakened from impact and thermal effects at the center of the south side of the core. Smaller displacements occurred in the global model due to the constraints of the hat truss and floors.

Finding 34: The WTC 2 isolated core subsystem analysis found that the core structure was unstable for the estimated structural damage to core columns. The core was most weakened from impact and thermal effects at the southeast corner and along the east side of the core. Larger displacements occurred in the global model as the isolated core model had lateral restraints imposed that were somewhat stiffer than in the global model.

10.7.2 Full Floor Subsystem

Finding 35: Floor sagging was caused primarily by either buckling of truss web diagonals or disconnection of truss seats at the exterior wall or the core perimeter. Except for the truss seat failures near the southeast corner of the core in WTC 2 following the aircraft impact, web buckling or truss seat failure was caused primarily by elevated temperatures of the structural components.

Finding 36: Analysis results from both the detailed truss model and the full floor models found that the floors began to exert inward pull forces when floor sagging exceeded approximately 25 in. for the 60 ft floor span.

Finding 37: Sagging at the floor edge was due to loss of vertical support at the truss seats. The loss of vertical support was caused in most cases by the reduction in vertical shear capacity of the truss seats due to elevated steel temperatures.

10.7.3 Isolated Exterior Wall Subsystem

Finding 38: Inward pull forces were required to produce inward bowing that was consistent with displacements measured from photographs. The inward pull was caused by sagging of the floors. Heating of the inside face of the exterior columns also contributed to inward bowing.

Finding 39: The observed inward bowing of the exterior wall indicated that most of the floor connections were intact to cause the observed bowing.

Finding 40: The floors that were identified through analysis to be affected by the fires and the dislodged insulation matched well with the floors that were observed to have participated in the inward bowing of the exterior walls.

Finding 41: The extent of floor sagging required at each floor was greater than that predicted by the full floor models. The estimates of the extent of sagging at each floor were governed by the combined effects of insulation damage and fire; insulation damage estimates were limited to areas subject to direct debris impact. Other sources of floor and insulation damage from the aircraft impact and fires (e.g., insulation damage due to shock and subsequent vibrations as a result of aircraft impact or concrete slab cracking and spalling as a result of thermal effects) were not included in the floor models.

10.8 STRUCTURAL RESPONSE TO AIRCRAFT IMPACT DAMAGE AND FIRE

Global analysis of WTC 1 and WTC 2 used final estimates of impact damage and elevated temperatures to determine the structural response and sequence of component and subsystem failures that led to collapse initiation.

10.8.1 General Findings

Finding 42: The structural analyses of WTC 1 and WTC 2 found that the collapse of the towers was due to the combined effects of structural and insulation damage from aircraft impact and the subsequent fires on the core, floor systems, and exterior walls. The towers collapsed when the weakened core and exterior columns could no longer redistribute or support the building loads with their reduced load carrying capacity.

Finding 43: Impact damage alone did not cause collapse of the towers, as they were stable after the aircraft impact. Global analyses showed that both towers had substantial reserve capacity after the aircraft impact.

Finding 44: The multi-floor fires alone did not cause collapse of the towers. Without impact damage to the insulation, the structural steel temperatures would have been generally less than 200 °C to 300 °C, with a few isolated locations of structural steel temperatures exceeding 400 ˚C in WTC 1 floors and 500 ˚C in WTC 2 floors. The core would not have weakened, the floor sag would have been insufficient to pull inward on the exterior columns, and the exterior walls would not have bowed inward.

Finding 45: The towers would likely not have collapsed under the combined effects of aircraft impact and the subsequent multi-floor fires if the insulation had not been dislodged or had been only minimally dislodged by aircraft impact. Had insulation not been dislodged by the debris field, temperature rise of structural components would likely have been insufficient to induce global collapse. Structural components that became thermally weakened were generally determined by impact of the debris field. The existing condition of the insulation prior to aircraft impact and the insulation thickness on the WTC floor system did not play a role in initiating collapse of the towers.

Finding 46: Creep strain was significant in the core and exterior columns over the 56 min to 102 min period of fire exposure in columns with temperatures greater than 500 ˚C to 600 ˚C and high stress. Columns with creep strains of sufficient magnitude to cause column shortening played a significant role in the collapse initiation.

Finding 47: The faces of the buildings that exhibited inward bowing were associated with the long span direction of the floor system. The primary direction of tilting at collapse initiation for WTC 1 and WTC 2 was in the direction of the bowed faces.

10.8.2 Performance with Intact Fire Protection

Finding 48: A detailed thermal-structural analysis, which did not include slab delamination/spalling effects, showed that a full collapse of the WTC floor system would not occur even with a number of failed trusses or connections.

Finding 49: Most of the horizontal and vertical capacity of the floor connections to the exterior and core columns significantly exceeded the demand under design load conditions.

10.9 PROBABLE COLLAPSE SEQUENCES

The results of structural analyses conducted in this study on components, subsystems, isolated exterior walls and cores, and global models of WTC 1 and WTC 2 showed that the collapses of the towers were initiated due to the combined effects of the structural and insulation damage from aircraft impact and the subsequent intense fires. The probable collapse sequences for WTC 1 and WTC 2 are based upon the collective consideration of structural analyses, statistical based methods, observations, and laboratory testing.

10.9.1 Role of the Building Core

Finding 50: The core columns were weakened significantly by the aircraft impact damage and thermal effects. Thermal effects dominated the weakening of WTC 1. As the fires moved from the north to the south side of the core, following the debris damage path, the core was weakened over time by significant creep strains on the south side of the core. Aircraft impact damage dominated the weakening of WTC 2. Immediately after impact, the vertical displacement at the southeast corner of the core increased 6 in. (from 4 in. to 10 in.). With the impact damage, the core subsystem leaned to the southeast and was supported by the south and east floors and exterior walls.

Finding 51: As the core was weakened from aircraft impact and thermal effects, it redistributed loads to the exterior walls primarily through the hat truss. Additional axial loads redistributed to the exterior columns from the core were not significant (only about 20 percent to 25 percent on average) as the exterior columns were loaded to approximately 20 percent of their capacity before the aircraft impact.

10.9.2 Role of the Building Floors

Finding 52: The primary role of the floors in the collapse of the towers was to provide inward pull forces that induced inward bowing of exterior columns (south face of WTC 1; east face of WTC 2).

Finding 53: Sagging floors continued to support floor loads as they pulled inward on the exterior columns. There would have been no inward pull forces if the floors truss seats had failed and disconnected.

10.9.3 Role of Exterior Frame-Tube

Finding 54: Column instability over an extended region of the exterior face ultimately triggered the global system failure as the loads could not be redistributed through the hat truss to the already weakened building core. In the area of exterior column buckling, load transferred through the spandrels to adjacent columns and adjacent exterior walls. As the exterior wall buckled (south face for WTC 1 and east face for WTC 2), the column instability propagated to adjacent faces and caused the initiation of the building collapse.

Finding 55: The exterior wall instability was induced by a combination of thermal weakening of the columns, inward pull forces from sagging floors, and to a lesser degree, additional axial loads redistributed from the core.

10.9.4 Probable Collapse Sequences

Finding 56: Although the north face of WTC 1 had extensive impact damage, thermal weakening of the core columns on the south side of the core and inward bowing of the south face caused the building to tilt to the south at collapse initiation. The extent of fires observed on all faces of WTC 1 was similar, although somewhat more extensive on the east and west faces (where short span floors were located) and somewhat less extensive on the north and south faces (where long span floors were located). Thermal weakening of exterior columns with floor sagging (which induced inward pull and occurred on the south side) caused inward bowing of the south face and tilting in the south direction.

Finding 57: Although the south face of WTC 2 had extensive impact damage, thermal weakening of the core columns on the east side of the core and inward bowing of the east face caused the building to tilt more to the east and less to the south at collapse initiation. Fires were more extensive along the east face and at the east side of the north and south faces. Thermal weakening of exterior columns with floor sagging (which induced inward pull and occurred on the east side) caused inward bowing of the east face and primary tilting in that direction (with additional southward tilting due to the aircraft impact damage).

Finding 58: The time it took for each WTC tower to collapse was due primarily to the differences in structural damage, the time it took the fires to travel from the impact area across the floors and core to critical locations, and the time it took to weaken the core and exterior columns. WTC 2 had asymmetric structural damage to the core, including the severing of a corner core column, and WTC 1 had more symmetrical damage. The fires in WTC 2 reached the east side of the building more quickly, within 10 min to 20 min, than the 50 min to 60 min it took the fires in WTC 1 to reach the south side.

Finding 59: NIST found no corroborating evidence for alternative hypotheses suggesting that the WTC towers were brought down by controlled demolition using explosives planted prior to September 11, 2001. NIST also did not find any evidence that missiles were fired at or hit the towers. Instead, photographs and videos from several angles clearly showed that the collapse initiated at the fire and

impact floors and that the collapse progressed from the initiating floors downward, until the dust clouds obscured the view.

This page intentionally left blank.

Appendix A
SUMMARY OF AIRCRAFT IMPACT DAMAGE FOR INITIAL CASES 1 TO 4

WTC 1 CASE A_I – THERMAL INSULATION AND PARTITION DAMAGE FOR OCCUPANCY FLOOR

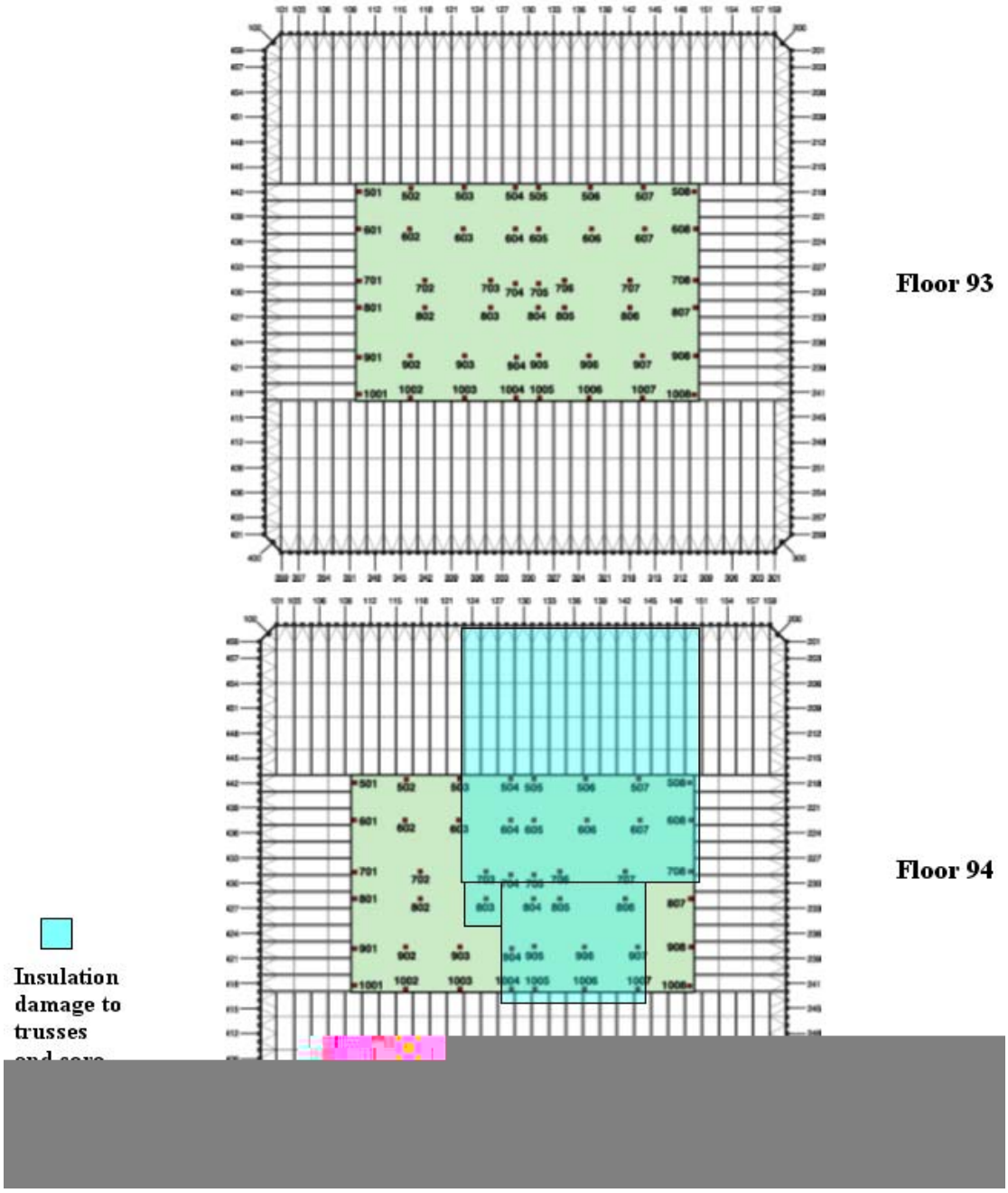

Figure A–1. WTC 1 Case A_i aircraft impact damage to Structural Floor 93 and 94.

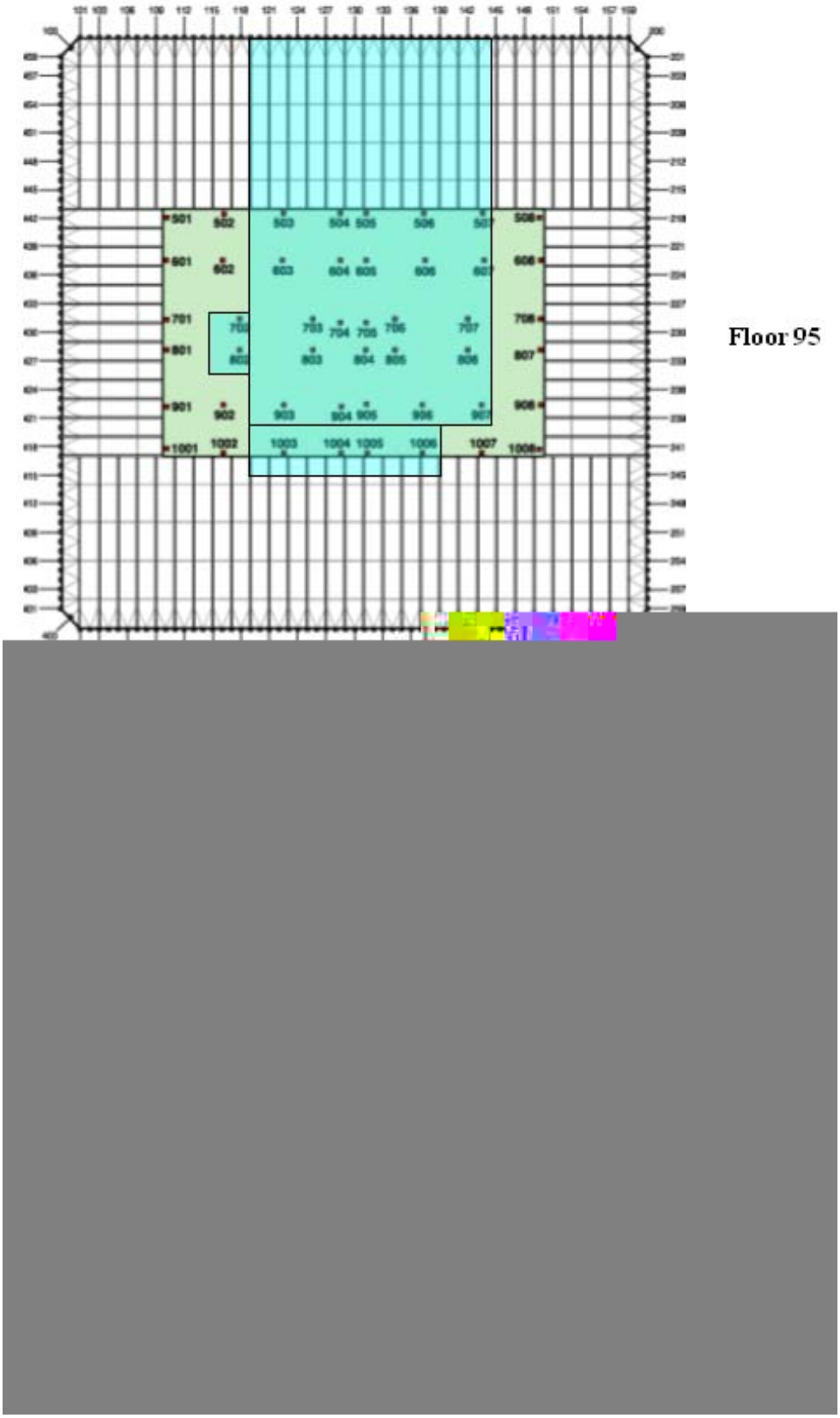

Figure A–2. WTC 1 Case A_i aircraft impact damage to Structural Floors 95 and 96.

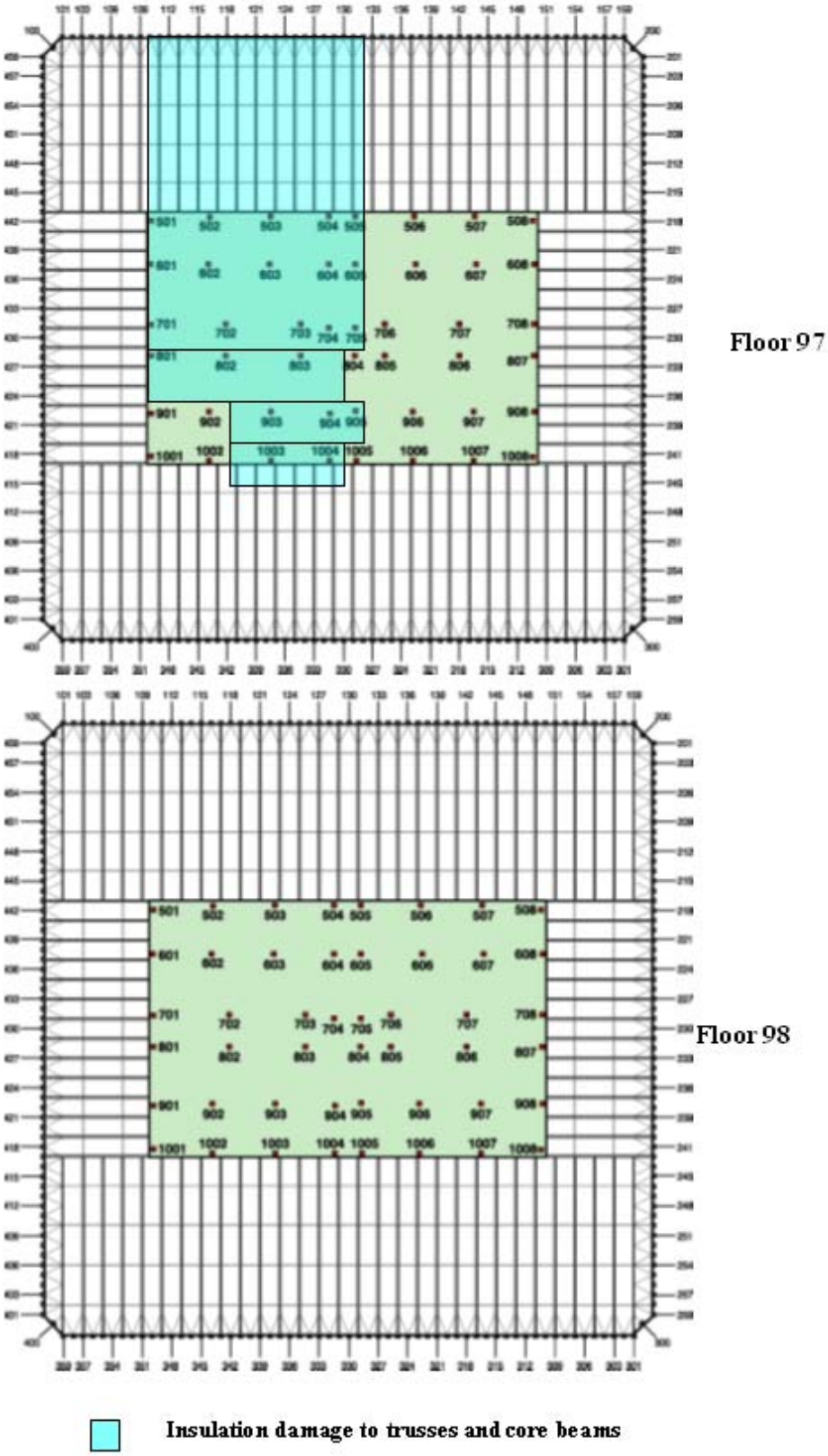

Figure A–3. WTC 1 Case A_i aircraft impact damage to Structural Floors 97 and 98.

WTC 1 CASE A_I – DAMAGE FOR STRUCTURAL FLOOR

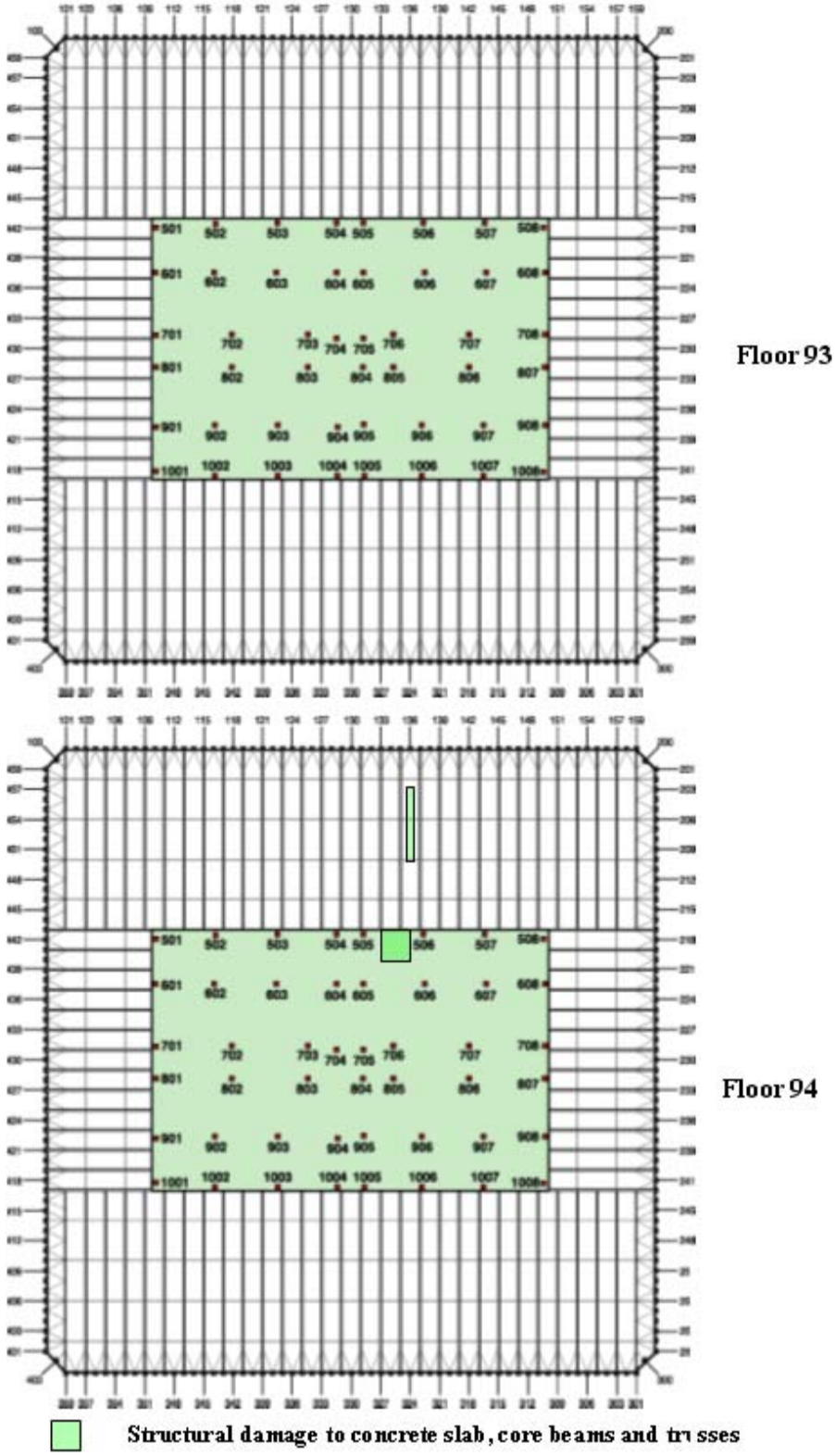

Figure A–4. WTC 1 Case A_i aircraft impact damage to Structural Floor 93 and 94.

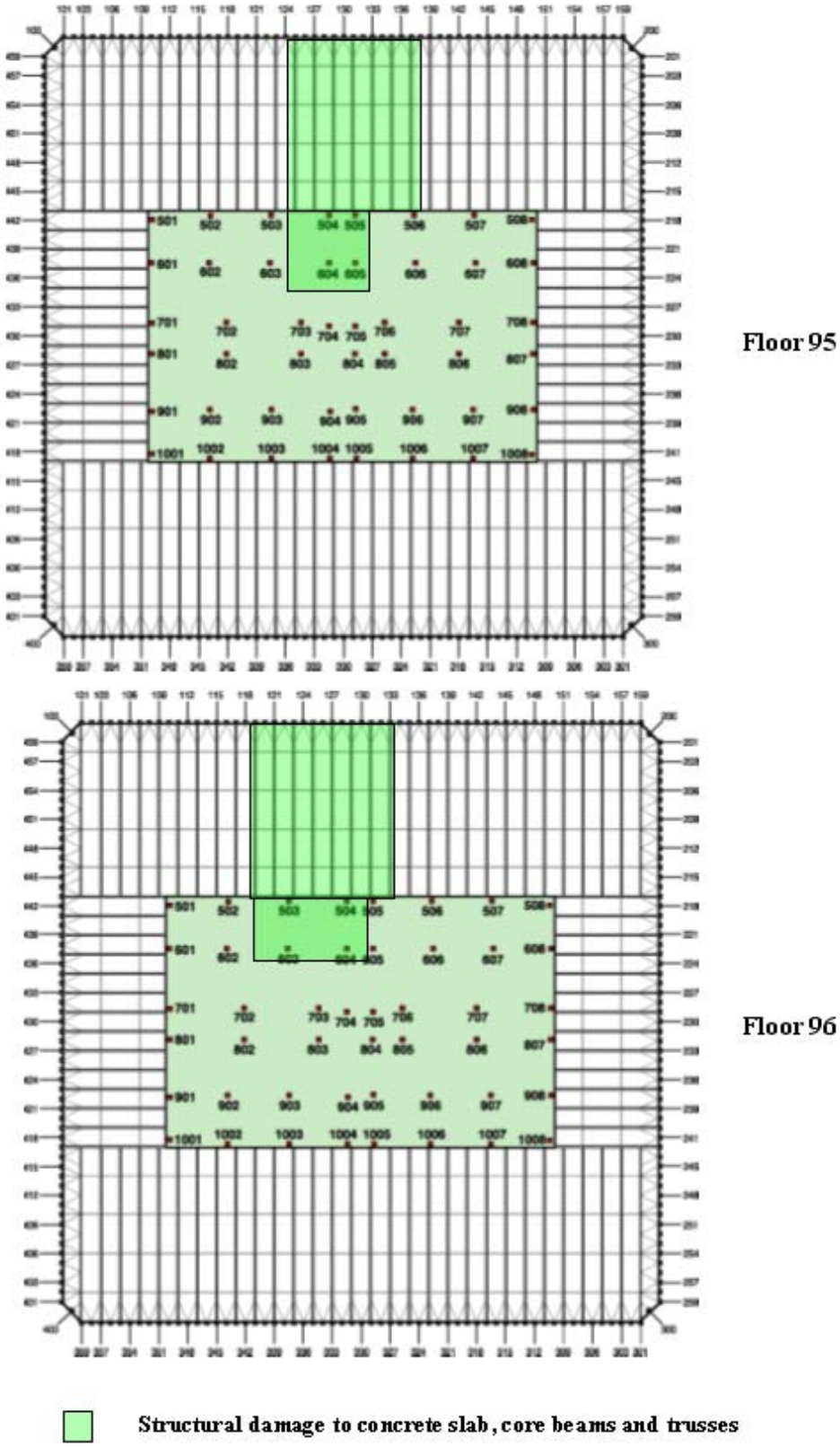

Figure A–5. WTC 1 Case A_i aircraft impact damage to Structural Floors 95 and 96.

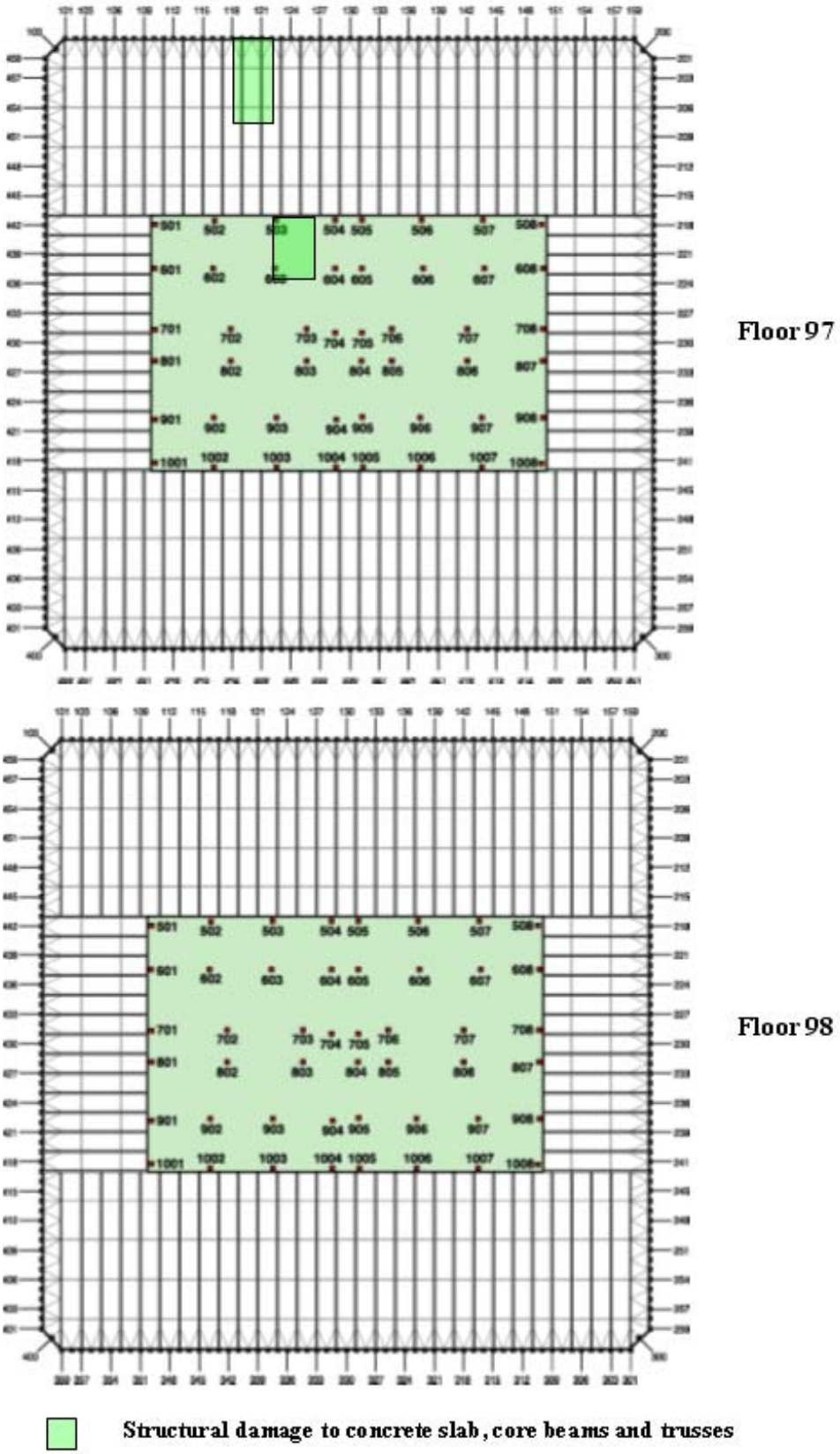

Figure A–6. WTC 1 Case A_i aircraft impact damage to Structural Floors 97 and 98.

WTC 1 CASE B_I – THERMAL INSULATION AND PARTITION DAMAGE FOR OCCUPANCY FLOOR

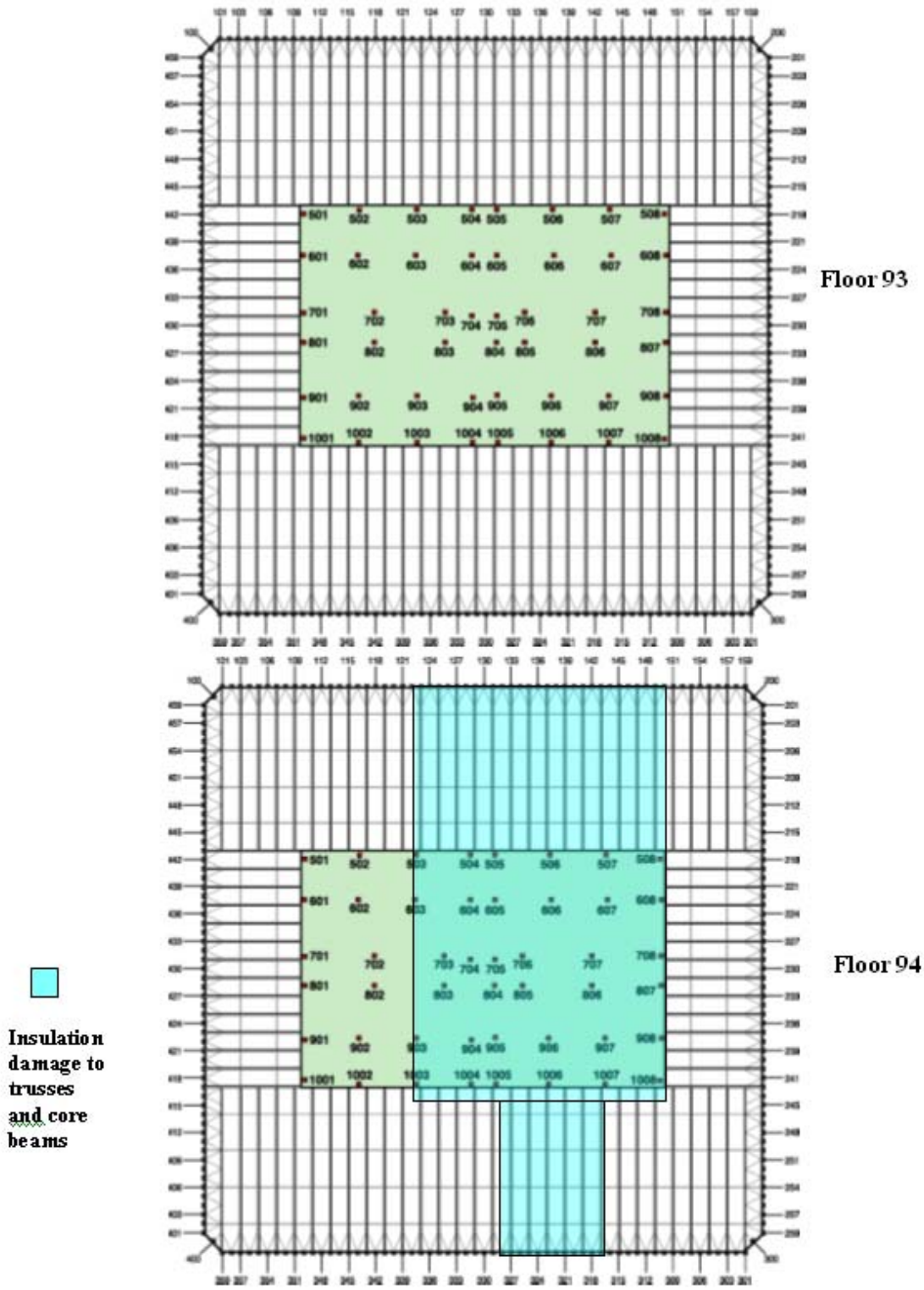

Figure A–7. WTC 1 Case B_i aircraft impact damage to Structural Floor 93 and 94.

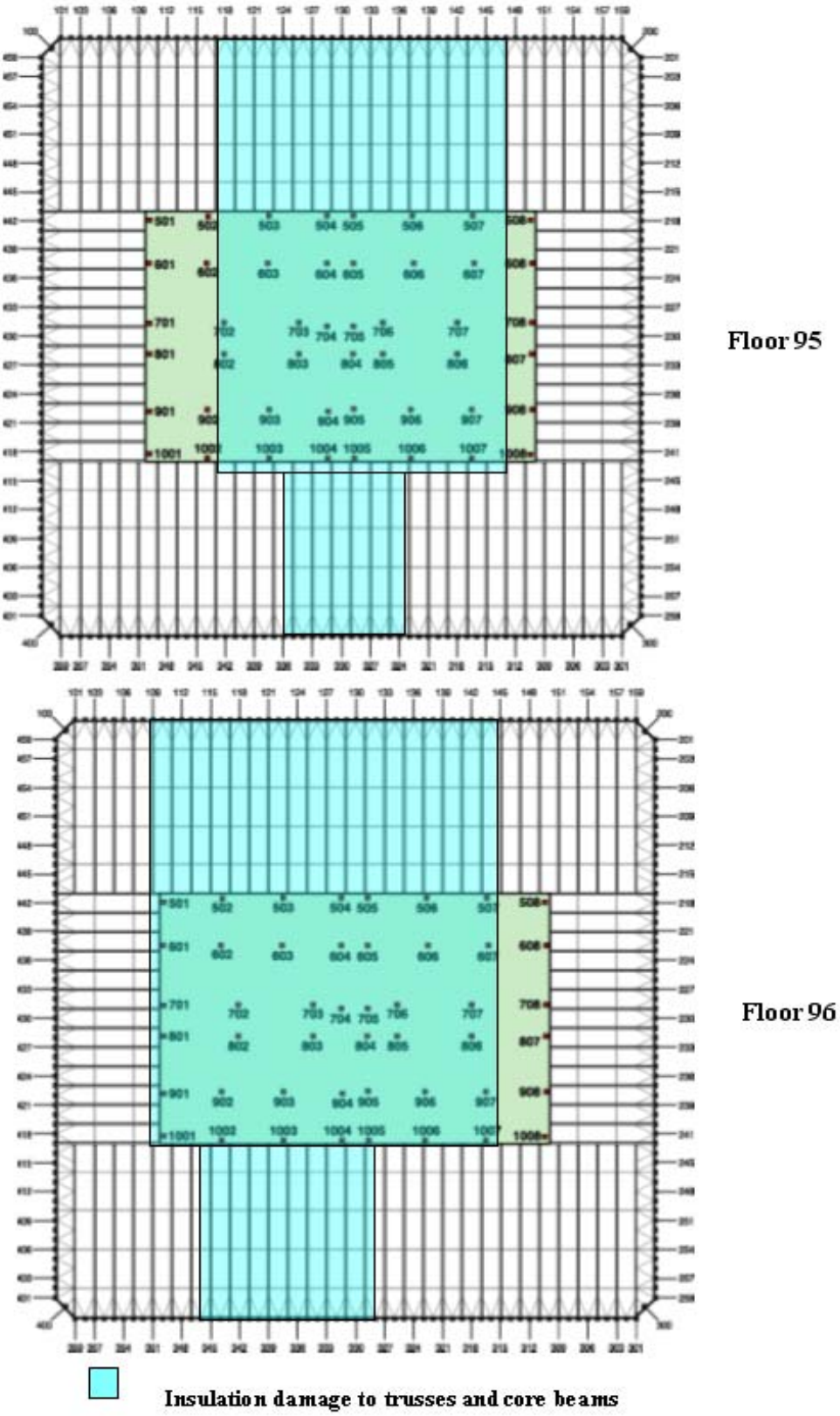

Figure A–8. WTC 1 Case B_i aircraft impact damage to Structural Floors 95 and 96.

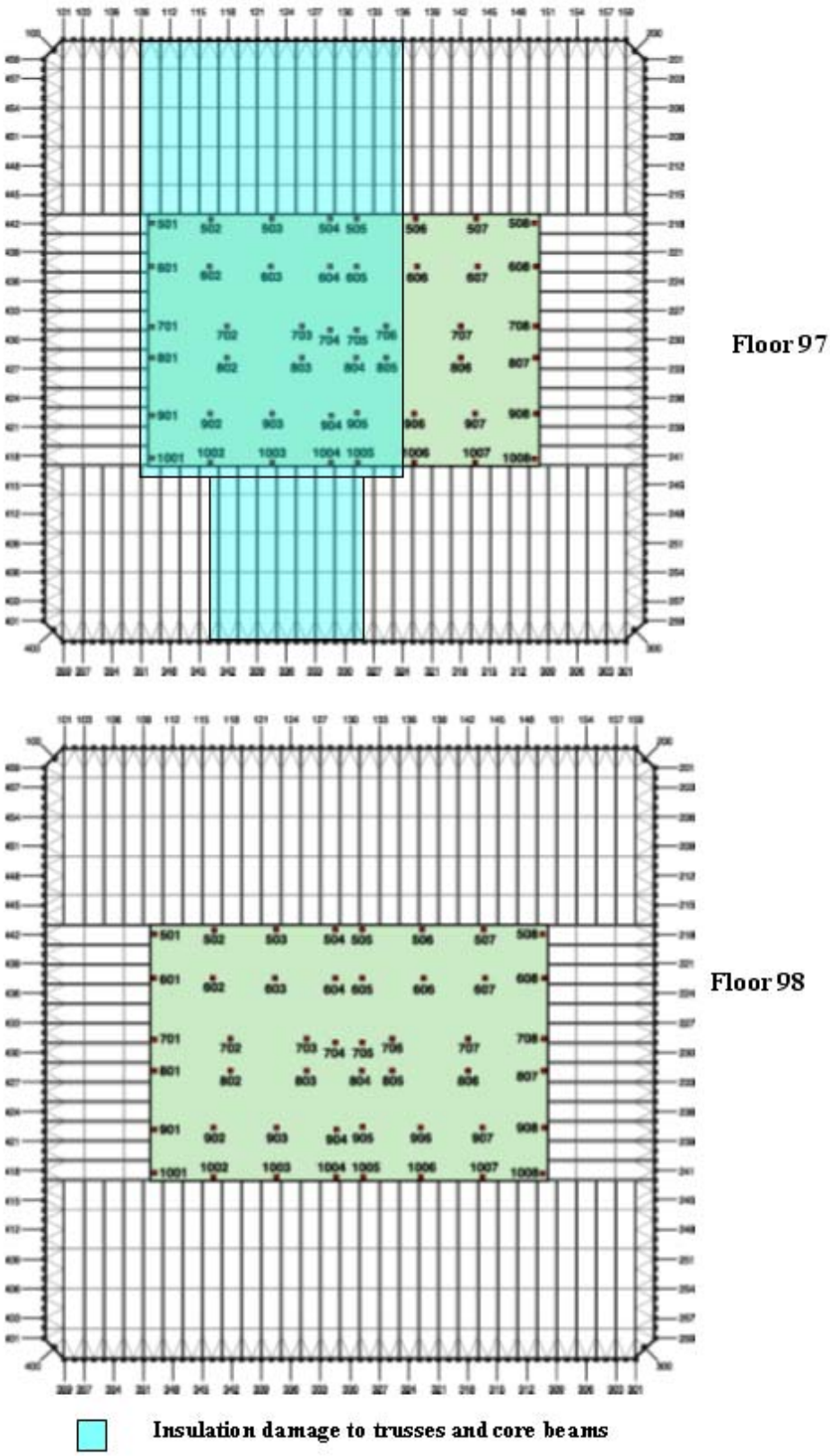

Figure A–9. WTC 1 Case B_i aircraft impact damage to Structural Floors 97 and 98.

WTC 1 CASE B_I – DAMAGE FOR STRUCTURAL FLOOR

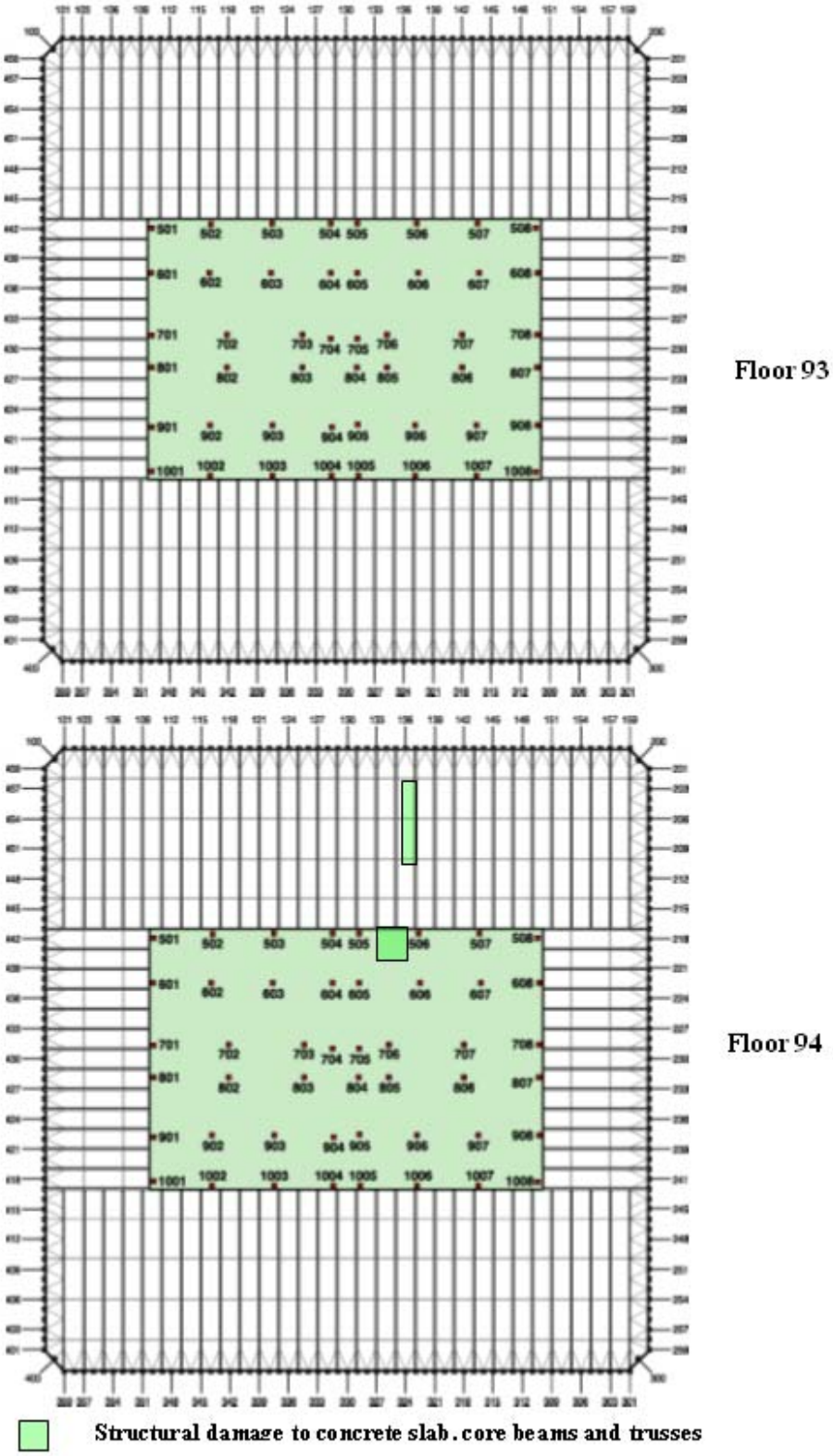

Figure A–10. WTC 1 Case B_i aircraft impact damage to Structural Floor 93 and 94.

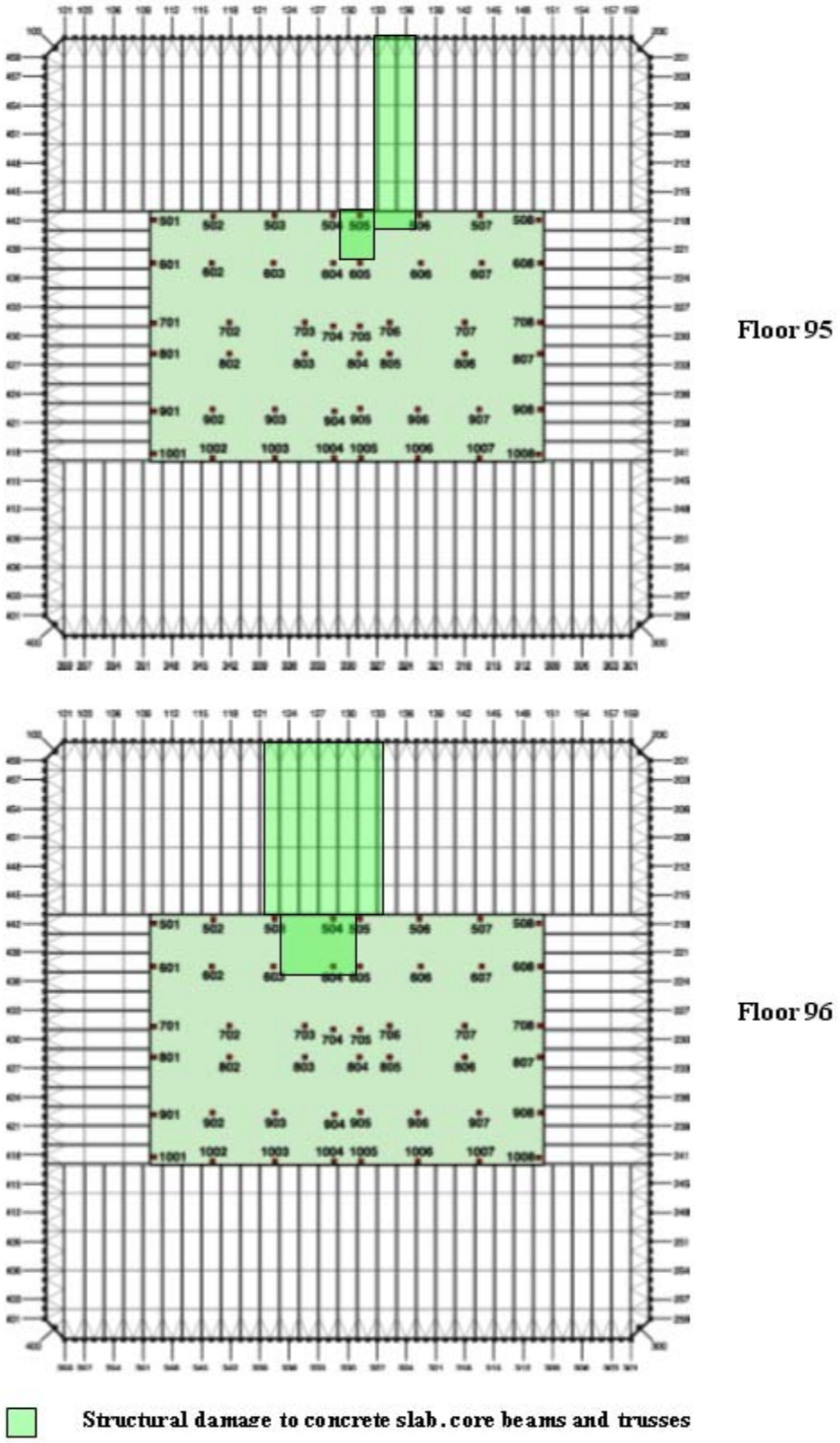

Figure A–11. WTC 1 Case B_i aircraft impact damage to Structural Floors 95 and 96.

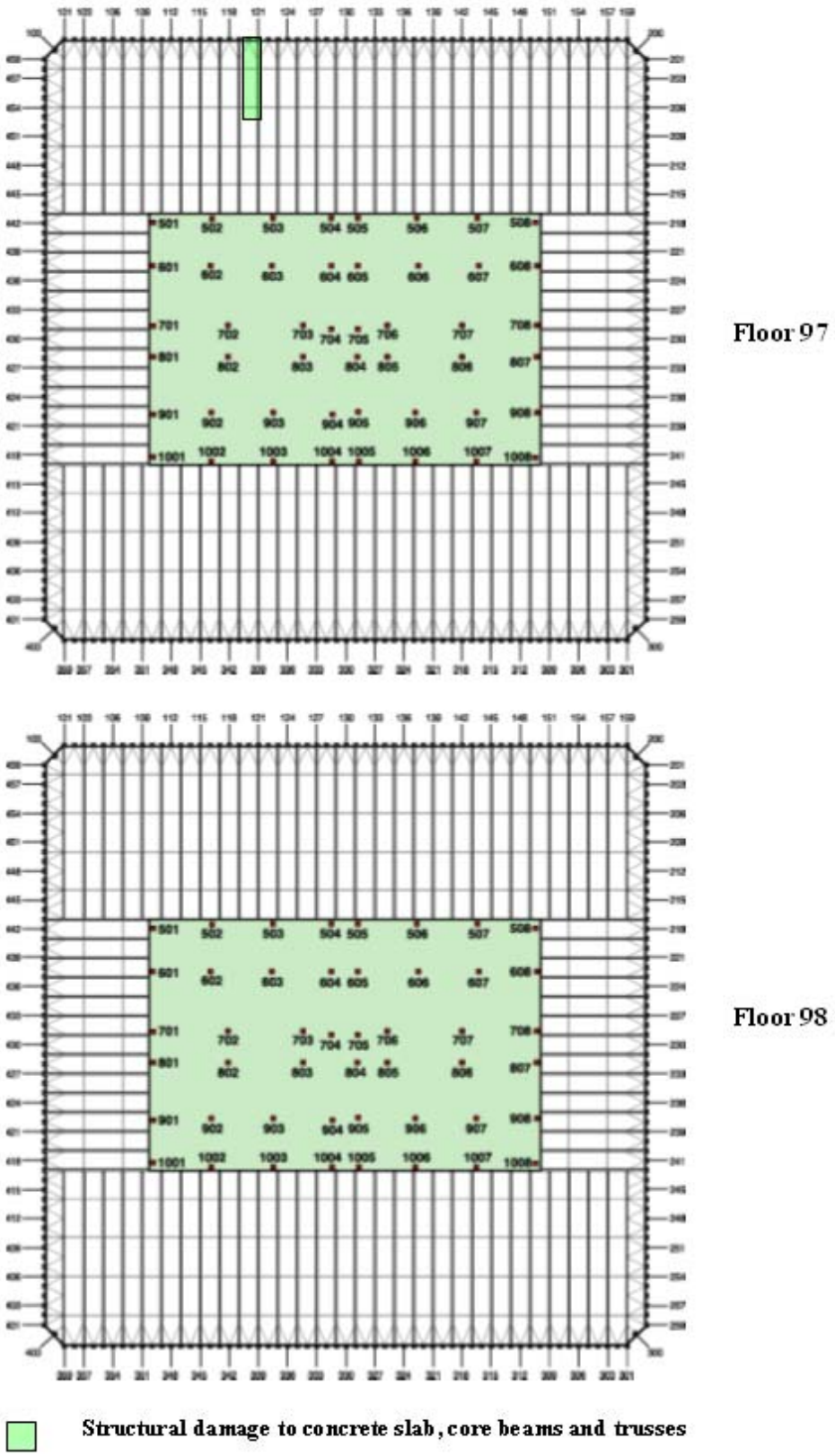

Figure A–12. WTC 1 Case B_i aircraft impact damage to Structural Floors 97 and 98.

WTC 2 CASE C_I – THERMAL INSULATION AND OCCUPANCY DAMAGE FOR OCCUPANCY FLOOR

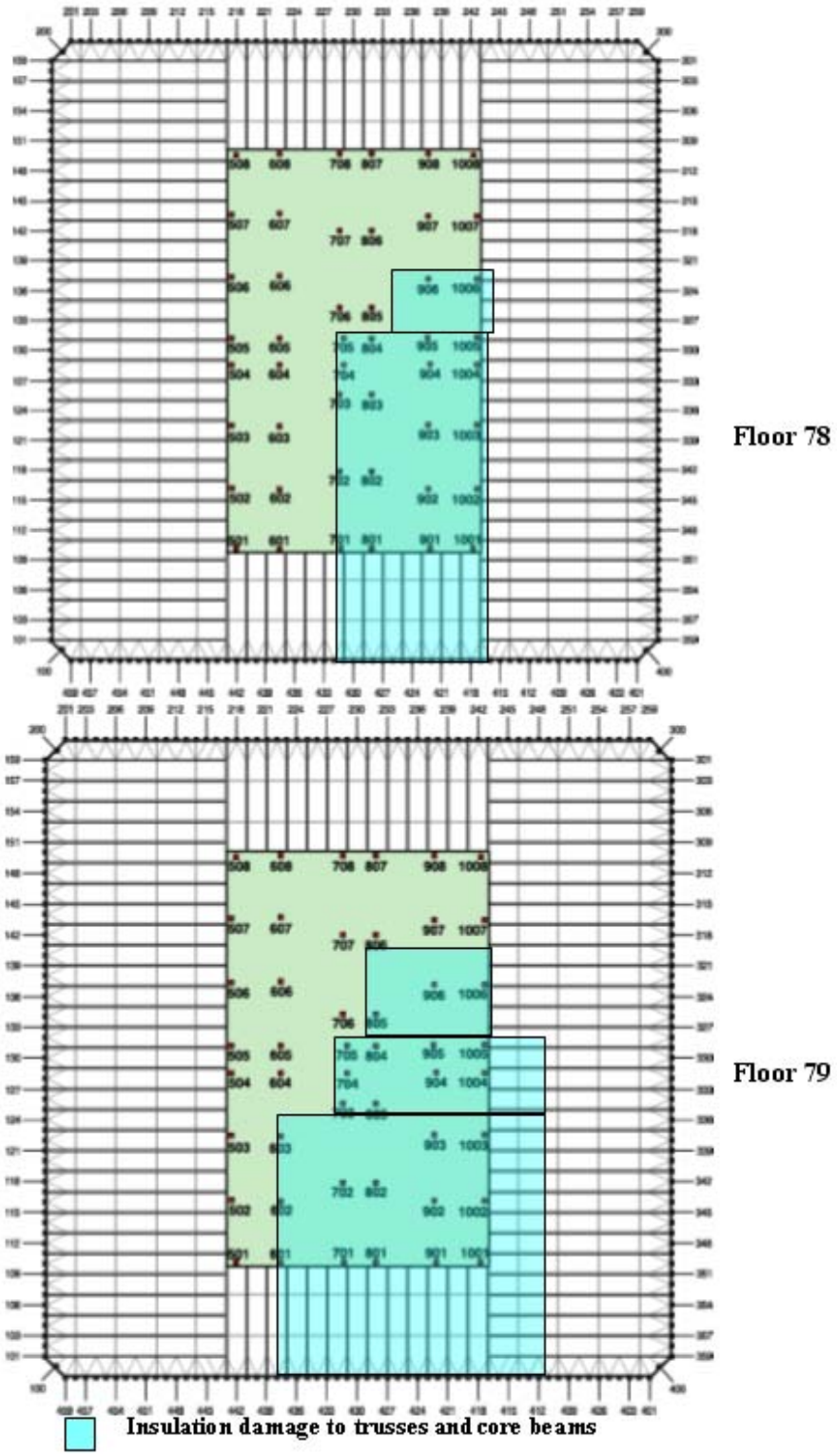

Figure A–13. WTC 2 Case C_i aircraft impact damage to Structural Floors 78 and 79.

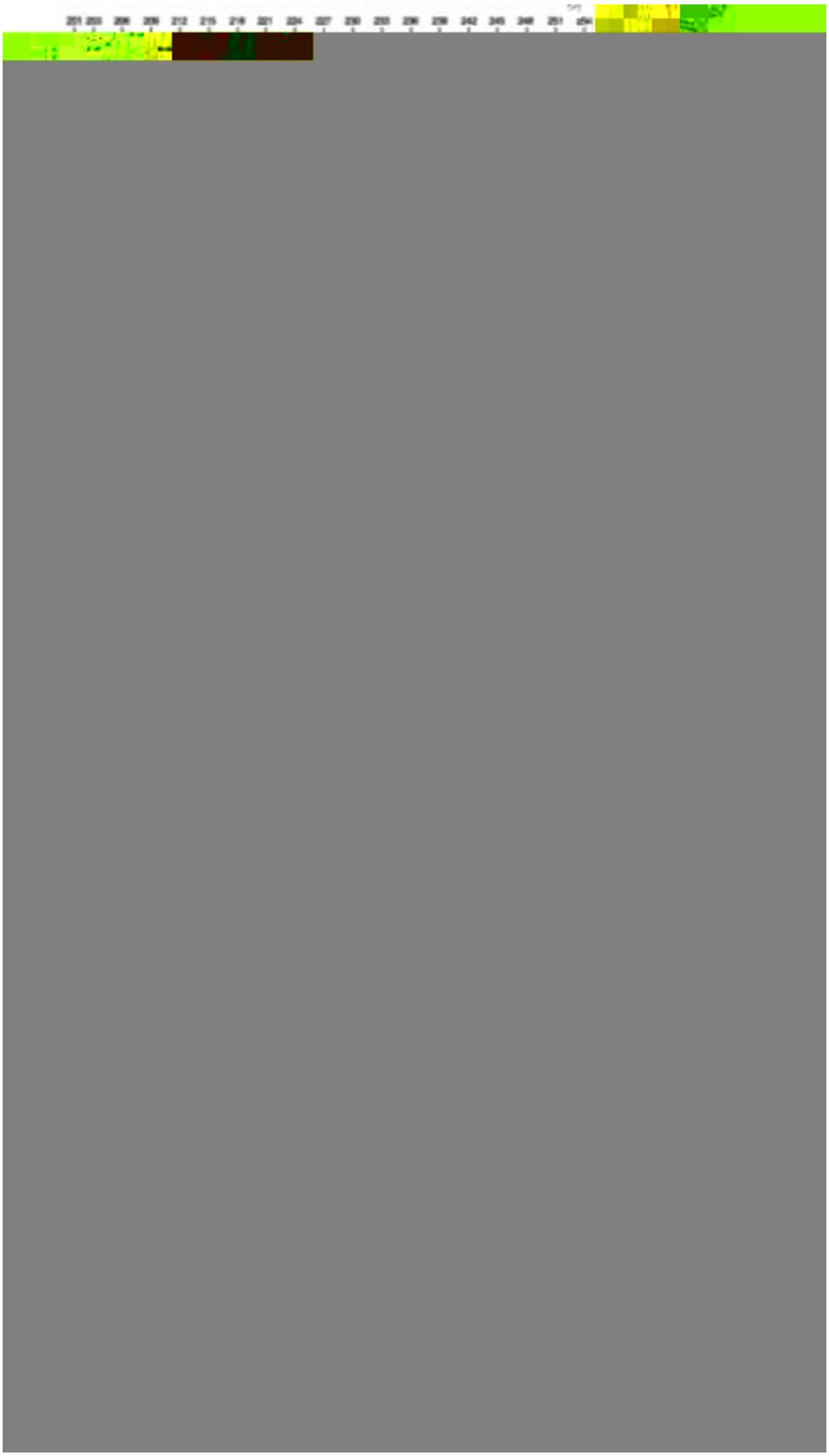

Figure A–14. WTC 2 Case C_i aircraft impact damage to Structural Floors 80 and 81.

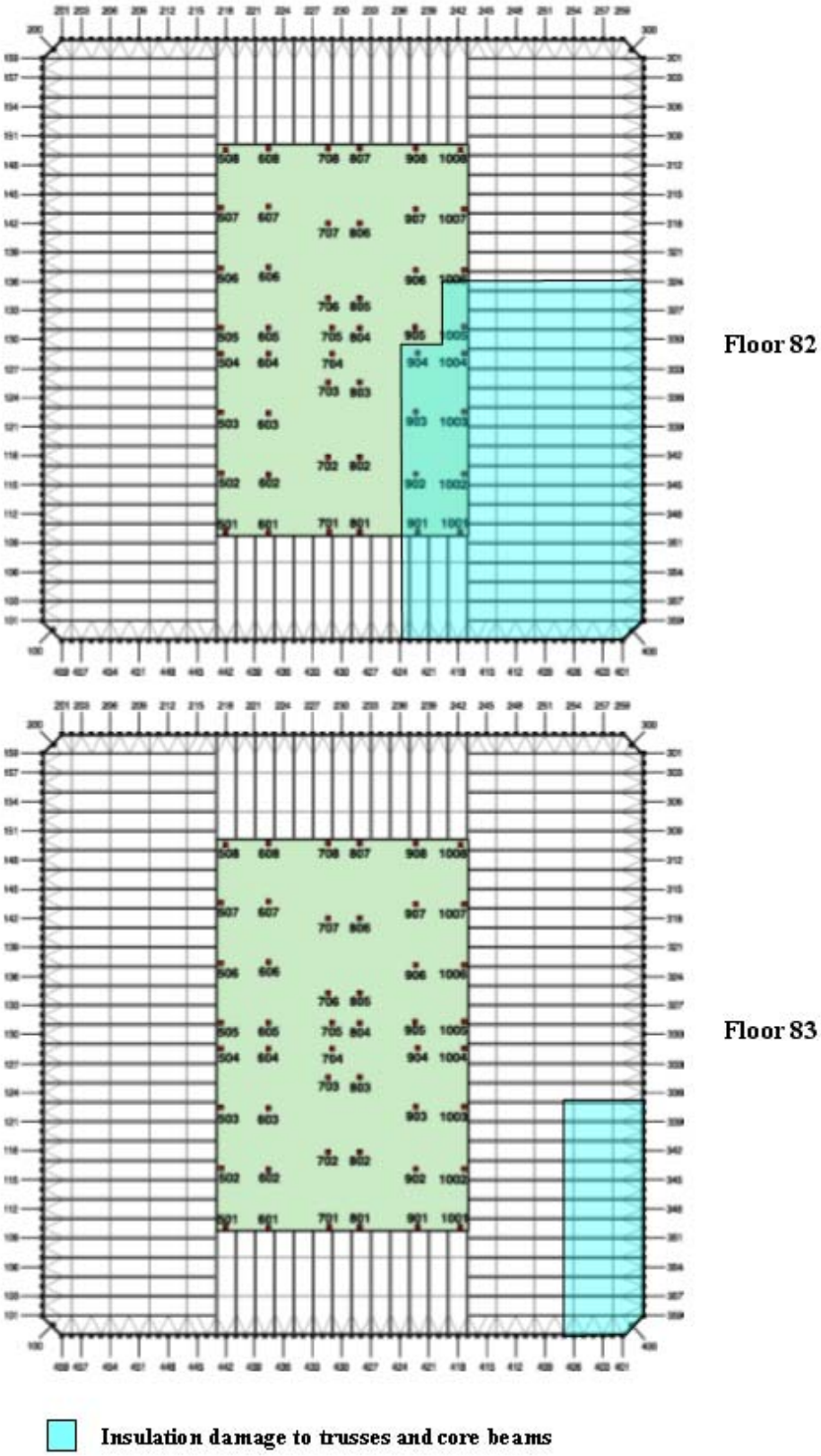

Figure A–15. WTC 2 Case C_i aircraft impact damage to Structural Floors 82 and 83.

WTC 2 CASE C_I – DAMAGE FOR STRUCTURAL FLOOR

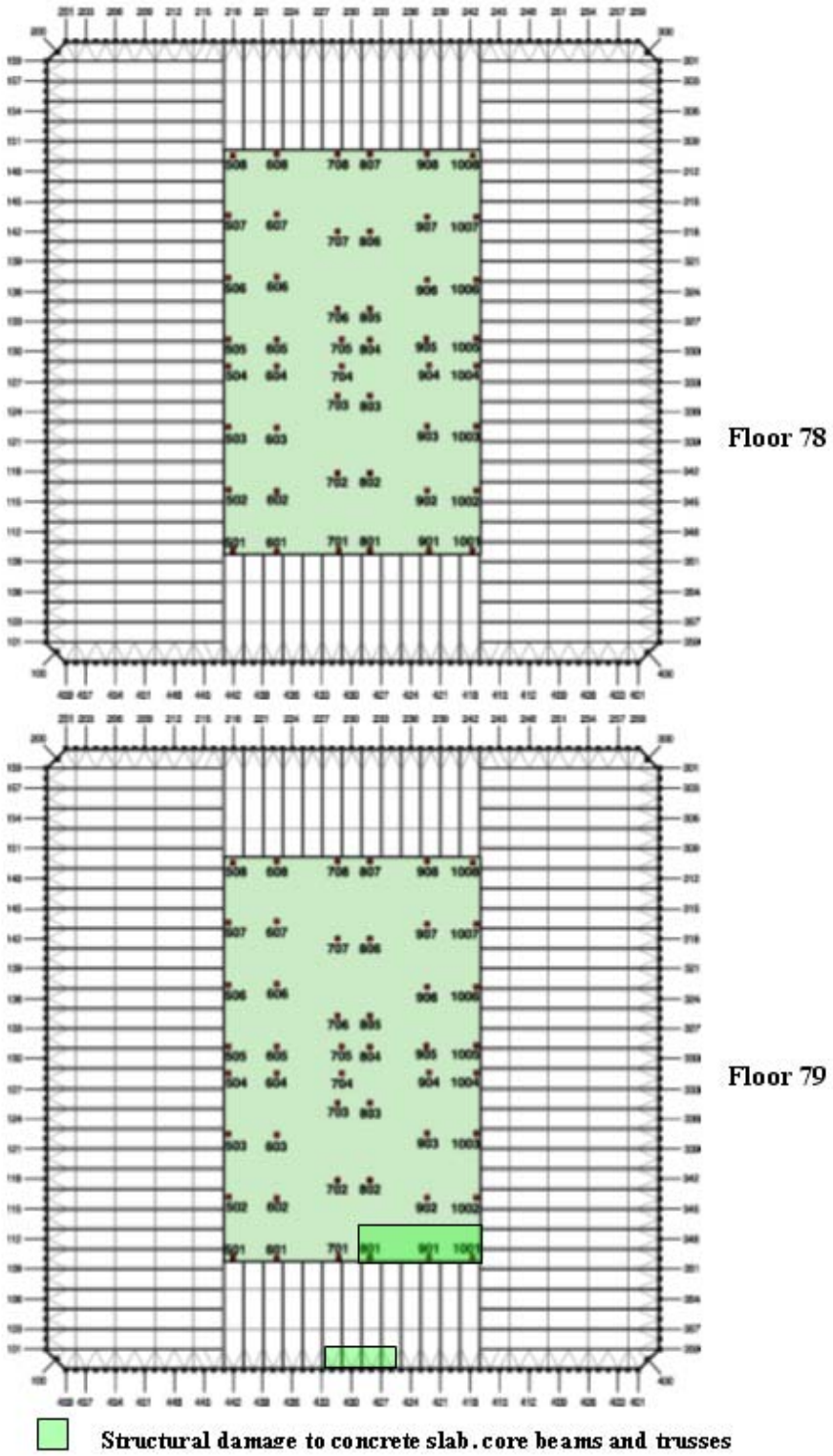

Figure A–16. WTC 2 Case C_i aircraft impact damage to Structural Floors 78 and 79.

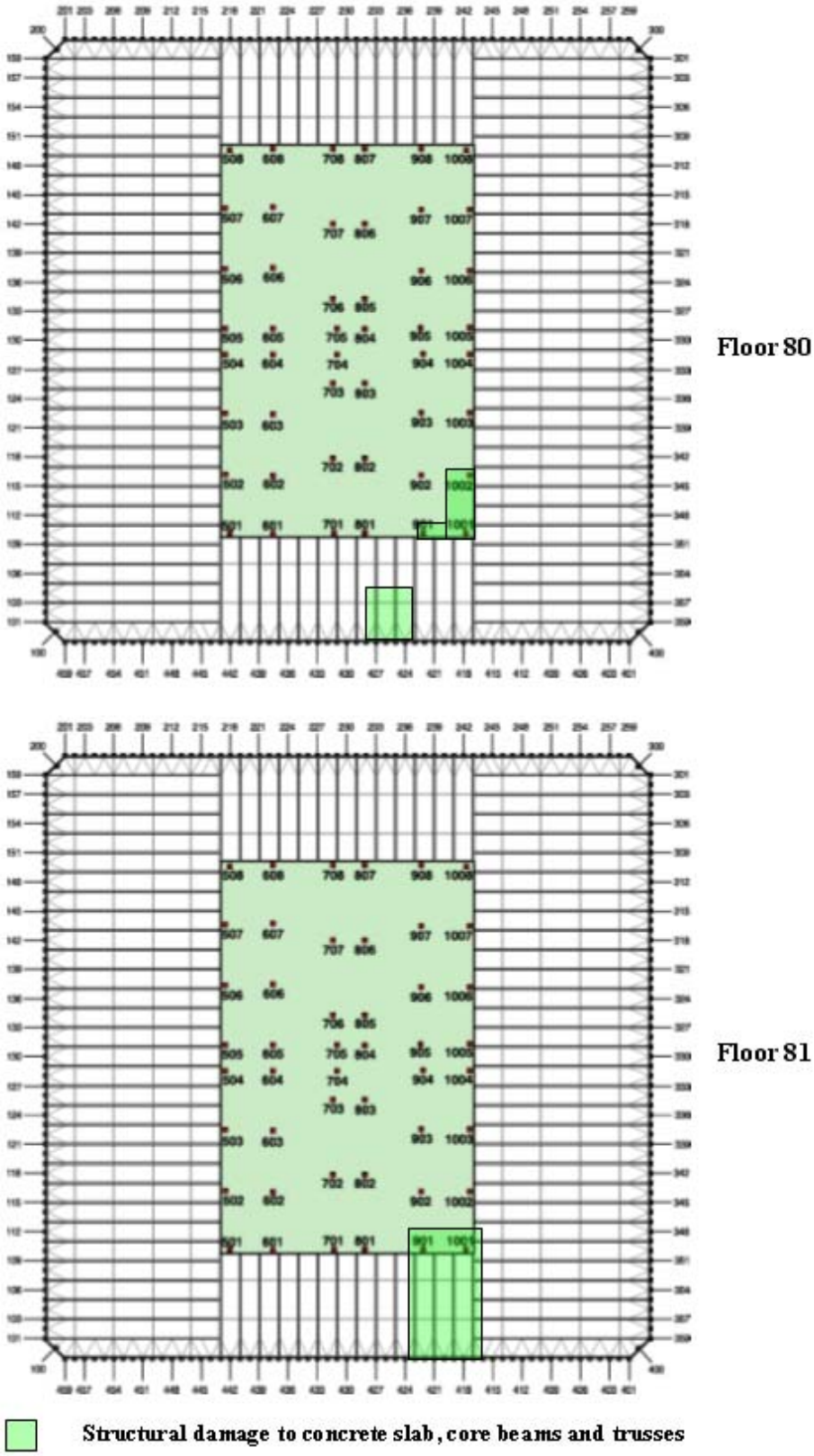

Figure A–17. WTC 2 Case C_i aircraft impact damage to Structural Floors 80 and 81.

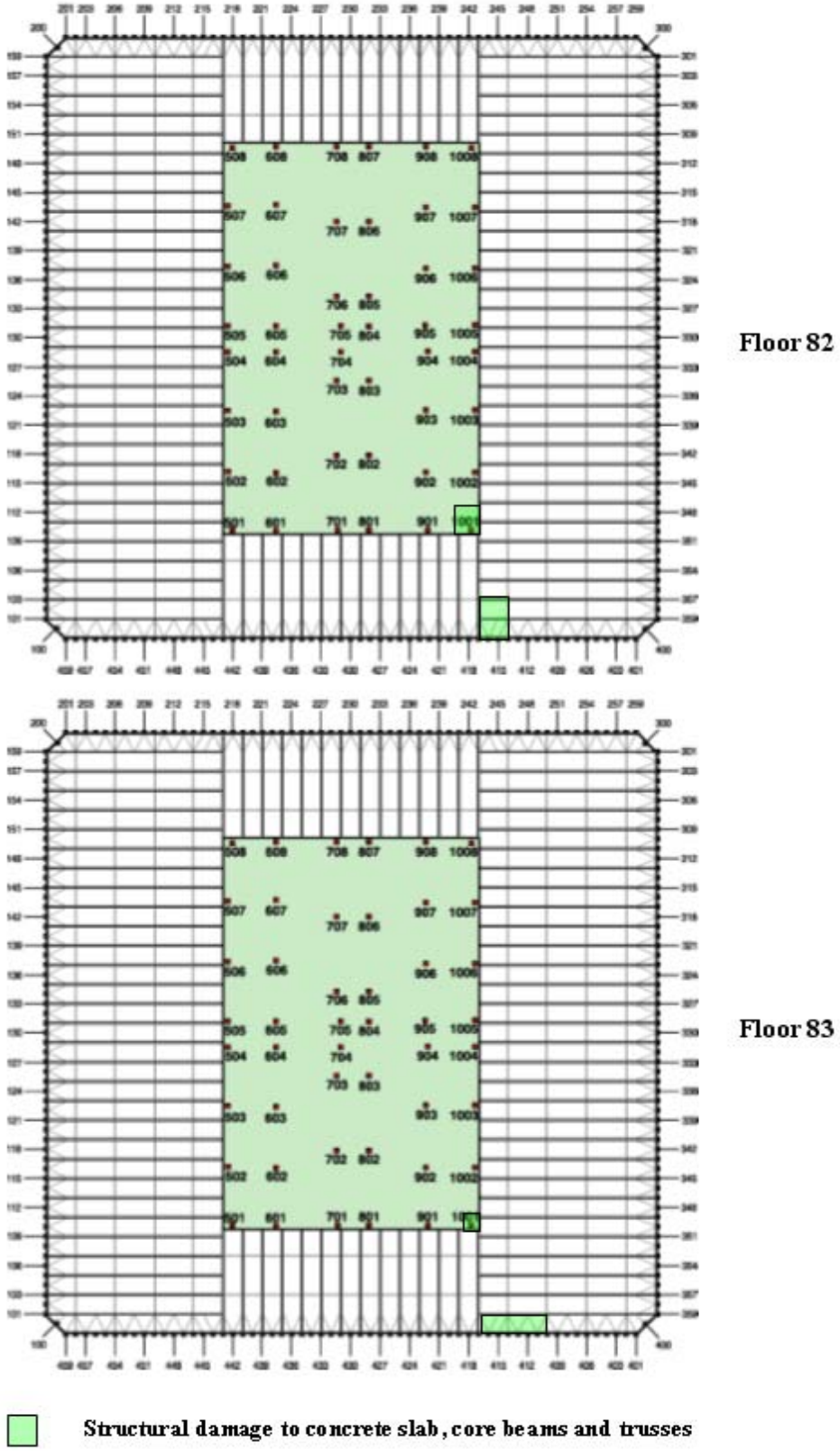

Figure A-18. WTC 2 Case C_i aircraft impact damage to Structural Floors 82 and 83.

WTC 2 CASE D_I – THERMAL INSULATION AND PARTITION DAMAGE FOR OCCUPANCY FLOOR

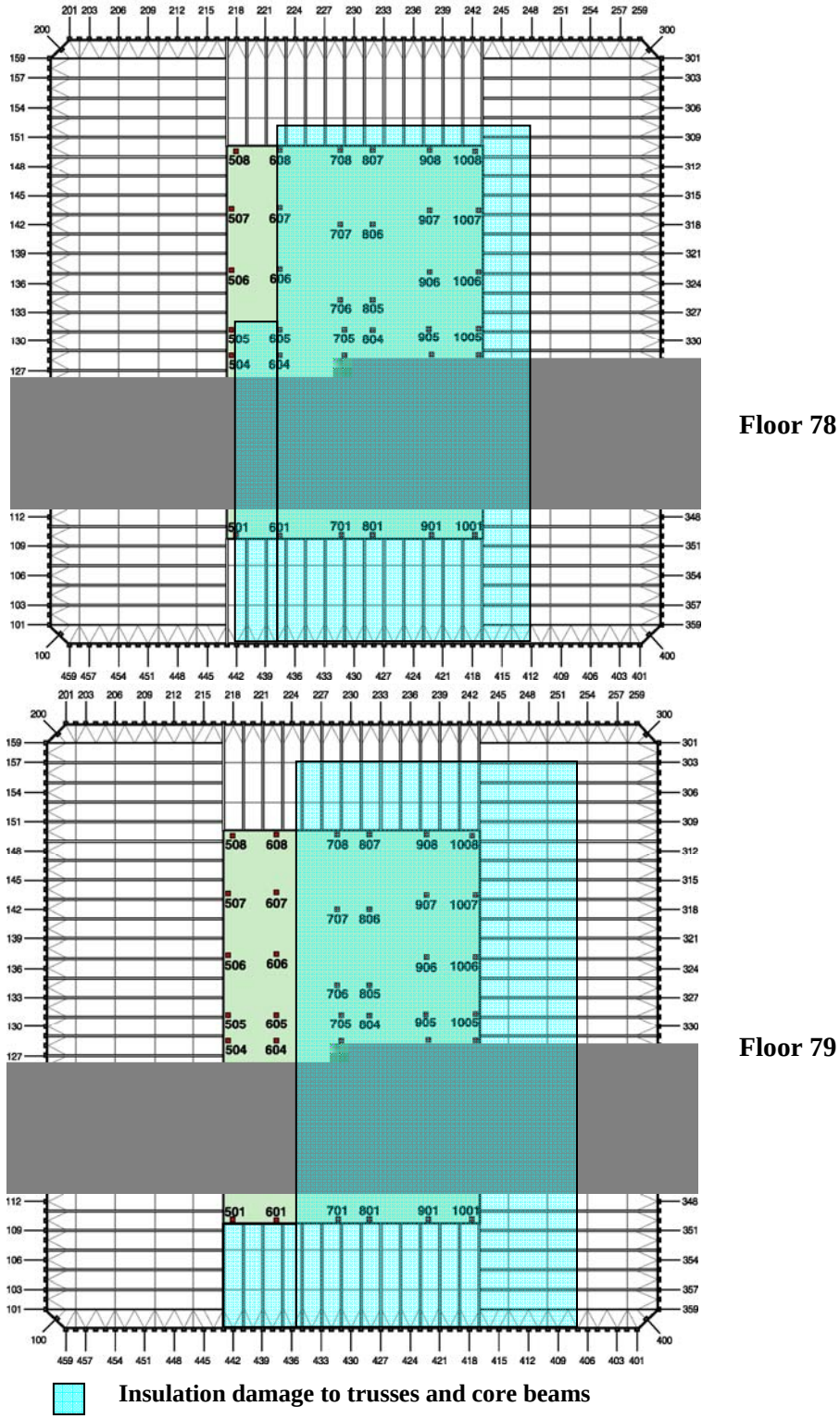

Figure A–19. WTC 2 Case D_i aircraft impact damage to Structural Floors 78 and 79.

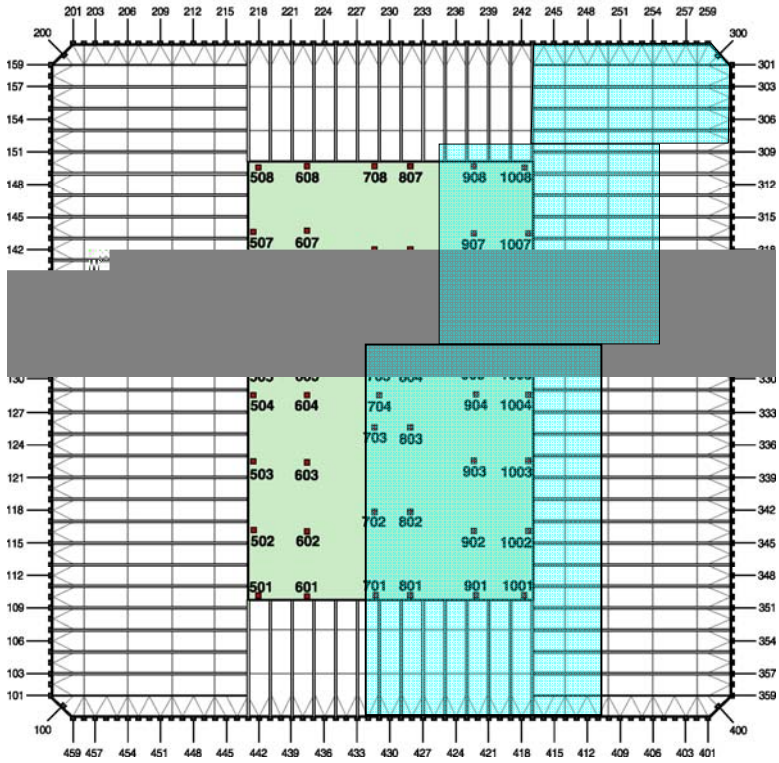

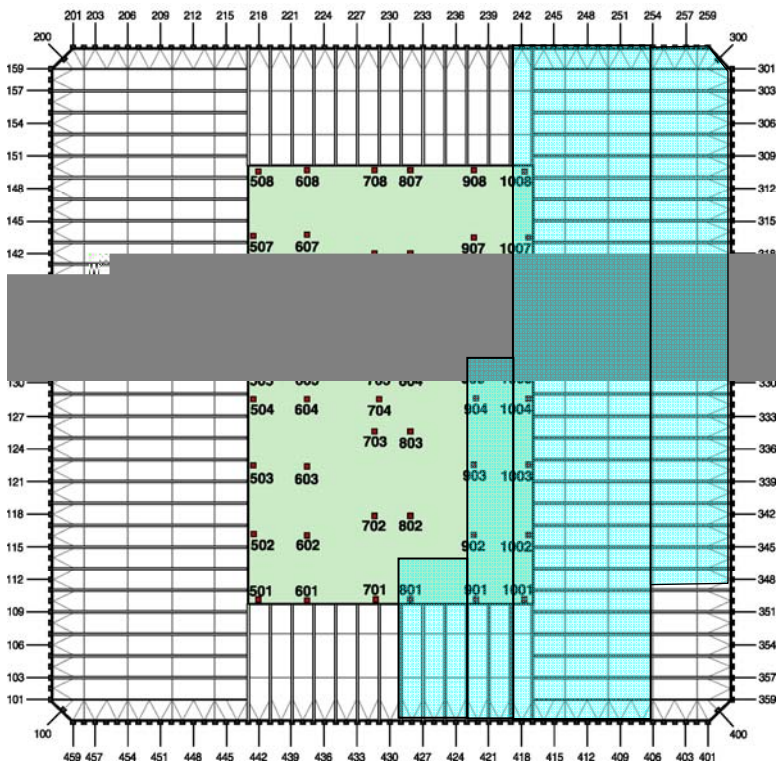

Insulation damage to trusses and core beams

Figure A–20. WTC 2 Case D_i aircraft impact damage to Structural Floors 80 and 81.

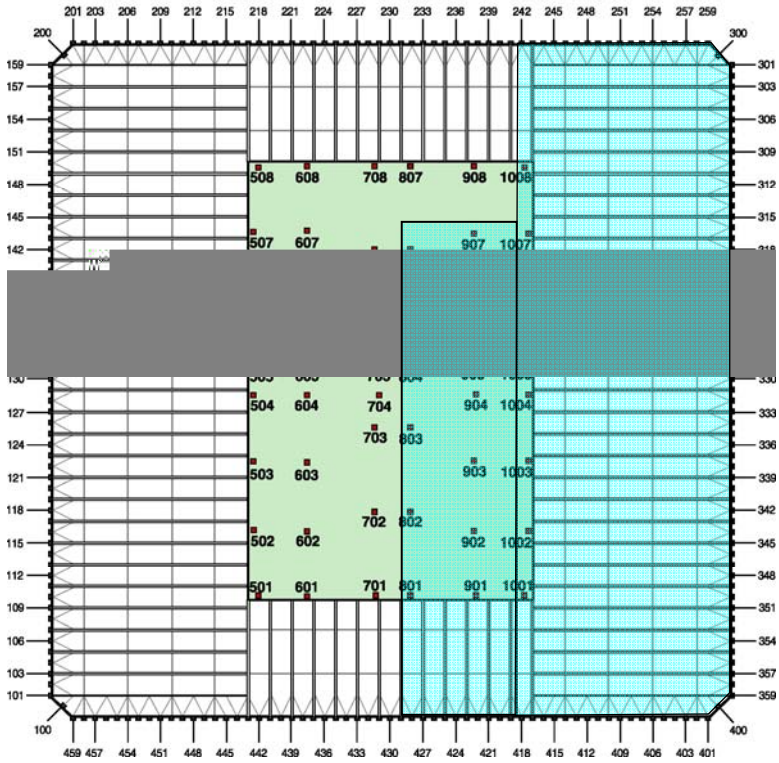

Floor 82

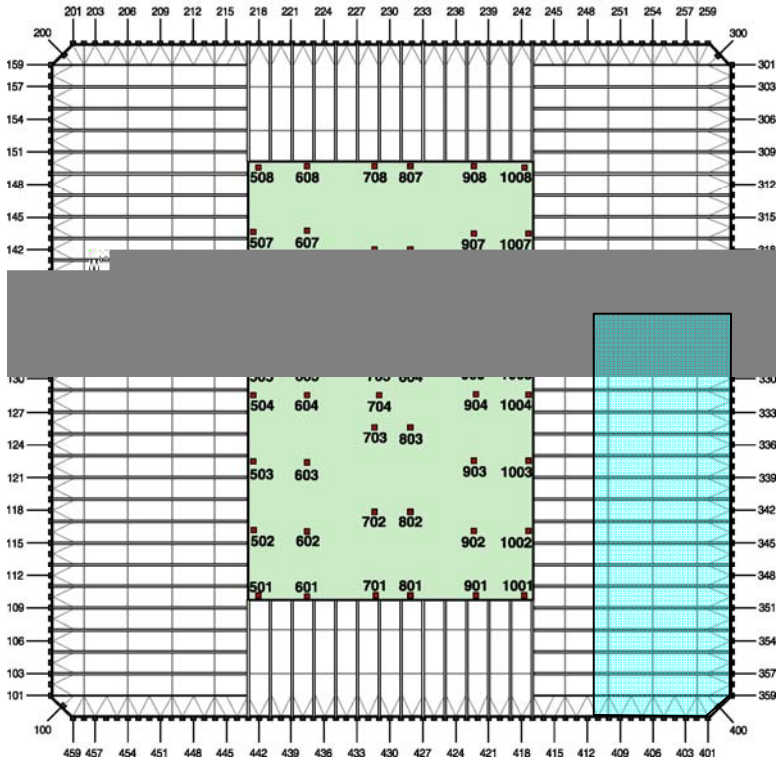

Floor 83

Insulation damage to trusses and core beams

Figure A–21. WTC 2 Case D_i aircraft impact damage to Structural Floors 82 and 83.

WTC 2 CASE D_I – DAMAGE FOR STRUCTURAL FLOOR

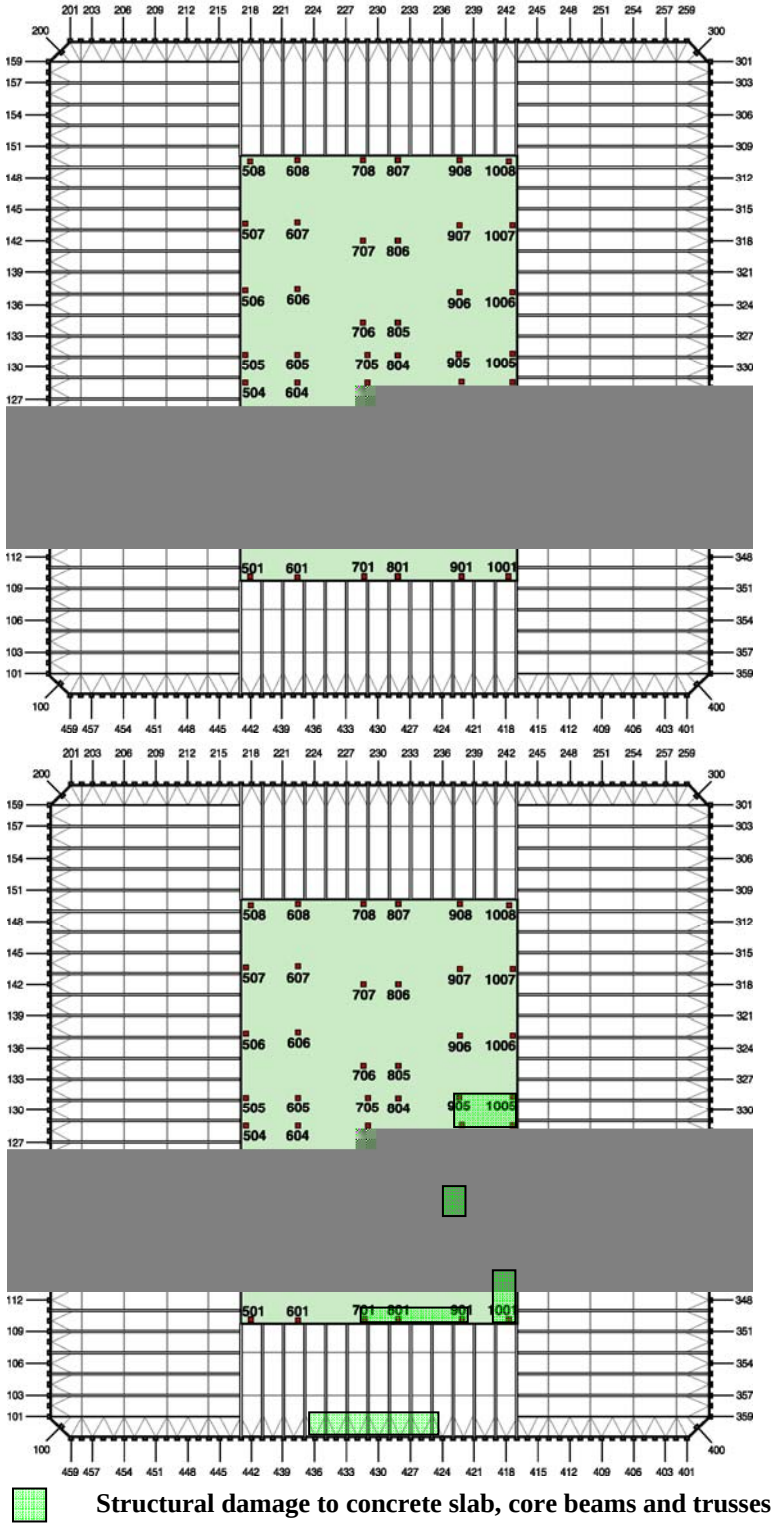

Figure A–22. WTC 2 Case D_i aircraft impact damage to Structural Floors 78 and 79.

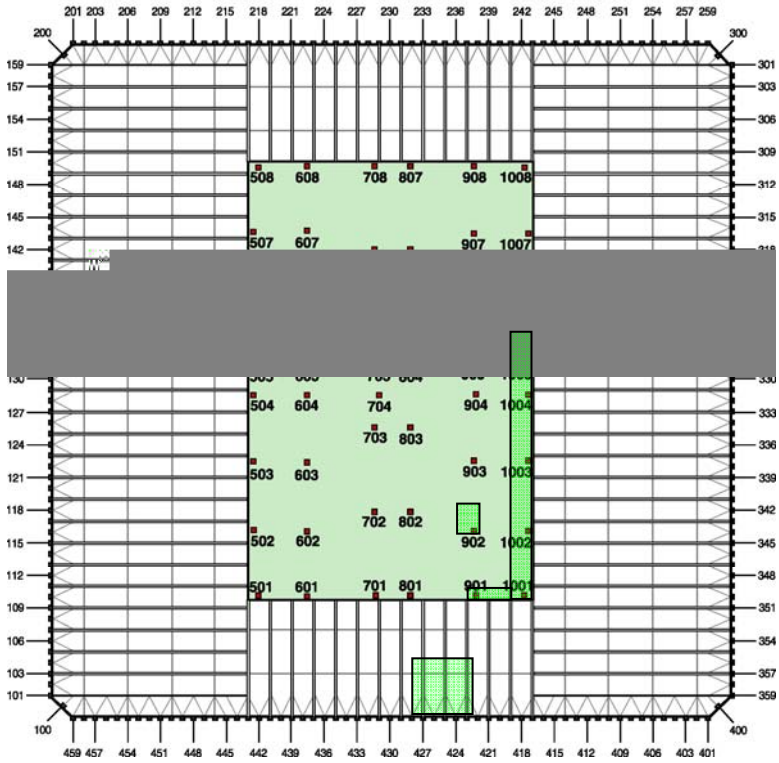

Floor 80

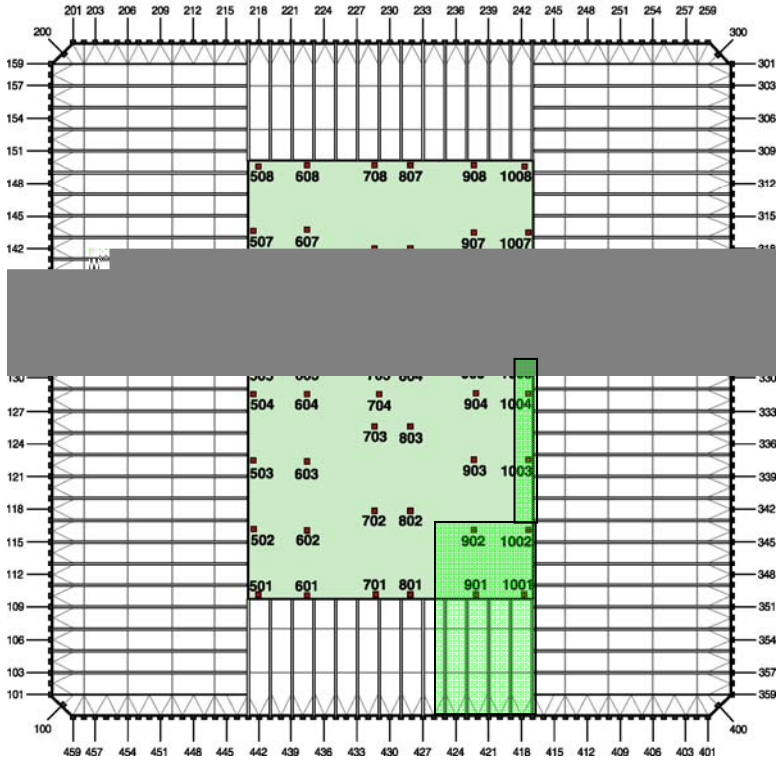

Floor 81

Structural damage to concrete slab, core beams and trusses

Figure A–23. WTC 2 Case D_i aircraft impact damage to Structural Floors 80 and 81.

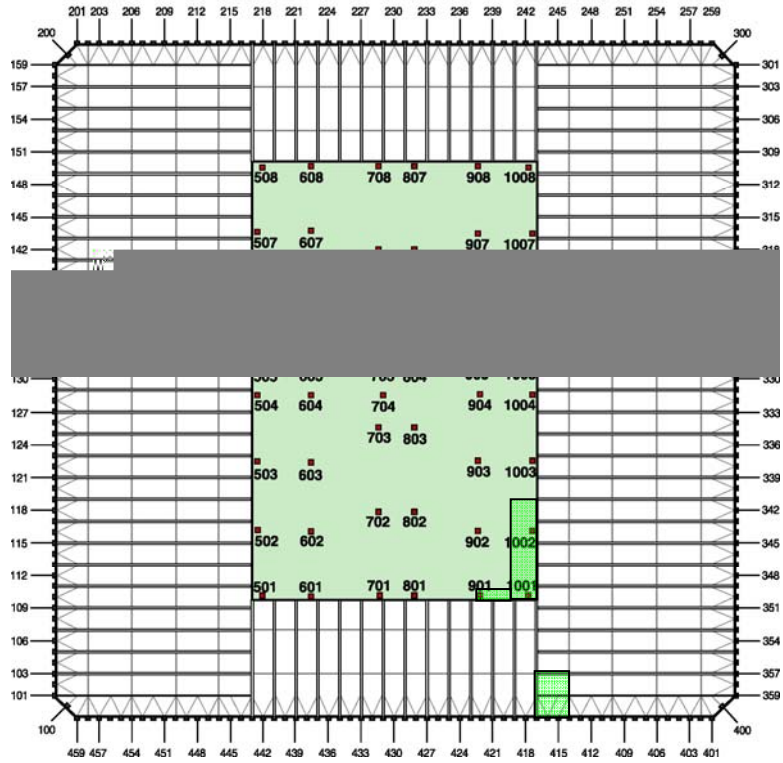

Floor 82

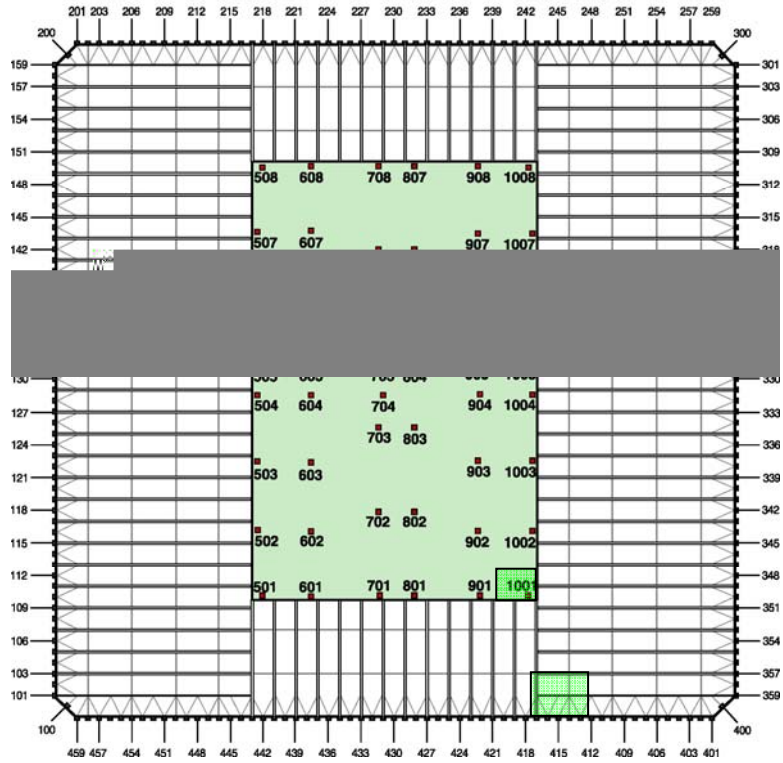

Floor 83

Structural damage to concrete slab, core beams and trusses

Figure A–24. WTC 2 Case D_i aircraft impact damage to Structural Floors 82 and 83.

Appendix B
SUMMARY OF AIRCRAFT IMPACT DAMAGE FOR FINAL CASES A TO D

WTC 1 CASE A - OCCUPANCY FLOOR GRAPHICS

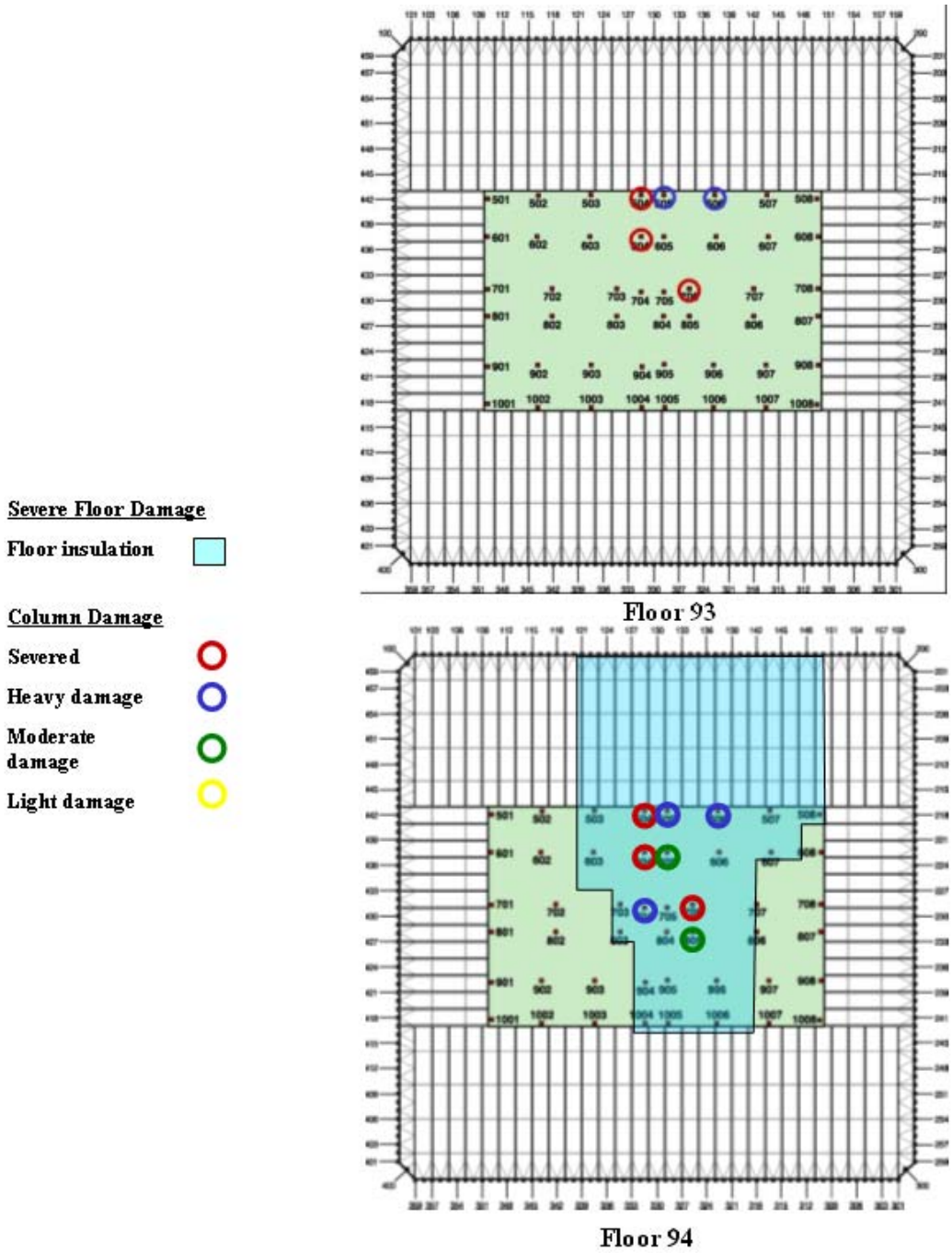

Figure B–1. WTC 1 Case A aircraft impact damage to Occupancy Floors 93 and 94.

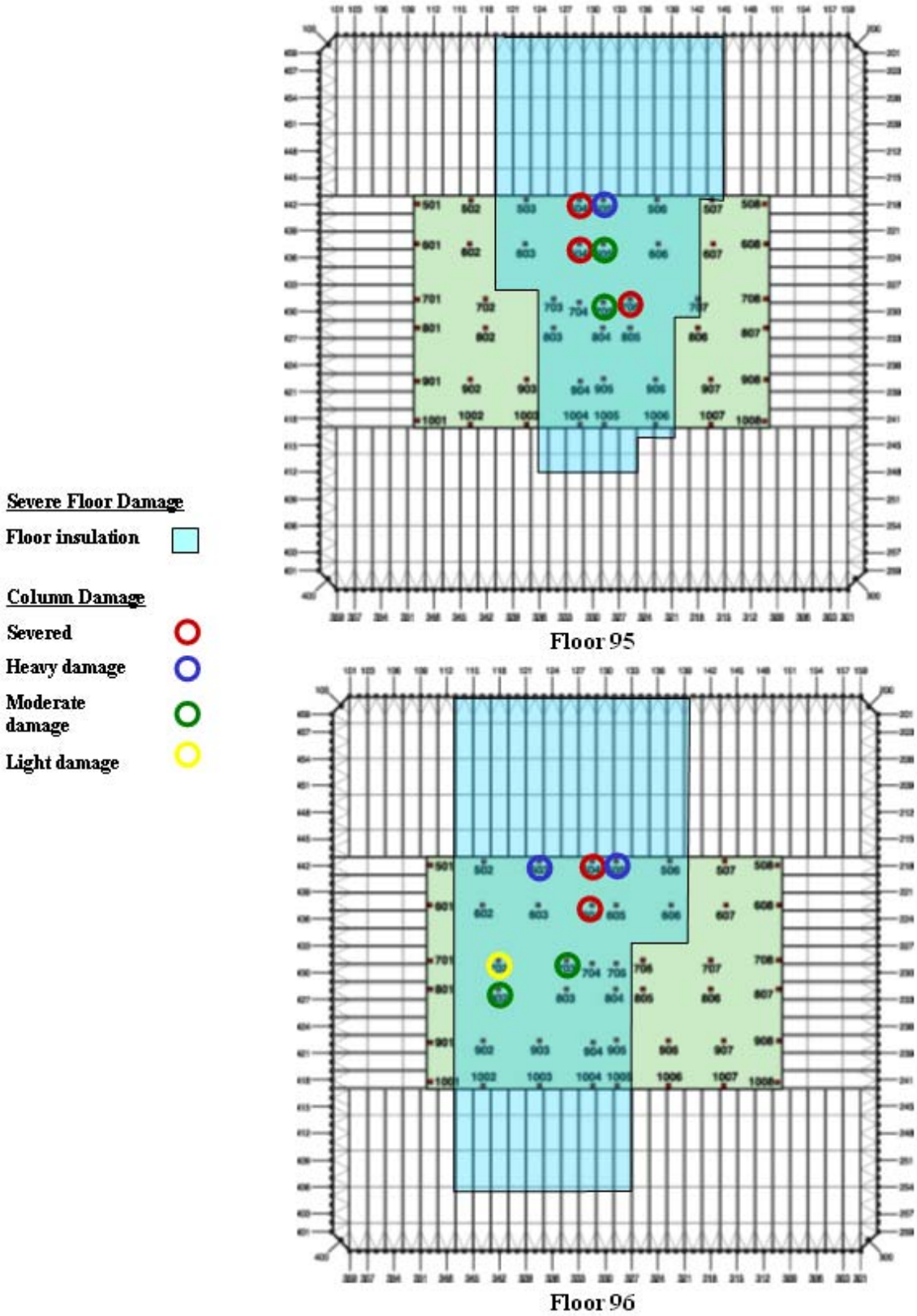

Figure B–2. WTC 1 Case A aircraft impact damage to Occupancy Floors 95 and 96.

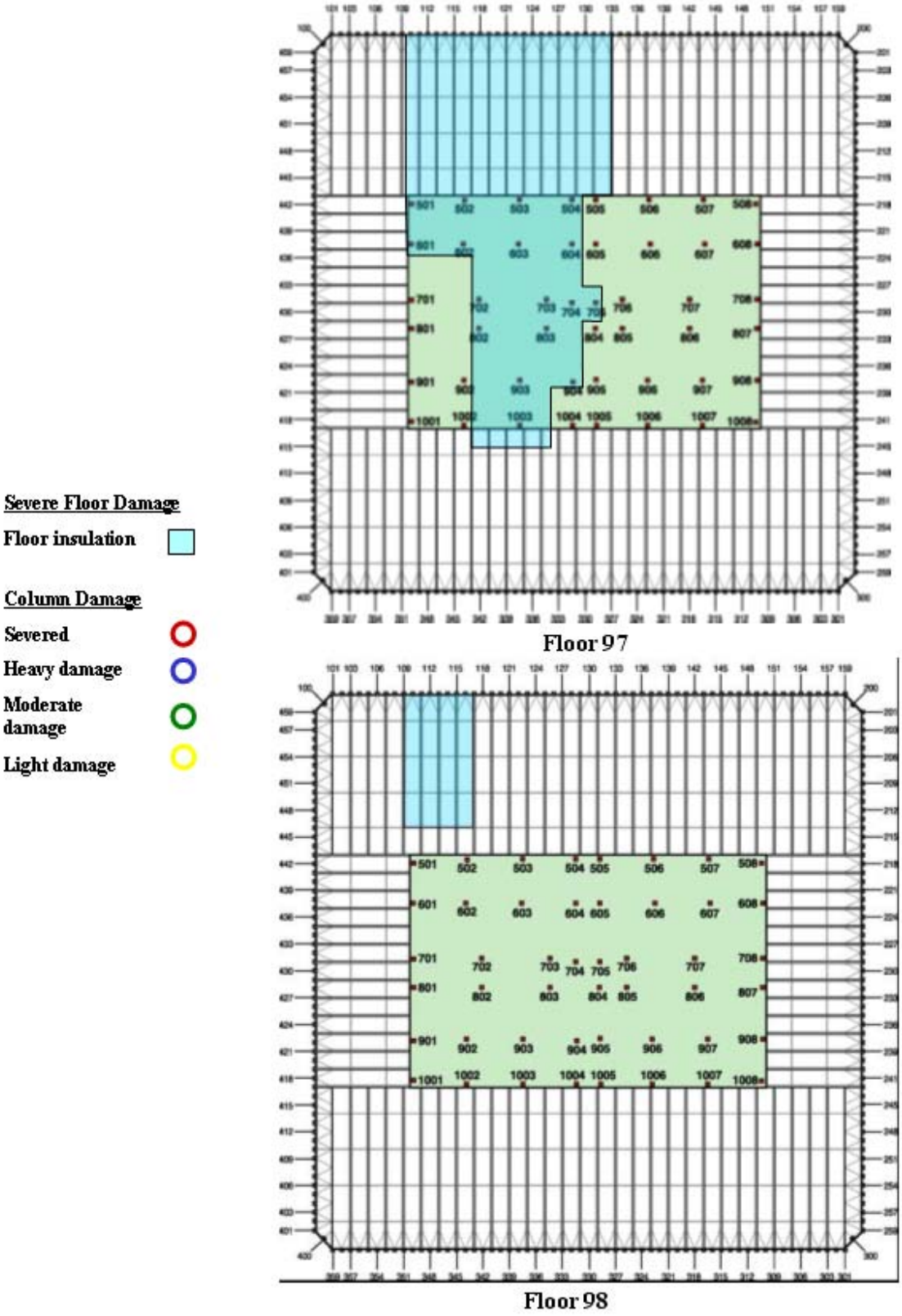

Figure B–3. WTC 1 Case A aircraft impact damage to Occupancy Floors 97 and 98.

WTC 1 CASE A - STRUCTURAL FLOOR GRAPHICS

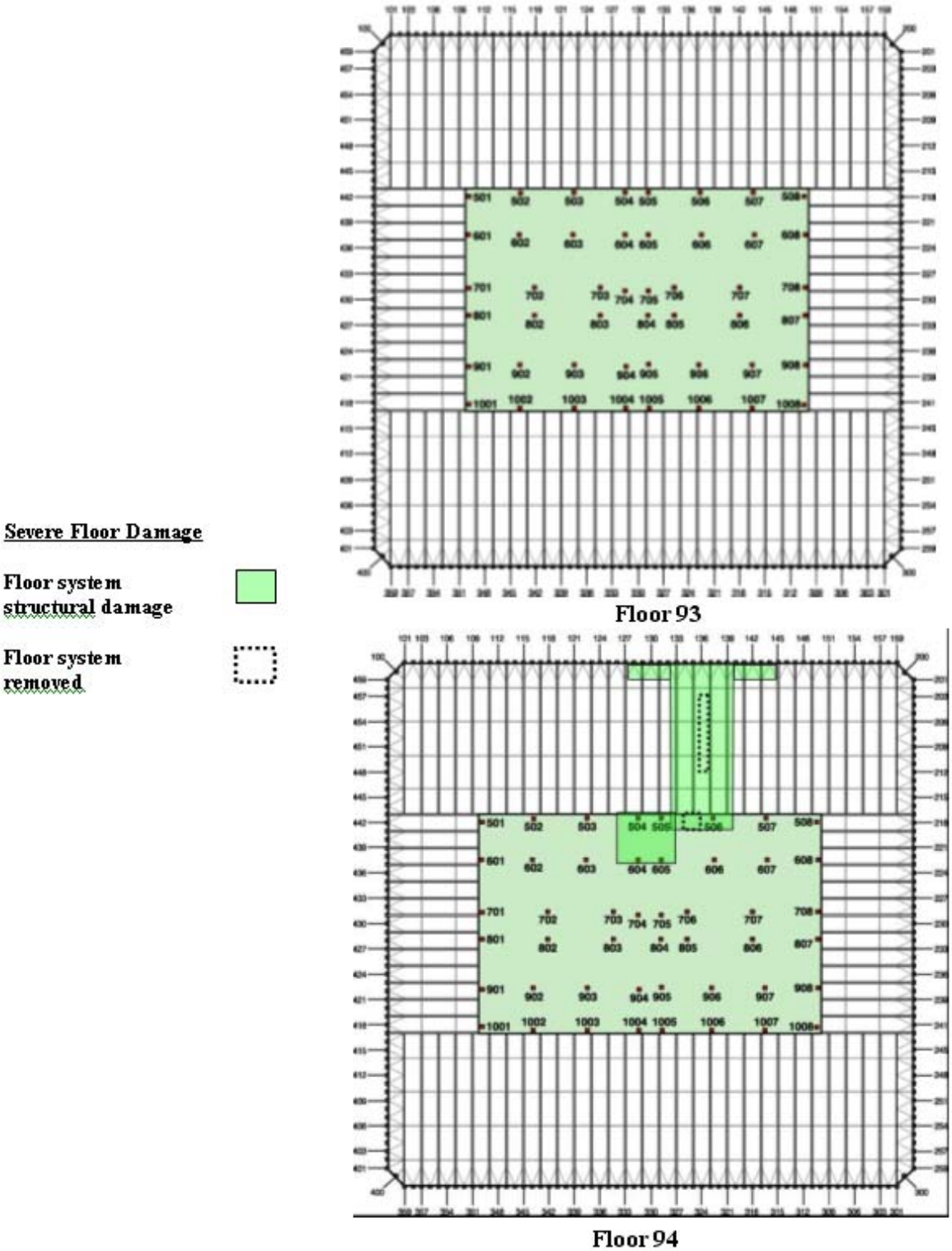

Figure B–4. WTC 1 Case A aircraft impact damage to Structural Floors 93 and 94.

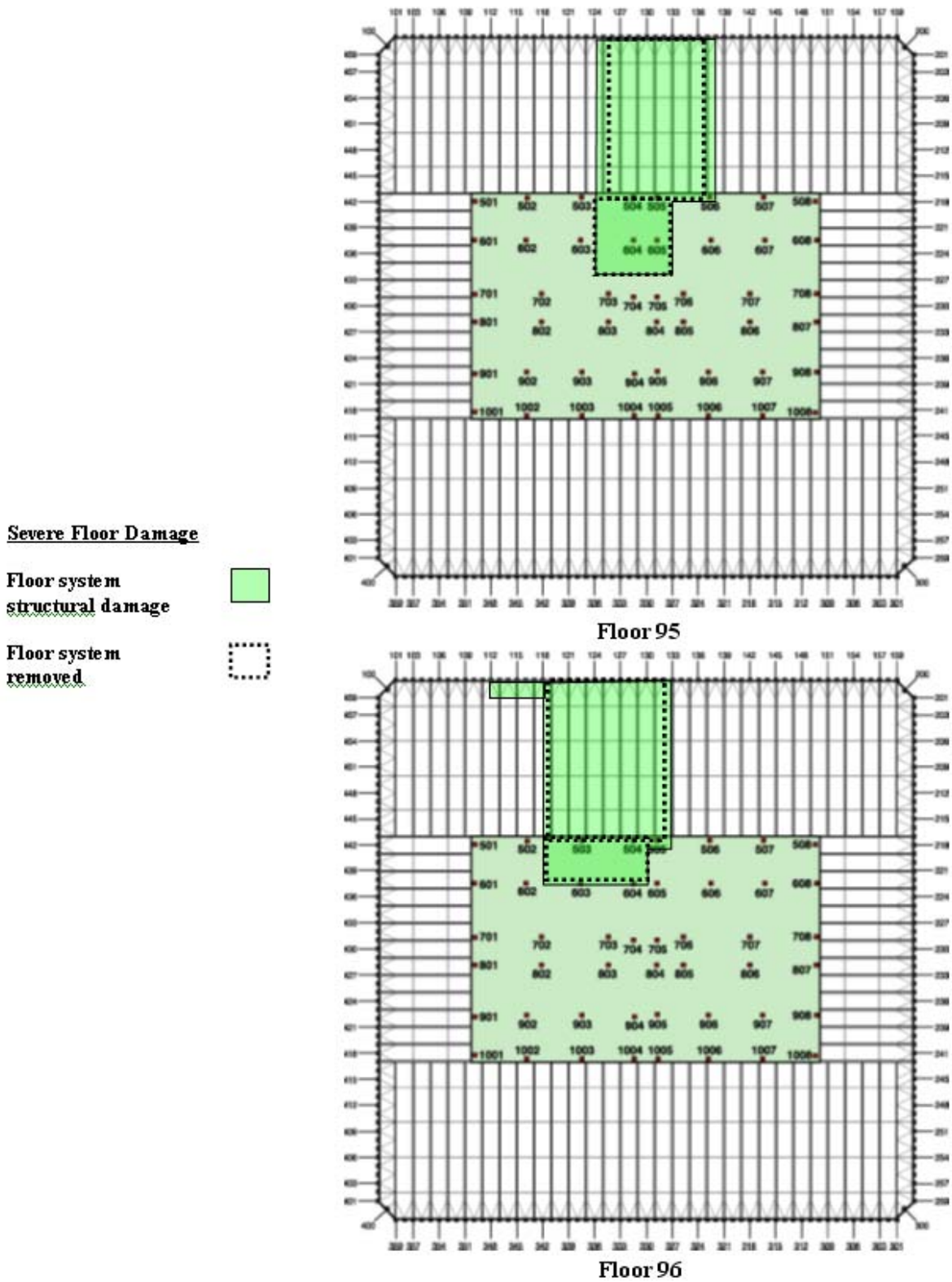

Figure B–5. WTC 1 Case A aircraft impact damage to Structural Floors 95 and 96.

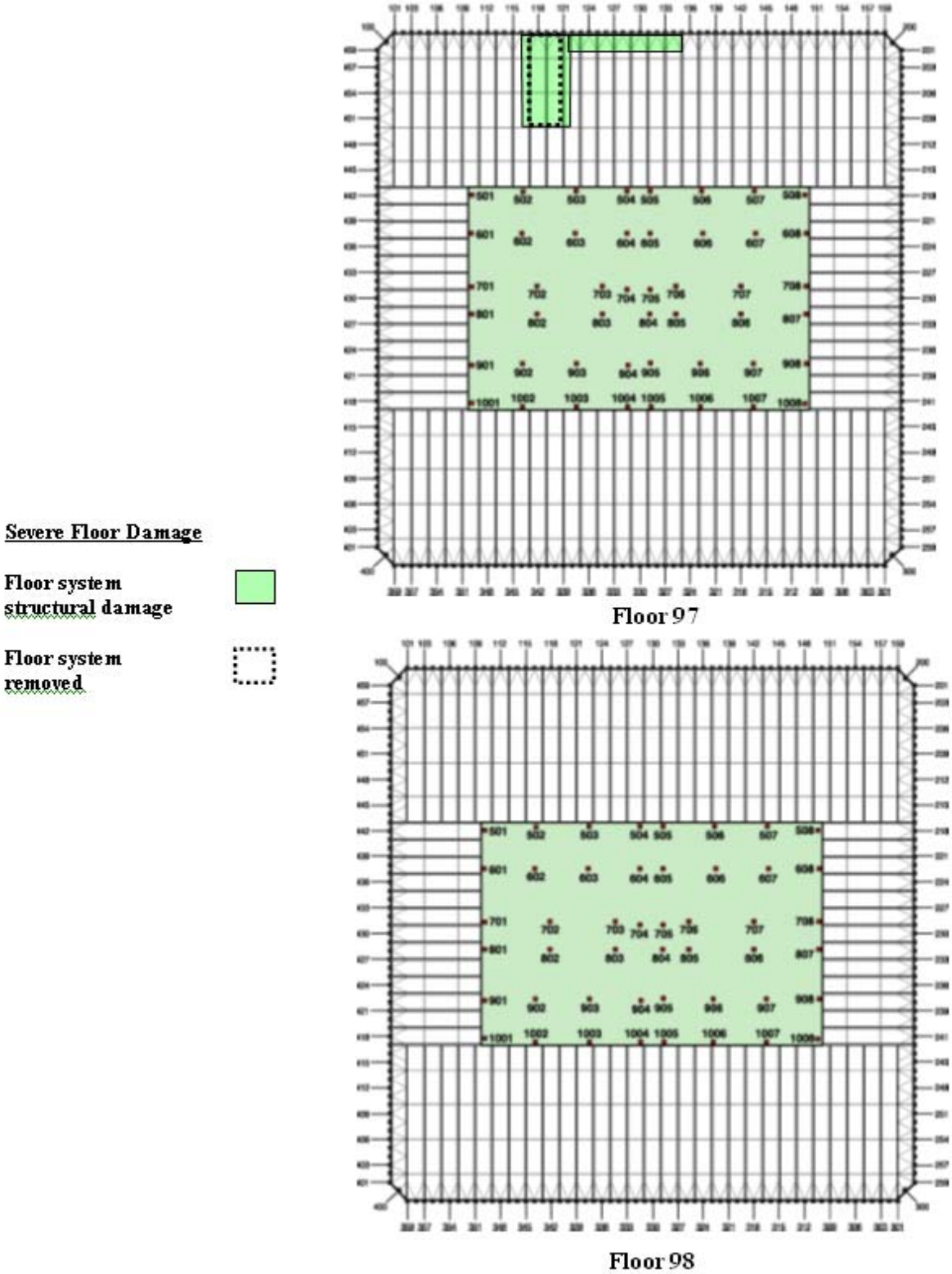

Figure B–6. WTC 1 Case A aircraft impact damage to Structural Floors 97 and 98.

WTC 1 CASE B - OCCUPANCY FLOOR GRAPHICS

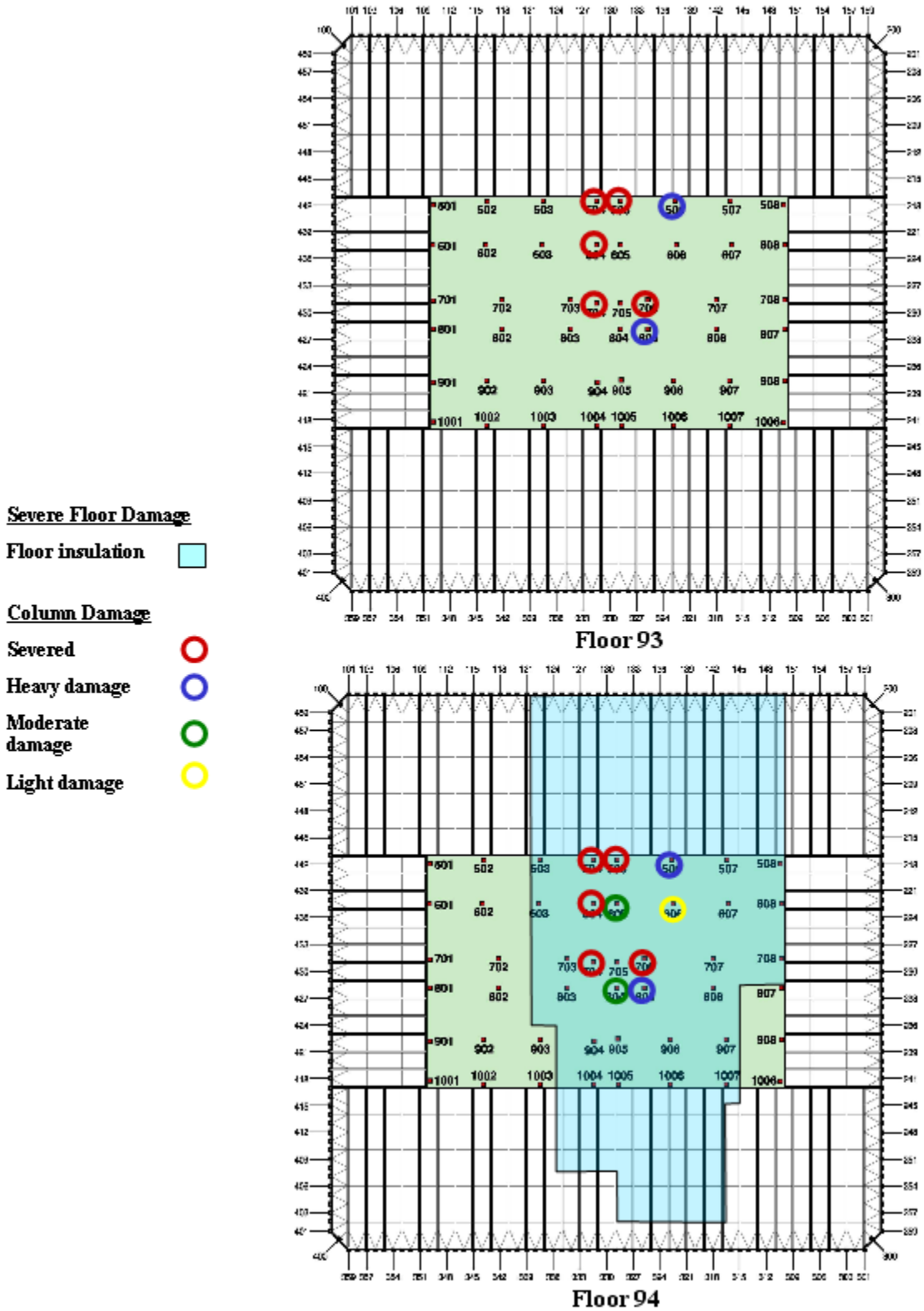

Figure B–7. WTC 1 Case B aircraft impact damage to Occupancy Floors 93 and 94.

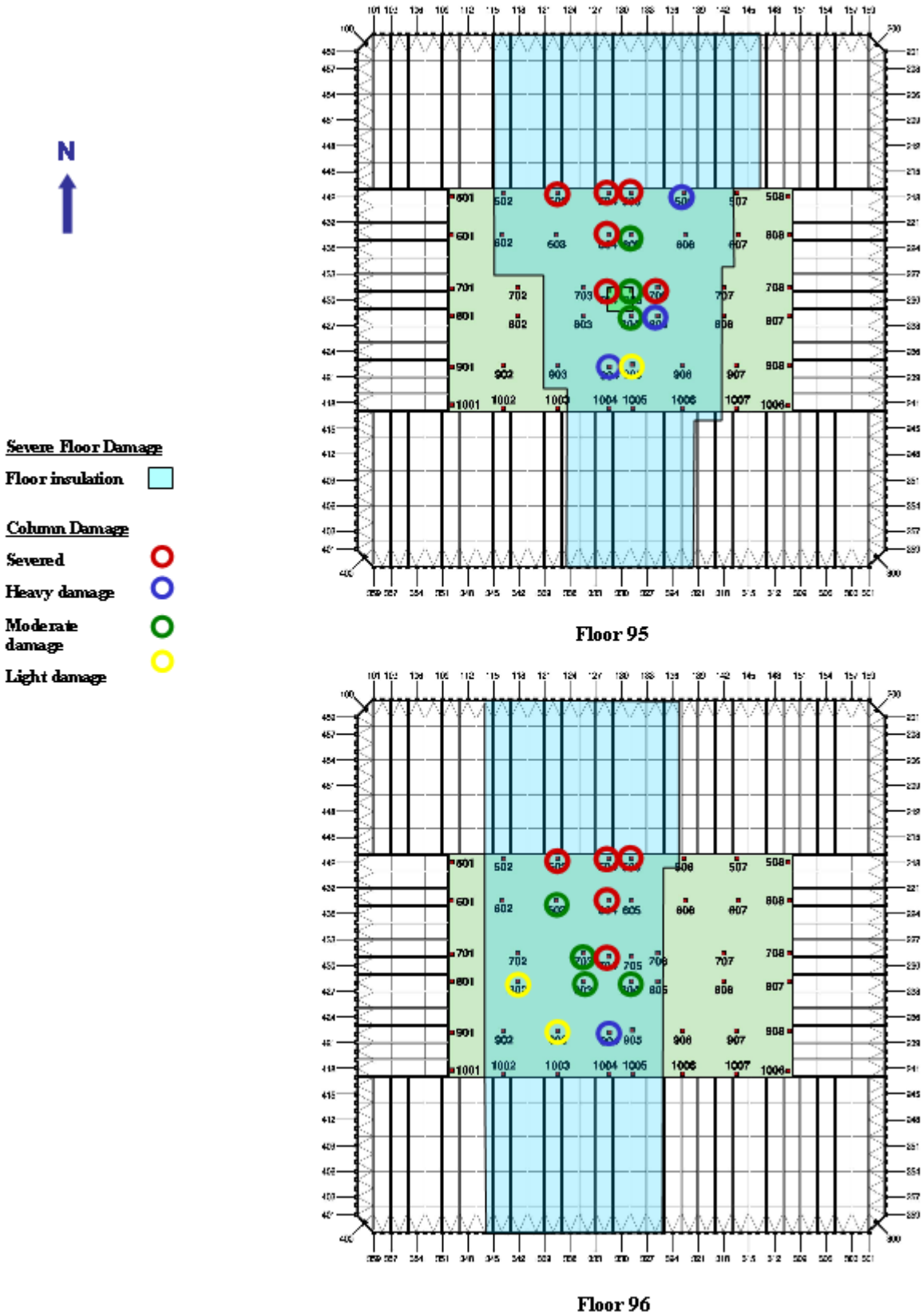

Figure B–8. WTC 1 Case B aircraft impact damage to Occupancy Floors 95 and 96.

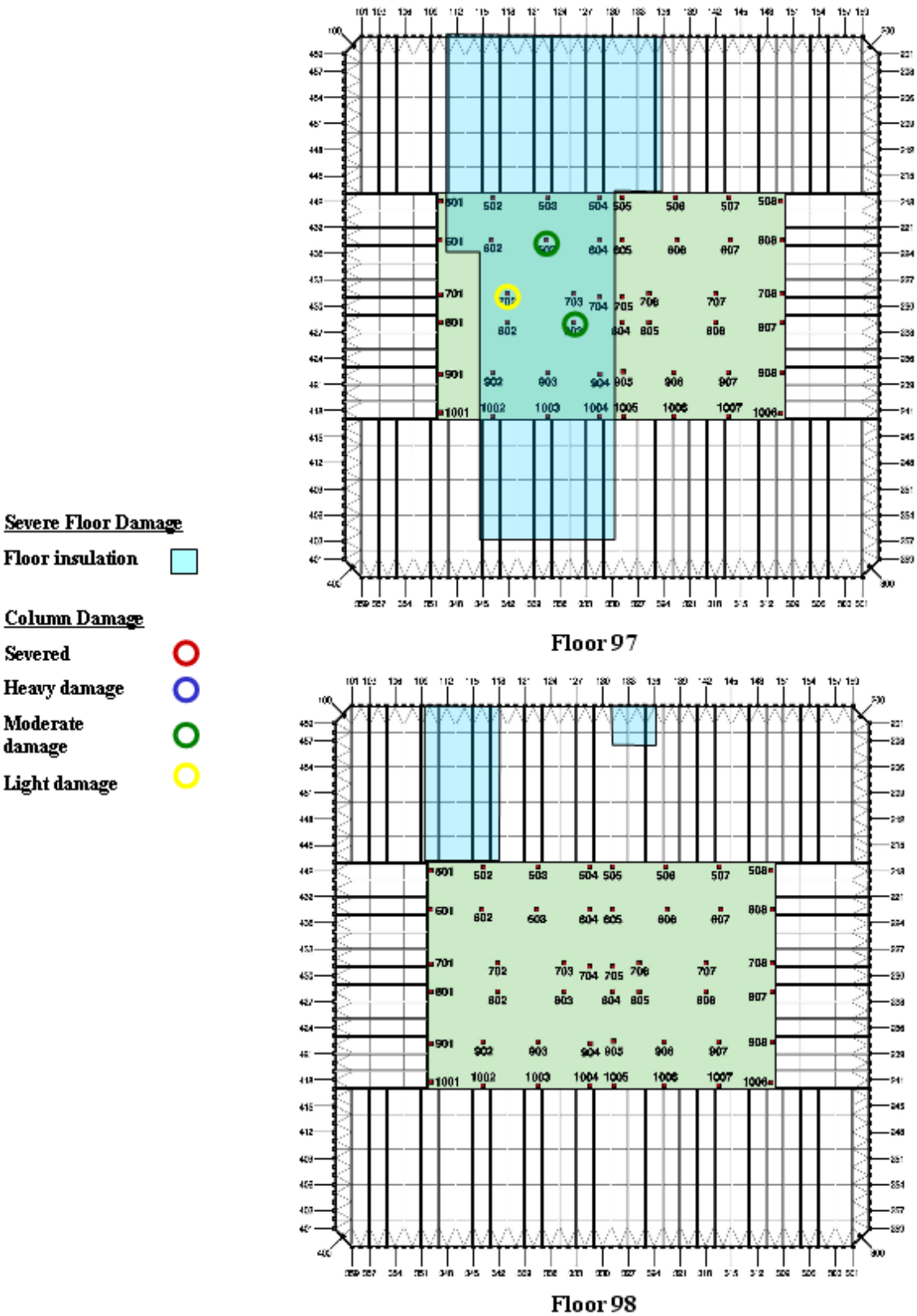

Figure B–9. WTC 1 Case B aircraft impact damage to Occupancy Floors 97 and 98.

WTC 1 CASE B - STRUCTURAL FLOOR GRAPHICS

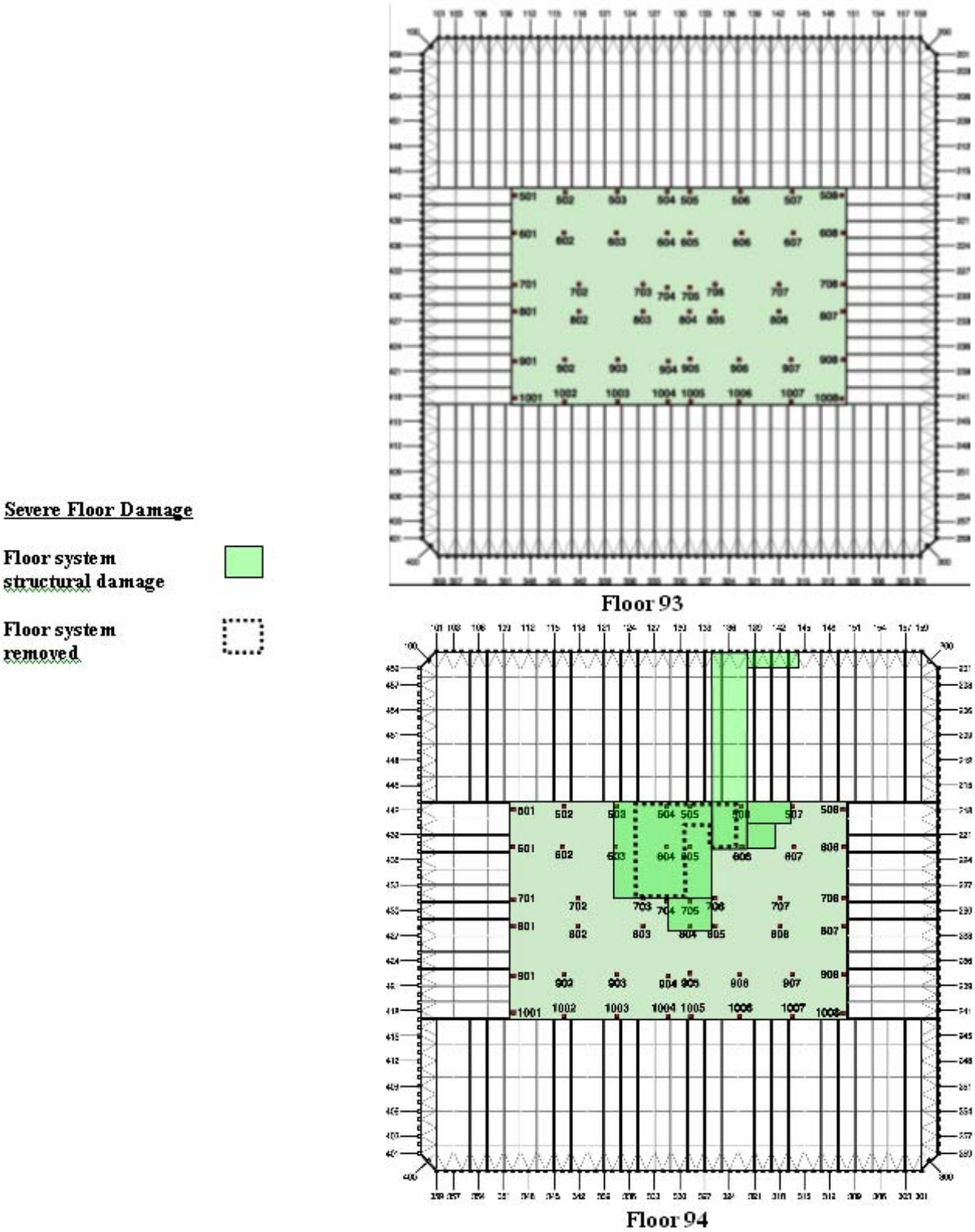

Figure B–10. WTC 1 Case B aircraft impact damage to Structural Floors 93 and 94.

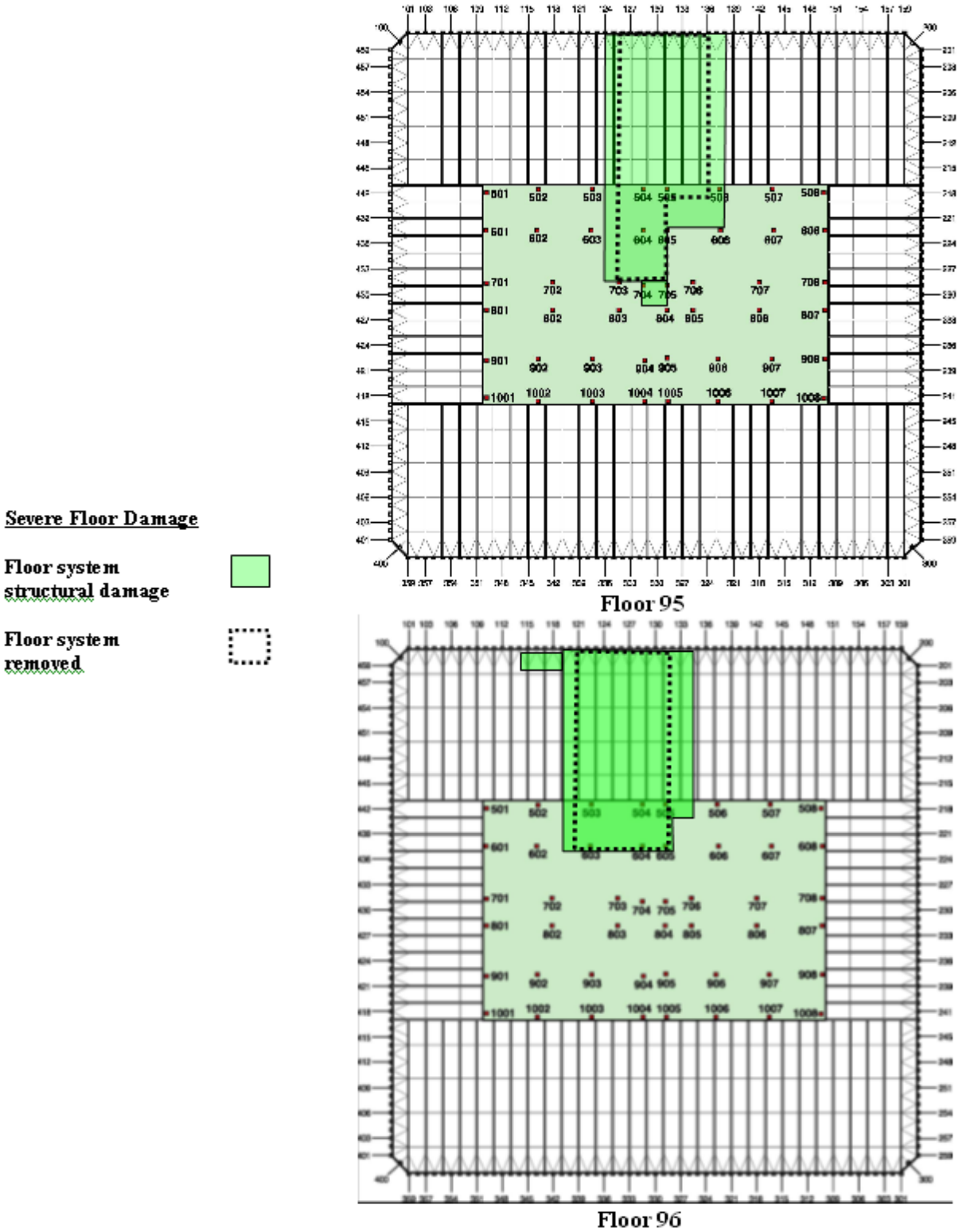

Figure B–11. WTC 1 Case B aircraft impact damage to Structural Floors 95 and 96.

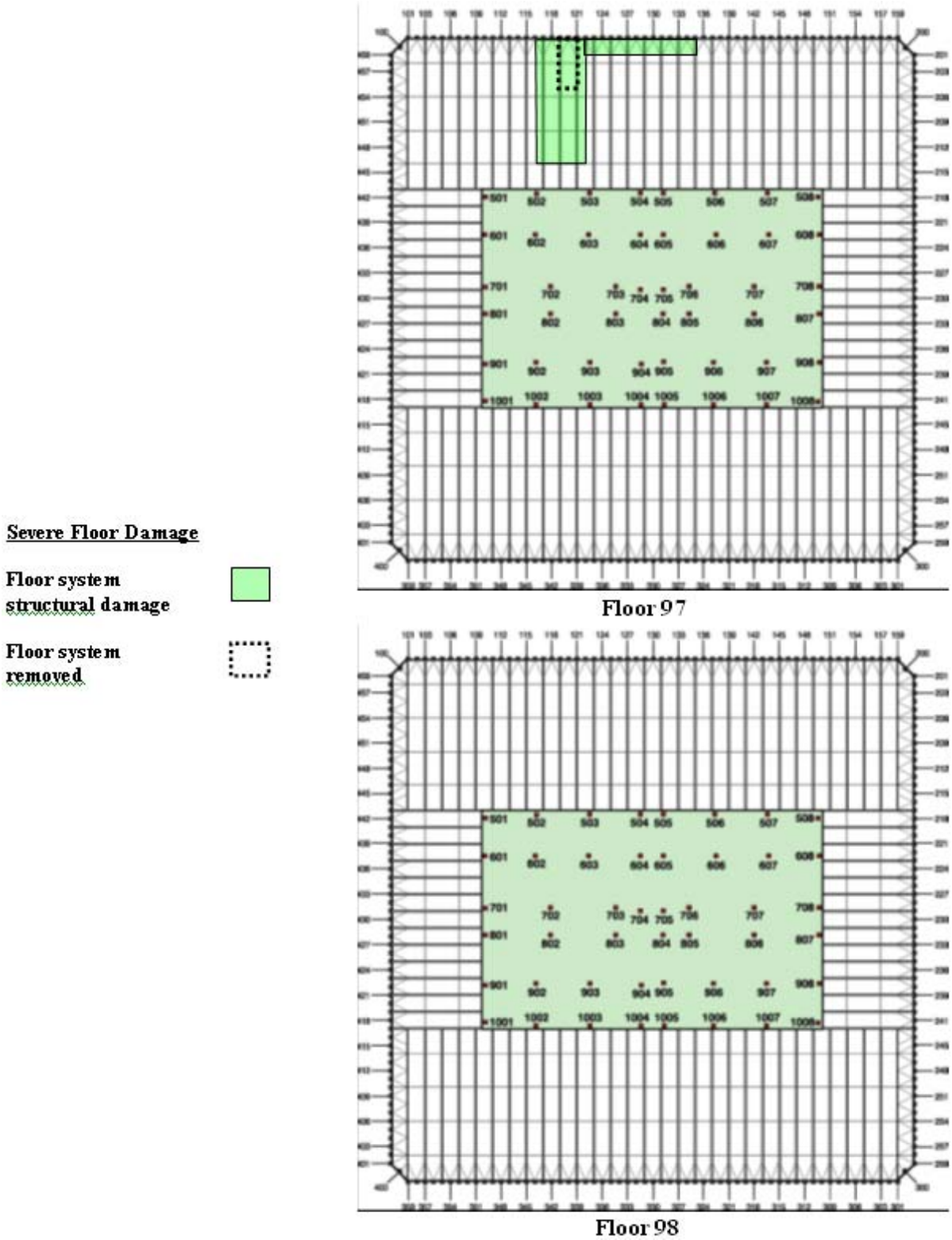

Figure B–12. WTC 1 Case B aircraft impact damage to Structural Floors 97 and 98.

WTC 2 CASE C – OCCUPANCY FLOOR GRAPHICS

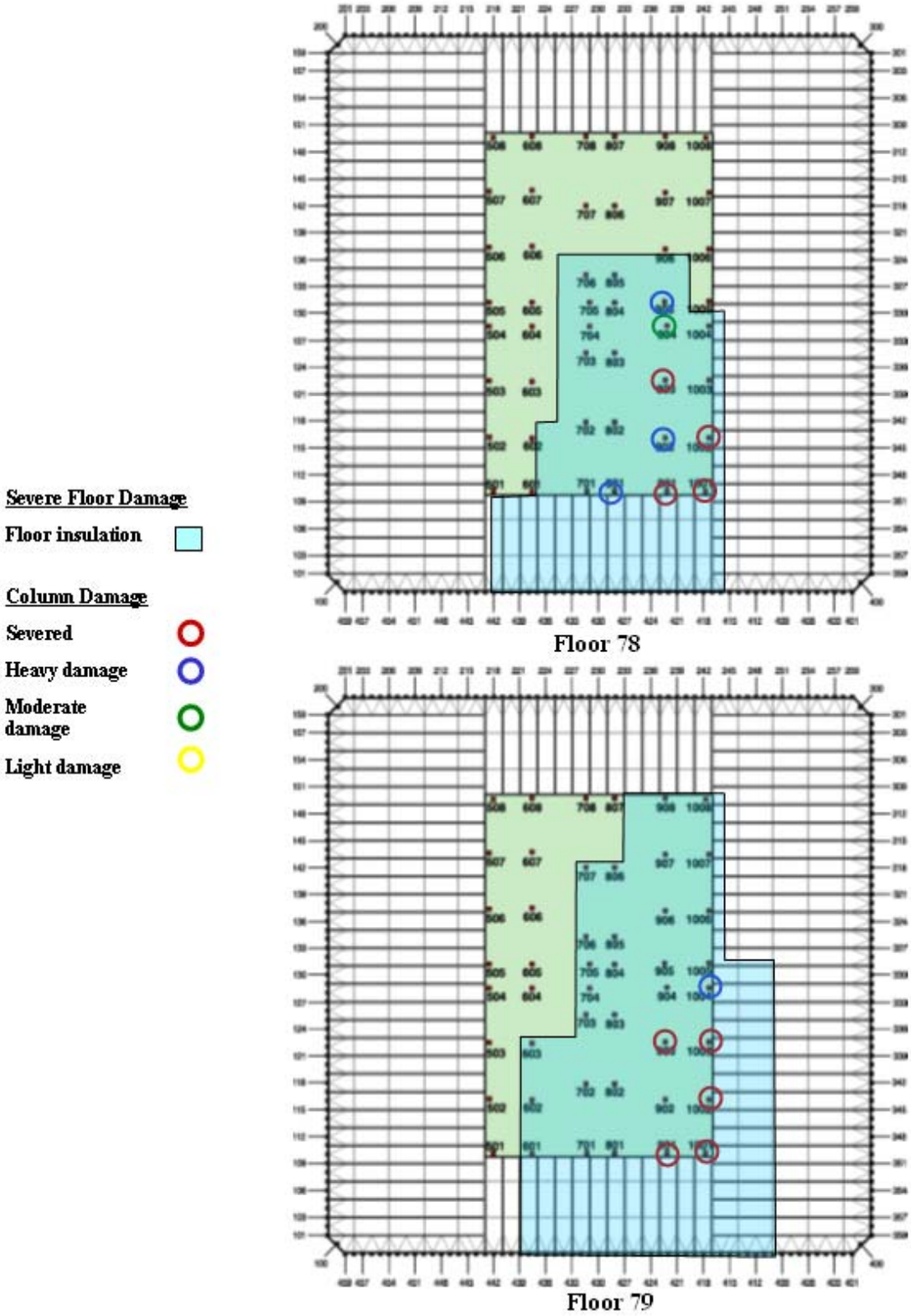

Figure B–13. WTC 2 Case C aircraft impact damage to Occupancy Floors 78 and 79.

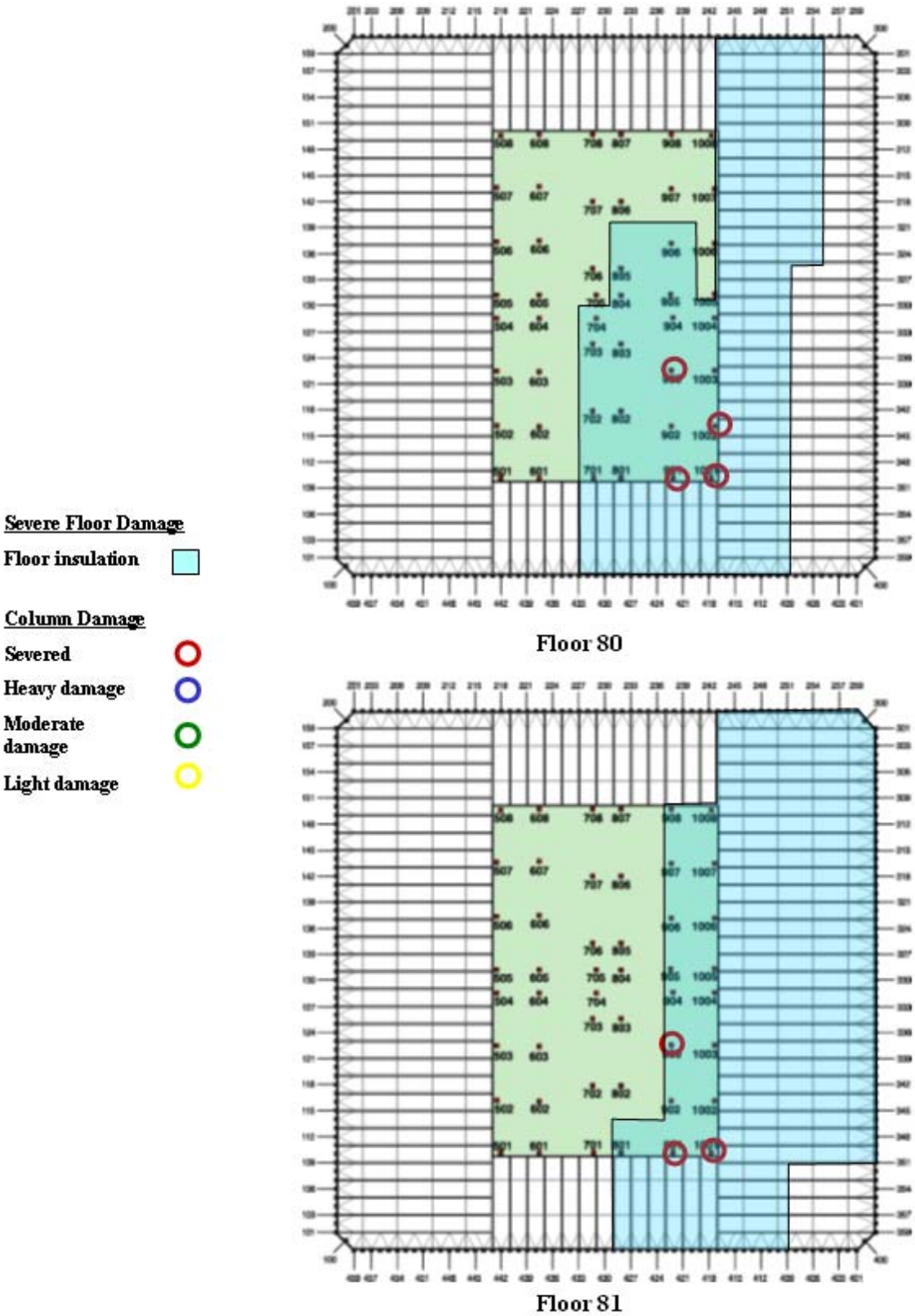

Figure B–14. WTC 2 Case C aircraft impact damage to Occupancy Floors 80 and 81.

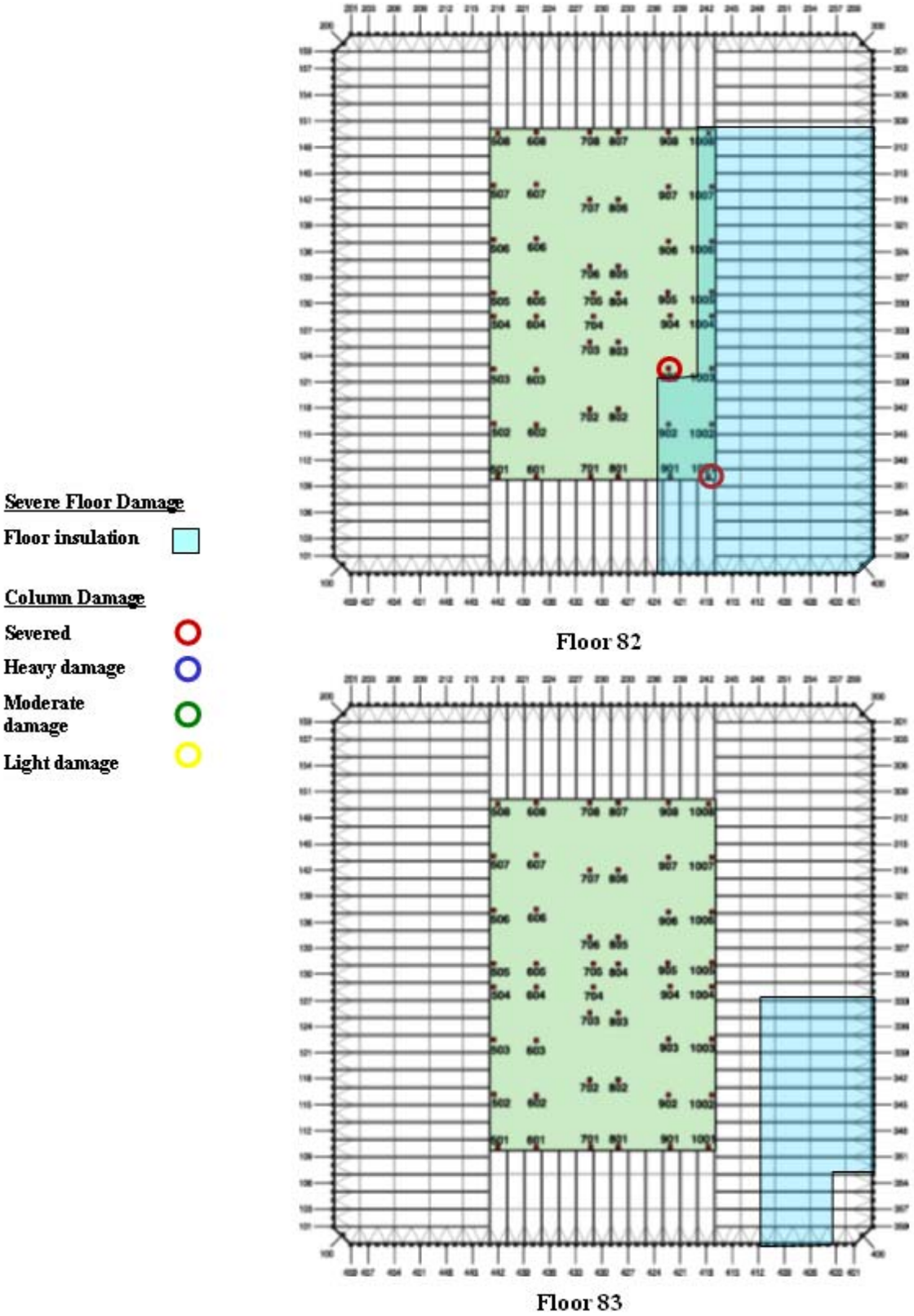

Figure B–15. WTC 2 Case C aircraft impact damage to Occupancy Floors 82 and 83.

WTC 2 CASE C – STRUCTURAL FLOOR GRAPHICS

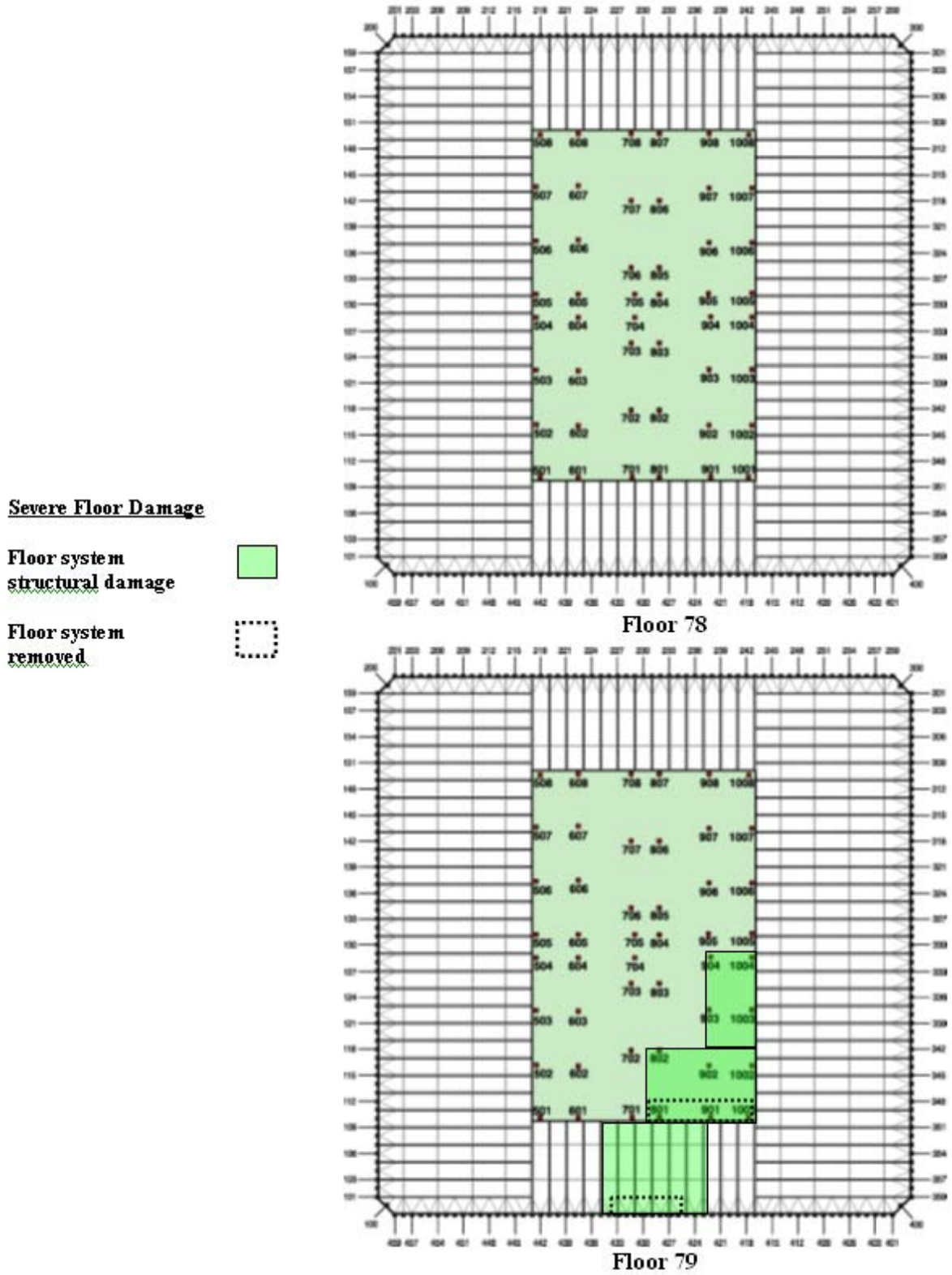

Figure B–16. WTC 2 Case C aircraft impact damage to Structural Floors 78 and 79.

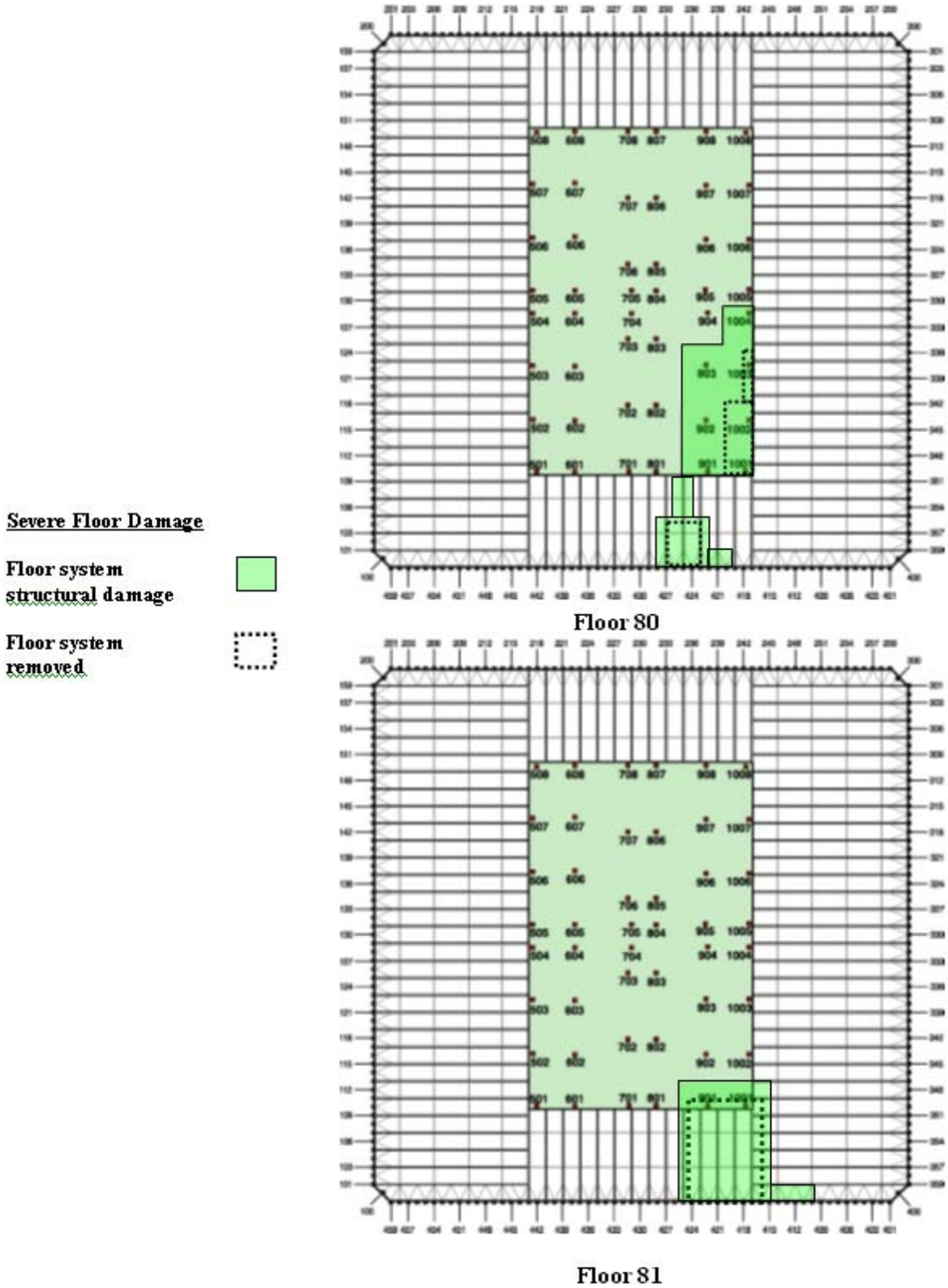

Figure B–17. WTC 2 Case C aircraft impact damage to Structural Floors 80 and 81.

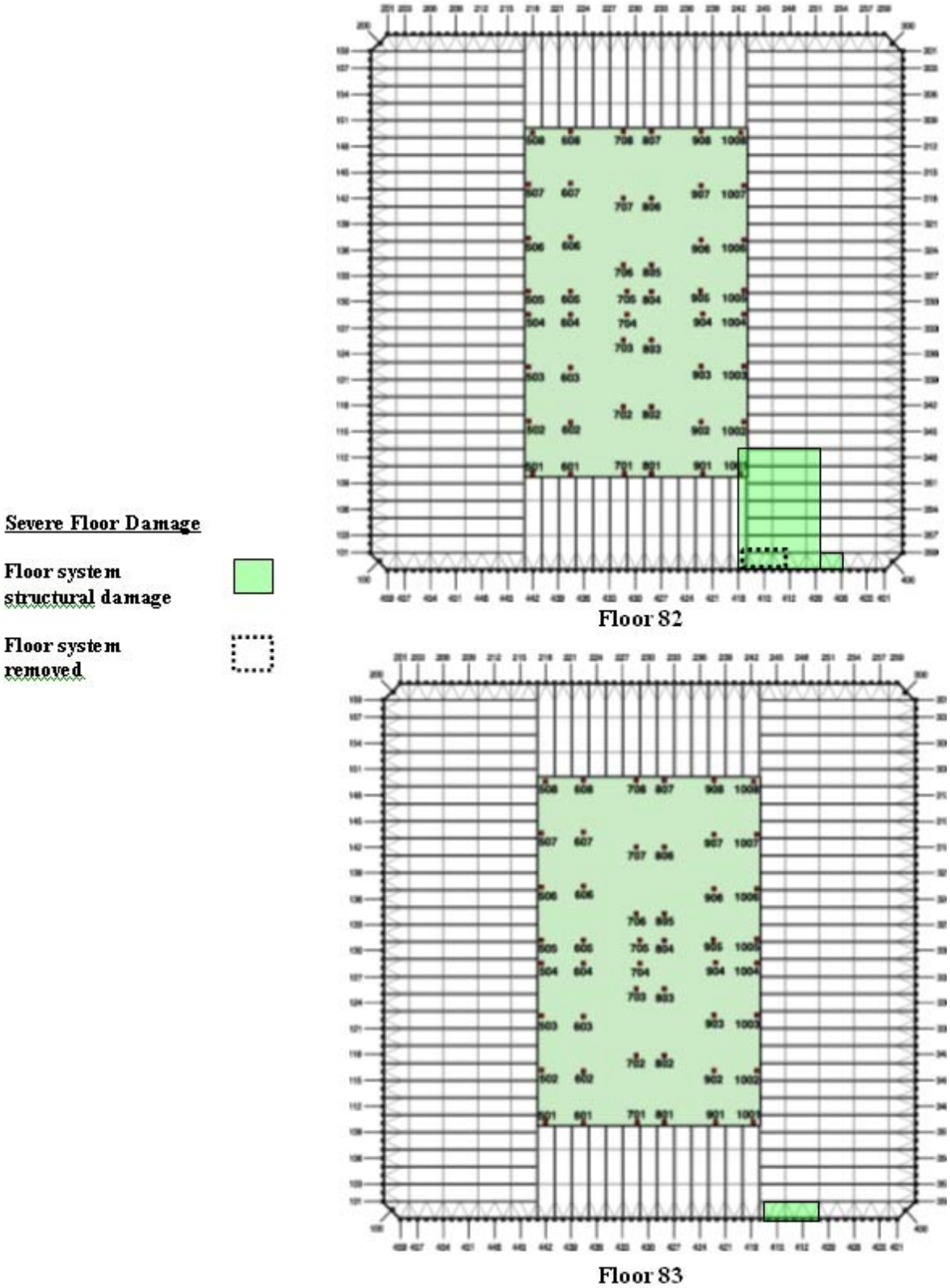

Figure B–18. WTC 2 Case C aircraft impact damage to Structural Floors 82 and 83.

WTC 2 CASE D – OCCUPANCY FLOOR GRAPHICS

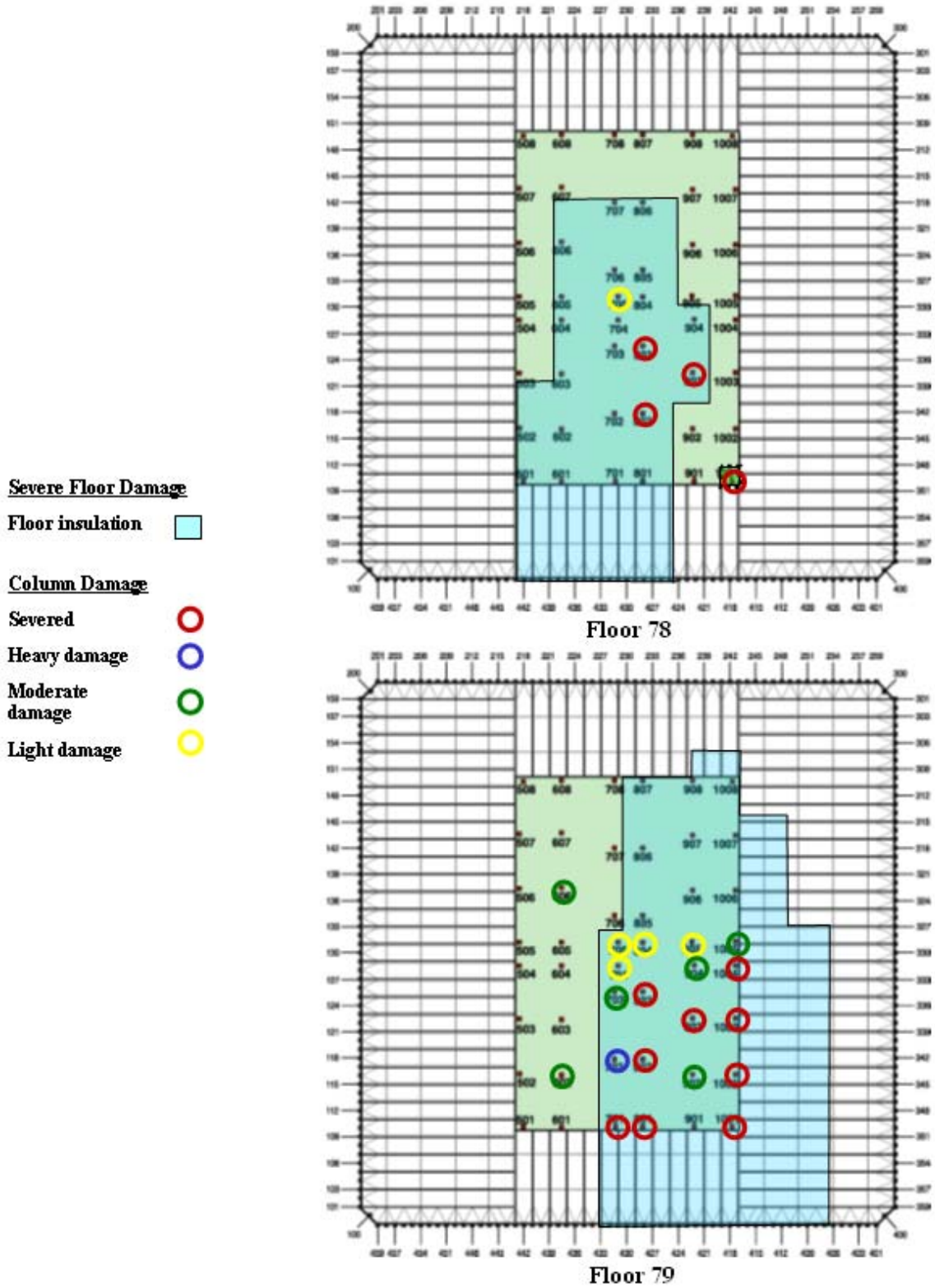

Figure B–19. WTC 2 Case D aircraft impact damage to Occupancy Floors 78 and 79.

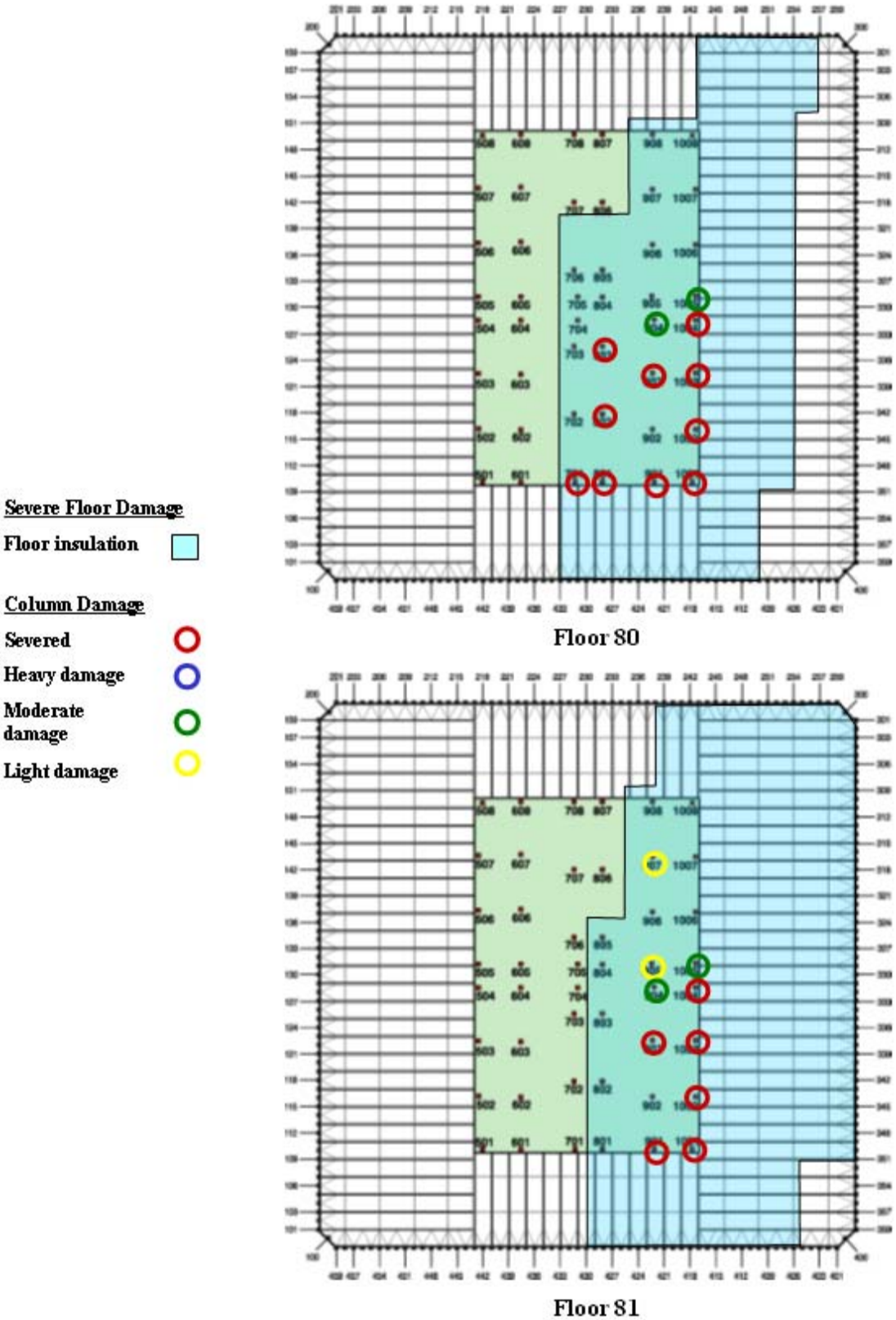

Figure B–20. WTC 2 Case D aircraft impact damage to Occupancy Floors 80 and 81.

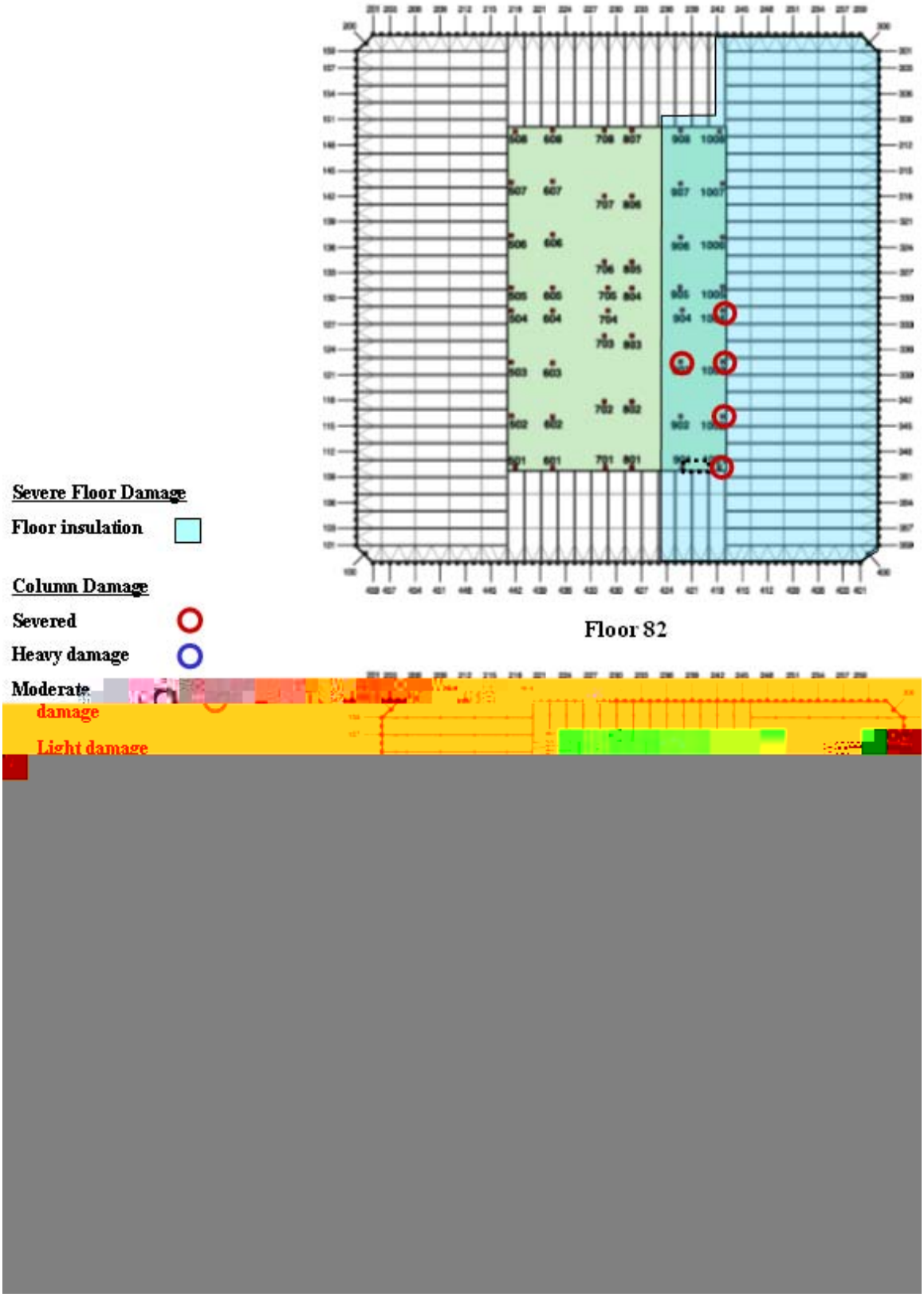

Figure B–21. WTC 2 Case D aircraft impact damage to Occupancy Floors 82 and 83.

WTC 2 CASE D – STRUCTURAL FLOOR GRAPHICS

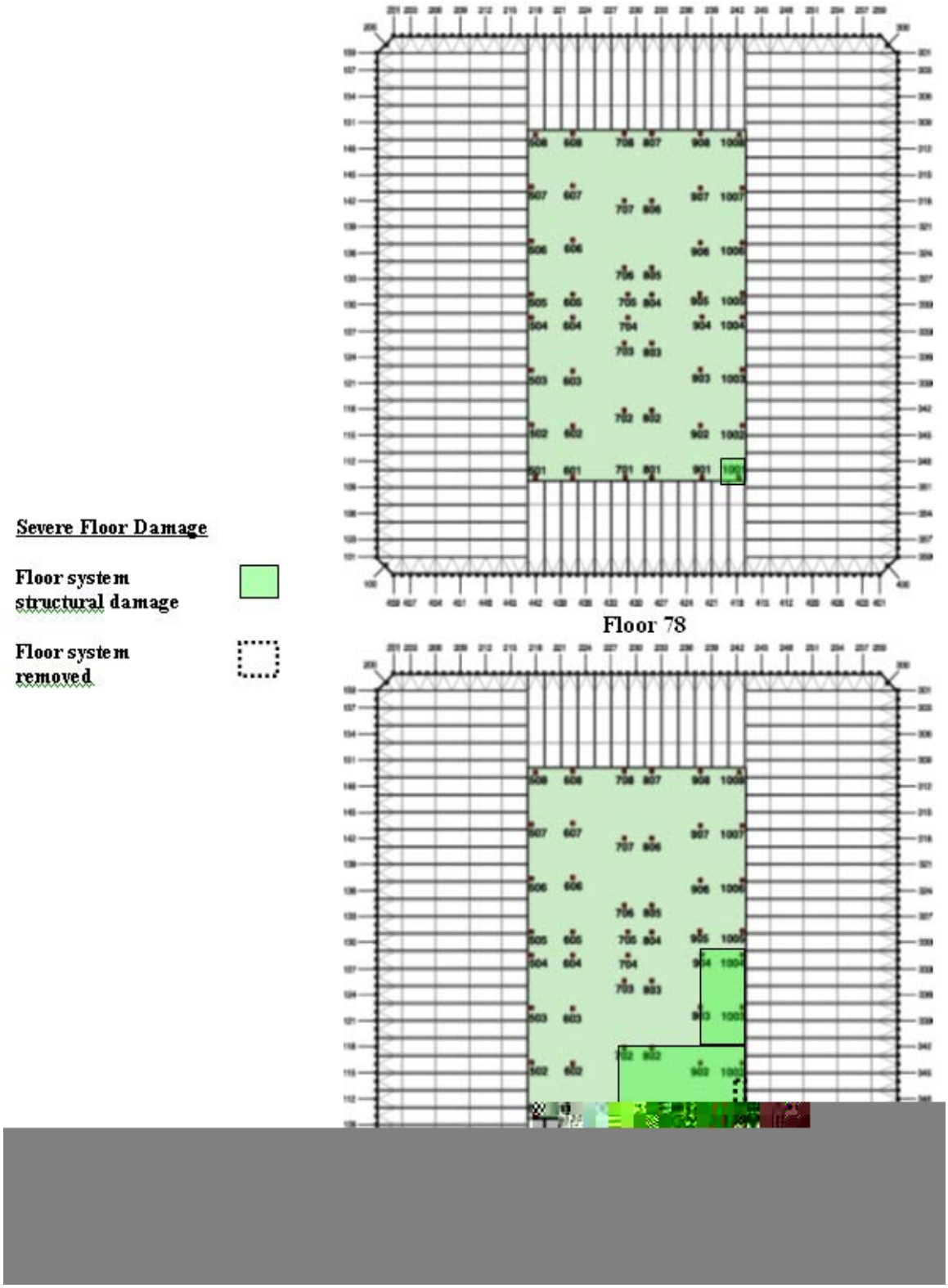

Figure B–22. WTC 2 Case D aircraft impact damage to Structural Floors 78 and 79.

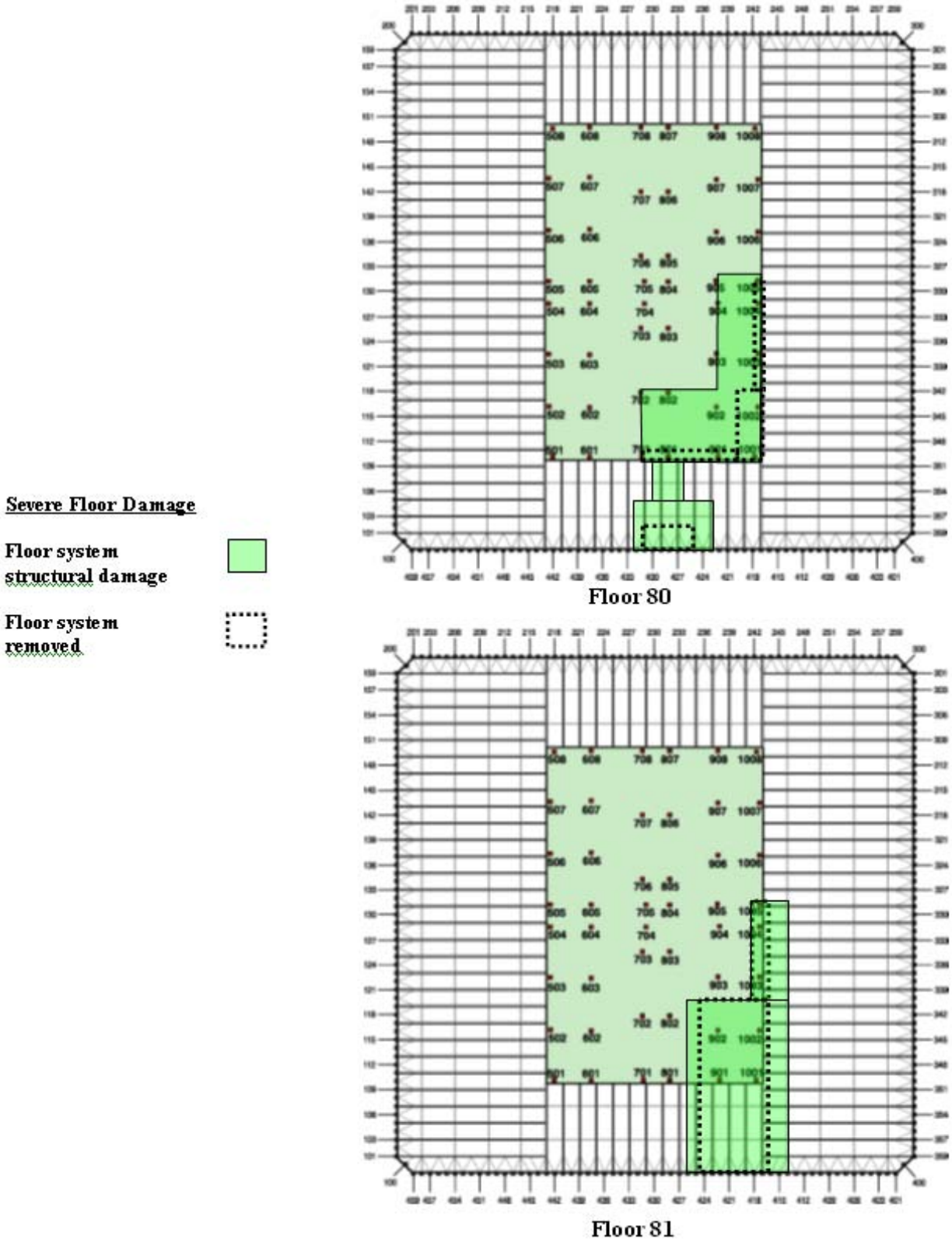

Figure B–23. WTC 2 Case D aircraft impact damage to Structural Floors 80 and 81.

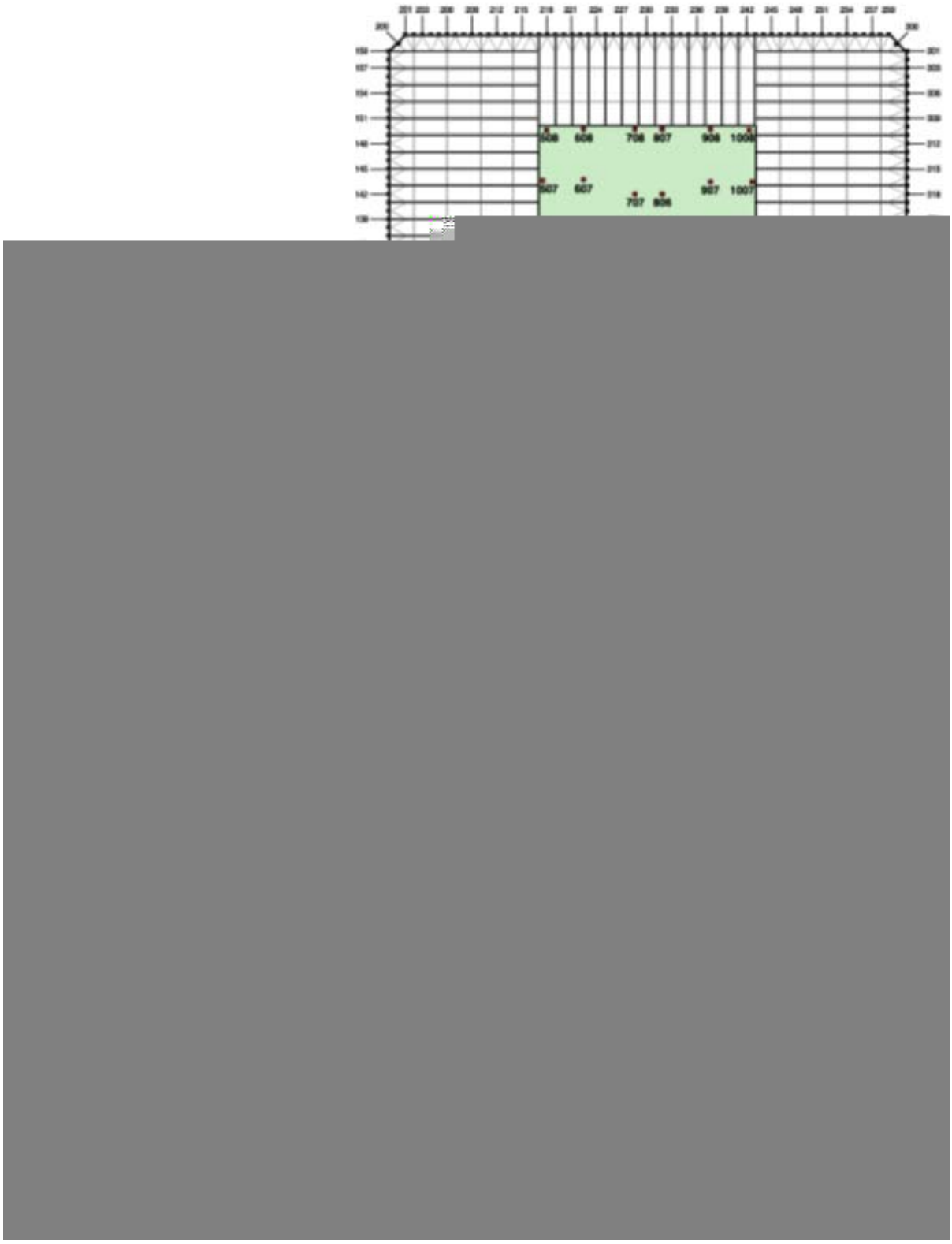

Figure B–24. WTC 2 Case D aircraft impact damage to Structural Floors 82 and 83.

NIST NCSTAR 1-6A

Federal Building and Fire Safety Investigation of the World Trade Center Disaster

Passive Fire Protection

Nicholas J. Carino
Monica A. Starnes
John L. Gross
Jiann C. Yang
Scott R. Kukuck
Kuldeep R. Prasad
Richard W. Bukowski

NIST National Institute of Standards and Technology • Technology Administration • U.S. Department of Commerce

NIST NCSTAR 1-6A

Federal Building and Fire Safety Investigation of the World Trade Center Disaster

Passive Fire Protection

Nicholas J. Carino*
Monica A. Starnes**
John L. Gross
Jiann C. Yang
Scott R. Kukuck***
Kuldeep R. Prasad
Richard W. Bukowski
Building and Fire Research Laboratory
National Institute of Standards and Technology

*Retired
**Current affiliation:
Johns Hopkins University
Applied Physics Laboratory
Laurel, Maryland

***Current affiliation:
U.S. Army Research Laboratory
Aberdeen Proving Grounds, Maryland

September 2005

U.S. Department of Commerce
Carlos M. Gutierrez, Secretary

Technology Administration
Michelle O' Neill, Acting Under Secretary for Technology

National Institute of Standards and Technology
William Jeffrey, Director

Disclaimer No. 1

Certain commercial entities, equipment, products, or materials are identified in this document in order to describe a procedure or concept adequately or to trace the history of the procedures and practices used. Such identification is not intended to imply recommendation, endorsement, or implication that the entities, products, materials, or equipment are necessarily the best available for the purpose. Nor does such identification imply a finding of fault or negligence by the National Institute of Standards and Technology.

Disclaimer No. 2

The policy of NIST is to use the International System of Units (metric units) in all publications. In this document, however, units are presented in metric units or the inch-pound system, whichever is prevalent in the discipline.

Disclaimer No. 3

Pursuant to section 7 of the National Construction Safety Team Act, the NIST Director has determined that certain evidence received by NIST in the course of this Investigation is "voluntarily provided safety-related information" that is "not directly related to the building failure being investigated" and that "disclosure of that information would inhibit the voluntary provision of that type of information" (15 USC 7306c).

In addition, a substantial portion of the evidence collected by NIST in the course of the Investigation has been provided to NIST under nondisclosure agreements.

Disclaimer No. 4

NIST takes no position as to whether the design or construction of a WTC building was compliant with any code since, due to the destruction of the WTC buildings, NIST could not verify the actual (or as-built) construction, the properties and condition of the materials used, or changes to the original construction made over the life of the buildings. In addition, NIST could not verify the interpretations of codes used by applicable authorities in determining compliance when implementing building codes. Where an Investigation report states whether a system was designed or installed as required by a code *provision*, NIST has documentary or anecdotal evidence indicating whether the requirement was met, or NIST has independently conducted tests or analyses indicating whether the requirement was met.

Use in Legal Proceedings

No part of any report resulting from a NIST investigation into a structural failure or from an investigation under the National Construction Safety Team Act may be used in any suit or action for damages arising out of any matter mentioned in such report (15 USC 281a; as amended by P.L. 107-231).

National Institute of Standards and Technology National Construction Safety Team Act Report 1-6A
Natl. Inst. Stand. Technol. Natl. Constr. Sfty. Tm. Act Rpt. 1-6A, 326 pages (September 2005)
CODEN: NSPUE2

U.S. GOVERNMENT PRINTING OFFICE
WASHINGTON: 2005

For sale by the Superintendent of Documents, U.S. Government Printing Office
Internet: bookstore.gpo.gov — Phone: (202) 512-1800 — Fax: (202) 512-2250
Mail: Stop SSOP, Washington, DC 20402-0001

ABSTRACT

This report deals with the passive fire protection used in the World Trade Center (WTC) towers. The main objective is to provide background information that can be used to assess the in-place conditions of the passive protection before and after aircraft impact. The report includes a review of key building code provisions related to structural fire protection. It also includes a review of key decisions related to passive fire protection made during design, construction, and occupancy of the towers. Copies of documents to support key findings are included in an Appendix. A summary is provided of available data on in-place measurements of the sprayed fire-resistive materials (SFRMs) applied to the floor trusses and to core members. Measurements of thermophysical properties of the passive fire protection materials, including gypsum panels, are presented. The effects of gaps in thermal insulation and the effects of variability of insulation thickness are evaluated. The rationale for selecting the effective thickness of thermal insulation for use in thermal-structural analyses is presented. Measurements of adhesive and cohesive strengths of a selected SFRM are summarized. Simplified models are presented for estimating the acceleration required to dislodge SFRM from planar surfaces and encased round bars. The report concludes with a summary of key findings.

Keywords: adhesive strength, building code, cohesive strength, construction classification, density, equivalent thickness, retrofit, specific heat capacity, sprayed fire-resistive materials (SFRM), thermal conductivity, thermal insulation, thickness, thickness variability, World Trade Center.

This page intentionally left blank.

TABLE OF CONTENTS

Abstract iii
List of Figures ix
List of Tables xiii
List of Acronyms and Abbreviations xv
Metric Conversion Table xvii
Preface xix
Acknowledgments xxix
Executive Summary xxxi

Chapter 1
Introduction 1
1.1 Fire-Resistive Materials 1
1.2 Scope of Report 2

Chapter 2
Building Code Concepts for Structural Fire Resistance 5
2.1 Origins and Intent of Building Codes 5
2.2 Construction Types 5
2.3 Fire Resistance of Structural Elements 6

Chapter 3
Historical Review Related to Passive Fire Protection of WTC Towers 9
3.1 Agreements Between Port Authority and New York City Department of Buildings and Fire Department 9
3.2 New York City Building Code Requirements 10
3.2.1 Occupancy Groups 10
3.2.2 Construction Classification and Fire Rating 11
3.3 Classification of WTC Towers 12
3.3.1 Specifications for Passive Fire Protection 12
3.3.2 Response to Local Law 5/1973 13
3.4 Selection of Fire-resistive Materials 14
3.4.1 Floor Trusses 14
3.4.2 Perimeter Columns 16
3.4.3 Core Columns 18

3.5 Specified Thickness of Fire-resistive Materials 18
3.5.1 During Construction 18
3.5.2 Report on 1975 Fire 21
3.5.3 In-Place Thickness and Upgrading of SFRM 24
3.5.4 Need for Fire Endurance Tests 26
3.5.5 Calculations of SFRM Thickness for Core Members 26
3.6 Maintenance of SFRM in Elevator Shafts 29
3.6.1 Bond Strength 29
3.6.2 Inspections 30
3.7 General Conditions of SFRM on Floor Trusses 30

Chapter 4
As-Applied Thickness of SFRM 37
4.1 Truss-Supported Floor System 37
4.2 Analysis of Photographs 40
4.3 Port Authority Data on Upgraded SFRM on Trusses 42
4.4 Column SFRM Thickness 49

Chapter 5
Effect of SFRM Geometry on Thermal Response 51
5.1 Effects of Thickness Variability and Gaps in SFRM 51
5.2 Equivalent Thickness 57
5.3 Recommended Thickness of SFRM for Thermal Analyses 60

Chapter 6
Thermophysical Properties 63
6.1 ASTM Test Methods for SFRMs 64
6.2 Reported SFRM Properties 65
6.3 Measured Thermophysical Properties of SFRMs 65
6.3.1 Sample Preparation 66
6.3.2 Thermal Conductivity Measurements 67
6.3.3 Specific Heat Capacity Measurements 69
6.3.4 Density Measurements 72
6.3.5 Concluding Remarks 74
6.4 Thermophysical Properties of Gypsum Panels 75
6.4.1 Samples 75
6.4.2 Thermal Conductivity Measurements 75

6.4.3 Specific Heat Capacity Measurements 78
6.4.4 Density Measurements 80

Chapter 7
Adhesive and Cohesive Strength 83
7.1 Reported In-Place Density and Bond Strength 83
7.2 Specimen Preparation and Test Procedures 87
7.2.1 Preparation of Test Plates 87
7.2.2 Test Methods 87
7.2.3 Preparation of Test Specimens 89
7.3 Test Results 95
7.3.1 Density 95
7.3.2 In-Plane Cohesive Strength 97
7.3.3 Adhesive Strength 98
7.3.4 Cohesive Strength Normal to Surface 104
7.3.5 Adhesive Strength Versus Cohesive Strength Normal to Surface 107
7.4 Simplified Approach to Predict Dislodging of SFRM 108
7.4.1 Debris Impact Study 113

Chapter 8
Summary 115
8.1 Findings 115

Chapter 9
References 119

Appendix A
Referenced Documents 123

Appendix B
Thermophysical Properties Test Data 253

Appendix C
Sprayed Fire-Resistive Material 263

This page intentionally left blank.

LIST OF FIGURES

Figure P–1. The eight projects in the federal building and fire safety investigation of the WTC disaster. xxi

Figure 1–1. Examples of sprayed fire-resistive materials: (left) material based on gypsum and vermiculite aggregate; (right) material based on mineral fibers and cementitious binder. 2

Figure 3–1. Mock up of floor truss system. 14

Figure 3–2. Schematic of composite floor truss system. 15

Figure 3–3. Demonstration of application of Monokote sprayed fire-resistive material to floor trusses. 16

Figure 3–4. Thermal insulation for perimeter columns. 17

Figure 3–5. Intersection of main truss and bridging truss showing generally good coverage of SFRM on truss members but thickness varies on web bars. 33

Figure 3–6. Intersection of main truss and bridging truss showing thinner SFRM on members of bridging truss. 33

Figure 3–7. Connection of main truss to spandrel beam showing relatively thin SFRM on truss seat and no SFRM on damper. 34

Figure 3–8. End of main truss showing low thickness of SFRM on truss members and no SFRM on damper saddle. 34

Figure 3–9. Intersection of main truss and bridging truss showing thin SFRM on the ends of some web bars; SFRM was not applied to the metal decking. 35

Figure 3–10. Example of damage to SFRM during installation of utilities. 35

Figure 4–1. (a) Dotplot of average thickness of floor trusses for floors 23 and 24, (b) normal probability plot of all average thickness values, and (c) normal probability plot of average thickness with four values (six points) excluded. 39

Figure 4–2. Example of measurement procedure used to estimate SFRM thickness from photographs. 41

Figure 4–3. (a) Normal probability plot of estimated SFRM thickness based on photographs, and (b) normal probability plot of natural logarithms of thickness (Data provided by PANYNJ). 43

Figure 4–4. (a) Dotplot of individual thickness measurements on floor trusses from Port Authority Construction Audit Reports, (b) histogram of thickness measurements, (c) normal probability plot of thickness measurements,

Figure 6–5. Comparison of BLAZE-SHIELD DC/F specific heat capacity measurements from Harmathy (1983) with present results from Laboratory A. 70

Figure 6–6. Comparison of specific heat capacity measurements from Laboratory B with results from Laboratory A. 71

Figure 6–7. Comparison of specific heat capacity measurements for BLAZE-SHIELD DC/F from

Figure 7–15. Results of second tests after repair: specimen on left had adhesive failure and specimen on right had cohesive failure. 94

Figure 7–16. SFRM specimen after measuring in-plane cohesive strength. 94

Figure 7–17. Density of BLAZE-SHIELD DC/F specimens. 96

Figure 7–18. Air-dry density of BLAZE-SHIELD DC/F from NIST/UL floor truss fire endurance tests (NIST NCSTAR 1-6B). 97

Figure 7–19. In-plane cohesive strength for BLAZE-SHIELD DC/F specimens. 98

Figure 7–20. Example of "adhesive" failure of SFRM (original location of test specimens are the gaps in the two strips); photo on left is magnified view of thin layer of paste and fibers (the marks around the perimeter is red ink used to locate field of view). 99

Figure 7–21. Example of lack of adhesion in 1½ in. SFRM on steel plate with primer. 100

Figure 7–22. Examples of good adhesion in specimens with unprimed steel plates: (top) ¾ in. SFRM specimen before testing; (bottom) 1½ in. SFRM specimen after completion of tests. 102

Figure 7–23. Adhesive strength of BLAZE-SHIELD DC/F specimens for primed and unprimed steel plates. 103

Figure 7–24. Examples of cohesive failure in 1½ in. SFRM specimens. 104

Figure 7–25. Comparative testing: current method versus ASTM E 736 method: (top) locations of two screw cap tests; (bottom) after completion of tests. 105

Figure 7–26. Cohesive strength normal to surface for BLAZE-SHIELD DC/F specimens for primed and unprimed steel plates. 106

Figure 7–27. Comparison of adhesive strength with cohesive strength normal to surface (P = primed steel, NP = bare steel). 108

Figure 7–28. Derivation of acceleration to dislodge SFRM from planar substrate. 110

Figure 7–29. Derivation of acceleration to dislodge SFRM surrounding a round bar. 111

LIST OF TABLES

Table P–1. Federal building and fire safety investigation of the WTC disaster. xx

Table P–2. Public meetings and briefings of the WTC Investigation. xxiii

Table 3–1. Area and height limitations for unsprinklered buildings for Noncombustible Construction (Group 1) with a Business occupancy (NYCBC 1968). 12

Table 3–2. Specified fire-resistive materials after April 1970. 21

Table 3–3. Information in Sweets Catalogs regarding BLAZE-SHIELD products applied directly to beams, girders, or spandrels (with protected deck) from 1960 to1972. 23

Table 3–4. Design thickness of thermal insulation for reapplication to accessible columns in elevator shafts 12 and 13 of WTC 1. 28

Table 3–5. Design thickness of thermal insulation for reapplication to accessible columns and beams in elevator shafts 6 and 7 of WTC1. 29

Table 4–1. Average fireproofing thickness from six measurements taken in 1994 on each of 16 random floor trusses on floors 23 and 24 of WTC 1. 38

Table 4–2. Summary of Port Authority test reports for upgraded SFRM on floor trusses (30-P). 45

Table 6–1. Summary of SFRMs used in WTC. 63

Table 6–2. Current ASTM test methods for SFRMs. 64

Table 6–3. Properties from tests of SFRMs reported by manufacturers. 65

Table 6–4. Measured thermal conductivity as a function of temperature. 68

Table 6–5. Calculated specific heat capacity of the three SFRMs. 69

Table 6–6. Mass loss of SFRMs with increasing temperature. 73

Table 6–7. Thermal expansion results of SFRMs. 73

Table 6–8. Calculated densities of SFRMs. 74

Table 6–9. Thermal conductivities of gypsum materials. 76

Table 6–10. Bulk densities of the four gypsum materials. 80

Table 7–1. Density and bond strength of SFRM on floor trusses reported by the Port Authority of New York and New Jersey (30-P). 85

Table 7–2. Test matrix. 95

Table 7–3. Density of BLAZE-SHIELD DC/F specimens. 95

Table 7–4. In-plane cohesive strength for BLAZE-SHIELD DC/F specimens. 98

Table 7–5. Adhesive strength of BLAZE-SHIELD DC/F specimens..... 103

Table 7–6. Summary of adhesive strength results..... 104

Table 7–7. Cohesive strength normal to surface for BLAZE-SHIELD DC/F specimens..... 106

Table 7–8. Summary of cohesive strengths normal to surface..... 107

Table 7–9. Comparison of average adhesive strength and average cohesive strength normal to surface. 108

Table 7–10. Acceleration required to dislodge SFRM from planar surface for different values of density, thickness, and bond strength (adhesive or cohesive). 110

Table 7–11. Acceleration required to dislodge SFRM from encased bar for different values of bar diameter, SFRM thickness, SFRM in-plane cohesive strength, and strength ratio (alpha). 112

LIST OF ACRONYMS AND ABBREVIATIONS

Acronyms

ASTM	ASTM International (formerly American Society for Testing and Materials)
BFRL	Building and Fire Research Laboratory
BOCA	Building Officials and Code Administrators
DSC	Differential Scanning Calorimetry
DTA	Differential Thermal Analysis
ER&S	Emory Roth & Sons
FDNY	New York City Fire Department
IBC	International Building Code
ICBO	International Conference of Building Officials
ICC	International Code Council
LERA	Leslie E. Robertson Associates
NCST	National Construction Safety Team
NIST	National Institute of Standards and Technology
NYCDOB	New York City Department of Buildings
SHCR	Skilling, Helle, Christiansen, & Robertson
SFRM	sprayed fire-resistive material
STA	Simultaneous Thermal Analyzer
TGA	Thermal Gravimetric Analysis
UBC	Uniform Building Code
UL	Underwriters Laboratories, Inc.
USM	United States Mineral Products Co.
WF	wide flange (a type of structural steel shape now usually called a W-shape). ASTM A 6 defines them as “doubly-symmetric, wide-flange shapes with inside flange surfaces that are substantially parallel.”
WTC	World Trade Center
WTC 1	World Trade Center 1 (North Tower)
WTC 2	World Trade Center 2 (South Tower)
WTC 7	World Trade Center 7

Abbreviations

a	acceleration
Btu	British thermal unit
°C	degrees Celsius
d_i	steel bar diameter
d_0	outside diameter of SFRM on round bar
°F	degrees Fahrenheit
f_b	cohesive strength normal to surface or adhesive strength
f_t	in-plane cohesive strength of SFRM
ft	foot
ft^2	square foot
g	acceleration of gravity
g	gram
h	hour
in.	inch
J	joule
K	kelvin (absolute temperature)
kg	kilogram
lb	pound
m	meter
m^2	square meter
m^3	cubic meter
min	minute
pcf	pounds per cubic foot
psf	pounds per square foot
psi	pounds per square inch
s	second
t	thickness of SFRM
W	watt
α	ratio of adhesive strength to in-plane cohesive strength of SFRM
ρ	mass density of SFRM

METRIC CONVERSION TABLE

To convert from	to	Multiply by
inch (in.)	meter (m)	2.54 E-02
degree Fahrenheit (°F)	degree Celsius (°C)	t/ °C = (t/ °F - 32)/1.8
foot (ft)	meter (m)	3.048 E-01
pcf (pound per cubic foot) (lb/ft^3)	kilogram per cubic meter (kg/m^3)	1.601 846 E+01
Btu_{IT} · in./(ft^2 · h · °F)	W/(m · K)	1.442 279 E-01
psf (pound-force per square foot) (lbf/ft^2)	kilopascal (kPa)	4.788 026 E-02
psi (pound-force per square inch) (lbf/in^2)	kilopascal (kPa)	6.894 757 E+00

This page intentionally left blank.

PREFACE

Genesis of This Investigation

Immediately following the terrorist attack on the World Trade Center (WTC) on September 11, 2001, the Federal Emergency Management Agency (FEMA) and the American Society of Civil Engineers began planning a building performance study of the disaster. The week of October 7, as soon as the rescue and search efforts ceased, the Building Performance Study Team went to the site and began its assessment. This was to be a brief effort, as the study team consisted of experts who largely volunteered their time away from their other professional commitments. The Building Performance Study Team issued its report in May 2002, fulfilling its goal "to determine probable failure mechanisms and to identify areas of future investigation that could lead to practical measures for improving the damage resistance of buildings against such unforeseen events."

On August 21, 2002, with funding from the U.S. Congress through FEMA, the National Institute of Standards and Technology (NIST) announced its building and fire safety investigation of the WTC disaster. On October 1, 2002, the National Construction Safety Team Act (Public Law 107-231), was signed into law. The NIST WTC Investigation was conducted under the authority of the National Construction Safety Team Act.

The goals of the investigation of the WTC disaster were:

- To investigate the building construction, the materials used, and the technical conditions that contributed to the outcome of the WTC disaster.
- To serve as the basis for:
  - Improvements in the way buildings are designed, constructed, maintained, and used;
  - Improved tools and guidance for industry and safety officials;
  - Recommended revisions to current codes, standards, and practices; and
  - Improved public safety.

The specific objectives were:

1. Determine why and how WTC 1 and WTC 2 collapsed following the initial impacts of the aircraft and why and how WTC 7 collapsed;
2. Determine why the injuries and fatalities were so high or low depending on location, including all technical aspects of fire protection, occupant behavior, evacuation, and emergency response;
3. Determine what procedures and practices were used in the design, construction, operation, and maintenance of WTC 1, 2, and 7; and
4. Identify, as specifically as possible, areas in current building and fire codes, standards, and practices that warrant revision.

NIST is a nonregulatory agency of the U.S. Department of Commerce's Technology Administration. The purpose of NIST investigations is to improve the safety and structural integrity of buildings in the United States, and the focus is on fact finding. NIST investigative teams are authorized to assess building performance and emergency response and evacuation procedures in the wake of any building failure that has resulted in substantial loss of life or that posed significant potential of substantial loss of life. NIST does not have the statutory authority to make findings of fault nor negligence by individuals or organizations. Further, no part of any report resulting from a NIST investigation into a building failure or from an investigation under the National Construction Safety Team Act may be used in any suit or action for damages arising out of any matter mentioned in such report (15 USC 281a, as amended by Public Law 107-231).

Organization of the Investigation

The National Construction Safety Team for this Investigation, appointed by the then NIST Director, Dr. Arden L. Bement, Jr., was led by Dr. S. Shyam Sunder. Dr. William L. Grosshandler served as Associate Lead Investigator, Mr. Stephen A. Cauffman served as Program Manager for Administration, and Mr. Harold E. Nelson served on the team as a private sector expert. The Investigation included eight interdependent projects whose leaders comprised the remainder of the team. A detailed description of each of these eight projects is available at http://wtc.nist.gov. The purpose of each project is summarized in Table P–1, and the key interdependencies among the projects are illustrated in Fig. P–1.

Table P–1. Federal building and fire safety investigation of the WTC disaster.

Technical Area and Project Leader	Project Purpose
Analysis of Building and Fire Codes and Practices; Project Leaders: Dr. H. S. Lew and Mr. Richard W. Bukowski	Document and analyze the code provisions, procedures, and practices used in the design, construction, operation, and maintenance of the structural, passive fire protection, and emergency access and evacuation systems of WTC 1, 2, and 7.
Baseline Structural Performance and Aircraft Impact Damage Analysis; Project Leader: Dr. Fahim H. Sadek	Analyze the baseline performance of WTC 1 and WTC 2 under design, service, and abnormal loads, and aircraft impact damage on the structural, fire protection, and egress systems.
Mechanical and Metallurgical Analysis of Structural Steel; Project Leader: Dr. Frank W. Gayle	Determine and analyze the mechanical and metallurgical properties and quality of steel, weldments, and connections from steel recovered from WTC 1, 2, and 7.
Investigation of Active Fire Protection Systems; Project Leader: Dr. David D. Evans; Dr. William Grosshandler	Investigate the performance of the active fire protection systems in WTC 1, 2, and 7 and their role in fire control, emergency response, and fate of occupants and responders.
Reconstruction of Thermal and Tenability Environment; Project Leader: Dr. Richard G. Gann	Reconstruct the time-evolving temperature, thermal environment, and smoke movement in WTC 1, 2, and 7 for use in evaluating the structural performance of the buildings and behavior and fate of occupants and responders.
Structural Fire Response and Collapse Analysis; Project Leaders: Dr. John L. Gross and Dr. Therese P. McAllister	Analyze the response of the WTC towers to fires with and without aircraft damage, the response of WTC 7 in fires, the performance of composite steel-trussed floor systems, and determine the most probable structural collapse sequence for WTC 1, 2, and 7.
Occupant Behavior, Egress, and Emergency Communications; Project Leader: Mr. Jason D. Averill	Analyze the behavior and fate of occupants and responders, both those who survived and those who did not, and the performance of the evacuation system.
Emergency Response Technologies and Guidelines; Project Leader: Mr. J. Randall Lawson	Document the activities of the emergency responders from the time of the terrorist attacks on WTC 1 and WTC 2 until the collapse of WTC 7, including practices followed and technologies used.

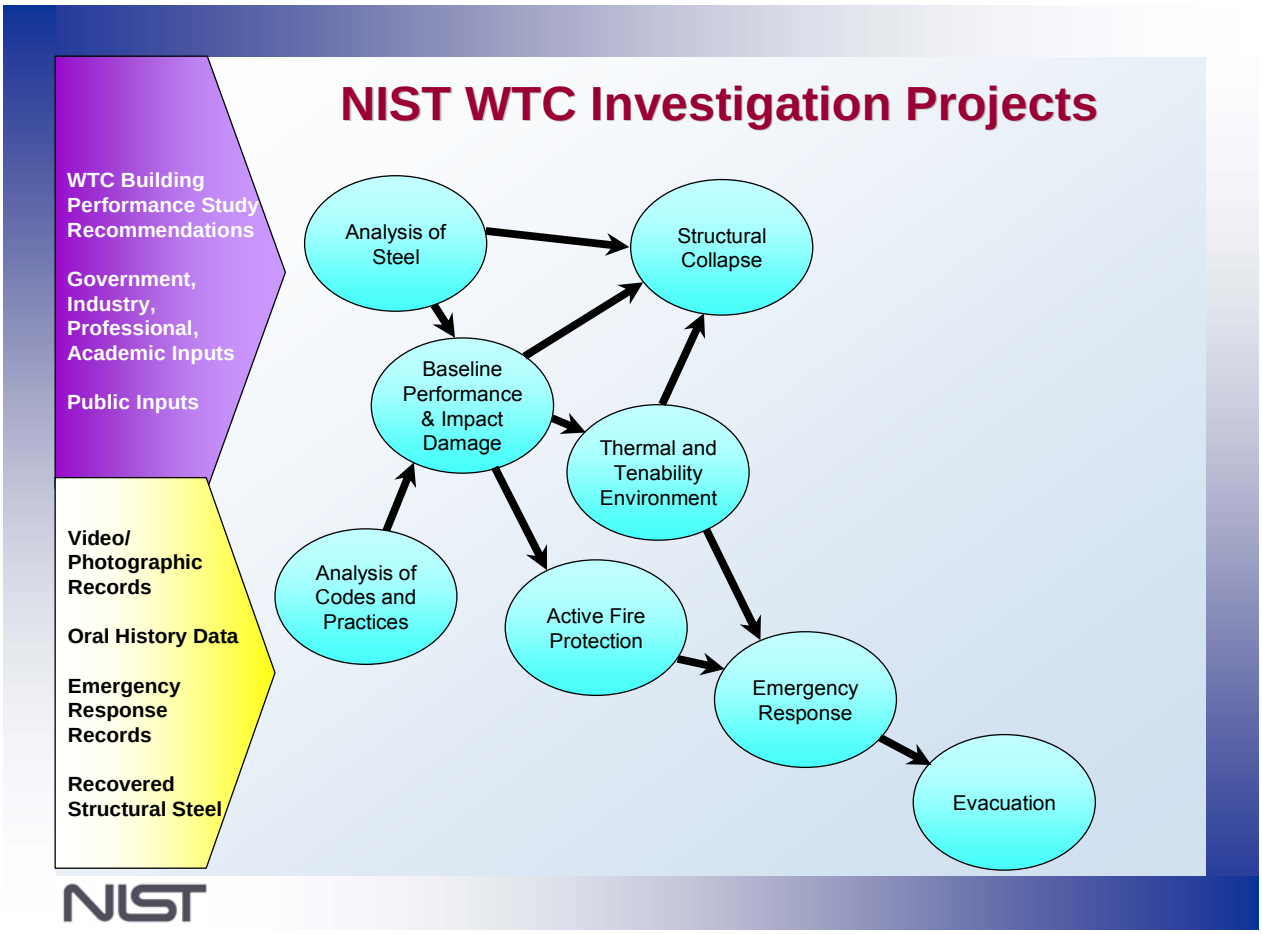

Figure P–1. The eight projects in the federal building and fire safety investigation of the WTC disaster.

National Construction Safety Team Advisory Committee

The NIST Director also established an advisory committee as mandated under the National Construction Safety Team Act. The initial members of the committee were appointed following a public solicitation. These were:

- Paul Fitzgerald, Executive Vice President (retired) FM Global, National Construction Safety Team Advisory Committee Chair
- John Barsom, President, Barsom Consulting, Ltd.
- John Bryan, Professor Emeritus, University of Maryland
- David Collins, President, The Preview Group, Inc.
- Glenn Corbett, Professor, John Jay College of Criminal Justice
- Philip DiNenno, President, Hughes Associates, Inc.

- Robert Hanson, Professor Emeritus, University of Michigan
- Charles Thornton, Co-Chairman and Managing Principal, The Thornton-Tomasetti Group, Inc.
- Kathleen Tierney, Director, Natural Hazards Research and Applications Information Center, University of Colorado at Boulder
- Forman Williams, Director, Center for Energy Research, University of California at San Diego

This National Construction Safety Team Advisory Committee provided technical advice during the Investigation and commentary on drafts of the Investigation reports prior to their public release. NIST has benefited from the work of many people in the preparation of these reports, including the National Construction Safety Team Advisory Committee. The content of the reports and recommendations, however, are solely the responsibility of NIST.

Public Outreach

During the course of this Investigation, NIST held public briefings and meetings (listed in Table P–2) to solicit input from the public, present preliminary findings, and obtain comments on the direction and progress of the Investigation from the public and the Advisory Committee.

NIST maintained a publicly accessible Web site during this Investigation at http://wtc.nist.gov. The site contained extensive information on the background and progress of the Investigation.

NIST's WTC Public-Private Response Plan

The collapse of the WTC buildings has led to broad reexamination of how tall buildings are designed, constructed, maintained, and used, especially with regard to major events such as fires, natural disasters, and terrorist attacks. Reflecting the enhanced interest in effecting necessary change, NIST, with support from Congress and the Administration, has put in place a program, the goal of which is to develop and implement the standards, technology, and practices needed for cost-effective improvements to the safety and security of buildings and building occupants, including evacuation, emergency response procedures, and threat mitigation.

The strategy to meet this goal is a three-part NIST-led public-private response program that includes:

- A federal building and fire safety investigation to study the most probable factors that contributed to post-aircraft impact collapse of the WTC towers and the 47-story WTC 7 building, and the associated evacuation and emergency response experience.
- A research and development (R&D) program to (a) facilitate the implementation of recommendations resulting from the WTC Investigation, and (b) provide the technical basis for cost-effective improvements to national building and fire codes, standards, and practices that enhance the safety of buildings, their occupants, and emergency responders.

Table P–2. Public meetings and briefings of the WTC Investigation.

Date	Location	Principal Agenda
June 24, 2002	New York City, NY	Public meeting: Public comments on the *Draft Plan* for the pending WTC Investigation.
August 21, 2002	Gaithersburg, MD	Media briefing announcing the formal start of the Investigation.
December 9, 2002	Washington, DC	Media briefing on release of the *Public Update* and NIST request for photographs and videos.
April 8, 2003	New York City, NY	Joint public forum with Columbia University on first-person interviews.
April 29–30, 2003	Gaithersburg, MD	NCST Advisory Committee meeting on plan for and progress on WTC Investigation with a public comment session.
May 7, 2003	New York City, NY	Media briefing on release of *May 2003 Progress Report.*
August 26–27, 2003	Gaithersburg, MD	NCST Advisory Committee meeting on status of the WTC investigation with a public comment session.
September 17, 2003	New York City, NY	Media and public briefing on initiation of first-person data collection projects.
December 2–3, 2003	Gaithersburg, MD	NCST Advisory Committee meeting on status and initial results and release of the *Public Update* with a public comment session.
February 12, 2004	New York City, NY	Public meeting on progress and preliminary findings with public comments on issues to be considered in formulating final recommendations.
June 18, 2004	New York City, NY	Media/public briefing on release of *June 2004 Progress Report.*
June 22–23, 2004	Gaithersburg, MD	NCST Advisory Committee meeting on the status of and preliminary findings from the WTC Investigation with a public comment session.
August 24, 2004	Northbrook, IL	Public viewing of standard fire resistance test of WTC floor system at Underwriters Laboratories, Inc.
October 19–20, 2004	Gaithersburg, MD	NCST Advisory Committee meeting on status and near complete set of preliminary findings with a public comment session.
November 22, 2004	Gaithersburg, MD	NCST Advisory Committee discussion on draft annual report to Congress, a public comment session, and a closed session to discuss pre-draft recommendations for WTC Investigation.
April 5, 2005	New York City, NY	Media and public briefing on release of the probable collapse sequence for the WTC towers and draft reports for the projects on codes and practices, evacuation, and emergency response.
June 23, 2005	New York City, NY	Media and public briefing on release of all draft reports for the WTC towers and draft recommendations for public comment.
September 12–13, 2005	Gaithersburg, MD	NCST Advisory Committee meeting on disposition of public comments and update to draft reports for the WTC towers.
September 13–15, 2005	Gaithersburg, MD	WTC Technical Conference for stakeholders and technical community for dissemination of findings and recommendations and opportunity for public to make technical comments.

- A dissemination and technical assistance program (DTAP) to (a) engage leaders of the construction and building community in ensuring timely adoption and widespread use of proposed changes to practices, standards, and codes resulting from the WTC Investigation and the R&D program, and (b) provide practical guidance and tools to better prepare facility owners, contractors, architects, engineers, emergency responders, and regulatory authorities to respond to future disasters.

The desired outcomes are to make buildings, occupants, and first responders safer in future disaster events.

National Construction Safety Team Reports on the WTC Investigation

A final report on the collapse of the WTC towers is being issued as NIST NCSTAR 1. A companion report on the collapse of WTC 7 is being issued as NIST NCSTAR 1A. The present report is one of a set that provides more detailed documentation of the Investigation findings and the means by which these technical results were achieved. As such, it is part of the archival record of this Investigation. The titles of the full set of Investigation publications are:

NIST (National Institute of Standards and Technology). 2005. *Federal Building and Fire Safety Investigation of the World Trade Center Disaster: Final Report on the Collapse of the World Trade Center Towers.* NIST NCSTAR 1. Gaithersburg, MD, September.

NIST (National Institute of Standards and Technology). 2006. *Federal Building and Fire Safety Investigation of the World Trade Center Disaster: Final Report on the Collapse of World Trade Center 7.* NIST NCSTAR 1A. Gaithersburg, MD.

Lew, H. S., R. W. Bukowski, and N. J. Carino. 2005. *Federal Building and Fire Safety Investigation of the World Trade Center Disaster: Design, Construction, and Maintenance of Structural and Life Safety Systems.* NIST NCSTAR 1-1. National Institute of Standards and Technology. Gaithersburg, MD, September.

Fanella, D. A., A. T. Derecho, and S. K. Ghosh. 2005. *Federal Building and Fire Safety Investigation of the World Trade Center Disaster: Design and Construction of Structural Systems.* NIST NCSTAR 1-1A. National Institute of Standards and Technology. Gaithersburg, MD, September.

Ghosh, S. K., and X. Liang. 2005. *Federal Building and Fire Safety Investigation of the World Trade Center Disaster: Comparison of Building Code Structural Requirements.* NIST NCSTAR 1-1B. National Institute of Standards and Technology. Gaithersburg, MD, September.

Fanella, D. A., A. T. Derecho, and S. K. Ghosh. 2005. *Federal Building and Fire Safety Investigation of the World Trade Center Disaster: Maintenance and Modifications to Structural Systems.* NIST NCSTAR 1-1C. National Institute of Standards and Technology. Gaithersburg, MD, September.

Grill, R. A., and D. A. Johnson. 2005. *Federal Building and Fire Safety Investigation of the World Trade Center Disaster: Fire Protection and Life Safety Provisions Applied to the Design and Construction of World Trade Center 1, 2, and 7 and Post-Construction Provisions Applied after Occupancy*. NIST NCSTAR 1-1D. National Institute of Standards and Technology. Gaithersburg, MD, September.

Razza, J. C., and R. A. Grill. 2005. *Federal Building and Fire Safety Investigation of the World Trade Center Disaster: Comparison of Codes, Standards, and Practices in Use at the Time of the Design and Construction of World Trade Center 1, 2, and 7*. NIST NCSTAR 1-1E. National Institute of Standards and Technology. Gaithersburg, MD, September.

Grill, R. A., D. A. Johnson, and D. A. Fanella. 2005. *Federal Building and Fire Safety Investigation of the World Trade Center Disaster: Comparison of the 1968 and Current (2003) New*

York City Building Code Provisions. NIST NCSTAR 1-1F. National Institute of Standards and Technology. Gaithersburg, MD, September.

Grill, R. A., and D. A. Johnson. 2005. *Federal Building and Fire Safety Investigation of the World Trade Center Disaster: Amendments to the Fire Protection and Life Safety Provisions of the New York City Building Code by Local Laws Adopted While World Trade Center 1, 2, and 7 Were in Use*. NIST NCSTAR 1-1G. National Institute of Standards and Technology. Gaithersburg, MD, September.

Grill, R. A., and D. A. Johnson. 2005. *Federal Building and Fire Safety Investigation of the World Trade Center Disaster: Post-Construction Modifications to Fire Protection and Life Safety Systems of World Trade Center 1 and 2*. NIST NCSTAR 1-1H. National Institute of Standards and Technology. Gaithersburg, MD, September.

Grill, R. A., D. A. Johnson, and D. A. Fanella. 2005. *Federal Building and Fire Safety Investigation of the World Trade Center Disaster: Post-Construction Modifications to Fire Protection, Life Safety, and Structural Systems of World Trade Center 7*. NIST NCSTAR 1-1I. National Institute of Standards and Technology. Gaithersburg, MD, September.

Grill, R. A., and D. A. Johnson. 2005. *Federal Building and Fire Safety Investigation of the World Trade Center Disaster: Design, Installation, and Operation of Fuel System for Emergency Power in World Trade Center 7*. NIST NCSTAR 1-1J. National Institute of Standards and Technology. Gaithersburg, MD, September.

Sadek, F. 2005. *Federal Building and Fire Safety Investigation of the World Trade Center Disaster: Baseline Structural Performance and Aircraft Impact Damage Analysis of the World Trade Center Towers.* NIST NCSTAR 1-2. National Institute of Standards and Technology. Gaithersburg, MD, September.

Faschan, W. J., and R. B. Garlock. 2005. *Federal Building and Fire Safety Investigation of the World Trade Center Disaster: Reference Structural Models and Baseline Performance Analysis of the World Trade Center Towers.* NIST NCSTAR 1-2A. National Institute of Standards and Technology. Gaithersburg, MD, September.

Kirkpatrick, S. W., R. T. Bocchieri, F. Sadek, R. A. MacNeill, S. Holmes, B. D. Peterson, R. W. Cilke, C. Navarro. 2005. *Federal Building and Fire Safety Investigation of the World Trade Center Disaster: Analysis of Aircraft Impacts into the World Trade Center Towers*, NIST NCSTAR 1-2B. National Institute of Standards and Technology. Gaithersburg, MD, September.

Gayle, F. W., R. J. Fields, W. E. Luecke, S. W. Banovic, T. Foecke, C. N. McCowan, T. A. Siewert, and J. D. McColskey. 2005. *Federal Building and Fire Safety Investigation of the World Trade Center Disaster: Mechanical and Metallurgical Analysis of Structural Steel.* NIST NCSTAR 1-3. National Institute of Standards and Technology. Gaithersburg, MD, September.

Luecke, W. E., T. A. Siewert, and F. W. Gayle. 2005. *Federal Building and Fire Safety Investigation of the World Trade Center Disaster: Contemporaneous Structural Steel Specifications.* NIST Special Publication 1-3A. National Institute of Standards and Technology. Gaithersburg, MD, September.

Banovic, S. W. 2005. *Federal Building and Fire Safety Investigation of the World Trade Center Disaster: Steel Inventory and Identification.* NIST NCSTAR 1-3B. National Institute of Standards and Technology. Gaithersburg, MD, September.

Banovic, S. W., and T. Foecke. 2005. *Federal Building and Fire Safety Investigation of the World Trade Center Disaster: Damage and Failure Modes of Structural Steel Components.* NIST NCSTAR 1-3C. National Institute of Standards and Technology. Gaithersburg, MD, September.

Luecke, W. E., J. D. McColskey, C. N. McCowan, S. W. Banovic, R. J. Fields, T. Foecke, T. A. Siewert, and F. W. Gayle. 2005. *Federal Building and Fire Safety Investigation of the World Trade Center Disaster: Mechanical Properties of Structural Steels.* NIST NCSTAR 1-3D. National Institute of Standards and Technology. Gaithersburg, MD, September.

Banovic, S. W., C. N. McCowan, and W. E. Luecke. 2005. *Federal Building and Fire Safety Investigation of the World Trade Center Disaster: Physical Properties of Structural Steels.* NIST NCSTAR 1-3E. National Institute of Standards and Technology. Gaithersburg, MD, September.

Evans, D. D., R. D. Peacock, E. D. Kuligowski, W. S. Dols, and W. L. Grosshandler. 2005. *Federal Building and Fire Safety Investigation of the World Trade Center Disaster: Active Fire Protection Systems.* NIST NCSTAR 1-4. National Institute of Standards and Technology. Gaithersburg, MD, September.

Kuligowski, E. D., D. D. Evans, and R. D. Peacock. 2005. *Federal Building and Fire Safety Investigation of the World Trade Center Disaster: Post-Construction Fires Prior to September 11, 2001.* NIST NCSTAR 1-4A. National Institute of Standards and Technology. Gaithersburg, MD, September.

Hopkins, M., J. Schoenrock, and E. Budnick. 2005. *Federal Building and Fire Safety Investigation of the World Trade Center Disaster: Fire Suppression Systems.* NIST NCSTAR 1-4B. National Institute of Standards and Technology. Gaithersburg, MD, September.

Keough, R. J., and R. A. Grill. 2005. *Federal Building and Fire Safety Investigation of the World Trade Center Disaster: Fire Alarm Systems.* NIST NCSTAR 1-4C. National Institute of Standards and Technology. Gaithersburg, MD, September.

Ferreira, M. J., and S. M. Strege. 2005. *Federal Building and Fire Safety Investigation of the World Trade Center Disaster: Smoke Management Systems.* NIST NCSTAR 1-4D. National Institute of Standards and Technology. Gaithersburg, MD, September.

Gann, R. G., A. Hamins, K. B. McGrattan, G. W. Mulholland, H. E. Nelson, T. J. Ohlemiller, W. M. Pitts, and K. R. Prasad. 2005. *Federal Building and Fire Safety Investigation of the World Trade Center Disaster: Reconstruction of the Fires in the World Trade Center Towers.* NIST NCSTAR 1-5. National Institute of Standards and Technology. Gaithersburg, MD, September.

Pitts, W. M., K. M. Butler, and V. Junker. 2005. *Federal Building and Fire Safety Investigation of the World Trade Center Disaster: Visual Evidence, Damage Estimates, and Timeline Analysis.* NIST NCSTAR 1-5A. National Institute of Standards and Technology. Gaithersburg, MD, September.

Hamins, A., A. Maranghides, K. B. McGrattan, E. Johnsson, T. J. Ohlemiller, M. Donnelly, J. Yang, G. Mulholland, K. R. Prasad, S. Kukuck, R. Anleitner and T. McAllister. 2005. *Federal Building and Fire Safety Investigation of the World Trade Center Disaster: Experiments and Modeling of Structural Steel Elements Exposed to Fire.* NIST NCSTAR 1-5B. National Institute of Standards and Technology. Gaithersburg, MD, September.

Ohlemiller, T. J., G. W. Mulholland, A. Maranghides, J. J. Filliben, and R. G. Gann. 2005. *Federal Building and Fire Safety Investigation of the World Trade Center Disaster: Fire Tests of Single Office Workstations.* NIST NCSTAR 1-5C. National Institute of Standards and Technology. Gaithersburg, MD, September.

Gann, R. G., M. A. Riley, J. M. Repp, A. S. Whittaker, A. M. Reinhorn, and P. A. Hough. 2005. *Federal Building and Fire Safety Investigation of the World Trade Center Disaster: Reaction of Ceiling Tile Systems to Shocks.* NIST NCSTAR 1-5D. National Institute of Standards and Technology. Gaithersburg, MD, September.

Hamins, A., A. Maranghides, K. B. McGrattan, T. J. Ohlemiller, and R. Anleitner. 2005. *Federal Building and Fire Safety Investigation of the World Trade Center Disaster: Experiments and Modeling of Multiple Workstations Burning in a Compartment.* NIST NCSTAR 1-5E. National Institute of Standards and Technology. Gaithersburg, MD, September.

McGrattan, K. B., C. Bouldin, and G. Forney. 2005. *Federal Building and Fire Safety Investigation of the World Trade Center Disaster: Computer Simulation of the Fires in the World Trade Center Towers.* NIST NCSTAR 1-5F. National Institute of Standards and Technology. Gaithersburg, MD, September.

Prasad, K. R., and H. R. Baum. 2005. *Federal Building and Fire Safety Investigation of the World Trade Center Disaster: Fire Structure Interface and Thermal Response of the World Trade Center Towers.* NIST NCSTAR 1-5G. National Institute of Standards and Technology. Gaithersburg, MD, September.

Gross, J. L., and T. McAllister. 2005. *Federal Building and Fire Safety Investigation of the World Trade Center Disaster: Structural Fire Response and Probable Collapse Sequence of the World Trade Center Towers.* NIST NCSTAR 1-6. National Institute of Standards and Technology. Gaithersburg, MD, September.

Carino, N. J., M. A. Starnes, J. L. Gross, J. C. Yang, S. Kukuck, K. R. Prasad, and R. W. Bukowski. 2005. *Federal Building and Fire Safety Investigation of the World Trade Center Disaster: Passive Fire Protection.* NIST NCSTAR 1-6A. National Institute of Standards and Technology. Gaithersburg, MD, September.

Gross, J., F. Hervey, M. Izydorek, J. Mammoser, and J. Treadway. 2005. *Federal Building and Fire Safety Investigation of the World Trade Center Disaster: Fire Resistance Tests of Floor Truss Systems.* NIST NCSTAR 1-6B. National Institute of Standards and Technology. Gaithersburg, MD, September.

Zarghamee, M. S., S. Bolourchi, D. W. Eggers, Ö. O. Erbay, F. W. Kan, Y. Kitane, A. A. Liepins, M. Mudlock, W. I. Naguib, R. P. Ojdrovic, A. T. Sarawit, P. R Barrett, J. L. Gross, and

T. P. McAllister. 2005. *Federal Building and Fire Safety Investigation of the World Trade Center Disaster: Component, Connection, and Subsystem Structural Analysis.* NIST NCSTAR 1-6C. National Institute of Standards and Technology. Gaithersburg, MD, September.

Zarghamee, M. S., Y. Kitane, Ö. O. Erbay, T. P. McAllister, and J. L. Gross. 2005. *Federal Building and Fire Safety Investigation of the World Trade Center Disaster: Global Structural Analysis of the Response of the World Trade Center Towers to Impact Damage and Fire.* NIST NCSTAR 1-6D. National Institute of Standards and Technology. Gaithersburg, MD, September.

McAllister, T., R. W. Bukowski, R. G. Gann, J. L. Gross, K. B. McGrattan, H. E. Nelson, L. Phan, W. M. Pitts, K. R. Prasad, F. Sadek. 2006. *Federal Building and Fire Safety Investigation of the World Trade Center Disaster: Structural Fire Response and Probable Collapse Sequence of World Trade Center 7.* (Provisional). NIST NCSTAR 1-6E. National Institute of Standards and Technology. Gaithersburg, MD.

Gilsanz, R., V. Arbitrio, C. Anders, D. Chlebus, K. Ezzeldin, W. Guo, P. Moloney, A. Montalva, J. Oh, K. Rubenacker. 2006. *Federal Building and Fire Safety Investigation of the World Trade Center Disaster: Structural Analysis of the Response of World Trade Center 7 to Debris Damage and Fire*. (Provisional). NIST NCSTAR 1-6F. National Institute of Standards and Technology. Gaithersburg, MD.

Kim, W. 2006. *Federal Building and Fire Safety Investigation of the World Trade Center Disaster: Analysis of September 11, 2001, Seismogram Data*. (Provisional). NIST NCSTAR 1-6G. National Institute of Standards and Technology. Gaithersburg, MD.

Nelson, K. 2006. *Federal Building and Fire Safety Investigation of the World Trade Center Disaster: The Con Ed Substation in World Trade Center 7.* (Provisional). NIST NCSTAR 1-6H. National Institute of Standards and Technology. Gaithersburg, MD.

Averill, J. D., D. S. Mileti, R. D. Peacock, E. D. Kuligowski, N. Groner, G. Proulx, P. A. Reneke, and H. E. Nelson. 2005. *Federal Building and Fire Safety Investigation of the World Trade Center Disaster: Occupant Behavior, Egress, and Emergency Communication.* NIST NCSTAR 1-7. National Institute of Standards and Technology. Gaithersburg, MD, September.

Fahy, R., and G. Proulx. 2005. *Federal Building and Fire Safety Investigation of the World Trade Center Disaster: Analysis of Published Accounts of the World Trade Center Evacuation.* NIST NCSTAR 1-7A. National Institute of Standards and Technology. Gaithersburg, MD, September.

Zmud, J. 2005. *Federal Building and Fire Safety Investigation of the World Trade Center Disaster: Technical Documentation for Survey Administration.* NIST NCSTAR 1-7B. National Institute of Standards and Technology. Gaithersburg, MD, September.

Lawson, J. R., and R. L. Vettori. 2005. *Federal Building and Fire Safety Investigation of the World Trade Center Disaster: The Emergency Response Operations.* NIST NCSTAR 1-8. National Institute of Standards and Technology. Gaithersburg, MD, September.

ACKNOWLEDGMENTS

Mr. Dale Bentz, Research Chemical Engineer in the Inorganic Materials Group of the Building and Fire Research Laboratory at NIST, is acknowledged for his contributions in conducting thermophysical property tests for gypsum materials.

This page intentionally left blank.

EXECUTIVE SUMMARY

The structural steel in the World Trade Center (WTC) towers was protected against the effects of fire with

higher risk of property loss in the event of failure of multiple floors. Fire resistance requirements,

WTC towers were classified as Occupancy Group E—Business. The 1968 Code identified two construction groups: Noncombustible Construction (Group 1) and Combustible Construction (Group 2). The WTC towers were classified as Construction Group 1 because their walls, exit ways, shafts, structural members, floors, and roofs were constructed of noncombustible materials. At the time of design and construction, the towers were not sprinklered.

The 1968 New York City Building Code defined five Classes within Construction Group 1. For Business occupancy, each Class required a fire endurance rating as follows:

- Class 1A: 4 hour protected
- Class 1B: 3 hour protected
- Class 1C: 2 hour protected
- Class 1D: 1 hour protected
- Class 1E: unprotected

Construction Classes 1A and 1B permitted buildings of unlimited height. Thus, the WTC towers could have been designed to meet either Class 1A or Class 1B requirements.

Classification of WTC Towers

It was the practice at the time, and continues to be the practice, for the architect to establish the building classification, fire rating of members and systems, and thermal protection requirements. The review of documents uncovered during the investigation indicated a discrepancy in the classification, and, therefore, in the fire ratings to be used in the design of the towers. Documents issued in the early stages of the design appear to indicate that the towers were classified as Class 1A. With the directive in 1965 to comply with the 1968 New York City Building Code, it appears that the towers were classified ultimately as Class 1B.

According to Section C26-314.1 of the 1968 New York City Building Code, construction classification 1B provided, in part, the following fire protection requirements:

- Columns, girders, trusses, other than roof trusses, and framing supporting more than one floor shall have 3 hour fire endurance;
- Columns, girders, trusses, other than roof trusses, and framing supporting one floor shall have 2 hour fire endurance
- Floor construction including beams shall have 2 hour fire endurance.
- Enclosure of vertical shafts, exits, passage-ways, and hoistways shall have 2 hour fire endurance; and

- Roof construction including beams, trusses, and framing including arches, domes, shells, cable supported roofs, and roof decks (for buildings over one story in height) shall have 2 hour fire endurance.

Thus, the columns were required to have a 3 hour fire endurance rating, and the floor system was required to a have a 2 hour rating when tested in accordance with ASTM E 119.

Response to Local Law 5/1973

In 1973, New York City Local Law No. 5 amended the New York City Building Code (effective January 18, 1973). Local Law No. 5 required, in part, the retrofit of existing unsprinklered office buildings 100 ft or higher. The New York City Department of Buildings permitted either:

- Subdividing the floor area into compartments of specified square footage by fire separations (1 h or 2 h fire rated depending on the size of the compartment), or

- Providing sprinkler protection.

A code compliance evaluation conducted in 1997 indicated that that all tenant floors in the two towers had been retrofitted with sprinklers (sprinklered) with the exception of four floors in WTC 1. In a 1999 update by the Port Authority it was noted that all tenant floors had been sprinklered and work was underway to complete sprinklering of the sky lobbies. In 2000, a property condition assessment report stated that the WTC towers were classified as "Class 1B – noncombustible, fire-protected, retrofitted with sprinklers in accordance with New York City Local Law 5/1973."

Selection of Fire-Resistive Materials

Classification of a building leads to its overall fire endurance rating and ratings of the various structural components. The New York City Building Code, however, does not prescribe how the required fire endurance rating is to be achieved. The Port Authority chose to protect the main structural components such as columns, spandrel beams, and floor trusses with sprayed fire-resistive material. This thermal protection technique was an established method for protecting columns, beams, and walls. In the 1960s, however, composite steel joist-supported floor systems were usually protected using "lath and plaster" enclosures or fire-rated ceiling tiles.

Since application of sprayed fire-resistive materials to floor trusses was an innovative fire protection method, the Port Authority arranged for demonstrations to establish its feasibility for the World Trade Center. The demonstrations were considered to be successful and in November 1968, the Port Authority awarded the contract for "spray fireproofing" of the interior portions (floor system and core) of the WTC towers. The fire protection of the exterior columns was included in the contract for the exterior aluminum cladding.

Several materials were considered for the sprayed thermal insulation. The exterior columns required insulation not only for fire protection but also to control column temperatures under service conditions. Alcoa recommended for the exterior columns the use of a sprayed material produced by U.S. Mineral Products, Co. known as BLAZE-SHIELD Type D. The same material was eventually selected for the floor trusses and core beams and columns. This product, however, contained asbestos fibers. On April

13, 1970, New York City issued restrictions on the application of sprayed thermal insulation containing asbestos. The use of BLAZE-SHIELD Type D was discontinued in 1970 at the 38th floor of WTC 1. The asbestos-containing material was subsequently encapsulated with a sprayed material that provided a hard coating. A green dye was added to the encapsulating material so that the asbestos containing SFRM could be identified. Thermal protection of the remaining floors of WTC 1 and all of WTC 2 was carried out using BLAZE-SHIELD Type DC/F, a product that contained mineral wool (glassy fibers) in place of the crystalline asbestos fibers. On the basis of tests, it was reported that the thermal properties of BLAZE-SHIELD Type DC/F were equal to or "slightly better" than those of BLAZE-SHIELD Type D.

Specified Thickness of Fire-Resistive Material

The thickness of fire-resistive material necessary to achieve the required fire endurance was assessed in 1965, more than three years before the award of the thermal protection contract. At that time, the Architect of Record recommended 1 in. of thermal protection for the top and bottom chords of the floor trusses and 2 in. for other members of the trusses. WTC project specifications for sprayed fire protection do not provide required material thickness or hourly ratings. In October 1969, the manager of project planning for the WTC provided the following instructions to the contractor applying the sprayed fire protection:

> "…Tower 'A' columns that are less than 14WF228 will require 2 3/16″ thick of 'Cafco Glaze [sic]-Shield 'Type D'' spray-on fireproofing. All Tower columns equal to or greater than 14WF228 will require 1 3/16″ of fireproofing…
>
> All Tower beams, spandrels and bar joists requiring spray-on fireproofing are to have a 1/2″ covering of 'Cafco.'
>
> The above requirements must be adhered to in order to maintain the Class 1-A Fire Rating of the New York City Building Code."

NIST's review of available documents has not uncovered the reasons for selecting BLAZE-SHIELD or the technical basis for specifying ½ in. thickness of insulation for the floor trusses. The last sentence in the above excerpt indicates that in October 1969, the towers were considered as Class 1A construction.

In February 1975, a fire occurred in WTC 1, spreading from the 9th to the 19th floor. After the fire, the Port Authority contracted Skilling, Helle, Christiansen, Robertson (SHCR), the Structural Engineer of Record for the design of the WTC towers, to assess the resulting structural damage and to report, in general, on the fire resistivity of the floor system. In its report dated April 1, 1975, SHCR communicated to the Port Authority that the fire did not cause structural damage, but it caused buckling of some top chord members of main trusses, buckling of bridging trusses, and distortion of deck support angles. The report provided valuable information on the history of the passive fire protection of the towers.

The 1975 post-fire report by SCHR stated further that thermal protection of the top chords of the floor trusses was not necessary, except for the corners of the buildings where the floor acted as a two-way system in bending. Additionally, it was stated that protection of the bridging trusses was not required because the bridging trusses were "not required as a part of the structural system."

In February 2003, NIST asked the Port Authority a series of questions related to the sprayed thermal protection for the floor system. The Port Authority replied in March that the top chords of the main trusses and the bridging trusses were protected.

Upgrading SFRM on Floor Trusses

In 1995, the Port Authority performed a study to establish requirements for retrofit of sprayed insulation to the floor trusses during major alterations (new construction) when tenants vacated spaces in the towers. The study estimated the thermal protection requirements based on "the fireproofing requirements" for Design No. G805 contained in the Fire Resistance Directory published by Underwriters Laboratories. The study concluded that "a two hour fire rating for the steel floor joist trusses can be achieved by applying a 1½ inch thickness of spray-on mineral fiber fire protection material directly to the steel truss chords and webs." In the years between 1995 and 2001, thermal protection was upgraded in a number of the floors affected by the fires on September 11, 2001. Specifically, in WTC 1, floors 92 through 100 and 102 were upgraded; and in WTC 2, floors 77, 78, 88, 89, 92, 96, and 97 were upgraded.

In 1999, the Port Authority established "guidelines regarding fireproofing repairs, replacement, and upgrades" for the towers. The guidelines for in tenant spaces may be summarized as follows:

- For full floors undergoing new construction or renovation, the floor trusses should be protected with 1½ in. of sprayed mineral fiber fire-resistive material. Retrofit of thermal protection requires removal of existing material and controlled inspection.

- For "tenant spaces less than a full floor undergoing either new construction or renovation," the floor trusses "need only meet the original construction standard. Fireproofing shall be inspected and patched as required to the greater of ¾ in. or to match existing" if it has already been upgraded to 1½ in.

In July 2000, an engineering consultant, commissioned by the Port Authority to conduct a fire-engineering assessment of the fire protection of the floor trusses, issued a report on the requirements of the fire resistance of the floor system of the towers. This report stated that BLAZE-SHIELD DC/F was used on the majority of the floor trusses. Based on calculations and risk assessment, the consultant concluded that:

- "The structural design has sufficient inherent fire performance to ensure that the fire condition is never the critical condition with respect to loading allowances.

- A single coat application is possible.

- Significant savings are possible.

- The target reduction of fiber content and increased long term durability can be achieved.

- Alternative materials should be considered."

As quoted, the report states that significant savings were possible by reducing the fiber content and considering alternative materials. The report suggested that the thickness of the SFRM could be reduced to ½ in. if the material properties at ambient temperature are applicable at higher temperatures. The

report recognized the lack of available temperature-dependent material data for BLAZE-SHIELD Type DC/F. Thus, considering the uncertainties in the material properties and having the understanding of material degradation with temperature and time, it was recommended that 1.3 in. of fire-resistive material be used for the floor trusses.

Later, in December 2000, the final draft of a report on *Property Condition Assessment of World Trade Center Portfolio* stated that, based on existing conditions "The rating of the structural fireproofing in the Towers and subgrade has been judged to be an adequate 1 hour rating considering the fact that all Tower floors are now sprinklered." The report also noted the ongoing Port Authority program to upgrade the fire-resistive material thickness to 1½ in. in order to achieve a 2 hour fire rating.

Need for Fire Endurance Tests

The fire protection of a truss-supported floor system by directly applying sprayed fire-resistive material to the trusses was innovative and not consistent with prevailing practice at the time the WTC towers were designed and constructed. While the benefits of conducting fire endurance tests were realized by individuals involved in the 1967 demonstrations of the application of SFRM, apparently no tests were conducted on the floor system used in the WTC towers. The Architect of Record and the Structural Engineer of Record stated that the fire rating of the floor system of the WTC towers could not be determined without testing. Communication from the Port Authority in 2003 confirms that there is no record of fire endurance testing of assemblies representing the thermally protected floor system.

Maintenance of SFRM in Elevator Shafts

Throughout the life of the WTC towers, the structural members that required the largest amount of inspection and maintenance within the core were the exposed columns and beams within the elevator shafts. These columns and beams were the only accessible fire-protected elements in the buildings. Adhesion failures were common, likely because of the exposed conditions of the columns and the inherently low strength of the SFRM.

Inspections of the shafts and accessible columns were reported as early as 1971. Problems were noted in the form of fallen insulation or with the over-spray material used to provide a harder surface. In 1993, the Port Authority commissioned Leslie E. Robertson Associates to carry out a continuing program to appraise the condition of the accessible columns located in the cores of the towers. The columns were inspected visually for signs of rusting, cracking, bowing, and loss of thermal insulation. During the first inspection, carried out in 1993, particular shafts were chosen based on the quantity and types of accessible columns, and the convenience to the Port Authority. Subsequent inspections involved sampling of the structural components and assemblies, which were more important to the structural integrity of the towers, and at locations with a relatively higher potential for defects and problems. The inspection report stated that the accessible columns in selected elevator shafts in WTC 1 and WTC 2 were "generally in good condition, no structural deficiencies such as cracking or bowing were found, the most common irregularities observed were missing fireproofing and light surface rusting of the exposed steel." Based on the inspections, LERA recommended "that remedial action to be taken where spray fireproofing is damaged, deteriorated or missing and where there is corrosion of the column base due to water leaks at elevator pits." Earlier in 1992, LERA performed calculations to determine the thickness of replacement thermal insulation for selected beams and columns within elevator shafts.

AS-APPLIED THICKNESS OF SFRM

1994 Measurements from WTC 1 Floors 23 and 24

In its search of documents, NIST found no information related to measurements of the thickness of thermal insulation taken during original construction. Reviewed documents, however, indicate that thickness appears to have been checked during construction. Recorded information on the in-place condition of the sprayed thermal insulation for the floor system first appeared in 1990 in the form of "Sample Area Data Sheets," which provided qualitative comments on the state of the in-place SFRM. Information regarding quantitative inspection of existing fire-resistive material appeared in documentation from 1994. That year, the Port Authority performed a series of thickness measurements of the existing SFRM on floors 23 and 24 of WTC 1. Six measurements were taken from "both flanges and web" of each of 16 randomly chosen trusses on each floor. Measured average thickness varied between 0.52 in. and 1.17 in. For the 32 measurements (16 on each floor), the overall average was 0.74 in., and the standard deviation of these averages was 0.16 in. Four of the 32 floor trusses had average thicknesses between 0.52 in. and 0.56 in. These measurements suggest that the minimum average thickness exceeded ½ in. Analysis of the reported mean thicknesses indicated that a lognormal distribution gave a better representation of the distribution rather than did a normal distribution.

Analysis of Photographs

Additional SFRM thickness data were developed by evaluating photographs of floor trusses taken during inspections. Two groups of photographs were used. The first group included images of floor trusses from WTC 1 (floors 22, 23, and 27). These photographs were taken in the mid-1990s and illustrated conditions before the upgrade carried out by the Port Authority. Thus, SFRM thickness on the photographed trusses would be expected be at least ½ in. The second group of photographs, taken in 1998, illustrated conditions after the upgrade program that was initiated in 1995. The photographs were of trusses for floor 31 and below in WTC 1. Selection of the photographs to be used to estimate thickness of SFRM was based on clarity of SFRM edges and the presence of a feature of known dimensions to provide a reference measurement.

For floors that had not been upgraded, it was observed that the estimated thickness of SFRM on the webs (inclined bars) of the main trusses tended to be greater than that on either the diagonal struts or on the webs of the bridging trusses. Hence, estimates of SFRM thickness for non-upgraded floors were divided into three groups:

- Webs (inclined bars) of main trusses,
- Webs (inclined bars) of bridging trusses, and
- Diagonal strut at the exterior wall end of the truss.

It was not possible to estimate the thickness of the SFRM on any truss element except the round web bars. Consequently, for the upgraded floors in WTC 1 that were included in the second group of photographs, only estimates of the thickness on the web bars of the main trusses were made. The average, standard

deviation, and coefficient of variation were computed for the total number of measurements in each of these groups. The results are summarized as follows:

- Main trusses before upgrade (85 measurements): Average thickness 0.6 in., standard deviation = 0.3 in., and coefficient of variation = 0.5.
- Bridging trusses before upgrade (52 measurements): Average thickness 0.4 in., standard deviation = 0.25 in., and coefficient of variation = 0.6.
- Diagonal struts before upgrade (26 measurements): Average thickness 0.4 in., standard deviation = 0.2 in., and coefficient of variation = 0.5.
- Main trusses after upgrade (52 measurements): Average thickness 1.7 in., standard deviation = 0.4 in., and coefficient of variation = 0.2.

Port Authority Data on Upgraded SFRM on Trusses

In the 1990s, the thermal protection for some floor trusses was upgraded to a specified thickness of 1½ in. as tenants vacated their spaces. According to the Port Authority, 18 floors of WTC 1 and 13 floors of WTC 2 were upgraded. The Port Authority also stated that: "The entire impact zone for Tower 1 (92-99) was upgraded with 1½" spray-on fireproofing. Only the 78th floor was upgraded with the 1½" spray-on fireproofing within the impact zone in Tower 2 (78-84)." The Port Authority provided Construction Audit Reports that included the density, average thickness, and strength characteristics of the upgraded SFRM (BLAZE-SHIELD II) as of 2000. In 2004, the Port Authority provided NIST reports of the individual measurements for many of the average thicknesses recorded in the Construction Audit Reports. These individual measurements permitted analysis of the variation of thickness at a cross section of a truss member and the variation in average thickness from truss to truss. A total of 18 data sets for WTC 1 (including floors 93, 95, 98, 99, and 100) and 14 data sets for WTC 2 (including floors 77, 78, 88, 89, and 92) were analyzed.

Data analysis indicated that the thickness measurements from the two towers represented similar distributions, and so the data were combined. It was also found that the distribution of thickness values could be approximated as lognormal distribution.

The overall average thickness determined from the 256 individual measurements was found to be 2.5 in. with a standard deviation of 0.6 in. Thus, the average thickness on the upgraded upper floors appears to be greater than that estimated from photographs taken on upgraded lower floors.

The overall standard deviation of 0.6 in. includes two contributions: (1) the variation of thickness at a cross section (within-truss variability), and (2) the variation of average thickness between trusses (between-truss variability). From analysis of variance, it was found that the within-truss standard deviation was 0.4 in., and the between-truss standard deviation was also 0.4 in. The within-truss standard deviation of 0.4 in. is similar to the standard deviation of the estimated individual thicknesses obtained from analysis of the photographs of upgraded main trusses.

Column SFRM Thickness

NIST requested that the Port Authority provide available information on the actual thickness of fire-resistive material on the exterior and interior columns of the WTC towers. The Port Authority replied that, due to inaccessibility of exterior columns and core columns, there were no records of SFRM thickness measurements for these elements. The only available measurements were for thickness of SFRM that was reapplied to accessible beams and columns within elevator shafts.

The most complete data set included measurements on beams and columns taken within shaft 10/11 in WTC 1. These measurements were taken in April 1999 and included measurements from floor 1 to floor 45. The thicknesses were recorded to the nearest 1/8 in., with a few thicknesses recorded to the nearest 1/16 in. The columns included 10 to 18 replicate measurements, and the beams included 11 to 16 replicate measurements.

The average thickness for the columns was found to be 0.82 in., with a standard deviation of 0.20, resulting in a coefficient of variation is 0.24. The average thickness for the beams was 0.97 in., with a standard deviation is 0.21 in., for a coefficient of variation is 0.21. The information from the Port Authority indicated that the minimum required thicknesses for the SFRM (Monokote Type Z-106) that was reapplied to the columns and beams were ½ in. and ¾ in., respectively.

The data described above may not have a direct bearing on the outcome of the investigation because they deal with lower stories. They do, however, provide some useful information on the variability of SFRM applied to beams and columns. As might be expected, the variation in thickness of SFRM for the beams and columns is lower than the variation computed for the floor trusses. The flat surfaces of the beams and columns result in more uniform application of the sprayed fire-resistive material than for the slender truss members.

EFFECT OF SFRM GEOMETRY ON THERMAL RESPONSE

As would be expected, and as confirmed by analyses of available data, the thickness of thermal insulation can have high variability. The effects of thickness variation on thermal response of a member are not well known. A sensitivity study using the finite element analysis to simulate heat transfer was conducted to investigate the sensitivity of steel temperature rise to the variability in SFRM thickness.

Effects of Thickness Variability and Gaps in SFRM

A finite element model for thermal analysis was developed for a plate protected on both faces with SFRM of variable thickness. A random number generator was used to assign a lognormally distributed random thickness of insulation along the length of the plate, and the plate was subjected to a thermal flux representative of a 1,100 °C fire. A parametric study was conducted with average thickness of fire-resistive material varying from 0 in. to 2 in. in increments of ¼ in. and a standard deviation varying from 0 to 1 in. Steel temperatures at five locations in the plate were recorded at 30 min, 60 min, 90 min, and 120 min of exposure to the thermal flux.

The simulations showed that when the SFRM thickness is variable, the isotherms in the steel follow the shape of the SFRM surface contour. Thus, the temperature history at any point in the steel depends on the

local thickness of the insulation. If the time to reach a specified high temperature is used as an indicator of protection efficiency, it was shown that an increase in thickness variability reduced the time to reach the critical temperature. Conversely, for a given time to reach a critical temperature, the required average thickness of thermal insulation increased with increasing variability in thickness of SFRM.

In addition to the effect of variation in thickness, the effect of missing SFRM over a portion of a member was studied. As expected, the bare steel at the missing insulation reached the gas temperature quickly, but more importantly the "gap" in the insulation led to transmission of heat into the interior steel.

The combined effects of variation in insulation thickness and extent of missing material were examined by a factorial study with the following factors:

- Average thickness of insulation varying from 0 in. to 2.0 in. in 1/4 in. increments;
- Standard deviation of insulation thickness of 0 in., 0.25 in., 0.5 in., 0.75 in., and 1.0 in.; and
- Length of missing insulation varying from 0 in. to 30 in., in 6 in. increments.

The results were summarized by a series of temperature-time plots representing the response for different combinations of the three factors. As expected, increasing the variability of insulation thickness or gap length reduced the time to reach a given critical temperature. Because there was not sufficient information to determine the frequency of occurrence of these gaps or their typical locations, gaps in insulation were not considered in the thermal modeling.

Thermally Equivalent Thickness of SFRM

The sensitivity study indicated that increased variation in thickness reduced the "effective thickness" of the SFRM. It would be impractical to attempt to account for the variation in SFRM thickness in the thermal modeling of the WTC towers by introducing variable thickness insulation material in the finite-element models. As an alternative, a "thermally equivalent uniform thickness" was determined that would result in the same thermo-mechanical response of a member as the variable thickness thermal protection. In the analyses, an insulated 1 in. diameter by 60 in. long steel bar was subjected to the heat flux arising from a 1,100 °C fire. The thermal history along the length of the bar was calculated, and that history was used to calculate the length change of the unrestrained bar under a tensile stress of 12,500 psi. The bar was assumed to be similar to the steel used in the WTC floor trusses, and the temperature dependence of the coefficient of thermal expansion and the modulus of elasticity were based on NIST measurements.

The average SFRM thickness and variability in thickness used in the models were based on the measurements for the web bars of the main trusses with both the original insulation and upgraded insulation. The following values were investigated:

- Original conditions: Average thickness = 0.75 in., standard deviation = 0.3 in., lognormal distribution.
- Upgraded conditions: Average thickness = 2.5 in., standard deviation = 0.6 in., lognormal distribution.

The variation of thermal insulation thickness along the length of the bar was established by using a pseudo random number generator to select values from a lognormal distribution with central value and dispersion consistent with the above average values and standard deviation. Three sets of random data were generated for each condition.

When the randomly selected thicknesses of each element were applied to the bar, it resulted in abrupt changes in insulation thickness along the length of the bar. This resulted in a "rough" surface texture that was not representative of actual conditions. As an alternative, five-point averaging was used to reduce the roughness of the insulation profile and produce a profile that was consistent with photographic evidence. Care was taken to ensure the "smoothed" profiles maintained the required dispersion.

The calculated thermal histories of the bar elements were used to calculate the unrestrained length changes of the bar due to thermal expansion and the applied stress. For comparison, elongations of the bar with different uniform thicknesses of thermal insulation were calculated. The "thermally equivalent thickness" was taken as the uniform thickness that resulted in approximately the same elongation of the bar as produced with the variable thickness insulation.

On the basis of these analyses, it was concluded that SFRM with an average thickness of 0.75 in. and a standard deviation of 0.3 in. provides protection equivalent to 0.6 in. of uniform thickness. Similarly, an average SFRM thickness of 2.5 in. with a standard deviation of 0.6 in. is equivalent to 2.2 in. of uniform thickness.

Recommended Thickness of SFRM for Thermal Analyses

Analyses of available data on SFRM thickness in the WTC towers and thermal modeling revealed the following:

- From measurements of SFRM thickness, the average values exceeded the specified thickness.
- SFRM thickness was variable, and the distribution of thickness in the floor trusses appeared to be described best by a lognormal distribution.
- The standard deviation of SFRM thickness on the trusses varied between about 0.3 in. and 0.6 in.
- The standard deviation of SFRM on columns and beams from the core tended to be lower, with a value of 0.2 in. for the available data.
- No information was available on the SFRM thickness on the exterior columns and spandrel beams.
- Variation in thickness reduces the effectiveness of SFRM, and the equivalent uniform thickness was less than the average thickness.

Based on findings stated above, the following uniform thicknesses for the undamaged SFRM were determined for use in calculating thermal response of the WTC towers under various fire scenarios:

- Original SFRM thickness on floor trusses: 0.6 in.

- Upgraded SFRM thickness on floor trusses: 2.2 in.
- Thermal protection on other elements: the specified thickness.

The choice of specified thickness for those members lacking data is justified by the following offsetting factors: (1) measured average thicknesses exceed specified values, and (2) variation in thickness reduces the effectiveness of the SFRM.

THERMOPHYSICAL PROPERTIES

To provide thermophysical property data for modeling the fire-structure interaction of the towers, the thermal conductivity, specific heat capacity, and density of the SFRMs used in the WTC towers were determined as a function of temperature up to 1,200 °C (2,190 °F). Since there are no ASTM test methods for characterizing the thermophysical properties of SFRMs as a function of temperature, ASTM test methods developed for other materials were used. Samples were prepared by the manufacturers of the fire-resistive materials, which included BLAZE-SHIELD DC/F, BLAZE-SHIELD II, and Monokote MK-5. Since Monokote MK-5 is no longer on the market, the samples were manufactured specially for this study according to the original MK-5 formulation. Testing services were provided under contract by a commercial testing agency.

Thermal Conductivity

The thermal conductivity measurements were performed according to ASTM C 1113, Standard Test Method for Thermal Conductivity of Refractories by Hot Wire (Platinum Resistance Thermometer Technique). The room temperature values were in general agreement with the manufacturer's published values for BLAZE-SHIELD DC/F and BLAZE-SHIELD II. No published values were available for Monokote MK-5. The thermal conductivities increased with temperature.

Specific Heat Capacity

Specific heat capacity determinations were made with the same instrument as for thermal conductivity with a slight modification. A thermocouple was added to the system, which permitted determination of the thermal diffusivity of the material. Knowing the thermal conductivity, the thermal diffusivity, and the density obtained from other tests, the specific heat capacity was calculated. The inherently indirect nature of the technique used precluded the direct measurements of specific heat capacity peaks associated with chemical reactions.

To examine the chemical reactions associated with heating of SFRMs, samples were sent to another laboratory under contract to perform differential scanning calorimetry (DSC) measurements in accordance with ASTM E 1269, Standard Test Method for Determining Specific Heat Capacity by Differential Scanning Calorimetry. Differential thermal analysis (DTA) is a "fingerprinting" technique that provides information on the chemical reactions, phase transformations, and structural changes that occur in a specimen during a heating or a cooling cycle. These tests revealed large peaks in the specific heat capacities in the range of 125 °C to 140 °C.

Density

Bulk densities of the SFRMs were not measured directly (except at room temperature) but were calculated from thermal gravimetric analysis (TGA) and thermal expansion measurements. The TGA tests to measure mass loss were performed according to ASTM E 1131, Standard Test Method for Compositional Analysis by Thermogravimetry. Thermal expansion measurements were performed according to ASTM E 228, Standard Test Method for Linear Thermal Expansion of Solid Materials. Since the materials were not isotropic, separate measurements were performed in the plane of the SFRM sample and perpendicular to the free surface of the sample. From the thermal expansion measurements, the change in volume for each material was calculated at each temperature. The density values were calculated from the results of the TGA and thermal expansion. The room temperature densities were 15.7 pcf for BLAZE-SHIELD DC/F, 20.8 pcf for BLAZE-SHIELD II, and 19.4 pcf for Monokote MK-5.

Thermophysical Properties of Gypsum Panels

Thermophysical properties of four representative types of commercially available gypsum panels were examined. The materials were:

1. 5/8 in. thick gypsum panel A,
2. ½ in. thick gypsum panel,
3. 5/8 in. thick gypsum panel B, and
4. 1 in. thick gypsum liner panel.

Thermal conductivity was measured using the heated probe technique described in ASTM D 5334, Standard Test Method for Determination of Thermal Conductivity of Soil and Soft Rock by Thermal Needle Probe Procedure. In general, the thermal conductivity initially decreased as the temperature increased to 200 °C and then increased with increasing temperature above 300 °C.

Specific heat capacities of the cores of the four gypsum panel samples were measured using a differential scanning calorimeter according to ASTM E 1269, Standard Test Method for Determining Specific Heat Capacity by Differential Scanning Calorimetry. The four panels had similar specific heat capacities as a function of temperature, with a high peak at about 150 °C and a smaller peak at about 250 °C.

Densities were calculated from the thermogravimetric analysis (TGA) and linear thermal expansion measurements. All four materials show the same trend as a function of temperature. The variation of density with temperature is associated with the mass loss and the change in volume of the gypsum material.

ADHESIVE AND COHESIVE STRENGTH

To analyze the thermo-structural response of the WTC towers during the fires after the aircraft impacts, it was necessary to estimate the extent of dislodged thermal insulation on structural members.

Dislodgement could occur as a result of direct impact by debris or due to inertial forces as a result of the aircraft impact. Photographic evidence suggested that thermal insulation was dislodged from portions of exterior columns of the towers that were likely not subjected to direct impact by debris. This study focused on dislodgement due to inertial forces.

The magnitude of the inertial forces depends on the density and thickness of the thermal insulation. The insulation would dislodge if the stresses resulting from inertial forces exceed the strength of the insulation. Therefore, the focus of the NIST study was to determine tensile strength characteristics of the thermal insulation. In addition, a simplified approach was developed for estimating the magnitude of accelerations required to dislodge thermal insulation.

In-place Density and Bond Strength

The Port Authority provided data on in-place density and bond strength characteristics of the thermal insulation (BLAZE-SHIELD II) applied to the floor trusses during tenant alterations. According to the manufacturer, BLAZE-SHIELD II is about 20 percent denser and has about 20 percent greater adhesive/cohesive strength than BLAZE-SHIELD DC/F. The Port Authority test reports indicate that bond strength was determined in accordance with ASTM E 736, Standard Test Method for Cohesion/Adhesion of Sprayed Fire Resistance Materials Applied to Structural Members. The method involves gluing a jar screw cap to the surface of the thermal insulation, and after the glue has cured, the cap is pulled. The force required to pull off the cap is divided by the area of the cap and reported as the "cohesive/adhesive strength." Failure is described as "cohesive" if it occurs within the insulation and is defined as "adhesive" if it occurs at the interface with the substrate.

Analysis of the reported density values indicated no statistically significant differences between the average SFRM densities in the two towers. The overall average density was 18.9 pcf with a standard deviation of 3.2 pcf, giving a coefficient of variation of 16 percent.

Analysis of the bond strength values indicated that there were statistically significant differences between the average bond strengths for the different floors, but there was no statistically significant difference between the average bond strengths for the two towers. The overall average bond strength was 302 psf, with a standard deviation of 91 psf, giving a coefficient of variation of 30 percent. This average value is less than the "tested performance" value of 360 psf indicated in the manufacturer's catalogs, but this published value is for tests under controlled conditions and may not be representative of field strengths. The manufacturer's product literature dated February 2002 refers to average bond strength of 150 psf as "standard performance," and the same value is used in its guide specification for BLAZE-SHEILD II.

Specimen Preparation and Test Procedures

While the in-place bond strength data for BLAZE-SHIELD II reported by the Port Authority appear to indicate acceptable performance, ASTM E 736 tests do not provide sufficient information for predicting whether insulation would be dislodged from structural members under various impact conditions. The standard test does not provide unambiguous values of cohesive and adhesive strengths and it does not provide tensile strength in a direction parallel to the surface, that is, the in-plane cohesive strength. Thus, tests were conducted by NIST to determine different tensile strength properties of sprayed thermal

insulation. BLAZE-SHIELD DC/F was used because the Port Authority data did not include tests of this material.

Test specimens were made by applying the SFRM to ¼ in. steel plates measuring 8 in. by 16 in. One half of the plates were coated with primer paint. Nominal SFRM thicknesses of ¾ in. and 1½ in. were applied. Thickness was built up in several passes of the spray nozzle. Gentle hand rubbing was used to remove local high spots and produce reasonably uniform thicknesses. The plate specimens were allowed to dry for over five months in the laboratory before testing. Companion specimens were weighed periodically for loss of water and it was found that the 1½ in. thick specimen reached equilibrium in about one month.

Tests were devised to determine adhesive strength, cohesive strength normal to the surface, and cohesive strength parallel to the surface of the SFRM. The first two properties were determined by adapting the pull-off test method described in ASTM C 1583, Standard Test Method for Tensile Strength of Concrete Surfaces and the Bond Strength or Tensile Strength of Concrete Repair and Overlay Materials by Direct Tension (Pull-off Method). The SFRM layer was cut carefully in two orthogonal directions to create a prismatic test specimen, and a 3/8 in. by 2.7 in. by 2.7 in. aluminum plate was glued to the surface. The advantages of this approach over the ASTM 736 technique are that the resisting area is easily determined and it offers the ability to measure both adhesive and cohesive strengths.

From each plate, three specimens were prepared for measuring both density and in-plane cohesive strength, and two specimens were prepared for measuring adhesive strength and cohesive strength normal to the surface. Prismatic specimens were prepared by carefully removing strips of SFRM from the steel plates and sanding them to obtain uniform thickness. These specimens were weighed to determine their densities. Then the specimens were glued to a steel plate and a small plate was glued to the other end for application of a tensile load.

The adhesive strength and cohesive strength normal to the surface were obtained using the modified pull-off procedure. An aluminum plate was bonded to the top surface of the SFRM using a fast curing, two-component urethane foam adhesive. After the adhesive had cured, the SFRM layer was cut to produce a prismatic test specimen. A hook was screwed into the aluminum plate, and a load was applied by hand using a 50-lb digital force gauge. The average length and width of the failure area was measured and used to compute the adhesive or cohesive strength. After the first test, the specimen was repaired with the same polyurethane adhesive and the test was repeated. If the first test was an adhesive failure, the second test of the repaired specimen measured cohesive strength of the bulk SFRM. If the first test resulted in cohesive failure, the specimens were repaired and retested until an adhesive failure was obtained.

Test Results

Table E–1 summarizes the results of the test described in the previous section.

Table E–1. Summary of physical characteristics of BLAZE-SHIELD DC/F specimens tested at NIST.

Property	Bare Steel		Primed Steel	
	¾ in.	1½ in	¾ in.	1½ in.
Density (pcf)			27.2 (0.8)[a]	29.7 (1.3)

In-plane cohesive strength (psf)			1120 (390)	1740 (540)
Adhesive strength (psf)	450 (63)	666 (151)	185 (96)	171[b](196)
Cohesive strength normal to surface (psf)	433 (99)	610 (142)	367 (79)	595 (163)

a. First number is the average and the number in parentheses is the standard deviation.
b. Based on testing selected samples.

The densities of the BLAZE-SHIELD DC/F measured in this study were higher than published in the manufacturer's catalogs and higher than the in-place average density of 18.9 pcf reported in Port Authority test reports for BLAZE-SHIELD II. The difference in average densities of the two thicknesses was statistically significant. The higher values in this study are attributed to the details of the specimen preparation procedures, which tended to result in denser test specimens than would be representative of field application.

The difference in average adhesive strength for the two SFRM thicknesses is statistically significant. The relative strengths are consistent with the difference in density for the two thicknesses.

The presence of primer reduced the adhesive strength, especially for the 1½ in. thick specimens. Two-thirds of the thicker SFRM plates had no adhesion to the coated steel plates.

Analysis of the cohesive strength normal to the surface indicated that there was no statistically significant effect due to the presence or absence of primer. This is logical, because the condition of the steel surface is not expected to influence the properties of the bulk SFRM. There was a statistically significant difference in the average strengths for the two thicknesses, with the 1½ in. SFRM having higher strength.

For comparison with the measured cohesive strength normal to the surface, two tests were done in accordance with ASTM E 736. The results of the two tests were in agreement with those obtained by the pull-off technique. This suggests that the ASTM E 736 procedure probably provides a measure of cohesive strength.

A comparison was made of the adhesive strength and cohesive strength normal to the surface for the plates made with bare steel. A formal analysis of variance indicated that there is an 8 percent probability that the difference could be the result of randomness. Generally, if this probability is greater than 5 percent, it can be concluded that the difference is not statistically significant. Thus, for the case of good adhesion, the test results do not contradict the assumption that the adhesive strength and cohesive strength normal to the surface are equal. If this assumption is accepted, the average of the adhesive and cohesive strengths is 409 psf for the ¾ in. SFRM, and the average is 622 psf for the 1½ in. SFRM. These values are considerably greater than the manufacturer's published strength of 295 psf obtained using the ASTM E 736 method under laboratory conditions.

Simplified Approach to Predict Dislodging of SFRM

When a member is subjected to an impact, it will undergo various modes of vibration. These vibrations result in local cyclic accelerations that are transferred to the SFRM by forces at the interface between the steel and the SFRM. The forces are proportional to the mass of the SFRM, and if they exceed the adhesive or cohesive strength of the SFRM, the SFRM will separate from the member. Two limiting cases are considered:

- Case 1 is a planar element with SFRM applied to one face of the element. This would be representative of SFRM applied to large webs and flanges of beams and columns. In this case, adhesive strength or cohesive strength normal to the surface would be the controlling SFRM properties.

- Case 2 is a slender bar encased with SFRM. This would be representative of SFRM applied to elements of the floor trusses. In this case, in-plane tensile strength and bond strength are the controlling SFRM properties.

To arrive at the ranges of accelerations that could be expected to dislodge SFRM from a planar surface, the following plausible ranges of values were assumed:

- SFRM thickness: 0.75 in and 2.5 in.;

- SFRM density: 15 pcf and 25 pcf [1];

- SFRM bond strength: 100 psf and 500 psf

For the combination of low thickness, low density, and high bond strength, the required acceleration is about 530 *g*, where *g* is the gravitational acceleration. For the other extreme combination of high thickness, high density, and low strength, the required acceleration is about 20 *g*. For values representative of the upgraded thermal insulation on the floor trusses, an acceleration of about 80 *g* would be required to dislodge a 2.5 in. thick layer of well-bonded SFRM from a planar surface.

To arrive at the ranges of accelerations that could be expected to dislodge SFRM from a round bar, the following ranges of values were assumed:

- Bar diameter: 0.9 in. and 1.2 in;

- SFRM thickness: 0.75 in. and 2.5 in.;

- Density: 15 pcf and 25 pcf;

- In-plane cohesive strength: 500 pcf and 2,000 psf; and

- Ratio of bond strength to in-plane cohesive strength: 0 and 0.3.

The smallest required acceleration is about 40 *g*, which corresponds to a large bar having a thick layer of the higher density SFRM with low strength. At the other extreme, the required acceleration is about 730 *g*. For a 1.2 in. diameter bar with 2.5 in. thickness of SFRM and density of 19 pcf, which are representative of the conditions of the upgraded insulation on the floor trusses, the acceleration required to dislodge the SFRM would vary from 55 *g* to 230 *g*, depending on the strength characteristics within the assumed ranges given above.

These simplified models are intended to provide insight into the important variables that affect the magnitude of the disturbance (that is, acceleration) required to dislodge SFRM from different kinds of

[1] These numbers need to be converted to units of mass by dividing by the gravitational acceleration.

structural members. These models do not consider the fact that the applied acceleration in an actual structure subjected to impact would vary with time. Also these models apply to members not directly impacted by debris.

Chapter 1
INTRODUCTION

When steel is heated it loses strength and stiffness. This characteristic allows steel to be formed into different shapes with relatively little effort. When steel is used in a structure, however, measures have to be taken to protect the steel from premature temperature rise in case of fire. The objective is for the structure to remain stable for the time needed to permit evacuation of occupants and for fire service personnel to complete search and rescue operations. This report deals with the passive fire protection materials used in the WTC towers.

1.1 FIRE-RESISTIVE MATERIALS

The investigation revealed that structural steel in the World Trade Center (WTC) towers was protected against the effects of fire with sprayed fire-resistive materials (SFRMs)[2] or rigid fire-rated gypsum panels. There are many types of SFRMs, but they can be characterized in terms of how they protect the steel and their density (Gewain et al. 2003). One class of SFRMs protects the steel by providing a material with a low thermal conductivity, such as mineral fibers. The fibers and binder are packaged as dry ingredients, and water is added by a pressurized system as the materials are sprayed onto the steel. The water mixes with the binder materials and provides "stickiness" that allows the SFRM to adhere weakly to the steel. With time, the binder hardens, and excess water evaporates. When dry, these SFRMs provide a low thermal conductivity barrier to reduce the rate of temperature rise during a fire.

The other class of SFRMs can be termed as "energy absorbing" (Gewain et al. 2003). This means that they incorporate cementitious materials that have chemically bound water (water of crystallization). When the material is heated, energy is absorbed in transforming the chemically bound water to free water, and this hinders the temperature rise of the coated steel. Examples of cementitious materials that have been used successfully include gypsum and magnesium oxychloride (Gewain et al. 2003). These types of SFRMs may also include very low-density aggregate particles, such as vermiculite or perlite, to reduce density and thermal conductivity. Cementitious SFRMs are typically mixed with water to produce a cohesive and pumpable mixture that is sprayed onto the steel.

Figure 1-1 is a photograph of two types of SFRMs. The material on the left is a gypsum based cementitious SFRM containing vermiculite aggregate, and the material on the right is a fibrous SFRM. Note that the cementitious SFRM specimen in the photograph was prepared by casting in a mold, not by spraying onto a surface. Thus, the surface texture is not representative of what would be obtained in the field.

Sprayed fire-resistive materials are also characterized by their density. Low-density materials have densities in the range of 15 lbs/ft^3 to 20 lbs/ft^3; medium density materials are generally in the range of 20 lbs/ft^3 to 40 lbs/ft^3. The density of the SFRM is closely related to its cohesive strength and its

[2] These sprayed fire-resistive materials are commonly referred to as "fireproofing." This term is, however, not used in the technical literature. In this report "SFRM" and "thermal insulation" are used to refer to the passive fire protection materials.

durability. Low-density SFRMs can be removed readily with hand tools and are not suitable for applications where the surface is exposed to weather or abrasion in service (Gewain et al. 2003).

Source: NIST.

Figure 1–1. Examples of sprayed fire-resistive materials: (left) material based on gypsum and vermiculite aggregate; (right) material based on mineral fibers and cementitious binder.

Analysis of the effects of the fires on the structural capacity of the damaged WTC towers as a function of time requires knowledge about the condition of fire-resistive materials on the various structural components, namely, the exterior columns, the spandrel beams, the floor trusses, and the core columns. Because of the method of application, sprayed fire-resistive material will have variable thickness, especially when applied to long, thin elements such as the diagonals and chords of the floor trusses. In addition, some insulation was dislodged during the impact, either from direct impact by debris or from vibrations of the members. The thermal properties of the insulation also need to be known as a function of temperature.

1.2 SCOPE OF REPORT

The thermal-structural analysis of the WTC towers focused on two objectives: (1) analysis of the undamaged buildings exposed to conventional building fires, and (2) analysis of the buildings damaged by the aircraft impact exposed to the subsequent fires. To reduce the uncertainties in the calculated thermal histories of various structural elements, the thermophysical properties and condition of the passive fire protection as it existed on September 11, 2001, had to be estimated as accurately as possible. In addition, reasonable estimates of the extent of SFRM dislodged by the aircraft impact and the resulting debris field had to be made.

To provide context for the information in this report, an overview of concepts used in U.S. building codes for structural fire resistance is presented first. This is followed with a summary of the construction history of the sprayed fire-resistive material in WTC 1 and WTC 2. To gain an understanding of the effect of SFRM thickness and its variability on the steel temperature during exposure to fire, results are presented of a sensitivity study based on a simple finite-element model. This is followed by a quantitative assessment of in-place thickness and its variability based on available data. The rationale for

the thickness of SFRM to be used in the structural fire endurance analyses is presented. The tests conducted to determine the thermal properties of insulation materials similar to those used in the WTC towers are reviewed. The results of mechanical property tests conducted on laboratory specimens are presented, and a simplified approach for estimating the acceleration required to dislodge thermal insulation during impact is discussed.

This page intentionally left blank.

Chapter 2
BUILDING CODE CONCEPTS FOR STRUCTURAL FIRE RESISTANCE

2.1 ORIGINS AND INTENT OF BUILDING CODES

Fire-induced collapse of buildings is regulated generally through limits on the height and the area per floor as a function of the types and degree of fire resistance of materials used in the structural elements. These material characteristics are categorized as types of construction, and the associated limits are contained in so-called "heights and areas tables," which are a cornerstone of most prescriptive building codes.

As discussed in NIST NCSTAR 1-1,[3] the origins of building codes in the United States can be traced to insurance regulations developed in the late 19th century to limit property losses in fires (Bukowski 1997). Thus, the intent of building height limits is to restrict taller buildings to non-combustible structural members, and the greatest fire resistance is assigned to members supporting multiple floors. The primary concern with combustible structural members is that they can become ignited by an exposing fire and can continue to burn (often in concealed spaces) even after the exposing fire has been extinguished, leading to collapse. The intent of increased fire resistance for members supporting multiple floors is directly related to the higher risk of property loss in the event of failure of multiple floors. Fire resistance requirements, however, do not take into account the actual number of stories being supported by these elements. Thus, the same ratings are required irrespective of whether columns support 10 stories or 100 stories.

The other important height factor is the definition of a high-rise building. This is based generally on the height above which fire department ladders will not reach, requiring that fires be fought from inside, which is significantly less effective (and more dangerous for the firefighters). In an exterior attack, hose streams can be brought to bear from several sides, and so-called master streams can apply large volumes of water. An interior attack is limited to hand-held hoses supplied from standpipes and working from interior stairways. Traditionally, high-rise buildings have been defined as those that exceed 75 ft (or six stories above grade) in height, but some newer model codes increase this height to 100 ft as modern fire department ladders are taller.

The intent of floor area limits is less obvious, but is generally attributed to limiting property risk and to limiting the size (area involved on any floor) of the fire to that which can be dealt with by the fire department, with the number of people and equipment typical of an initial response.

2.2 CONSTRUCTION TYPES

Construction types (or groups) are defined in the model building codes and in NFPA 220 (NFPA 220, 1999) and, while there are some variations in categories, they are reasonably consistent. The main

[3] This reference is to one of the companion documents from this Investigation. A list of these documents appears in the Preface to this report.

categories are Type I (fire resistive), Type II (non-combustible), Type III (ordinary), Type IV (heavy timber) and Type V (combustible).

Types I and II are constructed with non-combustible exterior and interior bearing walls and columns, where fire resistance ratings are greatest for Type I, and Type II is any (non-combustible) construction not meeting Type I requirements. Type III is where exterior bearing walls are non-combustible, and interior bearing walls and some columns may employ approved combustible materials. Type IV is known as heavy timber, which utilizes large, solid cross section wooden members such as in post-and-beam construction. Type V is traditional wood frame construction. Common non-combustible structural elements employ steel or reinforced concrete. Combustible structural elements are usually solid wood, engineered wood, and laminates.

Combustibility of the materials in the structural element is determined in accordance with ASTM E 136 (ASTM 2004a) in which the material is placed in a furnace at 750 °C (1,380 °F). Some minor surface burning (e.g., from paint or coatings) is allowed in the first 30 seconds, but there cannot be any significant energy released as determined by more than 30 °C (54 °F) increase in the furnace temperature, and the sample cannot lose more than half its initial mass. Materials that pass are designated non-combustible, and the rest are combustible. In 1973, an in-between category of "limited combustible" was added to ASTM E 136 to regulate some structural materials.

Within each construction type are several sub-categories determined by the fire resistance ratings of the columns (vertical structural elements that support predominantly gravity loads and the actions of lateral loads), beams (horizontal structural elements that support predominantly live loads), and floor supports. In some model codes these sub-categories are identified by letters following the type (e.g., IB or IIIA) (IBC 2003) or by a set of three numbers that represent the fire resistance required (in hours) of the exterior bearing walls; columns, beams, girders, trusses and arches supporting bearing walls, columns, or loads from more than one floor; and floor construction, respectively (e.g., Type I [3, 3, 2]) (NFPA 5000, 2003). The Annex of NFPA 220 (2006 Edition) includes a table that cross-references different construction types in various model codes.

2.3 FIRE RESISTANCE OF STRUCTURAL ELEMENTS

Building codes require that structural elements be protected to achieve a specified fire resistance rating, expressed in hours (Buchanan 2001; Bukowski 2003). The fire resistance rating of structural materials and assemblies is generally determined through testing, and in the United States, such testing is frequently conducted in accordance with ASTM Test Method E 119 (refer to NIST NCSTAR 1-6B[4] for a discussion of this procedure). The objective of requiring minimum fire ratings is for the building to support design loads (including fire) without local structural collapse until occupants can escape and the fire service can complete search and rescue operations. Further, in high-rise buildings, local collapse is to be prevented while the fire service undertakes suppression operations.

With regard to total collapse, the intent of the code is for this not to occur for any design condition (including design fires), but it is recognized that collapse might occur in an extreme event

[4] This reference is to one of the companion documents from this Investigation. A list of these comments appears in the Preface to this report.

(Buchanan 2001; Bukowski 2003). For an extreme event, collapse should not occur until the building has been evacuated of both occupants and firefighters.

Building codes generally require the highest fire resistance for columns and elements supporting multiple floors, and somewhat less resistance is required for columns supporting single floors, for beams, and for floors. For example, NFPA 5000, Building Construction and Safety Code (NFPA 5000, 2003), requires exterior bearing walls or columns supporting one or more floors to have the same fire resistance rating, but for interior bearing walls or columns the fire resistance rating is one hour less if only a single floor is supported. Historically, similar requirements were found in other model codes such as the Building Officials and Code Administrators (BOCA) *Basic Building Code* and the Southern Building Code Congress International (SBCCI) *Standard Building Code*, which have been replaced by the International Code Council's *International Building Code* (Bukowski 1997).

The required fire resistance ratings have been reduced in recent years as fire sprinklers have become universal in high-rise buildings and common in most other commercial buildings (Messersmith 2002). Where high-rise buildings generally required a 4 h rating for columns, this has been reduced to 3 h in recent codes, and can be as low as 2 h in current model codes based on the additional mandatory requirement for sprinklers. This reduction in fire rating requirements for structural components in sprinklered buildings is usually referred to as sprinkler "trade-offs" (Buchanan 2001; Messersmith 2002).

This page intentionally left blank.

Chapter 3
HISTORICAL REVIEW RELATED TO PASSIVE FIRE PROTECTION OF WTC TOWERS

3.1 AGREEMENTS BETWEEN PORT AUTHORITY AND NEW YORK CITY DEPARTMENT OF BUILDINGS AND FIRE DEPARTMENT

The World Trade Center (WTC) towers were built by the Port of New York Authority, which in 1972 became known as the Port Authority of New York and New Jersey and is hereinafter referred to as the Port Authority. As an interstate agency created under a clause of the U.S. Constitution permitting compacts between states, the Port Authority is not bound by any local authority having jurisdiction, in this case the New York City (City) Department of Buildings. Thus, the Port Authority was not required to comply with the New York City Building Code or any other building code; however, the Port Authority made explicit statements that it would comply with the Code.

In a letter dated May 15, 1963 (see Appendix A Fig. A-1), the Port Authority instructed its consulting engineers and architects to comply with the New York City Building Code. In the areas where the Code was not explicit or where technological advances made portions of the Code obsolete, it directed that design may be based on acceptable engineering practice. At that time, the 1938 edition of the New York Building Code was in effect, and a revised code was being drafted. On September 29, 1965, in a letter from Malcolm P. Levy to Minoru Yamasaki, the Port Authority instructed the designers of the WTC towers to revise the design plans to comply with the second and third drafts of the Code revision (see Appendix A Fig. A-2). The revised Building Code became effective in December 1968.

In 1993, the Port Authority and the New York City Department of Buildings entered into a Memorandum of Understanding (see Appendix A Fig. A-3) establishing procedures to be followed by the Port Authority for any building construction project undertaken by the Port Authority or any of its tenants at buildings owned or operated by the Port Authority and located in the City's jurisdiction. While the long-standing policy of the Port Authority was that its buildings meet or exceed the New York City Building Code (Code) requirements, the 1993 agreement restated the commitment. Among other key points, it was agreed that:

- Each project would be reviewed and examined for compliance with the Code;
- All plans would be prepared, sealed, and reviewed by New York State licensed professional engineers or architects; and,
- The Port Authority engineer or architect approving the plans would be licensed in the State of New York and would not have assisted in the preparation of the plans.

A supplement to this memorandum of understanding was executed in June 1995, which permitted tenants to use New York State licensed architects or engineers, in lieu of a Port Authority review, to certify that construction plans conformed to the Code and that construction was performed in accordance with the plans (see Appendix A Fig. A-4). In September 1995, the supplement was modified to permit a single

licensed consultant to certify the plans and the construction, except if the alteration would change the occupancy group of the space.

"In order to maintain and enhance the safety" of its facilities, the Port Authority "adopted a policy providing for the implementation of fire safety recommendations made by local government fire departments after a fire safety inspection of a Port Authority facility" as stated in the introduction of a Memorandum of Understanding between The Fire Department of the City of New York (FDNY) and the Port Authority of New York and New Jersey executed on December 30, 1993 (see Appendix A Fig. A-5). The purpose of the agreement was to restate the Port Authority's commitment to the policy, and the agreement included the following statements:

- "FDNY, acting through its Bureau of Fire Prevention ("BFP"), shall have the right to conduct fire safety inspections at any Port Authority facility located in the City of New York…"
- "BFP will issue a letterhead report of its fire safety findings and recommendations for corrective action with respect to any deficiencies forming a part of such findings addressed to the Port Authority's General Manager of Risk Management operations…"
- "…The Port Authority policy is and will continue to be to assure that such new or modified fire safety systems are in compliance with local codes and regulations…"

In 1995, the Memorandum of Understanding between FDNY and the Port Authority was amended with respect to additions to or modifications of fire safety systems. The Port Authority was required to notify the Bureau of Fire Protection prior to installing new systems or modifying existing systems. In addition, plans for these systems were to be prepared by New York State licensed professional engineers or architects (see Appendix A Fig. A-5).

3.2 NEW YORK CITY BUILDING CODE REQUIREMENTS

3.2.1 Occupancy Groups

Application of the New York City Building Code provisions affected, among other things, the assigned building classification and, thus, the required fire rating of the WTC towers and their structural members. It should be recalled that the Code was under revision during the design of the WTC towers.

Sub-article 301.0 of the 1968 New York City Building Code established occupancy classifications based on the use of a building and spaces. It divided occupancy into nine groups, A through I, as follows:

- A—High Hazard;
- B—Storage;
- C—Mercantile;
- D—Industrial;
- E—Business;

- F—Assembly;
- G—Educational;
- H—Institutional; and,
- I—Residential.

As office buildings, the WTC towers were classified as Occupancy Group E. This classification was confirmed in a letter dated May 14, 1969 from Malcolm P. Levy of the World Trade Department to Milton Gerstman of Tishman Realty & Construction Company, Inc. (see Appendix A Fig. A-6).

3.2.2 Construction Classification and Fire Rating

Additionally, there were other factors that determined the "classification" of a building and, consequently, its required fire rating: combustible versus noncombustible construction, sprinklered versus unsprinklered spaces, and building height and floor area limitations. Sub-articles 314.0 and 315.0 of the 1968 Code identified two construction groups: Noncombustible Construction (Group 1) and Combustible Construction (Group 2). The WTC towers were classified as Construction Group 1 because their walls, exit ways, shafts, structural members, floors, and roofs were constructed of noncombustible materials. The investigation revealed that at the time of design and construction, the towers were not sprinklered.

The 1968 New York City Building Code defined five Classes within Construction Group 1. For Business occupancy, each Class required a fire endurance rating as follows (NYCBC 1968):

- Construction Group 1A: 4 hour protected
- Construction Group 1B: 3 hour protected
- Construction Group 1C: 2 hour protected
- Construction Group 1D: 1 hour protected
- Construction Group 1E: unprotected

As mentioned in Section 2.3, fire endurance is a rating, given in hours, established in accordance with the ASTM E 119. Fire endurance is also referred to as fire rating or fire index.

To provide perspective, the 1961-1962 revision to the 1938 New York City Building Code required that the 110 story towers be classified as "Class 1 – Fireproof Structures," which includes office buildings (NYCBC 1961-1962). This meant that the columns were required to have 4 hour fire endurance while the floor system was required to have 3 hour fire endurance.

In Sub-articles 405.0 and 406.0 of the 1968 New York City Building Code, area and height limitations for unsprinklered buildings of Construction Group 1 with a Business Occupancy were as presented in Table 3–1 (NYCBC 1968). The WTC towers, WTC 1 and WTC 2, had roof heights of 1,368 ft and 1,362 ft, respectively, and each tower had a floor area of approximately 43,100 ft^2. As Table 3–1 indicates, the WTC towers could have been classified as either Class 1A or Class 1B.

Table 3–1. Area and height limitations for unsprinklered buildings for Noncombustible Construction (Group 1) with a Business occupancy (NYCBC 1968).

	Class 1A	Class 1B	Class 1C	Class 1D	Class 1E
Area	No Limit	No Limit	No Limit	17,500 ft^2	10,500 ft^2
Height	No Limit	No Limit	85 ft	75 ft	40 ft

3.3 CLASSIFICATION OF WTC TOWERS

It was the practice at the time, and continues to be the practice, for the architect to establish the building classification, fire rating of members and systems, and thermal protection requirements. On the subject of fire rating in accordance with the New York City Building Code revision effective December 6, 1968, a Port Authority memorandum dated January 15, 1987, from Lester S. Feld to Robert J. Linn states that Emery Roth & Sons (ER&S), the Architect of Record for the towers, had classified the WTC towers as Class 1B since there was "no economic advantage in using Class 1A Construction" (see Appendix A Fig. A-7).

According to the 1968 New York City Building Code, construction classification 1B provided, in part, the following fire protection requirements:

- Enclosure of vertical shafts, exits, passage-ways, and hoistways shall have a 2 hour fire endurance;
- Columns, girders, trusses, other than roof trusses, and framing supporting one floor shall have a 2 hour fire endurance;
- Columns, girders, trusses, other than roof trusses, and framing supporting more than one floor shall have a 3 hour fire endurance; and
- Floor construction including beams shall have a 2 hour fire endurance.
- Roof construction including beams, trusses, and framing including arches, domes, shells, cable supported roofs, and roof decks (for buildings over one story in height) shall have a 2 hour fire endurance.

Generally, fire ratings would appear on the application submitted for approval to the New York City Department of Buildings. In the case of the towers, however, no plans or forms were filed because the Port Authority was not subject to the New York City Building Code (see Appendix A Fig. A-7).

3.3.1 Specifications for Passive Fire Protection

In the case of the WTC towers, there appears to have been a problem related to the sprayed fire-resistive material specifications. A letter dated February 11, 1969, from Douglas Fernández of Emery Roth & Sons to Joseph A. Schwartzman of the Port Authority indicates that in early 1969 the Port Authority had rewritten the SFRM specifications (see Appendix A Fig. A-8). In the process of rewriting, the following key paragraph specifying the fire rating requirements for the structural members was apparently omitted:

> "Finished thicknesses of applied material over the various component steel parts requiring fireproofing shall be great enough to qualify the fireproofed parts for a three (3) hour rating (support beams, steel deck work) and a four (4) hour rating for all pick-up girders, if any, and columns."

ER&S continued:

> "We cannot be expected to accept responsibility for specifications which have been revised in such a manner; that which we originally stated clearly and simply, has become a meaningless document."

3.3.2 Response to Local Law 5/1973

In 1973, New York City Local Law No. 5 amended the New York City Building Code (effective January 18, 1973). Local Law No. 5/1973 required, in part, the retrofit of existing unsprinklered office buildings 100 ft or higher and having heating, ventilating, and air conditioning (HVAC) systems that serve more than the floor on which the equipment is located. To conform to Local Law 5/1973, the New York City Department of Buildings permitted either (NYCLL5/73 1973):

- Subdividing the floor area into compartments of specified square footage by fire separations (1 h or 2 h fire rated depending on the size of the compartment), or
- Providing sprinkler protection.

Owners of unsprinklered buildings were required to comply according to the following timetable from the effective date of the law (NYCLL5/73 1973):

- At least 1/3 of the non-complying floor area shall be completed in 5 years;
- At least 2/3 of the non complying floor area shall be completed in 10 years; and,
- The entire building shall be completed in 15 years.

A code compliance evaluation conducted in 1997 indicated that that all tenant floors in the two towers had been retrofitted with sprinklers (sprinklered) with the exception of four floors in WTC 1. In a 1999 update by the Port Authority it was noted that all tenant floors had been sprinklered and work was underway to complete sprinklering of the sky lobbies (see Appendix A Fig. A-9).

The 1999 revision of the New York City Building Code placed a 75 ft height limitation on unsprinklered buildings of Construction Groups 1A, 1B, 1C, and 1D. Sprinklered buildings, however, had no height limitations for Construction Group 1A, 1B, and 1C. Thus, the retrofitted WTC towers could have been reclassified as Class 1C (2 hour protected) (NYCBC 2001). As Class 1C, the columns and floor systems would have required 2 h and 1½ h fire ratings, respectively.

In preparation for leasing the WTC buildings to Silverstein Properties in 2000, the Port Authority commissioned a property condition assessment. The report titled "Property Condition Assessment of World Trade Center Portfolio," which was prepared for the Port Authority by Merritt & Harris, Inc. states

that the WTC towers were classified as “Class 1B – noncombustible, fire-protected, retrofitted with sprinklers in accordance with New York City Local Law 5/1973” (see Appendix A Fig. A-10).

3.4 SELECTION OF FIRE-RESISTIVE MATERIALS

3.4.1 Floor Trusses

Classification of a building leads to its overall fire endurance rating and ratings of the various structural components. The New York City Building Code, however, does not prescribe how the required fire endurance rating is to be achieved. Rather, the means for providing passive fire protection is established by the Architect of Record and depends, in part, on the structural materials used in the construction.

In the case of the WTC towers, the primary structural material was steel. Steel, in general, requires passive fire protection to achieve code-prescribed fire ratings. The Port Authority chose to protect the main structural components such as columns, spandrel beams, and floor trusses with sprayed fire-resistive material. This thermal protection technique was an established method for protecting columns, beams, and walls. In the 1960s, however, composite steel truss-supported floor systems were usually protected using “lath and plaster” enclosures or fire-rated ceiling tiles.

Based on copies of construction drawings provided to NIST, it was established that the floor system used in the towers consisted of open-web floor trusses acting as a composite system with a 4 in. thick reinforced lightweight concrete slab over metal decking. The main composite trusses, which were used in pairs, were spaced 6 ft 8 in. on center and had a nominal clear span of either 60 ft or 35 ft. The steel floor trusses were fabricated with double-angles for the top and bottom chords and round bars for the webs. Additionally, the floor system included bridging trusses (perpendicular to main trusses) spaced 13 ft 4 in. on center. Figure 3-1 shows a mock-up of the floor truss system that was manufactured for the WTC towers by Laclede Steel Co. Figure 3-2 shows the basic configuration of the composite floor truss system.

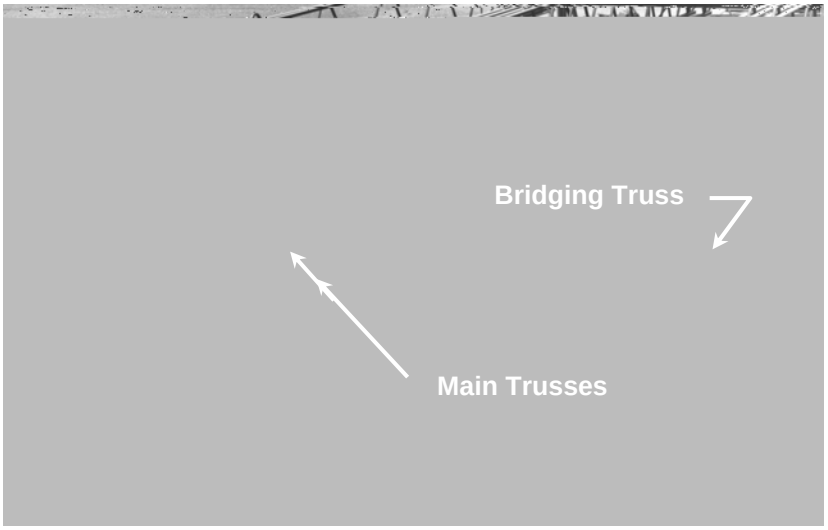

Source: Photograph from about 1967 from Laclede Steel Co.

Figure 3–1. Mock up of floor truss system.

Source: Provided by Laclede Steel Co.

Figure 3–3. Demonstration of application of Monokote sprayed fire-resistive material to floor trusses.

A similar demonstration of a sprayed thermal insulation from U.S. Mineral Products Co. was conducted in September 1967 (see Appendix A Fig. A-13). In other construction documents and correspondence reviewed by NIST, this material produced by U.S. Mineral Products Co. was identified typically as CAFCO D or CAFCO Type D.[5]

In November 1968, the Port Authority authorized award of Contract WTC-113.00 on Spray Fireproofing to Mario & Di Bono Plastering Co., Inc. (see Appendix A Fig. A-14). The company was the subcontractor to Alcoa for application of sprayed thermal insulation to the exterior columns, and the Port Authority reasoned that "contract administration problems would be minimized and coordination between fireproofing work on the interior structural steel and the exterior columns would be facilitated if a single contractor were to perform such work" (see Appendix A Fig. A-15).

3.4.2 Perimeter Columns

By May 1966, several thermal insulation materials were being considered for the perimeter columns (see Appendix A Fig. A-16). This insulation was needed not only for fire protection but also to control steel temperatures under service conditions (see next paragraph). The materials under consideration were Spraycraft (sprayed asbestos fiber), Monokote[6] (sprayed cementitious vermiculite), U.S. Gypsum Fire Code (laminated gypsum board), Vonco (sprayed magnesium oxychloride material), and BLAZE-

[5] CAFCO is the acronym for Columbia Acoustics and Fireproofing Co., a subsidiary of U.S. Mineral Products Co. In other NIST NCSTAR reports and elsewhere in this report, the same material may be referred to as BLAZE-SHIELD D (or BLAZE-SHIELD Type D).

[6] The document shown in Fig. A-16, refers to this material as "Monocoat."

SHIELD Type D. The thermal insulation for the inside face of the columns was assumed to be 1 3/8 in. gypsum plaster, having a conductivity of 1.56 Btu·in/hr·ft^2·°F. An overall transmission coefficient of 0.396 Btu/hr·ft^2·°F between the room and column was also assumed for calculation purposes (see Appendix A Fig. A-17).

In December 1966, Aluminum Company of America (Alcoa) presented its proposal for participation in the wall construction of the World Trade Center towers. The proposal stated (see Appendix A Fig. A-18):

> "The "insulation materials applied to the structural steel components of the wall (columns and spandrels) must serve to control column temperature to a minimum of 50° with 70° inside and 0° outside, provide fireproofing to meet a four hour test on a heavy column, and minimize heat loss and gain to satisfy HVAC requirements."

Alcoa proposed the application of BLAZE-SHIELD (of a type described in UL report R3749-10) to three sides of exterior columns. The fire-resistive material would be thick enough to provide 4 h fire rating. Specifically, Alcoa proposed fire-resistive material thicknesses of 1 7/16 in. for exterior columns and ½ in. for spandrels (see Appendix A Fig. A-18).

For the inside face of the columns, Alcoa proposed to apply a high "k" value (thermal conductivity) material. This application would provide thermal protection while permitting heat migration from the room air to the column steel under service conditions. Figure 3-4 illustrates the thermal protection design for the perimeter columns.

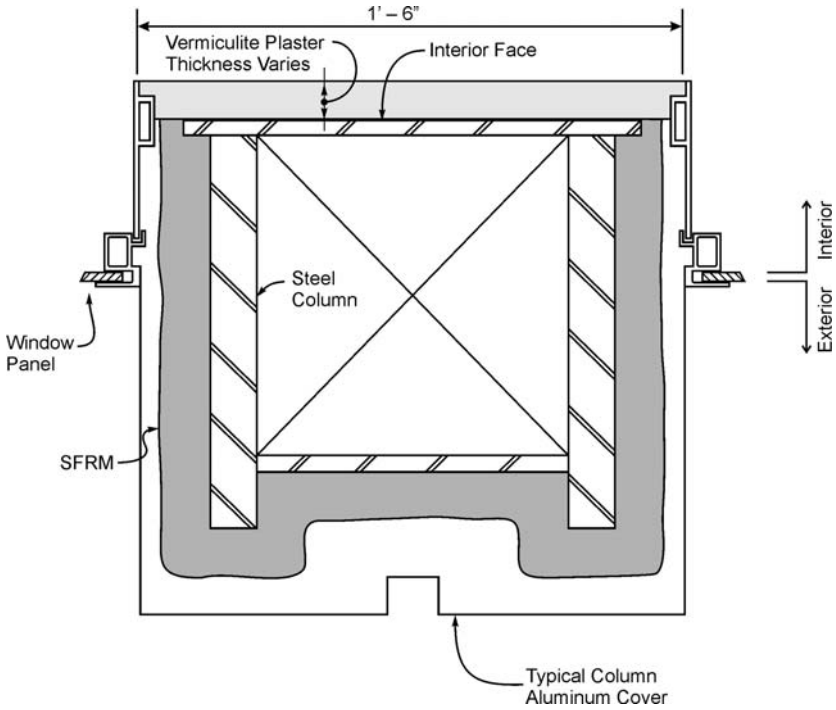

Figure 3–4. Thermal insulation for perimeter columns.

On August 3-4, 1967, an inspection of the quality of fire-resistive material application on an exterior column and spandrel was carried out on a mock-up developed at the Alcoa-Cupples plant in St. Louis, MO. Representatives of Mario & Di Bono Plastering Co., Inc, United States Mineral Products Co., and the Port Authority were present during the inspection. Columns and spandrels were sprayed using BLAZE-SHIELD Type D. In an internal Port Authority memorandum dated August 8, 1967, it was noted that the application of thermal insulation "was done in a workmanship like manner… with ease and very little spillage" (see Appendix A Fig. A-19).

3.4.3 Core Columns

Copies of architectural drawings provided to NIST indicated that the core columns were protected with fire-rated gypsum wallboard, sprayed fire-resistive material, or a combination of these. Core columns located in rentable and public spaces, in closets, and mechanical shafts were enclosed typically with two layers of ½ in. gypsum wallboard and were inaccessible for inspection. The extent of gypsum enclosure around a core column varied depending on the location of the column within the core (see NIST NCSTAR 1-6). In all cases, however, sprayed fire-resistive material was applied on those faces that were not in direct contact with the gypsum enclosure. Again, the selected sprayed fire-resistive material was BLAZE-SHIELD Type D.

Columns located at the elevator shafts were the only columns in the core that were not enclosed and thus were accessible for routine inspections. The columns located at the elevator shafts were protected originally with BLAZE-SHIELD Type D., but other materials were used when dislodged thermal insulation was reapplied (see Chapter 4).

3.5 SPECIFIED THICKNESS OF FIRE-RESISTIVE MATERIALS

3.5.1 During Construction

The thickness of fire-resistive material necessary to achieve the required fire endurance was being assessed in 1965, more than three years before the award of the thermal protection contract. Correspondence from Julian Roth (ER&S) to Malcolm P. Levy (Port Authority) stated that "the one-inch thick material meets the 3 hour requirements of both the new code and Underwriters. (See Appendix A Fig. A-20). Follow-on correspondence from Julian Roth to Malcolm Levy stated the following (see Appendix A Fig. A-21):

> "Although the one-inch spray-on fireproofing meets the 3 hour requirements of both the proposed Building Code and Underwriters, advance information from manufacturers indicates that if the truss were required to be fire-tested, then two inches of material would be required for the light angle members. We are therefore revising our working drawings to indicate a one inch thickness of spray-on fireproofing around the top and bottom chords of the trusses, and two-inch thickness for all other members of the trusses."

Neither of these communications identified the manufacturer or type of fire-resistive material.

WTC project specifications for spray-applied fire-resistive material do not provide required material thickness or hourly ratings. Correspondence in September 1969 from Mario & Di Bono Plastering Co. to Tishman Realty & Construction Co. indicated the following thicknesses (see Appendix A Fig. A-22):

> "1. Beams throughout buildings - ½ inch.
> 2. Columns 1 3/16 inches.
> 3. Elevator columns – 1 inch total including overspray.
> 4. Bar joist – 1 inch overall thickness.
> 5. All beams in MER rooms and utility rooms will be ½ inch thickness with overspray. No tamping or shaping of Cafco type D."

A letter dated October 30, 1969, from Robert J. Linn (manager, Project Planning, WTC) to Mario & Di Bono Plastering Co. stated, in part (see Appendix A Fig. A-23):

> "…Tower 'A' columns that are less than 14WF228 will require 2 3/16″ thick of 'Cafco Glaze-Shield 'Type D'' spray-on fireproofing. All Tower columns equal to or greater than 14WF228 will require 1 3/16″ of fireproofing…
>
> All Tower beams, spandrels and bar joists requiring spray-on fireproofing are to have a 1/2″ covering of 'Cafco.'
>
> The above requirements must be adhered to in order to maintain the Class 1-A Fire Rating of the New York City Building Code."

NIST's review of available documents has not uncovered the reasons for selecting BLAZE-SHIELD Type D or the technical basis for specifying ½ in. thickness of insulation for the floor trusses. Note that this letter indicates that in October 1969 it appeared that the towers were considered as Class 1A construction.

Technical literature from U. S. Mineral Products Co. (USM) dated 1966-1967, included a table indicating that ½ in. of BLAZE-SHIELD Type D would provide a 4 hour rating for beams, girders and spandrels, citing authority of UL tests performed according to ASTM E 119 (see Appendix A Fig. A-24). The 1966–1967 USM product literature does not address bar joists with thermal insulation sprayed directly on the truss members. Instead, the fire protection for joists was shown as an enclosure of thermal insulation. By way of comparison, the product catalog recommended 2-3/16 in. of BLAZE-SHIELD Type D for light columns (columns lighter than W14×228) to achieve the same 4 hour rating.

The October 30, 1969 letter from Linn to Di Bono did not make explicit reference to the required thickness of thermal insulation for core box columns or exterior built-up columns. Alcoa was the supplier of the aluminum cladding on the exterior columns (Contract WTC 400.00). As indicated in Fig. A-18 of Appendix A, Alcoa's contract included providing thermal insulation for the exterior columns and spandrels. The following "Note 11" was included among the "General Notes" of the Alcoa drawings for exterior cladding (See Appendix A Fig. A-25):

> 11. Exterior column and spandrel fireproofing–Cafco Blaze Shield Type D Fireproofing. Interior column and spandrel fireproofing–Vermiculite plaster aggregate fireproofing with finished plaster coat on exposed areas of columns. (3 hr on spandrels, 4 hr on cols)

	Fireproofing Thickness	
Rating	**Cafco**	**Vermiculite Aggregate**
4 hr (heavy column)	1 3/16″	7/8″
3 hr (spandrels)	1/2″	1/2″

Note the 4 h and 3 h ratings within the parentheses are consistent with Class 1A construction.

In a letter dated July 25, 1966, from Emery Roth and Sons to the Port of New York Authority, it is stated "Since the deck is non-structural it will not be fire proofed" (see Appendix A Fig. A-26). As discussed in Section 3.7, photographs taken after construction show that in some areas the underside of the metal deck was not protected, while in other areas fire-resistive material appears to be present but of undetermined thickness and possibly resulting from over spray. Photographs also show that the dampers and damper saddles were not protected. Additionally, it is unclear whether the bridging trusses were required to be protected in all areas.

On April 13, 1970, New York City issued restrictions on the application of sprayed thermal insulation containing asbestos. Since asbestos fiber was a key component of BLAZE-SHIELD Type D, the use of this material was discontinued in 1970 at the 38th floor of WTC 1 (see Appendix A Fig. A-27). The asbestos-containing material was "subsequently encapsulated with a spray-on hardening material" and left in place. Thermal protection of the remaining floors of WTC 1 and all of WTC 2 was carried out using BLAZE-SHIELD Type DC/F, a product that contained mineral wool (glassy fibers) in place of the crystalline asbestos fibers. In May 1970, the construction manager for the World Trace Center wrote a memorandum that summarized considerations in changing from Type D to Type DC/F (see Appendix A Fig. A-28). Correspondence dated April 24, 1970 from Underwriters Laboratories, Inc. to the Port Authority) stated that the thermal properties of BLAZE-SHIELD Type DC/F were equal to or "slightly better" than those of BLAZE-SHIELD Type D (see Appendix A Fig. A-29). There is no record that the required thickness of the fire-resistive material was reconsidered following the change to Type DC/F.

Table 3-2 summarizes information on the fire-resistive materials for the WTC towers after April 1970 based on the reviewed construction documents and correspondence. The "Implied Class" refers to the construction classification implied by the hourly ratings or classification mentioned in correspondence and construction documents.

Table 3–2. Specified fire-resistive materials after April 1970.

Structural Component	Members	Material	Thickness (in.)	Implied Class	Rating (h)
Floor trusses	All	BLAZE-SHIELD DC/F	½	1A	3
Interior columns	< 14WF228	BLAZE-SHIELD DC/F	2 3/16	1A	4
	≥ 14WF228	BLAZE-SHIELD DC/F	1 3/16	1A	4
	Box columns	BLAZE-SHIELD DC/F	NA[a]	1A	4
Interior beams	All	BLAZE-SHIELD DC/F	½	1A	3
Exterior columns	"Heavy" Exterior faces	BLAZE-SHIELD DC/F	1 3/16	1A	4
	"Heavy" Interior face	Vermiculite aggregate	7/8	1A	4
Spandrel beams	Exterior face	BLAZE-SHIELD DC/F	½	1A	3
	Interior face	Vermiculite aggregate	½	1A	3

a. NA, not available.

3.5.2 Report on 1975 Fire

In February 1975, a fire took place in WTC 1, spreading from the 9th to the 19th floor (Powers 1975)[7]. Most of the damage occurred on the 11th floor where the fire affected 9,000 ft^2. After the fire, the Port Authority contracted Skilling, Helle, Christiansen, Robertson (SHCR) to assess the resulting structural damage and to report, in general, on the fire resistance of the floor system. In its report dated April 1, 1975, SHCR communicated to the Port Authority that the fire did not cause structural damage, but it caused buckling of some top chord members of main trusses, buckling of bridging trusses, and distortion deck support angles (see Appendix A Fig. A-30). The SHCR transmittal letter for the report stated that it was "intended to provide background … as to the development of the fire-resistive standards for World Trade Center and looks also at the adequacy of existing systems."

In the transmittal letter, SHCR also indicated that it held itself "as a reporter of facts -- as presented in communications gleaned from the files of Port Authority," the architects, and its own files, and that it did "not purport to have any special expertise not commonly held by other structural engineers." Furthermore, the letter stated that "The only way to assure the existence of the fire safety of floor systems is to be found through the participation of a fire safety engineer and/or fire testing."

The SHCR report suggested that the required thickness of BLAZE-SHIELD for the various structural members could have been determined from catalog information (1966-1967 BLAZE-SHIELD product literature, U.S. Mineral Products Co. [USM]). As mentioned previously, USM's catalog from 1967 indicated that the product had been tested by Underwriters Laboratories, and that for beams, girders, and spandrels, a thickness of ½ in. of BLAZE-SHIELD Type D provided a 4 h rating. As mentioned, the catalog did not provide any information on thermal protection applied directly to members of bar joists.

[7] See also NIST NCSTAR 1-4A.

Table 3-3 summarizes the "fire retardant ratings" obtained from Sweets Catalogs[8] from about 1960 to 1972 for USM's BLAZE-SHIELD products applied directly to beams, girders, and spandrels. The information is based primarily on ASTM E 119 fire endurance tests. The table also presents the thermal conductivity, *k*, for some of the fire-resistive material (the higher the value of *k*, the lower the thermal insulation). Two items are particularly noteworthy. First, the thickness requirement was nearly halved for BLAZE-SHIELD Type D from 1965 to 1966 based on two different test results. Second, the 1966-1967 fire rating, based on two different test results, using ½ in. of the Standard product (with better insulation properties) is one-half of that with ½ in. of the BLAZE-SHIELD Type D product.

The 1975 post-fire report by SCHR stated further that thermal protection of the top chord of the floor trusses was not necessary, except for the corner 60 ft × 35 ft quadrants of the buildings, where the floor acted as a two-way system in bending. In the one-way portion of the floor, "the concrete slab becomes the dominant element of the top chord." Thus, if the shear knuckle remains intact, "the structural integrity of the top chord is not required." Additionally, for resistance to wind load "the structural steel top chord provides only a small increment in the diaphragm strength," so the insulation may be omitted. (see Appendix A Fig. A-30). The report also stated that fire protection of the bridging trusses was not required because they were used "for reduction in floor 'tremor' and to reduce the effects of differential deflections associated with gravity loads." Bridging trusses were "not required as a part of the structural system" and, therefore, insulation could be omitted from them.

The report also addressed the performance of the floor system in the 1975 fire, stating,

> "The fire of February, while reported in the press to have been very hot, did not damage a single primary, fireproofed element. Some top chord members (not needed for structural integrity), some bridging members (used to reduce floor tremor and the like), and some deck support angles (used only as construction devices) were buckled in the fire – all were unfireproofed steel."

In February 2003, NIST asked the Port Authority a series of questions related to the sprayed thermal protection for the floor system. The Port Authority replied in March, and indicated that the top chords of the main trusses and the bridging trusses were protected (see Appendix A Fig. A-31).

[8] McGraw Hill Construction, http://sweets.construction.com

Table 3–3. Information in Sweets Catalogs regarding BLAZE-SHIELD products applied directly to beams, girders, or spandrels (with protected deck) from 1960 to1972.

Year	Product	Reported Thermal Conductivity, *k* (Btu·in/(h·ft^2·°F))[†§]	Hour Rating (h)	SFRM Thickness (in.)	Authority	UL Design No.
1960	BLAZE-SHIELD	0.26	4	2 1/8	UL test R3749-3	
			3	1 7/16	UL test CR193-2	
			2	1 1/8	UL test CR193-3	
			1	3/4	Extr.BMS-92[‡]	
1965	BLAZE-SHIELD	0.27	4	1	ULI[*]#R3749-8	
			3	7/8	ULI# R3789-2	
			2	1/2	ULI# R3749-6	
	BLAZE-SHIELD Type D	None	4	7/8	ULI# R3749-11	
1966	BLAZE-SHIELD Type D	None	4	1/2	ULI# R3749-13	
1966-1967	BLAZE-SHIELD Standard	0.27	3	7/8	ULI# R3789-2	
			2	1/2	ULI# R3749-6	
	BLAZE-SHIELD Type D	0.34	4	1/2	ULI# R3749-13	
1968	BLAZE-SHIELD Standard	0.27	2	1/2	ULI# R3749-6	
	BLAZE-SHIELD Type D	0.34	4	9/16	ULI# R3749-20	
			4	1/2	ULI# R3749-13	
1970	BLAZE-SHIELD Type D	None	4	9/16		98-3 HR
			4	1/2		86-3 HR
			2	1/2		54-2 HR
1971	BLAZE-SHIELD Type DC/F	0.29	4	1/2		86-3 HR
			4	9/16		98-3 HR
			2	5/16		310-2 HR
1972	BLAZE-SHIELD Type DC/F	0.29	4	1/2		86-3 HR
			4	9/16		98-3 HR
			2	5/16		310-2 HR

[†] U.S. Mineral Products Co. catalogs incorrectly report units of thermal conductivity as Btu/in/hr/ft^2/°F.
[§] Thermal conductivities are reported only at ambient temperature.
[‡] Reported to be extrapolations based on formulae contained in National Bureau of Standards Report, *Fire Resistance Classifications of Building Constructions*, Building Materials Structures Report, BMS-92, Washington, DC 1942.
[*] Underwriters Laboratory Inc.

3.5.3 In-Place Thickness and Upgrading of SFRM

No information has been found related to the results of measurements during construction of the thickness of thermal insulation, although thickness appears to have been checked during construction (see Appendix A Fig. A-32). Recorded information on the in-place condition of the sprayed thermal insulation for the floor system first appears in Sample Area Data Sheets from 1990 (see Appendix A Fig. A-33). The data sheets commented on the state of the in-place SFRM. As an example, the data sheet for floor 29 of WTC 1 states the following for the South West quadrant of the floor:

> "Fluffy spray-on fireproofing coating the support beams, joists, and deck above the ceiling. The thickness of the material on the beams and joists was consistently about 1/2″. Regarding the deck it ranged from very sparse [*sic*] in areas to 1/4″ in other areas. The areas we sampled were coated with a light green encapsulant."

Similar statements were recorded for the remaining quadrants of the floor. These inspections were related to litigation related to asbestos and focused on the lower floors of WTC 1, where BLAZE-SHIELD Type D had been applied.

In 1995, the Port Authority performed a study to establish requirements for retrofit of sprayed insulation to the floor trusses during major alterations (new construction) when tenants vacated spaces in the towers (see Appendix A Fig. A-34). The study estimated the thermal protection requirements for the floor trusses of the towers based on "the fireproofing requirements" for Design No. G805 contained in the Fire Resistance Directory (UL 2002) published by Underwriters Laboratories (see Appendix A Fig. A-35). The study concluded that "a two hour fire rating for the steel floor joist trusses can be achieved by applying a 1½ inch thickness of spray-on mineral fiber fire protection material directly to the steel truss chords and webs." In the years between 1995 and 2001, thermal protection was upgraded in a number of the floors affected by the fires on September 11, 2001. Chapter 4 discusses data made available by the Port Authority on the thickness of the upgraded SFRM.

In 1999, the Port Authority established "guidelines regarding fireproofing repairs, replacement, and upgrades" for the towers (see Appendix A Fig. A-36). The guidelines for tenant spaces may be summarized as follows:

- For full floors undergoing new construction or renovation, the floor trusses should be protected with 1½ in. of sprayed mineral fiber fire-resistive material. Retrofit of thermal protection requires removal of existing material and controlled inspection.

- For "tenant spaces that are less than a full floor, undergoing either new construction or renovation," the floor trusses "need only meet the original construction standard. Fireproofing shall be inspected and patched as required to the greater of ¾" or to match existing" if it has already been upgraded to 1½ in.

While the primary material used to provide thermal protection to the floor system was BLAZE-SHIELD DC/F, small areas with damaged SFRM were patched using the Monokote fire-resistive material instead of BLAZE-SHIELD. For patching, Monokote was trowelled on rather than sprayed. In February 2000, a consultant to the Port Authority reported that, in the majority of the cases, the existing fire-resistive material required so much patching that it was more effective to replace it (see Appendix A Fig. A-37).

The same report stated that proper application of 1½ in. of BLAZE-SHIELD took between 2 and 3 passes. When fewer passes were used, the material usually failed the adhesion tests conducted after application.

The Port Authority provided examples of specifications used in alterations that required reapplication of thermal insulation. Figure A-38 in Appendix A is an excerpt from the specifications related to 1998 upgrades to public corridors and bathrooms on the 18th, 18th, and 22nd floors of WTC 2. In this case the specified fire resistive material was Monokote 6. Figure A-39 is an excerpt from the specifications for a tenant alteration in 2001 on the 48th floor of WTC 2. It is seen that the 2001 specifications are not as detailed as the 1998 specifications with respect to application of fire resistive material.

Buro Happold, an engineering consultant, was commissioned by the Port Authority to "conduct a fire-engineering assessment of the fire-proofing requirements of the open-web, steel joists that support the floors in the tenant areas of Towers 1 and 2 of the World Trade Center." The final report issued in July 2000, focused on the requirements of the fire resistance of the floor system of the towers. This report stated that BLAZE-SHIELD DC/F was used on the majority of the floor trusses. Based on calculations and risk assessment, the consultant concluded that (see Appendix A Fig. A-40).

- "The structural design has sufficient inherent fire performance to ensure that the fire condition is never the critical condition with respect to loading allowances.
- A single coat application is possible.
- Significant savings are possible.
- The target reduction of fiber content and increased long term durability can be achieved.
- Alternative materials should be considered."

As quoted, the report states that significant savings could be possible by reducing the fiber content and considering alternative materials. The report suggested that the thickness of the SFRM could be reduced to ½ in. if the material properties at ambient temperature are valid at higher temperatures (see Appendix A Fig. A-40). The report recognized the lack of available temperature-dependent material data for BLAZE-SHIELD Type DC/F. Thus, considering the uncertainties in the material properties and having the understanding of material degradation with temperature and time, Buro Happold recommended a thickness of 1.3 in. of fire-resistive material for the floor trusses.

Later, in December 2000, the final draft of the Property Condition Assessment of World Trade Center Portfolio, prepared by Merritt & Harris, Inc., was presented to the Port Authority. The report stated that, based on existing conditions (see Appendix A Fig. A-41), "The rating of the structural fireproofing in the Towers and subgrade has been judged to be an adequate 1 hour rating considering the fact that all Tower floors are now sprinklered." The report also noted the ongoing program, established by the Port Authority, to upgrade the fire-resistive material thickness to 1½ in. in order to achieve a 2 hour fire rating.

Table 3–4. Design thickness of thermal insulation for reapplication to accessible columns in elevator shafts 12 and 13 of WTC 1.

Floor	Monokote Type Z-106	
	UL-Design	Calculated Thickness
Column 601		
69–79	15/16 in.	15/16 in.
63–68	15/16 in.	13/16 in.
48–62	15/16 in.	11/16 in.
43–47	15/16 in.	9/16 in.
41, 42	15/16 in.	7/16 in.
33–40	15/16 in.	9/16 in.
18–32	15/16 in.	7/16 in.
7–17	3/8 in.	3/8 in.
Elevation 274 - 6	3/8 in.	3/8 in.
Column 602		
69–79	15/16 in.	7/8 in.
54–68	15/16 in.	5/8 in.
43–53	15/16 in.	9/16 in.
41, 42	3/8 in.	3/8 in.
36–40	15/16 in.	9/16 in.
18–35	15/16 in.	7/16 in.
7–17	3/8 in.	3/8 in.
Elevation 274 - 6	3/8 in.	3/8 in.
Columns 501 and 502		
Elevation 310	3/8 in.	3/8 in.

Source: 1992 LERA calculations (240-LERA).[11]

[11] This refers to the ID number in the NIST document database.

Table 3–5. Design thickness of thermal insulation for reapplication to accessible columns and beams in elevator shafts 6 and 7 of WTC1.

Floor	Column 903	Column 904	Beam A	Beam B
B2	3/8 in.	7/16 in.	Note 1	15/16 in.
B1	3/8 in.	7/16 in.	1/2 in.	Note 1
Elevation 294	3/8 in.	7/16 in.	7/16 in.	15/16 in.
1	3/8 in.	7/16 in.	7/16 in.	1 1/16 in.
Intermediate	3/8 in.	7/16 in.	1/2 in.	Note 1
2	3/8 in.	7/16 in.	1/2 in.	1 in.
3–7	3/8 in.	7/16 in.	1/2 in.	1 3/16 in.
8–18	3/8 in.	1/2 in.	1/2 in.	1 3/16 in.
19–33	3/8 in.	5/8 in.	1/2 in.	1 3/16 in.

Key: Note 1=Beams are concrete encased.
Source: 1994 LERA calculations (659-P).

3.6 MAINTENANCE OF SFRM IN ELEVATOR SHAFTS

Based on inspection reports reviewed by the investigation team, the structural members that required the largest amount of inspection and maintenance within the core were the exposed columns and beams within the elevator shafts (see also NIST NCSTAR 1-1C). These columns and beams were the only accessible fire-protected elements in the buildings. Adhesion failures were common, likely because of the exposed conditions of the columns (see Appendix A Fig. A-49) and the inherently low strength of the SFRM.

3.6.1 Bond Strength

Internal memoranda from U.S. Mineral Products Co., dating from 1960 to 1969, warned of the poor adherence or bond performance of BLAZE-SHIELD, and specifically BLAZE-SHIELD Type D. As communicated in an intra-office memorandum dated July 29, 1960, vibration tests performed in 1960 apparently indicated poor bond characteristics of CAFCCO BLAZE-SHIELD as manufactured in the plant compared with laboratory mixtures (see Appendix A Fig. A-50).

In March 1968, the Port Authority investigated the adherence of BLAZE-SHIELD Type D under field conditions. Based on letters from both U.S. Mineral Products Co. and Mario & Di Bono Plastering Co. relative to an “on-the-job” application of BLAZE-SHIELD in January 1968 to evaluate the ability of the material to adhere to the steel and to itself, the Port Authority stated in March 1968 that “this material can be applied successfully to the exterior steel under adverse weather conditions” (see Appendix A Fig. A-51). The Port Authority transmitted this information to the New York City Department of Buildings in January 1970 along with a U.S. Mineral Products Co. report on the material and application techniques and a product catalog (see Appendix A Fig. A-52).

Adhesion problems with BLAZE-SHIELD Type D, however, were reported in December 1969 during construction of the World Trade Center. U.S. Mineral Products Co. intra-office correspondence on December 11, 1969 stated that “Of the 20 tons [800 bags] of material sprayed to the 10th floor exterior

columns on this project, approximately 600-700 bags of the material washed off as clean as a whistle from the exterior columns on this job" (see Appendix A Fig. A-53).

3.6.2 Inspections

Personnel of the World Trade Center Department inspected sprayed thermal insulation during construction. After one of these inspections in 1971, the inspector wrote "it was noted that the Cafco fireproofing treated with Mark II overspray had not cured or hardened according to specifications" due to the extremely cold temperature conditions existing during construction (see Appendix A Fig. A-54). The inspector recommended that shafts 39, 40, and 41 of WTC 1 be re-sprayed with Mark II sealer. Additional WTC office correspondence dated September 24, 1973 mentioned that the sprayed thermal insulation had come loose and fallen from perimeter box beams in elevator shafts 10 and 11 of WTC 2 (see Appendix A Fig. A-55).

In 1993, the Port Authority commissioned Leslie E. Robertson Associates to carry out a continuing program to appraise the condition of the accessible columns in the World Trade Center complex. These inspection programs are described in greater detail in NIST NCSTAR 1-1C. Accessible columns were those columns that were not enclosed in any kind of architectural finish and could be inspected visually. All accessible columns were located in the core of the towers. The columns were inspected visually for signs of rusting, cracking, bowing, and loss of thermal insulation. During the first inspection, carried out in 1993, particular shafts were chosen based on the quantity and types of accessible columns, and convenience to the Port Authority. The findings were summarized in LERA's Structural Integrity Inspection Report for Accessible Columns at 1, 2, 4, and 5 WTC dated 29 January 1993 (see Appendix A Fig. A-56).

Subsequent inspections involved sampling of the structural components and assemblies, which were more important to the structural integrity of the towers, and at locations with a relatively higher potential for defects and problems. As indicated in the Structural Integrity Inspection Report dated 14 April 1995, a statistical sampling approach was used since concurrent visual inspection of all the accessible columns was "not a practical goal" (see Appendix A Fig. A-57). The report stated that the accessible columns in selected elevator shafts in WTC 1 and 2 were "generally in good condition, no structural deficiencies such as cracking or bowing were found, the most common irregularities observed were missing fireproofing and light surface rusting of the exposed steel." Based on the inspections, LERA recommended "that remedial action to be taken where spray fireproofing is damaged, deteriorated or missing and where there is corrosion of the column base due to water leaks at elevator pits." LERA also recommended painting steel with a zinc-rich paint on areas affected by water leaks prior to re-fireproofing. Refer to NIST NCSTAR 1-1C for a comprehensive discussion of the structural integrity inspection reports.

3.7 GENERAL CONDITIONS OF SFRM ON FLOOR TRUSSES

In accordance with the descriptions of the structural systems described in NIST NCSTAR 1-2A, it was estimated that each floor that was supported by trusses contained about 4,350 lineal ft of main trusses. Since main trusses are composed of two trusses side-by-side (see Fig. 3-2), there were over 8,700 ft of main trusses per floor. In addition, each floor contained about 2,000 lineal ft of bridging trusses. Thus, each floor contained over 10,500 lineal feet (or about two miles) of floor trusses. The actual length of members that had to be protected with SFRM was, however, at least twice this length, because each truss

cross section included two chord members and a web bar. In order to understand whether the condition of the thermal insulation played a dominant role in the outcomes on September 11, it was desirable to have information on the general conditions of the SFRM. Since the total collapses of the buildings dislodged the SFRM, it was necessary to rely on available photographic evidence.

Two series of photographs provided some insight on the prevailing conditions of the SFRM on the floor system. One of these was a series of photographs was taken in the mid-1990s by Morse Zehtner Associates and included images from floors 12, 22, 23, and 27 of WTC 1 and floor 26 of WTC 2. These photographs showed the following conditions of the thermal protection applied to the truss-supported floors:

- Some floor trusses had good coverage with SFRM, but the average thickness was not uniform along the lengths of web bars (see Fig. 3-5).
- Bridging trusses did not appear to have as much SFRM applied (see Fig. 3-6). As mentioned in Section 3.5.2, the Engineer of Record stated that bridging trusses did not require thermal protection.
- The SFRM applied to the truss seats at the spandrel beams appeared to be thin (see Fig. 3-7).
- In some cases, the ends of main trusses near the spandrel beams appeared to have thinner SFRM, and the saddles and dampers were not protected (see Fig. 3-7 and Fig. 3-8).
- The SFRM thickness on web bars appeared low in the vicinity of where they connected to the chords (see Fig. 3-5 and Fig. 3-9).
- The metal decking did not appear to have been protected, which is consistent with the requirements stated by the Architect of Record (see Section 3.5.1).
- Some damage to SRM was caused when utilities (HVAC, electrical, network cabling, and so forth) were installed within the ceiling space occupied by the floor trusses (see Fig. 3-10).

A second series of photographs showed the conditions on the 85th floor of WTC 2 prior to removal (by water blast) of SFRM by the tenant, who was conducting a major alteration of the space including an upgrade to the thermal insulation in accordance with the guidelines discussed in Section 3.5.3. Photographs[12] and video were taken on March 8, March 20, April 13, and July 17, 2001. The photographs include close-up views of different features of the thermal insulation applied to the floor trusses and overall views of large sections of the floor truss system, before and after removal of the SFRM. Based on these photographs, the following observations were made:

- There were no examples of total absence of SFRM on trusses that had not been cleaned by water blasting.

[12] Photographs and videotapes were provided by the former tenant, Harris Beach LLP. They were taken for the tenant by a hired photographer (Forensic Photography International). NIST was not able to locate the photographer to obtain permission to reproduce the photographs in this report. The photographs, however, are available for viewing at NIST and have been assigned ID number 223-I.

- Areas where SFRM had been dislodged had been repaired using a trowel-applied material. Some of the repairs on lower chords were incomplete, but it is not known whether these repairs had failed or if the repair material had purposely not been applied to some portions of the chords.

- There were many instances where SFRM had obviously been dislodged in the process of installing utilities. In some cases hardware was attached directly to the lower chords and SFRM was dislodged. These damaged areas should have been repaired when the various trades had completed their work.

- The overall views of the trusses showed that regions of missing insulation where minor in extent when compared with the total area of applied SFRM.

In comparing the overall condition of the SFRM as indicated by these two series of photographs, the following differences were noted:

- The photographs taken in the 1990s of the lower floors appeared to show more instances of thinly applied SFRM than the photographs of the 85th floor taken in 2001.

- The photographs taken in the 1990s appeared to show less damage as a result of installation of utilities and other services within the space occupied by the trusses.

Figure 3–5. Intersection of main truss and bridging truss showing general good coverage of SFRM on truss members but thickness varies on web bars.

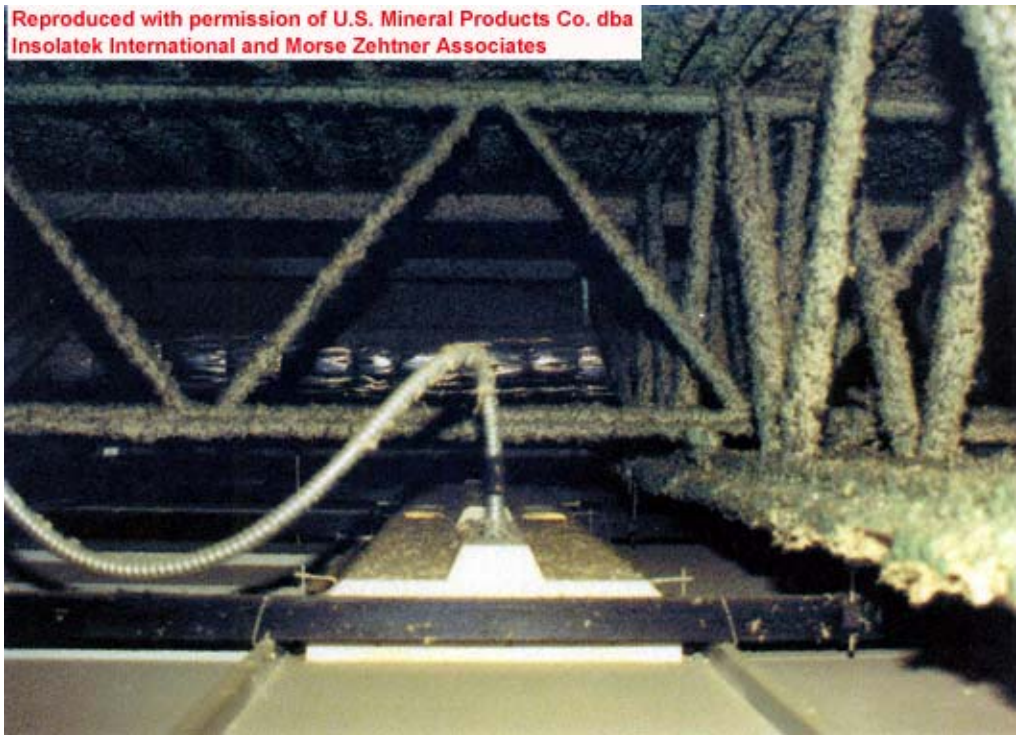

Figure 3–6. Intersection of main truss and bridging truss showing thinner SFRM on members of bridging truss.

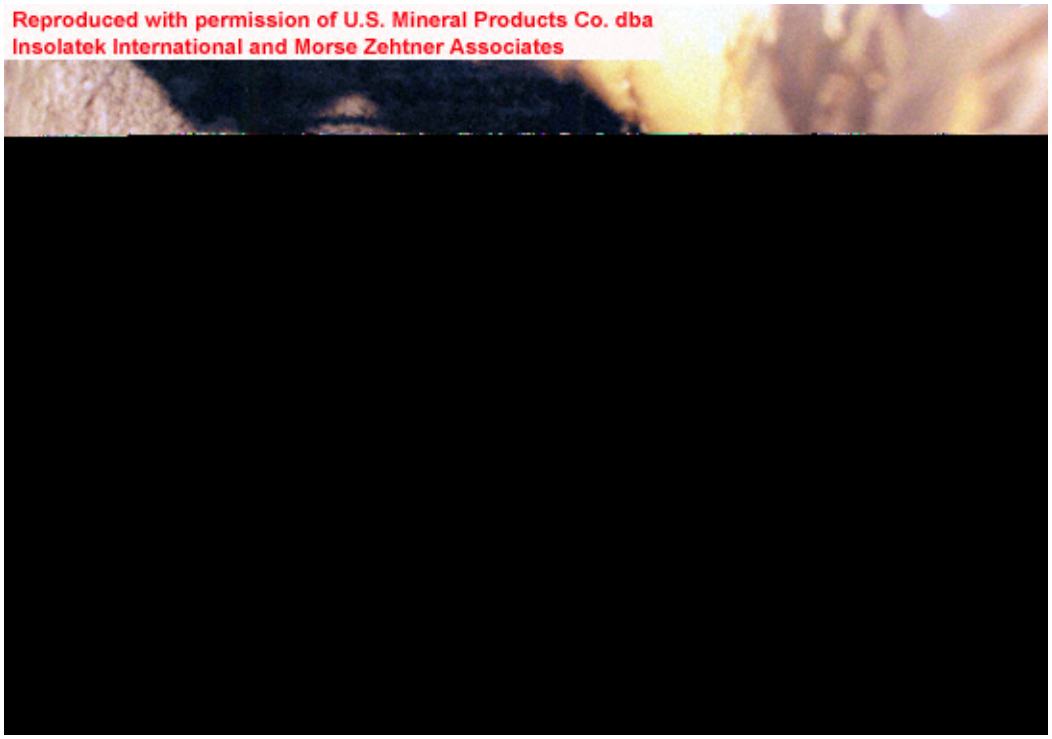

Figure 3–7. Connection of main truss to spandrel beam showing relatively thin SFRM on truss seat and no SFRM on damper.

Figure 3–8. End of main truss showing low thickness of SFRM on truss members and no SFRM on damper saddle.

Figure 3–9. Intersection of main truss and bridging truss showing thin SFRM on the ends of some web bars; SFRM was not applied to the metal decking.

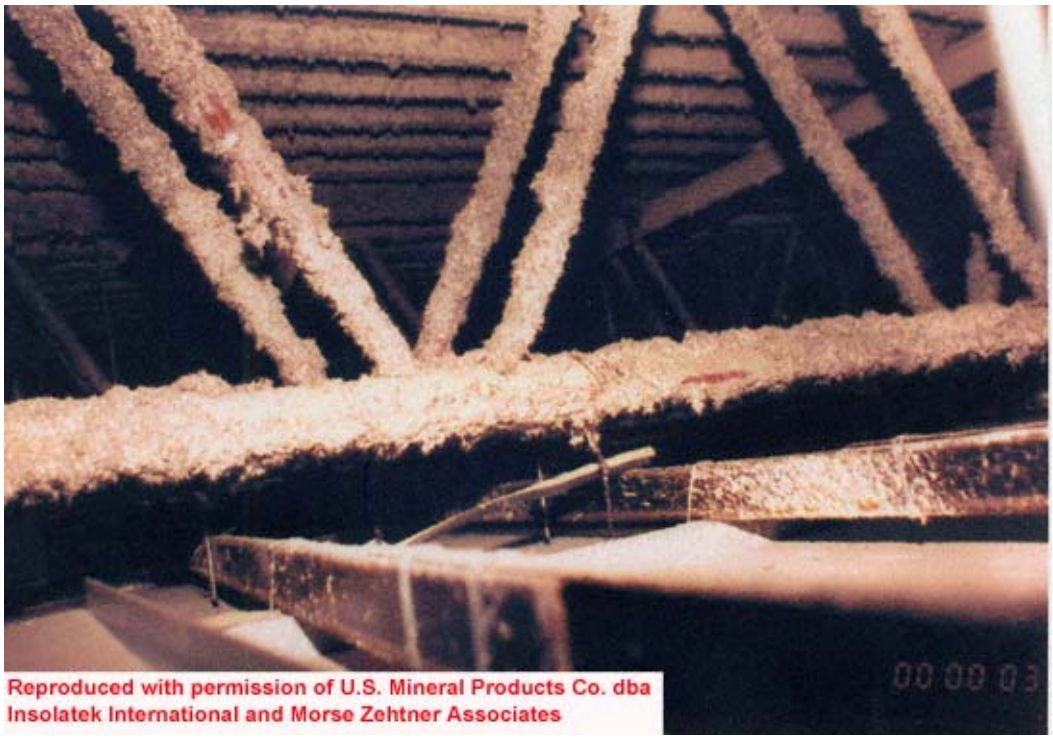

Figure 3–10. Example of damage to SFRM during installation of utilities.

This page intentionally left blank.

Chapter 4
AS-APPLIED THICKNESS OF SFRM

Because both towers collapsed totally on September 11, 2001, and most of the sprayed fire-resistive material (SFRM) was either dislodged or abraded (or scraped) off in the collapse, no examples remain of the "as installed" condition of the SFRM. To make an estimate of the as-applied thickness and variability in thickness, several sources of information were used, including measurements taken by the Port Authority, condition surveys and anecdotal information, and photographs and video clips showing the condition of the fire-resistive material in selected areas. Each of the structural components or systems is considered here separately.

4.1 TRUSS-SUPPORTED FLOOR SYSTEM

As mentioned in Section 3.5.3, qualitative information on the in-place condition of the SFRM for the floor system first appeared in Sample Area Data Sheets from 1990. Information regarding quantitative inspection of existing fire-resistive material appears in documentation from 1994. That year, the Port Authority performed a series of thickness measurements of the existing SFRM on floors 23 and 24 of WTC 1 (see Appendix A Fig. A-58). Six measurements were taken from "both flanges and web" of each of 16 randomly chosen trusses on each floor at those locations where the SFRM was not damaged or absent. The averages of six measurements per joist that were recorded on the two floors are presented in Table 4-1. Measured average thickness varied between 0.52 in. and 1.17 in. For the 32 measurements (16 on each floor), the overall average was 0.74 in. Four of the 32 floor trusses had average thicknesses between 0.52 in. and 0.56 in. These measurements suggest that the minimum average thickness exceeded 1/2 in.

As shown in Fig. A-58 in Appendix A, it was stated that, on floor 23,

> "... truss members located adjacent to the outside walls (within 3 ft) are devoid of fireproofing material. Visual inspection on floor 24 was not possible, as this area still has a lowered ceiling in place."

The data in Table 4-1 can be examined further to understand the variability of the SFRM thickness in the non-upgraded locations. Figure 4-1 (a) shows the average thicknesses measured on the floor trusses of floors 23 and 24. The values appear to be similar for the two locations in terms of overall average thicknesses and the variation in average thickness. A formal analysis of variance indeed indicated no statistically significant differences between the overall mean thicknesses for the two floors. Thus, the two groups of data can be combined into one group.

Figure 4-1(b) is a normal probability plot of the average thicknesses shown in Table 4-1. If the data were from the same distribution they would fall approximately on a straight line in the normal probability plot. This is expected from the *central limit theorem*, which states that the sampling distribution of the average of *N* samples from a distribution with mean μ and variance σ^2 approaches a normal distribution with mean μ and variance σ^2/N as N increases (Miller and Freund 1965). It is seen that four points deviate from an approximately linear relationship. It is, therefore, reasonable to conclude that those points do not

belong to the same distribution. These four values are identified with an asterisk in Table 4-1. Figure 4-1(c) is a normal probability plot with the four values (actually six points) excluded. It is seen that the remaining points fall close to a straight line. The intercept (0.74 in) and slope (0.12 in.) of the straight line are the mean and standard deviation of the distribution, respectively. Since each of the averages in Table 4-1 is obtained from six individual measurements, an estimate of the standard deviation of the individual measurements of SFRM thickness is $0.12\sqrt{6} \approx 0.3$ in.

Table 4–1. Average fireproofing thickness from six measurements taken in 1994 on each of 16 random floor trusses on floors 23 and 24 of WTC 1.

Fireproofing Thickness (in.)	
Floor 23	**Floor 24**
0.60	0.76
0.53*	0.60
0.70	0.90
0.76	0.72
0.88	0.64
0.89	0.80
0.83	0.68
1.17*	0.65
0.88	0.67
0.71	0.77
0.82	0.96
0.52*	0.66
0.69	0.65
0.52*	1.11*
0.64	0.95
0.52*	0.56

*Not considered in estimating thickness variability.
Source: Data provided by Port Authority of New York and New Jersey.

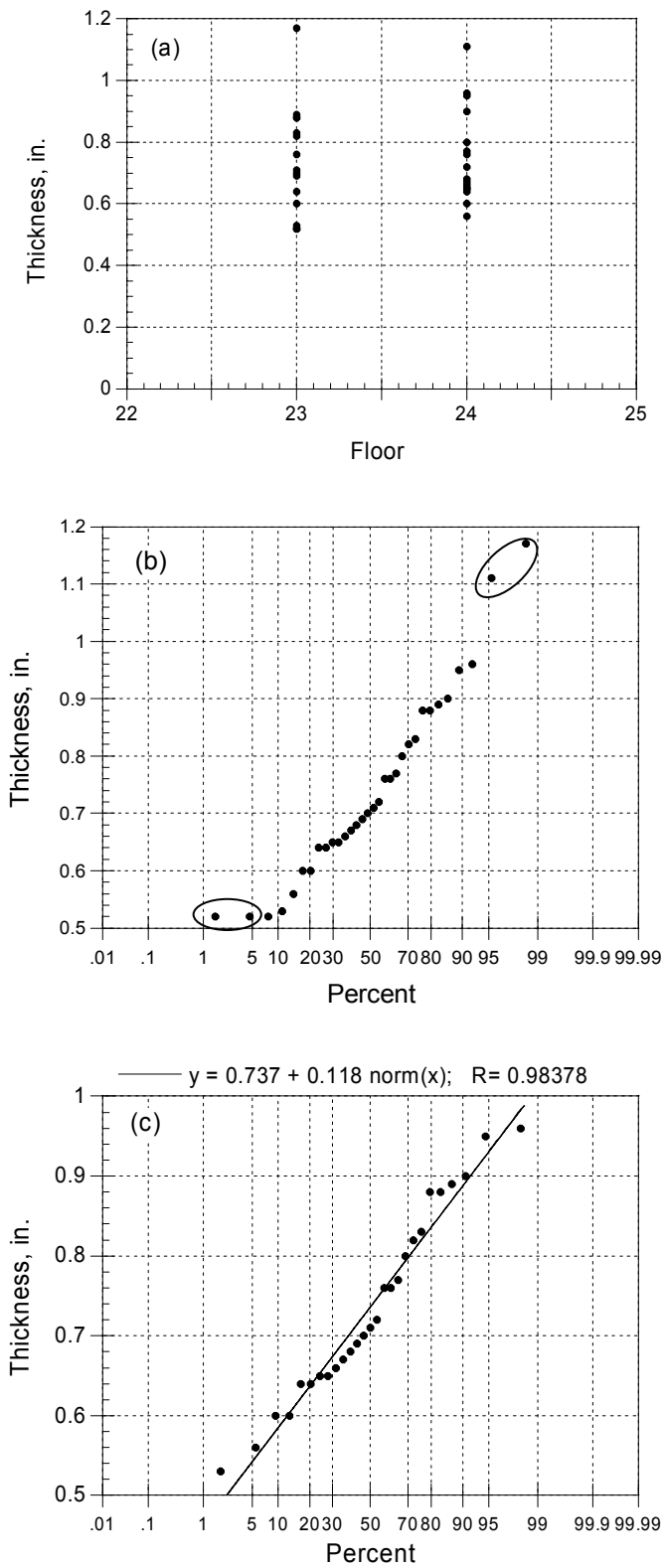

Figure 4–1. (a) Dotplot of average thickness from floor trusses for floors 23 and 24, (b) normal probability plot of all average thickness values, and (c) normal probability plot of average thickness with four values (six points) excluded.

4.2 ANALYSIS OF PHOTOGRAPHS

Additional data regarding the thickness of SFRM was gathered by evaluating photographic evidence. Although photographic evidence of the state of the SFRM was limited, two groups of photographs were located and used for estimating SFRM thickness.

The first group of photographs was provided to NIST by Morse Zehnter Associates and includes images of floor trusses from WTC 1 (floors 12, 22, 23, and 27) and WTC 2 (floor 26). From this group, only photographs from floors 22, 23, and 27 of WTC 1 were analyzed. Photographs provided by Morse Zehnter Associates were taken in the mid-1990s and illustrate the fire-resistive material conditions prior to the upgrade carried out by the Port Authority. Thus, SFRM thickness on the photographed trusses would be expected to be at least ½ in. as specified by the Port Authority on October 1969.

The second group of photographs, taken in 1998, was provided by Gilsanz Murray Steficek (consulting engineers). This group illustrates the state of fire-resistive material after the upgrade program that was initiated in 1995. The photographs were of trusses for floor 31 and below in WTC 1.

Selection of which photographed trusses were used to estimate thickness of SFRM was based on clarity of SFRM edges and whether a feature of known dimensions was present to provide a reference measurement. Thus, only photographs where reference measurements could be performed were used. The general approach to the analysis involved the estimation of distances based on the computed reference length per pixel. The procedure is summarized as follows:

- A feature of known dimension (based on construction drawings) that could be used as reference was located in the photograph. For example, the dimension of the bare vertical leg of a damper saddle was a dimension that could be obtained from shop drawings.

- In the photograph, the length of the reference dimension was measured in pixels.

- The scaling factor of length per pixel was computed by dividing the known dimension in inches by the number of pixels. For example, if the vertical leg of the damper saddle was measured as 48.2 pixels in the photograph, and it is known that the actual size of the leg was 3.13 in., the scaling factor would be 3.13 in./48.2 pixels = 0.065 in./pixel.

- Only truss webs or struts (diagonal bar at end of truss) located near and in the same plane as the reference object were selected for analysis. This selection was made to minimize error due to perspective.

- It was assumed that the fire-resistive material on web bars was applied evenly around the perimeter of the bar. Based on this assumption, a “virtual” centerline along the length of the bar was drawn in the photograph.

- Lines were drawn perpendicular to the “virtual” centerline. The number of pixels along the lines from the “virtual” centerline to the edge of the SFRM was determined from the cursor positions indicated by the software. Measurements were made at regularly spaced intervals to avoid bias. Figure 4-2 is an example of a series of measurements made on a strut.

- Each measurement in pixels was multiplied by the scaling factor (in./pixel) to estimate the bar radius plus SFRM thickness. This provides two measurements at each cross section.

- The radius of the bar was subtracted to provide the estimate of the SFRM thickness.

Figure 4–2. Example of measurement procedure used to estimate SFRM thickness from photographs.

For floors that had not been upgraded, it was observed that the estimated thickness of SFRM on the webs of the main trusses tended to be greater than that on either the diagonal struts or on the webs of the bridging trusses. Hence, estimates of SFRM thickness for non-upgraded floors were divided into three groups:

- Webs of main trusses,

- Webs of bridging trusses, and

- Diagonal strut at the exterior wall end of the truss.

It was not possible to estimate the thickness of the SFRM on any truss element except the round web bars. Consequently, for the upgraded floors in WTC 1 that were included in the second group of photographs, only estimates of the thickness on the web bars of the main trusses were made. Figure 4-3 (a) shows normal probability plots of the SFRM thickness estimated from the photographs. It is seen that the points for the "upgraded" main trusses follow a generally linear trend, which indicates that the estimated thicknesses for the upgraded main trusses are approximately normally distributed. The estimated thicknesses from the non-upgraded floors, however, do not follow linear trends on the normal probability plot. Figure 4-3 (b) shows normal probability plots of the natural logarithms of the thicknesses. The transformed values for the non-upgraded thermal protection now follow generally linear trends, which

means that a lognormal distribution is more appropriate for the non-upgraded floors. Thus, there is evidence that the original SFRM thickness on the floor trusses follows a log normal distribution.

The reason for a lognormal distribution for SFRM thickness on the non-upgraded floor trusses can be explained as follows. It is expected that the thickness of SFRM will be variable due to the difficulty in spraying the material on the relatively thin members. If the overall thickness is low and the variability is high, a normal distribution would require a fraction of the surfaces to have negative values of SFRM thickness, which is not possible. If the thickness distribution is lognormal, the thickness cannot be zero, and there is a low likelihood of having thickness close to zero. Thus, from a physical point of view, a log-normal distribution of SFRM thickness is more logical than a normal distribution. If the underlying distribution of SFRM thickness is lognormal, the average thickness overestimates the thickness expected to be exceeded with 50 percent probability, and the median is the appropriate statistic for the 50-percentile value (Melchers 1999).

The average, standard deviation, and coefficient of variation were computed for the total number of measurements in each of these groups. The results are summarized as follows:

- Main trusses before upgrade (85 measurements): Average thickness 0.6 in., standard deviation = 0.3 in., and coefficient of variation = 0.5; median = 0.55 in.

- Bridging trusses before upgrade (52 measurements): Average thickness 0.4 in., standard deviation = 0.25 in., and coefficient of variation = 0.6; median = 0.36 in.

- Diagonal struts before upgrade (26 measurements): Average thickness 0.4 in., standard deviation = 0.2 in., and coefficient of variation = 0.5; median = 0.38 in.

- Main trusses after upgrade (52 measurements): Average thickness 1.7 in., standard deviation = 0.4 in., and coefficient of variation = 0.2; median = 1.80 in.

4.3 PORT AUTHORITY DATA ON UPGRADED SFRM ON TRUSSES

In the 1990s, the floor trusses of several floors were upgraded to a specified thickness of 1½ in. of fire-resistive material as tenants vacated their space. According to correspondence in 2002 (see Appendix A Fig. A-59), the Port Authority indicated that 18 floors of WTC 1 and 13 floors of WTC 2 had been upgraded. The Port Authority also stated that: “The entire impact zone for Tower 1 (92-99) was upgraded with 1½" spray-on fireproofing. Only the 78th floor was upgraded with the 1½" spray-on fireproofing within the impact zone in Tower 2 (78-84).” The Port Authority provided information from Construction Audit Reports regarding the characteristics of SFRM that was upgraded as of 2000 in the aircraft impacted regions of the WTC towers. The provided test reports state that the material used for the upgrade was BLAZE-SHIELD II (see Appendix A Fig. A-60 for an example of such a report).

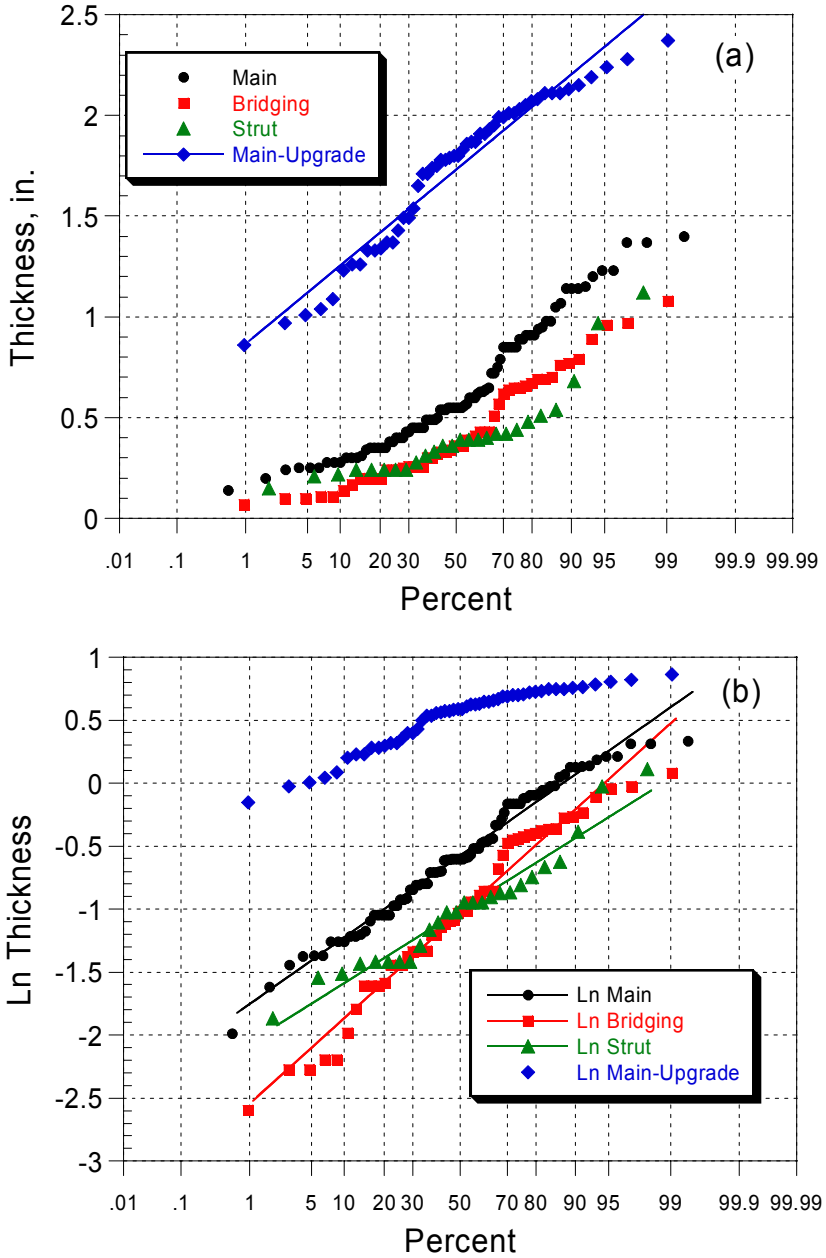

Figure 4–3. (a) Normal probability plot of estimated SFRM thickness based on photographs, and (b) normal probability plot of natural logarithms of thickness (Data provided by PANYNJ).

Port Authority test reports state that tests of upgraded SFRM were performed in accordance with ASTM E 605 for thickness and density (ASTM 1993) and in accordance with ASTM E 736 for adhesive/cohesive strength (ASTM 1992). Section 8.1.1 of ASTM E 605-93 requires that thickness measurements be taken at "One bay per floor or one bay for each 10,000 ft^2, whichever provides the greater number of tests." In addition, the test method states that: "Thickness determinations for the following structural elements shall be conducted in each randomly selected bay: one selected area of metal deck, concrete slab, or wall section; one column; and one beam (joist or truss)." For each

preselected joist (or truss), Section 8.1.5.2 of the test method requires that one 12 in. length be laid out and seven thickness measurements be taken at each end of the 12 in. length. Thus, two sets of thickness readings are expected for each truss if ASTM E 605-93 were followed. Figure 4 of ASTM E 605-93 shows that there should be seven measurements at each cross section, which are to be distributed as follows: two at the top chord, two at the web, and three at the bottom chord.

Table 4-2 shows the test data provided by the Port Authority for the impact-affected floors.[13] Shown are the average thickness, bond strength, and density for each test area on a given floor. The specified minimum requirements are 1½ in. for thickness, 150 psf for bond strength, and 15 lb/ft^3 for density. Correspondence from the Port Authority in March 2004, clarified that the words "bottom truss" in the test reports referred to the location of the bond test and where the sample was removed for density measurement (see Appendix A, Fig. A-61). Note that some of the average thicknesses shown in Table 4-2 equal or exceed 3.5 in. No photos were available of upgraded floors to show the appearance of a truss with such high average thickness of SFRM. There is no record in the test reports of whether the top chord and bridging trusses were protected in the upgraded floors.

In 2004, the Port Authority provided NIST reports of the individual measurements for many of the average thicknesses shown in Table 4-2.[14] With the individual measurements, it was possible to investigate the variation of thickness at a cross section of a truss member and the variation in average thickness from truss to truss. To permit such analyses, only those data having the same number of individual measurements at each cross section were used. This resulted in 18 data sets for WTC 1 (including floors 93, 95, 98, 99, and 100) and 14 data sets for WTC 2 (including floors 77, 78, 88, 89, and 92).

[13] Transmittal of construction audit material testing reports by Saroj Bhol (PANYNJ), January 21, 2003 (30-P).

[14] Electronic file of individual thickness values transmitted by Frank Lombardi (PANYNJ) to NIST on April 7, 2004 (682-P).

Table 4–2. Summary of Port Authority test reports for upgraded SFRM on floor trusses (30-P).

WTC Tower	Floor Number	Specific Location /Tenant	Date of Report	Average SFRM thickness (in.)	Adhesion/ Cohesion (lb/ft^2)	Density (lb/ft^3)
1	79	Multiple tenant floor	11/24/99	2.4	333	16.6
1	80	Multiple tenant floor				
1	81	Multiple tenant floor	10/24/96	2.7	270	19.0
1	81	Multiple tenant floor	7/16/99	2.3, 2.4, 3.0	352, 463, 315	17.4, 17.6, 17.4
1	83	Suite 8331	12/15/99	2.2	259	16.0
1	85	Multiple tenant floor	12/24/97	3.5, 2.9, 2.9	162, 180, 288	28.7, 23.7, 18.6
1	85	Multiple tenant floor	6/12/99	2.9	278	15.8
1	85	Multiple tenant floor Suite 8563	8/16/99	2.8	259	16.4
1	86	Julien Studley Inc. (7000 ft^2)				
1	92	Full floor	4/2/97	3.0, 2.8, 2.8	360, 324, 360	20.3, 15.4, 18.0
1	93	Full floor	8/28/98	1.8, 2.0, 1.8, 2.2, 1.8, 1.9, 2.9	117 (153)†, 207, 216, 234, 162, 180, 216	14.2, 16.6, 16.1, 18.4, 15.1, 17.4, 21.3
1	94	Full floor	12/27/96	4.3, 3.8, 4.3	486, 504, 288	21.2, 20.5, 20.1
1	95	Full floor	8/24/98	2.2, 2.4, 3.3	270, 306, 198	18.0, 20.1, 20.4
1	96	Full floor	10/22/98	3.0, 3.2, 3.2	486, 288, 324	20.5, 19.8, 19.9
1	97	Full floor	10/22/98	2.6, 2.2, 2.2	360, 468, 468	26.5, 20.0, 23.9
1	98	Full floor	11/19/98	2.9, 2.8, 2.5	407, 351, 518	31.3, 16.8, 19.6
1	99	Full floor	11/20/98	2.8, 2.2, 2.2	204, 222, 204	18.8, 16.6, 18.4
1	100	Full floor	11/20/98	2.8, 3.2, 3.4	278, 278, 333	16.4, 17.3, 19.9
1	102	Full floor	9/28/99	3.2, 3.2, 2.1	333, 333, 315	16.5, 16.9, 15.9
2	77	Full floor	6/9/98	2.7, 2.1, 2.6	351, 198, 297	19.4, 19.4, 17.2
2	78	Full floor	4/3/98	2.5, 2.8	288, 270	17.0, 18.1
2	85	Full Floor				
2	88	Full floor	7/5/00	1.9, 2.4, 2.1	167, 333, 157	18, 16, 15
2	89	Full floor	5/5/99	2.8, 2.7, 3.0	370, 333, 270	22.4, 15.8, 15.3
2	92	Full floor	2/26/98	2.8, 3.0, 2.7	342, 360, 297	19.7, 21.1, 19.7
2	96	Full floor				
2	97	Full floor				
2	98	?				
2	99	Half floor	7/28/97	2.1, 3.0	315, 252	19.5, 22.7
2	99	Half floor	4/3/98	1.8, 1.7	306, 270	21.9, 19.5

† Repeated test

An analysis of the individual measurements was carried out to determine the underlying distribution for the measured thicknesses. Figure 4-4(a) is a dotplot of the individual measurements in WTC 1 (144 measurements) and in WTC 2 (112 measurements). It is observed that the central values and ranges are similar for the two towers, and the two groups of measurements were combined into one group. Figure 4-4 (b) is the histogram of the individual measurements, and Fig. 4-4 (c) is the corresponding normal probability plot. A straight line fit to the normal probability plot shows a tendency of the points to deviate from the line. Figure 4-4 (d) is a histogram of the natural logarithms of the individual thickness values, and Fig. 4-4 (e) is the corresponding lognormal probability plot. A comparison of the probability plots shows that natural logarithms fall closer to a straight line. Thus, it appears that the thickness of the upgraded SFRM on the floor trusses is described by a lognormal distribution. This contradicts the observation based on analysis of photographs from lower floors discussed in the previous section. The overall average thickness of the 256 individual measurements is 2.5 in. with a standard deviation of 0.6 in. The median was also 2.5 in. Thus, the average thickness on the upgraded upper floors appears to be greater than that estimated from photographs taken on upgraded lower floors.

As shown in Fig. 4-4, there were a number of points representing individual thicknesses of 3 ½ in. or greater. As mentioned, there are no corroborating data, such as photographs, of such reported high thicknesses. The probability distributions in Fig. 4-4 show, however, that the high thicknesses were consistent with the remainder of the distributions. In any case, statistics were recomputed after removing thicknesses of 3 ½ in. and greater (this amounted to 20 out 256 points). The resulting average thickness was reduced to 2.4 in., and the standard deviation was reduced to 0.5 in. The median remained unchanged. Thus, it was concluded that the high reported thicknesses would not have a dramatic effect on the overall statistics of the SFRM thickness in the upgraded floors.

The overall standard deviation of 0.6 in. includes two contributions: (1) the variation of thickness at the cross section (within-truss variability), and (2) the variation of average thickness between trusses (between-truss variability). Figure 4-5 shows these two components of the thickness variability for the two towers. Figures 4-5 (a) and (c) show the within-truss variability, and Figs. 4–5 (b) and (d) show the variation of average thickness of each truss. From analysis of variance, it was found that the within-truss standard deviation is 0.4 in., and the between-truss standard deviation is also 0.4 in. The within-truss standard deviation of 0.4 in. is similar to the standard deviation of the estimated individual thicknesses obtained from analysis of the photographs of upgraded main trusses.

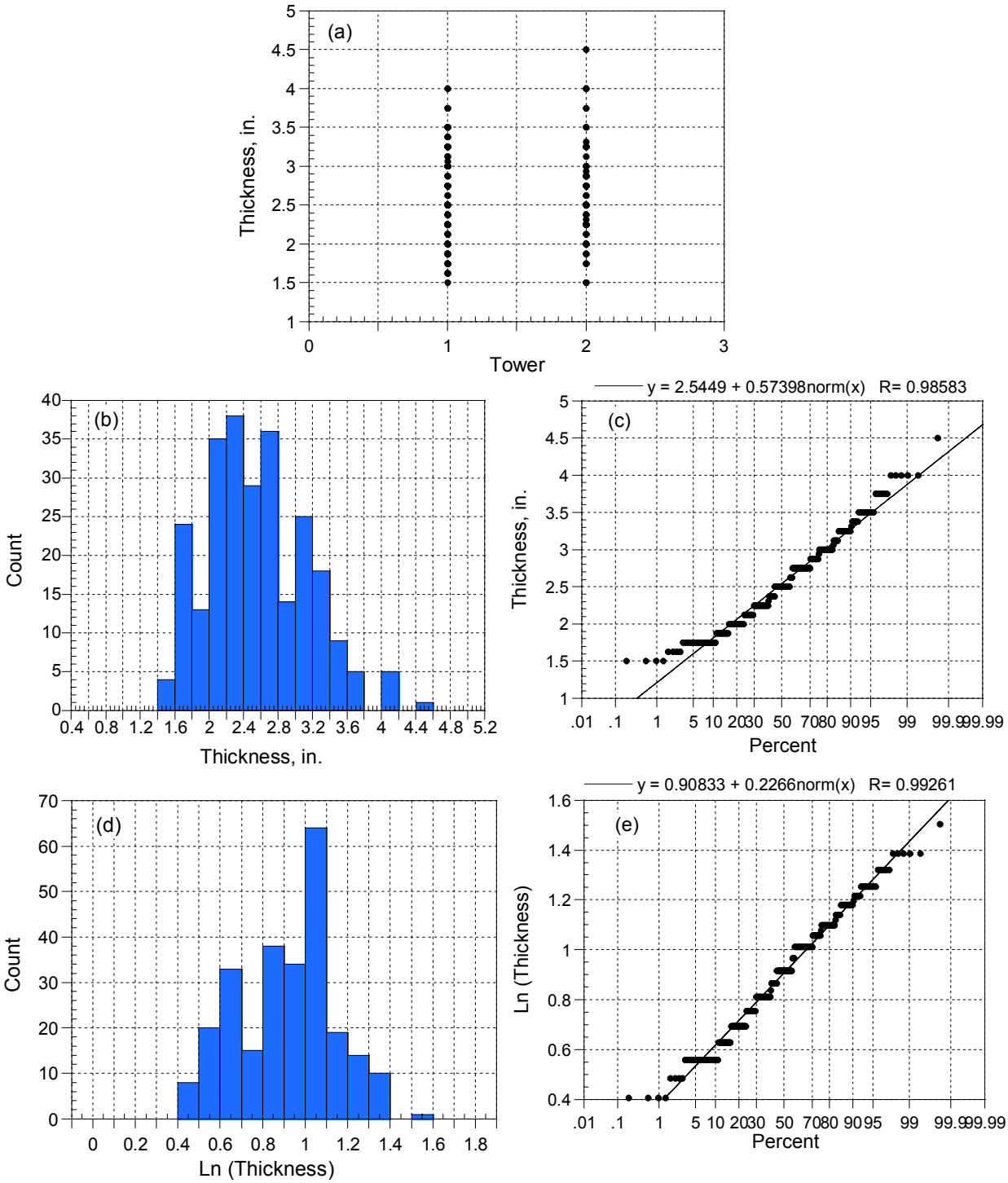

Figure 4–4. (a) Dotplot of individual thickness measurements on floor trusses from Port Authority Construction Audit Reports, (b) histogram of thickness measurements, (c) normal probability plot of thickness measurements, (d) histogram of natural logarithms of thickness measurements, and (e) normal probability plot of natural logarithm of thickness measurements.

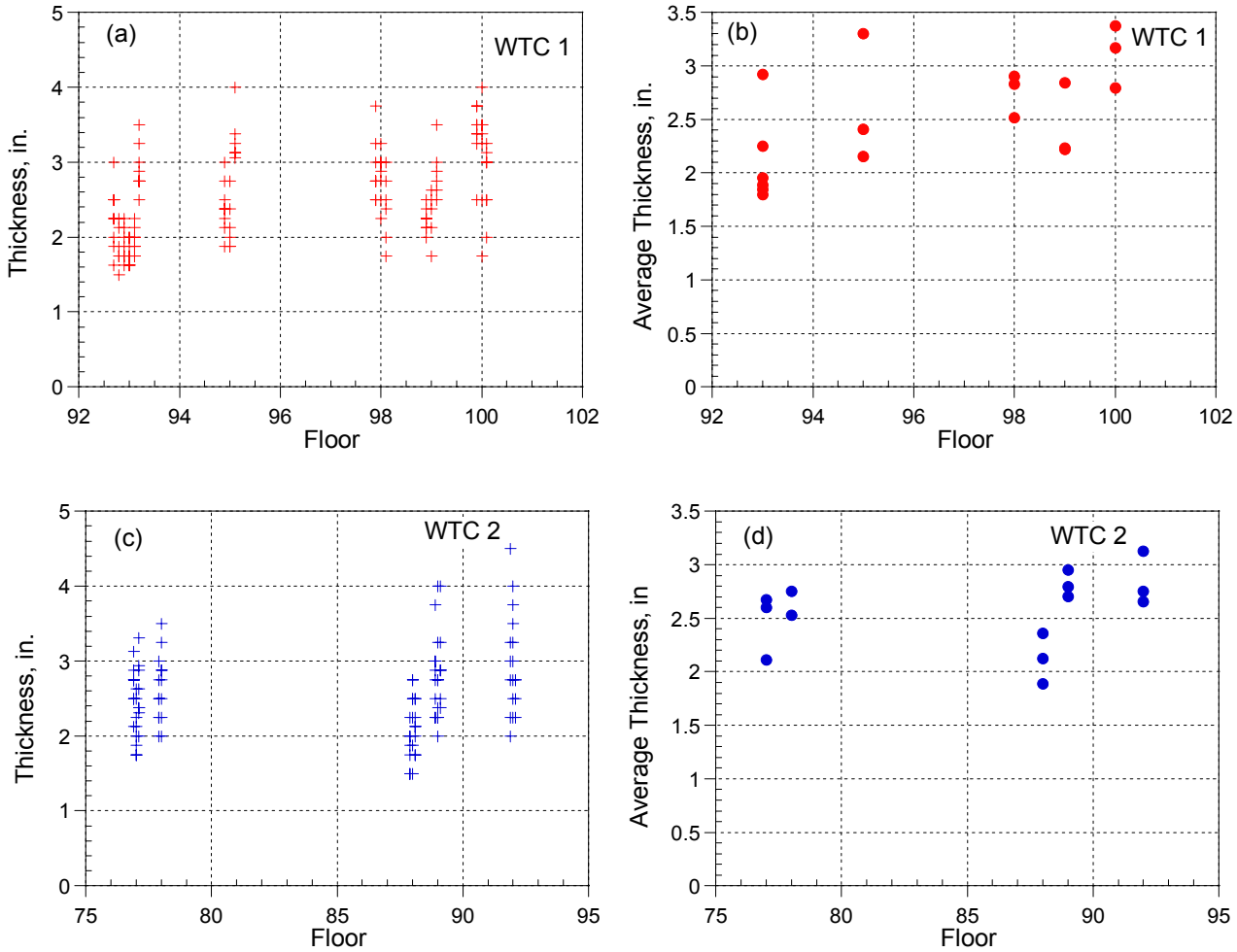

Figure 4–5. SFRM thickness on floor trusses in upgraded portions of WTC towers: (a) individual measurements in WTC 1, (b) average thickness in WTC 1, (c) individual measurements in WTC 2, and (d) average thickness in WTC 2 (data provided by PANYNJ).

4.4 COLUMN SFRM THICKNESS

NIST requested that the Port Authority provide available information on the thickness of fire-resistive material for the exterior and interior columns of the WTC towers (see Appendix A Fig. A-62). Specifically, the request included the following:

- The fire-resistive material used and the thickness on the various plates comprising the exterior columns and spandrels.
- The fire-resistive material used and the thickness on core columns.
- Confirmation that the wide flange column sections were protected with BLAZE-SHIELD Type DC/F with specified thickness of 2 3/16 in. for sections smaller than 14WF228 and 1 3/16 in. for 14WF228 and larger.
- Information on in-place SFRM thickness.

The Port Authority replied that, due to inaccessibility of exterior columns and core columns, there were no recent records of SFRM thickness for these elements (see Appendix A Fig. A-62). The only available measurements of SFRM thickness were for beams and columns accessible within elevator shafts. These measurements were, however, for re-applied thermal insulation.

The most complete data set included measurements on beams and columns taken within shaft 10/11 in WTC 1. These measurements were taken in April 1999 and included measurements from floor 1 to floor 45. The thicknesses were recorded to the nearest 1/8 in., with a few thicknesses recorded to the nearest 1/16 in. The columns included 10 to 18 replicate measurements, and the beams included 11 to 16 replicate measurements.

Figure 4-6 (a) shows the individual and average SFRM thickness on the core columns. Analysis of variance indicated no statistically significant differences among the average values, and all data were pooled together. The average thickness for the columns is 0.82 in., the standard deviation is 0.20, and the coefficient of variation is 0.24. The information from the Port Authority indicated that the “minimum thickness required” for the columns was ½ in. As noted in Appendix A Fig. A-62, the required thickness was based on calculations performed by LERA for re-applied thermal insulation (Monokote Type Z-106), similar to what was discussed in Section 3.5.5. Figure 4-6 (b) is the normal probability plot of the individual thickness measurements. Because most of the thicknesses were reported to the nearest 1/8 in., the points are staggered in steps instead of uniformly distributed. The plot, however, shows that the points follow a linear trend, and it appears that the thickness of the reapplied SFRM on the core columns could be described by a normal distribution. Figures 4-6 (c) and (d) show the corresponding plots for the thickness of SFRM reapplied to beams surrounding shaft 10/11 of WTC 1. The average thickness is 0.97 in., the standard deviation is 0.21 in. and the coefficient of variation is 0.21. The information from the Port Authority indicated that the “minimum thickness required” for the thermal insulation reapplied to the beams was 3/4 in.

The data described above may not have a direct bearing on the outcome of the investigation because they deal with lower stories. They do, however, provide some useful information on the variability of SFRM applied to beams and columns. The variation in SFRM thickness for the beams and columns shown in

Fig. 4-6 is lower than the variation observed in the floor trusses. This is not unexpected because the planar surfaces of the beams and columns result in more uniform application of the sprayed fire-resistive material than for the slender truss members. This results in reduced differences in the average thickness of SFRM on different members and less variability within a member.

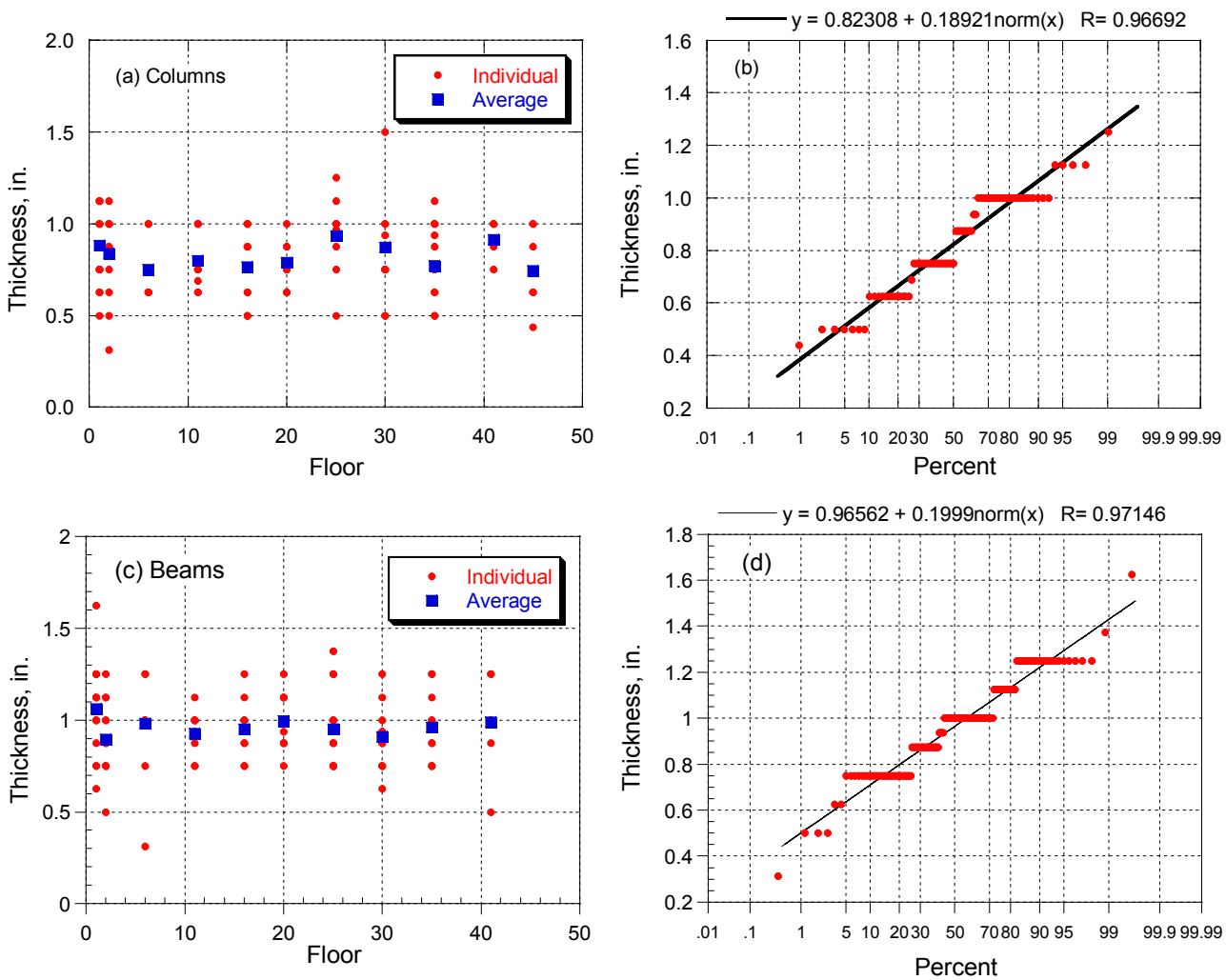

Figure 4–6. Thickness of re-applied SFRM in elevator shaft 10/11 of WTC 1: (a) Individual and average thickness for core columns, (b) normal probability plot of individual measurements on columns, (c) individual and average thickness for core beams, and (d) normal probability plot of individual measurements on beams (data provided by PANYNJ).

Chapter 5
EFFECT OF SFRM GEOMETRY ON THERMAL RESPONSE

The thickness of sprayed fire-resistive material (SFRM) has a great effect on the thermal response of the structural protected elements for a given fire condition. The effect of the variation of thickness along the length of a member is, however, not well known. A sensitivity study using finite element modeling of heat transfer was conducted to investigate the sensitivity of steel temperature to the variability in SFRM thickness.

5.1 EFFECTS OF THICKNESS VARIABILITY AND GAPS IN SFRM

The simplified model that was used is shown in Fig. 5-1. A 1 in. thick, 60 in. long steel plate (cyan color) was coated with fire-resistive material (purple color) and subjected to the uniform radiative flux arising from a 1,100 °C fire. As shown in Fig. 5-1 (b), the fire-resistive material is modeled with a layer of finite elements (0.125 in. thick and 0.6 in. long) having the thermal properties of fire-resistive material (purple). A parametric study was conducted with average thickness of fire-resistive material varying from 0 in. to 2 in. in increments of 1/4 in. The effect of variability in thickness was modeled by imposing a normal probability distribution on the SFRM thickness along the length of the steel plate. The assumed standard deviation varied from 0 in. (uniform thickness) to 1 in. A pseudo-random number generator was employed to determine the thickness at each cross section based on the assumed average thickness and standard deviation. The layer representing SFRM was taken to be twice the average thickness, and the thickness of SFRM at any cross section was modeled by assigning a low heat capacity and a high thermal conductivity to those elements that do not provide thermal protection. Figure 5-1 (c) shows an example of variable thickness SFRM; in this case, the average thickness is 1 in. and the standard deviation is 3/8 in.

When the model in Fig. 5-1 is exposed to the thermal flux representing a 1,100 °C fire, the surface of the insulation heats up quickly to the gas temperature (1,100 + 273 = 1,373 K). Numerical simulation was performed over a 2 h period, and the steel temperature at five locations was recorded at 30 min, 60 min, 90 min, and 120 min of exposure. The temperature recording locations are 6 in. from each end and at 12 in. intervals, which are shown as numbers 1 to 5 in Fig. 5-1 (a). The initial temperature of the model is 300 K.

Figure 5-2 shows temperature contours (in K) through the fire-resistive material and steel at 60 min after initial exposure for the model shown in Fig. 5-1 (a). The surface temperature of the fire-resistive material is close to the gas temperature of 1,373 K, while the steel temperature is 311 K. If the SFRM were of uniform thickness, the isotherms would be a series of lines parallel to the plate. It is seen that, when the thickness is variable, the isotherms follow the shape of the SFRM surface contour. Thus, the temperature history at any point in the steel depends on the local thickness of the fire-resistive material.

Figure 5-3 shows the steel temperature at the far sensor #1 (6 in. from the end) as a function of time for various insulation thicknesses ranging from 0 in. to 2 in. (the thickness is indicated by the numbers on the curves). For the case in Fig. 5-3 (a), the fire-resistive material is of uniform thickness, and for the cases in

Fig. 5-3 (b), the thickness varies with a standard deviation of 1 in. The time to reach a temperature of 600 °C is used as a measure of relative performance. It is seen that the presence of high variability in thickness has a detrimental effect on the protection provided by the fire-resistive material. For example, for a uniform thickness of 0.5 in., it takes about 60 min for the steel at point #1 to reach 600 °C, but when the standard deviation of the thickness is 1 in., the average thickness has to be 1.75 for the same level of thermal protection.

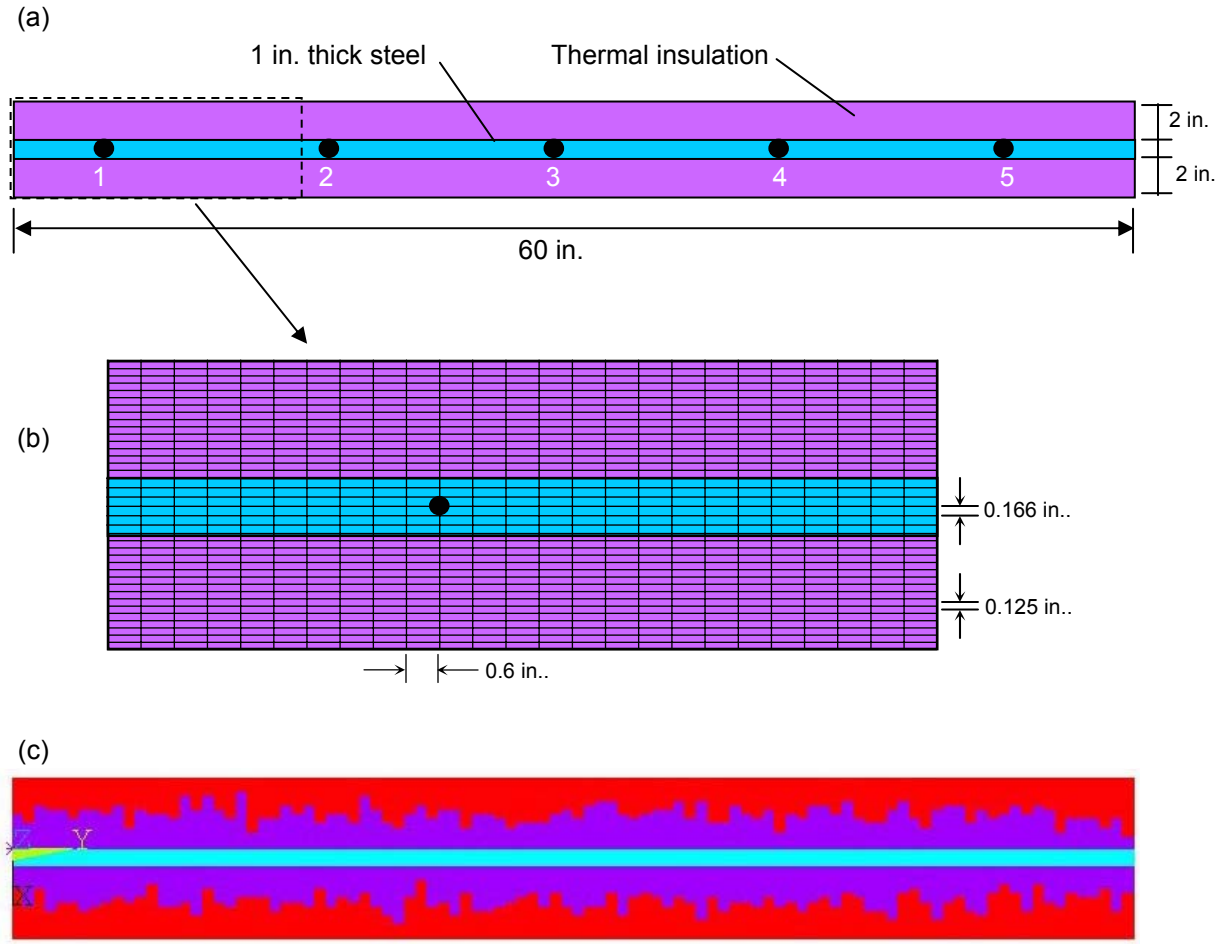

Figure 5–1. Model used to study effects of SFRM thickness and variability of thickness on steel temperature: (a) physical model used in analyses (points 1 to 5 are locations where temperatures are monitored), (b) finite element mesh used to represent physical model, and (c) finite element model to represent variable thickness of SFRM (purple) (the elements in red represent material of high thermal conductivity).

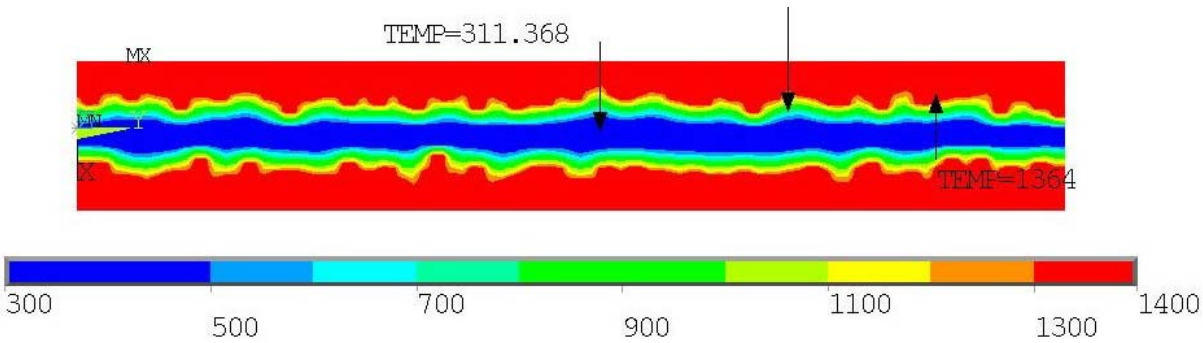

Figure 5–2. Temperature distribution after 1 h of exposure to gas temperature of 1,100 °C (1,373 K).

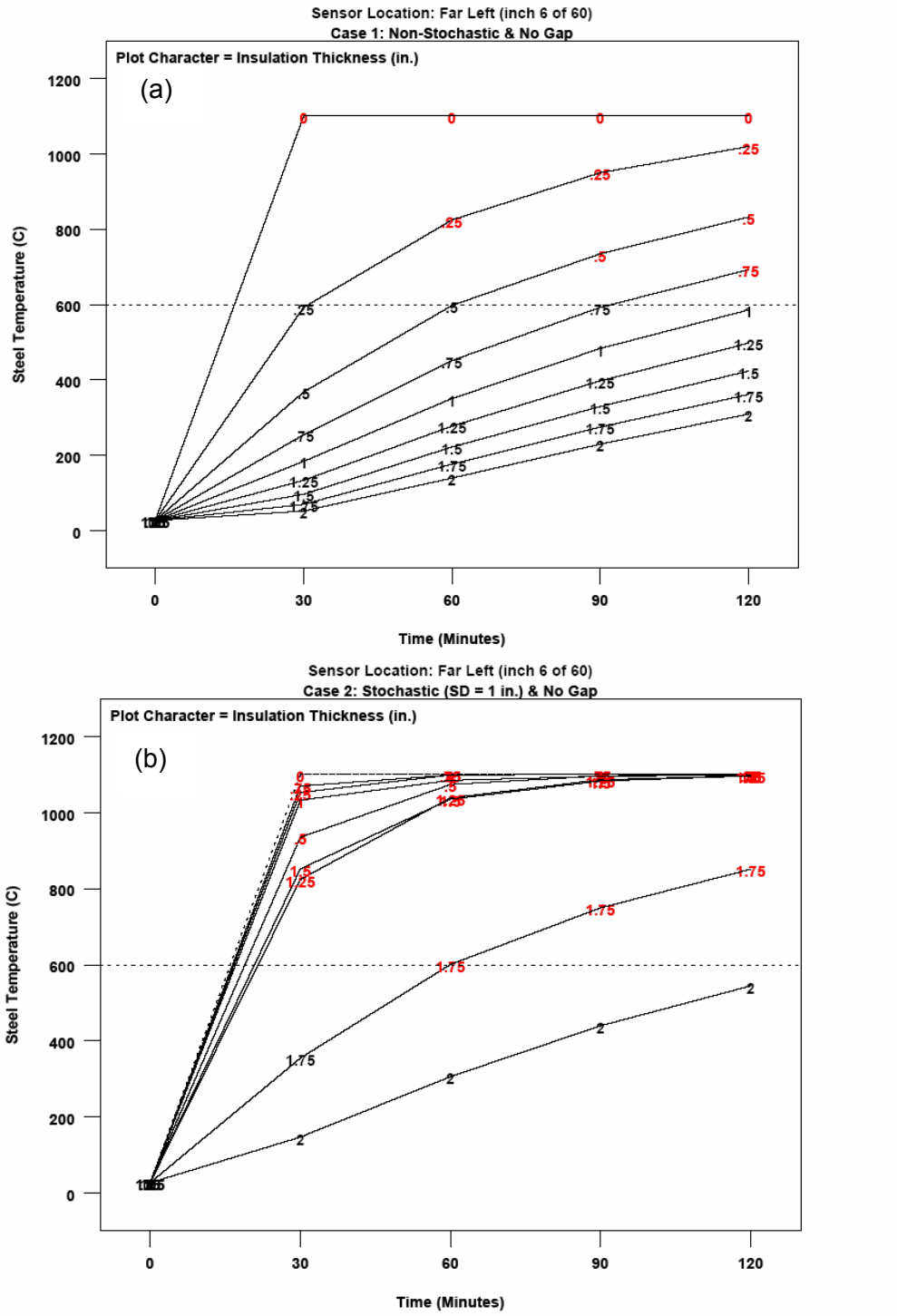

Figure 5–3. Variation of steel temperature (at a point 6 in. from end of plate) with time for different average thicknesses of fire-resistive material (shown as numbers on the curves): (a) uniform thickness, and (b) variable thickness with standard deviation = 1 in.

In addition to the effect of variation in thickness, it is important to understand the effect of missing SFRM over a portion of a member. As an example, Fig. 5-4 shows missing SFRM from a diagonal of a bridging truss of the WTC towers floor system. Note that this photograph is from a lower story and may not be representative of conditions in the upper stories, especially following the upgrade of thermal insulation. Figure 5-5 (a) shows an example of a numerical model with missing fire-resistive material. In this case, there is 12 in. of missing SFRM on the steel plate, which is otherwise protected by 2 in. of uniform thickness fire-resistive material. Figure 5-5 (b) shows the temperature contours (isotherms) at time equal to 50 min. For comparison, Fig. 5-5 (c) shows isotherms at the same time in a plate with no gap in the fire-resistive material. As expected, the bare steel at the missing fire-resistive material is at the gas temperature, but more importantly the "gap" in SFRM leads to a "leakage" of heat into the interior steel.

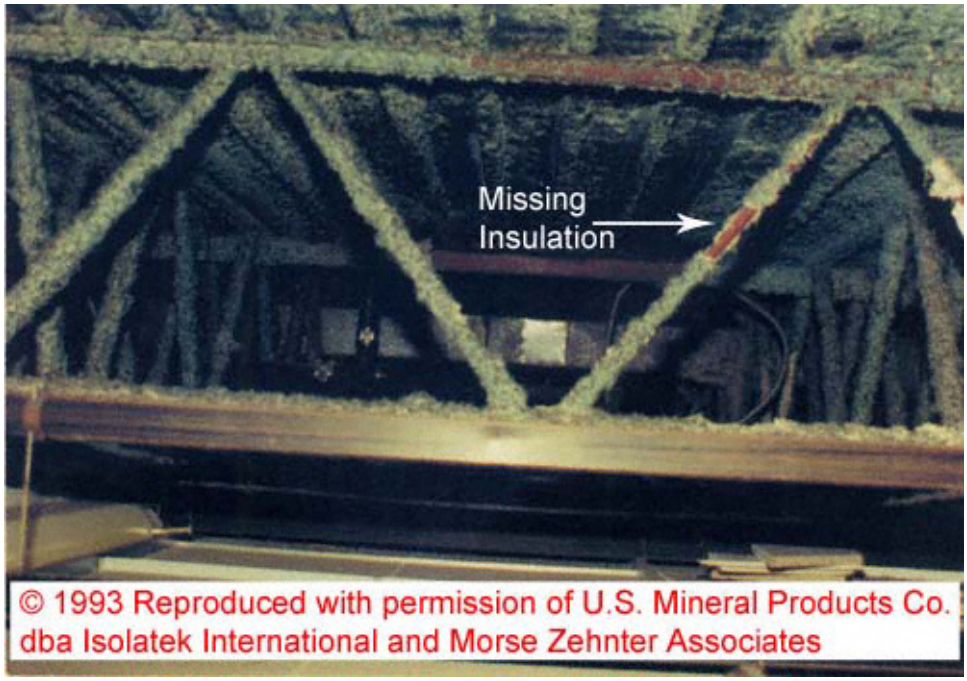

Figure 5–4. Example of "gap" in fire-resistive material on diagonal member of a bridging floor truss.

The combined effects of variation in thickness of the fire-resistive material and length of missing material were examined by a factorial study with the following factors:

- Average thickness of fire-resistive material varying from 0 in. to 2.0 in. in 1/4 in. increments;
- Standard deviation of fire-resistive material thickness of 0 in., 0.25 in., 0.5 in., 0.75 in. and 1.0 in.; and
- Length of missing fire-resistive material varying from 0 in. to 30 in., in 6 in. increments.

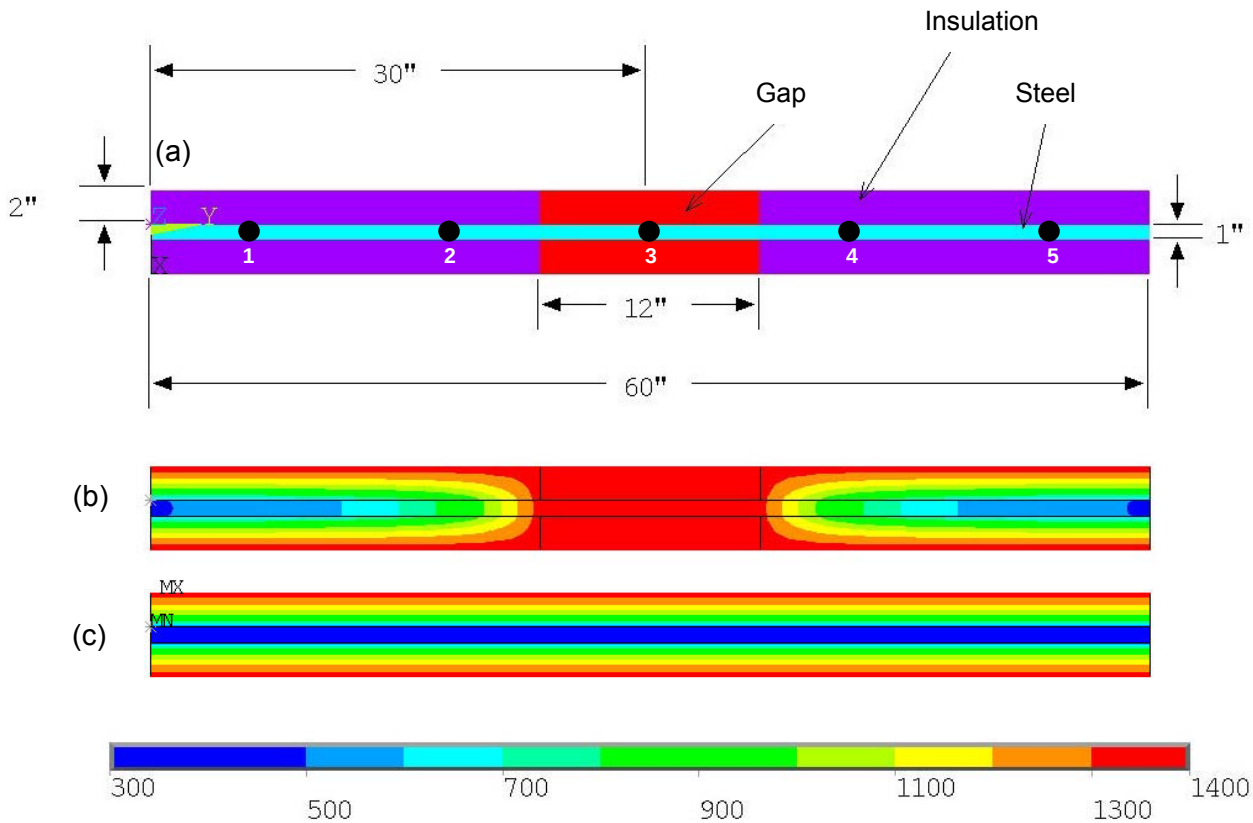

Figure 5–5. Effects of gap in fire-resistive material: (a) model of plate with SFRM having 2 in. uniform thickness and 12 in. gap, (b) isotherms (K) at time = 50 min with 12 in. gap, and (c) isotherms without gap.

The results of the sensitivity study can be summarized in a series of plot matrices, which show the time histories of the steel temperature for different combinations of gap length and variability in SFRM thickness. For example, Fig. 5-6 shows the plot matrix for the temperature history at point #2 (18 in. from the end of the plate). Each plot contains a series of curves representing different average thicknesses of fire-resistive material, as in Fig. 5-3. Each column of plots represents a constant value of thickness variability (standard deviation), and each row represents a constant gap length. The plot in the upper left corner represents the case of uniform thickness of SFRM and no gap, which is the same plot as in Fig. 5-3(a). (Note that for the case of uniform thickness and no gap, the steel temperature at any point in a cross section is the same along the length of the plate, as shown in Fig. 5-5(c).) For gaps of 24 in. and 30 in., the temperature at point #2 rises rapidly because there is no SFRM on the plate at that location. This explains the shapes of the curves in the two lower rows. In going from left to right in one of the top four rows it is seen that as variability of thickness increases, the time histories shift upward, thereby reducing the time to reach 600°C. This is the same observation as shown in Fig. 5-3. Moving from the top to the bottom in any column shows the effects of increasing gap length. The effect of gap length depends, of course, on where the steel temperature is measured. At a point within the portion of steel that is bare, the temperature rises quickly. At points within the steel that are surrounded with fire-resistive material, the gap provides a path for heat flow, as shown in Fig. 5-5 (b). As a result, points in the steel within the vicinity of the missing SFRM will experience higher temperatures, as indicated by the rising

trend of the curves in going downward from the top of a column in Fig. 5-6. The National Institute of Standards and Technology (NIST) does not have sufficient information to determine the frequency of occurrence of these gaps or their typical locations within the fire-affected floors. Therefore, gaps in insulation were not considered in the thermal modeling.

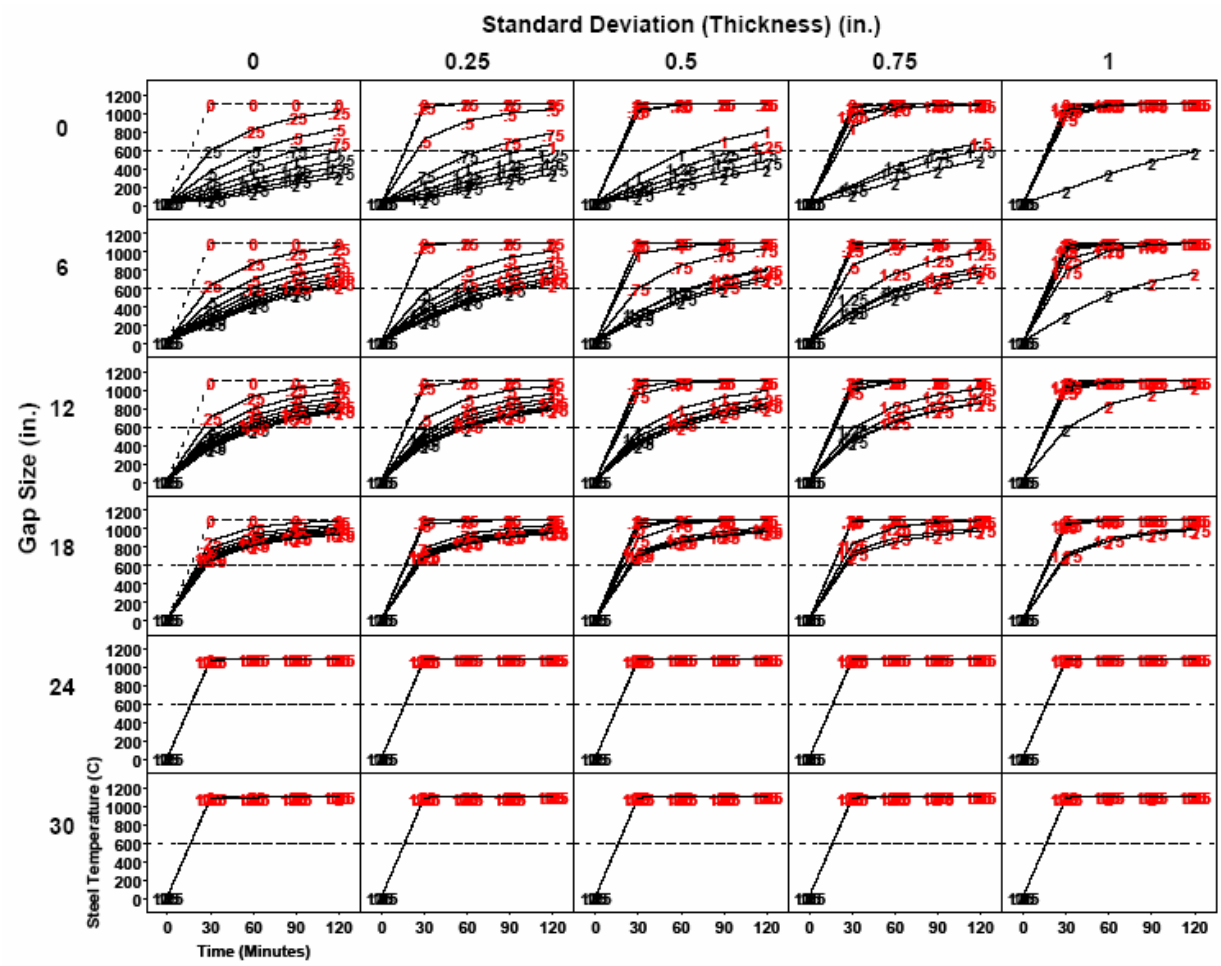

Figure 5–6. Example of plot matrix from sensitivity study of the effects of missing SFRM and variability of SFRM thickness on steel temperature. Each graph is a temperature history of the steel at point #2 (see Fig. 5-5 for location) for different thicknesses of SFRM.

5.2 EQUIVALENT THICKNESS

The sensitivity study summarized in Section 5.1 indicated that variation in the thickness of SFRM reduced the "effective thickness" of the material. It would be impractical to attempt to account for the variation in SFRM thickness in the thermal modeling by introducing variable thickness insulation material in the finite-element models. As an alternative, it was decided to attempt to determine the "equivalent uniform thickness" of fire-resistive material that would result in the same thermo-mechanical response of a member as variable thickness thermal protection. An approach similar to the methodology described in Section 5.1 was used to model a 1 in. diameter by 60 in. long bar with thermal insulation and subjected to the heat flux arising from a 1,100 °C fire. The bar was subdivided into 0.6 in. long elements,

so that there were 100 elements along the length of the bar. The thermal history of the bar was calculated, and that history was used to calculate the length change of the unrestrained bar under a tensile stress of 12,500 psi. The bar was assumed to be similar to the steel used in the floor trusses, and the temperature dependence of the coefficient of thermal expansion and the modulus of elasticity were based on NIST measurements.

The thermal insulation thickness in the models was based on the measurements summarized in Chapter 4 for the web bars of main trusses in the original condition and after the upgrade. Specifically, the following target values were investigated:

- Original: average thickness = 0.75 in., standard deviation = 0.3 in., lognormal distribution.
- Upgrade: average thickness = 2.5 in., standard deviation = 0.6 in., lognormal distribution.

The variation of thermal insulation thickness along the length of the bar was established by using a pseudo random number generator to select values from a lognormal distribution with central value and dispersion consistent with the above average values and standard deviation. Three sets of random data were generated for each condition.

When the randomly selected thicknesses of each element were applied to the bar, it resulted in sudden changes in insulation thickness along the length of the bar. This resulted in a “rough” surface texture as shown by the dotted thickness profile in Fig. 5-7 (a). It was felt that this rough texture (see also Fig. 5-1 (c) might not be representative of actual conditions, so an alternative approach was to use five-point averaging to reduce the roughness of the insulation profile. The solid line in Fig. 5-7 (a) shows such a “smooth” profile. The two profiles in Fig. 5-7 (a) have approximately the same average value and standard deviation and have similar cumulative distribution of thermal protection thickness as shown in Fig. 5-7 (b).

As stated, the calculated thermal histories of the bar elements were used to calculate the unrestrained length change of the bar due to thermal expansion and an applied stress of 12,500 psi. For comparison, the deformation of the bar with different but uniform thickness of thermal insulation was calculated. The “equivalent thickness” was taken as the uniform thickness that resulted in similar deformation as under the variable thickness conditions. Figure 5-7 (c) shows the results of these calculations for the original SFRM thickness. The three continuous curves are the deformation-time relationships for uniform thickness of 0.4 in., 0.5 in., and 0.6 in. The solid symbols represent the results for three cases with “rough” texture, and the open symbols are for the “smooth” texture. The following values summarize the six variable thickness profiles:

- Rough 1: average = 0.79 in., standard deviation = 0.29 in.
- Rough 2: average = 0.77 in., standard deviation = 0.27 in.
- Rough 3: average = 0.79 in., standard deviation = 0.31 in.

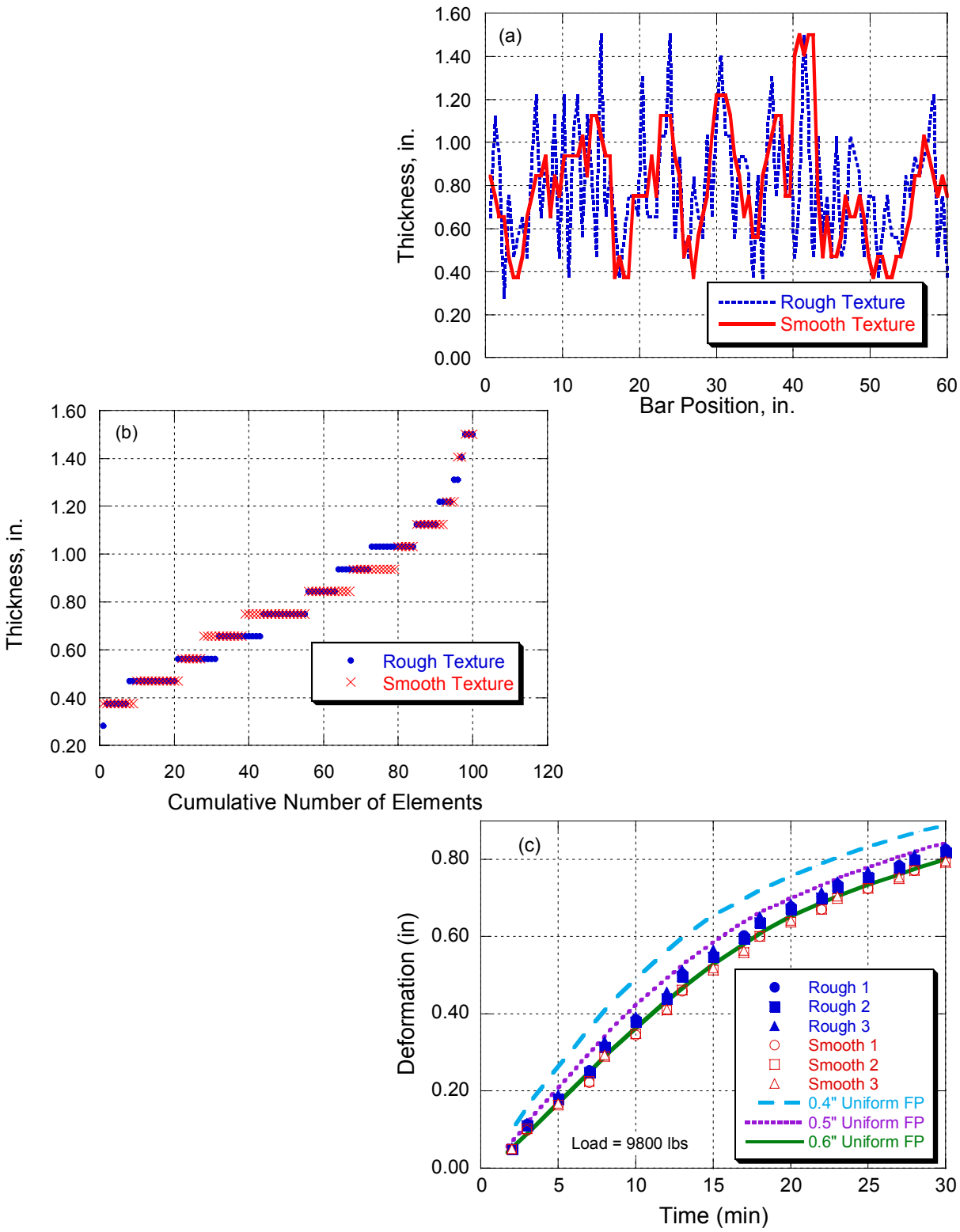

Figure 5–7. (a) Randomly generated thickness profiles with average thickness of 0.75 in. and standard deviation of 0.3 in., (b) cumulative element size, and (c) deformation of 1 in. bar compared with deformation for uniform thickness of thermal insulation.

- Smooth 1: average = 0.79 in., standard deviation = 0.28 in.
- Smooth 2: average = 0.78 in., standard deviation = 0.31 in.
- Smooth 3: average = 0.78 in., standard deviation = 0.32 in.

Figure 5-7 (c) shows that the "rough" texture reduces the effectiveness of the insulation by a small amount compared with the "smooth" texture. As noted above, it is believed that the "smooth" texture is more representative of the actual conditions. On the basis of these analyses, it is concluded that SFRM with an average thickness of 0.75 in. and a standard deviation of 0.3 in. provides protection equivalent to 0.6 in. of uniform thickness.

The results for the upgraded thermal protection are shown in Fig. 5-8. Only the "smooth" texture was used, and the values for the three cases are as follows:

- Case 1: average = 2.50 in., standard deviation = 0.71 in.
- Case 2: average = 2.43 in., standard deviation = 0.51 in.
- Case 3: average = 2.55 in., standard deviation = 0.63 in.

Figure 5-8 (a) shows the three profiles, and Fig. 5-8 (b) shows the normal probability plots of thickness values. Because the three randomly generated profiles do not have the same averages and dispersions, the responses show more scatter than in Fig. 5-7 (c). On the basis of these analyses, it is concluded that an average SFRM thickness of 2.5 in. with a standard deviation of 0.6 in. is equivalent to 2.2 in. of uniform thickness.

5.3 RECOMMENDED THICKNESS OF SFRM FOR THERMAL ANALYSES

Analyses of available data on SFRM thickness in the WTC towers and thermal modeling revealed the following:

- From measurements of SFRM thickness, the average values exceeded the specified thickness.
- SFRM thickness was variable, and the distribution of thickness in the floor trusses appears to be described best by a lognormal distribution.
- The standard deviation of SFRM thickness on the trusses varied between about 0.3 in. and 0.6 in.
- The standard deviation of SFRM on columns and beams from the core tended to be lower, with a value of 0.2 in. for the available data.
- No information is available on the SFRM thickness on the exterior columns and spandrel beams.
- Variation in thickness reduces the effectiveness of SFRM, and the equivalent uniform thickness is less than the average thickness.

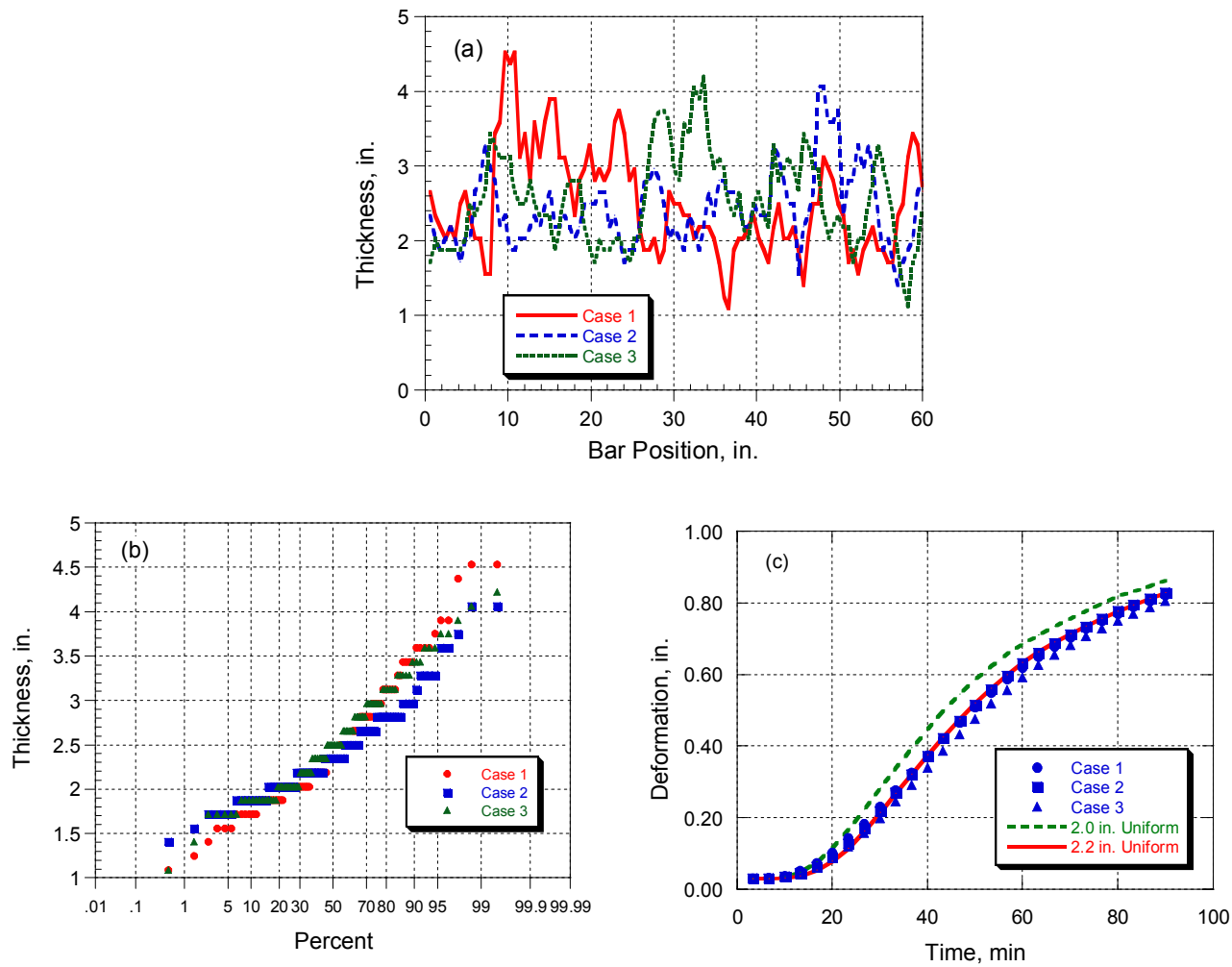

Figure 5–8. (a) Randomly generated thickness profiles with average thickness of 2.5 in. and standard deviation of 0.6 in., (b) normal probability plots of thickness values, and (c) deformation of 1 in. bar compared with deformation for uniform thickness of thermal insulation.

Based on the findings stated above, the following uniform thicknesses for the undamaged SFRM were determined for use in calculating thermal response of the WTC towers under various fire scenarios:

- Original SFRM thickness on floor trusses: 0.6 in.
- Upgraded SFRM thickness on floor trusses: 2.2 in.
- Thermal protection on other elements: the specified thickness.

The choice of specified thickness for those members lacking data is justified by offsetting factors as follows: (1) measured average thicknesses exceed specified values, and (2) variation in thickness reduces the effectiveness of the SFRM.

This page intentionally left blank.

Chapter 6
THERMOPHYSICAL PROPERTIES

Based on information reviewed in this investigation, five sprayed fire-resistive materials (SFRMs) have been identified in WTC 1, 2, and 7: (1) BLAZE-SHIELD Type D, (2) BLAZE-SHIELD Type DC/F, (3) BLAZE-SHIELD Type II, (4) Monokote MK-5, and (5) vermiculite aggregate plaster. As mentioned in Section 3.5.1, the use BLAZE-SHIELD Type D was discontinued in 1978, and it had been used only in the lower stories of WTC 1. Of the four SFRMs, only BLAZE-SHIELD Type II is sold currently in the U.S., and BLAZE-SHIELD Type DC/F is sold in Canada. Table 6-1 summarizes where these materials were used.

Table 6–1. Summary of SFRMs used in WTC.

	Fire-Resistive Material	Locations			
		Interior Columns	Floor Systems	Exterior Columns	
WTC 1	BLAZE-SHIELD DC/F	Yes	Yes	Outside	
	BLAZE-SHIELD II		Yes (Upgrade)		
	Vermiculite plaster				Inside
WTC 2	BLAZE-SHIELD DC/F	Yes	Yes	Outside	
	BLAZE-SHIELD II		Yes (Upgrade)		
	Vermiculite plaster				Inside
WTC 7	Monokote MK-5	Yes	Yes	Yes	Yes

BLAZE-SHIELD Type DC/F is manufactured by Isolatek International (formerly U.S. Mineral Products Co., Stanhope, New Jersey) and was used in the interior columns, floor systems, and the exterior faces of the exterior columns of WTC 1 and WTC 2. BLAZE-SHIELD Type II, also from Isolatek, was used in subsequent upgrades of the passive fire protection to WTC 1 and WTC 2 floor systems. BLAZE-SHIELD Type DC/F and Type II are portland cement based products in which mineral fibers are the primary insulation materials. Monokote MK-5, a gypsum-based SFRM containing vermiculite aggregate, was manufactured by W.R. Grace and Co. (Cambridge, Massachusetts) and used in WTC 7. W.R. Grace stopped the production of Monokote MK-5 in the 1980s. Vermiculite aggregate plaster, manufactured by W.R. Grace until the 1970s, was used on the interior faces of the exterior columns of WTC 1 and WTC 2 (see Fig. 3–4).

No information on the thermophysical properties of vermiculite plaster has been located in the open literature. During the construction of the WTC, the Monokote product was sometimes referred to as sprayed vermiculite. See, for example, Appendix A Fig. A-17, where the description "Sprayed (Cementitious) Vermiculite (Monokote)" is used. Discussions with a former researcher at W. R. Grace and Co. indicated that vermiculite plasters were used before the development of the Monokote product line, and these plasters had densities of 20 pcf to 25 pcf; any Monokote product used during construction of the WTC towers would probably have had similar density.[15] Based on this information, the

[15] Personal communication from Arnie Rosenberg, August 30, 2005 (242-I).

thermophysical properties of Monokote MK-5 will be taken to be representative of the vermiculite plaster specified for the interior face of the exterior columns.

In addition to the SFRMs, the thermophysical properties of four representative types of gypsum boards were examined to provide technical support to other aspects of the WTC investigation.

6.1 ASTM TEST METHODS FOR SFRMS

Since 1977, a number of ASTM test methods have been developed specifically for testing different characteristics of SFRMs. These methods were developed mainly for characterizing mechanical and physical properties. For completeness, these test methods are summarized in Table 6-2.

Table 6–2. Current ASTM test methods for SFRMs.

ASTM Designation	Summary of Test Method
ASTM E 605 – 93 (Reapproved 2000) Test Method for Thickness and Density of Sprayed Fire-Resistive Material (SFRM) Applied to Structural Members	Density and thickness are determined using a thickness gauge, scales, steel rules, and templates
ASTM E 736 – 00 Test Method for Cohesion/Adhesion of Sprayed Fire-Resistive Materials Applied to Structural Members	The cohesion/adhesion of SFRM to structural members is determined using a metal or plastic cap with a hook attached. The cap is attached to the SFRM with a suitable adhesive. An increasing load, measured by a scale, is applied manually until failure occurs.
ASTM E 759 – 92 (Reapproved 2000) Test Method for Effect of Deflection on Sprayed Fire-Resistive Material Applied to Structural Members	A cellular steel deck panel sprayed with SFRM is subjected to bending by a vertical center load while supported horizontally at its ends.
ASTM E 760 – 92 (Reapproved 2000) Test Method for Effect of Impact on Bonding of Sprayed Fire-Resistive Material Applied to Structural Members	A cellular steel deck with a concrete topping sprayed with SFRM is subjected to a leather bag drop impact while supported horizontally at its ends.
ASTM E 761 – 92 (Reapproved 2000) Test Method for Compressive Strength of Sprayed Fire-Resistive Material Applied to Structural Members	The compressive strength of SFRM applied to a steel sheet is determined by a compressive load normal to the surface of the specimen.
ASTM E 859 – 93 (Reapproved 2000) Test Method for Air Erosion of Sprayed Fire-Resistive Materials (SFRMs) Applied to Structural Members	The SFRM is subjected to a tangential air stream for a minimum of 24 h. Collection filters downstream from the specimen are weighed at frequent intervals to determine the amount of material removed from the specimen.
ASTM E 937 – 93 (Reapproved 2000) Test Method for Corrosion of Steel by Sprayed Fire-Resistive Material (SFRM) Applied to Structural Members	Replicate panels of bare, shop-coated, and galvanized steel are sprayed with SFRM and subjected to room temperature and humidity conditions and to 240 h of conditioning in a chamber with temperature and humidity control. Corrosion induced under these conditions is determined by mass loss of the sheets as related to sheets not so conditioned.

6.2 REPORTED SFRM PROPERTIES

For comparison with measurements to be reported in this Chapter, the nominal physical and mechanical characteristics taken from product literature (see Appendix A Fig. A-63)[16] of the manufacturers of the SFRMs are listed in Table 6-3.

Table 6–3. Properties from tests of SFRMs reported by manufacturers.

Characteristic	ASTM Method	SFRM		
		BLAZE-SHIELD DC/F	BLAZE-SHIELD II	Monokote MK 5
Cohesion/adhesion	E 736	300 psf[a]	360 psf[a]	320 psf
Deflection	E 759	No cracks or delaminations	No cracks or delaminations	No cracks or delaminations
Bond impact	E 760	No cracks or delaminations	No cracks or delaminations	No cracks or delaminations
Compressive strength	E 761	830 psf	2380 psf	3110 psf
Air erosion resistance	E 859	0.000 g/m^2	0.000 g/m^2	0.022 g/m^2
Density	E 605	13 pcf	16 pcf	20 to 25 pcf[b]
Corrosion resistance	E 937	Does not promote corrosion of steel	Does not promote corrosion of steel	Not available
Thermal conductivity	C 518	0.042 W/(m · K) @ 24 °C	0.043 W/(m · K) @ 24 °C	Not available

a. Based on laboratory tests under controlled conditions.
b. Based on information from former employee of W.R. Grace, see previous footnote.

6.3 MEASURED THERMOPHYSICAL PROPERTIES OF SFRMS

To provide thermophysical property data for modeling the fire-structure interaction of the towers, the thermal conductivity, specific heat capacity, and density of each SFRM were determined as a function of temperature up to 1,200 °C (2,190 °F). Since there are no ASTM test methods for characterizing the thermophysical properties of SFRMs as a function of temperature, ASTM test methods developed for other materials were used. Testing services were provided by a commercial testing laboratory, through a competitive open procurement. The laboratory (referred to as Laboratory A in this report) is an ISO 9002 certified company. Test results were presented to NIST in the form of a letter report with data and plots as attachments.

[16] In Fig. A-63, thermal conductivity is reported as an R-value per in. thickness. The inverse of this value is the thermal conductivity. Thus, a reported R value of 3.45 indicates a thermal conductivity of 0.29 Btu-in./(ft2 · °F · h) or 0.042 W/(m · K).

6.3.1 Sample Preparation

Samples of BLAZE-SHIELD DC/F and II were purchased from Isolatek, Inc. in Stanhope, New Jersey, and samples of Monokote MK-5 were purchased from W.R. Grace and Co. in Cambridge, Massachusetts, according to their respective application manuals. Since Monokote MK-5 is no longer on the market, it was manufactured specially by W.R. Grace according to the original MK-5 formulation. The samples were made from the same batch of raw materials, shipped to NIST for examination and documentation, and sent to Laboratory A for testing. The samples were 9 in. long, 4.5 in. wide, and 3 in. thick. These dimensions were dictated by the test methods used. Three samples of each material were sent for testing. Two of them were used for the thermal conductivity measurements, and the third was used to prepare specimens for the other measurements involved. Figures 6-1, 6-2, and 6-3 show photographs of samples of BLAZE-SHIELD DC/F, BLAZE-SHIELD II, and Monokote MK-5, respectively.

Source: NIST.

Figure 6–1. BLAZE-SHIELD DC/F sample used for thermophysical property measurements.

Source: NIST.

Figure 6–2. BLAZE-SHIELD II sample used for thermophysical property measurements.

Source: NIST.

Figure 6–3. Monokote MK-5 sample used for thermophysical property measurements.

6.3.2 Thermal Conductivity Measurements

The thermal conductivity measurements were performed according to ASTM C 1113 (ASTM 1999). This test method is based on heating two specimens with a platinum wire placed between them. The thin platinum wire serves not only as a heater, but also as a temperature sensor, since the variation of its electrical resistance during the test is converted into variation of temperature. Thermal conductivity is calculated based on the rate of temperature increase of the wire and power input.

Laboratory A reported that substantial shrinkage occurred during the measurements for the three materials. The two MK-5 specimens shrunk, exposing the platinum wire positioned between them. For this reason, no thermal conductivity measurement could be performed for this material at 1,200 °C. Table 6-4 summarizes thermal conductivity as a function of temperature. The results are plotted in Fig. 6-4, which also shows the results for BLAZE-SHIELD DC/F from Harmathy, which were obtained using a variable-state method (Harmathy 1983). The results show similar trends of increased thermal conductivity with increasing temperature; however, the Monokote MK-5 specimens had a different behavior than BLAZE-SHIELD Type DC/F and Type II at temperatures above 500 °C.

Table 6–4. Measured thermal conductivity as a function of temperature.

	Thermal Conductivity (W/(m · K))[a]		
Temperature (°C)	**BLAZE-SHIELD DC/F**	**BLAZE-SHIELD II**	**Monokote MK-5**
25	0.0460	0.0534	0.0954
50	0.0687	0.0745	0.0926
100	0.0628	0.0921	0.1252
200	0.0810	0.0895	0.0919
300	0.1106	0.1057	0.1214
400	0.1286	0.1362	0.1352
500	0.1651	0.1689	0.1504
600	0.2142	0.2156	0.1622
800	0.3380	0.2763	0.1895
1000	0.5010	0.3708	0.2618
1200	0.5329	0.4081	–

a. SI units are used because this system was used to make the measurements. To convert to Btu-in./(h · ft2 · °F) divide by 0.1442279.

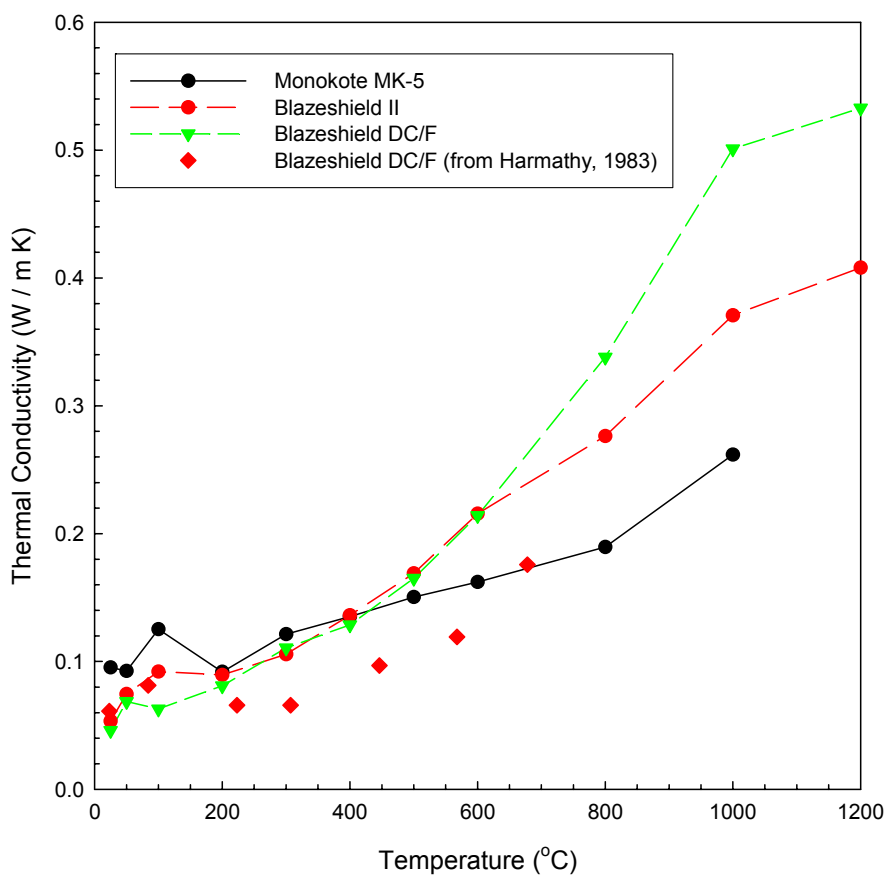

Figure 6–4. Thermal conductivities of the three SFRMs as a function of temperature.

6.3.3 Specific Heat Capacity Measurements

For the specific heat capacity measurements, the same instrument (Unitherm™ Model QL–3141) was used with a slight modification. A thermocouple was added to the system and mounted on the specimen, parallel with the platinum wire at a known distance from the wire. The test was performed in a similar manner as the thermal conductivity measurements, but from the thermocouple output the thermal diffusivity of the material was derived. Knowing the thermal conductivity, the thermal diffusivity, and the density calculated from the thermal expansion results and the thermogravimetric analysis (see Section 6.3.4), the specific heat capacity of the material was calculated. Table 6-5 tabulates the measurements. Figure 6-5 compares the present results for BLAZE-SHIELD DC/F with those from Harmathy, which were obtained using a DuPont 910 differential scanning calorimeter with a heating rate of 5 °C/min (Harmathy 1983). It is clear from the figure that the inherently indirect nature of the technique used by Laboratory A precludes the direct measurements of specific heat capacity associated with chemical reactions (peaks in the figure) when the SFRMs are subjected to heating.

Table 6–5. Calculated specific heat capacity of the three SFRMs.

	Specific heat capacity (J/(kg K))[a]		
Temperature (°C)	**BLAZE-SHIELD DC/F**	**BLAZE-SHIELD II**	**Monokote MK-5**
25	826.4	801.6	841.0
50	941.5	868.4	1045.8
100	723.9	708.4	1005.7
200	897.2	925.4	1205.5
300	1020.2	1084.7	1253.9
400	1070.6	1147.5	1302.9
500	1097.6	1255.3	1331.6
600	1189.7	1299.1	1400.8
800	1258.6	1369.6	1468.2
1000	1325.3	1411.3	1520.8
1200	1391.7	1461.3	–

a. SI units are used because this system was used to make the measurements. To convert to Btu /(lb · °F) divide by 4186.8.

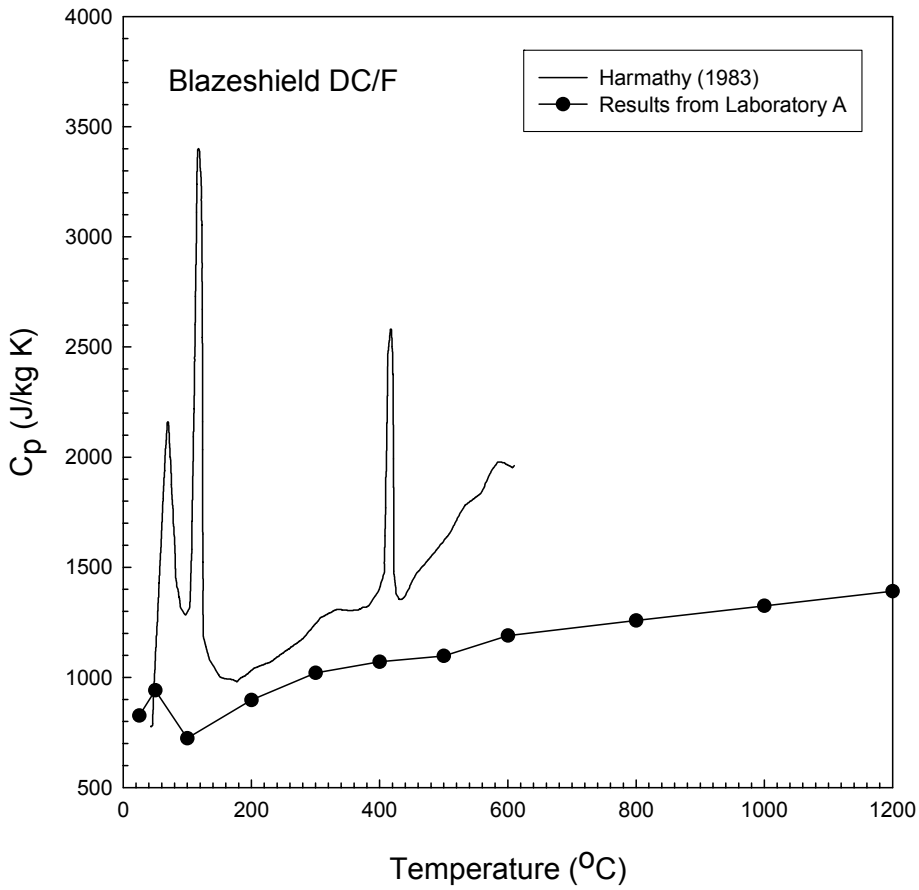

Figure 6–5. Comparison of BLAZE-SHIELD DC/F specific heat capacity measurements from Harmathy (1983) with present results from Laboratory A.

To examine the chemical reactions associated with heating of SFRMs, samples were sent to another laboratory (referred to as Laboratory B) to perform differential scanning calorimetry (DSC) because the DSC in the Building and Fire Research Laboratory at NIST was not working at that time. The specimens for DSC were prepared by removing small pieces from the bulk samples. The pieces were placed into small glass vials and sent to Laboratory B for analysis.

Specific heat capacity was measured in accordance with ASTM E 1269 (ASTM 2001) using a Perkin-Elmer Model DSC-2 Differential Scanning Calorimeter with sapphire as the reference material. The standard and SFRM specimens were subjected to the same heat flux as a blank specimen, and the differential powers required to heat the specimen and the standard at the same rate were determined using the digital data acquisition system. The specific heat capacity of the specimen was computed from the masses of the sapphire standard and the SFRM specimen, the differential power, and the known specific heat capacity of sapphire. The data were displayed visually as the test progressed. All measured quantities were directly traceable to NIST standards.

Differential thermal analysis (DTA), which is a “fingerprinting” technique that provides information on the chemical reactions, phase transformations and structural changes that occur in a specimen during a heat-up or a cool-down cycle, was used to locate the peaks and valleys during continuous heating to 600 ºC at a rate of 10 ºC/min. Once the peak and valley regions were identified, the sensitive DSC was

used to examine these regions further at a heating rate of 5 ºC/min, first from room temperature to 350 ºC and then from 300 ºC to 580 ºC. It was noted by Laboratory B, however, that the DSC results at temperatures greater than 350 ºC were of questionable quality and problematic. Only the results (up to 350 ºC) are tabulated in Appendix B Table B-1 and are displayed in Fig. 6-6, together with the results from Laboratory A for comparison.

Figure 6-7 shows a comparison of specific heat capacity data for BLAZE-SHIELD DC/F from Harmathy (1983) with the results from Laboratory B. For temperatures up to 350 °C, both results exhibit two peaks although their locations occur at different temperatures, and their magnitudes are different. In general, an increase in the heating rate results in a shift of the peaks toward higher temperatures and in increases of maxima or minima of peaks with narrowing peak widths. Both studies used the same heating rate of 5 °C/min, however, other procedural and operational factors could have affected the measurements. Since milligram quantities of SFRM are used in DSC, assurance of specimen homogeneity and representativeness of the bulk sample in the specimen holder is essential to the validity of the measurements, especially for inhomogeneous materials like SFRMs. In addition, mass loss from the specimen holder during heating could interfere with the measurements.

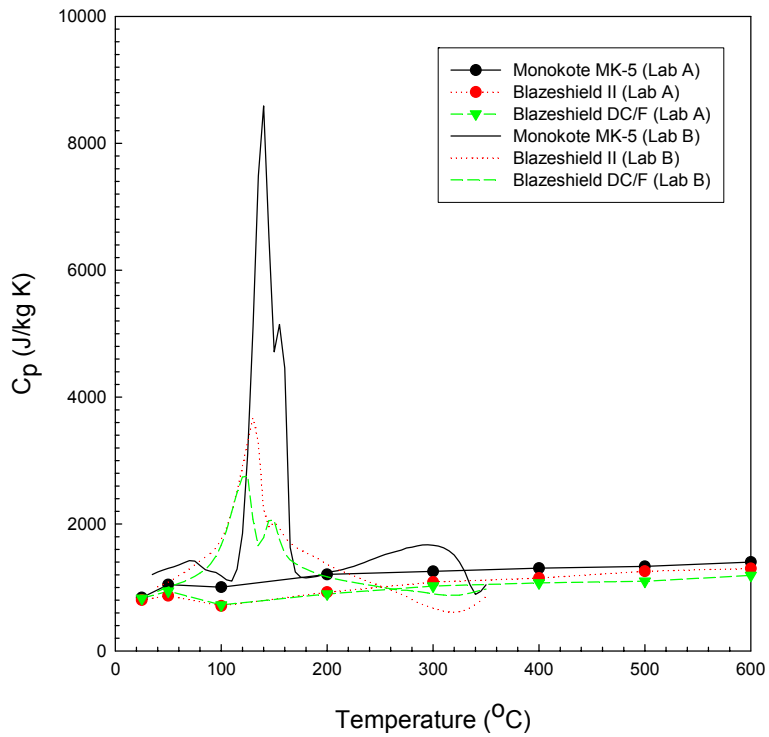

Figure 6–6. Comparison of specific heat capacity measurements from Laboratory B with results from Laboratory A.

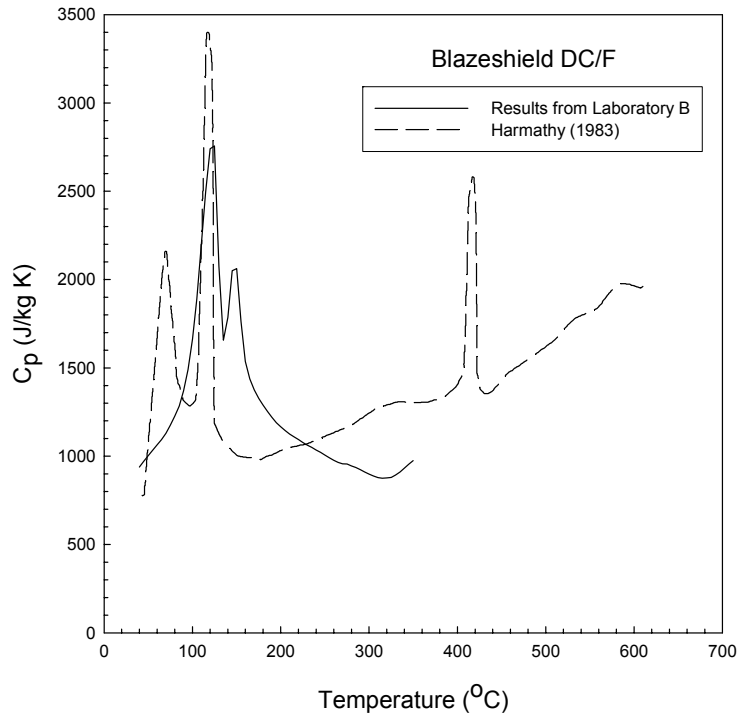

Figure 6–7. Comparison of specific heat capacity measurements for BLAZE-SHIELD DC/F from Laboratory B with the results from Harmathy (1983).

6.3.4 Density Measurements

Bulk densities of the SFRMs were not measured directly (except at room temperature) but were calculated from thermal gravimetric analysis (TGA) and thermal expansion measurements. The TGA tests were performed according to ASTM E 1131 (ASTM 1998) using an Orton Model ST-736 TGA. The resulting mass changes are shown in Table 6-6. The thermal expansion measurements were performed according to ASTM E 228 (ASTM 1995) using a Unitherm™ Model 1161 pushrod dilatometer. Since the materials were not isotropic, separate measurements had to be performed for the X and Z orientations. It was assumed that the X and Y directions had the same thermal expansion. The Z direction was defined as the direction perpendicular to the fibrous strands in the samples. The specimens were tested from room temperature to 1,200 °C at a heating rate of 2 °C/min. All of the specimens shrunk during the tests and in all cases lost contact with the pushrod at temperature about 1,100 °C before reaching the maximum test temperature. Table 6-7 shows the results of the thermal expansion measurements.

From the thermal expansion measurements, the change in volume for each material was calculated at each temperature. The density values were calculated from the results of the TGA and thermal expansion. Table 6-8 summarizes the calculations, and Fig. 6-8 displays the results. The shrinkage of the material and the specimen mass loss both contribute to the unrealistic variation in density at high temperatures. Thus, the density values are only valid up to 600 °C.

Table 6–6. Mass loss of SFRMs with increasing temperature.

	Mass Change (percent)		
Temperature (°C)	**BLAZE-SHIELD DC/F**	**BLAZE-SHIELD II**	**Monokote MK-5**
25	0.0	0.0	0.0
50	–0.2	–0.6	–0.5
100	–2.7	–3.9	–2.7
200	–5.1	–7.4	–15.0
300	–6.0	–8.7	–19.0
400	–6.7	–9.9	–22.0
500	–7.5	–11.0	–23.0
600	–8.6	–12.0	–24.0
800	–11.0	–16.0	–25.0
1000	–11.0	–16.0	–27.0
1200	–14.0	–20.0	–42.0

Table 6–7. Thermal expansion results of SFRMs.

	Thermal Expansion (percent)					
Temperature (°C)	**BLAZE-SHIELD DC/F**		**BLAZE-SHIELD II**		**Monokote MK-5**	
	X and Y Direction	**Z direction**	**X and Y Direction**	**Z direction**	**X and Y Direction**	**Z direction**
25	0.00	0.00	0.00	0.00	0.00	0.00
50	0.02	0.02	0.02	0.02	0.03	0.03
100	0.05	0.03	0.04	–0.04	0.08	0.09
200	0.10	–0.13	0.04	–0.36	–0.06	–0.13
300	0.17	–0.12	0.09	–0.48	–0.23	–0.23
400	0.23	–0.16	0.11	–0.63	–0.65	–0.92
500	0.19	–0.38	0.08	–0.98	–0.69	–0.97
600	0.06	–0.93	–0.07	–1.45	–0.69	–0.97
800	–10.95	–26.40	–12.56	–12.42	–1.22	–2.13
1000	–11.83	–27.86	–12.80	–13.63	–7.03	–8.32

Table 6–8. Calculated densities of SFRMs.

	Density (kg/m^3)[a]		
Temperature (°C)	**BLAZE-SHIELD DC/F**	**BLAZE-SHIELD II**	**Monokote MK-5**
25	236.8	313.7	292.4
50	236.1	311.5	290.5
100	230.1	301.3	283.8
200	224.6	291.3	249.1
300	222.1	287.2	238.5
400	220.3	283.7	233.2
500	219.0	281.5	230.5
600	218.2	280.5	227.5
800	361.1	393.4	229.6
1000	375.8	401.1	269.3
1200	432.1	436.7	369.4

a. To convert to pcf multiply by 0.062428.

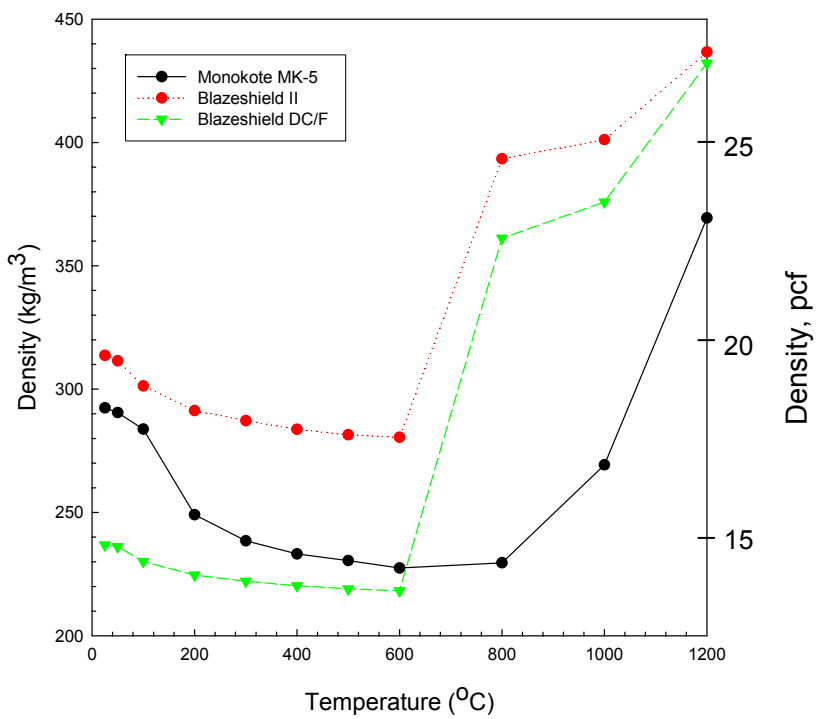

Figure 6–8. Bulk densities of the three SFRMs as a function of temperature.

6.3.5 Concluding Remarks

It should be noted that the thermal conductivity and bulk density depend on how the SFRM is sprayed or applied; therefore, it is expected that the results will vary from sample to sample. In general, the thermal conductivity of a porous material is a complex function of bulk density, porosity, and other material

properties (e.g., Stephenson and Mark 1961). Recent attempts to use existing predictive methods to estimate thermal conductivities of porous media for SFRMs show some promise, and alternative approaches have also been proposed for future research.[17]

6.4 THERMOPHYSICAL PROPERTIES OF GYPSUM PANELS

In this section, measurement results of the thermophysical properties of four gypsum materials will be presented. Unless stated otherwise, measurements were performed by Laboratory B. Four representative types of gypsum materials were examined. They were:

1. 5/8 in. thick gypsum panel A,
2. ½ in. thick gypsum panel,
3. 5/8 in. thick gypsum panel B, and
4. 1 in. gypsum liner panel.

6.4.1 Samples

The gypsum materials were all commercially available and were purchased from a local building supply store in Gaithersburg, Maryland. Samples were cut from the gypsum panel using a box cutter and then sent to the testing laboratory.

6.4.2 Thermal Conductivity Measurements

Thermal conductivity was measured using the heated probe technique described in ASTM D 5334 (ASTM 2000h). The following description of the heated probe method is provided by Laboratory B:[18]

> "In the heated probe method, which may be considered as a variant of the line source method, the line source and temperature sensor are combined in one small diameter probe. This probe is inserted into the sample and the heater turned on for a preselected time interval. During this time interval, the rate of heating of the probe is measured. This heating rate quickly becomes semi-logarithmic and from this semi-logarithmic rate, the thermal conductivity of the sample is calculated. The probe may be inserted into powders, fluids, small holes drilled into rocks, biological materials, etc. A variety of probe sizes, ranging from needle-shaped to rods are available. The data is collected by the PC based digital data acquisition system and the heating rate displayed visually. A semi-logarithmic portion of the heating curve is chosen using the mouse and the conductivity calculated based on this portion of the curve."

The measurement results are summarized in Table 6-9, and the results are plotted in Fig. 6-9.

---

[17] Bentz, D. P., Prasad, K. R. and Yang, J.C. 2004. Towards a Methodology for the Characterization of Fire Protection Materials with Respect to Thermal Performance Models. *Fire and Materials (*accepted for publication).

[18] www.tpfrl.com/heatprb.html

Table 6–9. Thermal conductivities of gypsum materials.

5/8 in. Panel A		½ in. Panel		5/8 in. Panel B		1 in. Liner Panel	
(°C)	(W/(m K))[a]	(°C)	(W/(m K)	(°C)	(W/(m K)	(°C)	(W/(m K)
23	0.156	23	0.194	23	0.154	23	0.133
45	0.1533	47	0.184	56	0.148	48	0.135
100	0.1558	97	0.188	103	0.156	97	0.136
222	0.0963	200	0.100	230	0.090	200	0.093
296	0.0976	299	0.097	318	0.105	293	0.089
384	0.0987	406	0.106	428	0.113	413	0.107
482	0.1102	496	0.113	508	0.113	508	0.116
591	0.1276	603	0.121	609	0.131	598	0.134

a. To convert to Btu · in./(h · ft^2 · °F) divide by 0.1442279.

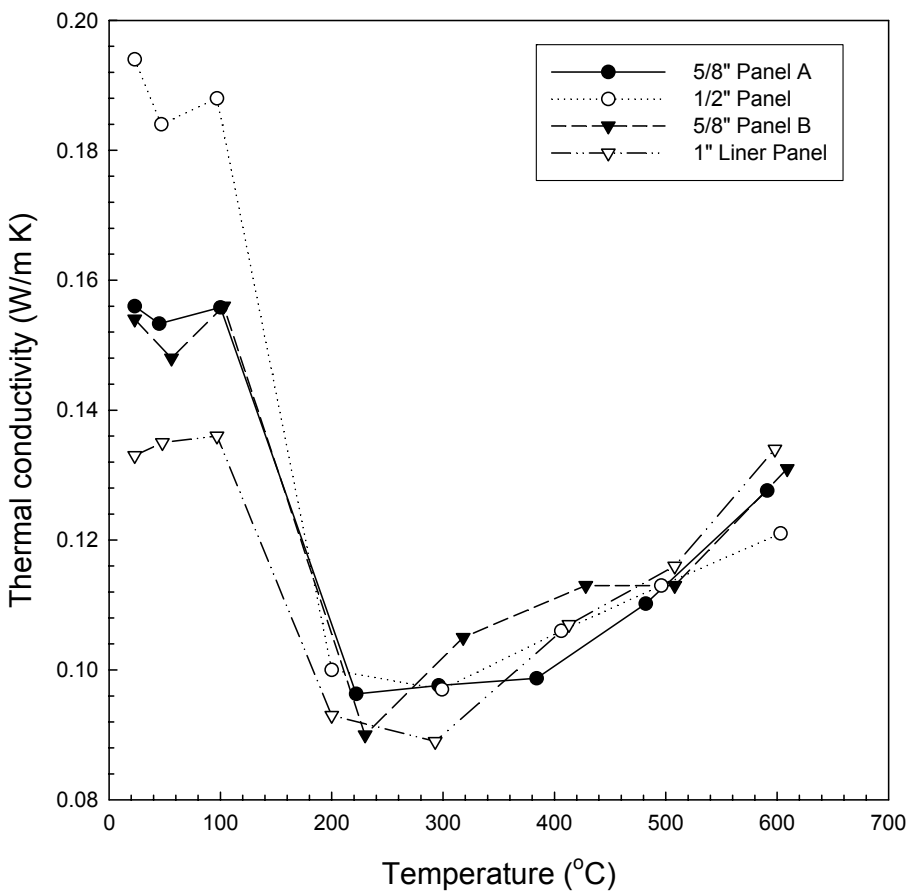

Figure 6–9. Thermal conductivities of the four gypsum materials as a function of temperature.

Figure 6-10 shows a comparison of the current thermal conductivity measurements with data from Mehaffey et al. (1994) for Firecode Core Type X gypsum panel. The data from Mehaffey et al. were obtained using a commercially available thermal conductivity meter. Both sets of data exhibit similar trends, although, in general, the values from Mehaffey et al. are higher.

A comparison of the current thermal conductivity results with the data obtained from Harmathy (1983) and Mehaffey et al. (1994) for Firecode C Core gypsum panel is shown in Fig. 6-11. The conductivities from Harmathy (1983) are higher than those obtained from other studies. In general, the thermal conductivity initially decreases and then increases with increasing temperature.

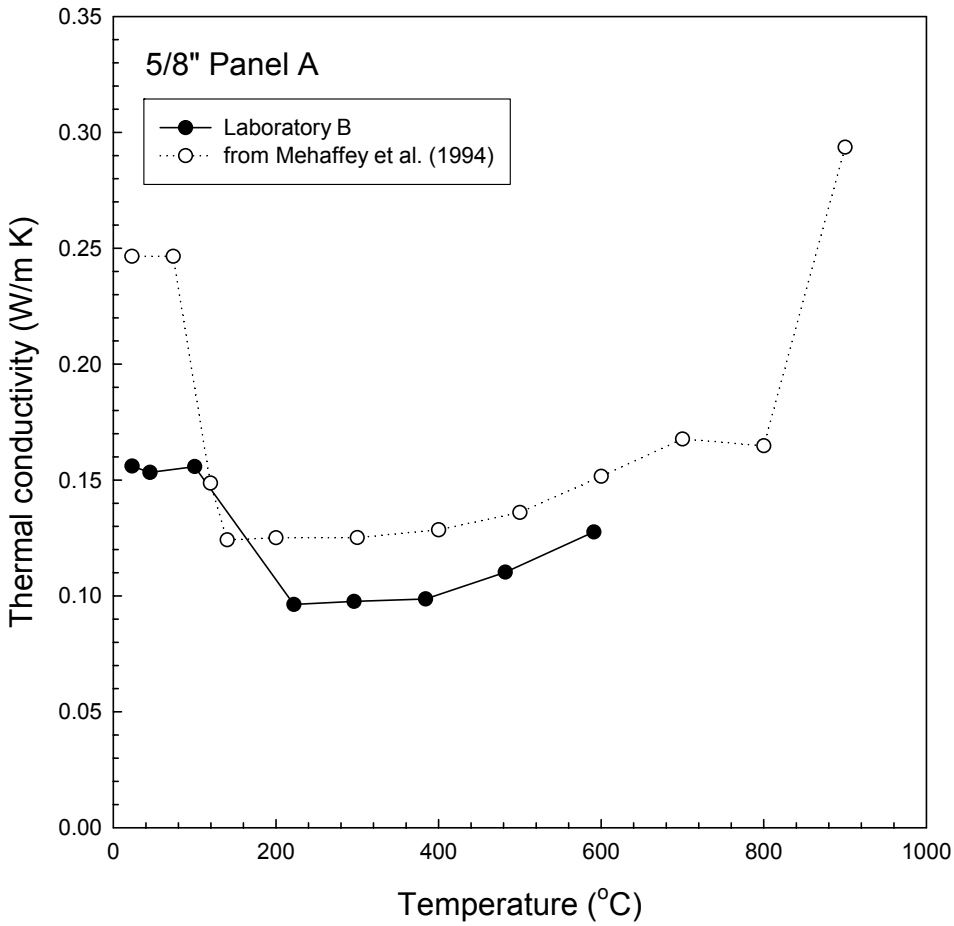

Figure 6–10. Comparison of the thermal conductivity measurements from Laboratory B with the data from Mehaffey et al. (1994) for 5/8 in. thick gypsum panel A.

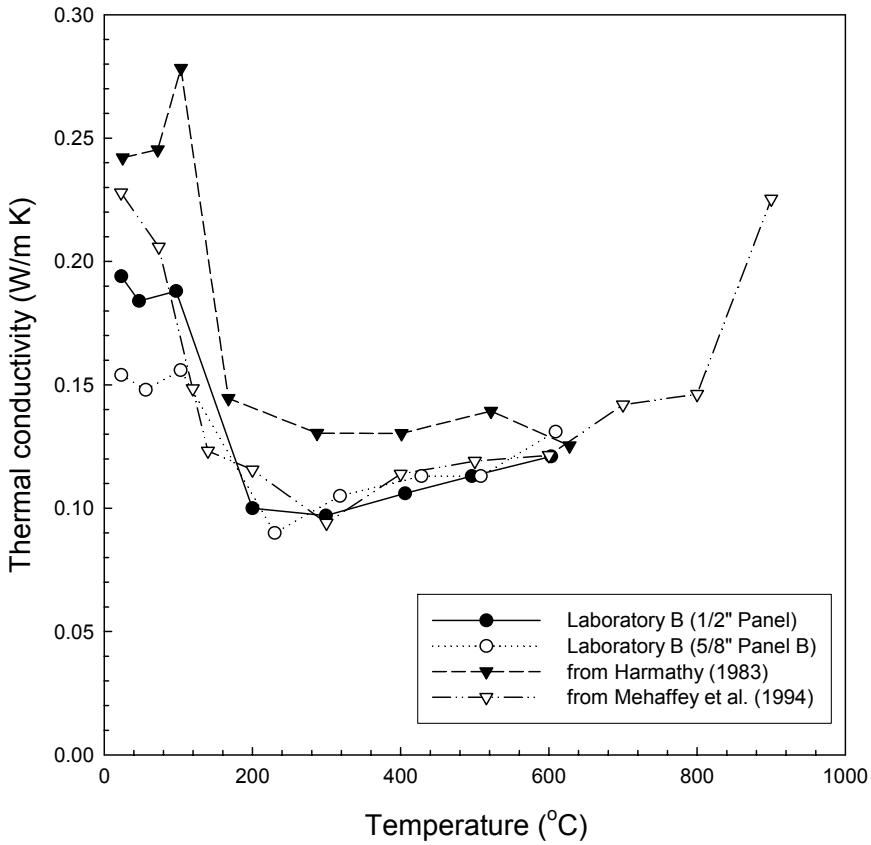

Figure 6–11. Comparison of thermal conductivity measurements from Laboratory B with other literature values for ½ in. thick gypsum panel and 5/8 in. thick gypsum panel B.

6.4.3 Specific Heat Capacity Measurements

Specific heat capacities of the cores of the four gypsum panel samples were measured using a TA Instruments DSC 2910 differential scanning calorimeter at NIST. Tests were conducted according to the procedure described in ASTM E 1269 (2001). Specimens of approximately 8.4 mg ± 0.1 mg in mass were held isothermally at 30 °C for 5 minutes. The temperatures were then increased at a rate of 20 °C/min to a maximum temperature of 600 °C, the operating limit of this instrument. The specimens were held isothermally at 600 °C for an additional 5 minutes. Single scans of both an empty pan and a pan containing standard reference material SRM 720 (sapphire or α-Al_2O_3) were conducted prior to testing and used to determine calorimetric sensitivity. The apparent specific heat capacity was calculated according to the formulas presented in the ASTM standard.

An additional modification to the ASTM test procedure was necessitated by the chemical nature of the material comprising the cores of the boards. The dominant material in the cores is gypsum, a naturally occurring mineral composed of calcium sulfate chemically bound to hydrated water (calcium sulfate dihydrate or $CaSO_4 \cdot 2H_2O$). As gypsum is heated, the hydrated water is liberated in two endothermic chemical reactions. If the core materials were contained within sealed hermetic pans, out-gassing of the liberated water would eventually increase the pressure beyond the accepted limits of the pans. Use of an

open pan is undesirable, however, as the dehydration reactions also depend on the partial pressure of water vapor in the gas surrounding the material. Therefore, aluminum hermetic pans with 50 μm diameter pinholes in the lids were used. The small diameter hole allowed pressure to dissipate from the pan, maintaining structural integrity, but retained sufficient water vapor to resolve the two dehydration processes. As the core of the gypsum panel is porous, having a porosity of approximately 0.3 (Blondeau et al. 2003), it is further expected that the liberated water will remain locally in the form of vapor even as pressure diffuses across the porous matrix. The procedure used should, therefore, provide a better estimate of the response of gypsum panel cores to the rapid heating observed in fires.

Results are presented as apparent specific heat capacity of the material with respect to the initial mass of the specimen. Clearly, as the water is driven from the samples and bleeds through the pinhole, the mass of the sample will decrease. Results of thermal gravimetric tests should also be used if the true specific heat capacity of the material is desired. The data are presented in Tables B-2, B-3, B-4 and B-5 and are plotted in Figs. B-1, B-2, B-3, and B-4 in Appendix B. Peaks and valleys attributed to chemical changes are labeled on each graph with the corresponding chemical reaction. Figure 6-12 is a plot of the results for all four gypsum materials. It is seen that the four panels had similar specific heat capacities as a function of temperature.

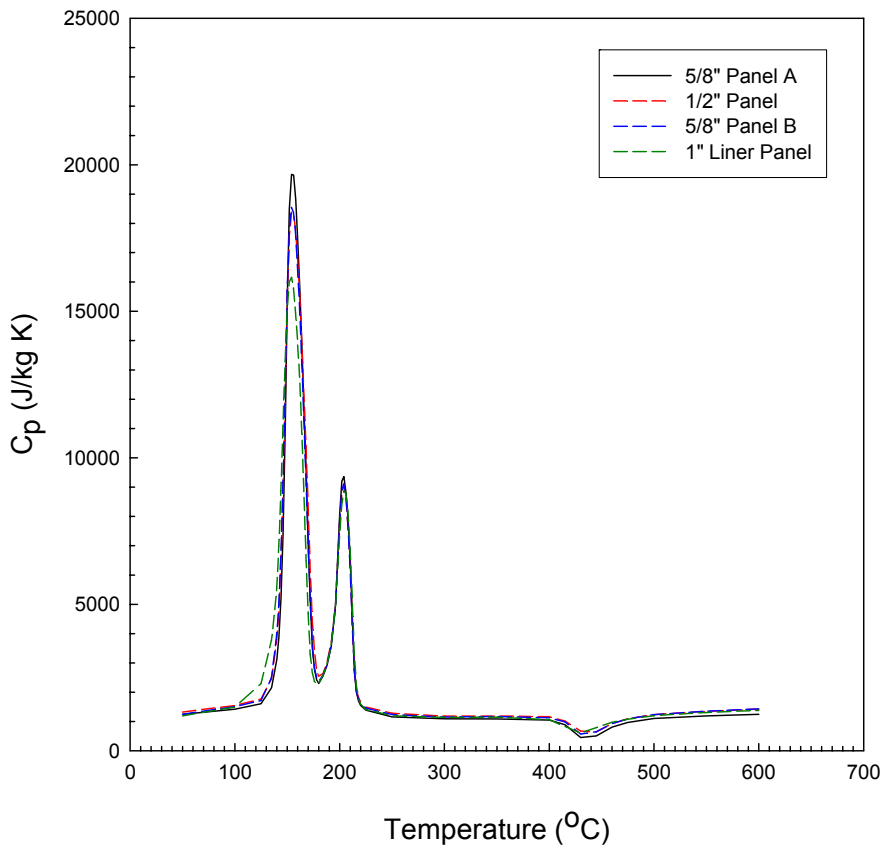

Figure 6–12. Comparison of specific heat capacities for the four gypsum materials.

6.4.4 Density Measurements

Laboratory B used a Netzsch Model 409 Simultaneous Thermal Analyzer (STA) equipped with both high and low temperature furnaces was used to determine mass changes as a function of temperature. The STA is vacuum tight, allowing specimens to be tested in pure inert, reducing, or oxidizing atmospheres as well as under vacuum. The unit can be operated in the differential scanning calorimetric (DSC) or thermogravimetric analysis (TGA) mode.

A dual push-rod dilatometer (Theta Dilatronics II) was used to measure linear thermal expansion following the procedure in ASTM E 228 (ATM 1995). The differential expansion between the gypsum specimen and a known standard reference material was measured as a function of temperature. The expansion of the specimen is computed from this differential expansion and the expansion of the standard. The measurements are made under computer control, and linear expansion is calculated at pre-selected temperatures. Six standard reference materials for expansion were obtained from NIST and these include materials with low, moderate, and large expansions. For the purposes of calibration and checkout, one NIST standard was measured against another NIST standard.

Densities were calculated from the TGA results and linear thermal expansion measurements. Table 6-10 summarizes the calculated results, which are also plotted in Fig. 6-13. All four materials show the same trend as a function of temperature. The variation of density with temperature is associated with the mass loss and the change in volume of the gypsum material.

Table 6–10. Bulk densities of the four gypsum materials.

	Density (kg/m^3)[a]			
Temperature (°C)	**5/8 in. Panel A**	**½ in. Panel**	**5/8 in. Panel B**	**1 in. Liner Panel**
23	709	760	787	770
50	706	759	785	767
100	680	754	780	759
150	629	725	752	721
200	586	668	691	664
250	580	636	656	638
300	581	634	654	636
350	582	634	654	638
400	597	659	679	659
450	600	665	684	663
500	600	664	682	664
550	599	663	681	664
600	605	663	682	664

a. To convert to pcf multiply by 0.062428.

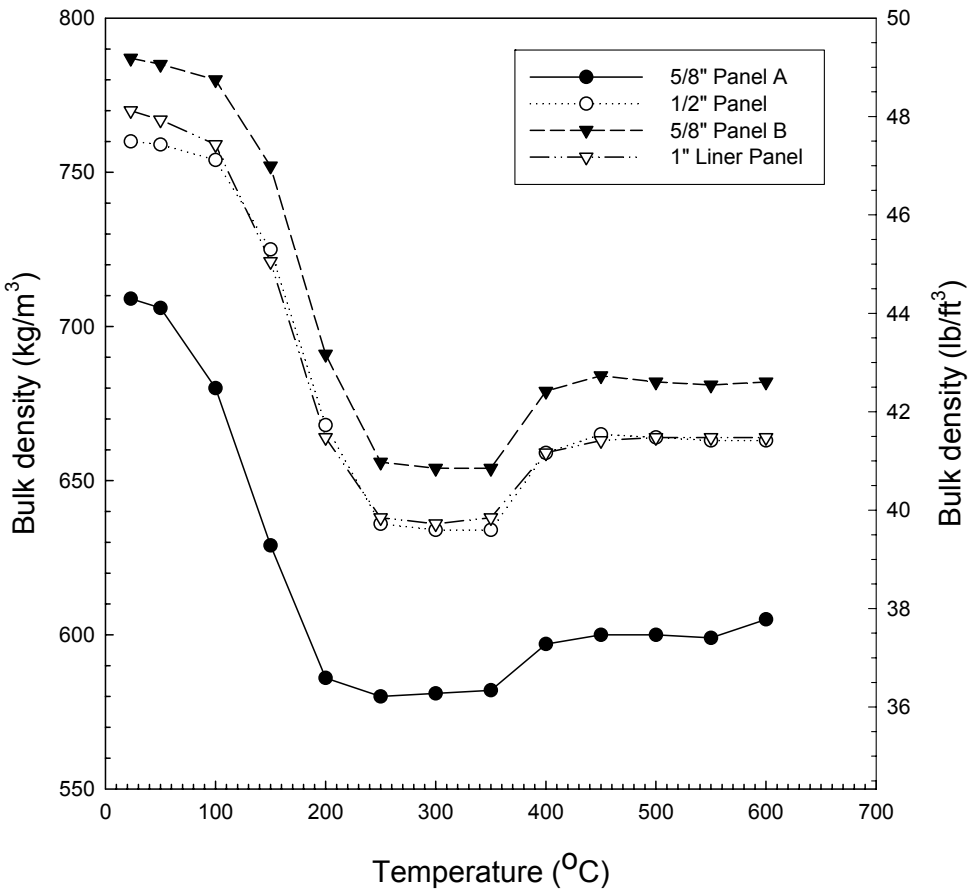

Figure 6–13. Bulk densities of the four gypsum materials as a function of temperature.

This page intentionally left blank.

Chapter 7
ADHESIVE AND COHESIVE STRENGTH

In order to analyze the thermo-structural response of the WTC towers during the fires after the aircraft impacts, it was necessary to estimate the extent of dislodged thermal insulation on structural members. Dislodgement could occur as a result of:

- Direct impact by debris resulting from breakup of the aircraft and its contents and breakup of structural elements, or
- Inertial forces due to vibration of members excited by the impact events.

For a given level of vibration, the magnitude of the inertial forces acting on the insulation depends on the density and thickness of the thermal insulation. The insulation would dislodge if the stresses resulting from inertial forces exceeded the strength of the insulation. The focus of the investigation reported in this chapter was to determine tensile strength characteristics of the thermal insulation. Information on in-place measurements provide by the Port Authority are reviewed. The experimental approach used to obtain additional information is presented along with test results. Finally, a simplified approach is presented for estimating the accelerations required to dislodge the thermal insulation.

7.1 REPORTED IN-PLACE DENSITY AND BOND STRENGTH

As was mentioned in Section 4.3, the Port Authority provided data on in-place density and tensile strength characteristics of the thermal insulation applied to the floor trusses during tenant alterations. Figure A-60 in Appendix A shows an example of such test reports. The reports indicated that tests were done in accordance with ASTM E 605 (density) and ASTM E 736 (cohesion/adhesion strength). As mentioned in Chapter 4, BLAZE-SHIELD II was used in the upgrade, and as noted previously in Table 6-3, the manufacturer indicated that BLAZE-SHIELD II is about 20 percent denser and has about 20 percent higher adhesive/cohesive strength compared with BLAZE-SHIELD DC/F.

According to ASTM E 605 (ASTM 2000a), density is determined by removing a rectangular portion of the insulation after taking 12 thickness measurements to obtain the average thickness. The length and width of the removed specimen are measured, and the volume is calculated. The equilibrium mass of the specimen is determined, and density is calculated by dividing the mass by the volume. The test reports provided by the Port Authority provided no notes to indicate deviations from the standard procedure.

The technique described in ASTM E 736 (ASTM 2000b) is illustrated in Fig. 7-1. A bottle screw cap is glued to the surface of the thermal insulation, and after the glue has cured, the cap is pulled. The force required to pull off the cap is divided by the area of the cap, and reported as the “cohesive/adhesive strength.” Failure is described as “cohesive” if it occurs within the insulation and is defined as “adhesive” if it occurs at the interface with the substrate. Figure 7-2 shows an example of a cohesive failure.

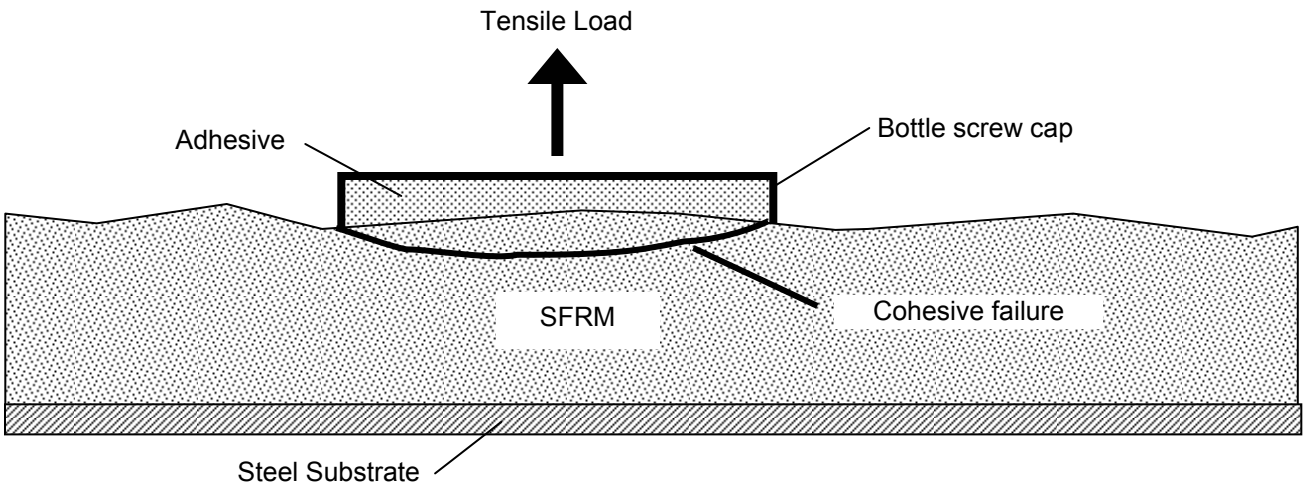

Figure 7–1. Bond strength test using screw cap in accordance with ASTM E 736.

Source: NIST.

Figure 7–2. Cohesive failure of SFRM using ASTM E 736 test (dashed circle is approximate location of cap before being pulled off.

Table 7-1 summarizes the density and strength data provided by the Port Authority (see also Table 4-2). The results of the tests are labeled as "bond strength." Test method ASTM E 736 calls for reporting the failure mode, but the Port Authority test reports did not include information on the nature of the failure associated with the reported strengths. The density values in Table 7-1 are plotted in Fig. 7-3 and the bond strength values are plotted in Fig. 7-4. Analysis of the density values indicated no statistically significant differences between the reported densities of the upgrade thermal insulation on floor trusses in the two towers. The overall average density was 18.9 pcf with a standard deviation of 3.2 pcf, giving a coefficient of variation of 16 percent.

Table 7–1. Density and bond strength of SFRM on floor trusses reported by the Port Authority of New York and New Jersey (30-P).

Tower	Floor	Density, pcf	Bond Strength, psf	Tower	Floor	Density, pcf	Bond Strength, psf
1	79	16.6	333	1	98	31.3	407
	81	19.0	270			16.8	351
		17.4	352			19.6	518
		17.6	463		99	18.8	204
		17.4	315			16.6	222
	83	16.0	259			18.4	204
	85	28.7	162		100	16.4	278
		23.7	180			17.3	278
		18.6	288			19.9	333
		15.8	278		102	16.5	333
		16.4	259			16.9	333
	92	20.3	360			15.9	315
		15.4	324	2	77	19.4	351
		18.0	360			19.4	198
	93	14.3	153			17.2	297
		16.6	207		78	17.0	288
		16.1	216			18.1	270
		18.4	234		88	18.0	167
		15.1	162			16.0	333
		17.4	180			15.0	157
		21.3	216		89	22.4	370
	94	21.2	486			15.8	333
		20.5	504			15.3	270
		20.1	288		92	19.7	342
	95	18.0	270			21.1	360
		20.1	306			19.7	297
		20.4	198		99	19.5	315
	96	20.5	486			22.7	252
		19.8	288			21.9	306
		19.9	324			19.5	270
	97	26.5	360				

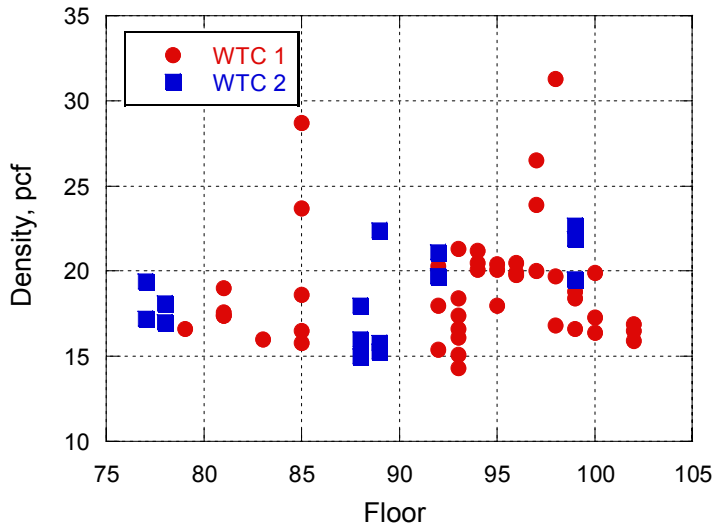

Figure 7–3. In-place density of BLAZE-SHIELD Type II on floor trusses from Port Authority test reports during the period 1997-1999.

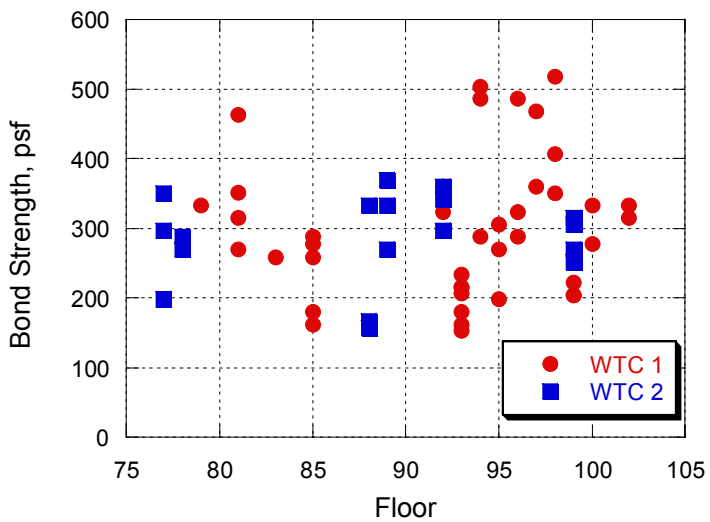

Figure 7–4. In-place bond strength of BLAZE-SHIELD Type II using ASTM E 736 from Port Authority test reports during the period 1997-1999.

Analysis of the bond strength values indicated that there were statistically significant differences between the average bond strengths for the different floors, but here was no statistically significant difference between the average bond strengths for the two towers. The overall average bond strength was 302 psf, with a standard deviation of 91 psf, giving a coefficient of variation of 30 percent. This value is less than the value of 360 psf indicated in Table 6-3, but the tabulated values is for tests under controlled conditions (referred to as “tested performance” in the manufacturer’s literature) and is not representative of field strengths. ISOLATEK product literature dated February 2002 refers to an average bond strength

of 150 psf as "standard performance" and this same value is used in its guide specification for BLAZE-SHEILD II.[19] Thus, the reported bond strengths shown in Fig. 7-4 are consistent with expectations.

7.2 SPECIMEN PREPARATION AND TEST PROCEDURES

While the in-place bond strength data of BLAZE-SHIELD II reported by the Port Authority appear to indicate acceptable performance, results of ASTM E 736 tests do not provide sufficient information for predicting whether insulation would be dislodged from structural members under various impact conditions. The standard test does not provide unambiguous values of cohesive and adhesive strengths, and it does not provide tensile properties in a direction parallel to the surface, that is, in-plane cohesive strength. As was mentioned in Section 6.3.4, because of the way a fibrous SFRM is installed, the resulting material is not isotropic. Layers of fiber bundles are deposited parallel to the surface of the substrate. It is expected that the strength perpendicular to the planes of the layers would be less than the strength parallel to the layers. Thus, a series of tests were conducted that would allow different strength properties to be determined. In addition, it was decided to test BLAZE-SHIELD DC/F because the Port Authority data did not include tests of this material.

7.2.1 Preparation of Test Plates

Test specimens were made by applying the SFRM to ¼ in. steel plates measuring 8 in. by 16 in. One half of the plates were coated with Series 10 Tnemec Primer (99 red)[20], which is the primer that was specified for the exterior columns (see Appendix A Fig. A-63). Nominal SFRM thicknesses of ¾ in. and 1½ in. were applied. Thickness was controlled by surrounding the steel plates with wood strips to form molds of the desired depth. Figure 7-5 shows the application of BLAZE-SHIELD DC/F to the steel plates positioned on the floor of the laboratory. Thickness was built up in several passes of the spray nozzle. Gentle hand rubbing was used to reduce local high spots and produce reasonably uniform thicknesses. The average thickness of SFRM for the ¾ in. plates was 0.85 in. with a standard deviation of 0.08 in. For the 1½ in. plates, the average thickness was 1.62 in. with a standard deviation of 0.16 in. The plate specimens were allowed to dry for over five months in the laboratory before testing. Companion specimens were weighed periodically for loss of water, and it was found that the 1½ in. thick specimen reached equilibrium in about one month.

7.2.2 Test Methods

It was desired to determine adhesive strength, cohesive strength normal to the surface, and cohesive strength parallel to the surface of the SFRM. Figure 7-6 is a schematic of the method used to measure the first two properties. This approach is based on the standard pull-off test method used in concrete technology to measure the bond strength of overlays applied to concrete substrates (ASTM 2004b). The SFRM layer was cut carefully in two directions, and a 3/8 in. by 2.7 in. by 2.7 in. aluminum plate was glued to the surface. After the adhesive had cured, a tensile load was applied to the plate, and the force required to pull off the SFRM was measured. The advantages of this approach over the ASTM 736

[19] Product Manual, Isolatek International, Stanhope, NJ, February, 2002.

[20] Purchased from Tnemec Company Inc., 6800 Corporate Drive, Kansas City, Missouri 64120-1372.

technique are that the resisting area is easily determined and it offers the ability to measure both adhesive and cohesive strengths.

Source: NIST.

Figure 7–5. Spraying steel plates with BLAZE-SHIELD DC/F.

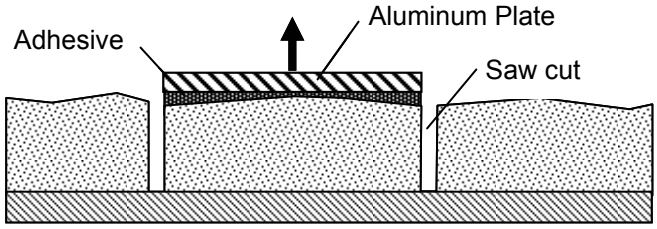

Figure 7–6. Schematic of "pull-off' test method used to measure cohesive and adhesive strengths.

In using the method shown in Fig. 7-6, one does not know beforehand what type of failure will occur, that is, whether it will be adhesive failure at the SFRM/steel interface or cohesive failure in the bulk SFRM. Failure occurs at the weakest link. It is possible, however, by a simple modification of the usual procedure to measure both strengths in the same specimen. This is accomplished by bonding together the failed specimen after the first test, and performing a second test on the repaired specimen. This approach is illustrated in Fig. 7-7, where the schematics on the left represent the first test and those on the right represent the re-test. Two cases are illustrated:

- Case 1: The initial failure is an adhesive failure near the SFRM/steel interface, and after repairing the specimen the second failure is a cohesive failure in the bulk SFRM.

- Case 2: The initial failure is a cohesive failure in the bulk SFRM, and after specimen repair the second failure is an adhesive failure near the SFRM/steel interface.

As will be seen, this approach works because adhesive and cohesive strengths are similar in magnitude.

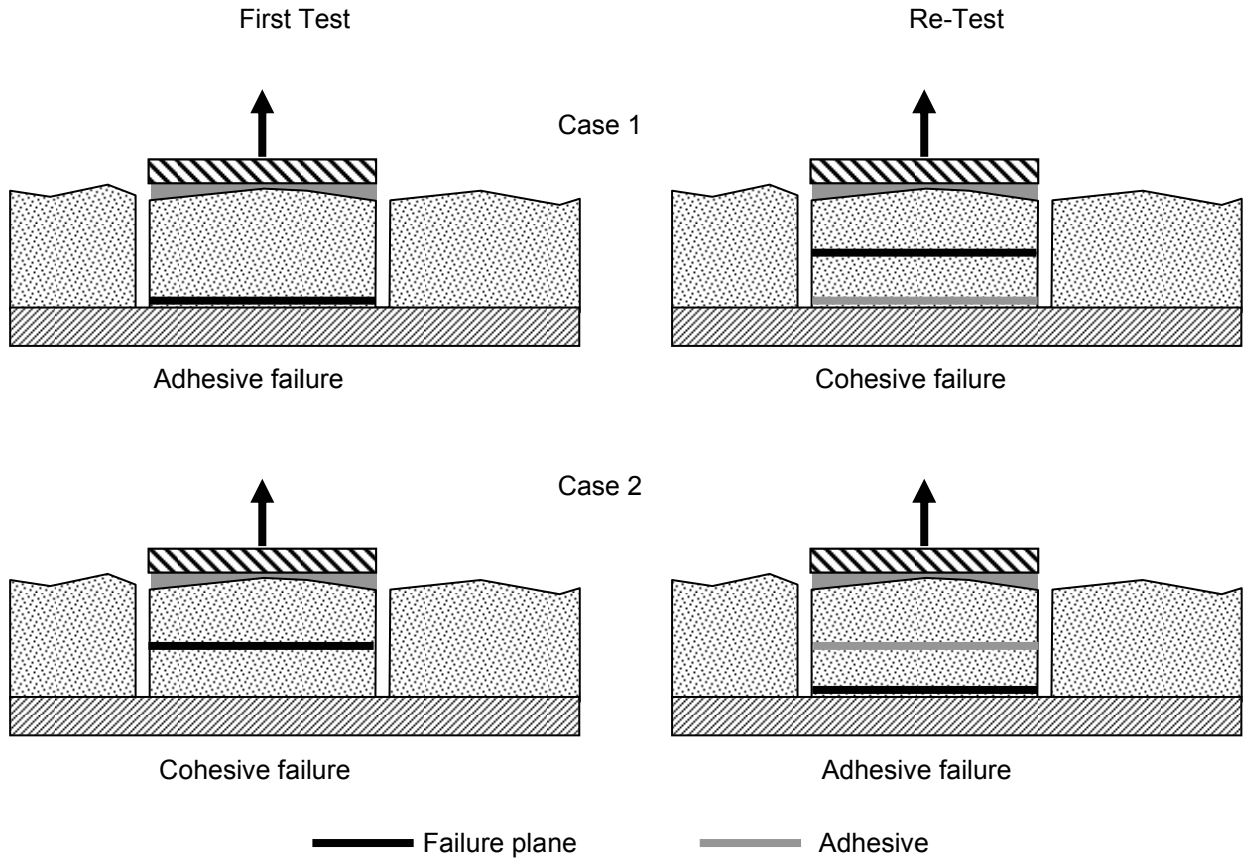

Figure 7–7. Technique used to measure both "adhesive" and "cohesive" strength in the same specimen.

The cohesive strength parallel to the surface was determined on specimens obtained by carefully removing the SFRM layer from the steel and preparing a prism that could be loaded as shown in Fig. 7-8. The following section describes how the test specimens were prepared.

7.2.3 Preparation of Test Specimens

From each plate, three specimens were prepared for measuring both density and in-plane cohesive strength, and two specimens were prepared for measuring adhesive strength and cohesive strength normal to the surface. The first step was to cut the SFRM layer into five 2.7 in. wide strips. A fine-toothed saw blade was used, and the sawing motion was done carefully so as to minimize damage to the SFRM (see Fig. 7-9). The two outer strips and the middle strip were debonded from the steel plate by using a sharpened putty knife. Care was taken to ensure that the two strips for adhesive/cohesive strength testing were not disturbed (see Fig. 7-10).

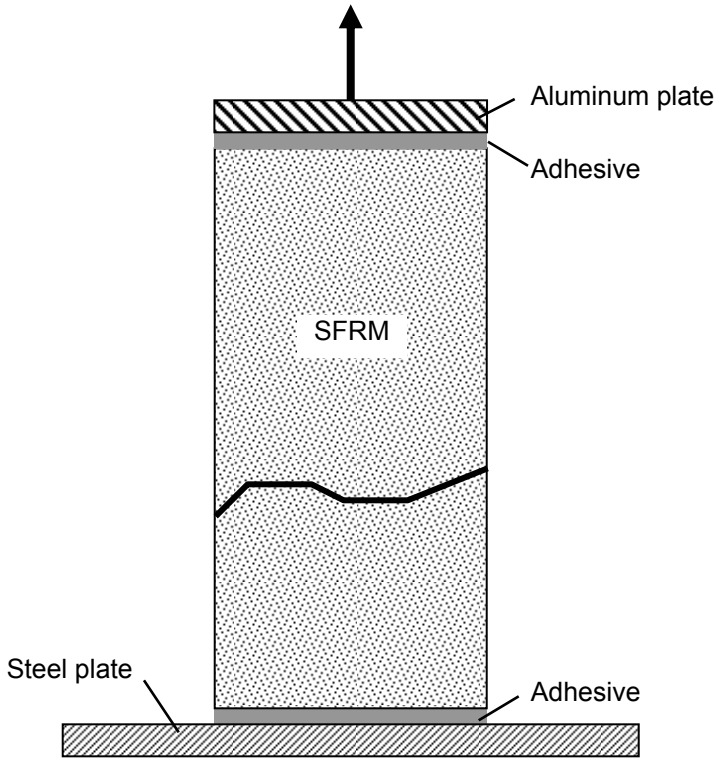

Figure 7–8. Method to measure cohesive strength parallel to SFRM surface (in-plane cohesive strength).

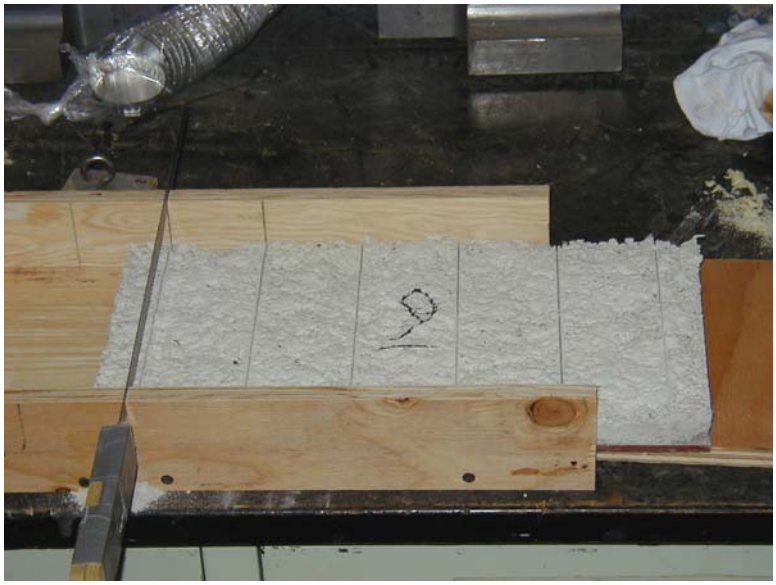

Source: NIST.

Figure 7–9. Cutting the SFRM layer into five strips.

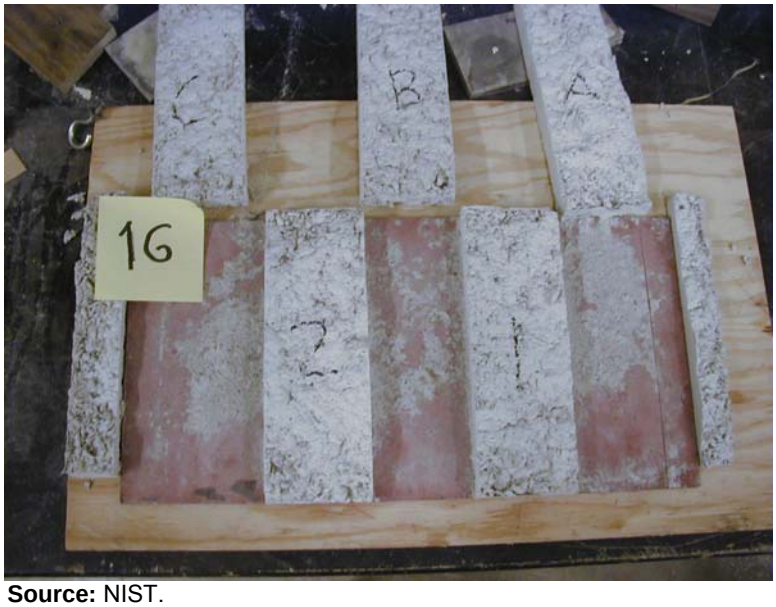

Source: NIST.

Figure 7–10. Five specimens obtained from single plate; top three specimens are used for density and in-plane cohesive strength, bottom specimens are used for adhesion/cohesion tests.

For the adhesive/cohesive strength tests, an aluminum plate was bonded to the top surface using a fast curing, two-component urethane foam adhesive. Fixtures were used to ensure that the bonded plate was parallel to the steel plate (see Fig. 7-11). After the adhesive had cured, the SFRM layer was cut as shown in Fig. 7-12 so as to produce a prismatic test specimen. A hook was screwed into the aluminum plate and a load was applied by hand using a 50 lb digital force gauge (see Fig. 7-13). The force gauge was able to store the peak load attained during the test. During loading, the steel plate was placed on the floor, and a foot was placed at each end of the plate to provide resistance to the applied tensile load. The average length and width of the failure area was measured and used to compute the adhesive or cohesive strength.

After the first test, the specimen was repaired with the same polyurethane adhesive, and the test was repeated as discussed in Section 7.2.2. Figure 7-14 shows two specimens after the first test. The specimen on the left failed in the bulk material, thereby giving a measure of the cohesive strength normal to the surface. The specimen on the right failed near the SFRM/steel interface, which is taken to be the adhesive strength. Figure 7-15 shows the same two specimens after they had been repaired and subjected to the second loading. Now the specimen on the right shows a crack in the bulk material, and the specimen on the left shows separation near the SFRM/steel interface. Note that for the specimen on the right, which had an adhesive failure during the first loading, the failed specimen was bonded to a bare steel plate (not shown) for the second test to measure cohesive strength. In some cases where the first failure was cohesive, the repeated test also resulted in cohesive failure. In these cases, the specimen was repaired as often as needed until an adhesive failure occurred.

Source: NIST.

Figure 7–11. Aluminum plate being bonded to the top surface of SFRM specimen; the wooden fixture is used to maintain the correct alignment of the plate.

Source: NIST.

Figure 7–12. Preparing the SFRM specimen for adhesion/cohesion test.

Source: NIST.

Figure 7–13. Manual application of tensile load using digital force gauge.

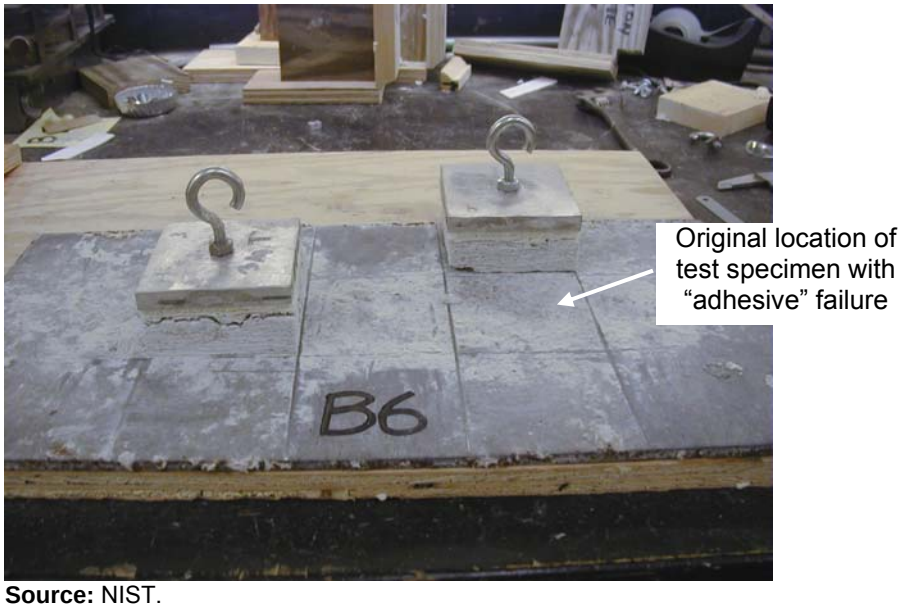

Source: NIST.

Figure 7–14. Results of first loading: specimen on left had a cohesive failure in the bulk SFRM, specimen on right failed near the SFRM/steel interface.

Source: NIST.

Figure 7–15. Results of second tests after repair: specimen on left had adhesive failure and specimen on right had cohesive failure.

The other three strips (see Fig. 7-10) were used for determining density and in-plane cohesive strength. First, the top surfaces of the debonded strips were sanded on a belt sander to obtain prismatic specimens. About 0.2 in. was removed from the ¾ in. plates, and about 0.4 in. was removed from the 1½ in. plates. The prisms were weighed and their average dimensions determined. The densities were obtained from the masses and computed volumes. Each prism was then bonded to a steel plate with the polyurethane adhesive. An aluminum plate was bonded to the other end of the specimen. After the adhesive had cured, a tensile load was applied to the aluminum plate until the SFRM failed (see Fig. 7-16). The area of the fracture plane was determined and the in-plane cohesive strength calculated from the recorded maximum load.

Source: NIST.

Figure 7–16. SFRM specimen after measuring in-plane cohesive strength.

7.3 TEST RESULTS

Table 7-2 summarizes the properties that were measured and the types of SFRM plates that were tested. It was assumed that the presence or absence of primer on the steel plates would not affect density or in-plane cohesive strength. Thus, only primed plates were used for these properties. The following sections summarize the test results.

Table 7–2. Test matrix.

Property	¾ in. Nominal Thickness		1½ in. Nominal Thickness	
	With Primer	Bare Steel	With Primer	Bare Steel
Density	X		X	
In-plane cohesive strength	X		X	
Adhesive/Cohesive (N)* strength	X	X	X	X

*N indicates normal to surface of SFRM

7.3.1 Density

As mentioned in Section 7.2.3, density was determined by weighing prismatic specimens prepared by sanding the irregular exposed surface of the SFRM. The specimens were about 5 months old when tested and had attained equilibrium water contents. Five plates with primed steel were chosen at random for each SFRM thickness. Table 7-3 lists the individual determinations, and Fig. 7-17 is a plot of the data. The average density of the ¾ in. thick specimens is 27.2 pcf, with a standard deviation of 0.8 pcf; and for the 1½ in. thick specimens the average density is 29.7 pcf with a standard deviation of 1.3 pcf. The difference in average values for the two thicknesses was found to be statistically significant.

Table 7–3. Density of BLAZE-SHIELD DC/F specimens.

Nominal Thickness	Specimen	Density, pcf	Nominal Thickness	Specimen	Density, pcf
¾ in.	7-a	26.1	1½ in.	24-a	29.5
	7-b	26.0		24-b	29.2
	7-c	26.6		24-c	29.3
	6-a	27.2		29-a	30.0
	6-b	27.2		29-b	29.0
	6-c	26.7		29-c	29.6
	18-a	26.2		10-a	31.2
	18-b	28.1		10-b	31.4
	18-c	27.2		10-c	29.9
	16-a	27.0		30-a	26.9
	16-b	28.2		30-b	27.7
	16-c	28.3		30-c	29.5
	2-a	27.9		11-a	31.5
	2-b	26.7		11-b	30.5
	2-c	28.0		11-c	29.7

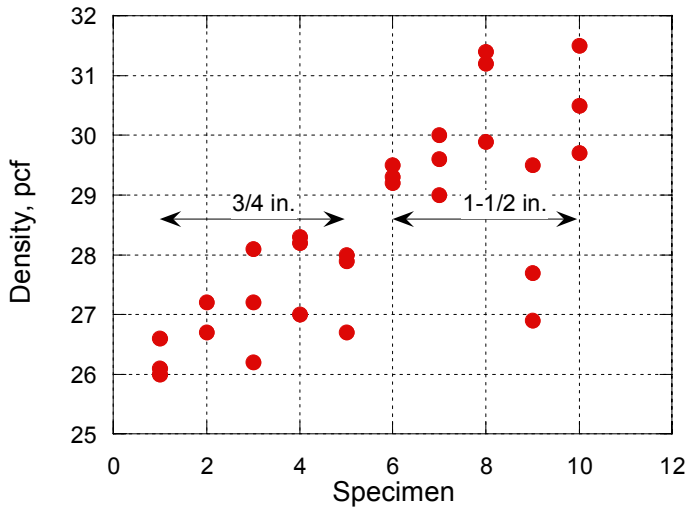

Figure 7–17. Density of BLAZE-SHIELD DC/F specimens.

These measured densities are unexpectedly high compared with published values and the values reported in Table 6-8, which indicates a room temperature density of 14.8 pcf. The 2001 ICBO Evaluation Service report E-R 1244, refers to a minimum average density of 13 pcf for BLAZE-SHIELD DC/F (ICBO 2001). The air-dry densities obtained in the NIST/UL fire endurance tests of floor truss assemblies (NIST NCSTAR 1-6B) are shown in Fig. 7-18. Again, those densities are lower than obtained in this study. The exact reason for the higher density in this study is not known, but possible reasons include the following:

- The use of forms, as opposed to only a piece of sheet metal (as in ASTM E 605), may have provided confinement during spraying leading to more consolidation of the SFRM.
- The smoothing of the top surface by sanding removed the less dense material. Recall that about 0.2 in. and 0.4 in. were removed from the ¾ in. and 1½ in. plates, respectively.
- The hand screening that was done to remove local high spots may have resulted in additional consolidation.

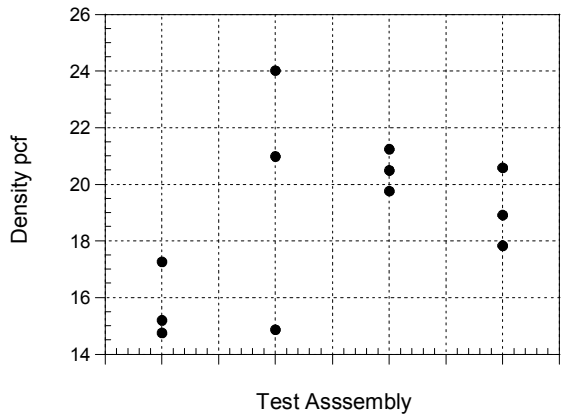

Figure 7–18. Air-dry density of BLAZE-SHIELD DC/F from NIST/UL floor truss fire endurance tests (NIST NCSTAR 1-6B).

7.3.2 In-Plane Cohesive Strength

After completing the density determinations the prismatic specimens of SFRM were bonded to a bare steel plate, and an aluminum plate was bonded to the other end (see Fig. 7-8). The steel plate was placed on the floor, and a tensile load was applied to the aluminum plate until the SFRM failed. The width and thickness of the specimen adjacent to the failure plane was measured, and the in-place cohesive strength was calculated.

Table 7-4 lists the individual values on in-plane cohesive strength, and Fig. 7-19 is a plot of the results. The average strength for the ¾ in. specimens is 1,120 psf with a standard deviation of 390 psf. For the 1½ in. specimens the average is 1,740 psf with a standard deviation of 540 psf. The difference in average strength is statistically significant. The relative strengths are consistent with the differences in density for the two thicknesses.

Table 7–4. In-plane cohesive strength for BLAZE-SHIELD DC/F specimens.

Nominal Thickness	Specimen	Cohesive Strength, psf	Nominal Thickness	Specimen	Cohesive Strength, psf
¾ in.	7-a	1095	1½ in.	24-a	2279
	7-b	1043		24-b	1607
	7-c	689		24-c	1687
	6-a	919		29-a	1473
	6-b	791		29-b	1986
	6-c	1512		29-c	3101
	18-a	1032		10-a	2006
	18-b	701		10-b	1876
	18-c	953		10-c	1304
	16-a	575		30-a	1579
	16-b	1500		30-b	636
	16-c	1254		30-c	1630
	2-a	1065		11-a	1902
	2-b	1875		11-b	1226
	2-c	1773		11-c	1861

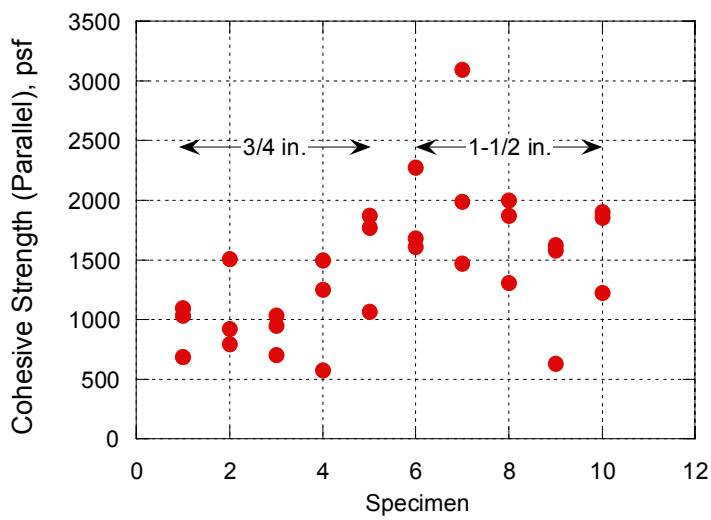

Figure 7–19. In-plane cohesive strength for BLAZE-SHIELD DC/F specimens.

7.3.3 Adhesive Strength

Adhesive failure is defined as failure near the SFRM/steel plate interface. In all cases where there was measurable adhesive strength a thin layer of cement paste and mineral fibers remained on the steel plate when the specimen separated. Figure 7-20 shows one of the ¾ in. specimens (with primed steel) after testing and illustrates “adhesive” failure. The photo on the left is a magnified view of about a 0.4 diameter region and shows the thin layer of mineral fibers and paste. Note in the in the right photograph that there are regions on the steel with no adhering paste, indicating essentially zero adhesive strength. The locations of the specimens for the adhesion/cohesion tests were chosen based on the

location of the regions with adhesive failure when the three strips used for density determination were removed. This is illustrated in Fig. 7-20, where the specimen on the right was located toward the top of the plate and the one on the left was located at the center.

The plan was to select five plates at random for each combination of SFRM thickness and condition of steel plate (bare versus primed). It was found that for the 1½ in. plates with primed steel two of the first three specimens had essentially zero bond strength because the SFRM strips were loose after cutting with the saw. Figure 7-21 shows an example of a plate with essentially zero adhesion strength. At this point in the testing, the remaining plates were examined by applying a small force by hand to the SFRM to check whether there was any significant adhesion. Ten of the 15 plates had no adhesion. Plates 30 and 11 appeared to have some adhesion, so these were selected to complete the 5 replicate plates for this group.

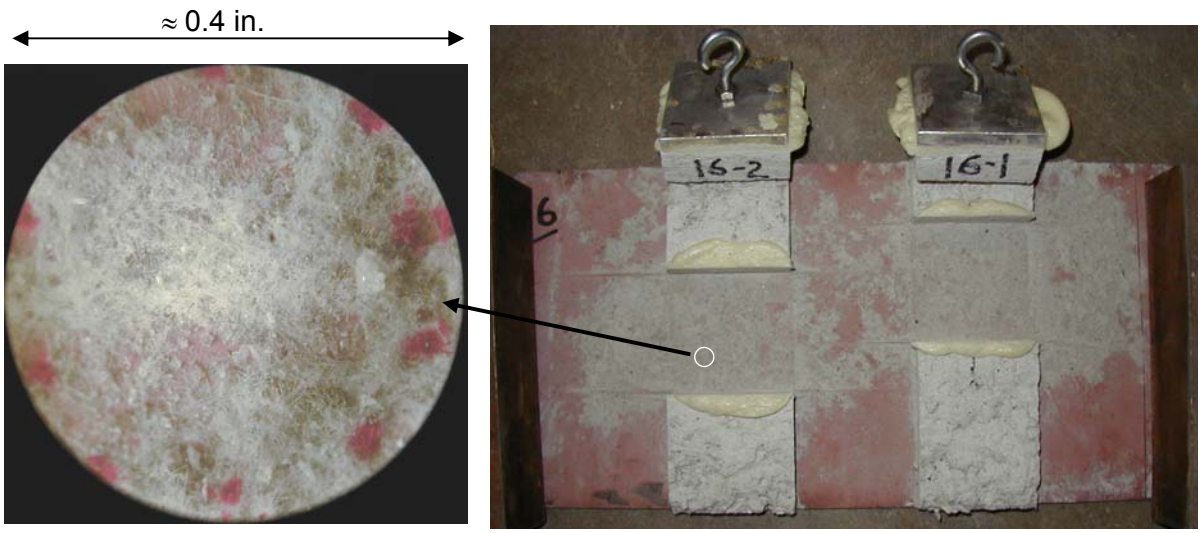

Source: NIST.

Figure 7–20. Example of "adhesive" failure of SFRM (original location of test specimens are the gaps in the two strips); photo on left is magnified view of thin layer of paste and fibers (the marks around the perimeter is red ink used to locate field of view).

Source: NIST.

Figure 7–21. Example of lack of adhesion in 1½ in. SFRM on steel plate with primer.

There were no adhesion problems in the specimens made with bare steel. Figure 7-22 shows examples of specimens with bare steel. The top photograph shows the appearance of a ¾ in. SFRM plate after removal of the three strips to be used for density testing. The regions of the plates with bare steel are due to the action of the putty knife used to debond the three strips. The lower photograph shows the appearance after completion of the adhesion tests on a 1½ in. SFRM specimen. Again the bare spots are due to scraping by the putty knife.

Table 7-5 shows the adhesive strength results and Fig. 7-23 is a plot of the data. Only four plates were selected for the ¾ in. SFRM with bare steel and only three were selected for the 1½ in. SFRM with bare steel. Table 7-6 summarizes the adhesive strength test results. As a point of reference, the manufacturer of BLAZE-SHIELD DC/F indicates an adhesion/cohesion value under controlled conditions in accordance with ASTM E 736 of 295 psf (see Appendix A Fig. A-63). In the ASTM standard procedure, the SFRM is applied to a 12 in. square galvanized steel sheet (0.060 in. thick) at a thickness of ½ in. to 1 in. Note however, that in the ASTM test method, failure can be cohesive (in the bulk SFRM) as well as combination of adhesive and cohesive failure.

It is clear that the condition of the steel has a significant effect on the SFRM adhesive strength. Typically, manufacturers require that compatibility with primed steel be evaluated to ensure that proper materials are used for adequate adhesion. For example, the following text is taken from the ICBO evaluation of different BLAZE-SHIELD products (ICBO 2001):

> **"2.2.5 Primed or Painted Surfaces:** CAFCO BLAZE-SHIELD materials are permitted to cover primed or painted wide flange shapes, subject to the following requirements:
>
> 1. Beam flange width is 12 inches (305 mm), maximum.
>
> 2. Column flange width is 16 inches (406 mm), maximum.

3. Beam or column web depth is 16 inches (406 mm), maximum.

4. Bond tests of five specimens in accordance with ASTM E 736 are used to verify the bond strength of the fire-protection material to a painted or primed steel beam or column at the jobsite. Condition of acceptance is that the average bond strength is 20 times the weight of in-place fire-protection material but not less than 150 psf (7.2 kN/m^2), or the minimum average bond strength is 80 percent, with a minimum individual bond strength of 50 percent of the bond strength of fire-protection material applied to bare, clean, 1/8 inch-thick (3.2 mm) steel plate, whichever is greater. Where bond-strength values are less than these minimums, CAFCO BOND-SEAL Type E.B.S. adhesive is applied to the primed or painted surfaces, and the bond-strength tests are repeated."

The results of these tests show that BLAZE-SHIELD DC/F is not compatible, from an adhesion point of view, with the Tnemec 99 Red Metal Primer used in this study and that was specified for the exterior columns of the WTC towers.

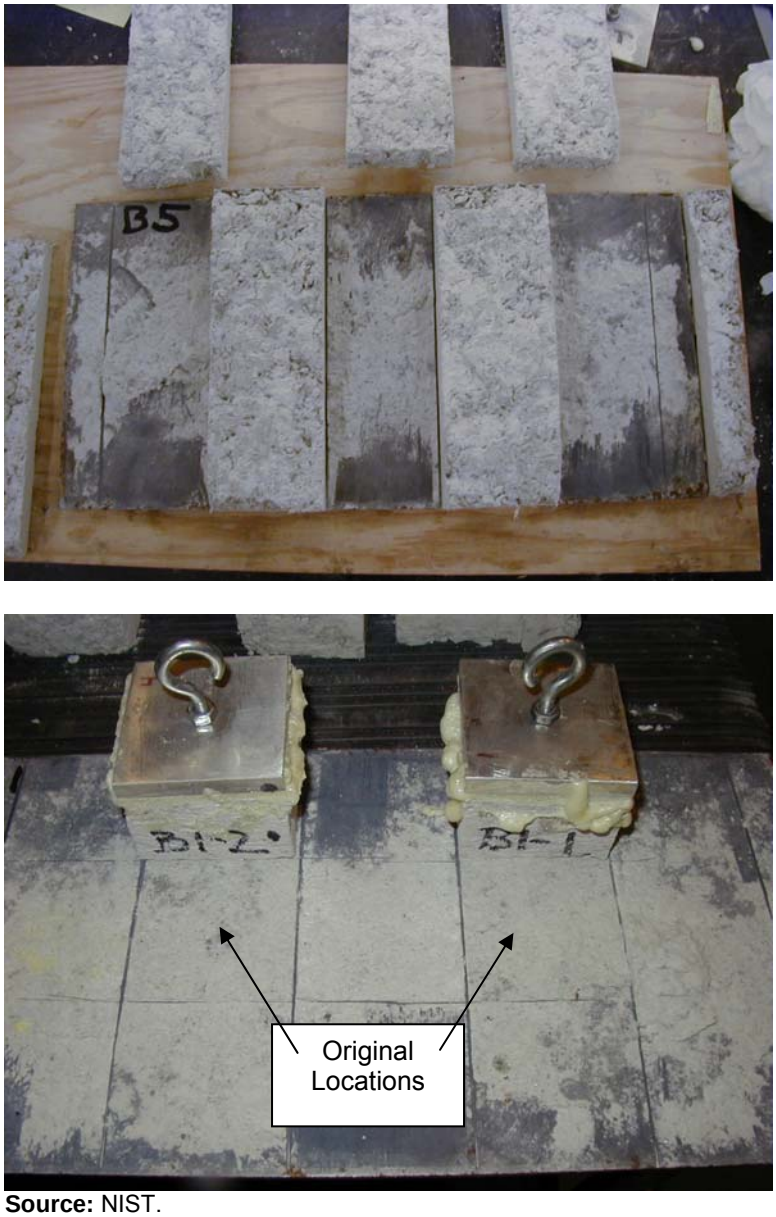

Source: NIST.

Figure 7–22. Examples of good adhesion in specimens with unprimed steel plates: (top) ¾ in. SFRM specimen before testing; (bottom) 1½ in. SFRM specimen after completion of tests.

Table 7–5. Adhesive strength of BLAZE-SHIELD DC/F specimens.

Nominal Thickness	Primer	Specimen	Adhesive Strength, psf	Nominal Thickness	Primer	Specimen	Adhesive Strength, psf
¾ in.	Yes	7-1	175	1½ in.	Yes	24-1	0
		7-2	234			24-2	0
		6-1	197			29-1	378
		6-2	267			29-2	401
		18-1	276			10-1	0
		18-2	164			10-2	0
		16-1	257			30-1[a]	501
		16-2	246			30-2[a]	253
		2-1	5			11-1[a]	130
		2-2	32			11-2[a]	44
	No	4-1	382		No	1-1	703
		4-2	423			1-2	651
		5-1	488			2-1	543
		5-2	493			2-2	767
		6-1	365			3-1	459
		6-2	552			3-2	876
		7-1	425				
		7-2	472				

a. Not selected randomly.

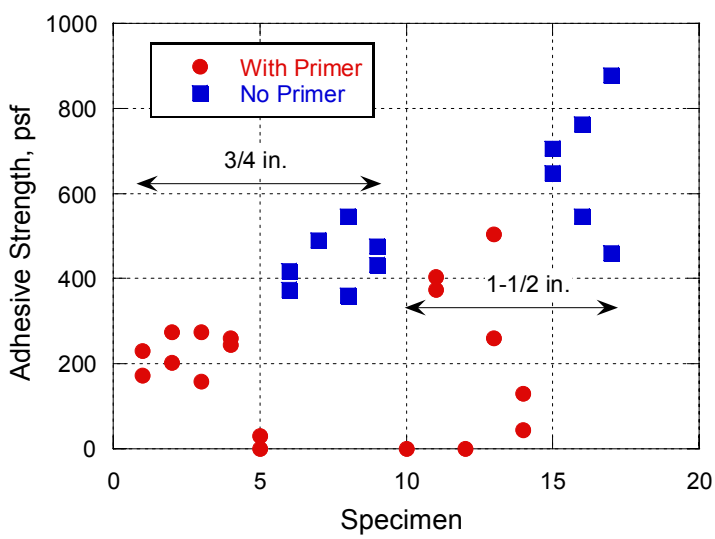

Figure 7–23. Adhesive strength of BLAZE-SHIELD DC/F specimens for primed and unprimed steel plates.

Table 7–6. Summary of adhesive strength results.

Nominal Thickness	Primer	Average, psf	Standard Deviation, psf	Coefficient of Variation, percent
¾ in.	Yes	185	96	52
	No	450	63	14
1½ in.	Yes	171[a]	196	115
	No	666	151	23

a. For selected specimens

7.3.4 Cohesive Strength Normal to Surface

As discussed in Section 7.2.3, the same specimens were tested twice (in some cases three times) so as to determine the adhesive and cohesive strength normal to the surface. Figure 7-24 shows examples of cohesive failures in 1½ in. SFRM specimens. These specimens were subsequently repaired with the polyurethane foam adhesive, and the adhesive strength was then determined. In general, cohesive failures tended to occur close to the surface of the SFRM layer. This is logical because less compaction would be expected near the surface and perhaps less hydration of cement due to drying.

Source: NIST.

Figure 7–24. Examples of cohesive failure in 1½ in. SFRM specimens.

To compare the results from the current test method, one of the ¾ in. plates with bare steel was also subjected to an ASTM E 736 type test with round screw cap bonded to the top surface. First, a screw-cap test was conducted at the center of the plate, and then three strips were cut as shown in top photo of Fig. 7-25. Another screw cap test was conducted on the right side of the plate, as shown in the bottom photo of Fig. 7-25. Finally, two tests with the current procedure were done on the strip on the left side of the plate. In the bottom photograph it is seen that the screw-cap pulled away in the bulk material near the top surface.

Source: NIST.

Figure 7–25. Comparative testing: current method versus ASTM E 736 method: (top) locations of two screw cap tests; (bottom) after completion of tests.

Table 7-7 shows the individual cohesive strengths normal to the surface, and Fig. 7-26 is a plot of the data. Table 7-8 summarizes the average strength and variability of test results.

Table 7–7. Cohesive strength normal to surface for BLAZE-SHIELD DC/F specimens.

Nominal Thickness	Primer	Specimen	Cohesive Strength psf	Thickness	Primer	Specimen	Cohesive Strength psf
¾ in.	Yes	7-1	318	1½ in.	Yes	24-1	538
		7-2	324			24-2	709
		6-1	507			29-1	463
		6-2	381			29-2	592
		18-1	503			10-1	680
		18-2	416			10-2	834
		16-1	401			30-1	458
		16-2	548			30-2	403
		2-1	340			11-1	755
		2-2	595			11-2	667
	No	4-1	412		No	1-1	464
		4-2	373			1-2	574
		5-1	349			2-1a	372
		5-2	366			2-2a	354
		6-1	373			2-1b	661
		6-2	264			2-2b	740
		7-1	372			3-1a	700
		7-2	430			3-2a	530
		7-3	419 [a]			3-2a	836
		7-4	369 [a]			3-2b	722

a. Using screw cap in accordance with ASTM E 736.

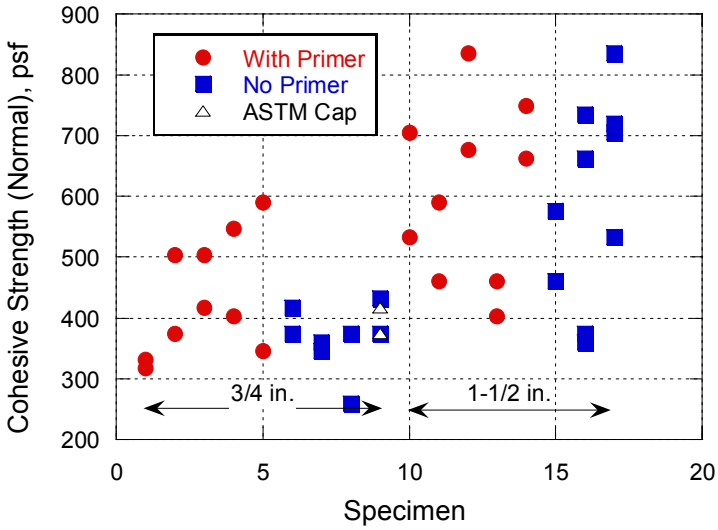

Figure 7–26. Cohesive strength normal to surface for BLAZE-SHIELD DC/F specimens for primed and unprimed steel plates.

Table 7–8. Summary of cohesive strengths normal to surface.

Nominal Thickness	Primer	Average, psf	Standard Deviation, psf	Coefficient of Variation, percent
¾ in.	Yes	433	99	23
	No	367	79	13
1½ in.	Yes	610	142	23
	No	595	163	27

Analysis of the results indicated that there was no statistically significant effect due to the presence or absence of primer. This is logical, because the condition of the steel surface is not expected to influence the properties of the bulk SFRM. There was a statistically significant difference in the average strengths for the two thicknesses, with the 1½ in. SFRM having higher strength. This difference is likely related to the observed difference in density.

Examination of Fig. 7-26, shows that the two results using the screw caps resulted in values similar to those obtained with the current test method. This agrees with the view that the ASTM E 736 procedure probably provides a measure of cohesive strength.

7.3.5 Adhesive Strength Versus Cohesive Strength Normal to Surface

A comparison was made of the adhesive strength and cohesive strength normal to the surface. The individual results previously shown in Fig. 7-23 and Fig. 7-26 are shown as “dotplots” in Fig. 7-27, and the average values from Tables 7-6 and 7-8 are shown in Table 7-9. In Fig. 7-27, the circles indicate results with bare steel plates, and the blue points (darker shade) indicate adhesive strength. For the specimens with primed steel, the average cohesive strength was much greater than the average adhesive strength. For the specimens made with bare steel the difference between the averages for the two types of strength was much smaller. Because of the high variability in individual test results, a formal analysis of variance indicates that there is an 8 percent probability that the difference could be the result of randomness. Generally, if this probability is greater than 5 percent, it can be concluded that the difference is not statistically significant. Thus, for the case of good adhesion, the test results do not contradict the assumption that the adhesive strength and cohesive strength normal to the surface are equal. If this assumption is accepted, the average of the adhesive and cohesive strengths is 409 psf for the ¾ in. SFRM, and the average is 622 psf for the 1½ in. SFRM.

From the measured strength properties, estimates were made of the local accelerations required to damage or dislodge the SFRM, as described in Section 7.4.

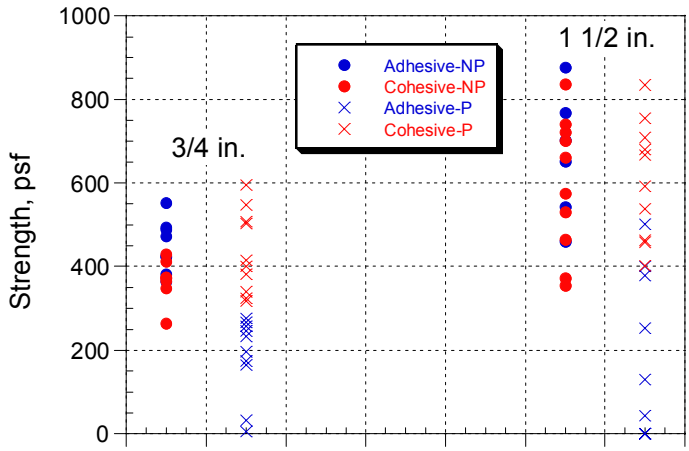

Figure 7–27. Comparison of adhesive strength with cohesive strength normal to surface (P = primed steel, NP = bare steel).

Table 7–9. Comparison of average adhesive strength and average cohesive strength normal to surface.

Primer	Nominal Thickness, in.	Average Adhesive Strength, psf	Standard Deviation, psf	Average Cohesive Strength, psf	Standard Deviation, psf
Yes	¾ in.	185	96	433	99
	1½ in.	171	196	610	142
No	¾ in.	450	63	367	79
	1½ in.	666	151	595	163

7.4 SIMPLIFIED APPROACH TO PREDICT DISLODGING OF SFRM

This section presents a simplified approach for estimating the acceleration required to dislodge SFRM from a structural element. When a member is subjected to an impact, it will undergo various modes of vibration. The vibrations result in local cyclic accelerations. These accelerations are transferred to the SFRM by forces applied at the interface between the steel and the SFRM. Two limiting cases are considered:

- Case 1 is a planar element with SFRM applied to one face of the element. This would be representative of SFRM applied to large webs and flanges of beams and columns. In this case, adhesive strength or cohesive strength normal to the surface would be the controlling SFRM properties.

- Case 2 is a slender bar encased with SFRM. This would be representative of SFRM applied to elements of the floor trusses. In this case, in-plane tensile strength and bond strength are the controlling SFRM properties.

CASE 1: Planar Element

The simplified model considers the substrate and SFRM as rigid bodies. The SFRM would dislodge when the inertial force exceeds the smaller of the adhesive bond strength or cohesive strength normal to the surface. Figure 7-28, shows the free body of the thermal insulation being acted upon by its inertial force and the adhesive force. The acceleration to dislodge the SFRM from the substrate is:

$$a = \frac{f_b}{\rho\, t} \tag{2}$$

where:

f_b = cohesive strength normal to surface or adhesive strength, whichever is smaller

t = thickness of SFRM

ρ = mass density of SFRM.

This equation shows that the acceleration to dislodge the SFRM from a planar surface is directly proportional to the smaller of adhesive or cohesive strength (normal to surface) and inversely proportional to the thickness and density.

To arrive at the ranges of accelerations that could be expected to dislodge SFRM from a planar surface, the following plausible ranges of values were assumed:

- SFRM thickness: 0.75 in. and 2.25 in.;
- SFRM density: 15 pcf and 25 pcf[21];
- SFRM bond strength: 100 psf and 500 psf

Table 7-10 shows the resulting accelerations expressed as a multiple of *g*, which is the gravitational acceleration. For the combination of low thickness, low density, and high bond strength, the required acceleration is about 530 *g*. For the other extreme combination of high thickness, high density, and low strength, the required acceleration is about 20 g. This simplified model, thus, gives an approximate range of the amplitude of accelerations required to dislodge the SFRM from a planar surface, depending on the actual values of the key parameters. For example, using the average values of in-place measurements for BLAZE-SHIELD II summarized in Section 7.1, for SFRM with a thickness of 2.5 in., a density of 19 pcf, and an adhesive strength of 300 psf, the SFRM would dislodge from a planar surface at an acceleration of about 80 *g*.

[21] These numbers need to be converted to units of mass by dividing by the gravitational acceleration.

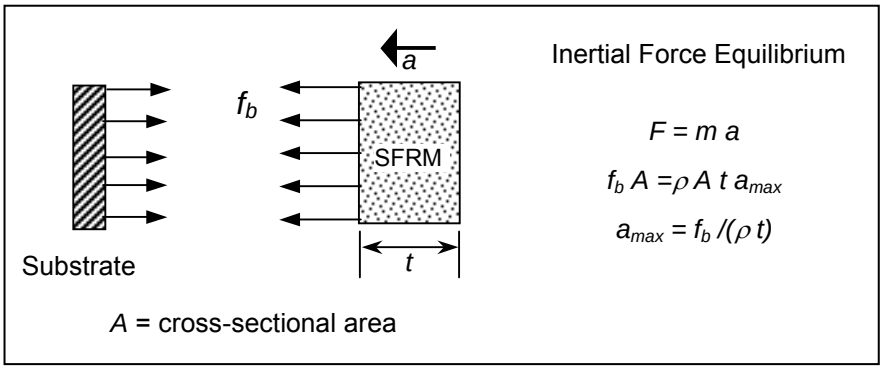

Figure 7–28. Derivation of acceleration to dislodge SFRM from planar substrate.

Table 7–10. Acceleration required to dislodge SFRM from planar surface for different values of density, thickness, and bond strength (adhesive or cohesive).

Density, pcf	Bond Strength, psf	Thickness, in.	Acceleration/g
15	100	0.75	107
15	100	2.25	32
15	500	0.75	533
15	500	2.25	160
25	100	0.75	64
25	100	2.25	19
25	500	0.75	320
25	500	2.25	96
19	300	2.5	76

Case 2: Encased Bar

The second case is representative of slender elements that would be surrounded by SFRM, such as the chords and diagonals of the floor trusses. In this case, adhesive strength is of minor importance, and the in-plane cohesive strength is of major importance. Figure 7–29 shows the derivation for the relationship between material strengths and acceleration to dislodge the SFRM from a round bar. The required acceleration is as follows:

$$a = \frac{4 f_t (d_0 + (\alpha - 1) d_i)}{(d_0^2 - d_i^2)\rho\pi} \tag{3}$$

where:

f_t = in-plane cohesive strength of SFRM

d_0 = outside diameter of SFRM

d_i = steel bar diameter

α = ratio of adhesive strength to in-plane cohesive strength of SFRM

ρ = density of SFRM

Inertial Force Equilibrium

$$\text{Mass} = m = \pi \frac{(d_o^2 - d_i^2)}{4} \rho$$

$$F = f_t(d_o - d_i) + f_b d_i$$

$$\text{Let} \quad f_b = \alpha \ f_t$$

$$F = f_t(d_o + (\alpha - 1)d_i) = \pi \frac{(d_o^2 - d_i^2)}{4} \rho \ a$$

$$a = \frac{4 f_t (d_o + (\alpha - 1)d_i)}{(d_o^2 - d_i^2)\rho\pi}$$

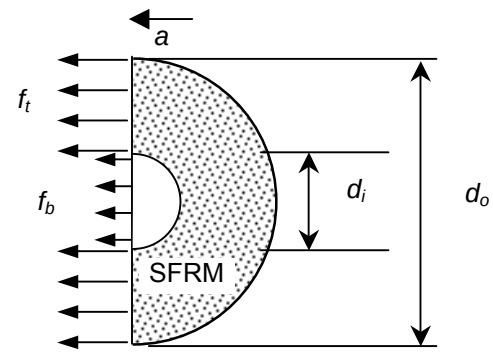

Figure 7–29. Derivation of acceleration to dislodge SFRM surrounding a round bar.

To arrive at the ranges of accelerations that could be expected to dislodge SFRM from a round bar, the following ranges of values were assumed:

- Bar diameter: 0.9 in. and 1.2 in;
- Thickness [$(d_0 - d_i)/2$]: 0.75 in and 2.5 in.;
- Density: 15 pcf and 25 pcf;
- In-plane cohesive strength: 500 psf and 2000 psf; and
- Strength ratio (α): 0 and 0.3.

Table 7-11 shows the results of using these limiting values in Eq. (3). The smallest required acceleration is about 40*g*, which corresponds to a large bar having a thick layer of the higher density SFRM with low strength. At the other extreme, the required acceleration is about 730*g*. For a 1.2 in. diameter bar with 2.5 in. thickness of SFRM and density of 19 pcf, the acceleration required to dislodge the SFRM would vary from 55*g* to 230*g*, depending on the strength characteristics within the assumed ranges given above.

These simplified models are intended to provide insight into the important variables that affect the magnitude of the disturbance (that is, acceleration) required to dislodge SFRM from different kinds of structural members. These models do not consider the fact that the applied acceleration in an actual structure subjected to impact would vary with time. Also, these models apply to members not directly impacted by debris. As discussed in NIST NCSTAR 1-3C, there was photographic evidence to suggest that thermal insulation was dislodged from exterior columns in regions not likely to have been impacted directly by debris.

Table 7–11. Acceleration required to dislodge SFRM from encased bar for different values of bar diameter, SFRM thickness, SFRM in-plane cohesive strength, and strength ratio (alpha).

Bar Diameter, in	Outer Diameter, in.	Density, pcf	Cohesive Strength, psf	Alpha	Acceleration/g
0.9	2.4	15	500	0	154
				0.3	182
			2000	0	617
				0.3	728
		25	500	0	93
				0.3	109
			2000	0	370
				0.3	437
	5.9	15	500	0	75
				0.3	79
			2000	0	300
				0.3	316
		25	500	0	45
				0.3	47
			2000	0	186
				0.3	189
1.2	2.7	15	500	0	131
				0.3	162
			2000	0	522
				0.3	648
		25	500	0	78
				0.3	97
			2000	0	313
				0.3	389
	6.2	15	500	0	69
				0.3	74
			2000	0	275
				0.3	295
		25	500	0	41
				0.3	44
			2000	0	165
				0.3	177

7.4.1 Debris Impact Study

A series of simulated debris impact tests were conducted using steel plates and bars covered with BLAZE-SHIELD DC/F. The experimental techniques and results are summarized in Appendix C.

This page intentionally left blank.

Chapter 8
SUMMARY

This report focused on the passive fire protection used in the WTC towers. Specifically, it sought to establish the likely characteristic of the sprayed fire-resistive materials (SFRMs) applied to the structural system. This information was required for calculating the thermal histories of structural members in a conventional building fire and during the fires after the aircraft impact.

To provide context, a brief review of code provisions related to structural fire protection was provided. An effort was made to document key decisions and actions related to passive fire protection during the design, construction, and subsequent occupancy of the towers. Copies of documents that support the findings are provided in Appendix A.

The NIST investigation sought available information on the in-place condition of the SFRM in the WTC towers. Some information was provided by the Port Authority in the form of thickness, density, and bond strength measurements on floor trusses taken at various times during the 1990s. Additional information was obtained from photographs of floor trusses provided to NIST. Analyses of the data indicated that fire-resistive material thickness was variable, as would be expected for application to floor truss members with small cross sections.

Results of simplified finite-element simulations of heat transfer under fire conditions showed that variability in thickness of SFRM reduced the effectiveness of the insulation so that protection was less than implied by the average thickness of the SFRM. A procedure was developed for estimating the equivalent uniform thickness of the variable thickness SFRM.

Tests were done on samples of SFRMs to establish the temperature dependencies of key thermophysical properties that were needed for calculating the thermal-structural response of the towers.

Tests were also done to establish basic tensile strength properties of SFRM, which are necessary to estimate the extent of dislodgement due to aircraft impact. Photographic evidence, documented in another phase of the investigations (see NIST NCSTAR 1-3C), suggested that thermal insulation was dislodged from visible portions of the exterior columns of WTC 1 and WTC 2 that were not impacted directly by debris.

8.1 FINDINGS

The following are the key findings based on the information discussed in this report.

- The reviewed documents appear to indicate that the initial design of the towers was based on the 1938 New York City Building Code and predicated on a Class 1A classification, which required a 4 h fire rating for columns and 3 h for the floor system. The WTC towers were classified subsequently as Class 1B, as defined by the 1968 New York City Building Code. This required a 3 h fire rating for columns and 2 h for the floor system. A condition assessment conducted in

2000 reported that the WTC towers were classified as Class-1B—noncombustible, fire-protected, retrofitted with sprinklers in accordance with Local Law 5/1973.

- The use of sprayed fire protection for floor trusses was innovative at the time of the design of the WTC and not consistent with prevailing practice, which used enclosures of fire-resistive materials to surround the floor trusses. Trial applications were performed to demonstrate that is was feasible and practicable to use this fire protection method for the composite floor truss system. Correspondence revealed that adhesion problems were encountered during application of the SFRM to the exterior columns.

- The 1968 New York City Building Code required testing of assemblies to establish that their fire rating conformed to Code requirements. The manufacturer of the floor trusses, the Architect of Record, and the Structural Engineer of Record recognized the need for such fire endurance testing of the composite floor system. There were no records of a fire endurance test of the WTC floor system.

- Fire protection of the exterior columns was the responsibility of Alcoa, which sub-contracted the work to Mario & Di Bono Plastering Co. (Mario & Di Bono) The sprayed fire protection of the floor trusses and core members was performed under a separate contract awarded to Mario & Di Bono. The project specifications for sprayed fire protection of the interior portions of the towers did not specify the type of material or thickness to be applied. Correspondence in 1969, from the construction manager to Mario & Di Bono, stated (see Appendix A Fig. A-23) that those portions of the floor system requiring thermal protection were "to have a ½ in. covering of 'Cafco.'" The product known as "Cafco" was BLAZE-SHIELD Type D supplied by U. S. Mineral Products Co., and was composed of asbestos fibers with a portland cement binder. No evidence was available to provide the technical basis for the value of ½ in. thickness indicated in the correspondence. Correspondence indicated that economics was an important factor in the Port Authority's decisions related to passive fire protection.

- Because of the asbestos fibers, the use of BLAZE-SHIELD Type D, was discontinued in 1970 at the 38th floor of WTC 1. The existing thermal insulation was encapsulated with a coating to contain the asbestos fibers. BLAZE-SHIELD Type DC/F was used as its replacement. This material contained mineral fibers instead of asbestos. Tests conducted by Underwriters Laboratories in 1970 indicated that BLAZE-SHIELD Type DC/F was at least as good as BLAZE-SHIELD Type D in terms of fire resistance."

- In 1975, the Structural Engineer of Record reported that in March of 1975 he was made aware of a fire endurance test of a floor assembly consisting of composite floor trusses with a normal weight concrete slab on a corrugated steel deck. The trusses were protected with "Mono-Kote," which was described as a "cementitious spray-applied fireproofing" (see Appendix A Fig. A-45). The members of the trusses were coated with 1½ in. of the insulation and the sheet metal deck had ½ in. The results of the fire endurance test assigned a 3 h rating to the floor system. It is noted that this test was not related in any way to the floor system in the WTC towers. The Structural Engineer of Record used this test result "with many simplifying assumptions" to demonstrate that ½ in. of BLAZE-SHIELD would provide the same 3 h rating when applied to 1 in. web bars (see Appendix A Fig. A-46). The calculations were said to be based on the differences in the room temperature thermal conductivity of the two insulation materials, with the

Mono-Kote product having about twice the thermal conductivity of the BLAZE-SHIELD product. He noted: "however, that theoretical extrapolations of fire endurance tests must the viewed with caution." He stated further that: "Without benefit of a full-scale fire test we cannot establish a rating for the floor assembly."

- In 1975, the Structural Engineer of Record reported that certain elements of the floor system did not require fire protection because those elements were not critical in supporting gravity loads. These included the bridging trusses and the top chords in the one-way portion of the floor system.

- Based on data provided by the Port Authority of insulation thickness on 16 trusses on each of floors 23 and 24 of WTC 1, the average thickness of the original thermal insulation on the floor trusses was estimated to be 0.75 in. with a standard deviation of 0.3 in. (coefficient of variation = 0.40). The reported average thicknesses ranged from 0.52 in. to 1.17 in.

- In 1995, the Port Authority performed a study to establish the thickness of fire protection to be applied to the floor trusses during major tenant renovations. On the basis of Design G805 listed in the UL *Fire Resistance Directory*, the thickness to achieve a 2 h fire rating was estimated to be 1½ in. At the time of the WTC disaster, fire protection had been upgraded on floors affected by the aircraft impact. According to information provided by the Port Authority, upgrading had occurred on floors 92 through 100 and 102 of WTC 1 and on floors 77, 78, 88, 89, 92, 96 and 97 of WTC 2.

- Based on analyses of insulation thickness data contained in Construction Audit Reports provided by the Port Authority, the average thickness of the upgraded thermal insulation (BLAZE-SHEILD II) on the floor trusses was estimated to be 2.5 in. with a standard deviation of 0.6 in. (coefficient of variation = 0.24). The reported average thicknesses ranged from 1.7 in. to 4.3 in.

- Based on finite element simulations of a 1 in. round bar covered with SFRM having lognormal distributions for thickness that were consistent with the average values and standard deviations noted above, it was concluded that the original thermal protection on the floor trusses was equivalent to a uniform thickness of 0.6 in. and that the upgraded insulation was equivalent to a uniform thickness of 2.2 in.

- No information is available on in-place conditions of the thermal protection on the exterior columns and spandrel beams, and little information is available on the conditions of fire-resistive material on core beams and columns. For thermal analyses of the towers, the thermal protection on these elements was taken to have uniform thicknesses equal to the specified values. This assumption is justified by the offsetting factors of measured average thicknesses tending to be greater than specified thicknesses and the reduced effectiveness of a given average thickness of SFRM due to thickness variability. These were ½ in. for beams and spandrels, 2 1/16 in. for columns lighter than 14WF228, and 1 3/16 in. for columns heavier than 14WF228.

- Data provided by the Port Authority on the thickness and density of the upgraded thermal insulation for floor trusses indicated that the average thicknesses exceeded the design thickness of 1½ in. and the bond strength measured according to ASTM E 736 exceeded 150 psf, which was stated to be the "standard performance" of BLAZE-SHIELD II.

- Results of NIST tests indicated that the thermal conductivity of SFRMs increased significantly at higher temperatures.

- Results of NIST tests indicated that the presence of primer paint caused significant reductions in the adhesive strength of BLAZE-SHIELD DC/F. Good adhesion was found with bare steel, in which case there was not a statistically significant difference between adhesive strength and cohesive strength normal to the surface.

- Results of NIST tests indicated that the in-plane cohesive strength of BLAZE-SHIELD DC/F was almost three times the cohesive strength normal to the surface.

- The density of BLAZE-SHIELD DC/F in the NIST tests for strength properties was greater than the densities in the Port Authority reports or in the manufacturer's catalogs. This may have accounted for the higher strength values obtained by NIST compared with the manufacturer's published values.

- Based on simplified models, the acceleration required to dislodge SFRM from planar surfaces might range from 20 *g* to 530 *g*, depending on the in-place density, thickness, and bond strength. For density of 19 pcf, thickness of 2.5 in., and bond strength of 300 psf, which are representative of the upgraded insulation on the floor trusses, an acceleration of about 40 *g* would dislodge the SFRM from a planar surface. For a round bar encased in SFRM, the estimates are 40 *g* to 730 *g*, depending on the bar diameter, insulation thickness, in-plane cohesive strength, and adhesive strength. For a 1.2 in. diameter bar, with 2.5 in. thickness of insulation, having a density of 19 pcf, the acceleration required to dislodge the SFRM was estimated to be between 55 *g* and 230 *g*, depending on the strength characteristics of the SFRM. These models provide insight into the factors that affect SFRM dislodgment due impact-induced vibration.

Chapter 9
REFERENCES

ASTM 1961. Standard Test Methods for Fire Tests of Building Construction and Materials. ASTM E 119-61, ASTM International, West Conshohocken, PA.

ASTM 1973. Standard Test Methods for Fire Tests of Building Construction and Materials, ASTM E 119-73. ASTM International, West Conshohocken, PA.

ASTM 1992. Standard Test Method for Cohesion/Adhesion of Sprayed Fire Resistance Materials Applied to Structural Members, ASTM E 736-92, ASTM International, West Conshohocken, PA.

ASTM 1993. Standard Test Methods for Thickness and Density of Sprayed Fire-Resistive Material (SFRM) Applied to Structural Members, ASTM E 605-93. ASTM International, West Conshohocken, PA.

ASTM 1995. Standard Test Method for Linear Thermal Expansion of Solid Materials With a Vitreous Silica Dilatometer, ASTM E 228-95, ASTM International, West Conshohocken, PA.

ASTM 1998. Standard Test Method for Compositional Analysis by Thermogravimetry, ASTM E 1131-98, ASTM International, West Conshohocken, PA.

ASTM 1999. Standard Test Method for Thermal Conductivity of Refractories by Hot Wire (Platinum Resistance Thermometer Technique), ASTM C 1113-99. ASTM International, West Conshohocken, PA.

ASTM 2000a. Standard Test Method for Thickness and Density of Sprayed Fire-Resistive Material (SFRM) Applied to Structural Members, ASTM E 605-93 (Reapproved 2000), ASTM International, West Conshohocken, PA.

ASTM 2000b. Standard Test Method for Cohesion/Adhesion of Sprayed Fire-Resistive Materials Applied to Structural Members, ASTM E 736-00, ASTM International, West Conshohocken, PA.

ASTM 2000c. Standard Test Method for Effect of Deflection on Sprayed Fire-Resistive Material Applied to Structural Members, ASTM E 759-92 (Reapproved 2000), ASTM International, West Conshohocken, PA.

ASTM 2000d. Standard Test Method for Effect of Impact on Bonding of Sprayed Fire-Resistive Material Applied to Structural Members, ASTM E 760-92 (Reapproved 2000), ASTM International, West Conshohocken, PA.

ASTM 2000e. Standard Test Method for Compressive Strength of Sprayed Fire-Resistive Material Applied to Structural Members, ASTM E 761-92 (Reapproved 2000), ASTM International, West Conshohocken, PA.

ASTM 2000f. Standard Test Method for Air Erosion of Sprayed Fire-Resistive Materials (SFRMs) Applied to Structural Members, ASTM E 859-93 (Reapproved 2000), ASTM International, West Conshohocken, PA.

ASTM 2000g. Standard Test Method for Corrosion of Steel by Sprayed Fire-Resistive Material (SFRM) Applied to Structural Members, ASTM E 937-93 (Reapproved 2000), ASTM International, West Conshohocken, PA.

ASTM 2000h. Standard Test Method for Determination of Thermal Conductivity of Soil and Soft Rock by Thermal Needle Probe Procedure, ASTM D 5334-00, ASTM International, West Conshohocken, PA.

ASTM 2001. Standard Test Method for Determining Specific Heat Capacity by Differential Scanning Calorimetry, ASTM E 1269-01, ASTM International, West Conshohocken, PA.

ASTM 2004a. Standard Test Method for Behavior of Materials in a Vertical Tube Furnace at 750 °C, ASTM E 136-04. ASTM International, West Conshohocken, PA.

ASTM 2004b. Standard Test Method for Tensile Strength of Concrete Surfaces and the Bond Strength or Tensile Strength of Concrete Repair and Overlay Materials by Direct Tension (Pull-off Method), ASTM C 1583-04. ASTM International, West Conshohocken, PA.

Blondeau P., A. L. Tiffonnet, A. Damian, O. Amiri, and J. L. Molina. 2003. Assessment of contaminant diffusivities in building materials from porosimetry tests. *Indoor Air*, 13, 302-310.

Buchanan, A. H. 2001, *Structural Design for Fire Safety*, John Wiley & Sons Ltd. West Sussex, England.

Bukowski, R. W. 2003. Prediction of the structural fire performance of buildings, Proceedings, Fire and Materials 2003, 8th International conference, Jan 27-28, 2003, San Francisco, CA Interscience Communications Limited, 8 pp. http://fire.nist.gov/bfrlpubs/fire03/art028.html

Bukowski, R.W. 1997. Progress toward a performance-based code system for the United States, Proc FORUM Symposium on Fire Safety Engineering, Tianjin China, 6-7 October 1997.

Gewain, R.G., Iwankiw, N.R. and Alfawakhiri, F., *Facts for Steel Buildings—Fire*, American Institute of Steel Construction, Chicago, IL, October 2003. 51 pp.

Harmathy, T. Z. 1983. *Properties of Building Materials at Elevated Temperatures*. DBR Paper No. 1080. National Research Council of Canada, Division of Building Research. Ottawa, March.

ICBO 2001. ES Report ER-1244, June 1, 2002, ICBO Evaluation Services, Inc., Whittier, CA.

ICC. 2003. *International Building Code 2003*. International Code Council, Alexandria, VA.

Mehaffey J. R., P. Cuerrier, and G. Carisse. 1994. A Model for Predicting Heat Transfer through Gypsum-Board/Wood-Stud Walls Exposed to Fire. *Fire and Materials*, 18, 297-305.

Melchers, R. E., 1999. *Structural Reliability Analysis and Prediction*. John Wiley & Sons, New York, NY.

Messersmith, J. J. 2002. Unwarranted relaxation. *Concrete Products*, September 1, 2002. http://concreteproducts.com/issue_20020901/

Miller, I. and Freund, J. E., 1965. *Probability and Statistics for Engineers*, Prentice-Hall, Inc., Englewood Cliffs, NJ.

NFPA 5000. 2003. *Building Construction and Safety Code, NFPA 5000*. National Fire Protection Assn., Quincy, MA.

NFPA.220, 1999. *Types of Building Construction*, NFPA 220(99), National Fire Protection Assn., Quincy, MA.

NYCBC 1961-1962. Administrative Building Code of the City of New York.

NYCBC 1968. Building Code—Local Law No. 76 of the City of New York. New York, NY.

NYCBC 2001. Building Code of the City of New York, 2001 Edition. Gould Publications, Binghamton, NY.

NYCLL5/73 1973. Local Laws of the City of New York for the year 1973, No.5. New York City Council, December 22, 1972. www.nyc.gov/html/dob/downloads/pdf/ll_0573.pdf

Powers, W. R. 1975. *One World Trade Center Fire*. Report of The New York Board of Fire Underwriters, New York, NY.

Stephenson, M. E., Jr., and M. Mark. 1961. Thermal Conductivity of Porous Materials. *ASHRAE Journal*, 3, 75-81.

UL 2002, "Design No. G805," *Fire Resistance Directory, Volume 1*, Underwriters Laboratories, Inc., pp.287-288.

This page intentionally left blank.

Appendix A
REFERENCED DOCUMENTS

R40-1

6211 - A1

A. SCHREIER

RECEIVED

THE PORT OF NEW YORK AUTHORITY

111 Eighth Avenue at 15th Street New York 11 NY

ALGONQUIN 5-1000

WORLD TRADE CENTER

Malcolm P. Levy
CHIEF, PLANNING DIVISION

Richard C. Sullivan
DIRECTOR

May 13, 1963

Mr. Minoru Yamasaki
Minoru Yamasaki & Associates
1025 East Maple Road
Birmingham, Michigan

Dear Yama:

At a recent meeting with Mr. John Kyle, Chief Engineer, the subject of New York City Code compliance was further amended as follows:

"All consulting engineers and architects working on the World Trade Center have been instructed to comply with the Code in preparing their designs. Questions have arisen, however, in areas where the Code is not explicit. It was agreed that in such cases and where techno-

Figure A–1. Port Authority letter instructing consultants to follow New York City Building Code (3-P).

6211
R 110-4

THE PORT OF NEW YORK AUTHORITY

111 Eighth Avenue at 15th Street New York NY 10011

620-8233

WORLD TRADE CENTER

Malcolm P. Levy
CHIEF, PLANNING DIVISION

Richard C. Sullivan
DIRECTOR

September 29, 1965

Mr. Minoru Yamasaki
Minoru Yamasaki & Associates
1025 East Maple Road
Birmingham, Michigan 48011

Dear Yama:

We have decided to adopt the new Building Code presently existing in second and third draft form for The World Trade Center.

The Roth office is requested to revise floor plans as quickly as possible and on an accelerated basis to comply with the provisions of this code. It is my understanding that the present drawings have been prepared to permit rapid conversion to the new code. Generally the tower core should be redesigned to eliminate the fire towers and to take advantage of the more lenient provisions regarding exit stairs. No other major change to the core should be undertaken without review by this office.

The structural consultants are instructed, by copy of this letter, to revise structural design in accordance with the more realistic criteria for partition weight allowance. The majority of interior partitions, as noted in a previous letter, will consist of reinforced gypsum plank.

The Roth office is requested to provide me with the dates on which we can expect revised floor plans and also to indicate any changes in design schedule caused by these instructions.

Sincerely,

Malcolm P. Levy

cc: R. Baum (JBB), J. Loring (JRLA), J. Roth (ERS), J. Skilling and L. Robertson (WSHJ)

Similar letter sent to Mr. Julian Roth (ERS)

Figure A–2. Port Authority letter instructing consultant to follow New York City Building Code under development (3-P).[22]

[22] Designation in parentheses refers to NIST catalog number for document or group of documents.

MEMORANDUM OF UNDERSTANDING BETWEEN THE NEW YORK CITY DEPARTMENT OF BUILDINGS AND THE PORT AUTHORITY OF NEW YORK AND NEW JERSEY

This Memorandum shall govern the relationship between the New York City Department of Buildings (the "Department") and the Port Authority of New York and New Jersey (the "Port Authority"), both parties entering into this agreement with the intention to establish procedures to be followed by the Port Authority for any building construction project ("Project"), to be undertaken by the Port Authority or any of its tenants at buildings owned or operated by the Port Authority and located in the City of New York (the "City), to assure conformance of Projects at such buildings with the standards set forth in the New York City Building Code (the "Code").

While the facilities of the Port Authority, an agency of the States of New York and New Jersey, are not technically subject to the requirements of local building codes, the long-standing policy of the Port Authority has been to assure that its facilities meet and, where appropriate, exceed Code requirements.

The purpose of this Memorandum is not only to restate that long-standing policy as part of an understanding with the City but to provide specific commitments to the Department, as the agency of the City responsible for assuring compliance with the Code, regarding procedures to be undertaken by the Port Authority for any Project at its facilities in the City to assure that the buildings owned or operated by the Port Authority within the City are in conformance with the Building Standards contained in the Code.

Accordingly, the Department and the Port Authority hereby agree as follows:

1. Port Authority Review. To assure conformance with the building standards set forth in the Code at the time of the design and construction of any Project, the Port Authority shall, in the case of each Project, thoroughly review and examine all plans in connection with such Project for conformance with the building standards set forth in the Code. Plans prepared for Projects to be undertaken by Port Authority tenants shall be prepared and sealed by a New York State licensed professional engineer or architect retained or employed by tenant; plans prepared for Projects to be undertaken by the Port Authority shall be prepared by a New York State licensed professional

Figure A–3. 1993 Memorandum of Understanding between Port Authority and New York City Department of Buildings (113-P).

prepared drawings, plans and any other documents required in connection with the review of the Project from the standpoint of Code conformance. In the case of any Project being effectuated by a tenant of the Port Authority (a "Tenant Project") such file shall also include the Tenant Alteration Application prepared by the Tenant. In the case of any project administered by a line department of the Port Authority, such file shall include any construction application prepared in connection with such Project. The Line Departments of the Port Authority are currently its World Trade, Aviation, Interstate Transportation, Port, and Regional Development Departments.

3. Project Certification. For each Tenant Project, the Port Authority shall require the Tenant to obtain the certification of a New York State licensed architect or engineer that such Project was constructed in accordance with the approved plans and specifications for such Project. For any Project effectuated by the Port Authority, the Chief Engineer or his successor in duties shall certify that the Project was constructed in accordance with the approved plans and specifications for the Project. Certifications for each Project shall be maintained in the Project File.

4. Copies of Project File. The Department may at any time request the Port Authority to provide it with a copy of any Project File and the Port Authority shall promptly provide a copy of the Project File to it.

5. Variances. The Port Authority shall promptly advise the Department of any Project approved by the Chief Engineer of the Port Authority which involves, in the judgment of the Chief Engineer of the Port Authority or his successor in duties, a variance from the clear requirements of the Code. In the event that the Department disagrees with the manner in which questions of Code conformance have been or are proposed to be dealt with in connection with such Project, it may so advise the Authority. The Port Authority shall seek expeditiously to resolve the matter. Any matter of Code conformance in connection with such Project which the Department believes involves an unacceptable variance from the requirements of the Code shall be subject to the further review of the Port Authority Board of Commissioners. The Commissioners shall be advised of the Department's views on the matter.

6. Inspections and Surveys. The Port Authority shall continue to conduct or cause to be conducted all building inspections, during both construction and post-construction periods, required under the Code. In addition, the Port Authority will continue to perform structural integrity inspections on a cyclical basis for all of its structures located in the City.

7. Port Authority Responsibility. As indicated above, the purpose of this Agreement is to set forth certain basic understandings between the Department and the Port Authority. It is understood, however, that the Port Authority with its tenants shall continue to bear the responsibility for life safety in buildings at its facilities and nothing in this Agreement is intended to impose any obligations of inspection or review on the Department. The Department shall refer back to the Chief Engineer of the Port Authority any requests for

2

Figure A–3 (Contd.). 1993 Memorandum of Understanding between Port Authority and New York City Department of Buildings (113-P).

information or interpretation which it may receive from tenants of the Port Authority with respect to any Project.

8. No Personal Liability. No Commissioner, officer, agent or employee of the Port Authority or the Department shall be held personally liable under any provision of this Agreement or because of its execution or attempted execution or because of any breach or alleged breach thereof.

IN WITNESS WHEREOF, the parties hereto have caused this instrument to be signed, sealed and attested.

ATTEST:

THE PORT AUTHORITY OF NEW YORK AND NEW JERSEY

Figure A–3 (Contd.). 1993 Memorandum of Understanding between Port Authority and New York City Department of Buildings (113-P).

SUPPLEMENT TO MEMORANDUM OF UNDERSTANDING
BETWEEN THE NEW YORK CITY DEPARTMENT OF
BUILDINGS AND THE PORT AUTHORITY OF NEW
YORK AND NEW JERSEY

In November, 1993 the New York City Department of Buildings (the "Department") and the Port Authority of New York and New Jersey (the "Port Authority") entered into the attached Memorandum of Understanding (the "Memorandum") establishing certain procedures for the purpose of helping to assure conformance of construction projects to be undertaken at buildings owned or operated by the Port Authority in New York City with the standards set forth in the New York City Building Code.

Recently, the Department implemented its own optional plan review system providing for professional certifications of applications and plans and subsequent construction work falling under its jurisdiction.

The purpose of this Supplement to the Memorandum is to provide under the Memorandum for the adoption by the Port Authority of a procedure under which any Port Authority tenants at the World Trade Center may utilize New York State licensed architects or engineers to certify, in lieu of any review by the Port Authority, that (i) the tenant's construction plans are in conformance with the standards set forth in the New York City Building Code, and (ii) construction has been performed in accordance with such plans, it being understood that the persons making the certifications described in (i) and (ii) shall not be the same.

Accordingly, the Department and the Port Authority hereby agree that the Memorandum is amended as follows:

1. Professional Certification. Notwithstanding anything to the contrary in the Memorandum, the Port Authority may, in lieu of any reviews or certifications by the Port Authority provided for in the Memorandum, provide procedures pursuant to which its tenants at the World Trade Center may utilize New York State licensed architects or engineers meeting qualifications to be established by the Port Authority to (A) prepare and review such tenant's plans for the construction of any project and certify that such plans conform with the building standards set forth in the New York City Building Code and (B) certify that such project has been constructed in accordance with the approved plans and specifications for such project. The person or firm performing the review and certification described in (A) above shall not be the same person or firm providing the certification described in (B) above.

2. Other Provisions. Except as provided herein, all the terms and conditions of the Memorandum shall remain in full force and effect.

3. No Personal Liability. No Commissioner, officer, agent or employee of the Port Authority or the Department shall be held personally

Figure A–4. 1995 Supplement to Memorandum of Understanding between Port Authority and New York City Department of Buildings (113-P).

liable under any provision of this Supplement or because of its execution or attempted execution or because of any breach or alleged breach thereof.

IN WITNESS WHEREOF, the parties hereto have caused this instrument to be signed, sealed and attested.

ATTEST:

SECRETARY

DATE: 6/7/95

THE PORT AUTHORITY OF NEW YORK AND NEW JERSEY

By: Executive Director

WITNESS:

FRANK M. SCHWARTZ
Notary Public, State of New York
No. 41-4632586
Qualified in Queens County
Commission Expires Jan. 31, 1997

DATE: 6/1/95

THE NEW YORK CITY DEPARTMENT OF BUILDINGS

By: Commissioner

Figure A–4(Contd.). 1995 Supplement to Memorandum of Understanding between Port Authority and New York City Department of Buildings (113-P).

THE PORT AUTHORITY OF NY & NJ

One World Trade Center
New York, N.Y. 10048

William H. Goldstein
Deputy Executive Director/
Capital Programs
(212) 435-8415
(201) 961-6000 x8415

September 15, 1995

Honorable Joel A. Miele, Sr., Commissioner
Department of Buildings
City of New York
60 Hudson Street
New York, New York 10013

Dear Commissioner Miele:

Figure A–4 (Contd.). 1995 Supplement to Memorandum of Understanding between Port Authority and New York City Department of Buildings (113-P).

MEMORANDUM OF UNDERSTANDING BETWEEN THE FIRE DEPARTMENT
OF THE CITY OF NEW YORK AND THE PORT AUTHORITY OF NEW YORK AND NEW JERSEY
EXECUTED AS OF DECEMBER 30, 1993

On April 15, 1993, the Port Authority, in order to maintain and enhance the safety of Port Authority facilities, adopted a policy providing for the implementation of fire safety recommendations made by local government fire departments after a fire safety inspection of a Port Authority facility and for the prior review by local fire safety agencies of fire safety systems to be introduced or added to a facility.

The purpose of this Memorandum of Understanding is to reiterate the Port Authority's commitment to this policy and to set forth certain procedures to facilitate the implementation of this policy for buildings at Port Authority facilities located in New York City.

Specifically, the Fire Department of the City of New York ("FDNY") and the Port Authority hereby agree as follows:

1. FDNY, acting through its Bureau of Fire Prevention ("BFP"), shall have the right to conduct fire safety inspections at any Port Authority facility located in the City of New York. These inspections will generally be coordinated with the Port Authority's General Manager of Risk Management operations, but the BFP, at its option, may conduct inspections without prior notice to the Port Authority.

2. BFP will issue a letterhead report of its fire safety findings and recommendations for corrective action with respect to any deficiencies forming a part of such findings addressed to the Port Authority's General Manager of Risk Management operations. The Port Authority will promptly undertake the implementation of such findings (including undertaking corrective action with respect to any deficiencies) and shall notify BFP of

Figure A–5. 1993 Memorandum of Understanding between Port Authority and The Fire Department of New York City and 1995 amendment (160-P).

4. The Port Authority and BFP will seek to expeditiously resolve any issues arising out of matters covered by this Memorandum of Understanding.

5. Nothing in this Memorandum of Understanding is intended to limit or modify in any way any arrangements which the Port Authority currently has with local fire companies in New York City regarding either facility inspections or joint training exercises or any other matters.

6. The Port Authority shall continue to be exempt from all inspection and permit fees for FDNY inspections at its facilities.

7. No Commissioner, officer, agent or employee of the Port Authority or FDNY shall be held personally liable under any provision of this Memorandum or because of its execution or attempted execution or because of any breach or alleged breach thereof.

IN WITNESS WHEREOF, the parties hereto have caused this instrument to be signed and sealed by duly authorized officers thereof.

THE PORT AUTHORITY OF NEW YORK AND NEW JERSEY

By: Stanley Brezenoff
Stanley Brezenoff
Executive Director

FIRE DEPARTMENT - CITY OF NEW YORK

By: William M. Feehan
William M. Feehan
Fire Commissioner
City of New York

Figure A–5 (Contd.). 1993 Memorandum of Understanding between Port Authority and The Fire Department of New York City and 1995 amendment (160-P).

FIRST AMENDMENT TO MEMORANDUM OF UNDERSTANDING BETWEEN THE FIRE DEPARTMENT OF THE CITY OF NEW YORK AND THE PORT AUTHORITY OF NEW YORK AND NEW JERSEY EXECUTED AS OF DECEMBER 30, 1993

On December 30, 1993, the Port Authority of New York and New Jersey (the "Port Authority") and the Fire Department of the City of New York ("FDNY") entered into a Memorandum of Understanding ("MOU") with respect to certain matters relating to the implementation of the policy adopted by the Port Authority on April 15, 1993 regarding the maintenance and enhancement of fire safety at Port Authority facilities.

Under paragraph 3 of the MOU, the FDNY, acting through its Bureau of Fire Prevention ("BFP") was to receive copies of the drawings and specifications of proposed new or modified fire safety systems for BFP's review and approval. FDNY has requested, and the Port Authority is agreeable, to the following changes to paragraph 3 of the MOU. Accordingly, effective January 1, 1995, FDNY and the Port Authority agree that paragraph 3 of the MOU shall be amended to read as follows:

3. The Port Authority shall notify the BFP in writing prior to the introduction of a new fire safety system or the introduction of modifications to an existing fire safety system at any building located at a Port Authority facility in the City of New York.

a. Port Authority Review: To assure conformance with the standards set forth in local codes and regulations at the time of the design and construction of any new or modified fire safety system, the Port Authority shall, in the case of each system, thoroughly review and examine all plans in connection with such system for conformance with the standards set forth in all applicable local codes and regulations. Plans prepared for new or modified systems to be undertaken by Port Authority tenants shall be prepared and sealed by a New York State licensed professional engineer or architect retained or employed by tenant; plans prepared for new or modified systems to be undertaken by the Port Authority shall be prepared by a New York State licensed professional engineer or architect employed or retained by the Port Authority. The Port Authority's examination of plans shall be conducted by New York State licensed architects and engineers retained or employed by the Port Authority. The Port Authority engineer or architect approving the plans for any new or modified system from the standpoint of Code conformance shall be a New York State licensed architect or engineer who shall not have assisted in the actual preparation of such plans.

b. New and/or Modified Fire Safety System File: The Port Authority shall maintain a file for each new or modified system which file shall at all times contain the most recently prepared drawings, plans and any other documents required in connection with the review of the systems from the standpoint of Code conformance. In the case of any new or modified system being effectuated by a tenant of the Port Authority, such file shall also include the Tenant Alteration Application prepared by the tenant. In the case of any new or modified system administered by a line department of the Port Authority, such file shall include any application prepared in connection with such new or modified system. The Line Departments of the Port Authority are currently its World Trade, Aviation, Interstate Transportation, Port and Regional Development Departments.

Figure A–5 (Contd.). 1993 Memorandum of Understanding between Port Authority and The Fire Department of New York City and 1995 amendment (160-P).

c. Fire Safety System Certification: For each Tenant System, the Port Authority shall require the Tenant to obtain the certification of a New York State licensed architect or engineer that such system was constructed in accordance with the approved plans and specifications. For any system effectuated by the Port Authority, Risk Management shall certify that the system was constructed in accordance with the approved plans and specifications. Certifications for each System shall be maintained in the New and/or Modified Fire Safety System File.

d. Copies of New and/or Modified Fire Safety System File: The BFP may at any time request the Port Authority to provide it with a copy of any Fire Safety System File and the Port Authority shall promptly provide a copy of the File as requested. The BFP reserves the right to audit any new or modified fire safety system to assure conformance with the standards set forth in local codes and regulations.

e. Variance: The Port Authority policy is and will continue to be to assure that such new or modified fire safety systems are in conformance with the local codes and regulations. When circumstances or conditions are unusual, the Port Authority shall have the right to petition the BFP for a variance in specific cases.

IN WITNESS WHEREOF, the Port Authority and FDNY have caused this First Amendment to the MOU to be signed by duly authorized officers thereof.

THE PORT AUTHORITY OF NEW YORK AND NEW JERSEY

Dated: 2/2/95 By: _____
Stanley Brezenoff,
Executive Director

Approved As To Form: WMF

Approved As To Form: [illegible]

FIRE DEPARTMENT - CITY OF NEW YORK

Dated: 1/27/95 By: _____
Howard Safir
Fire Commissioner
City of New York

Figure A–5 (Contd.). 1993 Memorandum of Understanding between Port Authority and The Fire Department of New York City and 1995 amendment (160-P).

28

PORT OF NEW YORK AUTHORITY

World Trade Department

REFERENCE #3 TO MEMO OF 1-14-87.

May 14, 1969

Mr. Milton Gerstman
Tishman Realty & Construction Co., Inc.
30 Church Street - 11th Floor
New York, New York 10007

Re: THE WORLD TRADE CENTER - New York City Building Code

Dear Milt:

A comparison of the recently revised New York City Building Code effective December 6, 1968 and The World Trade Center Design Standards, with respect to tenant demising walls, leads to some interesting questions.

The Code seems to indicate that the demising walls between tenant spaces in the Towers could be non-combustible and not fire-rated if the Code were applicable.

Page 39 - C26 - 301.1

4B3 - CLASS 1B

The World Trade Center Towers would be classified as Occupancy Group "E" (Business) with a fire index of 2 hours.

Page 39 - C26 - 301.4 (B)

In Occupancy Group "E", tenants shall be separated from each other by construction meeting the fire resistance rating requirement for a "Fire Separation".

4B3

Page 53 - C26 - 504 (B)

The minimum requirement for a "Fire Separation" is that it be non-combustible.

4B3 BUT DOES NOT HAVE 1 HOUR

NOTE: ABOVE APPLIES TO BUSINESS OCCUPANCY ONLY.

TIS

TISHMAN
MAY 15 1969
CONSTRUCTION DEPT.

Figure A–6. Letter from Port Authority to Tishman Realty & Construction Co. regarding Occupancy Group for WTC towers (3-P).

29

Mr. M. Gerstman - 2 - May 14, 1969

If we apply these interpretations to the World Trade Center, there would be savings in construction costs with respect to the following items:

a. Ordinary non-combustible partitions could be used in lieu of the one-hour rated tenant demising walls.

b. Standard non-combustible ceiling system could be used in lieu of the one-hour rated acoustical tile ceiling.

c. The deletion of all insulating batt fire protection at all air handling lighting fixtures in ceilings as well as the deletion of damper equipped return air troffers. These are presently proposed for fixtures within 10'-0" of a demising partition.

We would appreciate your opinion as to whether it would be appropriate to make the changes to the design noted in paragraphs a, b and c. By copy of this letter, the office of Emery Roth & Sons is also requested to comment.

Sincerely,

Malcolm P. Levy

cc: Mr. Joseph Solomon (ER&S)

Figure A–6 (Contd.). Letter from Port Authority to Tishman Realty and Construction Co. regarding Occupancy Group for WTC towers (3-P).

PORT AUTHORITY OF NY & NJ
OFFICE OF DIRECTOR OF DESIGN
INFRASTRUCTURE

M E M O R A N D U M

TO: Robert J. Linn, Deputy Director for Physical Facilities, WTD
FROM: Lester S. Feld
DATE: January 15, 1987

RECEIVED
NOTED:
REFERRED TO:

SUBJECT: THE WORLD TRADE CENTER - TOWERS & PLAZA BUILDINGS FIRE RATING PER NYC BUILDING CODE REVISION EFFECTIVE 12-6-68.

REFERENCE:
(1) - Memo - M. Levy to File - dated 4-20-65
(2) - Letter - L. Robertson (WSHJ) to M. Levy - dated 4-26-65
(3) - Letter - M. Levy to M. Gerstman (TRCC) - dated 5-14-69
(4) - Office Memo - W. Bracco (TRCC) to J. Endler (TRCC) - dated 5-26-69
(5) - UL Fire Test Report from T. P. Feit - dated 7-26-69
(6) - Letter - A. F. Abbasi (UL) to T. P. Feit (Zonolite) - dated 3-26-70
(7) - Buckslip - V. Dovletian to D. Bais - dated 1-9-87
(8) - Page 4 - Item 1C of Issue A entitled "Office Space Design Guide"

COPY TO: D. Bais, J. Carlock, A. Cracchiolo, V. Dovletian, P. Martinez (ER&S) D. Montalbano, A. Preschle, J. Pugh (LERA), L. Robertson (LERA) A. Vaccaro - All w/Reference 1 - 8 attached.

COPY TO
AGC
IL
AN
VAD
HR
ENRG

1/28 Please brief me. Tony C.

1. On January 13, 1987 I contacted Richard Roth, Jr. (ER&S) regarding the subject fire ratings, normally established by the Architect. Mr. Roth referred me to Phil Martinez for the required information.

2. Phil's recollection (since ER&S had given all their WTC tracings to our Planning Division) was as follows:

A. The egress requirement and fire ratings used to design the WTC Towers & Plaza Buildings were in accordance with the provisions of the planned NYC Building Code revisions effective December 8, 1968. Normally fire ratings are not shown on the Architectural Working Drawings or in the General Notes. The fire ratings are given only on the application forms filed with the plans for NYC Building Department Approval. Since the Port Authority is not subject to the NYC Building Code Requirements, no plans or forms were filed.

B. For office buildings there is no economic advantage in using

Figure A–7. Port Authority memorandum indicating that WTC towers were classified as Class 1B Construction (3-P).

4. For your information and use I have also attached References #5 & #6 on the UL Test of floor construction showing a 3 hour rating. Please note that the UL Test is based on the use of 1½" thick Monokote Fireproofing on joists and ½" thick Monokote on steel deck. Actually - Cafco - Type "D" spray-on was used at the WTC on joists only, in lieu of Monokote. In addition, the UL Test used stone-concrete slab with a thickness of 2' 3/4" over top of corrugated deck, as compared to the 4" lightweight concrete slab used at the WTC.

5. With regard to Reference #7, no joists were used in the floor construction of 3 WTC, 4 WTC, or 5 WTC - rolled beam are used in all Plaza Buildings. Mr. Martinez (ER&S) Mal Levy (Reference #3) & TRCC (Reference #4) all concur that the Plaza Buildings are Class 1B Construction.

6. In addition, Issue "A" of the "Tower Office Space Design Guide" prepared by the WTC Planning and Construction Division (with Errata Sheet #1 to Issue A - dated March 23, 1970) - Page 4 - Item C1 (attached as Reference #8) verifies that the towers are class 1B Construction.

Lester S. Feld
Chief Structural Engineer
World Trade Department

Figure A–7 (Contd.). Port Authority memorandum indicating that WTC towers were classified as Class 1B Construction (3-P).

COPY

EMERY ROTH & SONS
850 THIRD AVENUE
NEW YORK, N. Y. 10022

February 11, 1969

Mr. Joseph A. Schwartzman
The Port of New York Authority
111 Eighth Avenue
New York, N. Y. 10011

RE: WORLD TRADE CENTER
TOWERS "A" and "B"
SPRAY-ON FIREPROOFING

Dear Joe:

In checking out your printed copy of the "Spray-On Fireproofing" specification, it has been noticed that someone in your office has taken the liberty of rewriting the original specification, making it almost totally unrecognizable. In the process of rewriting the specification, a key paragraph seems to have been omitted in its entirety, reading as follows:

"Finished thicknesses of applied material over the various component steel parts requiring fireproofing shall be great enough to qualify the fireproofed parts for a three (3) hour rating (support beams, steel deck work) and a four (4) hour rating for all pick-up girders, if any, and columns".

We cannot be expected to accept responsibility for specifications which have been revised in such a manner; that which originally stated clearly and simply, has become a meaningless document.

Very truly yours,

EMERY ROTH & SONS

BY
DOUGLAS FERNANDEZ

DF:srf

Figure A–8. Letter from Emery Roth & Sons to Port Authority regarding specification for sprayed thermal insulation (3-P).

ATTACHMENT A PAGE 3

Standpipe Hose Stations

6. Several standpipe and auxiliary hose stations do not provide coverage of all portions of all floor areas within the required 145 feet of any given hose's effective reach. Further, some hose racks are equipped with 150 feet of hose in lieu of the standard 125 feet, and provide coverage for 170 feet.

It is recommended that the Port Authority establish a program to survey all tenanted floors to identify areas inadequately covered, and to remediate such inadequacies as quickly as possible.

Also, it is recommended that approval be obtained from the New York City Fire Department for the existing 150 foot long hoses.

Standpipe Telephone Jacks

7. **The requirement that permanent telephone jacks be installed on each floor near standpipe risers has been addressed.** Permanent standpipe telephone jacks have been installed and activated on each floor level of all fire stairways in both towers.

Smoke Vents

8. All closed shafts having a cross-section area exceeding four (4) square feet are required to be equipped with a smoke vent. Although the return air shafts currently have the means to exhaust smoke-laden air directly to the outside by mechanical means, **it is recommended that the Port Authority investigate methods by which this overall requirement maybe satisfied.**

Sprinkler Protection

9. At this writing, only four (4) tenanted floors (all in 1 WTC) have not been sprinklered.

Figure A–9. Excerpt from 1999 code compliance evaluation indicating progress since a similar 1997 evaluation (1999 evaluation is shown in bold-italic text) (161-P).

M&H

One World Trade Center

World Trade Center
New York, New York

The ADA sets forth "recommended priorities for public accommodations" to be accessible to the disabled. In general, the three priorities are as follows:

1. Access from public sidewalks, parking, or public transportation to a building entrance;
2. Access to any areas of goods and services that are made available to the public; and,
3. Access to rest room facilities.

During our tour of the project, we noted the following:

The building's primary entrance is from West Street into the Tower lobby through automatic power operated entrance doors. The path to the elevators is accessible. The Concourse entrance also has 2 sets of automatic doors.

The Plaza Level main entrance has 2 sets of swing doors, without automatic door opening hardware. Provide door-opening hardware on 1 set of swing doors to make the entrance accessible.

The banks of local elevators and mid-zone express elevators are equipped with car control panels that comply substantially with ADAAG. Two upper zone elevators (19 and 19) are not equipped with complying car controls.

Some (approximately 25%) toilet rooms have had upgrades for ADA requirements, but in most rooms observed, there were noncompliant items such as lack of full size ADA toilet stalls, and ADA compliant urinals. ADA compliance on most full tenant floors is reportedly the responsibility of the tenant under terms of the lease.

12. Code Compliance

Applicable Code	1968 NYC Building Code as Administered by the Port Authority of New York and New Jersey
Building Construction Classification	Class1-B - noncombustible, fire-protected, retrofitted with sprinklers in accordance with Local Law 5/1973
Occupancy Type	Group E - Business

December 6, 2000

20-251E - Section V-1 - Page 24

Figure A–10. Excerpt from 2000 property condition assessment of the WTC towers indicating construction classification (7-P).

Truss Fireproofing Systems

Early discussions for fireproofing systems for the floor truss work covered nearly every conceivable method. Port Authority staff as well as the architectural and structural consultants sought efficient and economical systems; the structural steel industry proposed alternative methods.

In early 1963 project estimates carried an allowance for a "demountable ceiling" providing the needed fire protection for the steel floor trusses. The problems of fire dampers for such a ceiling were discussed at length.

By late 1964 a series of alternate contact fireproofing systems had been investigated with some cost data assembled.

By late 1965 the use of a spray-on material similar to Cafco or Mono-Kote appears to have been selected. The ERS letters of December 14 and 23, 1965 are clear on this point. Only the required thickness appears to have been in doubt. (see pages 5.1 and 5.2).

"Demonstrations" of fireproofing systems were carried out by various vendors. For example, on Aug. 7 and 8, 1967, the application on Laclede trusses Mono-Kote fireproofing was demonstrated to Mr. Feld and others (1"thickness). In September of 1967 Messrs. Monti and Solomon appear to have wittnessed spray tests making use of U.S. Mineral Products Co. "Cafco".

-5-

SKILLING, HELLE, CHRISTIANSEN, ROBERTSON

Figure A–11. Excerpt from April 1, 1975 post-fire report prepared by Skilling, Helle, Christiansen, Robertson (3-P).

CC: W. M. Akin
P. B. Akin
H. R. Kilpatrick
A. C. Weber
R. D. Bay
J. R. Paul

August 10, 1967

OFFICE MEMORANDUM

BLOWN ON FIREPROOFING
LACLEDE STEEL JOISTS

During the past week two test applications of blown on fireproofing on Laclede joists and trusses have been accomplished by the U. S. Gypsum Company and the Zonolite Division of W. R. Grace and Company.

This testing, primarily concerned with the floor trusses of the World Trade Center, has been necessary to provide information to the Port of New York Authority engineers on the amount of loss they might expect from a spraying operation on open web structures.

The U. S. Gypsum Company materials, primarily a gypsum and asbestos combination of fibrous material, was applied at the Cupples Company plant of the Aluminum Company of America on Hanley Road on the wall structure that is currently being tested for wind and temperature variations.

The Zonolite Company material made up primarily of vermiculite and gypsum plaster is a much harder cementaecous coating that seems to apply better than the so-called Cafco (U. S. Gypsum material).

A set of 24H8 joists electro coated in the same fashion that the World Trade Center joists will be painted were set up at Madison and with 1/2" and 3/8" nozzles, the Leroy Thompson Plaster Company of Belleville, Illinois coated six joists, two of them with only a single coat to demonstrate the material adherence.

It is apparent that a single coating or scratch coat can be applied as quickly as a man can pass across web and chord sections of the joists leaving a thickness of 3/8" to 1/2" completely incasing all metal.

With a one to two day drying time, depending on the humidity, a second and final coat to a 1" thickness can be easily applied, and according to figures from the Zonolite engineers, a remarkably low percentage of material loss results. Less than 15% material was shot through the joists and lost. With this low material loss it has been pointed out that the use of material is far less than would be required for solid section beams previously considered for spray insulation and is no more than would be experienced with angle and flat section trusses.

Figure A–12. Intra-office correspondence at Laclede Steel Co. regarding 1967 demonstration of sprayed application of thermal insulation to floor trusses (70-I).

- 2 -

With the successful application of spray-on insulation an entire new scheme of fire safe building construction is possible for steel joists in that the fire protection of the joists would permit the installation of low cost acoustical ceilings with access to utility lines that have not be possible in the two hour rated buildings before.

It is anticipated that the U. S. Gypsum Company will be doing further testing on small web trusses at their plant in Stanhope, New Jersey since Ray Monti the general superintendent of the World Trade Center called yesterday to ask if we would provide joists similar to those used by Zonolite for U. S. Gypsum. A New York plastering contractor that is normally the applicator for U. S. Gypsum products in New York, Mario DeBono, is the contractor with whom we would be working if U. S. Gypsum material would be specified.

Mr. DeBono is to call us with an order for electro coated 24" trusses, and according to the Port Authority, will be paying for them since this is a research that U. S. Gypsum is intending to perform without others observing the results. From what I gather, various types of surrounding nozzles are proposed by the DeBono people and they are not anxious to have their competitors learn of their application plans.

In any event, the fireproofing of joists seems to be a problem now solved, and in the World Trade Center as well as in other steel joist structures, we may be sure that an economical fireproofing can be effected in the field without the expense of a heavy ceiling construction.

A. C. Weber

ACW:pjz

Figure A–12 (Contd.). Intra-office correspondence at Laclede Steel Co. regarding 1967 demonstration of sprayed application of thermal insulation to floor trusses (70-I).

PA 36
12-54

THE PORT OF NEW YORK AUTHORITY

Sept. 20, 1967

To: Malcolm P. Levy

From: R. M. MONTI (Ext. 7918 — Room 300)

cc: Mr. H. Tessler

Attached brochure was given to me and

Figure A–13. Port Authority intra-office memorandum indicating demonstration of the application of thermal insulation from U.S. Mineral Products Co. was completed in August 1967 (176-ITK).

AGENDA
COMMITTEE ON CONSTRUCTION
January 29, 1969

0036579

TITLE NO. THE WORLD TRADE CENTER - NORTH AND SOUTH TOWER BUILDINGS - SPRAY FIREPROOFING - CONTRACT WTC-113.00 - SUPPLEMENTAL AGREEMENT

RECOMMENDATION: That the Committee authorize a Supplemental Agreement to Contract WTC-113.00 - Spray Fireproofing, North and South Tower Buildings, The World Trade Center - with Mario and DiBono Plastering Company, Inc., providing for fireproofing isolated steel box columns in the North and South Towers, at a cost of $85,000.

REPORT: The Board, at its meeting on November 14, 1968, authorized the award of Contract WTC-113.00 to Mario and DiBono Plastering Company, Inc., at a price of $1,725,000, and including an allowance of $80,000 for extra work and extra materials. Contract WTC-113.00 provides for the spray fireproofing of interior steel work in the North and South Tower Buildings.

At the time of award of Contract WTC-113.00, it was planned to fireproof certain interior columns by enclosing them with gypsum plank partitioning and wall board. These columns form the framework for the elevator shafts. This work was to be performed under Contract WTC-110.00 - Carpentry, North and South Towers and Below Grade - which was awarded to Star Circle Wall Systems, Inc. by the Board at its meeting on November 27, 1968.

During the contract discussions with Star Circle, evaluation of the fireproofing requirements showed that sufficient protection would be provided by spray fireproofing these columns and that this method would be more economical. Therefore, applying gypsum plank and wall board fireproofing to the columns was deleted from Contract WTC-110.00, resulting in a reduction in their proposal.

Mario and DiBono Plastering Company, Inc. has agreed to spray fireproof the columns at a price of $85,000 which is considered reasonable. It is, therefore, proposed to include this work in a supplemental agreement to Contract WTC-113.00.

Figure A–14. Agenda item for January 29, 1969 meeting of Committee on Construction regarding modification to sprayed fire protection contract (120-ITK).

7. The World Trade Center - North and South Tower Buildings - Spray Fireproofing - Contract WTC-113.00

It was reported to the Committee that Contract WTC-113.00 requires the contractor to spray the structural steel of the North and South Tower Buildings of The World Trade Center with a mixture of asbestos, cement and water, which, when hardened, will provide the necessary fire protection for the structure.

The Board, at its meeting on January 12, 1967, authorized the award of Contract WTC-400.00 - North and South Tower Buildings, Curtain Wall, The World Trade Center - to Aluminum Company of America. Under this contract, Alcoa will provide spray-on fireproofing and plastering to the exterior columns of the North and South Tower Buildings. Alcoa sub-contracted this work to Mario and DiBono Plastering Company, Inc., who performed extensive tests of various methods of providing fireproofing which would meet specifications.

The fireproofing mixture will be applied to the erected steel on each floor and must be completed before any other work on a floor can proceed. In view of this, it was evident that the interior and exterior fireproofing applications would have to be closely coordinated. Staff determined that contract administration problems would be minimized and coordination between the fireproofing work on the interior structural steel and the exterior columns would be facilitated if a single contractor [illegible] to perform such work. Therefore, discussions were held with Mario and Di Bono on the interior fireproofing work and resulted in the submission of a proposal of $1,725,000, including $925,000 for work and $800,000 for sale.

The Project Estimate for Contract WTC-113.00 is $1,625,000, exclusive of an allowance of 5% for extra work and extra materials.

Mario and DiBono Plastering Company, Inc., is qualified to perform the work under Contract WTC-113.00. In the past, they have provided all interior finish plastering, exterior cement plastering and interior and exterior fireproofing for such projects as the International Arrivals Building at Kennedy International Airport; Madison Square Garden; Two Penn Plaza; Rochdale Village, Jamaica, Long Island, consisting of twenty 14-story buildings; and Co-op City in the Bronx, New York.

Recommendation was made that the Committee recommend to the Board that the Board authorize the award of Contract WTC-113.00 - Spray Fireproofing, North and South Tower Buildings, The World Trade Center - to Mario and DiBono Plastering Company, Inc., at a price of $1,725,000 and an allowance of $80,000 for extra work and extra materials.

Approved and recommended to the Board.

Figure A–15. Excerpt from October 30, 1968 minutes of the Committee on Construction regarding the sprayed fire protection contract (123-ITK).

TISHMAN REALTY & CONSTRUCTION CO., INC.
666 FIFTH AVENUE
NEW YORK, N.Y. 10019

OWNERS AND BUILDERS SINCE 1898

JUDSON 2-6700

THE PORT OF NEW YORK AUTHORITY
RECEIVED
APR 1 1966
WORLD TRADE DEPARTMENT
WORLD TRADE CENTER
PLANNING DIVISION

MARCH 30, 1966

PORT OF NEW YORK AUTHORITY
111 EIGHTH AVENUE
NEW YORK, NEW YORK 10011

ATTENTION: MR. R. M. MONTI, RES. ENGINEER - WORLD TRADE CENTER

RE: FIREPROOFING COST COMPARISON
WORLD TRADE CENTER

DEAR RAY:

WE ARE TRANSMITTING HEREWITH OUR COST COMPARISON AND RECOMMENDATIONS FOR SPRAYED FIREPROOFING. THIS ANALYSIS COMPARES THE COSTS AND MERITS OF VONCO 2, CAFCO TYPE D, SPRAY-CRAFT, FIRECODE V AND MONOCOAT SPRAY MATERIALS. WE HAVE SELECTED FOR COMPARISON, ONLY THOSE SYSTEMS FOR WHICH UNDERWRITERS' LABORATORIES INC. AND/OR NEW YORK BOARD OF STANDARDS AND APPEALS APPROVALS ALREADY EXIST OR ARE IMMINENTLY EXPECTED.

THE ANALYSIS SHOWS AUTHORITY, STRUCTURAL MEMBER SIZE AND FUNCTIONAL FIREPROOFING THICKNESS REQUIRED, FIRE RATING IN HOURS, AS WELL AS COST PER SQUARE FOOT FOR MATERIAL AND LABOR AT THE INDICATED THICKNESS. WE HAVE ALSO INTERJECTED BY NOTE, INFORMATION WHICH WE FEEL IS PERTINENT TO PERFORMANCE AS WELL AS POSSIBLE, HIDDEN ECONOMIES OR EXPENSES.

VERY TRULY YOURS,

TISHMAN REALTY & CONSTRUCTION CO., INC.

JAMES R. ENDLER
ASSISTANT VICE PRESIDENT

ENCL.
DU

USM-002657

DEFENDANT'S
EXHIBIT
DX 282

Figure A–16. Correspondence related to economic study of alternative thermal insulation materials (432-P).

WORLD TRADE CENTER FIREPROOFING COST ANALYSIS

LABOR AND MATERIAL COSTS REFLECT SPRAYED SQUARE FOOT CONTACT AREA, INCLUDING OVERHEAD AND PROFIT AND N.Y.C. SALES TAX FOR THE INDICATED THICKNESS AND ASSUME LARGE UNCLUTTERED AREAS WHERE FULL PRODUCTION IS ASSURED, BUT DOES NOT PROVIDE FOR EXCESSIVE CLEAN-UP OR SCAFFOLDING. THESE COSTS SHOULD NOT BE USED FOR SPRAY REQUIREMENTS BETWEEN EXTERIOR COLUMN OR SPANDRELS AND THE CURTAIN WALL, SINCE ACTUAL PRODUCTION CANNOT BE DETERMINED.

MATERIAL DESCRIPTION	AUTHORITY (U.L.I.) (B.S.A.)	SIZE OF MEMBER TESTED	INCHES REQ.	FIRE RATING IN HOURS	MAT. $/SQ.FT.	LABOR $/SQ.FT.	TOTAL $/SQ.FT.
"VONCO 2 AND 4 W"	ULI-48-3	8" BEAM	9/16"	5	.225*	.057**	.282
MAGNESIUM OXYCHLORIDE SPRAY MATERIAL AS MANUFACTURED BY THE MD CORP. OF 101 EMPIRE BUILDING, SPRINGFIELD, MISSOURI.	ULI-29-4	10WF49 COL.	2 5/16"	4	.925*	.210	1.135
	ULI-2-1½	10WF49 COL.	1"	1½	.400*	.091	.491
	UNLISTED***	10WF49 COL.	1 3/4"	4	.700*	.159	.859
	UNLISTED***	10WF49 COL.	1½"	3	.600*	.136	.736
	UNLISTED***	10WF49 COL.	1¼"	2	.500*	.113	.613

* MATERIAL COSTS MAY BE REDUCED FROM .05 TO .06 PER BOARD FT. IF A VONCO PLANT IS LOCATED IN THE EAST AS INDICATED BY MR. HARVEY DAVIS OF THE MD CORP.

** LABOR COSTS WERE ASSUMED THE SAME AS THOSE USED FOR SPRAYED CEMENTATIOUS MATERIALS SINCE NO ACTUAL APPLICATION COSTS ARE AVAILABLE FOR VONCO.

*** ULI FIRE TESTS WERE CONDUCTED AND APPROVED, BUT WERE NOT INCLUDED IN THE 1966 ULI BUILDING MATERIALS' LIST OR THE FEBRUARY BI-MONTHLY SUPPLEMENT.

NOTE No.1 - THIS COMPANY HAS ALSO CONDUCTED THE FOLLOWING ULI FIRE TESTS ON A 10WF49 COLUMN. THESE APPROVALS ARE NOT LISTED TO DATE.
A) ½" THICKNESS FAILED @ 50 MINUTES
B) 1" THICKNESS FAILED @ 1 HOUR AND 55 MINUTES
C) 2¼" THICKNESS FAILED @ 6 HOURS AND 14 MINUTES

NOTE No.2 - THIS MATERIAL IS REPORTED ACCEPTABLE FOR EXTERIOR APPLICATION AT OUTSIDE TEMPERATURES OF 0°F.

CAFCO TYPE "D" CRYSOTILE ASBESTOS AND MINERAL FIBER FIREPROOFING AS MANUFACTURED BY THE UNITED STATES MINERAL PRODUCTS CO., STANHOPE, N.J. AND CALLED "BLAZE SHIELD".	ULI-86-3 195-65-SM	8" BEAM	½"	4	.075	.041	.116
	ULI-19-3 195-65-SM	14WF228 COL.	1 1/8"	3	.169	.092	.261
	ULI-20-4 195-65-SM	14WF228 COL.	1 3/4"	4	.262	.144	.406

NOTE No.1 - AS PER CAFCO FILE No. C-409, FIELD PAINTING OF STRUCTURAL STEEL MAY BE ELIMINATED WHEN "CAFCO" IS APPLIED DIRECT.

NOTE No.2 - NO TAMPING OR ADHESIVE IS REQUIRED.

USM-002658

Figure A–16 (Contd.). Correspondence related to economic study of alternative thermal insulation materials (432-P).

NOTE No. 3 - MAY BE SPRAYED BY POLE-FIBER-GUN WHICH SHOULD EFFECT SCAFFOLDING COSTS.

TERIAL DESCRIPTION	AUTHORITY (U.L.I.) (B.S.A.)	SIZE OF MEMBER TESTED	INCHES REQ.	FIRE RATING IN HOURS	MAT. $/SQ.FT.	LABOR $/SQ.FT.	TOTAL $/SQ.FT
SPRAY CRAFT ASBESTOS FIBER MANUFACTURED BY THE SMITH & KANZLER CORP., 1414 EAST LINDEN AVENUE LINDEN, N.J.	ULI-203-2 502-53-SM	10" BEAM	½"	3	.075	.041	.116
	ULI-81-3	10WF29 BEAM	7/8"	4	.131	.072	.203
	ULI-76-3 502-53-SM	10" BEAM	3/4"	4	.113	.062	.175
	ULI-25-5	8" BEAM	1 7/8"	5	.281	.154	.435
	R2923-12 (OBSOLETE)	COLUMN	3"	4	.450	.246	.696
	UNLISTED*	14WF228 COL.	1 3/4"	5	.263	.144	.407
	UNLISTED*	14WF228 COL.	1 3/16"	4	.178	.097	.275
	UNLISTED*	14WF228 COL.	7/8"	3	.131	.072	.203

* ULI FIRE TESTS WERE CONDUCTED AND APPROVED BUT WERE NOT INCLUDED IN THE 1966 ULI BUILDING MATERIALS LIST OR THE FEBRUARY BI-MONTHLY SUPPLEMENT.

NOTE No. 1 - NO TAMPING OR ADHESIVE IS REQUIRED.

NOTE No. 2 - MAY BE APPLIED WITH POLE-FIBER-GUN, WHICH SHOULD EFFECT SCAFFOLDING COSTS.

FIRE CODE "D" OR "V" SPRAY CEMENTATIOUS AS MANUFACTURED BY THE UNITED STATES GYPSUM CO., CHICAGO, ILL.	ULI-37-5	8" BEAM ONLY	1¼"	5	.108	.119	.227
	ULI-22-3	8" BEAM	1¼"	4	.108	.119	.227
	ULI-24-3	8" BEAM	1½"	4	.124	.136	.260
	ULI-32-3	12" BEAM	1¼"	3	.108	.119	.227
	ULI-67-3	8" BEAM ONLY	1"	3	.077	.091	.168
	ULI-70-3	8" BEAM	1½"	5	.124	.136	.260
	ULI-30-4	10WF49 COL.	2¼"	4	.186	.204	.390
	ULI-13-3	COLUMN	2 1/8"	3	.175	.193	.368
	ULI-23-3	14WF228 COL.	7/8"	3	.072	.079	.151
	ULI-25-3	10WF49 COL.	1 7/8"	3	.154	.170	.324
	ULI-229-2	8 WF BEAM	3/4"	3	.062	.068	.130

-2-

USM-002659

Figure A–16 (Contd.). Correspondence related to economic study of alternative thermal insulation materials (432-P).

MATERIAL DESCRIPTION	AUTHORITY (U.L.I.) (B.S.A.)	SIZE OF MEMBER TESTED	INCHES REQ.	FIRE RATING IN HOURS	MAT. $/SQ.FT.	LABOR $/SQ.FT.	TOTAL $/SQ.FT.
	UL1-31-4 UNLISTED*	10WF228 COL.	1¼"	4	.108	.113	.221
	UNLISTED*	10WF228 COL.	1 1/8"	4	.092	.102	.194
	UNLISTED*	10WF228 COL.	13/16"	3	.066	.075	.141

* ULI FIRE TESTS WERE CONDUCTED AND APPROVED BUT WERE NOT INCLUDED IN THE 1966 - ULI BUILDING MATERIALS' LIST OR THE FEBRUARY BI-MONTHLY SUPPLEMENT.

NOTE No. 1 - COSTS INDICATED DO NOT INCLUDE POSSIBLE REQUIRED SCAFFOLDING OR EXCESSIVE CLEAN-UP AND/OR PROTECTION FOR OVERSPRAY.

NOTE No. 2 - MATERIAL COSTS WERE INDICATED BY THE N.Y.C. REPRESENTATIVE OF U.S. GYPSUM CO. (REVISED PRICES).

MONOCOAT	UL1-248-2*	8WF28 BEAM	3/4"	4	.062	.068	.130
CEMENTATIOUS SPRAY FIREPROOFING AS MANUFACTURED BY THE ZONOLITE DIVISION OF THE W.R. GRACE & CO. CHICAGO, ILL.	UL1-23-3**	14WF228 COL.	7/8"	3	.070	.079	.149
	UL1-27-4**	14WF228 COL.	1¼"	4	.108	.119	.227

* ULI FIRE TESTS WERE CONDUCTED AND APPROVED BUT
** WERE NOT INCLUDED IN THE 1966 ULI BUILDING MATERIALS' LIST OR THE FEBRUARY BI-MONTHLY SUPPLEMENT. (3/4" THICKNESS FAILED @ 4 HOURS AND 10 MINUTES.)

NOTE No. 1 - COSTS INDICATED DO NOT INCLUDE POSSIBLE REQUIRED SCAFFOLDING OR EXCESSIVE CLEAN-UP AND/OR PROTECTION FOR OVERSPRAY.

NOTE No. 2 - MATERIAL COSTS WERE INDICATED BY THE W.R. GRACE & CO.

-3-

USM-002660

Figure A–16 (Contd.). Correspondence related to economic study of alternative thermal insulation materials (432-P).

WORLD TRADE CENTER - FIREPROOFING ANALYSIS

RECOMMENDATIONS

PRESENTLY, IT APPEARS THAT THE SPRAYED FIBER MATERIALS (CAFCO AND SPRAY CRAFT) ENJOY A SLIGHTLY MORE ECONOMICAL APPLIED COST PER SQUARE FOOT THAN THE SPRAYED CEMENTITIOUS (FIRECODE V AND MONOCOAT) MATERIALS BUT NOT ENOUGH TO PRECLUDE KEEPING BOTH IN COMPETITION UNTIL A FINAL BUY IS MADE. NOTE THAT THE FIBER SUPPLIERS HAVE NOT CONDUCTED AS EXTENSIVE A FIRE TESTING PROGRAM AS HAVE THE CEMENTITIOUS MATERIAL MANUFACTURERS. SINCE MORE DATA IS AVAILABLE IN THE LATTER INSTANCE, MORE ACCURATE INTERPOLATION IS POSSIBLE HERE WITHOUT EXPENSIVE ADDITIONAL TESTING.

THE REMOVAL OF BOTH THE TAMPING AND ADHESIVE REQUIREMENTS (BY ACTUAL U.L.I. AUTHORITY) FROM THE FIBER APPLICATIONS, THE APPARENT ABILITY TO SPRAY FIBER WITH ACCURACY FROM THE FLOOR USING THE NEWLY DEVELOPED POLE-FIBER-GUN AND THE RELATIVE EASE OF CLEAN-UP WITHOUT SCRAPING OF OVER SPRAYED MATERIAL, GENERALLY CONTRIBUTES TO THE EDGE IN ECONOMY OF THE FIBER MATERIALS.

THE POSSIBLE REQUIREMENT (ASSUMING THAT AN EXTERIOR GYPSUM BOARD ASSEMBLY PROVES ITSELF) OF CONFINED SPRAYING BETWEEN THE CURTAIN WALL AND EXTERIOR BOX COLUMNS AS WELL AS BETWEEN THE CURTAIN WALL AND EXTERIOR SPANDREL MEMBERS, COULD GIVE THE FIBER MATERIAL AN ADDED ADVANTAGE OVER CEMENTITIOUS, SINCE FIBER EQUIPMENT APPEARS MORE VERSATILE AND EASILY ADAPTABLE TO FAN SPRAYS, NOZZLE MIXING OR SLURRY MIXING (GROUT), SIMPLY BY CHANGING EXISTING SPRAY HEADS OR ADAPTING NEW HEAD CONFIGURATIONS IF EXISTING EQUIPMENT CANNOT BE SATISFACTORILY CONTROLLED.

THE ABILITY OF THE CEMENTITIOUS MATERIAL TO HARDEN OR CRUST AFTER APPLICATION IS A PLUS FOR THIS MATERIAL SINCE DUCT WORK GENERALLY IS SCHEDULED FOR INSTALLATION (BETWEEN TRUSSES) AFTER THE FIREPROOFING OF STEEL, WITH RESULTING DAMAGE TO FIREPROOFING BEING MINIMIZED. MATERIAL COSTS HAVE BEEN DROPPING AND MAY NOT HAVE REACHED BOTTOM.

IT IS RECOMMENDED THAT BOTH SPRAYED FIBER AND SPRAYED CEMENTITIOUS SUBCONTRACTORS BE PLACED IN A COMPETITION WITH EACH OTHER WITH INSTRUCTIONS FOR LOGICAL INTERPOLATION OF REQUIRED THICKNESS OF THEIR RESPECTIVE MATERIALS BASED ON ACTUAL OR UNPUBLISHED UNDERWRITERS' LABORATORIES APPROVALS.

WE ARE IN THE PROCESS OF EVALUATING THE ECONOMICS OF VONCO MAGNESIUM SPRAY VERSUS A SPECIAL WATERPROOFED LAMINATED ASSEMBLY OF GYPSUM BOARD SHEETS FOR THE EXTERIOR OF THE COLUMNS AND SPANDRELS ONLY (WHERE MOISTURE OR TEMPERATURE PRECLUDES OTHER MATERIALS, IN OUR OPINION, WITHOUT EXCESSIVE RE-WORK).

VONCO IS TOO COSTLY FOR FURTHER CONSIDERATION FOR INTERIOR FIREPROOFING APPLICATION.

WHEN THIS ANALYSIS IS COMPLETE, WE WILL RECOMMEND THE MOST ECONOMICAL APPROACH TO THE PROJECT'S EXTERIOR FIREPROOFING REQUIREMENTS. AT THIS TIME, THERE APPEARS JUSTIFICATION TO PURSUE THE INVESTIGATION OF THIS PREFABRICATED LAMINATED ASSEMBLY OF EITHER THE STANDARD 5/8" FIRECODE GYPSUM BOARD OR A SPECIAL BOARD MADE OF FIRECODE V MATERIAL WHICH CONCEIVABLY WILL PERMIT A 4 HOUR RATING WITH A SINGLE 1 1/8" THICK BOARD (U.L.I. 31-4 REVISED) FOR APPLICATION TO THE EXTERIOR FACE OF THE EXTERIOR BOX COLUMNS, PERMITTING THE ERECTION OF CURTAIN WALL AND THE CLOSING IN OF THE TOWER STRUCTURE PRIOR TO APPLICATION OF THE INTERIOR SPRAYED

USM-002661

Figure A–16 (Contd.). Correspondence related to economic study of alternative thermal insulation materials (432-P).

FIREPROOFING. IF THE BUILDING CAN BE ENCLOSED EARLY IN THE CONSTRUCTION CYCLE, INTERIOR FIREPROOFING WITH EITHER FIBER OR CEMENTITIOUS MATERIAL WILL BE MORE EFFICIENT AND THUS MORE ECONOMICAL.

Figure A–16 (Contd.). Correspondence related to economic study of alternative thermal insulation materials (432-P).

6. MR. H. S. GROPP
U.S. MIN. PROD. CO.
STANHOPE, N.J. 07874
12-DI-7-439
N.J. 201-347-1200

10TH
SMITH & KANELOK CO.
1414 EAST LINDEN AVE
LINDEN, N.J.
N.Y.C. 212-WO4-5265
N.J. 201-925-2100

WORLD TRADE CENTER

EXTERIOR WALL, SPANDRELS AND EXTERIOR COLUMN INSULATIONS

THERMAL CONDUCTIVITY AND HEAT TRANSMISSION COEFFICIENTS

Value Based on Wall & Column Design As of 5/5/66
Drawing A-A-314

Fireproofing Material	Conductivity (k) BTU / HR-SF-8F-IN	"U" - Coefficient Transmission - BTU/HR-SF-OF: At Sides of Column: With 1 5/8" F. P.& Air Space	At Sides of Column: 1 5/8" F. P.+ 3/8" Urethane No Air Space	At Outside Face of Column (W/Air Space): With 1 5/8" F. P.	At Outside Face of Column (W/Air Space): 1 5/8" F. P.+ 3/8" Urethane	At Outside Face of Column (W/Air Space): With 2" F.P. and 3/8" Polyurethane
1. Sprayed Mineral Fiber (Spraycraft)	.26	0.135	0.116	.136	.104	.092
2. Sprayed (Cementitious) Vermiculite (Monokote)	.75	0.302	.221	.302	.182	0.167
3. Laminated Gypsum Board (U.S.G. Fire Code)	1.11	0.385	.261	.385	.209	.195
4. Concrete (L.W. 100 PCF)	3.57	0.630	.353	.625	.264	.256
5. Vonco	.38	0.185	.151	.185	.131	0.116
6. Cafco	.27	0.140	.119	.140	0.107	0.093

Notes:

1. Fireproofing for inside face of column is assumed to be 1 3/8" gupsum plaster having conductivity of 1.56 and the overall transmission coeff. of .396 between the room and column steel.
2. Inside still air film resistance is taken as .68
3. Outside air film resistance is taken as .17
4. Air space resistance is taken as .97
5. Conductivity of polyurethane is taken as .17

NC:rt,dd,fk

Figure A–17. Thermal conductivity and heat transfer coefficients used in 1966 study of candidate thermal insulation materials for exterior columns (437-P).

THERMAL INSULATION

The insulation materials applied to the structural steel components of the wall (columns and spandrels) must serve to control column temperature to a minimum of 50° with 70° inside and 0° outside, provide fireproofing to meet a four hour test on a heavy column, and minimize heat loss and gain to satisfy HVAC requirements. After extensive testing of many insulating and fireproofing materials, a sprayed mineral fibre has been selected to meet all requirements of the three purposes above. It will be used on the three exterior sides of the column and both sides of the spandrel plate. The *room* side of the column will be covered with gypsum plaster to meet fireproofing requirements with a relatively high "K" value to permit heat migration to the steel. This migration is necessary to hold steel temperatures above specified minimum during extreme and prolonged cold periods.

Thermal Testing

The minimum column steel temperatures of 50°F requires strategic use of both high "K" and low "K" fireproofing. Since the required thermal balance results from a combination of many factors, calculations can be only a rough guide to design and true performance can be determined only by actual test.

Such tests have been performed at Cupples on three 5' sections of columns completed in full detail typical of the 100th floor. Two units were assembled in a dividing partition of the thermal chamber at Cupples with thermocouples mounted on the steel, top and bottom and inside to outside. "Outside" temperature on one side of the partition was reduced to 0°F and "Inside" temperature was controlled at 70°F until steel had reached thermal balance when results were recorded. A third unit was tested similarly at Pennsylvania State University in the thermal chambers of the Institute for Building Research.

Complete details of tests and results are included in the pocket at the back of this book.

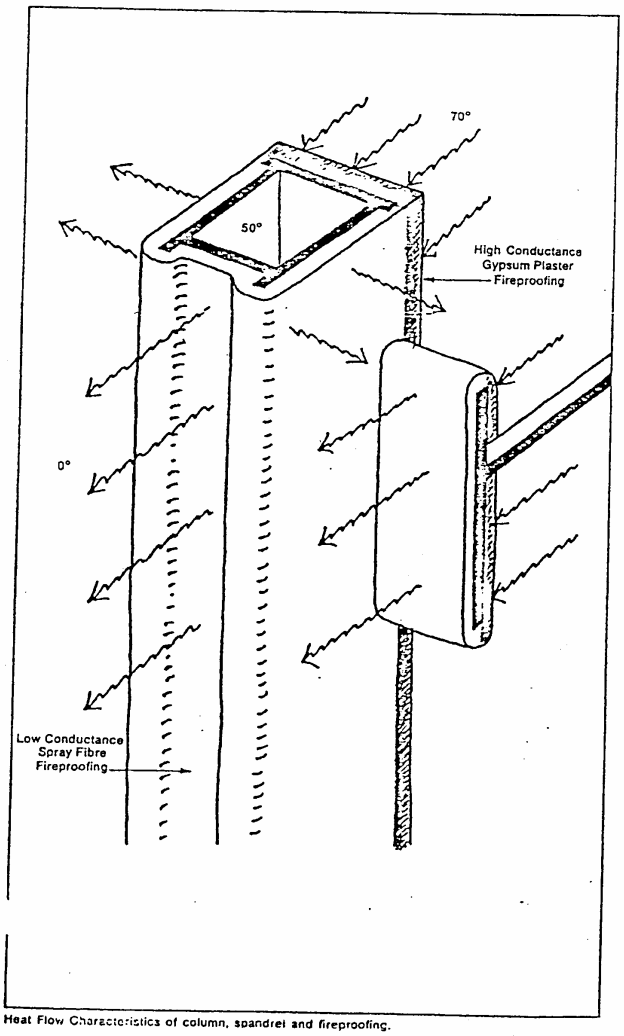

Heat Flow Characteristics of column, spandrel and fireproofing.

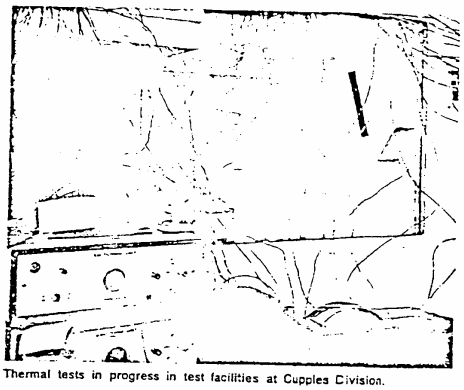

Thermal tests in progress in test facilities at Cupples Division.

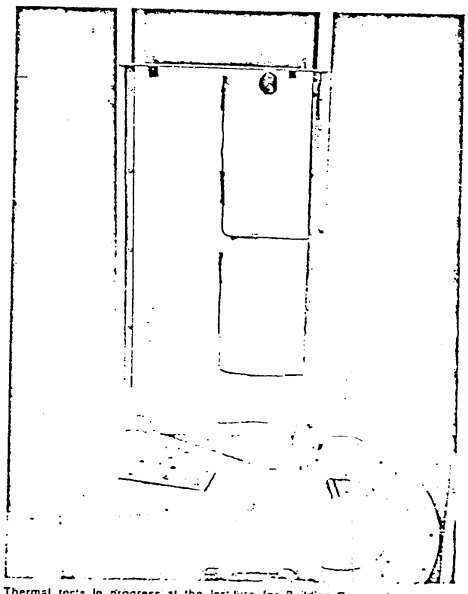

Thermal tests in progress at the Institute for Building Research, Pennsylvania State University.

Figure A–18. Excerpts from December 1996 Alcoa proposal for exterior wall of WTC (448-P).

Hoisting—All hoisting would be done after regular working hours from 4 P.M. to approximately 8 P.M. Assuming the inside dimension of the hoist platform to be 7'4" x 13'3", each lift will include one mobile cart carrying two 1800# packages.

Distribution and Floor Storage—On the designated floor the mobile carts would be moved to storage areas allotted for the purpose. A minimum of six and as many as ten floors of material would be so stored ahead of the actual erection. Glass would be handled on the inside job hoist in cases weighing 3,600 lb. The cases would be handled, moved and stored on the floors in the same manner as the metal components.

FIREPROOFING

Sprayed fiber material as manufactured by CAFCO and of a type described in Underwriters Laboratories report R 3749-10 will be applied to three sides of the exterior columns thick enough to provide four hour fire protection and to maintain the proper thermal insulations. The required thicknesses to meet fireproofing requirements are 1 7/16" for exterior columns and ½" for spandrels. As space permits, the thickness can be increased to obtain the required thermal characteristics.

On the inner side of the columns, a high "K" value material will be applied to provide fireproofing while also permitting heat migration from room air to column steel.

The sprayed fiber will resist the elements during construction of the curtain wall, remain firm to the touch and will not reduce in thickness with time. (See copy of CAFCO Bulletin C-940 in pocket at rear of book). Application would be accomplished with a special nozzle and a transportable cage to safely project the applicator to the exterior of the building. Adjustable vertically, the cage would permit complete coverage of the outer faces of columns and spandrel beams. A screen would be provided around the spray zone to prevent the "blow-by" of fiber material to the exterior of the building and the street below.

Fireproofing in progress would be approximately ten floors above the aluminum wall,

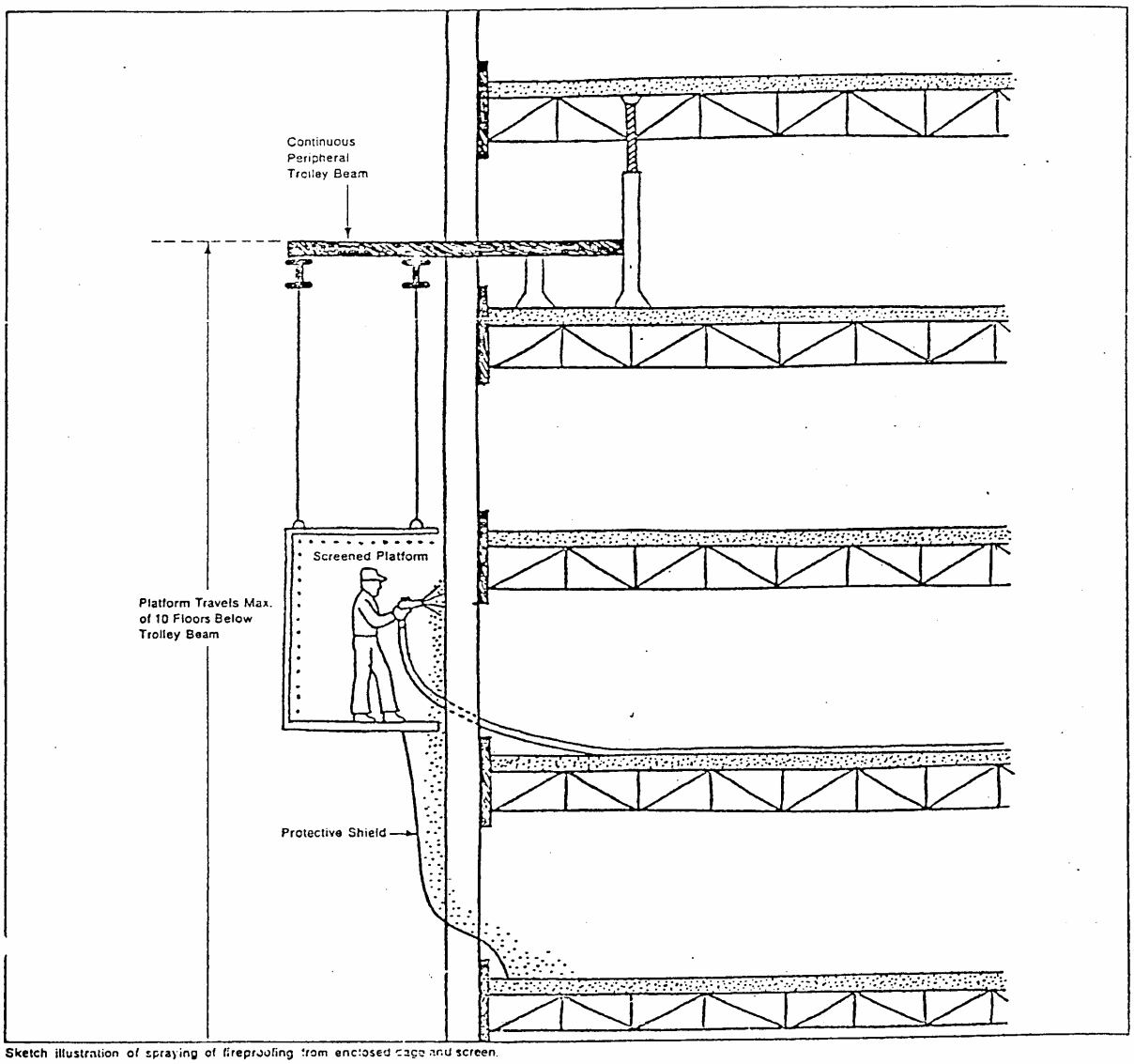

Sketch illustration of spraying of fireproofing from enclosed cage and screen.

Figure A–18 (Contd.). Excerpts from December 1996 Alcoa proposal for exterior wall of WTC (448-P).

PA 90-A
5-63

MEMORANDUM

0011788

REFER		NOTED	
TO	DATE	BY	DATE
RETURN TO		FILE	

TO: Mr. R. M. Monti
FROM: A. J. Calabrese
DATE: August 8, 1967
SUBJECT: COLUMN AND SPANDREL FIREPROOFING OBSERVED AT ALCOA PLANT

REFERENCE:

COPY TO:

File ALCOA

I went to Alcoa-Cupples plant in St. Louis on August 3, 1967 on an inspection of column and spandrel fireproofing of mock-up.

Mario and D'Bono - plasterer - contractor representative was a Mr. Louis D'Bono and Cafco representative was a Mr. A. Bessemer.

The above mentioned and I were present when columns and spandrels were sprayed with Cafco Blaze Shield Fireproofing Type "D" on August 3 and 4, 1967.

It is my opinion that the method of applying was done in a workmanship like manner. It is also my opinion that the method of applying was done with ease and very little spillage.

A. J. Calabrese

AJC/eam

THE PORT OF NEW YORK AUTHORITY
RECEIVED
AUG 8 1967
WORLD TRADE DEPARTMENT
WORLD TRADE CENTER
PLANNING DIVISION

PLAINTIFF'S EXHIBIT
PX-470

A-B-C-F
1-4-5F-5G
5J-5K-6-7-8
9-10B-10C
II1-II3-II4 II2
10

Figure A–19. Port Authority correspondence related to demonstration of application of BLAZE-SHIELD Type D to mockup of exterior columns and spandrels (384-P).

December 14, 1965

Mr. Malcolm P. Levy
The Port of New York Authority
241 Eighth Avenue
New York, N. Y. 10011

Re: Sprayed-on Fireproofing
World Trade Center

Dear Mal:

On Friday, December 10, 1965, a meeting was held in our office to discuss the fireproofing requirements of the floor trusses. The meeting was attended by Messrs. Solomon, ??????, Soffer and Brewer. This letter confirms what was discussed at the meeting.

Our present design concept, and the one which we are continuing with, is based upon the use of a maximum thickness of one inch sprayed-on fireproofing material around the individual components of the floor trusses. This concept is based upon the original standards for the project wherein we would either meet the New York City code or Underwriter's requirements.

To date, the one inch thick material meets the 3-hour requirements of both the new code and Underwriter's using previously approved assemblies tested by the "load criteria" but ignoring the more stringent time-temperature-rate-of-rise criteria which is an alternate testing procedure not required by the new code or by Underwriter's, and which we do not consider necessary.

On Friday, December 10, 1965, a meeting was held in our office to discuss the fireproofing requirements of the floor trusses. The meeting was attended by Messrs. Solomon, ??????, Soffer, and Brewer. This letter confirms what was discussed at the meeting.

Our present design concept, and the one we are continuing with, is based upon the use of a maximum thickness of one inch sprayed-on fireproofing material around the individual components of the floor trusses. This concept is based upon the original standards for the project where in we would either meet the New York City code or Underwriter's requirements.

To date, the one inch thick material meets the 3 hour requirements of both the new code and Underwriter's using previously approved assemblies tested by the "load criteria" but ignoring the more stringent time-temperature-rate-of-rise criteria which is an alternate testing procedure not required by the new code or by Underwriter's, and which we do not consider necessary.

Figure A–20. Correspondence from Emery Roth & Sons to Port Authority related to thickness of thermal insulation for floor trusses (text in box was typed by NIST since copy of document is of poor quality) (3-P).

COPY

EMERY ROTH & SONS, ARCHITECTS
850 THIRD AVENUE
NEW YORK 22, N. Y.

December 23, 1965

Mr. Malcolm F. Levy
The Port of New York Authority
111 Eighth Avenue
New York, N.Y. 10011

Re: Sprayed-on Fireproofing
World Trade Center

Dear Mal:

This supplements my December 14th letter to you.

Although the one-inch thick sprayed-on fireproofing meets the 3-hour requirements of both the proposed Building Code and Underwriters, advance information from manufacturers indicates that if the truss were required to be fire-tested, then two inches of material would be required for the light angle members. We are therefore revising our working drawings to indicate a one-inch thickness of sprayed-on fireproofing around the top and bottom chords of the trusses, and a two-inch thickness for all other members of the trusses.

By informational copy of this letter, all consultants are requested to review their designs and drawings, and to make all necessary changes to meet this new criteria.

Sincerely,

EMERY ROTH & SONS

BY: _____
JULIAN ROTH

JR:ml
cc: Leslie Robert
Aaron Schreie
Joseph R. Lor
Jaros, Baum &
J. Solomon

This supplements my December 14th letter to you.

Although the one-inch thick sprayed fireproofing meets the 3 hour requirements of the proposed building code and Underwriters, advance information form the manufacturers indicates that if the truss were required to be fire-tested, the two inches of material would be required for the light angle members. We are therefore revising our working drawings to indicate a one-inch thickness of sprayed-on fireproofing around the top and bottom chords of the trusses, and a two-inch thickness for all other members of the trusses.

By informational copy of this letter, all consultants are requested to review their designs and drawings, and to make all necessary changes to meet his new criteria.

(5.2)

Figure A–21. Correspondence from Emery Roth & Sons. to Port Authority on thickness of thermal insulation for floor trusses (text in box was typed by NIST since copy of document is of poor quality) (3-P).

732-5222-3-4

Mario & Di Bono

Plastering Co., Inc.

136 LIBERTY STREET NEW YORK, N. Y. 10006

September 15, 1969

Mr. Milt Gerstman
Tishman Realty & Construction Co., Inc.
30 Church Street
New York, New York

RE: Fireproofing thickness' to be sprayed on steel

Dear Mr. Gerstman:

This list is being submitted for your approval.

1. Beams throughout buildings - 1/2 inch. No tamping or shaping of Cafco type D.

2. Columns 1 3/16 inches. No tamping or shaping of Cafco type D.

3. Elevator columns - 1 inch total including overspray. No tamping or shaping of Cafco type D.

4. Bar joist - 1 inch overall thickness. No tamping or shaping of Cafco type D.

Very truly yours,

MARIO & DI BONO PLASTERING CO., INC.

Louis Di Bono

LD/cz

TISHMAN REALTY & CONST. CO., INC.

SEP 15 1969

DEFENDANT'S EXHIBIT DX 434

USM-002883

Figure A–22. Correspondence from thermal insulation contractor to Tishman Realty & Construction Co. related to insulation thickness (255-ITK).

732-5222-3-4

Mario & Di Bono
Plastering Co., Inc.
136 LIBERTY STREET NEW YORK, N. Y. 10006

September 18, 1969

A-49

Mr. Milt Gerstman
Tishman Realty & Construction Co., Inc.
30 Church Street
New York, New York

RE: Fireproofing thickness' to be sprayed on steel

Dear Mr. Gerstman:

In regard to our letter dated September 15, 1969 concerning the thickness of fireproofing material, please add the following paragraph:

5. All beams in MER rooms and utility rooms will be 1/2 inch thickness with overspray. No tamping or shaping of Cafco type D.

Very truly yours,

MARIO & DI BONO PLASTERING CO., INC.

Louis DiBono

LD/cz

DEFENDANT'S EXHIBIT DX 438

TISHMAN REALTY & CONST. CO., INC.

SEP 22 1969

USM-002884

Figure A–22 (Contd.). Correspondence from thermal insulation contractor to Tishman Realty & Construction Co. related to insulation thickness (255-ITK).

October 30, 1969

Mr. Louis DiBono
Mario & DiBono Plastering Co., Inc.
370 Northern Boulevard
Great Neck, Long Island, New York 11021

Re: THE WORLD TRADE CENTER - Contract WTC 113.00-
Spray-On Fireproofing - Towers A & B

Dear Lou:

As a result of your meeting with Mr. Levy on October 21, 1969 I am enclosing a list of Tower "A" columns that are less than 14WF228 which will require 2 3/16" thick of "Cafco Glaze-Shield 'TypeD'" spray-on fireproofing. All Tower columns equal to or greater than 14WF228 will require 1 3/16" of fireproofing. Both of the above thicknesses develop the required 4-hour rating.

All Tower beams, spandrels and bar joists requiring spray-on fireproofing are to have a ½" covering of "Cafco".

The above requirements must be adhered to in order to maintain the Class 1-A Fire Rating of the New York City Building Code.

Sincerely,

Robert J. Linn
Manager, Project Planning
The World Trade Center

cc: Messrs. M. Gerstman (TRCC), J. Solomon (ER&S)

Figure A–23. Correspondence from World Trade Center Department to the thermal insulation contractor specifying the required insulation thickness (3-P).

BLAZE-SHIELD
fireproofing **STANDARD**

[illegible] is a mill quality control blend of virgin asbestos fiber, highly refined white mineral fiber and proprietary binders. Tested and listed by Underwriters' Laboratories, Inc. (ULI) and Underwriters' Laboratories of Canada (ULC) for fireproofing applications, code acceptance has been registered by major municipal building departments throughout the United States and Canada and in many countries overseas.

PRODUCT FEATURES

[illegible] — An improved BLAZE-SHIELD STANDARD formulation eliminates application dustiness generally associated with conventional sprayed fiber products. Respiratory hazards, clean-up time and expenses are minimized.

[illegible] — BLAZE-SHIELD STANDARD out-performed other fireproofing media when exposed to severe fire temperatures on major high-rise structures. CAFCO applications have been credited with restricting fire spread and preventing serious damage.

[illegible] — Tested in accordance with ASTM B-117 and Federal Specification MIL-E-5272A, CAFCO protected, shop painted steel evidenced no corrosion under severe exposure conditions. Rust preventive properties are superior to the combination of shop and field painting; costly field painting may be eliminated.

[illegible] — CAFCO treated spandrels, roof decks and floor units reduce heating and air conditioning costs; [illegible]d insulation at roof set backs may be eliminated. BLAZE-[illegible]ELD STANDARD provides a thermal conductivity (k) value of 0.27.

[illegible]

ALL-WEATHER APPLICATION
REDUCTION IN DEAD LOAD
PERMANENCE OF PROTECTION
ACOUSTICAL ABSORPTION

ARCHITECTURAL SPECIFICATIONS
BLAZE-SHIELD STANDARD

GENERAL

[illegible] — See BLAZE-SHIELD Type D specification
[illegible] — See BLAZE-SHIELD Type D specification
[illegible] — See BLAZE-SHIELD Type D specification

MATERIALS

[illegible] — Bonding adhesive, where required, shall be a milky white, latex-type water emulsion which shall be unaffected by water, water vapor, condensation, aging or freezing once it has set. Shall be CAFCO ADHESIVE as supplied by the United States Mineral Products Company (Canadian subsidiary—Columbia Acoustics & Fireproofing Co. (Canada) Ltd.), or approved equal.

[illegible] — The fiber shall be a factory quality controlled and formulated mix consisting of 100% inorganic virgin Crysolite asbestos fiber and small pellet, white mineral fiber, combined with 100% inorganic binders. Fibers shall be CAFCO BLAZE-SHIELD STANDARD as manufactured by United States Mineral Products Company (Canadian subsidiary—Columbia Acoustics & Fireproofing Company (Canada) Ltd.), or approved equal, and shall be supplied to the job site in sealed bags, properly marked and labeled to show the inspection of Underwriters' Laboratories, Inc. or Underwriters' Laboratories of Canada for the application specified.

[illegible] — Overspray, where required, shall be transparent and unaffected by moisture; shall be CAFCO SEALER as supplied by United States Mineral Products Company (Canadian subsidiary—Columbia Acoustics & Fireproofing Company (Canada) Ltd.), or approved equal.

WORK OF OTHER SECTIONS

[illegible] — See BLAZE-SHIELD Type D specification
[illegible] — See BLAZE-SHIELD Type D specification
[illegible] — See BLAZE-SHIELD Type D specification

INSTALLATION

[illegible] — See BLAZE-SHIELD Type D specification
[illegible] — See BLAZE-SHIELD Type D specification
[illegible] — All surfaces to be treated shall be primed with CAFCO ADHESIVE. Fibers shall be applied and tamped to required thickness and oversprayed, where required, with CAFCO SEALER.
[illegible] — See BLAZE-SHIELD Type D specification

SYSTEM	HOURS	THICKNESS	AUTHORITY	BLAZE-SHIELD Type D	BLAZE-SHIELD Standard	CONSTRUCTION
BEAMS — GIRDERS — SPANDRELS						
BEAMS, GIRDERS, SPANDRELS	2	1/2"	ULI#R3749-6		X	
	3	7/8"	ULI#R3789-2		X	
	4	1 1/2"	ULI#R3749-13 N605	X		
WRAPPED BEAMS, GIRDERS, SPANDRELS, JOISTS	3	9/16"	ULI#R3749-18	X		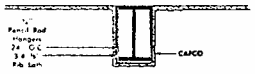
	4	1"	ULC#60197	X	X	
COLUMNS						
COLUMNS AND COLUMN CAPS	3	1 1/8"	ULI#R3749-10† X807	X		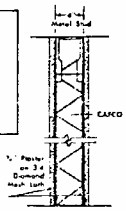
	4	1 7/16"	ULI#R3749-9† X807	X		
	2	1 1/4"	ULI#R3749-19 X818	X	X	
	3	1 3/4"	ULI#R3749-19 X818	X	X	
	4	2 3/16"	ULI#R3749-19 X801	X	X	
WALLS						
WALLS	4	4"	ULI#R3749-21	X		

† For application to columns 14WF228 or greater
ULC — Underwriters' Laboratories of Canada / ULI — Underwriters' Laboratories, Inc.
All tests conducted in accordance with ASTM E-119

Figure A–24. Excerpt from 1966-67 U.S. Mineral Products Co. catalog for BLAZE-SHIELD indicating thermal insulation thickness for various applications (3-P).

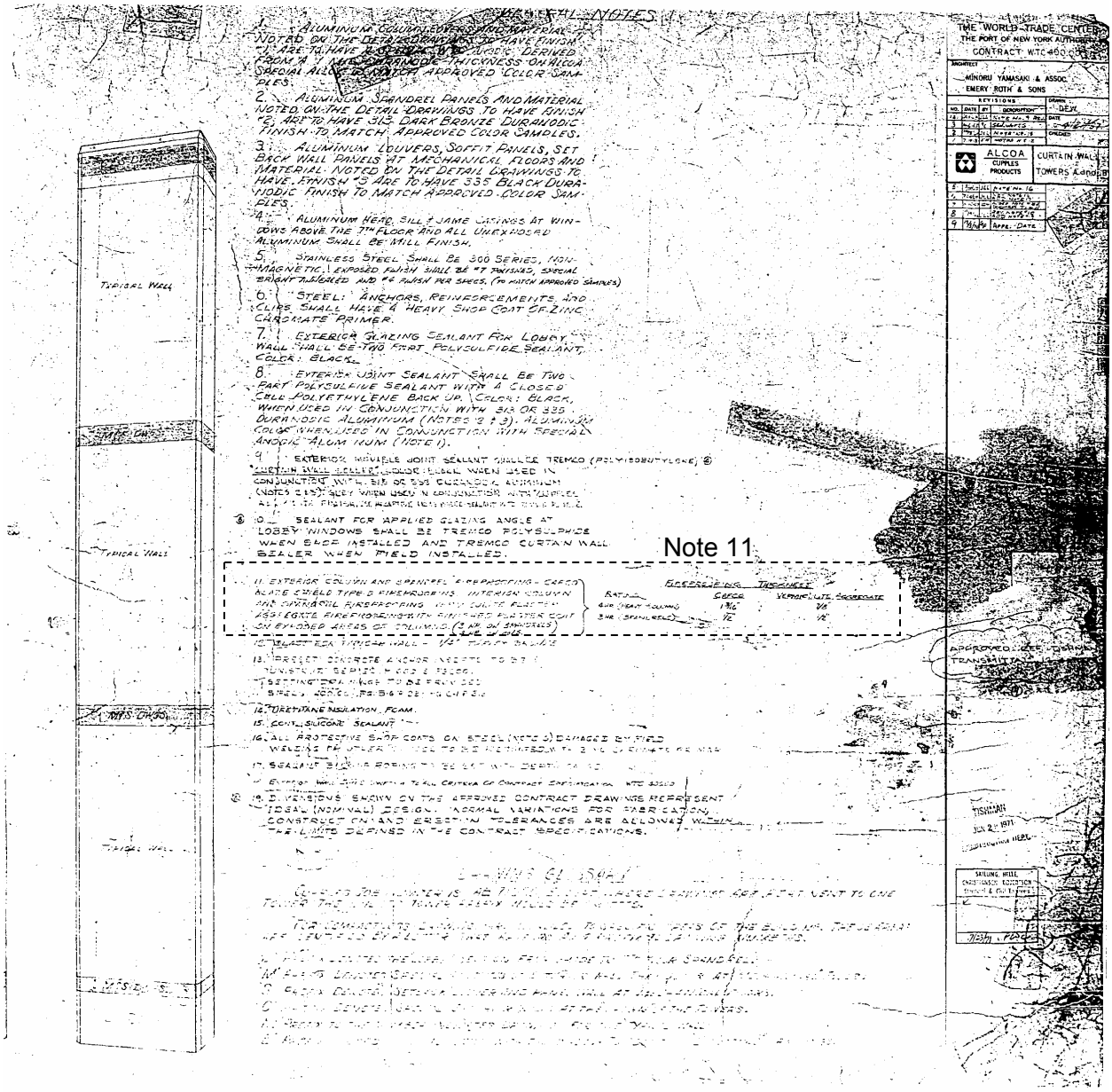

Figure A–25. Portion of "General Notes" page of the Alcoa curtain wall drawings and blow-up of Note 11 indicating the thermal insulation thickness for the exterior columns and spandrels (116-LERA).

11. EXTERIOR COLUMN AND SPANDREL FIREPROOFING - CAFCO PLATE SHIELD TYPE-D FIREPROOFING. INTERIOR COLUMN AND SPANDREL FIREPROOFING: VERMICULITE PLASTER AGGREGATE FIREPROOFING WITH FINISHED PLASTER COAT ON EXPOSED AREAS OF COLUMNS. (3 HR. ON SPANDRELS, 4 HR. ON COLS.)

FIREPROOFING THICKNESS

RATING	CAFCO	VERMICULITE AGGREGATE
4 HR (HEAVY COLUMN)	1 3/16"	7/8"
3 HR. (SPANDRELS)	1/2"	1/2"

2/1/70	7 PTS	ERECTION	CPD-NY.
5/5/70	10 PTS 2 SEPIA	FILE & RECORD	TRUMAN

GENERAL NOTES

JOB NUMBER AB71060 SHEET 1 of 1

THE WORLD TRADE CENTER
THE PORT OF NEW YORK AUTHORITY
CONTRACT WTC 400.00

ARCHITECT
MINORU YAMASAKI & ASSOC.
EMERY ROTH & SONS

REVISIONS				DRAWN: D.E.W.
NO.	DATE	BY	DESCRIPTION	DATE 4/20/67
(4)	2/14/69	JLL	NOTE No. 9 REV.	
3	11-6-68	RC	GEN. NOTES	CHECKED
2	7/28/67	JLL	NOTE NO. 18	
1	7-19-67	SW	NOTES 11 & 12	

ALCOA CUPPLES PRODUCTS — CURTAIN WALL TOWERS A and B

5	3/26/69	JLL	NOTE No. 16
6	7/24/69	JLL	ADD NOTE 17
7	5/26/69	SW	ADD NOTE 18 THICKNESS TABLE
8	11/19/69	JLL	ADD NOTE 19
9	12/16/69	RP	APPR: DATE

Figure A–25 (Contd.). Portion of "General Notes" page of the Alcoa curtain wall drawings and blow-up of Note 11 indicating the thermal insulation thickness for the exterior columns and spandrels (title blocks of drawing are also shown) (116-LERA).

COPY

EMERY ROTH & SONS, ARCHITECTS
850 THIRD AVENUE
NEW YORK 22, N. Y.

111 Eighth Avenue
New York, New York 10011

Re: World Trade Center

Dear Mal:

Figure A–26. Letter from Emery Roth & Sons to Port Authority regarding the application of thermal insulation to the bottom of the concrete floor slabs (3-P).

THE PORT AUTHORITY OF NY & NJ

One World Trade Center
New York, N.Y. 10048
(212) 466-7000
(201) 622-6600

PORT AUTHORITY OF N. Y. & N. J.
RECEIVED
MAR 17 1983
WORLD TRADE DEPARTMENT
DEP. DIR. PHYS. FAC.

March 14, 1983

Mr. Jerry Silecchia
National Cleaning Contractors, Inc.
60 Madison Avenue
New York, New York 10010

Dear Jerry:

As you know, during the construction of the World Trade Center the use of asbestos fireproofing was discontinued at the 38th floor of the World Trade Center. Those areas were subsequently encapsulated with a spray-on hardening material. The Port Authority has, on occasion, reviewed the asbestos fiber count above the ceiling in these areas and found these counts to be well below the OSHA standards.

However, in the interest of safety for all, you should direct your employees to use OSHA approved dust filter masks, provided by the Port Authority, when working above the ceilings in these areas.

Kindly advise your employees as needed.

Sincerely,

Daniel J. Censullo
Manager, WTC Operations
The World Trade Center

bcc: T. Cancelliere, J. Grismer, R. Linn, A. Rhome, J. Ritter, J. Verbist

Writer's direct dial telephone: 466-3585

Figure A–27. Correspondence indicating that use of BLAZE-SHIELD Type D was discontinued at the 38th floor of WTC 1 (229-ITK).

MEMORANDUM

PA 90-A
3-63

REFER		NOTED	
TO	DATE	BY	DATE
RETURN TO			

TO: File
FROM: R. M. Monti
DATE: May 15, 1970
SUBJECT: THE WORLD TRADE CENTER - SPRAY FIREPROOFING - CONTRACTS WTC 400.00, WTC 113.00, WTC 120.00
REFERENCE:

COPY TO: Messrs. Levy, Tozzoli, Falvey, Werneke, Raiola, DeConzo (All W/Ref.)

At the present time there are two contracts involved in spray fireproofing: 1) WTC 400.00 with ALCOA, and 2) Port Authority Contract WTC 113.00 for fireproofing of floor trusses in the towers, core column in the towers, below grade areas of the bathtub area, and the Northeast Plaza Building. In the immediate future there will be a third subcontract (WTC 120.00) for fireproofing the Customs building.

ALCOA Contract WTC 400.00

From the inception of studies on this contract ALCOA proposed the use of Cafco type D spray fireproofing which conforms to the fire requirements, but more important to ALCOA, conforms to the required K factor for thermal conductivity. ALCOA is a performance type contract and they proposed to use this material which met their performance requirements and contained asbestos fibers. On all other contracts the Port Authority likewise specified Cafco type D spray fireproofing which contained asbestos fibers.

Port Authority knew

What about Selikoff Hearing

For the last six months there has been a certain amount of interest developed in the New York City area on the potential health problems caused by asbestos fibers. This study was conducted primarily by Dr. I. Selikoff of Mt. Sinai School of Medicine in conjunction with the New York City Air Pollution Department. Early in April, New York City promulgated a set of emergency instructions regarding the application and use of spray fireproofing containing asbestos fibers (Enclosure 1 is a copy of said regulations). On the World Trade Center, the Port Authority complied to the best of its ability and was praised as the best job in the city in conforming with the regulations for the application of this material. However, item No. 10 of Enclosure 1 indicates potential problems of exposed fireproofing containing asbestos which is installed in return air plenum ceilings. It was maintained by Dr. Selikoff that studies performed by his staff indicated that exposure over a considerable number of years of people sitting in an office, where the return air passed by exposed spray fireproofing containing asbestos, could cause health problems. Item No. 10 of Enclosure 1 specifies that such asbestos products in return plenums should be sealed with an appropriate sealant to prevent dusting of asbestos particles. At this point the Port Authority started studying possible sealants that could be applied, should it be decided to proceed in this matter. Enclosure 2 is a letter from Mario & DiBono Plastering Company, listing the components of a possible sealant manufactured by U. S. Mineral Products for areas already sprayed with asbestos. Enclosure 3 is a letter from R. M. Monti to Dr. Selikoff regarding the possible use of a sealant and asking that he advise us of his opinion before we proceed further.

Knew before then-Asbestos

DEFENDANT'S EXHIBIT DX 589

Figure A–28. Port Authority memorandum summarizing the factors considered in choosing BLAZE-SHIELD Type DC/F as a replacement for the asbestos-fiber containing Type D (185-ITK).

File - 2 - May 15, 1970

Enclosure 4 is a letter from Dr. Selikoff, Mt. Sinai School of Medicine, to R. M. Monti, dated April 16, 1970, indicating that our proposal to use a sealant on areas sprayed with mineral fireproofing containing asbestos is the best technical means available at this time to prevent dusting, and it has his concurrence.

On April 17, 1970 the spray fireproof contractor, Mario & DiBono Plastering Co. who is a subcontractor to ALCOA under WTC 400.00 and also the Port Authority's contractor under WTC 113.00, was served with five summonses, one for each day of the week of April 13th. These summonses stated that he was in violation of the regulations listed in Enclosure 1. On April 17th, Mario & DiBono also received a Show Cause order returnable before the Commissioner of the Department of Air Resources on April 24th in connection with the fireproofing work being performed at the World Trade Center, as to why the job should not be sealed off. On April 20, 1970 I was advised by Mario & DiBono that he had received said Show Cause order and asked my advice. I immediately contacted Pat Falvey, Assistant General Counsel of the Port Authority, and discussed it with him. A meeting regarding this Show Cause order was held with Pat Falvey on April 21, 1970, at which time Mr. Falvey called Mr. Fabricant, General Counsel of the New York City Environmental Protection Administration, and requested that said Show Cause order be indefinitely postponed. Mr. Fabricant agreed, providing he received said request in writing from Mr. Falvey. Enclosure 5 is a copy of Mr. Falvey's letter to Mr. Fabricant requesting said adjournment. This letter states that should we resume spraying with asbestos we would give the City a two day notice, and should we resume spraying with non-asbestos material we would give them a one day notice of our intentions.

As of April 20, 1970 all spray fireproofing operations at the World Trade Center site were suspended.

On April 20, 1970 I also went to the office of U. S. Mineral Products Company in Stanhope, New Jersey where I observed a test demonstration on Cafco type D which had been sealed with a sealant to prevent its dusting. Enclosure 6 is a copy of results of tests conducted on mineral fiber fireproofing in accordance with GSA specifications regarding dusting. I was advised by the Research Director of U. S. Mineral Products that the application of a sealant on top of the Cafco type D would reduce the dusting to a negligible amount. Tests on Cafco type D for dusting, due to air velocity without a sealant, have been conducted and documented as listed in Enclosure 6. These tests indicated that the amount of asbestos particles dusting off due to air velocity are well within the standards set by the Environmental Health Department of the United States and also the British standard. It is also concluded and concurred in by Dr. Selikoff as indicated in the aforementioned Enclosure 4, that the use of a sealant is the best way to control dusting for work already installed that contains asbestos.

While at Stanhope, New Jersey, I also inquired into their research of an asbestos free material which would perform the same functions as Cafco-D. I was advised that they have such a material which had passed

Figure A–28 (Contd.). Port Authority memorandum summarizing the factors considered in choosing BLAZE-SHIELD Type DC/F as a replacement for the asbestos-fiber containing Type D (185-ITK).

File - 3 - May 15, 1970

preliminary tests and which they were working on final tests for all the requirements. The tests that are required for approval of this material are as follows:

1. A fire rating test.
2. An adhesion under fire test.
3. A K factor or thermal conductivity test.
4. A bonding strength test.
5. Confirmation regarding the components of the material that could possibly be alleged to have health hazards.

Cafco research lab advised me that they had performed all of the above tests in their own laboratory, and that their material without asbestos, known as Cafco type D-CF, was equivalent to their previous Cafco type D with asbestos in all aspects. I advised Cafco representatives that I could not accept only the findings of their own laboratory but must have independent laboratory tests. They said they would arrange for all such tests and send reports directly to me. On April 23, 1970 Cafco called me and advised me that the fire rating tests being conducted by Underwriters Laboratory in Chicago had passed all the requirements. I requested that this be put in writing. On April 24, 1970 I received a telephone call from an engineer in Underwriters Laboratory, Inc., Mr. S. Bell, who advised me that the fire resistance tests on Cafco type D-CF were at least equivalent and probably 5% better than Cafco type D. I requested confirmation in writing. Attached is Enclosure 7 from Underwriters Laboratory attesting to this finding.

Enclosure 8 is a letter from U. S. Mineral Products dated April 30, 1970 attaching a copy of a test made by Dynatech of Cambridge, Massachusetts on the thermal conductivity of type D-CF. The test indicates that type D-CF is equivalent or better to regular type D.

Cafco also advised that they had performed bonding tests on type D-CF and these were successful. However, I requested independent laboratory tests. Enclosure 9 is a report from International Testing Laboratories, Inc. of Newark, New Jersey which reports the tensile strength in pounds per square foot of type D-CF to be within a range of 19.9 to 22.40. This tensile strength indicates that type D-CF is able to support its own weight approximately 20 times. Regular type D Cafco is advertised to support its own weight 10 to 12 times. Therefore, type D-CF results indicated it to be better than regular type D for bond strength.

I had previously been advised by Cafco representatives that two samples of type D-CF had been sent to Dr. Selikoff at Mt. Sinai for his examination. On April 23, 1970 I called Dr. Selikoff and asked him if he ever had examined Type D-CF. He advised me that he had not, but he had examined some similar material and he had found it to contain certain particles of asbestos. He advised that if I were to deliver to him a sample of this type, which I had taken personally out of a bag, he would re-examine same. I had a bag of type D-CF delivered to my office and one of my inspectors removed from the bag a one gallon canister of this material with rubber gloves, sealed it and delivered it to Mt. Sinai Hospital. Enclosure 10 is a memorandum to file from my inspector, R. Kalenborn, confirming said delivery.

Figure A–28 (Contd.). Port Authority memorandum summarizing the factors considered in choosing BLAZE-SHIELD Type DC/F as a replacement for the asbestos-fiber containing Type D (185-ITK).

File - 4 - May 15, 1970

On the afternoon of April 24, 1970 Dr. Nicholson, assistant to Dr. Selikoff at Mt. Sinai Hospital, called me and advised me that a preliminary analysis of the material indicated that it was free of asbestos fibers except for possibly a few fibers that could have been picked up in the production line of the previous type D material. Dr. Nicholson gave me a good report on the material and further stated that it appeared to be much better in all respects to type D. I asked Dr. Nicholson if he would put this in writing to me. He said he would and he further stated that in his opinion this material did not present a health hazard due to asbestos, but of course we should maintain tarpaulins during installation and thorough cleanup as you would do with any material. He even said that it would not be necessary to comply with the City regulations listed in Enclosure 1 for this material. Dr. Nicholson did say that he would do further analysis of the material to check for its other constituent parts. I received a letter dated April 29, 1970 from Dr. Nicholson, Enclosure 11 hereto, regarding the examination of this material, which indicates the material is free from asbestos and excellent in other respects. However, Dr. Nicholson stated that "while no direct evidence exists linking mineral wool fibers to disease its extensive use has not been of sufficient duration to say that there could not be such disease." This statement merely allows Mt. Sinai to keep the door open on research of this material.

I have also received other preliminary verbal reports on extensive previous research performed by independent outside agencies on any deleterious health problems due to the mineral wool fibers in Cafco D-CF. These reports, to date, are very encouraging in that they are all negative. When written reports are received, copies will be sent to all interested parties.

On April 27, 1970 Mr. Sorrell and Mr. Roby of ALCOA requested my acquiescence to allow them to resume spraying and/or patching on floors 16 to 19 with type D-CF to permit continued erection of aluminum column covers. At this time all the required test reports indicated above had not been received by me and therefore I merely indicated my acquiescence to their request to proceed with the understanding that this change in material for these floors or for any subsequent change for their material under their performance type contract would not entail any additional costs to the Port Authority. Mr. Sorrell agreed to no cost for floors 16 to 19 but said "let's not talk about the rest." I repeated my statement that there would be no consideration of additional costs under their performance type contract for changing the materials. Enclosure 12 hereto is a copy of my letter to ALCOA dated April 27, 1970, confirming the aforementioned discussions and restating the Port Authority's position on no additional compensation for change in material, should ALCOA desire to do so. Enclosure 12 was reviewed by Tony Raiola and Pat Falvey of the Port Authority Law Department prior to its issuance.

Enclosure 13 attached hereto is a copy of a letter from ALCOA to Mr. Tozzoli, dated April 23, 1970, requesting consideration of additional compensation of $173,000 for their corporate decision to change the material to type D-CF. This letter was received in Mr. Tozzoli's office on April 27. This is an attempt by ALCOA, as I discussed with Mr. Tozzoli, to see if one letter they can possibly get consideration of $173,000. I understand that ALCOA has made a corporate decision to change this material on

Figure A—28 (Contd.). Port Authority memorandum summarizing the factors considered in choosing BLAZE-SHIELD Type DC/F as a replacement for the asbestos-fiber containing Type D (185-ITK).

File - 5 - May 15, 1970

on their own, regardless of the fact whether they get additional compensation, because they do not want to get involved with the bad public relations that would be associated with their continuing the two towers with an asbestos material, even if they were able to continue, by conforming to the regulations in Enclosure 1. It is interesting to note that since April 20 all jobs in New York City using asbestos material have been stopped, and to the best of my knowledge, as of this date have not resumed spraying. Enclosure 14 is a reply by Mr. Tozzoli to ALCOA dated May 8 substantiating the Port Authority's position as stated in Mr. Monti's letter to Mr. Sorrell of ALCOA, dated April 27, 1970, in that the Port Authority does not accept any responsibility for any additional costs ALCOA may incur due to their performance type contract. On May 1, 1970 Mr. Sorrell of ALCOA hand delivered to me a letter dated May 1, 1970 requesting Port Authority approval to use type D-CF in lieu of type D for the entire project. This is Enclosure 15 hereto. Since on May 1, 1970 I did not have in my hands all complete reports listed above, I annotated said ALCOA letter and gave verbal approval to proceed with type D-CF only for Tower "A" floors 20 through 25 inclusive, pending receipt of final reports. Mr. Sorrell concurred with this and advised that by the time he reached the 25th floor, maybe all reports would be in and we could give him an unqualified proceed for the entire two towers.

In the interim Tishman Realty & Construction Co., Inc. proceeded on a separate course of investigating other sources of spray material which would be free from asbestos. Enclosure 16 is a copy of a letter from Tishman to ALCOA dated May 1, 1970, reporting on their investigations with W. R. Grace Company on a material called Monacote and coming to the conclusions that the K factor of the material that they investigated did not meet the requirements and therefore concluded that Monacote would not be considered any further for application.

Contract WTC 113.00

Mario & DiBono Plasterinc Company includes the spraying for Towers "A" & "B" and below grade. This contract was awarded specifying asbestos spray materials (Cafco type D) for floor trusses, columns and beams. Certain specific columns in the elevator shafts are required, under the original contract, to be coated with Cafco Mark II hard finish coating due to the high velocity of air caused by the elevators. Thus, if we continued spraying with Cafco type D, the elevator shafts specified to be hard finished are already sealed and would not require a sealant on top of same. All other areas which were to be sprayed with type D asbestos material would require a sealant.

During the week of April 13, 1970, I started discussions with the contractor regarding the possibility of applying a sealant to all areas of both Towers "A" & "B" and below grade which are not required to have Cafco Mark II hard finish coating. The contractor originally indicated that the going price for sealants per square foot would result in a total compensation of approximately $605,000 for sealing the entire project. The contractor
'icated, however, he was willing to cooperate. Using an estimated cost
9 en to me by Dr. Neuman of Tishman Realty & Construction Co., Inc. of

Figure A–28 (Contd.). Port Authority memorandum summarizing the factors considered in choosing BLAZE-SHIELD Type DC/F as a replacement for the asbestos-fiber containing Type D (185-ITK).

File - 6 - May 15, 1970

3½ cents per square foot as an equitable price, I was able to convince the contractor to agree at a lump sum proposal of $350,000 for sealing all areas of Towers "A" & "B" and below grade. The contractor also agreed that he would release the Port Authority of his existing claim for excessive rust scaling on steel, which is outside of the scope of his contract, and was estimated by him to run $160,000. My staff indicated to me that based on T&M slips submitted to date that this item of removing excessive rust could run as high as $200,000.

Subsequent to the above discussions, the problem of continued use of asbestos material arose; therefore, I proceeded to discuss costs of substituting type D-CF fireproofing and only sealing the areas that had previously been sprayed with the asbestos material, plus continued release of the claims for excessive rusting of the steel. The contractor's proposal for this work, including changing the material on the U. S. Customs Building and the Northeast Building, amounted to $442,425. I offered the contractor $296,500. After further review with the contractor and a review of the numbers with Mr. Tozzoli, I made a final offer to the contractor of $320,000. The contractor accepted same. This cost covers the following items of work in Towers "A" & "B" and below grade, the Norhteast Plaza Building and the U. S. Customs Building:

1. From the times that we allow him to proceed to resume spray operations he will use asbestos free Cafco type D-CF in all spray work.

2. He will apply a sealant to all areas that have previously been sprayed with asbestos material, except for those areas which receive Cafco Mark II hard finish, in both Tower "A" and below grade, and should any be done in Tower "B", in that area also.

3. He releases the Port Authority by signed release from any further claim regarding removal of excessive rusting from the steel. Clause 13.03 subparagraph 2 on page 123 of Contract WTC 113.00 must be amended or deleted so that no further recourse to said statements can be made by the contractor.

R. M. Monti
Construction Manager
The World Trade Center

RMM:rd

Figure A–28 (Contd.). Port Authority memorandum summarizing the factors considered in choosing BLAZE-SHIELD Type DC/F as a replacement for the asbestos-fiber containing Type D (185-ITK).

UNDERWRITERS' LABORATORIES, INC.

an independent, not-for-profit organization testing for public safety

April 24, 1970

L3749

Port of New York Authority
111 8th Avenue, Room 300
New York, New York

Attention: Mr. R. Monti, Construction Manager
World Trade Center

Subject: Fire Resistance Evaluation of Cafco CF Type "D" vs Cafco Type "D"

Gentlemen:

Confirming our telephone conversation of April 23, the Subject investigation is approximately 80 per cent completed. All of our test results to date indicate that Cafco CF Type "D" sprayed fiber is at least as good as Cafco Type "D" in regard to fire resistance. The CF Type "D" may even be slightly better from this standpoint.

Although our test results to date are not 100 per cent conclusive, the indications are that Cafco CF Type "D" will be approved for all of the Floor and Ceiling Designs for which Cafco Type "D" is currently Listed, particularly those incorporating a 1 to 1 blend of cellular and fluted steel deck units and normal weight concrete.

If you should have any further questions regarding this investigation, we would be happy to try to answer them for you so long as we have the permission of United States Mineral Products Company to release our testing information.

Very truly yours,

S. W. BELL
Assistant Engineer
Fire Protection Department

SWB/klr

cc: Mr. Frank M. Stumpf

USM-007234

Figure A–29. Correspondence indicating BLAZE-SHIELD Type DC/F as a suitable replacement for Type D (180-ITK).

SKILLING, HELLE, CHRISTIANSEN, ROBERTSON

Consulting Structural and Civil Engineers · 230 Park Avenue, New York, N. Y. 10017 · MU. 9-8874

John B. Skilling · Helge J. Helle · John V. Christiansen · Leslie E. Robertson

Manager
Wayne A. Brewer

April 1, 1975
File: WTC-Fire

Mr. Malcolm P. Levy
Chief, Planning and Construction
Port Authority of New York & New Jersey
1 World Trade Center - 63rd floor
New York, New York 10048

Dear Mal:

Attached to this letter is a report dealing with the fire safety of specific facets of the twin towers of the World Trade Center.

The report deals with the general topic of the fire resistivity of the floor system. Questions of structural integrity and of heat transmission through the floor are examined. The report is intended to provide background to the reader as to the development of the fire-resistive standards for World Trade Center and looks also at the adequacy of the existing systems.

In preparing these documents, SHCR holds itself out as a reporter of facts--as they are presented in communications gleaned from the files of Port Authority, ERS, MYA and SHCR. It does not purport to have any special expertise not commonly held by other structural engineers. No new literature search or research was accomplished for purposes of this report.

Finally, the data contained in the report is based on logic and analysis and, as such, is not definitive or conclusive. The only way to assure the existence of the fire safety of floor systems is to be found through the participation of a fire safety engineer and/or fire testing.

Please feel free to call on us should you have any questions.

Very truly yours,

SKILLING, HELLE, CHRISTIANSEN, ROBERTSON

Leslie E. Robertson
Enclosure
LER/amh
c.c. Mr. Julian Roth, ERS (Encl)
Mr. M. Yamasaki, MYA (Encl)

RICHARD W. CHAUNER
PAUL S. A. FOSTER
FRANK HOELTERHOFF
ERNEST T. LIU
KENT R. ROGERS
CHARLES A. SANDUSKY
WILLIAM D. WARD
E. J. WHITE, JR.

LORENTS L. WIDING
PETER W. CHEN
ROBERT O. FOWLER, JR.
V. A. PRISADSKY
MICHAEL B. RIGO
HAROLD D. ROET
ROBERT P. ST. GERMAIN
RICHARD E. TAYLOR

ARTHUR J. BARKSHIRE — MANAGER, ALASKA
EDWARD R. WOLFE — BUSINESS MANAGER

SEATTLE OFFICE: 1215 FOURTH AVENUE, SEATTLE, WASHINGTON 98161
ALASKA OFFICE: 601 WEST FIFTH AVENUE, ANCHORAGE, ALASKA 99501

Figure A–30. Excerpts from April 1, 1975 post-fire report prepared by Skilling, Helle, Christiansen, Robertson (3-P).

MANUFACTURERS CATALOGUES

The fireproofing contract was accepted on the basis of the Mario and DiBono Plastering Co., Inc. proposal dated March 17, 1969. While SHCR is not privy to the contents of that proposal, it is likely that it contains only finanical and catalogue information.

The only Cafco catalogue available to SHCR (excluding current issues of 1975) is the one supplied by Mr. Monti to Mr. Levy in September 20, 1967 (see -appendix). The catalogue cites ULI #R3749-6, ULI R3789-2 and ULI #R3749-13 for the spray fireproofing of beams. From the catalogue one can determine that:

(1) The product has been subject to extensive ULI testing; and
(2) for "beams, girders and spandrels", a thickness of 1/2 inch of Blaze-Shield Type D (the product used in World Trade Center) provides a 4 hour rating.

The catalogue does not report on fireproofing of trusses.

-11-

SKILLING, HELLE, CHRISTIANSEN, ROBERTSON

Figure A–30 (Contd.). Excerpts from April, 1 1975 post-fire report prepared by Skilling, Helle, Christiansen, Robertson (3-P).

LACLEDE COMPOSITE FLOOR TRUSSES

FIRE RESISTIVITY - TOP CHORD

Introduction

The Laclede trusses used in the construction of The World Trade Center are a standard product manufactured from specially-rolled angles used in conjunction with round-bar webs. To achieve composite action the webs extend into the concrete slab so as to effect the required shear transfer.

In The World Trade Center the top chords are not spray fireproofed for selected areas of the work. Specifically, for the most of the one-way span areas directly out from the service core, the top chords are not always spray fireproofed. Also bridging trusses are not spray fireproofed.

This paper addresses itself to reasons of structural engineering as to why spray fireproofing may not be required.

Structural System - Top Chord

First, a discussion of the role of the steel top chord in the overall structural system:

1) Construction Period:

a) Acting in conjunction with the bottom chord and the web, the steel top chord completes the trusswork providing primary structural support for the concrete slab until such time as the slab has achieved design strength.

Fireproofing of the steel top chord is not required for reasons of construction loading.

b) Acting as a beam, spanning from truss panel point to truss panel point, the top chord supports a small amount of concrete until such time as the concrete has attained design strength.

Fireproofing of the steel top chord is not required for reasons of construction loading.

2) Supporting Gravity Loads:

a) Once concrete strength has been achieved, the capabilities cited under 1) are modified. The concrete slab becomes the dominant element of the top chord. So long as the shear knuckle is maintained, the structural integrity of the steel top chord is not required.

-13-

SKILLING, HELLE, CHRISTIANSEN, ROBERTSON

Figure A–30 (Contd.). Excerpts from April, 1 1975 post-fire report prepared by Skilling, Helle, Christiansen, Robertson (3-P).

Since the top chord may be cut without loss of structural integrity, we concur that fireproofing of the steel top chord is not required for this purpose.

b) Where a given shear knuckle is not adequate to transfer panel point loads directly into the slab, then an increment of the load must be taken down the steel top chord to the next knuckle. This condition exists only in the corner, two-way portion of the floor. We concur that fireproofing of the steel top chord is required and is provided for this purpose.

3) Assisting in Diaphragm Strength:

a) The concrete slab, with its mesh and bar reinforcing provides for diaphragm strength within the building. As structure sway under wind load increases, the need for diaphragm strength increases. Structural steel top chords provide a kind of reinforcing steel and add to diaphragm strength. While diaphragm strength is not required by Code, we know it to be essential to the proper behavior of the structural system. We do not believe it to be proper to design for the combined circumstance of an extreme wind and an extreme fire with the same factor of safety as that associated with the single event alone.

Since the structural steel top chord provides only a small increment in the diaphragm strength, we concur that fireproofing may be omitted for this purpose.

Structural System - Bridging

The bridging system is used only to provide for the reduction in floor "tremor" and to reduce the effects of differential deflections associated with heavy gravity loads.

Since it is not required as a part of the structural system, we concur that fireproofing may be omitted for these members.

Conclusions

Fireproofing of the top chords of floor trusses is required and is provided in the two-way portions of the floor systems.

A logical analysis indicates that fireproofing of the structural steel top chord and of the bridging is not required so long as the risk of the joint occurrence of an extreme value wind storm and a fire is accepted. Over much of the two buildings, fireproofing has been provided.

-14-

SKILLING, HELLE, CHRISTIANSEN, ROBERTSON

Figure A–30 (Contd.). Excerpts from April 1, 1975 post-fire report prepared by Skilling, Helle, Christiansen, Robertson (3-P).

PERFORMANCE IN SERVICE

The fire of February, while reported in the press to have been very hot, did not damage a single primary, fireproofed element. Some top chord members (not needed for structural integrity, some bridging members (used to reduce floor tremor and the like) and some deck support angles (used only as construction devices) were buckled in the fire--all were unfireproofed steel.

The SHCR report of fire damage, including all repairs, is attached in the appendix.

As requeste by Port Authority Engineering Department and by SHCR, shores were placed in the vicinity of repairwork. This was done, not because of concern for damaged structure, but as a matter of prudence to avoid the accidental destruction of needed structure by over-zealous steel workers.

It is likely that this fire did not provide the ultimate test of fire-resistivity. More severe fires will likely strike the project. However, since only non-essential, non-fireproofed elements of the floor assembly were damaged, some optimism can be expressed.

SKILLING, HELLE, CHRISTIANSEN, ROBERTSON

Figure A–30 (Contd.). Excerpts from April, 1 1975 post-fire report prepared by Skilling, Helle, Christiansen, Robertson (3-P).

March 7, 2003

John L. Gross, Ph.D., P.E.
Leader, Structures Group
National Institute of Standards and Technology
100 Bureau Drive, Stop 8611
Gaithersburg, MD 20899-8611

Re: Confidential and Pre-decisional Communication – Questions on Fire Resistance of the WTC Floor System

Dear John:

Following are the Port Authority (PA) responses to your questions:

Questions to the Port Authority of New York & New Jersey, February 26, 2003

1. In a letter from ERS (Julian Roth) to PoNYA (Malcolm Levy) dated December 14, 1965, it had apparently been decided that the fire protection of the WTC floor system would involve "the use of a maximum thickness of one inch spray-on fireproofing material around the individual components of the floor trusses." It was further stated that "one inch material meets the 3-hour requirements of both the new code (New York City Building Code under revision in 1965 and ultimately published in 1968) and Underwriter's (Underwriter Laboratories, Inc.) using previously approved assemblies tested by the 'load criteria' method but ignoring the more stringent time-temperature-rate-of-rise criteria which is an alternate testing procedure not required by the new code or by Underwriter's, and which we do not consider necessary."

   In a follow-up letter from ERS (Julian Roth) to PoNYA (Malcolm Levy) dated December 22, 1965, the PA is advised that "advance information from manufacturers indicates that if the truss were required to be fire-tested, then two inches of material would be required for light angle members."

   In a letter from ERS (Harry Harman) to PoNYA (Malcolm Levy) dated July 25, 1966, it is stated "Obviously, with so many penetrations of the floor system [4" concrete slab over a metal deck] the fire rating of the floor construction is of an indeterminate value unless tested."

   1) Were tests performed on the fire resistance of the composite floor system during the design or construction phase of the project?

   PA Response: **There are no test records in our files.**

Figure A–31. Response from Port Authority regarding the applied thermal insulation (678-P).

2. In a letter dated October 30, 1969, from PoNYA (Robert Linn) to Mario & DiBono Plastering Co., Inc, the contractor is directed as follows: "bar joists requiring spray-on fireproofing are to have 1/2" covering of 'Cafco'."

   2) Was ½ inch of Cafco Type-D fireproofing specified for the floor trusses requiring spray-on fireproofing?

   PA Response: Thickness was not specified on the drawings. PA is still trying to locate the original specifications, which NIST is aware of. The letters you reference and quote in your questions are snapshots in time. The culmination of these written exchanges led to what was finally called for in the original specifications that were part of the contract documents. In the absence of the original specifications, we must rely on the actual measured thickness of the fireproofing. Over the years, this has been documented to be a nominal ¾ inches.

   It should be kept in mind that the fireproofing determinations were made in the context of buildings that were to be constructed without a sprinkler system. Following the enactment of Local Law 5 in New York City, a complete sprinkler system was added to the towers over a period of years, thus reducing the overall reliance on the truss joist fireproofing for fire protection.

3. In a report by SHCR prepared for the PANYNJ dealing with "the fire safety of specific facets of the twin towers of the World Trade Center" following the 1975 fire, it is stated that the 4 inch slab exceeds the commonly used (and therefore accepted by the NYC Building Dept.) 3-1/4 inch slab on metal deck without fireproofing.

   3) Was the underside of the floor slab (metal deck) fireproofed?

   PA Response: No.

4. In this same report by SHCR prepared for the PANYNJ, it is stated that, fireproofing of the top chord of the floor trusses is not necessary (except for the two-way portion of the floor). Additionally, it is stated that fireproofing of the bridging system is not required.

   4a) In the one-way portions of the floor system, were the top chords of the composite floor trusses fireproofed?

   PA Response: Yes.

   4b) In the one-way portions of the floor system, were the bridging trusses fireproofed?

Figure A–31 (Contd.). Response from Port Authority regarding the applied thermal insulation.

PA Response: **Yes.**

5. It is our understanding that initially the spray-on fireproofing contained asbestos. We also understand that, at some point, asbestos was not permitted and a Cafco product that contained mineral wool instead of asbestos was substituted.

5a) Is the situation stated here correct?

PA Response: **Yes.**

If so,

5b) What floors of which towers were fireproofed with the asbestos-containing product?

PA Response: **For the tower floor system, only steel trusses in Zone 1(44th floor and below) in Tower 1 were fireproofed with asbestos containing product.**

5c) Was the asbestos-containing "fireproofing" removed?

PA Response: **Yes.**

I hope these responses are helpful. If you have any further questions please send them to us.

Sincerely,

o/s/b

Joseph M. Englot, P.E.
Asst. Chief Engineer/Design

CC: F. Lombardi

Figure A–31 (Contd.). Response from Port Authority regarding the applied thermal insulation.

.O: B. Weinstien, Project Manager (TRCC) DATE: March 25, 1970
FROM: D. L. Brown
SUBJECT: THE WORLD TRADE CENTER CONTRACT 113.00 - MARIO DIBONO PLASTERING CO. SPRAY ON FIREPROOFING - TOWER A & B - INSPECTION
REFERENCE:

COPIES: P. Balduzzi, R. Linn, M. Levy, R. Monti, T. Calabrese, F. Werneke

During a routine inspection trip on March 19, 1970, I had occasion to discuss with Frank Tartamella, superintendent, the status of work under the subject contract. In the course of this conversation I reminded Frank Tartamella that Mario DiBono still had to complete the core columns spray-on fireproofing of Tower A core columns up to the 28th floor as these columns are unsatisfactory having only ½" to 3/4" of fireproofing not the 1 3/16 inches required. He stated that I should direct this matter to his office as he did not plan to do any further work on these members. Please again remind the contractor that this work is not acceptable to this office, also that they are to fireproof the under side of the electrical header ducts.

D. L. Brown
Supervising Engineer
The World Trade Center

DLB:mb

Figure A–32. Correspondence indicating that thickness of thermal insulation was being checked during construction (256-P).

K-127

(212) 964-2691

Tishman Realty & Construction Co., Inc.

AS AGENTS FOR THE PORT OF NEW YORK AUTHORITY
WORLD TRADE CENTER
30 CHURCH STREET, NEW YORK, N.Y. 10007

MARCH 30, 1970

R. Brown
~~FOLLOW-UP~~
4/6/70 ~~Call to D. Brown~~

MARIO & DIBONO PLASTERING
136 LIBERTY STREET
NEW YORK, NEW YORK 10006

ATTENTION: MR. F. TARTAMELLO

RE: WTC/113.00 9
INSUFFICIENT THICKNESS

GENTLEMEN:

REFERENCE IS MADE TO OUR LETTER DATED JANUARY 9, 1970 WITH FOLLOW-UP COPIES SENT DATED JANUARY 19TH AND FEBRUARY 6TH, IN ADDITION TO PHONE CALLS ON THE SUBJECT, ADVISING YOU OF THE INSUFFICIENT THICKNESS OF SPRAY-ON FIREPROOFING ON CORE COLUMNS.

WE ARE NOW IN RECEIPT OF A COMMUNICATION FROM THE PORT OF NEW YORK AUTHORITY REITERATING THE SAME ITEM.

BE ADVISED THAT TO CONTINUE TO IGNORE THESE COMMUNICATIONS WILL REQUIRE US TO ADVISE THE PORT OF NEW YORK AUTHORITY TO SEEK COMPENSATION AMOUNTS FROM YOUR CONTRACT PRICE, COMMENSURATE WITH THE WORK WHICH IS INCOMPLETE PLUS ANY COSTS INVOLVED IN REMOVING AND REPLACING WORK BY OTHERS WHICH MAY, DUE TO THIS LONG DELAY, COVER YOUR WORK.

VERY TRULY YOURS,

TISHMAN REALTY & CONSTRUCTION CO., INC.

BERT WEINSTEIN
PROJECT MANAGER

BW/BMS

CC: MESSRS. MONTI, WERNEKE, P/A

Figure A–32 (Contd.). Correspondence indicating that thickness of thermal insulation was being checked during construction (256-P).

ORIGINAL

Port Authority of N.Y and N.J.
Litigation Sampling Program

JOB NUMBER 115-245

Sample Area Data Sheet

Facility: ONE World TRADE Center Building: Tower Building One

Building No: 1 Floor: 29th Floor Sample Size Vial, 4OZ.

Description of Sampling Area: 29th Floor

Sample Numbers: Additional Sample #'s on the following page →

LL-389-WTC-A,B,C	LL-395-WTC-A,B,C	LL-401-WTC-A,B,C	LL-
LL-390-WTC-V,A,B,C	LL-396-WTC-A,B,C	LL-402-WTC-V,A,B,C	LL-
LL-391-WTC-A,B,C	LL-397-WTC-A,B,C	LL-403-WTC-A,B,C	LL-
LL-392-WTC-A,B,C	LL-398-WTC-A,B,C	LL-404-WTC-A,B,C	LL-
LL-393-WTC-V,A,B,C	LL-399-WTC-V,A,B,C	LL-	LL-
LL-394-WTC-A,B,C	LL-400-WTC-A,B,C	LL-	LL-

Form of Asbestos Material	Location of Asbestos Material
✓ Sprayed-On	✓ Support Beams/Columns
✓ Troweled-On/Cementitious	✓ Concrete Slab/Metal Decking
___ Plaster	___ Cable
___ Acoustical Plaster	___ Duct/Breeching
___ Air Cell	___ Floors
___ Molded Sections/Pads	___ Heating/Cooling Equiptment
___ VAT	___ Ceilings
___ Ceiling Tile	___ Piping/Fittings
___ Other:	✓ Other: Troweled on wall support Be

Comments: (Indicate any unique characteristics of the material which may help identify the manufacturer.)

Sample taken by: Frantz Dambreville, Frank Pergola Date: 03/12/90.

Persons Present Frantz Dambreville, Frank Pergola, Charles Kondakjia

Photographs Taken By: Frantz Dambreville, Frank Pergola

1 1 D 0 Signature Frank Pergola 03/14/90

Figure A–33. Example of "Sample Area Data Sheet" used to record condition of sprayed thermal insulation (212 ITK).

ORIGINAL

Job Number 115 • 245

COMMENTS

South West quadrant → fluffy spray-on fireproofing coating the support Beams, joists, and deck above the ceiling. the thickne of the material on the Beams and joists was consistently about ½". Regarding the deck it ranged from very sparce in areas to ¼" in other areas. The Areas we sampled were coated with a Light green encapsulant.

NorthWEST quadrant → Fluffy spray-on fireproofing. The Beams and joists were coated with about ½" of material. the deck ranged from ¼" to Barely nothing. this Section was also coated with a Light green encapsulant.

North East quadrant → Fluffy spray-on fire proofing the Beams and joists were coated with @ ½" of material the deck was coated with @ ¼" of material in this section. the Light green encapsulant was presEnt in this area.

South East quadrant → fluffy spray-on fire proofing. Beams and Joists were coated with @ ½" of material the deck was coated with ¼" of material. Sample area was coated with encapsulant. One Sample from a Vertical Support Beam on the outermost wall, was a grayish cementitious material @ ¼" thick.

* the only Samples that were free from the encapsulant were those taken from the top of the Support Beam. (LL-395-WTC LL-397-WTC)

Figure A–33 (Contd.). Example of "Sample Area Data Sheet" used to record condition of sprayed thermal insulation (212 ITK).

THE PORT AUTHORITY OF NEW YORK & NEW JERSEY

MEMORANDUM

TO: Peter Sweeney, Engineering Program Manager
FROM: Joseph M. Englot
DATE: August 18, 1995
SUBJECT: **STEEL JOIST SPRAY-ON REQUIREMENTS FOR NEW CONSTRUCTION IN WORLD TRADE CENTER TOWERS**

COPY TO: R. Davidson, J. Lin, F. Lombardi, E. Ramabhushanam, O. Suros

Attached is a white paper summarizing a study to determine the spray-on thickness required to achieve the required two hour rating for steel joist trusses in the towers of the World Trade Center. This is intended for any new construction for which the Engineering Department is engineer-of-record. It concludes that 1-1/2 inches of spray-on mineral fiber is sufficient when applied directly to chords and web members.

Joseph M. Englot, P.E.
Chief Structural Engineer

JME:ng

Attachment

Figure A–34. Results of 1995 study of thermal insulation for floor trusses during new construction when tenants vacated spaces (3-P).

FIREPROOFING REQUIREMENTS FOR WORLD TRADE CENTER TENANT FLOOR JOIST CONSTRUCTION THAT REQUIRES INSTALLATION DUE TO ASBESTOS REMOVAL OR LOCAL REMOVAL TO FACILITATE CONSTRUCTION

This serves as a basis for determining the minimum requirements for installing sprayed mineral fiber fireproofing on the steel floor joist trusses supporting typical tenant floor areas within the towers of the World Trade Center. Its purpose is to establish requirements for new construction that meet local codes and ordinances.

The technical basis for the fireproofing requirement is Design No. G805 in the Fire Resistance Directory (BXRH) Published by Underwriters Laboratories. This UL design is based upon fire tests conducted as per ASTM E-119 which is a basic Reference Standard (No. RS5-2) in the New York City Building Code for structural members and assemblies. Reference standard RS5-1F, "Methods of Analytical Determination of Fire Resistance of Load Bearing Steel Truss Assemblies", is not applied since it is intended for large trusses (i.e., deep trusses), too large to fit in the fire test compartments. Since there is a wealth of fire tests on steel joists which approximate the ones used in the World Trade Center, joist test results are interpreted to arrive at an appropriate spray-on protection thickness.

There are various parameters in the G805 design which have to be interpreted or approximated in the case of World Trade Center construction. Each parameter will be discussed individually.

Joist Spacing

G805: 48 inch and 66 inch spacing.
Actual: Double joist system - average joist spacing is 40 inches (spacing alternates between 8 inches and 72 inches). Conservatively, use values for 66 inches since actual spacing is not uniform.

Metal Deck Protection

G805: Values tabulated with or without spray-on applied to bottom of metal deck.
Actual: Use values without spray-on applied to deck. Spray-on is only used in the World Trade Center below trench headers. Follow design values without protected deck.

Concrete Topping

G805: Values tabulated for lightweight concrete, 117 pcf unit weight, 3500 psi compressive strength and a thickness of topping over the metal deck of 3-7/8 inches to achieve a 2 hour rating.
Actual: Lightweight concrete, 110 pcf unit weight, 3000 psi compressive strength and a thickness of topping over the metal deck of 4 inches. The actual is judged equivalent to the G805 design for 2 hour rating.

Wire Mesh Location

G805: Provides a thickness of concrete from the top plane of the metal deck to the wire fabric of 1-1/4 inches for a 2 hour rating with 1-5/16 inch deep steel form unit.
Actual: Has two layers of wire mesh. Thickness from top plane of 1-1/2 inch metal deck to center of wire mesh layers is 1.22 inches. Where rebar is used instead of wire mesh, 1-1/4 inch thickness

Figure A–34 (Contd.). Results of 1995 study of thermal insulation for floor trusses during new construction when tenants vacated spaces (3-P).

is provided. This is judged to be equivalent to the G805 design for 2 hour rating.

Steel Joist Parameters

G805: Composite steel joist with a minimum area of steel (double angles) for top and bottom chords (each) of 0.708 sq. inches and minimum steel area of web members of 0.442 sq. inches in conjunction with the "thinner" layer of spray-on (1-1/2 inches) applied directly to the joist without lath.

Actual: Minimum area of chords is 0.813 sq. inches and the minimum area of web steel is 0.665 sq. inches with composite behavior. 1-1/2 inches applied directly to the joist steel yields a two hour assembly rating whether restrained or unrestrained.

Ceiling

G805: A ceiling is not relied upon for fire protection in the design.

Actual: All occupied areas in the World Trade Center have ceilings and they will add to the fire rating of the floor system, however, a stringent study of what rating values could be achieved for existing types of ceilings is beyond the scope of this study.

Conclusion

It is concluded that a two hour fire rating for the steel floor joist trusses can be achieved by applying a 1-1/2 inch thickness of spray-on mineral fiber fire protection material directly to the steel truss chords and webs. The value of the ceiling as a fire protection element is not relied upon to achieve this fire rating.

Attachments:

1. Excerpted pages from N.Y.C. Building Code.
2. G805 Design from U.L. Directory

Figure A–34 (Contd.). Results of 1995 study of thermal insulation for floor trusses during new construction when tenants vacated spaces (3-P).

Design No. G805

Restrained Assembly Ratings — 1, 1-1/2, 2 or 3 Hr (See Items 1, 4 and 5)
Unrestrained Assembly Ratings — 1, 1-1/2 or 2 Hr (See Items 1, 4 and 5)
Unrestrained Beam Ratings — 1, 1-1/2 or 2 Hr (See Item 5)

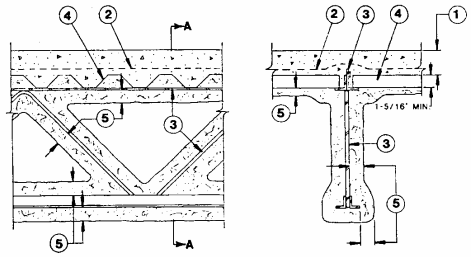

SECTION A-A

1. **Normal-Weight Or Lightweight Aggregate Concrete** — Normal weight concrete carbonate or siliceous aggregate, 150 pcf unit weight, 3500 psi compressive strength, vibrated. Lightweight concrete, expanded shale, clay or slate aggregate by rotary-kiln method, 117 pcf unit weight 3500 psi compressive strength, vibrated, 2 oz air entrainment per bag of cement. The thickness of concrete topping over the top plane of the steel deck varies according to the spacing of the structural steel members, the hourly ratings and whether or not the steel deck is protected. When no Spray-Applied Fire Resistive Materials protection is used on the steel deck, the thickness of concrete topping over the top plane of the steel deck shall be as specified in the following table:

Restrained or Unrestrained Assembly Rating Hr	Normal Weight Concrete Topping Thk In Joist Spacing 48 In. OC Max	Normal Weight Concrete Topping Thk In Joist Spacing 66 In. OC Max	Lightweight Concrete Topping Thk In Joist Spacing 48 In. OC Max	Lightweight Concrete Topping Thk In Joist Spacing 66 In. OC Max	Min Thk of Concrete From Top Plane of Steel Deck to Bottom of Reinforcement In.
1 h	3-1/8	3-7/8	2-3/8	3-7/8	1
1-1/2 h	3-7/8	3-7/8	2-7/8	3-7/8	1-1/8
2 h	4-5/8	4-5/8	3-3/8	3-7/8	1-1/4

When the steel deck is protected with the Spray-Applied Fire Resistive Materials, the min thickness of normal weight or lightweight concrete topping above the top plane of the steel deck, and the min thickness of concrete from the top plane of steel deck to the wire fabric, shall be as follows:

Restrained or Unrestrained Assembly Rating Hr	Min Concrete Topping Thk In Joist Spacing 48 In. OC Max	Min Concrete Topping Thk In Joist Spacing 66 In. OC Max	Min Thk of Concrete From Top Plane of Steel Deck to Bottom of Reinforcement In.
2 h or less	2-3/8	2-3/8	1-1/8
3 h	2-3/8	3-7/8	1-1/4

2. **Welded Wire Fabric/Reinforcing Bars** — As required, to develop the structural capacity of the floor in accordance with the applicable ACI specifications.
3. **Structural Steel Members*** — Composite joists with vertical leg of top chord angles embedded in concrete slab. Min area of steel angles for the top and bottom chord members shall be 0.708 sq in. each, and the min area of web members shall be 0.442 sq in. when the sprayed material is applied directly to the joists. Min area of steel angles for the top and bottom chord members may be reduced to 0.560 sq in. each, and the min area of web members to 0.299 sq in. when the joists are protected with greater thickness of Spray-Applied Fire Resistive Materials with or without the metal lath or the nonmetallic fabric, as covered in

the Table under Item 5. Max joist spacing is 48 or 66 in. O. C. depending on the thickness and type of concrete topping, the hourly ratings, and the thickness of Spray-Applied Fire Resistive Materials applied to the steel deck (see Items 1 and 5).

VESCOM STRUCTURAL SYSTEMS INC —Type V.

3A. **Steel Joists — (Not Shown)** — As alternate to Item 3, Min size 16K6 or heavier K-Series joist with min 3/4 in. diam or larger cross sectional area web members.

3B. **Horizontal Bridging — (Not Shown)** — Min 1-1/4 by 1-1/4 by 1/8 in. thick steel angles for use with steel joists (Item 3A). Size and spacing per Steel Joist Institute specifications. Welded to top and bottom chords of each joist. Min thickness of Spray-Applied Fire Resistive Materials on bridging angles is 1-1/2 in.

4. **Steel Floor and Form Units** — For max 2 h ratings, nom 1-5/16 in. deep uncoated or galv corrugated steel form units. For 3 h ratings, composite or noncomposite, min 1-1/2 in. deep, 22 gauge uncoated or galv fluted steel floor units. The steel floor and form units are not considered in calculating the load carrying capacity of the floor.
5. **Spray-Applied Fire Resistive Materials*** — All surfaces to which material is applied must be free of dirt, loose scale and oil before spraying. Applied by mixing with water and spraying in more than one coat to the required thickness on the joists and the steel form units as tabulated below:

Min Area of Joist Chord Sq In.	Min Area of Joist Web Sq In.	Thk of Spray Applied Fire Resistive Mtl In. on Steel Deck: Normal Weight Concrete Topping	Lightweight Concrete Topping	on Joist	Hr Rating: Restrained Assembly Rating Hr	Unrestrained Assembly Rating Hr	Unrestrained Beam Rating Hr
0.708	0.442	3/8	—	1-1/2	1	1	1
0.708	0.442	3/4*	3/8	1-1/2	2	2*	2*
0.708	0.442	1-1/4	1	1-1/2	3	2	2
0.560	0.299	3/8	—	2-1/2**	1	1	1
0.560	0.299	3/4	3/8	2-1/2**	2	2	2

Min avg and min ind density of 13/11 pcf, respectively for Types II or DC/F. Min avg and min ind densities of 22 and 19 pcf, respectively, for Type HP. For method of density determination, see Design Information Section, Sprayed Materials.

*The 3/4 in. thickness may be reduced to 1/2 in. when (a) the joist spacing does not exceed 48 in. O. C. or (b) the Unrestrained Assembly and Beam ratings are reduced from 2 to 1-1/2 h.

**The 2-1/2 in. thickness of Spray-Applied Fire Resistive Materials shown may be reduced to 2 in. when the metal lath or the nonmetallic fabric mesh is used.

ISOLATEK INTERNATIONAL —Type D-C/F, HP or Type II, Type EBS or Type X adhesive/sealer optional.

6. **Metal Lath** — (Optional, not shown) — Metal lath may be used to facilitate the spray application of Spray-Applied Fire Resistive Materials to steel bar joists. The diamond mesh, 3/8 in. expanded steel lath, 1.7 to 3.4 lbs per sq yd should be secured to one side of each steel joist with 18 SWG galv steel wire at joist web and bottom chord members, spaced 15 in. O. C. max. When used, the metal lath is to be fully covered with Spray-Applied Fire Resistive Materials with no min thickness requirements.
7. **Non-Metallic Fabric Mesh** — (Optional, not shown) — As an alternate to metal lath, glass fiber fabric mesh — weighing approximately 2.5 oz per sq yd, polypropylene fabric mesh — weighing approximately 1.25 oz per sq yd, or equivalent, may be used to facilitate the spray application. The mesh should be secured to each joist web member and/or the chords to hold the mesh and the Spray-Applied Fire Resistive Materials material in place during application. One method for attaching the mesh is by embedding it in 1/4 in. long beads of hot melted glue spaced a max of 12 in. O. C. along the top chord of the bar joist. Another method is by using 1-1/4 in. long by 1/2 in. wide hairpin clips formed from 18 SWG or heavier steel wire.

*Bearing the UL Classification Mark

Figure A–35. Underwriters Laboratories Design No. G805 used as the basis for Port Authority determination of retrofit thermal insulation thickness for floor trusses (213-I).

THE PORT AUTHORITY OF NEW YORK AND NEW JERSEY

CHIEF ENGINEER'S OFFICE
P.A. OF N.Y. & N.J.
RECEIVED

BUCKSLIP

1999 MAR 25 PM 3:28

J. Spencer
Div Mgrs
Dinkelo
Eyler
FYI
3/26

TO: John Castaldo, Kent Piatt
FROM: Alan L. Reiss
DATE: March 24, 1999
SUBJECT: **World Trade Center Fireproofing Guidelines For Tenant Spaces**

COPY TO: E. McGinley, T. Kobel, F. Lombardi J. Richardson, J. Napolitano, R. Rafferty, L. Menno, E. Moscovitz, C. Nanninga, N. Seliga, T. Stam

In order to establish clear and consistent guidelines regarding fireproofing repairs, replacement, and upgrades at the World Trade Center Towers, the following guidelines have been established with the concurrence of the Chief Engineer.

1) Full floors being demolished for new construction or renovation shall have the fireproofing on trusses checked and upgraded if it has not already been done to the attached 1995 Engineering Department Engineered Solutions Standard. Adequate time must be allowed in any schedule to accommodate this work, typically two weeks. This work may be performed by either the tenant or us but is a landlord obligation and reimbursable to the tenant (typically $5/sq. ft.) if the work is performed by the tenant. Refireproofing requires removal of existing material to insure adequate bonding and is subject to a controlled inspection.

2) Tenant spaces that are less than a full floor, undergoing either new construction or renovation, need only meet the original construction standard. Fireproofing shall be inspected and patched as required to the greater of ¾" or to match existing (it may already have been upgraded to the Engineered Solutions Standard.)

3) On a new lease, trusses requiring patching at the time of tender of the space are a landlord obligation, however, we normally will reimburse fair and reasonable costs if performed by the tenant after authorization. For existing tenant space being renovated, careful judgement should be used to determine if the need for the work arose as a result of a tenant action, i.e. previous construction work, or our obligation because of our work over the years in the ceiling. Any recommendation should be discussed with project and property management prior to being discussed with the tenant.

AT	AF	BF	CJL	RP	SB	
2D	MAR 26 1999					MA
						RS
FILE	C. JOHN LIN MANAGER Q.A.D.					IR
POST						RTN

Alan L. Reiss
Director
World Trade Department

Figure A–36. Port Authority 1999 guidelines for thermal insulation on floor trusses (3-P).

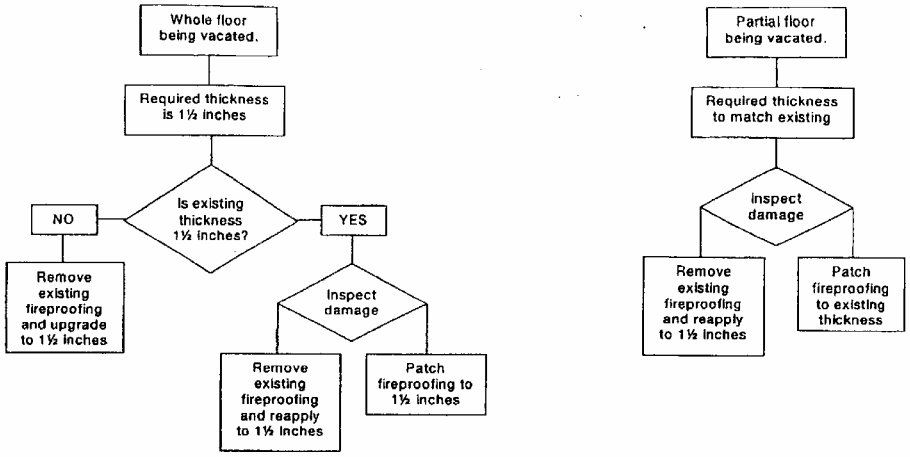

Figure 1: Fireproofing assessment process

Damage of existing fireproofing

Significant amounts of damage to the existing fireproofing occur during demolition after tenants move out. The product used in the past can be easily dislodged as ductwork, partitions, hangers, etc. are removed. Additional damage that happened during tenant fit-out or later modifications that may not have been repaired at the time.

As we understand it, in the majority of cases, the existing fireproofing requires so much patching that it is more cost-effective to replace it.

Repairs

If the damaged fireproofing is to be patched rather than replaced, the cementitious Monokote product is generally used regardless of what the in situ fireproofing material is. This can result in joists that are fireproofed by a combination of materials. This patching is generally done by hand rather than spray application. Repairs are made such that a constant thickness of fireproofing is provided to all joist members.

Removal

The Cafco Blaze-Shield fireproofing is readily removed using a high-powered water jet. The water from the jet is soaked up by the fireproofing which falls to the floor in a damp state. Usually all the water is absorbed by the fire proofing, however, on occasion water does leak onto the floor below. The floor is covered with protective sheets. The fireproofing is collected from these sheets and transported in waste buckets to a waste disposal area.

Any portions of fireproofing that are not removed by the jet are scraped away by hand. This often happens if there are sections of Monokote fireproofing and in the troughs that are formed at the bottom flange of the joist by the back-to-back angles. If the Monokote cannot be removed by hand, it is assumed to be fixed in place and is covered by the new fireproofing applications.

Application

When the fireproofing needs replacing, new fireproofing is applied to a thickness of 1½ inches. While equivalent products are permitted, Cafco Blaze-Shield mineral fiber spray is generally used as the replacement fireproofing.

It is estimated that 60-70% of the material is lost to overspray.

It can take 2-3 passes to apply 1½ inches. If it is done in fewer passes, the fireproofing tends to fail the adhesion tests that are conducted after application. Sometimes ten feet fall off at once when tested.

Figure A–37. Excerpt from draft report on the assessment of thermal protection of steel in WTC (73-LERA).

SECTION 07250 – FIREPROOFING

Work includes, but is not necessarily limited to, the following:

Patching fireproofing damaged by installation of new construction.

Patching or replacing of existing or new fireproofing where required to meet code.

Single Source Responsibility: Obtain fireproofing materials from a single manufacturer for each different product.

Fire Resistance Ratings: As indicated by reference to design designation in UL "Fire Resistance Directory" for fire-rated assemblies in which fireproofing serves as direct-applied protection, tested per ASTM E 119.

Minimum fire resistance rating shall be 2 hours on decking floor assemblies, 3 hours on bearing columns, unless indicated on the drawings otherwise.

Provide appropriate MEA/BSA numbers for approved use in New York City.

Underwriters' Laboratories, Inc. – Fire Resistance Index.

JOB CONDITIONS

Provide ventilation in area to receive sprayed fireproofing, introducing fresh air and exhausting air continuously during and 24 hours after application to maintain non-toxic, unpolluted, safe working area.

Provide temporary enclosures to prevent spray from contaminating air.

WARRANTY

On completion, furnish a certificate confirming that work complies with these Specifications.

FIREPROOFING MATERIALS

Cementitious self-adhesive compound containing no asbestos, no free crystalline silica and no mica, for spray application, minimum density 13-15 pounds per cubic foot: "Monokote 6" by W.R. Grace, conforming to the following:

Dry density as required for prescribed rating and thickness: ASTM E605.

Minimum acceptable bond strength 100 psf: ASTM E736.

No cracking or delamination under deflection of 1/120 of span or under impact of 60lb.: ASTM E759, E760.

10% maximum acceptable deformation: ASTM E761.

Maximum acceptable weight loss .02 gms/sq. ft.: ASTM E859.

Bonding adhesive and sealer for fireproofing: Cafco Bond Seal, diluted 3 parts to 1 part clean potable water.

MIXES: In accordance with manufacturer's instructions.

APPLICATION

Apply bonding adhesive or primer to substrate as recommended by manufacturer.

Apply fireproofing over substrate, building up to required thickness with as many passes or stages necessary to cover substrate with monolithic blanket of uniform density and texture.

Tamp fireproofing after application to provide a dense, medium smooth surface.

Apply sealer or curing compound to surface of fireproofing if recommended by manufacturer, in a space serving as a plenum.

Provide protection to space and occupants when working adjacent to or over tenant areas. Work shall be done off hours if directed by the Landlord.

Patching

Patch damage to this work caused by other trades before fireproofing is covered up.

Uncover work covered before final approval for inspection before acceptance is granted.

Patch existing sprayed fireproofing which has been removed for attachment of new construction, and restore to required fire resistant rating.

Figure A–38. Excerpt from 1998 specification related to SFRM for upgrade of public corridors and bathrooms on 15th, 18th, and 22nd floors of WTC 2 (3-P).

SECTION 07250 – FIREPROOFING

SUMMARY
1. Patch fireproofing disturbed by remodeling operations.

PRODUCTS
1. Fire Performance: ASTM E 119, and local regulations. Cementitious Type for Concealed Use: 15 pounds per cubic foot dry density,
2. ASTM E 605.
3. Mineral Fiber Type for Concealed Use: 15 pounds per cubic foot dry density, ASTM E 605.
4. Exposed Sprayed–On Fireproofing: Match existing.

INSTALLATION
1. Inspect existing and new structural members for proper fireproofing prior to close–in of ceilings and walls.
2. Provide material thicknesses necessary to provide fire–resistance ratings indicated or required by authorities having jurisdiction.

SECTION 07270 – FIRESTOPPING SUMMARY

1. Provide Firestopping at the Following Locations: Penetrations through fire–resistance–rated floor and roof construction; Penetrations through fire–resistance–rated walls and partitions; Penetrations through smoke barriers and construction enclosing compartmentalized areas; Sealant joints in fire–resistance–rated construction.

PRODUCTS
1. Fire Performance: ASTM E 119, ASTM E 814, and local regulations.
2. Through–Penetration Firestop Systems: Ceramic–Fiber and Mastic Coating; Endothermic, Latex Compounds; Intumescent Latex Sealant; Intumescent Putty.
3. Fire–Resistive Elastomeric Joint Sealants: Single–component, neutral–curing, silicone sealant; Multicomponent, nonsag, urethane sealant; Single–component, nonsag, urethane sealant.

INSTALLATION
1. Inspect existing and new work for proper firestopping prior to close–in of ceilings and walls.
2. Provide material thicknesses necessary to provide fire–resistance ratings indicated or required by authorities having jurisdiction.

Figure A–39. Excerpt from 2001 specification related to SFRM for upgrade on 48th floor of WTC 2 (3-P).

Executive Summary

The development of fire safety engineering and in particular the performance of structure during fire has been developing rapidly over the last 5 years. Buro Happold has identified the value and benefits of this work to many of our global clients. This has required major investment in research and development, involvement with the development of new codes, working with government and the employment of staff as part of a technology transfer from the universities carrying out this research. The ultimate aim is to ensure that the research and development is used in practical way for real buildings in a short but realistic time scale. The extent to which fire safety engineering can be used in this respect has to be based on the local code development, the attitude of the client and the authorities having jurisdiction.

The USA has been party to this development and now has its own performance based design codes. Historically fire safety engineering in the USA has only been done on special or difficult projects. However as the benefits are understood and are more widely accepted the quantity of performance based design is likely to increase significantly. This work on the World Trade Centre is significant and well contained example of what is possible now as a relatively low risk early development.

The components of this global development that have been most important from the point of view of the World Trade Centre are.

1. Better understanding and the analysis of natural fires.
2. Analysis of structures at high temperatures during fire.
3. Improving relationship and understanding between the supplier and the designer
4. More data relating to the performance of materials.
5. The development of the fire safety engineering discipline and the risk assessment process.

On the basis of the current calculations and the risk assessment whilst taking a reasonably conservative view the following conclusions can be drawn for the open web joists on the tenant floors of World Trade Center Towers 1 and 2.

- The structural design has sufficient inherent fire performance to ensure that the fire condition is never the critical condition with respect to loading allowances.
- A single coat application is possible.
- Significant savings are possible.
- The target reduction of fiber content and increased long term durability can be achieved.
- Alternative materials should be considered.

World Trade Center
Fire Engineering of Steelwork - Final Report
\\barry\project\99177 wtc fire study\reports\r000727 final.doc

Rev A.
July 2000
Page iii

Figure A–40. Excerpts from 2000 report on thermal protection of floor trusses (3-P).

7 Recommendations

The calculations, the reliability of information, the conservative assumptions, and the risk assessment have been carefully judged to determine a reasonable compromise between the following: -

- Compliance with the defined performance criteria and a reasonable level of safety.
- Value engineering to reduce costs or improve performance. Performance can be based on long term durability and robustness, reduction in fibre content, insulation of steelwork during fire and ease of application.
- The need for margins of safety to ensure that the decision making and the approvals process are more straightforward. This in combination with the sensitivity tests covers the fact that the calculations and predictions for the phenomena of fire can never be exact.

If the most optimistic assumptions are made the thickness of the fire protection can be as low as 30% of the current thickness. However taking into account the variables, the following recommendations can be made.

7.1 Thickness

For the existing material, there is some uncertainty about the performance of this material due to lack of available data. If the material performs to the insulation standard defined at ambient temperature in the manufacturers data a thickness of 0.5 inches can be used whilst still maintaining a reasonable margin of safety. If however the material does degrade to some extent as suggested by the UL listings then a greater thickness of up to 1.3 inches is recommended. Further tests or test data would be required to achieve the lower thicknesses. The issues of reduced fibre content and long term durability have not been addressed with this selection. It is likely that only a single coat will be required for the 0.5 inch case.

7.2 Choice of System

The true cost of a system can only be accurately determined following a market test. The long term costs are a complex and are a function of the following:

- Material cost
- Required thickness
- Maximum thickness per application
- Time before the next layer can be applied
- Volume of dry material required
- Volume of water required in spraying procedure
- Overspray and other wastage
- Durability
- Etc.

An assessment of a variety of materials has been carried out in this report and judging from the results alternative materials should be considered for use in the World Trade Center. For example, the Carboline Pyrocrete 239 could be applied to a thickness of 0.75 inches, subject to receipt of confirmatory test data. This product is significantly more durable than the current product and therefore could reduce the overall life-cycle costs of the fireproofing system.

Figure A–40 (Contd.). Excerpts from 2000 report on thermal protection of floor trusses (3-P).

M&H

Executive Summary

World Trade Center
New York, New York

Structural

The building structures appear to be in adequate overall condition. Major structural repairs following the 1993 bomb blast were successfully completed and signed-off by a Permit to Occupy or Use issued by the Port Authority Office of the Chief Engineer on October 10, 1997. The repairs appear to have been properly engineered and executed. Following the bombing incident, stringent security measures were implemented at the vehicular entrances to the Plaza and subgrade facilities.

In the buildings we observed only minor cracking in some slabs, partitions or in stairwells of the buildings. Some minor slab cracks have been noted which should be monitored by the PA's structural consultant. The slabs at the truck dock and delivery area on level B-1 have deteriorated due to ice-melting salts that enter the building on vehicles during the winter. A slab replacement program is ongoing and should be continued until all of the damaged slabs are replaced. The monitoring of the visco-elastic movement dampers in the two Towers is an essential program that has been strongly recommended for continuation by the PA's outside structural consultant. Building movement is monitored by analysis of measurements taken and recorded by devices located in the 108th floor of 1 WTC. Analysis of these records is done by the Port Authority's independent engineer (LERA) and should continue in the future. In addition, physical sampling and analysis of the condition of the visco-elastic dampers is reportedly continuing on a 5-year cycle, with the next sampling to be done in 2001. The slurry wall that surrounds and contains the subgrade levels of the complex has some seepage that is contained by curbing and leaders, and is discharged by sump pumps in the lowest levels.

The slurry wall and the adjacent floor slabs that brace the wall are inspected on an ongoing basis to ensure that unsafe conditions do not develop. Structural Integrity Inspection (SII) Report I-38, dated April 3, 1998, provided in the Data Room, found the conditions to be acceptable. These periodic inspections should continue.

The rating of the structural fireproofing in the Towers and subgrade has been judged to be an adequate 1-hour rating considering the fact that all Tower floors are now sprinklered. An ongoing program of re-fireproofing the structural steel to the full thickness for 2-hour rating is in place. This work is done on a lease rollover basis whenever there is a full floor of space being built out for new occupancy. To date approximately 30 floors have been completed in the two towers. The PA will require this program to continue. The presence of asbestos containing

December 6, 2000

20-251E - Sections I-IV - Page 15

Figure A–41. Excerpt from 2000 report on condition assessment of the World Trade Center (7-P).

CC: A. C. WEBER
J. R. PAUL

August 10, 1967

Mr. M. Malter
Zonolite Division
W. R. Grace & Company
135 South LaSalle Street
Chicago, Illinois 60603

Dear Marty:

It was nice to get together with you and your good associates this week at Madison to see the spraying of your fireproofing on steel joists.

I think the people from the Port Authority were impressed with the good job you did on our joists, and I hope that you are successful in your effort with the Authority and the plastering contractors in New York.

Mr. Ray Monti, the general superintendent of the World Trade Center towers, called yesterday to ask if we could furnish some trusses similar to those you had used in the spray application, so I presume there will be considerable activity regarding the spray-on material in the next few weeks.

If there is anything further we can be doing for you, do not hesitate to call upon us. I know Jim Paul is expecting a call from you concerning what effort might be made to run some fire tests on the coated trusses and joists. Give us a call the next time you are in town.

Best personal regards.

Yours very truly,

LACLEDE STEEL COMPANY

A. Carl Weber
Vice President

ACW:pjz

Figure A–42. Example of correspondence referring to fire endurance testing of coated floor trusses (70-I).

FIRE TESTING

While not advocating the omission of fire testing, it is clear that numerous examples of non-tested assemblies are incorporated into major buildings--under the watchful eye of responsible building officials and with the full knowledge of designers, builders and constructors. Obvious examples include:

(1) The floor assembly of the Sears Tower; and
(2) Typical composite beams supporting composite deck construction, with unsprayed steel deck.

The latter is an example of industry "standard" construction, accepted on a nationwide basis, but not supported by fire testing.

Reasons for this lack of testing of special construction (such as Sears and World Trade Center floors) is not to be found on account of a lack of desire on the part of designers or builders. The problem is quite straightforward:

(1) It is not possible to test all products and all combinations of products prior to contract award. For example, Leclede trusses were accepted on October 4, 1967 and Cafco fireproofing on March 26, 1969.
(2) Proper testing of the one-way World Trade Center floors would have required a floor furnace capable of testing an assembly 60'x15'.
(3) Proper testing of the two-way World Trade Center floors would have required a floor furnace capable of testing an assembly 60'x80'.
(4) With the limited availability of such furnaces, it is nearly impossible to schedule a test program in time to meet construction requirements.

These special floor assemblies would best be fire tested--since actual testing is the only known, reliable method known to assure compliance with fire resisting requirements. At the same time the writer knows of no example wherein testing has been accomplished--the problems of time and scheduling appear to preclude such testing.

-10-

SKILLING, HELLE, CHRISTIANSEN, ROBERTSON

Figure A–43. Excerpts from 1975 post fire report indicating need for fire endurance testing to establish a fire rating for the floor system (3-P).

Early drafts of the revised Code required the 3-hour rating. Later drafts and the final version of the Code allow a 2-hour rating.

It is unlikely that a fire test of the 4-inch World Trade Center slab, making use of materials actually incorporated into the work, will pass a 3-hour test. It will almost surely pass a 2-hour test and would not be challenged on this account.

The World Trade Center construction of 4-inch reinforced concrete slab atop 1 1/2 inch steel deck formwork is more fire-resistive then the most commonly used construction of today (1975)--a 3 1/4 inch slab atop 1 1/2 inch composite steel deck without benefit of spray fireproofing.

Available Fire Rating

The fire resistive requirements for the project were subjected to continuous modification as a result of the development of the new Building Code.

The decision to provide for 1/2 inch of Cafco was made in full realization that:

(1) the floor slab provided only a 2-hour rating; and
(2) the new Code provided for a 2-hour rating.

We presume, but do not know, that the Cafco decision was based on the need for a 2-hour rating. Even without benefit of full scale testing we do know that a 3-hour rating cannot be achieved by the floor slab. We know also that the basic World Trade Center floor slab is superior to construction provided commonly throughout the country and does exceed a 2-hour requirement. Without benefit of a full-scale fire test we cannot establish a rating for the floor assembly.

Fire Performance

The construction performed as expected during the fire of February, 1975. While some reports indicated that the fire was very hot, no evidence of temperatures reached is available to the writer. In any event, at the very least, it can be said that the February fire provided no evidence that the construction was not satisfactory for its intended purpose.

- -

We hope that this report will provide some insight into the fire-

SKILLING, HELLE, CHRISTIANSEN, ROBERTSON

Figure A–43 (Contd.). Excerpts from 1975 post fire report indicating need for fire endurance testing to establish a fire rating for the floor system (3-P).

Fire Testing

While it is difficult to document through the media of project correspondence, the question of full scale fire testing occupied the minds of the planners and designers of The World Trade Center.

In March of 1964 Mr. C. H. Yuill, Manager Fire Research Section, Southwest Research Institute wrote to SHCR in response to its inquiry. The tone of the letter reflects a little the many problems associated with such tests; size of furnace, non-standard test procedures, long waiting time and the like (see page 8.1 and 8.2).

In June 2, 1965, SHCR transmitted truss loads for use in a fire test by U.S. Mineral Products Co. Designs of that era assumed conventional trusses--not the Laclede variety actually incorporated into the work. While not privy to the results of the test we understand(from discussions with Mr. Soffer of Port Authority) that another test program was carried out in small scale using Mono-Kote spray-on materials.

The Underwriters' Laboratories, Inc., test of July 26, 1969 (Fire TEst R4374; 68NK2435) makes use of Mono-Kote materials and Laclede trusses and provides a 3-hour rating. A copy of that report is attached (appendex). The test is not completely representative of World Trade Center trusses in that the members are lighter, the span is shorter (16'-10") and the trusses are shallower. (see page 8.3). It should be noted also that the test was conducted subsequent to the contracting for World Trade Center fireproofing. There is no evidence of when the report came to the attention of Port Authority; it was given to SHCR on March 24, 1975.

-8-

SKILLING, HELLE, CHRISTIANSEN, ROBERTSON

Figure A–44. Excerpt from April, 1 1975 post-fire report referring to fire endurance test of floor truss system with sprayed thermal insulation (3-P).

GRACE

ZONOLITE

ONSTRUCTION PRODUCTS DIVISION

G E N E R A L

The subject of this report is a 3-hour fire endurance rated assembly composed of Laclede Composite Joists supporting a concrete slab over corrugated steel centering, protected with Mono-Kote cementitious fireproofing spray-applied directly to the surfaces of the joists and to the underside of the steel centering.

The object of the investigation was to establish a 3-hour fire resistance classification for the assembly, constructed with the materials and in the manner as herein described, by means of the Fire Test of Building Construction and Materials, ASTM E-119 (UL 263).

D E S C R I P T I O N

MATERIALS:

The following materials were used in the test assembly.

Laclede Composite Joists - Type 10H5C, spaced 3 ft. 6 in. on center with a 16 ft. 10 in. clear span.

Corrugated Centering - No. 28 gauge steel attached to joists with welding washers.

Concrete - Average 28 day strength of 4290 psi, ready-mixed concrete, poured to a thickness of 2-3/4" as measured over the crests of the corrugated centering.

Temperature Reinforcement - No. 8 SWG, 6 in. by 6 in. wire mesh.

Mono-Kote Cementitious Spray-Applied Fireproofing - Applied directly to the surfaces of the joists to a thickness of 1-1/2" and to the underside of the centering to a thickness of 1/2", following the contours of the joists and the corrugated centering. Bags of Mono-Kote contained the UL label for "Cementitious Mixture."

Figure A–45. Reports of 1970 fire endurance test of floor truss system with sprayed thermal insulation (3-P).

GRACE
ZONOLITE
CONSTRUCTION PRODUCTS DIVISION

ERECTION OF TEST ASSEMBLY:

The assembly was constructed at the Northbrook, Illinois, testing facility of Underwriters' Laboratories, Inc. in accordance with the attached construction drawing Nos. UL 100-1 and -2, dated 2/27/70, under the observation of members of the staff of Underwriters' Laboratories, Inc.

FIRE ENDURANCE TEST:

The test was conducted in accordance with the Fire Test of Building Construction and Materials, ASTM E-119 (UL 263 test method).

The assembly was loaded to provide a uniformly distributed live load of 126 psf or a combined live and dead load of 169 psf, producing a maximum stress of 30,000 psi in the joists.

R E S U L T S

Observations of the Exposed Surface - All of the Mono-Kote cementitious fireproofing remained in place throughout the 3 hour 13 minute test duration.

Temperatures of the Assembly - The initial average temperatures of the unexposed surface was 69F. Based, therefore, on a maximum average temperature rise of 250F and a maximum individual temperature rise of 325F, the average limiting temperature was 319F and the individual maximum limiting temperature was 394F. At 180 minutes (3-hours), the average limiting temperature of 319F was reached. At this time the maximum individual temperature was 352F.

Figure A–45 (Contd.). Reports of 1970 fire endurance test of floor truss system with sprayed thermal insulation (3-P).

GRACE
ZONOLITE
NSTRUCTION PRODUCTS DIVISION

Deflection of the Assembly

Time	Deflection
60 min	2 "
90 min	2-1/2"
120 min	3 "
150 min	3-3/8"
180 min	4-3/4"

Temperatures of the Joists -

Time	Top Chord	Diagonal Web	Bottom Chord	Average
60 min	235F	485F	485F	301F
90 min	395F	915F	1,150F	814F
120 min	486F	972F	1,243F	900F
150 min	550F	1,200F	1,543F	1,095F
180 min	622F	1,280F	1,580F	1,160F

C O N C L U S I O N S

The assembly achieved a 3-hour fire endurance rating in accordance with ASTM E-119 and as verified by the attached letter dated March 26, 1970, from A. F. Abbasi of Underwriters' Laboratories, Inc.

Submitted by:
Thomas P. Feit

Thomas P. Feit - Manager
Technical Services

TPF/jac

Figure A–45 (Contd.). Reports of 1970 fire endurance test of floor truss system with sprayed thermal insulation (3-P).

UNDERWRITERS' LABORATORIES, INC.
333 PFINGSTEN ROAD · NORTHBROOK, ILLINOIS 60062

an independent, not-for-profit organization testing for public safety

AIR MAIL

March 26, 1970

in reply, please refer to

R4374
68NK2453

CAMBRIDGE

Zonolite Construction Products Div.
W. R. Grace & Co.
62 Whittemore Ave.
Cambridge, Massachusetts 02140

Subject: Fire Endurance Test of Composite Bar Joist and Concrete Deck

Attention: Mr. T. P. Feit

Gentlemen:

This letter summarizes the results of the fire endurance test of floor assembly of the subject matter.

The floor assembly was constructed according to Drawing No. LS101UL dated July 26, 1969 of Laclede Steel Company. It consisted of 3 bar joists type 10H5C with 3 ft 6 in. spacing on centers and 16 ft 10 in. clear span, supporting concrete deck over corrugated centering. The thickness of concrete was 2 3/4 in. over the crests and 3 1/4 in. over the valleys, and was reinforced with 6 by 6 in. No. 8/8 wire mesh. The bar joists and the corrugated centering were sprayed with Mono-Kote MK of the following thicknesses:

1. Bar Joists - An average of 1 1/2 in. thick directly applied over all the exposed surfaces of bottom and top chords and webs.
2. Corrugated Centering - An average of 1/2 in. thick following the contours of the exposed surface of the corrugations.

The average strength of concrete at 28 days was 4290 psi. The equivalent uniform live load of 126 p. s. f. was applied on the assembly. The total live and dead load was 169 p. s. f. which produced a maximum stress of 30,000 psi in the bottom chord of the bar joist.

Figure A–45 (Contd.). Reports of 1970 fire endurance test of floor truss system with sprayed thermal insulation (3-P).

UNDERWRITERS' LABORATORIES, INC.

- 2 - March 26, 1970

The floor assembly was tested on February 27, 1970, and the test was continued for 3 hours 13 minutes and 10 seconds. The structural performance of the floor assembly during the test was considered satisfactory. The average temperature of the unexposed surface before the fire test was 69F. At 3 hours of test time the average temperature of the unexposed surface reached 319 F and the maximum individual temperature was 352 F. The maximum deflection of the unexposed surface at 3 hours was 4.76 in.

The assembly was further loaded with an additional live load of 126 p. s. f. on March 2, 1970 which increased the maximum deflection by 0.35 in. without any apparent structural damage.

We shall be preparing a formal report which will contain details of the test.

Very truly yours,

A. F. ABBASI
Fire Protection Department

AFA:ck

Figure A–45 (Contd.). Reports of 1970 fire endurance test of floor truss system with sprayed thermal insulation (3-P).

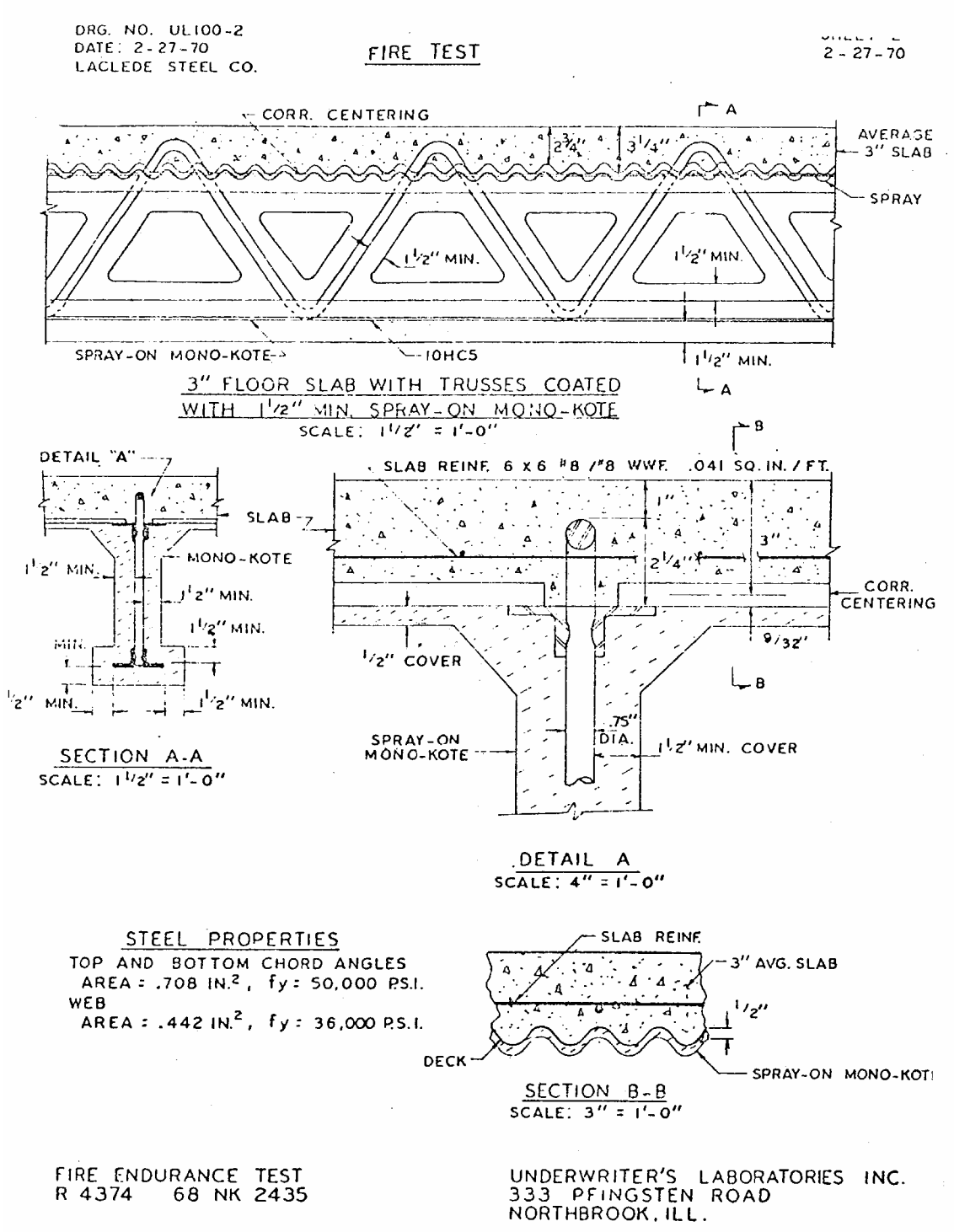

Figure A–45 (Contd.). Reports of 1970 fire endurance test of floor truss system with sprayed thermal insulation (3-P).

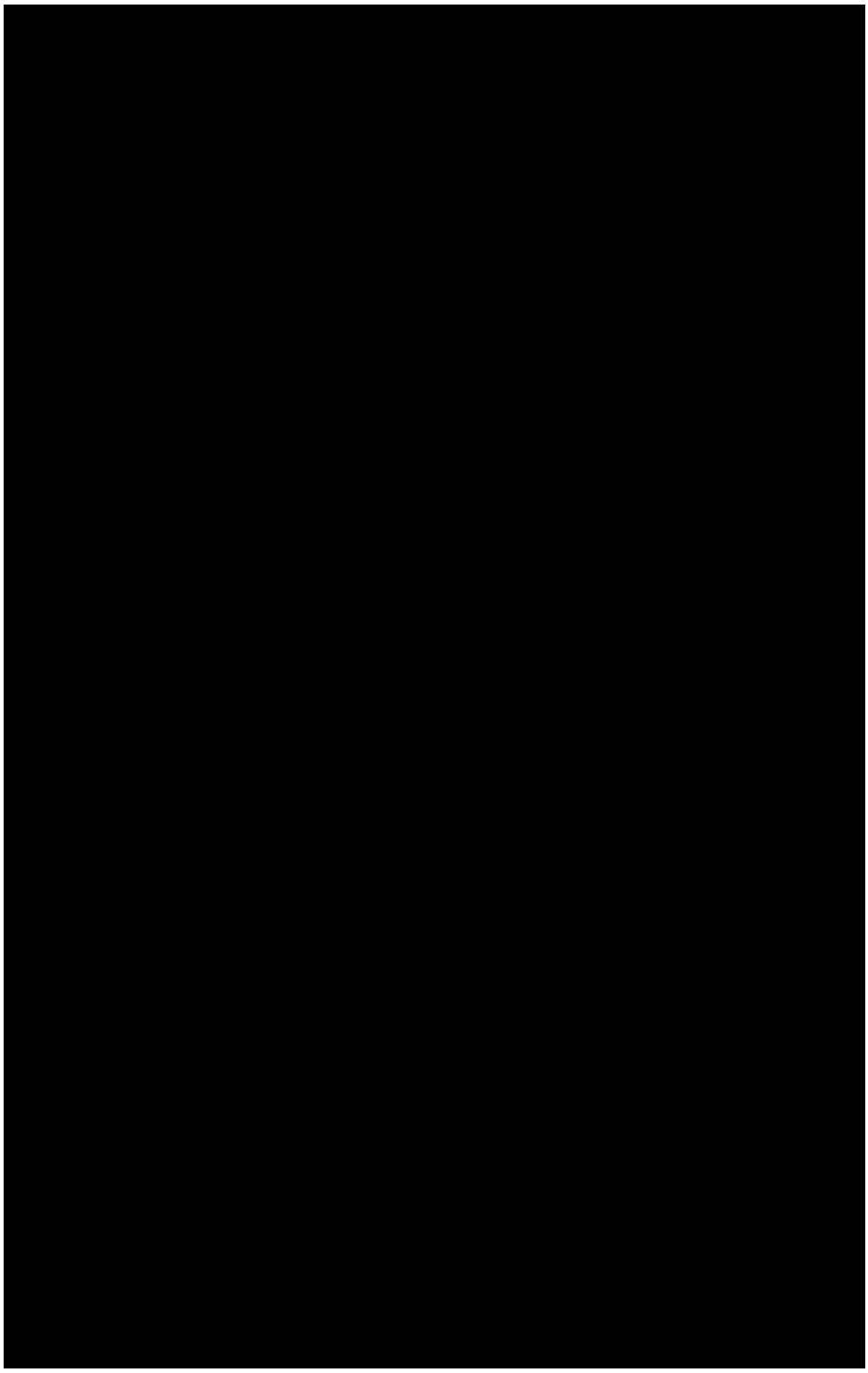

Figure A–46. Excerpt from 1975 post-fire report indicating interpretation of 1970 fire endurance test of truss floor system with sprayed thermal insulation (3-P).

REV.	LERA LESLIE E. ROBERTSON ASSOCIATES CONSULTING STRUCTURAL ENGINEERS	P 1003114	DRAWING NO.
	WTC-REFIREPROOF ELEVATOR SHAFTS 12+13	DRAFT	2/37
	INTRODUCTION	DESIGN WPM	
		CHECK	12/9/92

DISCUSSION (CONTINUED)

A REVIEW OF THE APPROPRIATE DRAWINGS, REFERENCES (B), (D), (F) AND (G) IDENTIFIED WHICH BEAMS AND COLUMNS WERE ACCESSABLE FROM INSIDE THE ELEVATOR SHAFTS. BEAMS SEPARATING SHAFTS PE12 & PE 13 ARE NOT FIREPROOFED.

ASSUMPTIONS: THE FOLLOWING ASSUMPTIONS WERE USED IN THIS CALCULATION:

- THE FIREPROOFING THICKNESS FOR COLUMNS WAS CALCULATED FOR GROUPS OF FLOORS IN ORDER TO SAVE TIME. THE GROUPS WERE DETERMINED BY LUMPING TOGETHER ALL COLUMNS WITH PLATE THICKNESSES WITHIN 1/2" OF EACH OTHER. BECAUSE FIREPROOFING THICKNESS INCREASES WITH SMALLER CROSS-SECTIONS, THE SMALLEST CROSS SECTION IN EACH GROUP WAS USED.

- SOME BEAMS HAD ADDITIONAL STIFFENING PLATES AND MOUNTING BRACKETS WELDED TO A PORTION OF THEIR SPAN. THIS EXTRA MATERIAL WAS NOT INCLUDED IN THE CALCULATION. AGAIN, THIS WAS DONE TO SAVE TIME AND IT SHOULD BE NOTED THAT THE ADDITION OF THESE PLATES WOULD TEND TO INCREASE THE BEAM'S CROSS SECTION AND THEREBY REDUCE THE THICKNESS OF FIREPROOFING REQUIRED.

- A 2 HOUR RATING FOR BEAMS IS REQUIRED. BEAMS ARE RESTRAINED AGAINST THERMAL EXPANSION.

- A 3 HOUR RATING FOR COLUMNS IS REQUIRED.

Figure A–47 (Contd.). Excerpts from 1992 report on thermal insulation thickness for repair of missing insulation (240-LERA).

REV.	LERA LESLIE E. ROBERTSON ASSOCIATES CONSULTING STRUCTURAL ENGINEERS	P/003114	DRAWING NO.
	WTC - REFIREPROOF ELEVATOR SHAFTS 12 & 13	DRAFT	4/37
	BEAMS	DESIGN WPM	
		CHECK	12/3/92

BEAMS

THE FOLLOWING CALCULATIONS WILL DETERMINE THE THICKNESS OF FIREPROOFING REQUIRED FOR BEAMS EXPOSED IN ELEVATOR SHAFTS PE12 & PE 13. FROM THE SKETCH BELOW, THERE ARE 5 BEAMS EXPOSED IN THE SHAFTS. BEAMS A AND E ARE NORMALLY ENCLOSED IN CONCRETE AND DO NOT REQUIRE SPRAY ON FIREPROOFING. BEAM C SEPARATES THE ELEVATOR SHAFTS AND IS NOT FIREPROOFED. ONLY BEAMS B AND D REQUIRE SPRAY ON FIREPROOFING.

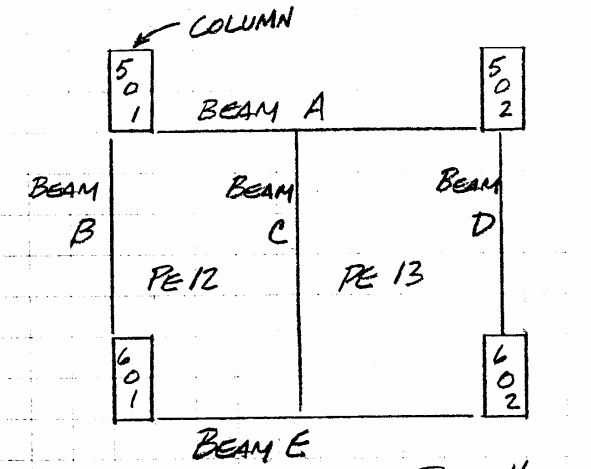

PLAN VIEW

SEE REFERENCE (D) FOR EXTENT OF FIREPROOFING ON BEAMS.

A 2 HOUR RATING FOR BEAMS (RESTRAINED) IS DESIRED.

SEE REFERENCES (F) AND (G) FOR BEAM DETAILS.

Figure A–47 (Contd.). Excerpts from 1992 report on thermal insulation thickness for repair of missing insulation (240-LERA).

[redacted]

Figure A–47 (Contd.). Excerpts from 1992 report on thermal insulation thickness for repair of missing insulation (240-LERA).

[redacted]

Figure A–47 (Contd.). Excerpts from 1992 report on thermal insulation thickness for repair of missing insulation (240-LERA).

REV.	LERA LESLIE E. ROBERTSON ASSOCIATES CONSULTING STRUCTURAL ENGINEERS	P 1003114	DRAWING NO.
	WTC - REFIREPROOF ELEVATOR SHAFTS 12+13	DRAFT	10/37
	[redacted] BEAM B	DESIGN WPM	
		CHECK	12/4/92

BEAM B, CAFCO 560 MATERIAL

UL DESIGN N714

2 HOUR RESTRAINED TEST BEAM W 8X28, W/D = .80

AS BEFORE, ALL FLOORS EXCEPT THE 8TH MAY USE DESIGN N714 THICKNESS OF 7/8".

FLOOR 8 REQUIRES AN INCREASE IN THICKNESS AND THE REMAINING FLOORS MAY BE REDUCED, ALL BY USING THE BEAM SUBSTITUTION EQUATION.

REVISED THICKNESSES (USE THE BEAM SUBSTITUTION EQUATION)

FLOOR	W/D	THICKNESS	FLOOR	W/D	THICKNESS
ELEV 294'	1.2	11/16"	41, 43, 44	1.03	13/16"
ELEV 310'	1.18	3/4"	42	.85	NO CHANGE 7/8"
INTER.	2.18	1/2"	45-66	1.01	13/16"
2	1.28	11/16"	67	1.26	11/16"
3-6	1.78	9/16"	68-74	1.01	13/16"
7	1.18	3/4"	75	1.28	11/16"
8	.57	1 11/16" REQ'D	76	.85	NO CHANGE 7/8"
9	1.13	3/4"	77	1.28	11/16"
10-39	1.26	11/16"	78	1.65	9/16"
40	1.01	13/16"	79	1.43	5/8"

Figure A–47 (Contd.). Excerpts from 1992 report on thermal insulation thickness for repair of missing insulation (240-LERA).

REV.	LERA LESLIE E. ROBERTSON ASSOCIATES CONSULTING STRUCTURAL ENGINEERS	P 1003114	DRAWING NO.
	WTC - REFIREPROOF ELEVATOR SHAFTS 12+13	DRAFT	11/37
	BEAM B	DESIGN WPM	
		CHECK	12/4/92

BEAM B ALBI DURASPRAY

UL DESIGN N711

2 HOUR RESTRAINED TEST BEAM W8X28 W/D = .80

SIMILAR TO THE TWO PREVIOUS CASES, ALL FLOORS EXCEPT 8TH MAY USE THE N711 DESIGN THICKNESS OF 1". FLOOR 8 REQUIRES AN INCREASED THICKNESS.
THE REVISED THICKNESSES AND THE REQUIREMENT FOR FLOOR 8 ARE BELOW.

REVISED THICKNESSES (USE THE BEAM SUBSTITUTION EQUATION)

FLOOR	W/D	THICKNESS	FLOOR	W/D	THICKNESS
ELEV 294'	1.2	13/16"	42	.85	NO CHANGE 1"
ELEV 310'	1.18	13/16"	45-66	1.01	7/8"

[redacted]

Figure A–47 (Contd.). Excerpts from 1992 report on thermal insulation thickness for repair of missing insulation (240-LERA).

REV.	LERA LESLIE E. ROBERTSON ASSOCIATES CONSULTING STRUCTURAL ENGINEERS	P 1003114	DRAWING NO.
	WTC-REFIREPROOF ELEVATOR SHAFTS 12+13	DRAFT	19/37
	COLUMN 601	DESIGN WPM	
		CHECK	12/8/92

COLUMNS

THE FOLLOWING CALCULATIONS WILL DETERMINE THE THICKNESS OF FIREPROOFING REQUIRED FOR COLUMNS 601, 602, 501 AND 502 FOR ALL 3 FIREPROOFING MATERIALS. COLUMN SIZES ARE FROM REFERENCE (B).

A) MONOKOTE TYPE Z-106, MANUFACTURED BY W.R. GRACE

COLUMN 601

UL DESIGN X738

THE UL DIRECTORY, REFERENCE (A), PROVIDES AN EQUATION FOR DETERMINING THE THICKNESS OF TYPE 106 MATERIAL REQUIRED. THIS EQUATION IS BASED ON THE W/D RATIO. BECAUSE THIS COLUMN'S CROSS SECTION CHANGES OVER ITS HEIGHT, SO WILL THE W/D RATIO.

IN AN ATTEMPT TO REDUCE THE NUMBER OF THICKNESS CHANGES, THE W/D RATIO WILL BE CALCULATED FOR GROUPS OF COLUMNS WHOSE PLATE THICKNESSES ARE WITHIN 1/2" OF EACH OTHER. BECAUSE FIREPROOFING THICKNESS INCREASES WITH SMALLER W/D RATIOS, THE LIGHTEST COLUMN IN EACH GROUP WILL BE USED.

ALTHOUGH DIFFERENT SIDES OF THE SAME COLUMN ARE EXPOSED AT DIFFERENT ELEVATIONS WITHIN THE SHAFT, THE CALCULATION WILL ASSUME A FIRE AROUND THE FULL PERIMETER OF THE COLUMN. THIS IS CONSERVATIVE AS IT WILL TEND TO LOWER THE W/D RATIO.

Figure A–47 (Contd.). Excerpts from 1992 report on thermal insulation thickness for repair of missing insulation (240-LERA).

REV.	LERA LESLIE E. ROBERTSON ASSOCIATES CONSULTING STRUCTURAL ENGINEERS	P 1003114	DRAWING NO.
	WTC-REFIREPROOF ELEVATOR SHAFTS 12413	DRAFT	20/37
	COLUMN 601	DESIGN WPM	
		CHECK	12/8/92

THE UL EQUATION TO DETERMINE TYPE Z-106 FIREPROOFING IS:

$$h = \frac{R}{1.05(W/D) + .61}$$

WHERE:

h = THICKNESS OF FIREPROOFING, INCHES
R = RESISTANCE TIME IN HOURS
W/D = WITHIN THE RANGE OF .33 TO 6.62

NOTE THAT THE USE OF THIS EQUATION IS NOT MANDATORY FOR W/D RATIOS GREATER THAN THOSE IN THE UL DESIGN. IT MUST BE USED FOR W/D RATIOS SMALLER THAN THOSE IN THE UL DESIGN.

FLOORS 69 → 79

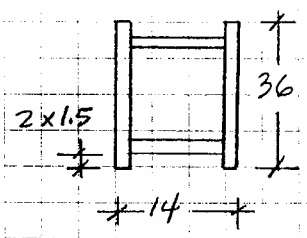

ALL PL IS .8125" THICK

$$W = [(36 \times 2) + (14 - .8125(2))2] \cdot .8125 \times 12 \times \frac{490}{1728} =$$

268 lb/ft

$$W/D = \frac{268}{(36 + 14 + 3)2} = 2.52$$

THE UL DESIGN THICKNESS IS 15/16" ...

APPLYING THE EQUATION h = .92 USE 15/16"

Figure A–47 (Contd.). Excerpts from 1992 report on thermal insulation thickness for repair of missing insulation (240-LERA).

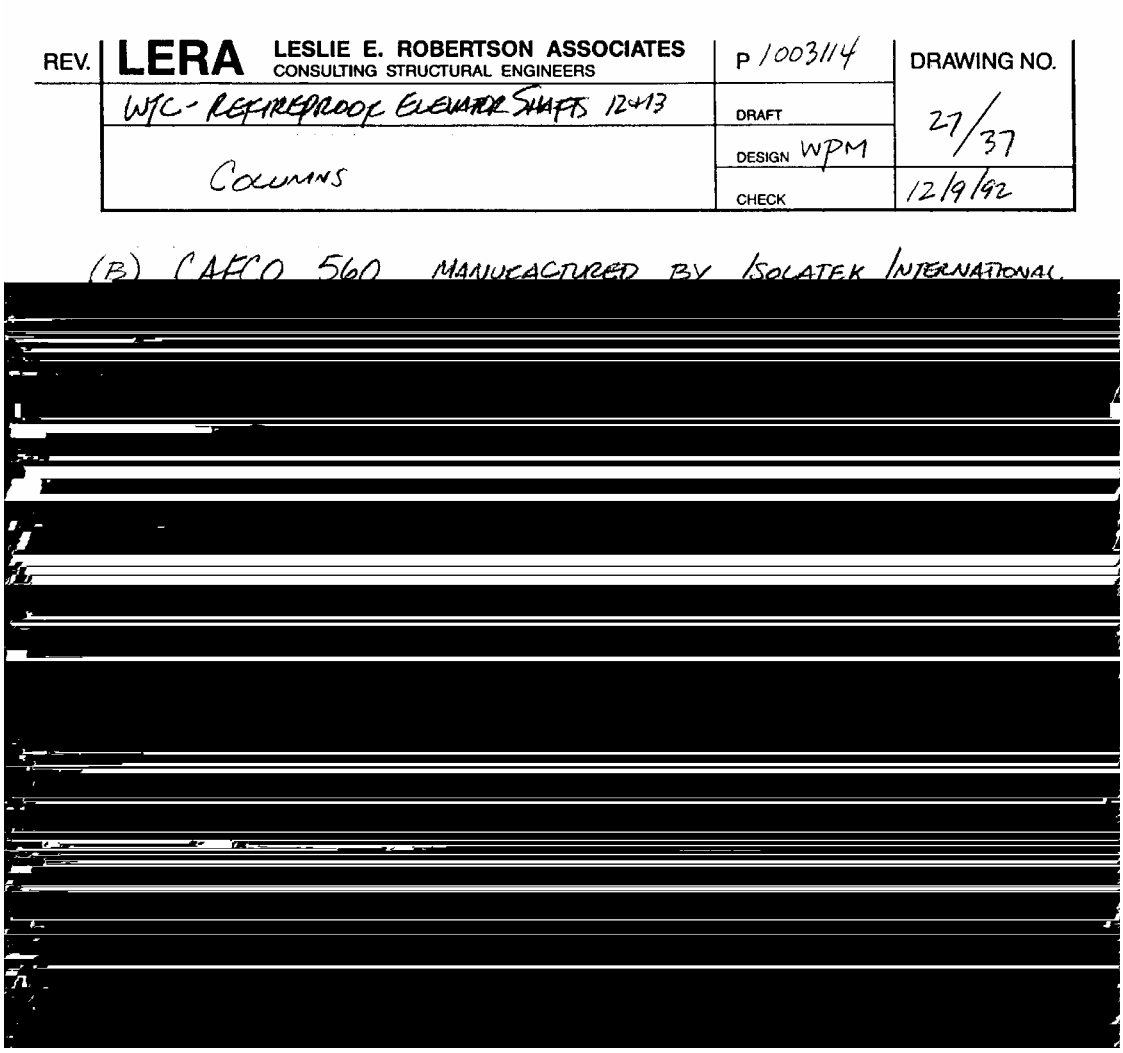

REV.	LERA LESLIE E. ROBERTSON ASSOCIATES CONSULTING STRUCTURAL ENGINEERS	P 1003114	DRAWING NO.
	WTC - REFIREPROOF ELEVATOR SHAFTS 12+13	DRAFT	27/37
	COLUMNS	DESIGN WPM	
		CHECK	12/9/92

(B) CAFCO 560 MANUFACTURED BY ISOLATEK INTERNATIONAL

Figure A–47 (Contd.). Excerpts from 1992 report on thermal insulation thickness for repair of missing insulation (240-LERA).

REV.	LERA LESLIE E. ROBERTSON ASSOCIATES CONSULTING STRUCTURAL ENGINEERS	P 1003114	DRAWING NO.
	WTC ~~[illegible]~~ ELEVATOR SHAFTS 12+13	DRAFT	28/37
	COLUMNS	DESIGN WPM	
		CHECK	12/9/92

c) ALBI DURA SPRAY AND DURASPRAY 30 UL DESIGN X-730 MANUFACTURED BY STANCHEM, INC

ALTHOUGH THIS DESIGN IS FOR A METAL LATH ENCLOSED W-SHAPE COLUMN, THE VENDOR RECOMMENDS THIS DESIGN FOR TUBE COLUMNS. FOR A 3 HOUR RATING, THE DESIGN SPECIFIED THICKNESS IS

1 1/16" FOR ALL COLUMNS.

CHECK W/D

THE TEST COLUMN IS A W10x49, ENCLOSED IN A BOX. THIS SHAPE HAS A HEIGHT AND FLANGE WIDTH OF 10".

$W/D = \frac{49}{10(4)} = 1.23$, THIS IS LESS THAN THE W/D FOR COLUMNS 501, 502, 601 & 602, SO THE TEST THICKNESS IS ACCEPTABLE.

NO EQUATIONS ARE AVAILABLE FOR REDUCING THIS THICKNESS.

Figure A–47 (Contd.). Excerpts from 1992 report on thermal insulation thickness for repair of missing insulation (240-LERA).

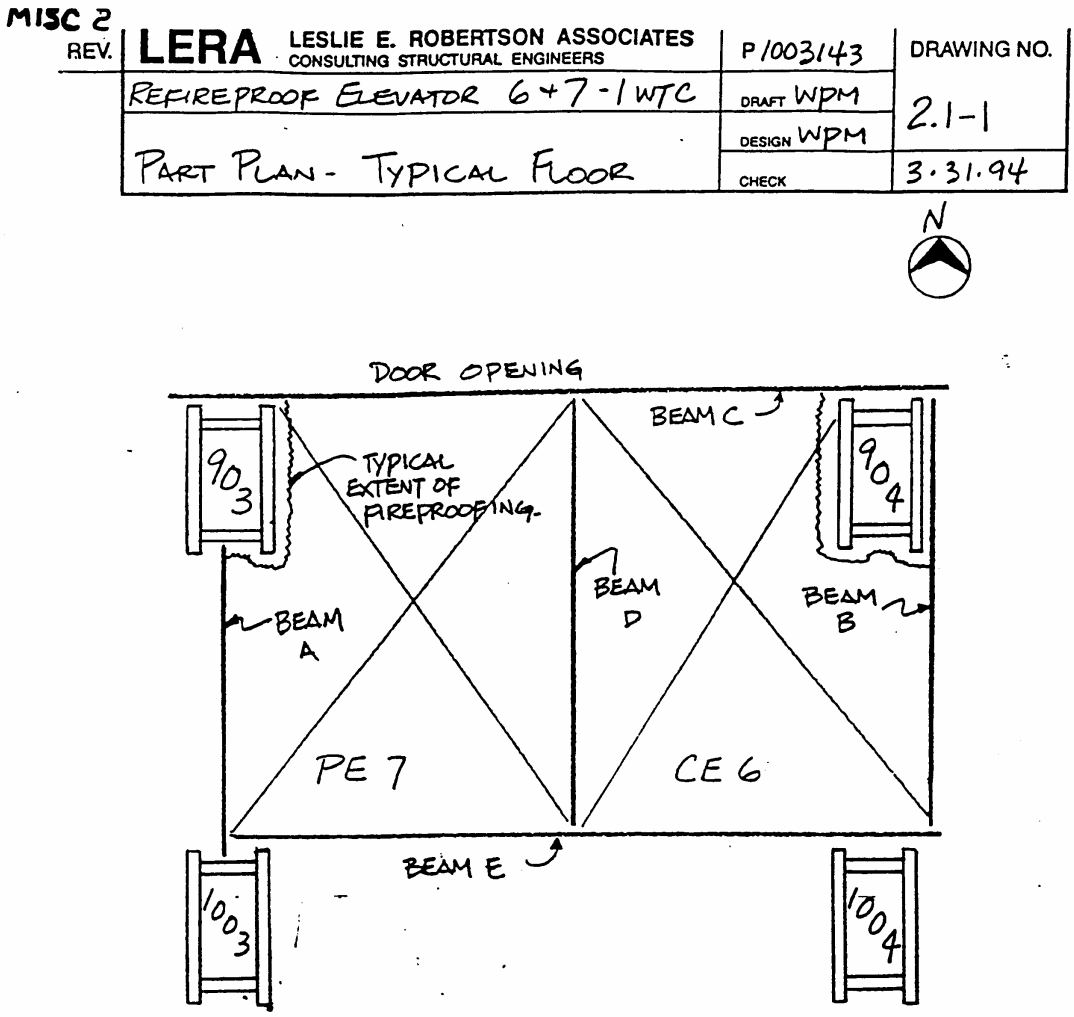

- BEAMS A AND B, AND COLUMNS 903 AND 904 TO BE FIREPROOFED. SEE SCHEDULE ON PAGE 2.2-1.
- BEAMS C AND E ARE CONCRETE ENCASED AND DO NOT RECEIVE FIREPROOFING. BEAM D IS NOT FIREPROOFED.
- COLUMNS 1003 AND 1004 ARE NOT ACCESSIBLE FROM THE ELEVATOR SHAFTS.

Figure A–48. Excerpt from 1994 design document related to reapplication of SFRM to accessible members in elevators shafts of WTC 1 (659-P).

TO: M. Gerstman

FROM: E. J. Boland

DATE: April 12, 1973

SUBJECT: THE WORLD TRADE CENTER - CONTRACT WTC 320.00 - ELEVATORS AND CONTRACT WTC 113.00 - SPRAY-ON FIREPROOFING - TOWERS A & B

REFERENCE: Letter M. Gerstman to Otis - dated 3/22/72

COPIES: R. Belsky, R. Linn, C. A. Smith, F. H. Werneke; G. Hughes, B. Weinstein (TRCC); File

As reported to this office, the slack condition in compensating cables, especially on shuttle cars, is causing a chafing condition against finished spray-on fireproofing on structural steel within hoistways.

The chafing has caused extensive damage to the spray-on which has been patched at considerable expense in the past. However, the damage re-occurs.

As evidenced in the referenced letter, TRCC has previously pursued this slack condition problem with Otis but it has not been corrected to date.

Patching costs due to cable chafing should be backcharged to

[redacted]

Figure A–49. Correspondence indicating that slack cables within elevator shafts damaged the thermal insulation (246-I).

R. E. Schlemmer

F. M. Stumpf July 29, 1960

CAFCO Bond Strength

In our recent vibration tests we have noted some poor bond characteristics of our CAFCO BLAZE and HEAT-SHIELD. This was contrary to work which we had done in the past on laboratory mixes. Since this difference was noted several times in the past, we decided to see if there was any difference in bond strength between plant and lab mixed formulas. As will be seen in the attached data sheet, there is quite a difference and most of it is in favor of the lab mixed formulas. This is particularly true in the critical low density ranges of HEAT and BLAZE-SHIELD for both wet and dry conditions.

This low bond strength can be a very serious defect to our products since at 11 lbs. per square foot bond, reasonable vibration should shake the mass loose. At a wet strength of 3½ lbs. per square foot, installed CAFCO which becomes wet and is subject to moderate vibration should delaminate. All specimens were sprayed under ideal laboratory conditions which means they were given the proper amount of water, proper spraying angle, and proper tamping. In the field, most of these conditions are not met which would further indicate poor performance of the product. It just happens that CAFCO is usually applied in areas where there is not excessive vibration and its weight is below the 3 lbs. per square foot range.

Before we start determining the difference in mixing procedures, changing formulas, etc., this appears to be a good time to set a minimum bond strength standard of perhaps 20 lbs. per square foot and that this check be a part of the quality control procedure. Next, we can study the mixing which appears to be non-uniform as evidenced by previous difficulties with SOUND-SHIELD variations and with the research wood fiber formula which never resulted in the uniform blend. We think it is also mandatory to regulate the nodule size of wool entering the mixer rather than depending upon the mixer to do this. In the lab mixer, with its tumbling action, the wool asbestos and binders gently tumble which results in uniform coating. In the plant mixer the constant breaking up of the wool nodule is never permited to be coated with the asbestos fibers and binders. This may be a key to our problem.

Under Section B of the attached data sheet is data of bond tests run previously, namely an audit in July 1959 and the original audit in February 1956. We can not answer why the bond strengths for the 1956 audit were as good as they were except that in these days we were using steam blown wool.

FMS/ad
CC - J. F. Verhalen

F. M. Stumpf

PLAINTIFF'S EXHIBIT
PX-24

Figure A–50. Correspondence indicating poor bond performance of sprayed thermal insulation during vibration testing (51-ITK).

MAR 7 1968

MEMORANDUM

0011814

TO: Mr. R. M. Monti, Construction Manager
FROM: F. H. Werncke
DATE: March 6, 1968
SUBJECT: THE WORLD TRADE CENTER - FIELD TEST APPLICATION CAFCO TYPE "D" FIREPROOFING

REFERENCE:

COPY TO: Messrs. Levy w/att., Endler (TRCC) w/att.

The attached are letters dated March 1, 1968, from both United States Mineral Products Company and Mario & DiBono Plastering Company,

Figure A–51. Correspondence indicating acceptable performance of BLAZE-SHIELD Type D when applied under adverse weather conditions (250-P).

January 14, 1970

Mr. Joseph Ferro
Deputy Commissioner
The City of New York
Department of Buildings
2 Lafayette Street
New York, New York 10007

RE: THE WORLD TRADE CENTER - FIREPROOFING

My dear Commissioner:

Transmitted herewith is a record of a sprayed fireproofing test conducted by the Port Authority. The material was applied on January 29, 1968 under adverse weather conditions and was subsequently inspected on July 22, 1968 and found to be in good condition. There is also attached a report from the U. S. Mineral Products Company on the material and techniques used in the application. The material used was a cementacious asbestos fiber whose trade name is Cafco Type D. I am also enclosing a copy of the U. S. M. catalog. You will also note from the report that pictures were taken of the installation. I am obtaining copies and will forward them to you in the near future.

I hope this information will be useful to you. Any additional information we have is, of course, at your disposal.

Sincerely,

Malcolm P. Levy

Encl.

MPL:fg:jtm

bcc: Messrs. J. Kyle, R. Monti

Figure A–52. Correspondence sent to New York City Department of Buildings in 1970 providing information on the performance of BLAZE-SHIELD Type D (92-ITK).

INTER-OFFICE MEMORANDUM

J.P. Verhulen

Harry Cropp

Date: Dec. 11, 1969

Last shipment of special Type D to World Trade Center

The last 800 bag shipment (20 tons) shipped to the World Trade Center was sprayed on Friday, Dec. 5th, Saturday, Dec. 6th and half of Sunday, Dec. 7th.

Of the 20 tons of material sprayed to the 10th floor exterior columns on this project, approximately 600-700 bags of the material washed off as clean as a whistle from the exterior columns on this job.

On reporting this experience to Frank Stumpf, he couldn't believe that this could happen. On Dec. 9th, 1969, Frank Stumpf and Siggy Sumski visited the World Trade Center in the company of Allen Bassemer to view this [illegible]. As Allen reports to me, he got the usual dribble of suggestions as to how to cure the problem. Such as, we are spraying too wet, we should change the disperser tip from a 60° to a 75° tip and there was too much hose on the floor.

As Allen knows, as I know, as you know, as Frank Stumpf knows, and as Bob Rath knows, none of those suggestions are going to cure what is the real problem of this material on the World Trade Center. Since we all know the problem, but unfortunately don't have the guts to tell each other in our own company. We know that the real problem is the lousy, poor, sub-standard product that we are trying to get our customers to accept and apply, and don't give me that the weather may have been cold, or the distance of the spray nozzle may be incorrect, or the amount of the blower pressure may be off, or the disperser tip may be the wrong one, because all of these things have been actually field tried on this job and we are headed for potential disaster - to put it very bluntly.

If this company doesn't realize now, that the product we are shipping to our customers is poor quality, inferior quality for which we are asking list prices or prices above what is asked for by our competitors, and for which we are asking our applicators to apply 20 to 30 per cent [illegible]

[redacted]

Figure A–53. Intra-office correspondence dealing with adhesion problems during spraying of exterior columns in WTC 1 (248-ITK).

- 2 -

For over one year, the Sales Department has lived with sub-standard, sub-par, below quality material products. My man, and myself, have overcome complaint upon complaint with very few contractors asking for compensation for experiences due to rocks, wire, nuts, bolts, lath, paper bags in the product. I feel we have come to the end of the line. Our contractors feel we have come to the end of the line. Please, no further ambiguous excuses. You want a company - then let's make the product.

Harry Gropp

cc: R. Rath
F. Stumpf
A. Bessemer
M & D File
WTC file
HSG

Figure A–53 (Contd.). Intra-office correspondence dealing with adhesion problems during spraying of exterior columns in WTC 1 (248-ITK).

MEMORANDUM

REFER		NOTED	
TO	DATE	BY	DATE
RETURN TO			

TO: E. Boland
FROM: L. Guadagno
DATE: March 15, 1971
SUBJECT: THE WORLD TRADE CENTER - CONTRACT WTC-113.00 - TOWER A - ELEVATOR BANK C SHAFTS 39, 40 & 41
REFERENCE:
COPY TO: G.A. Smith, File

Spray-on fireproofing work was performed by Mario & DiBono in Shafts 39, 40 & 41 from 2/4/71 to 2/17/71. This work was done during extremely cold temperatures in an attempt to meet existing construction schedules.

During a recent inspection of these shafts, it was noted that the Cafco fireproofing treated with Mark II overspray has not cured or hardened according to specifications. The writer believes that this improper hardening was caused by the low temperatures during which the Mark II sealer was applied.

This inspector recommends that shafts 39, 40 & 41 be re-sprayed with Mark II sealer.

L. Guadagno
Construction Inspector IV
The World Trade Center

LG/mk

Figure A–54. Correspondence related to inadequate hardening of thermal insulation applied to core columns (660-P).

A-54580

FILE: WTC 113.00

TO: D. Meyers

DATE: September 24, 1973

FROM: E. J. Boland

SUBJECT: THE WORLD TRADE CENTER - CONTRACT WTC 113.00 - TOWER "B" ELEVATOR SHAFTS #10 & #11 - LOOSE AND FALLING SPRAY-ON FIREPROOFING

REFERENCE: Photos attached, B-1, B-2, B-3, B-4

COPIES: R. Linn, C. A. Smith; B. Weinstein (TRCC); File

Our inspection of the above mentioned shafts indicates that the spray-on fireproofing has been improperly applied in several areas.

The fireproofing has come loose and fallen at floors 35, 40 and 43 in shaft #10 and at floor 31 in shaft #11. Also several small sections have come loose from perimeter box beams in both shafts.

We request that you direct the contractor Mario & DiBono, to re-spray the above mentioned areas as required under their Contract. Please refer to Chapter II, Page 123, Section 13.03 - Product Qualifications, "...the material shall resist the normal abuse resulting from the construction work of subsequent trades, shall not crack, craze, dust or disintegrate and shall adhere to the base surfaces with sufficient strength to insure against any loosing and falling off of

Figure A–55. Correspondence related to dislodged thermal insulation within elevator shafts of WTC 2 (658-P).

LERA

WORLD TRADE CENTER
Structural Integrity Inspection
Accessible Columns @ 1,2,4 and 5 WTC

P1103904 & 3927
29 January 1993
Page 1 of 9

EXECUTIVE SUMMARY

This report details the findings of the inspection of accessible columns in the elevator shafts of 1, 2 and 5 World Trade Center.

No structural deficiencies such as cracking or bowing were found in any of the columns inspected.

The most common irregularities observed were missing fireproofing and light surface rusting of exposed steel.

We recommend that fireproofing be repaired on all columns in the elevator shaft

Figure A–56. Excerpts from 1993 structural integrity inspection report related to condition of thermal protection on accessible columns (16-FEMA).

LERA

WORLD TRADE CENTER P1103904 & 3927
Structural Integrity Inspection 29 January 1993
Accessible Columns @ 1,2,4 and 5 WTC Page 5 of 9

PROCEDURE & LIST OF INSPECTED COLUMNS

The visual assessment of the accessible columns in the elevator shafts was carried out from top of the elevator cars. The elevator was operated by a field inspector from National Elevators.

The operator ran the elevator at a very slow speed from top to bottom and if any irregularity was noticed the car was stopped and the defect was duly noted and, at times, recorded using a 35mm camera.

A total of 10 elevator shafts were selected. This selection included 8 local elevators and 2 express elevators. Table A gives a listing of all the elevators and columns inspected during this survey.

Figure A–56 (Contd.). Excerpts from 1993 structural integrity inspection report related to condition of thermal protection on accessible columns (16-FEMA).

LERA

WORLD TRADE CENTER
Structural Integrity Inspection
Accessible Columns @ 1,2,4 and 5 WTC

P1103904 & 3927
29 January 1993
Page 6 of 9

TABLE A

Tower	Elevator Shaft Number	Floors Inspected	Adjacent Column Number	Face of Column Inspected
A (1 WTC)	21	4-78	606	East
		4-78	607	West
	36	1-32	701	East, South
		1-32	801	East, North
	63	45-67	701	East, South
		45-67	801	East, North
	73	43-74	703	North, West
		43-74	803	North, West
	83	78-93	701	East, South
		78-93	801	East, North
B (2 WTC)	15	4-78	602	North
		4-78	603	South, West
	29	1-16	707	South, East
		1-16	806	South, West
	56	45-54	707	South, East
		45-54	806	South, West
	78	78-86	707	South, East
		78-86	806	South, West
Northeast Plaza (5 WTC)	E-7 / 28	1-9	E-7 / 28	W

See Appendix A for the plan locations of the above columns.

Figure A–56 (Contd.). Excerpts from 1993 structural integrity inspection report related to condition of thermal protection on accessible columns (16-FEMA).

LERA

WORLD TRADE CENTER P1103904 & 3927
Structural Integrity Inspection 29 January 1993
Accessible Columns @ 1,2,4 and 5 WTC Page 7 of 9

OBSERVATION

Appendix B-2 shows the typical cross sections of columns used

Figure A–56 (Contd.). Excerpts from 1993 structural integrity inspection report related to condition of thermal protection on accessible columns (16-FEMA).

LERA

One and Two World Trade Center
Strucural Integrity Inspection
Accessible Columns

14 April 1995
File: P1113903
Page 1 of 10

Executive Summary

Leslie E. Robertson, R.L.L.P., (LERA) carried out a survey of the accessible columns in the elevator shafts of One and Two World Trade Center as part of the ongoing structural integrity inspections. This survey was undertaken for the purpose of ascertaining the condition of the accessible columns in the elevator shafts in terms of the overall structural integrity of the accessible columns, for signs of rust or cracking, bowing, or deviation from plump, to identify specific locations of structural distress or damage, to identify locations of damage to the fireproofing envelopes, for lateral displacement or rotation of the column about a vertical axis where the column is braced directly on only one axis by connecting beams or abutting concrete slabs due to large beam offset dimensions, for signs of rust, or deformation of the slabs on ground surrounding each column at sub-level, and to provide recommendations for remedial work for both structural and fireproofing damage.

Most of the information presented in this report originates from on-site observations of selected columns within elevator shafts made by LERA during March 1995. The visual assessment of the accessible columns in the elevator shaft was carried out from the top of the elevator cars, by a field inspector. A total of 24(Twenty-four) elevator shafts and 56(Fifty-six) elevator pits were selected, this selection included 10 local elevators and 14 express elevators.

The accessible columns in the selected elevator shafts of One and Two World Trade Center are generally in good condition, no structural deficiencies such as cracking or bowing were found, the most common irregularities observed were missing fireproofing and light surface rusting of the exposed steel.

Figure A–57. Excerpts from 1995 structural integrity inspection report dealing with accessible columns (17-FEMA).

LERA

One and Two World Trade Center
Strucural Integrity Inspection
Accessible Columns

14 April 1995
File: P1113903
Page 5 of 10

INSPECTION METHODOLOGY

Since the concurrent visual inspection of all the accessible columns or even a major portion of them is not a practical goal, a statistical approach is followed. This approach involves the sampling of those components and systems which are more important to structural integrity, and at locations with a relatively higher potential for occurrence of defects or problems. A visual inspection of the accessible columns located in the rectangular core (the elevator area) was made from the top of the elevator cars and from a walk-through of the elevator pits. The elevator car was operated by a field

Figure A–57 (Contd.). Excerpts from 1995 structural integrity inspection report dealing with accessible columns (17-FEMA).

LERA

One and Two World Trade Center
Strucural Integrity Inspection
Accessible Columns

14 April 1995
File: P1113903
Page 7 of 10

DETAILED INSPECTION FINDINGS

This report details the findings of the inspection of the selected accessible columns within elevator shafts. Our inspection findings and our opinions concerning the findings

[redacted]

Figure A–57 (Contd.). Excerpts from 1995 structural integrity inspection report dealing with accessible columns (17-FEMA).

LERA

One and Two World Trade Center
Strucural Integrity Inspection
Accessible Columns

14 April 1995
File: P1113903
Page 9 of 10

CONCLUSIONS AND RECOMMENDATIONS

Our opinions concerning the findings and our recommendations for remedial action are summarized below. Detailed suggested remedial action can be found in Appendix B, E and F.

Based on the survey data we collected and our evaluations of this data, we believe that the structural integrity of the accessible column in the selected elevator shafts is satisfactory. We recommend that remedial action to be taken where spray fireproofing is damaged, deteriorated or missing and where there is corrosion of the column base due to water leaks in the elevator pits.

The following are our specific recommendations for the structural and fireproofing damage we observed.

Spalling, Missing and Damaged Fireproofing

[redacted]

Figure A–57 (Contd.). Excerpts from 1995 structural integrity inspection report dealing with accessible columns (17-FEMA).

THE PORT AUTHORITY OF NY AND NJ MEMORANDUM

TO: E. Ramabhushanam
FROM: S.M. Solomon
DATE: March 17. 1994
SUBJECT: WTC Existing Fireproofing

REFERENCE:

COPY TO: V. Berndt, C. Bognacki, Eng. Files

As requested, the Chemical Division performed numerous thickness measurements on existing fireproofing located on the 23rd and 24th floors of the WTC North.

Damaged and/or absent fireproofed areas on the 23rd Floor were repaired with patch material; These areas were not measured. Truss members located adjacent to the outside walls (within 3 feet) are devoid of fireproofing material. Visual inspection of the truss members on the 24th floor was not possible, as this area still has a lowered ceiling in place. Tests were taken through areas where ceiling tiles were removed. Thickness readings were taken on 16 random truss members on each floor. Measurements were taken from both flanges and webs of the truss member.

At each of these locations, a total of six individual measurements were made and averaged. These mini averages are listed on the attached table along with a total average, standard deviation, high value and low value for each floor.

S.M. Solomon
Chief of Chemical/
Environmental Testing

RG

Figure A–58. Correspondence and data related to 1994 measurements of thermal insulation thickness on floor trusses for 23rd and 24th floors in WTC 1(3-P).

MAR-17-1995 16:31 FROM PA MATERIALS DIV. TO 108555 P.003/003

41

NUMBER TWO WTC
EXISTING FIREPROOFING THICKNESS

	23rd Floor	24th Floor
Readings, inches:	0.60	0.76
	0.53	0.60
	0.70	0.90
	0.76	0.72
	0.88	0.64
	0.89	0.80
	0.83	0.68
	1.17	0.65
	0.88	0.67
	0.71	0.77
	0.82	0.96
	0.52	0.66
	0.69	0.65
	0.52	1.11
	0.84	0.95
	0.52	0.56
Average	0.73	0.76
Standard Deviation	0.14	0.15
High	1.17	1.11
Low	0.52	0.56

Figure A–58 (Contd.). Correspondence and data related to 1994 measurements of thermal insulation thickness on floor trusses for 23rd and 24th floors in WTC 1 (3-P).

Lombardi, Frank

From: Lombardi, Frank
Sent: Tuesday, February 12, 2002 3:03 PM
To: 'edepaola@severud.com'
Subject: WTC - 1 1/2" SPRAY ON FIREPROOFING UPGRADE

[redacted]

Figure A–59. Port Authority correspondence indicating number of floors where thermal insulation on floor trusses was upgraded to 1½ in. (73-LERA).

THE PORT AUTHORITY OF NY AND NJ MEMORANDUM

TO: Eli Moscovitz
FROM: Dorian Bailey
DATE: September 28, 1999
SUBJECT: World Trade Center: Test of Fire Resistive Material
Contract WTC - 697.00 W.O. #4682 Charge #W02-857090
COPY TO: C. Bognacki, J. Bullard, P. Ortiz, J. Shanahan, M.Young, E.F.

As requested, the Materials Engineering Division has tested the application of the sprayed-on fireproofing, CAFCO Blaze-Shield II for conformance to Port Authority specifications. The material was applied at the 102nd floor of WTC #1.

The tests were performed in accordance with ASTM E-605, "Thickness and Density" and ASTM E-736 "Adhesion/Cohesion" of Sprayed Fire Resistive Materials Applied to Structural Steel Members".

The results are as follows:

	Density lb./cu. ft.	Adhesion/ Cohesion lb./sq. ft.	Thickness Inches
Minimum Requirements	***15.00***	***150***	***1.50***
TEST AREA #1 1WTC 102nd Floor Truss 131 North Bottom of truss	16.47	333	3.25
TEST AREA #2 1WTC 102nd Floor Truss 231 East Bottom of truss	16.87	333	3.25
TEST AREA #3 1WTC 102nd Floor Truss 313 South Bottom of truss	15.93	315	2.11

Figure A–60. Example of test report on upgraded thermal insulation for floor trusses (3-P).

The test results indicate that the applied fireproof material, CAFCO Blaze-Shield II meets Port Authority specifications. Therefore the Materials Engineering Division recommends the acceptance of the fireproofing material.

Dorian Bailey
Staff Services Engineer

Figure A–60 (Contd.). Example of test report on upgraded thermal insulation for floor trusses (3-P).

THE PORT AUTHORITY OF NY & NJ

FRANCIS J. LOMBARDI, P.E.
CHIEF ENGINEER
225 PARK AVENUE SOUTH, 18TH FLOOR
NEW YORK, NY 10003
(212) 435-7449
(212) 435-6689 FAX
flombard@panynj.gov

March 23, 2004

John L. Gross, Ph.D., P.E.
Leader, Structures Group
United States Department of Commerce
National Institute of Standards and Technology
Gaithersburg, MD 20899-0001

Dear Dr. Gross:

Following are responses to your questions, which are repeated here in bold italics. The PDF file attached has information previously submitted to NIST as a reference to some of your questions.

In 1994, the Port Authority's Chemical Division carried out measurements of existing fireproofing on the 23rd and 24th floors of WTC 1. Averages of 6 individual measurements at 16 random locations on each floor (for a total of 32 locations) were reported in a memorandum of 17 March, 1994. While the information reported is useful, additional information is necessary to determine the true statistics of the fireproofing thickness. NIST would like to request the following:

1. ***Please provide individual measurements, rather than the averages, for all the tested locations.***

The current supervisor and staff of our Chemical/Environmental Testing Laboratory cannot find the supporting information for Mr. Solomon's memo of March 17, 1994. They do, however, state that the procedures similar to those described below in response to question 2 were followed at the time to establish the average thickness data listed in the table.

Construction audit reports of upgraded fireproofing thickness (floors 92-100 of WTC 1 and floors 77-78, 88-89, 92, 96-97 of WTC 2) indicate that thickness measurements were performed in accordance with ASTM E-605. There is, however, a discrepancy between the required procedure established by ASTM and the Port Authority's audit report data, which states that values were recorded only at the "Bottom of Truss" (see for example, memorandum of November 24, 1999, regarding material applied on 79th floor of WTC 1). Regarding this discrepancy, NIST would like to request the following:

Figure A–61. Correspondence from Port Authority addressing questions related to thickness of thermal insulation on floor trusses (681-P)

THE PORT AUTHORITY OF NY & NJ

John L. Gross, Ph.D., P.E.
National Institute of Standards and Technology
March 23, 2004
Page 2

2. Please clarify specifically what procedures were used to measure the fireproofing thickness.

A depth gage is used to determine thickness as follows: A thickness probe made of a needle that extends out along a measured scale is inserted into the fireproof material and stopped at the surface of the steel. The reading of how deep the needle extended into the fireproofing material is shown on the probe and recorded by an inspector. Thickness measurements are taken around the entire member. For the report in question of 11/24/99, 8 discrete measurements were taken to support the result of an average thickness measurement of 2.36 inches.

3. Please clarify why only data from the "Bottom of Truss" were reported.

The labeling of "Bottom of Truss" pertains to the location of collection of the physical sample, not field-testing of thickness. A test sample was obtained from the bottom of the truss for density testing, and also represents the location of the pull test. Fireproofing thickness measurements were taken from the truss diagonals as well as the upper and lower truss members, not only at the "Bottom of Truss".

4. Please provide individual measurements rather than averages.

The original thickness measurements taken from this report are: 2⅛, 2¼, 2½, 2¾, 1½, 1¾, 1¾, 2¼ inches.

Finally, in 1995 the Port Authority stated in a memorandum and white paper (memorandum dated August 18, 1995 by Joseph M. Englot) that 1.5 inch thickness of spray-on mineral fiber was required to achieve a 2-hour rating for steel joist trusses in WTC 1 and 2. Based on the 1995 information, guidelines for fireproofing repairs were established in 1999 (buckslip dated March 24, 1999 by Alan L. Reiss).

5. Please clarify what is meant by the requirement that 1.5 inches of spray on fireproofing was to be required only on "new construction."

The term "new construction" means any construction performed in the World Trade Center through a contract or work order that required the application of fireproofing. For example, re-fireproofing floors that have had asbestos mitigation, or otherwise re-fireproofing truss joists where the removal of old ceilings, ducts, light fixtures, and installation of new finishes required

Figure A–61 (Contd.). Correspondence from Port Authority addressing questions related to thickness of thermal insulation on floor trusses (681-P).

THE PORT AUTHORITY OF NY & NJ

John L. Gross, Ph.D., P.E.
National Institute of Standards and Technology
March 23, 2004
Page 4

Therefore, in consultation with the Office of the Chief Engineer, the 1999 policy was developed to address this issue. It was based on an overall fire-engineering approach, namely:

1. The sprinklerization of tenant spaces.
2. The new redundant decentralized fire alarm systems with consoles located in each tower.
3. Monitoring of the tower fire alarm systems around the clock by FDNY.
4. Certified fire safety directors (whose only responsibility was watching the fire alarm system). Port Authority Police who were stationed at the WTC were trained in structural fire fighting and were immediately notified of any alarm.
5. PA Police had a direct hot line with the Manhattan Fire Dispatchers so they knew what they were responding to, i.e. water flow alarm on a floor or multiple smoke detectors, etc.
6. The removal from the lobbies for tenanted space such as the airline counters and package counters.
7. Periodic testing of the sprinkler system and its components.

There were many occasions where small sections of the original fireproofing had been dislodged by work in the ceiling and it was feasible to patch these areas using a troweled-on patch to the original ¾" thickness, but not to 1.5 inches. Hence, the 1999 policy was developed with the above factors in mind, along with operational test procedures. This provided a process for the phased upgrade of the entire fireproofing system in the World Trade Center in accordance with the Chief Engineer's new requirements, while ensuring the overall safety program was maintained.

These requirements were written into the net lease documents for the World Trade Center to make sure the process continued after the transition from Port Authority operation and management of the WTC. The following is from section 6.2.1:

1. *One World Trade Center and Two World Trade Center Fireproofing – The existing policy of the Port Authority to upgrade steel fireproofing to 1½" thick (based on UL Guideline G508) on the earlier to occur of (i) a full floor becoming vacant, (ii) a full floor being completely renovated or (iii) for any remaining non-compliance office space, within twenty-five (25) years from the Commencement Date, unless the tenant never does a major alteration, shall be applicable to the Lessee, provided the following standards remain in force:*

   a) *all floors in One World Trade Center and Two World Trade Center, including Mechanical Equipment Rooms (once the work described in paragraph 7 of Schedule 6.2.3 has been completed) and Sky Lobbies, are sprinkled in conformance with the Port Authority Manual and NFPA 13;*

   b) *the Fire Command Centers in the lobby shall be (i) staffed with a New York City Certified "Fire Safety Director" at all times, and (ii) a total video surveillance system is installed and operating and is being monitored at all times, then the sprinkler plan may exclude the*

Figure A–61 (Contd.). Correspondence from Port Authority addressing questions related to thickness of thermal insulation on floor trusses (681-P).

THE PORT AUTHORITY OF NY & NJ

John L. Gross, Ph.D., P.E.
National Institute of Standards and Technology
March 23, 2004
Page 5

310 level of both One World Trade Center and Two World Trade Center. There will be no other permanent or temporary uses within the lobby, other than (i) the Command Center(s), visitors' desk(s), and mail boxes, provided each such area contains steel frames with marble fronts and composite/laminate tops, and (ii) temporary holiday displays composed of non-flammable materials;

c) the Lessee continues the current programs and implements additional programs as necessary to ensure the inspection, testing, and maintenance procedures of and for the sprinkler systems and the components thereof, which include, but are not limited to, the water supply, fire pumps, gravity tanks, piping and valving.

These programs shall be designed to comply with the intent of NFPA 25 and the other requirements contained in the Port Authority Manual; and

d) when the Lessee is performing the testing of the sprinkler system's water flow and alarm transmission, the specific system pressure indicated at the gage downstream of the pressure-reducing valve shall be recorded at the time of such testing, to ensure conformance with the minimums/maximums indicated on the valves.

If the practices described in clauses (a) through (d) above are not adhered to, the Lessee shall immediately begin such fireproofing, even if such work causes the Lessee to relocate the affected Space Tenants.

I hope this answers your questions. Please call or reply otherwise if you need further information.

Very truly yours,

Francis J. Lombardi, PE
Chief Engineer

Attachment

PA memoranda.pdf

Figure A–61 (Contd.). Correspondence from Port Authority addressing questions related to thickness of thermal insulation on floor trusses (681-P).

[redacted]

Figure A–62. Correspondence from Port Authority dealing with thermal insulation on WTC columns (672-P).

THE PORT AUTHORITY OF NY & NJ

John L. Gross, Ph.D., P.E.
National Institute of Standards and Technology
April 14, 2004
Page two

We have no records in our Materials Division of ever repairing or replacing fireproofing on core columns due to their inaccessibility (other than columns which are accessible within the elevator shafts) and, therefore, have no recent thickness measurements of any re-applied fireproofing for core columns.

The only records of thickness measurements we could find were for the columns that are accessible within the elevator shafts. The Port Authority Materials Engineering Division took them and they correspond to World Trade Center Tower 1 elevator shafts. Discrete readings were taken at shaft 10/11 from the basement to the 45th Floor in Tower 1 in a report dated 4/7/1999. Mean thickness values were found for shaft 14/15 from the basement to the 80th Floor in Tower 1 in a report dated 8/4/1997. These measurements cover the full extent of these two elevator shafts. One was an express from the concourse lobby to 44 with a machine room on 47 and the other was express from the concourse to 78 with an EMR on 81. The readings for both of these shafts are attached (Excel file).

Discussions with Engineering Department staff and former World Trade Department staff indicate that these two shafts had asbestos abatement and were re-fireproofed. The measurements also show a "Minimum Thickness Required" of fireproofing. Staff members recall that there was a schedule of replacement fireproofing thickness that was prepared by the firm Leslie E. Robertson Associates (LERA). One staff member located a copy of one schedule, which will be forwarded under separate cover as a sample. We have contacted William Faschan of LERA and it appears that the "Minimum Thickness Required" is the thickness called for in a schedule that appeared in documents for the work that was prepared by LERA. The sample schedule indicates that the fireproofing applied was "Type Z-106". We will try to locate the specification book for this material. This information may be among the documents that LERA assembled for NIST at the Port Authority's 225 Park Avenue South office. We will continue to search for more complete sets of this information.

In the meantime, I hope this answers your questions. Please call or reply otherwise if you need further information.

Very truly yours,

Francis J. Lombardi, PE
Chief Engineer

Att.

Figure A–62 (Contd.). Correspondence from Port Authority dealing with thermal insulation on WTC columns (657-P).

Physical Performance*

	ASTM Method	BLAZE-SHIELD DC/F	BLAZE-SHIELD II	BLAZE-SHIELD HP
Surface Burning	CAN/ULC-S102 E84	Flame: 0 Smoke: 0	Flame: 0 Smoke: 0	Flame: 0 Smoke: 0
Combustibility	CAN4-S114 E136	Noncombustible	Noncombustible	Noncombustible
Density	E605	13 pcf (208 kg/m³)	16.0 pcf (256 kg/m³)	26.2 pcf (419.2 kg/m³)
Cohesion/Adhesion	E736	295 psf (14.2 kPa)	360 psf (17.2 kPa)	1,421 psf (68 kPa)
Deflection	E759	No Cracks or Delaminations	No Cracks or Delaminations	No Cracks or Delaminations
Bond Impact	E760	No Cracks or Delaminations	No Cracks or Delaminations	No Cracks or Delaminations
Compressive Strength	E761	828 psf (39.6 kPa)	2,380 psf (113.9 kPa)	7,980 psf (382 kPa)
Air Erosion Resistance	E859	0.000 g/ft² (0.000 g/m²)	0.000 g/ft² (0.000 g/m²)	0.000 g/ft² (0.000 g/m²)
Corrosion Resistance	E937 or Mil Std 810	Does Not Promote Corrosion of Steel	Does Not Promote Corrosion of Steel	Does Not Promote Corrosion of Steel
Sound Absorption	C423	0.85 NRC 1/2" (12.7 mm) onto deck & beam	0.75 NRC 1/2" (12.7 mm) onto deck & beam	0.85 NRC 1/2" (12.7 mm) onto deck & beam
Thermal Conductivity	C518	3.45 R Value	3.33 R Value	2.43 R Value

* Values represent independent laboratory tests under controlled conditions. Refer to individual product brochures for standard values which indicate average performance to be specified.

Figure A–63. Excerpt from manufacturer's product catalog showing properties of BLAZE-SHIELD DC/F obtained from independent testing under controlled conditions (Source: www.buildcore.com/c0cafco.htm).

Pacific Car and Foundry Company

March 5, 1968 PCF #D666-69

THE PORT OF NEW YORK AUTHORITY
Office of the Construction Manager
30 Church Street - Room 1119
New York, New York 10007

Attention: Mr. R.M. Monti
Construction Manager

Reference: World Trade Center
Contract WTC-214.00
Project D679

Gentlemen:

Please find enclosed 2 copies of PCF painting specifications for Contract WTC-214.00.

A copy of this letter and specifications has been forwarded directly to Mr. J. White (SHCR).

Please note particularly Clause 5.3 which we believe satisfies the erector's requirements for these panels.

We are about to paint our first production panels and request your early approval of this specification.

Yours very truly,

PACIFIC CAR & FOUNDRY COMPANY

R.C. Symes, Project Engineer
Structural Steel Division

RCS/dv
Encl.
cc: J. White (SHCR)
J. Endler/A. Guttentag (TRCC)

Figure A–64. Letter from Pacific Car and Foundry regarding painting specification and excerpt from that specification (656-P).

5.0 PAINT, INHIBITORS AND PRESERVATIVES

5.1 Tnemec 99 Red Metal Primer is the only paint approved for use on this project.

5.2 Milled surfaces and bevels for field welds shall be treated with one coat Texaco #LB rust proofing compound.

5.3 All panels shall be stencilled, showing full engineering panel number and weight of panel in tons, thus:

103-22-19(12^T)

Weight shall be taken to nearest ton above actual weight. Stencilled marks shall be placed on Plate 3, center column of panel, directly above the bottom hand-hole. Tnemec 99-G Green Metal Primer shall be used for all stencilled marks and letters and numbers shall be 3" high.

Figure A–63 (Contd.). Letter from Pacific Car and Foundry regarding painting specification and excerpt from that specification.

This page intentionally left blank.

Appendix B
THERMOPHYSICAL PROPERTIES TEST DATA

Table B–1. Specific heat capacity results of the three SFRMs from Laboratory B DSC.

	Specific heat capacity (J/kg K)		
Temperature (^{o}C)	**BLAZE-SHIELD DC/F**	**BLAZE-SHIELD II**	**Monokote MK-5**
35	--------	--------	1204
40	939	1009	1243
45	972	1047	1276
50	1004	1087	1302
55	1034	1134	1325
60	1064	1186	1355
65	1094	1237	1391
70	1130	1295	1423
75	1175	1355	1415
80	1227	1417	1348
85	1284	1479	1279
90	1369	1546	1253
95	1491	1623	1236
100	1663	1755	1183
105	1892	1945	1122
110	2187	2199	1100
115	2495	2528	1290
120	2740	2908	1851
125	2756	3298	3094
130	2074	3672	5117
135	1658	3293	7488
140	1785	2235	8589
145	2050	1937	6528
150	2062	2038	4713
155	1763	1934	5146
160	1536	1796	4459
165	1437	1700	1629
170	1375	1637	1244
175	1328	1587	1162
180	1289	1546	1152
185	1254	1506	1161
190	1220	1466	1174

	Specific heat capacity (J/kg K)		
Temperature (^oC)	**BLAZE-SHIELD DC/F**	**BLAZE-SHIELD II**	**Monokote MK-5**
195	1190	1414	1196
200	1167	1368	1226
205	1145	1320	1251
210	1125	1284	1266
215	1110	1248	1283
220	1094	1217	1309
225	1077	1183	1332
230	1063	1149	1364
235	1050	1112	1393
240	1035	1082	1428
245	1022	1053	1460
250	1006	1025	1492
255	991	996	1521
260	977	961	1544
265	965	926	1567
270	958	891	1590
275	956	857	1622
280	945	807	1636
285	936	765	1656
290	924	729	1669
295	911	701	1673
300	899	675	1665
305	888	649	1651
310	878	627	1625
315	876	613	1578
320	877	610	1512
325	880	620	1400
330	893	642	1245
335	911	682	1042
340	932	734	892
345	955	789	940
350	975	857	1042

Table B–2. Specific heat capacity of 5/8 in. gypsum panel A.

Temperature (°C)	Cp (J/kg K)		Temperature (°C)	Cp (J/kg K)
50	1248		192	3569
100	1416		196	5020
125	1608		200	8087
135	2155		202	9200
140	3118		204	9356
142	3890		206	8816
144	5210		208	7948
146	7428		210	6497
148	11148		212	4496
150	15341		214	2771
152	18490		216	2010
154	19671		218	1695
156	19648		220	1550
158	18822		225	1389
160	17476		250	1156
162	15728		300	1094
164	13734		350	1089
166	11553		400	1046
168	9436		415	890
170	7034		430	453
172	5107		445	506
174	3501		460	808
176	2768		475	966
178	2417		500	1104
180	2297		550	1192
184	2544		600	1245
188	2923			

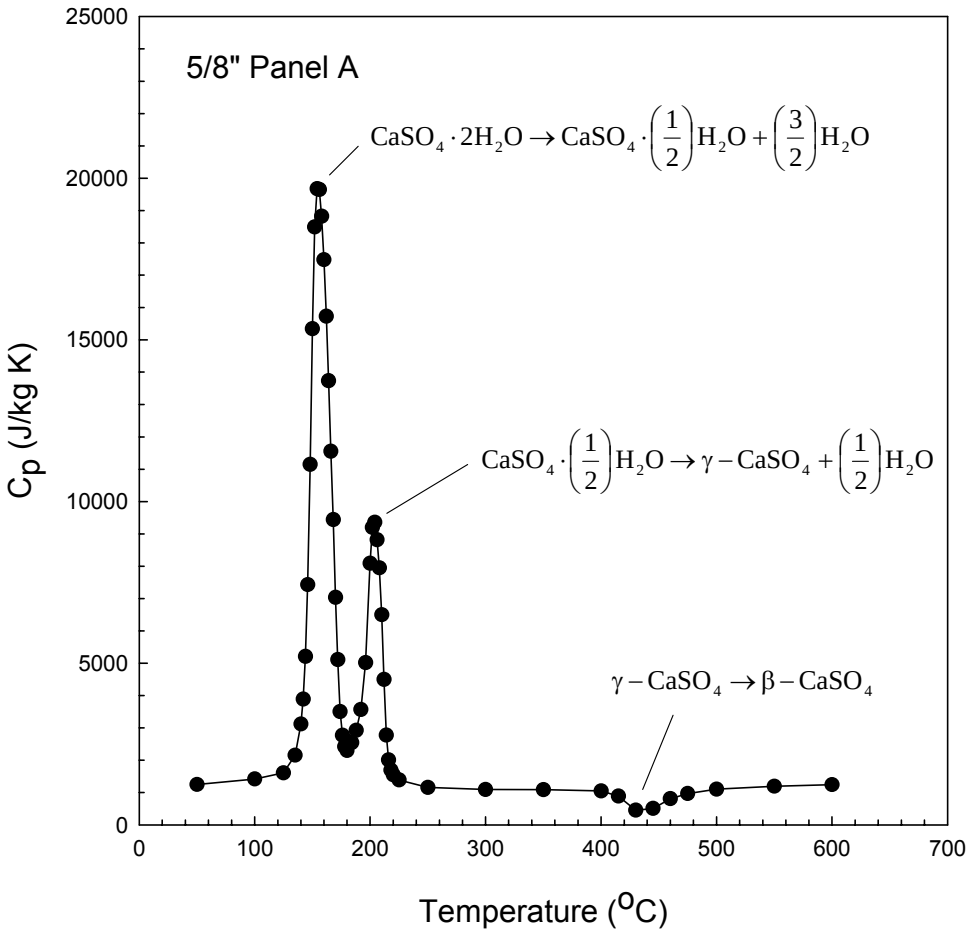

Figure B–1. Specific heat capacity of 5/8 in. gypsum panel A.

Table B–3. Specific heat capacity of ½ in. gypsum panel.

Temperature (°C)	Cp (J/kg K)		Temperature (°C)	Cp (J/kg K)
50	1325		192	3693
100	1544		196	4957
125	1764		200	7730
135	2457		202	8774
140	3801		204	9088
142	4769		206	8644
144	6418		208	7693
146	8787		210	6364
148	12015		212	4487
150	15429		214	2888
152	17532		216	2090
154	18399		218	1828
156	18349		220	1672
158	17769		225	1495
160	16776		250	1278
162	15564		300	1185
164	13895		350	1188
166	12124		400	1159
168	10357		415	1015
170	8263		430	667
172	6180		445	642
174	4459		460	930
176	3383		475	1091
178	2768		500	1235
180	2545		550	1350
184	2632		600	1416
188	3006			

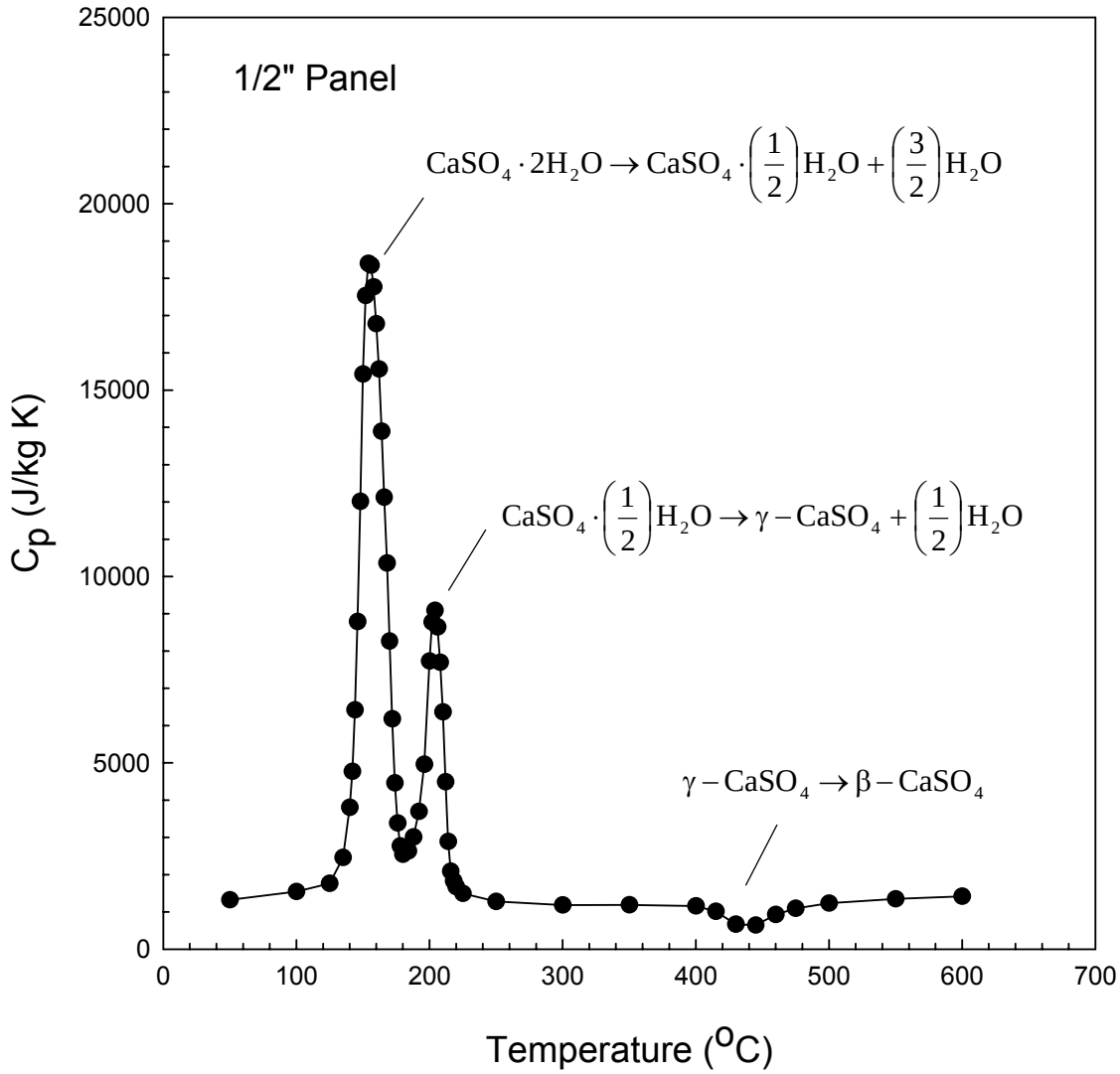

Figure B–2. Specific heat capacity of 1/2 in. gypsum panel.

Table B–4. Specific heat capacity of 5/8 in. gypsum panel B.

Temperature (°C)	Cp (J/kg K)		Temperature (°C)	Cp (J/kg K)
50	1250		192	3624
100	1507		196	4886
125	1711		200	7769
135	2486		202	8848
140	3966		204	9102
142	5001		206	8727
144	6728		208	7705
146	9142		210	6210
148	12341		212	4342
150	15681		214	2775
152	17740		216	2052
154	18550		218	1770
156	18374		220	1621
158	17667		225	1451
160	16401		250	1233
162	14914		300	1148
164	13190		350	1168
166	11251		400	1130
168	9096		415	984
170	7108		430	568
172	5091		445	646
174	3658		460	930
176	2814		475	1084
178	2516		500	1232
180	2364		550	1347
184	2567		600	1432
188	2936			

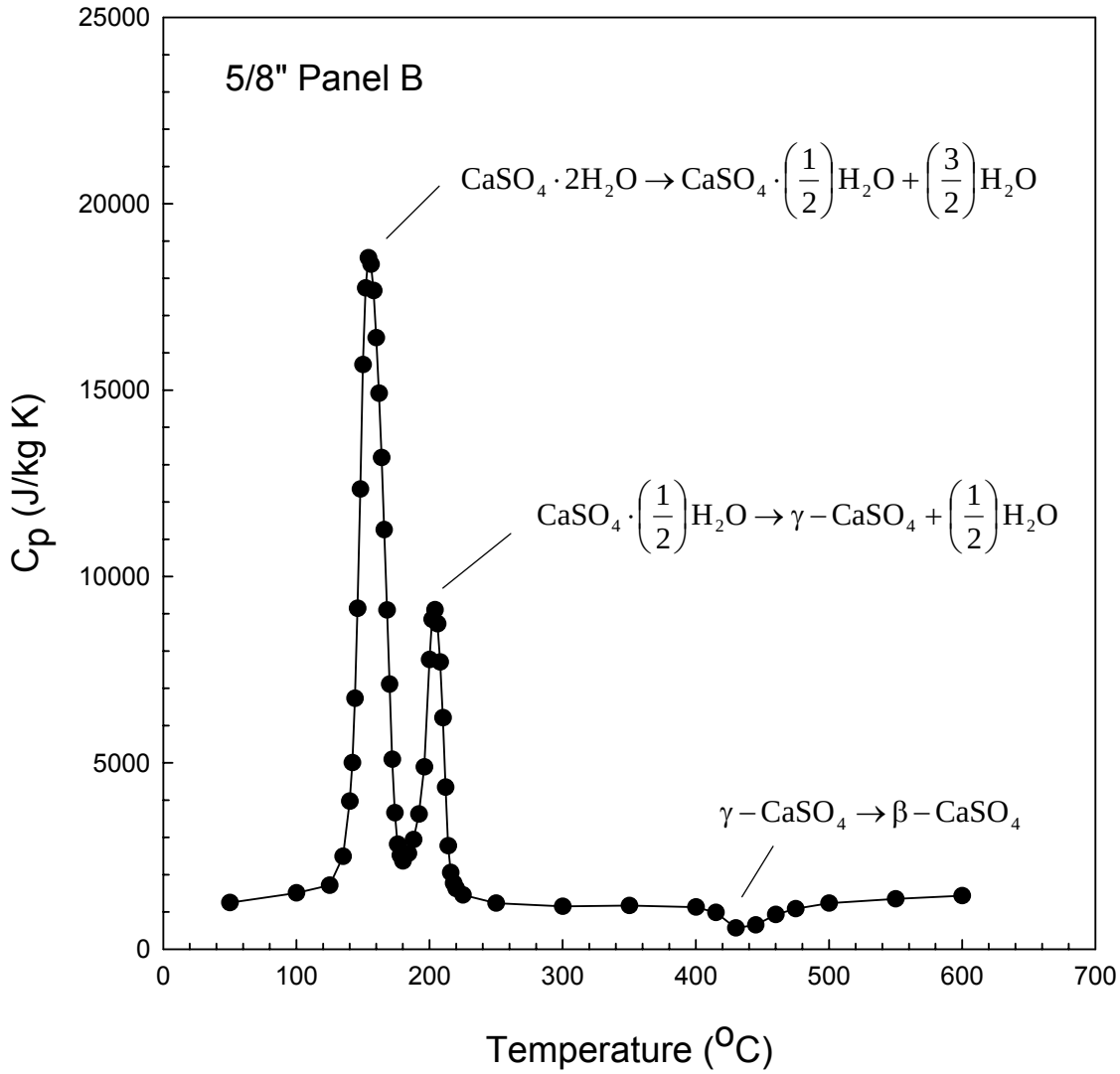

Figure B–3. Specific heat capacity of 5/8 in. gypsum panel B.

Table B–5. Specific heat capacity of 1 in. gypsum liner panel.

Temperature (°C)	Cp (J/kg K)		Temperature (°C)	Cp (J/kg K)
50	1192		192	3583
100	1495		196	4876
125	2293		200	7346
135	3766		202	8360
140	5548		204	8872
142	6987		206	8787
144	8876		208	8164
146	11092		210	6847
148	13303		212	5256
150	15076		214	3305
152	15999		216	2260
154	16160		218	1787
156	15787		220	1597
158	14949		225	1408
160	13925		250	1192
162	12577		300	1137
164	10840		350	1146
166	8755		400	1060
168	6481		415	822
170	4676		430	609
172	3296		445	794
174	2685		460	971
176	2369		475	1079
178	2252		500	1200
180	2288		550	1306
184	2577		600	1378
188	2959			

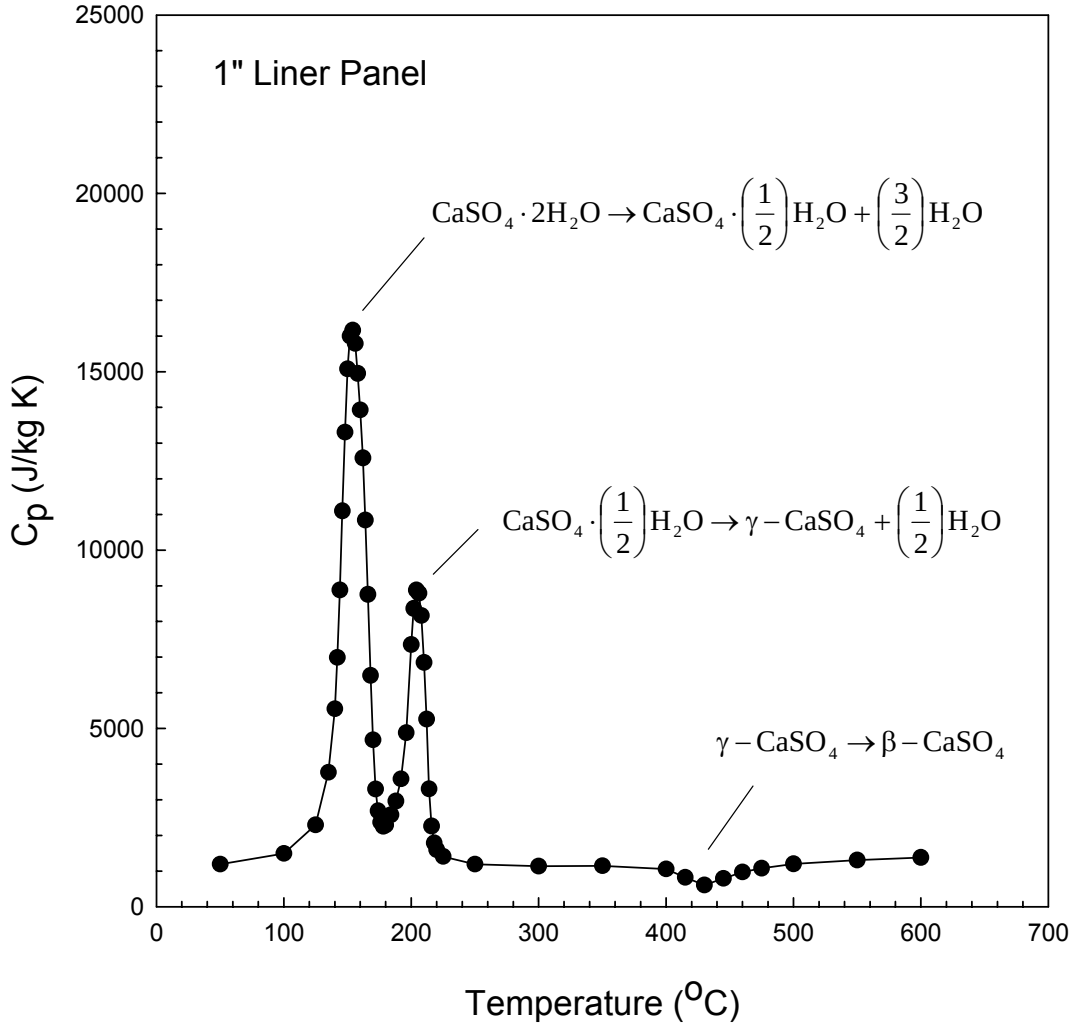

Figure B–4. Specific heat capacity of gypsum 1 in. liner panel.

Appendix C
DEBRIS IMPACT TESTS OF BLAZE-SHIELD DC/F SPRAYED FIRE-RESISTIVE MATERIAL

INTRODUCTION

This appendix presents experimental observations obtained from a series of debris impact tests on steel plates and bars with the sprayed fire-resistive material (SFRM) BLAZE-SHIELD DC/F. The tests were performed to provide evidence regarding the assumption that, within the debris field created by the aircraft impact into WTC 1 and WTC 2, the SFRM used for thermal insulation of structural members was damaged and dislodged.

Engineering judgment, based on the aircraft impact damage analysis (NIST NCSTAR 1-2), was used to develop test parameters that were also within the limitations of the experimental facility. Two sets of controlled experiments were designed: a high-speed low-mass test, which used uniform size lead pellets (buckshot) for debris and high-speed impact, and a low-speed high-mass test, which used a lower speed and several types of projectiles to simulate a random debris size distribution.

The SFRM on the steel plates and bars was subjected to a field of impacting projectiles fired from a universal receiver (a modified gun) at various orientations. For the high-speed low-mass impact, a debris field was simulated by buckshot fired from a modified shotgun. Since firing of conventional shotgun shells would result in average buckshot speed in excess of 682 mph (304 m/s), controlled firing with custom-made shot shells was needed to reduce the impact speed within the range found for the debris field in the aircraft impact analyses of the WTC towers (NIST NCSTAR 1-2).

The speed of the aircraft at impact was estimated to be 443 mph (198 m/s) for WTC 1 and 542 mph (242 m/s) for WTC 2. Therefore, the speed of the debris field in each tower ranged between the maximum aircraft speed at impact and zero, when the debris came to a rest. As no single speed or debris size could represent the debris field in the towers, a range of debris speeds and sizes were selected that were within the limitations of the test facility, as noted above. An average speed of 341 mph (152 m/s) was chosen for the debris impact velocity for the high-speed low-mass impact tests. For low-speed high-mass impact tests, an average speed of the projectiles ranging between 112 mph (50 m/s) and 201 mph (90 m/s) was selected.

The desired impact speed was achieved but the universal receiver could only accommodate small projectiles, which did not represent actual debris shapes and sizes. Therefore, *the impact kinetic energies from the projectiles were significantly lower than those from actual impacting debris in the WTC towers due to differences in size (mass)*. However, when the impact kinetic energies were normalized by the impact area, the impact conditions used in the tests approximated those in the towers, based on the following order-of-magnitude analysis.

The kinetic energies of the two aircraft before they impacted the WTC towers differed somewhat, but were of the same order of magnitude. Based on the aircraft masses and initial speeds reported in NIST NCSTAR 1-2, the kinetic energy of the impacting aircraft were approximately 3.4×10^9 ft lb (2.5×10^9 J)

and 5 x 10^9 ft lb (3.7 x 10^9 J) for WTC 1 and WTC 2, respectively. Based on the aircraft impact analysis (NIST NCSTAR 1-2), the speed of the aircraft fragments as they approached the core were about 0.4 to 0.7 of the initial impact speed for WTC 1 and WTC 2, respectively (energy is proportional to the square of the speed). In addition, portions of the aircraft masses were stopped prior to reaching the core. As a result, it might be expected that the energy associated with the aircraft debris at the core were on the order of 10^8 ft lb to 10^9 ft lb (10^8 J to 10^9 J).

For the purpose of this study, it was assumed that the energy of the debris impacting the SFRM was distributed throughout a debris area that was about five floors high (60 ft or 18 m) and 150 ft (45 m) wide, or an area of about 9 x 10^3 ft^2 (8 x 10^2 m^2). Thus, the energy per unit area would be on the order of $O(10^4$ to 10^5 ft lb/ft^2) ($O(10^5$ to 10^6 J/m^2)). The total kinetic energy of the buckshot impact per unit area in the experiments was estimated, based on an average pellet size of 0.33 in. (8.4 mm), a mass of 0.1 oz (3.5 g), and a speed of 341 mph (152 m/s), to be of the same order of magnitude, $O(10^4$ to 10^5 ft lb/ft^2) ($O(10^5$ to 10^6 J/m^2)). Therefore, the impact parameters (impact speed and kinetic energy per unit area) used in the experiments are considered representative of these parameters in the aircraft impact analysis of the WTC towers. *However, the debris impact test condition simulated an instantaneous impact by a burst of debris whereas the actual scenario involved a three dimensional field of debris, with a depth, width, and height, continuously impacting the target(s) for a finite duration over a large area.* In addition, since the samples used in the tests were not restrained in the same way as actual structural elements would be, the response of the steel component and SFRM to debris impact in terms of dislodgement of SFRM may differ somewhat from that of an actual structural member.

EXPERIMENTAL APPARATUS AND TEST PROCEDURE

The experimental set-up and procedure used to perform the debris impact tests are described here. All ballistic tests on the SFRM were performed at the ballistic research test facility at NIST.

Ballistic research test facility

The facility consists of two pieces of ballistic firing equipment (small and large universal receivers), an optical device (two optical interrupters) to measure average projectile speed, an adjustable platform to mount the target, and a projectile trap. Figure C-1 shows a schematic of the facility.

The small universal receiver was configured to a 12-gauge shotgun using a custom-made barrel. This universal receiver was remotely triggered in the adjacent control room. The shells used No. 00 lead buckshot with a diameter of 0.33 in. (8.4 mm). The shot shells were specifically tailored to achieve nominal average projectile speeds between 307 mph (137 m/s) and 375 mph (168 m/s) by adjusting the amount of gunpowder and the number of buckshot used in the shells. For all tests using the small universal receiver, 0.3 oz (10 g) of gunpowder (Hodgdon Titegroup) and 2 oz (63 g) of buckshot were used.

The large universal receiver was configured to have a custom-made barrel with an inside diameter of 3.15 in. (80 mm). The receiver was air operated and could be triggered only at the gun station. The shot shells consisted of two halves of Styrofoam wads that held 2.2 lb (1,000 g) of projectiles. The projectiles were comprised of a random combination of steel bolts and hexagon nuts that were larger and heavier than the buckshot (the largest nut size was 2 in. (50 mm) wide by 1.2 in. (30 mm) thick hexagon nuts for a 1 ¼ in. (32 mm) bolt). Air pressure was adjusted to achieve nominal average projectile speeds between

112 mph (50 m/s) and 201 mph (90 m/s). Thus, the large receiver simulated impact by fields of projectiles with larger mass density than those of the small receiver, but at slower speeds. Photos of the typical shot shells for ballistic impact tests using the large universal receiver are shown in Fig. C-2.

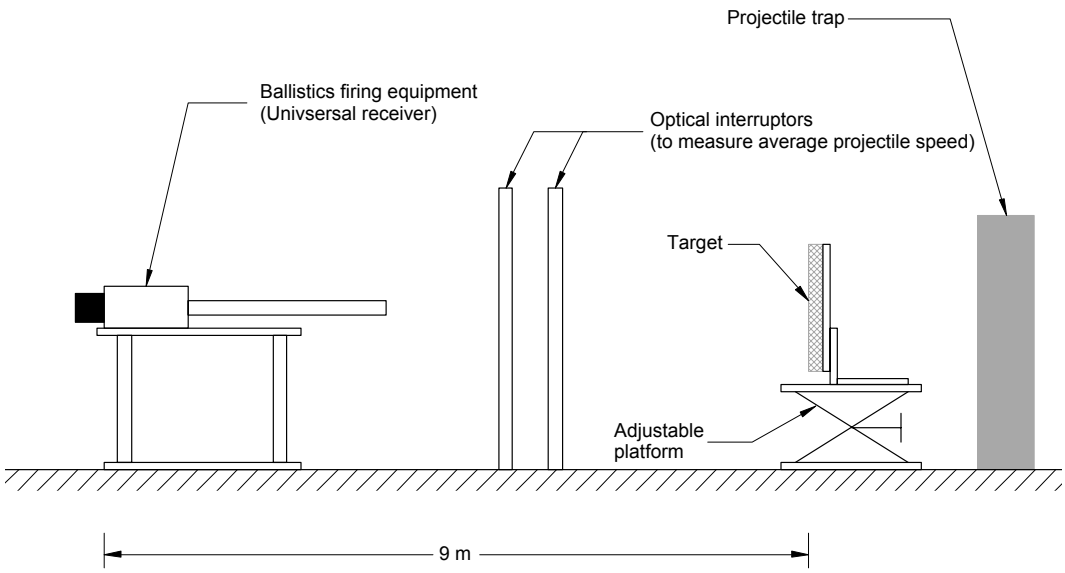

Figure C-1. Schematic of the ballistic research test facility.

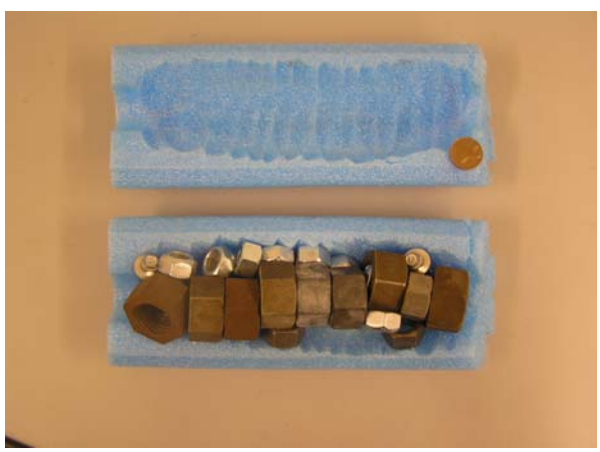

Figure C-2. Typical shot shells used in the large universal receiver. A penny is also shown for comparison.

The target was mounted 29.5 ft (9 m) from the universal receiver for testing of the steel plate specimens and 15.7 ft (4.8 m) for testing of the steel bar specimens. A plywood enclosure was built around the target area to contain ricocheted buckshot. A laser sight was used to position the target area with respect to the barrel. The impact angle was varied from a 0 degree (target perpendicular to the barrel) to 60 degree angle (measured from the 0 degree position).

Sample (impact target) preparation

The steel plates were ¼ in. × 12 in. × 12 in. (6 mm × 300 mm × 300 mm) and unprimed. Four nuts, arranged in a square pattern, 8 in. × 8 in. (200 mm. × 200 mm), were welded on one side of the plate to mount the sample for testing. The 1 in. (25.4 mm) diameter bars were 20 in. (508 mm) long for the small universal receiver tests and 36 in. (914 mm) long for the large universal receiver tests. The steel plates and the 36 in. long bars were shipped to Isolatek, Inc. in Stanhope, New Jersey, for application of BLAZE-SHIELD DC/F to a thickness of 1.5 in. (38 mm). The 20 in. (0.5 m) long bars had been previously prepared and sprayed by Isolatek at NIST with a nominal thickness of 1.5 in. (38 mm). Figure C-3 shows a steel plate with SFRM mounted in the ballistic research test facility ready for a test.

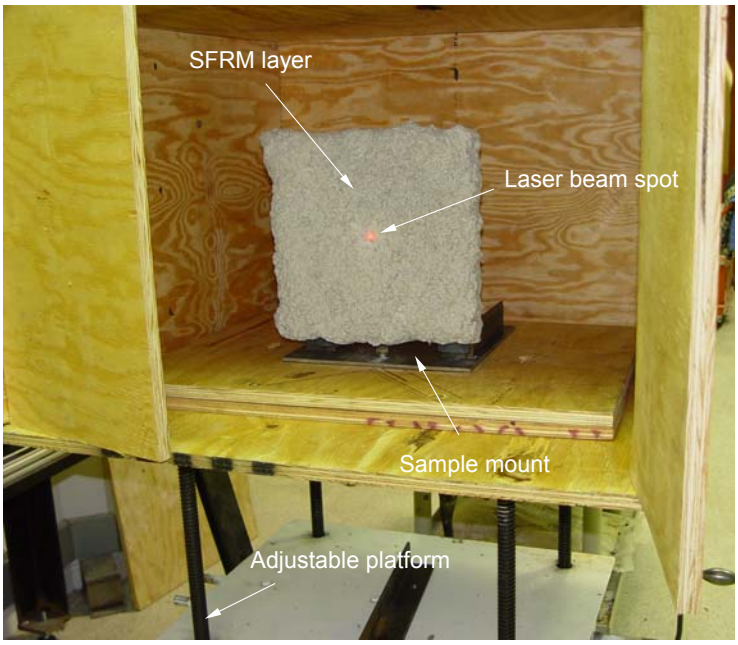

Figure C-3. Photograph of a steel plate with SFRM mounted in the ballistic research test facility.

Test matrix

Table C-1 summarizes the tests conducted in the debris impact tests.

Table C-1. Test matrix.

Debris speed/mass	Universal receiver	Test Specimen	Impact Angle				
			0°	*20°*	*30°*	*45°*	*60°*
High speed/low mass	Small	Steel plate (unprimed)	××××	××		××	××
	Small	Steel bar (unprimed)	×				
	Small	Steel bar (primed)	××				
Low speed/high mass	Large	Steel bar (unprimed)	××				

'×' = 1 run

Test procedure

Each sample was photographed before and after each test. The steel plate or bar test sample was first mounted on two parallel L-brackets at the target location. The L-brackets were attached to a base plate, which could be rotated to adjust the impact orientation. A laser sight was then loaded into the chamber to center the target with respect to the barrel. The sample impact angle (0 degree, 20 degree, 30 degree, 45 degree, or 60 degree) was set using a protractor. Impact angle was measured with respect to the leading edge of the adjustable platform, which was set to be perpendicular to the laser beam. A 0 degree impact angle was defined as the target oriented perpendicular to the direction of the projectiles. Other impact angles were measured with respect to 0 degree.

After the impact angle was set, the laser sight was removed from the chamber of the barrel. The shot shells were prepared in the ammunition laboratory. The receiver was fired and the average projectile speed was recorded. The impact tests were viewed through a bulletproof observation window in the control room. After the test, the sample was examined and photographed to assess damage to the SFRM by the projectiles.

The nominal impact area by the buckshot fired from the small universal receiver at a distance of 29.5 ft (9 m) had a diameter of approximately 6 in. to 8 in. (0.15 m to 0.2 m). For the large universal receiver, the nominal impact area by the projectiles (bolts, nuts, and buckshot) had a diameter of approximately 24 in. (0.6 m). For the steel bars, the impact area was reduced to about a 4 in. (0.1 m) diameter, which was approximately the diameter of the SFRM layer on the bar, by moving the bar closer to the receiver to increase the likelihood of projectiles hitting the target.

TEST RESULTS AND DISCUSSION

In this section, damage to the SFRM due to debris impact is assessed and photographic evidence is provided.

Steel plate and SFRM specimens

All tests on steel plates were performed using the small universal receiver (high-speed low-mass). In these tests, the impact area was much smaller than the sample surface area. Table C-2 summarizes the test parameters for the steel plates with an SFRM layer. The kinetic energy per unit impact area was estimated based on the projectile speed, an average pellet mass of 0.1 oz (3.5 g), and an impact area equivalent to the cross section area of the pellet 0.09 in^2 (5.52 mm^2). Tests at a 0 degree impact orientation had damage to the SFRM at the points of projectile impact, which was marked by distinct, approximately circular indentations on the layer. The vibration of the plate caused by the impact was severe enough to break the adhesive bond and completely separate the SFRM from the unprimed steel plate (see Figure C-4). Similar observations were made for tests at a 20 degree and 40 degree impact angle, as shown in Figure C-5 and Figure C-6, respectively. However, at a 60 degree impact orientation, the SFRM remained attached to the steel plate. Several projectile exit points were noted, which were due to projectiles ricocheting off the steel surface. Figure C-7 shows the entry points of the projectiles and the damage to the SFRM, and illustrates the size of the debris impact field relative to the specimen size. Two 0 degree impact tests were also conducted with the four edges of the SFRM layer taped to the steel plate (see Figure C-8) to simulate better adhesion to the plate and to prevent the separation of the SFRM from

the plate upon impact of the projectiles. However, when the tape was carefully removed after the test, no adhesion of the SFRM to the steel plate was found; this also occurred for the 0 degree impact test without duct tape.

Table C-2. Summary of test parameters for using unprimed steel plates with SFRM.

Test #		Impact orientation (degree)	Average projectile speed (ft/s (m/s))	Kinetic energy per impact area (ft lb/ft^2 (J/m^2))
Small universal receiver (low mass, high impact velocity)	PL01	0	511 (155.8)	5.3 x 10^4 (7.7 × 10^5)
	PL02	55	346 (105.5)	2.4 x 10^4 (3.5 × 10^5)
	PL03	60	574(175)	6.7 x 10^4 (9.7 × 10^5)
	PL04	0	541(165)	5.9 x 10^4 (8.6 × 10^5)
	PL05	20	469(143)	4.5 x 10^4 (6.5 × 10^5)
	PL06	20	563 (171.6)	6.4 x 10^4 (9.3 × 10^5)
	PL07	40	561(171)	6.4 x 10^4 (9.3 × 10^5)
	PL08	40	568(173)*	6.5 x 10^4 (9.5 × 10^5)
	PL09**	0	558(170)	6.3 x 10^4 (9.2 × 10^5)
	PL10**	0	225 (69)	1.0 x 10^4 (1.5 × 10^5)

* Receiver misfired initially at 102 ft/s (31 m/s); a few shots hit but there was no visible damage to SFRM; sample reused for 2nd shot.

** The edges of the SFRM layer were taped to the steel plate using duct tape.

Figure C-4. Photograph showing damage to the SFRM after a ballistic impact at 0 degree. The SFRM layer completely separated from the steel plate.

Figure C-5. Photograph showing damage to the SFRM after a ballistic impact at 20 degree. The SFRM layer completely separated from the steel plate and landed on the floor.

Figure C-6. Photograph showing damage to the SFRM after a ballistic impact at 40 degree. The SFRM layer completely separated from the steel plate.

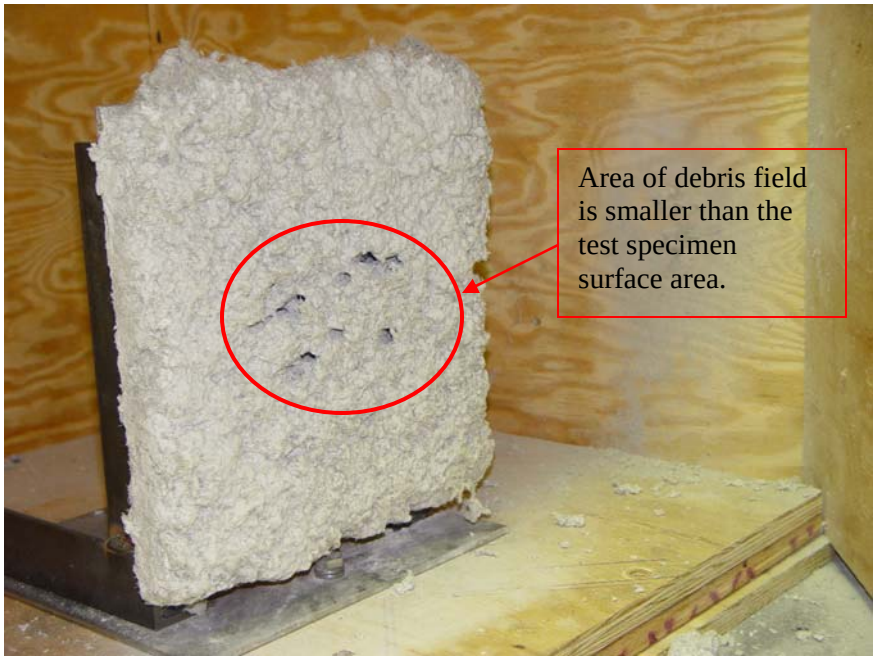

Figure C-7. Photograph showing damage to the SFRM after a ballistic impact at 60 degree. The SFRM layer did not separate from the steel plate.

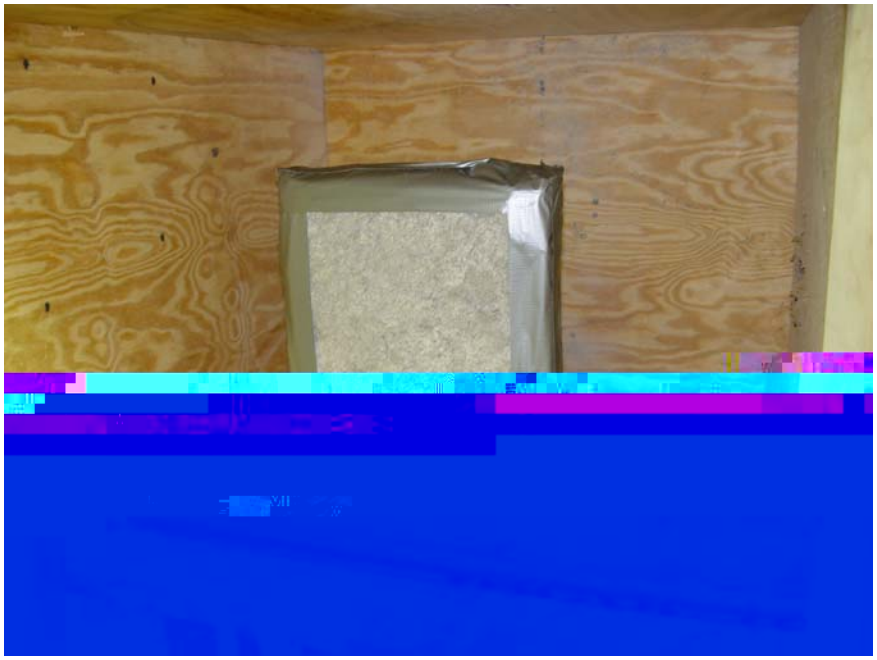

Figure C-8. Photograph showing the edges of the SFRM duct taped to the steel plate before the ballistic tests at 0 degree.

Steel bar and SFRM specimens

The ballistic impact tests for the steel bars were performed using both the small and large universal receivers. A summary of the test parameters used for the steel bars with SFRM is given in Table C-3. For these tests, the adjustable mounting table was moved closer to the receiver to reduce the number of projectiles that might have missed the target bar. The distance from the chamber of the universal receivers to the target was 15.7 ft (4.8 m).

In tests using the small universal receiver (high-speed low-mass), the projectiles dislodged the SFRM completely at the impact area of both the primed and unprimed bars, exposed the steel bar, and resulted in loss of adhesion (not cohesion) of the remaining SFRM on the bar. After the ballistic impact, the remaining SFRM rotated freely with respect to the bar. Figure C-9 and Figure C-10 show the damage to the SFRM on the unprimed and primed bars, respectively, which were tested with the small universal receiver. In Figure C-9, the projectiles impacted the upper portion of the bar specimen and missed the center and lower portions.

Similar results were observed for tests with the large universal receiver (low-speed high-mass). The projectiles dislodged the SFRM completely at the impact area of the bars, resulting in exposed steel bar and loss of adhesion of the remaining undamaged SFRM on both sides of the impact area. Figure C-11 and Figure C-12 show the damage to the SFRM on unprimed steel bars tested with the large universal receiver. In Figure C-12, the projectiles also missed the lower portion of the specimen.

Table C-3. Summary of test parameters used for the steel bars with SFRM.

Test #		Configuration	Impact orientation (degree)	Total mass of projectiles (oz (g))	Average projectile speed (ft/s (m/s))	Kinetic energy / impact area (ft lb/ft^2 (J/m^2))
Small Universal Receiver	BAR01	unprimed	0	2 (63)*	443 (135)	4.0×10^4 (5.8×10^5)
	BAR02	primed	0	2 (63)*	556 (170)	6.2×10^4 (9.1×10^5)
	BAR03	primed	0	2 (63)*	543 (166)	5.9×10^4 (8.7×10^5)
Large Universal Receiver	BAR04	unprimed	0	32 (1,000)**	282 (86)	$3.2 \times 10^4 – 5.3 \times 10^4$ ($4.6 \times 10^5 – 7.8 \times 10^5$)
	BAR05	unprimed	0	32 (1,000)**	344 (105)	$4.6 \times 10^4 – 8.0 \times 10^5$ ($6.8 \times 10^5 – 1.2 \times 10^6$)

* Projectiles consisted of only No. 00 lead buckshot.

** Projectiles consisted of a combination of hexagon steel nuts of different sizes. The minimum and maximum kinetic energy per unit impact area were estimated based on the smallest and the largest nuts and the minimum and maximum nut cross sections as impact areas.

Figure C-9. Photograph showing damage to the SFRM on an unprimed steel bar (BAR01) after a ballistic impact at 0 degree using the small universal receiver.

Figure C-10. Photograph showing damage to the SFRM on a primed steel bar (BAR02) after a ballistic impact at 0 degree using the small universal receiver.

Figure C-11. Photograph showing damage to the SFRM on unprimed steel bar (BAR04) after a debris impact at 0 degree using the large universal receiver.

Figure C-12. Photograph showing damage to the SFRM on unprimed steel bar (BAR05) after a debris impact at 0 degree using the large universal receiver.

SUMMARY OF FINDINGS

Based on the observations made in the ballistic impact tests, the SFRM was dislodged by direct impact with solid objects that had a kinetic energy per unit impact area approaching 10^4 to 10^5 ft lb/ft^2 (10^5 to 10^6 J/m^2). In addition, SFRM that was not dislodged after the debris impact lost its adhesion to the steel surface in all but one test. The SFRM on the steel plate was dislodged upon impact of the projectiles, except for the ballistic impact at a 60 degree angle to the plate. When the SFRM was taped to the steel plate and the tape carefully removed after debris impact at 0 degree, no adhesion of the SFRM to the steel plate was found, the same result found for the 0 degree impact test without duct tape. For SFRM on steel bars, the remaining SFRM after impact rotated freely with respect to the bar.

When the debris field dimensions were similar to the specimen dimensions, the SFRM was dislodged completely from the steel component. For instance, the SFRM was dislodged over the width of the steel bar specimen when the debris field was centered over the specimen width. However, the steel plate dimensions were much larger than the debris field dimensions and the SFRM was damaged only where the impact occurred; the surrounding SFRM remained cohesively intact but lost its adhesive bond to the steel plate.

The test results demonstrated that there was dislodgment of SFRM at locations subject to direct debris impact. For direct debris impact up to a 60 degree orientation, the SFRM adhesive bond to the steel component was lost, but there was no loss of the SFRM cohesive bond.

In the WTC towers, where the debris fields were larger than the dimensions of steel components (i.e., such as trusses, beams, and columns), these tests show that SFRM would have been dislodged for a wide range of debris sizes and speeds. The test results support the assumption that, within the debris field created by the aircraft impact into WTC 1 and WTC 2, the SFRM used for thermal insulation of structural members was damaged and dislodged.

NIST NCSTAR 1-6B

Federal Building and Fire Safety Investigation of the World Trade Center Disaster

Fire Resistance Tests of Floor Truss Systems

John Gross
Frederick Hervey
Mark Izydorek
John Mammoser
Joseph Treadway

NIST National Institute of Standards and Technology • Technology Administration • U.S. Department of Commerce

NIST NCSTAR 1-6B

Federal Building and Fire Safety Investigation of the World Trade Center Disaster

Fire Resistance Tests of Floor Truss Systems

John Gross
Building and Fire Research Laboratory
National Institute of Standards and Technology

Frederick Hervey
Mark Izydorek
John Mammoser
Joseph Treadway
Underwriters Laboratories, Inc.

September 2005

U.S. Department of Commerce
Carlos M. Gutierrez, Secretary

Technology Administration
Michelle O'Neill, Acting Under Secretary for Technology

National Institute of Standards and Technology
William Jeffrey, Director

Disclaimer No. 1

Certain commercial entities, equipment, products, or materials are identified in this document in order to describe a procedure or concept adequately or to trace the history of the procedures and practices used. Such identification is not intended to imply recommendation, endorsement, or implication that the entities, products, materials, or equipment are necessarily the best available for the purpose. Nor does such identification imply a finding of fault or negligence by the National Institute of Standards and Technology.

Disclaimer No. 2

The policy of NIST is to use the International System of Units (metric units) in all publications. In this document, however, units are presented in metric units or the inch-pound system, whichever is prevalent in the discipline.

Disclaimer No. 3

Pursuant to section 7 of the National Construction Safety Team Act, the NIST Director has determined that certain evidence received by NIST in the course of this Investigation is “voluntarily provided safety-related information” that is “not directly related to the building failure being investigated” and that “disclosure of that information would inhibit the voluntary provision of that type of information” (15 USC 7306c).

In addition, a substantial portion of the evidence collected by NIST in the course of the Investigation has been provided to NIST under nondisclosure agreements.

Disclaimer No. 4

NIST takes no position as to whether the design or construction of a WTC building was compliant with any code since, due to the destruction of the WTC buildings, NIST could not verify the actual (or as-built) construction, the properties and condition of the materials used, or changes to the original construction made over the life of the buildings. In addition, NIST could not verify the interpretations of codes used by applicable authorities in determining compliance when implementing building codes. Where an Investigation report states whether a system was designed or installed as required by a code *provision*, NIST has documentary or anecdotal evidence indicating whether the requirement was met, or NIST has independently conducted tests or analyses indicating whether the requirement was met.

Use in Legal Proceedings

No part of any report resulting from a NIST investigation into a structural failure or from an investigation under the National Construction Safety Team Act may be used in any suit or action for damages arising out of any matter mentioned in such report (15 USC 281a; as amended by P.L. 107-231).

National Institute of Standards and Technology National Construction Safety Team Act Report 1-6B
Natl. Inst. Stand. Technol. Natl. Constr. Sfty. Tm. Act Rpt. 1-6B, 202 pages (September 2005)
CODEN: NSPUE2

U.S. GOVERNMENT PRINTING OFFICE
WASHINGTON: 2005

For sale by the Superintendent of Documents, U.S. Government Printing Office
Internet: bookstore.gpo.gov — Phone: (202) 512-1800 — Fax: (202) 512-2250
Mail: Stop SSOP, Washington, DC 20402-0001

ABSTRACT

The National Institute of Standards and Technology (NIST) review of available documents related to the design and construction of the World Trade Center (WTC) towers indicated that the fire performance of the composite floor system of the WTC towers was an issue of concern to the building owners and designers from the original design and throughout the service life of the buildings. However, NIST found no evidence that fire resistance tests of the WTC floor system were ever conducted. As a result, NIST conducted a series of four standard fire resistance tests (ASTM E 119). In this series of tests, the effects of three factors were studied: (1) thickness of sprayed fire-resistive material (SFRM), (2) test restraint conditions, and (3) scale of the test. The tests were conducted by Underwriters Laboratories, Inc. under a NIST contract and represented both full-scale (35 ft span) and reduced-scale (17 ft span) floor assemblies constructed to represent the original design as closely as practical. For three of the tests, the thickness of the sprayed fire resistive material was ¾ in. which represented the average thickness applied in the original construction. In the fourth test, the thickness of applied SFRM was ½ in. which was the thickness specified for the original design. Tests were conducted in both the restrained and unrestrained condition to provide bounds on the expected performance of the floor system under the standard fire exposure. The restrained full-scale floor system obtained a fire resistance rating of 1½ h, while the unrestrained floor system achieved a 2 h rating. For the unrestrained test condition, specimens protected with ¾ in. thick sprayed fire resistive material were able to sustain the maximum design load for approximately 2 h without collapsing; in the unrestrained test, the load was maintained without collapsing for 3½ h. Past experience with the ASTM E 119 test method would lead investigators to expect that the unrestrained floor assembly would not perform as well as the restrained assembly, and therefore, would receive a lower fire rating. A fire rating of 2 h was determined from the reduced-scale test with the average applied SFRM thickness of ¾ in., while a fire rating of 1½ h was determined from the full-scale test with the same SFRM thickness. This finding raises the question of whether or not a fire rating based on the ASTM E 119 performance of a 17 ft span floor assembly is scalable to a larger floor system such as found in the WTC towers where spans ranged from 35 ft to 60 ft.

Keywords: ASTM E 119, fire testing, floor systems, sprayed fire-resistive materials, standard fire test, steel, structural behavior, testing, trusses, World Trade Center.

This page intentionally left blank.

TABLE OF CONTENTS

Abstract iii
List of Figures ix
List of Tables xiii
List of Acronyms and Abbreviations xv
Preface xvii
Acknowledgments xxvii
Executive Summary xxix

Chapter 1
Introduction 1
1.1 Motivation for Conducting Standard Fire Tests of the WTC Floor System 1
1.2 Purpose of the Standard Fire Tests 2
1.3 Test Variables 2
1.3.1 SFRM Thickness 2
1.3.2 Restraint Conditions 3
1.3.3 Scale 3
1.4 Test Program 3

Chapter 2
ASTM Standard Fire Test 5
2.1 General Description 5
2.2 Restraint Conditions 5
2.3 Conditions of Acceptance 5

Chapter 3
Description of WTC Floor System and SFRM 7
3.1 Composite Slab Floor System 7
3.2 Steel Trusses 7
3.3 SFRM Thickness 8

Chapter 4
Floor Test Assemblies 9
4.1 Design of Tests 9
4.1.1 Span of Test Assembly 9

4.1.2 Geometric Scaling of Floor Trusses 9
4.1.3 Concrete Slab Thickness 10
4.1.4 Steel Truss Sections 10
4.1.5 Applied Load 10
4.2 Materials of Construction 11
4.2.1 Fabrication of Trusses 11
4.2.2 Steel Grade 12
4.2.3 Truss Welds 12
4.2.4 Metal Deck 14
4.2.5 Welded Wire Fabric 21
4.2.6 Concrete 21
4.2.7 Primer 21
4.2.8 Sprayed Fire-Resistive Materials 21
4.2.9 Miscellaneous Steel 21
4.3 Construction of Test Assemblies 22
4.3.1 Construction of 35 Ft Assemblies 22
4.3.2 Construction of 17 Ft Assemblies 35
4.4 Loading of Test Assemblies 43
4.4.1 Loading of 35 Ft Assemblies 43
4.4.2 Loading of 17 Ft Assemblies 44
4.5 Instrumentation 46
4.5.1 Deflection Instrumentation 46
4.5.2 Furnace Thermocouples 46
4.5.3 Radiometers 47

Chapter 5
Test Results 49
5.1 Fire Test of Assembly No. 1 49
5.1.1 Test Observations 49
5.1.2 Data 51
5.1.3 Post-Test Observations 57
5.2 Fire Test of Assembly No. 2 63
5.2.1 Test Observations 63
5.2.2 Data 64
5.2.3 Post-Test Observations. 71

5.3 Fire Test of Assembly No. 3 73
5.3.1 Test Observations 73
5.3.2 Data 75
5.3.3 Post-Test Observations 81
5.4 Fire Test of Assembly No. 4 83
5.4.1 Test Observations 83
5.4.2 Data 85
5.4.3 Post-Test Observations 91
5.5 Fire Resistance Ratings 94
5.5.1 Test Assembly No. 1 94
5.5.2 Test Assembly No. 2 94
5.5.3 Test Assembly No. 3 94
5.5.4 Test Assembly No. 4 95
5.5.5 Summary Table 95

Chapter 6
Discussion of Results 97
6.1 Comparison of Results 97
6.1.1 Furnace Control Temperatures 97
6.1.2 Furnace Thermal Environment 98
6.1.3 Steel Temperatures 100
6.1.4 Unexposed Surface Temperatures 104
6.1.5 Deflections of Floor Assembly 104
6.2 Observations 105
6.3 Areas of Further Study 106

Chapter 7
References 107

Appendix A
Certified Mill Test Reports (CMTRs)

Appendix B
Primer Paint Specification

Appendix C
Construction Drawings for 35 Ft Test Assemblies

Appendix D
Instrumentation for 35 Ft Test Assemblies

Appendix E
Construction Drawings for 17 Ft Test Assemblies

Appendix F
Instrumentation for 17 Ft Test Assemblies

Appendix G
Truss Calculation Sheets

Appendix H
Unreliable Data

Appendix I
Units Conversions

LIST OF FIGURES

Figure P–1. The eight projects in the federal building and fire safety investigation of the WTC disaster xix

Figure 5–55. Assembly No. 4 – average and maximum individual temperatures on east main truss. 86
Figure 5–56. Assembly No. 4 – overall average and maximum individual temperatures on west and east main trusses. 86
Figure 5–57. Assembly No. 4 – average and maximum individual temperatures on south bridging truss. 87
Figure 5–58. Assembly No. 4 – average and maximum individual temperatures on south bridging truss. 87
Figure 5–59. Assembly No. 4 – average and maximum individual temperatures on unexposed surface. 88
Figure 5–60. Assembly No. 4 – average temperatures on steel deck. 88
Figure 5–61. Assembly No. 4 – bottom chord deflection measurements. 89
Figure 5–62. Assembly No. 4 – temperatures of bottom chord deflection rods. 89
Figure 5–63. Assembly No. 4 – unexposed surface deflection measurements. 90
Figure 5–64. Assembly No. 4 – additional instrumentation through south opening. 90
Figure 5–65. Assembly No. 4 – additional instrumentation through south opening. 91
Figure 5–66. Unexposed surface of Assembly No. 4 after loading equipment was removed. 91
Figure 5–67. Unexposed surface of Assembly No. 4, view of concrete spalling on west side of assembly. 92
Figure 5–68. Unexposed surface of Assembly No. 4, close-up of concrete spalling on west side of assembly. 92
Figure 5–69. Intersection of north bridging and west main truss on Assembly 4. 93
Figure 5–70. View looking north of south bridging truss at location where concrete spalling occurred on Assembly 4. 93

Figure 6–1. Comparison of average furnace temperatures. 97
Figure 6–2. Temperatures measured at the bottom chord by the plate thermocouple in the ULC furnace (Test No. 2) and ULN furnace (Test No. 4). 98
Figure 6–3. Temperatures measured at the underside of the metal deck by the plate thermocouple at the ULC furnace (Test No. 2) and ULN furnace (Test No. 4). 99
Figure 6–4. Average temperatures of the bottom chord for Test Nos. 1, 2 and 3 (3/4 in. thick SFRM). 100
Figure 6–5. Average temperature of web diagonals for Test Nos. 1, 2 and 3 (3/4 in. thick SFRM). 101
Figure 6–6. Average temperature of the top chord for Test Nos. 1, 2 and 3 (3/4 in. thick SFRM). 102
Figure 6–7. Average temperature of the bottom chord for Test No. 3 (3/4 in. thick SFRM) and No. 4 (1/2 in. thick SFRM). 103
Figure 6–8. Average temperature of the unexposed surface for all four tests. 104
Figure 6–9. Deflection measured at the center of each assembly. 105
Figure 6–10. Deflection measured at the center of each assembly divided by the span. 105

LIST OF TABLES

Table P–1. Federal building and fire safety investigation of the WTC disaster. xviii
Table P–2. Public meetings and briefings of the WTC Investigation. xxi

Table 4–1. Redistance Weld Data. 13
Table 4–2. Concrete mix design per cubic yard of concrete. 21
Table 4–3. General construction details. 22
Table 4–4. Details of concrete placement. 30
Table 4–5. SFRM Thickness measurements on Assembly No. 1. 33
Table 4–6. Air dry density of spray applied fire resistive material on Assembly No. 1. 33
Table 4–7. Thickness measurements on Assembly No. 2. 35
Table 4–8. Air dry density of spray applied fire resistive material on Assembly No. 2. 35
Table 4–9. Details of concrete. 40
Table 4–10. SFRM Thickness measurements on Assembly No. 3. 42
Table 4–11. Air dry density of spray applied fire resistive material on Assembly No. 3. 42
Table 4–12. Thickness measurements on Assembly No. 4. 42
Table 4–13. Air dry density of spray applied fire resistive material on Assembly No. 4. 42
Table 4–14. Summary of analysis for maximum load condition for 35 ft assembly. 44
Table 4–15. Summary of analysis for maximum load condition for 17 ft assembly. 45
Table 4–16. Summary of radiometers. 47

Table 5–1. Test observations – Assembly 1 49
Table 5–2. Test observations – Assembly No. 2 63
Table 5–3. Test observations – Assembly No. 3 74
Table 5–4. Test observations – Assembly No. 4 84
Table 5–5. Times to reach ASTM E 119 end-point criteria and ASTM E 119 hourly ratings. 96

This page intentionally left blank.

LIST OF ACRONYMS AND ABBREVIATIONS

Acronyms

ASTM	American Society for Testing and Materials, ASTM International
CMTR	Certified Mill Test Report
MIG	Metal Inert Gas (welding)
NIST	National Institute of Standards and Technology
PANYNJ	Port Authority of New York and New Jersey
SFRM	sprayed fire-resistive material
STS	STS Consultants, Ltd.
SMAW	shielded metal arc welding
ULC	Underwriters Laboratories of Canada, Toronto, Ontario, Fire Test Facility
ULN	Underwriters Laboratories, Inc., Northbrook, Illinois, Fire Test Facility
UL	Underwriters Laboratories Inc.
USM	United States Minerals Products, Co.
WJE	Wiss Janey Elstner & Associates
WTC	World Trade Center
WWF	welded wire fabric

Abbreviations

°C	degrees Celsius (centigrade)
°F	degrees Fahrenheit
ft	feet
in.	inch
lb	pound (force)
min	minute
o.c.	on center
pcf	pounds per cubic foot (1 pcf = 16.03 kg/m^3)
psf	pounds per square foot (1 psf = 0.0479 kN/m^2)
psi	pounds per square inch (1 psi = 0.006895 N/mm^2 or 0.006895 MPa)
s	second

This page intentionally left blank.

PREFACE

Genesis of This Investigation

Immediately following the terrorist attack on the World Trade Center (WTC) on September 11, 2001, the Federal Emergency Management Agency (FEMA) and the American Society of Civil Engineers began planning a building performance study of the disaster. The week of October 7, as soon as the rescue and search efforts ceased, the Building Performance Study Team went to the site and began its assessment. This was to be a brief effort, as the study team consisted of experts who largely volunteered their time away from their other professional commitments. The Building Performance Study Team issued its report in May 2002, fulfilling its goal "to determine probable failure mechanisms and to identify areas of future investigation that could lead to practical measures for improving the damage resistance of buildings against such unforeseen events."

On August 21, 2002, with funding from the U.S. Congress through FEMA, the National Institute of Standards and Technology (NIST) announced its building and fire safety investigation of the WTC disaster. On October 1, 2002, the National Construction Safety Team Act (Public Law 107-231), was signed into law. The NIST WTC Investigation was conducted under the authority of the National Construction Safety Team Act.

The goals of the investigation of the WTC disaster were:

- To investigate the building construction, the materials used, and the technical conditions that contributed to the outcome of the WTC disaster.
- To serve as the basis for:
  - Improvements in the way buildings are designed, constructed, maintained, and used;
  - Improved tools and guidance for industry and safety officials;
  - Recommended revisions to current codes, standards, and practices; and
  - Improved public safety.

The specific objectives were:

1. Determine why and how WTC 1 and WTC 2 collapsed following the initial impacts of the aircraft and why and how WTC 7 collapsed;
2. Determine why the injuries and fatalities were so high or low depending on location, including all technical aspects of fire protection, occupant behavior, evacuation, and emergency response;
3. Determine what procedures and practices were used in the design, construction, operation, and maintenance of WTC 1, 2, and 7; and
4. Identify, as specifically as possible, areas in current building and fire codes, standards, and practices that warrant revision.

NIST is a nonregulatory agency of the U.S. Department of Commerce's Technology Administration. The purpose of NIST investigations is to improve the safety and structural integrity of buildings in the United States, and the focus is on fact finding. NIST investigative teams are authorized to assess building performance and emergency response and evacuation procedures in the wake of any building failure that has resulted in substantial loss of life or that posed significant potential of substantial loss of life. NIST does not have the statutory authority to make findings of fault nor negligence by individuals or organizations. Further, no part of any report resulting from a NIST investigation into a building failure or from an investigation under the National Construction Safety Team Act may be used in any suit or action for damages arising out of any matter mentioned in such report (15 USC 281a, as amended by Public Law 107-231).

Organization of the Investigation

The National Construction Safety Team for this Investigation, appointed by the then NIST Director, Dr. Arden L. Bement, Jr., was led by Dr. S. Shyam Sunder. Dr. William L. Grosshandler served as Associate Lead Investigator, Mr. Stephen A. Cauffman served as Program Manager for Administration, and Mr. Harold E. Nelson served on the team as a private sector expert. The Investigation included eight interdependent projects whose leaders comprised the remainder of the team. A detailed description of each of these eight projects is available at http://wtc.nist.gov. The purpose of each project is summarized in Table P–1, and the key interdependencies among the projects are illustrated in Fig. P–1.

Table P–1. Federal building and fire safety investigation of the WTC disaster.

Technical Area and Project Leader	Project Purpose
Analysis of Building and Fire Codes and Practices; Project Leaders: Dr. H. S. Lew and Mr. Richard W. Bukowski	Document and analyze the code provisions, procedures, and practices used in the design, construction, operation, and maintenance of the structural, passive fire protection, and emergency access and evacuation systems of WTC 1, 2, and 7.
Baseline Structural Performance and Aircraft Impact Damage Analysis; Project Leader: Dr. Fahim H. Sadek	Analyze the baseline performance of WTC 1 and WTC 2 under design, service, and abnormal loads, and aircraft impact damage on the structural, fire protection, and egress systems.
Mechanical and Metallurgical Analysis of Structural Steel; Project Leader: Dr. Frank W. Gayle	Determine and analyze the mechanical and metallurgical properties and quality of steel, weldments, and connections from steel recovered from WTC 1, 2, and 7.
Investigation of Active Fire Protection Systems; Project Leader: Dr. David D. Evans; Dr. William Grosshandler	Investigate the performance of the active fire protection systems in WTC 1, 2, and 7 and their role in fire control, emergency response, and fate of occupants and responders.
Reconstruction of Thermal and Tenability Environment; Project Leader: Dr. Richard G. Gann	Reconstruct the time-evolving temperature, thermal environment, and smoke movement in WTC 1, 2, and 7 for use in evaluating the structural performance of the buildings and behavior and fate of occupants and responders.
Structural Fire Response and Collapse Analysis; Project Leaders: Dr. John L. Gross and Dr. Therese P. McAllister	Analyze the response of the WTC towers to fires with and without aircraft damage, the response of WTC 7 in fires, the performance of composite steel-trussed floor systems, and determine the most probable structural collapse sequence for WTC 1, 2, and 7.
Occupant Behavior, Egress, and Emergency Communications; Project Leader: Mr. Jason D. Averill	Analyze the behavior and fate of occupants and responders, both those who survived and those who did not, and the performance of the evacuation system.
Emergency Response Technologies and Guidelines; Project Leader: Mr. J. Randall Lawson	Document the activities of the emergency responders from the time of the terrorist attacks on WTC 1 and WTC 2 until the collapse of WTC 7, including practices followed and technologies used.

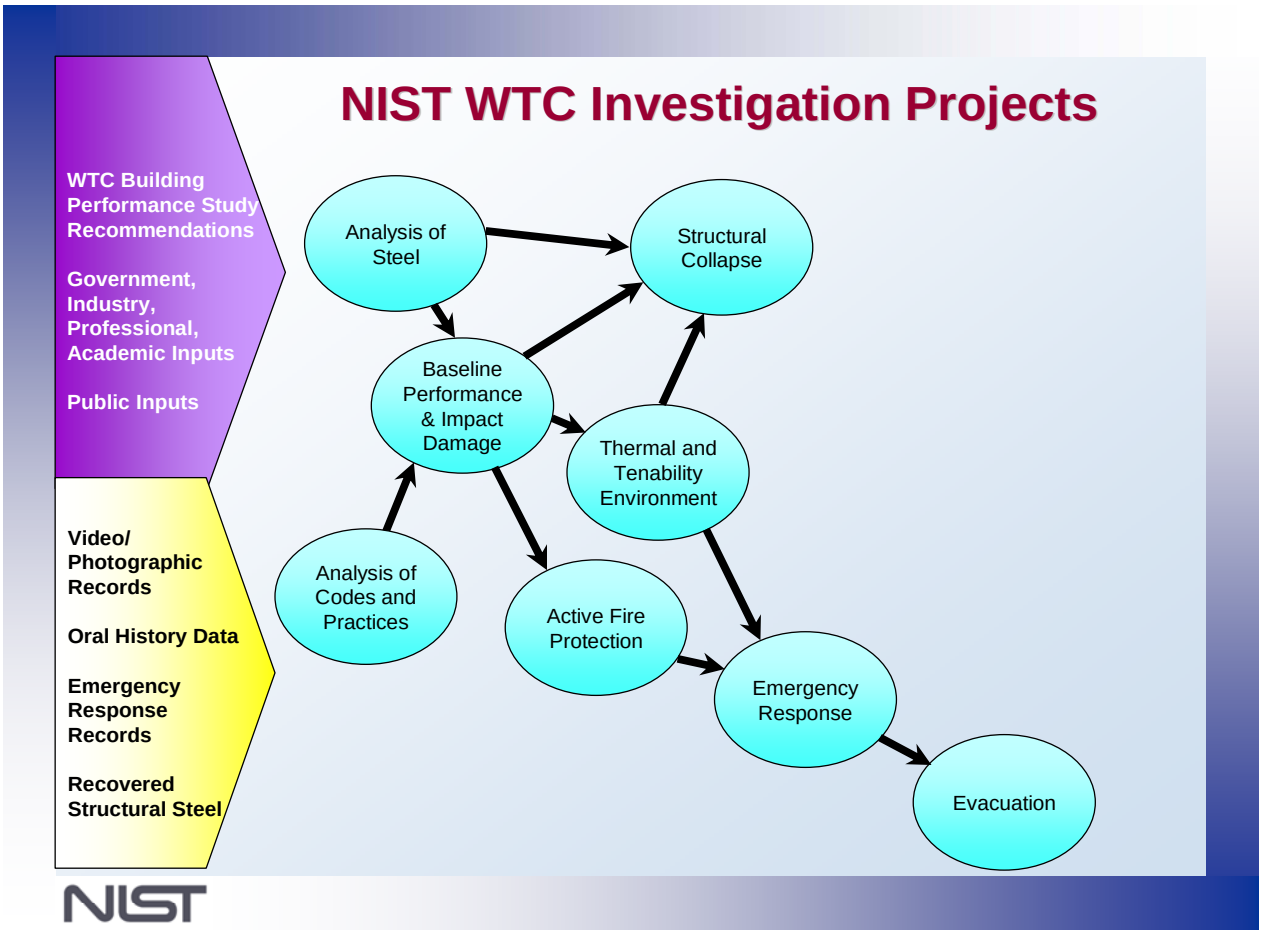

Figure P–1. The eight projects in the federal building and fire safety investigation of the WTC disaster.

National Construction Safety Team Advisory Committee

The NIST Director also established an advisory committee as mandated under the National Construction Safety Team Act. The initial members of the committee were appointed following a public solicitation. These were:

- Paul Fitzgerald, Executive Vice President (retired) FM Global, National Construction Safety Team Advisory Committee Chair
- John Barsom, President, Barsom Consulting, Ltd.
- John Bryan, Professor Emeritus, University of Maryland
- David Collins, President, The Preview Group, Inc.
- Glenn Corbett, Professor, John Jay College of Criminal Justice
- Philip DiNenno, President, Hughes Associates, Inc.

- Robert Hanson, Professor Emeritus, University of Michigan
- Charles Thornton, Co-Chairman and Managing Principal, The Thornton-Tomasetti Group, Inc.
- Kathleen Tierney, Director, Natural Hazards Research and Applications Information Center, University of Colorado at Boulder
- Forman Williams, Director, Center for Energy Research, University of California at San Diego

This National Construction Safety Team Advisory Committee provided technical advice during the Investigation and commentary on drafts of the Investigation reports prior to their public release. NIST has benefited from the work of many people in the preparation of these reports, including the National Construction Safety Team Advisory Committee. The content of the reports and recommendations, however, are solely the responsibility of NIST.

Public Outreach

During the course of this Investigation, NIST held public briefings and meetings (listed in Table P–2) to solicit input from the public, present preliminary findings, and obtain comments on the direction and progress of the Investigation from the public and the Advisory Committee.

NIST maintained a publicly accessible Web site during this Investigation at http://wtc.nist.gov. The site contained extensive information on the background and progress of the Investigation.

NIST's WTC Public-Private Response Plan

The collapse of the WTC buildings has led to broad reexamination of how tall buildings are designed, constructed, maintained, and used, especially with regard to major events such as fires, natural disasters, and terrorist attacks. Reflecting the enhanced interest in effecting necessary change, NIST, with support from Congress and the Administration, has put in place a program, the goal of which is to develop and implement the standards, technology, and practices needed for cost-effective improvements to the safety and security of buildings and building occupants, including evacuation, emergency response procedures, and threat mitigation.

The strategy to meet this goal is a three-part NIST-led public-private response program that includes:

- A federal building and fire safety investigation to study the most probable factors that contributed to post-aircraft impact collapse of the WTC towers and the 47-story WTC 7 building, and the associated evacuation and emergency response experience.
- A research and development (R&D) program to (a) facilitate the implementation of recommendations resulting from the WTC Investigation, and (b) provide the technical basis for cost-effective improvements to national building and fire codes, standards, and practices that enhance the safety of buildings, their occupants, and emergency responders.

Table P–2. Public meetings and briefings of the WTC Investigation.

Date	Location	Principal Agenda
June 24, 2002	New York City, NY	Public meeting: Public comments on the *Draft Plan* for the pending WTC Investigation.
August 21, 2002	Gaithersburg, MD	Media briefing announcing the formal start of the Investigation.
December 9, 2002	Washington, DC	Media briefing on release of the *Public Update* and NIST request for photographs and videos.
April 8, 2003	New York City, NY	Joint public forum with Columbia University on first-person interviews.
April 29–30, 2003	Gaithersburg, MD	NCST Advisory Committee meeting on plan for and progress on WTC Investigation with a public comment session.
May 7, 2003	New York City, NY	Media briefing on release of *May 2003 Progress Report.*
August 26–27, 2003	Gaithersburg, MD	NCST Advisory Committee meeting on status of the WTC investigation with a public comment session.
September 17, 2003	New York City, NY	Media and public briefing on initiation of first-person data collection projects.
December 2–3, 2003	Gaithersburg, MD	NCST Advisory Committee meeting on status and initial results and release of the *Public Update* with a public comment session.
February 12, 2004	New York City, NY	Public meeting on progress and preliminary findings with public comments on issues to be considered in formulating final recommendations.
June 18, 2004	New York City, NY	Media/public briefing on release of *June 2004 Progress Report.*
June 22–23, 2004	Gaithersburg, MD	NCST Advisory Committee meeting on the status of and preliminary findings from the WTC Investigation with a public comment session.
August 24, 2004	Northbrook, IL	Public viewing of standard fire resistance test of WTC floor system at Underwriters Laboratories, Inc.
October 19–20, 2004	Gaithersburg, MD	NCST Advisory Committee meeting on status and near complete set of preliminary findings with a public comment session.
November 22, 2004	Gaithersburg, MD	NCST Advisory Committee discussion on draft annual report to Congress, a public comment session, and a closed session to discuss pre-draft recommendations for WTC Investigation.
April 5, 2005	New York City, NY	Media and public briefing on release of the probable collapse sequence for the WTC towers and draft reports for the projects on codes and practices, evacuation, and emergency response.
June 23, 2005	New York City, NY	Media and public briefing on release of all draft reports for the WTC towers and draft recommendations for public comment.
September 12–13, 2005	Gaithersburg, MD	NCST Advisory Committee meeting on disposition of public comments and update to draft reports for the WTC towers.
September 13–15, 2005	Gaithersburg, MD	WTC Technical Conference for stakeholders and technical community for dissemination of findings and recommendations and opportunity for public to make technical comments.

- A dissemination and technical assistance program (DTAP) to (a) engage leaders of the construction and building community in ensuring timely adoption and widespread use of proposed changes to practices, standards, and codes resulting from the WTC Investigation and the R&D program, and (b) provide practical guidance and tools to better prepare facility owners, contractors, architects, engineers, emergency responders, and regulatory authorities to respond to future disasters.

The desired outcomes are to make buildings, occupants, and first responders safer in future disaster events.

National Construction Safety Team Reports on the WTC Investigation

A final report on the collapse of the WTC towers is being issued as NIST NCSTAR 1. A companion report on the collapse of WTC 7 is being issued as NIST NCSTAR 1A. The present report is one of a set that provides more detailed documentation of the Investigation findings and the means by which these technical results were achieved. As such, it is part of the archival record of this Investigation. The titles of the full set of Investigation publications are:

NIST (National Institute of Standards and Technology). 2005. *Federal Building and Fire Safety Investigation of the World Trade Center Disaster: Final Report on the Collapse of the World Trade Center Towers.* NIST NCSTAR 1. Gaithersburg, MD, September.

NIST (National Institute of Standards and Technology). 2008. *Federal Building and Fire Safety Investigation of the World Trade Center Disaster: Final Report on the Collapse of World Trade Center 7.* NIST NCSTAR 1A. Gaithersburg, MD, November.

Lew, H. S., R. W. Bukowski, and N. J. Carino. 2005. *Federal Building and Fire Safety Investigation of the World Trade Center Disaster: Design, Construction, and Maintenance of Structural and Life Safety Systems.* NIST NCSTAR 1-1. National Institute of Standards and Technology. Gaithersburg, MD, September.

Fanella, D. A., A. T. Derecho, and S. K. Ghosh. 2005. *Federal Building and Fire Safety Investigation of the World Trade Center Disaster: Design and Construction of Structural Systems.* NIST NCSTAR 1-1A. National Institute of Standards and Technology. Gaithersburg, MD, September.

Ghosh, S. K., and X. Liang. 2005. *Federal Building and Fire Safety Investigation of the World Trade Center Disaster: Comparison of Building Code Structural Requirements.* NIST NCSTAR 1-1B. National Institute of Standards and Technology. Gaithersburg, MD, September.

Fanella, D. A., A. T. Derecho, and S. K. Ghosh. 2005. *Federal Building and Fire Safety Investigation of the World Trade Center Disaster: Maintenance and Modifications to Structural Systems.* NIST NCSTAR 1-1C. National Institute of Standards and Technology. Gaithersburg, MD, September.

Grill, R. A., and D. A. Johnson. 2005. *Federal Building and Fire Safety Investigation of the World Trade Center Disaster: Fire Protection and Life Safety Provisions Applied to the Design and Construction of World Trade Center 1, 2, and 7 and Post-Construction Provisions Applied after Occupancy*. NIST NCSTAR 1-1D. National Institute of Standards and Technology. Gaithersburg, MD, September.

Razza, J. C., and R. A. Grill. 2005. *Federal Building and Fire Safety Investigation of the World Trade Center Disaster: Comparison of Codes, Standards, and Practices in Use at the Time of the Design and Construction of World Trade Center 1, 2, and 7*. NIST NCSTAR 1-1E. National Institute of Standards and Technology. Gaithersburg, MD, September.

Grill, R. A., D. A. Johnson, and D. A. Fanella. 2005. *Federal Building and Fire Safety Investigation of the World Trade Center Disaster: Comparison of the 1968 and Current (2003) New*

York City Building Code Provisions. NIST NCSTAR 1-1F. National Institute of Standards and Technology. Gaithersburg, MD, September.

Grill, R. A., and D. A. Johnson. 2005. *Federal Building and Fire Safety Investigation of the World Trade Center Disaster: Amendments to the Fire Protection and Life Safety Provisions of the New York City Building Code by Local Laws Adopted While World Trade Center 1, 2, and 7 Were in Use*. NIST NCSTAR 1-1G. National Institute of Standards and Technology. Gaithersburg, MD, September.

Grill, R. A., and D. A. Johnson. 2005. *Federal Building and Fire Safety Investigation of the World Trade Center Disaster: Post-Construction Modifications to Fire Protection and Life Safety Systems of World Trade Center 1 and 2*. NIST NCSTAR 1-1H. National Institute of Standards and Technology. Gaithersburg, MD, September.

Grill, R. A., D. A. Johnson, and D. A. Fanella. 2005. *Federal Building and Fire Safety Investigation of the World Trade Center Disaster: Post-Construction Modifications to Fire Protection, Life Safety, and Structural Systems of World Trade Center 7*. NIST NCSTAR 1-1I. National Institute of Standards and Technology. Gaithersburg, MD, September.

Grill, R. A., and D. A. Johnson. 2005. *Federal Building and Fire Safety Investigation of the World Trade Center Disaster: Design, Installation, and Operation of Fuel System for Emergency Power in World Trade Center 7*. NIST NCSTAR 1-1J. National Institute of Standards and Technology. Gaithersburg, MD, September.

Sadek, F. 2005. *Federal Building and Fire Safety Investigation of the World Trade Center Disaster: Baseline Structural Performance and Aircraft Impact Damage Analysis of the World Trade Center Towers.* NIST NCSTAR 1-2. National Institute of Standards and Technology. Gaithersburg, MD, September.

Faschan, W. J., and R. B. Garlock. 2005. *Federal Building and Fire Safety Investigation of the World Trade Center Disaster: Reference Structural Models and Baseline Performance Analysis of the World Trade Center Towers.* NIST NCSTAR 1-2A. National Institute of Standards and Technology. Gaithersburg, MD, September.

Kirkpatrick, S. W., R. T. Bocchieri, F. Sadek, R. A. MacNeill, S. Holmes, B. D. Peterson, R. W. Cilke, C. Navarro. 2005. *Federal Building and Fire Safety Investigation of the World Trade Center Disaster: Analysis of Aircraft Impacts into the World Trade Center Towers*, NIST NCSTAR 1-2B. National Institute of Standards and Technology. Gaithersburg, MD, September.

Gayle, F. W., R. J. Fields, W. E. Luecke, S. W. Banovic, T. Foecke, C. N. McCowan, T. A. Siewert, and J. D. McColskey. 2005. *Federal Building and Fire Safety Investigation of the World Trade Center Disaster: Mechanical and Metallurgical Analysis of Structural Steel.* NIST NCSTAR 1-3. National Institute of Standards and Technology. Gaithersburg, MD, September.

Luecke, W. E., T. A. Siewert, and F. W. Gayle. 2005. *Federal Building and Fire Safety Investigation of the World Trade Center Disaster: Contemporaneous Structural Steel Specifications.* NIST Special Publication 1-3A. National Institute of Standards and Technology. Gaithersburg, MD, September.

Banovic, S. W. 2005. *Federal Building and Fire Safety Investigation of the World Trade Center Disaster: Steel Inventory and Identification.* NIST NCSTAR 1-3B. National Institute of Standards and Technology. Gaithersburg, MD, September.

Banovic, S. W., and T. Foecke. 2005. *Federal Building and Fire Safety Investigation of the World Trade Center Disaster: Damage and Failure Modes of Structural Steel Components.* NIST NCSTAR 1-3C. National Institute of Standards and Technology. Gaithersburg, MD, September.

Luecke, W. E., J. D. McColskey, C. N. McCowan, S. W. Banovic, R. J. Fields, T. Foecke, T. A. Siewert, and F. W. Gayle. 2005. *Federal Building and Fire Safety Investigation of the World Trade Center Disaster: Mechanical Properties of Structural Steels.* NIST NCSTAR 1-3D. National Institute of Standards and Technology. Gaithersburg, MD, September.

Banovic, S. W., C. N. McCowan, and W. E. Luecke. 2005. *Federal Building and Fire Safety Investigation of the World Trade Center Disaster: Physical Properties of Structural Steels.* NIST NCSTAR 1-3E. National Institute of Standards and Technology. Gaithersburg, MD, September.

Evans, D. D., R. D. Peacock, E. D. Kuligowski, W. S. Dols, and W. L. Grosshandler. 2005. *Federal Building and Fire Safety Investigation of the World Trade Center Disaster: Active Fire Protection Systems.* NIST NCSTAR 1-4. National Institute of Standards and Technology. Gaithersburg, MD, September.

Kuligowski, E. D., D. D. Evans, and R. D. Peacock. 2005. *Federal Building and Fire Safety Investigation of the World Trade Center Disaster: Post-Construction Fires Prior to September 11, 2001.* NIST NCSTAR 1-4A. National Institute of Standards and Technology. Gaithersburg, MD, September.

Hopkins, M., J. Schoenrock, and E. Budnick. 2005. *Federal Building and Fire Safety Investigation of the World Trade Center Disaster: Fire Suppression Systems.* NIST NCSTAR 1-4B. National Institute of Standards and Technology. Gaithersburg, MD, September.

Keough, R. J., and R. A. Grill. 2005. *Federal Building and Fire Safety Investigation of the World Trade Center Disaster: Fire Alarm Systems.* NIST NCSTAR 1-4C. National Institute of Standards and Technology. Gaithersburg, MD, September.

Ferreira, M. J., and S. M. Strege. 2005. *Federal Building and Fire Safety Investigation of the World Trade Center Disaster: Smoke Management Systems.* NIST NCSTAR 1-4D. National Institute of Standards and Technology. Gaithersburg, MD, September.

Gann, R. G., A. Hamins, K. B. McGrattan, G. W. Mulholland, H. E. Nelson, T. J. Ohlemiller, W. M. Pitts, and K. R. Prasad. 2005. *Federal Building and Fire Safety Investigation of the World Trade Center Disaster: Reconstruction of the Fires in the World Trade Center Towers.* NIST NCSTAR 1-5. National Institute of Standards and Technology. Gaithersburg, MD, September.

Pitts, W. M., K. M. Butler, and V. Junker. 2005. *Federal Building and Fire Safety Investigation of the World Trade Center Disaster: Visual Evidence, Damage Estimates, and Timeline Analysis.* NIST NCSTAR 1-5A. National Institute of Standards and Technology. Gaithersburg, MD, September.

Hamins, A., A. Maranghides, K. B. McGrattan, E. Johnsson, T. J. Ohlemiller, M. Donnelly, J. Yang, G. Mulholland, K. R. Prasad, S. Kukuck, R. Anleitner and T. McAllister. 2005. *Federal Building and Fire Safety Investigation of the World Trade Center Disaster: Experiments and Modeling of Structural Steel Elements Exposed to Fire.* NIST NCSTAR 1-5B. National Institute of Standards and Technology. Gaithersburg, MD, September.

Ohlemiller, T. J., G. W. Mulholland, A. Maranghides, J. J. Filliben, and R. G. Gann. 2005. *Federal Building and Fire Safety Investigation of the World Trade Center Disaster: Fire Tests of Single Office Workstations.* NIST NCSTAR 1-5C. National Institute of Standards and Technology. Gaithersburg, MD, September.

Gann, R. G., M. A. Riley, J. M. Repp, A. S. Whittaker, A. M. Reinhorn, and P. A. Hough. 2005. *Federal Building and Fire Safety Investigation of the World Trade Center Disaster: Reaction of Ceiling Tile Systems to Shocks.* NIST NCSTAR 1-5D. National Institute of Standards and Technology. Gaithersburg, MD, September.

Hamins, A., A. Maranghides, K. B. McGrattan, T. J. Ohlemiller, and R. Anleitner. 2005. *Federal Building and Fire Safety Investigation of the World Trade Center Disaster: Experiments and Modeling of Multiple Workstations Burning in a Compartment.* NIST NCSTAR 1-5E. National Institute of Standards and Technology. Gaithersburg, MD, September.

McGrattan, K. B., C. Bouldin, and G. Forney. 2005. *Federal Building and Fire Safety Investigation of the World Trade Center Disaster: Computer Simulation of the Fires in the World Trade Center Towers.* NIST NCSTAR 1-5F. National Institute of Standards and Technology. Gaithersburg, MD, September.

Prasad, K. R., and H. R. Baum. 2005. *Federal Building and Fire Safety Investigation of the World Trade Center Disaster: Fire Structure Interface and Thermal Response of the World Trade Center Towers.* NIST NCSTAR 1-5G. National Institute of Standards and Technology. Gaithersburg, MD, September.

Gross, J. L., and T. McAllister. 2005. *Federal Building and Fire Safety Investigation of the World Trade Center Disaster: Structural Fire Response and Probable Collapse Sequence of the World Trade Center Towers.* NIST NCSTAR 1-6. National Institute of Standards and Technology. Gaithersburg, MD, September.

Carino, N. J., M. A. Starnes, J. L. Gross, J. C. Yang, S. Kukuck, K. R. Prasad, and R. W. Bukowski. 2005. *Federal Building and Fire Safety Investigation of the World Trade Center Disaster: Passive Fire Protection.* NIST NCSTAR 1-6A. National Institute of Standards and Technology. Gaithersburg, MD, September.

Gross, J., F. Hervey, M. Izydorek, J. Mammoser, and J. Treadway. 2005. *Federal Building and Fire Safety Investigation of the World Trade Center Disaster: Fire Resistance Tests of Floor Truss Systems.* NIST NCSTAR 1-6B. National Institute of Standards and Technology. Gaithersburg, MD, September.

Zarghamee, M. S., S. Bolourchi, D. W. Eggers, Ö. O. Erbay, F. W. Kan, Y. Kitane, A. A. Liepins, M. Mudlock, W. I. Naguib, R. P. Ojdrovic, A. T. Sarawit, P. R Barrett, J. L. Gross, and

T. P. McAllister. 2005. *Federal Building and Fire Safety Investigation of the World Trade Center Disaster: Component, Connection, and Subsystem Structural Analysis.* NIST NCSTAR 1-6C. National Institute of Standards and Technology. Gaithersburg, MD, September.

Zarghamee, M. S., Y. Kitane, Ö. O. Erbay, T. P. McAllister, and J. L. Gross. 2005. *Federal Building and Fire Safety Investigation of the World Trade Center Disaster: Global Structural Analysis of the Response of the World Trade Center Towers to Impact Damage and Fire.* NIST NCSTAR 1-6D. National Institute of Standards and Technology. Gaithersburg, MD, September.

Averill, J. D., D. S. Mileti, R. D. Peacock, E. D. Kuligowski, N. Groner, G. Proulx, P. A. Reneke, and H. E. Nelson. 2005. *Federal Building and Fire Safety Investigation of the World Trade Center Disaster: Occupant Behavior, Egress, and Emergency Communication.* NIST NCSTAR 1-7. National Institute of Standards and Technology. Gaithersburg, MD, September.

Fahy, R., and G. Proulx. 2005. *Federal Building and Fire Safety Investigation of the World Trade Center Disaster: Analysis of Published Accounts of the World Trade Center Evacuation.* NIST NCSTAR 1-7A. National Institute of Standards and Technology. Gaithersburg, MD, September.

Zmud, J. 2005. *Federal Building and Fire Safety Investigation of the World Trade Center Disaster: Technical Documentation for Survey Administration.* NIST NCSTAR 1-7B. National Institute of Standards and Technology. Gaithersburg, MD, September.

Lawson, J. R., and R. L. Vettori. 2005. *Federal Building and Fire Safety Investigation of the World Trade Center Disaster: The Emergency Response Operations.* NIST NCSTAR 1-8. National Institute of Standards and Technology. Gaithersburg, MD, September.

McAllister, T., R. G. Gann, J. D. Averill, J. L. Gross, W. L. Grosshandler, J. R. Lawson, K. B. McGrattan, H. E. Nelson, W. M. Pitts, K. R. Prasad, F. H. Sadek. 2008. *Federal Building and Fire Safety Investigation of the World Trade Center Disaster: Structural Fire Response and Probable Collapse Sequence of World Trade Center Building 7.* NIST NCSTAR 1-9. National Institute of Standards and Technology. Gaithersburg, MD, November.

MacNeill, R., S. Kirkpatrick, B. Peterson, and R. Bocchieri. 2008. *Federal Building and Fire Safety Investigation of the World Trade Center Disaster: Global Structural Analysis of the Response of World Trade Center Building 7 to Fires and Debris Impact Damage.* NIST NCSTAR 1-9A. National Institute of Standards and Technology. Gaithersburg, MD, November.

ACKNOWLEDGMENTS

The National Institute of Standards and Technology would like to acknowledge the many individuals who contributed substantially to the successful completion of four ASTM E 119 Standard Fire Tests conducted by Underwriters Laboratories, Inc. (UL) under contract to NIST and reported herein. Specifically, the laboratory staff at UL including William Joy, Aldo Jimenez, and Romuald Bolewski did an outstanding and highly professional job. Colleagues at NIST who contributed both technically as well as administratively include Dr. Nicholas Carino, Dr. William Grosshandler, and Dr. Monica Starnes.

This page intentionally left blank.

EXECUTIVE SUMMARY

E.1 OBJECTIVES OF THE FIRE RESISTANCE TESTS

One of the objectives of the National Institute of Standards and Technology (NIST) Investigation was to determine why and how the World Trade Center (WTC) towers collapsed following the initial impact of the aircraft. A key aspect of this work was to differentiate the factors that most influenced the collapse of the WTC towers as they may relate to normal building and fire safety considerations and those unique to the terrorist attacks of September 11, 2001. Another of the NIST Investigation objectives was to study the procedures and practices that were used in the design, construction, operation, and maintenance of the WTC buildings. As an important public safety objective, it was necessary to establish the facts regarding the acceptance procedures for innovative materials, technologies, and systems. Past building and fire safety investigations have shown that such studies help to identify improvements to practices, standards, and codes that may be warranted.

NIST review of available documents had indicated that the fire performance of the composite floor system of the WTC towers was an issue of concern to the building owners and designers not only during the original design phase but throughout the service life of the buildings. NIST found no evidence regarding the technical basis for the selection of sprayed fire-resistive material (SFRM) for the WTC floor trusses and for the SFRM thickness to achieve a 2 h rating. Further, no evidence was found that fire resistance tests of the WTC floor system were conducted. Review of documents related to the WTC has not identified a similar concern for other structural components of the WTC towers.

To address, in part, the investigation objectives cited above, NIST conducted a series of four standard fire resistance tests of the composite floor system used in the towers. The fire resistance tests were conducted to study three factors: the effect of (1) SFRM thickness, (2) test restraint conditions, and (3) scale of the test. The tests were conducted by Underwriters Laboratories, Inc. (UL) under contract to NIST at UL's Northbrook (Illinois) fire testing facility and at its affiliate's, Underwriters Laboratories of Canada, fire testing facilities in Toronto.

E.2 THE WTC FLOOR SYSTEM AND SFRM

The floor system design for the world trade center consisted of a lightweight concrete floor slab supported by steel trusses bridging between the building's core columns and exterior wall columns. The main composite trusses, which were used in pairs, spanned either 60 ft or 35 ft. Steel double-angles formed the top and bottom chords of the trusses, while round bars were used for the webs. The web members protruded above the top chord in the form of a "knuckle" which was embedded in the concrete slab to develop composite action. Additionally, the floor system included bridging trusses perpendicular to the main trusses. In the corners of the towers, the bridging trusses acted with the main trusses to provide two-way slab action.

Passive fire protection was provided by sprayed fire-resistive materials (SFRM), commonly referred to as "fireproofing," applied directly to the steel bars of the trusses. The Port Authority of New York and New Jersey (PANYNY or Port Authority) specified U.S. Minerals Products Cafco BLAZE-SHIELD Type D as

the sprayed fire-resistive material and in a letter to the fireproofing contractor stated that "All Tower beams, spandrels, and bar joists requiring spray-on fireproofing are to have a ½″ [1/2 in] covering of Cafco[1]". Measured thicknesses of the applied SFRM were found to vary between 0.52 in. and 1.17 in. with an overall average of approximately 0.75 in. These two thicknesses, ½ in. representing specified thickness and ¾ in. representing average applied thickness, were used in the standard fire resistance tests described here.

E.3 FIRE RESISTANCE TESTING

The fire rating of structural materials and assemblies is generally determined through testing, and in the United States, such testing is frequently conducted in accordance with ASTM E 119, "Standard Test Methods for Fire Tests of Building Construction and Materials." The test methods described in ASTM E 119 prescribe a standard fire exposure for comparing the test results of building construction assemblies. For the tests of floors and roofs, a test assembly is structurally loaded and the standard fire exposure is applied to the underside of the specimen. The assembly is evaluated for its ability to contain the fire by limiting flame spread (hot gasses) and heating of the unexposed surface while maintaining the applied load. The assembly is given a rating, expressed in hours, based on these conditions of acceptance.

Since 1971, versions of the ASTM E 119 Standard differentiate between testing and classifying thermally restrained and unrestrained floor assemblies. A thermally restrained specimen is "one in which expansion at the support of a load carrying element resulting from the effects of fire is resisted by forces external to the element." In an unrestrained condition, the element is free to expand and rotate at its supports. It is customary in the United States to conduct standard fire tests of floor assemblies in the restrained condition.

The current standard describes a means to establish restrained and unrestrained ratings for floor assemblies from restrained test samples. For restrained ratings from restrained test samples, the conditions of acceptance are based on limiting the passage of flame and hot gasses, limiting temperatures on the unexposed surface of the slab, and failure of the assembly to sustain the applied load. For an unrestrained rating determined from a restrained test sample, the conditions of acceptance are based on the same criteria and, in addition, temperature limitations are placed on the main structural members.

In addition, since 1971, the ASTM E 119 Standard describes a means to establish unrestrained ratings from unrestrained test samples. For unrestrained samples, the fire resistance rating is again based on limiting passage of flame and hot gasses, exceeding temperatures on the unexposed surface of the slab, and failure to sustain the applied load; there are no limiting temperatures on the steel structural members when the test sample is installed in an unrestrained condition.

Prior to 1970, there was no distinction between restraint conditions, nor were restrained and unrestrained ratings defined in ASTM E 119. Fire resistance ratings were determined based upon the same requirements as for restrained assemblies described above, and no limitations were placed on temperature of structural steel.

[1] Cafco was the manufacturer of the SFRM used for fire protection of structural steel in the WTC.

In practice, a floor assembly such as that used in the WTC towers is neither restrained nor unrestrained but is likely somewhere in between. Testing under both restraint conditions, then, bounds expected performance under the standard fire exposure. In addition, it provides a comparison of unrestrained ratings developed from both restrained and unrestrained test conditions.

The ASTM E 119 Standard requires that, for floor and roof assembly tests, the area exposed to fire be a minimum of 180 ft^2 and neither dimension of the furnace less than 12 ft. Traditionally, relatively small scale assemblies have been tested, and results have been scaled to practical floor system spans.

The Underwriters Laboratories of Canada fire testing facility in Toronto, has a furnace with nominal dimensions of 35 ft by 14 ft. Thus, full- or large-scale tests of floor assemblies can be tested in this furnace. Availability of the 35 ft span furnace in UL's Toronto facility, in addition to the 17 ft span furnace its Northbrook, Illinois, facility allowed NIST to conduct tests to compare the effect of scale.

E.4 TEST PROGRAM

To limit the number of tests and obtain information of greatest value to meet the investigation objectives, NIST conducted four tests to study the effect of three factors: SFRM thickness, scale of the test, and test restraint conditions. To this end, four tests were designed and conducted as follows:

- Test #1: Full-scale, restrained test condition, ¾ in. thick SFRM.
- Test #2: Full-scale, unrestrained test condition, ¾ in. thick SFRM.
- Test #3: Reduced-scale, restrained conditions, ¾ in. thick SFRM.
- Test #4: Reduced-scale, restrained conditions, ½ in. thick SFRM.

The full-scale tests were conducted at the Underwriters Laboratories of Canada fire testing facility in Toronto . Loading of the floor slab with an applied load to "simulate a maximum load condition," as required by ASTM E 119, was accomplished through a combination concrete blocks and containers filled with water. The water containers were tied-off with steel cables to prevent them from falling into the furnace and causing damage to the fire brick and instrumentation in the event of a catastrophic failure of the floor system.

For the reduced-scale test specimens, the size of the truss members and thickness of concrete slab were selected to allow the most information to be extracted as practicably possible considering that the Standard Fire Resistance Test is a test of the assembly's ability to contain a fire and is based on both thermal response (flame spread and heating of the unexposed surface) and structural response (support the applied load) to the standard fire exposure. The sizes of the steel members, thickness of concrete slab, and truss spacing were selected to be the same as in the full-scale tests. Otherwise, the geometry was scaled by roughly half. This scaling required that the loading be increased by a factor of two.

E.5 TEST RESULTS

Results of the four tests are summarized as follows:

- The test assemblies were able to withstand standard fire conditions for between ¾ h and 2 h without exceeding the limits prescribed by ASTM E 119.
- Test specimens protected with ¾ in. thick spray applied fire-resistive material were able to sustain the maximum design load for approximately 2 hours without collapsing; in the unrestrained test, the load was maintained for 3½ h without collapsing.
- The restrained full-scale floor system obtained a fire resistance rating of 1½ h while the unrestrained floor system achieved a 2 h rating. Past experience with the ASTM E 119 test method would lead investigators to expect that the unrestrained floor assembly would not perform as well as the restrained assembly, and therefore, would receive a lower fire rating.
- A fire rating of 2 h was determined from the reduced-scale test with the average applied SFRM thickness of ¾ in., while a fire rating of 1½ h was determined from the full-scale test with the same SFRM thickness.
- The result stated above raises the question of whether or not a fire rating based on the ASTM E 119 performance of a 17 ft span floor assembly is scalable to a larger floor system such as found in the WTC towers where spans ranged from 35 ft to 60 ft.
- A fire rating of ¾ h was determined from the reduced-scale test with the specified SFRM thickness of ½ in.

The tested floor assemblies were similar, though not identical, to steel joist and concrete floor systems that are widely used in low rise construction. The test results provide valuable insight into the behavior of these widely used assemblies and also identify issues regarding scaling, restraint, and SFRM thickness that require further study for floor systems and other types of structural components such as beams, girders, columns, trusses, etc.

The NIST tests identified areas where further study related to the Standard Fire Resistance Test method may be warranted. The issues related to the test method that NIST will consider in formulating its recommendations include:

- the scale of the test for prototype assemblies that are much larger than the tested assemblies,
- the effect of restraint conditions on test results,
- the repeatability of test results (e.g., do multiple fire resistance tests conducted under the same conditions yield the same results?),
- the effects of test scale, end restraint, and test repeatability on other types of structural components (beams, girders, columns, etc.), and

- the acceptance criteria to evaluate the load carrying capacity of the tested assemblies (currently tests are stopped before the load carrying capacity of the assembly is reached because other acceptance criteria are met or because the deflection becomes excessive and assembly failure could damage the furnace).

This page intentionally left blank.

Chapter 1
INTRODUCTION

The need to perform fire resistance rating tests of the floor system developed for the World Trade Center (WTC) towers was raised several times during the design stage as well as after completion of the towers. National Institute of Standards and Technology (NIST) NCSTAR 1-6A[2] contains a detailed chronicle of the procedures and practices used for passive fire protection of the floor system of the WTC towers. The report summarizes factual data contained in documents provided to NIST by The Port Authority of New York and New Jersey (Port Authority) and its contractors and consultants; by Laclede Steel Company, the firm that supplied the floor trusses for the WTC towers; and by United States Mineral Products Co. (USM), the manufacturer of the SFRM. Review of the information collected revealed no evidence that testing was ever conducted to determine the fire endurance of the WTC floor system fireproofed with sprayed fire-resistive materials (SFRM).

1.1 MOTIVATION FOR CONDUCTING STANDARD FIRE TESTS OF THE WTC FLOOR SYSTEM

The first of the four NIST investigation objectives *(see Preface)* was to determine why and how the WTC towers collapsed following the initial impact of the aircraft. A key aspect of this work was to differentiate the factors that most influenced the collapse of the WTC towers as they may relate to normal building and fire safety considerations and those unique to the terrorist attacks of September 11, 2001.

Another of the four NIST investigation objectives was to study the procedures and practices that were used in the design, construction, operation, and maintenance of the WTC buildings. A key aspect was to study the acceptance procedures for innovative materials, technologies, and systems. Past building and fire safety investigations have shown that studies of procedures and practices help to identify improvements to practices, standards, and codes that may be warranted.

A third investigation objective was to identify, as specifically as possible, areas in national building and fire codes, standards, and practices that warrant revision.

NIST review of available documents related to the design and construction of the WTC towers indicated that the fire performance of the composite floor system of the WTC towers was an issue of concern to the building owners and designers from the original design and throughout the service life of the buildings (NIST NCSTAR 1-6A). NIST found no evidence to determine the technical basis for the selection of SFRM for the WTC floor trusses and of the thickness required to achieve a 2 hour rating. Further, NIST found no evidence that fire resistance tests of the WTC floor system were ever conducted. Review of the documents has not identified a similar concern for other structural components of the WTC towers.

[2] This reference is to one of the companion documents from this Investigation. A list of these documents appears in the Preface to this report.

1.2 PURPOSE OF THE STANDARD FIRE TESTS

To address these three investigation objectives, NIST conducted a series of four standard fire tests as described herein. The purpose of this series of tests was as follows:

- to establish the baseline performance of the floor system of the WTC towers as they were originally designed,
- to differentiate the factors that most influenced the collapse of the WTC towers as they may relate to normal building and fire safety considerations and those unique to the terrorist attacks of September 11, 2001,
- to determine whether there was an adequate technical basis for the original SFRM specification, and
- to study the procedures and practices used to accept an innovative structural and fire protection system.

1.3 TEST VARIABLES

To obtain information of greatest value to meet the investigation objectives, while limiting the number of tests to a practical number, NIST studied the effects of three factors: (1) SFRM thickness, (2) test restraint conditions, and (3) scale of the test. These factors are described more fully in this section.

1.3.1 SFRM Thickness

The Port Authority and its consultants sought an efficient and economical method to provide fire protection for the floor system and, by late 1965, the use of a fire-resistive material that was applied directly to the bars of the steel trusses was selected[3]. The Port Authority specified U.S. Minerals Products Cafco BLAZE-SHIELD Type D[4] as the sprayed fire-resistive material and, in a letter to the fireproofing contractor stated,

> "All Tower beams, spandrels, and bar joists requiring spray-on fireproofing are to have a ½″ covering of Cafco."[5]

Fire protection of a truss-supported floor system using a fire-resistive material applied directly to the steel trusses was innovative and not consistent with the practice at the time. Fire resistance testing of the floor assemblies constructed to represent as closely as practical those used in the WTC towers provides information to evaluate the procedures and practices used to accept an innovative system and to determine if there is a need for changes to those practices.

---

[3] See NIST NCSRAT 1-6A for a detailed chronicle of the procedures and practices used for fire protection of structural steel in the WTC towers

[4] This U.S. Minerals Products SFRM has been cited in WTC correspondence and documents using several designations. For consistency with other WTC Investigation reports, it is referred to herein as BLAZE-SHIELD D.

[5] Letter dated October 30, 1969 from Robert J. Linn (Manager, Project Planning, The World Trade Center) to Mr. Louis DiBono (Mario & DiBono Plastering Co., Inc.).

The BLAZE-SHIELD D product originally specified contained asbestos and its use was discontinued in 1970 at the 38th floor of WTC 1. Thermal protection of the remaining floors of WTC 1 and all of WTC 2 was carried out using BLAZE-SHIELD DC/F, a product that contained mineral wool fibers in place of the asbestos fibers.

In 1994, the Port Authority performed a series of thickness measurements of the existing SFRM on floors 23 and 24 of WTC 1. Six measurements were taken from "both flanges and web" of each of 16 random trusses on each floor at those locations where the SFRM was not damaged or absent. Measured average thickness varied between 0.52 in. and 1.17 in. and for the 32 measurements (16 on each floor) the overall average was 0.74 in. Four of the 32 trusses, had an average thicknesses between 0.52 in. and 0.56 in. This limited set of data suggests that the average thickness of SFRM as originally installed (as contrasted with SFRM that was upgraded in thickness beginning in the 1990s) was approximately 0.75 in.

1.3.2 Restraint Conditions

It is customary in the United States to conduct standard fire tests of floor assemblies in the restrained condition; that is, the condition in which expansion at the support of the floor test assembly resulting from the effects of the exposing fire is resisted by forces external to the element. In practice, a floor assembly such as that used in the WTC towers is neither restrained nor unrestrained, but likely its restraint condition lies somewhere in between. Testing under both restraint conditions, then, provides bounds on the expected performance of the floor system under the standard fire exposure. In addition, it provides a comparison of unrestrained ratings developed from both restrained and unrestrained test conditions.

1.3.3 Scale

Traditionally, relatively light assemblies have been tested with spans less than 18 ft, and results have been scaled up to practical floor system dimensions and spans. The Underwriters Laboratories of Canada fire testing facility in Toronto (ULC) has a furnace with nominal long dimension of 35 ft. Thus, full- or large-scale tests of floor assemblies can be tested in this furnace. Availability of the 35 ft span furnace at ULC, in addition to the 17 ft span furnace at UL's Northbrook, Illinois, facility (ULN) allowed NIST to conduct comparison tests to study the effect of scale[6].

1.4 TEST PROGRAM

Four tests as noted above were designed and conducted as follows:

- Test No. 1: Full-scale, restrained test condition, ¾ in. thick SFRM.
- Test No. 2: Full-scale, unrestrained test condition, ¾ in. thick SFRM.
- Test No. 3: Reduced-scale, restrained conditions, ¾ in. thick SFRM.

[6] ULC is used in this report to identify the fire testing facility operated by UL's affiliate, Underwriters Laboratories of Canada, while ULN is used to identify UL's Northbrook (Illinois) fire testing facility.

- Test No. 4: Reduced-scale, restrained conditions, ½ in. thick SFRM.

The objective of the full-scale restrained test with ¾ in. thick SFRM, Test 1, was to determine the baseline fire resistance of the floor system with average as-applied SFRM thickness. This test also demonstrated whether the fire resistance of such a system was significantly different from that of a system with the specified SFRM thickness of ½ in.

The test conditions for Test 2, full-scale unrestrained test with ¾ in. thick SFRM, were the same as those for Test 1 except that the specimen was supported to allow thermal expansion and, therefore, represented the unrestrained test condition. Results of this test allowed a determination of the unrestrained rating by test and, by comparing with the results of Test 1, a comparison of unrestrained ratings from both a restrained and unrestrained assembly test.

Test 3 was a reduced-scale test which, other than scale, was the same as Test 1. Thus, a comparison of the results of these two tests allowed an examination of whether test results are independent of test assembly scale.

Test assemblies for Tests 1, 2 and 3 were fire protected in the same manner, with ¾ in. thick SFRM representing the average SFRM thickness in the impact and fire affected floors of WTC 2. Measurements taken from photographs of the originally applied SFRM indicated that, while the SFRM thickness on main the trusses was approximately ¾ in., the thickness on the bridging trusses was approximately half that value (see NIST NCSTAR 1-6A). Also, photographs indicated that the metal deck was sometimes sprayed and sometimes not. For these three tests (Tests 1, 2, and 3), then, the main trusses were protected with ¾ in. thick SFRM, the bridging trusses with ⅜ in. thick SFRM, and the metal deck was not intentionally sprayed but was also not masked from overspray and thereby had, in most instances, at least a light covering of SFRM. These conditions best represented the thickness of the SFRM as it was originally applied in the one-way slab areas.

The objective of the test with the ½ in. SFRM (Test 4) was to determine whether or not there was adequate technical basis for the original SFRM specification. As explained by the designer, it was not necessary to fire protect the bridging trusses in the one-way areas nor was it necessary to spray the metal deck (see NIST NCSTAR 1-6A). Consequently, the Test 4 specimen had ½ in. thick SFRM applied to the main trusses and no SFRM applied to either the bridging trusses or the underside of the metal deck. Both the bridging trusses and metal deck were masked to prevent overspray as well. These conditions best represented the SFRM that was necessary, in the opinion of the designer, to provide the required level of passive fire protection.

Chapter 2
ASTM STANDARD FIRE TEST

The fire rating of structural materials and assemblies is generally determined through testing, and in the United States, such testing is frequently conducted in accordance with the ASTM International standard, ASTM E 119, "Standard Test Methods for Fire Tests of Building Construction and Materials" (ASTM 2000). This standard was first published in 1917 as a tentative standard, ASTM C 19, and was first adopted as ASTM E 119 in 1933. Since its introduction, the test method has been modified and updated, although its essential character has remained unchanged.

2.1 GENERAL DESCRIPTION

The test methods described in ASTM E 119 prescribe a standard fire exposure for comparing the test results of building construction assemblies. For the tests of floors and roofs, a test assembly is structurally loaded and the standard fire exposure is applied to the underside of the specimen. The assembly is evaluated for its ability to contain a fire by limiting passage of flame or hot gasses, and limiting heating of the unexposed surface, while maintaining the applied load. The assembly is given a rating, expressed in hours, based on these acceptance, or end-point, criteria. Revisions to the ASTM E 119 Standard in 1971, introduced the concept of fire endurance classifications based on two conditions of support: restrained and unrestrained.

2.2 RESTRAINT CONDITIONS

According to Appendix A4 of ASTM E 119-73, a restrained condition is "one in which expansion at the support of a load carrying element resulting from the effects of fire is resisted by forces external to the element." In an unrestrained condition, the element is free to expand and rotate at its supports. The Standard does not address how to achieve restraint at the assembly's supports, nor does it specify, in the case of floor assemblies, the stiffness characteristics of the restraining frame used to support an assembly.

The current standard describes a means to establish restrained and unrestrained ratings for floor assemblies from restrained test samples. The conditions of acceptance are based on limiting passage of flame or hot gasses, limiting temperatures on the unexposed surface of the slab, and failure to sustain the applied load. In addition, temperature limitations are placed on the main structural members. The location of temperature measurements on the structural members is specified in the ASTM E 119 Standard.

2.3 CONDITIONS OF ACCEPTANCE

The ASTM Standard Fire Test (ASTM 2000) is conducted by exposing a specimen to a standard fire controlled to achieve specified temperatures throughout a specified time period. It is emphasized in the Standard that the fire exposure "is not representative of all fire conditions because conditions vary with changes in the amount, nature and distribution of fire loading, ventilation, compartment size and configuration, and heat sink characteristics of the compartment." The conditions of acceptance relate

directly to the fire by limiting passage of flame or hot gasses and heating of the unexposed surface while maintaining the applied load. For floor and roof assemblies, the Standard provides for:

- Measurement of transmission of heat,
- Measurement of the transmission of hot gasses,
- Measurement of the load carrying ability of the test specimen during the test exposure.

Further, the Standard states specifically that it does not provide for, among other things, the following:

- Full information as to performance of assemblies constructed with components or lengths other than those tested,
- The effect of fire endurance of conventional openings in the assembly, that is, electrical receptacle outlets, plumbing pipe, etc., unless specifically provided for in the construction.

For tests of floors and roofs, a superimposed load is applied “to simulate a maximum load condition,” which is determined as “the maximum load condition allowed under nationally recognized structural design criteria.”

Temperatures of the floor assembly are measured during the fire exposure using thermocouples located on both the supporting steel members and top and bottom of the concrete slab.

Chapter 3
DESCRIPTION OF WTC FLOOR SYSTEM AND SFRM

3.1 COMPOSITE SLAB FLOOR SYSTEM

The floor system design for the World Trade Center (WTC) towers consisted of a lightweight concrete floor slab supported by steel trusses bridging between the building's core columns and exterior wall columns[7]. The main composite trusses, which were used in pairs, were spaced at 6 ft 8 in. on center (o.c.) and had a nominal clear span of either 60 ft or 35 ft. The steel trusses were fabricated using double angles for the top and bottom chords, and round bars for the webs. The web members protruded above the top chord in the form of a "knuckle" which was embedded in the concrete slab to develop composite action. Additionally, the floor system included bridging trusses (perpendicular to main trusses) spaced 13 ft 4 in. o.c. In the corners of the towers, the bridging trusses acted with the main trusses to provide two-way slab action, i.e., bending moments existed in both principal directions. Figure 3–1 is a cut-away of the composite floor system showing the main and bridging trusses, metal deck, and concrete slab.

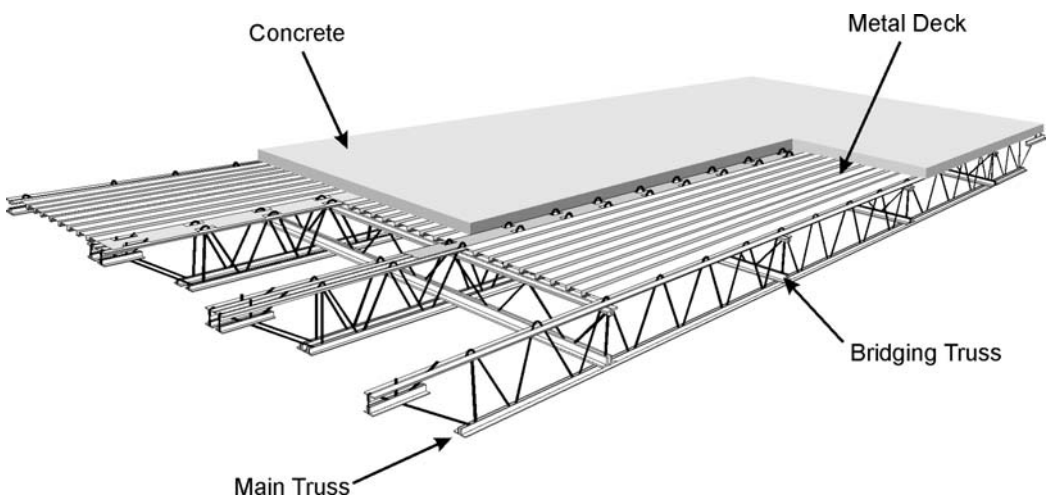

Figure 3–1. Floor system of the WTC towers.

3.2 STEEL TRUSSES

The steel trusses for the floor system were manufactured by Laclede Steel Co. using the resistance welding process to join the web, generally formed by bending a single steel rod, to the double angles forming the chord members. Resistance welding melts the two pieces being joined and fuses them to make the weld. The angles, which were produced by Laclede Steel Co., were specially rolled with a

[7] All information and data related to the design and construction of the WTC floor system were obtained from contract drawings provided to NIST by The Port Authority of New York and New Jersey. Refer to NIST NCSTAR 1-2A for a complete description of the WTC structural system and index of all structural drawings.

convex protrusion on the outside surface of one leg which melted locally where the angle leg was joined to the round bar webs.

3.3 SFRM THICKNESS

As noted in Section 1.3, the average thickness of SFRM as originally installed was approximately ¾ in. The thicknesses of ½ in. representing the specified thickness, and ¾ in. representing average applied thickness, were used in the standard fire resistance tests described here (see NIST NCSTAR 1-6A).

Chapter 4
FLOOR TEST ASSEMBLIES

4.1 DESIGN OF TESTS

For floor and roof assemblies, the ASTM E 119 Standard requires that the area exposed to fire be a minimum of 180 ft^2 and that neither dimension of the furnace be less than 12 ft. Furnaces available today (2005) in the United States for conducting standardized fire resistance tests of floor and roof assemblies have a maximum span less than 18 ft (Beitel 2002). Traditionally, relatively light construction floor assemblies have been tested, and results have been scaled to practical floor system dimensions.

4.1.1 Span of Test Assembly

The floor system used in the World Trade Center (WTC) spanned either 35 ft or 60 ft. The Underwriters Laboratories of Canada fire testing facility in Toronto (ULC) has a furnace with nominal dimensions of 35 ft by 14 ft, thereby allowing full-scale tests of the 35 ft span floor assemblies. For this series of tests, the floor truss designated on Laclede drawings as C32T5 was selected. This truss type was the most common 35 ft-span truss in the floors affected by the aircraft impact and subsequent fires (see Appendix G of NIST NCSTAR 1-2A).

As noted in Section 1.1, one of the motivations for conducting the standard fire resistance tests was to determine the technical basis for the selection of the SFRM for the WTC floor trusses and of the thickness to achieve a 2 h rating. Since test furnaces available at the time of the initial design of the WTC towers had a maximum span on the order of 18 ft, it would have been impractical to test a full-scale assembly although that possibility was raised in discussions between the Port Authority, the building designer, and steel truss fabricator (see NIST NCSTAR 1-6A). In designing a reduced-scale test, it is important to scale appropriately to capture, as nearly as practical, the conditions used for rating an assembly, namely the transmission of heat, the transmission of hot gasses, and the load-carrying ability of the test assembly during the period of fire exposure.

Both the thermal and mechanical properties of the materials and components used in the test assembly are important to its performance in a standard fire test. Likewise, the geometry of the test assembly, including steel member sizes, thickness of concrete slab, and overall geometric scale are determining factors in the thermal and structural performance of a test assembly. Finally, the magnitude of the applied load that represents the maximum load condition affects the structural performance of the test assembly. The fire exposure must follow the prescribed time-temperature curve given in the ASTM E 119 Standard.

4.1.2 Geometric Scaling of Floor Trusses

The prototype truss, designated C32T5, has an overall length of 35 ft 8 in. and a distance between centerlines of the bolts at the end supports of 35 ft ¾ in. The trusses for the “full-scale” test assembly had an overall length of 35 ft 0 in. as determined by the inside dimension of the reaction frame at the ULC fire test facility. The overall length of the reduced-scale specimens is 17 ft 5½ in., also limited by the largest

dimension of the reaction frame used at the ULN fire test facility. Thus, the span of the reduced-scale specimen was 17.46/35.00 = 0.50, or half that of the full-scale, or prototype, span.

A structural element in flexure, such as the floor system under study, carries both shear force and bending moment. The shear force, which governs the design of the truss web diagonals, is proportional to the magnitude of the uniform applied load on the slab multiplied by the span. If the span is reduced by one half, then the maximum shear force is reduced by one half. The bending moment controls the design of the truss chords and concrete slab and is proportional to the magnitude of the uniform applied load multiplied by the square of the span. Thus, if the span is reduced by one half, the maximum moment would be one quarter that in the prototype.

4.1.3 Concrete Slab Thickness

The heating rate of the unexposed surface of the floor assembly depends on the thermal properties of the lightweight concrete, the thickness of the floor slab, and profile of the supporting metal deck. Since the thermal properties of concrete are not easily changed, the slab thickness and deck must remain the same in the scaled specimen as in the prototype, or full-scale, specimen.

4.1.4 Steel Truss Sections

The structural response of a floor assembly subjected to an exposing fire depends on the rate at which the steel heats up since both the stiffness and strength of the steel decrease with increasing temperature. The rate at which the steel heats up is, in turn, a function of the thermal properties of the SFRM which change with temperature, the thickness of the applied SFRM, and the thermal conductivity of the steel. Since both the mechanical and thermal properties of steel and the SFRM are not easily changed, to preserve the rate at which the steel heats up and, therefore, the rate at which the steel loses its stiffness and strength, both the size of the steel sections and thickness of SFRM must be the same in the reduced-scale specimen as in the full-scale specimen.

4.1.5 Applied Load

The structural response of a floor assembly is also determined by the applied load, which the ASTM E 119 Standard defines as the maximum load condition allowed under nationally recognized structural design criteria. For the correct structural response to be captured, the stresses in the reduced-scale test assembly resulting from the applied load should match, as closely as practical, those of the prototype floor system. It is this principal upon which the loading for the reduced-scale tests was calculated.

As discussed under geometric scaling, the shear force, which is a function of the applied load and the section properties of the members, determine the stresses in the truss web diagonals. If the scale factor is one half, the applied load must be doubled to produce the same shear force. Because the section properties are not scaled, doubling the magnitude of the applied load produces the same forces in the diagonals of the reduced-scale assembly as in the prototype. The allowable compressive stress is governed by inelastic buckling and does not scale in exactly the same way, that is, the allowable compressive stress for the web diagonals in the reduced-scale assembly is greater than that for the web diagonals in the full-scale assembly.

The stresses in the chord members and in the concrete slab are a function of the applied load and span (bending moment) and the geometry of the assembly and geometric section properties of the structural elements. Because the bending moment is a function of the applied load and the square of the span (see above), for a scale factor of 0.50 and an applied load approximately twice that of the prototype design load, the bending moment is half that of the prototype. The force in the chord members is computed from statics and is a function of the applied load and the depth of the truss. Since the moment is one half and the depth of the floor section is approximately one half, the stresses in the truss chord members of the reduced-scale assembly are roughly equal to those of the prototype.

The loading was calculated to satisfy design requirements of the *Specification for the Design, Fabrication & Erection of Structural Steel for Buildings*, which were the nationally recognized structural design criteria under which the floor system for the WTC towers was designed (AISC 1963). A complete description of the specimen loading is presented in Section 4.4

Doubling of the applied load (expressed in force per unit length) on a composite double truss floor system as discussed above is achievable with the loading devices available. However, if the distance between trusses is scaled by the factor of one half, then the load per unit area would be four times that applied to the prototype full-scale assembly. Since this magnitude of loading would be difficult to achieve and the consequences of a structural failure at elevated temperatures would be catastrophic under such a load, the truss spacing for the reduced-scale tests was not scaled from the full-scale configuration. Since the trusses are each loaded to their design capacity, the spacing would not be expected to influence the test results significantly.

4.2 MATERIALS OF CONSTRUCTION

Every attempt was made to duplicate conditions that existed at the time of construction of the WTC floor system, including geometry and section properties of structural components, materials of construction, and fabrication and construction techniques. This chapter addresses the selection of materials and components and the level of care taken to insure faithful duplication of the floor system found in the WTC towers. Properties of the steels, concrete, metal deck, welded wire fabric, etc. used in the construction of all four test assemblies are documented in this section. Properties of concrete and sprayed fire-resistive material, which varied for each test specimen, are reported in the next section.

4.2.1 Fabrication of Trusses

As will be addressed in Section 4.2.3, resistance welding, which was used in the fabrication of the WTC trusses, was not employed in the fabrication of the test assembly trusses. Consequently, the specially rolled angles with a convex protrusion were not necessary. Conventional hot-rolled steel angles were used and, since unequal-leg angles were not available in the size required, equal-leg angles were cut (sheared) to the appropriate dimension.

The main and bridging trusses were fabricated by Canam Steel Co. under subcontract to Underwriters Laboratories Inc. (UL). Dimensions were taken from Laclede Steel shop drawings and scaled for the 35 ft and 17 ft span test frames. The 35 ft long trusses, Test Specimens 1 and 2, were scaled from 35 ft 8 in., the total length of the C32T5 truss, to a length of 35 ft 5 in. to fit the dimensions of UL's test

frame in the Toronto fire test facility. The overall depth of the truss was scaled accordingly. Figures 4–1 and 4–2 show the dimensions of the full-scale test specimen main trusses.

The 17 ft trusses, Test Specimens 3 and 4, were scaled to fit the test frame in UL's Northbrook facility; that is, by the ratio of 17 ft 5½ in. to 35 ft 8 in. The height of the knuckle was not changed since the depth of concrete slab was the same for both full- and reduced-scale tests. All member sizes, both chord and web, were unchanged. Figures 4–3 and 4–4 show the dimensions of the reduced-scale test specimen main trusses.

The bridging trusses for the full-scale test assembly were scaled in the same manner as the main trusses. For the reduced-scale tests, since the truss spacing was not scaled (see Section 4.1.5) the depth of the truss was scaled per the main trusses but the length (i.e., spacing of knuckles) was not. Figures 4–5 and 4–6 show the dimensions of the full- and reduced-scale bridging trusses, respectively.

4.2.2 Steel Grade

The original C32T5 trusses in the WTC were fabricated from ASTM A242 grade steel according to WTC contract drawings and confirmed by NIST (see NIST NCSTAR 1-3D). Since this steel is no longer produced, it was determined that ASTM A 572 Gr. 50 was an acceptable substitute, considering both chemistry and mechanical properties. The truss fabricator was not able to obtain the steel used for the web members in A572 grade steel in a time frame that would not impact the project. It was further decided that ASTM A529 grade steel was an acceptable substitute and would be used for the truss webs while, ASTM A572 grade steel would be used for the chord members. Chemistry, mechanical properties, and weldability were all considered in making this determination. Certified Mill Test Reports (CMTR) for the steel used to fabricate the main trusses and bridging trusses are shown in Appendix A.

4.2.3 Truss Welds

Most of the original WTC truss welds were made using resistance welding and the remainder using the submerged metal arc welding (SMAW) process (see Jefferson, 1962). Resistance welding is no longer widely used in practice, and no fabricator could be located that employed this technique. It was determined that metal inert gas (MIG) welding (Jefferson, 1962) could be used for all welds to fabricate the trusses.

The specification for the fabrication of the floor trusses[8] states, in section 105 Quality Control and Inspection of Resistance Welding,

> "All interior truss panel points will be connected by electronically controlled resistance welding designed to provide a minimum of two times the strength of the connected members at full design load."

The strength of a resistance weld is a function of the size of the pieces being joined, and parameters of the welding process such as heat (current), applied pressure, holding time, etc. For the WTC contract, Laclede developed 29 resistance weld designations for the various combinations of double chord angle

[8] World Trade Center Contract WTC-221.00, Fabricated Steel Floor Trusses, Bridging, Beams and Bracing for Prefabricated floor Units for North and South Towers, dated October, 1967 (WTCI-71-I

size and web rod size (see Table 4–1) Test Weld Strengths for many of the designations were found in a review of Laclede WTC Quality Control program documents and are also shown in Table 4–1. Welds designated R-22 were used for the fabrication of the C32T5 and are reported as having a Test Weld Strength (design strength) of 24 kips. Laclede WTC Quality Control Data (load test data) were found for 20 of the 29 designations; R-22 was not among them. The test data found showed results for ten load tests and the average load at failure is reported in Table 4–1. Dividing the failure load by the design load one obtains, in essence, a factor of safety which is also reported in the last column of Table 4–1. The average of these values was found to be 2.02. Thus, it could be concluded that the resistance weld procedure used by Laclede Steel Company in the fabrication of the floor trusses, produced welds with two times the design strength as called for in the contract specification.

Table 4–1. Redistance Weld Data.

Resistance Weld Designation	Double ChordAngle Size	Web Rod Size (in.)	Test Weld Strength (Kip)	Average Load (Kip)	F.S.
R-1	3 x 2 x 0.37	1.14	45	81	1.80
R-2	3 x 2 x 0.37	1.09	45	82	1.82
R-3	3 x 2 x 0.37	0.98		68	
R-4	3 x 2 x 0.37	0.92		63	
R-5	3 x 2 x 0.33	1.14	40	77.5	1.94
R-6	3 x 2 x 0.33	1.09	40	73.6	1.84
R-7	3 x 2 x 0.33	0.98	32	65.6	2.05
R-8	3 x 2 x 0.33	0.92	28	62.4	2.23
R-9	2 x 1-1/2 x 0.37	1.14	38	67.1	1.76
R-10	2 x 1-1/2 x 0.37	1.09		65.8	
R-11	2 x 1-1/2 x 0.37	0.98		60.7	
R-12	2 x 1-1/2 x 0.37	0.92		56.9	
R-13	2 x 1-1/2 x 0.37	0.75			
R-14	2 x 1-1/2 x 0.31	1.14	40	66.5	1.66
R-15	2 x 1-1/2 x 0.31	1.09	38	65.2	1.71
R-16	2 x 1-1/2 x 0.31	0.98	30	60.1	2.00
R-17	2 x 1-1/2 x 0.31	0.92	25	56.8	2.27
R-18	2 x 1-1/2 x 0.31	0.75	40		
R-19	2 x 1-1/2 x 0.25	1.14	40	75.4	1.88
R-20	2 x 1-1/2 x 0.25	1.09	40	73.7	1.84
R-21	2 x 1-1/2 x 0.25	0.98	29		
R-22	2 x 1-1/2 x 0.25	0.92	25		
R-23	2 x 1-1/2 x 0.25	0.75			

Resistance Weld Designation	Double ChordAngle Size	Web Rod Size (in.)	Test Weld Strength (Kip)	Average Load (Kip)	F.S.
R-24	1-1/2 x 1-1/4 x 0.275	0.98	18	44.8	2.49
R-25	1-1/2 x 1-1/4 x 0.275	0.92	18	41.1	2.28
R-26	1-1/2 x 1-1/4 x 0.275	0.75			
R-27	1-1/2 x 1-1/4 x 0.230	0.98	16	38.5	2.40
R-28	1-1/2 x 1-1/4 x 0.230	0.92	16	37.9	2.37
R-29	1-1/2 x 1-1/4 x 0.230	0.75	16		
				Average	2.02

The inherent factor of safety of welds designed in accordance with AISC, may be estimated by dividing the nominal strength of a groove weld in shear (AISC 1999) by the allowable stress of a groove weld in shear (AISC 2001), or $0.6\ F_y / 0.3\ F_y = 2.0$. To reproduce, approximately, the strengths of the resistance welds used in the fabrication of the WTC floor trusses, NIST used metal inert gas (MIG) welds designed to meet the strength requirements of AISC specifications (AISC 2001). The MIG process uses small gauge wire, well suited for producing the flare-bevel groove welds joining the round web bars to the double chord angles.

4.2.4 Metal Deck

The non-composite deck consisted of 1½ in. No. 22 gauge galvanized sheet metal floor units. Each full panel measured 35 ft 2 in. long by 3 ft 1½ in. wide for Assembly Nos. 1 and 2, and 17 ft 8 in. by 3 ft 1½ in. wide for Assembly Nos. 3 and 4. The original deck used for the floor system in the WTC towers was custom produced specifically for the WTC buildings. The steel deck was rolled in widths that spanned between trusses without a longitudinal seam. It was not possible to obtain deck in the desired span, and therefore, it was determined that typical Type B steel deck, seamed per the manufacturer's recommendation, would be acceptable.

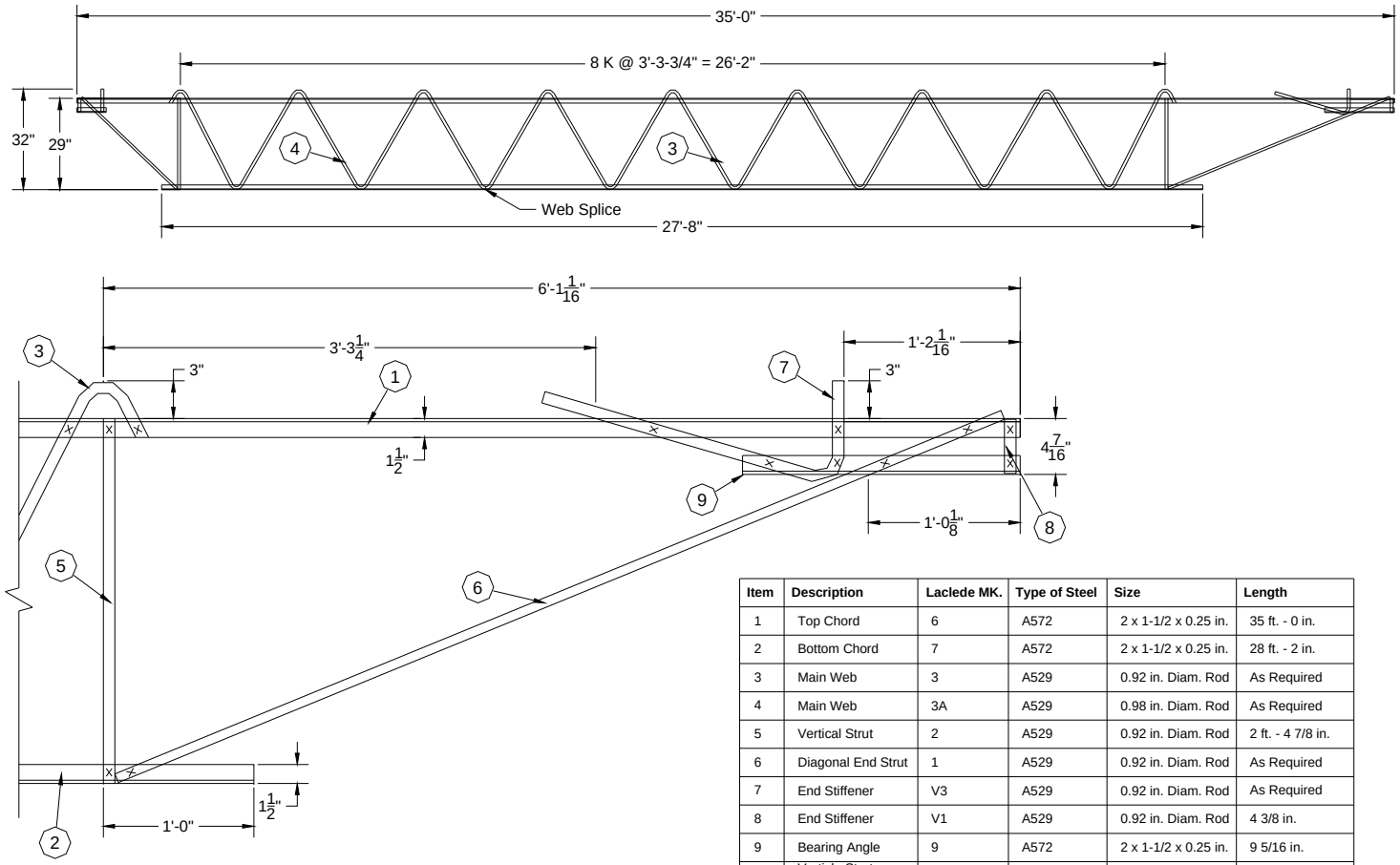

Item	Description	Laclede MK.	Type of Steel	Size	Length
1	Top Chord	6	A572	2 x 1-1/2 x 0.25 in.	35 ft. - 0 in.
2	Bottom Chord	7	A572	2 x 1-1/2 x 0.25 in.	28 ft. - 2 in.
3	Main Web	3	A529	0.92 in. Diam. Rod	As Required
4	Main Web	3A	A529	0.98 in. Diam. Rod	As Required
5	Vertical Strut	2	A529	0.92 in. Diam. Rod	2 ft. - 4 7/8 in.
6	Diagonal End Strut	1	A529	0.92 in. Diam. Rod	As Required
7	End Stiffener	V3	A529	0.92 in. Diam. Rod	As Required
8	End Stiffener	V1	A529	0.92 in. Diam. Rod	4 3/8 in.
9	Bearing Angle	9	A572	2 x 1-1/2 x 0.25 in.	9 5/16 in.
10	Verticle Strut Core Side	5	A529	0.98 in. Diam. Rod	As Required
11	Diagonal Strut	10	A529	0.98 in. Diam. Rod	As Required
12	End Stiffener	V2	A529	0.98 in. Diam. Rod	7 3/8 in.
13	End Stiffener	V1	A529	0.98 in. Diam. Rod	As Required

Figure 4–1. 35 ft main truss, column end.

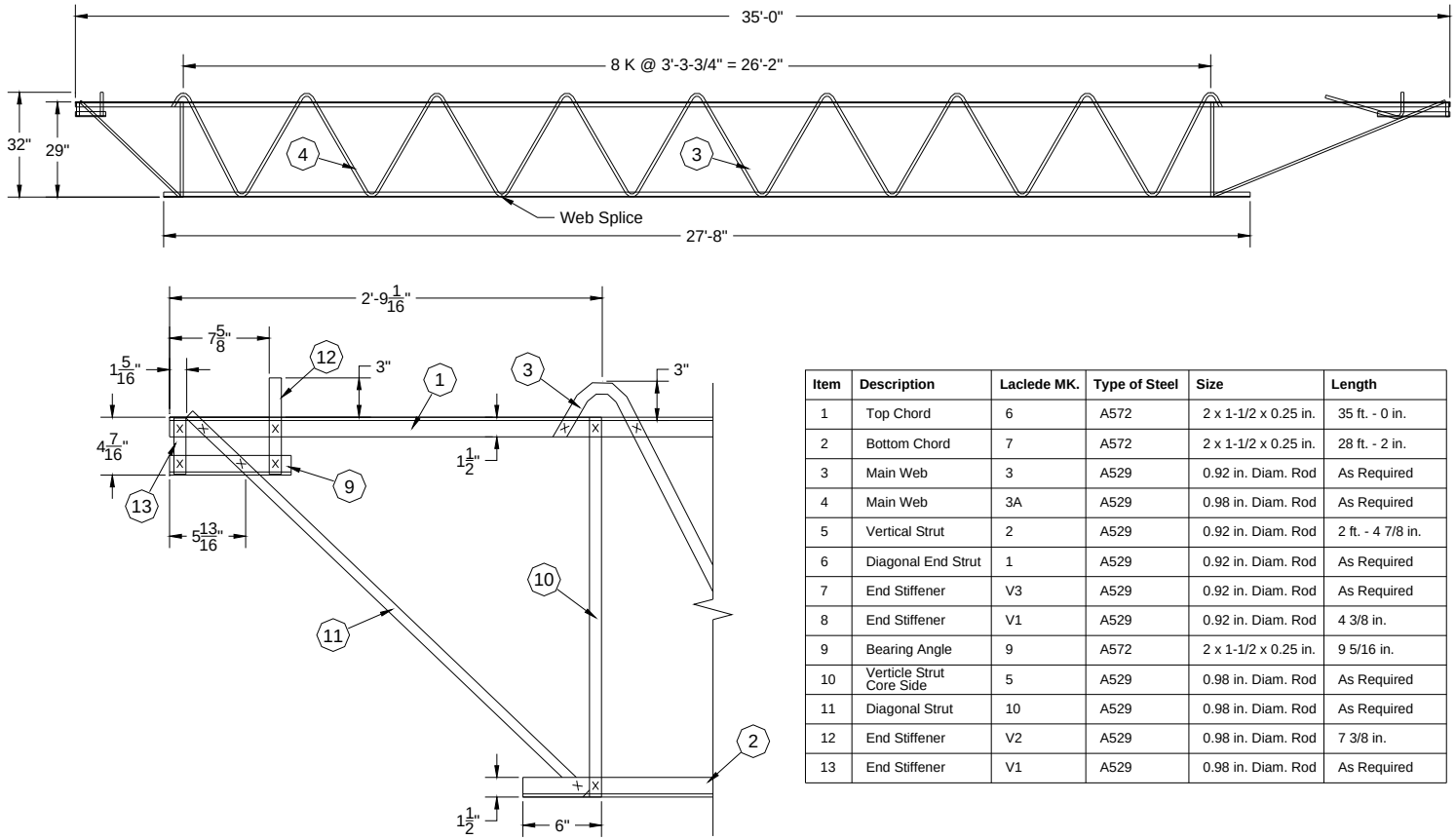

Item	Description	Laclede MK.	Type of Steel	Size	Length
1	Top Chord	6	A572	2 x 1-1/2 x 0.25 in.	35 ft. - 0 in.
2	Bottom Chord	7	A572	2 x 1-1/2 x 0.25 in.	28 ft. - 2 in.
3	Main Web	3	A529	0.92 in. Diam. Rod	As Required
4	Main Web	3A	A529	0.98 in. Diam. Rod	As Required
5	Vertical Strut	2	A529	0.92 in. Diam. Rod	2 ft. - 4 7/8 in.
6	Diagonal End Strut	1	A529	0.92 in. Diam. Rod	As Required
7	End Stiffener	V3	A529	0.92 in. Diam. Rod	As Required
8	End Stiffener	V1	A529	0.92 in. Diam. Rod	4 3/8 in.
9	Bearing Angle	9	A572	2 x 1-1/2 x 0.25 in.	9 5/16 in.
10	Verticle Strut Core Side	5	A529	0.98 in. Diam. Rod	As Required
11	Diagonal Strut	10	A529	0.98 in. Diam. Rod	As Required
12	End Stiffener	V2	A529	0.98 in. Diam. Rod	7 3/8 in.
13	End Stiffener	V1	A529	0.98 in. Diam. Rod	As Required

Figure 4–2. 35 ft main truss, core end.

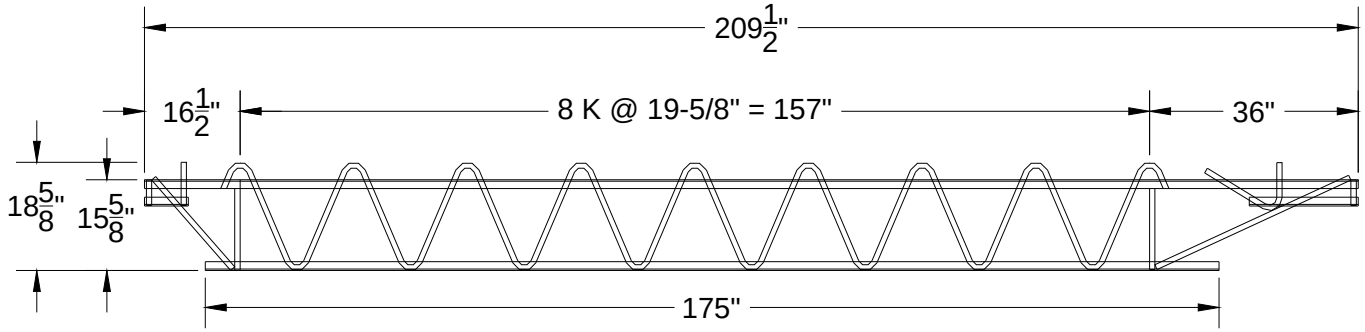

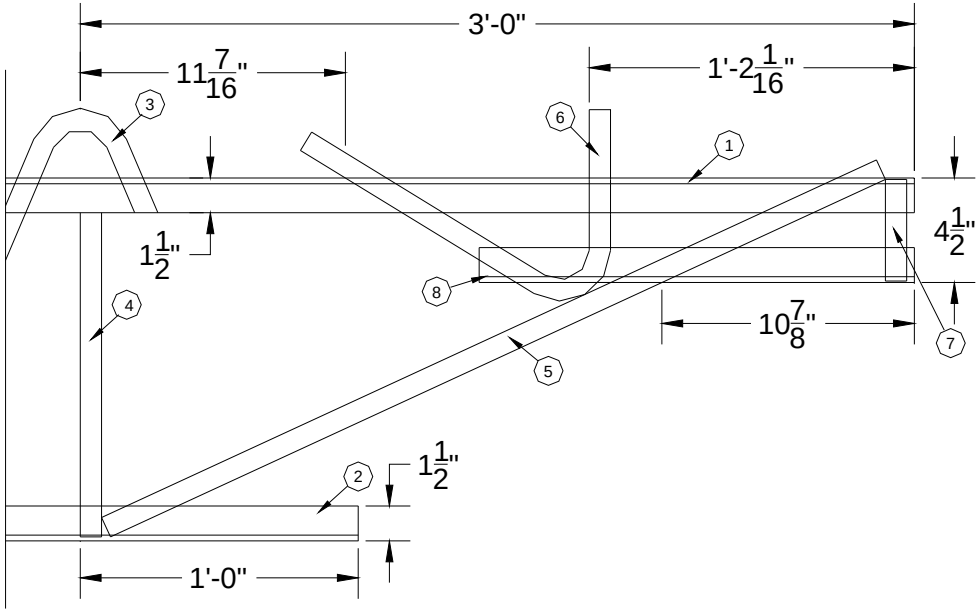

Item	Description	Laclede MK.	Type of Steel	Size	Length
1	Top Chord	6	A572	2 x 1-1/2 x 0.25 in.	17 ft. - 5 1/2 in.
2	Bottom Chord	7	A572	2 x 1-1/2 x 0.25 in.	14 ft. - 10 in.
3	Knuckle Chord	3	A529	0.98 in. Diam. Rod	As Required
4	Vertical Strut	2	A529	0.92 in. Diam. Rod	2 ft. - 4 7/8 in.
5	Diagonal End Strut	1	A529	0.92 in. Diam. Rod	As Required
6	End Stiffener	V3	A529	0.92 in. Diam. Rod	As Required
7	End Stiffener	V1	A529	0.92 in. Diam. Rod	4-3/8 in.
8	Bearing Angle	9	A572	2 x 1-1/2 x 0.25 in.	9 3/16 in.
9	Vertical Strut Core Side	5	A529	0.98 in. Diam. Rod	2ft. - 4 7/8 in.
10	Diagonal Strut	10	A529	0.98 in. Diam. Rod	As Required
11	End Stiffener	V2	A529	0.98 in. Diam. Rod	As Required
12	End Stiffener	V1	A529	0.98 in. Diam. Rod	As Required

Figure 4–3. 17 ft main truss, column end.

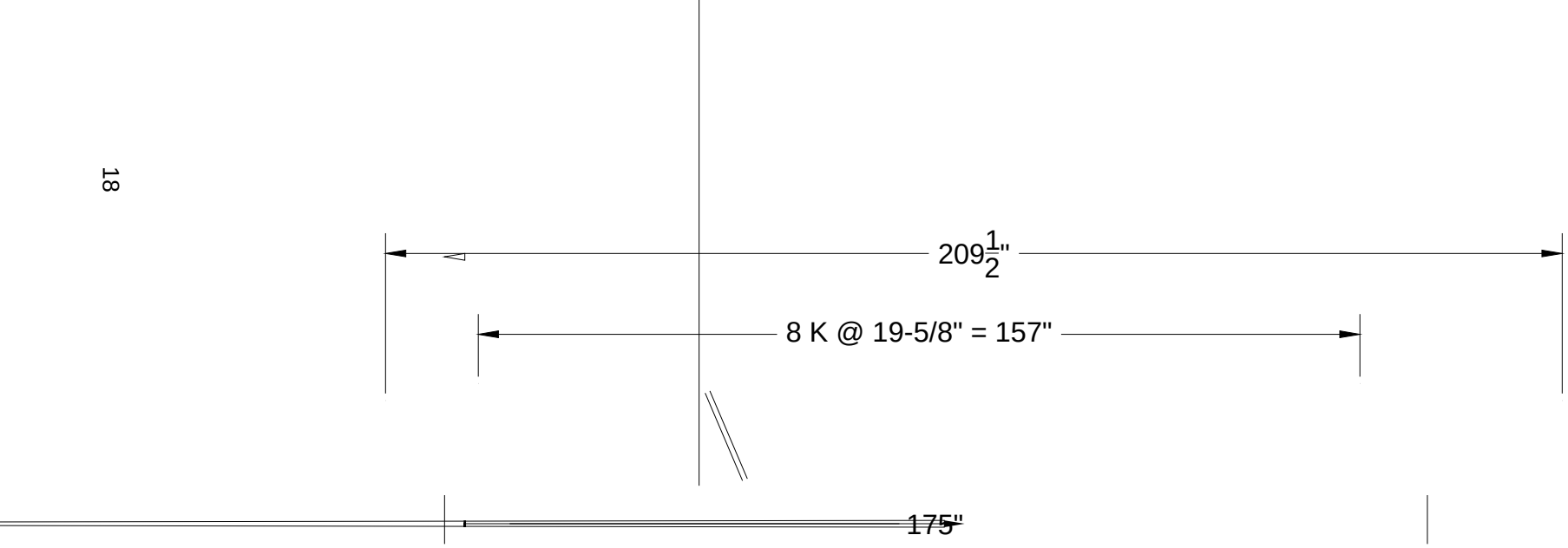

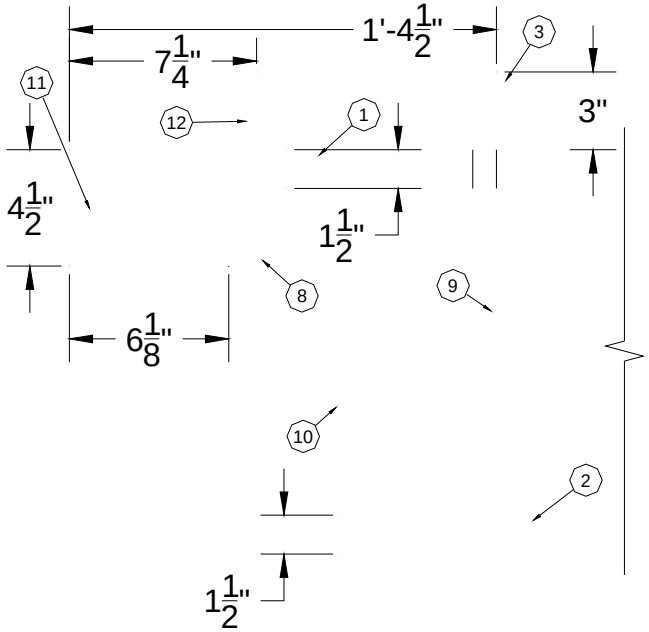

Item	Description	Laclede MK.	Type of Steel	Size	Length
1	Top Chord	6	A572	2 x 1-1/2 x 0.25 in.	17 ft. - 5 1/2 in.
2	Bottom Chord	7	A572	2 x 1-1/2 x 0.25 in.	14 ft. - 10 in.
3	Knuckle Chord	3	A529	0.98 in. Diam. Rod	As Required
4	Vertical Strut	2	A529	0.92 in. Diam. Rod	2 ft. - 4 7/8 in.
5	Diagonal End Strut	1	A529	0.92 in. Diam. Rod	As Required
6	End Stiffener	V3	A529	0.92 in. Diam. Rod	As Required
7	End Stiffener	V1	A529	0.92 in. Diam. Rod	4-3/8 in.
8	Bearing Angle	9	A572	2 x 1-1/2 x 0.25 in.	9 3/16 in.
9	Vertical Strut Core Side	5	A529	0.98 in. Diam. Rod	2ft. - 4 7/8 in.
10	Diagonal Strut	10	A529	0.98 in. Diam. Rod	As Required
11	End Stiffener	V2	A529	0.98 in. Diam. Rod	As Required
12	End Stiffener	V1	A529	0.98 in. Diam. Rod	As Required

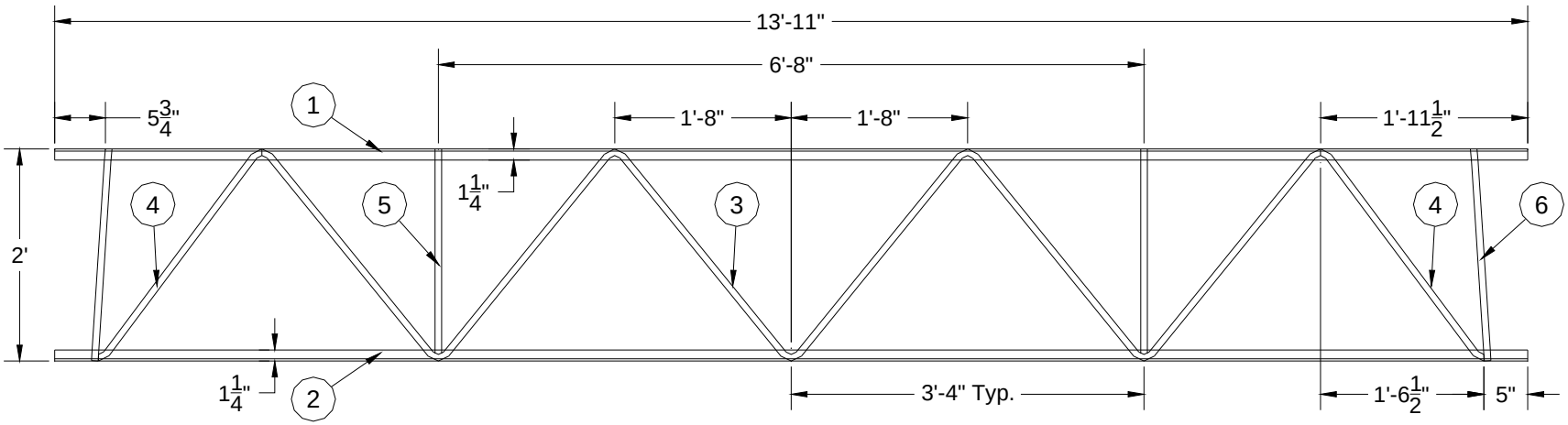

Item	Description	Laclede MK.	Type of Steel	Size	Length
1	Top Chord	6	A572	1-1/2 x 1-1/4 x 0.230 in.	13 ft. - 8 in.
2	Bottom Chord	7	A572	1-1/2 x 1-1/4 x 0.230 in.	13 ft. - 8 in.
3	Main Web	3	A572	0.75 in. Diam. Rod	As Required
4	Web Chord	4	A572	0.75 in. Diam. Rod	As Required
5	Vertical Strut	12	A572	0.75 in. Diam. Rod	1 ft. - 10-7/8 in.
6	Inclined End Strut	2	A572	0.75 in. Diam. Rod	1 ft. - 11-3/4 in.

Figure 4–5. Bridging truss for Assemblies Nos. 1 and 2.

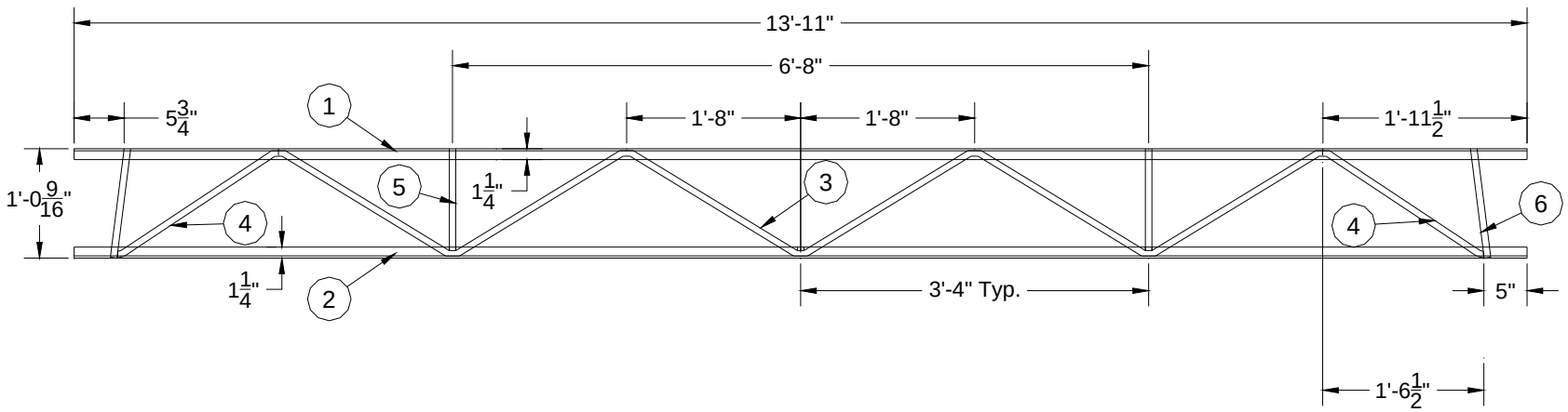

Item	Description	Laclede MK.	Type of Steel	Size	Length
1	Top Chord	6	A572	1-1/2 x 1-1/4 x 0.230 in.	13 ft. - 11 in.
2	Bottom Chord	7	A572	1-1/2 x 1-1/4 x 0.230 in.	13 ft. - 11 in.
3	Main Web	3	A572	0.75 in. Diam. Rod	As Required
4	Web Chord	4	A572	0.75 in. Diam. Rod	As Required
5	Vertical Strut	12	A572	0.75 in. Diam. Rod	As Required
6	Inclined End Strut	2	A572	0.75 in. Diam. Rod	As Required

Figure 4–6. Bridging truss for Assemblies Nos. 3 and 4.

4.2.5 Welded Wire Fabric

The welded wire fabric used in the concrete was 10 in. by 4 in. W4.2/W4.3 welded steel mesh. Steel wire was supplied by Insteel Wire Products and its strength shown in Appendix A.

4.2.6 Concrete

The concrete design strength for a typical office floor of the WTC was specified to be 3,000 psi, and the lightweight density was specified as 100 pcf. The concrete for the floor slab consisted of ¾ in. lightweight haydite aggregate, sand, Type I Portland cement and water. No records of actual mixture proportions or cylinder strengths were found in NIST's review of available documents. The mix design shown in Table 4–2 was determined by the concrete supplier to produce a 3,000 psi 28-day strength using lightweight aggregate.

Table 4–2. Concrete mix design per cubic yard of concrete.

Cement (lb)	Haydite "C" (lb)	Sand (lb)	Entrained Air (%)	Water (lb)
522	940	1300	6	281*

* Includes 40 lb of water in sand

4.2.7 Primer

The trusses supplied by Laclede Steel were shop primed during production using an electro-deposition process. The formulation for the primer was designated as Formula LREP – 10001 and was found in Laclede files (see Appendix B). The exact formulation could not be reproduced due to current environmental considerations. A stock structural steel primer, manufactured by Sherwin Williams and designated Type B50NV11 (recommended by Isolatek International, the manufacturer of the sprayed fire-resistive material used in these tests and in the original construction of the WTC towers) was determined to be an acceptable substitute. The primer was field applied to the trusses after assembly in the ULN and ULC fire test facilities.

4.2.8 Sprayed Fire-Resistive Materials

The sprayed fire resistive material used on the test assemblies was BLAZE-SHIELD DC/F which is manufactured by Isolatek International, and is the same product as that applied during original construction.

4.2.9 Miscellaneous Steel

Miscellaneous steel including rebar, pourstop coverplates, and support angles used during construction are described in Section 4.3.

4.3 CONSTRUCTION OF TEST ASSEMBLIES

The construction of each assembly was conducted by UL technical staff and under the supervision of NIST at Underwriters' Laboratories of Canada (ULC), and Underwriters Laboratories Inc. in Northbrook, Illinois (ULN). All welds were made by certified welders and inspected by STS Consultants Ltd. (STS) under sub-contract to UL. Table 4–3 lists the construction periods and test dates for the four assemblies tested.

Table 4–3. General construction details.

Assembly No.	Description	Location	Construction Dates	Test Date
1	35 ft Restrained	Toronto, ON, Canada	1/20/2004 - 1/27/2004	8/7/2004
2	35 ft Unrestrained	Toronto, ON, Canada	1/28/2004 - 2/04/2004	8/11/2004
3	17 ft Restrained	Northbrook, IL, U.S.	2/13/2004 - 2/22/2004	8/19/2004
4	17 ft Restrained w/ unprotected bridging trusses	Northbrook, IL, U.S.	2/13/2004 - 2/22/2004	8/25/2004

4.3.1 Construction of 35 Ft Assemblies

Assembly No. 1 was restrained from thermal expansion. The trusses were welded to steel support angles that were attached to the test frame, and the concrete was poured in contact with the frame. Assembly No. 2 was unrestrained. The trusses were bolted to steel support angles having a 2⅞ in. slot to allow for unrestrained thermal expansion. The concrete was poured with a 1½ in. gap between the concrete and the frame. Figure 4–7 shows the assembly of the steel support system for test Assembly No. 1. Refer to Appendix C for construction drawings.

Structural Steel Frame and Deck

The two nominal 35 ft by 14 ft floor assemblies were constructed of the same materials and in the same manner, with the exception of the restraint condition, provided by the attachment of the main trusses to the test frame as described above. Two main trusses were symmetrically positioned in the test frame, 6 ft 8 in. o.c.

The ends of the main trusses in Test Assembly No. 1 were supported by L6×4×1 structural angles 12 in. long welded to the test frame. The bearing length for each main truss was 3½ in. The ends of the main trusses were welded with a ½ in. fillet along the entire bearing length on each side of the trusses (see Fig. 4–8). Steel plates were placed between the ends of the main trusses and the test frame, filling the gap and, thus, preventing thermal expansion.

Source: NIST.

Figure 4–7. Structural steel frame of Assembly No. 1.

Source: NIST.

Figure 4–8. Restrained end condition of Assembly No. 1 prior to shimming.

The ends of the main trusses in Test Assembly No. 2 were supported on L7×4×1 structural angles, 14 in. long welded to the test frame. Slotted holes, 2 7/8 in. long, were provided in the steel angles, and the

centerline of each slot was located 3 in. from the edge of the angle. The edge distance of the slotted holes was 1¼ in. The bolt holes in the truss bearing angles were 15/16 in. in diameter. The main trusses were bolted to the support angles using two ⅞ in. diameter by 2½ in. long ASTM A325 bolts with ASTM F436 washers and ASTM A563 nuts as seen in Fig. 4–9. The nuts were hand tightened to provide connection stability without hindering thermal expansion. Also, the trusses and supports were designed so that the bolts were installed close to the inside edge of the slot, thus allowing the maximum unrestrained outward movement as the test specimens heated and expanded. The slots extending beyond the edge of the truss support angles are just visible in Fig. 4–13.

Source: NIST.

Figure 4–9. Unrestrained end condition of Assembly No. 2.

Two bridging trusses, one located 9 ft 4 in. from the west test frame edge and one located 12 ft 7¼ in. from the east test frame edge were installed in the assembly. The bridging trusses were welded to 6 in. long L2½×1½×½ angles that were welded to the bottom chord of each main truss. The top of the bridging truss was welded to the top chord of the main truss. All welds were ¼ in. fillets.

Three L3×2×¼ in. steel deck support angles, one located 3 ft ¾ in. from the west test frame edge, one at 16 ft 1 in. from the west test frame edge, and one at 6 ft 5 in. from the east test frame edge were welded to the bottom of the top chord of the main truss (see Fig. 4–10).

Source: NIST.

Figure 4–10. Intersection of deck support angle and main truss.

At the intersection of the bridging trusses, steel deck support angles, and main trusses, a 3 in. by 3 in. by ⅜ in. steel plate was welded to the top side of the bottom chord of the main truss with ¼ in. fillet on the east and west sides of the plate. There was no steel plate welded to the bottom chord at the location of the center steel deck support angle.

Cover plates made from A36 steel, 7 in. wide and 0.116 in. thick were welded to the full length of the top chords of the main trusses to prevent the wet concrete from passing through (Fig. 4–10). Steel cover plates measuring 3½ in. by 7 in. by 0.116 in. thick were welded under each web knuckle for the same purpose. A 2 in. by 7 in. by ¼ in. steel plate was welded to adjacent knuckles (Fig. 4–11) per Laclede shop drawings. The plates were located at the knuckles immediately above the intersection of bridging trusses and deck support angles with the main trusses (see Fig. 4–12). A 6¼ in. long piece of No. 8 reinforcing steel bar was welded to each end stiffener at both ends of the truss (see Fig. 4–13).

Source: NIST.

Figure 4–11. Cover plates on main truss.

Source: NIST.

Figure 4–12. Intersection of main and bridging truss, bottom chord.

Source: NIST.

Figure 4–13. Detail of rebar welded to end stiffener.

The steel floor deck was placed on the assembly in 3 ft 1½ in. widths, 35 ft lengths, with the crests and valleys parallel to the main trusses (Fig. 4–14). Near the east-west centerline of the assembly the deck was overlapped and secured with ⅝ in. long self-taping hex-head screws spaced 18 in. o.c., beginning 16 in. from the east edge of the frame. At the interface of the steel deck edge and the upper chords of the main trusses, the deck was secured to the chords with ½ in. puddle welds spaced 6 in. o.c. Where the deck met the north and south test frame edges, 4¼ in. by 96 in. by 0.116 in. thick steel plate was secured to the top of the steel deck with 1¼ in. long by 5/32 in. shank hex-head, self-tapping screws spaced 18 in. o.c., located 1½ in. from the edge of the steel plate. The steel plate was installed so that it was flush against the test frame surface.

Source: NIST.

Figure 4–14. Placement of steel form deck.

Chairs, ¾ in. high measuring 60 in. long, with 12 legs per chair spaced 5 in. o.c. and 2¾ in. from each end, were placed and taped on alternating deck crests along the full length of the assembly (see Fig. 4–15). Welded wire fabric (WWF), 10 in. by 4 in. W4.2/W4.3, supplied in 60 in. widths, was placed on the chairs with the 4 in. dimension running the length of the assembly (east to west). The WWF was notched to fit around the knuckles and instrumentation sleeves. Adjacent sections of WWF were overlapped nominally 12 in. per ACI 318-63 (ACI, 1963). At the overlaps, the mesh was secured with 18 gauge wire twist-ties spaced approximately 24 in. o.c.

No. 4 (½ in. or 13 mm diameter) steel reinforcing bar was placed on top of the first layer of welded wire fabric, 3 in. from the east and west ends of the test frame. A second layer of welded wire fabric was installed with overlaps and fastened with wire ties as described above for the first layer. Two lengths of No. 5 (⅝ in. or 16 mm diameter) steel reinforcing bar were placed on both sides of each bridging truss over the second layer of wire fabric (Fig. 4–16). The rebar was secured to the top layer of welded wire fabric with 18 gauge wire twist-tied approximately 24 in. o.c.

Source: NIST.

Figure 4–15. Chairs for welded wire fabric.

Source: NIST.

Figure 4–16. Welded wire fabric.

Concrete Placement

The ready-mixed concrete was poured to an average depth of 4 in. measured from the top plane of the 1½ in. deep steel deck. Details of the concrete mix and compressive strengths are given in Table 4–4. The concrete was finished to a flat, smooth surface with a wooden trowel. Placement of concrete is shown in Fig. 4–17.

Table 4–4. Details of concrete placement.

Assembly No.	Concrete Pour Date	Wet Unit Weight* (lb/ft^3)	Slump* (in.)	Air Content* (%)	Water Added (gal)	Compressive Strength at 28 Days (psi)	Compressive Strength at 56 days (psi)
1	1/27/2004	114.2/114.8 l	6/8	4.5/5.75	4	4177	4735
2	2/4/2004	109.4 lb/ft^3	7.5	8.75%	–	2937	3893

*Results before and after water added

Source: NIST.

Figure 4–17. Concrete placement.

Curing of Concrete

The ASTM E 119 test standard requires the average relative humidity of the concrete slab to be 70 percent +/-5 percent. In order to accelerate the process of driving the moisture out of the concrete slab, the assemblies were placed in a high temperature, low humidity environment following an initial 28 day curing at ambient environment. The relative humidity of each slab was monitored regularly in accordance with the method described in ASTM E 119-2000a, paragraph 12.1.3, Note 6.

Preparation of Trusses

Prior to the application of primer to the structural steel members, the steel was sand blasted (Fig. 4–18) to the Society of Protective Coatings SSPC-SP6 specification in accordance with the product specification sheet of the primer. Following the sand blasting, the steel was primed (Fig. 4–19) with Sherwin Williams Type B50NV11 at an approximate dry film thickness of 0.003 in.

Source: NIST.

Figure 4–18. Sandblasted assembly.

Source: NIST.

Figure 4–19. Primer on bridging truss.

Instrumentation

Prior to the concrete pour, four 18-gauge Type K thermocouples were attached to the steel form deck at each of three locations, near the center point and quarter points in the east-west direction. At each location, a thermocouple was placed in the valley, sidewall, crest, and next adjacent valley of the deck. Refer to Appendix D for locations of deck thermocouples.

After priming of the structural steel, 18-gauge Type K thermocouples were attached to each main and bridging truss (see Fig. 4–20). Eight thermocouples were peened into the steel at each cross section, located approximately at the quarter and center points on each main truss (see Appendix D for exact locations). Additionally, 10 thermocouples were located at the intersections of each main and bridging truss. In total, 44 thermocouples were attached to each main truss, for a total of 88 thermocouples.

On each bridging truss, four thermocouples were attached at each cross section located at the center of the truss, at the intersections of the main and bridging trusses, and approximately halfway between the main truss and the end of the bridging truss (see Appendix D for exact locations). In total, 16 thermocouples were attached to each bridging truss, for a total of 32 thermocouples.

Strain gauges were attached on the bottom chords of the main trusses to measure strain as each test assembly was loaded. A pre-wired 350 Ω resistance strain gauge was placed, per the manufacturer's instructions, on the top surface and bottom surface of the bottom chord angle. The strain gauges were symmetrically opposed, at the mid-length of the bottom chord of each main truss. Each pair of gauges was wired to a half-bridge amplifier prior to loading of the assembly. Strain gauge readings were used to confirm proper loading of the assemblies, and the wiring was cut and bridge circuit removed prior to the start of the tests.

Source: NIST.

Figure 4–20. Peened thermocouples on truss.

Application of Sprayed Fire Resistive Materials

Application of the sprayed fire resistive materials was conducted by the manufacturer of the SFRM under a sub-contract to UL and witnessed by representatives of UL and NIST. On the underside of the assembly, the BLAZE-SHIELD DC/F sprayed fire resistive material was applied to the main and bridging trusses in multiple coats. No attempt was made to control overspray of material onto the deck of the 35 ft test assemblies.

Thickness and density measurements were taken in accordance with ASTM E 605 Standard Test Methods for Thickness and Density of Sprayed Fire-Resistive Material (SFRM) Applied to Structural Members (ASTM 2000a). The average SFRM thicknesses on the trusses are shown in Table 4-5 for Test Assembly No. 1. Figure 4–21 shows the SFRM on main trusses after achieving the desired thickness. Figure 4–22 shows SFRM thickness measurements being made on the bottom chord of a main truss.

Table 4–5. SFRM Thickness measurements on Assembly No. 1.

Location	Nominal Thickness (in.)	Final Average Measured Thickness (in.)	Basis: No. of Thickness Measurements
North Main Truss	3/4	0.756	254
South Main Truss	3/4	0.750	254
East Bridging Truss	3/8	0.385	72
West Bridging Truss	3/8	0.385	72

The air dry density of the Type DC/F sprayed fire resistive material was determined using 12 in. by 12 in. samples. The air dry densities are shown in Table 4–6 for Assembly No. 1. The average air dry density was found to be 15.73 pcf.

Table 4–6. Air dry density of spray applied fire resistive material on Assembly No. 1.

Material Type	Nominal Thickness (in.)	Measured Density (pcf)
DC/F	3/4	17.27
DC/F	3/4	15.19
DC/F	3/4	14.73

Source: NIST.

Figure 4–21. SFRM on main truss.

Source: NIST.

Figure 4–22. Measurement of SFRM thickness on truss chord.

SFRM thickness measurements for Test Assembly No. 2 are given in Table 4–7. Air dry density of spray applied fire resistive material on Assembly No. 2 is given in Table 4–8; the average air dry density was found to be 19.95 pcf.

Table 4–7. Thickness measurements on Assembly No. 2.

Location	Nominal Thickness (in.)	Final Average Measured Thickness (in.)	Basis: No. of Thickness Measurements
North Main Truss	3/4	0.756	254
South Main Truss	3/4	0.755	254
East Bridging Truss	3/8	0.393	72
West Bridging Truss	3/8	0.391	72

Table 4–8. Air dry density of spray applied fire resistive material on Assembly No. 2.

Material Type	Nominal Thickness, in.	Measured Density, pcf
DC/F	3/4	20.98
DC/F	3/4	24.01
DC/F	3/4	14.87

4.3.2 Construction of 17 Ft Assemblies

Structural Steel Frame and Deck

Assembly Nos. 3 and 4 were both restrained from thermal expansion by welding the trusses to the steel support angles that were attached to the test frame and by casting the concrete in contact with the frame. The sprayed fire resistive material was applied to Assembly No. 3 in the same way as for Assembly Nos. 1 and 2. Assembly No. 4 was protected with ½ in. of SFRM on the main trusses, while the bridging trusses were left unprotected, and the deck and deck support angles were shielded from any overspray (see Section 1.4). Refer to Appendix E for construction drawings.

The two nominal 17 ft by 14 ft floor assemblies were constructed in the test frames to fill the openings. Both assemblies were constructed of the same materials and in the same manner. The two main trusses were symmetrically positioned in the test frame 6 ft 8 in. o.c. (see Fig. 4–23).

Source: NIST.

Figure 4–23. Steel framing of 17 ft assembly.

The ends of the main trusses were supported on structural steel support angles installed at the north and south walls of the test frame. The resulting bearing length at each end of the main trusses was 3½ in. The ends of the main trusses were welded with ½ in. fillets along the entire bearing length on each side of the truss bearing angles. Steel plates were placed between the ends of the main trusses and the test frame, filling the gap and, thus, preventing thermal expansion.

Each test assembly had two bridging trusses, one located 4 ft 9⅝ in. from the north test frame edge and one located 6 ft 5⅝ in. from the south test frame edge. The bridging trusses were welded to 6 in. long by 1½ in. by 2½ in. by ¼ in. thick angles welded to the bottom chord of each main truss. The top of the bridging truss was welded to top chord of the main truss. All welds were ¼ in. fillets.

Three 2 in. by 3 in. steel deck support angles, one located 1 ft 8 1/16 in. from the north test frame edge, one at 8 ft 1⅝ in. from the north test frame edge, and one at 6 ft 5⅝ in. from the south test frame edge, were welded to the bottom of the top chord of the main truss (see Fig. 4–24).

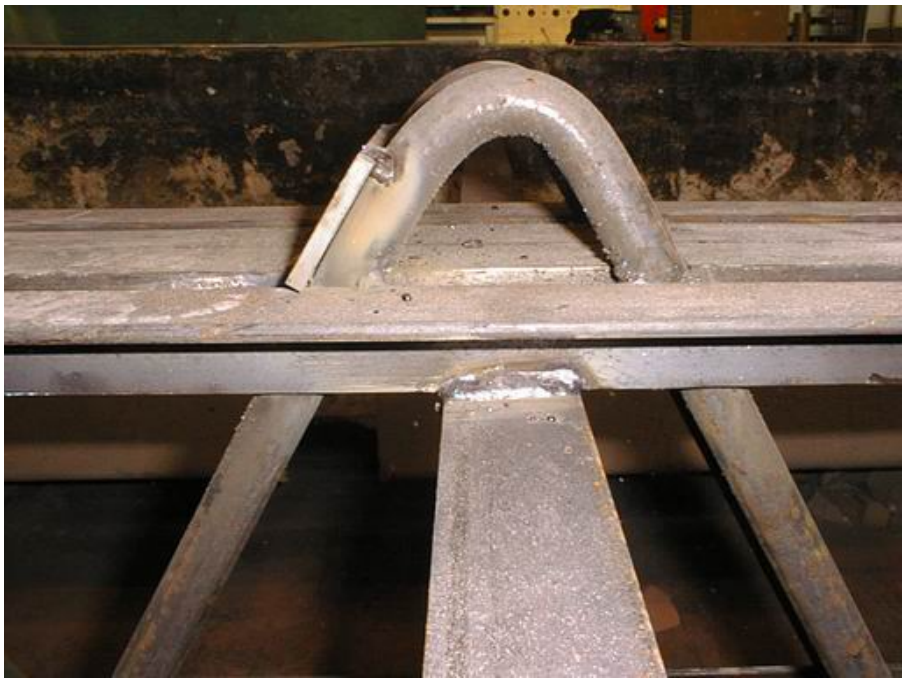

Source: NIST.

Figure 4–24. Intersection of main truss and deck support angle.

At the intersection of the bridging trusses, steel deck support angles, and main trusses, a 3 in. by 3 in. by ⅜ in. steel plate was welded to the top side of the bottom chord of the main truss with ¼ in. fillet on the east and west sides of the plate (see Fig. 4–25). There was no steel plate welded to the bottom chord at the location of the center steel deck support angle.

Source: NIST.

Figure 4–25. Intersection of main and bridging truss bottom chord.

Cover plates made from A36 steel, 7 in. wide and 0.116 in. thick, were welded to the full length of the top chords of the main trusses to prevent concrete from passing through (see Fig. 4–26). Steel cover plates measuring 3½ in. by 7 in. by 0.116 in. thick were welded under each web knuckle for the same purpose. A 6¼ in. length of No. 8 reinforcing steel rod was welded to each end stiffener at both ends of the truss.

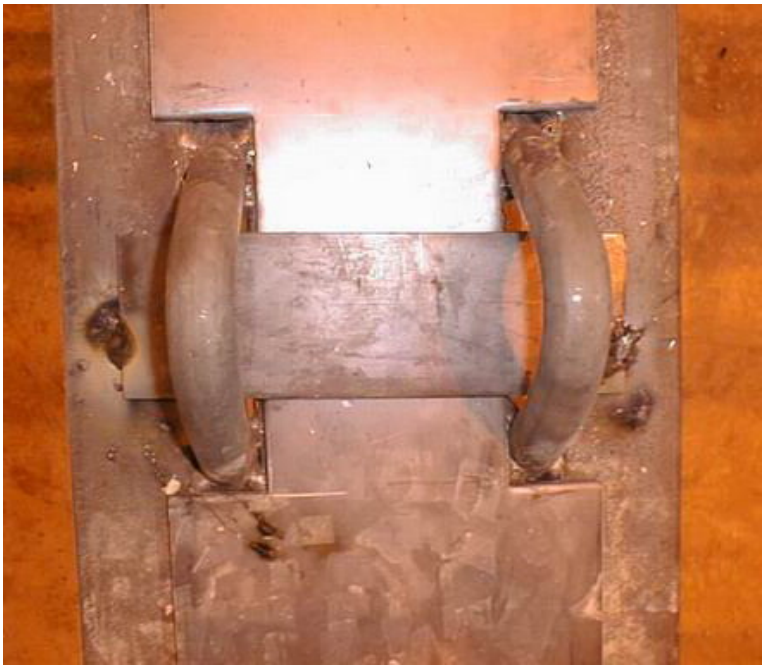

Source: NIST.

Figure 4–26. Cover plate detail.

The steel floor deck was placed on the assembly in 3 ft 1½ in. widths, 18 ft lengths, with the crests and valleys parallel to the main trusses (Fig. 4–27). At the interface of the steel deck edge and the upper chords of the main trusses, the deck was secured to the chords with ½ in. puddle welds spaced 6 in. o.c.

Source: NIST.

Figure 4–27. Steel floor deck placement.

Chairs, ¾ in. high measuring 60 in. long, with 12 legs per chair spaced 5 in. o.c. and 2¾ in. from each end, were placed and taped on alternating deck crests along the full 17 ft length of the assembly (see Fig. 4–28). Welded wire fabric, 10 in. by 4 in. W4.2/W4.3, supplied in 60 in. widths, was placed on the chairs, with the 4 in. dimension running the length of the assembly (north to south). The wire fabric was notched to fit around the knuckles and instrumentation sleeves. Adjacent sections of WWF were overlapped nominal 12 in. per ACI 318-63 (ACI 1963). At the overlaps, the mesh was secured with 18 gauge wire twist-ties spaced approximately 24 in. o.c.

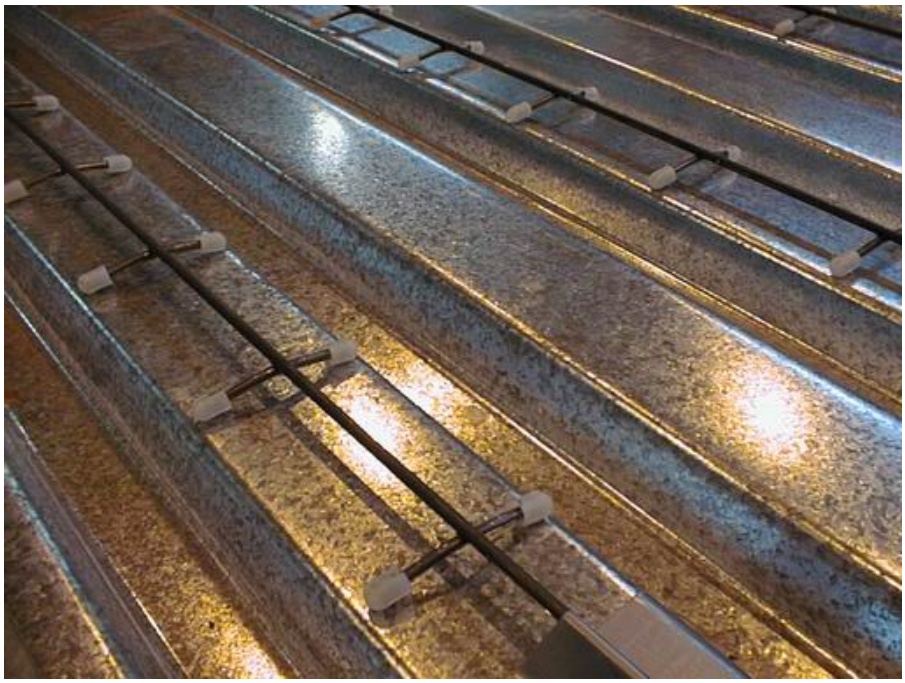

Source: NIST.

Figure 4–28. Chairs on steel deck.

No. 4 steel reinforcing bar was placed on top of the first layer of welded wire fabric, 3 in. from the east and west ends of the test frame. A second layer of welded wire fabric was installed with overlaps and fastened with wire ties as described above for the first layer. No. 5 steel reinforcing bar was placed on both sides of each bridging truss over the second layer of WWF (Fig. 4–29). The rebar was secured to the top layer of welded wire fabric with 18 gauge wire twist-ties approximately 24 in. o.c.

Source: NIST.

Figure 4–29. Welded wire fabric and rebar.

Concrete Placement

The ready-mixed concrete was poured to an average depth of 4 in. measured from the top plane of the 1½ in. deep steel deck. The concrete was finished to a flat, smooth surface with a wooden trowel. Details of the concrete for test Assemblies 3 and 4 are shown in Table 4–9.

Table 4–9. Details of concrete.

Assembly No.	Concrete Pour Date	Wet Unit Weight (lb/ft^3)	Slump(in.)	Air Content (%)	Water Added (gal)	Compressive Strength at 28 Days (psi)	Compressive Strength at 56 Days (psi)
3	2/20/2004	113.8	8	7	9	3370	3995
4	2/20/2004	111.6	7.5	8	0	2320	3220

Preparation of Trusses

Prior to the application of primer to the structural steel members, the steel was sand blasted to the Society of Protective Coatings SSPC-SP6 specification in accordance with the product specification sheet of the

primer. Following the sand blasting, the steel was primed with Sherwin Williams Type B50NV11 at an approximate dry film thickness of 0.003 in.

Instrumentation

Prior to the concrete pour, four 18-gauge Type K thermocouples were attached to the steel form deck at each of three locations, near the center point and quarter points in the north-south direction. At each location, a thermocouple was placed in the valley, sidewall, crest, and next adjacent valley of the deck. Refer to Appendix F for locations of deck thermocouples.

After priming of the structural steel, 18-gauge Type K thermocouples were installed on each main and bridging truss. Eight thermocouples were peened into the steel at each cross section, located approximately at the quarter and center points on each main truss (see Appendix F for exact locations). Additionally, ten thermocouples were located at the intersections of each main and bridging truss. In total, 44 thermocouples were installed on each main truss, for a total of 88 thermocouples.

On each bridging truss, four thermocouples were peened into the steel at each cross section located at the center of the truss, at the intersections of the main and bridging trusses, and approximately halfway between the main truss and the end of the bridging truss (see Appendix F for exact locations). In total, 16 thermocouples were installed on each bridging truss, for a total of 32 thermocouples.

Strain gauges were attached on the bottom chord of the main trusses to measure strain as each test assembly was loaded. A pre-wired 350 Ω resistance strain gauge was placed, per the manufacturer's instructions, on the top surface and bottom surface of the bottom chord angle. The strain gauges were symmetrically opposed, at the mid-length of the bottom chord of each main truss. Each pair of gauges would later be wired to a half-bridge amplifier prior to loading of the assembly. Strain gauge readings were used to confirm proper loading of the assemblies, and the circuitry was removed prior to the start of the tests.

Application of Sprayed Fire-Resistive Materials

The application of the sprayed fire resistive materials was conducted by the manufacturer of the sprayed fire resistive material under a sub-contract to UL and observed by representatives of UL and NIST. On the underside of the assembly, the BLAZE-SHIELD DC/F was applied to the main and bridging trusses in multiple coats. For Test Assembly No. 3, which had ¾ in. thick SFRM on the steel trusses, no attempt was made to control overspray on the metal deck. For Test Assembly No. 4, with ½ in. thick SFRM, the metal deck was masked to prevent overspray.

Thickness and density measurements were taken in accordance with ASTM E 605 (ASTM 2000a). The average SFRM thicknesses on the trusses are shown in Table 4–10 for Test Assembly No. 3.

Table 4–10. SFRM Thickness measurements on Assembly No. 3.

Location	Nominal Thickness (in.)	Final Average Measured Thickness (in.)	Basis: No. of Thickness Measurements
East Main Truss	3/4	0.766	128
West Main Truss	3/4	0.763	128
North Bridging Truss	3/8	0.397	66
South Bridging Truss	3/8	0.387	66

The air dry density of the BLAZE-SHIELD DC/F sprayed fire resistive material was determined using twelve 12 in. by 12 in. samples of various thickness. The air dry densities are shown in Table 4–11 for Assembly No. 3. The average air dry density was found to be 20.49 pcf.

Table 4–11. Air dry density of spray applied fire resistive material on Assembly No. 3.

Material Type	Nominal Thickness (in.)	Measured Density (pcf)
DC/F	3/4	21.23
DC/F	3/4	19.76
DC/F	3/4	20.49

SFRM thickness measurements for Test Assembly No. 4 are given in Table 4–12. Air dry density of spray applied fire resistive material on Assembly No. 4 is given in Table 4–13, and the average air dry density was found to be 19.10 pcf. There was no sprayed fire resistive material applied to the bridging trusses on Assembly No. 4

Table 4–12. Thickness measurements on Assembly No. 4.

Location	Nominal Thickness (in.)	Final Average Measured Thickness (in.)	Basis: No. of Thickness Measurements
East Main Truss	1/2	0.514	128
West Main Truss	1/2	0.512	128

Table 4–13. Air dry density of spray applied fire resistive material on Assembly No. 4.

Material Type	Nominal Thickness (in.)	Measured Density (pcf)
DC/F	1/2	20.57
DC/F	1/2	18.90
DC/F	1/2	17.83

4.4 LOADING OF TEST ASSEMBLIES

The test assemblies were loaded in accordance with ASTM E 119. That is, a superimposed load was applied "to simulate a maximum load condition," which was determined as "the maximum load condition allowed under nationally recognized structural design criteria" (ASTM 2000). In this section, the analysis for this maximum load condition is given, and the procedures used to apply the computed loads are explained for both the full- and reduced-scale test assemblies. The structural analysis and test loading procedure was performed by Wiss Janey Elstner & Associates (WJE) under sub-contract to Underwriters Laboratories Inc.

4.4.1 Loading of 35 Ft Assemblies

Table 4–14 details the demand-to-capacity ratio of key elements of the trusses for Assembly Nos. 1 and 2. Demand-to-capacity ratios for the original C32-T5 truss design are given in the last column and were computed from Laclede design calculation sheets (see Appendix G). The compression web diagonal at the vertical strut was the limiting member with a demand-to-capacity ratio of 1.01. The calculations indicate that the maximum load condition is achieved with a uniform load of 104 psf.

The test load was applied to the assembly in a sequence that generally proceeded outwards from the center. Concrete blocks, which had first been weighed, were placed between the truss lines starting at the midspan and working symmetrically to the east and west ends of the test assembly. Next, empty water tubs were placed symmetrically outward to the ends of the span, alternating between the truss lines from the midspan. Finally, concrete blocks were placed between the water tubs and the longitudinal edges of the assembly, again alternating along both edges, working symmetrically from midspan to the ends of the assembly. The last set of blocks was placed as close as practicable to the water tubs to minimize bending of the cantilevered deck slab. The water tubs were filled from the center of the assembly outward toward the edges. The amount of water was calculated for each location to insure the same load was applied at each section since the weight of the concrete blocks varied slightly.

Table 4–14. Summary of analysis for maximum load condition for 35 ft assembly.

	Test Assembly	35 Foot		Laclede WTC Design
	Load Case	Uniform Load		Calculations
	Uniform Self Weight Construction Load (psf)	48		46
	Additional Superimposed Load (psf)	104*		108
Top Chord Panel Point	Truss Member	Member DCR		Member DCR
A: Short End of truss				
B: Bearing point				
	#5: End Diagonal at short end	0.50		0.58**
	#2A: Vertical at short end	0.85		NA***
C: At vertical strut				0.97
	#4:Compression web diagonal	1.01		
D:				NA***
	#4A: Compression web diagonal	0.76		
E: At bridging Truss				
F:				
G: Near midspan				
H:				
J: At bridging Truss				
	#3A: Compression web diagonal	0.65		NA***
K:				
	#3: Compression web diagonal	0.97		0.99
L: At vertical strut				
	#2: Vertical at long end	0.87		1.00
	#1: End diagonal at long end	0.88		0.99
M: Bearing point				
N: Long end of truss				
Bottom Chord	#7: Tension chord near midspan	0.63		0.81

* Includes 2 psf representing weight of SFRM

** The original Laclede calculations use a slope factor of 1.90, whereas the slope factor for Member 5 should be on the order of 1.45 according to truss geometry. The original Laclede DCR of 0.76 has been adjusted as follows:0.76*1.45/1.90=0.58

*** Not Applicable: The Laclede calculations do not include a design for this member.

4.4.2 Loading of 17 Ft Assemblies

Table 4–15 details the demand-to-capacity ratio of key elements of the trusses for Assembly Nos. 3 and 4. The long end web diagonal at the vertical strut was the limiting member with a demand-to-capacity ratio of 1.00. The calculations indicate that the maximum load condition is achieved with a uniform load of 293 psf and concentrated loads applied at the truss panel points averaging to 86 psf.

Table 4–15. Summary of analysis for maximum load condition for 17 ft assembly.

Test Assembly		17 Foot			Laclede WTC Design
Load Case		Uniform Load	Concentrated Load		Calculations
Uniform Self Weight Construction Load (psf)		48	48		46
Additional Superimposed Load (psf)		293	86*		108
Top Chord Panel Point	Truss Member	Member DCR	Load(lbs)	Member DCR	Member DCR
A: Short End of truss					
B: Bearing point					
	#5: End Diagonal at short end	0.58		0.58	0.58**
	#2A: Vertical at short end	0.60		0.60	NA***
C: At vertical strut			4100		0.97
	#4:Compression web diagonal	0.46		0.38	
D:			0		NA***
	#4A: Compression web diagonal	0.34		0.34	
E: At bridging Truss			4100		
F:			0		
G: Near midspan			4100		
H:			0		
J: At bridging Truss			3800		
	#3A: Compression web diagonal	0.35		0.37	NA***
K:			0		
	#3: Compression web diagonal	0.53		0.43	0.99
L: At vertical strut			3800		
	#2: Vertical at long end	0.55		0.55	1.00
	#1: End diagonal at long end	1.00		1.00	0.99
M: Bearing point					
N: Long end of truss					
Bottom Chord	#7: Tension chord near midspan	0.70		0.64	0.81

*Includes 2 psf representing weight of SFRM

** The original Laclede calculations use a slope factor of 1.90, whereas the slope factor for Member 5 should be on the order of 1.45 according to truss geometry. The original Laclede DCR of 0.76 has been adjusted as follows:0.76*1.45/1.90=0.58

*** Not Applicable: The Laclede calculations do not include a design for this member.

The test load was applied to the assembly in a sequence that generally proceeded outward from the center of the deck. First, empty water tubs were placed between the truss lines, starting at midspan and working symmetrically to the ends of the span. Next concrete blocks were placed, working both truss lines simultaneously from mid-span symmetrically outward to the ends of the span. After the concrete blocks were placed, the water tubs were filled to calculated depth. The hydraulic ram loads were applied last using four electric driven hydraulic pumps with pressure gauges.

4.5 INSTRUMENTATION

Prior to testing of each assembly, instrumentation was installed to measure vertical deflections of the unexposed surface and the bottom chords of the main trusses. Instruments were also added to characterize the furnace environment as well as to measure temperature on the unexposed surface of the test assembly.

4.5.1 Deflection Instrumentation

The deflection on the unexposed surface was measured using nine transducers, located approximately at the center and quarter points in the long span direction and center and quarter points in the short span direction. The locations of the deflection transducers are given in Appendix D for the 35 ft test assemblies and Appendix F for the 17 ft test assemblies.

The deflection of the bottom chord of the main truss was measured at six locations by means of thin round bars, welded at one end to the bottom chord of the main truss and protruding through sleeves in the concrete slab. Displacement transducers were attached to the rods and to a stationary frame. To account for any thermal expansion of the round bar, 20 gauge Inconel thermocouples were attached approximately at the midpoint of the depth of the main truss to measure temperatures throughout the duration of the test.

4.5.2 Furnace Thermocouples

The furnace temperature at UL's Toronto fire test facility was measured by means of twenty-four, 16 gauge Type K thermocouples, sheathed in Inconel pipe symmetrically located in the furnace chamber. Sixteen furnace thermocouples, made from similar materials, were used at UL's Northbrook furnace. In addition to the furnace thermocouples required by the ASTM E 119 Standard, Wickstrom plate thermocouples and aspirated thermocouples were located at the level of the bottom chord of the main truss and at the valley of the steel form deck. The locations of the aspirated and plate thermocouples are given in Appendix D for the 35 ft test assemblies and Appendix F for the 17 ft test assemblies..

The Wickstrom plate thermocouples were made of a stainless steel sheet, on which an 18 gauge Type K, Inconel sheathed thermocouple was attached to the back side. An insulating pad, approximately 4 in. by 4 in. by ¼ in. was placed over the thermocouple. The non-insulated stainless steel side was positioned horizontally, receiving a furnace exposure similar to the tested assembly.

The double walled aspirated thermocouple consisted of two concentric stainless steel tubes, approximately 0.435 in. ID and 0.1875 in. ID, with an 18 gauge Type K thermocouple bead located approximately ⅛ in. inside the end of the center tube. Furnace gasses were drawn through both tubes past

the thermocouple bead using a Venturi air amplifier. At room temperature, air was measured at approximately 30 ft/s at the tip of the concentric tubes.

4.5.3 Radiometers

To also characterize the furnace environment, both Gardon Gauge and Schmidt-Boelter types of heat flux gauges were mounted to the assembly (see Fig. 4–30). Table 4–16 summarizes the type of radiometer gauges used for each test.

Table 4–16. Summary of radiometers.

Assembly No.	Location	Type: Gardon Gauge (GG) or Schmidt-Boelter (SB)
1	Bottom Chord	SB
	Deck	SB
2	Bottom Chord	– *
	Deck	– *
3	Bottom Chord	GG
	Deck	GG
4	Bottom Chord	GG
	Deck	SB

* Due to significant damage to the heat flux probes during testing of Assembly 1, no heat flux probes were available at the time when testing Assembly 2

Similar to the plate and aspirated thermocouples, the heat flux probes were placed at two locations in the furnace: at the bottom chord level of the main trusses and at the valley of the steel deck. The locations of the sensors are given in Appendix D for the 35 ft test assemblies and Appendix F for the 17 ft test assemblies.

The Schmidt-Boelter radiometers were 1 in. diameter, 4 ft long, water and air cooled furnace probes with Schmidt-Boelter heat flux sensors. The sensors were capable of measuring heat fluxes up to 25 BTU/ft^2-s (284 kW/m^2) and had a view angle of 150 degrees. An air purged zinc selenide window was attached to the sensor, blocking convective flux, thus the sensor measured only radiative flux.

Gardon Gauge sensors, used in two of the tests, were 1 in. diameter, internally water cooled, with the wire leads air purged and insulated. The sensors were capable of measuring heat fluxes up to 15 BTU/ft^2-s (170 kW/m^2) and had a view angle of 180 degrees. No window was attached to the sensor, thus total (radiative and convective) heat flux was measured.

Source: NIST.

Figure 4–30. View of radiometer and plate thermocouple.

Chapter 5
TEST RESULTS

The tests described herein were conducted in accordance with the Standard Test Methods for Fire Tests of Building Construction and Materials, ASTM E 119-2000a. Results of all four fire resistance tests are presented in this chapter; each test is discussed separately.

5.1 FIRE TEST OF ASSEMBLY NO. 1

The fire resistance test of Assembly No. 1 was conducted at Underwriter Laboratories Toronto, Canada facility (ULC) on August 7, 2004 under the observation of representatives of Underwriters Laboratories Inc., Underwriters' Laboratories of Canada, and NIST.

The relative humidity of the concrete slab met the requirements prescribed in ASTM E 119.

5.1.1 Test Observations

Table 5–1 presents observations that were recorded during the conduct of the test. All dimensions given are approximate since they were estimated by making observations through furnace viewports. Times were generally recorded to the nearest minute. The term "report" is used to describe a loud sound, which might be described as a "bang" or a "pop." Because these loud reports were often accompanied by observed movement of the metal deck and the dislodging of SFRM, it is asumed that the reports signaled explosive spalling of the concrete. It was not possible to ascertain the exact location and extent of any spalling.

Table 5–1. Test observations – Assembly 1.

Test Time, Min	Exposed (E) or Unexposed (U) Surface	Observations
0.5	E	There was slight discoloration of the SFRM on the west side of the assembly.
7	E	The east center steel deck seam began to separate.
11	E	The deck buckled west of the west bridging truss running in a north-south direction.
14	E	The east steel deck seam had a 3/8 in. opening
16		The vertical member on the east bridging truss where it intersects the south main truss had buckled.
17	E/U	Reports heard with the SFRM deck over-spray falling simultaneously.
19	E/U	Same observation as 17 minutes.
19	E	The east steel deck seam had a 5/8 in. opening
20	E/U	Same observation as 17 minutes and could visually see deck moving simultaneously.
21	E/U	Reports becoming louder and more frequent.
21	U	The concrete was spalling near the west end of the assembly.

Test Time, Min	Exposed (E) or Unexposed (U) Surface	Observations
23	E/U	Same observation as 21 minutes.
24	U	The concrete continued to spall.
25	E	Visual deflection was observed in the bottom chords of the bridging trusses.
26	E/U	Same observation as 21 minutes.
26	E	Visual deflection was observed on the deck spans between the trusses. Separation was observed in the deck seam above the center deck support angle.
27	E	The southeast metal deck seams began to separate.
29	E	Visual deflection was observed in the center deck support angle. The SFRM was turning brown in color.
33	E	The bridging trusses became more deformed. The vertical member on the west bridging truss where it intersects the south main truss was heavily deformed.
37	E	The deflection in the center deck support angle was more pronounced.
38	E/U	Reports heard.
44	E	The vertical members on all of the bridging trusses where they intersect the main trusses were deformed.
45	E	Large reports heard.
49	E/U	A loud report was heard near the center of assembly and a visible drop was observed.
53	E	One-half of the SFRM on the vertical member noted at 33 min. had fallen.
60	E	No additional fall off of SFRM on the bridging trusses.
63	E	The steel deck between west bridging truss and the deck support angle was 1/2 in. from the furnace thermocouple. The long diagonal web member on the south main truss was slightly bent.
68	E/U	Large report heard.
78	E/U	Large report heard.
78	E	The bottom chord of the north main truss, approximately 36 in. west of the assembly centerline, was deformed.
87	E	A 10 in. long piece of SFRM on the inner most angle of the lower chord on the north truss, 36 in west of the north-south centerline of the assembly fell.
88	E	A 7 to 10 in. long piece of SFRM on the inner most angle of the lower chord on the north truss, 36 in east of the north-south centerline of the assembly fell.
90	E	Additional SFRM at the area described at 87 min. peeling away but has not fallen.
92	E	A 12 in. long piece of SFRM on the inner most angle of the lower chord on the south truss, 36 in west of the north-south centerline of the assembly fell.
93	E	The area of fall off described at 87 min. had expanded to the three inner most angles.
109	E/U	A very large report was heard.
111	E/U	A very large report was heard.
116	E/U	Gas off, furnace fire extinguished.

5.1.2 Data

All data shown in the following figures (Figures 5–1 through 5–12) are unedited for the entire duration of the test. However, not all data shown is reliable due to the limitations of the instrumentation, i.e. thermocouples, radiometers, and calorimeters. Data may become unreliable past the rating period when structural events occur that can dislodge the instrumentation. Also, protective insulation of the thermocouple wire may burn away, and the individual wires can make contact with themselves and/or neighboring wires rendering the data unreliable. Appendix H gives a listing of the times that various instrumentation failed to give reliable data, as determined by UL.

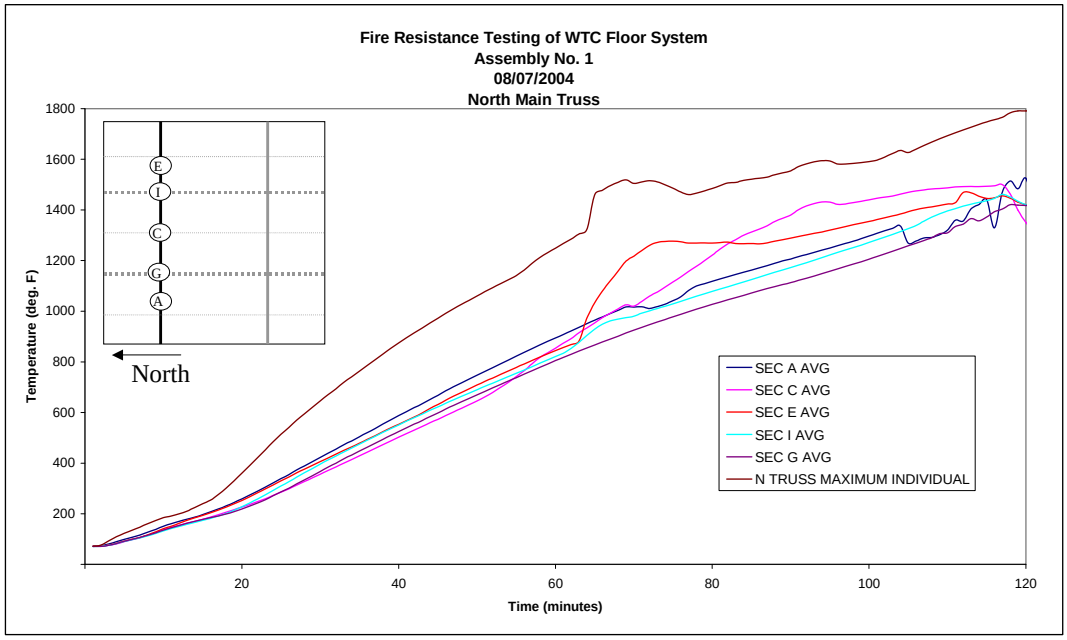

Figure 5–1. Assembly No. 1 – average and maximum individual temperatures on north main truss.

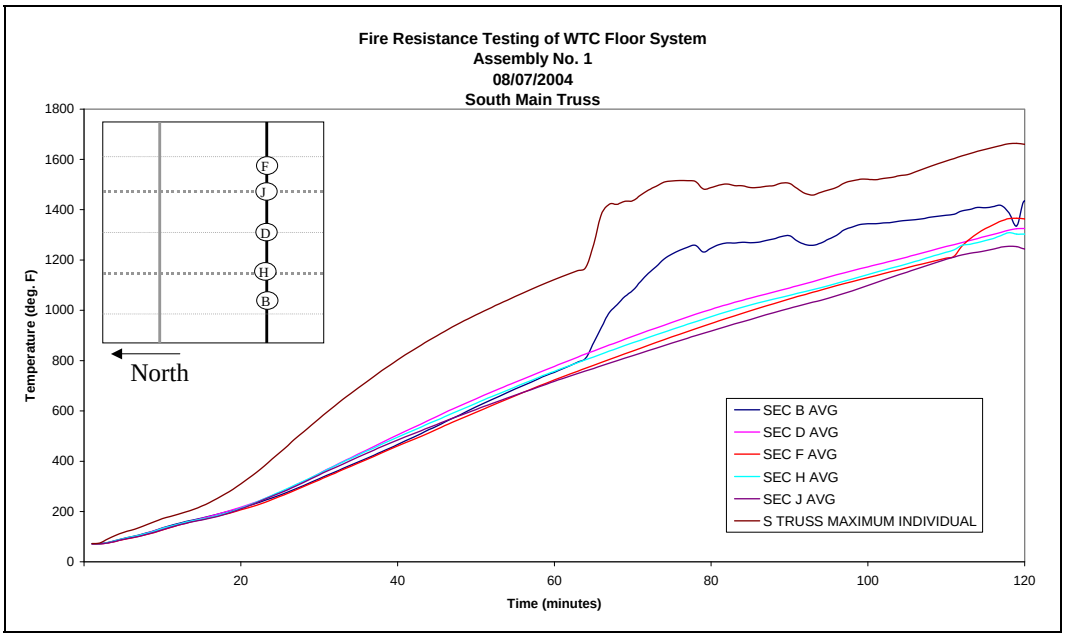

Figure 5–2. Assembly No. 1 – average and maximum individual temperatures on south main truss.

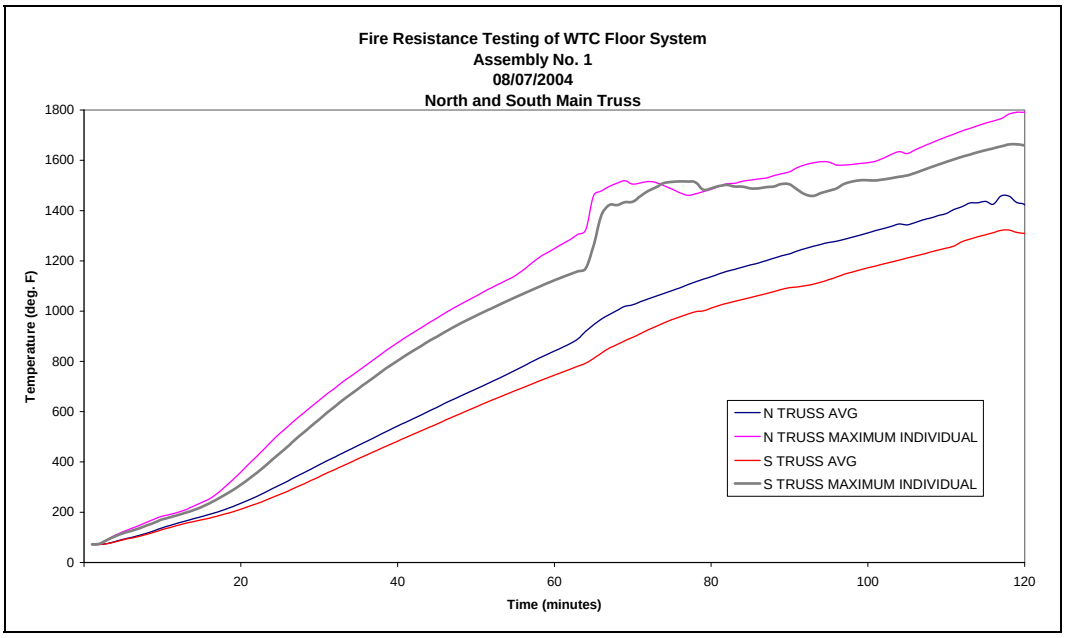

Figure 5–3. Assembly No. 1 – overall average and maximum individual temperatures on north and south main trusses.

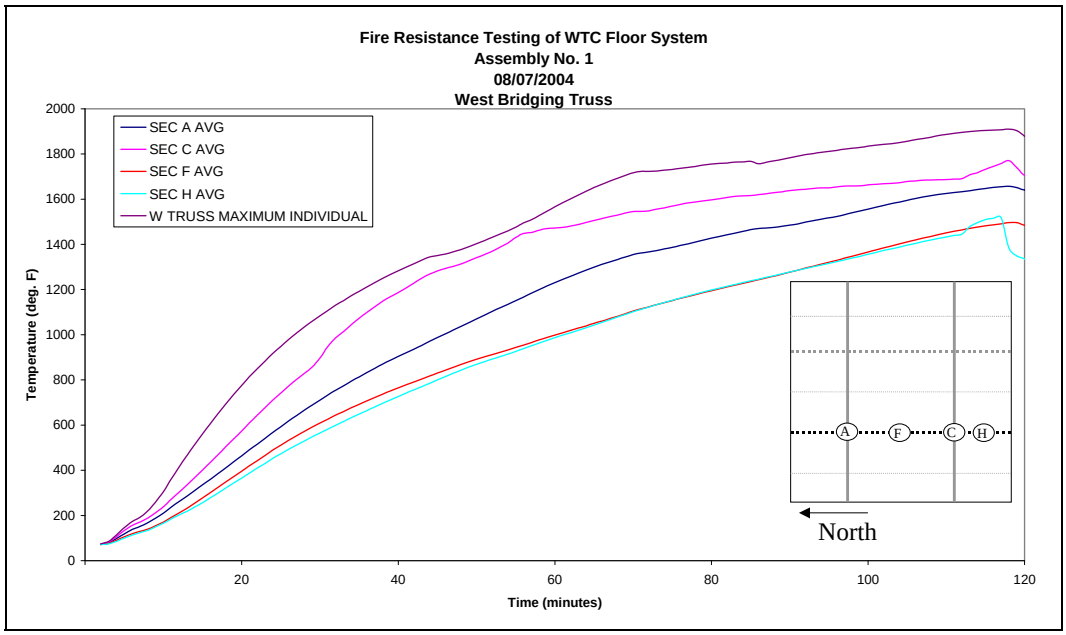

Figure 5–4. Assembly No. 1 – average and maximum individual temperatures on west bridging truss.

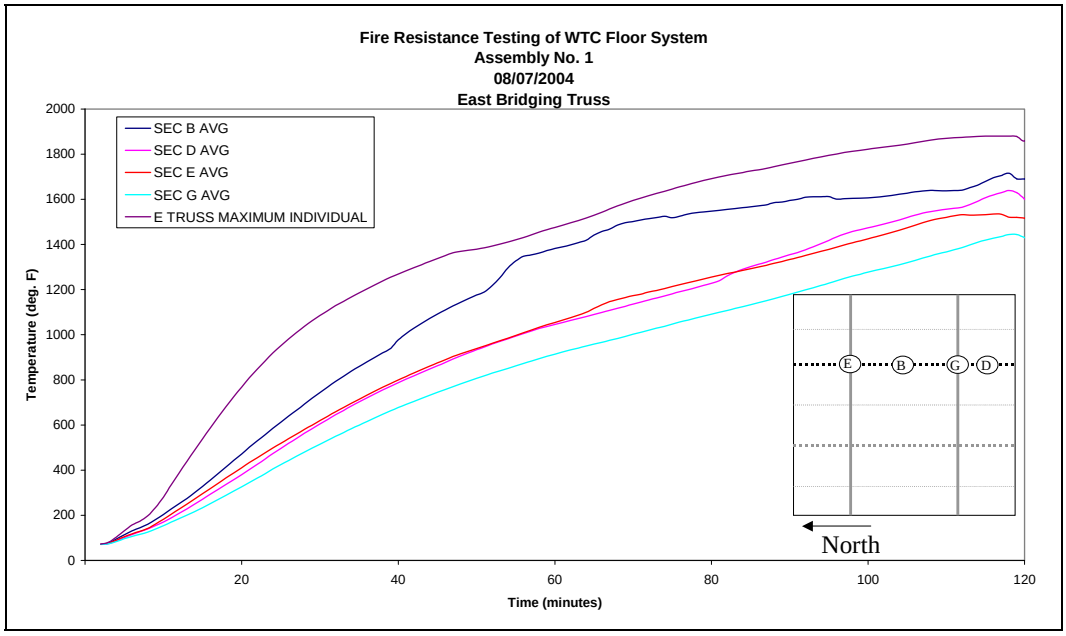

Figure 5–5. Assembly No. 1 – average and maximum individual temperatures on east bridging truss.

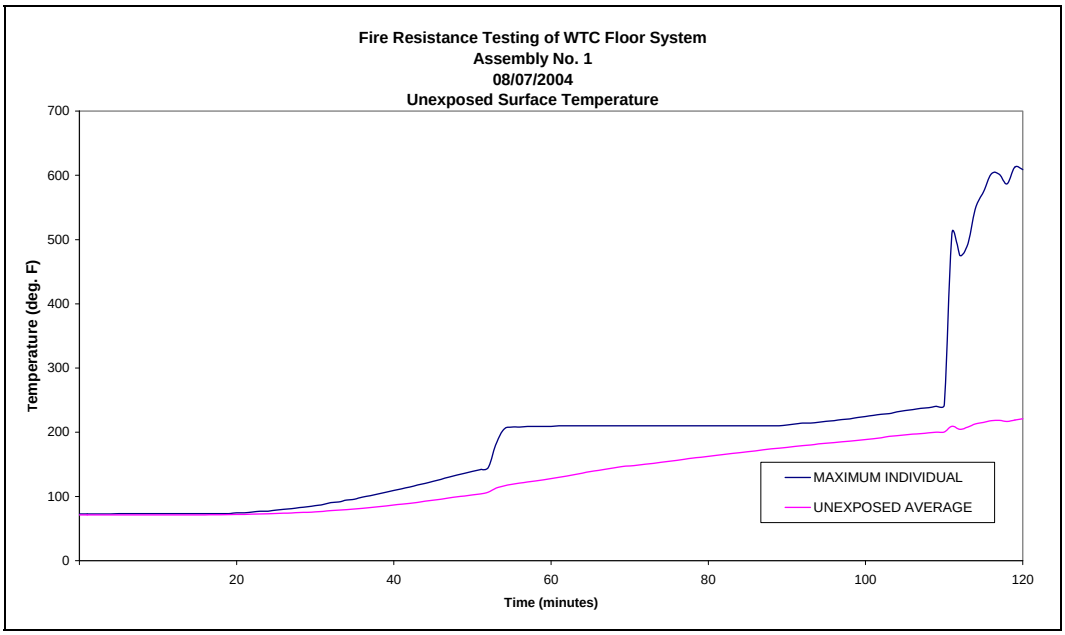

Figure 5–6. Assembly No. 1 – average and maximum individual temperatures on unexposed surface.

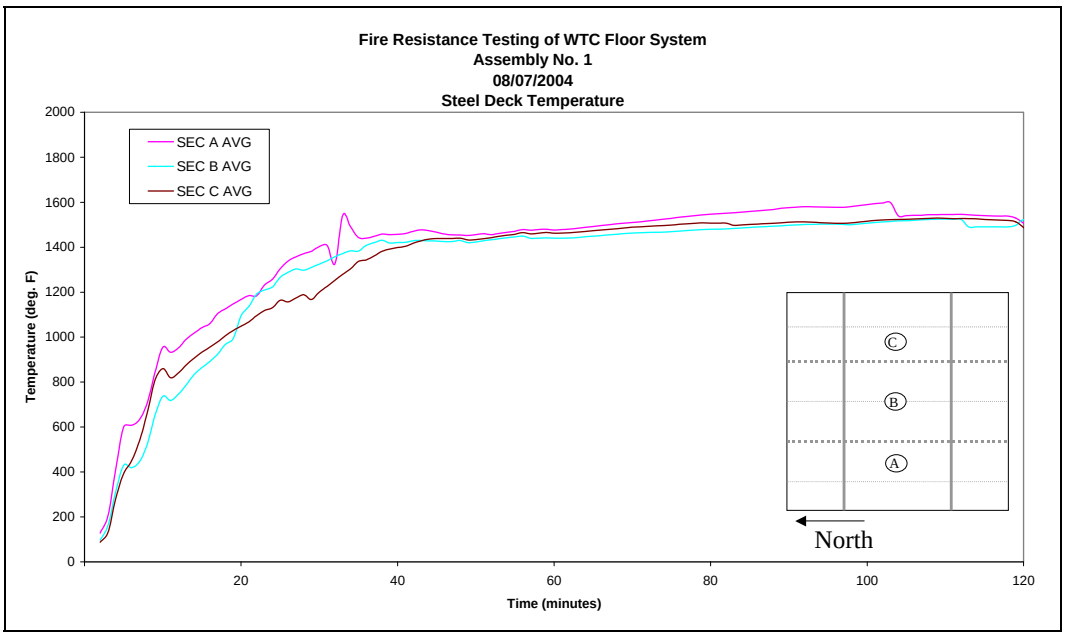

Figure 5–7. Assembly No. 1 – average temperatures on steel deck.

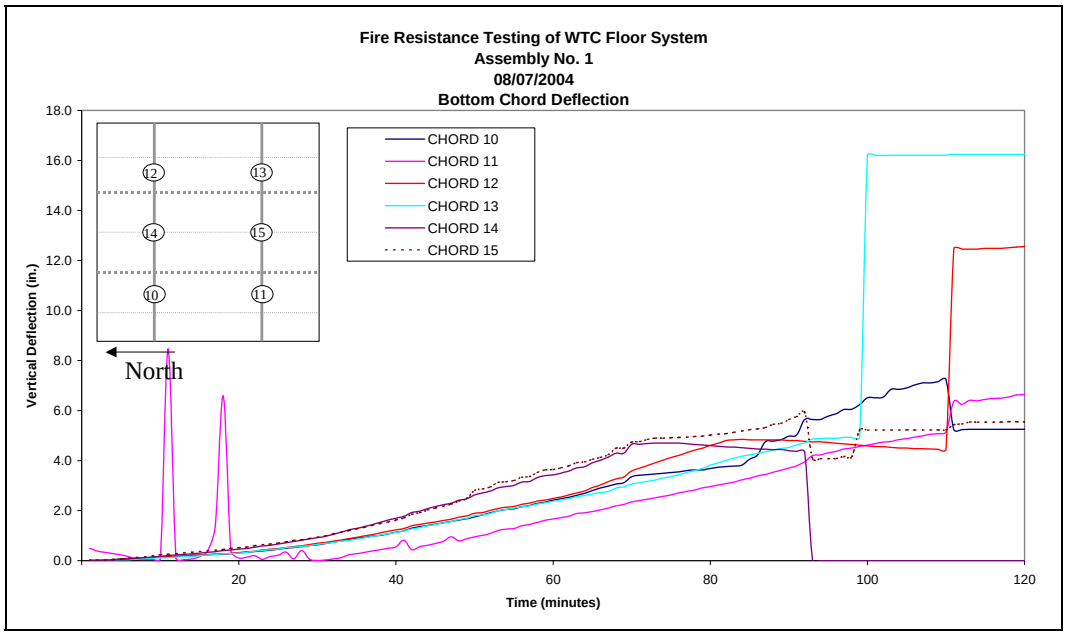

Figure 5–8. Assembly No. 1 – bottom chord deflection measurements.

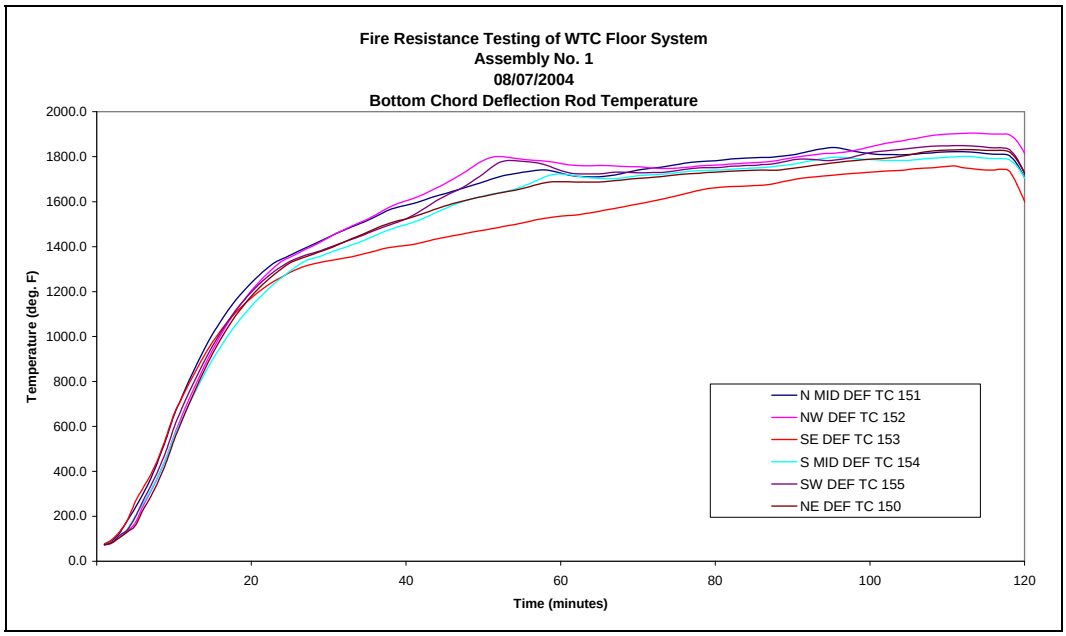

Figure 5–9. Assembly No. 1 – temperatures of bottom chord deflection rods.

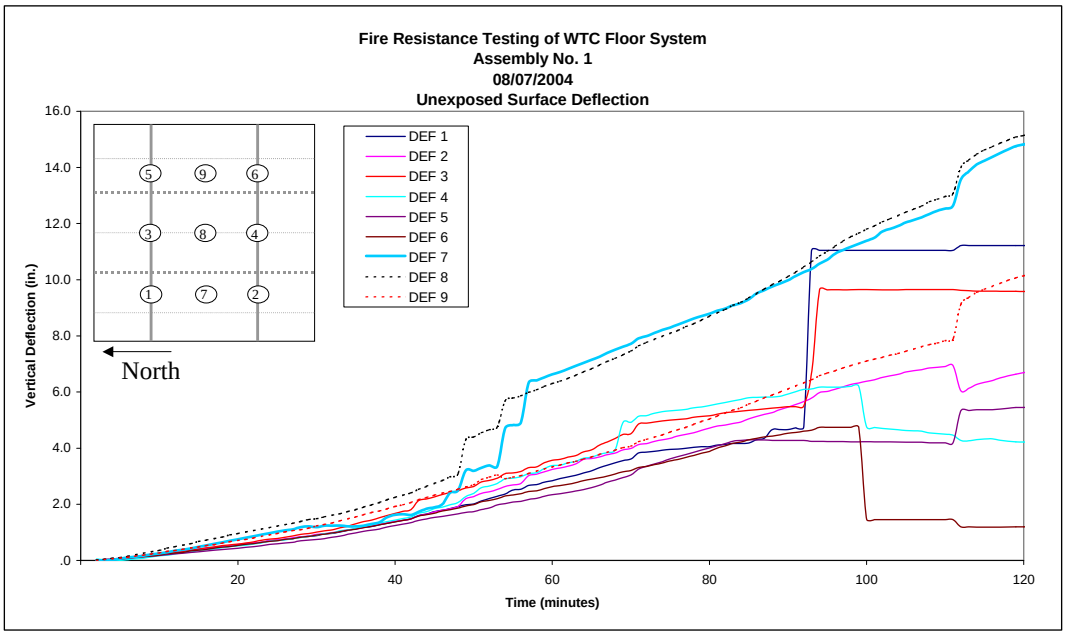

Figure 5–10. Assembly No. 1 – unexposed surface deflection measurements.

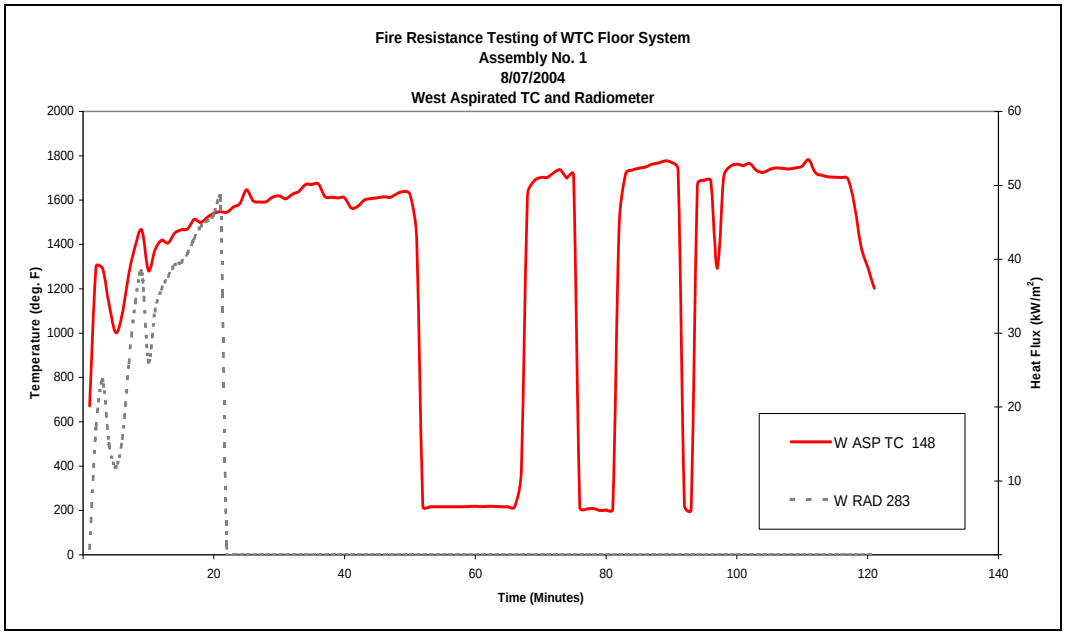

Figure 5–11. Assembly No. 1 – additional instrumentation through west opening.

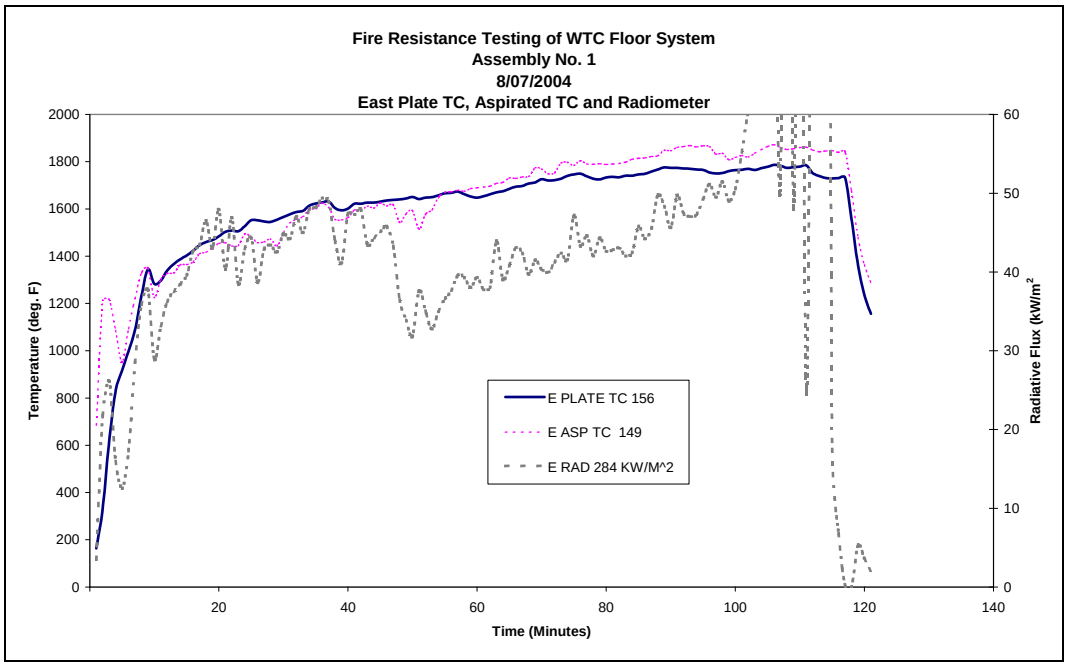

Figure 5–12. Assembly No. 1 – additional instrumentation through east opening.

5.1.3 Post-Test Observations

Figure 5–13 shows the unexposed surface of the assembly after all loading equipment had been removed (view looking east). Numbers shown at the centerline and quarter points are vertical deflections after cooling. All other numbers are reference dimensions as measured from the edge of the slab.
Figures 5–14 through 5–19 are additional views of the top of the specimen, showing the cracked and spalled concrete, and of the underside, showing bulging of the metal deck and deformations of the steel trusses after the test specimen had cooled and had been removed from the furnace. To confirm the spalling of the bottom side of the concrete slab and to quantify the depth of spalling, sections of the slab were cut using a diamond concrete wet saw (see Fig. 5–20). The depth of the delamination spalling varied but was on the order of 2 in. as seen in Fig. 5–21.

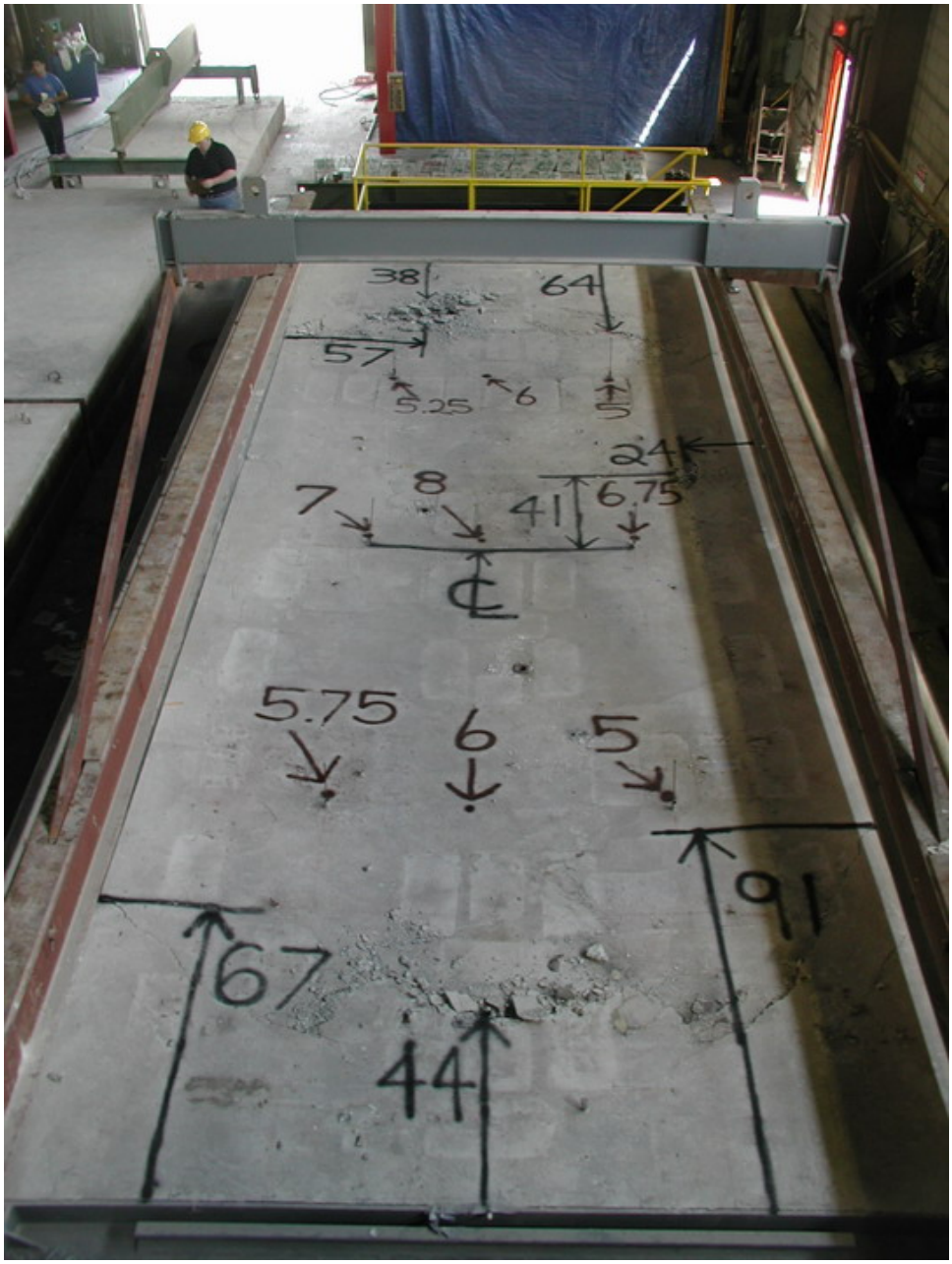

Source: NIST.

Figure 5–13. Unexposed surface of Assembly No. 1 after loading equipment was removed.

Source: NIST.

Figure 5–14. Detail of spalling concrete at west end of Assembly No. 1.

Source: NIST.

Figure 5–15. Detail of spalling concrete at east end of Assembly No. 1.

Source: NIST.

Figure 5–16. Close-up of spalling concrete at east end of Assembly No. 1.

Source: NIST.

Figure 5–17. View looking east of the exposed side of Assembly No. 1– south main truss seen at right side.

Source: NIST.

Figure 5–18. Intersection of north main and east bridging trusses on Assembly No. 1.

Source: NIST.

Figure 5–19. View of core-end diagonal strut of south main truss on Assembly No. 1.

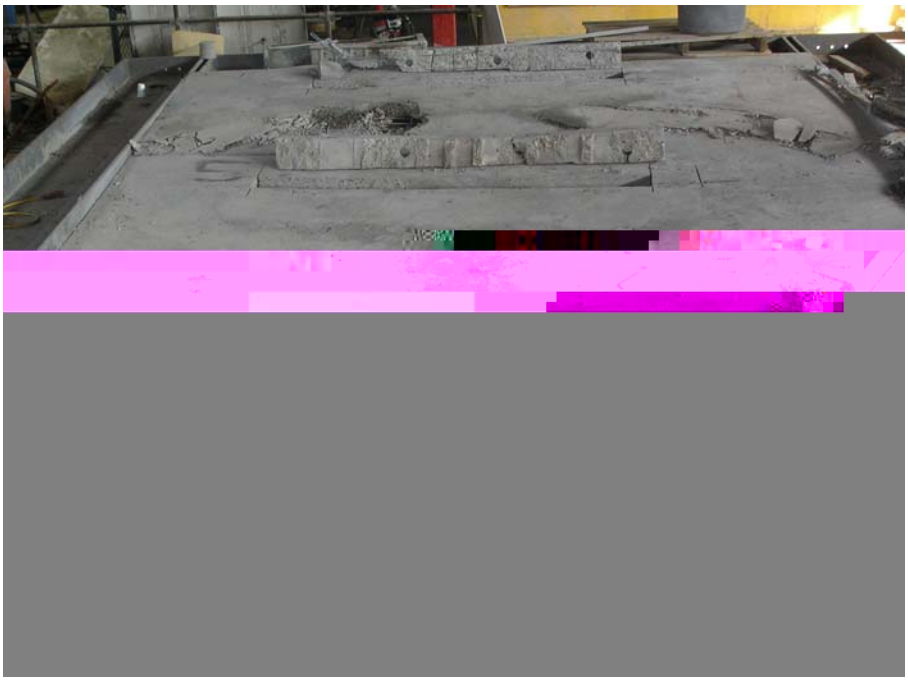

Source: NIST.

Figure 5–20. Sections cut through concrete slab to confirm delamination spalling.

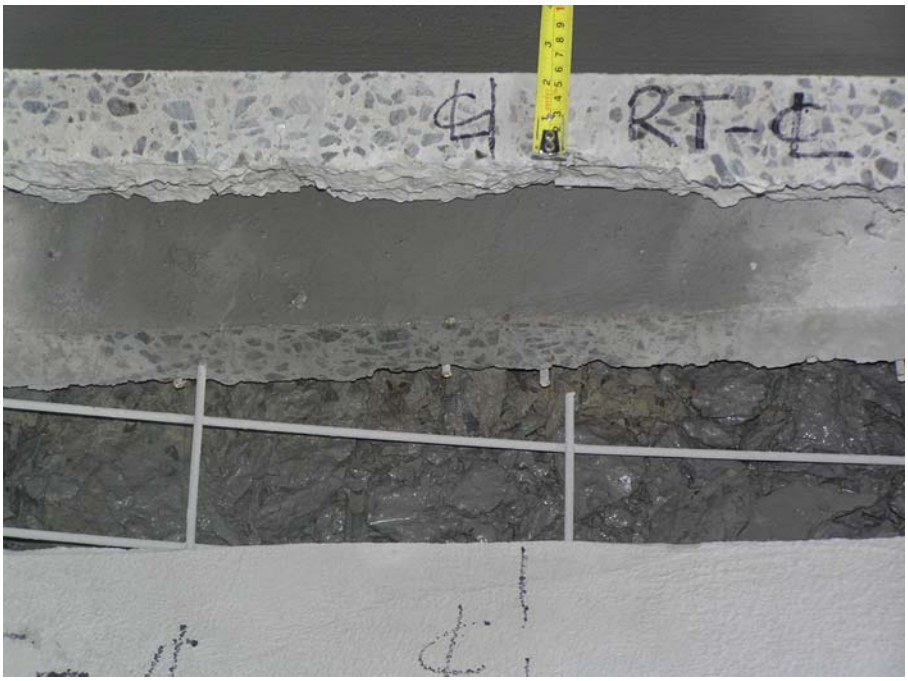

Source: NIST.

Figure 5–21. Measurement of depth of delamination spalling.

5.2 FIRE TEST OF ASSEMBLY NO. 2

The fire resistance test of Assembly No. 2 was conducted at the (ULC) facility on August 11, 2004 under the observation of representatives of Underwriters Laboratories Inc., Underwriters Laboratories of Canada, NIST, and a member of the National Construction Safety Team Advisory Committee.

The relative humidity of the concrete slab met the requirements prescribed in ASTM E 119.

5.2.1 Test Observations

Table 5–2 presents observations that were recorded during the conduct of the test. All dimensions given are approximate since they were estimated by making observations through furnace viewports. Times were generally recorded to the nearest one half minute. The term "report" is used to describe a loud sound, which might be described as a "bang" or a "pop." Because these loud reports were often accompanied by observed movement of the metal deck and the dislodging of SFRM, it is assumed that the reports signaled explosive spalling of the concrete. It was not possible to ascertain the exact location and extent of any spalling. The reports heard during the test of Assembly No. 2 were generally not as loud as those heard during the test of Assembly No. 1.

Table 5–2. Test observations – Assembly No. 2.

Test Time, min	Exposed (E) or Unexposed (U) Surface	Observations
1	E & U	Faint reports heard.
1	E	The SFRM began to discolor.
3	E & U	A faint report was heard.
3	E	SFRM over-spray on the steel deck began to fall when report was heard.
5	E	The steel deck began to deform east of the east bridging truss and west of the west bridging truss.
10	E	A buckle in the steel deck was observed. The buckle was located 1 ft west of the center deck support angle and ran in a north–south direction. The length of the buckle spanned from the north truss to the south truss.
12	E	The steel deck was bowing downward between the bridging trusses and the center deck support angle.
15	E & U	A faint report was heard.
16	E & U	A faint report was heard.
18	E & U	Reports became slightly louder. There were three reports in a row, approx. 5 seconds apart.
22	E & U	Reports continued and became slightly louder.
22	E	There was minor fall off of the SFRM on the top angle of the east bridging truss. The fall off was partial and did not result in bare steel being exposed.
23	E & U	Reports continued.
30	E & U	Reports continued.
34	E	Visual deformation of the top angles of bridging trusses was observed.
36	E	There was no visual buckling of the bridging truss web members.

Test Time, min	Exposed (E) or Unexposed (U) Surface	Observations
40	E & U	A large report was heard. Pronounced deck bow at the area noted in the 10 min. observation.
43	E	The web members of the bridging trusses began to deform.
46	E	The steel deck continued to deform.
48	E & U	Reports continued.
48.5	E & U	A report was heard.
50	E & U	A report was heard.
51.5	E & U	A report was heard.
53	E	Visual deflection of the center deck support angle was observed.
54	E & U	A report was heard.
56.5	E & U	A report was heard.
57	E & U	Three reports in a row were heard, approx. 1 second apart.
59.5	E & U	A report was heard.
60	E	All SFRM remained in place besides what was previously noted on the bridging trusses.
61	E & U	A report was heard.
63	E & U	A report was heard.
64	E & U	A report was heard.
72	E & U	A report was heard.
74	E	2 1/2 ft length of SFRM fell from the top angle of the east bridging truss.
75	E & U	A report was heard.
78	E & U	A report was heard.
84	E & U	A report was heard.
108	E	All SFRM remained on the main trusses.
120	E	All SFRM remained on the main trusses.
130	E & U	All observations were terminated due to safety precautions.
146	E & U	Gas off, fire test terminated.

5.2.2 Data

All data shown in the following figures (Figures 5–22 through 5–33) are unedited for the entire duration of the test. However, not all of the data shown is reliable due to the limitations of the instrumentation, i.e. thermocouples, radiometers, and calorimeters. Data may become unreliable past the rating period when structural events occur that can dislodge the instrumentation. Also, protective insulation of the thermocouple wire may burn away, and the individual wires make contact with themselves and/or neighboring wires rendering the data unreliable. Appendix H gives a listing of the times that instrumentation failed to give reliable data, as determined by UL.

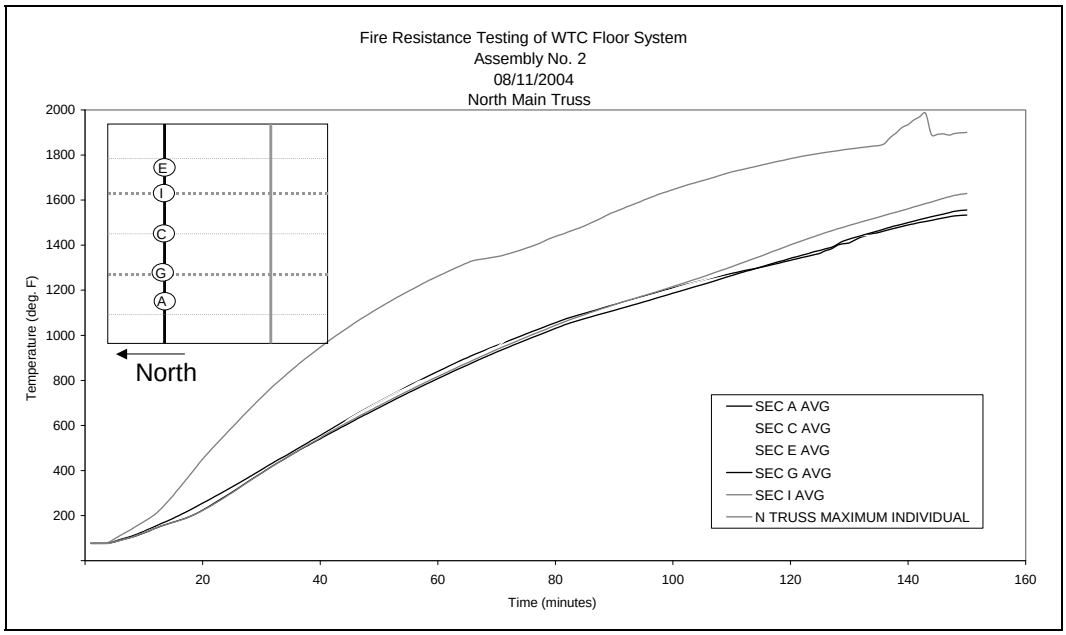

Figure 5–22. Assembly No. 2 – average and maximum individual temperatures on north main truss.

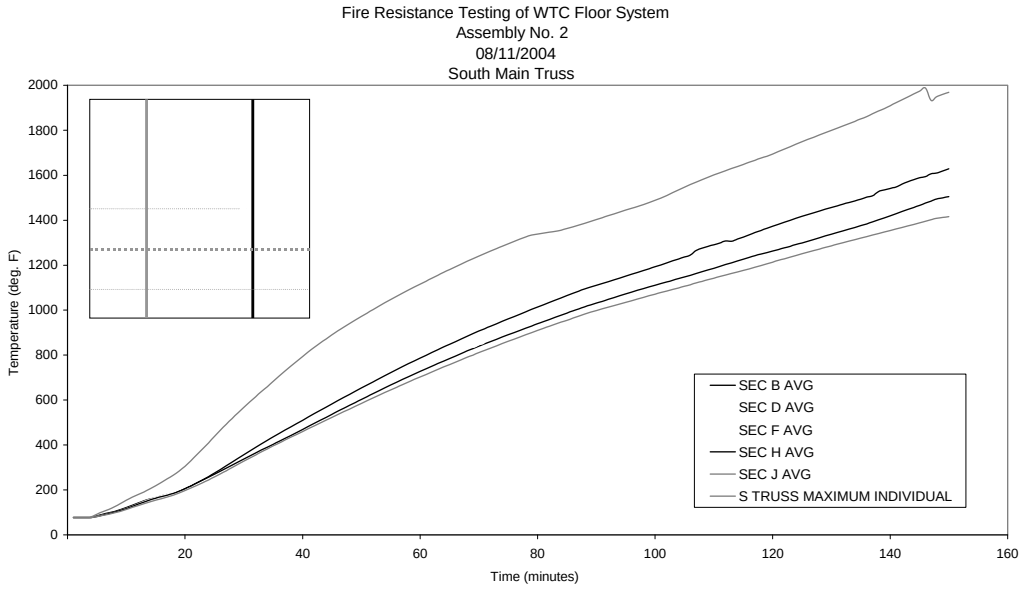

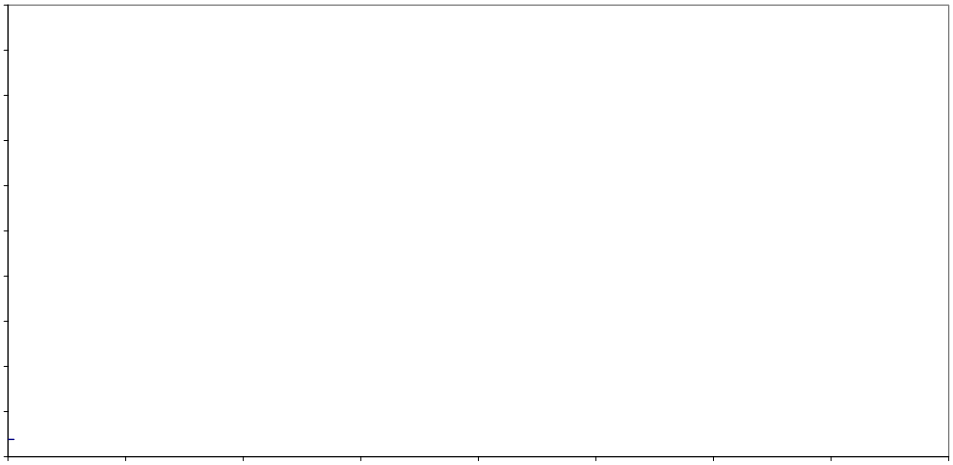

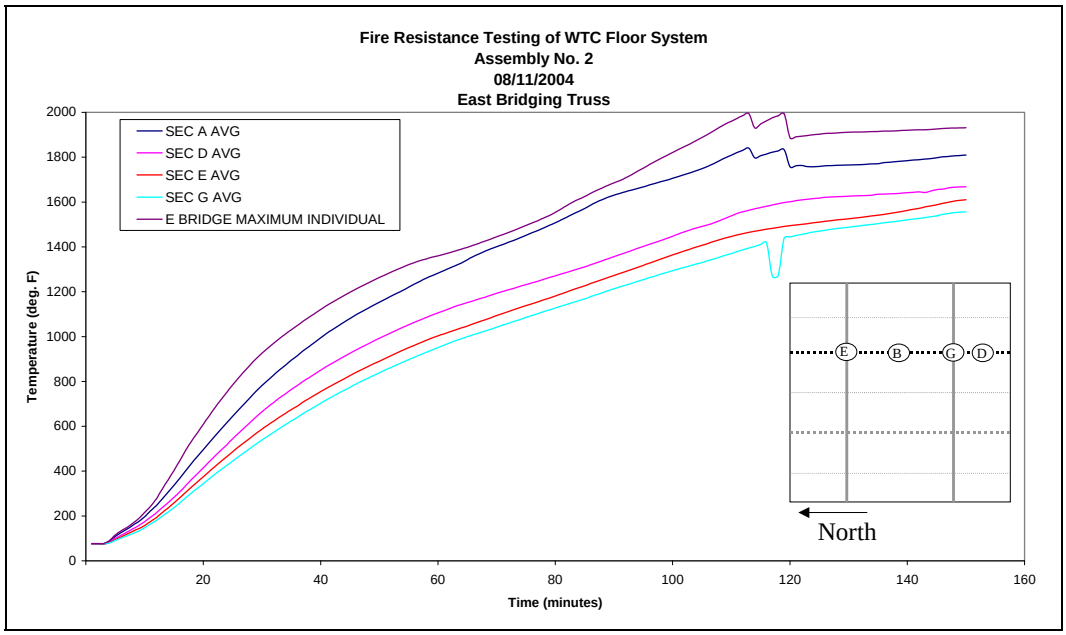

Figure 5–26. Assembly No. 2 – average and maximum individual temperatures on east bridging truss.

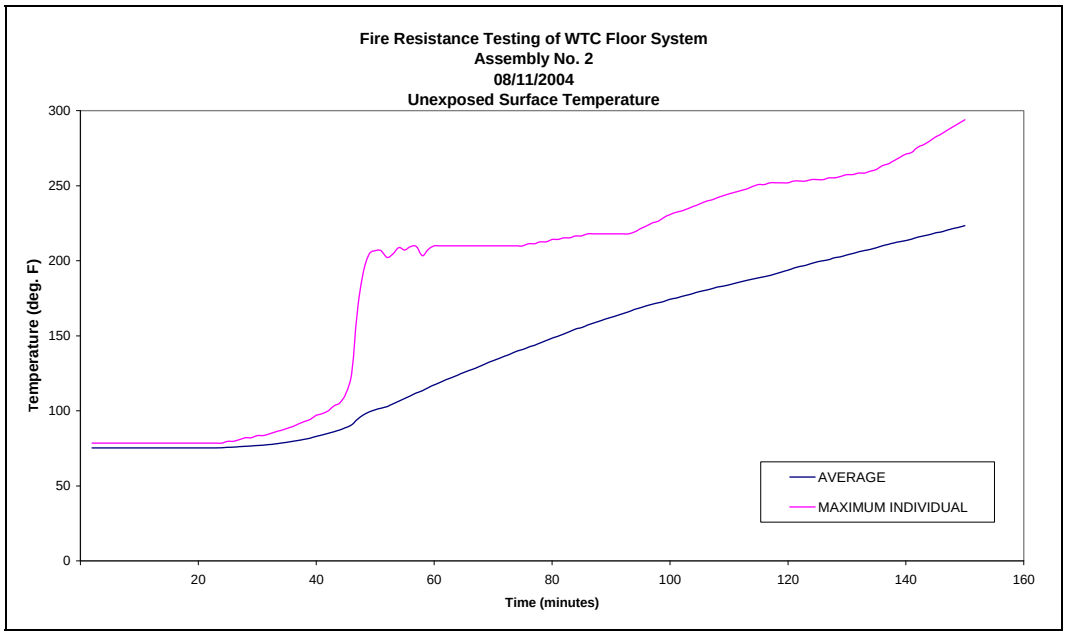

Figure 5–27. Assembly No. 2 – average and maximum individual temperatures on unexposed surface.

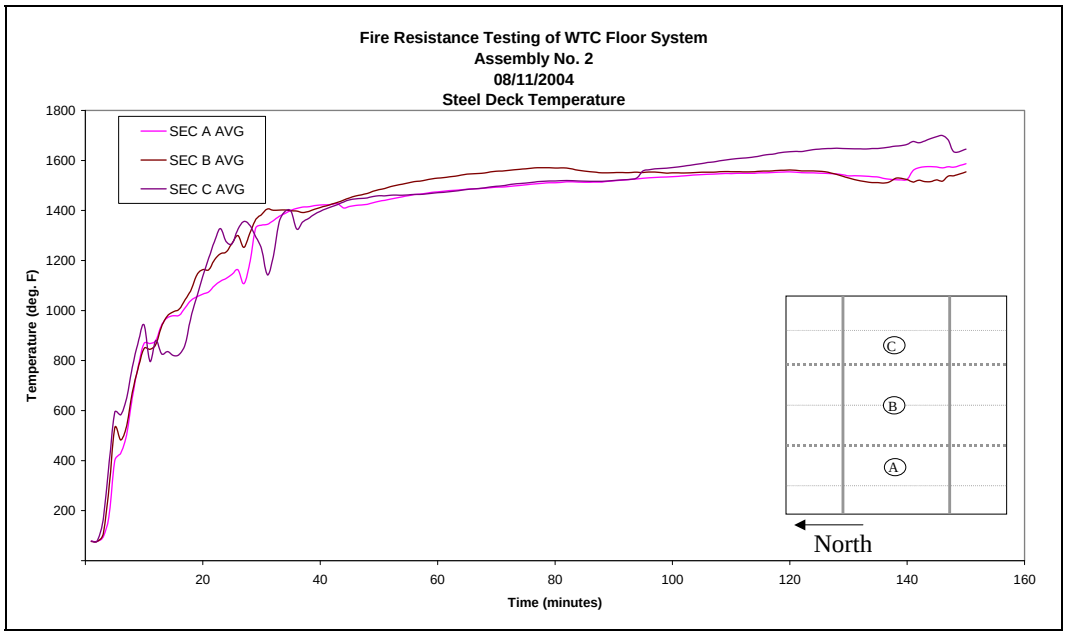

Figure 5–28. Assembly No. 2 – average temperatures on steel deck.

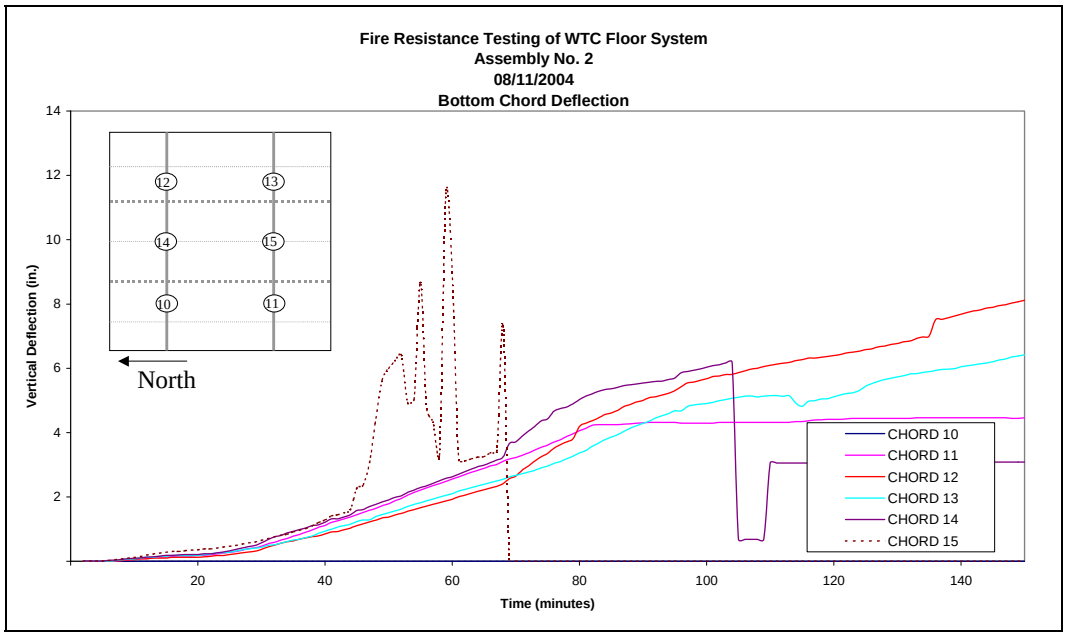

Figure 5–29. Assembly No. 2 – bottom chord deflection measurements.

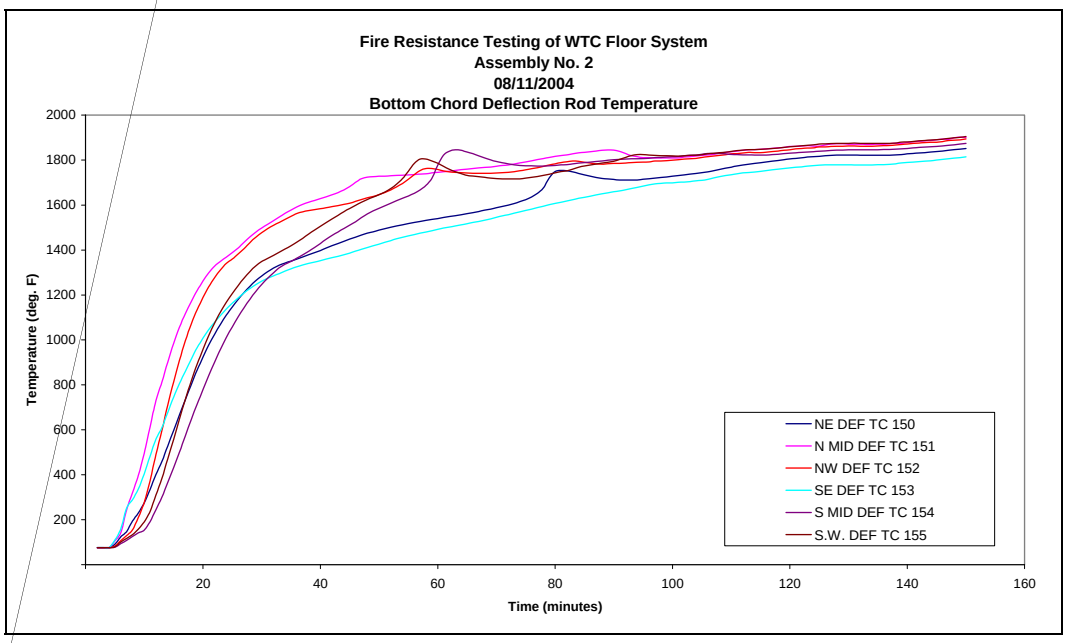

Figure 5–30. Assembly No. 2 – temperatures of bottom chord deflection rods.

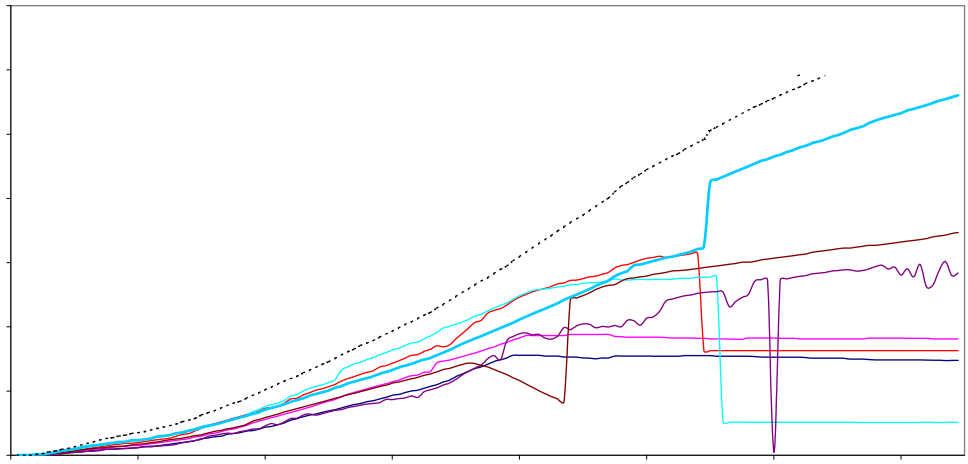

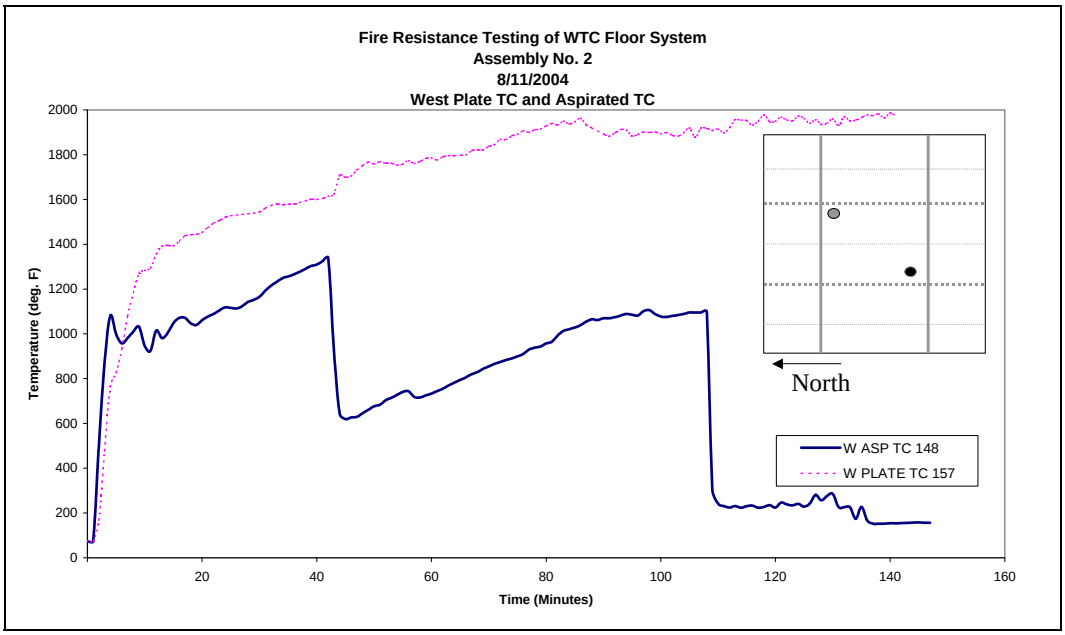

Figure 5–32. Assembly No. 2 – additional instrumentation through west opening.

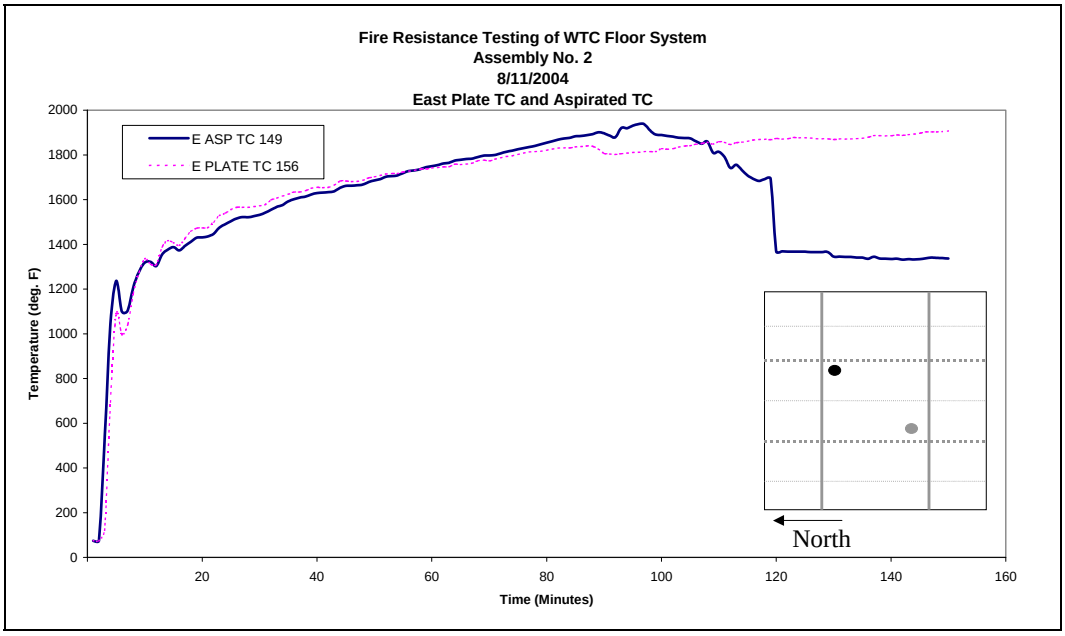

Figure 5–33. Assembly No. 2 – additional instrumentation through east opening.

5.2.3 Post-Test Observations.

Figure 5–34 shows the unexposed side of the floor assembly after all loading equipment had been removed (view looking east). Numbers shown at the centerline and quarter points are vertical deflections after cooling. All other numbers are reference dimensions as measured from the edge of the slab. Figures 5–35 through 5–37 are views of the underside of the test specimen, showing bulging of the metal deck, and deformations of the steel trusses after the test specimen had cooled and had been removed from the furnace.

Source: NIST.

Figure 5–34. Unexposed surface of Assembly No. 2 after loading equipment was removed.

Source: NIST.

Figure 5–35. View of core end diagonal strut of north main truss on Assembly No. 2.

Source: NIST.

Figure 5–36. South main truss of Assembly No. 2, looking east.

Source: NIST.

Figure 5–37. Intersection of east bridging and north main trusses on Assembly No. 2.

5.3 FIRE TEST OF ASSEMBLY NO. 3

The fire resistance test of Assembly No. 3 was conducted at the (ULC) facility on August 19, 2004 under the observation of representatives of Underwriters Laboratories Inc. and NIST.

The relative humidity of the concrete slab met the requirements prescribed in ASTM E 119.

5.3.1 Test Observations

Table 5–3 presents observations that were recorded during the conduct of the tests. All dimensions given are approximate since they were estimated by making observations through furnace viewports. Times were generally recorded to the nearest one half minute. The term “report” is used to describe a loud sound, which might be described as a “bang” or a “pop.” Because these loud reports were often accompanied by observed movement of the metal deck and the dislodging of SFRM, it is assumed that the reports signaled explosive spalling of the concrete. It was not possible to ascertain the exact location and extent of any spalling.

Table 5–3. Test observations – Assembly No. 3.

Test Time, Min	Exposed (E) or Unexposed (U) Surface	Observations
5.5	E	The steel desk buckled between the south bridging truss and the center deck support angle.
8.5	E	The steel desk buckled between the north bridging truss and the center deck support angle.
10	E	The north-south deck seam between the south bridging truss and the center deck support angle began to separate.
14	E & U	A minor report was hear and there was visual movement of the steel deck with fall off of the SFRM over-spray from the steel deck.
16	E	The center deck support angle was twisting.
19	E & U	A minor report was heard.
21	E & U	A minor report was heard.
22.5	E & U	Two minor reports were heard.
23	E & U	A minor report was heard.
26	E & U	Three minor reports were heard.
27	E & U	Two minor reports were heard.
27	E	The steel deck was becoming more deformed.
31	E	The third and forth vertical members north of center deck support angle on the west main truss appear to be bent.
35	E & U	A minor report was heard.
55	U	Hairline cracks were observed in the concrete surface on both the east and west sides of the assembly between the edges of the loading blocks and the edges of the test frame. The cracks were more pronounced on the east side.
59	E	Visual deflection was observed on the bridging trusses.
60	E	All of the SFRM remained in place.
82	E & U	A very large report was heard. Pieces on concrete fell to the lower part of the furnace area were observations were being observed.
90	E	All of the SFRM remained in place.
92	E	The bridging trusses were becoming deformed. The deformation of the steel deck was more pronounced.
120	E	No significant changes were observed besides increased deflection. All of the SFRM remained in place.
140	E	The SFRM had separated from the bottom chord of the north bridging truss but had not fallen to the furnace floor.
152	E	The area, approximately 8 inched long, described in the 140 min. observation fell to the furnace floor.
180	E	No significant changes were observed besides increased deflection.
210	E	No significant changes were observed.
210.75	E & U	Furnace fire extinguished. Fire test terminated.

5.3.2 Data

All data shown in the following figures (Figures 5–38 through 5–49) are unedited for the entire duration of the test. However, not all data shown is reliable due to the limitations of the instrumentation, i.e. thermocouples, radiometers, and calorimeters. Data may become unreliable past the rating period when structural events occur that can dislodge the instrumentation. Also, protective insulation of the thermocouple wire may burn away, and the individual wires make contact with themselves and/or neighboring wires rendering the data unreliable. Appendix H gives a listing of the times that instrumentation failed to give reliable data, as determined by UL.

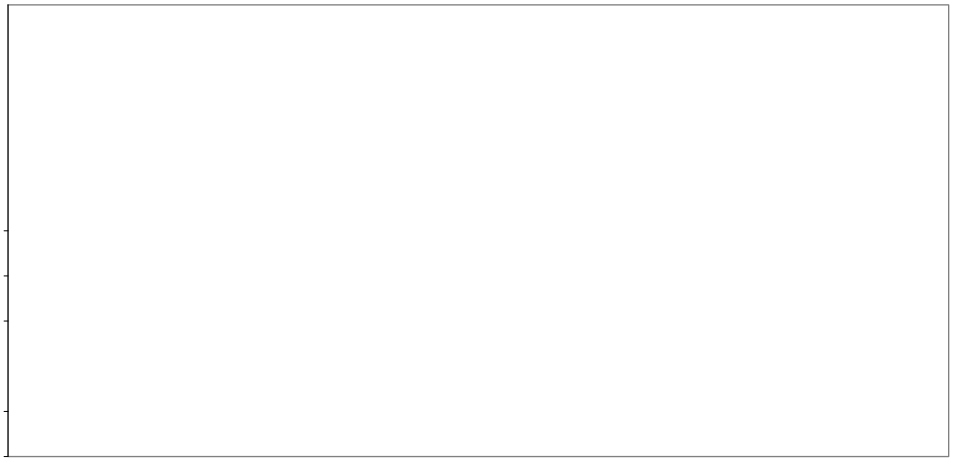

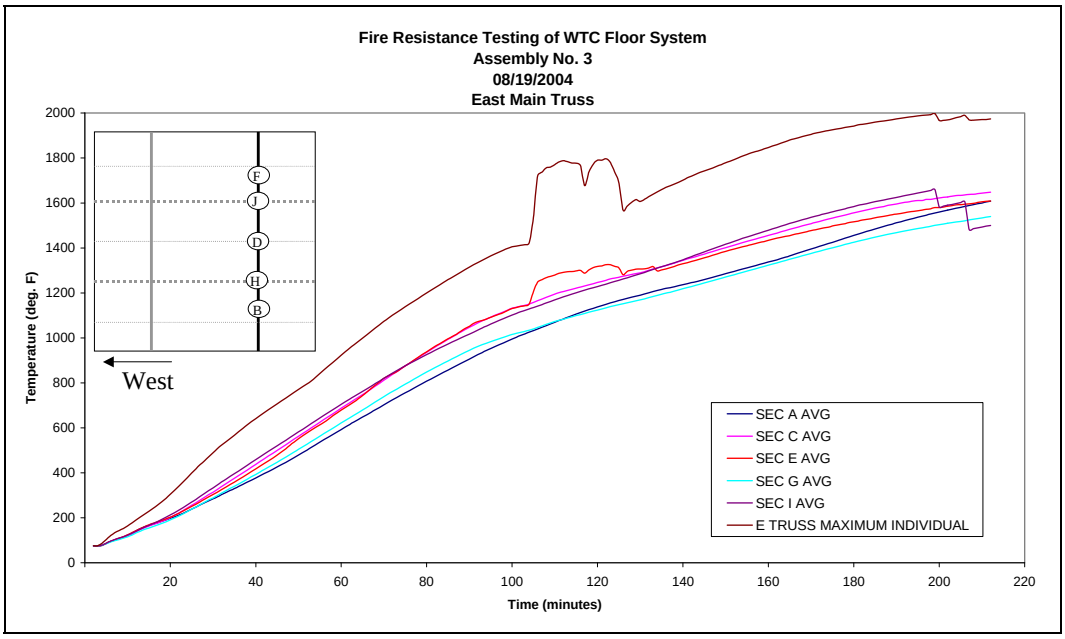

Figure 5–39. Assembly No. 3 – average and maximum individual temperatures on east main truss.

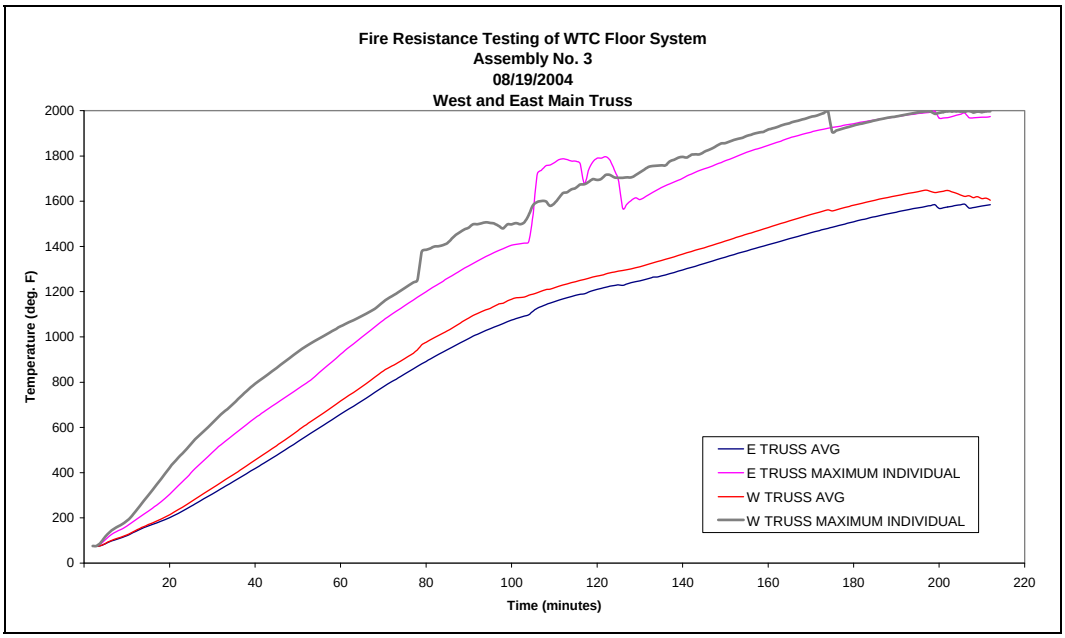

Figure 5–40. Assembly No. 3 – overall average and maximum individual temperatures on west and east main trusses.

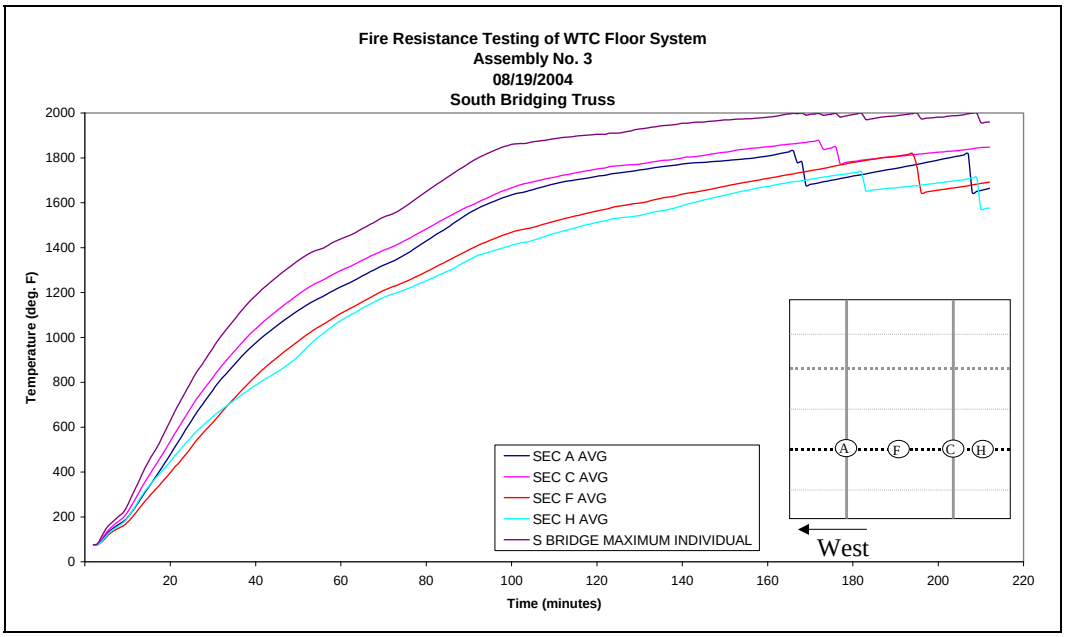

Figure 5–41. Assembly No. 3 – average and maximum individual temperatures on south bridging truss.

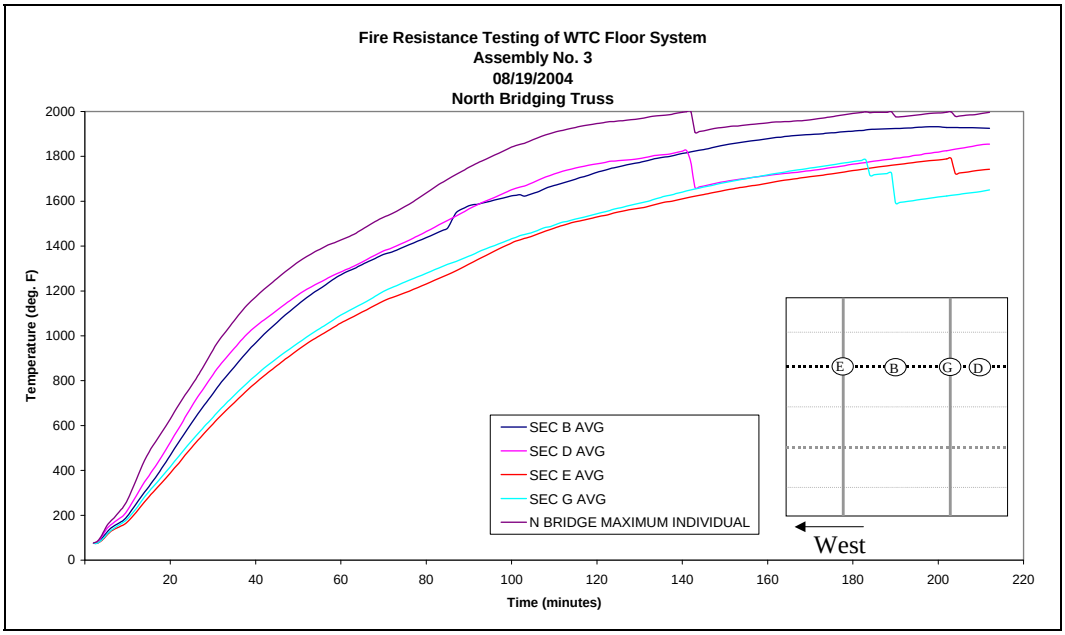

Figure 5–42. Assembly No. 3 – average and maximum individual temperatures on north bridging truss.

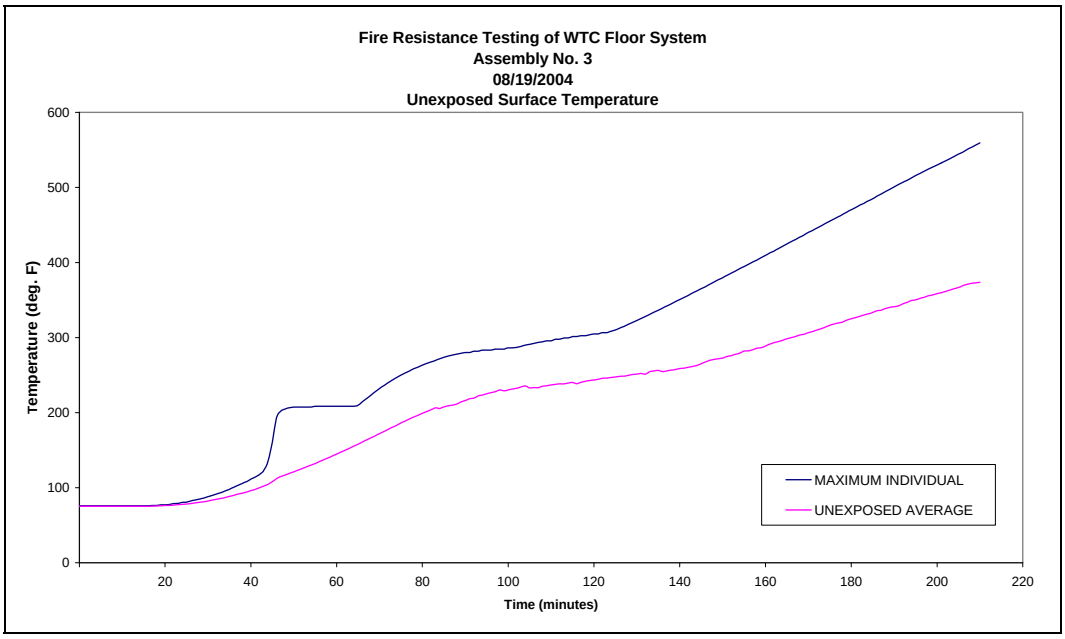

Figure 5–43. Assembly No. 3 – average and maximum individual temperatures on unexposed surface.

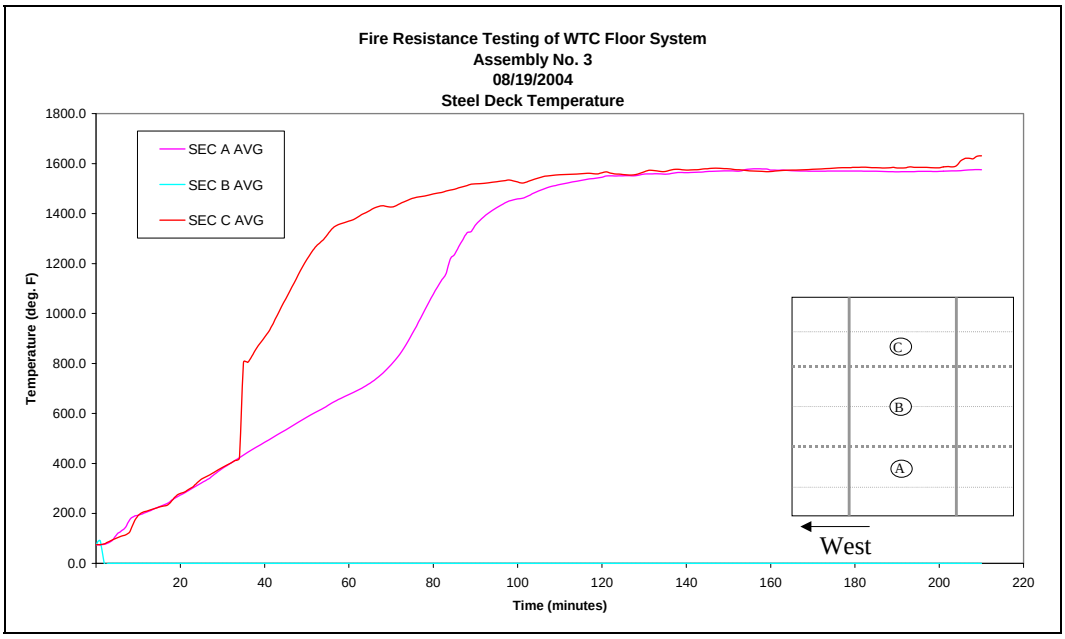

Figure 5–44. Assembly No. 3 – average temperatures on steel deck.

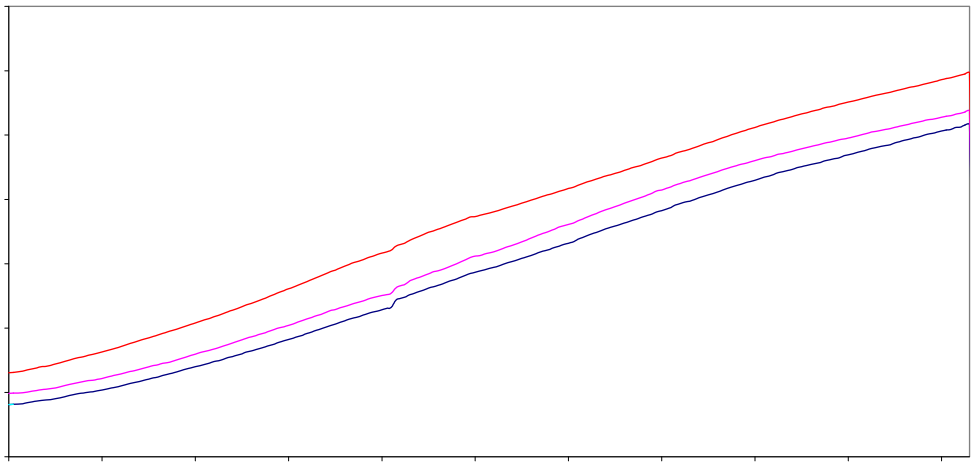

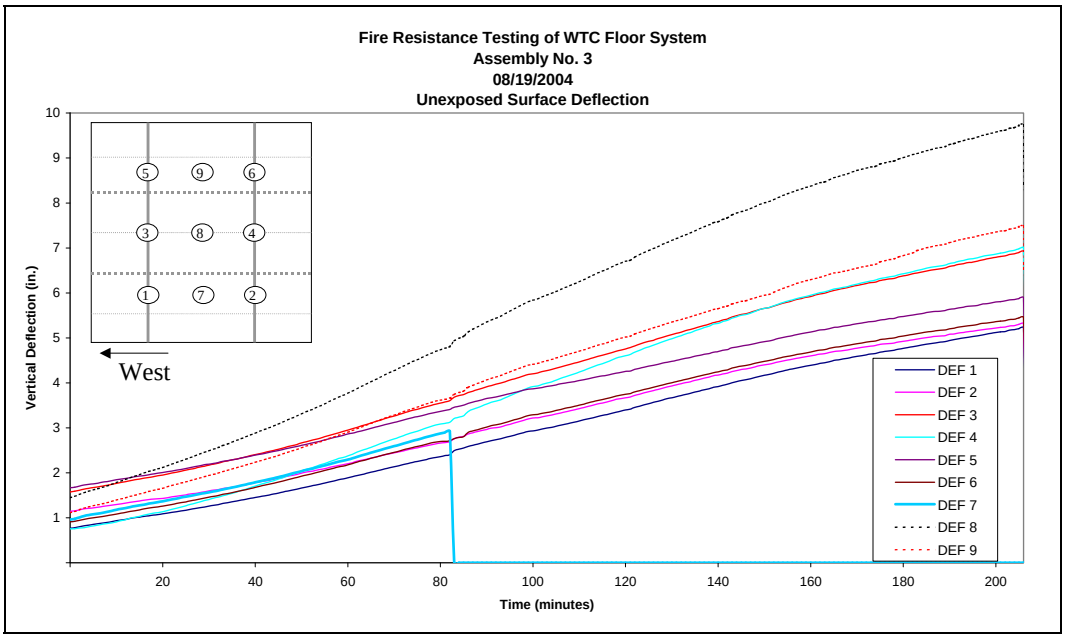

Figure 5–47. Assembly No. 3 – unexposed surface deflection measurements.

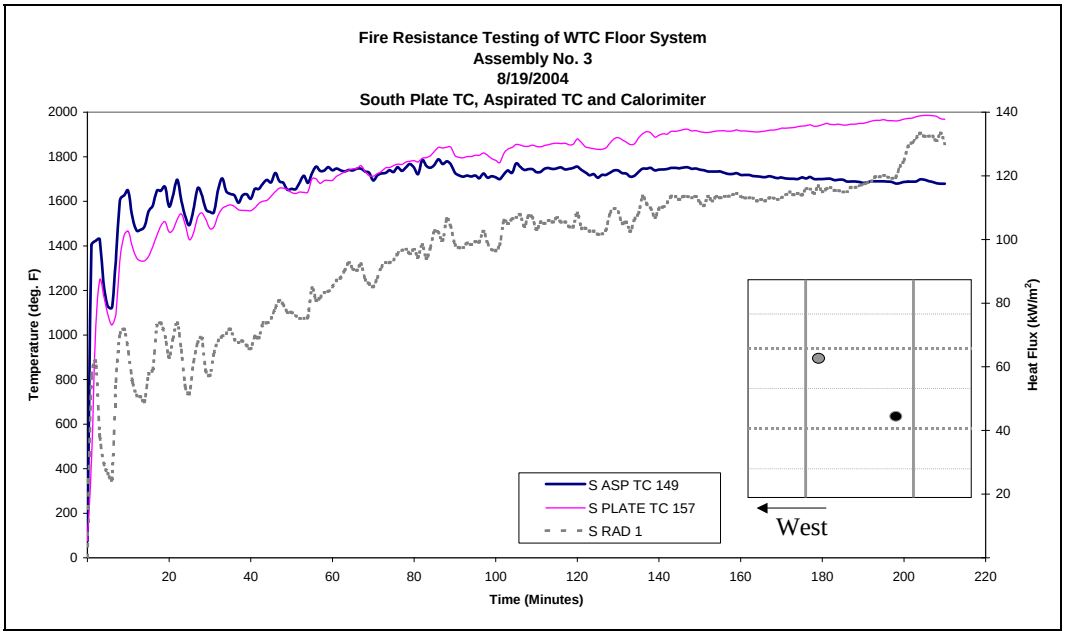

Figure 5–48. Assembly No. 3 – additional instrumentation through south opening.

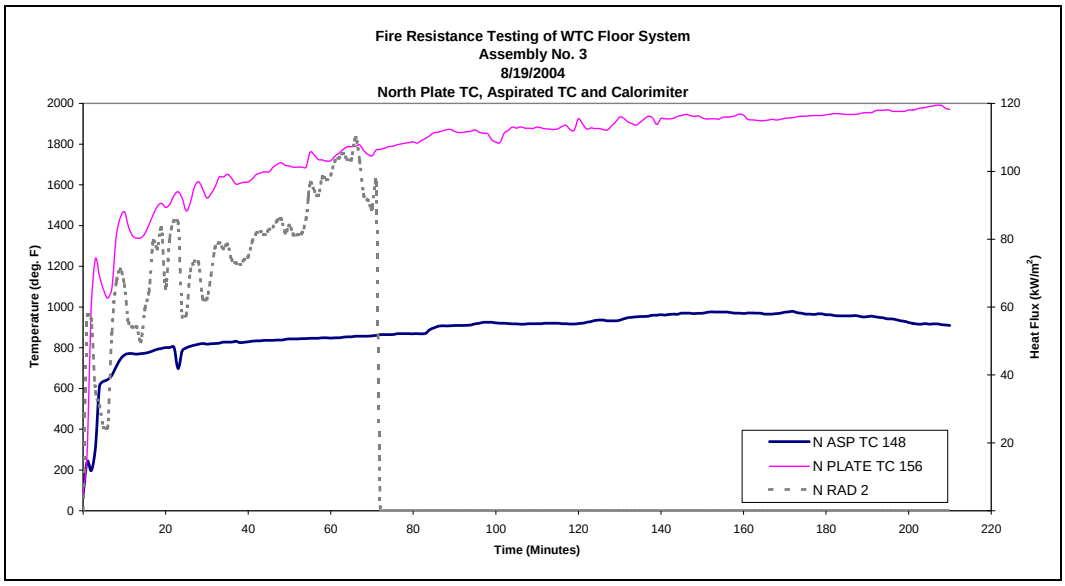

Figure 5–49. Assembly No. 3 – additional instrumentation through north opening.

5.3.3 Post-Test Observations

Figure 5–50 shows the unexposed side of floor assembly No. 3 after all loading equipment had been removed (view looking north). Numbers shown at the centerline and quarter points are vertical deflections after cooling. All other numbers are reference dimensions as measured from the edge of the slab. Figures 5–51 through 5–53 are additional views of the post-test condition of the test specimen.

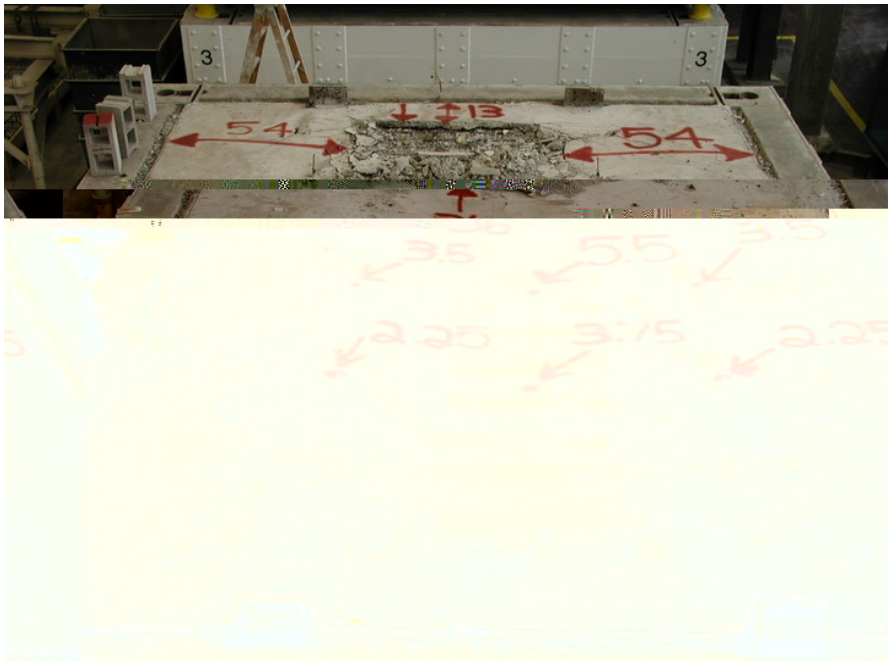

Source: NIST.

Figure 5–50. Unexposed surface of Assembly No. 3 after loading equipment was removed.

Source: NIST.

Figure 5–51. Detail of spalling concrete at north end of Assembly No. 3.

Source: NIST.

Figure 5–52. View of column-end diagonal strut of west main truss on Assembly No. 3.

Source: NIST.

Figure 5–53. Intersection of north bridging and west main truss on Assembly 3.

5.4 FIRE TEST OF ASSEMBLY NO. 4

The fire resistance test of Assembly No. 4 was conducted at the UL Northbrook facility (ULN) on August 25, 2004 under the observation of representatives of Underwriters Laboratories Inc., and NIST.

The relative humidity of the concrete slab met the requirements prescribed in ASTM E 119.

5.4.1 Test Observations

Table 5–4 presents observations that were recorded during the conduct of the test. All dimensions given are approximate since they were estimated by making observations through furnace viewports. Times were generally recorded to the nearest one quarter minute. The term “report” is used to describe a loud sound, which might be described as a “bang” or a “pop.” Because these loud reports were often accompanied by observed movement of the metal deck and the dislodging of SFRM, it is assumed that the reports signaled explosive spalling of the concrete. It was not possible to ascertain the exact location and extent of any spalling. After the concrete spalling at approximately 55 minutes, ceramic fiber insulation was placed over the opening in the concrete to protect the hydraulic loading equipment from the heat escaping the furnace, thereby, allowing the test to continue.

Table 5–4. Test observations – Assembly No. 4.

Test Time, Min	Exposed (E) or Unexposed (U) Surface	Observations
4.25	E	Slight buckling of the steel deck was observed near the bridging trusses. The buckling was more pronounced near the north bridging truss.
7	E	There was heavy deck buckling in a east-west direction 1 ft south of the center deck support angle.
8	E	The center deck support angle was bowing towards the north.
9.5	E	The finish on the bridging trusses was peeling away.
14	E/U	A minor report was heard.
14.75	E/U	Two minor reports were heard approximately 1 second apart.
15.5	E/U	Two minor reports were heard approximately 1 second apart.
15.75	E/U	A report was heard.
16	E	The reports were becoming louder and more frequent.
17.5	E	Over spray of the SFRM on the steel deck was falling from the assembly.
18.25	E	The top chord of the south bridging truss was becoming deformed.
20	E/U	The reports were becoming less frequent and louder.
20.5	E	The steel deck became heavily deformed south of the center deck support angle.
22	E/U	The reports were more frequent.
23	E/U	A loud report was heard.
24.75	E	The top chord of the north bridging truss was becoming deformed.
31.5	E	The reports were becoming less frequent.
35.75	E	The SFRM became darker in color.
41	E/U	A report was heard. It was the first one since the 31.5 minute observation.
42	E/U	A loud report was heard.
44.75	E/U	Three reports were heard approximately 1 second apart.
48.5	E/U	A loud report was heard.
51	E/U	A very loud report was heard.
51	E	Visible steel deck deflection between the center deck support angles and the bridging trusses.
54	E	The bridging trusses were bowing downward near their centers.
55.25	E/U	A very loud report was heard. Pieces on concrete fell to the lower part of the furnace area were observations were being observed.
56	E	The center deck span west of the west main truss was bowing downward past the lower chord of the main truss.
60	E	All of the SFRM on the main trusses remained in place.
60.25	E	The center deck support angle was twisting where it interfaced with the main trusses.
73	E	Visual deck deflection near the center of the assembly continued.
88	E/U	No reports were heard since the 55.25 minute observation.
90	E	All of the SFRM on the main trusses remained in place.
110	E	A minor report was heard.
120	E	All of the SFRM on the main trusses remained in place.
120	E/U	Furnace Fire extinguished at the request of the submitter.

5.4.2 Data

All data shown in the following figures (Figures 5–54 through 5–65) are unedited for the entire duration of the test. However, not all data shown is reliable due to the limitations of the instrumentation, i.e. thermocouples, radiometers, and calorimeters. Data may become unreliable past the rating period when structural events occur that can dislodge the instrumentation. Also, protective insulation of the thermocouple wire may burn away, and the individual wires make contact with themselves and/or neighboring wires rendering the data unreliable. Appendix H gives a listing of the times that instrumentation failed to give reliable data, as determined by UL.

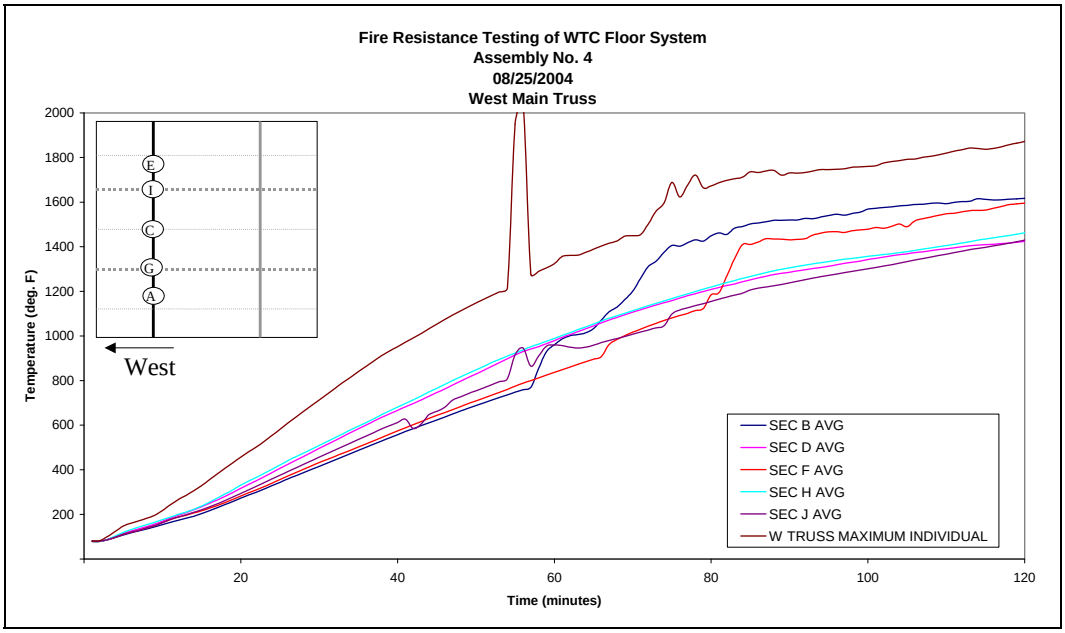

Figure 5–54. Assembly No. 4 – average and maximum individual temperatures on west main truss.

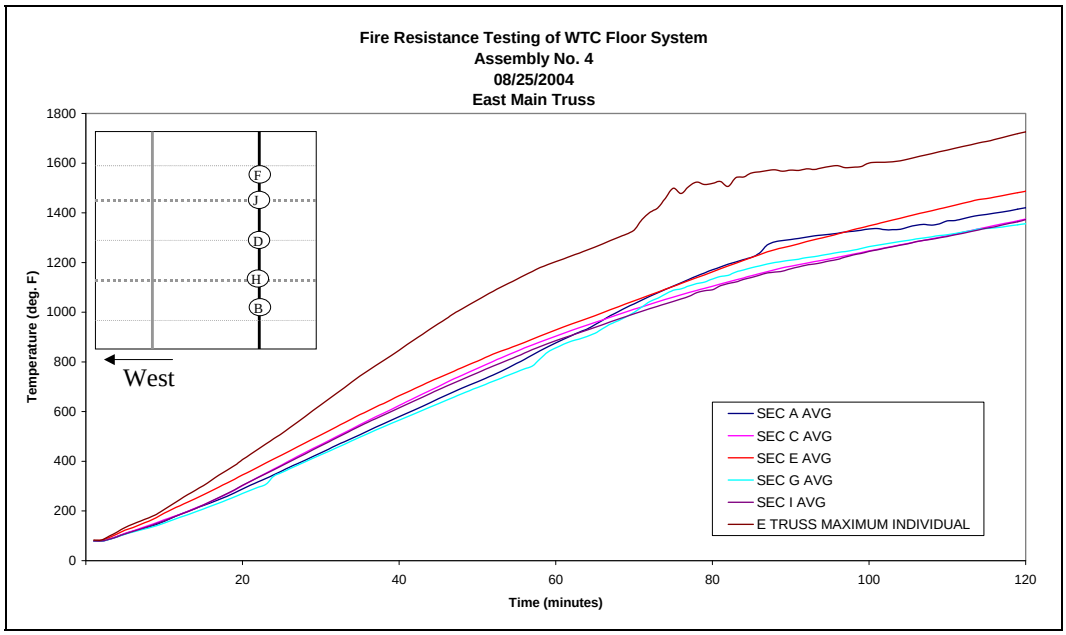

Figure 5–55. Assembly No. 4 – average and maximum individual temperatures on east main truss.

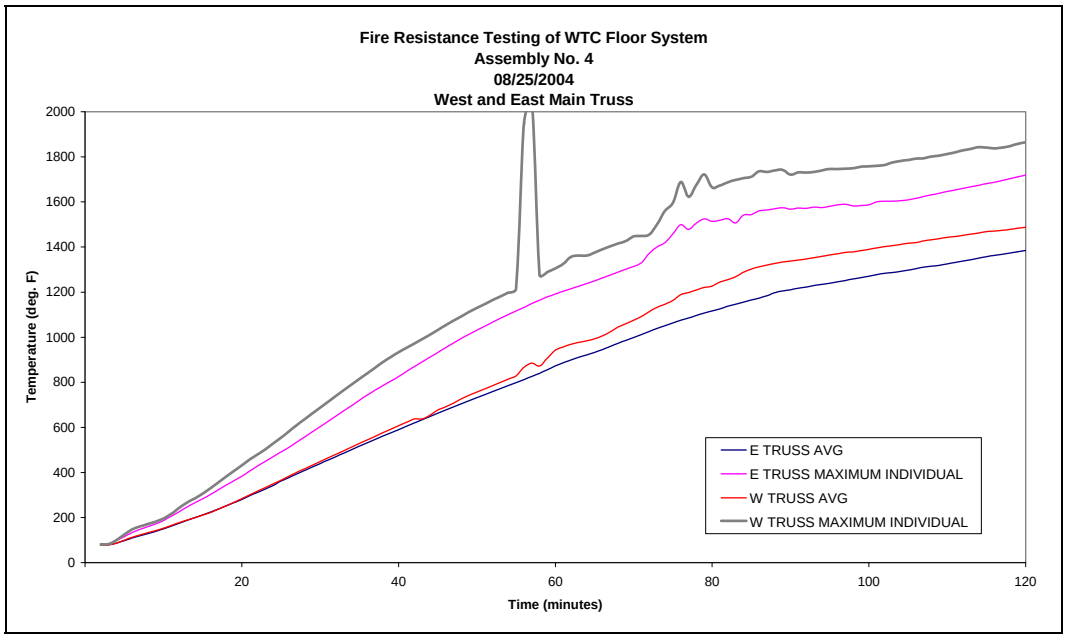

Figure 5–56. Assembly No. 4 – overall average and maximum individual temperatures on west and east main trusses.

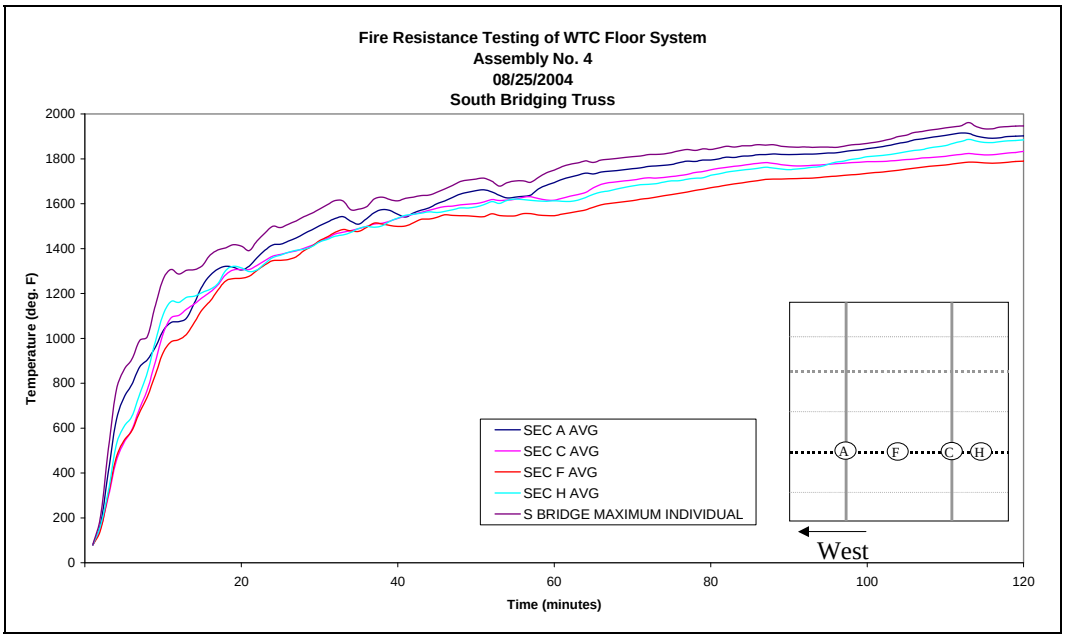

Figure 5–57. Assembly No. 4 – average and maximum individual temperatures on south bridging truss.

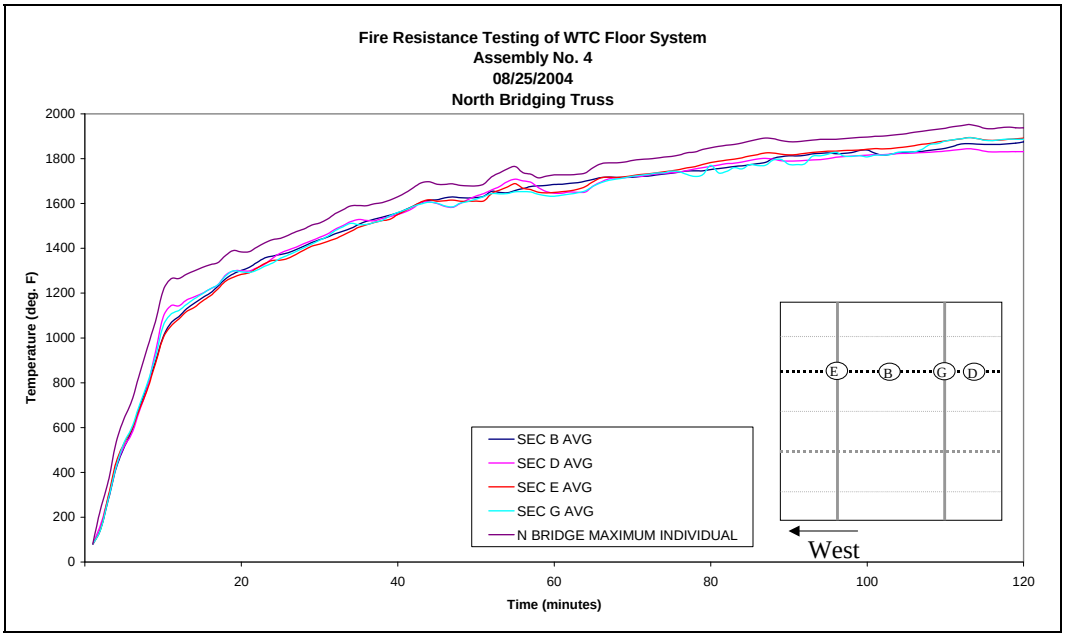

Figure 5–58. Assembly No. 4 – average and maximum individual temperatures on south bridging truss.

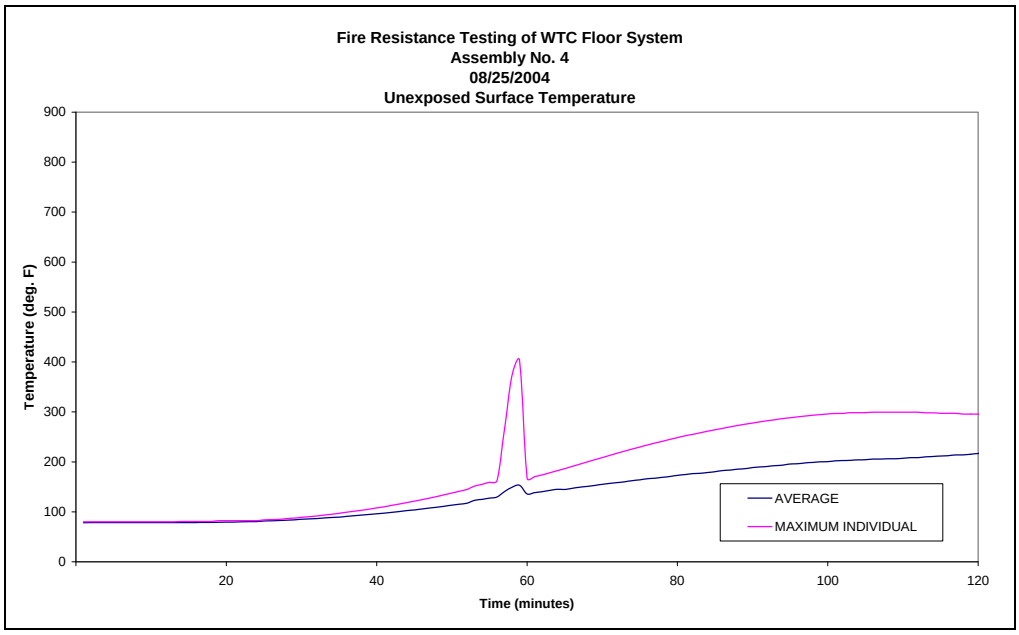

Figure 5–59. Assembly No. 4 – average and maximum individual temperatures on unexposed surface.

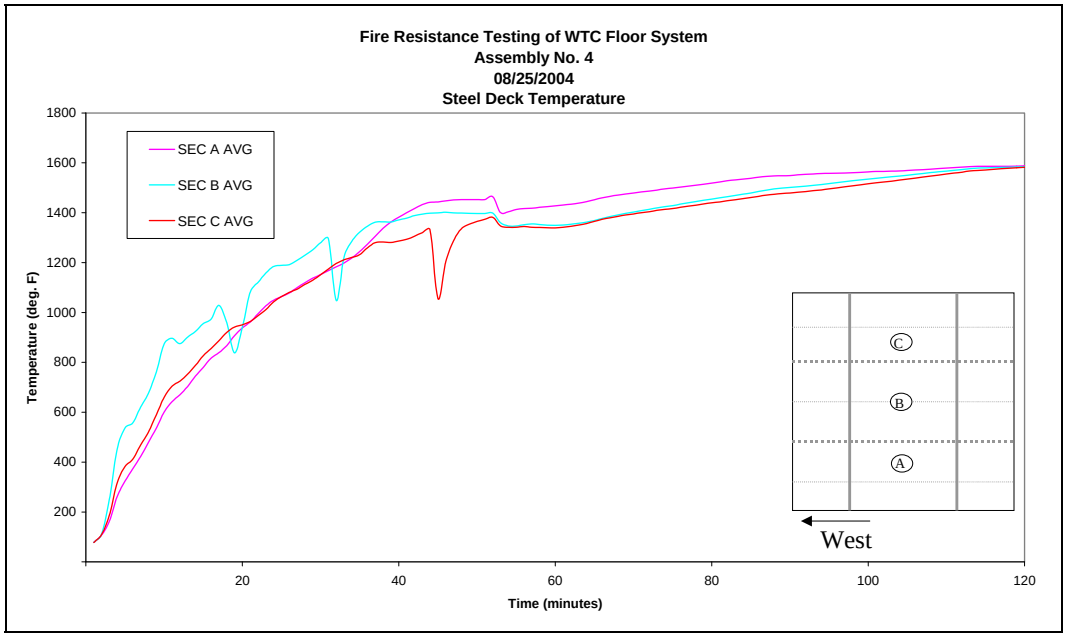

Figure 5–60. Assembly No. 4 – average temperatures on steel deck.

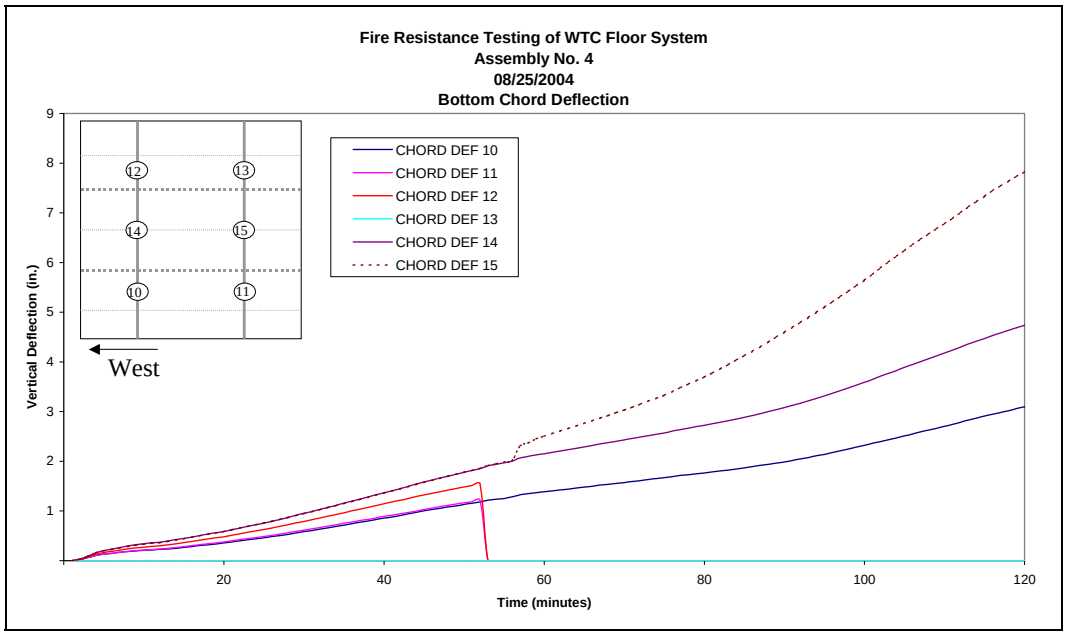

Figure 5–61. Assembly No. 4 – bottom chord deflection measurements.

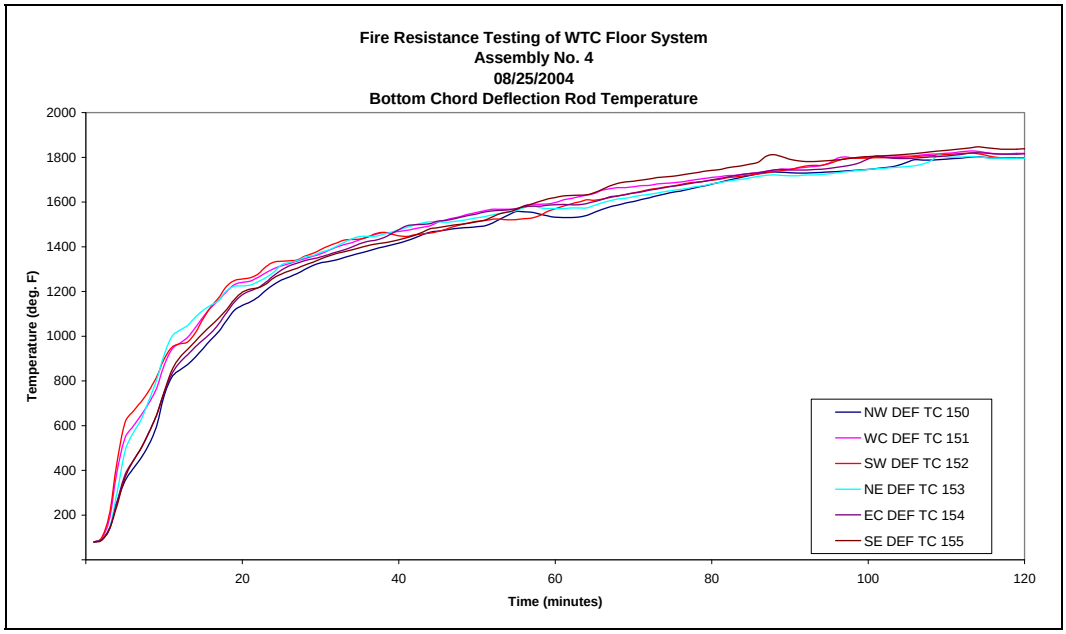

Figure 5–62. Assembly No. 4 – temperatures of bottom chord deflection rods.

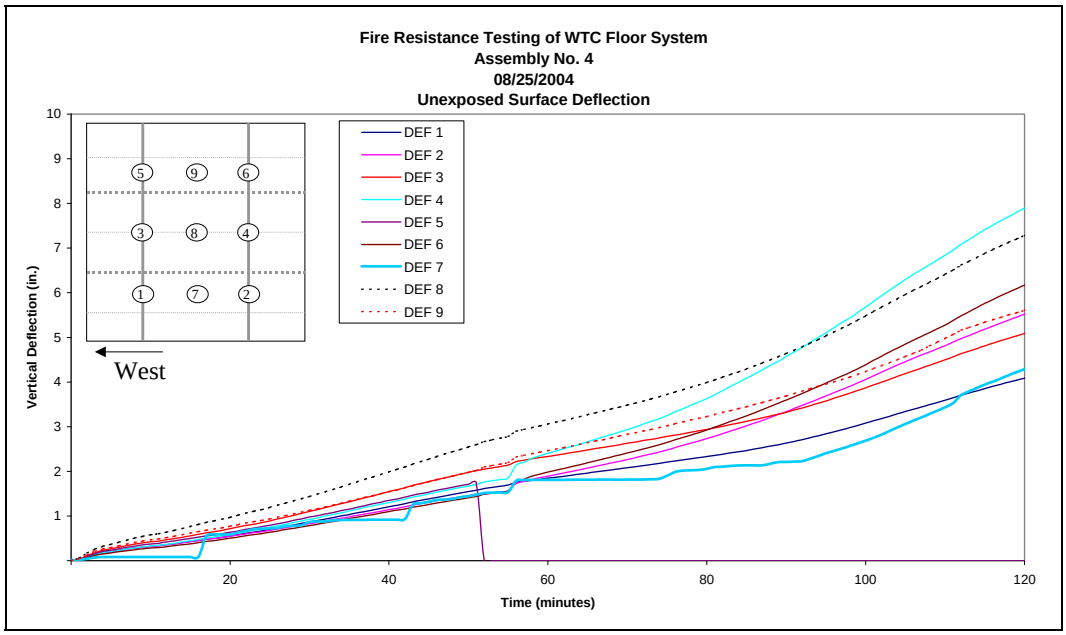

Figure 5–63. Assembly No. 4 – unexposed surface deflection measurements.

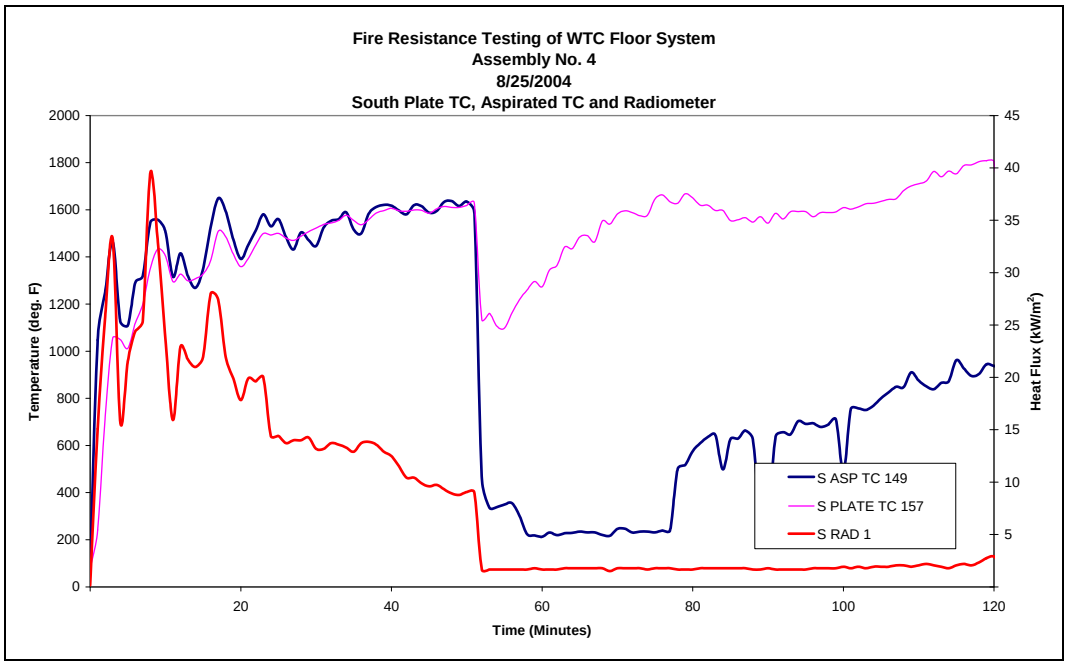

Figure 5–64. Assembly No. 4 – additional instrumentation through south opening.

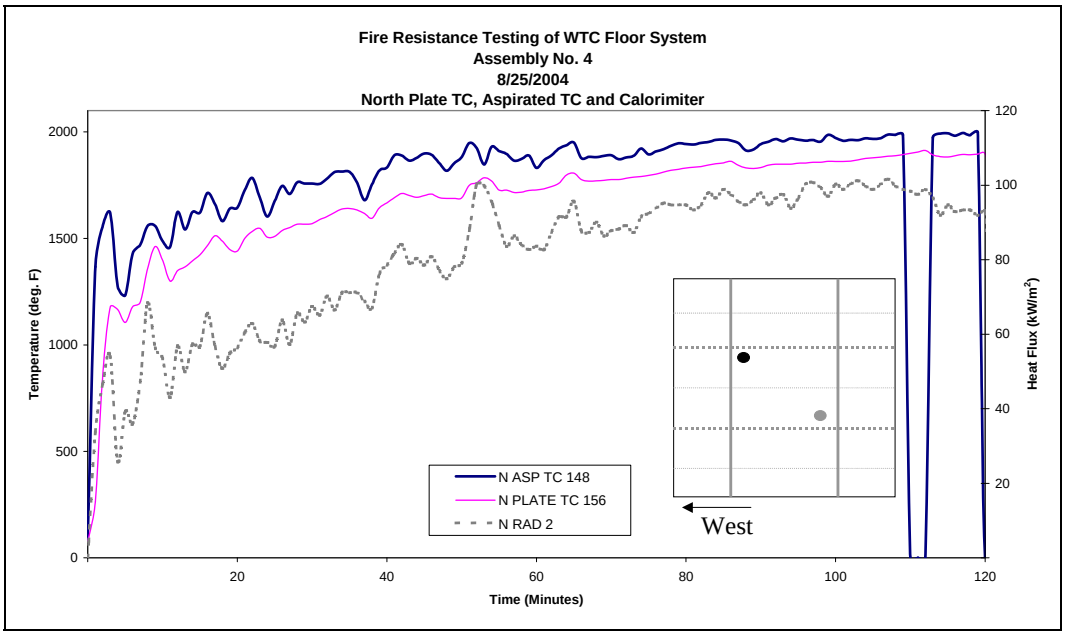

Figure 5–65. Assembly No. 4 – additional instrumentation through north opening.

5.4.3 Post-Test Observations

Figure 5–66 shows the unexposed side of the assembly after all loading equipment was removed (view looking north). Numbers shown at the centerline and quarter points are vertical deflections after cooling. All other numbers are reference dimensions as measured from the edge of the slab. Figures 5–67 through 5–70 are additional views of the post-test condition of the test specimen.

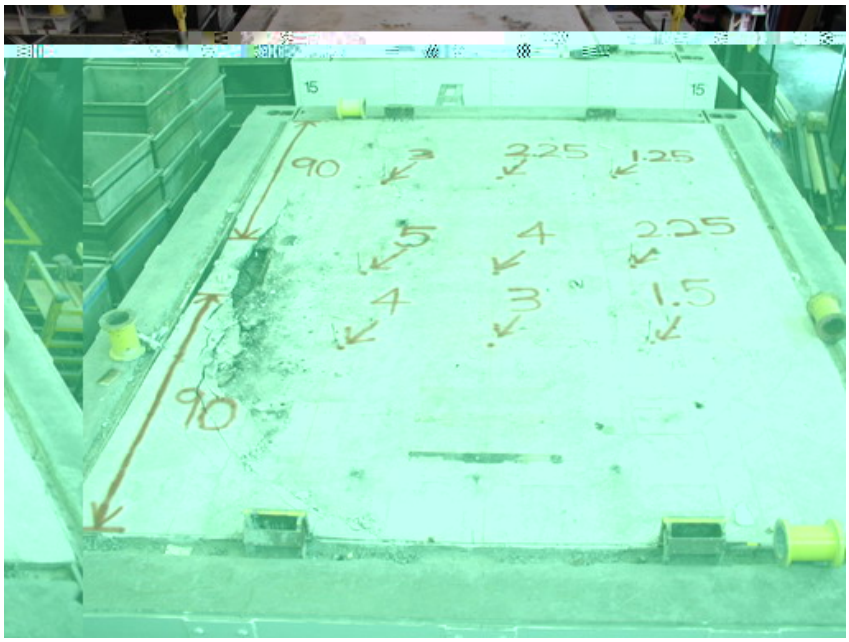

Source: NIST.

Figure 5–66. Unexposed surface of Assembly No. 4 after loading equipment was removed.

Source: NIST.

Figure 5–67. Unexposed surface of Assembly No. 4, view of concrete spalling on west side of assembly.

Source: NIST.

Figure 5–68. Unexposed surface of Assembly No. 4, close-up of concrete spalling on west side of assembly.

Source: NIST.

Figure 5–69. Intersection of north bridging and west main truss on Assembly 4.

Source: NIST.

Figure 5–70. View looking north of south bridging truss at location where concrete spalling occurred on Assembly 4.

5.5 FIRE RESISTANCE RATINGS

All four fire resistance tests were conducted for as long as practical to obtain as much information as possible. As such, the tests were not stopped when the first end-point criteria was reached. Rather, the tests were continued until it was determined that collapse of the test specimen was imminent or until instrumentation critical to the determination of safe continuation of the test had failed to provide reliable readings. Additionally, excessive deflection of the floor system would sometimes contact and damage furnace instrumentation making it impractical to continue the test.

5.5.1 Test Assembly No. 1

Assembly No. 1 was fire tested on August 7, 2004 in accordance with ASTM E 119-61 and ASTM E 119-00a. The test was continued for 116 minutes and terminated when collapse of the assembly was imminent. The main trusses reached a maximum individual temperature of 1,300 ^{o}F (704 ^{o}C) (at thermocouple No. 18), as defined in Paragraph 32.1.3 of ASTM E 119-00a, at 62 min. The average limiting temperature of 1,100 ^{o}F (593 ^{o}C), as defined in Paragraph 32.1.3 of ASTM E 119, was reached at 66 minutes at section E. The unexposed surface temperatures exceeded the maximum individual requirement of 325 ^{o}F (163 ^{o}C) rise over ambient temperatures as defined in Paragraphs 7.4 and 32.1.2 of ASTM E 119-00a at 111 minutes. For safety reasons, access to the top of the floor assembly was not permitted during the test and, consequently, testing for unexposed surface conditions that would ignite cotton waste was not done.

5.5.2 Test Assembly No. 2

Assembly No. 2 was fire tested on August 11, 2004 in accordance with ASTM E 119-61 and ASTM E 119-00a. The test was continued for 146 minutes and terminated when the vertical deflection of the assembly exceeded the capability of the instrumentation to accurately measure the deflection at the center of the test assembly. The main trusses reached maximum individual temperature of 1,300 ^{o}F (704 ^{o}C) at 62 minutes. The average limiting temperature of 1,100 ^{o}F (593 ^{o}C) was reached at 76 minutes at Section C. Neither the maximum or average unexposed surface temperatures were exceeded throughout the duration of the fire test. As described for the test of Assembly No. 1, testing for unexposed surface conditions that would ignite cotton waste was not done.

5.5.3 Test Assembly No. 3

Assembly No. 3 was fire tested on August 19, 2004 in accordance with ASTM E 119-61 and ASTM E 119-00a. The test was continued for 210 minutes and terminated when the vertical deflection of the assembly exceeded the capability of the instrumentation to accurately measure the deflection at the center of the test assembly. The main trusses reached a maximum individual temperature of 1,300 ^{o}F (704 ^{o}C) at 80 minutes. The average limiting temperature of 1,100 ^{o}F (593 ^{o}C) was reached at 86 minutes at Section F. The unexposed surface temperatures exceeded the maximum individual temperature requirement of 325 ^{o}F (163 ^{o}C) rise over ambient temperature at 157 min. The average temperature of the unexposed surface limit was reached at 180 minutes. Since the top of the floor assembly was loaded with concrete block , water containers, and hydraulic actuators, access to most of the concrete surface was limited and testing for unexposed surface conditions that would ignite cotton waste was not done.

5.5.4 Test Assembly No. 4

Assembly No. 4 was fire tested on August 25, 2004 in accordance with ASTM E 119-61 and ASTM E 119-00a. The test was continued for 120 minutes and terminated when collapse of the assembly was imminent. The main trusses reached a maximum individual temperature of 1,300 ^{o}F (704 ^{o}C) at 58 minutes. The average limiting temperature of 1,100 ^{o}F (593 ^{o}C) was reached at 66 minutes at Section B. The unexposed surface temperatures exceeded the maximum individual requirement of 325 ^{o}F (163 ^{o}C) rise over ambient temperatures at 58 minutes. As described for the test of Assembly No. 3, testing for unexposed surface conditions that would ignite cotton waste was not done.

5.5.5 Summary Table

Based on the results of the fire tests, assemblies 1 through 4 achieved the hourly ratings shown in Table 5–5.

Table 5–5. Times to reach ASTM E 119 end-point criteria and ASTM E 119 hourly ratings.

Test	Description	Times to Reach End-Point Criteria (min)					Test Terminated (min)	Standard Fire Test Rating (hr)		
		Temperature on Unexposed Surface		Steel Temperatures		Failure to Support Load		ASTM E 119-61	ASTM E 119-00	
		Average (Ambient +250ºF)	Maximum (Ambient +325ºF)	Average (1100ºF)	Maximum (1300ºF)			Rating	Restrained Rating	Unrestrained Rating
1	35 ft restrained ¾ in SFRM	---	111 (see Fig. 5-6)	66 (see Fig. 5-1)	62 (see Fig. 5-1)	(3)	116(1)	1½	1½	1
2	35 ft unrestrained ¾ in SFRM	---	---	76 (Fig. 5-20)	62 (Fig. 5-20)	(3)	146(2)	2	---	2
3	17 ft restrained ¾ in SFRM	180 (see Fig. 5-41)	157 (Fig. 5-41)	86 (Fig. 5-36)	76 (Fig. 5-36)	(3)	210(2)	2	2	1
4	17 ft restrained ½ in SFRM	---	58 (Fig. 5-57)	66 (Fig. 5-52)	58 (Fig. 5-52)	(3)	120(1)	¾	¾	¾

Notes: (1) Test terminated due to imminent collapse
(2) Test terminated when vertical displacement exceeded capability to measure accurately
(3) Did not occur

Chapter 6
DISCUSSION OF RESULTS

6.1 COMPARISON OF RESULTS

Results of the four fire resistance tests are compared in this section. First, it is useful to compare the fire environment for all four tests. The ASTM E 119 Standard requires that the prescribed time-temperature relationship be followed as determined by the average of individual temperature measurements within the furnace. For the tests conducted here, additional instrumentation was installed to characterize the thermal environment and, in particular, the exposure at different locations relative to the floor assembly. Lastly, the performance of the floor assembly, as evidenced by temperatures on the unexposed side of the floor slab, temperatures of the steel trusses, and by the deflections of the slabs and supporting steel members, is presented.

6.1.1 Furnace Control Temperatures

The average furnace temperatures during all four tests and the target time-temperature relationship prescribed by ASTM E 119 are shown in Fig. 6–1. It is seen that the average furnace control temperatures were very similar and indeed met the requirements of ASTM E 119.

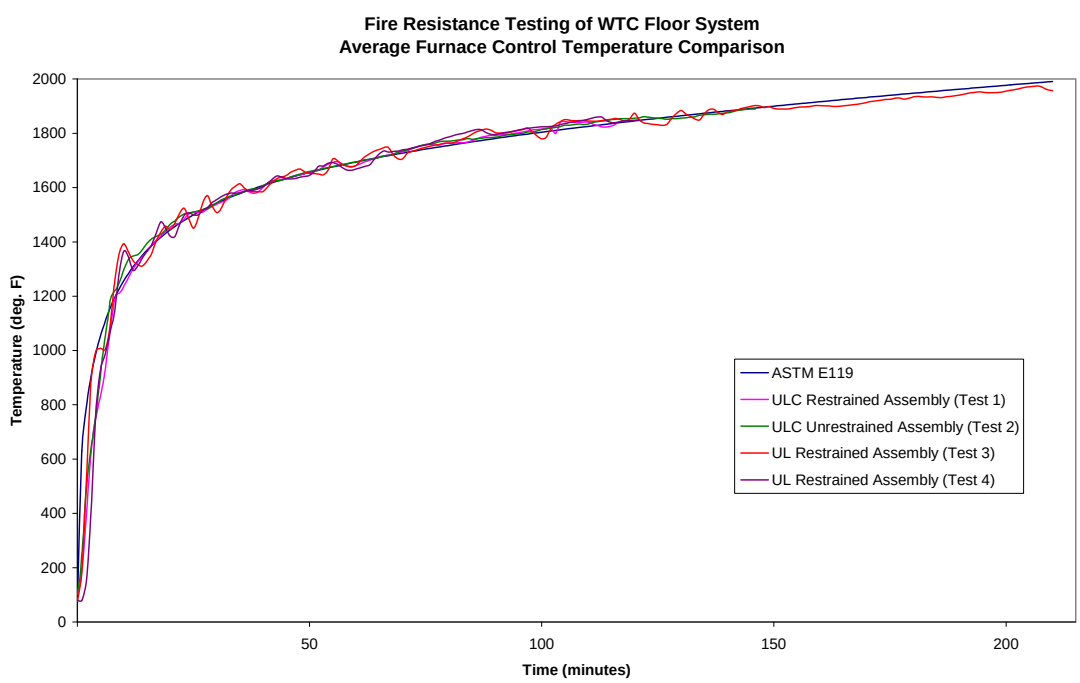

Figure 6–1. Comparison of average furnace control temperatures.

6.1.2 Furnace Thermal Environment

Additional instrumentation was included in all four tests to further characterize the thermal environment of the exposing fire. Aspirated thermocouples, plate thermocouples and radiometers were located at the underside of the metal deck and at the elevation of the bottom chord and recordings were made throughout the duration of the tests.

Plate Thermocouple Measurements

Figures 6–2 and 6–3 show temperatures recorded by the plate thermocouples for Test No. 2 (ULC furnace) and Test No. 4 (ULN furnace). Temperatures recorded at the bottom chord are presented in Fig. 6–2, and those recorded at the underside of the metal deck are shown in Fig. 6–3. These two plots show that temperatures measured at two locations are very similar between the two furnaces. Note that the plate TC at the metal deck in Test 4 (ULN) gave unreliable data after approximately 50 min. This time is consistent with observations of very loud report and visible steel deck deflection recorded at 51 min (see Table 5–4). This plate TC was dislodged from its initial position, relative to the metal deck, and readings beyond 50 min cannot be interpreted.

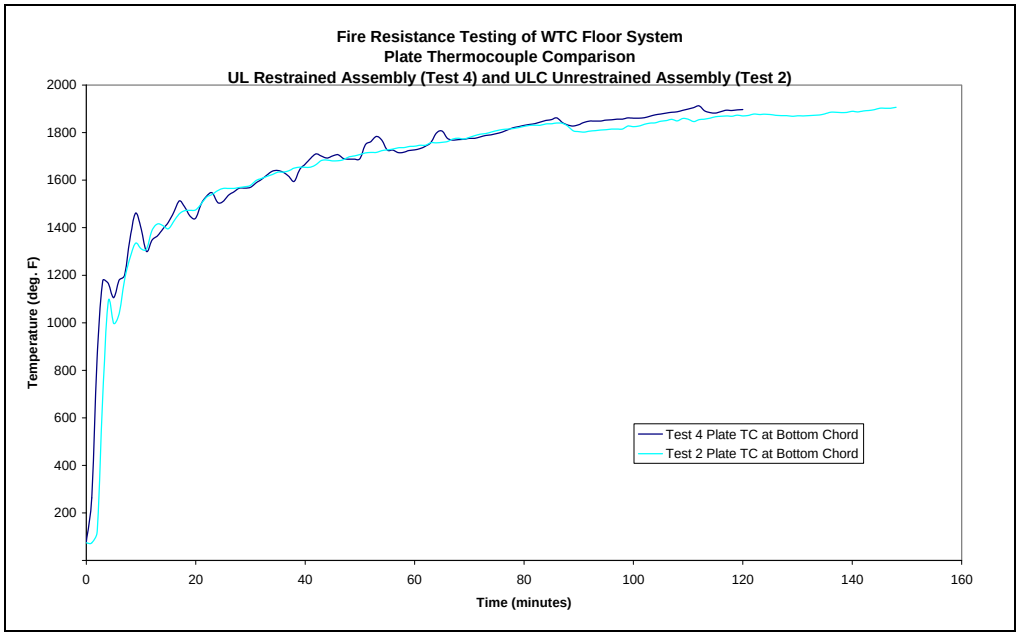

Figure 6–2. Temperatures measured at the bottom chord by the plate thermocouple in the ULC furnace (Test No. 2) and ULN furnace (Test No. 4).

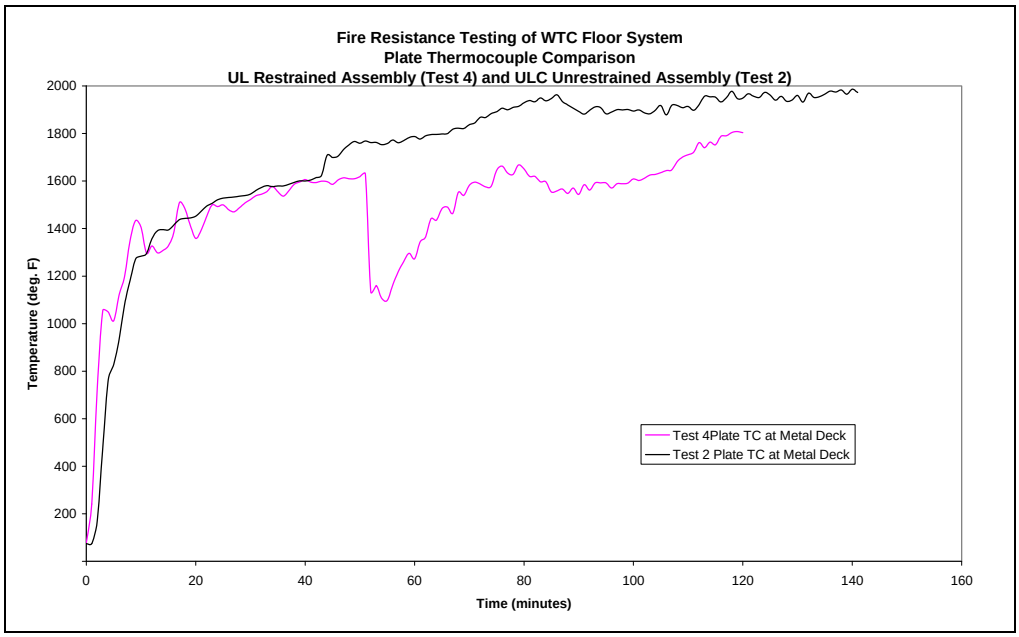

Figure 6–3. Temperatures measured at the underside of the metal deck by the plate thermocouple at the ULC furnace (Test No. 2) and ULN furnace (Test No. 4).

Radiometer Measurements

Thermal radiation is the dominant mode of heat transfer from the furnace to the test specimen. Hence, heat flux measured by radiometers should provide a better indication of how quickly a specimen will heat up than temperature of the surrounding gas as measured by furnace control thermocouples. Comparing the radiant flux measured in the larger (ULC) furnace (see Figs. 5–11 and 5–12) to the radiant heat flux measured in the smaller (ULN) furnace (see Figs. 5–48, 5–49, and 5–65), one observes that smaller furnace produced a radiant heat flux somewhat higher than the larger furnace, in spite of the fact that the temperatures used to control both furnaces followed the ASTM E 119 time-temperature curve (Fig. 6–1). Comparison of overall average temperatures of the main trusses, protected with 3/4 in. fireproofing (see Figs. 5–3, 5–24, and 5–40) indicates that, at 60 minutes, average steel temperatures are on the order of 700 ^{o}F to 800 ^{o}F for all three test specimens (furnace temperature at 60 min is prescribed to be 1700 ^{o}F).

The above observations are based on a limited number of measurements, and, for Test No. 2, there were no radiometer readings due to damage to the radiometers in Test No. 1. In addition, factors such as heat loss must also be taken into account when comparing differences in furnace exposures to assess reproducibility of test results.

6.1.3 Steel Temperatures

Steel temperatures were recorded at several locations on the main and bridging trusses. Average temperatures of the bottom chord, web diagonal, and top chord are presented here.

Figure 6–4 shows a comparison of the average temperature of the bottom chord for the three tests in which the thickness of the SFRM was ¾ in. Temperatures are seen to be very comparable up to about 75 min, which is around the time when SFRM began to dislodge.

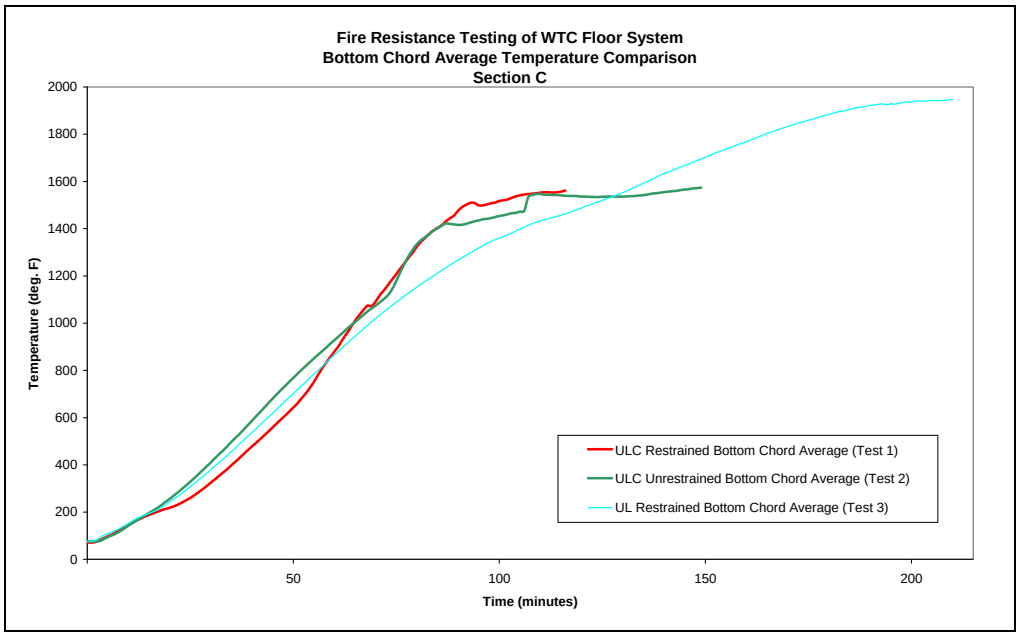

Figure 6–4. Average temperatures of the bottom chord for Test Nos. 1, 2, and 3 (3/4 in. thick SFRM).

Figure 6–5 presents a comparison of temperatures of the truss web diagonals for the three tests in which the thickness of the SFRM was ¾ in. The web temperatures for the two full-scale tests (35 ft span assemblies) were greater than those for the reduced-scale test (17 ft span assembly) after about 15 min. The reason for this difference is not clear but is possibly due to the relationship between the SFRM thickness and scale of the steel trusses. Comparison of Figs. 5–35 and 5–53 illustrates the difference in the buildup of SFRM at the intersections of the webs and chord members between the full- and reduced-scale test specimens, which may affect the rate of heating of the truss web diagonals. These results illustrate that thermal scaling is an issue that needs to be addressed.

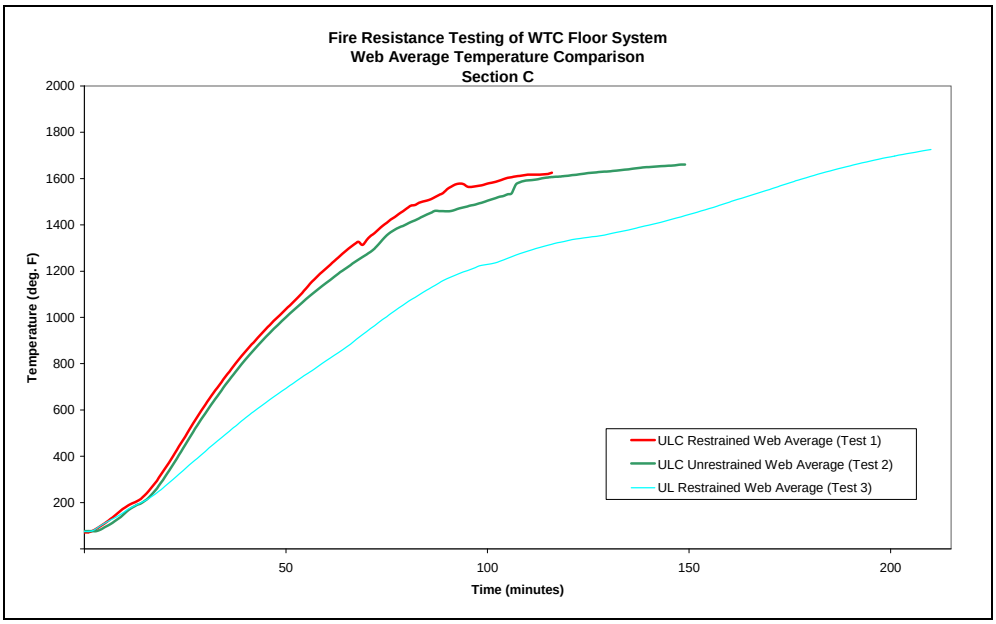

Figure 6–5. Average temperature of web diagonals for Test Nos. 1, 2, and 3 (3/4 in. thick SFRM).

The average temperature of the top chord is plotted in Figure 6–6 for the three test assemblies with ¾ in. of SFRM. The average top chord temperature for the two full-scale tests (35 ft span test assemblies) was greater than the average temperature recorded for the reduced-scale test (17 ft span assembly) after about 50 min. Because of the comparatively abrupt changes in average temperature beginning around 50 min, the difference may be explained by sudden changes such as the onset of spalling of concrete and attendant loss of fire protection. However, since the steel temperatures in the reduced-scale test generally tend to be lower than in the full-scale test, this trend may be explained by a scale-related factor such as the difference in the buildup of SFRM affecting the rate of heating of the steel as noted above. Further, it is possible that the overspray on the metal deck was greater for test Specimen No. 3 than for the other two tests since the lower chord is closer to the metal deck. This, too, would be a geometrical scaling effect.

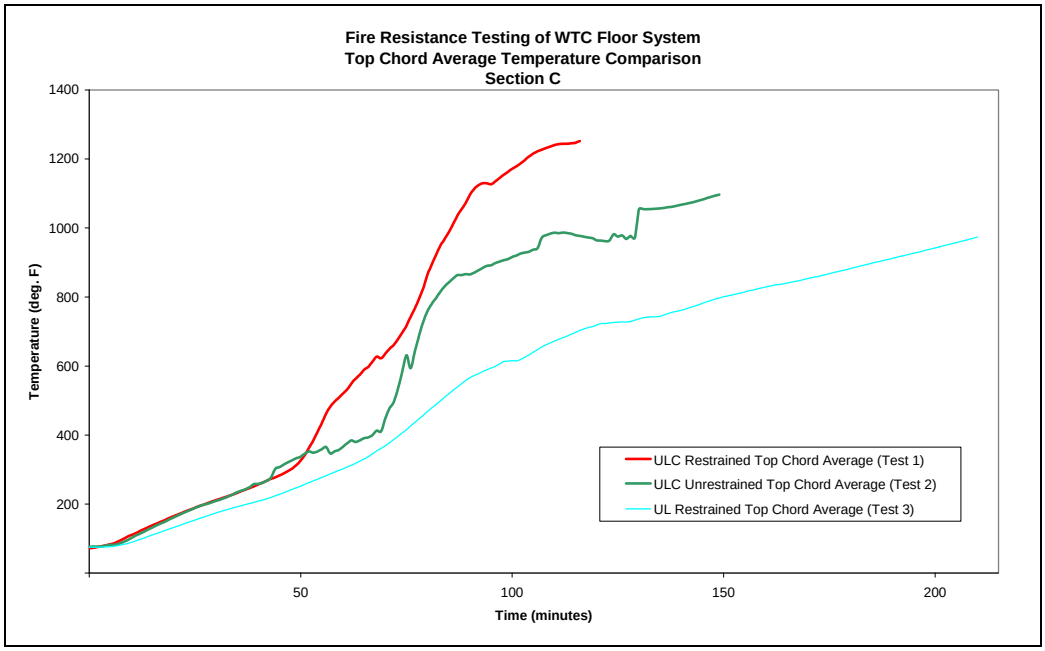

Figure 6–6. Average temperature of the top chord for Test Nos. 1, 2, and 3 (3/4 in. thick SFRM).

Average temperature of the bottom chord at Section C (center of west truss) for Test No. 3 (¾ in. thick SFRM) and Test No. 4 (½ in. thick SFRM) is plotted in Fig. 6–7. As expected, the steel temperatures for the specimen with ½ in. of SFRM were higher than those for the specimen with ¾ in. of SFRM. Here, the same furnace (ULN) was used for the comparison.

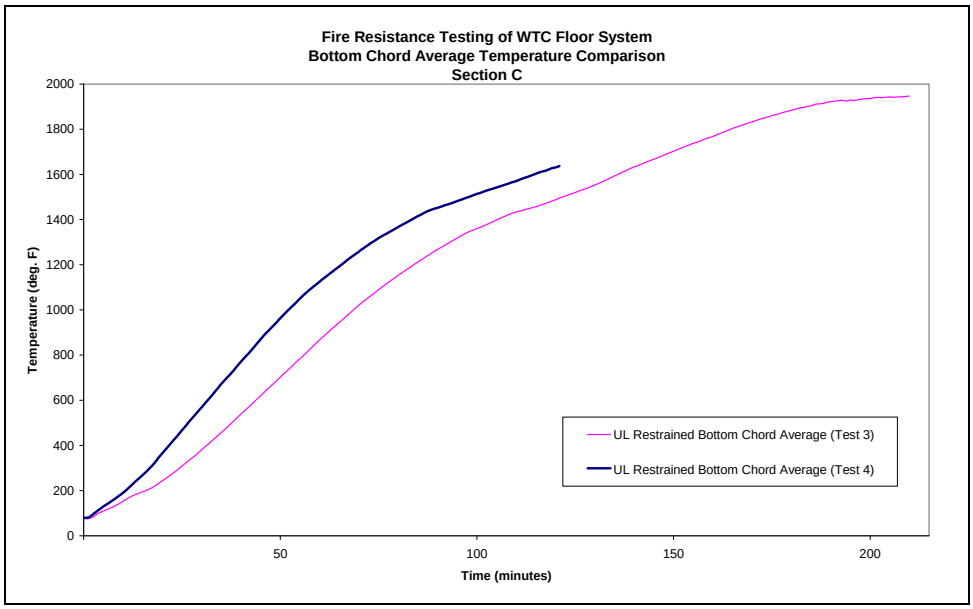

Figure 6–7. Average temperature of the bottom chord for Test No. 3 (3/4 in. thick SFRM) and No. 4 (1/2 in. thick SFRM).

6.1.4 Unexposed Surface Temperatures

The temperature of the unexposed surface of the floor assemblies is plotted in Fig 6–8. It is observed that the unexposed surface temperatures of all four test assemblies were similar prior to the onset of significant concrete spalling at around 50 min. In Test 4, the surface-mounted TC on the west edge near the center of the span was affected by the explosive failure of the slab and recorded hot gas temperatures.

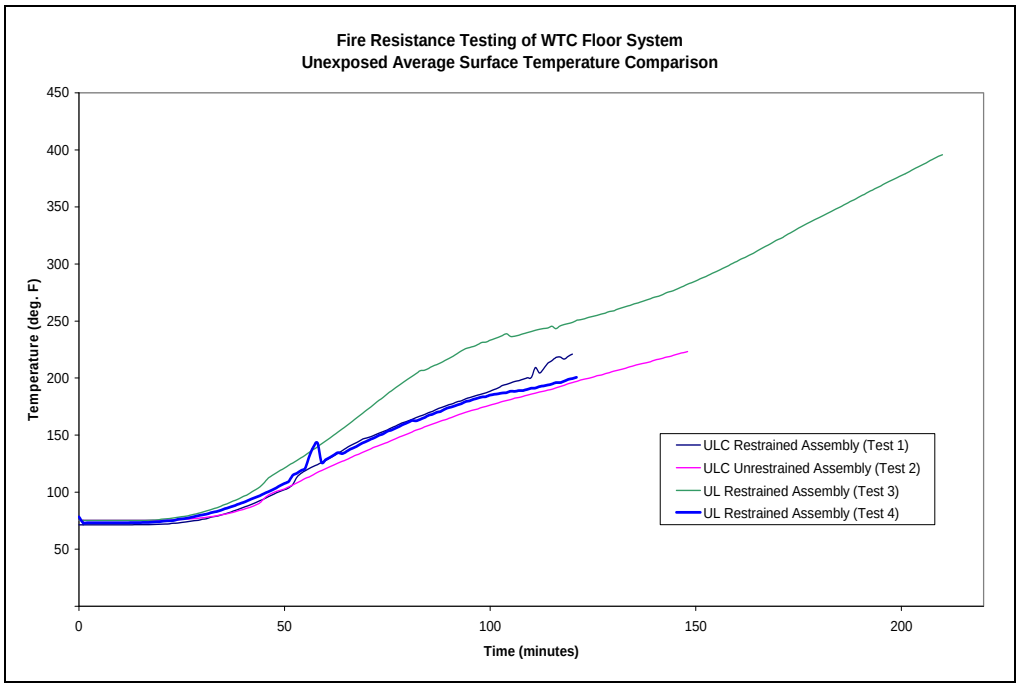

Figure 6–8. Average temperature of the unexposed surface for all four tests.

6.1.5 Deflections of Floor Assembly

The following plots show the vertical deflection measured at the center of each assembly. Figure 6–9 shows the deflection, while Fig. 6–10 shows a plot of the deflection normalized by the span. It is seen that test Assembly No. 1 experienced a significant increase in vertical deflection at 49 min, which corresponds directly to a loud report and visible deflection noted in the test observations. Figure 5–13 shows the damage to the top side of the concrete slab that occurred with the sudden increases in deflection. The normalized curves show good agreement throughout the duration of the tests.

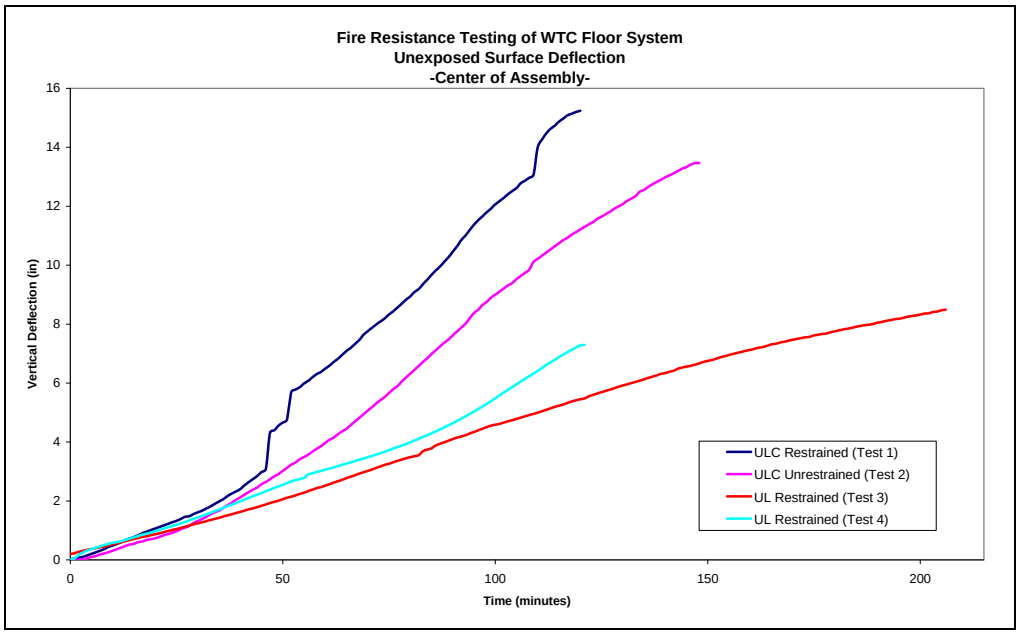

Figure 6–9. Deflection measured at the center of each assembly.

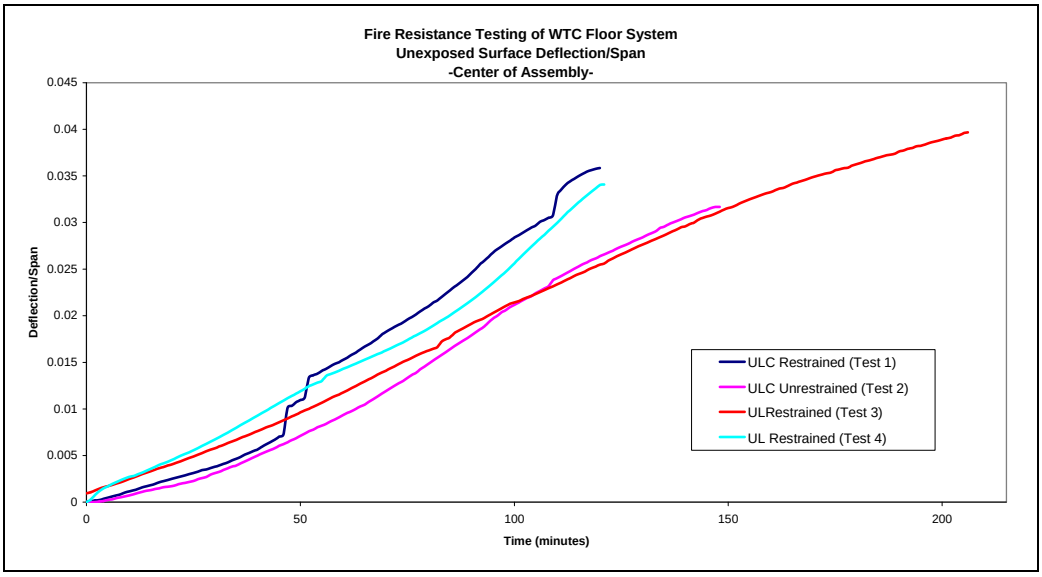

Figure 6–10. Deflection measured at the center of each assembly divided by the span.

6.2 OBSERVATIONS

Several observations can be made from the results presented in Chapter 5 for each test, the summary table of hourly ratings (Table 5–5), and the comparisons discussed above.

- The test assemblies were able to withstand standard fire conditions for between ¾ h and 2 h without exceeding the limits prescribed by ASTM E 119.

- Test specimens protected with ¾ in. thick sprayed fire-resistive material were able to sustain the maximum design load for approximately 2 hours (the minimum was 116 min) without collapsing; in the reduced-scale restrained test, the load was maintained for 3½ h (210 min) without collapsing.

- The restrained full-scale floor system obtained a fire resistance rating of 1½ h while the unrestrained floor system achieved a 2 h rating. Past experience with the ASTM E 119 test method would lead investigators to expect that the unrestrained floor assembly would not perform as well as the restrained assembly, and therefore, would receive a lower fire rating.

- A fire rating of 2 h was determined from the reduced-scale restrained test with the average applied SFRM thickness of ¾ in., while a fire rating of 1½ h was determined from the full-scale restrained test with the same SFRM thickness.

- The result stated above raises the question of whether or not a fire rating based on the ASTM E 119 performance of a 17 ft span floor assembly is scalable to a larger floor system such as that found in the WTC towers where spans ranged from 35 ft to 60 ft.

- A fire rating of ¾ h was determined from the reduced-scale restrained test with the specified SFRM thickness of ½ in.

6.3 AREAS OF FURTHER STUDY

The NIST tests have identified areas where further study related to the Standard Fire Resistance Test method may be warranted. The issues related to the test method that NIST considered in formulating its recommendations include:

- Criteria for determining structural limit states, including failure, and means for measurement

- Scale of test assembly versus prototype application

- Effect of end restraint conditions (restrained and unrestrained) on test results, including the influence of stiffness

- Structural connections (not currently addressed in ASTM E 119)

- Combination of loading and exposure (temperature profile) adequately represent expected conditions

- Procedures to analyze and evaluate data from fire resistance tests of other building components and assemblies to qualify an untested building element

- Repeatability of test results (single test currently defines rating for system)

- Reproducibility of heat flux environment between different furnaces and laboratories.

- Relationships between prescriptive ratings and performance of the assembly in realistic building fires.

Chapter 7
REFERENCES

ACI 318-63 (1963). Building Code Requirements for Reinforced Concrete, American Concrete Institute, Detroit, MI.

AISC 1963 (1963). *Manual of Steel Construction*, Sixth Edition, American Institute of Steel Construction, Chicago, IL.

AISC 2001 (1989). *Manual of Steel Construction: Allowable stress Design*, Ninth Edition, American Institute of Steel Construction, Chicago, IL.

AISC 2001 (2001). *Manual of Steel Construction: Load and Resistance Factor Design*, Third Edition, American Institute of Steel Construction, Chicago, IL.

ASTM (1973). Standard Test Methods for Fire Tests of Building Construction and Materials, ASTM E 119-73, ASTM International, Conshohocken, PA.

ASTM (2000). Standard Test Methods for Fire Tests of Building Construction and Materials, ASTM E 119-00, ASTM International, Conshohocken, PA.

ASTM (2000a). Standard Test Methods for Thickness and Density of Sprayed Fire-Resistive Material (SFRM) Applied to Structural Members, ASTM E 605-93 (Reapproved 2000), ASTM International, Conshohocken, PA.

Beitel, J, and Iwankiw, N. (2002). "Analysis of Needs and Existing Capabilities for Full-Scale Fire Resistance Testing," NIST GCR 02-843, National Institute of Standards and Technology, Gaithersburg, MD.

Jefferson, T. B. and Woods, G. (1962). *Metals and How to Weld Them*, Second edition, The James F. Lincoln Arc Welding Foundation, Cleveland, OH.

This page intentionally left blank.

Appendix A
CERTIFIED MILL TEST REPORTS (CMTRS)

This page intentionally left blank.

BAYOU STEEL CORPORATION
RIVER ROAD P.O. BOX 5000
LA PLACE, LOUISIANA 70069-1156
Telephone (985) 652-4900

MATERIAL CERTIFICATION REPORT

THE A588 & A572 STEEL CO
133 SABAGO LAKE DRIVE
SEWICKLY, PA 15143

THE A588 & A572 STEEL CO
10 ARCH STREET EXT.
CARNEGIE, PA 15106

TESTED IN ACCORDANCE WITH ASTM A6

INVOICE NO.
PRODUCT ANGLES
HEAT NO. 18040S 83 Pcs
Length 40'0"

DATE 09/17/03
Cust A-0005 -0000
GRADE A588B -01
SIZE L 2 X 2 X 1/4 X 3.19

PO:2032

Metals USA 9239
PO# BAL821

CHEMICAL ANALYSIS	
C	.16
Mn	.94
P	.008
S	.03
Si	.25
Cu	.37
Ni	.13
Cr	.50
Mo	.045
Cb	.000
V	.035
B	
Al	
Sn	.005
N	
Ti	

CI	6.3
CE	

MECHANICAL PROPERTIES	TEST 1 IMPERIAL	TEST 1 METRIC	TEST 2 IMPERIAL	TEST 2 METRIC	TEST 3 IMPERIAL	TEST 3 METRIC
YIELD STRENGTH	61,245 PSI	422 MPa	62,178 PSI	429 MPa	PSI	MPa
TENSILE STRENGTH	92,502 PSI	638 MPa	92,389 PSI	637 MPa	PSI	MPa
ELONGATION	30.0 %	30.0 %	25.0 %	25.0 %	%	%
GUAGE LENGTH	8 in	203 mm	8 in	203 mm	in	mm
BEND TEST DIAMETER	d	d	d	d	d	d
BEND TEST RESULTS						
SPECIMEN AREA	sq in	sq mm	sq in	sq mm	sq in	sq mm
REDUCTION OF AREA	%	%	%	%	%	%
IMPACT STRENGTH	ft-lbs	J	ft-lbs	J	ft-lbs	J

IMPACT STRENGTH	IMPERIAL	METRIC
AVERAGE	ft-lbs	J
TEST TEMP	F	C
ORIENTATION		

INTERNAL CLEANLINESS	
SEVERITY	
FREQUENCY	
RATING	

GRAIN SIZE	
HARDNESS	
GRAIN PRACTICE	
REDUCTION RATIO	

Customer Grade & Specs: A588B NO WELD REPAIR
AASHTO M270 GRADE 50W, 345MPA, ASTM GRADE A572 GRADE 50
FULLY KILLED FINE GRAIN PRACTICE

I HEREBY CERTIFY THAT THE MATERIAL TEST RESULTS PRESENTED HERE ARE FROM THE REPORTED HEAT AND ARE CORRECT. ALL TESTS WERE PERFORMED IN ACCORDANCE TO THE SPECIFICATIONS REPORTED ABOVE. ALL STEEL IS ELECTRIC FURNACE MELTED, MANUFACTURED, PROCESSED, AND TESTED IN THE U.S.A WITH SATISFACTORY RESULTS, AND IS FREE OF MERCURY CONTAMINATION IN THE PROCESS.

NOTARIZED UPON REQUEST:
SWORN TO AND SUBSCRIBED BEFORE ME IN AND FOR ST. JOHN PARISH ON THIS _____ DAY OF _____, 20____

(NOTARY PUBLIC)

SIGNED Timothy R. White
TIMOTHY R. WHITE, QUALITY ASSURANCE MANAGER

DIRECT ANY QUESTIONS OR NECESSARY CLARIFICATIONS CONCERNING THIS REPORT TO THE SALES DEPARTMENT.
1-800-535 7692 (USA)

ROANOKE ELECTRIC STEEL CORPORATION

P.O. BOX 13948 ROANOKE, VIRGINIA 24038-3948

Test and Inspection Report

NO. 47405-1
ROANOKE

METALS USA P&S LANGHORNE
50 CABOT BOULEVARD
LANGHORNE PA 19047-0000

Date 3/05/03

HEAT NUMBER	SIZE	1-YIELD Pt. KSI	ULTIMATE KSI	ELONG 8 IN.	BEND TEST	GRADE
JD4165	ANGLES 1 1/2 X 1 1/2 X 1/4	61.7	79.2	23.1		AH36
PURCHASE ORDER NUMBER	NUMBER PIECES	2-YIELD PT. KSI	ULTIMATE KSI	ELONG 8 IN.	BEND TEST	GRADE
W6095	251 PIECES 20'	63.4	80.7	23.1		AH36

HEAT NUMBER	SIZE	1-YIELD Pt. MPA	ULTIMATE MPA	ELONG 203mm	BEND TEST	GRADE
JD4165	ANGLES 38.1 X 38.1 X 6.4	425.4	546.1	23.1		AH36
PURCHASE ORDER NUMBER	NUMBER PIECES	2-YIELD PT. MPA	ULTIMATE MPA	ELONG 203mm	BEND TEST	GRADE
W6095	251 PIECES 20'	437.1	556.4	23.1		AH36

C	MN	S	P	SI	CR	NI	MO	CU	V	NB
.15	1.10	.020	.008	.21	.08	.09	.02	.24	.060	.001

METALS USA
Northeast Heavy Carbon Group
Test Reports for
CANAM
Your Order # R6517
Requisition #
Our Invoice # PHI-60847

MERCURY, RADIUM OR OTHER ALPHA SOURCE MATERIALS IN ANY FORM HAVE NOT BEEN USED IN THE PRODUCTION OF THIS MATERIAL. NO WELD REPAIR HAS BEEN PERFORMED. MATERIAL MANUFACTURED IN ACCORDANCE WITH OUR QUALITY MANUAL REVISION 9 DATED 5-1-1998, BASED UPON ISO 9002-1994, ASME SECTION III DIV I NCA3800, ANSI-45.2 10CFR50 AND 10CFR21.

Approved ABS QA Mill. Certificate No. 00NN10108-X.

This material was melted and manufactured in the USA by basic Electric Furnace processes to meet specification: ASTM A572-99A GR 50 TYPE 2

The tensile values stated in either inch-pound units or SI units are to be regarded as separate as defined in the ASTM scope for this material. Unless a metric specification is ordered, this material has been tested and meets the requirements of the inch-pound ranges.

This is to certify the above to be a true and accurate report as contained in the records of this company.

Engineer of Tests: Charles R. Charlton

SMI Steel - Alabama and South Carolina

SMI Steel - Alabama
P.O. Box 321188
Birmingham, AL 35232-1188
www.smi-al.com

SMI Steel - South Carolina
Box 2005
Cayce, SC 29171-2005
www.smi-sc.com

CERTIFIED MILL TEST REPORT

For additional copies call (800) 637-3227

We hereby certify that the test results presented here are accurate and conform to the reported grade specification

Richard B. Ray
Quality Assurance Manager

HEAT NO.: 48361
SECTION: RD 15/16x40'0"
23.81mm RDx12.192
GRADE: ASTM A529-00 GRADE 50
ASTM A529M-00 GRADE 50

SOLD TO:
CANAM STEEL CORPORATION
P.O. BOX 285
POINT OF ROCKS, MD 21777-0285

SHIP TO:
CANAM STEEL CORP
4010 CLAY ST.-RT. 28
POINT OF ROCKS, MD 21777-

SHIP#: 101196/150
BOL #: 185997
INV #:
CUST PO#: R6450
CUST P/N:

CHEMICAL ANALYSIS	%
C	0.21
Mn	0.92
P	0.006
S	0.031
Si	0.19
Cu	0.34
Cr	0.11
Ni	0.11
Mo	0.031
Cb	0.000
V	0.000
Sn	
B	
Ti	
C.Eq.	0.45

MECHANICAL PROPERTIES	TEST 1 IMPERIAL	TEST 1 METRIC	TEST 2 IMPERIAL	TEST 2 METRIC	TEST 3 IMPERIAL	TEST 3 METRIC
Yield Strength	58.4 KSI	402.5 MPA				
Tensile Strength	80.7 KSI	556.4 MPA				
Elongation	25 %	25 %				
Gauge Length	8 INS	203 MM				
Reduction of Area	43 %	43 %				
Bend Test						
Diameter						
Charpy Impact						
Test Temp						
Sample Size						
Orientation						
Hardness						

JOMINY RESULTS - Rockwell C hardness at 1/16th Inch Increments

1	2	3	4	5	6	7	8	9	10	11	12
13	14	15	16	18	20	22	24	26	28	30	32

GRAIN SIZE
METHOD
RESULT

INCLUSION RATING

METHOD				
TYPE				
SIZE	T H	T H	T H	T H

100% MELTED AND MANUFACTURED IN THE USA AND FREE OF MERCURY CONTAMINATION IN THE PROCESS

REMARKS:

SEP-30-2003 18:53

SMI Steel - Alabama and South Carolina

SMI Steel - Alabama
P.O. Box 321188
Birmingham, AL 35232-1188
www.smi-al.com

SMI Steel - South Carolina
Box 2005
Cayce, SC 29171-2005
www.smi-sc.com

CERTIFIED MILL TEST REPORT

For additional copies call (800) 637-3227

We hereby certify that the test results presented here are accurate and conform to the reported grade specificatio

Richard S. Ray
Quality Assurance Manager

HEAT NO.: 53143
SECTION: RD 1x40'0"
25.4mm RDx12.192
GRADE: ASTM A529-00 GRADE 50
ASTM A529M-00 GRADE 50

SOLD TO: CANAM STEEL CORPORATION
P.O. BOX 285
POINT OF ROCKS, MD 21777-0285

SHIP TO: CANAM STEEL CORP
4010 CLAY ST.--RT. 28
POINT OF ROCKS, MD 21777-

SHIP#: 101195/168
BOL #: 185864
INV #:
CUST PO#: R6338
CUST P/N:

CHEMICAL ANALYSIS

	%
C	0.21
Mn	0.94
P	0.009
S	0.042
Si	0.19
Cu	0.24
Cr	0.16
Ni	0.11
Mo	0.026
Cb	0.000
V	0.000
Sn	
B	
Ti	
C.Eq.	0.46

PROPERTIES

MECHANICAL	TEST 1 IMPERIAL	TEST 1 METRIC	TEST 2 IMPERIAL	TEST 2 METRIC	TEST 3 IMPERIAL	TEST 3 METRIC
Yield Strength	54.0 KSI	372.1 MPA				
Tensile Strength	78.6 KSI	541.9 MPA				
Elongation	23 %	23 %				
Gauge Length	8 INS	203 MM				
Reduction of Area	42 %	42 %				
Bend Test						
Diameter						
Charpy Impact						
Test Temp						
Sample Size						
Orientation						
Hardness						

JOMINY RESULTS - Rockwell C hardness at 1/16th inch increments

1	2	3	4	5	6	7	8	9	10	11	12
13	14	15	16	18	20	22	24	26	28	30	32

GRAIN SIZE
METHOD
RESULT

INCLUSION RATING

METHOD				
TYPE				
SIZE	T H	T H	T H	T H

100% MELTED AND MANUFACTURED IN THE USA AND FREE OF MERCURY CONTAMINATION IN THE PROCESS

REMARKS:

INSTEEL WIRE PRODUCTS

Mount Airy, North Carolina

DISCRETE JOB # 161663

This is to certify that the manufacturing processes for the reinforcement material described below occurred in the United States of America and was made in accordance with and conforms to the following specifications:

ASTM -A 82 Tensile & Bend Tests
ASTM-A 185 Weld Shear Tests

Conf Number: 164877
Cust. Order No:
Sales Order No:

Item Number: **533-061358**

Product Style: 10X4-W4.2/W4.3-60"X18'2"(1+1) W4.2/W4.3

TENSILE TESTS

WIRE SIZES		Test No.	Pounds / Foot "Deformed Wire Only"		WIRE DIA.	ACTUAL AREA	TENSILE POUNDS/ SQ. IN.	ROA %	YIELD STRENGTH P.S.I.
Longitudunal	Transverse		Actual	Nominal	(Inches)	(Sq. In.)			
W4.2	XXXXXXX	1			0.230	0.04155	96,412	61%	71,361
W4.2	XXXXXXX	2			0.230	0.04155	94,450	61%	71,361
XXXXXXX	W4.3	1			0.234	0.04301	95,076	59%	72,198
XXXXXXX	W4.3	2			0.234	0.04301	96,117	59%	72,198

ALL WIRES LISTED ABOVE MEET A.S.T.M. A-82 OR A-496 BEND TEST REQUIREMENTS

WELD SHEAR TESTS

WIRE SIZES: W4.2 / W4.3

Test Number	1	2	3	4
Break Load (Lbs. Of Force)	2764	2215	3608	3477

MINIMUM BREAK LOAD REQUIRED 1505 **LBS. OF FORCE**

RAW MATERIALS - HEAT NUMBER INFORMATION

Longitudinal Wires	Heat No's.:
Code: W17516	164877

Transverse Wires	Heat No's.:
Code: W17516	164877

Date: 12/13/2003

Quality Assurance
Insteel Wire Products
Wesley Knott

INSTEEL WIRE PRODUCTS

Mount Airy, North Carolina

DISCRETE JOB # 161664

This is to certify that the manufacturing processes for the reinforcement material described below occurred in the United States of America and was made in accordance with and conforms to the following specifications:

ASTM -A 82 Tensile & Bend Tests
ASTM-A 185 Weld Shear Tests

Conf Number: 164877
Cust. Order No:
Sales Order No:

Item Number: **533-061359** Product Style: 10x4-W4.2/W4.3-60"(+)X36'2"(1+1) W4.2/W4.3

TENSILE TESTS

WIRE SIZES		Test No.	Pounds / Foot "Deformed Wire Only"		WIRE DIA.	ACTUAL AREA	TENSILE POUNDS/	ROA %	YIELD STRENGTH
Longitudunal	Transverse		Actual	Nominal	(Inches)	(Sq. In.)	SQ. IN.		P.S.I.
W4.2	XXXXXXX	1			0.230	0.04155	96,281	61%	71,361
W4.2	XXXXXXX	2			0.230	0.04155	94,936	61%	71,361
XXXXXXX	W4.3	1			0.234	0.04301	95,169	59%	72,198
XXXXXXX	W4.3	2			0.234	0.04301	96,047	59%	72,198

ALL WIRES LISTED ABOVE MEET A.S.T.M. A-82 OR A-496 BEND TEST REQUIREMENTS

WELD SHEAR TESTS

WIRE SIZES: W4.2 / W4.3

Test Number	1	2	3	4
Break Load (Lbs. Of Force)	2562	3635	3708	3608

MINIMUM BREAK LOAD REQUIRED 1505 **LBS. OF FORCE**

RAW MATERIALS - HEAT NUMBER INFORMATION

Longitudinal Wires	Heat No's.:
Code: W17516	164877

Transverse Wires	Heat No's.:
Code: W17516	164877

Date: 12/13/2003

Quality Assurance
Insteel Wire Products Wesley Knott

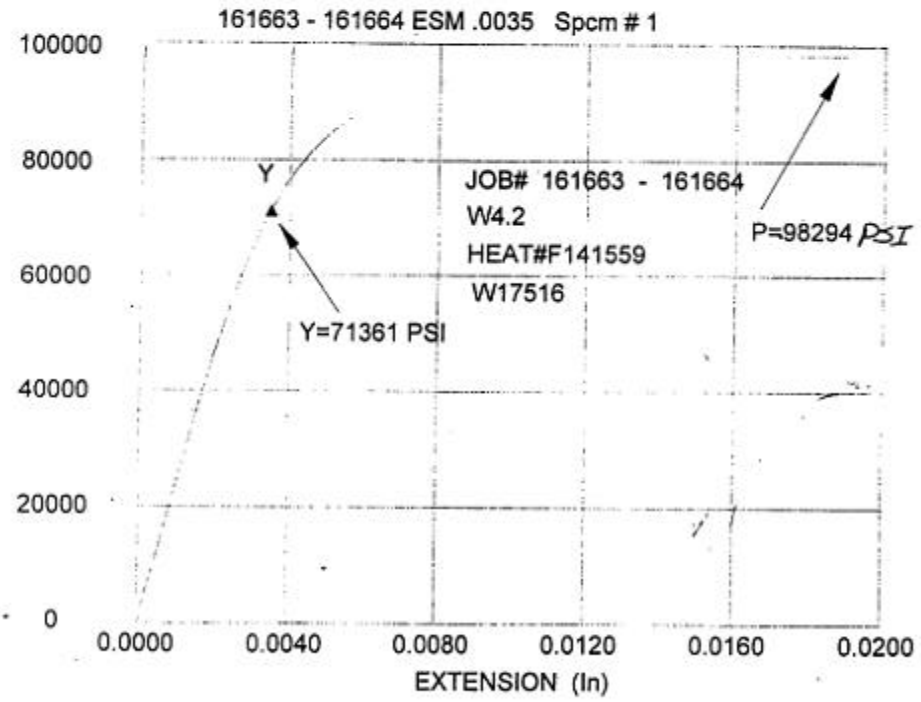
161663 - 161664 ESM .0035 Spcm # 1
100000
80000
60000
40000
20000
0
0.0000
0.0040
0.0080
0.0120
0.0160
0.0200
EXTENSION (In)
Y
JOB# 161663 - 161664
W4.2
HEAT#F141559
W17516
P=98294 PSI
Y=71361 PSI

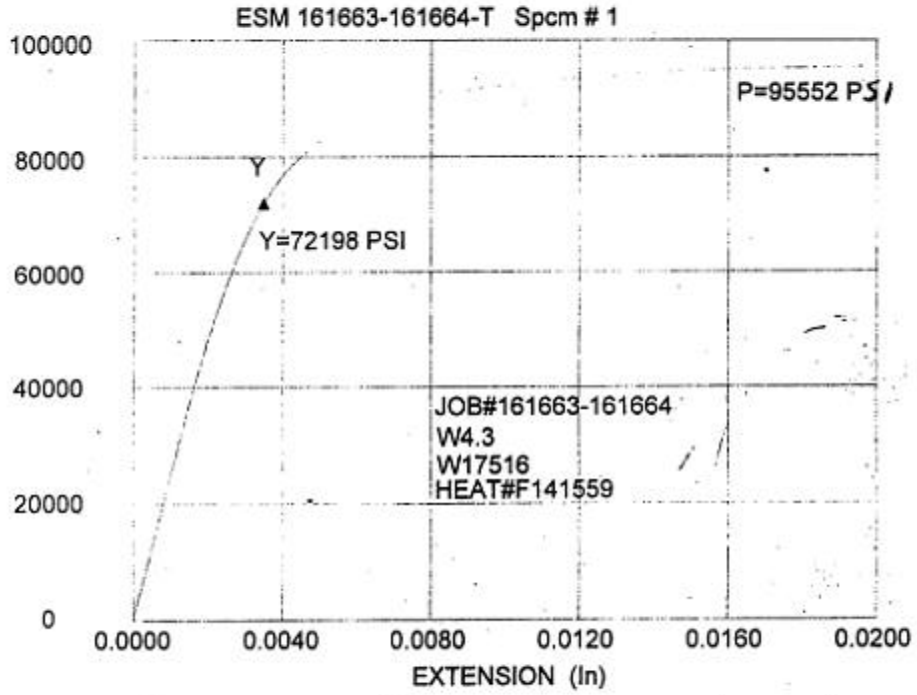
ESM 161663-161664-T Spcm # 1
100000
80000
60000
40000
20000
0
P=95552 PSI
Y
Y=72198 PSI
JOB#161663-161664
W4.3
W17516
HEAT#F141559
0.0000
0.0040
0.0080
0.0120
0.0160
0.0200
EXTENSION (In)

Appendix B
PRIMER PAINT SPECIFICATION

This page intentionally left blank.

LACLEDE STEEL COMPANY

September 1, 1967

Laclede Standard Steel Joist Paint
(FORMULA LREP - 10001)

Title: Standard Protective Red Chromate Primer No. 10001

Formulation:

Pigment		28.5%
Iron Oxide	55.0%	
Aluminum Silicate	41.0%	
Strontium Chromate	4.0%	
Total Pigment	100.0%	
Vehicle		71.5%
Unmodified Epoxy Amine	45.0%	
Deionized Water and Amine	55.0%	
Total Vehicle	100.0%	
		100.0%

Wt/Gal	9.3 Lbs.
Solids	52% by wt.
Grind	#4 Hegman Gauge
Viscosity	3600 cps. at 77° F.
Bake	Metal temperature 20 minutes at 350° F.
Weatherability	ASTM B-117-64 passes 150 hrs. on specified clean steel panel at 1 mil film thickness unscribed
Film Thickness	Dry 1.0 plus or minus 0.2 mils
Gloss	30 - 50
Pencil Hardness	F - H

Folder
From WTC221.00 PAINTING
2002-NOV-20
1 9

July 17, 1967

RECOMMENDED PAINT SPECIFICATION

Steel Joists and Accessories

Steel joists, bridging and accessories shall receive one uniform coat of protective paint before shipment, applied by the electrophoresces or similar process, providing a dense coating with a minimum dry film thickness of one mil.

The shop paint or primer shall be furnished in accordance with Pittsburgh Plate Glass Company Standard V.C. 41901 or equal. The finish applied paint shall be subject to a 350° Fahrenheit baking for a minimum of 10 minutes.

The paint shall be furnished in the manufacturer's standard red or gray color as specified.

Paint shall be applied thoroughly and evenly to clean chord angle and web sections with a resultant film not detrimental to the quality of field welding or field applied insulation or paint. The painted surfaces shall be free from oil, grease, dirt and foreign material.

The shop coating shall withstand 150 hours of 5% salt fog when applied to a clean rolled steel panel at 1.0 mil dry film thickness and tested according to ASTM B-117 salt fog test. Maximum failure allowed will be 6F according to ASTM D-714-56.

Appendix C
CONSTRUCTION DRAWINGS FOR 35 FT TEST ASSEMBLIES

This page intentionally left blank.

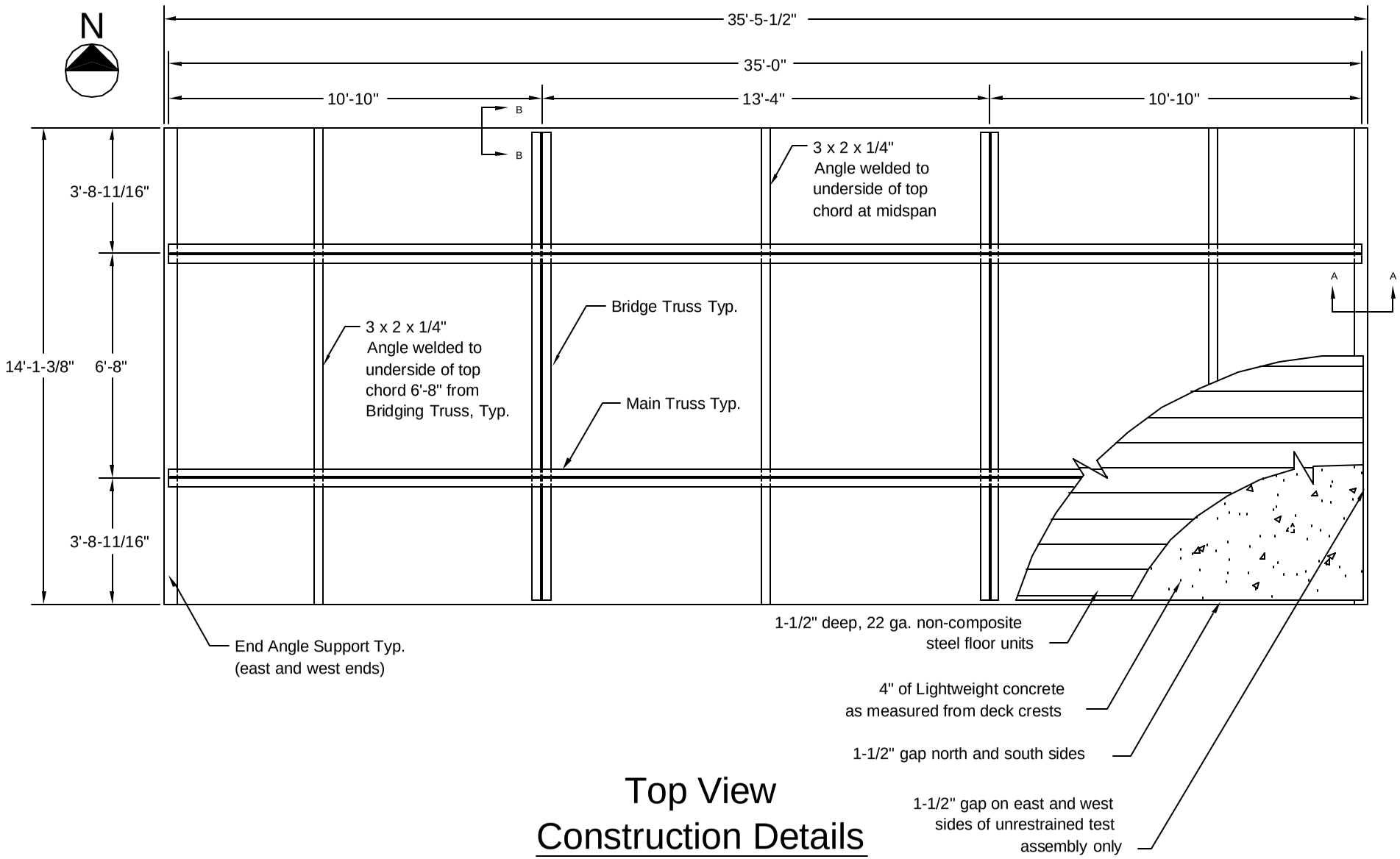

Top View
Construction Details

ULC CONSTR01.DWG

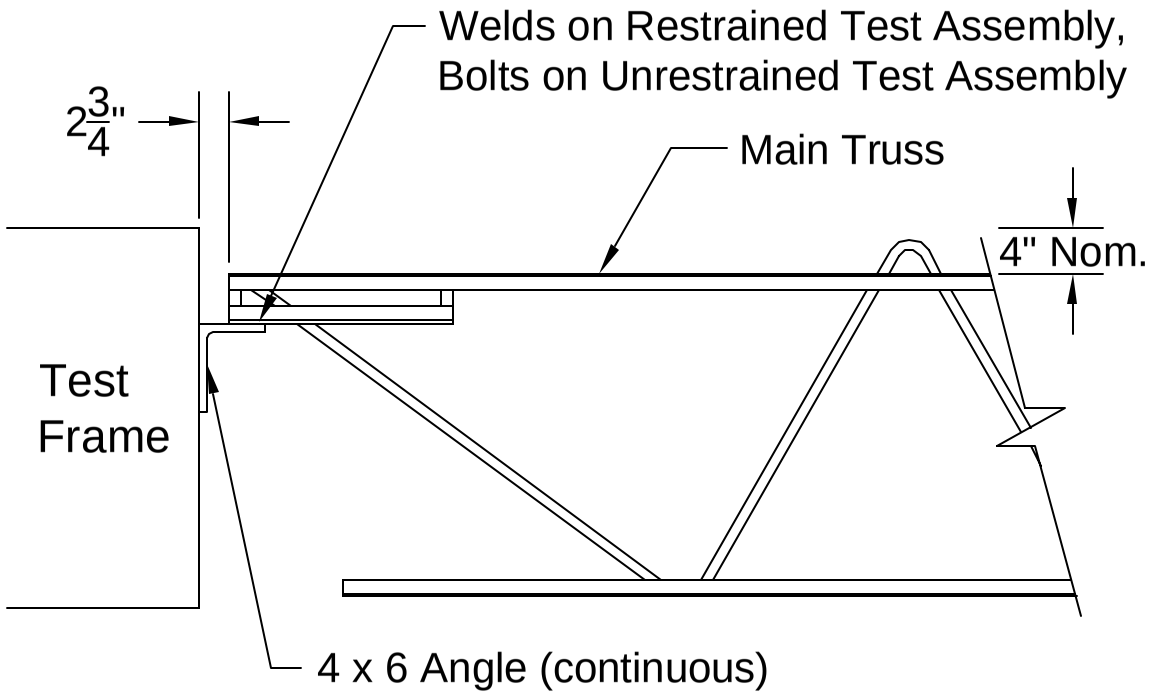

Section A-A

Construction Details

UL CONSTR02.DWG

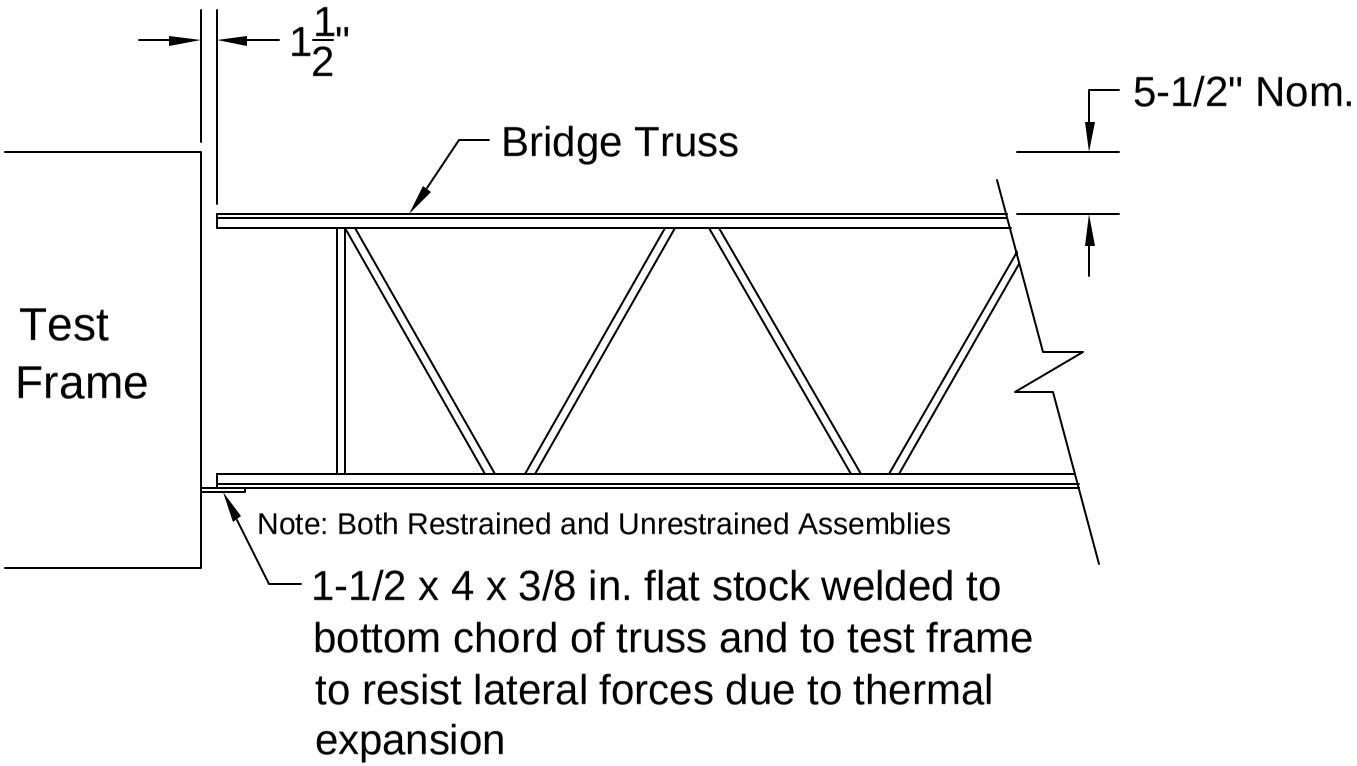

Section B-B

Construction Details

UL CONSTR03.DWG

This page intentionally left blank.

Appendix D
INSTRUMENTATION FOR 35 FT TEST ASSEMBLIES

This page intentionally left blank.

						*	*	*	*
A	B	C	D	E	F	G	H	I	J
1	9	17	25	33	41	49	59	69	79
2	10	18	26	34	42	50/51	60/61	70/71	80/81
3	11	19	27	35	43	52	62	72	82
4	12	20	28	36	44	53	63	73	83
5	13	21	29	37	45	54	64	74	84
6	14	22	30	38	46	55/56	65/66	75/76	85/86
7	15	23	31	39	47	57	67	77	87
8	16	24	32	40	48	58	68	78	88

* = Lower number to the East of the Bridging Truss and Higher number to the West of the Bridging Truss

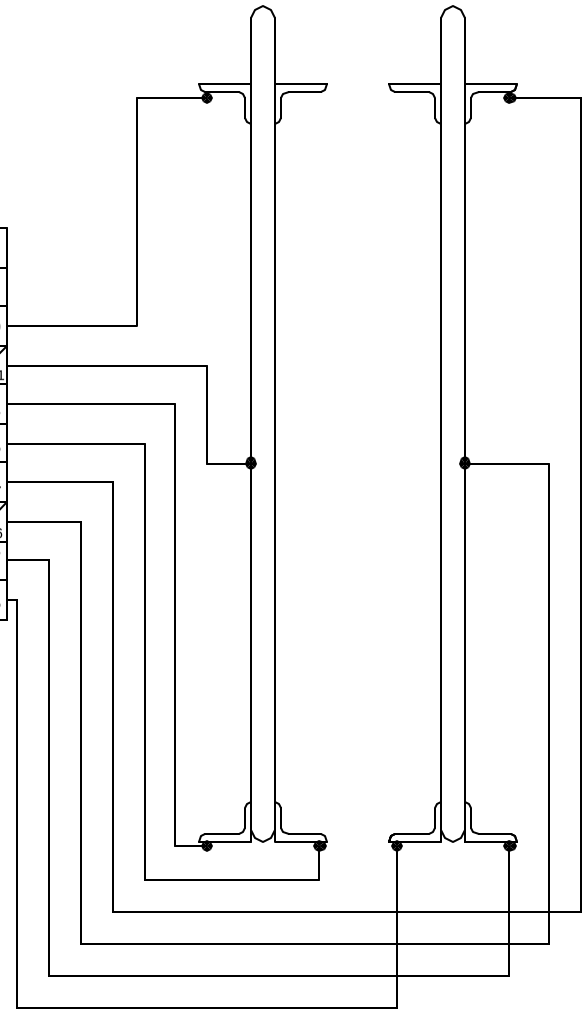

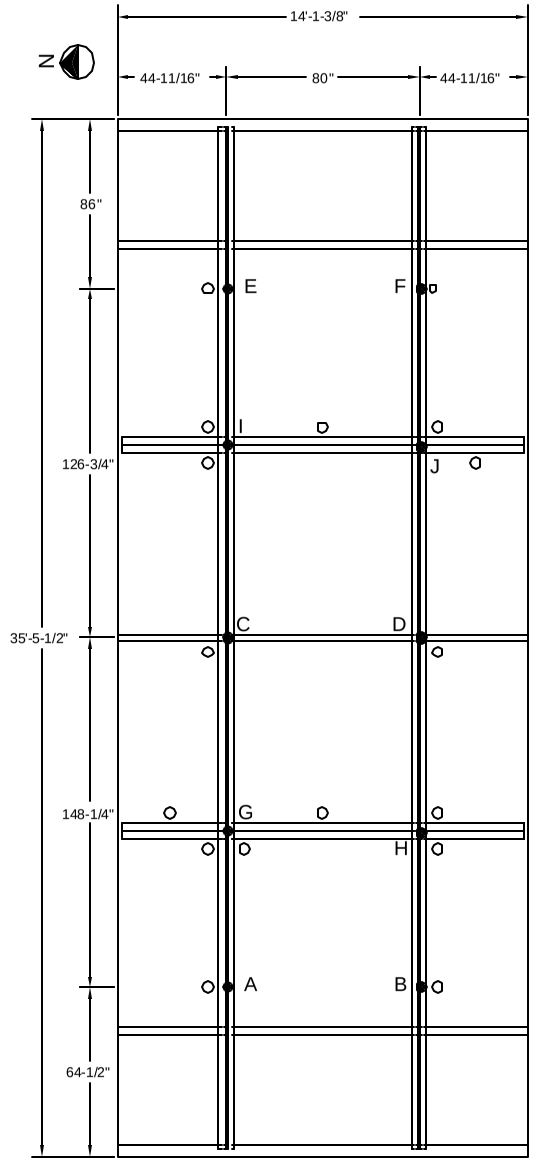

o - 1" diameter opening for themocouple wires on main and bridge trusses.

Main Truss Thermocouple Locations

ULC MAINTRUSSTC.DWG

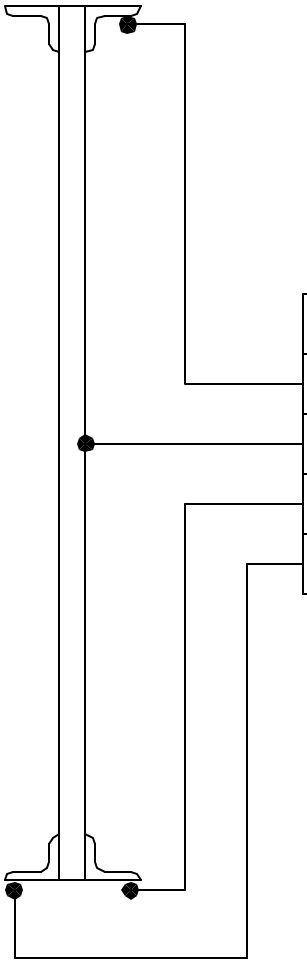

A	B	C	D	E	F	G	H
89	93	97	101	105	109	113	117
90	94	98	102	106	110	114	118
91	95	99	103	107	111	115	119
92	96	100	104	108	112	116	120

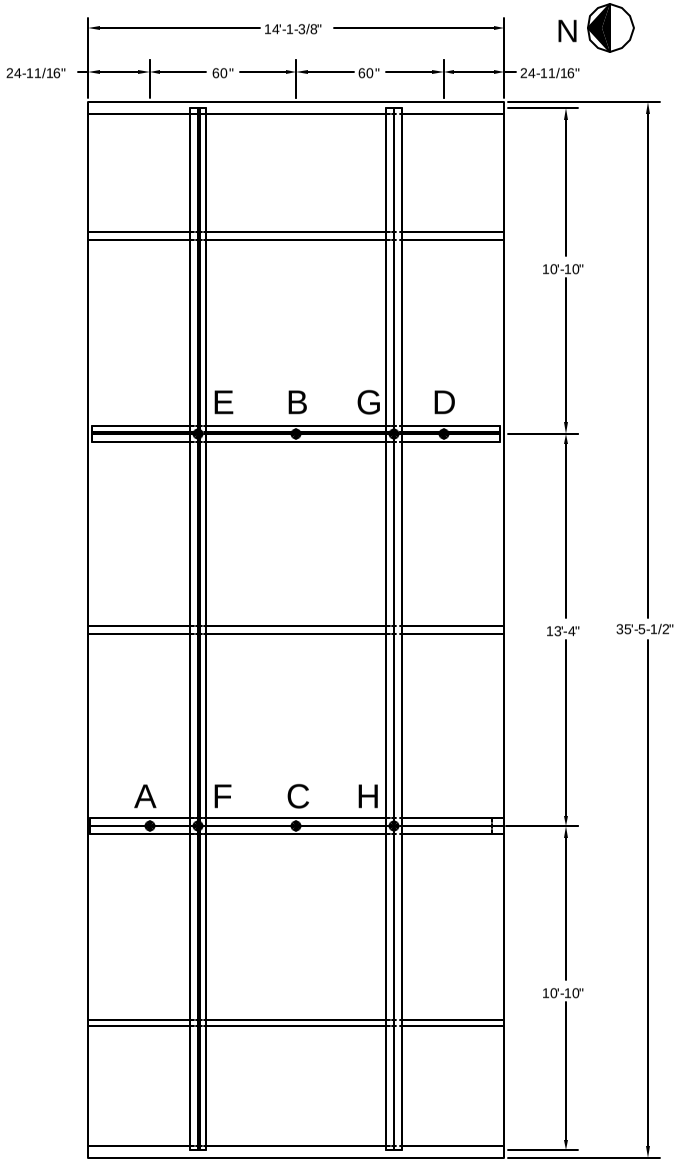

Bridging Truss Thermocouple Locations

ULC BRIDTC.DWG

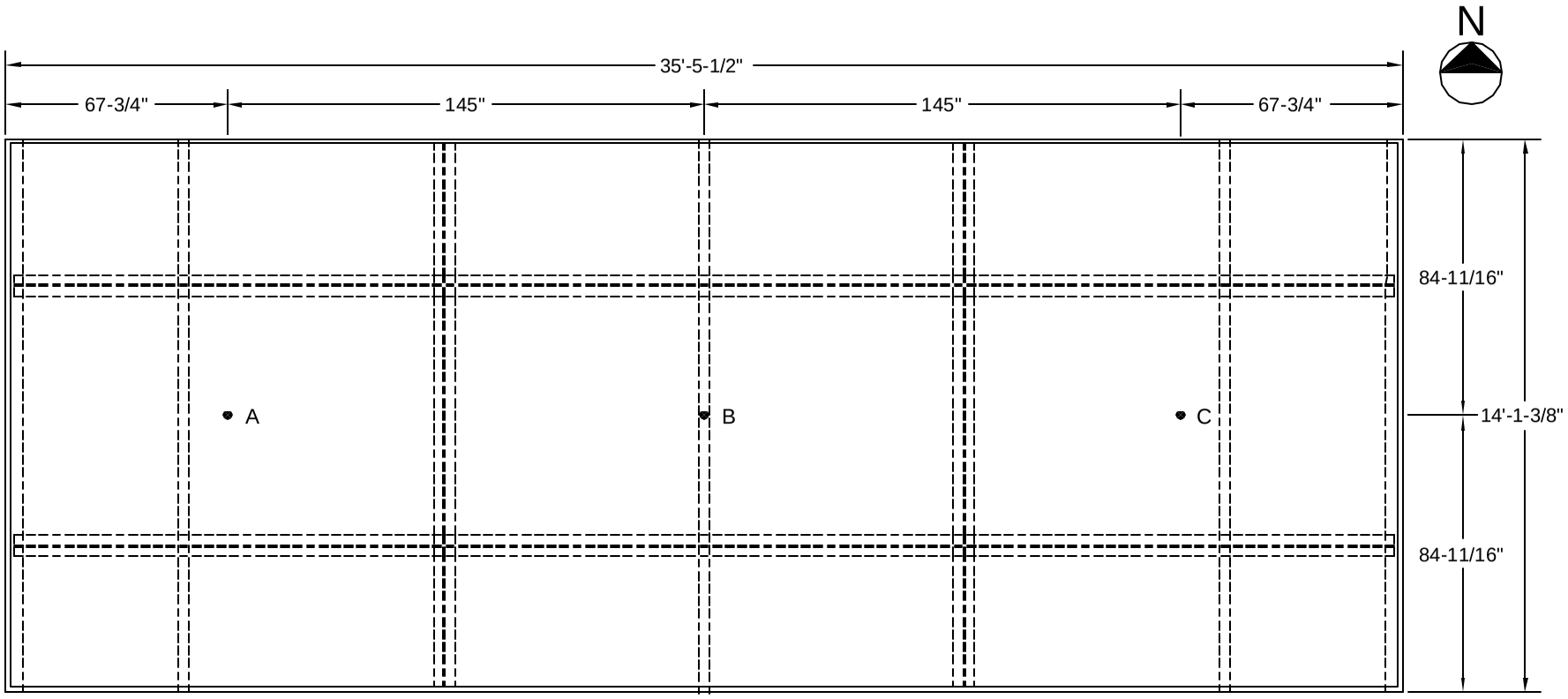

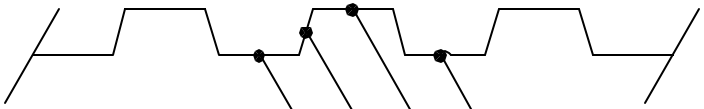

Note: Dimensions for locations may vary slightly depending on deck valley and crest occurance in actual construction

A	B	C	
121	125	129	Joint
122	126	130	Crest
123	127	131	Side
124	128	132	Valley

Steel Deck Thermocouple Locations

ULC DECKTC.DWG

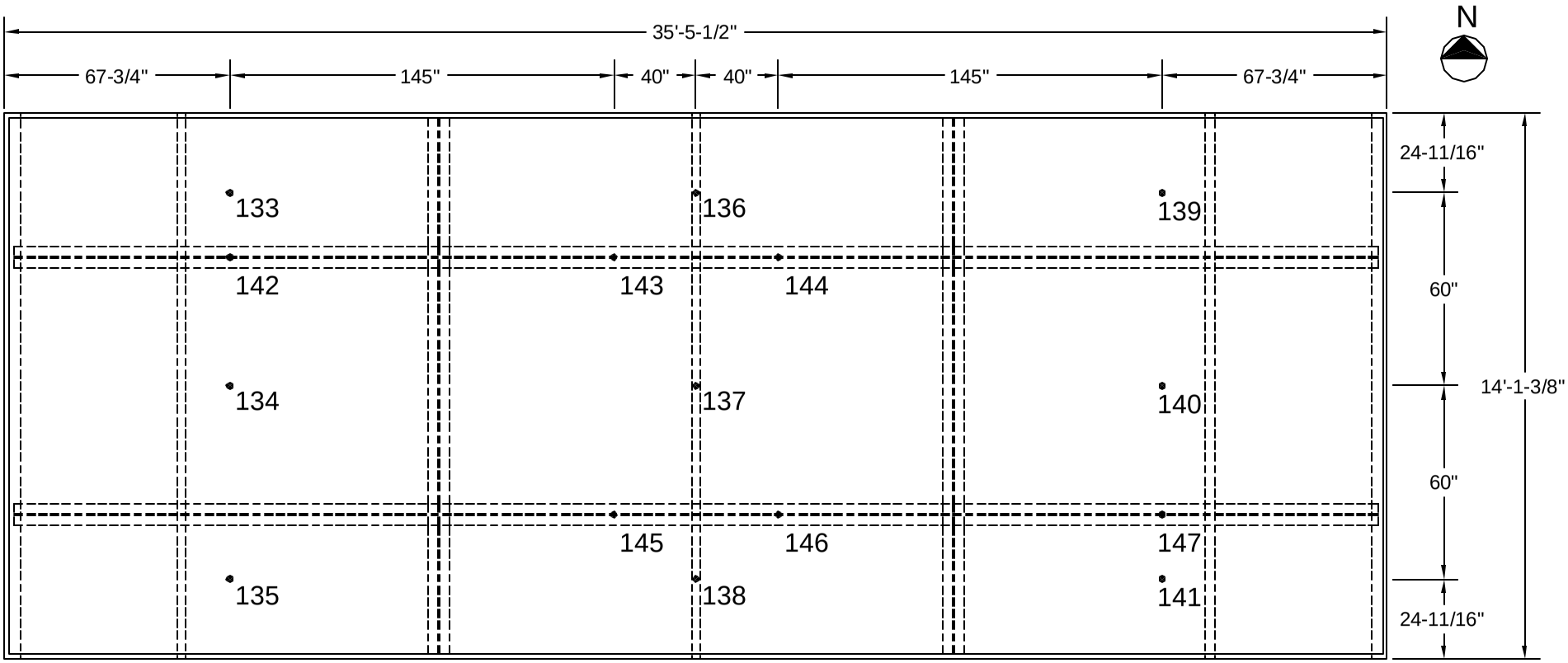

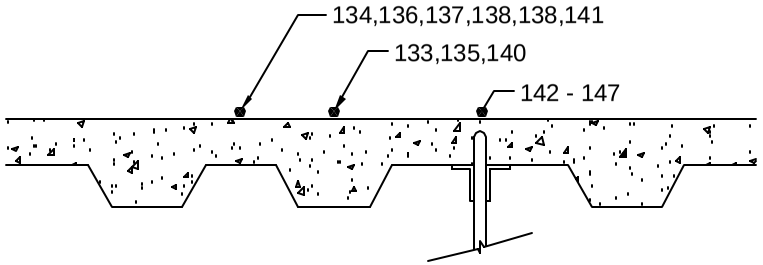

Note: Dimensions for locations may vary slightly depending on deck valley and crest occurance, and main truss knuckle location in actual construction

Unexposed Surface Thermocouple Locations

ULC UNEXPTC.DWG

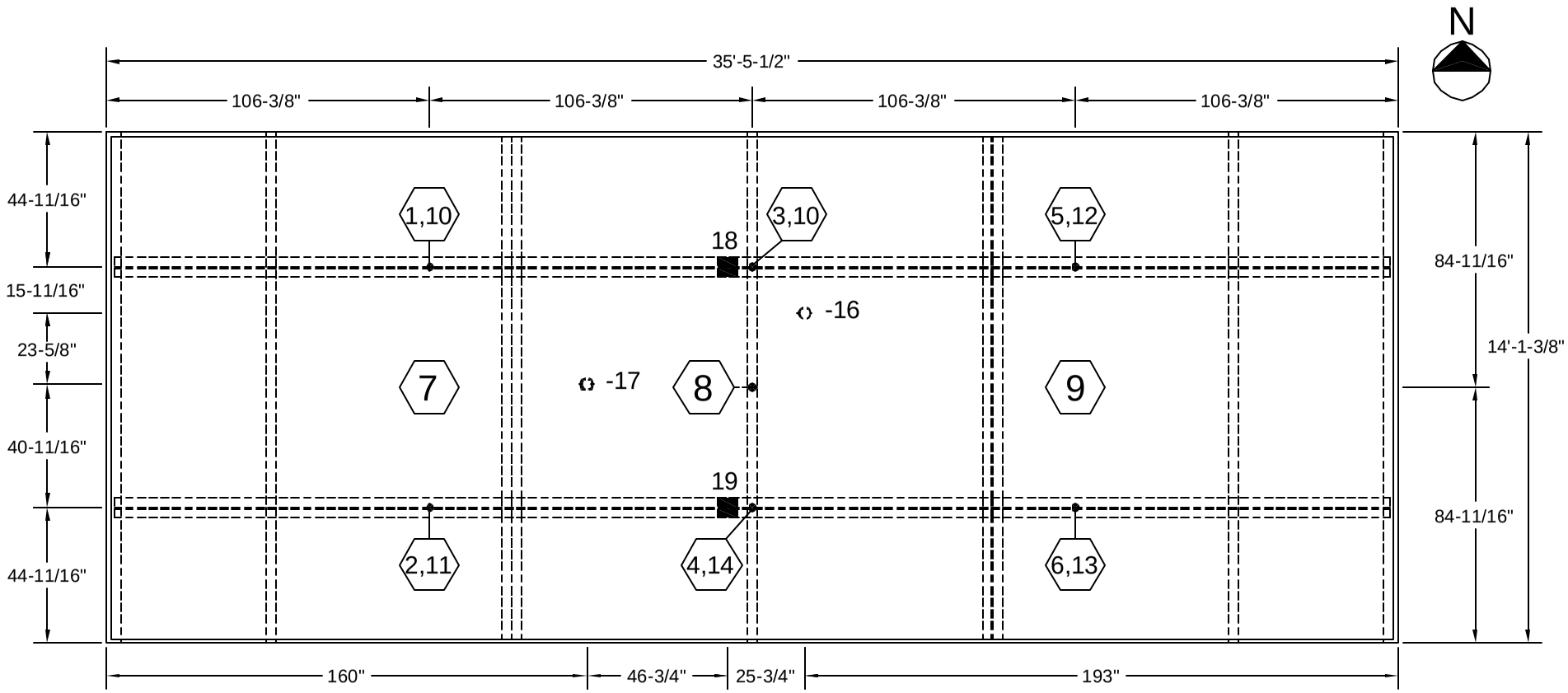

DEFLECTION TRANSDUCERS = ⬡ STRAIN GAUGES = ■ RADIOMETER = ⬭

Nos. 1 - 9 on unexposed surface
Nos. 10 - 15 on bottom chord of main truss

Note: Number 17 on Test Assembly No. 2 was moved 6 inches South from the location shown on drawing due to Steel Deck Thermocouple Locations

Additional Instrumentation Locations

ULC DEFL.DWG

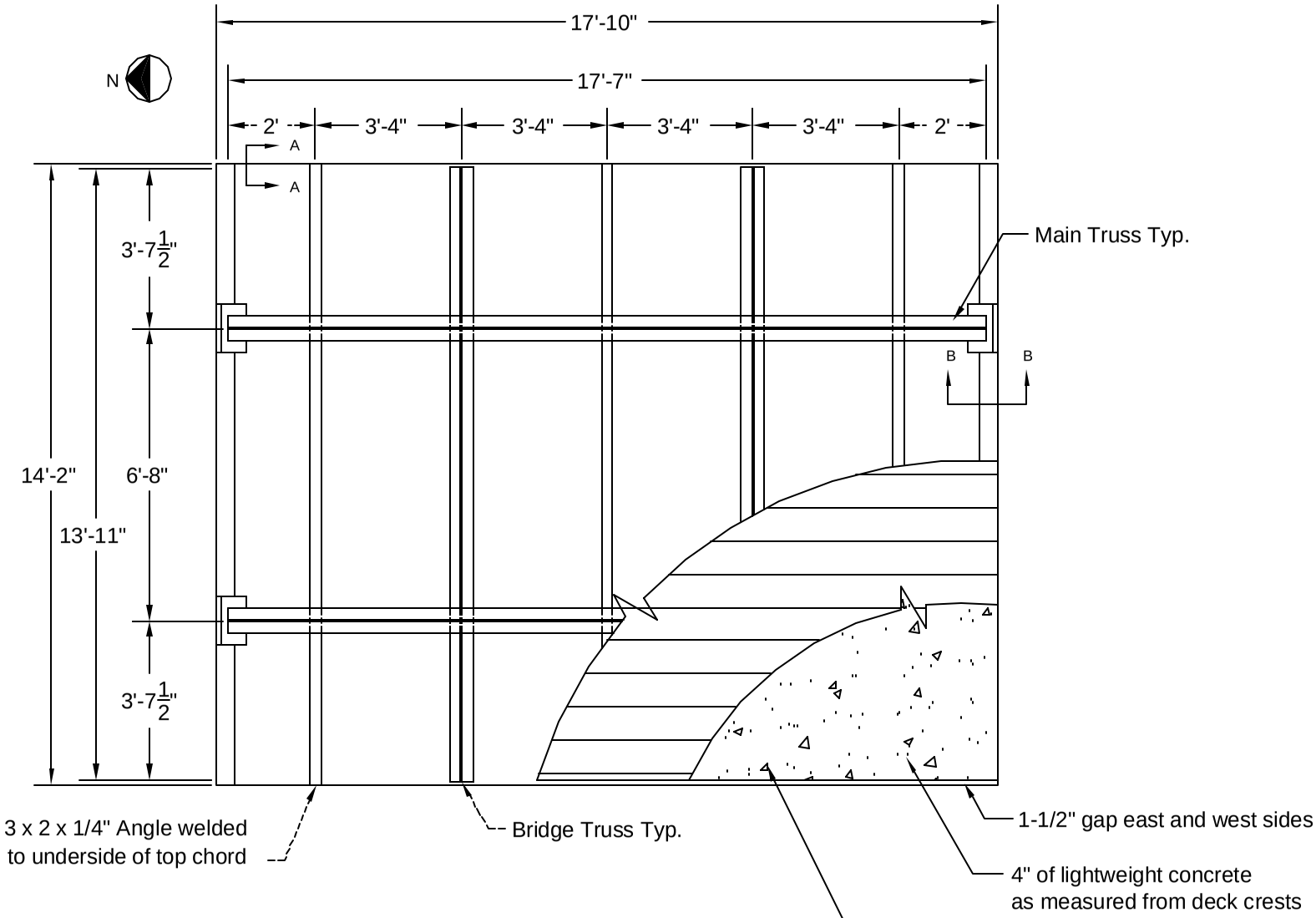

Note: All Connections
outside of fire area

Top View
Construction Details

UL CONSTR01.DWG

Appendix E
CONSTRUCTION DRAWINGS FOR 17 FT TEST ASSEMBLIES

This page intentionally left blank.

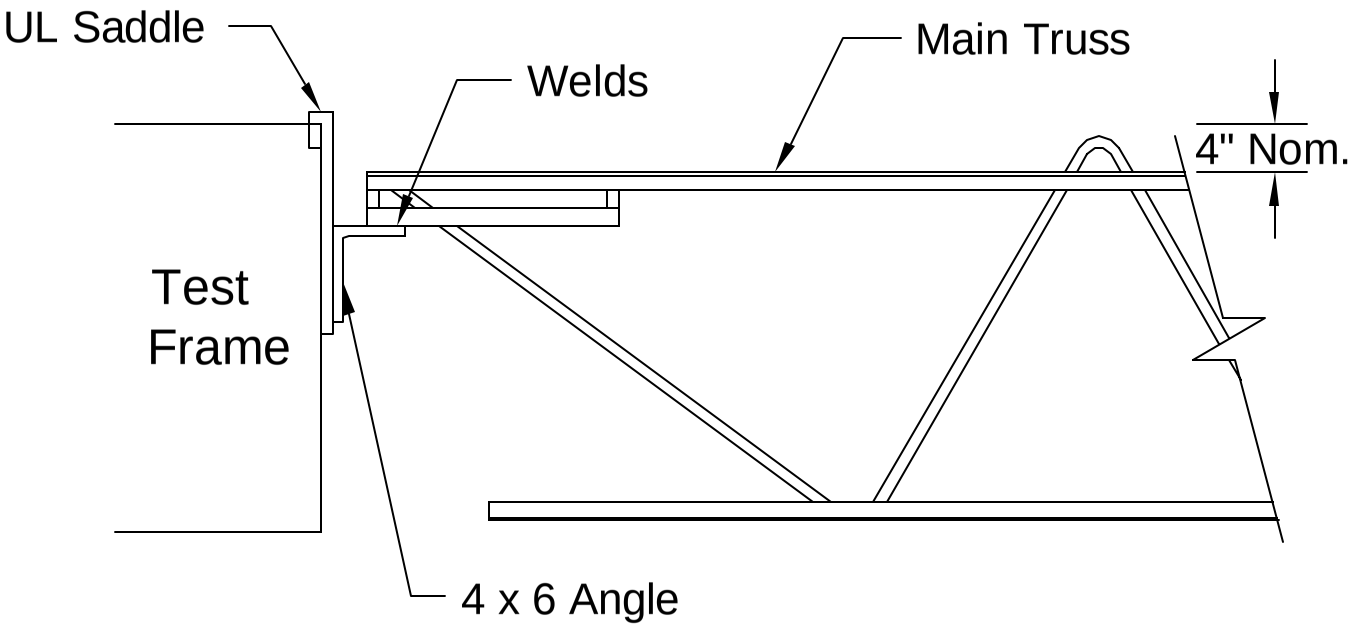

Section A-A

Construction Details

UL CONSTR02.DWG

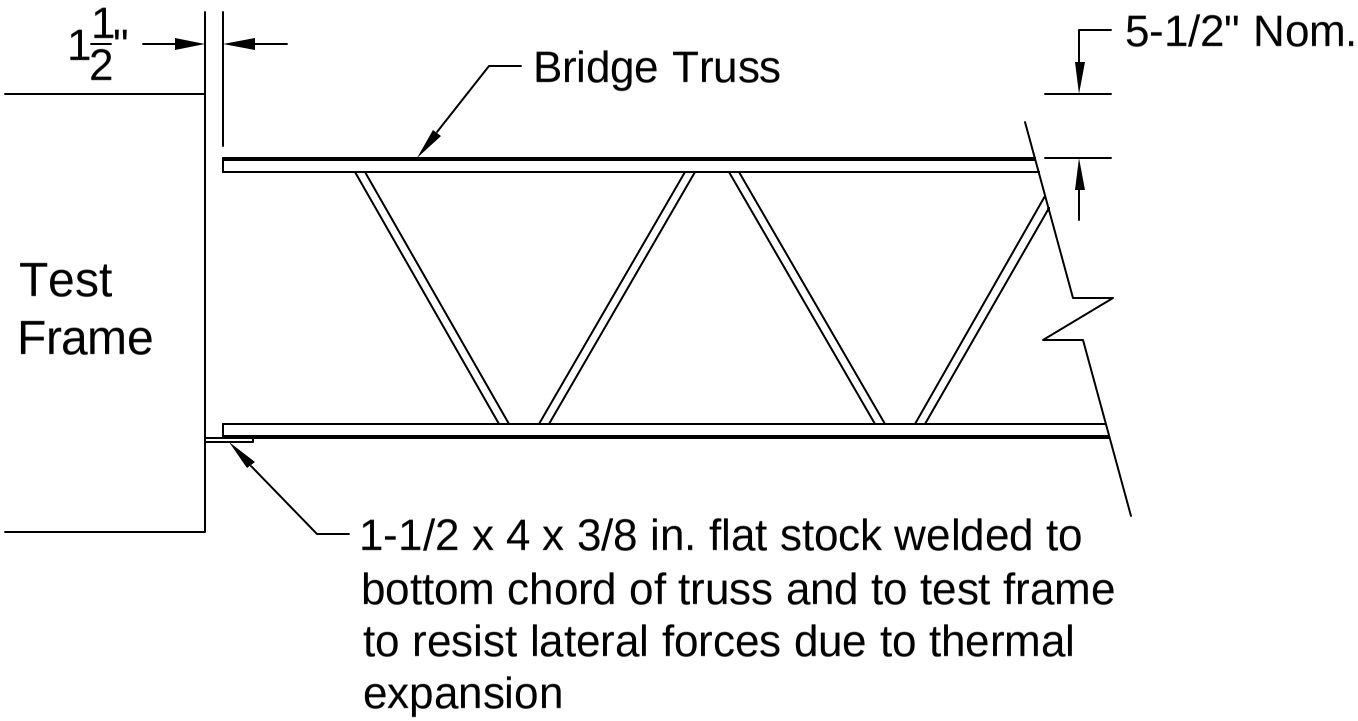

Section B-B

Construction Details

UL CONSTR03.DWG

Appendix F
INSTRUMENTATION FOR 17 FT TEST ASSEMBLIES

This page intentionally left blank.

A	B	C	D	E	F	G	H	I	J
1	9	17	25	33	41	49	57	65	73
2	10	18	26	34	42	50	58	66	74
3	11	19	27	35	43	51	59	67	75
4	12	20	28	36	44	52	60	68	76
5	13	21	29	37	45	53	61	69	77
6	14	22	30	38	46	54	62	70	78
7	15	23	31	39	47	55	63	71	79
8	16	24	32	40	48	56	64	72	80

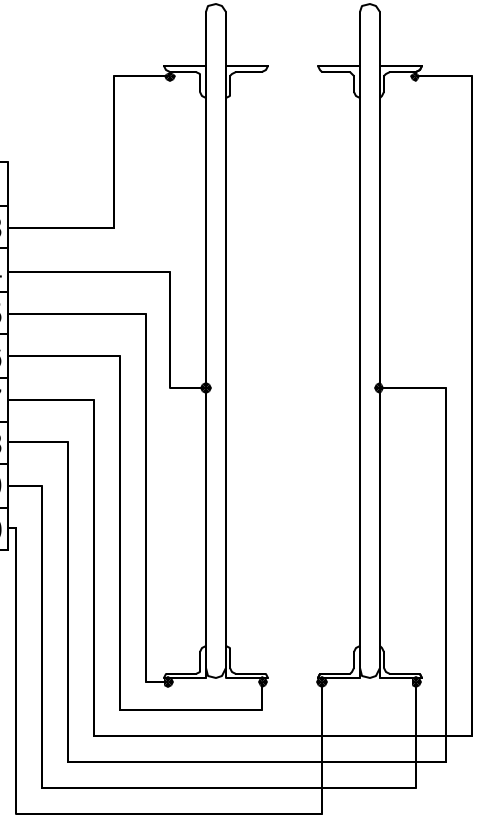

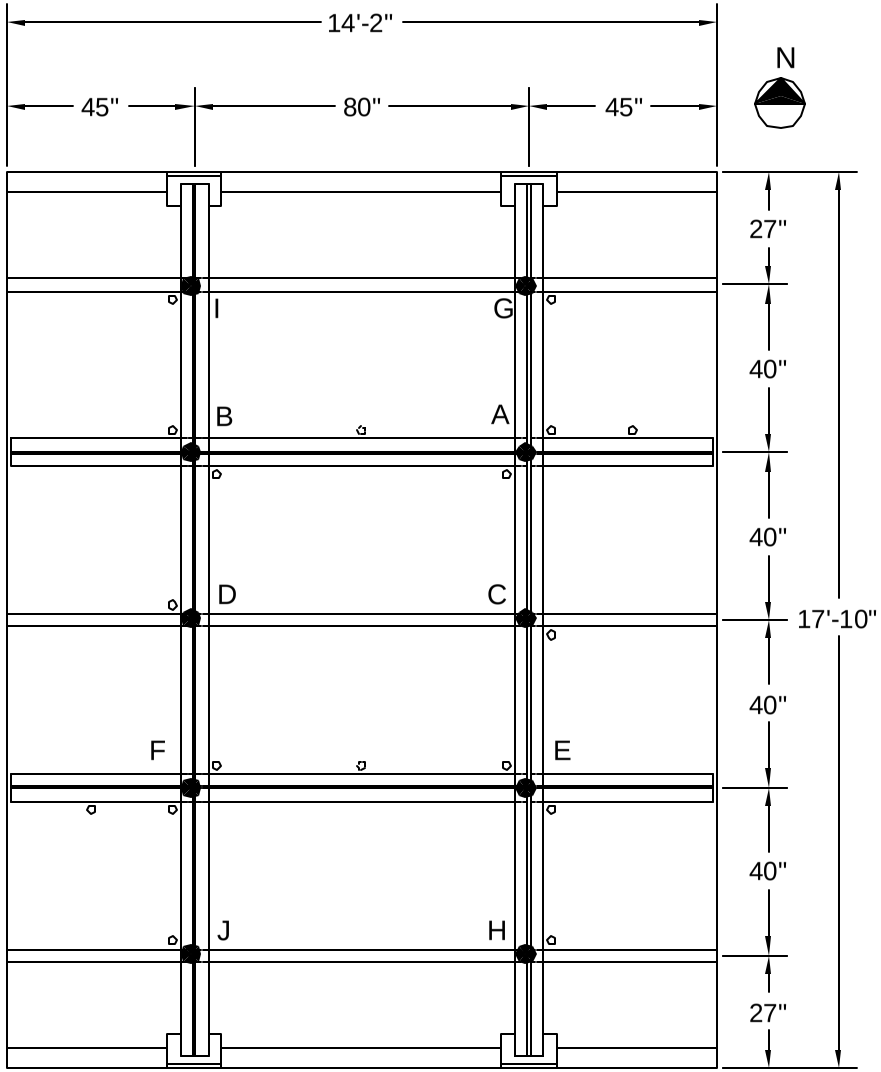

- 1" diameter opening for thermocouple wires on main and bridging trusses.

Main Truss Thermocouple Locations

UL MAINTRUSSTC.DWG

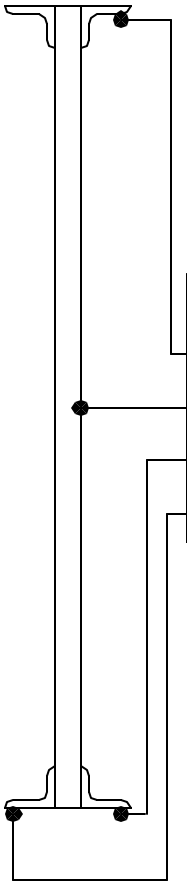

A	B	C	D	E	F	G	H
81	85	89	93	97	101	105	109
82	86	90	94	98	102	106	110
83	87	91	95	99	103	107	111
84	88	92	96	100	104	108	112

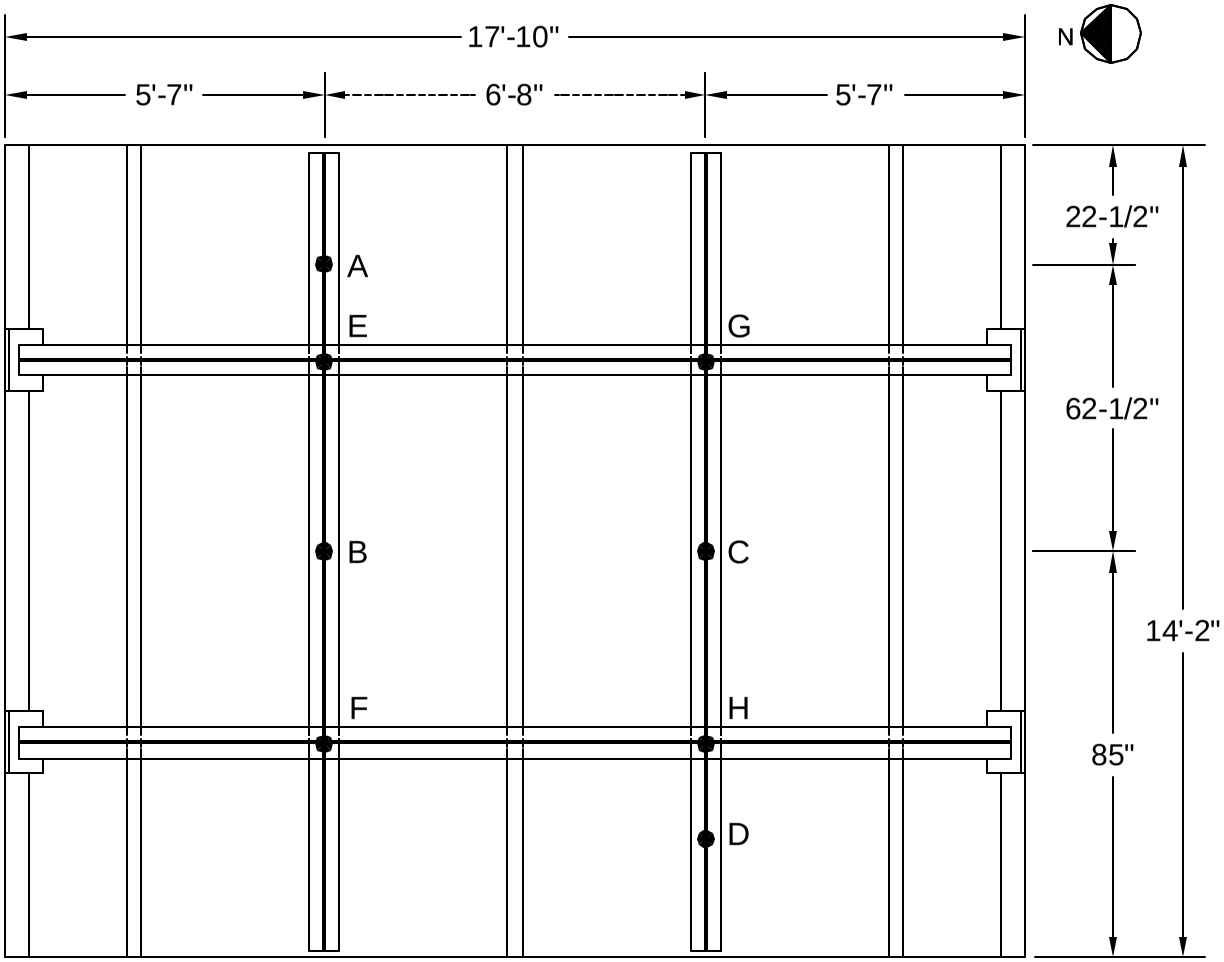

Bridging Truss Thermocouple Locations

UL BRIDTC.DWG

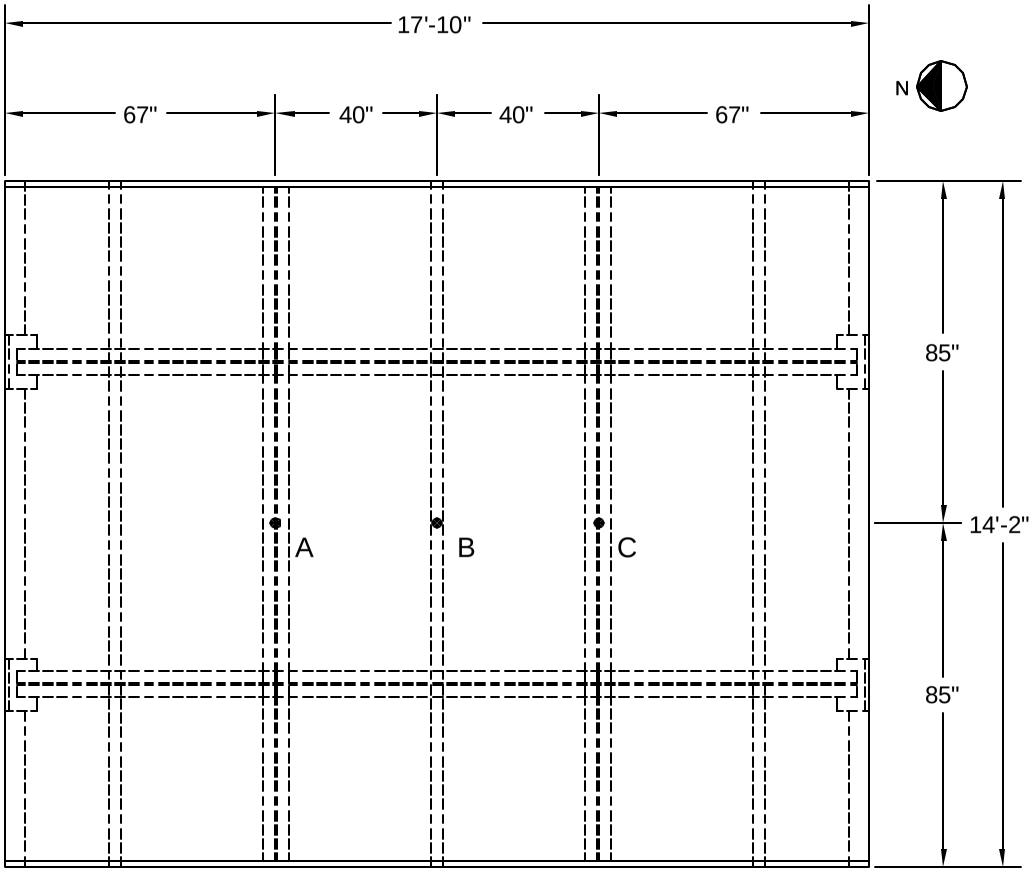

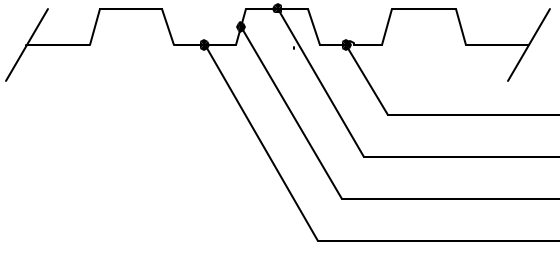

A	B	C	
113	117	121	JOINT
114	118	122	CREST
115	119	123	SIDE
116	120	124	VALLEY

Note: Dimensions for locations may vary slightly depending on deck valley and crest occurance in actual construction

Steel Deck Thermocouple Locations

UL DECKTC.DWG

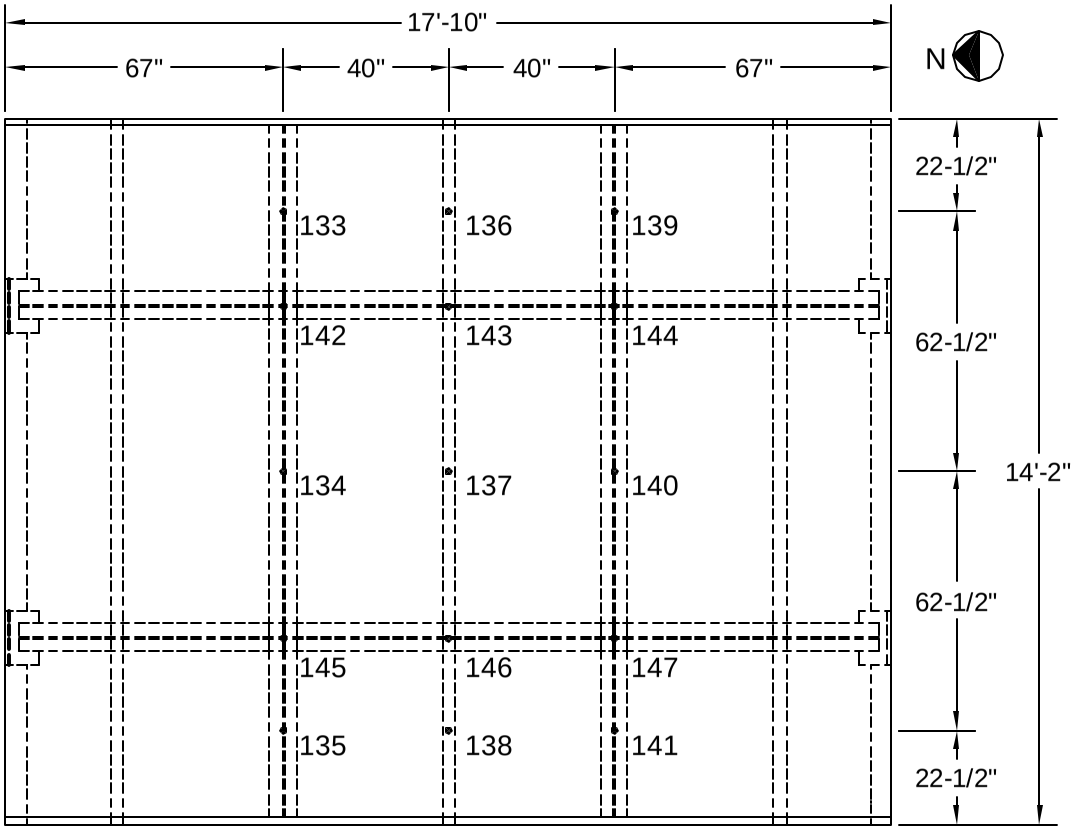

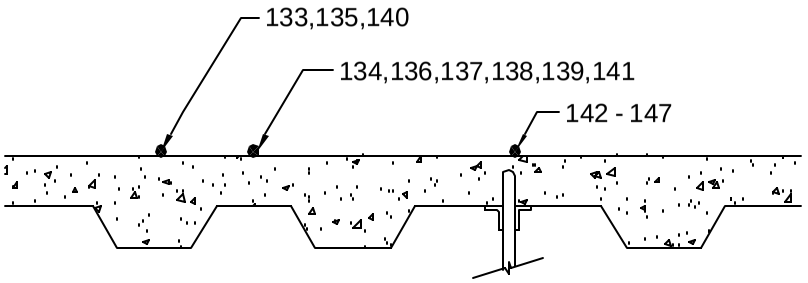

Note: Dimensions for locations may vary slightly depending on deck, valley and crest occurance, and main truss knuckle location in actual construction

Unexposed Surface Thermocouple Locations

UL UNEXPTC.DWG

ILL. 15

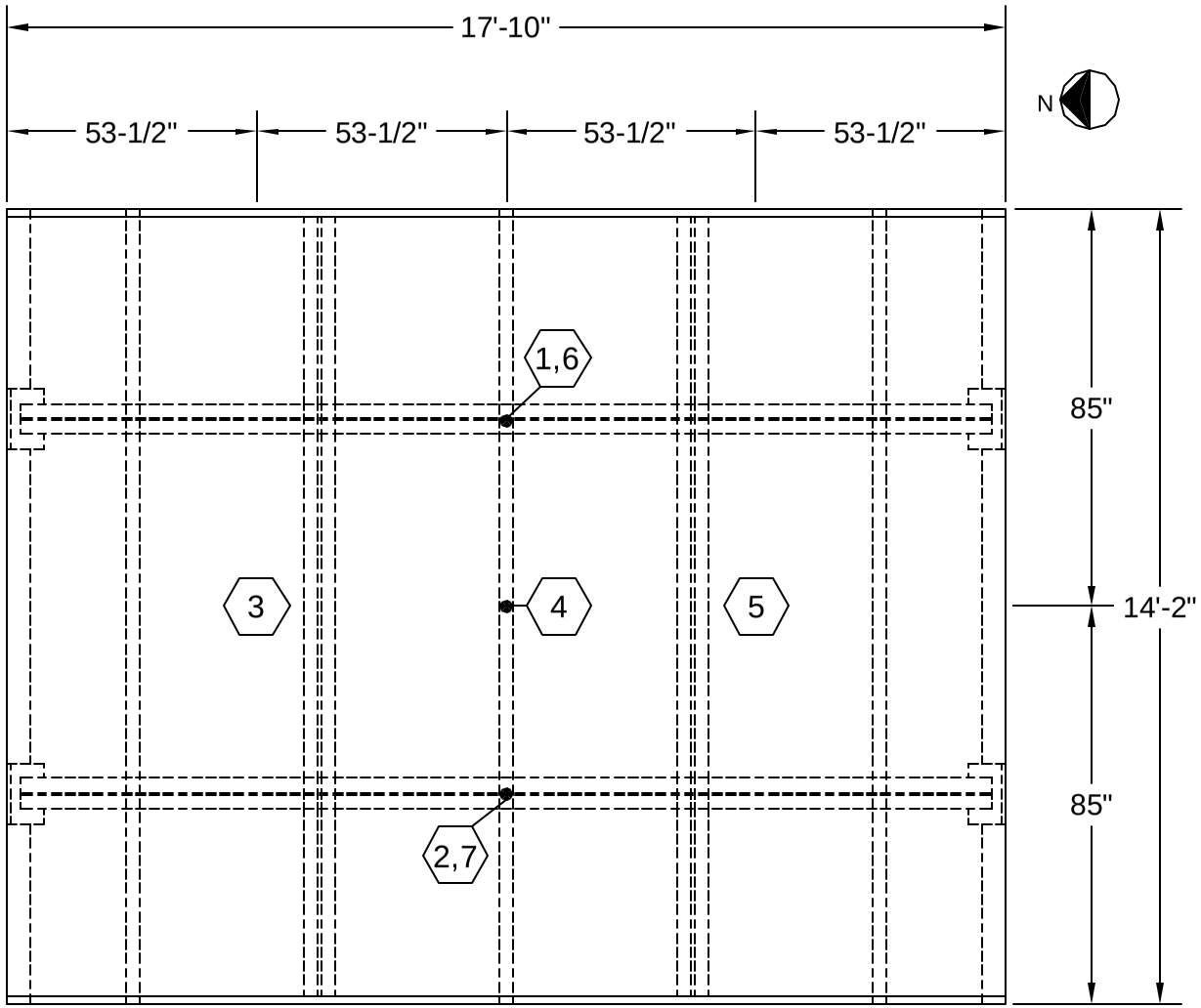

Nos. 1-5 on unexposed surface
Nos. 6 & 7 on bottom chord of main truss

Deflection Transducer Locations

UL DEFL.DWG

This page intentionally left blank.

Appendix G
TRUSS CALCULATION SHEETS

This page intentionally left blank.

REVISED 3-15-67

LACLEDE STEEL COMPANY

D105- T 5 -Sheet 1

WORLD TRADE CENTER
FLOOR GRID TRUSSES
DESIGN DATA

Truss Mk. 2C32T5-358

Truss Component Mk. C32T5-358

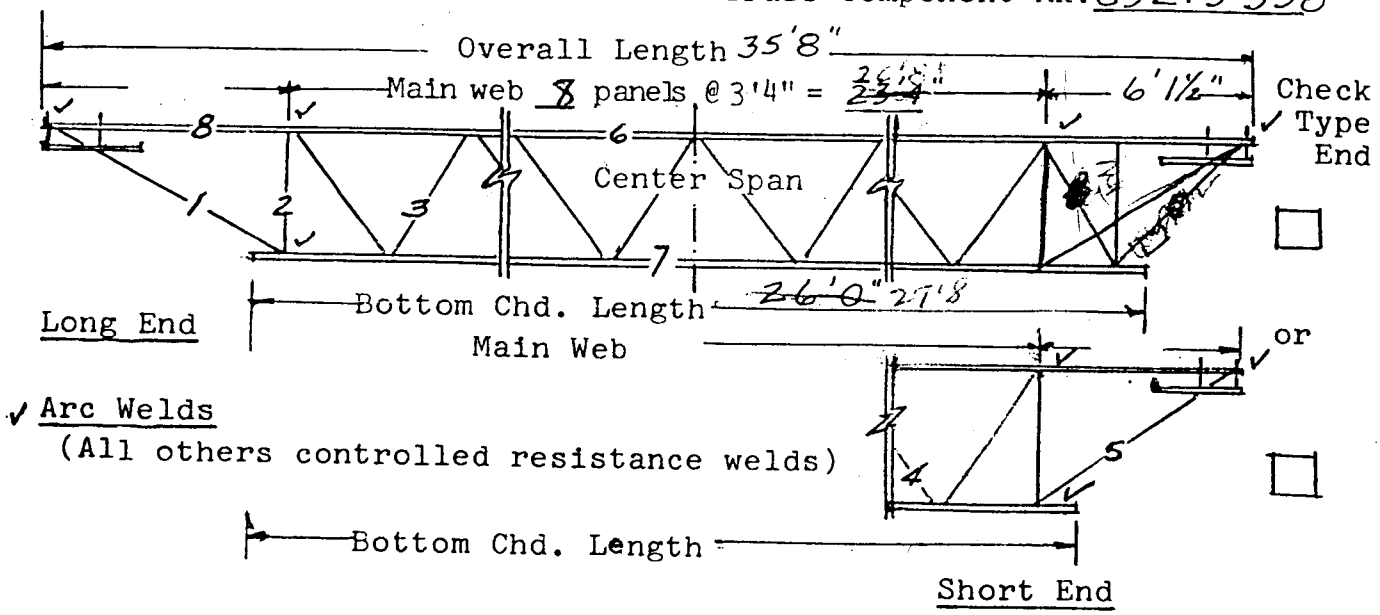

NOTES:

Main Web - Continuous uniform section throughout Member Mk. 3. (Top chord fillers same section as Main Web - at midpoint center web panels minimum.) NONE

Vertical Struts Mk. 2 - Same size as main web.

End Bearing Struts - Same size as main web.

Composite Type - Webs extend above top chord 3 ".

MEMBERS REQUIRED PER TRUSS COMPONENT S____ or C ✓

Member	Mk.No.	Grade of Steel	Size	Total Length Member	Weight Member
Top Chord	6-8	A-441	2-2" x 1½" x 0.25" ⊲		
Bottom Chord	7	A-36	2-2" x 1½" x 0.25" ⊲		
Main Web	3	A-36	0.92" DIA.		
Compression Web	4	A-441	0.98" DIA.		
Vertical End Struts	2	A-36	0.92" DIA.		
Long End Diagonal	1	A-441	0.92" DIA.		
Short End Diagonal	5	A-441	0.92" DIA.		

WORLD TRADE CENTER
FLOOR GRID TRUSSES
DESIGN DATA

TRUSS UNIT MARKED 2C32T5 Refer to drawings ST 101,6,8 .

Clearspan "L" = 34.83 ft. Spacing = 6.67 ft.

Applicable Total Moment = 1,920,000 inch pounds.

Based on 154 lbs./sq. ft. Total Load "w". [31' PARTIAL LOADING]

Applicable End Reaction = 18,000 pounds.

Based on 154 lbs./sq. ft. Total Load "w".

Applicable Total Constr. Moment = 585,000 inch pounds.

Based on 46 lbs./sq. ft. Construction Load.

Applicable Constr. End Reaction = 5470 pounds.

Based on 46 lbs./sq. ft. Construction Load.

"V" Shear at End Panel = 14,920 pounds. ED = 3.0 ft.

WEB MEMBER #1 Distance from End Panel = 0.0 ft.

Applicable Shear V_x = 14,920 lbs. f_y = 50,000 psi

Slope = 2.65 f_s = 30,000 psi

ℓ = — in. f_{sc} = — psi

Reqd. Area = 1.32 sq. in. Use 2-0.92" DIA Area = 1.33 sq. in.

WEB MEMBER #2 Distance from End Panel = 0.0 ft.

Applicable Shear V_x = 14,920 lbs. f_y = 36,000 psi

Slope = 1.00 f_s = — psi

ℓ = 26.0 in. f_{sc} = 11,200 psi

Reqd. Area = 1.33 sq. in. Use 2-0.92" DIA Area = 1.33 sq. in.

WEB MEMBER #3 Distance from End Panel = 4.87 ft.

Applicable Shear V_x = 9,920 lbs. f_y = 36,000 psi

Slope = 1.162 f_s = — psi

ℓ = 30.0 in. f_{sc} = 8,750 psi

Reqd. Area = 1.32 sq. in. Use 2-0.92" DIA Area = 1.33 sq. in.

WEB MEMBER #4 Distance from End Panel = 3.21 ft. (ED = 2.08')

Applicable Shear V_x = 12,570 lbs. f_y = 50,000 psi

Slope = 1.162 f_s = — psi

ℓ = 30.0 in. f_{sc} = 9,970 psi

Reqd. Area = 1.47 sq. in. Use 2-0.98" DIA Area = 1.51 sq. in.

WEB MEMBER #5 Distance from End Panel = 0.0 ft. (ED = 2.08')

Applicable Shear V_x = 15,865 lbs. f_y = 50,000 psi

Slope = 1.90 f_s = 30,000 psi

ℓ = — in. f_{sc} = — psi

Reqd. Area = 1.01 sq. in. Use 2-0.92" DIA Area = 1.33 sq. in.

CHORD MEMBER #6 Consists of 4 - 2" x 1½" x 0.25" Angles

Construction Load Design Area = 3.60 sq. in.

Applicable Moment = 685,000 in. lbs. f_y = 50,000 psi

ℓ = 33.375 in. f_s = — psi

r_x = 0.44 in. f_{sc} = 12,930 psi

r_z = 0.31 in. (~~with fillers in middle 60% of span~~)

$\frac{\ell}{r_x}$ = 75.8

$\frac{\ell}{r_z}$ = 107.5

$$\frac{f_a}{F_a} + \frac{f_b\ C_m}{F_b\left(1 - \frac{f_a}{F'_e}\right)} = 0.477 \text{ less than 1}$$

f_a = 5,800 psi

F_a = 12,930 psi

f_b = 748 psi

F_b = 30,000 psi

F'_e = 25,950 psi

Use 4 - 2" x 1½" x 0.25" ∡'s Area = 3.60 sq. in.

CHORD MEMBER #7 Consists of 4 - 2" x 1½" x 0.25" Angles

Total Load Design Area = 3.60 sq. in.

CHORD MEMBER #7 (CONTD.)

Applicable Moment = 1,920,000 in lbs. f_y = 36,000 psi

f_s = 22,000 psi

D_t = 33.00 in. f_{sc} = — psi

B_{eff} = 64.00 in.

t = 4.00 in.

y_1 = 2.00 in. d_2 = 2.46 in.

y_2 = 4.44 in. d_3 = 25.66 in.

y_3 = 32.56 in. c_1 = 6.90 in.

d_1 = 4.90 in. c_2 = 26.10 in.

$$I_s = \sum\left[(I_c + A_c d_1^2) + (I_{TCA} + A_{TCA} d_2^2) + I_{BCA} + A_{BCA} d_3)\right]$$

$$\bar{y} = \frac{\sum(A_c y_1 + A_{TCA} y_2 + A_{BCA} y_3)}{\sum(A_c + A_{TCA} + A_{BCA})}$$

$\bar{y}$ = 6.90 in.

I_s = 2826 in.^{4} (2C32T5)

Resisting Moment = $f_s \times \frac{I_s}{c_2}$ = 2,380,000 in. lbs.

Use 4-2"x 1½" x 0.25" ∠'s Area = 3.60 sq. in.

Composite Design Top Chord Check

Total Load Design f_c = 3,000 psi

Applicable Moment = 1,920,000 in. lbs. f'_c = 1,350 psi

$$f'_{cc} = \frac{M_c c_1}{15 I_s} = 312 \text{ psi}$$

CHORD MEMBER #8 Consists of 4-2"x 1½" x 0.25" Angles

Area = 3.60 sq. in.

(SAME AS MEMBER 6)

Appendix H
UNRELIABLE DATA

This page intentionally left blank.

Test 1

Test Time (min)	Location	Unreliable Data
0	Unexposed Surface	Thermocouple 133
1	Bottom Chord Deflection	Deflection 11
1	West Instrumentation	Plate Thermocouple
15	Steel Deck	Thermocouple 123
18	Steel Deck	Thermocouple 126
20	Steel Deck	Thermocouple 122
21	West Instrumentation	Radiometer Thermocouple
23	West Instrumentation	Radiometer
27	East Instrumentation	Radiometer Thermocouple
28	Steel Deck	Section C-C
32	Steel Deck	Section A-A
39	East Instrumentation	Radiometer
50	Unexposed Surface	Thermocouple 145
52	West Instrumentation	Aspirated Thermocouple
68	North Main Truss	Thermocouple 40
68	North Main Truss	Thermocouple 18
68	North Main Truss	Thermocouple 19
68	North Main Truss	Thermocouple 2
68	North Main Truss	Thermocouple 32
68	North Main Truss	Thermocouple 8
69	North Main Truss	Thermocouple 3
69	North Main Truss	Thermocouple 72
70	North Main Truss	Section A-A
70	Unexposed Surface	Thermocouple 139
72	North Main Truss	Thermocouple 33
73	North Main Truss	Thermocouple 17
73	East Bridging Truss	Thermocouple 95
74	North Main Truss	Thermocouple 36
76	North Main Truss	Section E-E
78	Bottom Chord Deflection	Deflection 14
78	Steel Deck	Thermocouple 131
79	South Main Truss	Section B-B
82	North Main Truss	Thermocouple 35
83	West Bridging Truss	Thermocouple 90
84	South Main Truss	Thermocouple 13
86	South Main Truss	Thermocouple 11
86	South Main Truss	Thermocouple 14
87	South Main Truss	Thermocouple 15
87	South Main Truss	Thermocouple 12
87	South Main Truss	Thermocouple 16
87	South Main Truss	Thermocouple 10
89	Unexposed Surface Deflection	Deflection 1
89	Unexposed Surface Deflection	Deflection 3
90	South Main Truss	Thermocouple 9
90	East Bridging Truss	Thermocouple 94
90	Steel Deck	Thermocouple 132
93	Bottom Chord Deflection	Deflection 15

Test Time (min)	Location	Unreliable Data
94	North Main Truss	Thermocouple 22
94	North Main Truss	Thermocouple 20
95	North Main Truss	Section C-C
96	Unexposed Surface Deflection	Deflection 4
96	Unexposed Surface Deflection	Deflection 6
100	Bottom Chord Deflection	Deflection 13
102	Steel Deck	Thermocouple 121
103	North Main Truss	Thermocouple 6
108	Unexposed Surface Deflection	Deflection 5
108	Unexposed Surface Deflection	Deflection 2
111	South Main Truss	Thermocouple 84
111	Bottom Chord Deflection	Deflection 10
111	Bottom Chord Deflection	Deflection 12
111	Steel Deck	Thermocouple 125
111	Unexposed Surface	Thermocouple 144
111	Unexposed Surface	Thermocouple 140
111	Unexposed Surface	Thermocouple 141
112	Unexposed Surface	Thermocouple 138
114	Unexposed Surface	Thermocouple 134

Test 2

Test Time (min)	Location	Unreliable Data
0	Steel Deck	Thermocouple 129
0	Steel Deck	Thermocouple 123
0	Steel Deck	Thermocouple 124
0	Steel Deck	Thermocouple 131
4	Steel Deck	Thermocouple 121
18	Steel Deck	Thermocouple 127
21	Steel Deck	Thermocouple 125
32	South Main Truss	Thermocouple 31
40	North Main Truss	Thermocouple 17
43	West Bridging Truss	Thermocouple 99
43	West Bridging Truss	Section C-C
43	West Instrumentation	Aspirated Thermocouple
46	South Main Truss	Thermocouple 30
46	Bottom Chord Deflection	Deflection 15
49	Steel Deck	Thermocouple 132
65	Steel Deck	Thermocouple 122
73	Steel Deck	Thermocouple 130
74	Unexposed Surface Deflection	Deflection 6
77	Steel Deck	Thermocouple 128
82	Unexposed Surface Deflection	Deflection 1
82	Unexposed Surface Deflection	Deflection 2
83	Bottom Chord Deflection	Deflection 11
84	Unexposed Surface Deflection	Deflection 5
87	North Main Truss	Thermocouple 18
87	North Main Truss	Thermocouple 23
88	North Main Truss	Thermocouple 20
88	North Main Truss	Thermocouple 24
93	East Instrumentation	Aspirated Thermocouple
96	West Bridging Truss	Thermocouple 92
105	Bottom Chord Deflection	Deflection 14
107	Unexposed Surface	Thermocouple 137
109	South Main Truss	Thermocouple 62
110	North Main Truss	Thermocouple 21
110	Unexposed Surface Deflection	Deflection 7
110	Unexposed Surface Deflection	Deflection 3
110	Unexposed Surface Deflection	Deflection 4
112	West Bridging Truss	Thermocouple 120
113	East Bridging Truss	Thermocouple 96
113	East Bridging Truss	Section A-A
114	Bottom Chord Deflection	Deflection 13
116	East Bridging Truss	Thermocouple 116
119	East Bridging Truss	Thermocouple 95
121	Steel Deck	Thermocouple 126
122	East Bridging Truss	Thermocouple 93
124	East Bridging Truss	Thermocouple 103
128	North Main Truss	Thermocouple 7
128	North Main Truss	Thermocouple 39

Test Time (min)	Location	Unreliable Data
128	North Main Truss	Thermocouple 34
128	North Main Truss	Thermocouple 38
128	West Bridging Truss	Thermocouple 112

Test 3

Test Time (min)	Location	Unreliable Data
0	East Main Truss	Thermocouple 58
1	Steel Deck	Thermocouple 126
1	Steel Deck	Thermocouple 127
1	North Instrumentation	Aspirated Thermocouple
2	Steel Deck	Thermocouple 128
2	Steel Deck	Thermocouple 125
8	Steel Deck	Thermocouple 129
19	Steel Deck	Thermocouple 132
71	East Main Truss	Thermocouple 37
72	North Instrumentation	Calorimeter
83	Unexposed Surface Deflection	Deflection 7
83	Bottom Chord Deflection	Deflection 14
84	Unexposed Surface	Thermocouple 142
85	Steel Deck	Thermocouple 121
87	Unexposed Surface	Thermocouple 143
90	West Main Truss	Thermocouple 13
95	West Main Truss	Thermocouple 46
95	West Main Truss	Thermocouple 48
96	West Main Truss	Thermocouple 44
96	West Main Truss	Thermocouple 42
100	West Main Truss	Thermocouple45
100	West Main Truss	Thermocouple 47
100	East Main Truss	Thermocouple 17
101	North Bridging Truss	Thermocouple 93
101	North Bridging Truss	Section B-B
101	North Bridging Truss	Thermocouple 96
101	North Bridging Truss	Thermocouple 95
105	Unexposed Surface	Thermocouple 134
107	North Bridging Truss	Thermocouple 116
111	East Main Truss	Thermocouple 33
111	East Main Truss	Thermocouple 36
115	West Main Truss	Thermocouple 59
115	East Main Truss	Thermocouple 76
115	East Main Truss	Section E-E
116	Unexposed Surface	Thermocouple 140
132	Unexposed Surface	Thermocouple 139
140	North Bridging Truss	Thermocouple 104
141	North Bridging Truss	Thermocouple 103
141	North Bridging Truss	Section D-D
165	South Bridging Truss	Thermocouple 91
165	South Bridging Truss	Section A-A
167	South Bridging Truss	Thermocouple 92
171	South Bridging Truss	Thermocouple 99
171	South Bridging Truss	Section C-C
175	South Bridging Truss	Thermocouple 100
175	South Bridging Truss	Thermocouple 119
181	South Bridging Truss	Thermocouple 120

Test Time (min)	Location	Unreliable Data
182	North Bridging Truss	Thermocouple 115
191	North Bridging Truss	Thermocouple 94
193	South Bridging Truss	Thermocouple 112
193	South Bridging Truss	Section F-F
194	South Bridging Truss	Thermocouple 110
195	West Main Truss	Thermocouple 43
196	West Main Truss	Thermocouple 67
202	North Bridging Truss	Section E-E
202	North Bridging Truss	Thermocouple 108
206	South Bridging Truss	Thermocouple 90

Test 4

Test Time (min)	Location	Unreliable Data
0	East Main Truss	TC 58
0	East Main Truss	TC 40
0	East Main Truss	TC 39
0	East Main Truss	TC 38
0	East Main Truss	TC 37
1	East Main Truss	TC 6
1	Unexposed Surface	TC 143
10	South Instrumentation	Radiometer
22	East Main Truss	TC 51
51	Steel Deck	TC 121
51	Steel Deck	TC 122
51	Steel Deck	TC 123
51	Steel Deck	TC 124
51	Steel Deck	TC 125
51	Steel Deck	TC 126
51	Steel Deck	TC 127
51	Steel Deck	TC 128
51	Steel Deck	TC 129
51	Steel Deck	TC 130
51	Steel Deck	TC 131
51	Steel Deck	TC 132
51	South Instrumentation	Aspirated Thermocouple
51	South Instrumentation	Plate Thermocouple
52	Bottom Chord Deflection	Deflection 12
52	Bottom Chord Deflection	Deflection 11
52	Unexposed Surface Deflection	Deflection 5
63	Unexposed Surface	TC 144
88	East Main Truss	TC 70
89	East Main Truss	TC 1
97	East Main Truss	TC 5

This page intentionally left blank.

Appendix I
UNITS CONVERSIONS

U.S. Customary Units to S. I. units

°F	=	°C ×(9/5)+32
1 in.	=	25.4 mm
1 in.^{2}	=	645.2 mm^2
1 ft	=	0.3048 m
1 ft^2	=	0.0929 m^2
1 lb	=	4.448 N
1 kip	=	4.448 kN
1 fb/ft	=	14.59 kN/m
1 psi	=	0.006895 N/mm^2 or 0.006895 MPa
1 ksi	=	6.895 MPa
1 psf	=	0.04788 kN/m^2
1 pcf	=	0.1571 kN/m^3
1 BTU/s	=	1.055 kW
1 BTU/s/ft^2	=	11.357 kW/m^2

S. I. Units to U. S. Customary Units

°C	=	(°F-32) × (5/9)
1 mm	=	0.0394 in.
1 m	=	3.281 ft
1 MPa	=	145.0 psi
1 kN/m^2	=	20.88 lb/ft^2 (psf)
1 kW	=	0.948 BTU/s
1 kW/m^2	=	0.088 $BTU/s/ft^2$

Table I–1. Temperature conversions.

°F	°C
70	21
100	38
200	93
300	149
400	204
500	260
600	316
700	371
800	427
900	482
1000	538
1100	593
1200	649
1300	704
1400	760
1500	816
1600	871
1700	927
1800	982
1900	1038
2000	1093

NIST NCSTAR 1-6C

Federal Building and Fire Safety Investigation of the World Trade Center Disaster

Component, Connection, and Subsystem Structural Analysis

Mehdi S. Zarghamee,
Said Bolourchi
Daniel W. Eggers
Ömer O. Erbay
Frank W. Kan
Yasuo Kitane

Peter R. Barrett

John L. Gross
Therese P. McAllister

Atis A. Liepins
Michael Mudlock
Wassim I. Naguib
Rasko P. Ojdrovic
Andrew T. Sarawit

NIST National Institute of Standards and Technology • Technology Administration • U.S. Department of Commerce

NIST NCSTAR 1-6C

Federal Building and Fire Safety Investigation of the World Trade Center Disaster

Component, Connection, and Subsystem Structural Analysis

Mehdi S. Zarghamee
Said Bolourchi, Daniel W. Eggers, Ömer O. Erbay, Frank W. Kan, Yasuo Kitane,
Atis A. Liepins, Michael Mudlock, Wassim I. Naguib, Rasko P. Ojdrovic, and Andrew T. Sarawit
Simpson Gumpertz & Heger Inc.

Peter R. Barrett
Computer Aided Engineering Associates, Inc.

John L. Gross
Therese P. McAllister
Building and Fire Research Laboratory
National Institute of Standards and Technology

September 2005

U.S. Department of Commerce
Carlos M. Gutierrez, Secretary

Technology Administration
Michelle O'Neill, Acting Under Secretary for Technology

National Institute of Standards and Technology
William Jeffrey, Director

Disclaimer No. 1

Certain commercial entities, equipment, products, or materials are identified in this document in order to describe a procedure or concept adequately or to trace the history of the procedures and practices used. Such identification is not intended to imply recommendation, endorsement, or implication that the entities, products, materials, or equipment are necessarily the best available for the purpose. Nor does such identification imply a finding of fault or negligence by the National Institute of Standards and Technology.

Disclaimer No. 2

The policy of NIST is to use the International System of Units (metric units) in all publications. In this document, however, units are presented in metric units or the inch-pound system, whichever is prevalent in the discipline.

Disclaimer No. 3

Pursuant to section 7 of the National Construction Safety Team Act, the NIST Director has determined that certain evidence received by NIST in the course of this Investigation is “voluntarily provided safety-related information” that is “not directly related to the building failure being investigated” and that “disclosure of that information would inhibit the voluntary provision of that type of information” (15 USC 7306c).

In addition, a substantial portion of the evidence collected by NIST in the course of the Investigation has been provided to NIST under nondisclosure agreements.

Disclaimer No. 4

NIST takes no position as to whether the design or construction of a WTC building was compliant with any code since, due to the destruction of the WTC buildings, NIST could not verify the actual (or as-built) construction, the properties and condition of the materials used, or changes to the original construction made over the life of the buildings. In addition, NIST could not verify the interpretations of codes used by applicable authorities in determining compliance when implementing building codes. Where an Investigation report states whether a system was designed or installed as required by a code *provision*, NIST has documentary or anecdotal evidence indicating whether the requirement was met, or NIST has independently conducted tests or analyses indicating whether the requirement was met.

Use in Legal Proceedings

No part of any report resulting from a NIST investigation into a structural failure or from an investigation under the National Construction Safety Team Act may be used in any suit or action for damages arising out of any matter mentioned in such report (15 USC 281a; as amended by P.L. 107-231).

National Institute of Standards and Technology National Construction Safety Team Act Report 1-6C
Natl. Inst. Stand. Technol. Natl. Constr. Sfty. Tm. Act Rpt. 1-6C, 251 pages (September 2005)
CODEN: NSPUE2

U.S. GOVERNMENT PRINTING OFFICE
WASHINGTON: 2005

For sale by the Superintendent of Documents, U.S. Government Printing Office
Internet: bookstore.gpo.gov — Phone: (202) 512-1800 — Fax: (202) 512-2250
Mail: Stop SSOP, Washington, DC 20402-0001

ABSTRACT

Simpson Gumpertz & Heger, Inc. (SGH) developed finite element models of the components, connections and subsystems of the World Trade Center (WTC) towers to study their structural performance in the fire environment that followed the aircraft impact to the towers. The results of this study were used to develop global models that captured with numerical efficiency the important failure modes and sequential failures of components and subsystems and to determine the probable sequence of structural responses that let to the global collapse initiation. The study was conducted as part of the investigation on the WTC disaster by the National Institute of Standards and Technology (NIST).

The structural response to the fire environment was established by hand calculations and finite element analyses (FEA) for: connections including interior and exterior truss seats, knuckles, column splices, and spandrel splices; components including a section of the floor system, including concrete slab and a single truss and a single column, and subsystems including full floors and a section exterior wall. The key structural responses, failure modes, and failure loads were identified.

The finite element models, developed in ANSYS, captured the nonlinear responses of the connections, components, and subsystems, including temperature-dependent material properties such as thermal expansion, plasticity and creep of metals, large deflection and the resulting instability, and failure modes of members and connections, modeled by *break elements* developed for this purpose. The models were subjected to gravity and thermal loads. Construction sequence was included in component models. NIST provided temperature-dependent nonlinear material properties, aircraft impact damage to structural members, and temperature time histories of structural elements for subsystems, which were used as input in this study.

The nonlinear analysis of a section of floor system, including break elements that represented the structural performance of interior and exterior truss seats and knuckles, showed that the floor sagged when subjected to high temperatures beyond 600 ˚C; the main cause of the floor sagging was buckling of truss web diagonals. The sagging floors pulled in the exterior walls. Floor/wall disconnections occurred by the truss walking off their seats after failure of all horizontal connections between the floor and the exterior wall, or by the vertical shear failure of the truss seat, as its capacity was reduced by heat.

The column analysis showed that exterior columns spanning a single floor at low temperatures were susceptible to premature buckling initiated by local buckling of plates with rapid reduction of load carrying capacity in the post-buckling regime. This failure mode did not exist when the column was spanning more than one floor or was at high temperatures.

The nonlinear model of the full floor system was developed in ANSYS by converting the existing linear SAP2000 model and by modifying the model to capture the failure modes and the failure loads calculated in the study of components in the fire environment and to enhance computational efficiency. The enhancement was achieved for example by combining double trusses into a single truss to enhance computational efficiency. The model was subjected to the gravity loads and the temperature time histories provided by NIST. The results of analyses performed for all floors with thermal loads showed that the key structural responses of the floors under fire were 1) floor sagging resulting in pull-in forces between the floor and the exterior wall, and 2) disconnections of the floors from the exterior walls.

A nonlinear model of a section of the exterior wall subsystem consisting of nine floors in height and nine columns in width was developed, including large deflection and inelastic buckling of columns and spandrels and failure of their splices. The model was subjected to gravity loads, including the column loads and NIST provided temperature time histories. The results of the analyses showed that instability of the wall system did not occur when the wall was braced at every floor or when the floor did not restrain the out-of-plane motion of the exterior wall for up to three floors. Bowing and buckling occurred when the wall was subjected to increased column loads or to floor/wall pull-in forces. Furthermore, the exterior column splice failure was rare and occurred by opening of the splices in bending; only in one case was sliding experienced without bolt failure at high temperatures and high vertical loads. Large deformation and buckling of spandrels and partial separations of the spandrel splices were also found in the analysis, but they did not significantly affect the stability of the exterior columns.

Keywords: Collapse, creep, large deflection, nonlinear finite element analysis, plasticity, structural response to damage, structural response to fire, stability, World Trade Center.

TABLE OF CONTENTS

Abstract iii
List of Figures ix
List of Tables xvii
List of Acronyms and Abbreviations xix
Preface xxi
Acknowledgements xxxi
Executive Summary xxxiii

Chapter 1
Introduction 1
1.1 Purpose 1
1.2 Scope of Work 1
1.3 Report Organization 1

Chapter 2
Description of Subsystem Structures 3
2.1 Full Floor Subsystem Description 3
2.2 Exterior Wall Subsystem Description 6
2.3 Loads 7

Chapter 3
Materials 9
3.1 Concrete 9
3.1.1 Concrete Properties 9
3.1.2 Concrete Stress-Strain Relationships 10
3.1.3 Concrete Failure Criteria 13
3.2 Steel 13
3.2.1 Steel Properties 13
3.2.2 Stress-Strain Relationship 13
3.2.3 Steel Failure Criteria 19
3.3 Welds 21
3.4 Bolts 21
3.5 Coefficient of Friction 22

3.6 Symbols 22

Chapter 4
Model Conversion From SAP to ANSYS 25

4.1 Translation Procedure 25

4.2 Validation 28

4.2.1 Floor Model Validation 28

4.2.2 Global Model Validation 33

4.3 Summary 37

Chapter 5
Full Floor Subsystem 39

5.1 Objective 39

5.2 Truss Seats 39

5.2.1 Description of Truss Seats 39

5.2.2 Truss Seat Material Properties 41

5.2.3 Truss Seat Failure Modes and Sequence 42

5.2.4 Truss Seat Capacity Calculations 46

5.2.5 Modeling Failure by Break Elements 53

5.2.6 Summary of Failure Modes and Finite Element Models of Truss Seats 55

5.2.7 Summary of Failure Modes and Finite Element Models of the Stud on Strap Anchor and Spandrel Stud 59

5.3 Knuckle Analysis 61

5.3.1 Description of Knuckle 61

5.3.2 Failure Modes of Knuckle 61

5.3.3 Knuckle Shear Tests 61

5.3.4 Finite Element Model for Knuckle Test 63

5.3.5 Material Properties for Knuckle Analysis 63

5.3.6 Results from Knuckle Analysis 64

5.3.7 Summary of Failure Modes and Finite Element Models of Knuckle Model for Truss Model 67

5.4 Truss Model 69

5.4.1 Model Description 69

5.4.2 Failure Modes 71

5.4.3 Boundary Conditions 71

5.4.4 Loads 73

5.4.5 Material Properties 73

5.4.6 Resistance Welds ... 74
5.4.7 Model Verification ... 75
5.4.8 Truss Analysis for Debris Load ... 75
5.4.9 Truss Analysis for Gravity and Thermal Loads ... 77
5.4.10 Simplified Truss Model ... 84
5.5 Full Floor Model ... 86
5.5.1 Objective ... 86
5.5.2 Failure Modes ... 86
5.5.3 Model Description ... 86
5.5.4 Material Properties ... 90
5.5.5 User-Defined Break Elements ... 91
5.5.6 Impact Damage ... 95
5.5.7 Gravity and Thermal Loads ... 107
5.5.8 Boundary Conditions ... 117
5.5.9 Results from WTC 1 Floor 96 under Case A_i Temperature Condition ... 117
5.5.10 Results from Other WTC 1 Floors under Case A_i Temperature Condition ... 122
5.5.11 Results from WTC 1 Floors under Case B_i Temperature Condition ... 127
5.5.12 Results from WTC 2 Floor 82 under Case C_i Temperature Condition ... 133
5.5.13 Results from Other WTC 2 Floors under Case C_i Temperature Condition ... 138
5.5.14 Results from WTC 2 Floors under Case D_i Temperature Condition ... 142
5.5.15 Creep Effect ... 148
5.5.16 Effect of Column Boundary Conditions ... 148
5.5.17 Floor Subsystem in Global Models ... 149
5.5.18 Summary of Results and Discussion ... 155

Chapter 6
Exterior Wall Subsystem ... 157
6.1 Objective ... 157
6.2 Exterior Wall Subsystem Description ... 157
6.3 Failure Modes ... 161
6.4 Model Validation ... 161
6.4.1 Description of Models ... 161
6.4.2 Validation Results ... 164
6.5 Finite-Element Model of Exterior Wall Subsystem ... 165
6.5.1 Elements and Meshing ... 165

6.5.2 Boundary Conditions 166
6.5.3 One-, Two-, and Three-Story High Columns 168
6.5.4 Spandrel Splices 171
6.5.5 Column Splices 173
6.5.6 Loads 174
6.6 Analysis Cases 176
6.7 Analysis Results 177
6.7.1 Columns Braced at All Floors 177
6.7.2 Columns Not Braced at Floors 95 and 96 185
6.7.3 Columns Not Braced at Floors 95, 96, and 97 186
6.7.4 Columns Not Braced and Pulled at Unbraced Floors 95, 96, and 97 188
6.7.5 Columns Not Braced at Floors 95, 96, and 97 and Pushed Down at Top 191
6.8 Summary and Discussion of Exterior Wall Analysis Results 196
6.8.1 Columns Braced at All Floors 196
6.8.2 Columns Not Braced at Floors 95 and 96 196
6.8.3 Columns Not Braced at Floors 95, 96, and 97 196
6.8.4 Columns Not Braced and Pulled in at Floors 95, 96, and 97 197
6.8.5 Columns Not Braced at Floors 95, 96, and 97 and Columns Pushed Down at Top 197
6.8.6 Summary of Analysis Results 198
6.9 Summary of Results 198

Chapter 7
Modeling Details for Subsystems in Global Models 201

Chapter 8
References 203

LIST OF FIGURES

Figure P–1. The eight projects in the federal building and fire safety investigation of the WTC disaster. xxiii

Figure 2–1. Mock up of office floor framing system (Photograph from about 1967 provided by Laclede Steel Co.). 4

Figure 2–2. Floor plan of Floor 96 of WTC 1. 5

Figure 2–3. Exterior wall construction with prefabricated wall panels. 7

Figure 3–1. Properties of concrete that vary with temperature. 11

Figure 3–2. Concrete stress-strain relationships at different temperatures. 12

Figure 3–3. Properties for all steel types that vary with temperature. 14

Figure 3–4. Steel (Material ID 1) stress-strain relationships at different temperatures. 16

Figure 3–5. Comparison of creep strains with $a(T)$ given by (7-a) and (7-d) for Material ID 1 steel subject to 15 ksi for 1,800 s at a given temperature. 18

Figure 3–6. Creep behavior at elevated temperatures for Material ID 1 steel. 19

Figure 3–7. Maximum plastic strain from the finite element analysis and limiting plastic strain. 21

Figure 3–8. 7/8 in. A325 bolt load-elongation curves at elevated temperatures. 22

Figure 4–1. Converted ANSYS model for Floor 96 of WTC 1: overall view. 28

Figure 4–2. Converted ANSYS model for Floor 96 of WTC 1: partial view near corner of building. 29

Figure 4–3. Converted ANSYS model for Floor 96 of WTC 1: close-up view at corner of building. 29

Figure 4–4. Converted ANSYS model for Floor 96 of WTC 1: view of floor beams and columns. 30

Figure 4–5. Deformed shape (x100) of gravity load case for SAP floor model (downward displacement is negative). 30

Figure 4–6. Deformed shape (x100) of gravity load case for ANSYS floor model (total displacements are shown). 31

Figure 4–7. Dominant mode shape (frequency = 4.32 Hz) of floor structure for SAP floor model. 32

Figure 4–8. Dominant mode shape (frequency = 4.43 Hz) of floor structure for ANSYS floor model. 32

Figure 4–9. Converted ANSYS model of WTC 1. 34

Figure 4–10. Converted ANSYS model of WTC 2. 34

Figure 4–11. Displaced shape of WTC 1 at the end of gravity analysis. 35

Figure 4–12. Displaced shape of WTC 2 at the end of gravity analysis. 35

Figure 5–1. Interior truss seat. 40
Figure 5–2. Exterior truss seat. 40
Figure 5–3. Truss seat detail location on northeast quadrant of Floor 96 of WTC 1. 41
Figure 5–4. Finite element model of exterior truss seat. 43
Figure 5–5. Failure sequence of the exterior truss seats against tensile force. 44
Figure 5–6. Capacity of exterior truss seat for tensile force (Path (A) in Fig. 5–5 for Detail 1411). 45
Figure 5–7. Truss seat capacity for vertical force 48
Figure 5–8. Truss seat capacity for horizontal tensile force. 51
Figure 5–9. Capacity of interior truss seat against vertical and horizontal force (for Detail 22). 52
Figure 5–10. Basic mathematical model of connection failure. 54
Figure 5–11. Representation of interior truss seat by break elements. 56
Figure 5–12. Results of interior truss seat model capturing failure from truss walking off the seat at 500 ˚C. 57
Figure 5–13. Results of interior truss seat model capturing failure from exceeding the vertical shear capacity at 500 ˚C. 57
Figure 5–14. Representation of exterior truss seat by break elements. 58
Figure 5–15. Location of stud on strap anchor and spandrel stud. 59
Figure 5–16. Representation of stud shear connector by break elements. 60
Figure 5–17. Longitudinal shear test of a knuckle. 62
Figure 5–18. Transverse shear test of a knuckle. 63
Figure 5–19. Finite element models of knuckle shear tests. 64
Figure 5–20. Compressive stresses in longitudinal shear finite element model (4,100 psi concrete). 65
Figure 5–21. Shear force versus displacement from finite element model for longitudinal shear of two knuckles (4,100 psi concrete). 65
Figure 5–22. Compressive stresses in transverse shear finite element model (2,500 psi concrete). 66
Figure 5–23. Shear force versus displacement from finite element model for transverse shear of two knuckles (2,500 psi concrete). 66
Figure 5–24. Representation of knuckle by break elements. 68
Figure 5–25. Truss model. 70
Figure 5–26. Boundary conditions. 72
Figure 5–27. Break elements at the interior end of slab. 72
Figure 5–28. Assumed Temperature Distribution in the Truss Model at 30 min. 73

Figure 5–29. Comparison of resistance weld strength and yield strength of web member at elevated temperatures. 75
Figure 5–30. Finite element analysis results from increasing gravity. 76
Figure 5–31. Vertical displacement at 700 ˚C (downward displacement is negative). 77
Figure 5–32. Displacement versus temperature of steel. 78
Figure 5–33. Element numbers and locations of elements examined for axial force. 79
Figure 5–34. Axial force in truss members versus temperature of steel. 80
Figure 5–35. Axial stress contour in the truss members at 700 ˚C (tension is positive; 1.0x displacement magnification). 81
Figure 5–36. Force in the knuckles versus temperature of steel. 82
Figure 5–37. Horizontal reaction forces. 83
Figure 5–38. Comparison of detailed and simplified truss models. 85
Figure 5–39. Full floor model without impact damage. 88
Figure 5–40. Full floor model after removal of deck support angles, spandrel studs, bridging trusses outside of two-way zones, and strap anchors. 90
Figure 5–41. Bilinear material model for concrete slab in the full floor model. 91
Figure 5–42. Bilinear material model in the spandrel. 91
Figure 5–43. Summary of user-defined break element locations in the full floor model. 93
Figure 5–44. User-defined break element locations in the full floor model (Floor 96, WTC 1). 94
Figure 5–45. Case A_i insulation damage condition for WTC 1 floor trusses and beams. 96
Figure 5–46. Case A_i structural damage condition for WTC 1 floors. 97
Figure 5–47. Structural damage to exterior walls of WTC 1 for Case A_i and Case B_i impact damage conditions. 98
Figure 5–48. Structural damage to core columns of WTC 1 for Case A_i impact damage condition. 99
Figure 5–49. Case C_i insulation damage condition for WTC 2 floor trusses and beams. 100
Figure 5–50. Case C_i structural damage condition for WTC 2 floors. 101
Figure 5–51. Case D_i insulation damage condition for WTC 2 floor trusses and beams. 102
Figure 5–52. Case D_i structural damage condition for WTC 2 floors. 103
Figure 5–53. Structural damage to exterior walls of WTC 2 for Case C_i and Case D_i impact damage conditions. 104
Figure 5–54. Structural damage to core columns of WTC 2 for Case C_i impact damage condition. 104
Figure 5–55. Case A_i structural impact damage condition for exterior columns of the north face in the WTC 1 Floor 96 model. 105
Figure 5–56. Case A_i structural impact damage condition for exterior columns of the south face in the WTC 1 Floor 96 model. 105
Figure 5–57. Case A_i structural impact damage condition for floor trusses in the WTC 1 Floor 96 model. 106

Figure 5–58. Case A_i structural impact damage condition for the concrete slab in the WTC 1 Floor 96 model. 106

Figure 5–59. Case A_i structural impact damage condition for core beams in the WTC 1 Floor 96 model. 107

Figure 5–60. Case A_i structural impact damage condition for core columns in the WTC 1 Floor 96 model. 107

Figure 5–61. Design live load distribution in Floor 96 of WTC 1. 108

Figure 5–62. Case A_i temperature condition for Floor 96 of WTC 1 at 10 min, 50 min, and 100 min. 109

Figure 5–63. Case A_i temperature distribution in the slab for Floor 96 of WTC 1 at 10 min, 50 min, and 100 min. 110

Figure 5–64. Case B_i temperature condition for Floor 96 of WTC 1 at 10 min, 50 min, and 100 min. 111

Figure 5–65. Case B_i temperature distribution in the slab for Floor 96 of WTC 1 at 10 min, 50 min, and 100 min. 112

Figure 5–66. Case C_i temperature condition for Floor 82 of WTC 2 at 10 min, 30 min, and 60 min. 113

Figure 5–67. Case C_i temperature distribution in the slab for Floor 82 of WTC 2 at 10 min, 30 min, and 60 min. 114

Figure 5–68. Case D_i temperature condition for Floor 82 of WTC 2 at 10 min, 30 min, and 60 min. 115

Figure 5–69. Case D_i temperature distribution in the slab for Floor 82 of WTC 2 at 10 min, 30 min, and 60 min. 116

Figure 5–70. Vertical displacement of WTC 1 Floor 96 for Case A_i temperature condition at 10 min, 50 min, and 100 min (downward displacement is negative; 5x displacement magnification). 119

Figure 5–71. Horizontal displacement of exterior columns of Floor 96 of WTC 1 for Case A_i temperature condition at 10 min, 50 min, and 100 min. 120

Figure 5–72. Horizontal reaction force per column of WTC 1 Floor 96 for Case A_i temperature condition. 121

Figure 5–73. User-defined break elements that failed by 100 min in the model of WTC 1 Floor 96 for Case A_i temperature condition. 121

Figure 5–74. Vertical displacement of WTC 1 Floor 93 for Case A_i temperature condition at 30 min (downward displacement is negative; 5x displacement magnification). 123

Figure 5–75. Vertical displacement of WTC 1 Floor 94 for Case A_i temperature condition at 100 min (downward displacement is negative; 5x displacement magnification). 124

Figure 5–76. Vertical displacement of WTC 1 Floor 95 for Case A_i temperature condition at 10 min (downward displacement is negative; 5x displacement magnification). 124

Figure 5–77. Vertical displacement of WTC 1 Floor 97 for Case A_i temperature condition at 60 min (downward displacement is negative; 5x displacement magnification). 125

Figure 5–78. Vertical displacement of WTC 1 Floor 98 for Case A_i temperature condition at 30 min (downward displacement is negative; 5x displacement magnification). 125

Figure 5–79. Vertical displacement of WTC 1 Floor 99 for Case A_i temperature condition at 50 min (downward displacement is negative; 5x displacement magnification). 126

Figure 5–80. Average thermal expansion of WTC 1 floors at 100 min for Case A_i temperature condition. 126

Figure 5–81. Horizontal reaction force per column of WTC 1 Floor 97 for Case A_i temperature condition. 127

Figure 5–82. Vertical displacement of WTC 1 Floor 93 for Case B_i temperature condition at 100 min (downward displacement is negative; 5x displacement magnification). 128

Figure 5–83. Vertical displacement of WTC 1 Floor 94 for Case B_i temperature condition at 100 min (downward displacement is negative; 5x displacement magnification). 129

Figure 5–84. Vertical displacement of WTC 1 Floor 95 for Case B_i temperature condition at 10 min (downward displacement is negative; 5x displacement magnification). 129

Figure 5–85. Vertical displacement of WTC 1 Floor 96 for Case B_i temperature condition at 10 min (downward displacement is negative; 5x displacement magnification). 130

Figure 5–86. Vertical displacement of WTC 1 Floor 97 for Case B_i temperature condition at 100 min (downward displacement is negative; 5x displacement magnification). 130

Figure 5–87. Vertical displacement of WTC 1 Floor 98 for Case B_i temperature condition at 100 min (downward displacement is negative; 5x displacement magnification). 131

Figure 5–88. Vertical displacement of WTC 1 Floor 99 for Case B_i temperature condition at 100 min (downward displacement is negative; 5x displacement magnification). 131

Figure 5–89. Loss of vertical supports in Floor 97 and Floor 98 of WTC 1 for Case B_i temperature condition at 100 min (1x displacement magnification)..... 132

Figure 5–90. Thermal expansion of WTC 1 floors at 100 min for Case B_i conditions. 132

Figure 5–91. Horizontal reaction force per column of WTC 1 Floor 96 for Case B_i temperature condition. 133

Figure 5–92. Horizontal reaction force per column of WTC 1 Floor 98 for Case B_i temperature condition. 133

Figure 5–93. Vertical displacement of WTC 2 Floor 82 for Case C_i temperature condition at 10 min, 30 min, and 60 min (downward displacement is negative; 5x displacement magnification). 135

Figure 5–94. Horizontal displacement of exterior columns of WTC 2 Floor 82 for Case C_i temperature condition at 10 min, 30 min, and 60 min. 136

Figure 5–95. Total horizontal reaction at exterior columns on east and west faces of WTC 2 Floor 82 for Case C_i conditions. 137

Figure 5–96. User-defined break elements that failed by 60 min in the model of WTC 2 Floor 82 for Case C_i temperature condition..... 137

Figure 5–97. Loss of vertical supports in Floor 82 of WTC 2 for Case C_i temperature condition at 60 min (1x displacement magnification)..... 138

Figure 5–98. Vertical displacement of WTC 2 Floor 79 for Case C_i temperature condition at 60 min (downward displacement is negative; 5x displacement magnification). 139

Figure 5–99. Vertical displacement of WTC 2 Floor 80 for Case C_i temperature condition at 60 min (downward displacement is negative; 5x displacement magnification). 140

Figure 5–100. Vertical displacement of WTC 2 Floor 81 for Case C_i temperature condition at 60 min (downward displacement is negative; 5x displacement magnification). 140

Figure 5–101. Vertical displacement of WTC 2 Floor 83 for Case C_i temperature condition at 60 min (downward displacement is negative; 5x displacement magnification). 141

Figure 5–102. Average thermal expansion of WTC 2 floors at 60 min under Case C_i temperature condition. 141

Figure 5–103. Horizontal reaction force per column of WTC 2 Floor 81 for Case C_i temperature condition. 142

Figure 5–104. Loss of vertical supports in Floor 83 of WTC 2 for Case C_i temperature condition at 60 min (3X displacement magnification)..... 142

Figure 5–105. Vertical displacement of WTC 2 Floor 79 for Case D_i temperature condition at 60 min (downward displacement is negative; 5x displacement magnification). 144

Figure 5–106. Vertical displacement of WTC 2 Floor 80 for Case D_i temperature condition at 40 min (downward displacement is negative; 5x displacement magnification). 144

Figure 5–107. Vertical displacement of WTC 2 Floor 81 for Case D_i temperature condition at 50 min (downward displacement is negative; 5x displacement magnification). 145

Figure 5–108. Vertical displacement of WTC 2 Floor 82 for Case D_i temperature condition at 60 min (downward displacement is negative; 5x displacement magnification). 145

Figure 5–109. Vertical displacement of WTC 2 Floor 83 for Case D_i temperature condition at 60 min (downward displacement is negative; 5x displacement magnification). 146

Figure 5–110. Horizontal reaction force per column of WTC 2 Floor 80 for Case D_i temperature condition. 146

Figure 5–111. Horizontal reaction force per column of WTC 2 Floor 82 for Case D_i temperature condition. 147

Figure 5–112. Average thermal expansion of WTC 2 floors at 60 min for Case D_i temperature condition. 147

Figure 5–113. Vertical displacement of a simplified truss model at Column 333 extracted from the full floor model of Floor 96 of WTC 1 under Case B_i temperature condition at 40 min (downward displacement is negative). 148

Figure 5–114. Conditions of connections between the exterior wall and the floors of WTC 1 for Case A_i temperature condition at 100 min. 151

Figure 5–115. Conditions of connections between the exterior wall and the floors of WTC 1 for Case B_i temperature condition at 100 min. 152

Figure 5–116. Conditions of connections between the exterior wall and the floors of WTC 2 for Case C_i temperature condition at 60 min. 153

Figure 5–117. Conditions of connections between the exterior wall and the floors of WTC 2 for Case D_i temperature condition at 60 min. 154

Figure 6–1. Exterior wall subsystem structure. 158

Figure 6–2. Columns, spandrels, and splices: type and material assignments. 159
Figure 6–3. Schematic of column cross section. 160
Figure 6–4. SAP2000 model of prefabricated panel. 162
Figure 6–5. ANSYS model of prefabricated panel showing meshing. 163
Figure 6–6. ANSYS model of prefabricated panel showing boundary conditions and loading (loads applied separately)..... 163
Figure 6–7. Deflection of prefabricated panel under 100 kip lateral load..... 164
Figure 6–8. Deflection of prefabricated panel under 100 kip transverse load..... 164
Figure 6–9. Deflection of prefabricated panel under 10 kip vertical load..... 165
Figure 6–10. Exterior wall subsystem model with boundary conditions. 166
Figure 6–11. Typical meshing of exterior wall model components. 167
Figure 6–12. Schematic representation of columns used in the exterior wall model. 167
Figure 6–13. One-story exterior column model. 169
Figure 6–14. Load-deflection of column at room temperature and 700 °C. 169
Figure 6–15. Local buckling of column at room temperature. 170
Figure 6–16. Plastic hinge in column at room temperature..... 170
Figure 6–17. Deformed shape of column at maximum axial load at 700 °C. 171
Figure 6–18. Typical spandrel splice layout for exterior wall subsystem. 172
Figure 6–19. Modeling of a typical interior spandrel splice in the exterior wall model. 172
Figure 6–20. Column splice model used in exterior wall model..... 173
Figure 6–21. Exterior wall model temperature time-histories..... 175
Figure 6–22. Structural response for temperature time history D with all floors supported. 178
Figure 6–23. Structural response for temperature time history DBARE with all floors supported. 179
Figure 6–24. Structural response for temperature time history E (hot bolts) with all floors supported..... 181
Figure 6–25. Structural response for temperature time history E119 with all floors supported..... 182
Figure 6–26. Structural response for temperature time history F with all floors supported..... 184
Figure 6–27. Structural response for temperature time history DBARE with two unbraced floors..... 185
Figure 6–28. Structural response for time history DBARE with three unbraced floors..... 187
Figure 6–29. Structural response for temperature time history DBARE with pull-in forces at three floors (10X displacement magnification)..... 189
Figure 6–30. Column splice bolt stresses for temperature time history and DBARE with pull-in forces at three floors..... 190
Figure 6–31. Column splice contact element status for temperature time history and DBARE with pull-in forces at three floors. 190

Figure 6–32. Structural response for temperature time history DBARE and push-down with three unbraced floors (10X displacement magnification). 192

Figure 6–33. Column splice response for temperature time history DBARE and push-down with three unbraced floors. 192

Figure 6–34. Sum of total column reaction forces at base during push-down after application of temperature DBARE with three unbraced floors. 193

Figure 6–35. Sum of additional vertical reaction forces at base induced by imposed displacement during push-down after application of temperature DBARE with three unbraced floors. 193

Figure 6–36. Individual total column reaction forces at base during push-down after application of temperature DBARE with three unbraced floors. 194

Figure 6–37. Individual additional column reaction forces at base induced by imposed vertical displacement during push-down after application of temperature DBARE with three unbraced floors. 194

Figure 6–38. Difference between the additional individual column reaction forces at base and the vertical force applied at the top of each column during push-down after application of temperature DBARE with three unbraced floors. 195

Figure 6–39. Transverse deflection during push-down after application of temperature DBARE with three unbraced floors. 195

LIST OF TABLES

Table P–1. Federal building and fire safety investigation of the WTC disaster. xxii

Table P–2. Public meetings and briefings of the WTC Investigation. xxv

Table 3–1. Steel types used in WTC 1 and WTC 2. 15

Table 3–2. Parameters for *K(T)* and *n(T)*. 16

Table 3–3. Uniaxial plastic strain at fracture by Eq. (11). 20

Table 4–1. Element types used in ANSYS models. 27

Table 4–2. Comparison of SAP and ANSYS results for gravity load case 28

Table 4–3. Comparison of SAP and ANSYS floor model modal analysis results. 31

Table 4–4. Comparison of maximum displacements and base reactions of WTC 1 from translated ANSYS and SAP2000 models. 36

Table 4–5. Comparison of maximum displacements and base reactions of WTC 2 obtained from translated ANSYS and SAP2000 models. 36

Table 4–6. Comparison of axial forces in randomly selected elements from WTC 1 model at the end of gravity analysis. 36

Table 4–7. Comparison of axial forces in randomly selected elements from WTC 2 model at the end of gravity analysis. 37

Table 5–1. Materials used for truss seat calculations. 42

Table 5–2. Exterior truss seat capacity for vertical force. 47

Table 5–3. Interior truss seat capacity for vertical force. 47

Table 5–4. Exterior truss seat capacity for horizontal tensile force. 50

Table 5–5. Interior truss seat capacity against horizontal tensile force 50

Table 5–6. Compression strength of gusset plate. 52

Table 5–7. Temperature-dependent knuckle capacity for assumed temperatures. 67

Table 5–8. Material assignments in truss model. 74

Table 5–9. Resistance weld strength. 74

Table 5–10. Types of user-defined break elements. 92

Table 5–11. Number of user-defined break elements in the full floor model (Floor 96, WTC 1). 94

Table 5–12. List of full floor model analyses performed. 117

Table 5–13. Number of failed user-defined break elements in the model of WTC 1 Floor 96 for Case A_i temperature condition. 122

Table 5–14. Maximum vertical displacement of WTC 1 floors for Case A_i temperature condition. ... 123

Table 5–15. Maximum vertical displacement of WTC 1 floors for Case B_i temperature condition..... 128

Table 5–16. Number of failed user-defined break elements in the model of WTC 2 Floor 82 for Case C_i temperature condition. 138

Table 5–17. Maximum vertical displacement of WTC 2 floors for Case C_i temperature condition..... 139

Table 5–18. Maximum vertical displacement of WTC 2 floors for Case D_i temperature condition. 143

Table 6–1a. Column sectional properties..... 160

Table 6–1b. Column splice details. 160

Table 6–1c. Spandrel splice details..... 161

Table 6–2. Prefabricated panel validation results. 165

Table 6–3. Thermal loading conditions used in the exterior wall model. 175

Table 6–4. Analysis cases for exterior wall subsystem model..... 177

Table 6–5. Summary of spandrel splice break elements for temperature time history D with all floors supported. 178

Table 6–6. Summary of spandrel splice break elements for temperature time history DBARE with all floors supported. 180

Table 6–7. Summary of spandrel splice break elements for temperature time-history E (hot bolts) with all floors supported. 181

Table 6–8. Summary of spandrel splice break elements for temperature time history E119 with all floors supported. 183

Table 6–9. Summary of spandrel splice break elements for temperature time history F with all floors supported. 184

Table 6–10. Summary of spandrel splice break elements for temperature time history DBARE with 2 unbraced floors..... 186

Table 6–11. Spandrel splice break elements for temperature time history DBARE with 3 unbraced floors..... 187

Table 6–12. Summary of exterior wall model results. 198

LIST OF ACRONYMS AND ABBREVIATIONS

Acronyms

ARA	Applied Research Associates, Inc.
ASTM	American Society for Testing and Materials
BPS	Building Performance Study
CAEAI	Computer Aided Engineering Associates, Inc.
FEMA	Federal Emergency Management Agency
FEA	Finite element analysis
LERA	Leslie E. Robertson Associates
NIST	National Institute of Standards and Technology
PANYNJ	The Port Authority of New York and New Jersey
SEAoNY	Structural Engineers Association of New York
SGH	Simpson Gumpertz & Heger Inc.
USC	United States Code
WTC	World Trade Center
WTC 1	World Trade Center 1 (North Tower)
WTC 2	World Trade Center 2 (South Tower)
WTC 7	World Trade Center 7

Abbreviations

˚C	degrees Celsius
°F	degrees Fahrenheit
ft	feet
in.	inch
L	liter
m	meter
μm	micrometer
h	hour
min	minute
s	second
lb	pound

kip	kilo pounds
pcf	pound per cubic foot
psf	pound per square foot
psi	pound per square inch
ksi	kilo pounds per square inch

PREFACE

Genesis of This Investigation

Immediately following the terrorist attack on the World Trade Center (WTC) on September 11, 2001, the Federal Emergency Management Agency (FEMA) and the American Society of Civil Engineers began planning a building performance study of the disaster. The week of October 7, as soon as the rescue and search efforts ceased, the Building Performance Study Team went to the site and began its assessment. This was to be a brief effort, as the study team consisted of experts who largely volunteered their time away from their other professional commitments. The Building Performance Study Team issued its report in May 2002, fulfilling its goal "to determine probable failure mechanisms and to identify areas of future investigation that could lead to practical measures for improving the damage resistance of buildings against such unforeseen events."

On August 21, 2002, with funding from the U.S. Congress through FEMA, the National Institute of Standards and Technology (NIST) announced its building and fire safety investigation of the WTC disaster. On October 1, 2002, the National Construction Safety Team Act (Public Law 107-231), was signed into law. The NIST WTC Investigation was conducted under the authority of the National Construction Safety Team Act.

The goals of the investigation of the WTC disaster were:

- To investigate the building construction, the materials used, and the technical conditions that contributed to the outcome of the WTC disaster.
- To serve as the basis for:
  - Improvements in the way buildings are designed, constructed, maintained, and used;
  - Improved tools and guidance for industry and safety officials;
  - Recommended revisions to current codes, standards, and practices; and
  - Improved public safety.

The specific objectives were:

1. Determine why and how WTC 1 and WTC 2 collapsed following the initial impacts of the aircraft and why and how WTC 7 collapsed;
2. Determine why the injuries and fatalities were so high or low depending on location, including all technical aspects of fire protection, occupant behavior, evacuation, and emergency response;
3. Determine what procedures and practices were used in the design, construction, operation, and maintenance of WTC 1, 2, and 7; and
4. Identify, as specifically as possible, areas in current building and fire codes, standards, and practices that warrant revision.

NIST is a nonregulatory agency of the U.S. Department of Commerce's Technology Administration. The purpose of NIST investigations is to improve the safety and structural integrity of buildings in the United States, and the focus is on fact finding. NIST investigative teams are authorized to assess building performance and emergency response and evacuation procedures in the wake of any building failure that has resulted in substantial loss of life or that posed significant potential of substantial loss of life. NIST does not have the statutory authority to make findings of fault nor negligence by individuals or organizations. Further, no part of any report resulting from a NIST investigation into a building failure or from an investigation under the National Construction Safety Team Act may be used in any suit or action for damages arising out of any matter mentioned in such report (15 USC 281a, as amended by Public Law 107-231).

Organization of the Investigation

The National Construction Safety Team for this Investigation, appointed by the then NIST Director, Dr. Arden L. Bement, Jr., was led by Dr. S. Shyam Sunder. Dr. William L. Grosshandler served as Associate Lead Investigator, Mr. Stephen A. Cauffman served as Program Manager for Administration, and Mr. Harold E. Nelson served on the team as a private sector expert. The Investigation included eight interdependent projects whose leaders comprised the remainder of the team. A detailed description of each of these eight projects is available at http://wtc.nist.gov. The purpose of each project is summarized in Table P–1, and the key interdependencies among the projects are illustrated in Fig. P–1.

Table P–1. Federal building and fire safety investigation of the WTC disaster.

Technical Area and Project Leader	Project Purpose
Analysis of Building and Fire Codes and Practices; Project Leaders: Dr. H. S. Lew and Mr. Richard W. Bukowski	Document and analyze the code provisions, procedures, and practices used in the design, construction, operation, and maintenance of the structural, passive fire protection, and emergency access and evacuation systems of WTC 1, 2, and 7.
Baseline Structural Performance and Aircraft Impact Damage Analysis; Project Leader: Dr. Fahim H. Sadek	Analyze the baseline performance of WTC 1 and WTC 2 under design, service, and abnormal loads, and aircraft impact damage on the structural, fire protection, and egress systems.
Mechanical and Metallurgical Analysis of Structural Steel; Project Leader: Dr. Frank W. Gayle	Determine and analyze the mechanical and metallurgical properties and quality of steel, weldments, and connections from steel recovered from WTC 1, 2, and 7.
Investigation of Active Fire Protection Systems; Project Leader: Dr. David D. Evans; Dr. William Grosshandler	Investigate the performance of the active fire protection systems in WTC 1, 2, and 7 and their role in fire control, emergency response, and fate of occupants and responders.
Reconstruction of Thermal and Tenability Environment; Project Leader: Dr. Richard G. Gann	Reconstruct the time-evolving temperature, thermal environment, and smoke movement in WTC 1, 2, and 7 for use in evaluating the structural performance of the buildings and behavior and fate of occupants and responders.
Structural Fire Response and Collapse Analysis; Project Leaders: Dr. John L. Gross and Dr. Therese P. McAllister	Analyze the response of the WTC towers to fires with and without aircraft damage, the response of WTC 7 in fires, the performance of composite steel-trussed floor systems, and determine the most probable structural collapse sequence for WTC 1, 2, and 7.
Occupant Behavior, Egress, and Emergency Communications; Project Leader: Mr. Jason D. Averill	Analyze the behavior and fate of occupants and responders, both those who survived and those who did not, and the performance of the evacuation system.
Emergency Response Technologies and Guidelines; Project Leader: Mr. J. Randall Lawson	Document the activities of the emergency responders from the time of the terrorist attacks on WTC 1 and WTC 2 until the collapse of WTC 7, including practices followed and technologies used.

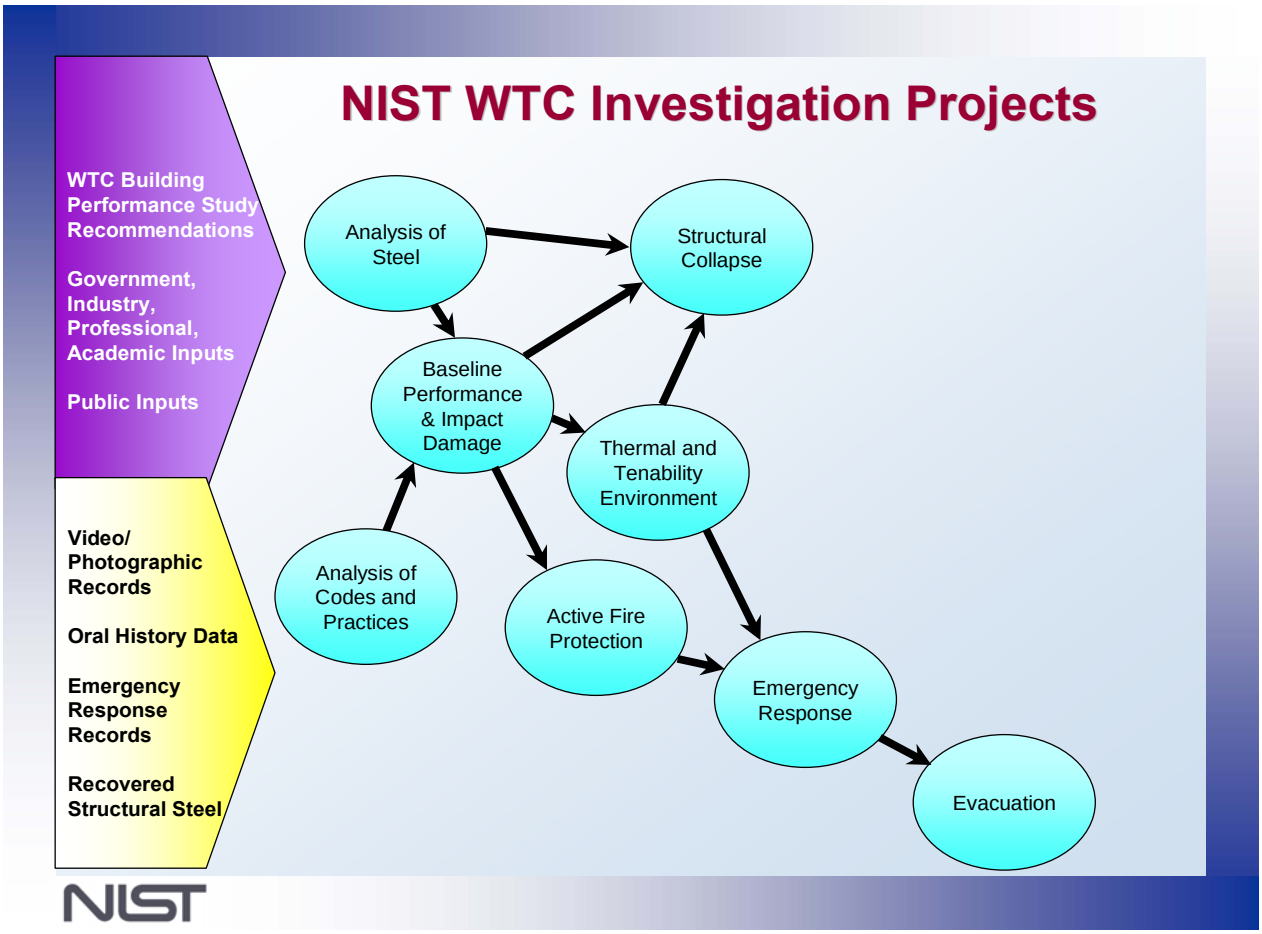

Figure P–1. The eight projects in the federal building and fire safety investigation of the WTC disaster.

National Construction Safety Team Advisory Committee

The NIST Director also established an advisory committee as mandated under the National Construction Safety Team Act. The initial members of the committee were appointed following a public solicitation. These were:

- Paul Fitzgerald, Executive Vice President (retired) FM Global, National Construction Safety Team Advisory Committee Chair
- John Barsom, President, Barsom Consulting, Ltd.
- John Bryan, Professor Emeritus, University of Maryland
- David Collins, President, The Preview Group, Inc.
- Glenn Corbett, Professor, John Jay College of Criminal Justice
- Philip DiNenno, President, Hughes Associates, Inc.

- Robert Hanson, Professor Emeritus, University of Michigan
- Charles Thornton, Co-Chairman and Managing Principal, The Thornton-Tomasetti Group, Inc.
- Kathleen Tierney, Director, Natural Hazards Research and Applications Information Center, University of Colorado at Boulder
- Forman Williams, Director, Center for Energy Research, University of California at San Diego

This National Construction Safety Team Advisory Committee provided technical advice during the Investigation and commentary on drafts of the Investigation reports prior to their public release. NIST has benefited from the work of many people in the preparation of these reports, including the National Construction Safety Team Advisory Committee. The content of the reports and recommendations, however, are solely the responsibility of NIST.

Public Outreach

During the course of this Investigation, NIST held public briefings and meetings (listed in Table P–2) to solicit input from the public, present preliminary findings, and obtain comments on the direction and progress of the Investigation from the public and the Advisory Committee.

NIST maintained a publicly accessible Web site during this Investigation at http://wtc.nist.gov. The site contained extensive information on the background and progress of the Investigation.

NIST's WTC Public-Private Response Plan

The collapse of the WTC buildings has led to broad reexamination of how tall buildings are designed, constructed, maintained, and used, especially with regard to major events such as fires, natural disasters, and terrorist attacks. Reflecting the enhanced interest in effecting necessary change, NIST, with support from Congress and the Administration, has put in place a program, the goal of which is to develop and implement the standards, technology, and practices needed for cost-effective improvements to the safety and security of buildings and building occupants, including evacuation, emergency response procedures, and threat mitigation.

The strategy to meet this goal is a three-part NIST-led public-private response program that includes:

- A federal building and fire safety investigation to study the most probable factors that contributed to post-aircraft impact collapse of the WTC towers and the 47-story WTC 7 building, and the associated evacuation and emergency response experience.
- A research and development (R&D) program to (a) facilitate the implementation of recommendations resulting from the WTC Investigation, and (b) provide the technical basis for cost-effective improvements to national building and fire codes, standards, and practices that enhance the safety of buildings, their occupants, and emergency responders.

Table P–2. Public meetings and briefings of the WTC Investigation.

Date	Location	Principal Agenda
June 24, 2002	New York City, NY	Public meeting: Public comments on the *Draft Plan* for the pending WTC Investigation.
August 21, 2002	Gaithersburg, MD	Media briefing announcing the formal start of the Investigation.
December 9, 2002	Washington, DC	Media briefing on release of the *Public Update* and NIST request for photographs and videos.
April 8, 2003	New York City, NY	Joint public forum with Columbia University on first-person interviews.
April 29–30, 2003	Gaithersburg, MD	NCST Advisory Committee meeting on plan for and progress on WTC Investigation with a public comment session.
May 7, 2003	New York City, NY	Media briefing on release of *May 2003 Progress Report.*
August 26–27, 2003	Gaithersburg, MD	NCST Advisory Committee meeting on status of the WTC investigation with a public comment session.
September 17, 2003	New York City, NY	Media and public briefing on initiation of first-person data collection projects.
December 2–3, 2003	Gaithersburg, MD	NCST Advisory Committee meeting on status and initial results and release of the *Public Update* with a public comment session.
February 12, 2004	New York City, NY	Public meeting on progress and preliminary findings with public comments on issues to be considered in formulating final recommendations.
June 18, 2004	New York City, NY	Media/public briefing on release of *June 2004 Progress Report.*
June 22–23, 2004	Gaithersburg, MD	NCST Advisory Committee meeting on the status of and preliminary findings from the WTC Investigation with a public comment session.
August 24, 2004	Northbrook, IL	Public viewing of standard fire resistance test of WTC floor system at Underwriters Laboratories, Inc.
October 19–20, 2004	Gaithersburg, MD	NCST Advisory Committee meeting on status and near complete set of preliminary findings with a public comment session.
November 22, 2004	Gaithersburg, MD	NCST Advisory Committee discussion on draft annual report to Congress, a public comment session, and a closed session to discuss pre-draft recommendations for WTC Investigation.
April 5, 2005	New York City, NY	Media and public briefing on release of the probable collapse sequence for the WTC towers and draft reports for the projects on codes and practices, evacuation, and emergency response.
June 23, 2005	New York City, NY	Media and public briefing on release of all draft reports for the WTC towers and draft recommendations for public comment.
September 12–13, 2005	Gaithersburg, MD	NCST Advisory Committee meeting on disposition of public comments and update to draft reports for the WTC towers.
September 13–15, 2005	Gaithersburg, MD	WTC Technical Conference for stakeholders and technical community for dissemination of findings and recommendations and opportunity for public to make technical comments.

- A dissemination and technical assistance program (DTAP) to (a) engage leaders of the construction and building community in ensuring timely adoption and widespread use of proposed changes to practices, standards, and codes resulting from the WTC Investigation and the R&D program, and (b) provide practical guidance and tools to better prepare facility owners, contractors, architects, engineers, emergency responders, and regulatory authorities to respond to future disasters.

The desired outcomes are to make buildings, occupants, and first responders safer in future disaster events.

National Construction Safety Team Reports on the WTC Investigation

A final report on the collapse of the WTC towers is being issued as NIST NCSTAR 1. A companion report on the collapse of WTC 7 is being issued as NIST NCSTAR 1A. The present report is one of a set that provides more detailed documentation of the Investigation findings and the means by which these technical results were achieved. As such, it is part of the archival record of this Investigation. The titles of the full set of Investigation publications are:

NIST (National Institute of Standards and Technology). 2005. *Federal Building and Fire Safety Investigation of the World Trade Center Disaster: Final Report on the Collapse of the World Trade Center Towers.* NIST NCSTAR 1. Gaithersburg, MD, September.

NIST (National Institute of Standards and Technology). 2006. *Federal Building and Fire Safety Investigation of the World Trade Center Disaster: Final Report on the Collapse of World Trade Center 7.* NIST NCSTAR 1A. Gaithersburg, MD.

Lew, H. S., R. W. Bukowski, and N. J. Carino. 2005. *Federal Building and Fire Safety Investigation of the World Trade Center Disaster: Design, Construction, and Maintenance of Structural and Life Safety Systems.* NIST NCSTAR 1-1. National Institute of Standards and Technology. Gaithersburg, MD, September.

Fanella, D. A., A. T. Derecho, and S. K. Ghosh. 2005. *Federal Building and Fire Safety Investigation of the World Trade Center Disaster: Design and Construction of Structural Systems.* NIST NCSTAR 1-1A. National Institute of Standards and Technology. Gaithersburg, MD, September.

Ghosh, S. K., and X. Liang. 2005. *Federal Building and Fire Safety Investigation of the World Trade Center Disaster: Comparison of Building Code Structural Requirements.* NIST NCSTAR 1-1B. National Institute of Standards and Technology. Gaithersburg, MD, September.

Fanella, D. A., A. T. Derecho, and S. K. Ghosh. 2005. *Federal Building and Fire Safety Investigation of the World Trade Center Disaster: Maintenance and Modifications to Structural Systems.* NIST NCSTAR 1-1C. National Institute of Standards and Technology. Gaithersburg, MD, September.

Grill, R. A., and D. A. Johnson. 2005. *Federal Building and Fire Safety Investigation of the World Trade Center Disaster: Fire Protection and Life Safety Provisions Applied to the Design and Construction of World Trade Center 1, 2, and 7 and Post-Construction Provisions Applied after Occupancy*. NIST NCSTAR 1-1D. National Institute of Standards and Technology. Gaithersburg, MD, September.

Razza, J. C., and R. A. Grill. 2005. *Federal Building and Fire Safety Investigation of the World Trade Center Disaster: Comparison of Codes, Standards, and Practices in Use at the Time of the Design and Construction of World Trade Center 1, 2, and 7*. NIST NCSTAR 1-1E. National Institute of Standards and Technology. Gaithersburg, MD, September.

Grill, R. A., D. A. Johnson, and D. A. Fanella. 2005. *Federal Building and Fire Safety Investigation of the World Trade Center Disaster: Comparison of the 1968 and Current (2003) New*

York City Building Code Provisions. NIST NCSTAR 1-1F. National Institute of Standards and Technology. Gaithersburg, MD, September.

Grill, R. A., and D. A. Johnson. 2005. *Federal Building and Fire Safety Investigation of the World Trade Center Disaster: Amendments to the Fire Protection and Life Safety Provisions of the New York City Building Code by Local Laws Adopted While World Trade Center 1, 2, and 7 Were in Use*. NIST NCSTAR 1-1G. National Institute of Standards and Technology. Gaithersburg, MD, September.

Grill, R. A., and D. A. Johnson. 2005. *Federal Building and Fire Safety Investigation of the World Trade Center Disaster: Post-Construction Modifications to Fire Protection and Life Safety Systems of World Trade Center 1 and 2*. NIST NCSTAR 1-1H. National Institute of Standards and Technology. Gaithersburg, MD, September.

Grill, R. A., D. A. Johnson, and D. A. Fanella. 2005. *Federal Building and Fire Safety Investigation of the World Trade Center Disaster: Post-Construction Modifications to Fire Protection, Life Safety, and Structural Systems of World Trade Center 7*. NIST NCSTAR 1-1I. National Institute of Standards and Technology. Gaithersburg, MD, September.

Grill, R. A., and D. A. Johnson. 2005. *Federal Building and Fire Safety Investigation of the World Trade Center Disaster: Design, Installation, and Operation of Fuel System for Emergency Power in World Trade Center 7*. NIST NCSTAR 1-1J. National Institute of Standards and Technology. Gaithersburg, MD, September.

Sadek, F. 2005. *Federal Building and Fire Safety Investigation of the World Trade Center Disaster: Baseline Structural Performance and Aircraft Impact Damage Analysis of the World Trade Center Towers.* NIST NCSTAR 1-2. National Institute of Standards and Technology. Gaithersburg, MD, September.

Faschan, W. J., and R. B. Garlock. 2005. *Federal Building and Fire Safety Investigation of the World Trade Center Disaster: Reference Structural Models and Baseline Performance Analysis of the World Trade Center Towers.* NIST NCSTAR 1-2A. National Institute of Standards and Technology. Gaithersburg, MD, September.

Kirkpatrick, S. W., R. T. Bocchieri, F. Sadek, R. A. MacNeill, S. Holmes, B. D. Peterson, R. W. Cilke, C. Navarro. 2005. *Federal Building and Fire Safety Investigation of the World Trade Center Disaster: Analysis of Aircraft Impacts into the World Trade Center Towers,* NIST NCSTAR 1-2B. National Institute of Standards and Technology. Gaithersburg, MD, September.

Gayle, F. W., R. J. Fields, W. E. Luecke, S. W. Banovic, T. Foecke, C. N. McCowan, T. A. Siewert, and J. D. McColskey. 2005. *Federal Building and Fire Safety Investigation of the World Trade Center Disaster: Mechanical and Metallurgical Analysis of Structural Steel.* NIST NCSTAR 1-3. National Institute of Standards and Technology. Gaithersburg, MD, September.

Luecke, W. E., T. A. Siewert, and F. W. Gayle. 2005. *Federal Building and Fire Safety Investigation of the World Trade Center Disaster: Contemporaneous Structural Steel Specifications.* NIST Special Publication 1-3A. National Institute of Standards and Technology. Gaithersburg, MD, September.

Banovic, S. W. 2005. *Federal Building and Fire Safety Investigation of the World Trade Center Disaster: Steel Inventory and Identification.* NIST NCSTAR 1-3B. National Institute of Standards and Technology. Gaithersburg, MD, September.

Banovic, S. W., and T. Foecke. 2005. *Federal Building and Fire Safety Investigation of the World Trade Center Disaster: Damage and Failure Modes of Structural Steel Components.* NIST NCSTAR 1-3C. National Institute of Standards and Technology. Gaithersburg, MD, September.

Luecke, W. E., J. D. McColskey, C. N. McCowan, S. W. Banovic, R. J. Fields, T. Foecke, T. A. Siewert, and F. W. Gayle. 2005. *Federal Building and Fire Safety Investigation of the World Trade Center Disaster: Mechanical Properties of Structural Steels.* NIST NCSTAR 1-3D. National Institute of Standards and Technology. Gaithersburg, MD, September.

Banovic, S. W., C. N. McCowan, and W. E. Luecke. 2005. *Federal Building and Fire Safety Investigation of the World Trade Center Disaster: Physical Properties of Structural Steels.* NIST NCSTAR 1-3E. National Institute of Standards and Technology. Gaithersburg, MD, September.

Evans, D. D., R. D. Peacock, E. D. Kuligowski, W. S. Dols, and W. L. Grosshandler. 2005. *Federal Building and Fire Safety Investigation of the World Trade Center Disaster: Active Fire Protection Systems.* NIST NCSTAR 1-4. National Institute of Standards and Technology. Gaithersburg, MD, September.

Kuligowski, E. D., D. D. Evans, and R. D. Peacock. 2005. *Federal Building and Fire Safety Investigation of the World Trade Center Disaster: Post-Construction Fires Prior to September 11, 2001.* NIST NCSTAR 1-4A. National Institute of Standards and Technology. Gaithersburg, MD, September.

Hopkins, M., J. Schoenrock, and E. Budnick. 2005. *Federal Building and Fire Safety Investigation of the World Trade Center Disaster: Fire Suppression Systems.* NIST NCSTAR 1-4B. National Institute of Standards and Technology. Gaithersburg, MD, September.

Keough, R. J., and R. A. Grill. 2005. *Federal Building and Fire Safety Investigation of the World Trade Center Disaster: Fire Alarm Systems.* NIST NCSTAR 1-4C. National Institute of Standards and Technology. Gaithersburg, MD, September.

Ferreira, M. J., and S. M. Strege. 2005. *Federal Building and Fire Safety Investigation of the World Trade Center Disaster: Smoke Management Systems.* NIST NCSTAR 1-4D. National Institute of Standards and Technology. Gaithersburg, MD, September.

Gann, R. G., A. Hamins, K. B. McGrattan, G. W. Mulholland, H. E. Nelson, T. J. Ohlemiller, W. M. Pitts, and K. R. Prasad. 2005. *Federal Building and Fire Safety Investigation of the World Trade Center Disaster: Reconstruction of the Fires in the World Trade Center Towers.* NIST NCSTAR 1-5. National Institute of Standards and Technology. Gaithersburg, MD, September.

Pitts, W. M., K. M. Butler, and V. Junker. 2005. *Federal Building and Fire Safety Investigation of the World Trade Center Disaster: Visual Evidence, Damage Estimates, and Timeline Analysis.* NIST NCSTAR 1-5A. National Institute of Standards and Technology. Gaithersburg, MD, September.

Hamins, A., A. Maranghides, K. B. McGrattan, E. Johnsson, T. J. Ohlemiller, M. Donnelly, J. Yang, G. Mulholland, K. R. Prasad, S. Kukuck, R. Anleitner and T. McAllister. 2005. *Federal Building and Fire Safety Investigation of the World Trade Center Disaster: Experiments and Modeling of Structural Steel Elements Exposed to Fire.* NIST NCSTAR 1-5B. National Institute of Standards and Technology. Gaithersburg, MD, September.

Ohlemiller, T. J., G. W. Mulholland, A. Maranghides, J. J. Filliben, and R. G. Gann. 2005. *Federal Building and Fire Safety Investigation of the World Trade Center Disaster: Fire Tests of Single Office Workstations.* NIST NCSTAR 1-5C. National Institute of Standards and Technology. Gaithersburg, MD, September.

Gann, R. G., M. A. Riley, J. M. Repp, A. S. Whittaker, A. M. Reinhorn, and P. A. Hough. 2005. *Federal Building and Fire Safety Investigation of the World Trade Center Disaster: Reaction of Ceiling Tile Systems to Shocks.* NIST NCSTAR 1-5D. National Institute of Standards and Technology. Gaithersburg, MD, September.

Hamins, A., A. Maranghides, K. B. McGrattan, T. J. Ohlemiller, and R. Anleitner. 2005. *Federal Building and Fire Safety Investigation of the World Trade Center Disaster: Experiments and Modeling of Multiple Workstations Burning in a Compartment.* NIST NCSTAR 1-5E. National Institute of Standards and Technology. Gaithersburg, MD, September.

McGrattan, K. B., C. Bouldin, and G. Forney. 2005. *Federal Building and Fire Safety Investigation of the World Trade Center Disaster: Computer Simulation of the Fires in the World Trade Center Towers.* NIST NCSTAR 1-5F. National Institute of Standards and Technology. Gaithersburg, MD, September.

Prasad, K. R., and H. R. Baum. 2005. *Federal Building and Fire Safety Investigation of the World Trade Center Disaster: Fire Structure Interface and Thermal Response of the World Trade Center Towers.* NIST NCSTAR 1-5G. National Institute of Standards and Technology. Gaithersburg, MD, September.

Gross, J. L., and T. McAllister. 2005. *Federal Building and Fire Safety Investigation of the World Trade Center Disaster: Structural Fire Response and Probable Collapse Sequence of the World Trade Center Towers.* NIST NCSTAR 1-6. National Institute of Standards and Technology. Gaithersburg, MD, September.

Carino, N. J., M. A. Starnes, J. L. Gross, J. C. Yang, S. Kukuck, K. R. Prasad, and R. W. Bukowski. 2005. *Federal Building and Fire Safety Investigation of the World Trade Center Disaster: Passive Fire Protection.* NIST NCSTAR 1-6A. National Institute of Standards and Technology. Gaithersburg, MD, September.

Gross, J., F. Hervey, M. Izydorek, J. Mammoser, and J. Treadway. 2005. *Federal Building and Fire Safety Investigation of the World Trade Center Disaster: Fire Resistance Tests of Floor Truss Systems.* NIST NCSTAR 1-6B. National Institute of Standards and Technology. Gaithersburg, MD, September.

Zarghamee, M. S., S. Bolourchi, D. W. Eggers, Ö. O. Erbay, F. W. Kan, Y. Kitane, A. A. Liepins, M. Mudlock, W. I. Naguib, R. P. Ojdrovic, A. T. Sarawit, P. R Barrett, J. L. Gross, and T. P. McAllister. 2005. *Federal Building and Fire Safety Investigation of the World Trade Center*

Disaster: Component, Connection, and Subsystem Structural Analysis. NIST NCSTAR 1-6C. National Institute of Standards and Technology. Gaithersburg, MD, September.

Zarghamee, M. S., Y. Kitane, Ö. O. Erbay, T. P. McAllister, and J. L. Gross. 2005. *Federal Building and Fire Safety Investigation of the World Trade Center Disaster: Global Structural Analysis of the Response of the World Trade Center Towers to Impact Damage and Fire.* NIST NCSTAR 1-6D. National Institute of Standards and Technology. Gaithersburg, MD, September.

McAllister, T., R. W. Bukowski, R. G. Gann, J. L. Gross, K. B. McGrattan, H. E. Nelson, L. Phan, W. M. Pitts, K. R. Prasad, F. Sadek. 2006. *Federal Building and Fire Safety Investigation of the World Trade Center Disaster: Structural Fire Response and Probable Collapse Sequence of World Trade Center 7.* (Provisional). NIST NCSTAR 1-6E. National Institute of Standards and Technology. Gaithersburg, MD.

Gilsanz, R., V. Arbitrio, C. Anders, D. Chlebus, K. Ezzeldin, W. Guo, P. Moloney, A. Montalva, J. Oh, K. Rubenacker. 2006. *Federal Building and Fire Safety Investigation of the World Trade Center Disaster: Structural Analysis of the Response of World Trade Center 7 to Debris Damage and Fire*. (Provisional). NIST NCSTAR 1-6F. National Institute of Standards and Technology. Gaithersburg, MD.

Kim, W. 2006. *Federal Building and Fire Safety Investigation of the World Trade Center Disaster: Analysis of September 11, 2001, Seismogram Data*. (Provisional). NIST NCSTAR 1-6G. National Institute of Standards and Technology. Gaithersburg, MD.

Nelson, K. 2006. *Federal Building and Fire Safety Investigation of the World Trade Center Disaster: The Con Ed Substation in World Trade Center 7*. (Provisional). NIST NCSTAR 1-6H. National Institute of Standards and Technology. Gaithersburg, MD.

Averill, J. D., D. S. Mileti, R. D. Peacock, E. D. Kuligowski, N. Groner, G. Proulx, P. A. Reneke, and H. E. Nelson. 2005. *Federal Building and Fire Safety Investigation of the World Trade Center Disaster: Occupant Behavior, Egress, and Emergency Communication.* NIST NCSTAR 1-7. National Institute of Standards and Technology. Gaithersburg, MD, September.

Fahy, R., and G. Proulx. 2005. *Federal Building and Fire Safety Investigation of the World Trade Center Disaster: Analysis of Published Accounts of the World Trade Center Evacuation.* NIST NCSTAR 1-7A. National Institute of Standards and Technology. Gaithersburg, MD, September.

Zmud, J. 2005. *Federal Building and Fire Safety Investigation of the World Trade Center Disaster: Technical Documentation for Survey Administration.* NIST NCSTAR 1-7B. National Institute of Standards and Technology. Gaithersburg, MD, September.

Lawson, J. R., and R. L. Vettori. 2005. *Federal Building and Fire Safety Investigation of the World Trade Center Disaster: The Emergency Response Operations.* NIST NCSTAR 1-8. National Institute of Standards and Technology. Gaithersburg, MD, September.

ACKNOWLEDGEMENTS

The assistance of SGH internal Structural Performance Review Committee (Glenn R. Bell, Ronal O. Hamburger, and Pedro J. Sifre) is gratefully acknowledged. Authors would also like to thank the technical staff of Computer Aided Engineering Associates, Inc., for their effort at converting SAP2000 finite element models to ANSYS and for their assistance in finite element modeling in ANSYS.

This page intentionally left blank.

EXECUTIVE SUMMARY

E.1 INTRODUCTION

Simpson Gumpertz & Heger Inc. (SGH) developed finite-element models of the components, connections and subsystems of the World Trade Center (WTC) towers to study their structural performance in the fire environment that followed the aircraft impact to the towers. The results of this study were used to develop global models that ran efficiently and captured the important failure modes and sequential failures of components and subsystems and to determine the probable sequence of structural responses that let to the global collapse initiation.

SGH performed this study under a NIST contract as part of Project 6 of the investigation on the WTC disaster by the National Institute of Standards and Technology (NIST). This report constitutes SGH report on Task 1 of the SGH contract with NIST and Part 1 of the SGH two-part report.

This study completed the following:

- Developed and validated ANSYS models of the full floor and exterior wall subsystems.
- Evaluated structural responses of components, connections, and subsystems to service loads due to gravity (dead and live loads) and elevated temperatures.
- Identified the likely failure modes and failure sequences of components, connections, and subsystems.
- Identified modeling details of the floor and exterior wall subsystems for the global models of the WTC towers.

All analyses used the nominal dimensions and design details shown on the WTC design and construction drawings. Material properties were based on information provided from NIST Project 3 study.

E.2 FULL FLOOR SUBSYSTEM

Floor 96 of WTC 1 was identified as an office floor with typical floor construction and loading; therefore, it was selected as the basis for modeling floor response. Figure E–1 shows a floor plan of Floor 96 of WTC 1. The full floor subsystem included office area and core area floor framing, as well as core and exterior columns extending to floors immediately above and below this floor.

The floor system in the office area consisted of lightweight concrete slab supported by steel floor trusses. The steel trusses for the floor system were manufactured by Laclede Steel Co. in Saint Louis, Missouri. Steel trusses spanned nominally 60 ft in the long-span area and 36 ft in the short-span area between exterior walls and the central core. Typically, a pair of primary trusses was supported at odd-numbered columns at 6 ft 8 in. on center. Each of these primary trusses consisted of top and bottom chords fabricated from double steel angles and web diagonals fabricated from round bars (see Fig. E–2). Web diagonals extended 3 in. above the top chord at the panel points into the concrete slab to form a knuckle and to provide shear transfer between the truss and the concrete slab (see Fig. E–2).

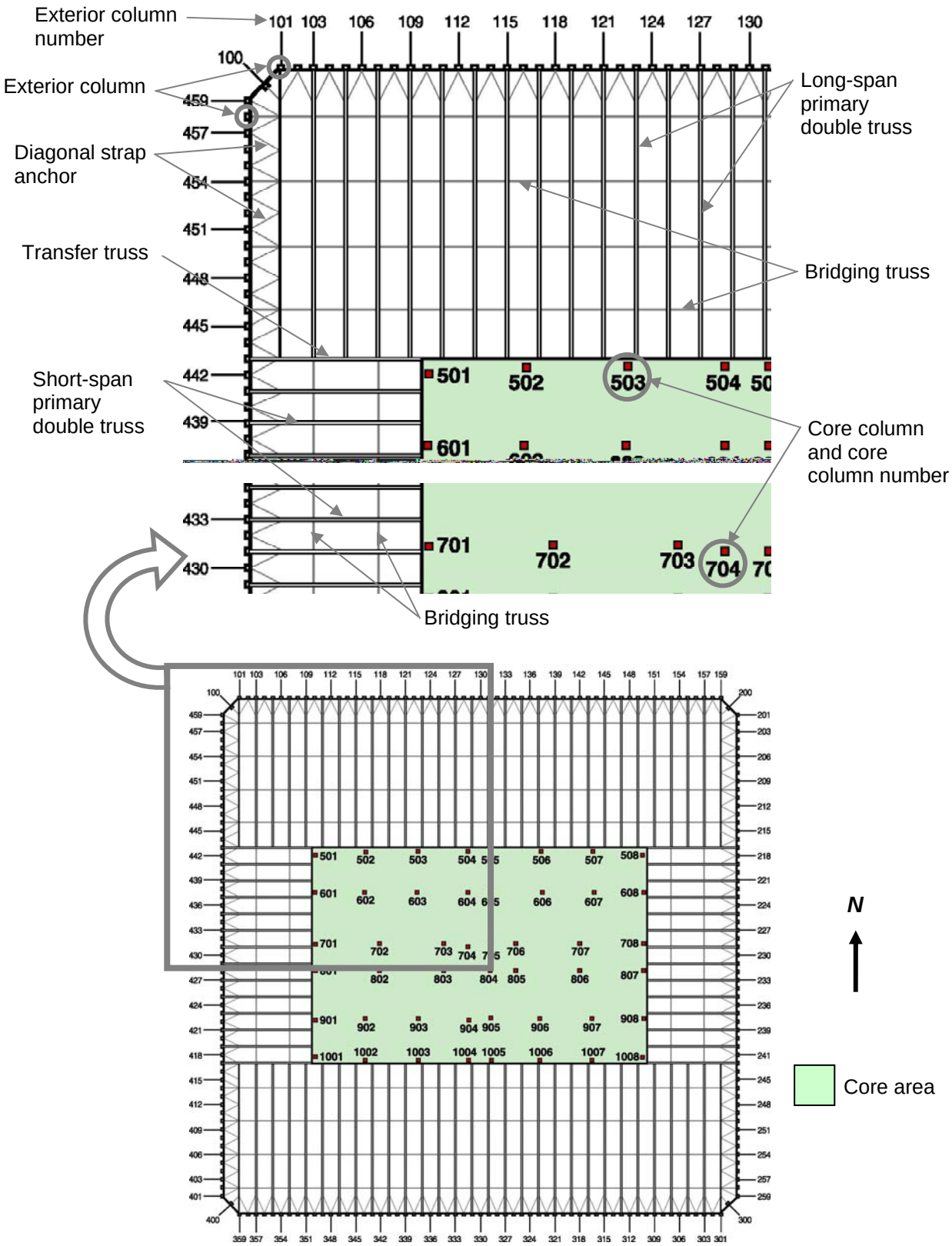

Figure E–1. Floor plan of Floor 96 of WTC 1.

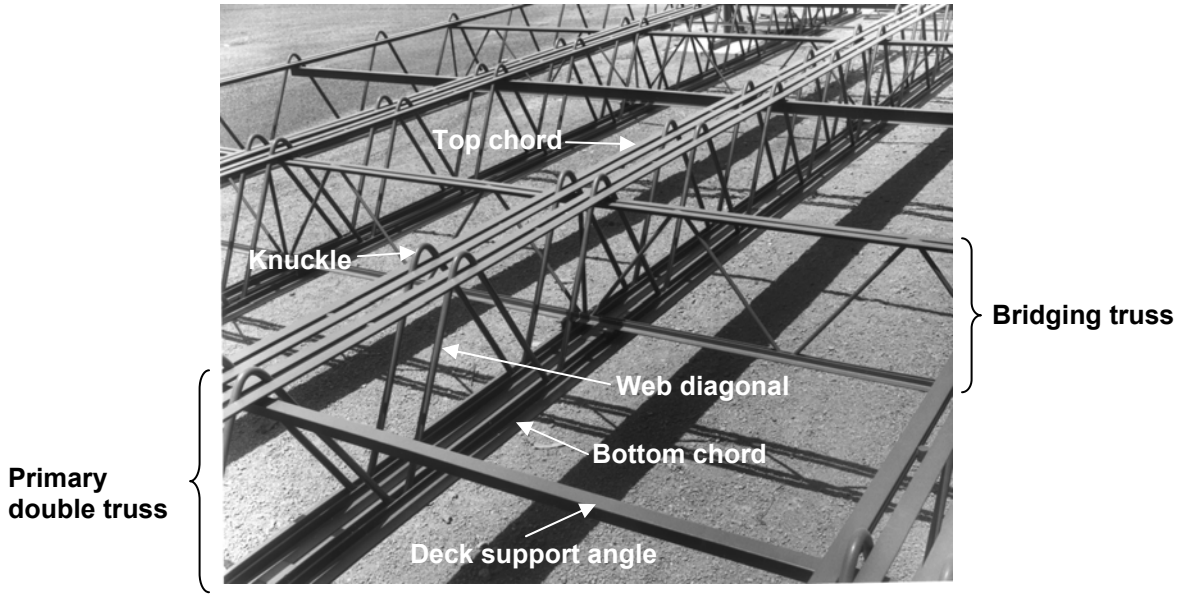

Figure E–2. Mock up of office floor framing system (Photograph from about 1967 provided by Laclede Steel Co.).

The top chords of a pair of trusses (double truss) were supported at the central core by an interior truss seat (Fig. E–3) welded to steel channels that ran continuously around the core floor area. Each pair of trusses was fastened to a horizontal plate of the interior truss seat by two 5/8 in. bolts (one bolt in each truss) in 1 3/4 in. long slotted holes. At the exterior wall, each pair of trusses was supported by an exterior truss seat (Fig. E–4), which fastened to a seat angle with two 5/8 in. diameter bolts in 2 in. long slotted holes. A pair of stand-off plates welded the seat angle to the spandrel. In addition, a gusset plate welded to the spandrel and to the truss top chord tied the truss to the supporting column, and a pair of diagonal strap anchors, welded to the top chords and to the adjacent columns, tied these columns to the primary trusses. Diagonal strap anchors will be referred to as “strap anchors” hereafter.

Primary trusses were interconnected by a transverse system of bridging trusses and deck support angles. These bridging trusses were of similar construction to the primary trusses, except the knuckles did not project above the top chords. The top chord of the bridging trusses sat 1 1/2 in. below the top chord of the primary trusses and provided support for the 4 in. thick lightweight concrete slab on the 1 1/2 in., 22 gauge steel deck with 2 in. wide at the top, 1.25 in. wide at the bottom, and 1.5 in. high flutes at 6.8 in. on center running parallel to the primary trusses. At each corner of the building core, a 36 ft long transfer truss extended out from the corner core column to the exterior wall and supported the 60 ft long primary trusses. The floor in the core consisted of a 4.5 in. thick lightweight concrete slab supported by wide flange girders and beams connected to the core columns with bolted connections. Reinforcement between the core area floor and the office area floor (#3 bars at 10 in. at the top and #4 bars at 12 in. at the bottom, respectively) provided continuity between the two areas and restrained the truss from walking off the interior seat.

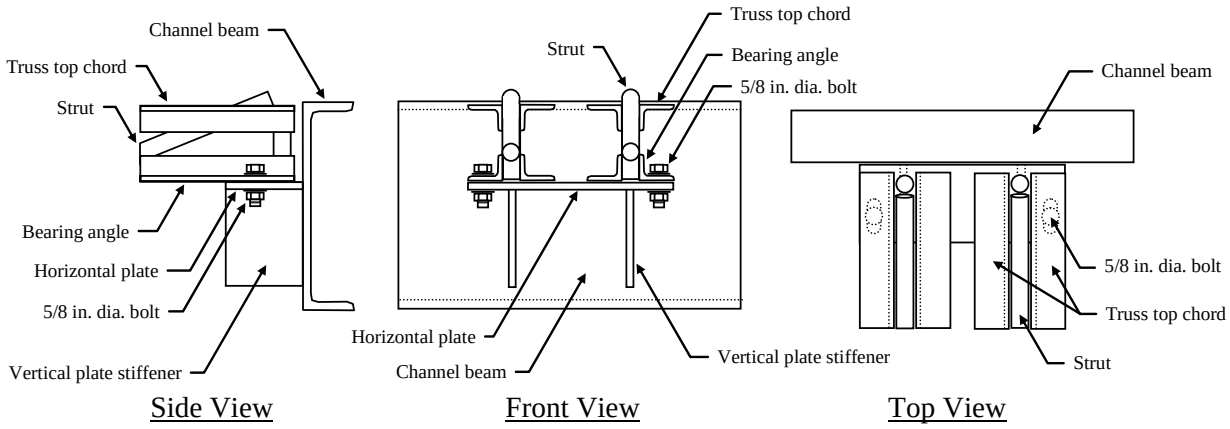

Figure E–3. Interior truss seat.

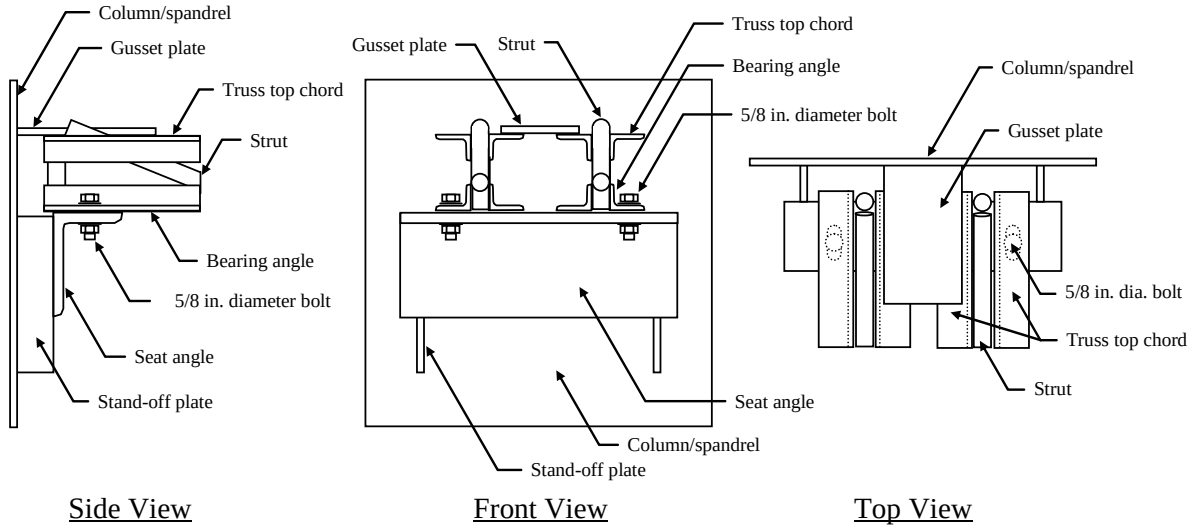

Figure E–4. Exterior truss seat.

E.2.1 Truss Seat Analysis

Failure Modes: The failure modes for truss seats were identified for vertical force, horizontal tensile force, horizontal compressive force, and combined vertical and horizontal force, and the corresponding capacities were calculated for different temperatures as follows:

- *Vertical Force*: The failure mode of exterior truss seats for vertical force was identified as fracture of the fillet welds between the stand-off plates and spandrel, which resulted in loss of truss vertical support. The failure mode of interior truss seats for vertical force was fracture of the fillet welds at the vertical plate to the channel beam. This failure mode results in loss of truss vertical support.
- *Horizontal Tensile Force*: The failure sequence of the exterior truss seats for horizontal tensile force differed for different seat details at different temperatures although the final failure mode was truss walk-off for all details. The typical failure sequence of the exterior truss seat was as follows: the gusset plate yielded, the groove weld yielded, the groove weld fractured, the truss bearing angle slid, seat bolts came to bear against the slotted hole, the

bolts sheared off, and finally the truss walked off the seat angle. The failure sequence of the interior truss seats for horizontal tensile force was bolt shear-off, resulting in truss walk-off.

- *Horizontal Compressive Force*: Even after the concrete slab failed in compression, additional resistance was developed from the spandrel at the exterior seat or from the channel beam at the interior seat after contact. Under compressive force, the truss did not lose its vertical support.
- *Combined Vertical and Horizontal Forces*: Under combined vertical and horizontal forces, the failure modes were a combination of the failure modes for vertical and horizontal forces. The vertical shear strength of the truss seats was reduced due to the additional horizontal tensile force. The horizontal tensile strength was not reduced by the additional vertical force on the seat.

Truss Seat Model for Truss Model: Truss seat capacities corresponding to the failure modes were computed for the different types of the truss seats at different temperatures. Finite element models of the exterior and interior truss seats were developed for incorporation in the floor truss analysis using "break elements." Break elements are unidirectional linear springs that were turned off and did not resist any force after the connection forces reached predefined temperature-dependent capacities.

E.2.2 Knuckle Analysis

Failure Modes: The failure modes of knuckles are:

- Horizontal shear failure due to shear crack or crushing of concrete
- Pullout failure due to vertical tension

The capacities of knuckles were determined based on shear test results conducted by Laclede Steel Co., the results of finite element analysis simulating the shear tests, and hand calculations. Knuckle shear and pullout capacity at room temperature were determined as 30 kip and 15 kip, respectively. Capacities at elevated temperatures were calculated based on knock-down factor on concrete strength at given temperatures.

Knuckle Model for Truss Model: A model of knuckle was also developed for the truss model, using break elements.

E.2.3 Truss Analysis

A finite element model of a section of a floor system, which consisted of a single floor truss and a section of concrete slab with a tributary width, was developed in ANSYS to capture the potential failure modes and failure sequence of the truss under gravity load and thermal load. The model is referred to as "truss model" in this report.

Failure Modes: Two possible failure modes were identified for the truss model: 1) softening and sagging of the truss caused by plasticity, creep, and buckling of web diagonal members at high temperatures; and 2) loss of truss vertical support resulting either from seat failure caused by loss of vertical shear capacity at high temperatures or from truss walking-off truss seat due to large sagging.

Model Description: The truss model included the following:

- A single typical long-span truss (C32T1) of the primary double truss at Column 143 at Floor 96 of WTC 1. All steel truss members were modeled by 3-D quadratic finite strain beam elements.
- Two exterior columns (Columns 143 and 144) with half the area and bending properties, and a length of 24 ft (12 ft above and below the floor level), using elastic beam elements.
- The portion of the spandrel between the two exterior columns, using elastic shell elements.
- The portion of the slab (40 in. wide) between the two exterior columns. The concrete slab was modeled with 4 layers of 3-D, 8-node structural solid elements for an equivalent thickness of 4.35 in.
- One strap anchor connected to the truss top chord, concrete slab, and the adjacent exterior column (Column 144). 3-D quadratic finite strain beam elements were used.
- Exterior and interior truss seats and the gusset plate at the exterior end. Break elements were used to model failures of these connections.
- Spandrel studs, studs on the strap anchor, and knuckles. Break elements were used to model failures of these connections.

Materials: Temperature-dependent elastic, plastic, and creep properties were included in steel members except for columns and spandrels. The Hjelm plasticity model was used for the solid elements of the concrete slab that allowed different "yield strengths" in tension and compression.

Boundary Conditions: The entire top chord of the truss was restrained against the movement transverse to the truss axis. The bottom chord was restrained against the movement transverse to the truss axis at four bridging truss locations. The two edges of the concrete slab parallel to the truss were restrained against rotations about the truss axis and the vertical axis, but were free in the translation along the truss axis. The interior truss seat was fixed in all directions. The exterior truss seat was attached to the spandrel. The truss was pinned at both exterior and interior truss seats. The interior end of the slab was fixed in the vertical direction. In the truss axis direction at the interior end of slab, break elements were implemented to represent temperature-dependent tensile capacities of steel reinforcement.

Loads: The loading on the truss model consisted of dead load and 13.75 psf of live load (equal to 25 percent of design live load for the WTC towers) and temperature time-histories for all truss components including the truss seats and concrete slab. Thermal loads were assumed for exercising the truss model. The temperature was ramped from 20 ˚C to 700 ˚C in steel members, from 20 ˚C to 700 ˚C at the bottom of the slab, and from 20 ˚C to 300 ˚C at the top of the slab for the period from 0 min to 30 min; thereafter, the temperatures were linearly increased by an additional 200 ˚C at 40 min. A linear temperature gradient through the thickness of the slab was assumed. Temperature was not applied to the columns and spandrel.

Summary of Results: Key structural response of the truss model to "assumed temperature conditions" can be summarized as follows:

- The stud on the spandrel and studs on the strap anchor failed in shear below 275 ˚C.
- The first knuckle from the interior end failed in vertical tension at around 100 ˚C.
- Top chords yielded above 300 ˚C due to the difference in coefficients of thermal expansion of steel and concrete.

- The floor sagged into a catenary shape as four compression diagonals buckled due to high axial compressive force at 565 ˚C.
- The interior truss seat bolts sheared off, and the second and third knuckles from the interior end failed in the horizontal shear at 566 ˚C.
- The gusset plate fractured, and the exterior truss seat bolts sheared off at around 680 ˚C.
- The truss walked off the exterior truss seat at 730 ˚C.

Simplified Truss Model: The truss model was modified for use in the full floor subsystem model to enhance computational efficiency. Characteristics captured by the simplified truss model were: (1) total horizontal reaction force under the thermal loading and (2) vertical deflection under the thermal loading. The simplified truss model had the following features:

- Double primary truss was combined into a single truss. Areas of truss members were doubled.
- The top and bottom chords and diagonals were modeled by 3-D linear finite strain beam elements. Only one element was used for a member between two panel points.
- Break elements were used to model the following failure modes: (a) seat bolt shear-off, (b) gusset plate fracture, (c) truss walk-off, (d) web diagonal buckling/resistance weld failure, (e) failure of spandrel studs and studs on strap anchors, and (f) weld failure between strap anchors and top chords. Knuckles were not modeled by break elements.
- Temperature-dependent elastic and plastic material properties of steel were used.
- Creep in steel was included in the simplified truss model; however, it was not included when the simplified truss model was incorporated in the full floor model because of convergence problems inherent to 3-D linear finite strain beam elements.
- The concrete slab was modeled by 4-node finite strain shell elements with a temperature-dependent bilinear material model that had the same yield strength in both tension and compression. The yield strength was set to the compressive strength.

E.2.4 Full Floor Analysis

The full floor models were developed and analyzed using ANSYS to identify the most likely failure modes and the fire-induced damage to be incorporated in the global model along with impact damage and to modify the floors in the global models to enhance computational efficiency.

Failure Modes: Possible failure modes of the floor subsystem were identified as follows:

- *Sagging of the Floor System:* Floor sagging caused by loss of stiffness, plastic bending, or buckling of web diagonal members resulted in tension in the floor subsystem, tension in the connections to the exterior walls, and lateral forces (pull-in forces) on columns.
- *Loss of Support:* Loss of a truss support could be caused by (1) vertical shear load due to debris and/or impact load of the dropping floor above, (2) reduced resistance of truss seats under elevated temperatures, (3) tension acting on truss seats caused by floor sagging, (4) cooling of a truss already shortened due to plastic deformation resulting from thermal

loading, and (5) aircraft impact. Loss of support will reduce buckling strength of exterior columns.

Model Description: The base floor model developed was for Floor 96 of WTC 1 with columns extending from Floor 95 to Floor 97. The full floor model included the following structural members:

- Both exterior and core columns extending from one floor below to one floor above, modeled by 3-D quadratic finite strain beam elements.
- Spandrels of the floor of interest, modeled by four-node finite strain shell elements (eight elements between two columns and four elements along the height), which were tied to exterior columns by rigid beam elements.
- Floor slab was modeled by four-node finite strain shell elements with four layers through the thickness.
- Floor trusses including primary and bridging trusses. Two primary trusses supported by the same column were combined into a single truss. Truss members (top and bottom chords and web diagonals) were modeled by 3-D linear finite strain beam elements.
- Strap anchors, modeled by 3-D linear finite strain beam elements.
- Core beams, modeled by 3-D linear finite strain beam elements. They were placed at their centroids and were connected to the slab by rigid beam elements.
- Deck support angles, modeled by 3-D linear finite strain beam elements.

Break elements were incorporated into the model to represent: 1) buckling of web diagonals, 2) gusset plate fracture, 3) truss seat bolt shear-off, 4) truss seat failure, 5) failure of connections between primary and bridging trusses, 6) failure of connections between primary long-span and transfer trusses, 7) failure of studs connecting the slab and the spandrel, and 8) failure of welds between strap anchors and top chords of primary trusses. Break elements were not used for representing knuckle failure as the truss analysis found that buckling of web diagonal members preceded knuckle failures. The concrete slab was always attached to primary trusses at knuckle locations in the full floor model.

Subsequent to the initial thermal response analysis, the following members were removed from the model to enhance computational efficiency: 1) deck support angles, 2) bridging trusses outside of the two-way zones, 3) spandrel studs connecting the slab and the spandrel, and 4) strap anchors. These members were found to fail in the early stage of thermal loading, caused the analysis to slow down due to the large residual nonlinearities in the subsequent stages of analysis. Deck support angles and bridging trusses buckled between primary trusses due to thermal expansion. Most spandrel studs and welds between strap anchors and truss top chords failed due to lateral shear force in the plane of slab caused by the difference in the thermal expansion between the floor and the exterior wall in the direction transverse to the truss axis. As a result of the removal of strap anchors and spandrel studs, the only connections between the exterior wall and the floor were gusset plates and exterior truss seats in the full floor models.

Materials: Temperature-dependent elastic and plastic material properties of steel provided by NIST were assigned to each structural member according to the PANYNJ drawings. It was found that creep in 3-D linear/quadratic finite strain beam elements would cause convergence problems when those elements experience thermally-induced buckling. Therefore, creep could not be included in the full floor models. For the concrete slab, a bilinear stress-strain relationship with a yield point at its compressive strength was used, where the yield strength was the same in both tension and compression.

Impact Damage: Elements corresponding to structural members that sustained severe structural damage were removed from the model. Based on the aircraft impact analysis, NIST identified two sets of structural and thermal insulation impact damage for each floor. These impact cases were designated as "Case A_i impact damage condition" and "Case B_i impact damage condition" for WTC 1, and "Case C_i impact damage condition" and "Case D_i impact damage condition" for WTC 2.

Boundary Conditions: Both core and exterior columns were fixed in the vertical direction at the bottom. When the column below the floor was severed by aircraft impact, the top of the column above the floor was supported in the vertical direction. Core columns were free in the horizontal directions and fixed for all rotations at the top and bottom ends. Exterior columns were fixed for translation perpendicular to the face of building and from rotating about the axis parallel to the face of the building at the top and bottom. They were also fixed in torsion at the top and bottom.

Loads: The full floor model was first analyzed for dead load and 25 percent of design live load of the WTC towers, and then temperature time histories representative of the WTC fire conditions were applied. Vertical loads to columns were not applied. NIST provided temperatures of structural components from reconstructed fires in the WTC towers based on the impact damage conditions; therefore, the impact damage condition and the temperature condition had one-to-one correspondence. Temperature cases provided were "Case A_i temperature condition" and "Case B_i temperature condition" for WTC 1, and "Case C_i temperature condition" and "Case D_i temperature condition" for WTC 2. Temperature data sets were provided at 10 min time intervals up to 100 min for WTC 1 and up to 60 min for WTC 2 for each temperature condition.

Summary of Results: The behaviors of the floor subsystem found in the full floor models subjected to impact damage and fire conditions can be summarized as follows:

- Bridging trusses subjected to elevated temperatures buckled between primary trusses.
- When significant differences in the thermal expansion occurred between the floors and the exterior wall in the direction transverse to the primary trusses, spandrel studs, strap anchors, gusset plates, and seat bolts failed due to lateral shear force.
- Floor sagged as the web diagonals of floor trusses buckled in the heated area where the thermal insulation was damaged.
- The floors were disconnected from the exterior wall in some areas due to failure of exterior truss seats.

Pull-in forces were expected to develop whenever the floor sagged. Although the floor sagging was captured by the full floor models, the pull-in force was not captured in most of the full floor model analyses. To accurately calculate pull-in forces between the floor and the exterior columns in the full floor model, much more detailed modeling was required. Such modeling included accurate boundary conditions on columns, creep in steel, friction at the truss seats, and accurate evaluation of failure of strap anchors and stud, and concrete cracking and spalling. In addition, temperatures of structural members might be low due to conservative assumption of limiting the insulation damage to debris abrasion and neglecting the effect of aircraft shock and vibration.

Floor Subsystem in Global Models: To enhance computational efficiency, floors in the global models were modeled by shell elements to have the following functions: 1) diaphragm action and 2) transfer of the load from the core to the exterior wall system by a membrane action. Since the floors modeled by shell elements cannot capture key failure modes under elevated temperatures, including sagging of floors

and disconnection of floors from the exterior wall, their effects need to be implemented in the global model as fire-induced damage at appropriate points in time.

E.3 EXTERIOR WALL SUBSYSTEM

The exterior wall subsystem was a nine-column (three-panel) wide by nine-story (three-panel) high section of WTC 1 between Floor 91 and Floor 100 and Column 150 and Column 158 as shown Fig. E–5. This area, typical of the exterior walls of the towers, connected to a part of the floor system near the corner.

Each face of the towers' exterior wall consisted of fifty-nine 14 in. square box columns spaced at 3 ft 4 in. on center, with 52 in. deep spandrel plates at each floor level. The exterior wall was constructed with shop-welded prefabricated panels, each consisting of three columns and three spandrel beams, 13 ft 4 in. wide by 36 ft high. Except at mechanical floors and the base and top of the structure, vertical splices (column splices) in prefabricated panels were staggered such that within any story, every third prefabricated panel had a column splice (see Fig. E–5). Exterior column splices at the upper stories typically consisted of four 7/8 in. diameter ASTM A325 bolts fastened through the welded butt plates at the tops and bottoms of adjoining columns. Special prefabricated panels existed for the mechanical floors where no stagger existed at Floors 7, 41, 75, and 108. At these mechanical floors, the column splice detail included supplemental field welding in addition to the bolted connection. Horizontal (spandrel-to-spandrel) connections between prefabricated panels were all field-bolted using splice plates. Corner panels that connected the orthogonal walls at corners were two-story tall (24 ft) and consisted of two columns, two spandrel plates, and a third column midway between the two columns on alternate floors.

Various grades of steel, having yield strengths ranging between 42 ksi and 100 ksi, were specified for the exterior column and spandrel plates. Column plate thickness also varied, both vertically and around the building perimeter. Column plate thickness was as thin as 1/4 in. at the upper stories and increased toward the base of the building.

E.3.1 Single Column Analysis

A single exterior column model was developed to examine column behavior under compression at different temperatures. The model included a one story high portion of Column 151 extending from Floor 95 to Floor 96 and portions of spandrels at Floor 95 and Floor 96. Four-node finite strain shell elements were used to model the plates of the column and the spandrels. Nodes of column plates at the top and the bottom of the model were rigidly tied to the center of gravity of the column cross section. The column was pinned at the bottom and fixed in the two horizontal directions at the top. Increments of axial displacement were applied at the top of the model at room temperature and 700 ˚C.

The calculated capacity of the columns spanning a single floor occurred after local buckling of plates and the subsequent kinking of the cross section at 1,030 kip at room temperature, well below the inelastic buckling strength of the column, and 270 kip for 700 ˚C. Since the compressive force demand on this particular column was estimated at 175 kip, the compressive strength of the column is greater than the demand even at 700 ˚C. The column underwent kink-type buckling at room temperature, and the load-carrying capacity in the post-buckling regime decreased rapidly; however, it decreased much more gradually at 700 ˚C.

Axial load-displacement behaviors of two and three-story single column models were also examined. As the unsupported length became longer and temperature increased, local buckling of plates and the resulting kinking of the cross section did not occur, and the negative slope of the axial load-deflection curve in the post-buckling regime became less steep.

E.3.2 Column Splices

Failure Modes: Failure modes identified for column splices were: (1) failure of bolts in tension, (2) failure of bolts in shear, (3) bending failure controlled by tension in bolts. Tension capacity was calculated as the ultimate tension capacity of four bolts. Shear capacity was calculated as the addition of bolt shear capacity and splice friction. The ultimate moment capacity was obtained prior to failure of two bolts with some capacity remaining on other two bolts.

Column Splice Model for Exterior Wall Model: Two 3-D quadratic finite strain beam elements for each of the four bolts, four pairs of 3-D node-to-node contact elements at the faying (contact) surfaces, and rigid beam elements, modeled by 3-D elastic beam elements, connecting the tops of the bolts to the contact elements, were used to model the column splice. Break elements were used to model the fracture of the column splice bolts based on data from bolt tests provided by NIST and on shear failure of the splice. A coefficient of friction of 0.35 was used for the contact elements. The 7/8 in. diameter column splice bolts were preloaded to 36.05 kip at 20ºC.

E.3.3 Spandrel Splices

Failure Modes: Failure modes identified for spandrel splices were: (1) bolt shear, (2) tearing of the spandrel plate, and (3) tearing of the splice plates at the bolt holes. Capacities of these failure modes at different temperatures were estimated by hand calculations.

Spandrel Splice Model for Exterior Wall Model: Break elements were used to model the spandrel splice connections in the model. At each splice location, eleven break elements were used. Nodal couples were used to model the spandrel splice connections on the boundaries of the model.

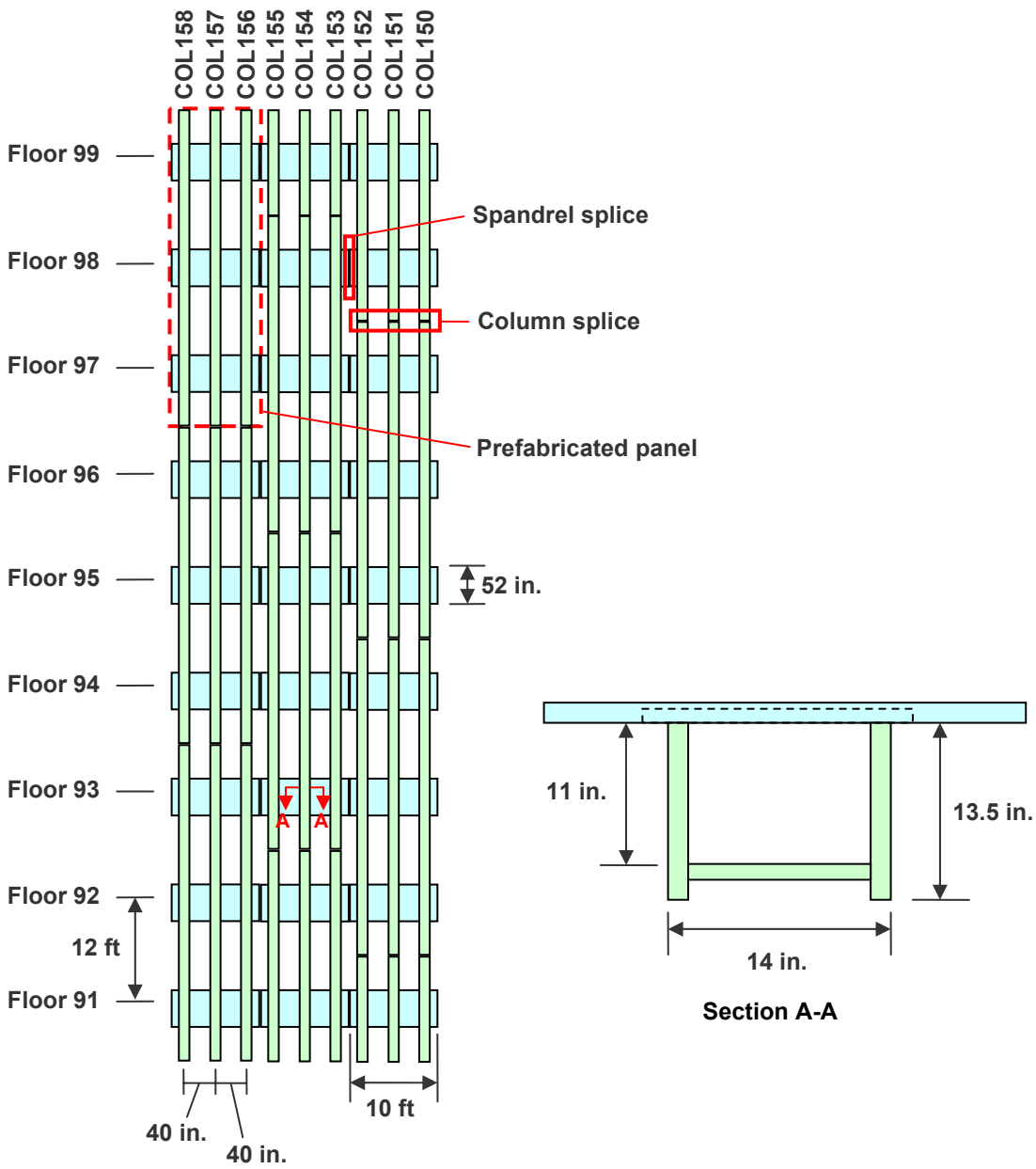

Figure E–5. Exterior wall subsystem.

E.3.4 Exterior Wall Analysis

Failure Modes: The exterior wall subsystem model captured the following failure modes:

- Inelastic buckling of columns from large lateral deformations,
- Inelastic buckling of columns from loss of support at floor truss seats and diagonal straps,
- Failure of column splice bolts, and
- Failure of spandrel splice bolts or tearing of spandrel or splice plates at bolt holes.

The model did not capture the local buckling of the column plates and the resulting kinking of the cross section. This was justified because the exterior walls were observed to have bowed inward over more than three floors prior to the collapse, and temperatures of the columns of these walls were high. In these cases, the kink-type buckling of columns did not occur.

Model Description: BEAM189 elements modeled the columns. Above and below spandrels, 3-D quadratic finite strain beam elements modeled the complete cross sections of the columns. Four-node finite strain shell elements modeled the spandrels. Rigid beam elements connected nodes on the axis of the columns to nodes located in the mid-plane of the spandrels.

Materials: Temperature-dependent elastic and plastic material properties of steel provided by NIST were assigned to each structural member according to the drawings. Creep in steel was included unless the analysis was a displacement-controlled analysis.

Boundary Conditions: The bottoms of all columns in the model were restrained in the vertical direction. The top and the bottom of all columns in the model were restrained in the direction normal to the wall. In addition, the bottom of central column was restrained in the plane of the wall. Symmetry boundary conditions were imposed on the spandrels at the boundaries of the model, except that the spandrels were free to expand in the plane of the wall. Motion out of the plane of the wall was restrained at all floor truss seats and straps. In several analyses, such restraints were removed at two or three floors (either Floors 95 and 96 or Floors 95, 96, and 97) to investigate the effect of floor sagging and floor/wall disconnection on stability of the exterior wall system.

Loads: The loads on the model were applied sequentially in the following order:

- Self weight of the exterior wall components,
- Column splice bolt preload,
- Dead load of the floor system, including 8 psf superimposed dead load,
- 25 percent of WTC floor design live loads,
- Temperatures of fire scenarios provided by NIST, and
- Transverse pull loading from sagging trusses or additional vertical deflection from a potential redistribution of forces to this portion of the exterior wall.

To represent a range of thermal conditions expected in the WTC towers, NIST provided five thermal load conditions: D, DBARE, E, E119, and F. These load conditions differed in fire behavior, intensity, location in the towers, and time. Thermal load DBARE assumed steel without insulation. Thermal load E119 corresponded to the standard ASTM E119 fire load.

Summary of Results: The response of the exterior wall model subjected to thermal loads can be summarized as follows:

- Large inelastic buckling of spandrels occurred at elevated temperatures.
- Although partial separations of the spandrel splices occurred at elevated temperatures, complete separation did not occur.
- Instability of the exterior wall subsystem did not occur at elevated temperatures when the wall was supported laterally at every floor. Instability of the exterior wall subsystem occurred when at least three floors were unbraced and the exterior wall subsystem was subjected to additional vertical load or pull-in force.

- All column splices remained closed, except near the points of instability of the exterior wall with three floors unbraced and subjected to additional vertical load or pull-in force where calculations showed opening and sliding of the splice with no bolt fracture.

Exterior Wall Subsystem in Global Models: The analyses of the exterior wall model support the following conclusions for modeling the towers:

1. Large inelastic deformations and buckling of the spandrels do not significantly affect the stability of the exterior columns and need not be accurately modeled in the global models.
2. Partial separations of the spandrel splices do not significantly affect the stability of the exterior columns and need not be accurately modeled in the global models.
3. Exterior column splices can be expected to fail by sliding or opening at elevated temperatures when subjected to increased vertical loading or pull-in forces. Since complete failure was not found before the exterior wall became unstable, column splice failure may not be modeled in the global models to enhance computational efficiency.

E.4 RECOMMENDED MODELING DETAILS FOR SUBSYSTEMS IN GLOBAL MODELS

Based on the results of finite-element analyses performed on components, connections, and subsystems, the following recommendations can be made for modeling of the subsystems in the global models to enhance numerical efficiency.

Floor Subsystem

Floors in the global model may be modeled by shell elements, which have their membrane stiffness equal to that of the full floor system. Floors in the global model function as diaphragms and transfer load between the exterior wall system and the core.

The global model cannot be constructed with the same level of detail in all floors subjected to thermal loading as the full floor model developed here. To enhance computational efficiency, the pull-in forces and disconnections of floors from the exterior walls may be implemented in the global models as “fire-induced damage” at appropriate times. Since the full floor models could not be used to calculate accurately the pull-in forces at floor/wall connections, the fire-induced damage obtained from the full floor model analyses needs to be modified by the results of “actual observations” obtained from the examination of photographs and videos performed by NIST (NIST NCSTAR 1-5A).

Exterior Wall Subsystem

The exterior and interior columns must be modeled with fidelity of their inelastic buckling behavior. To capture the premature buckling of the single span exterior columns at low temperatures, which occurs at the onset of plate buckling and results in kinking of the cross section, a fine mesh is needed. However, observations of photographs and videos show that bowing is extended over several floors and column temperatures are not low. Therefore, kink-type buckling of the exterior columns may be neglected.

Exterior column splices need not be modeled in the global models.

Spandrels can be modeled by beam elements capable of resisting shear and bending moment. The spandrel splices need not be modeled in the global analyses.

Chapter 1
INTRODUCTION

1.1 PURPOSE

Simpson Gumpertz & Heger Inc. (SGH) developed finite-element models of the components, connections, and subsystems of the World Trade Center (WTC) towers to study their structural performance in the fire environment that followed the aircraft impact to the towers. The results of this study were used to develop global models that ran efficiently and captured the important failure modes and sequential failures of components and subsystems and to determine the probable sequence of structural responses that let to the global collapse initiation.

SGH performed this study as part of Project 6 of the investigation on the WTC disaster by the National Institute of Standards and Technology (NIST). This report constitutes the SGH's report on Task 1 of the SGH contract with NIST and Part 1 of the SGH two-part report. The Task 2 and 3 report deals with the global analysis of the WTC towers (NIST NCSTAR 1-6D[1]).

1.2 SCOPE OF WORK

SGH in Task 1 performed the following:

- Developed and validated ANSYS models of the full floor and exterior wall subsystems.
- Evaluated structural responses of components, connections, and subsystems to service loads due to gravity (dead and live loads) and elevated temperatures.
- Identified the likely failure modes and failure sequences of components, connections, and subsystems.
- Identified modeling details of the floor and exterior wall subsystems in the global models of the WTC towers.

The analyses performed as part of this Task 1 report used the nominal dimensions and design details shown on the PANYNJ drawings[2]. Material properties were based on information provided from the NIST Project 3 study (NIST NCSTAR 1-3, NIST NCSTAR 1-3D).

1.3 REPORT ORGANIZATION

This report consists of eight chapters:

- Chapter 1 serves as an introduction to this report and describes purpose and scope of this study.

---

[1] This reference is to one of the companion documents from this Investigation. A list of these documents appears in the Preface to this report.

[2] The technical data required to conduct the analyses of the WTC towers reported herein were obtained from drawings that were provided by the Port Authority of New York and New Jersey (PANYNJ) and their contractors.

- Chapter 2 introduces a floor subsystem and an exterior wall subsystem of the WTC towers and provides descriptions of their structural details.
- Chapter 3 summarizes temperature-dependent material properties of steel and concrete used in this study.
- Chapter 4 describes a conversion process from SAP2000 reference models to ANSYS models and presents validation studies of the converted ANSYS models.
- Chapter 5 presents results from a study on the full floor subsystem.
- Chapter 6 presents results from a study on the exterior wall subsystem.
- Chapter 7 summarizes recommendations for modeling details of the full floor subsystem and the exterior wall subsystem in the global models.
- Chapter 8 provides a list of references.

Chapter 2
DESCRIPTION OF SUBSYSTEM STRUCTURES

The finite-element models of the full floor subsystem and the exterior wall subsystem of the World Trade Center (WTC) towers were developed to calculate the structural response of these subsystems to impact damage and to the fire environments that followed the aircraft impact. The full floor subsystem is a model of Floor 96 of WTC 1. The model is believed to be typical of the upper floors in both towers. The exterior wall subsystem is a nine-column (three-panel) wide by nine-story (three-panel) high section of WTC 1 between Floor 91 and Floor 100 and Column 150 and Column 158. This area is typical of the exterior walls of the towers and connects to a part of the floor system near the corner with different types of trusses.

2.1 FULL FLOOR SUBSYSTEM DESCRIPTION

Floor 96 of WTC 1 was identified as an office floor with typical floor construction and loading; therefore, it was selected as the basis for modeling floor response. The full floor subsystem included office area and core area floor framing, as well as core and exterior columns extending to floors immediately above and below this floor. The floor system in the office area consisted of lightweight concrete slab supported by steel floor trusses. Steel trusses spanned nominally 60 ft in the long-span area and 36 ft in the short-span area between exterior walls and the central core. Typically, a pair of primary trusses (double truss) was supported at odd-numbered columns at 6 ft 8 in. on center.

Each of these primary trusses consisted of top and bottom chords fabricated from double steel angles and web diagonals fabricated from round bars (see Fig. 2–1). Web diagonals extended 3 in. above the top chord at the panel points into the concrete slab to form a knuckle and to provide shear transfer between the truss and the concrete slab (see Fig. 2–1).

Hand calculations and finite-element analyses of components of the full floor subsystem and their connections were performed under gravity loads and fire-induced temperature time-histories to capture the different failure modes and loads at failure. Then the results of these calculations and analyses were used to develop the full floor subsystem model.

The top chords of a pair of trusses were supported at the central core by an interior truss seat (Fig. 2–1) welded to steel channels that ran continuously around the core floor area. Each pair of trusses was fastened to a horizontal plate of the interior truss seat by two 5/8 in. bolts (one bolt in each truss) in 1 3/4 in. long slotted holes. At the exterior wall, each pair of trusses was supported by an exterior truss seat (Fig. 2–1), which fastened to a seat angle with two 5/8 in. diameter bolts in 2 in. long slotted holes. A pair of stand-off plates welded the seat angle to the spandrel. In addition, a gusset plate welded to the spandrel and to the truss top chord tied the truss to the supporting column, and a pair of diagonal strap anchors, welded to the top chords and to the adjacent columns, tied these columns to the primary trusses.

Figure 2–2 shows a floor plan of Floor 96 of WTC 1. Primary trusses were interconnected by a transverse system of bridging trusses and deck support angles. These bridging trusses were of similar construction to the primary trusses, except the knuckles did not project above the top chords. The top chord of the bridging trusses sat 1 1/2 in. below the top chord of the primary trusses and provided support for the 4 in. thick lightweight concrete slab on the 1 1/2 in., 22 gauge steel deck with 2 in. wide at the top, 1.25 in.

wide at the bottom, and 1.5 in. high flutes at 6.8 in. on center running parallel to the primary trusses. At each corner of the building core, a 36 ft long transfer truss extended out from the corner core column to the exterior wall and supported the 60 ft long primary trusses. The floor in the core consisted of a 4.5 in. thick lightweight concrete slab supported by wide flange girders and beams connected to the core columns with bolted connections. Reinforcement between the core area floor and the office area floor (#3 bars at 10 in. at the top and #4 bars at 12 in. at the bottom) provided continuity between the two areas and restrained the truss from walking off the interior seat.

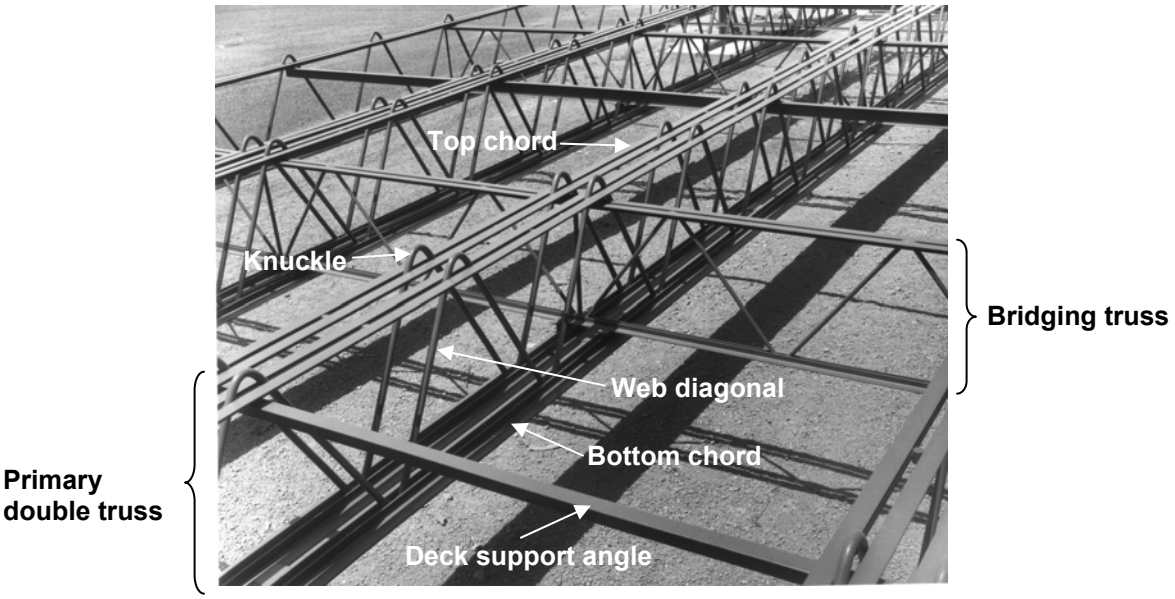

Figure 2–1. Mock up of office floor framing system (Photograph from about 1967 provided by Laclede Steel Co.).

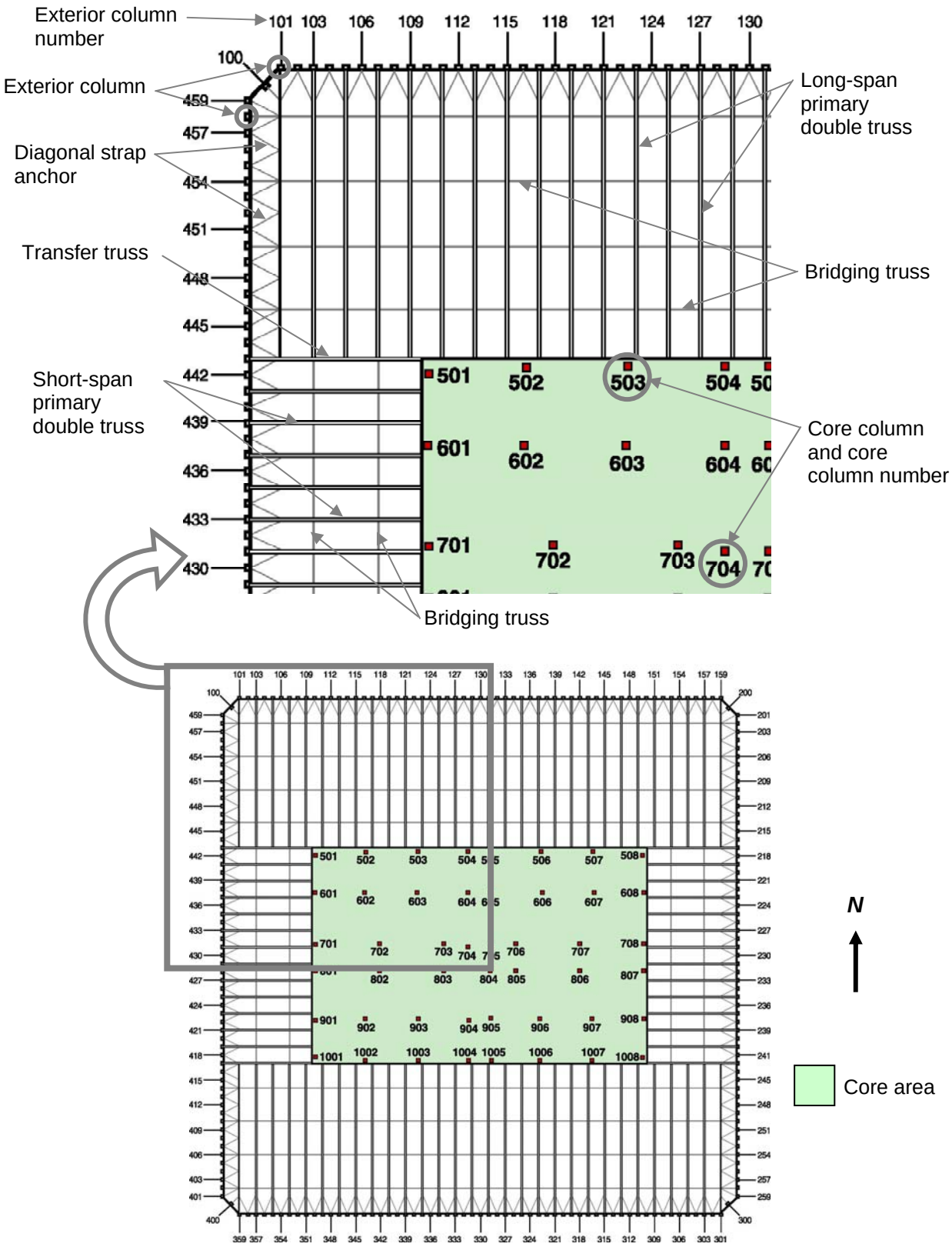

Figure 2–2. Floor plan of Floor 96 of WTC 1.

2.2 EXTERIOR WALL SUBSYSTEM DESCRIPTION

Each exterior wall of the towers consisted of fifty-nine 14 in. square box columns spaced at 3 ft 4 in. on center, with 52 in. deep spandrel plates at each floor level. The exterior wall was constructed with shop-welded prefabricated panels, each consisting of three columns and three spandrel beams, 13 ft 4 in. wide by 36 ft high. Except at mechanical floors and the base and top of the structure, vertical splices (column splices) in prefabricated panels were staggered such that within any story, every third prefabricated panel had a column splice (see Fig. 2–3). Exterior column splices at the upper stories typically consisted of four 7/8 in. diameter ASTM A325 bolts fastened through the welded butt plates at the tops and bottoms of adjoining columns. Special prefabricated panels existed for the mechanical floors where no stagger existed at Floors 7, 41, 75, and 108. At these mechanical floors, the column splice detail included supplemental field welding in addition to the bolted connection. Horizontal (spandrel-to-spandrel) connections between prefabricated panels were all field-bolted using splice plates. Corner panels that connected the orthogonal walls at corners were two-story tall (24 ft) and consisted of two columns, two spandrel plates, and a third column midway between the two columns on alternate floors.

Various grades of steel, having yield strengths ranging between 42 ksi and 100 ksi, were specified for the exterior column and spandrel plates. However, fewer grades were actually used than specified by supplying a single grade steel for the 3 highest specified yield strengths. Column plate thickness also varied, both vertically and around the building perimeter. Column plate thickness was as thin as 1/4 in. at the upper stories and increased toward the base of the building. The specified plate thickness and material yield strength for each column differed between the two towers primarily due to the 90-degree change in the building orientation between the two towers and computed wind loads (NIST NCSTAR 1-2).

The model of the exterior wall subsystem was a nine-column (three-panel) wide by nine-story (three-panel) high section of WTC 1 between Floor 91 and Floor 100 and Column 150 and Column 158 as shown Fig. 2–3. This area, typical of the exterior walls of the towers, connected to a part of the floor system near the corner. (Column 159 is at the corner of the north face of WTC 1, see Fig. 2–3). Using this model, the structural behavior and failure modes of the exterior wall system were evaluated in the fire environment.

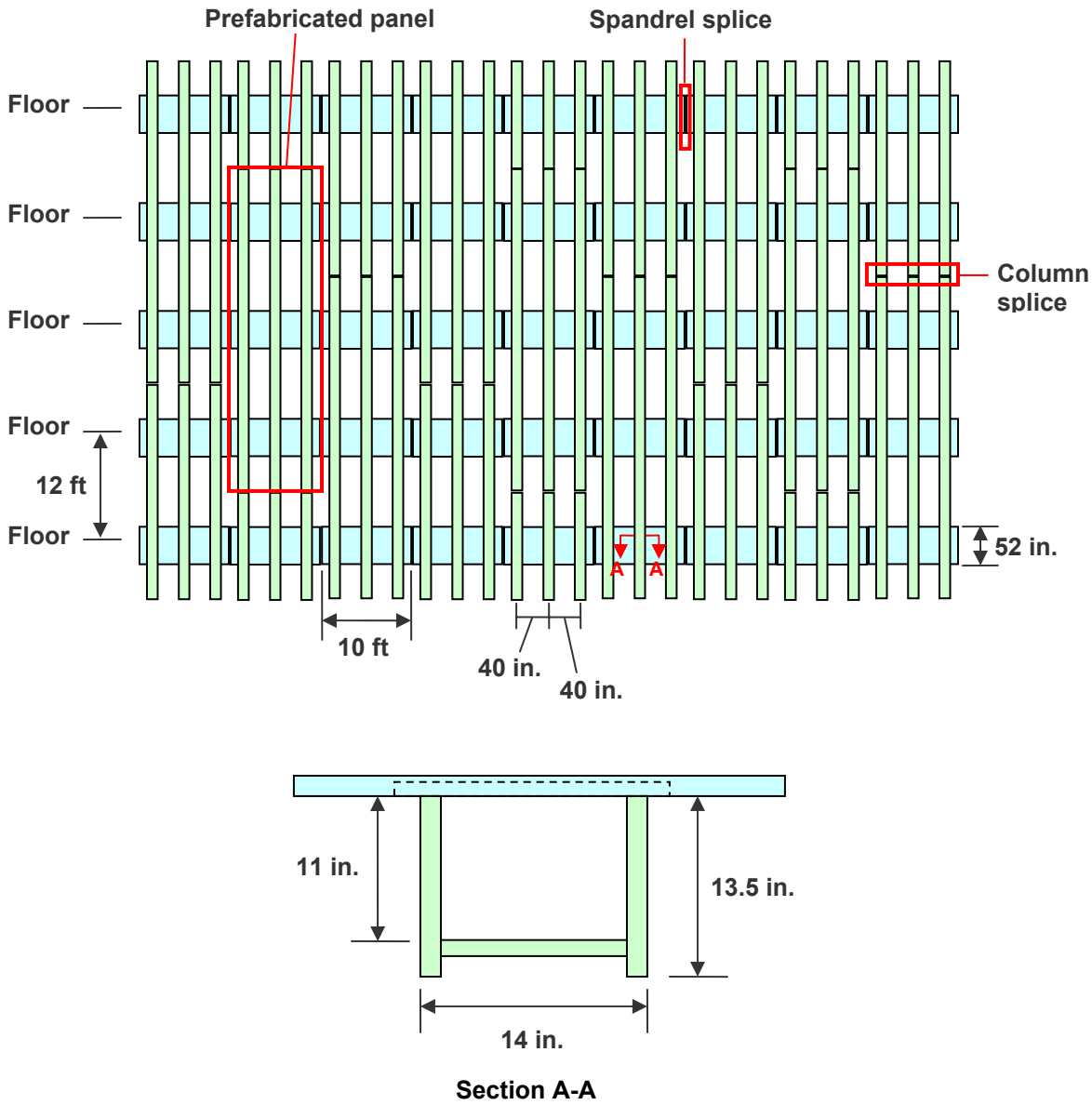

Figure 2–3. Exterior wall construction with prefabricated wall panels.

2.3 LOADS

The subsystems and components were analyzed for dead (D), live (L), and thermal (T_a) loads. The dead load consisted of structural weight and superimposed dead loads. The superimposed dead load and design live load were defined in the World Trade Center Design Criteria (LERA 2003). The superimposed dead loads for floors outside the core consisted of the weights of ceiling, mechanical and electrical equipment, passive fire protection (also referred to as thermal insulation or fireproofing), and floor finish, and were estimated at 8 psf. Twenty five (25) percent of the design live load was selected as a reasonable approximation of the load that likely existed at the time of the collapse. (For example, 25 percent of the design live load resulted in a load of 13.75 psf for the long-span trusses in the two way zone of Floor 96

with 55 psf design live load.) The service dead and live loads were applied first, followed by the thermal loads.

The dead and live loads were defined as weights, so that during the collapse process, the gravity loads remained acting on the structure. The weight of debris from the plane provided by Project 2 (NIST NCSTAR 1-2) was found to be negligible relative to the dead and service live loads and was not included in the analysis.

The thermal loads, T_a, were temperature time histories for all structural members provided by Project 5 (NIST NCSTAR 1-5, NIST NCSTAR 1-5G).

For analysis of some of the components, discrete values of temperature or temperature distributions were linearly ramped from 20 °C to 700 °C (or to a temperature below 700 °C that results in the failure of the component) over 30 min. Failure modes of the components were evaluated at room temperature and at different elevated temperatures, as failure modes and failure loads may change with increasing temperature.

Although wind may have had a minor role in the collapse of the towers, all analyses performed in this study did not include wind load effects.

Chapter 3
MATERIALS

The mechanical properties of both steel and concrete are affected significantly by temperature. In the following sections, the material properties used in this study are specified as a function of temperature. For finite element analysis (FEA) of components, subsystems, and global models of the World Trade Center (WTC) towers, a material properties catalog was developed. Each material model was identified with a number in ANSYS; steels were Material ID 1 through Material ID 29, and concretes were Material ID 51 through Material ID 83. The details of different materials are discussed for concrete and steel separately in this chapter.

3.1 CONCRETE

Two types of concrete were generally used for the flooring inside the towers: lightweight concrete and normal weight concrete. Thermal properties of normal weight concrete depend on the type of aggregate. Petrographic inspection by Simpson Gumpertz & Heger Inc. of two samples of concrete taken from the debris at NIST showed siliceous sand. Because the source of coarse and fine aggregates for a construction site is usually the same, available data for siliceous aggregates were used.

3.1.1 Concrete Properties

The unit weight of the lightweight concrete was specified at 100 pcf by the WTC Design Criteria (LERA 2003); however, 110 pcf was used in the analysis based on the density of the two concrete samples examined by SGH. The unit weight of the normal weight concrete was specified at 150 pcf by the WTC Design Criteria (LERA 2003).

Poisson's ratio, ν_c, of 0.17 was used for both normal weight and lightweight concrete at all temperatures.

The specified concrete strength was 3,000 psi for the lightweight concrete, and either 3,000 psi or 4,000 psi for the normal weight concrete, as shown on Drawing Book 8, Sheet AB1–2.1 (SHCR 1973). The actual strength, f_a, of in-place concrete at room temperature was calculated from the specified strength, f_c', as follows:

$$f_a = f_c' \cdot F_1 \cdot F_2 \cdot F_3 \tag{1}$$

where the factor F_1 = the ratio of the average strength of 28-day cylinders to specified strength, F_2 = the ratio of in-situ 28-day strength to 28-day cylinder strength, and F_3 = factor that accounts for the change in concrete strength with age.

By using F_1 = 1.25 and F_2 = 0.95 (Bartlett and MacGregor 1996) and F_3 = 1.16, based on the formula specified in Section 2.2.1 of American Concrete Institute (ACI) 209 for the change of concrete strength with age, the mean of the ratio of actual strength of in-place concrete to the specified concrete strength was determined to be f_a / f_c' = 1.38. Based on this mean value, the actual strengths of in-place concretes are f_a = 5,500 psi for the specified 4,000 psi normal weight concrete, 4,100 psi for the specified 3,000 psi normal weight concrete, and 4,100 psi for the specified 3,000 psi lightweight concrete.

Temperature-dependent properties of concrete used in this study were modulus of elasticity, instantaneous coefficient of thermal expansion, compressive strength, and tensile strength.

Modulus of elasticity at room temperature was evaluated by the following formula:

$$E_c(RT) = 33\gamma_c^{1.5}\sqrt{f_a} \tag{2}$$

For the compressive strength, the actual strength, f_a, was used as the compressive strength at room temperature. The tensile strength at room temperature was evaluated by:

$$f_t(RT) = 5\sqrt{f_a} \tag{3}$$

The effects of elevated temperature on concrete properties are based on the work of Phan (1996) as shown in Fig. 3–1.

3.1.2 Concrete Stress-Strain Relationships

The compressive stress-strain relationship for concrete, formulas expressed by Seanz (1964), is given by

$$\sigma = \frac{K_c f_a \left(\dfrac{\varepsilon}{\varepsilon_{c1}}\right)}{1 + a\left(\dfrac{\varepsilon}{\varepsilon_{c1}}\right) + b\left(\dfrac{\varepsilon}{\varepsilon_{c1}}\right)^2 + c\left(\dfrac{\varepsilon}{\varepsilon_{c1}}\right)^3} \tag{4}$$

Where,

$$c = \frac{K_s - 1}{(K_e - 1)^2}K_c - \frac{1}{K_e}\ , \quad b = 1 - 2c\ , \quad a = c + K_c - 2\ ,$$

$$K_c = 2\ , \quad K_s = \frac{1}{0.85}\ , \quad K_e = 1.41\ , \text{ and } \quad \varepsilon_{c1} = K_c\frac{f_a}{E_c}$$

In tension, stress increases linearly up to the tensile strength. When concrete is strained in tension beyond its strength, it softens, and the stress drops. However, the descending branch of stress-strain relationship caused significant numerical problems which were avoided by assuming, with little error, that concrete becomes plastic in tension. The assumption of concrete plasticity after the onset of micro-cracking is valid for reinforced concrete with a reinforcement ratio of about a ratio of the tensile strength of concrete to the yield strength of reinforcement, which is 0.46 percent. The reinforcement ratio in the typical concrete slab in the WTC towers was 0.21 percent in the primary truss direction and 0.74 percent in the direction transverse to the primary trusses. Although the reinforcement ration in the truss direction was smaller than 0.46 percent, the resulting error was not significant. Figure 3–2 shows stress-strain curves of concrete with 3,000 psi specified compressive strength at room and elevated temperatures.

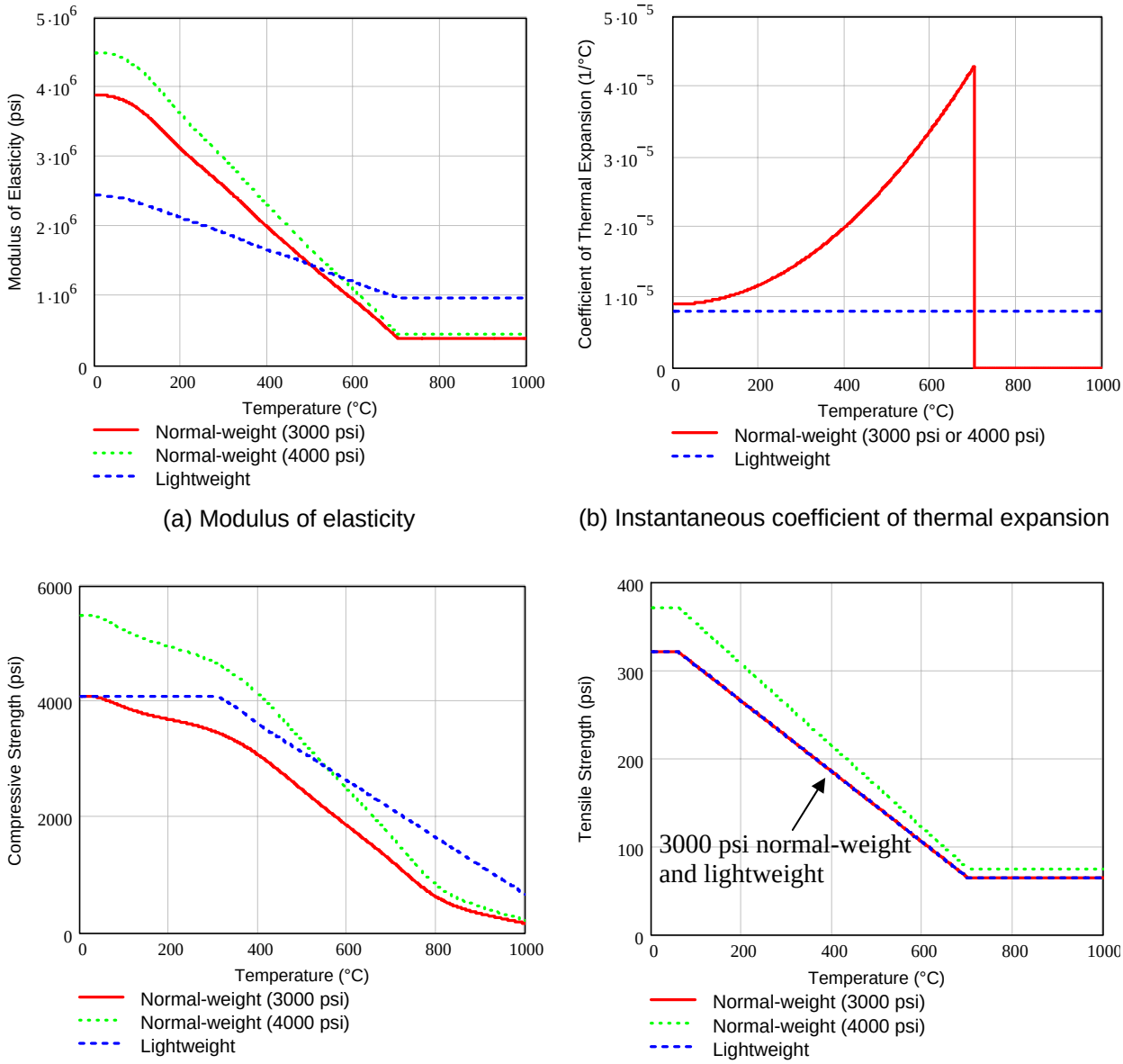

(a) Modulus of elasticity

(b) Instantaneous coefficient of thermal expansion

(c) Compressive strength

(d) Tensile strength

Figure 3–1. Properties of concrete that vary with temperature.

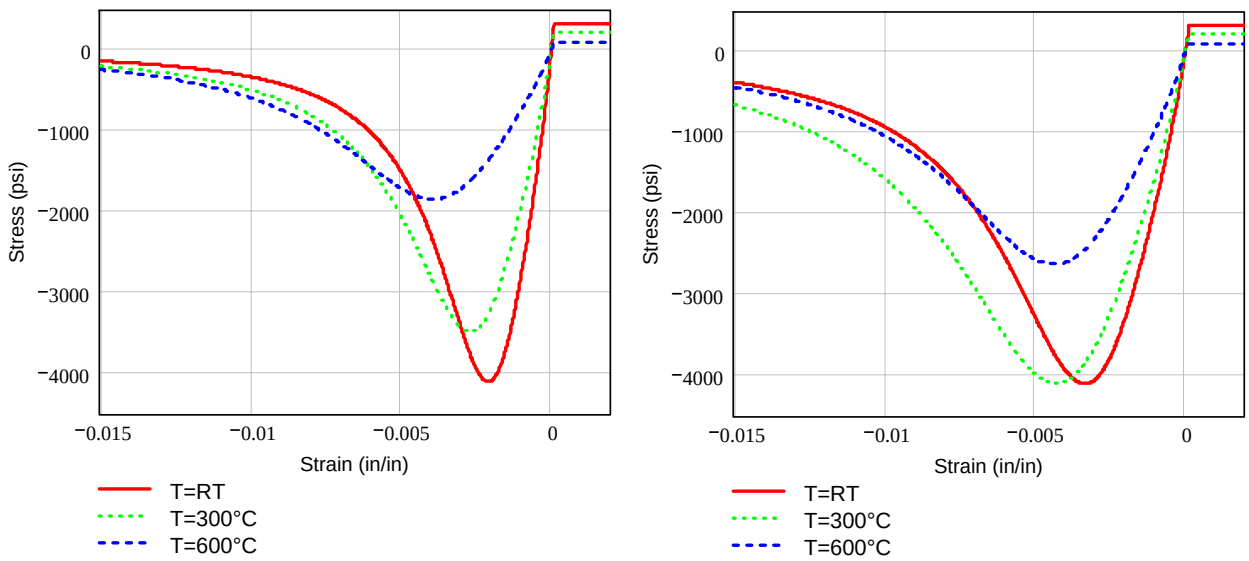

(a) Normal-weight concrete (3,000 psi) (b) Lightweight concrete

Figure 3–2. Concrete stress-strain relationships at different temperatures.

For the knuckle model in LS-DYNA, solid concrete elements were used with Pseudo Tensor material model (Livermore Software Technology Corporation 2003). The response mode II default concrete option was used. Properties of welded wire fabric were smeared into the concrete material properties, assuming a steel reinforcement of 0.47 percent and a yield strength of wire of 70 ksi, where 0.47 percent steel reinforcement was the average of the reinforcement in the two horizontal directions. Since material properties cannot be defined as temperature-dependent properties in this model, different material types were specified for the lightweight concrete at 20 ˚C, 150 ˚C, 300 ˚C, 450 ˚C, 600 ˚C, and 750 ˚C (Material IDs 51 through 56) with different stress-strain relationships.

The concrete floor slab in the truss model was modeled with eight-node solid elements (SOLID185) with a material model that accounts for different behaviors in tension and compression. One such material model in ANSYS is the Hjelm plasticity model with different yield properties in tension and compression. A low "yield stress in tension" was used to simulate cracking of concrete. The Hjelm model uses the Rankine maximum stress criterion in tension and the von Mises yield criterion in compression (ANSYS, Inc. 2004). Concrete material models with the Hjelm model for the specified 3,000 psi normal weight concrete, the specified 4,000 psi normal weight concrete, and the specified 3,000 psi lightweight concrete were assigned to Material ID 81, 82, and 83, respectively. To improve convergence in analysis, the negative slope in the stress-strain relationship after cracking or crushing in compression was removed, and the concrete was assumed to be plastic after cracking or crushing.

Isotropic hardening von Mises plasticity with a bilinear stress-strain relationship was used for the shell element modeling of the concrete slab in the full floor model. The model was elastic until the stress reached the compressive strength. It has the same yield strength in both tension and compression and, thus, did not accurately represent the tensile softening of concrete. This model did have temperature-dependent material properties.

3.1.3 Concrete Failure Criteria

The Mohr-Coulomb failure surface with end caps (a tensile cut-off stress and a compressive failure end cap) was used in the Pseudo Tensor material model in the knuckle analysis (Livermore Software Technology Corporation 2003). The cut-off stress for tensile failure was set as

$$\sigma_{cut} = 1.7(f_a)^{2/3} \tag{5}$$

3.2 STEEL

Steel types used in WTC 1 and WTC 2 are listed in Table 3–1 along with the actual yield and tensile strengths used in analysis. NIST examined the WTC steels in Project 3 and determined their material properties (NIST NCSTAR 1-3). There were a number of steel suppliers and the multiple sources for steel components of the same grade resulted in different strengths.

3.2.1 Steel Properties

Figure 3–3 shows mechanical properties of steel that are affected by elevated temperatures: (a) modulus of elasticity, (b) Poisson's ratio, (c) yield strength reduction factor, (d) tensile strength reduction factor, and (e) instantaneous coefficient of thermal expansion. All steel properties, except yield and tensile strength reduction factors for bolt steels, are the same for all steels shown in Table 3–1.

3.2.2 Stress-Strain Relationship

Plasticity: Stress-strain relationships at room temperature were provided by Project 3. They were constructed from mill reports, actual test data, and literature information using the Voce hardening law.

Stress-strain relationships at elevated temperatures, without consideration of creep, were obtained from the power law:

$$\sigma = R_{TS} R_C K(T) \varepsilon_{ep}^{n(T)} \tag{6}$$

where:

$$K(T) = (k4 - k0)\exp\left\{-0.5\left[\left(\frac{T}{tk1}\right)^{k1} + \left(\frac{T}{tk2}\right)^{k2}\right]\right\} + k0$$

$$n(T) = (n4 - n0)\exp\left\{-0.5\left[\left(\frac{T}{tn1}\right)^{n1} + \left(\frac{T}{tn2}\right)^{n2}\right]\right\} + n0$$

The steel stress-strain relationships at different temperatures varied depending on the type of steel used in the construction of the towers. Values for R_{TS} and R_C are given in Table 3–1, and parameters of functions $K(T)$ and $n(T)$, which were provided by Project 3, are given in Table 3–2. The stress-strain curve is linear with Young's modulus up to the "linearity limit." At the linearity limit, the linear stress-strain curve intersects the power law stress strain curve. (Stress at the linearity limit at elevated temperature was not necessarily equal to the yield stress at the given temperature. The linearity limit was required for ANSYS input.)

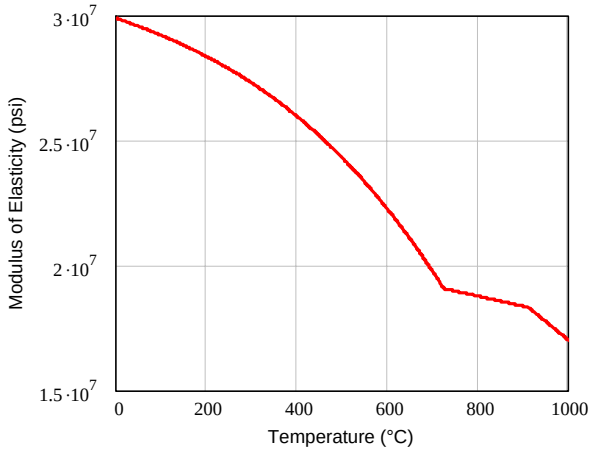

(a) Modulus of elasticity

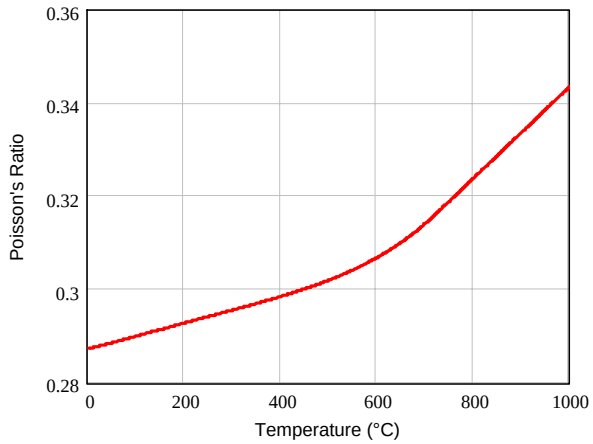

(b) Poisson's ratio

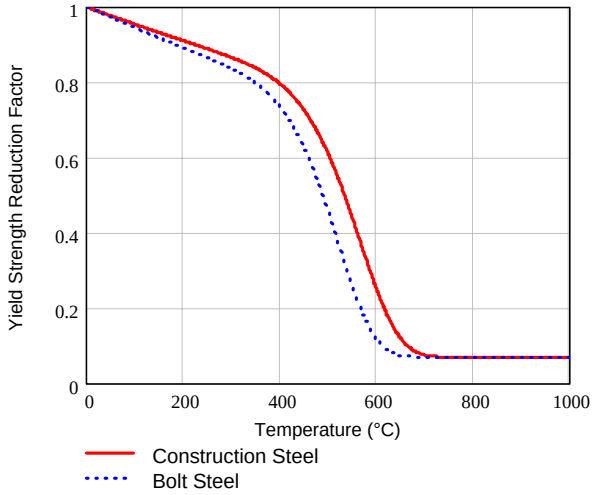

(c) Yield strength reduction factor

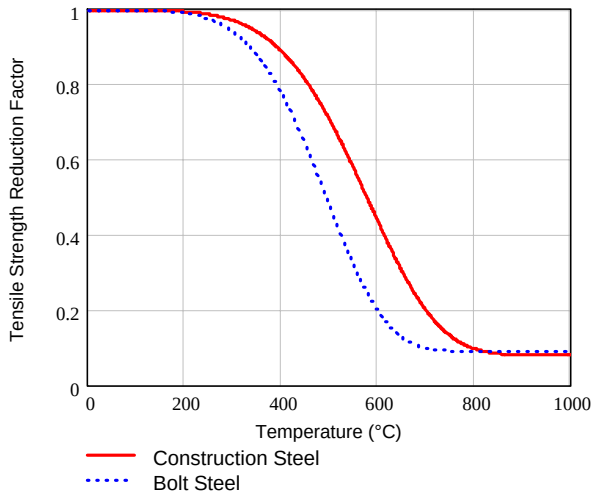

(d) Tensile strength reduction factor

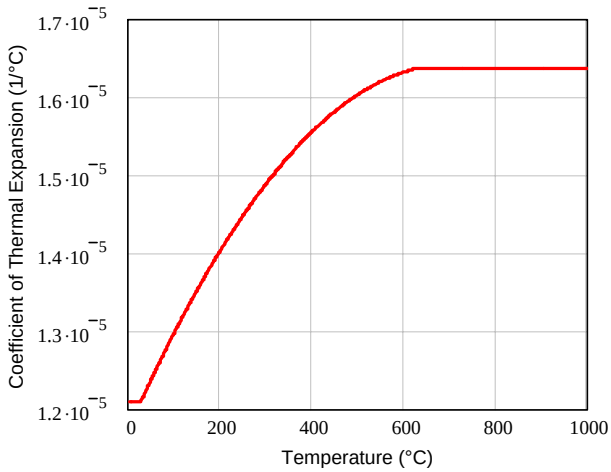

(e) Instantaneous coefficient of thermal expansion

Figure 3–3. Properties for all steel types that vary with temperature.

Table 3–1. Steel types used in WTC 1 and WTC 2.

Material ID	Description	σ_{yRT} (psi)	σ_{uRT} (psi)	R_{TS}	R_C
1	All 36 ksi core box columns, plates, straps[a]	36,720	64,470	1.086	0.857
2	All 36 ksi core WF, channels, and tubes 36 ksi large area and large inertia "rigid" beams in SAP2000 model[a]	37,000	63,450	1.069	0.954
3	All 42 ksi box columns (1<=0.75 in.)	51,400	79,200	1.070	0.884
4	All 42 ksi box columns (0.75 in. < t <= 1.5 in.)	47,000	74,800	1.010	0.884
5	All 42 ksi box columns (t > 1.5 in.)	42,600	70,400	0.951	0.880
6	42 ksi or 45 ksi Group 3 WF core columns	53,800	74,400	1.005	0.977
7	42 ksi or 45 ksi Group 3 WF core columns	49,000	71,040	0.960	0.954
8	42 ksi Group 4&5 WF core columns	44,200	66,640	0.900	0.948
9	45 ksi Group 4&5 WF core columns	47,800	71,074	0.960	0.939
10	All 36 ksi Plates 1, 2, and 4 in perimeter columns	35,630	61,170	1.031	0.875
11	All (42, 45, or 46) ksi Plates 1, 2, and 4 in. perimeter columns	53,051	74,864	1.011	0.948
12	All 50 ksi Plates 1, 2, and 4 in. perimeter columns. All 50 ksi channels and plates[a]	53,991	75,618	1.021	0.978
13	All 55 ksi Plates 1, 2, and 4 with t<=1.5 in. in perimeter columns	60,817	82,558	1.115	0.903
14	All 60 ksi Plates 1, 2, and 4 with t<=1.25 in. in perimeter columns	62,027	87,250	1.178	0.894
15	All 65 ksi Plates 1, 2, and 4 with t<=0.5 in. in perimeter columns[b]	69,642	90,442	1.221	0.979
16	All 70 ksi Plates 1, 2, and 4 in. perimeter columns	76,735	91,951	1.242	0.955
17	All 75 ksi Plates 1, 2, and 4 in perimeter columns	82,469	96,821	1.308	0.936
18	All 80 ksi perimeter columns steels, regardless of plate	91,517	99,442	1.343	0.987
19	All (85, 90, 100) ksi perimeter column steels, regardless of plate	104,783	115,983	1.566	0.976
20	Laclede truss web bar rounds specified as A36	38,067	59,567	1.004	0.935
21	Laclede truss chord angels (regardless of ASTM Spec) and all rounds specified as A242	55,332	74,050	1.000	0.959
22	A325 bolts[c]	104,783	115,983	1.566	0.976
23	All 42 ksi Plate 3 in perimeter columns	42,600	67,216	0.900	0.912
24	All 45 ksi Plate 3 in perimeter columns	45,900	69,831	0.940	0.921
25	All 50 ksi Plate 3 in perimeter columns	51,400	74,188	1.000	0.935
26	All 55 ksi Plate 3 in perimeter columns	56,900	78,546	1.070	0.906
27	All 60 ksi Plate 3 in perimeter columns	62,400	83,903	1.130	0.949
28	All 65 ksi Plate 3 in perimeter columns	67,900	87,261	1.190	0.975
29	All 70 ksi and 75 ksi Plate 3 in perimeter columns	78,900	95,976	1.310	0.997

a. Steels in the following members are assumed to have the properties shown in the table:
36 ksi plates and straps (Material 1).
36 ksi channels, tubes, and "rigid" beams (Material 2).
50 ksi channels and plates (Material 12).

b. 65 ksi steels in perimeter columns with t>0.5 in. are assumed to have the same properties as those in Material 15.

c. In the column model, stress-strain relationships of bolts are used.

Note: Bolt properties are assumed to be the same as those in Material 19.

Creep: Steel creeps at elevated temperatures ($T \geq 350$ ˚C). The creep behavior of the steels in the WTC towers was expressed by NIST as follows:

$$\varepsilon_{cr}(t,T,\sigma) = \frac{1}{100} a(T) \left(\frac{t}{60}\right)^{b(T)} \left(70.5 \frac{\sigma}{\sigma_{uRT}}\right)^{c(T)} \tag{7}$$

where:

$$a(T) = \begin{cases} 0 & \text{for} \quad T < 350^\circ C \\ 10^{-(6.1+0.00573T)} & \text{for} \quad 350^\circ C \leq T < 500^\circ C \\ 10^{-(13.25-0.00851T)} & \text{for} \quad 500^\circ C \leq T < 725^\circ C \end{cases} \tag{7-a}$$

$$b(T) = -1.1 + 0.0035T \quad \text{for} \quad T < 725^\circ C \tag{7-b}$$

$$c(T) = 2.1 + 0.0064T \quad \text{for} \quad T < 725^\circ C \tag{7-c}$$

The creep model was validated against experimental data by NIST (NIST NCSTAR 1-3D). The creep model was derived by modifying the creep model already developed by Fields and Fields (1991). In this original model, the stress was scaled by yield strength at room temperature. The original model was used in the truss model and the exterior wall model.

The function, $a(T)$, is not smooth at T = 500 °C. To enhance numerical efficiency, $a(T)$ was modified by smoothing it as follows:

$$a(T) = \begin{cases} 10^{-(13.25-0.00851\times 20)} & \text{for} \quad T < 20^\circ C \\ 10^{-(13.25-0.00851T)} & \text{for} \quad 20^\circ C \leq T < 725^\circ C \end{cases} \tag{7-d}$$

A comparison of creep strains calculated from Eq. (7) with $a(T)$ given by Eqs. (7-a) and (7-d) is shown in Fig. 3–5. For 350 °C $\leq$ T $\leq$ 500 °C, creep strain is underestimated with $a(T)$ by Eq. (7-d). However, the difference is small, and creep strains for temperatures below 500 ˚C are usually negligible. Figure 3–6 illustrates creep behavior of steel at elevated temperatures for Material ID 1. Figure 3–6 (a) shows creep strain rate at different stress levels and different temperatures, and Fig. 3–6 (b) compares elastic, plastic, creep, elastic plus plastic, and total strains at T = 600 °C and after loading at a constant stress level for 1,800 s. The creep model expressed by Eq. (7) with $a(T)$ given by Eq. (7-d) was used in the global models.

In ANSYS analysis, the "time hardening" implicit creep model was used for BEAM188 and BEAM189 elements, where creep strain rate was given by:

$$\frac{d\varepsilon_{cr}}{dt} = C_1(T)\sigma^{C_2(T)} t^{C_3(T)} \tag{8}$$

and $C_1(T)$, $C_2(T)$, and $C_3(T)$ are temperature-dependent parameters derived from the creep model expressed by Eq. (7) with the following relationships:

$$C_1(T) = \frac{1}{100} a(T) b(T) \left(\frac{1}{60}\right)^{b(T)} \left(\frac{70.5}{\sigma_{uRT}}\right)^{c(T)}$$
$$C_2(T) = c(T)$$
$$C_3(T) = b(T) - 1$$

For BEAM24 elements in ANSYS, the primary explicit creep model was used. Creep strain rate was specified by

$$\frac{d\varepsilon_{cr}}{dt} = M(T) K(T) \sigma^{N(T)} t^{M(T)-1} \tag{9}$$

where

$$M(T) = b(T)$$
$$N(T) = c(T)$$
$$K(T) = \frac{1}{100} a(T) \left(\frac{1}{60}\right)^{b(T)} \left(\frac{70.5}{\sigma_{uRT}}\right)^{c(T)}$$

The truss model and the exterior wall subsystem model included creep with BEAM188 and 189 elements. The global model included creep with BEAM24 elements, as they were more numerically stable for creep and post-buckling behaviors.

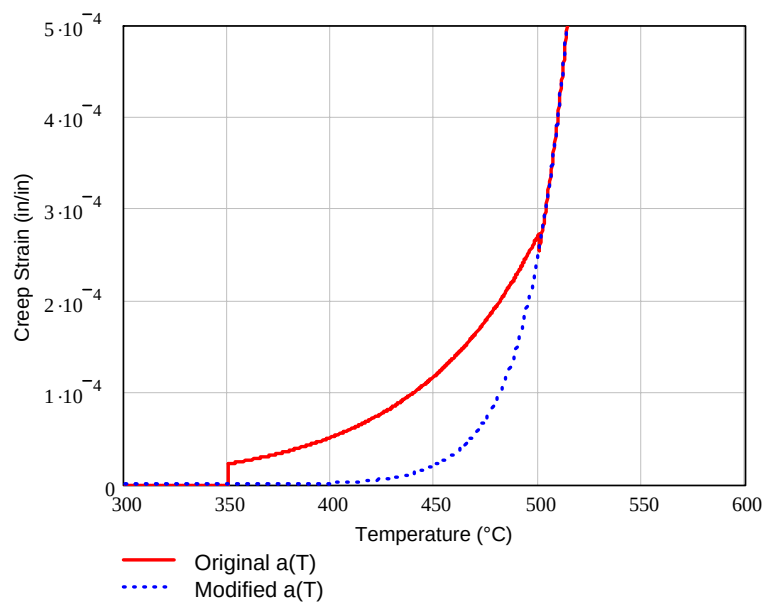

Figure 3–5. Comparison of creep strains with $a(T)$ given by (7-a) and (7-d) for Material ID 1 steel subject to 15 ksi for 1,800 s at a given temperature.

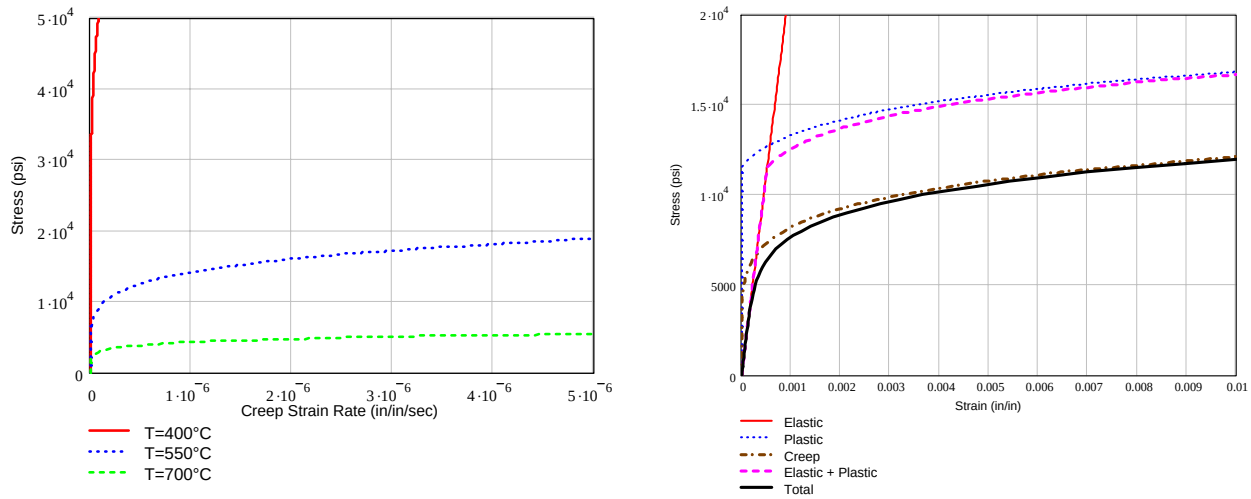

(a) Creep strain rate

(b) Comparison of different strains at T = 600 ˚C and t = 1,800 s

Figure 3–6. Creep behavior at elevated temperatures for Material ID 1 steel.

3.2.3 Steel Failure Criteria

The tensile failure criteria for steel were defined in terms of plastic strains. The multi-axial fracture strain criterion for different steels and temperatures in terms of true stress and true strain (NIST NCSTAR 1-3D) can be expressed as follows:

$$\bar{\varepsilon}_f = \alpha(T)\exp\left[-\frac{3}{2}\frac{\sigma_m}{\bar{\sigma}}\right] \tag{10}$$

$\alpha(T)$ is a temperature dependent material property, values of which can be calculated from Table 3–3 by using Eq. (11). For the uniaxial stress condition, where $\bar{\sigma} = \sigma$ and $\sigma_m = \sigma/3$, the plastic strain at fracture reduces to:

$$\bar{\varepsilon}_{f_uni} = \alpha(T)\exp(-0.5) \tag{11}$$

Table 3–3 shows the uniaxial plastic strain at fracture, $\bar{\varepsilon}_{f_uni}$, calculated by Eq. (11) for different temperatures. This criterion is valid for a finite element analysis (FEA) with a very fine mesh. For a coarser mesh, the equivalent steel fracture criterion was determined numerically as follows. A standard tension test specimen was modeled in ANSYS. The gauge length, width, and thickness of the specimen were 8 in, 1.5 in, and 1 in., respectively, and steel properties of Material ID 1 were used. Six different models (Model 0 to 5) were created, each having a different mesh size. Element sizes of Models 0 to 5 were 0.025 in., 0.050 in., 0.0125 in., 0.250 in., 0.375 in., and 0.75 in. It was assumed that Model 0 was a fine mesh that was able to capture tensile fracture in uniaxial tension.

Model 0 was subjected to tension until the maximum plastic strain in the direction of applied displacement reached the uniaxial fracture strain determined by Eq. (11) for uniaxial stress condition, and the corresponding elongation of the specimen, Δ_0, was obtained. Models 1 to 5 were then subjected to the same elongation, Δ_0, and the maximum plastic strain in the direction of applied displacement was measured for each model. The maximum plastic strain due to the elongation of Δ_0 was defined as the limiting plastic strain (equivalent fracture plastic strain) for the corresponding element size.

From these six cases, a relationship between element size and equivalent uniaxial fracture plastic strain was established. This process was repeated for temperatures 20 °C, 100 °C, 300 °C, 500 °C, and 700 °C. Figure 3–7 (a) shows the ratio of the maximum plastic strain in the direction of applied displacement due to displacement Δ_0 to uniaxial plastic strain by Eq. (11) vs. element size at different temperatures. The FEA results were extrapolated up to the element size of 50 in. Plastic strain shown in Fig. 3–7 (b) was used as the failure criterion for the corresponding element size in the FEA. Note that Fig. 3–7 (b) shows the failure criterion for element size larger than 0.375 in.

The compressive failure criteria for steel were not specified explicitly in terms of plastic strains because the information was not available. However, failure of compressive members was expressed by elastic buckling and plastic kink-type buckling (see Chapter 6) of compression members.

Table 3–3. Uniaxial plastic strain at fracture by Eq. (11).

Material ID	Plastic Strain at Fracture in the Uniaxial Test, $\bar{\varepsilon}_{f_uni}$					
	20 ˚C	100 ˚C	300 ˚C	500 ˚C	700 ˚C	1000 ˚C
1	0.8411	0.6989	0.6610	1.0446	1.8100	3.5862
2	0.8411	0.6989	0.6610	1.0446	1.8100	3.5862
3	0.4908	0.4078	0.3857	0.6095	1.0561	2.0924
4	0.4908	0.4078	0.3857	0.6095	1.0561	2.0924
5	0.4908	0.4078	0.3857	0.6095	1.0561	2.0924
6	0.4908	0.4078	0.3857	0.6095	1.0561	2.0924
7	0.4908	0.4078	0.3857	0.6095	1.0561	2.0924
8	0.4908	0.4078	0.3857	0.6095	1.0561	2.0924
9	0.4908	0.4078	0.3857	0.6095	1.0561	2.0924
10	0.8891	0.7388	0.6987	1.1042	1.9142	3.7907
11	0.4908	0.4078	0.3857	0.6095	1.0561	2.0924
12	0.4908	0.4078	0.3857	0.6095	1.0561	2.0924
13	0.2846	0.2364	0.2236	0.3534	0.6123	1.2132
14	0.3774	0.3136	0.2965	0.4686	0.8120	1.6088
15	0.5338	0.4436	0.4195	0.6629	1.1486	2.2758
16	0.5623	0.4672	0.4418	0.6983	1.2099	2.3972
17	0.7752	0.6442	0.6092	0.9628	1.6681	3.3051
18	0.6545	0.5439	0.5143	0.8129	1.4084	2.7906
19	0.4254	0.3535	0.3343	0.5283	0.9154	1.8137
20	0.8411	0.6989	0.6610	1.0446	1.8100	3.5862
21	0.4908	0.4078	0.3857	0.6095	1.0561	2.0924

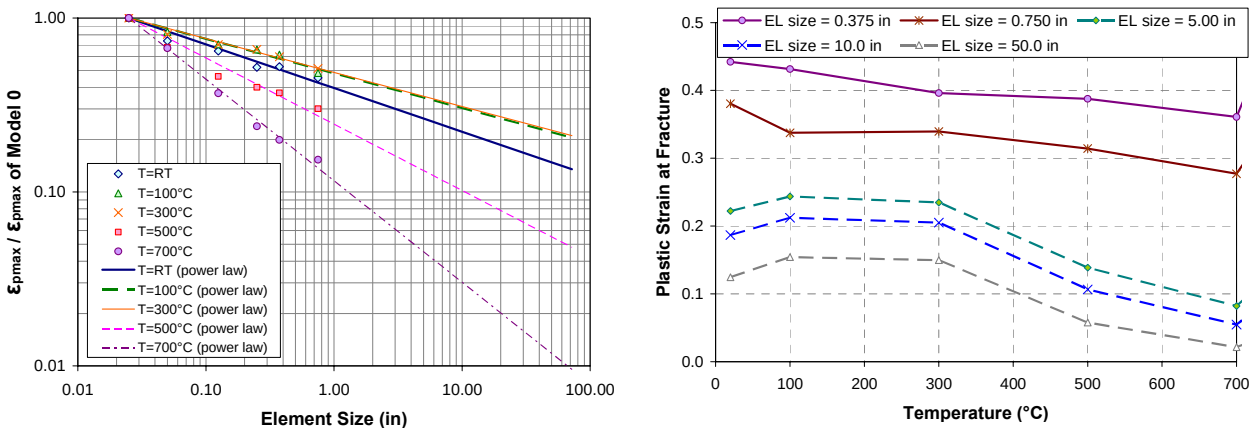

(a) FEA results and extrapolation

(b) Recommended limiting plastic strain

Figure 3–7. Maximum plastic strain from the finite element analysis and limiting plastic strain.

3.3 WELDS

The weld properties at all temperatures were assumed to be the same as those of the base metal of the same ultimate tensile strength as determined by Project 3. High temperature properties of the weld metals were not found in the literature. Susceptibility of existing cracks in the welds to growth (fracture toughness) does not increase with temperature (Stevick 1994). This assumption was supported by the following observations in the recovered WTC steel: the exterior column welds were strong enough to fail the base metal, the observed fractures in the exterior columns were mostly through the base metal, and the welds in trusses were resistance welds with no filler added. For the core columns, the area of the welds was significantly less than that of the base metal, and several fractures through the welds were observed. Fractures in the truss seats and truss connections were also observed.

3.4 BOLTS

A load-elongation relationship for a 7/8 in. A325 bolt with 4 in. length at room temperature was provided by Project 3. Load-elongation relationships at elevated temperatures are constructed by scaling the loads by the yield and ultimate tensile strength reduction factors for bolt steels shown in Fig. 3–3 (c) and (d). Figure 3–8 shows the load-elongation relationships of a 7/8 in. bolt at different temperatures. Load-elongation relationships of A325 bolts of different size were created by proportioning the load by the net area.

The load-elongation relationship for bolts with a different length than 4.0 in. is expected to be very similar to the load-elongation relationship for 4.0 in. length since bolt deformations are localized.

Based on the AISC formulas (AISC 2003), C-J3–2 to C-J3–4, the shear strength for a single shear plane is calculated as 0.67 of the tensile strength given in Fig. 3–8 when threads are excluded from the shear plane. When threads are not excluded from the shear plane, the nominal shear strength for a single shear plane is 0.53 of the tensile strength given in Fig. 3–8. These factors were obtained by a ratio between the shear strength and the tensile strength evaluated by the AISC formulas. No shear ductility was assumed at failure.

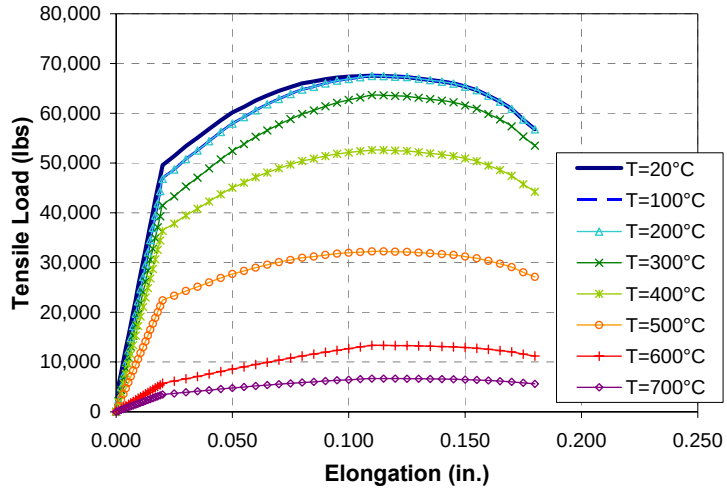

Figure 3–8. 7/8 in. A325 bolt load-elongation curves at elevated temperatures.

3.5 COEFFICIENT OF FRICTION

The coefficient of friction of 0.33 for calculation of shear in friction-type connections was used. This value was taken from the AISC LRFD (2003) friction coefficient for uncoated clean mill scale steel surfaces, or surfaces with Class A coatings on blast-cleaned steel surfaces.

3.6 SYMBOLS

$\alpha(T)$ = temperature-dependent material property that defines fracture criterion

$\alpha_c(T)$ = instantaneous coefficient of thermal expansion of concrete

$\alpha_s(T)$ = instantaneous coefficient of thermal expansion of steel

$\beta_y(T)$ = steel yield strength reduction factor due to elevated temperature

$\beta_u(T)$ = steel ultimate strength reduction factor due to elevated temperature

γ_c = unit weight of concrete (110 pcf and 150 pcf for lightweight and normal weight concrete, respectively)

γ_s = unit weight of steel (490 pcf = 0.284 pci for all steel types at any temperature)

ε_{c1} = concrete strain at maximum compressive stress

ε_{cr} = creep strain of steel

ε_e = elastic strain

ε_{ep} = elastic plus plastic strain

$\bar{\varepsilon}_f$ = effective plastic strain at fracture

$\bar{\varepsilon}_{f_uni}$ = uniaxial plastic strain at fracture

ε_p = plastic strain

ε_t = concrete strain at maximum tensile stress

ε_{tu} = concrete strain at full crack formation (separation) in tension

ν_c	=	Poisson's ratio of concrete
ν_s	=	Poisson's ratio of steel
$\bar{\sigma}$	=	effective von Mises stress
σ_m	=	mean stress
σ_{yRT}	=	room temperature yield strength of steel
σ_{uRT}	=	room temperature tensile strength of steel
$E_s(T)$	=	modulus of elasticity of steel
$E_c(T)$	=	modulus of elasticity of concrete
F_1	=	mix design factor = ratio of the actual 28 day cylinder strength to f_c'
F_2	=	in-situ factor = ratio of in-situ 28 day strength to the 28 day cylinder strength
F_3	=	aging factor = ratio of mature concrete strength to 28 day concrete strength
f_a	=	actual strength of in-place concrete
f_c'	=	specified 28 day strength
$f_c(T)$	=	compressive strength of concrete
$f_t(T)$	=	tensile strength of concrete
$K(T)$	=	sigmoidal function of temperature with six parameters
$n(T)$	=	sigmoidal function of temperature with six parameters
R_C	=	correction factor that has the following two functions: (1) to correct the strain rate effect introduced in the material testing and create the stress-strain curve for zero strain rate, and (2) to match the room temperature stress-strain curve at strain of 0.05
R_{TS}	=	ratio of the room temperature tensile strength of the steel of interest to the room temperature tensile strength of the steel used to develop the power law model
RT	=	room temperature (20 °C)

This page intentionally left blank.

Chapter 4
MODEL CONVERSION FROM SAP TO ANSYS

Reference structural models were developed under Project 2 in SAP2000 (SAP) for traceability to a verified data set (NIST NCSTAR 1-2, NIST NCSTAR 1-2A). The SAP2000 Floor 96 model of WTC 1 and the SAP global models of WTC 1 and WTC 2 were converted into ANSYS 8.1 (ANSYS) and used as a foundation for developing detailed structural models. The converted ANSYS models were modified to incorporate the nonlinear behaviors of the components for the thermal/structural evaluation of collapse initiation.

4.1 TRANSLATION PROCEDURE

An automatic translation software was developed to partially convert the floor model and global models from SAP to ANSYS:

- The Joints, Frames, and Shells in the SAP model were translated into ANSYS Keypoints, Lines, and Areas. Translation using geometry definition, instead of nodes and elements, allowed for easy mesh refinement, where needed.
- Lines were meshed with both section properties and real constants so that a translation between 3-D elastic beam (BEAM44) elements and 3-D inelastic finite strain beam (BEAM188/BEAM189) elements was achieved by simply changing element types. Areas were meshed with elastic shell (SHELL63) elements in ANSYS to match the Shell elements in SAP. Lines and Areas were able to be changed to nonlinear beam (BEAM188) and nonlinear shell (SHELL181) elements simply by changing an element type.
- Material properties were assigned as described in Chapter 3 based on the material definitions and Frame section properties in SAP.
- Frame section properties in SAP were converted into Real Constants for BEAM44 in ANSYS. Cross section properties in SAP were retained for future conversion into cross section data for BEAM188 elements. Shell thicknesses in SAP were converted into Real Constants for SHELL63 in ANSYS.
- Joint restraints in SAP were translated into DOF constraints in ANSYS.
- Frame distributed loads and area uniform loads were translated into surface loads on Lines and Areas in ANSYS.
- The ANSYS BEAM44 elements support element moment releases, but the ANSYS nonlinear BEAM188 elements do not. Therefore, Frame releases in SAP were modeled by coincident nodes with coupled (CP) degrees of freedom in ANSYS.
- The ANSYS BEAM44 elements allow beam end offsets in three directions, but the ANSYS nonlinear BEAM188 elements only allow beam end offsets perpendicular to the element axis through section offset (SECOFFSET) command. Frame insertion points in SAP were converted in two ways. For offsets along the element axis, additional nodes and rigid MPC184 elements with the proper lengths were used in ANSYS. For offsets perpendicular to

the element axis, beam end offsets were defined using Real Constants for BEAM44, and were defined using SECOFFSET command for BEAM188.

- Frame offsets and rigid panel factor in SAP were modeled by adding additional nodes and rigid beam MPC184 elements with the proper lengths in ANSYS.

During the conversion of the SAP floor model, the following conditions were encountered and were resolved:

- The SAP floor model allowed automatic division of the frames at joints. This caused problems in the translation software, because the frame connectivities in the Graphical User Interface did not show the actual internal element connectivities used in the SAP analysis engine. In order to resolve this problem, the translation software was modified to use the internal element connectivities. The table of internal connectivities was exported from the SAP model after the execution of the SAP analysis.
- Information on automatic offsets in the SAP model were not available in the SAP input file. The table of element offsets was exported after the execution of the SAP analysis.
- There were both intentional and unintentional duplicate elements in the SAP floor model that led to problems in the translator since ANSYS cannot have duplicate lines sharing the same keypoints. Some duplicate elements were used to model additional steel plates at the ends of trusses. The duplicate elements were manually deleted, and the section properties of the remaining elements were modified to account for the additional steel. Some duplicate elements were from frame elements with different lengths that overlapped. These were manually corrected.

Those parts of the model that were not converted by the translation software were converted manually.

Table 4–1 presents the descriptions of finite elements used in ANSYS models, such as BEAM188 (ANSYS, Inc. 2004). All structural elements listed in the table including link, beam, shell, and solid elements can be used with temperature-dependent material properties.

Table 4–1. Element types used in ANSYS models.

Name	Element Type	Description
LINK8	3-D truss	LINK8 is a uniaxial tension-compression element with three degrees of freedom at each node. It has plasticity, creep, and large deflection capabilities.
BEAM4	3-D elastic beam	BEAM4 is a 3-D elastic Euler beam element. The element has six degrees of freedom at each node. Large deflection capability is included.
BEAM44	3-D elastic tapered unsymmetric beam	BEAM44 is a 3-D elastic Euler beam element and allows a different unsymmetrical geometry at each end. The element has six degrees of freedom at each node. Large deflection capability is included.
BEAM188	3-D linear finite strain beam	BEAM188 is a linear (2-node) or a quadratic beam element in 3-D based on Timoshenko beam theory. Each node has six degrees of freedom or seven degrees of freedom (6+warping). Shear deformation effects are included. This element is supported for plasticity, creep, large deflection. A cross section can be a built-up section referencing more than one material. Creep strain is calculated by implicit time integration method.
BEAM189	3-D quadratic finite strain beam	BEAM189 is a quadratic (3-node) beam element in 3-D based on Timoshenko beam theory. Each node has six degrees of freedom or seven degrees of freedom (6+warping). This element is supported for plasticity, creep, large deflection. A cross section can be a built-up section referencing more than one material. Creep strain is calculated by implicit time integration method.
SHELL63	4-node elastic shell	SHELL63 has both bending and membrane capabilities. The element has six degrees of freedom at each node: three translations and three rotations. Large deflection capability is also included.
SHELL181	4-node finite strain shell	SHELL181 is a 4-node shell element with six degrees of freedom at each node: three translations and three rotations. Plasticity, creep, and large deflection capabilities are supported. In nonlinear analyses, change in shell thickness is accounted for. SHELL181 may be used for layered applications.
SOLID185	3-D 8-node structural solid	SOLID185 is an 8-node structural solid element and has three degrees of freedom at each node (three translations). Plasticity, creep, and large deflection capabilities are supported.
COMBIN37	Control element	COMBIN37 is a unidirectional element with the capability of turning on and off during an analysis. The element has one degree of freedom at each node.
MPC184	Multipoint constraint element	MPC184 comprises a general class of multi constraint elements that implement kinematic constraints using Lagrange multipliers. Depending on the option that the user selects, the element can be used as a rigid link element, a rigid beam element, a slider element, a spherical element, a revolute joint element, and a universal joint element.

4.2 VALIDATION

4.2.1 Floor Model Validation

Figures 4–1 through 4–4 show the converted floor model.

The following analyses were performed to validate the converted ANSYS floor model against the original SAP model.

- One static analysis with gravity loads, defined in SAP as Load Case "DEAD," included self-weight plus 3.5 psf uniform load in the office area.
- One modal analysis, using structural mass only.

Table 4–2 summarizes the comparison of the SAP and ANSYS results for the gravity load case. The total reactions for the SAP and ANSYS models were within 0.1 percent of each other. The maximum slab displacement predicted by the ANSYS model was 3.2 percent smaller than that obtained from the SAP model. The deformed shapes of the gravity load case for the SAP and ANSYS models are shown in Figs. 4–5 and 4–6.

Table 4–2. Comparison of SAP and ANSYS results for gravity load case.

	SAP	ANSYS
Total reaction, kip	2,212.81	2,210.85 (-0.09 %)
Maximum slab displacement, in.	0.718	0.695 (-3.2 %)

Figure 4–1. Converted ANSYS model for Floor 96 of WTC 1: overall view.

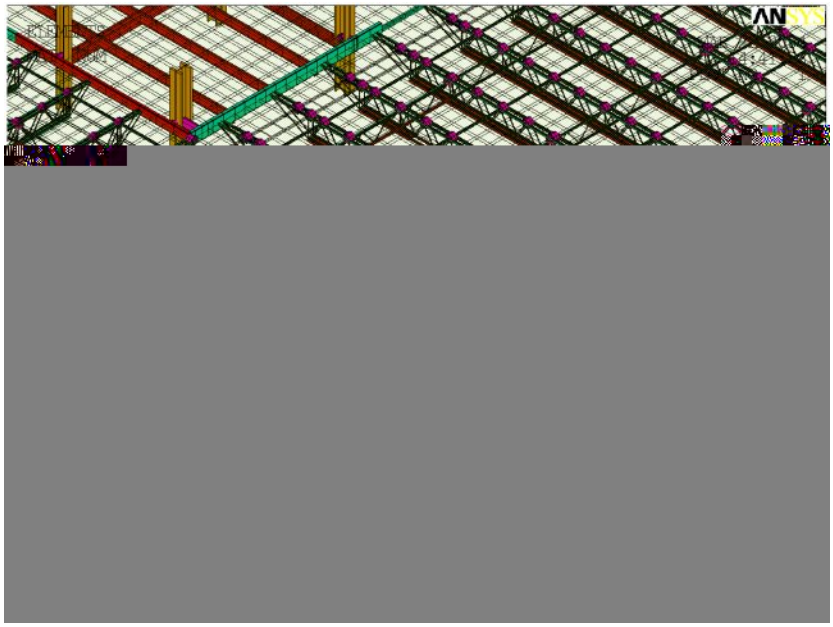

Figure 4–2. Converted ANSYS model for Floor 96 of WTC 1: partial view near corner of building.

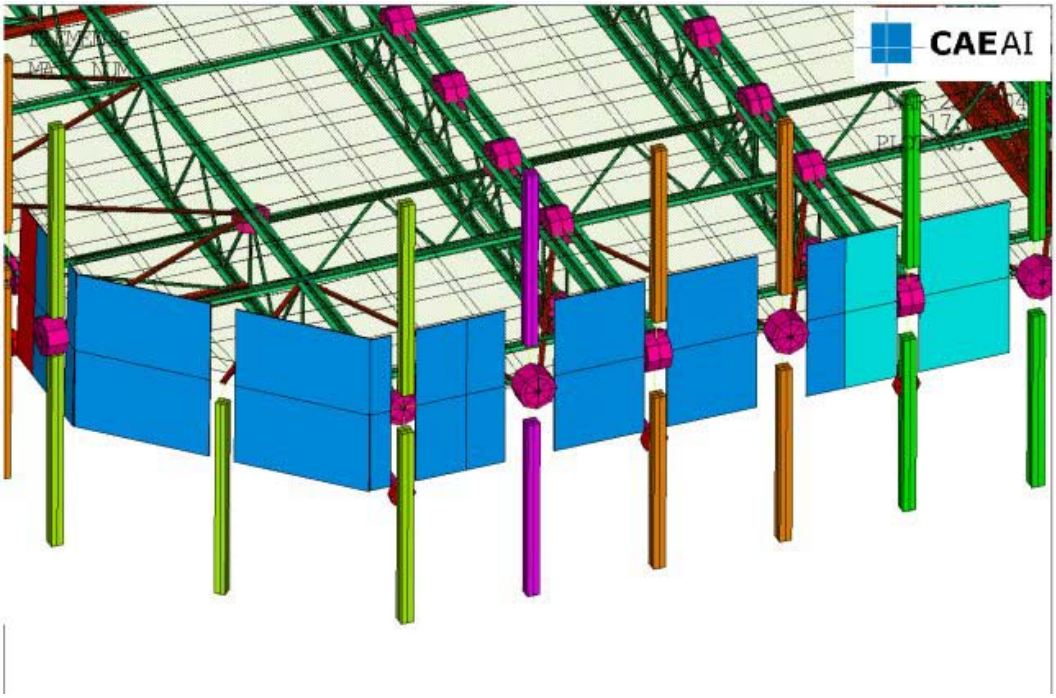

Figure 4–3. Converted ANSYS model for Floor 96 of WTC 1: close-up view at corner of building.

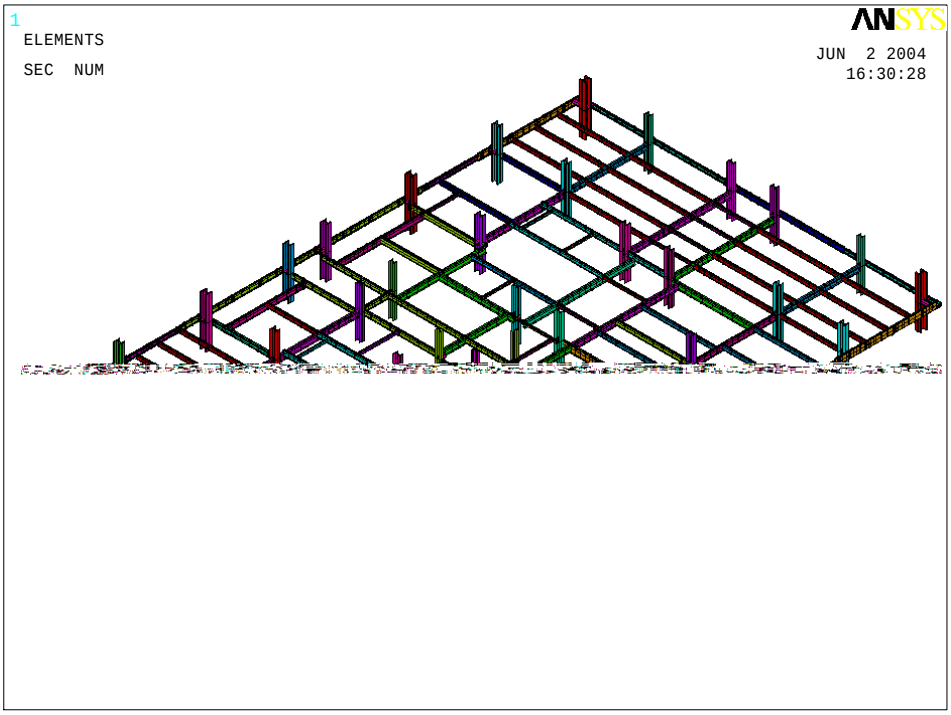

Figure 4–4. Converted ANSYS model for Floor 96 of WTC 1: view of floor beams and columns.

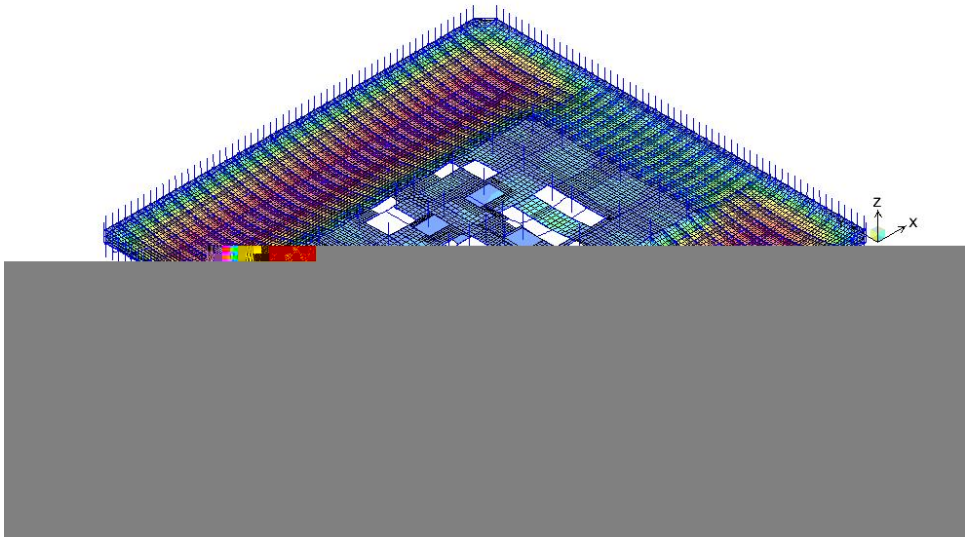

(in.)

Figure 4–5. Deformed shape (x100) of gravity load case for SAP floor model (downward displacement is negative).

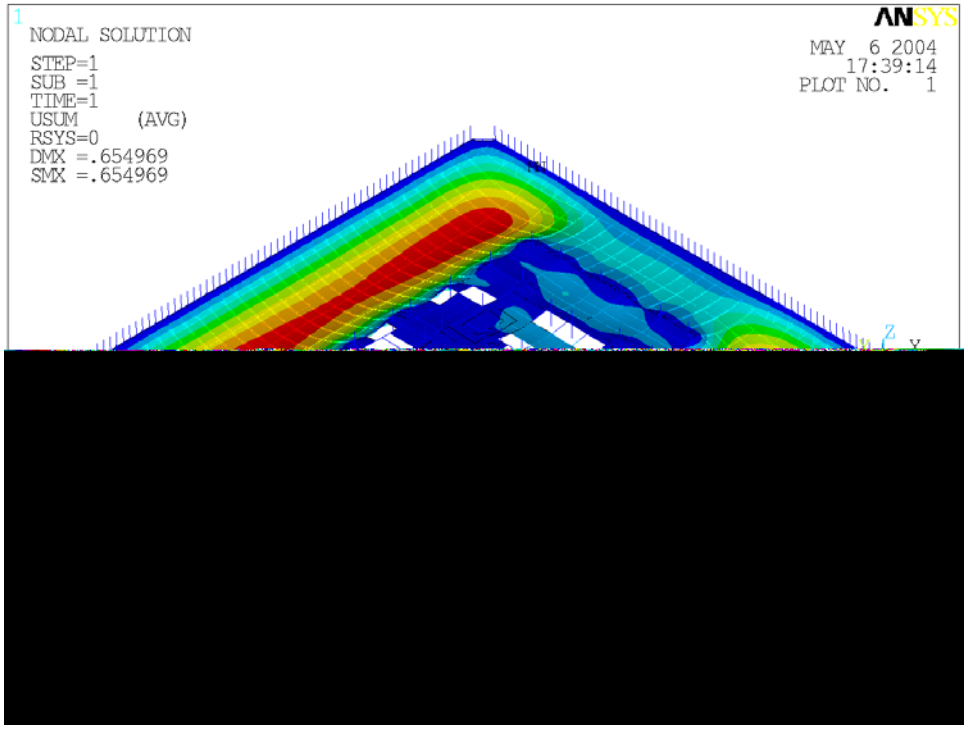

Figure 4–6. Deformed shape (x100) of gravity load case for ANSYS floor model (total displacements are shown).

Table 4–3 summarizes the comparison of the SAP and ANSYS results for the modal analysis of the floor models. The total masses of the SAP and ANSYS models were within 0.02 percent of each other. The dominant natural frequency of the floor predicted by the ANSYS model was 2.5 percent higher than that obtained from the SAP model. This discrepancy is consistent with the discrepancy observed for gravity displacement. The dominant mode shapes of the floor for SAP and ANSYS models are shown in Figs. 4–7 and 4–8.

Table 4–3. Comparison of SAP and ANSYS floor model modal analysis results.

	SAP	ANSYS
Total mass, lb·sec^2/in.	5448.7	5447.7 (-0.02 %)
Dominant natural frequency of floor, Hz	4.32	4.43 (+2.5 %)

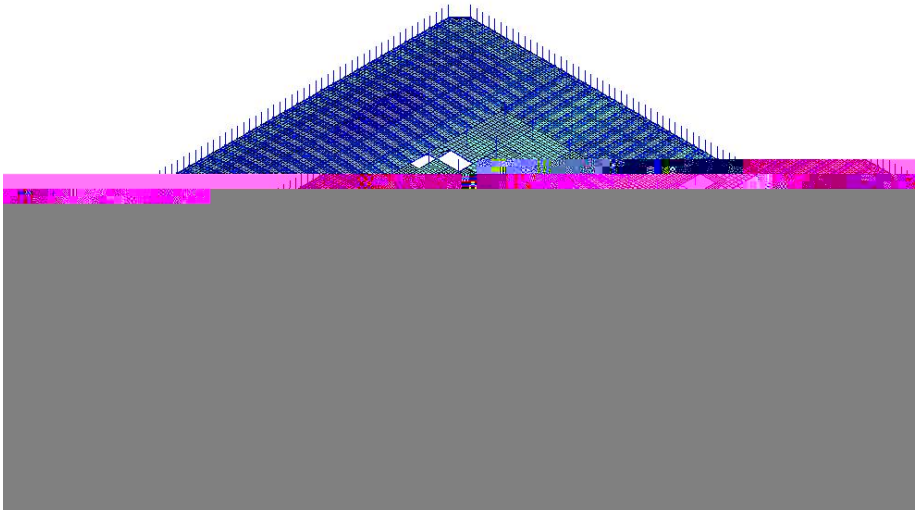

Figure 4–7. Dominant mode shape (frequency = 4.32 Hz) of floor structure for SAP floor model.

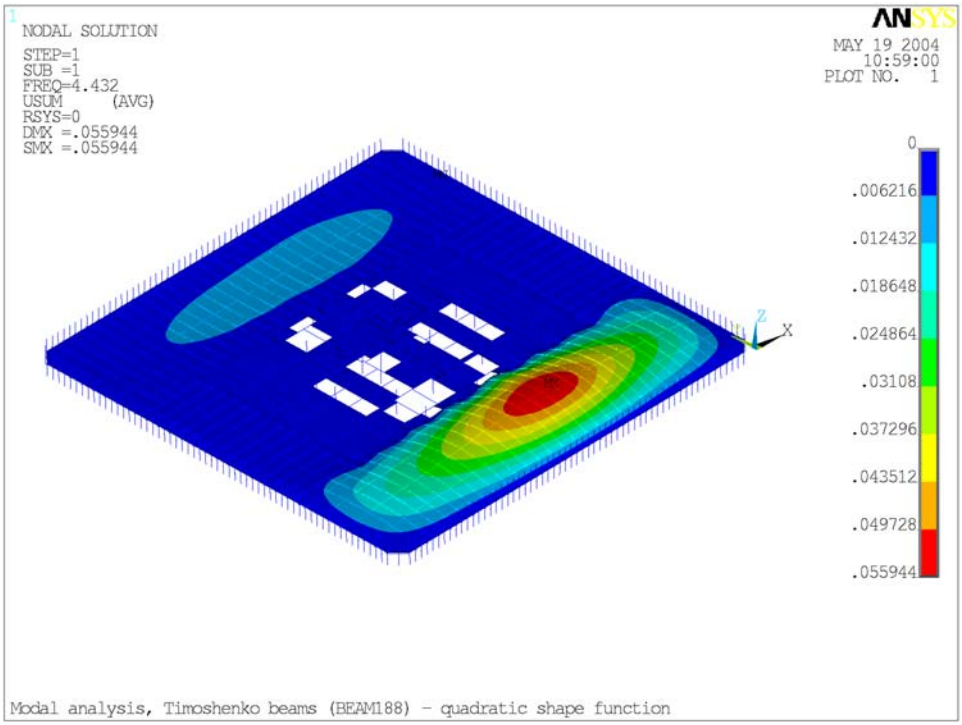

Figure 4–8. Dominant mode shape (frequency = 4.43 Hz) of floor structure for ANSYS floor model.

4.2.2 Global Model Validation

The translated ANSYS models were subjected to gravity dead and live loads and the results were compared to the results of SAP2000 global models (Figures 4–9 and 4–10). This comparison was performed to verify the accuracy of the translation of the SAP2000 models into ANSYS. The overall displaced shapes, the maximum displacements and vertical base reactions at each construction stage, and element forces for a set of randomly selected members from different parts of the buildings were compared.

The gravity analysis consisted of three stages that simulated the construction sequence of the buildings. Stage 1 was the analysis of the parts of the towers up to and including Floor 106 under their self weight. In Stage 2, the members above Floor 106 in unstressed states were added to the parts of the towers up to and including Floor 106, which had already deformed under their self-weight, and the towers were subjected to and analyzed for the dead load of the newly added members. In Stage 3, the towers were subjected to and analyzed for the additional load consisting of the superimposed dead load and 25 percent of the design live loads were added to the existing dead loads.

Figures 4–11 and 4–12 compare the deformed shapes of WTC 1 and WTC 2 obtained from the translated ANSYS models to the ones obtained from the SAP models at the end of Stage 3 of the gravity analysis. Table 4–4 and Table 4–5 summarize the maximum displacement and vertical reactions at the base for all stages of the gravity analysis. As can be seen, the deformed shapes and the maximum displacements and vertical reactions obtained from the analyses performed with the translated ANSYS models agree well with the results of the SAP analyses. The maximum differences between the two models were less than 1.4 percent for WTC 1 and 0.7 percent for WTC 2 for the displacements, and 1.2 percent for WTC 1 and 0.3 percent for WTC 2 for the base reactions.

Table 4–6 and Table 4–7 show the comparisons of the axial forces computed from ANSYS and SAP2000 for a randomly selected set of elements from different parts of each building. In Table 4–6 and Table 4–7, the axial force values that are less then 0.5 kip are shown as 0.0 kip. There is good agreement between the results obtained from ANSYS and SAP models.

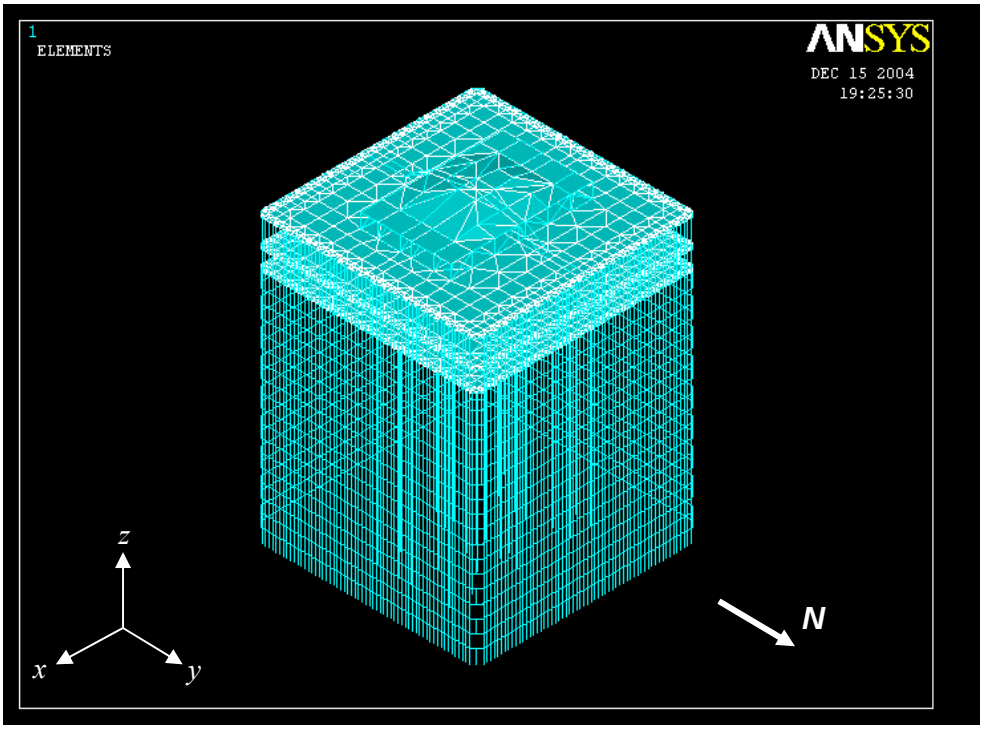

Figure 4–9. Converted ANSYS model of WTC 1.

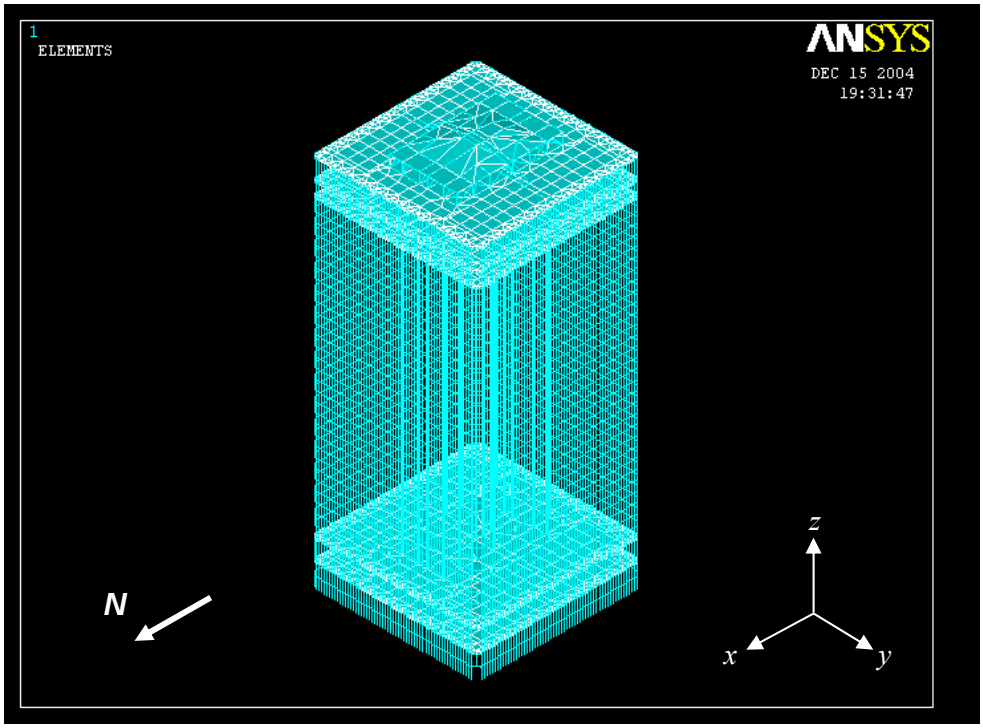

Figure 4–10. Converted ANSYS model of WTC 2.

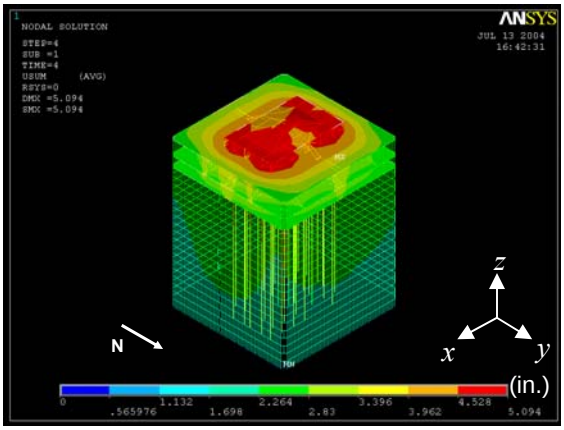

(a) WTC 1 ANSYS Model at Stage 3

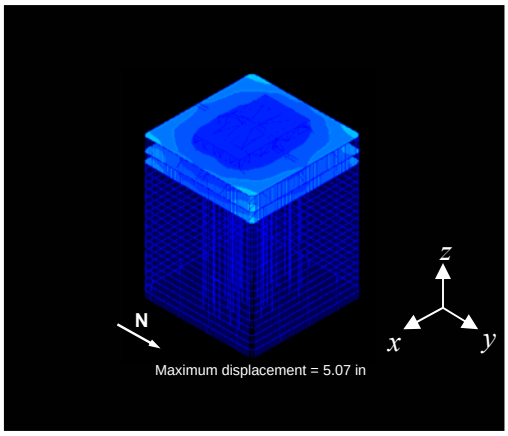

(b) WTC 1 SAP2000 Model at Stage 3 (Displacement contour is only shown on floor (shell) elements.)

Figure 4–11. Displaced shape of WTC 1 at the end of gravity analysis.

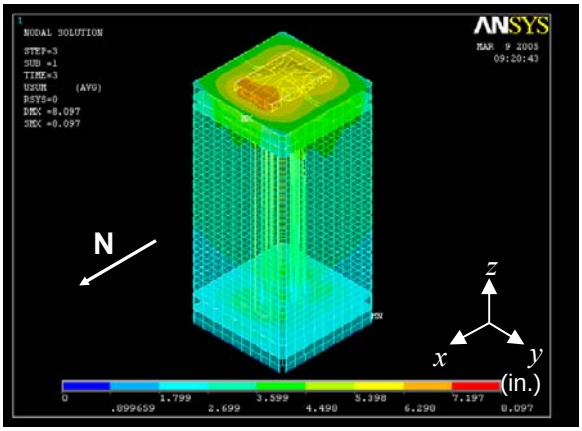

(a) WTC 2 ANSYS Model at Stage 3

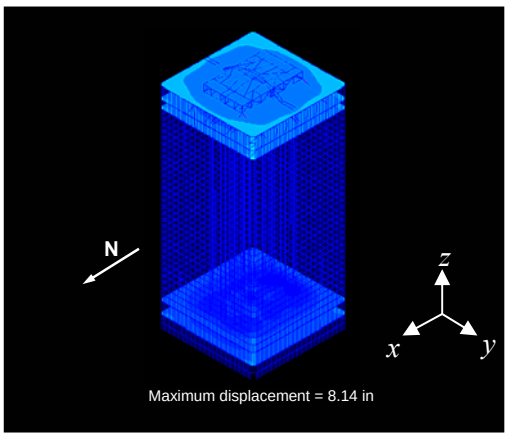

(b) WTC 2 SAP2000 Model at Stage 3 (Displacement contour is only shown on floor (shell) elements.)

Figure 4–12. Displaced shape of WTC 2 at the end of gravity analysis.

Table 4–4. Comparison of maximum displacements and base reactions of WTC 1 from translated ANSYS and SAP2000 models.

Stage	Maximum Vertical Displacement (in.)			Base Reaction Sum (kip)		
	ANSYS	SAP2000	Percent Difference	ANSYS	SAP2000	Percent Difference
1	-2.87	-2.83	1.4	55,600	54,940	1.2
2	-4.76	-4.74	0.4	98,470	97,850	0.6
3	-5.09	-5.07	0.4	107,040	106,450	0.6

Table 4–5. Comparison of maximum displacements and base reactions of WTC 2 obtained from translated ANSYS and SAP2000 models.

Stage	Maximum Vertical Displacement (in.)			Base Reaction Sum (kip)		
	ANSYS	SAP2000	Percent Difference	ANSYS	SAP2000	Percent Difference
1	-5.87	-5.91	-0.7	125,050	124,680	0.3
2	-7.67	-7.71	-0.5	166,950	166,980	0.0
3	-8.10	-8.14	-0.5	180,250	180,360	-0.1

Table 4–6. Comparison of axial forces in randomly selected elements from WTC 1 model at the end of gravity analysis.

Location and Type of Selected Element	Axial Force (kip)	
	ANSYS	SAP2000
Exterior Column 302 at Floor 104	-77	-69
Spandrel between Columns 124 and 125 at Floor 102	0	0
Outrigger member between at Floor 110	-39	-48
Vertical hat-truss member at 1005 core column line at Floor 109	-74	-91
Horizontal hat-truss member at Floor 107	21	19
Horizontal hat-truss member at Floor 108	170	150
Core Column 602 at Floor 97	-738	-745
Core Column 501 at Floor 93	-2,180	-2,190
Core Column 1001 at Floor 89	-2,570	-2,590
Spandrel between Columns 339 and 340 at Floor 100	0*	0

* Axial force values less than 0.5 kip are shown as 0.0 kip.

Table 4–7. Comparison of axial forces in randomly selected elements from WTC 2 model at the end of gravity analysis.

Location and Type of Selected Element	Axial Force (kip)	
	ANSYS	SAP2000
Core beam at Floor 107	11	6
Inclined truss member at hat-truss at Floor 107	-34	-4
Inclined truss member at hat-truss at Floor 108	36	8
Inclined truss member at hat-truss at Floor 108	-580	-670
Core Column 502 at Floor 87	-1,930	1,940
Core Column 1001 at Floor 82	-3,270	-3,290
Core Column 1002 at Floor 87	-1,910	-1,920
Core Column 1008 at Floor 82	-3,400	3,520
Core Column 1003 at Floor 107	-590	-608
Exterior Column 122 at Floor 82	-313	-313
Exterior Column 329 at Floor 82	-228	-230
Exterior Column 130 at Floor 107	-222	-202
Spandrel between Columns 138 and 139 at Floor 83	0*	0
Spandrel between Columns 447 and 448 at Floor 87	0	0

* Axial force values less than 0.5 kip are shown as 0.0 kip.

4.3 SUMMARY

In general, the results from the translated ANSYS floor and global models showed good agreement with the results obtained form the SAP models. For the floor model, the calculated base reactions and displacements due to gravity load showed a 3 percent difference between the ANSYS and SAP models. Similarly, the modal analysis results showed a 3 percent difference in calculated total mass and the fundamental frequency between the ANSYS and SAP floor models.

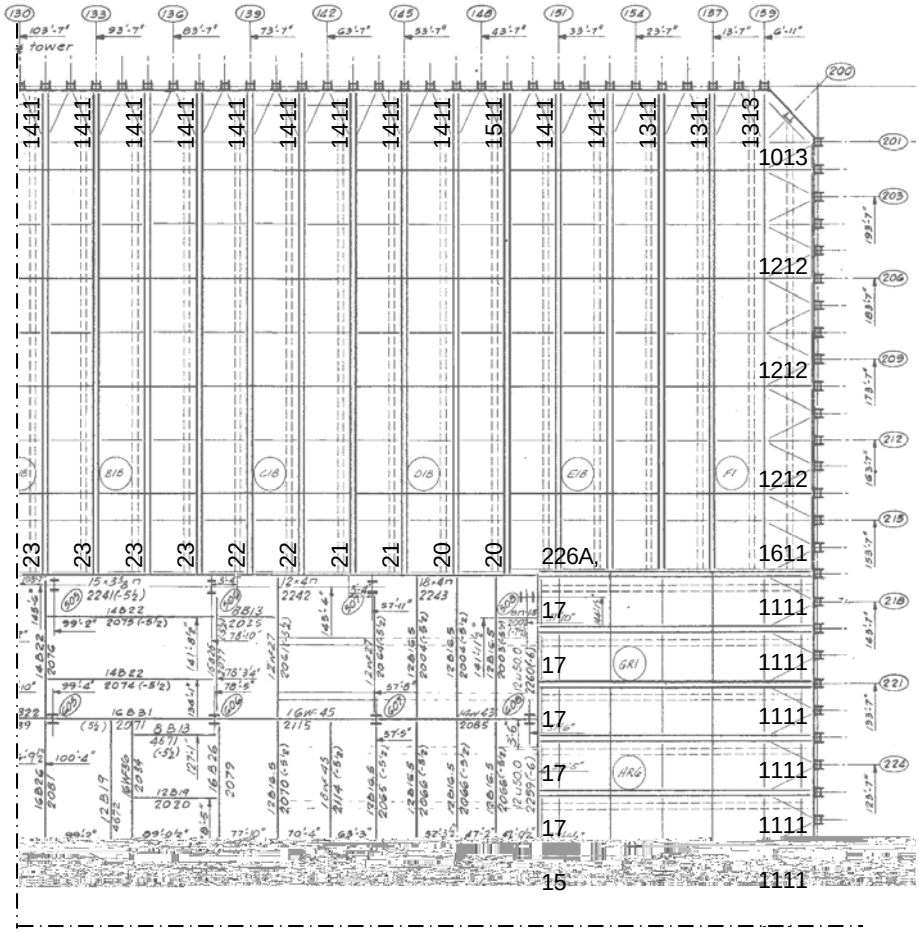

Reproduced with permission of The Port Authority of New York and New Jersey.

Figure 5–3. Truss seat detail location on northeast quadrant of Floor 96 of WTC 1.

5.2.2 Truss Seat Material Properties

The material properties used in the calculations were selected from Table 3–1 to best match the material properties indicated on the design drawings. Figure 3–3 was used to determine the mechanical properties at high temperature. The materials used for truss seat calculations are shown in Table 5–1.

Table 5–1. Materials used for truss seat calculations.

Description		Selected Material ID
Exterior and interior truss seat	A325 bolts	Material 22
	Fillet welds	Material 7
	Truss bearing angles	Material 21
Exterior truss seat	Seat angle	Material 1
	Gusset plate	Material 12
	Stand-off	Material 23
	Truss top chord angles	Material 21
	Cover plate for bridging truss top chord	Material 1
Interior truss seat	Vertical plate stiffener	Material 12
	Horizontal plate	Material 12

5.2.3 Truss Seat Failure Modes and Sequence

Possible failure modes for truss seats were identified for vertical force, horizontal tensile force, horizontal compressive force, and combined vertical and horizontal force. For each failure mode, the truss seat capacity was determined at different temperatures.

Failure Modes of Exterior Truss Seats for Vertical Force: The vertical load on the seat was eccentric to the plane of connection between the seat and the spandrel. Because of this eccentricity, the truss seat resisted to combined effect of both shear and bending. Finite element analysis of the truss seat was performed to determine load paths and evaluate the behavior of the seat connection.

Figure 5–4 shows the finite element model of the exterior truss seat connection. Half of the truss seat was modeled and symmetry boundary conditions were applied to all nodes in the plane of symmetry. The results of the finite element analysis showed that shear force was carried primarily by the stand-off plates, while the bending moment was resisted by tensile force in the gusset plate and compressive force in the stand-off plate. The seat angle restrained the moment until horizontal force in the connection caused slippage between the seat angle and bearing angle. The truss seat capacity was governed by the capacities of fillet welds at the stand-off plate to spandrel connection subjected to shear, bending, and compression. The failure mode was the fracture of the fillet welds between the stand-off plates and spandrel, resulting in loss of vertical support.

Failure Modes of Interior Truss Seats for Vertical Force: The vertical load on the truss seat was eccentric to the plane of fillet weld connection between the truss seat vertical plate stiffeners and the channel beam. Calculations showed that the truss seat capacity was governed by the capacities of the fillet welds at this joint subjected to shear and bending. The failure mode was the fracture of the fillet welds between the vertical plate stiffeners and the channel beam, resulting in loss of vertical support.

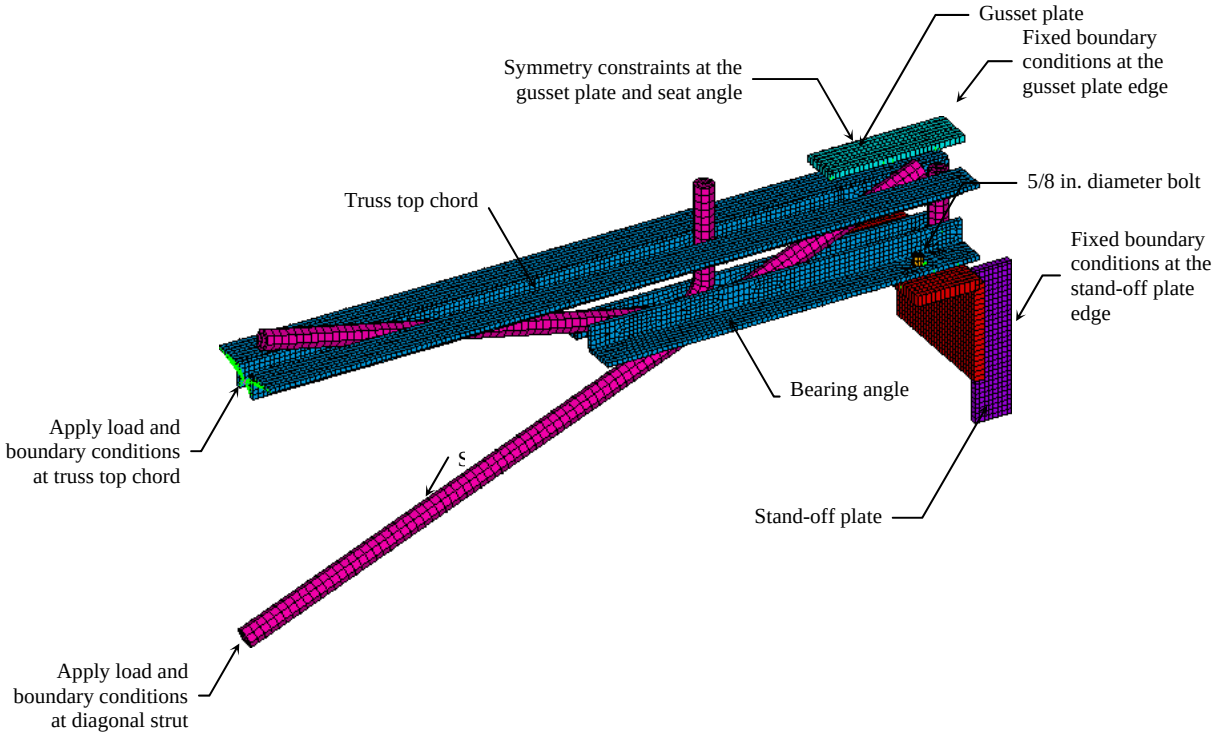

Figure 5–4. Finite element model of exterior truss seat.

Failure Modes of Exterior Truss Seats for Horizontal Tensile Force: The failure of exterior truss seats subjected to a horizontal tensile force can occur in the following modes: (1) fracture of the groove weld between the gusset plate and spandrel, (2) fracture of the fillet weld between the gusset plate and the truss top chord, (3) tensile fracture of the gusset plate, and (4) shear failure of the bolted connection by bolt shear, bolt bearing, tear-out, and block shear. For calculation purposes, the bolts were assumed to be centered in the slotted holes. The typical failure sequence of the exterior truss seat was as follows: (1) the gusset plate yielded, (2) the groove weld fractured, (3) the truss bearing angle slid so that the bolts were bearing against the slotted holes and then the bolts sheared off, and (4) the truss walked off the seat angle. The travel distance for the truss to walk off the seat angle was 4 5/8 in. This failure sequence is illustrated in Fig. 5–5 as path (A). The relationship between the tensile force resistance and the truss travel distance is plotted in Fig. 5–6 for path (A) in Fig. 5–5. In this figure, frictional resistance between the seat angle and bearing angle was not included.

Seat details 1212 and 1313 had a wider gusset plate and followed path (D), where the bolts bore against the slotted hole then sheared off before the gusset plate connection failed. The failure sequence of seat detail 1013 was temperature-dependent. At temperatures below 100 ˚C, the fillet weld connection between the gusset plate and the truss top chord fractured before the bolts sheared off. At temperatures greater than or equal to 100 ˚C, the failure sequence was the same as that for Details 1212 and 1313.

Failure Modes of Interior Truss Seats for Horizontal Tensile Force: The failure of interior truss seats subjected to a horizontal tensile force can occur in the following modes: (1) shear failure of the bolted connection by bolt shear, bolt bearing, tear-out, block shear, and (2) fracture of fillet weld connection between the truss seat and the channel beam. Calculations showed that the bolt shear strength controlled the truss seat capacity. Bolt shear by itself, however, did not cause the truss to lose its vertical support,

but it was the prerequisite to the truss walking off the seat. The travel distance required for the truss to walk off the seat was 4 in.

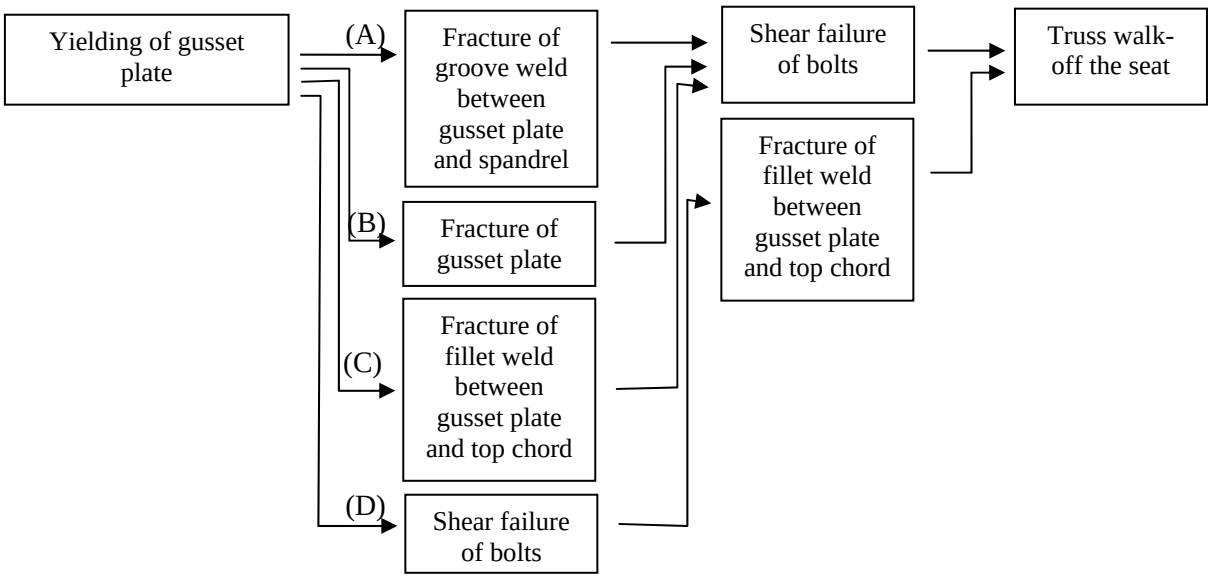

(A) Seat details 1311, 1411, 1511, and 1611 at all temperatures.

(B) Seat detail 1111 at all temperatures.

(C) Seat detail 1013 at temperatures below 100 °C.

(D) Seat details 1212 and 1313 at all temperatures, and detail 1013 at temperatures more than or equal to 100 °C.

Figure 5–5. Failure sequence of the exterior truss seats against tensile force.

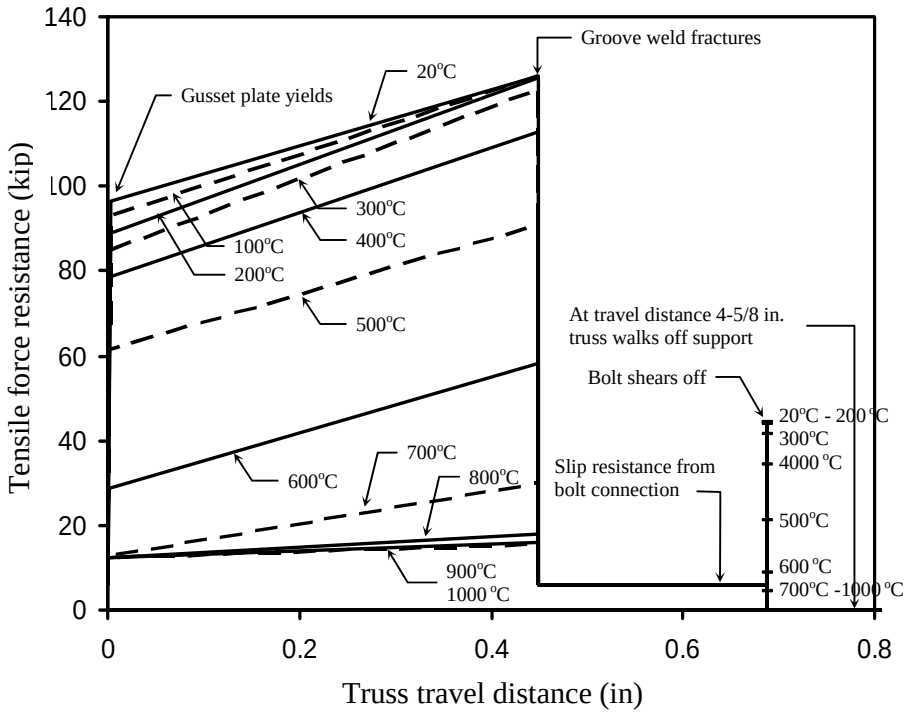

Figure 5–6. Capacity of exterior truss seat for tensile force (Path (A) in Fig. 5–5 for Detail 1411).

Failure Modes of Exterior Truss Seats for Horizontal Compressive Force: The concrete slab above the truss seat connection provided the compressive force resistance. In the absence of the concrete slab, the truss seat resistance against compressive force was provided by the gusset plate until it buckled, and by bolt shear when the bolt bore against the slotted hole. Surface friction between the seat angle and bearing angles also provided some resistance. Additional resistance developed when the truss came into contact with the spandrel. Travel distance for the truss to contact the column spandrel was 1 1/2 in. Under compressive force, the truss did not lose its vertical support.

Failure Modes of Interior Truss Seats for Horizontal Compressive Force: The reinforced concrete slab above the truss seat connection provided the compressive force resistance. In the absence of the concrete slab, the truss seat resistance against compressive force came from surface friction between the seat horizontal plate and bearing angles. Additional resistance was developed when the truss came into contact with the channel beam. Travel distance for the truss to contact the channel beam was 1/2 in. Under compressive force, the truss did not lose its vertical support.

Failure Modes of Interior and Exterior Truss Seats for Combined Vertical and Horizontal Forces: The failure modes of the interior and exterior truss seats when subjected to combined vertical and horizontal forces were a combination of the failure modes for vertical and horizontal forces. The vertical shear strengths of fillet welds in both the interior and exterior truss seats were reduced by the horizontal tensile force. This fillet weld was between the vertical plate and channel beam for interior truss seats and between the stand-off plate and spandrel for exterior truss seats. The horizontal tensile strengths of the truss seats were not reduced by the additional vertical forces on the truss seats.

5.2.4 Truss Seat Capacity Calculations

In this section, truss seat capacities corresponding to the failure modes described in the previous section are given. The capacities were computed for different types of truss seats at different temperatures. Calculation of the capacities was performed using the methods in the *Manual of Steel Construction: Load and Resistance Factor Design* (AISC 2001) with the resistance factor, ϕ, assumed to be equal to one.

Capacity of Exterior Truss Seats for Vertical Force: The failure mode of the truss seat against vertical force was fracture of the fillet welds at the stand-off plate to spandrel connection. Strength of the fillet welds at this connection is summarized in Table 5–2 and Fig. 5–7. The symbol # in this table refers to seat detail number.

Capacity of Interior Truss Seats for Vertical Force: Failure mode of the truss seat against vertical force was fracture of the fillet welds between the seat vertical plate stiffener and channel beam. Strengths of the fillet welds at this joint are summarized in Table 5–3 and Fig. 5–7.

Table 5–2. Exterior truss seat capacity for vertical force.

Temp. (˚C)	Connection Detail Capacity for Vertical Force (kip)							
	#1013	#1111	#1212	#1311	#1313	#1411	#1511	#1611
20	94	94	111	94	94	140	193	207
100	94	94	111	94	94	140	193	207
200	93	93	110	93	93	139	192	206
300	91	91	108	91	91	136	187	201
400	84	84	100	84	84	126	172	184
500	69	69	81	69	69	102	136	146
600	45	58	53	60	45	78	84	90
700	29	26	34	27	29	35	38	41
800	14	13	17	13	14	17	19	20
900	12	11	14	11	12	14	16	17
1000	12	11	14	11	12	14	15	17

Table 5–3. Interior truss seat capacity for vertical force.

Temp. (˚C)	Connection Detail Capacity for Vertical Force (kip)						
	#15	#17	#20	#21	#22	#23	#226A
20	233	233	274	229	194	194	395
100	233	233	274	229	194	194	395
200	232	232	273	228	194	194	393
300	226	226	267	223	189	189	384
400	207	207	244	204	173	173	352
500	164	164	194	162	137	137	279
600	101	101	119	100	85	85	172
700	46	46	54	45	39	39	78
800	23	23	27	22	19	19	38
900	19	19	22	18	16	16	32
1000	19	19	22	18	16	16	32

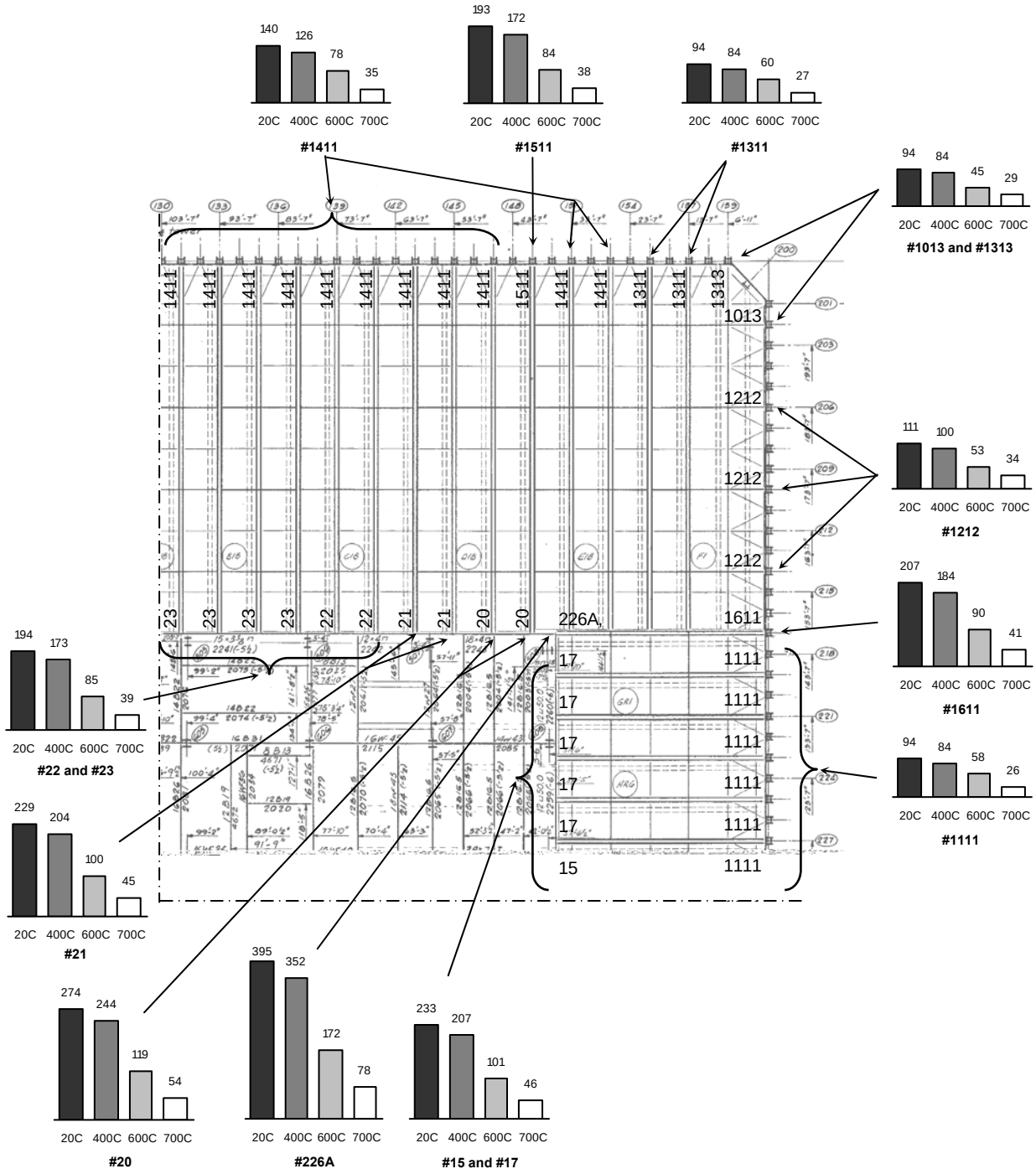

Original document reproduced with permission of The Port Authority of New York and New Jersey.

Figure 5–7. Truss seat capacity for vertical force

Capacity of Exterior Truss Seats for Horizontal Tensile Force: The capacities of truss seats that followed failure sequence (A), as shown in Fig. 5–5, were governed by the fracture strength of the groove weld between the gusset plate and the spandrel. The capacities of truss seats that followed failure sequence (B) were governed by the tensile fracture strength of the gusset plate, and truss seats that followed failure sequence (C) were governed by the fracture strength of the fillet weld between the gusset plate and the truss top chord. The capacities of truss seats that followed failure sequence (D) were governed by a combination of shear strength of bolts and tension developed in the gusset plate. The results of the exterior truss seat capacity calculations are summarized in Table 5–4 and Fig. 5–8. Note that the strength of the truss seat #1013 at 100 ˚C is higher than that at 20 ˚C by about 38 percent. For temperatures less than 100 ˚C, the capacity was controlled by the fillet weld strength, and for temperatures in excess of 100 ˚C, the bolt reached the end of its travel in the elongated bolt hole, thus providing a stiffer load path and higher load capacity of the connection.

Capacity of Interior Truss Seats for Horizontal Tensile Force: Failure loads were computed for the failure modes described above, including shear failure of the bolted connection by bolt shear, bolt bearing, tear-out, block shear, and fracture of fillet weld connection between the truss seat and the channel beam. The results showed that the shear strength of the two bolts controlled the horizontal tensile strength of the truss seat connection for all seat details including 15, 17, 20, 21, 23, and 226 A. Table 5–5 and Fig. 5–8 summarize the capacities of interior truss seats for horizontal tensile force. As can be seen from this table, at temperature 500 ˚C, bolt shear capacity was reduced by half, and at 600 ˚C it was reduced to less than a quarter of the original capacity at room temperature.

Capacity of Exterior Truss Seats for Horizontal Compressive Force: Under compressive force, the gusset plate buckled before the bolts sheared off. Compression strength of the gusset plate governed the exterior truss seat capacity. The compressive strength of gusset plate is summarized in Table 5–6.

Capacity of Interior Truss Seats for Horizontal Compressive Force: Under compressive force, the truss came into contact with the channel beam before the bolt bore against the slotted hole. The interior truss seat did not fail under compressive force.

Capacity of Interior Truss Seats for Combined Vertical and Horizontal Force: A typical interaction relationship for the combined vertical and horizontal tensile force is shown in Fig. 5–9.

Table 5–4. Exterior truss seat capacity for horizontal tensile force.

Temp. (˚C)	Connection Detail Capacity for Horizontal Tensile Force (kip)							
	#1013	#1111	#1212	#1311	#1313	#1411	#1511	#1611
	Fracture of Fillet Weld/ Shear Failure of Bolts	Fracture of Gusset Plate	Shear Failure of Bolts	Fracture of Groove Weld	Shear Failure of Bolts	Fracture of Groove Weld	Fracture of Groove Weld	Fracture of Groove Weld
20	100	104	182	126	182	126	126	126
100	138	104	181	126	181	126	126	126
200	135	103	180	126	180	126	126	126
300	130	101	174	123	174	123	123	123
400	115	93	156	113	156	113	113	113
500	84	75	117	91	117	91	91	91
600	42	49	67	58	67	58	58	58
700	20	25	32	30	32	30	30	30
800	14	16	19	18	19	18	18	18
900	13	14	17	16	17	16	16	16
1000	13	14	17	16	17	16	16	16

Table 5–5. Interior truss seat capacity against horizontal tensile force.

Temp. (˚C)	Capacity (kip)
	Shear Failure of Bolts
20	44
100	44
200	44
300	42
400	34
500	21
600	9
700	4
800	4
900	4
1000	4

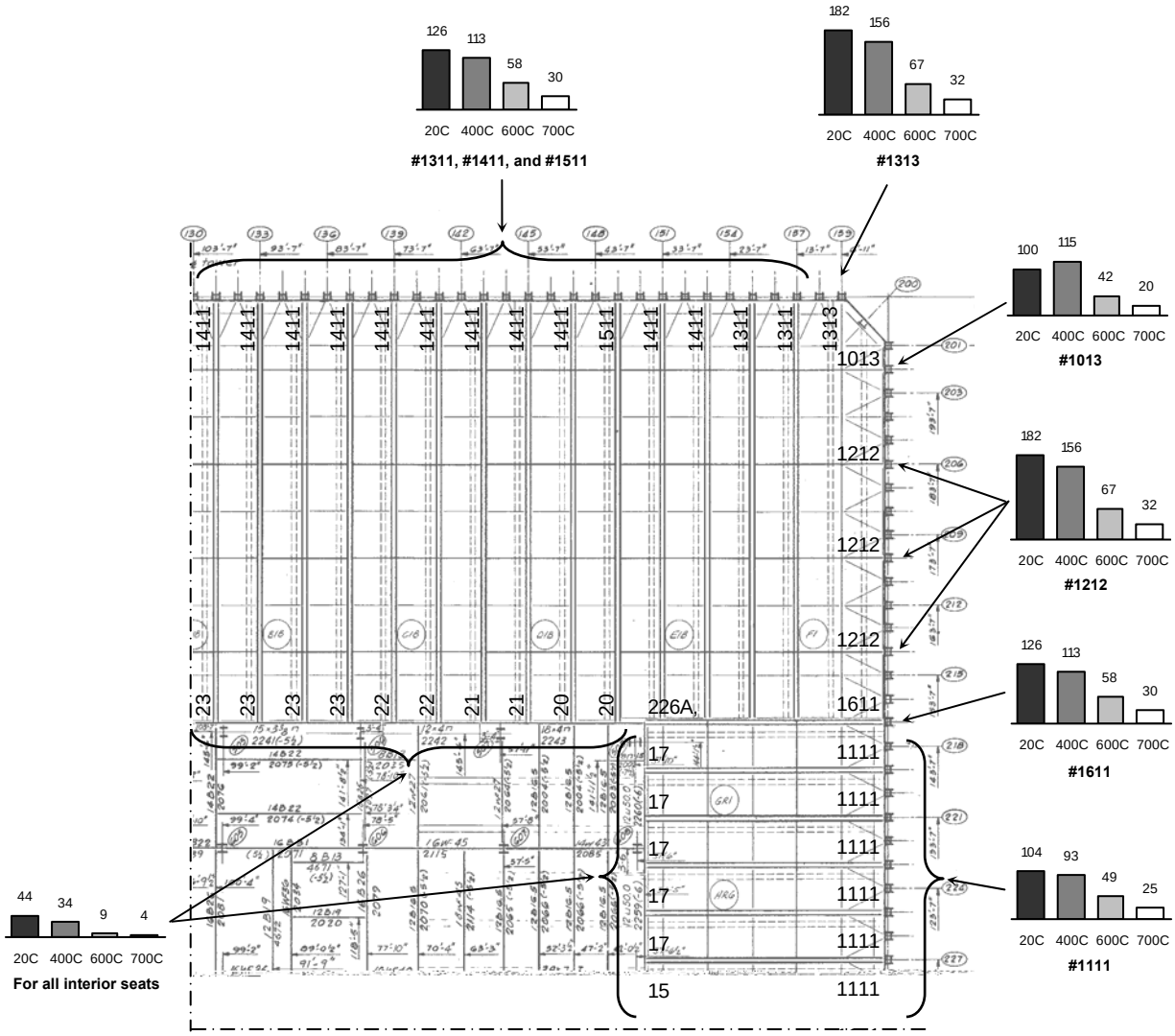

Original document reproduced with permission of The Port Authority of New York and New Jersey.

Figure 5–8. Truss seat capacity for horizontal tensile force.

Table 5–6. Compression strength of gusset plate.

Temp. (°C)	Compression Strength of Gusset Plate (kip)							
	#1013	#1111	#1212	#1311	#1313	#1411	#1511	#1611
20	74	68	98	90	98	90	90	90
100	71	66	95	86	95	86	86	86
200	68	63	90	82	90	82	82	82
300	65	60	86	78	86	78	78	78
400	60	55	79	72	79	72	72	72
500	46	42	60	55	60	55	55	55
600	19	17	25	22	25	22	22	22
700	6	5	8	7	8	7	7	7
800	6	5	7	6	7	6	6	6
900	6	5	7	6	7	6	6	6
1000	6	5	7	6	7	6	6	6

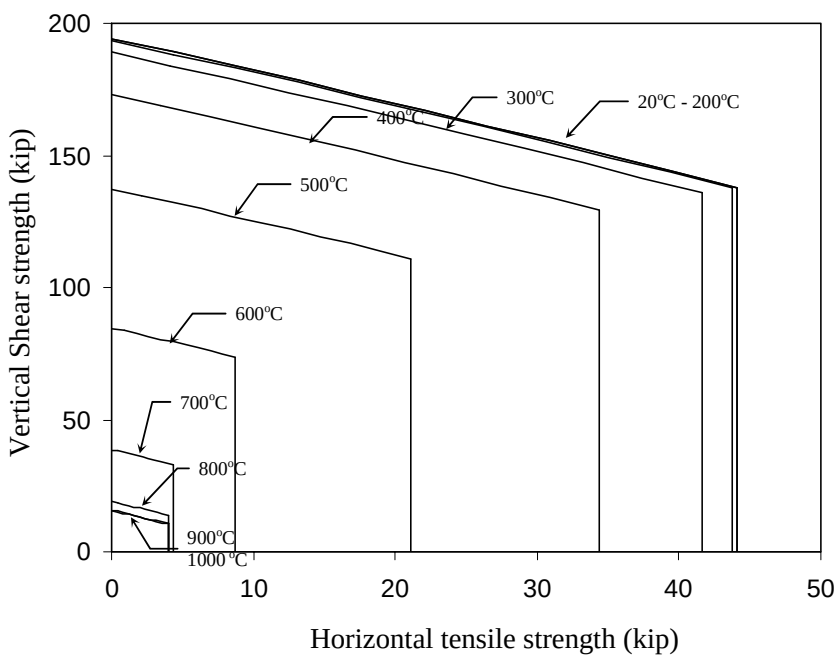

Figure 5–9. Capacity of interior truss seat against vertical and horizontal force (for Detail 22).

5.2.5 Modeling Failure by Break Elements

In this section, the finite element models developed to capture failure modes of the exterior and interior truss seats, studs on strap anchors, and studs on spandrels are described. These models were developed for incorporation in the floor truss analysis to capture the connection failure modes, failure loads as a function of temperature, and failure sequences.

The models of these connections simulated the loss of connection resistance after their failure either from exceeding the connection force capacity or from exceeding the allowable deformation (for example, truss walking off the seat). The connection capacity was also temperature-dependent. The finite element modeling assumptions are as follows:

A control element (COMBIN37), a unidirectional linear spring element with the capability of turning on and off during an analysis, was used for modeling connection failure. The element is referred to as "break element" in this report. The element is a part of the structure that connects two "active" nodes in the "on" mode and disconnects them in the "off" mode, depending on the relative displacement of two "control" nodes. The break element is defined as follows:

$$B_m[(i,j,dof_{ij});(k,l,dof_{kl});(K,\Delta_0)] \tag{12}$$

where m is the break element number, i and j are the active nodes, dof_{ij} is the degree of freedom for the active nodes, k and l are the control nodes, dof_{kl} is the degree of freedom for the control nodes, K is the elastic stiffness of the break element, and Δ_0 is the differential displacement limit of the control nodes.

To make the connection capacity temperature-dependent, a beam element with temperature-dependent coefficient of thermal expansion was added to the break element. This was done by using the deformation of a beam element from thermal expansion to control the status (on/off) of the break element. Figure 5–10 illustrates the basic mathematical model of the connection using break elements.

Multiple connection failure modes require use of different break elements that are connected together in a logical manner. For example, to model independent failure modes, that is, one failure mode that does not cause other failures, break elements are connected in parallel so that when one break element turns "off", the other break elements remain "on". For dependent failure modes, break elements are connected in series so that when one break element turns "off", all elements turn "off".

Basic mathematical model:

– Let node *l* and *i* have same displacement.

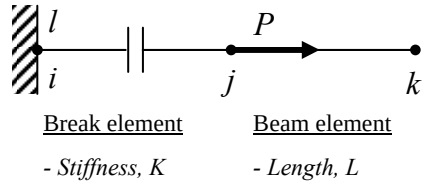

– In this example, control nodes *k* and *l* relative displacement has the form:

$$U_k - U_l = \frac{P}{K} + \alpha L \Delta T$$

– Break element status is by definition

$$U_k - U_l \le \Delta_0, \text{ status : on}$$
$$U_k - U_l > \Delta_0, \text{ status : off}$$

– Define break element to turn off when capacity, P_u, has been reached

$$\Delta_0 = \frac{P_u}{K} + \alpha L \Delta T$$

– Element capacity at room temperature is given as

$$P_{u.rm} = K\Delta_0$$

– Hence for a given P_u and ΔT relationship, the required thermal expansion to turn the break element off can be found by

$$\alpha = \frac{P_{u.rm} - P_u}{KL\Delta T}$$

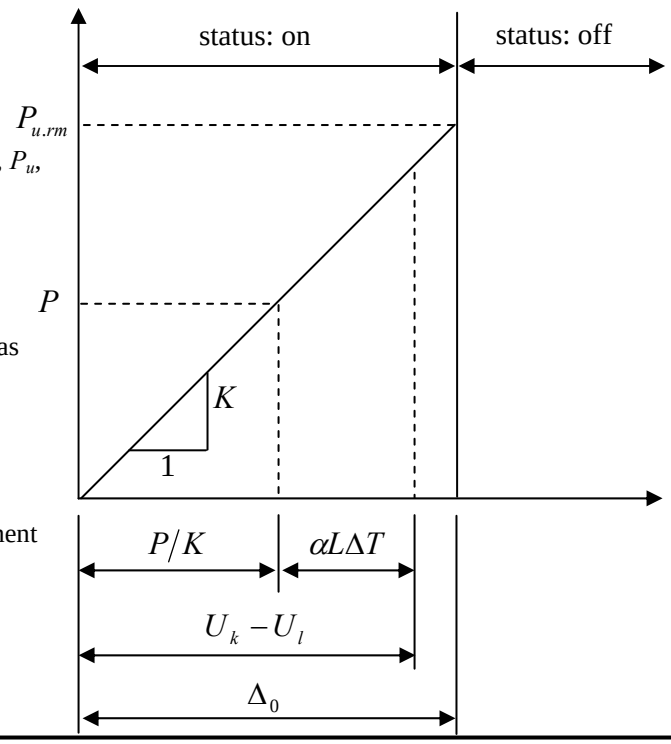

Figure 5–10. Basic mathematical model of connection failure.

5.2.6 Summary of Failure Modes and Finite Element Models of Truss Seats

The failure modes of the interior truss seats include (1) truss walking off the seat, (2) exceeding the vertical temperature-dependent shear capacity of the fillet welds between the seat vertical plate stiffeners and channel beam, and (3) exceeding temperature-dependent shear capacity of bolts when they bear against the slotted holes. These failure modes were modeled by using four break elements and two beam elements as shown in Fig. 5–11. The interior seat model was tested in ANSYS, and results are shown in Figs. 5–12 and 5–13. These figures depict the relationship between the horizontal and vertical seat forces and the horizontal truss travel distance.

Figure 5–12 shows the results from analysis where the truss seat was subjected to a constant vertical load and horizontal displacement increments at 500 ˚C. When a truss seat is subjected to a large horizontal tension and small vertical shear, the failure is by two bolts shearing off followed by the truss walking off the seat, as shown in Fig. 5–12. The shear strength of the bolts controls the truss seat horizontal tension capacity. The bolt shear by itself does not cause the truss to lose its vertical support, but it is the prerequisite for the truss walking off the seat. The travel distance for a truss to walk off a truss seat is 4 in. for an interior seat and 4 5/8 in. for an exterior seat.

Figure 5–13 shows the results from analysis where the truss seat was subjected to a constant horizontal load and vertical displacement increments at 500 ˚C. When a truss seat is subjected to a large vertical shear and small horizontal tension, the failure is by the fracture of fillet welds between the vertical plate stiffeners and the channel beam at an interior seat and between the stand-off plates and the spandrel at an exterior seat, resulting in loss of both vertical and horizontal support, as shown in Fig. 5–13.

The finite element models of the exterior truss seats were similar to those for the interior truss seats, except for an additional beam element and a break element to model failure of the gusset plate, as shown in Fig. 5–14.

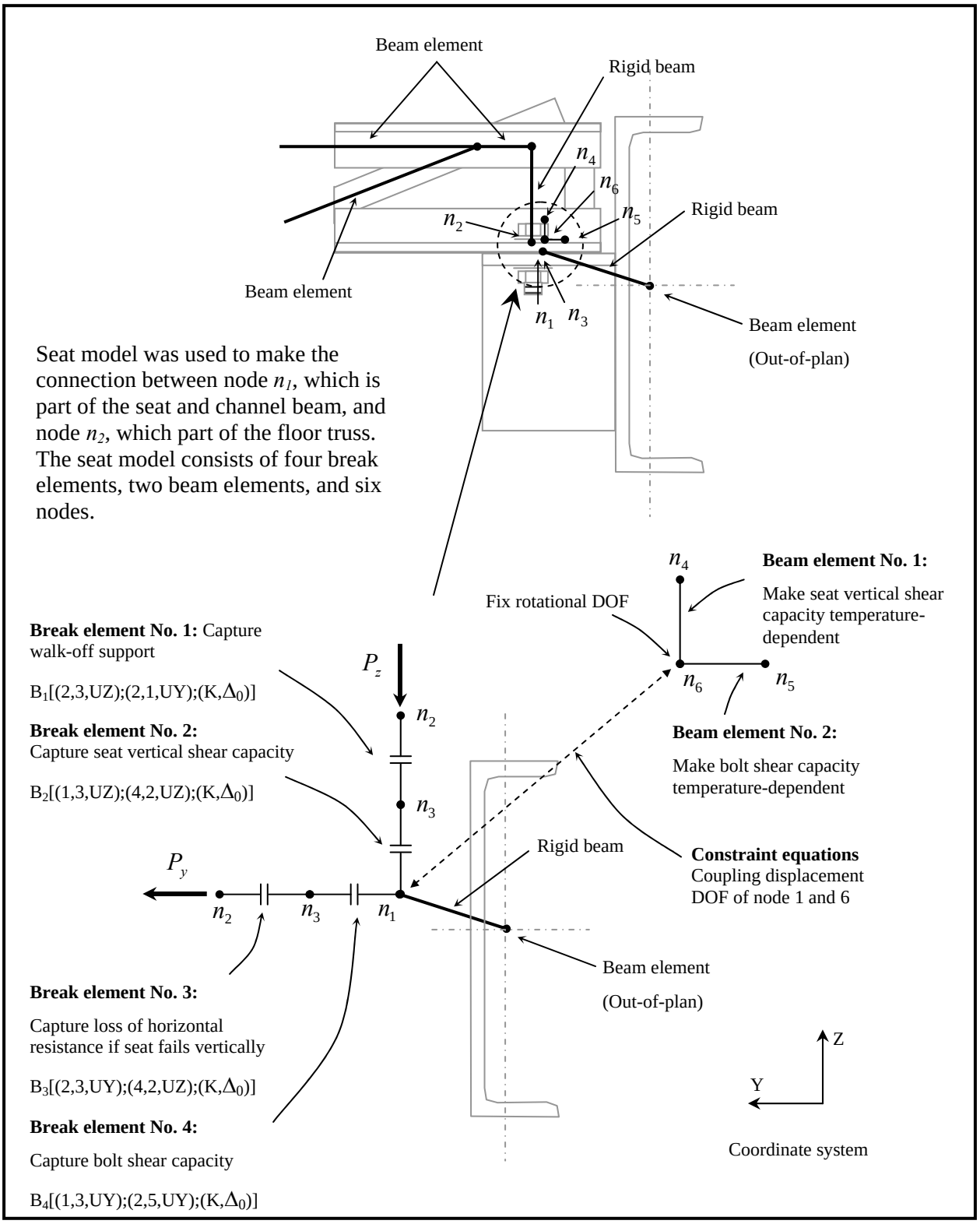

Figure 5–11. Representation of interior truss seat by break elements.

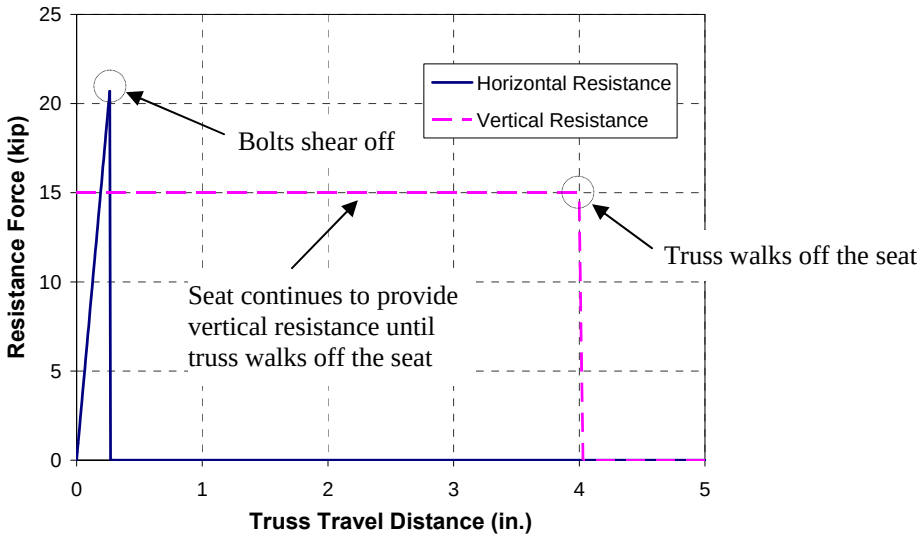

Figure 5–12. Results of interior truss seat model capturing failure from truss walking off the seat at 500 ˚C.

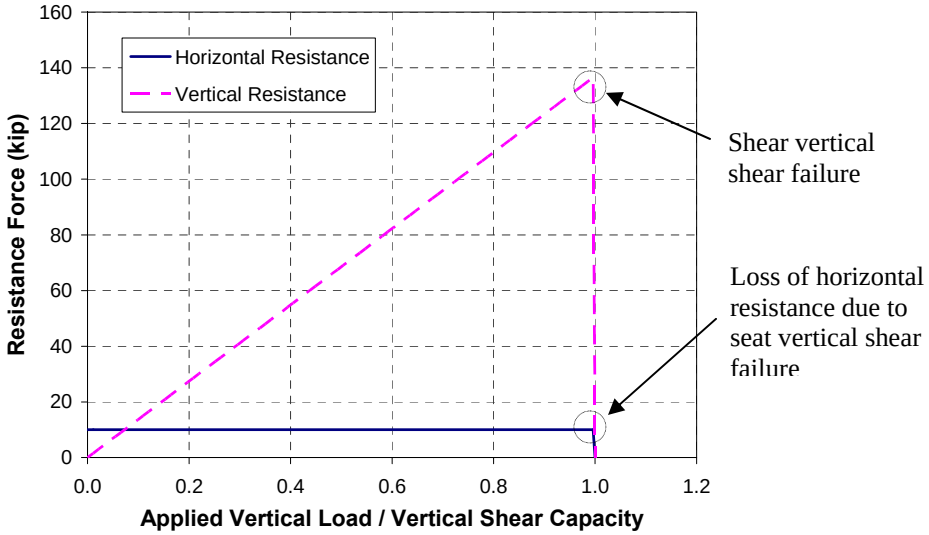

Figure 5–13. Results of interior truss seat model capturing failure from exceeding the vertical shear capacity at 500 ˚C.

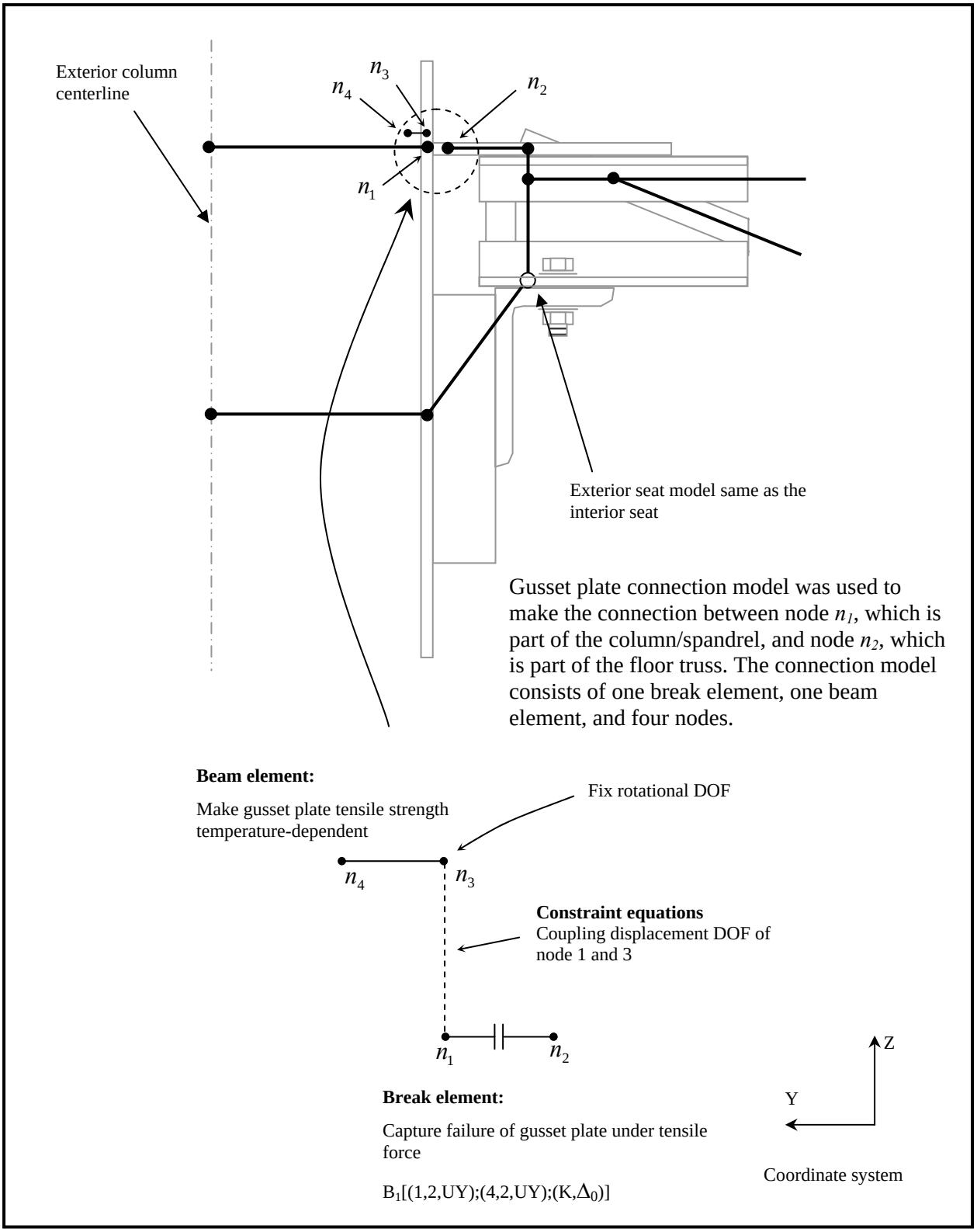

Figure 5–14. Representation of exterior truss seat by break elements.

5.2.7 Summary of Failure Modes and Finite Element Models of the Stud on Strap Anchor and Spandrel Stud

Stud on Strap Anchor: There were four 5/8 in. × 2.5 in. studs on each strap anchor as shown in Fig. 5–15. Calculations were carried out to compute the lateral shear capacity of these stud shear connectors using the procedure in *Building Code Requirements for Structural Concrete* (ACI 318-02) at different temperatures. The following failure modes were considered in the calculation: steel shear failure, concrete pryout, and concrete breakout. The capacity of the stud close to the edge of the slab was governed by concrete breakout at all temperatures, while those of the other three studs located farther from the concrete edge were governed by concrete pryout at temperatures below 700 ˚C and steel shear failure at temperature equal to and above 700 ˚C.

Spandrel Stud: There was one 3/4 in. × 6 in. spandrel stud located between two adjacent exterior columns as shown in Fig. 5–15. Calculations were carried out to compute the shear capacity and tensile capacity of the spandrel stud at different temperatures. For shear capacity, the following failure modes were considered: steel shear failure, concrete pryout, and concrete breakout. For tensile capacity, the following failure modes were considered: steel tensile failure, concrete breakout, pullout strength, and concrete side-face blowout. The shear and tensile capacities of the spandrel stud were both governed by concrete breakout strength.

Finite element models of studs on strap anchors and studs on spandrels were developed using break elements. The stud model included 8 break elements and 4 beam elements, as shown in Fig. 5–16.

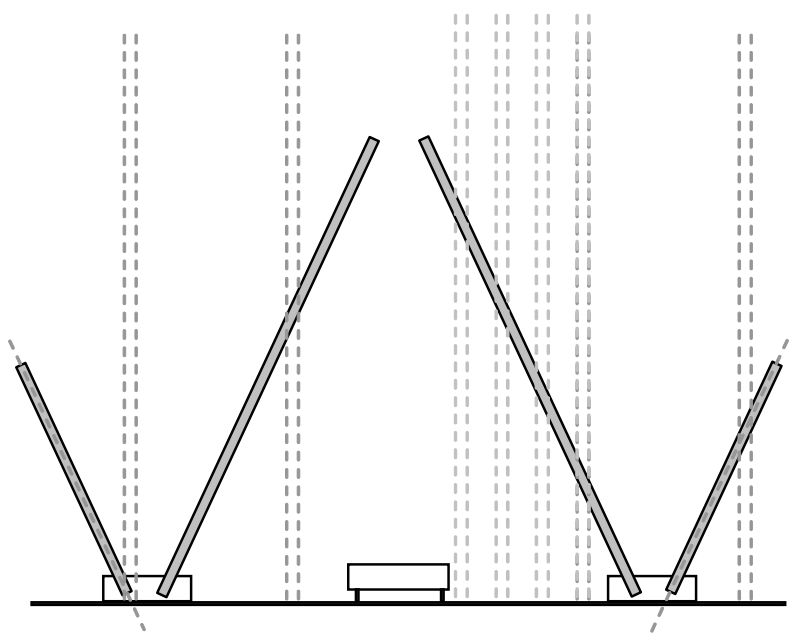

Figure 5–15. Location of stud on strap anchor and spandrel stud.

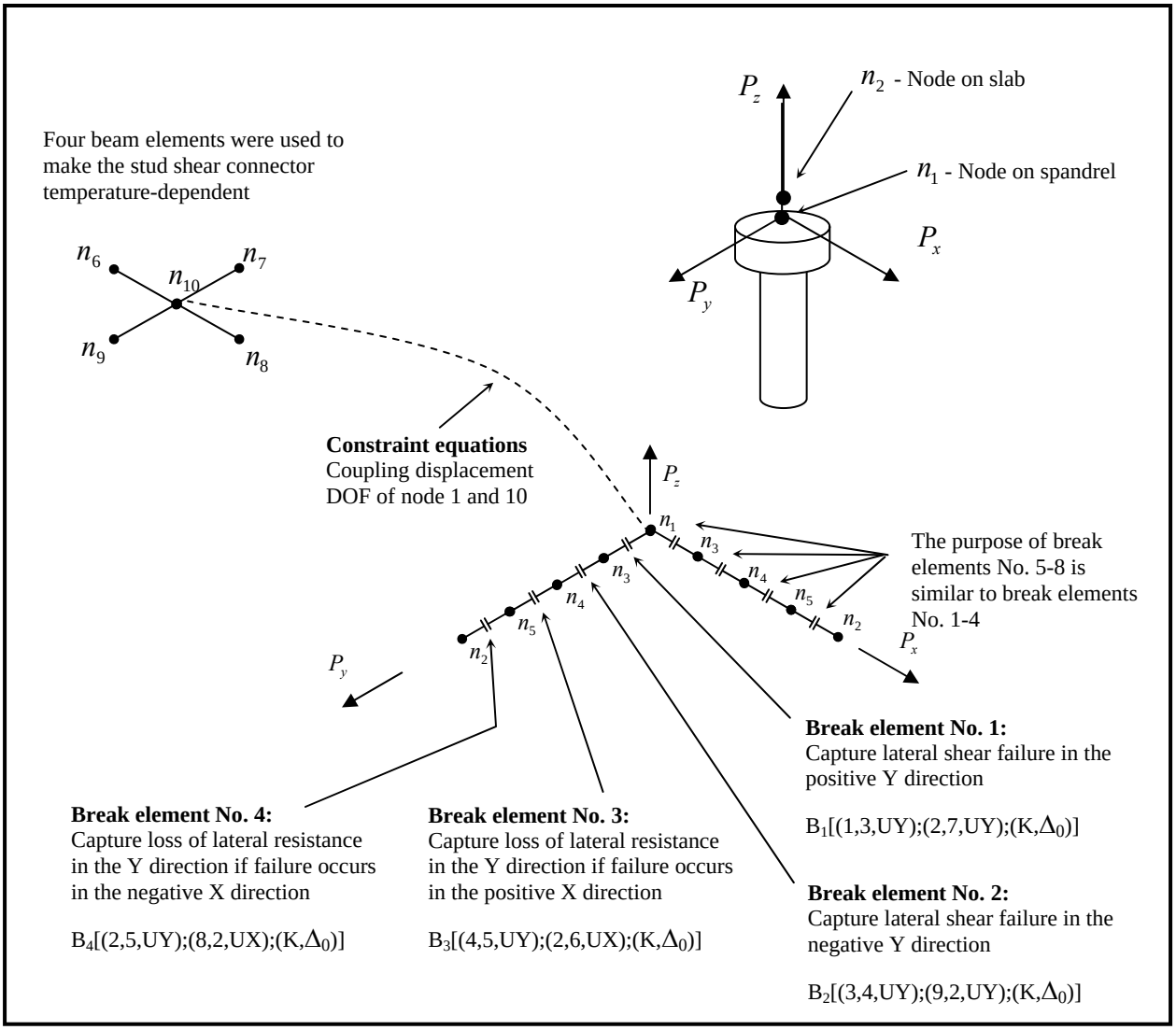

Figure 5–16. Representation of stud shear connector by break elements.

5.3 KNUCKLE ANALYSIS

The objective of this analysis was to predict the capacity of the knuckle subjected to loads between the truss and the concrete slab and to develop a finite element model of the knuckle to be included in the full floor subsystem model.

5.3.1 Description of Knuckle

The "knuckle" was formed by the extension of the truss web diagonals into the concrete slab. It provides for composite action of the steel truss and concrete slab (see Fig. 2–1) as it allows shear transfer in both the transverse and longitudinal directions.

5.3.2 Failure Modes of Knuckle

Failure modes of knuckles are:

- Horizontal shear failure due to crack or crushing of concrete
- Pullout failure due to vertical tension

5.3.3 Knuckle Shear Tests

Two sets of experiments were performed in 1967 at Laclede Steel Company in Saint Louis, Missouri, to determine the transverse and longitudinal shear capacities of the knuckle.

The longitudinal shear test consisted of double knuckles cast into two concrete blocks as shown in Fig. 5–17. The test specification showed corner angles confining the concrete blocks and no reinforcement in concrete. However, the test pictures showed reinforcement in both directions for each concrete block, with the corner angles dismantled. The test specification called for concrete density of 152 pcf, which corresponds to a normal weight concrete. The slab in the office areas was made from lightweight concrete. Three specimens were tested: two specimens after 28-day curing and one after 96-day curing. The average compressive strength of two 28-day cylinders tested was 4,290 psi. A third sample, tested after 96 days, showed a strength of 2,850 psi. No reason is known for the compressive strength in the third test being less than the other two tests. The test specification did not identify the weld size connecting the inner ends of the two knuckles to two channels. However, the primary failure mode observed in the third test was weld failure. Weld failure was not identified as the failure mode of the knuckle for the other two tests. The results of the longitudinal shear strengths of the knuckle based on the first two tests were approximately 28.3 kip per knuckle. The strength of in-place, mature, lightweight concrete is 4,100 psi, and the 28-day corrected average strength of the normal weight concrete used in the test was 3,707 psi. After adjusting for the strength of in-place, mature, lightweight concrete by multiplying by the ratio of 4,100 psi to 3,707 psi, the longitudinal shear capacity of the knuckle in the WTC floor systems was determined at approximately 31 kip per knuckle.

The transverse shear test consisted of double knuckles cast into two reinforced concrete blocks that were confined at the corners by angles as shown in Fig. 5–18. The concrete density was 110 pcf, corresponding to a lightweight concrete. Two tests were conducted, seven and 27 days after casting concrete. The concrete compressive strengths reported for seven-day and 27-day cylinder tests were 1,330 psi, and 2,600 psi, respectively. The inner ends of the two knuckles were connected through channels to a #11 rebar, and the rebar was loaded until the concrete failed. The tests were conducted at concrete ages of six and 27 days. The primary failure mode observed was concrete shear failure. The pictures from the tests showed formation of a shear crack in one of the concrete blocks. The transverse

shear capacity of the knuckle, as the average of the two reported tests, was 16.9 kip per knuckle. For the WTC floor system, the knuckle transverse shear capacity was determined by adjusting the strength of in-place, mature, lightweight concrete of 4,100 psi relative to the average strength of the lightweight concrete used in the test of 1,965 psi. Multiplying by the ratio of 4,100 to 1,965 psi, the transverse shear capacity of the knuckle in the WTC floor system was determined at approximately 35 kip per knuckle.

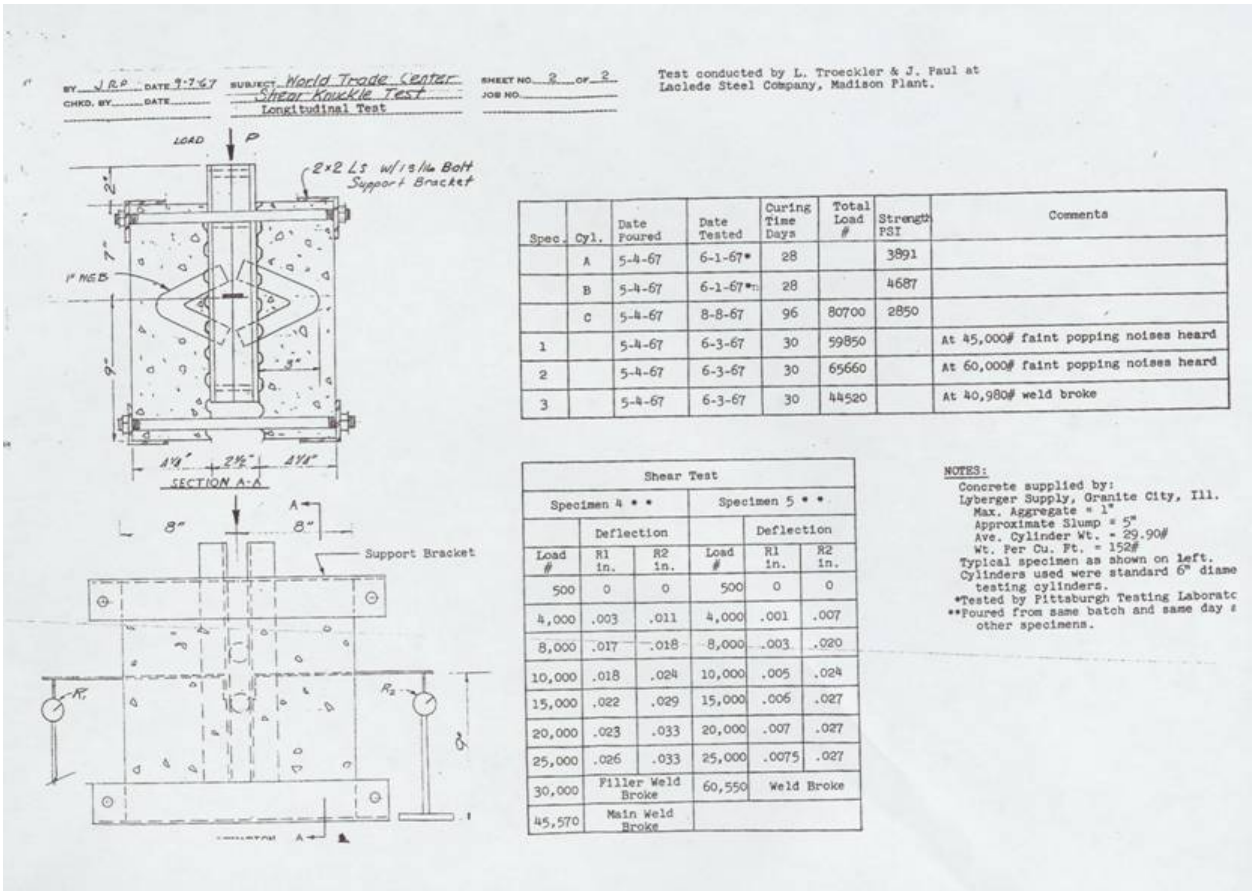

Spec.	Cyl.	Date Poured	Date Tested	Curing Time Days	Total Load #	Strength PSI	Comments
	A	5-4-67	6-1-67*	28		3891	
	B	5-4-67	6-1-67*	28		4687	
	C	5-4-67	8-8-67	96	80700	2850	
1		5-4-67	6-3-67	30	59850		At 45,000# faint popping noises heard
2		5-4-67	6-3-67	30	65660		At 60,000# faint popping noises heard
3		5-4-67	6-3-67	30	44520		At 40,980# weld broke

Shear Test					
Specimen 4 **			Specimen 5 **		
	Deflection			Deflection	
Load #	R1 in.	R2 in.	Load #	R1 in.	R2 in.
500	0	0	500	0	0
4,000	.003	.011	4,000	.001	.007
8,000	.017	.018	8,000	.003	.020
10,000	.018	.024	10,000	.005	.024
15,000	.022	.029	15,000	.006	.027
20,000	.023	.033	20,000	.007	.027
25,000	.026	.033	25,000	.0075	.027
30,000	Filler Weld Broke		60,550	Weld Broke	
45,570	Main Weld Broke				

Information provided by Laclede Steel

Figure 5–17. Longitudinal shear test of a knuckle.

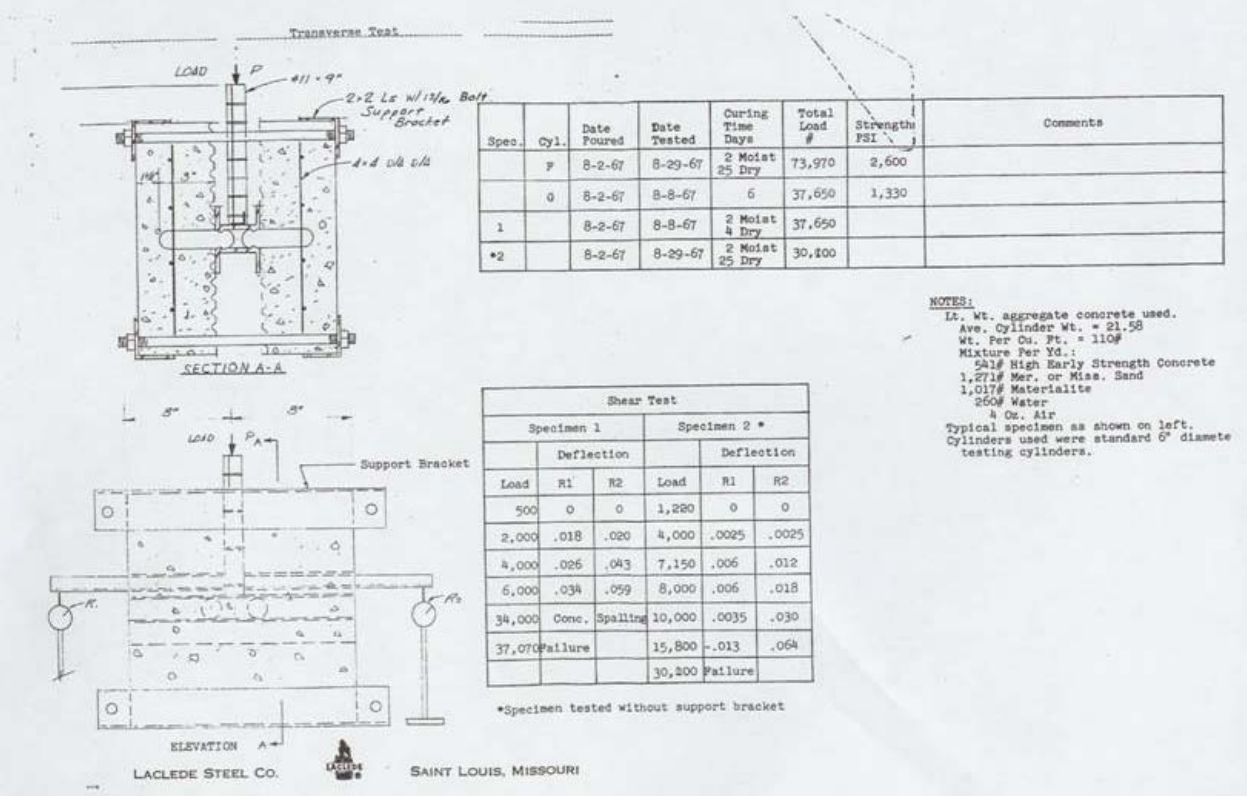

Spec.	Cyl.	Date Poured	Date Tested	Curing Time Days	Total Load #	Strength PSI	Comments
	9	8-2-67	8-29-67	2 Moist 25 Dry	73,970	2,600	
	0	8-2-67	8-8-67	6	37,650	1,330	
1		8-2-67	8-8-67	2 Moist 4 Dry	37,650		
*2		8-2-67	8-29-67	2 Moist 25 Dry	30,100		

Shear Test					
Specimen 1			Specimen 2 *		
	Deflection			Deflection	
Load	R1	R2	Load	R1	R2
500	0	0	1,220	0	0
2,000	.018	.020	4,000	.0025	.0025
4,000	.026	.043	7,150	.006	.012
6,000	.034	.059	8,000	.006	.018
34,000	Conc.	Spalling	10,000	.0035	.030
37,070	Failure		15,800	-.013	.064
			30,200	Failure	

Information provided by Laclede Steel

Figure 5–18. Transverse shear test of a knuckle.

5.3.4 Finite Element Model for Knuckle Test

The LS-DYNA computer program was used for the analysis. Finite element models, shown in Fig. 5–19, represent one quarter of the knuckle test specimens. The knuckle and channel members in the test set-up were modeled with solid elements with steel material properties. Concrete was also modeled with solid elements with the Pseudo Tensor material model described in Chapter 3. Two different assumptions were made about the interface condition between the concrete and the steel, namely, fully bonded or frictionless. Boundary conditions are also shown in Fig. 5–19. Displacement was imposed in a form of a ramp to the angles.

5.3.5 Material Properties for Knuckle Analysis

The concrete strengths used in the finite element model were 4,100 psi for the longitudinal shear test and 2,500 psi for the transverse shear test. In addition, 0.47 percent steel reinforcement, representing the welded wire reinforcement of the slab, was added in a distributed way to the concrete.

Angles were modeled with Material 21 (see Chapter 3 for description).

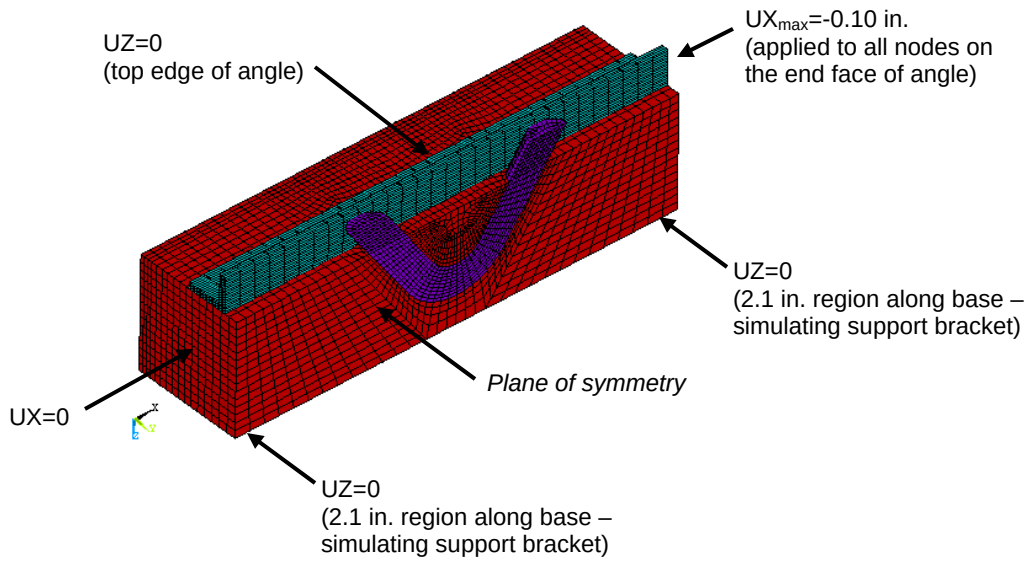

(a) Longitudinal sheat test model

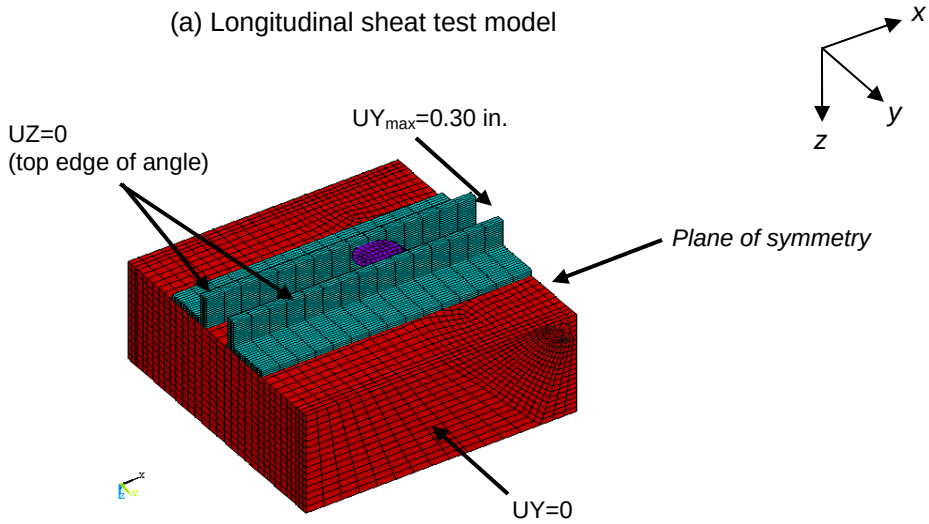

(b) Transverse sheat test model

Figure 5–19. Finite element models of knuckle shear tests.

5.3.6 Results from Knuckle Analysis

Finite Element Analysis (FEA) of Tests

The results of FEA of the tests are shown in Figs. 5–20 through 5–23. The results showed significant dependence on the interface characteristics between the steel and the concrete. The results of FEA of the longitudinal shear test (Fig. 5–21) showed that each knuckle had strength in the range of 15 kip to 35 kip, depending on the interface condition. When the analysis results are compared to the test results, the interface appears to be closer to the fully bonded case.

The transverse shear FEA results (Fig. 5–23) showed that transverse knuckle strength was about 24 kip for the frictionless condition with 2,500 psi concrete, which corresponds to 39 kip for 4,100 psi concrete. For the full bonded case, the analysis was terminated at 20 kip per knuckle before reaching the ultimate

strength. The transverse shear FEA results (Fig. 5–22) showed that concrete was crushed in a small region next to the knuckle and extended in front of the shear load. Figure 5–22 also shows large regions of crushed concrete at the lower portion of the model. (Note that the boundary condition UY=0, although realistic for the test, would not occur in a pair of transversely loaded knuckles in the two actual trusses.) The small crushed regions indicate that a pair of knuckles can be expected to behave nearly independently of each other and, therefore, have nearly double the capacity of a single knuckle.

Although the analysis showed the sensitivity of the results to the steel-concrete interface assumptions, it supported the shear capacities determined from test results.

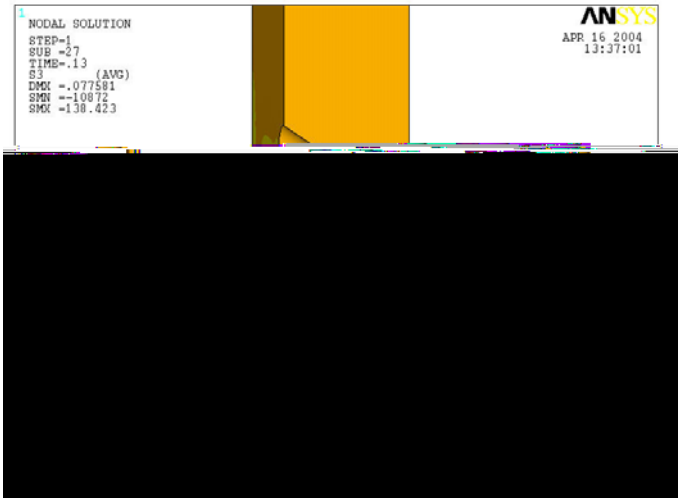

Figure 5–20. Compressive stresses in longitudinal shear finite element model (4,100 psi concrete).

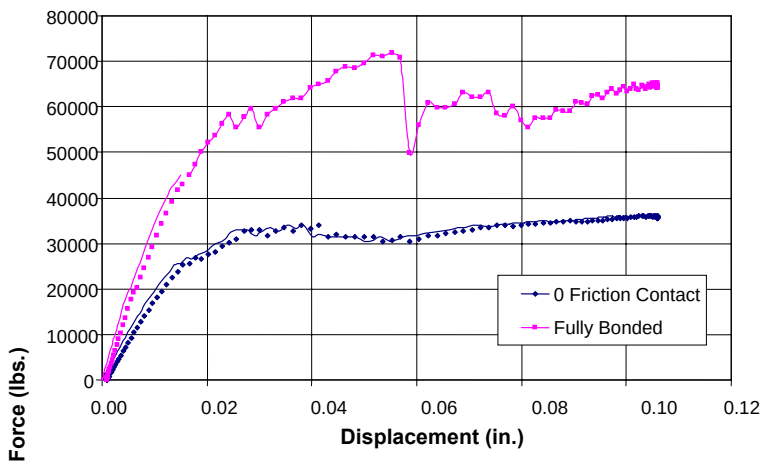

Figure 5–21. Shear force versus displacement from finite element model for longitudinal shear of two knuckles (4,100 psi concrete).

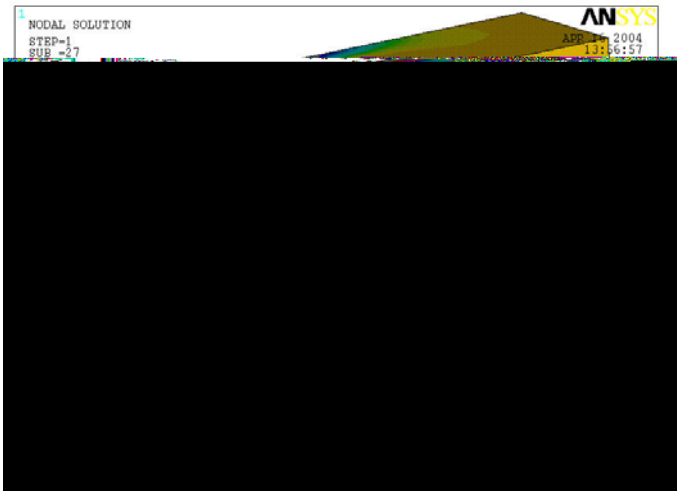

Figure 5–22. Compressive stresses in transverse shear finite element model (2,500 psi concrete).

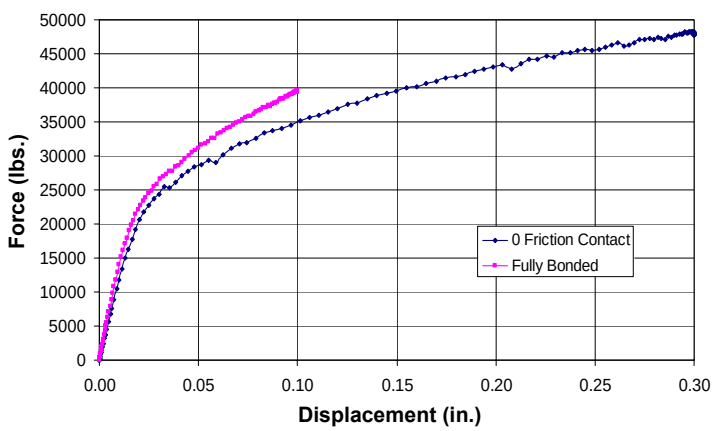

Figure 5–23. Shear force versus displacement from finite element model for transverse shear of two knuckles (2,500 psi concrete).

Analysis of Temperature Effects

Temperature effects on knuckles were evaluated based on hand calculations and engineering judgment. The effects can be summarized as follows:

- The steel knuckle heated rapidly and reached the temperature of the truss web diagonal member without much loss of heat into the relatively cool concrete slab. Concrete had a low coefficient of conductivity and did not respond as rapidly as steel to the rise of temperature.
- Concrete in the immediate proximity of the steel knuckle heated to a temperature close to that of the steel.
- Shear failure of the knuckle was initiated by the failure of concrete in close proximity to the knuckle. Final failure engaged not only the hot concrete in close proximity to the knuckle, but the cooler concrete farther away.

- It was assumed that for gas temperatures of 20 ˚C to 450 ˚C, 650 ˚C, 850 ˚C, and 1,050 ˚C, the knuckle steel temperatures would be lower at 20 ˚C to 375 ˚C, 550 ˚C, 725 ˚C, and 900 ˚C, and average concrete temperatures would be even lower at 20 ˚C to 300 ˚C, 450 ˚C, 600 ˚C, and 750 ˚C, respectively.

Neglecting the difference in thermal expansion of concrete and steel, for gas temperatures of 20 ˚C to 450 ˚C, 650 ˚C, 850 ˚C, and 1,050 ˚C, the expected concrete strength at the knuckle is in the range of 4,100 psi, 3,300 psi, 2,600 psi, and 2,000 psi based on the expected concrete temperature. Based on the results of tests performed and bracketing of test results by the finite element analysis, the knuckle capacities in either longitudinal or transverse direction are 30 kip, 24 kip, 19 kip, and 15 kip for the average concrete temperature of 20 ˚C to 300 ˚C, 450 ˚C, 600 ˚C, and 750 ˚C, respectively. Temperature-dependent knuckle shear capacities for the assumed temperatures are summarized in Table 5–7.

For the pullout failure mode, the capacity was estimated at 15 kip at room temperature. Based on concrete temperature and concrete strength, temperature-dependent capacity for pullout was calculated as shown in Table 5–7.

Table 5–7. Temperature-dependent knuckle capacity for assumed temperatures.

Gas temperature (˚C)	Steel temperature (˚C)	Concrete temperature (˚C)	Knuckle shear capacity (kip)	Knuckle pullout capacity (kip)
20 - 450	20 - 375	20 - 300	30	15
650	550	450	24	12
850	725	600	19	10
1,050	900	750	15	7

5.3.7 Summary of Failure Modes and Finite Element Models of Knuckle Model for Truss Model

Knuckle failure modes captured by the finite element models of knuckles in the truss model were the horizontal shear failure and vertical tensile pullout failure, which are both temperature-dependent. Finite element modeling assumptions for the knuckle are: (1) the knuckle has resistance in all translational degree of freedom, (2) the knuckle does not have a vertical compression capacity limit, (3) capacities in the horizontal shear and vertical tension are temperature-dependent, and (4) vertical compression resistance is independent of the capacities in the other directions. A finite element knuckle model was constructed by using 15 break elements and five beam elements for incorporation into the truss model, as shown in Fig. 5–24.

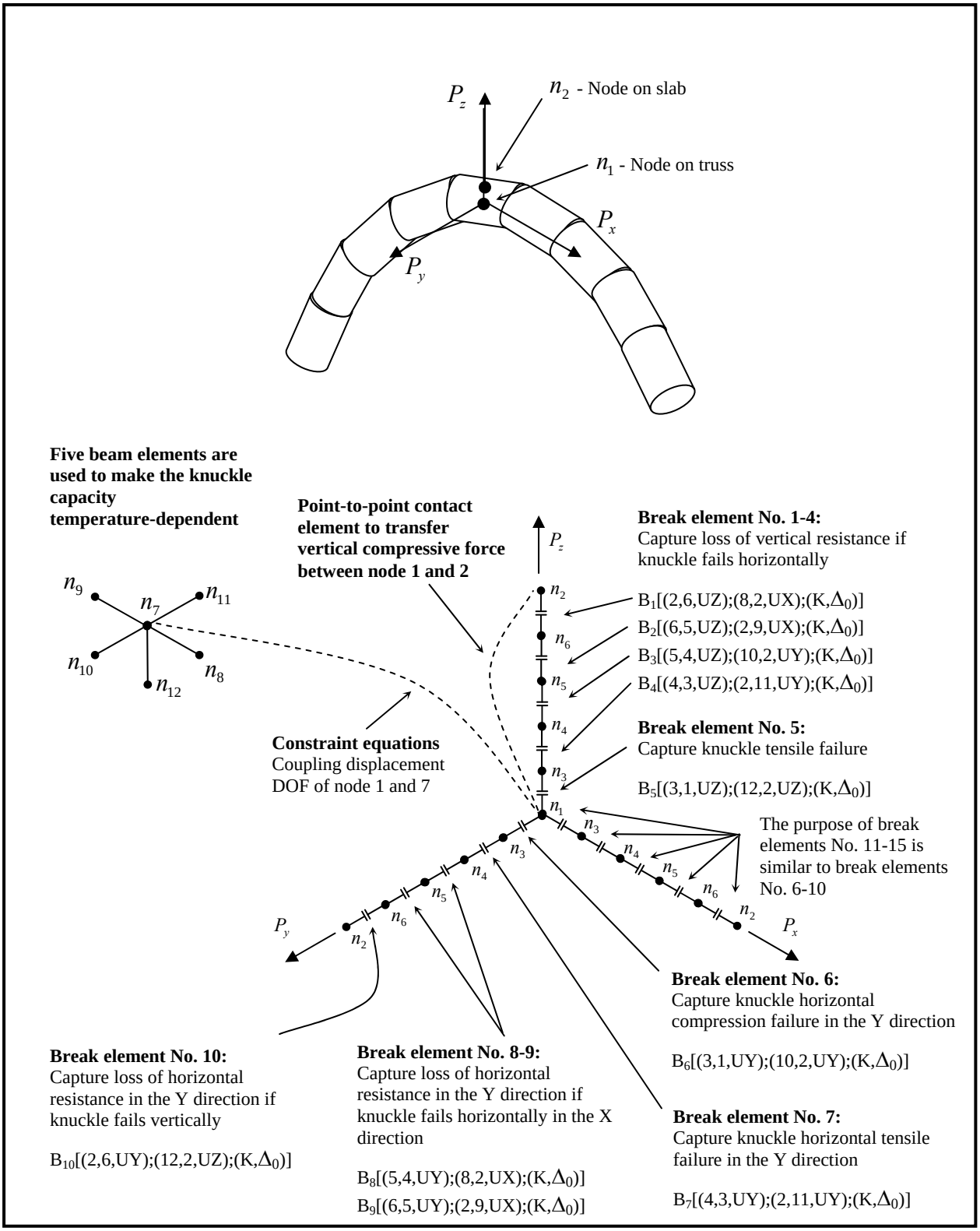

Figure 5–24. Representation of knuckle by break elements.

5.4 TRUSS MODEL

The truss model is a section of a floor system, which consists of a single floor truss and a corresponding section of the concrete slab. The objectives of the truss model study were to:

- Capture the potential failure modes and failure sequence of the truss model subjected to gravity load and temperature time histories,
- Determine failure loads for different failure modes, and
- Develop a simplified model that replicates the expected failure modes of the truss model for use in the full floor subsystem model.

5.4.1 Model Description

Figure 5–25 shows the truss model. The truss model is a cut-out section of the office area floor system. A typical long-span truss designated C32T1 (SHCR 1973:WTC Drawing Book 7, Sheet AB1–2) was modeled. The model used symmetry and included the following:

- One of the two primary trusses at Column 143 at Floor 96 of WTC 1,
- Two exterior columns (Columns 143 and 144) at the plane of symmetry with half the area and the moment of inertia and with a length of 24 ft (each column extends over the full height of a floor),
- Part of the spandrel between the two planes of symmetry,
- Part of the slab (40 in. wide) between the two plane of symmetry,
- Strap anchor attached on one end to the truss top chord and the concrete slab and on the other end to the adjacent exterior column (Column 144), and
- Halves of exterior and interior truss seats and the gusset plate at the exterior end.

The slab was 4 in. thick lightweight concrete on 22 gauge steel deck with flutes 6.8 in. on center running parallel to the primary trusses. Two layers of welded wire reinforcement were provided in the slab. The reinforcement ratios were 0.21 percent and 0.735 percent in the directions parallel and transverse to the truss, respectively. A flute was 2 in. wide at the top, 1.25 in. wide at the bottom, and 1.47 in. high.

The finite element model of the concrete slab had an equivalent thickness of 4.35 in. By using the equivalent thickness, the bending stiffness in the direction transverse to the truss became about 15 percent higher than the actual stiffness. However, since the bending in the transverse direction to the truss was small, the concrete slab was modeled as an isotropic plate. The steel deck and the welded wire fabric were not included in the truss model either explicitly or implicitly by modification of concrete stress-strain relationship. The concrete slab was modeled with four layers of 3-D eight-node structural solid (SOLID185) elements. The Hjelm plasticity model as described in Section 3.1.2 was used for the solid elements that allowed different “yield strengths” in tension and compression.

The top chord of truss C32T1 consisted of double angles of 1 1/2 × 2 × 0.25 (long legs horizontal), and the bottom chord consisted of double angles of 3 × 2 × 0.37 (long legs horizontal). Web diagonal members were round bars of either 1.09 in. or 1.14 in. diameter. Most web diagonal members had a 1.09 in. diameter.

The top and bottom chords and the web diagonals were modeled by BEAM189 elements with temperature-dependent elastic, plastic, and creep material properties. Top and bottom chords were

divided into four elements between panel points; panel points are those where web diagonals attached to chord members. Web diagonals were also divided into four elements between top and bottom chords.

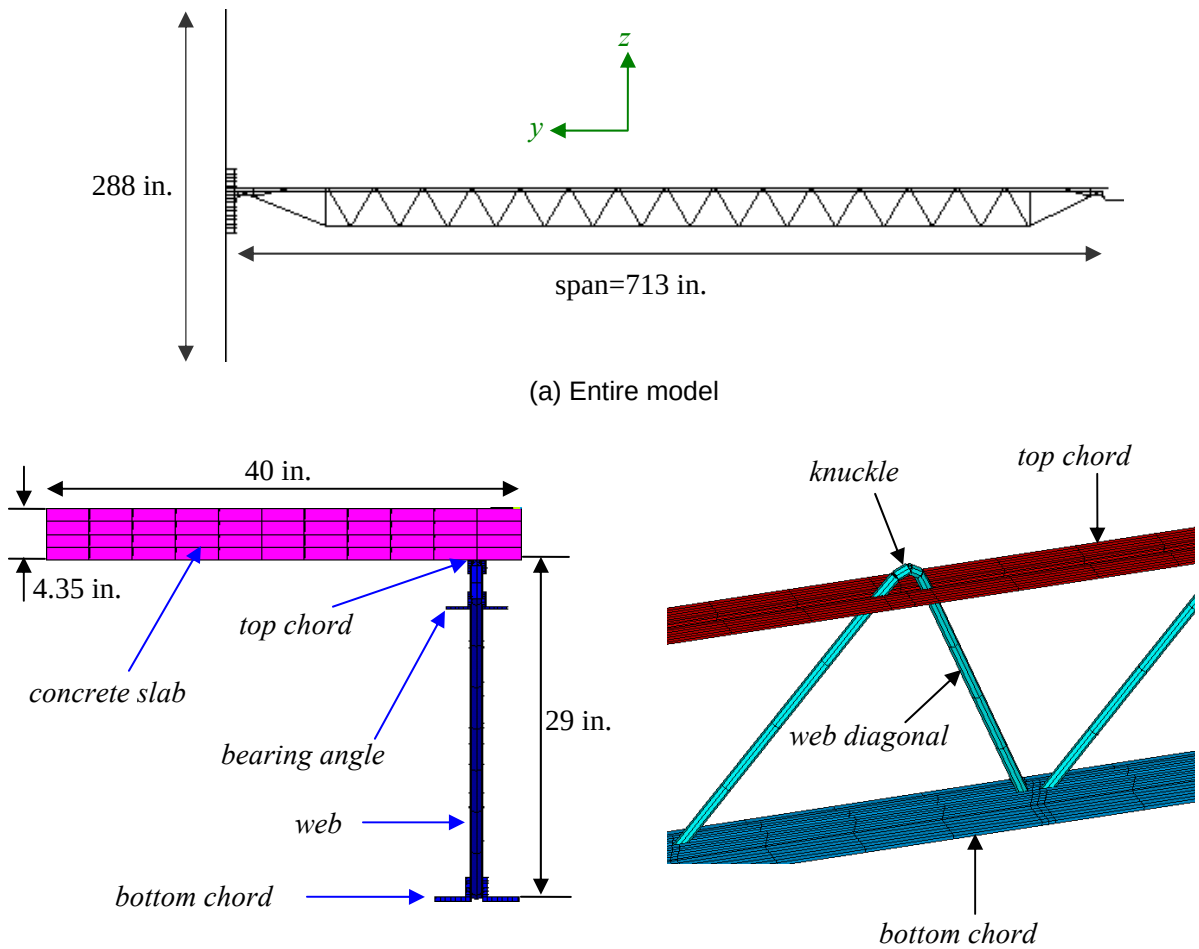

Figure 5–25. Truss model.

At knuckle locations, elements representing the top chord and the concrete slab were connected by break elements (COMBIN37) with capacities determined from the knuckle analysis. By including point-to-point contact (CONTA178) elements, compression was transferred even after failure of knuckles. The studs on the strap anchor between the top chord and column 144 were also modeled by break elements (COMBIN37) that connected the strap anchor to the slab and had temperature-dependent capacities. The slab and the strap anchor were tied by the COMBIN37 break elements horizontally while their vertical displacements were coupled. The exterior and interior truss seats were modeled by COMBIN37 break elements that had temperature-dependent capacities determined from the truss seat analysis. A stud on the spandrel was also modeled by COMBIN37 break elements, which tied the spandrel with the slab and had temperature-dependent capacities.

The visco-elastic damping unit that connected the truss bottom chord to the spandrel plate was not included in the truss model because the dampers were expected to be soft when subjected to very slow loading rates.

Elastic BEAM44 elements were used to model the exterior columns. Elastic SHELL63 elements were used to model the spandrel.

A camber of 2.0 in. at midspan was not included in the truss model.

5.4.2 Failure Modes

Two possible failure modes were identified for the truss model:

Sagging of Truss: The top and bottom chords and web diagonals were exposed to the hot gas layer that accumulated below the floor slab. The steel in the truss exhibited stiffness degradation, yield strength reduction, plastic softening, and creep at high temperatures. A truss with softened chords and diagonals would sag. As the concrete slab was heated, its stiffness and strength were reduced, especially at its bottom layer where temperatures were the highest due to exposure to hot gas and around the knuckles where concrete temperature rose by conduction through the steel.

In addition to direct thermal effects, sagging and weakening of the truss were caused by the following component failures:

- Buckling of web diagonal members,
- Yielding of the chord members,
- Knuckle failure and loss of composite action between the concrete slab and the steel truss (see Section 5.3), and/or
- Weld failure between the web diagonal members and the chord members.

Loss of Truss Support: The truss can fail by loss of support. Loss of support at either the exterior or interior truss seats was caused by the loss of vertical shear capacity of the seats at elevated temperatures or by the truss walking-off the seat due to large sagging.

As discussed in Section 5.4.3, the bottom chord of the truss model was restrained in the direction transverse to the truss at the bridging truss locations. Although the out-of-plane deformation of the bottom chord due to thermal expansion of bridging trusses may result in a reduction of the vertical load capacity of a primary truss, the use of symmetry in the truss model prevents its application to cases with lateral loads. The interaction between the bridging trusses and the primary trusses was captured in the full floor model.

5.4.3 Boundary Conditions

Boundary conditions for the truss model are shown in Fig. 5–26.

The entire top chord of the truss was restrained against lateral movement in the x direction. The bottom chord was restrained against lateral movement in the *x* direction at four bridging truss locations. The two edges of the concrete slab parallel to the truss were restrained against rotations about the *y* and *z* axes, but were free in the *x* direction.

The interior truss seat was fixed in all directions. The exterior truss seat was attached to the spandrel. The truss was supported by break elements to capture failure modes of the truss seats, and break elements were connected to beam elements representing the seats.

The exterior end of the slab was tied to the spandrel by contact elements to prevent the slab from penetrating the spandrel and break elements representing tension and shear failures of the spandrel stud.

The interior end of the slab was fixed in the *z* direction, but connected to break elements with temperature-dependent tensile capacities of the slab in the *y* direction, as shown in Fig. 5–27. Therefore, the interior slab end was fixed in the *y* direction as long as the tensile force was within the tensile capacity of the slab calculated for the actual steel reinforcement in the region between office area and core slabs (#3@10 in. top and #4@12 in. bottom).

The top and bottom ends of the columns were restrained against all rotations and against the translation in the *y*-direction. In addition, the lower columns were restrained against the translation in the vertical direction. The end restraint conditions of columns affect the magnitude of the horizontal reaction to thermal expansion of the floor section. A quantitative study of the effect of column boundary conditions is discussed in Section 5.5.16.

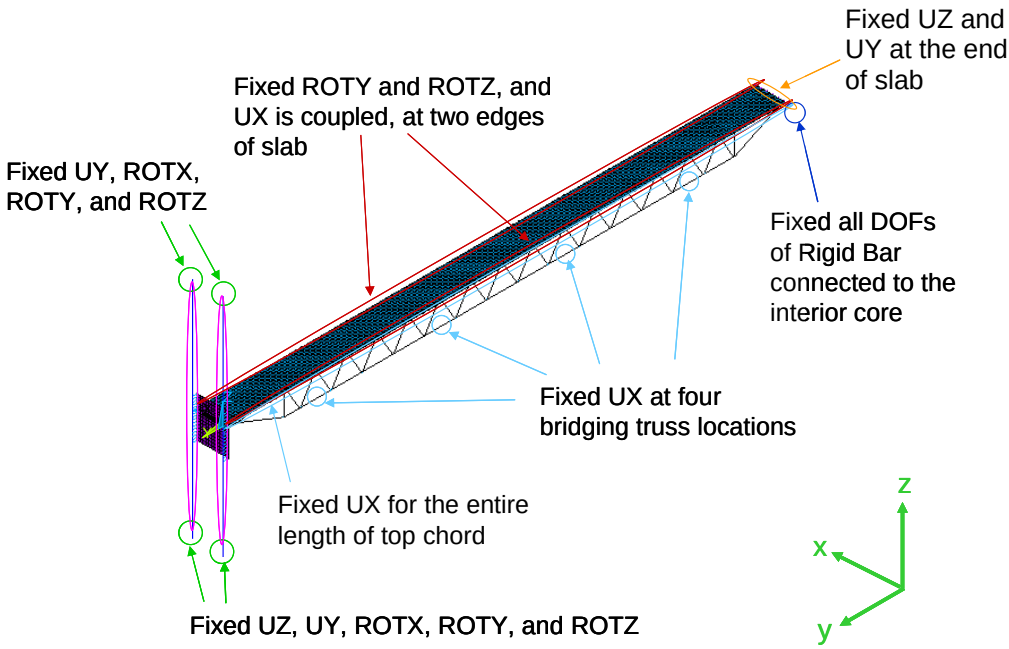

Figure 5–26. Boundary conditions.

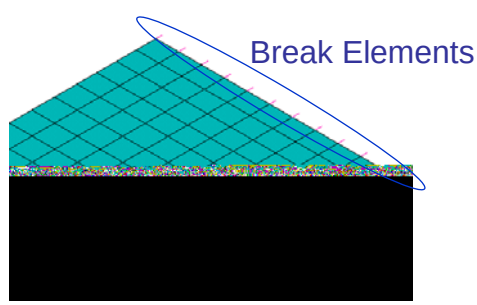

Figure 5–27. Break elements at the interior end of slab.

5.4.4 Loads

Loads on the truss model consisted of dead and live loads and temperature time histories for all truss components including the truss seats and concrete slab. The gravity loads included the weight of the structure, 8 psf superimposed dead load (including nonstructural dead loads due to architectural items and fixed service equipment), and 13.75 psf of live load equal to 25 percent of design live load of 55 psf.

A temperature time history was used for exercising the truss model (Figure 5–28). It was not obtained from fire dynamics or heat conduction analyses. The temperature was ramped over the first 30 min linearly from 20 ˚C to 700 ˚C in truss members, from 20 ˚C to 700 ˚C at the bottom surface of the concrete slab, and from 20 ˚C to 300 ˚C at the top surface of the concrete slab; thereafter, the maximum temperatures were linearly increased at a rate of 20 ˚C per min. At 40 min temperatures increased by 200 ˚C from those at 30 min. A linear gradient through the thickness of the slab was assumed. No temperature load was applied to the columns or spandrel.

The effects of construction sequence were included by using "element birth and death" for the concrete slab. In the first step, the self-weight of truss members and concrete slab was applied to the truss without the concrete slab. In the second step, the concrete slab was placed stress-free, and the superimposed dead and live load were applied to the model.

To determine the effect of debris load on the truss behavior, the gravity was increased until the analysis failed to converge at room temperature.

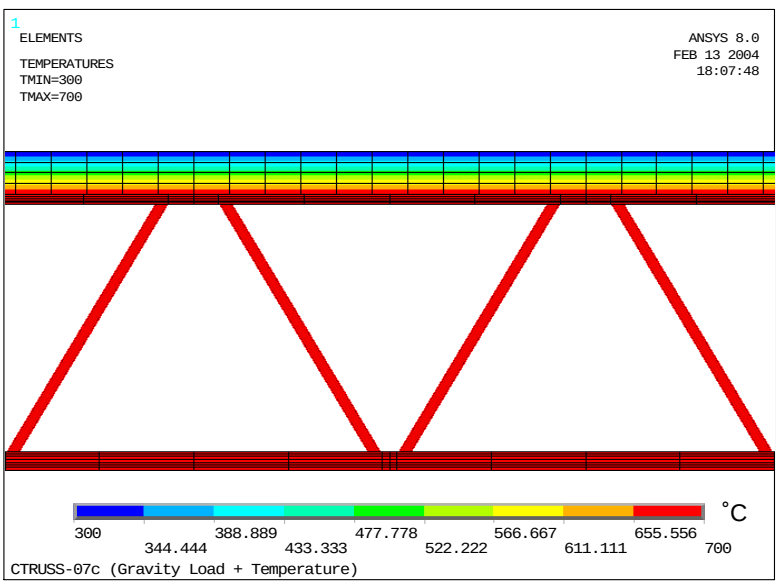

Figure 5–28. Assumed Temperature Distribution in the Truss Model at 30 min.

5.4.5 Material Properties

Table 5–8 shows material assignments for structural components in the truss model.

Elastic properties were assigned to the elements for Columns 143 and 144 and the spandrel. As described in Section 3.1.2, the Hjelm material model was used for the concrete model, which allowed different yield strengths for tension and compression. To improve convergence in the analysis, the negative slope after cracking in tension or crushing in compression was removed, and the concrete was assumed to be plastic after cracking or crushing.

Creep in steel was included in the analysis; however, the creep formulation was slightly different from Eq. (7) in Section 3.2.2. A ratio of room temperature yield strengths (i.e., $35.5/\sigma_{yRT}$) was used as the scaling factor of stress in the creep formulation for the truss model. NIST later changed the scaling factor from what was used here to the ratio of room temperature ultimate strengths (i.e., $70.5/\sigma_{uRT}$) as shown in Eq. (7).

Table 5–8. Material assignments in truss model.

Structural Component	Specified Yield Strength	Material ID
Top chord	50 ksi	21
Bottom chord	50 ksi	21
1.09 in. diameter web	36 ksi	20
1.14 in. diameter web	50 ksi	21
Strap	36 ksi	1
Column 143	65 ksi	15
Column 144	65 ksi	15
Spandrel	42 ksi	11
Lightweight concrete slab	3,000 psi (f'c)	83

5.4.6 Resistance Welds

Table 5–9 shows the resistance weld strength between a double angle chord and a web diagonal[3]. Weld strengths shown in Table 5–9 were the sum of the capacities of two resistance welds, one on each side of the web diagonal to each angle. Figure 5–29 compares resistance weld strength at the top or bottom chord with the yield strength of a web diagonal at elevated temperatures. As shown in Fig. 5–29 (a), a typical web diagonal (1.09 in. diameter) yields before the resistance weld fails. For a 1.14 in. diameter web diagonal, the resistance weld strength is less than the web diagonal yield strength at temperatures below 550 ˚C, as can be seen in Fig. 5–29 (b). However, shop drawings showed additional arc welds between the chord and 1.14 in. diameter bar at most locations.[4]

Table 5–9. Resistance weld strength.

Chord	Size of Web Diagonal (in.)	Average Weld Strength (kip)
Top chord	1.09	36.9
Top chord	1.14	37.7
Bottom chord	1.09	41.0
Bottom chord	1.14	40.5

[3] Based on the test data from Laclede Steel Co.

[4] Based on the test data from Laclede Steel Co.

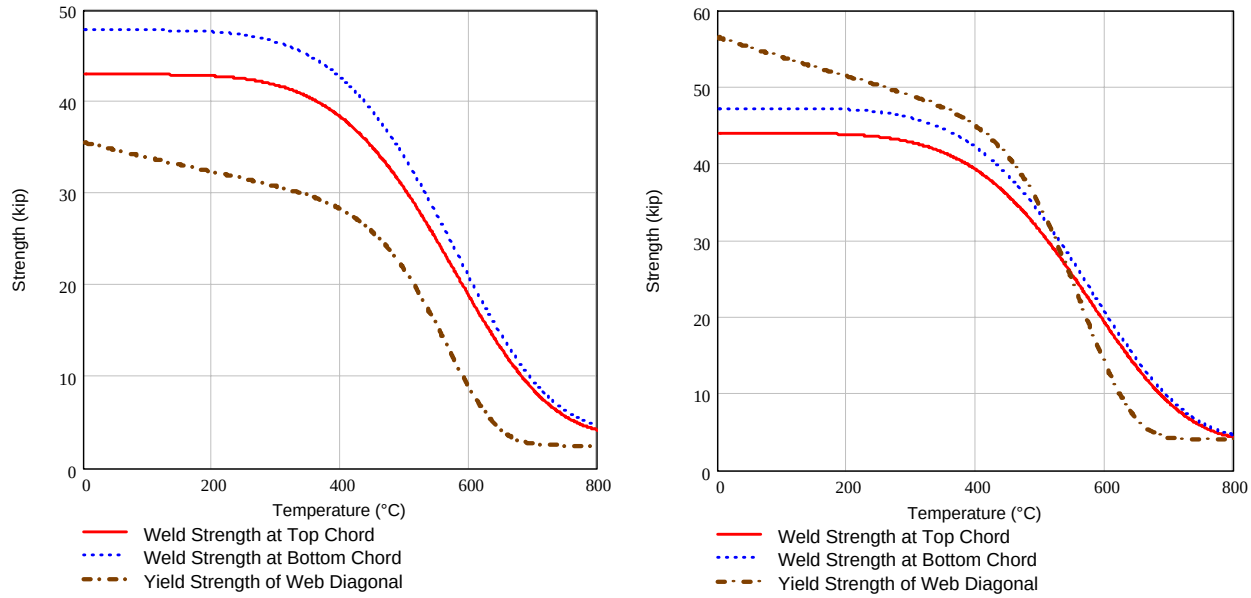

(a) 1.09 in. diameter bar (b) 1.14 in. diameter bar

Figure 5–29. Comparison of resistance weld strength and yield strength of web member at elevated temperatures.

5.4.7 Model Verification

Before analyzing the truss model response to elevated temperatures, the maximum vertical displacement under dead and live loads was verified against the single truss model extracted from the ANSYS full floor model. The maximum difference in the vertical displacement was found to be 3.5 percent. In this comparison, the effects of construction sequence were not included in either model.

5.4.8 Truss Analysis for Debris Load

The capacity of the truss model against additional debris load was determined by increasing the gravity loads. When this analysis was performed, the truss model was still under development and somewhat different from the model described in Section 5.4.1. Break elements were not used for studs, interior, or exterior truss seats, nor for reinforcement at the interior end of the slab. The slab was modeled by SHELL181 elements with elastic material properties. Boundary conditions of the slab were also slightly different from those described in Section 5.4.3. The exterior end of the slab was tied to the spandrel without break elements and contact elements, and the interior end of the slab was fixed in the y and z directions and against rotations about the x and z axes without break elements.

The analysis was terminated at a load factor of 3.4. Load factor is the ratio of the gravity load plus debris weight to the gravity load. Figure 5–30 (a) shows midspan vertical displacement versus load factor. At a load factor of 2.4, Knuckles 5 to 15 failed due to horizontal shear in the truss direction. At a load factor of 2.8, Knuckle 4 failed. Figure 5–30 (b) shows the sum of the horizontal reaction forces measured at the exterior columns, where a positive value is used when columns are pulled in by the truss. After twelve of fifteen knuckles failed, the model lost its composite action, and the vertical displacement increased significantly. As a result, horizontal reaction forces at the exterior columns also increased.

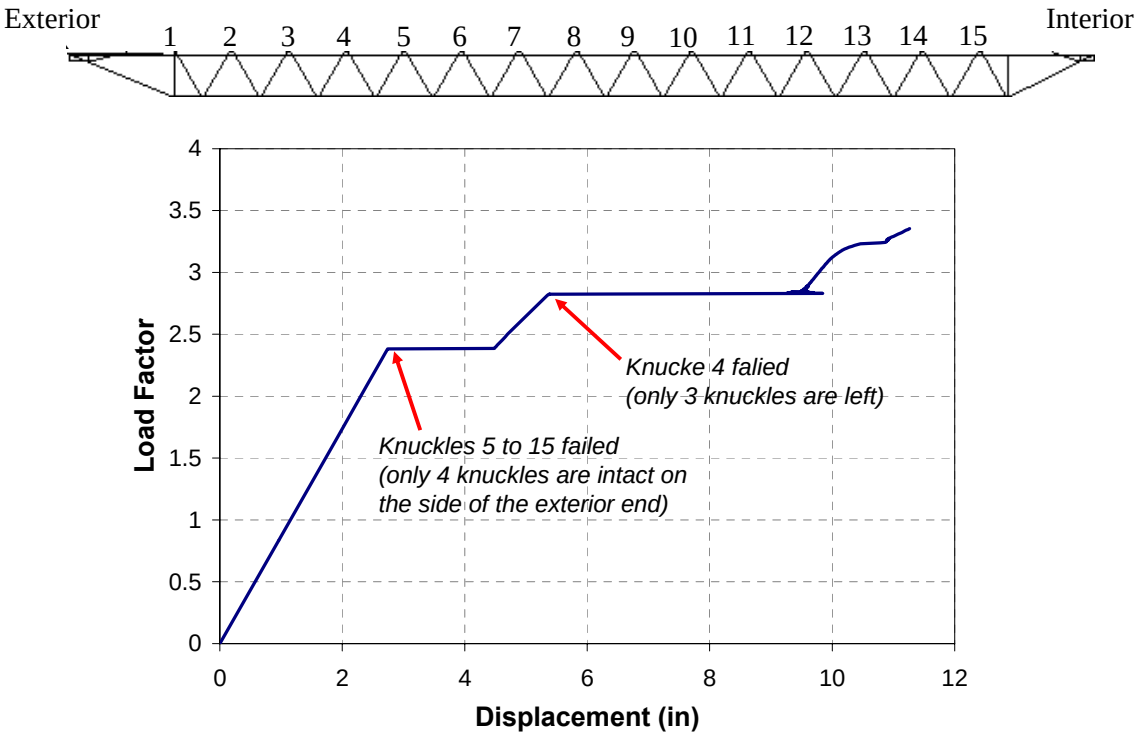

(a) Load factor versus midspan vertical displacement

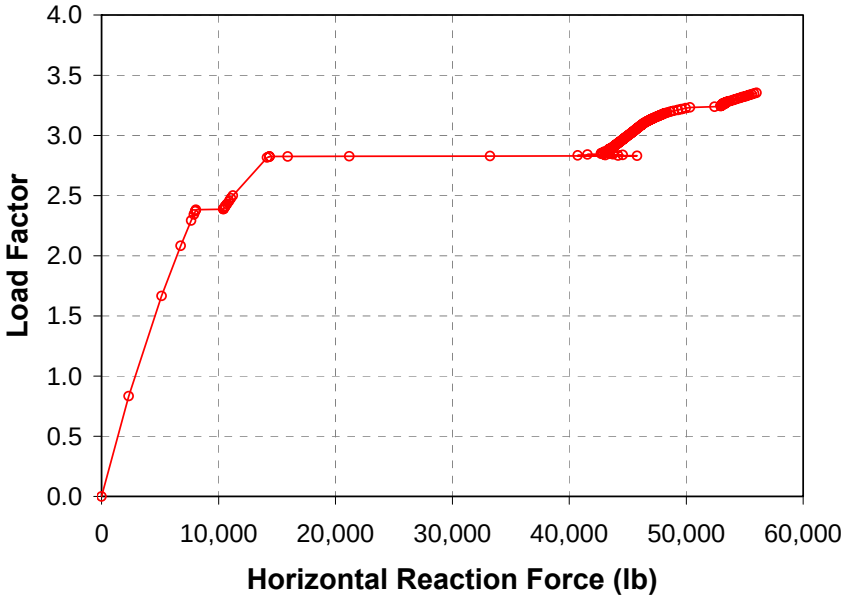

(b) Load factor versus horizontal reaction force

Figure 5–30. Finite element analysis results from increasing gravity.

5.4.9 Truss Analysis for Gravity and Thermal Loads

Gravity Loading: The maximum calculated vertical deflection due to the self-weight of the structure, which occurred when the concrete was still wet, was 1.7 in. downward. When the superimposed dead and live loads were applied to the truss with hardened concrete slab, the maximum vertical deflection became 2.0 in., and the maximum horizontal column deflection was 0.05 in. inward. The maximum forces in the top chord, bottom chord, web diagonal, and end diagonal strut were -25.7 kip, 41.3 kip, -6.9 kip, and 16.0 kip, respectively, which translate to average stresses of 14.8 ksi, 11.6 ksi, 6.7 ksi, and 15.7 ksi, respectively. The yield strength of top and bottom chords and end diagonal struts was 55.3 ksi. The yield strength of web diagonals was 38.1 ksi, except for the first compressive web diagonal at the interior end, which had a yield strength of 55.3 ksi. Therefore, the maximum stress level was about 30 percent of yield strength.

Gravity Plus Thermal Loading: The analysis of the truss model subjected to temperature time history was carried out statically; however, when the solution process did not converge, to overcome the convergence problem, the problem was solved dynamically with a 5 percent Rayleigh damping. The static analysis was then resumed when acceleration and velocity became small. The analysis proceeded in this fashion until the temperature of the steel became 727 ˚C. Figure 5–31 shows the vertical displacement of the truss at 700 ˚C, and Fig. 5–32 shows the horizontal displacement of Column 143 at the floor level and vertical displacement of the bottom chord at midspan with temperature of steel. The zero vertical displacement in this figure represents the initial displacement after the self-weight was applied. A positive horizontal displacement indicates that the exterior columns were pushed out, and a negative vertical displacement indicates that the truss was deflected downward. At 445 ˚C, when the end diagonal struts began to yield, the horizontal displacement at the exterior column began to decrease. At 565 ˚C, the truss sag became large due to the buckling of web diagonals, and the exterior columns were pulled in.

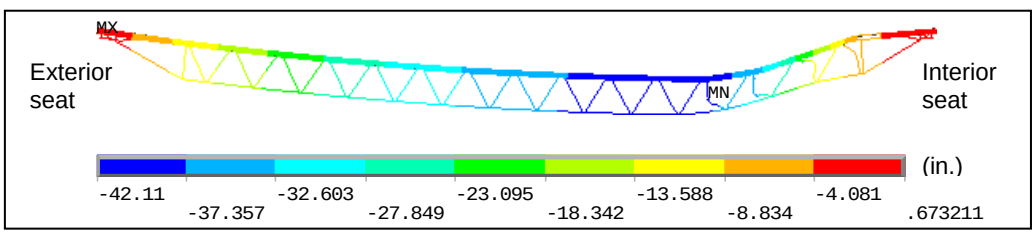

Figure 5–31. Vertical displacement at 700 ˚C (downward displacement is negative).

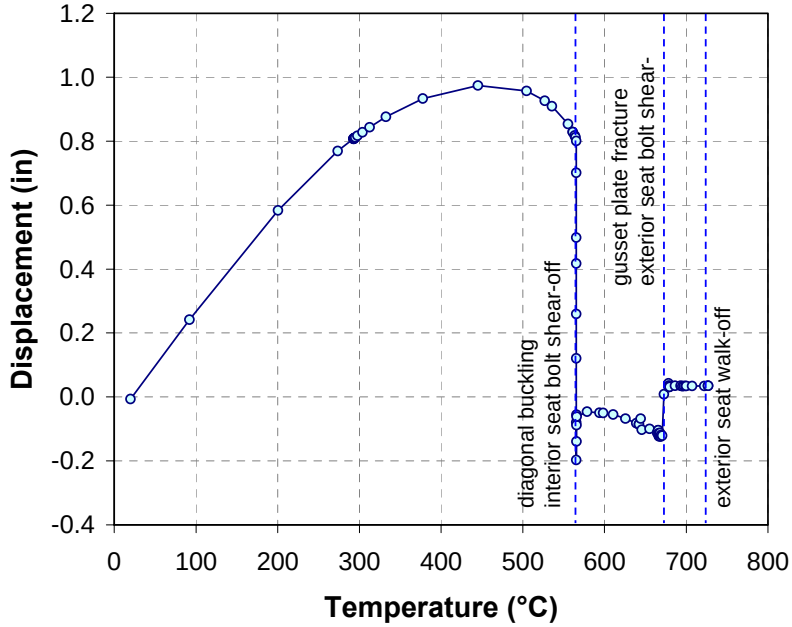

(a) Horizontal displacement at Column 143

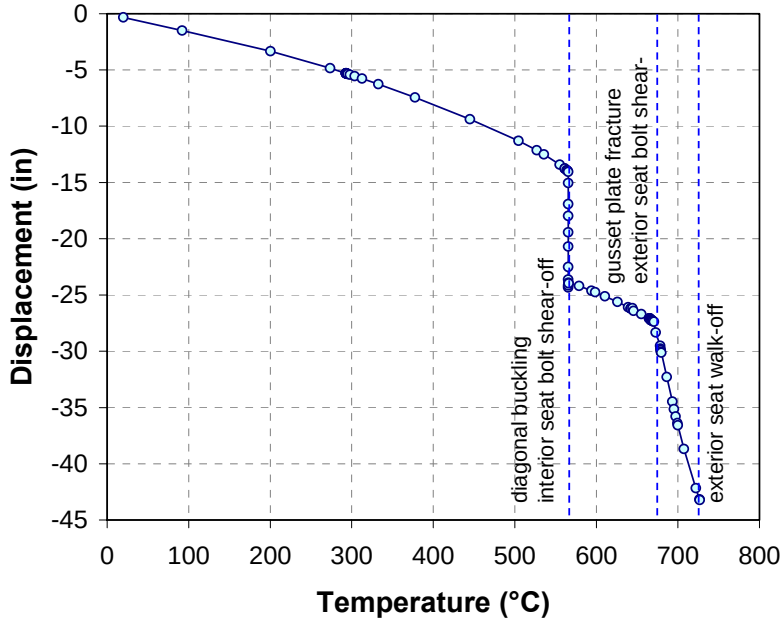

(b) Vertical displacement at midspan

Figure 5–32. Displacement versus temperature of steel.

Figure 5–33 shows selected truss members. Figure 5–34 shows the axial forces in selected truss members Fig. 5–33. In Fig. 5–34, Py is the axial force at yield and equals the product of the net area of the member and the yield strength which varies with temperature. Pc in Fig. 5–34 (c) is the compressive strength calculated per the American Institute of Steel Construction's Manual of Steel construction, Load and Resistance Factor Design (AISC 2003) for fixed end conditions. Because the top chord was tied to the concrete in the vertical direction and was restrained in the direction transverse to the truss in this model, the failure of the top chord was by yielding, Py, rather than buckling, Pc.

Figure 5–34 (a) shows yielding of the top chords between knuckles beyond 300 ˚C, resulting from the significant difference in coefficients of thermal expansion between concrete and steel. At 500 ˚C, the coefficient of thermal expansion of steel was twice that of lightweight concrete. Yielding of the top chord did not play a significant role in the truss response because of its minor contribution to the composite area of the concrete slab and steel truss. Bottom chords were still in the elastic range at the end of analysis. Buckling of web diagonals started at approximately 565 ˚C. Several web diagonals were bent significantly in the plane of the truss by the high compressive axial force (see Fig. 5–35 for the deformed shape at the interior end).

Figure 5–36 shows knuckle forces in the longitudinal truss direction and the vertical direction. The capacity of a knuckle was 30 kip in shear and 15 kip in tension at room temperature. Knuckle 15 failed due to tension around 100 ˚C. Knuckles 13 and 14 failed due to shear in the longitudinal truss direction at about 566 ˚C.

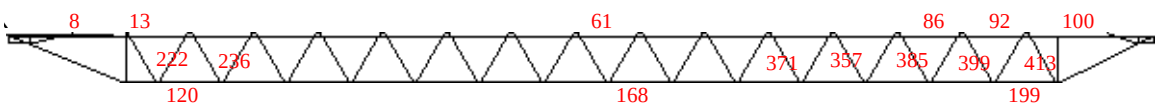

Figure 5–33. Element numbers and locations of elements examined for axial force.

(a) Top chord

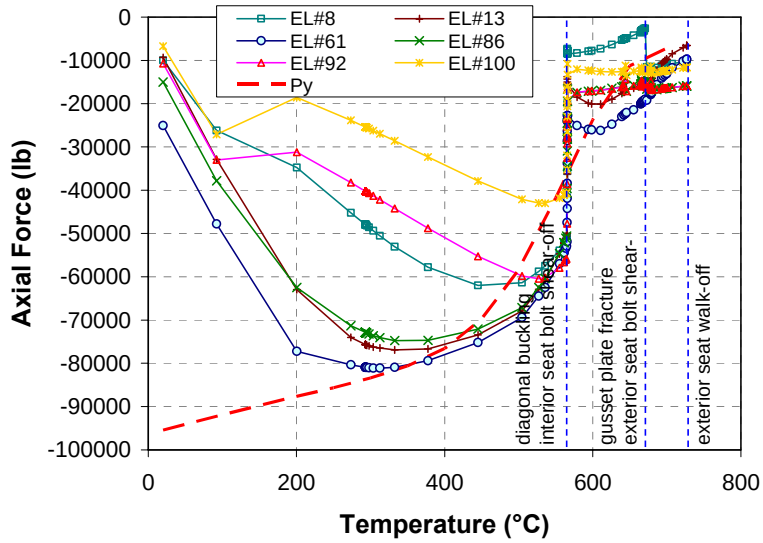

(b) Bottom chord

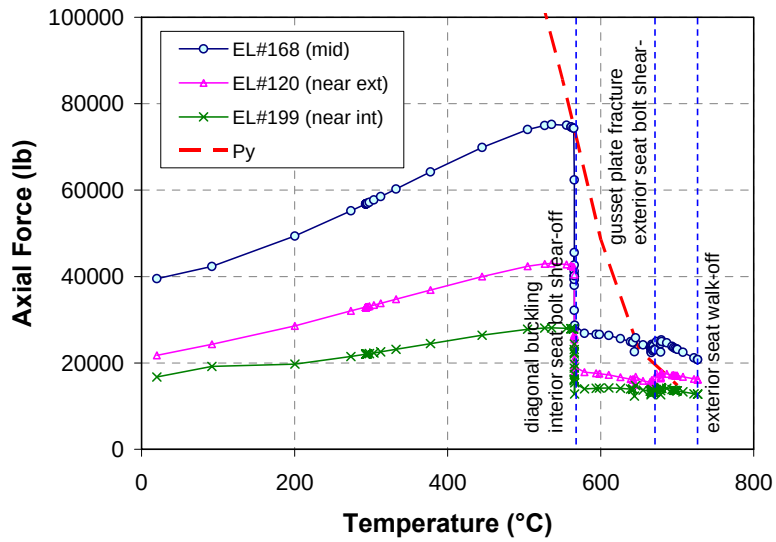

(c) Compression web diagonal

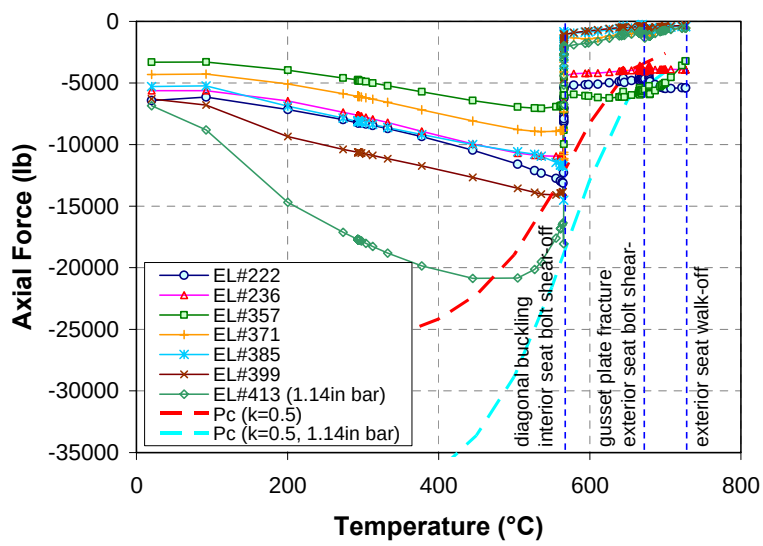

Figure 5–34. Axial force in truss members versus temperature of steel.

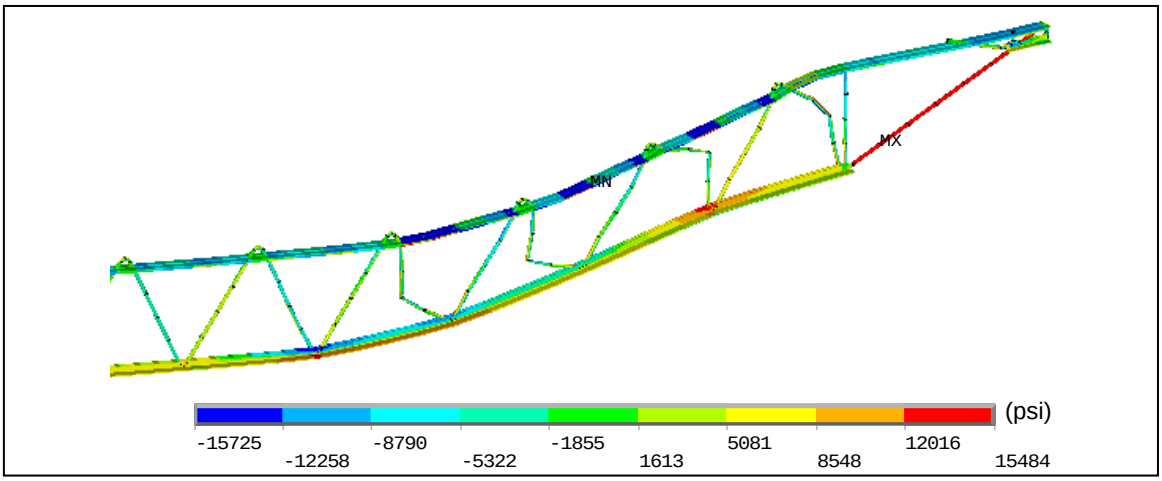

Figure 5–35. Axial stress contour in the truss members at 700 ˚C (tension is positive; 1.0x displacement magnification).

Figure 5–37 (a) and (b) show the horizontal reaction forces at exterior and interior truss seats and exterior columns, respectively. At 566 ˚C, the interior truss seat bolts sheared off, without loss of vertical support. At 670 ˚C, the gusset plate at the exterior truss seat fractured, followed by shearing of the exterior seat bolt. At 730 ˚C, the truss walked off the exterior truss seat. At about 600 ˚C before failures of the gusset plate and the exterior seat bolts, the tension between the truss and the exterior columns was about 12 kip, which was through the gusset plate and the strap anchor. At about 700 ˚C after failure of the gusset plate and the exterior truss seat bolts, the tension became about 10 kip, which was only through the strap anchor. It was found that 10 kip tension in the strap anchor was larger than the strength at 700 ˚C (7.5 kip) of the weld (a size of 5/16 in. and a length of 4 in.) between the strap anchor and the top chord. The failure of this weld was not modeled by break elements in the truss model. If the failure of this weld had been modeled in the truss model, the walk-off could have occurred at a temperature lower than 730 ˚C.

Failure modes and failure sequence of the truss model subjected to “assumed temperature conditions” were as follows:

- The stud on the spandrel and studs on the strap anchor failed in shear below 275 ˚C.
- Knuckle 15 failed in vertical tension at around 100 ˚C, and Knuckles 13 and 14 failed in the horizontal shear at 566 ˚C.
- Top chords yielded above 300 ˚C due to the difference in coefficients of thermal expansion of steel and lightweight concrete.
- Four compression web diagonals buckled due to high axial compressive force at 565 ˚C.
- The interior truss seat bolts sheared off at 566 ˚C.
- The gusset plate fractured and the exterior truss seat bolts sheared off at around 680 ˚C.
- The truss walked off the exterior truss seat at 730 ˚C.

The actual failure modes and failure sequence in the WTC towers may have been different due to the difference in actual and assumed temperature time histories. The truss model was simplified as described in the next section and incorporated in the full floor model and analyzed for the actual estimates of temperature time histories.

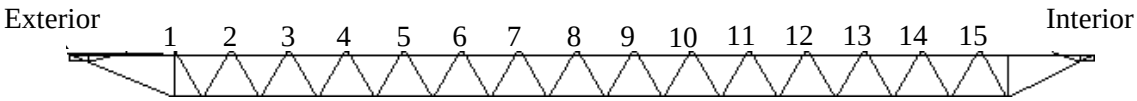

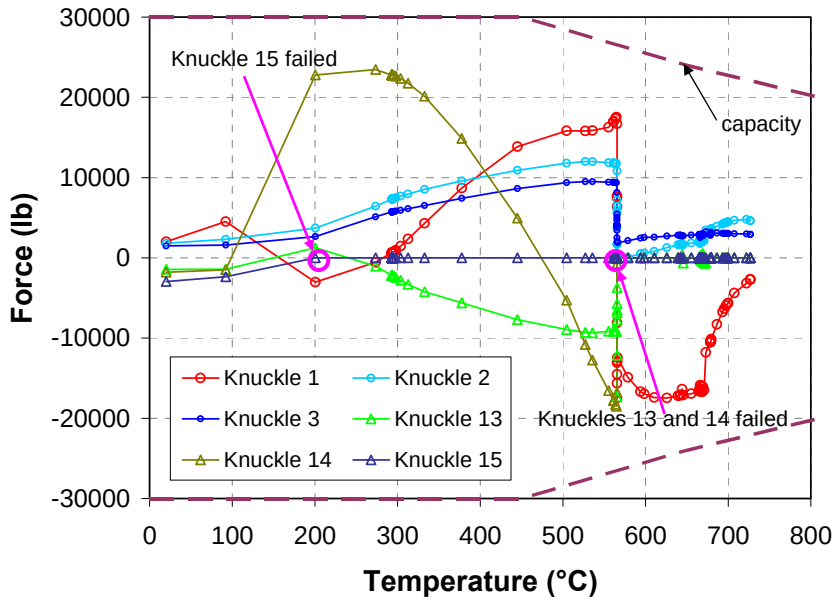

(a) Horizontal force

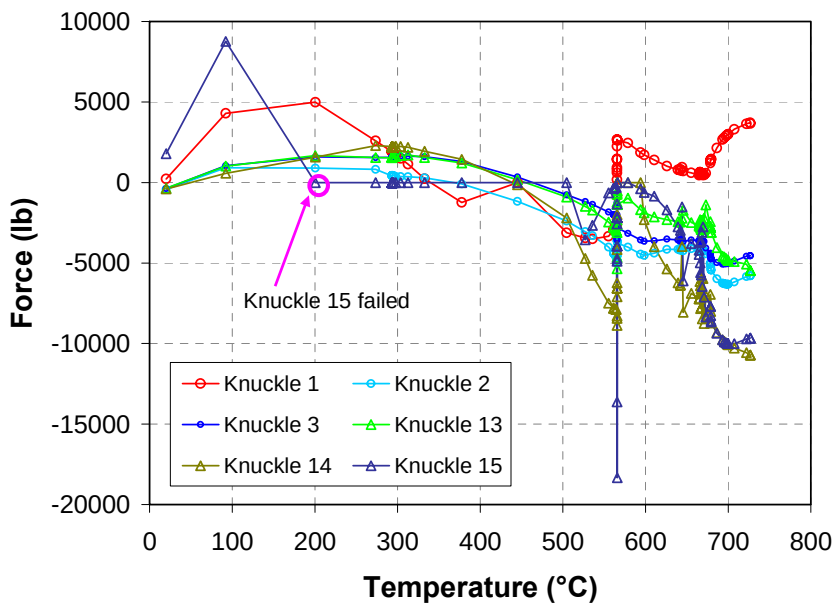

(b) Vertical force

Figure 5–36. Force in the knuckles versus temperature of steel.

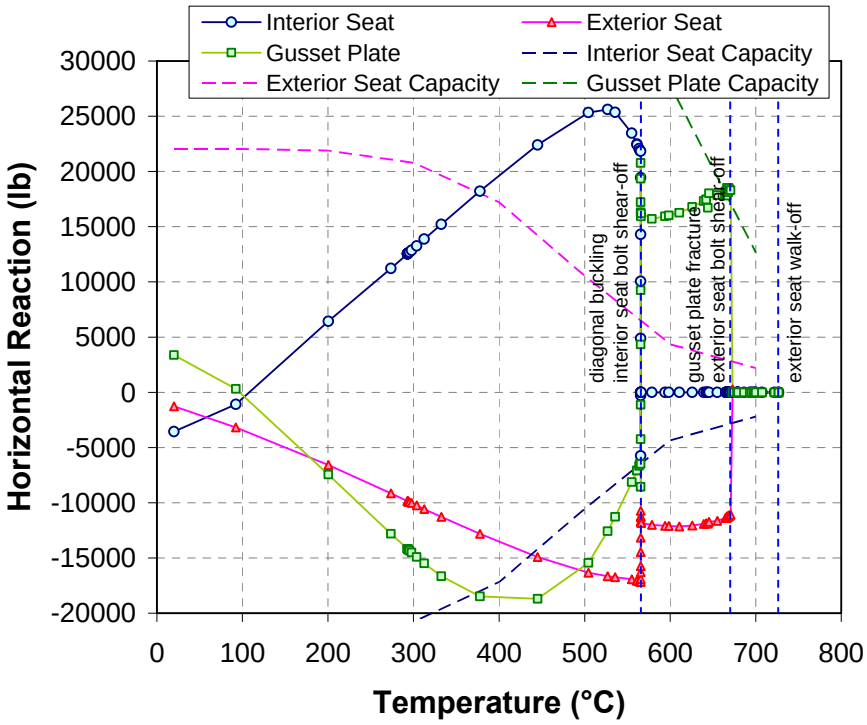

(a) At truss seats

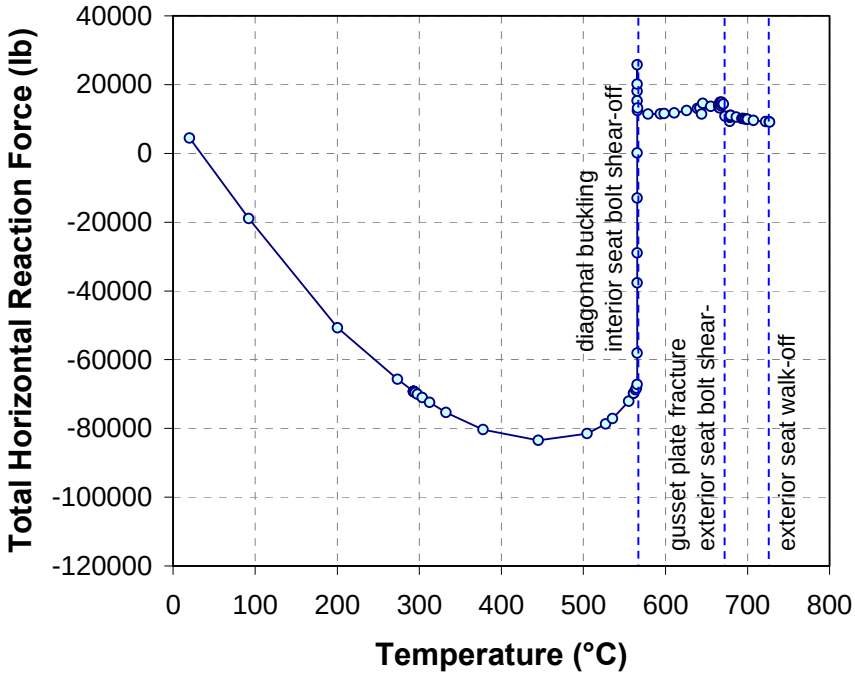

(b) At exterior columns

Figure 5–37. Horizontal reaction forces.

5.4.10 Simplified Truss Model

The truss model was simplified for use in the full floor subsystem model. Characteristics of the truss model captured by the simplified truss model were: (1) total horizontal reaction force under the thermal loading and (2) vertical deflection at midspan under the thermal loading. The simplified truss model had the following features:

- The geometry of the truss was preserved.
- A pair of primary trusses at each exterior column was combined into one truss. Cross sections of truss members were doubled.
- The top and bottom chords and web diagonals were modeled by BEAM188 elements. A member between two panel points was modeled by one element only.
- Break elements modeled by ANSYS user-defined elements were used to model the following failure modes: (a) seat bolt shear-off, (b) gusset plate fracture, (c) truss walk-off, (d) web diagonal buckling/resistance weld failure, (e) failure of studs on the spandrel and strap anchors, and (f) weld failure between strap anchors and top chords. User-defined break elements will be further discussed in Section 5.5.5.
- Knuckles were not modeled by break elements. It was found that neglecting knuckle failure did not significantly change truss behavior subjected to thermal loads.
- Steel had temperature-dependent elastic and plastic material properties.
- Creep in steel was included in the simplified truss model; however, it was not included when the simplified truss model was incorporated in the full floor model, because of convergence problems inherent in BEAM188 elements.
- The concrete slab was modeled by SHELL181 elements with a temperature-dependent bilinear material model that had the same yield strength in both tension and compression. The yield strength was set to the compressive strength.
- Construction sequence was not considered.

Figure 5–38 shows the vertical deflection at midspan and the horizontal reaction at exterior columns of the truss model and simplified truss model subjected to the gravity load and the assumed thermal load described in Section 5.4.4. Vertical displacement in this figure is the displacement that occurred during thermal loading. The simplified truss model predicted the buckling of web diagonals at 530 ˚C, which is about 35 ˚C lower than the temperature at which web diagonal buckling was predicted by the truss model. The tension at 700 ˚C in the simplified truss model was about 2 kip, which was less than 10 kip in the truss model. Overall truss behaviors as predicted by the simplified truss model subjected to gravity and the assumed thermal loading were in good agreement with the truss model.

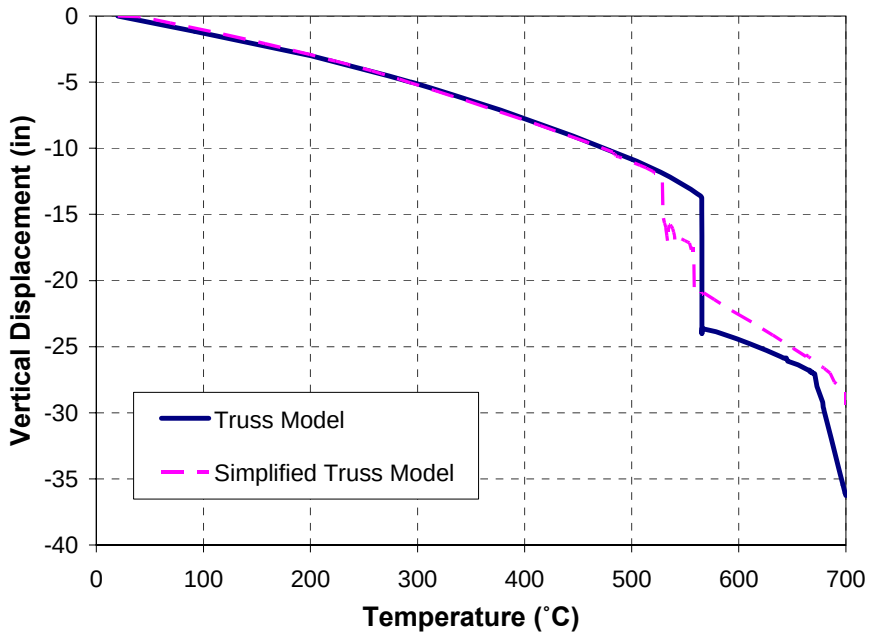

(a) Midspan vertical deflection

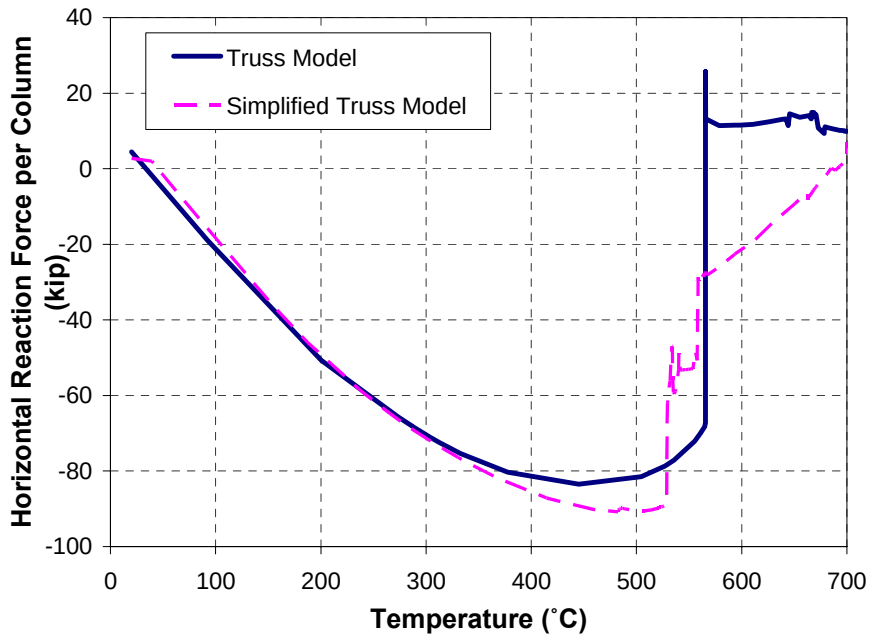

(b) Horizontal reaction force at exterior columns

Figure 5–38. Comparison of detailed and simplified truss models.

5.5 FULL FLOOR MODEL

5.5.1 Objective

The full floor model was developed and analyzed using the ANSYS general purpose finite element program Version 8.1. The objectives of the full floor model analysis were:

- To identify the most likely failure modes,
- To evaluate
  - Failure loads,
  - Temperatures at failure,
  - Time-to-failure, and
  - Changes in mechanical properties and geometry at failure.
- To identify the fire-induced damage to be incorporated along with impact-induced damage in the global model
- To develop computationally efficient modeling details of the floor subsystem for incorporation into the global model.

5.5.2 Failure Modes

Failure modes that the full floor models captured were as follows:

- Floor Sagging: Floor sagging was caused by loss of stiffness and softening of truss at high temperature, by yielding and buckling of truss members, and by the impact damage to truss seats. These were discussed in some detail under truss failure modes. Floor sagging resulted in tension in the floor subsystem, tension on the connections to the exterior walls, and lateral forces (pull-in forces) on exterior columns.
- Loss of Support: Loss of a truss support was caused by reduced vertical shear resistance of truss seats at elevated temperatures, by tension acting on truss seats caused by floor sagging, and by aircraft impact.

5.5.3 Model Description

The base floor model developed was for Floor 96 of WTC 1 with columns extending from Floor 95 to Floor 97. The model was developed based on the converted SAP2000 model for Floor 96 of WTC 1, with the following modifications:

1. Two adjacent trusses supported by the same column were combined into a single truss. The areas of members in a truss were doubled to create a combined truss.
2. Spandrels were defined as beam sections in the SAP2000 model, and were replaced with SHELL181 elements (eight elements between two columns and four elements along the height). This modification eliminated the need for defining panel zone stiffness at the interface between spandrel and exterior column.
3. Elastic column elements were changed to BEAM189 elements with user-defined composite sections and nonlinear material properties.

4. Section offsets of exterior columns were removed, and nodes were placed at centroids of their cross sections.
5. Spandrels were tied to exterior columns by rigid beam elements as described in Section 6.4.1 of this report.
6. Core floor slab was remeshed with a more uniform mesh.
7. Section offsets of core beams were removed to eliminate the end bending moment due to eccentricity. Core beams were placed at their centroids and were connected to the slab by rigid beam elements.
8. Where there was more than one beam element representing a top chord between two adjacent panel points, the beam elements were merged into one to prevent the top chord from buckling upward and penetrating the slab.
9. Web diagonals were modeled by BEAM188 elements.
10. Coincident nodes were provided for user-defined break elements.
11. User-defined break elements were incorporated into the model to represent:
    a. buckling of web diagonals,
    b. gusset plate fracture,
    c. truss seat bolt shear-off,
    d. truss seat failure,
    e. failure of connections between primary and bridging trusses,
    f. failure of connections between primary long-span and transfer trusses,
    g. failure of studs connecting the slab and the spandrel, and
    h. failure of welds between strap anchors and top chords of primary trusses.
12. The ANSYS floor model translated from the SAP model had the bottom chord connection at every intersection of primary and bridging trusses. Some of the bottom chord connections between primary and bridging trusses were removed according to the PANYNJ drawings.

The full floor model, as shown in Fig. 5–39, included the following structural members:

a. both exterior and core columns extending from one floor below to one floor above,
b. spandrels of the floor modeled,
c. floor slab,
d. floor trusses including primary and bridging trusses,
e. strap anchors,
f. core beams, and
g. deck support angles.

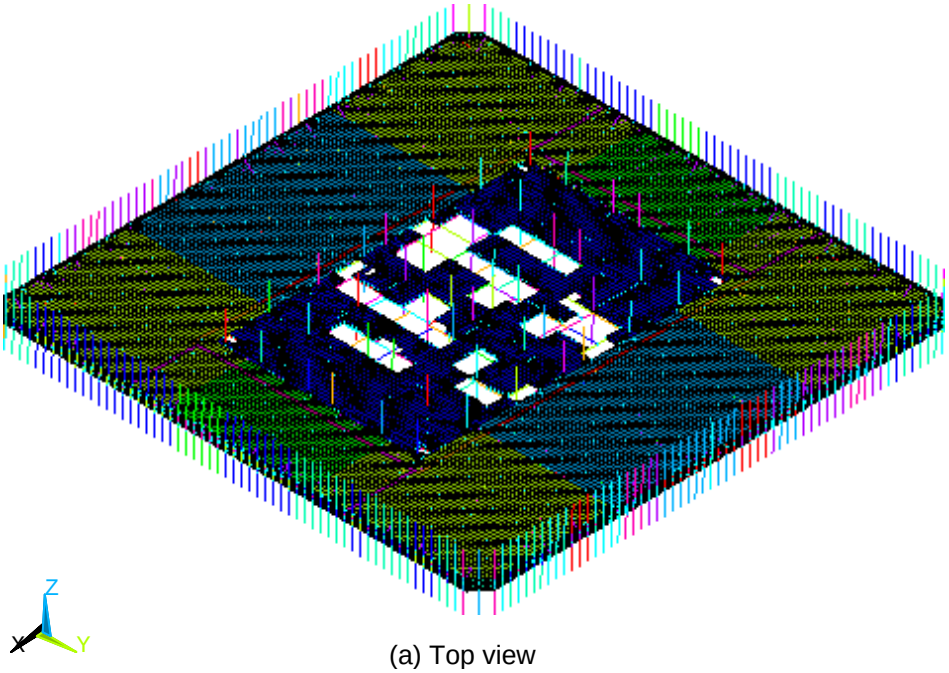

(a) Top view

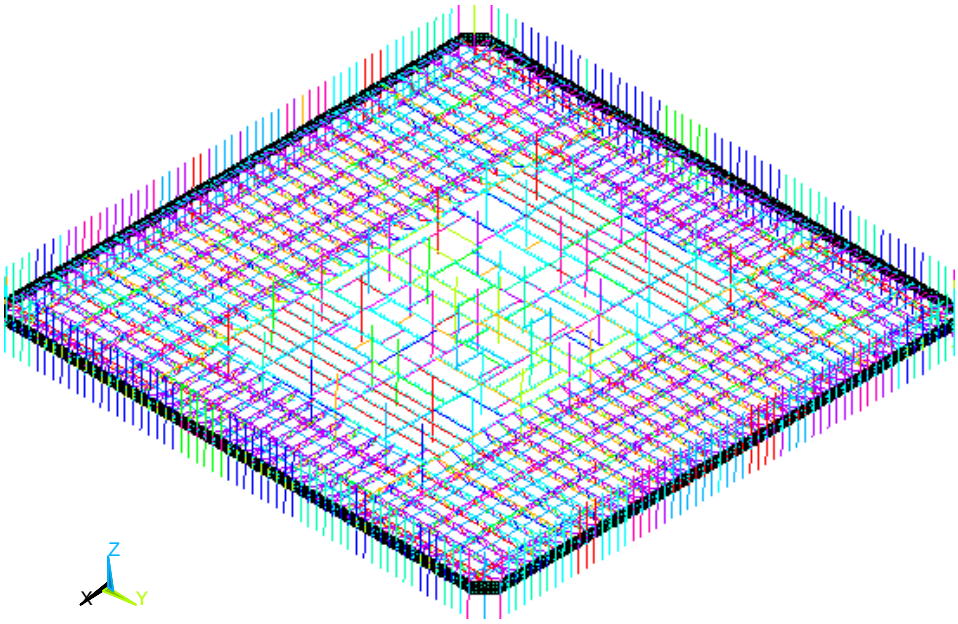

(b) Top view without concrete slab

Figure 5–39. Full floor model without impact damage.

The size of the full floor model was as follows:

- Number of elements: 46,280
- Number of nodes: 61,251
- Number of degrees of freedom: 269,926

Truss members (top and bottom chords and web diagonals) were modeled by BEAM188 elements. Columns were modeled by BEAM189 elements. Spandrels were modeled by SHELL181 elements. The concrete slab was modeled by SHELL181 elements with four layers through the thickness. Each layer of the shell element for the slab had one integration point.

The full floor model was validated against the SAP floor model by performing the two analyses described in Section 4.2.1. To compare the full floor model with the SAP floor model, density of lightweight concrete was changed from 110 pcf to 100 pcf. Under gravity loads, the maximum displacement of the full floor model was 0.722 in., which is only 0.56 percent smaller than that of the SAP floor model. The first vibration mode of the full floor model was not the vertical deflection of the office floor, but the lateral vibration of the bridging trusses in the short-span truss area. This was a result of removing some of the bottom chord connections between the primary and bridging trusses. The natural frequency of the vertical deflection mode was 4.41 Hz, which is only 2 percent higher than that of the SAP floor model.

Subsequent to initial full floor analysis with thermal loads, the members listed below were removed from the model to enhance computational efficiency without loss of accuracy of prediction of final failure modes and failure sequence, as shown in Fig. 5–40.

- Deck support angles
- Bridging trusses outside of the two-way zones
- Spandrel studs connecting the slab and the spandrel
- Strap anchors

These elements failed in the early stage of thermal loading and caused the analysis to slow down due to large nonlinearities of the failed elements. Deck support angles and bridging trusses buckled between the primary trusses due to thermal expansion. Many shear studs and welds between strap anchors and truss top chords failed due to lateral shear force in the direction transverse to the primary trusses caused by the difference in thermal expansion between the floor and the exterior wall. These members were removed from the model to enhance computational efficiency. As a result of removal of strap anchors and spandrel studs, the only connections between the exterior wall and the floor were gusset plates and exterior truss seats.

The visco-elastic dampers that connected the truss bottom chords to the spandrels were not included in the full floor model because dampers were expected to be soft when subjected to very slow loading rates.

The concrete slab was attached to primary trusses at knuckle locations. Break elements were not used for representing knuckle failure as the truss analysis found that web diagonal buckling rather than knuckle failure caused floors to sag. The concrete slab and trusses were always connected in the analysis.

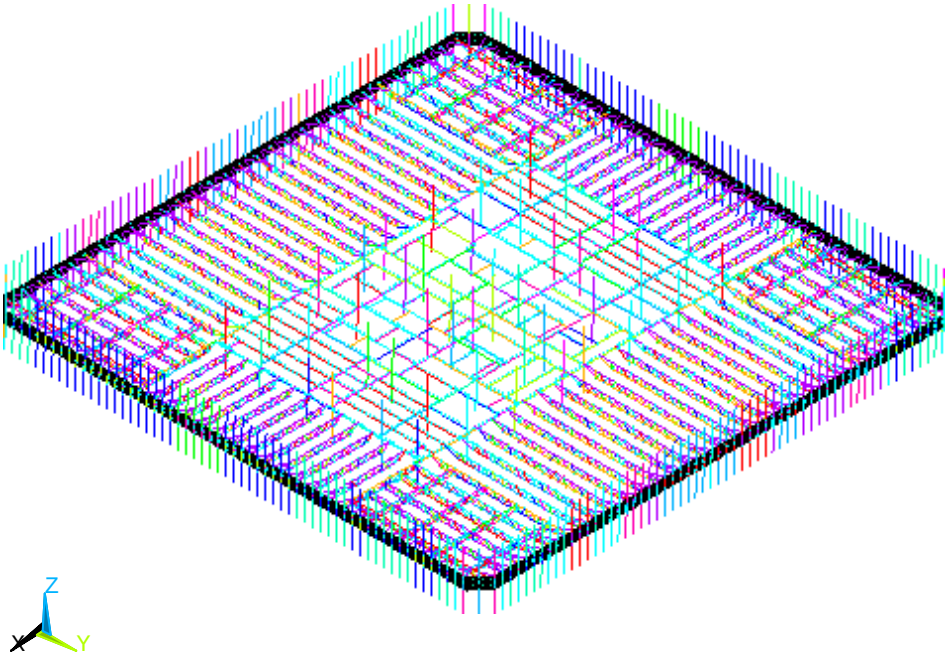

Figure 5–40. Full floor model after removal of deck support angles, spandrel studs, bridging trusses outside of two-way zones, and strap anchors.

5.5.4 Material Properties

Material properties from Table 3–1 were assigned to each steel member according to the PANYNJ drawings. The Hjelm plasticity model used for the concrete slab in the truss model can be used only with solid elements. Since the concrete slab in the full floor model was modeled by shell elements to enhance computational efficiency, a bilinear model with a yield point at its compressive strength was created and assigned to the shell elements for the concrete slab. This material model required the same yield strength values in both tension and compression, as shown in Fig. 5–41. With this material model, tensile strength of the concrete slab was not represented accurately, and the actual floor stiffness was overestimated. In the full floor models, bending stresses in the concrete slab that exceeded the actual tensile strength of concrete were found in few locations. This phenomenon was typically observed when the temperature of the top of the slab was higher than the temperature at the bottom of the slab, and the concrete slab still deflected down due to large thermal expansion of the truss. However, when the temperature is higher at the bottom, the simplified truss model with this material model showed a very similar behavior to the detailed truss model, and the key failure modes of the floors were not significantly affected.

Thermal expansion of the spandrel would cause the spandrel to buckle between columns at early stages of thermal loading and slow down the computation, causing severe convergence problems. To enhance computational efficiency, a bilinear material model with a yield strength lower than the elastic buckling strength was incorporated in the spandrel to prevent its elastic buckling. Figure 5–42 shows the bilinear model in the spandrel and the location of elements with this material model.

It was found that creep in BEAM188/189 elements would cause severe convergence problems when those elements experience thermally-induced buckling. Therefore, creep was not included in any of the full floor analyses.

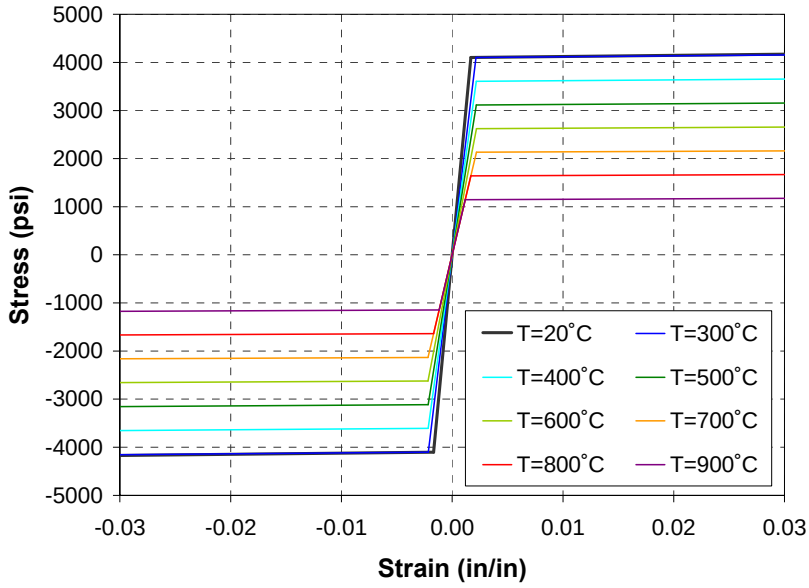

Figure 5–41. Bilinear material model for concrete slab in the full floor model.

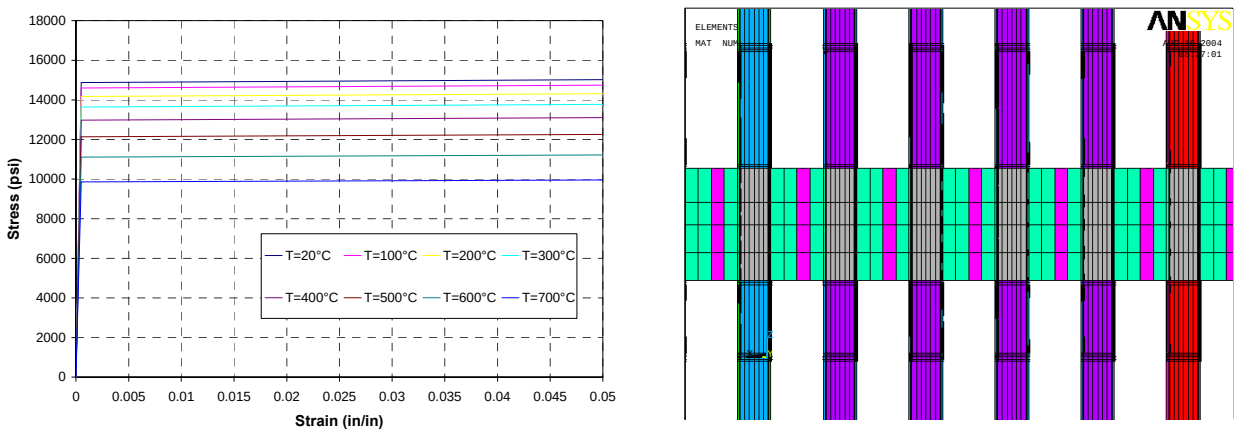

(a) Bilinear material model for spandrel (only tension side is shown)

(b) Elements with the bilinear material model (shown in pick)

Figure 5–42. Bilinear material model in the spandrel.

5.5.5 User-Defined Break Elements

Break elements were used to represent component failures. Break elements for the full floor model were recreated by using user-defined elements in ANSYS. Basically, a user-defined break element is an elastic spring. When the force or the moment in a certain direction in the element reaches its capacity, the spring stiffnesses in all directions are reduced to the predefined post-failure stiffnesses. Initial and post-failure stiffnesses are defined as temperature-independent properties, while the capacity can be defined as temperature-dependent properties. Different capacities can be assigned to tension and compression. There are differences between the break elements defined by COMBIN37 elements described in Section 5.2.5 and the break elements defined by user-defined elements. First, the user-defined break

element has stiffness even after failure of the element although the post-failure stiffness is set significantly small, usually 10^{-4} to 10^{-6} times the initial stiffness. Second, only one user-defined break element is usually required to model one failure mode, while many COMBIN37 break elements along with elastic beam elements are required to model one failure mode.

Four different types of user-defined break elements were developed for the full floor model and the exterior wall model, and their features are summarized in Table 5–10. Figure 5–43 shows a summary of user-defined break element locations in the full floor model.

Table 5–10. Types of user-defined break elements.

Type	Degrees of Freedom.	Capacities to be defined	Stiffness to be defined	Description	Usage in the floor model
102	UX UY UZ ROTX ROTY ROTZ	Positive FX Negative FX Positive FY Negative FY Positive FZ Negative FZ MX MY MZ	Initial stiffness for UX Post-failure stiffness for UX Initial stiffness for UY Post-failure stiffness for UY Initial stiffness for UZ Post-failure stiffness for UZ Initial stiffness for ROTX Post-failure stiffness for ROTX Initial stiffness for ROTY Post-failure stiffness for ROTY Initial stiffness for ROTZ Post-failure stiffness for ROTZ	All force and moment components are checked with corresponding capacities.	Failure of seats Fracture of gusset plates Failure of connections between primary and bridging trusses Failure of connections between long-span and transfer trusses
103	UX UY UZ	Positive F Negative F	Initial stiffness for UX, UY, and UZ Post-failure stiffness for UX, UY, and UZ	SRSS* of three force components is checked with the capacity. The sign of force is determined by the direction specified by the user.	Failure of strap anchor welds
104	UX UY UZ	Positive FX Negative FX Positive FY Negative FY Positive FZ Negative FZ	Initial stiffness for UX Post-failure stiffness for UX Initial stiffness for UY Post-failure stiffness for UY Initial stiffness for UZ Post-failure stiffness for UZ	All force components are checked with corresponding capacities.	Failure of studs connecting the spandrel and the slab
105	UX UY UZ ROTX ROTZ ROTZ	Positive F Negative F	Initial stiffness for UX, UY, and UZ Post-failure stiffness for UX, UY, and UZ Initial stiffness for ROTX, ROTY, and ROTZ Post-failure stiffness for ROTX, ROTY, and ROTZ	SRSS* of three force components is checked with the capacity. The sign of force is determined by the direction specified by the user.	Buckling of web diagonals Failure of resistance weld between web diagonals and chords

*SRSS: square-root-of-sum-of-square

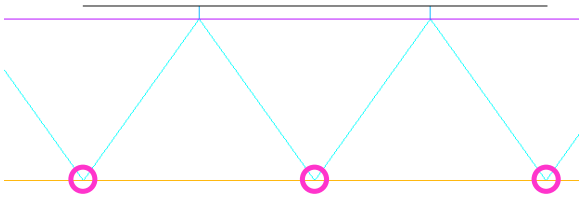

(a) Web diagonal buckling or weld failure

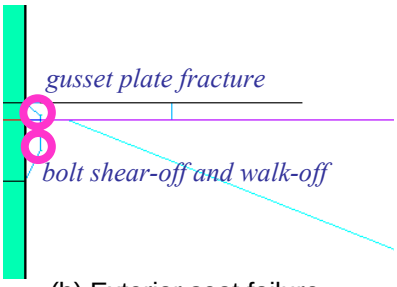

(b) Exterior seat failure

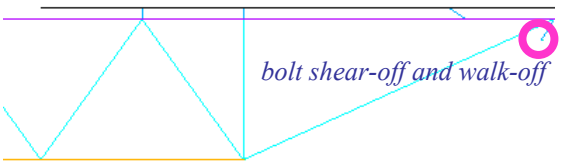

(c) Interior seat failure

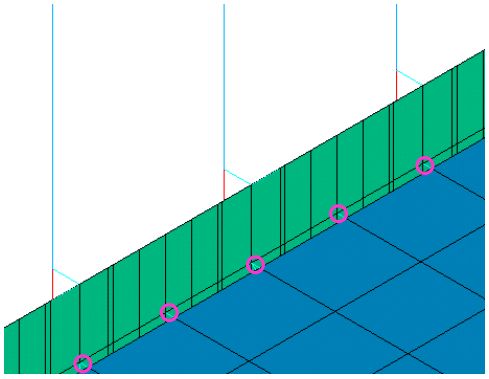

(d) Stud failure

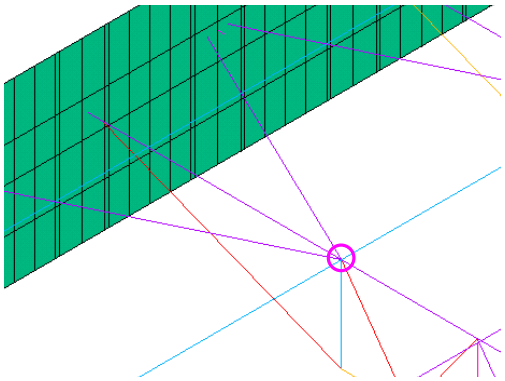

(d) Strap anchor weld failure

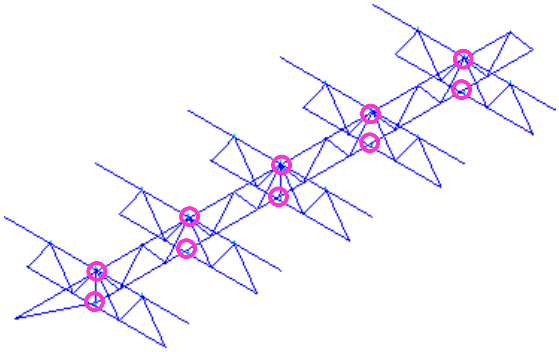

(e) Connection failure between primary and bridging trusses

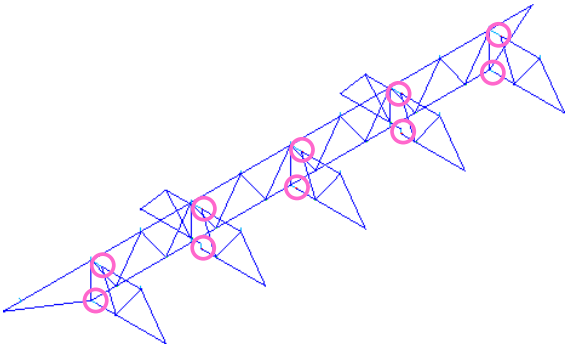

(f) Connection failure between long-span and transfer trusses

Figure 5–43. Summary of user-defined break element locations in the full floor model.

Table 5–11 gives the number of user-defined break elements in the WTC 1 Floor 96 model after the removal of studs, strap anchors, bridging trusses, and severed members by aircraft impact, and Fig. 5–44 shows locations of the user-defined break elements.

Table 5–11. Number of user-defined break elements in the full floor model (Floor 96, WTC 1).

	Number of break elements
Web diagonals	1,264
Studs	0
Strap anchor welds	0
Seats and gusset plates	564
Connections between primary and bridging trusses	200
Connections between long-span and transfer trusses	40
Total	2,068

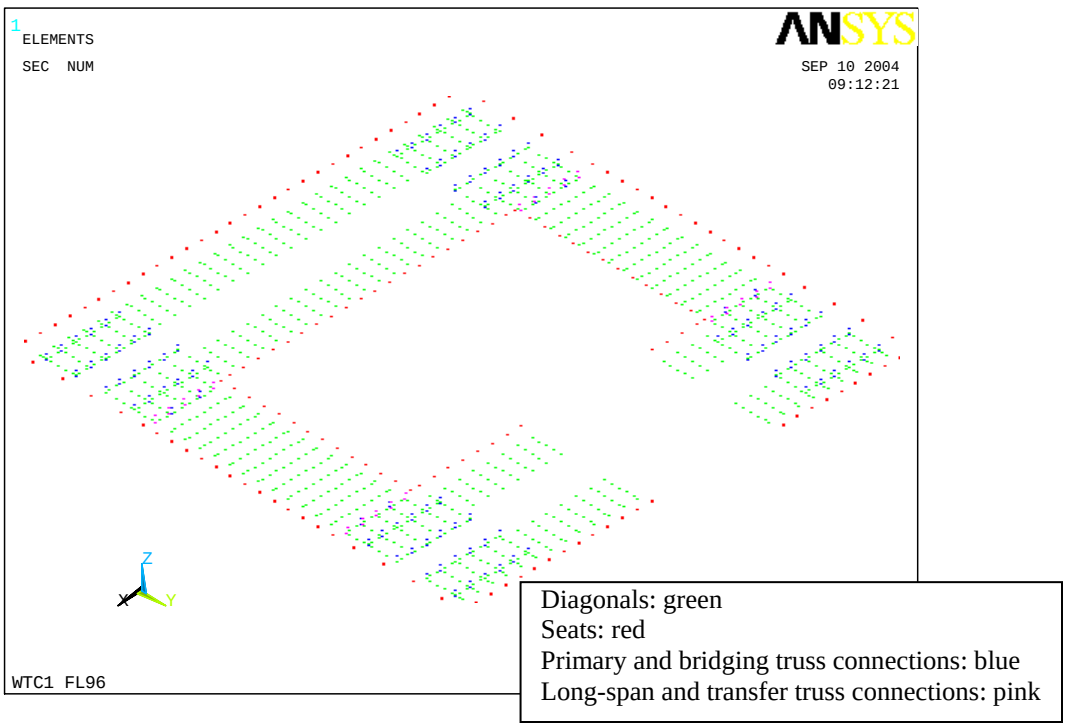

Figure 5–44. User-defined break element locations in the full floor model (Floor 96, WTC 1).

5.5.6 Impact Damage

Elements corresponding to structural members that sustained severe structural damage were removed from the model. Based on the aircraft impact analysis, NIST identified two sets of impact damage (structural damage and insulation damage) for each of the two WTC towers. These two cases represented a *base case* and a *more severe* case of damage estimates, and they were designated as "Case A_i impact damage condition" and "Case B_i impact damage condition" for WTC 1, and "Case C_i impact damage condition" and "Case D_i impact damage condition" for WTC 2. The floor model analyses were performed by using these impact damage conditions. However, NIST later refined these impact damage conditions, and refined cases are referred to as "Case A impact damage condition" and "Case B impact damage condition" for WTC 1, and "Case C impact damage condition" and "Case D impact damage condition" for WTC 2. Refined impact damage conditions were never used in the full floor model. Figures 5–45 to 5–54 show structural impact damage conditions for different cases. Structural impact damage to exterior columns did not change between Case A_i and Case B_i or between Case C_i and Case D_i. Only columns that were indicated as "severed" were removed from the model, and those columns that were damaged but not severed were retained as undamaged in the analysis. Figures 5–55 through 5–60 show floor models of WTC 1 Floor 96 with and without impact damage for Case A_i impact damage condition.

Using the base floor model (WTC 1 Floor 96) as a basis, seven floor models from Floor 93 to Floor 99 of WTC 1 were created for Case A_i structural damage condition. Each model had the same geometry, but different impact damages were incorporated. Since Case B_i structural damage condition was not provided by NIST at the time of computation, the same structural damage as Case A_i was assumed for Case B_i condition. The WTC 2 Floor 81 model was developed by changing only column properties of the base floor model (WTC 1 Floor 96). Floor models of other floors of WTC 2 (Floor 79, Floor 80, Floor 82, and Floor 83) had the same geometry as the WTC 2 Floor 81 model, but had different impact damage. For WTC 2, a total of ten models were created: five models for Case C_i impact damage condition and five for Case D_i impact damage condition.

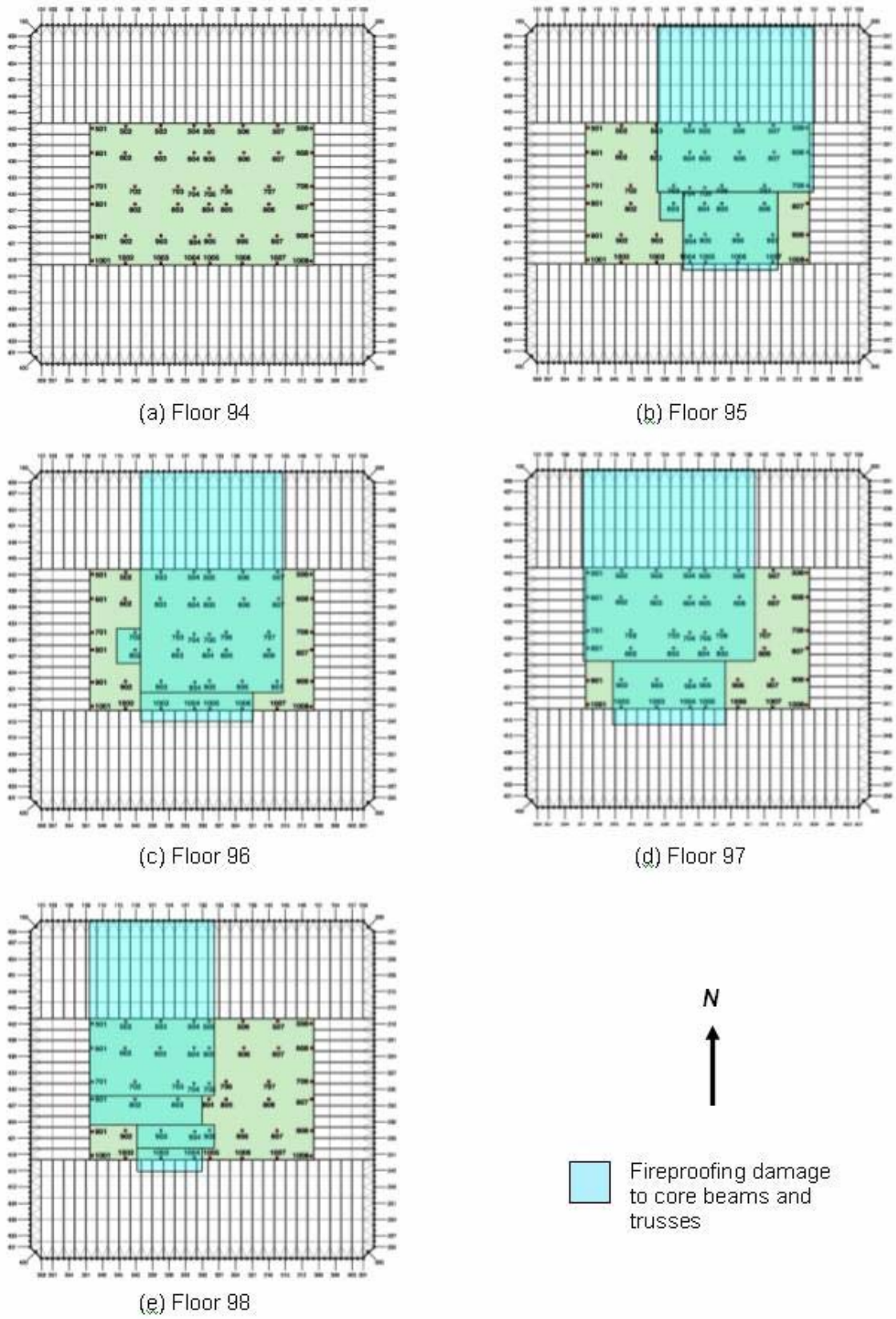

Figure 5–45. Case A_i insulation damage condition for WTC 1 floor trusses and beams.

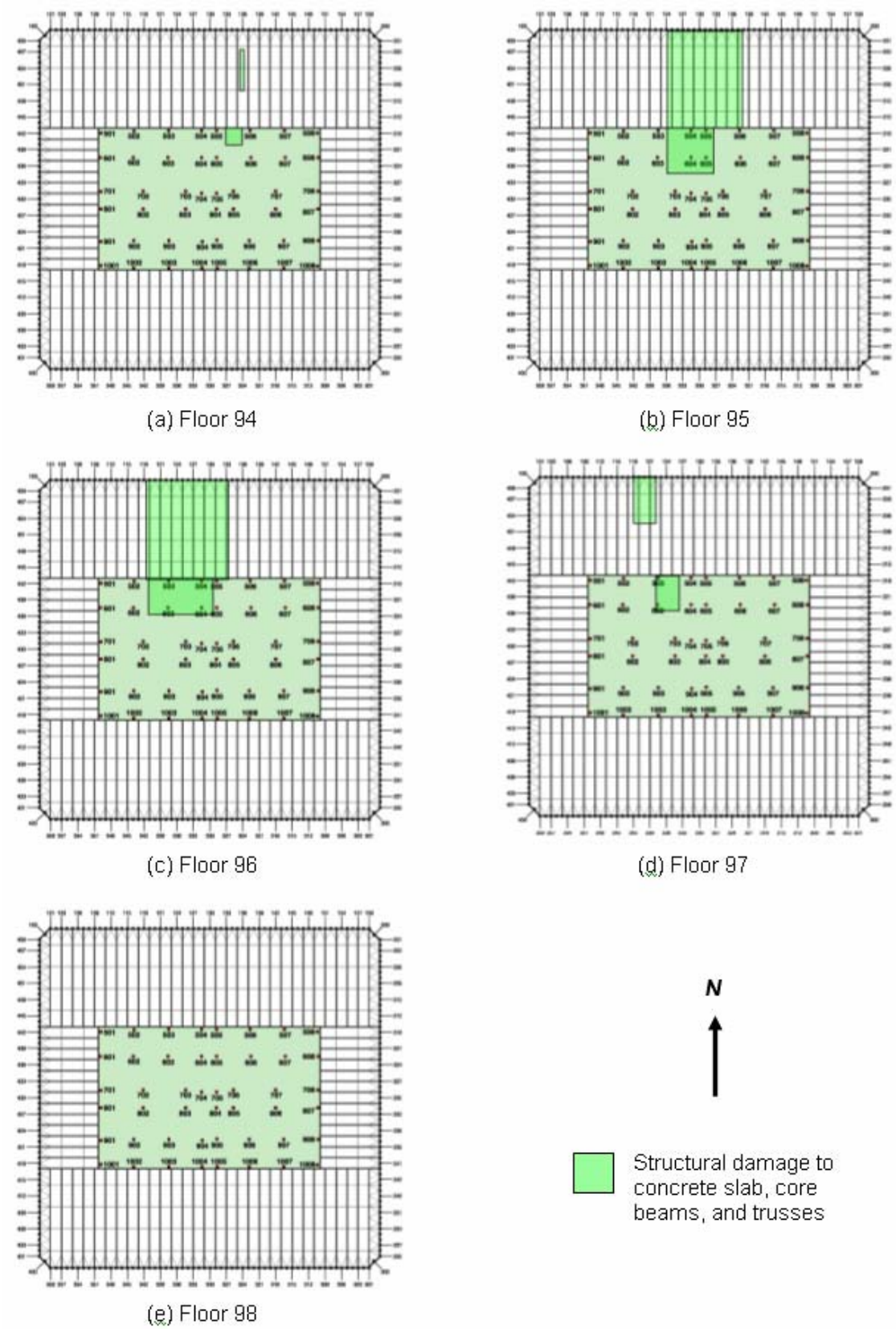

Figure 5–46. Case A_i structural damage condition for WTC 1 floors.

Column	200	159	158	157	156	155	154	153	152	151	150	149	148	147	146	145	144	143	142	141	140	139	138	137	136	135	134	133	132	131	130	129	128	127	126	125	124	123	122	121	120	119	118	117	116	115	114	113	112	111	110	109	108	107	106	105	104	103	102	101	100
Floor																																																														
99 Spandrel																																																														
Column																																																														
98 Spandrel																																													S	S	S	S	S													
Column																											S	S	S				S	S	S			D	D	S	S	S	S	S	S	D															
97 Spandrel																											S	S	S				S	S	S			D	S	S	S	S																			
Column																											S	S	S	S	S	S	S	S	S	S	S	S	S	S	S																				
96 Spandrel																											S	S	S	S	S	S	S	S	S	S	S	S	D																						
Column															S	S	S							S	S	S	S	S	S	S	S	S	S	S	S	S	S	S																							
95 Spandrel																					D	D	D	S	S	S	S	S	S				S	S	S																									
Column										S			D	D	D	D	S	S	S	S	S	S	S	S	S	S	S	S	S				S	S	S																									
94 Spandrel																																																														
Column																																																														
93 Spandrel																																																														
Column																																																														
92 Spandrel																																																														

(a) North face

	400	359	358	357	356	355	354	353	352	351	350	349	348	347	346	345	344	343	342	341	340	339	338	337	336	335	334	333	332	331	330	329	328	327	326	325	324	323	322	321	320	319	318	317	316	315	314	313	312	311	310	309	308	307	306	305	304	303	302	301	300
Floor																																																														
99 Spandrel																																																														
Column																																																														
98 Spandrel																																																														
Column																																																														
97 Spandrel																																																														
Column																																																														
96 Spandrel																														S	S	S																														
Column																														S	S	S																														
95 Spandrel																														S	S	S																														
94 Spandrel																														S	S	S																														
Column																																																														
93 Spandrel																																																														
Column																																																														
92 Spandrel																																																														

(b) South face

S: severed; D: damaged

Figure 5–47. Structural damage to exterior walls of WTC 1 for Case A_i and Case B_i impact damage conditions.

	COL501	COL601	COL701	COL801	COL901	COL1001
FL100						
FL99	I	I	I	I	I	I
FL98	D*	I	I	I	I	D*
FL97	I	I	I	I	I	I
FL96	I	I	I	I	I	I
FL95	I	I	I	I	I	I
FL94	I	I	I	I	I	I
FL93	I	I	I	I	I	I
FL92	D*	I	I	I	I	D*

	COL502	COL602	COL702	COL802	COL902	COL1002
FL100						
FL99	I	I	I	I	I	I
FL98	D*	I	I	I	I	I
FL97	I	I	I	I	I	I
FL96	I	I	I	I	I	I
FL95	I	I	I	I	I	I
FL94	I	I	I	I	I	I
FL93	I	I	I	I	I	I
FL92	I	I	I	I	I	I

	COL503	COL603	COL703	COL803	COL903	COL1003
FL100						
FL99	I	I	I	I	I	I
FL98	I	I	I	I	I	I
FL97	I	I	I	I	I	I
FL96	D	I	I	I	I	I
FL95	I	I	I	I	I	I
FL94	I	I	I	I	I	I
FL93	I	I	I	I	I	I
FL92	I	I	I	I	I	I

	COL504	COL604	COL704		COL904	COL1004
FL100						
FL99	I	I	I		I	I
FL98	I	I	I		I	I
FL97	I	I	I		I	I
FL96	S	A	D		D	I
FL95	S	S	D		I	I
FL94	S	S	I		I	I
FL93	S	I	I		I	I
FL92	R	I	I		I	I

	COL505	COL605	COL705	COL804	COL905	COL1005
FL100						
FL99	I	I	I	I	I	I
FL98	I	I	I	I	I	I
FL97	I	I	I	I	I	I
FL96	D	I	I	I	I	I
FL95	D	I	I	I	I	I
FL94	I	I	I	I	I	I
FL93	I	I	I	I	I	I
FL92	I	I	I	I	I	I

	COL506	COL606	COL706	COL805	COL906	COL1006
FL100						
FL99	I	I	I	I	I	I
FL98	I	I	I	I	I	I
FL97	I	I	I	I	I	I
FL96	I	I	I	I	I	I
FL95	I	I	S	I	I	I
FL94	D	I	S	D	I	I
FL93	I	I	S	I	I	I
FL92	I	I	R	I	I	I

	COL507	COL607	COL707	COL806	COL907	COL1007
FL100						
FL99	I	I	I	I	I	I
FL98	I	I	I	I	I	I
FL97	I	I	I	I	I	I
FL96	I	I	I	I	I	I
FL95	I	I	I	I	I	I
FL94	I	I	I	I	I	I
FL93	I	I	I	I	I	I
FL92	I	I	I	I	I	I

	COL508	COL608	COL708	COL807	COL908	COL1008
FL100						
FL99	I	I	I	I	I	I
FL98	D*	I	I	I	I	D*
FL97	I	I	I	I	I	I
FL96	I	I	I	I	I	I
FL95	I	I	I	I	I	I
FL94	I	I	I	I	I	I
FL93	I	I	I	I	I	I
FL92	D*	I	I	I	I	D*

I: intact	A: alignment affected
D: damaged (plastic strain present)	S: severed
R: rotated	*: column connections show plastic strains

Figure 5–48. Structural damage to core columns of WTC 1 for Case A_i impact damage condition.

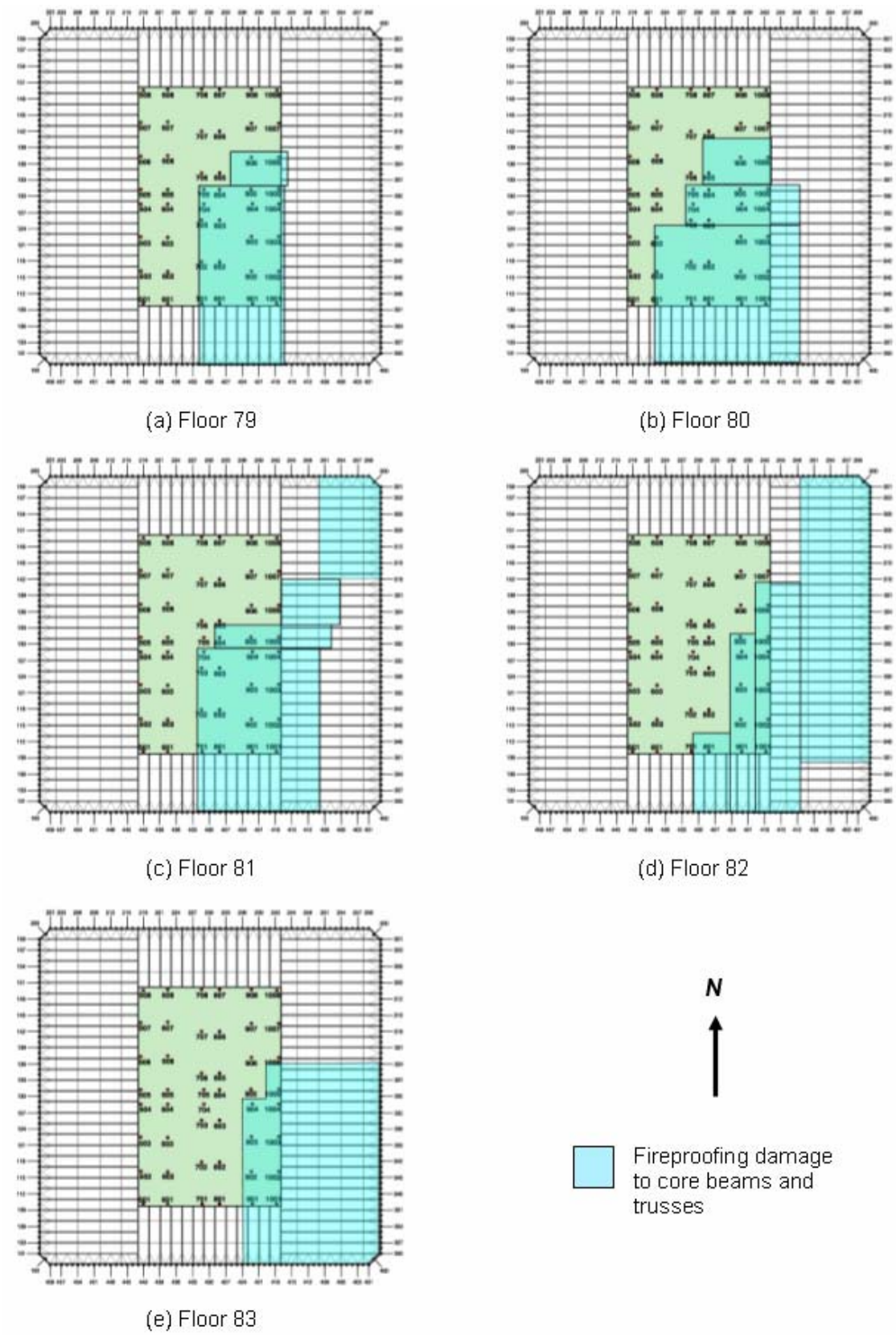

Figure 5–49. Case C_i insulation damage condition for WTC 2 floor trusses and beams.

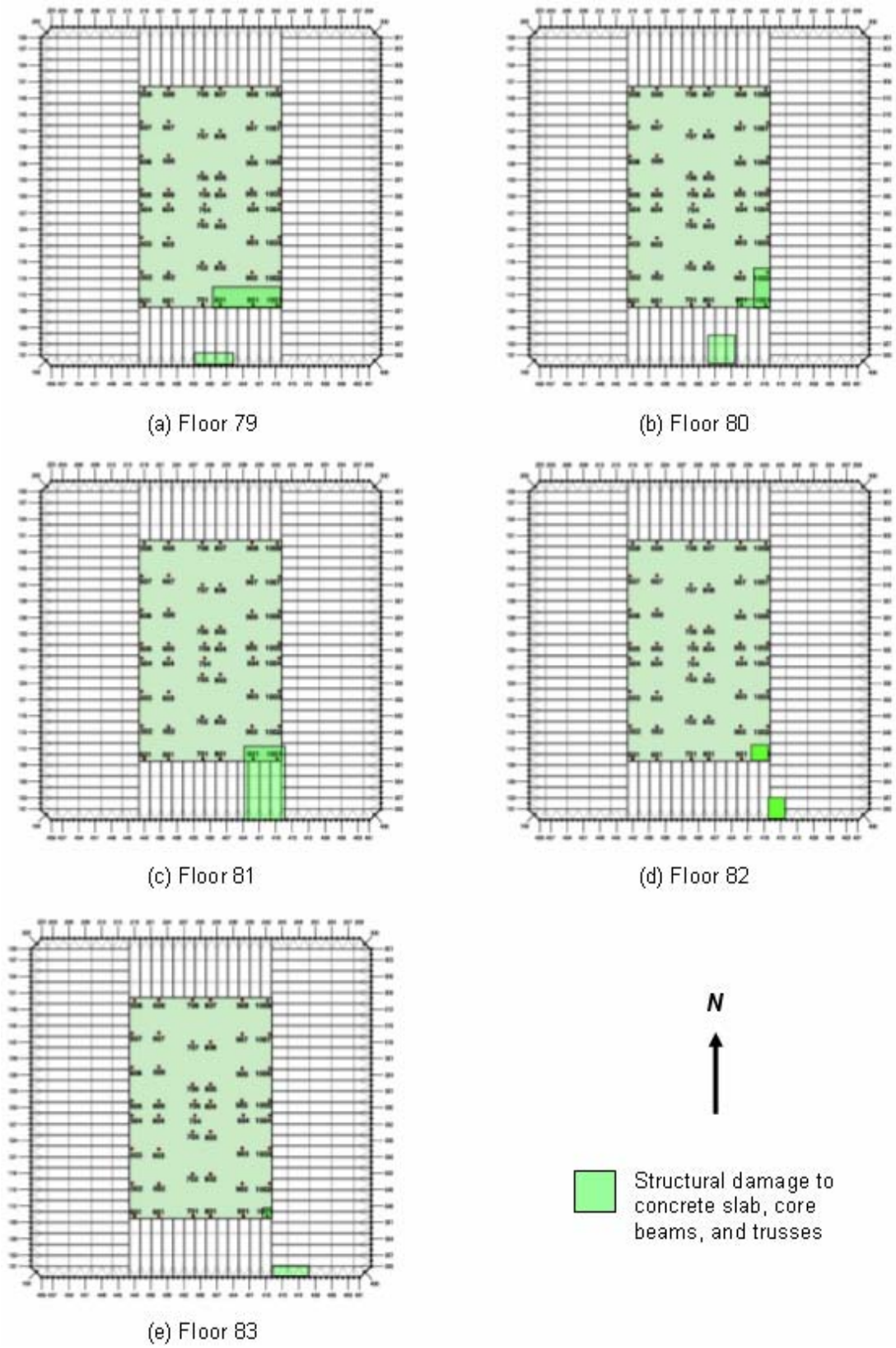

Figure 5–50. Case C_i structural damage condition for WTC 2 floors.

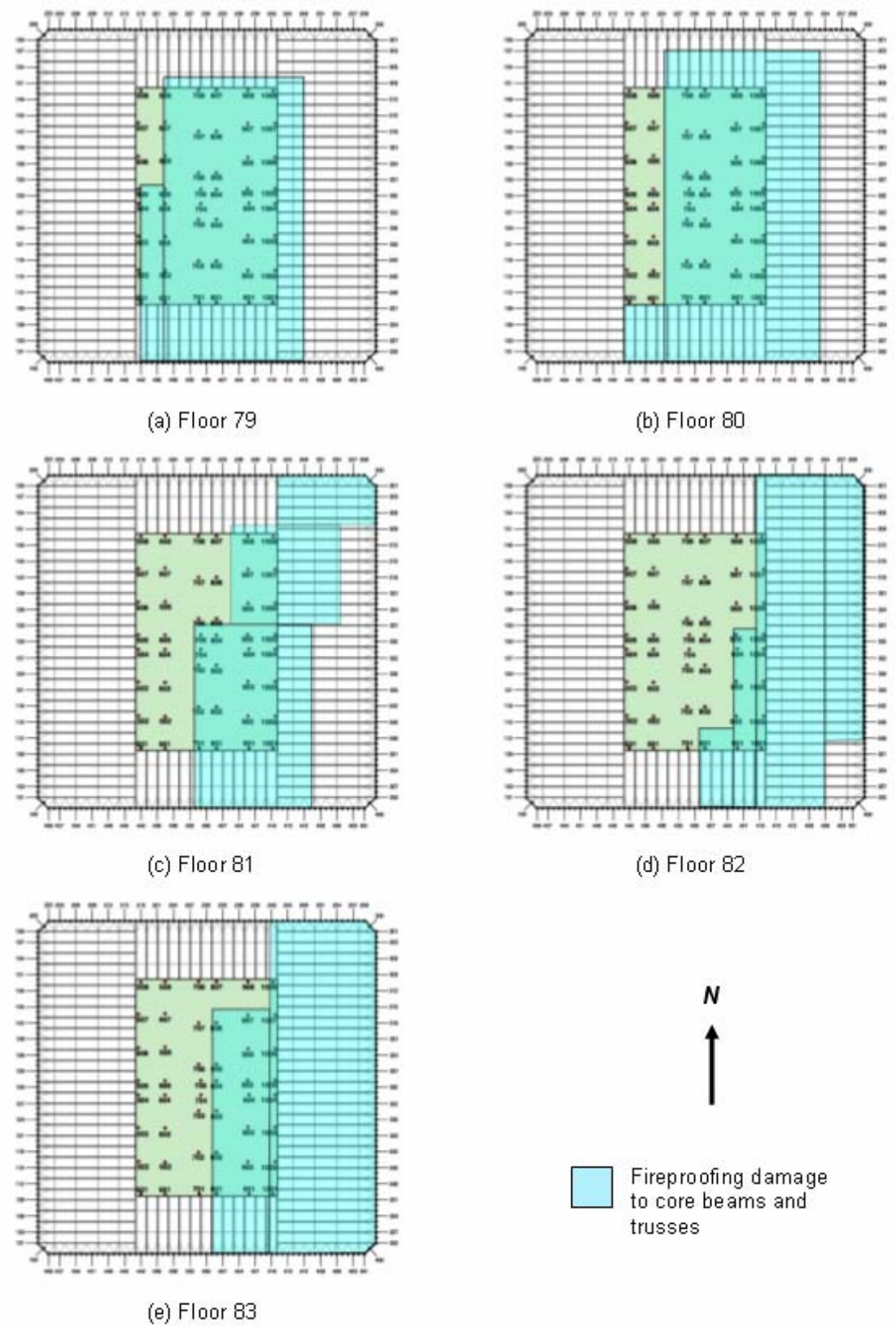

Figure 5–51. Case D_i insulation damage condition for WTC 2 floor trusses and beams.

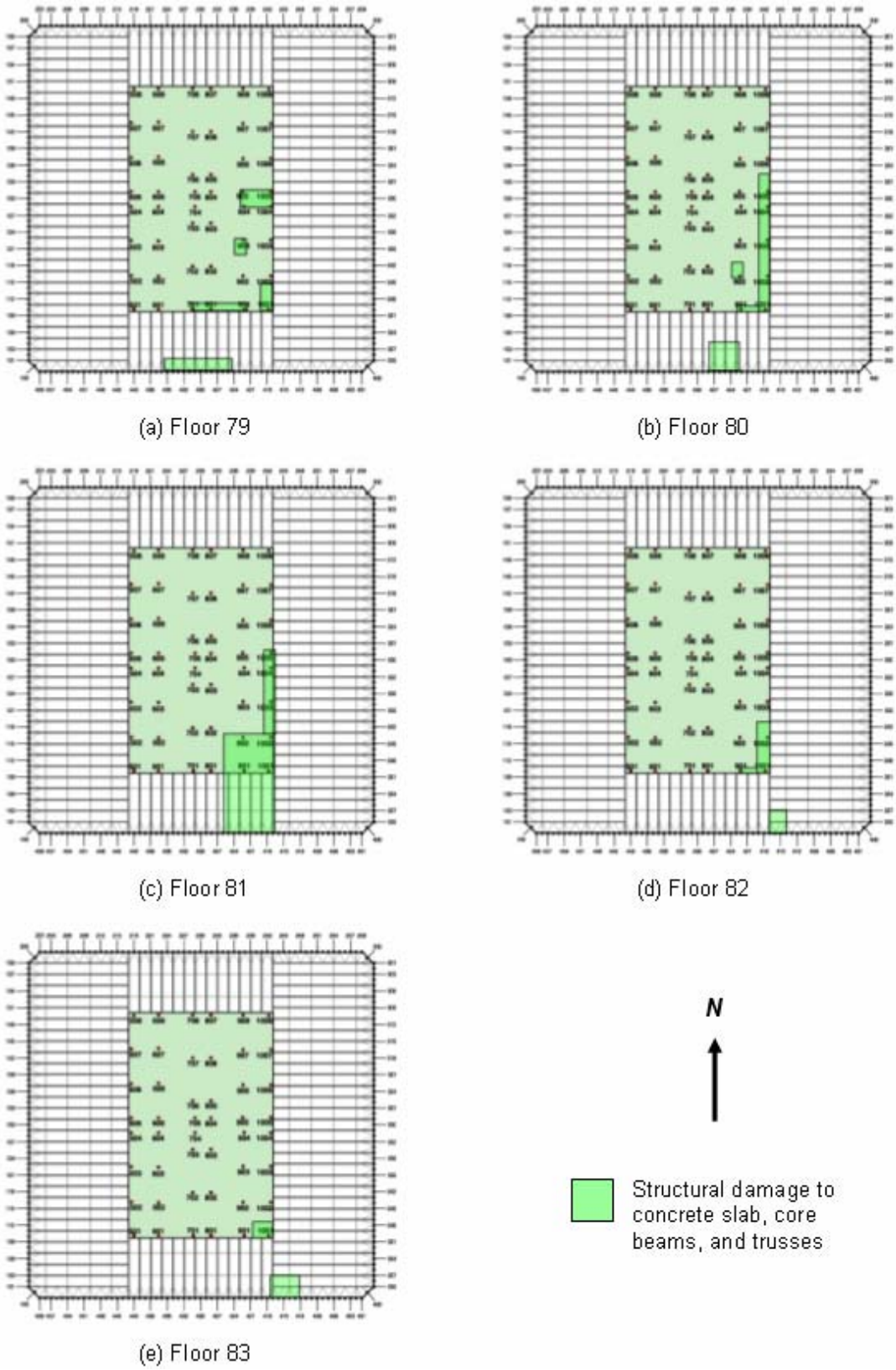

Figure 5–52. Case D_i structural damage condition for WTC 2 floors.

Column	300	259	258	257	256	255	254	253	252	251	250	249	248	247	246	245	244	243	242	241	240	239	238	237	236	235	234	233	232	231	230	229	228	227	226	225	224	223	222	221	220	219	218	217	216	215	214	213	212	211	210	209	208	207	206	205	204	203	202	201	200
Floor																																																															
85 Spandrel																																																															
Column																																																															
84 Spandrel																																																															
Column																																																															
83 Spandrel																																																															
Column																																																															
82 Spandrel																																																															
Column																																																															
81 Spandrel																																																															
Column							D	S																																																						
80 Spandrel																																																															
Column																																																															
79 Spandrel																																																															
Column																																																															
78Spandrel																																																															
Column																																																															
77 Spandrel																																																															

(a) North face

Column	100	459	458	457	456	455	454	453	452	451	450	449	448	447	446	445	444	443	442	441	440	439	438	437	436	435	434	433	432	431	430	429	428	427	426	425	424	423	422	421	420	419	418	417	416	415	414	413	412	411	410	409	408	407	406	405	404	403	402	401	400
Floor																																																															
85 Spandrel																																																															
Column																																																									s	s					
84 Spandrel																																																															
Column																																																		s	S	s											
83 Spandrel																																													S	S	S	S	S	s		d	d										
Column																																										S	S	S	S	S	S	S	S												
82 Spandrel																																					D	D	D	D	D	S	S	S	S	S	S	S													
Column																																					S	S	S	S	S	S	S	S	S	S	S	S													
81 Spandrel																																				D	S	S	S	S	S	S	S	S																		
Column																																				S	S	S	S	S	S	S	S	S																	
80 Spandrel																															D	D	D	D	S	S	S	S	D	D	D	S	S	S															
Column																											S	S	S	S	S	S	S	S	S	S	S	S				S	S	S														
79 Spandrel																											S	S	S	S	S	S	S	D	D	D																						
Column																						S	S		S	S	S	S	D	S	S	S	D	D																								
78Spandrel																																																															
Column																																																															
77 Spandrel																																																															

(b) South face

S: severed; D: damaged

Figure 5–53. Structural damage to exterior walls of WTC 2 for Case C_i and Case D_i impact damage conditions.

	COL1001	COL1002	COL1003	COL1004	COL1005	COL1006	COL1007	COL1008
FL85								
FL84	I	I	I	I	I	I	I	I
FL83	S	I	I	I	I	I	I	I
FL82	S	I	I	I	I	I	I	I
FL81	S	S	I	I	I	I	I	I
FL80	S	S	I	I	I	I	I	I
FL79	S	S	I	I	I	I	I	I
FL78	S	D	I	I	I	I	I	I
FL77	S	I	I	I	I	I	I	I

	COL701	COL702	COL703	COL704	COL705	COL706	COL707	COL708
FL85								
FL84	I	I	I	I	I	I	I	I
FL83	I	I	I	I	I	I	I	I
FL82	I	I	I	I	I	I	I	I
FL81	I	I	I	I	I	I	I	I
FL80	I	I	I	I	I	I	I	I
FL79	I	I	I	I	I	I	I	I
FL78	I	I	I	I	I	I	I	I
FL77	I	I	I	I	I	I	I	I

	COL901	COL902	COL903	COL904	COL905	COL906	COL907	COL908
FL85								
FL84	I	I	I	I	I	I	I	I
FL83	I	I	I	I	I	I	I	I
FL82	I	I	I	I	I	I	I	I
FL81	D	I	I	I	I	I	I	I
FL80	S	S	I	I	I	I	I	I
FL79	S	D	I	I	I	I	I	I
FL78	I	D	I	I	I	I	I	I
FL77	I	I	I	I	I	I	I	I

	COL601	COL602	COL603	COL604	COL605	COL606	COL607	COL608
FL85								
FL84	I	I	I	I	I	I	I	I
FL83	I	I	I	I	I	I	I	I
FL82	I	I	I	I	I	I	I	I
FL81	I	I	I	I	I	I	I	I
FL80	I	I	I	I	I	I	I	I
FL79	I	I	I	I	I	I	I	I
FL78	I	I	I	I	I	I	I	I
FL77	I	I	I	I	I	I	I	I

	COL801	COL802	COL803	COL804	COL805	COL806	COL807
FL85							
FL84	I	I	I	I	I	I	I
FL83	I	I	I	I	I	I	I
FL82	I	I	I	I	I	I	I
FL81	I	I	I	I	I	I	I
FL80	I	I	I	I	I	I	I
FL79	I	I	I	I	I	I	I
FL78	I	I	I	I	I	I	I
FL77	I	I	I	I	I	I	I

	COL501	COL502	COL503	COL504	COL505	COL506	COL507	COL508
FL85								
FL84	I	I	I	I	I	I	I	I
FL83	I	I	I	I	I	I	I	I
FL82	I	I	I	I	I	I	I	I
FL81	I	I	I	I	I	I	I	I
FL80	I	I	I	I	I	I	I	I
FL79	I	I	I	I	I	I	I	I
FL78	I	I	I	I	I	I	I	I
FL77	I	I	I	I	I	I	I	I

I: Intact
D: Damaged (plastic strain present)
R: Rotated
A: Alignment affected
S: Severed

Figure 5–54. Structural damage to core columns of WTC 2 for Case C_i impact damage condition.

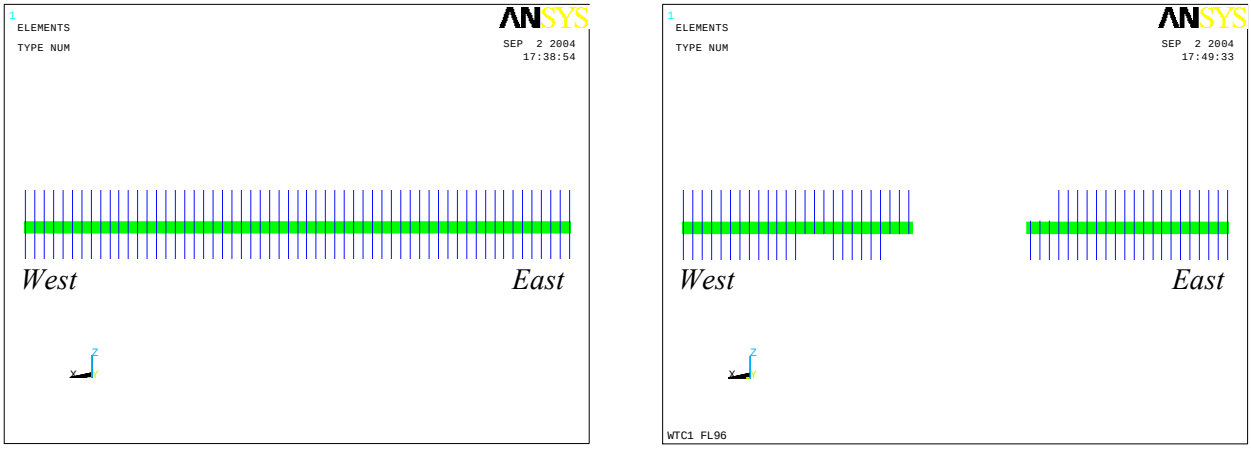

(a) Model without damage (b) Model with damage

Figure 5–55. Case A_i structural impact damage condition for exterior columns of the north face in the WTC 1 Floor 96 model.

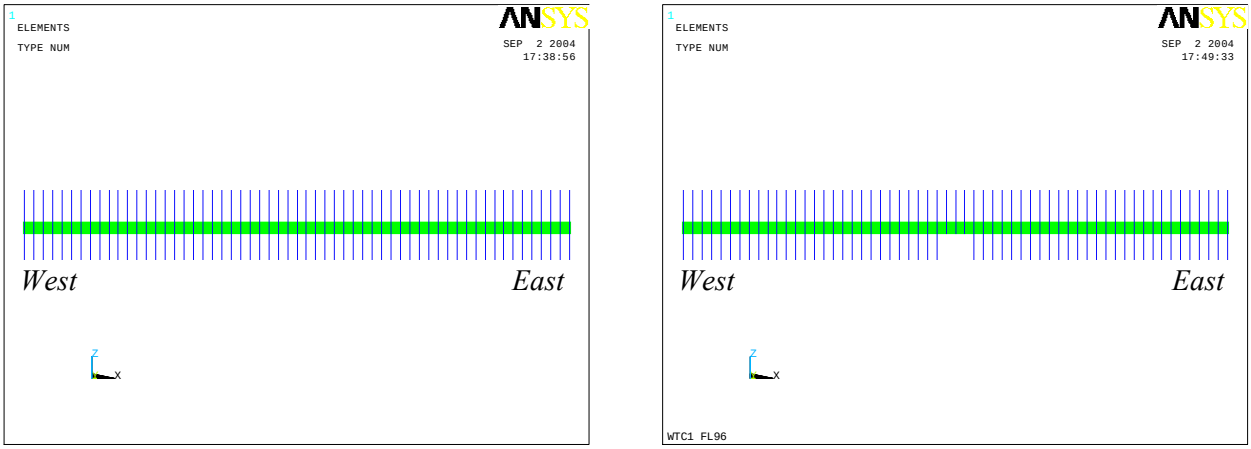

(a) Model without damage (b) Model with damage

Figure 5–56. Case A_i structural impact damage condition for exterior columns of the south face in the WTC 1 Floor 96 model.

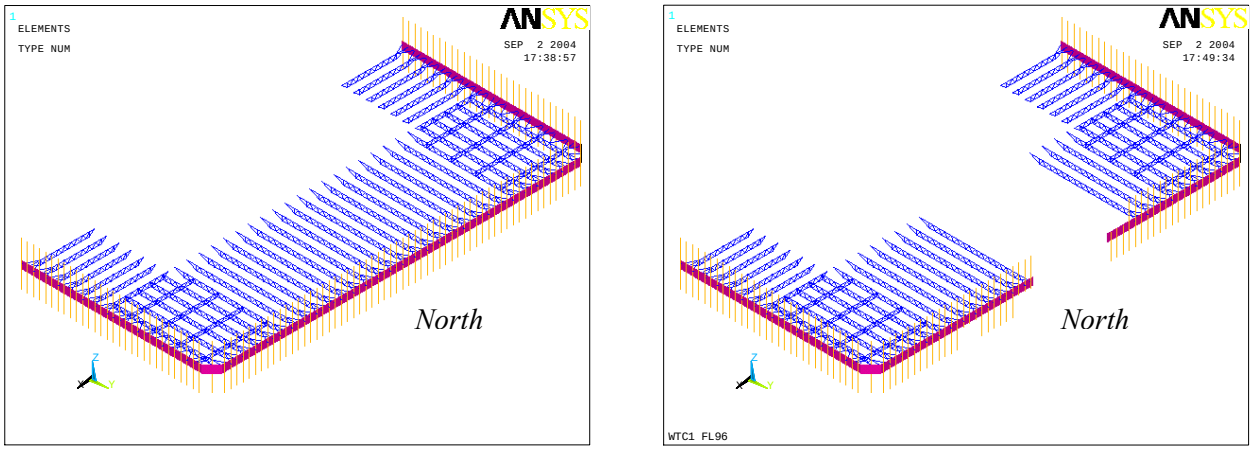

(a) Model without damage (b) Model with damage

Figure 5–57. Case A_i structural impact damage condition for floor trusses in the WTC 1 Floor 96 model.

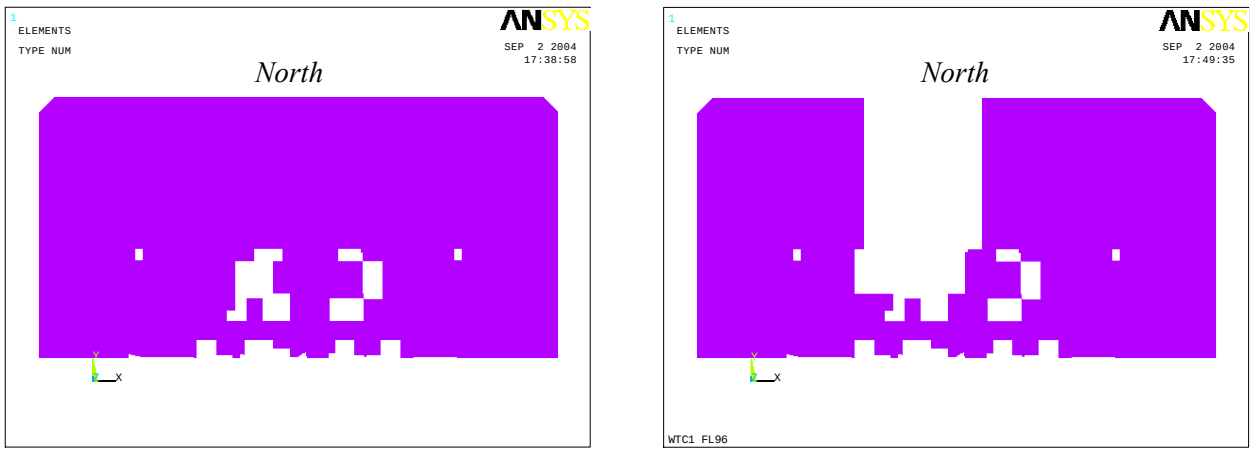

(a) Model without damage (b) Model with damage

Figure 5–58. Case A_i structural impact damage condition for the concrete slab in the WTC 1 Floor 96 model.

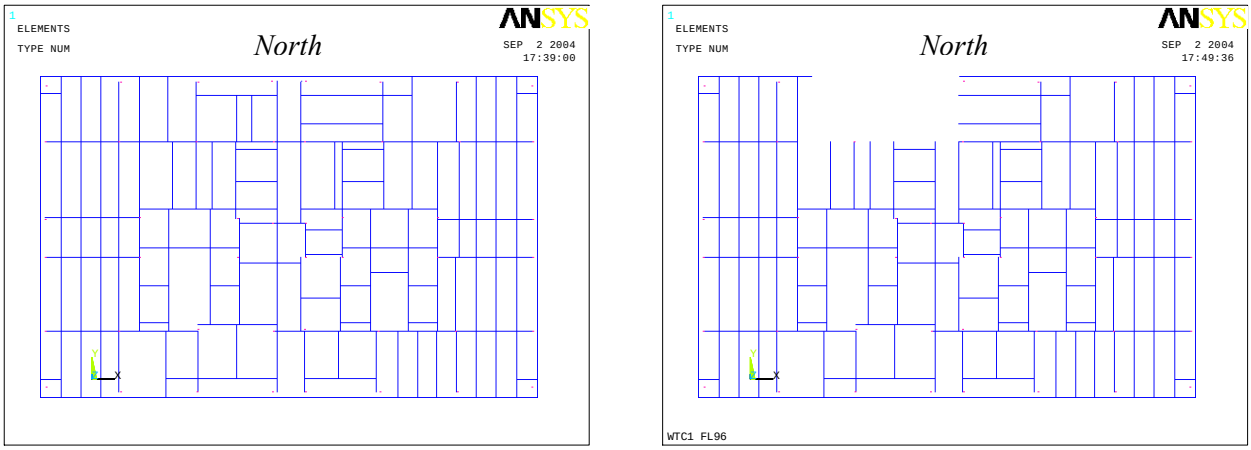

(a) Model without damage (b) Model with damage

Figure 5–59. Case A_i structural impact damage condition for core beams in the WTC 1 Floor 96 model.

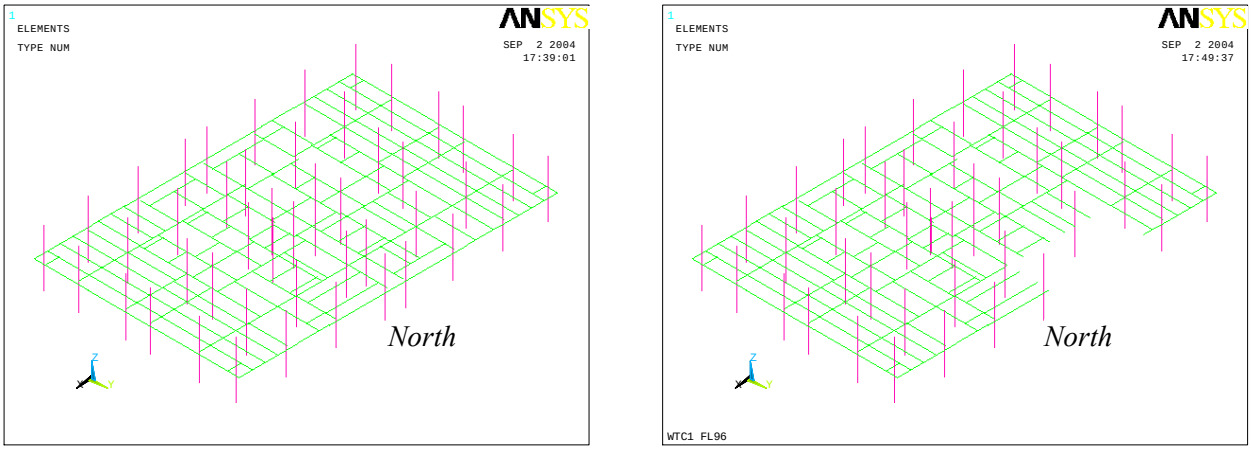

(a) Model without damage (b) Model with damage

Figure 5–60. Case A_i structural impact damage condition for core columns in the WTC 1 Floor 96 model.

5.5.7 Gravity and Thermal Loads

The full floor model with impact damage included was first analyzed for gravity dead and live loads, and then temperature time histories representative of the WTC fire conditions were applied to analyze its path-dependent nonlinear structural response. Gravity dead and live loads consisted of self-weight, 8 psf superimposed dead load, and 25 percent of design live loads. Design live loads varied from 55 psf to 85 psf as shown in Fig. 5–61. Vertical loads were not applied to the top of columns.

NIST derived the temperatures of structural components from fire models of the WTC towers and the thermal insulation damage conditions. Temperature cases provided by NIST were "Case A_i temperature condition" and "Case B_i temperature condition" for WTC 1, and "Case C_i temperature condition" and

"Case D_i temperature condition" for WTC 2.[5] The floor model analyses were performed by using these temperature conditions. However, NIST later refined these temperature conditions based on the refined impact damage conditions, and the refined cases were "Case A temperature condition" and "Case B temperature condition" for WTC 1, and "Case C temperature condition" and "Case D temperature condition" for WTC 2. For the WTC 1 Floor 97 full floor model only, Case A temperature condition was also used. Since the results from the WTC 1 Floor 97 analysis for Case A temperature condition was very similar to those for Case A_i, it was concluded that the refined temperature cases would not change the floor behavior significantly. Therefore, other floors were not run with the refined temperature conditions. Temperature data sets were provided at 10 min intervals up to 100 min for WTC 1 and up to 60 min for WTC 2 for each temperature condition. In the first step of thermal loading, temperatures were linearly ramped from room temperature (20 ˚C) to the temperatures specified at 10 min. After the first step, temperatures were varied linearly to the next specified temperatures. Figures 5–62 to 5–65 show Case A_i and Case B_i temperature conditions for Floor 96 of WTC 1, and Figs. 5–66 to 5–69 show Case C_i and Case D_i temperature conditions for Floor 82 of WTC 2. These figures show that high temperature occurs in trusses where there is insulation damage. Severed members are also shown in these figures; however, severed members were not included in the analysis. Table 5–12 shows a list of full floor analyses performed in this study.

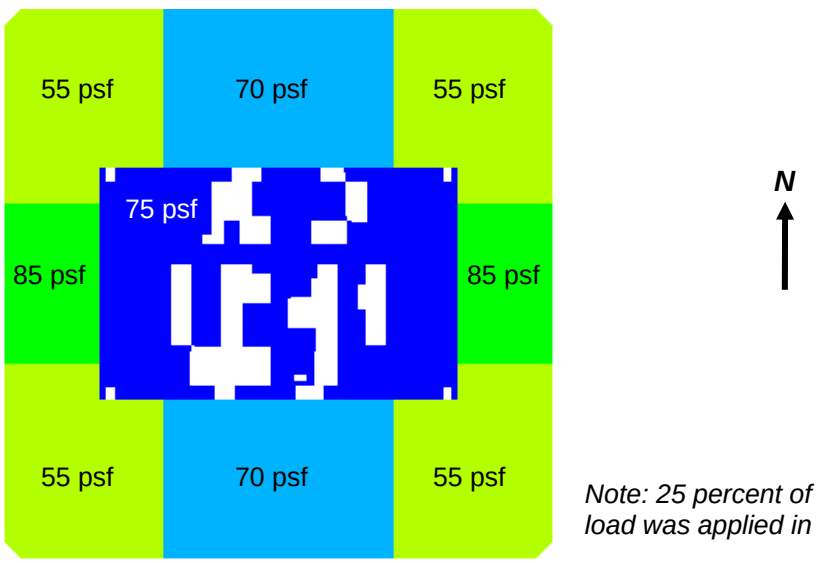

Note: 25 percent of the design live load was applied in the analysis.

Figure 5–61. Design live load distribution in Floor 96 of WTC 1.

Temperatures were assigned at node locations for beam elements. Only columns had temperature gradients across their cross sections; trusses and spandrels had uniform temperatures within their cross sections. Slab temperatures were assigned at node locations. Shell elements for the slab had four layers through thickness, and there were five points across the thickness to define the temperature distribution through the thickness at each node location.

[5] Temperature cases were formerly called by different names. Case D_i and Case C_i conditions were called "baseline case", and Case B_i and Case D_i conditions were called "maximum damage case". Case A and Case C conditions were called "best estimate case" or "realistic case", and Case B and Case D conditions were called "upper bound case" or "severe case". These former temperature case names may appear on graphics produced in ANSYS.

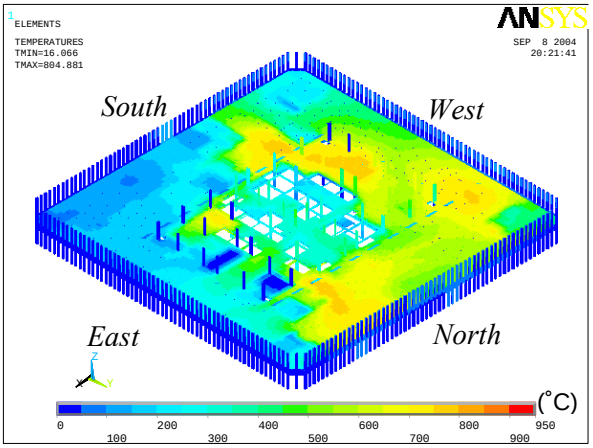

(a) Top view at 10 min

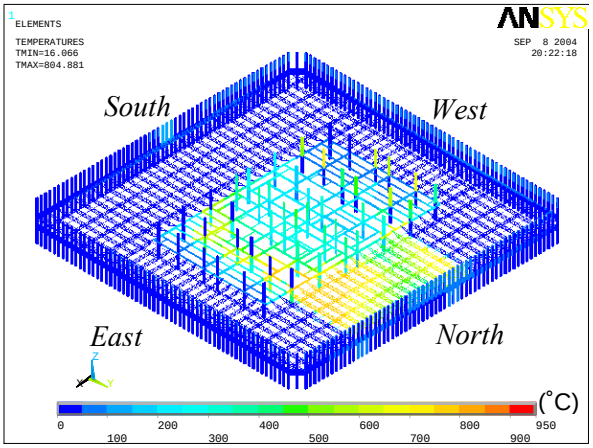

(b) Top view without concrete slab at 10 min

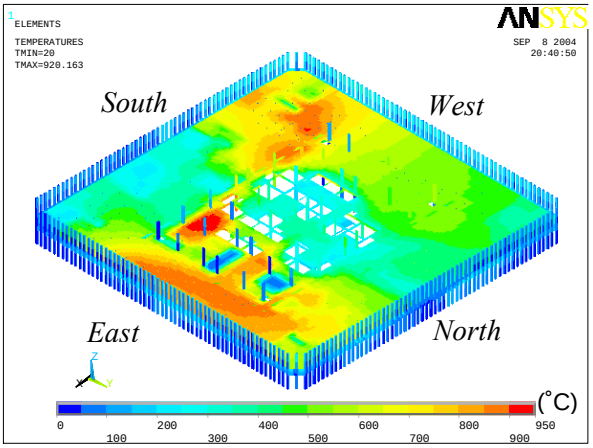

(c) Top view at 50 min

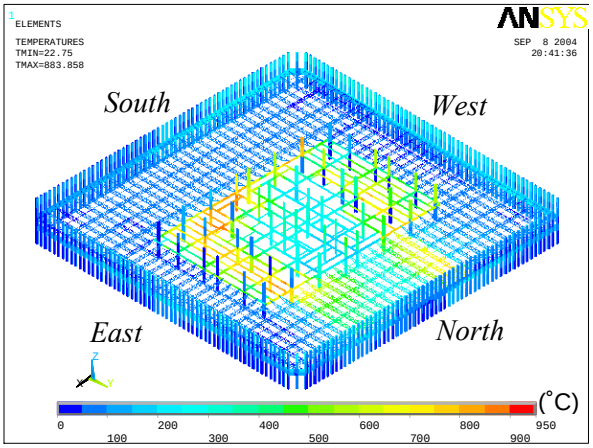

(d) Top view without concrete slab at 50 min

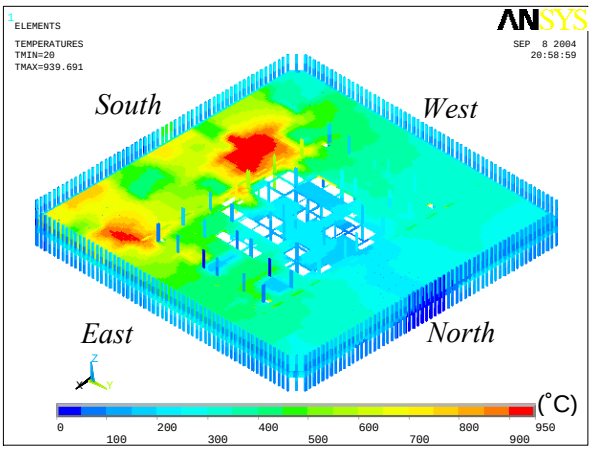

(e) Top view at 100 min

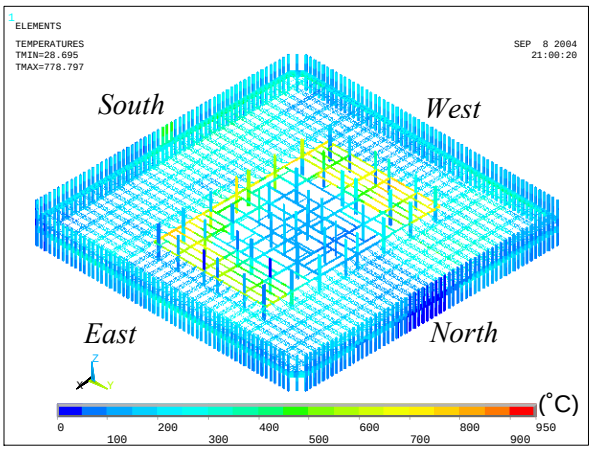

(f) Top view without concrete slab at 100 min

Figure 5–62. Case A_i temperature condition for Floor 96 of WTC 1 at 10 min, 50 min, and 100 min.

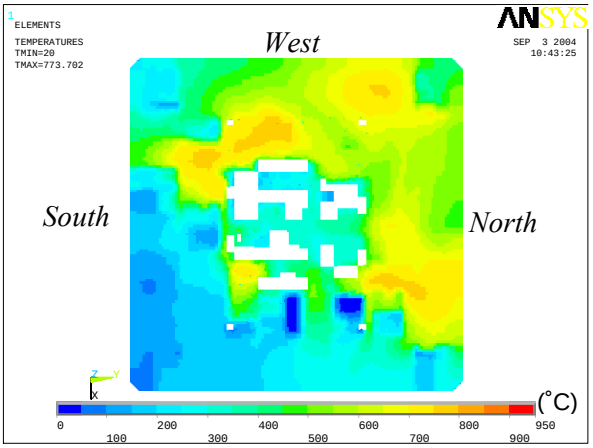

(a) Top surface at 10 min

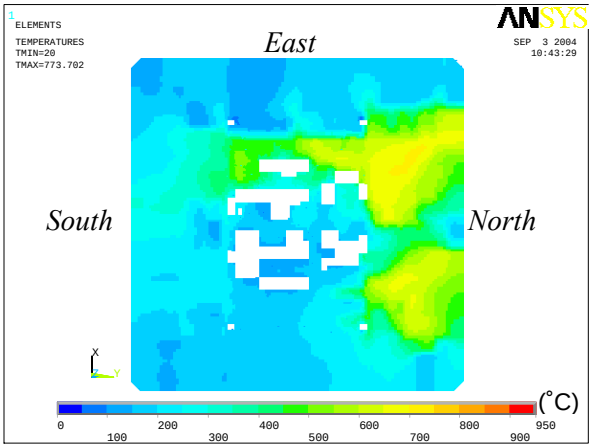

(b) Bottom surface at 10 min

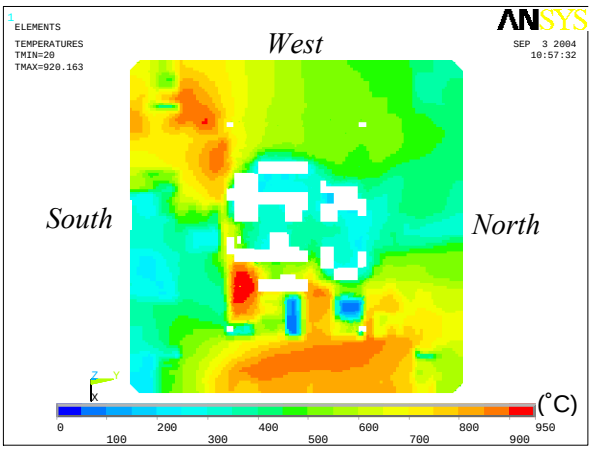

(c) Top surface at 50 min

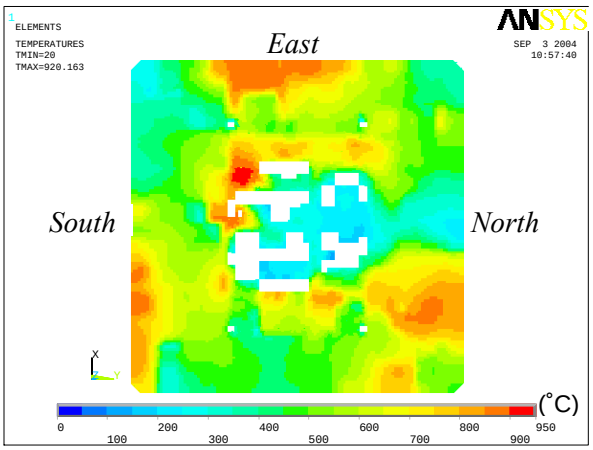

(d) Bottom surface at 50 min

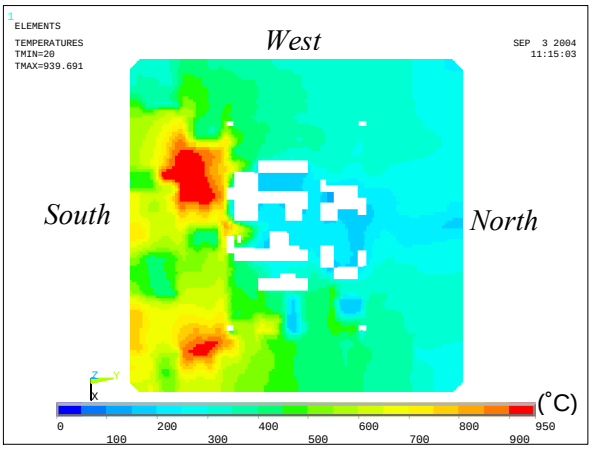

(e) Top surface at 100 min

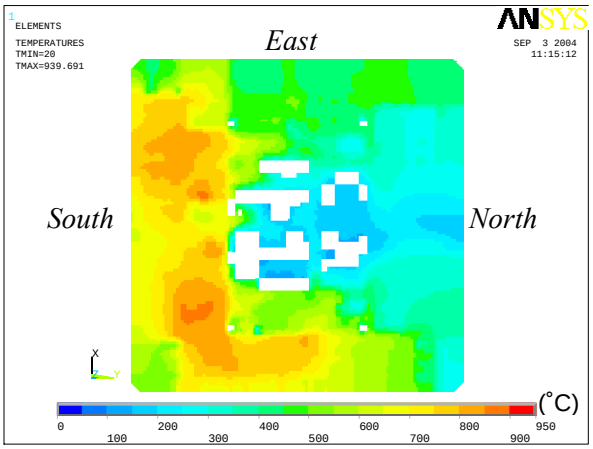

(f) Bottom surface at 100 min

Figure 5–63. Case A_i temperature distribution in the slab for Floor 96 of WTC 1 at 10 min, 50 min, and 100 min.

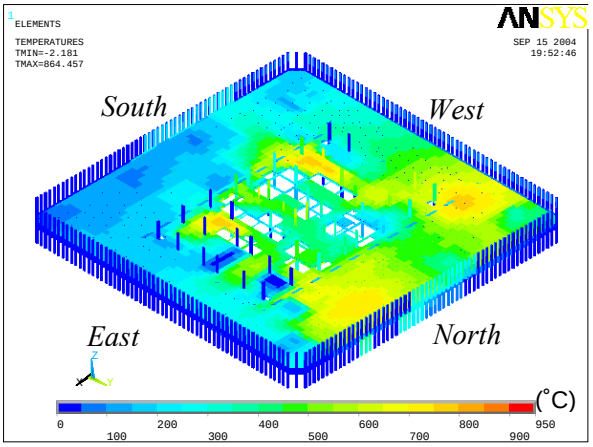

(a) Top view at 10 min

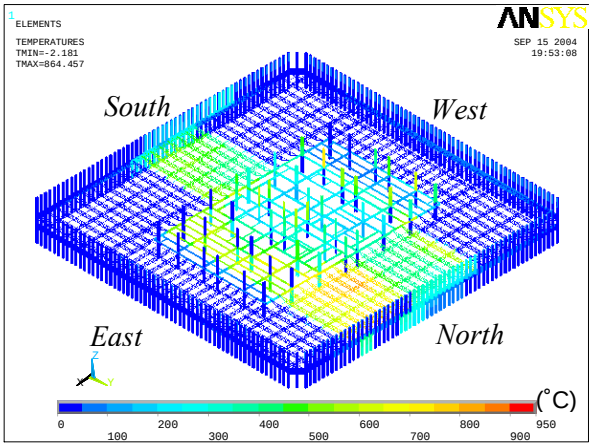

(b) Top view without concrete slab at 10 min

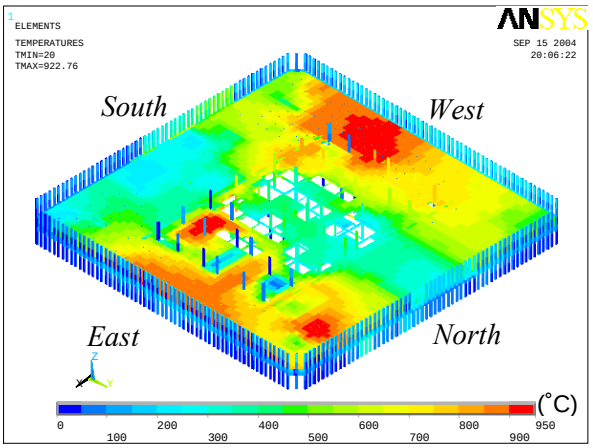

(c) Top view at 50 min

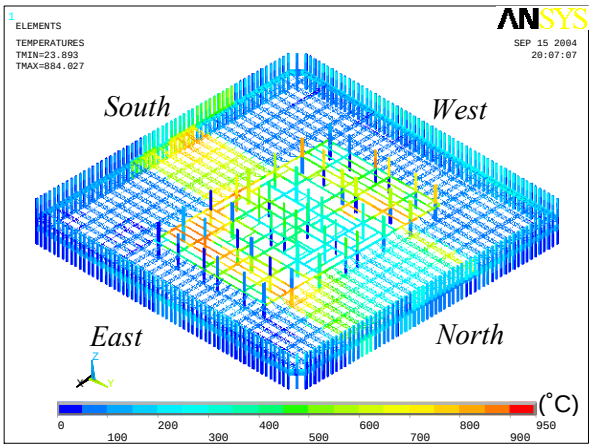

(d) Top view without concrete slab at 50 min

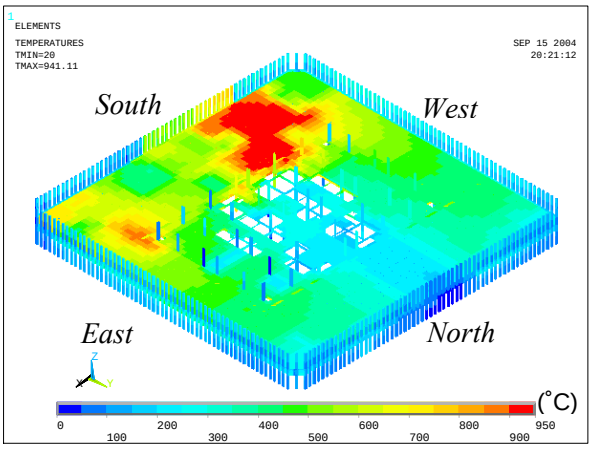

(e) Top view at 100 min

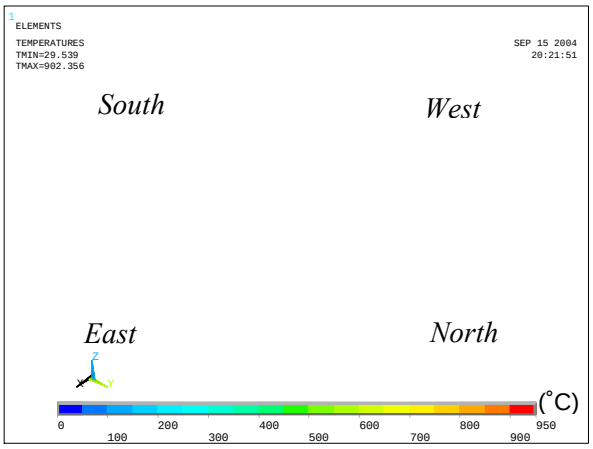

(f) Top view without concrete slab at 100 min

Figure 5–64. Case B_i temperature condition for Floor 96 of WTC 1 at 10 min, 50 min, and 100 min.

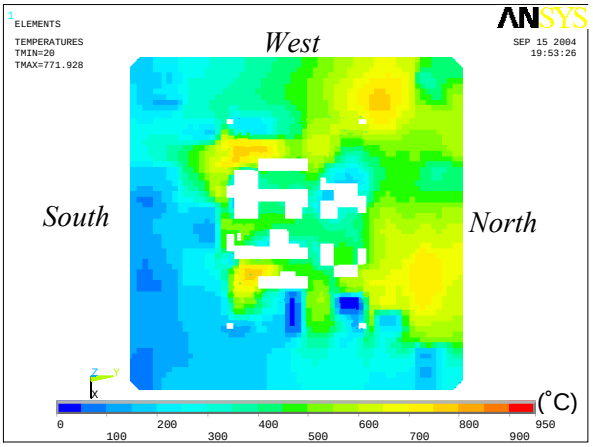

(a) Top surface at 10 min

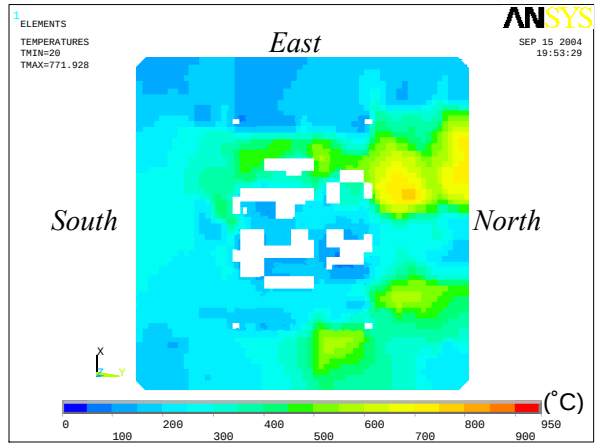

(b) Bottom surface at 10 min

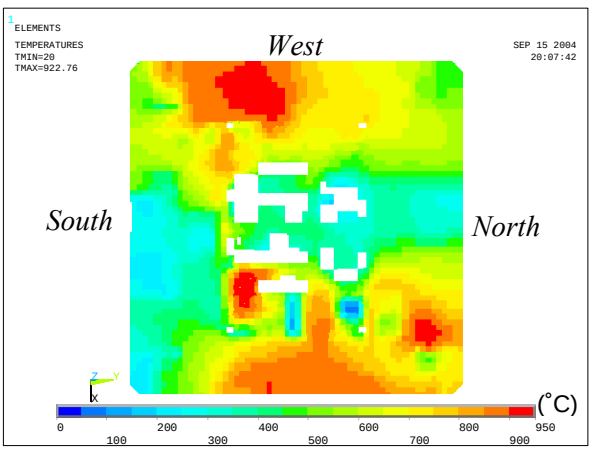

(c) Top surface at 50 min

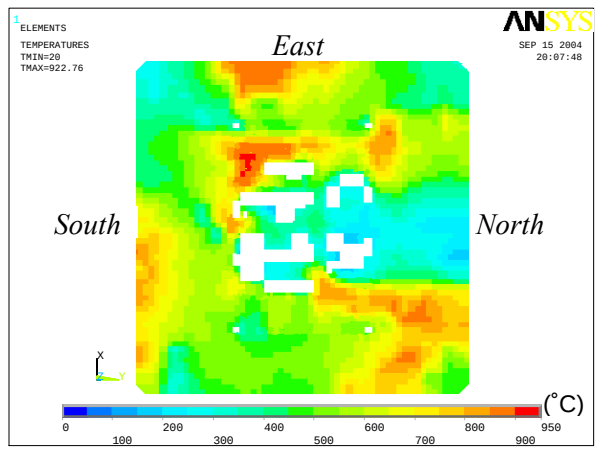

(d) Bottom surface at 50 min

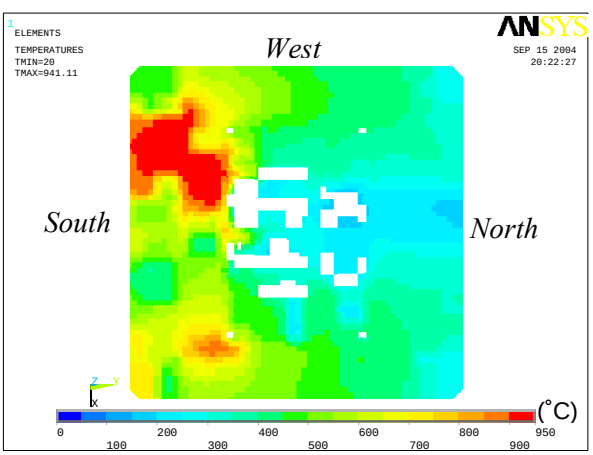

(e) Top surface at 100 min

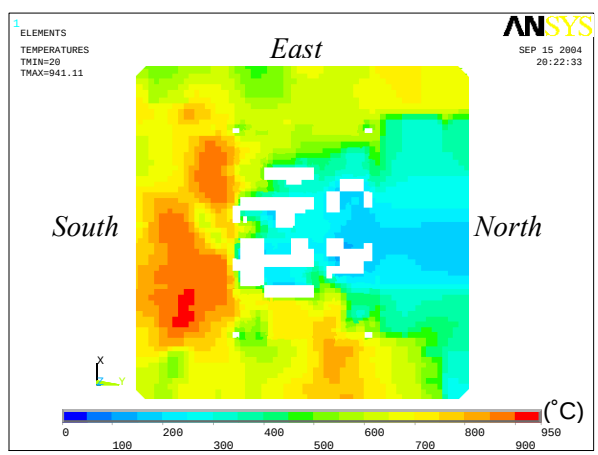

(f) Bottom surface at 100 min

Figure 5–65. Case B_i temperature distribution in the slab for Floor 96 of WTC 1 at 10 min, 50 min, and 100 min.

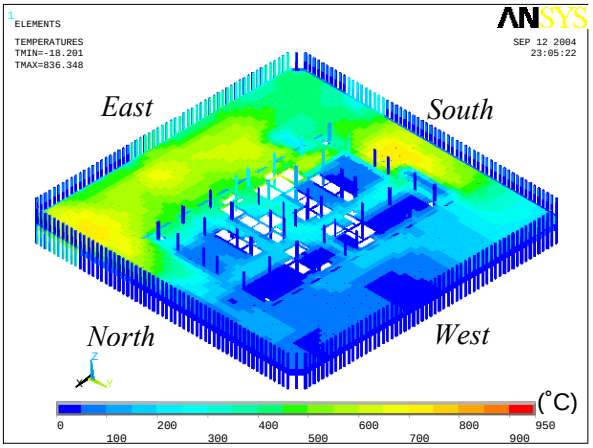

(a) Top view at 10 min

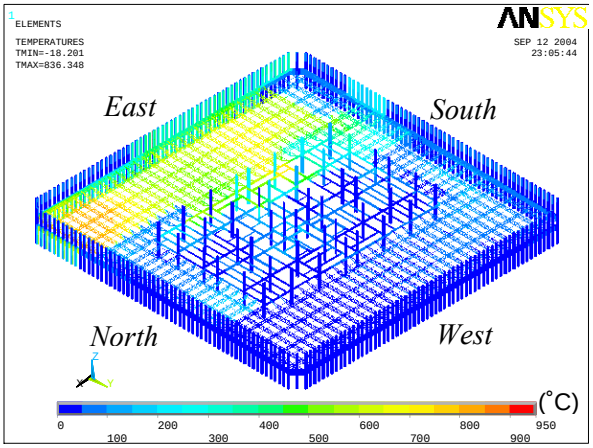

(b) Top view without concrete slab at 10 min

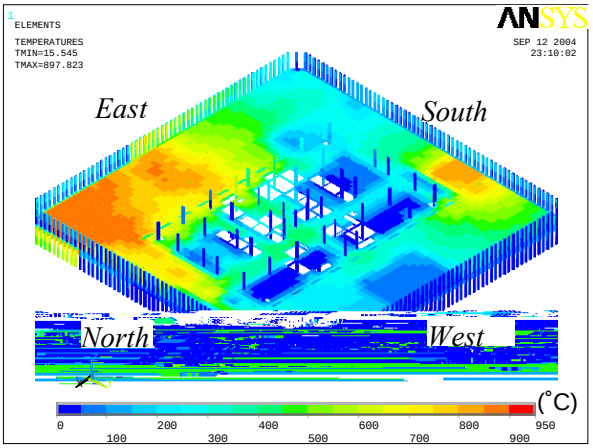

(c) Top view at 30 min

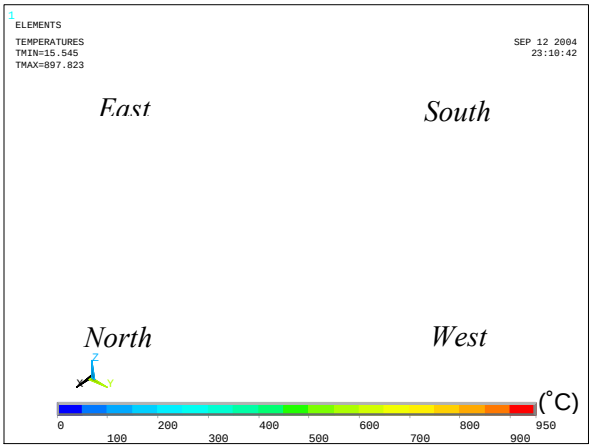

(d) Top view without concrete slab at 30 min

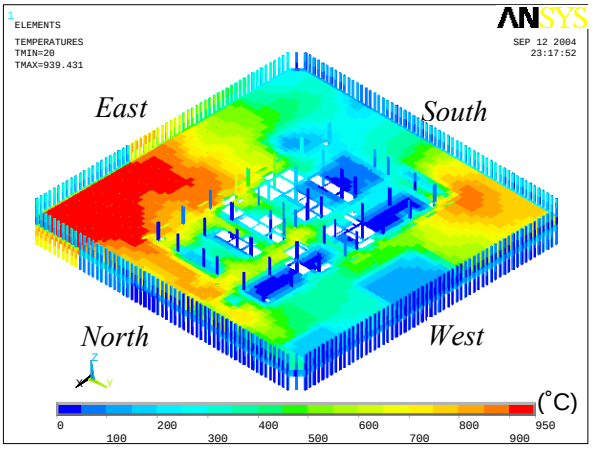

(e) Top view at 60 min

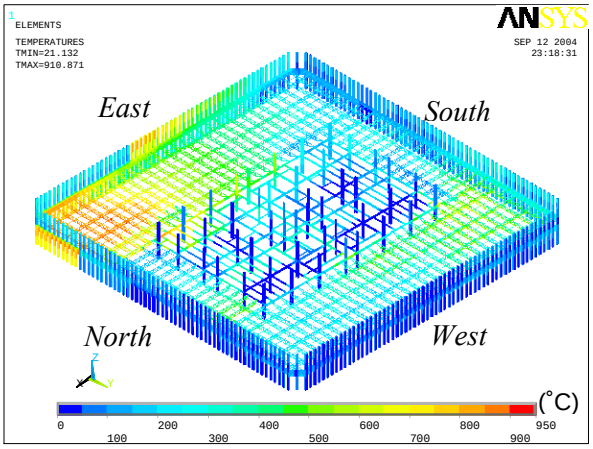

(f) Top view without concrete slab at 60 min

Figure 5–66. Case C_i temperature condition for Floor 82 of WTC 2 at 10 min, 30 min, and 60 min.

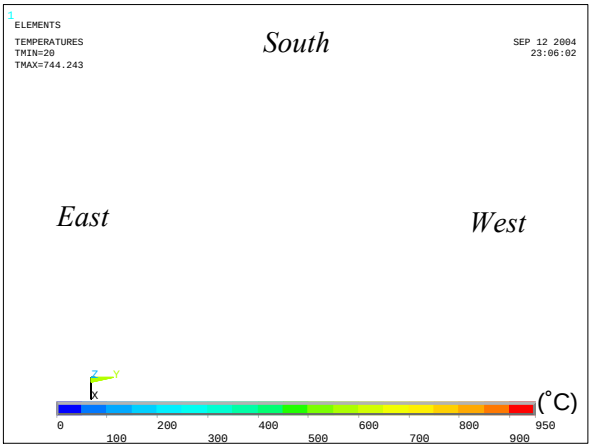

(a) Top surface at 10 min

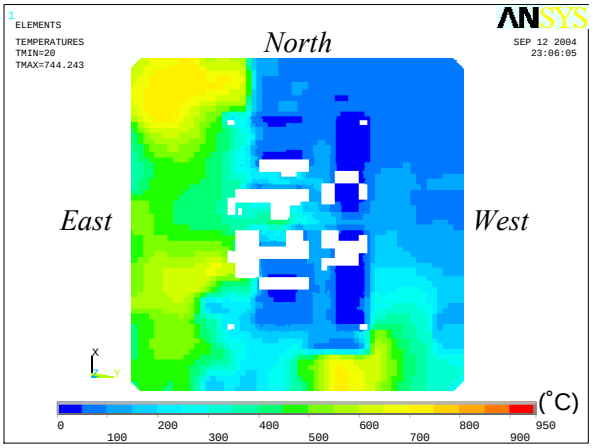

(b) Bottom surface at 10 min

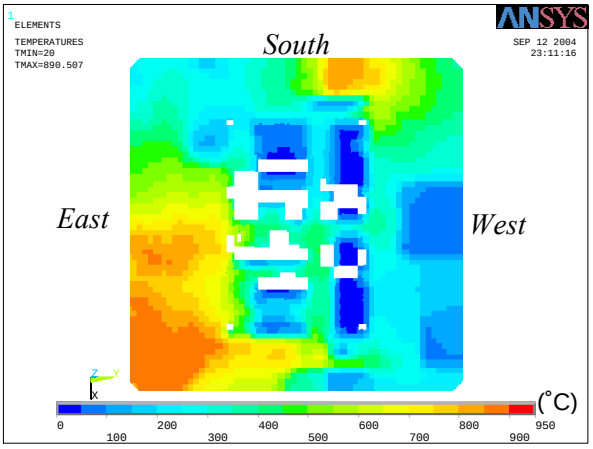

(c) Top surface at 30 min

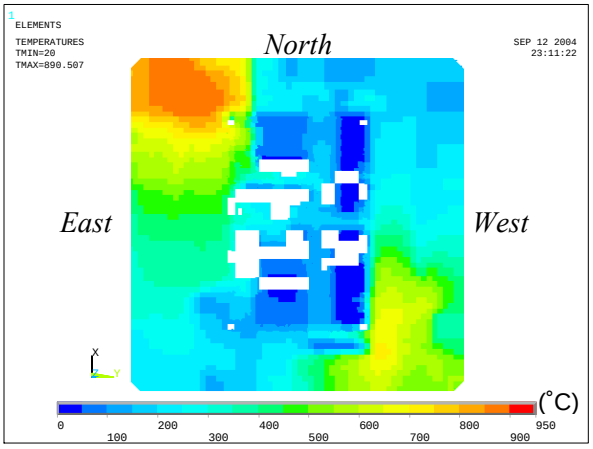

(d) Bottom surface at 30 min

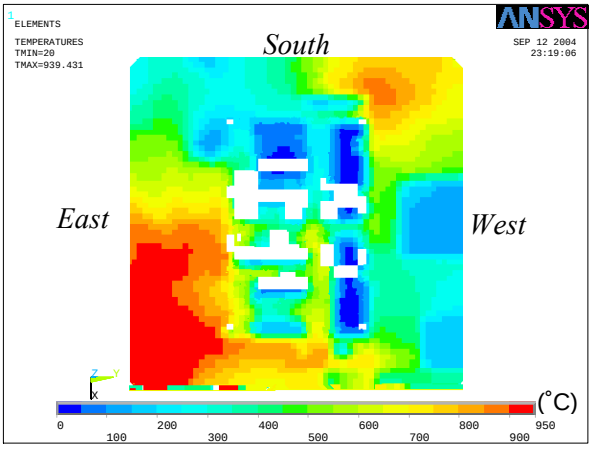

(e) Top surface at 60 min

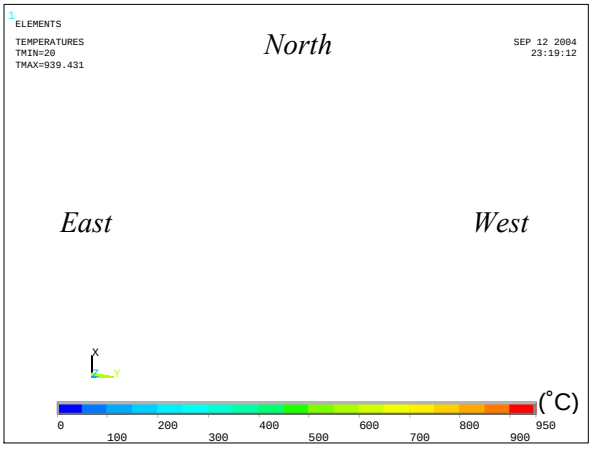

(f) Bottom surface at 60 min

Figure 5–67. Case C_i temperature distribution in the slab for Floor 82 of WTC 2 at 10 min, 30 min, and 60 min.

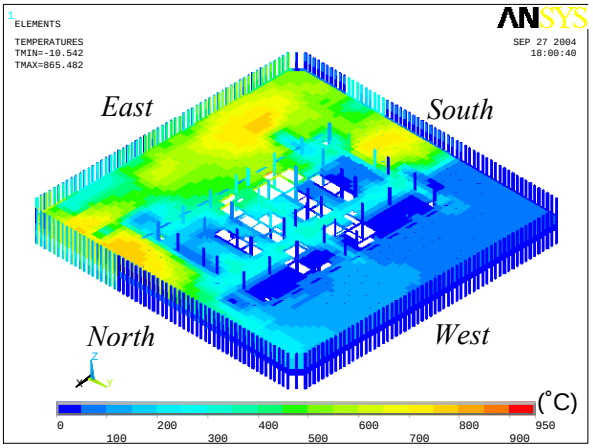

(a) Top view at 10 min

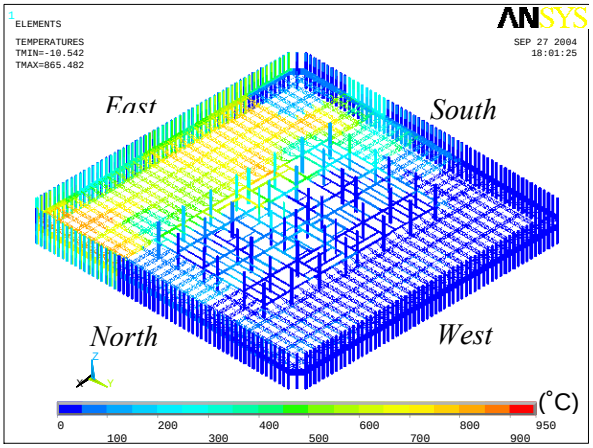

(b) Top view without concrete slab at 10 min

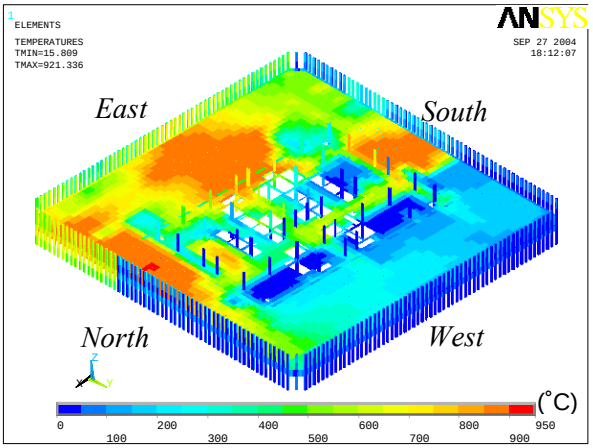

(c) Top view at 30 min

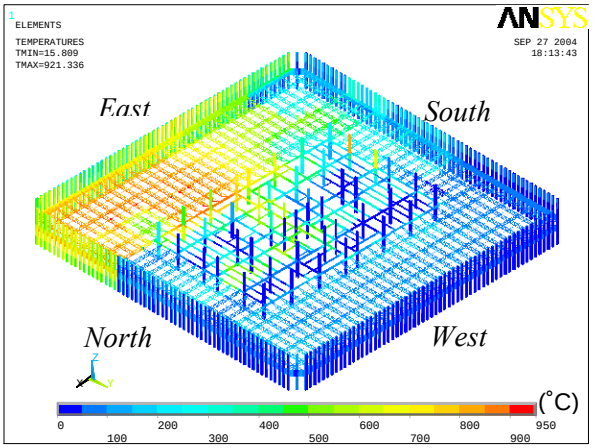

(d) Top view without concrete slab at 30 min

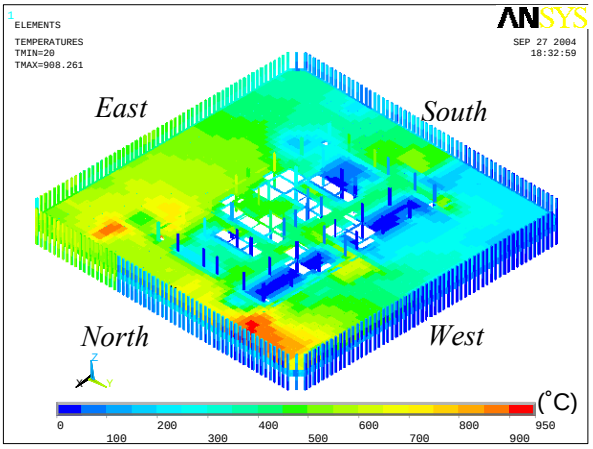

(e) Top view at 60 min

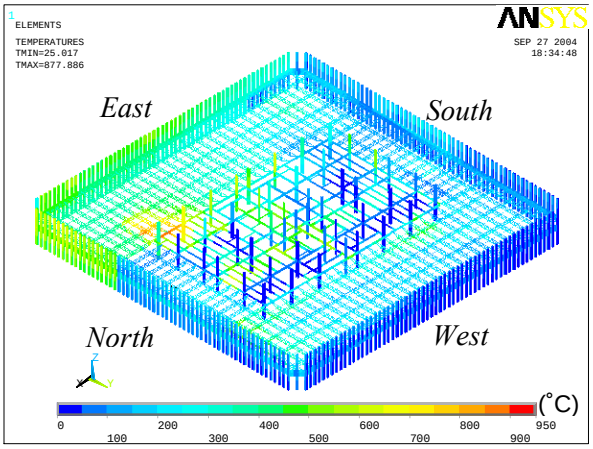

(f) Top view without concrete slab at 60 min

Figure 5–68. Case D_i temperature condition for Floor 82 of WTC 2 at 10 min, 30 min, and 60 min.

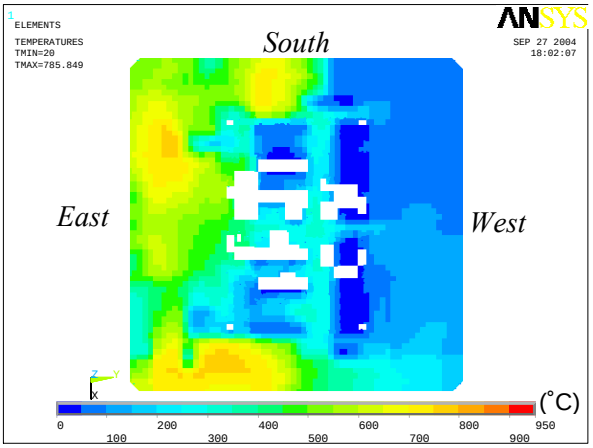

(a) Top surface at 10 min

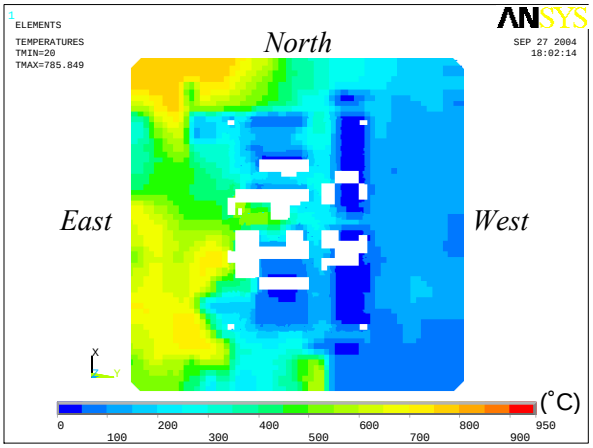

(b) Bottom surface at 10 min

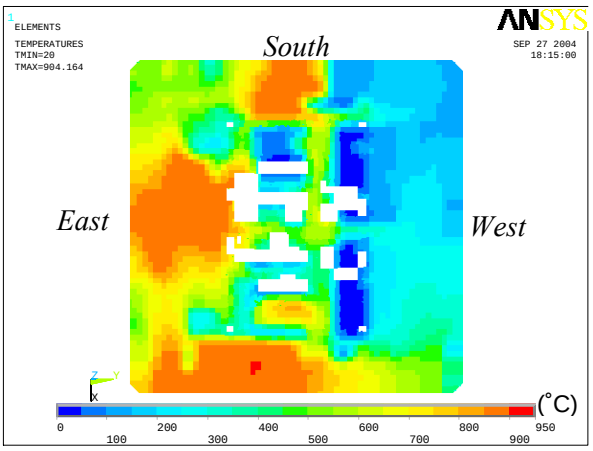

(c) Top surface at 30 min

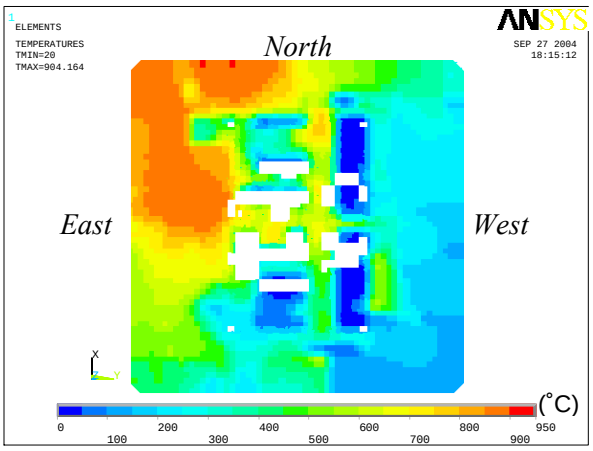

(d) Bottom surface at 30 min

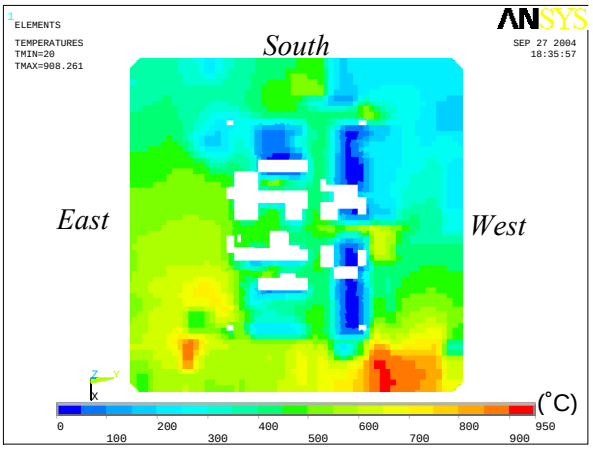

(e) Top surface at 60 min

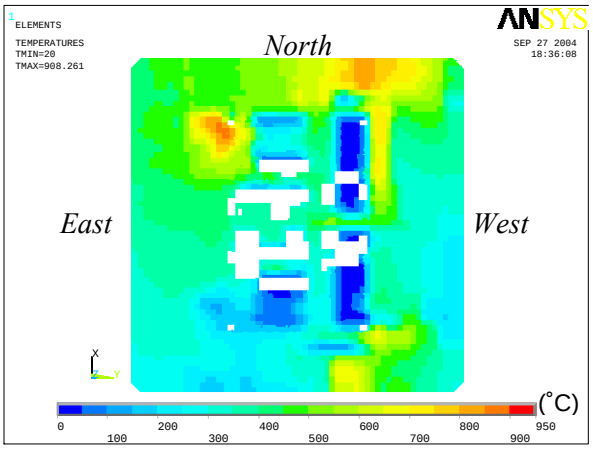

(f) Bottom surface at 60 min

Figure 5–69. Case D_i temperature distribution in the slab for Floor 82 of WTC 2 at 10 min, 30 min, and 60 min.

Table 5–12. List of full floor model analyses performed.

Analysis #	Tower	Floor	Impact Damage	Temperature
1	WTC 1	Floor 93	Case A_i	Case A_i
2	WTC 1	Floor 94	Case A_i	Case A_i
3	WTC 1	Floor 95	Case A_i	Case A_i
4	WTC 1	Floor 96	Case A_i	Case A_i
5	WTC 1	Floor 97	Case A_i	Case A_i
6	WTC 1	Floor 98	Case A_i	Case A_i
7	WTC 1	Floor 99	Case A_i	Case A_i
8	WTC 1	Floor 93	Case A_i	Case B_i
9	WTC 1	Floor 94	Case A_i	Case B_i
10	WTC 1	Floor 95	Case A_i	Case B_i
11	WTC 1	Floor 96	Case A_i	Case B_i
12	WTC 1	Floor 97	Case A_i	Case B_i
13	WTC 1	Floor 98	Case A_i	Case B_i
14	WTC 1	Floor 99	Case A_i	Case B_i
15	WTC 2	Floor 79	Case C_i	Case C_i
16	WTC 2	Floor 80	Case C_i	Case C_i
17	WTC 2	Floor 81	Case C_i	Case C_i
18	WTC 2	Floor 82	Case C_i	Case C_i
19	WTC 2	Floor 83	Case C_i	Case C_i
20	WTC 2	Floor 79	Case D_i	Case D_i
21	WTC 2	Floor 80	Case D_i	Case D_i
22	WTC 2	Floor 81	Case D_i	Case D_i
23	WTC 2	Floor 82	Case D_i	Case D_i
24	WTC 2	Floor 83	Case D_i	Case D_i
25	WTC 1	Floor 97	Case A_i	Case A

5.5.8 Boundary Conditions

Both core and exterior columns were supported in the vertical direction at the bottom. When the column below the floor was severed by aircraft impact, the top of the column above the floor was supported in the vertical direction. Core columns were free in the horizontal directions and fixed against all rotations at the top and bottom ends. Exterior columns were fixed for translation perpendicular to the face of the building and against rotation about the axis parallel to the face of the building at the top and bottom. They were also fixed in torsion at the top and bottom. A quantitative study of the effect of column boundary conditions is discussed in Section 5.5.16.

5.5.9 Results from WTC 1 Floor 96 under Case A_i Temperature Condition

Vertical Displacement: Figure 5–70 shows the vertical displacements of Floor 96 for Case A_i temperature condition at 10 min, 50 min, and 100min. The maximum displacement of 23 in. occurred at 10 min in the north office area. Then, the vertical displacement decreased in the north office area as the fire moved away from the area. The floor in the south office area started to deflect upward at 20 min, and part of the

south office area deflected upward at 70 min. Most short-span trusses also deflected upward. In the early stage of Case A_i temperature condition, the temperature in the slab was much higher than that in the trusses in the south office area as can be seen in Figs. 5–62 and 5–63 because the insulation was intact on the trusses in the south office area. Although the coefficient of thermal expansion (CTE) of steel is larger than that of concrete (50 percent larger at room temperature; the difference increases as temperature becomes higher), when the difference in temperature between the slab and the trusses becomes large enough to cause the thermal expansion of the slab to be greater than that of trusses, the floor deflects upward. At 80 min, several trusses in the south office area started to deflect downward, which was caused by the buckling of the floor due to compression in the east-west direction. At 100 min, the maximum downward displacement of the floor in the north area was 12.8 in., reflecting the cooling that took place, and the maximum vertical displacements in the south office area were 4.8 in. upward and 6.4 in. downward.

Behavior of Exterior Columns on North and South Faces*:* Figure 5–71 shows the displacements of exterior columns normal to the face of the building at 10 min, 50 min, and 100 min. The maximum outward displacements were 5.8 in. and 3.7 in. for the north and south faces, which occurred at 70 min and 90 min after the impact, respectively. Exterior columns were pushed out by the floor throughout the duration of the thermal loading. Figure 5–72 shows the horizontal reaction at each column on the north and south faces. Since even number columns were not connected to trusses and spandrel studs and strap anchors were removed, reaction forces at even number columns were small. In the figure, the reaction force is positive when the floor pulls the exterior column in. Since exterior columns were always pushed out by the floor during the analysis, reaction forces were always negative. Sagged floors did not pull in the exterior wall in this analysis.

Break Elements: Figure 5–73 shows the locations of user-defined break elements that failed by 100 min. Table 5–13 gives the number of failed user-defined break elements. Many web diagonals buckled in the northeast half of the office area where the insulation on the trusses was removed by the aircraft impact. In the south office area, there were only a few web diagonals that buckled because the insulation on the trusses was not damaged by the aircraft impact for Case A_i impact damage condition. By 100 min, about 70 percent of all the primary and bridging truss connections in the two-way zones and the long-span and transfer truss connections had failed at their top chord connections, but remained connected at their bottom chord connections at most of these locations. None of the truss seats failed during the analysis; therefore, all trusses were still connected to the exterior wall.

Effect of Vertical Loads to Columns*:* Another analysis was made with vertical loads applied to columns that were obtained from the SAP2000 floor model without impact damage. Core columns yielded when their temperatures exceeded 600 ˚C. However, the floor behavior did not change significantly from the analysis without the vertical loads on columns.

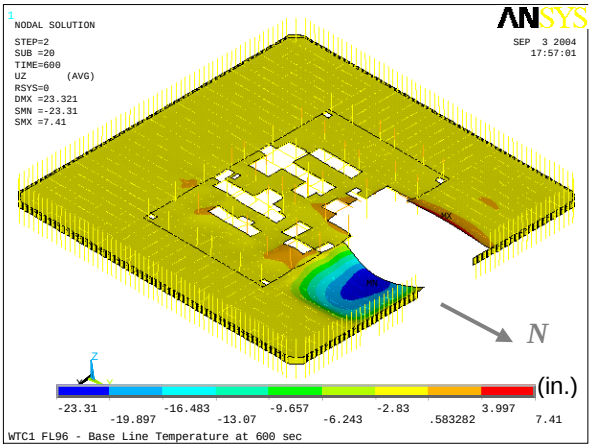

(a) Entire model at 10 min

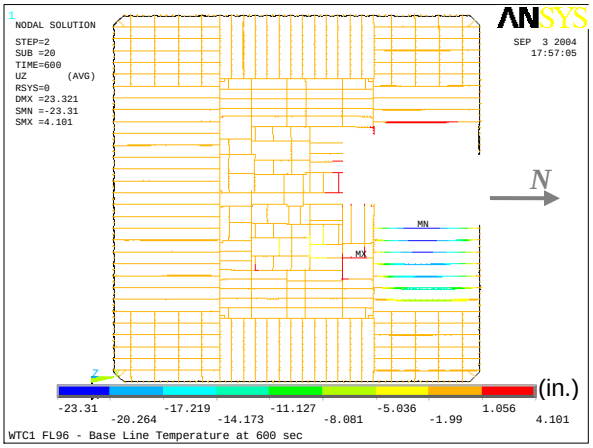

(b) Top view without concrete slab at 10 min

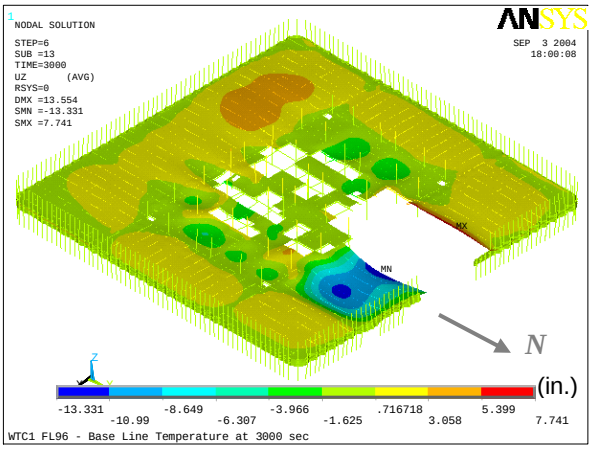

(c) Entire model at 50 min

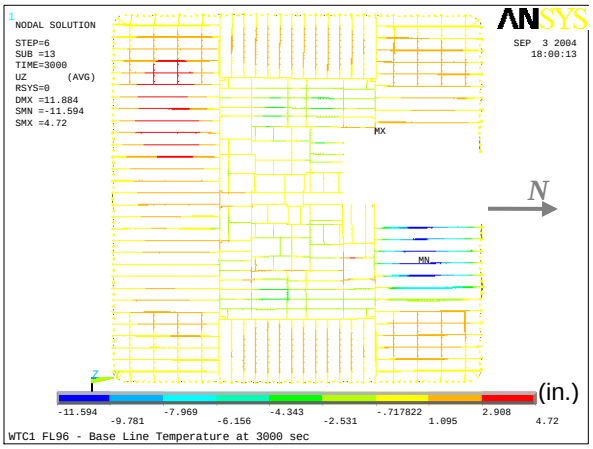

(d) Top view without concrete slab at 50 min

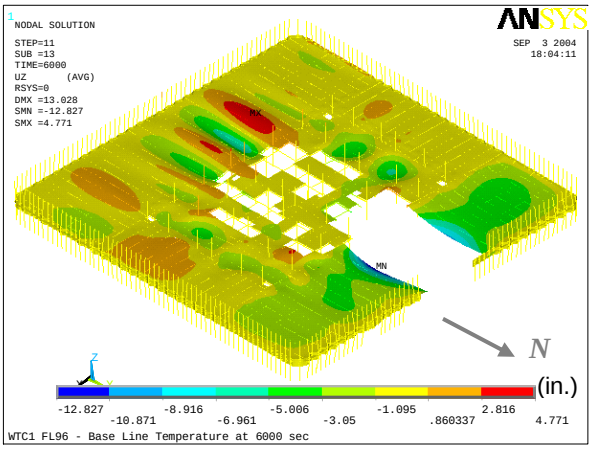

(e) Entire model at 100 min

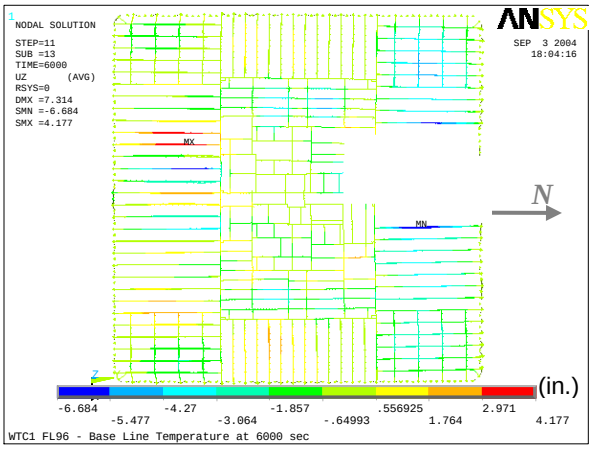

(f) Top view without concrete slab at 100 min

Figure 5–70. Vertical displacement of WTC 1 Floor 96 for Case A_i temperature condition at 10 min, 50 min, and 100 min (downward displacement is negative; 5x displacement magnification).

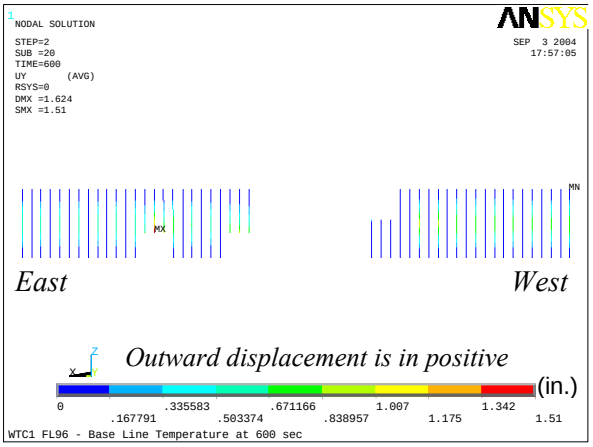

(a) North face at 10 min

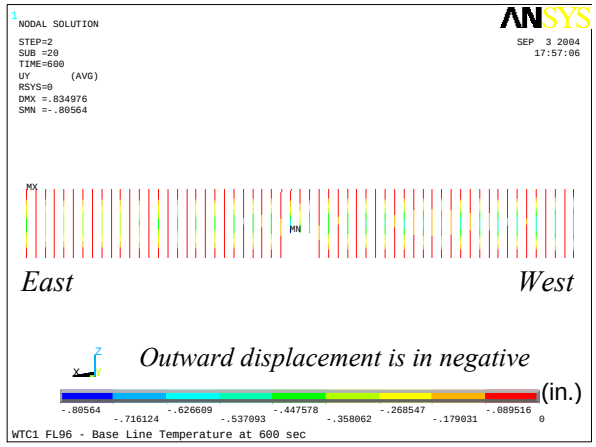

(b) South face at 10 min

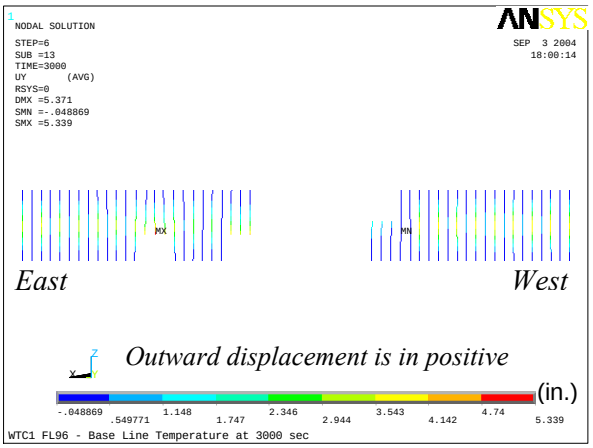

(c) North face at 50 min

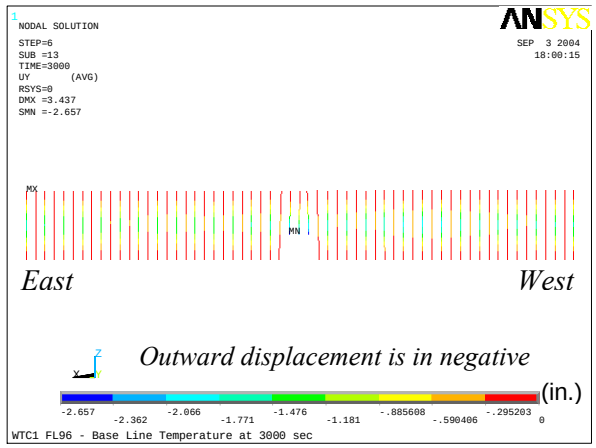

(d) South face at 50 min

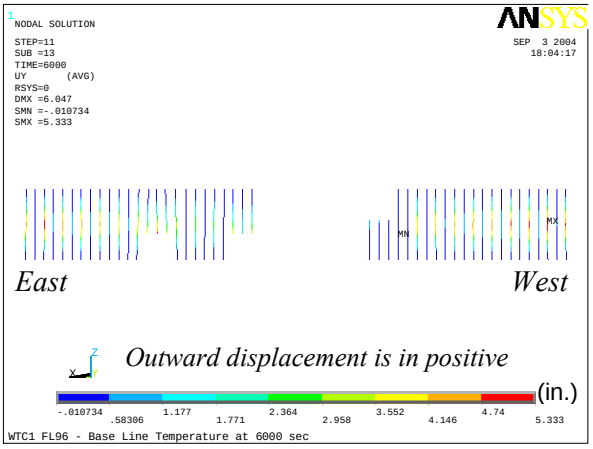

(e) North face at 100 min

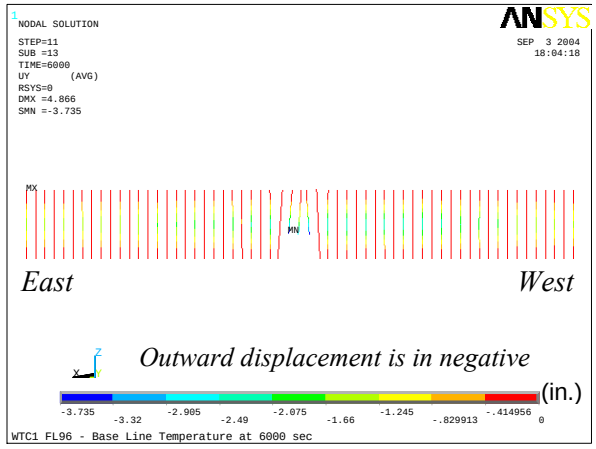

(f) South face at 100 min

Figure 5–71. Horizontal displacement of exterior columns of Floor 96 of WTC 1 for Case A_i temperature condition at 10 min, 50 min, and 100 min.

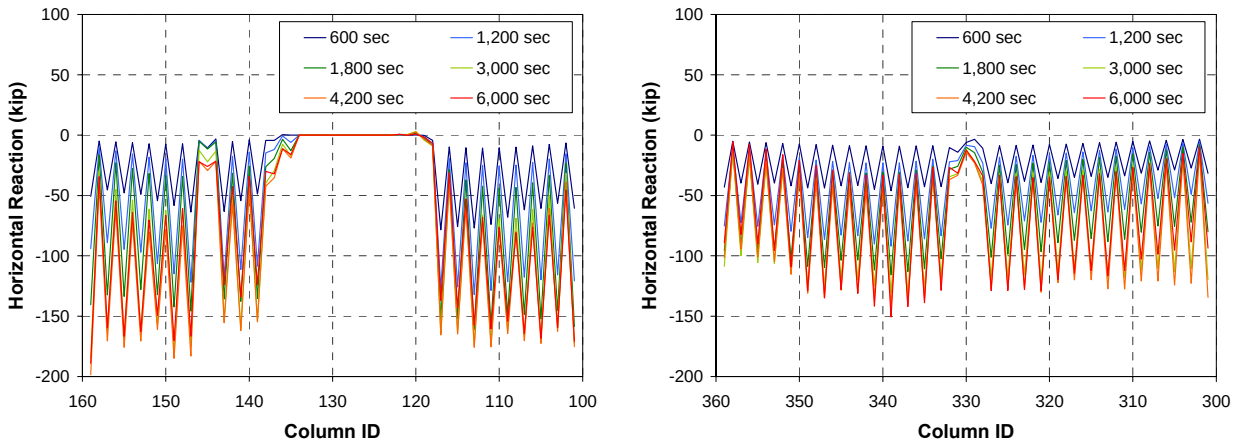

(a) North face (b) South face

Figure 5–72. Horizontal reaction force per column of WTC 1 Floor 96 for Case A_i temperature condition.

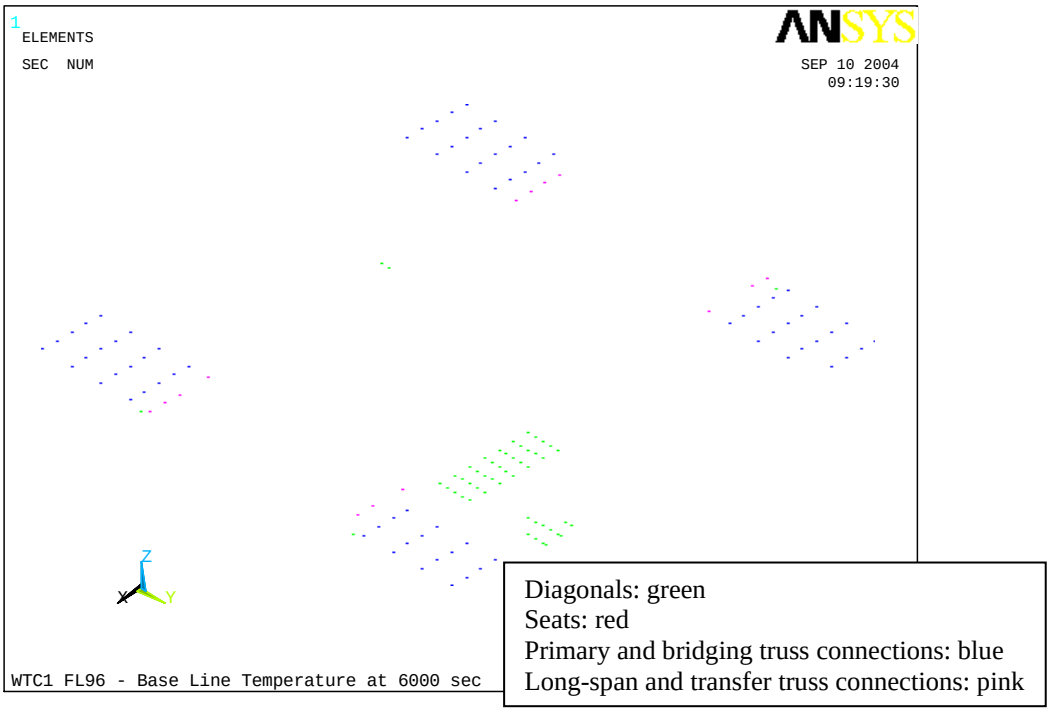

Figure 5–73. User-defined break elements that failed by 100 min in the model of WTC 1 Floor 96 for Case A_i temperature condition.

Table 5–13. Number of failed user-defined break elements in the model of WTC 1 Floor 96 for Case A_i temperature condition.

	Number of Break Elements
Web diagonals	56
Seats and gusset plates	0
Connections between primary and bridging trusses	75
Connections between long-span and transfer trusses	14
Total	145

5.5.10 Results from Other WTC 1 Floors under Case A_i Temperature Condition

Table 5–14 summarizes the maximum vertical displacements of WTC 1 floors for Case A_i temperature condition. Figures 5–74 to 5–79 show vertical displacements of WTC 1 floors under Case A_i temperature condition when each floor experienced the maximum displacement. Floor 95 to Floor 98 showed a significant vertical displacement in the north office area near the impact damage where truss insulation was damaged. The maximum vertical displacement of all floors was 32 in. at Floor 97 at 60 min. The vertical displacement in the south office area was found to be insignificant on all the floors throughout the thermal loading. Note that no truss insulation was damaged in the south office area of WTC 1 floors for Case A_i temperature condition.

Figure 5–80 (a) shows the average horizontal displacement due to thermal expansion of floors at 100 min on each face, while Fig. 5–80 (b) shows the average total thermal expansion of floors at 100 min in two orthogonal directions. The total floor expansion ranged from 4 in. to 8 in. Figure 5–81 shows horizontal reaction force at individual columns of the north and south faces of Floor 97. In this figure, the reaction is positive when the column is pulled inward by the floor. As can be seen in the figure, almost all the columns were pushed outward by the floor. This was also the case for other floors.

Many web diagonals of Floor 95 to Floor 98 buckled in the hot zones of the north office area where the truss insulation was damaged. Although gusset plates at the exterior truss seats fractured at several locations, a complete disconnection of the floor from the exterior wall was not found in any floor.

Results from WTC 1 Floor 97 under Case A temperature condition were found to be very close to those from WTC 1 Floor 97 under Case A_i temperature condition, and, hence, will not be presented separately in this report.

Table 5–14. Maximum vertical displacement of WTC 1 floors for Case A_i temperature condition.

Floor	Max. Displacement (in.)	Time at the Maximum (min)
93	5.4	30
94	13.5	100
95	30.9	10
96	23.3	10
97	31.5	60
98	26.4	30
99	7.0	50

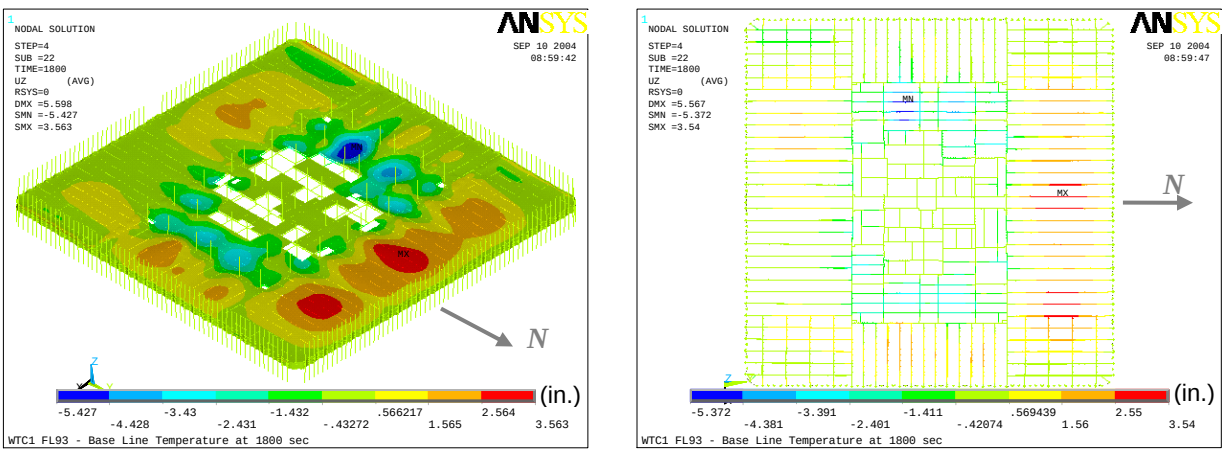

(a) Entire model (b) Top view without slab

Figure 5–74. Vertical displacement of WTC 1 Floor 93 for Case A_i temperature condition at 30 min (downward displacement is negative; 5x displacement magnification).

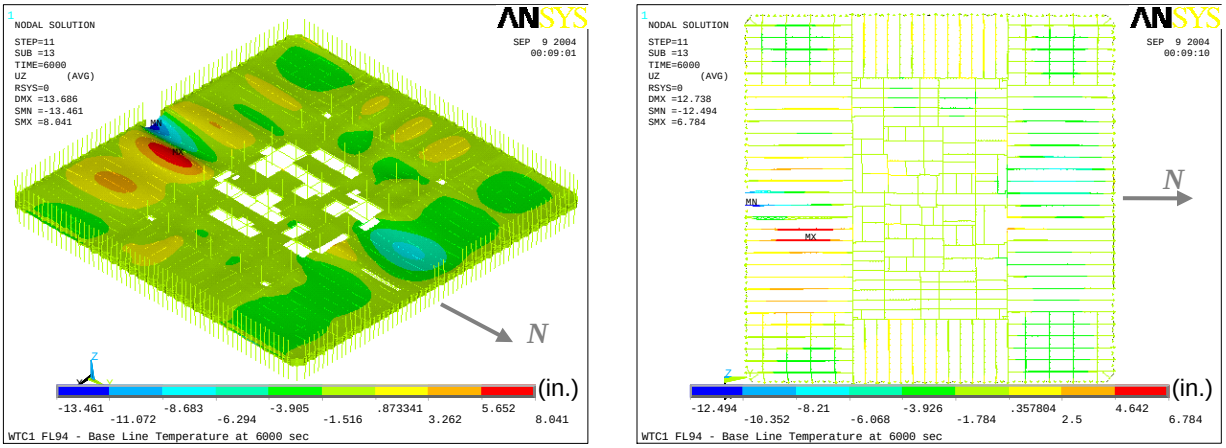

(a) Entire model (b) Top view without slab

Figure 5–75. Vertical displacement of WTC 1 Floor 94 for Case A_i temperature condition at 100 min (downward displacement is negative; 5x displacement magnification).

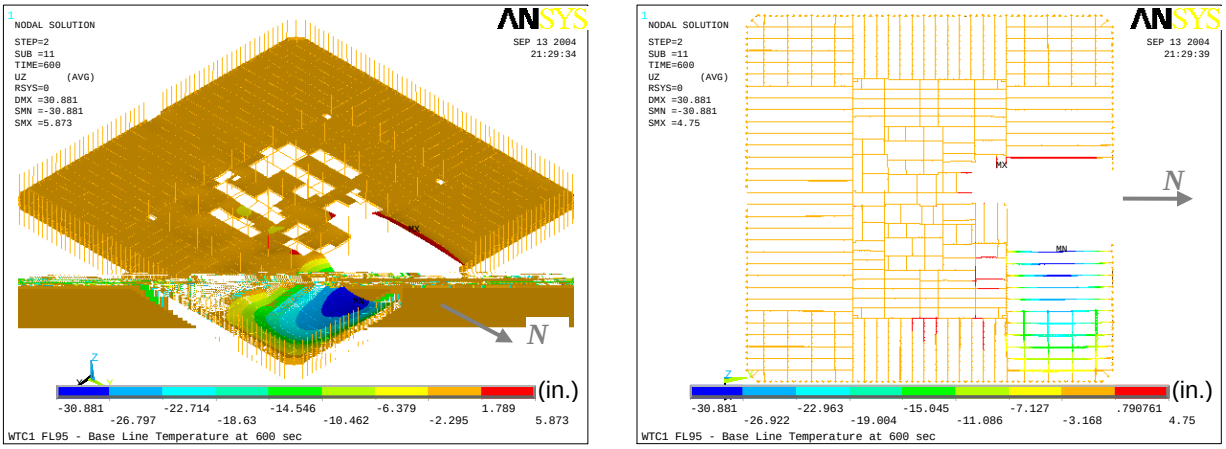

(a) Entire model (b) Top view without slab

Figure 5–76. Vertical displacement of WTC 1 Floor 95 for Case A_i temperature condition at 10 min (downward displacement is negative; 5x displacement magnification).

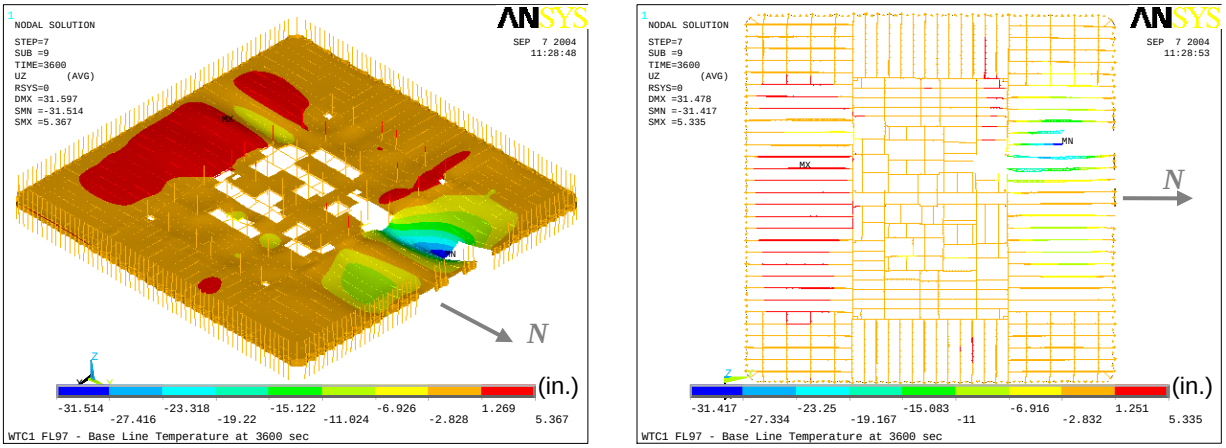

(a) Entire model (b) Top view without slab

Figure 5–77. Vertical displacement of WTC 1 Floor 97 for Case A_i temperature condition at 60 min (downward displacement is negative; 5x displacement magnification).

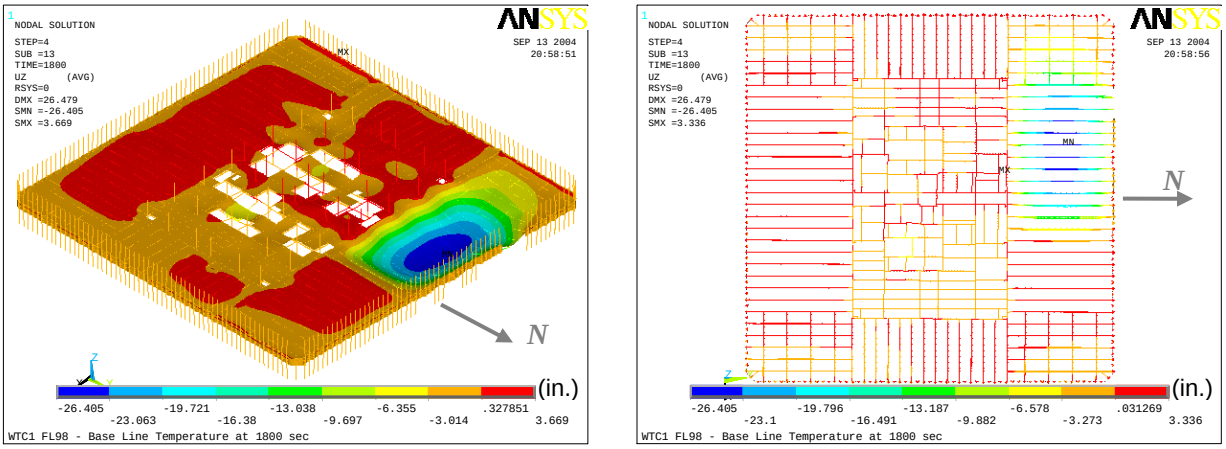

(a) Entire model (b) Top view without slab

Figure 5–78. Vertical displacement of WTC 1 Floor 98 for Case A_i temperature condition at 30 min (downward displacement is negative; 5x displacement magnification).

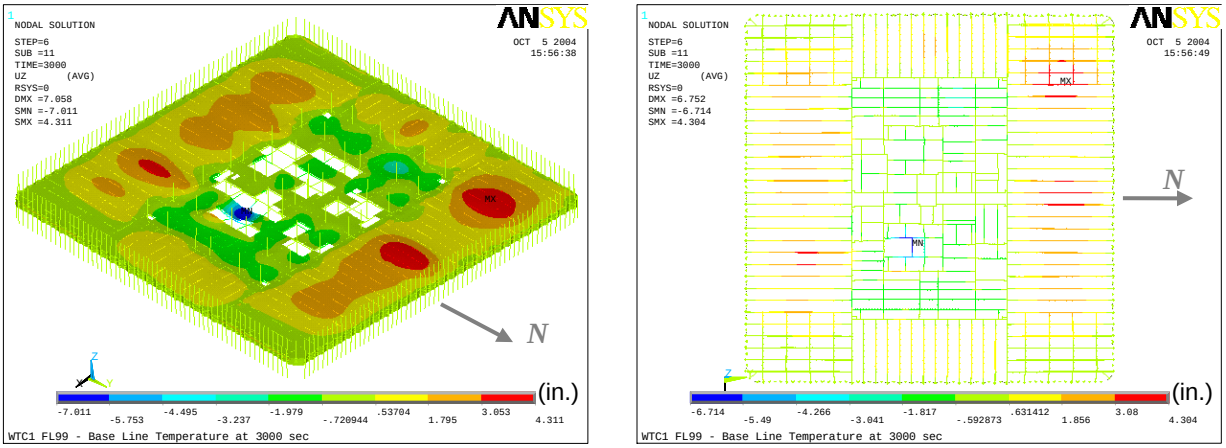

(a) Entire model (b) Top view without slab

Figure 5–79. Vertical displacement of WTC 1 Floor 99 for Case A_i temperature condition at 50 min (downward displacement is negative; 5x displacement magnification).

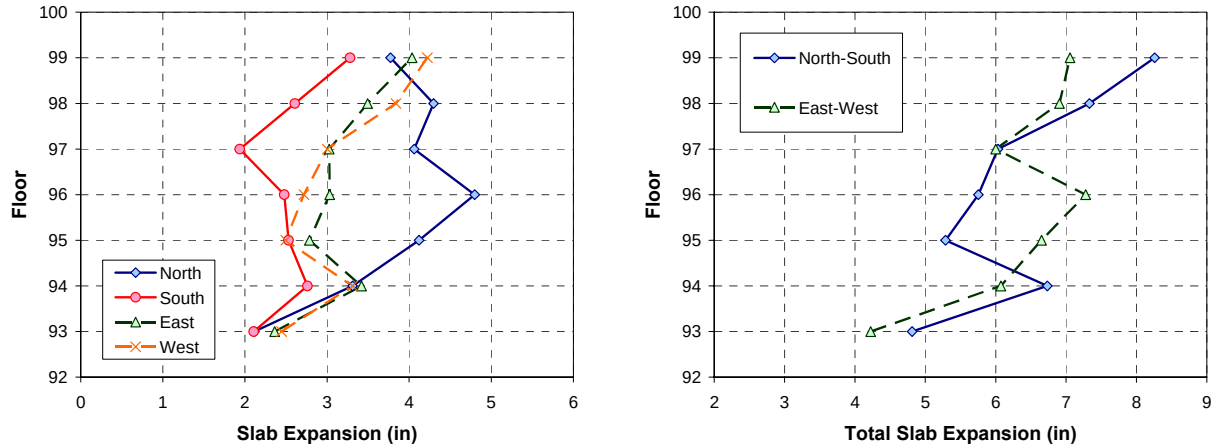

(a) Average displacement of each face (b) Average slab expansion in each direction

Figure 5–80. Average thermal expansion of WTC 1 floors at 100 min for Case A_i temperature condition.

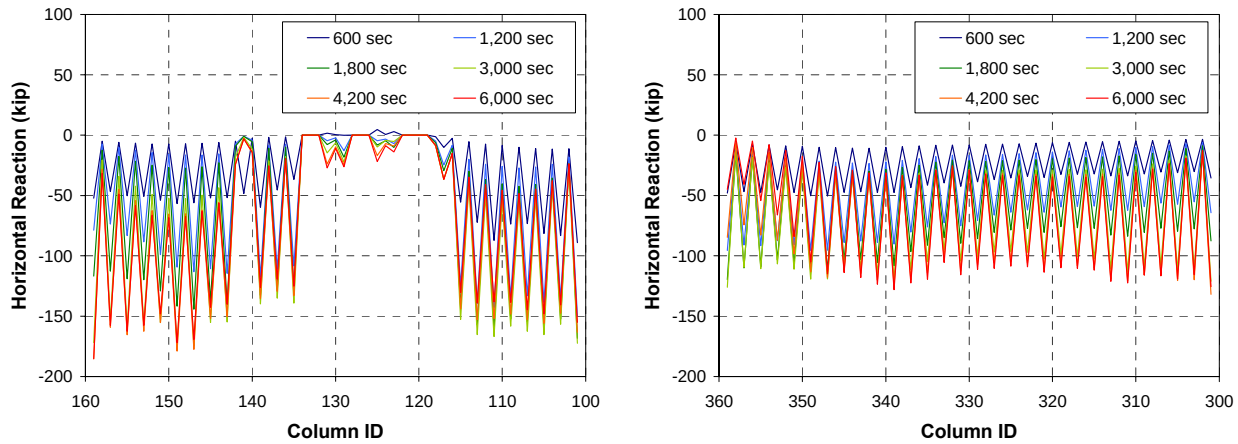

(a) North face (b) South face

Figure 5–81. Horizontal reaction force per column of WTC 1 Floor 97 for Case A_i temperature condition.

5.5.11 Results from WTC 1 Floors under Case B_i Temperature Condition

Table 5–15 summarizes the maximum vertical displacement of WTC 1 floors for Case B_i temperature condition, and Figs. 5–82 to 5–88 show the vertical displacements of WTC 1 floors when each floor experienced the maximum displacement. The maximum vertical displacements of Floor 95 to Floor 98 increased due to higher temperatures when compared to those for Case A_i temperature condition, especially in the south office area. The increase in temperatures in the south office area was a result of impact damage to insulation on floor trusses in the area. The maximum vertical displacement among all floors was 49 in. in the south office area of Floor 98, as shown in Fig. 5–87. The large displacement on the south side of Floor 98 was caused by the exterior truss seat failures between Column 329 and Column 343 that started between 80 min and 90 min. Exterior truss seats at Column 337 to Column 347 of Floor 97 also failed, which caused 37 in. of vertical displacement in the south office area. These exterior truss seats failed by losing vertical shear strength due to extreme temperatures of greater than 800 ˚C. Exterior seat failures of Floor 97 and Floor 98 are shown in Fig. 5–89.

Figure 5–90 (a) shows the average horizontal displacement due to thermal expansion of floors at 100 min on each face, while Fig. 5–90 (b) shows the average total thermal expansion of floors at 100 min in two orthogonal directions. The total floor expansion ranged from 5 in. to 8.5 in. Figures 5–91 and 5–92 show the horizontal reaction force at individual columns of north and south faces of Floor 96 and Floor 98. In these figures, the reaction is positive when the column is pulled inward by the floor. Although almost all the columns were pushed outward by the floor, it was found that large vertical displacement of the floor would reduce the compression between the floor and the exterior wall. By comparing Fig. 5–72 (b) and Fig. 5–91 (b), one can see that the compressive forces at Columns 323 to 337 on the south face decreased significantly for Case B_i temperature condition. It should be also noted in Fig. 5–92 (b) that the compressive forces became almost zero at columns where the floor was disconnected.

Many web diagonals of Floor 95 to Floor 98 buckled in the hot zones of the north and south office areas where the truss insulation was damaged. In addition to exterior seat failures (see Fig. 5–89) that occurred on the south face, gusset plates and seat bolts at the exterior truss seats failed at several locations on the north face; however, failures of gusset plates and seat bolts did not cause complete disconnection of the floor from the exterior wall.

Table 5–15. Maximum vertical displacement of WTC 1 floors for Case B_i temperature condition.

Floor	Max. Displacement (in.)	Time at the Maximum (min)
93	-5.8	100
94	12.7	100
95	29.2	10
96	28.6	10
97	37.4	100
98	49.0	100
99	6.8	100

Note: Negative value represents upward displacement in this table.

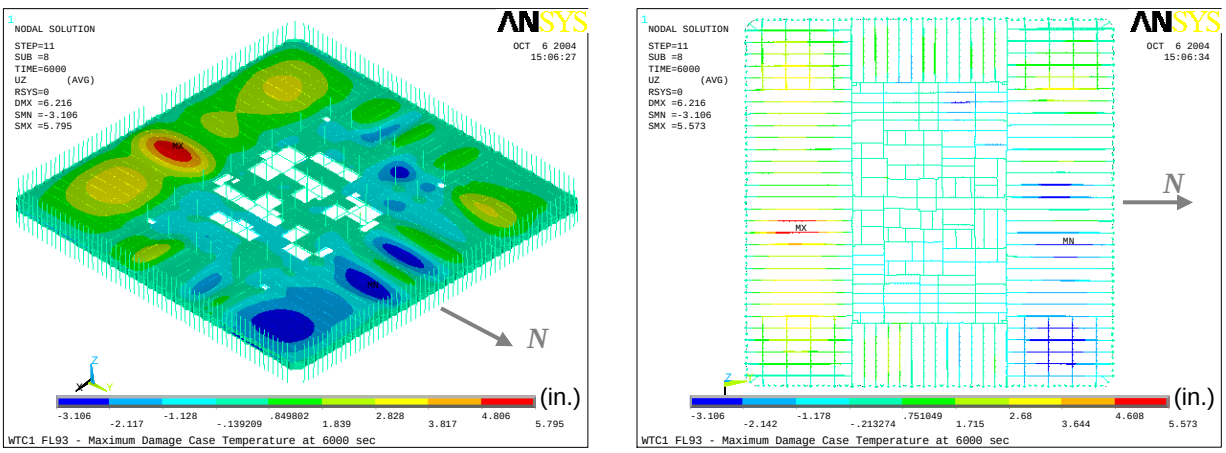

(a) Entire model (b) Top view without slab

Figure 5–82. Vertical displacement of WTC 1 Floor 93 for Case B_i temperature condition at 100 min (downward displacement is negative; 5x displacement magnification).

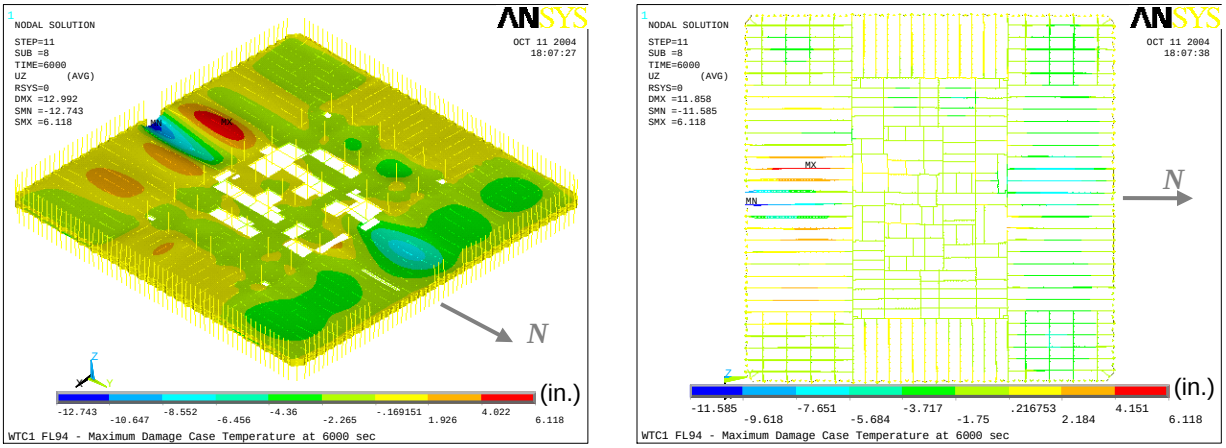

(a) Entire model (b) Top view without slab

Figure 5–83. Vertical displacement of WTC 1 Floor 94 for Case B_i temperature condition at 100 min (downward displacement is negative; 5x displacement magnification).

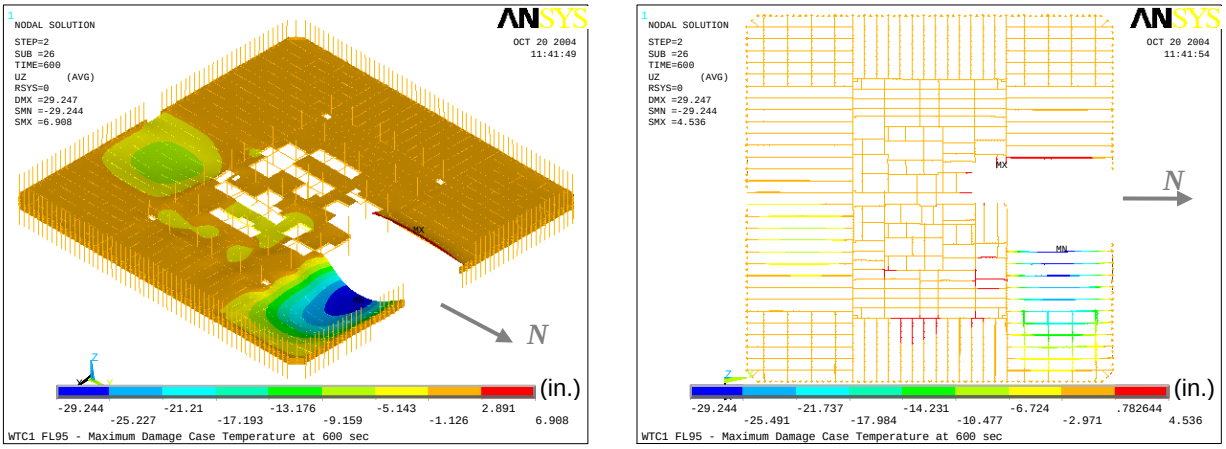

(a) Entire model (b) Top view without slab

Figure 5–84. Vertical displacement of WTC 1 Floor 95 for Case B_i temperature condition at 10 min (downward displacement is negative; 5x displacement magnification).

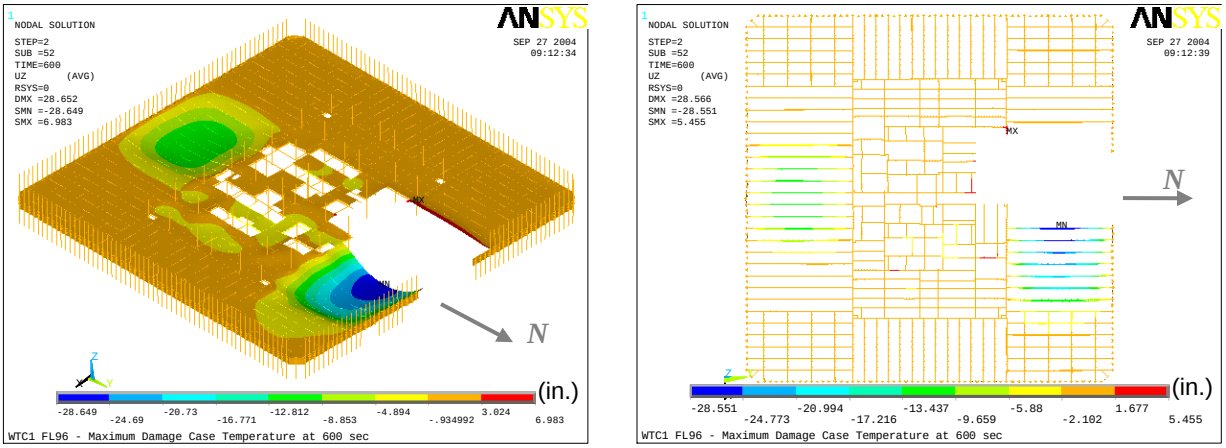

(a) Entire model (b) Top view without slab

Figure 5–85. Vertical displacement of WTC 1 Floor 96 for Case B_i temperature condition at 10 min (downward displacement is negative; 5x displacement magnification).

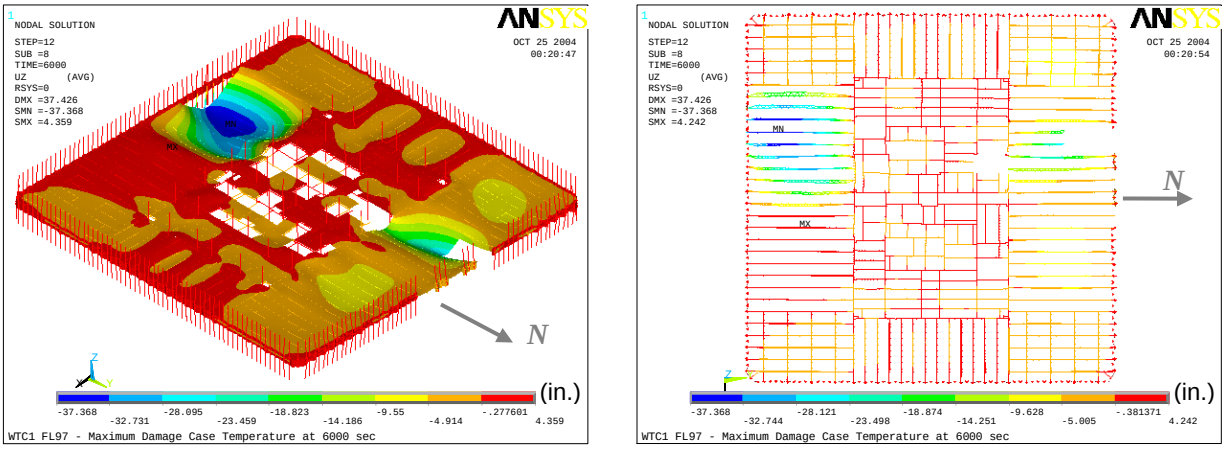

(a) Entire model (b) Top view without slab

Figure 5–86. Vertical displacement of WTC 1 Floor 97 for Case B_i temperature condition at 100 min (downward displacement is negative; 5x displacement magnification).

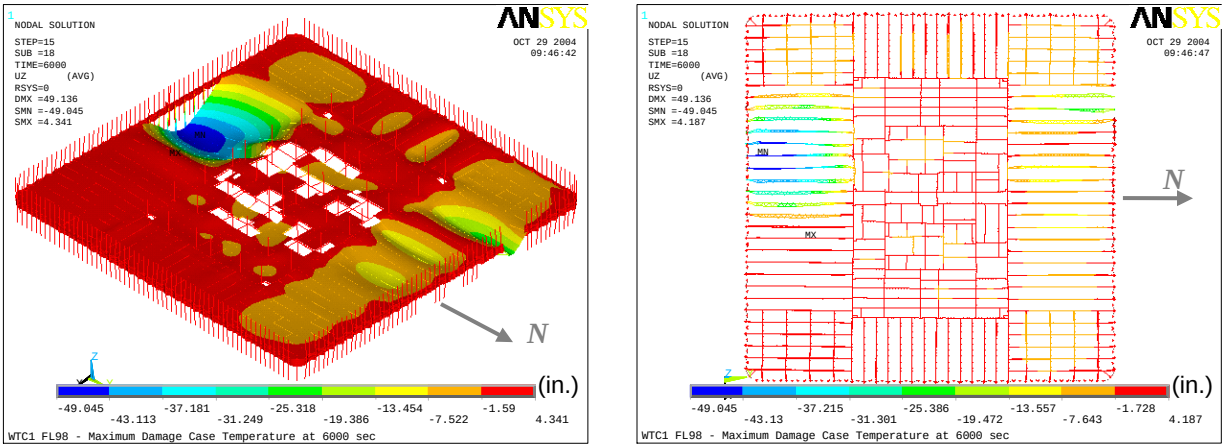

(a) Entire model (b) Top view without slab

Figure 5–87. Vertical displacement of WTC 1 Floor 98 for Case B_i temperature condition at 100 min (downward displacement is negative; 5x displacement magnification).

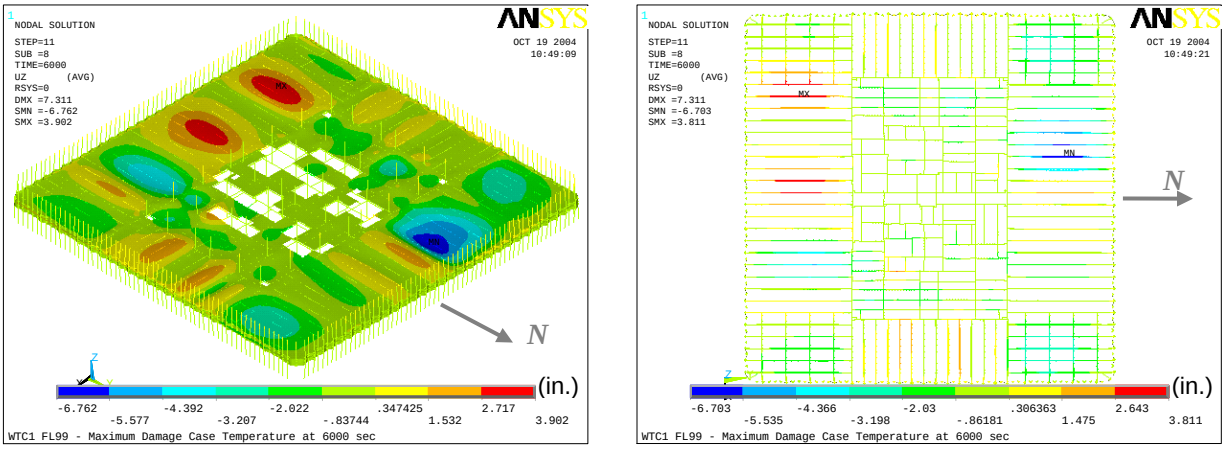

(a) Entire model (b) Top view without slab

Figure 5–88. Vertical displacement of WTC 1 Floor 99 for Case B_i temperature condition at 100 min (downward displacement is negative; 5x displacement magnification).

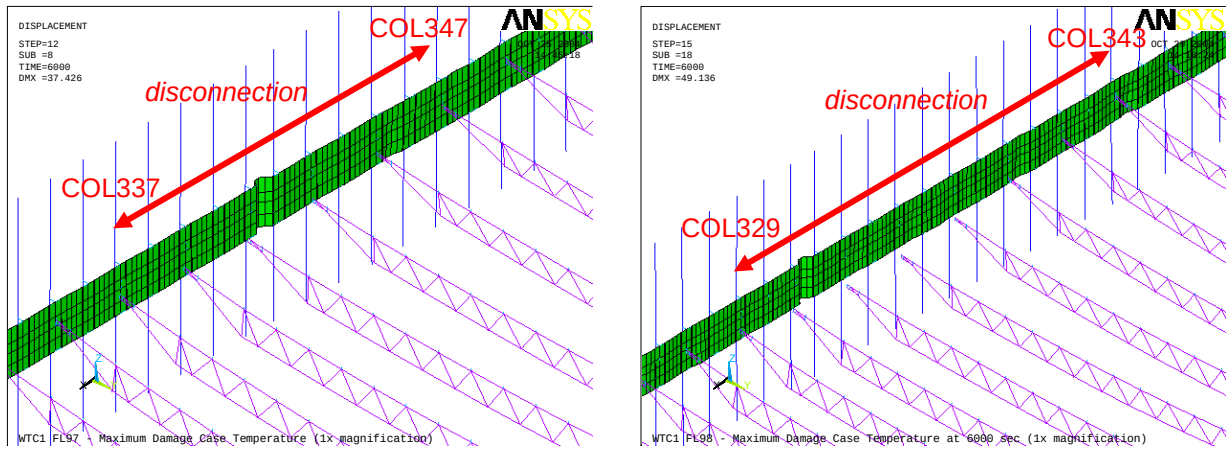

(a) Floor 97 (b) Floor 98

Figure 5–89. Loss of vertical supports in Floor 97 and Floor 98 of WTC 1 for Case B_i temperature condition at 100 min (1x displacement magnification).

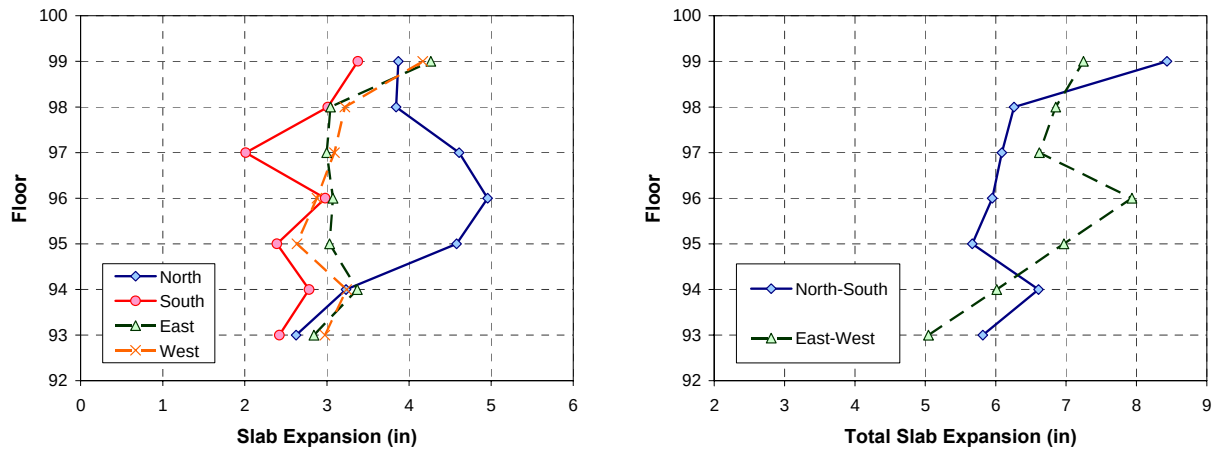

(a) Average displacement of each face (b) Average slab expansion in each direction

Figure 5–90. Thermal expansion of WTC 1 floors at 100 min for Case B_i conditions.

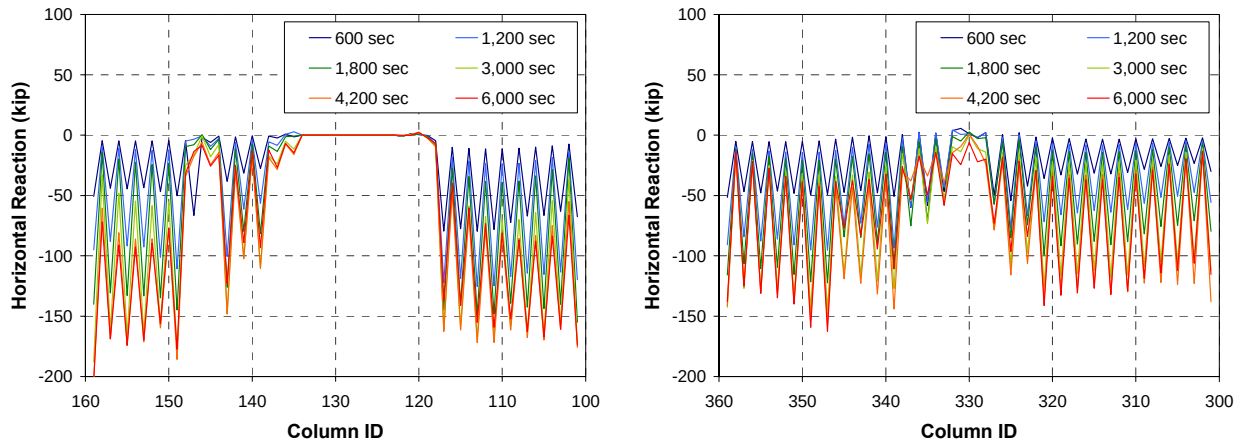

(a) North face (b) South face

Figure 5–91. Horizontal reaction force per column of WTC 1 Floor 96 for Case B_i temperature condition.

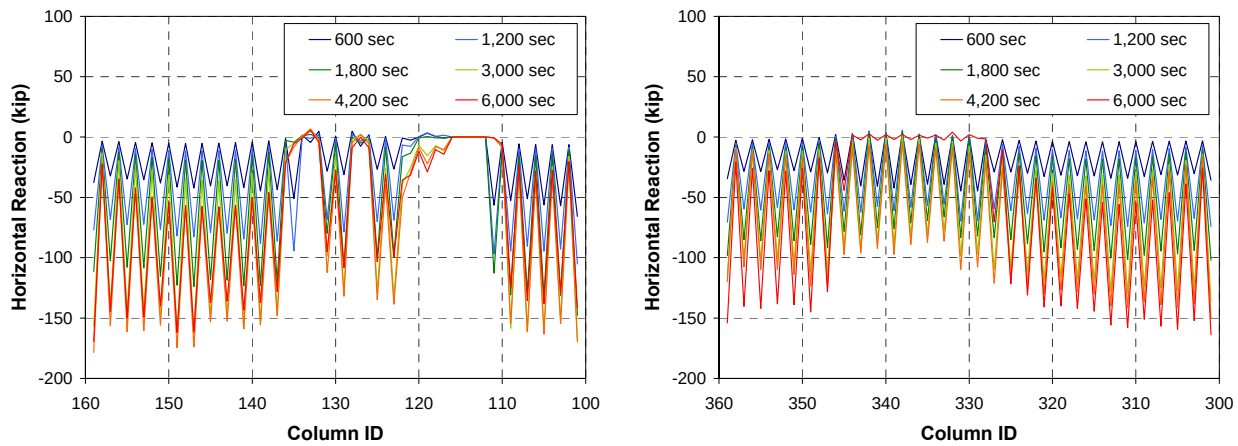

(a) North face (b) South face

Figure 5–92. Horizontal reaction force per column of WTC 1 Floor 98 for Case B_i temperature condition.

5.5.12 Results from WTC 2 Floor 82 under Case C_i Temperature Condition

Vertical Displacement: Figure 5–93 shows the vertical displacements of WTC 2 Floor 82 at 10 min, 30 min, and 60 min. The maximum vertical displacement after the impact was 5 in. in the southeast area near the impact damage. At 50 min, trusses at Column 301 to Column 317 near the northeast corner lost their vertical support at the exterior truss seats, and the vertical displacement in this area increased significantly. A maximum displacement of 45 in. occurred at 60 min in the northeast corner area. The west office area did not show significant vertical displacement because the insulation on trusses was intact.

Behavior of Exterior Columns on East and West Faces*:* Figure 5–94 shows the horizontal displacements of the exterior columns normal to the face of the building at 10 min, 30 min, and 60 min.

The maximum outward displacements were 3.8 in. and 1.6 in. for the east and west faces, respectively, at 60 min after the impact. In general, the exterior columns had outward displacement except for the north side of the east face where there was an inward displacement of about 0.8 in. at 10 min. This inward displacement was caused by the temperature gradient in the cross section of the exterior columns. Figure 5–95 shows the horizontal reaction at each column on the north and south faces. Since even number columns were not connected to trusses and spandrel studs and strap anchors were removed, reaction forces at even number columns were small. In the figure, the reaction force is positive when the floor pulls the exterior column in. It was found that both faces experienced compression from the floor throughout the thermal loading; however, several columns of the east face near the northeast corner lost lateral support from the floor, and the reaction forces at these columns became very small.

Break Elements: Figure 5–96 shows the locations of user-defined break elements that failed by 60 min. Table 5–16 summarizes the number of failed user-defined break elements during the analysis. A significant number of web diagonals buckled in the east office area where insulation on the trusses was damaged by the aircraft impact. By 60 min, about 70 percent of all the primary and bridging truss connections in the two-way zones and the long-span and transfer truss connections failed at their top chord connections; however, at the majority of these locations, they were still connected at their bottom chord connections. By the end of the thermal loading, gusset plates fractured at 19 exterior truss seats, bolts sheared off at 18 exterior truss seats and 1 interior truss seat, and 8 exterior truss seats failed in vertical shear. Figure 5–97 shows the deformed shape of the floor trusses after loss of their vertical support at the exterior truss seats.

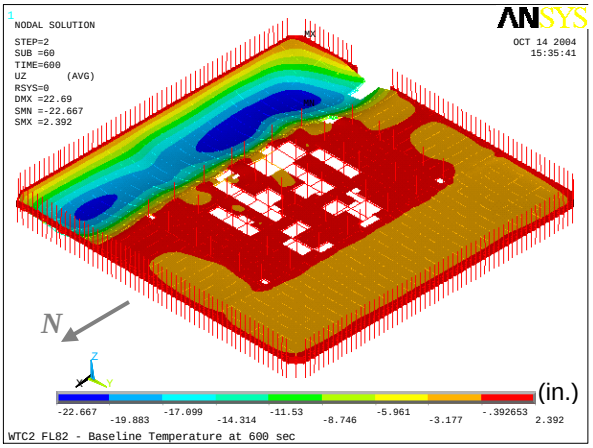

(a) Entire model at 10 min

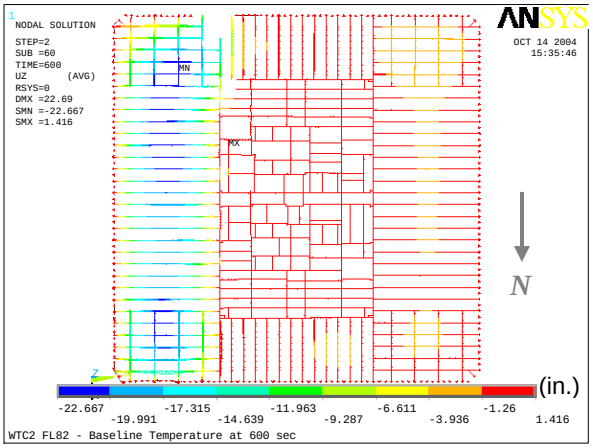

(b) Top view without concrete slab at 10 min

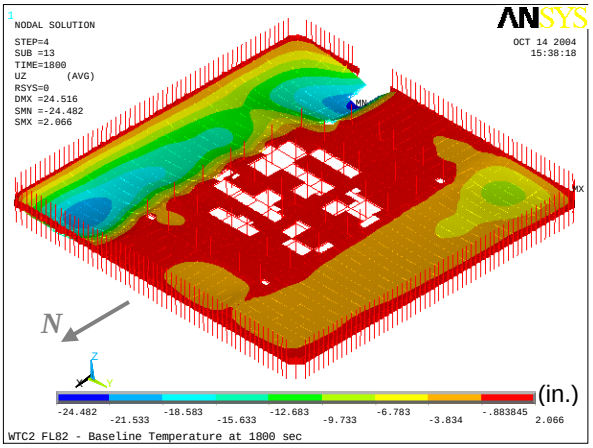

(c) Entire model at 30 min

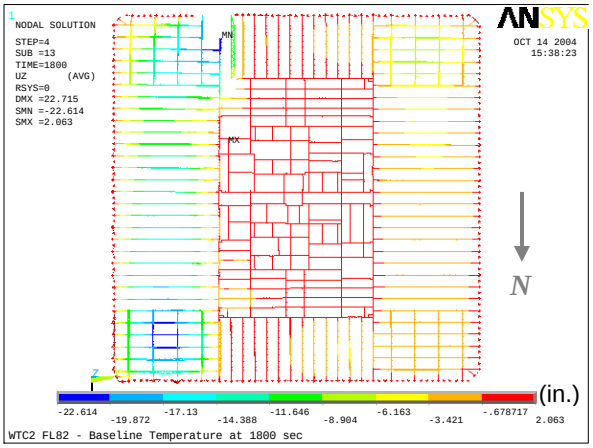

(d) Top view without concrete slab at 30 min

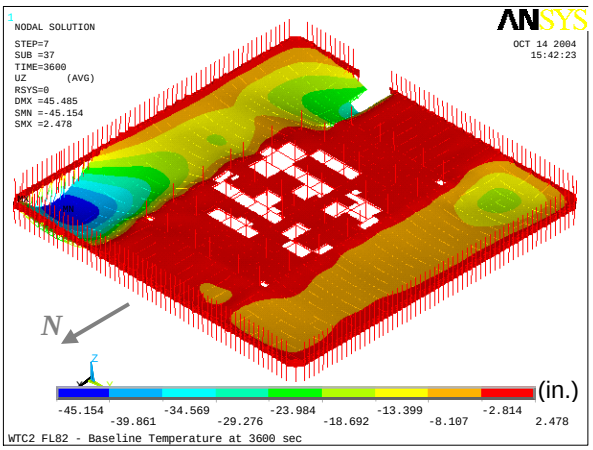

(e) Entire model at 60 min

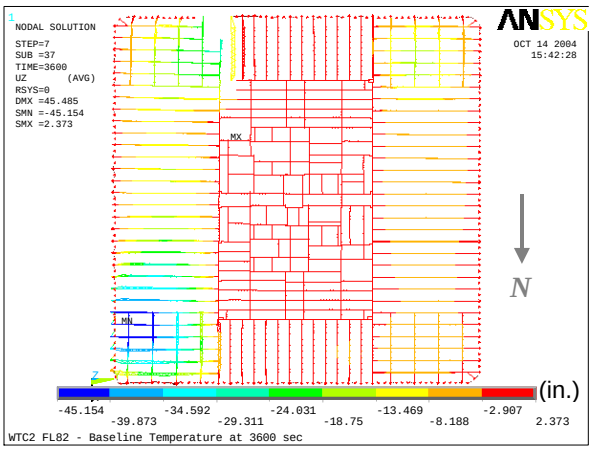

(f) Top view without concrete slab at 60 min

Figure 5–93. Vertical displacement of WTC 2 Floor 82 for Case C_i temperature condition at 10 min, 30 min, and 60 min (downward displacement is negative; 5x displacement magnification).

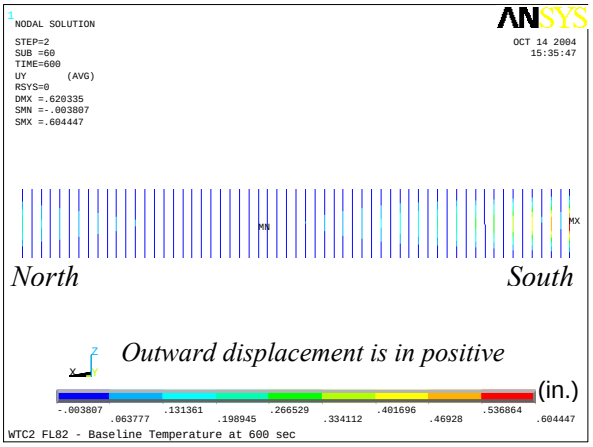

(a) West face at 10 min

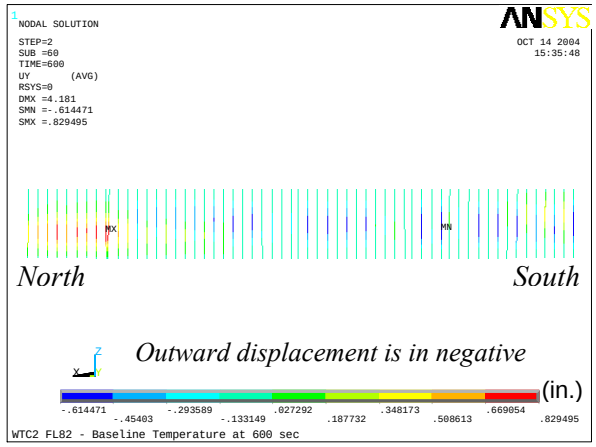

(b) East face at 10 min

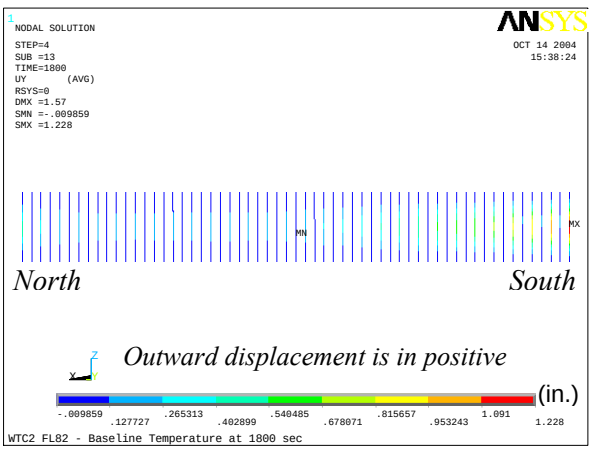

(c) West face at 30 min

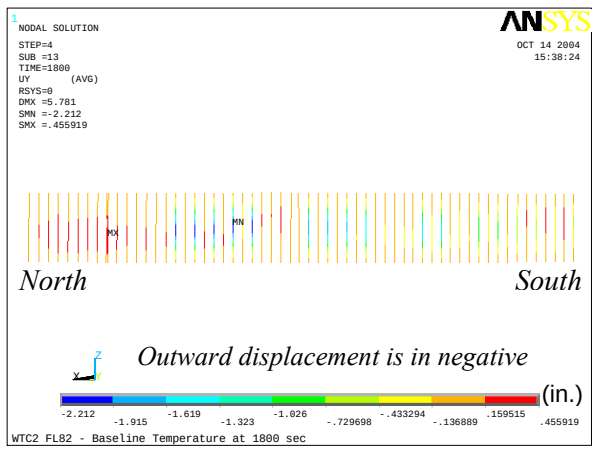

(d) East face at 30 min

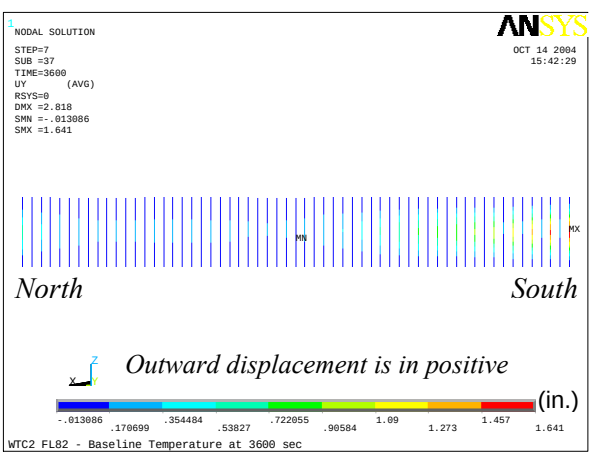

(e) West face at 60 min

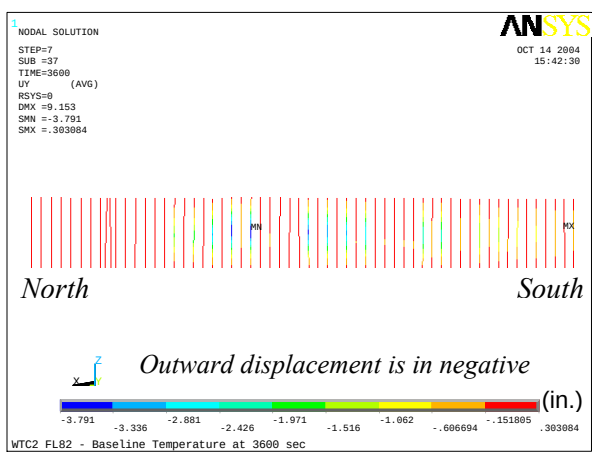

(f) East face at 60 min

Figure 5–94. Horizontal displacement of exterior columns of WTC 2 Floor 82 for Case C_i temperature condition at 10 min, 30 min, and 60 min.

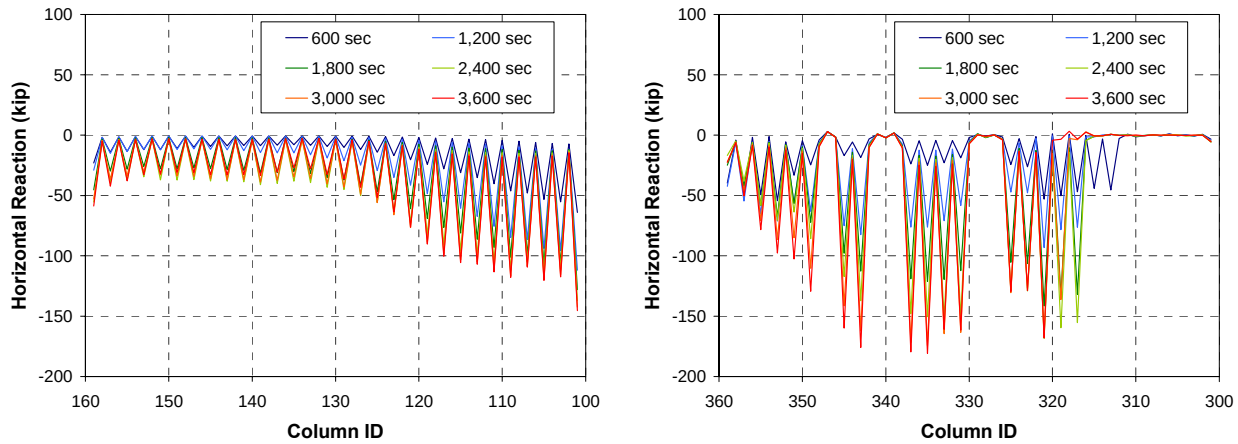

(a) West face (b) East face

Figure 5–95. Total horizontal reaction at exterior columns on east and west faces of WTC 2 Floor 82 for Case C_i conditions.

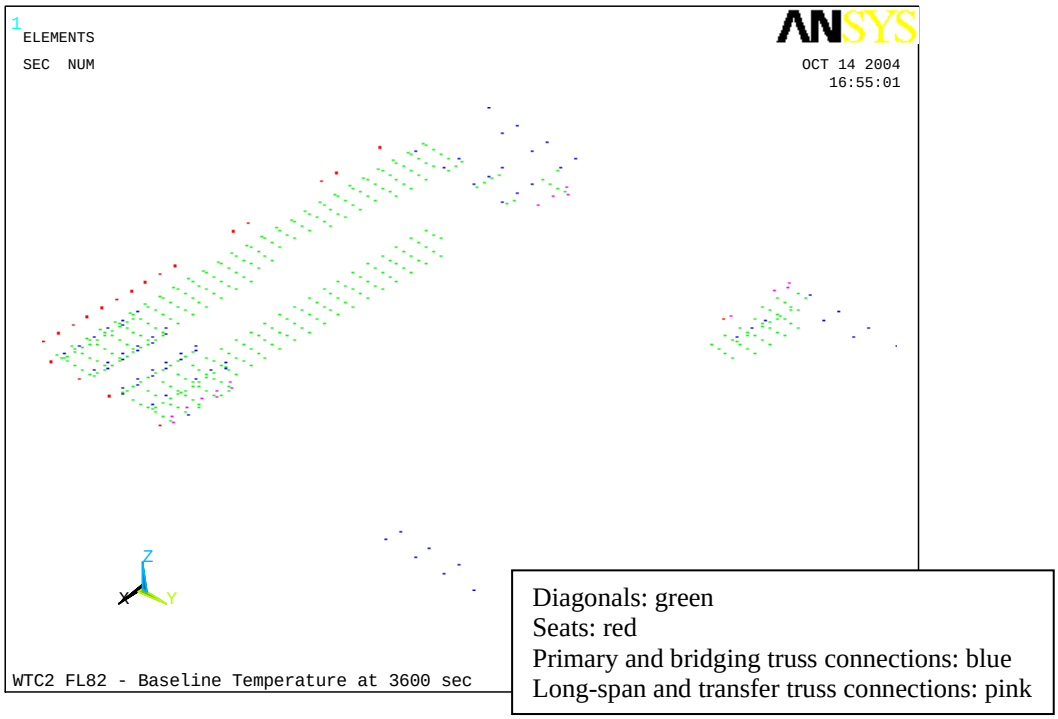

Figure 5–96. User-defined break elements that failed by 60 min in the model of WTC 2 Floor 82 for Case C_i temperature condition.

Table 5–16. Number of failed user-defined break elements in the model of WTC 2 Floor 82 for Case C_i temperature condition.

	Number of Break Elements
Web diagonals	381
Seats and gusset plates	46
Connections between primary and bridging trusses	70
Connections between long-span and transfer trusses	16
Total	513

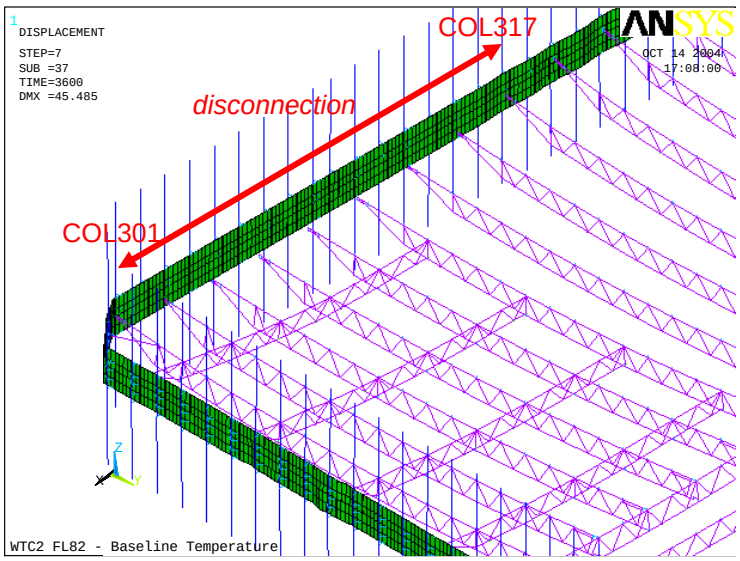

Figure 5–97. Loss of vertical supports in Floor 82 of WTC 2 for Case C_i temperature condition at 60 min (1x displacement magnification).

5.5.13 Results from Other WTC 2 Floors under Case C_i Temperature Condition

Table 5–17 gives the maximum vertical displacement of WTC 2 floors for Case C_i temperature condition, and Figs. 5–98 to 5–101 show the vertical displacements of WTC 2 floors when each floor experienced the maximum displacement. Except for Floor 82, the maximum vertical displacement occurred in the southeast area near the impact damage. The maximum displacement occurred at 60 min on all floors. The vertical displacement in the west office area was found to be insignificant on all the floors except Floor 80 throughout the thermal loading because the insulation on floor trusses was intact in the west office area. In Floor 80, the maximum vertical displacement of the west office area became about 20 in. at 60 min.

Figure 5–102 (a) shows the average thermal expansion of floors at 60 min on each face, while Fig. 5–102 (b) shows the average total thermal expansion of floors at 60 min in two orthogonal directions. The total slab expansion ranged from 2.5 in. to 5.5 in. Figure 5–103 shows the horizontal reaction at each column on the north and south faces of Floor 82. (The reaction force is positive when the floor pulls the exterior column in.) It was found that Columns 353 to 359 were pulled in by the floor due to the

significant sag in the southeast area caused by the impact damage to the transfer truss and interior truss seats in this area.

Web diagonals of Floor 81 to Floor 83 buckled in the hot zones of the east office area where the insulation on the trusses was damaged. Failures of the exterior truss seats, gusset plates, or seat bolts were not observed on Floor 79 to Floor 81. Trusses at Column 325 to Column 333 on the east face of Floor 83 lost their vertical support at the exterior truss seats at 50 min, as shown in Fig. 5–104.

Table 5–17. Maximum vertical displacement of WTC 2 floors for Case C_i temperature condition.

Floor	Max. Displacement (in.)	Time at the Maximum (min)
79	19.0	60
80	30.1	60
81	31.0	60
82	45.2	60
83	38.9	60

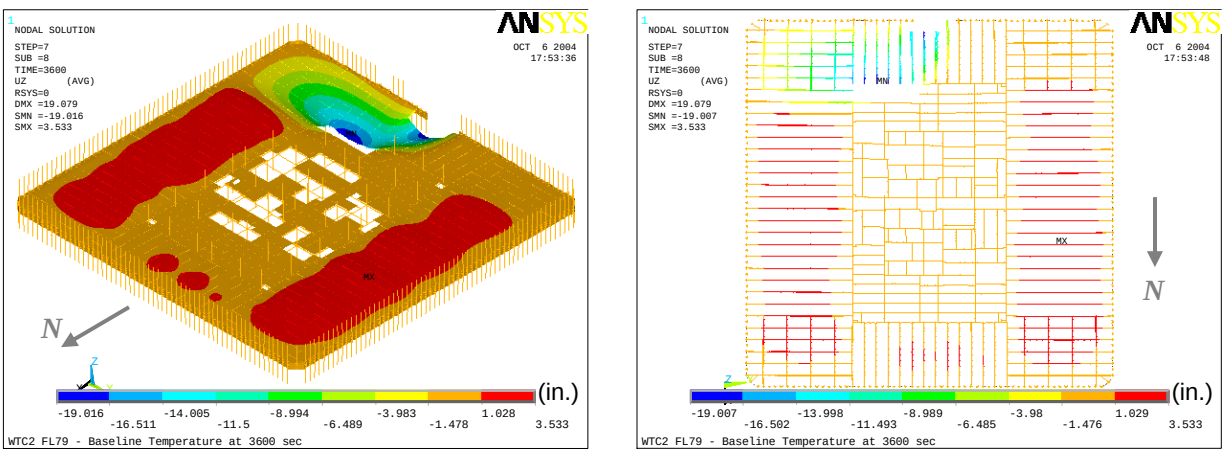

(a) Entire model (b) Top view without slab

Figure 5–98. Vertical displacement of WTC 2 Floor 79 for Case C_i temperature condition at 60 min (downward displacement is negative; 5x displacement magnification).

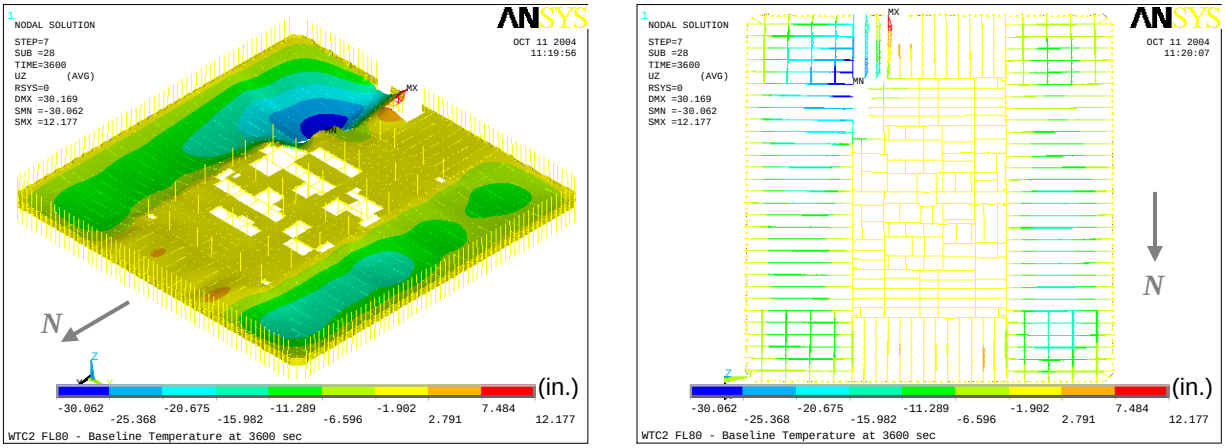

(a) Entire model (b) Top view without slab

Figure 5–99. Vertical displacement of WTC 2 Floor 80 for Case C_i temperature condition at 60 min (downward displacement is negative; 5x displacement magnification).

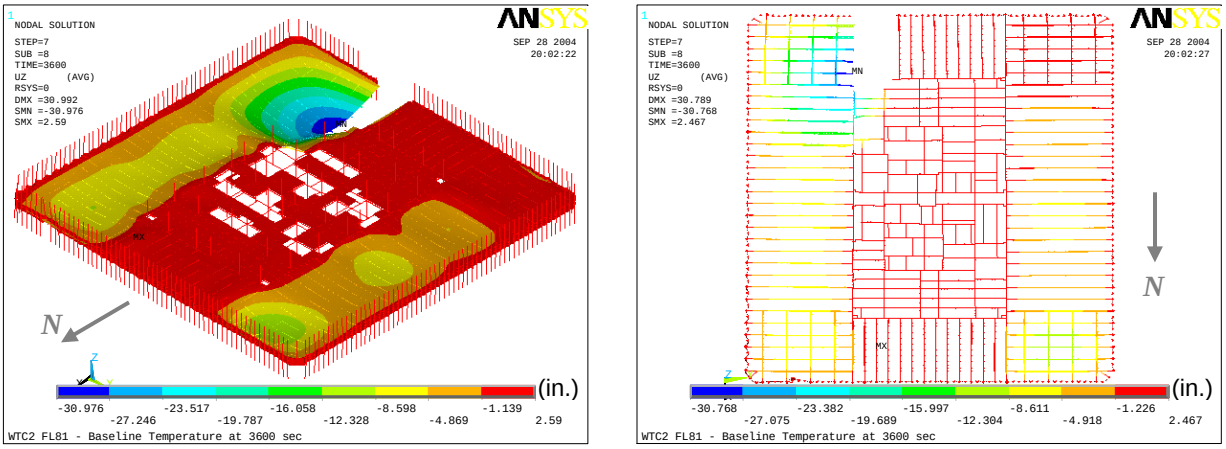

(a) Entire model (b) Top view without slab

Figure 5–100. Vertical displacement of WTC 2 Floor 81 for Case C_i temperature condition at 60 min (downward displacement is negative; 5x displacement magnification).

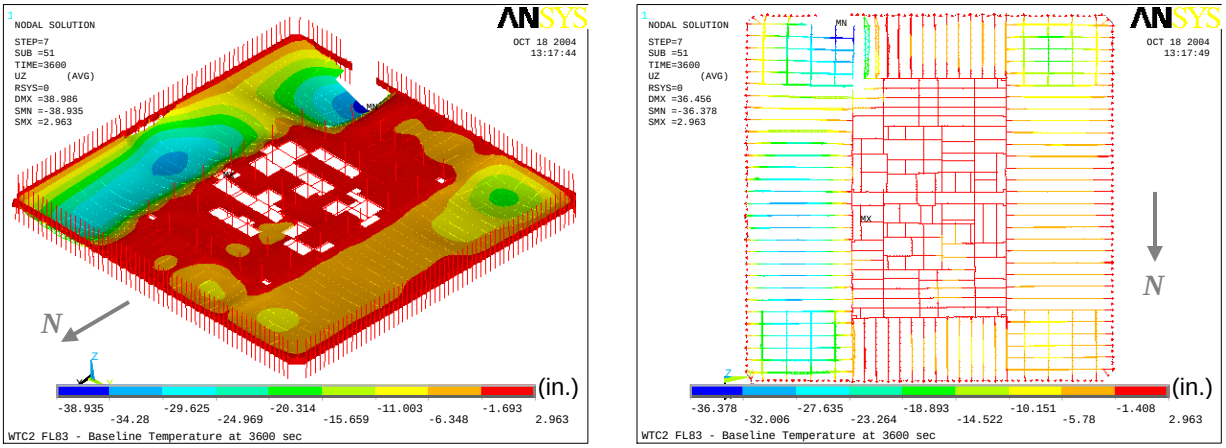

(a) Entire model (b) Top view without slab

Figure 5–101. Vertical displacement of WTC 2 Floor 83 for Case C_i temperature condition at 60 min (downward displacement is negative; 5x displacement magnification).

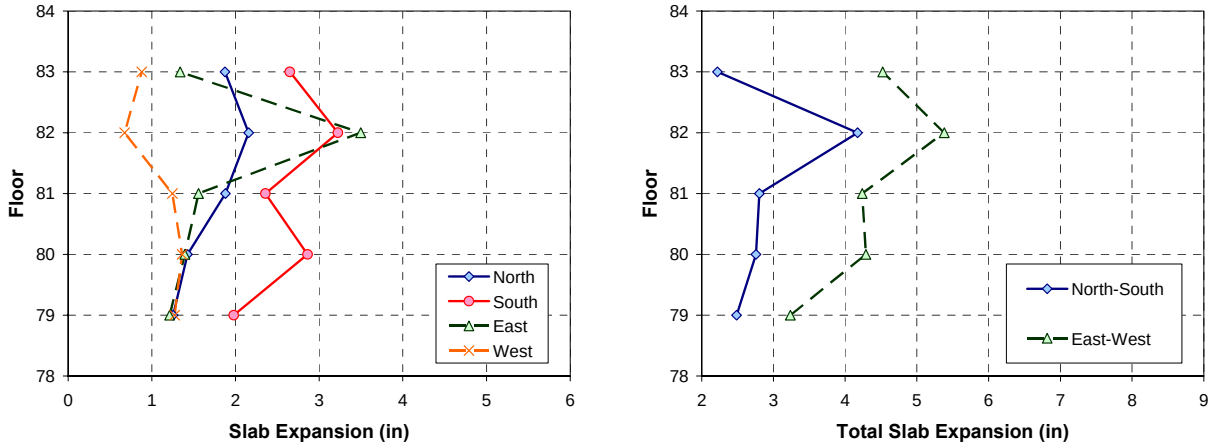

(a) Average displacement of each face (b) Average slab expansion in each direction

Figure 5–102. Average thermal expansion of WTC 2 floors at 60 min under Case C_i temperature condition.

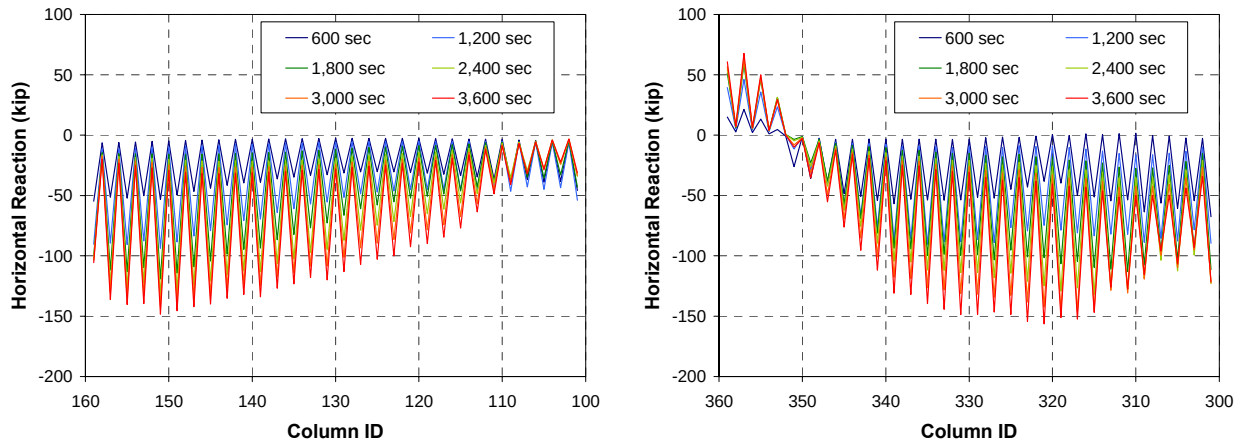

(a) West face (b) East face

Figure 5–103. Horizontal reaction force per column of WTC 2 Floor 81 for Case C_i temperature condition.

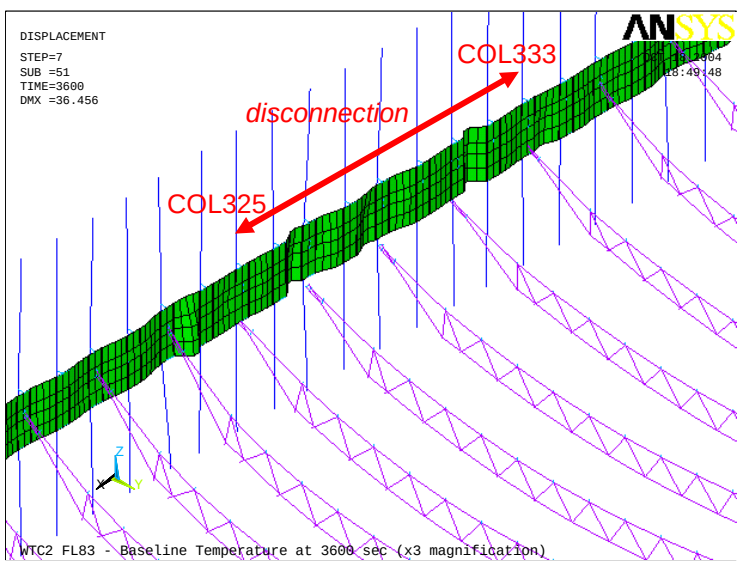

Figure 5–104. Loss of vertical supports in Floor 83 of WTC 2 for Case C_i temperature condition at 60 min (3X displacement magnification).

5.5.14 Results from WTC 2 Floors under Case D_i Temperature Condition

Table 5–18 summarizes the maximum vertical displacement of WTC 2 floors under Case D_i temperature condition, and Figs. 5–105 to 5–109 show the vertical displacements of WTC 2 floors when each floor experienced the maximum displacement. Due to the more extensive impact damage and higher temperatures than Case C_i conditions, all floors had larger vertical displacement. Floor 80 and Floor 81 suffered impact damage to transfer trusses and many interior truss seats in the southeast area. Bridging trusses that had been removed in the analyses with Case C_i conditions were replaced in these two floors to provide support to the primary trusses in the east office area after aircraft impact. A maximum vertical

displacement of 97 in. occurred at Floor 81 near the impact damage at 50 min as shown in Fig. 5–107. Similar sagging of the floor was found in other floors.

Gusset plates and bolts at more than 75 percent of all the exterior seats of the east face of Floor 82 and Floor 83 failed due to horizontal shear force that was caused by the difference in the thermal expansion between the floor and the exterior wall in the direction transverse to primary trusses. The truss at Column 357 of Floor 81 was the only truss that lost its vertical support at the exterior truss seat among all floors. This truss walked off the truss seat.

Floor sagging caused pull-in forces. For instance, Column 101 to Column 111 on the west face and Column 347 to Column 359 on the east face were pulled in by the floor at 60 min on Floor 80 as shown in Fig. 5–110 because of the floor sagging occurring in the southeast area. Since core columns were not restrained in the horizontal directions, when the floor pulled in one face of exterior wall, the opposite face of the exterior wall was also pulled in. Columns at the southeast corner were pulled in by the floor at Floor 79 and Floor 81. Many columns of the west face of Floor 82 were pulled in. The reaction forces at many columns of the east face of Floor 82 were close to zero, as shown in Fig. 5–111 (b). The gusset plates and seat bolts failed at a number of trusses on the east face of Floor 82. Since columns at these locations were not supported in the horizontal direction by the floor, the reaction force became close to zero at these columns.

Figure 5–112 shows the average thermal expansion of floors at 60 min of Case D_i temperature condition. The average total floor expansion ranged from 1 in. to 5 in.

Table 5–18. Maximum vertical displacement of WTC 2 floors for Case D_i temperature condition.

Floor	Max. Displacement (in.)	Time at the Maximum (min)
79	35.8	60
80	65.6	40
81	96.7	50
82	49.4	60
83	44.6	60

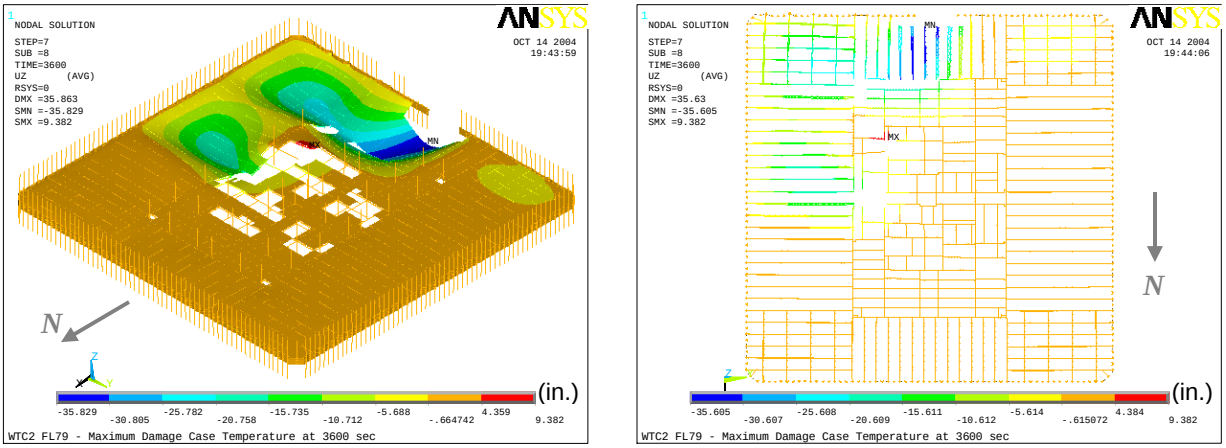

(a) Entire model (b) Top view without slab

Figure 5–105. Vertical displacement of WTC 2 Floor 79 for Case D_i temperature condition at 60 min (downward displacement is negative; 5x displacement magnification).

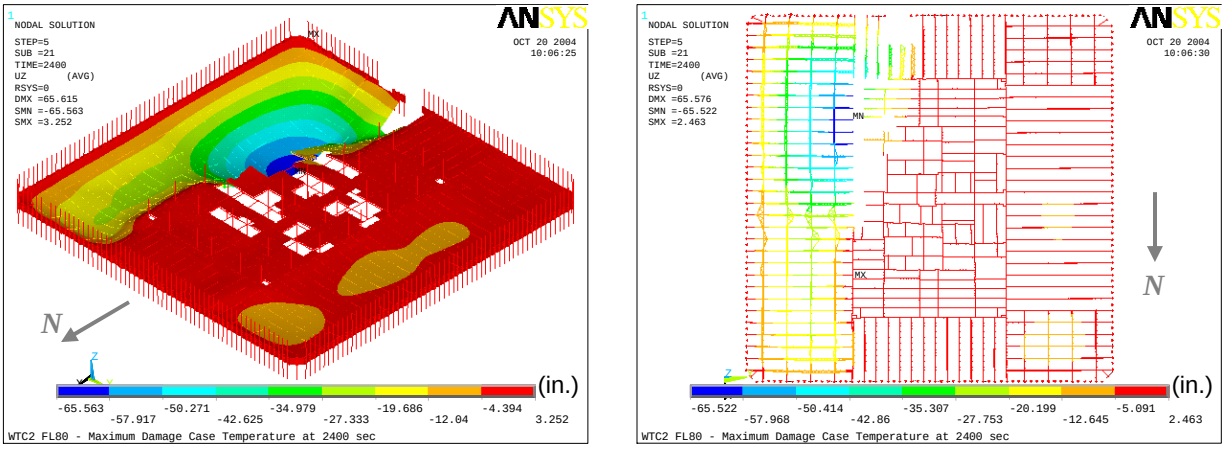

(a) Entire model (b) Top view without slab

Figure 5–106. Vertical displacement of WTC 2 Floor 80 for Case D_i temperature condition at 40 min (downward displacement is negative; 5x displacement magnification).

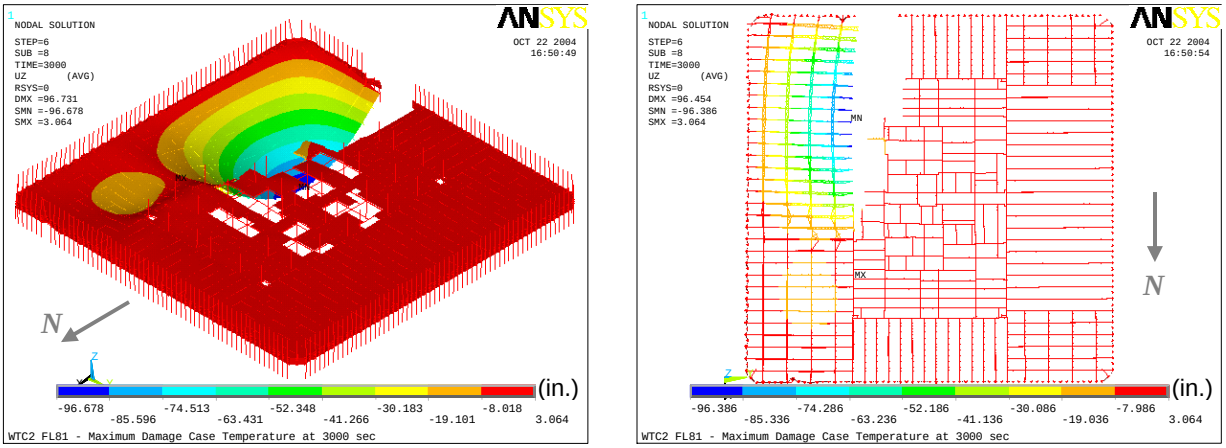

(a) Entire model (b) Top view without slab

Figure 5–107. Vertical displacement of WTC 2 Floor 81 for Case D_i temperature condition at 50 min (downward displacement is negative; 5x displacement magnification).

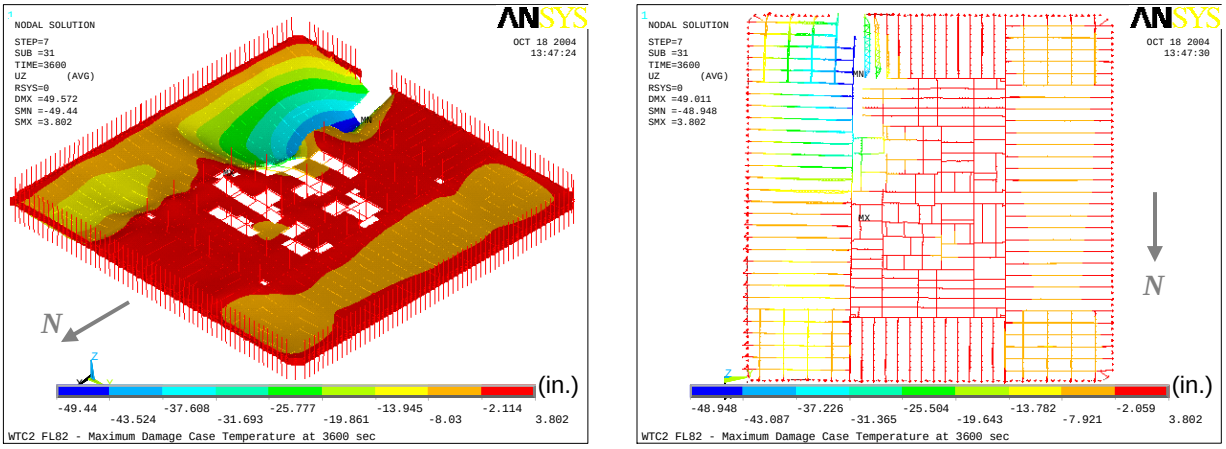

(a) Entire model (b) Top view without slab

Figure 5–108. Vertical displacement of WTC 2 Floor 82 for Case D_i temperature condition at 60 min (downward displacement is negative; 5x displacement magnification).

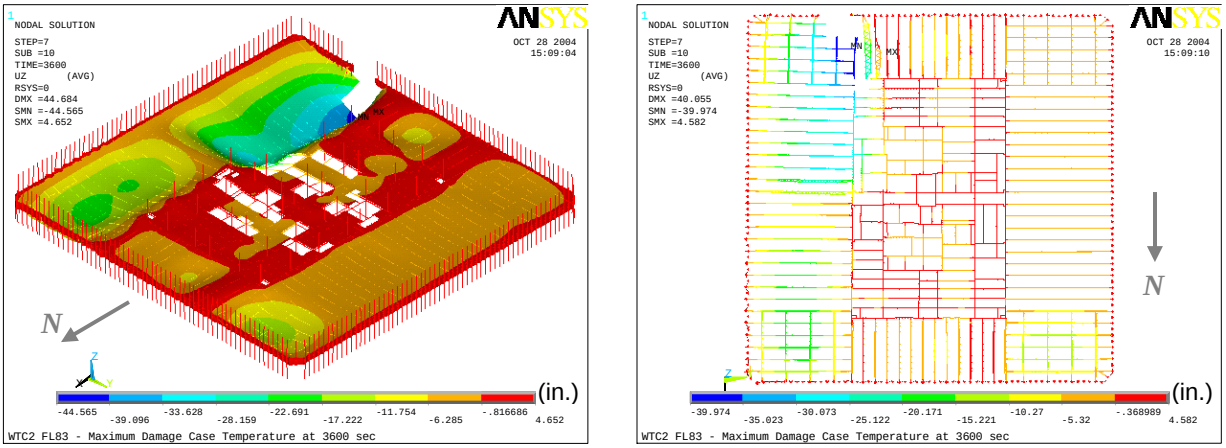

(a) Entire model (b) Top view without slab

Figure 5–109. Vertical displacement of WTC 2 Floor 83 for Case D_i temperature condition at 60 min (downward displacement is negative; 5x displacement magnification).

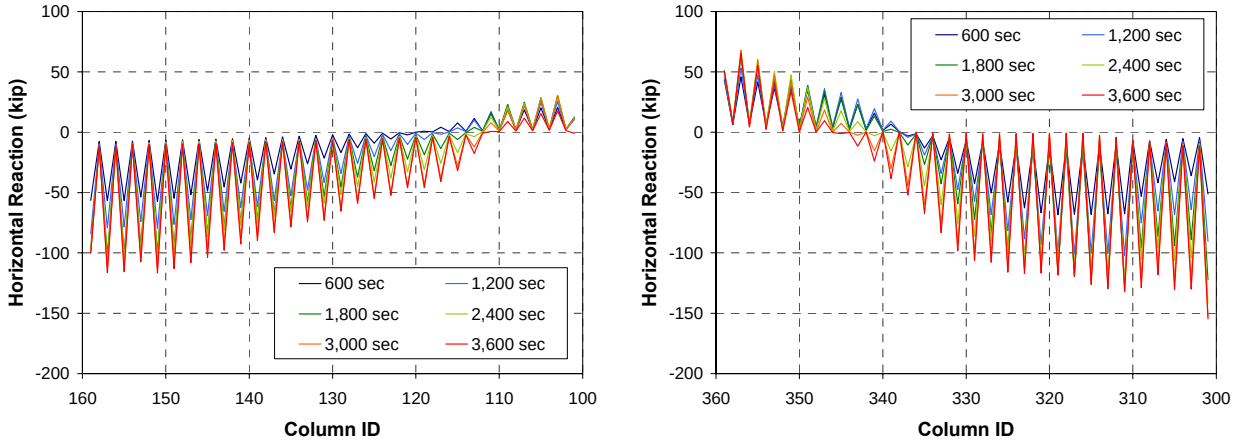

(a) West face (b) East face

Figure 5–110. Horizontal reaction force per column of WTC 2 Floor 80 for Case D_i temperature condition.

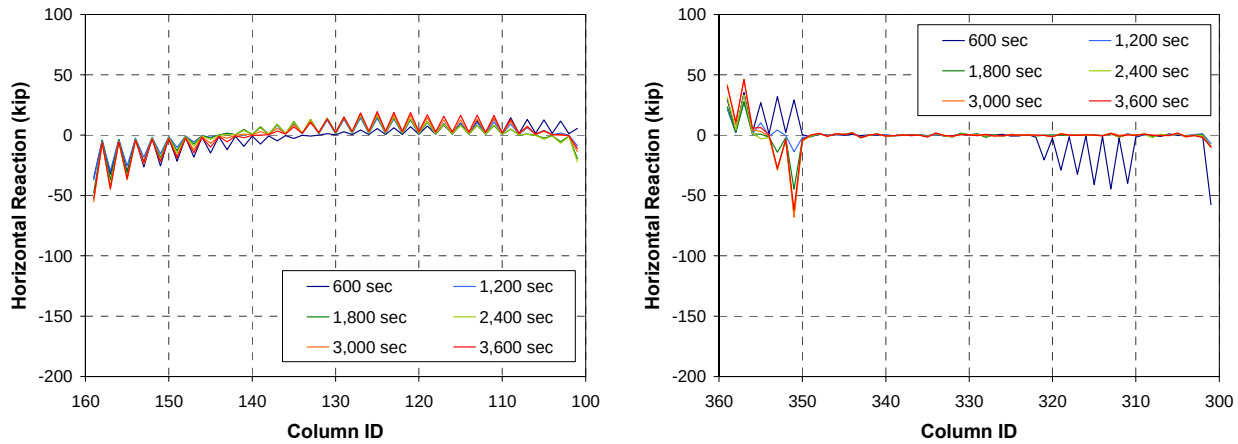

(a) West face (b) East face

Figure 5–111. Horizontal reaction force per column of WTC 2 Floor 82 for Case D_i temperature condition.

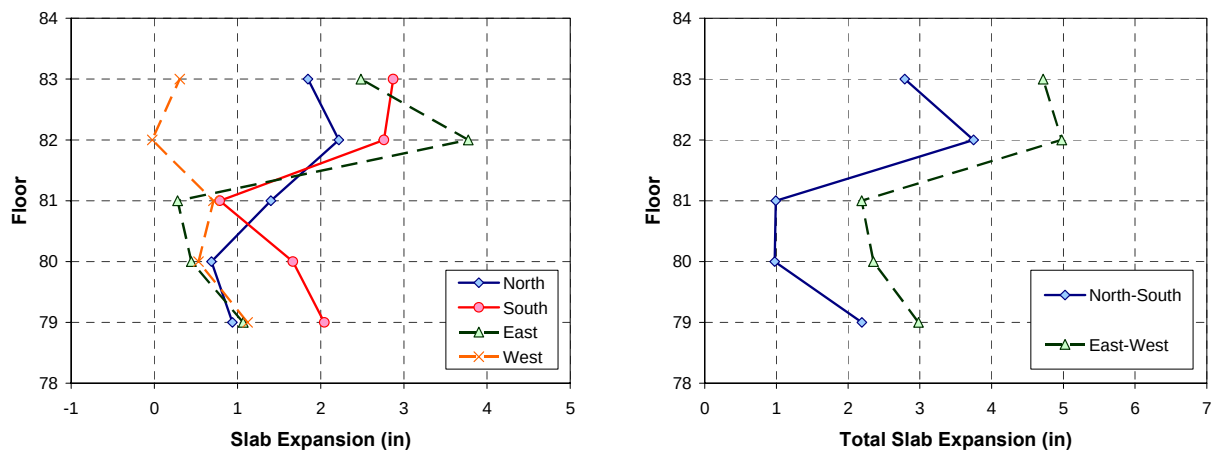

(a) Average displacement of each face (b) Average slab expansion in each direction

Figure 5–112. Average thermal expansion of WTC 2 floors at 60 min for Case D_i temperature condition.

5.5.15 Creep Effect

Full floor models were not run with creep due to the inherent convergence problems of BEAM188/189 elements under thermal loadings with materials with temperature-dependent creep. To evaluate the effect of creep, a simplified truss model at Column 333 of Floor 96 was extracted from the full floor model and was subjected to Case B_i temperature condition. The model was analyzed with and without creep in the steel.

Vertical displacements at 40 min are shown in Fig. 5–113. The maximum displacements at 40 min were 44 in. for the model with creep and 26 in. for the model without creep. After 40 min, the model with creep walked off the exterior truss seat, while the model without creep did not walk off the exterior truss seat, and the vertical displacement increased with time and reached 31 in. at 100 min. The maximum pull-in forces were 14 kip for the model with creep and 8 kip for the model without creep. The interface force between the exterior columns and the truss became compression in the model without creep after 37 min because the thermal expansion overcame the shortening caused by the sagging.

Based on this study of the simplified truss model, creep in steel would significantly increase the existing floor sag at high temperatures. Therefore, the sagging of floors was underestimated in the full floor model analyses performed without creep.

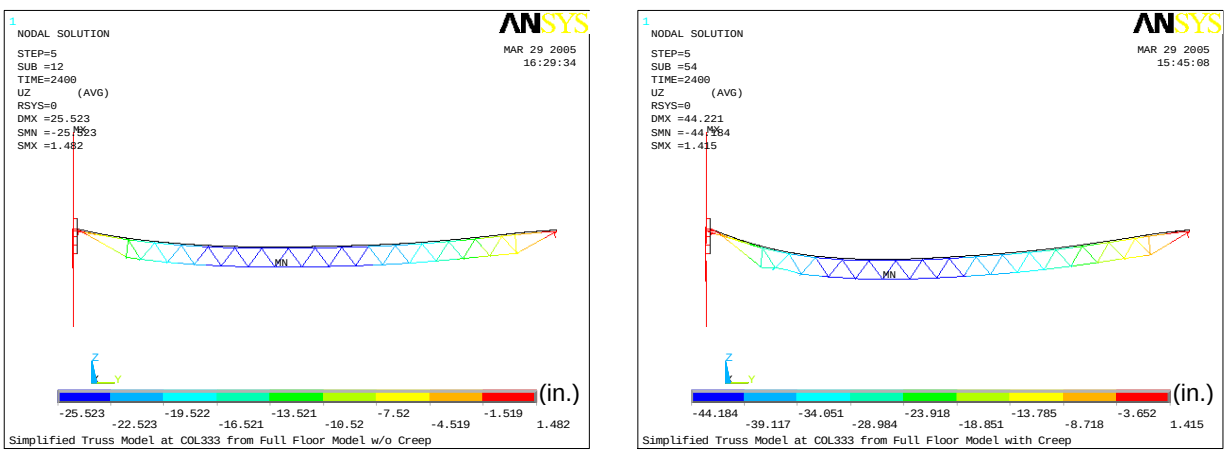

(a) Model without creep (b) Model with creep

Figure 5–113. Vertical displacement of a simplified truss model at Column 333 extracted from the full floor model of Floor 96 of WTC 1 under Case B_i temperature condition at 40 min (downward displacement is negative).

5.5.16 Effect of Column Boundary Conditions

The boundary conditions at the ends of columns and column length affect the horizontal force between the floors and the exterior walls resulting from the thermal expansion of the floor. The fixed boundary conditions and single story column length assumed in the floor analyses shown in this report represent a relatively high degree of lateral restraint. The effect of reducing the degree of lateral restraint was evaluated by performing nonlinear static finite element analysis with two story and three story column lengths.

The results showed that the reduced restraint did not significantly affect the overall structural performance of the floors although it decreased the vertical deflection of the floor by less than 20 percent and it

decreased the magnitude of the lateral force by as much as 85 percent. (Note that this decrease in deflection compensates partially for the additional deflection expected due to creep, as discussed in Section 5.5.15.)

5.5.17 Floor Subsystem in Global Models

Floor: The floors in the global models were modeled by SHELL181 elements with temperature-dependent elastic properties to enhance computational efficiency. Their functions were to:

1. Simulate the diaphragm action of floors
2. Simulate the load transfer from the core to the exterior wall system when the core experiences significant downward displacement due to shortening of core columns

The membrane stiffness of shell elements for the office area was determined by calculating the longitudinal stiffness of the composite floor using the single truss model which included not only the stiffness of the truss but also the stiffness of the connections between the truss and the exterior wall.

Fire-Induced Damage: Floors modeled by shell elements could not capture failure modes of floors under elevated temperatures; therefore, key failure modes were implemented in the global models at appropriate points in time as fire-induced damage. Two different behaviors were considered based on conditions of connections between the floor and the exterior wall: 1) the floor sagged and pulled the exterior wall in and 2) the floor was disconnected from the exterior wall. The locations of floor/wall disconnections and the locations and magnitudes of pull-in forces in the sagging floor areas were determined using not only the full floor model results but also the actual observations from photographs and videos and the analyses performed on isolated exterior wall models, as discussed in Section 2.5 of NIST NCSTAR1-6D.

Results from the full floor model analyses are presented in Figs. 5–114 to 5–117 only at the end of time histories for the conditions of the connections between the exterior wall and the floors. The figures show the following conditions:

- Condition 1: gusset plate failure + seat failure due to vertical shear (loss of vertical support)
- Condition 2: gusset plate failure + seat bolt shear-off + truss walk-off (loss of vertical support)
- Condition 3: gusset plate failure + seat bolt shear-off + significant vertical displacement (>25 in.) of the floor in that area (floor remains vertically supported)
- Condition 4: tensile force between the exterior wall and the floor system (floor remains vertically connected, but exerts pull-in force on the exterior wall)

Conditions 1 and 2 were treated as the case of floor/wall disconnections. Conditions 3 and 4 were treated as the case where the floor pulled in the exterior wall. Owing to the failure of the gusset plate and seat bolts (Condition 3), the floor in this model cannot pull in the exterior wall at these connections. In reality, in addition to studs and diagonal strap anchors that may not have failed, there was friction between the truss bearing angles and the exterior truss seat angle. For these reasons, Condition 3 was treated as the case where the floor pulled in the exterior wall. More discussion on the pull-in force can be found in Section 2.5 of NIST NCSTAR1-6D.

In the full floor model, every other exterior column was connected to the floor because spandrel studs and strap anchors were removed from the model. The four conditions above were defined for columns at primary trusses; however, they are shown in Figs. 5–114 to 5–117 for all columns because there were

strap anchors connecting the floor to the columns located between primary trusses. When the same condition of the connection was found for two adjacent truss locations, the column between the two trusses was assumed to have the same condition as the adjacent columns in these figures. For example, failure of exterior seats (Condition 1) occurred at Columns 329 and 331 of Floor 98 of WTC 1 for Case B_i temperature condition. In Fig. 5–115, Column 330 is also indicated as Condition 1, although there was no truss located at Column 330.

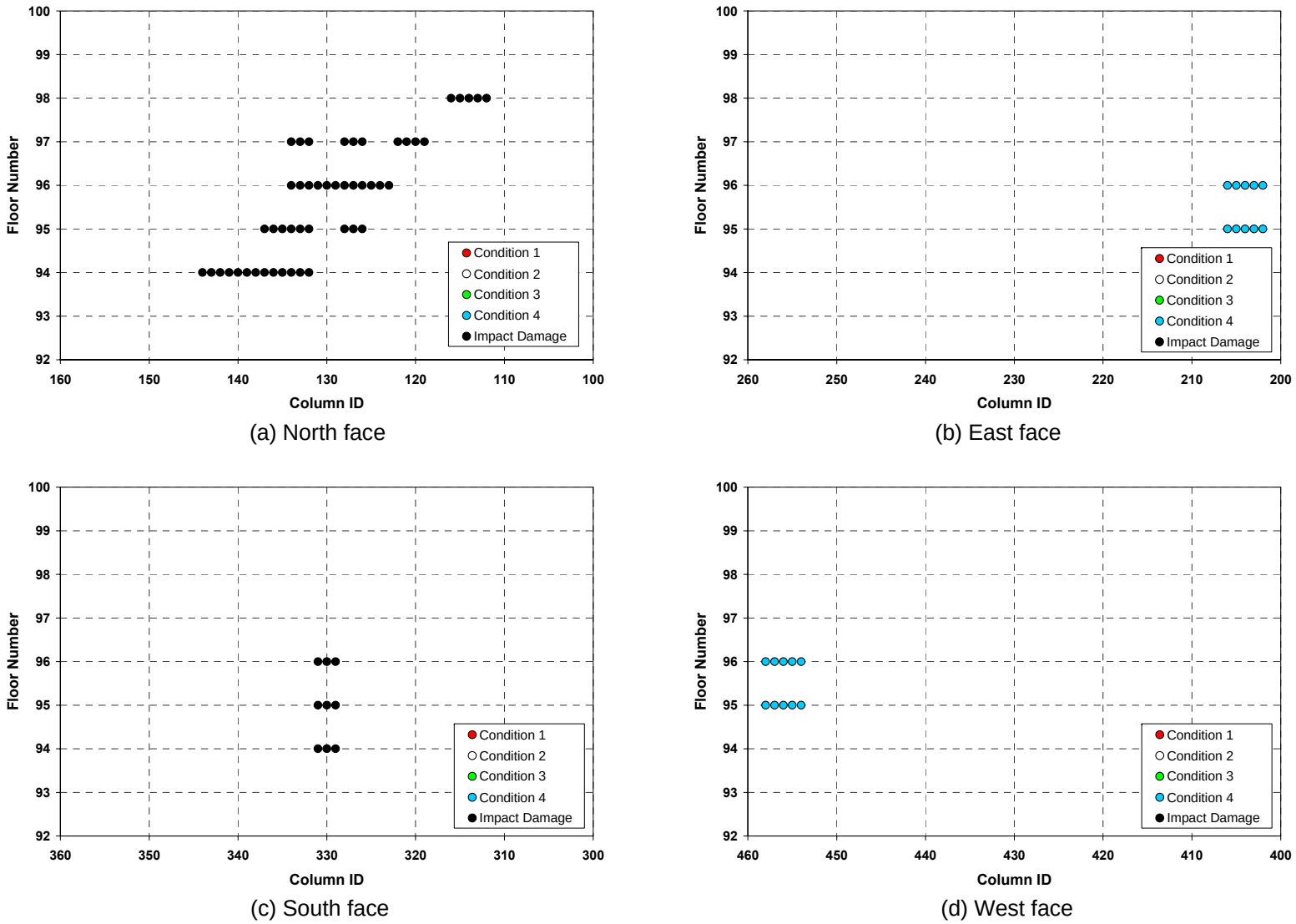

Figure 5–114. Conditions of connections between the exterior wall and the floors of WTC 1 for Case A_i temperature condition at 100 min.

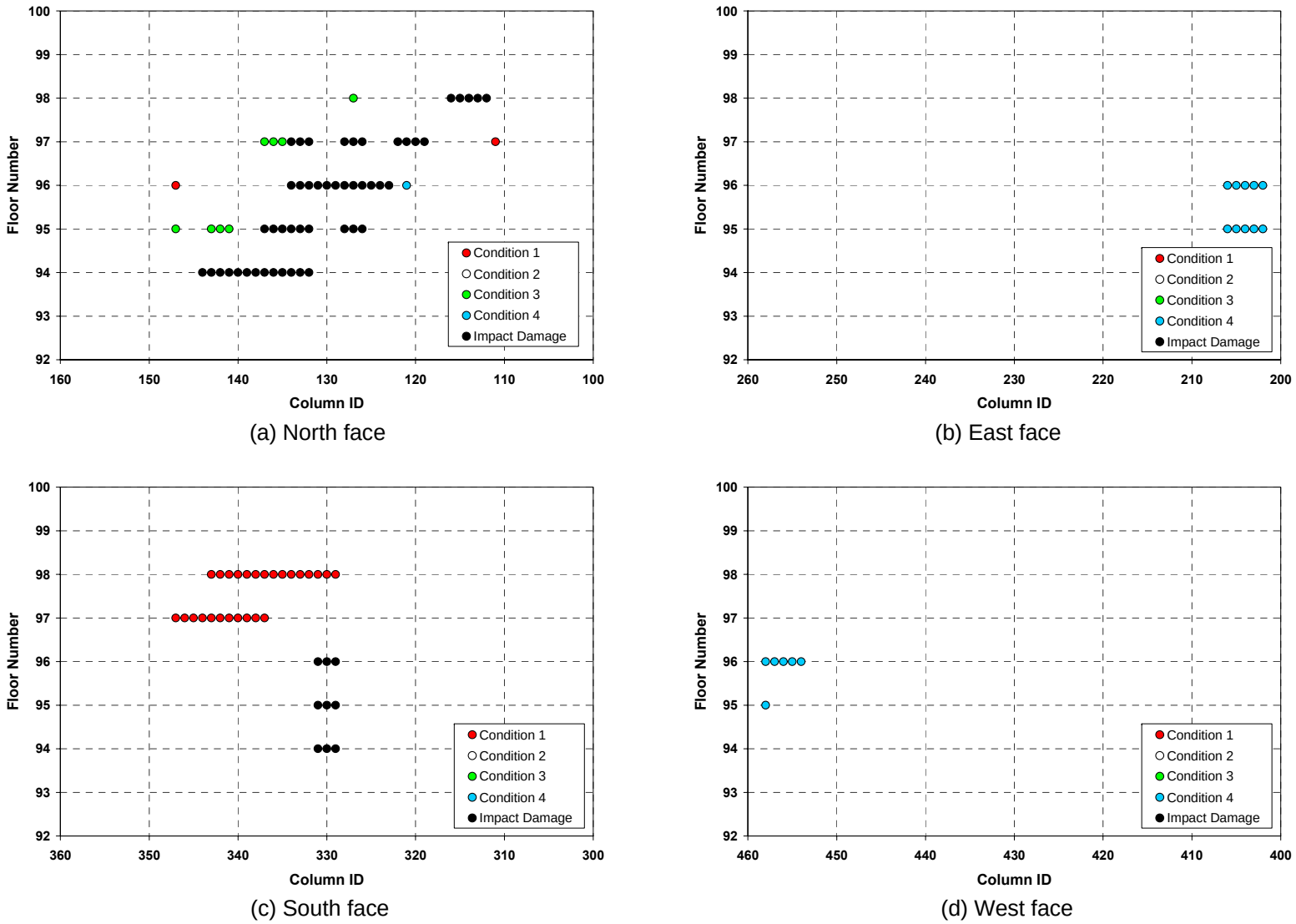

Figure 5–115. Conditions of connections between the exterior wall and the floors of WTC 1 for Case B_i temperature condition at 100 min.

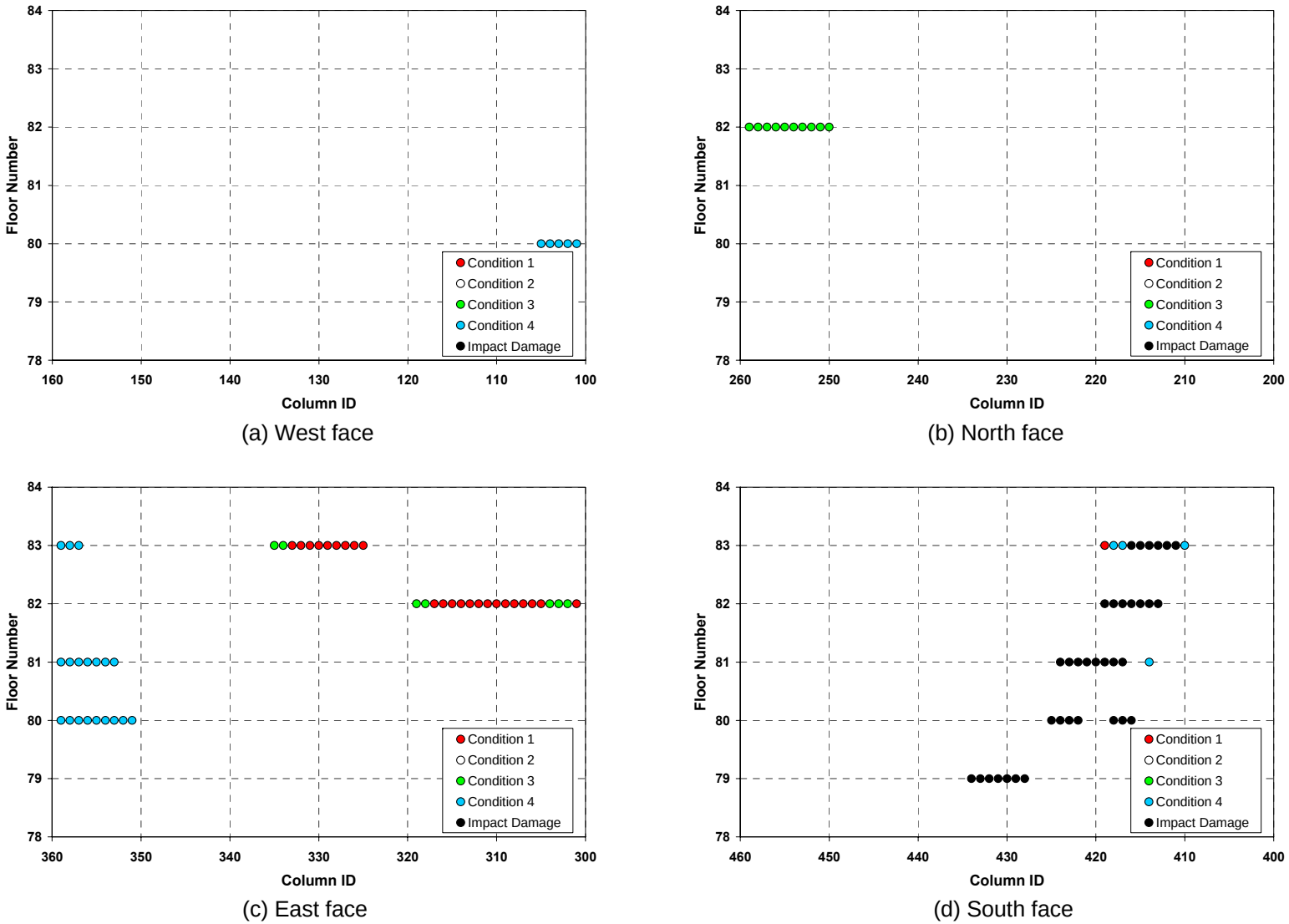

Figure 5–116. Conditions of connections between the exterior wall and the floors of WTC 2 for Case C_i temperature condition at 60 min.

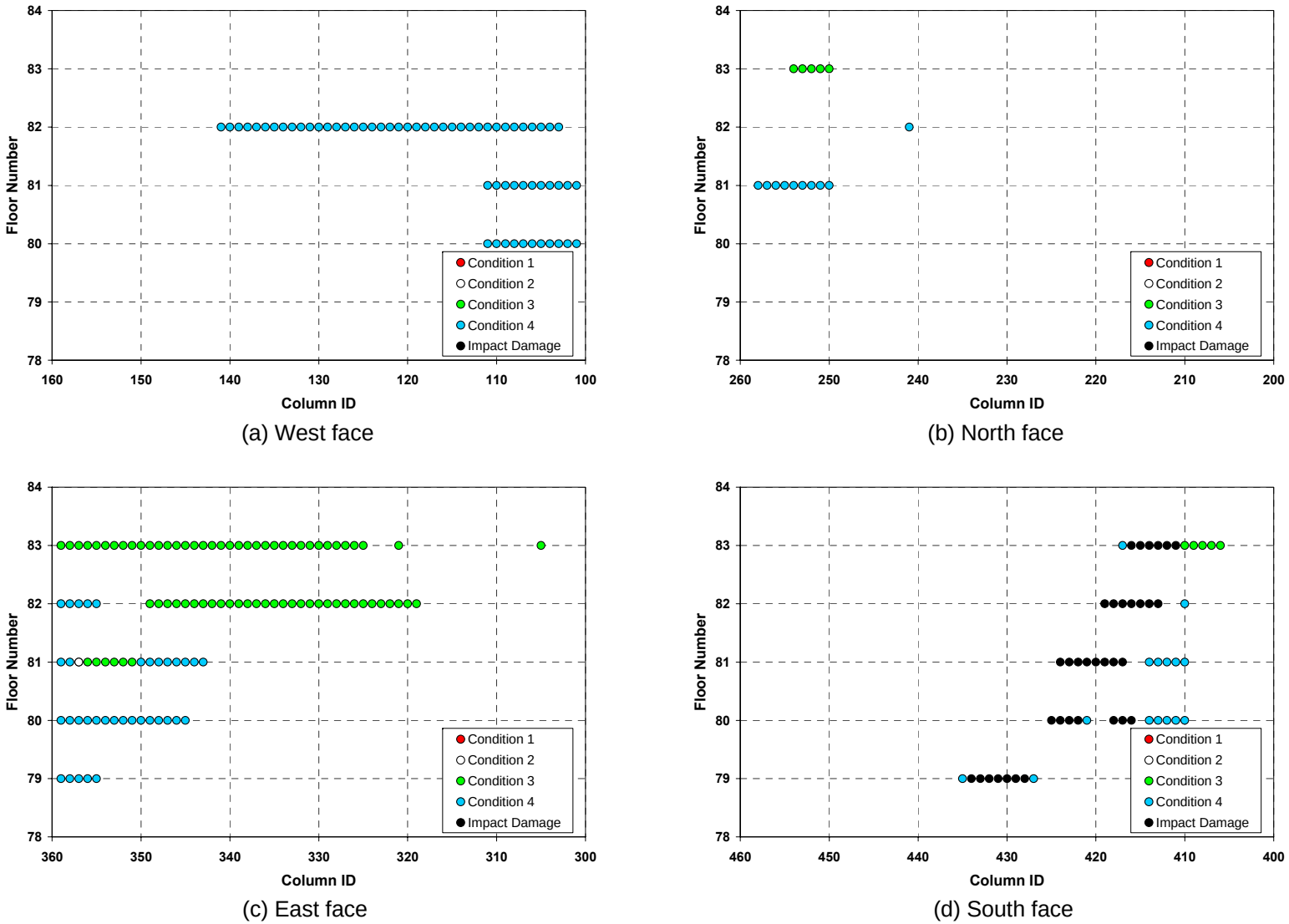

Figure 5–117. Conditions of connections between the exterior wall and the floors of WTC 2 for Case D_i temperature condition at 60 min.

5.5.18 Summary of Results and Discussion

The behaviors of the floor system found in the full floor models subjected to impact damage and elevated temperatures from the fires can be summarized as follows:

Bridging trusses subjected to elevated temperatures buckled between primary trusses.

When significant differences in thermal expansion of the floors and exterior walls in the direction transverse to the axes of primary trusses occurred near the corners, studs, diagonal strap anchors, gusset plates, and seat bolts at exterior truss seats failed due to the lateral shear.

Web diagonals of floor trusses with damaged insulation buckled.

Floors sagged as they lost bending stiffness resulting from web diagonal buckling, and they pulled the exterior wall in.

Truss seats disconnected from the exterior walls.

Pull-in forces were expected to develop whenever the floor sagged. Although the floor sagging was captured by the floor models in the heated area, the pull-in force on the exterior columns was not captured in most of the full floor model analyses. To accurately calculate pull-in forces between the floors and the exterior columns in the full floor model, much more detailed modeling will be required. Such modeling includes accurate boundary conditions on columns, creep in steel, friction at the truss seats, accurate evaluation of failure of strap anchors and studs, and concrete cracking and spalling. In addition, temperature time histories that were used in the full floor model analyses may have been conservative estimates, which were derived from conservative estimates of impact damage to the insulation. Further discussion on the pull-in force can be found in Section 2.5.2 of NIST NCSTAR1-6D.

This page intentionally left blank.

Chapter 6
EXTERIOR WALL SUBSYSTEM

6.1 OBJECTIVE

The objective of the exterior wall subsystem model was to study the performance of the exterior wall subjected to the combined effects of gravity and thermal loads for the following conditions:

- all floors provide lateral support,
- two adjacent floors do not provide lateral support,
- three adjacent floors do not provide lateral support,
- in addition to loss of lateral support at three floors, the exterior wall is subjected to pull-in forces by the sagging floors, and
- in addition to loss of lateral support at three floors, the exterior wall is subjected to additional gravity loads.

The following temperature-dependent nonlinearities and material properties were included in the exterior wall model:

- Large deflections and buckling
- Material plasticity
- Creep
- Material failure
- Column splice failure
- Spandrel splice failure

6.2 EXTERIOR WALL SUBSYSTEM DESCRIPTION

The exterior walls of the towers were constructed with prefabricated wall panels, referred to hereafter as panels. Typical panels contained three-column segments spanning three stories with three spandrels extending one half-span past the outer columns. The panels were arranged such that the spandrel splices between panels aligned vertically, and the column splices between panels were offset by one story.

The modeled exterior wall subsystem was located on the north face of WTC 1 toward the east side and included nine columns, extending vertically from the column splice located below Floor 91 to the column splice above Floor 99, and nine spandrels extending horizontally from the spandrel splice between Columns 149 and 150 to the spandrel splice between Columns 158 and 159. This exterior wall subsystem model included seven full panels and portions of four other panels.

Figure 6–1 shows the subsystem pictorially. Figures 6–2 (a) and 6–2 (b) give the types and yield strengths of the columns and spandrels and the types of column and spandrel splices. Figure 6–3 shows the column plate notation used. Tables 6–1a through 6–1c give the geometry and material properties of the plates in the columns, the spandrels, and the column and spandrel splices.

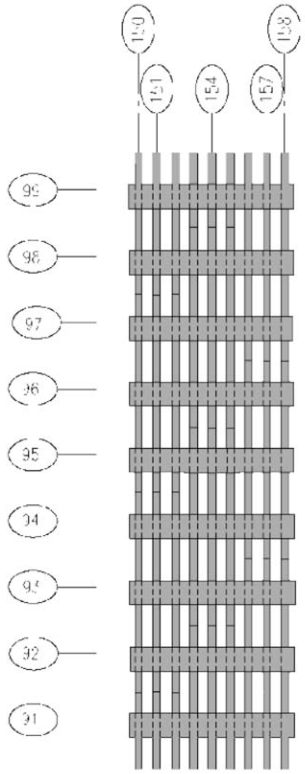

Figure 6–1. Exterior wall subsystem structure.

The odd-numbered columns supported the floor trusses. Pairs of strap anchors extended diagonally from the top chords of truss pairs to the even-numbered columns. The trusses and the strap anchors partially braced the columns both in-plane and out-of-plane of the exterior wall.

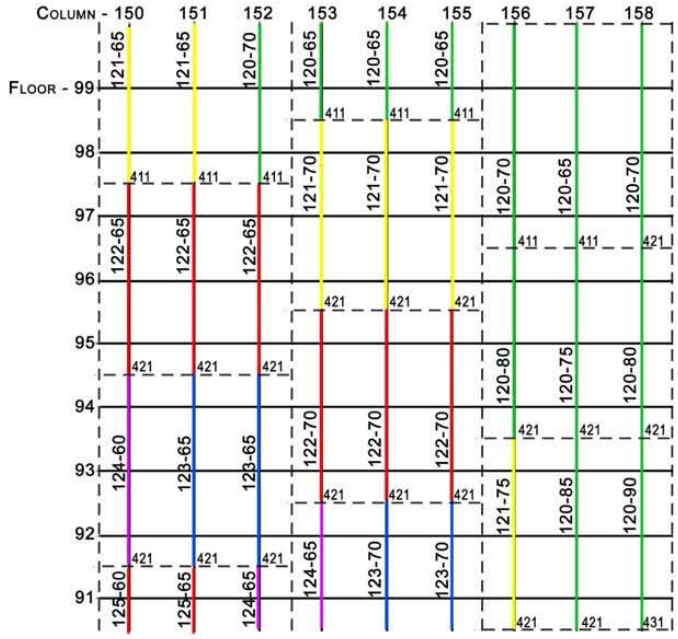

XXX-XX indicates type and nominal yield strength of column (ksi)
xxx indicates type of colum splice

(a) Columns and column splices

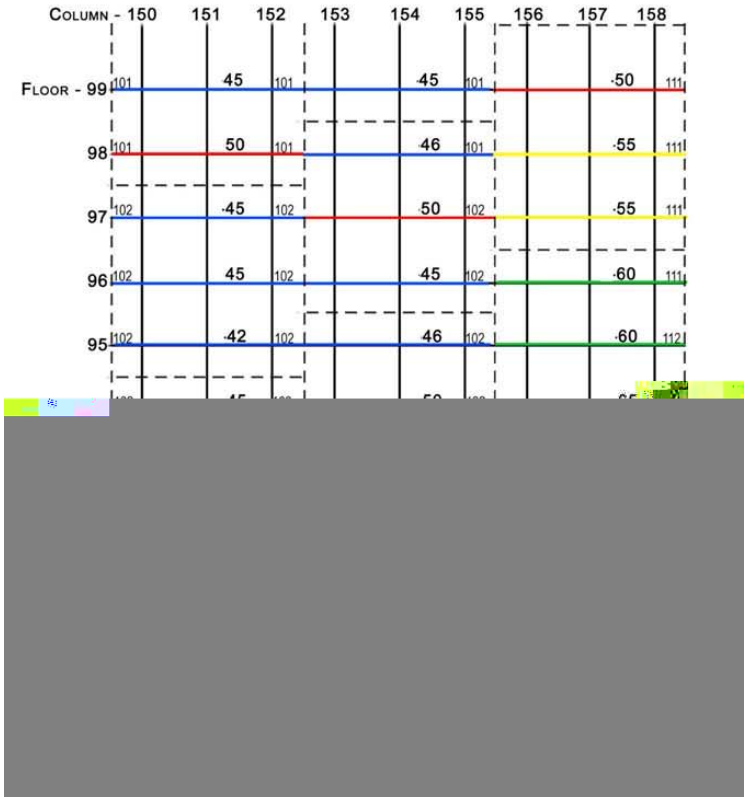

Figure 6–2. Columns, spandrels, and splices: type and material assignments.

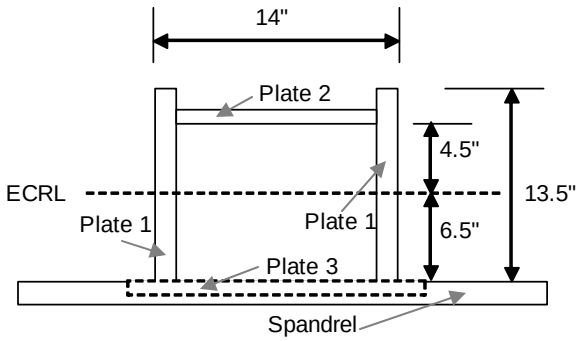

Figure 6–3. Schematic of column cross section.

Table 6–1a. Column sectional properties.

Column Type	Plate 1 l x t (in. x in.)	Plate 2 l x t (in. x in.)	Plate 3. l x t (in. x in.)
120	13.5 x 0.25	13.5 x 0.25	15.75 x 0.25
121	13.5 x 0.3125	13.375 x 0.25	15.75 x 0.25
122	13.5 x 0.375	13.25 x 0.25	15.75 x 0.25
123	13.5 x 0.4375	13.125 x 0.25	15.75 x 0.25
124	13.5 x 0.5	13 x 0.25	15.75 x 0.25
125	13.5 x 0.5625	12.875 x 0.25	15.75 x 0.25

[1]All spandrels in model are 52 in. deep x 3/8 in. thick.

Table 6–1b. Column splice details.

Column Splice Type	Butt Plate Thickness (in.)	Number of Bolts	Bolt Diameter (in.)	Gage (in.)	Bolt Spacing (in.)	Column Splice ID
411	1.375	4	0.875	3.5	6	411
421	1.625	4	0.875	3.5	6	421
431	1.875	4	1	3.5	6	431

[1]Butt plates have specified yield strength of 50 ksi.
[2]Bolts are A325.

Table 6–1c. Spandrel splice details.

Spandrel Splice Type	Number of Bolts/Row	Total Number of Rows	Bolt Spacing (in.)	Gage (in.)	Overall Splice Plate Dimensions (in. x in. x in.)	Bolt to Centerline of Splice (in.)	Gap B/W Spandrels (in.)	Spandrel Splice ID
101	6	2	5@9		49x6.75x.25	1.875	0.75	101
102	8	2	3,6,3@9,6,3		49x6.75x.25	1.875	0.75	102
111	6	4	5@9	3	49x12.75x.25	1.875	0.75	111
112	8	4	3,6,3@9,6,3	3	49x12.75x.25	1.875	0.75	112

[1]All spandrel splices use 7/8 in. A325 bolts; specified spandrel splice plate yield strength is 36 ksi.
[2]Holes in spandrel are 1/4 in. larger than bolts; holes in plates are bolt + 1/16 in. or option to match spandrel holes.

6.3 FAILURE MODES

The exterior wall subsystem model can capture the following failure modes:

- Column buckling from large lateral deformations,
- Column buckling from loss of support at floor truss seats and strap anchors,
- Failure of column splice bolts, and
- Failure of spandrel splice bolts or tearing of spandrel or splice plates at bolt holes.

The model does not capture the local buckling of column plates or the formation of plastic hinges (kinking) from the interaction of local plate buckling and general stability of the column when subjected to combined axial load and bending moments.

Several of the later analyses did not include the effects of creep. Displacement control analysis in ANSYS did not function properly when strain rate effects of creep were included.

6.4 MODEL VALIDATION

6.4.1 Description of Models

Validation of the exterior wall model was performed by comparing the stiffness of an ANSYS model of a single exterior wall panel with beam and shell elements to a SAP2000 shell model of the same panel developed by Leslie E. Robertson Associates under a contract from NIST.

Figure 6–4 shows the SAP2000 shell model of a typical prefabricated panel at Floors 79 to 82 provided by NIST. The model was modified as follows:

1. Eliminated self-weight from loading conditions.
2. Provided a stiff member at the top of the columns.
3. Added out-of-plane wall supports (UY) at the top of the columns for stability under out-of-plane loading.

Figure 6–5 shows the ANSYS prefabricated panel model. BEAM189 elements modeled the columns, SHELL181 elements modeled the spandrels, and BEAM4 elements connected nodes on the axis of the columns to nodes located in the mid-plane of the spandrels.

Figure 6–6 shows the various boundary conditions. Out of plane displacement (UY) was restrained at the tops of the columns. All three directions of translation were restrained at the bottoms of the columns. The spandrels were free at the boundaries of the model.

Both models were subjected to three loading cases at room temperature, as shown in Fig. 6–6:

1. A vertical force (FZ) at the top of one of the outside columns.
2. A horizontal force in the plane of the wall (FX) at the top of one of the outside columns. The stiff members described previously distributed this shear load evenly to the tops of all three columns.
3. A transverse force (FY) on the middle column at Floor 81 (middle floor).

The loads described above did not include self-weight.

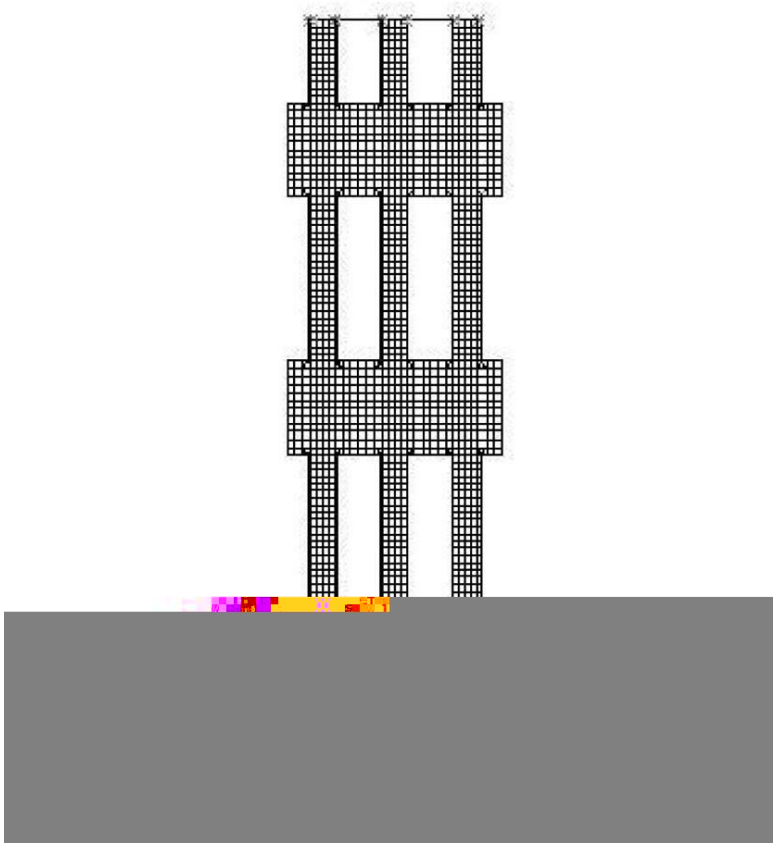

Figure 6–4. SAP2000 model of prefabricated panel.

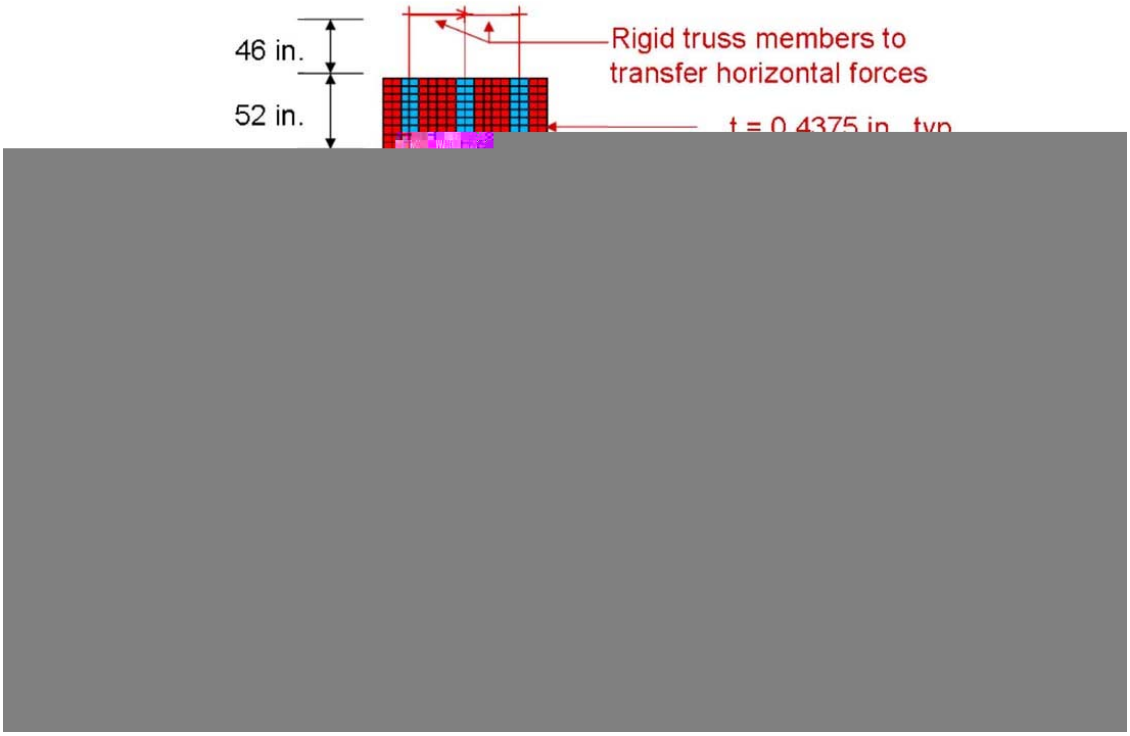

Figure 6–5. ANSYS model of prefabricated panel showing meshing.

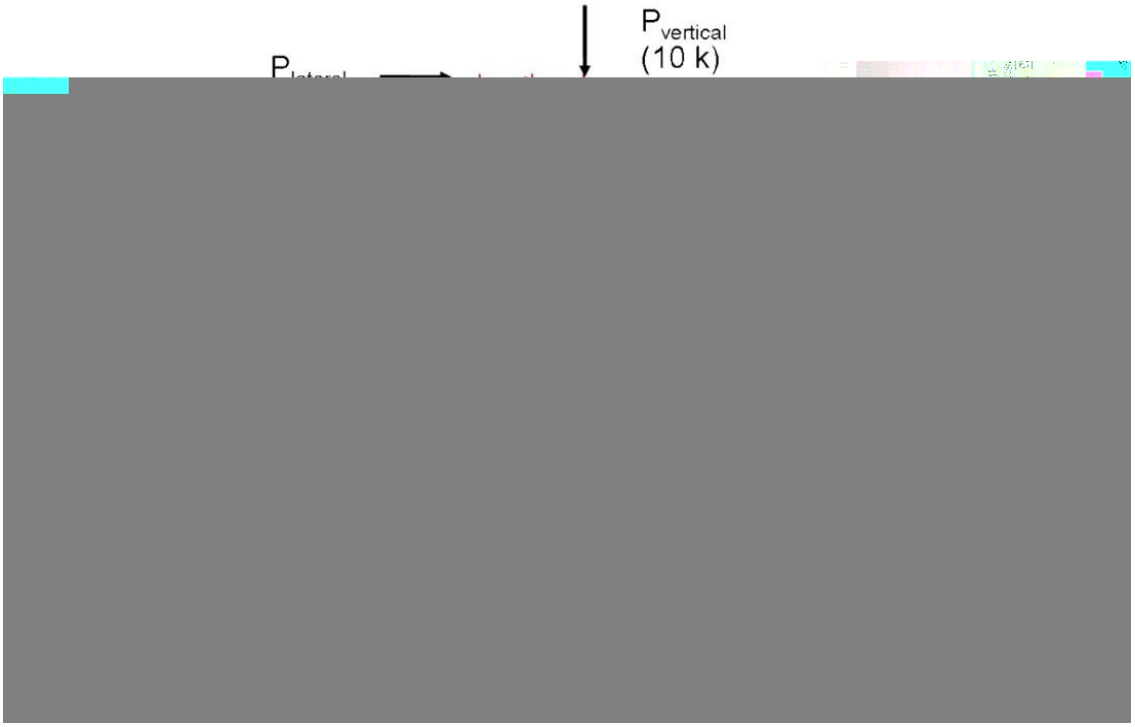

Figure 6–6. ANSYS model of prefabricated panel showing boundary conditions and loading (loads applied separately).

6.4.2 Validation Results

Figures 6–7 through 6–9 show deflected shapes and indicate the displacement at the points of applied load for the SAP2000 and ANSYS models. Table 6–2 summarizes the differences in reactions and displacements between the SAP2000 and ANSYS models. The table indicates that these differences were small.

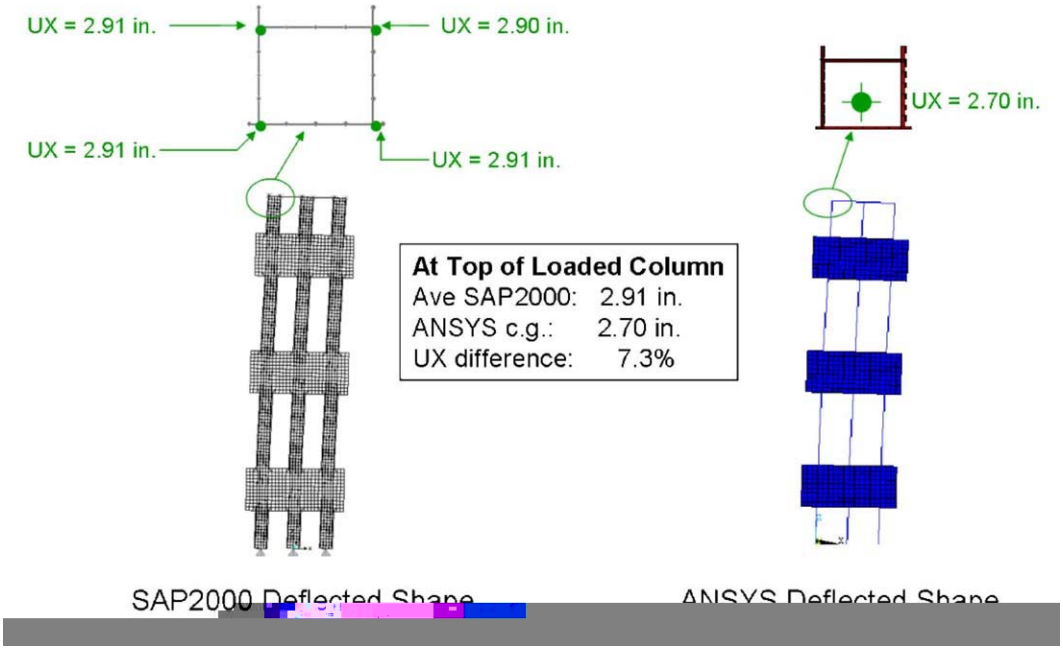

Figure 6–7. Deflection of prefabricated panel under 100 kip lateral load.

Figure 6–8. Deflection of prefabricated panel under 100 kip transverse load.

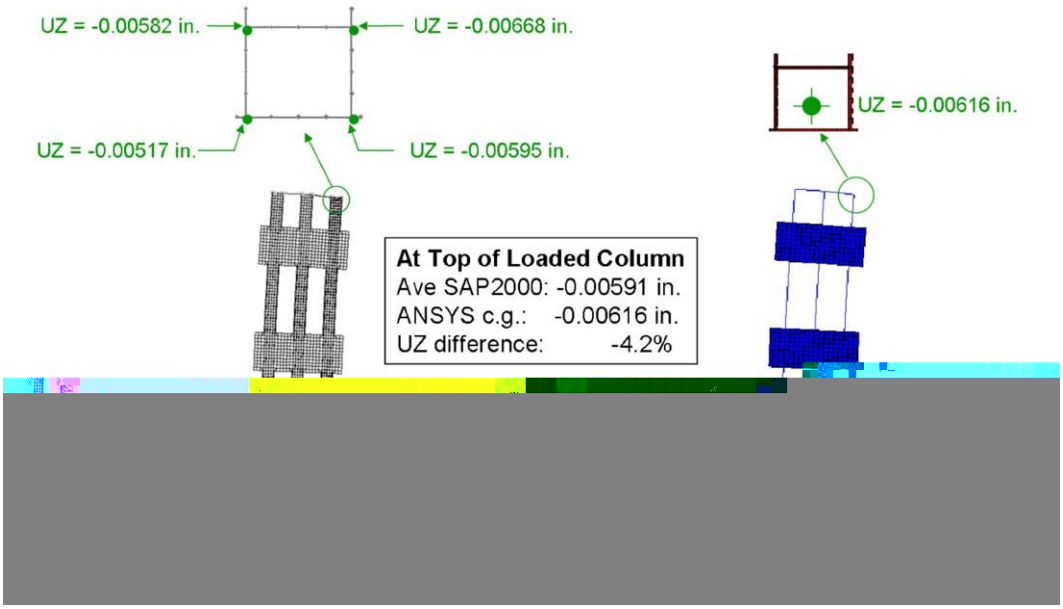

Figure 6–9. Deflection of prefabricated panel under 10 kip vertical load.

Table 6–2. Prefabricated panel validation results.

Loading Condition	SAP2000/ANSYS Difference Range	
	Reactions[1]	Displacements[2]
Lateral FX	RX: -2% to +1%	UX: 7%
Transverse FY	RY: -6% to +7%	UY: -13%
Vertical FZ	RZ: -1% to +2%	UZ: -7%

[1]Range considers maximum disparities between results for all support reactions.

[2]Displacements considered at tops of columns for FX and FZ, and at points of load application for FY.

6.5 FINITE-ELEMENT MODEL OF EXTERIOR WALL SUBSYSTEM

6.5.1 Elements and Meshing

Figure 6–10 shows the model in elevation. BEAM189 elements modeled the columns. Above and below spandrels, BEAM189 elements modeled the complete cross sections of the columns. At spandrels, BEAM189 elements modeled cross sections where the interior plate thickness of the column was reduced to 0.005 in. to maintain a closed section yet allowed for a continuous spandrel. Since neutral axis location of column shifted in the column elements in the spandrel zone, MPC184 rigid elements were used to connect the neutral axes of column elements where this shift occurred. SHELL181 elements modeled the spandrels. Figure 6–11 shows the number of elements used to model columns and spandrels. BEAM4 elements connected nodes on the axis of the columns to nodes located in the mid-plane of the spandrels. Figure 6–12 shows this use of the BEAM4 elements.

BEAM4 elements are two-node Euler (elastic) elements with large deflection capability. BEAM189 elements are three-node (quadratic) Timoshenko beam elements with large deflection, plasticity, and creep capabilities. SHELL181 elements are four-node multi-layer elements with large deflection,

plasticity, and creep capabilities. MPC184 elements are multipoint constraint elements that implement kinematic constraints using Lagrange multipliers. These element types and their features are summarized in Table 4–1.

Material IDs, as described in Chapter 3, were assigned to the elements. The properties (e.g. stiffness) and behavior (e.g. plasticity) of the elements vary with temperature as the assigned material properties vary with temperature.

6.5.2 Boundary Conditions

The bottoms of all columns in the model were restrained in the vertical direction. The top and the bottom of all columns in the model were restrained in the direction normal to the wall. In addition, the bottom of central Column 154 was restrained in the in-plane horizontal direction. Symmetry boundary conditions were imposed on the spandrels at the boundaries of the model, except that the spandrels were free to expand in the plane of the wall. Motion out of the plane of the wall was restrained at all floor truss seats and strap anchors. In several analyses, such restraints were removed at two or three floors (either Floors 95 and 96 or Floors 95, 96, and 97) to investigate the effect of floor sagging and floor/wall disconnection on stability of the exterior wall system.

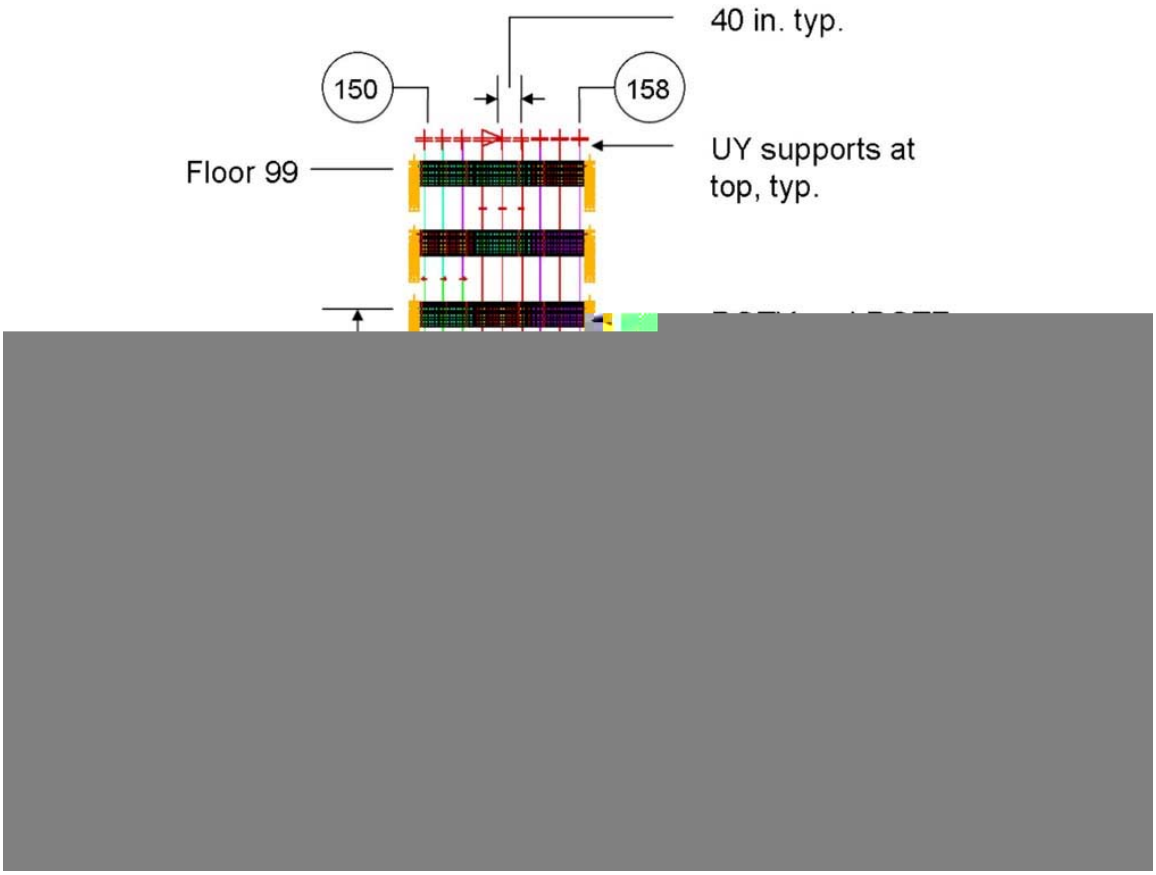

Figure 6–10. Exterior wall subsystem model with boundary conditions.

Figure 6–11. Typical meshing of exterior wall model components.

Figure 6–12. Schematic representation of columns used in the exterior wall model.

6.5.3 One-, Two-, and Three-Story High Columns

Figure 6–13 shows the model of a one-story high exterior column. The model included a one-story high portion of Column 151 extending from Floor 95 to Floor 96 and portions of spandrels at Floor 95 and Floor 96. The model also represented Column 151 from Floor 96 to Floor 97 since the dimensions, plate thicknesses, and material properties were identical to those of Column 151 from Floor 95 to 96. SHELL181 plate elements modeled the plates of columns and spandrels. CERIG rigid elements connected the center of gravity of the column to its component plates and to the spandrel at both the top and the bottom of the model. The column was pinned at the bottom and restrained in the two horizontal directions at the top. Axial displacement was applied incrementally at the top of the model.

Figure 6–14 shows the variation of axial load with the imposed axial displacement and the resulting lateral deflection at room temperature (RT) and 700 °C. This figure also shows the hand calculated theoretical column load levels at room temperature (RT) and 700 °C for:

1. Local buckling of Plate 2 and Plate 3.
2. Uniform yielding of the column.
3. Axial load demand due to gravity dead and live loads at Floor 96.

Figure 6–15 shows the local bucking deformation of Plate 2 and Plate 3 at the maximum load at room temperature. Figure 6–16 shows a plastic hinge at mid-height of the column for an imposed axial displacement of 2 in. Figure 6–17 shows local buckling in Plate 2 and Plate 3 at maximum load at 700 °C.

Figure 6–14 shows that at room temperature Plate 2 and Plate 3 buckle locally at a load that is less than the maximum column load, but at 700 °C the column yields before it buckles locally. This figure also shows that the expected column demand load of 175 kip is substantially lower than the local buckling load at room temperature and the column yield load at 700 °C.

At room temperature, the load-carrying capacity in the post-buckling regime decreased rapidly; however, it decreased much more gradually at 700 °C.

Axial load-displacement behaviors of two- and three-story models were also examined, and the results are shown in Fig. 6–14. As the unsupported length became longer and the temperature became higher, the negative slope of the axial load-deflection curve in the post-buckling regime became less steep.

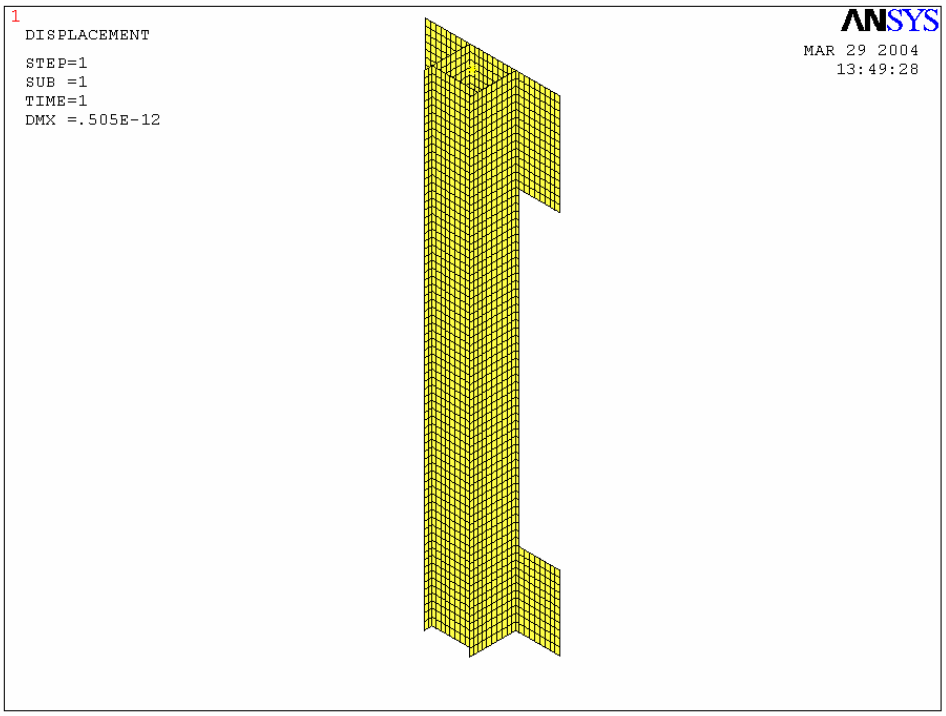

Figure 6–13. One-story exterior column model.

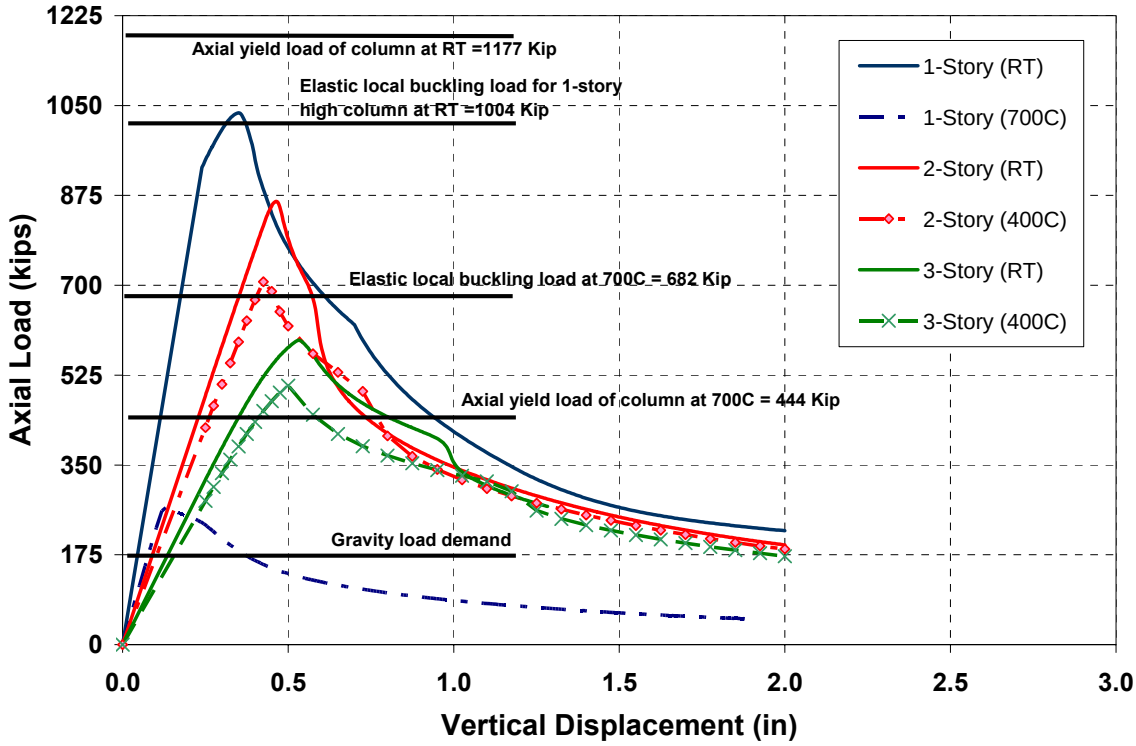

Figure 6–14. Load-deflection of column at room temperature and 700 °C.

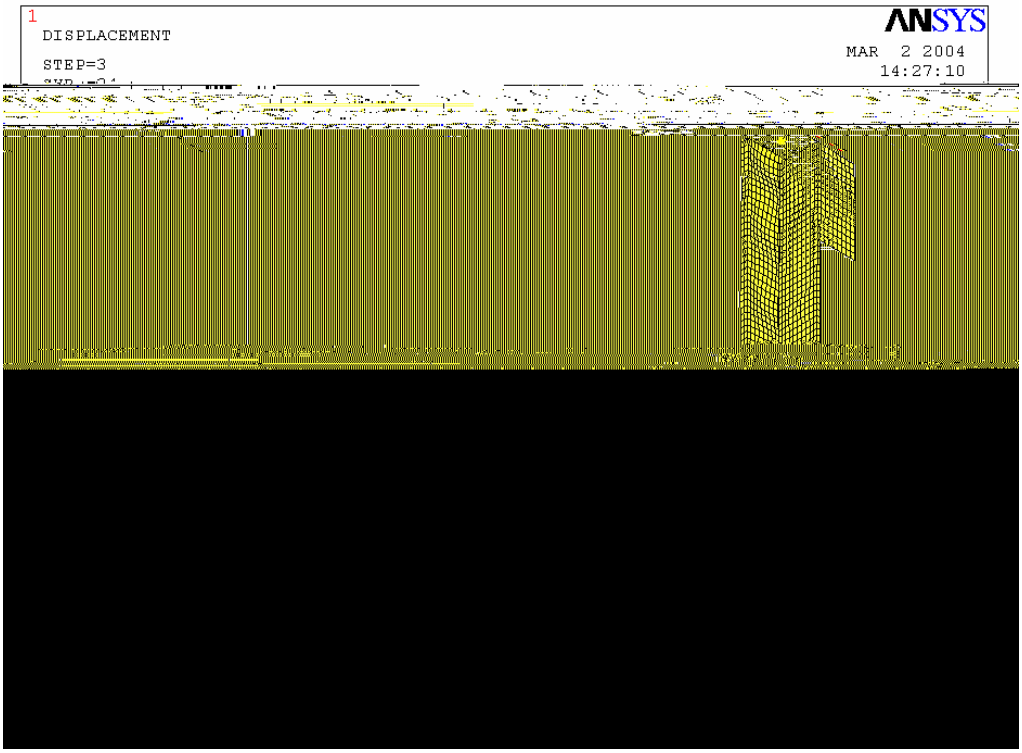

Figure 6–15. Local buckling of column at room temperature.

Figure 6–16. Plastic hinge in column at room temperature.

Figure 6–17. Deformed shape of column at maximum axial load at 700 °C.

6.5.4 Spandrel Splices

Figure 6–18 shows the typical layout of the spandrel splices in the model. User-defined break elements were used to model the interior spandrel splice connections, and nodal couples were used to model the exterior spandrel splice connections. An interior spandrel splice occurs between Columns 150 and 158, and an exterior spandrel splice occurs at the end of the model outside of Columns 150 and 158. Figure 6–19 shows the modeling of an interior spandrel splice. User-defined break elements at each node through the depth of a spandrel allowed the modeling of failure connection failure modes including (1) bolt shear, (2) tearing of the spandrel plate, and (3) tearing of the splice plates at the bolt holes. The exterior wall model contains 18 interior spandrel splices with 11 break elements at each splice for a total of 198 spandrel splice break elements. With initial failure stiffness values and temperature-dependent capacities defined by the user, the user-defined break elements transfer forces and moments between nodes according to the initial stiffness values until the element reaches its capacity in one direction. Upon reaching the capacity in one direction, the stiffness of the element in all directions changes to the corresponding failure stiffness, and the element sheds load to other load paths. The models used user-defined break elements that had the capability to fail in translation or rotation.

6.5.5 Column Splices

Two BEAM189 elements for each of the four bolts, four pairs of CONTA178 contact elements at the faying (contact) surfaces, and stiff BEAM4 elements connecting the tops of the bolts to the CONTA178 contact elements were used to model the column splice. COMBIN37 elements modeled the fracture of the column splice bolts based on data from bolt tests provided by NIST and on shear failure of the splice. Figure 6–20 shows a schematic view of the column splice. A coefficient of friction of 0.35 was used for the contact elements. The 7/8 in. diameter column splice bolts were preloaded to 36.05 kip at 20 ˚C (AISC 1964).

The column splice model cannot fail in compression. In tension, the bolts and ,therefore, the entire splice will disconnect at 0.18 in. deflection beyond the ultimate capacity of the bolts. In shear, the column splice will disconnect after 1.1 in. deflection. The shear capacity is the summation of bolt shear capacity and splice friction. In bending, the capacity is controlled by bolt tension. The peak moment capacity occurs prior to failure of the first set of bolts with some capacity remaining on the second set of bolts.

The column splice model was verified by subjecting it to three displacement controlled load cases under two temperature conditions and comparing the results with hand calculated maximum capacities for each case. The load cases examined were: axial extension, to determine a maximum tensile load; applied rotation with 175 kip axial compression, to determine a maximum moment; and applied lateral displacement with 175 kip axial compression, to determine a maximum shear. Each load case was performed at 20 ˚C and 300 ˚C. The maximum difference between the finite element model and calculated capacities was 4 percent under the tensile load case. All other cases showed agreement to within 2.5 percent. The load-displacement response of the splice model to each load case was in agreement with the predicted behavior.

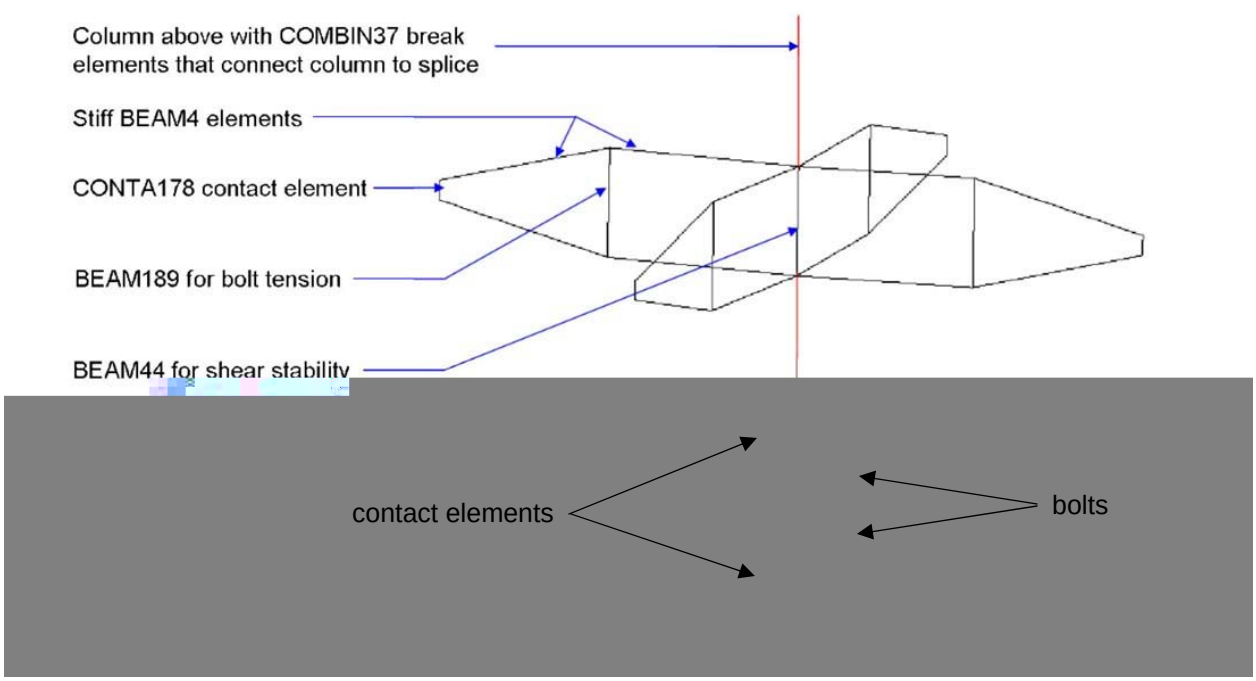

Figure 6–20. Column splice model used in exterior wall model.

6.5.6 Loads

The loads on the model were applied sequentially in the following order:

- Self weight of the exterior wall components,
- Column splice bolt preload,
- Gravity dead and live loads of the floor system,
- Temperature time histories provided by NIST, and
- Transverse pull-in force from sagging floors or additional vertical load from a potential redistribution of gravity loads to this portion of the exterior wall

Gravity Loads

Gravity loading was obtained from two sources: the LERA SAP2000 global model and the LERA SAP2000 floor model. To capture the gravity load effects from upper floors (those above Floor 99), internal forces and moments at midheight of the columns between Floors 99 and 100 in the LERA SAP2000 global model, caused by dead plus 25 percent of design live load, were applied as loads at the tops of the corresponding columns in the exterior wall model at the center of gravity of the columns. To capture the gravity load effects from individual floors, floor loads were extracted from the LERA SAP2000 floor model and applied to each column. Also, a moment about the plane of the wall, based on the vertical force from the floor and the eccentricity of the truss seats, was applied to each odd-numbered column at the mid-plane of the spandrel.

Thermal Loads

To represent a range of thermal conditions expected in the WTC towers, NIST provided five thermal load conditions based upon fire conditions in the towers. These were labeled D, DBARE, E, E119, and F, and are described in Table 6–3. These load conditions differed in fire behavior, intensity, location in the towers, and time. Thermal load DBARE assumed steel without thermal insulation. Thermal load E119 corresponded to the standard ASTM-E119 fire load. Figure 6–21 shows how the maximum temperature in each thermal loading condition varied with time.

For columns that were modeled by BEAM189 elements, temperatures were provided for nodes at the center of gravity of the column, and their linear gradients transverse to the exterior wall were also provided. Gradients parallel to the wall were found to be negligible. Temperatures for SHELL181 elements were provided at each node. NIST did not always provide temperatures for the bolts at column splices. When bolt temperatures were provided, they matched temperatures at the nearest interior or exterior tips of columns.

Table 6–3. Thermal loading conditions used in the exterior wall model.

Thermal Loading Condition	Building and Location	Columns	Floors	Thermal insulation	Time Duration	Maximum Temperature °C
D	WTC 1 South face towards West	340 – 348	91 – 99	as specified	90 min	537 °C
DBARE	WTC 1 Same as D	340 – 348	91 – 99	none – bare steel	90 min	598 °C
E	WTC 1 East face towards North	221 – 229	91 – 99	as specified	90 min	871 °C
E119	WTC 1			as specified	90 min	418 °C
F	WTC 2 North face East corner	250 – 258	76 – 84	as specified	60 min	382 °C

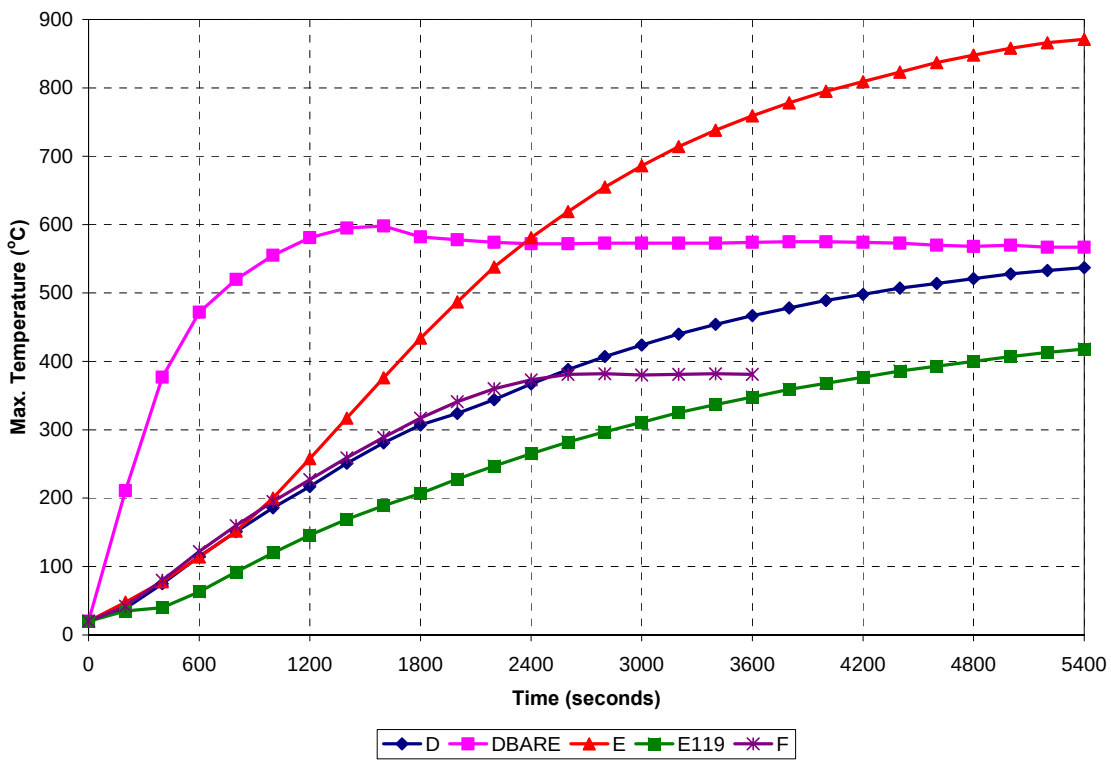

Figure 6–21. Exterior wall model temperature time-histories.

Transverse Pull at Disconnected Floors

When floors sag, they begin to pull in the columns. The results of truss component analyses indicated approximately 14 kip of pull-in force per truss. Strap anchors distributed this pull to the columns that did not support trusses. A 15 kip pull-in force was applied to each column of laterally-unsupported floors to model the effect of the sagging floor.

Push-down Loading

Exterior wall columns were subjected to additional gravity loads that were redistributed due to weakening of other exterior walls and/or the core by the aircraft impact or temperature effects through the hat truss and spandrels. To simulate a redistribution of gravity loads, equal vertical displacements were imposed at the top of each column to push the model down. The imposed vertical displacements induced additional gravity loads in the columns.

6.6 ANALYSIS CASES

The loading sequence described in Section 6.5.6 is the same for all exterior wall analyses. Table 6–4 summarizes the different loadings and boundary conditions of the exterior wall subsystem.

As shown in Table 6–4, Case 6 and Case 7 used thermal condition DBARE with two and three floors not bracing the exterior wall system. Case 8 used DBARE, where the columns were not braced at three floors, and transverse loads (pull-in forces) were applied. Case 9 used DBARE, where the columns were not braced at three floors and vertical displacement was applied to the top of each column until unloading of the columns and instability was detected.

The analyses of Case 1, Case 5, and Case 6 through Case 9 were completed for the entire temperature time history of each case provided by NIST. The analysis of Case 2 was inadvertently stopped at 83 min of its temperature history; the temperature time history at 83 min was flat, and no significant change in the results was expected. Case 3, at 70 min of its temperature history, reached a temperature of 800 °C, beyond which material properties were not defined, and the computation was terminated. Case 4 could not be advanced past 83 min of its temperature time history, because the creep algorithm failed. The temperature difference between the temperatures at 83 min and 90 min was not significant for this case.

Table 6–4. Analysis cases for exterior wall subsystem model.

Analysis Case	Thermal Loading	Bolt Temperatures	Creep Effects	Floor Supports	Pull-in Force	Push Down
1	D	No	Yes	All		
2	DBARE	No	Yes	All		
3	E	Yes	Yes	All		
4	E119	No	Yes	All		
5	F	No	Yes	All		
6	DBARE	Yes	Yes	All but 95 and 96		
7	DBARE	Yes	No	All but 95, 96, and 97		
8	DBARE	Yes	No	All but 95, 96, and 97	X	
9	DBARE	Yes	No	All but 95, 96, and 97		X

6.7 ANALYSIS RESULTS

6.7.1 Columns Braced at All Floors

This group of analyses includes Analysis Case 1 through Case 5.

Analysis Case 1 (Fire Scenario D) Figures 6–22 (a) through 6–22 (c) show the total displacement, von Mises stress, and plastic strain, respectively, for the entire model. Figure 6–22 (a) shows that the maximum displacement of 1.53 in. occurred at Floor 98 near Column 158. Figure 6–22 (b) shows that the maximum von Mises stress in the spandrels of 49 ksi occurred at Floor 95 and Column 156. Figure 6–22 (c) shows that plasticity in the spandrels was confined to Floors 95 and 96, with the highest plastic strain occurring at Floor 96 near Column 155. Figure 6–22 (d) shows the deformation of the spandrel at Floor 94. Table 6–5 summarizes the status of the spandrel splice break elements. All failed break elements indicated tearing failure.

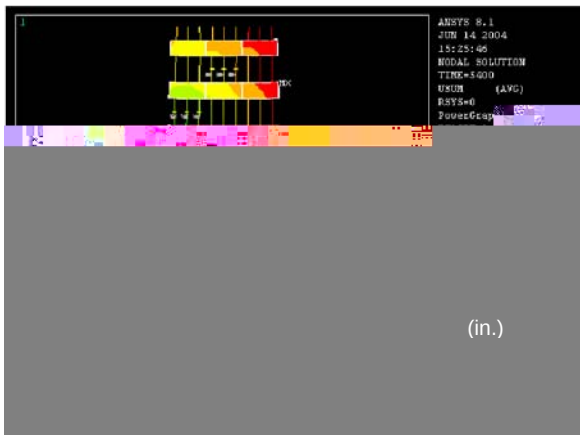

(a) Total deflection

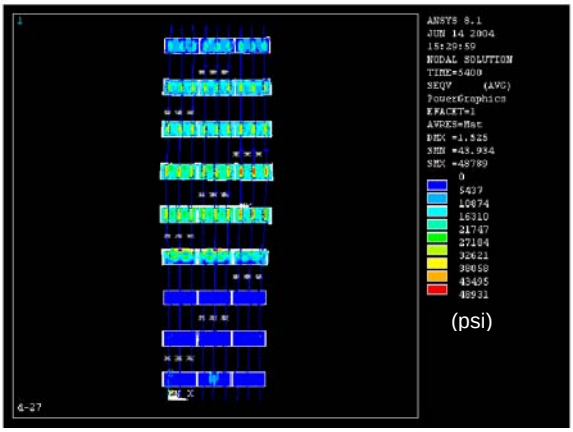

(b) von Mises stress

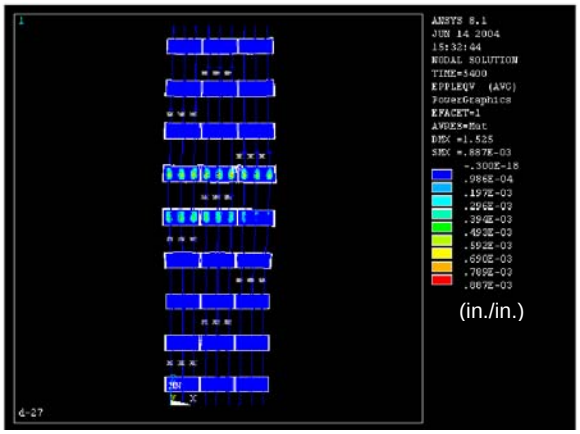

(c) Plastic strain

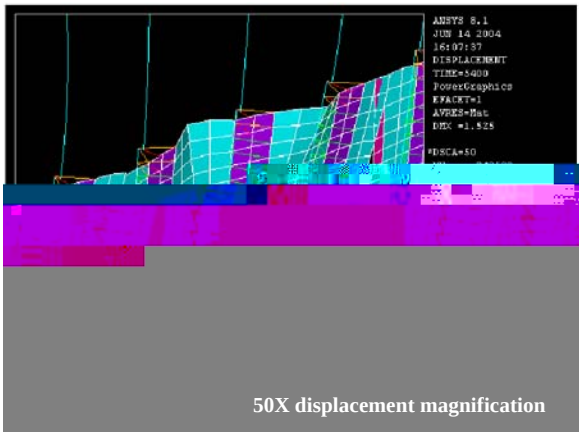

(d) Spandrel deformation at Floor 94

Figure 6–22. Structural response for temperature time history D with all floors supported.

Table 6–5. Summary of spandrel splice break elements for temperature time history D with all floors supported.

	Number of failed elements	
Floor	**West Interior Splice**	**East Interior Splice**
99	3	3
98	0	0
97	2	1
96	1	2
95	0	0
94	0	0
93	0	0
92	0	0
91	0	0
Total	6	6

Analysis Case 2 (Fire Scenario DBARE) Figures 6–23 (a) through 6–23 (c) shows the total displacement, von Mises stress, and plastic strain, respectively, for the entire model. Figure 6–23 (a) indicates the maximum displacement of 3.74 in. occurred at the roof Column 158. Figure 6–23 (b) shows that the maximum von Mises stress in the spandrels of 49 ksi occurred at Floor 94 and Column 156. Figure 6–23 (c) shows plastic strain in spandrels at Floors 94 through 98, with the highest value at Floor 95 and Column 152.

Table 6–6 summarizes the status of the spandrel break elements. All failed break elements indicated tearing failure.

(a) Total deflection

(b) von Mises stress

(c) Plastic strain

Figure 6–23. Structural response for temperature time history DBARE with all floors supported.

Analysis Case 4 (Fire Scenario E119) Figure 6–25 (a) through 6–25 (c) show the total displacement, von Mises stress, and plastic strain, respectively, for the entire model. Figure 6–25 (a) shows that the maximum displacement of 2.07 in. occurred at Floor 99 near Column 158. Figure 6–25 (b) indicates that maximum von Mises stress in the spandrels of 53 ksi occurred at Floor 94 and Column 158. Figure 6–25 (c) shows plastic strain in spandrels between Floors 93 through 99, with the highest value occurring at Floor 93 between Columns 154 and 155. Figure 6–25 (d) shows the deformation of the spandrel at Floor 93. Table 6–8 summarizes the status of the spandrel splice break elements. All failed break elements indicated tearing failure.

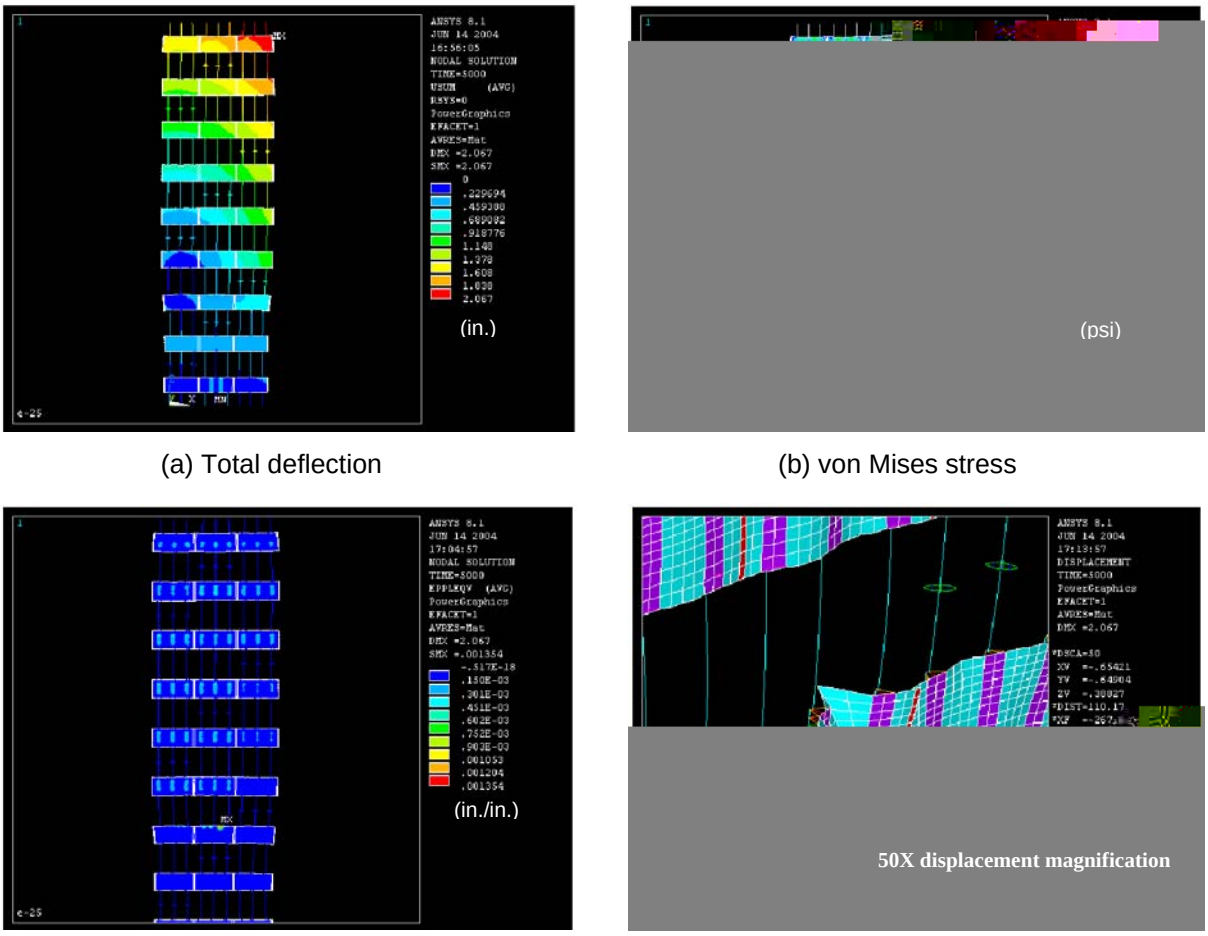

(a) Total deflection

(b) von Mises stress

(c) Plastic strain

(d) Spandrel deformation at Floor 93

Figure 6–25. Structural response for temperature time history E119 with all floors supported.

Table 6–8. Summary of spandrel splice break elements for temperature time history E119 with all floors supported.

	Number of failed elements	
Floor	**West Interior**	**East Interior Splice**
99	3	3
98	0	0
97	0	0
96	0	0
95	0	0
94	0	0
93	0	0
92	0	0
91	0	0
Total	3	3

Analysis Case 5 (Fire Scenario F) Figures 6–26 (a) through 6–26 (c) show the total displacement, von Mises stress, and plastic strain, respectively, for the entire model. Figure 6–26 (a) shows that the maximum displacement of 1.57 in. occurred at Floor 99 near Column 158. Figure 6–26 (b) indicates that the maximum von Mises stress in the spandrels of 46 ksi occurred at Floor 96 and Column 158. Figure 6–26 (c) shows plastic strain in spandrels between Floors 96 through 99 with the highest value occurring at Floor 97 at Column 151. Figure 6–26 (d) shows the deformation of the spandrel at Floor 99. Table 6–9 summarizes the status of the spandrel splice break elements. All failed break elements indicated tearing failure.

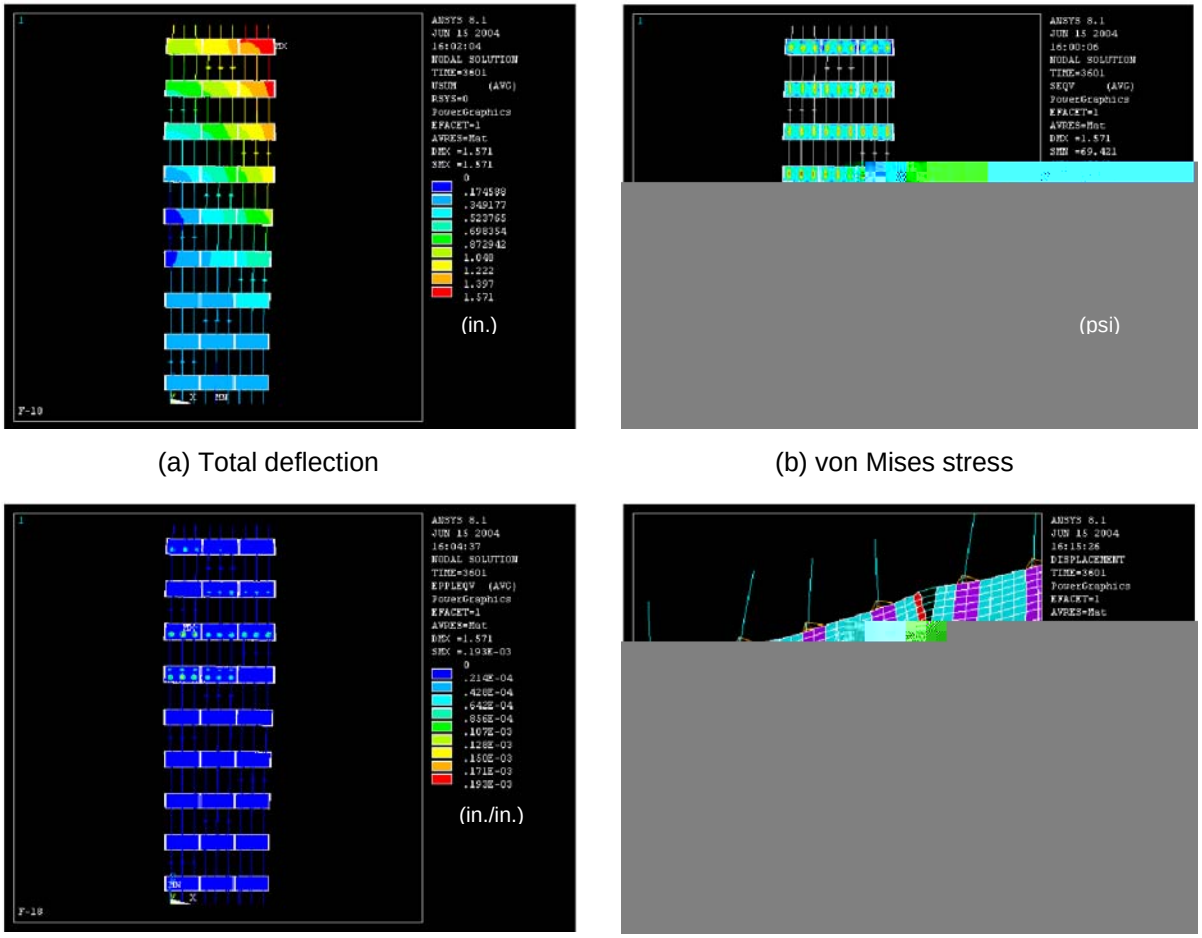

(a) Total deflection

(b) von Mises stress

(c) Plastic strain

(d) Spandrel deformation at Floor 99

Figure 6–26. Structural response for temperature time history F with all floors supported.

Table 6–9. Summary of spandrel splice break elements for temperature time history F with all floors supported.

	Number of failed elements	
Floor	**West Interior**	**East Interior Splice**
99	3	3
98	0	0
97	0	0
96	0	0
95	0	0
94	0	0
93	0	0
92	0	0
91	0	0
Total	3	3

6.7.2 Columns Not Braced at Floors 95 and 96

Analysis Case 6 (Fire Scenario DBARE) Figures 6–27 (a) and 6–27 (b) show the total displacement and von Mises stress, respectively, for the entire model. Figure 6–27 (a) shows that the maximum displacement of 3.76 in. occurred above Floor 99. Figure 6–27 (b) indicates that the maximum von Mises stress in the spandrels of 23 ksi occurred at Floor 94 between Columns 154 and 155. Figure 6–27 (c) shows normal (transverse to the plane of the wall) displacement of the entire model. This figure shows a maximum outward displacement of 0.34 in. at Floor 96 and Column 154 and a maximum inward displacement of 0.45 in. at Floor 95 and Column 158. Table 6–10 summarizes the status of the spandrel splice break elements. Failed break elements at Floors 97 through 99 indicated tearing failure, and failed break elements at Floors 96 and below indicated bolt shear failure.

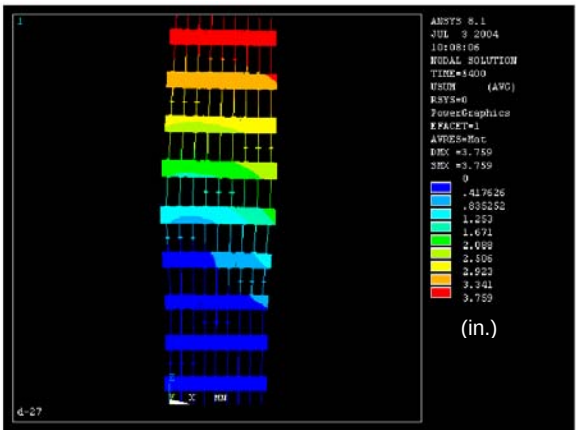

(a) Total deflection

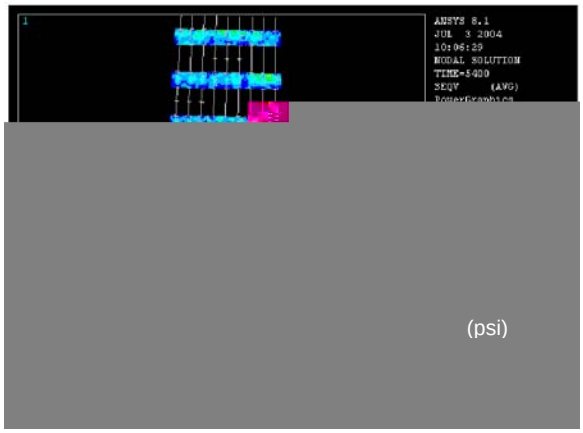

(b) von Mises stress

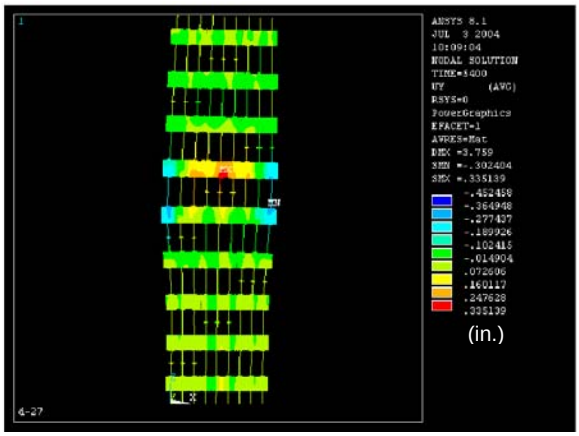

(c) Transverse displacement
(outward displacement is positive)

Figure 6–27. Structural response for temperature time history DBARE with two unbraced floors.

Table 6–10. Summary of spandrel splice break elements for temperature time history DBARE with 2 unbraced floors.

	Number of failed elements	
Floor	West Interior	East Interior Splice
99	1	3
98	3	3
97	1	0

6.7.4 Columns Not Braced and Pulled at Unbraced Floors 95, 96, and 97

Analysis Case 8 (Fire Scenario DBARE) Figures 6–29 (a) through 6–29 (d) show the total displacement, von Mises stress, and plastic strain, respectively, for the entire model. Figure 6–29 (a) shows that the maximum displacement of 10.4 in. occurred at Floor 96. Figures 6–29 (b) through 6–29 (c) indicate that the maximum von Mises stress occurred at Floor 94 and Column 156. Figure 6–29 (d) shows that plastic strain is limited to the portion of the spandrel at Floor 96 and Column 152. Figure 6–29 (e) shows transverse (to the plane of the wall) displacement of the entire model. This figure shows a maximum inward displacement of 10.2 in. at Floor 96. Figure 6–30 shows the maximum column splice bolt stresses, which occurred between Floors 96 and 97 at Columns 156 through 158. Figure 6–31 shows column splice contact status for those column splices occurring between Floors 94 and 97. This figure indicates that column splices had opened or nearly opened at eight of the nine columns within this group of floors.

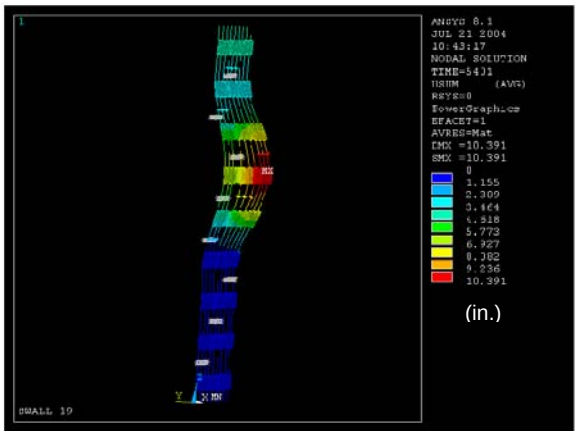

(a) Total deflection

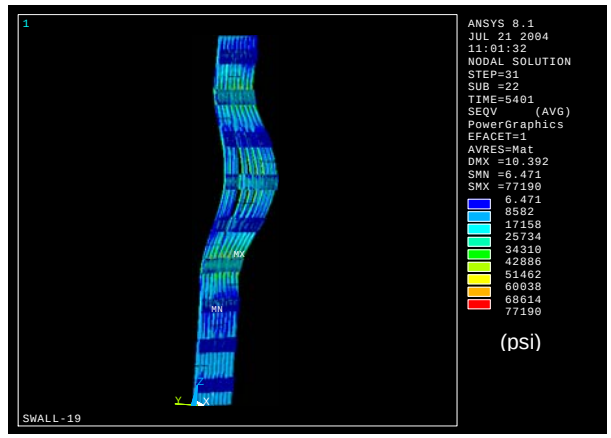

(b) von Mises stress

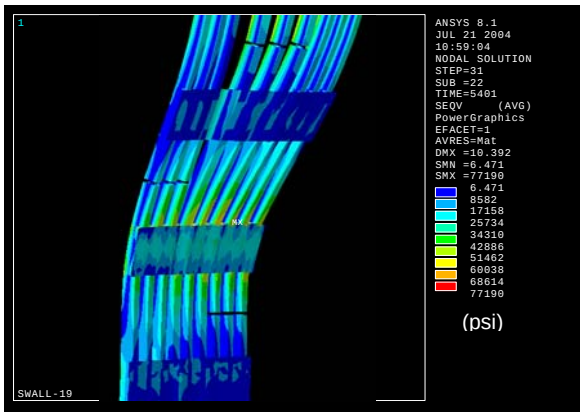

(c) von Mises stress

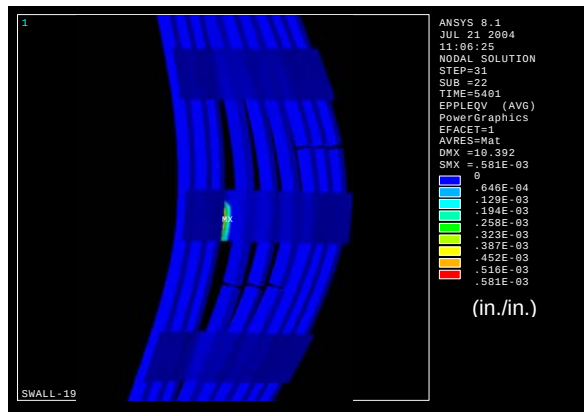

(d) Plastic strain

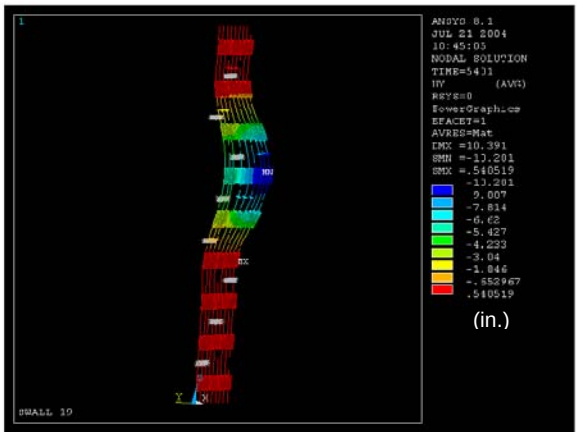

(e) Transverse displacement
(outward displacement is positive)

Figure 6–29. Structural response for temperature time history DBARE with pull-in forces at three floors (10X displacement magnification).

(psi)

Figure 6–30. Column splice bolt stresses for temperature time history and DBARE with pull-in forces at three floors.

Figure 6–31. Column splice contact element status for temperature time history and DBARE with pull-in forces at three floors.

Figure 6–32. Structural response for temperature time history DBARE and push-down with three unbraced floors (10X displacement magnification).

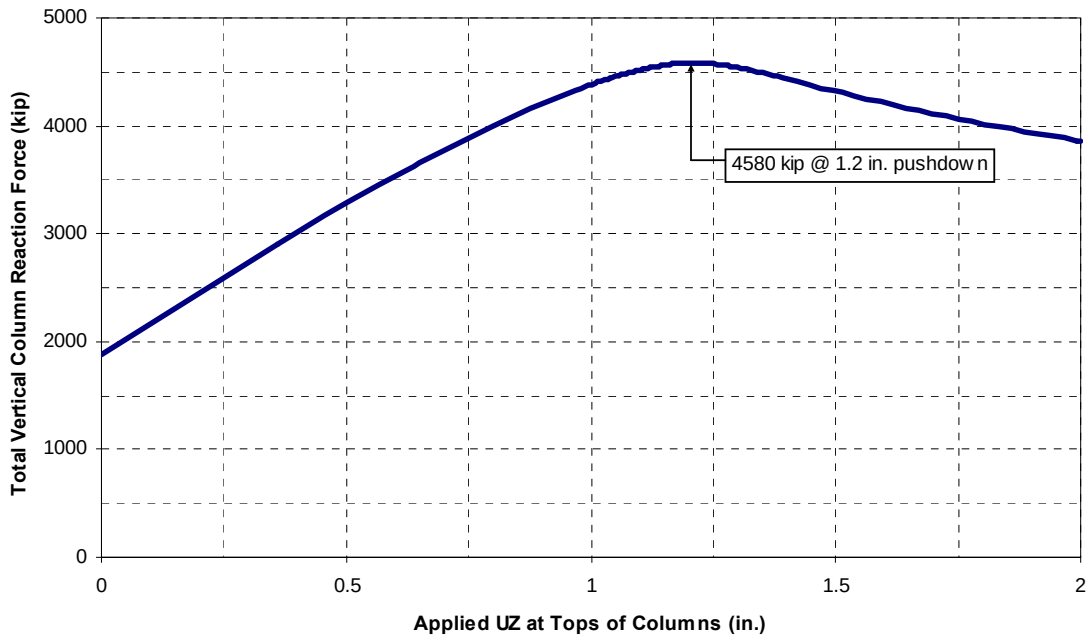

Figure 6–34. Sum of total column reaction forces at base during push-down after application of temperature DBARE with three unbraced floors.

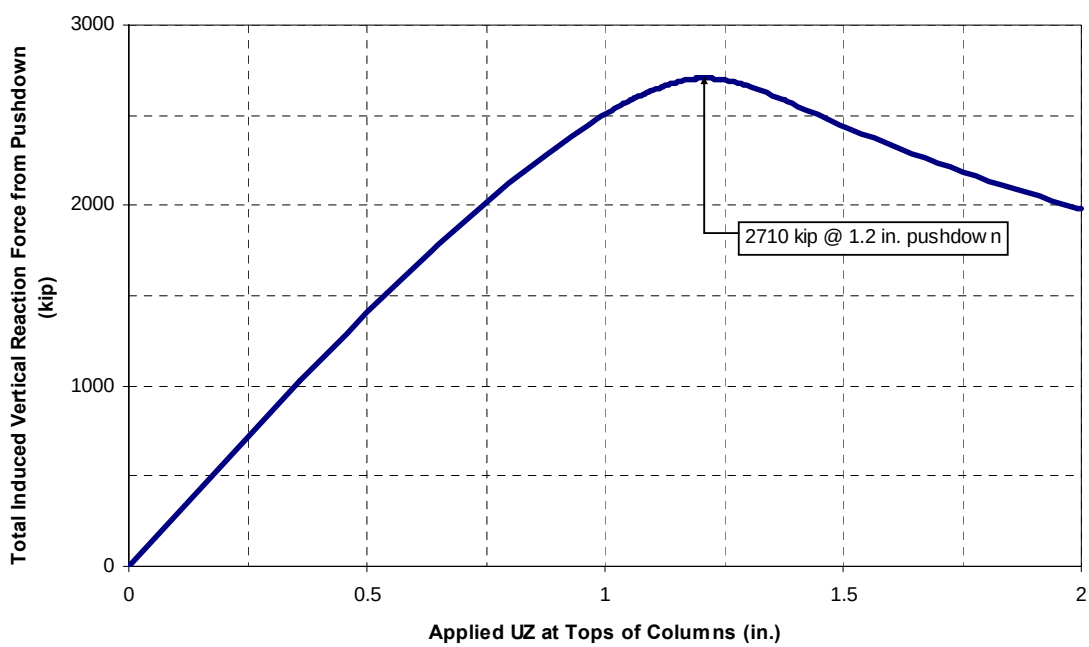

Figure 6–35. Sum of additional vertical reaction forces at base induced by imposed displacement during push-down after application of temperature DBARE with three unbraced floors.

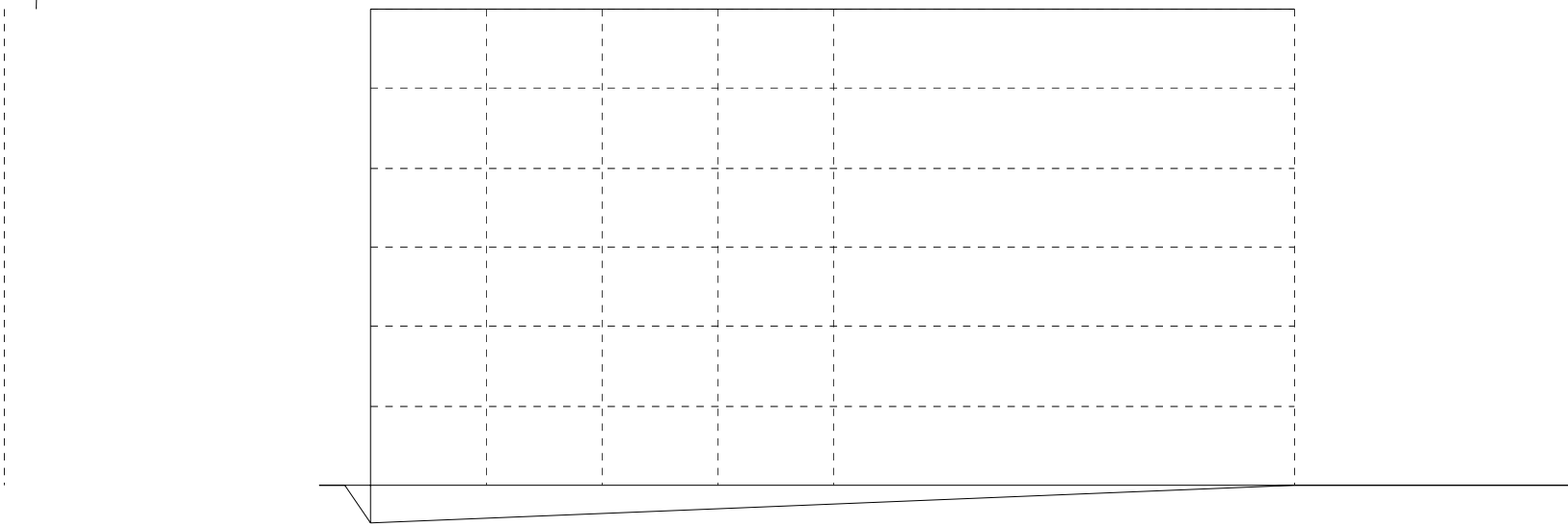

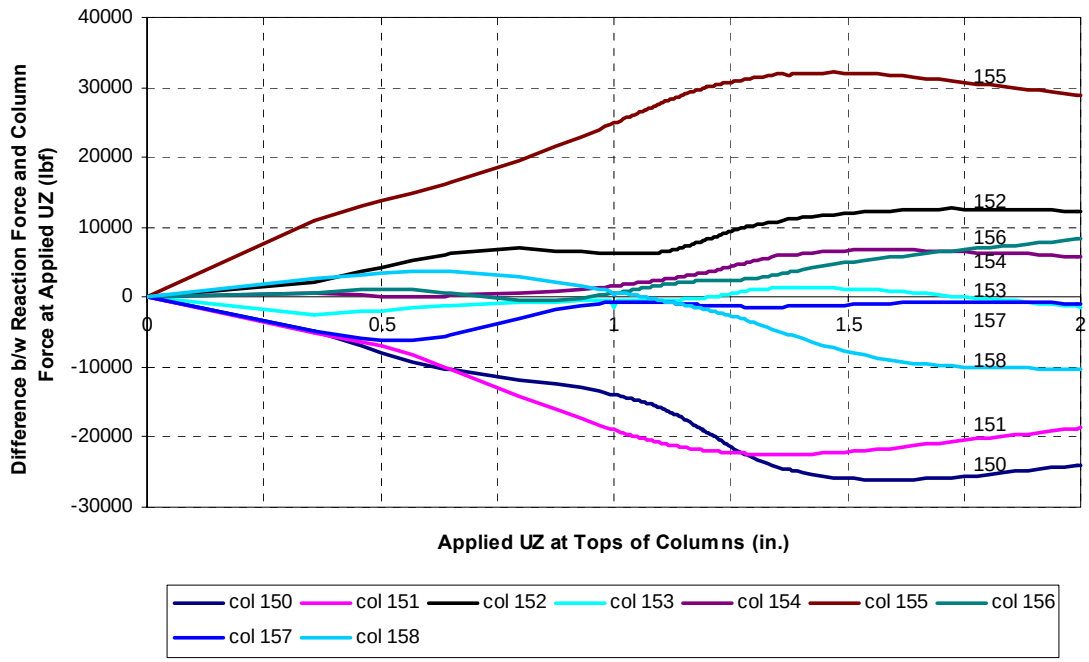

Figure 6–38. Difference between the additional individual column reaction forces at base and the vertical force applied at the top of each column during push-down after application of temperature DBARE with three unbraced floors.

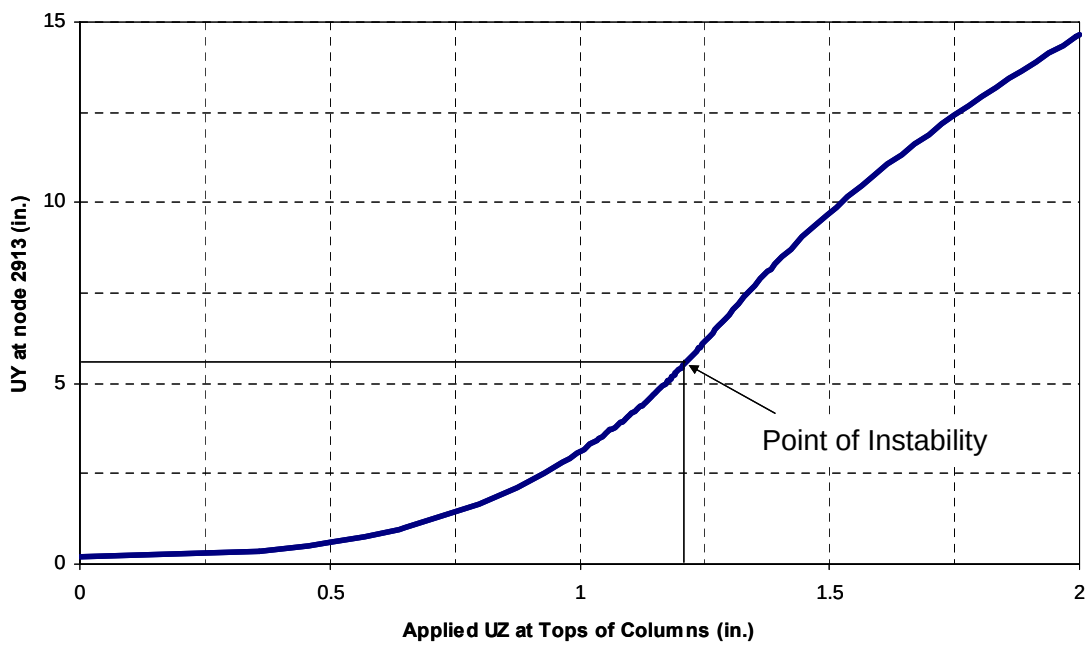

Figure 6–39. Transverse deflection during push-down after application of temperature DBARE with three unbraced floors.

6.8 SUMMARY AND DISCUSSION OF EXTERIOR WALL ANALYSIS RESULTS

6.8.1 Columns Braced at All Floors

The analysis results presented above for the exterior wall subsystem with columns braced at all floors, Analysis Case 1 through Case 5, indicate the following:

1. Spandrels had the maximum stress in each Case.
2. The maximum spandrel stresses were at the columns.
3. The maximum spandrel strains were plastic.
4. Spandrels experienced large lateral distortions, indicative of lateral buckling.
5. Spandrel splices partially separated, but no spandrel splice separated completely in any of the five Cases. Partial failure of spandrel splices typically indicated tearing failures at Floor 97 and above and bolt shear failures at Floor 96 and below.
6. Lateral deflections of columns did not exceed 1 in.
7. The principal contributor to the total vertical deflection of the columns was the unrestrained vertical expansion due to thermal effects.
8. General instability of the exterior wall did not occur.

The model was unrestrained against in-plane deflection at both edges. In-plane deflection restraint from the remaining wall can further increase the lateral distortions, possibly buckle the spandrels, and fail additional spandrel splices from thermal expansion effects.

6.8.2 Columns Not Braced at Floors 95 and 96

The analysis results for the exterior wall subsystem with columns not braced at Floors 95 and 96, Analysis Case 6, indicate the following:

1. Lateral deflections of the columns were less than 1 in.
2. There was no plastic strain in the columns and spandrels.
3. All column-splice contacts remained closed.
4. There was additional partial spandrel splice separation at Floors 95, 96, 97, and 99.
5. No spandrel splice separated completely. Partial failure of spandrel splices indicated tearing failures at Floor 97 and above and bolt shear failures at Floor 96 and below.
6. General instability of the exterior wall did not occur.

6.8.3 Columns Not Braced at Floors 95, 96, and 97

The analysis results for the exterior wall subsystem with columns not braced at Floors 95, 96, and 97, Analysis Case 7, indicate the following:

1. Lateral deflections of the columns were less than 1 in.
2. There was no plastic strain in the columns and spandrels.
3. All column-splice contacts remained closed.

4. There was additional partial spandrel splice separation at Floors 95, 96, 97, and 99.
5. No spandrel splice separated completely. Partial failure of spandrel splices indicated tearing failures at Floor 97 and above and bolt shear failures at Floor 96 and below.
6. General instability of the exterior wall did not occur.

6.8.4 Columns Not Braced and Pulled in at Floors 95, 96, and 97

The analysis results for the exterior wall subsystem with columns not braced at Floors 95, 96, and 97 and subjected to pull-in force after DBARE temperature condition, Analysis Case 8, indicate the following:

1. A converged solution could not be obtained at the point of instability with a pull-in force greater than 12.6 kip.
2. At 12.6 kip pull-in force, the inward bowing of the exterior wall was 10.2 in.
3. The maximum column stress of 77.2 ksi was at Floor 94
4. Column-splice contacts slid or opened at several columns.
5. No column splice bolts fractured.
6. There were local plastic strains in the spandrel at Floor 94.
7. There was additional partial spandrel splice plate separation at Floor 99, but no spandrel splice separated completely.
8. Instability of the exterior wall with 12.6 kip pull-in force was likely for the temperature condition at the end of DBARE temperature.

6.8.5 Columns Not Braced at Floors 95, 96, and 97 and Columns Pushed Down at Top

The analysis results for the exterior wall subsystem with columns not braced at Floors 95, 96, and 97 and subjected to push-down displacement after DBARE temperature condition, Analysis Case 9, indicate the following:

1. The maximum sum of total reaction forces resulting from self weight, column and floor loads, and push-down force and was 4,580 kip, for nine columns.
2. The maximum individual total column reaction force was approximately 570 kip.
3. The maximum sum of additional column reaction force induced from push-down was 2,710 kip for nine columns.
4. The maximum individual additional column reaction force induced from push-down was approximately 350 kip.
5. Point of general instability, i.e. the maximum sum of column reaction forces was obtained at a push-down vertical deflection of 1.2 in.
6. The lateral deflection at point of instability was 5.2 in.
7. At an imposed downward vertical displacement of 2.0 in. (i.e., at the end of the push-down analysis), the sum of additional vertical reaction forces was reduced from 2,710 kip to approximately 2,000 kip.

8. At an imposed downward vertical displacement of 2.0 in., the lateral deflection increased from 5.2 in. at the maximum load to deflection 14.7 in.
9. Instability of the exterior wall was reached at a downward deflection of 1.2 in. when the push-down force was approximately about 150 percent of the initial gravity dead and live loads.

6.8.6 Summary of Analysis Results

Table 6-12 provides a brief summary of the exterior wall model analysis results.

Table 6–12. Summary of exterior wall model results.

Analysis Case	Total Deflection (in.)	Maximum Stress (ksi)	Plastic Strain?	Number of Spandrel Splice Break Element Failures[1]	Spandrel Splice Failure Type
1	1.53	49	YES	12	Tearing
2	3.74	49	YES	11	Tearing
3	1.87	57	YES	48	Tearing and Bolt Shear
4	2.07	53	YES	6	Tearing
5	1.57	46	YES	6	Tearing
6	3.76	23	NO	14	Tearing and Bolt Shear
7	3.79	23	NO	15	Tearing and Bolt Shear
8	10.4	77	YES	-	-
9	14.8	69	YES	-	-

[1]198 total possible break element failures

6.9 SUMMARY OF RESULTS

The analyses of the exterior wall model support the following conclusions for modeling the towers:

1. Large inelastic deformations of the spandrels and buckling at elevated temperatures can be expected, but they do not significantly affect the stability of the exterior columns and need not be accurately modeled for the global analyses.
2. Partial separations of the spandrel splices can be expected at elevated temperatures, but they do not significantly affect the stability of the exterior columns and need not be accurately modeled for the global analyses.
3. Exterior column splices can be expected to fail by sliding or opening at elevated temperatures and increased vertical loading. However, failure of column splices is expected only in the final phases of collapse sequence and need not be accurately modeled for global analyses.
4. Instability of exterior wall subsystem is expected when at least three floors are unbraced and the exterior wall subsystem is subjected to additional vertical load or pull-in forces.

5. Plastic buckling by kinking with rapid reduction of load capacity in the post-buckling regime of exterior columns is expected at high column loads and at low temperatures. At lower loads and at high temperatures, plastic buckling with some reduction of load-carrying capacity as expected by P-delta effect occurs. Hence, the kinking-type plastic buckling need not be accurately modeled for global models.

This page intentionally left blank.

Chapter 7
MODELING DETAILS FOR SUBSYSTEMS IN GLOBAL MODELS

Structural analyses performed for components, connections, and subsystems revealed their key structural responses and failure modes. The results of analyses performed on the exterior wall subsystem showed that when the exterior wall subsystem was subjected to fires it would become unstable either when three or more floors were disconnected from the exterior wall and the exterior wall was subjected to additional vertical loads or when sagging floors exerted pull-in forces on the exterior wall. The results of the full floor subsystem analyses showed that the floor disconnected from the exterior wall when the sagging floor walked off the truss seat or the exterior truss seat failed under the combined action of vertical gravity loads and high temperatures.

Based on the results of the finite-element analyses performed on components, connections, and subsystems, a decision was made to use the following modeling details for the subsystems in the global models to enhance numerical efficiency.

Floor Subsystem

Floors in the global model were modeled by shell elements, which have their membrane stiffness equal to that of the full floor system. Floors in the global model function as diaphragms and transfer load between the exterior wall system and the core.

The global model cannot be constructed with the same level of detail in all floors subjected to thermal loading as the full floor model developed in this report. It was not practical, or in some cases not possible, to create computationally efficient global models that included all details of the floor system. The BEAM188/189 elements used in the full floor model caused severe convergence problems when creep was included and those elements experience thermally-induced buckling. Also, the extent of pull-in forces from sagging floors in the full floor models was less than estimated from the observed bowing of the exterior walls in photographs and videos because the aircraft impact damage to thermal insulation of the floors was conservatively estimated by limiting the dislodged thermal insulation to regions of direct debris impact.

To enhance computational efficiency and perform the computations in a reasonable time span, it was decided to model the pull-in forces and disconnections of floors from the exterior walls in the global models as “fire-induced damage” at appropriate times. Since the full floor models did not accurately estimate the pull-in forces at floor/wall connections, the fire-induced damage obtained from the full floor model analyses were modified by “actual observations” obtained from the examination of photographs and videos performed by NIST (NIST NCSTAR 1-5A).

Exterior Wall Subsystem

The exterior and interior columns were modeled with fidelity of their inelastic buckling behavior. To capture the premature buckling of the single span exterior columns at low temperatures, which would occur at the onset of plate buckling and results in kinking of the cross section, a fine mesh was needed. However, observations of photographs and videos showed that bowing was extended over several floors

and column temperatures were not low. Therefore, kink-type buckling of the exterior columns was neglected, and was not modeled.

Exterior column splices were not modeled in the global models as failure of columns splices did not occur in the exterior wall subsystem analyses and was not observed in either tower prior to collapse initiation.

Spandrels were modeled by beam elements capable of resisting shear and bending moment. The spandrel splices were not modeled in the global analyses as complete separation of spandrel splices did not occur in the exterior wall studies and was not observed in either tower prior to collapse initiation.

Chapter 8
REFERENCES

ACI Committee 209 (1992), "Prediction of Creep, Shrinkage, and Temperature Effects in Concrete Structures," *ACI 209R-92*, ACI.

ACI Committee 318 (2002), "Building Code Requirements for Structural Concrete and Commentary," *ACI 318-02*, ACI.

American Institute for Steel Construction (2003), *Manual of Steel Construction, Load and Resistance Factor Design*, 3rd Edition, AISC.

American Institute for Steel Construction (2001), *Manual of Steel Construction, Load and Resistance Factor Design*, 2nd Edition, AISC.

American Institute for Steel Construction (1964), *Manual of Steel Construction, Allowable Stress Design*, 6th Edition, AISC.

ANSYS, Inc. 2004. *ANSYS Release 8.1 Documentation*. ANSYS, Inc., Canonsburg, PA.

ANSYS, Inc. 2004. *Theory Reference*, ANSYS, Inc.

Bartlett, F. M. and MacGregor, J. G. (1996), "Statistical Analysis of the Compressive Strength of Concrete in Structures," *ACI Materials Journal*, March-April, pp. 158-168.

Fields, B. A. and Fields, R. J. (1991), *The Prediction of Elevated Temperature Deformation of Structural Steel Under Anisothermal Conditions*, NIST.

LERA (2003), *Development of Structural Databases and Baseline Models for the World Trade Center (WTC) Towers - Progress Report #4: Structural Analysis Computer Models*.

Livermore Software Technology Corporation. 2003. *LS-DYNA User's Manual*. Livermore Software Technology Corporation. Livermore, CA.

Phan, Long T. (1996), *Fire Performance of High-Strength Concrete: A Report of the State-of-the-Art*, NIST.

Seanz, L. P. (1964), "Discussion of Equation of the Stress-Strain Curve of Concrete by Desayi and Krishman," *Journal of the American Concrete Institute*, Col. 61, No. 9, pp. 1229-1235.

Stevick, G. R. (1994), "Failure of Welds at Elevated Temperatures," *Welded Research Council Bulletin 390*, Welding Research Council, pp. 1-39.

This page intentionally left blank.

NIST NCSTAR 1-6D

Federal Building and Fire Safety Investigation of the World Trade Center Disaster

Global Structural Analysis of the Response of the World Trade Center Towers to Impact Damage and Fire

Mehdi S. Zarghamee
Yasuo Kitane
Ömer O. Erbay
Therese P. McAllister
John L. Gross

NIST National Institute of Standards and Technology • Technology Administration • U.S. Department of Commerce

NIST NCSTAR 1-6D

Federal Building and Fire Safety Investigation of the World Trade Center Disaster

Global Structural Analysis of the Response of the World Trade Center Towers to Impact Damage and Fire

Mehdi S. Zarghamee
Yasuo Kitane
Ömer O. Erbay
Simpson Gumpertz & Heger Inc.

Therese P. McAllister
John L. Gross
Building and Fire Research Laboratory
National Institute of Standard and Technology

September 2005

U.S. Department of Commerce
Carlos M. Gutierrez, Secretary

Technology Administration
Michelle O'Neill, Acting Secretary for Technology

National Institute of Standards and Technology
William Jeffrey, Director

Disclaimer No. 1

TABLE OF CONTENTS

Abstract iii
List of Figures vii
List of Tables xxv
List of Acronyms and Abbreviations xxix
Preface xxxi
Acknowledgments xli
Executive Summary xliii

Chapter 1
Introduction 1
1.1 Objective 1
1.2 Background 1
1.3 Method of Approach 3
1.4 Report Organization 4

Chapter 2
Global Models 7
2.1 Description of Global Models 7
2.2 Impact Damage 12
2.2.1 Introduction 12
2.2.2 Initial Damage Sets 12
2.2.3 Final Damage Sets 23
2.3 Temperature Effects 34
2.4 Thermal Behavior of Floors 35
2.5 Fire-Induced Damage 36
2.5.1 Floor/Wall Disconnections 36
2.5.2 Pull-in Forces 37
2.5.3 Floor/Wall Disconnections and Pull-in Forces Included in the Global Model 39

Chapter 3
Isolated Wall and Core Model Analyses 61
3.1 Introduction 61
3.2 Exterior Wall Buckling 61

3.2.1 Finite Element Analysis of WTC 1 Exterior Wall 65
3.2.2 FEA of WTC 2 Exterior Wall 102
3.3 Core Column Shortening and Downward Displacement of Core 134
3.3.1 FEA of WTC 1 Core 135
3.3.2 FEA of WTC 2 Core 154

Chapter 4
Global Analysis 167
4.1 Conversion from SAP2000 to ANSYS 167
4.1.1 ANSYS Models 168
4.1.2 Validation of Translated ANSYS Global Models 170
4.2 Global Analysis with Creep 173
4.2.1 Introduction 173
4.2.2 Modifications to the Global Model with Creep and Inelastic Buckling of Columns 173
4.2.3 Boundary Conditions and Loading Steps 179
4.2.4 Simulation of WTC 1 Collapse 179
4.2.5 Simulation of WTC 2 Collapse 245

Chapter 5
Collapse Sequence 309
5.1 Introduction 309
5.2 WTC 1 Collapse Sequence 312
5.3 WTC 2 Collapse Sequence 319
5.4 Discussion 329

Appendix A
FEA of Floors 331

Appendix B
Floor Truss Dynamic Response Due to Impact of Dropping Floor 373

Appendix C
Global Analysis Without Creep 377

LIST OF FIGURES

Figure P–1. The eight projects in the federal building and fire safety investigation of the WTC disaster. xxxiii

Figure 2–1. Column designations. 11

Figure 2–2. Structural damage condition on the exterior walls of WTC 1 for all cases of impact damage. 13

Figure 2–3. Structural damage condition on the exterior walls of WTC 2 for all cases of impact damage. 14

Figure 2–4. Core columns and core beams in the WTC 1 global model without aircraft impact damage. 14

Figure 2–5. Core columns and core beams in the WTC 2 global model without aircraft impact damage. 15

Figure 2–6. Case A_i structural damage condition on the core columns of WTC 1. 15

Figure 2–7. Case C_i structural damage condition on the core columns of WTC 2. 16

Figure 2–8. Revised Case C_i structural damage condition on the core columns of WTC 2. 16

Figure 2–9. Case A_i insulation damage conditions for WTC 1 floor trusses and beams. 17

Figure 2–10. Case A_i structural damage conditions for WTC 1. 18

Figure 2–11. Case C_i insulation damage conditions for WTC 2 floor trusses and beams. 19

Figure 2–12. Case C_i Structural damage conditions for WTC 2 floors. 20

Figure 2–13. Case D_i insulation damage conditions for WTC 2 floor trusses and beams. 21

Figure 2–14. Case D_i Structural damage conditions for WTC 2 floors. 22

Figure 2–15. Case A structural damage condition on the core columns of WTC 1. 23

Figure 2–16. Case C structural damage condition on the core columns of WTC 2. 24

Figure 2–17. Case B structural damage condition on the core columns of WTC 1 (including heavily damaged columns). 24

Figure 2–18. Case D structural damage condition on the core columns of WTC 2 (including heavily damaged columns). 25

Figure 2–19. Case A insulation damage condition for WTC 1 floor trusses and beams. 26

Figure 2–20. Case A structural damage condition for WTC 1 floors. 27

Figure 2–21. Case C insulation damage condition for WTC 2 floor trusses and beams. 28

Figure 2–22. Case C structural damage condition for WTC 2 floors. 29

Figure 2–23. Case B insulation damage conditions for WTC 1 floor trusses and beams. 30

Figure 2–24. Case B structural damage conditions for WTC 1 floors. 31

Figure 2–25. Case D insulation damage conditions for WTC 2 floor trusses and beams. 32

Figure 2–26. Case D structural damage conditions for WTC 2 floors. 33

Figure 2–27. Comparison of vertical displacement of a simplified truss model at Column 333 extracted from the full floor model of Floor 96 of WTC 1 for Case B_i temperature condition at 40 min with and without creep. 39

Figure 2–28. Locations of floor/wall disconnections and pull-in forces for the global analysis of WTC 1 between 0 min and 10 min for Case B conditions. 41

Figure 2–29. Locations of floor/wall disconnections and pull-in forces for the global analysis of WTC 1 between 10 min and 20 min for Case B conditions. 42

Figure 2–30. Locations of floor/wall disconnections and pull-in forces for the global analysis of WTC 1 between 20 min and 30 min for Case B conditions. 43

Figure 2–31. Locations of floor/wall disconnections and pull-in forces for the global analysis of WTC 1 between 30 min and 40 min for Case B conditions. 44

Figure 2–32. Locations of floor/wall disconnections and pull-in forces for the global analysis of WTC 1 between 40 min and 50 min for Case B conditions. 45

Figure 2–33. Locations of floor/wall disconnections and pull-in forces for the global analysis of WTC 1 between 50 min and 60 min for Case B conditions. 46

Figure 2–34. Locations of floor/wall disconnections and pull-in forces for the global analysis of WTC 1 between 60 min and 70 min for Case B conditions. 47

Figure 2–35. Locations of floor/wall disconnections and pull-in forces for the global analysis of WTC 1 between 70 min and 80 min for Case B conditions. 48

Figure 2–36. Locations of floor/wall disconnections and pull-in forces for the global analysis of WTC 1 between 80 min and 90 min for Case B conditions. 49

Figure 2–37. Locations of floor/wall disconnections and pull-in forces for the global analysis of WTC 1 between 90 min and 100 min for Case B conditions. 50

Figure 2–38. Locations of floor/wall disconnections and pull-in forces for the global analysis of WTC 2 between 0 min and 10 min for Case D conditions. 54

Figure 2–39. Locations of floor/wall disconnections and pull-in forces for the global analysis of WTC 2 between 10 min and 20 min for Case D conditions. 55

Figure 2–40. Locations of floor/wall disconnections and pull-in forces for the global analysis of WTC 2 between 20 min and 30 min for Case D conditions. 56

Figure 2–41. Locations of floor/wall disconnections and pull-in forces for the global analysis of WTC 2 between 30 min and 40 min for Case D conditions. 57

Figure 2–42. Locations of floor/wall disconnections and pull-in forces for the global analysis of WTC 2 between 40 min and 50 min for Case D conditions. 58

Figure 2–43. Locations of floor/wall disconnections and pull-in forces for the global analysis of WTC 2 between 50 min and 60 min for Case D conditions. 59

Figure 3–1. Isolated exterior wall segments from WTC 1 and WTC 2 (horizontal lines show spandrels and vertical lines show column). 62

Figure 3–2. Boundary conditions applied on the isolated exterior wall segment on the south wall of WTC 1. 62

Figure 3–3. Case A temperature condition of south wall columns of WTC 1 at 10 min. 66
Figure 3–4. Case A temperature condition of south wall columns of WTC 1 at 20 min. 66
Figure 3–5. Case A temperature condition of south wall columns of WTC 1 at 30 min. 67
Figure 3–6. Case A temperature condition of south wall columns of WTC 1 at 40 min. 67
Figure 3–7. Case A temperature condition of south wall columns of WTC 1 at 50 min. 67
Figure 3–8. Case A temperature condition of south wall columns of WTC 1 at 60 min. 68
Figure 3–9. Case A temperature condition of south wall columns of WTC 1 at 70 min. 68
Figure 3–10. Case A temperature condition of south wall columns of WTC 1 at 80 min. 68
Figure 3–11. Case A temperature condition of south wall columns of WTC 1 at 90 min. 69
Figure 3–12. Case A temperature condition of south wall columns of WTC 1 at 100 min. 69
Figure 3–13. Case A temperature condition of south wall spandrels of WTC 1 at 10 min..... 69
Figure 3–14. Case A temperature condition of south wall spandrels of WTC 1 at 20 min..... 70
Figure 3–15. Case A temperature condition of south wall spandrels of WTC 1 at 30 min..... 70
Figure 3–16. Case A temperature condition of south wall spandrels of WTC 1 at 40 min..... 70
Figure 3–17. Case A temperature condition of south wall spandrels of WTC 1 at 50 min..... 71
Figure 3–18. Case A temperature condition of south wall spandrels of WTC 1 at 60 min..... 71
Figure 3–19. Case A temperature condition of south wall spandrels of WTC 1 at 70 min..... 71
Figure 3–20. Case A temperature condition of south wall spandrels of WTC 1 at 80 min..... 72
Figure 3–21. Case A temperature condition of south wall spandrels of WTC 1 at 90 min..... 72
Figure 3–22. Case A temperature condition of south wall spandrels of WTC 1 at 100 min..... 72
Figure 3–23. Response of Isolated south wall model of WTC 1 after aircraft impact. 73
Figure 3–24. Vertical displacements of isolated south wall model of WTC 1 for Case A temperature condition (downward displacement is negative)..... 74
Figure 3–25. Out-of-plane displacements of isolated south wall model of WTC 1 for Case A temperature condition (inward displacement is positive). 75
Figure 3–26. Axial load in columns of isolated south wall model of WTC 1 for Case A temperature condition (compression is negative). 76
Figure 3–27. Plastic strain in columns of isolated south wall model of WTC 1 for Case A temperature condition at 100 min (compressive strain is negative)..... 77
Figure 3–28. Axial load in columns of south wall of WTC 1 at 100 min: isolated wall model for Case A temperature condition compared to global model without creep for Case Ai conditions (compression is positive)..... 77
Figure 3–29. Responses of isolated south wall model of WTC 1 after corrective loads from the global model were applied (Case A temperature condition at 100 min)..... 78
Figure 3–30. Total additional vertical load versus additional vertical displacement during push-down analysis of isolated south wall model of WTC 1 for Case A temperature condition (compression is positive). 79

Figure 3–31. Additional vertical load per column at different additional vertical displacements during push-down analysis of isolated south wall model of WTC 1 for Case A temperature condition (compression is positive). 79

Figure 3–32. Response of isolated south wall model of WTC 1 to Case A temperature condition and push down at the end of the push-down analysis. 80

Figure 3–33. Location of the out-of-plane supports and floor/wall disconnections between exterior wall and the floor (WTC 1 south wall for Case B conditions at 100 min)..... 82

Figure 3–34. Case B temperature condition of south wall columns of WTC 1 at 10 min. 82

Figure 3–35. Case B temperature condition of south wall columns of WTC 1 at 20 min. 83

Figure 3–36. Case B temperature condition of south wall columns of WTC 1 at 30 min. 83

Figure 3–37. Case B temperature condition of south wall columns of WTC 1 at 40 min. 83

Figure 3–38. Case B temperature condition of south wall columns of WTC 1 at 50 min. 84

Figure 3–39. Case B temperature condition of south wall columns of WTC 1 at 60 min. 84

Figure 3–40. Case B temperature condition of south wall columns of WTC 1 at 70 min. 84

Figure 3–41. Case B temperature condition of south wall columns of WTC 1 at 80 min. 85

Figure 3–42. Case B temperature condition of south wall columns of WTC 1 at 90 min. 85

Figure 3–43. Case B temperature condition of south wall columns of WTC 1 at 100 min..... 85

Figure 3–44. Case B temperature condition of south wall spandrels of WTC 1 at 10 min. 86

Figure 3–45. Case B temperature condition of south wall spandrels of WTC 1 at 20 min. 86

Figure 3–46. Case B temperature condition of south wall spandrels of WTC 1 at 30 min. 86

Figure 3–47. Case B temperature condition of south wall spandrels of WTC 1 at 40 min. 87

Figure 3–48. Case B temperature condition of south wall spandrels of WTC 1 at 50 min. 87

Figure 3–49. Case B temperature condition of south wall spandrels of WTC 1 at 60 min. 87

Figure 3–50. Case B temperature condition of south wall spandrels of WTC 1 at 70 min. 88

Figure 3–51. Case B temperature condition of south wall spandrels of WTC 1 at 80 min. 88

Figure 3–52. Case B temperature condition of south wall spandrels of WTC 1 at 90 min. 88

Figure 3–53. Case B temperature condition of south wall spandrels of WTC 1 at 100 min. 89

Figure 3–54. Vertical displacement of isolated south wall model of WTC 1 for Case B temperature condition (downward displacement is negative). 90

Figure 3–55. Out-of-plane displacement of isolated south wall model of WTC 1 for Case B temperature condition (inward displacement is positive). 91

Figure 3–56. Axial load in columns of isolated south wall model of WTC 1 for Case B temperature condition (compression is negative). 92

Figure 3–57. Plastic strain in columns of isolated south wall model of WTC 1 for Case B temperature condition at 100 min (compressive strain is negative). 93

Figure 3–58. Axial load in columns of south wall of WTC 1 at 100 min: isolated wall model for Case B temperature condition compared to global model without creep for Case A_i conditions (compression is positive). 93

Figure 3–59. Response of isolated south wall model of WTC 1 after corrective loads from the global model were applied (Case B temperature condition at 100 min). 94

Figure 3–60. Total additional vertical load versus additional vertical displacement during push-down analysis of isolated south wall model of WTC 1 for Case B temperature condition (compression is positive). 95

Figure 3–61. Additional load per column at different additional vertical displacements during push-down analysis of isolated south wall model of WTC 1 for Case B temperature condition (compression is positive). 95

Figure 3–62. Response of isolated south wall model of WTC 1 to Case B temperature condition and push-down. 96

Figure 3–63. Locations of floor/wall disconnections and pull-in forces used between 80 min and 100 min of Case B temperature for south wall of WTC 1. 98

Figure 3–64. Response of isolated south wall model of WTC 1 at 80 min of Case B temperature condition with floor/wall disconnections and 6 kip pull-in forces over five floors. 99

Figure 3–65. Response of isolated south wall model of WTC 1 at 90 min of Case B temperature condition with floor/wall disconnections and 6 kip pull-in forces over five floors. 100

Figure 3–66. Response of isolated south wall model of WTC 1 at 100 min of Case B temperature condition with floor/wall disconnections and 6 kip pull-in forces over five floors. 101

Figure 3–67. Axial load in columns between Floors 98 and 99 of isolated south wall model of WTC 1 at 80 min, 90 min, and 100 min of Case B temperature condition with floor/wall disconnections and 6 kip pull-in forces over five floors (compression is positive). 102

Figure 3–68. Column temperatures on the east wall of WTC 2 for Case C temperature condition at 10 min, 20 min, and 30 min. 104

Figure 3–69. Column temperatures on the east wall of WTC 2 for Case C temperature condition at 40 min, 50 min, and 60 min. 105

Figure 3–70. Location of the out-of-plane supports and floor/wall disconnections between exterior wall and the floor (WTC 2 east wall for Case C conditions at 60 min). 106

Figure 3–71. Vertical displacement of isolated east wall model of WTC 2 for Case C temperature distribution (downward displacement is negative; displacements scaled ten times). 107

Figure 3–72. Vertical displacement of isolated east wall model of WTC 2 for Case C temperature distribution at 60 min (downward displacement is negative; displacements scaled ten times). 108

Figure 3–73. Out-of-plane displacement of isolated east wall model of WTC 2 for Case C temperature condition (inward displacement is positive; displacements scaled ten times). 109

Figure 3–74. Out-of-plane displacement of isolated east wall model of WTC 2 for Case C temperature distribution at 60 min (inward displacement is positive; displacements scaled ten times). 110

Figure 3–75. Axial load on columns of isolated east wall model of WTC 2 under Case C temperature condition (compression is negative). 111

Figure 3–76. Axial load on columns of isolated east wall model of WTC 2 for Case C temperatures distribution at 60 min (compression is negative). 112

Figure 3–77. Comparison of axial load in columns at Floor 83 of isolated east wall model of WTC 2 at 60 min for Case C temperature conditions and the global model without creep for Case C_i conditions (compression is positive). 113

Figure 3–78. Vertical and out-of-plane displacements of isolated east wall model of WTC 2 after column forces were corrected to those of global modal without creep for Case C_i conditions (displacements scaled ten times). 113

Figure 3–79. Vertical and out-of-plane displacements of isolated east wall model of WTC 2 after Case C temperature condition and push down analysis (displacements scaled five times)..... 114

Figure 3–80. Axial load on east wall columns of isolated east wall model of WTC 2 after Case C temperature condition and push-down (compression is negative). 114

Figure 3–81. Additional vertical load versus additional vertical displacement during push–down analysis of isolated east wall model of WTC 2 for Case C temperature condition..... 115

Figure 3–82. Variation of additional vertical load applied to columns of isolated east wall model of WTC 2 at different levels of additional vertical displacements imposed after Case C temperature condition (compression is positive). 115

Figure 3–83. Column temperatures on the east wall of WTC 2 for Case D temperature condition at 10 min, 20 min, and 30 min. 117

Figure 3–84. Column temperatures on the east wall of WTC 2 for Case D temperature condition at 40 min, 50 min, and 60 min. 118

Figure 3–85. Location of the out-of-plane supports and floor/wall disconnections between exterior wall and the floor (WTC 2 east wall for Case D conditions at 60 min)..... 119

Figure 3–86. Vertical displacement of isolated east wall model of WTC 2 for Case D temperature condition (downward displacement is negative; displacements scaled ten times)..... 120

Figure 3–87. Vertical displacement of isolated east wall model of WTC 2 for Case D temperature condition at 60 min (downward displacement is negative; displacements scaled ten times)..... 121

Figure 3–88. Out-of-plane displacement of isolated east wall model of WTC 2 for Case D temperature condition (inward displacement is positive; displacements scaled ten times)..... 122

Figure 3–89. Out-of-plane displacement of isolated east wall model of WTC 2 for Case D temperature condition at 60 min (inward displacement is positive; displacements scaled ten times)..... 123

Figure 3–90. Axial load on east wall columns of isolated east wall model of WTC 2 for Case D temperature condition (compression is negative). 124

Figure 3–91. Axial load on east wall columns of isolated east wall model of WTC 2 for Case D temperature condition at 60 min (compression is negative). 125

Figure 3–92. Comparison of axial load in columns at Floor 83 of isolated east wall model of WTC 2 at 60 min for Case D temperature conditions and the global model without creep for Case C_i structural damage condition and Case D_i temperature condition (compression is positive). 126

Figure 3–93. Vertical and out-of-plane displacements of columns of isolated east wall model of WTC 2 after column forces were corrected to those of global model without creep for Case C_i structural damage condition and Case D_i temperature condition (displacements scaled ten times). 126

Figure 3–94. Vertical and out-of-plane displacements of isolated east wall model of WTC 2 after Case D temperature condition and push down (displacements scaled five times). 127

Figure 3–95. Axial load on east wall columns of isolated east wall model of WTC 2 after Case D temperature condition and push down (compression is negative). 127

Figure 3–96. Additional vertical load applied to columns versus additional vertical during displacement for push-down analysis of isolated east wall model of WTC 2 for after Case D temperature condition (compression is positive; see Fig. 3–95 for column locations). 128

Figure 3–97. Variation of additional vertical load applied to columns of isolated east wall model of WTC 2 at different levels of additional vertical displacements imposed after Case D temperature condition (compression is positive). 128

Figure 3–98. Out-of-plane displacements of the east wall of WTC 2 estimated by NIST from photographs (inward displacement is positive; displacements are in in.). 129

Figure 3–99. Out-of-plane displacement of isolated east wall model of WTC 2 with 0.5 kip and 5.0 kip pull-in force with uniform magnitude distribution at 20 min and 18 min (inward displacement is positive). 130

Figure 3–100. Out-of-plane displacement of isolated east wall model of WTC 2 with 0.5 kip pull-in force with uniform magnitude distribution at 32 min (inward displacement is positive). 130

Figure 3–101. Out-of-plane displacement of isolated east wall model of WTC 2 with nonuniform pull-in force with magnitude of 1.0 kip on the south half and 4.0 kip on the north half (inward displacement is positive). 132

Figure 3–102. Out-of-plane displacement of isolated east wall model of WTC 2 with nonuniform pull-in force with magnitude of 1.5 kip on the south half and 5.0 kip on the north half (inward displacement is positive). 133

Figure 3–103. Isolated core models. 134

Figure 3–104. Vertical displacement of isolated core model of WTC 1 after aircraft impact (downward displacement is negative). 136

Figure 3–105. Vertical displacement of isolated core model of WTC 1 for Case A temperature condition at 10 min (downward displacement is negative). 136

Figure 3–106. Vertical displacement of isolated core model of WTC 1 for Case A temperature condition at 20 min (downward displacement is negative). 137

Figure 3–107. Vertical displacement of isolated core model of WTC 1 for Case A temperature condition at 30 min (downward displacement is negative). 137

Figure 3–108. Vertical displacement of isolated core model of WTC 1 for Case A temperature condition at 40 min (downward displacement is negative). 138

Figure 3–109. Vertical displacement of isolated core model of WTC 1 for Case A temperature condition at 50 min (downward displacement is negative). 138

Figure 3–110. Vertical displacement of isolated core model of WTC 1 for Case A temperature condition at 70 min (downward displacement is negative). 139

Figure 3–111. Vertical displacement of isolated core model of WTC 1 for Case A temperature condition at 100 min (downward displacement is negative). 139

Figure 3–112. Horizontal displacement of isolated core model of WTC 1 for Case A temperature condition at 100 min. 140

Figure 3–113. Axial load in columns of isolated core model of WTC 1 after aircraft impact (compression is negative). 141

Figure 3–114. Axial load in columns of isolated core model of WTC 1 for Case A temperature condition at 100 min (compression is negative). 142

Figure 3–115. Plastic strain in columns of isolated core model of WTC 1 for Case A temperature condition at 100 min (compressive strain is negative). 143

Figure 3–116. Vertical displacement after push down of isolated core model of WTC 1 for Case A temperature condition (downward displacement is negative). 144

Figure 3–117. Total additional vertical load versus additional vertical displacement during push-down analysis of isolated core model of WTC 1 for Case A temperature condition (compression is positive). 144

Figure 3–118. Additional axial load (kip) in columns at Floor 98 when the total axial load reached the maximum during push down analysis of isolated core model of WTC 1 for Case A temperature condition (compression is positive). 145

Figure 3–119. Vertical displacement of isolated core model of WTC 1 for Case B temperature condition at 10 min (downward displacement is negative). 146

Figure 3–120. Vertical displacement of isolated core model of WTC 1 for Case B temperature condition at 20 min (downward displacement is negative). 146

Figure 3–121. Vertical displacement of isolated core model of WTC 1 for Case B temperature condition at 30 min (downward displacement is negative). 147

Figure 3–122. Vertical displacement of isolated core model of WTC 1 for Case B temperature condition at 40 min (downward displacement is negative). 147

Figure 3–123. Vertical displacement of isolated core model of WTC 1 for Case B temperature condition at 50 min (downward displacement is negative). 148

Figure 3–124. Vertical displacement of isolated core model of WTC 1 for Case B temperature condition at 70 min (downward displacement is negative). 148

Figure 3–125. Vertical displacement of isolated core model of WTC 1 for Case B temperature condition at 100 min (downward displacement is negative). 149

Figure 3–126. Horizontal displacement of isolated core model of WTC 1 for Case B temperature condition at 100 min. 150

Figure 3–127. Axial load in columns of isolated core model of WTC 1 for Case B temperature condition at 100 min (compression is negative). 151

Figure 3–128. Plastic strain in columns of isolated core model of WTC 1 for Case B temperature condition at 100 min (compressive strain is negative). 152

Figure 3–129. Vertical displacement after push down of isolated core model of WTC 1 for Case B temperature condition (downward displacement is negative). 153

Figure 3–130. Total additional vertical load versus additional vertical displacement relationship obtained from push down analysis of isolated core model of WTC 1 for Case B temperature condition (compression is positive). 153

Figure 3–131. Additional axial load (kip) in columns at Floor 98 when the total axial load reached the maximum during push down analysis of the WTC 1 core for Case B temperature condition (compression is positive). 154

Figure 3–132. Vertical displacement of isolated core model of WTC 2 for Case C temperature condition (downward displacement is negative)..... 156

Figure 3–133. Vertical displacement of isolated core model of WTC 2 for Case C temperature condition at 60 min (downward displacement is negative)..... 157

Figure 3–134. Axial load in core columns of isolated core model of WTC 2 for Case C temperature condition at 60 min (compression is negative). 158

Figure 3–135. Axial plastic strains in core columns of isolated core model of WTC 2 for Case C temperature condition at 60 min (compressive strain is negative)..... 159

Figure 3–136. Vertical displacement after push down of isolated core model of WTC 2 for Case C temperature condition (downward displacement is negative)..... 160

Figure 3–137. Additional average vertical load versus additional vertical displacement during push-down analysis of isolated core model of WTC 2 for Case C temperature condition (compression is positive; core column locations are shown in Fig. 3–136). 160

Figure 3–138. Vertical displacement of isolated core model of WTC 2 for Case D temperature condition (downward displacement is negative)..... 162

Figure 3–139. Vertical displacement of isolated core model of WTC 2 for Case D temperature condition at 60 min (downward displacement is negative)..... 163

Figure 3–140. Axial load in core columns of isolated core model of WTC 2 for Case D temperature condition at 60 min (compression is negative). 164

Figure 3–141. Axial plastic strains in core columns of isolated core model of WTC 2 for Case D temperature condition at 60 min (compressive strain is negative)..... 165

Figure 3–142. Vertical displacement after push down of isolated core model of WTC 2 for Case D temperature condition (downward displacement is negative)..... 166

Figure 3–143. Additional average vertical load versus additional vertical displacement during push-down analysis of isolated core model of WTC 2 for Case D temperature condition..... 166

Figure 4–1. Coordinate system used in the analysis models. 167

Figure 4–2. Office and core area floors and core beams. 169

Figure 4–3. Location and IDs of outriggers and supporting columns. 170

Figure 4–4. Displaced shape of WTC 1 at the end of gravity analysis. 171

Figure 4–5. Displaced shape of WTC 2 at the end of gravity analysis. 171

Figure 4–6. Comparison of vertical displacement between WTC 1 models with and without construction sequence. 177

Figure 4–7. Comparison of vertical displacement between WTC 2 models with and without construction sequence. 178

Figure 4–8. Vertical displacement of exterior wall of WTC 1 before aircraft impact (downward displacement is negative). 186

Figure 4–9. Vertical displacement of exterior wall of WTC 1 after aircraft impact for Case B conditions (downward displacement is negative). 187

Figure 4–10. Vertical displacement of exterior wall of WTC 1 at 80 min for Case B conditions (downward displacement is negative). 188

Figure 4–11. Vertical displacement of exterior wall of WTC 1 at 100 min for Case B conditions (downward displacement is negative). 189

Figure 4–12. Vertical displacement of north wall of WTC 1 before aircraft impact. 190

Figure 4–13. Vertical displacement of north wall of WTC 1 after aircraft impact for Case B conditions (downward displacement is negative). 190

Figure 4–14. Vertical displacement of north wall of WTC 1 at 80 min for Case B conditions (downward displacement is negative). 191

Figure 4–15. Vertical displacement of north wall of WTC 1 at 100 min for Case B conditions with 5 kip pull-in forces (downward displacement is negative). 191

Figure 4–16. Vertical displacement of east wall of WTC 1 before aircraft impact (downward displacement is negative). 192

Figure 4–17. Vertical displacement of east wall of WTC 1 after aircraft impact for Case B conditions (downward displacement is negative). 192

Figure 4–18. Vertical displacement of east wall of WTC 1 at 80 min for Case B conditions (downward displacement is negative). 193

Figure 4–19. Vertical displacement of east wall of WTC 1 at 100 min for Case B conditions with 5 kip pull-in forces (downward displacement is negative). 193

Figure 4–20. Vertical displacement of south wall of WTC 1 before aircraft impact (downward displacement is negative). 194

Figure 4–21. Vertical displacement of south wall of WTC 1 after aircraft impact for Case B conditions (downward displacement is negative). 194

Figure 4–22. Vertical displacement of south wall of WTC 1 at 80 min for Case B conditions (downward displacement is negative). 195

Figure 4–23. Vertical displacement of south wall of WTC 1 at 100 min for Case B conditions with 5 kip pull-in forces (downward displacement is negative). 195

Figure 4–24. Vertical displacement of core of WTC 1 before aircraft impact (downward displacement is negative). 196

Figure 4–25. Vertical displacement of core of WTC 1 after aircraft impact for Case B conditions (downward displacement is negative). 197

Figure 4–26. Vertical displacement of core of WTC 1 at 50 min for Case B conditions (downward displacement is negative). 198

Figure 4–27. Vertical displacement of core of WTC 1 at 80 min for Case B conditions (downward displacement is negative). 199

Figure 4–28. Vertical displacement of core of WTC 1 at 100 min for Case B conditions with 5 kip pull-in forces (downward displacement is negative). 200

Figure 4–29. Vertical displacement of core columns of WTC 1 before aircraft impact (downward displacement is negative). 201

Figure 4–30. Vertical displacement of core columns of WTC 1 after aircraft impact for Case B conditions (downward displacement is negative). 202

Figure 4–31. Vertical displacement of core columns of WTC 1 at 80 min for Case B conditions (downward displacement is negative). 203

Figure 4–32. Vertical displacement of core columns of WTC 1 at 100 min for Case B conditions with 5 kip pull-in forces (downward displacement is negative). 204

Figure 4–33. Vertical displacement at Floor 99 of WTC 1 before aircraft impact. 205

Figure 4–34. Change in vertical displacement at Floor 99 of WTC 1 from the time before impact to the time after impact for Case B conditions. 205

Figure 4–35. Change in vertical displacement at Floor 99 of WTC 1 from the time before impact to 50 min for Case B conditions. 206

Figure 4–36. Change in vertical displacement at Floor 99 of WTC 1 from the time before impact to 80 min for Case B conditions. 206

Figure 4–37. Change in vertical displacement at Floor 99 of WTC 1 from the time before impact to 100 min for Case B conditions with 5 kip pull-in forces. 207

Figure 4–38. Out-of-plane displacement of south wall of WTC 1 before aircraft impact (inward displacement is positive). 208

Figure 4–39. Out-of-plane displacement of south wall of WTC 1 after aircraft impact for Case B conditions (inward displacement is positive). 208

Figure 4–40. Out-of-plane displacement of south wall of WTC 1 at 80 min (at the end of Analysis Step 17) for Case B conditions (inward displacement is positive). 209

Figure 4–41. Out-of-plane displacement of south wall of WTC 1 at 100 min for Case B conditions with 5 kip pull-in forces (inward displacement is positive). 209

Figure 4–42. Time history of maximum out-of-plane displacement of south wall of WTC 1 for Case B conditions with 5 kip pull-in forces (from Analysis Step 18 to Step 21). 210

Figure 4–43. Out-of-plane displacement of south wall of WTC 1 at 100 min for Case B conditions with 4 kip pull-in forces (inward displacement is positive). 210

Figure 4–44. Axial load in exterior columns of north wall of WTC 1 before aircraft impact (compression is negative). 211

Figure 4–45. Axial load in exterior columns of north wall of WTC 1 after aircraft impact for Case B conditions (compression is negative). 211

Figure 4–46. Axial load in exterior columns of north wall of WTC 1 at 80 min for the Case B conditions (compression is negative). 212

Figure 4–47. Axial load in exterior columns of north wall of WTC 1 at 100 min for Case B conditions with 5 kip pull-in forces (compression is negative). 212

Figure 4–48. Axial load in exterior columns of east wall of WTC 1 before aircraft impact (compression is negative). 213

Figure 4–49. Axial load in exterior columns of east wall of WTC 1 after aircraft impact for Case B conditions (compression is negative). 213

Figure 4–107. Axial load in the south wall of WTC 2 for Case D conditions (compression is negative). 274
Figure 4–108. Axial load in the north wall of WTC 2 for Case D conditions (compression is negative). 275
Figure 4–109. Axial load in the north wall of WTC 2 for Case D conditions (compression is negative). 276
Figure 4–110. Axial load in the east and the west wall columns at Floor 83 of WTC 2 for Case D conditions (compression is positive). 277
Figure 4–111. Axial load in the south and the north wall columns at Floor 83 of WTC 2 for Case D conditions (compression is positive). 278
Figure 4–112. Axial load in 800 series core columns of WTC 2 for Case D conditions (compression is negative). 279
Figure 4–113. Axial load in 800 series core columns of WTC 2 for Case D conditions (compression is negative). 280
Figure 4–114. Axial load in 900 series core columns of WTC 2 for Case D conditions (compression is negative). 281
Figure 4–115. Axial load in 900 series core columns of WTC 2 for Case D conditions (compression is negative). 282
Figure 4–116. Axial load in 1000 series core columns of WTC 2 for Case D conditions (compression is negative). 283
Figure 4–117. Axial load in 1000 series core columns of WTC 2 for Case D conditions (compression is negative). 284
Figure 4–118. Core column loads (kip) at Floor 83 of WTC 2 for Case D conditions (compression is positive). 285
Figure 4–119. Core column loads (kip) at Floor 83 of WTC 2 for Case D conditions (compression is positive). 286
Figure 4–120. Axial load in Floor 83 columns of WTC 2 for Case D conditions (compression is positive). 287
Figure 4–121. Maximum elastic-plus-plastic strains for columns between Floor 78 and Floor 83 of WTC 2 for Case D conditions (compressive strain is positive; strain values are in percent). 288
Figure 4–122. Maximum elastic-plus-plastic strains for columns between Floor 78 and Floor 3 of WTC 2 for Case D conditions (compressive strain is positive; strain values are in percent). 289
Figure 4–123. Maximum elastic-plus-plastic-plus-creep strains for columns between Floor 78 and Floor 83 of WTC 2 for Case D conditions (compressive strain is positive; strain values are in percent). 290
Figure 4–124. Axial load in core columns (kip) at Floor 105 (at hat truss level) of WTC 2 for Case D conditions (compression is positive). 291
Figure 4–125. Axial load in core columns (kip) at Floor 105 (at hat truss level) of WTC 2 for Case D conditions (compression is positive). 292

Figure 4–126. Progressive failure of core column splices at Floor 105 of WTC 2 (compression is positive; values are in kip). 293
Figure 4–127. State of core column splices at Floor 105 of WTC 2. 294
Figure 4–128. Axial force in hat truss members of WTC 2 for Case D conditions (tension is positive). 295
Figure 4–129. Axial force in hat truss members of WTC 2 for Case D conditions (tension is positive). 296
Figure 4–130. Axial stress in hat truss members of WTC 2 for Case D conditions (tension is positive). 297
Figure 4–131. Axial stress in hat truss members of WTC 2 for Case D conditions (tension is positive). 298
Figure 4–132. Primary load path within the hat truss of WTC 2. 301
Figure 4–133. Location of hat truss connections that were in the primary load path. 301

Figure 5–1. Vertical displacement of the truss model under thermal loading. 311
Figure 5–2. Catenary action in the floor system. 311
Figure 5–3. Total column loads at Floor 98 of the south wall of WTC 2 global model for Case B conditions (compression is positive). 315
Figure 5–4. Vertical displacements of full floor models of WTC 1 for Case Bi temperature condition at 100 min (downward displacement is negative). 316
Figure 5–5. Loss of vertical supports obtained in Floor 97 and Floor 98 full floor models of WTC 1 for Case Bi temperature condition at 100 min (1x displacement magnification). 316
Figure 5–6. Inward bowing of exterior columns of the South wall of WTC 1 at 10:23 a.m. (97 min after impact). Displacements were estimated by NIST from the analysis of this photograph. 317
Figure 5–7. Inward bowing of south wall of WTC 1 global model with creep at 100 min for Case B conditions with 5 kip pull-in forces (5x displacement magnification). 318
Figure 5–8. Collapse initiation and tilting of WTC 1 (view from the northeast). 318
Figure 5–9. Vertical displacements of full floor models of WTC 2 for Case D_i temperature condition at 40 min (downward displacement is negative). 323
Figure 5–10. Floor sagging observed on the east wall of WTC 2 at different times. 324
Figure 5–11. Total column loads at Floor 83 of the east wall of WTC 2 global model for Case D conditions (compression is positive). 325
Figure 5–12. Maximum elastic + plastic + creep strain magnitudes for columns between Floor 78 and Floor 83 of WTC 2 global model for Case D conditions at 20 min, 30 min, and 40 min (compressive strain is positive; strain values are in percent). 326
Figure 5–13. Inward bowing of the east wall of WTC 2 global model for Case D conditions at 43 min at the instant of collapse initiation (deformed shape scaled four times). 327
Figure 5–14. Inward bowing of exterior columns of the west wall of WTC 2 just before collapse. 327

Figure 5–15. Total displacements of WTC 2 global model above Floor 86 for Case D conditions at 43 min at collapse initiation (note the tilt toward east and south; deformed shape magnified 20 times). 328

Figure 5–16. Initiation of Collapse of WTC 2. Note the tilt toward east and south. 328

Figure 5–17. Full floor model of Floor 96 of WTC 1 for Case B_i temperature condition at 100 min. ... 330

This page intentionally left blank.

LIST OF TABLES

Table P–1 Federal building and fire safety investigation of the WTC disaster xxxii

Table P–2 Public meetings and briefings of the WTC Investigation xxxv

Table 2–1. Element types used in the global models. 8

Table 2–2. Temperatures of exterior seats at east wall of Floor 82 of WTC 2. 51

Table 2–3. Demand-to-capacity ratios of exterior seats at east wall of Floor 82 of WTC 2 predicted by the full floor model. 52

Table 3–1. Analysis steps conducted on WTC 1 isolated exterior wall model. 64

Table 3–2. Analysis steps conducted on WTC 2 isolated exterior wall model. 64

Table 4–1. Conversion from SAP2000 element types to ANSYS element types. 168

Table 4–2. Comparison of maximum displacements and base reactions of WTC 1 from translated ANSYS and SAP2000 models. 172

Table 4–3. Comparison of maximum displacements and base reactions of WTC 2 obtained from translated ANSYS and SAP2000 models. 172

Table 4–4. Comparison of axial forces in randomly selected elements from WTC 1 model at the end of gravity analysis. 172

Table 4–5. Comparison of axial forces in randomly selected elements from WTC 2 model at the end of gravity analysis. 173

Table 4–6. Global model properties before and after modifications for computational efficiency. 174

Table 4–7. Comparison of total column loads between WTC 1 models with and without construction sequence 176

Table 4–8. Comparison of total column loads between WTC 2 models with and without construction sequence 176

Table 4–9. Analysis steps of WTC 1 ANSYS global model. 180

Table 4–10. Total column loads at Floor 98 of WTC 1 for Case B conditions. 225

Table 4–11. Total column loads at Floor 105 of WTC 1 for Case B conditions. 225

Table 4–12. Total column loads on the north wall of WTC 1 for Case B conditions. 226

Table 4–13. Change in total column loads on the north wall of WTC 1 for Case B conditions from the state before aircraft impact. 226

Table 4–14. Total column loads on the east wall of WTC 1 for Case B conditions. 227

Table 4–15. Change in total column loads on the east wall of WTC 1 for Case B conditions from the state before aircraft impact. 227

Table 4–16. Total column loads on the south wall of WTC 1 for Case B conditions..... 228

Table 4–17. Change in total column loads on the south wall of WTC 1 for Case B conditions from the state before aircraft impact..... 228

Table 4–18. Summation of total column loads on the west wall of WTC 1 for Case B conditions..... 229

Table 4–19. Change in total column loads on the west wall of WTC 1 for Case B conditions from the state before aircraft impact..... 229

Table 4–20. Total column loads on the core of WTC 1 for Case B conditions. 230

Table 4–21. Change in total column loads on the core of WTC 1 for Case B conditions from the state before aircraft impact..... 230

Table 4–22. Change in total column loads before and after aircraft impact. (Loads after impact) – (Loads before impact) 231

Table 4–23. Change in total column loads after aircraft impact and at 80 min for Case B conditions. (Loads at 80 min) – (Loads After Impact)..... 231

Table 4–24. Change in total column loads at 80 min and at 100 min for Case B conditions. (Loads at 100 min) – (Loads at 80 min)..... 231

Table 4–25. Tension capacity of core column splices at Floor 106 239

Table 4–26. Axial load in core columns at Floor 105 of WTC 1 for Case B conditions 240

Table 4–27. Demand-to-capacity ratio for axial load in outriggers of WTC 1 for Case B conditions (outrigger IDs are indicated in Fig. 4–3). 242

Table 4–28. Demand to capacity ratio for axial load in exterior columns supporting outriggers at Floor 107 of WTC 1 for Case B conditions. 242

Table 4–29. Demand and capacity of the hat truss connections (kip) in the primary load path at 80 min (connection IDs are shown in Fig. 4–85)..... 244

Table 4–30. Analysis Steps of WTC 2 ANSYS global model with Case D conditions. 245

Table 4–31. Total column loads (kip) at Floor 105 at different stages of splice failures at 40 min (compression is positive). 294

Table 4–32. Demand-to-capacity ratios for outriggers of WTC 2 for Case D conditions (outrigger IDs are shown in Fig. 4–3)..... 299

Table 4–33. Demand to capacity ratios for columns supporting outriggers at Floor 107 of WTC 2 for Case D conditions..... 300

Table 4–34. Demand and capacity of the hat truss connections (kip) in the primary load path at 40 min (connection IDs are shown in Fig. 4–133)..... 302

Table 4–35. Total column loads at Floor 83 of WTC 2 for Case D conditions. 302

Table 4–36. Total column loads at Floor 105 of WTC 2 for Case D conditions. 303

Table 4–37. Change in total column loads before and after aircraft impact. (Loads After Impact) – (Loads Before Impact) 303

Table 4–38. Change in total column loads between 40 min and 43 min. (Loads at 43 min) – (Loads at 40 min) 303

Table 4–39. Total column loads over the height for the east wall of WTC 2 for Case D conditions. ... 304

Table 4–40. Total column loads over the height for the south wall of WTC 2 for Case D conditions. 305
Table 4–41. Total column loads over the height for the north wall of WTC 2 for Case D conditions. 306
Table 4–42. Total column loads over the height for the west wall of WTC 2 for Case D conditions. 307
Table 4–43. Total column loads over the height for the core of WTC 2 for Case D conditions. 308

Table 5–1. Summary of main events that led to the collapse of WTC 1. 312
Table 5–2. Observations on WTC 1 provided by NIST. 312
Table 5–3. Total column loads at Floor 98 and Floor 105 of WTC 1 global model for Case B conditions. 315
Table 5–4. Summary of main events that led to the collapse of WTC 2 319
Table 5–5. Observations on WTC 2 provided by NIST. 319
Table 5–6. Total column loads at Floor 83 and Floor 105 of WTC 2 for Case D conditions. 322

This page intentionally left blank.

LIST OF ACRONYMS AND ABBREVIATIONS

Acronyms

ARA	Applied Research Associates, Inc.
ASTM	American Society for Testing and Materials
BPS	Building Performance Study
CAEAI	Computer Aided Engineering Associates, Inc.
FEMA	Federal Emergency Management Agency
FEA	finite element analysis
LERA	Leslie E. Robertson Associates
NIST	National Institute of Standards and Technology
PANYNJ	The Port Authority of New York and New Jersey
SEAoNY	Structural Engineers Association of New York
SGH	Simpson Gumpertz & Heger Inc.
USC	United States Code
WTC	World Trade Center

Abbreviations

°C	degrees Celsius
°F	degrees Fahrenheit
ft	feet
in.	inch
L	liter
m	meter
μm	micrometer
min	minute
s	second
lb	pound
kip	a force equal to 1,000 pounds
pcf	pound per cubic foot

psf	pound per square foot
psi	pound per square inch
ksi	1,000 pounds per square inch

PREFACE

Genesis of This Investigation

Immediately following the terrorist attack on the World Trade Center (WTC) on September 11, 2001, the Federal Emergency Management Agency (FEMA) and the American Society of Civil Engineers began planning a building performance study of the disaster. The week of October 7, as soon as the rescue and search efforts ceased, the Building Performance Study Team went to the site and began its assessment. This was to be a brief effort, as the study team consisted of experts who largely volunteered their time away from their other professional commitments. The Building Performance Study Team issued its report in May 2002, fulfilling its goal "to determine probable failure mechanisms and to identify areas of future investigation that could lead to practical measures for improving the damage resistance of buildings against such unforeseen events."

On August 21, 2002, with funding from the U.S. Congress through FEMA, the National Institute of Standards and Technology (NIST) announced its building and fire safety investigation of the WTC disaster. On October 1, 2002, the National Construction Safety Team Act (Public Law 107-231), was signed into law. The NIST WTC Investigation was conducted under the authority of the National Construction Safety Team Act.

The goals of the investigation of the WTC disaster were:

- To investigate the building construction, the materials used, and the technical conditions that contributed to the outcome of the WTC disaster.
- To serve as the basis for:
  - Improvements in the way buildings are designed, constructed, maintained, and used;
  - Improved tools and guidance for industry and safety officials;
  - Recommended revisions to current codes, standards, and practices; and
  - Improved public safety.

The specific objectives were:

1. Determine why and how WTC 1 and WTC 2 collapsed following the initial impacts of the aircraft and why and how WTC 7 collapsed;
2. Determine why the injuries and fatalities were so high or low depending on location, including all technical aspects of fire protection, occupant behavior, evacuation, and emergency response;
3. Determine what procedures and practices were used in the design, construction, operation, and maintenance of WTC 1, 2, and 7; and
4. Identify, as specifically as possible, areas in current building and fire codes, standards, and practices that warrant revision.

NIST is a nonregulatory agency of the U.S. Department of Commerce's Technology Administration. The purpose of NIST investigations is to improve the safety and structural integrity of buildings in the United States, and the focus is on fact finding. NIST investigative teams are authorized to assess building performance and emergency response and evacuation procedures in the wake of any building failure that has resulted in substantial loss of life or that posed significant potential of substantial loss of life. NIST does not have the statutory authority to make findings of fault nor negligence by individuals or organizations. Further, no part of any report resulting from a NIST investigation into a building failure or from an investigation under the National Construction Safety Team Act may be used in any suit or action for damages arising out of any matter mentioned in such report (15 USC 281a, as amended by Public Law 107-231).

Organization of the Investigation

The National Construction Safety Team for this Investigation, appointed by the then NIST Director, Dr. Arden L. Bement, Jr., was led by Dr. S. Shyam Sunder. Dr. William L. Grosshandler served as Associate Lead Investigator, Mr. Stephen A. Cauffman served as Program Manager for Administration, and Mr. Harold E. Nelson served on the team as a private sector expert. The Investigation included eight interdependent projects whose leaders comprised the remainder of the team. A detailed description of each of these eight projects is available at http://wtc.nist.gov. The purpose of each project is summarized in Table P–1, and the key interdependencies among the projects are illustrated in Fig. P–1.

Table P–1. Federal building and fire safety investigation of the WTC disaster.

Technical Area and Project Leader	Project Purpose
Analysis of Building and Fire Codes and Practices; Project Leaders: Dr. H. S. Lew and Mr. Richard W. Bukowski	Document and analyze the code provisions, procedures, and practices used in the design, construction, operation, and maintenance of the structural, passive fire protection, and emergency access and evacuation systems of WTC 1, 2, and 7.
Baseline Structural Performance and Aircraft Impact Damage Analysis; Project Leader: Dr. Fahim H. Sadek	Analyze the baseline performance of WTC 1 and WTC 2 under design, service, and abnormal loads, and aircraft impact damage on the structural, fire protection, and egress systems.
Mechanical and Metallurgical Analysis of Structural Steel; Project Leader: Dr. Frank W. Gayle	Determine and analyze the mechanical and metallurgical properties and quality of steel, weldments, and connections from steel recovered from WTC 1, 2, and 7.
Investigation of Active Fire Protection Systems; Project Leader: Dr. David D. Evans; Dr. William Grosshandler	Investigate the performance of the active fire protection systems in WTC 1, 2, and 7 and their role in fire control, emergency response, and fate of occupants and responders.
Reconstruction of Thermal and Tenability Environment; Project Leader: Dr. Richard G. Gann	Reconstruct the time-evolving temperature, thermal environment, and smoke movement in WTC 1, 2, and 7 for use in evaluating the structural performance of the buildings and behavior and fate of occupants and responders.
Structural Fire Response and Collapse Analysis; Project Leaders: Dr. John L. Gross and Dr. Therese P. McAllister	Analyze the response of the WTC towers to fires with and without aircraft damage, the response of WTC 7 in fires, the performance of composite steel-trussed floor systems, and determine the most probable structural collapse sequence for WTC 1, 2, and 7.
Occupant Behavior, Egress, and Emergency Communications; Project Leader: Mr. Jason D. Averill	Analyze the behavior and fate of occupants and responders, both those who survived and those who did not, and the performance of the evacuation system.
Emergency Response Technologies and Guidelines; Project Leader: Mr. J. Randall Lawson	Document the activities of the emergency responders from the time of the terrorist attacks on WTC 1 and WTC 2 until the collapse of WTC 7, including practices followed and technologies used.

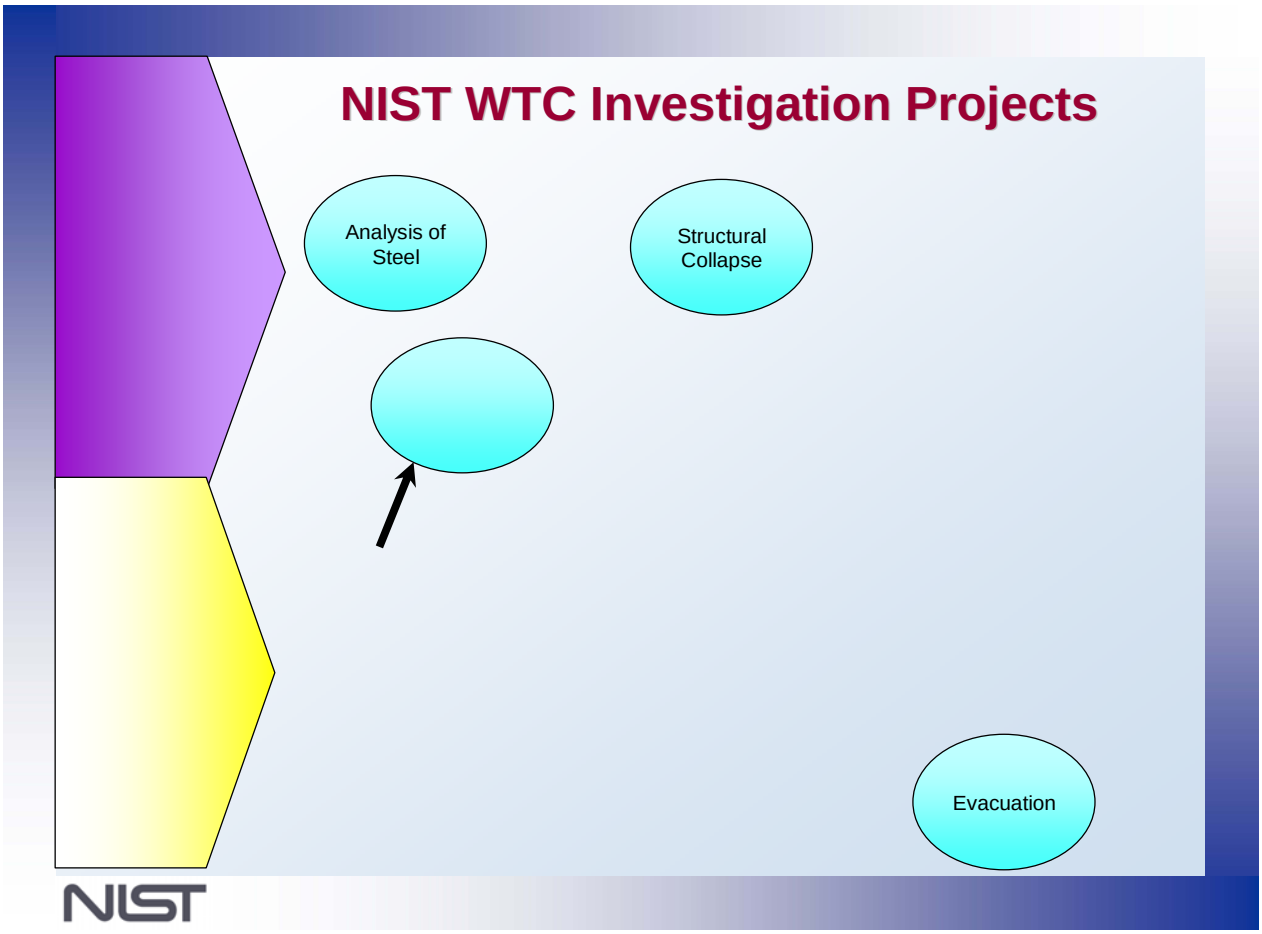
NIST WTC Investigation Projects
Analysis of Steel
Structural Collapse
Evacuation
NIST

- Robert Hanson, Professor Emeritus, University of Michigan
- Charles Thornton, Co-Chairman and Managing Principal, The Thornton-Tomasetti Group, Inc.
- Kathleen Tierney, Director, Natural Hazards Research and Applications Information Center, University of Colorado at Boulder
- Forman Williams, Director, Center for Energy Research, University of California at San Diego

This National Construction Safety Team Advisory Committee provided technical advice during the Investigation and commentary on drafts of the Investigation reports prior to their public release. NIST has benefited from the work of many people in the preparation of these reports, including the National Construction Safety Team Advisory Committee. The content of the reports and recommendations, however, are solely the responsibility of NIST.

Public Outreach

During the course of this Investigation, NIST held public briefings and meetings (listed in Table P–2) to solicit input from the public, present preliminary findings, and obtain comments on the direction and progress of the Investigation from the public and the Advisory Committee.

NIST maintained a publicly accessible Web site during this Investigation at http://wtc.nist.gov. The site contained extensive information on the background and progress of the Investigation.

NIST's WTC Public-Private Response Plan

The collapse of the WTC buildings has led to broad reexamination of how tall buildings are designed, constructed, maintained, and used, especially with regard to major events such as fires, natural disasters, and terrorist attacks. Reflecting the enhanced interest in effecting necessary change, NIST, with support from Congress and the Administration, has put in place a program, the goal of which is to develop and implement the standards, technology, and practices needed for cost-effective improvements to the safety and security of buildings and building occupants, including evacuation, emergency response procedures, and threat mitigation.

The strategy to meet this goal is a three-part NIST-led public-private response program that includes:

- A federal building and fire safety investigation to study the most probable factors that contributed to post-aircraft impact collapse of the WTC towers and the 47-story WTC 7 building, and the associated evacuation and emergency response experience.
- A research and development (R&D) program to (a) facilitate the implementation of recommendations resulting from the WTC Investigation, and (b) provide the technical basis for cost-effective improvements to national building and fire codes, standards, and practices that enhance the safety of buildings, their occupants, and emergency responders.

Table P–2. Public meetings and briefings of the WTC Investigation.

Date	Location	Principal Agenda
June 24, 2002	New York City, NY	Public meeting: Public comments on the Draft Plan for the pending WTC Investigation.
August 21, 2002	Gaithersburg, MD	Media briefing announcing the formal start of the Investigation.
December 9, 2002	Washington, DC	Media briefing on release of the Public Update and NIST request for photographs and videos.
April 8, 2003	New York City, NY	Joint public forum with Columbia University on first-person interviews.
April 29–30, 2003	Gaithersburg, MD	

York City Building Code Provisions. NIST NCSTAR 1-1F. National Institute of Standards and Technology. Gaithersburg, MD, September.

Grill, R. A., and D. A. Johnson. 2005. *Federal Building and Fire Safety Investigation of the World Trade Center Disaster: Amendments to the Fire Protection and Life Safety Provisions of the New York City Building Code by Local Laws Adopted While World Trade Center 1, 2, and 7 Were in Use*. NIST NCSTAR 1-1G. National Institute of Standards and Technology. Gaithersburg, MD, September.

Grill, R. A., and D. A. Johnson. 2005. *Federal Building and Fire Safety Investigation of the World Trade Center Disaster: Post-Construction Modifications to Fire Protection and Life Safety Systems of World Trade Center 1 and 2*. NIST NCSTAR 1-1H. National Institute of Standards and Technology. Gaithersburg, MD, September.

Grill, R. A., D. A. Johnson, and D. A. Fanella. 2005. *Federal Building and Fire Safety Investigation of the World Trade Center Disaster: Post-Construction Modifications to Fire Protection, Life Safety, and Structural Systems of World Trade Center 7*. NIST NCSTAR 1-1I. National Institute of Standards and Technology. Gaithersburg, MD, September.

Grill, R. A., and D. A. Johnson. 2005. *Federal Building and Fire Safety Investigation of the World Trade Center Disaster: Design, Installation, and Operation of Fuel System for Emergency Power in World Trade Center 7*. NIST NCSTAR 1-1J. National Institute of Standards and Technology. Gaithersburg, MD, September.

Sadek, F. 2005. *Federal Building and Fire Safety Investigation of the World Trade Center Disaster: Baseline Structural Performance and Aircraft Impact Damage Analysis of the World Trade Center Towers.* NIST NCSTAR 1-2. National Institute of Standards and Technology. Gaithersburg, MD, September.

Faschan, W. J., and R. B. Garlock. 2005. *Federal Building and Fire Safety Investigation of the World Trade Center Disaster: Reference Structural Models and Baseline Performance Analysis of the World Trade Center Towers.* NIST NCSTAR 1-2A. National Institute of Standards and Technology. Gaithersburg, MD, September.

Kirkpatrick, S. W., R. T. Bocchieri, F. Sadek, R. A. MacNeill, S. Holmes, B. D. Peterson, R. W. Cilke, C. Navarro. 2005. *Federal Building and Fire Safety Investigation of the World Trade Center Disaster: Analysis of Aircraft Impacts into the World Trade Center Towers*, NIST NCSTAR 1-2B. National Institute of Standards and Technology. Gaithersburg, MD, September.

Gayle, F. W., R. J. Fields, W. E. Luecke, S. W. Banovic, T. Foecke, C. N. McCowan, T. A. Siewert, and J. D. McColskey. 2005. *Federal Building and Fire Safety Investigation of the World Trade Center Disaster: Mechanical and Metallurgical Analysis of Structural Steel.* NIST NCSTAR 1-3. National Institute of Standards and Technology. Gaithersburg, MD, September.

Luecke, W. E., T. A. Siewert, and F. W. Gayle. 2005. *Federal Building and Fire Safety Investigation of the World Trade Center Disaster: Contemporaneous Structural Steel Specifications.* NIST Special Publication 1-3A. National Institute of Standards and Technology. Gaithersburg, MD, September.

Banovic, S. W. 2005. *Federal Building and Fire Safety Investigation of the World Trade Center Disaster: Steel Inventory and Identification.* NIST NCSTAR 1-3B. National Institute of Standards and Technology. Gaithersburg, MD, September.

Banovic, S. W., and T. Foecke. 2005. *Federal Building and Fire Safety Investigation of the World Trade Center Disaster: Damage and Failure Modes of Structural Steel Components.* NIST NCSTAR 1-3C. National Institute of Standards and Technology. Gaithersburg, MD, September.

Luecke, W. E., J. D. McColskey, C. N. McCowan, S. W. Banovic, R. J. Fields, T. Foecke, T. A. Siewert, and F. W. Gayle. 2005. *Federal Building and Fire Safety Investigation of the World Trade Center Disaster: Mechanical Properties of Structural Steels.* NIST NCSTAR 1-3D. National Institute of Standards and Technology. Gaithersburg, MD, September.

Banovic, S. W., C. N. McCowan, and W. E. Luecke. 2005. *Federal Building and Fire Safety Investigation of the World Trade Center Disaster: Physical Properties of Structural Steels.* NIST NCSTAR 1-3E. National Institute of Standards and Technology. Gaithersburg, MD, September.

Evans, D. D., R. D. Peacock, E. D. Kuligowski, W. S. Dols, and W. L. Grosshandler. 2005. *Federal Building and Fire Safety Investigation of the World Trade Center Disaster: Active Fire Protection Systems.* NIST NCSTAR 1-4. National Institute of Standards and Technology. Gaithersburg, MD, September.

Kuligowski, E. D., D. D. Evans, and R. D. Peacock. 2005. *Federal Building and Fire Safety Investigation of the World Trade Center Disaster: Post-Construction Fires Prior to September 11, 2001.* NIST NCSTAR 1-4A. National Institute of Standards and Technology. Gaithersburg, MD, September.

Hopkins, M., J. Schoenrock, and E. Budnick. 2005. *Federal Building and Fire Safety Investigation of the World Trade Center Disaster: Fire Suppression Systems.* NIST NCSTAR 1-4B. National Institute of Standards and Technology. Gaithersburg, MD, September.

Keough, R. J., and R. A. Grill. 2005. *Federal Building and Fire Safety Investigation of the World Trade Center Disaster: Fire Alarm Systems.* NIST NCSTAR 1-4C. National Institute of Standards and Technology. Gaithersburg, MD, September.

Ferreira, M. J., and S. M. Strege. 2005. *Federal Building and Fire Safety Investigation of the World Trade Center Disaster: Smoke Management Systems.* NIST NCSTAR 1-4D. National Institute of Standards and Technology. Gaithersburg, MD, September.

Gann, R. G., A. Hamins, K. B. McGrattan, G. W. Mulholland, H. E. Nelson, T. J. Ohlemiller, W. M. Pitts, and K. R. Prasad. 2005. *Federal Building and Fire Safety Investigation of the World Trade Center Disaster: Reconstruction of the Fires in the World Trade Center Towers.* NIST NCSTAR 1-5. National Institute of Standards and Technology. Gaithersburg, MD, September.

Pitts, W. M., K. M. Butler, and V. Junker. 2005. *Federal Building and Fire Safety Investigation of the World Trade Center Disaster: Visual Evidence, Damage Estimates, and Timeline Analysis.* NIST NCSTAR 1-5A. National Institute of Standards and Technology. Gaithersburg, MD, September.

Hamins, A., A. Maranghides, K. B. McGrattan, E. Johnsson, T. J. Ohlemiller, M. Donnelly, J. Yang, G. Mulholland, K. R. Prasad, S. Kukuck, R. Anleitner and T. McAllister. 2005. *Federal Building and Fire Safety Investigation of the World Trade Center Disaster: Experiments and Modeling of Structural Steel Elements Exposed to Fire.* NIST NCSTAR 1-5B. National Institute of Standards and Technology. Gaithersburg, MD, September.

Ohlemiller, T. J., G. W. Mulholland, A. Maranghides, J. J. Filliben, and R. G. Gann. 2005. *Federal Building and Fire Safety Investigation of the World Trade Center Disaster: Fire Tests of Single Office Workstations.* NIST NCSTAR 1-5C. National Institute of Standards and Technology. Gaithersburg, MD, September.

Gann, R. G., M. A. Riley, J. M. Repp, A. S. Whittaker, A. M. Reinhorn, and P. A. Hough. 2005. *Federal Building and Fire Safety Investigation of the World Trade Center Disaster: Reaction of Ceiling Tile Systems to Shocks.* NIST NCSTAR 1-5D. National Institute of Standards and Technology. Gaithersburg, MD, September.

Hamins, A., A. Maranghides, K. B. McGrattan, T. J. Ohlemiller, and R. Anleitner. 2005. *Federal Building and Fire Safety Investigation of the World Trade Center Disaster: Experiments and Modeling of Multiple Workstations Burning in a Compartment.* NIST NCSTAR 1-5E. National Institute of Standards and Technology. Gaithersburg, MD, September.

McGrattan, K. B., C. Bouldin, and G. Forney. 2005. *Federal Building and Fire Safety Investigation of the World Trade Center Disaster: Computer Simulation of the Fires in the World Trade Center Towers.* NIST NCSTAR 1-5F. National Institute of Standards and Technology. Gaithersburg, MD, September.

Prasad, K. R., and H. R. Baum. 2005. *Federal Building and Fire Safety Investigation of the World Trade Center Disaster: Fire Structure Interface and Thermal Response of the World Trade Center Towers.* NIST NCSTAR 1-5G. National Institute of Standards and Technology. Gaithersburg, MD, September.

Gross, J. L., and T. McAllister. 2005. *Federal Building and Fire Safety Investigation of the World Trade Center Disaster: Structural Fire Response and Probable Collapse Sequence of the World Trade Center Towers.* NIST NCSTAR 1-6. National Institute of Standards and Technology. Gaithersburg, MD, September.

Carino, N. J., M. A. Starnes, J. L. Gross, J. C. Yang, S. Kukuck, K. R. Prasad, and R. W. Bukowski. 2005. *Federal Building and Fire Safety Investigation of the World Trade Center Disaster: Passive Fire Protection.* NIST NCSTAR 1-6A. National Institute of Standards and Technology. Gaithersburg, MD, September.

Gross, J., F. Hervey, M. Izydorek, J. Mammoser, and J. Treadway. 2005. *Federal Building and Fire Safety Investigation of the World Trade Center Disaster: Fire Resistance Tests of Floor Truss Systems.* NIST NCSTAR 1-6B. National Institute of Standards and Technology. Gaithersburg, MD, September.

Zarghamee, M. S., S. Bolourchi, D. W. Eggers, Ö. O. Erbay, F. W. Kan, Y. Kitane, A. A. Liepins, M. Mudlock, W. I. Naguib, R. P. Ojdrovic, A. T. Sarawit, P. R Barrett, J. L. Gross, and

T. P. McAllister. 2005. *Federal Building and Fire Safety Investigation of the World Trade Center Disaster: Component, Connection, and Subsystem Structural Analysis.* NIST NCSTAR 1-6C. National Institute of Standards and Technology. Gaithersburg, MD, September.

Zarghamee, M. S., Y. Kitane, Ö. O. Erbay, T. P. McAllister, and J. L. Gross. 2005. *Federal Building and Fire Safety Investigation of the World Trade Center Disaster: Global Structural Analysis of the Response of the World Trade Center Towers to Impact Damage and Fire.* NIST NCSTAR 1-6D. National Institute of Standards and Technology. Gaithersburg, MD, September.

McAllister, T., R. W. Bukowski, R. G. Gann, J. L. Gross, K. B. McGrattan, H. E. Nelson, L. Phan, W. M. Pitts, K. R. Prasad, F. Sadek. 2006. *Federal Building and Fire Safety Investigation of the World Trade Center Disaster: Structural Fire Response and Probable Collapse Sequence of World Trade Center 7.* (Provisional). NIST NCSTAR 1-6E. National Institute of Standards and Technology. Gaithersburg, MD.

Gilsanz, R., V. Arbitrio, C. Anders, D. Chlebus, K. Ezzeldin, W. Guo, P. Moloney, A. Montalva, J. Oh, K. Rubenacker. 2006. *Federal Building and Fire Safety Investigation of the World Trade Center Disaster: Structural Analysis of the Response of World Trade Center 7 to Debris Damage and Fire*. (Provisional). NIST NCSTAR 1-6F. National Institute of Standards and Technology. Gaithersburg, MD.

Kim, W. 2006. *Federal Building and Fire Safety Investigation of the World Trade Center Disaster: Analysis of September 11, 2001, Seismogram Data*. (Provisional). NIST NCSTAR 1-6G. National Institute of Standards and Technology. Gaithersburg, MD.

Nelson, K. 2006. *Federal Building and Fire Safety Investigation of the World Trade Center Disaster: The Con Ed Substation in World Trade Center 7.* (Provisional). NIST NCSTAR 1-6H. National Institute of Standards and Technology. Gaithersburg, MD.

Averill, J. D., D. S. Mileti, R. D. Peacock, E. D. Kuligowski, N. Groner, G. Proulx, P. A. Reneke, and H. E. Nelson. 2005. *Federal Building and Fire Safety Investigation of the World Trade Center Disaster: Occupant Behavior, Egress, and Emergency Communication.* NIST NCSTAR 1-7. National Institute of Standards and Technology. Gaithersburg, MD, September.

Fahy, R., and G. Proulx. 2005. *Federal Building and Fire Safety Investigation of the World Trade Center Disaster: Analysis of Published Accounts of the World Trade Center Evacuation.* NIST NCSTAR 1-7A. National Institute of Standards and Technology. Gaithersburg, MD, September.

Zmud, J. 2005. *Federal Building and Fire Safety Investigation of the World Trade Center Disaster: Technical Documentation for Survey Administration.* NIST NCSTAR 1-7B. National Institute of Standards and Technology. Gaithersburg, MD, September.

Lawson, J. R., and R. L. Vettori. 2005. *Federal Building and Fire Safety Investigation of the World Trade Center Disaster: The Emergency Response Operations.* NIST NCSTAR 1-8. National Institute of Standards and Technology. Gaithersburg, MD, September.

ACKNOWLEDGMENTS

The Authors would like to thank Glenn R. Bell and Ronald O. Hamburger of Simpson Gumpertz & Heger Inc. (SGH) for reviewing the report and assisting in its revision. The assistance of the SGH internal Structural Performance Review Committee (Glenn R. Bell, Ronal O. Hamburger, and Pedro J. Sifre) and the Computation/Modeling Review Committee (Said Bolourchi, Atis A. Liepins, and Peter R. Barrett of Computer Aided Engineering Associates, Inc., an SGH subconsultant in this project) is acknowledged. The authors would also like to thank the technical staff of Computer Aided Engineering Associates, Inc., for their effort at converting SAP2000 finite element models to ANSYS and for their assistance in finite element modeling in ANSYS.

This page intentionally left blank.

EXECUTIVE SUMMARY

E.1 INTRODUCTION

Simpson Gumpertz & Heger Inc. (SGH) developed global models of the World Trade Center (WTC) towers using finite elements and performed analyses of the global models to gain an understanding of the roles of the aircraft impact damage and the subsequent fires in the WTC towers in the structural stability and sequential failures of components and subsystems and to determine the probable sequence of structural responses that let to the global collapse initiation. The study was conducted as part of the investigation of the WTC disaster by the National Institute of Standards and Technology (NIST).

The work presented in this report was performed as a part of Project 6 of the NIST WTC investigation. This report complements the work performed by SGH on the structural response to the fire environment of connections such as truss seats and knuckles, components such as trusses and columns, and subsystems including full floors and exterior walls of the WTC towers.

Global analyses of the WTC towers were also guided by observations. NIST examined photos and videos for visual evidence, damage estimates, and timeline of the collapse process in NIST NCSTAR 1-5A. A trial and error procedure was used in this study, which was (1) to identify the major observations at different times during the collapse process, (2) to determine the deviation between the observations and calculations, and to identify the likely assumptions that led to such deviations, and (3) to use the observations to correct the state of the structure at that time and continue the calculation to collapse initiation point. Actual observations based on NIST's examination of photos and videos are summarized in Tables E–1 and E–2 for WTC 1 and WTC 2, respectively. Columns that are referenced by column numbers can be located in Fig. E–1.

Table E–1. Observations on WTC 1 provided by NIST.

Time	Time from Impact (min)	Observation
8:46:26	0	Aircraft impact on the north wall of WTC 1 between Floor 93 and Floor 99 and Columns 112 and 151.
9:25:28	39	Fire on west side of south wall.
9:40	54	No bowing of columns was observed between Columns 301 and 323 on the east side of south wall.
10:18:43	92	Smoke suddenly expelled on Floor 92 north wall; Floor 94 east side of north wall; Floor 95 to Floor 98 on west side of north wall; Floor 95 and Floor 98 on north side of west wall; lower floor on south side.
10:22:59	97	Inward bowing from Floor 95 to about Floor 99 between Columns 308 and 326 (maybe to 340) on the south wall, maximum amplitude approximately 55 in. at Floor 97.
10:28:18	102	Smoke puff out of north edge and center of west wall; smoke and debris clouds out of the north, east, and west walls on Floor 98. Fire out of windows on the north, east, west, and south walls between Floor 92 and Floor 98, and on Floor 104.
10:28:20	102	WTC 1 began to collapse. First exterior sign of collapse was at Floor 98. Rotation of at least 8 degrees to the south occurred before the building section began to fall vertically under gravity.

Table E–2. Observations on WTC 2 provided by NIST.

Time	Time from Impact (min)	Observation
9:03	0	Aircraft impact on the south wall of WTC 2 between Floors 77 and 85, Columns 404 to 443.
9:21	18	Columns of the east wall bowed inward over the entire width of Floors 78 to 83; maximum of 7–9 in. at Floor 80.
9:38	35	Floor 83 disconnections on the east wall appeared to extend.
9:54	51	Columns of the east wall bowed inward between Floor 78 and Floor 84, 12–20 in. at Floor 80. East side of Floor 83 draped between Columns 310 to 342.
9:59	56	WTC 2 began to collapse. Column splices failed at every third panel and columns sprung back from inward bowing as collapse initiated on the east wall near the northeast corner Smoke and debris clouds were expelled from Floor 81 on the east, north, and west walls of the building. WTC 2 appeared to tilt around the base of Floor 82 and initial downward motion was visible at the same location. Tilt of approximately 3 to 4 degrees to the south and 7 to 8 degrees to the east occurred before building section fell. Kink (change in slope) on the southeast corner near Floor 94 (halfway along building section above failure). Kink (change in slope) and offset about at the Floor 106.

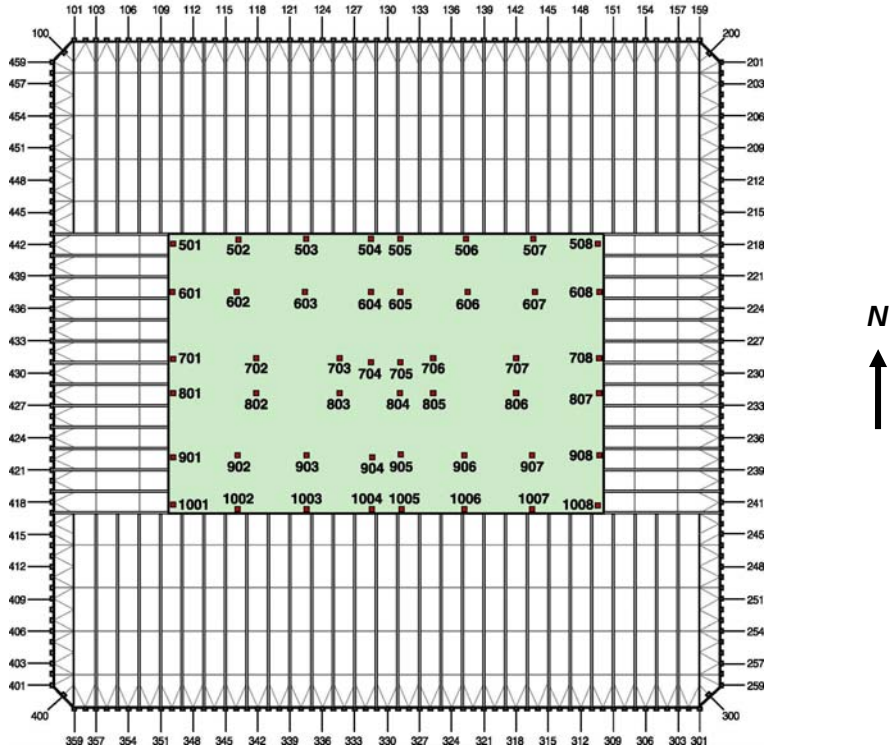

(a) WTC 1

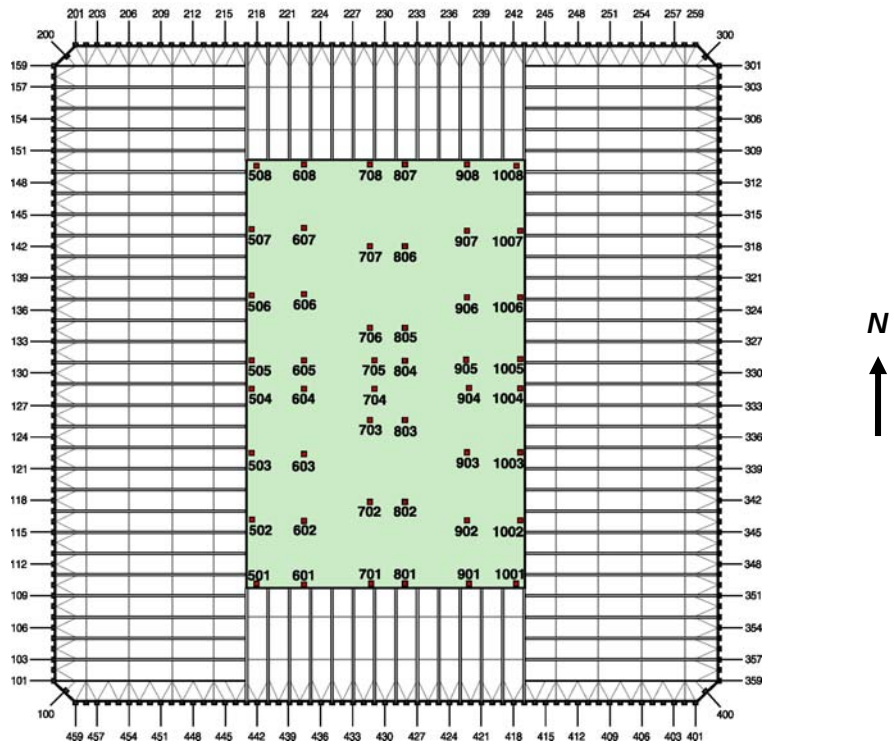

(b) WTC 2

Figure E–1. Column designations.

E.2 GLOBAL MODEL ANALYSIS

E.2.1 Global Models

SGH developed global finite-element structural models of WTC towers in ANSYS to perform collapse analysis of WTC 1 and WTC 2 subjected to the combined effects of gravity and thermal loads. The geometry, the connectivity, and the member shapes of the global models for WTC 1 and WTC 2 were obtained from an ANSYS model converted from the reference SAP2000 model developed by NIST (NIST NCSTAR 1-2) and the study conducted by SGH on components and subsystems of the WTC towers. The global models were then modified by truncating the models below the aircraft impact zone and including changes to the modeling of columns, trusses, and slabs to capture the failure modes calculated in the structural analysis of components, connections, and subsystems of the WTC towers. Material properties of steel were modified to include: temperature-dependent material properties, such as thermal expansion, elastic properties, isotropic hardening plasticity, and creep. In addition, global models allowed geometrically nonlinear analysis and large deflection effects needed for elastic and inelastic structural instability at high temperatures.

E.2.2 Impact Damage

Aircraft impact damage to the structural members and the fireproofing of steel members of the WTC towers were determined in NIST NCSTAR 1-2 and NIST NCSTAR 1-6. In the global analysis the severed exterior wall columns, spandrels, core columns, core beams, and parts of the floors were removed at the appropriate stage of analysis.

The NIST investigation identified four aircraft impact damage sets (two damage sets for each tower) consisting of an impact damage condition and a fireproofing damage condition. These damage sets were named Case A and Case B for WTC 1 and Case C and Case D for WTC 2. Case B and Case D damage sets were used in the final global analyses. Case B and Case D impact damage sets for columns are shown in Figs. E–2 to E–5, where severed columns are shown as missing vertical lines. For comparison, core columns and beams before aircraft impact are shown in Figs. E–6 and E–7 for WTC 1 and WTC 2, respectively. (Note that the global models included only core beams that had moment connections; hence, Figs E-3 and E-5 do not show all the core beams that existed in the WTC towers.)

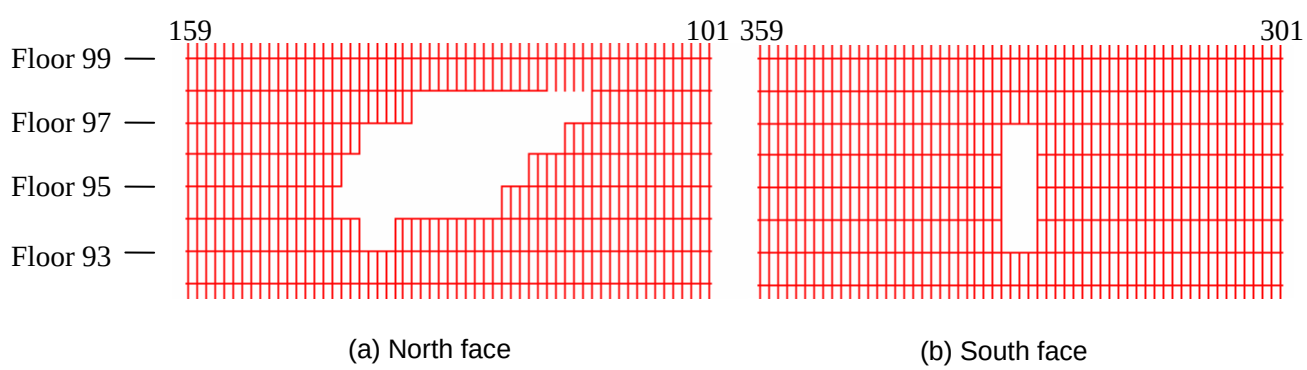

Figure E–2. Structural damage condition on the exterior walls of WTC 1 for all cases of impact damage.

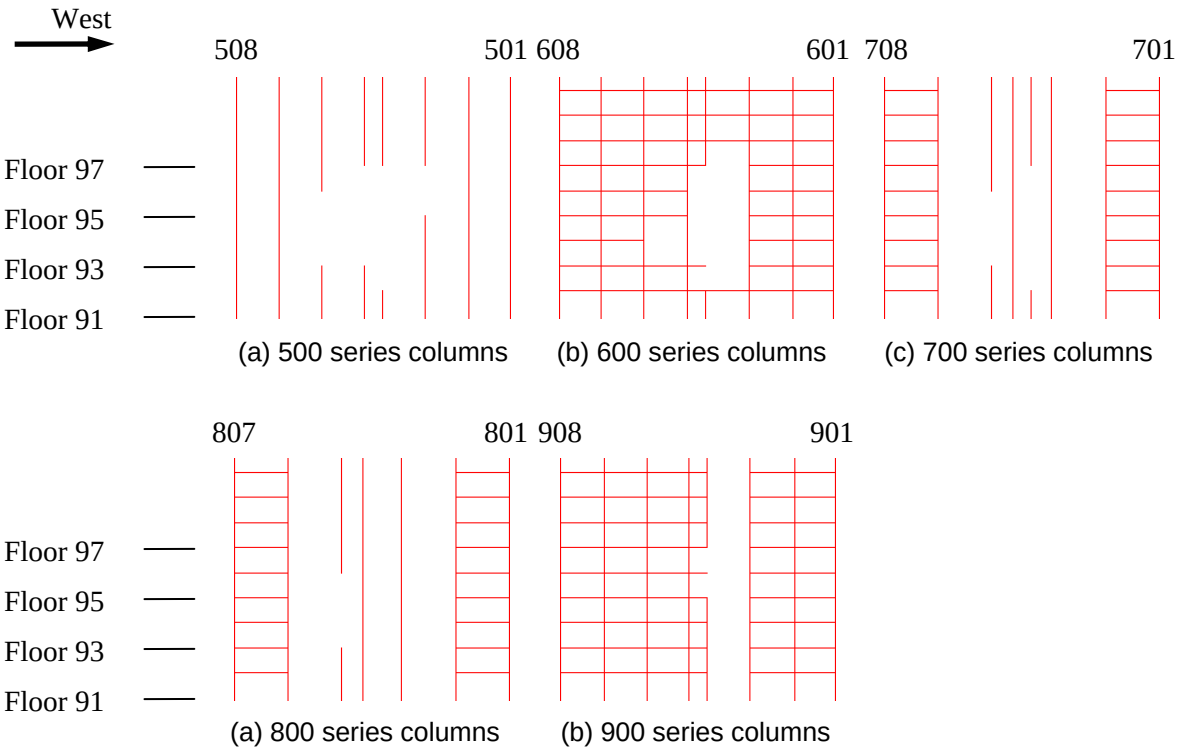

Figure E–3. Case B structural damage condition on the core columns of WTC 1 (including heavily damaged columns).

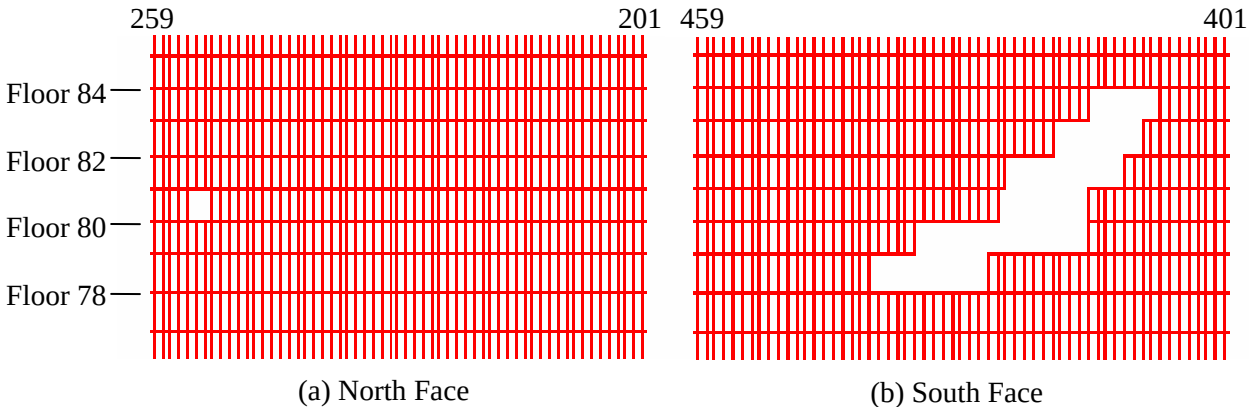

Figure E–4. Structural damage condition on the exterior walls of WTC 2 for all cases of impact damage.

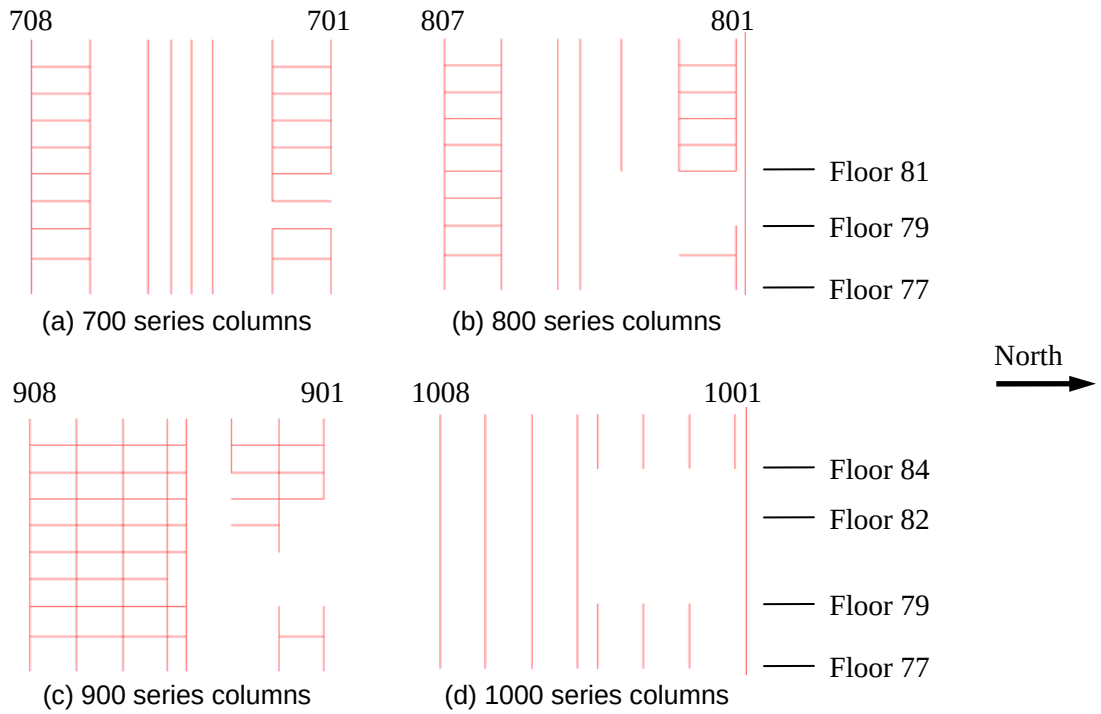

Figure E–5. Case D structural damage condition on the core columns of WTC 2 (including heavily damaged columns).

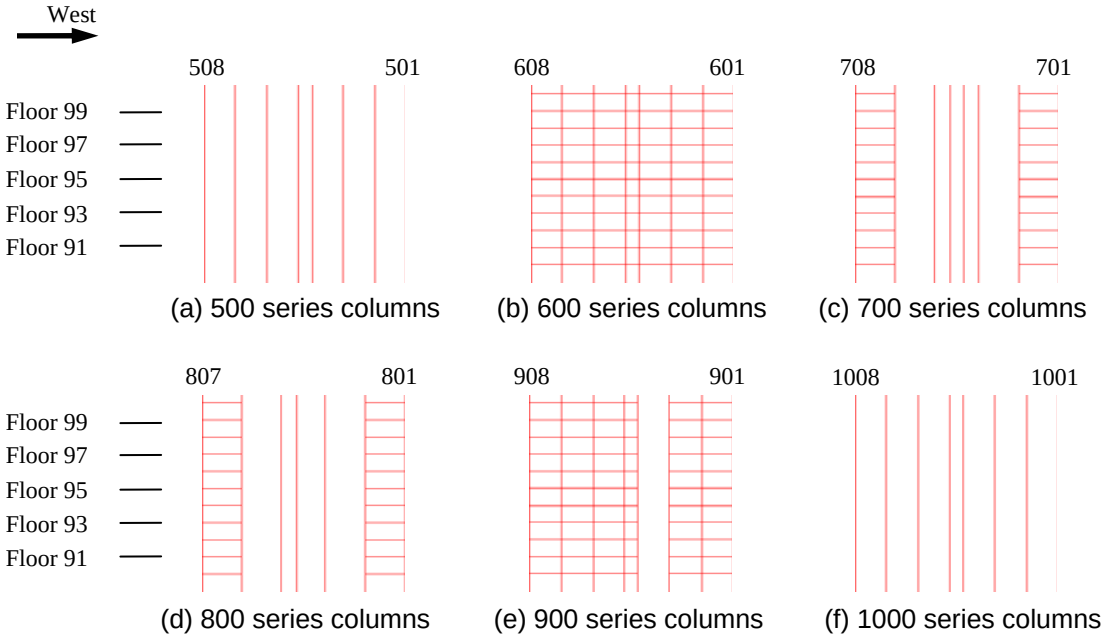

Figure E–6. Core columns and core beams in the WTC 1 global model without aircraft impact damage.

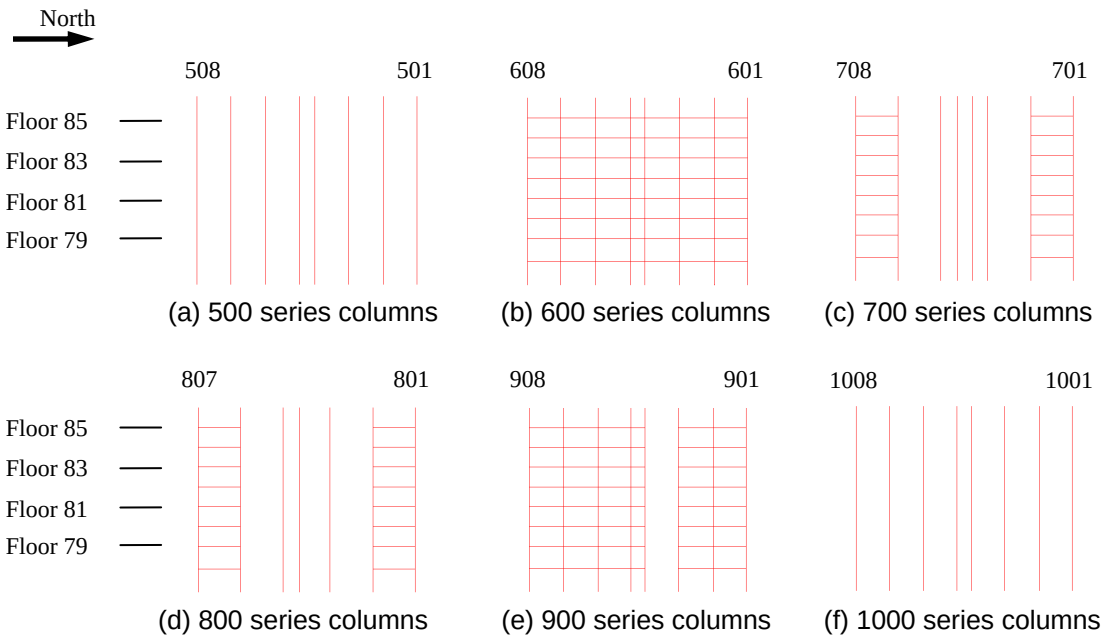

Figure E–7. Core columns and core beams in the WTC 2 global model without aircraft impact damage.

E.2.4 Loads and Boundary Conditions in the Global Models

The global models were fully restrained at the base of the vertical springs. The loads on the structure consisted of gravity loads and temperature loads. The gravity loads included dead load and live load (equal to 25 percent of the design live load). Temperature loads consisted of temperature time histories provided by NIST based on their fire dynamics and heat transfer analyses performed for different conditions of structural and fireproofing damage. Temperature data were provided for every structural node at 10 min intervals. Temperatures between the 10 min intervals were determined by linear interpolation.

E.2.5 Fire-Induced Damage

It was not practical to develop global models that could capture all the failure modes found in the study of components, connections, and subsystems, and to perform global analyses within a reasonable time period. Since detailed modeling of the floors was not included in the global models, important floor behavioral modes could not be captured directly from the global analyses. Key floor behavioral modes include sagging that imposed pull-in forces on the exterior wall and failure of support of the trusses at the exterior wall resulting in local disconnection of the floor from the exterior wall. Moreover, the sagging and the resulting bowing of the exterior walls calculated from the full floor model did not match the observed inward bowing. To account for these effects, the pull-in forces on the exterior wall and floor/wall disconnections were input into the global models as fire-induced damage at certain points in time, as illustrated in Figure E–8. Fire-induced damage calculated by the full floor models were then calibrated to the damage observed by NIST through their examination of photographs and videos during the heating period up to the final collapse. In addition, the magnitudes of pull-in forces were determined

by trial and error to match the observed inward bowing of exterior walls using the isolated exterior wall models from the global models.

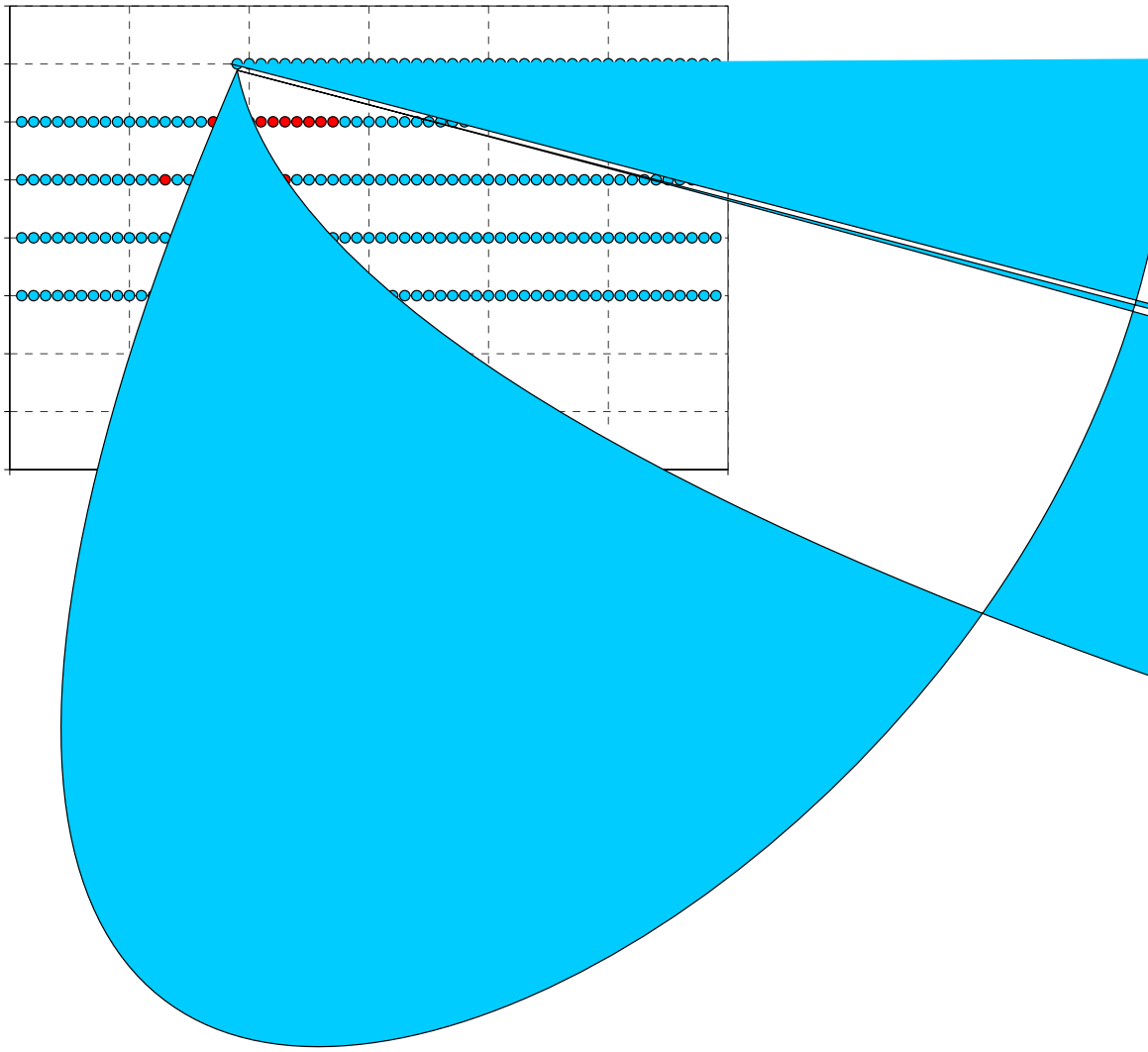

Figure E–8. Examples of locations of floor/wall disconnections and pull-in forces used in the collapse analyses of the global model with creep.

E.3 COLLAPSE SEQUENCE

The final global models were developed based on the following assumptions:

- Floor subsystem was modeled by plate elements with elastic properties without ability to simulate sagging and its effect on the development of pull-in forces and floor/wall disconnections. Pull-in forces resulting from floor sagging and floor/wall disconnections were determined based on the results of full floor models and isolated wall models and modified by visual observations. They were input in the global model analyses at different times as fire-induced damage.

- Spandrels were modeled by beam elements. Axial degree of freedom of the beam elements representing spandrels was released to enhance numerical efficiency and avoid thermally-induced buckling. The exterior wall subsystem analysis showed that large deformations and buckling of spandrels would not affect the stability of exterior columns significantly.

- Columns were modeled to capture inelastic buckling, but not the kink-type buckling initiated by the local buckling of plates and resulting in significant distortion of the cross section. The analysis of columns showed that when buckling occurs on a column that spans several floors and is at high temperatures, inelastic buckling, rather than kink-type buckling, governs its load deformation characteristic.

- The sections below the impact zones were removed, and the vertical stiffness of the removed sections was replaced with equivalent vertical springs. Preliminary analyses of the global models showed that sections below the impact zone did not contribute much to the overall behavior of the towers.

- Construction sequence was not considered to enhance computational efficiency. A comparative study showed that the total column load on each face of the exterior wall increased by 7 to 15 percent, and the total column load on the core decreased by about 10 percent, by neglecting the construction sequence.

- Structural members that were severed or heavily damaged by aircraft impact were removed from the final global models before gravity loads were applied to enhance computational efficiency.

- Break elements were not used in the final global models to represent component failures such as failure of column splices. However, the results of the global model analyses were examined to determine whether any component failure occurred and to what extent its failure impacted the collapse sequence.

The key structural events common to both towers are discussed below.

- Sagging of floors caused by the elevated steel temperatures resulting from loss of fireproofing. Elevated temperature caused buckling of the truss web diagonals, with the floor deforming into a catenary. The catenary action in this study refers to the combined action that results when the bending capacity of the truss is exceeded and additional load is carried

by the floor system acting as a tensile structure. Sagging of the floor resulted in pull-in forces at floor/exterior wall connections, and led to inward bowing of the exterior wall

- Bowing and buckling of the entire exterior wall of a tower under the combined effects of temperature, the redistributed gravity load, pull-in force from sagging floors, and loss of lateral support due to sagging or floor/wall disconnections. Floors deformed into catenaries did not restrain the exterior wall columns from buckling.

- Downward displacement of the core due to severed core columns from the aircraft impact and redistributed column loads to non-severed core columns, and shortening of the core columns caused by buckling, plasticity, and creep of core columns at elevated temperatures.

- Redistribution of gravity loads among exterior and interior columns resulting from damage due to aircraft impact, restrained thermal expansion, shortening of core columns, tilting of the tower above the impact region, and bowing and buckling of exterior walls. Redistribution of the loads from aircraft impact or fire-induced damaged columns, both in the core and exterior walls, was primarily to the neighboring columns. Redistribution of gravity loads from the core to the exterior walls and from the exterior walls to the core was primarily through the hat truss. Redistribution between adjacent exterior walls was primarily through the spandrels, and to a lesser extent through the hat truss. Major load redistribution mechanisms were as follows:

  – Aircraft impact reduced the load on the impacted wall and on the opposite wall through the pivoting action of the hat truss, and increased the load on side walls.

  – Thermal expansion caused increased loads in thermally restrained members.

  – Shortening of core columns caused a redistribution of the load from the core to the exterior walls.

  – Tilting of the tower redistributed the load among the exterior walls, resulting in increased load on the compressed part of the exterior walls.

  – Buckling of the exterior wall caused rapid unloading of the buckled wall and of the opposite wall through the pivoting action of the stiff hat truss and increased the load on the other two exterior walls.

The collapse sequences of the two towers are discussed separately below.

E.3.1 WTC 1 Collapse Sequence

The aircraft impacted the north wall of WTC 1 at 8:46 a.m. The aircraft severed exterior columns and floors on the north side of the tower and core columns and floor members between Floor 93 and Floor 98. The subsequent fires weakened structural subsystems, including the core columns, floors, and exterior walls. The core displaced downward, the floors sagged, and the south exterior wall bowed inward. At 10:28 a.m., about 102 min after the aircraft impact, WTC 1 began to collapse. The collapse sequence of WTC 1 consists of five main structural events: 1) aircraft impact, 2) unloading of core, 3) sagging of floors and floor/wall disconnections, 4) inward bowing of south wall, and 5) buckling of south wall and collapse initiation.

Aircraft Impact. The aircraft impacted WTC 1 at the north wall. The aircraft severed or heavily damaged Columns 112 to 151 between Floors 94 and 98 on the north wall. After breaching the building's perimeter, the aircraft continued to penetrate into the building. The north office area floor system sustained severe structural damage between Columns 112 and 145 at Floors 94 to 98. Core Columns 503, 504, 505, 506, 604, 704, 706, 805, and 904 were severed or heavily damaged between Floor 92 and Floor 97. The aircraft also severed a single exterior panel at the center of the south wall from Columns 329 to 331 between Floor 93 and Floor 96. In summary, 38 of 59 columns of the north wall, three of 59 columns of the south wall, and nine of 47 core columns were severed or heavily damaged. In addition, thermal insulation on floor framings and columns were damaged from the impact area to the south perimeter wall, primarily through the center of WTC 1 and over one-third to one-half of the core width.

Gravity loads in the columns that were severed were redistributed mostly to the neighboring columns. Due to the severe impact damage to the north wall, the wall section above the impact zone moved downward. The hat truss resisted the downward movement of the north wall and rotated about its east-west axis, which reduced the load on the south wall. As a result, the north and south walls each carried about 7 percent less gravity loads at Floor 98 after impact, the east and west walls each carried about 7 percent more loads, and the core carried about 1 percent more gravity loads at Floor 98 after impact. Column 705 buckled, and Columns 605 and 804 showed minor buckling.

Unloading of Core. Temperatures in the core area rose quickly, and thermal expansion of the core was greater than the thermal expansion of the exterior walls in early stages of the fire. This increased the gravity loads in the core columns until 10 min after impact. The additional gravity loads from adjacent severed columns and high temperatures caused high plastic and creep strains to develop in the core columns in the early stages of the fire. More columns buckled inelastically due to high temperatures. Creep strain continued to increase to the point of collapse. By 30 min, the plastic-plus-creep strains exceeded thermal expansion strains. Due to high plastic and creep strains and inelastic buckling of core columns, the core columns shortened, and the core displaced downward. At 100 min, the downward displacement of the core at Floor 99 became 2.0 in. on the average.

The shortening of core columns was resisted by the hat truss, which unloaded the core with time and redistributed the gravity loads from the core to the exterior walls. As a result, the north, east, south, and west walls at Floor 98 carried about 12 percent, 27 percent, 10 percent, and 22 percent more gravity loads, respectively, at 80 min than the state immediately after the impact, and the core carried about 20 percent less loads. The net increase in the total column load on the south wall, where exterior wall failure initiated, was only about 10 percent due to core downward displacement. At 80 min, the total core column loads reached their maximum. As the floor pulled in starting at 80 min on in the south side, the south exterior wall began to shed load to adjacent walls and the core.

Sagging of Floors and Floor/Wall Disconnections. The long-span trusses of Floor 95 through Floor 99 sagged due to high temperatures. While the fires were on the north side and the floors on the north side sagged first, the fires later reached the south side and the floors on the south side sagged. Full floor models underestimated the extent of sagging because cracking and spalling of concrete and creep in steel under high temperatures were not modeled, and because the extent of insulation damage was conservatively estimated. The sagging floors pulled in the south wall columns over Floors 95 to 99. In addition, the exterior seats on the south wall in the hot zone of Floors 97 and 98 began to fail due to their reduced vertical shear capacity at around 80 min, and by 100 min about 20 percent of the exterior seats on

the south wall of Floors 97 and 98 failed. Partial collapse of floor may have occurred at Floors 97 and 98, resulting from the exterior seat failures, as indicated by the observed smoke puff at 92 min (10:19 a.m.), but this phenomenon was not modeled.

Bowing of South Wall. The exterior columns on the south wall bowed inward as they were subjected to high temperatures, pull-in forces from the floors beginning at 80 min, and additional gravity loads redistributed from the core. Figure E–9 shows the observed and the estimated inward bowing of the south wall at 97 min after impact (10:23 a.m.). Since no bowing was observed on the south wall at 69 min (9:55 a.m.), it is estimated that the south wall began to bow inward at around 80 min when the floors on the south side began to substantially sag. The inward bowing of the south wall increased with time due to continuing floor sagging and increased temperatures on the south wall (Fig. E–10). At 97 min (10:23 a.m.), the maximum bowing observed was about 55 in.

Buckling of South Wall and Collapse Initiation. With continuously increased bowing, as more columns buckled, the entire width of the south wall buckled inward. Instability started at the center of the south wall and rapidly progressed horizontally toward the sides. As a result of the buckling of the south wall, the south wall significantly unloaded, redistributing its load to the softened core through the hat-truss and to the south side of the east and west walls through the spandrels. At 100 min, the north, east, and west walls at Floor 98 carried about 7 percent, 35 percent, and 30 percent more gravity loads than the state immediately after impact, and the south wall and the core carried about 7 percent and 20 percent less loads, respectively. The section of the building above the impact zone tilted to the south (observed at about 8˚) as column instability progressed rapidly from the south wall along the adjacent east and west walls (see Fig. E–11), resulting in increased gravity load on the core columns. The release of potential energy due to downward movement of building mass above the buckled columns exceeded the strain energy that could be absorbed by the structure. Global collapse ensued.

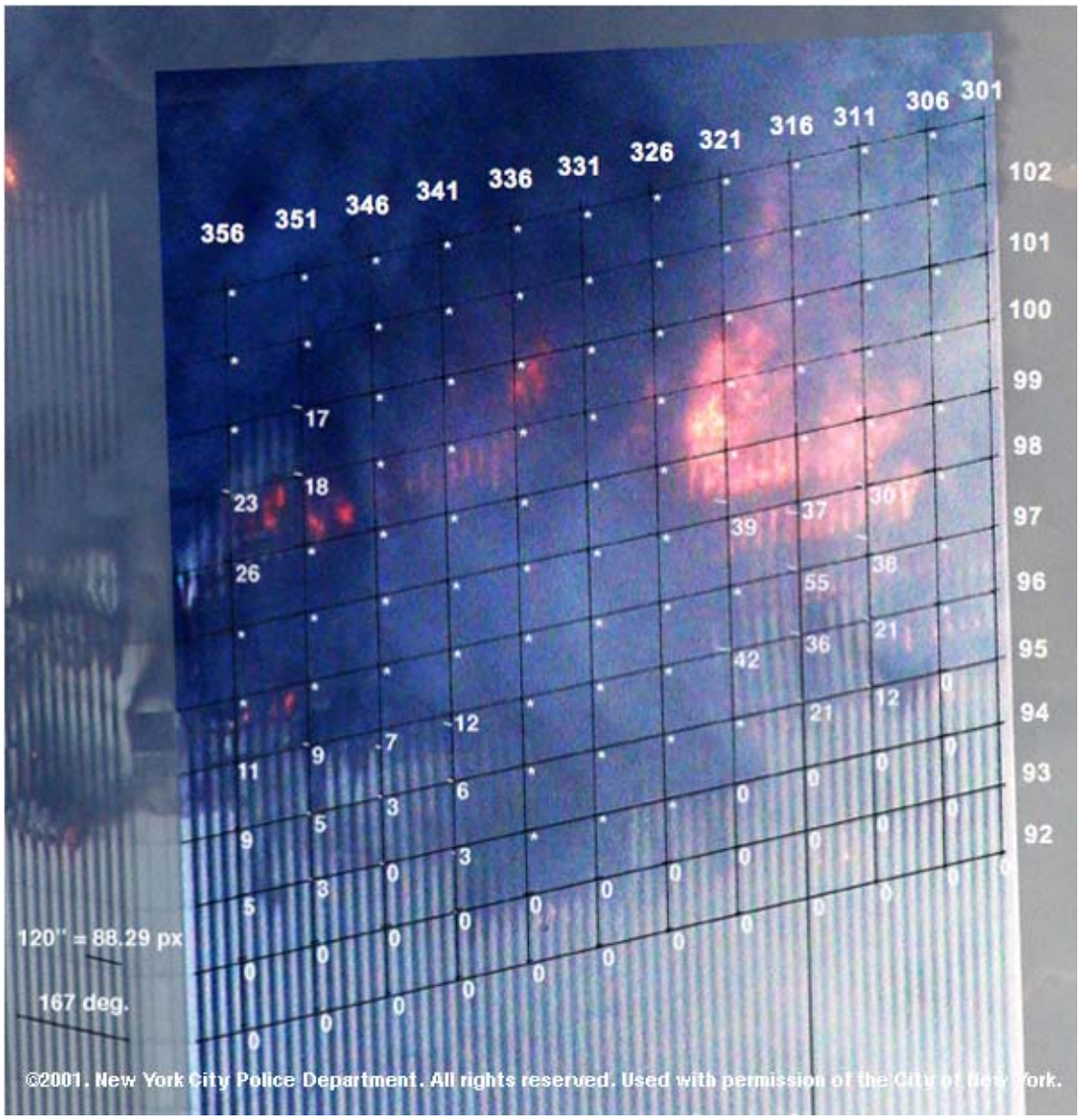

Figure E–9. Inward bowing of the south wall of WTC 1 at 10:23 a.m. Displacement estimated by NIST.

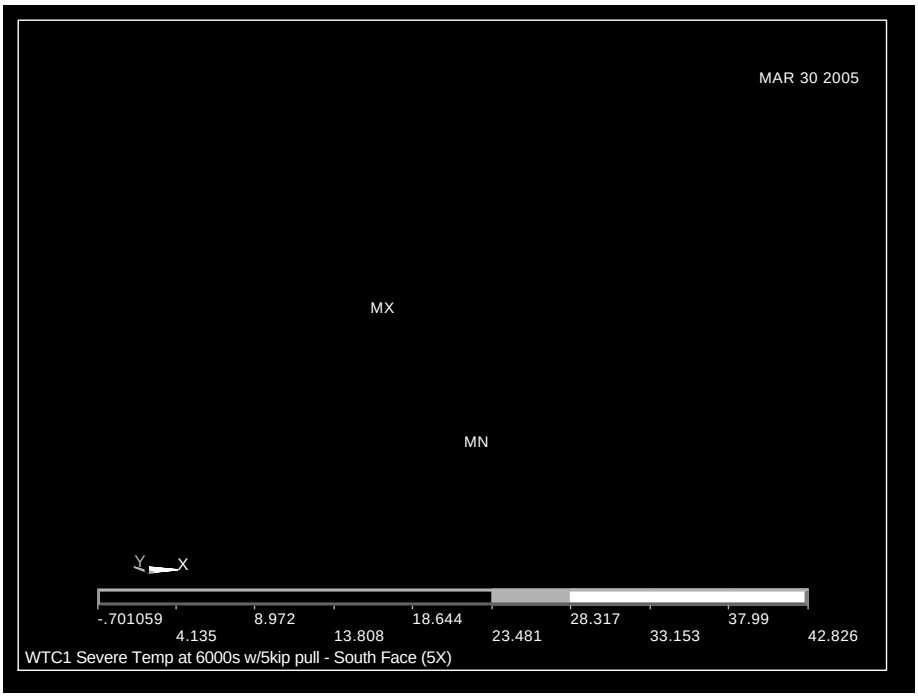

Figure E–10. Inward bowing of south wall of WTC 1 global model with creep at 100 min for Case B conditions with 5 kip pull-in forces (5x displacement magnification).

Figure E–11. Collapse initiation and tilting of WTC 1 (view from the northeast).

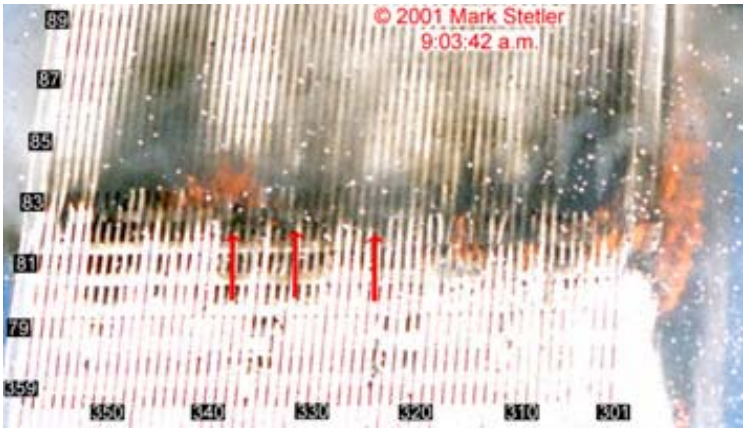

(a) After impact damage

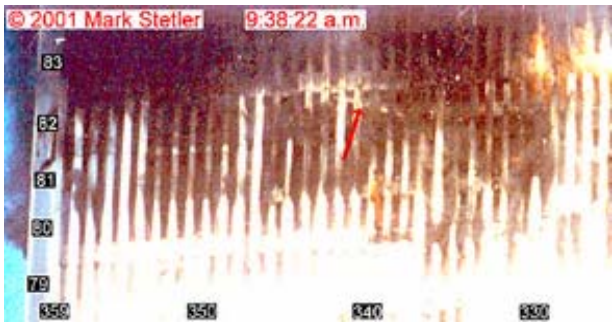

(b) South side at 9:38 a.m.
(35 min after impact)

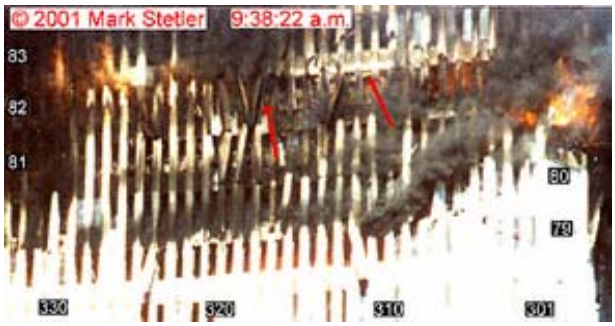

(c) North side at 9:38 a.m.
(35 min after impact)

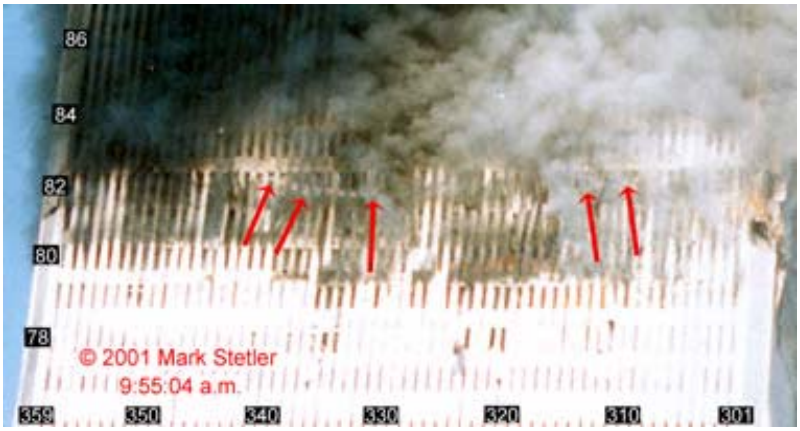

(d) At 9:54 a.m.
(51 min after impact)

Figure E–12. Floor sagging observed on the east wall of WTC 2 at different times.

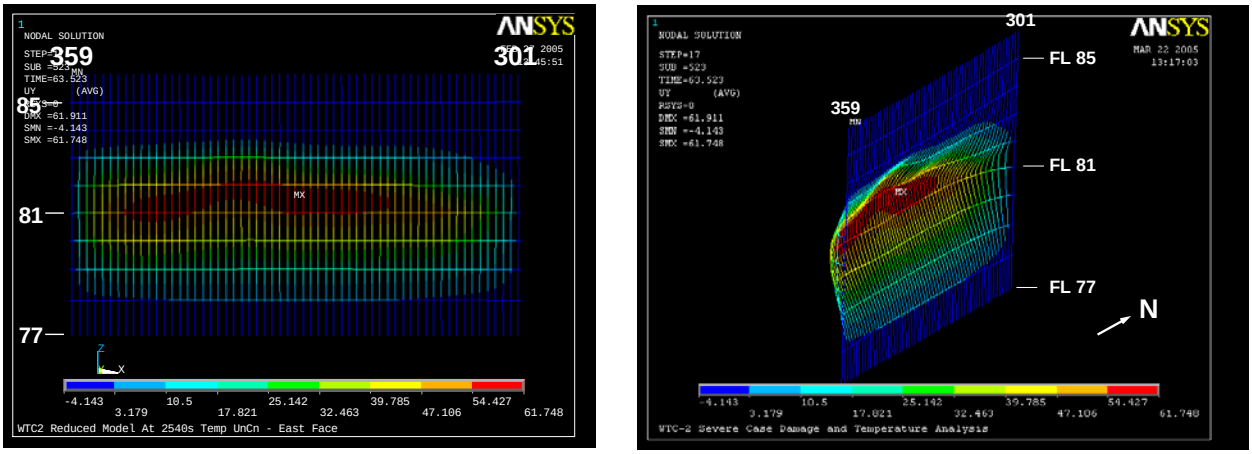

(a) View from east (b) View from southeast

Figure E–13. Inward bowing of the east wall of WTC 2 global model for Case D conditions at 43 min at the instant of collapse initiation (deformed shape scaled four times).

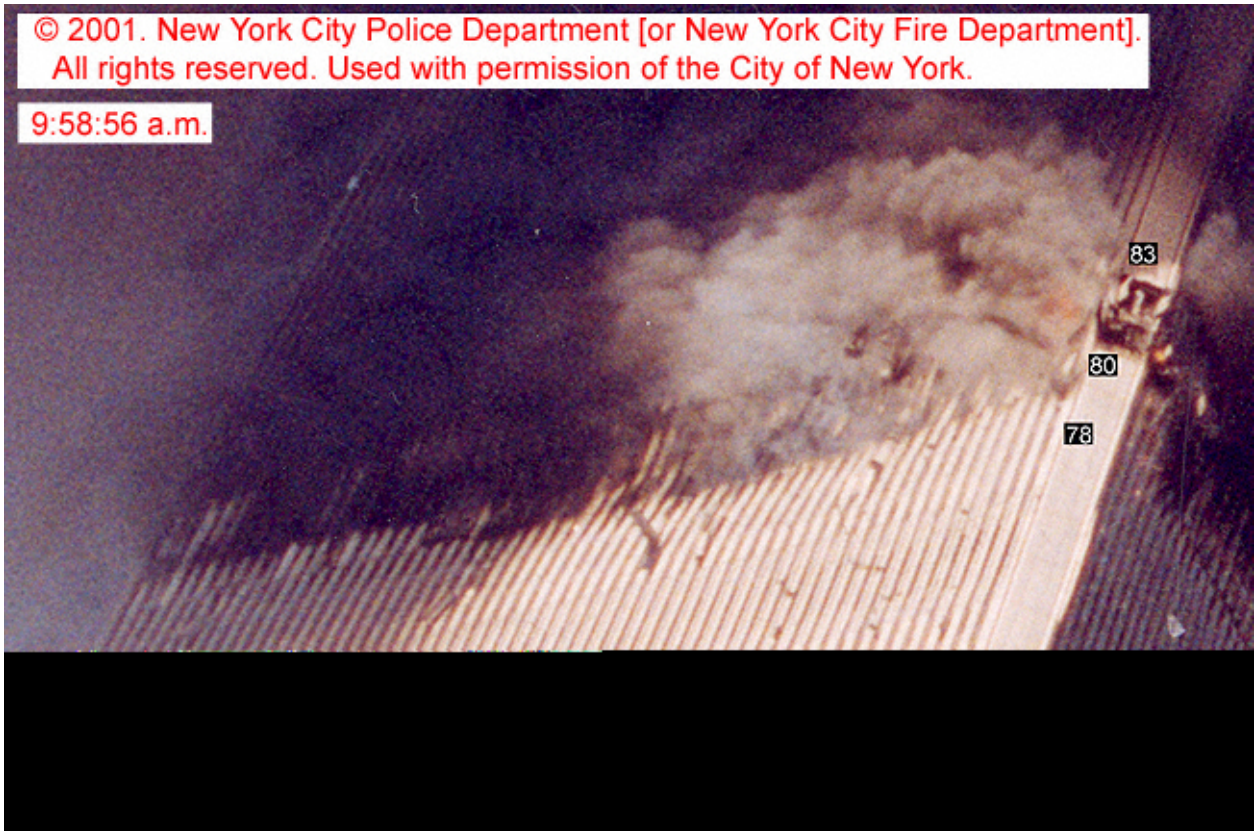

Figure E–14. Inward bowing of exterior columns of the west wall of WTC 2 just before collapse.

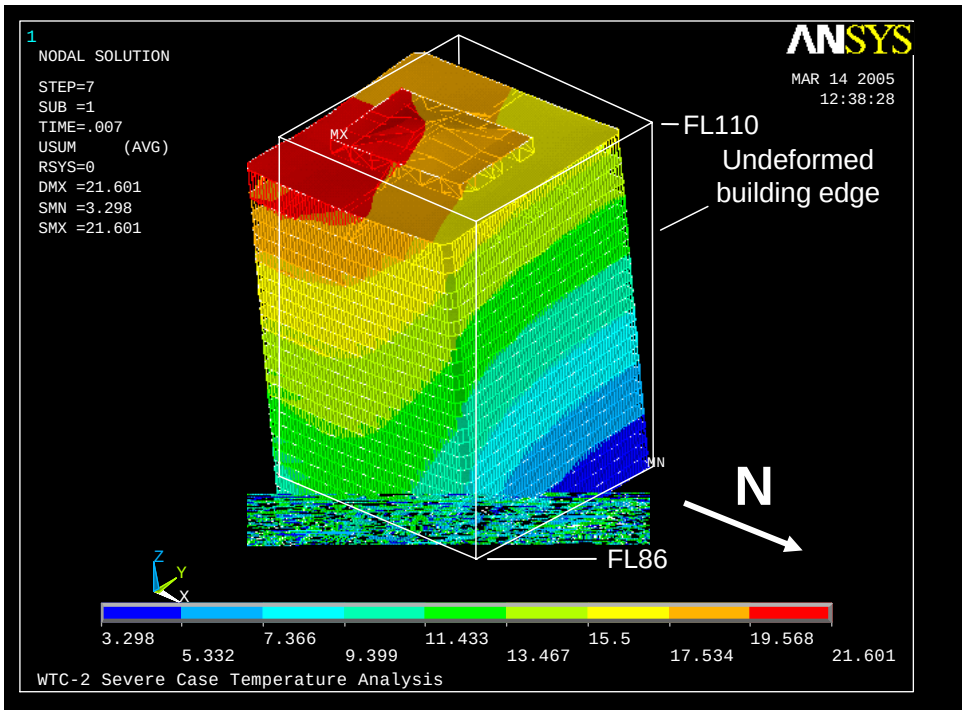

Figure E–15. Total displacements of WTC 2 global model above Floor 86 for Case D conditions at 43 min at collapse initiation (note the tilt toward east and south; deformed shape magnified 20 times).

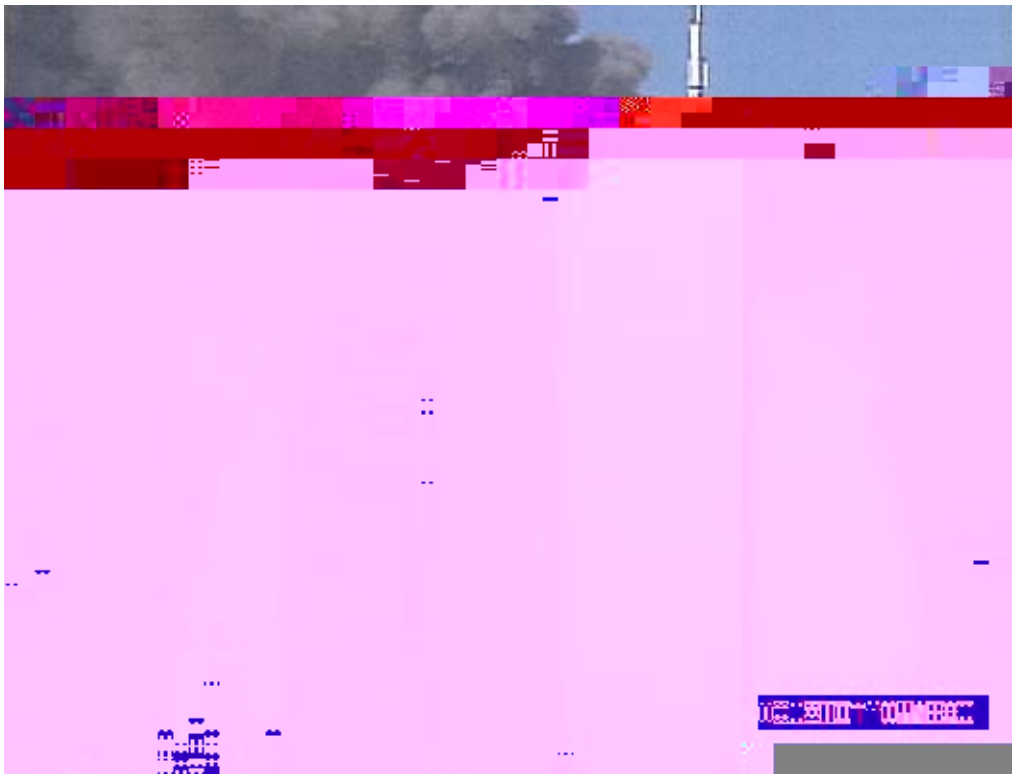

Figure E–16. Initiation of collapse of WTC 2. Note the tilt toward east and south.

This page intentionally left blank.

Chapter 1
INTRODUCTION

1.1 OBJECTIVE

The objective of this report is to present the results of finite element analyses (FEA) performed by Simpson Gumpertz and Heger Inc. (SGH) on global models of the World Trade Center (WTC) towers. The purpose of the analyses is to determine the roles of aircraft impact damage and of subsequent fires in the probable sequence of structural responses that led to global collapse of the WTC towers.

This report complements the work that SGH performed on the structural response of components in the WTC towers, such as trusses and columns, connections such as truss seats and knuckles, and subsystems including full floors and exterior walls to the fire environment. Results were reported in NIST NCSTAR 1-6C[1].

1.2 BACKGROUND

On the morning of September 11, 2001, two Boeing 767 aircraft were hijacked after they left Boston's Logan International Airport for Los Angeles. At 8:46 a.m., American Airline Flight 11, traveling from the north at an estimated speed of 440 miles per hour, impacted near the center of the north face of WTC 1 between Floor 94 and Floor 98, 1,100 ft above the plaza level. At 9:03 a.m., United Airlines Flight 175, traveling at an estimated speed of 540 miles per hour from the south, impacted the south face of WTC 2 between Floor 78 and Floor 84, 901 ft above the plaza level (NIST NCSTAR 1).

Although both WTC towers suffered substantial damage over several floors, they withstood the aircraft impact damage without global collapse. Subsequent fires, ignited with aircraft fuel and fed by the building and aircraft contents, led to the collapse of the two towers. The collapse of WTC 2 occurred at 9:59 a.m., 56 min after impact, and the collapse of WTC 1 occurred at 10:28 a.m., 102 min after impact (NIST NCSTAR 1).

Since the collapse of these tall steel frame buildings were unprecedented, questions were raised about the safety of tall steel buildings in fires. Before drawing conclusions regarding the safety of tall steel buildings in fire, it is necessary to understand how and why the WTC towers collapsed. Various aspects of the WTC towers and their collapses have been investigated by many researchers and engineers (Bažant and Zhou 2002, FEMA 2002, Kausel et al. 2002, Levy and Abboud 2002, Usmani et al. 2003). NIST initiated a comprehensive investigation of the WTC disaster on August 21, 2002, and SGH was retained under contract in October, 2003. The work presented in this report was performed by SGH as part of Project 6 of the NIST WTC Investigation.

[1] This reference is to one of the companion documents from this Investigation. A list of these documents appears in the Preface to this report.

Aircraft impact damage to the structural components of the WTC buildings were investigated and reported in NIST NCSTAR 1-2 and NIST NCSTAR 1-2B. These studies assessed structural damage and thermal insulation damage caused by aircraft impact. Although the computed aircraft impact damage to the exterior wall system of each building can be validated from the many photographs and videos taken, aircraft impact damage to the interior columns and floor systems and to the insulation cannot be validated using this same technique.

NIST performed a fire dynamics study to estimate the thermal input to the building following the aircraft impact. The fire dynamics analysis depends on the distribution of the building and aircraft contents following the impact, the spread of aircraft fuel throughout the structure upon impact, the amount of fuel that ignited and burned off immediately upon impact, and the availability of air in fire-involved areas, flowing through broken windows and through damaged interior partitions and structures to support continued combustion. Of these factors, only the distribution of broken windows on the exterior of the building can be verified, through examination of photographic and video evidence. Other factors were estimated and validated against recorded smoke plumes and other data. These calculations were performed by NIST and were reported in NIST NCSTAR 1-5 and NIST NCSTAR 1-5F.

Based on the results of the fire dynamics model, NIST calculated the steel and concrete temperatures at various times from the time of aircraft impact for the estimated extent of remaining insulation. Before aircraft impact, WTC 1 had thicker insulation on floor trusses in the areas principally involved in the fires than did WTC 2. The columns, spandrels, and core beams had similar insulation in both of the towers. No insulation had been applied to the steel deck supporting the concrete slabs in either building, though there was overspray from application of insulation to the trusses. Based on the path of the debris determined from the aircraft impact analysis, NIST estimated the extent of the insulation that was dislodged from the structural components of the WTC towers. These estimates considered insulation to be removed only in areas where direct impact from debris was predicted. Possible additional dislodgement of insulation due to the shock and resulting vibration from the aircraft impact was neglected. The extent of dislodged insulation predicted by the aircraft impact analysis is discussed in NIST NCSTAR 1-6A, and the calculation of steel and concrete temperatures is presented in NIST NCSTAR 1-5G.

NIST determined mechanical and metallurgical properties of structural steel recovered from the WTC towers. NIST also estimated the mechanical properties of WTC steel for elevated temperatures. Results were reported in NIST NCSTAR 1-3 and NIST NCSTAR 1-3D. Temperature-dependent mechanical properties of WTC steel include modulus of elasticity, Poisson’s ratio, coefficient of thermal expansion, yield strength, tensile strength, and nonlinear stress-strain relationship. NIST also predicted temperature-dependent creep properties for the WTC steels.

Prior to the development of the global finite element models of the WTC towers, SGH used hand and finite element analyses to study the structural behavior of subcomponents such as knuckles and connections, components, and subsystems. Results from structural analyses of truss seats and knuckles were used in a detailed model of a slice of a floor that included a single truss and a section of slab, which was referred to as the truss model. It was found that when subjected to elevated temperatures, the trusses sagged after diagonal web members buckled. Based on the truss model analyses, a simplified truss model was constructed and used in a model of a typical full floor. Full floor model analyses showed that in a fire environment floors sagged significantly at areas where insulation was dislodged, and exterior seats failed under extreme temperatures causing floors to disconnect from the exterior wall. The structural

performance of columns and exterior walls was studied with the analysis of single column and exterior wall subsystem models, which gave guidance in choosing element size and type for exterior columns in the global model that captured inelastic buckling behavior under elevated temperatures.

SGH developed global models that would simulate the key failure modes discovered in the analysis of components and subsystems. In addition, certain damage that could not be accurately modeled without significant loss of computational efficiency, such as certain fire-induced damage, were introduced to the global models at appropriate times. Types of fire-induced damage that were important in the collapse analysis of the global model included sagging of the floors that applied pull-in forces on the exterior columns and disconnections of floors from the exterior walls. The fire-induced damage incorporated in the global model is discussed in detail in Section 2.5.

1.3 METHOD OF APPROACH

SGH developed global finite element structural models of the WTC towers in ANSYS, based on reference structural models developed in SAP2000 (NIST NCSTAR 1-2A), and based on the studies that SGH conducted on components and subsystems of the WTC towers (NIST NCSTAR 1-6C). Owing to the existing limits of computational software and hardware, all potential structural behaviors and failure modes that could contribute to the collapse of the WTC towers were not explicitly included in the global models. A single global model that included all structural behaviors and failure modes would not be practical due to the extremely large time period required for analyses.

An alternative approach, a trial and error procedure, was used in this study to (1) perform global structural time history analyses for an assumed set of fire-induced damage, (2) identify major observations of subsequent fire-induced structural damage at different times up to the initiation of collapse, (3) determine the deviation between the calculated and observed fire-induced damage, (4) develop a structural explanation of the deviation, and (5) use the observed fire-induced damage to correct the state of the structure at that time and continue the calculation. This approach reduced the error margin (hence increased the accuracy) of the results due to epistemic uncertainties in modeling and load estimation by updating the response of the WTC towers according to observed facts at specific time points.

In developing the global models, the knowledge obtained from extensive investigation of components' and subsystems' responses to various temperature-dependent nonlinear actions was utilized. The pertinent structural actions and failure modes between and within components and subsystems that were obtained from the isolated model investigations allowed us to include or represent in a more efficient way all essential nonlinear responses in the global models without sacrificing accuracy and computation time. The important features of the detailed component and subsystem models and their influence on the global building response during the collapse process are discussed in NIST NCSTAR 1-6C. Similar discussions for two additional substructure models isolated from the global models (isolated core and exterior wall models) are provided in Chapter 3 of this report.

As discussed earlier, collapse analyses of the WTC towers were also guided by observations from the photos and videos taken during the collapse process. Visual evidence, damage estimates, and the timeline of the collapse process are reported in NIST NCSTAR 1-5A. The key observations of collapse sequences of the WTC towers are presented in Chapter 5.

The global and subsystem models were capable of capturing material nonlinearities due to plasticity and creep in steel, geometric nonlinearities due to large deflection, and elastic and inelastic buckling of the columns and other structural members at high temperatures.

The global models developed in this study were first validated against the SAP2000 models under gravity loads. Then, aircraft impact damage was included in these models by removing corresponding elements based on results from Project 2. Impact damage is discussed in detail in Section 2.2. The global models with impact damage were then subjected to temperature time histories derived from reconstructed fires in the WTC towers in Project 5.

Based on the results from FEA of the isolated and global models and the results of component and subsystem models, collapse sequences of WTC 1 and WTC 2 were identified as a conclusion of this study.

1.4 REPORT ORGANIZATION

This report presents results from the isolated models and the global models of the WTC towers. All the results are based on FEA and hand calculations. The "observed values" when used refer to the estimates obtained from photographs and videos.

This report consists of six chapters:

- Chapter 1 serves as an introduction of this report and includes objectives, background, and methods of approach of this study.
- Chapter 2 introduces the global models of WTC 1 and WTC 2. It gives general descriptions of the global models and of temperatures and aircraft impact and fire-induced damage used in the global model analyses.
- Chapter 3 gives the results from FEA of isolated wall and core models subjected to gravity and thermal loadings. The results shown in this chapter do not form a major link in the chain of collapse sequence arguments and may be skipped by those interested only in this chain of arguments.
- Chapter 4 describes the details of the global models and presents the results of FEA of the global models with creep subjected to gravity and thermal loadings.
- Chapter 5 presents the collapse sequences of WTC 1 and WTC 2 concluded from this study and provides supporting evidence.
- Chapter 6 provides a list of references.

This report also includes three appendices:

- Appendix A summarizes the results from FEA of full floor models.
- Appendix B summarizes a study on dynamic response of a floor to impact from collapse of a floor above.

- Appendix C summarizes the results of FEA of the global models without creep subjected to gravity and thermal loadings. The analyses presented in this appendix are preliminary global analyses and were primarily used to get a better understanding of the interaction between various structural components in the overall global response of the towers.

This page intentionally left blank.

Chapter 2
GLOBAL MODELS

2.1 DESCRIPTION OF GLOBAL MODELS

Simpson Gumpertz& Heger Inc. (SGH) developed two different finite element models to simulate the global structural behavior of the World Trade Center towers, WTC 1 and WTC 2, incorporating the aircraft impact damage and the fire environment that followed the impact. The finite element models of the towers were developed using ANSYS commercial structural analysis software package. The finite element models were developed to determine the roles of aircraft impact damage and of subsequent fires in the probable sequence of structural responses that led to global collapse of the WTC towers.

SGH obtained the basic building geometry, member types and cross sections, and their connectivity from models developed by Leslie E. Robertson Associates (LERA) as described in Chapter 4 of the National Instiutute of Standards and Technology (NIST) NCSTAR 1-6C. LERA developed the original models using SAP2000 structural analysis software.

The observation of photographic and video evidence of the behavior of both structures, following the time of aircraft impact and until collapse initiation, strongly suggested that nonlinear behavior and structural collapse initiation occurred within the upper portions of the structures, generally above the zone of aircraft impact. Therefore, to reduce the model size and improve solution time, the model of WTC 1 was truncated at Floor 89, five floors below the zone of impact, and a series of equivalent vertical linear springs were introduced at the base of this truncated model to represent the stiffness of the interior columns and exterior walls beneath the level of truncation. Similarly, the model of WTC 2 was truncated at Floor 73. This truncation is believed to have negligible effect on the predicted behavior of the structure.

As a first step in the analyses, the truncated SAP2000 models were converted to ANSYS. While the geometry from the SAP2000 model was directly transferable to ANSYS, it was necessary to substitute the elements with those from ANSYS element library. Table 2–1 summarizes the element types used in the ANSYS global models. The element names used in the table correspond to specific ANSYS (ANSYS, Inc. 2004) element formulations. All element types listed in Table 2–1 have temperature-dependent material properties.

In the original SAP2000 models, LERA represented the structural floors as rigid constraints with no out-of-plane stiffness. In order to capture the potential behavior of the floor slabs in transferring loads between the core and the exterior walls, these rigid constraints were replaced with grids of plate elements with the same membrane stiffness as the composite floor system (slab and trusses). Floors in the global models were not intended to capture floor response and failure modes during fires. Important failure modes were identified in the truss and full floor analyses and incorporated into the global models as floor/wall disconnections and pull-in forces at appropriate time intervals. See Chapter 7 in NIST NCSTAR 1-6C and Chapter 2 in this report for a detailed discussion of how floor behavior was modeled in the global analyses.

SGH next performed a series of modifications to the models, to simulate the structural damage resulting from the aircraft impacts and the effects of fire. The damage to the exterior walls was modeled by removing structural elements in a pattern that replicated the damage observed in available photographic and video evidence. The damage to interior structural elements was modeled based on aircraft impact simulations reported in NIST NCSTAR 1-2. The effects of fire damage to the structure were also included in the global models, based on thermal predictions developed by NIST, and the results of structural analyses performed by SGH of individual structural subsystems, including individual floor trusses, entire floor assemblies, and portions of exterior walls. Since projection of these subsystem analyses to global behavior entailed substantial uncertainty, visual photographic and video evidence of the behavior of the exterior structure were also used to benchmark the projections from the subsystem analyses.

The models were also modified to include a number of nonlinear behavioral modes including:

- Geometric nonlinearity associated with large deflections,
- Nonlinearity in stress-strain behavior as a function of applied loading and thermal effects, as described in Chapter 3 of NIST NCSTAR 1-6C,
- Creep behavior as the time-dependent effect of sustained stress and elevated temperatures on strain as described in Chapter 3 of NIST NCSTAR 1-6C,
- Failure of a connection between elements, resulting in a complete loss of load transfer ability and deformation compatibility.

The converted ANSYS models were validated against the SAP2000 models by comparing gravity load response, natural frequencies, and mode shapes.

Table 2–1. Element types used in the global models.

Name	Element Type	Description	Usage in the Model
BEAM188	3-D linear finite strain beam	BEAM188 is a linear (2-node) or a quadratic beam element in 3-D based on Timoshenko beam theory. Each node has six degrees of freedom or seven degrees of freedom (6+warping). Shear deformation effects are included. This element is supported for plasticity, creep, large deflection. A cross-section can be a built-up section referencing more than one material. Creep strain is calculated by implicit time integration method.	Exterior columns Core columns Core beams Spandrels Hat truss members
BEAM24	3-D thin-walled beam	BEAM24 is a 3-D beam element of arbitrary open or closed cross-section with axial, bending, and St. Venant torsional capabilities. Each node has six degrees of freedom. The element has plastic, creep, large deflection, and shear deflection capabilities. Creep strain is calculated by explicit time integration method.	Exterior columns Core columns
SHELL63	4-node elastic shell	SHELL63 has both bending and membrane capabilities. The element has six degrees of freedom at each node: three translations and three rotations. Large deflection capability is also included.	Floors

Name	Element Type	Description	Usage in the Model
SHELL181	4-node finite strain shell	SHELL181 is a 4-node shell element with six degrees of freedom at each node: three translations and three rotations. Plasticity, creep, and large deflection capabilities are supported. In nonlinear analyses, change in shell thickness is accounted for. SHELL181 may be used for layered applications.	Floors
LINK8	3-D truss	LINK8 is a uniaxial tension-compression element with three degrees of freedom at each node. It has plasticity, creep, and large deflection capabilities.	Vertical springs at the base

Damage modified the geometry and connectivity of and load distribution in the towers. Types of damage included in the global models were aircraft impact damage to the exterior wall that were visible and documented by photos and videos and interior damage resulting from the movement of aircraft impact debris through the interior space of the towers which were obtained from the aircraft impact analyses.

Structural damage caused by the fires, such as disconnection of the floor from the exterior wall, was determined from the structural analysis of the full floor subsystems. Some structural behaviors caused by the fires were not adequately captured by the full floor analysis, such as pull-in forces at the floor/wall connections. The pull-in forces were estimated through additional analyses with exterior wall models that were conducted to estimate the pull-in force required to match the observed inward bowing of the exterior walls.

The models were then analyzed for the effects of gravity and temperature loads. Gravity loads considered included: the dead load of the structure itself; superimposed dead load consisting of the estimated weights of ceilings, mechanical and electrical equipment, thermal insulation, and floor finishes; and live load, taken as 25 percent of design live load specified in the original construction documents. The use of 25 percent of the design live load as service live loads is discussed in NIST NCSTAR 1-2. Wind loads were negligible and were not considered (see NIST NCSTAR 1-6 for the recorded wind data).

Due to the height of the structures, substantial column shortening occurred under the application of dead loads. If these loads were applied to the model while the stiffness of the hat trusses was present, the hat trusses would restrain the downward deflection of the columns and in the process experience higher levels of stress. These stresses did not occur in the real buildings, because the columns experienced most of their dead load-induced shortening before the hat trusses were erected. In order to account for this effect, except for those simulations in which the effect of creep was also considered, the sequence of construction was considered during gravity load application. The loading of the structure was staged so that the stiffness of the hat trusses was not present when dead loads below Floor 106 level were applied. Construction sequence effects were not considered in the global analyses that included creep effects to enhance computational efficiency. The effect of construction sequence is discussed in more detail in Section 4.2.2.

Thermal loading of a structure resulted in several effects:

- restrained axial thermal expansion of members causing local redistribution of loads, e.g., heated columns of WTC towers that attracted more load,
- differential thermal expansion across member depth, resulting in bowing if unrestrained or bending moment if restrained,
- reduction in the stiffness and strength of members, and
- high creep strain when accompanied by high stress.

SGH applied thermal loading in the form of temperature time histories. NIST developed these temperature time histories using gas dynamic and heat transfer models. Each temperature time history corresponded to a unique set of assumptions regarding the extent of impact damage to the structure, glazing, fire separation elements, and insulation. Each temperature time history was defined discretely at 10 min time intervals which were linearly interpolated for times in between.

The behavior of columns in the two structures was significant to the collapse behavior of the towers. Throughout this report reference is made to the behavior of various columns and lines of columns, using the specific column numbering system found in the original PANYNJ structural drawings[1]. In WTC 1, columns in the exterior north wall were assigned a number ranging from 101 at the west end to 159 at the east end. Columns in the exterior east wall were assigned a number ranging from 201 at the north end to 259 at the south end. Columns in the exterior south wall were assigned a number ranging from 301 at east end to 359 at the west end. Columns in the west wall were numbered sequentially from 401 at the south end to 459 at the north end. Columns 100, 200, 300 and 400 were located, respectively, at the northwest, northeast, southeast and southwest building corners. Within the rectangular core of the structure, there were six rows of either seven or eight columns each. Columns of the northern-most row were numbered 501 through 508 with column 501 located at the west end and 508 at the east end. Successive rows of columns, reading from north to south were designated 601-608, 701-708, 801-807, 901-908, and 1001-1008. This numbering scheme is illustrated in Fig. 2–1 (a). The column numbering system used for WTC 2 is similar. However, for WTC 2 Columns 101-159 were located along the west wall, Columns 201-259 along the north wall, 301-359 along the east wall, and Columns 401-459 along the south wall. Column 100 was located at the southwest corner, 200 at the northwest corner, 300 at the northeast corner and 400 at the southeast corner. In the core of WTC 2, Columns 501-508 were located along the extreme west side of the core and Columns 1000-1008 along the extreme east side of the core with the 600, 700, 800, and 900 series columns arranged progressively from west to east. Figure 2–1 (b) illustrates the column numbering system used in WTC 2.

[1] The technical data required to conduct the analyses of the WTC towers reported herein were obtained from drawings that were provided by the Port Authority of New York and New Jersey (PANYNJ) and their contractors.

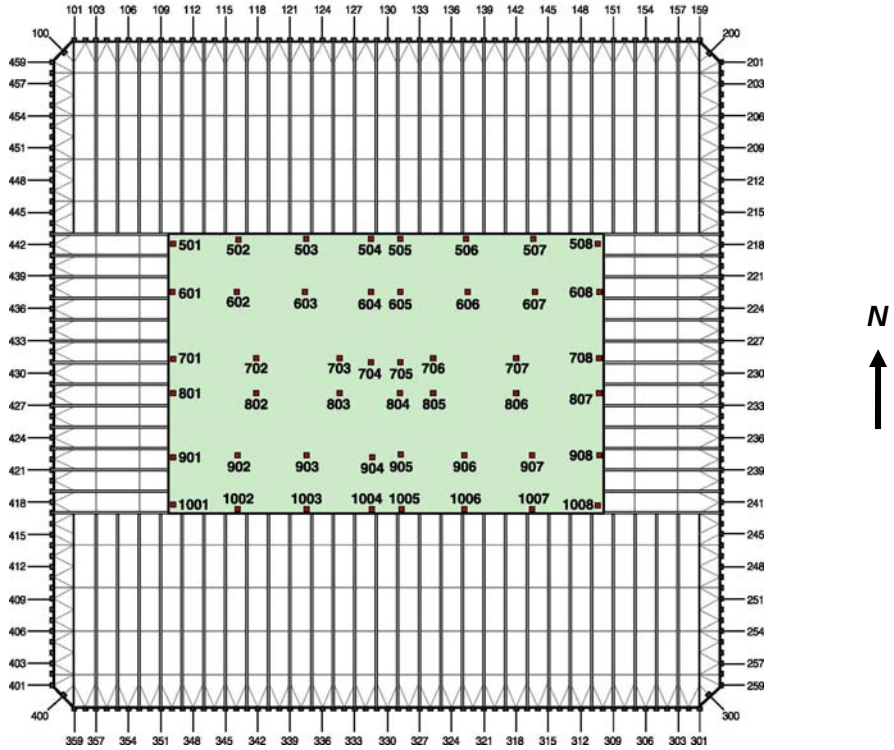

(a) WTC 1

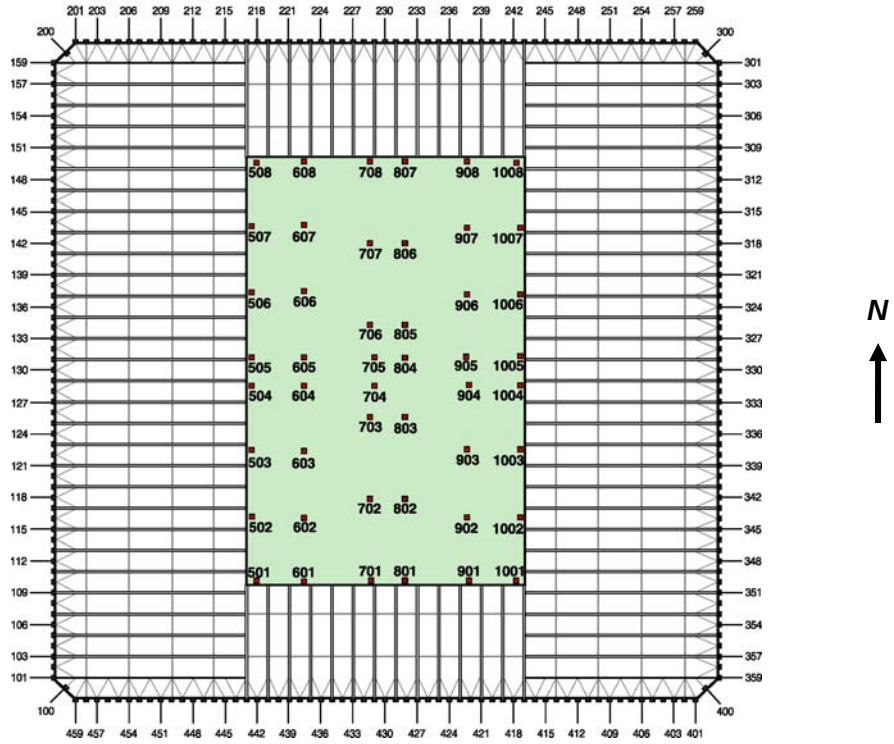

(b) WTC 2

Figure 2–1. Column designations.

2.2 IMPACT DAMAGE

2.2.1 Introduction

The extent of aircraft impact damage to the structural components of the WTC towers has been separately investigated as part of NIST Project 2 and reported in NIST NCSTAR 1-2 and NIST NCSTAR 1-2B. SGH incorporated the results of the studies into the global models of the WTC towers to characterize the aircraft impact damage to exterior columns and spandrels, core columns, beams, and floors. Specifically, those elements identified in the aircraft impact studies as severed or heavily damaged were removed from the global models.

NIST's investigation initially identified two sets of aircraft impact damage for each of the two towers, consisting of a structural damage condition, which was damage to the structure, and a insulation damage condition, which affected the temperature of members. These damage sets represented a case and a more severe case of damage estimates. They were named as Case A and Case B for WTC 1 and Case C and Case D for WTC 2. These initial damage sets were used in early analyses to study the structural response of full floor subsystem models and global models without creep. The results of the full floor subsystem analyses were presented in Section 5.4 of NIST NCSTAR 1-6C and summarized in Appendix A of this report. The results of the global model analyses without creep are discussed in Section 4.1 of this report.

NIST refined the initial damage sets at later stages of the investigation and renamed them as Case A and Case B for WTC 1 and Case C and Case D for WTC 2. These damage sets were used in isolated wall and isolated core models and global models with creep. The results of the isolated wall and core models are discussed in Chapter 3, and the results of the global model analyses with creep are discussed in Section 4.2 of this report.

For each tower, the impact damage on the exterior columns and spandrels was primarily obtained from photographs and video footage that were taken before and during the collapse of the buildings. For this reason, the impact damage on the exterior columns a

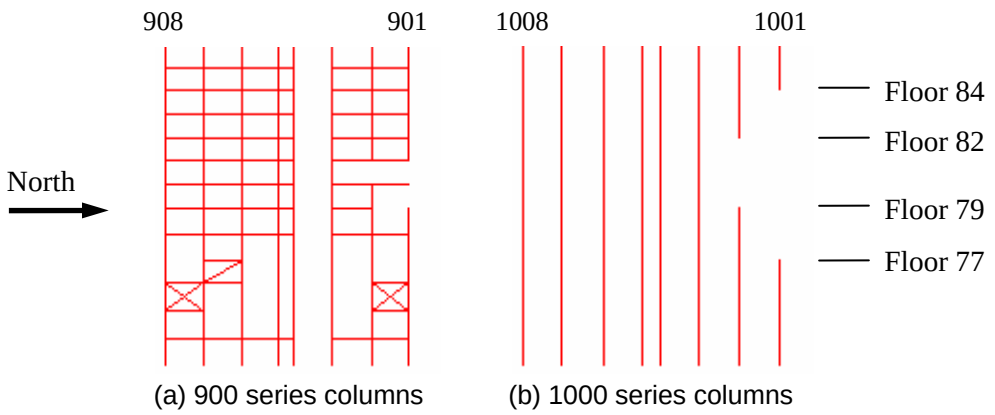

Figure 2–7. Case C_i structural damage condition on the core columns of WTC 2.

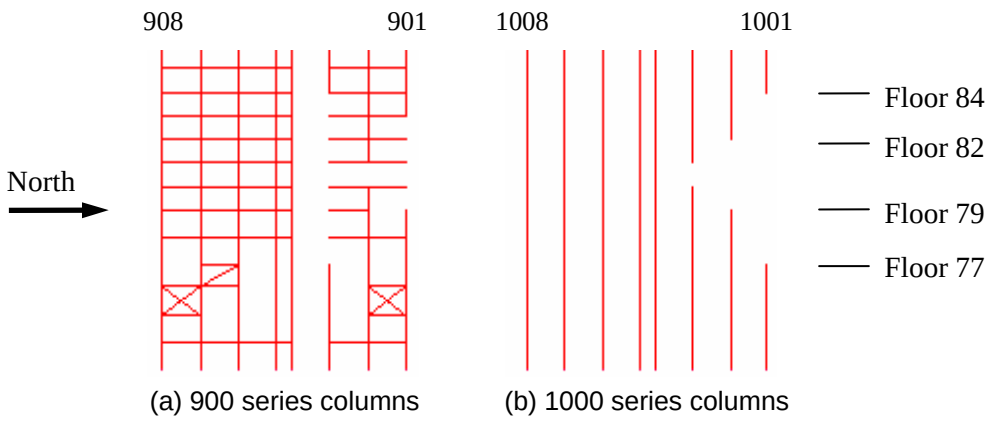

Figure 2–8. Revised Case C_i structural damage condition on the core columns of WTC 2.

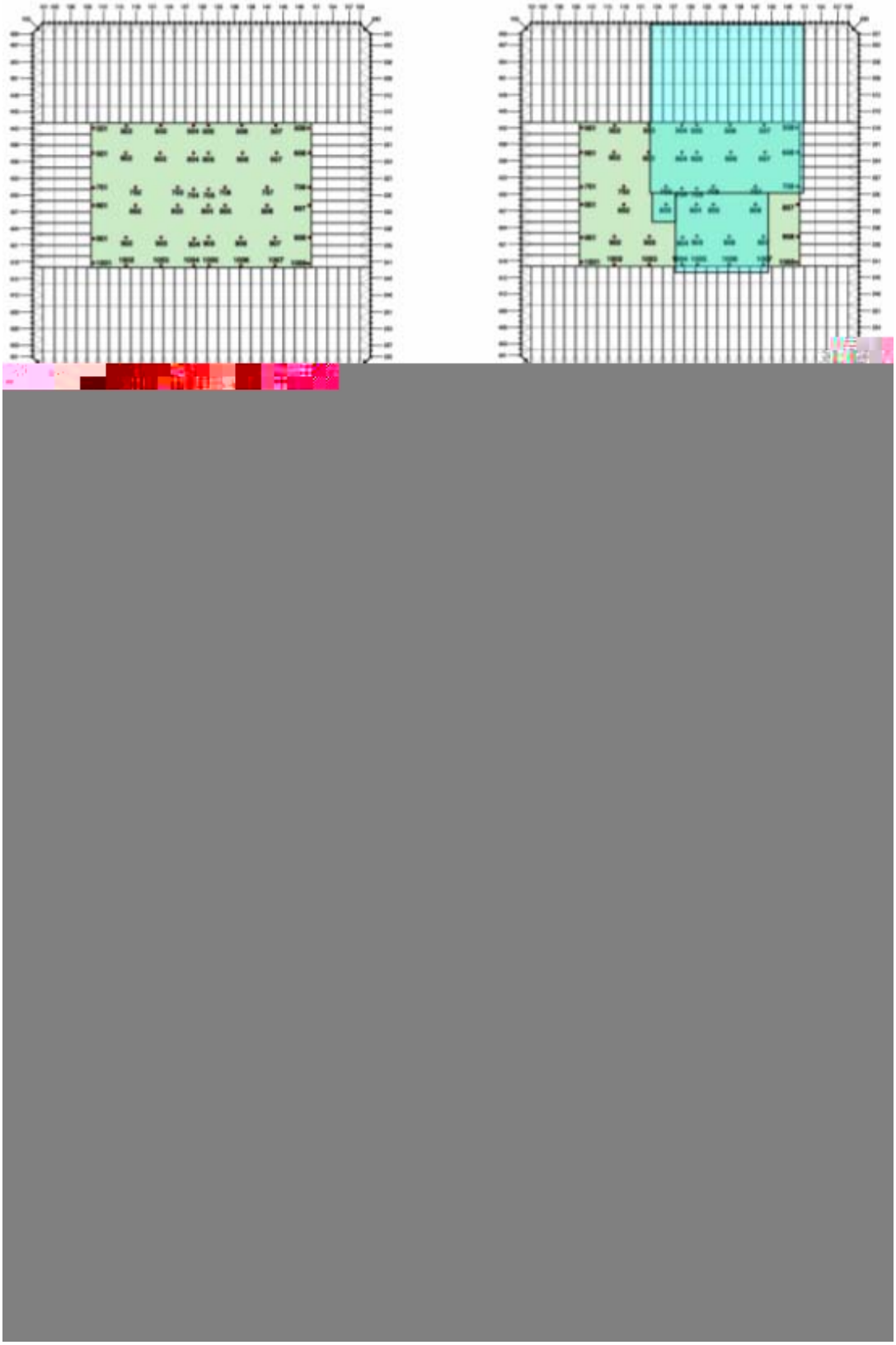

Figure 2–9. Case A_i insulation damage conditions for WTC 1 floor trusses and beams.

Figure 2–11. Case C_i insulation damage conditions for WTC 2 floor trusses and beams.

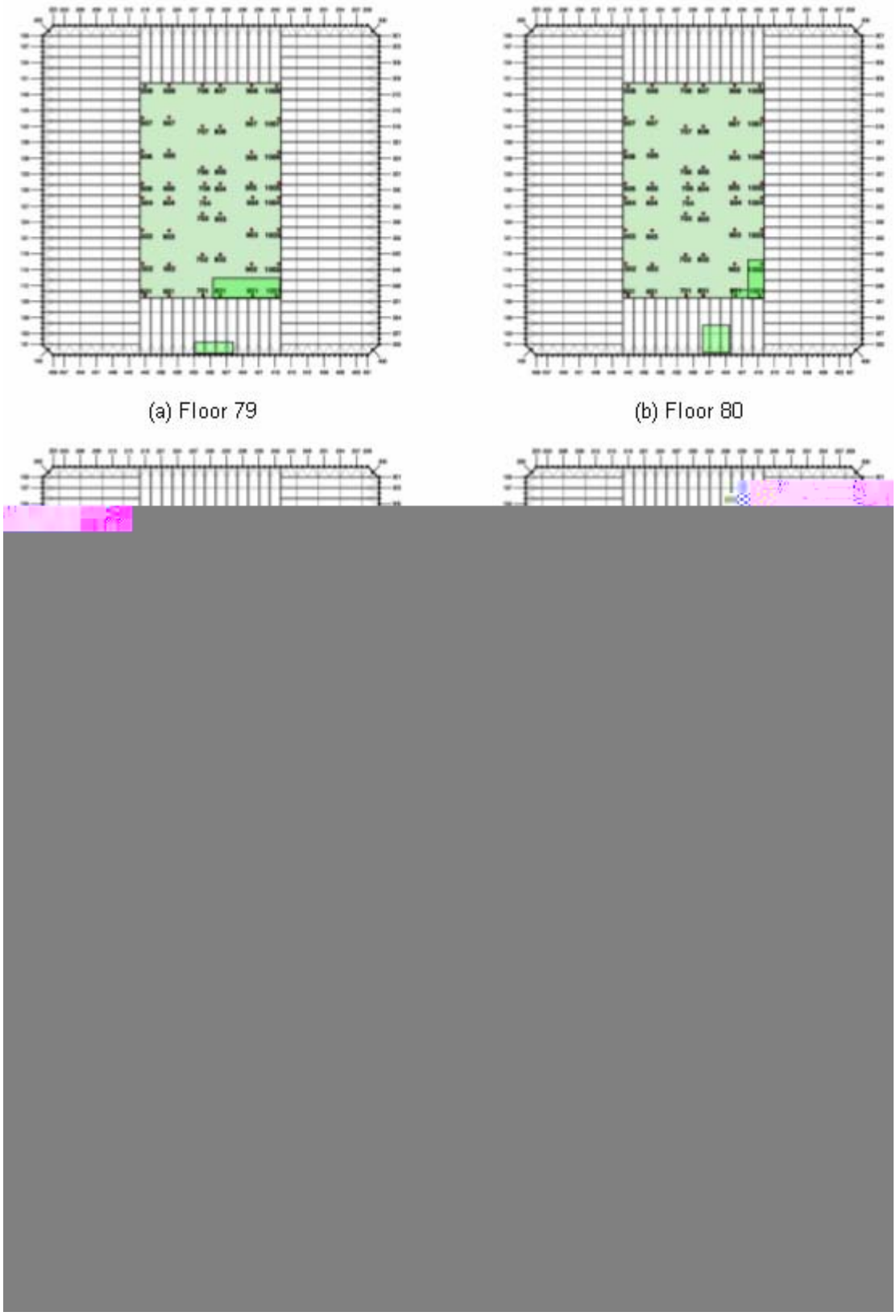

Figure 2–12. Case C_i Structural damage conditions for WTC 2 floors.

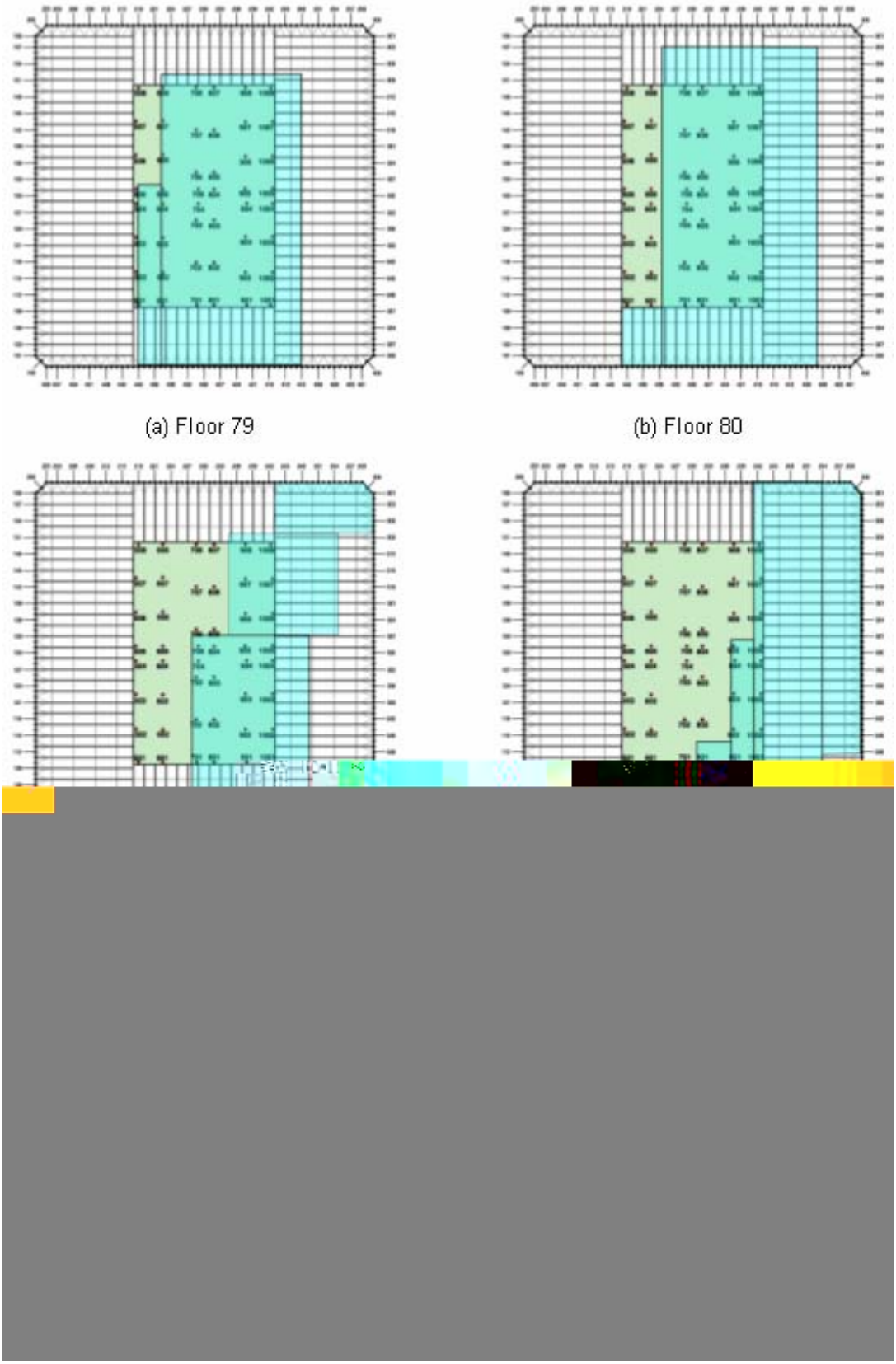

Figure 2–13. Case D_i insulation damage conditions for WTC 2 floor trusses and beams.

Figure 2–14. Case D_i Structural damage conditions for WTC 2 floors.

2.2.3 Final Damage Sets

NIST provided a series of final damage sets for use in the global analyses. Two sets were provided for each of the two buildings, together with temperature time history data sets computed by NIST based on the damage set. The final damage sets for WTC 1 were designated Case A and Case B, respectively, representing different scenarios of aircraft impact damage to the structure and thermal insulation. The final damage sets for WTC 2 were designated Case C and Case D. The exterior wall damage contained in the final damage sets are identical to those in the contained in the initial damage sets, described in the previous section and illustrated in Figs. 2–2 and 2–3. However, the projected damage to floor and core elements differed from the initial damage sets. The final damage sets were used in SGH analyses of the isolated wall models, the isolated core models, and the global analyses with creep.

The severed columns in the core area of WTC 1 for Case A and Case B and WTC 2 for Case C and Case D are shown in Figs. 2–15 through 2–18. For Case B and Case D structural damage condition, heavily damaged core columns were also considered as severed and removed from the analysis. Columns removed from the global models are shown as missing vertical lines in these figures. For WTC 2, core column 902 was assigned a moderate damage state after aircraft impact at Floor 79 and Floor 80 by NIST. The preliminary analyses showed that this column buckled after aircraft impact and caused numerical problems in the temperature time history analyses. Therefore, in the Case D damage set, this column was also treated as heavily damaged and removed from the model. The core column series that are not shown in Figs. 2–15 through 2–18 did not include severed columns for all the cases or heavily damaged columns for Case B of WTC 1 and Case D of WTC 2.

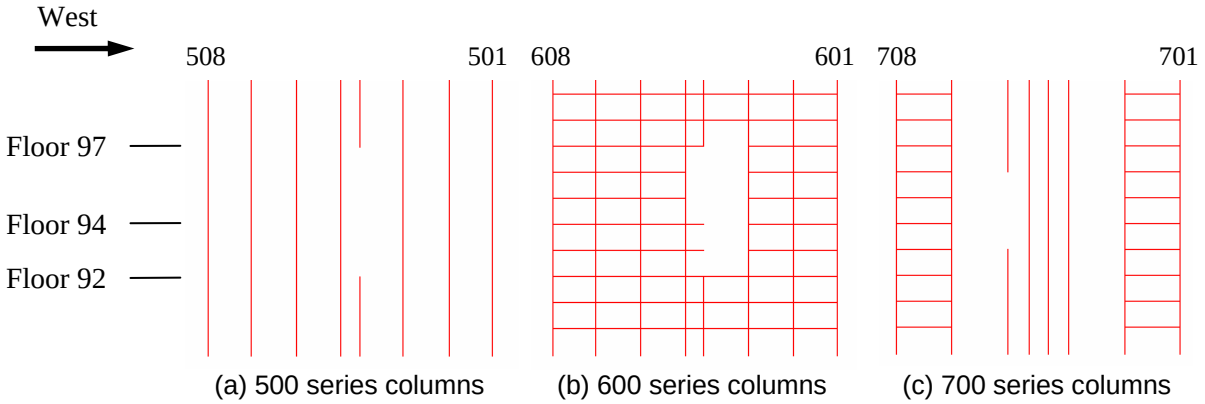

Figure 2–15. Case A structural damage condition on the core columns of WTC 1.

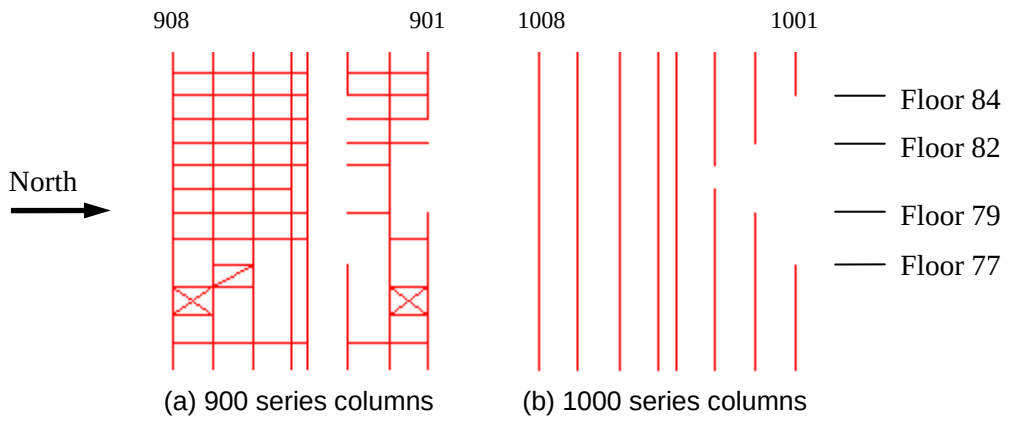

Figure 2–16. Case C structural damage condition on the core columns of WTC 2.

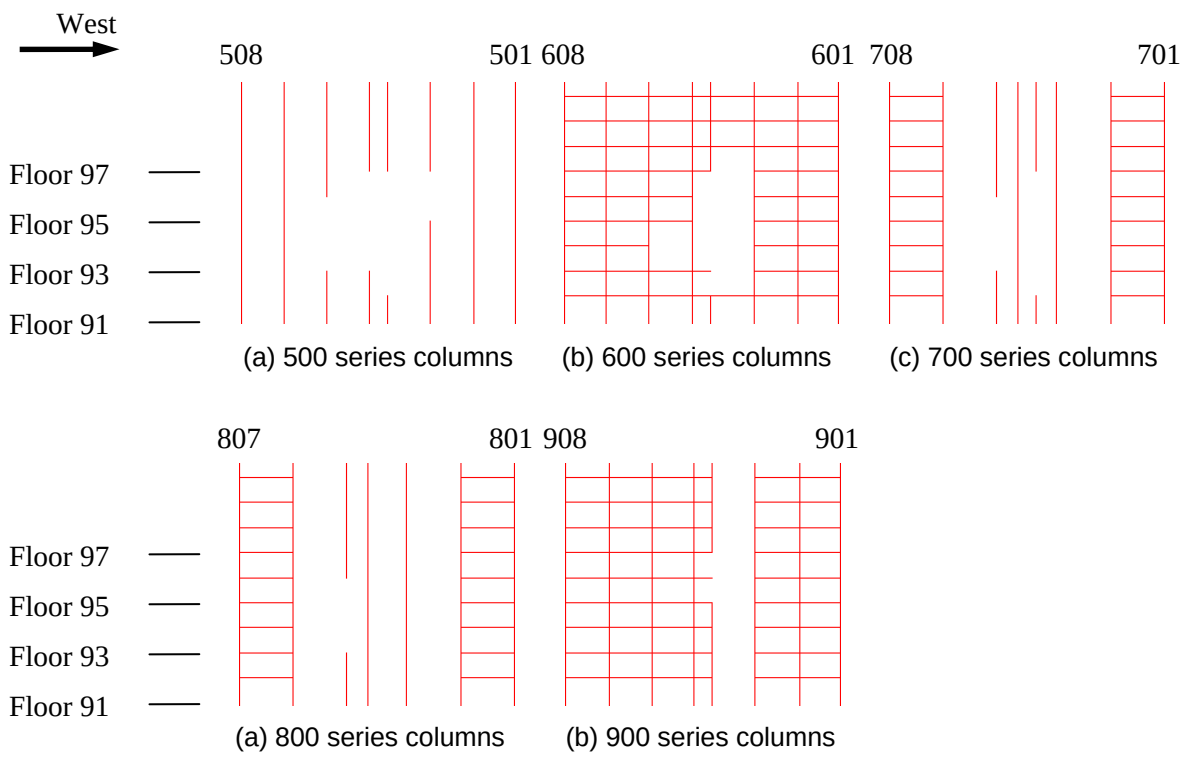

Figure 2–17 Case B structural damage condition on the core columns of WTC 1 (including heavily damaged columns).

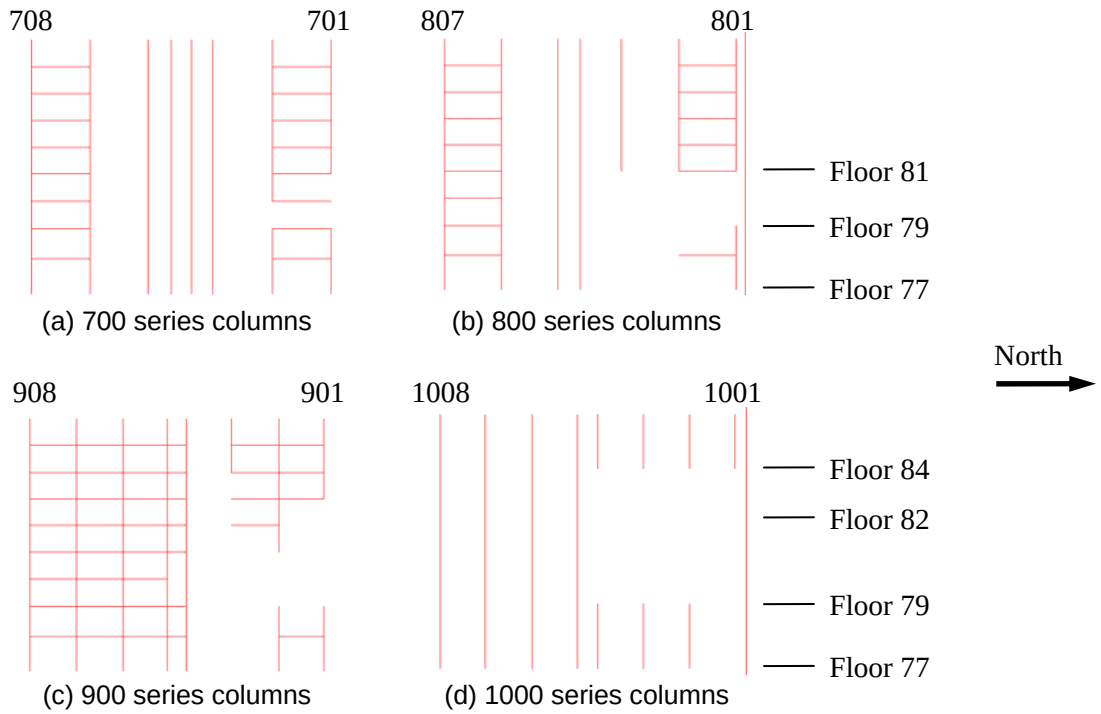

Figure 2–18. Case D structural damage condition on the core columns of WTC 2 (including heavily damaged columns).

The floor insulation and structural damage conditions are shown in Figs. 2–19 and 2–20 for Case A, in Figs. 2–23 and 2–24 for Case B, in Figs. 2–21 and 2–22 for Case C, and in Figs. 2–25 and 2–26 for Case D.

The shell elements of the floors and beam elements of core beams were removed from the global models at appropriate locations to replicate the areas of structural floor damage indicated in these figures. For the regions where the floor slab was coarsely meshed, the elements were removed in such a way as to capture force discontinuities resulting from the structural damage in that region. This sometimes resulted somewhat larger floor openings than indicated in Figs. 2–20, 2–22, 2–24, and 2–26. However, as discussed in Chapter 4, the dead and live loads of the floor system were applied as concentrated loads to the connecting columns; this minimized the effect of slightly larger floor openings.

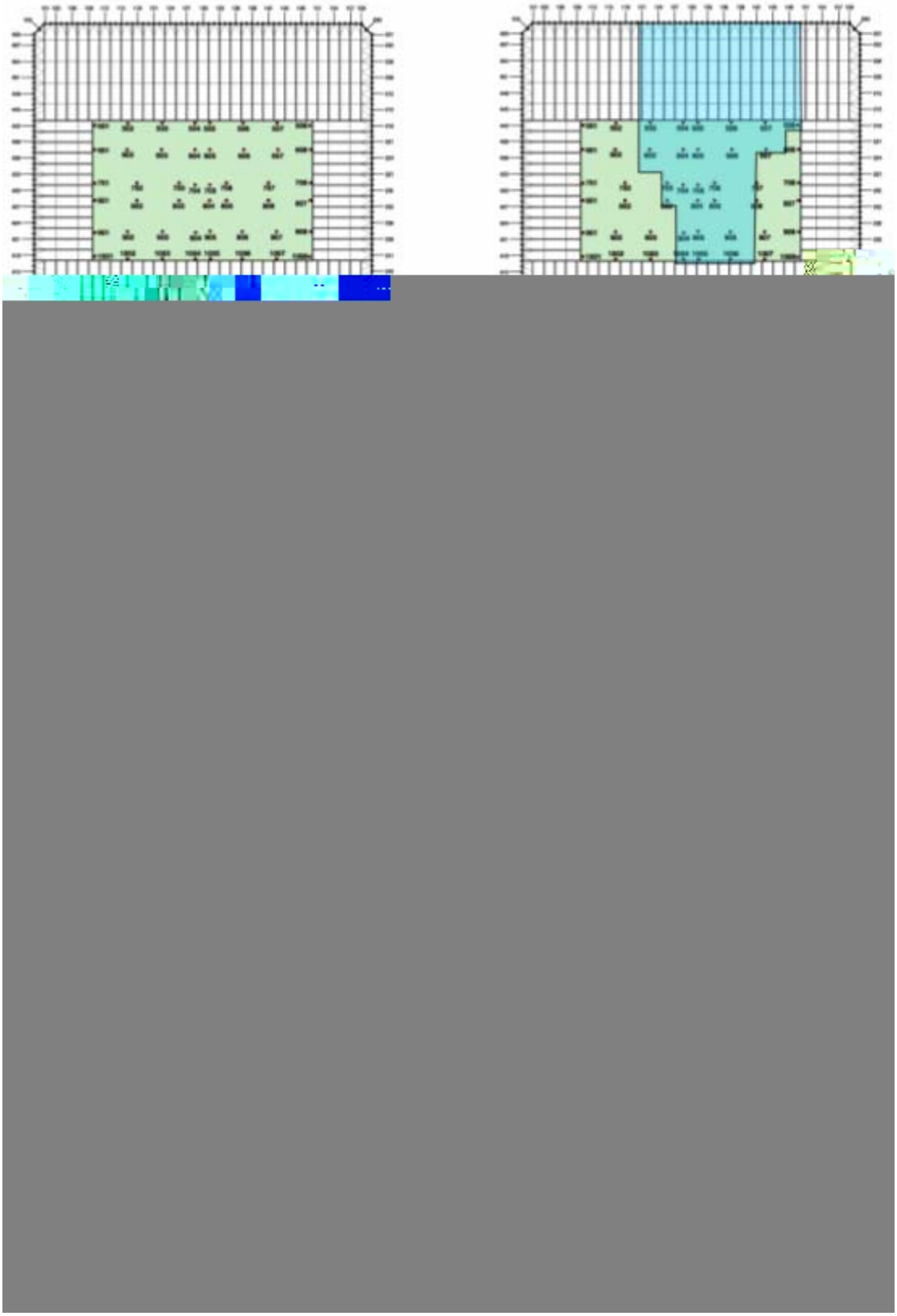

Figure 2–19. Case A insulation damage condition for WTC 1 floor trusses and beams.

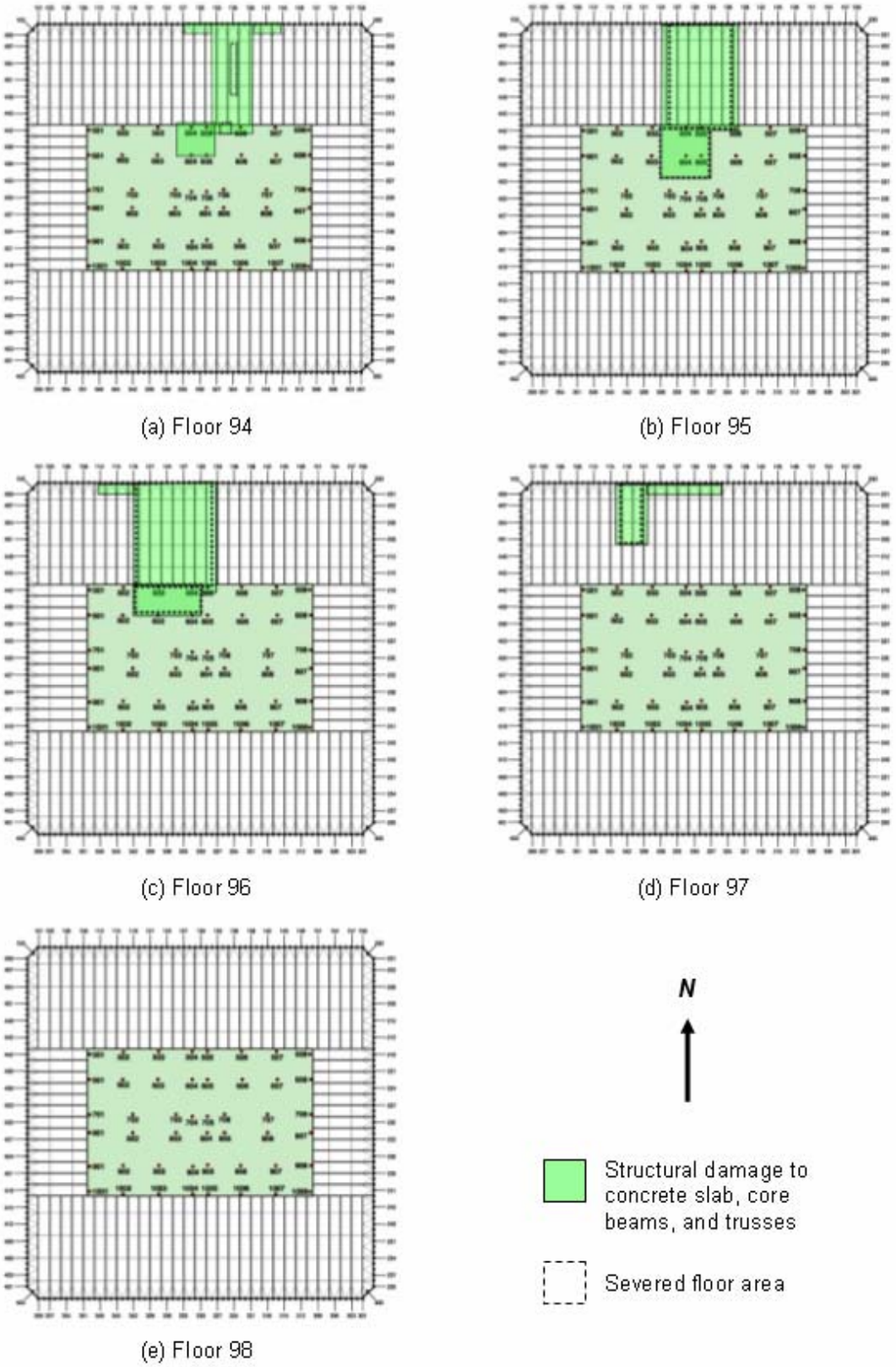

Figure 2–20. Case A structural damage condition for WTC 1 floors.

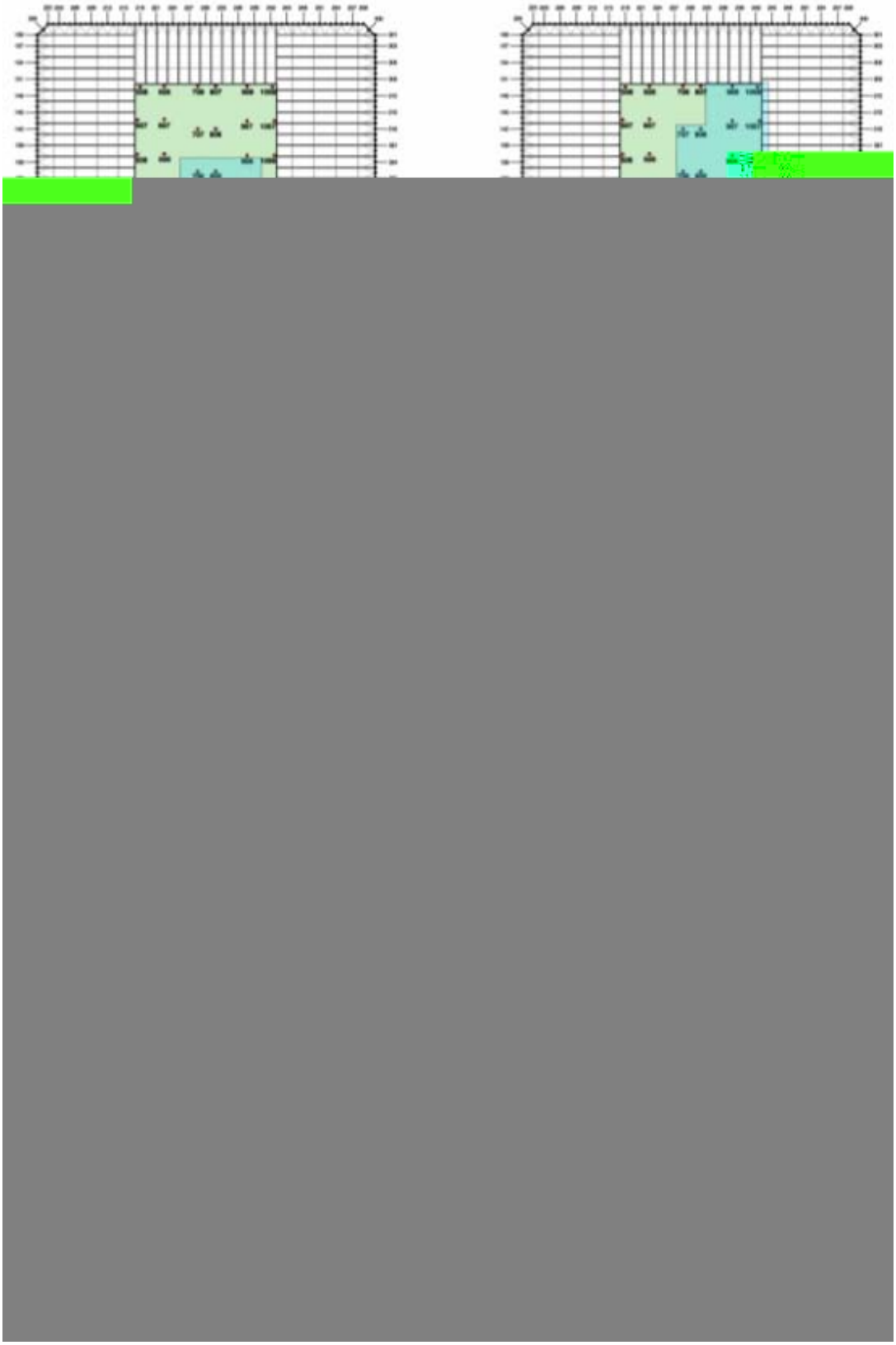

Figure 2–21. Case C insulation damage condition for WTC 2 floor trusses and beams.

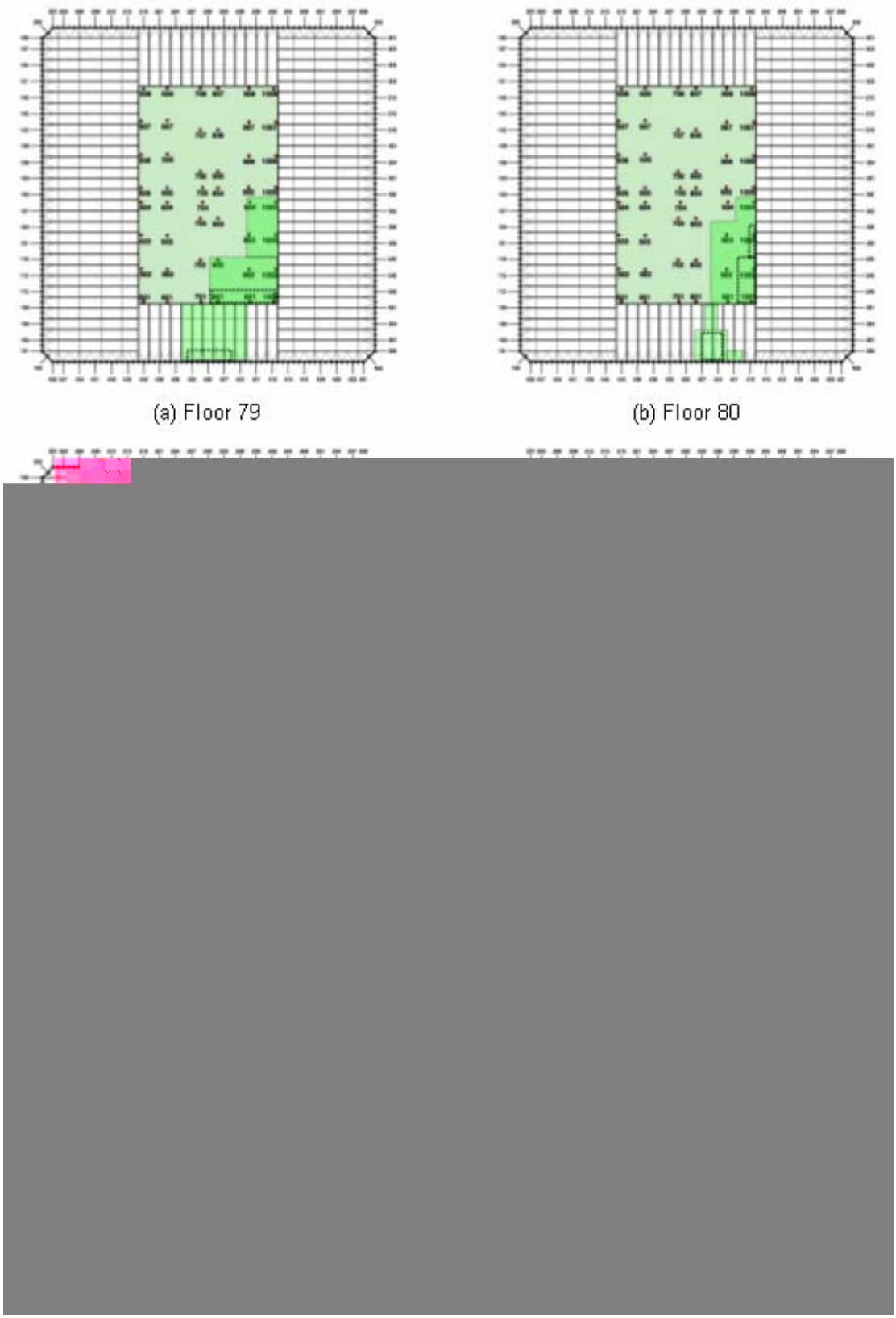

Figure 2–22. Case C structural damage condition for WTC 2 floors.

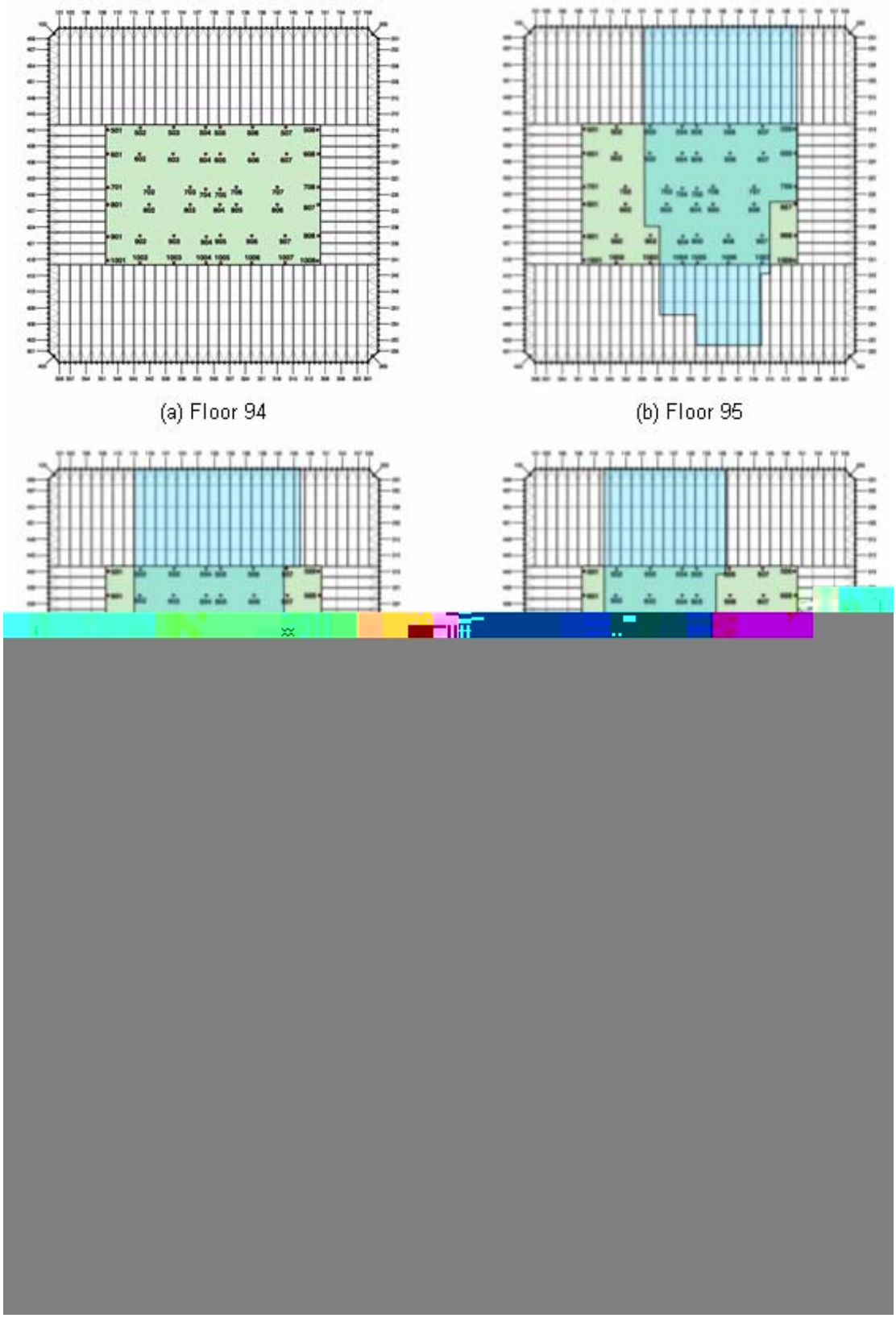

Figure 2–23. Case B insulation damage conditions for WTC 1 floor trusses and beams.

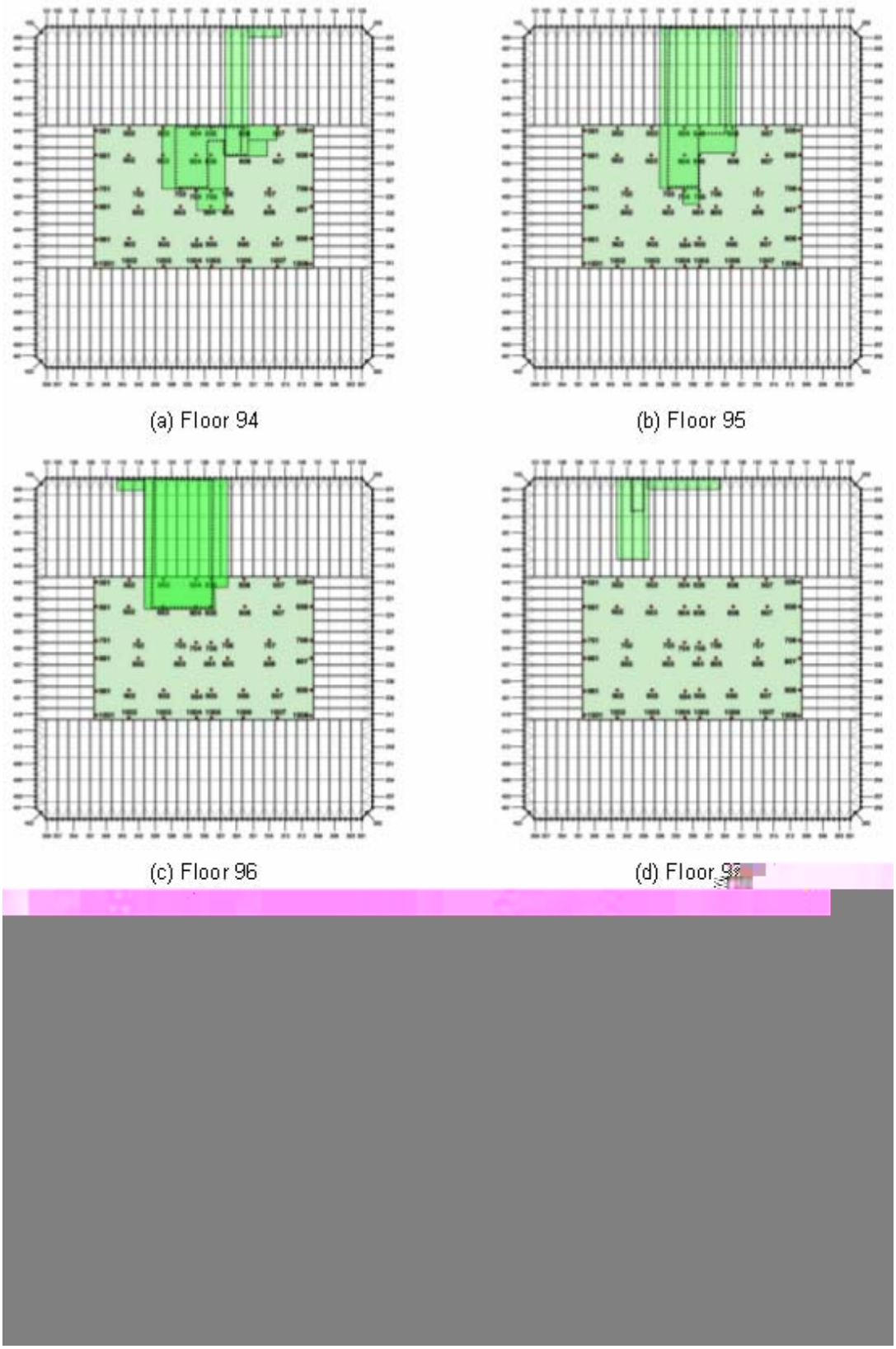

Figure 2–24. Case B structural damage conditions for WTC 1 floors.

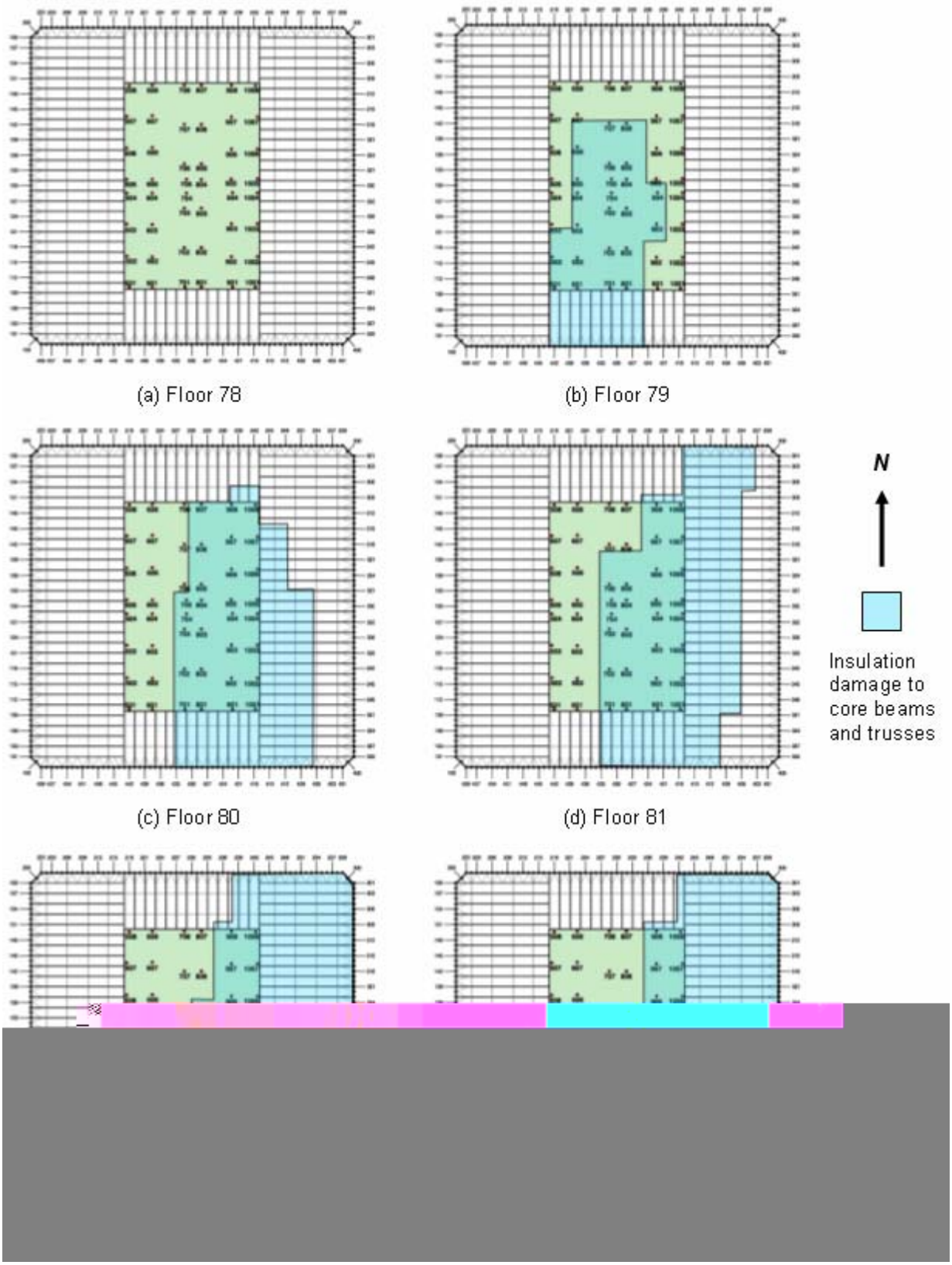

Figure 2–25. Case D insulation damage conditions for WTC 2 floor trusses and beams.

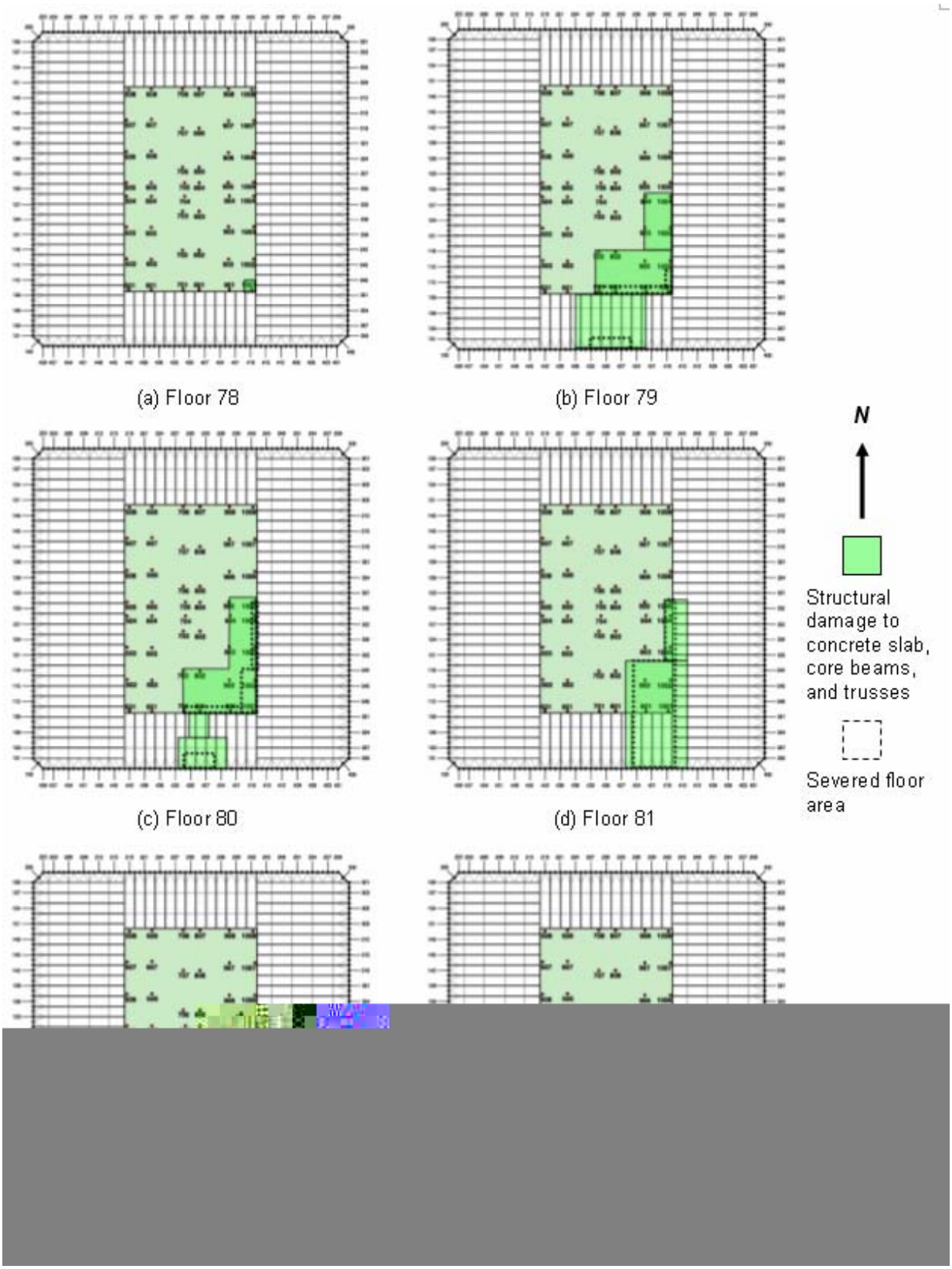

Figure 2–26. Case D structural damage conditions for WTC 2 floors.

2.3 TEMPERATURE EFFECTS

The fires resulting from the combustion of the jet fuel, followed by the combustion of building contents and the debris from the aircraft produced high-temperature gases that in turn increased the temperature of the exposed structural members. Fire is dynamic in nature. As fire consumes combustible materials in the area of ignition, the high temperature gases produced by the fire spread to other areas of the building, heating the structure and igniting combustible contents in these other areas. Even as the fire spreads, it consumes the fuel in areas already involved, extinguishing itself and allowing the structure in those areas to cool. As a result of this behavior, the temperature of the exposed structural members in the two towers varied with time, from the instant of aircraft impact until the final collapse. NIST performed a series of computational fluid dynamics analyses to predict the distribution with time of gas temperatures in various locations in the structures and also to produce temperature time histories for the structural members in the affected areas of the buildings. These analyses are reported in NIST NCSTAR 1-5.

In the analyses performed by NIST, a key factor in the calculation of the temperature distribution for the structural members was the extent of insulation that was in place after the impact. NIST assumed that any damage to the insulation was by direct abrasion from flying debris created as the aircraft impacted, disintegrated, and transited across the building. A series of aircraft impact analyses were performed to predict the pattern of debris flow as well as the probable damage to structural members inside the building. In these analyses, the trajectories of the debris flow and, therefore, of the extent and distribution of insulation damage predicted was dependent on the estimted values for aircraft speed and direction of travel, point of impact on the structure, and impact trajectory. The several damage sets (Case A_i, Case B_i, Case C_i, etc.) resulted from variation in the values of these parameters and, therefore, the estimated damage and temperature time histories. One temperature time history data set was derived for each set of structural and insulation damage[2]. As discussed in Section 2.2, Case C_i and revised Case C_i have the same temperature time histories for structural components.

The high temperature gases produced by the fires primarily heated the floor trusses and the bottom face of the slabs through convection and the top face of the slabs through radiation. The temperatures predicted in the structural members depended on the extent of insulation assumed to be in place and on the material properties and geometry of the structural members. In the actual buildings, the temperature in the structural members varied through the length and cross section and changed with time. The temperature at every node in the global models was calculated by interpolation of temperatures from the thermal analysis, which had a much finer mesh than the global structural models. A linear temperature gradient was assumed across column cross sections and along the length of members. To reduce data handling, the continuous temperature time histories were replaced with piecewise linear time-histories without significant loss of accuracy. Consequently, snapshots of the spatial distribution of temperature were taken at 10 min intervals, initiating at the time of impact and extending through the time of collapse (or approximately the time of collapse) for each of the buildings (see NIST NCSTAR 1-5G for more discussion of the 10 min intervals).

[2] Temperature cases were formerly called by different names. Case A_i and Case C_i conditions were called “baseline case”, and Case B_i and Case D_i conditions were called “maximum damage case”. Case A and Case C conditions were called “best estimate case” or “realistic case”, and Case B and Case D conditions were called “upper bound case” or “severe case”. These former temperature case names may appear on graphics produced in ANSYS.

Structural response of a building to fire-induced temperature is a complex phenomenon involving the following phenomena:

- Axial thermal expansion of members as they heat and thermal contraction of members as they cool; if these members are restrained, this expansion and contraction can induce a change in the stress distribution in the structure.
- Differential thermal expansion of members across their cross section if they are heated unevenly, resulting in bowing of the members along their length; if members are under significant compression, this bowing can lead to onset of buckling.
- Significant reduction in modulus of elasticity and strength of steel and concrete as temperature increases beyond 500 ˚C (NIST NCSTAR 1-6C).
- Creep in steel at high stresses and high temperatures.

Creep is a time-dependent phenomenon and, in the analyses that SGH performed, was found to have resulted in shortening of core columns with high temperatures and high stresses.

In the global models, NIST-provided temperatures were applied to structural members between Floor 93 and Floor 99 in WTC 1 and between Floor 79 and Floor 83 in WTC 2. In each case, the temperatures were applied to exterior columns, spandrels, core columns and beams, and floor slabs.

In general, temperatures were assigned to the node locations in the global models. The distribution of temperature was assumed to be uniform throughout the member cross section except in the case of the exterior columns where temperature gradients within the cross section were considered in the direction normal to the exterior walls.

All temperatures reported in this study are in units of ˚C.

2.4 THERMAL BEHAVIOR OF FLOORS

It was not practically possible to develop global models that could capture all structural behaviors or failure modes found in the study of components and subsystems and to perform the global analysis within a reasonable time period. To enhance computational efficiency, selected modeling details were omitted in the global models, and structural behaviors or failure modes that could not be captured by the global models were introduced in the global analysis as fire-induced damage at appropriate points in time.

Key failure modes of the floor subsystem were identified in NIST NCSTAR 1-6C for components and subsystems subjected to temperature time histories. These analyses indicated that as floor system temperature increased, web diagonals in the floor trusses buckled, allowing the floors to sag. In extreme cases, the analyses showed loss of vertical support for individual trusses, as either the truss seats supporting the trusses lost strength and failed under the influence of vertical gravity loads or sagging of the trusses caused them to walk off the supporting seats.

This floor truss behavior was incorporated into the finite element models of entire individual floors that are referred to as full floor models. The models included representation of the floor slabs, trusses, beams, and columns that extended full height to the floors immediately above and below the level under

consideration. When an entire full floor model was subjected to the temperature time histories, the analyses showed that the floors sagged in areas where insulation was damaged and that individual floor trusses lost their vertical support at the exterior wall in some areas. However, it was found that these full floor models could not accurately capture the pull-in forces that the sagging floors were expected to apply to the exterior walls. Discussions on these pull-in forces can be found in Section 2.5.2.

Since detailed modeling of the floors was not included in the global analysis models, important floor behavioral modes could not be captured in these global analyses. Key floor behavioral modes include floor sagging that imposes pull-in forces on the exterior wall and loss of support of the trusses at the exterior wall resulting in local disconnection of the floor from the exterior wall. To account for these effects, pull-in forces on the exterior wall and disconnections of the floors from the wall were introduced in the global analyses at appropriate times as fire-induced damage. In the process of developing the fire-induced damage, the behaviors predicted by the full floor model analyses as well as the damage observed by NIST in their review of photographic and video evidence were both considered.

2.5 FIRE-INDUCED DAMAGE

Disconnections of the floors from the exterior walls caused by fire-induced connection failure between the floor and the exterior wall and pull-in forces on the exterior wall exerted by sagging floors were included in the global analyses as fire-induced damage. The locations of the floor/wall disconnections and the locations and magnitudes of the pull-in forces were determined based on a combination of the results from the full floor model analyses, the results from the isolated wall model analyses, and the actual observations in photographic and video evidence of WTC 1 and WTC 2.

2.5.1 Floor/Wall Disconnections

In areas where the connection of the floor to the exterior wall failed and the floor was locally disconnected from the exterior wall, the floor could no longer provide out-of-plane support for the wall at the locations of floor/wall disconnections, which resulted in a reduction of the buckling capacity of the exterior columns. In order to simulate this behavior in the global analyses, the connection between floor and wall elements was removed. When either one of the following conditions was encountered in the full floor analyses, the floor was disconnected from the exterior wall in the global model as it lost vertical support:

- Gusset plate failure + seat failure due to vertical shear
- Gusset plate failure + bolt shear-off + truss walk off the truss seat

Most disconnections obtained in the full floor models were due to the first of these conditions.

NIST performed extensive review of the available photographic and video evidence of the condition of the two towers prior to their collapse. Some of the photographs NIST reviewed were taken immediately after the aircraft impacts, while others were taken at various times leading up to the collapse. From this visual evidence, NIST constructed a time-variant map of the locations of observed floor/wall disconnections. During the global analyses, floor/wall disconnections were introduced at those locations and those times indicated in NIST's damage maps, if these disconnections had not previously been

indicated by the full-floor analyses. Although FEA results and the observations were generally in good agreement, the visual evidence suggested a somewhat greater extent of floor/wall disconnections.

2.5.2 Pull-in Forces

When the floor sagged while it was still connected to the exterior wall, the floor developed tensile forces that tended to pull the exterior wall inward. There were four types of structural elements that connected the floor system to the exterior wall system: 1) diagonal strap anchors that extended from the top chords of trusses to the spandrel (they are referred to as strap anchors in this report), 2) headed studs on the spandrels that extended into the floor slab edges, 3) gusset plates that were horizontal field-welded plates that joined the top chords of the trusses to the spandrels, and 4) seat bolts that fastened bearing angles to the seats that were attached to the spandrels.

Pull-in force was applied to the exterior column in the global analyses, where either one of the following conditions was encountered in the full floor analyses:

- Gusset plate failure + bolt shear-off + significant deflection (>25 in.) of the floor slab in that area (floor remains vertically connected)

- Tensile force between the exterior wall and the floor system

However, locations and magnitudes of pull-in forces were not accurately simulated by the full floor models for the following reasons:

- The full floor models did not and could not have an accurate set of boundary conditions on the columns. Columns extended from one floor below to one floor above, and the top and bottom of exterior columns were restrained in the direction normal to the exterior wall. These boundary conditions could not accurately portray the thermally-induced movements of floors above and below the floor being analyzed and could not accurately capture the stiffness of columns in the exterior walls. Photographs of the towers taken before collapse indicated that the exterior walls bowed inward over a height of several floors. Bowing of exterior columns as observed could not be captured in the floor model because the boundary condition of a full floor model could not be formulated to represent the observed bowing of the exterior wall over several floors.

- In the actual buildings, the strap anchors and studs must have been capable of transmitting a significant amount of force between the floor system and exterior wall. However, the full floor analysis with the strap anchors and studs resulted in sequential failure of these components and an extremely slow convergence in the analyses. Because these components were found to fail at early stages of fire, these elements were then removed from all the full floor models to obtain solution within a reasonable period of time. Therefore, in these analyses, the only structural elements in the full floor model that could transfer horizontal interface forces between the floor system and the exterior walls were the gusset plates and seat bolts. This caused premature failure of the gusset plates and seat bolts in the analyses, which resulted in horizontal floor/wall disconnections. In addition, friction between bearing angles and seats was not modeled in the full floor analyses. Therefore, the full-floor model did not show significant tension at the floor/exterior wall interface. In the real structures,

tension forces could develop between the floor system and walls following failure of the gusset plates and seat bolts through the mechanism of friction between the truss seats and bearing angles and through the strap anchors that had not failed.

- There is considerable uncertainty as to what the actual capacity of the strap anchor system was to transfer pull-in forces from the floors to the walls. Assuming that the strap anchors were installed as shown on the PANYNJ drawings, with only the minimum length and size of welds specified actually installed, the tensile capacity of the strap anchor system was controlled by the strength of weld at the strap anchors to the truss the top chords. Typically, 5/16 in., 4 in long fillet welds were specified for this joint. For a pair of floor trusses, joined to the wall by a pair of diagonal strap anchors, this translates into a computed tensile capacity of 68 kip at room temperature and 6.6 kip at 800 ˚C. In full floor model analyses that incorporated the strap anchors, these capacities were used. However, if longer welds were provided, say in excess of 6 in., or somewhat larger fillets were actually placed, the ultimate tensile strength of the strap anchor (1-1/2 in. x 5/8 in. flat plate) could have controlled the capacity of this system. In such a case, the strap anchors for a pair of floor trusses could develop a 101 kip tension force at room temperature and a 9.8 kip tension force at 800 ˚C.
- Assuming a coefficient of friction of 0.33 and vertical reaction at an exterior seat of 13 kip, the friction force can be as much as 4.3 kip for a pair of trusses. The capacity of the two 5/8 in.-diameter seat bolts present in each pair of trusses in shear is 44 kip at room temperature and 4.0 kip at 800 ˚C. Therefore, at elevated temperature, the combined action of friction and bolts could develop on the order of an 8 kip tension force at the exterior seat.

- Creep at high temperature was found to significantly increase the sag of a floor system. A thermal response analysis of a simplified truss model removed from the full floor model showed a significant increase in vertical deflection when creep was considered, as shown in Fig. 2–27. However, full floor models were made with BEAM188/189 element types and were not run with creep due to inherent convergence problems of BEAM188/189 when used under thermal loadings with materials having temperature-dependent creep property.

- In the full floor models, crushing or cracking of the concrete slab was neglected. Extreme temperatures can crack and spall concrete, further reducing the floor stiffness, and increasing both the floor sag and the floor/wall pull-in forces.

- NIST may have underestimated the amount of thermal insulation that was damaged by the aircraft impacts. The estimates developed by NIST were limited to the insulation on sections of framing that were exposed to direct abrasion by the debris field, predicted in the impact analyses. Potential loss of insulation due to impact shock and vibration effects was not included. More severe insulation damage would have resulted in higher temperatures of the trusses than those used in the full floor analyses. This in turn would result in larger areas in which the floors would have sagged.

Figure 2–27. Comparison of vertical displacement of a simplified truss model at Column 333 extracted from the full floor model of Floor 96 of WTC 1 for Case B_i temperature condition at 40 min with and without creep.

Given these uncertainties and inaccuracies in the evaluation of the likely magnitude and location of pull-in forces on the exterior wall, in the global analyses, pull-in forces were applied in some locations where the full floor analyses did not predict the development of such behavior. The magnitude and location of pull-in forces were selected by trial and error to produce a computed bowing of the exterior walls that matched that observed in the photographic and video evidence, as discussed in Chapter 3.

In the actual buildings, floor attachment to the exterior wall occurred continuously along the length of the wall. Headed studs were spaced uniformly along the length of the wall. Pairs of trusses, with truss seats and gusset plates were present at alternate column locations, and diagonal strap anchors connected to the columns between those supporting trusses. Therefore, pull-in forces were applied to columns attached to trusses as well as those attached to strap anchors.

2.5.3 Floor/Wall Disconnections and Pull-in Forces Included in the Global Model

In the global models, nodal couplings tied the exterior columns to the floors. The nodal couplings were removed at locations of floor/wall disconnections. If disconnections were projected to occur or were observed in visual evidence at a time intermediate to the 10 min intervals used in the analyses, for example, between 10 min and 20 min, they were imposed starting at the earlier time point, in this example, at 10 min. Once a portion of a floor was disconnected from the exterior wall, it remained disconnected for the remainder of the analysis. Similarly, pull-in forces were also applied to the global models at the beginning of the 10 min time intervals in which they were predicted to occur or were observed, and they were maintained at a constant level for the 10 min time interval.

Outward expansion of the floors was not included in the global models. Floor analyses showed that the floors initially pushed exterior column outward by a few inches. However, significant outward bowing was not observed and several inches of outward deflection of exterior columns would not affect the global stability of the towers.

WTC 1

Figures 2–28 to 2–37 show the locations of floor/wall disconnections and pull-in forces imposed on the WTC 1 global model for Case B conditions. Each figure covers a 10 min time interval, the first initiating at 0 min, when the initial impact occurred, and the last initiating at 90 min. Until 80 min, the locations of floor/wall disconnections and pull-in forces were determined solely on the basis of full floor model analyses. After 80 min, the observations from the photographic and video evidence were also considered in determining these events to capture floor/wall disconnections and pull-in locations that were not evident in the full floor analyses. Section 3.2.1 discusses the process used to incorporate the actual observations.

As is discussed in Chapter 5, inward bowing of the exterior south wall of WTC 1 was actually observed at 10:23 a.m., about 97 min after the aircraft impact (NIST NCSTAR 1-6), while inward bowing of the south wall was not observed in photos or videos at 9:55 a.m. (about 69 min after the aircraft impact). The observed inward bowing extended from Floors 95 to 99 between Columns 308 to 326 (possibly to 340), and the maximum bowing estimated by NIST from photographs was about 55 in. at Floor 97. Subsystem analyses of the full floors and the exterior walls suggested that this observed bowing of the south wall was caused by sagging of the floors. As the floors sagged, they imposed tension force on the exterior wall, and the exterior wall was pulled in. However, sagging of floors in such a wide range over five floors was not predicted by the full floor model analyses. Possible reasons for floor sagging in areas not predicted by the full floor analyses include loss of insulation outside of the areas considered by NIST when formulating the temperature time histories, the additional structural softening caused by concrete cracking and spalling, and debris weight from different sources including the aircraft, accumulation of debris from the impact, and partial floor collapse, none of which were modeled in the full floor analyses. To match the observations, the south wall was assumed to be pulled in by the floors between Floor 95 and Floor 99 across the entire width of the wall except at locations of floor/wall disconnections, starting at 80 min. The magnitude of the pull-in force was determined, by trial and error, by matching the observed bowing magnitude as discussed in Section 3.2.1. The pull-in forces were selected as 4 or 5 kip per column. Results from the analysis with 5 kip pull-in forces are presented in Chapter 4.

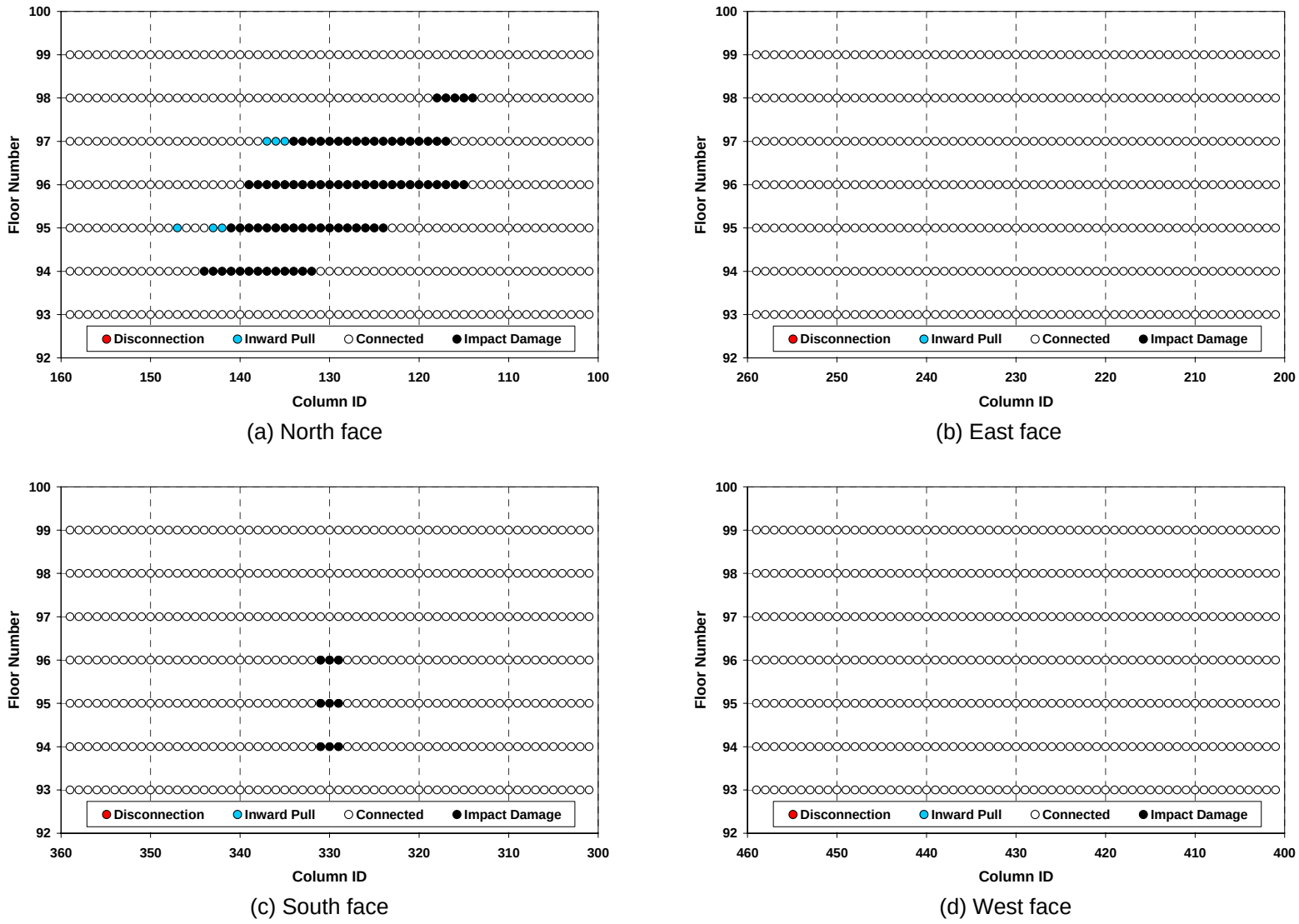

Figure 2–28. Locations of floor/wall disconnections and pull-in forces for the global analysis of WTC 1 between 0 min and 10 min for Case B conditions.

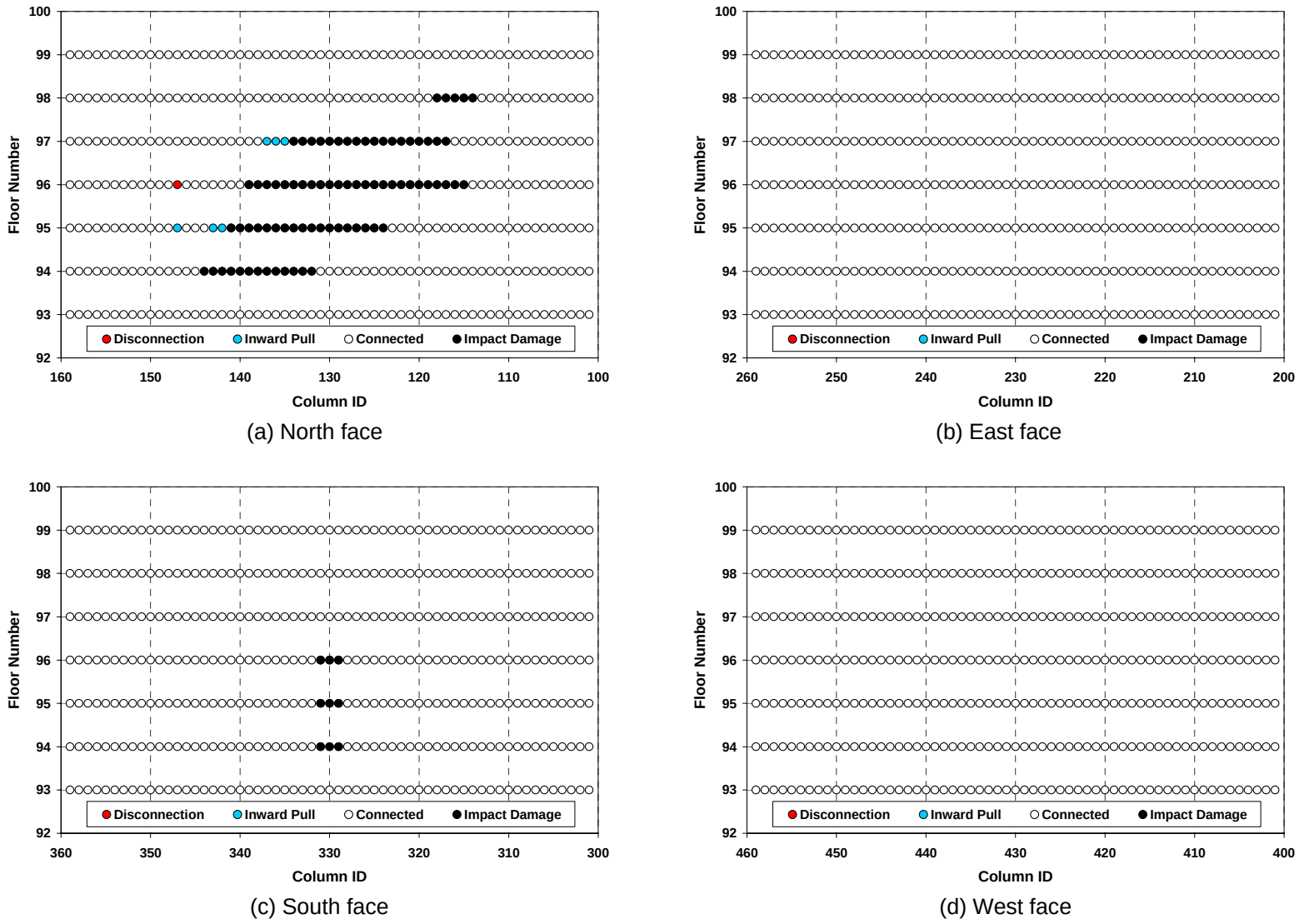

Figure 2–29. Locations of floor/wall disconnections and pull-in forces for the global analysis of WTC 1 between 10 min and 20 min for Case B conditions.

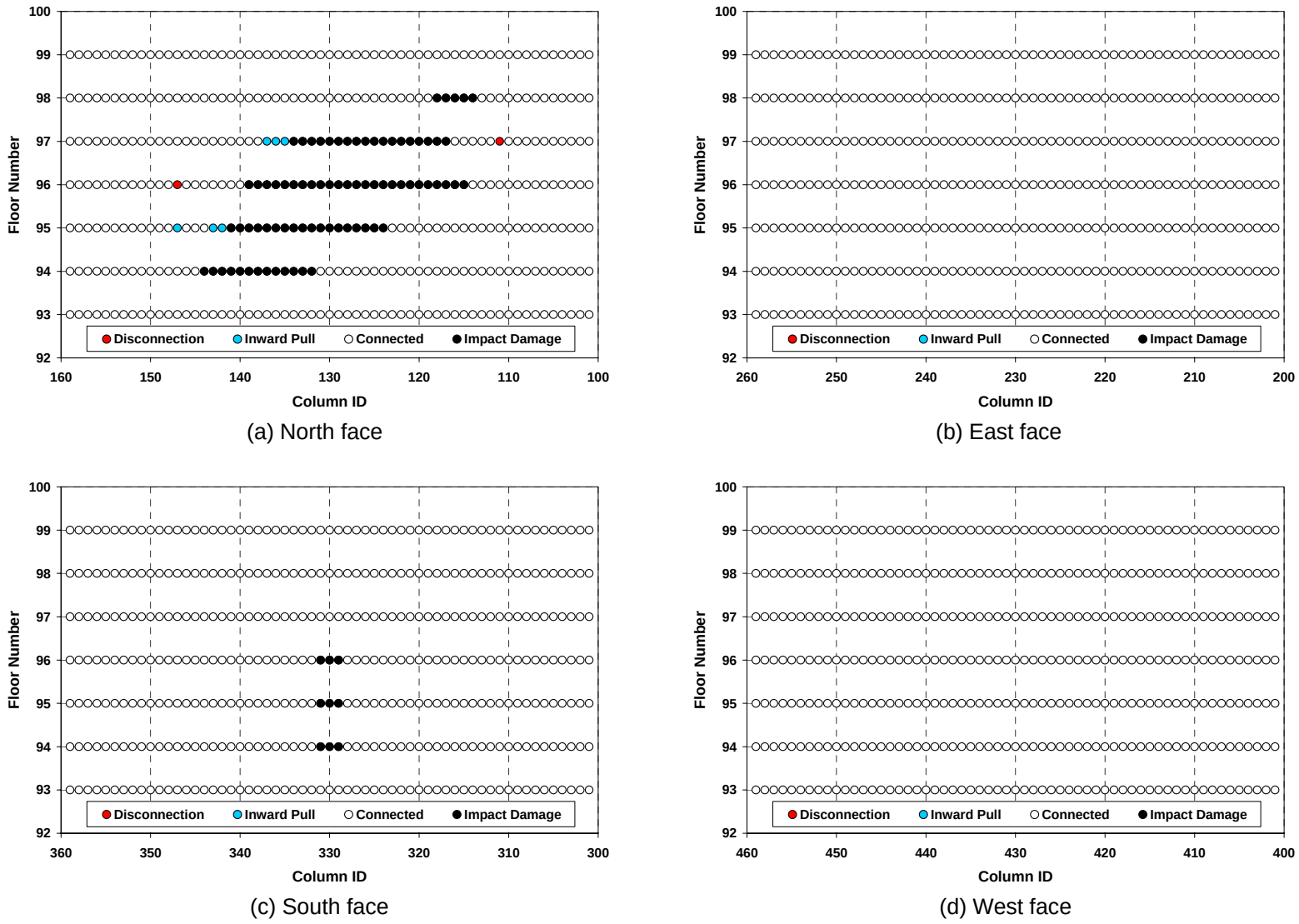

Figure 2–30. Locations of floor/wall disconnections and pull-in forces for the global analysis of WTC 1 between 20 min and 30 min for Case B conditions.

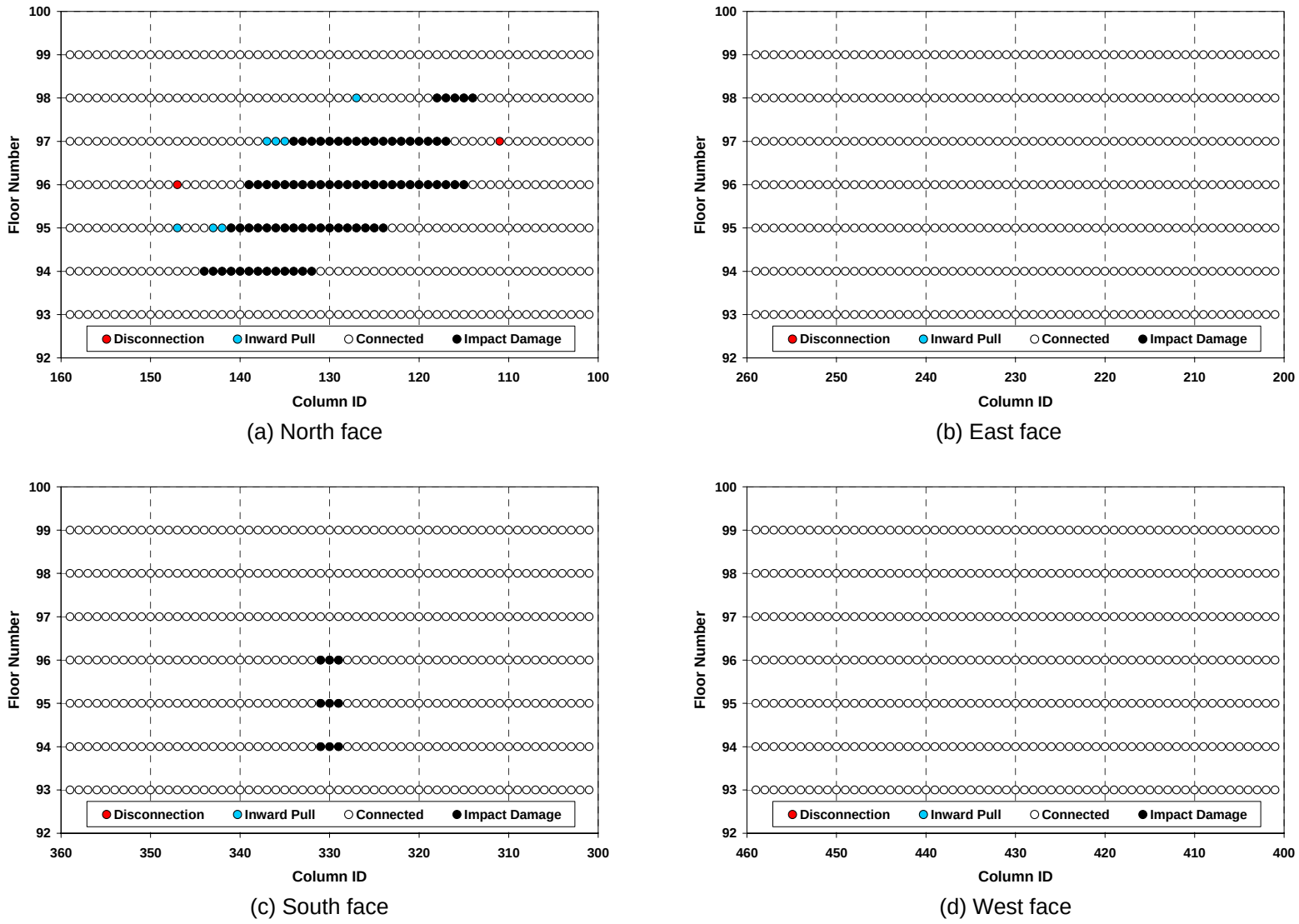

Figure 2–31. Locations of floor/wall disconnections and pull-in forces for the global analysis of WTC 1 between 30 min and 40 min for Case B conditions.

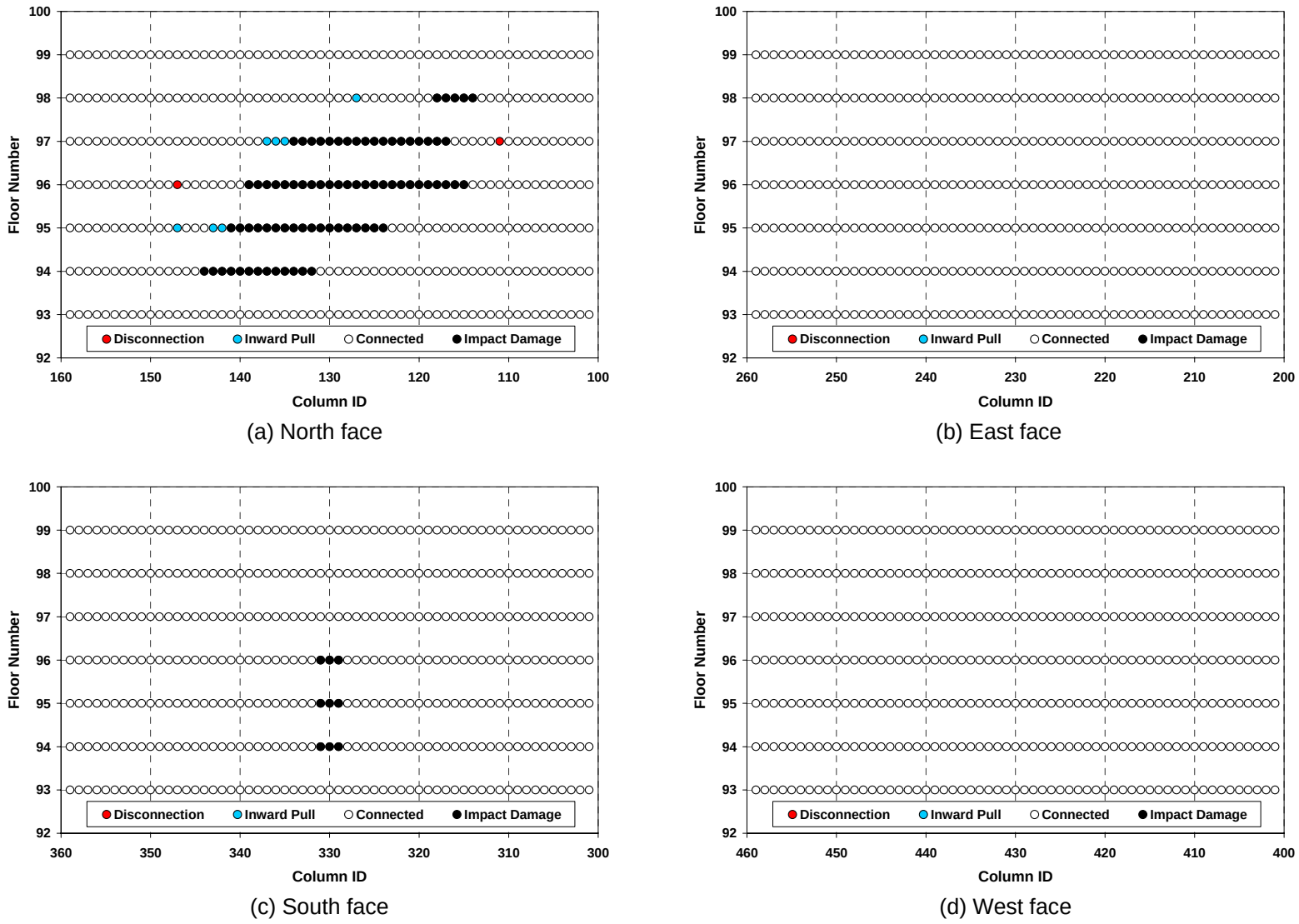

Figure 2–32. Locations of floor/wall disconnections and pull-in forces for the global analysis of WTC 1 between 40 min and 50 min for Case B conditions.

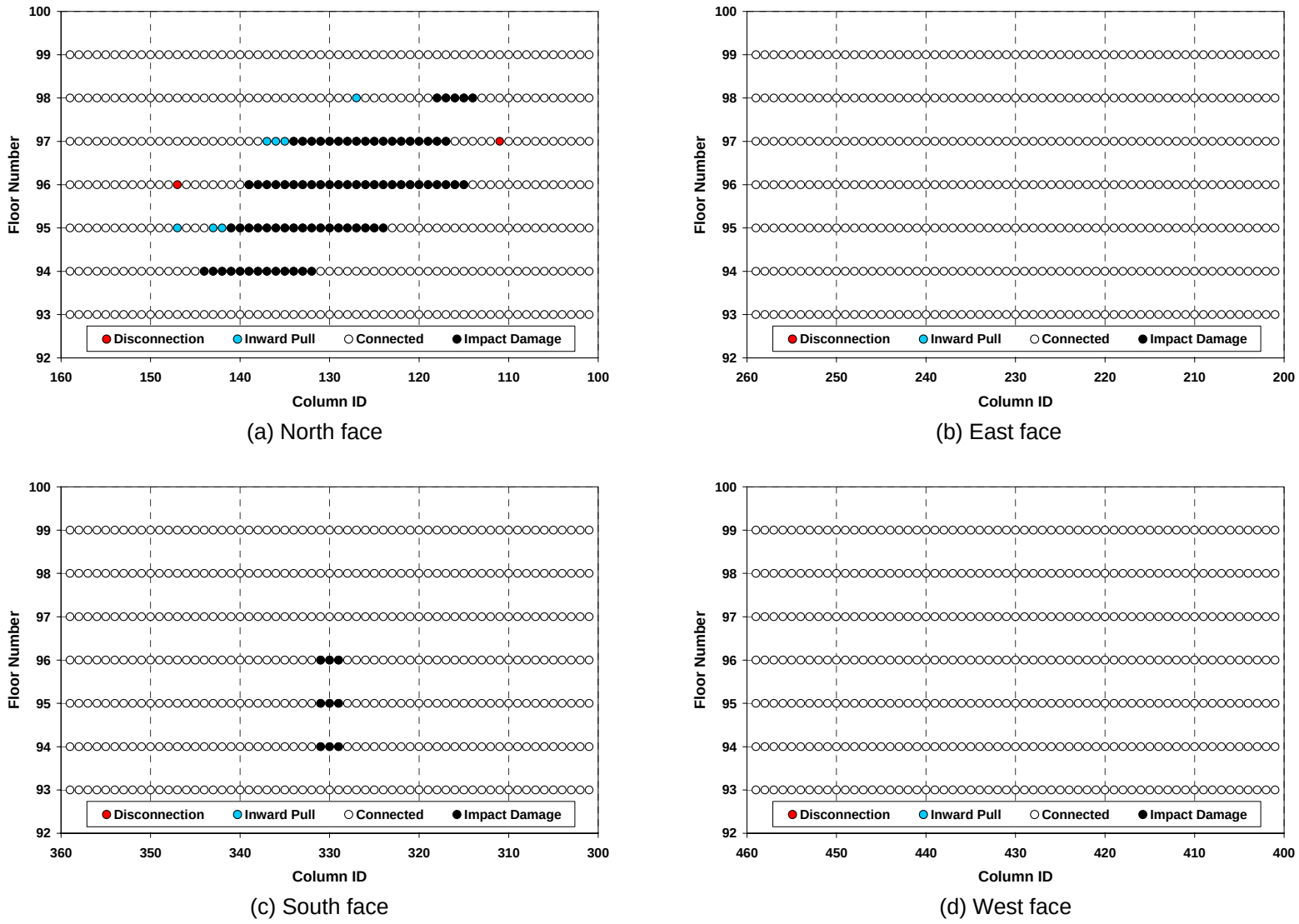

Figure 2–33. Locations of floor/wall disconnections and pull-in forces for the global analysis of WTC 1 between 50 min and 60 min for Case B conditions.

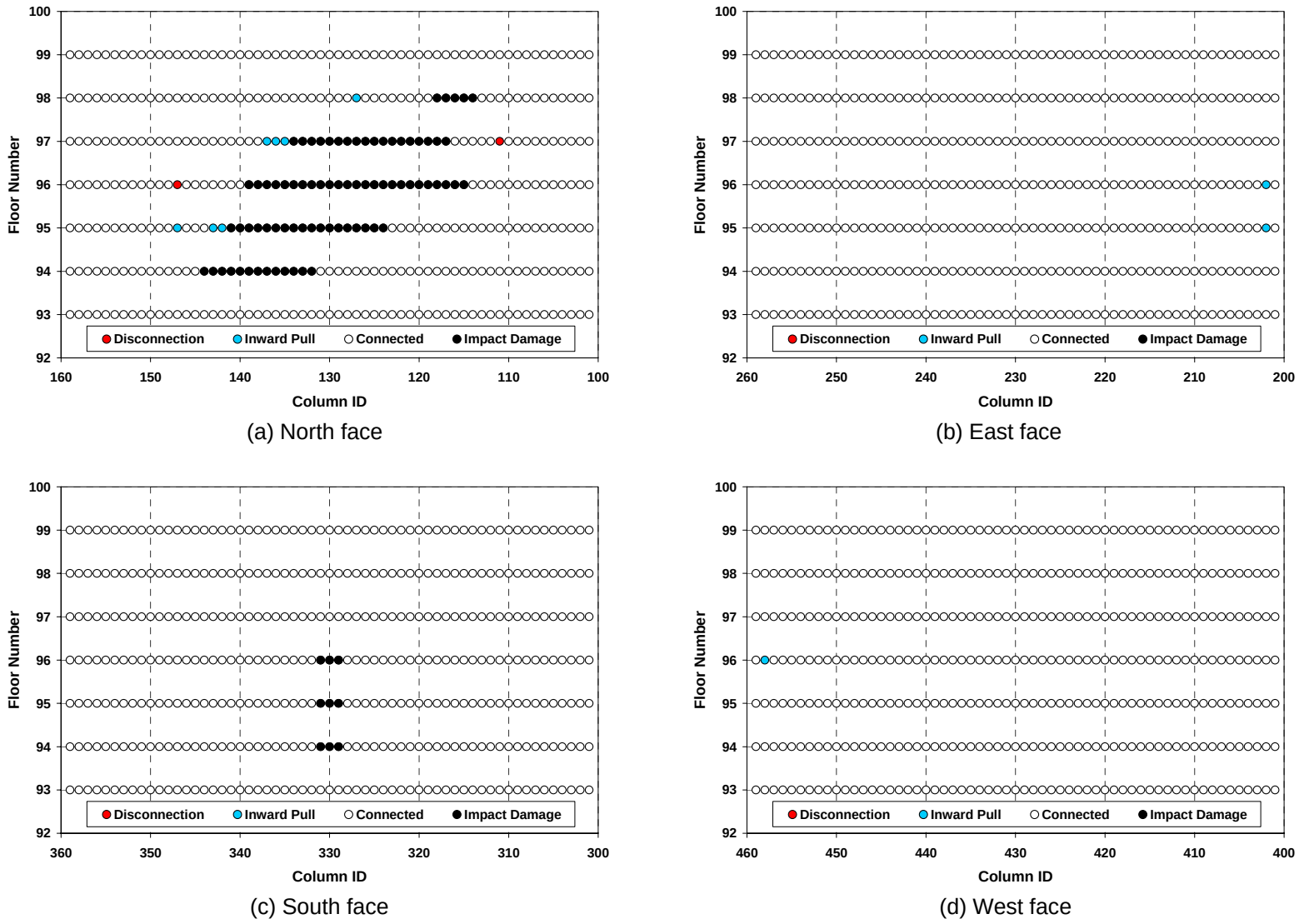

Figure 2–34. Locations of floor/wall disconnections and pull-in forces for the global analysis of WTC 1 between 60 min and 70 min for Case B conditions.

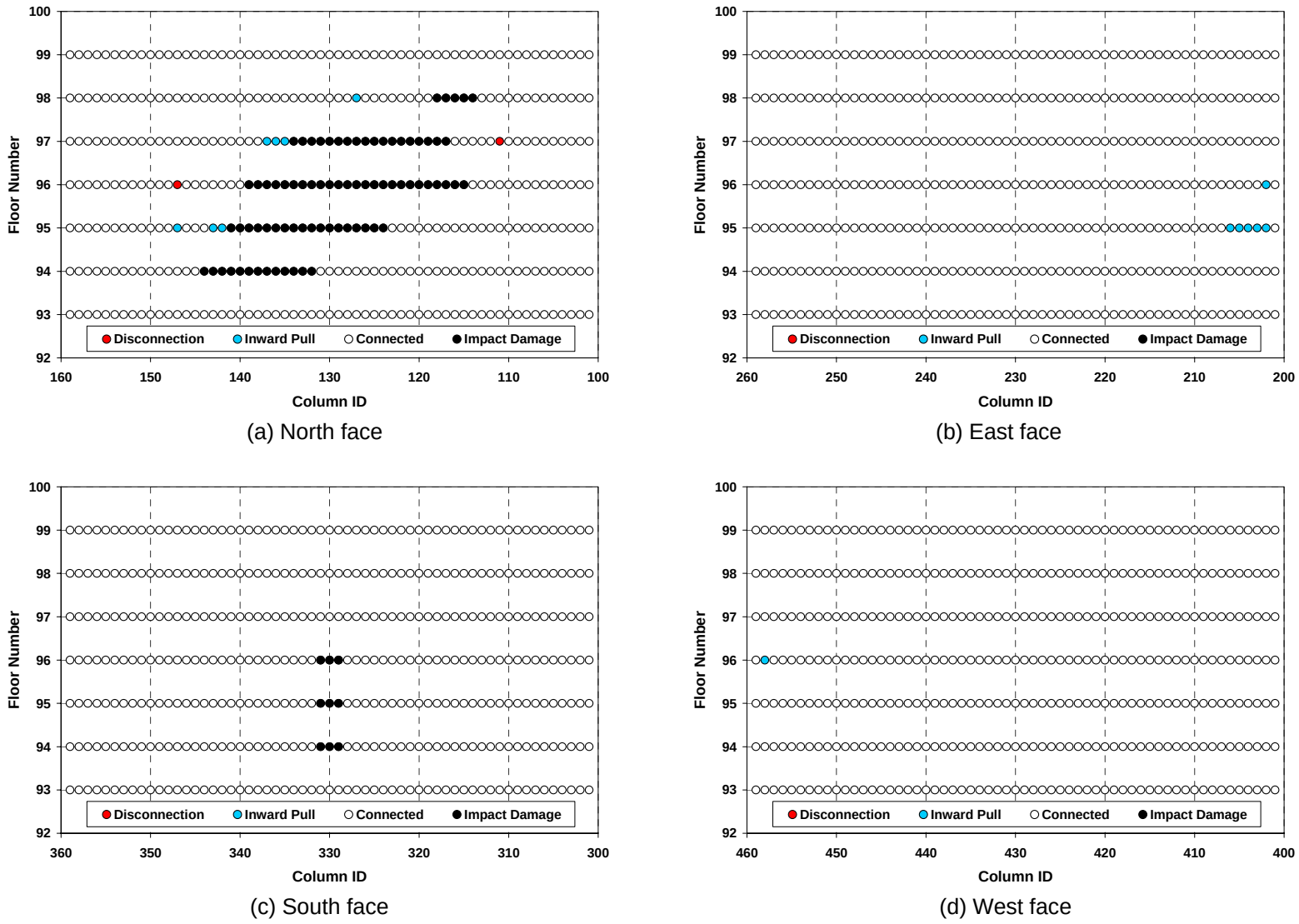

Figure 2–35. Locations of floor/wall disconnections and pull-in forces for the global analysis of WTC 1 between 70 min and 80 min for Case B conditions.

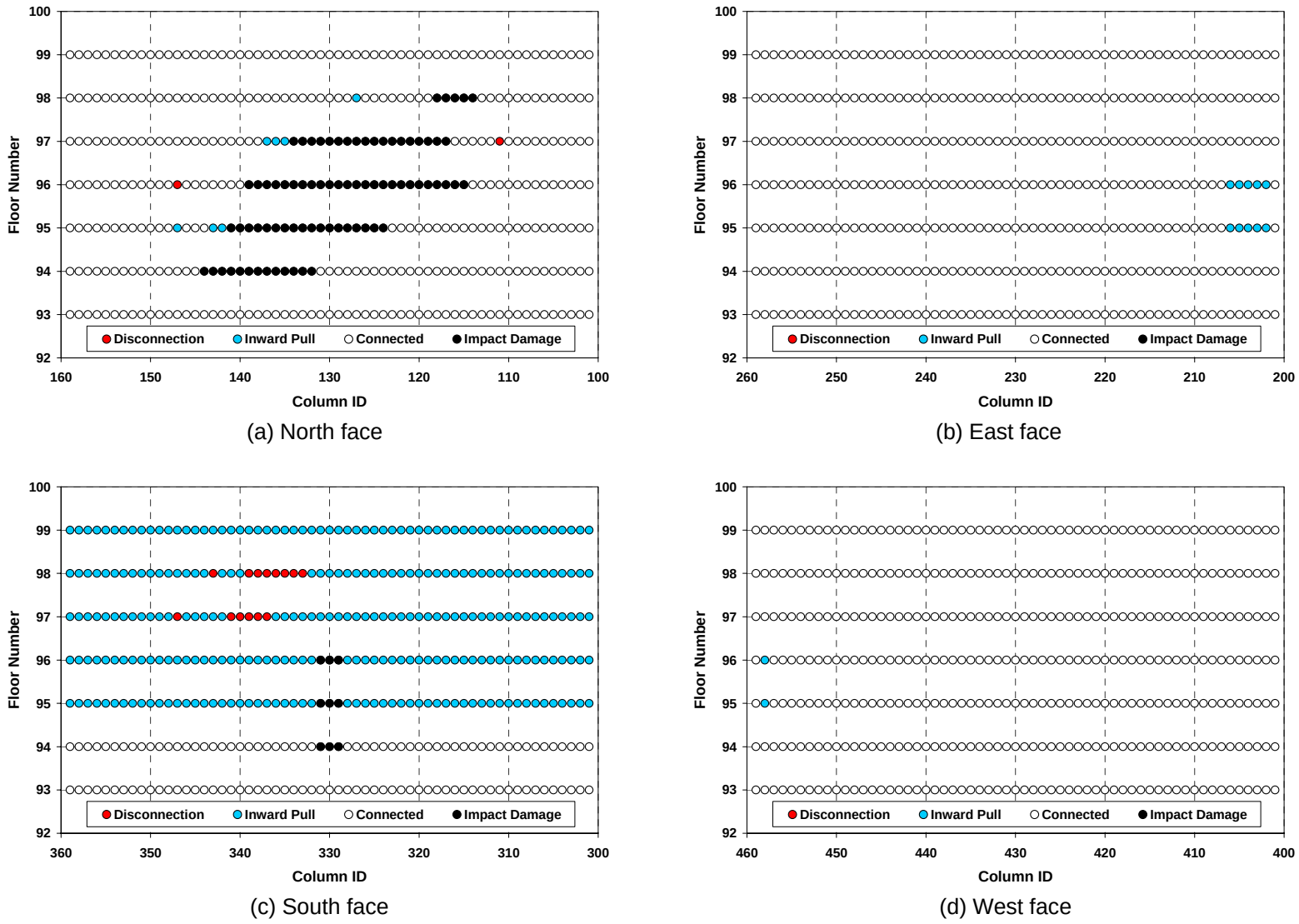

Figure 2–36. Locations of floor/wall disconnections and pull-in forces for the global analysis of WTC 1 between 80 min and 90 min for Case B conditions.

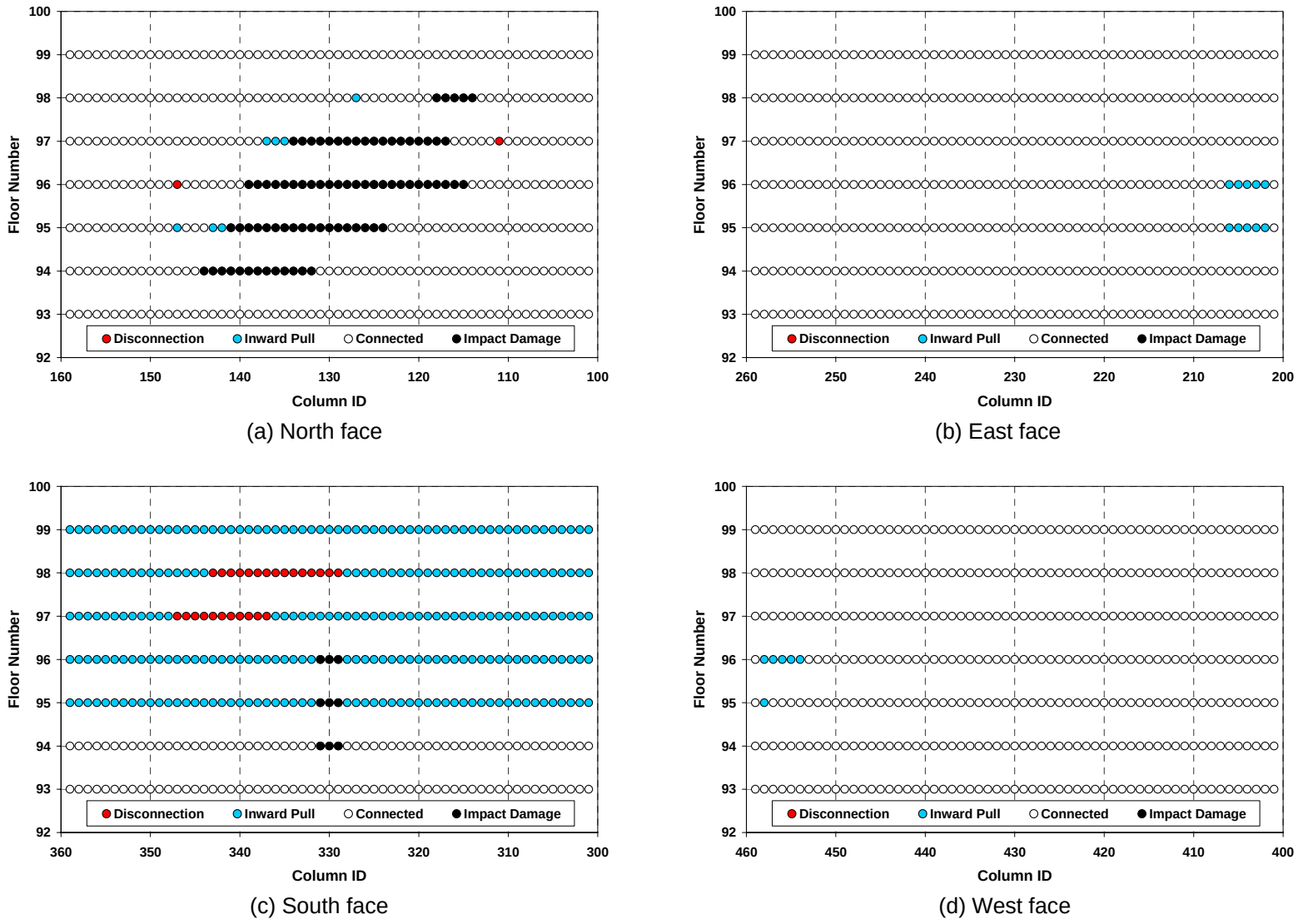

Figure 2–37. Locations of floor/wall disconnections and pull-in forces for the global analysis of WTC 1 between 90 min and 100 min for Case B conditions.

WTC 2

Figures 2–38 to 2–43 show the locations of floor/wall disconnections and pull-in forces imposed on the WTC 2 global model for Case D conditions. Each figure covers a 10 min time interval, the first initiating at 0 min, when the initial impact occurred, and the last initiating at 50 min.

In determining the locations of floor/wall disconnections from the full floor models, the results of Case C_i and Case D_i temperature conditions were considered jointly for the uncertainties in truss seat temperatures. This uncertainty is illustrated in Tables 2–2 and 2–3. Table 2–2 compares the temperature predicted for the exterior truss seats at selected columns of the east wall at Floor 82 at times of 30 min, 40 min, 50 min, and 60 min. Table 2–3 shows demand-to-capacity ratios for vertical support of these same exterior seats. Temperatures of the exterior seats at the east wall of Floor 82 rapidly dropped after 40 min in Case D_i; whereas, in Case C_i they continued to increase with time. Due to this difference, the truss seats that were very close to failure (such as the seat at Column 303) at 40 min of Case D_i did not fail at 50 min in the full floor analysis. If high temperatures had continued for a few more minutes for Case D_i, these seats would have failed. The actual temperature time history may not have descended rapidly between 40 min and 50 min, as is deduced from the consideration of piecewise linear temperature time history in this study.

The state of the floor/wall connections in the full floor analysis were reevaluated considering the effects of uncertainties in the seat capacities by comparing the demands to the seat capacities that were 10 percent lower than the calcuated seat capacities. As a result of this comparison, the seats adjacent to the already disconnected seats at Floors 82 and 83 were found to be progressively failing, and the extent of floor/wall disconnection was extended to nearly the entire width of the east wall. These worst-case floor/wall disconnections were included in the floor/wall disconnections for Case D conditions in the global analysis.

Table 2–2. Temperatures of exterior seats at east wall of Floor 82 of WTC 2.

Column ID	Case C_i Temperatures (°C)				Case D_i Temperatures (°C)			
	30 min	40 min	50 min	60 min	30 min	40 min	50 min	60 min
301	763	788	811	813	818	819	507	345
303	752	774	809	808	822	820	509	348
305	750	769	807	804	823	821	513	348
307	750	769	804	799	823	821	511	342
309	727	748	787	790	822	816	485	334
311	677	698	738	758	816	804	458	328
313	636	657	700	724	809	803	487	342
315	591	605	632	662	816	794	481	347
317	574	580	615	637	815	799	494	351

Table 2–3. Demand-to-capacity ratios of exterior seats at east wall of Floor 82 of WTC 2 predicted by the full floor model.

Column ID	Case C_i Temperatures (°C)				Case D_i Temperatures (°C)			
	30 min	40 min	50 min	60 min	30 min	40 min	50 min	60 min
301	0.35	0.31	failed	failed	0.63	0.54	0.02	0.08
303	0.66	0.81	failed	failed	0.92	0.97	0.18	0.14
305	0.39	0.53	failed	failed	0.63	0.70	0.20	0.19
307	0.41	0.51	failed	failed	0.59	0.60	0.15	0.13
309	0.35	0.43	failed	failed	0.60	0.60	0.13	0.13
311	0.38	0.46	failed	failed	0.87	0.71	0.09	0.05
313	0.23	0.27	failed	failed	0.64	0.48	0.10	0.09
315	0.20	0.24	failed	failed	0.49	0.41	0.08	0.09
317	0.10	0.09	0.96	failed	0.45	0.50	0.14	0.13

In addition to the reevaluation of the seat capacities, the location of floor/wall disconnections estimated from full floor analyses were compared and were updated based on the floor/wall disconnections observed in the photographs and videos. Observed floor/wall disconnections were provided for the east wall at 9:03 a.m., 9:38 a.m., and 9:55 a.m. and for the north wall at 9:10 a.m., 9:14 a.m., and 9:58 a.m. All observed floor/wall disconnections were included in the global analysis for Case D conditions at appropriate points in time, whether predicted by the full floor analyses or not.

As previosusly described above for the case of WTC 1, the photographic and video evidence was also reviewed by NIST to determine the extent of inward bowing of the east wall of WTC 2. These displacement measurements were used to update the location and the magnitude of the pull-in forces applied to the global model. The earliest observations of inward bowing for WTC 2 were made at 9:21 a.m., 18 min after impact (NIST NCSTAR 1-6), when the east wall was observed to be bowing inward between Column 301 and Column 345 between Floor 78 and Floor 83. At this time, NIST estimated the maximum inward deformation to be about 10 in. at Floors 80 and 81 between Column 322 and Column 329. To replicate this inward bowing, pull-in forces were applied at Floors 79, 80, 81, and 82. The full floor analyses correctly predicted the floors that were pulled in, but underestimated the location of the pull-in forces across the width of the east wall, relative to that required to replicate the observed bowing. The locations of pull-in forces predicted by the full-floor analyses were concentrated toward the south side of the east wall and typically ranged between Columns 329 and 359 at Floor 82 and between Columns 357 and 359 at Floor 79. The locations of pull-in forces estimated from the observation were used to augment those obtained from the full floor analyses. Based on this augmented data, at 20 min after imact, pull-in forces were applied over the entire width of the east wall at Floors 79, 80, 81, and 82 in the global analysis.

The photographic and video evidence, obtained at 9:53 a.m., about 50 min after impact (NIST NCSTAR 1-6), show the east wall bowing inward from Column 301 to Column 353 between Floor 77 and Floor 84. At this instant, NIST estimated the maximum inward deformation to be about 15 in. to 20 in. at Floor 81 between Column 320 and Column 330. To replicate this observed bowing geometry, a combination of pull-in forces and floor/wall disconnections were applied between Floor 77 and Floor 84. Except for Floor 78, which was not analyzed using a full floor model, the full floor analyses correctly predicted the floor levels at which the exterior wall was observed to be pulled in, but underestimated the locations of pull-in forces. The locations of the pull-in forces estimated from the full floor analyses were

concentrated toward the south side of the east wall and typically ranged between Column 333 and Column 359 at Floor 81 and between Column 355 and Column 359 at Floor 79. Based on the full floor analyses and the reevaluated seat capacities, Floor 83 was disconnected from the east wall between Column 302 and Column 357, and Floor 82 was disconnected between Column 301 and Column 349. For this reason, no pull-in forces were applied at these column locations. The locations of the pull-in forces estimated from the observations at 50 min were used to augment those estimated from the full floor analyses. As a result of this addition, at 50 min after impact, pull-in forces were applied over the entire width of the east wall at Floors 78, 79, 80, and 81, and between Column 350 and Column 359 at Floor 82.

As is discussed in Section 3.2.2, the magnitude of the pull-in force was estimated through a trial and error process by applying different levels of pull-in forces to the isolated wall models and by comparing the resulting inward bowing to that estimated from observations at 9:21 a.m. and 9:53 a.m. From these comparative analyses, the magnitude of pull-in forces were determined to range from 1.0 to 2.0 kip on the south side of the east wall and 4.0 to 5.0 kip on the north side of the east wall. It was necessary to apply larger pull-in forces on the north side than on the south side of the east wall because column temperatures on the north side were higher than the column temperatures on the south side of the east wall. Higher temperatures resulted in more outward bowing of columns, and thus larger pull-in forces were required to overcome this outward bowing.

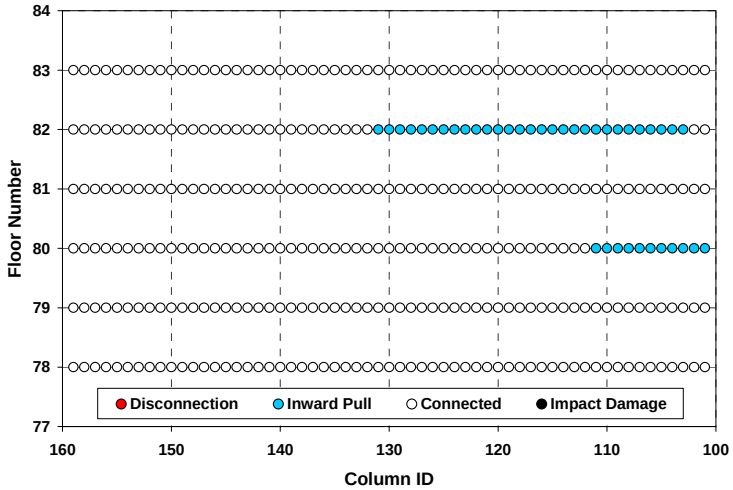

(a) West face

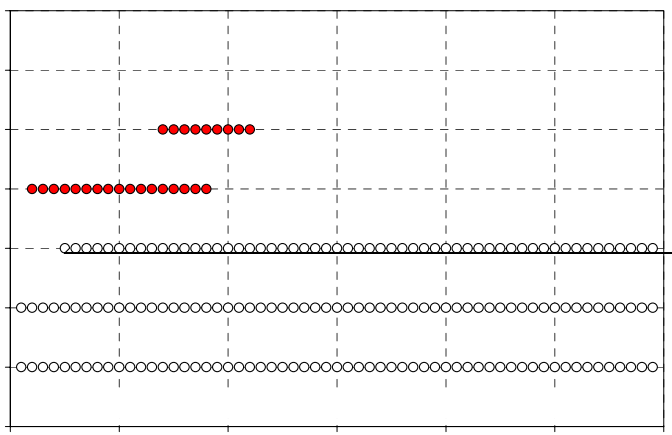

(b) North face

(c) East face

(d) South face

Figure 2–38. Locations of floor/wall disconnections and pull-in forces for the global analysis of WTC 2 between 0 min and 10 min for Case D conditions.

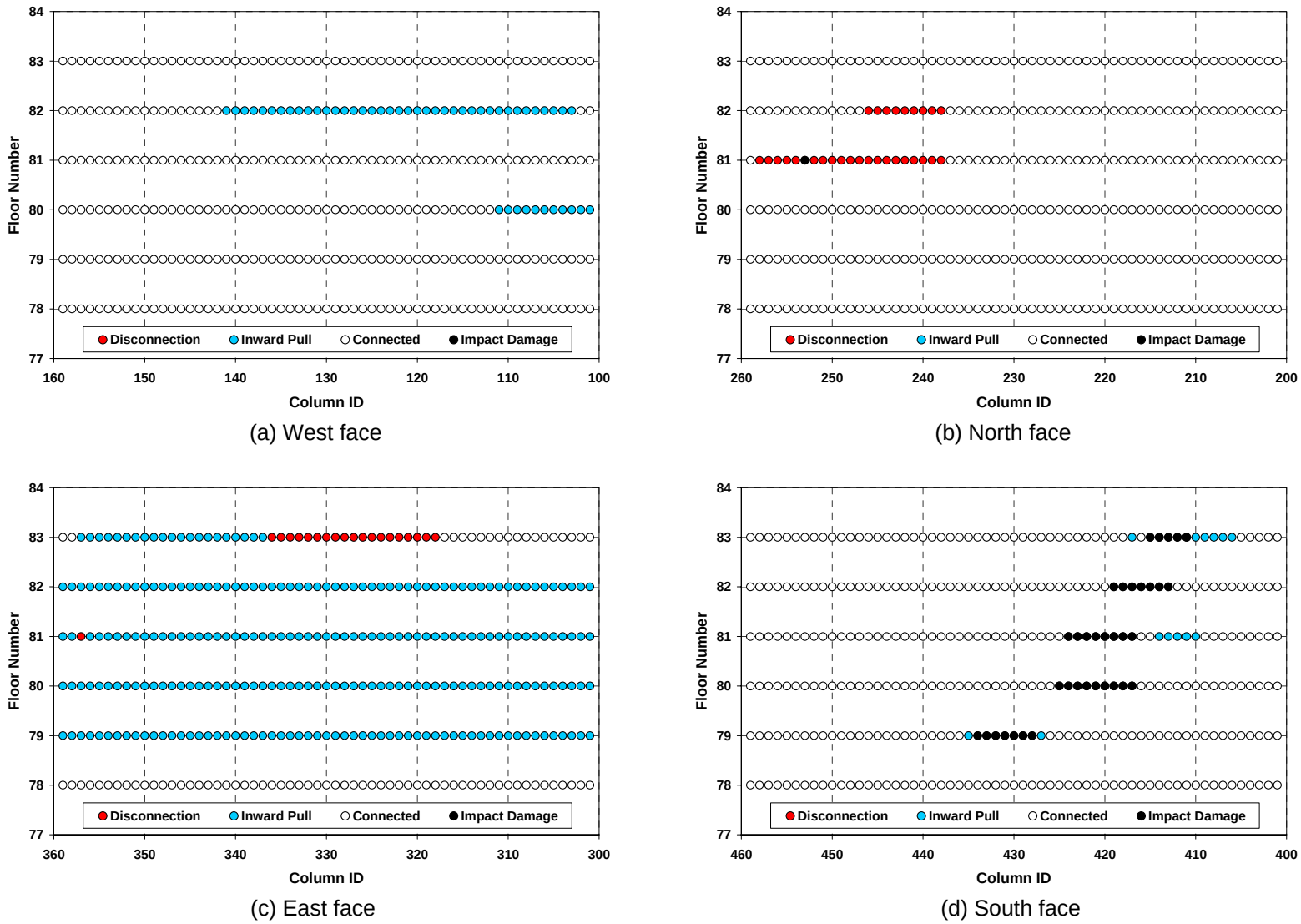

Figure 2–39. Locations of floor/wall disconnections and pull-in forces for the global analysis of WTC 2 between 10 min and 20 min for Case D conditions.

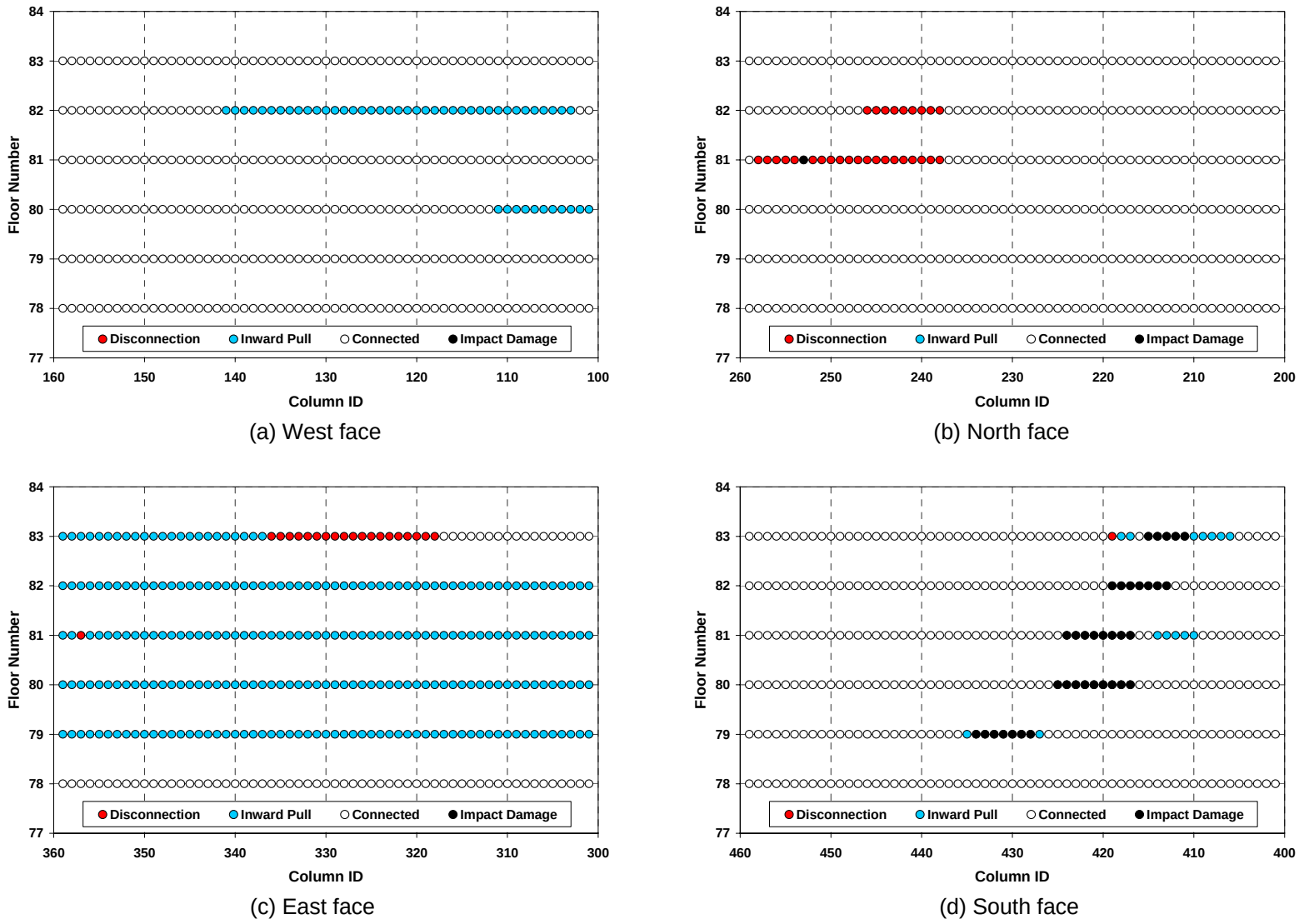

Figure 2–40. Locations of floor/wall disconnections and pull-in forces for the global analysis of WTC 2 between 20 min and 30 min for Case D conditions.

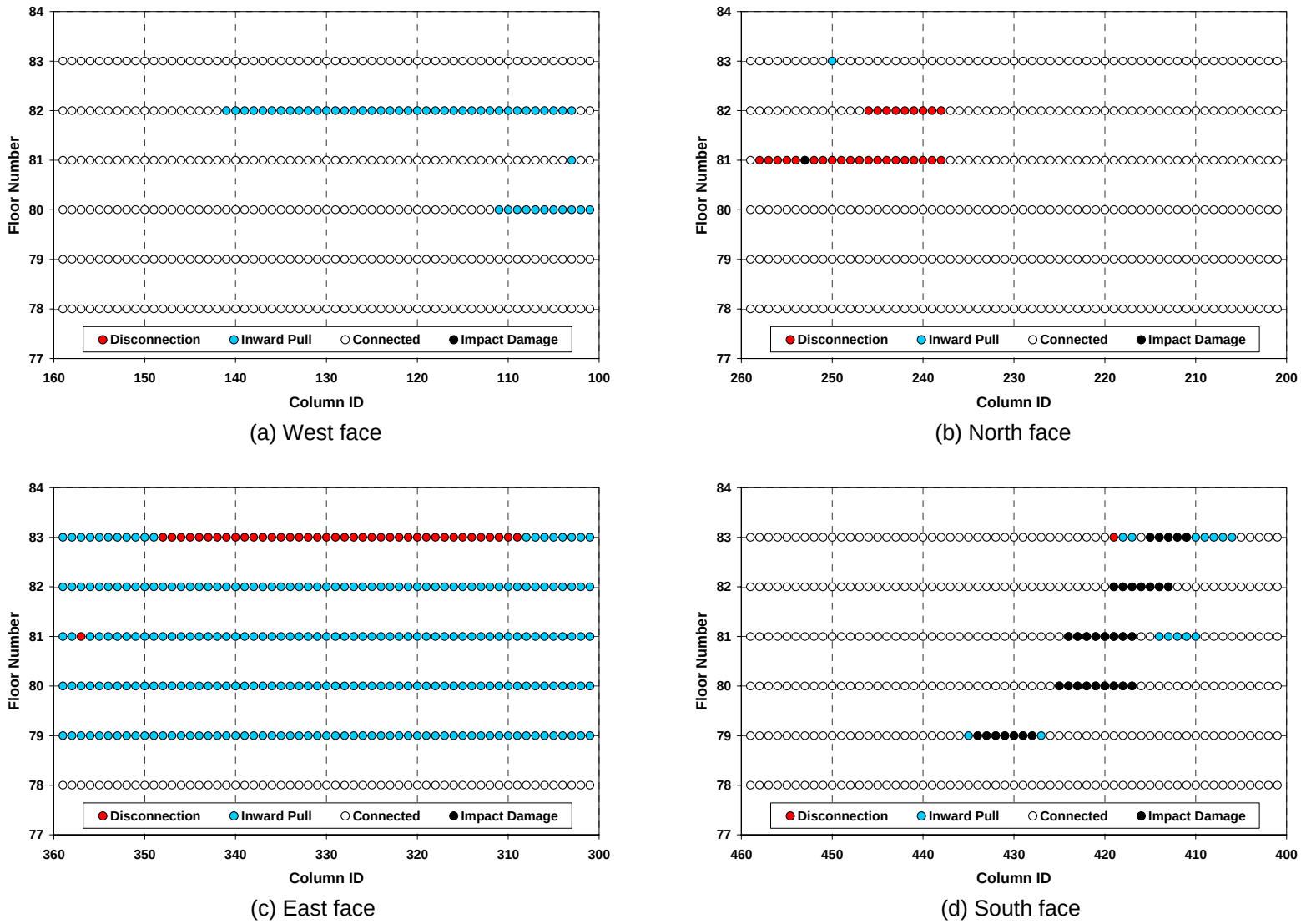

Figure 2–41. Locations of floor/wall disconnections and pull-in forces for the global analysis of WTC 2 between 30 min and 40 min for Case D conditions.

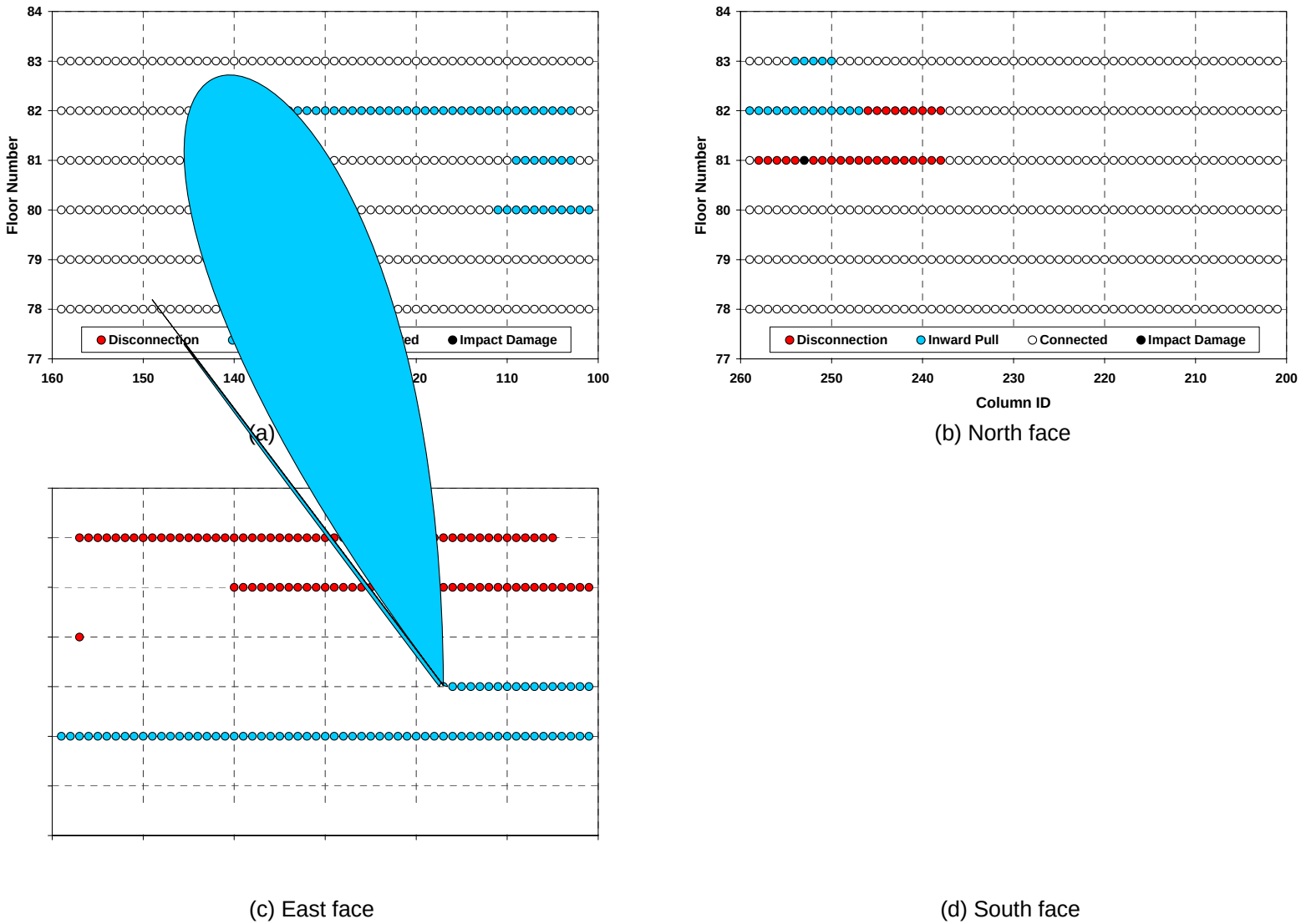

Figure 2–42. Locations of floor/wall disconnections and pull-in forces for the global analysis of WTC 2 between 40 min and 50 min for Case D conditions.

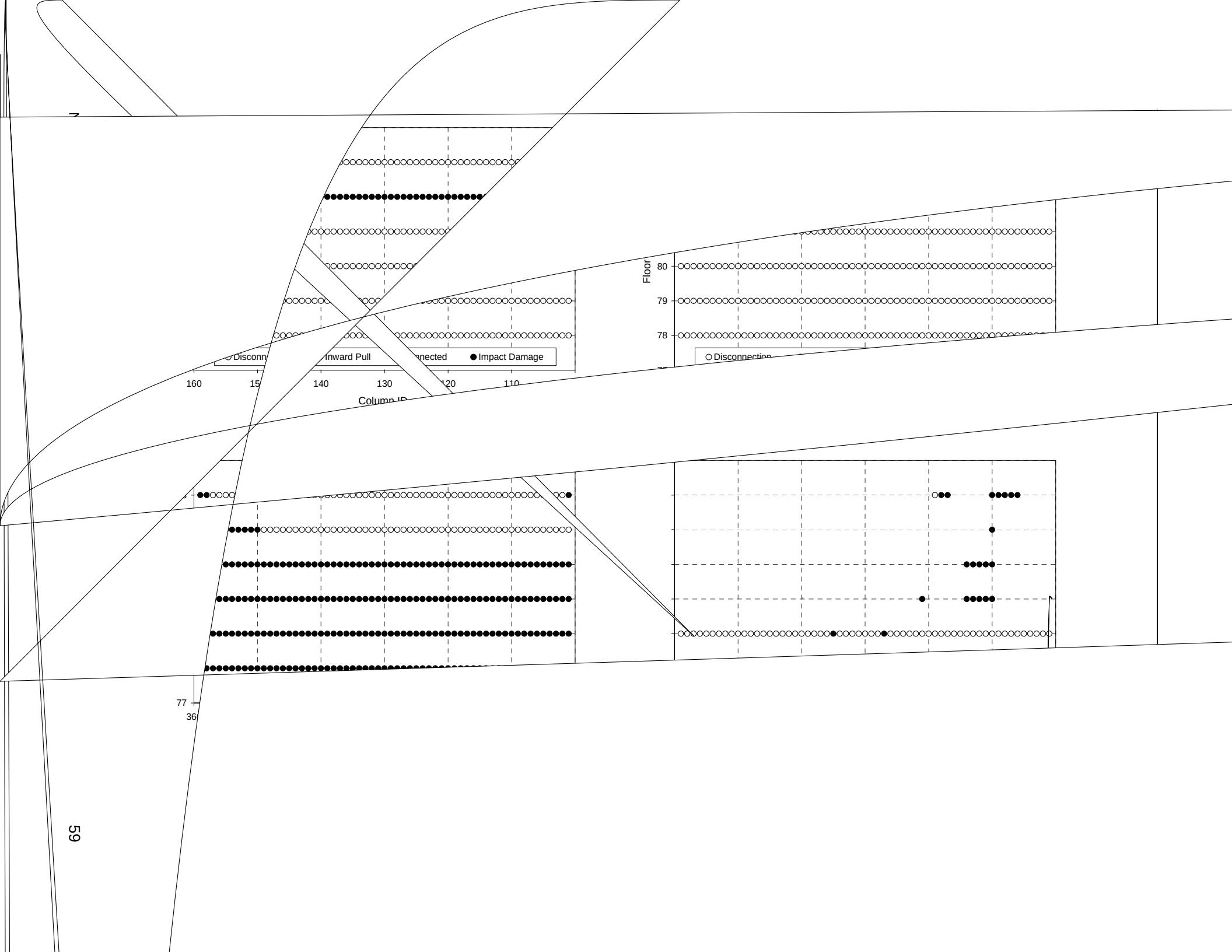
Floor
80
79
78
77
Disconnection
Inward Pull
Impact Damage
160
140
130
120
110
Column ID

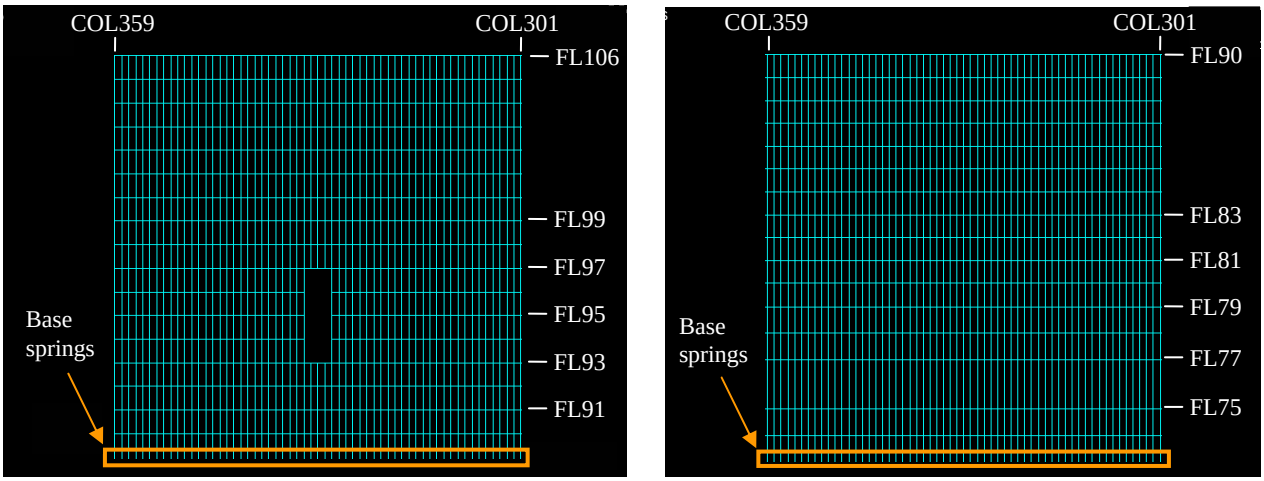

(a) Segment from South wall of WTC 1

(b) Segment from East wall of WTC 2

Figure 3–1. Isolated exterior wall segments from WTC 1 and WTC 2 (horizontal lines show spandrels and vertical lines show column).

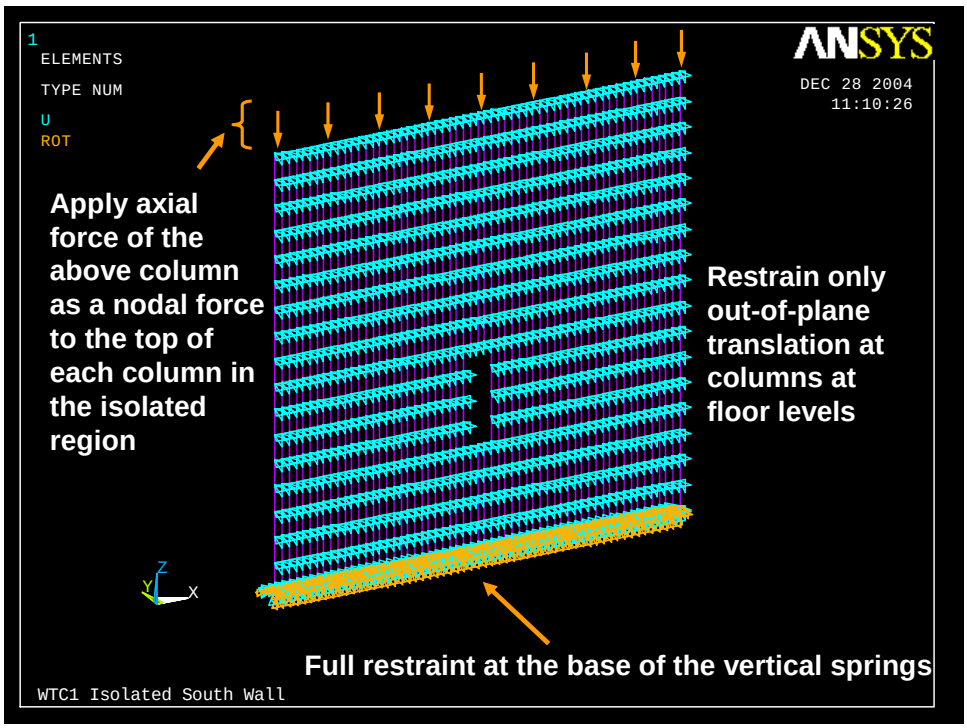

Figure 3–2. Boundary conditions applied on the isolated exterior wall segment on the south wall of WTC 1.

The applied boundary conditions for both isolated exterior wall models were identical and are shown for WTC 1 in Fig. 3–2. The isolated exterior wall models were fully restrained at the base of the vertical

springs. In the out-of-plane direction (direction y) they were supported at floor levels. At predetermined points in times, these supports were removed at locations where either calculations or observations showed floor/wall disconnections. For the east wall of WTC 2, there were floor/wall disconnections or pull-in forces calculated by the full floor models along the edges of the model (Column 301 and Column 359). In the analyses of the isolated wall model for Case C and Case D temperature conditions, the out-of-plane supports were removed at disconnections located on the edges of the model. However, in the analysis of the pull-in forces needed to match the observed bowing (see Section 3.2.2), the disconnections on the edges of the model were not modeled, and all nodes along the vertical edges of the model were restrained.

To represent the column loads after aircraft impact, a set of axial loads and moments were applied at the top of the isolated wall segments. These axial loads and moments, taken from the preliminary global model analyses with Case A (for WTC 1) and Case C and Case D (for WTC 2) structural damage conditions, represented the axial load and moment in the columns at the floor right above the top of the isolated wall segments after aircraft impact. For instance, for the WTC 2 exterior wall segment, the isolated wall terminates at Floor 90. In order to represent the axial load coming from Floor 90 and above, the axial loads from the columns between Floor 90 and Floor 91 of the global model were extracted at the end of the aircraft impact analysis and were applied on the top of the isolated wall model of WTC 2. In addition to the set of vertical loads applied at the top of the isolated walls, loads representing the dead and 25 percent of the design live loads of the floors were applied at each column node at floor levels.

The isolated exterior wall models were subjected to a set of loading conditions as summarized in Table 3–1 for WTC 1 and Table 3–2 for WTC 2. After the gravity analysis, the isolated exterior wall models were subjected to temperature loads at 10 min increments. The analyses were conducted with Case A and Case B temperature conditions for WTC 1 and Case C and Case D temperature conditions for WTC 2. For each temperature analysis, the column and spandrel temperatures at time t were ramped to the column and spandrel temperatures at time = t + 10 min. Before applying the temperatures, the out-of-plane supports were removed at disconnected column to exterior wall connections at or prior to t + 10 min. Once the temperature analyses were completed (WTC 1 was analyzed to 100 min and WTC 2 to 60 min), both isolated exterior wall models were pushed down by imposing additional displacements to determine additional axial-load-carrying capacity remaining in the exterior wall system. For push-down analysis, the vertical displacements at the top of the isolated exterior wall models at the end of temperature analyses were extracted. These displacements were applied on top of the isolated exterior wall models, and additional uniform displacement increments were imposed in a displacement-controlled analysis. During push-down analysis, the temperature of the columns and spandrels were kept constant at the values specified at the end of the temperature analyses (WTC 1 column and spandrel temperatures were kept at 100 min temperatures and WTC 2 column and spandrel temperatures were kept at 60 min temperatures). The results of isolated exterior wall model analyses are discussed in the following sections.

Table 3–1. Analysis steps conducted on WTC 1 isolated exterior wall model.

Analysis Step		Description
1	Gravity	Apply gravity loads with aircraft impact
2	Temperature at 10 min	Remove the out-of-plane supports at floor to exterior wall connections disconnected at or prior to 10 min. Apply column and spandrel temperatures at 10 min.
3	Temperature at 20 min	Remove the out-of-plane supports at floor to exterior wall connections disconnected at or prior to 20 min. Apply column and spandrel temperatures at 20 min.
4	Temperature at 30 min	Remove the out-of-plane supports at floor to exterior wall connections disconnected at or prior to 30 min. Apply column and spandrel temperatures at 30 min.
5	Temperature at 40 min	Remove the out-of-plane supports at floor to exterior wall connections disconnected at or prior to 40 min. Apply column and spandrel temperatures at 40 min.
6	Temperature at 50 min	Remove the out-of-plane supports at floor to exterior wall connections disconnected at or prior to 50 min. Apply column and spandrel temperatures at 50 min.
7	Temperature at 60 min	Remove the out-of-plane supports at floor to exterior wall connections disconnected at or prior to 60 min. Apply column and spandrel temperatures at 60 min.
8	Temperature at 70 min	Remove the out-of-plane supports at floor to exterior wall connections disconnected at or prior to 70 min. Apply column and spandrel temperatures at 70 min.
9	Temperature at 80 min	Remove the out-of-plane supports at floor to exterior wall connections disconnected at or prior to 80 min. Apply column and spandrel temperatures at 80 min.
10	Temperature at 90 min	Remove the out-of-plane supports at floor to exterior wall connections disconnected at or prior to 90 min. Apply column and spandrel temperatures at 90 min.
11	Temperature at 100 min	Remove the out-of-plane supports at floor to exterior wall connections disconnected at or prior to 100 min. Apply column and spandrel temperatures at 100 min.
12	Push Down	Extract the vertical displacements at the top of the isolated wall model and impose these displacements and additional uniform displacement increments with column and spandrel temperatures kept at 100 min.

Table 3–2. Analysis steps conducted on WTC 2 isolated exterior wall model.

Analysis Step		Description
1	Gravity	Apply gravity loads right after aircraft impact
2	Temperature at 10 min	Remove the out-of-plane supports at floor to exterior wall connections that were disconnected at or prior to 10 min. Apply column and spandrel temperatures at 10 min.
3	Temperature at 20 min	Remove the out-of-plane supports at floor to exterior wall connections that were disconnected at 20 min. Apply column and spandrel temperatures at 20 min.
4	Temperature at 30 min	Remove the out-of-plane supports at floor to exterior wall connections that were disconnected at 30 min. Apply column and spandrel temperatures at 30 min.
5	Temperature at 40 min	Remove the out-of-plane supports at floor to exterior wall connections that were disconnected at 40 min. Apply column and spandrel temperatures at 40 min.
6	Temperature at 50 min	Remove the out-of-plane supports at floor to exterior wall connections that were disconnected at 50 min. Apply column and spandrel temperatures at 50 min.
7	Temperature at 60 min	Remove the out-of-plane supports at floor to exterior wall connections that were disconnected at 60 min. Apply column and spandrel temperatures at 60 min.
8	Push Down	Extract the vertical displacements at the top of the isolated wall model and impose these displacements and additional uniform displacement increments with column and spandrel temperatures kept at 60 min.

3.2.1 Finite Element Analysis of WTC 1 Exterior Wall

Case A Temperature Condition

As calculated in the full-floor model analyses for Case A_i condition, described in Appendix A, the floors were assumed to remain connected to the south wall of WTC 1 throughout the temperature history for Case A condition.

Figures 3–3 to 3–12 show the temperature distributions of Case A condition in columns of the WTC 1 south wall from 10 min to 100 min. A linear temperature gradient in the direction normal to the exterior wall was assumed to exist in the cross section of beam elements for exterior columns. As Figs. 3–3 to 3–12 show, temperatures on the south wall were not very high; the peak temperature was only 455°C for Case A temperature condition. The temperature distributions of Case A condition in spandrels are shown in Figs. 3–13 to 3–22. Temperatures were assumed to be uniform over the entire cross section of beam elements for spandrels.

Figure 3–23 shows vertical displacements, out-of-plane displacements, and axial loads in columns of the WTC 1 south wall after the impact. In contour plots created by ANSYS, “MN” and “MX” indicate the locations of the minimum and maximum values, respectively. Columns from Column 329 to Column 331 between Floor 93 and Floor 97 were severed by the aircraft impact, and the maximum displacement occurred at Column 330 at Floor 106. Column 328 and Column 332 between Floor 93 and Floor 97 on both sides of the aircraft impact damage area were heavily loaded, and the maximum axial load was 377 kip at Column 332.

Figures 3–24 to 3–26 show vertical displacements, out-of-plane displacements, and axial loads in the columns of the WTC 1 south wall for Case A temperature condition, respectively. At 100 min, the maximum vertical displacement was nearly the same as the vertical displacement of 2.6 in. after the impact. The out-of-plane displacement was insignificant during thermal loading. The maximum out-of-plane displacement was 0.35 in. outward, occurring at Column 332 between Floor 96 and Floor 97. During thermal loading, the axial load in Column 332 between Floor 96 and Floor 97 increased from 377 kip to 756 kip.

Figure 3–27 shows plastic strains in columns at 100 min. The maximum plastic strain of 4 percent occurred in Column 332 between Floor 96 and Floor 97.

As described in Appendix C for the preliminary global model without creep and in Chapter 4 for the final global model with creep, gravity loads on the south wall varied under thermal loads as the loads were redistributed within the tower through the hat truss and the spandrels. Figure 3–28 compares the axial loads in columns derived from the preliminary global model without creep and with Case A_i structural damage condition to those of the isolated model wall model with Case A structural damage and temperature conditions. The preliminary global model without creep was the only available source for this comparison at that time. The differences in the axial loads were applied to the columns at Floor 99 as corrective loads. Figure 3–29 shows the response of the south wall after applying these corrective loads. The WTC 1 south wall remained stable after the application of these corrective loads.

To determine the additional load-carrying capacity of the south wall at the end of the temperature analysis at 100 min, the top of the isolated exterior wall model was pushed down by converting the model from a

force-control analysis to a displacement-control analysis and by imposing additional vertical displacement increments on top of the isolated model. The analysis was terminated at an additional vertical displacement of 13.2 in. This model reached a peak total vertical load at an additional vertical displacement of 11.3 in. Figure 3–30 shows the relationship between the total additional vertical load and the additional vertical displacement. Figure 3–31 shows additional vertical load per column at different additional vertical displacements of 2 in., 4 in., 6 in., 8 in., and 10 in. Figure 3–32 shows the response of the WTC 1 south wall at the additional displacement of 13.2 in. When an additional 2 in. of vertical displacement was imposed, the variation among the additional vertical loads on columns was within 50 kip for the average additional vertical load of about 160 kip. However, at an additional displacement of 10 in., the variation became large, indicating some columns were softer than others; the softer columns had reached their load-carrying capacities and were in the post-buckling regime. The WTC 1 south wall model carried an additional vertical load of 33,000 kip (560 kip per column on the average). Therefore, the south wall possessed significant reserve capacity after the application of Case A temperature condition.

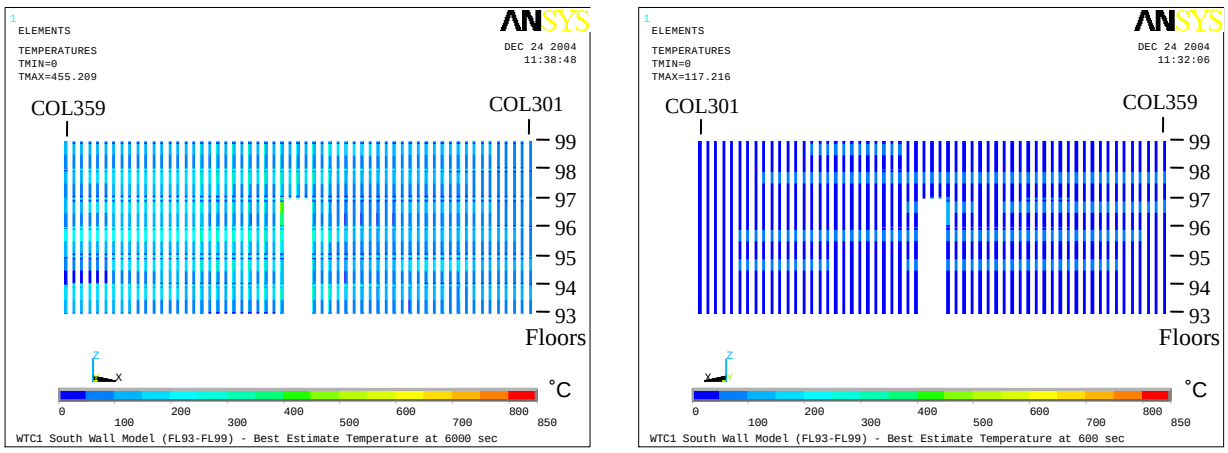

(a) Outside (b) Inside

Figure 3–3. Case A temperature condition of south wall columns of WTC 1 at 10 min.

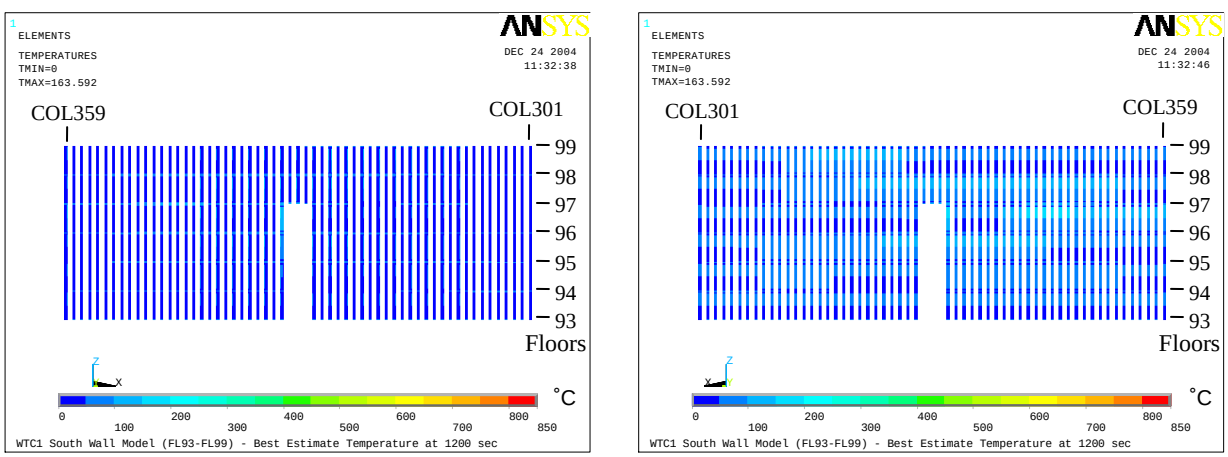

(a) Outside (b) Inside

Figure 3–4. Case A temperature condition of south wall columns of WTC 1 at 20 min.

Figure 3–5. Case A temperature condition of south wall columns of WTC 1 at 30 min.

Figure 3–6. Case A temperature condition of south wall columns of WTC 1 at 40 min.

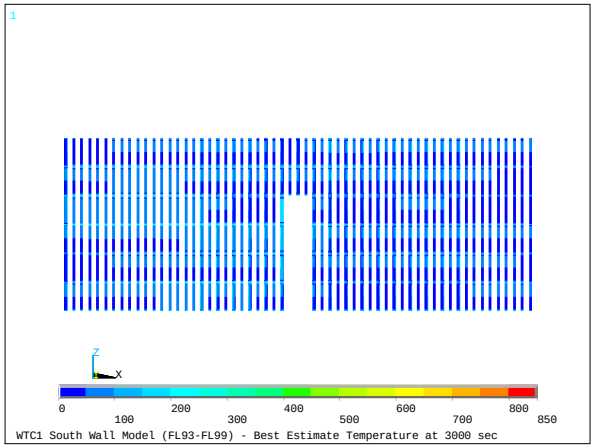

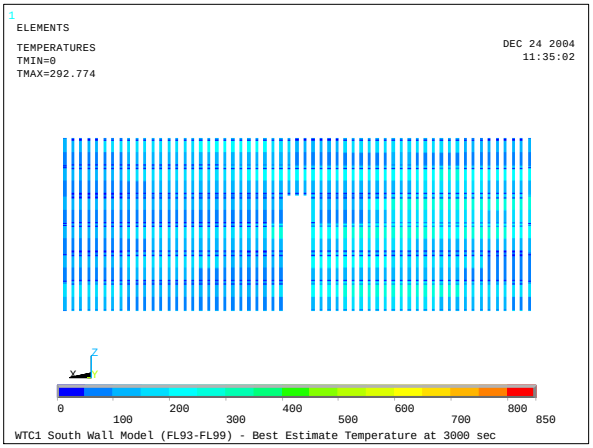

Figure 3–7. Case A temperature condition of south wall columns of WTC 1 at 50 min.

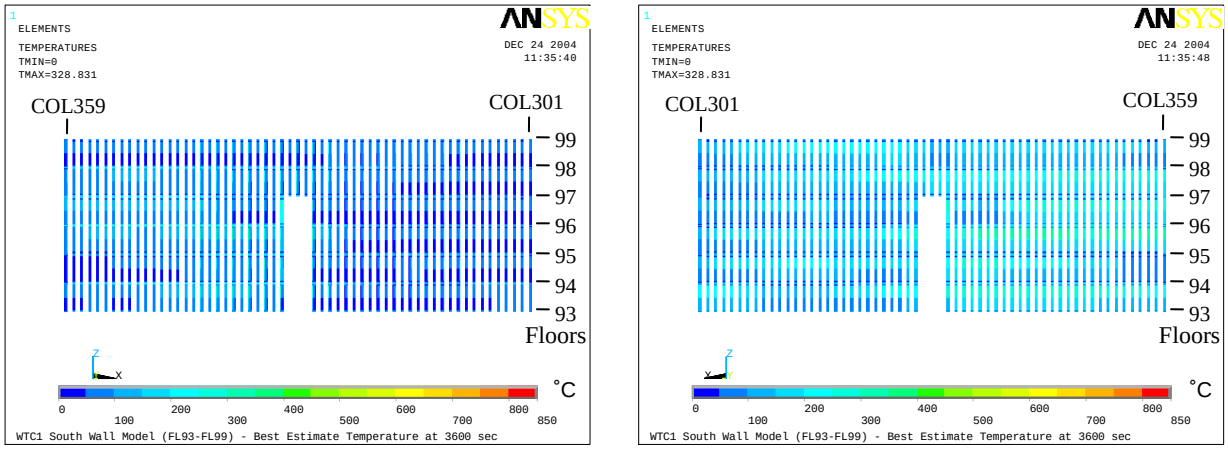

(a) Outside (b) Inside

Figure 3–8. Case A temperature condition of south wall columns of WTC 1 at 60 min.

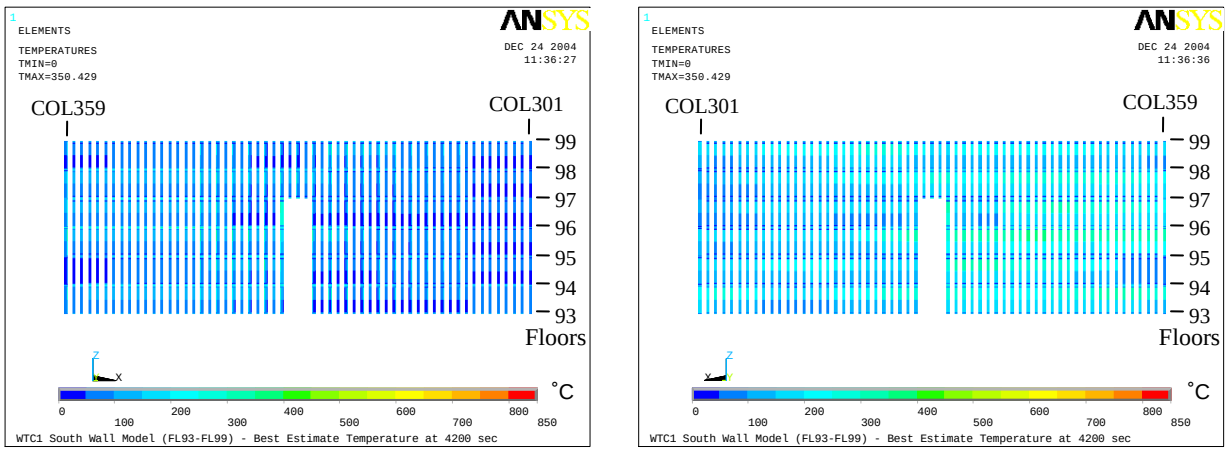

(a) Outside (b) Inside

Figure 3–9. Case A temperature condition of south wall columns of WTC 1 at 70 min.

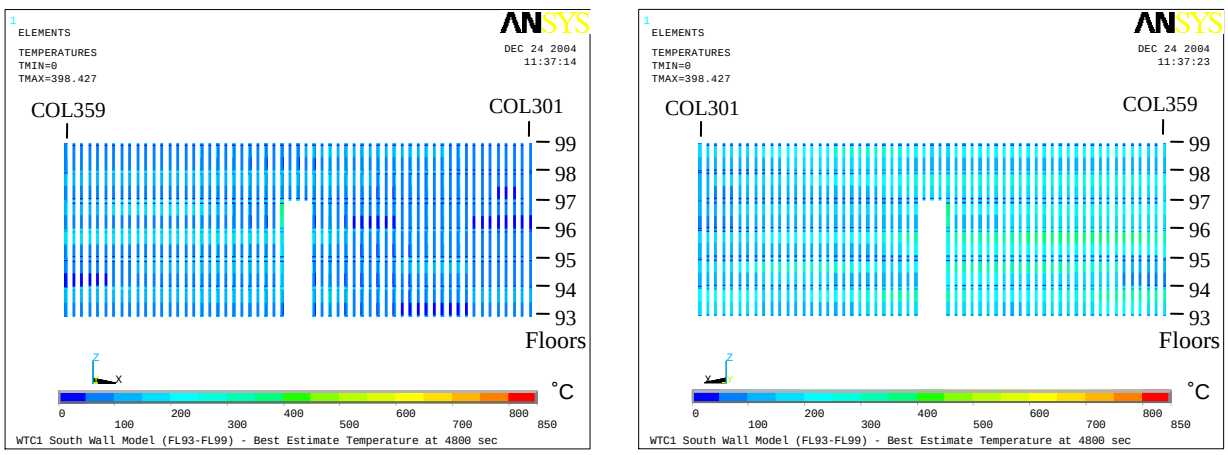

(a) Outside (b) Inside

Figure 3–10. Case A temperature condition of south wall columns of WTC 1 at 80 min.

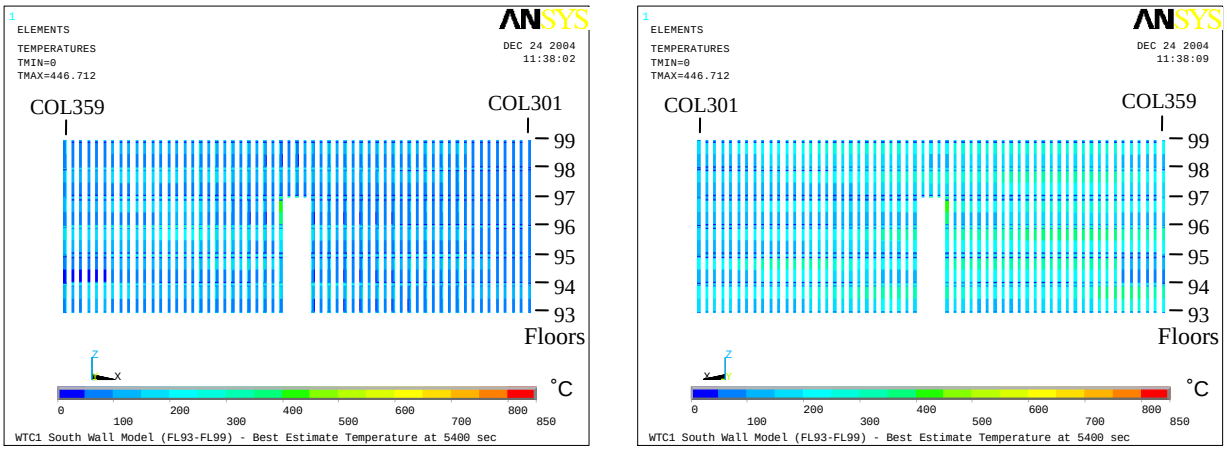

(a) Outside (b) Inside

Figure 3–11. Case A temperature condition of south wall columns of WTC 1 at 90 min.

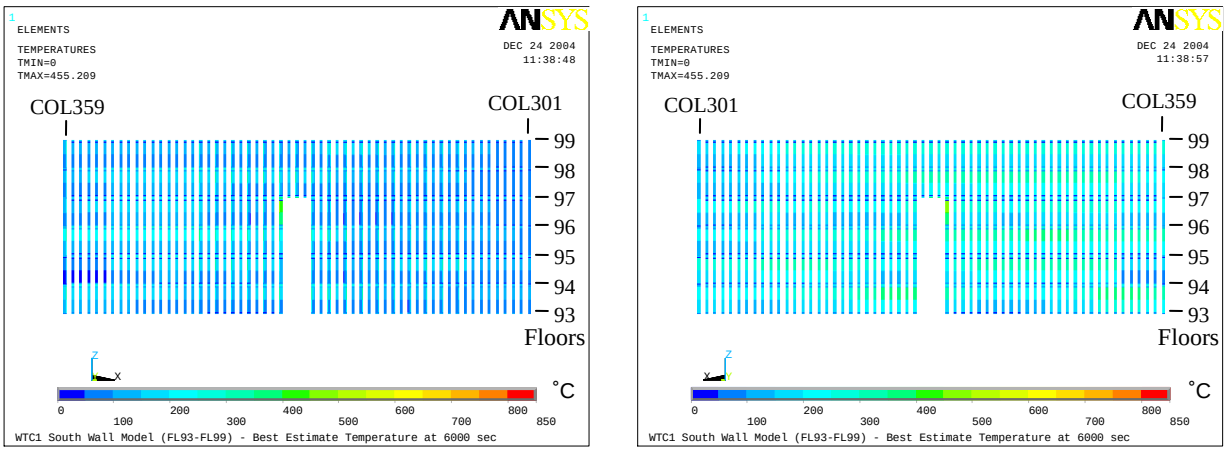

(a) Outside (b) Inside

Figure 3–12. Case A temperature condition of south wall columns of WTC 1 at 100 min.

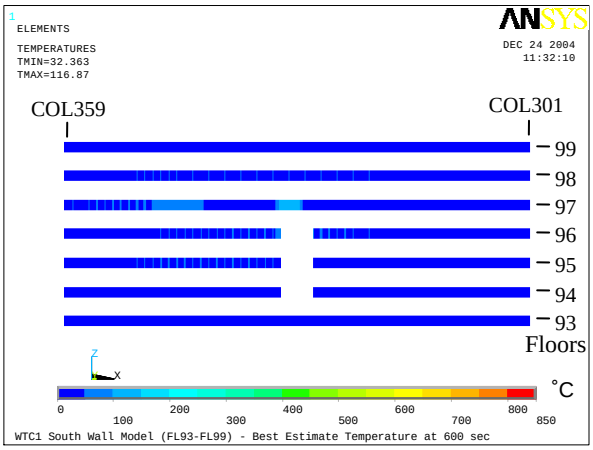

Figure 3–13. Case A temperature condition of south wall spandrels of WTC 1 at 10 min.

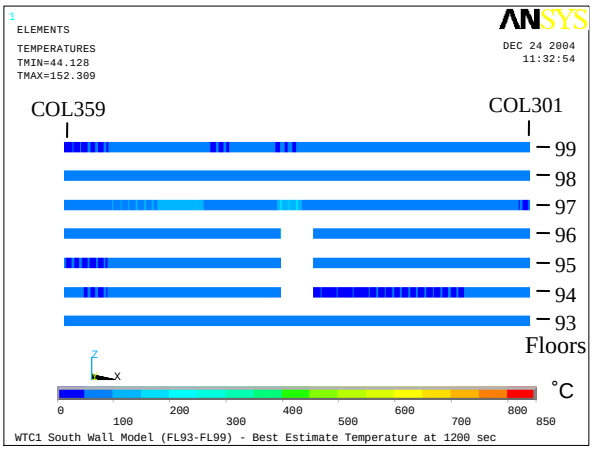

Figure 3–14. Case A temperature condition of south wall spandrels of WTC 1 at 20 min.

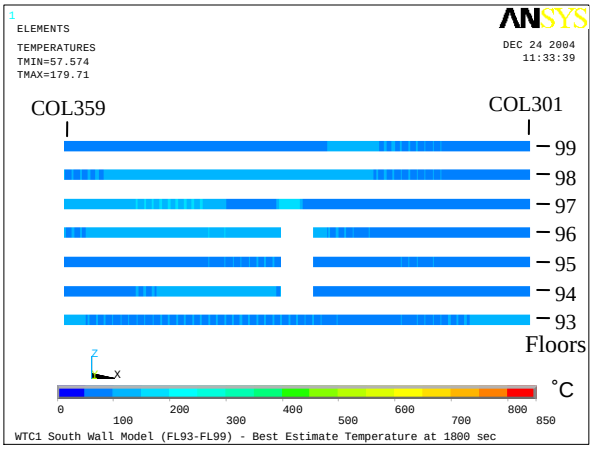

Figure 3–15. Case A temperature condition of south wall spandrels of WTC 1 at 30 min.

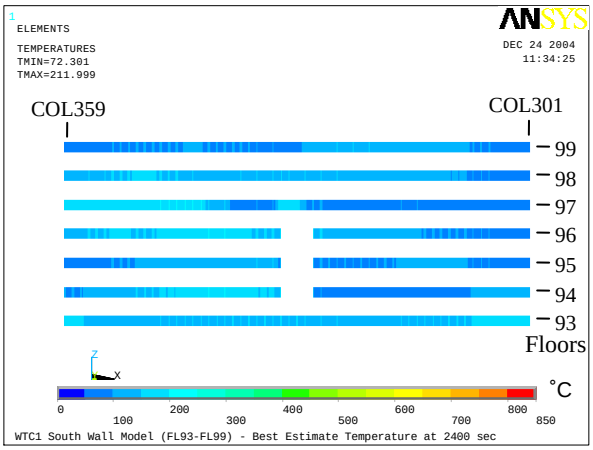

Figure 3–16. Case A temperature condition of south wall spandrels of WTC 1 at 40 min.

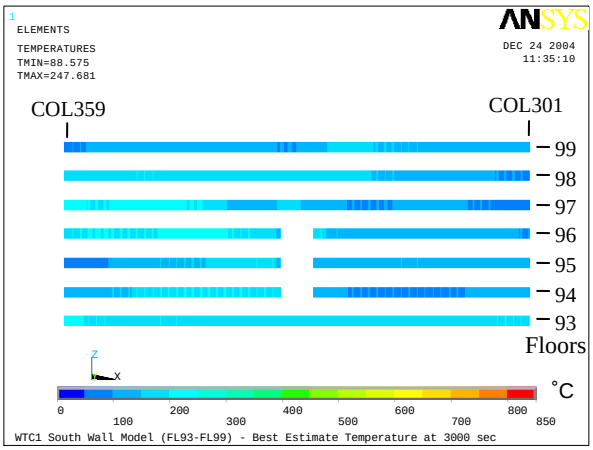

Figure 3–17. Case A temperature condition of south wall spandrels of WTC 1 at 50 min.

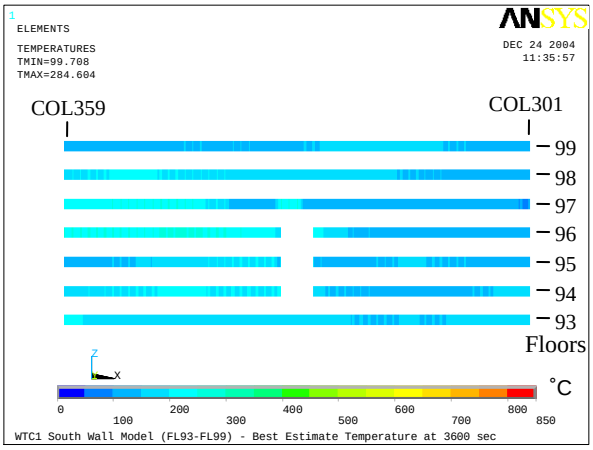

Figure 3–18. Case A temperature condition of south wall spandrels of WTC 1 at 60 min.

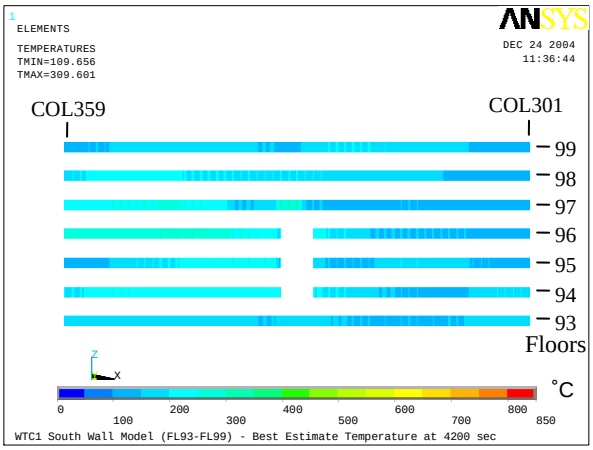

Figure 3–19. Case A temperature condition of south wall spandrels of WTC 1 at 70 min.

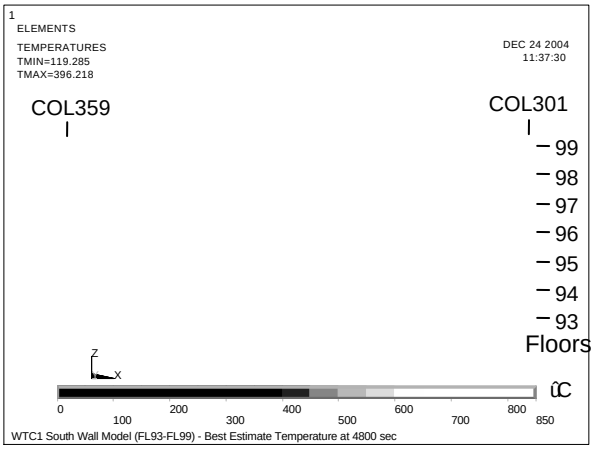

Figure 3–20. Case A temperature condition of south wall spandrels of WTC 1 at 80 min.

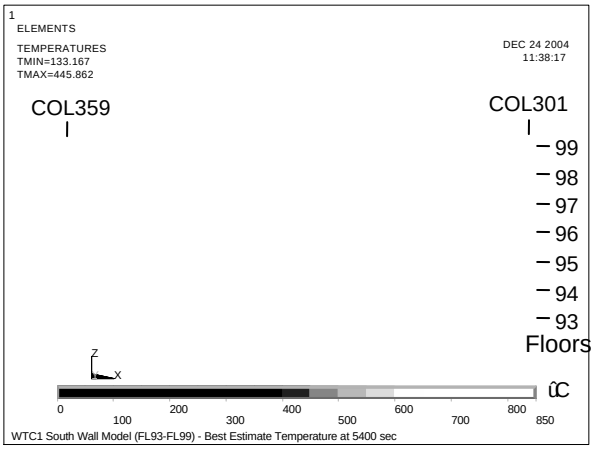

Figure 3–21. Case A temperature condition of south wall spandrels of WTC 1 at 90 min.

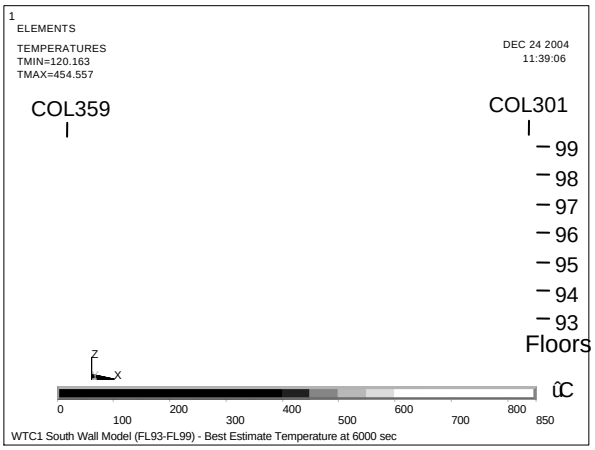

Figure 3–22. Case A temperature condition of south wall spandrels of WTC 1 at 100 min.

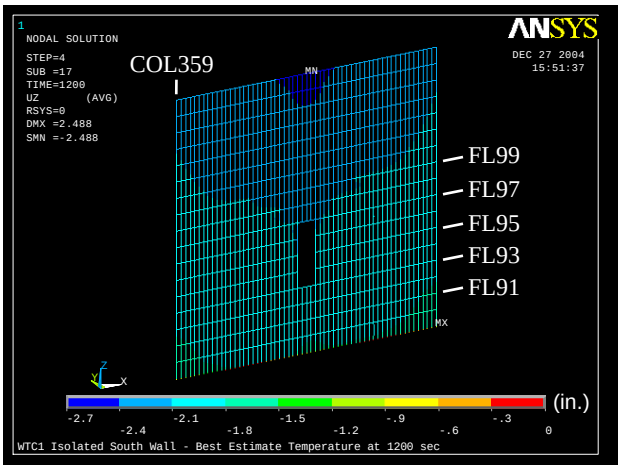

(a) At 20 min

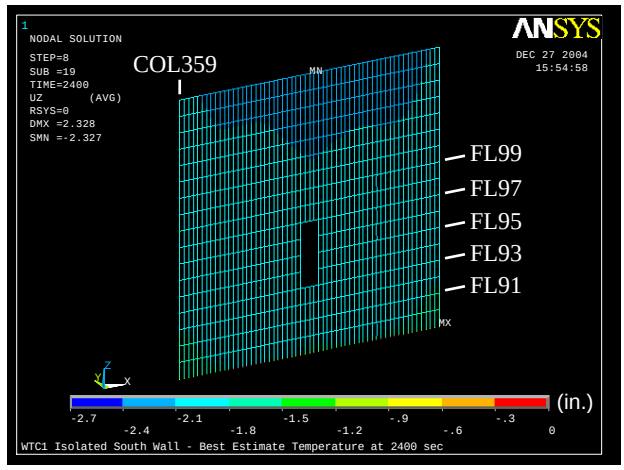

(b) At 40 min

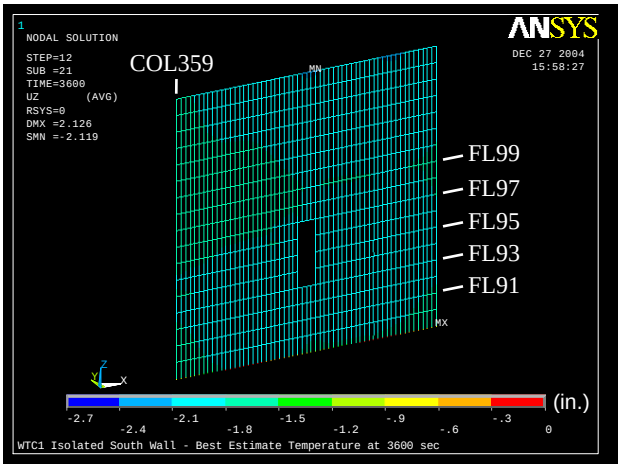

(c) At 60 min

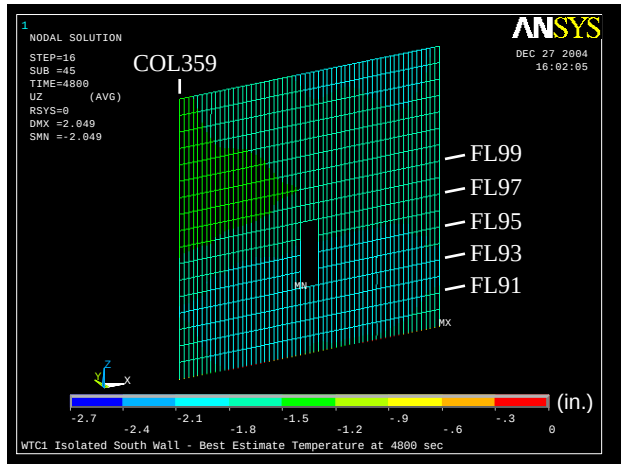

(d) At 80 min

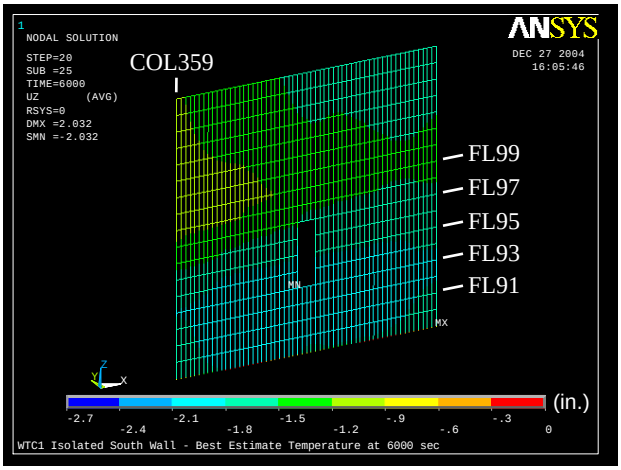

(e) At 100 min

Figure 3–24. Vertical displacements of isolated south wall model of WTC 1 for Case A temperature condition (downward displacement is negative).

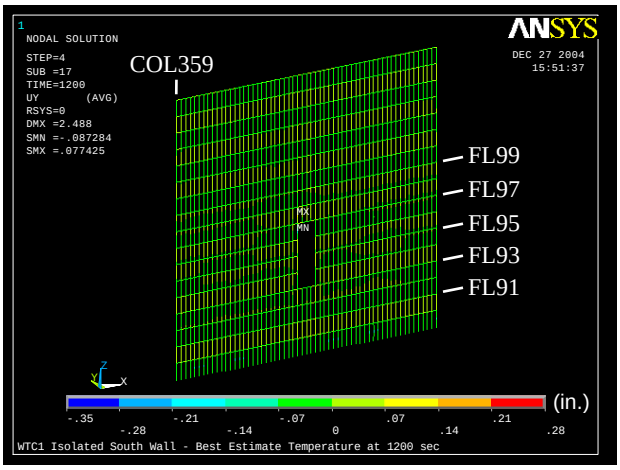

(a) at 20 min

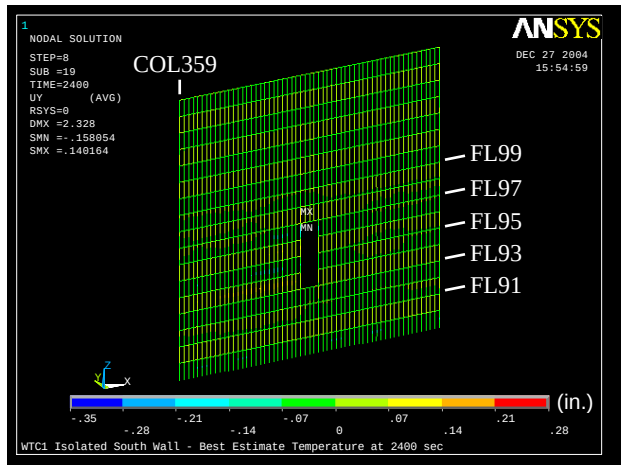

(b) at 40 min

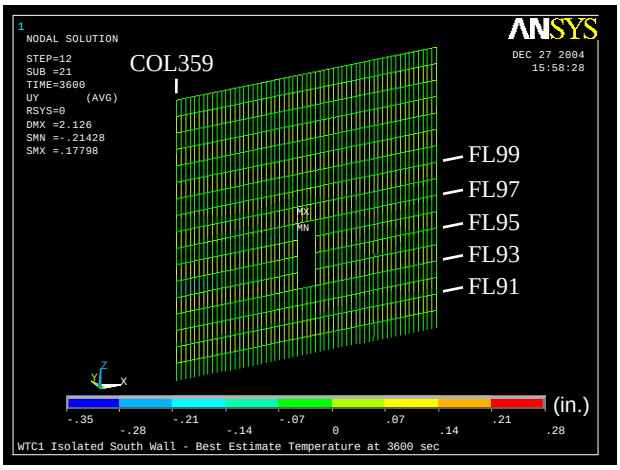

(c) at 60 min

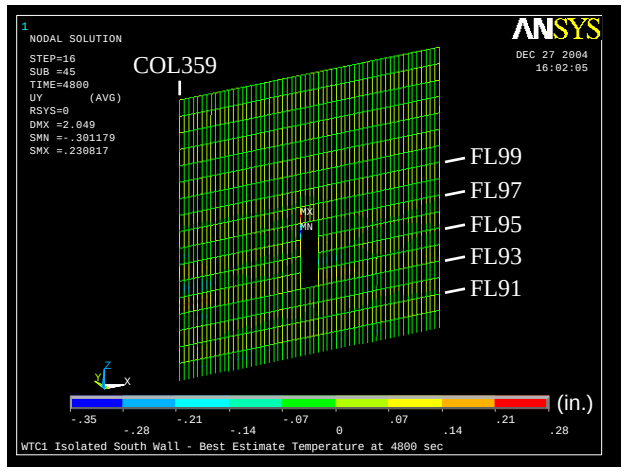

(d) at 80 min

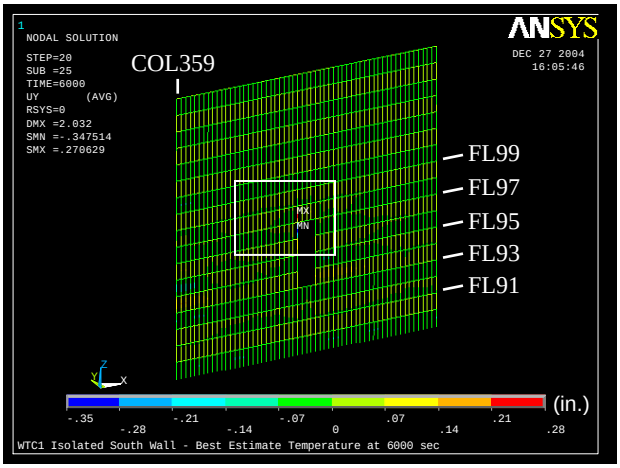

(e) at 100 min

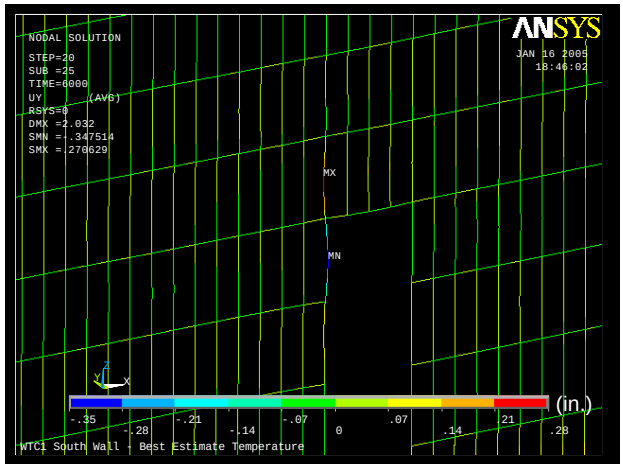

(f) Close-up view at 100 min
(30X displacement magnification)

Figure 3–25. Out-of-plane displacements of isolated south wall model of WTC 1 for Case A temperature condition (inward displacement is positive).

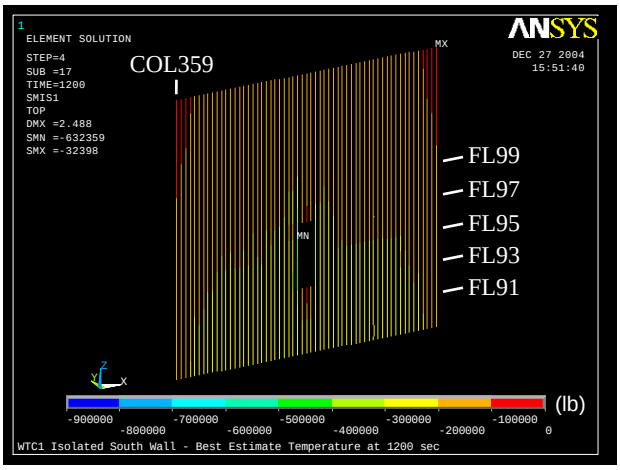

(a) at 20 min

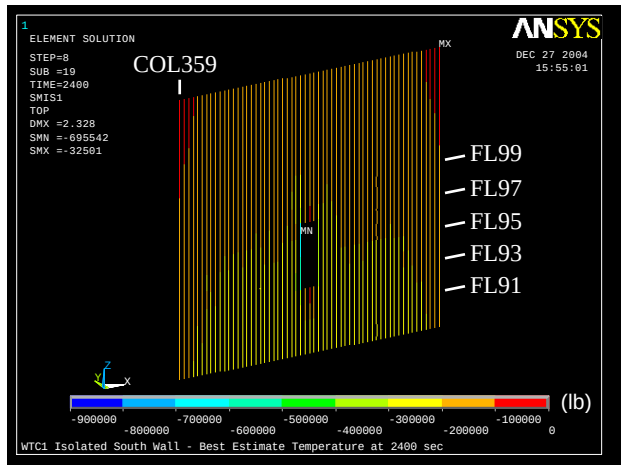

(b) at 40 min

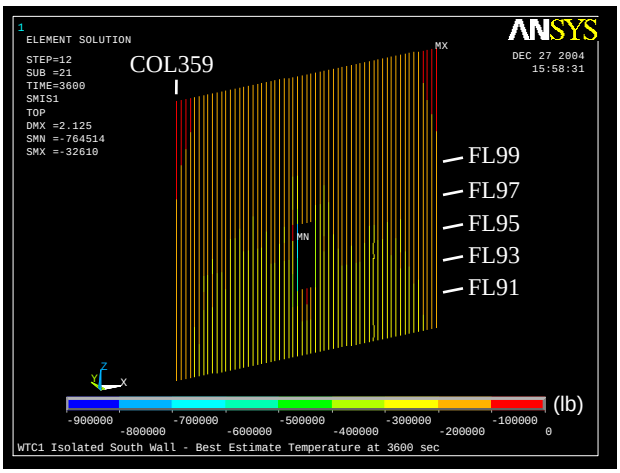

(c) at 60 min

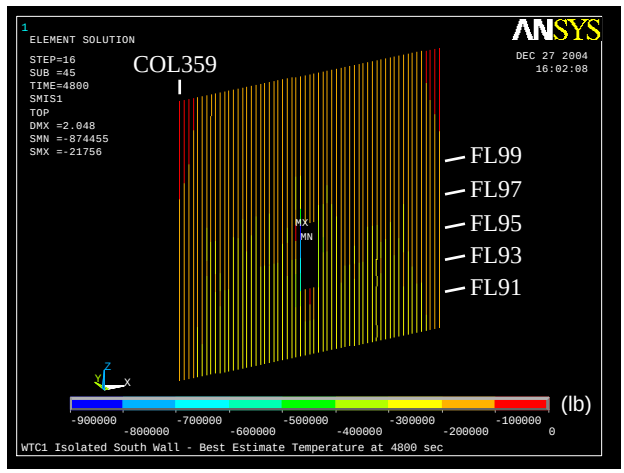

(d) at 80 min

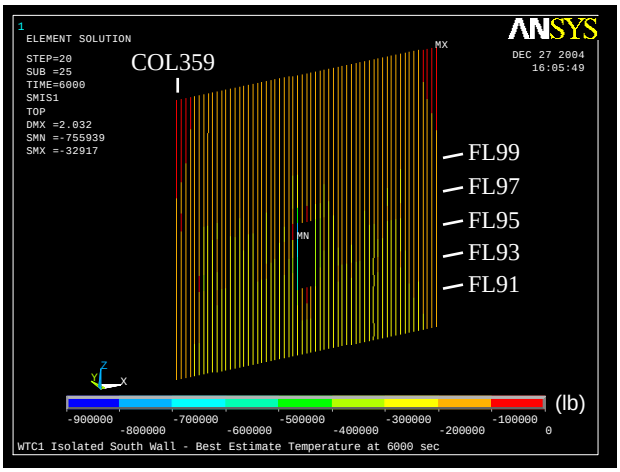

(e) at 100 min

Figure 3–26. Axial load in columns of isolated south wall model of WTC 1 for Case A temperature condition (compression is negative).

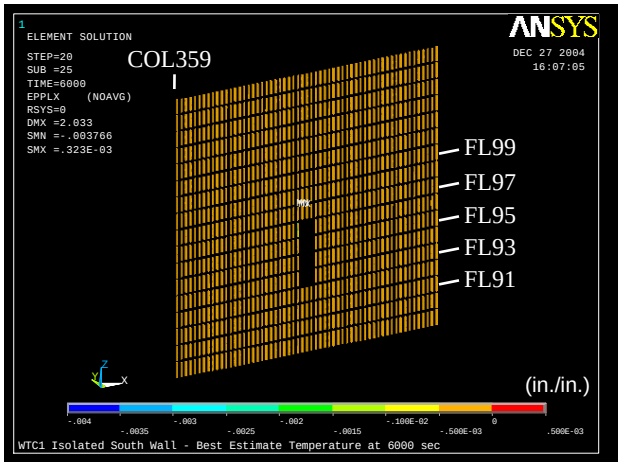

Figure 3–27. Plastic strain in columns of isolated south wall model of WTC 1 for Case A temperature condition at 100 min (compressive strain is negative).

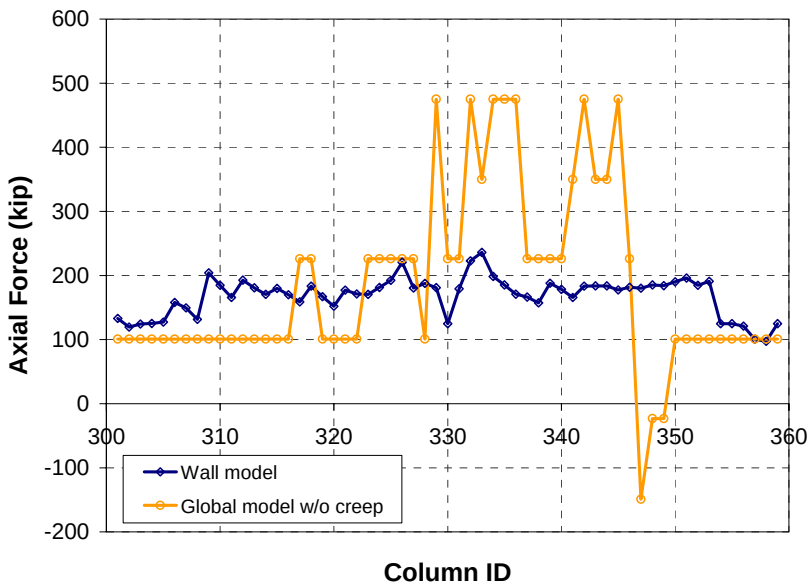

Figure 3–28. Axial load in columns of south wall of WTC 1 at 100 min: isolated wall model for Case A temperature condition compared to global model without creep for Case A_i conditions (compression is positive).

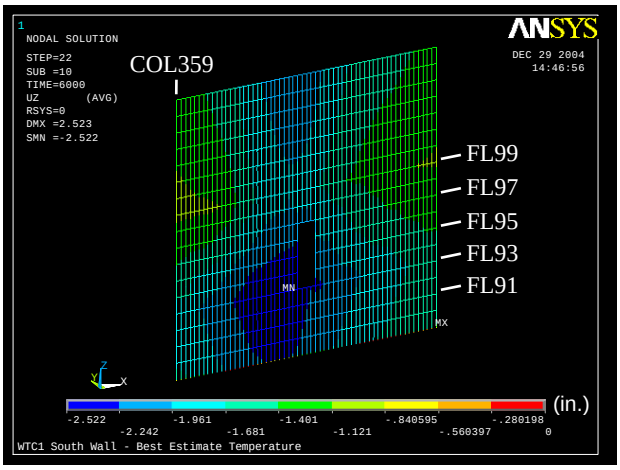

(a) Vertical displacement
(downward displacement is negative)

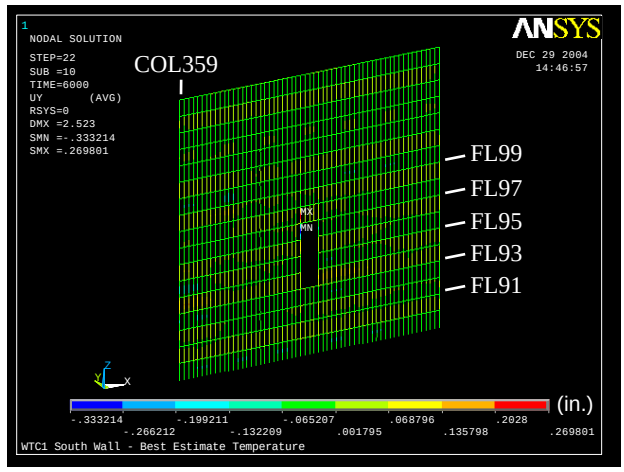

(b) Out-of-plane displacement
(inward displacement is positive)

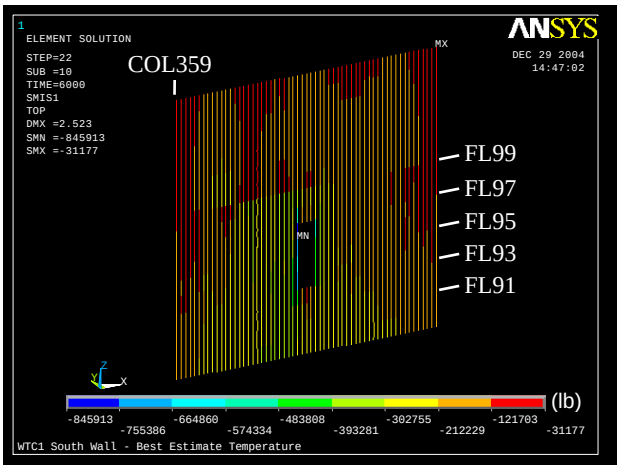

(c) Axial force in columns
(compression is negative)

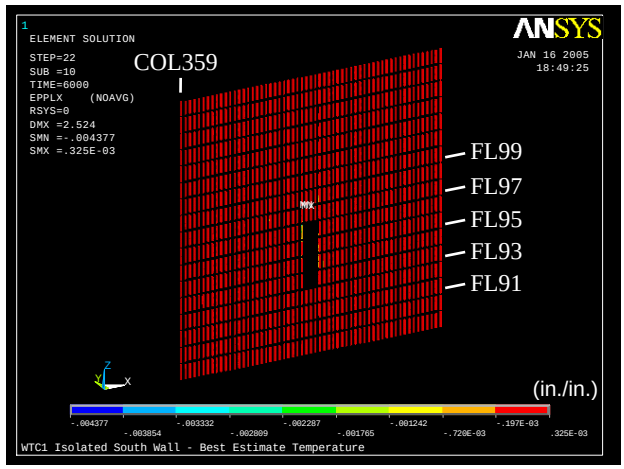

(d) Plastic strain in columns
(compressive strain is negative)

Figure 3–29. Responses of isolated south wall model of WTC 1 after corrective loads from the global model were applied (Case A temperature condition at 100 min).

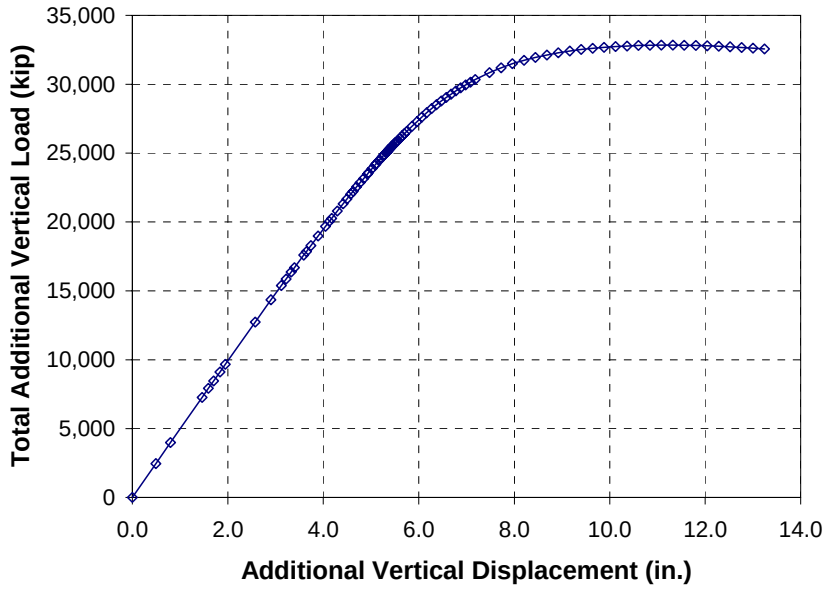

Figure 3–30. Total additional vertical load versus additional vertical displacement during push-down analysis of isolated south wall model of WTC 1 for Case A temperature condition (compression is positive).

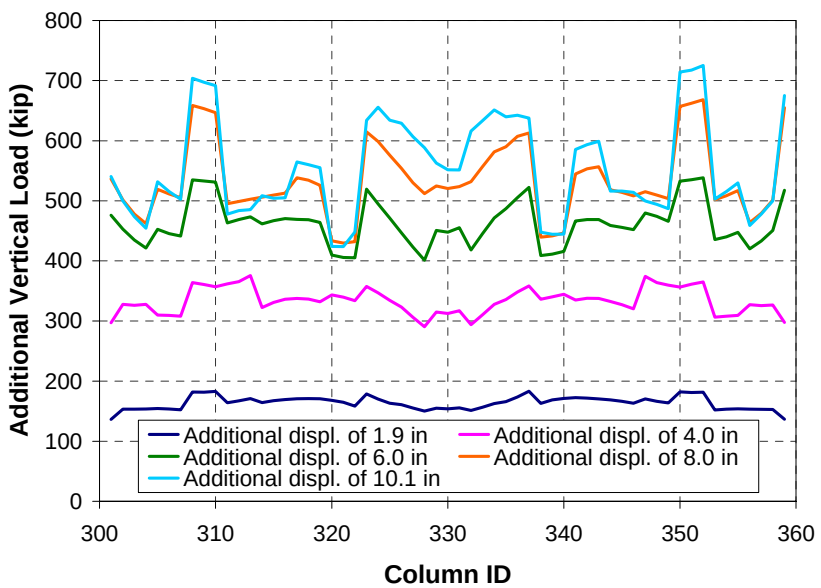

Figure 3–31. Additional vertical load per column at different additional vertical displacements during push-down analysis of isolated south wall model of WTC 1 for Case A temperature condition (compression is positive).

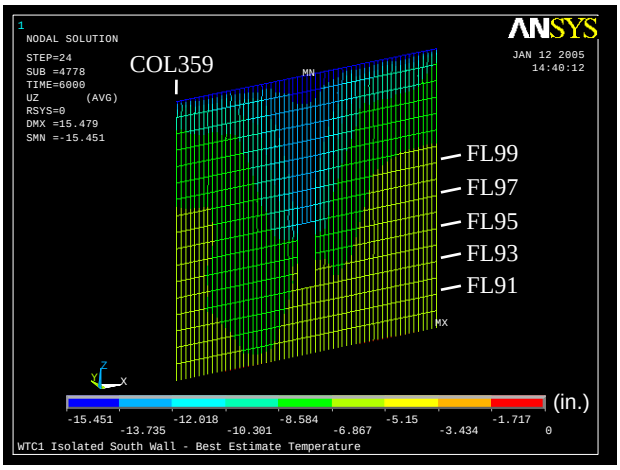

(a) Vertical displacement
(downward displacement is negative)

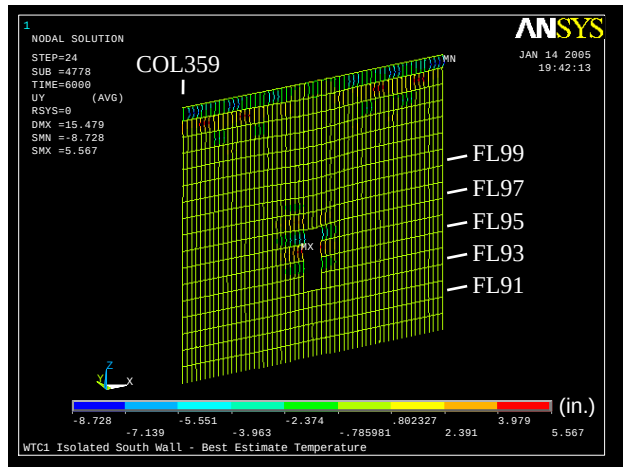

(b) Out-of-plane displacement
(inward displacement is positive,
5X displacement magnification)

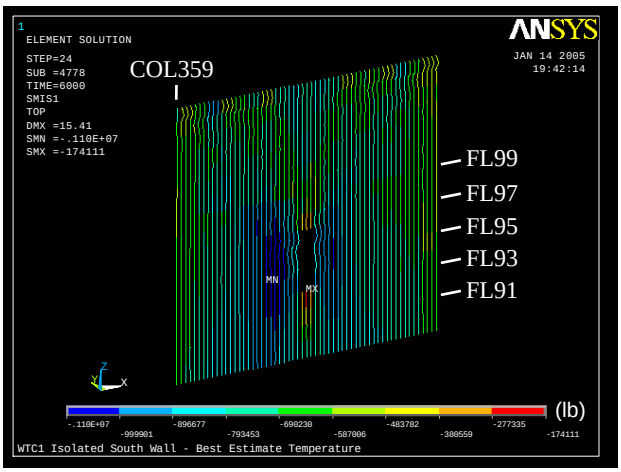

(c) Axial force in columns
(compression is negative,
5X displacement magnification)

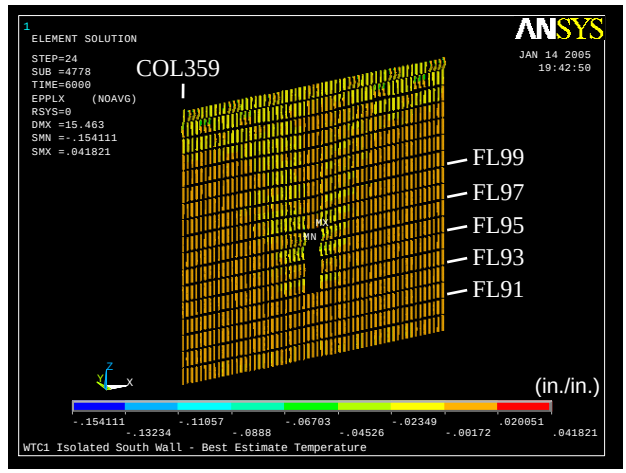

(d) Plastic strain in columns
(compressive strain is negative,
5X displacement magnification)

Figure 3–32. Response of isolated south wall model of WTC 1 to Case A temperature condition and push down at the end of the push-down analysis.

Case B Temperature Condition

In the full floor model analyses, described in Appendix A, Floors 97 and 98 disconnected from the exterior walls at several columns between 80 min and 90 min. Figure 3–33 shows locations of the out-of-plane supports of the exterior wall model of WTC 1 at 100 min.

Figures 3–34 to 3–43 show the temperature distributions of Case B condition in the south wall columns of WTC 1 from 10 min to 100 min. Figures 3–34 to 3–43 show that temperatures on the south wall became very high near the impact damage area, reaching 801°C. Figures 3–44 to 3–53 show the temperature distributions of Case B condition in spandrels. The temperatures of the spandrels are also quite high, reaching 778°C.

Figures 3–54 to 3–56 show the vertical displacements, the out-of-plane displacements, and the axial loads, respectively, in the south wall columns of WTC 1 for Case B temperature condition. Throughout the temperature time history the maximum vertical displacement changed negligibly, starting at 2.64 in. immediately after impact and ending at 2.60 in. at 100 min. The maximum inward out-of-plane displacement was 0.66 in. at Column 336 at Floor 98 at 100 min, while the maximum outward out-of-

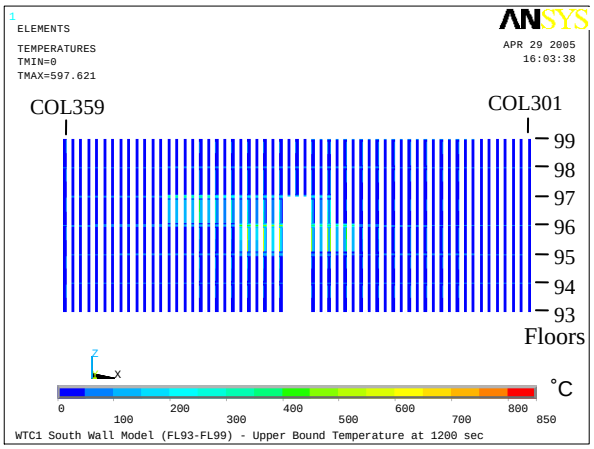

(a) Outside

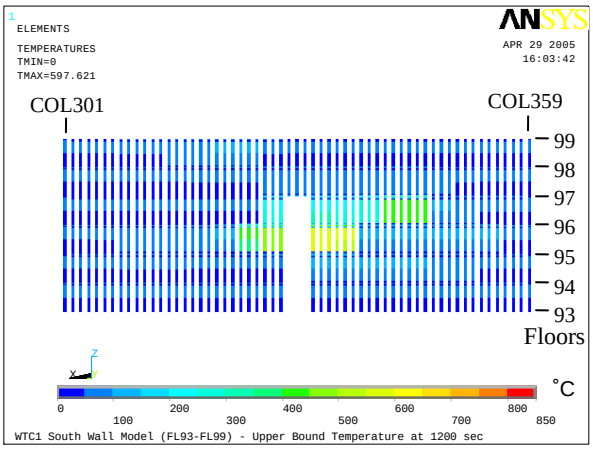

(b) Inside

Figure 3–35. Case B temperature condition of south wall columns of WTC 1 at 20 min.

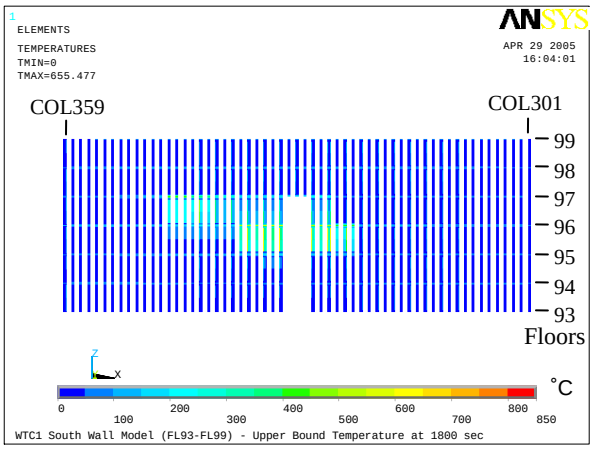

(a) Outside

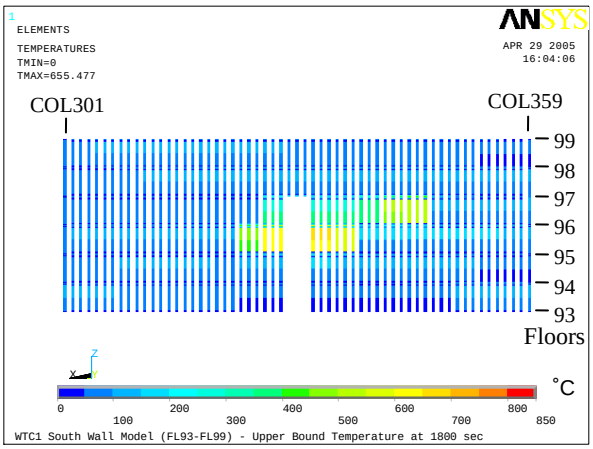

(b) Inside

Figure 3–36. Case B temperature condition of south wall columns of WTC 1 at 30 min.

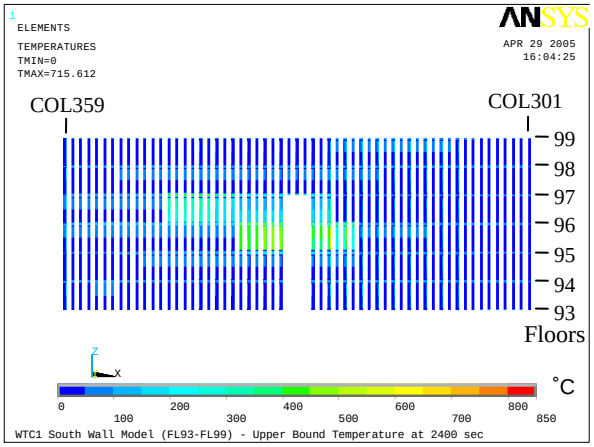

(a) Outside

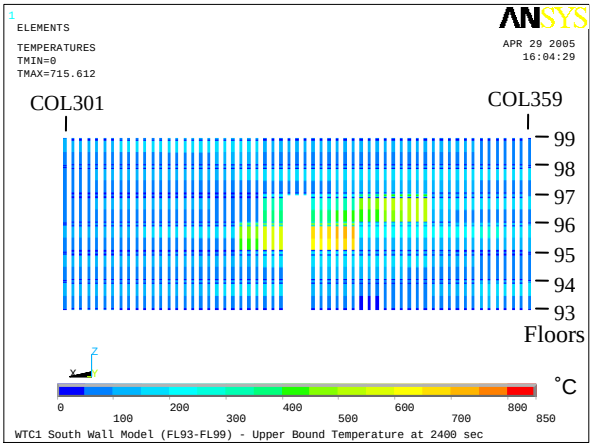

(b) Inside

Figure 3–37. Case B temperature condition of south wall columns of WTC 1 at 40 min.

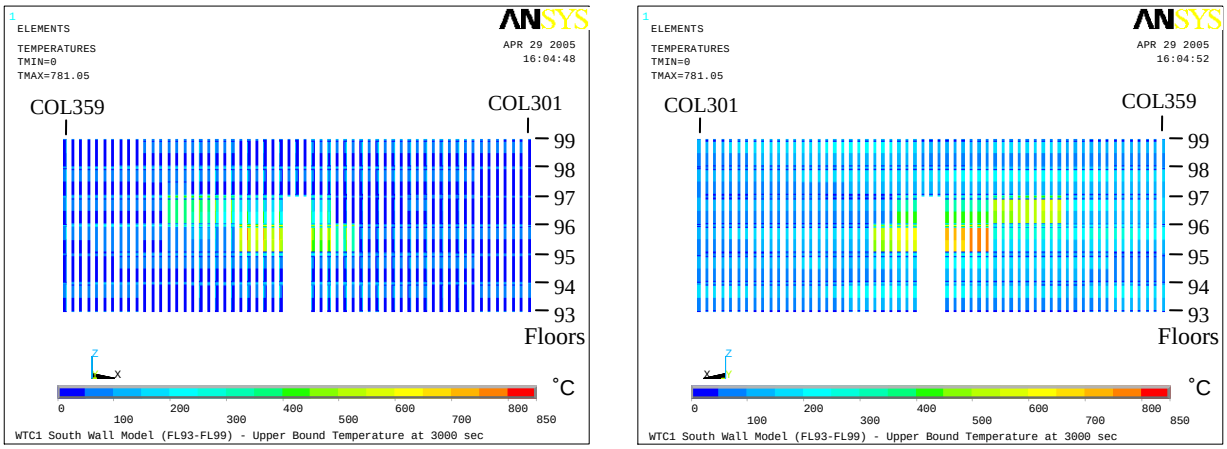

(a) Outside (b) Inside

Figure 3–38. Case B temperature condition of south wall columns of WTC 1 at 50 min.

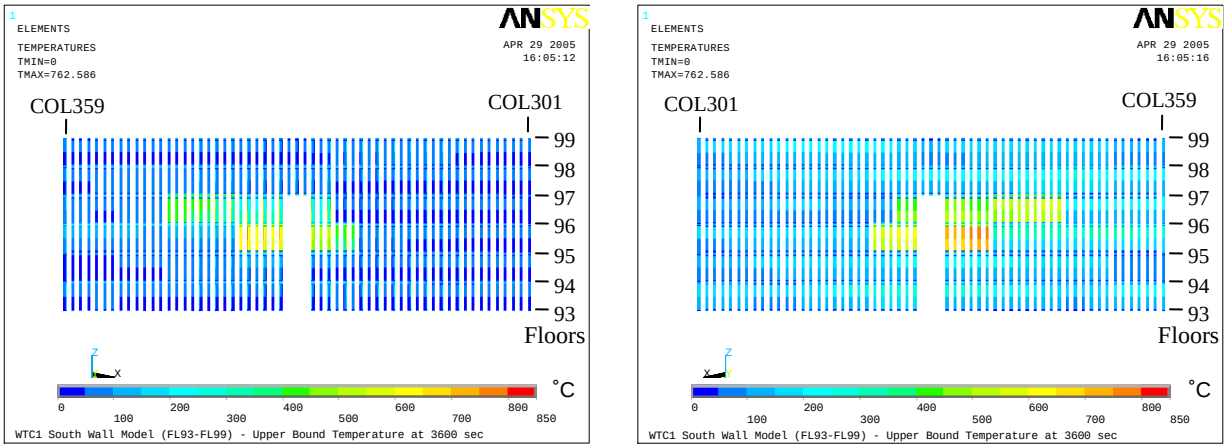

(a) Outside (b) Inside

Figure 3–39. Case B temperature condition of south wall columns of WTC 1 at 60 min.

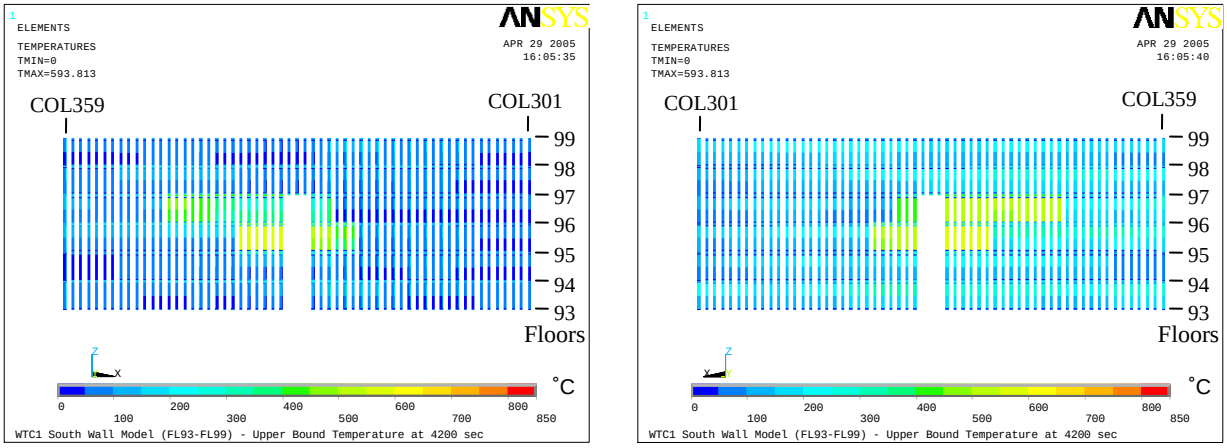

(a) Outside (b) Inside

Figure 3–40. Case B temperature condition of south wall columns of WTC 1 at 70 min.

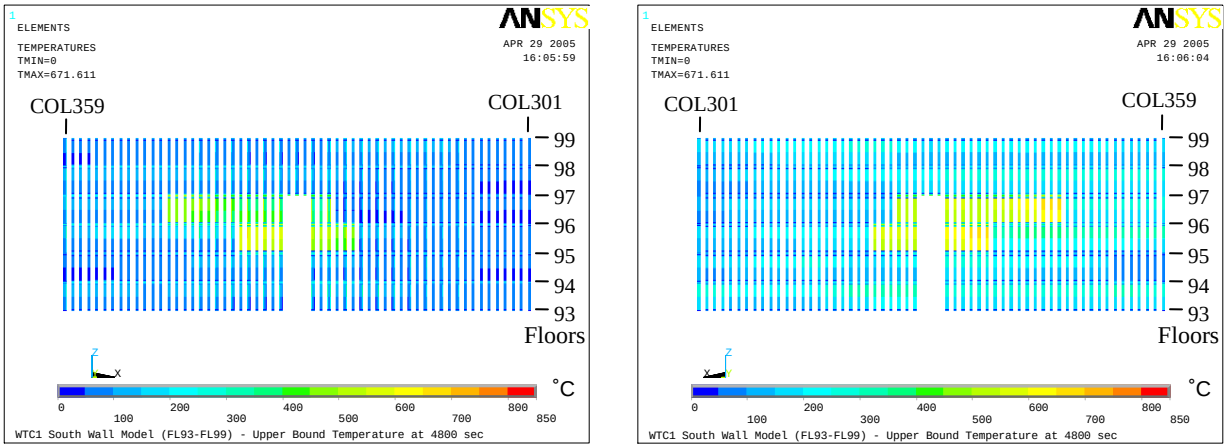

(a) Outside (b) Inside

Figure 3–41. Case B temperature condition of south wall columns of WTC 1 at 80 min.

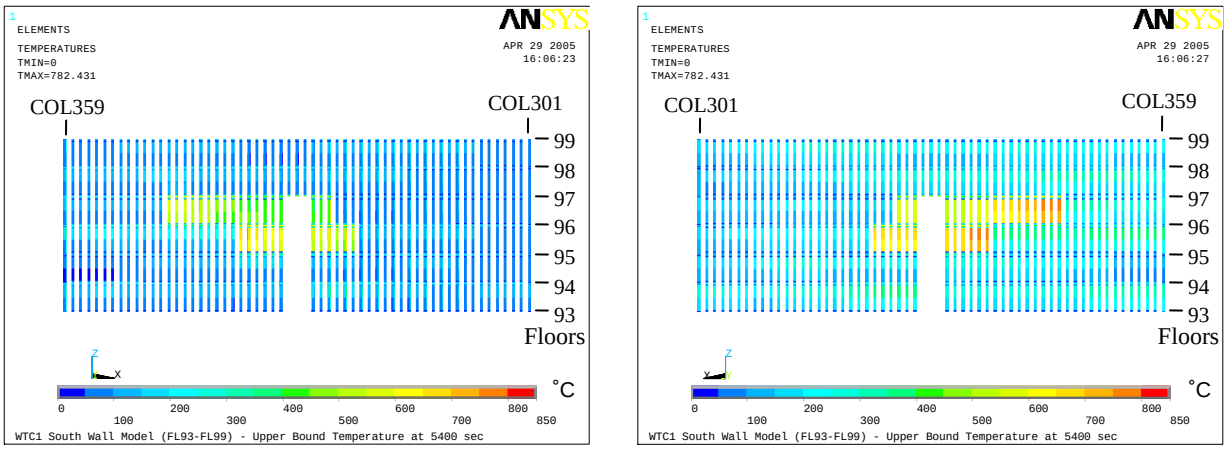

(a) Outside (b) Inside

Figure 3–42. Case B temperature condition of south wall columns of WTC 1 at 90 min.

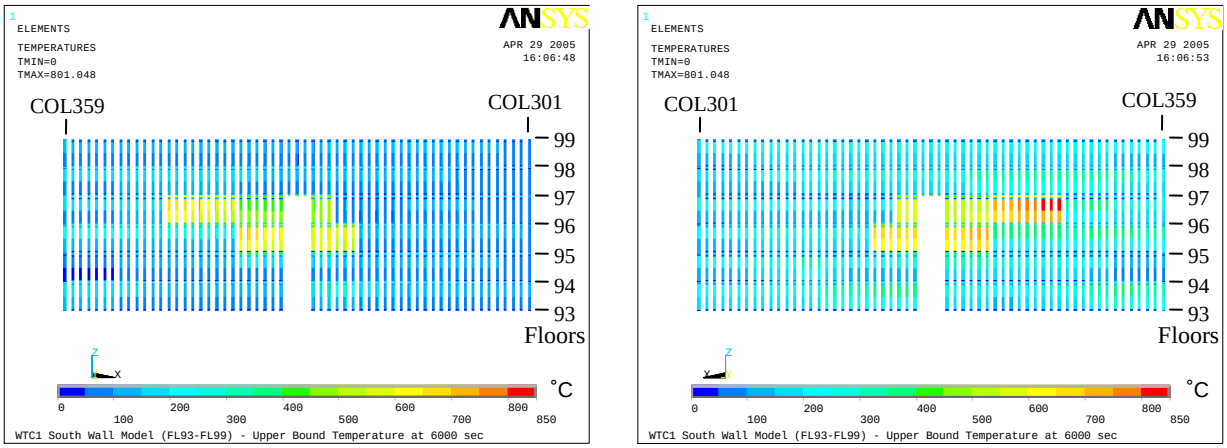

(a) Outside (b) Inside

Figure 3–43. Case B temperature condition of south wall columns of WTC 1 at 100 min.

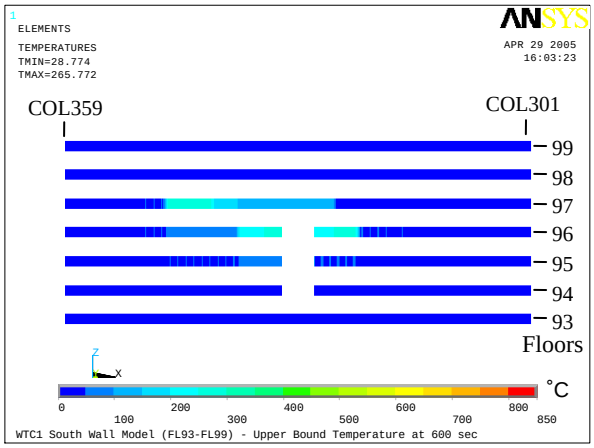

Figure 3–44. Case B temperature condition of south wall spandrels of WTC 1 at 10 min.

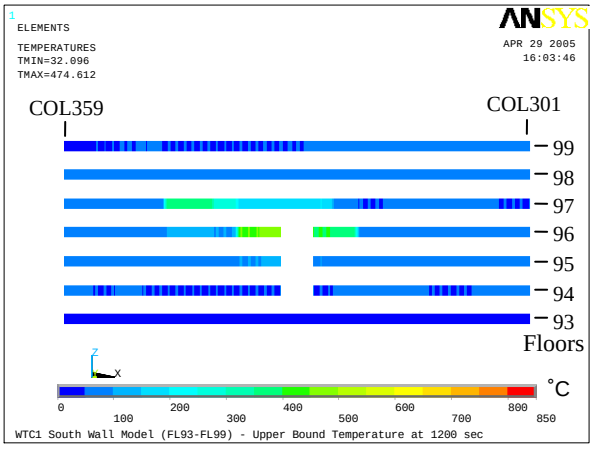

Figure 3–45. Case B temperature condition of south wall spandrels of WTC 1 at 20 min.

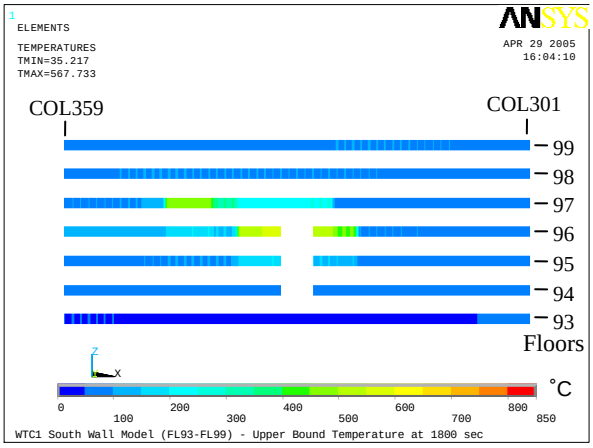

Figure 3–46. Case B temperature condition of south wall spandrels of WTC 1 at 30 min.

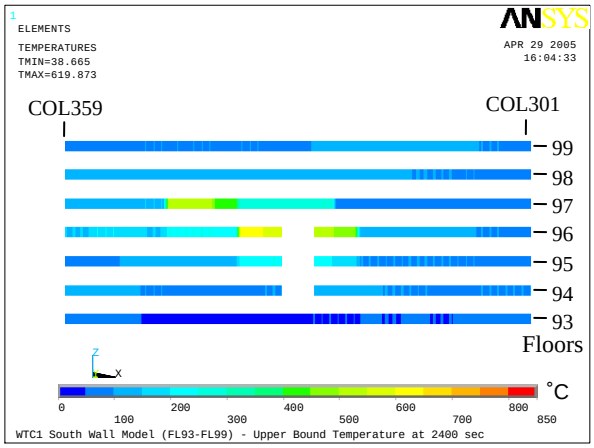

Figure 3–47. Case B temperature condition of south wall spandrels of WTC 1 at 40 min.

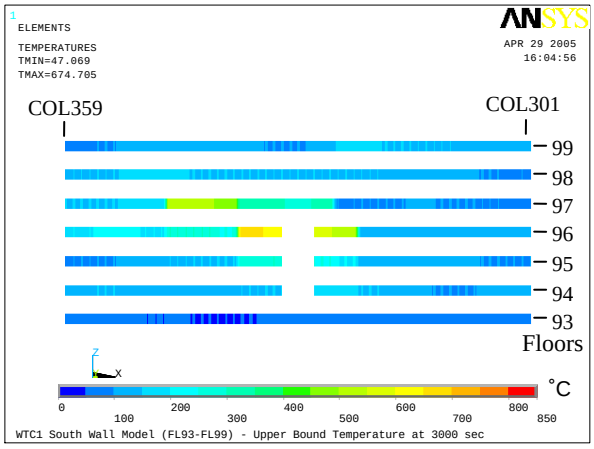

Figure 3–48. Case B temperature condition of south wall spandrels of WTC 1 at 50 min.

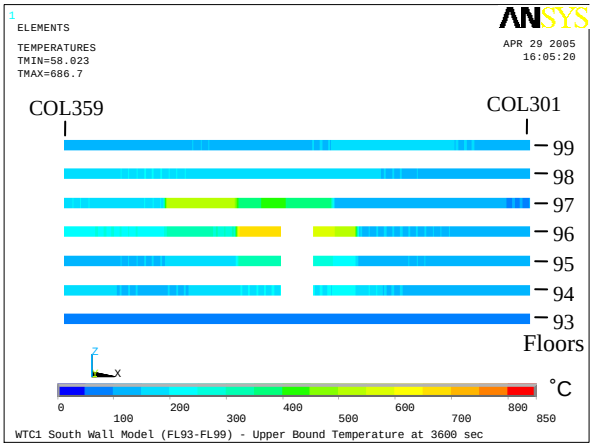

Figure 3–49. Case B temperature condition of south wall spandrels of WTC 1 at 60 min.

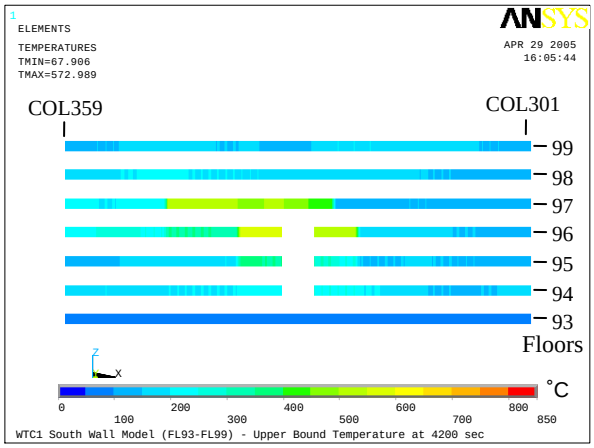

Figure 3–50. Case B temperature condition of south wall spandrels of WTC 1 at 70 min.

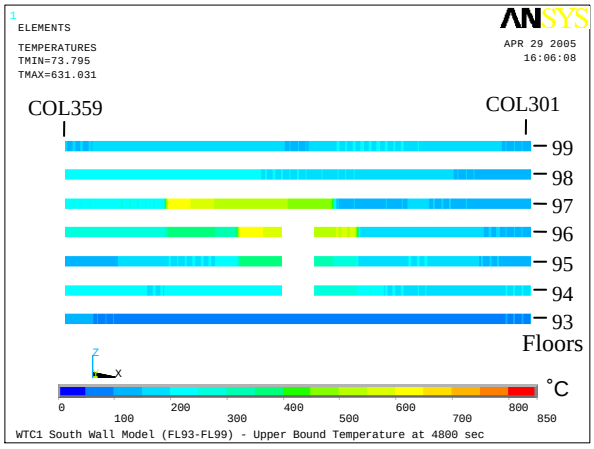

Figure 3–51. Case B temperature condition of south wall spandrels of WTC 1 at 80 min.

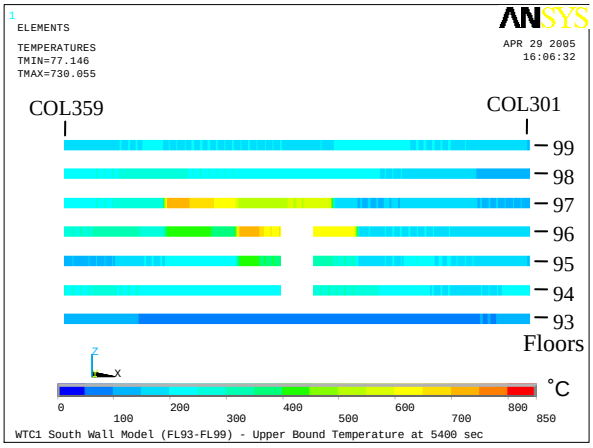

Figure 3–52. Case B temperature condition of south wall spandrels of WTC 1 at 90 min.

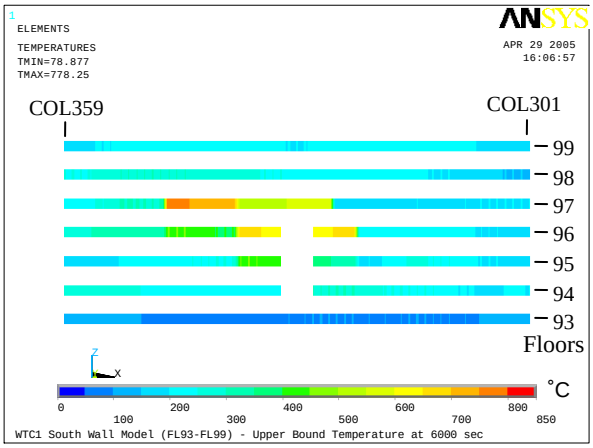

Figure 3–53. Case B temperature condition of south wall spandrels of WTC 1 at 100 min.

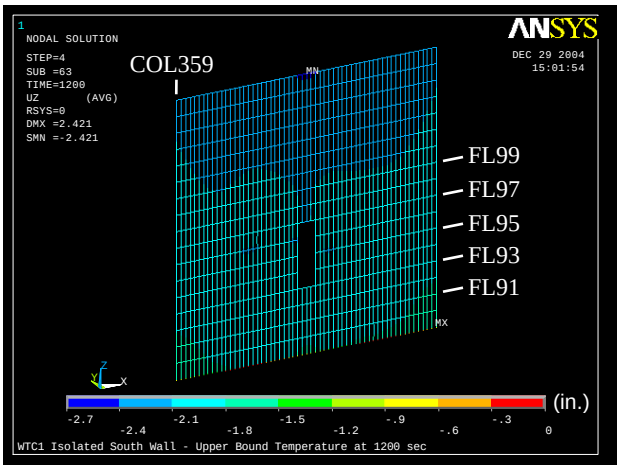

(a) At 20 min

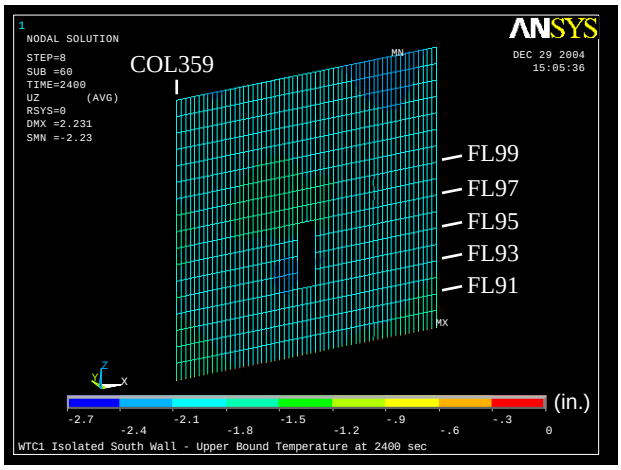

(b) At 40 min

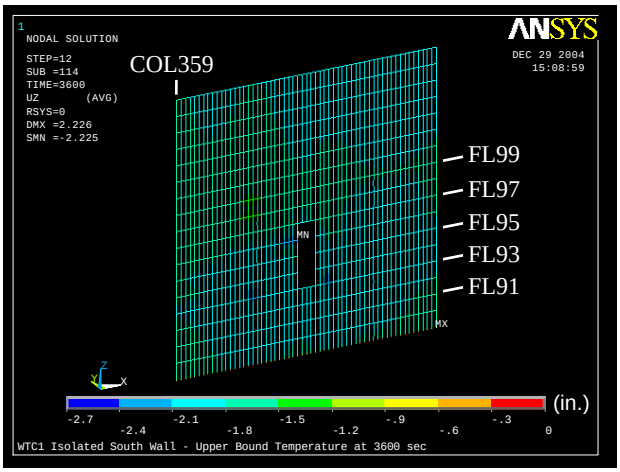

(c) At 60 min

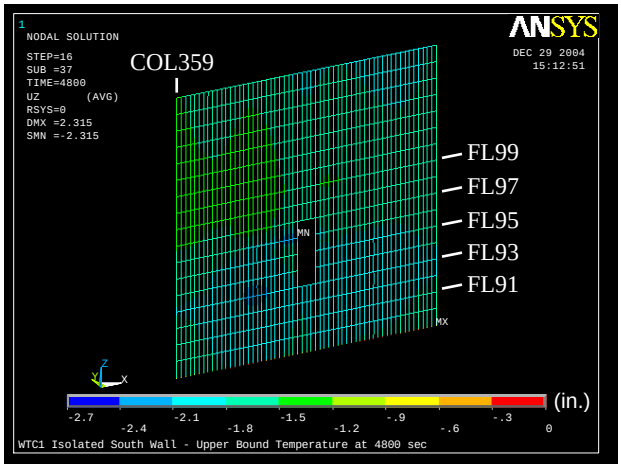

(d) At 80 min

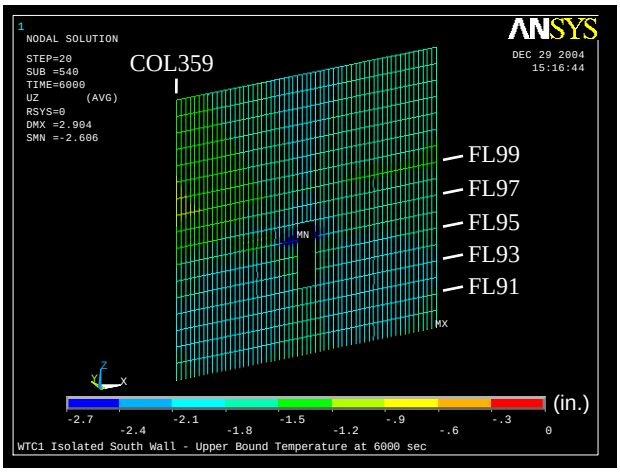

(e) At 100 min

Figure 3–54. Vertical displacement of isolated south wall model of WTC 1 for Case B temperature condition (downward displacement is negative).

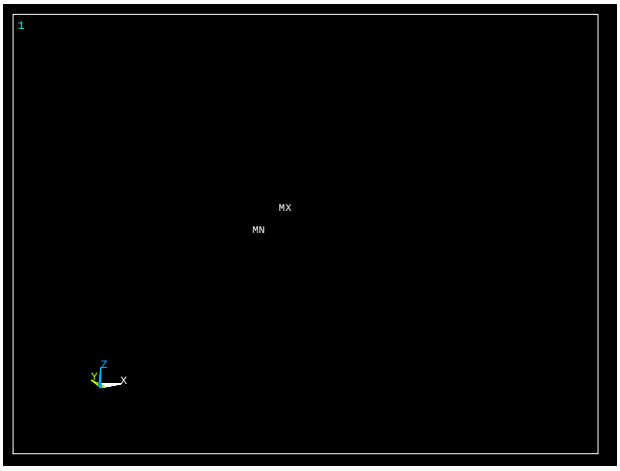

Figure 3–55. Out-of-plane displacement of isolated south wall model of WTC 1 for Case B temperature condition (inward displacement is positive).

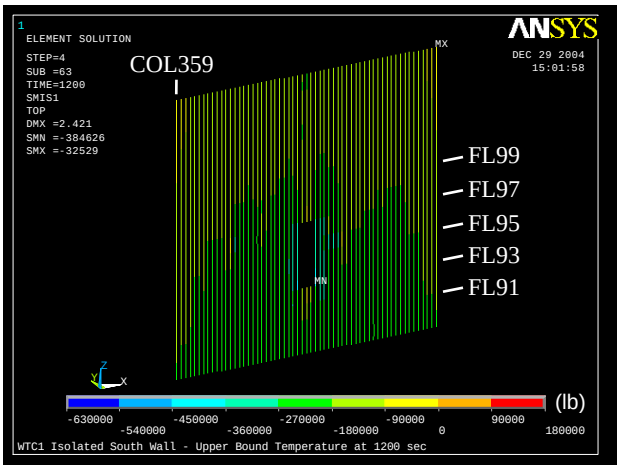

(a) At 20 min

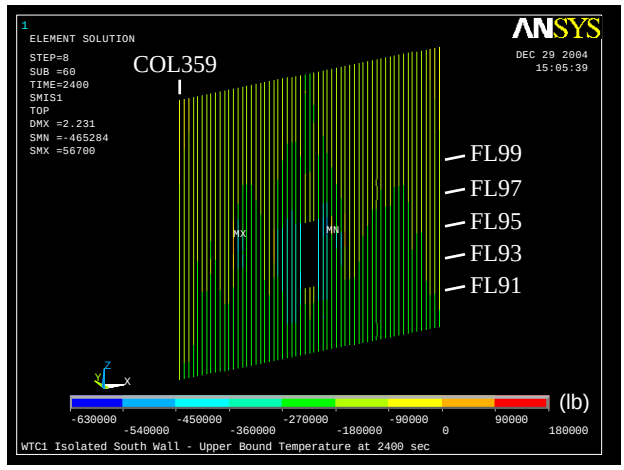

(b) At 40 min

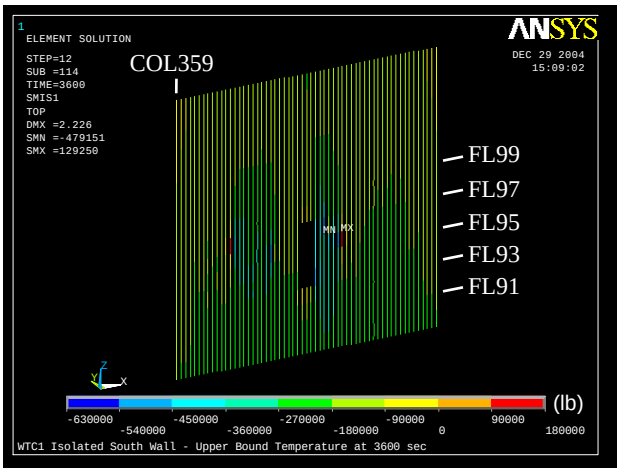

(c) At 60 min

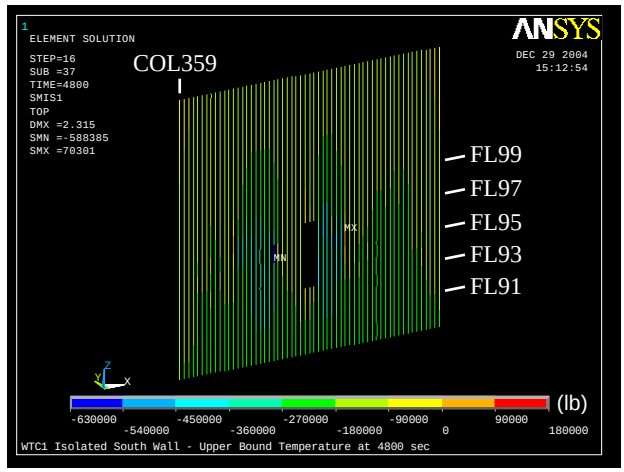

(d) At 80 min

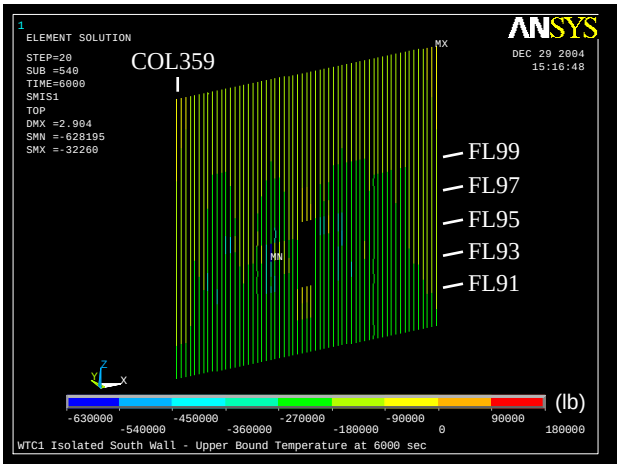

(e) At 100 min

Figure 3–56. Axial load in columns of isolated south wall model of WTC 1 for Case B temperature condition (compression is negative).

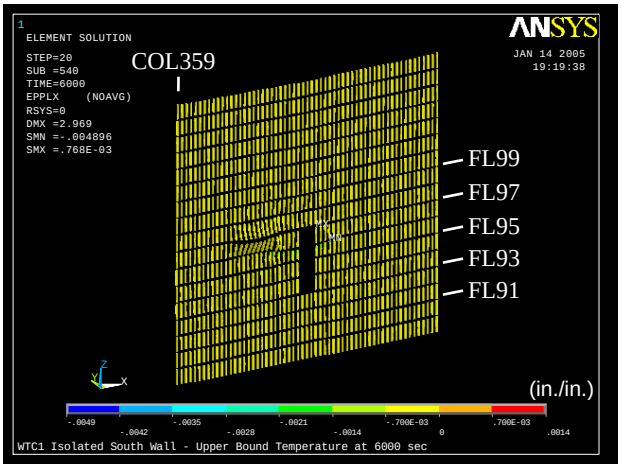

(30X displacement magnification)

Figure 3–57. Plastic strain in columns of isolated south wall model of WTC 1 for Case B temperature condition at 100 min (compressive strain is negative).

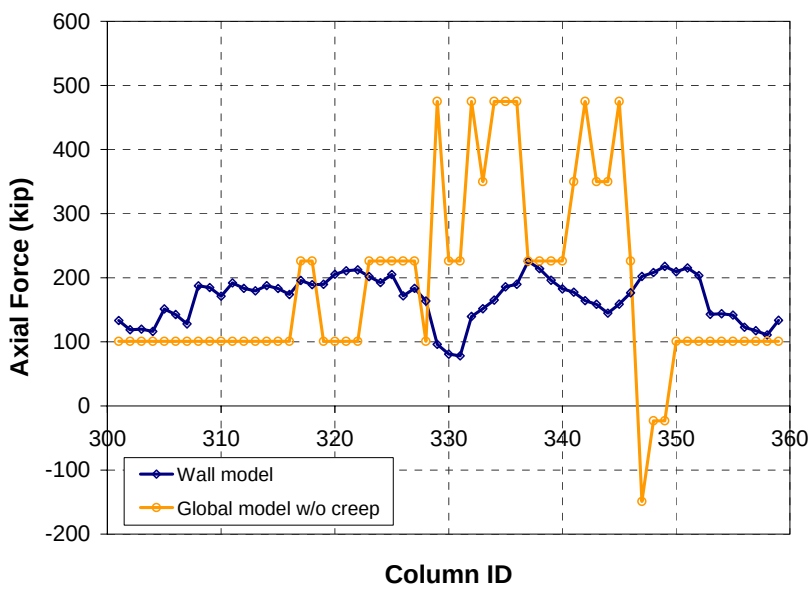

Figure 3–58. Axial load in columns of south wall of WTC 1 at 100 min: isolated wall model for Case B temperature condition compared to global model without creep for Case A_i conditions (compression is positive).

(a) Vertical displacement
(downward displacement is negative)

(b) Out-of-plane displacement
(inward displacement is positive)

(c) Axial force in columns
(compression is negative)

(d) Plastic strain in columns
(compressive strain is negative)

Figure 3–59. Response of isolated south wall model of WTC 1 after corrective loads from the global model were applied (Case B temperature condition at 100 min).

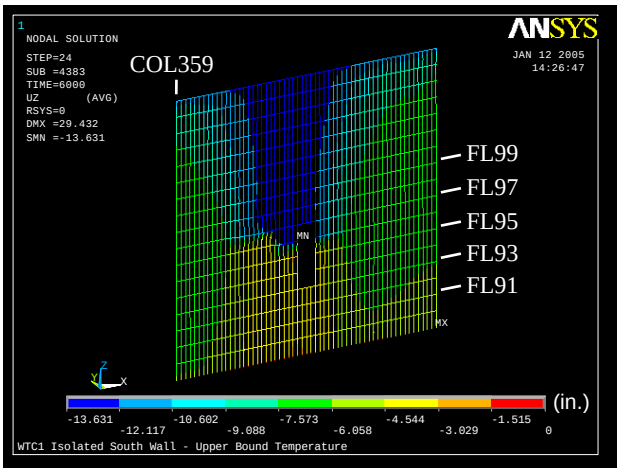

(a) Vertical displacement
(downward displacement is negative)

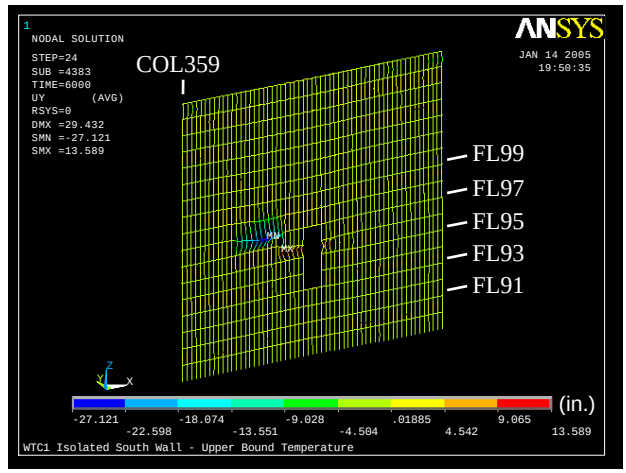

(b) Out-of-plane displacement
(inward displacement is positive,
3X displacement magnification)

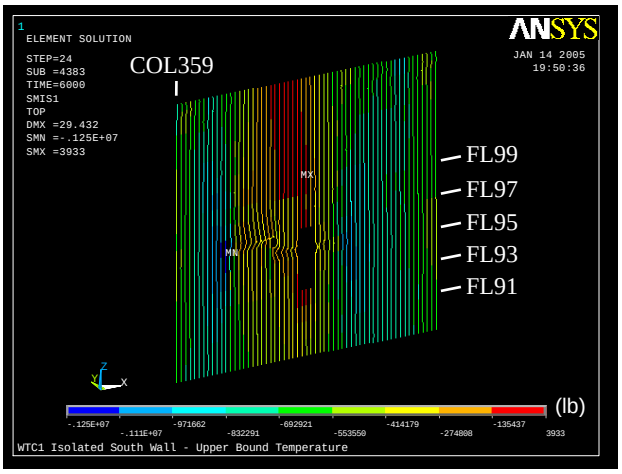

(c) Axial force in columns
(compression is negative,
3X displacement magnification)

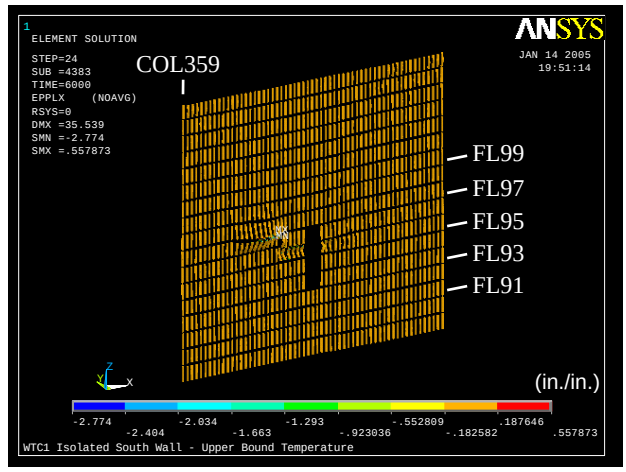

(d) Plastic strain in columns
(compressive strain is negative,
3X displacement magnification)

Figure 3–62. Response of isolated south wall model of WTC 1 to Case B temperature condition and push-down.

Pull-in Forces to Cause Observed Bowing

As discussed in Chapter 5, inward bowing of the exterior wall on the south face of WTC 1 can be seen in photographs of the event at 10:23 am (about 97 min after the aircraft impact), while no bowing of the south wall is evident at 9:55 am (about 68 min after the aircraft impact). The inward bowing at 97 min extended from Floors 95 to 99 between Columns 308 to 326 (possibly to 340); NIST estimated the maximum bowing to be 55 in. at Floor 97.

The isolated south wall model of WTC 1 did not bow inward under Case A temperature condition, and it bowed slightly over a very limited area under Case B temperature condition. The isolated wall model results did not capture the actual bowing.

The most plausible explanation for the discrepancy between the observed and modeled bowing of the exterior walls is that the pull-in forces were not captured in the full floor models, and floors sagged to a greater extent than these models predicted. Following are reasons the floor models likely underestimated sagging and did not accurately calculate pull-in forces.

- The exterior wall boundary conditions used in the floor models were realistic only if a single floor was heated. The floor trusses were supported on exterior columns that extended one story above and one story below the floor modeled. The far ends of the columns were restrained against translation in the direction normal to the exterior wall and rotation about the axis parallel to the exterior wall. This boundary condition was much stiffer in translation normal to the exterior wall than actually occurred for sequential floors heating simultaneously.
- The floor models did not include creep behavior in the steel or cracking of the concrete floors.
- The floor models did not include strap anchors or studs.
- More thermal insulation may have been dislodged from the trusses than estimated from the impact analysis. The impact analysis did not account for the effect of impact or vibrations on dislodging insulation.
- The floor models assumed a uniform live load. Debris accumulated in large piles was observed in some floor areas.

To model the effect of pull-in forces on inward bowing of the columns, trial values of pull-in forces were applied to the exterior columns of the south wall over five floors from Floor 95 to Floor 99 where bowing was observed.

The magnitudes of the pull-in forces were determined by trial and error, matching the observed inward bowing of exterior walls for Case B temperature condition. The Case B temperature condition was used because temperatures of the south office area floors and south wall columns were much higher than those of the Case A temperature condition, and because the full floor models with the Case B_i temperature condition showed much larger floor sagging in the south office area than did the floor models with the Case A_i temperature condition.

The floor models for Case B temperature condition showed that floors began to disconnect from the south wall about 80 min after impact. In the temperature time histories of the Case B condition, temperatures of the south wall and south office area had begun to rise again after 80 min, having been relatively constant for some time. Consequently, pull-in forces were applied to the exterior wall model starting at 80 min and, the temperature time history was analyzed with these pull-in forces to 100 min. Figure 3–63 shows locations of floor/wall disconnections and pull-in forces for this analysis.

Figures 3–64, 3–65, and 3–66 show the results of the analysis performed with a 6 kip pull-in force per column. After applying 6 kip pull-in forces at 80 min, the maximum inward bowing increased to 12.2 in. as shown in Fig. 3–64. At 90 min, the maximum inward bowing became 19.0 in., and at 100 min, it reached 31.3 in., as shown in Figs. 3–65 and 3–66. The thermal loading from 80 min to 100 min increased the inward bowing significantly where there was inward bowing initially. Figure 3–67 shows the axial loads in columns between Floors 98 and 99 at 80 min, 90 min, and 100 min. At 100 min,

Columns 320 to 346 were in the post-buckling regime and were unloading. The maximum bowing of 31.3 in. was smaller than the observed maximum bowing of 55 in.. The wall remained stable at 100 min.

In the global model, the exterior wall boundary conditions were different from the isolated wall model: generally the stiffness against inward bowing in the global models was softer. In addition, the exterior walls were expected to carry additional gravity loads redistributed from the core due to downward displacement of the core resulting from creep and inelastic buckling. Consequently, it is likely that the inward bowing of the global model would be significantly larger than 31 in. with the same 6 kip pull-in forces. Therefore, 4 or 5 kip pull-in forces were selected for the WTC 1 global analysis.

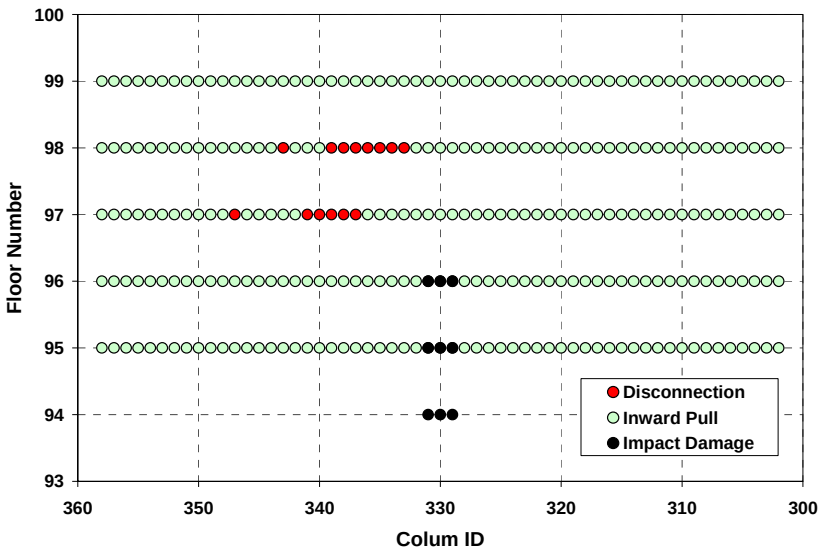

(a) Between 80 min and 90 min

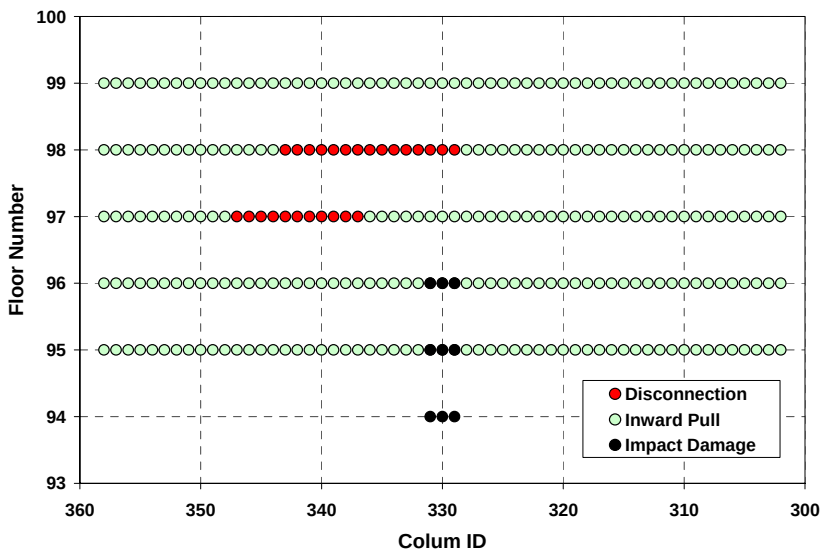

(b) Between 90 min and 100 min

Figure 3–63. Locations of floor/wall disconnections and pull-in forces used between 80 min and 100 min of Case B temperature for south wall of WTC 1.

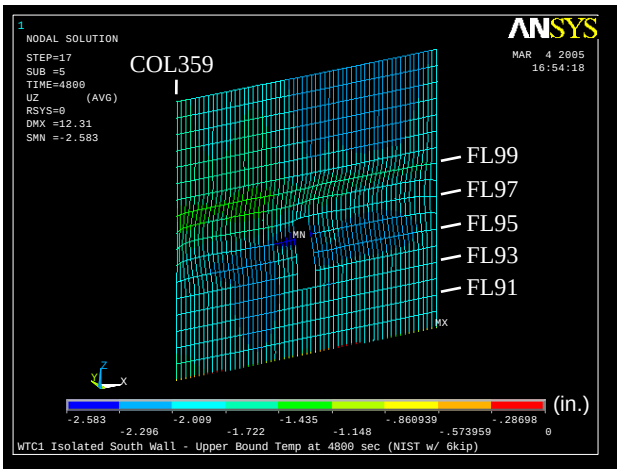

(a) Vertical displacement (downward displacement is negative, 10X displacement magnification)

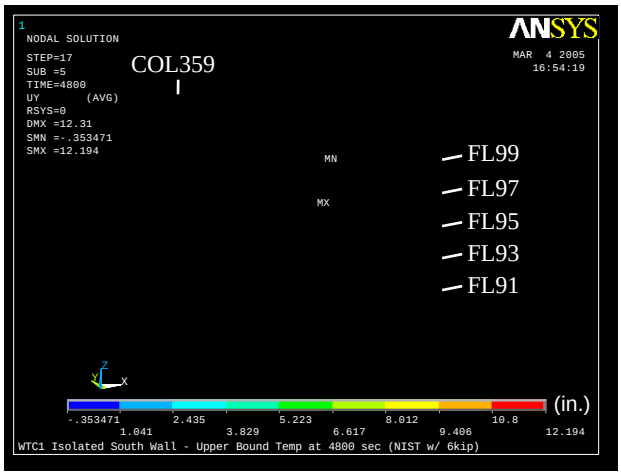

(b) Out-of-plane displacement (inward displacement is positive, 10X displacement magnification)

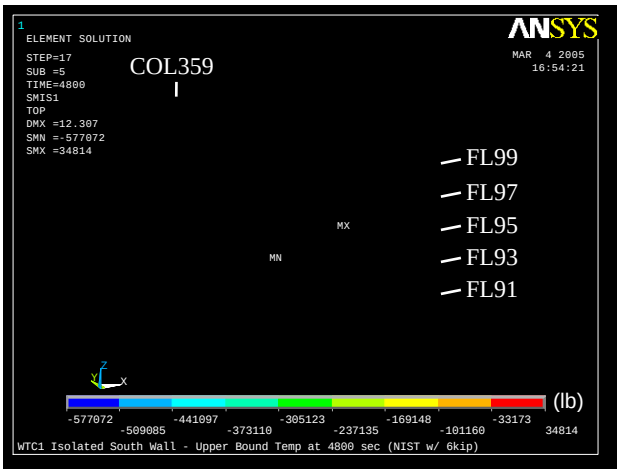

(c) Axial force in columns (compressive is negative, 10X displacement magnification)

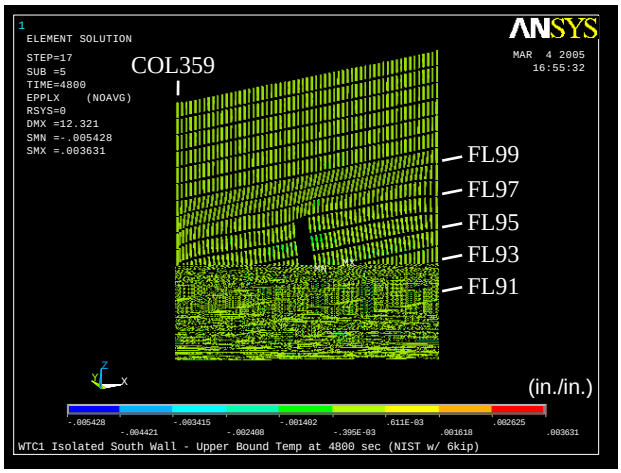

(d) Plastic strain in columns (compressive strain is negative, 10X displacement magnification)

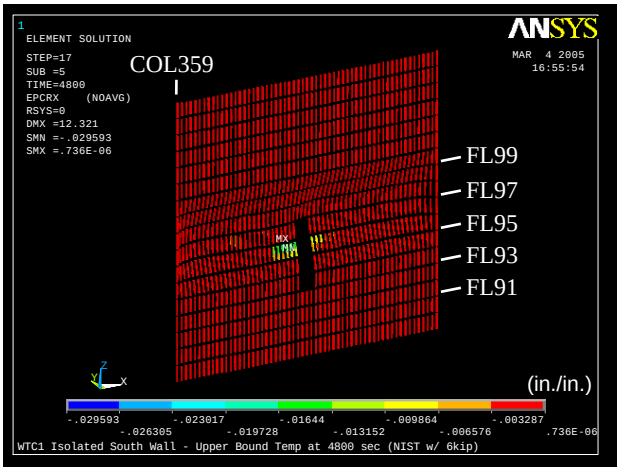

(e) Creep strain in columns (compressive strain is negative, 10X displacement magnification)

Figure 3–64. Response of isolated south wall model of WTC 1 at 80 min of Case B temperature condition with floor/wall disconnections and 6 kip pull-in forces over five floors.

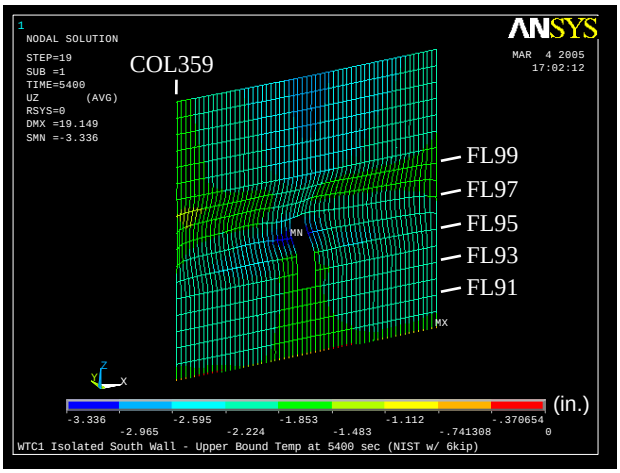

(a) Vertical displacement (downward displacement is negative, 10X displacement magnification)

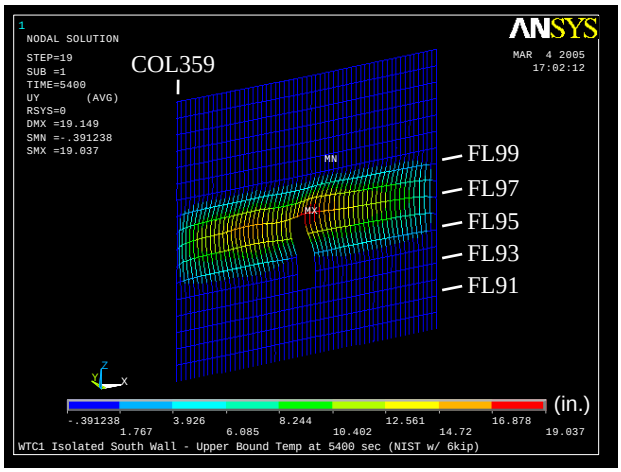

(b) Out-of-plane displacement (inward displacement is positive, 10X displacement magnification)

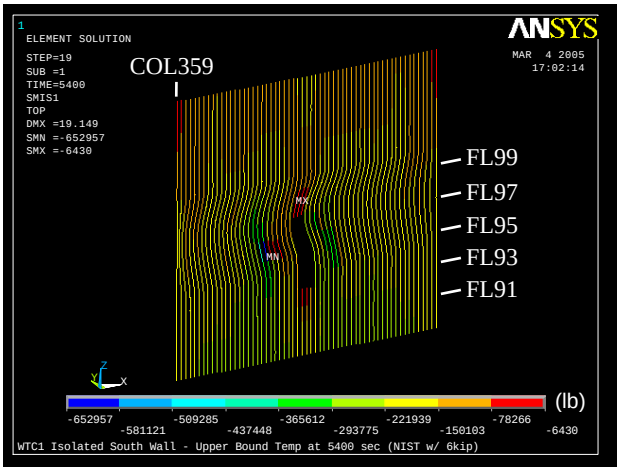

(c) Axial force in columns (compressive is negative, 10X displacement magnification)

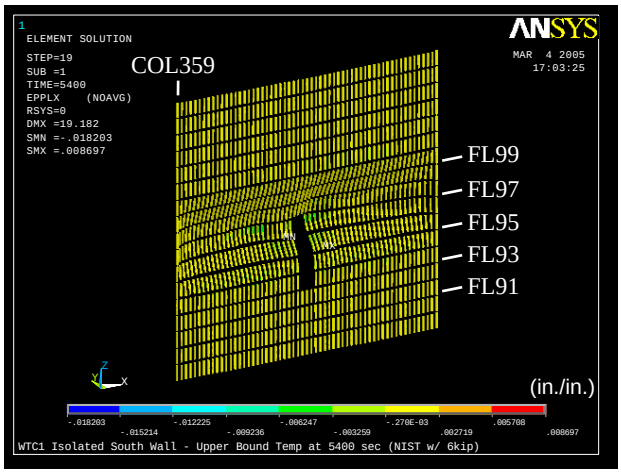

(d) Plastic strain in columns (compressive strain is negative, 10X displacement magnification)

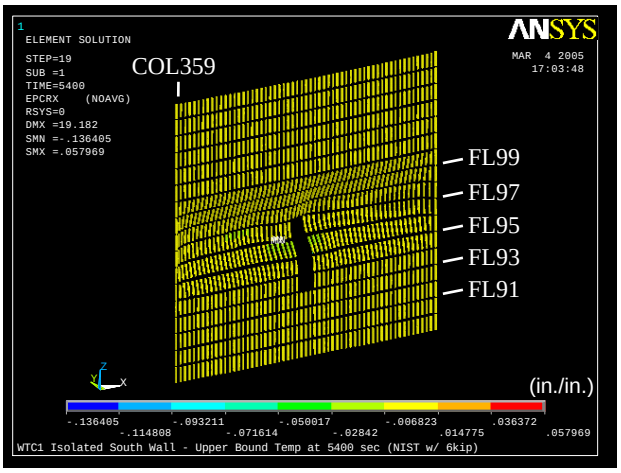

(e) Creep strain in columns (compressive strain is negative, 10X displacement magnification)

Figure 3–65. Response of isolated south wall model of WTC 1 at 90 min of Case B temperature condition with floor/wall disconnections and 6 kip pull-in forces over five floors.

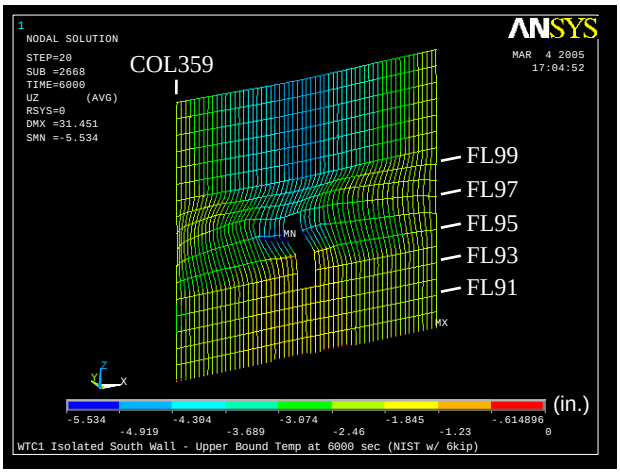

(a) Vertical displacement (downward displacement is negative, 10X displacement magnification)

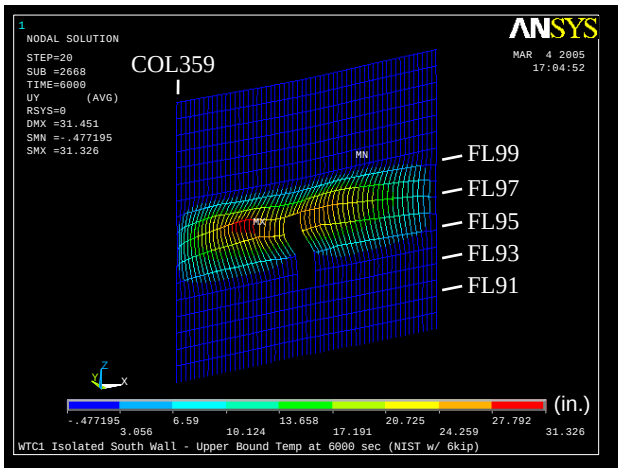

(b) Out-of-plane displacement (inward displacement is positive, 10X displacement magnification)

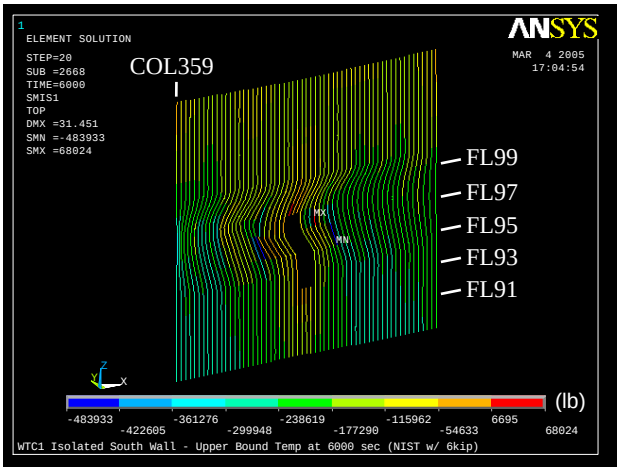

(c) Axial force in columns (compressive is negative, 10X displacement magnification)

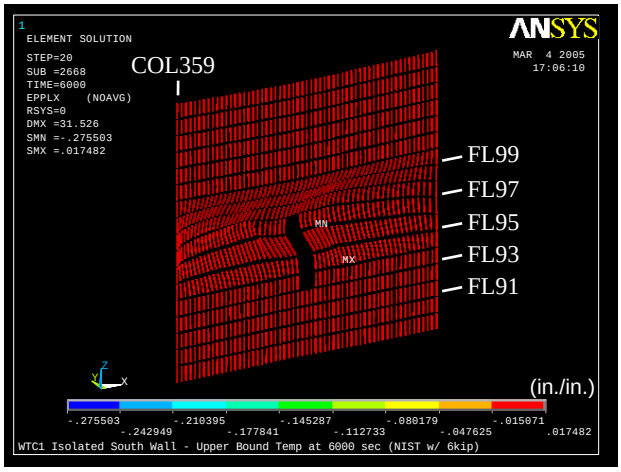

(d) Plastic strain in columns (compressive strain is negative, 10X displacement magnification)

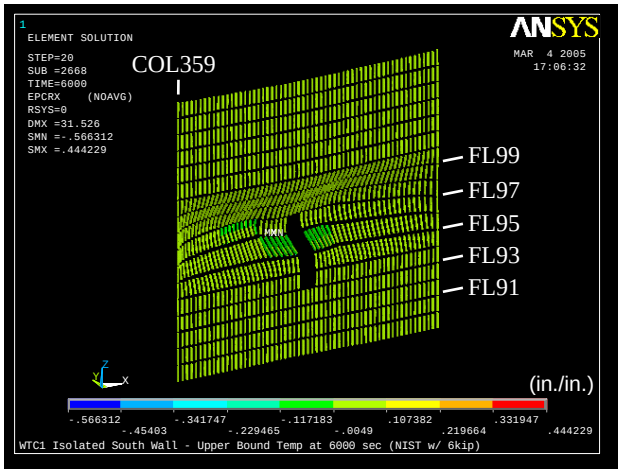

(e) Creep strain in columns (compressive strain is negative, 10X displacement magnification)

Figure 3–66. Response of isolated south wall model of WTC 1 at 100 min of Case B temperature condition with floor/wall disconnections and 6 kip pull-in forces over five floors.

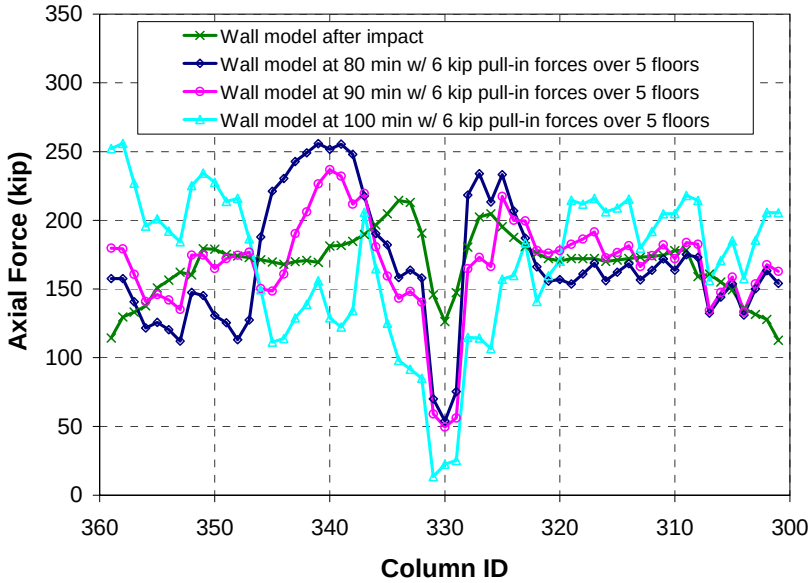

Figure 3–67. Axial load in columns between Floors 98 and 99 of isolated south wall model of WTC 1 at 80 min, 90 min, and 100 min of Case B temperature condition with floor/wall disconnections and 6 kip pull-in forces over five floors (compression is positive).

3.2.2 FEA of WTC 2 Exterior Wall

Case C Temperature Condition

Figures 3–68 and 3–69 show Case C temperature distributions in the columns of the isolated east exterior wall of WTC 2. The highest temperature, 850°C, occurred at 60 min in Column 303 between Floor 81 and Floor 82 for Case C temperature condition. Column temperatures were higher on the inside face of the exterior wall. Figure 3–70 shows the locations of the out-of-plane supports for Case C conditions at 60 min.

The vertical and the out-of-plane displacements at the end of the gravity load step after aircraft impact and at the end of each temperature step are shown in Figs. 3–71, 3–72, 3–73, and 3–74. The maximum vertical displacement of 3.6 in. occurred at Column 301 at Floor 90 at 60 min. The maximum out-of-plane deflection of 4.0 in. occurred at Column 302 at Floor 82 at 60 min (out-of-plane displacement is positive outward). The south side of the isolated east exterior wall displaced vertically after aircraft impact more than other parts of the east wall, as the impact damage was concentrated mostly on the southeast corner of the WTC 2. The maximum vertical displacement shifted to the north during the heating period. As time approached 60 min after the aircraft impact, the columns on the north side buckled, and the out-of-plane displacement increased.

The axial load distributions of the columns at the end of the gravity load step and each 10 min time interval are shown in Figs. 3–75 and 3–76. The maximum axial load occurred at Column 332 between Floor 83 and Floor 84 at 50 min. The axial load in this column increased from 330 kip after the aircraft

impact to 750 kip at 50 min. The axial load on the buckled columns on the north side of the isolated wall remained approximately constant throughout the temperature time history.

To consider the effect of load redistribution within the tower, the same corrective technique described earlier in this chapter for WTC 1 was used. The axial loads in columns between Floor 83 and Floor 84 in the isolated east wall model were compared with those obtained from the preliminary global model analysis without creep and with Case C_i temperature and impact damage conditions (Appendix C). Column loads obtained from the preliminary global model and isolated exterior wall model at 60 min are shown in Fig. 3–77. The difference between the two column loads was applied to the columns of the isolated wall model at Floor 84 as corrective loads. The resulting vertical and out-of-plane displacements are shown in Fig. 3–78. The additional column loads increased the maximum vertical displacement by only 0.1 in., and the maximum out-of-plane displacement by less than 0.1 in.

Also as described earlier for the WTC 1 isolated wall model, a push-down analysis of the WTC 2 isolated exterior wall model was performed. At an additional 5.6 in. of vertical displacement the model failed to converge, and the analysis was terminated. The vertical and out-of-plane displacements at the end of 5.6 in. of push down are shown in Fig. 3–79. At the end of push down, the maximum total vertical displacement increased to 9.4 in., and the maximum out-of-plane displacement increased to 17.2 in. Axial column loads are shown in Fig. 3–80. This figure also shows the location of the columns for which the load-deflection relationships are shown in Fig. 3–81. As can be seen from Fig. 3–81, the buckled columns on the north side of the isolated east exterior wall carried, on average, an additional 300 kip at 60 min temperatures, compared to 470 kip for the average of the entire east wall columns. The additional axial loads on individual columns at different additional vertical displacements are shown in Fig. 3–82.

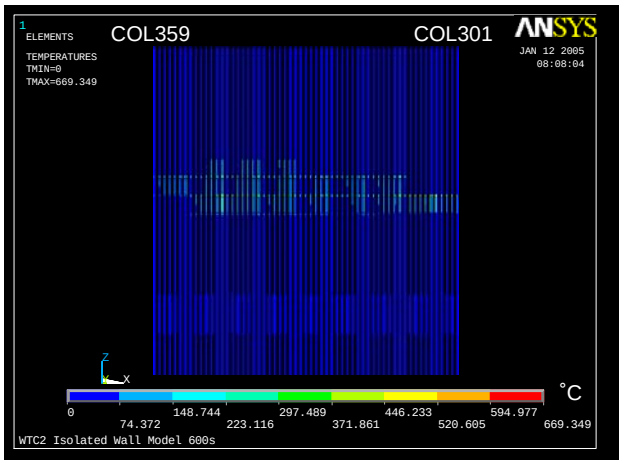

(a) Outside at 10 min

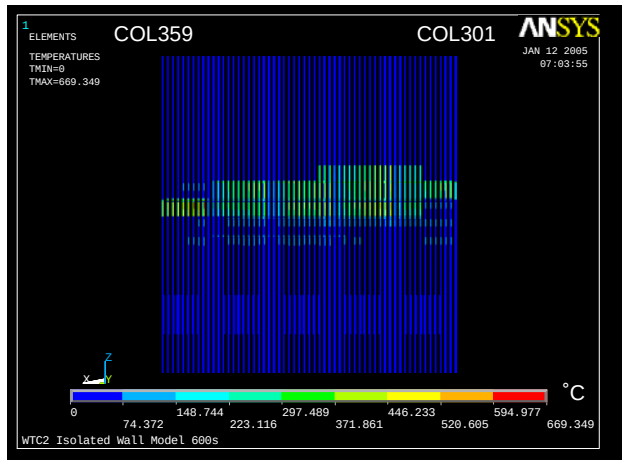

(b) Inside at 10 min

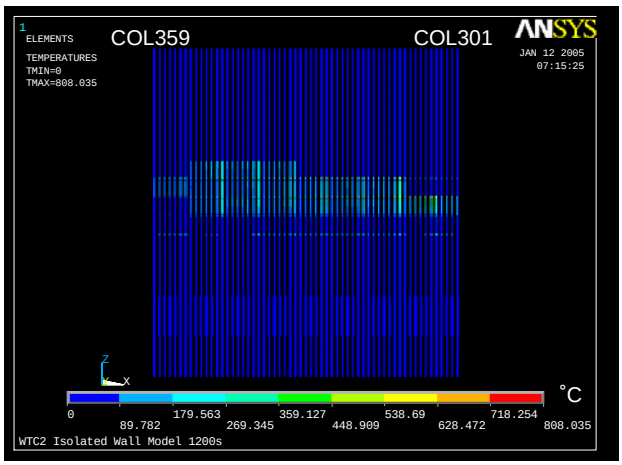

(c) Outside at 20 min

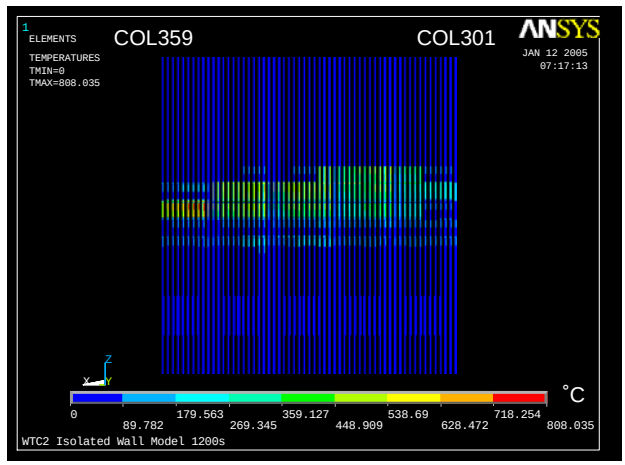

(d) Inside at 20 min

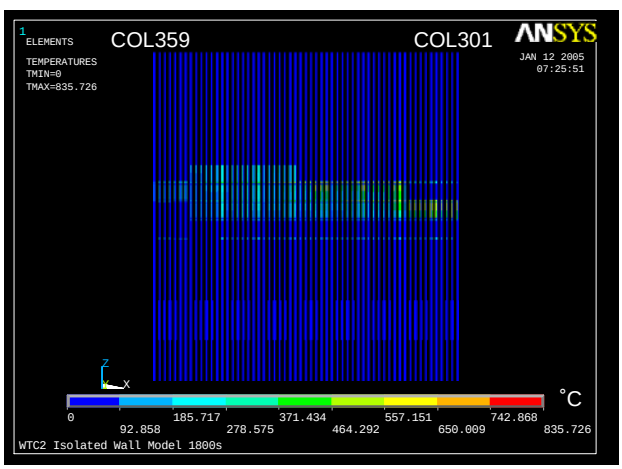

(e) Outside at 30 min

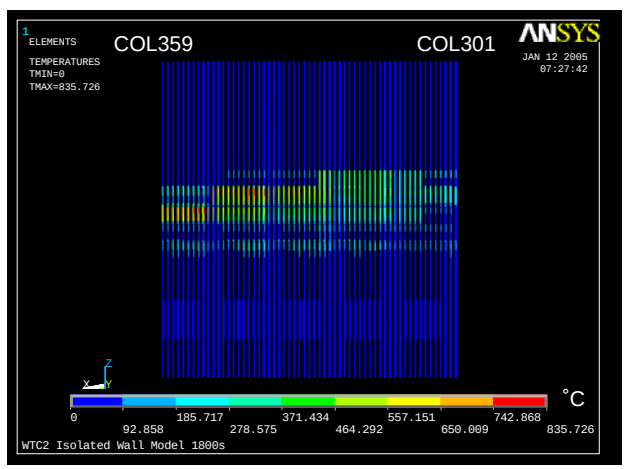

(f) Inside at 30 min

Figure 3–68. Column temperatures on the east wall of WTC 2 for Case C temperature condition at 10 min, 20 min, and 30 min.

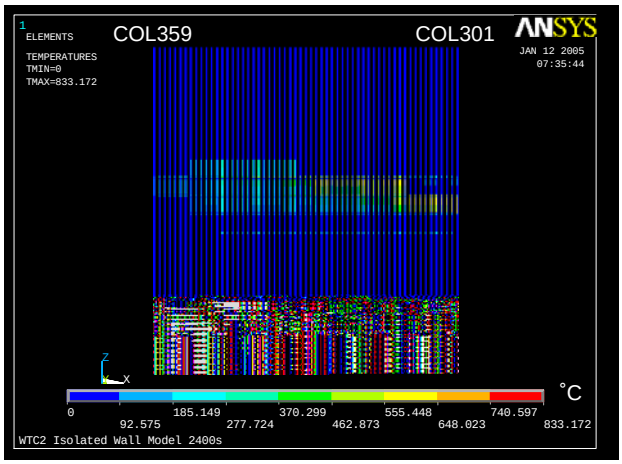

(a) Outside at 40 min

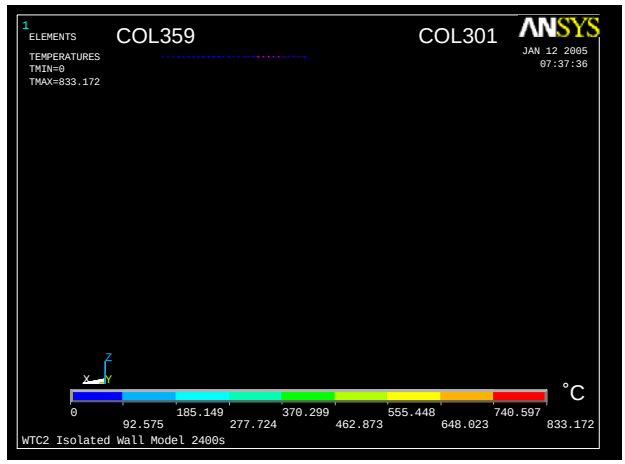

(b) Inside at 40 min

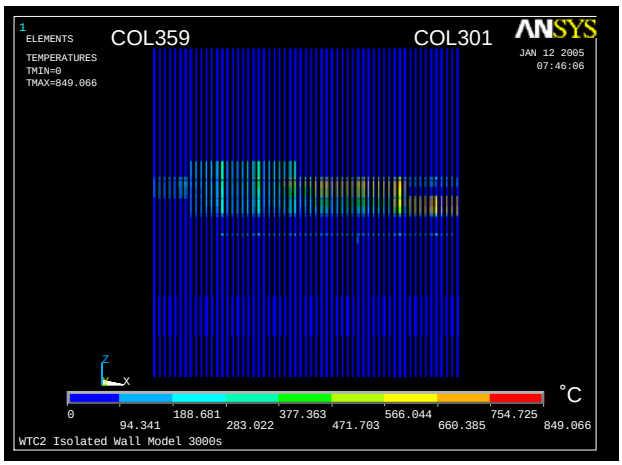

(c) Outside at 50 min

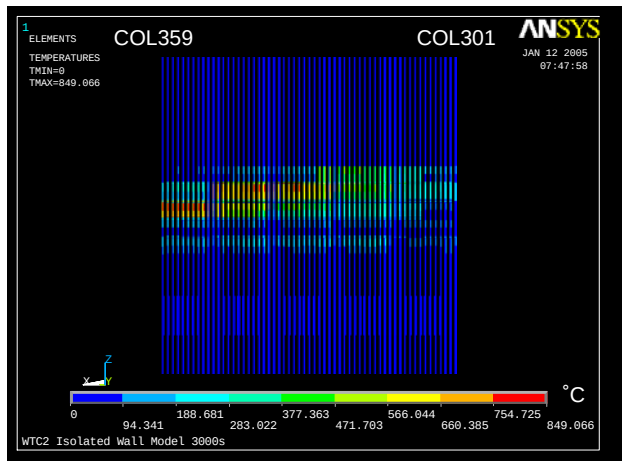

(d) Inside at 50 min

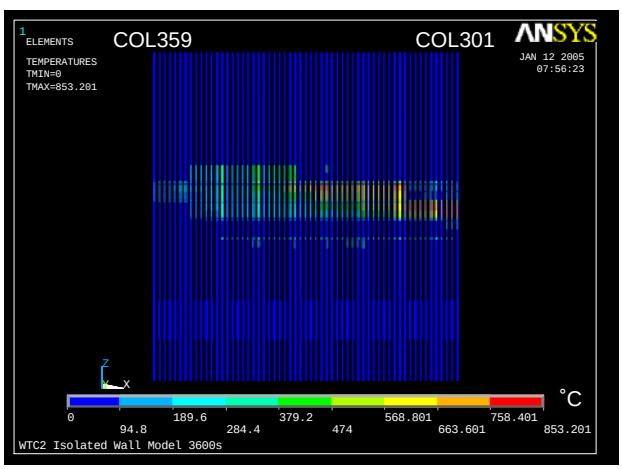

(e) Outside at 60 min

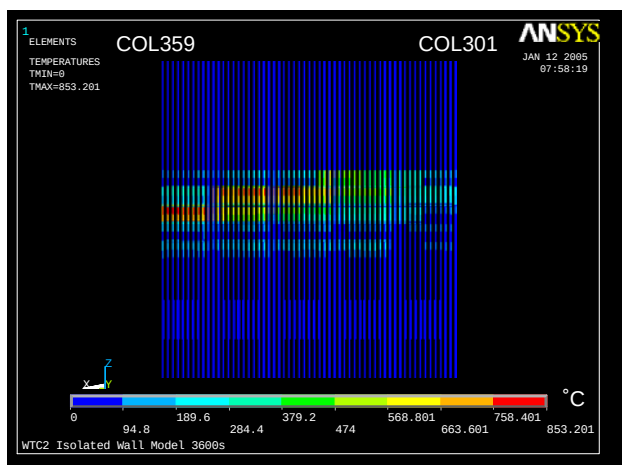

(f) Inside at 60 min

Figure 3–69. Column temperatures on the east wall of WTC 2 for Case C temperature condition at 40 min, 50 min, and 60 min.

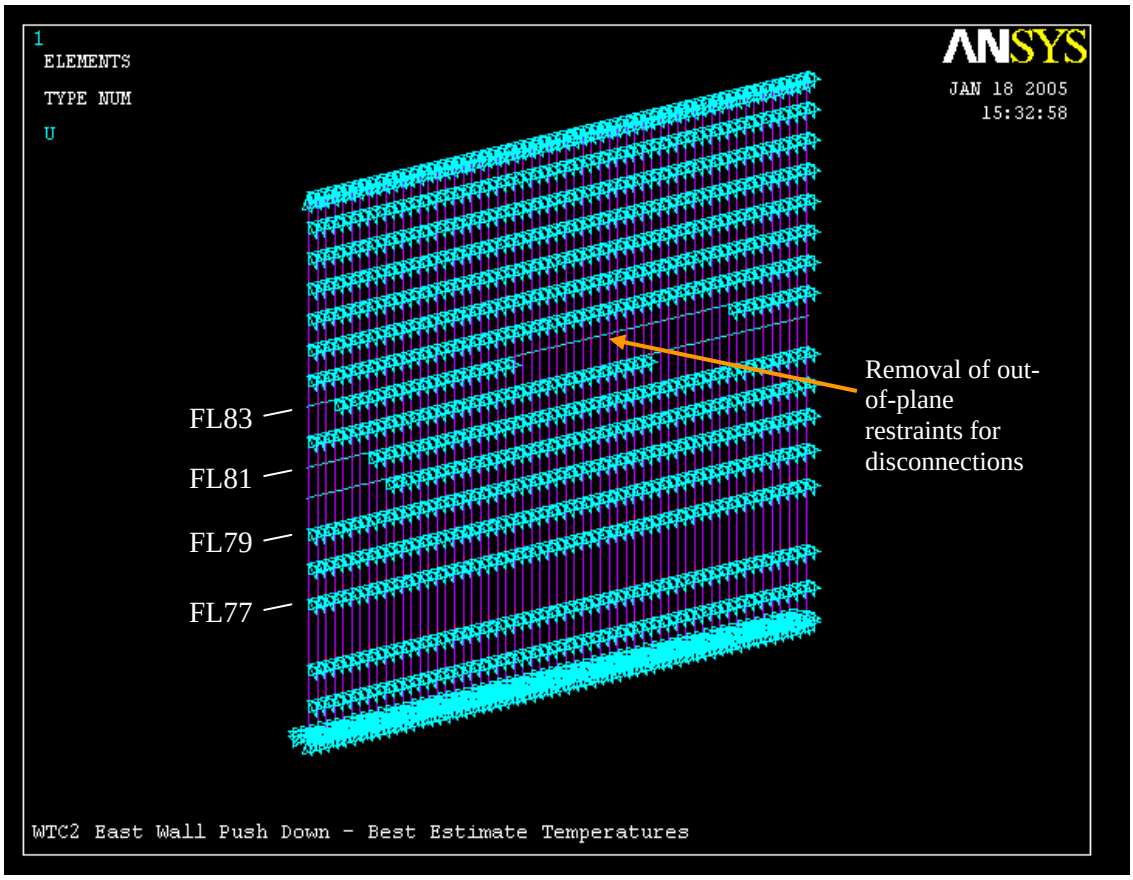

Figure 3–70. Location of the out-of-plane supports and floor/wall disconnections between exterior wall and the floor (WTC 2 east wall for Case C conditions at 60 min).

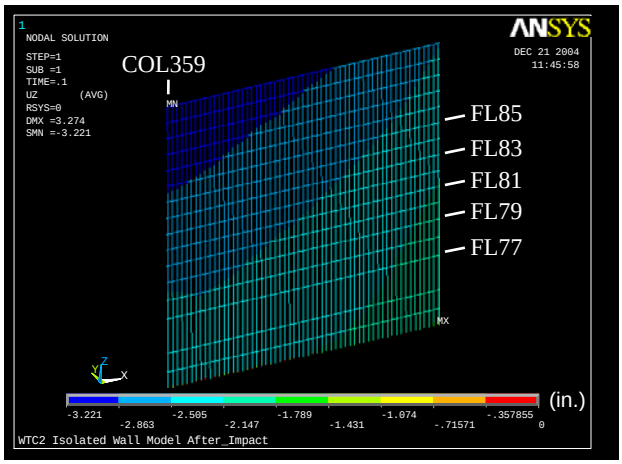

(a) After aircraft impact

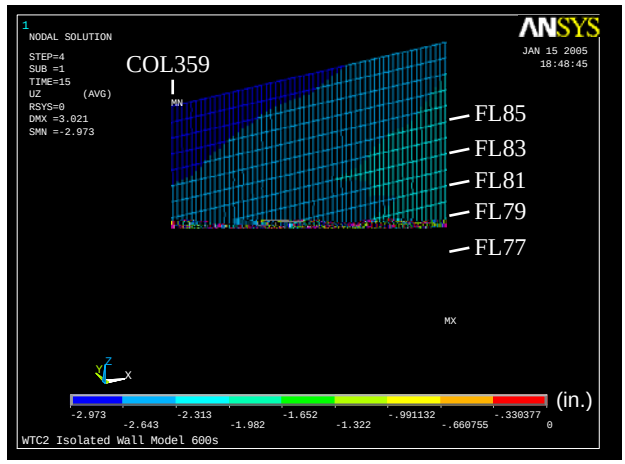

(b) At 10 min

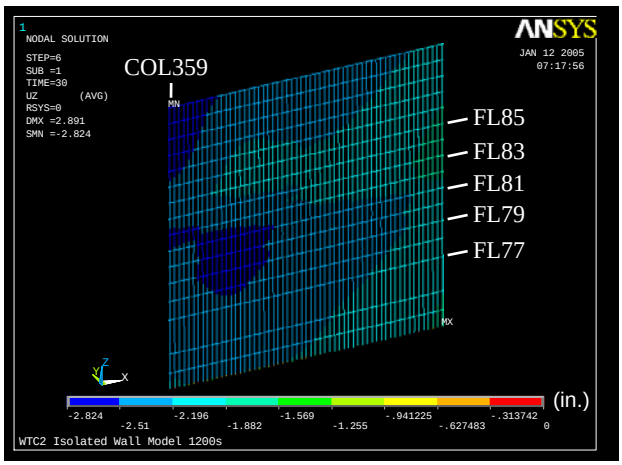

(c)At 20 min

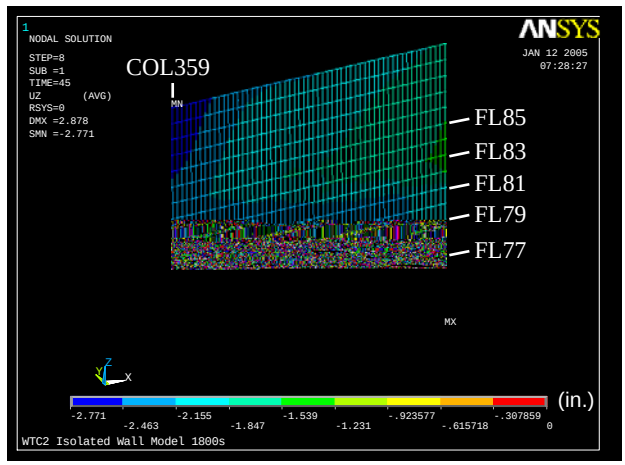

(d) At 30 min

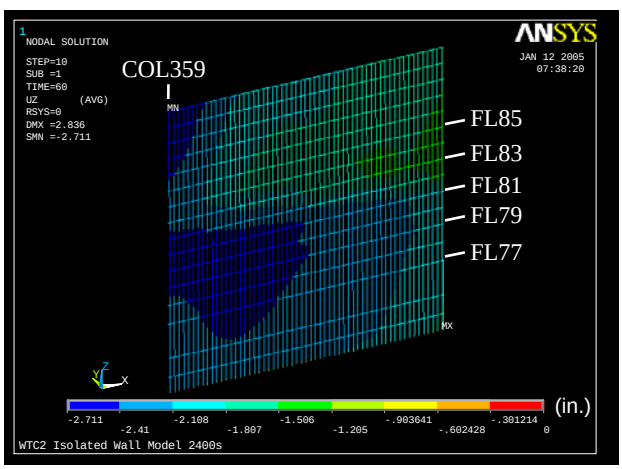

(e) At 40 min

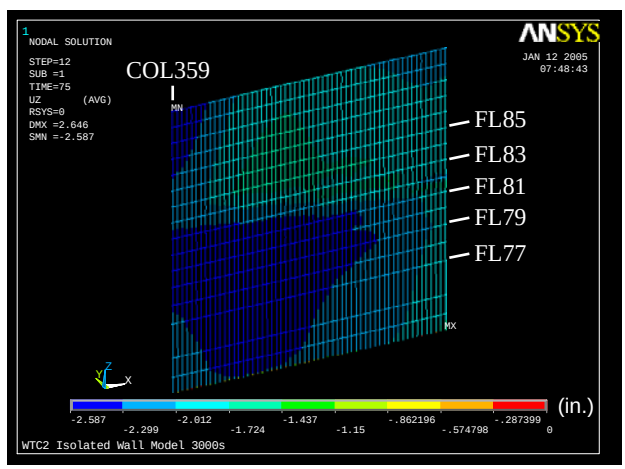

(f) At 50 min

Figure 3–71. Vertical displacement of isolated east wall model of WTC 2 for Case C temperature distribution (downward displacement is negative; displacements scaled ten times).

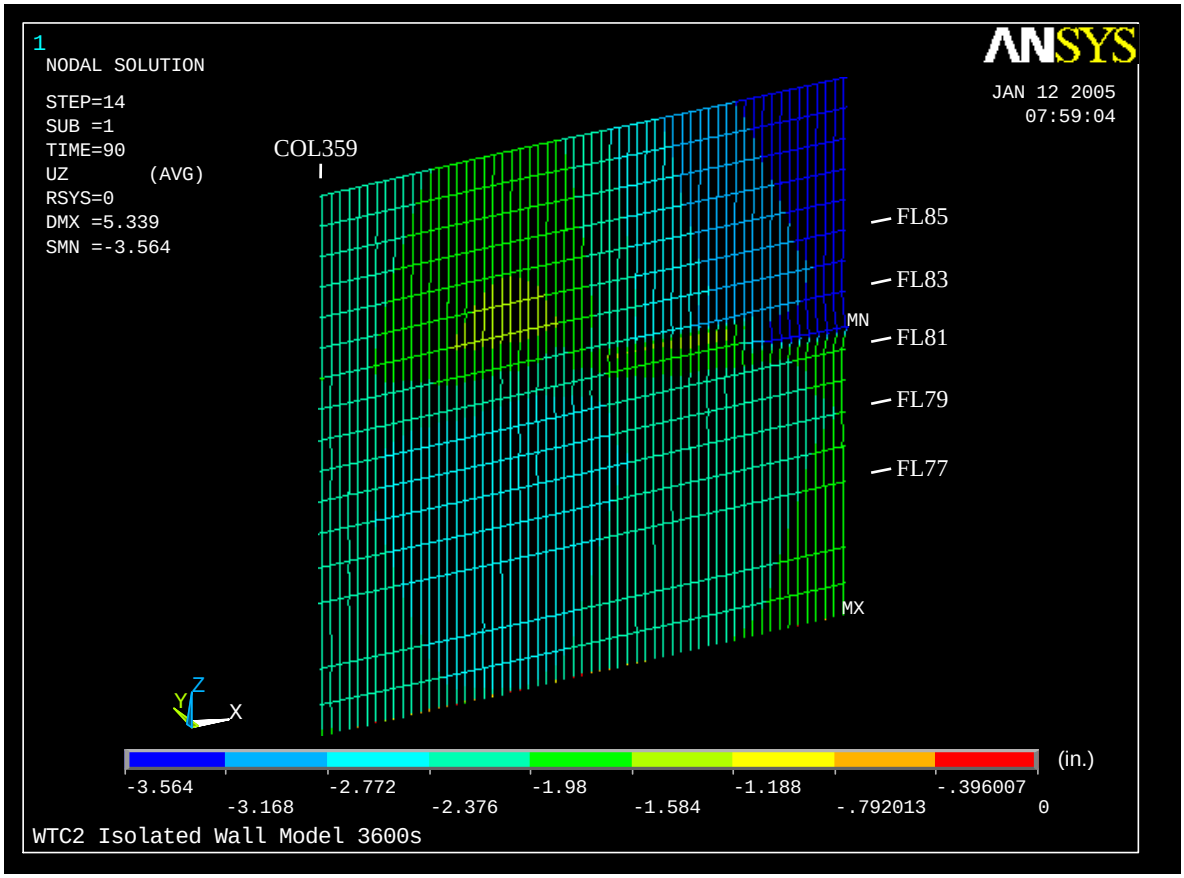

Figure 3–72. Vertical displacement of isolated east wall model of WTC 2 for Case C temperature distribution at 60 min (downward displacement is negative; displacements scaled ten times).

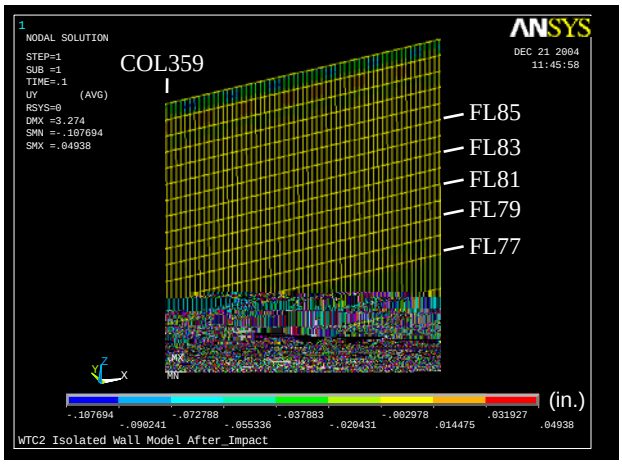

(a) After aircraft impact

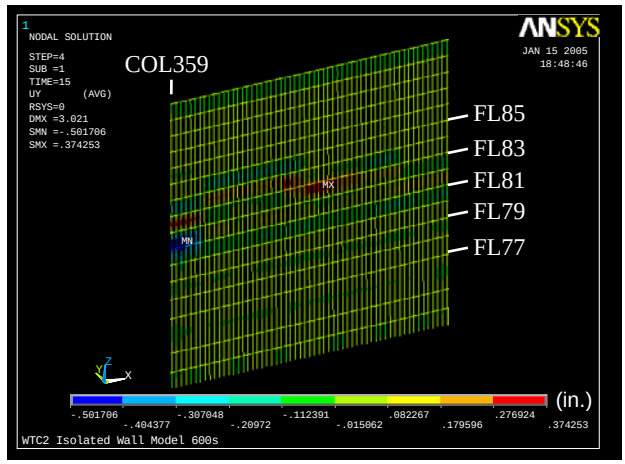

(b) At 10 min

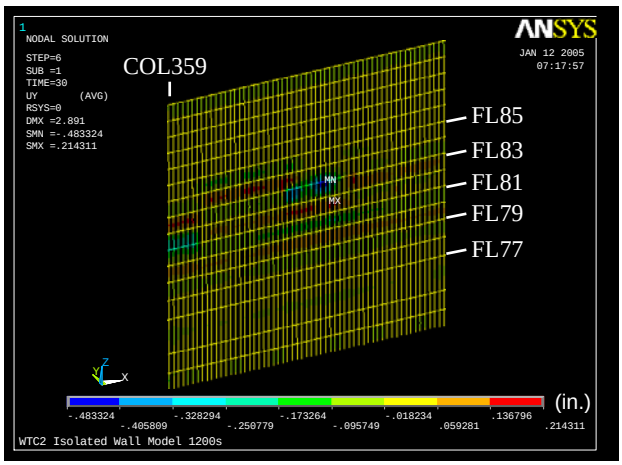

(c) At 20 min

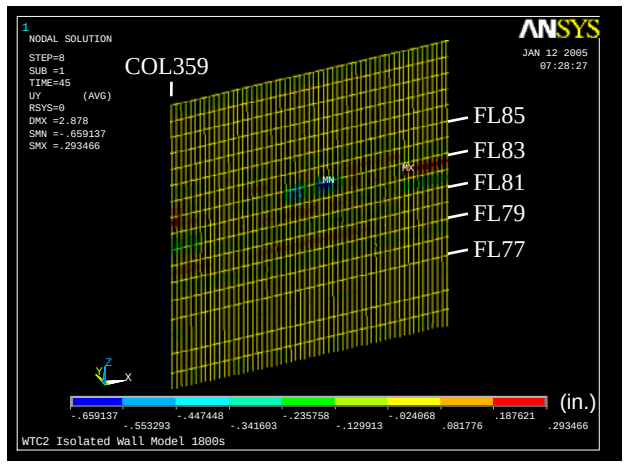

(d) At 30 min

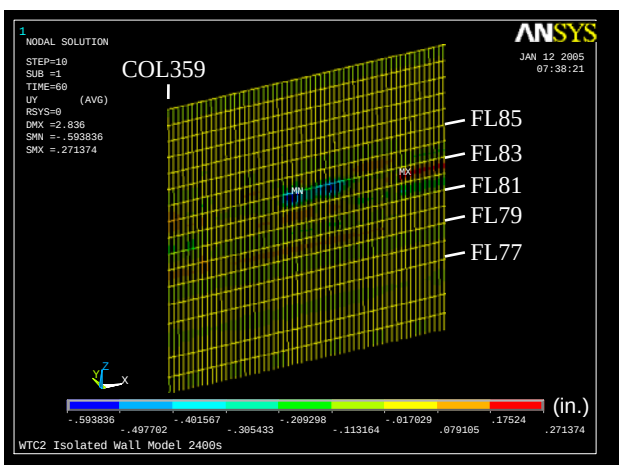

(e) At 40 min

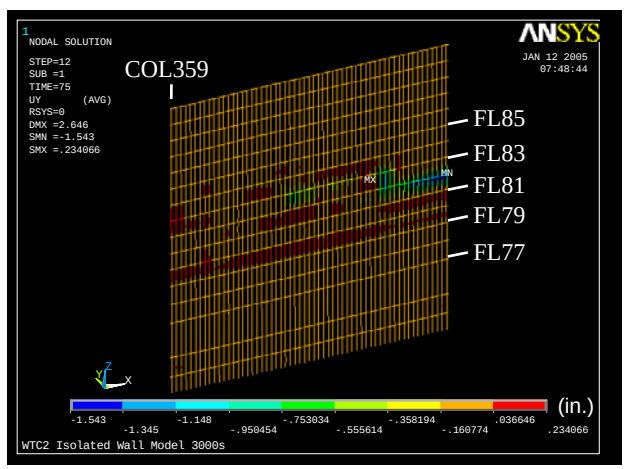

(f) At 50 min

Figure 3–73. Out-of-plane displacement of isolated east wall model of WTC 2 for Case C temperature condition (inward displacement is positive; displacements scaled ten times).

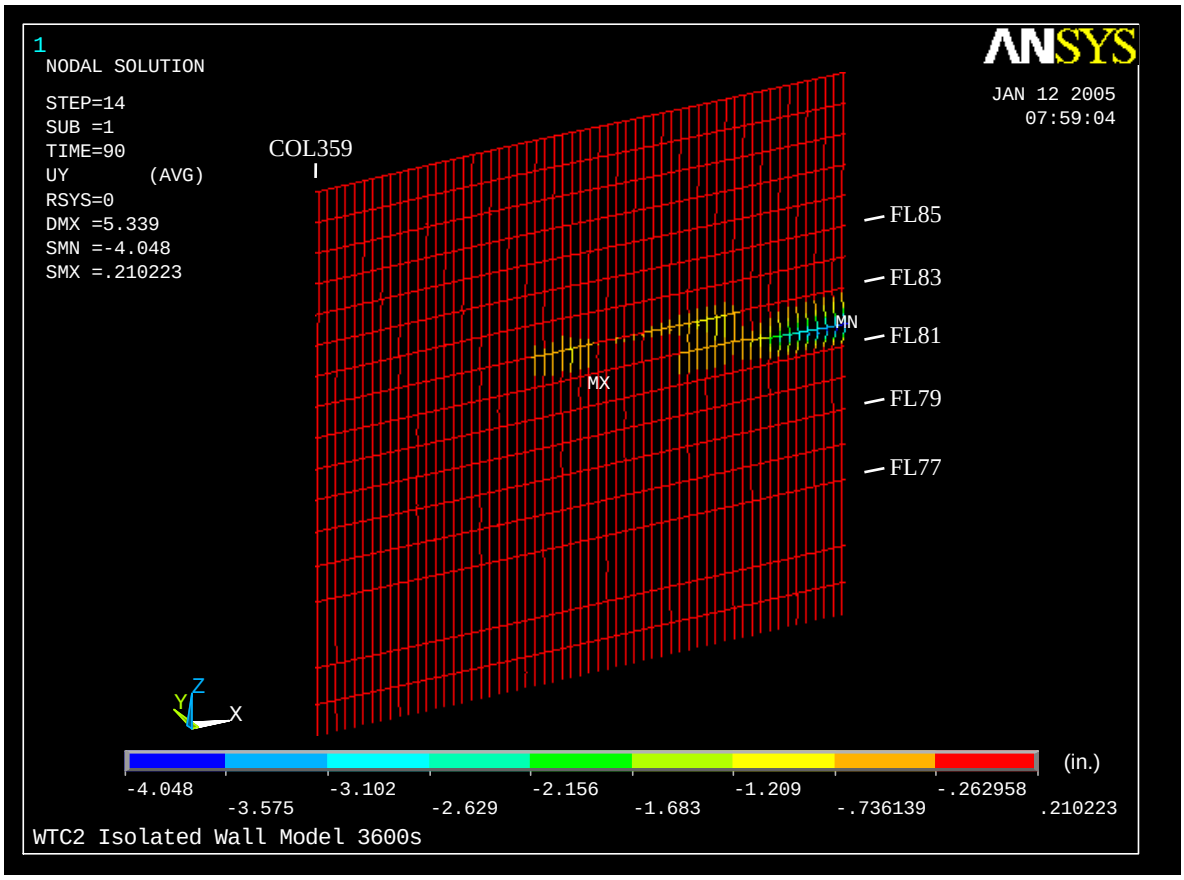

Figure 3–74. Out-of-plane displacement of isolated east wall model of WTC 2 for Case C temperature distribution at 60 min (inward displacement is positive; displacements scaled ten times).

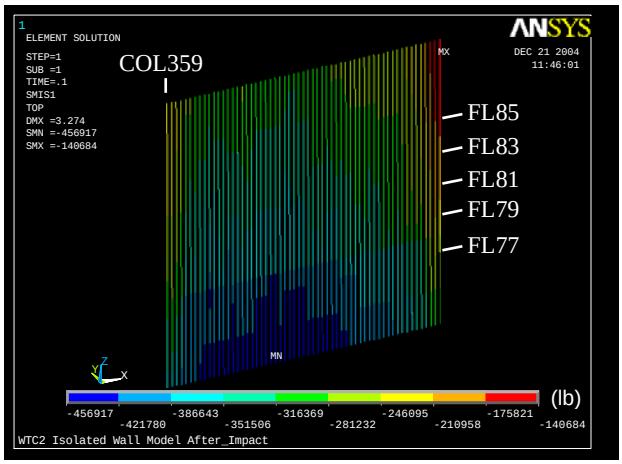

(a) After aircraft impact

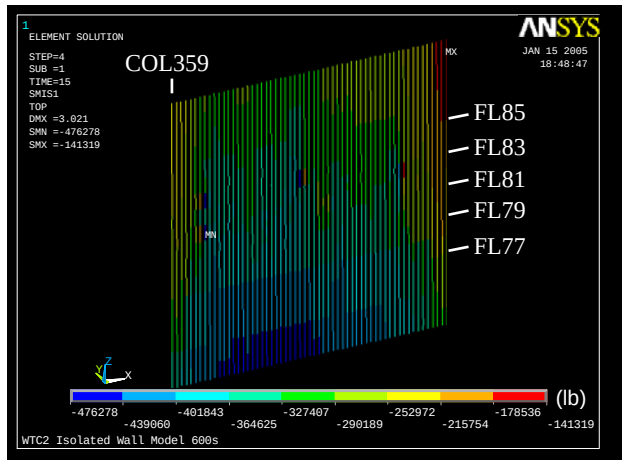

(b) At 10 min

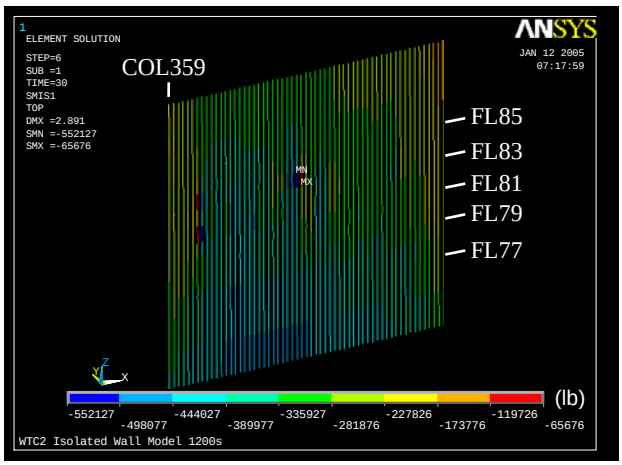

(c) At 20 min

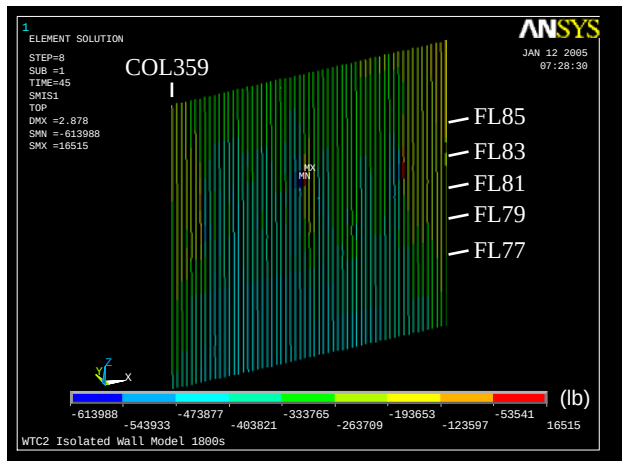

(d) At 30 min

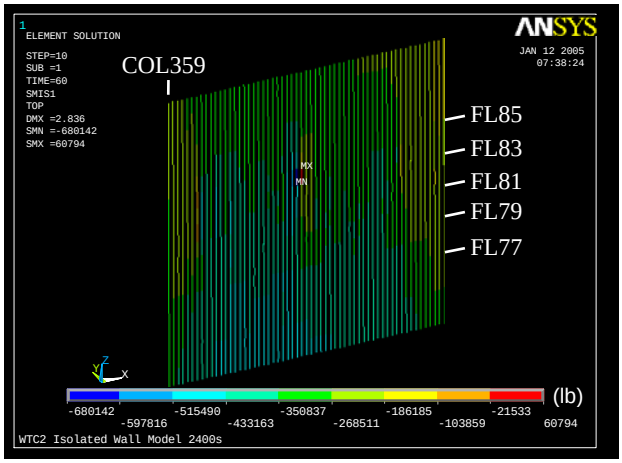

(e) At 40 min

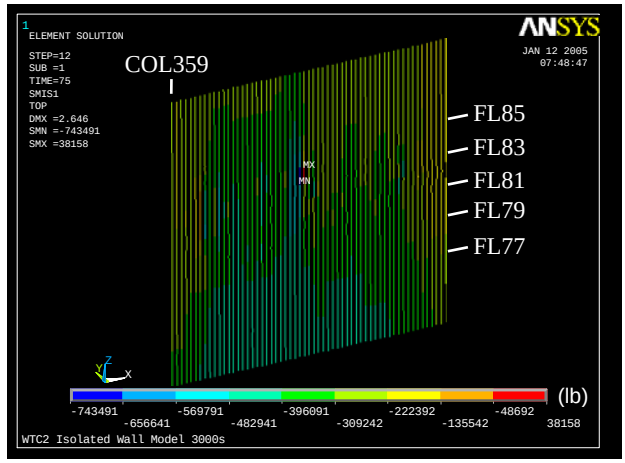

(f) At 50 min

Figure 3–75. Axial load on columns of isolated east wall model of WTC 2 under Case C temperature condition (compression is negative).

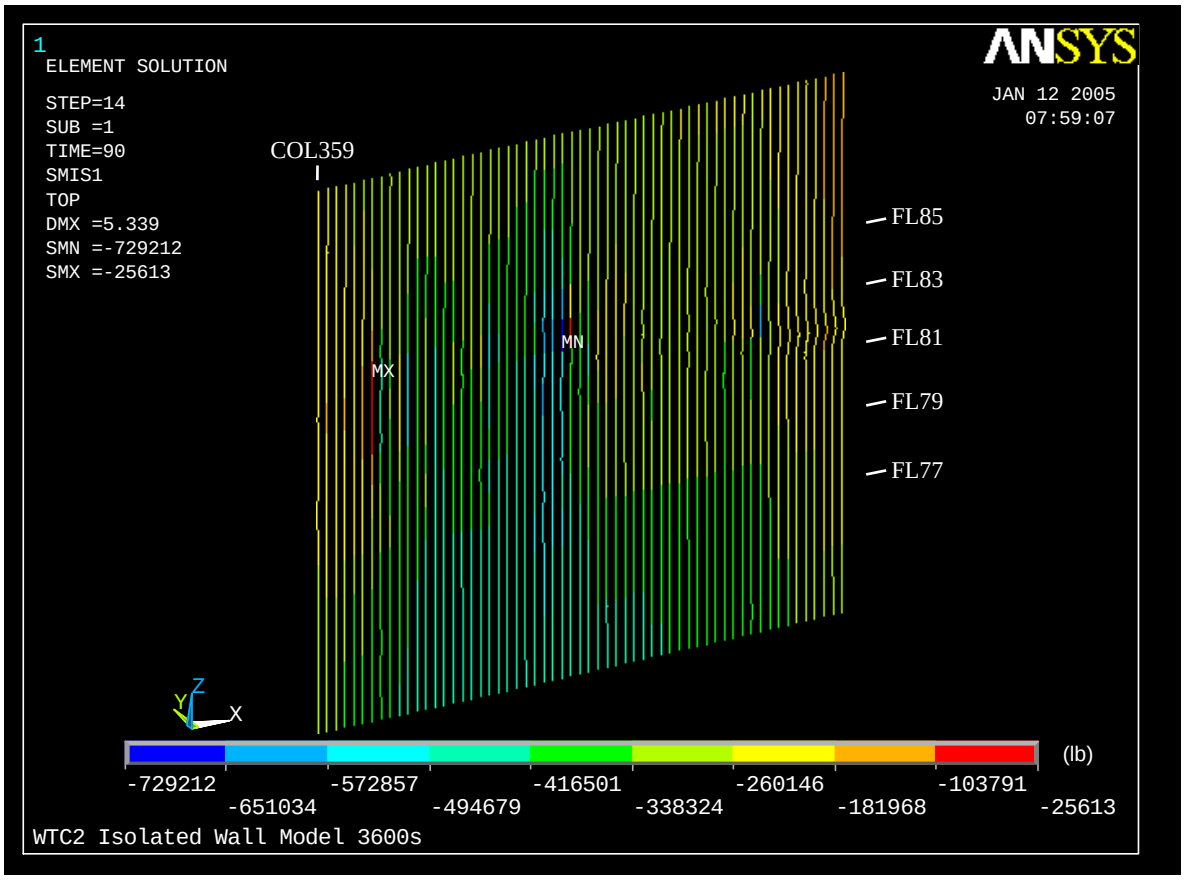

Figure 3–76. Axial load on columns of isolated east wall model of WTC 2 for Case C temperatures distribution at 60 min (compression is negative).

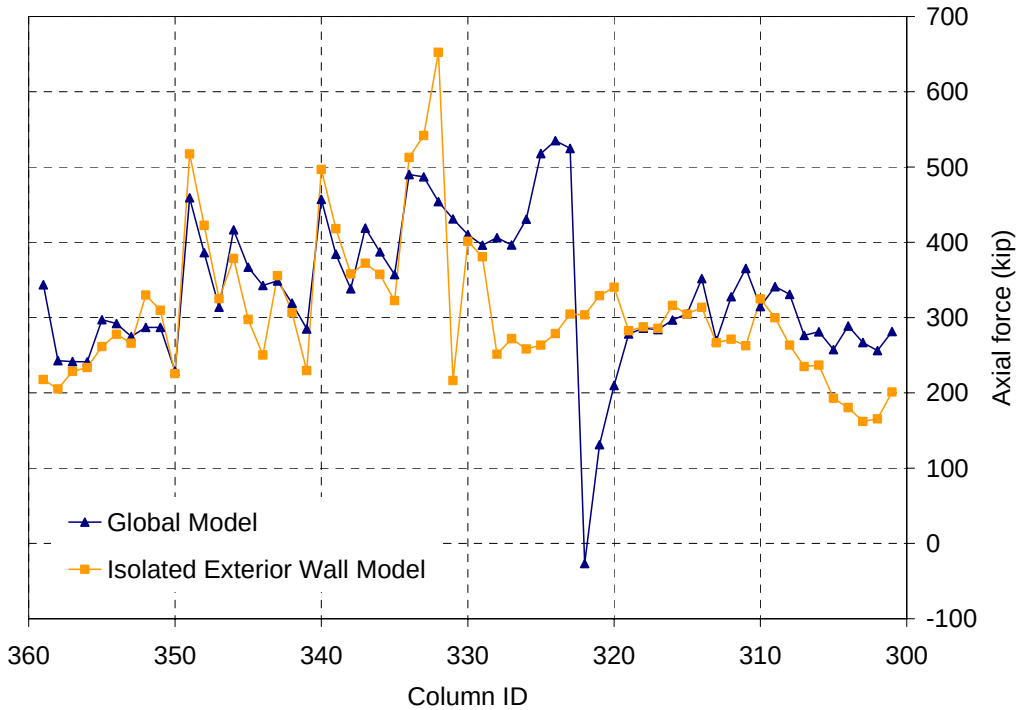

Figure 3–77. Comparison of axial load in columns at Floor 83 of isolated east wall model of WTC 2 at 60 min for Case C temperature conditions and the global model without creep for Case C_i conditions (compression is positive).

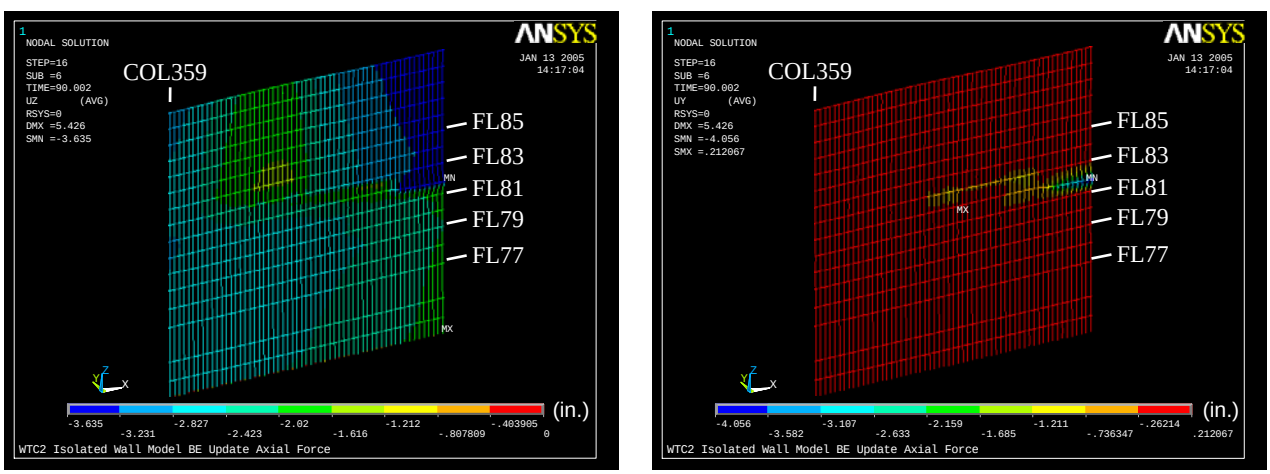

(a) Vertical displacement
(Downward displacement is negative)

(b) Out-of-plane displacement
(Inward displacement is positive)

Figure 3–78. Vertical and out-of-plane displacements of isolated east wall model of WTC 2 after column forces were corrected to those of global modal without creep for Case C_i conditions (displacements scaled ten times).

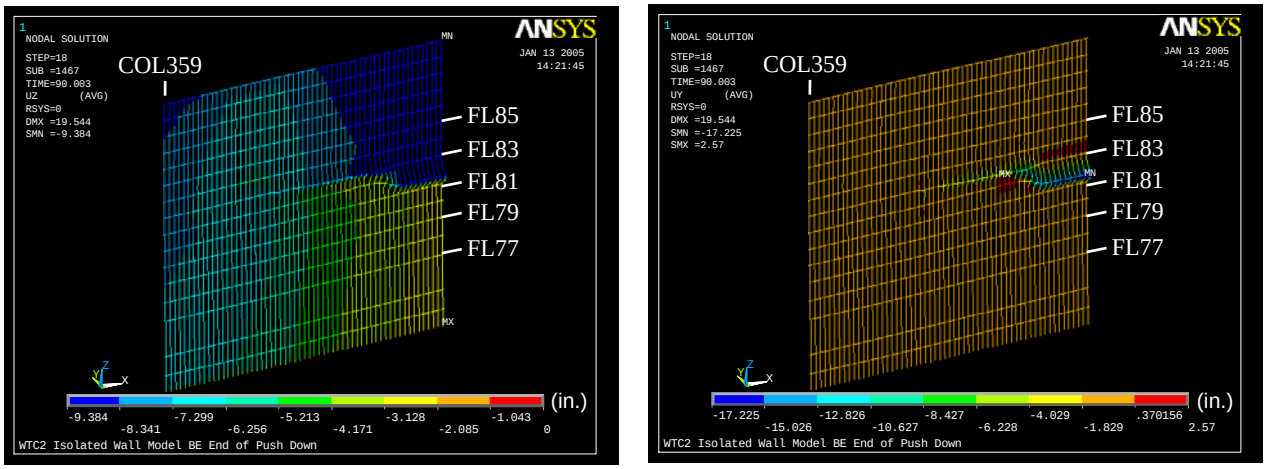

(a) Vertical displacement
(downward displacement is negative)

(b) Out-of-plane displacement
(Inward displacement is positive)

Figure 3–79. Vertical and out-of-plane displacements of isolated east wall model of WTC 2 after Case C temperature condition and push down analysis (displacements scaled five times).

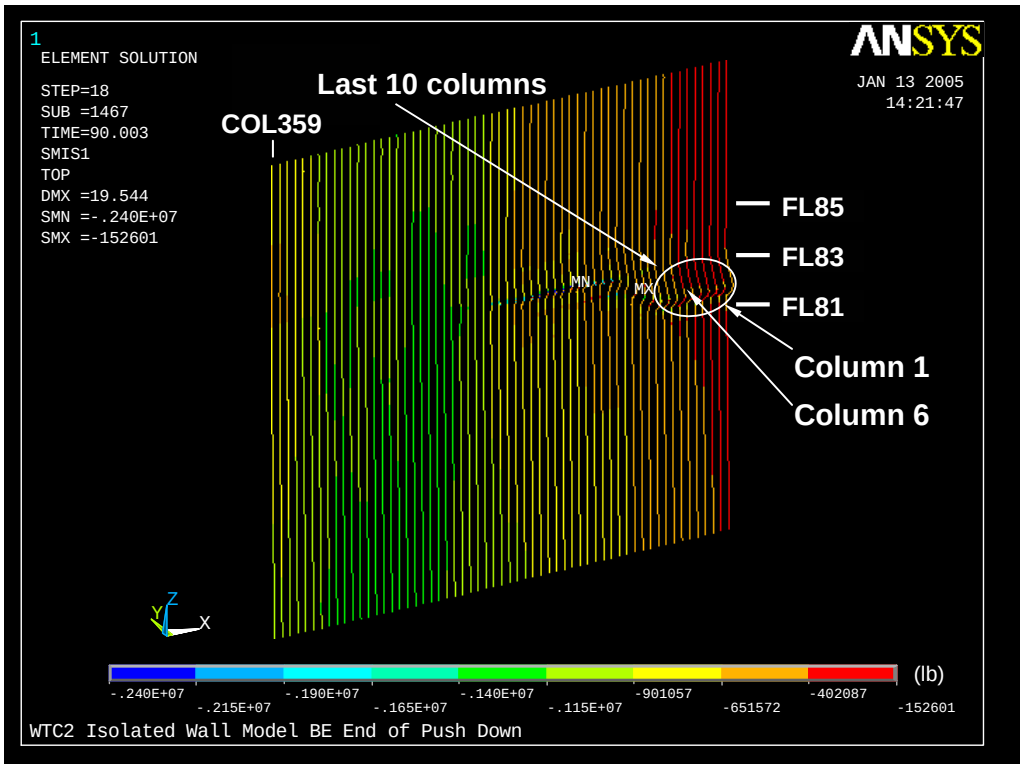

Figure 3–80. Axial load on east wall columns of isolated east wall model of WTC 2 after Case C temperature condition and push-down (compression is negative).

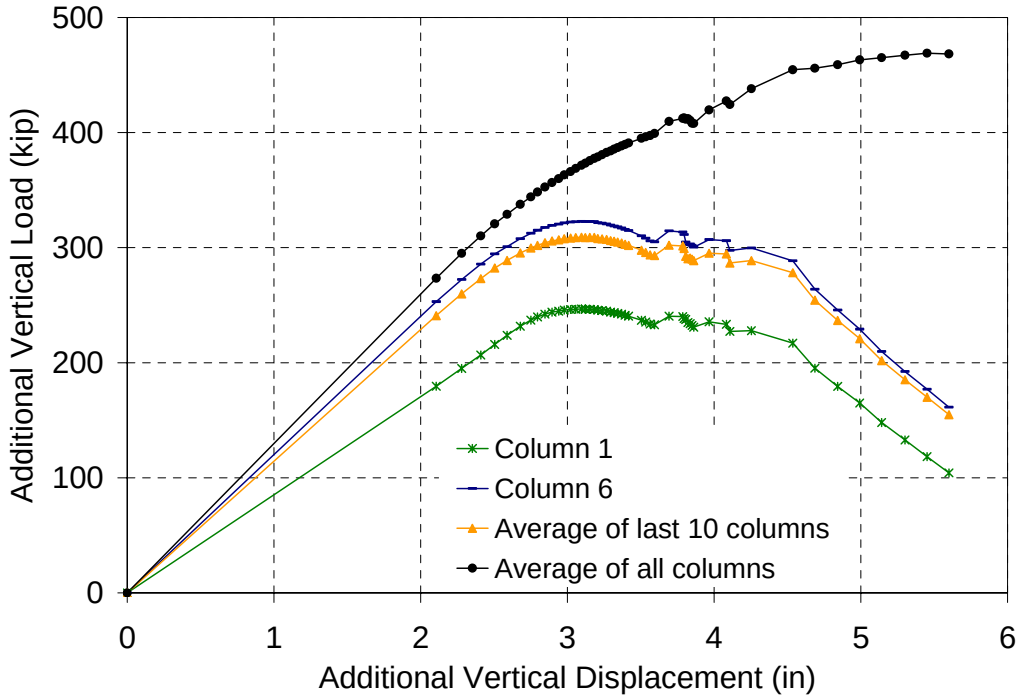

Figure 3–81. Additional vertical load versus additional vertical displacement during push–down analysis of isolated east wall model of WTC 2 for Case C temperature condition (compression is positive; see Fig. 3–80 for column locations).

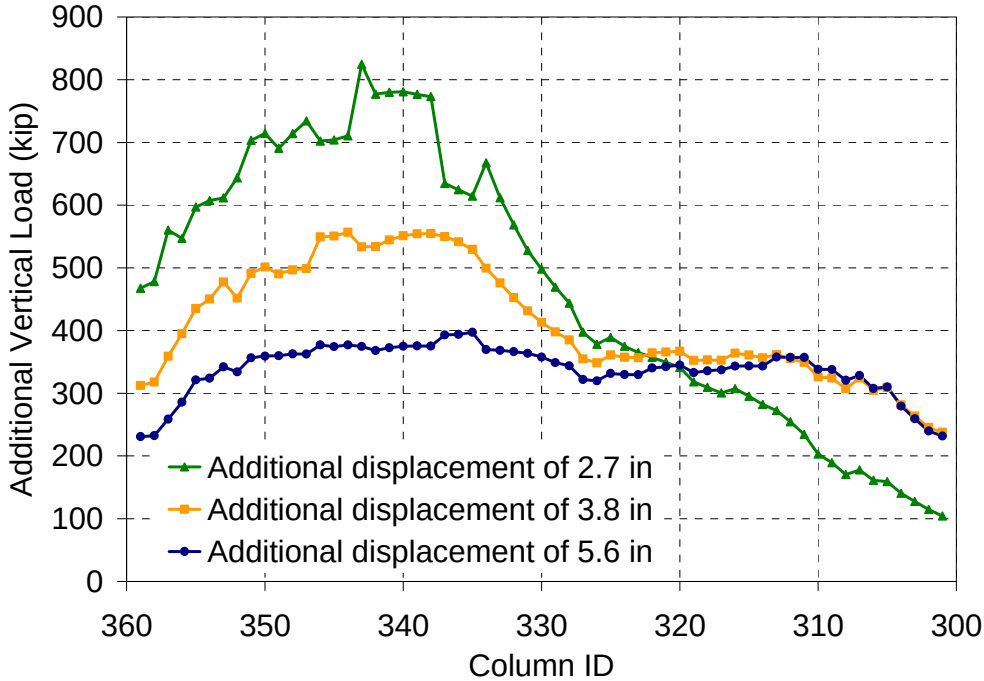

Figure 3–82. Variation of additional vertical load applied to columns of isolated east wall model of WTC 2 at different levels of additional vertical displacements imposed after Case C temperature condition (compression is positive).

Case D Temperature Condition

Figures 3–83 and 3–84 show Case D temperature distributions in the columns of the isolated east exterior wall model of WTC 2. The highest temperature, 845°C, occurred at 20 min in Column 307 between Floor 81 and Floor 82. Column temperatures were higher on the inside face of the exterior wall. Figure 3–85 shows the locations of the out-of-plane supports for Case D conditions at 60 min.

The vertical and the out-of-plane displacements at the end of the gravity load step after aircraft impact and at the end of each temperature step are shown in Figs. 3–86, 3–87, 3–88, and 3–89. The maximum vertical displacement of 3.2 in. occurred at Column 359 at Floor 90 immediately after aircraft impact. The maximum out-of-plane displacement of 7.8 in. occurred at Column 359 at Floor 81 at 60 min. (The out-of-plane displacement is positive inward.) The south side of the isolated exterior wall displaced vertically after aircraft impact more than other parts of the east wall, as impact damage was concentrated mostly on the southeast corner of the WTC 2. As time approached 60 min, the columns on the south side buckled, and the out-of-plane displacements increased.

The axial load distributions on the columns at the end of the gravity load step and each time interval are shown in Figs. 3–90 and 3–91. The maximum axial load occurred at Column 301 between Floor 82 and Floor 83 at 10 min. The axial load in this column increased from 200 kip after aircraft impact to 920 kip at 10 min. The axial load of 920 kip was very close to the theoretical local buckling load of 985 kip for Column 301 at 314 ˚C and less than the yielding or Euler buckling load of the column. Since local buckling of plates in exterior columns could not be captured by the beam elements that were used in the model of the exterior wall, the model overestimated the buckling capacity of exterior columns. The axial loads on the buckled columns on the south side of the isolated wall remained approximately constant throughout the temperature time history.

To consider the effect of load redistribution within WTC 2, the same corrective technique as described earlier in this chapter for WTC 1 was used. The axial loads at 60 min in columns between Floor 83 and Floor 84 in the isolated exterior wall model were compared to the corresponding values from the global model without creep and with Case C_i structural damage condition and Case D_i temperature condition, as shown in Fig. 3–92. The difference between the two curves in Fig. 3–92 was then applied to the columns at Floor 84 as corrective loads. The resulting vertical and out-of-plane displacements are shown in Fig. 3–93. As can be seen, the additional loads increased the maximum vertical displacement by 0.4 in. and the maximum out-of-plane displacement by about 0.8 in.

Also as described earlier for the WTC 1 isolated wall models, a push-down analysis of the WTC 2 isolated exterior wall model was performed. At an additional 5.3 in. of vertical displacement the model failed to converge, and the analysis was terminated. The vertical and out-of-plane displacements at the end of 5.3 in. of push down are shown in Fig. 3–94. At the end of push down, the maximum vertical displacement reached 8.0 in. and the maximum out-of-plane displacement reached 26.1 in. Figure 3–95 shows the column loads. This figure also shows the location of the columns, for which the load-deflection relationships are shown in Fig. 3–96. As can be seen from Fig. 3–96, the buckled columns on the south side of the isolated east exterior wall carried, on the average, an additional load of 410 kip at 60 min, compared to 630 kip for the average of the entire east wall columns. The additional axial loads on individual columns at different levels of additional vertical displacements are shown in Fig. 3–97.

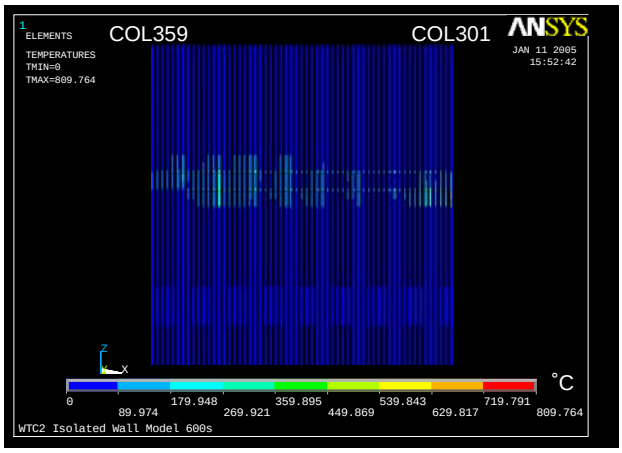

(a) Outside at 10 min

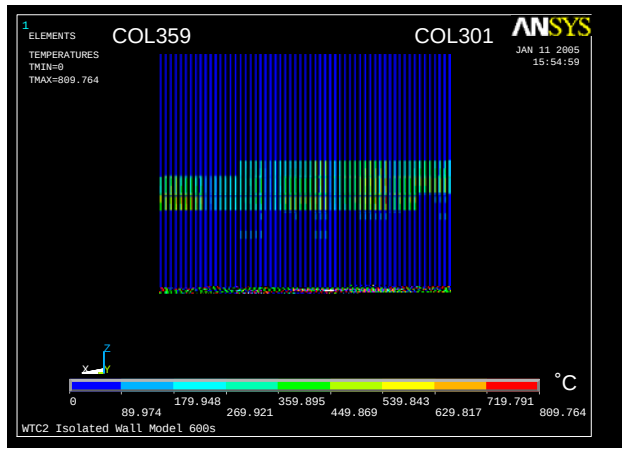

(b) Inside at 10 min

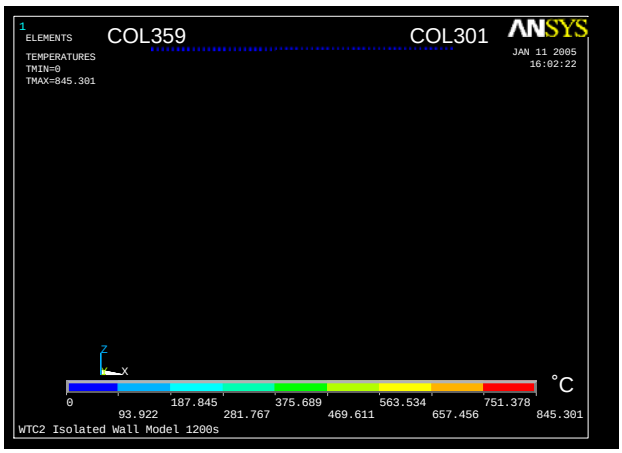

(c) Outside at 20 min

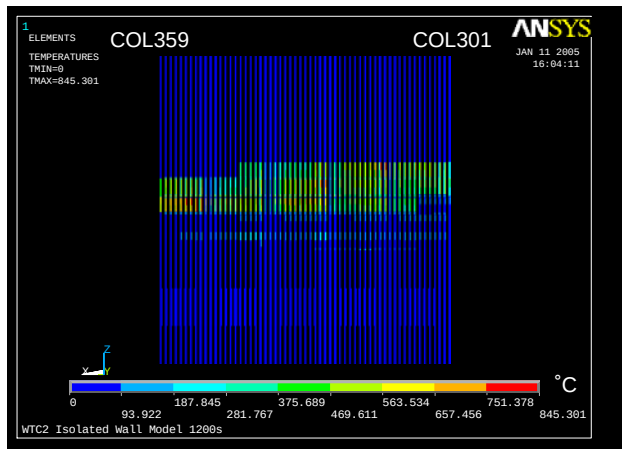

(d) Inside at 20 min

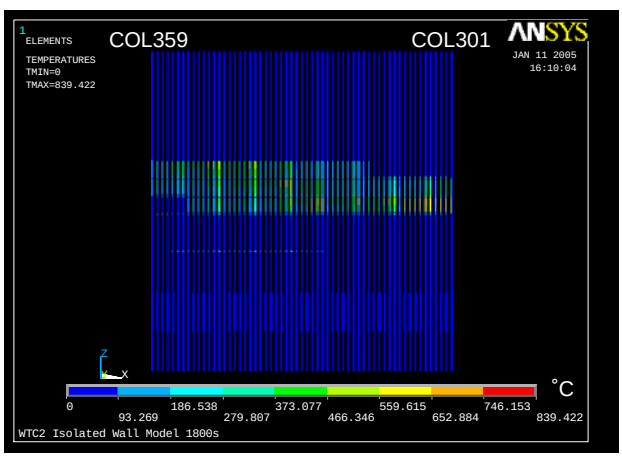

(e) Outside at 30 min

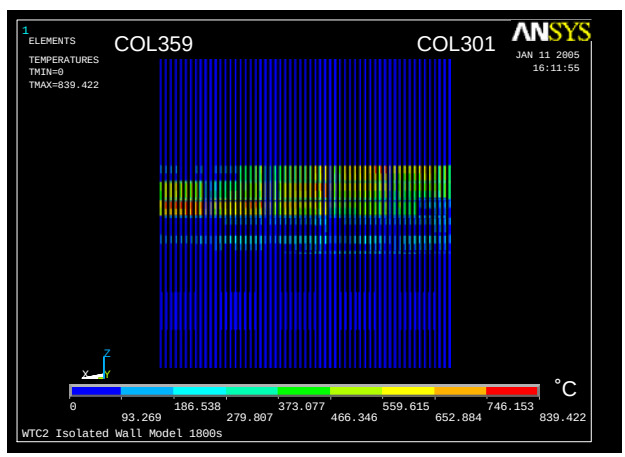

(f) Inside at 30 min

Figure 3–83. Column temperatures on the east wall of WTC 2 for Case D temperature condition at 10 min, 20 min, and 30 min.

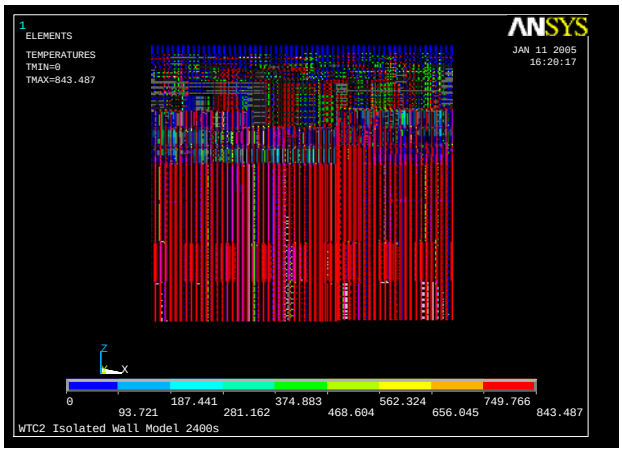

(a) Outside at 40 min

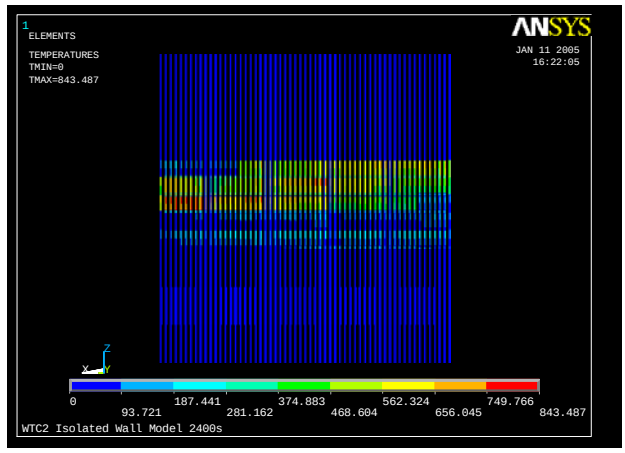

(b) Inside at 40 min

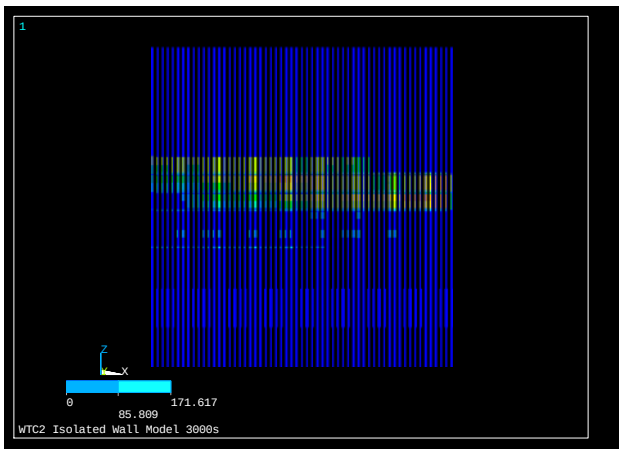

(c) Outside at 50 min

(d) Inside at 50 min

(e) Outside at 60 min

(f) Inside at 60 min

Figure 3–84. Column temperatures on the east wall of WTC 2 for Case D temperature condition at 40 min, 50 min, and 60 min.

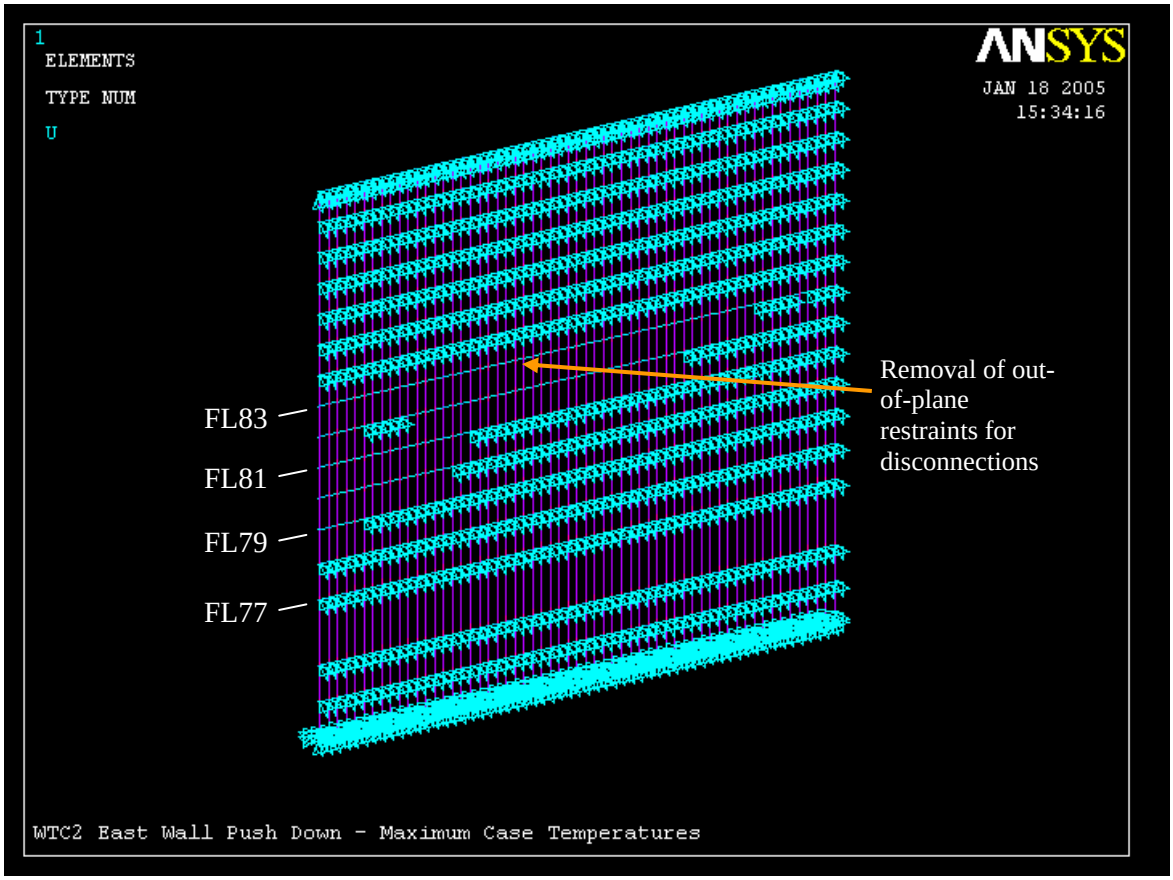

Figure 3–85. Location of the out-of-plane supports and floor/wall disconnections between exterior wall and the floor (WTC 2 east wall for Case D conditions at 60 min).

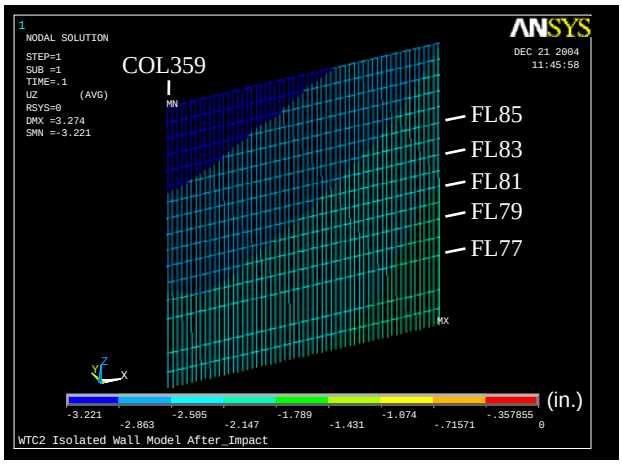

(a) After aircraft impact

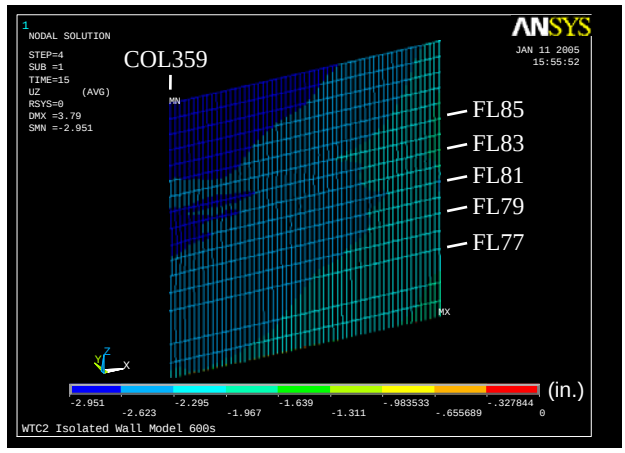

(b) At 10 min

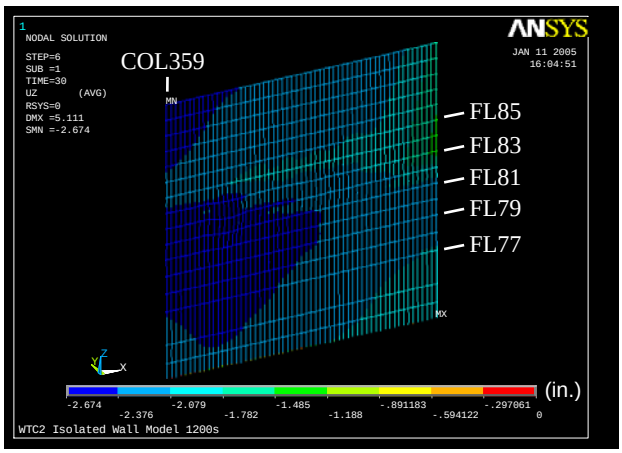

(c) At 20 min

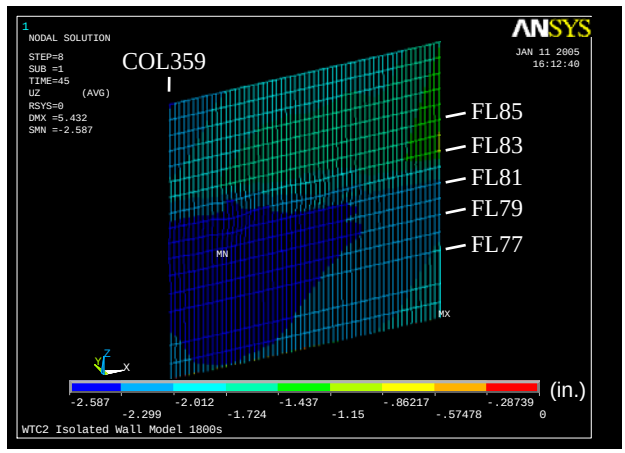

(d) At 30 min

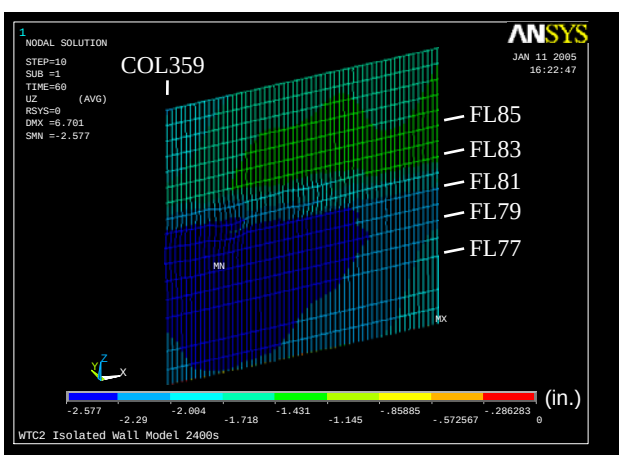

(e) At 40 min

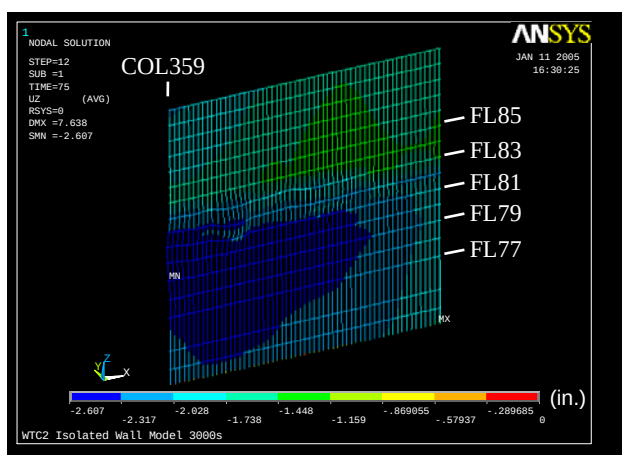

(f) At 50 min

Figure 3–86. Vertical displacement of isolated east wall model of WTC 2 for Case D temperature condition (downward displacement is negative; displacements scaled ten times).

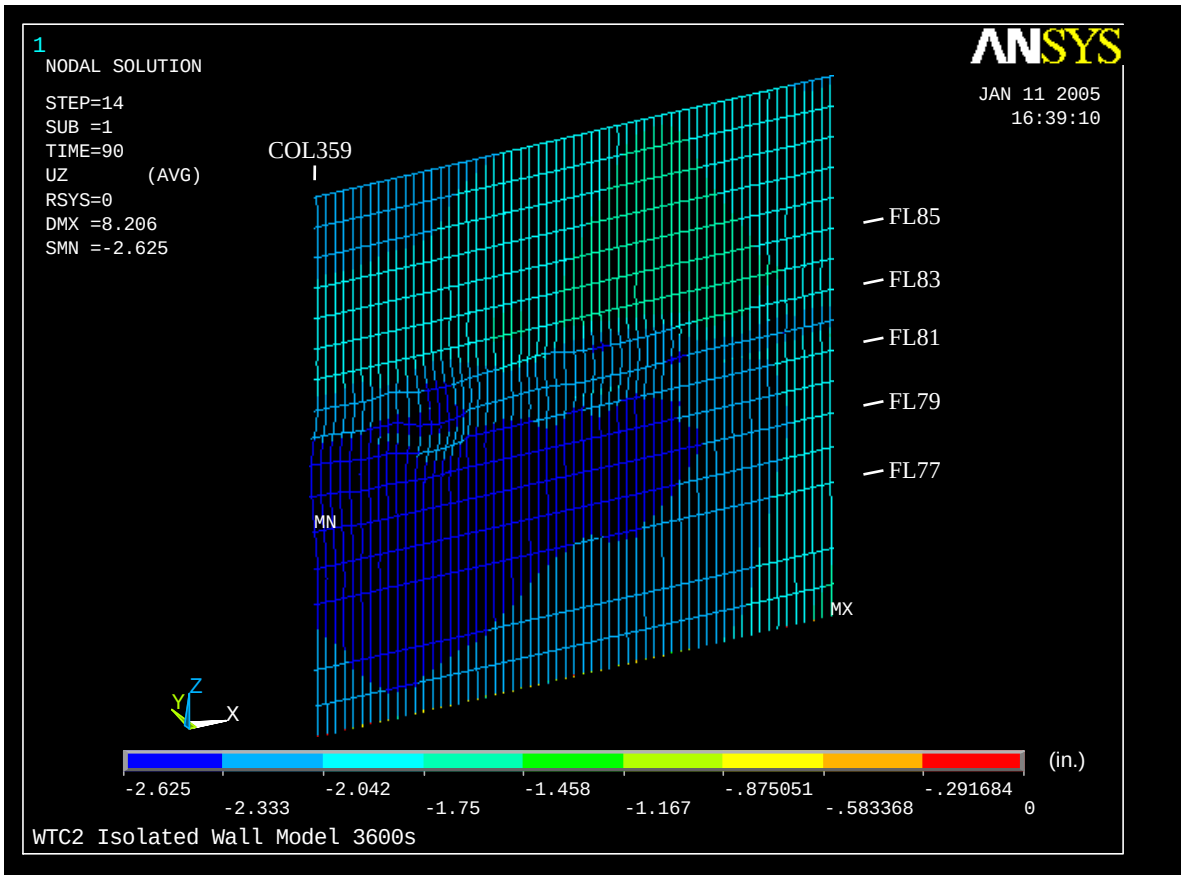

Figure 3–87. Vertical displacement of isolated east wall model of WTC 2 for Case D temperature condition at 60 min (downward displacement is negative; displacements scaled ten times).

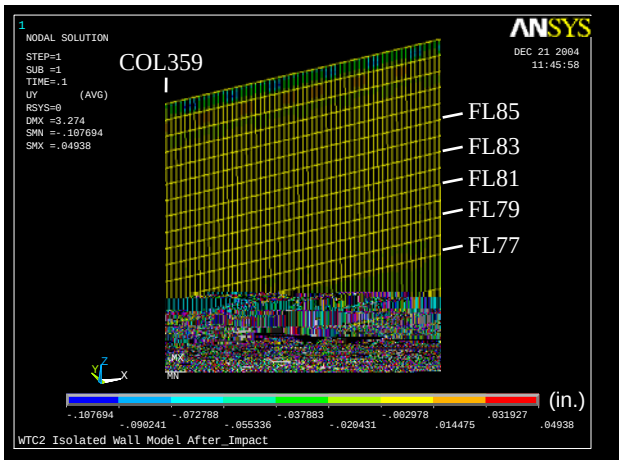

(a) After aircraft impact

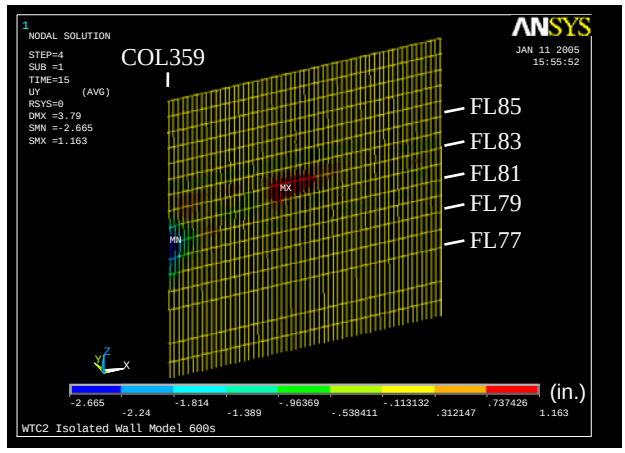

(b) At 10 min

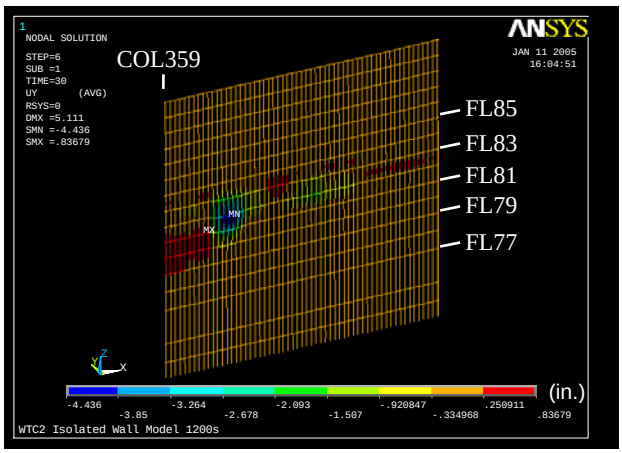

(c) At 20 min

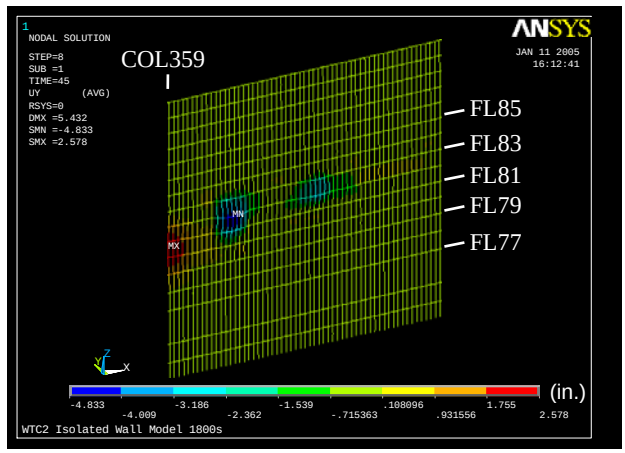

(d) At 30 min

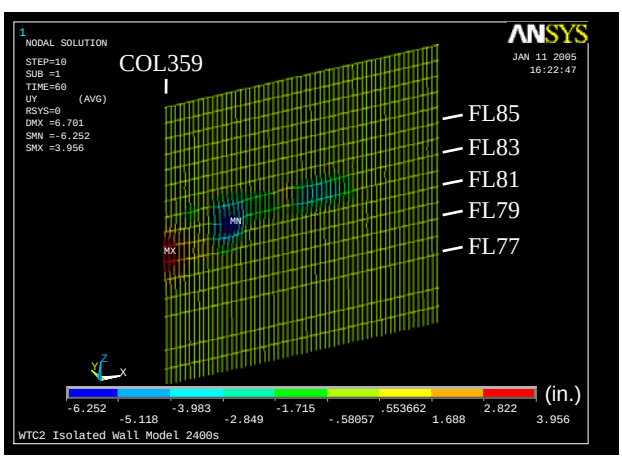

(e) At 40 min

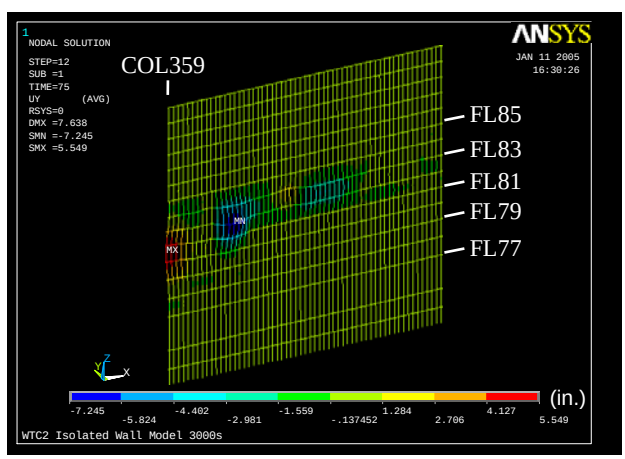

(f) At 50 min

Figure 3–88. Out-of-plane displacement of isolated east wall model of WTC 2 for Case D temperature condition (inward displacement is positive; displacements scaled ten times).

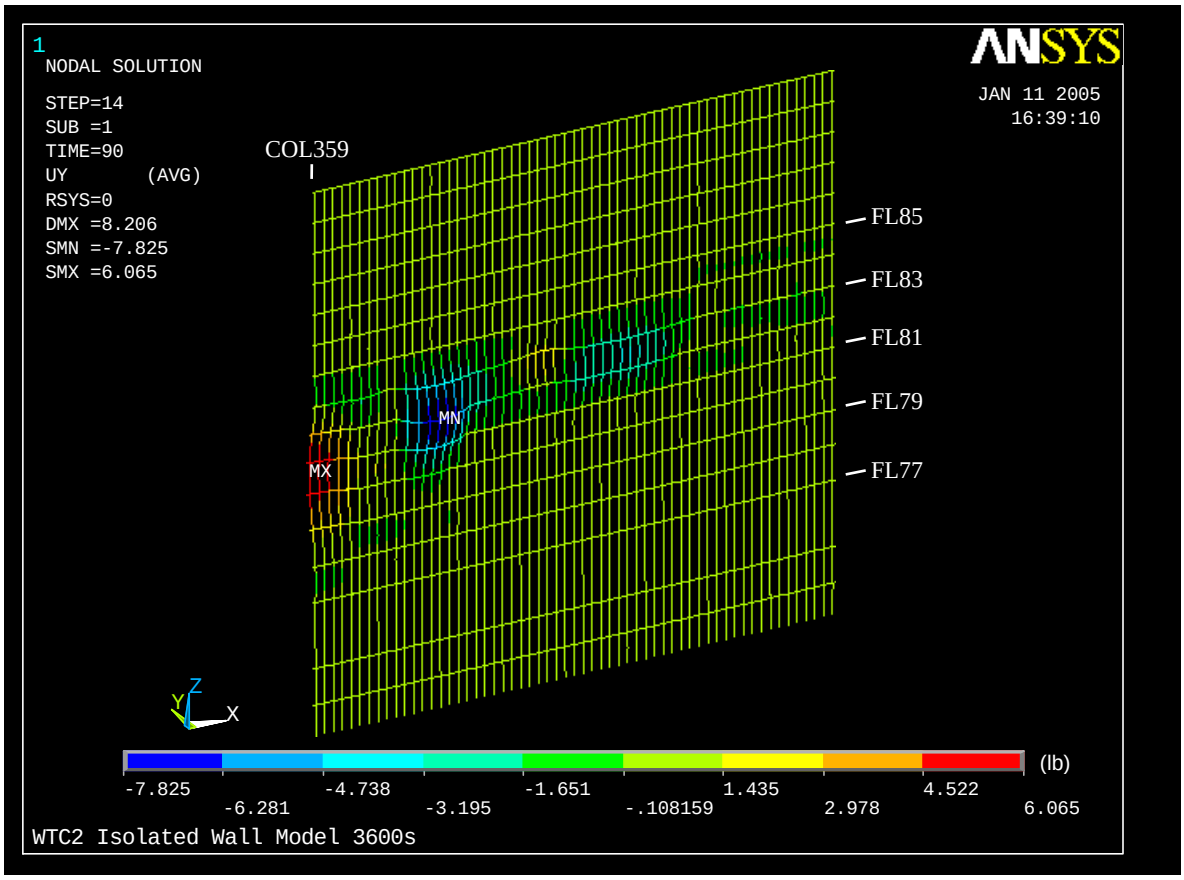

Figure 3–89 Out-of-plane displacement of isolated east wall model of WTC 2 for Case D temperature condition at 60 min (inward displacement is positive; displacements scaled ten times).

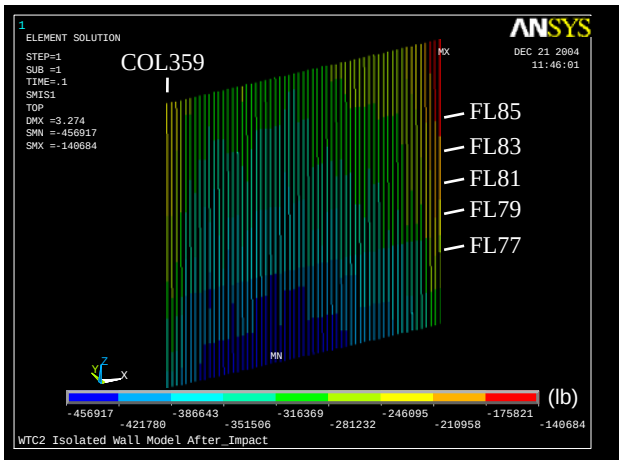

(a) After aircraft impact

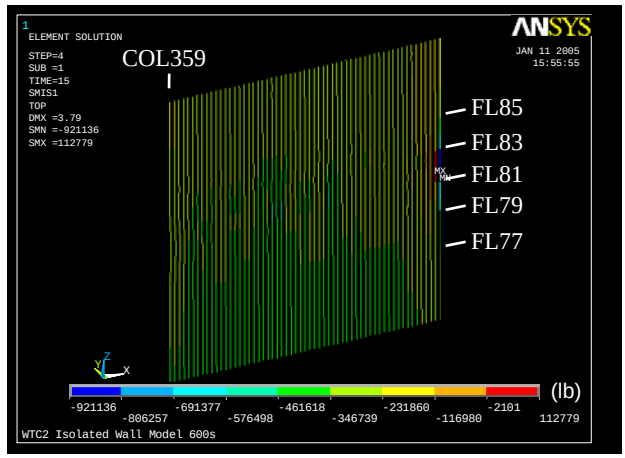

(b) At 10 min

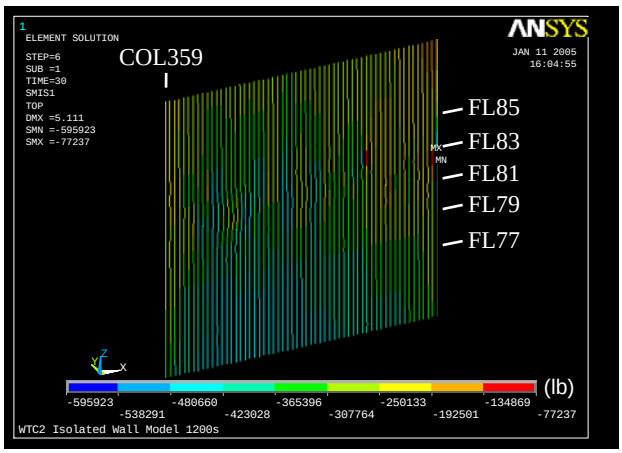

(c) At 20 min

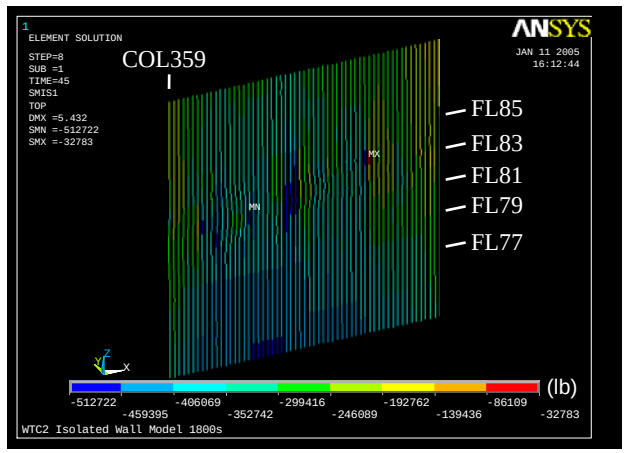

(d) At 30 min

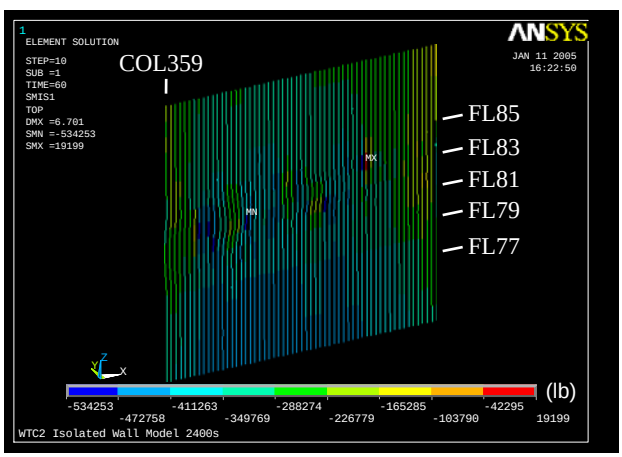

(e) At 40 min

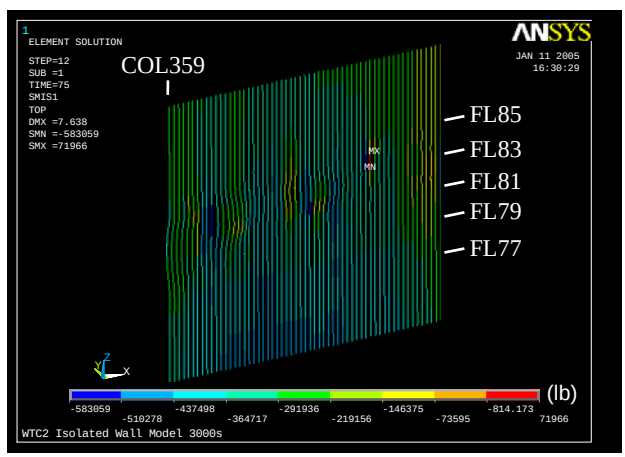

(f) At 50 min

Figure 3–90. Axial load on east wall columns of isolated east wall model of WTC 2 for Case D temperature condition (compression is negative).

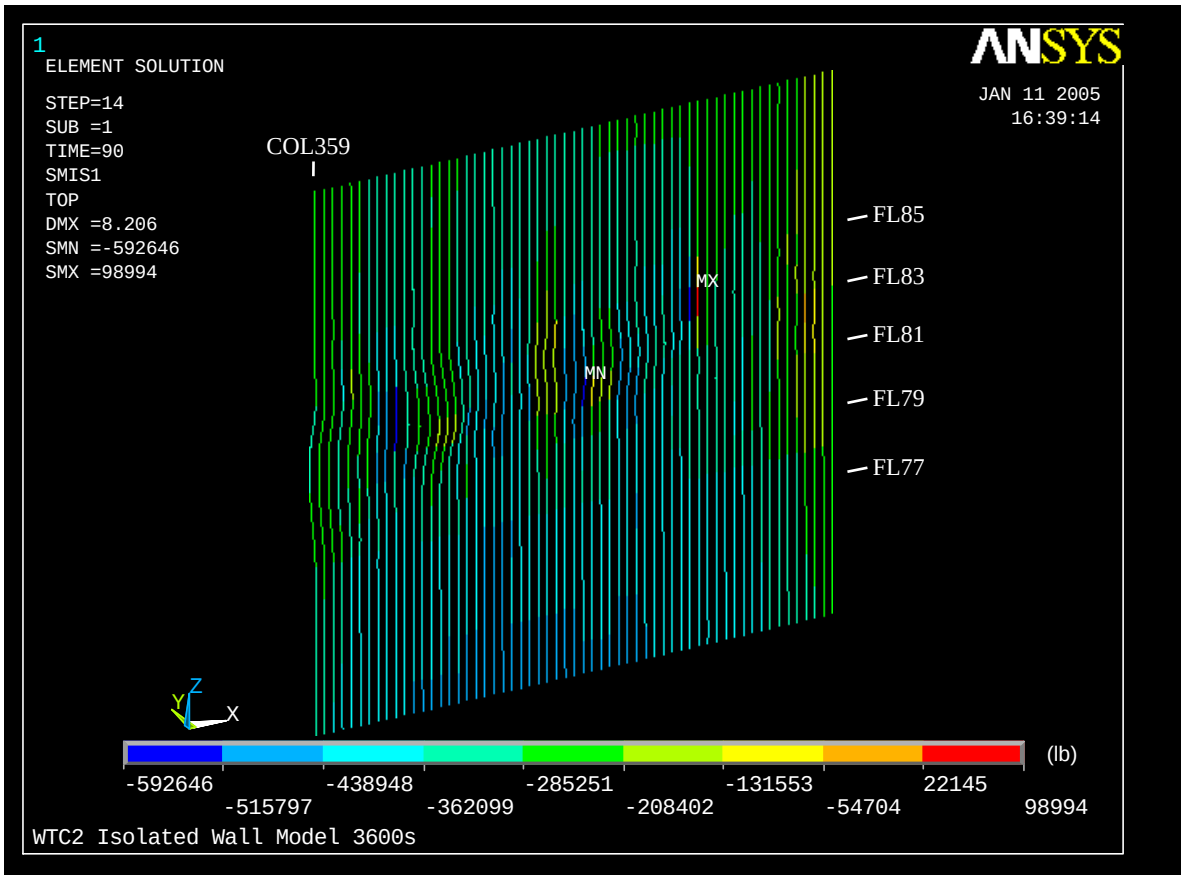

Figure 3–91. Axial load on east wall columns of isolated east wall model of WTC 2 for Case D temperature condition at 60 min (compression is negative).

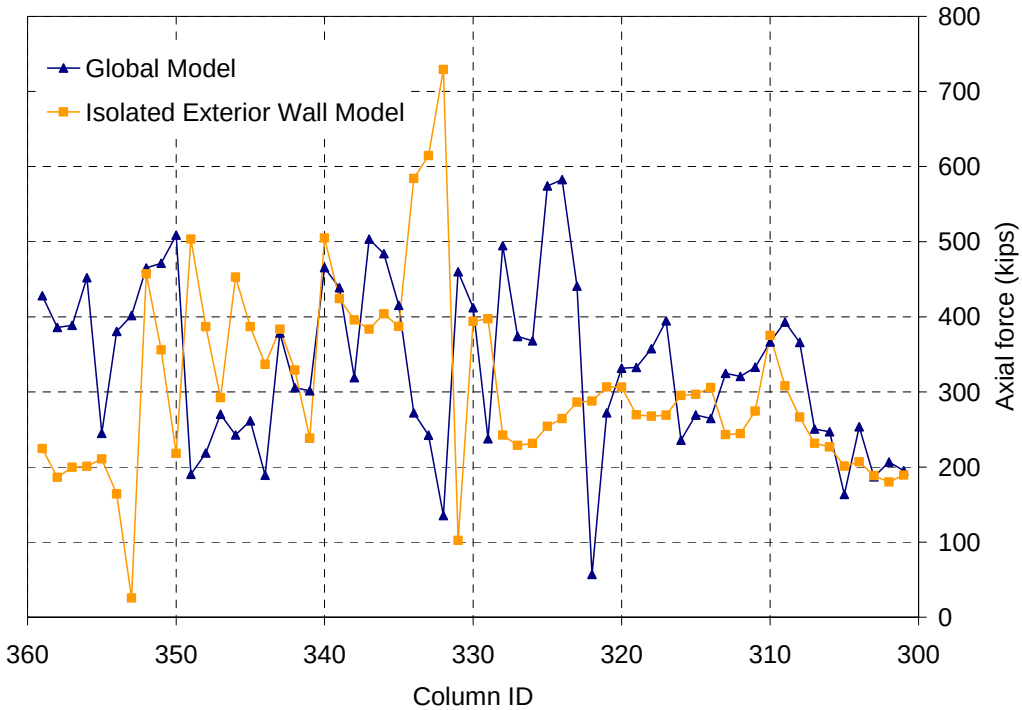

Figure 3–92. Comparison of axial load in columns at Floor 83 of isolated east wall model of WTC 2 at 60 min for Case D temperature conditions and the global model without creep for Case C_i structural damage condition and Case D_i temperature condition (compression is positive).

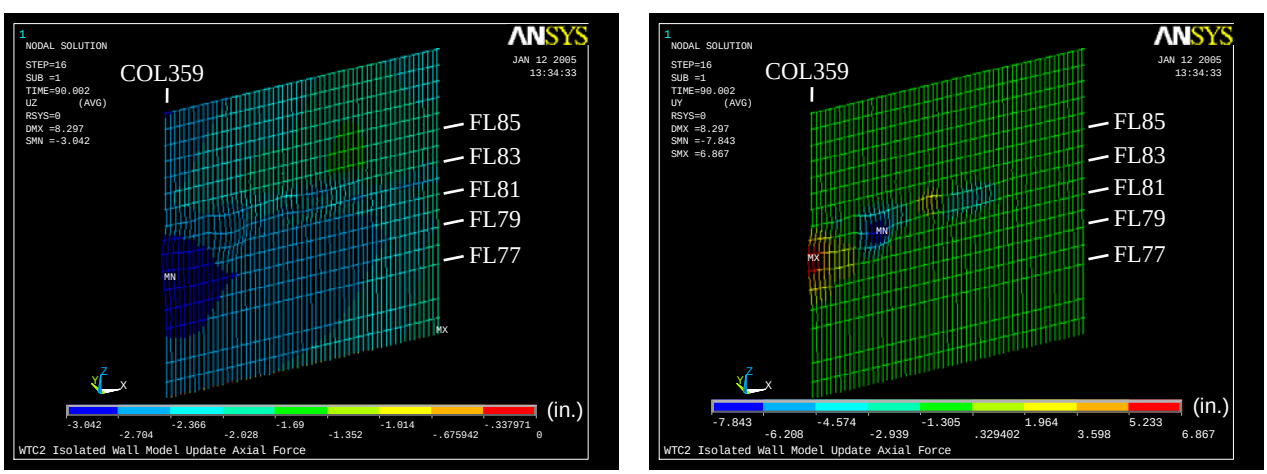

(a) Vertical displacement
(downward displacement is negative)

(b) Out-of-plane displacement
(inward displacement is positive)

Figure 3–93. Vertical and out-of-plane displacements of columns of isolated east wall model of WTC 2 after column forces were corrected to those of global model without creep for Case C_i structural damage condition and Case D_i temperature condition (displacements scaled ten times).

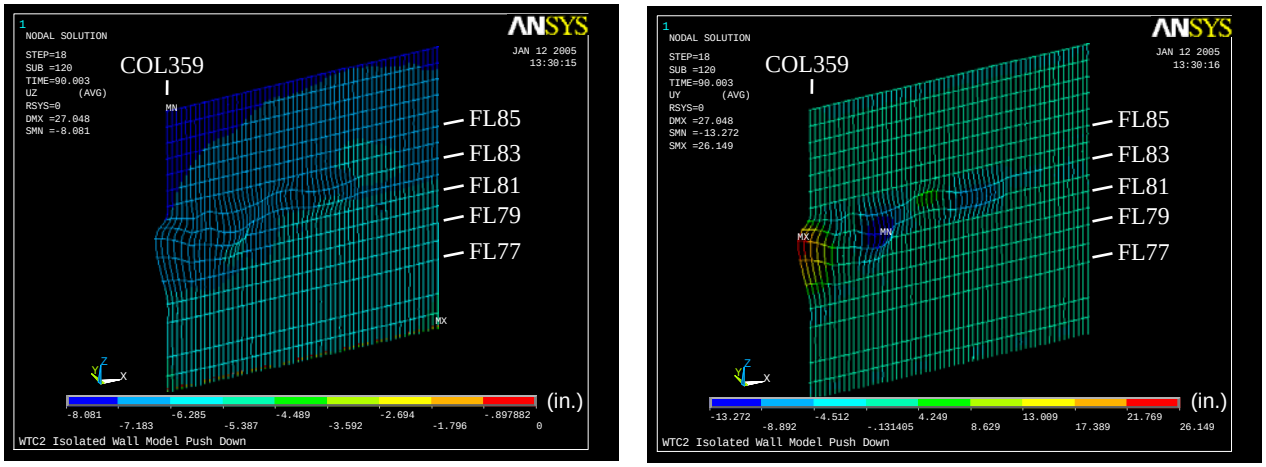

(a) Vertical displacement
(downward displacement is negative)

(b) Out-of-plane displacement
(inward displacement is positive)

Figure 3–94. Vertical and out-of-plane displacements of isolated east wall model of WTC 2 after Case D temperature condition and push down (displacements scaled five times).

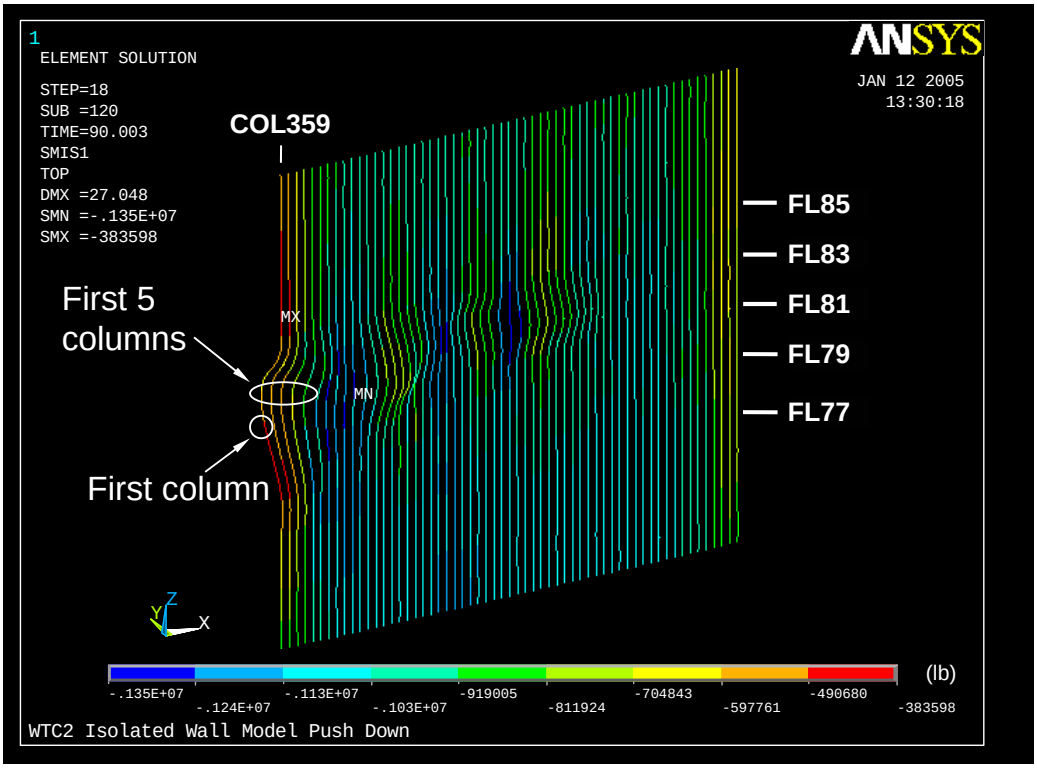

Figure 3–95. Axial load on east wall columns of isolated east wall model of WTC 2 after Case D temperature condition and push down (compression is negative).

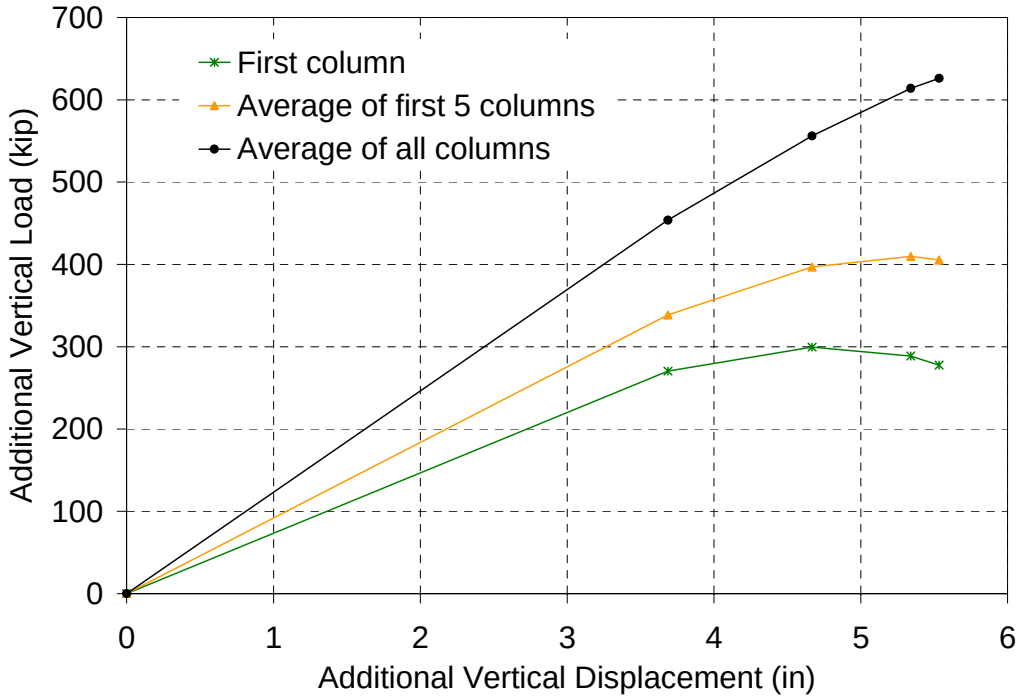

Figure 3–96. Additional vertical load applied to columns versus additional vertical during displacement for push-down analysis of isolated east wall model of WTC 2 for after Case D temperature condition (compression is positive; see Fig. 3–95 for column locations).

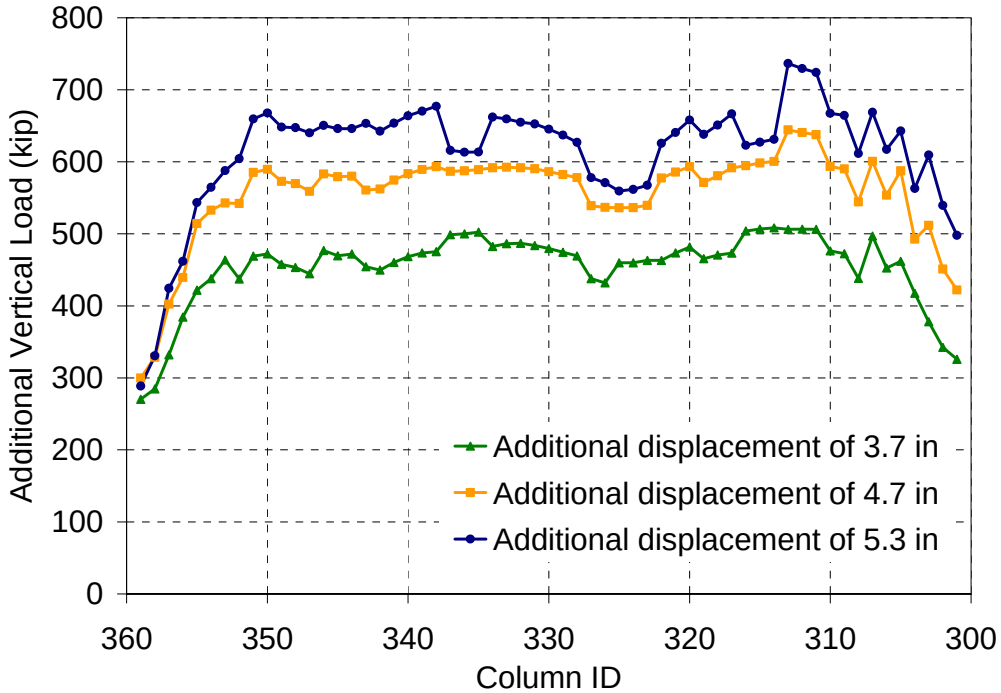

Figure 3–97. Variation of additional vertical load applied to columns of isolated east wall model of WTC 2 at different levels of additional vertical displacements imposed after Case D temperature condition (compression is positive).

Pull-in Forces to Cause Observed Bowing

As discussed in Section 2.5, the pull-in forces and their locations and the calculated floor/wall disconnections and pull-in locations were updated based on the observations from the photographs and videos. This section describes the analyses performed on the isolated wall model to estimate the magnitude of pull-in forces on the east wall of WTC 2, which would result in an inward bowing shape similar to that estimated from the photographs and videos. The estimated pull-in forces were used in the global analysis with Case D temperature condition.

The load steps that were used in the current analyses are similar to the load steps used in the earlier wall runs. At the beginning of each temperature load step, disconnections and lateral pull-in forces were applied to each floor connection to the east wall, as shown in Section 2.5. The magnitude and the distribution of the pull-in forces were obtained by trial and error. The magnitude of the pull-in force was kept constant till the end of the analysis, unless the column-floor connection fully disconnected before the analysis ended; at which point the pull-in force was set to zero. For each trial, the wall model was analyzed from the beginning (time = 0 min), accounting for large deflections and temperature-dependent plasticity and creep. The out-of-plane displacements calculated at the end of 20 min and 50 min were compared to the displacements estimated at the same points in time from the photographs, as shown in Fig. 3–98.

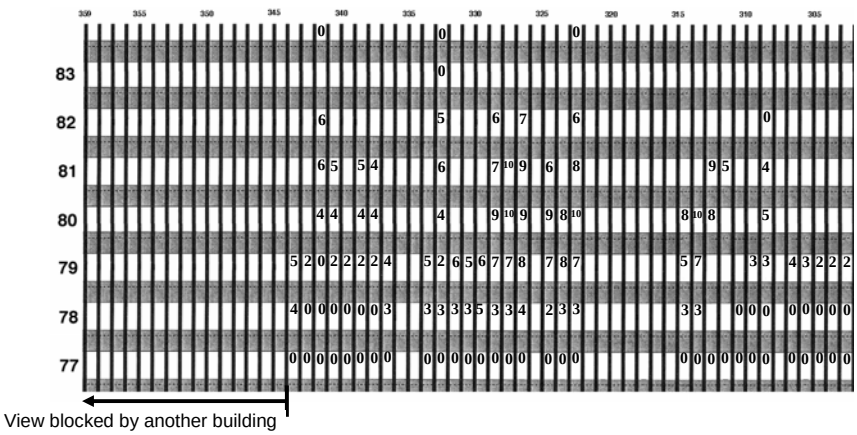

(a) Displacement measurements at 9:21 a.m. (18 min after impact)

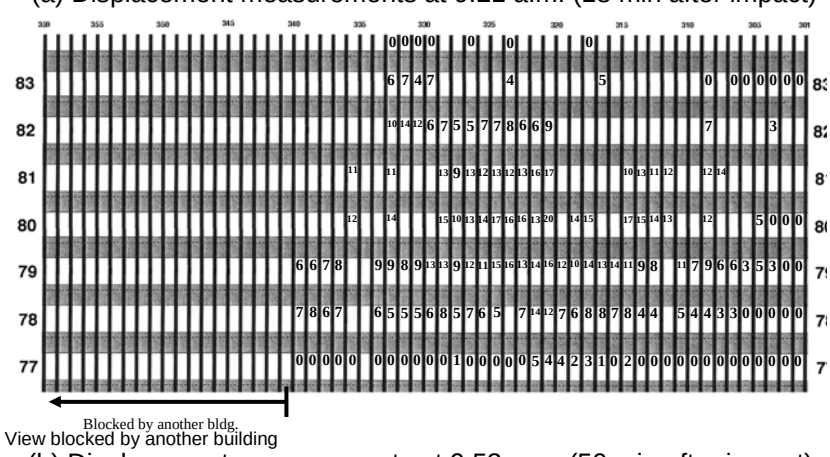

(b) Displacement measurements at 9:53 a.m. (50 min after impact)

Figure 3–98. Out-of-plane displacements of the east wall of WTC 2 estimated by NIST from photographs (inward displacement is positive; displacements are in in.).

For the first set of trials, the pull-in forces were assumed to be uniformly distributed over the entire width of the model. Two different magnitudes for pull-in forces were tried: 0.5 kip and 5.0 kip. The analysis for 0.5 kip ran to 32 min, at which point it failed to converge. As shown in Fig. 3–99(a), the wall primarily bowed outward at 20 min (positive displacement direction is inward). These results disagreed with what was observed in the photographs and videos, indicating that the assumed magnitude of pull-in force of 0.5 kip was not sufficient to cause inward bowing. In a second trial, the 5.0 kip pull-in force was used. This analysis ran to 18 min, at which point it failed to converge. Contrary to the first trial with 0.5 kip pull-in force, the wall bowed inward, as shown in Fig. 3–99(b). The maximum inward displacement in this trial was 31 in. This value is about three times larger than the displacement estimated from photographs, indicating that the 5.0 kip pull-in force is greater than the actual magnitude of pull-in force. Based on these two runs, it was concluded that the magnitude of the pull-in forces for a uniform distribution is between 0.5 kip and 5.0 kip.

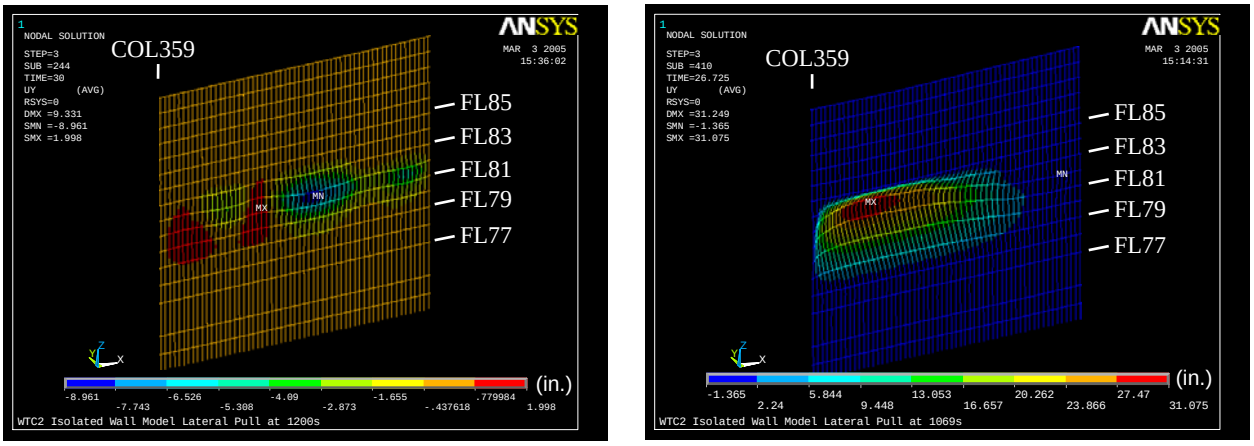

(a) Pull-in force = 0.5 kip
t = 20 min

(b) Pull-in force = 5.0 kip
t = 18 min

Figure 3–99. Out-of-plane displacement of isolated east wall model of WTC 2 with 0.5 kip and 5.0 kip pull-in force with uniform magnitude distribution at 20 min and 18 min (inward displacement is positive).

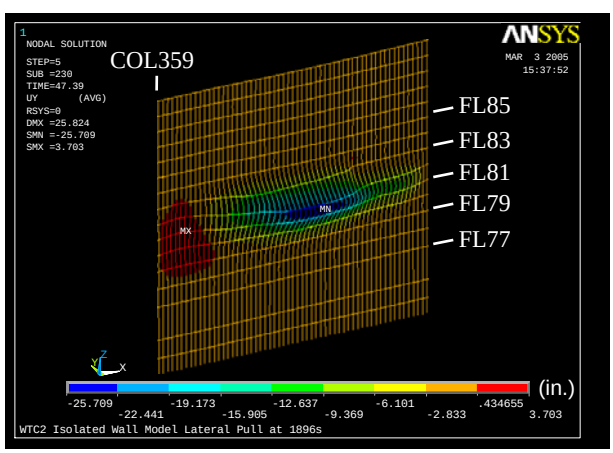

Pull-in force = 0.5 kip
t = 32 min

Figure 3–100. Out-of-plane displacement of isolated east wall model of WTC 2 with 0.5 kip pull-in force with uniform magnitude distribution at 32 min (inward displacement is positive).

From these two runs, it was also possible to learn about the distribution of the pull-in forces over the width of the east wall. When a uniform distribution of a 0.5 kip pull-in force was used at 20 min over the entire width of the east wall, the resulting out-of-plane displacements were inward on the south side and outward on the north side of the wall, as shown in Fig. 3–99. The primary reasons for the outward bowing on the north side of the east wall are as follows: (1) the higher temperatures in the north side of the wall resulted in restrained thermal expansion and larger column loads; (2) the higher temperatures of the inside face of the columns, relative to the outside, caused higher plastic and creep strains and resulted in differential shortening of the inside relative to the outside; and (3) the plastic softening and creep of the inside caused an outward shift in the neutral axis, and a resulting outward bow of the columns. This phenomenon can be seen in the displacement results presented in Figs. 3–99 and 3–100, where inward displacements on the south side of the east wall became smaller and smaller and eventually changed to outward displacements toward the north side of the east wall. Consequently, a simple non-uniform pull-in force distribution was selected with higher loads on the north side to ensure inward bowing as observed in photographs and videos.

Two cases were analyzed for the second set of trials. In the first case, the magnitude of the pull-in forces on the south half of the east wall was set to 1.0 kip and the magnitude of the pull-in forces on the north half was set to 4.0 kip. The wall analysis with these pull-in force magnitudes ran to 60 min. Figure 3–101 shows the out-of-plane displacements at different stages of the analysis. As can be seen, the maximum inward bowing was 7.5 in. at 20 min, located approximately at the middle of Floor 81 of the east wall. This agreed well with the observed displacements, which showed maximum inward displacement of about 10 in. around the middle of Floor 81. In the earlier trial with a uniform 0.5 kip magnitude of pull-in force, the inward bowing started to decrease with increasing time after 20 min, and at around 40 min it bowed outward The bowing at 50 min was mostly outward, disagreeing with the observed displacements. In the second trial, the magnitude of the pull-in force on the south half was increased from 1.0 to 1.5 kip, and on the north half was increased from 4.0 to 5.0 kip. This analysis ran to 50 min, at which point the analysis failed to converge. Figure 3–102 shows the magnitude of inward bowing at different stages of the analysis. The maximum inward bowing in this trial was 9.5 in. at 20 min, located approximately at the middle of Floor 81 of the east wall. This result agreed well with the observed displacements. The inward bowing continued to increase with time and reached a maximum of 37 in. at 50 min. As seen in Fig. 3–102, the location of the maximum displacements agreed well with the observations. However, the magnitude of the calculated displacements was about twice the magnitude of the observed displacements.

From these trial runs, it was concluded that the magnitude of pull-in forces ranged from 1.0 kip to 1.5 kip on the south half and from 4.0 kip to 5.0 kip on the north half of the east wall. Based on these ranges, and also considering the possible increase in column loads of the east face after impact for Case D conditions, a pull-in force of 1.0 kip on the south half and 4.0 kip on the north half of the east wall was initially selected for the global model analysis with creep. As will be discussed in Chapter 4, at 30 min, the magnitude of the pull-in force was increased to 1.5 kip on the south half and decreased to 3.0 kip on the north half of the east wall and kept constant after that time.

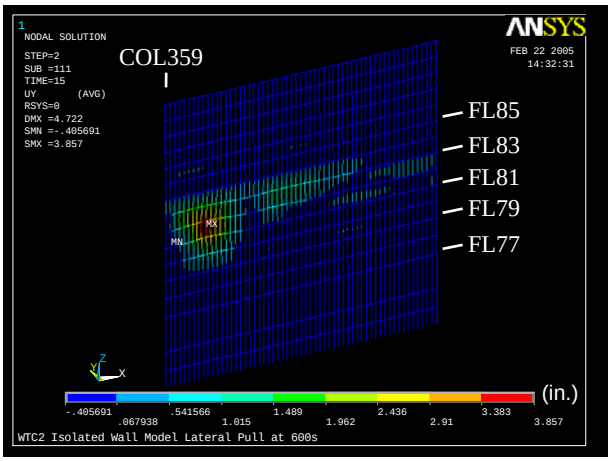

(a) At 10 min

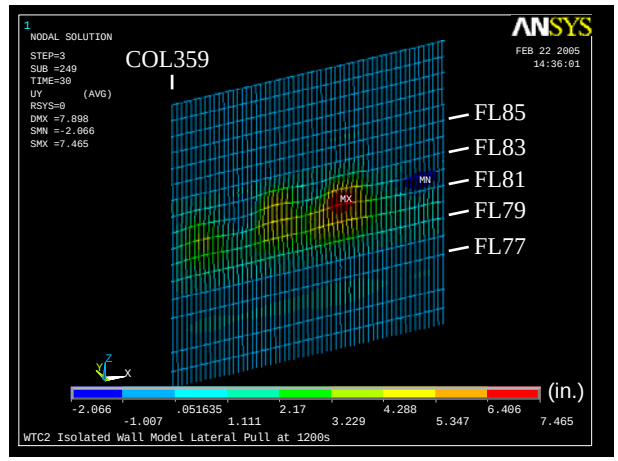

(b) At 20 min

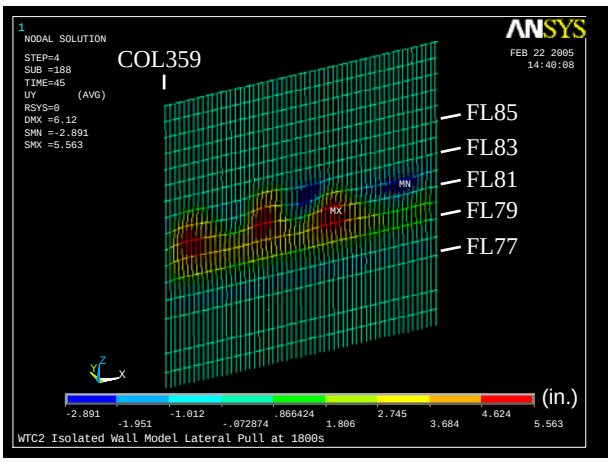

(c) At 30 min

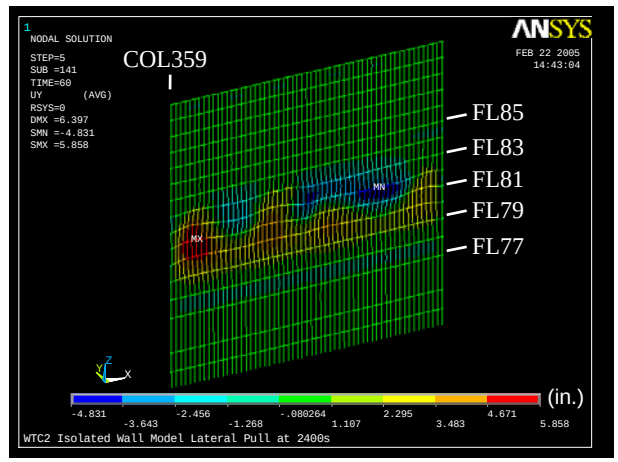

(d) At 40 min

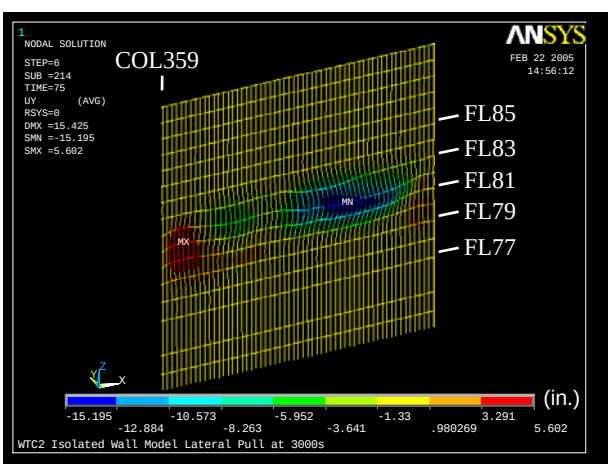

(e) At 50 min

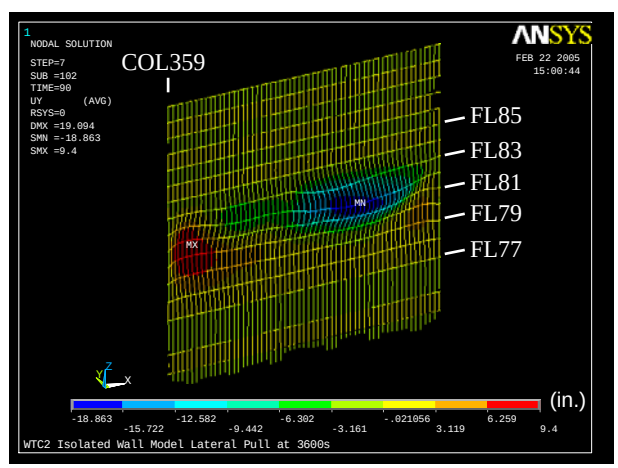

(f) At 60 min

Figure 3–101. Out-of-plane displacement of isolated east wall model of WTC 2 with nonuniform pull-in force with magnitude of 1.0 kip on the south half and 4.0 kip on the north half (inward displacement is positive).

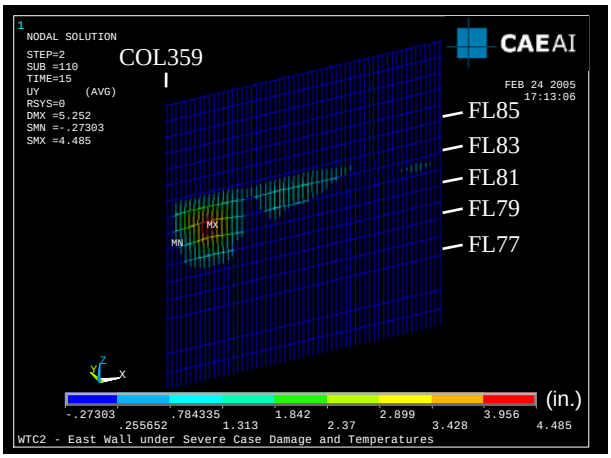

(a) At 10 min

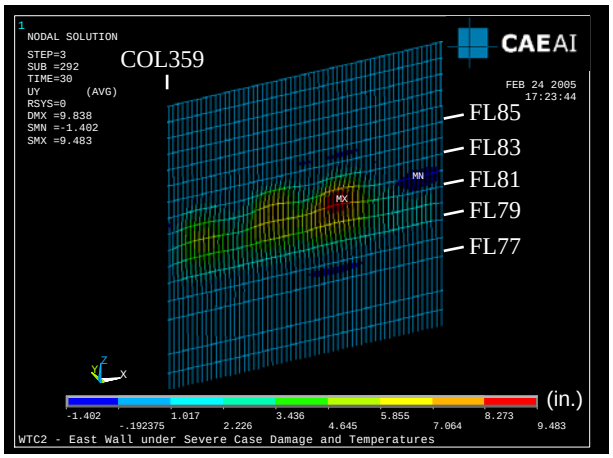

(b) At 20 min

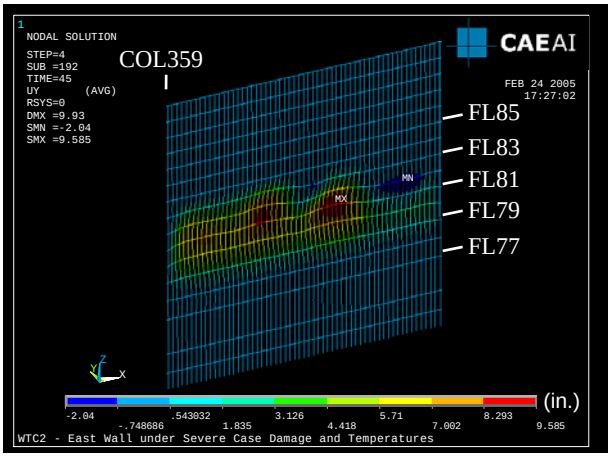

(c) At 30 min

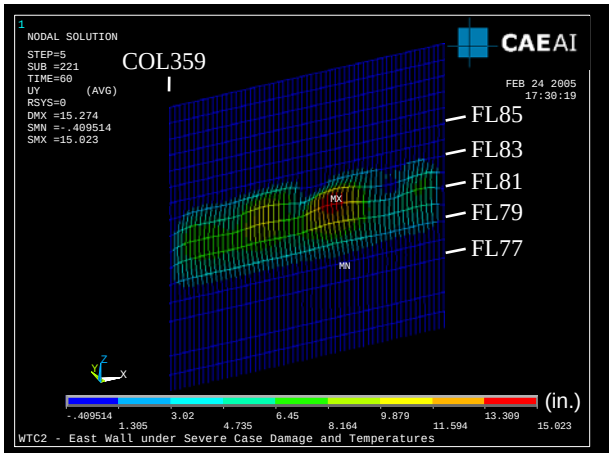

(d) At 40 min

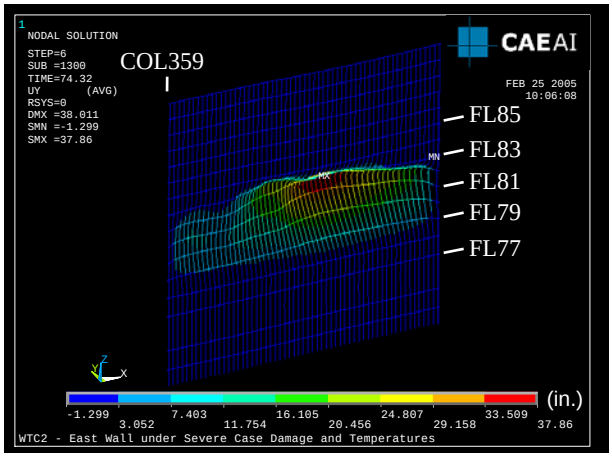

(e) At 50 min

Figure 3–102. Out-of-plane displacement of isolated east wall model of WTC 2 with nonuniform pull-in force with magnitude of 1.5 kip on the south half and 5.0 kip on the north half (inward displacement is positive).

3.3 CORE COLUMN SHORTENING AND DOWNWARD DISPLACEMENT OF CORE

To examine whether or not the core columns shortened and the core displaced downward when subjected to fire-induced temperature loads, the core models were isolated from the global models of WTC 1 and WTC 2. The isolated core models extended from Floor 89 to Floor 106 for WTC 1 and from Floor 73 to Floor 106 for WTC 2, and did not include any parts of their hat trusses. At the base of the models, vertical springs connected Floor 89 and Floor 73 to fixed ground; the spring stiffness represented the vertical stiffness of the columns below. The isolated core models included core columns, core beams, and core slabs, as in the global models (see Chapter 4 for details).

The WTC 2 core model was restrained in two horizontal directions at every floor level to represent the lateral restraint of the exterior walls. Without the lateral restraints, the WTC 2 core model would tilt significantly, due to the extensive impact damage to the southeast part of the core. The WTC 1 core model was not restrained in the horizontal directions at floor levels.

Gravity dead and live loads were directly obtained from the global models and applied to the core model nodes. Internal forces and moments of the columns of Floor 106 of the global models after aircraft impact were imposed at the ends of the Floor 106 columns of the isolated core models. Only the Case A structural damage condition was used for the WTC 1 core model, and only the Case C structural damage condition was used for the WTC 2 core model. The isolated core models with Case B and Case D structural damage conditions were also run, but the models did not converge, even with lateral restraints.

The models were then subjected to two temperature conditions for each tower: Case A and Case B (for WTC 1) and Case C and Case D (for WTC 2). Temperature data were provided at 10 min intervals up to 100 min for WTC 1 and up to 60 min for WTC 2.

Since the models included only the core, the load transfer between the core and the exterior wall through either the hat truss or floors was not captured.

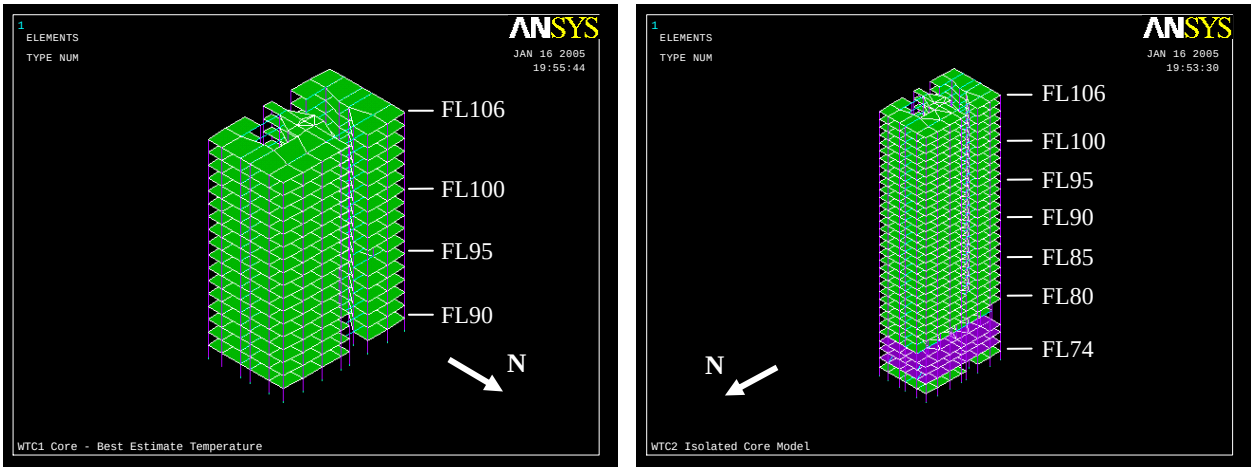

(a) WTC 1 (b) WTC 2

Figure 3–103. Isolated core models.

3.3.1 FEA of WTC 1 Core

Case A Temperature Condition

Figures 3–104 to 3–111 show the vertical displacements of the WTC 1 isolated core model subjected to Case A temperatures from aircraft impact to 100 min. At 30 min, the vertical displacement of the northwest corner at Column 501 became large above Floor 98, and grew larger with time. The core started to tilt toward the northwest corner at 30 min, and the analysis was terminated due to nonconvergence. The analysis was restarted at 30 min by restraining corner Column 501 in the horizontal directions at floor levels above Floor 98 to represent lateral restraint from the exterior walls and office floors. At 100 min, the maximum vertical displacement of 21.7 in. occurred at Column 501. Figures 3–114 and 3–115 show axial loads and plastic strains in the core columns at 100 min. Columns at the northwest corner experienced large plastic strains. The maximum plastic strain was about 14 percent.

The vertical displacement at Floor 106 at 100 min ranged from 3.3 in. to 21.7 in. The maximum vertical displacement of the south side was limited to 11.2 in. at Column 1004. The average vertical displacement of Floor 106 was 7.4 in. The average vertical displacement of the south side at Floor 106 was 6.0 in. Considering the average vertical displacement of 5 in. after the aircraft impact, the average additional downward displacement of the core due to thermal loads was about 2 in.

To determine the additional axial load-carrying capacity of the core, the isolated core model at 100 min was pushed down by imposing additional incremental vertical displacement. The analysis was converted from a force-control analysis to a displacement-control analysis by imposing the vertical displacements calculated at 100 min under force control and then imposing additional vertical displacement increments on the top of the columns at Floor 106. The analysis was terminated when the additional vertical displacement reached 9.5 in. Figure 3–116 shows the total vertical displacements of the model at the end of the push-down analysis. Figure 3–117 shows the relationship between the total additional vertical force and the additional vertical displacement. The additional vertical force reached its maximum at 7.2 in. of additional vertical displacement. Figure 3–118 shows the additional axial loads in columns of Floor 98 when the total additional vertical force is at its maximum. The maximum total additional vertical force of 37,142 kip was about 95 percent of the total column force at Floor 98 prior to push-down. Therefore, the core still had significant reserve capacity at the end of Case A temperature condition.

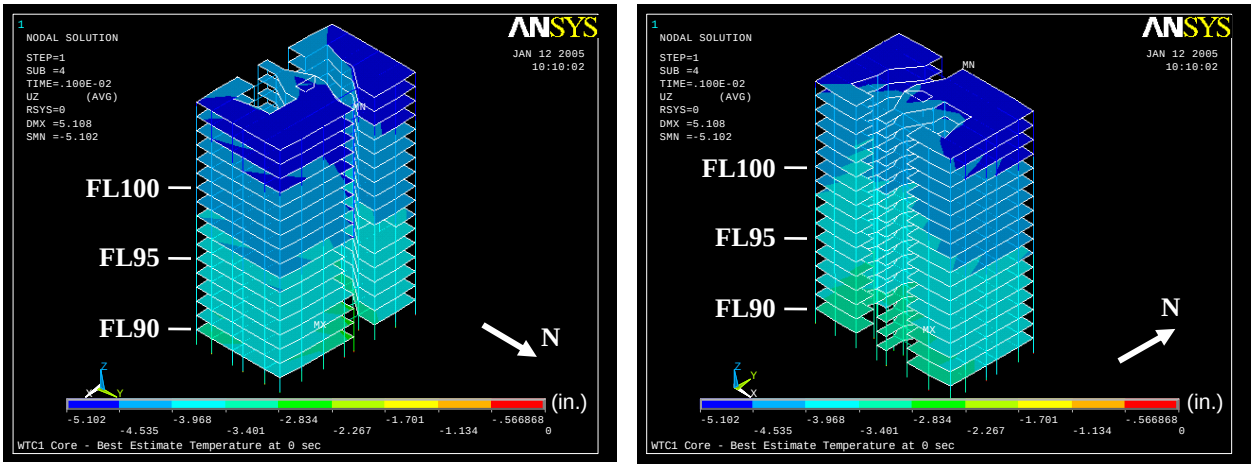

(a) North and east sides (b) South and east sides

Figure 3–104. Vertical displacement of isolated core model of WTC 1 after aircraft impact (downward displacement is negative).

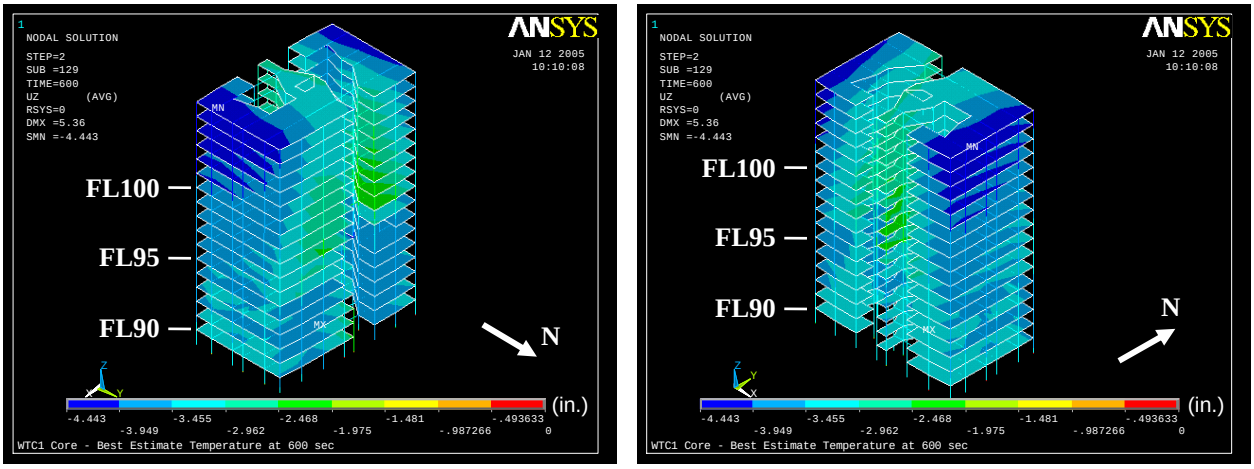

(a) North and east sides (b) South and east sides

Figure 3–105. Vertical displacement of isolated core model of WTC 1 for Case A temperature condition at 10 min (downward displacement is negative).

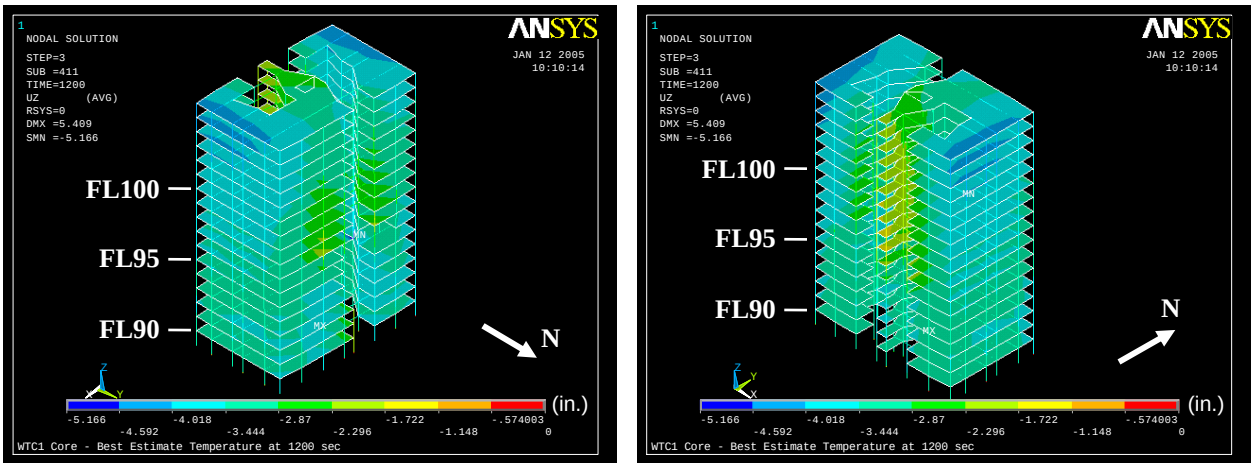

(a) North and east sides (b) South and east sides

Figure 3–106. Vertical displacement of isolated core model of WTC 1 for Case A temperature condition at 20 min (downward displacement is negative).

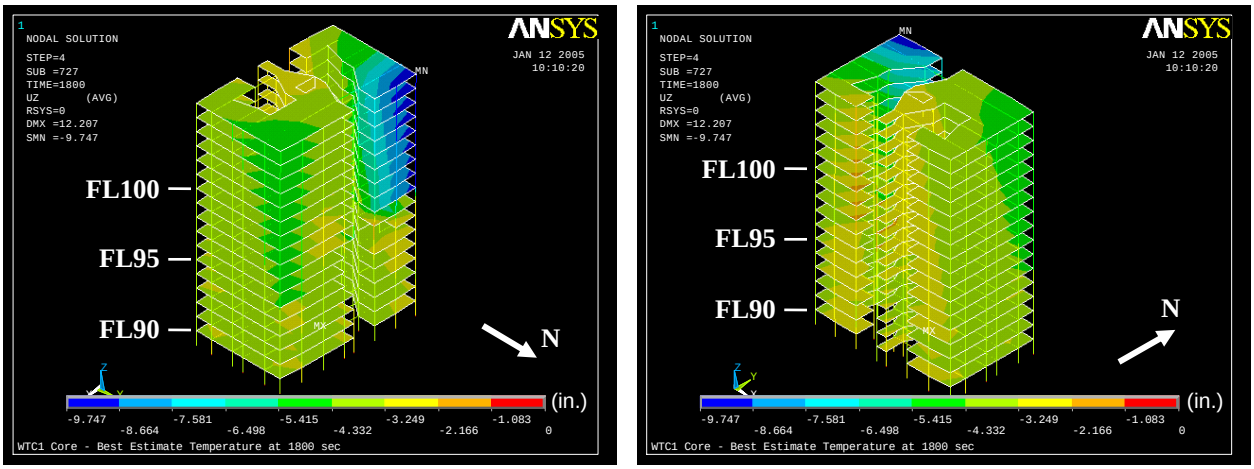

(a) North and east sides (b) South and east sides

Figure 3–107. Vertical displacement of isolated core model of WTC 1 for Case A temperature condition at 30 min (downward displacement is negative).

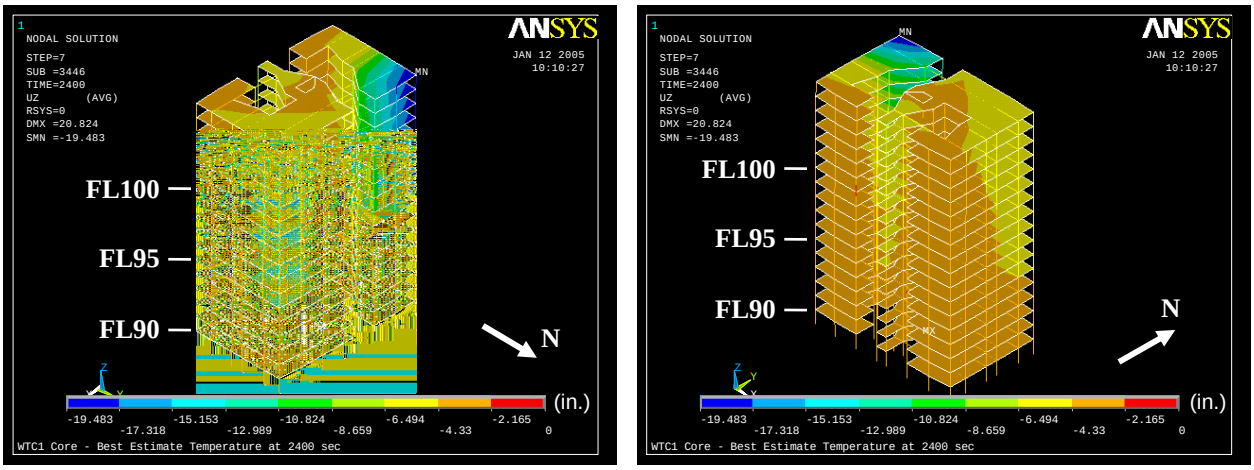

(a) North and east sides (b) South and east sides

Figure 3–108. Vertical displacement of isolated core model of WTC 1 for Case A temperature condition at 40 min (downward displacement is negative).

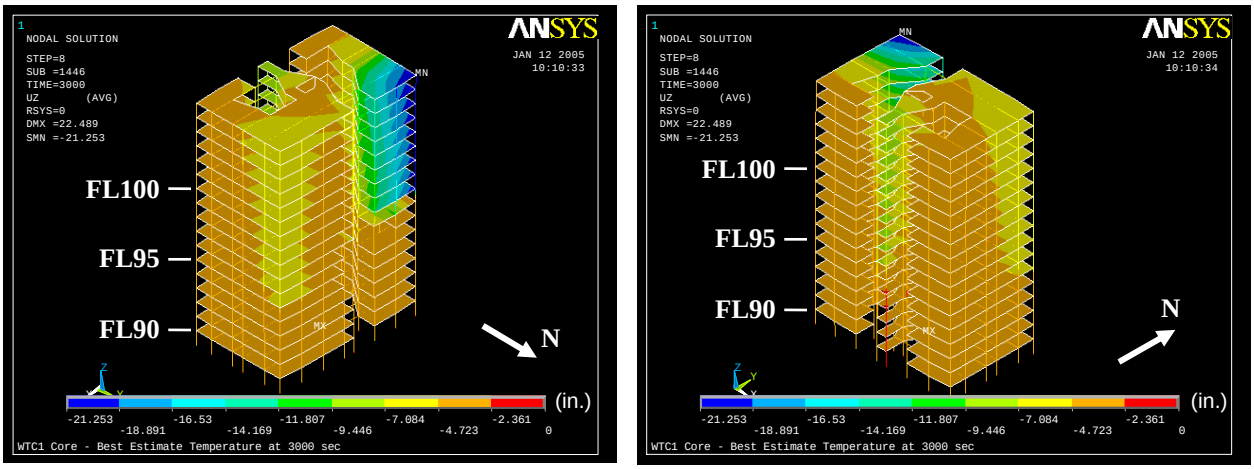

(a) North and east sides (b) South and east sides

Figure 3–109. Vertical displacement of isolated core model of WTC 1 for Case A temperature condition at 50 min (downward displacement is negative).

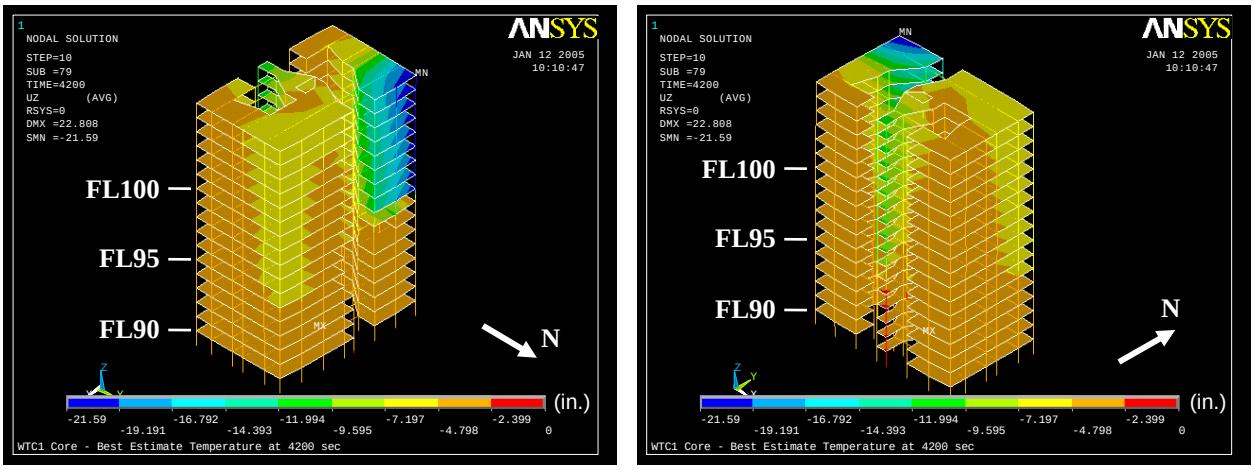

(a) North and east sides (b) South and east sides

Figure 3–110. Vertical displacement of isolated core model of WTC 1 for Case A temperature condition at 70 min (downward displacement is negative).

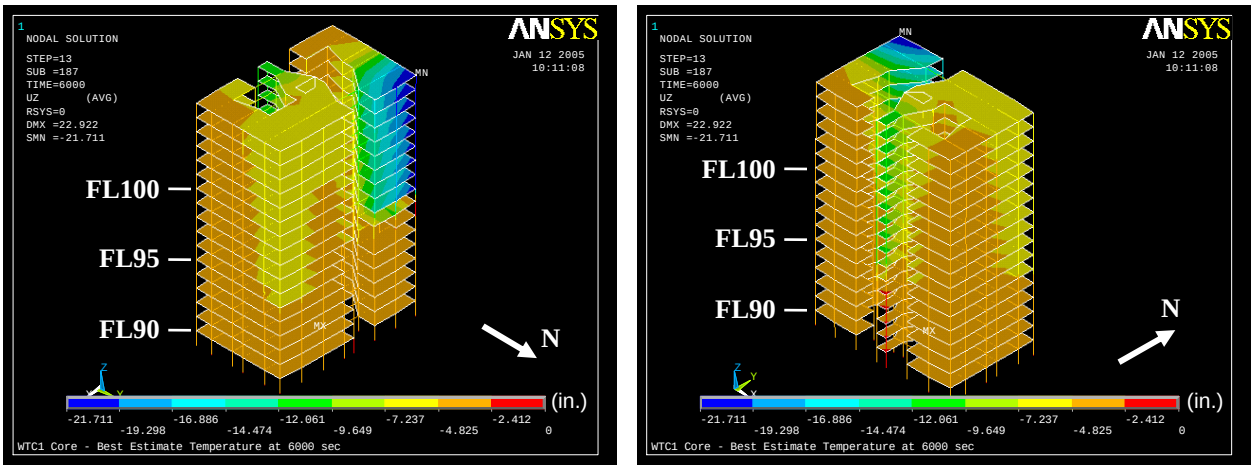

(a) North and east sides (b) South and east sides

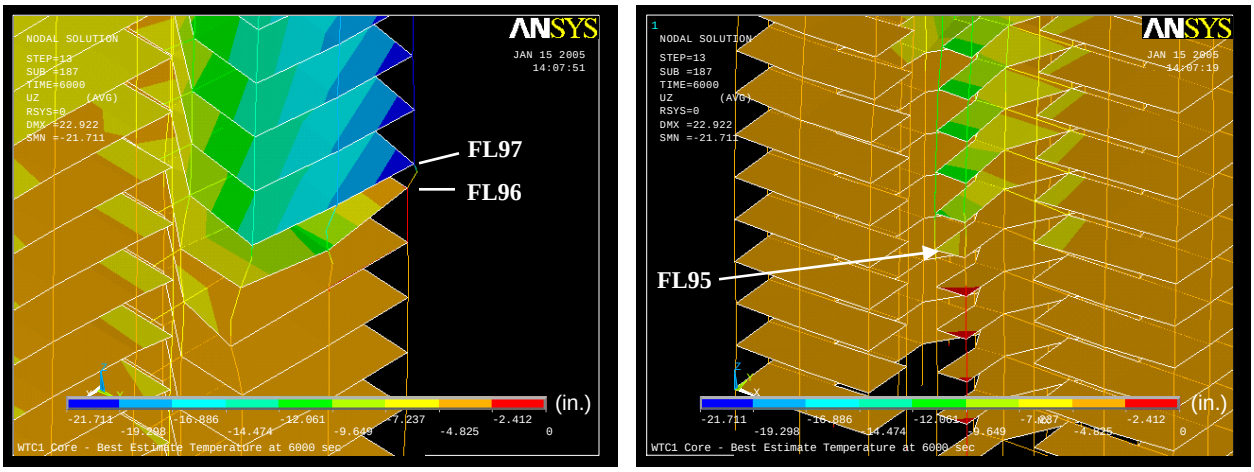

(c) Northwest corner
(5X displacement magnification)

(b) South side
(5X displacement magnification)

Figure 3–111. Vertical displacement of isolated core model of WTC 1 for Case A temperature condition at 100 min (downward displacement is negative).

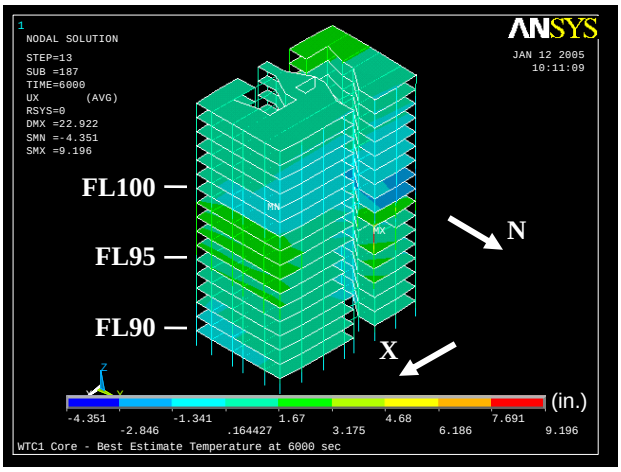

(a) X-displacement of north and east sides

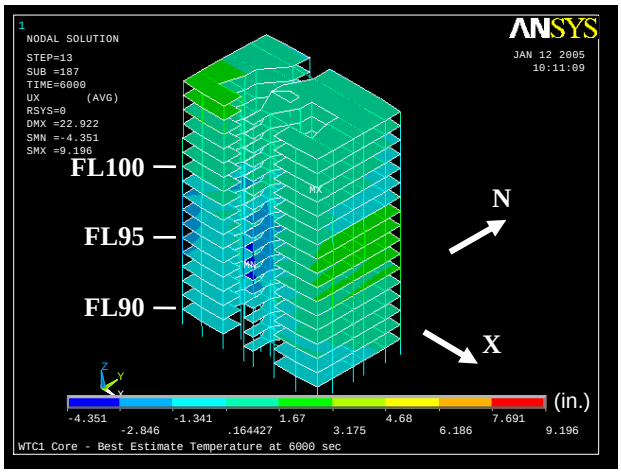

(b) X-displacement of south and east sides

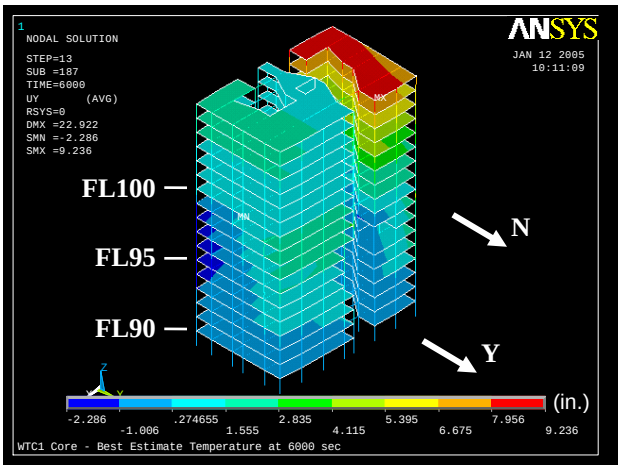

(c) Y-displacement of north and east sides

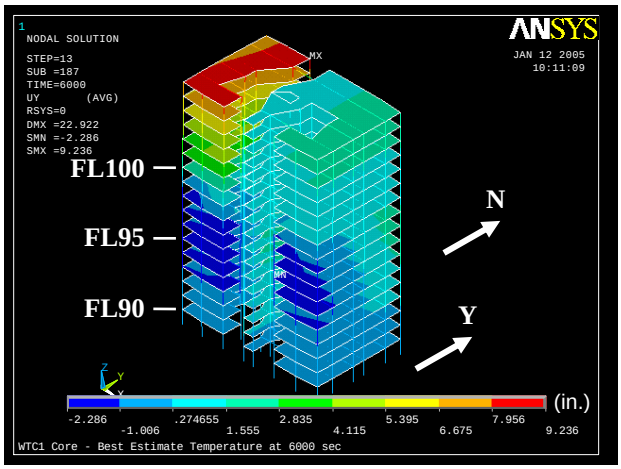

(d) Y-displacement of south and east sides

Figure 3–112. Horizontal displacement of isolated core model of WTC 1 for Case A temperature condition at 100 min.

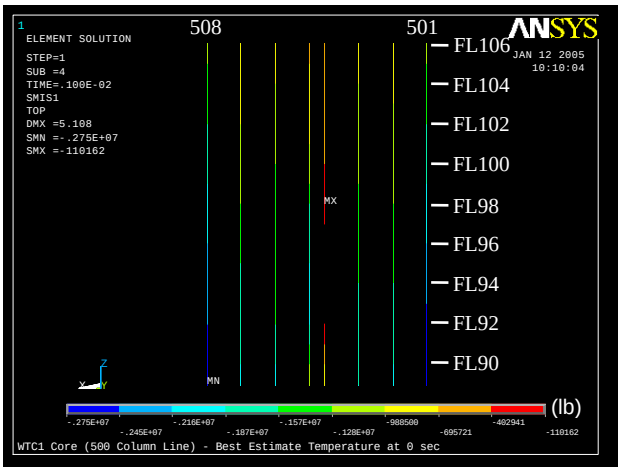

(a) 500 series columns

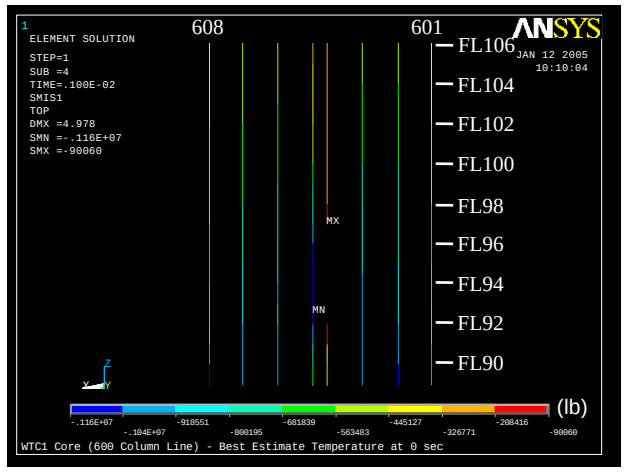

(b) 600 series columns

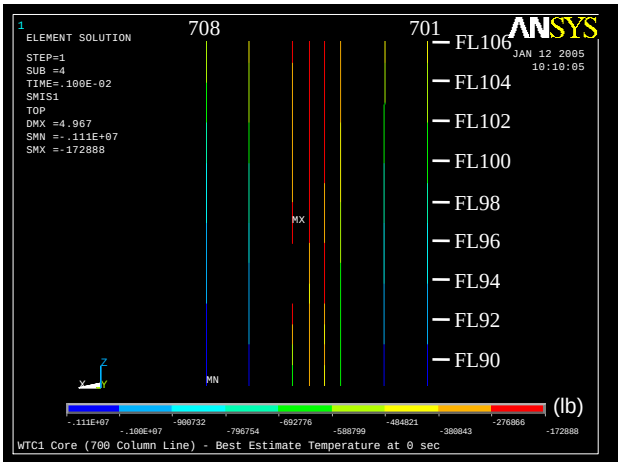

(c) 700 series columns

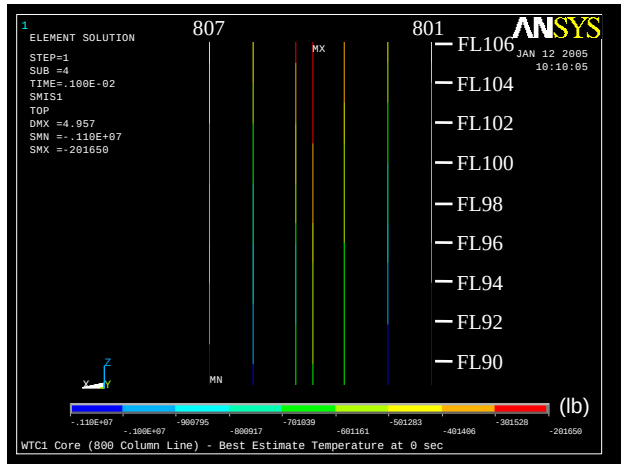

(d) 800 series columns

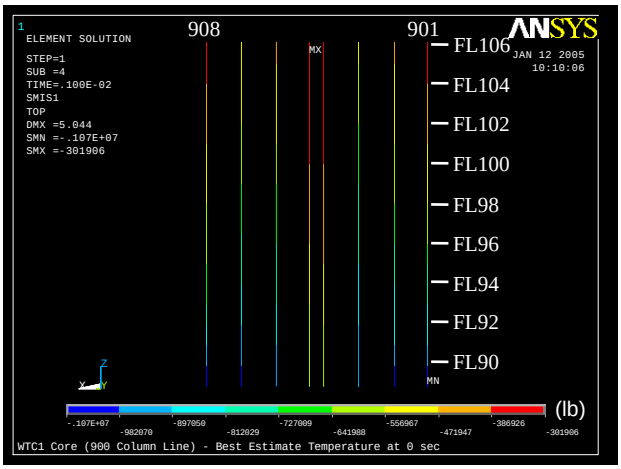

(e) 900 series columns

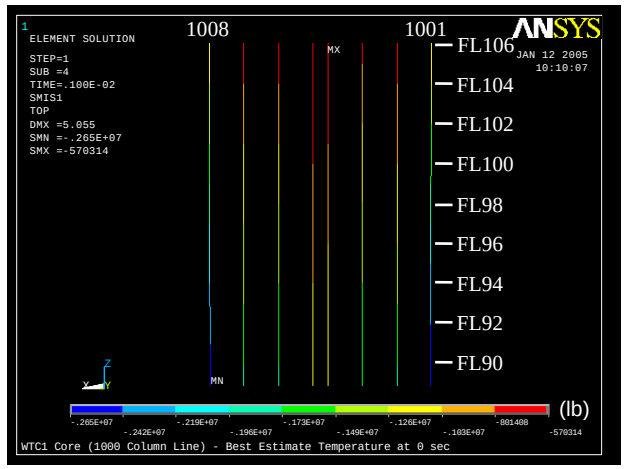

(f) 1000 series columns

Figure 3–113. Axial load in columns of isolated core model of WTC 1 after aircraft impact (compression is negative).

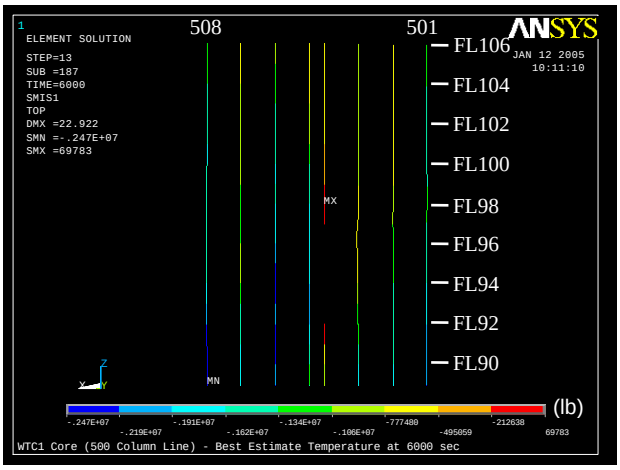

(a) 500 series columns

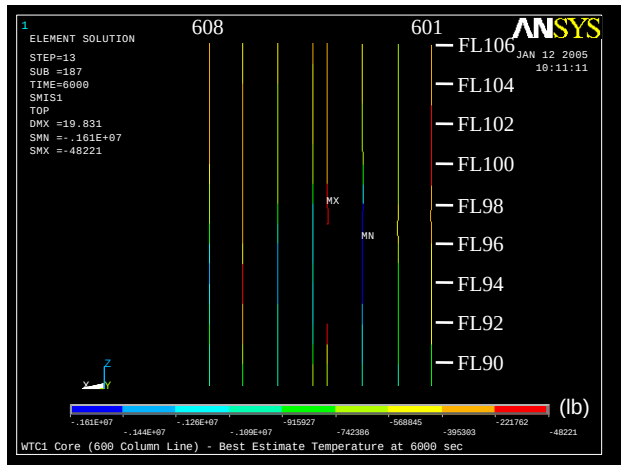

(b) 600 series columns

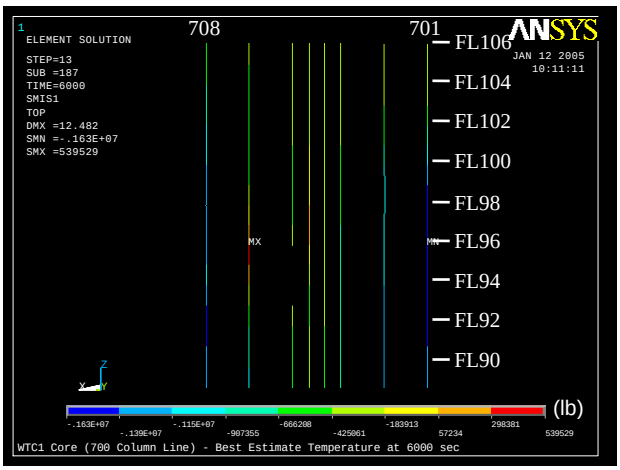

(c) 700 series columns

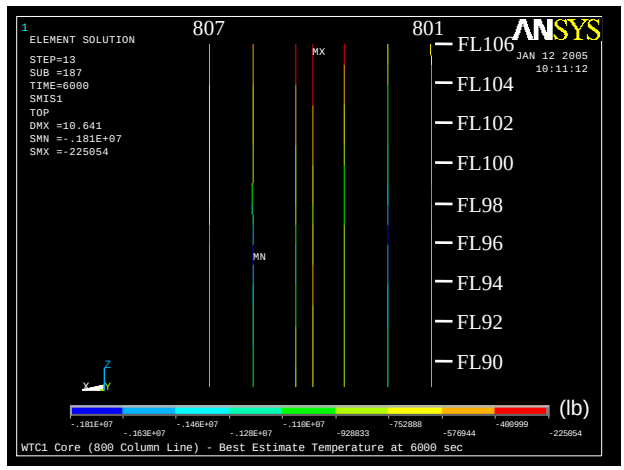

(d) 800 series columns

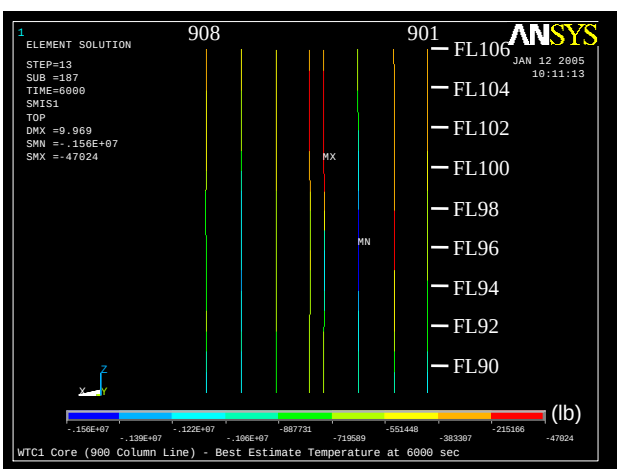

(e) 900 series columns

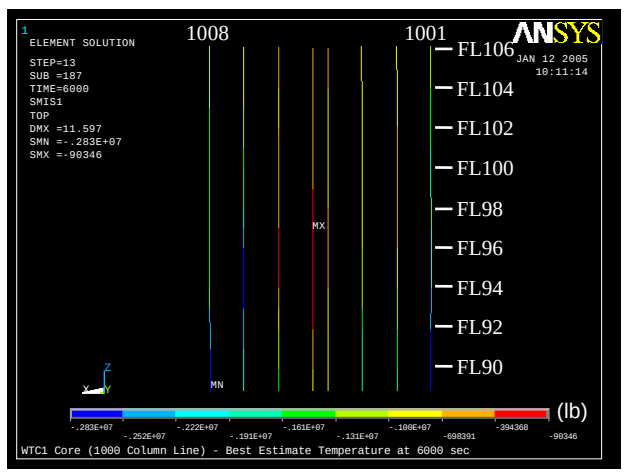

(f) 1000 series columns

Figure 3–114. Axial load in columns of isolated core model of WTC 1 for Case A temperature condition at 100 min (compression is negative).

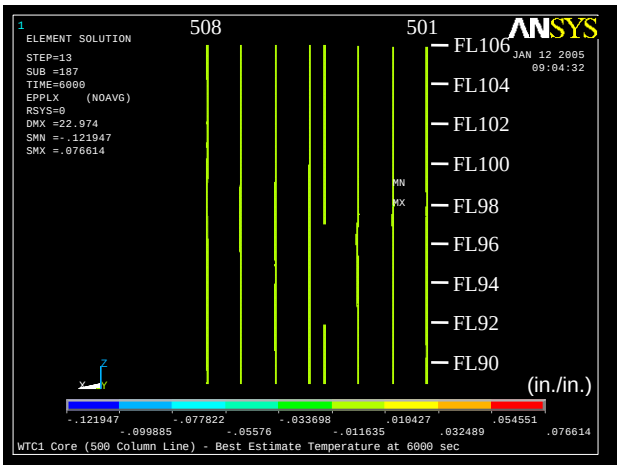

(a) 500 series columns

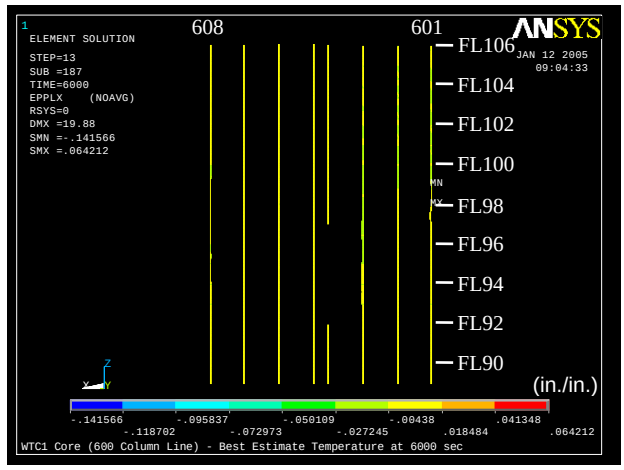

(b) 600 series columns

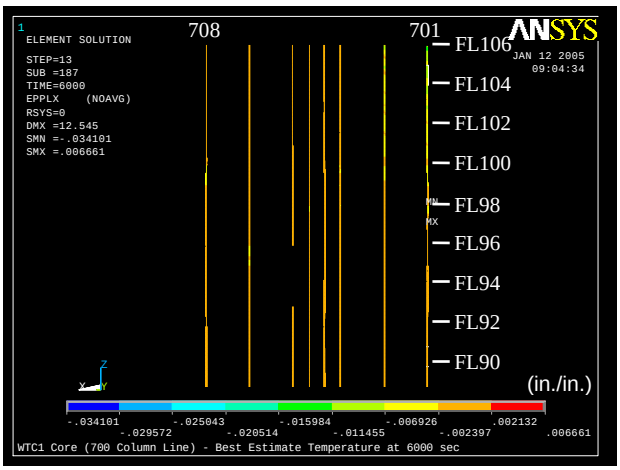

(c) 700 series columns

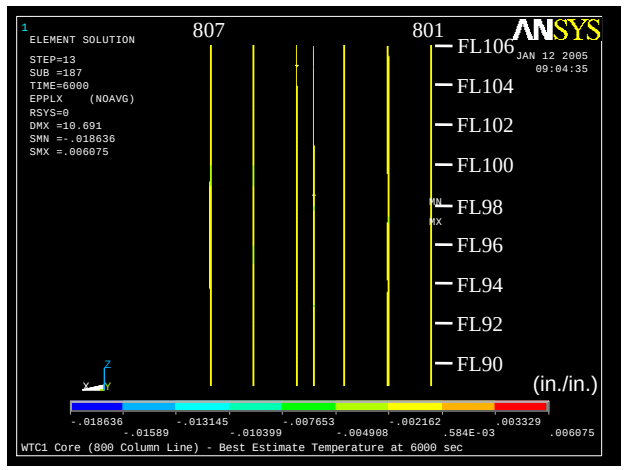

(d) 800 series columns

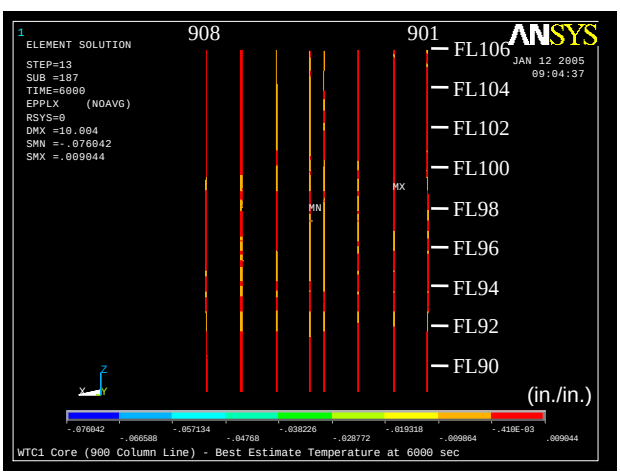

(e) 900 series columns

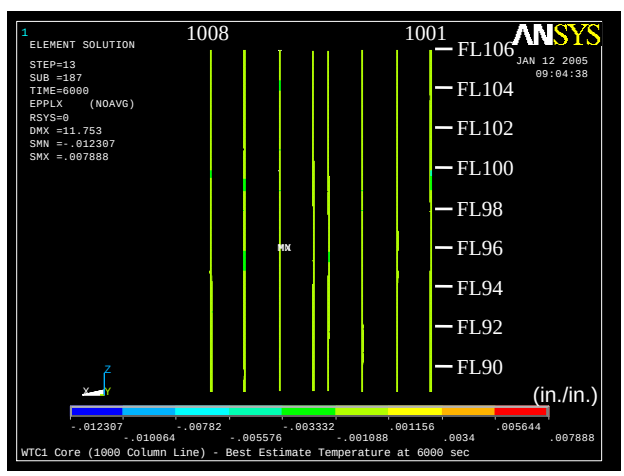

(f) 1000 series columns

Figure 3–115. Plastic strain in columns of isolated core model of WTC 1 for Case A temperature condition at 100 min (compressive strain is negative).

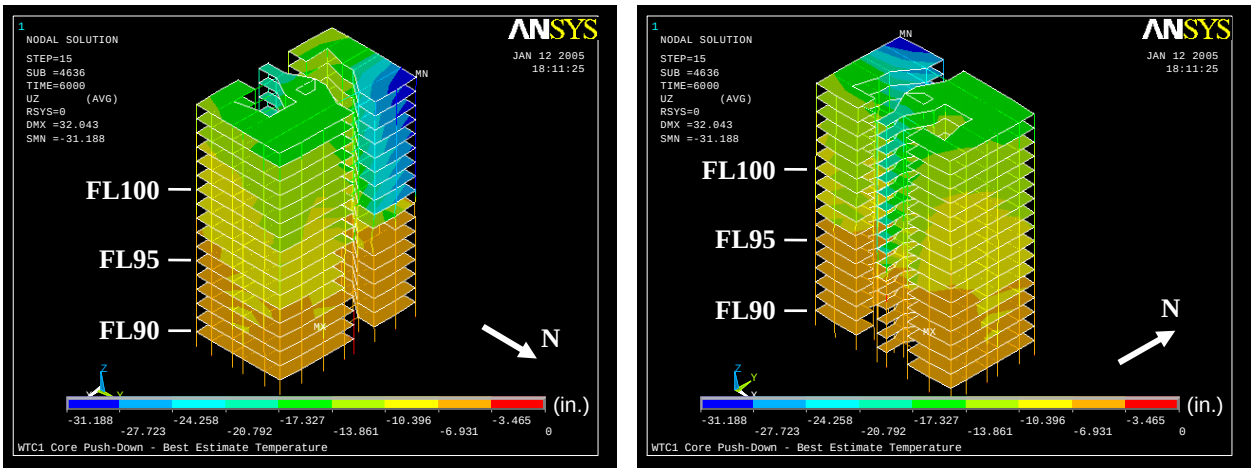

(a) North and east sides (b) South and east sides

Figure 3–116. Vertical displacement after push down of isolated core model of WTC 1 for Case A temperature condition (downward displacement is negative).

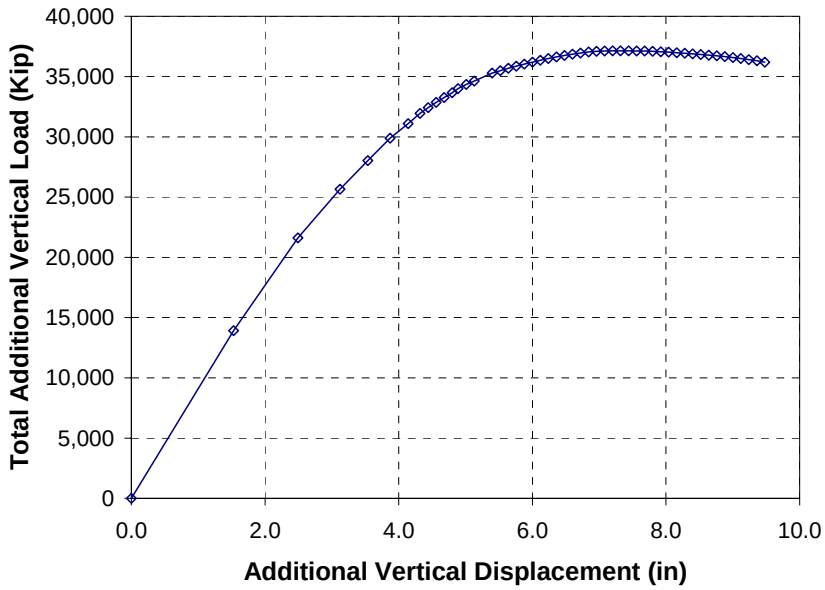

Figure 3–117. Total additional vertical load versus additional vertical displacement during push-down analysis of isolated core model of WTC 1 for Case A temperature condition (compression is positive).

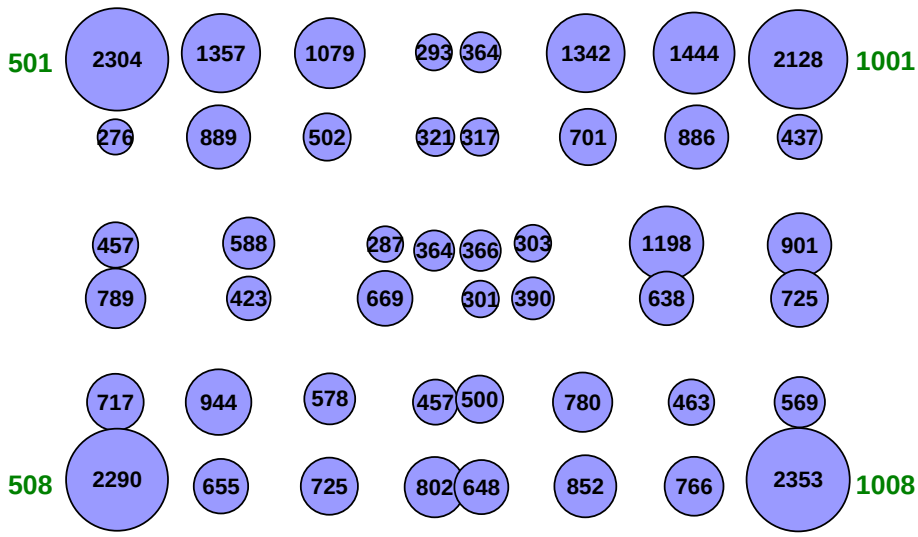

Figure 3–118. Additional axial load (kip) in columns at Floor 98 when the total axial load reached the maximum during push down analysis of isolated core model of WTC 1 for Case A temperature condition (compression is positive).

Case B Temperature Condition

Figures 3–119 to 3–125 show the vertical displacements of the WTC 1 isolated core model subjected to Case B temperature condition. At 30 min, the vertical displacement of the south side above Floor 96 between Column 1004 and Column 1005 became large. At 100 min, the maximum vertical displacement was 44.2 in. on the south side at Column 1005.

Figures 3–127 and 3–128 show axial loads and plastic strains in columns at 100 min. The following columns buckled: Column 904 spanning Floor 97 and Floor 98, Column 1004 spanning Floor 97 and Floor 98, Column 1005 spanning Floor 95 and Floor 96, and Column 1006 spanning Floor 95 and Floor 96. These columns also experienced large localized plastic strains.

The northeast corner, where the largest displacement occurred for Case A temperature condition, did not displace significantly for Case B temperature condition. The vertical displacement at Floor 106 ranged from 4.8 to 44.2 in. The average vertical displacement of Floor 106 was 11.9 in. The average displacement of the south face was 20 in. Considering the 5 in. displacement after the aircraft impact, the average additional downward displacement of the core due to thermal loads was about 7 in.

To determine the additional axial load-carrying capacity of the core, a push-down analysis was performed for Case B temperature condition in the same manner as described for the isolated core model for Case A temperature condition. The analysis was terminated when an additional vertical displacement of 9.4 in. was applied to the top. Figure 3–129 shows vertical displacements of the model at the end of analysis. Figure 3–130 shows the relationship between the total additional vertical force and the additional vertical displacement. The total additional vertical force reached its maximum at an additional displacement of 4.9 in. Figure 3–131 shows the additional axial loads in columns of Floor 98 when the total additional vertical force was at its maximum. The maximum total additional vertical force of 24,002 kip was about

61 percent of the total column force at Floor 98 prior to push-down. Thus, the reserve capacity of the core at the end of Case B temperature condition was substantial, but less than that of Case A temperature condition.

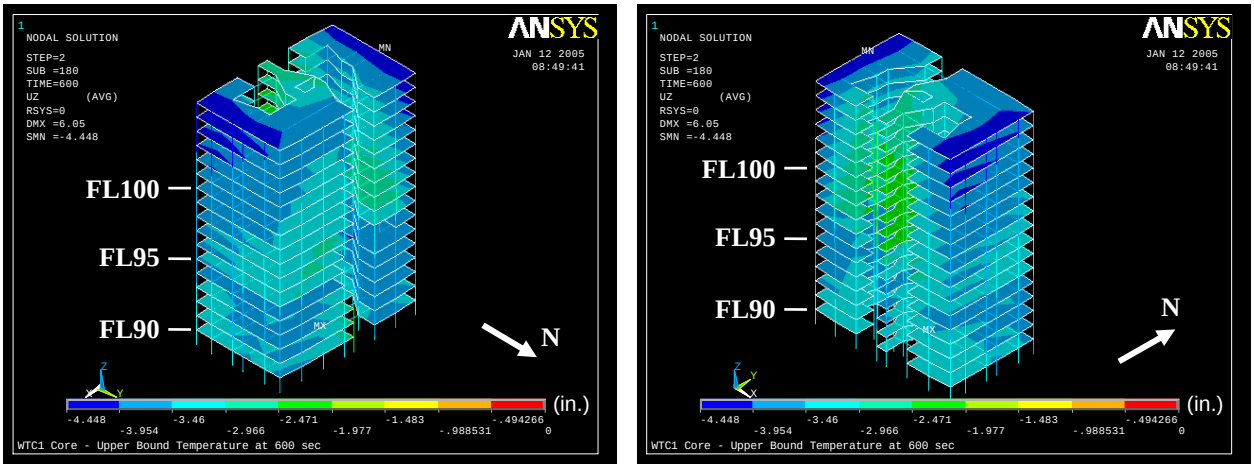

(a) North and east sides (b) South and east sides

Figure 3–119. Vertical displacement of isolated core model of WTC 1 for Case B temperature condition at 10 min (downward displacement is negative).

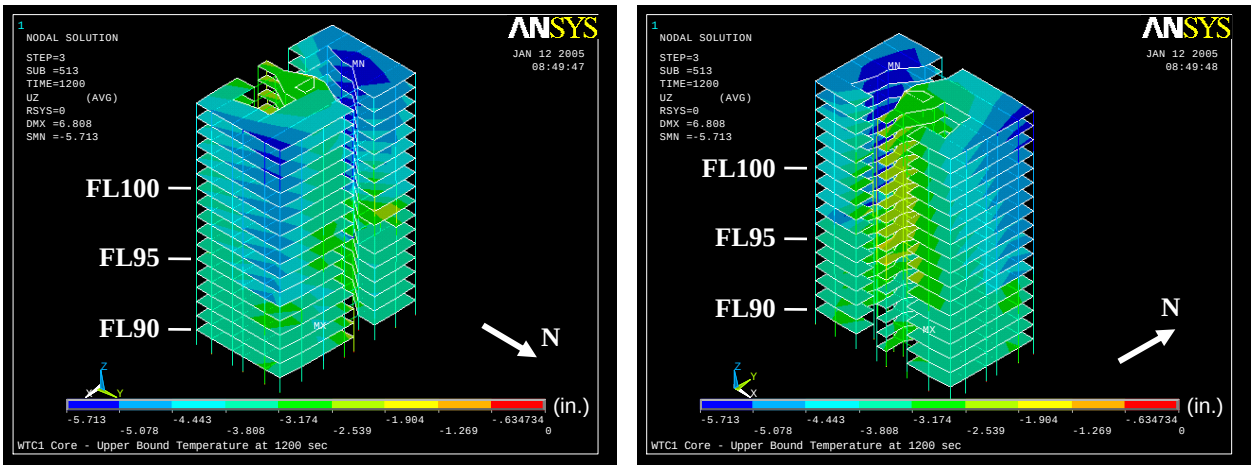

(a) North and east sides (b) South and east sides

Figure 3–120. Vertical displacement of isolated core model of WTC 1 for Case B temperature condition at 20 min (downward displacement is negative).

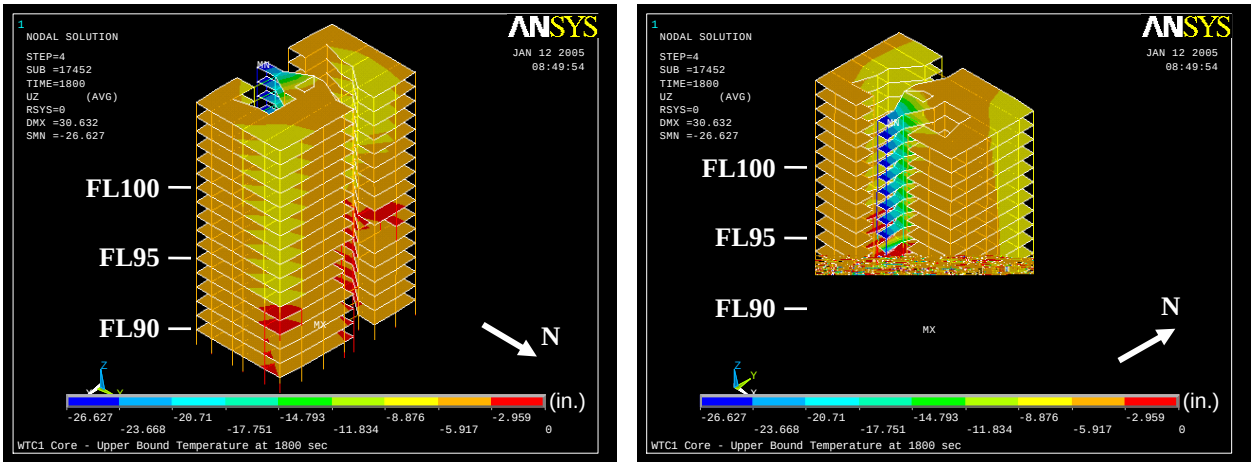

(a) North and east sides (b) South and east sides

Figure 3–121. Vertical displacement of isolated core model of WTC 1 for Case B temperature condition at 30 min (downward displacement is negative).

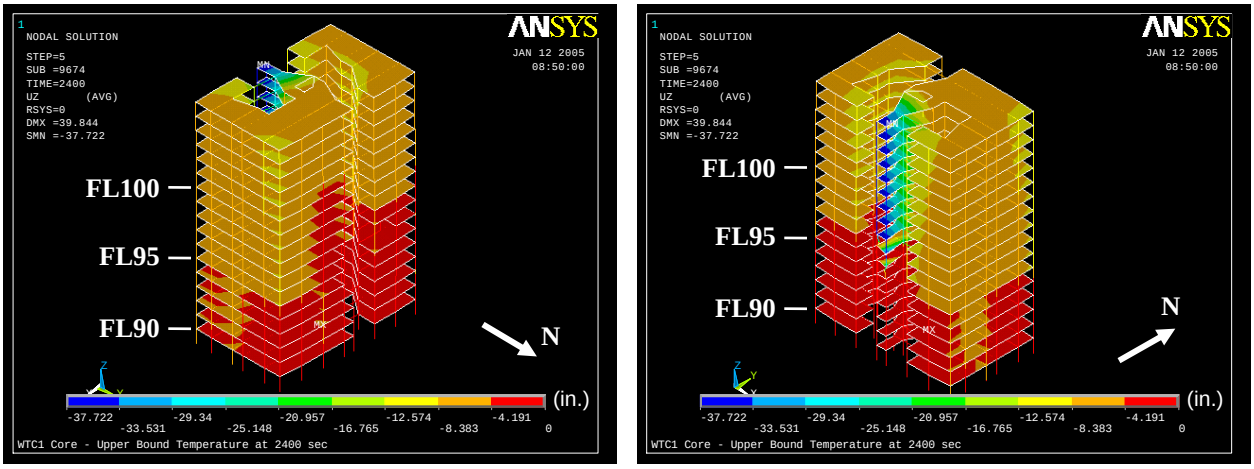

(a) North and east sides (b) South and east sides

Figure 3–122. Vertical displacement of isolated core model of WTC 1 for Case B temperature condition at 40 min (downward displacement is negative).

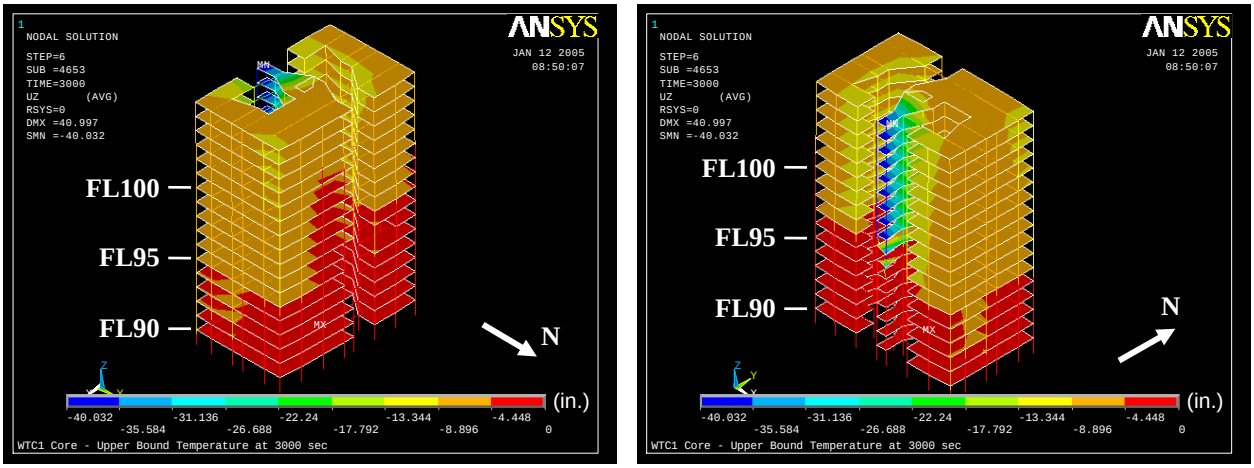

(a) North and east sides (b) South and east sides

Figure 3–123. Vertical displacement of isolated core model of WTC 1 for Case B temperature condition at 50 min (downward displacement is negative).

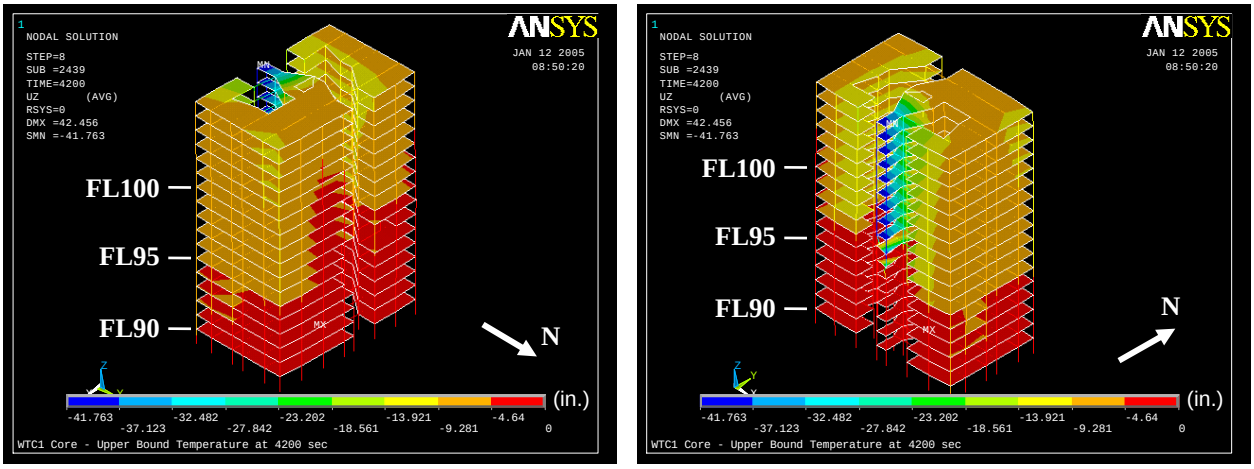

(a) North and east sides (b) South and east sides

Figure 3–124. Vertical displacement of isolated core model of WTC 1 for Case B temperature condition at 70 min (downward displacement is negative).

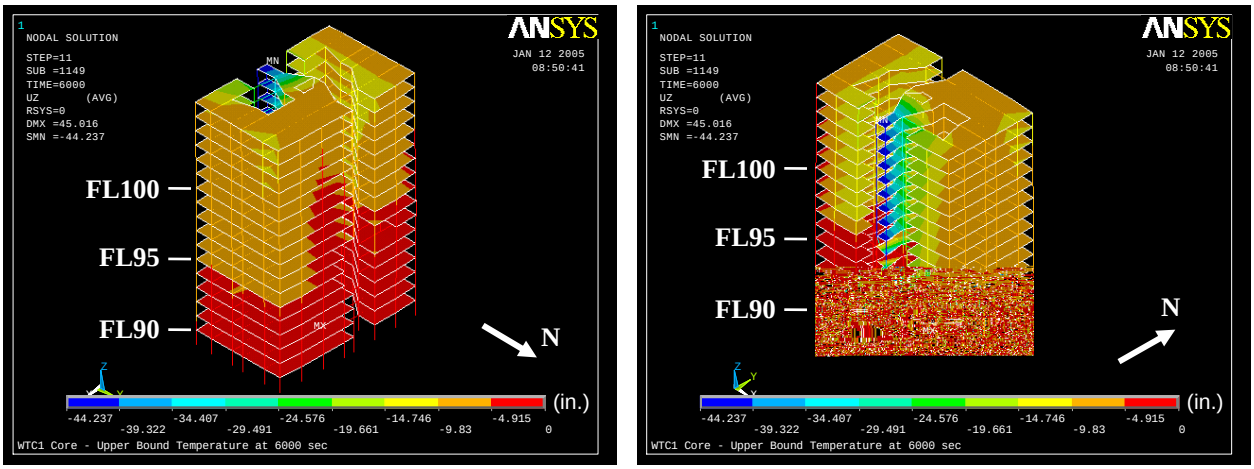

(a) North and east sides

(b) South and east sides

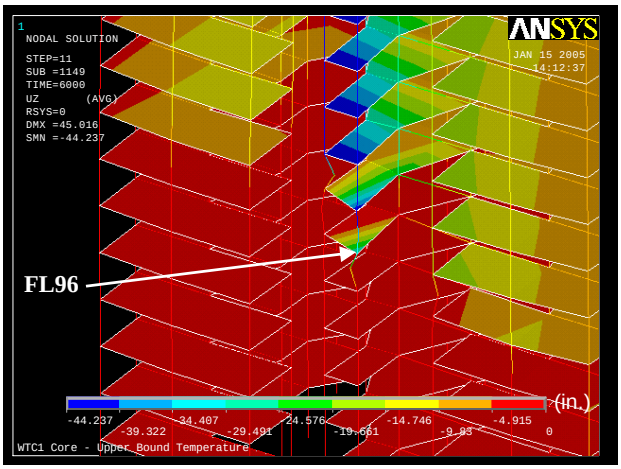

(c) South side
(1X displacement magnification)

Figure 3–125. Vertical displacement of isolated core model of WTC 1 for Case B temperature condition at 100 min (downward displacement is negative).

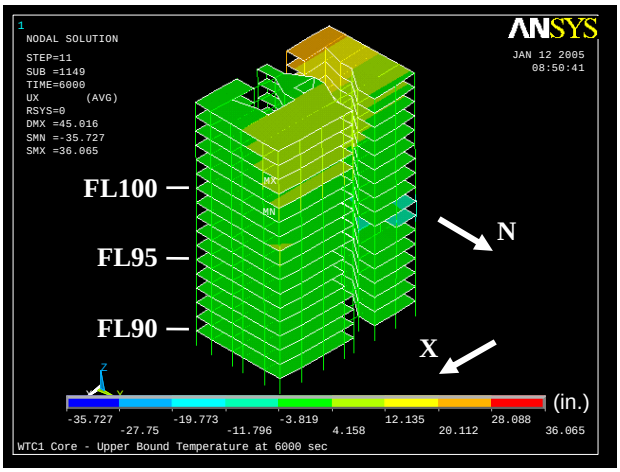

(a) X-displacement of north and east sides

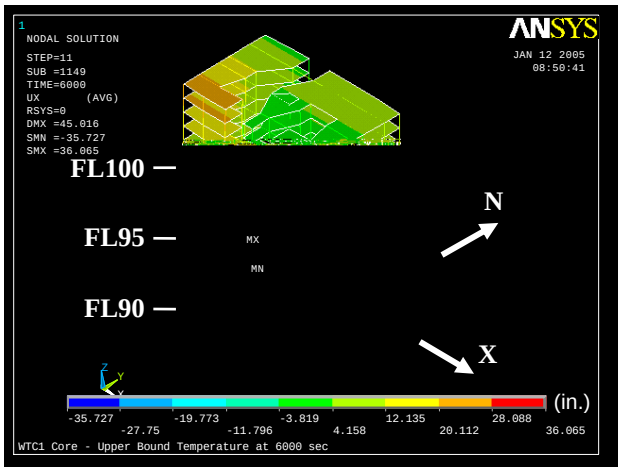

(b) X-displacement of south and east sides

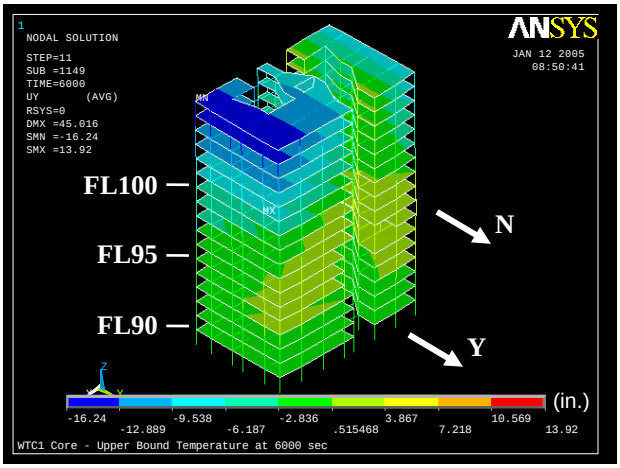

(c) Y-displacement of north and east sides

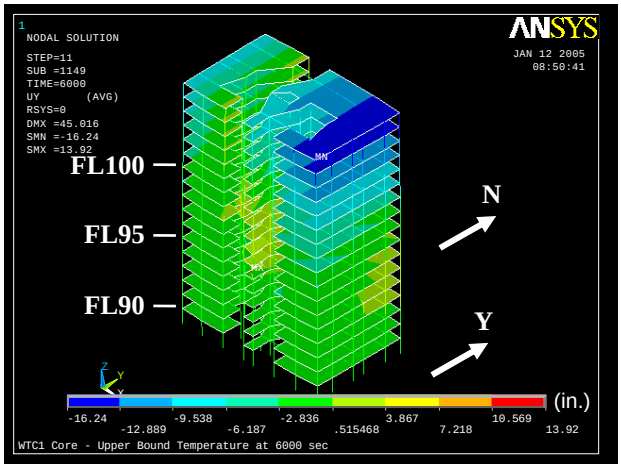

(d) Y-displacement of south and east sides

Figure 3–126. Horizontal displacement of isolated core model of WTC 1 for Case B temperature condition at 100 min.

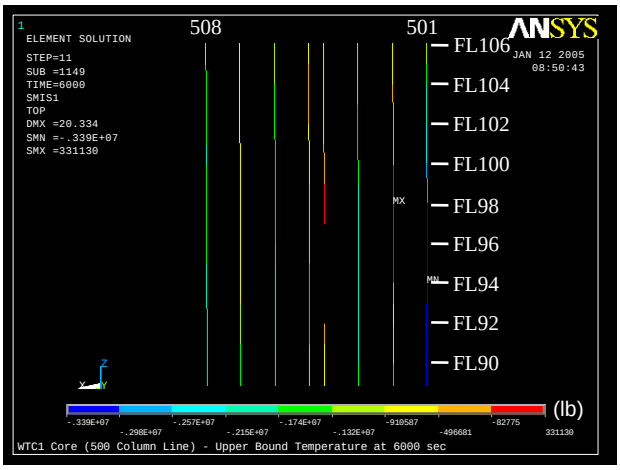

(a) 500 series columns

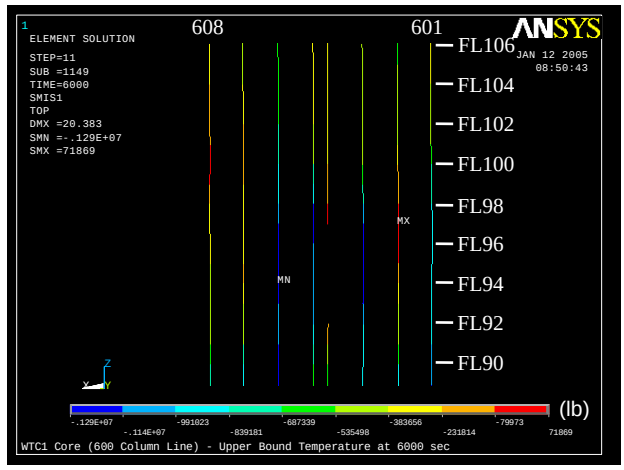

(b) 600 series columns

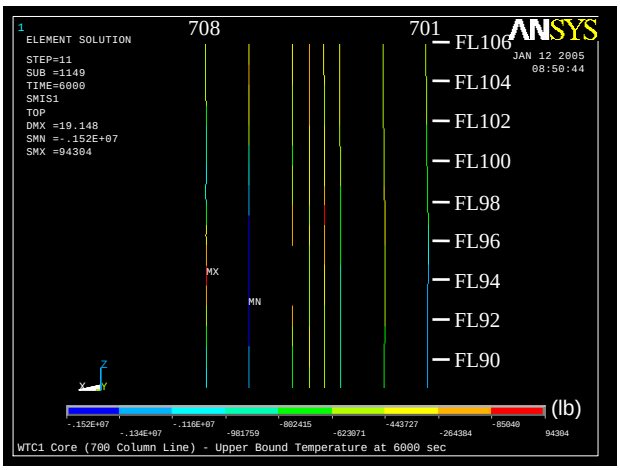

(c) 700 series columns

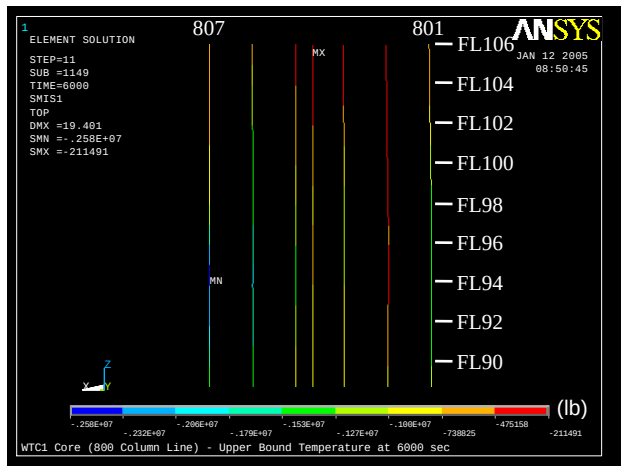

(d) 800 series columns

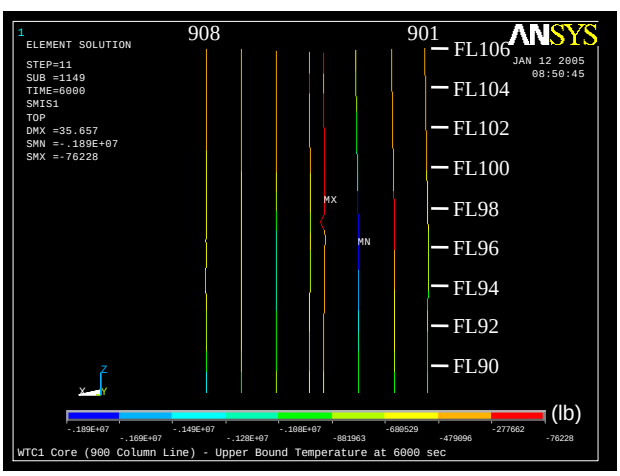

(e) 900 series columns

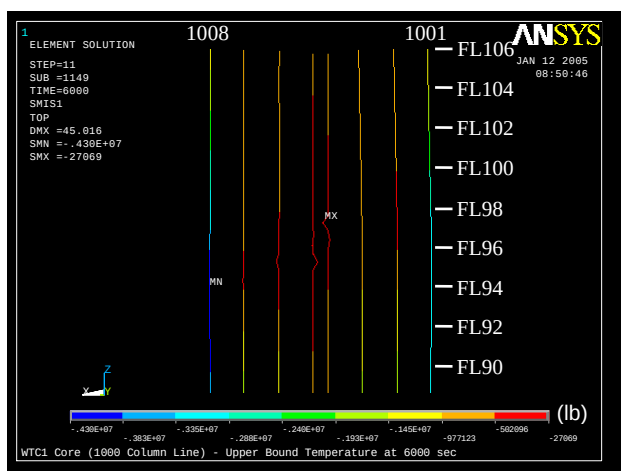

(f) 1000 series columns

Figure 3–127. Axial load in columns of isolated core model of WTC 1 for Case B temperature condition at 100 min (compression is negative).

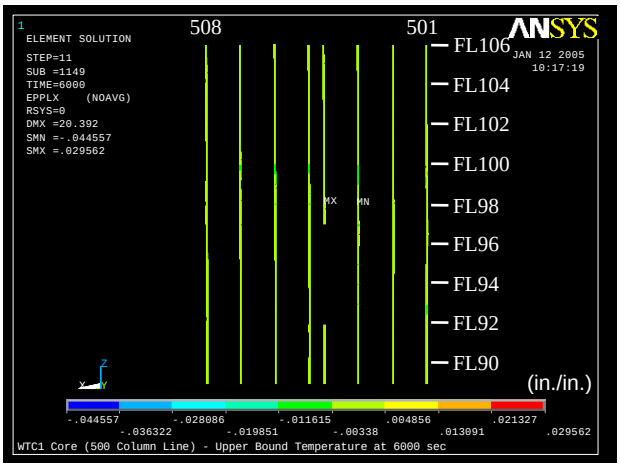

(a) 500 series columns

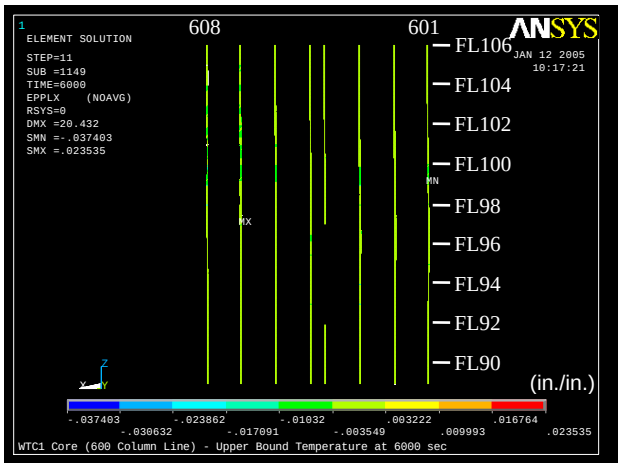

(b) 600 series columns

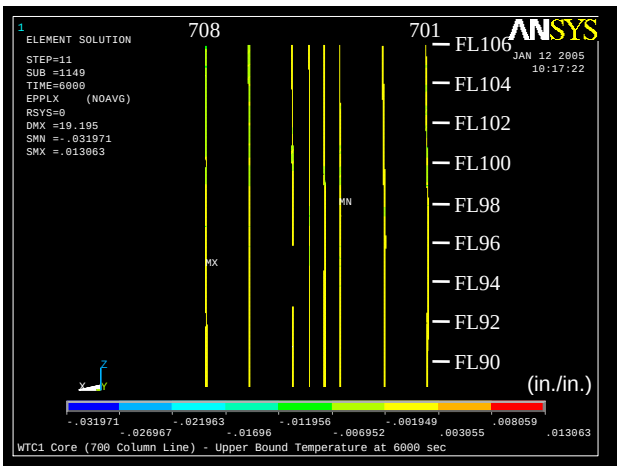

(c) 700 series columns

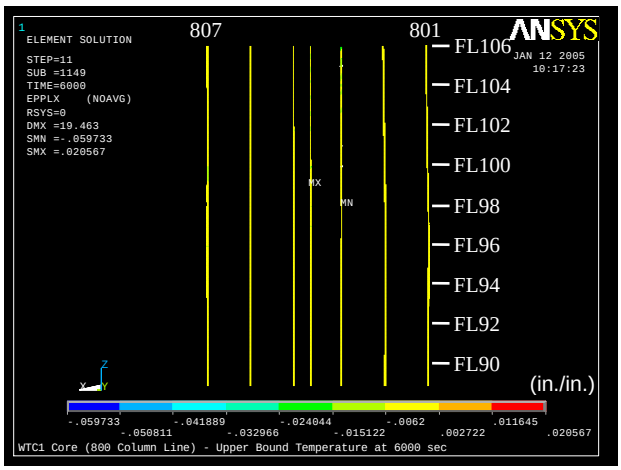

(d) 800 series columns

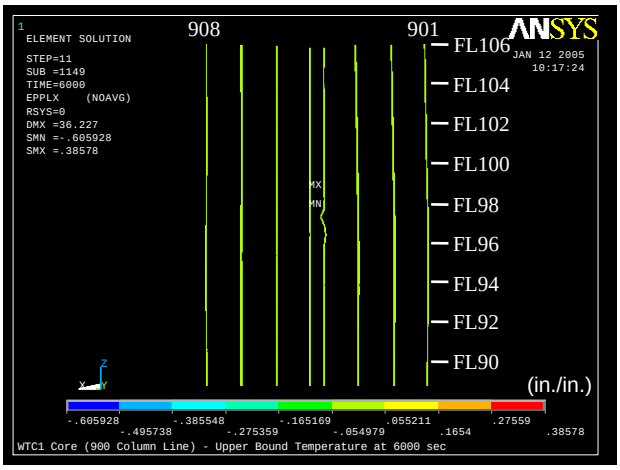

(e) 900 series columns

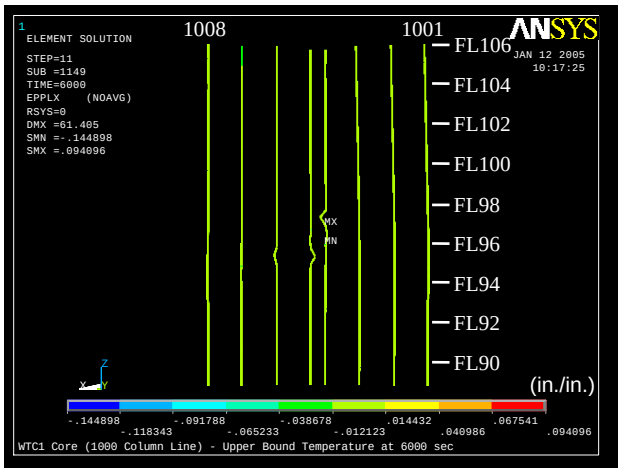

(f) 1000 series columns

Figure 3–128. Plastic strain in columns of isolated core model of WTC 1 for Case B temperature condition at 100 min (compressive strain is negative).

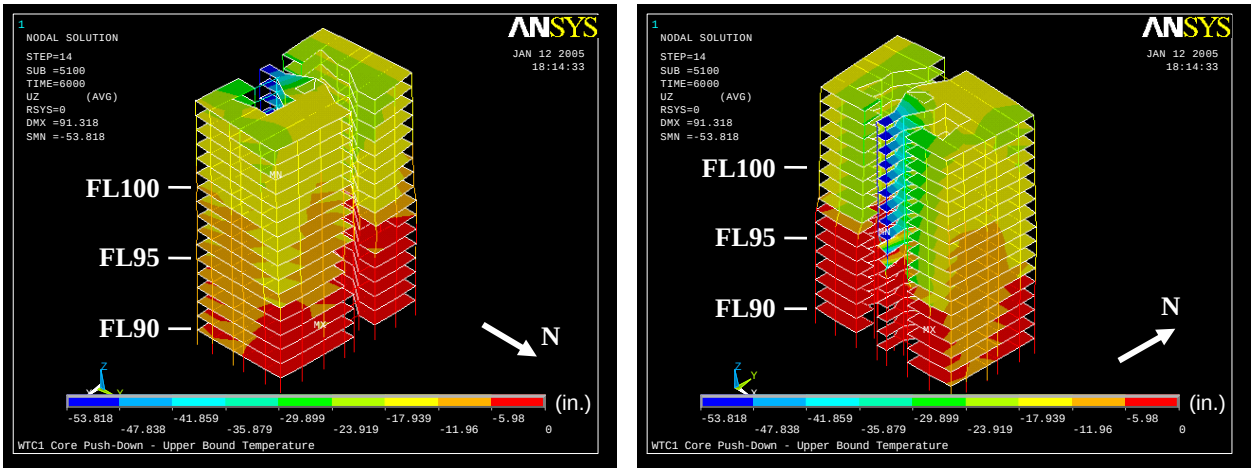

(a) North and east sides (b) South and east sides

Figure 3–129. Vertical displacement after push down of isolated core model of WTC 1 for Case B temperature condition (downward displacement is negative).

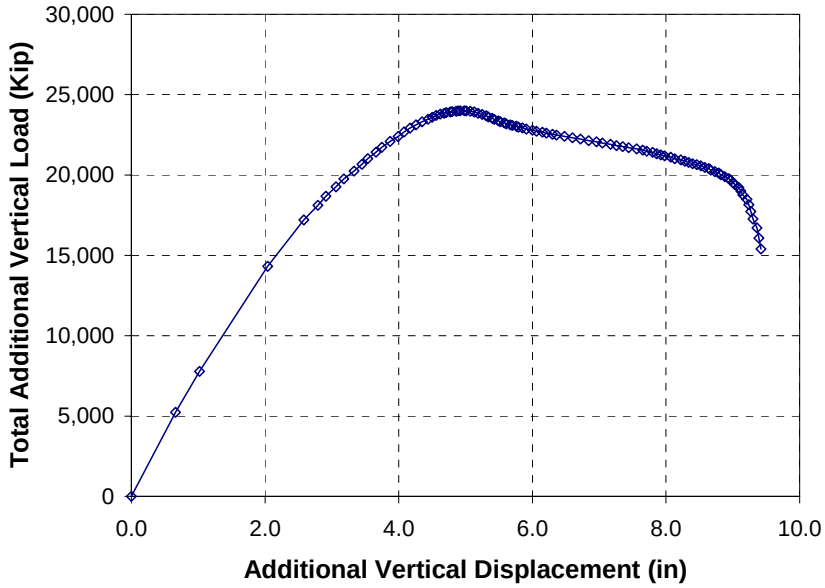

Figure 3–130. Total additional vertical load versus additional vertical displacement relationship obtained from push down analysis of isolated core model of WTC 1 for Case B temperature condition (compression is positive).

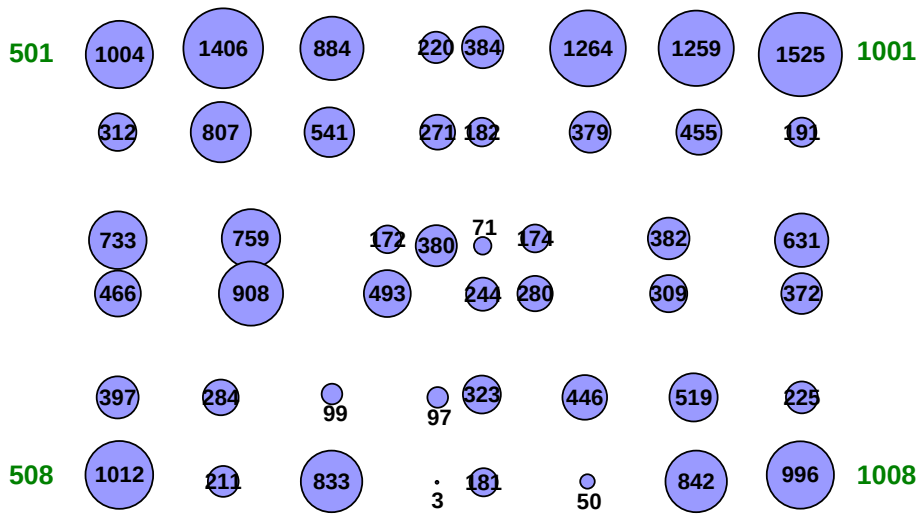

Figure 3–131. Additional axial load (kip) in columns at Floor 98 when the total axial load reached the maximum during push down analysis of the WTC 1 core for Case B temperature condition (compression is positive).

3.3.2 FEA of WTC 2 Core

Case C Temperature Condition

The isolated core model of WTC 2 was unstable after the aircraft impact damage, tilting excessively towards the southeast corner. To simulate the restraining effect of office floors and the exterior walls, the isolated core model was restrained in the horizontal directions at all floors.

Figures 3–132 to 3–133 show the vertical displacements of the WTC 2 isolated core model when subjected to Case C temperature condition from just after the aircraft impact to 60 min. The vertical displacement was always the highest at the southeast corner of the core as the aircraft impact severed the southeast corner core columns in Floors 79 to 82. After aircraft impact damage, the vertical displacement of the southeast corner was 5.6 in. This displacement increased to 6.1 in. at 60 min. Figures 3–134 and 3–135 show axial load and plastic strain in columns at 60 min. Columns at the southeast corner experienced plastic strains immediately following aircraft impact. The maximum plastic strain in the 900-series core columns was 1.2 percent, and 0.5 percent in the 1000 series core.

The vertical displacement of the core at Floor 106 at 60 min ranged from 2.3 in. to 5.3 in. The maximum vertical displacement of the southeast corner was less than 5.3 in. at Column 1001. The average vertical displacement of Floor 106 at 60 min was 3.7 in., close to the 3.9 in. average vertical displacement after the aircraft impact. None of core columns buckled during thermal loading.

Similar to the WTC 1 isolated core models, the WTC 2 isolated core model was pushed down following the analysis for Case C temperature condition to determine the additional axial load-carrying capacity of the core. The analysis was terminated at an additional vertical displacement of 17.0 in. even though the core was still continuing to carry more axial load. The vertical displacements at the end of 17.0 in. push-down are shown in Fig. 3–136. Figure 3–137 shows the relationship between the additional

displacements and the average additional vertical load of corner columns, corner and middle columns on the east face, and all core columns (there column locations are shown in Fig. 3–136). The columns on the southeast corner of the isolated core at 60 min temperature condition carried an additional load of about 900 kip without failure, compared to about 1,500 kip for the average of the entire core columns prior to push-down. The additional load was about 1.6 times that of the average load in Floor 82 columns at 60 min temperature condition.

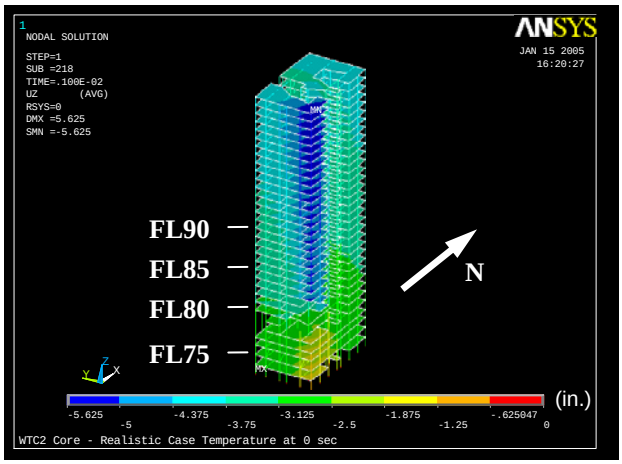

(a) After aircraft impact

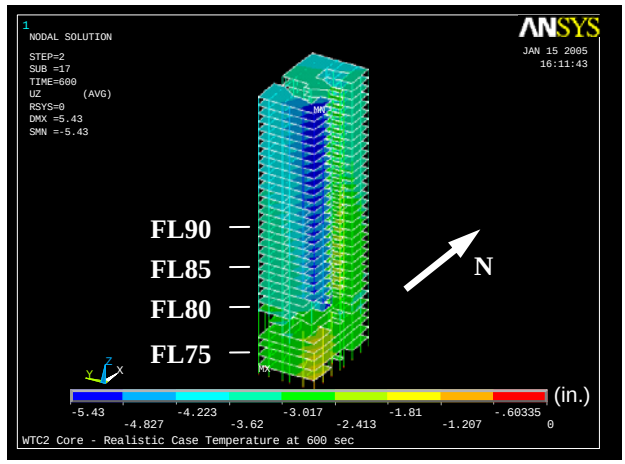

(b) At 10 min

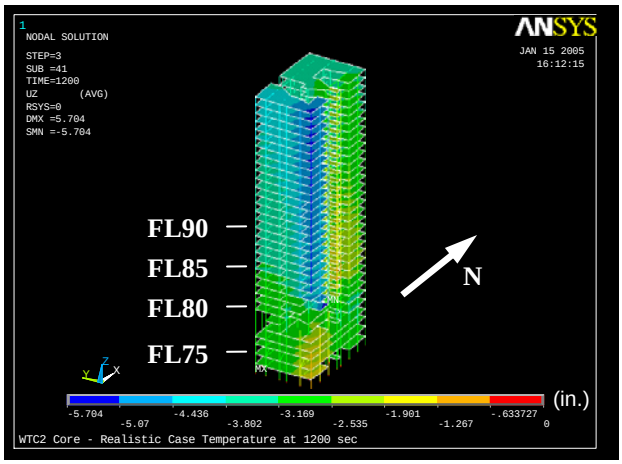

(c) At 20 min

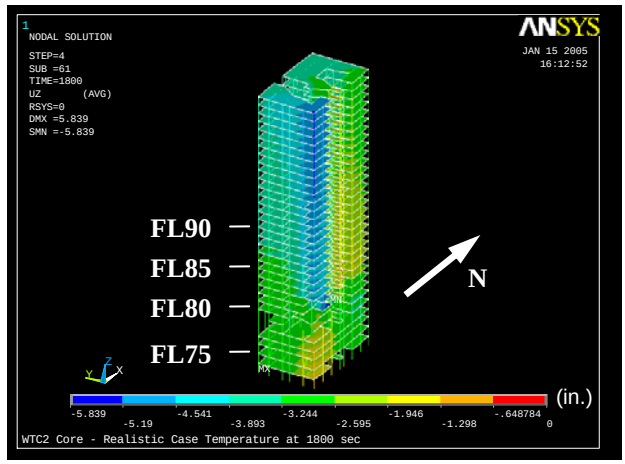

(d) At 30 min

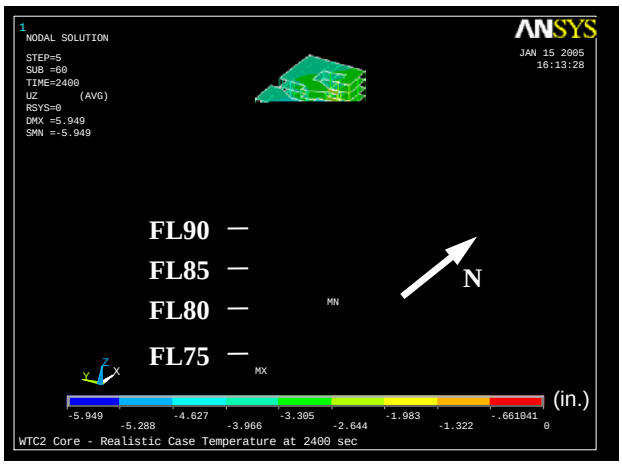

(e) At 40 min

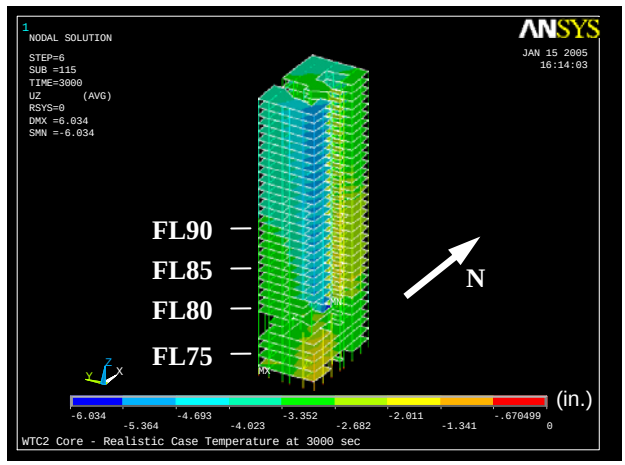

(f) At 50 min

Figure 3–132. Vertical displacement of isolated core model of WTC 2 for Case C temperature condition (downward displacement is negative).

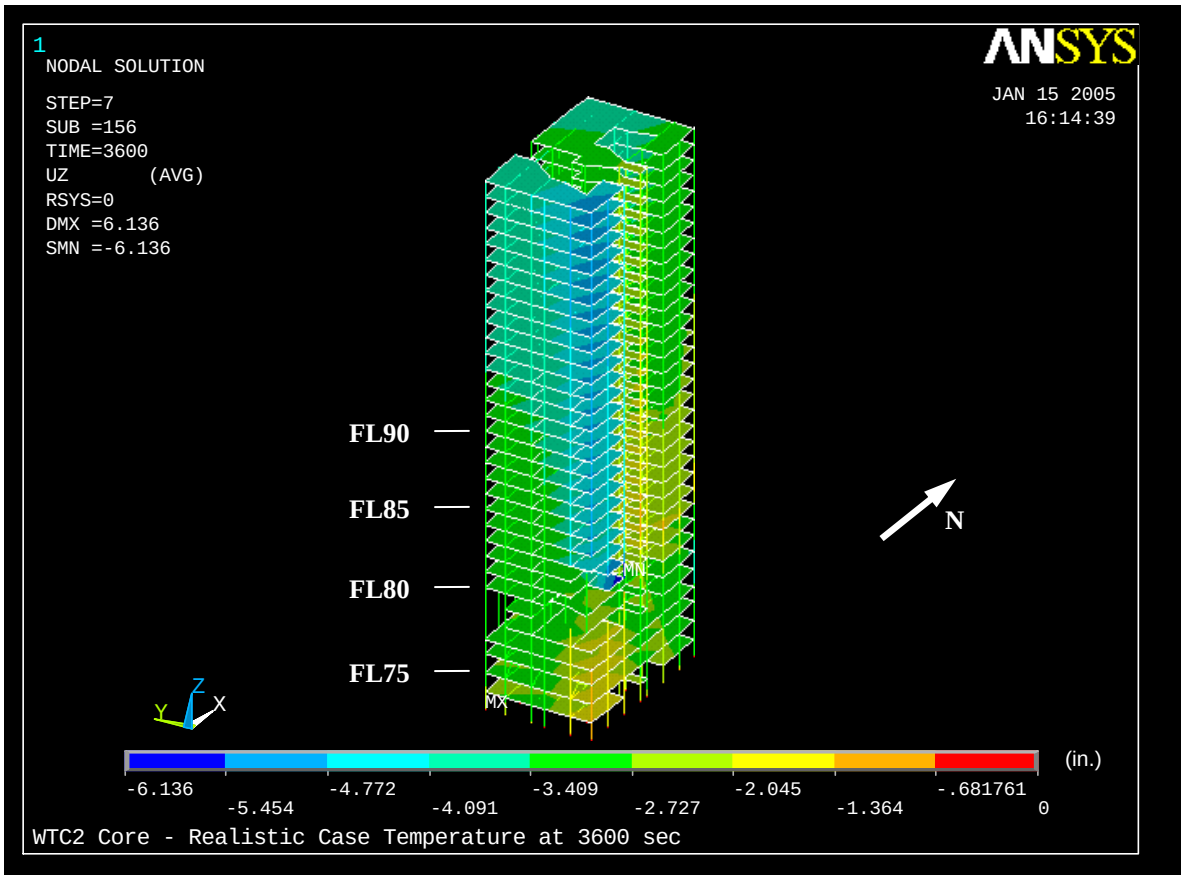

Figure 3–133. Vertical displacement of isolated core model of WTC 2 for Case C temperature condition at 60 min (downward displacement is negative).

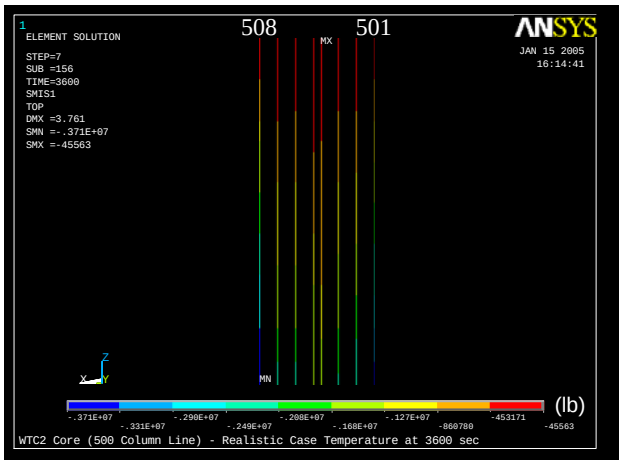

(a) 500 series columns

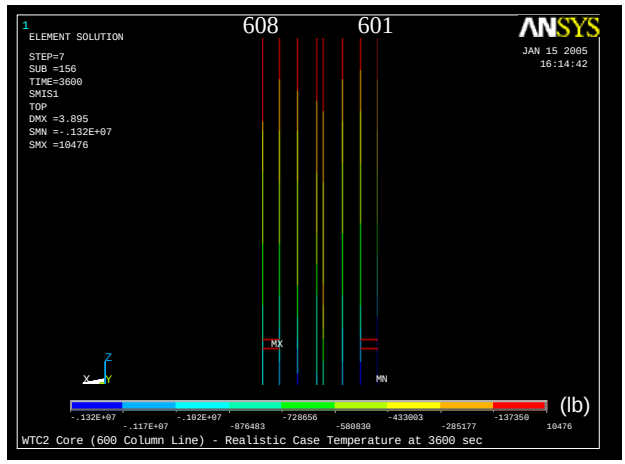

(b) 600 series columns

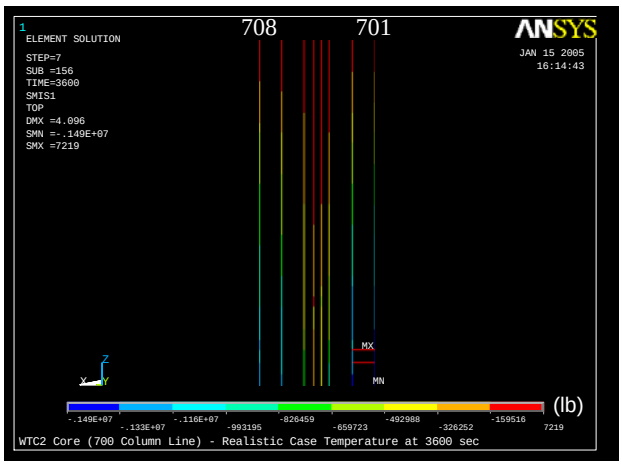

(c) 700 series columns

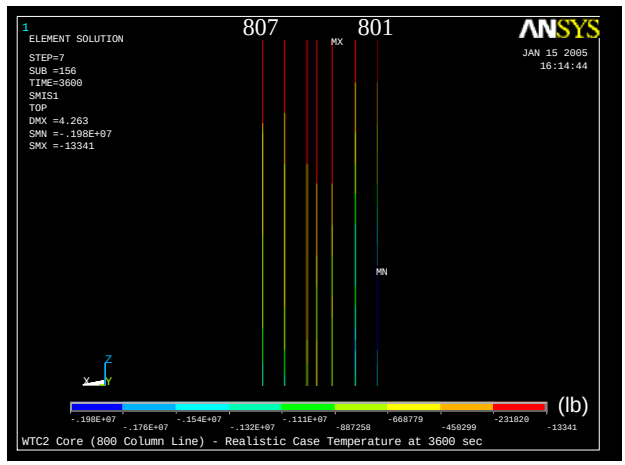

(d) 800 series columns

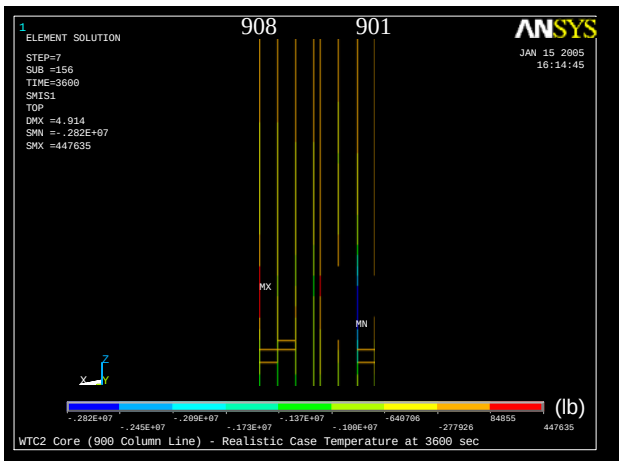

(e) 900 series columns

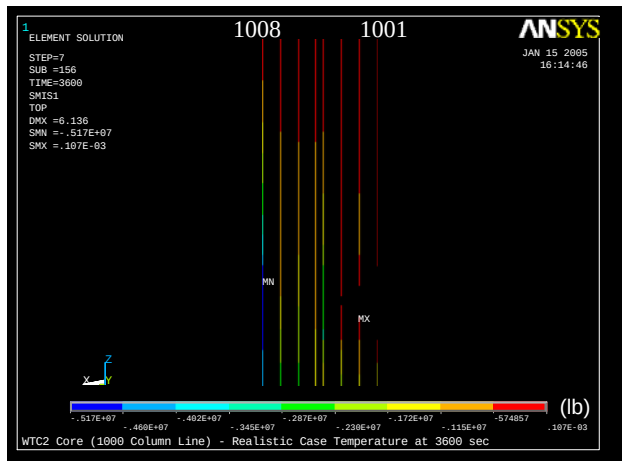

(f) 1000 series columns

Figure 3–134. Axial load in core columns of isolated core model of WTC 2 for Case C temperature condition at 60 min (compression is negative).

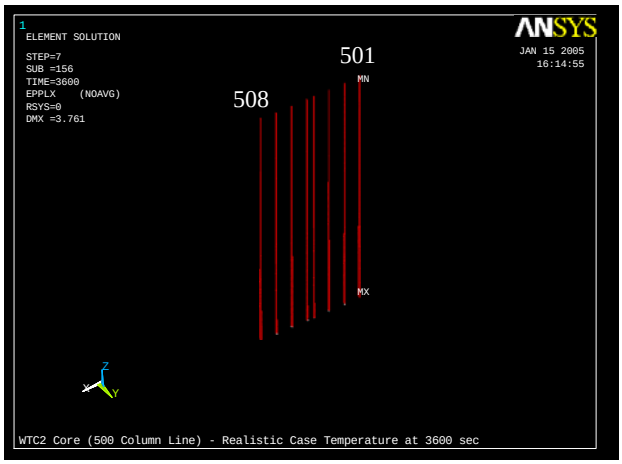

(a) 500 series columns

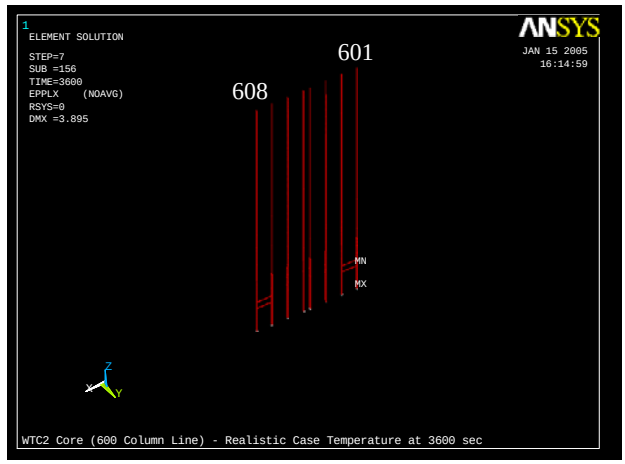

(b) 600 series columns

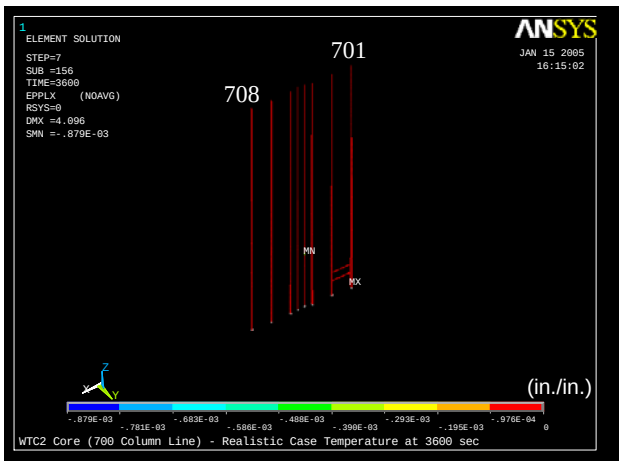

(c) 700 series columns

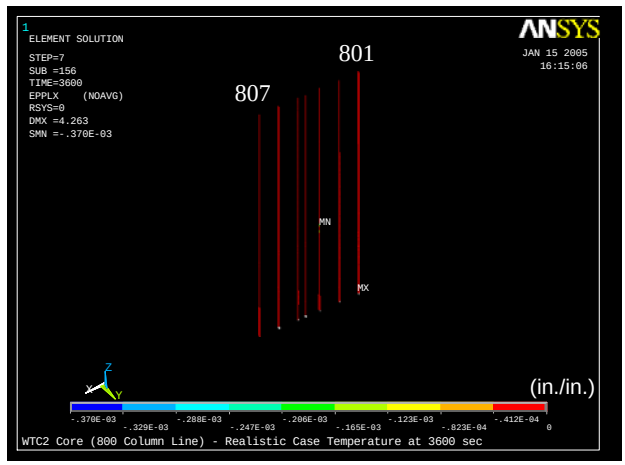

(d) 800 series columns

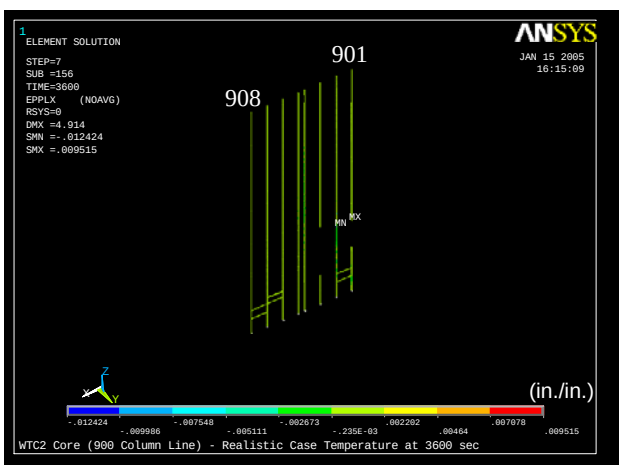

(e) 900 series columns

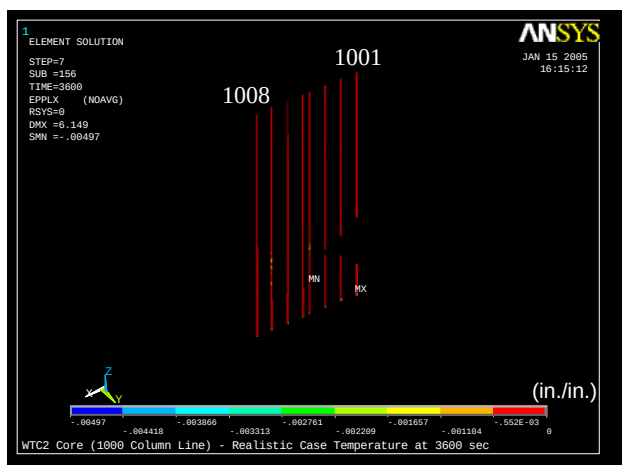

(f) 1000 series columns

Figure 3–135. Axial plastic strains in core columns of isolated core model of WTC 2 for Case C temperature condition at 60 min (compressive strain is negative).

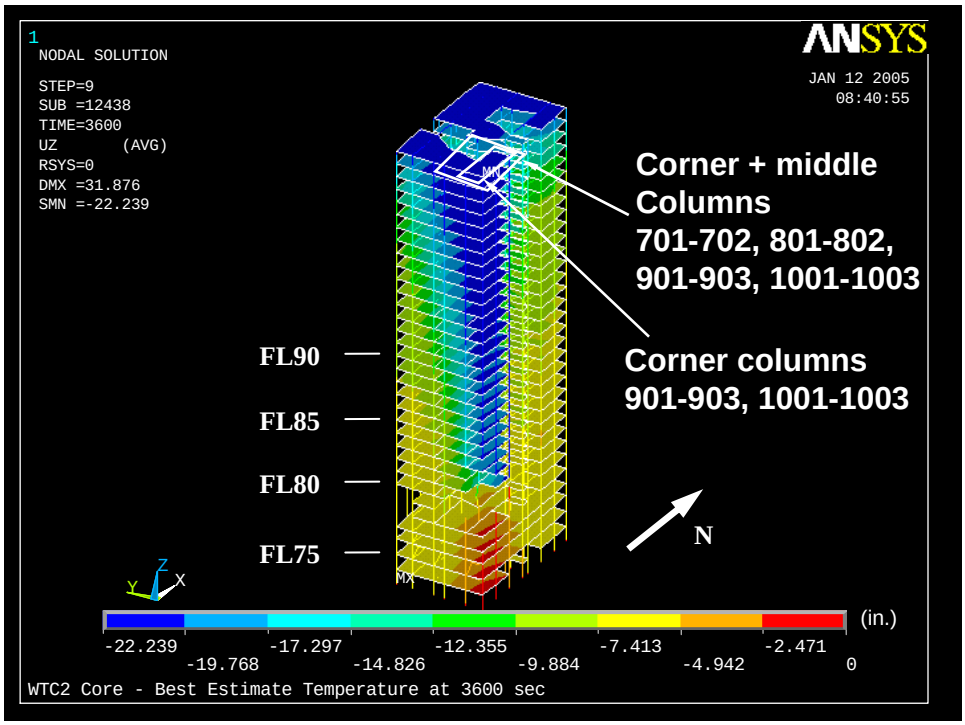

Figure 3–136. Vertical displacement after push down of isolated core model of WTC 2 for Case C temperature condition (downward displacement is negative).

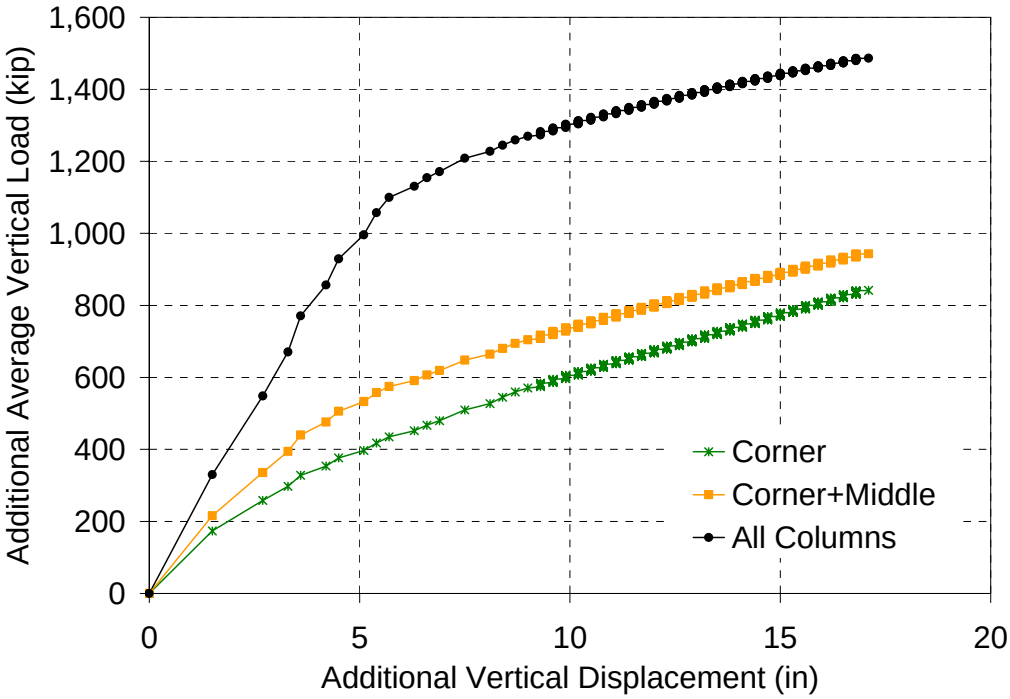

Figure 3–137. Additional average vertical load versus additional vertical displacement during push-down analysis of isolated core model of WTC 2 for Case C temperature condition (compression is positive; core column locations are shown in Fig. 3–136).

Case D Temperature Condition

As mentioned in the previous section for Case C temperature condition, the isolated core model of WTC 2 was unstable after the aircraft impact damage, so the model was restrained in the horizontal directions.

Figures 3–138 to 3–139 show the vertical displacements of the WTC 2 isolated core model subjected to Case D temperature condition from just after the aircraft impact to 60 min. The vertical displacement was always the highest at the southeast corner of the core as the aircraft impact severed the southeast corner core columns in Floors 79 to 82. After aircraft impact damage, the vertical displacement of the southeast corner was 5.6 in. This displacement increased to 8.2 in. at 60 min. Figures 3–140 and 3–141 show axial load and plastic strain in columns at 60 min. Columns at the southeast corner experienced plastic strains immediately following aircraft impact. The maximum plastic strain in the 900-series core columns was 2.5 percent, and 0.7 percent in the 1000 series core columns.

The vertical displacement of the core at Floor 106 at 60 min ranged from 3.3 in. to 6.0 in. The maximum vertical displacement of the southeast corner was less than 6.0 in. at Column 1001. The average vertical displacement of Floor 106 after thermal loading at 60 min was 4.1 in., similar to the 3.9 in. average vertical displacement after the aircraft impact. None of core columns buckled during thermal loading.

To determine the additional axial load-carrying capacity of the core, the isolated core model was pushed down following the analysis for Case D temperature condition as described before. The top of the isolated core was pushed down an additional 30.0 in. The analysis was stopped even though the core was continued to carry additional load. The vertical displacement at the end of 30.0 in. push-down is shown in Fig. 3–142. Figure 3–143 shows the relationship between the additional vertical displacement and the average additional vertical load on core columns, the corner columns, and the corner and middle columns shown in Fig. 3–143. As it can be seen from Fig. 3–143 at 60 min temperature condition, the columns on the southeast corner of the isolated core continued to carry, on the average, an additional load of about 1,200 kip without failure, compared to about 1,700 kip for the average of the entire core columns prior to push down. The additional load on the core columns was about 1.8 times that of the average load in Floor 82 columns at 60 min temperature condition.

The results of the isolated core models of WTC 2 show that significant downward displacement of the core and core column buckling are not likely to occur for WTC 2 during the global analysis.

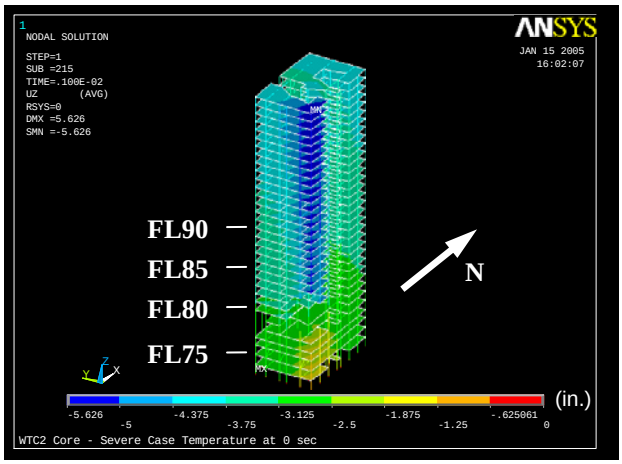

(a) After aircraft impact

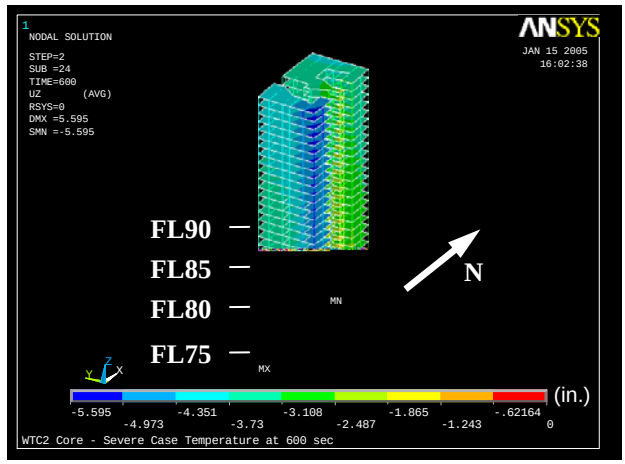

(b) At 10 min

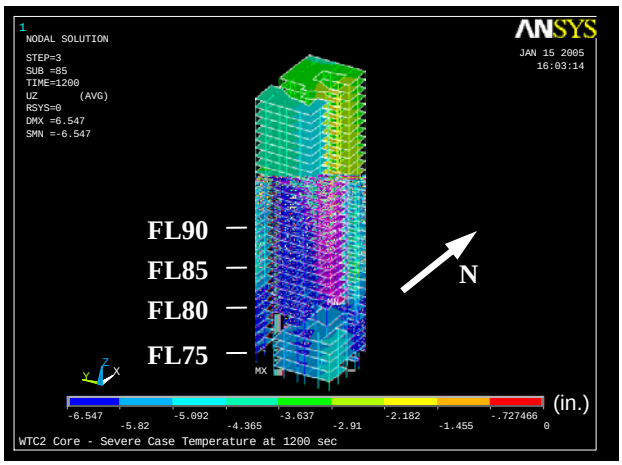

(c) At 20 min

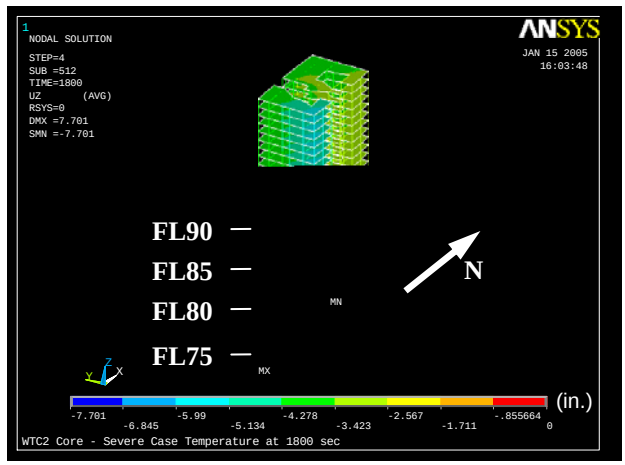

(d) At 30 min

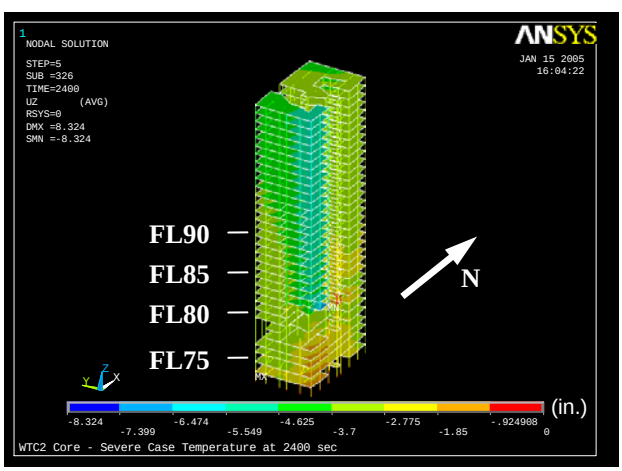

(e) At 40 min

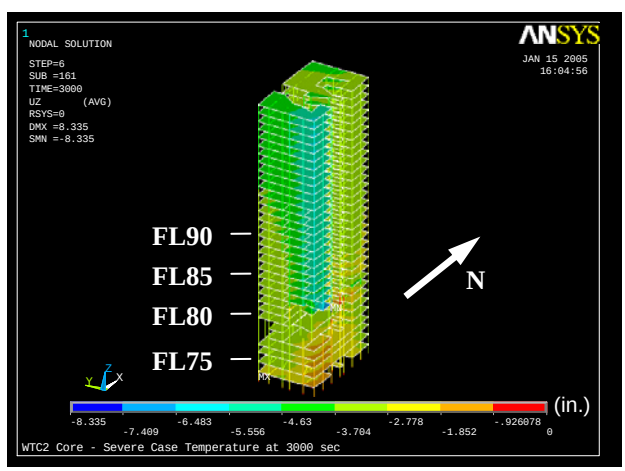

(f) At 50 min

Figure 3–138. Vertical displacement of isolated core model of WTC 2 for Case D temperature condition (downward displacement is negative).

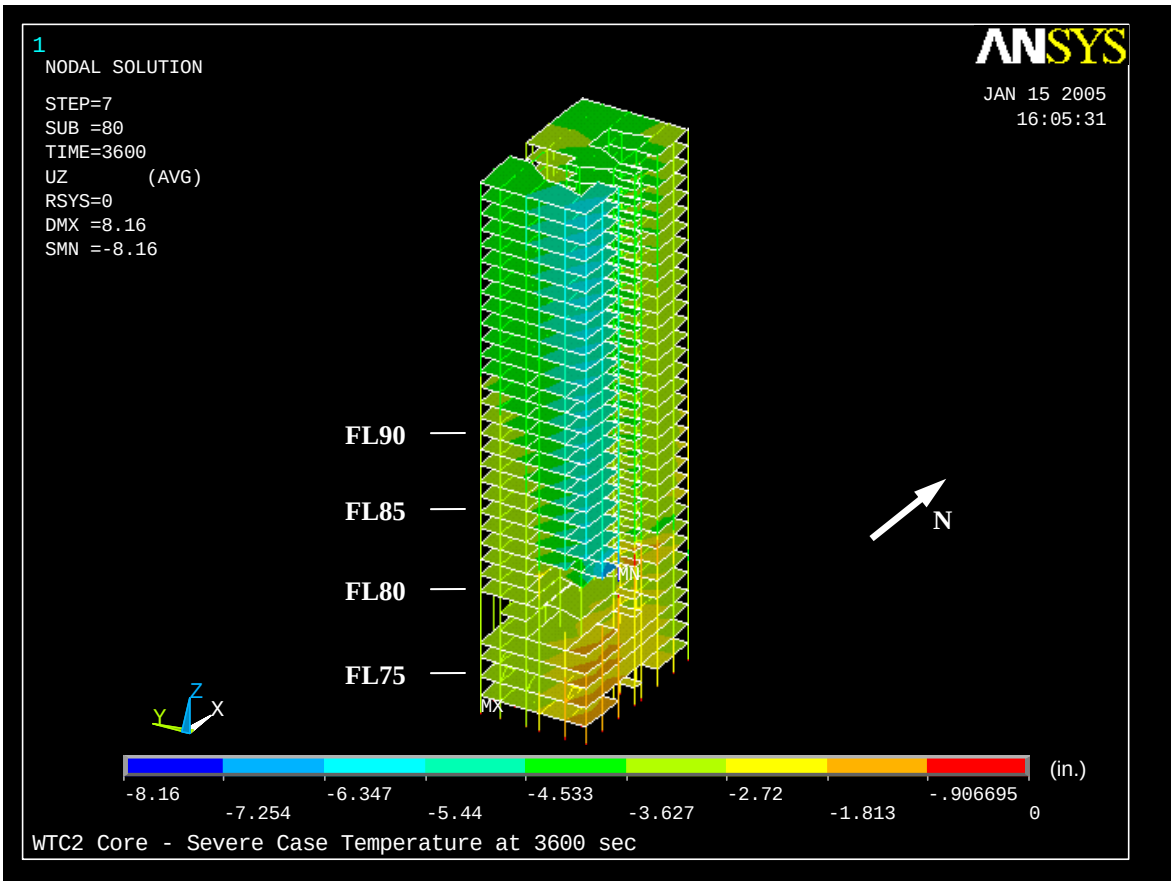

Figure 3–139. Vertical displacement of isolated core model of WTC 2 for Case D temperature condition at 60 min (downward displacement is negative).

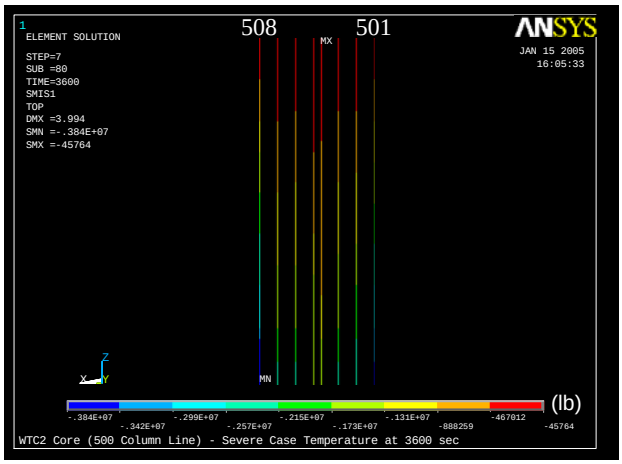

(a) 500 series columns

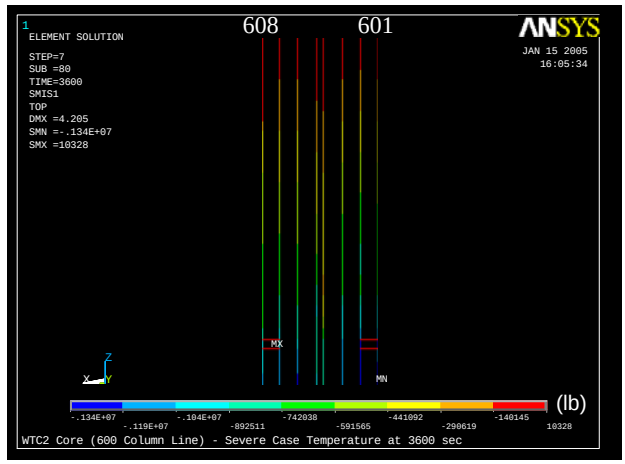

(b) 600 series columns

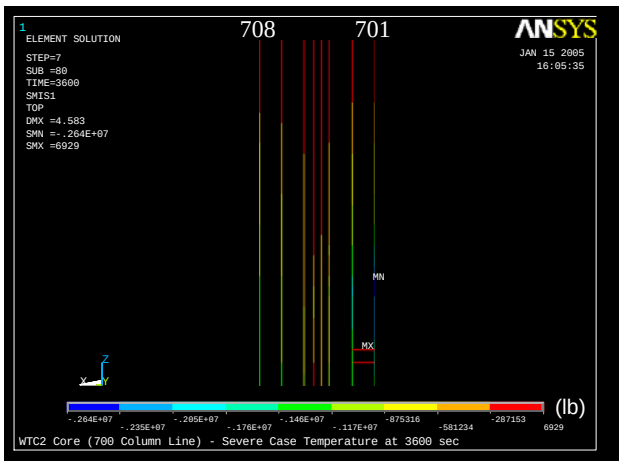

(c) 700 series columns

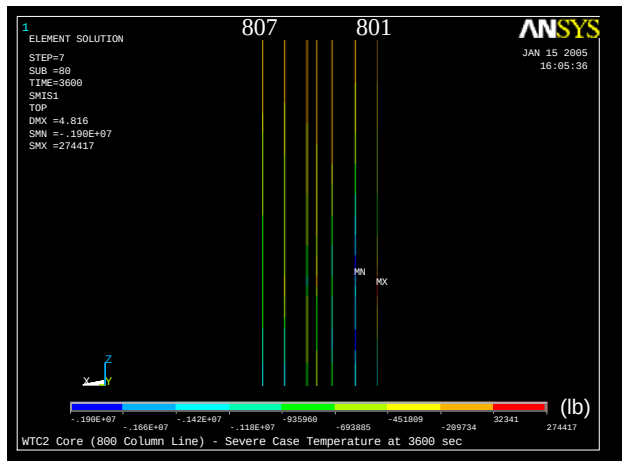

(d) 800 series columns

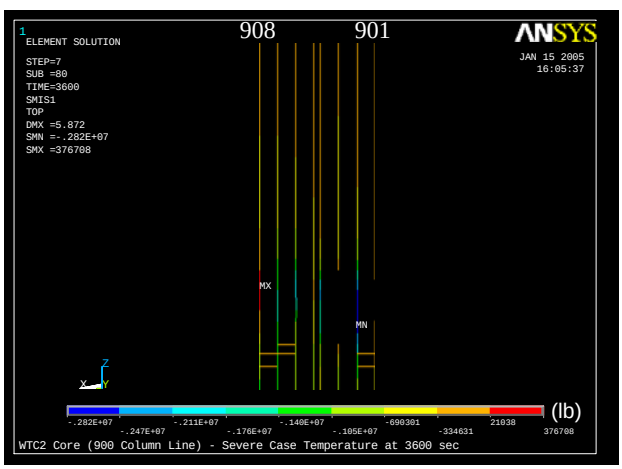

(e) 900 series columns

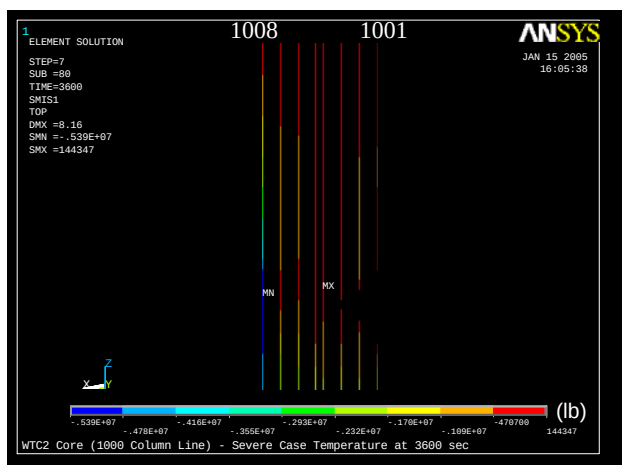

(f) 1000 series columns

Figure 3–140. Axial load in core columns of isolated core model of WTC 2 for Case D temperature condition at 60 min (compression is negative).

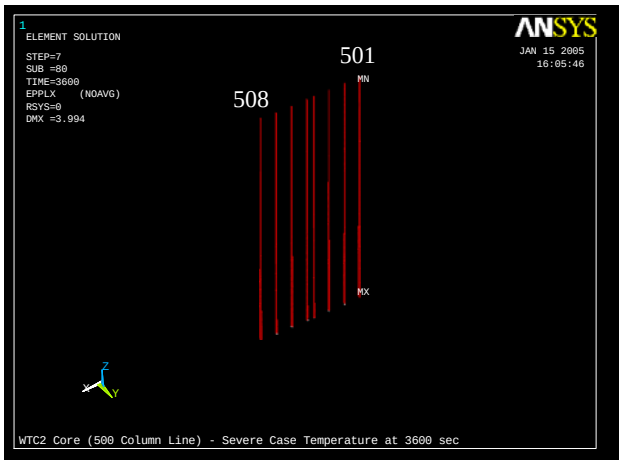

(a) 500 series columns

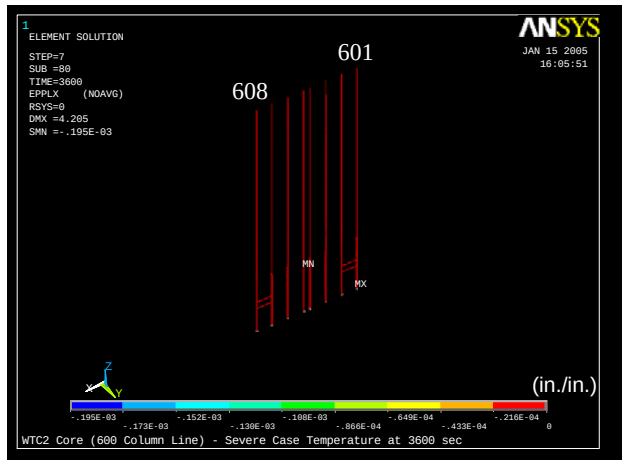

(b) 600 series columns

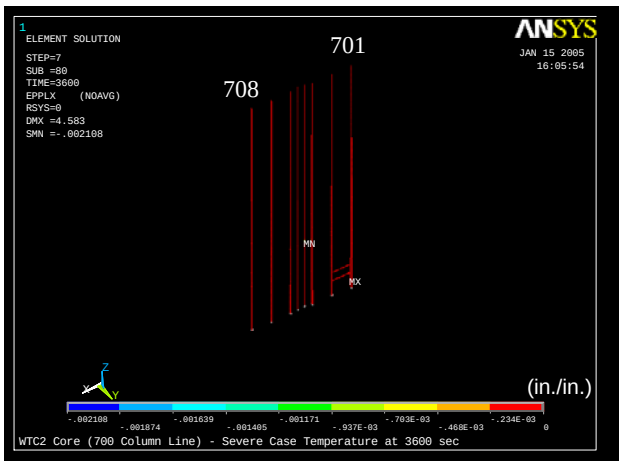

(c) 700 series columns

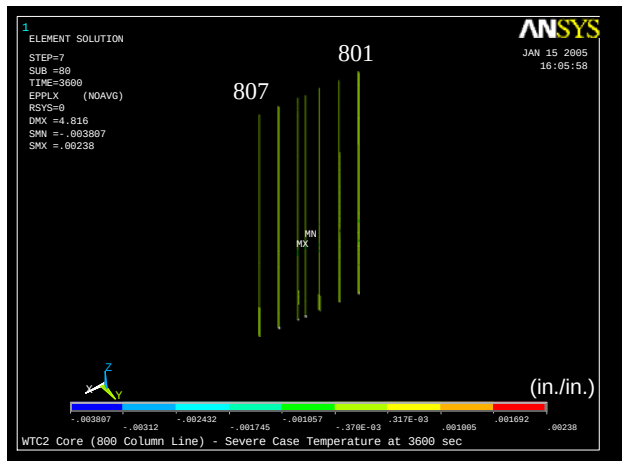

(d) 800 series columns

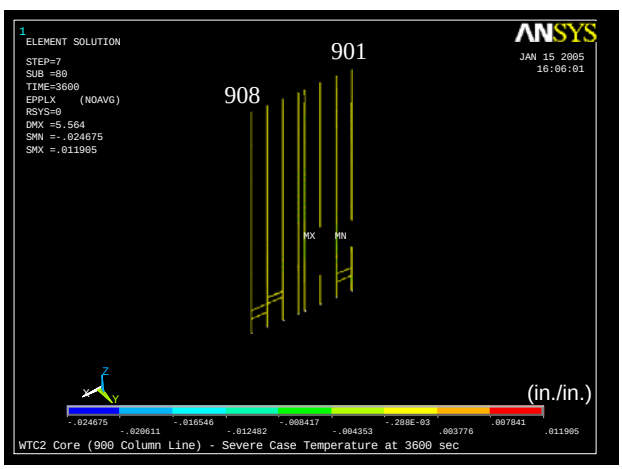

(e) 900 series columns

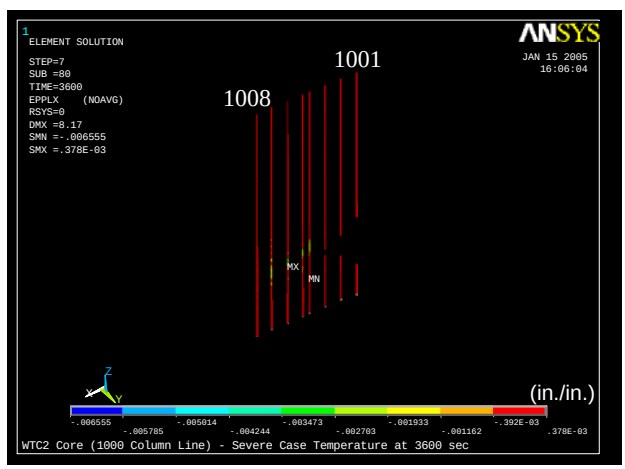

(f) 1000 series columns

Figure 3–141. Axial plastic strains in core columns of isolated core model of WTC 2 for Case D temperature condition at 60 min (compressive strain is negative).

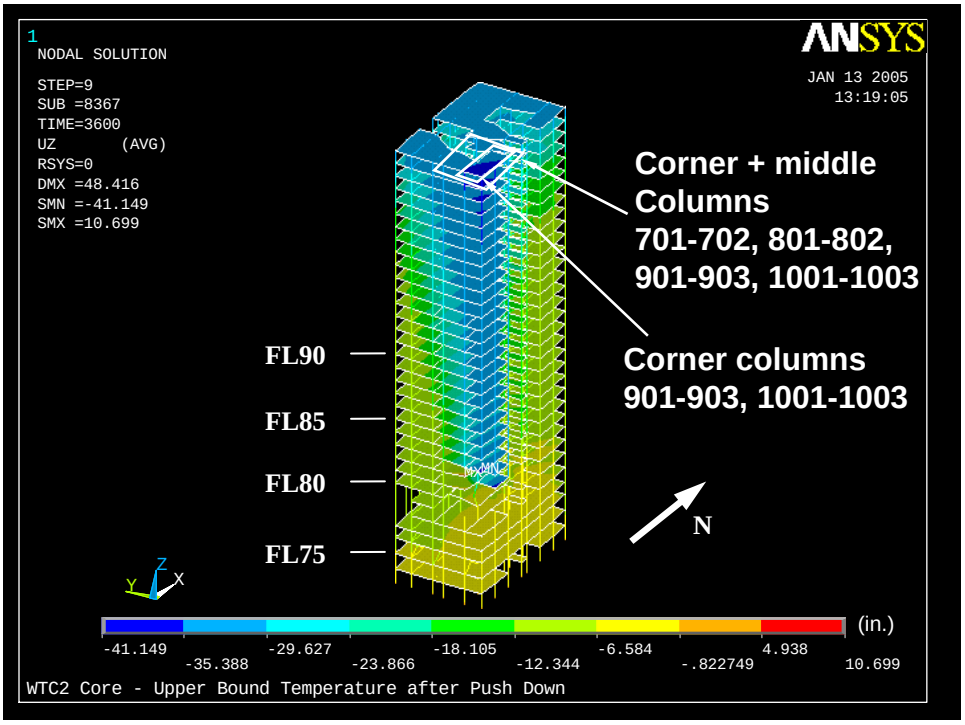

Figure 3–142. Vertical displacement after push down of isolated core model of WTC 2 for Case D temperature condition (downward displacement is negative).

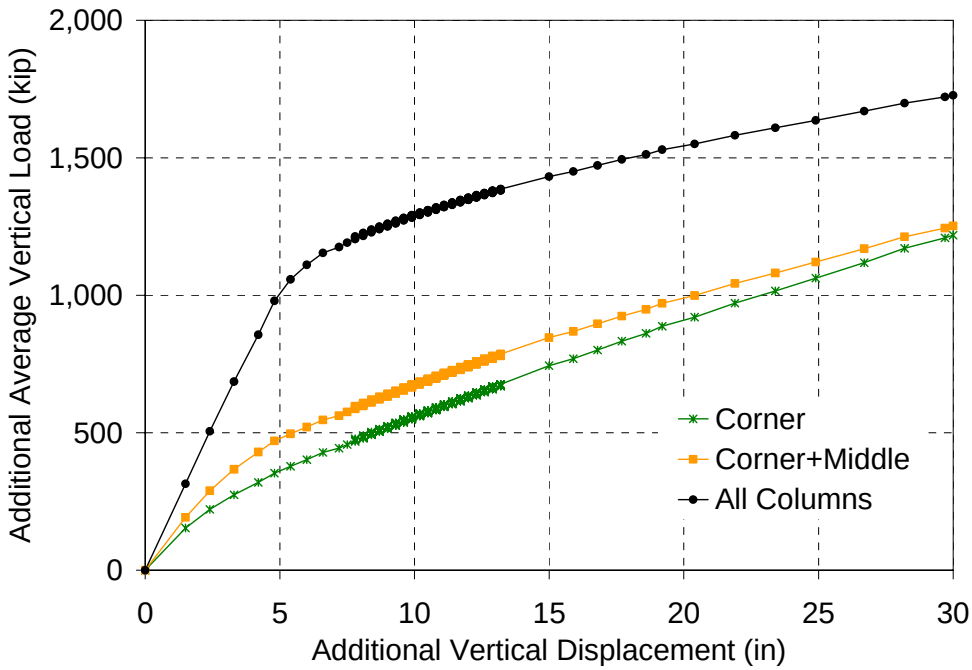

Figure 3–143. Additional average vertical load versus additional vertical displacement during push-down analysis of isolated core model of WTC 2 for Case D temperature condition. (compression is positive; core column locations are indicated in Fig. 3–142.)

Chapter 4
GLOBAL ANALYSIS

4.1 CONVERSION FROM SAP2000 TO ANSYS

Simpson, Gumpertz & Heger, Inc. (SGH) performed global analysis of the WTC 1 and WTC 2 towers using global models of the two towers developed in ANSYS as described in Chapter 2. The models were subjected to the aircraft impact damage and the temperature time histories resulting from the ensuing fire environments. The global models described in this report, and the reference models in NIST NCSTAR 1-2A, used the same coordinate system. As illustrated in Fig. 4–1, the z-axis in this coordinate system is parallel to the vertical axis of the building, the x axis is parallel to the long direction of the building's central core, and the y-axis is parallel to the short direction of the central core. In the WTC 1 models, the origin of the coordinate system is located at the southeast corner of the building with the y-axis extending to the north. In the WTC 2 models, the origin is located at the northeast corner of the building with the y-axis extending west.

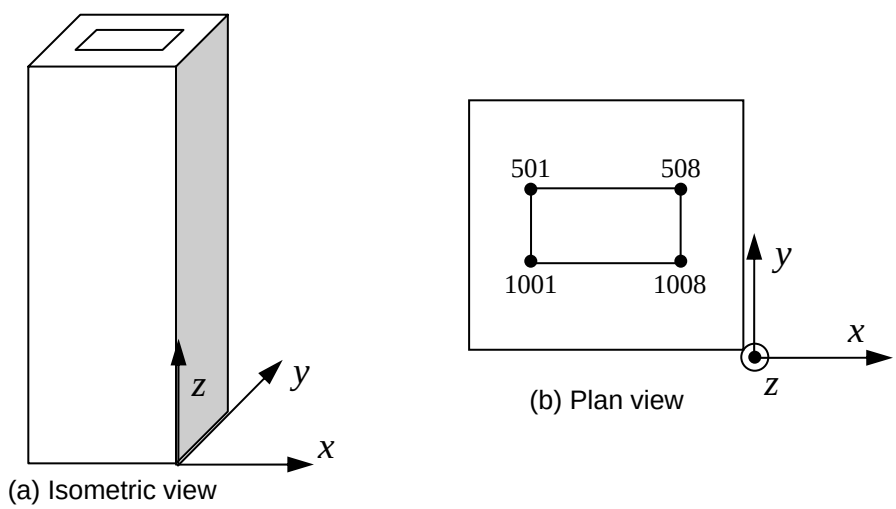

Figure 4–1. Coordinate system used in the analysis models.

The SAP2000 global models in NIST NCSTAR 1-2A were linearly elastic and included interior and exterior columns, spandrels, hat truss members, and floor slabs at mechanical floors. Only the mechanical floors were individually modeled. The other floor slabs were modeled using a set of coupling equations in the software to slave the displacement of certain nodes to the displacement of other nodes. In this case, these coupling equations provided full rigidity within the plane of the floor slabs (the x-y plane) and full flexibility out of this plane.

As most of the structural action that led to the collapse of the buildings took place within and above the aircraft-impacted floors, the reference models were truncated for each building below the lowest damaged floors. The model of WTC 1 was truncated at Floor 89, five floors below the zone of impact, and a series of equivalent vertical linear springs were introduced at the base of this truncated model to represent the

stiffness of the interior columns and exterior walls beneath the level of truncation. Similarly, the model of WTC 2 was truncated at Floor 73.

The truncated SAP2000 models were converted to ANSYS and modified to capture the failure modes of floors and columns and to enhance numerical efficiency. The global models included geometric and temperature-dependent material nonlinearities, including creep.

4.1.1 ANSYS Models

The ANSYS models were the direct translation of the truncated SAP2000 models. During the translation of the models, the coordinates of the nodes, cross sectional properties of members, including orientation and offset of the cross sections, nodal loads, material properties, and member end releases were automatically converted from each SAP2000 database into an ANSYS database. Table 4–1 summarizes the conversion used in translating the element types between SAP2000 and ANSYS. Comparison of the results obtained for the gravity analysis of WTC 1 and WTC 2 from the SAP2000 models and translated ANSYS models are discussed in the next section.

Table 4–1 summarizes the correspondence between element types containd in the SAP2000 model and those in the converted ANSYS model. Table 2–1 previously presented a description of the various ANSYS elements used in the global models. Gravity load analyses of the two buildings were then performed using both the truncated SAP2000 and converted ANSYS models to verify the fidelity of the conversion.

Table 4–1. Conversion from SAP2000 element types to ANSYS element types.

SAP2000 Element Types	ANSYS Element Types
Frame/Cable elements	BEAM188/189 later changed to BEAM24
Shell elements	SHELL63 later changed to SHELL181
Springs	LINK8

Following these analyses, the linear, elastic material properties of the converted ANSYS models were replaced with temperature-dependent inelastic material properties as defined for all material types in Chapter 3 of NIST NCSTAR 1-6C. These material types were assigned to the elements according to their material and cross sectional properties and their locations in the buildings. In the SAP2000 global model, each cross section was assigned a yield value representing the material capacity for that cross section. During the translation to ANSYS, a different name was given to each cross section and material combination, which resulted in a unique material index. Using this material index, the material properties of all elements were replaced with temperature-dependent inelastic material properties. In the actual buildings, the rectangular tube columns in the exterior wall were typically fabricated from four plates, Plate 1 (see Chapter 6 of NIST NCSTAR 1-6C for more information) and could have a different specified yield strength than the rest (Plates 2 and 3). Examination of drawings in the region of interest showed that all these plates had the same yield strength. Therefore, in the translation process, all plates in the same column cross section were considered to be of the same material.

The ANSYS models were also modified to include representation of the floor slabs, which except at mechanical floors, were not included in the SAP2000 models. Floor elements added into the ANSYS model included the core slabs, those core beams that were framed with moment connections at their ends,

and the office area slabs. Figure 4–2 shows the analytical representation of the core and office area floors and the core beams included in the models. Beams in the core that were framed without moment connections were not included in the model because they cannot transfer shear between columns without significant relative displacement. However, their axial stiffness was combined with in-plane stiffness of the floor slab, and then shell elements with this composite in-plane stiffness were used to model the floor.

An equivalent concrete thickness and modulus was calculated for the office area floors to match the in-plane stiffness of the composite floor system which included the concrete slab, the floor trusses, and the floor seats. The thickness of the core slab was taken from the PANYNJ drawings, but the elastic modulus was adjusted to match the in-plane stiffness of the composite floor that included the steel beams and the concrete slab. Both core and office area floor slabs were modeled with linear-elastic material properties for lightweight concrete. Later analyses with these models indicated that these slabs, composite with their framing members, could redistribute load locally amongst neighboring columns and transfer lateral loads to the exterior walls as collapse initiated and WTC 2 began to tilt.

Floors in the global models also provided diaphragm stiffness at each level. However, the floors were not modeled with sufficient detail to capture such floor behaviors under elevated temperatures as sagging and failure of floor-wall connections. Instead, these effects were incorporated into the global analyses as fire-induced damage, as described in Section 2.5.

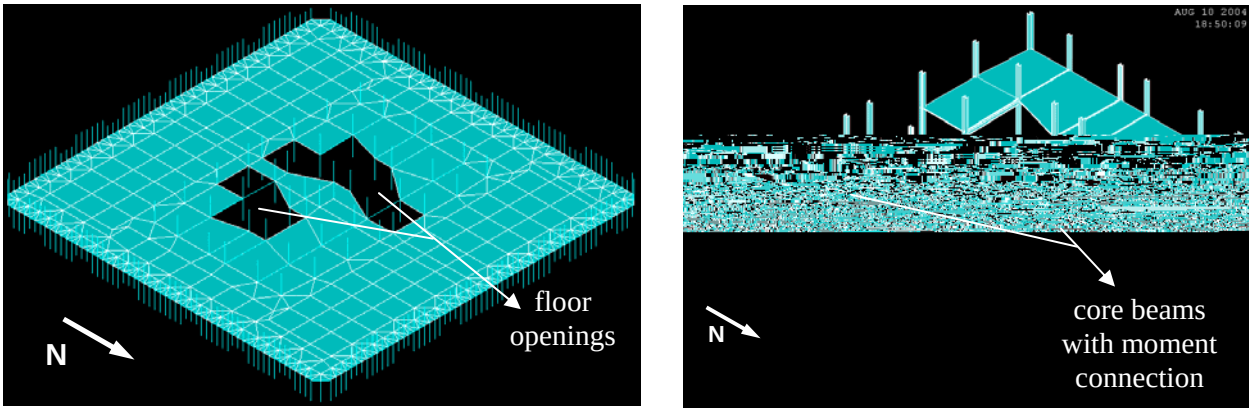

(a) Office and core area floor

(b) Core area floor and core beams

Figure 4–2. Office and core area floors and core beams.

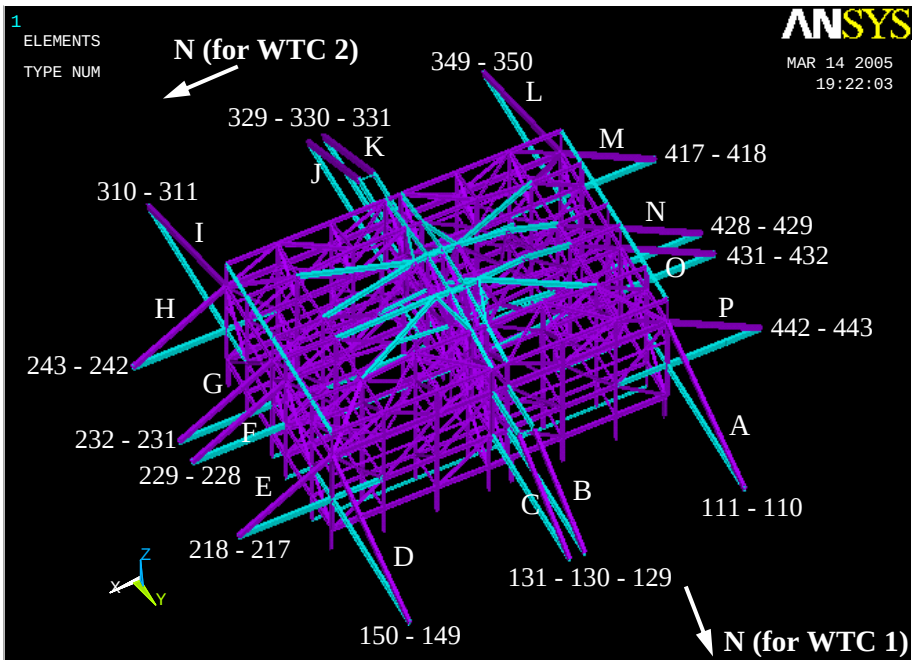

Figure 4–3. Location and IDs of outriggers and supporting columns.

Due to the limitations of the BEAM188 element used to model spandrels, columns, and truss members, a set of preliminary global analyses were conducted without including creep and inelastic buckling in the core and exterior wall columns, as discussed in Appendix C of this report. Plasticity and large deflection were the only nonlinearities included in those analyses. Later, the BEAM188 element was replaced with the BEAM24 element to eliminate the limitations on creep and inelastic buckling. As shown in the global analyses that included consideration of creep and buckling, described in Section 4.2, creep strains and inelastic column buckling played a very significant role in the collapse of the towers.

Figure 4–3 shows the hat trusses in the global models. The hat trusses connected the exterior walls and the core columns. As seen in the figure, four outrigger members on each face of the core extended outward from the core to the exterior walls. Hat truss members were provided with plasticity in the preliminary global models without creep and in the final WTC 1 global model with creep. The hat truss of the WTC 2 global model with creep was part of the "superstructure" where elastic properties were used. Further discussion of this is presented in Section 4.2.2. The hat trusses were not modeled with sufficient detail to capture the onset of buckling. However, the yield strength of the outrigger elements in the final WTC 1 model was set so that compressive yielding would occur when axial load reached the compressive capacity of the members.

4.1.2 Validation of Translated ANSYS Global Models

In order to verify the accuracy of the conversion of the building models from SAP2000 to ANSYS, prior to adding material nonlinearities and elements representing the floor slabs to the ANSYS models, the translated ANSYS models were subjected to gravity dead and live loads, and the ANSYS results were compared to the results of SAP2000 global models. The comparison included the calculated overall displaced shapes, the maximum displacements, vertical base reactions at each construction stage, and element forces for a set of randomly selected members from different parts of the buildings.

The gravity analysis was performed in three stages to simulate construction sequencing in the actual erection of the buildings. In Stage 1 the portion of the towers up to and including Floor 106 was analyzed under self-weight. In Stage 2 the members above Floor 106 were added, and the analysis was performed for the effects of dead loads of the newly added members. In Stage 3, the superimposed dead load and 25 percent of the design live load was added at each floor level to obtain an estimate of the deformations and stresses in each building under normal occupancy conditions.

Figure 4–4 shows the deformed shape calculated for WTC 1 by the ANSYS model and the truncated SAP 2000 model, following Stage 3 analysis. Figure 4–5 provides a similar comparison for WTC 2.

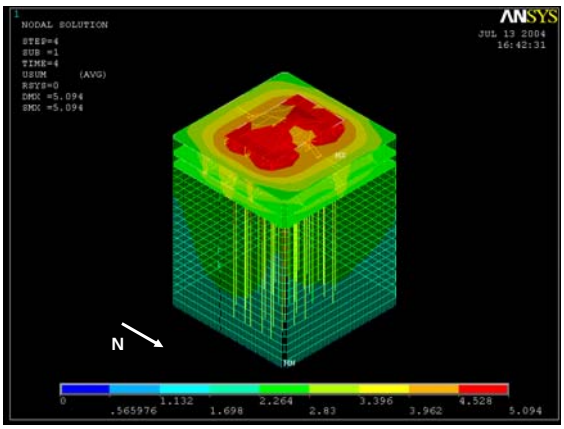

(a) WTC 1 ANSYS Model at Stage 3

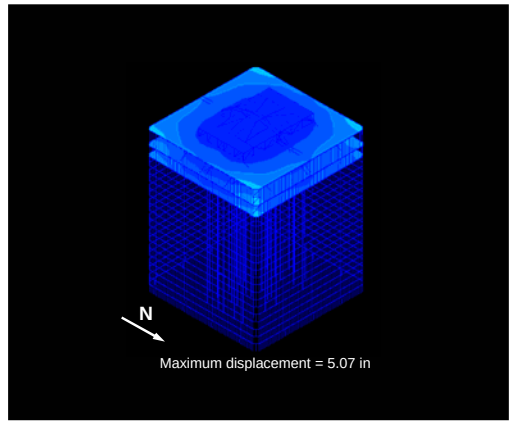

(b) WTC 1 SAP2000 Model at Stage 3
(Displacement is only shown on shell elements.)

Figure 4–4. Displaced shape of WTC 1 at the end of gravity analysis.

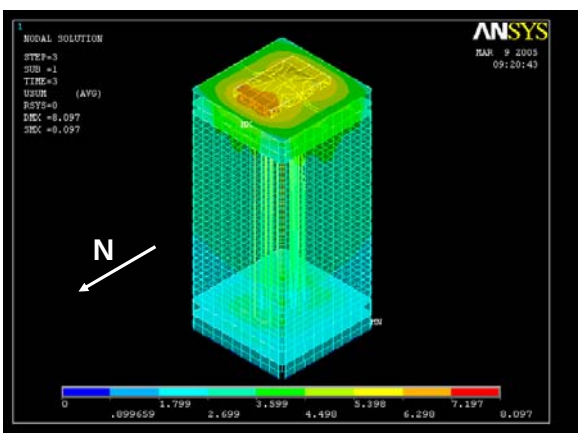

(a) WTC 2 ANSYS Model at Stage 3

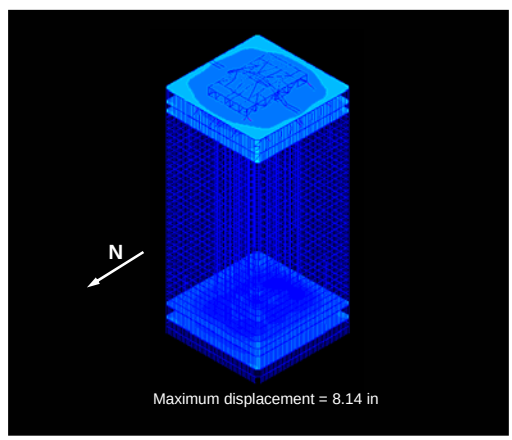

(b) WTC 2 SAP2000 Model at Stage 3
(Displacement is only shown on shell elements.)

Figure 4–5. Displaced shape of WTC 2 at the end of gravity analysis.

Table 4–2 summarizes the maximum displacement and vertical reactions at the base for all stages of the gravity analysis of WTC 1, and Table 4–3 presents similar data for WTC 2. As can be seen, the deformed shapes as well as the maximum displacements and vertical reactions obtained from the analyses performed with the ANSYS models agree well with the results of the similar analyses performed with

SAP2000. The maximum difference in displacements between the two models was less than 1.4 percent for WTC 1 and 0.7 percent for WTC 2. The maximum difference between base reactions predicted by the two analyses was 1.2 percent for WTC 1 and 0.3 percent for WTC 2.

Table 4–4 presents a comparison of the axial forces computed from the ANSYS and SAP2000 analyses for a randomly selected set of elements from different parts of WTC 1. Table 4–5 presents similar data for WTC 2. The agreement between the results obtained from the ANSYS and SAP2000 analyses is quite good.

Table 4–2. Comparison of maximum displacements and base reactions of WTC 1 from translated ANSYS and SAP2000 models.

Stage	Maximum Vertical Displacement (in.)			Base Reaction Sum (kip)		
	ANSYS	SAP2000	Percent Difference	ANSYS	SAP2000	Percent Difference
1	-2.87	-2.83	1.4	55,600	54,940	1.2
2	-4.76	-4.74	0.4	98,470	97,850	0.6
3	-5.09	-5.07	0.4	107,040	106,450	0.6

Table 4–3. Comparison of maximum displacements and base reactions of WTC 2 obtained from translated ANSYS and SAP2000 models.

Stage	Maximum Vertical Displacement (in.)			Base Reaction Sum (kip)		
	ANSYS	SAP2000	Percent Difference	ANSYS	SAP2000	Percent Difference
1	-5.87	-5.91	-0.7	125,050	124,680	0.3
2	-7.67	-7.71	-0.5	166,950	166,980	-0.02
3	-8.10	-8.14	-0.5	180,250	180,360	-0.06

Table 4–4. Comparison of axial forces in randomly selected elements from WTC 1 model at the end of gravity analysis.

Location and Type of Selected Element	Axial Force (kip)	
	ANSYS	SAP2000
Exterior Column 302 at Floor 104	-77	-69
Spandrel between Columns 124 and 125 at Floor 102	0	0
Outrigger member between at Floor 110	-39	-48
Vertical hat truss member at 1005 core column line at Floor 109	-74	-91
Horizontal hat truss member at Floor 107	21	19
Horizontal hat truss member at Floor 108	170	150
Core Column 602 at Floor 97	-738	-745
Core Column 501 at Floor 93	-2,180	-2,190
Core Column 1001 at Floor 89	-2,570	-2,590
Spandrel between Columns 339 and 340 at Floor 100	0	0

Table 4–5. Comparison of axial forces in randomly selected elements from WTC 2 model at the end of gravity analysis.

Location and Type of Selected Element	Axial Force (kip)	
	ANSYS	SAP2000
Core beam at Floor 107	11	6
Inclined truss member at hat truss at Floor 107	-34	-4
Inclined truss member at hat truss at Floor 108	36	8
Inclined truss member at hat truss at Floor 108	-580	-670
Core Column 502 at Floor 87	-1,930	1,940
Core Column 1001 at Floor 82	-3,270	-3,290
Core Column 1002 at Floor 87	-1,910	-1,920
Core Column 1008 at Floor 82	-3,400	3,520
Core Column 1003 at Floor 107	-590	-608
Exterior Column 122 at Floor 82	-313	-313
Exterior Column 329 at Floor 82	-228	-230
Exterior Column 130 at Floor 107	-222	-202
Spandrel between Columns 138 and 139 at Floor 83	0	0
Spandrel between Columns 447 and 448 at Floor 87	0	0

4.2 GLOBAL ANALYSIS WITH CREEP

4.2.1 Introduction

This section presents the results of analyses conducted with global models that included consideration of plasticity, geometric nonlinearity relating to large displacements, inelastic buckling, and creep, and are referred to hereafter as global models or global analysis with creep. As noted earlier, a preliminary set of global analyses were conducted on models that did not include creep and could not simulate inelastic buckling of columns with fidelity. The results of these preliminary analyses are presented in Appendix C of this report, and are referred to as global analysis without creep. Due to the limited non-linear features in the preliminary global models without creep, global instability could not be captured during temperature time history analyses.

The results of the global analyses with creep are presented in Section 4.2.4 for WTC 1 and in Section 4.2.5 for WTC 2.

4.2.2 Modifications to the Global Model with Creep and Inelastic Buckling of Columns

Preliminary global analyses with creep resulted in an unacceptably slow rate of convergence. This was due to the size of the models and the nonlinear effects of temperature-dependent material properties, especially creep. To reduce the size of the global models and to enhance the computational efficiency without adversely affecting the fidelity of the results, a set of modifications were made. These modifications and their effects on the analysis results are discussed in this section. Table 4–6 summarizes the number of degrees of freedom, number of elements, and number of constraint equations in WTC 1 and WTC 2 global models before and after the modifications.

Table 4–6. Global model properties before and after modifications for computational efficiency.

Item	WTC 1		WTC 2	
	Before Modifications	After Modifications	Before Modifications	After Modifications
Number of Degrees of Freedom	291,670	265,760	487,260	196,900
Number of Constraint Eqs.	31,680	28,330	53,890	12,560
Number of Elements	63,880	57,680	106,460	38,130
Number of Beam Elements	48,200	43,600	81,280	32,540
Number of Shell Elements	15,680	14,080	25,180	5,490

Removal of Floors below Impact Zone

The parts of structures below the impact zones (Floor 89 to Floor 91 in WTC 1 and Floor 73 to Floor 77 in WTC 2) contributed little to the overall behavior of the buildings. Previous analyses of subsystem models and preliminary global models showed that the elements below the impact zone did not experience plastic deformations or buckling. Therefore, they were eliminated to further reduce the size of the models. With this modification, the global model for WTC 2 was truncated at Floor 77 just above the mechanical floors and the global model for WTC 1 was truncated at Floor 91.

Release of Axial Degree of Freedom of Spandrels

The spandrel elements in the exterior wall were modeled using BEAM188 elements. These elements caused convergence problems when thermal expansion caused buckling of spandrels. Based on visual evidence, buckling of spandrels did not compromise their ability to transfer shear and bending moment and did not play a very important role in the collapse sequence. Therefore, the axial degree of freedom was released on these spandrel elements, avoiding buckling due to development of large axial force in the spandrels. However, these BEAM188 elements could still transfer shear and bending moments. The coefficient of thermal expansion of spandrels was also removed so that the spandrels would not expand with temperatures.

Removal of Coefficient of Thermal Expansion from the Slab in the Office Area

Since trusses were not modeled individually, the office area slab buckled easily when thermal expansion was restrained by the exterior wall. Artificial buckling of the slab caused convergence problems in the global analysis. Since buckling of the slab in the actual buildings was resisted by the joists, and was not observed in any of the detailed full floor models, this slab buckling mode was considered unlikely to represent real building behavior. Consequently, the coefficient of thermal expansion for the slab in the office area was set to zero.

Neglecting the thermal expansion of the office area slabs did introduce small errors in the out-of-plane bending of columns extending between a hot floor and a cool floor, but such errors were small for columns extending between two hot floors. The error introduced by this modification was not expected to change failure modes or collapse sequence in the global analysis, because thermal expansion of floors was limited to less than a few inches (see Appendix A). The full floor models thermally expanded and pushed

outward on the columns until the thermal expansion was overcome by the floor sagging and the floors pulled inward on the exterior columns..

Use of Superelement in WTC 2

The term “superelement” is used to indicate substructuring, in which a portion of a large model expected to remain elastic is condensed out from the model as a whole. In this technique, the stiffness, damping and mass matrices for the substructure elements are calculated once and used throughout the analysis without any further change. One can calculate stresses and strains in individual elements in the superelement allowing verification of the assumption that the substructure elements remain elastic, or nearly so. The WTC 2 model was suitable for such modification as earlier analyses indicated that the section of the building above Floor 86 would remain nearly elastic. Therefore, this portion of the structure was converted into a superelement.

The use of this superelement in the WTC 2 analyses reduced the solution time required to complete a single iteration by a factor of three. However, it was recognized that if the hat truss members became inelastic and highly nonlinear, such nonlinearities could not be captured. Moreover, when the superelement is used, the effects of construction sequence on the load distribution between core and wall elements cannot be represented, since the birth and death option cannot be used in a superelement. As shown below, the effect of not including construction sequence was evaluated and found to introduce an error of less than 12 percent for vertical displacement.

To evaluate whether any member in the hat truss exceeded its elastic limits, the stresses in all elements within the superelement were calculated at the end of each time interval. For this purpose, a separate model that included the elements at and above Floor 86 was created. In this model, the material properties of all elements were replaced with elastic material properties. At each time interval, the displacements that were obtained from the global model at Floor 86 were imposed on the new model at the same level. Dead and live loads were also applied on the model. Member forces were calculated and compared with their capacities. The results are discussed in Section 4.2.5.

Change from BEAM188 to BEAM24 Elements

In the global models without creep, columns were modeled by BEAM188 (3D linear finite strain beam) elements. The analysis could not be conducted with elements of this type capturing time dependent creep behavior of steel. Frequent convergence problems occurred when thermally induced creep and buckling of columns was in process. Different element types were tested to determine whether thermally induced buckling and creep could be captured. Finally, BEAM24 element was selected, and the element type for the columns was changed from BEAM188 to BEAM24 (3D thin-walled beam).

Construction Sequence

Construction sequence was not included in the global models with creep. The effect of neglecting construction sequence was examined for both buildings. When construction sequence was not included in the analysis, the total axial loads in columns along the exterior walls increased by 7 percent to 15 percent. Similarly, the total column loads supported by the core columns decreased by about 10 percent.

Tables 4–7 and 4–8 indicate the differences in column loads when construction sequence either was or was not considered.

Table 4–7. Comparison of total column loads between WTC 1 models with and without construction sequence

	North		South		East		West		Core	
	w/ Const	w/o Const	w/ Const	w/o Const	w/ Const	w/o Const	w/ Const	w/o Const	w/ Const	w/o Const
Floor 93 - 94	12,307	13,145	12,383	13,191	8,910	10,036	8,933	10,049	47,525	43,638
Floor 94 - 95	11,922	12,760	11,999	12,806	8,580	9,708	8,605	9,723	45,573	41,682
Floor 95 - 96	11,450	12,281	11,530	12,329	8,339	9,475	8,365	9,492	43,598	39,703
Floor 96 - 97	11,065	11,895	11,145	11,944	8,012	9,151	8,040	9,170	41,633	37,735
Floor 97 - 98	10,602	11,426	10,686	11,478	7,763	8,911	7,793	8,932	39,669	35,767
Floor 98 - 99	10,217	11,040	10,302	11,092	7,439	8,591	7,471	8,613	37,714	33,808

Note: Compression is positive. Units are in kip.

Table 4–8. Comparison of total column loads between WTC 2 models with and without construction sequence

	North		South		East		West		Core	
	w/ Const	w/o Const	w/ Const	w/o Const	w/ Const	w/o Const	w/ Const	w/o Const	w/ Const	w/o Const
Floor 78 - 79	13,536	15,304	13,442	15,000	18,861	20,169	18,805	20,119	78,104	72,156
Floor 79 - 80	12,965	14,723	12,877	14,424	18,650	19,970	18,596	19,923	76,197	70,246
Floor 80 - 81	12,892	14,675	12,810	14,379	17,959	19,257	17,903	19,207	74,160	68,206
Floor 81 - 82	12,367	14,141	12,292	13,851	17,728	19,036	17,673	18,989	71,824	65,866
Floor 82 - 83	12,279	14,078	12,208	13,789	17,064	18,353	17,008	18,301	69,777	63,815
Floor 83 - 84	11,775	13,567	11,712	13,284	16,816	18,114	16,761	18,114	67,793	61,828

Note: Compression is positive. Units are in kip.

The calculations showed that the outriggers in the WTC 1 simulations were more highly stressed when the construction sequence was not considered. Since it was believed that the hat truss played an important role in transferring loads in WTC 1, the yield strengths of the materials for these outriggers in WTC 1 were artificially increased to account for the incorrect increase in compressive stresses when construction sequence was not considered.

The difference in maximum displacement calculated with and without consideration of construction sequence was within 12 percent for both WTC 1 and WTC 2. Figures 4–6 and 4–7 present the differences in calculated displacements for analyses in which construction sequence either was or was not considered, respectively, for WTC 1 and WTC 2. In these figures, the results presented for global analyses with creep for the state of the structure before aircraft impact are for the analyses in which construction sequence was neglected; they differ from the corresponding results presented in Appendix C for global analyses without creep as those analyses included the effects of the construction sequence.

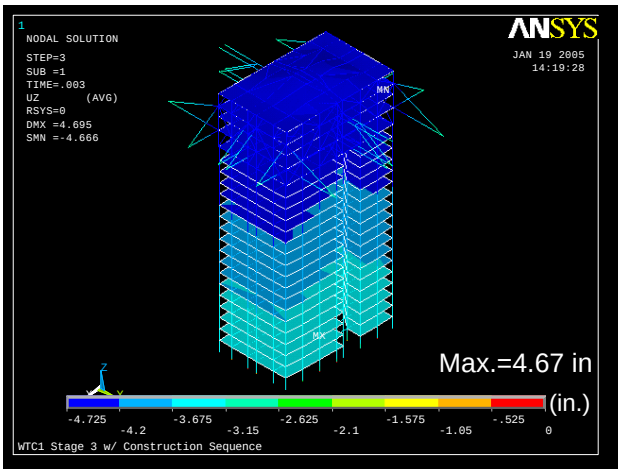

(a) Core w/ construction sequence

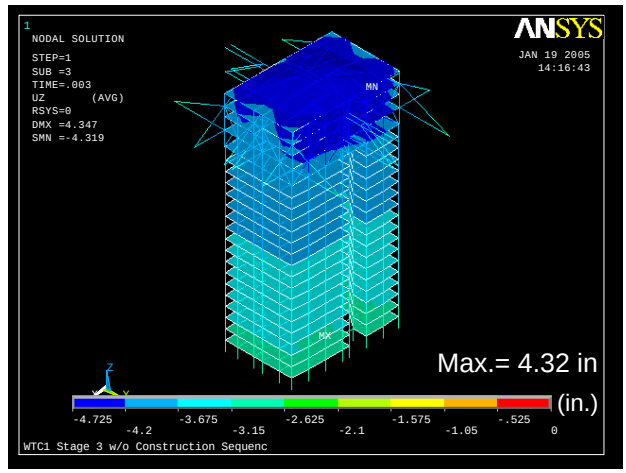

(b) Core w/o construction sequence

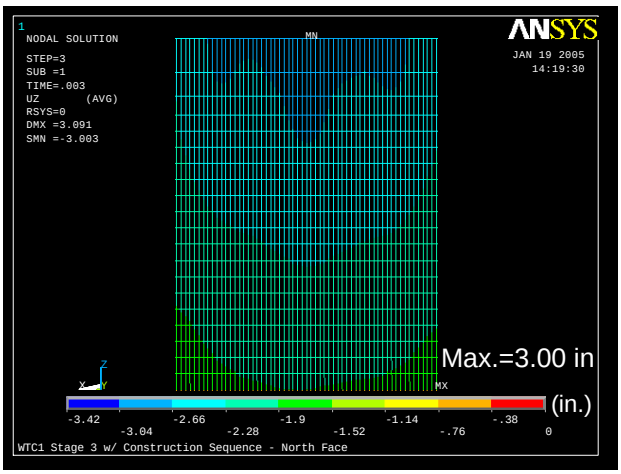

(c) North face w/ construction sequence

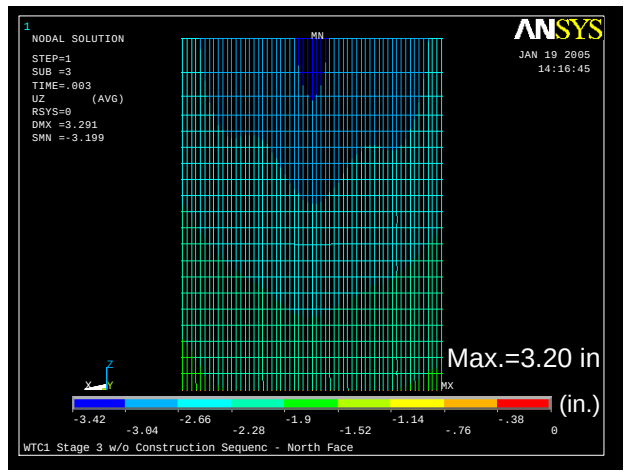

(d) North face w/o construction sequence

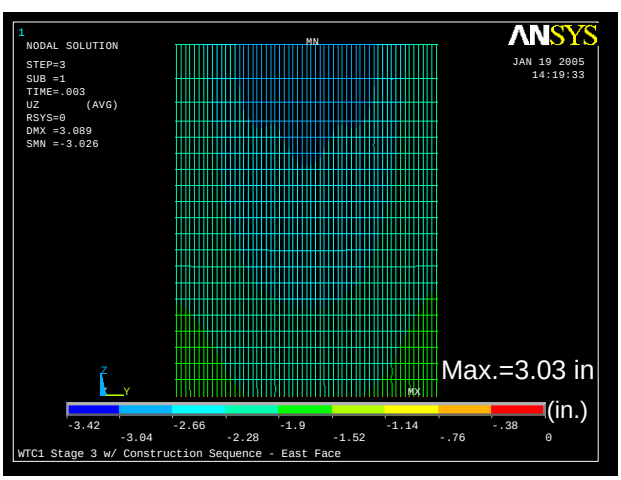

(e) East face w/ construction sequence

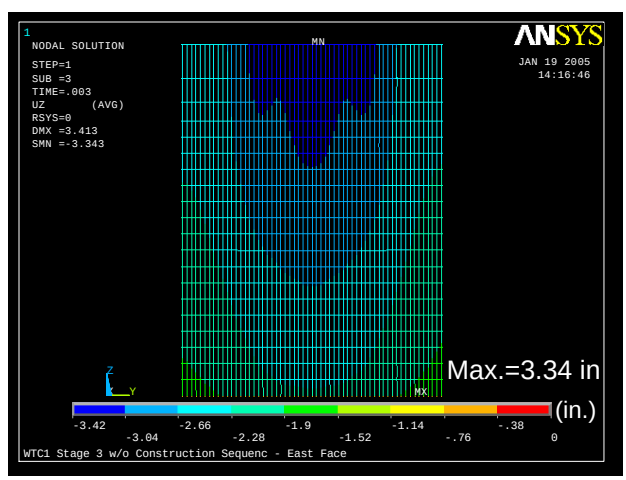

(f) East face w/o construction sequence

Figure 4–6. Comparison of vertical displacement between WTC 1 models with and without construction sequence.

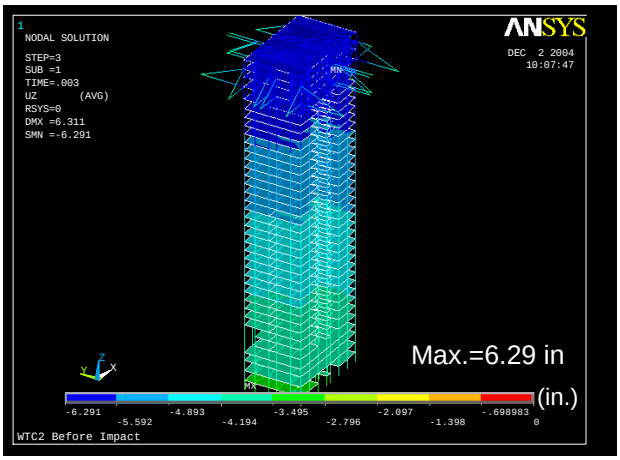

(a) Core w/ construction sequence

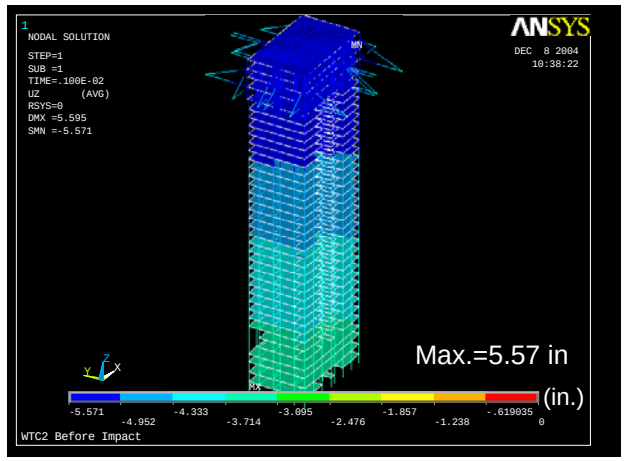

(b) Core w/o construction sequence

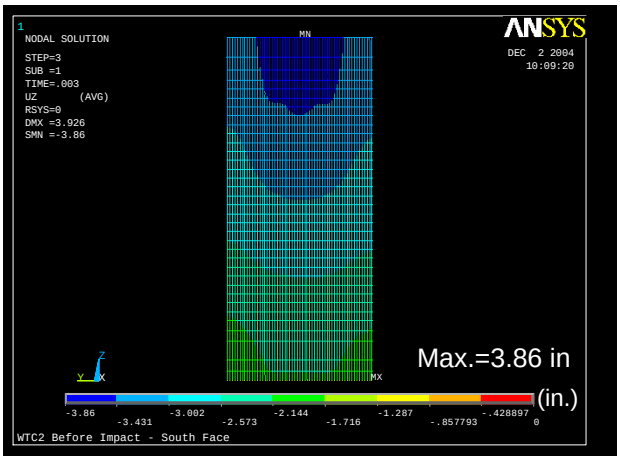

(c) South face w/ construction sequence

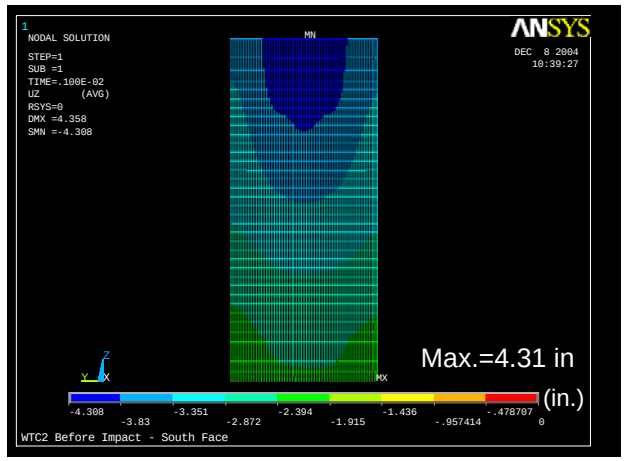

(d) South face w/o construction sequence

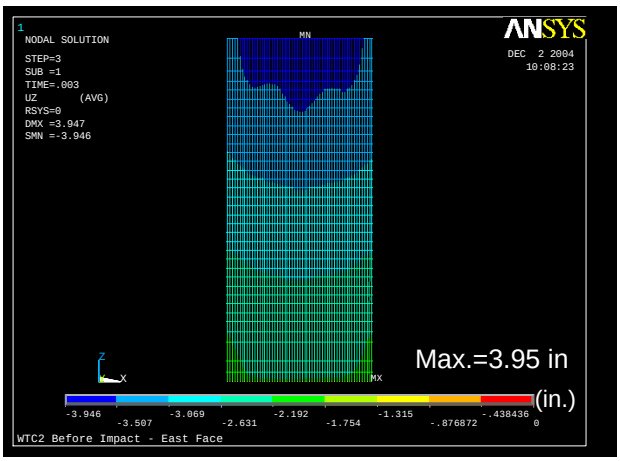

(e) East face w/ construction sequence

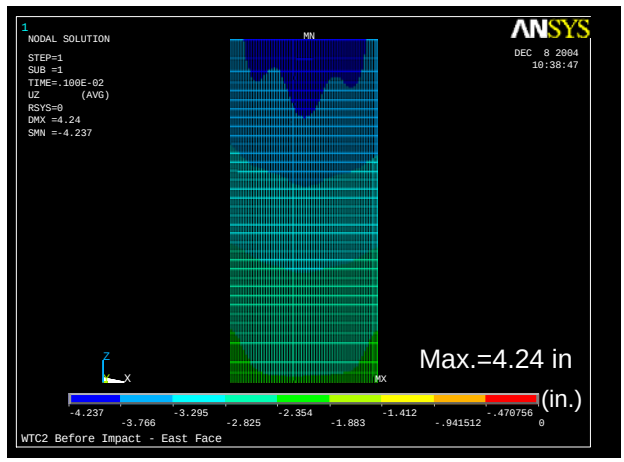

(f) East face w/o construction sequence

Figure 4–7. Comparison of vertical displacement between WTC 2 models with and without construction sequence.

4.2.3 Boundary Conditions and Loading Steps

The global models with creep were vertically supported on elastic springs at Floor 91 for WTC 1 and Floor 77 for WTC 2. These elastic springs represented the axial flexibility of the portion of the building below these floors. The models were fixed against horizontal translation at these floors.

The collapse analysis of WTC 1 considered creep and was performed only for Case B damage conditions and temperature time histories; and that for WTC 2 was only performed for Case D. Section 2.2.3 of this report provides a description of these damage conditions. Severed and heavily damaged core columns were removed in the global model with creep, while only severed columns were removed in the global models without creep.

To reduce the size of the global models as much as possible, members that were predicted to have been severed or heavily damaged by the aircraft impact were removed from the models before applying the gravity load. The floor dead and live loads were applied at each column node at the floor levels. These forces were taken directly from the ANSYS global models converted from the reference SAP2000 global models. WTC 1 and WTC 2 global models were then subjected to Case B and Case D temperature conditions, respectively. NIST provided temperature data at 10 min intervals ranging from 0 min to 100 min for WTC 1 and to 60 min for WTC 2. For the first loading step of temperature analysis, temperatures of the structural elements were linearly ramped up from room temperature to the temperatures at 10 min. After the first step, the temperatures were linearly ramped from the temperatures at the end of the previous time step to those at the end of current time step.

4.2.4 Simulation of WTC 1 Collapse

The global model of WTC 1, described in the previous section, was used to simulate the response of the building to aircraft impact damage and the ensuing fire environment. Studies performed on the isolated exterior wall and core models and on the full floor subsystem models indicated that the calculated response of these models to the Case B impact damage and temperature time history set, as described in Section 2.2.3, more closely matched the structural behavior observed in the visual evidence than did analyses using the Case A data set. Therefore, only the Case B impact damage and temperature time history set was used in the final global analyses.

The gravity loading, consisting of the structure's self weight, superimposed dead load, and 25 percent of the design live loads, was applied as a concentrated joint load at each column-floor node, without consideration of construction sequence effects. Then the temperature time history was applied in a series of load steps. Table 4–9 summarizes the sequence of analyses that were performed. The results of each analysis step were used as the initial conditions for the next analysis step. The steps consisted of alternate applications of fire damage, in the form of floor/wall disconnections or pull-in forces, followed by application of temperature change. Section 2.5 describes the methods by which floor/wall disconnections and pull-in forces were determined and applied.

After application of the Case B aircraft impact damage set, which included severe damage on the north face and to the north side of the core, the results of analysis showed slight tilting of the portion of the structure above the damaged area, to the north. In early stages of the application of the temperature time history, temperatures increased significantly in the core columns where thermal insulation was projected to be damaged. The resulting thermal expansion of these core columns was larger than the thermal

expansion of the exterior walls which occurred at the same time. Therefore, as the core columns in the model expanded, they were restrained by the stiff hat truss, resulting in increased compressive forces in the core columns. This effect first became significant at 20 min. By 50 min some of the core columns under the influence of the high temperatures and high compressive loads began to exhibit buckling and large creep strains. As buckling and creep strains accumulated, the core began to displace downward. Again, the movement of the tops of the core columns was restrained by the hat truss which now began to redistribute loads from the core columns to the exterior walls. At 80 min, pull-in forces were applied to the south wall, based on the observed evidence. At 87 min, the south wall started to bow inward significantly, initiating the buckling of the south wall that triggered the collapse sequence.

Table 4–9. Analysis steps of WTC 1 ANSYS global model.

Analysis Step	Description
1	Dead and 25 percent of the design live loads were applied on the model of WTC 1 with impact damage.
2	Floor/wall disconnections and pull-in forces that were projected to occur between 0 min and 10 min were applied.
3	Column and spandrel temperatures were linearly ramped up from room temperature of 20°C to temperatures at 10 min.
4	Floor/wall disconnections and pull-in forces that were projected to occur between 10 min and 20 min were applied.
5	Column and spandrel temperatures were linearly changed from temperatures at 10 min to 20 min.
6	Floor/wall disconnections and pull-in forces that were projected to occur between 20 min and 30 min were applied.
7	Column and spandrel temperatures were linearly changed from temperatures at 20 min to 30 min.
8	Floor/wall disconnections and pull-in forces that were projected to occur between 30 min and 40 min were applied.
9	Column and spandrel temperatures were linearly changed from temperatures at 30 min to 40 min.
10	Floor/wall disconnections and pull-in forces that were projected to occur between 40 min and 50 min were applied.
11	Column and spandrel temperatures were linearly changed from temperatures at 40 min to 50 min.
12	Floor/wall disconnections and pull-in forces that were projected to occur between 50 min and 60 min were applied.
13	Column and spandrel temperatures were linearly changed from temperatures at 50 min to 60 min.
14	Floor/wall disconnections and pull-in forces that were projected to occur between 60 min and 70 min were applied.
15	Column and spandrel temperatures were linearly changed from temperatures at 60 min to 70 min.
16	Floor/wall disconnections and pull-in forces that were projected to occur between 70 min and 80 min were applied.
17	Column and spandrel temperatures were linearly changed from temperatures at 70 min to 80 min.
18	Floor/wall disconnections and pull-in forces that were projected to occur between 80 min and 90 min were applied.
19	Column and spandrel temperatures were linearly changed from temperatures at 80 min to 90 min.
20	Floor/wall disconnections and pull-in forces that were projected to occur between 90 min and 100 min were applied.
21	Column and spandrel temperatures were linearly changed from temperatures at 90 min to 100 min.

Figures 4–8 to 4–23 show the calculated vertical displacements for the exterior walls of WTC 1, before the aircraft impact, immediately after impact, at 80 min after impact (at the end of Step 17), and 100 min after impact. Figures 4–24 to 4–32 show similar data for the core columns. Figure 4–33 shows the calculated vertical displacement of Floor 99 before the aircraft impact. Figures 4–34 to 4–37 show changes in vertical displacement at Floor 99 from the state before the aircraft impact. Before aircraft impact, the maximum vertical displacements of the exterior walls and the core were respectively calculated as 3.3 in. and 4.2 in. (see Figs. 4–8 and 4–24). As indicated in Fig. 4–33, the core had larger vertical displacements by about 1 in. than the exterior walls at Floor 99. Since the construction sequence was not considered in the analysis, this difference in the vertical displacements changed initial loading conditions of columns. As shown in Table 4–7, the total column loads on the north and south walls increased by 7 percent at the impacted floors, the total column loads on the east and west walls increased by about 14 percent, and the total column loads on the core decreased by about 9 percent, by ignoring the construction sequence. Owing to impact damage on the north face and the north side of the core, WTC 1 tilted slightly to the north after the aircraft impact as can be seen in Fig. 4–34. The maximum calculated displacement of the north wall increased from 3.1 in. to 5.9 in. as shown in Figs. 4–12 and 4–13, and the maximum displacement of the south wall decreased from 3.2 in. to 3.0 in. as shown in Figs. 4–20 and 4–21. The calculated vertical displacement for the east and west walls only increased slightly.

In the early stages of thermal loading, the temperatures in the core area were rising. At 50 min, the calculated downward displacement of the core from plasticity, creep, and buckling of core columns was 1.6 in. on average at Floor 99, as shown in Fig. 4–35. At 100 min, the downward displacement of the core was at 2.0 in. on average at Floor 99. Average increases of the downward vertical displacement at Floor 99 of the north, east, south, and west faces were 1.7 in., -0.24 in., -0.51 in., and -0.24 in. at 100 min, respectively. As the bowing of the south wall increased, a section of the south wall above the bowed-in area moved downward as shown in Fig. 4–37.

Figures 4–38 to 4–41 show the calculated out-of-plane displacements for the south wall before and after the aircraft impact, at 80 min (at the end of Step 17), and 100 min after impact. In these figures, inward displacement is shown as positive. Figure 4–42 shows a plot of the variation of maximum calculated out-of-plane displacement in the south wall between 80 min and 100 min. Until pull-in forces were applied to the columns on the south wall over Floor 95 to Floor 99 at 80 min (Step 18), no inward bowing had occurred. This matches the available video evidence. After the pull-in forces were applied, the bow initiated and grew to 15.5 in. At about 87 min into the analysis, the inward bow began to increase significantly. By 90 min, the rate of increase in inward bowing of the south wall slowed, and gravity loads were redistributed to the east and west walls and the core. The predicted inward bowing gradually increased to approximately 43 in. at 100 min. However, the south wall did not show instability (buckling) at 100 min.

Analyses of isolated exterior wall substructure models and of the global model showed that the amount of inward bowing predicted for the wall was highly sensitive to the magnitude of the applied pull-in forces. For a comparison, when pull-in forces were revised from the 5 kip magnitude used in the analyses discussed above to 4 kip, the predicted inward bowing of the south wall decreased dramatically from nearly 43 in. at 100 min to approximately 15 in. Minor upward adjustment of the pull-in forces, from the 5 kip used in the analyses, would have produced wall instability by 100 min. It is likely that the pull-in forces in the actual building increased with time, and that likely, this inward bowing of the south wall did trigger instability, which initiated the global structural collapse.

Figures 4–44 to 4–55 show calculated axial loads in exterior columns before and after the aircraft impact, at 80 min (at the end of Step 17), and 100 min after impact. Figures 4–56 to 4–59 show the variation of calculated axial loads in exterior columns along the different building faces at Floor 98 at different points in time. Figures 4–60 to 4–63 show axial loads for the core columns before and after the aircraft impact, at 80 min (at the end of Step 17), and 100 min. Figures 4–64 to 4–67 show the magnitude of axial load in each column at Floor 98; the size of axial load is proportional to the size of the circles. Tables 4–10 and 4–11 show the total column loads on each of the exterior walls and the core at Floor 98 and Floor 105, respectively. Tables 4–12, 4–14, 4–16, 4–18, and 4–20 show total column loads on each of the exterior walls and the core at different floors from Floor 93 to Floor 105. Tables 4–13, 4–15, 4–17, 4–19, and 4–21 show the predicted changes in the total column loads of each of the exterior walls and the core at various times in the analysis. Tables 4–22 to 4–24 show the difference in total column loads at Floor 98 and Floor 105 between the states before and after aircraft impact, just after aircraft impact to 80 min (at the end of Step 17), and between 80 min (at the end of Step 17) and 100 min.

After aircraft impact, gravity loads that were previously carried by severed columns were redistributed to other columns within the building. For example, Table 4–10 shows that the exterior columns of the north wall at Floor 98 carried 10,974 kip load before the aircraft impact, and 10,137 kip just after aircraft impact, a net reduction of 837 kip. Table 4–11 shows that columns along the north wall at Floor 105 lost 732 kip of column loads as a result of the impact damage. Therefore, 732 kip out of 837 kip was transferred by the hat truss to other portions of the structure, and the rest was redistributed to the adjacent walls by the Vierendeel behavior of the walls themselves. Table 4–22 shows this load redistribution. Due to the impact damage and the northward tilting of the building after impact, the south wall also lost gravity loads. Approximately 600 kip was transferred from the south wall by the hat truss. The east and west walls and the core gained respectively gained 466 kip, 472 kip, and 400 kip, respectively.

As described above, during early stages of the thermal analysis, thermal expansion of the core area was greater than that of the exterior walls. As this expansion occurred, the total column loads in the core increased until 20 min into the analysis, as shown in Tables 4–20 and 4–21. After 20 min, the core began to shed gravity loads as it displaced downward, under the influence of column creep and buckling. This behavior continued until the south wall initiated inward bowing. At 80 min, about 6,800 kip of the gravity load in the core was transferred by the hat truss to the exterior walls, as shown in Table 4–11. The north, east, south, and west walls respectively gained 1,234 kip, 2,470 kip, 1,063 kip, and 2,021 kip from this behavior. As shown in Table 4–23, the primary load redistribution path during the thermal loading up to 80 min was through the hat truss.

Figure 4–58 shows that after 80 min, Columns 318 to 346 on the south wall unloaded as they bowed inward. The vertical displacement of the south wall simultaneously increased as shown in Figs. 4–23 and 4–37, and the south wall shed 1,485 kip of the gravity load between 80 min and 100 min. As a result, the east and west walls and the core all gained gravity loads. Figure 4–58 also shows load redistribution within the south wall. As the columns near the center of the south wall unloaded after 80 min, the axial loads on the columns on the east and west sides of the south wall increased.

Figures 4–68 to 4–71 show the calculated axial load demand-to-capacity ratio of each core column before and after the aircraft impact, at 80 min (at the end of Step 17), and 100 min. Compressive capacities of the core columns were calculated using Eq. E2-1 in the American Institute of Steel Construction's Manual of Steel Construction Load and Resistance Factor Design (AISC LRFD) for inelastic buckling with an effective length factor, K, of unity and a resistance factor of unity. At 100 min, a large number of core

columns (501, 601, 603, 606, 701, 703, 705, 707, 801, 804, 806, 807, 901, 903, 904, 905, 906, 908, and 1001) exhibited demand-to-capacity ratios larger than 0.7. Eight columns (501, 606, 705, 707, 804, 806, 807, and 908) exhibited ratios larger than 1.0. Although there is some significant uncertainty associated with calculation of both the load on these columns and the buckling capacity, this indicates that at this time step, the core had either initiated or was close to initiating buckling-induced failure.

Figures 4–72 to 4–77 show the maximum strains in each column between Floor 93 and Floor 99 before and after aircraft impact, at 10 min (at the end of Step 3), 40 min (at the end of Step 9), 80 min (at the end of Step 18), and 100 min. These figures include elastic and inelastic strain, but no creep effects. Figures 4–78 to 4–81 show the same data, but include the additional effects of creep. Before the aircraft impact, all of the columns were loaded within their elastic range. After the aircraft impact, columns close to removed columns (which included both severed and highly damaged columns) developed plastic strain. Plastic strain of the core columns increased significantly for the first 40 min, and then remained almost constant until 100 min. At 100 min, the maximum elastic-plus-plastic strain was 0.98 percent at Column 603. From 80 min to 100 min, plastic strain increased in almost all the bowed columns on the south face. However, creep strain was found to be far greater than plastic strain as can be seen in Figs. 4–78 to 4–81, especially in the core. At 40 min, 22 of 38 core columns that were not severed or highly damaged by aircraft impact had creep strains larger than 1.0 percent. After 40 min, the creep strains of core columns on the south side of the core slowly increased. The maximum elastic-plus-plastic-plus-creep strain at 100 min was 7.3 percent in Column 1006. As temperature increased on the south wall in the later times, creep strain in columns on the south wall also increased. By 100 min, creep strain increased in about 20 columns on the south face; the maximum elastic-plus-plastic-plus-creep strain in the columns on the south face reached 2.9 percent.

At 100 min, the core was weakened on the south side and had shortened by 1.6 in., and the south wall had bowed inward to approximately 43 in. from pull-in forces at Floors 95 to 99 and was unloading to the core and the adjacent east and west walls.

Based on the observations and the calculated results of the analysis, reported above, the following sequence of events likely occurred as the south wall reached instability and buckled:

- As columns buckled, they shed load through Vierendeel action to adjacent columns in the south wall, in turn buckling these columns.
- The inward bowing of the south wall increased as additional columns buckled.
- As a result of this behavior, instability progressed horizontally across the wall.
- When instability engulfed the entire south wall, the wall continued to shed load to the east and west walls and to the core.

The onset of this load redistribution can be found in Table 4–24. The section of the building above the impact zone began tilting to the south as column instability progressed rapidly from the south wall along the adjacent east and west walls, resulting in increase of the gravity load on the core columns and in turn contributing to the buckling failure of these columns and initiating global collapse of the structure.

Since the global model did not include elements capable of capturing failure of column or hat truss element splices, nor buckling of hat truss outriggers, the conditions of the connections and the members in the primary load path to and through the hat truss were evaluated at different time intervals. This evaluation included the core column splices for tension, outriggers and supporting columns for compression, and the hat truss connections that were in the primary load path for tension.

Before the aircraft impact, core column splices were under compression. After the impact and with increasing plastic and creep strains, the core displaced downward, and some core columns became suspended from the hat truss. In fact, as shown in Table 4–26 and Fig. 4–82, Columns 503, 504, 505, 602, 603, 604, 605, 702, and 802 were calculated to be in tension at Floor 105 at 100 min. To evaluate the condition of the core column splices at Floor 106, the tension capacities of these splices were calculated using the AISC LRFD procedures and compared to the calculated tensile forces at each time interval. Table 4–25 shows the calculated tension capacities of core column splices at Floor 106, and Fig. 4–83 shows tensile demand-to-capacity ratios for the core column splices at Floor 106 at 100 min. It was found that tension forces in core columns were less than the capacities of the splices.

Sixteen outrigger members (four on each face) were present and participated in transfer of gravity loads between the core columns and the exterior walls, as shown in Fig. 4–3. In the global model, each of these outriggers was represented by one BEAM24 element; therefore, buckling of the member could not be captured, although material nonlinearity was included. Table 4–27 presents axial load demand-to-capacity ratios of the outrigger members. Capacities of outriggers were calculated using AISC LRFD Eq. E2-1 with an effective length factor K=0.75 and a resistance factor of unity. To check against calculated capacities, axial loads obtained from the global model were adjusted for the additional axial load caused by ignoring construction sequence. Analyses predicted that Outrigger E reached its axial load capacity (see Fig. 4–3 for designations of outrigger members). Because the material properties of the outriggers in the global model were set so that they would yield when the axial load in the outrigger reached its compressive capacity, the axial load in Outrigger E did not change after reaching its capacity as unloading in the post-buckling regime was not modeled. This may have resulted in an underestimate of the force redistribution to the other outriggers.

Table 4–28 shows the computed demand-to-capacity ratios for axial loads of exterior columns supporting the outriggers. Each of these exterior columns was also modeled by only one element (BEAM188) in the global model; therefore, buckling of the columns were not captured in the analysis. Compressive capacities of these columns were also calculated using AISC LRFD Eq. E2-1 with an effective length factor K=0.75 and a resistance factor of unity. This analysis showed that the axial loads in these columns were well below their inelastic buckling capacities.

For effective load transfer from the core columns to the outriggers to occur, the capacities of the hat truss connections in the intermediate load path could not be exceeded. To investigate this issue, the hat truss connections that were in this load path were identified, and their capacities were compared to the calculated forces transferred through them. The load path was identified by selecting the hat truss members that were predicted to have an absolute axial stress of 25 ksi or more. The hat truss stresses were evaluated at 80 min (at the end of Step 17) as at this time they had reached their predicted maxima. Only the connections that were transferring tensile forces were evaluated. Figure 4–84 shows the members determined to be in the primary load path. Figure 4–85 shows the location of the critical hat truss connections that were evaluated. The capacities of the connections were calculated using the AISC LRFD procedures. Table 4–29 summarizes capacities, demands, and the conditions of the connections

identified in Fig. 4–85. As can be seen in Table 4–29, none of the connections exceeded their capacities. The state of the outriggers and core column splices at Floor 105 were discussed in the earlier paragraphs.

Based on these evaluations, it can be stated that even though one outrigger reached its capacity, the hat truss was capable of redistributing loads between the core and the exterior walls, and therefore, the evaluations described above are valid.

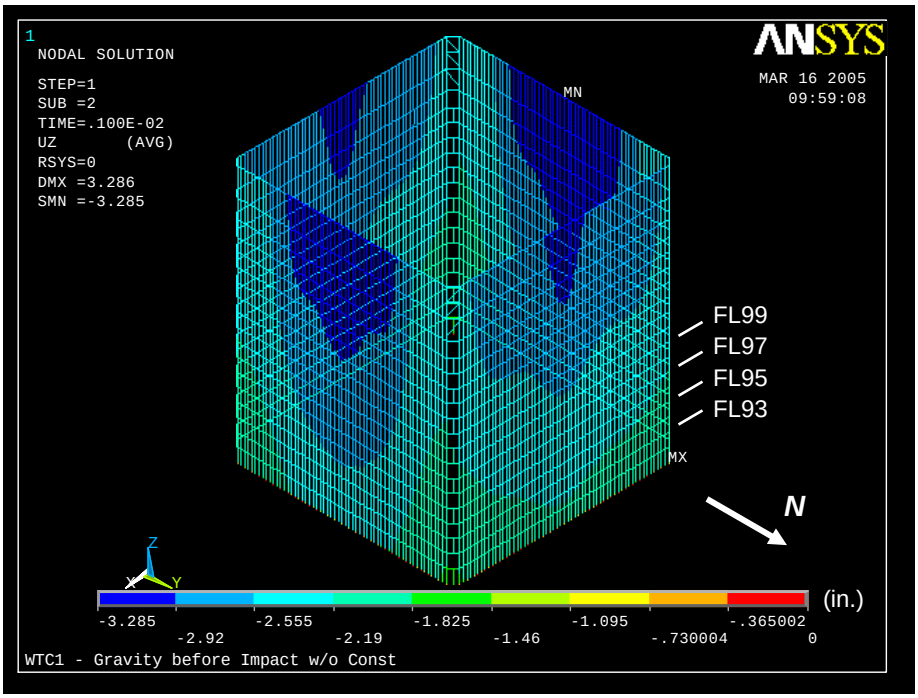

(a) North and east sides

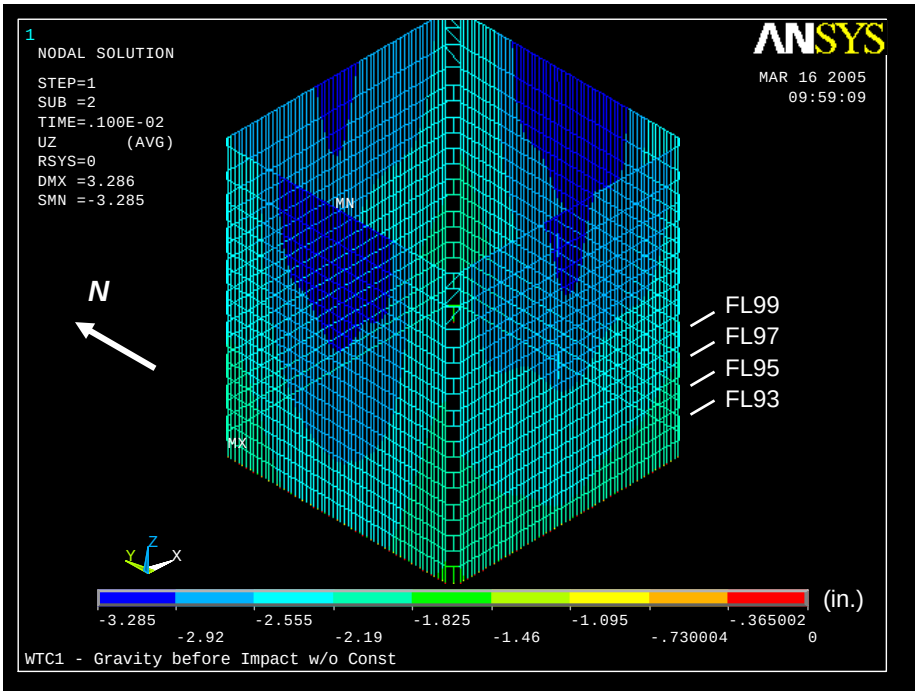

(b) South and west sides

Figure 4–8. Vertical displacement of exterior wall of WTC 1 before aircraft impact (downward displacement is negative).

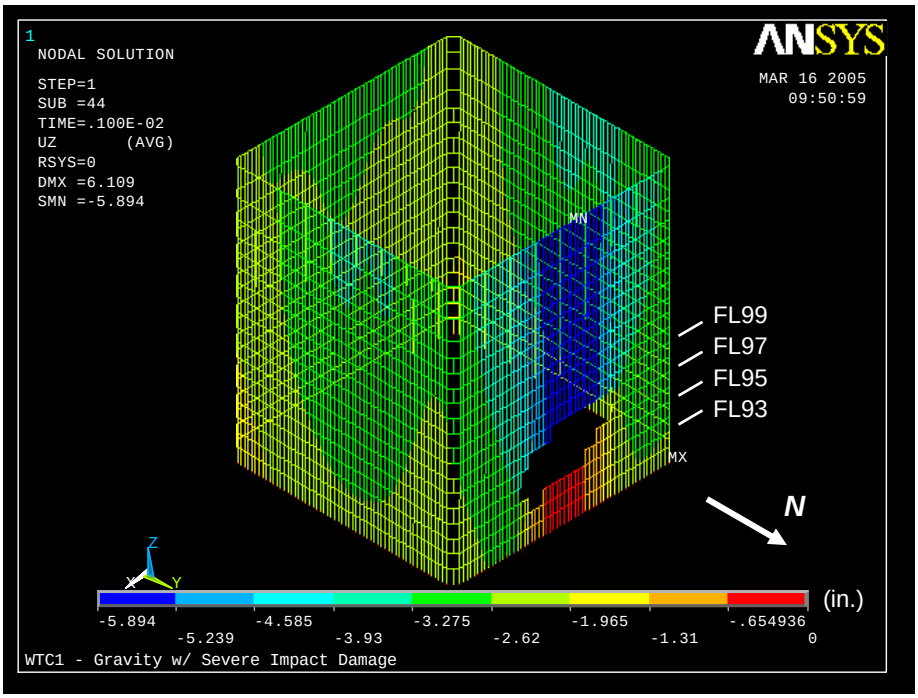

(a) North and east sides

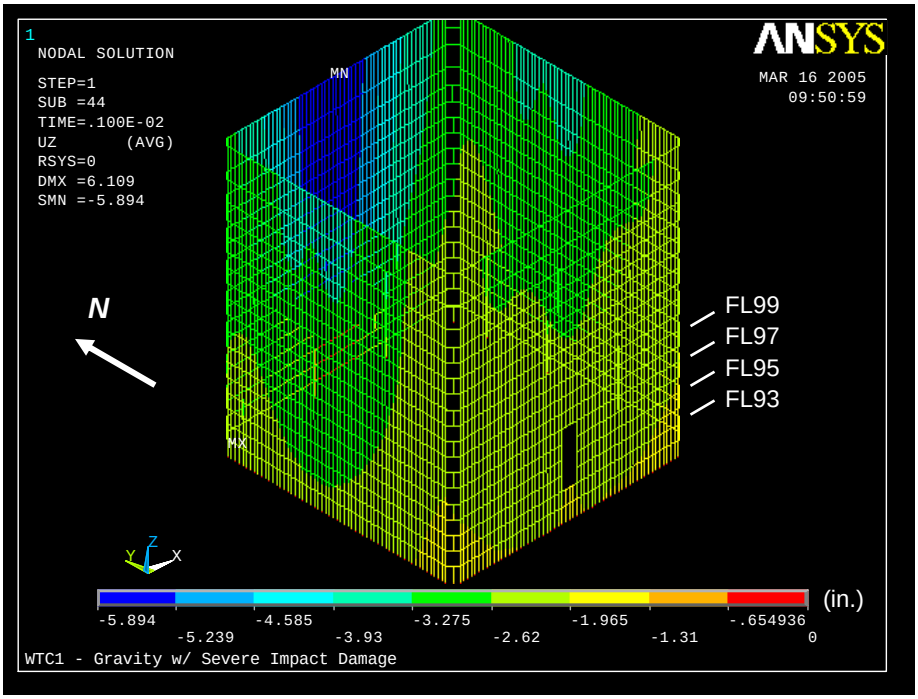

(b) South and west sides

Figure 4–9. Vertical displacement of exterior wall of WTC 1 after aircraft impact for Case B conditions (downward displacement is negative).

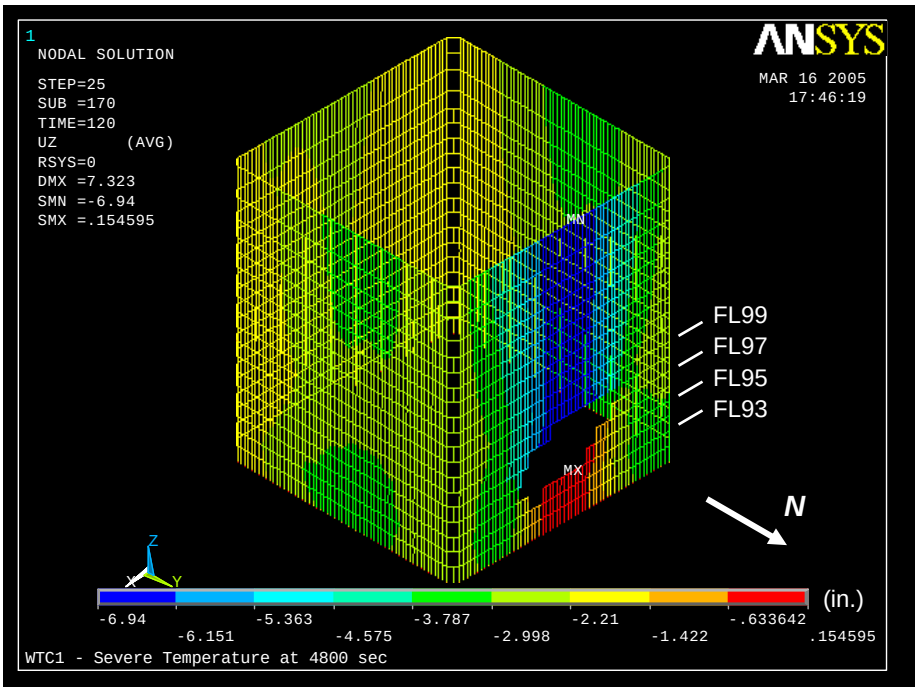

(a) North and east sides

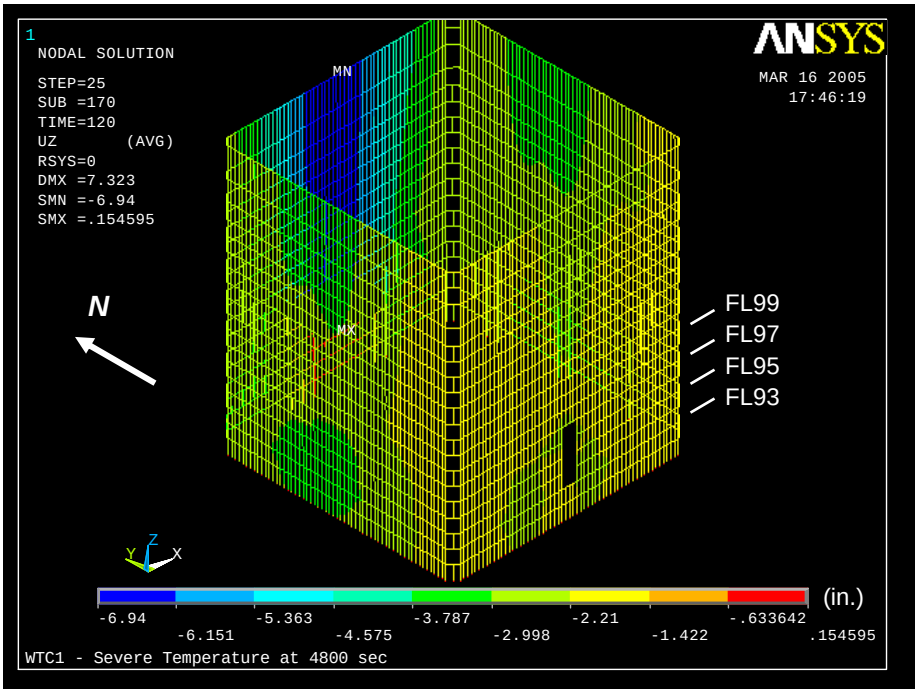

(b) South and west sides

Figure 4–10. Vertical displacement of exterior wall of WTC 1 at 80 min for Case B conditions (downward displacement is negative).

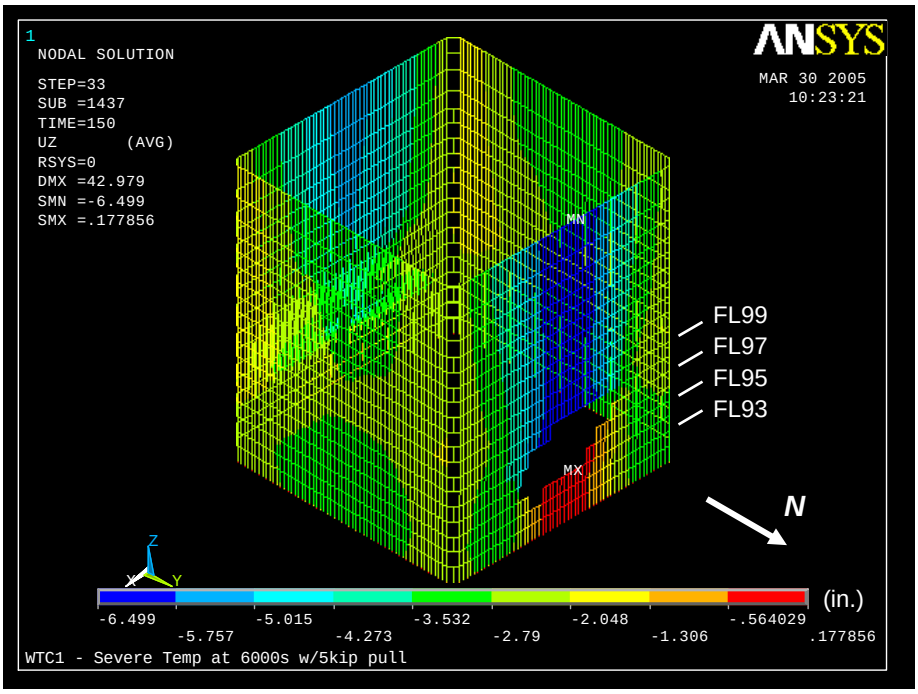

(a) North and east sides

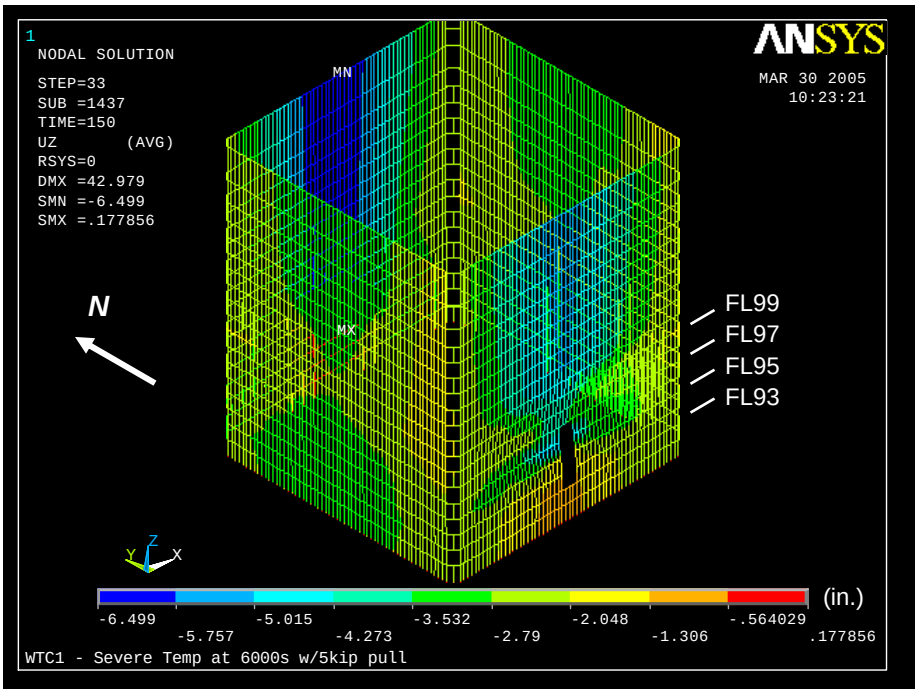

(b) South and west sides

Figure 4–11. Vertical displacement of exterior wall of WTC 1 at 100 min for Case B conditions (downward displacement is negative).

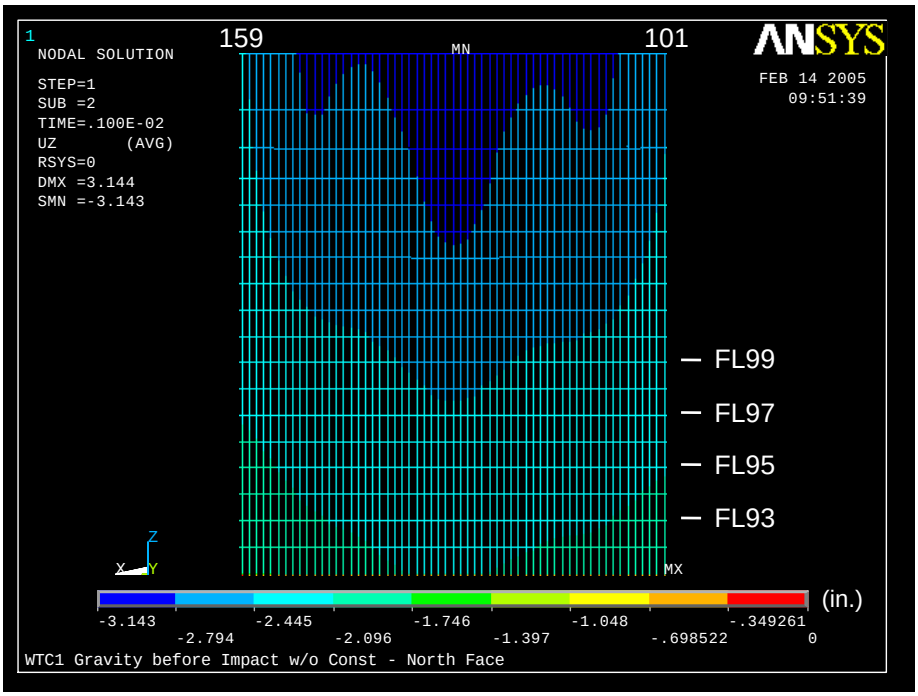

Figure 4–12. Vertical displacement of north wall of WTC 1 before aircraft impact.

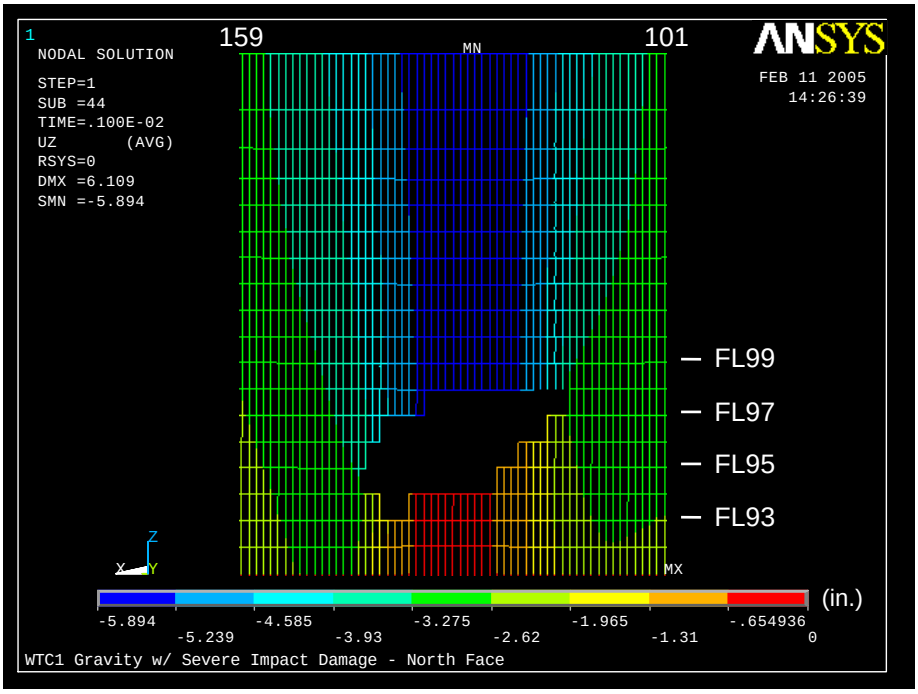

Figure 4–13. Vertical displacement of north wall of WTC 1 after aircraft impact for Case B conditions (downward displacement is negative).

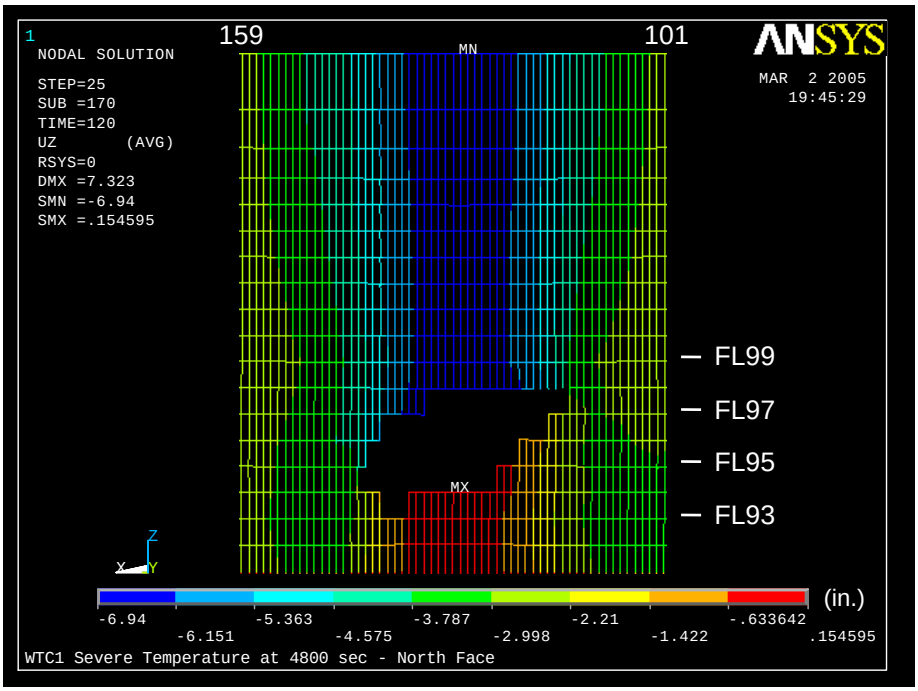

Figure 4–14. Vertical displacement of north wall of WTC 1 at 80 min for Case B conditions (downward displacement is negative).

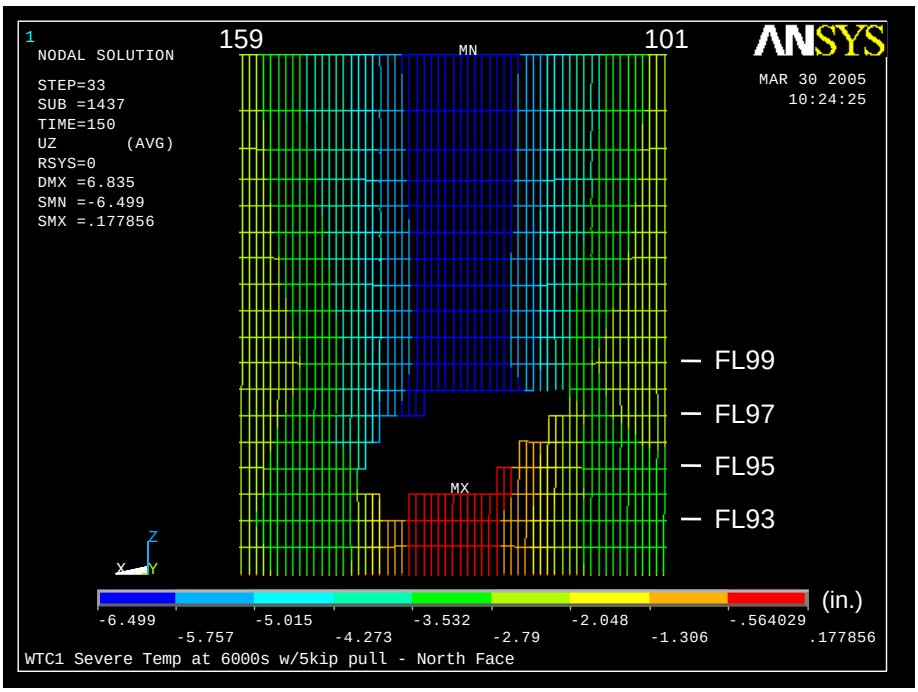

Figure 4–15. Vertical displacement of north wall of WTC 1 at 100 min for Case B conditions with 5 kip pull-in forces (downward displacement is negative).

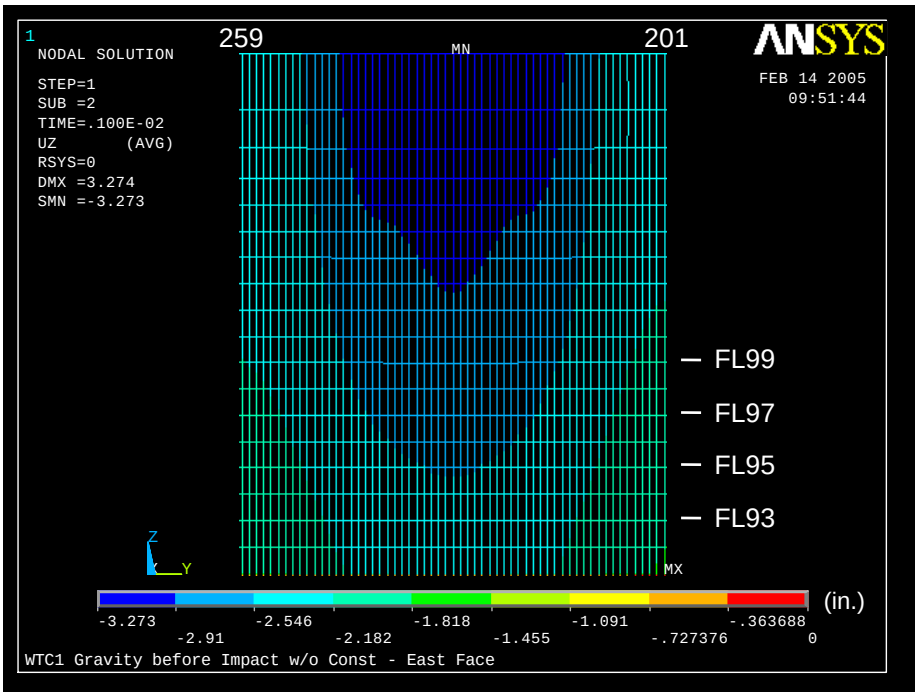

Figure 4–16. Vertical displacement of east wall of WTC 1 before aircraft impact (downward displacement is negative).

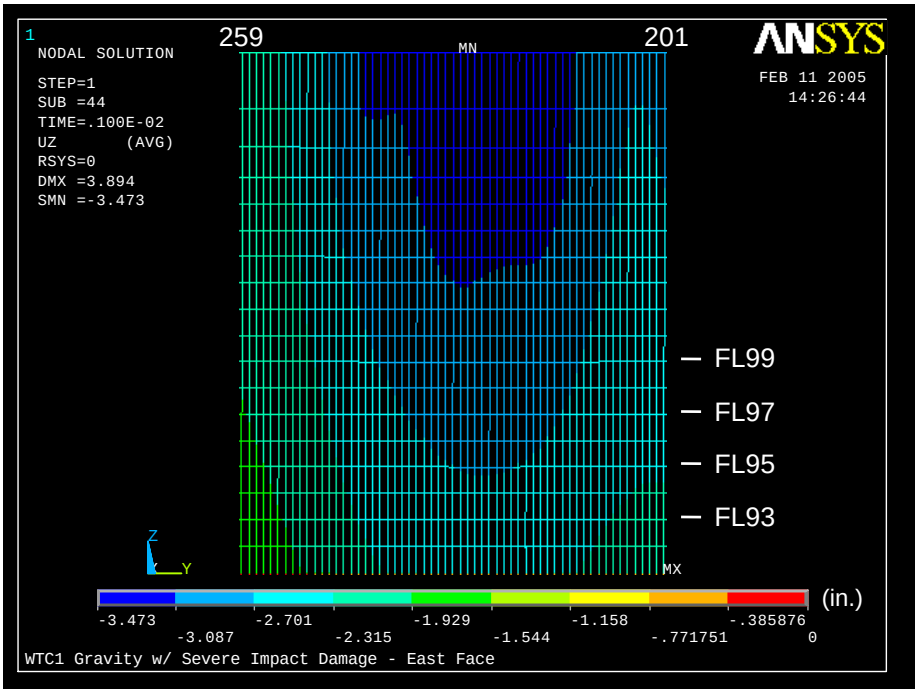

Figure 4–17. Vertical displacement of east wall of WTC 1 after aircraft impact for Case B conditions (downward displacement is negative).

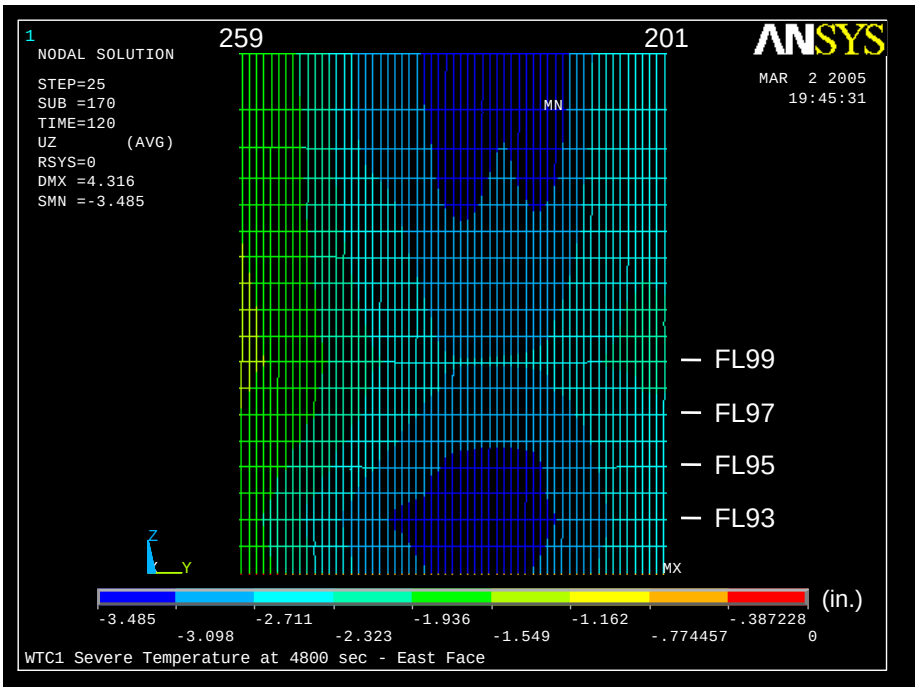

Figure 4–18. Vertical displacement of east wall of WTC 1 at 80 min for Case B conditions (downward displacement is negative).

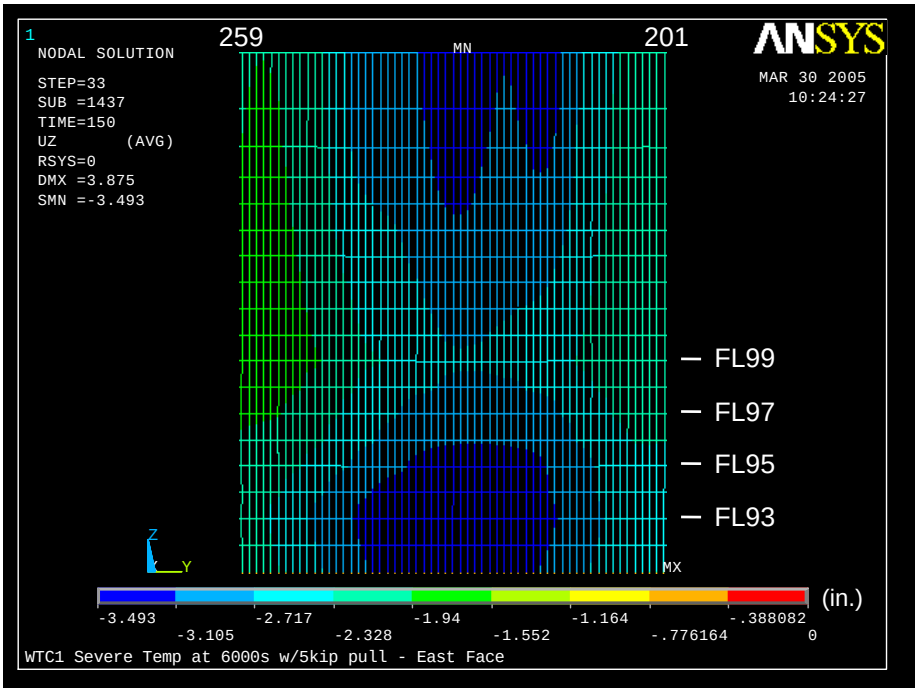

Figure 4–19. Vertical displacement of east wall of WTC 1 at 100 min for Case B conditions with 5 kip pull-in forces (downward displacement is negative).

Figure 4–20. Vertical displacement of south wall of WTC 1 before aircraft impact (downward displacement is negative).

Figure 4–21. Vertical displacement of south wall of WTC 1 after aircraft impact for Case B conditions (downward displacement is negative).

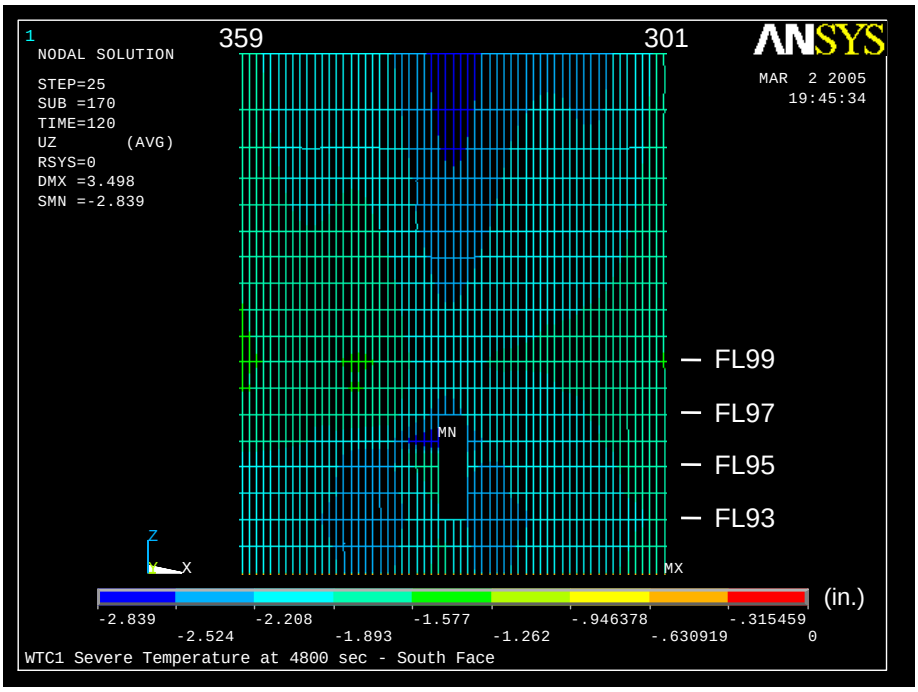

Figure 4–22. Vertical displacement of south wall of WTC 1 at 80 min for Case B conditions (downward displacement is negative).

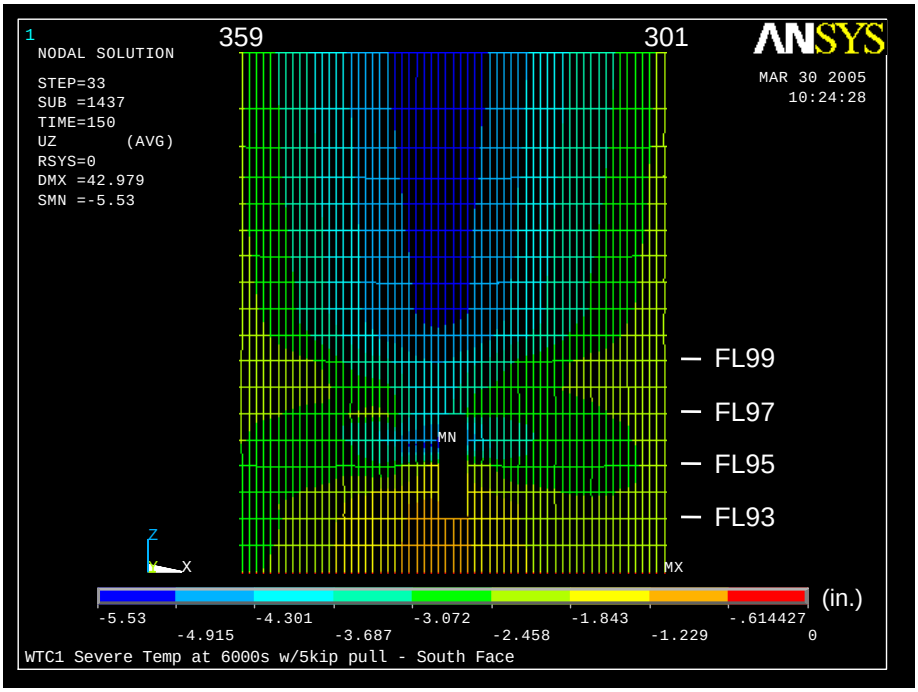

Figure 4–23. Vertical displacement of south wall of WTC 1 at 100 min for Case B conditions with 5 kip pull-in forces (downward displacement is negative).

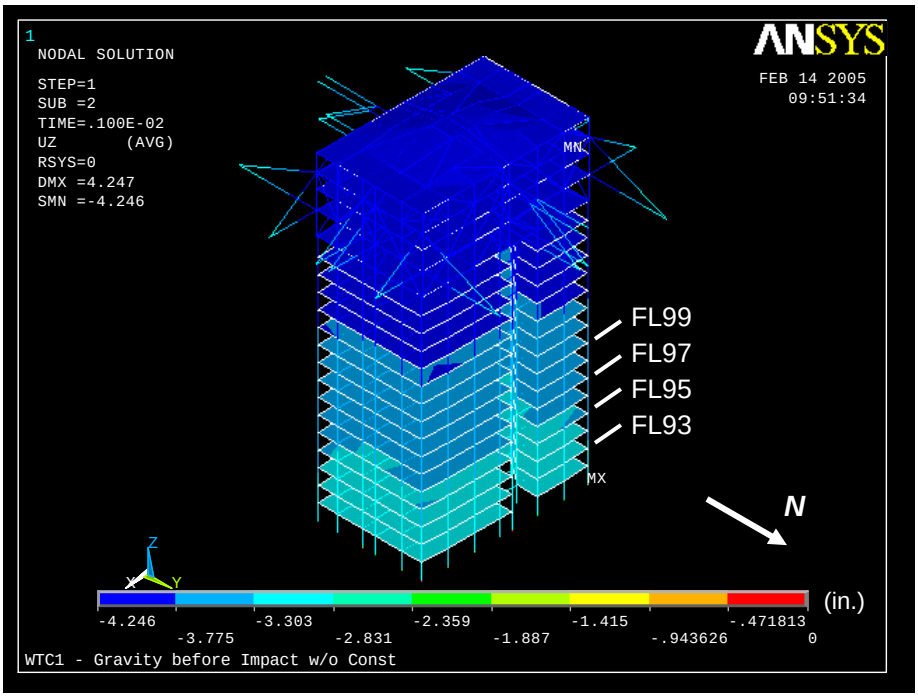

(a) North and east sides

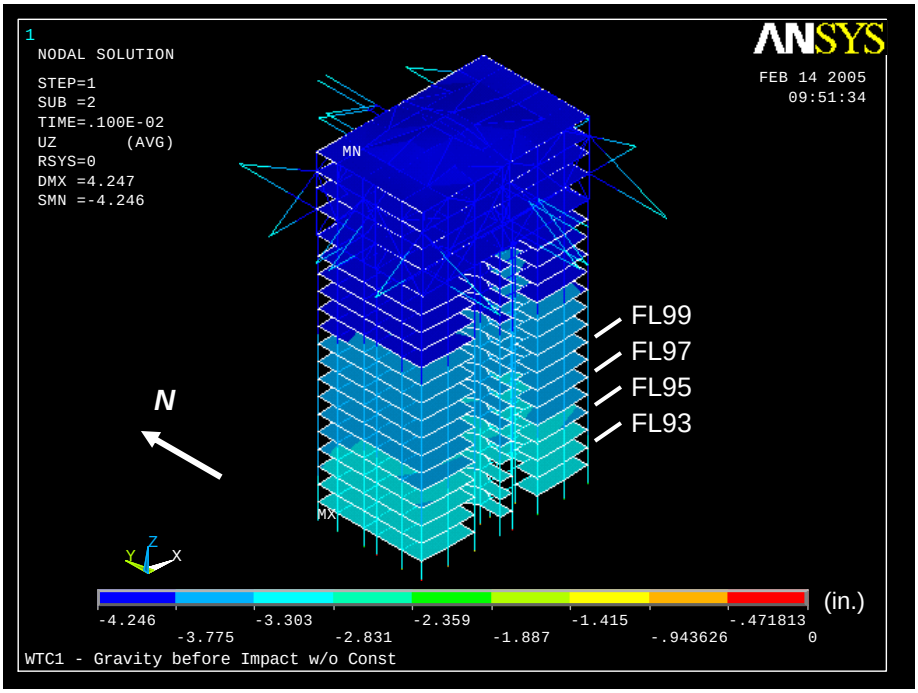

(b) South and west sides

Figure 4–24. Vertical displacement of core of WTC 1 before aircraft impact (downward displacement is negative).

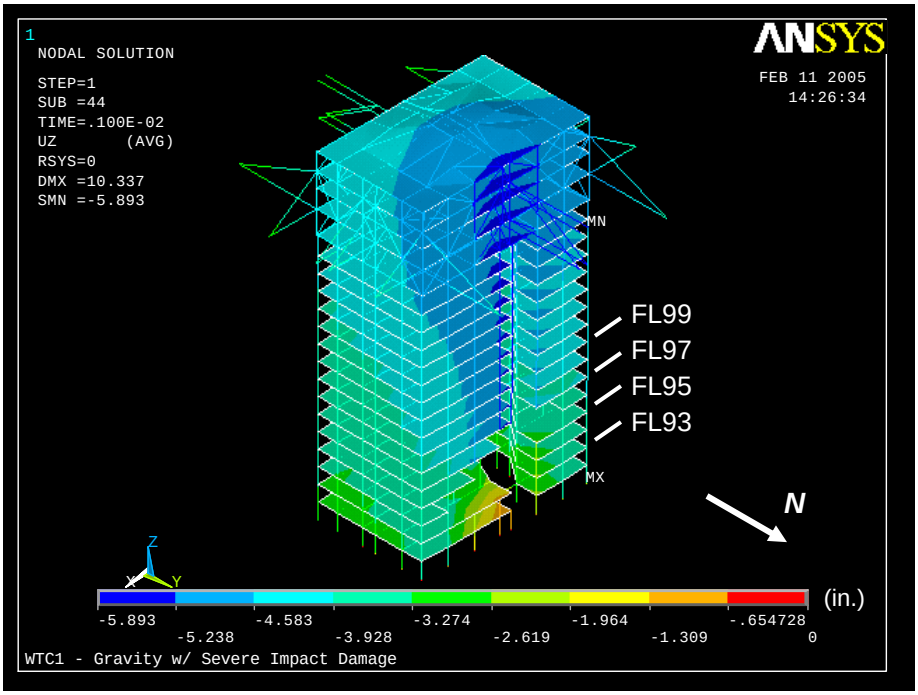

(a) North and east sides

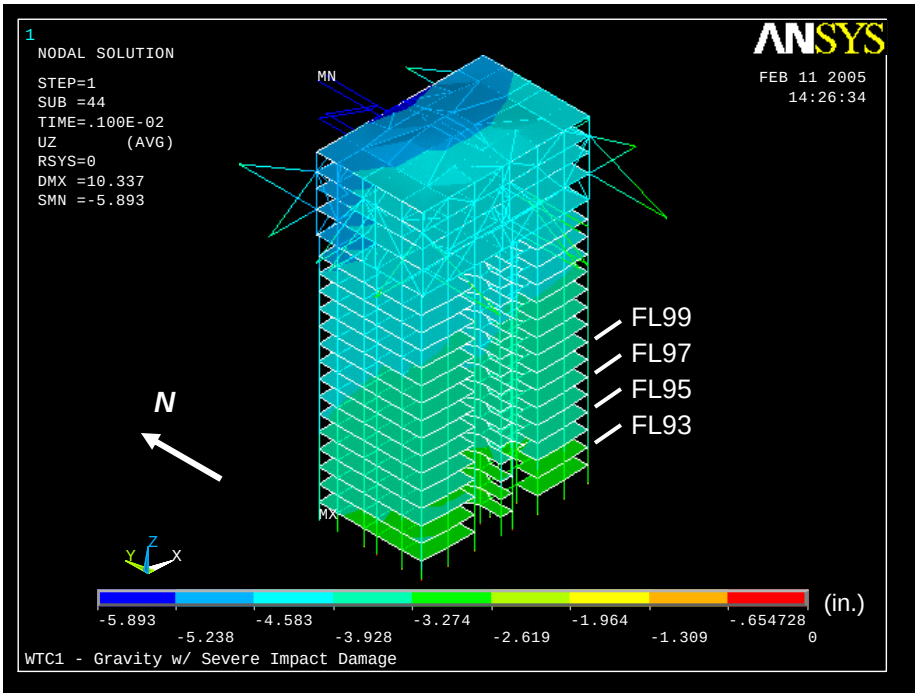

(b) South and west sides

Figure 4–25. Vertical displacement of core of WTC 1 after aircraft impact for Case B conditions (downward displacement is negative).

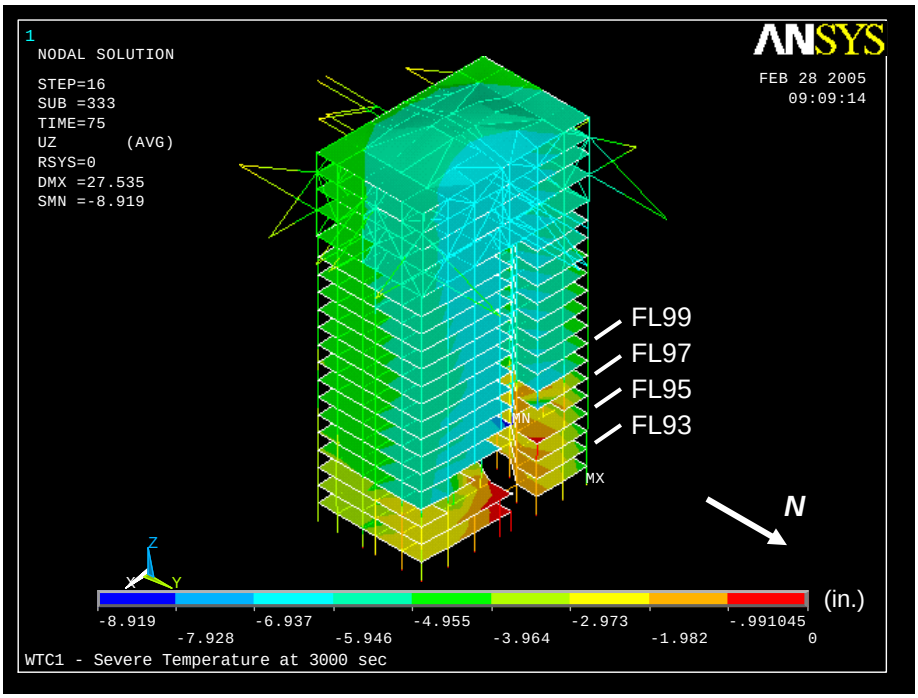

(a) North and east sides

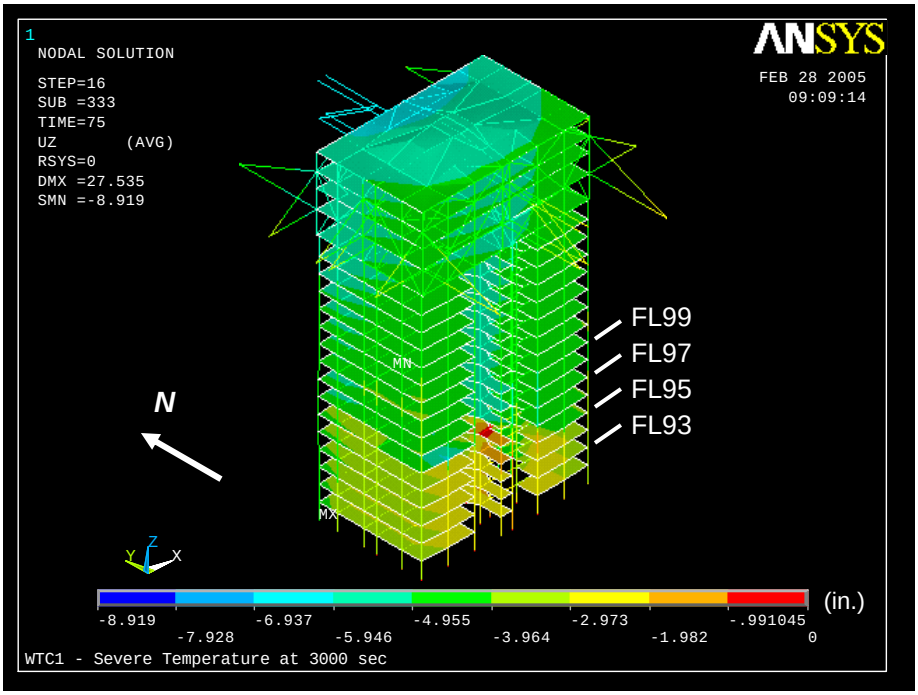

(b) South and west sides

Figure 4–26. Vertical displacement of core of WTC 1 at 50 min for Case B conditions (downward displacement is negative).

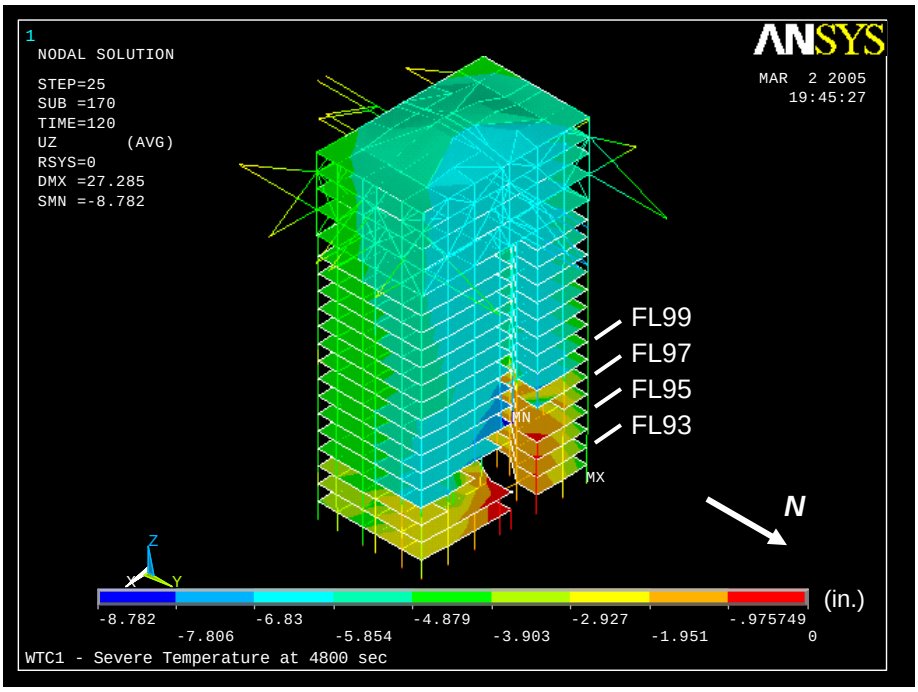

(a) North and east sides

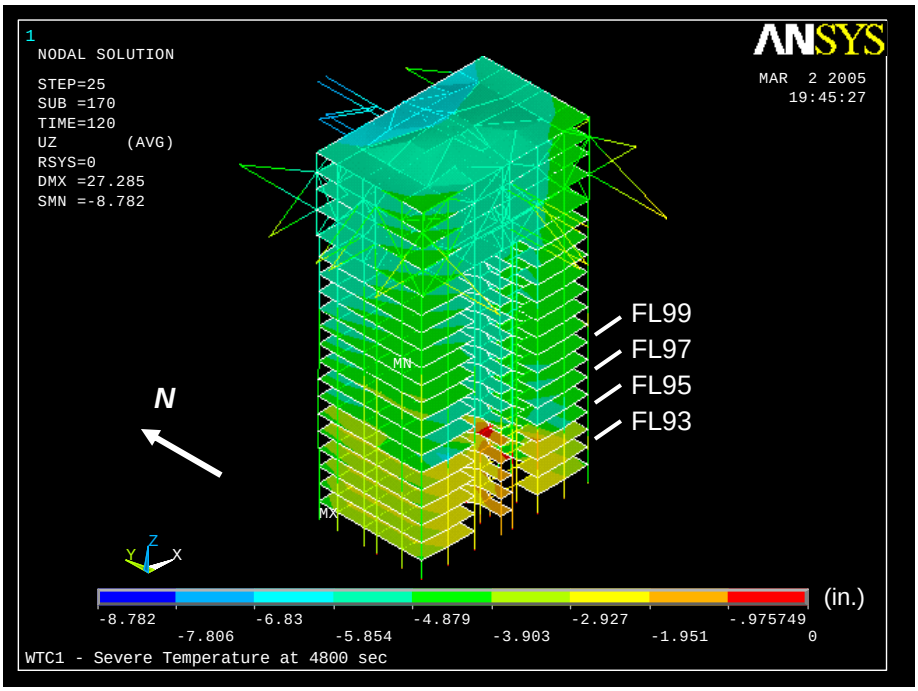

(b) South and west sides

Figure 4–27. Vertical displacement of core of WTC 1 at 80 min for Case B conditions (downward displacement is negative).

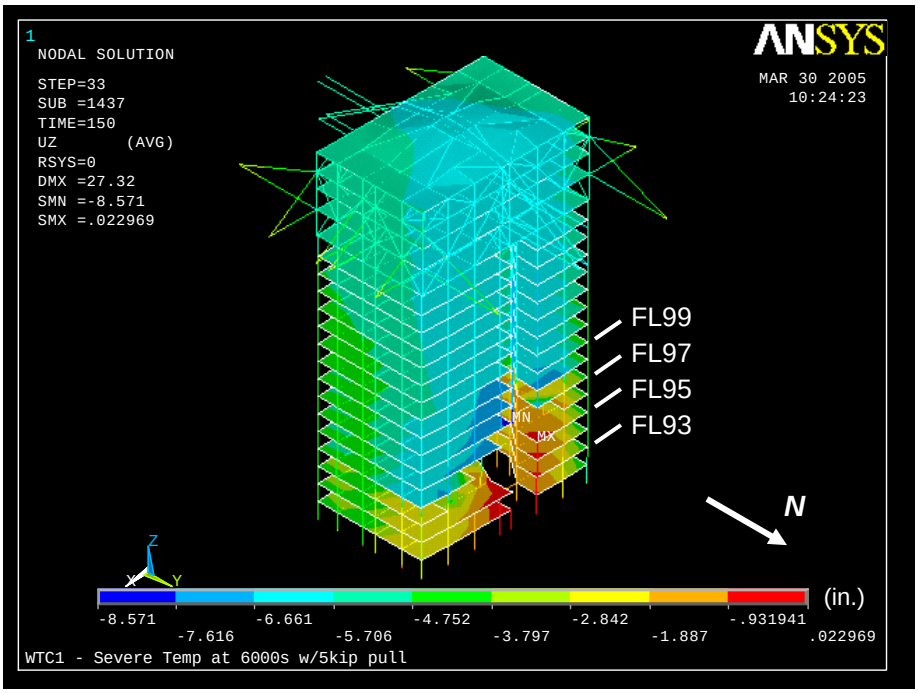

(a) North and east sides

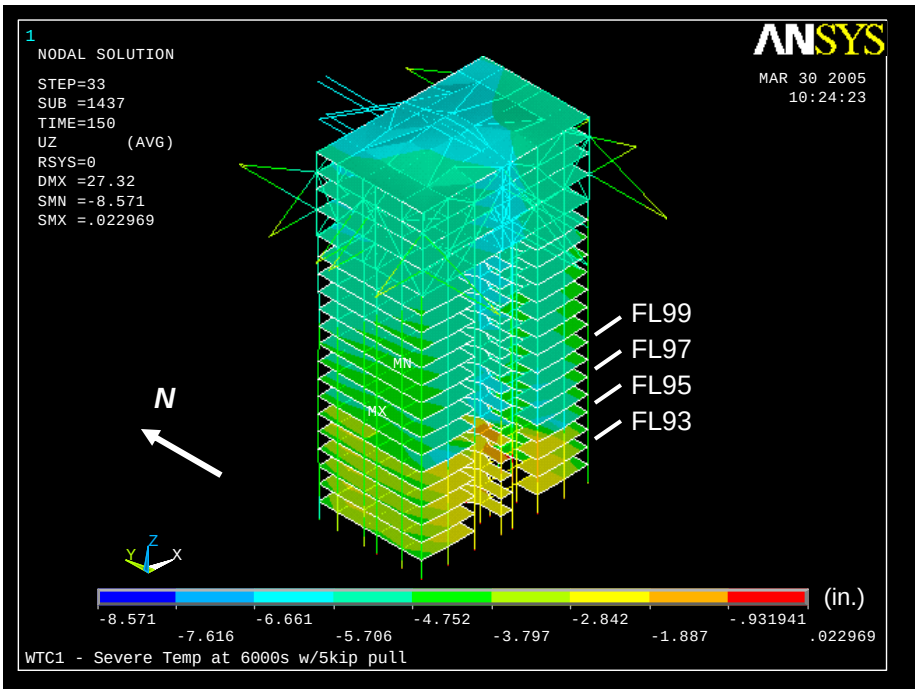

(b) South and west sides

Figure 4–28. Vertical displacement of core of WTC 1 at 100 min for Case B conditions with 5 kip pull-in forces (downward displacement is negative).

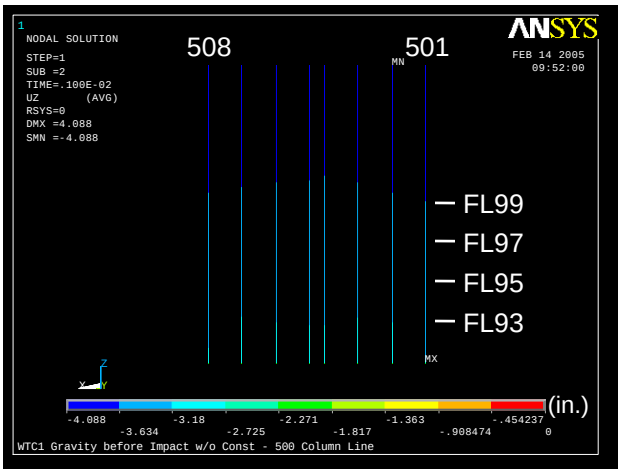

(a) 500 series columns

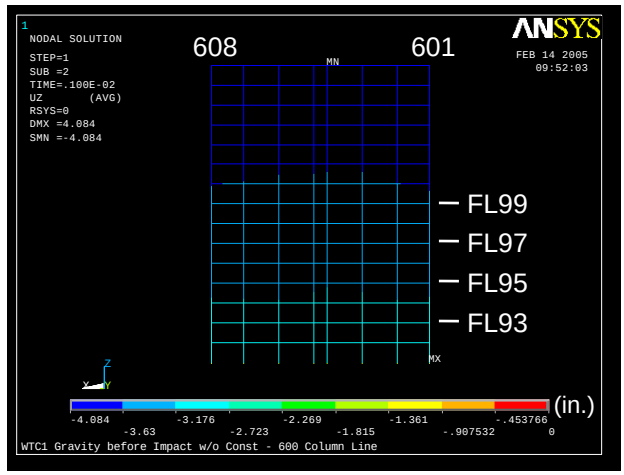

(b) 600 series columns

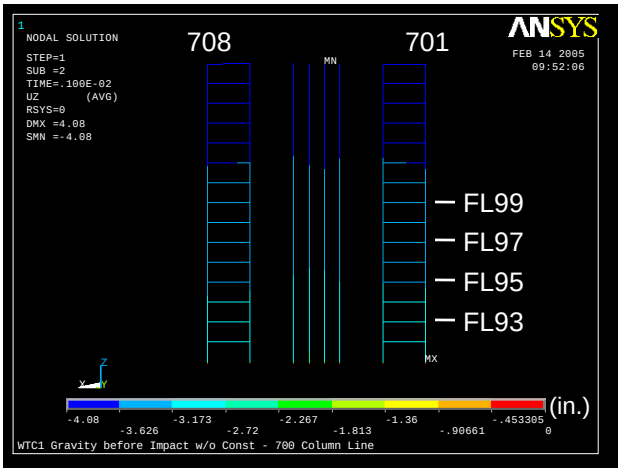

(c) 700 series columns

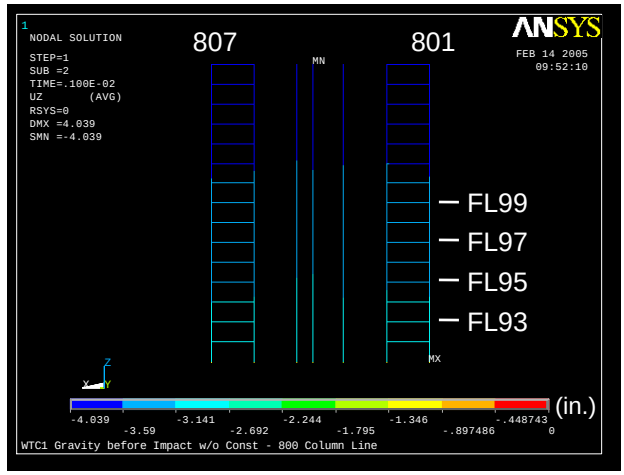

(d) 800 series columns

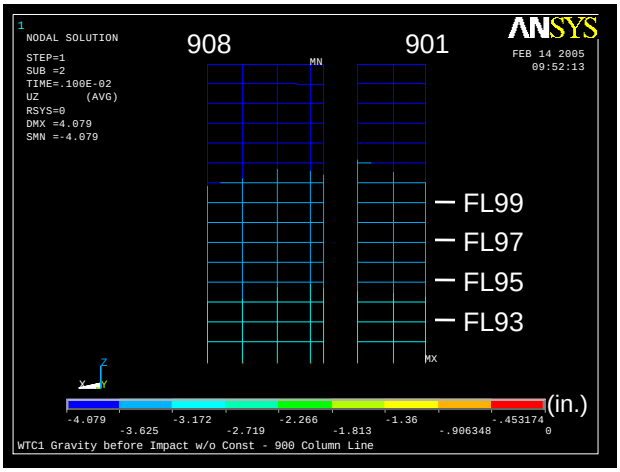

(e) 900 series columns

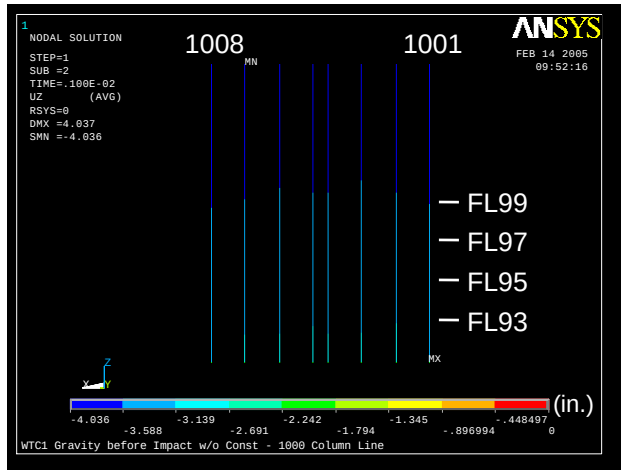

(f) 1000 series columns

Figure 4–29. Vertical displacement of core columns of WTC 1 before aircraft impact (downward displacement is negative).

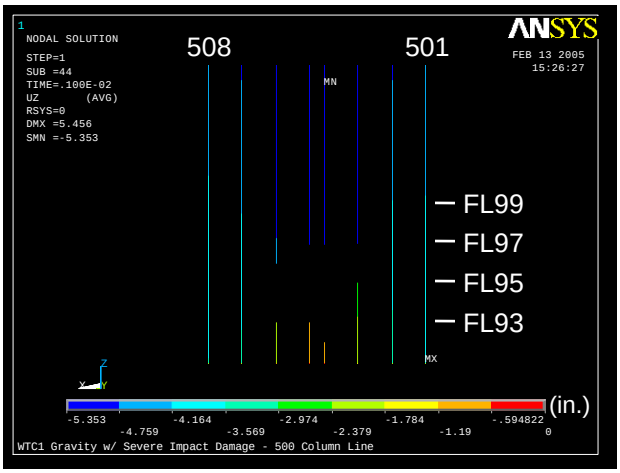

(a) 500 series columns

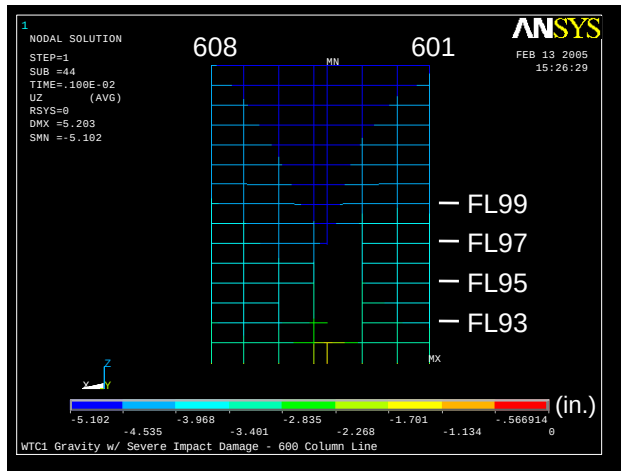

(b) 600 series columns

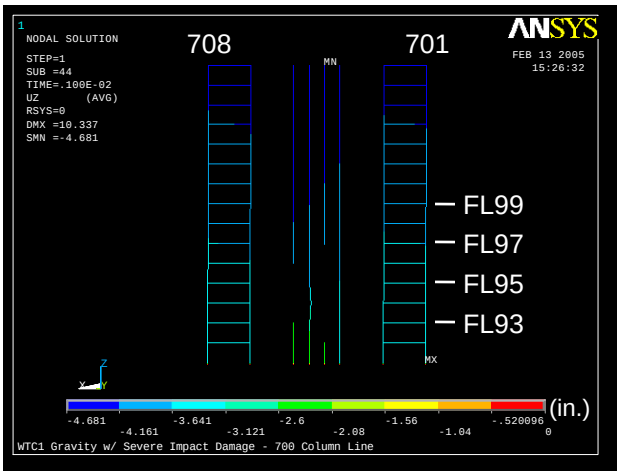

(c) 700 series columns

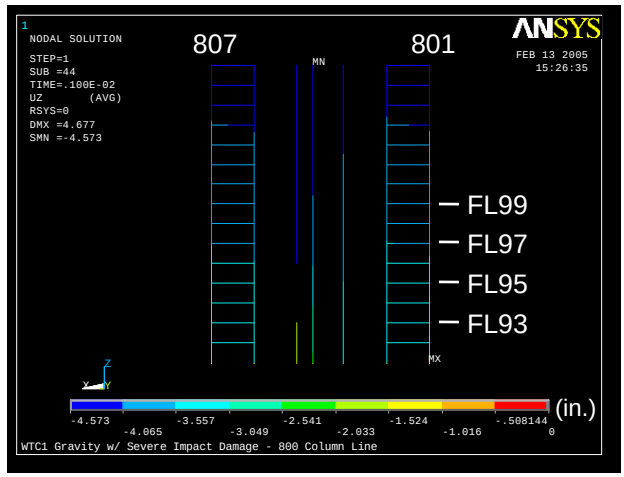

(d) 800 series columns

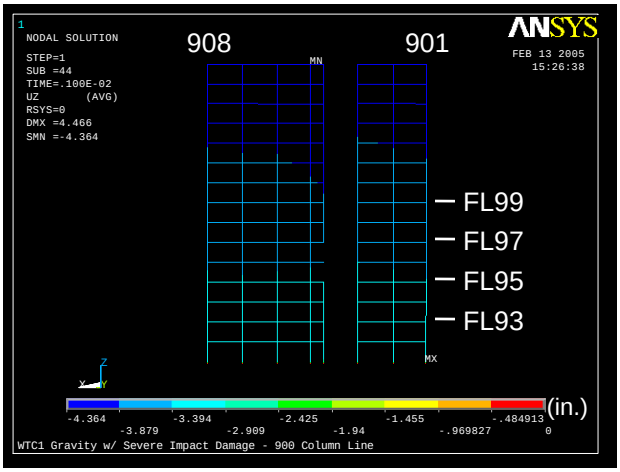

(e) 900 series columns

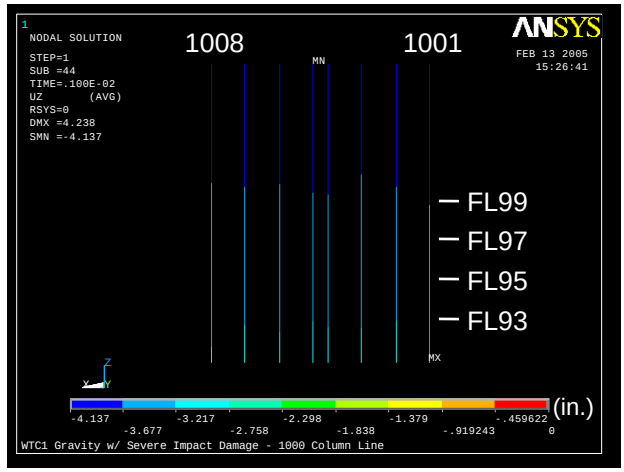

(f) 1000 series columns

Figure 4–30. Vertical displacement of core columns of WTC 1 after aircraft impact for Case B conditions (downward displacement is negative).

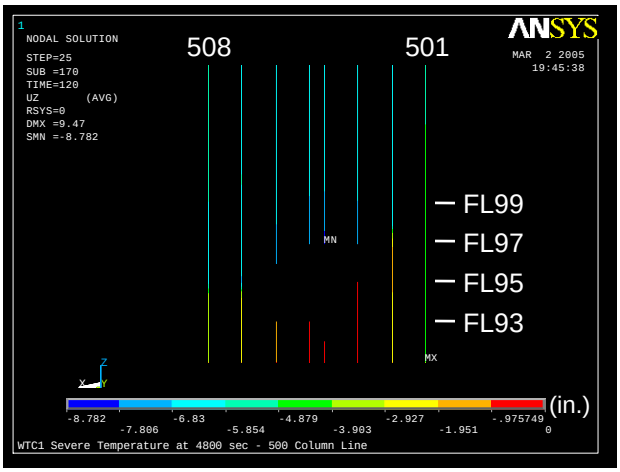

(a) 500 series columns

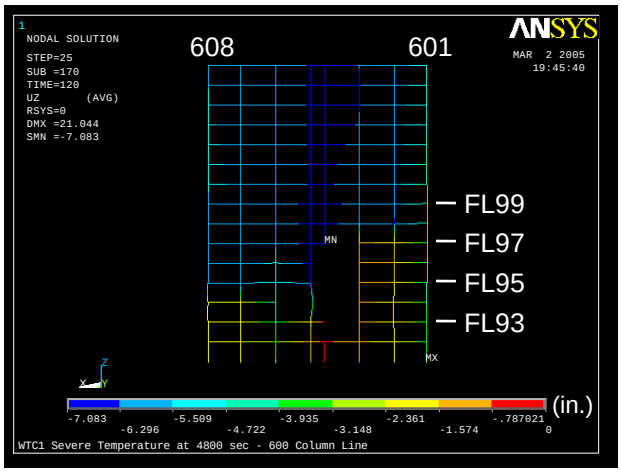

(b) 600 series columns

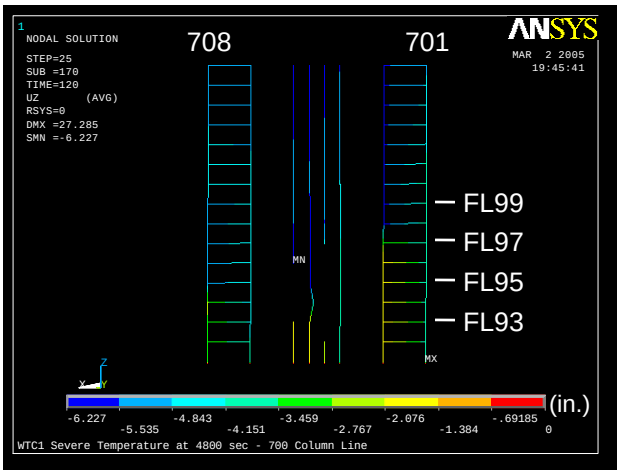

(c) 700 series columns

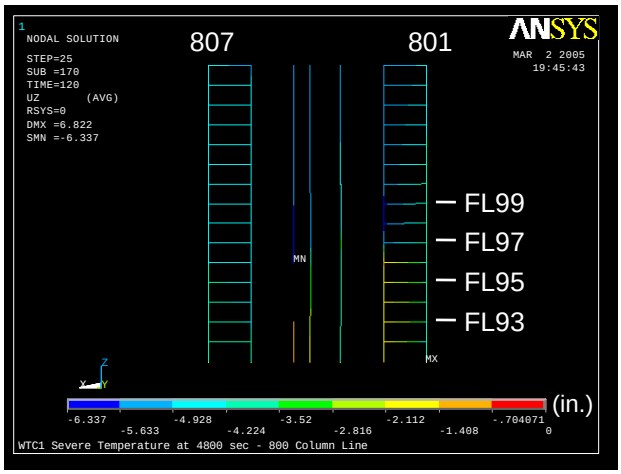

(d) 800 series columns

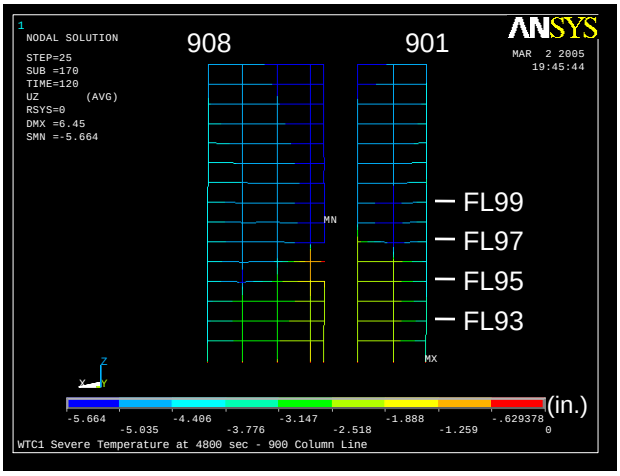

(e) 900 series columns

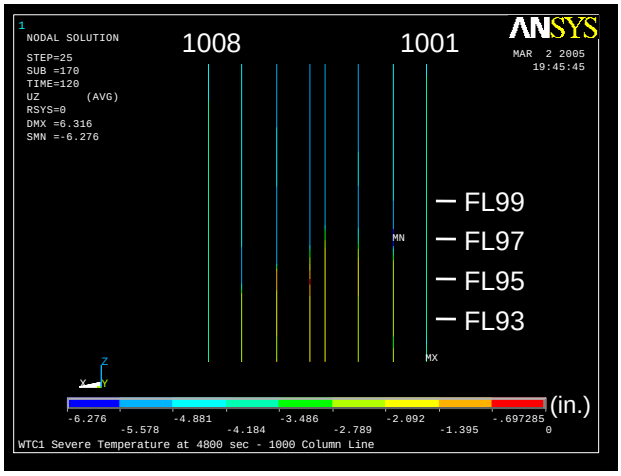

(f) 1000 series columns

Figure 4–31. Vertical displacement of core columns of WTC 1 at 80 min for Case B conditions (downward displacement is negative).

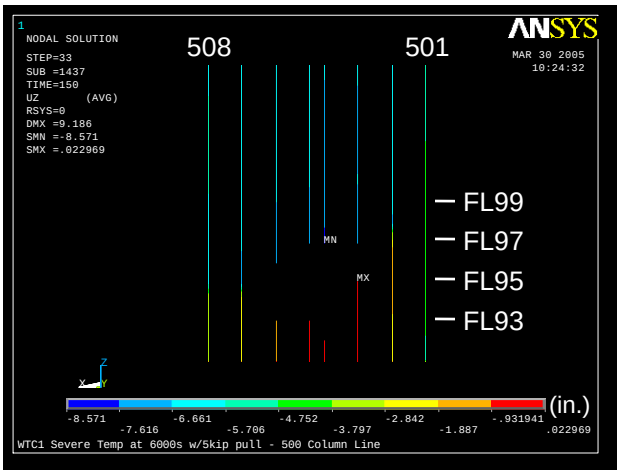

(a) 500 series columns

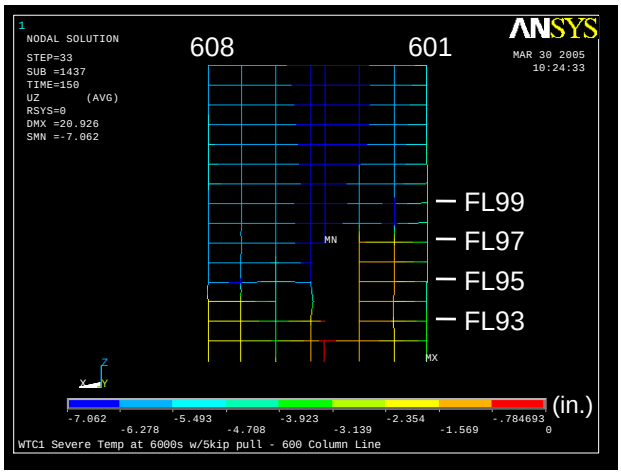

(b) 600 series columns

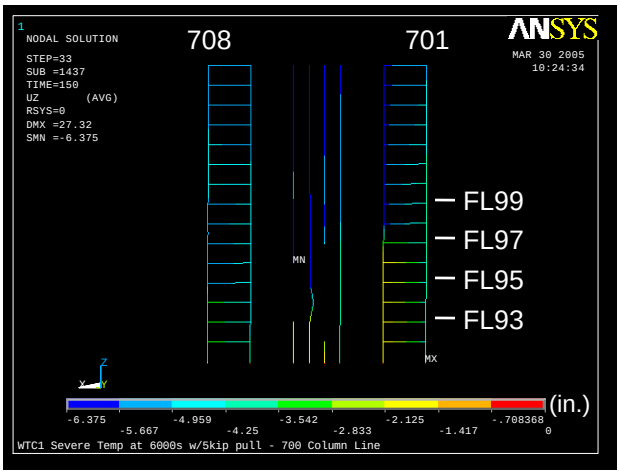

(c) 700 series columns

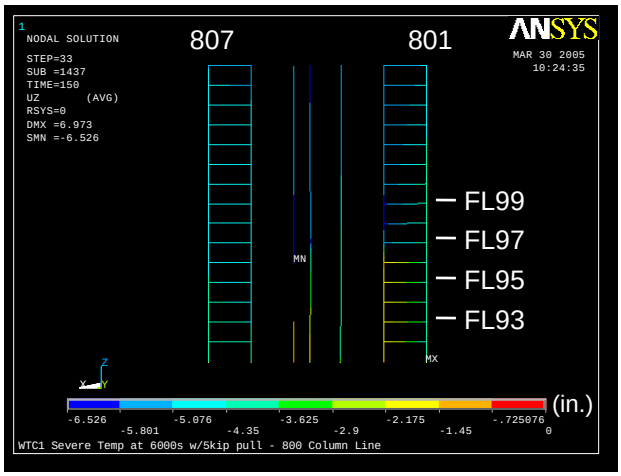

(d) 800 series columns

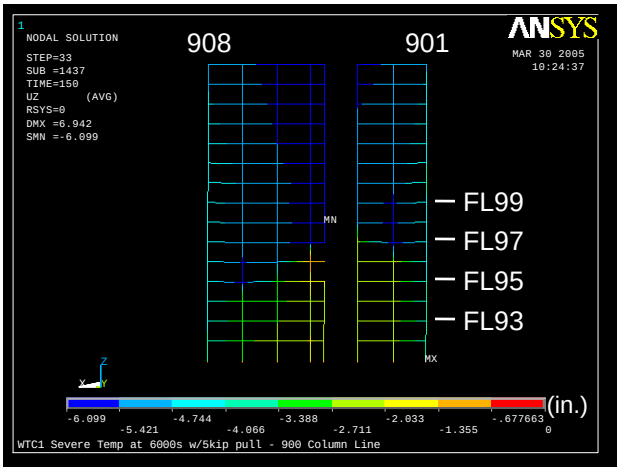

(e) 900 series columns

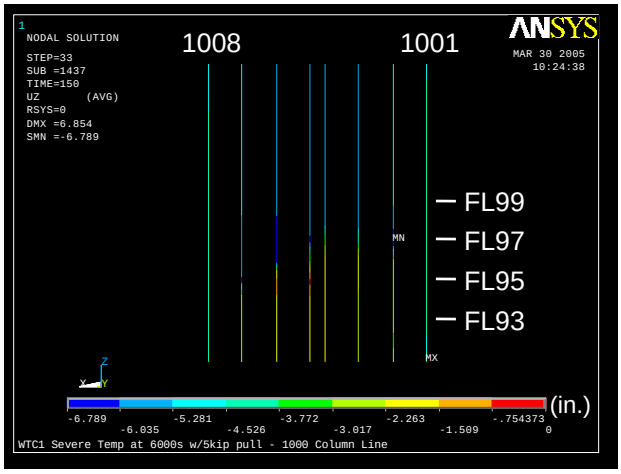

(f) 1000 series columns

Figure 4–32. Vertical displacement of core columns of WTC 1 at 100 min for Case B conditions with 5 kip pull-in forces (downward displacement is negative).

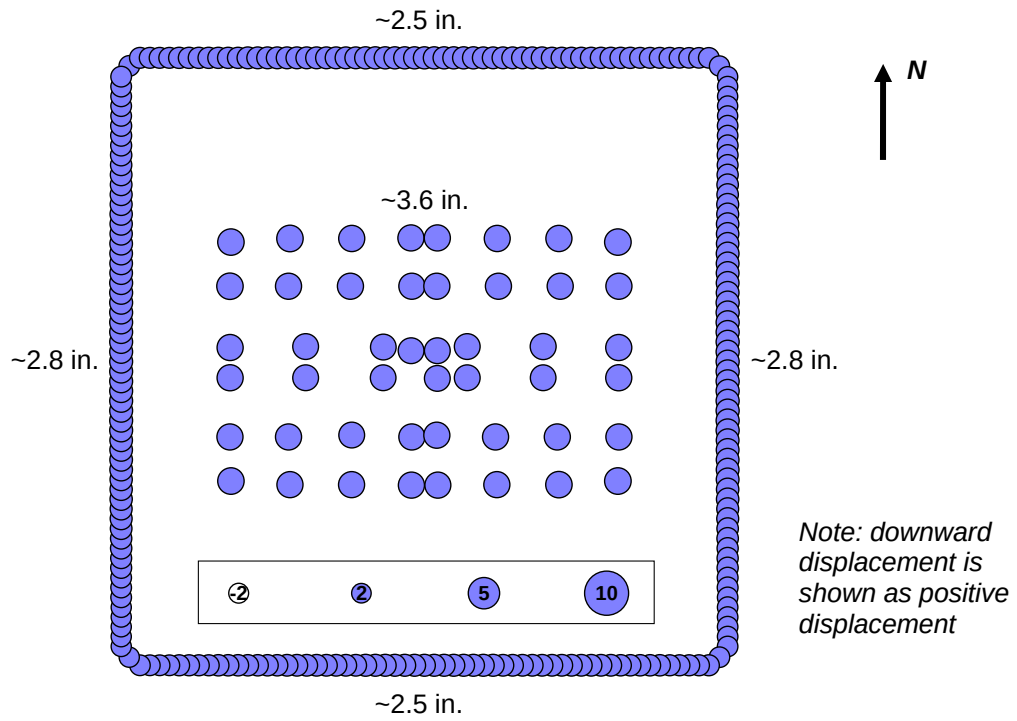

Figure 4–33. Vertical displacement at Floor 99 of WTC 1 before aircraft impact.

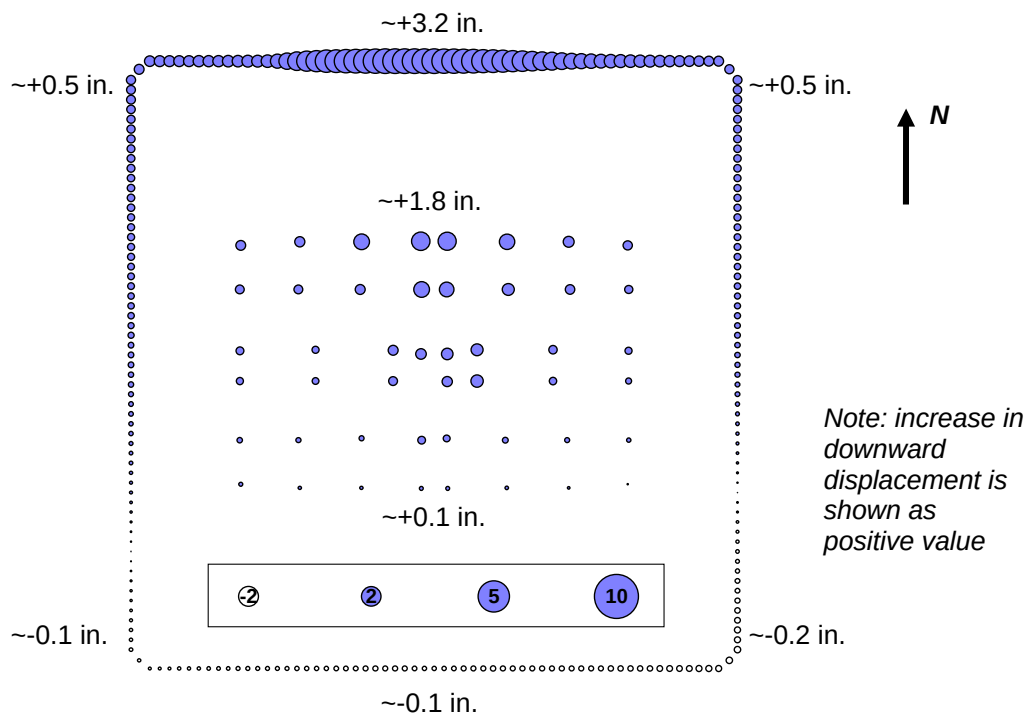

Figure 4–34. Change in vertical displacement at Floor 99 of WTC 1 from the time before impact to the time after impact for Case B conditions.

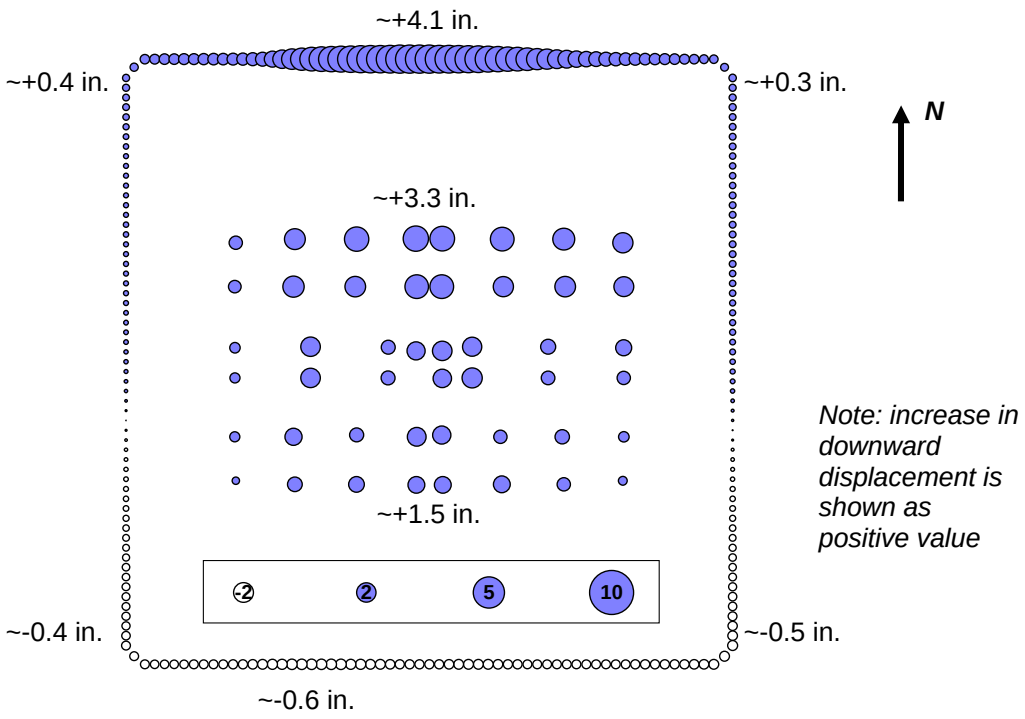

Figure 4–35. Change in vertical displacement at Floor 99 of WTC 1 from the time before impact to 50 min for Case B conditions.

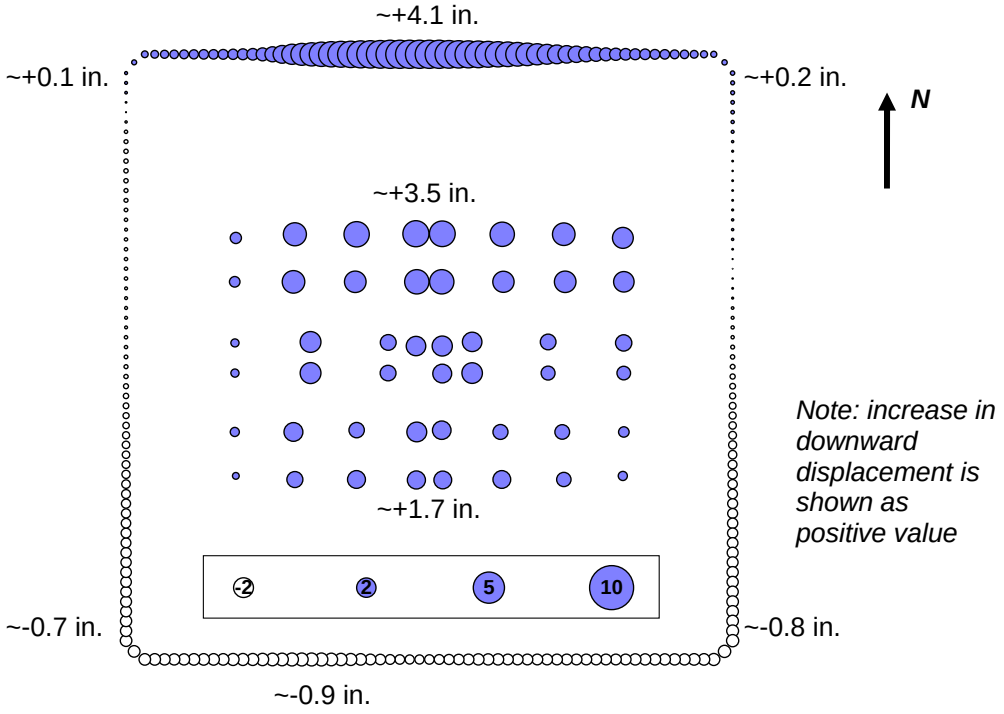

Figure 4–36. Change in vertical displacement at Floor 99 of WTC 1 from the time before impact to 80 min for Case B conditions.

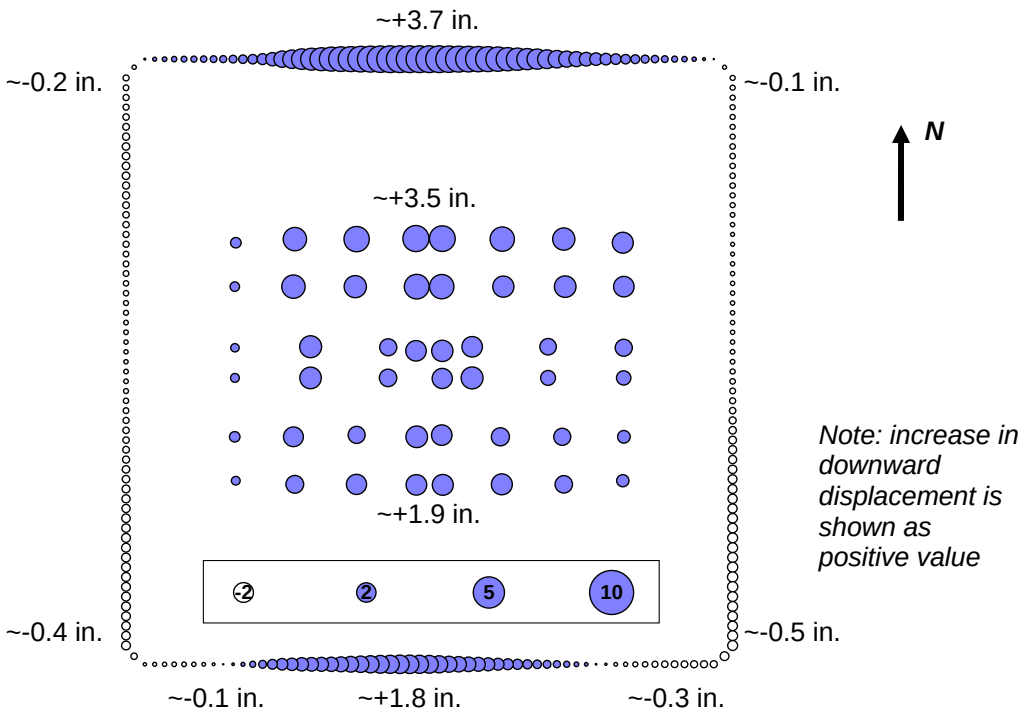

Figure 4–37. Change in vertical displacement at Floor 99 of WTC 1 from the time before impact to 100 min for Case B conditions with 5 kip pull-in forces.

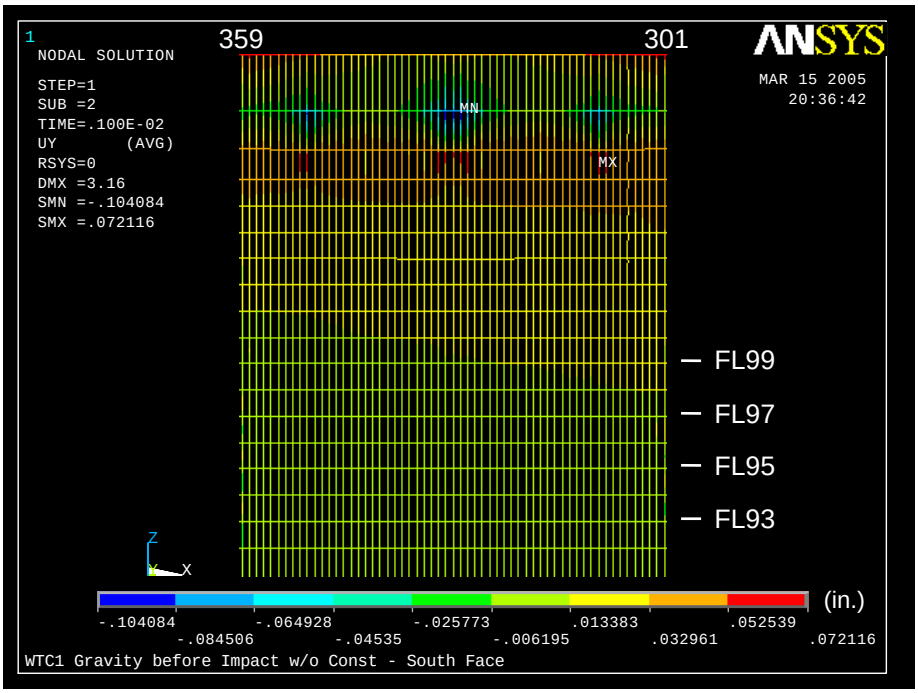

Figure 4–38. Out-of-plane displacement of south wall of WTC 1 before aircraft impact (inward displacement is positive).

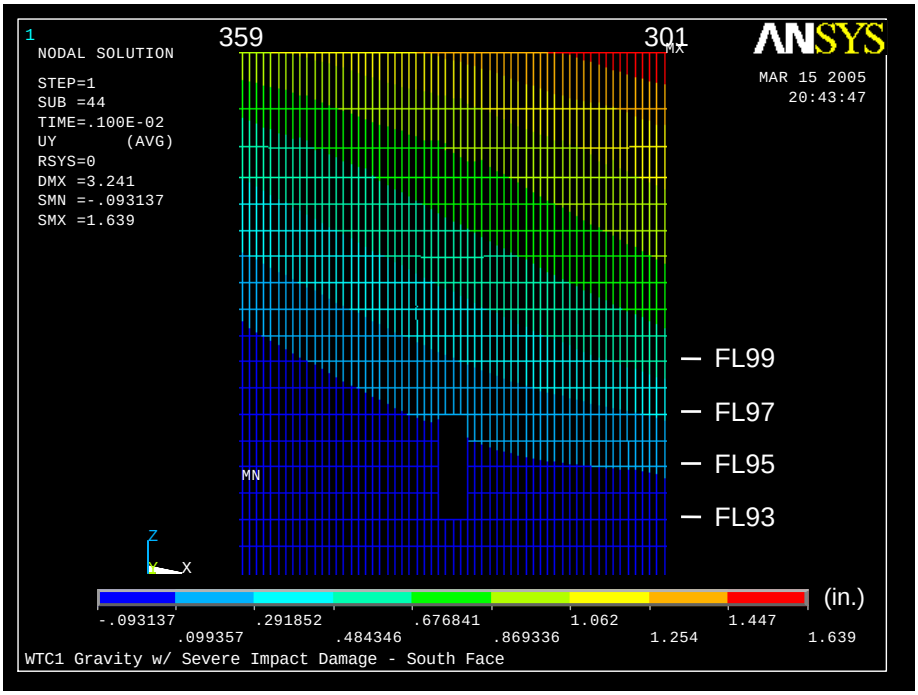

Figure 4–39. Out-of-plane displacement of south wall of WTC 1 after aircraft impact for Case B conditions (inward displacement is positive).

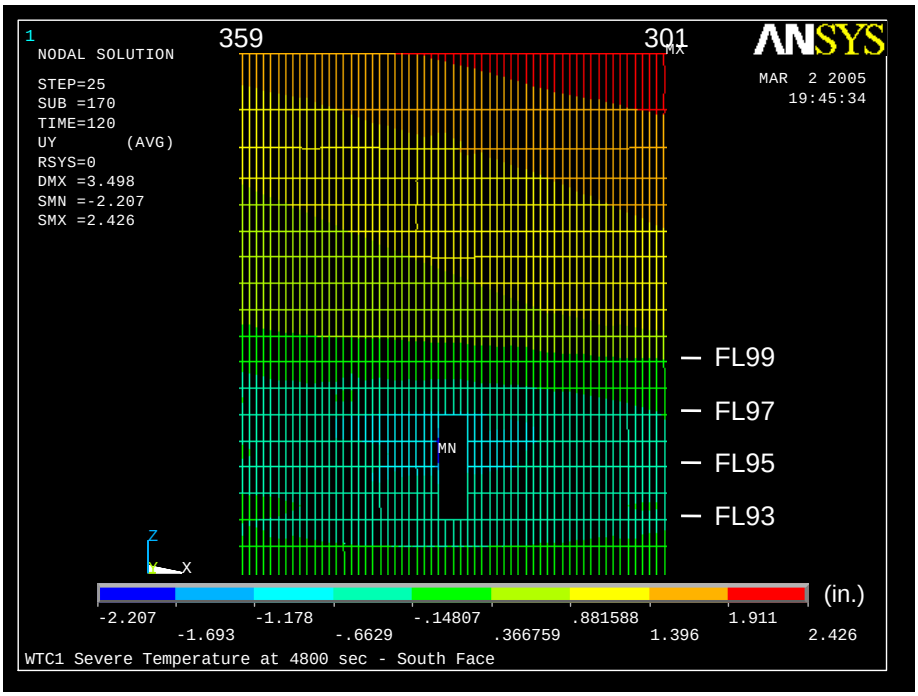

Figure 4–40. Out-of-plane displacement of south wall of WTC 1 at 80 min (at the end of Analysis Step 17) for Case B conditions (inward displacement is positive).

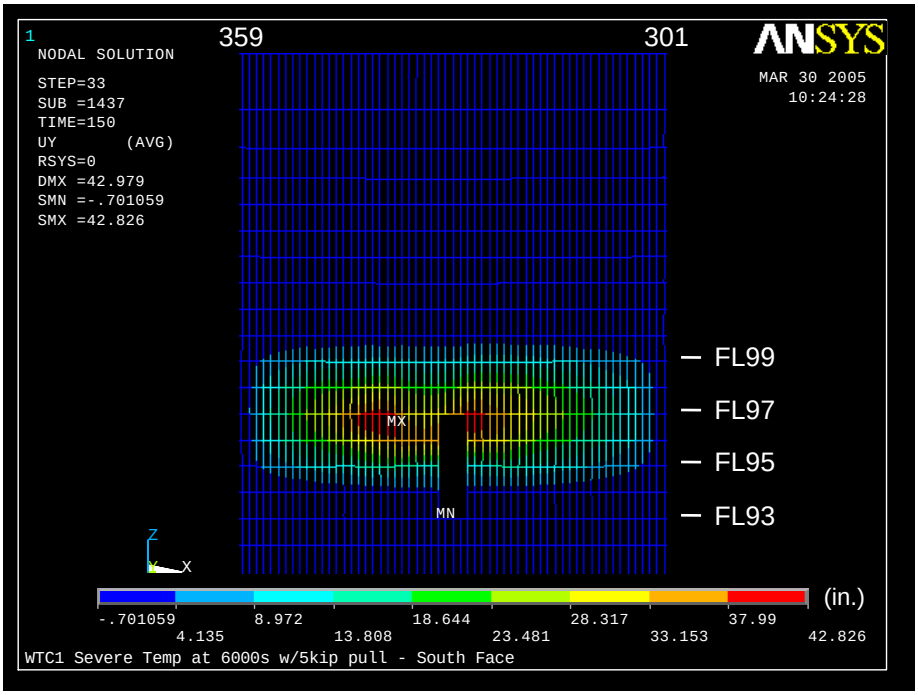

Figure 4–41. Out-of-plane displacement of south wall of WTC 1 at 100 min for Case B conditions with 5 kip pull-in forces (inward displacement is positive).

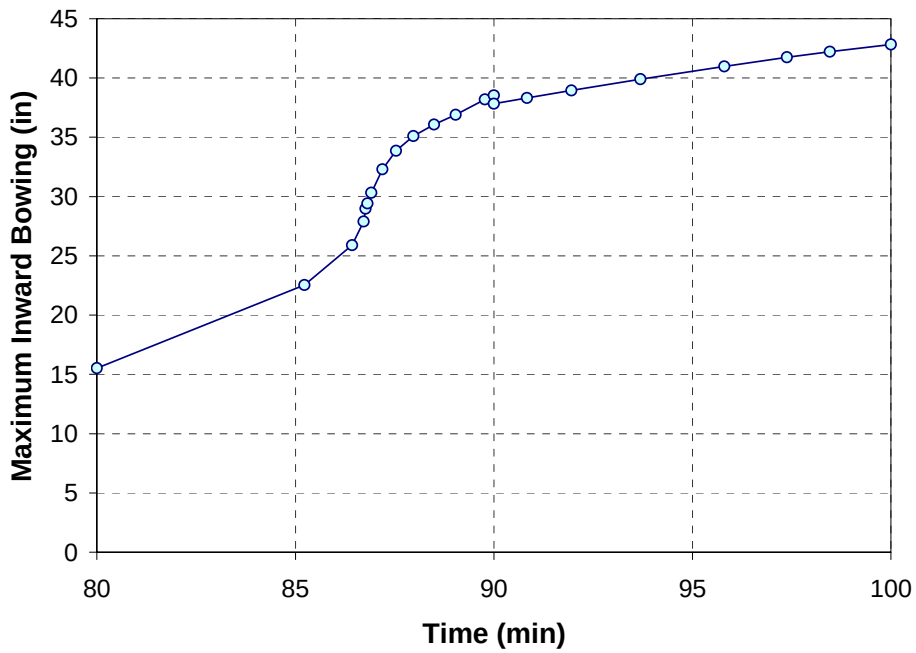

Figure 4–42. Time history of maximum out-of-plane displacement of south wall of WTC 1 for Case B conditions with 5 kip pull-in forces (from Analysis Step 18 to Step 21).

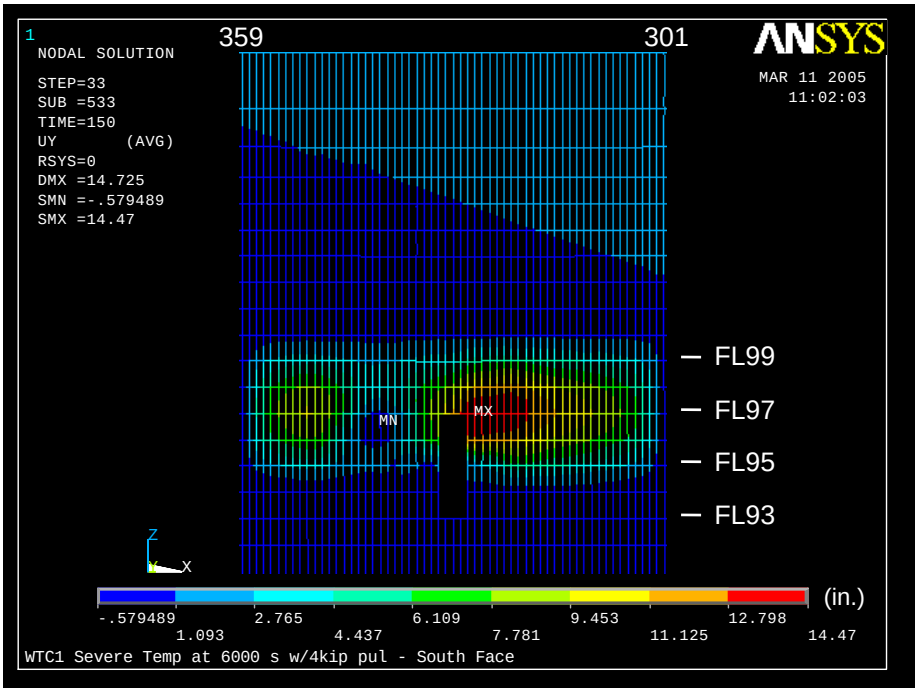

Figure 4–43. Out-of-plane displacement of south wall of WTC 1 at 100 min for Case B conditions with 4 kip pull-in forces (inward displacement is positive).

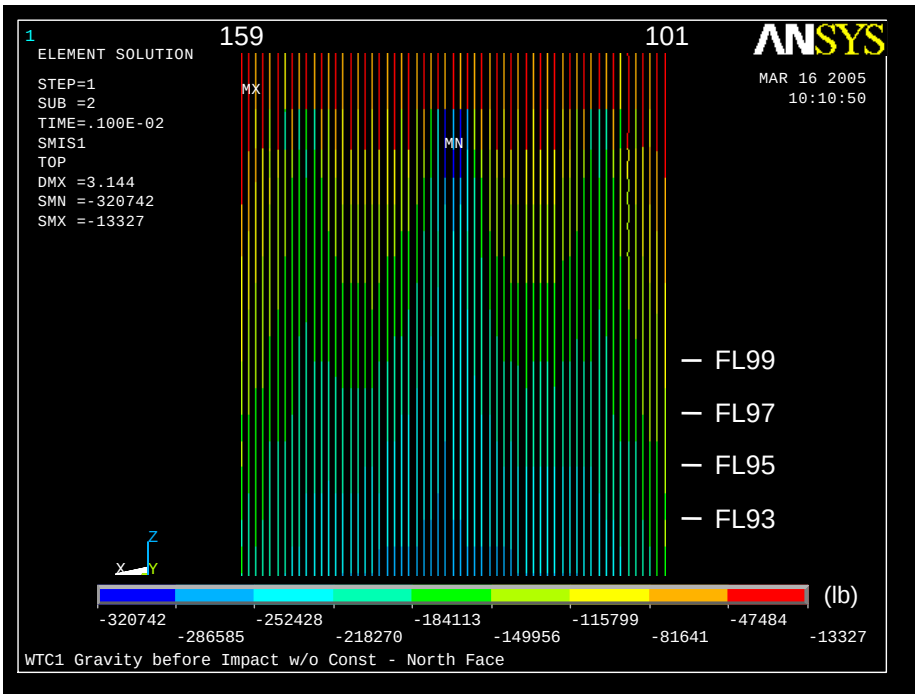

Figure 4–44. Axial load in exterior columns of north wall of WTC 1 before aircraft impact (compression is negative).

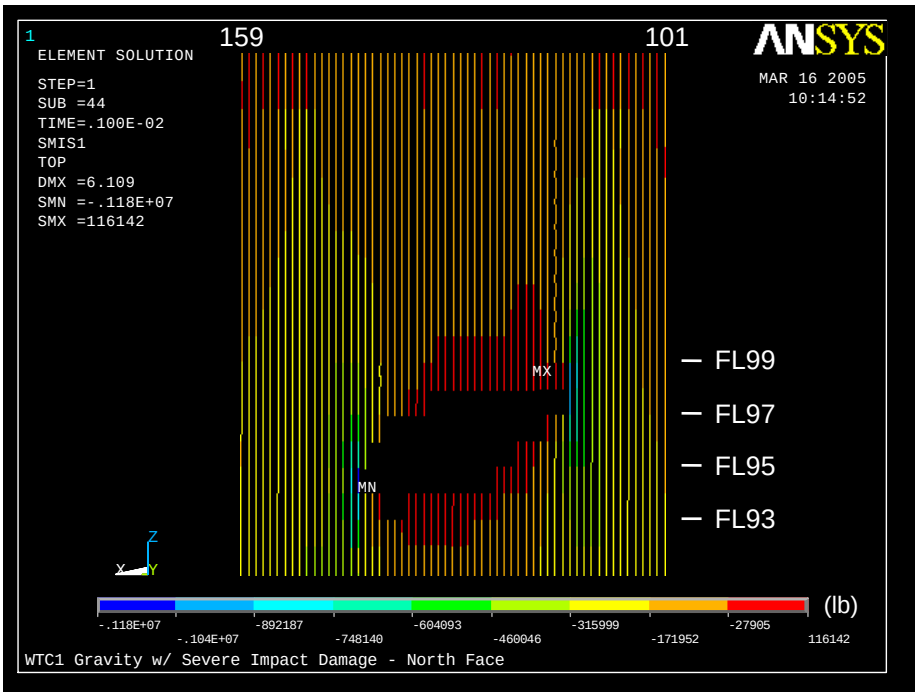

Figure 4–45. Axial load in exterior columns of north wall of WTC 1 after aircraft impact for Case B conditions (compression is negative).

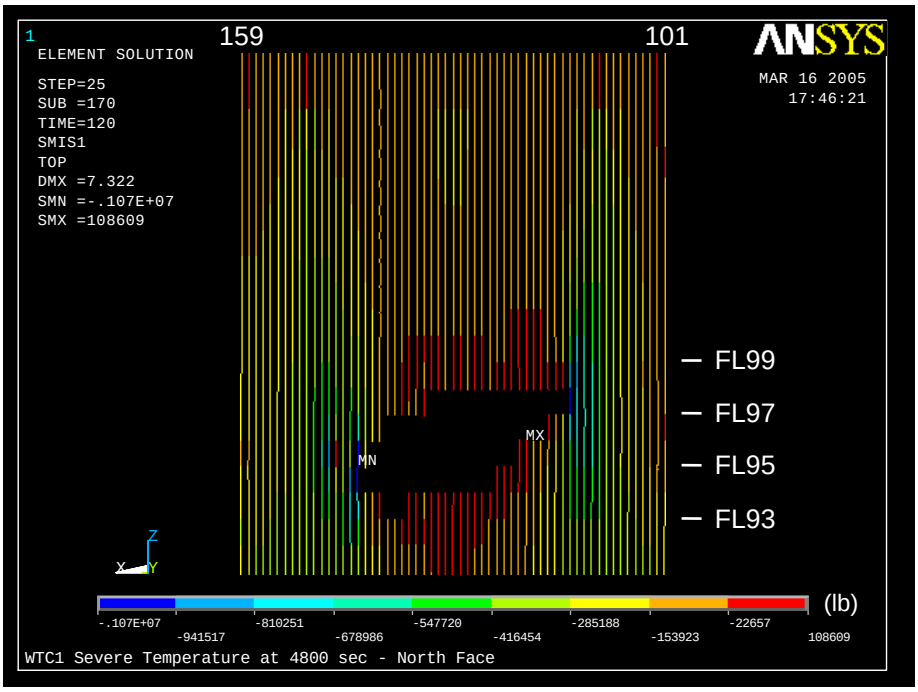

Figure 4–46. Axial load in exterior columns of north wall of WTC 1 at 80 min for the Case B conditions (compression is negative).

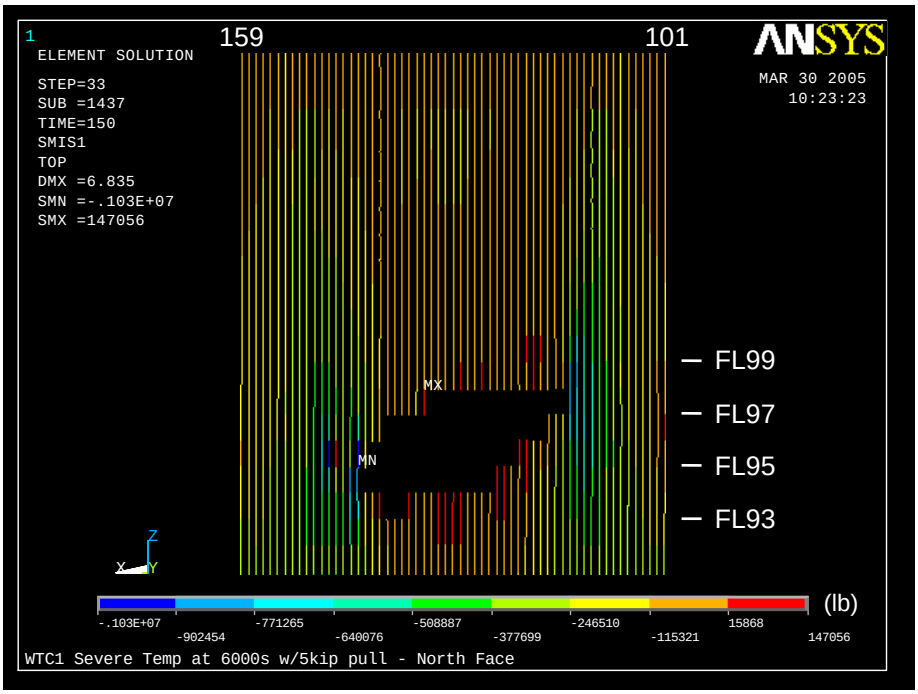

Figure 4–47. Axial load in exterior columns of north wall of WTC 1 at 100 min for Case B conditions with 5 kip pull-in forces (compression is negative).

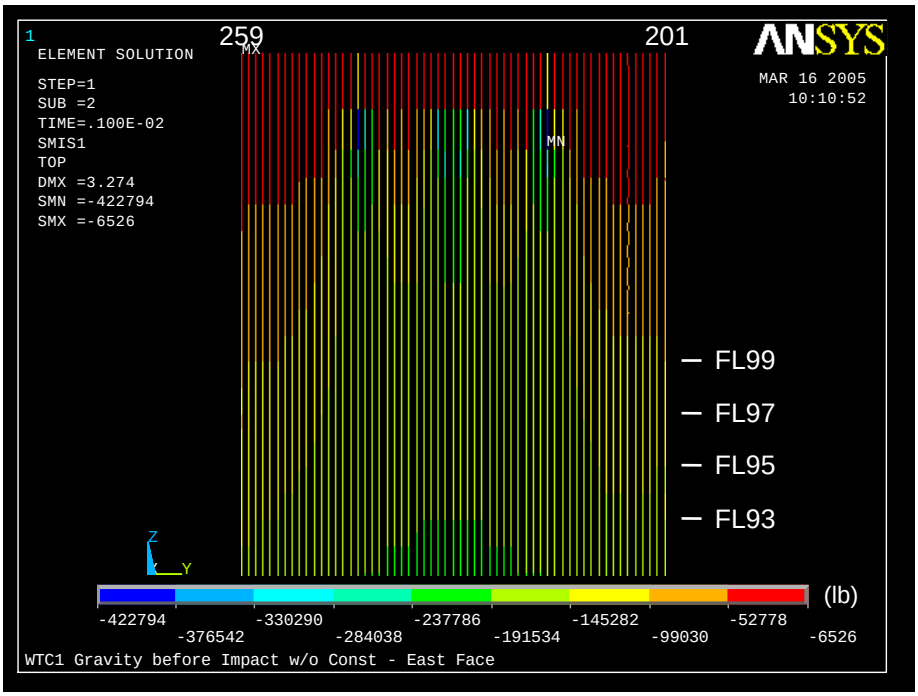

Figure 4–48. Axial load in exterior columns of east wall of WTC 1 before aircraft impact (compression is negative).

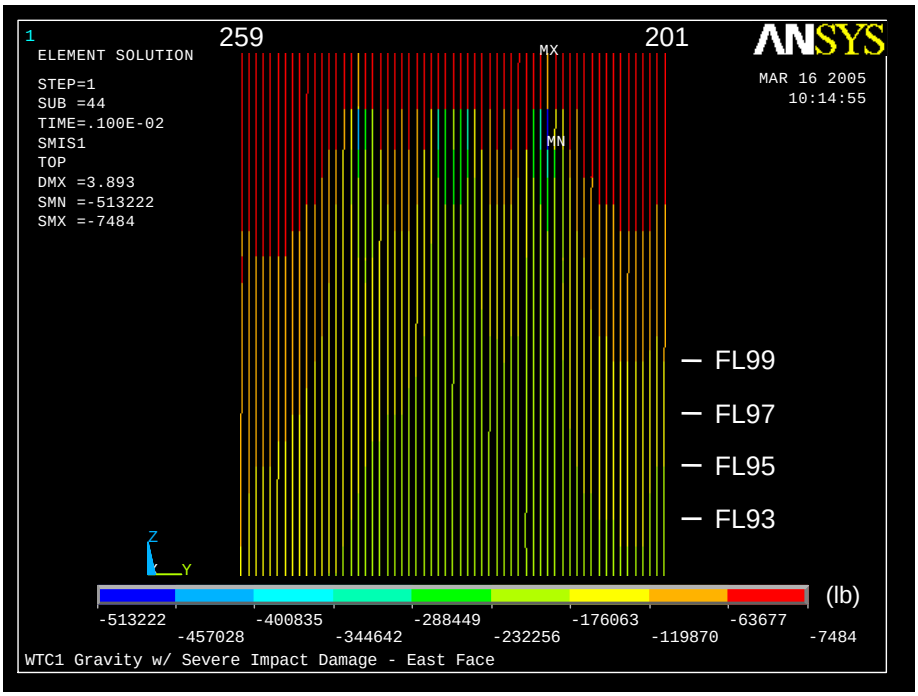

Figure 4–49. Axial load in exterior columns of east wall of WTC 1 after aircraft impact for Case B conditions (compression is negative).

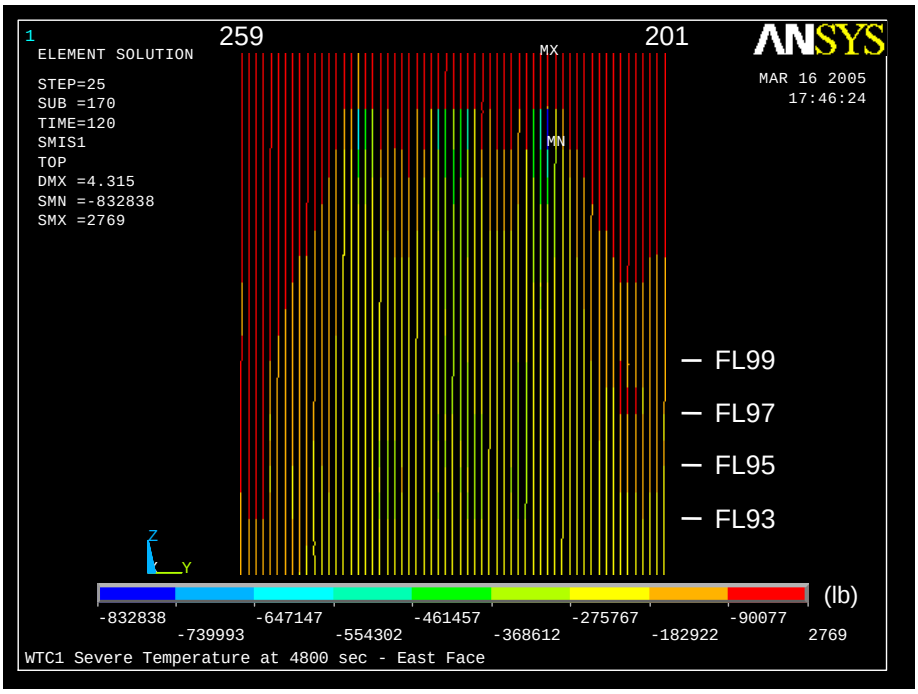

Figure 4–50. Axial load in exterior columns of east wall of WTC 1 at 80 min for the Case B conditions (compression is negative).

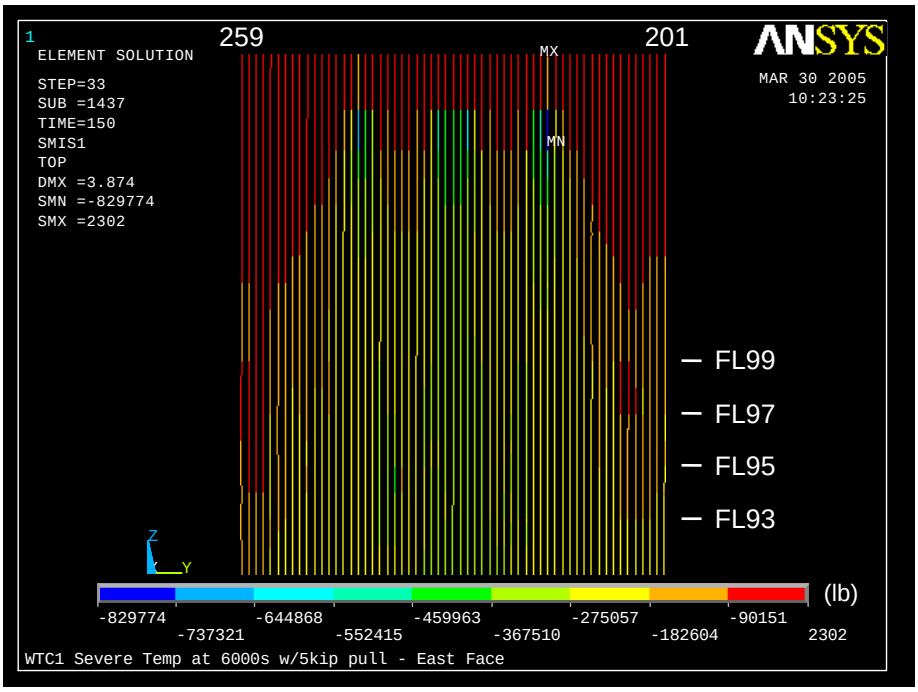

Figure 4–51. Axial load in exterior columns of east wall of WTC 1 at 100 min for the Case B conditions with 5 kip pull-in forces (compression is negative).

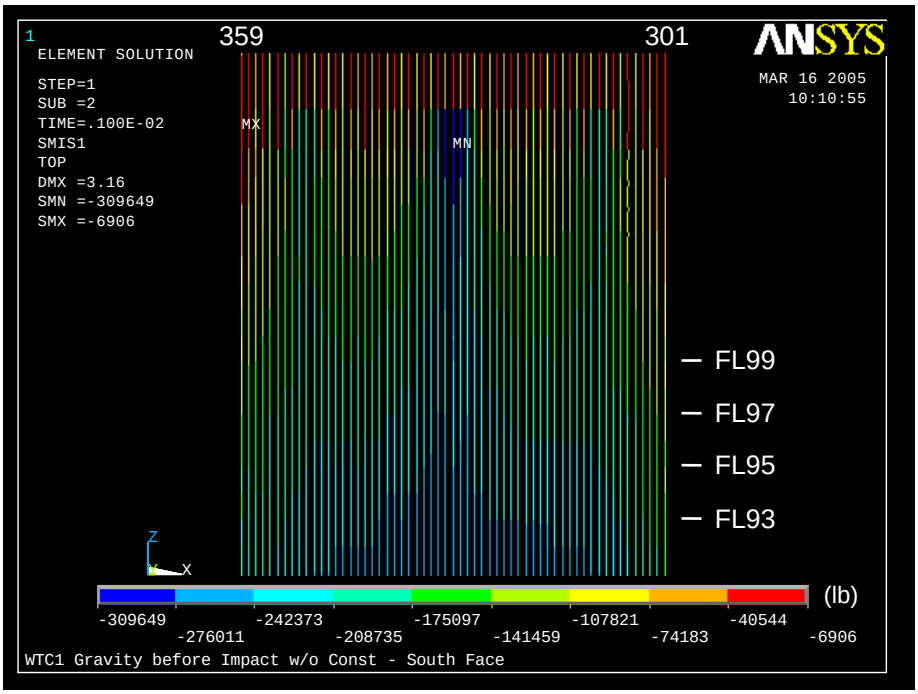

Figure 4–52. Axial load in exterior columns of south wall of WTC 1 before aircraft impact (compression is negative).

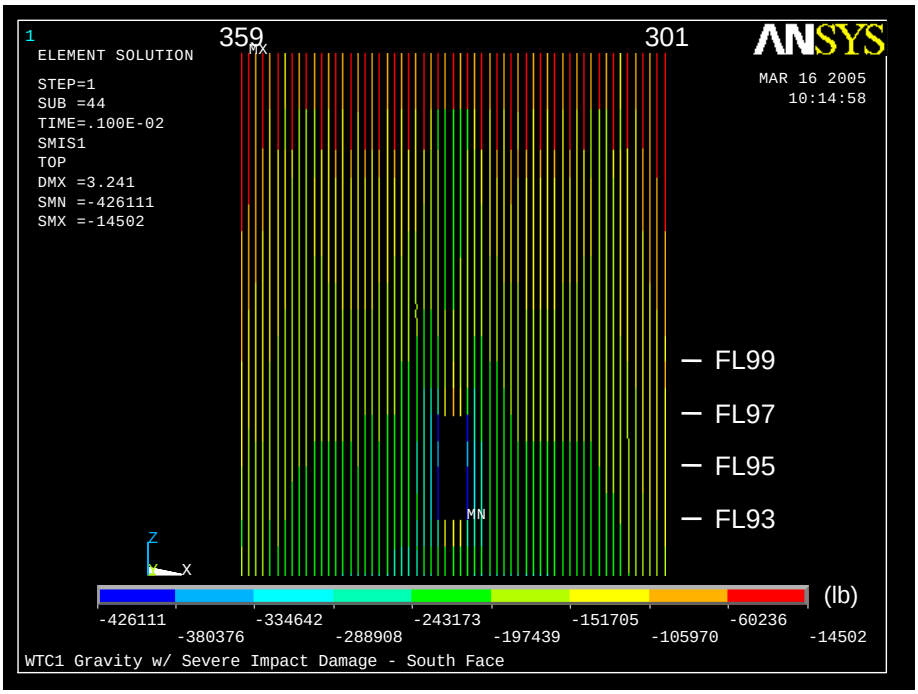

Figure 4–53. Axial load in exterior columns of south wall of WTC 1 after aircraft impact for Case B conditions (compression is negative).

Figure 4–54. Axial load in exterior columns of south wall of WTC 1 at 80 min for Case B conditions (compression is negative).

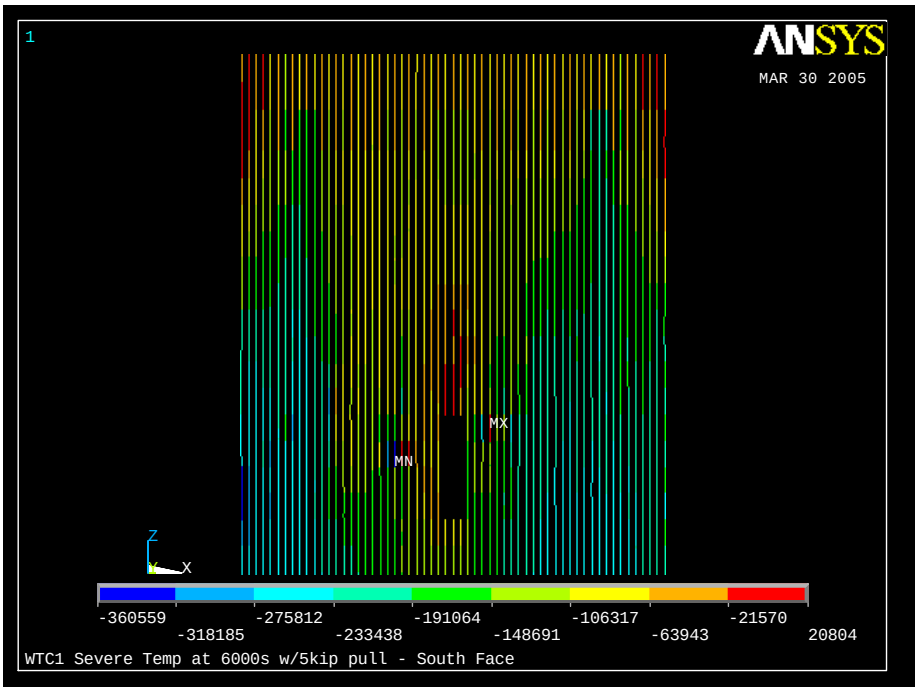

Figure 4–55. Axial load in exterior columns of south wall of WTC 1 at 100 min for Case B conditions with 5 kip pull-in forces (compression is negative).

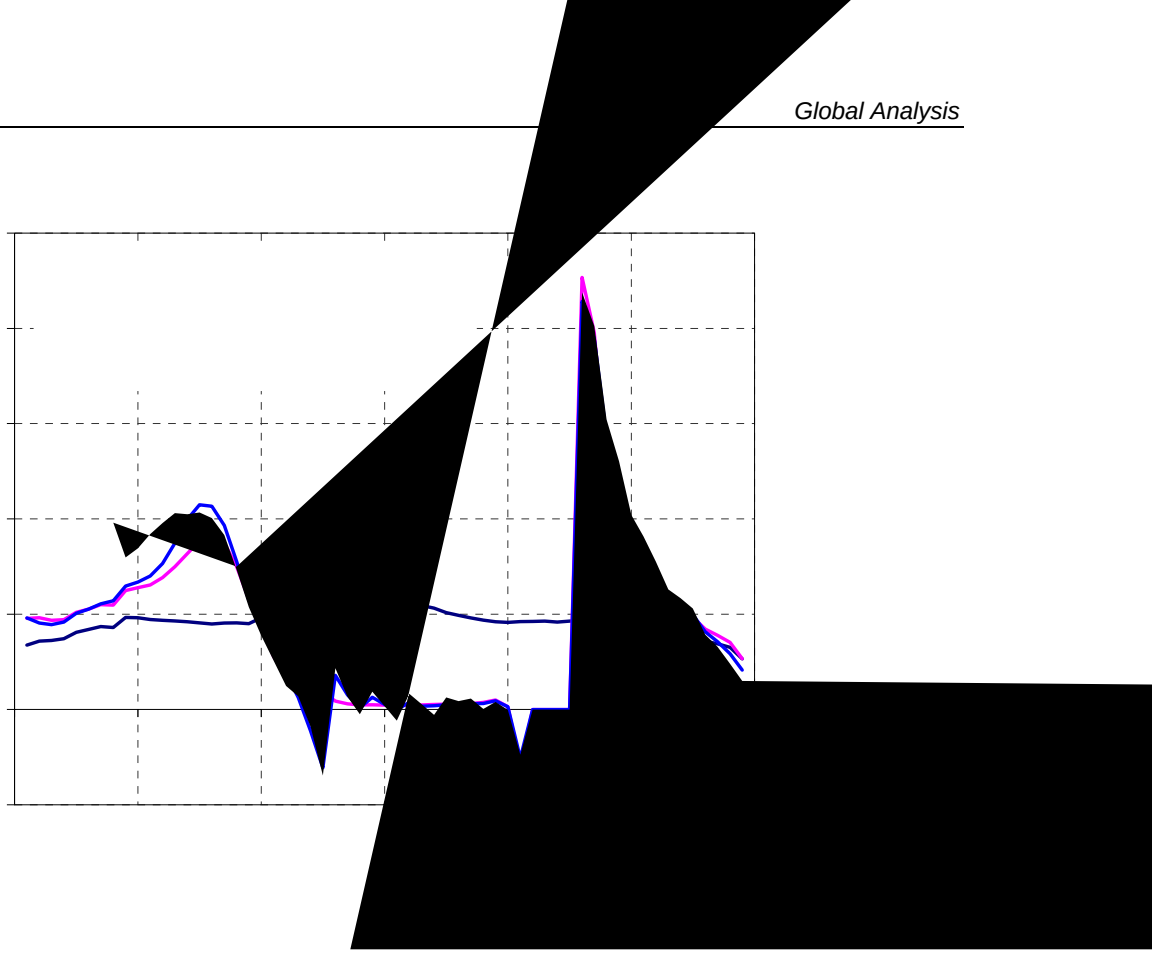

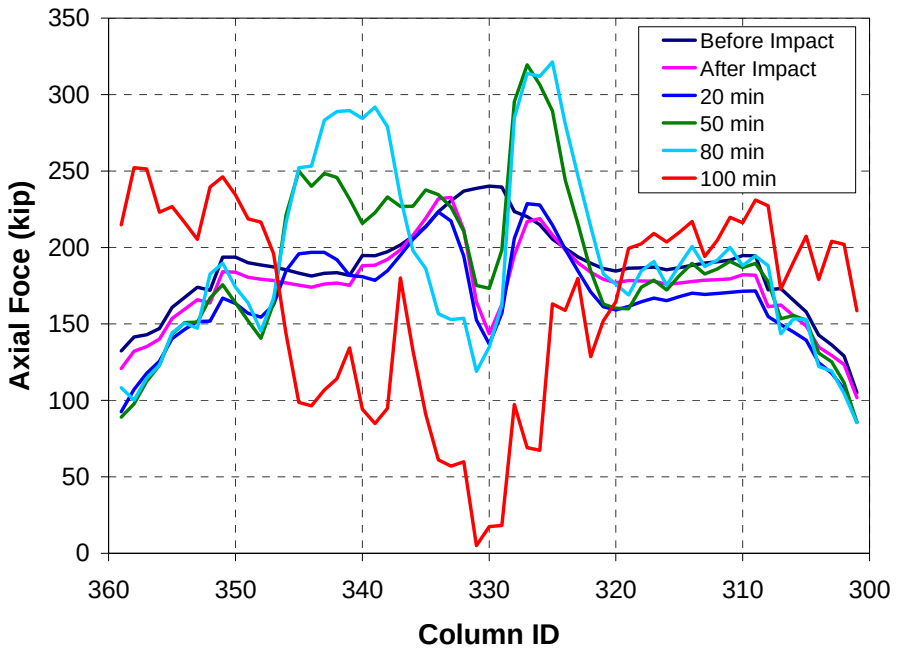

Figure 4–58. Variation of axial load in exterior columns at Floor 98 of south wall of WTC 1 for Case B conditions with 5 kip pull-in forces (compression is positive).

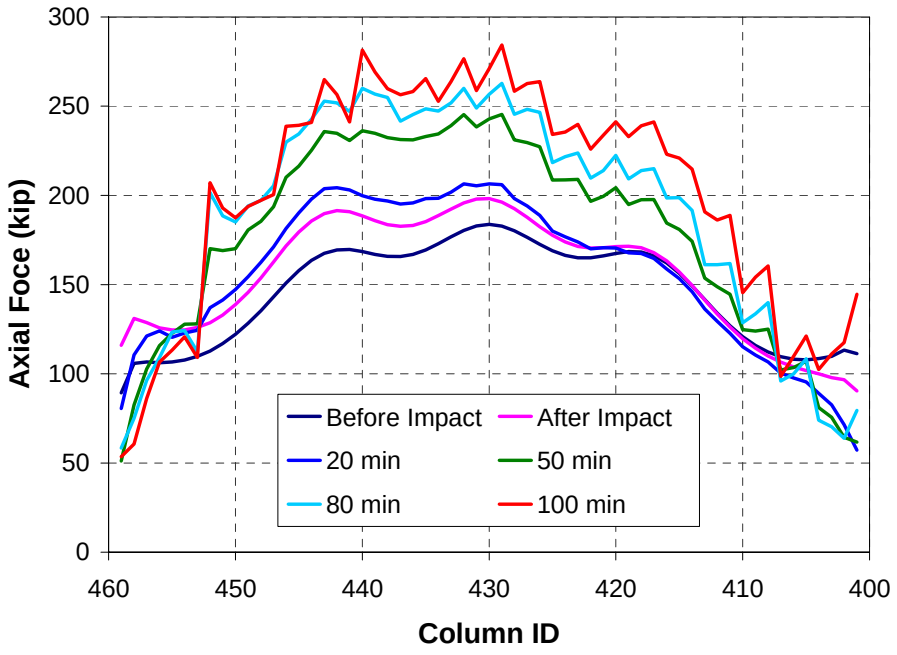

Figure 4–59. Variation of axial load in exterior columns at Floor 98 of west wall of WTC 1 for Case B conditions with 5 kip pull-in forces (compression is positive).

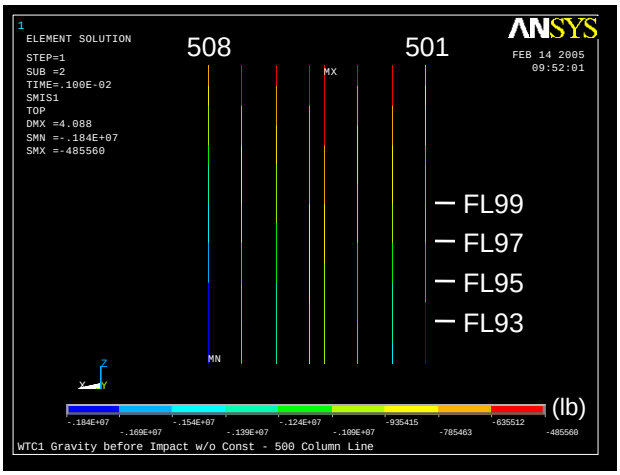

(a) 500 series columns

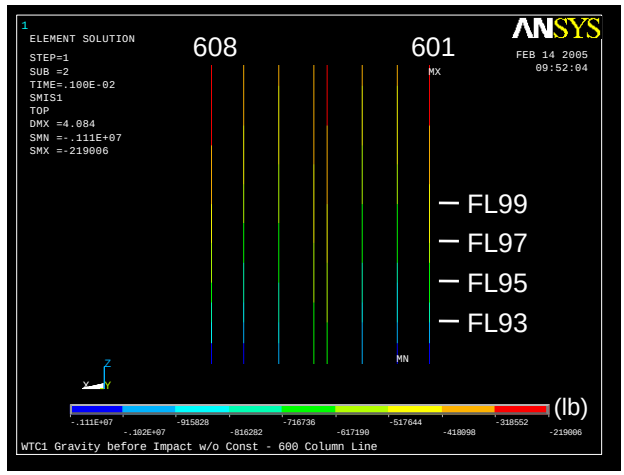

(b) 600 series columns

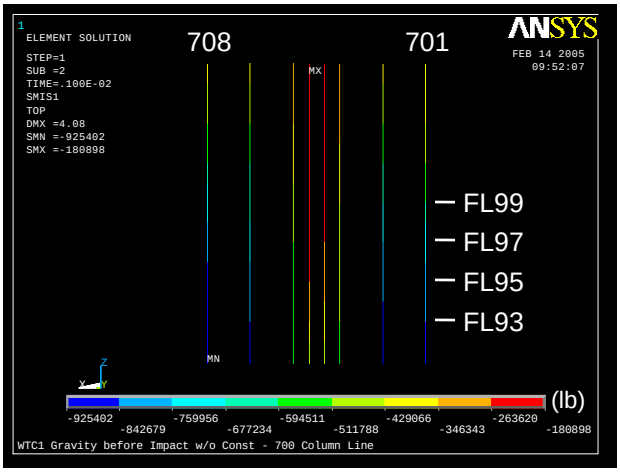

(c) 700 series columns

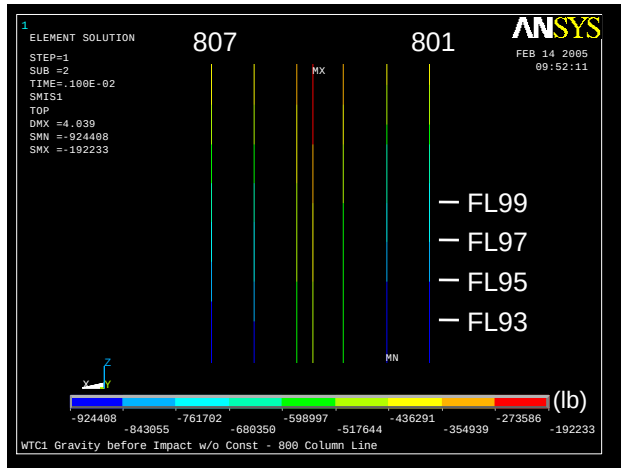

(d) 800 series columns

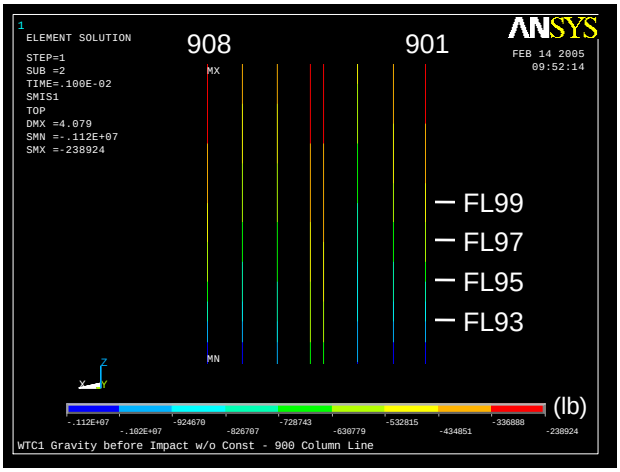

(e) 900 series columns

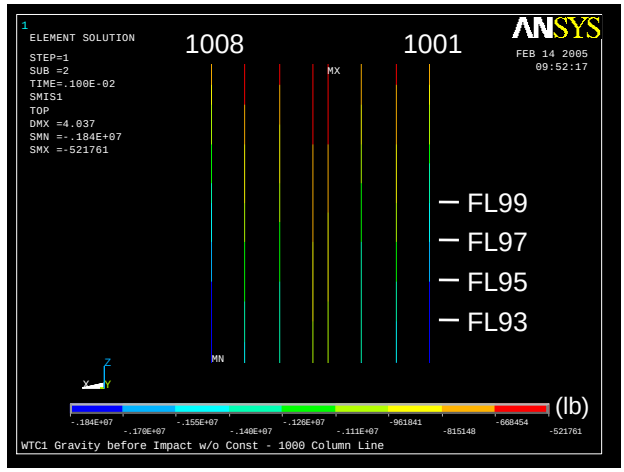

(f) 1000 series columns

Figure 4–60. Axial load in core columns of WTC 1 before aircraft impact (compression is negative).

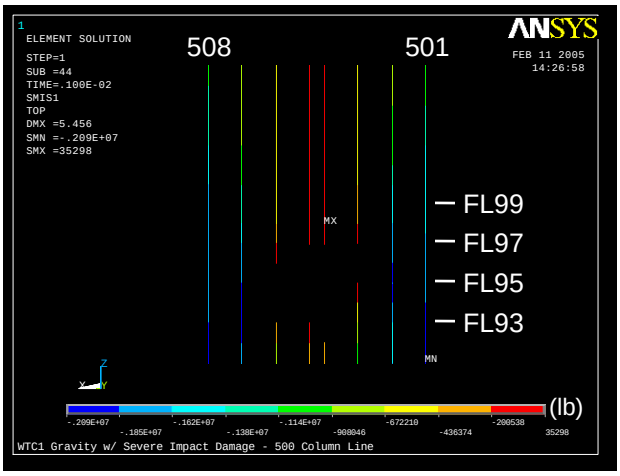

(a) 500 series columns

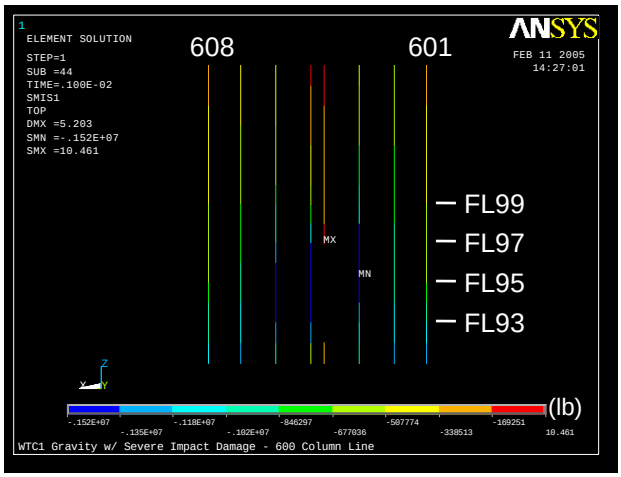

(b) 600 series columns

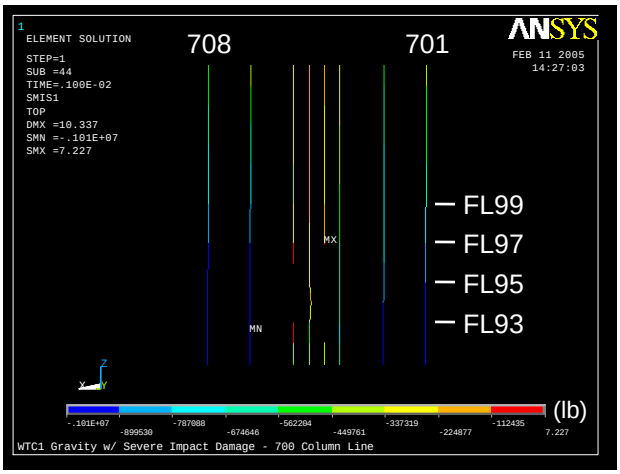

(c) 700 series columns

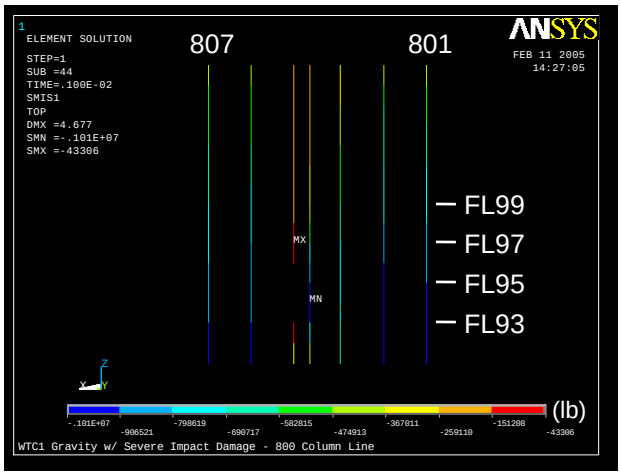

(d) 800 series columns

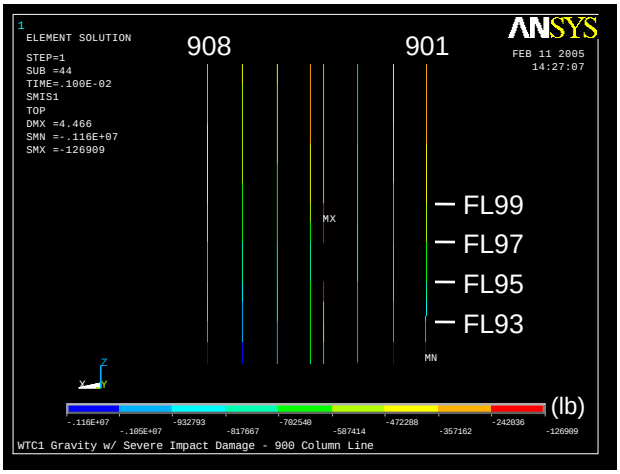

(e) 900 series columns

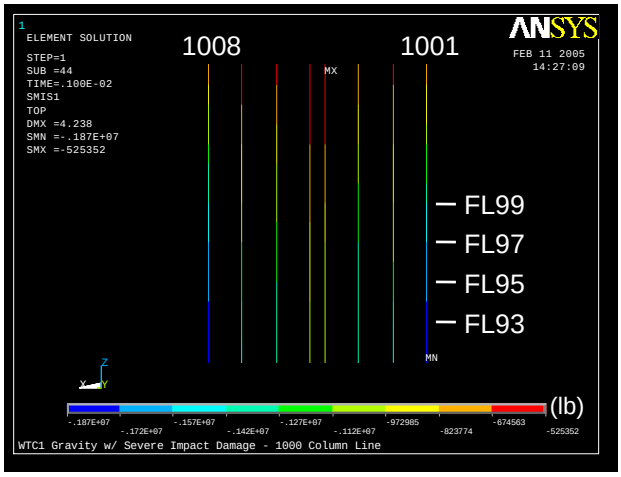

(f) 1000 series columns

Figure 4–61. Axial load in core columns of WTC 1 after aircraft impact for Case B conditions (compression is negative).

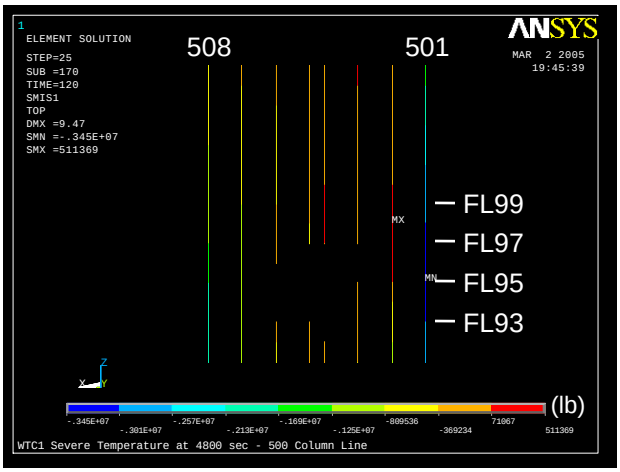

(a) 500 series columns

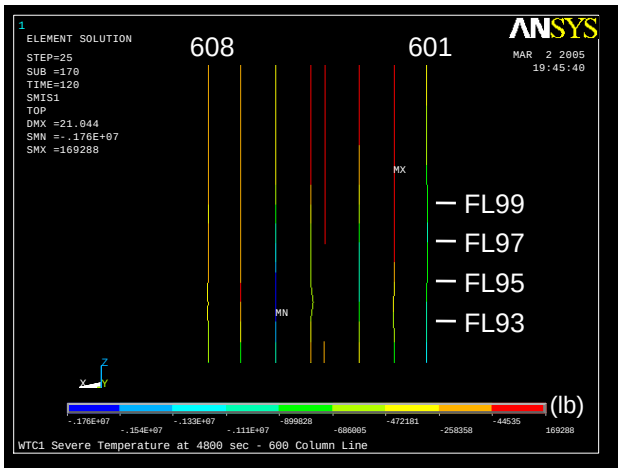

(b) 600 series columns

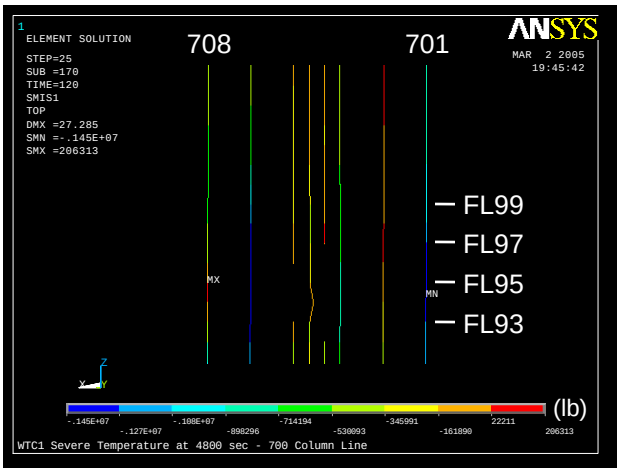

(c) 700 series columns

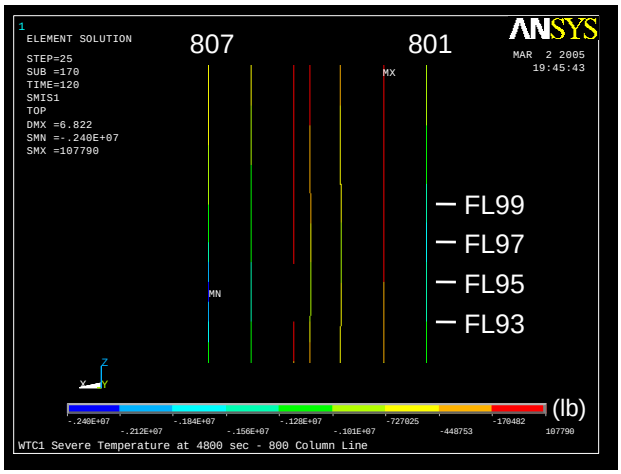

(d) 800 series columns

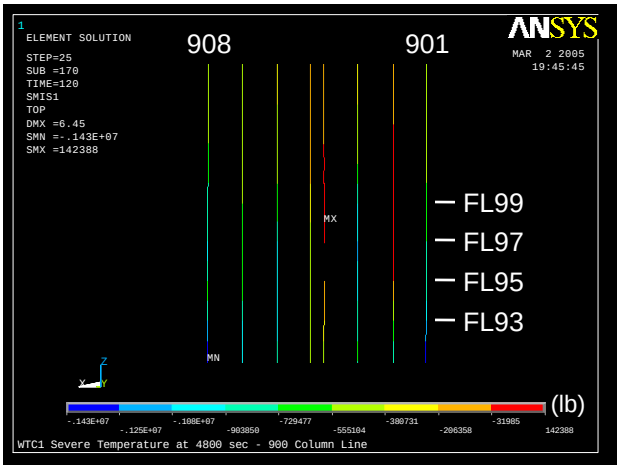

(e) 900 series columns

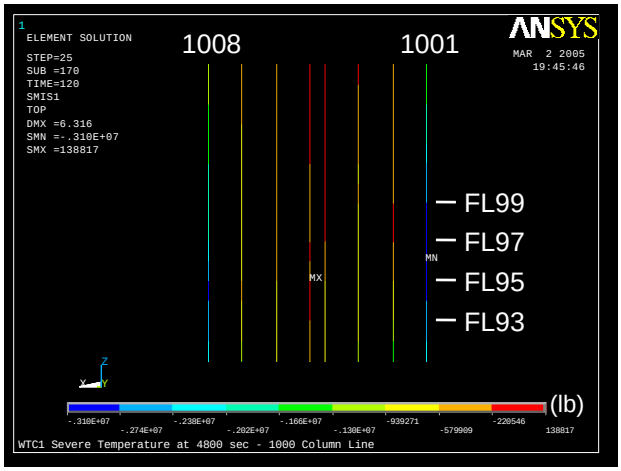

(f) 1000 series columns

Figure 4–62. Axial load in core columns of WTC 1 at 80 min for Case B conditions (compression is negative).

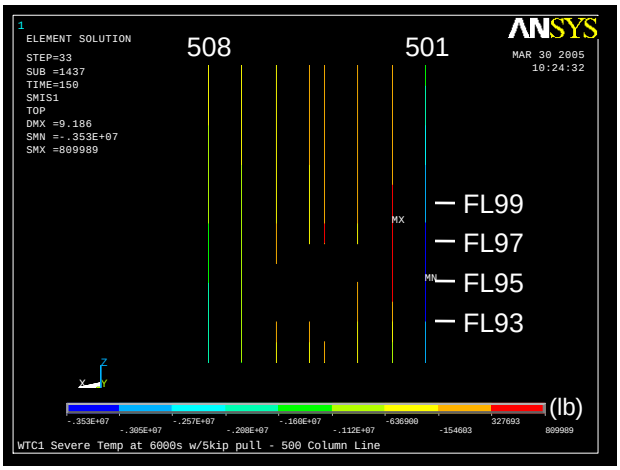

(a) 500 series columns

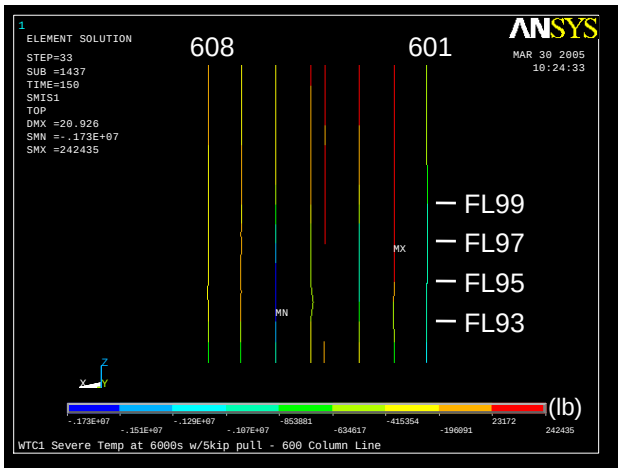

(b) 600 series columns

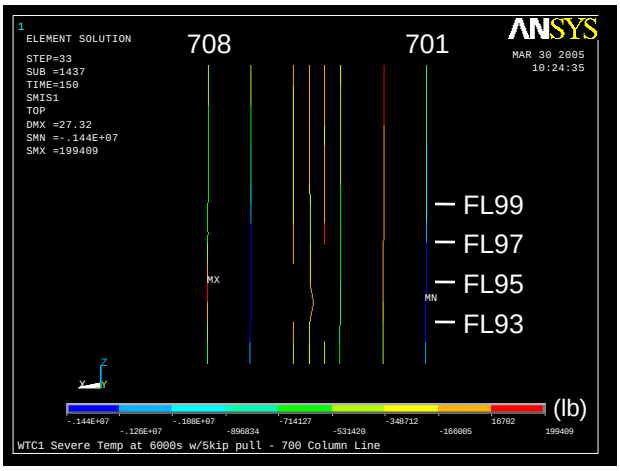

(c) 700 series columns

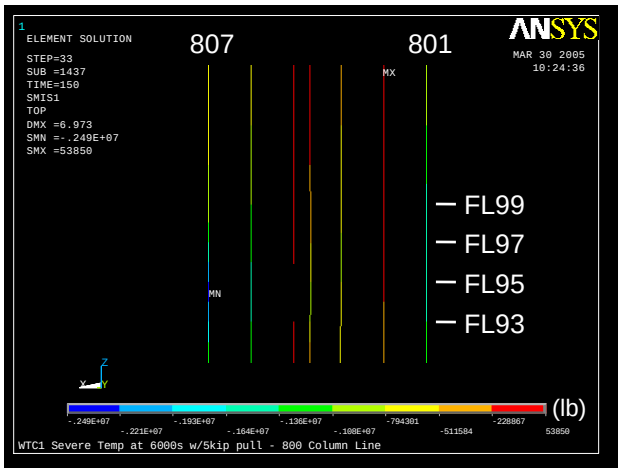

(d) 800 series columns

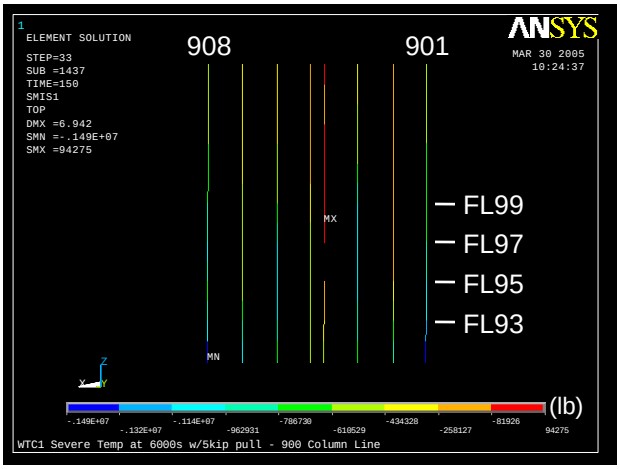

(e) 900 series columns

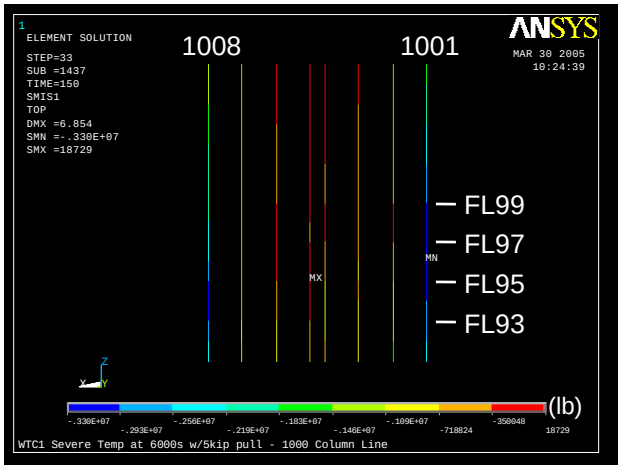

(f) 1000 series columns

Figure 4–63. Axial load in core columns of WTC 1 at 100 min for Case B conditions with 5 kip pull-in forces (compression is negative).

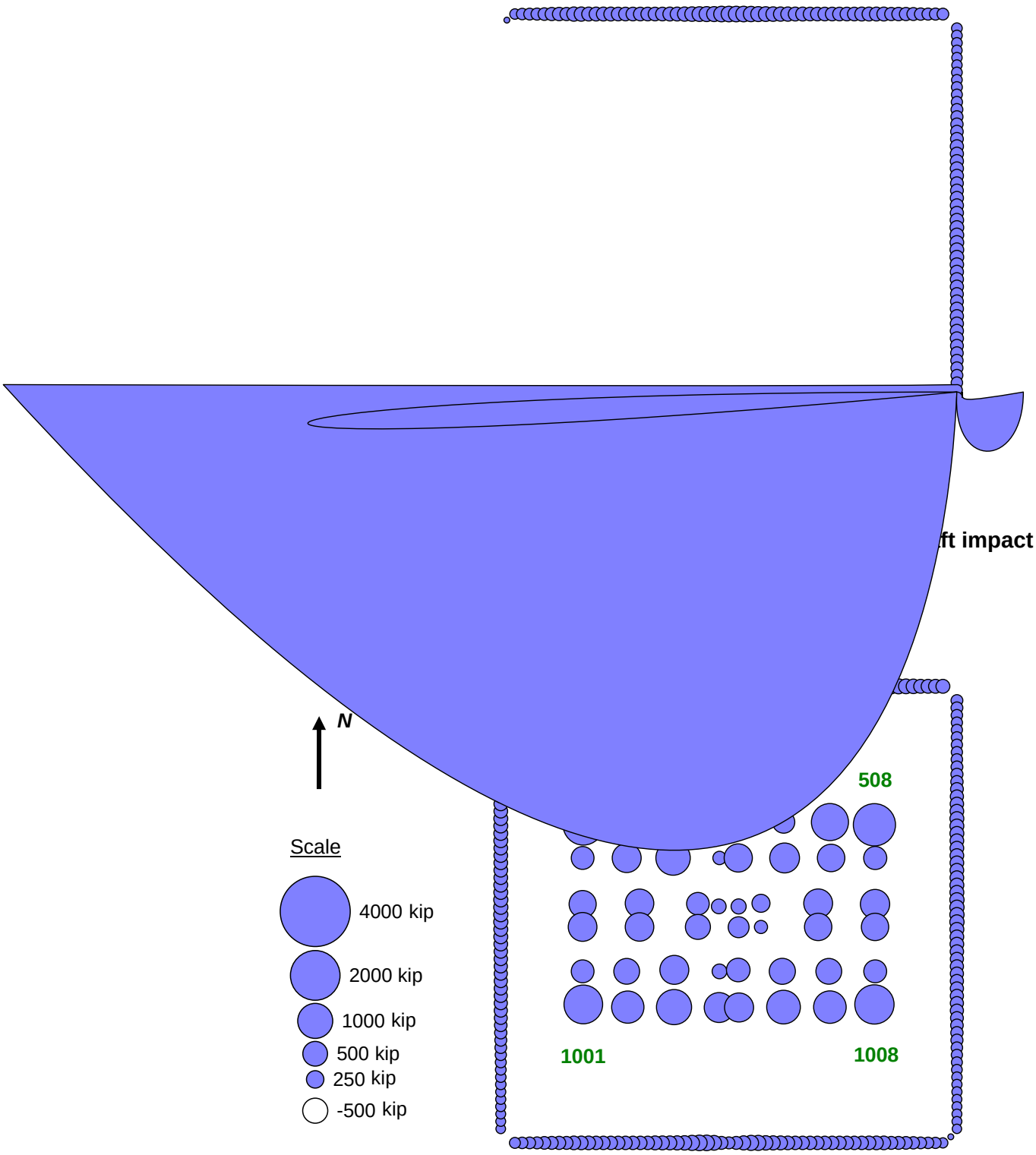

Figure 4–65. Axial load in columns at Floor 98 of WTC 1 after aircraft impact for Case B conditions (compression is positive).

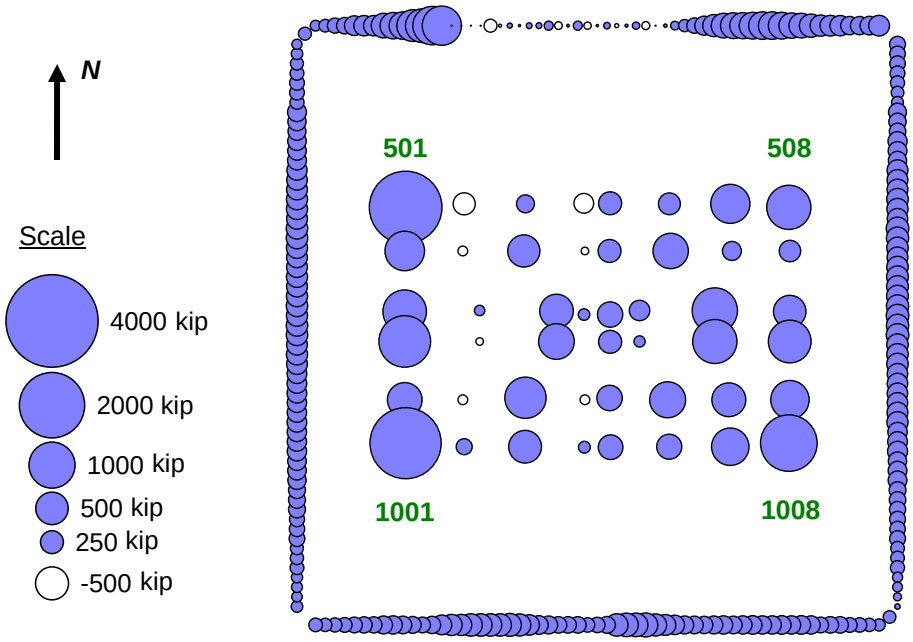

Figure 4–66. Axial load in columns at Floor 98 of WTC 1 at 80 min for Case B conditions (compression is positive).

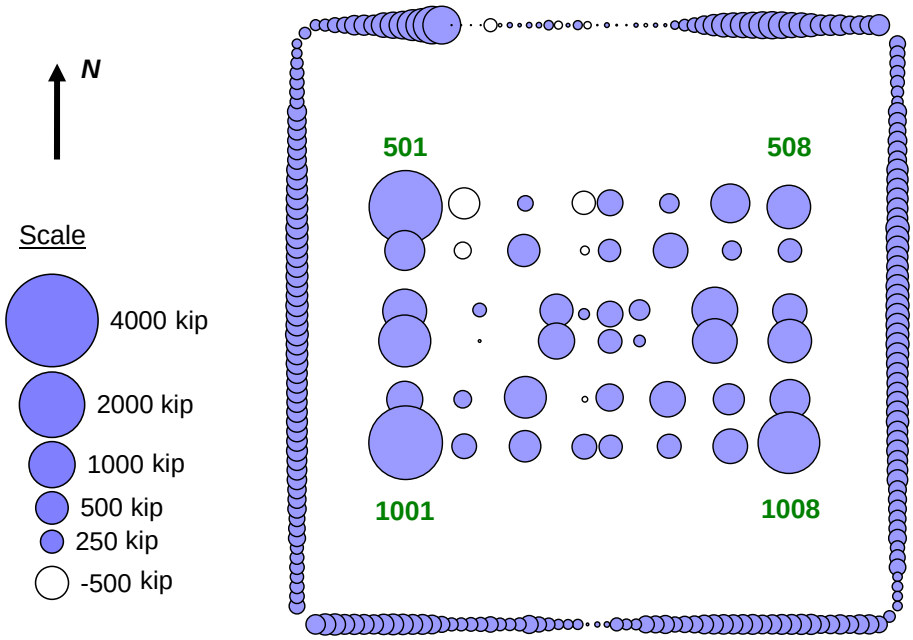

Figure 4–67. Axial load in columns at Floor 98 of WTC 1 at 100 min for Case B conditions with 5 kip pull-in forces (compression is positive).

Table 4–10. Total column loads at Floor 98 of WTC 1 for Case B conditions.

Row	Analysis Step	North	East	South	West	Core	Total
(1)	Before Impact	10,974	8,545	11,025	8,572	34,029	73,144
(2)	After Impact	10,137	9,071	10,356	9,146	34,429	73,139
(3)	10 min	9,796	8,490	9,848	8,536	36,473	73,143
(4)	20 min	10,437	9,108	9,900	9,202	34,495	73,143
(5)	30 min	10,913	10,034	10,420	9,715	32,060	73,142
(6)	40 min	11,068	10,599	11,004	10,178	30,294	73,142
(7)	50 min	11,149	10,908	11,192	10,458	29,435	73,141
(8)	60 min	11,205	11,168	11,285	10,716	28,766	73,141
(9)	70 min	11,286	11,366	11,343	10,939	28,205	73,138
(10)	80 min	11,376	11,555	11,409	11,119	27,681	73,140
(11)	90 min	10,916	11,991	9,949	11,657	28,587	73,099
(12)	100 min	10,828	12,249	9,638	11,905	28,478	73,098
(13)	(2) - (1)	-837	526	-668	574	400	-5
(14)	(10) - (2)	1,239	2,484	1,052	1,973	-6,748	1
(15)	(12) - (2)	692	3,178	-719	2,759	-5,951	-41
(16)	(12) - (10)	-548	694	-1,771	786	797	-42

Note: Compression is positive. Units are in kip.

Table 4–11. Total column loads at Floor 105 of WTC 1 for Case B conditions.

Row	Analysis Step	North	East	South	West	Core	Total
(1)	Before Impact	8,026	6,562	8,092	6,604	20,361	49,645
(2)	After Impact	7,294	7,028	7,488	7,076	20,761	49,646
(3)	10 min	6,944	6,461	6,981	6,469	22,790	49,646
(4)	20 min	7,551	7,075	7,057	7,158	20,806	49,647
(5)	30 min	8,020	7,998	7,569	7,685	18,377	49,648
(6)	40 min	8,193	8,571	8,129	8,147	16,608	49,649
(7)	50 min	8,285	8,878	8,315	8,428	15,743	49,650
(8)	60 min	8,351	9,130	8,414	8,687	15,069	49,650
(9)	70 min	8,435	9,319	8,481	8,914	14,502	49,651
(10)	80 min	8,528	9,497	8,551	9,097	13,978	49,651
(11)	90 min	8,096	9,847	7,327	9,506	14,876	49,652
(12)	100 min	8,023	10,076	7,066	9,720	14,767	49,653
(13)	(2) - (1)	-732	466	-604	472	400	1
(14)	(10) - (2)	1,234	2,470	1,063	2,021	-6,783	5
(15)	(12) - (2)	730	3,048	-422	2,644	-5,993	7
(16)	(12) - (10)	-504	579	-1,485	623	790	2

Note: Compression is positive. Units are in kip.

Table 4–12. Total column loads on the north wall of WTC 1 for Case B conditions.

Floor	Before Impact	After Impact	10 min	20 min	30 min	40 min	50 min	60 min	70 min	80 min	90 min	100 min
105	8,026	7,294	6,944	7,551	8,020	8,193	8,285	8,351	8,435	8,528	8,096	8,023
104	8,470	7,723	7,373	7,984	8,453	8,623	8,715	8,779	8,863	8,956	8,521	8,447
103	8,868	8,102	7,752	8,363	8,830	8,997	9,087	9,150	9,233	9,325	8,888	8,813
102	9,307	8,529	8,179	8,795	9,264	9,429	9,518	9,580	9,663	9,755	9,314	9,238
101	9,696	8,897	8,545	9,161	9,627	9,787	9,873	9,933	10,015	10,106	9,663	9,586
100	10,143	9,334	8,982	9,605	10,073	10,230	10,315	10,374	10,455	10,546	10,094	10,017
99	10,527	9,700	9,347	9,970	10,436	10,590	10,672	10,726	10,802	10,890	10,437	10,359
98	10,974	10,137	9,796	10,437	10,913	11,068	11,149	11,205	11,286	11,376	10,916	10,828
97	11,359	10,370	10,027	10,649	11,112	11,258	11,329	11,387	11,467	11,558	11,103	11,024
96	11,826	10,648	10,235	10,982	11,472	11,634	11,712	11,762	11,838	11,920	11,449	11,359
95	12,211	10,827	10,404	11,124	11,593	11,749	11,825	11,880	11,963	12,052	11,589	11,501
94	12,688	11,132	10,739	11,442	11,928	12,091	12,179	12,244	12,326	12,415	11,941	11,846
93	13,072	11,349	10,934	11,599	12,062	12,217	12,301	12,358	12,439	12,527	12,069	11,984

Note: Compression is positive. Units are in kip.

Table 4–13. Change in total column loads on the north wall of WTC 1 for Case B conditions from the state before aircraft impact.

Floor	After Impact	10 min	20 min	30 min	40 min	50 min	60 min	70 min	80 min	90 min	100 min
105	-732	-1,082	-475	-6	167	259	325	409	502	70	-3
104	-747	-1,096	-486	-17	154	245	310	393	486	51	-22
103	-765	-1,116	-505	-38	130	219	282	365	457	20	-54
102	-778	-1,128	-512	-43	122	211	273	356	448	7	-69
101	-798	-1,151	-534	-69	92	178	237	319	410	-33	-109
100	-809	-1,160	-538	-70	88	172	231	313	404	-49	-126
99	-827	-1,180	-557	-92	63	144	199	275	362	-91	-168
98	-837	-1,178	-537	-61	94	175	231	312	402	-58	-145
97	-988	-1,332	-710	-247	-101	-29	28	108	199	-256	-335
96	-1,178	-1,590	-844	-354	-192	-114	-64	12	94	-377	-467
95	-1,383	-1,807	-1,087	-618	-462	-386	-331	-247	-159	-622	-710
94	-1,556	-1,949	-1,247	-760	-598	-510	-445	-362	-273	-748	-843
93	-1,724	-2,138	-1,474	-1,011	-855	-772	-714	-634	-546	-1,004	-1,089

Note: Compression is positive. Units are in kip.

Table 4–14. Total column loads on the east wall of WTC 1 for Case B conditions.

Floor	Before Impact	After Impact	10 min	20 min	30 min	40 min	50 min	60 min	70 min	80 min	90 min	100 min
105	6,562	7,028	6,461	7,075	7,998	8,571	8,878	9,130	9,319	9,497	9,847	10,076
104	6,840	7,316	6,748	7,363	8,287	8,861	9,168	9,421	9,612	9,792	10,152	10,386
103	7,153	7,641	7,072	7,690	8,617	9,192	9,501	9,757	9,949	10,131	10,505	10,744
102	7,416	7,911	7,342	7,961	8,888	9,462	9,771	10,028	10,223	10,406	10,792	11,035
101	7,731	8,240	7,669	8,294	9,226	9,802	10,113	10,373	10,570	10,756	11,154	11,404
100	7,987	8,501	7,930	8,556	9,488	10,063	10,376	10,637	10,836	11,024	11,439	11,691
99	8,305	8,831	8,256	8,886	9,822	10,399	10,715	10,982	11,188	11,381	11,797	12,051
98	8,545	9,071	8,490	9,108	10,034	10,599	10,908	11,168	11,366	11,555	11,991	12,249
97	8,866	9,397	8,811	9,443	10,384	10,963	11,284	11,543	11,741	11,931	12,353	12,608
96	9,108	9,633	9,038	9,642	10,562	11,121	11,429	11,689	11,890	12,082	12,512	12,767
95	9,432	9,960	9,374	9,990	10,927	11,491	11,803	12,061	12,255	12,445	12,874	13,137
94	9,667	10,192	9,611	10,204	11,119	11,670	11,969	12,221	12,412	12,593	13,004	13,266
93	9,995	10,527	9,965	10,579	11,511	12,067	12,366	12,618	12,810	12,995	13,445	13,709

Note: Compression is positive. Units are in kip.

Table 4–15. Change in total column loads on the east wall of WTC 1 for Case B conditions from the state before aircraft impact.

Floor	After Impact	10 min	20 min	30 min	40 min	50 min	60 min	70 min	80 min	90 min	100 min
105	466	-101	513	1,436	2,009	2,316	2,568	2,757	2,935	3,285	3,514
104	475	-92	523	1,447	2,020	2,328	2,581	2,772	2,952	3,312	3,545
103	488	-81	538	1,465	2,039	2,348	2,604	2,797	2,978	3,352	3,592
102	496	-74	545	1,473	2,046	2,356	2,612	2,807	2,991	3,376	3,620
101	509	-62	563	1,495	2,071	2,383	2,643	2,840	3,025	3,424	3,673
100	514	-57	569	1,501	2,076	2,389	2,650	2,849	3,036	3,452	3,704
99	526	-49	581	1,517	2,094	2,410	2,676	2,883	3,075	3,491	3,745
98	526	-55	564	1,489	2,054	2,363	2,623	2,821	3,010	3,446	3,704
97	531	-55	577	1,518	2,097	2,418	2,677	2,875	3,065	3,487	3,742
96	525	-70	535	1,454	2,013	2,321	2,582	2,782	2,975	3,404	3,659
95	528	-59	558	1,494	2,059	2,371	2,629	2,823	3,012	3,442	3,705
94	525	-56	538	1,453	2,004	2,302	2,554	2,745	2,927	3,337	3,600
93	532	-30	584	1,516	2,072	2,370	2,623	2,815	3,000	3,450	3,714

Note: Compression is positive. Units are in kip.

Table 4–16. Total column loads on the south wall of WTC 1 for Case B conditions.

Floor	Before Impact	After Impact	10 min	20 min	30 min	40 min	50 min	60 min	70 min	80 min	90 min	100 min
105	8,092	7,488	6,981	7,057	7,569	8,129	8,315	8,414	8,481	8,551	7,327	7,066
104	8,532	7,918	7,411	7,484	7,996	8,560	8,746	8,844	8,909	8,979	7,729	7,462
103	8,929	8,307	7,800	7,869	8,382	8,947	9,133	9,230	9,295	9,364	8,077	7,799
102	9,365	8,734	8,226	8,292	8,806	9,375	9,562	9,658	9,722	9,789	8,478	8,194
101	9,753	9,114	8,605	8,667	9,180	9,751	9,937	10,032	10,094	10,161	8,808	8,514
100	10,197	9,548	9,038	9,094	9,608	10,182	10,368	10,463	10,523	10,590	9,229	8,932
99	10,581	9,924	9,414	9,466	9,979	10,554	10,738	10,829	10,886	10,951	9,504	9,194
98	11,025	10,356	9,848	9,900	10,420	11,004	11,192	11,285	11,343	11,409	9,949	9,638
97	11,409	10,736	10,224	10,262	10,761	11,327	11,503	11,586	11,638	11,703	10,278	9,959
96	11,874	11,167	10,664	10,713	11,230	11,811	11,996	12,087	12,145	12,198	10,765	10,454
95	12,258	11,518	11,007	11,044	11,548	12,116	12,293	12,380	12,436	12,488	11,004	10,676
94	12,733	11,954	11,451	11,498	12,016	12,601	12,790	12,885	12,946	13,007	11,505	11,175
93	13,116	12,309	11,795	11,832	12,339	12,913	13,094	13,181	13,239	13,291	11,850	11,518

Note: Compression is positive. Units are in kip.

Table 4–17. Change in total column loads on the south wall of WTC 1 for Case B conditions from the state before aircraft impact.

Floor	After Impact	10 min	20 min	30 min	40 min	50 min	60 min	70 min	80 min	90 min	100 min
105	-604	-1,111	-1,035	-523	37	223	322	389	459	-765	-1,026
104	-614	-1,121	-1,048	-536	28	214	312	377	447	-803	-1,070
103	-622	-1,129	-1,060	-548	18	204	301	366	435	-852	-1,130
102	-632	-1,140	-1,074	-560	10	196	293	356	424	-887	-1,171
101	-639	-1,148	-1,087	-573	-2	184	279	341	408	-945	-1,239
100	-650	-1,160	-1,103	-590	-15	171	266	326	392	-968	-1,266
99	-656	-1,166	-1,115	-601	-27	157	249	305	370	-1,077	-1,387
98	-668	-1,176	-1,125	-605	-21	167	260	319	384	-1,075	-1,387
97	-673	-1,185	-1,147	-648	-82	94	177	229	294	-1,131	-1,450
96	-707	-1,210	-1,161	-644	-62	122	213	271	324	-1,109	-1,420
95	-740	-1,251	-1,214	-710	-142	35	122	178	230	-1,254	-1,582
94	-779	-1,283	-1,236	-717	-132	57	152	213	274	-1,229	-1,558
93	-808	-1,321	-1,284	-778	-204	-23	65	122	175	-1,266	-1,598

Note: Compression is positive. Units are in kip.

Table 4–18. Summation of total column loads on the west wall of WTC 1 for Case B conditions.

Floor	Before Impact	After Impact	10 min	20 min	30 min	40 min	50 min	60 min	70 min	80 min	90 min	100 min
105	6,604	7,076	6,469	7,158	7,685	8,147	8,428	8,687	8,914	9,097	9,506	9,720
104	6,880	7,365	6,759	7,447	7,973	8,436	8,717	8,977	9,204	9,387	9,814	10,031
103	7,190	7,689	7,085	7,773	8,299	8,763	9,045	9,306	9,533	9,716	10,168	10,391
102	7,451	7,964	7,360	8,046	8,570	9,035	9,317	9,577	9,804	9,987	10,455	10,681
101	7,764	8,292	7,690	8,376	8,902	9,367	9,650	9,912	10,139	10,322	10,821	11,052
100	8,018	8,561	7,961	8,644	9,168	9,634	9,918	10,180	10,407	10,589	11,103	11,335
99	8,334	8,893	8,293	8,973	9,495	9,963	10,248	10,512	10,740	10,924	11,460	11,702
98	8,572	9,146	8,536	9,202	9,715	10,178	10,458	10,716	10,939	11,119	11,657	11,905
97	8,892	9,483	8,875	9,551	10,073	10,539	10,823	11,087	11,315	11,500	12,025	12,270
96	9,132	9,742	9,114	9,767	10,267	10,719	11,000	11,260	11,485	11,675	12,234	12,487
95	9,455	10,087	9,464	10,142	10,656	11,119	11,402	11,662	11,887	12,075	12,636	12,889
94	9,688	10,341	9,713	10,386	10,891	11,344	11,616	11,862	12,082	12,266	12,848	13,112
93	10,015	10,698	10,076	10,775	11,297	11,764	12,047	12,306	12,531	12,719	13,308	13,571

Note: Compression is positive. Units are in kip.

Table 4–19. Change in total column loads on the west wall of WTC 1 for Case B conditions from the state before aircraft impact.

Floor	After Impact	10 min	20 min	30 min	40 min	50 min	60 min	70 min	80 min	90 min	100 min
105	472	-135	554	1,081	1,543	1,824	2,083	2,310	2,493	2,902	3,116
104	485	-121	567	1,094	1,557	1,838	2,097	2,324	2,507	2,934	3,152
103	499	-105	583	1,109	1,573	1,855	2,116	2,343	2,526	2,978	3,201
102	514	-91	595	1,120	1,584	1,866	2,127	2,354	2,536	3,004	3,230
101	528	-73	612	1,138	1,603	1,886	2,148	2,376	2,558	3,057	3,289
100	543	-57	626	1,150	1,616	1,900	2,162	2,389	2,572	3,085	3,318
99	558	-41	638	1,161	1,628	1,913	2,177	2,406	2,589	3,126	3,368
98	574	-36	630	1,143	1,606	1,886	2,145	2,367	2,547	3,085	3,333
97	592	-17	660	1,182	1,647	1,931	2,195	2,424	2,608	3,133	3,378
96	611	-18	636	1,135	1,587	1,868	2,128	2,354	2,544	3,103	3,355
95	632	9	687	1,201	1,664	1,947	2,207	2,431	2,620	3,181	3,434
94	654	25	698	1,203	1,657	1,929	2,174	2,394	2,578	3,160	3,425
93	683	61	760	1,282	1,749	2,032	2,291	2,515	2,704	3,293	3,556

Note: Compression is positive. Units are in kip.

Table 4–20. Total column loads on the core of WTC 1 for Case B conditions.

Floor	Before Impact	After Impact	10 min	20 min	30 min	40 min	50 min	60 min	70 min	80 min	90 min	100 min
105	20,361	20,761	22,790	20,806	18,377	16,608	15,743	15,069	14,502	13,978	14,876	14,767
104	22,340	22,740	24,771	22,786	20,355	18,586	17,720	17,045	16,478	15,953	16,853	16,744
103	24,311	24,712	26,744	24,758	22,326	20,555	19,690	19,014	18,447	17,922	18,821	18,712
102	26,267	26,668	28,701	26,715	24,282	22,510	21,644	20,968	20,401	19,875	20,775	20,666
101	28,228	28,628	30,663	28,677	26,242	24,469	23,603	22,926	22,359	21,833	22,734	22,625
100	30,177	30,576	32,614	30,628	28,192	26,420	25,554	24,876	24,310	23,783	24,686	24,577
99	32,127	32,525	34,565	32,579	30,139	28,363	27,497	26,819	26,250	25,724	26,634	26,524
98	34,029	34,429	36,473	34,495	32,060	30,294	29,435	28,766	28,205	27,681	28,587	28,478
97	35,988	36,387	38,425	36,458	34,031	32,275	31,422	30,760	30,203	29,674	30,592	30,487
96	37,956	38,217	40,264	38,305	35,878	34,129	33,279	32,617	32,060	31,540	32,455	32,349
95	39,925	39,872	41,961	39,998	37,573	35,816	34,974	34,314	33,758	33,240	34,151	34,044
94	41,903	41,551	43,648	41,681	39,251	37,503	36,655	35,995	35,441	34,924	35,847	35,742
93	43,859	43,304	45,394	43,429	40,998	39,247	38,400	37,742	37,188	36,673	37,561	37,455

Note: Compression is positive. Units are in kip.

Table 4–21. Change in total column loads on the core of WTC 1 for Case B conditions from the state before aircraft impact.

Floor	After Impact	10 min	20 min	30 min	40 min	50 min	60 min	70 min	80 min	90 min	100 min
105	400	2,430	445	-1,984	-3,752	-4,617	-5,292	-5,858	-6,383	-5,484	-5,593
104	400	2,431	446	-1,985	-3,754	-4,620	-5,295	-5,862	-6,387	-5,487	-5,596
103	400	2,432	447	-1,985	-3,756	-4,622	-5,297	-5,864	-6,390	-5,490	-5,599
102	400	2,433	448	-1,986	-3,757	-4,623	-5,300	-5,867	-6,392	-5,492	-5,601
101	400	2,435	449	-1,986	-3,758	-4,624	-5,301	-5,868	-6,395	-5,493	-5,603
100	399	2,436	451	-1,985	-3,757	-4,623	-5,301	-5,867	-6,394	-5,491	-5,600
99	399	2,438	452	-1,988	-3,763	-4,630	-5,308	-5,876	-6,402	-5,493	-5,602
98	400	2,444	466	-1,969	-3,735	-4,594	-5,263	-5,824	-6,348	-5,443	-5,552
97	399	2,437	470	-1,956	-3,713	-4,566	-5,228	-5,785	-6,314	-5,396	-5,501
96	261	2,307	349	-2,079	-3,827	-4,677	-5,339	-5,897	-6,417	-5,501	-5,607
95	-53	2,037	73	-2,352	-4,108	-4,950	-5,610	-6,167	-6,685	-5,773	-5,880
94	-352	1,745	-223	-2,653	-4,401	-5,248	-5,908	-6,462	-6,979	-6,056	-6,162
93	-556	1,534	-431	-2,861	-4,613	-5,460	-6,117	-6,671	-7,186	-6,298	-6,405

Note: Compression is positive. Units are in kip.

Table 4–22. Change in total column loads before and after aircraft impact. (Loads after impact) – (Loads before impact)

Row	Floor	North	East	South	West	Core
(1)	Floor 98	-837	526	-668	574	400
(2)	Floor 105	-732	466	-604	472	400
(3)	(2) - (1)	105	-60	64	-103	0

Note: Increase in compression is shown as positive. Units are in kip.

Table 4–23. Change in total column loads after aircraft impact and at 80 min for Case B conditions. (Loads at 80 min) – (Loads After Impact)

Row	Floor	North	East	South	West	Core
(1)	Floor 98	1,239	2,484	1,052	1,973	-6,748
(2)	Floor 105	1,234	2,470	1,063	2,021	-6,783
(3)	(2) - (1)	-5	-15	11	48	-35

Note: Increase in compression is shown as positive. Units are in kip.

Table 4–24. Change in total column loads at 80 min and at 100 min for Case B conditions. (Loads at 100 min) – (Loads at 80 min)

Row	Floor	North	East	South	West	Core
(1)	Floor 98	-548	694	-1,771	786	797
(2)	Floor 105	-504	579	-1,485	623	790
(3)	(2) - (1)	44	-115	285	-163	-7

Note: Increase in compression is shown as positive. Units are in kip.

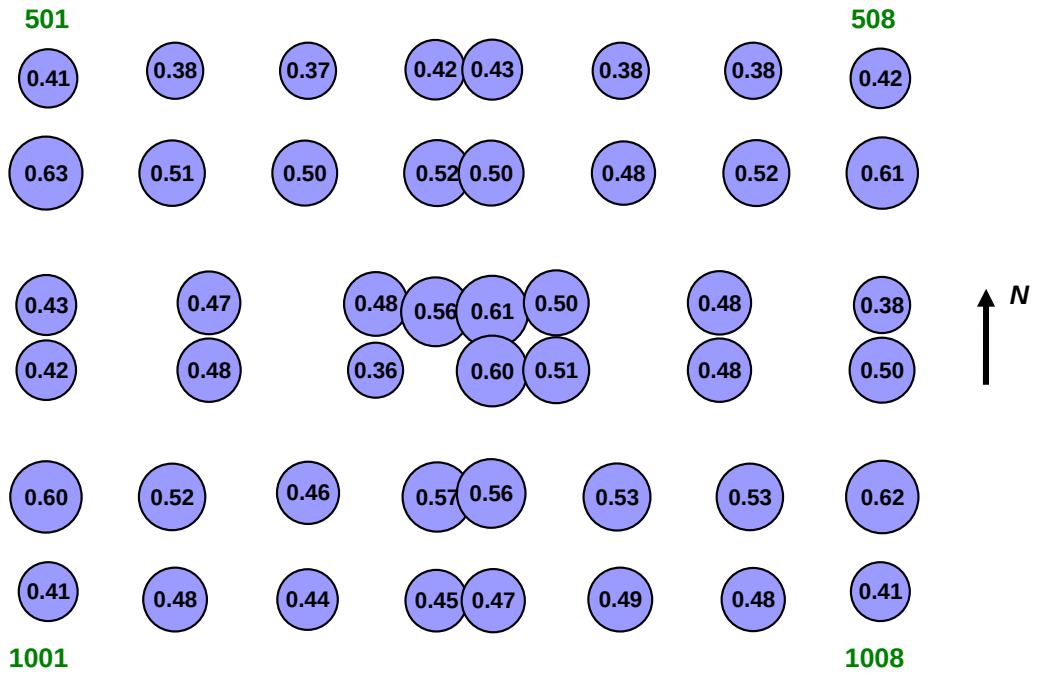

Figure 4–68. Maximum demand-to-capacity ratio for axial load in core columns between Floor 93 and Floor 99 of WTC 1 before aircraft impact.

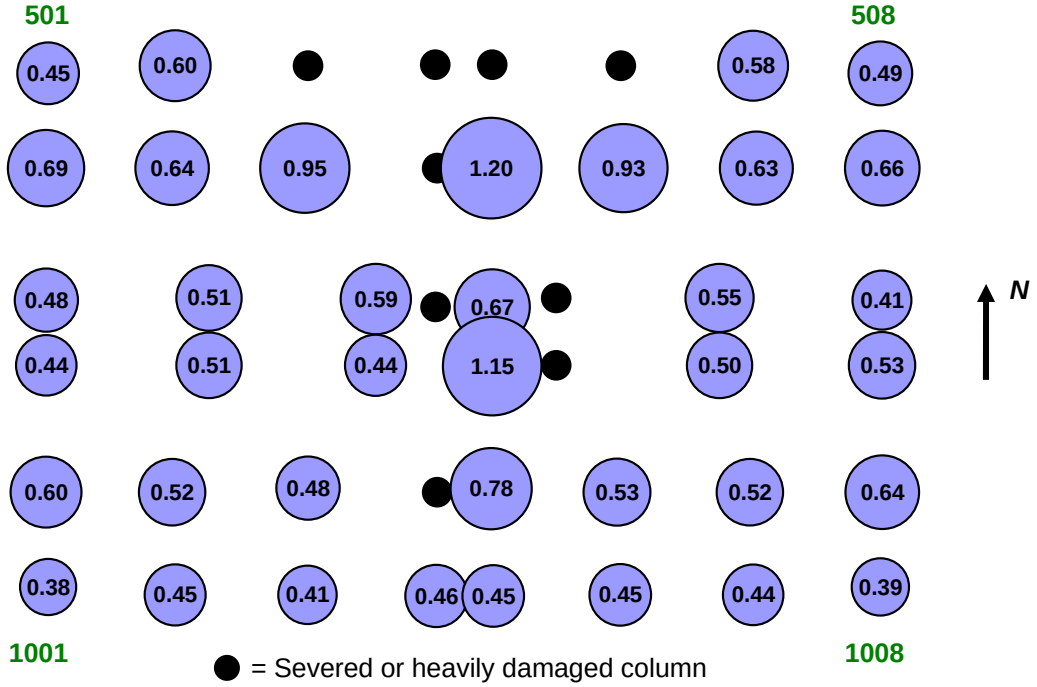

Figure 4–69. Maximum demand-to-capacity ratio for axial load in core columns between Floor 93 and Floor 99 of WTC 1 after aircraft impact for Case B conditions.

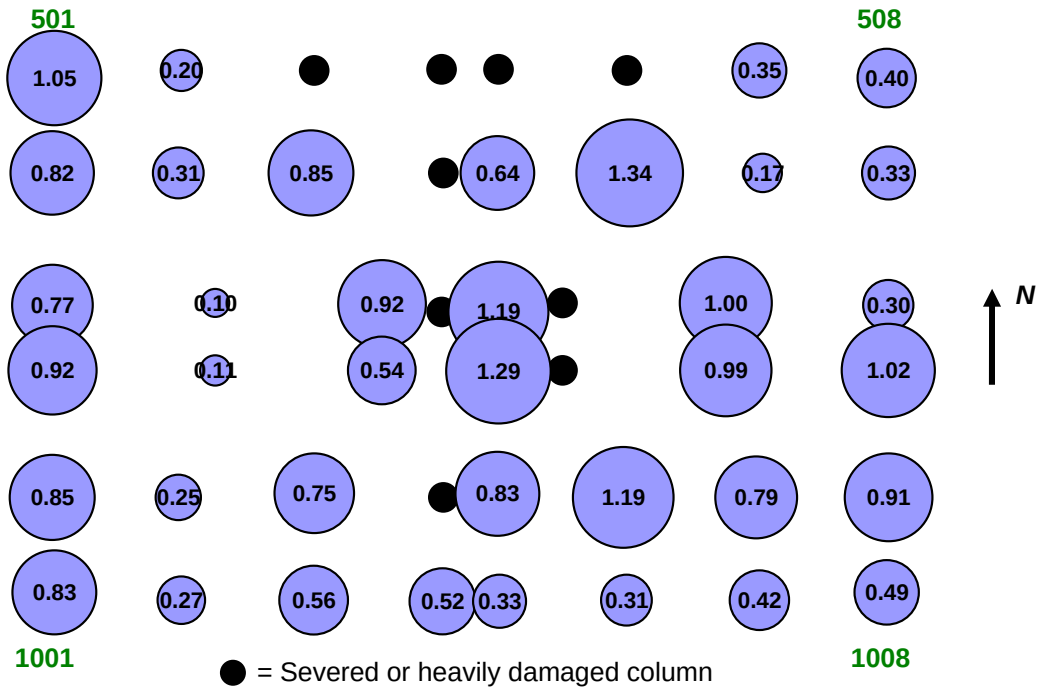

Figure 4–70. Maximum demand-to-capacity ratio for axial load in core columns between Floor 93 and Floor 99 of WTC 1 at 80 min for Case B conditions.

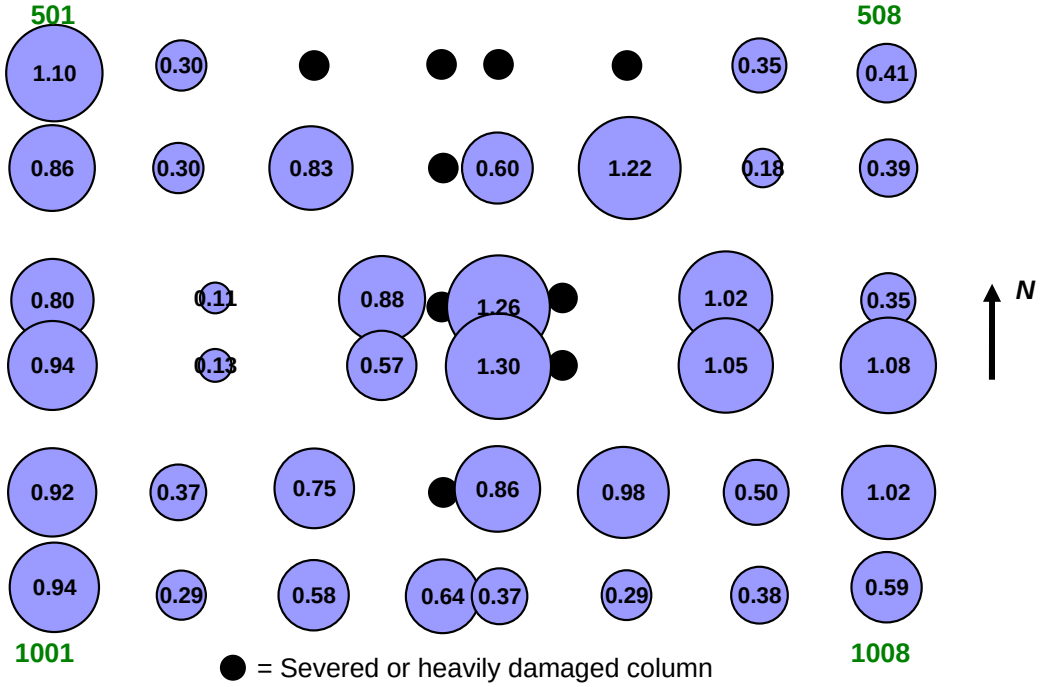

Figure 4–71. Maximum demand-to-capacity ratio for axial load in core columns between Floor 93 and Floor 99 of WTC 1 at 100 min for Case B conditions with 5 kip pull-in forces.

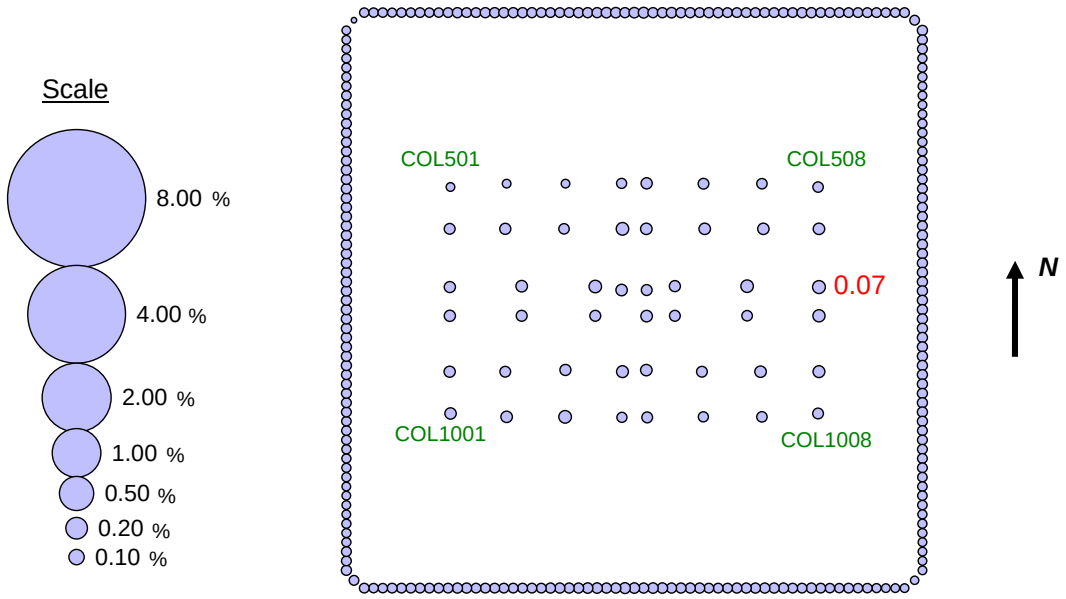

Figure 4–72. Maximum elastic-plus-plastic strain for columns between Floor 93 and Floor 99 of WTC 1 before aircraft impact (compressive strain is positive; strain values are in percent).

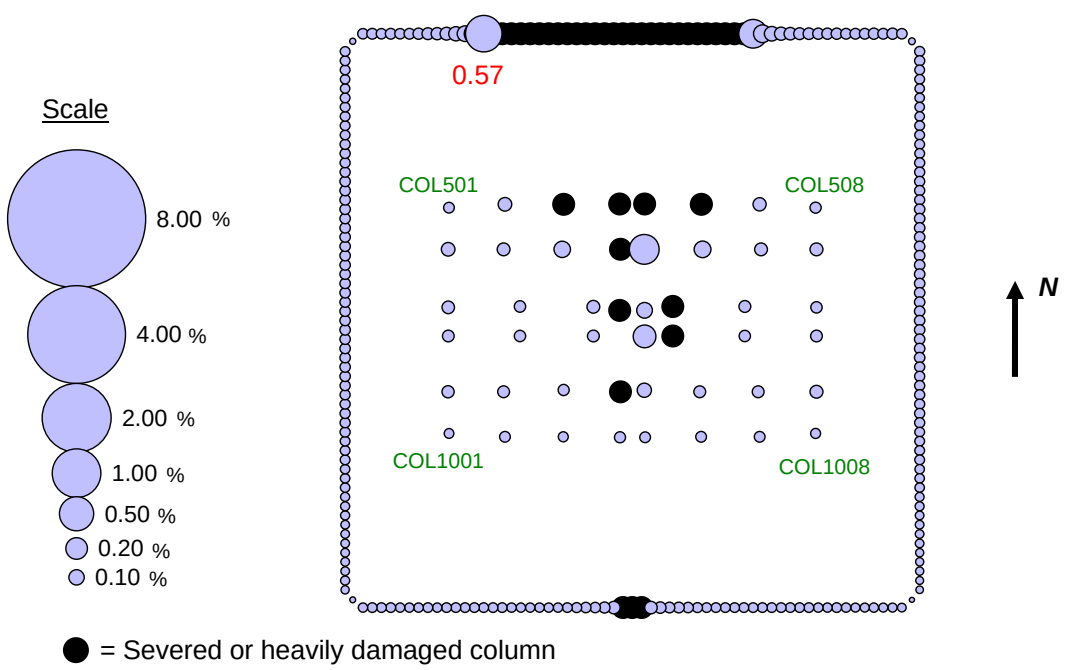

Figure 4–73. Maximum elastic-plus-plastic strain for columns between Floor 93 and Floor 99 of WTC 1 after aircraft impact for Case B conditions (compressive strain is positive; strain values are in percent).

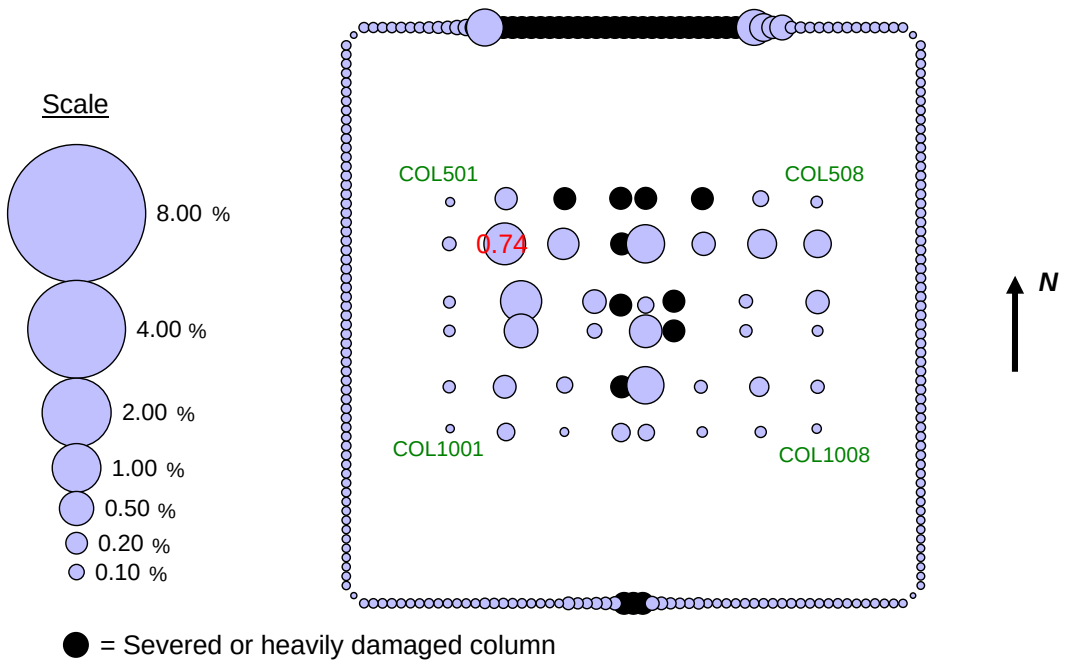

Figure 4–74. Maximum elastic-plus-plastic strain for columns between Floor 93 and Floor 99 of WTC 1 at 10 min for Case B conditions (compressive strain is positive; strain values are in percent).

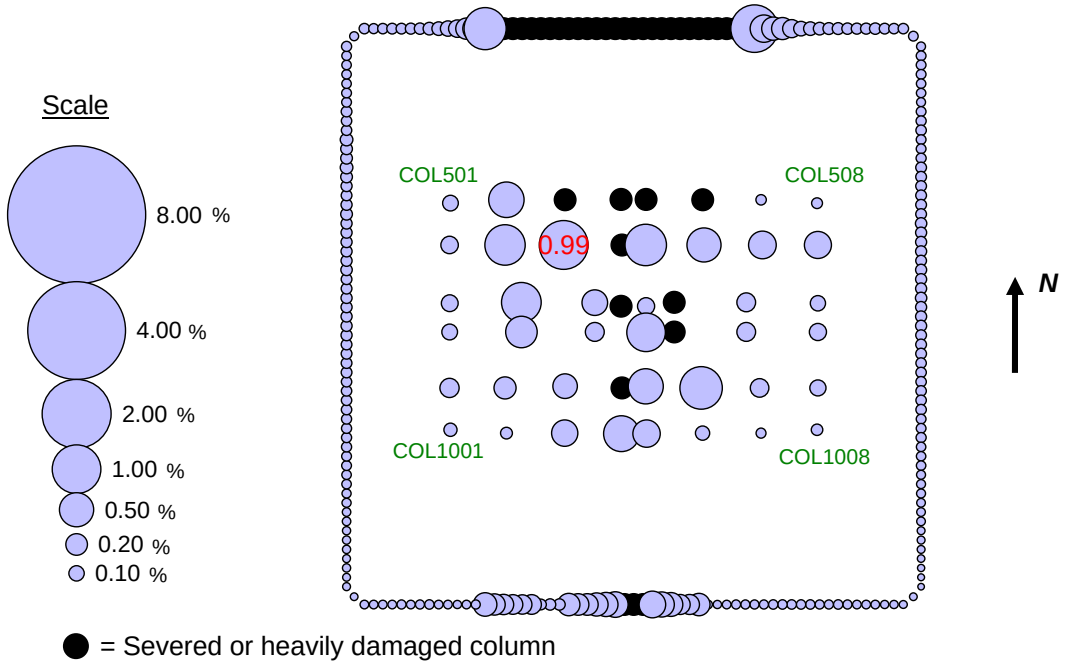

Figure 4–75. Maximum elastic-plus-plastic strain for columns between Floor 93 and Floor 99 of WTC 1 at 40 min for Case B conditions (compressive strain is positive; strain values are in percent).

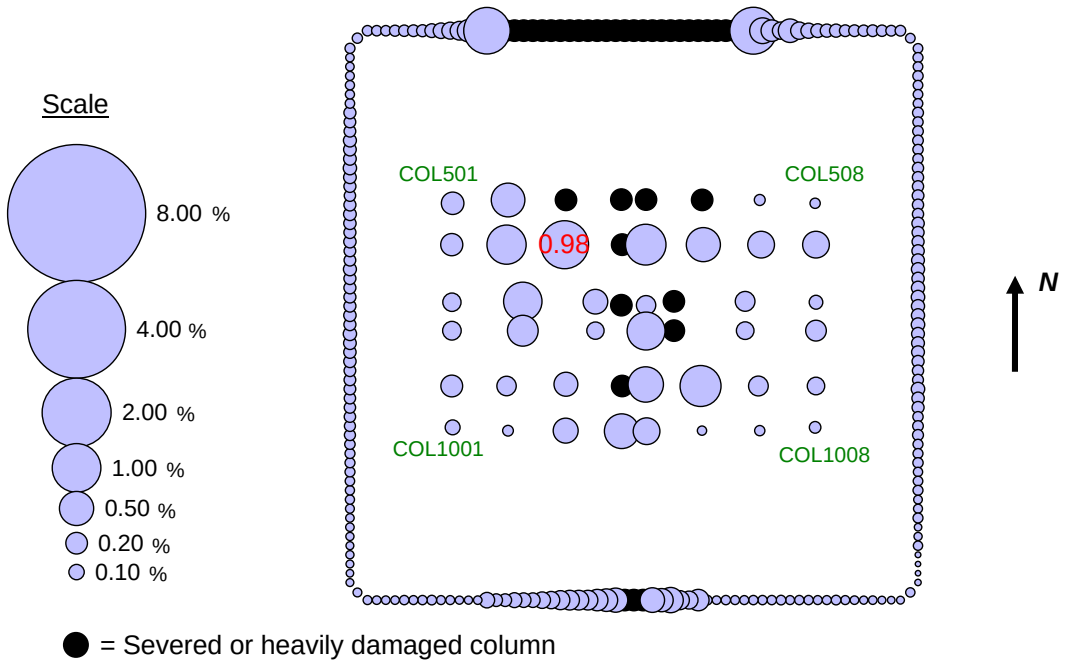

Figure 4–76. Maximum elastic-plus-plastic strain for columns between Floor 93 and Floor 99 of WTC 1 at 80 min for Case B conditions (compressive strain is positive; strain values are in percent).

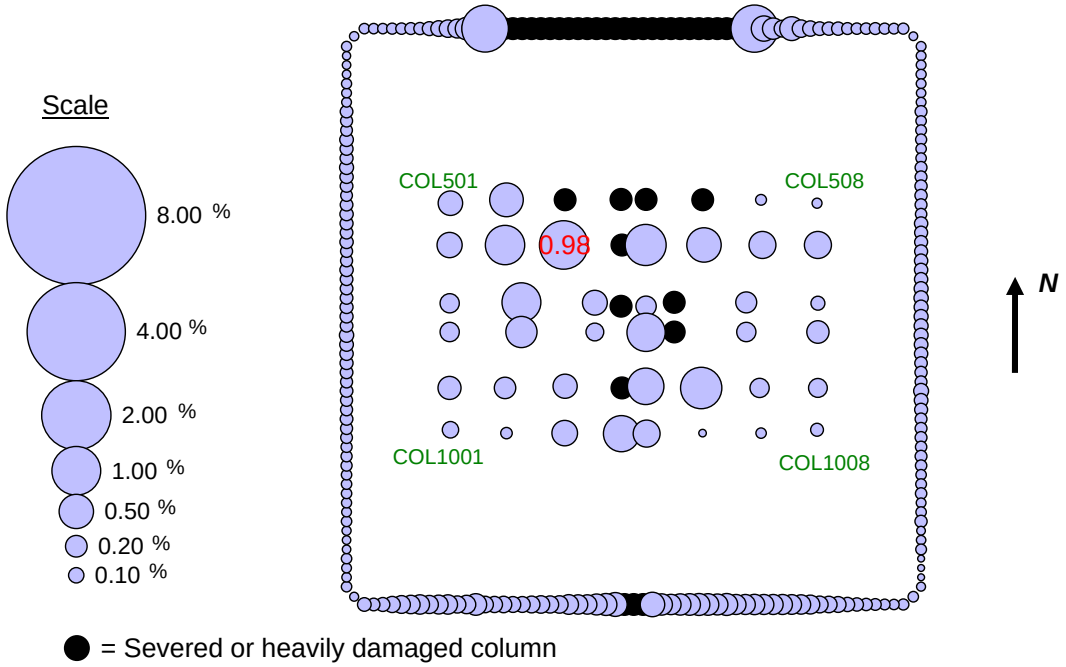

Figure 4–77. Maximum elastic-plus-plastic strain for columns between Floor 93 and Floor 99 of WTC 1 at 100 min for Case B conditions with 5 kip pull-in forces (compressive strain is positive; strain values are in percent).

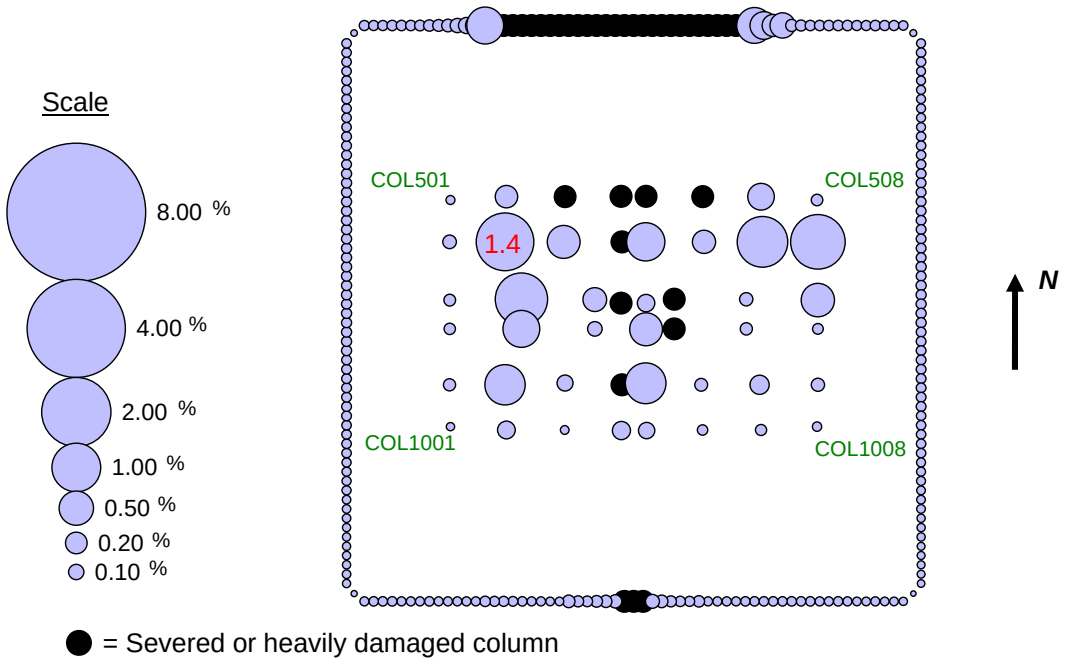

Figure 4–78. Maximum elastic-plus-plastic-plus-creep strain for columns between Floor 93 and Floor 99 of WTC 1 at 10 min for Case B conditions (compressive strain is positive; strain values are in percent).

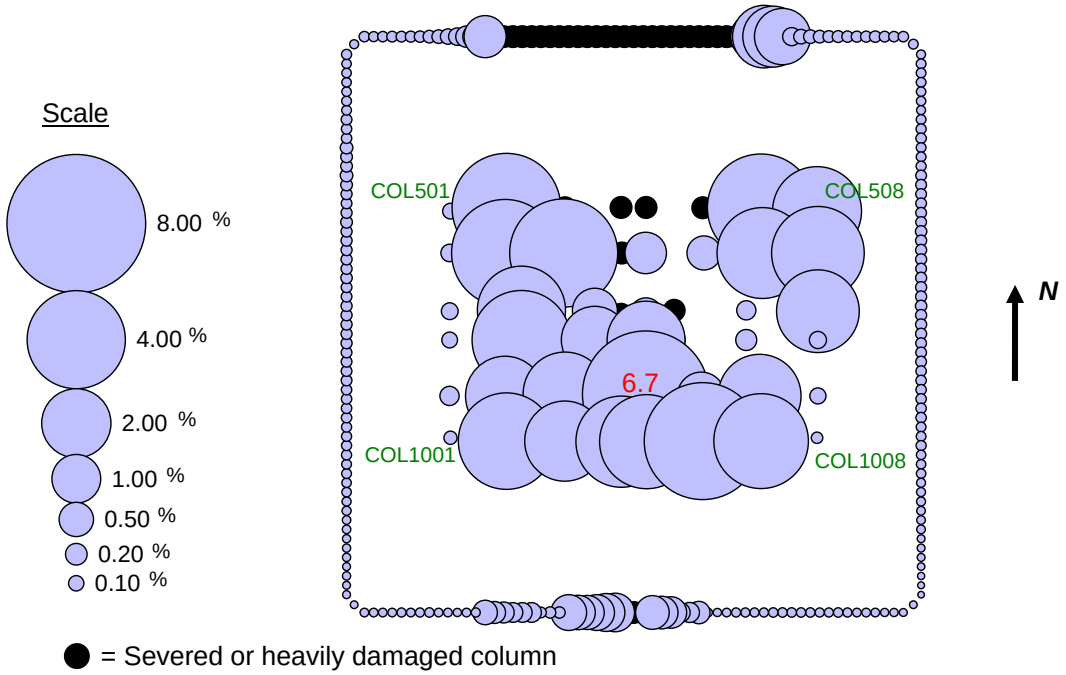

Figure 4–79. Maximum elastic-plus-plastic-plus-creep strain for columns between Floor 93 and Floor 99 of WTC 1 at 40 min for Case B conditions (compressive strain is positive; strain values are in percent).

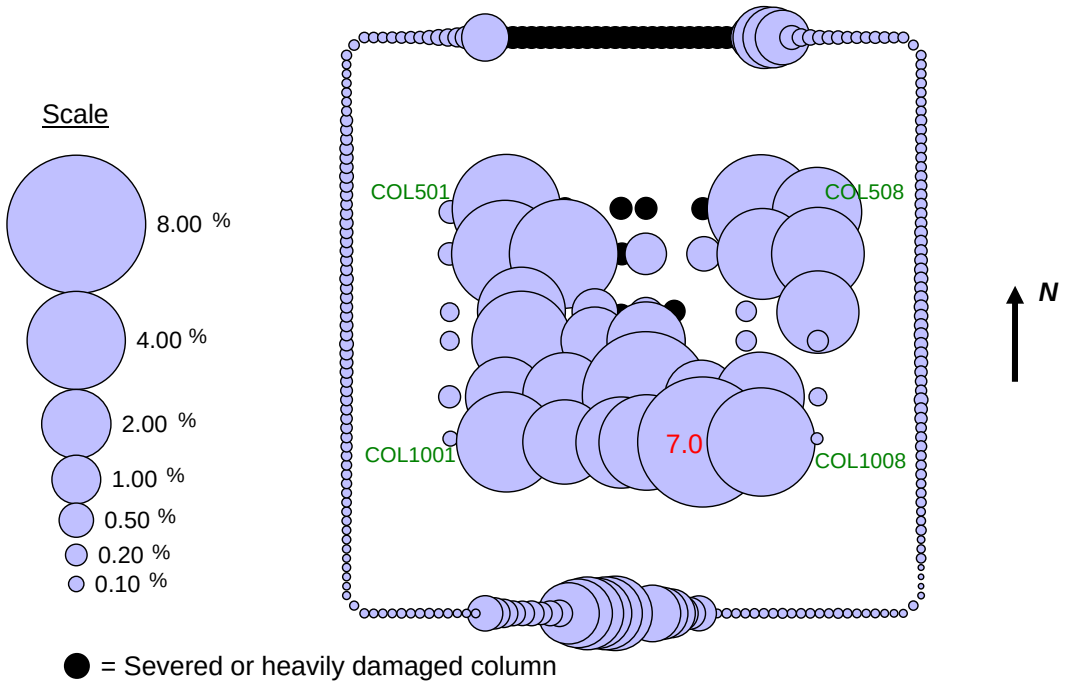

Figure 4–80. Maximum elastic-plus-plastic-plus-creep strain for columns between Floor 93 and Floor 99 of WTC 1 at 80 min for Case B conditions (compressive strain is positive; strain values are in percent).

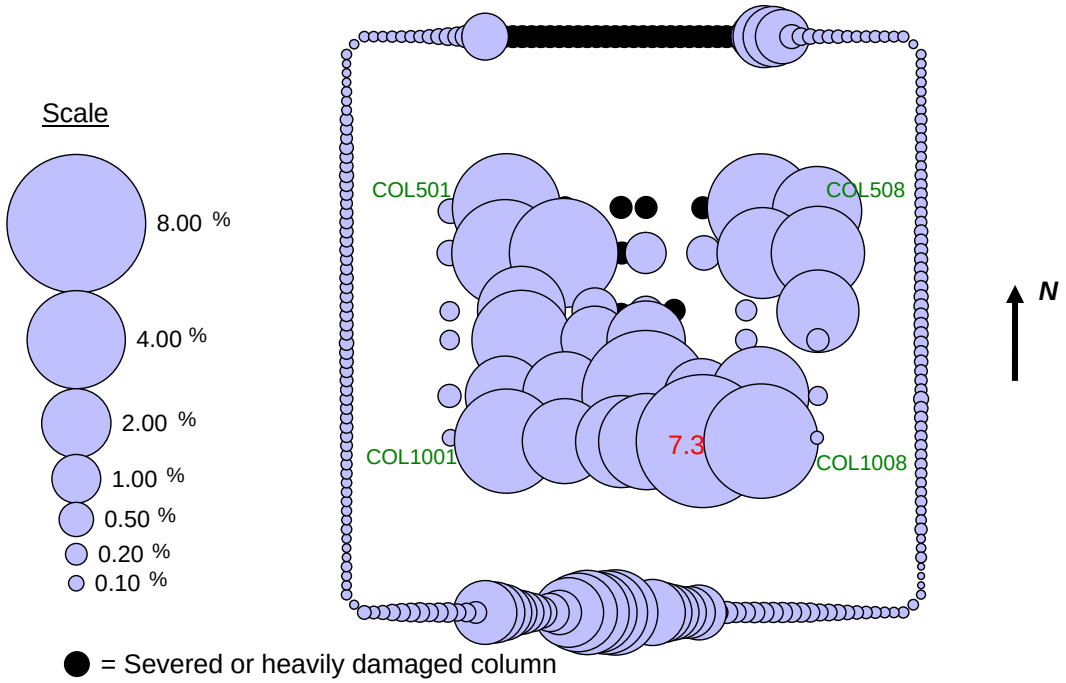

Figure 4–81. Maximum elastic-plus-plastic-plus-creep strain for columns between Floor 93 and Floor 99 of WTC 1 at 100 min for Case B conditions with 5 kip pull-in forces (compressive strain is positive; strain value are in percent).

Table 4–25. Tension capacity of core column splices at Floor 106

	Column Line					
Col #	**500**	**600**	**700**	**800**	**900**	**1000**
1	460	335	335	335	335	460
2	335	335	335	335	335	335
3	335	335	335	335	460	460
4	335	335	335	335	335	335
5	335	335	335	335	335	335
6	335	335	335	335	335	335
7	335	335	335	335	335	335
8	460	335	335		335	460

Note: Units are in kip.

Table 4–26. Axial load in core columns at Floor 105 of WTC 1 for Case B conditions

Column ID	Before Impact	After Impact	10 min	20 min	30 min	40 min	50 min	60 min	70 min	80 min	90 min	100 min
501	753	1,033	976	1,326	1,504	1,634	1,690	1,703	1,661	1,635	1,595	1,563
502	567	751	996	569	416	353	303	266	210	156	90	44
503	632	469	631	312	129	57	23	-13	-63	-118	-190	-240
504	486	1	-49	-17	-34	-39	-32	-34	-36	-44	-70	-82
505	576	82	27	18	3	-8	-8	-8	-8	-16	-42	-52
506	629	512	544	311	311	324	320	313	314	315	281	266
507	558	676	774	466	328	313	304	296	303	312	284	275
508	743	1,057	1,185	1,108	587	493	469	455	448	430	399	389
601	219	272	239	341	383	413	423	432	432	427	427	420
602	395	524	612	310	206	153	103	69	30	-5	-21	-45
603	408	475	525	315	118	15	-28	-64	-94	-126	-130	-137
604	275	131	85	45	7	-16	-28	-38	-45	-51	-50	-52
605	320	149	70	20	-3	-17	-23	-28	-34	-38	-36	-37
606	408	428	415	334	327	325	313	303	295	291	298	299
607	371	447	470	350	286	268	247	232	224	222	230	235
608	224	296	335	255	165	149	134	123	116	113	123	128
701	355	418	363	518	594	658	684	705	718	722	733	733
702	395	529	652	232	145	85	17	-34	-73	-98	-88	-89
703	266	288	380	456	456	425	407	387	368	351	344	334
704	224	221	237	214	189	165	147	132	121	113	119	117
705	181	159	146	135	125	117	110	103	99	96	98	95
706	276	227	195	178	167	161	153	146	141	137	138	133
707	386	447	472	514	524	514	491	471	456	445	448	449
708	391	491	540	420	448	470	462	451	446	445	470	482
801	398	450	374	536	630	706	742	762	777	788	818	834
802	398	473	622	167	110	69	1	-55	-91	-108	-73	-54
803	298	298	417	542	521	470	445	423	402	383	389	383
804	192	173	179	166	146	136	125	119	119	116	127	127
805	329	188	145	105	85	85	76	72	73	71	86	86
806	395	454	502	567	631	652	642	635	630	620	626	624
807	362	432	439	399	449	480	489	493	497	498	528	540
901	253	273	217	280	343	398	422	436	450	460	496	517
902	385	425	470	268	241	193	152	112	95	88	135	167
903	523	606	833	847	653	491	435	393	358	336	358	349
904	298	287	397	322	192	116	71	47	43	42	76	77
905	278	271	332	259	150	96	66	55	60	59	89	89
906	406	464	507	646	616	516	477	455	409	354	351	319
907	413	457	485	534	513	468	456	458	455	441	438	425
908	239	274	242	274	321	350	366	378	387	392	425	438
1001	762	735	605	721	915	1,112	1,212	1,301	1,370	1,405	1,595	1,685
1002	614	611	759	560	527	432	405	382	367	353	453	465
1003	745	744	855	1,079	990	555	426	286	214	182	299	271
1004	522	525	809	719	416	194	106	46	15	15	148	150
1005	534	546	830	685	359	176	94	50	27	20	135	132
1006	637	634	682	904	661	408	348	321	288	242	273	230
1007	587	578	582	727	624	500	478	476	463	435	438	408
1008	758	785	687	770	902	991	1,030	1,055	1,067	1,070	1,216	1,274

Note: Compression is positive. Units are in kip.

Note: Shading indicates when core columns were in tension.

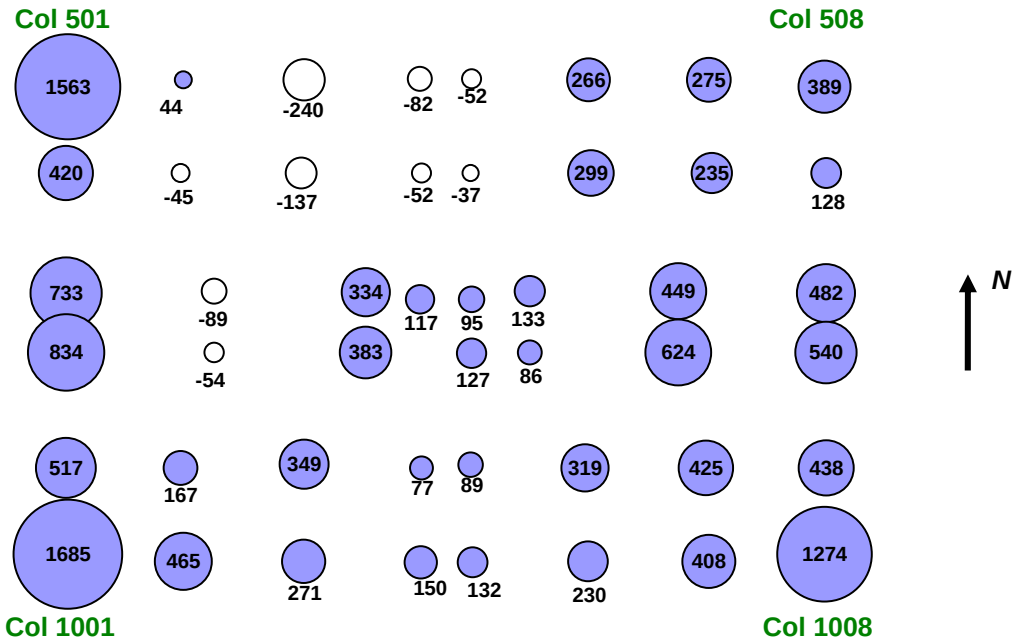

Figure 4–82. Axial load (kip) in core columns at Floor 105 of WTC 1 at 100 min for Case B conditions with 5 kip pull-in forces (compression is positive).

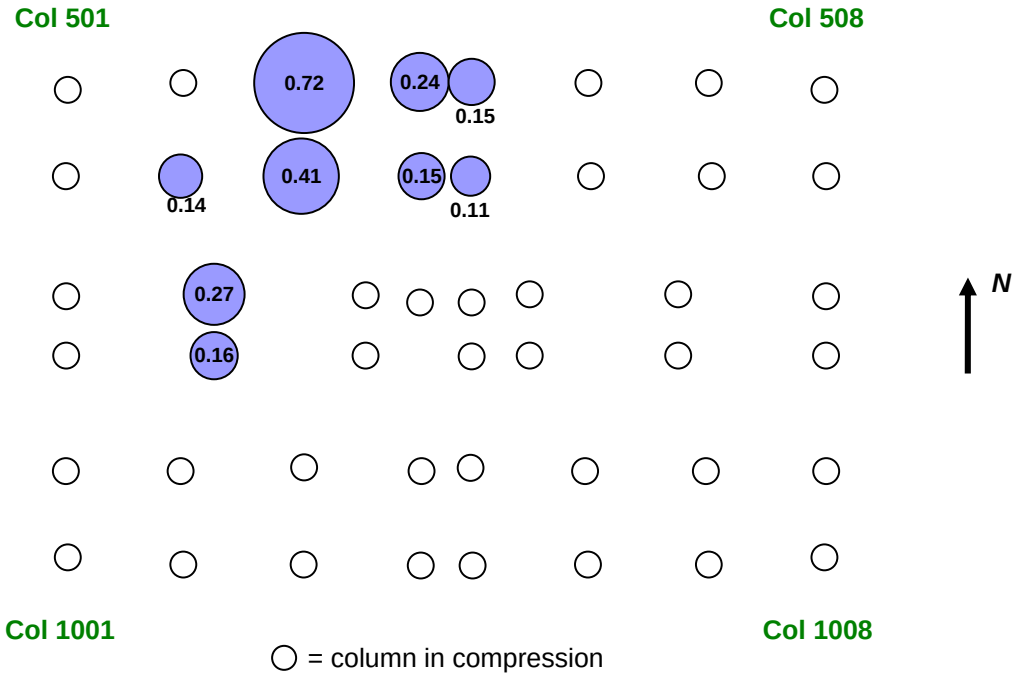

Figure 4–83. Tension demand-to-capacity ratio for core column splices at Floor 106 of WTC 1 at 100 min for Case B conditions with 5 kip pull-in forces.

Table 4–27. Demand-to-capacity ratio for axial load in outriggers of WTC 1 for Case B conditions (outrigger IDs are indicated in Fig. 4–3).

Outrigger ID	Bfr Imp	Aftr Imp	10 min	20 min	30 min	40 min	50 min	60 min	70 min	80 min	90 min	100 min
North												
A	0.26	0.35	0.26	0.40	0.49	0.53	0.56	0.59	0.62	0.65	0.54	0.52
B	0.22	-0.07	-0.13	-0.04	0.02	0.04	0.06	0.07	0.08	0.09	0.03	0.03
C	0.21	-0.05	-0.11	-0.02	0.04	0.06	0.08	0.08	0.09	0.11	0.05	0.04
D	0.25	0.35	0.29	0.45	0.61	0.67	0.70	0.72	0.73	0.75	0.65	0.63
East												
E	0.32	0.48	0.38	0.56	0.75	0.83	0.88	0.92	0.94	0.97	0.95	0.96
F	0.23	0.28	0.21	0.30	0.41	0.48	0.52	0.55	0.57	0.59	0.62	0.64
G	0.23	0.26	0.20	0.26	0.35	0.42	0.46	0.49	0.51	0.54	0.58	0.61
H	0.33	0.31	0.23	0.25	0.36	0.46	0.51	0.55	0.58	0.60	0.72	0.77
South												
I	0.25	0.12	0.04	0.03	0.12	0.20	0.23	0.26	0.27	0.28	0.28	0.28
J	0.21	0.10	0.01	0.03	0.13	0.24	0.28	0.29	0.30	0.31	0.04	-0.02
K	0.21	0.10	0.01	0.03	0.13	0.24	0.27	0.28	0.30	0.31	0.02	-0.04
L	0.26	0.12	0.02	0.05	0.11	0.20	0.24	0.27	0.29	0.31	0.19	0.18
West												
M	0.33	0.33	0.22	0.29	0.36	0.44	0.49	0.53	0.56	0.58	0.69	0.73
N	0.24	0.27	0.20	0.28	0.34	0.40	0.44	0.47	0.50	0.52	0.56	0.58
O	0.24	0.29	0.22	0.31	0.38	0.43	0.47	0.50	0.53	0.55	0.59	0.61
P	0.33	0.48	0.39	0.54	0.64	0.71	0.75	0.79	0.83	0.87	0.88	0.90

Table 4–28. Demand to capacity ratio for axial load in exterior columns supporting outriggers at Floor 107 of WTC 1 for Case B conditions.

Column ID	Bfr Imp	Aftr Imp	10 min	20 min	30 min	40 min	50 min	60 min	70 min	80 min	90 min	100 min
North												
110	0.30	0.40	0.35	0.43	0.48	0.51	0.53	0.54	0.56	0.58	0.52	0.51
111	0.24	0.31	0.28	0.33	0.36	0.37	0.38	0.39	0.40	0.41	0.37	0.37
129	0.28	0.00	-0.05	0.02	0.08	0.10	0.11	0.11	0.12	0.14	0.09	0.08
130	0.30	0.04	0.00	0.06	0.11	0.13	0.14	0.15	0.16	0.17	0.12	0.11
131	0.30	0.02	-0.03	0.04	0.10	0.12	0.13	0.13	0.14	0.16	0.10	0.10
149	0.25	0.30	0.28	0.33	0.39	0.41	0.42	0.43	0.43	0.44	0.41	0.40
150	0.25	0.31	0.29	0.36	0.43	0.46	0.48	0.49	0.49	0.50	0.45	0.44
East												
217	0.20	0.26	0.23	0.29	0.38	0.41	0.43	0.45	0.46	0.47	0.46	0.47
218	0.25	0.34	0.28	0.38	0.51	0.57	0.60	0.63	0.65	0.67	0.66	0.67
228	0.30	0.35	0.28	0.36	0.47	0.53	0.57	0.59	0.62	0.64	0.67	0.69
229	0.22	0.25	0.20	0.26	0.34	0.38	0.41	0.43	0.45	0.46	0.49	0.50
231	0.22	0.25	0.20	0.25	0.32	0.37	0.40	0.42	0.43	0.45	0.48	0.49
232	0.30	0.33	0.27	0.33	0.42	0.48	0.52	0.55	0.57	0.59	0.63	0.65
242	0.25	0.25	0.20	0.21	0.28	0.33	0.36	0.39	0.40	0.42	0.50	0.53
243	0.20	0.20	0.17	0.18	0.22	0.25	0.27	0.29	0.30	0.31	0.36	0.38
South												
310	0.30	0.23	0.19	0.19	0.23	0.28	0.29	0.31	0.31	0.32	0.33	0.33
311	0.24	0.20	0.18	0.17	0.20	0.22	0.23	0.24	0.24	0.25	0.25	0.25
329	0.27	0.17	0.10	0.12	0.20	0.29	0.32	0.33	0.33	0.34	0.10	0.05
330	0.34	0.23	0.14	0.16	0.26	0.37	0.40	0.41	0.41	0.43	0.13	0.07
331	0.27	0.18	0.10	0.12	0.21	0.30	0.32	0.32	0.33	0.34	0.10	0.05
349	0.24	0.20	0.17	0.18	0.20	0.22	0.23	0.25	0.25	0.26	0.22	0.22
350	0.31	0.23	0.18	0.20	0.23	0.27	0.30	0.31	0.33	0.33	0.28	0.28
West												
417	0.21	0.21	0.17	0.19	0.22	0.25	0.27	0.29	0.30	0.31	0.35	0.37
418	0.25	0.25	0.19	0.23	0.27	0.32	0.34	0.37	0.38	0.40	0.46	0.49
428	0.30	0.34	0.27	0.35	0.41	0.46	0.49	0.52	0.55	0.56	0.60	0.62
429	0.23	0.26	0.20	0.26	0.31	0.35	0.37	0.40	0.41	0.43	0.46	0.47
431	0.23	0.26	0.21	0.27	0.32	0.36	0.39	0.41	0.43	0.44	0.47	0.48
432	0.30	0.35	0.28	0.37	0.43	0.48	0.51	0.54	0.57	0.59	0.62	0.64
442	0.25	0.34	0.28	0.37	0.44	0.48	0.51	0.54	0.57	0.59	0.60	0.62
443	0.21	0.26	0.23	0.29	0.33	0.36	0.37	0.39	0.41	0.43	0.43	0.44

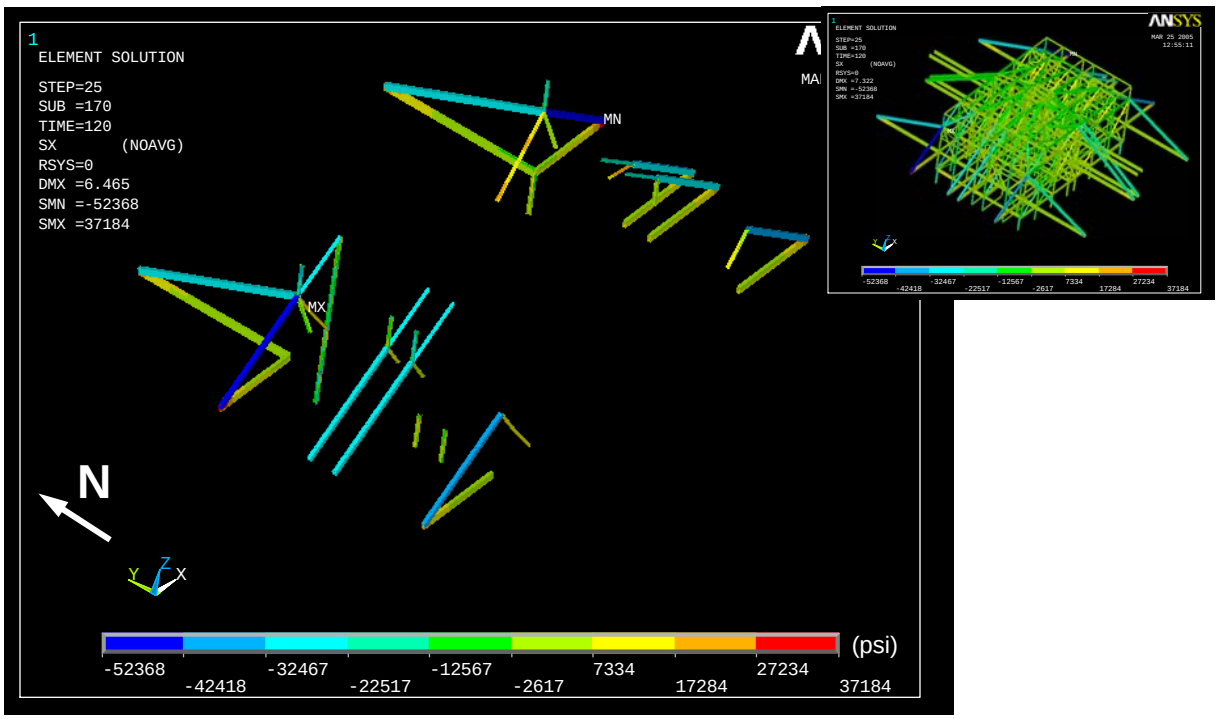

Figure 4–84. Primary load path within the hat truss of WTC 1.

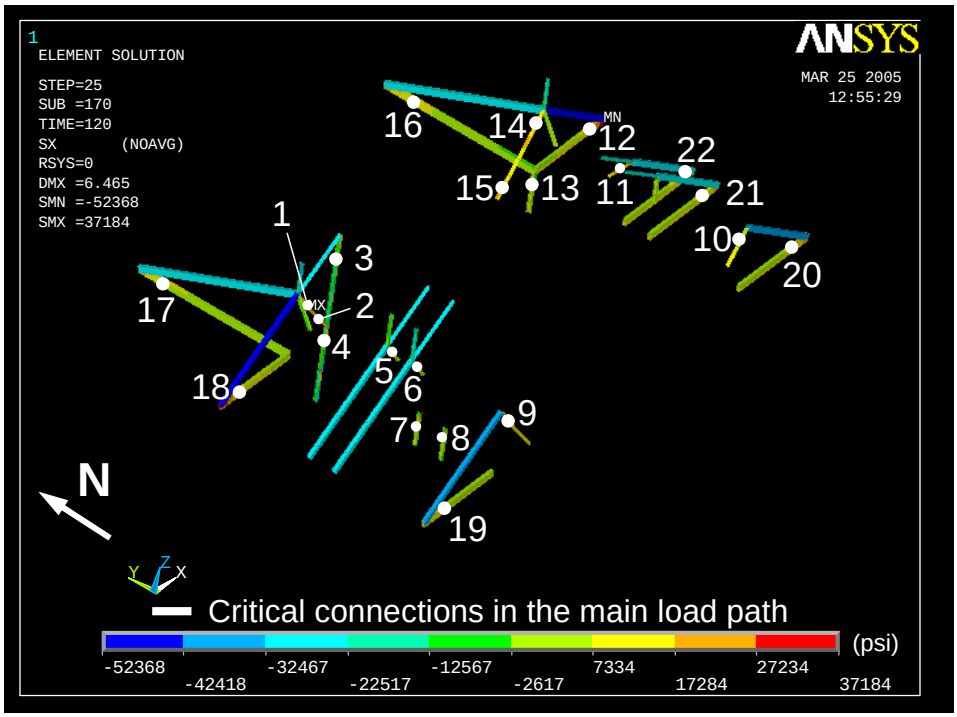

Figure 4–85. Location of the hat truss connections in the primary load path.

Table 4–29. Demand and capacity of the hat truss connections (kip) in the primary load path at 80 min (connection IDs are shown in Fig. 4–85).

Connection	Location		Tension Capacity		Demand Force	State
ID	Floor	Column	Yield	Ultimate	(tension)	
1	110	501	1,250	1,250	680	Safe
2	108	502	1,250	1,250	680	Safe
3	111	502	1,930	1,930	80	Safe
4	108	502	520	520	100	Safe
5	110	701	1,340	1,340	390	Safe
6	107	702	950	950	370	Safe
7	110	801	1,340	1,340	140	Safe
8	107	802	335	260	140	Safe
9	110	1001	1,250	1,250	400	Safe
10	110	1008	1,250	1,250	290	Safe
11	110	708	1,340	1,340	360	Safe
12	108	217-218	4,520	5,880	1,810	Safe
13	108	508	870	760	410	Safe
14	110	508	1,250	1,250	530	Safe
15	108	507	1,250	1,250	530	Safe
16	108	149-150	2,640	2,640	1,310	Safe
17	108	110-111	2,640	2,640	1,170	Safe
18	108	442-443	4,520	5,880	1,650	Safe
19	108	417-418	4,520	5,880	1,200	Safe
20	108	242-243	4,520	5,880	1,230	Safe
21	108	231-232	3,010	3,920	1,070	Safe
22	108	228-229	3,010	3,920	1,150	Safe

4.2.5 Simulation of WTC 2 Collapse

The global model of WTC 2, as described in Sections 4.1.1 to 4.2.3, was used to simulate the response of the building to aircraft impact damage and the ensuing fire environment. Studies performed on the isolated exterior wall and core models and on the full floor subsystem models indicated that the calculated response of these models to the Case D damage and temperature time history set more closely matched the structural behavior observable in photographic and video evidence than did analyses using Case C. Therefore, in this global analysis only the Case D damage and temperature time history set were used. Section 2.2 of this report provides a description of the Case D structural impact damage set. The analysis started with dead and 25 percent of the design live loads taken directly from the reference SAP2000 models and applied as concentrated loads at each column-floor node. Table 4–30 summarizes the sequence of analyses that were performed. Section 2.5 gives the locations of floor/wall disconnections and pull-in forces at different analysis steps. The results of each analysis step were used as the initial conditions for the next analysis step.

Table 4–30. Analysis Steps of WTC 2 ANSYS global model with Case D conditions.

Analysis Step	Description
1	Dead and 25 percent of the design live loads were applied on the model of WTC 2 with impact damage.
2	Floor/wall disconnections and pull-in forces that were projected to occur between 0 min and 10 min were applied.
3	Column and spandrel temperatures were linearly ramped up from room temperature of 20 °C to temperatures at 10 min.
4	Floor/wall disconnections and pull-in forces that were projected to occur between 10 min and 20 min were applied.
5	Column and spandrel temperatures were linearly changed from temperatures at 10 min to 20 min.
6	Floor/wall disconnections and pull-in forces that were projected to occur between 20 min and 30 min were applied.
7	Column and spandrel temperatures were linearly changed from temperatures at 20 min to 30 min.
8	Floor/wall disconnections and pull-in forces that were projected to occur between 30 min and 40 min were applied.
9	Column and spandrel temperatures were linearly changed from temperatures at 30 min to 40 min.
10	Floor/wall disconnections and pull-in forces that were projected to occur between 40 min and 50 min were applied.
11	Column and spandrel temperatures were linearly changed from temperatures at 40 min to 50 min.

Figures 4–86 through 4–133 summarize the results of the global analyses with creep for the analysis steps described in Table 4–30. The vertical displacements of the exterior wall and the core area are presented in Figs. 4–86 through 4–98. For the exterior wall, the vertical displacements were about 2.0 in. to 3.0 in. before the aircraft impact. As indicated in Fig. 4–88, the core had larger vertical displacements by about 1 in. than the exterior walls at Floor 83 before aircraft impact. Since construction sequence was not considered in the analysis, this difference in the vertical displacements changed initial loading conditions of the columns. As shown in Table 4–8, the total column loads on the east and west walls increased by 7 percent at the impacted floors, the total column loads on the north and south walls increased by about 13 percent, and the total column loads on the core decreased by about 8 percent, by ignoring the construction sequence. After aircraft impact, the vertical displacements increased to 7.4 in. on the south wall

(Fig. 4–86). Due to thermal expansion of columns, the vertical downward displacements recovered slightly initially and eventually increased as shortening due to plastic and creep deformations became larger than the thermal expansion. However, the vertical displacements remained around 7.5 in. until 43 min at which point they increased rapidly to 11.3 in. on the east and south faces with the bowing of the east wall. When the east wall reached instability and buckled, the northwest corner of the exterior wall lifted up about 2.0 in., which indicated that the tower was tilting toward the southeast around an axis passing through the southwest and the northeast corners (Fig. 4–87). The tilting of the tower is also illustrated in Figs. 4–88 and 4–89, where the vertical displacements at Floor 83 are presented. As can be seen, with increasing time the displacements on the southeast corner increased, whereas the displacements on the northwest corner decreased. The likely axis about which the tower was tilted is indicated in Fig. 4–89. The axis location in Fig. 4–89 was based upon the distribution of plastic and creep strains, which is presented later in this Section. Figure 4–90 shows the total displacements above Floor 86 when the east wall buckled and collapse initiated. For reference, the undeformed tower is also shown. The tilt toward the southeast is clearly visible.

Analysis of the structure without aircraft impact damage indicates vertical displacements at the top of the building of approximately 4 in. (Figs. 4–91, 4–93, 4–95, and 4–97). Analysis with the estimated aircraft impact damage in place indicates that vertical displacements at the southeast corner of the core increased to approximately 10 in. (Figs. 4–91 and 4–97). As with displacements on the exterior wall, vertical downward displacement of the core was predicted to be somewhat recovered in the initial periods of the fire, due to thermal expansion, and then increased with time as inelastic and creep deformations of the heated and heavily loaded columns increased substantially. When the east wall reached instability and buckled, at 43 min, the core displacements suddenly increased to 13 in. at the southeast corner (Figs. 4–92, 4–94, 4–96, and 4–98).

Figures 4–99 through 4–101 show the out-of-plane displacements of the east wall at various analysis steps. As shown in Fig. 4–99, there was no out-of-plane displacement on the east wall before the aircraft impact. After aircraft impact, the south side of the east wall at Floor 86 displaced outward about 2.0 in., whereas the north side at the same floor remained approximately at the same displacement as before aircraft impact. This shows a slight twist about the z-axis. With increasing time and temperatures, the east wall bowed and the inward displacements increased (Fig. 4–100). At 20 min the maximum inward displacement reached 9.5 in. toward the center of the east wall. This maximum inward displacement agrees well with the maximum inward displacement (~10 in.) that was measured from the photographs and videos at the same time (at 9:21 am which is approximately 18 minutes after the aircraft impact). After 20 min, the inward displacements steadily increased until at 43 min they rapidly increased to 62 in. (Figs. 4–100 and 4–101). At this point, the east wall reached instability and buckled over the entire width of the wall.

Figures 4–102 and 4–103 show the lateral displacements of the exterior wall above Floor 86 after aircraft impact and at the instant of the east wall buckling. After aircraft impact, Floor 110 moved toward the east about 5.0 in. and toward the south about 5.1 in. There was also a slight twist about the z-axis of the tower which was about 0.0007 radian at Floor 110. The twist about the z-axis was calculated by taking the difference between the average in-plane displacement of the two opposing exterior walls (such as the east and the west walls) at Floor 110 and dividing the result by the distance between these walls (~200 ft). With the buckling of the east wall, the lateral displacements increased rapidly. The lateral displacements

of the north exterior wall increased to 15.2 in. toward the east, and of the south exterior wall increased to 6.7 in. toward south. The twist around the z-axis of the tower increased to 0.0010 radian at Floor 110.

Figures 4–104 through 4–111 show the variation of axial loads on the exterior wall columns at different analysis steps. Typically, before aircraft impact, the load distribution along the width of the walls was symmetric with respect to the centerline of each wall. After aircraft impact, the loads in the severed columns redistributed. As a result of this redistribution, the column loads on the south side of the east and west walls and on the east side of south wall increased. This was due to leaning of the tower toward the southeast as the aircraft impact severed columns on the east side of the south wall and on the southeast corner of the core (Figs. 4–104, 4–106, 4–108, 4–110, and 4–111). After redistribution, at Floor 83 the column loads on the south wall increased from about 250 kip before aircraft impact to 400 kip to 800 kip in general and to 1,500 kip at the edges of the severed area after aircraft impact. The column loads on the south side of the east wall at Floor 83 increased from about 350 kip before aircraft impact to about 450 kip after aircraft impact. The column loads on the east side of the north wall at Floor 83 did not change significantly; however, the column loads on the west side of the north wall at Floor 83 decreased from about 250 kip before aircraft impact to about 200 kip after aircraft impact. The column loads on the south side of the west wall at Floor 83 increased from about 300 kip before aircraft impact to about 380 kip after aircraft impact. The column loads on the north side of the west wall at Floor 83, however, decreased from about 300 kip before aircraft impact to 250 kip after aircraft impact. Over the duration of the fires the column load distributions remained constant except for some localized changes due to relative temperatures. When the east wall buckled, the load distribution significantly changed. The columns over nearly the whole width of the east wall unloaded about 400 kip on the average at Floor 83. Similarly, the columns on the west face unloaded about 65 kip on the average. This was due to the increased tilting of the tower toward the east, as the east wall buckled. A part of the loads from the east and the west walls were redistributed to the east side of the south and the north walls. The column loads on the east side of the south wall increased from about 500 kip to 800 kip after aircraft impact, and to 800 kip to 1,100 kip after east wall buckling. The column loads on the east side of the north wall increased from about 200 kip to 250 kip after aircraft impact, and to 300 kip to 500 kip after east wall buckling.

Figures 4–112 through 4–119 show the core column loads at different analysis steps. Before the aircraft impact the loads on the core columns were distributed symmetrically with respect to the center of the core. The slight difference between corner columns on the south side (Columns 501 and 1001) and north side (Columns 508 and 1008) of the core was due to slightly higher dead and live loads in the north side columns. After aircraft impact, some portion of the loads in the severed columns was redistributed to the adjacent intact columns within the core. The tilt toward the southeast also influenced the load redistribution within the core. Columns 506, 507, 508, and 1008 at the northwest and northeast corners unloaded; other intact core columns increased in load (Fig. 4–118). The maximum load in the 800 series core columns increased from about 1,400 kip before aircraft impact to about 1,700 kip after aircraft impact (Fig. 4–112). The maximum load in the 900 series core columns increased from about 1,250 kip before aircraft impact to about 1,900 kip after aircraft impact (Fig. 4–114). Although the maximum load in the 1000 series core columns reduced from about 4,300 kip before aircraft impact to about 3,000 kip after aircraft impact (Fig. 4–116), the average load on the remaining intact 1000 series columns increased about 360 kip at Floor 83 (Fig. 4–118).

Over the duration of the fires, some of the core columns, especially the ones on the east side of the core, unloaded due to yielding and creeping at high temperatures. Loads in softening columns were

redistributed to the adjacent columns with lower temperatures. During buckling of the east wall, the loads in the core columns, especially the ones at the northeast corner of the core, increased significantly. For instance, at Floor 83 the load in core column 1008 increased from 2,820 kip after aircraft impact to 5,320 kip at 43 min, the load in core column 907 increased from 1,290 kip to 2,330 kip, and the load in core column 805 increased from 950 kip to 1,480 kip (Figs. 4–118 and 4–119).

Figure 4–120 shows the axial loads in the columns at Floor 83 before aircraft impact and after the buckling of the east wall. This figure illustrates the load redistribution among the exterior wall and core columns. The tilting of the building about an axis likely located through the shaded area occurred after the buckling of the east wall and weakening of the core. Comparison of column loads before aircraft impact and after the east wall buckled clearly shows the unloading over the entire width of the east wall and increased loads at the east side of the south and north walls.

Figures 4–121, 4–122, and 4–123 show the maximum of the elastic-plus-plastic strains and elastic-plus-plastic-plus-creep strains in the columns between Floor 78 and Floor 83 for different analysis steps. The elastic-plus-plastic strains, which were less than 0.05 percent before the aircraft impact, reached about 0.60 percent in the exterior columns and about 0.35 percent in the core columns after the aircraft impact. With increasing temperatures the plastic strains increased, especially on the east wall and the east side of the core. When the east wall buckled, the elastic-plus-plastic strains reached their maximum of 2.2 percent in the east wall and 0.9 percent in the east side core columns. The creep strains also increased with increasing temperatures to the same level as the elastic-plus-plastic strains in the east wall (1.0 percent to 2.0 percent), to about 2 to 6 times that in the core columns (2.0 percent to 6.0 percent), and to about 10 times that in the east side of the north wall (4.0 percent to 5.0 percent).

The state of the hat truss members and the connections were checked as the global model did not include break elements to capture column and hat truss splice failures or sufficient beam elements to capture buckling of hat truss outriggers. The condition of the connections and the members in the primary load path of the hat truss was evaluated at different time intervals. Evaluations were performed for the core column splices for tensile capacity, outriggers and supporting columns for compressive capacity, and hat truss connections in the primary load path for tensile capacity. The demand forces that were used in the evaluation were obtained from the “superelement” since the hat truss was part of it for the WTC 2 global model with creep. The results for elements within the superelement were obtained by back-substitution. For this purpose the elastic model that was used to generate the stiffness matrix for the superelement was used. This elastic model essentially represents the portion of the building from Floor 86 and above and is referred to as the “top model” hereinafter. The displacements obtained at the interface nodes between the “superelement” and the nonlinear portion of the building (Floor 86 and below) were applied to the base of the “top model” at the end of each analysis step together with the nodal loads representing the dead and the 25 percent of the design live loads.

Figures 4–124 and 4–125 show the loads on the core column splices at the hat truss level at different analysis steps. As can be noticed, each splice was under compressive load before the aircraft impact. After the aircraft impact, the splices at severed core column lines started to carry tensile loads. To evaluate the condition of the core column splices at Floor 106, the tensile capacities of these splices were determined using the AISC LRFD procedures and were compared to the tensile forces obtained at 40 min, since at this time point the tensile forces at core column splices were at their maxima. The evaluation of core column splices required an iterative procedure as splice failures were not modeled in the “top model”. The iteration procedure was required due to the slight nonlinearity of the problem where the

failure of a few splices did not alter boundary conditions of the "top model" significantly. In the first iteration, the state of the "top model" was calculated using the interface nodal displacements at 40 min. Once equilibrium was reached, the columns exceeding their splice capacity were identified (in the first iteration Columns 1001 and 1002 were identified (see Fig. 4–126) and removed). This removal represented the splice failure at that column location. Before removing the columns, the displacement boundary conditions applied at the bottom of these column lines (at Floor 86) were replaced with the reaction forces that were obtained at the end of the first iteration. This conversion from displacement to force boundary condition allowed the remaining portion of the column lines to displace in the vertical direction when the columns were removed at Floor 105 to simulate splice failure. After the removal of the columns, the "top model" was reanalyzed to redistribute the released tensile force due to splice failure. Once equilibrium was reached, the remaining core column splices were reevaluated and any additional splice failures were identified. This iterative procedure was repeated until none of the remaining splices exceeded their tension capacity. A stable state was reached at the end of the fourth iteration. Figure 4–126 summarizes the iteration sequence and the splices that failed at each iteration. Figure 4–127 shows the state of the core column splices at the end of the fourth iteration.

In the global analyses, none of the splice failures were represented as those elements were part of the "superelement" which remained elastic throughout the analysis. However, the inclusion of splice failures is not expected to significantly affect the load redistribution in the global analysis. The loads on columns with failed splices would have redistributed through the core slab and core beams with moment connections to adjacent core columns, which in turn would transfer these extra loads to the hat truss. To quantify the amount of load that was redistributed to the hat truss through the adjacent core columns, the total column loads on each face and at the core area were extracted at Floor 105 at the end of each iteration. Table 4–31 summarizes these total column loads together with the magnitude of total tensile load released and total tensile load retransferred to the hat truss at each iteration. In Table 4–31, the Column "TTLRSF" represents the total tensile load that was released due to splice failure and is equal to the summation of the load carried by the circled columns in Fig. 4–126 up to and including the current iteration. In Table 4–31, the Column "Core" between Rows 6 and 9 represents the load that was transferred to the base of the "top model" through the core columns. The sum of Column "TTLRSF" and Column "Core" represents the total tensile load that was transferred to the hat truss after the splice failures (labeled as "TTLRHT" in Table 4–31). As can be seen, about 73 percent (= 2,728 kip /3,717 kip) of the released tension load was transferred to the hat truss after the fourth iteration. The core slab and the core beams with moment connections were the primary components that transferred the released load to the adjacent core columns and to the hat truss. Capacity calculations have shown that the core slab and the core beams in the top 20 stories had enough cumulative capacity to redistribute the released load to the adjacent core columns. As a result of load redistribution, the loads on the southeast corner outriggers were reduced, but the loads on adjacent outriggers increased.

Figures 4–128 through 4–130 show the axial loads and stresses in the hat truss members at different analysis steps. With the aircraft impact, the maximum axial load on the outriggers, which was about 1,900 kip before the aircraft impact, increased to about 3,400 kip at the southeast corner. This increase remained almost constant over the duration of the fires. After the buckling of the east wall the maximum load slightly increased to 3,500 kip. The axial stresses in the outriggers also increased as a result of the aircraft impact. The maximum axial stress of 28.4 ksi before aircraft impact increased to 55.0 ksi after the buckling of the east wall. The specified grade of steel for the outriggers was 50 ksi. The tests conducted on this grade of steel showed an average yield strength of about 54 ksi. Considering this yield

strength and the 10 percent increase in the hat truss forces due to neglecting construction sequence, it was concluded that the outriggers of the hat truss did not exceed their elastic limits. To check against buckling, the buckling capacities of these outriggers as well as the supporting columns were calculated. The buckling calculations were performed using the AISC LRFD Eqs. E2-1 and E2-3 with an effective length factor "K" of 0.75 and a resistance factor of 1.0. The calculated capacities were then compared with the axial compressive forces obtained from the analysis and corrected to account for the load increase due to construction sequence. The location of the outriggers and the supporting columns are shown in Fig. 4–3. Tables 4–32 and 4–33 summarize the resulting demand-to-capacity ratios for the outriggers and the supporting columns, respectively. Except for one outrigger, designated Outrigger L, none of the outriggers or supporting columns was predicted to buckle.

Outrigger L was located at the southeast corner of the core, and above the severed core columns. With the splice failures in Columns 1001, 1002, and adjacent core columns, the load on this outrigger reduced and the load redistributed to other outriggers. With the load redistribution after splice failures, the demand-to-capacity ratio on Outrigger L reduced from 1.3 to 1.1 (Col "40* min" in Table 4–32). To investigate whether the buckling of the Outrigger L would cause additional outriggers to buckle, the element representing Outrigger L was removed from the "top model." Removal of Outrigger L from the "top model" represents an upper bound solution as the load in the outrigger would not drop to zero after buckling. After removal of Outrigger L, the adjacent outriggers increased in load however, as presented in Col "40** min" of Table 4–32, none of the remaining outriggers exceeded their buckling or yield capacities.

In the global analysis, it was assumed that the connections in the hat truss area were adequate to transfer the loads from the core columns to the outriggers. The structural adequacy of the "primary" connections, those hat truss connections between members that were predicted to have axial tensile or compressive stress of 25 ksi or more, was evaluated. To perform this evaluation, the results at 40 min were used, since at 40 min the stresses in the hat truss members were at their maxima. Only connections that transferred tensile forces were evaluated. Figure 4–132 shows the members in the primary load path. Figure 4–133 shows the location of the critical hat truss connections that were evaluated in this study. The connections between the horizontal tie-backs and the outriggers were not evaluated as they were found to have significant capacity in the WTC 1 connection evaluations. Connection capacities were calculated using AISC LRFD procedures. Table 4–34 summarizes capacities, demands, and the predicted condition of the evaluated connections. As can be seen in Table 4–34, before redistribution of load due to column splice failure, none of the connections exceeded their capacities except the connections associated with the 1001 core column line. After load redistribution, the demand was less than the yield capacities for all connections. Based on this, and the other evaluations of column splices and hat truss members discussed above, it was concluded that the hat truss was capable of transferring loads from core columns to the outriggers without any connection failures.

Tables 4–35 and 4–36 summarize the total column loads at each exterior face and the core for Floor 83 and Floor 105. The first seven rows of Tables 4–35 and 4–36 provide the total loads at each analysis step. The rows from 8 through 13 give the change in total column loads at each analysis step with respect to the total column loads before aircraft impact. For instance, Row 8 gives the difference between the total column loads before and after aircraft impact. A positive value between Row 8 and Row 13 indicates that the total compressive load has increased in that analysis stage as compared to the total compressive load before the aircraft impact. Based on these tables, after the aircraft impact, the core and the north wall

unloaded and their loads were redistributed to the south, west, and especially to the east wall at Floor 83. A similar load redistribution pattern was found for Floor 105. The comparison of the total column loads before and after aircraft impact at Floor 83 and Floor 105 is presented in Table 4–37. The second row in this table represents the amount of load redistributed through the hat truss, and the third row represents the amount of load redistributed through the spandrels and the floors. Based on this table, it can be stated that about 94 percent (3,740 kip/4,000 kip) of the load that was unloaded from the core was redistributed through the hat truss to the east, south, and west walls, and the remaining 6 percent was redistributed through the floors to the exterior walls. A similar calculation for the east wall indicates that about 62 percent (2,699 kip/4,368 kip) of the load increase on the east wall came through the hat truss and the remaining 38 percent came through the Vierendeel action of the wall. Rows 8, 9, 10, and 11 of Table 4–35, show that the loads in the various walls and the core itself did not significantly change until the core unloaded at about 30 min. At 30 min the total column loads on the east wall increased by about 1,200 kip (from 5,567 kip to 4,368 kip) and the core unloaded about 850 kip (from 4,861 kip to 4,007 kip) and the north wall unloaded about 420 kip (from 1,797 kip to 1,374 kip) at Floor 83. Similarly, at Floor 105 and at 30 min the total column loads in the various walls and core remained almost constant until initiation of buckling of the east wall. After 40 min, the east wall suddenly unloaded about 8,540 kip, the west wall unloaded about 2,860 kip, the core experienced a load increase of about 5,600 kip, the north wall increased by about 2,310 kip, and the south wall increased by about 2,820 kip at Floor 83 (Table 4–38). Comparison of the load redistribution that took place at Floor 105 with the one at Floor 83 indicates that about 100 percent of the additional core load came from the east and the west walls through the hat truss. For the east wall, about 46 percent (3,901 kip/8,539 kip) of the relieved load was redistributed through the hat truss to the core, and the remainder was redistributed through Vierendeel action to the south and north walls. After the redistribution, at 43 min, the load in the core had recovered to the same level as the total load before the aircraft impact.

Tables 4–39 through 4–43 summarize the loads in the east, south, north, west walls, and the core at several floor levels. The tables also indicate the change in column load at each stage of the analysis, compared to the load present before aircraft impact. These load changes are provided in Columns 8 through 13. As described before, the changes in loads at Floor 105 represent the load redistribution through the hat truss. The changes in loads along the height of the tower indicate the load redistribution through the exterior wall and the floor system. In referring to the changes in loads after the aircraft impact (Col 8 in the tables), it can be concluded that the total column loads along the height of the core and the west wall remained almost constant. This indicates that almost all load redistribution from and to these portions of the tower went through the hat truss. The total column loads in the east wall increased at the hat truss level and continued to increase with distance from the hat truss. The north wall showed the opposite trend; at the hat truss level the wall unloaded and continued to unload further with distance from the hat truss. The unloading took place primarily through Vierendeel action, to the east wall. After the buckling of the east wall, the change in loads (Col 13 in the tables) indicates that the hat truss was the primary load path for the portion of the load picked up by the core. The east and west walls unloaded at the hat truss level and at lower floors. Both walls steadily picked up more load at lower floors through the action of spandrels.

During the load redistribution, the floor slabs played a significant role in restraining the core in the lateral direction. The aircraft impact damage to the core and the ensuing fire environment caused the core to lean toward the south and east. In fact, calculations show that the isolated core would not have been stable. The resistance to core leaning was provided by the exterior wall. The load was transferred to the

exterior walls by shear either through slabs or hat truss. To identify the contribution of the floor slabs to the lateral restraint of the core, the moment of the core column loads around the center of the building in the x- and y-directions at Floor 83 and Floor 105 were computed for WTC 2. Before impact, there was no eccentricity in the load, and the moments thus calculated were small. After impact and at the end of temperature histories, the moment in the x-direction was 5,905,640 kip-in at Floor 83 and 2,282,320 kip-in at Floor 105. Similarly, the moment in the y-direction was 5,051,130 kip-in at Floor 83 and 2,196,440 kip-in at Floor 105. The change in moment from Floors 83 to 105 was due to the lateral resistance of provided by the slabs and the exterior walls to the core. The results of calculations show that the overturning moment reduced by about 55 percent to 60 percent along the height of the tower. This reduction was due to the lateral resistance provided by the floor slabs. The remaining 40 percent to 45 percent was resisted by the hat truss.

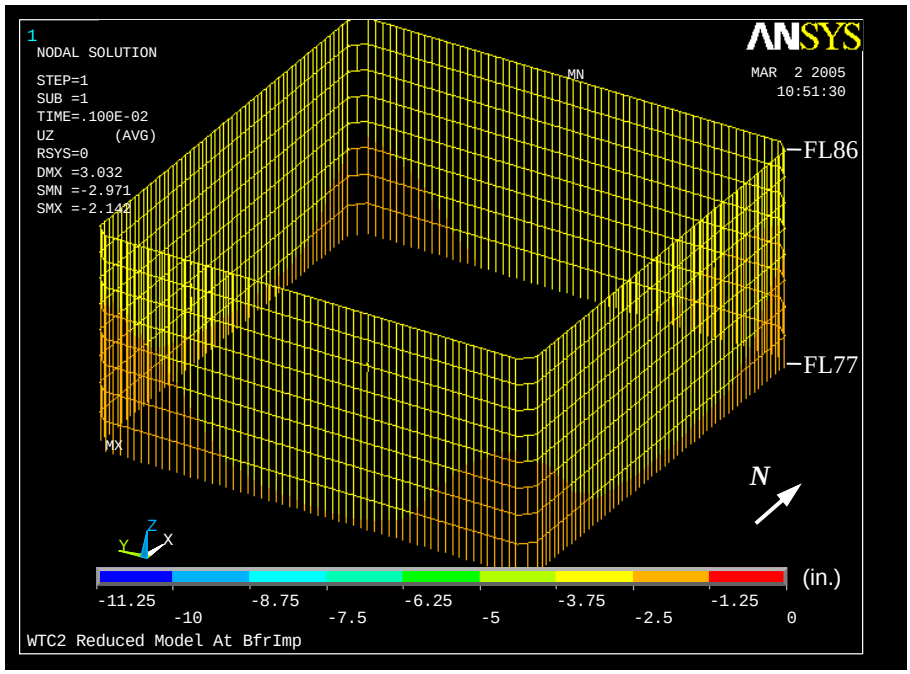

(a) Before impact

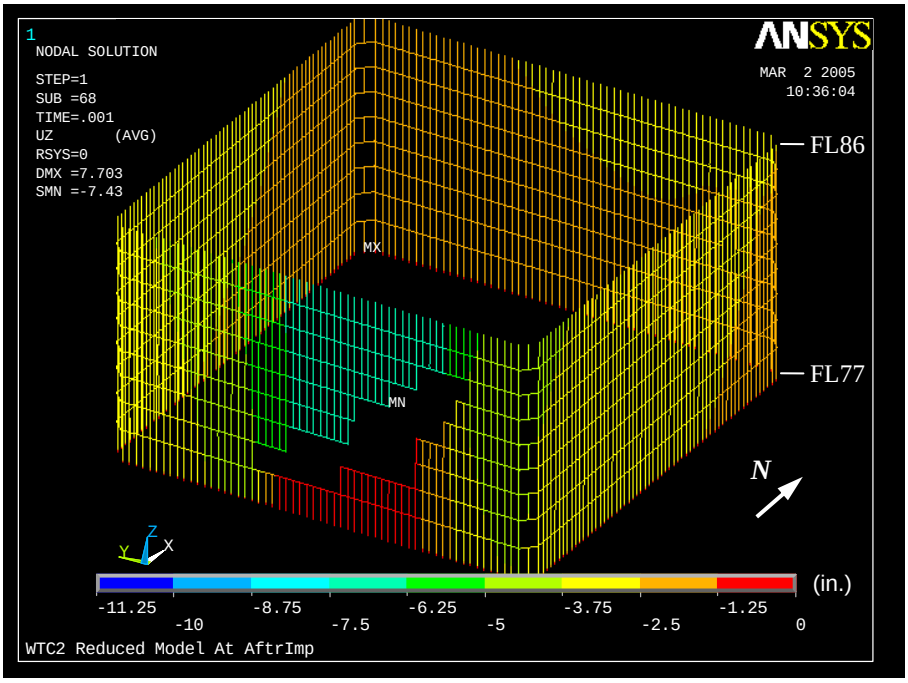

(b) After impact

Figure 4–86. Vertical displacement of exterior wall of WTC 2 for Case D conditions (downward displacement is negative).

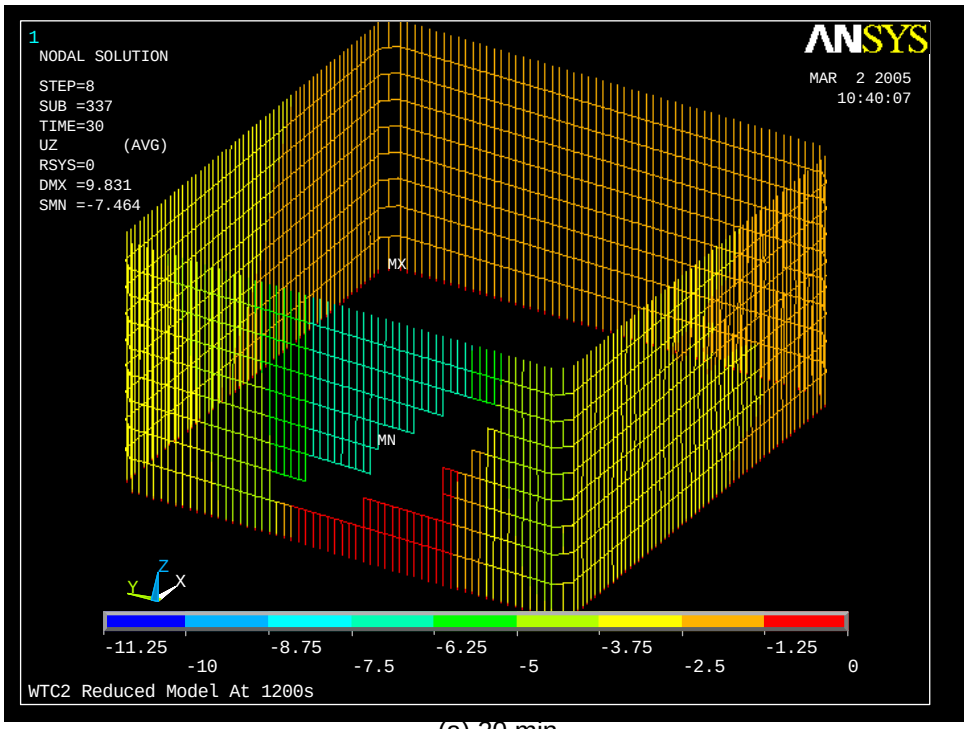

(a) 20 min

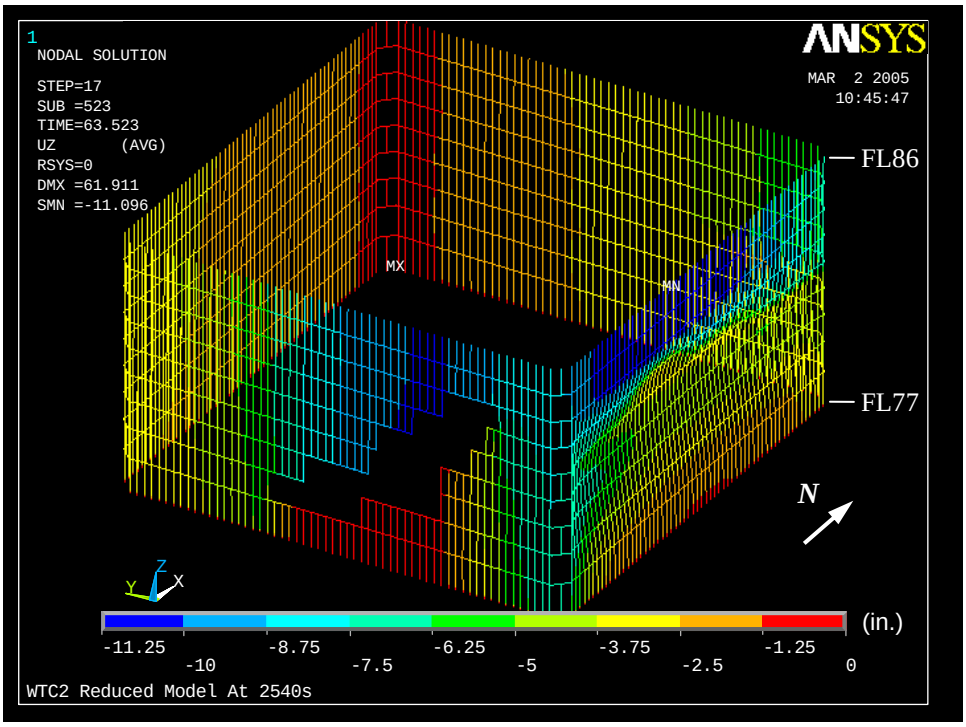

(b) 43 min

Figure 4–87. Vertical displacement of exterior wall of WTC 2 for Case D conditions (downward displacement is negative).

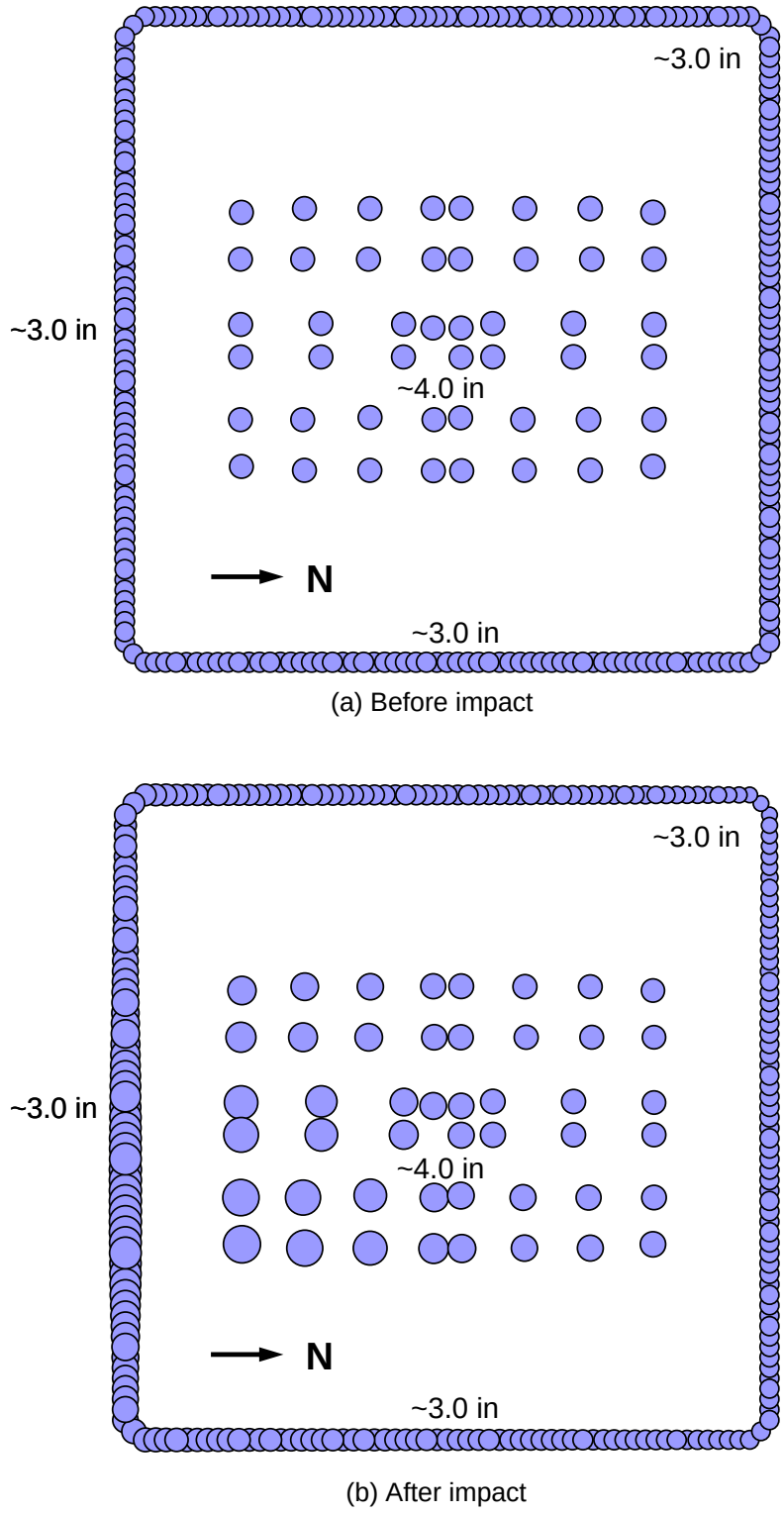

Figure 4–88. Vertical displacement at Floor 83 of WTC 2 for Case D conditions (downward displacement is positive).

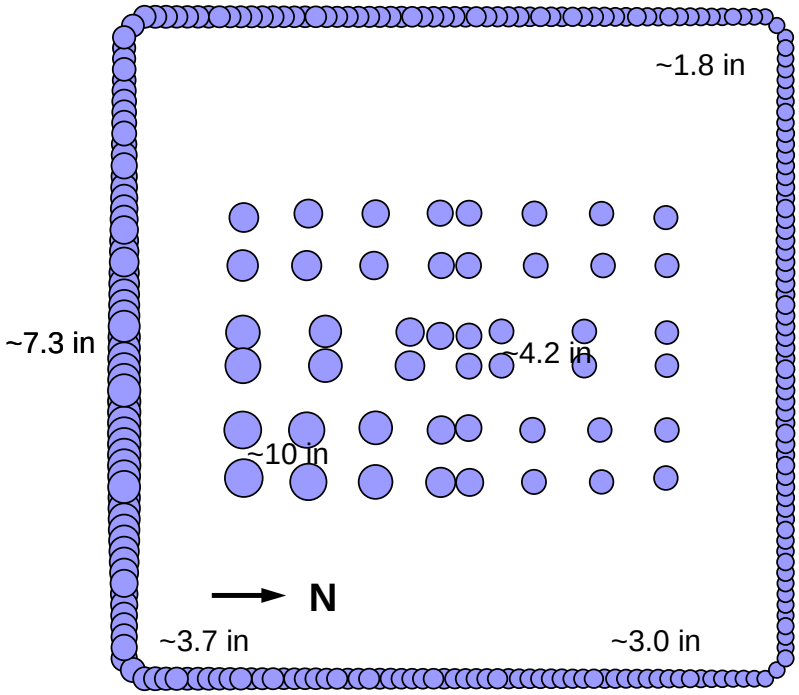

(a) 20 min

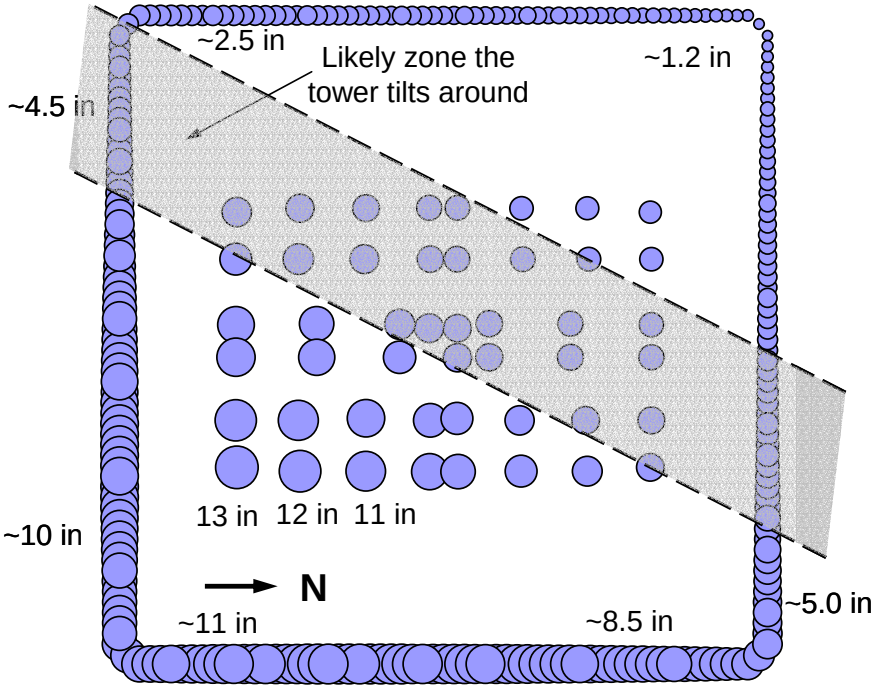

(b) 43 min

Figure 4–89. Vertical displacement at Floor 83 of WTC 2 for Case D conditions (downward displacement is positive; note the tilt toward east and south).

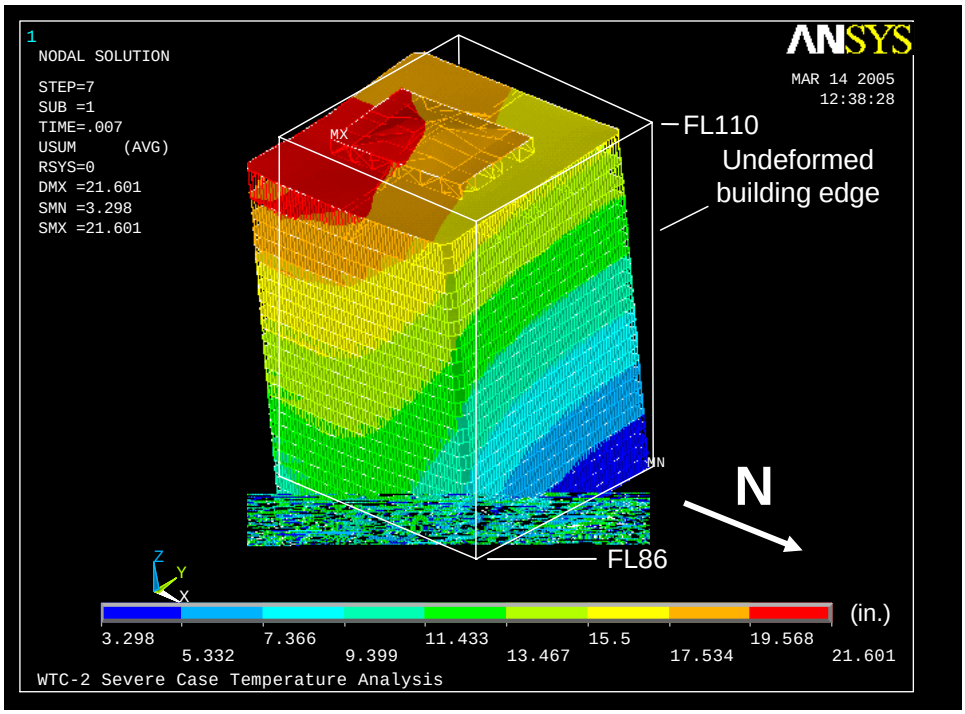

Figure 4–90. Total displacements of WTC 2 above Floor 86 at 43 min of Case D conditions (deformed shape magnified 20 times). Note the tilt toward east and south.

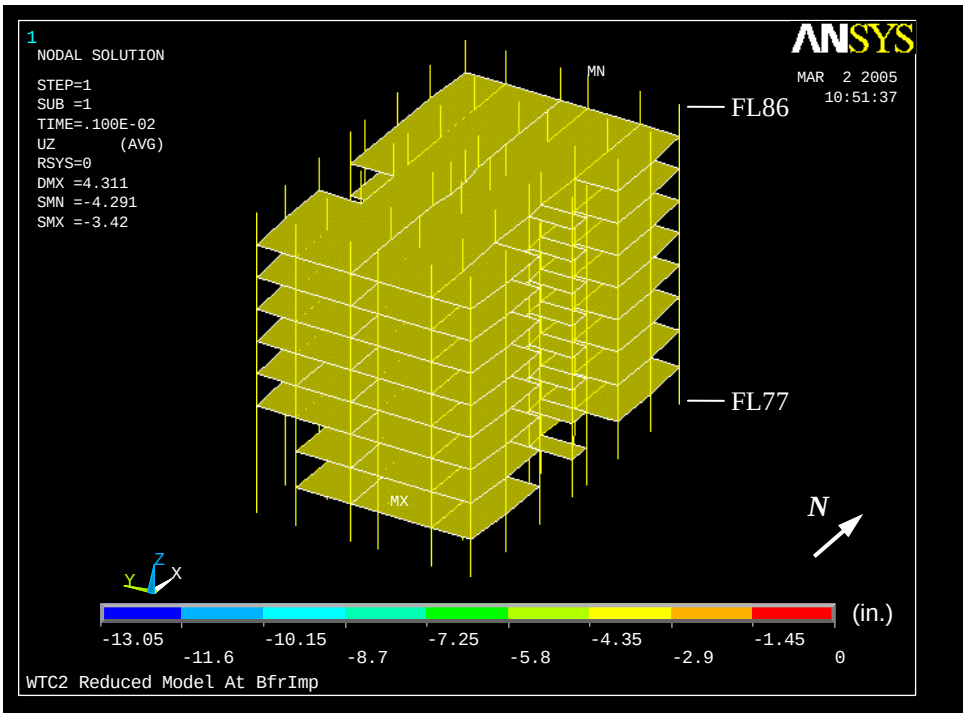

(a) Before impact

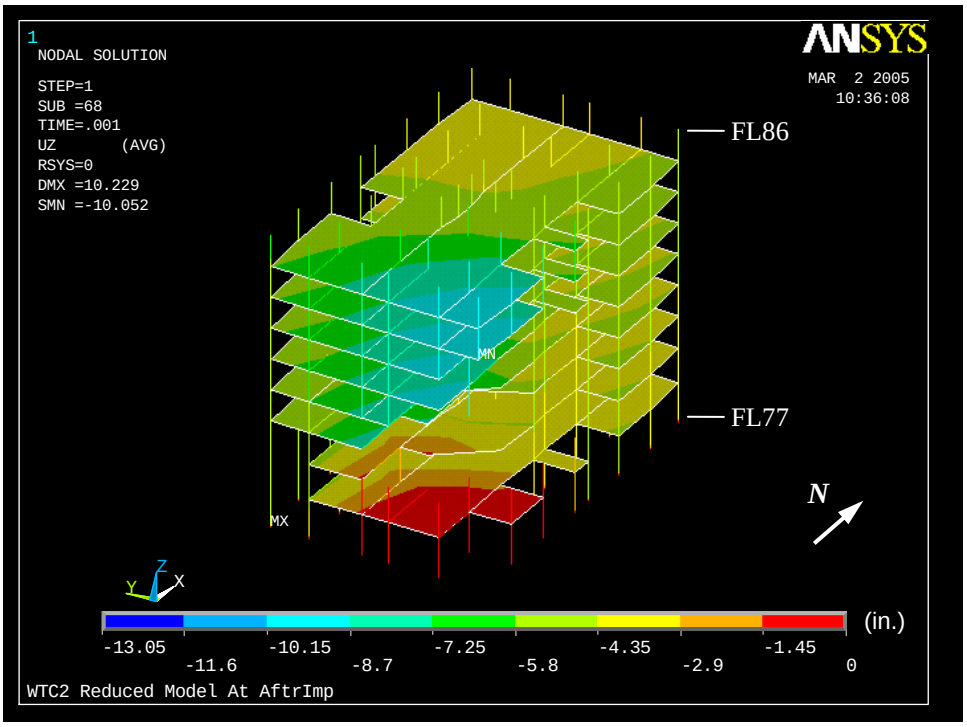

(b) After impact

Figure 4–91. Vertical displacement of core of WTC 2 for Case D conditions (downward displacement is negative).

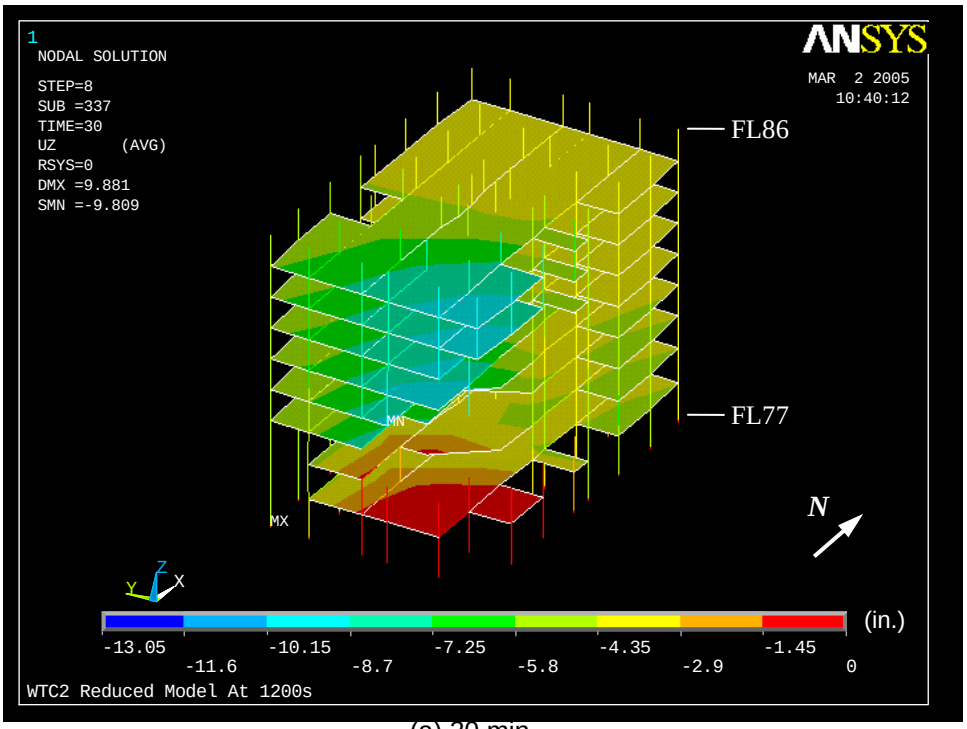

(a) 20 min

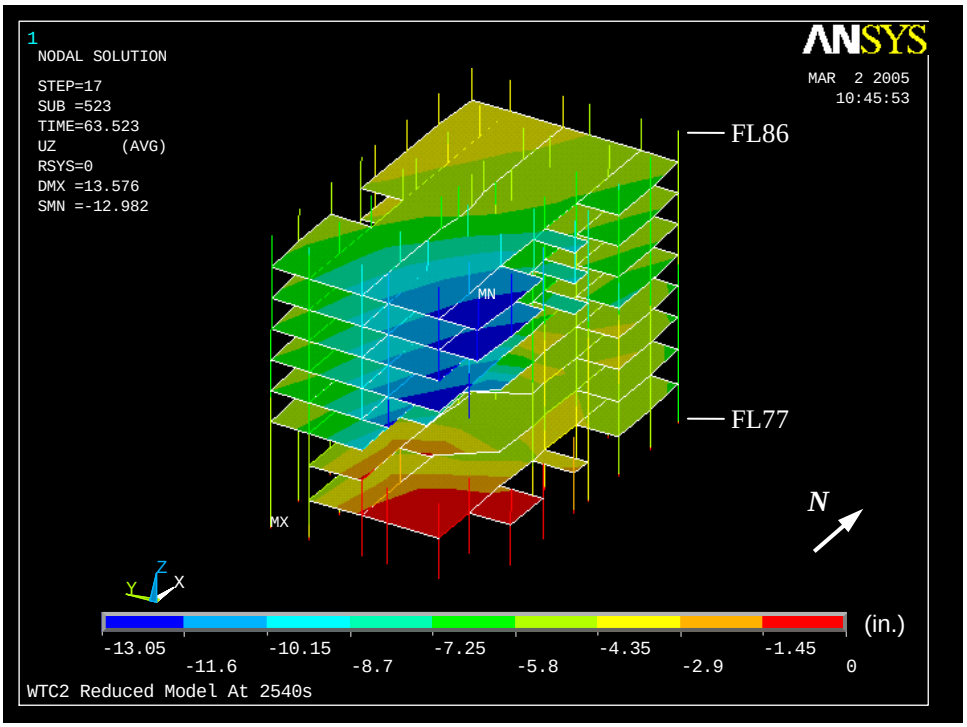

(b) 43 min

Figure 4–92. Vertical displacement of core of WTC 2 for Case D conditions (downward displacement is negative).

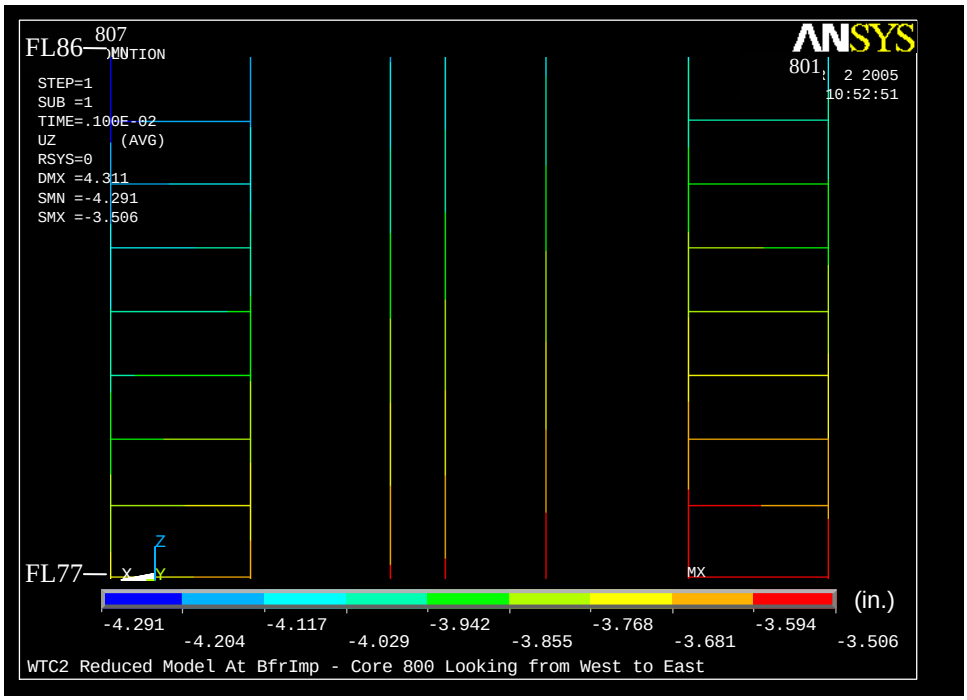

(a) Before impact

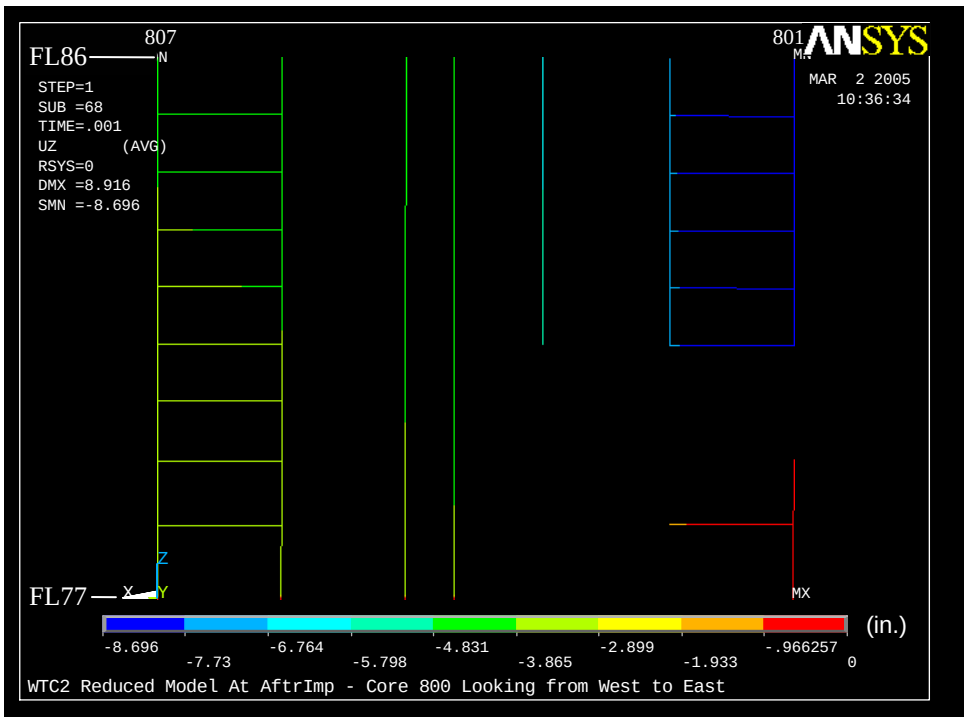

(b) After impact

Figure 4–93. Vertical displacement of 800 series core columns of WTC 2 for Case D conditions (downward displacement is negative).

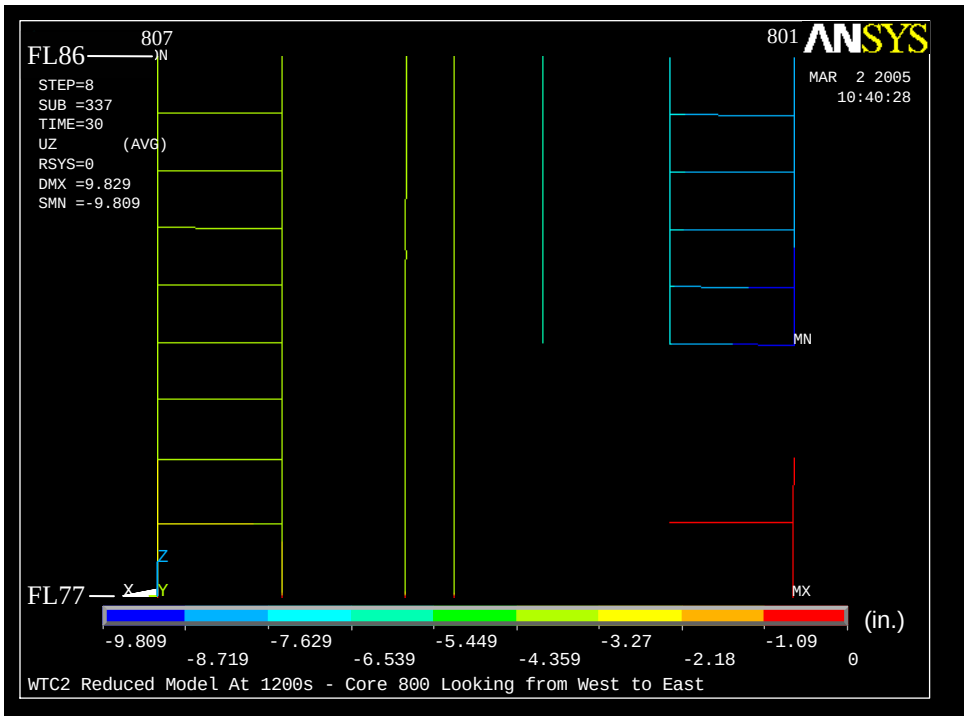

(a) 20 min

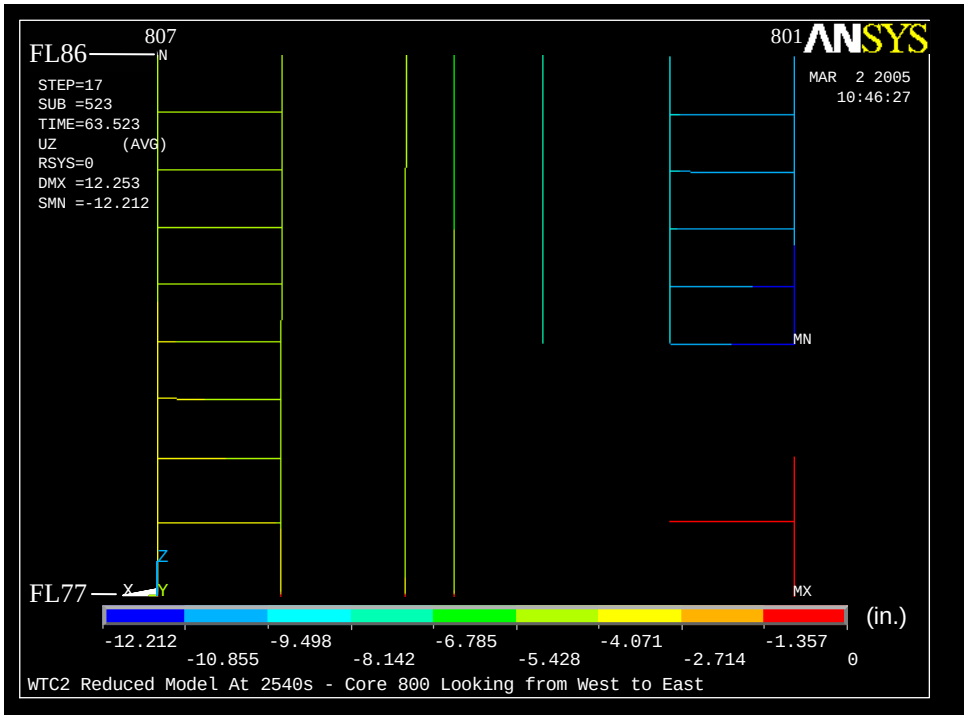

(b) 43 min

Figure 4–94. Vertical displacement of 800 series core columns of WTC 2 for Case D conditions (downward displacement is negative).

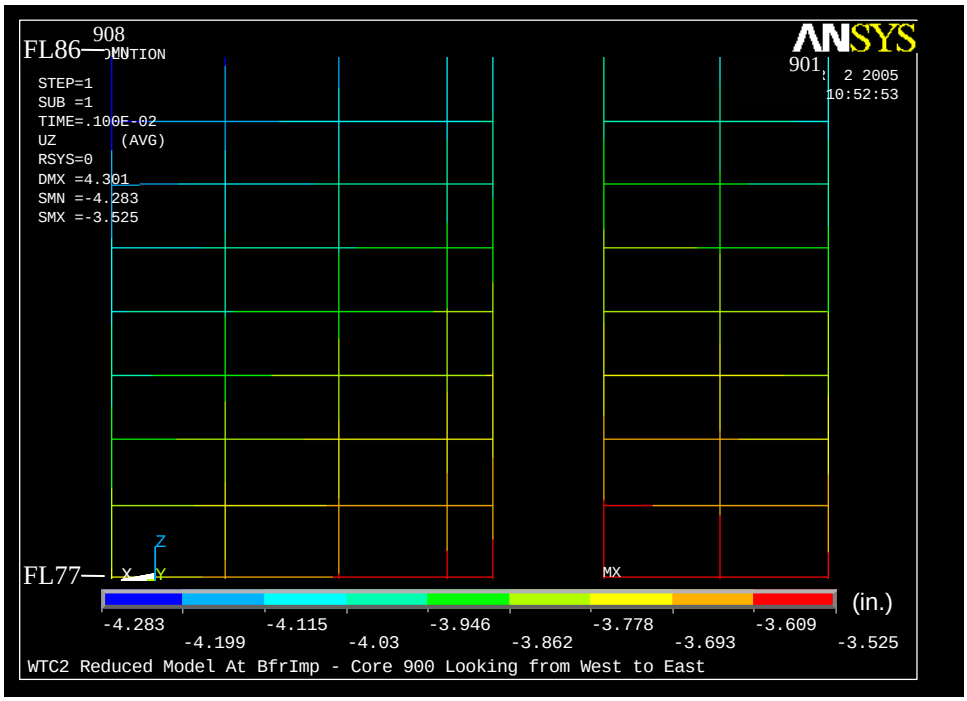

(a) Before impact

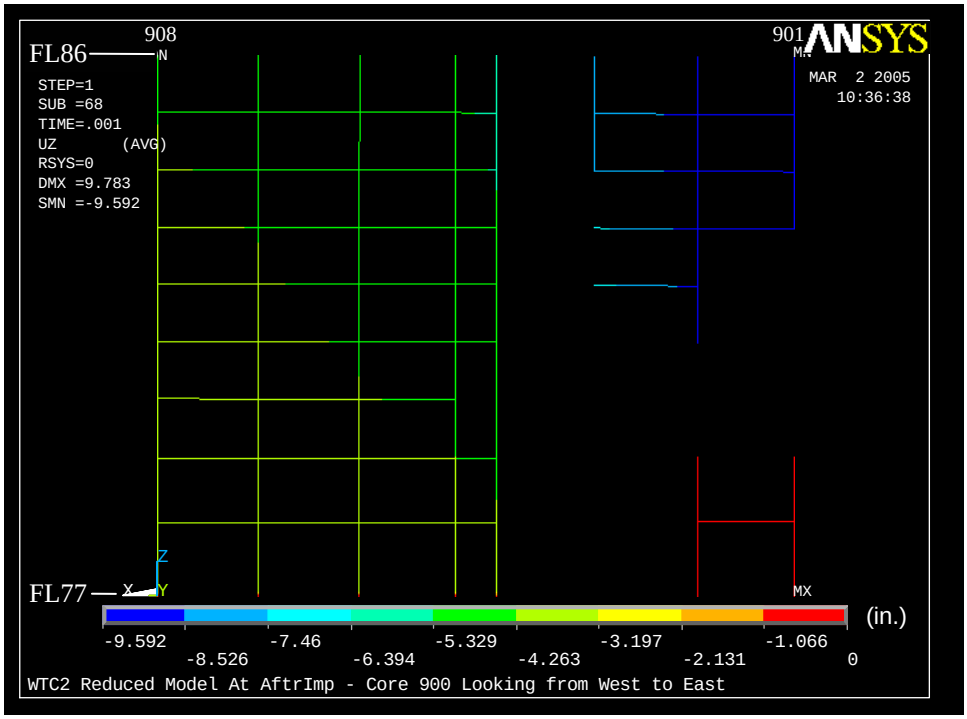

(b) After Impact

Figure 4–95. Vertical displacement of 900 series core columns of WTC 2 for Case D conditions (downward displacement is negative).

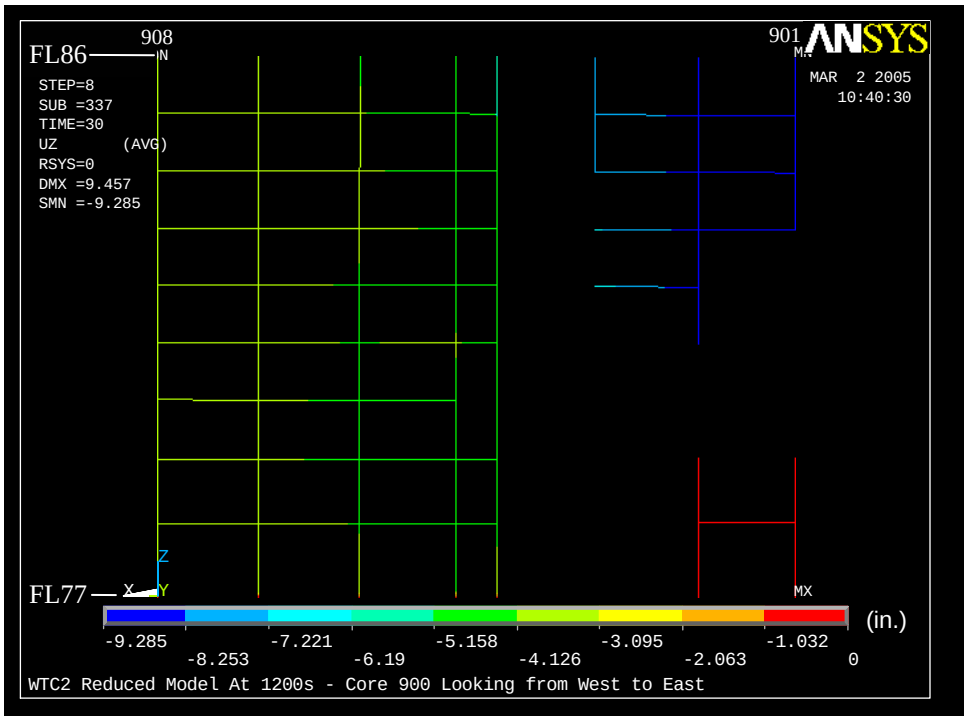

(a) 20 min

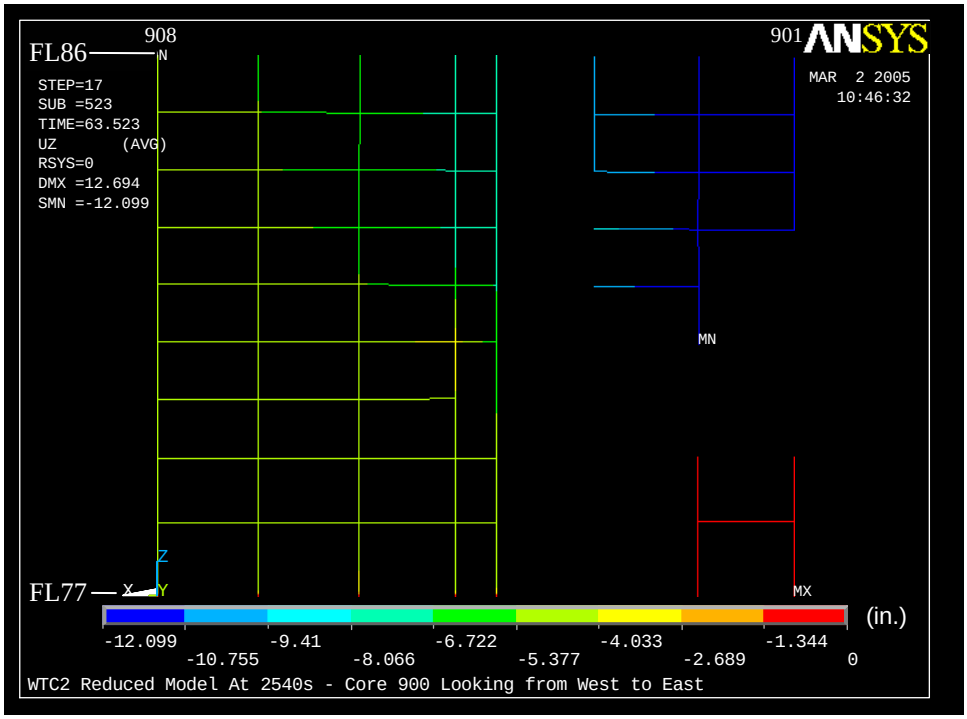

(b) 43 min

Figure 4–96. Vertical displacement of 900 series core columns of WTC 2 for Case D conditions (downward displacement is negative).

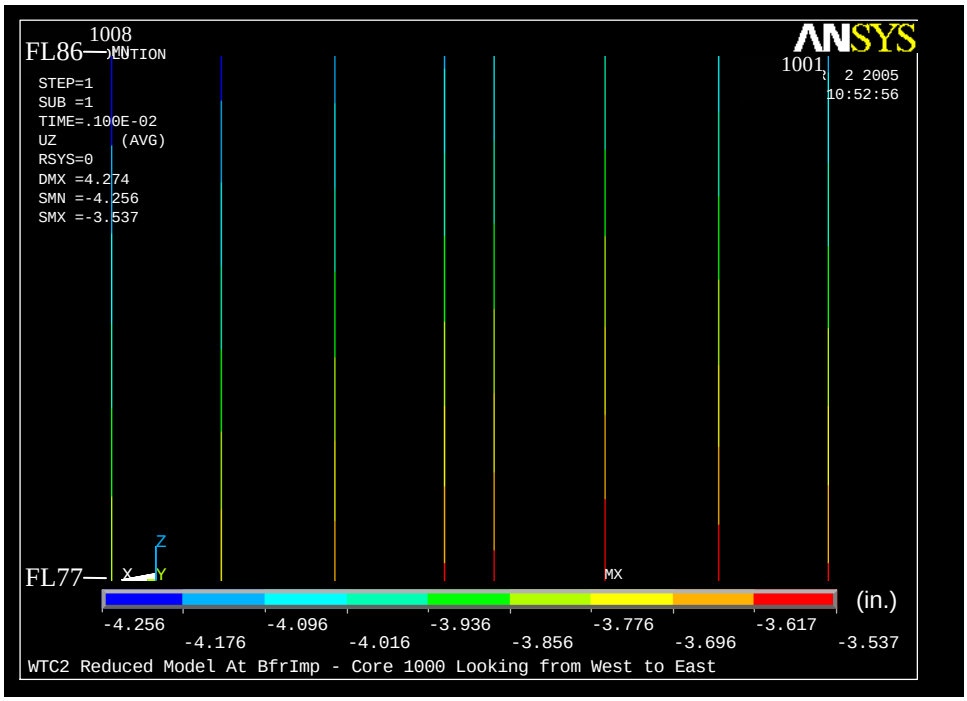

(a) Before impact

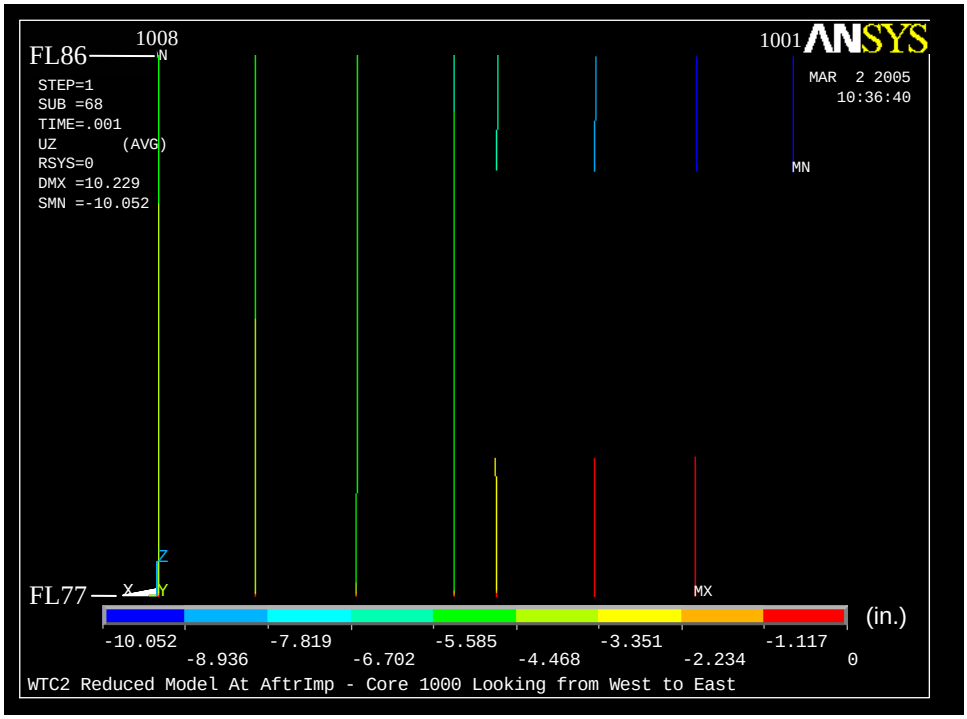

(b) After impact

Figure 4–97. Vertical displacement of 1000 series core columns of WTC 2 for Case D conditions (downward displacement is negative).

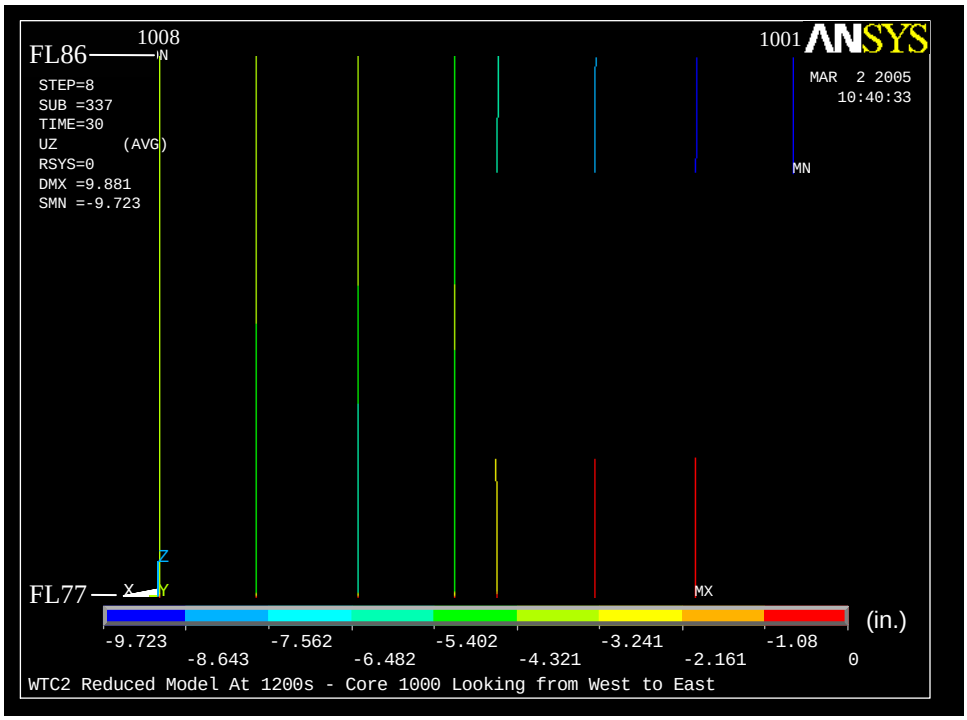

(a) 20 min

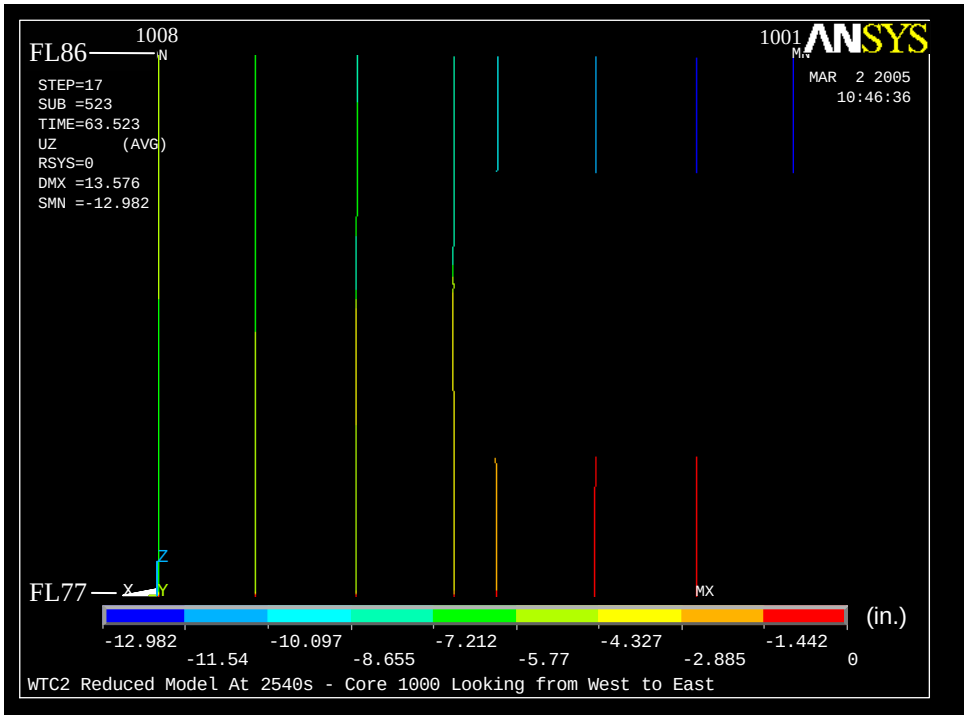

(b) 43 min

Figure 4–98. Vertical displacement of 1000 series core columns of WTC 2 for Case D conditions (downward displacement is negative).

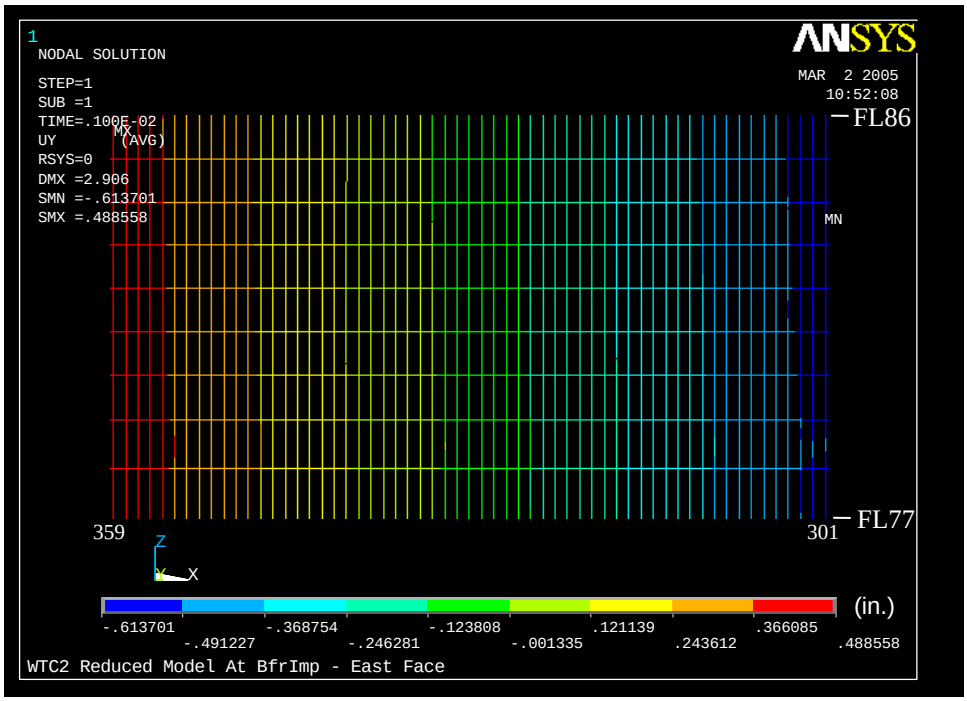

(a) Before impact

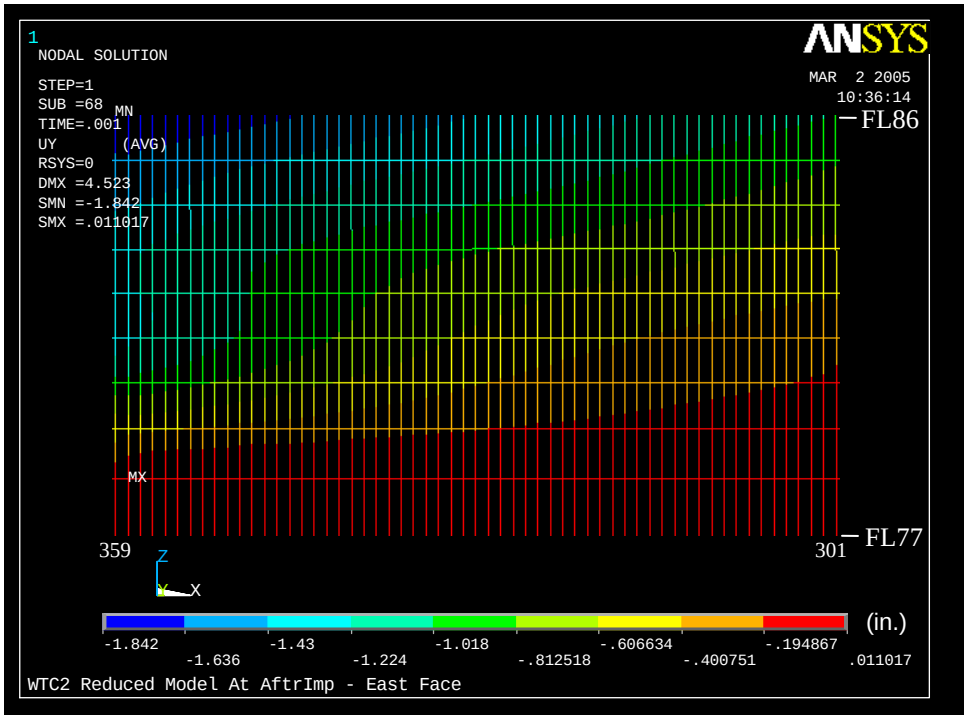

(b) After impact

Figure 4–99. Out-of-plane displacement of the east wall of WTC 2 for Case D conditions (inward displacement is positive).

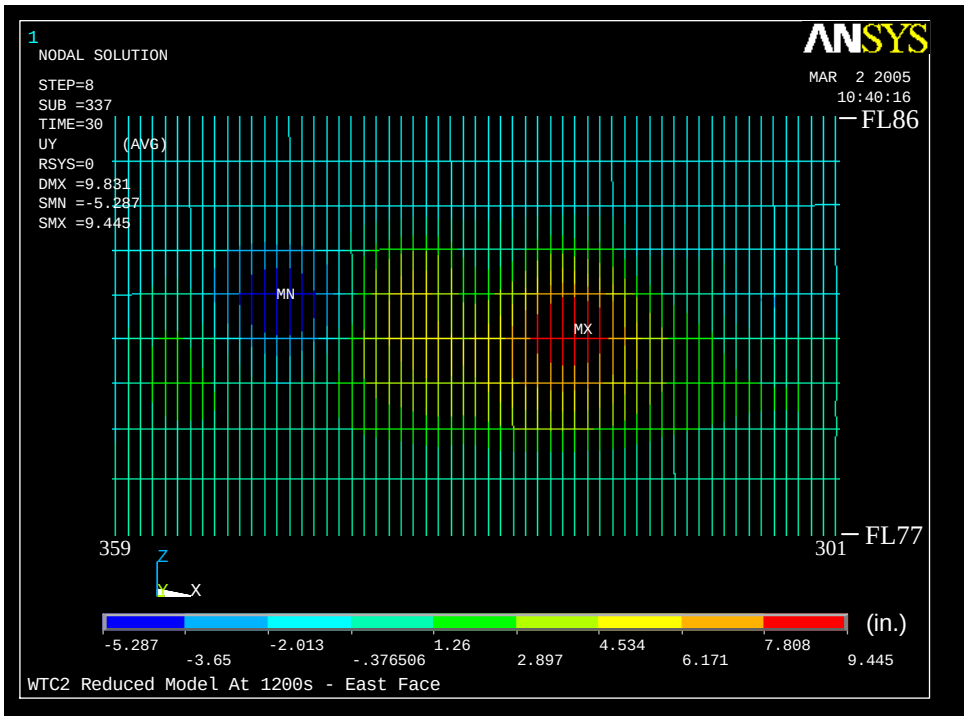

(a) 20 min

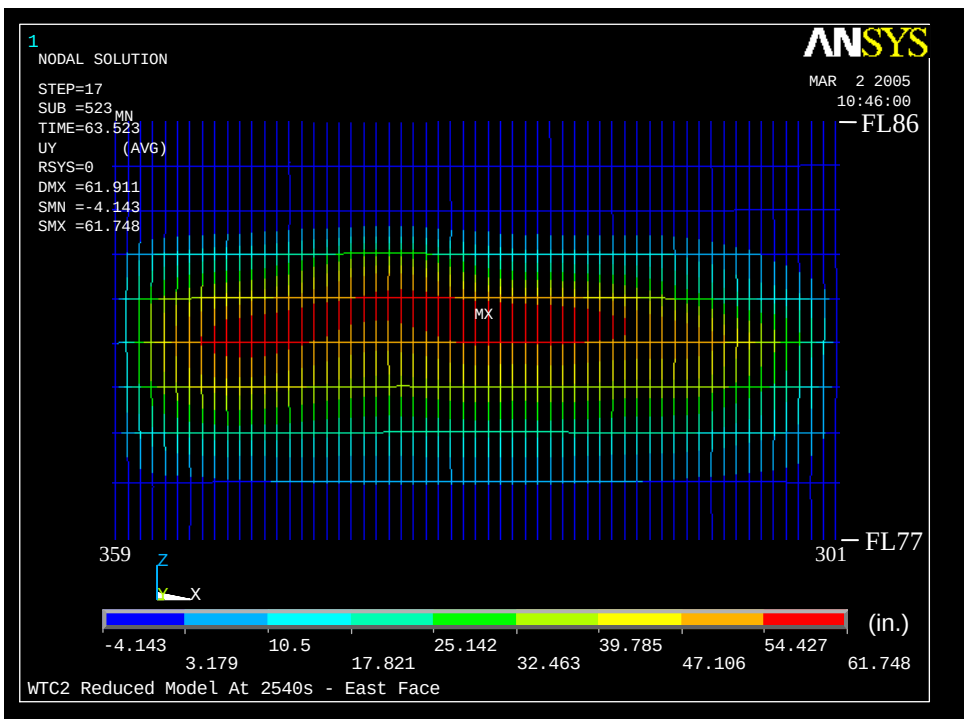

(b) 43 min

Figure 4–100. Out-of-plane displacement of the east wall of WTC 2 for Case D conditions (inward displacement is positive).

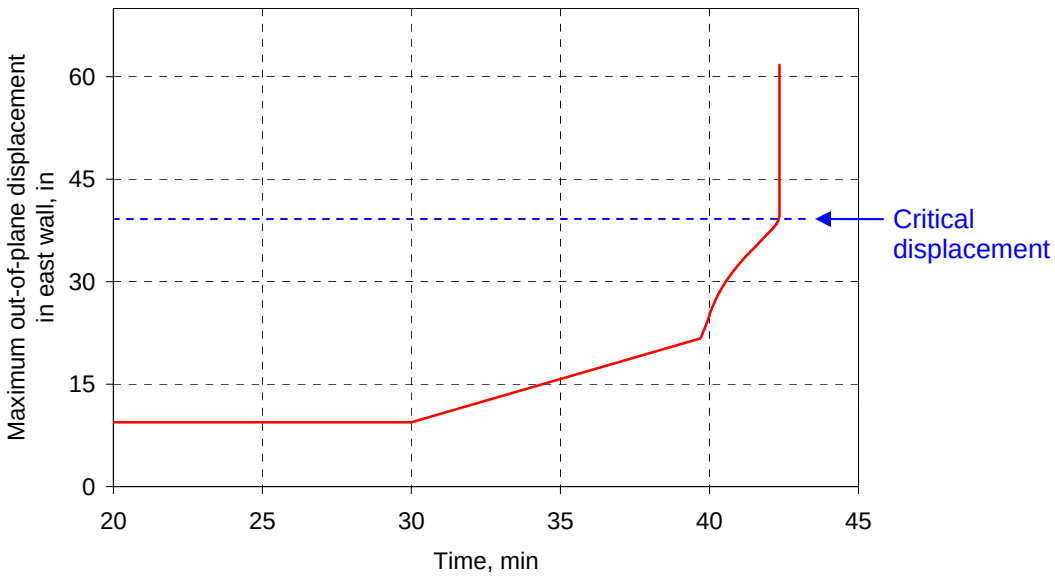

Figure 4–101. Variation of maximum inward bowing of the east wall of WTC 2 over time for Case D conditions.

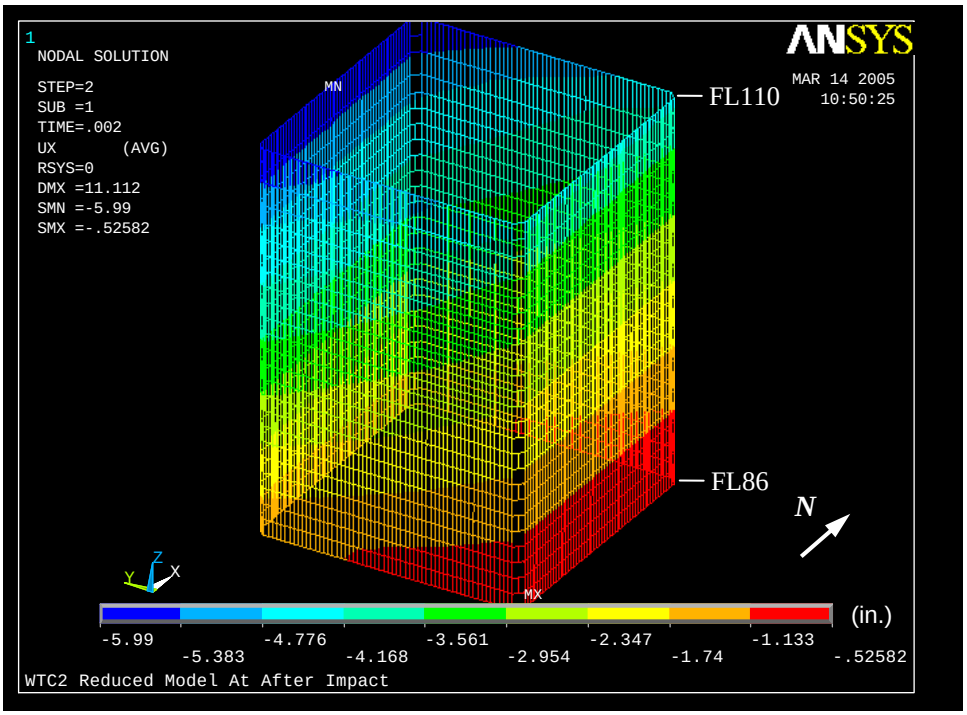

(a) After impact

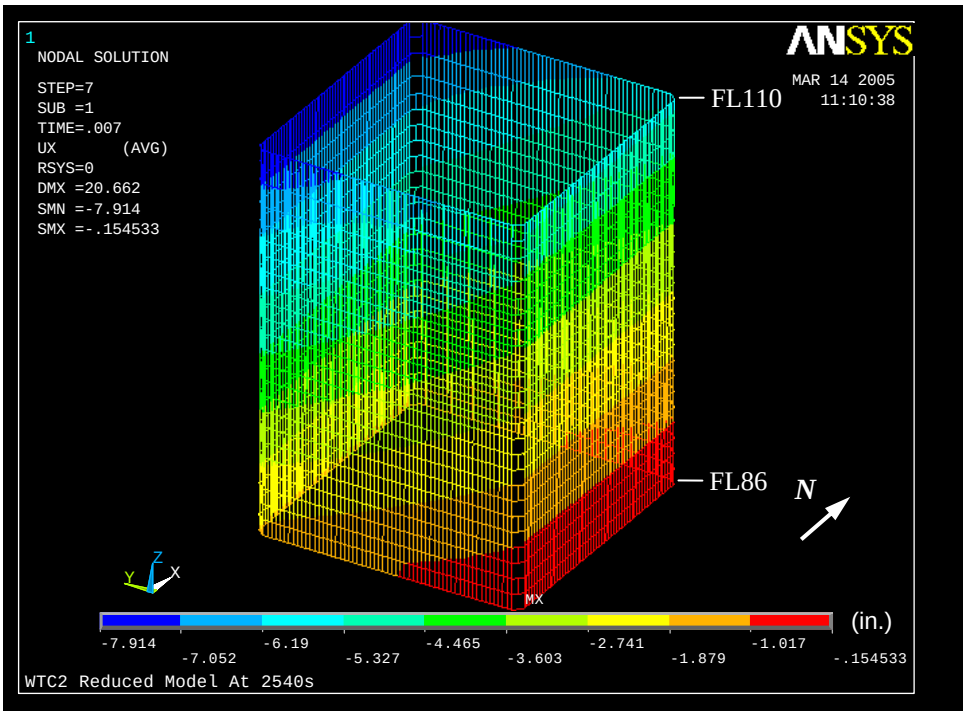

(b) 43 min

Figure 4–102. Lateral displacements above Floor 86 of WTC 2 in the x-direction (north-south) for Case D conditions.

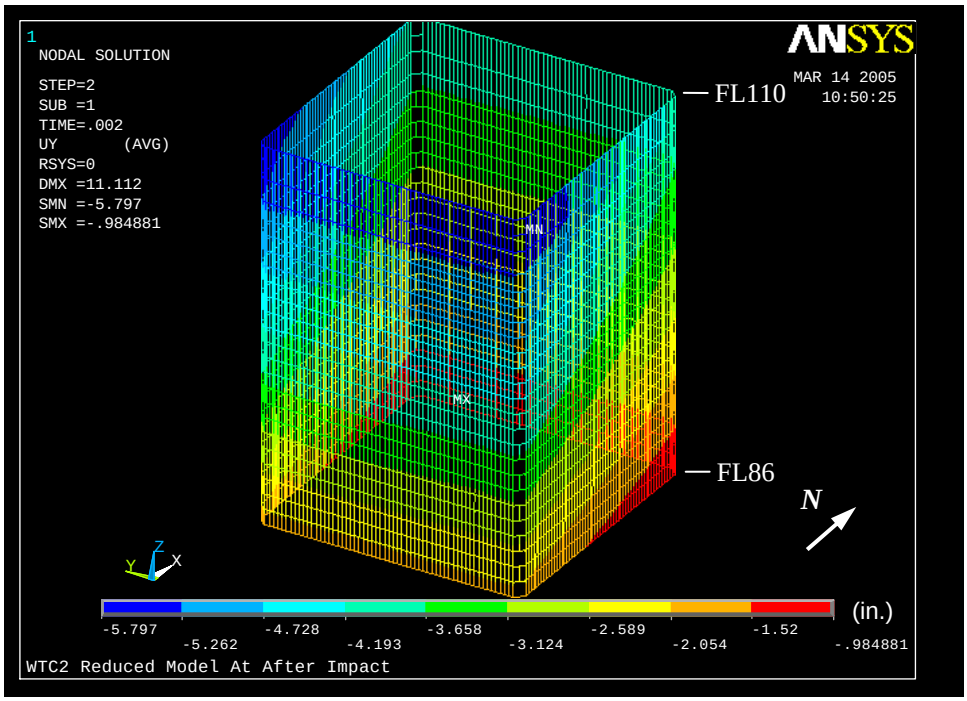

(a) After impact

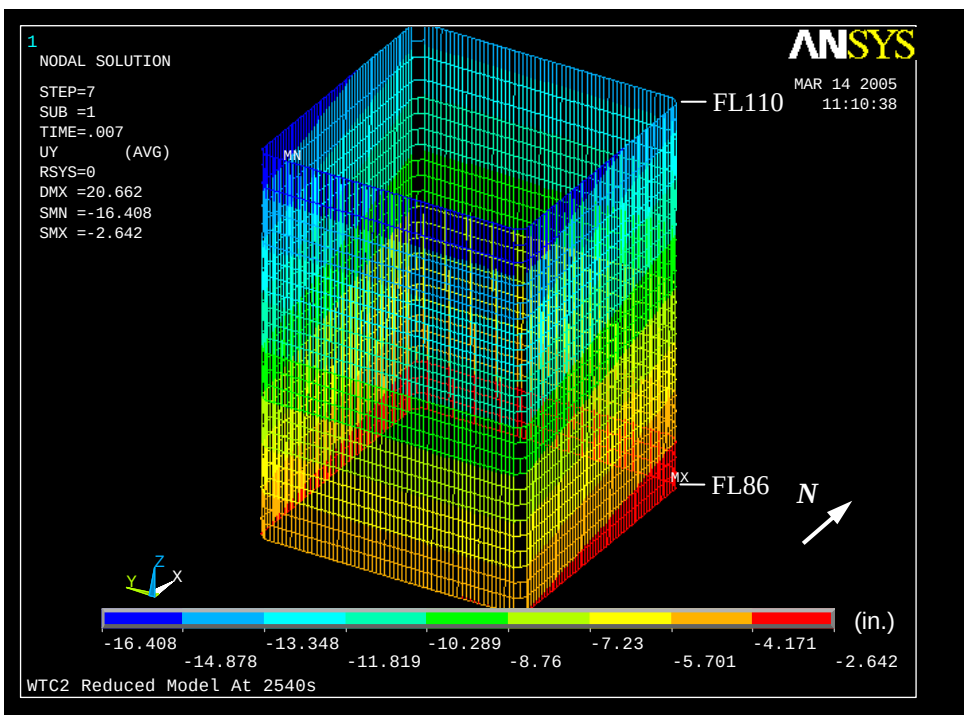

(b) 43 min

Figure 4–103. Lateral displacements above Floor 86 of WTC 2 in the y-direction (east-west) for Case D conditions.

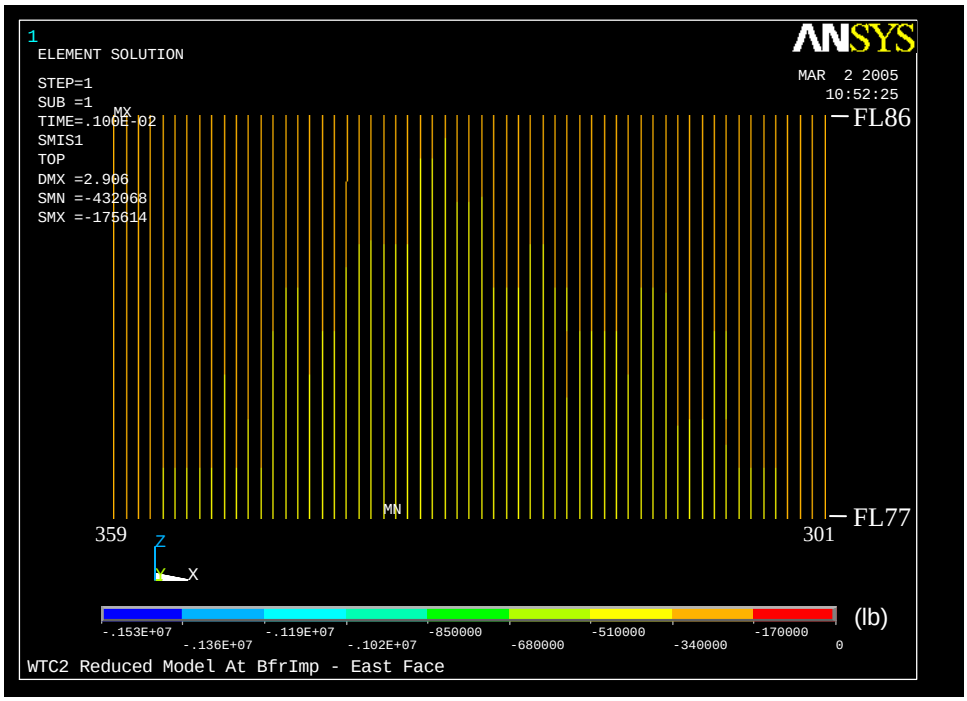

(a) Before impact

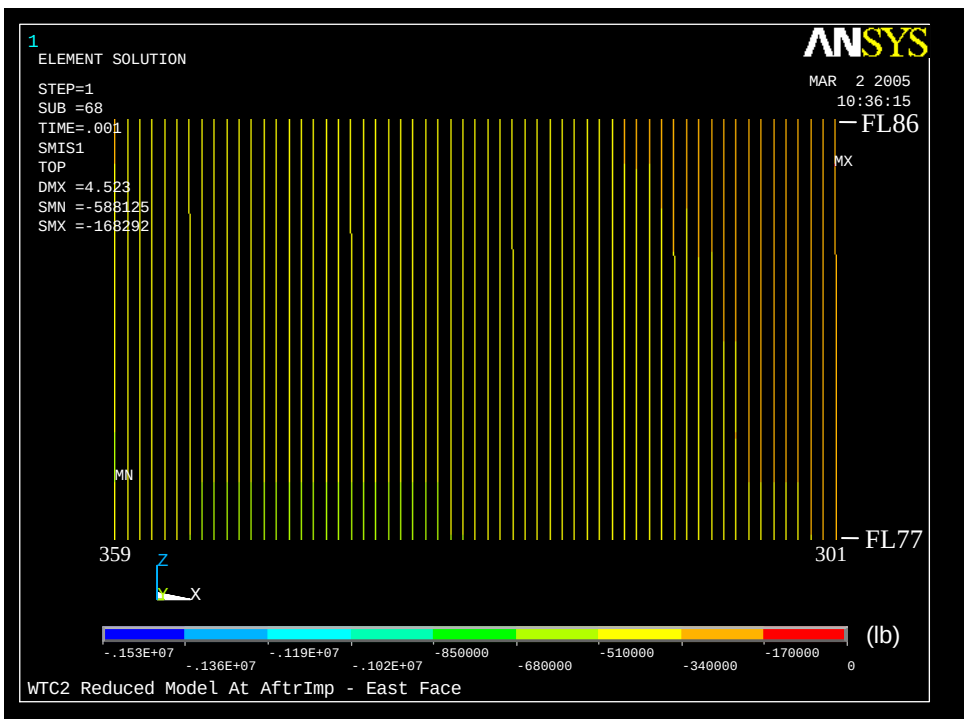

(b) After impact

Figure 4–104. Axial load in the east wall of WTC 2 for Case D conditions (compression is negative).

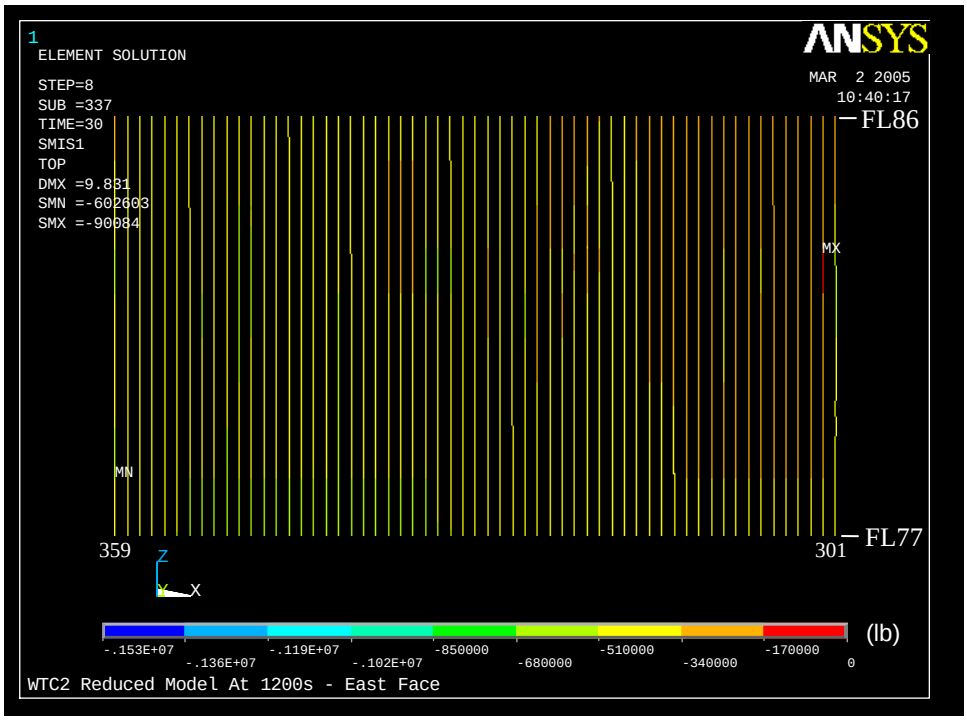

(a) 20 min

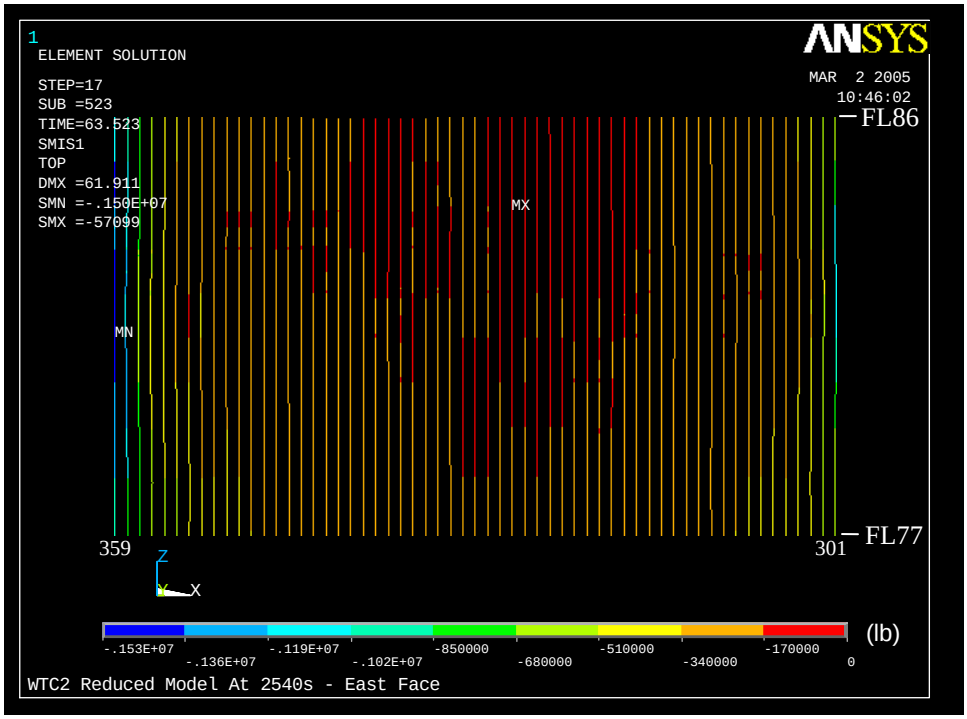

(b) 43 min

Figure 4–105. Axial load in the east wall of WTC 2 for Case D conditions (compression is negative).

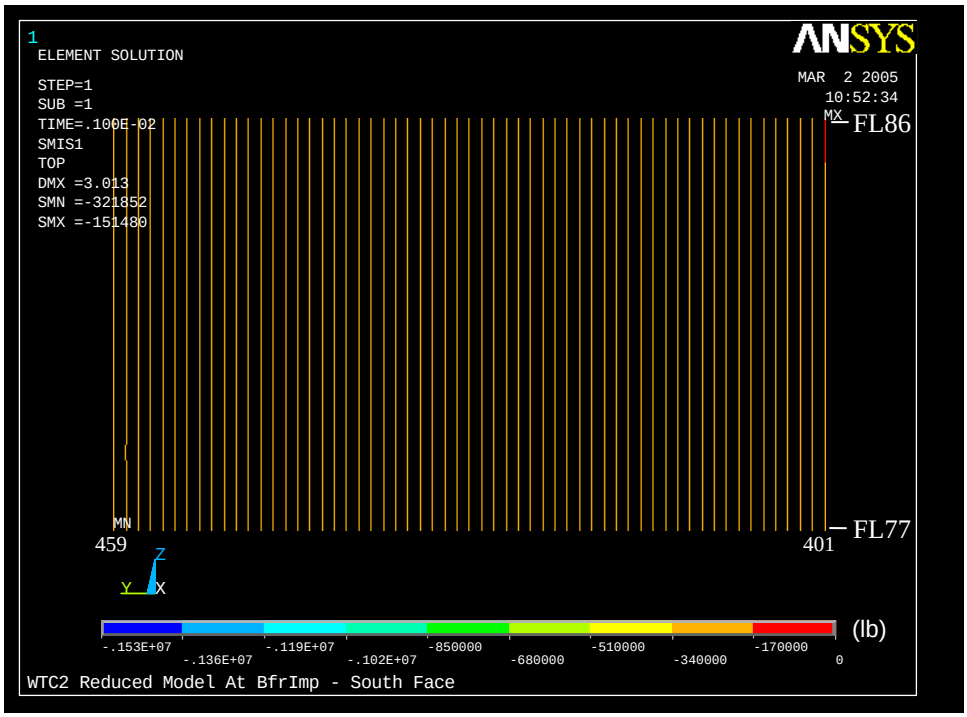

(a) Before impact

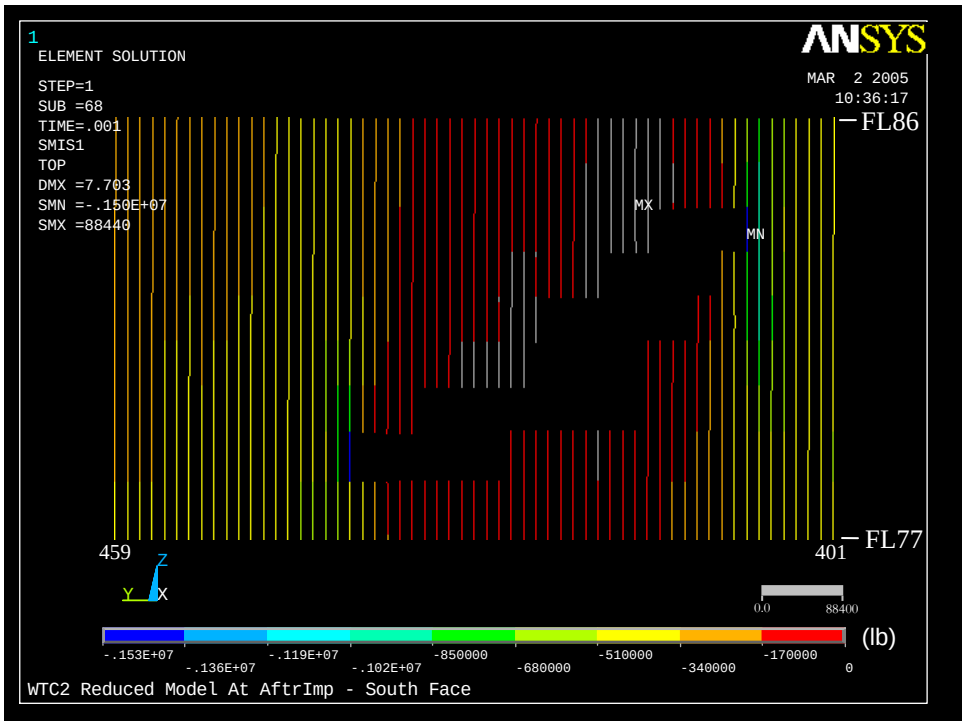

(b) After impact

Figure 4–106. Axial load in the south wall of WTC 2 for Case D conditions (compression is negative).

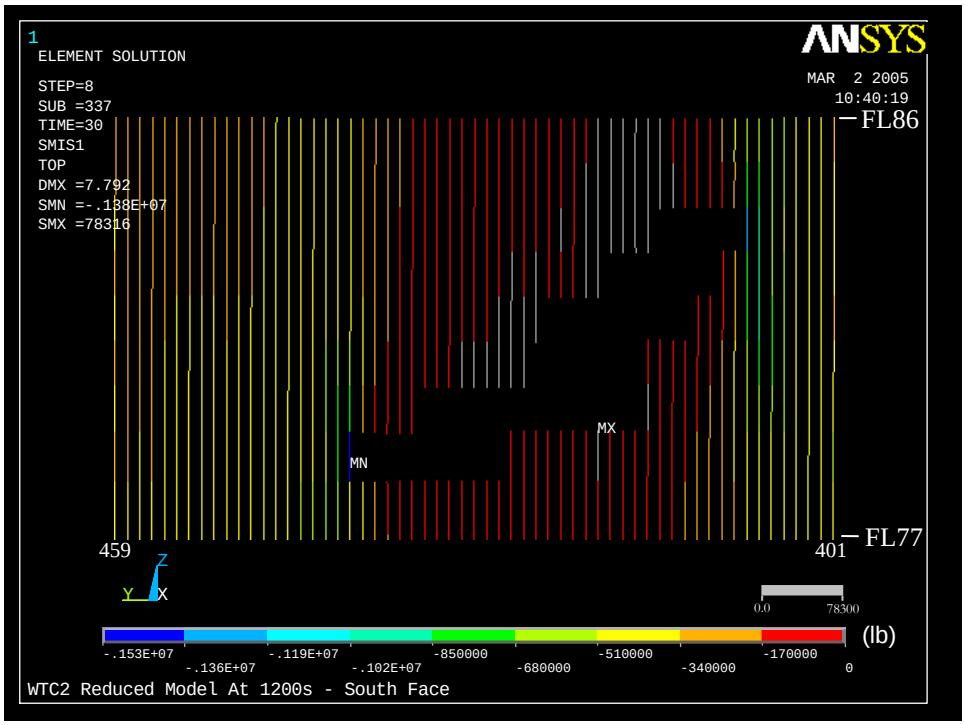

(a) 20 min

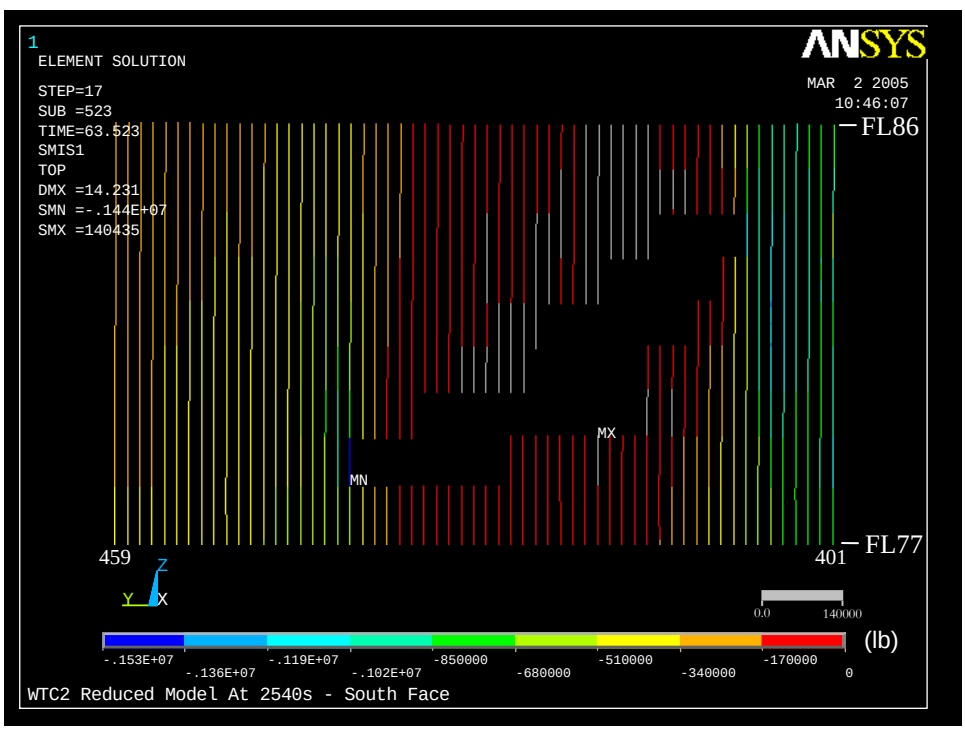

(b) 43 min

Figure 4–107. Axial load in the south wall of WTC 2 for Case D conditions (compression is negative).

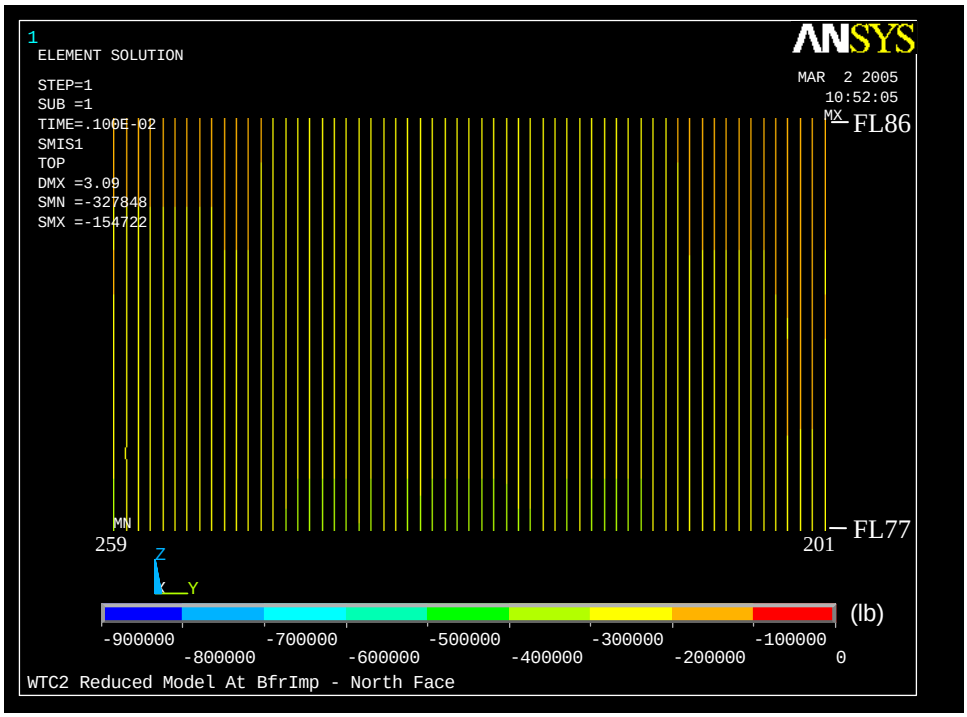

(a) Before impact

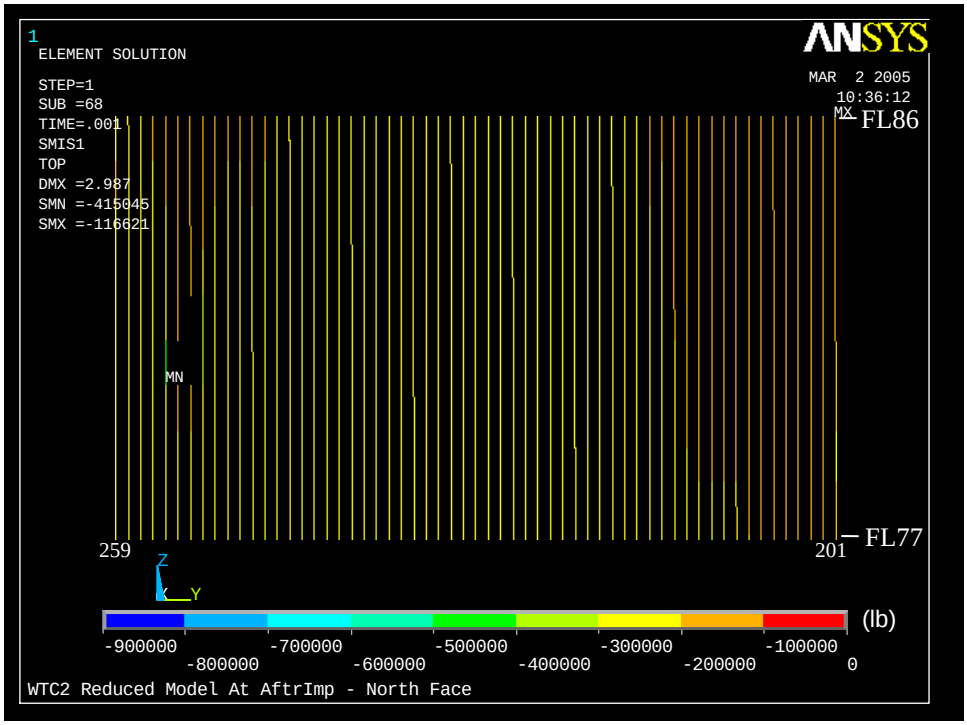

(b) After impact

Figure 4–108. Axial load in the north wall of WTC 2 for Case D conditions (compression is negative).

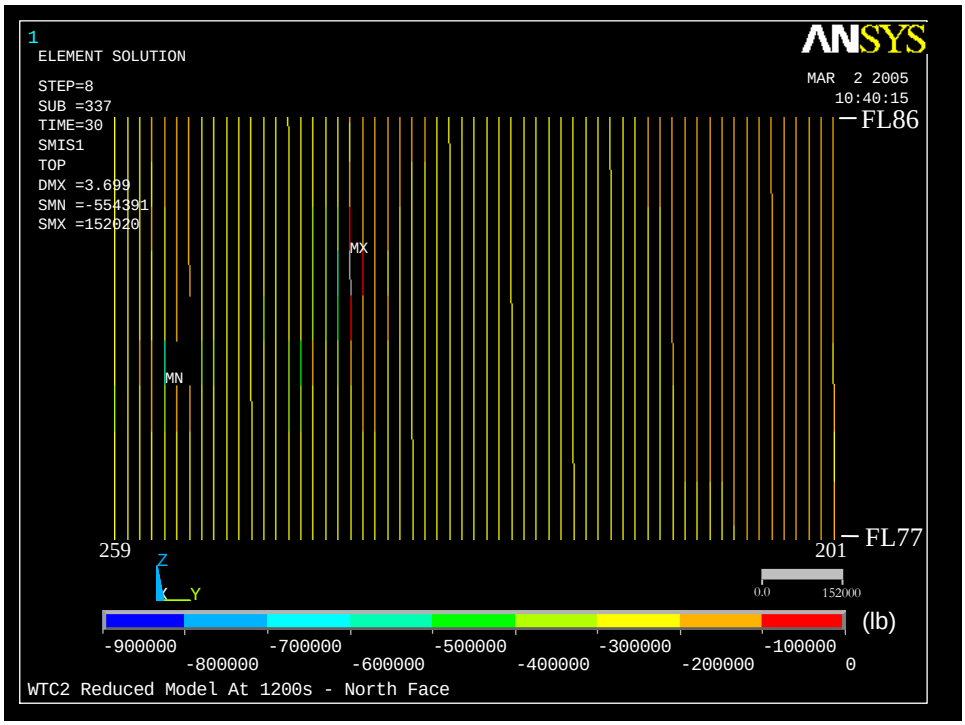

(a) 20 min

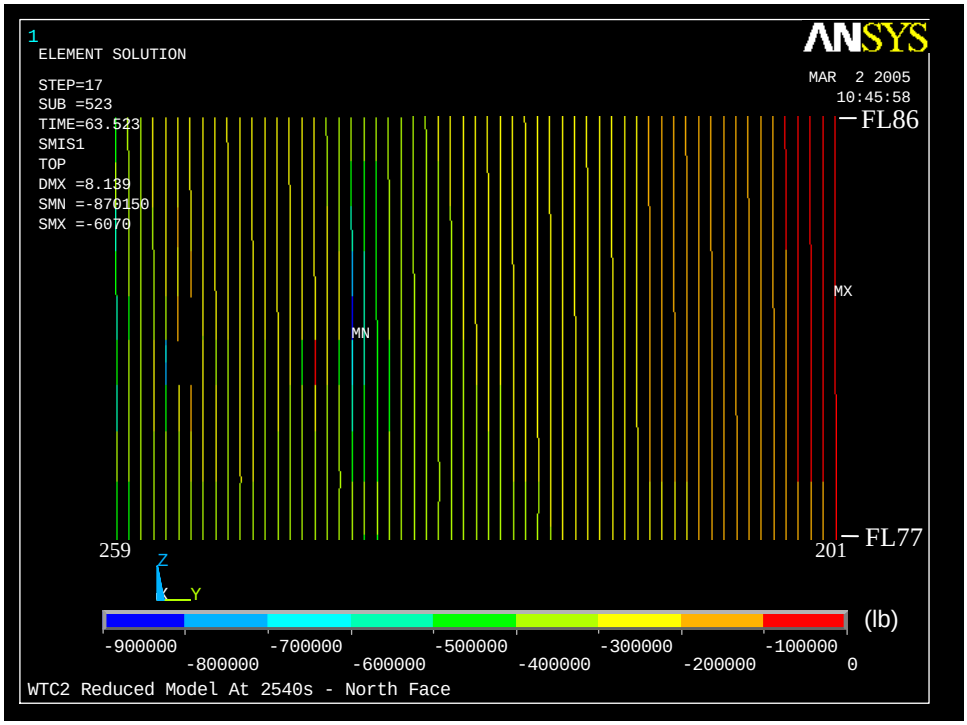

(b) 43 min

Figure 4–109. Axial load in the north wall of WTC 2 for Case D conditions (compression is negative).

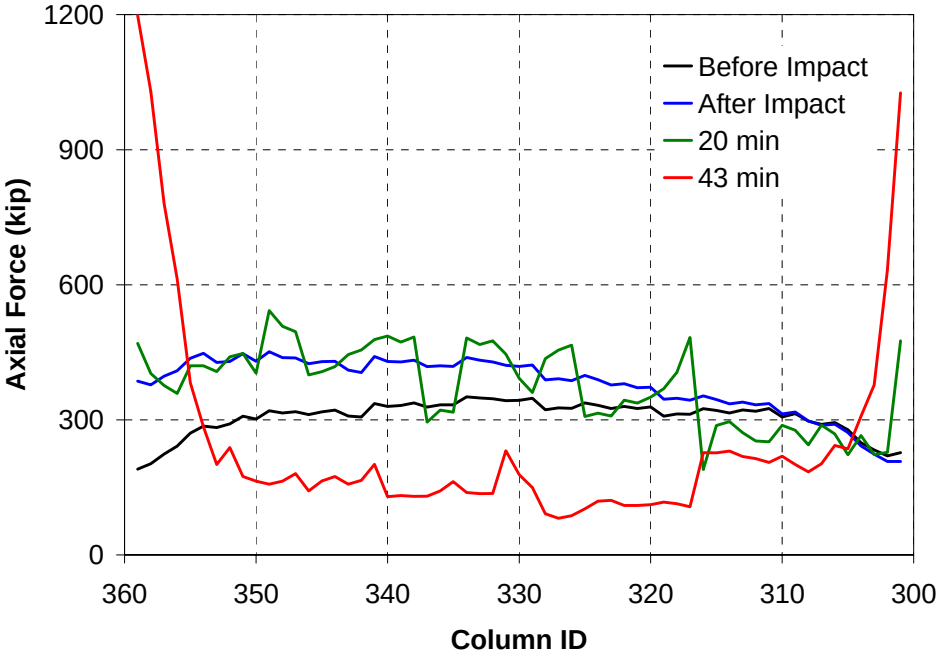

(a) East wall

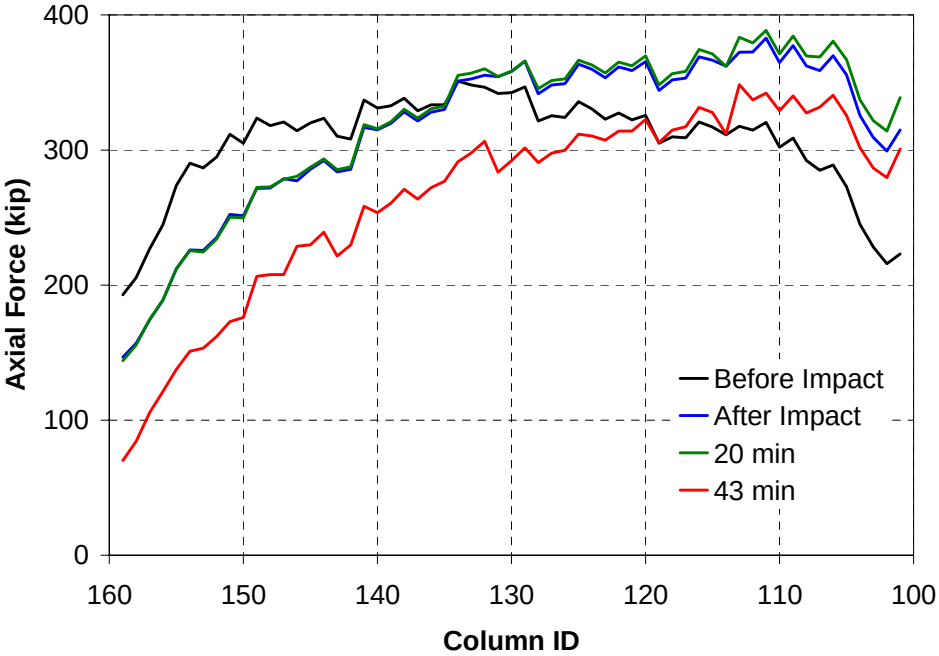

(b) West wall

Figure 4–110. Axial load in the east and the west wall columns at Floor 83 of WTC 2 for Case D conditions (compression is positive).

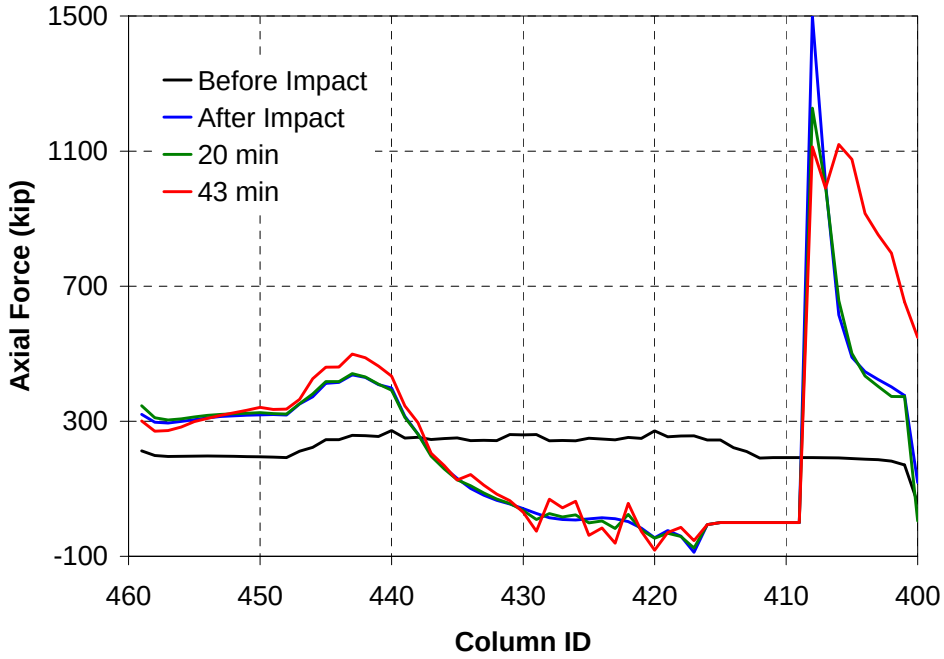

(a) South wall

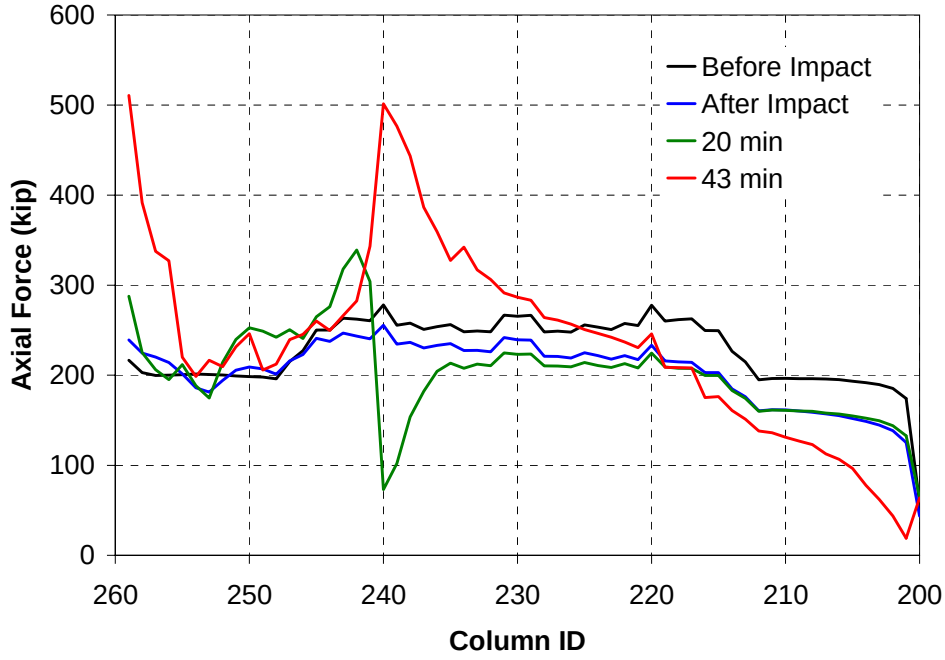

(b) North wall

Figure 4–111. Axial load in the south and the north wall columns at Floor 83 of WTC 2 for Case D conditions (compression is positive).

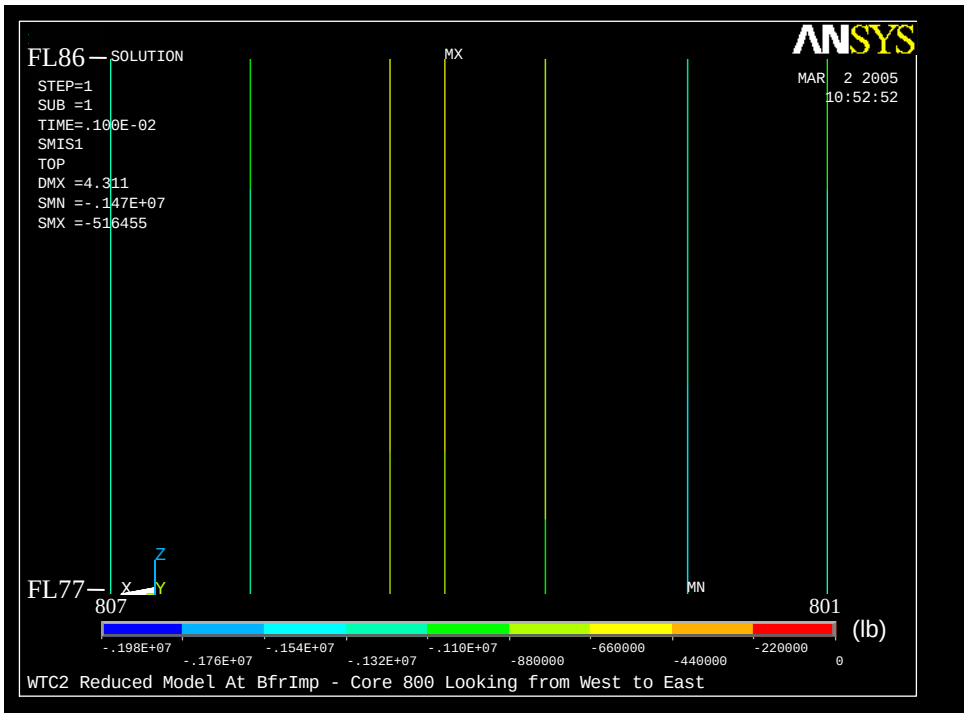

(a) Before impact

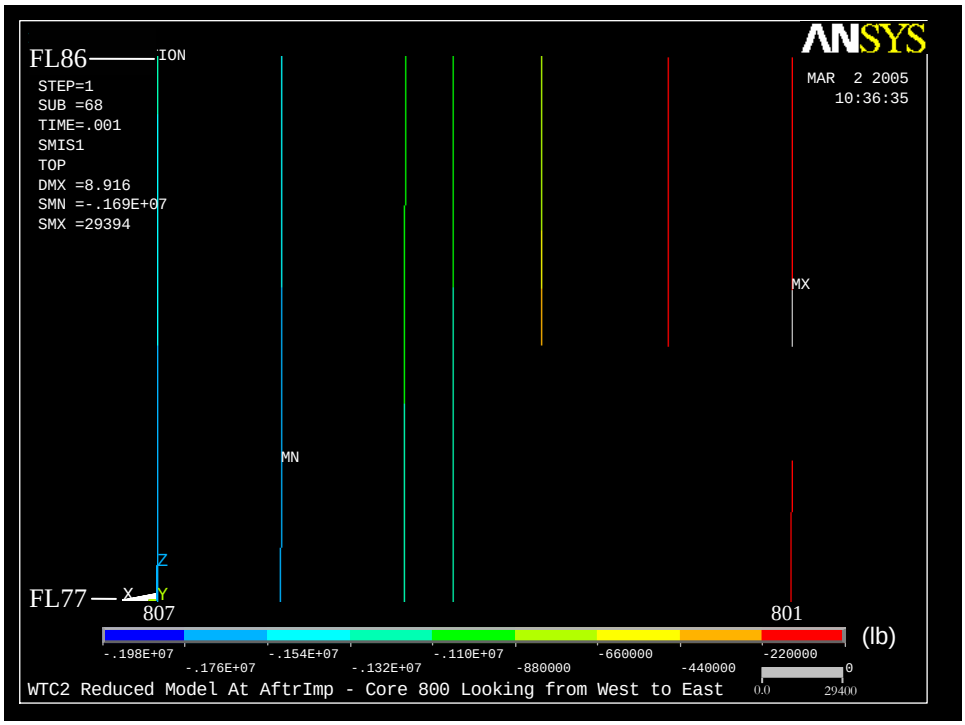

(b) After impact

Figure 4–112. Axial load in 800 series core columns of WTC 2 for Case D conditions (compression is negative).

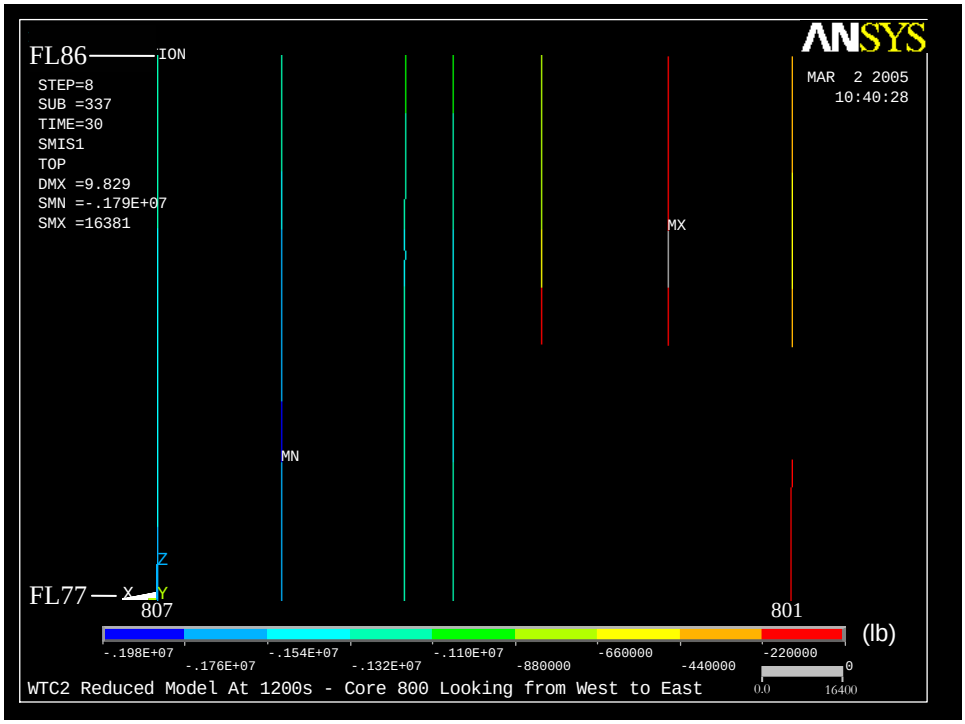

(a) 20 min

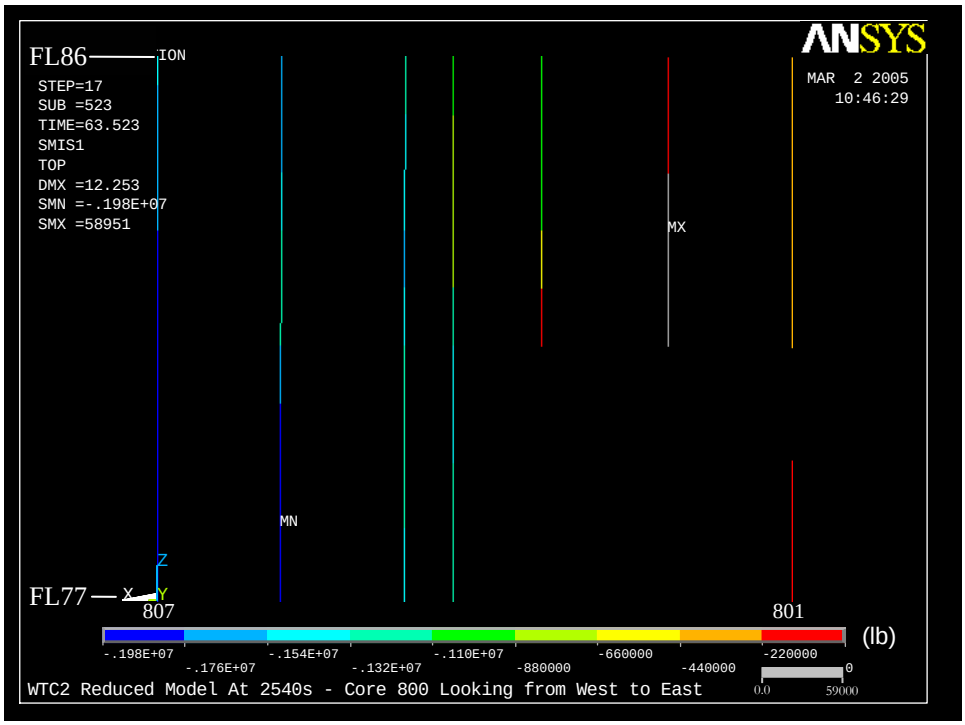

(b) 43 min

Figure 4–113. Axial load in 800 series core columns of WTC 2 for Case D conditions (compression is negative).

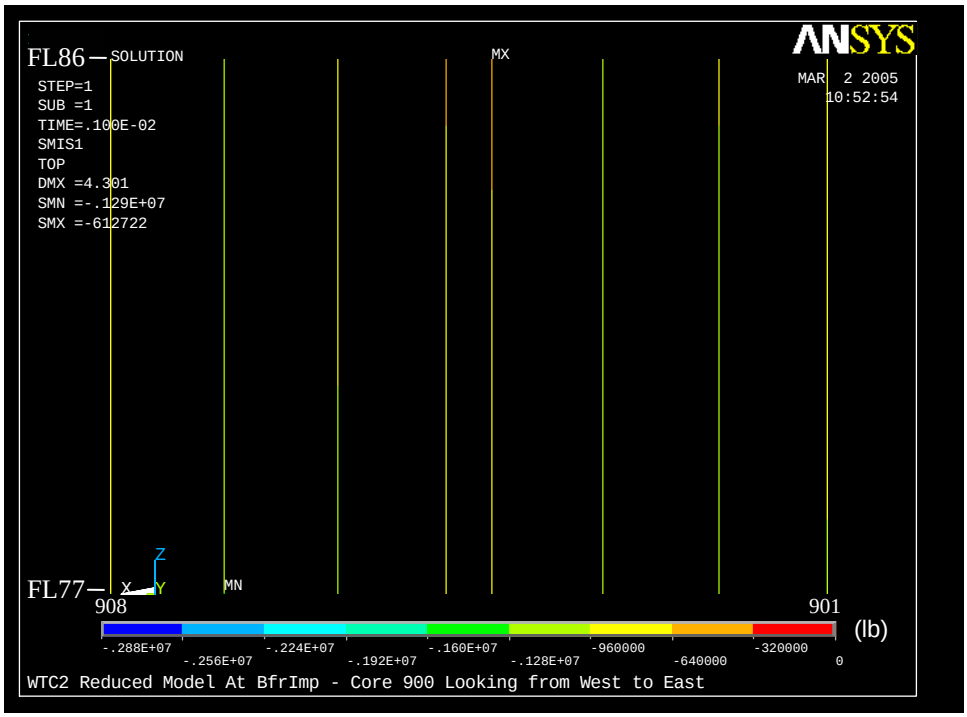

(a) Before impact

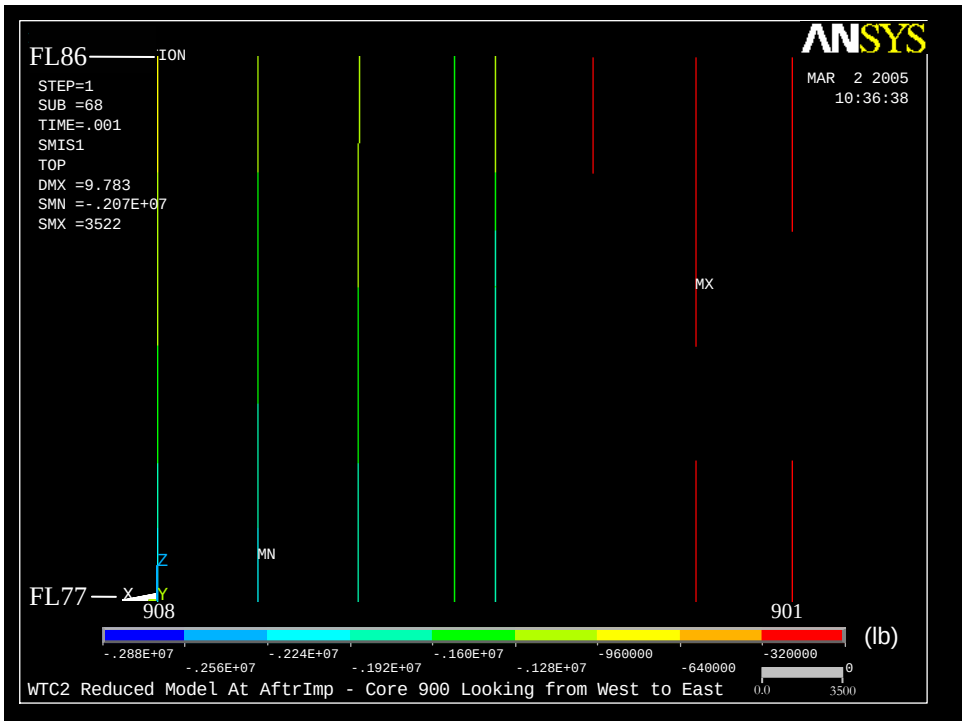

(b) After impact

Figure 4–114. Axial load in 900 series core columns of WTC 2 for Case D conditions (compression is negative).

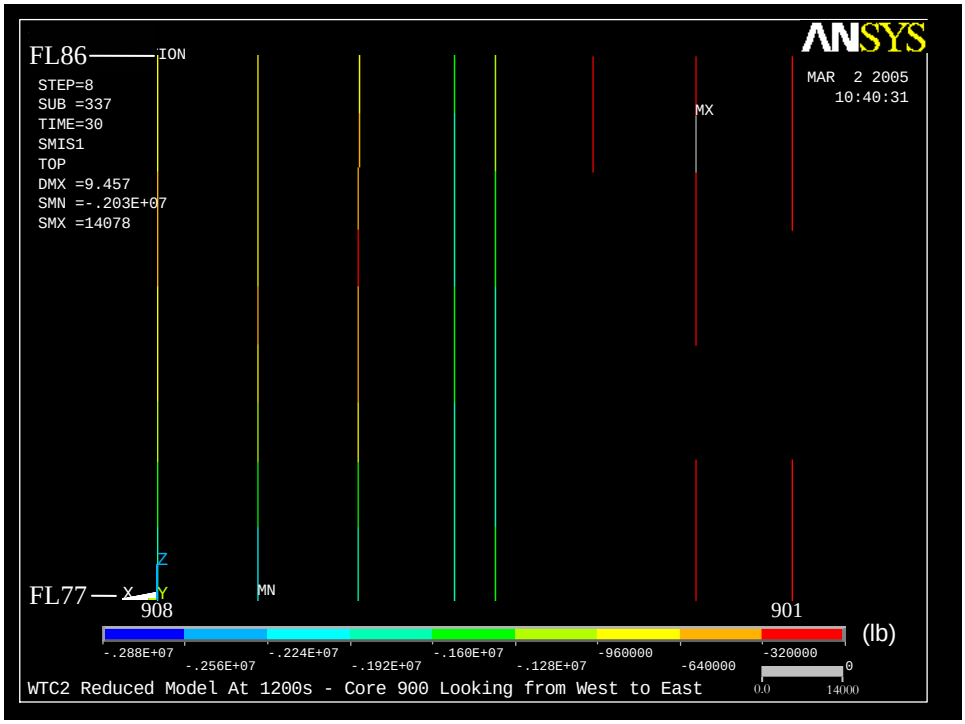

(a) 20 min

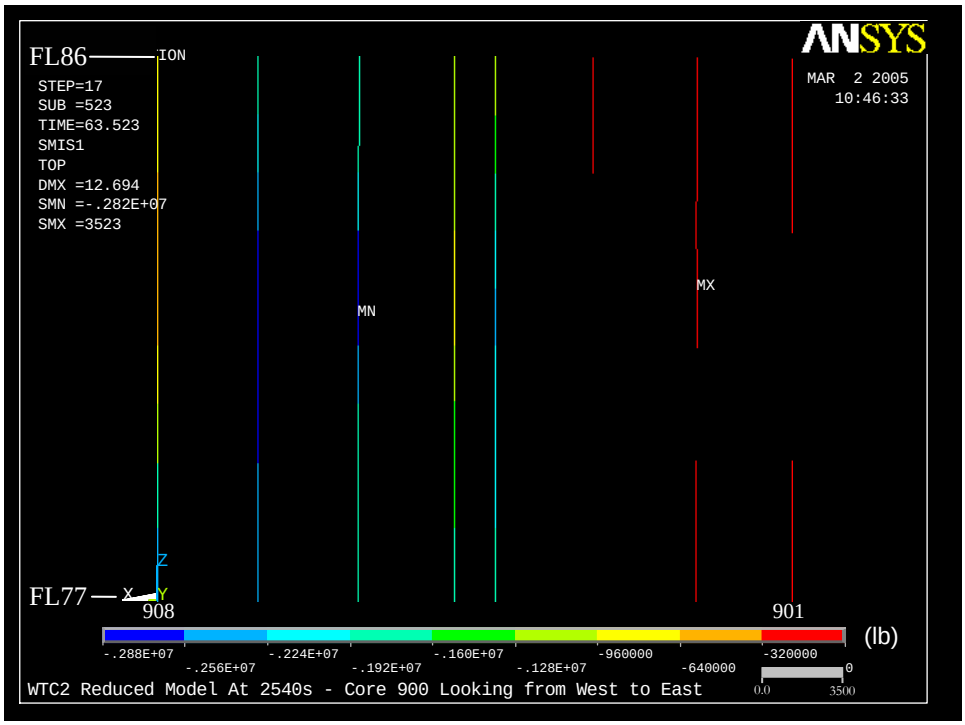

(b) 43 min

Figure 4–115. Axial load in 900 series core columns of WTC 2 for Case D conditions (compression is negative).

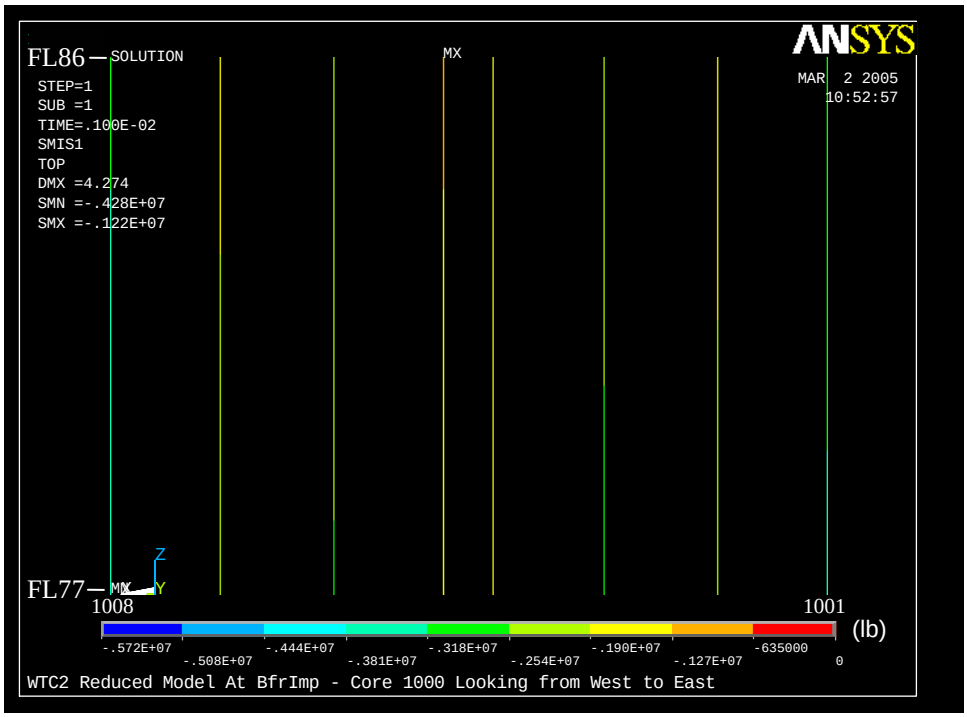

(a) Before impact

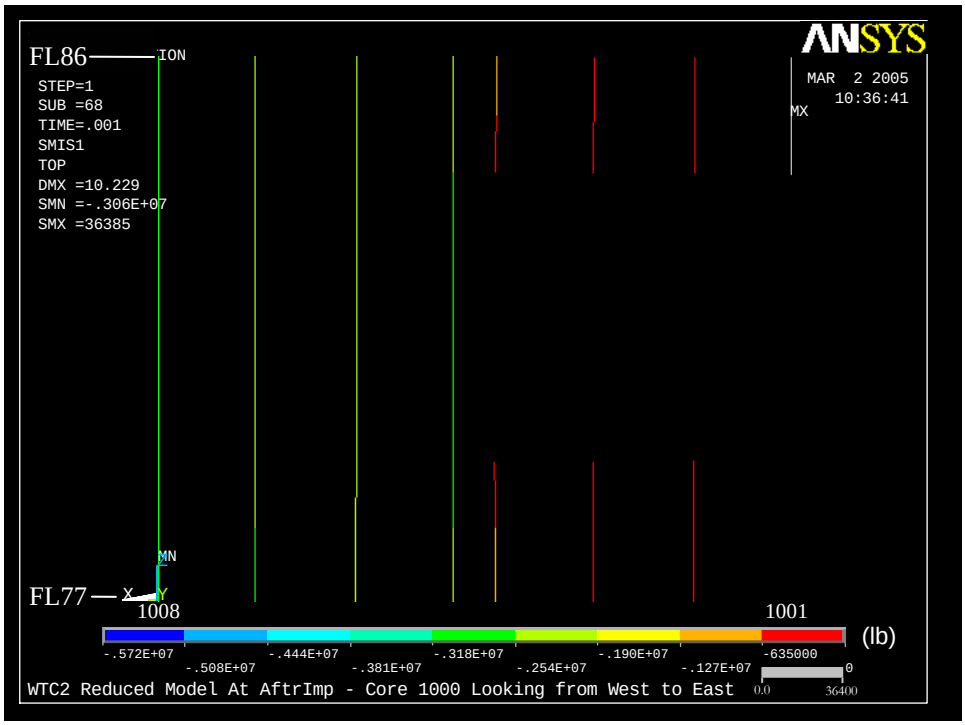

(b) After impact

Figure 4–116. Axial load in 1000 series core columns of WTC 2 for Case D conditions (compression is negative).

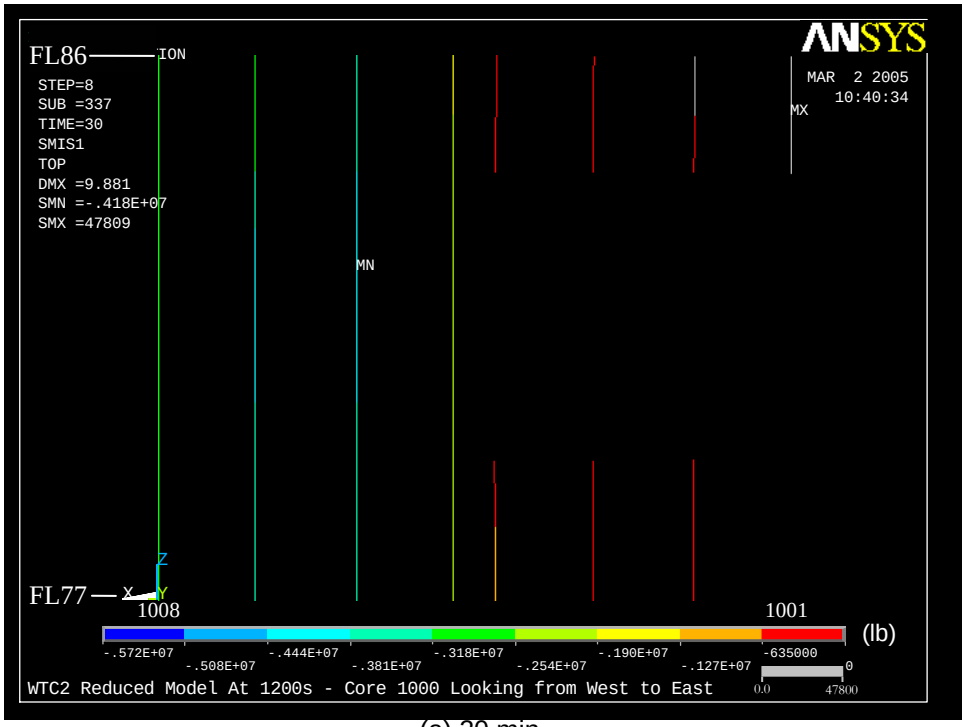

(a) 20 min

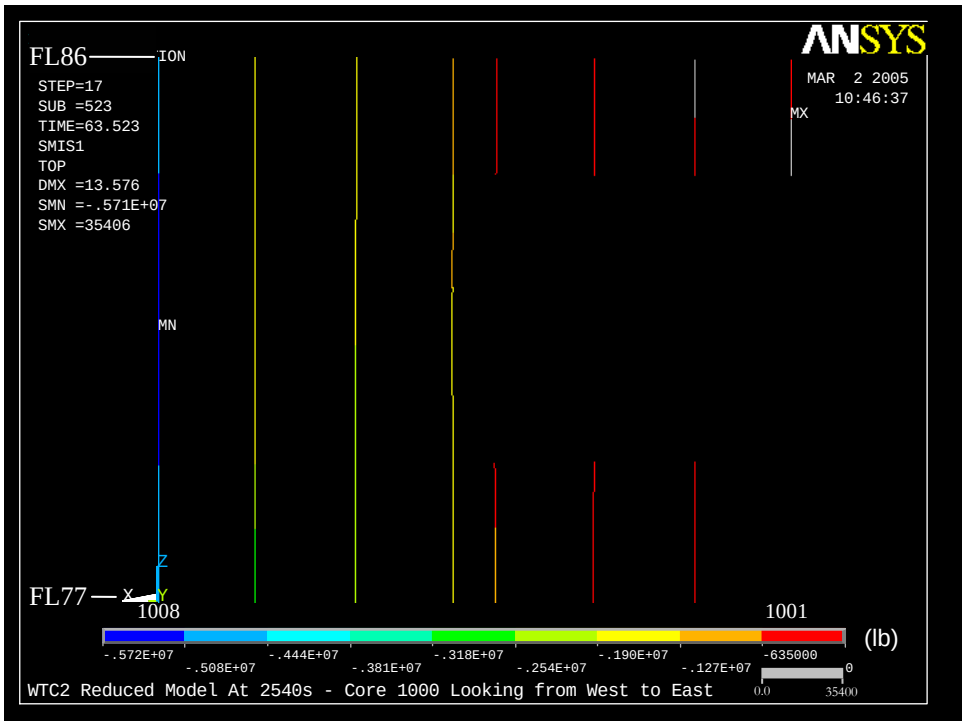

(b) 43 min

Figure 4–117. Axial load in 1000 series core columns of WTC 2 for Case D conditions (compression is negative).

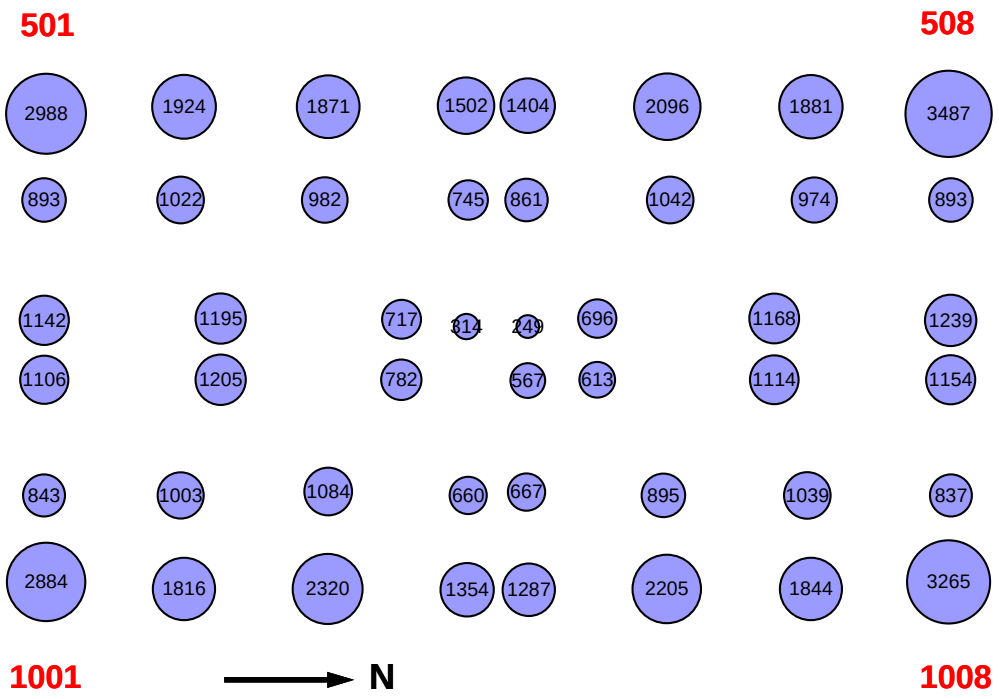

(a) Before impact

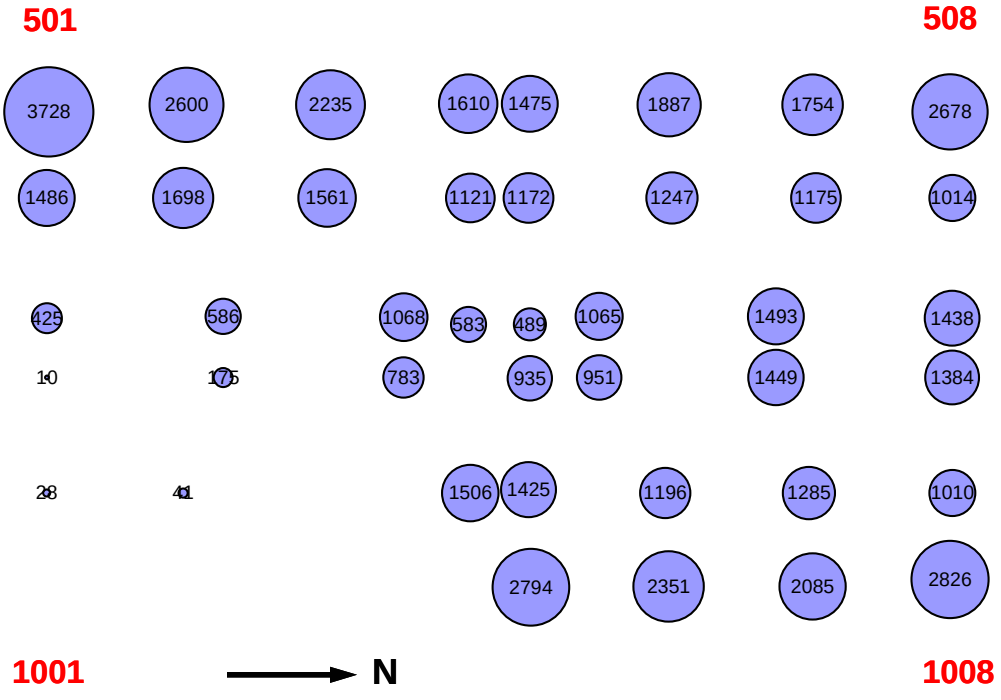

(b) After impact

Figure 4–118. Core column loads (kip) at Floor 83 of WTC 2 for Case D conditions (compression is positive).

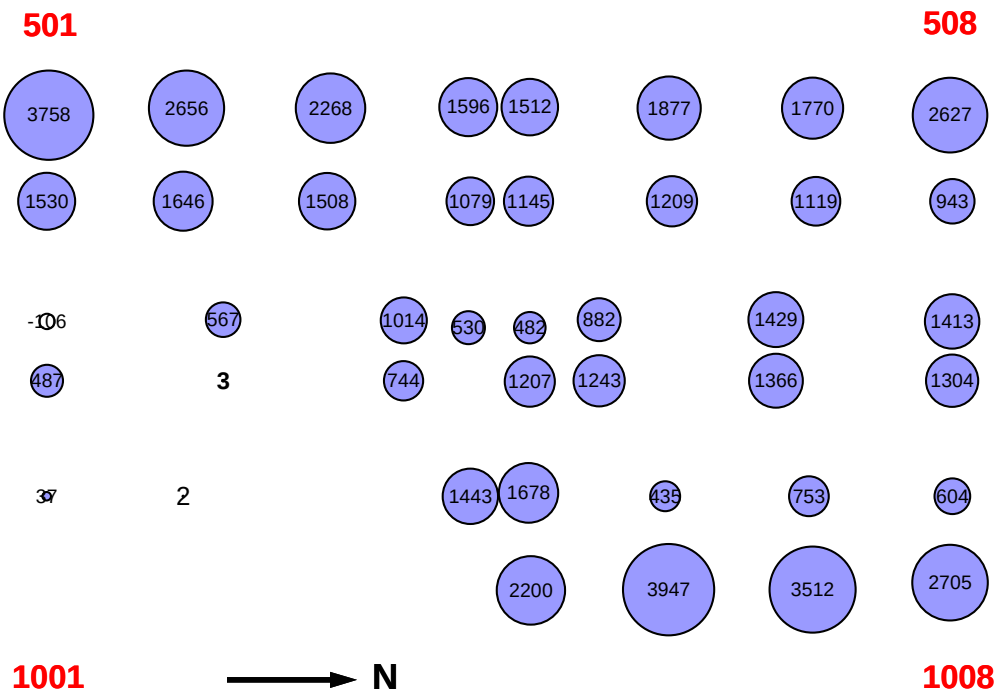

(a) 20 min

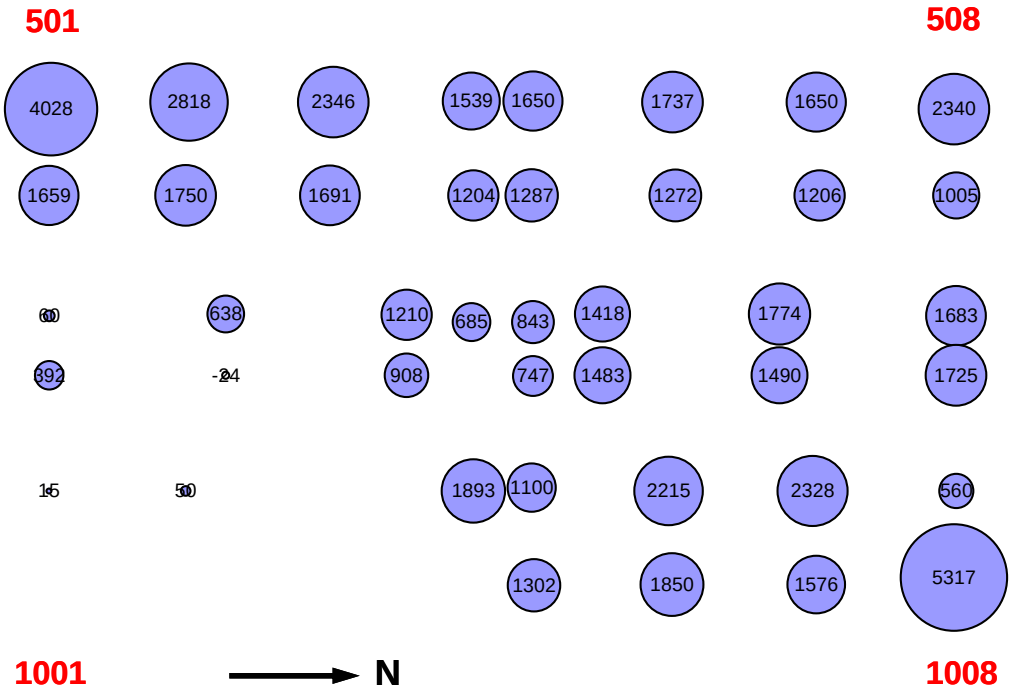

(b) 43 min

Figure 4–119. Core column loads (kip) at Floor 83 of WTC 2 for Case D conditions (compression is positive).

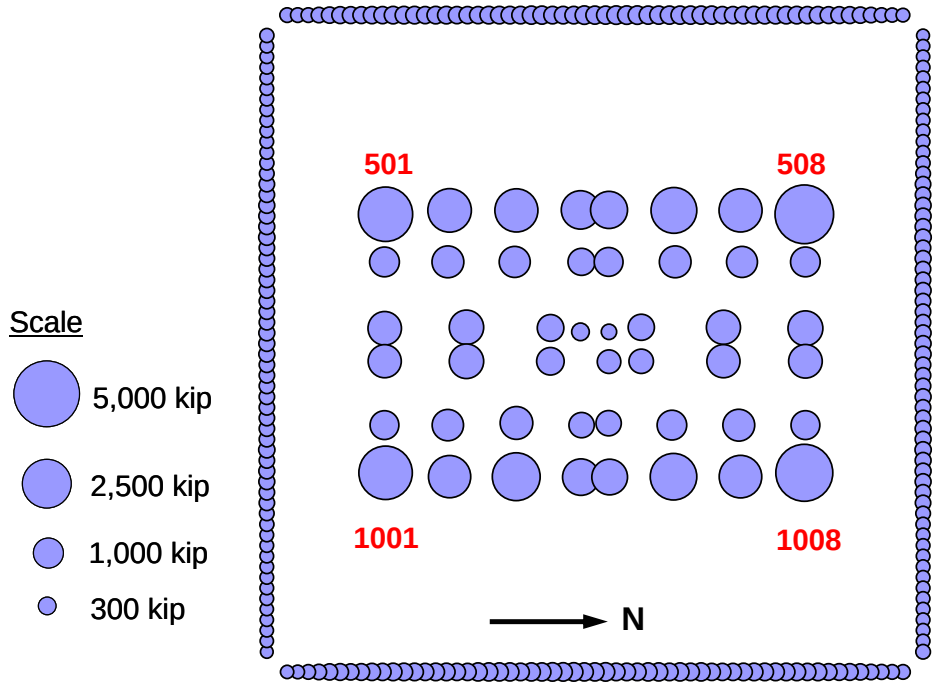

(a) Before impact

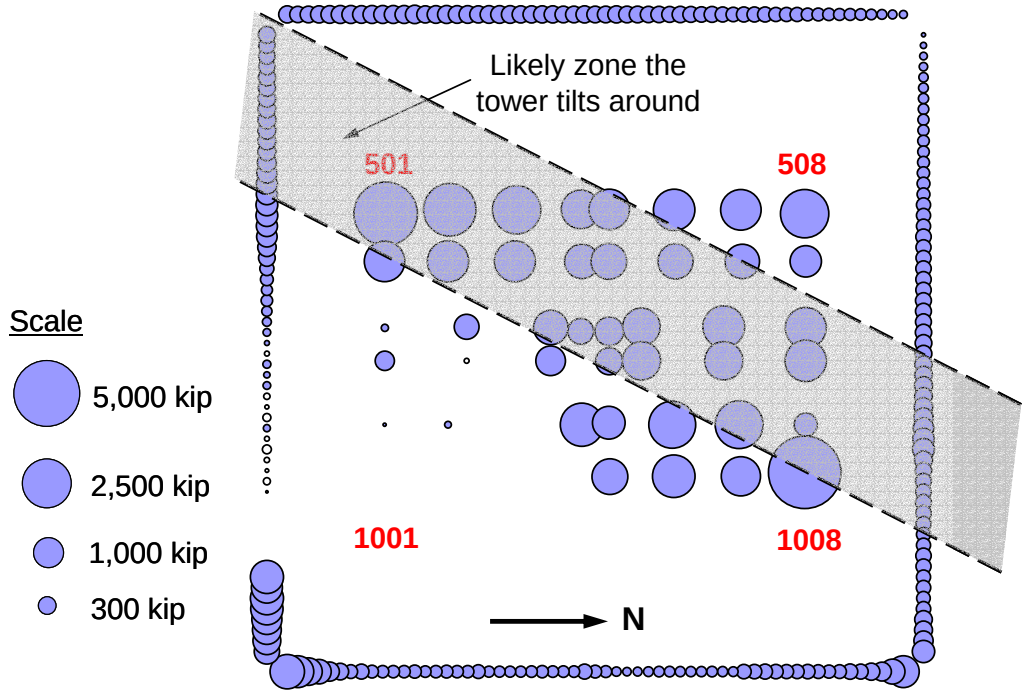

(b) 43 min

Figure 4–120. Axial load in Floor 83 columns of WTC 2 for Case D conditions (compression is positive).

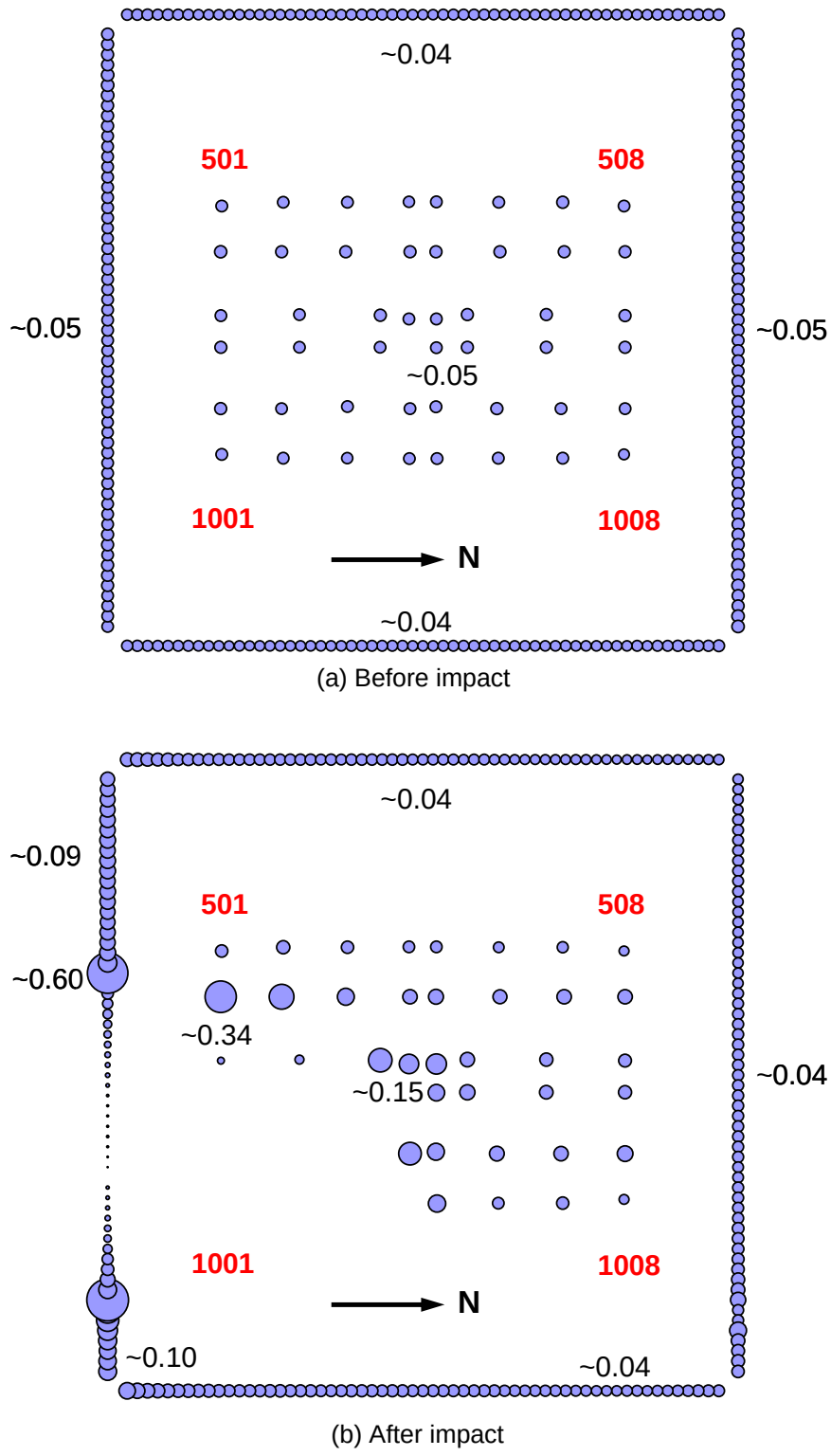

Figure 4–121. Maximum elastic-plus-plastic strains for columns between Floor 78 and Floor 83 of WTC 2 for Case D conditions (compressive strain is positive; strain values are in percent).

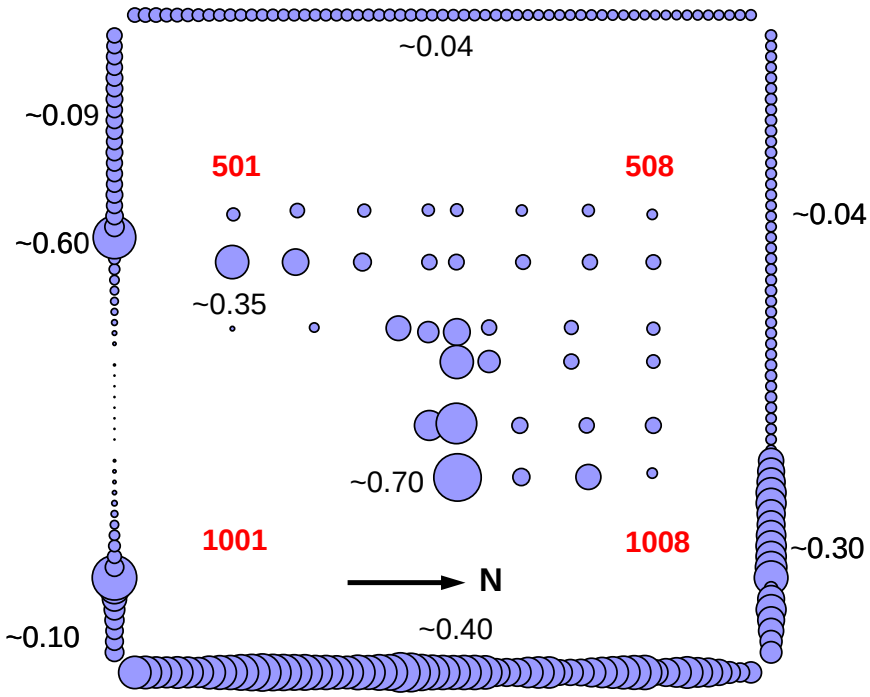

(a) 20 min

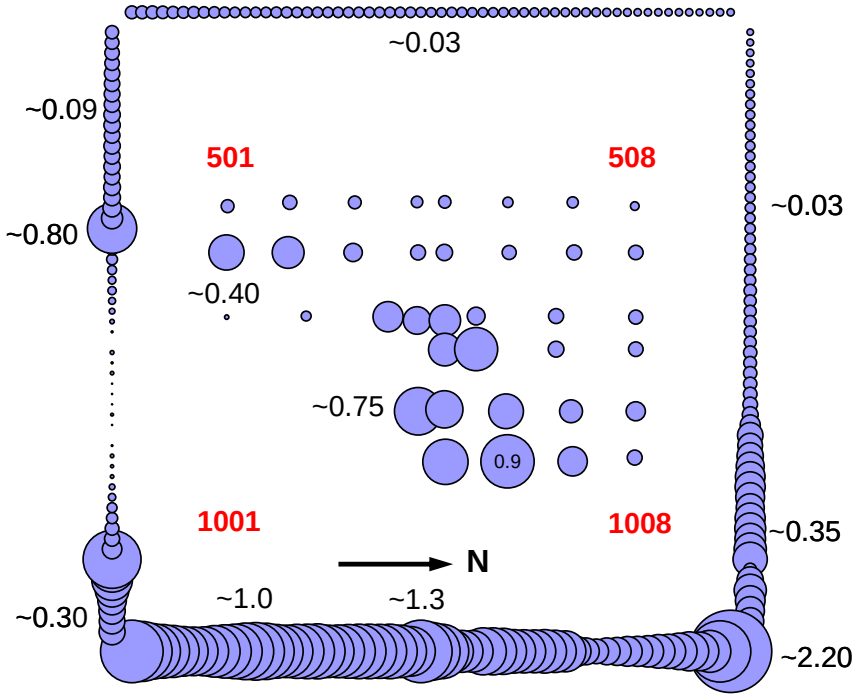

(b) 43 min

Figure 4–122. Maximum elastic-plus-plastic strains for columns between Floor 78 and Floor 3 of WTC 2 for Case D conditions (compressive strain is positive; strain values are in percent).

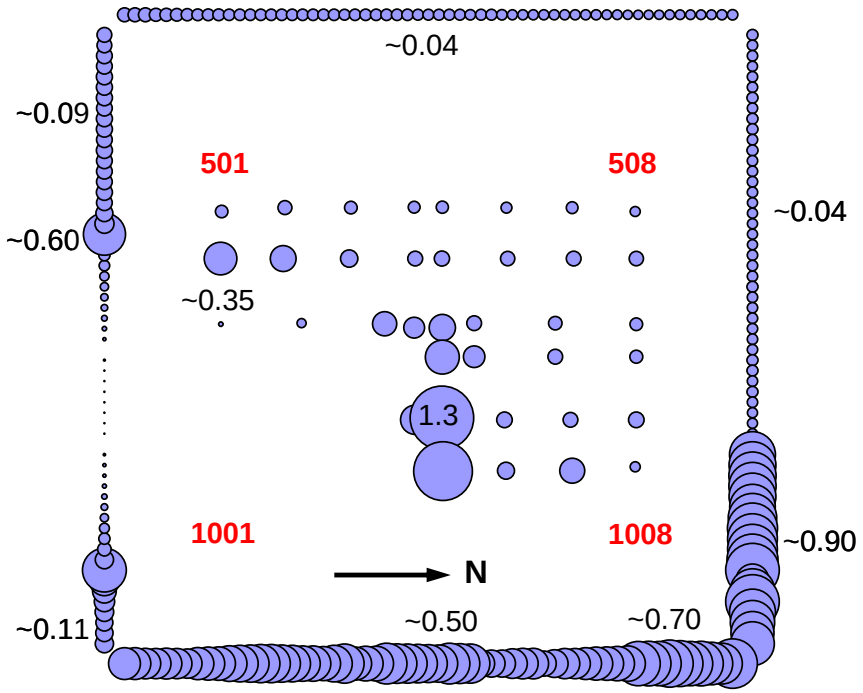

(a) 20 min

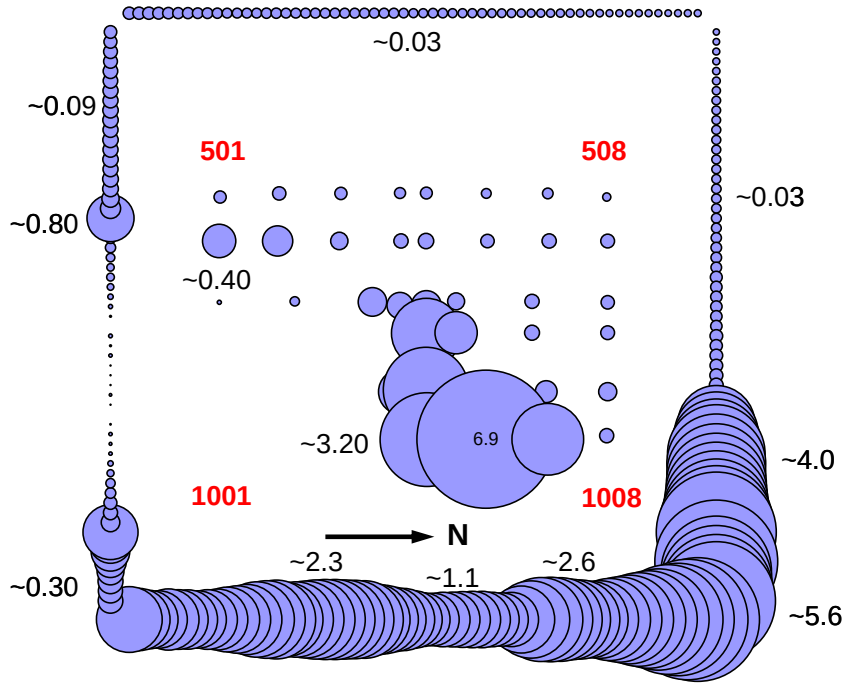

(b) 43 min

Figure 4–123. Maximum elastic-plus-plastic-plus-creep strains for columns between Floor 78 and Floor 83 of WTC 2 for Case D conditions (compressive strain is positive; strain values are in percent).

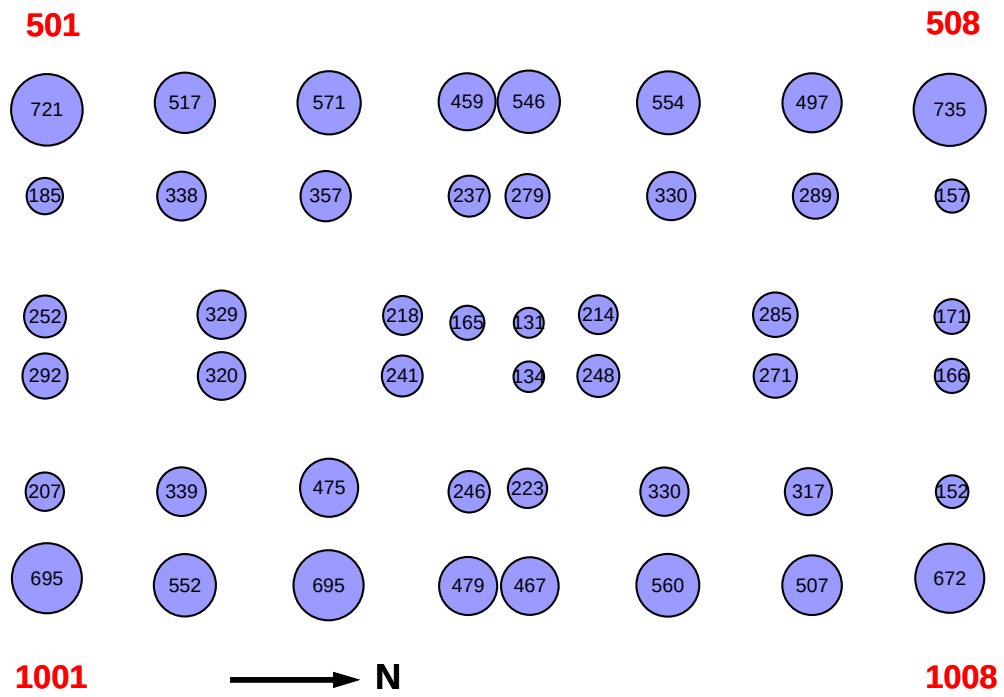

(a) Before impact

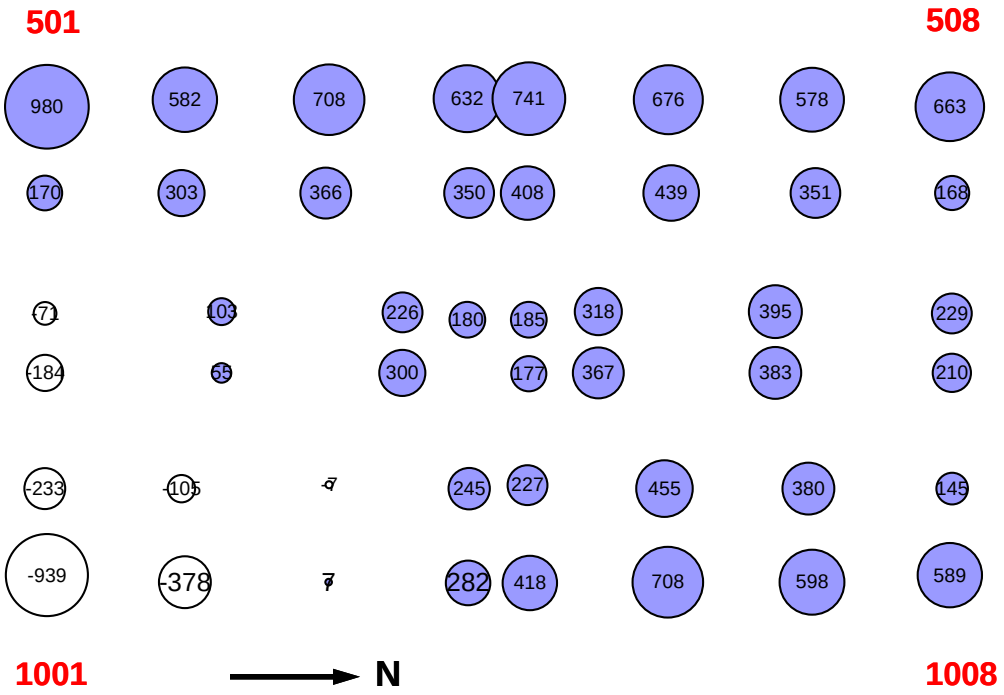

(b) After impact

Figure 4–124. Axial load in core columns (kip) at Floor 105 (at hat truss level) of WTC 2 for Case D conditions (compression is positive).

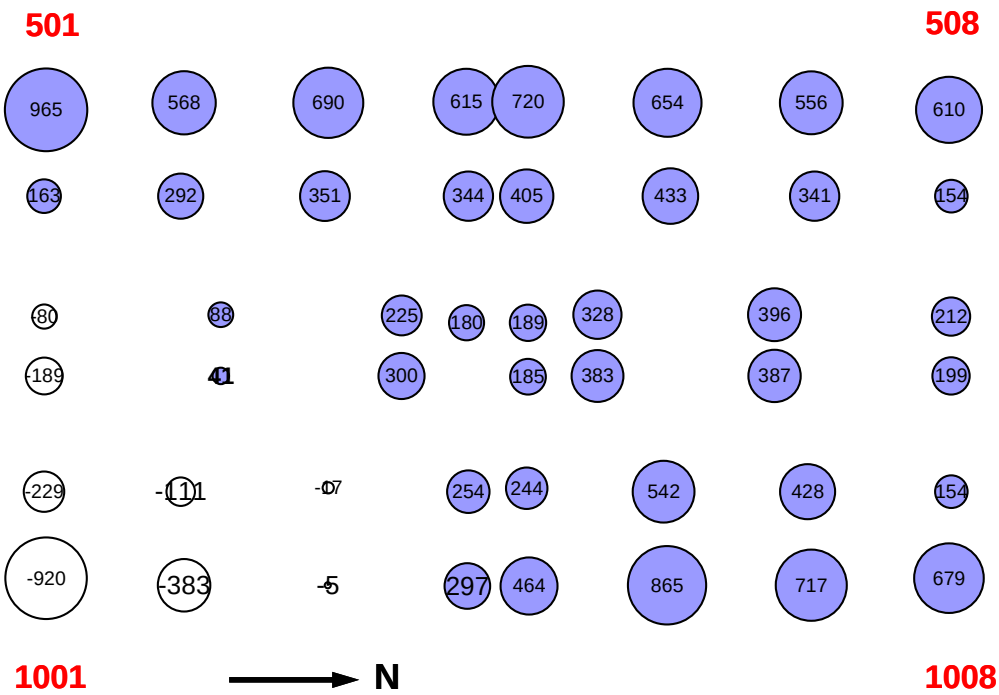

(a) 20 min

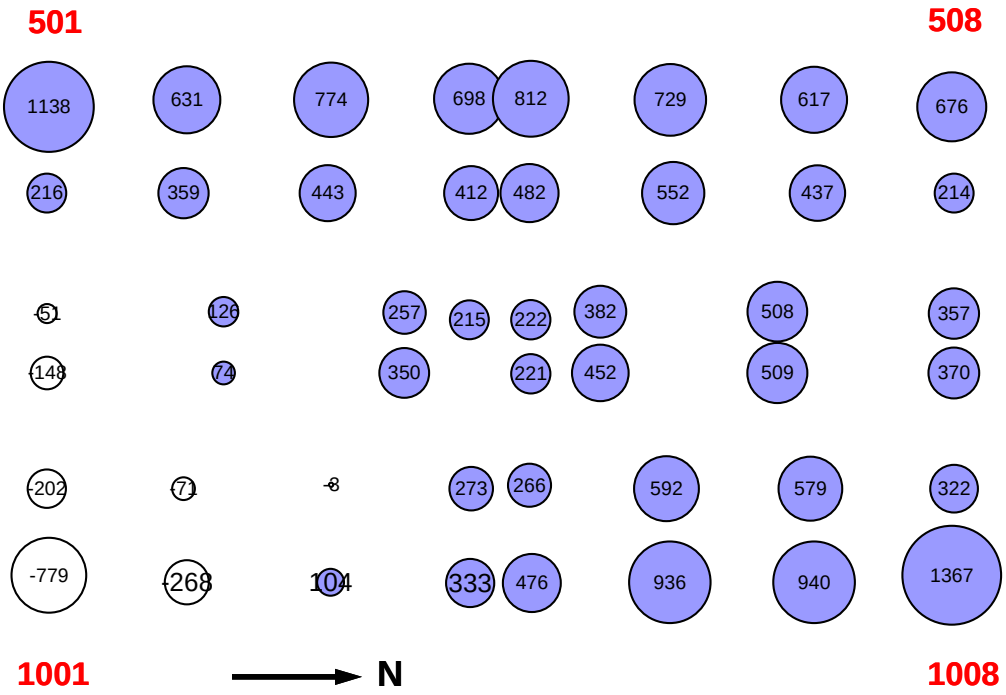

(b) 43 min

Figure 4–125. Axial load in core columns (kip) at Floor 105 (at hat truss level) of WTC 2 for Case D conditions (compression is positive).

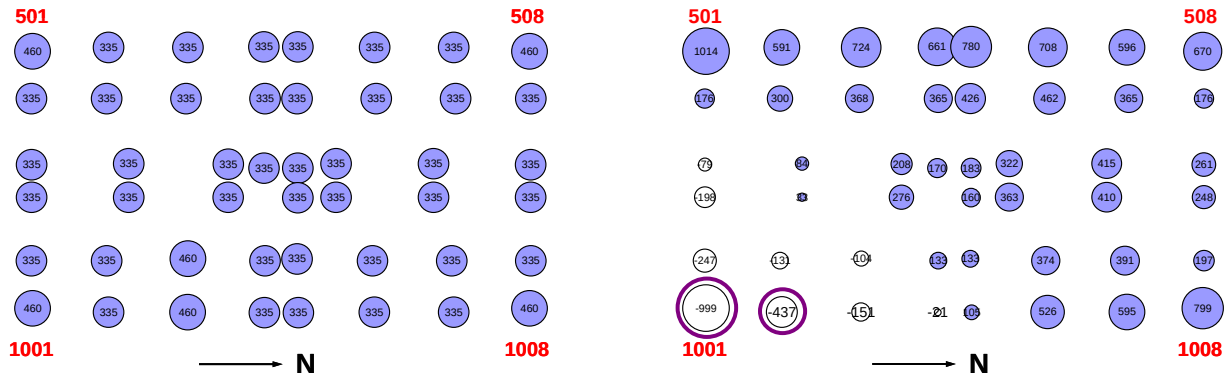

(a) Tension capacities of core column splices

(b) Before splices 1001 and 1002 fail (t = 40 min)

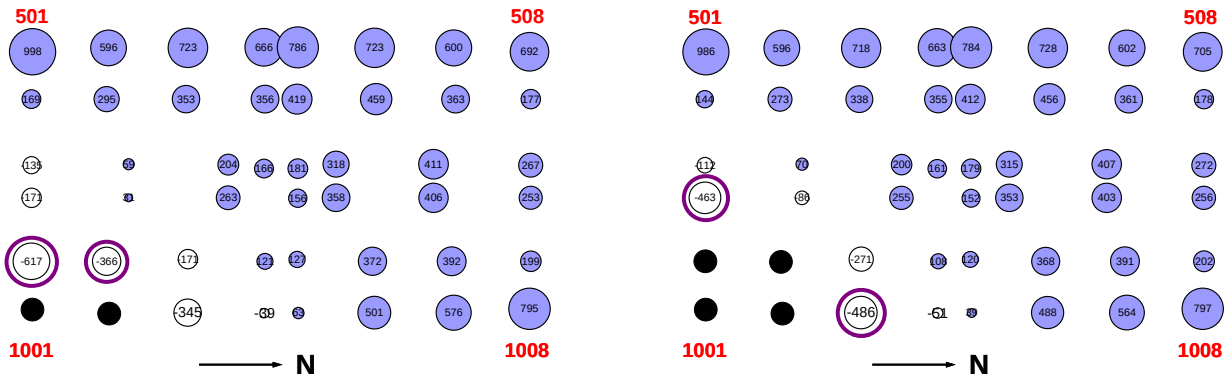

(c) After splices 1001 and 1002 fail (t = 40 min) (1st iteration)

(d) After splices 901 and 902 fail (t = 40 min) (2nd iteration)

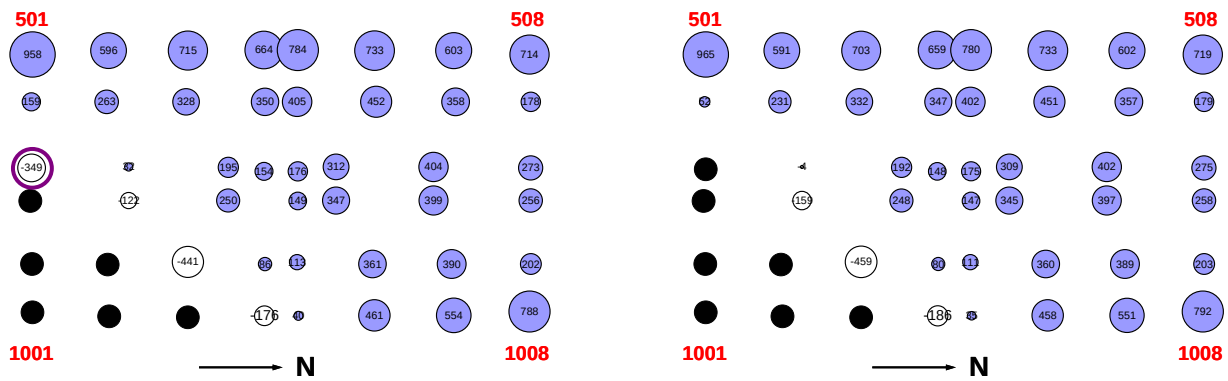

(e) After splices 801 and 1003 fail (t = 40 min) (3rd iteration)

(f) After splice 701 fails (t = 40 min) (4th iteration)

Splices exceeding their tension capacity at that iteration

Already failed splices

Figure 4–126. Progressive failure of core column splices at Floor 105 of WTC 2 (compression is positive; values are in kip).

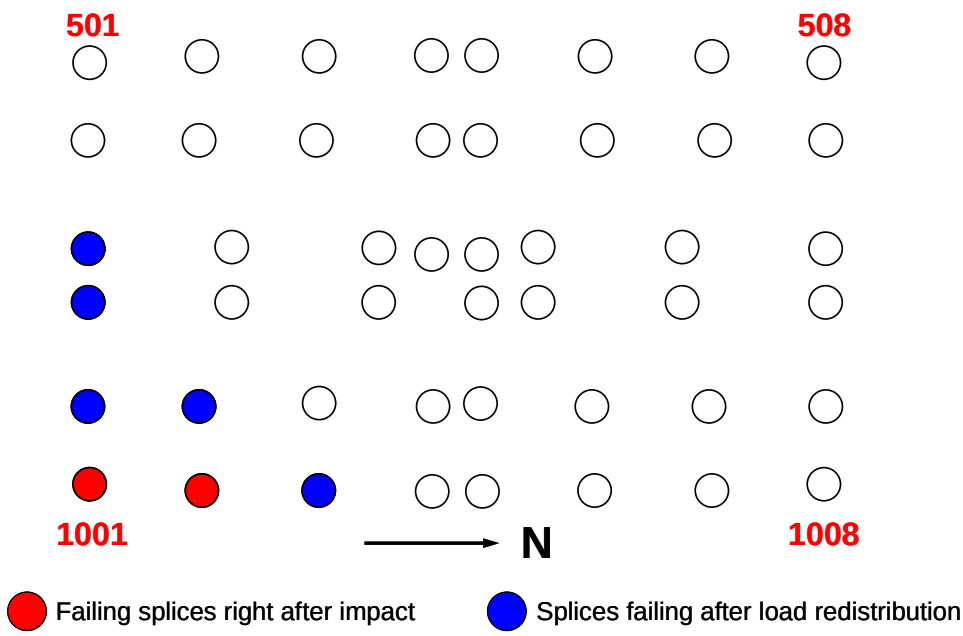

Figure 4–127. State of core column splices at Floor 105 of WTC 2.

Table 4–31. Total column loads (kip) at Floor 105 at different stages of splice failures at 40 min (compression is positive).

Row	Analysis Status	West	East	North	South	Core	TLRSF*	TLRHT**
(1)	Before Splice Failure (t = 40 min)	9185	11913	6537	8706	12402	0	0
(2)	Splices 1001 and 1002 fail	9221	11747	6577	8432	12761	-1436	-1077
(3)	Splices 901 and 902 fail	9227	11644	6612	8206	13045	-2419	-1776
(4)	Splices 801 and 1003 fail	9241	11550	6629	8043	13267	-3368	-2503
(5)	Splice 701 fails	9229	11533	6649	7925	13391	-3717	-2728
(6)	(2)-(1)	36	-166	40	-274	359	-1436	-1077
(7)	(3)-(2)	6	-103	35	-226	284	-983	-699
(8)	(4)-(3)	13	-93	17	-163	222	-949	-727
(9)	(5)-(4)	-11	-17	20	-117	124	-349	-225
(10)	(6)+(7)+(8)+(9)	44	-380	112	-780	989	-3717	-2728

* Total load released by the splice failure

** Total load retransferred to the hat-truss

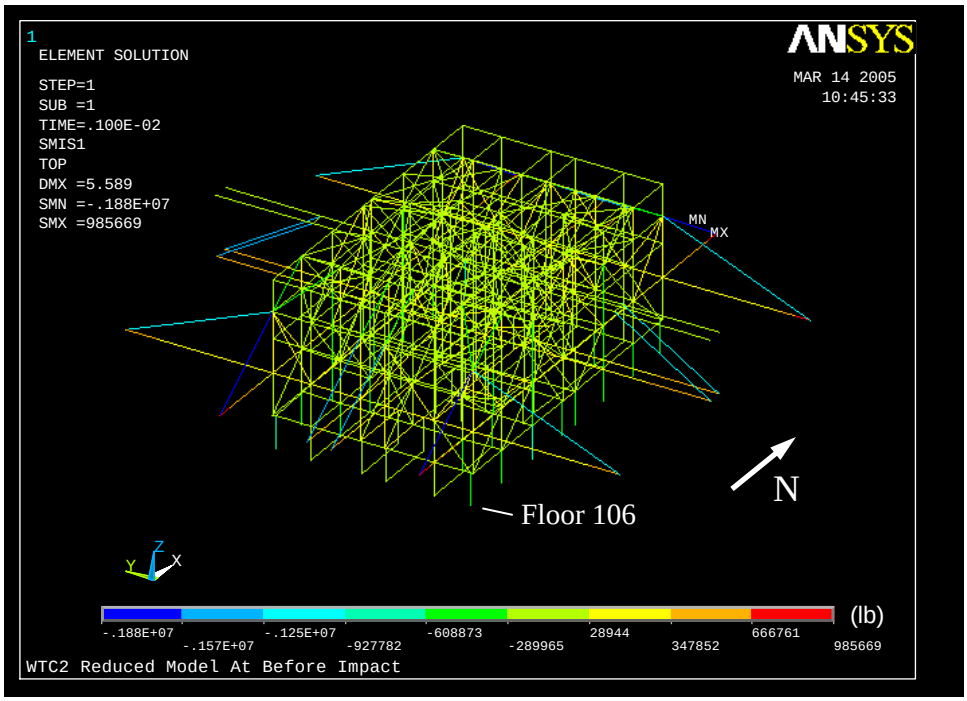

(a) Before impact

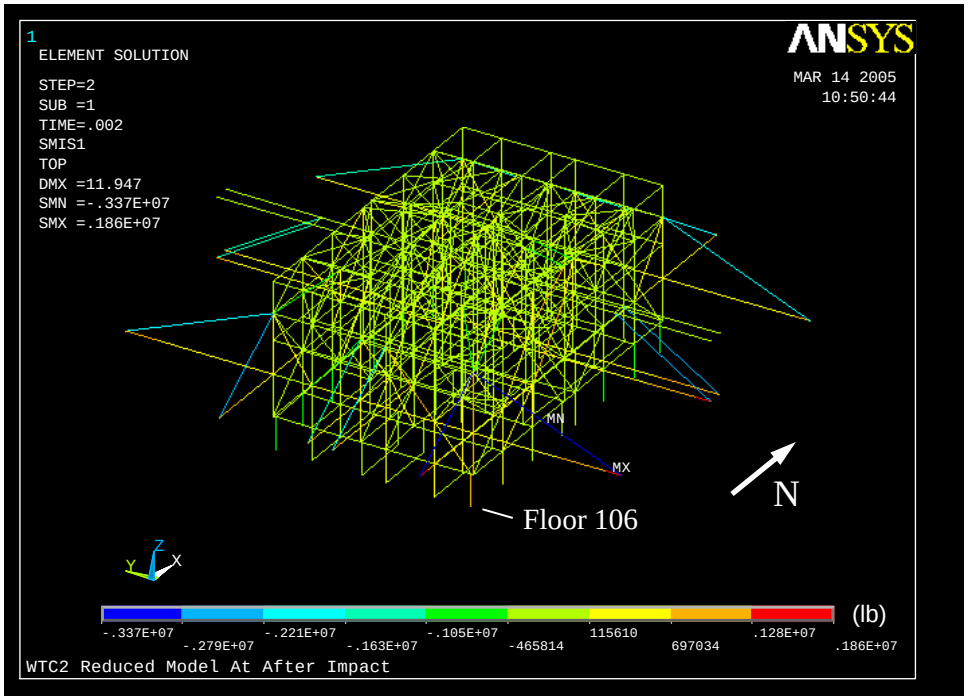

(b) After impact

Figure 4–128. Axial force in hat truss members of WTC 2 for Case D conditions (tension is positive).

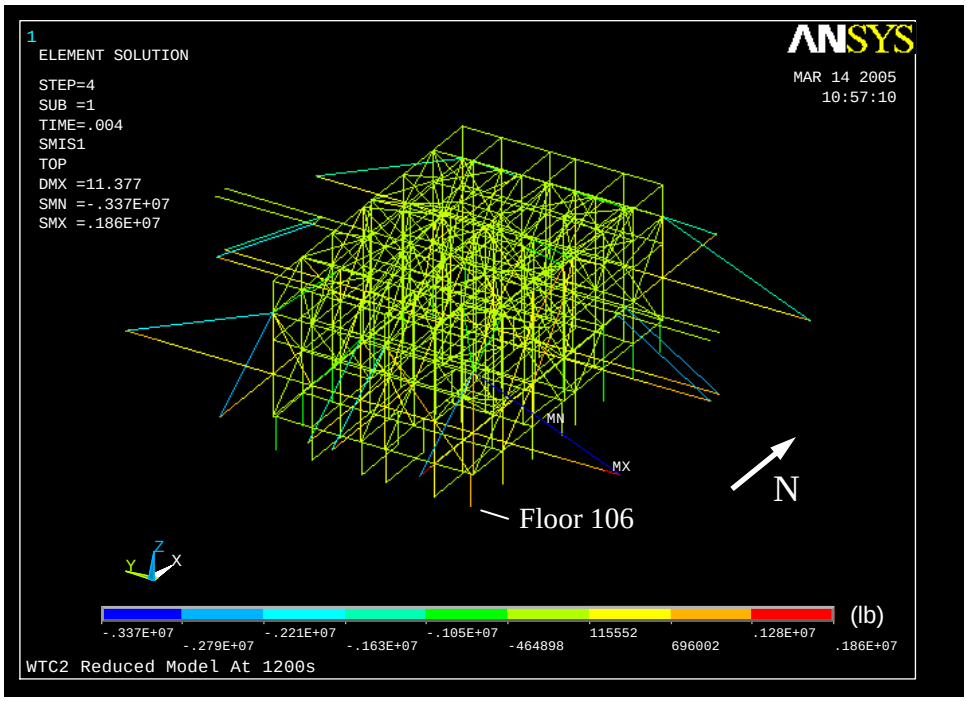

(a) 20 min

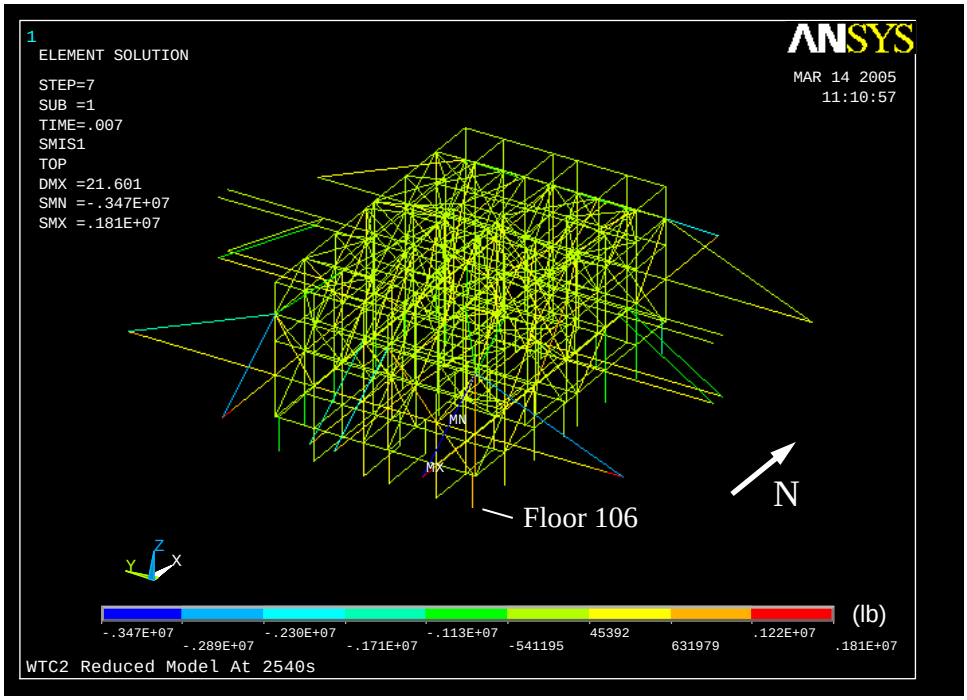

(b) 43 min

Figure 4–129. Axial force in hat truss members of WTC 2 for Case D conditions (tension is positive).

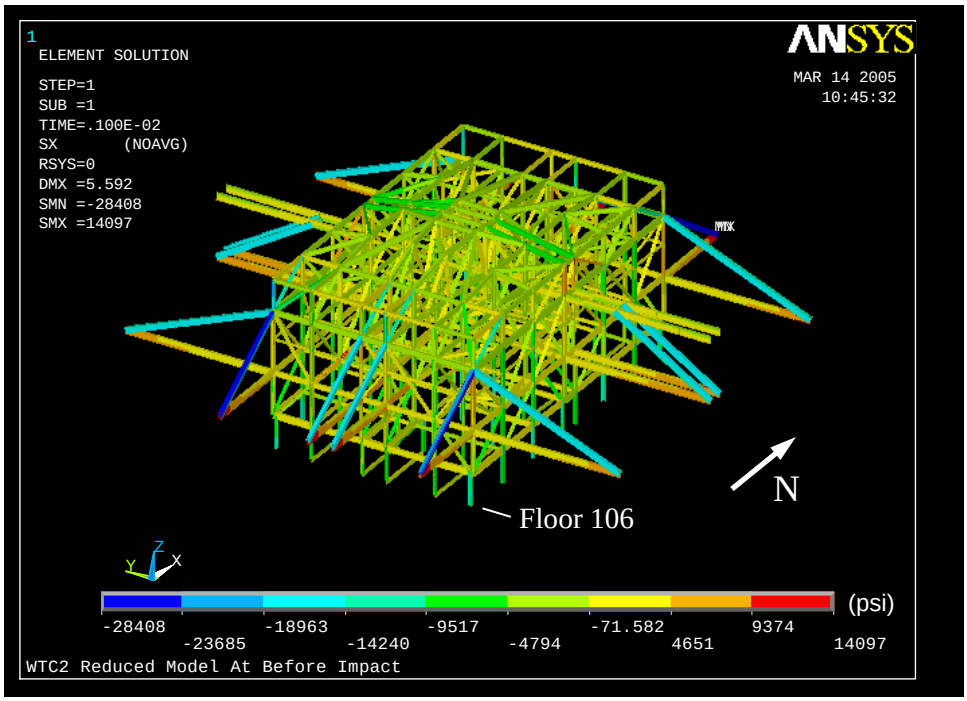

(a) Before impact

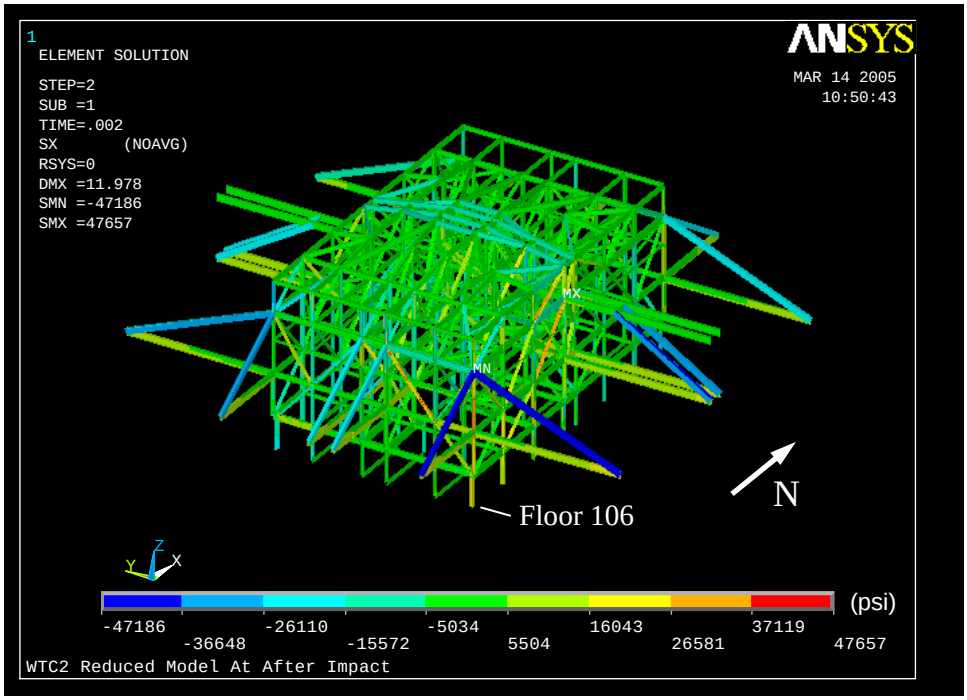

(b) After impact

Figure 4–130. Axial stress in hat truss members of WTC 2 for Case D conditions (tension is positive).

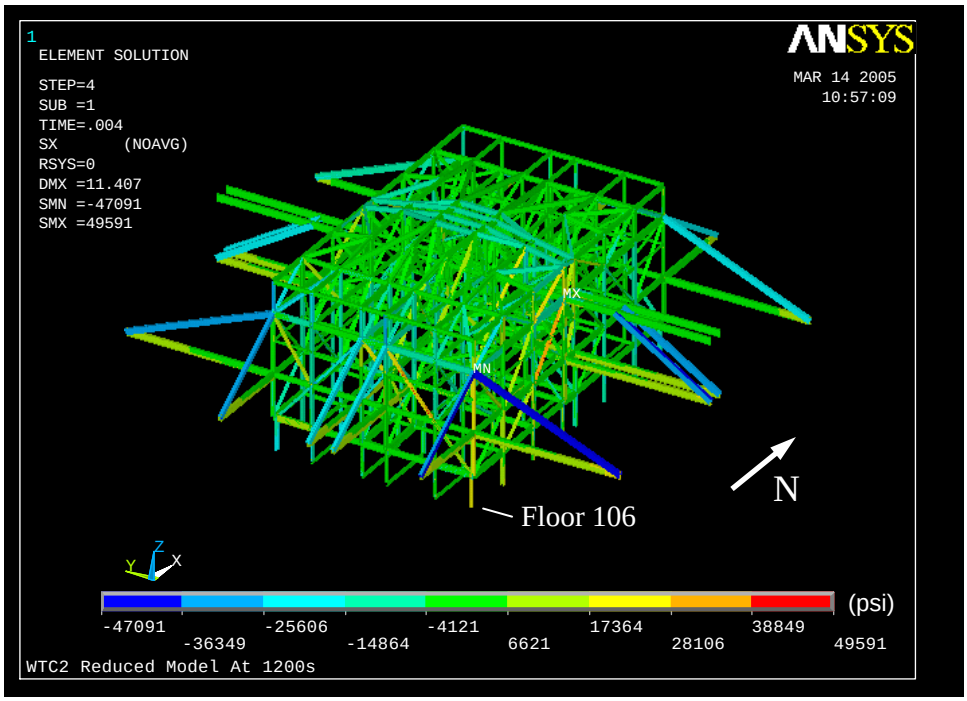

(a) 20 min

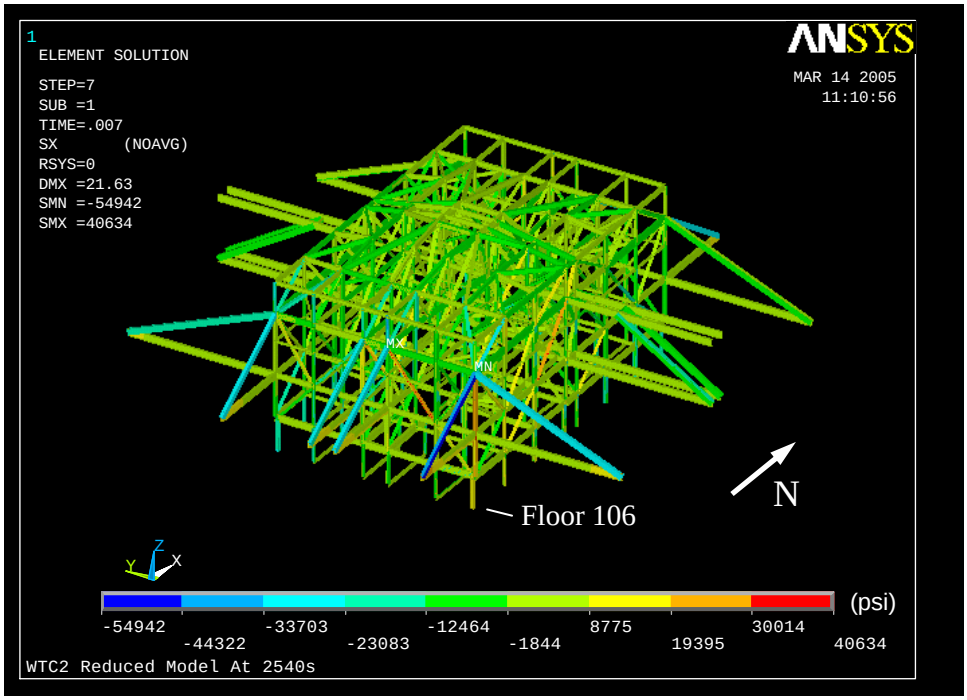

(b) 43 min

Figure 4–131. Axial stress in hat truss members of WTC 2 for Case D conditions (tension is positive).

Table 4–32. Demand-to-capacity ratios for outriggers of WTC 2 for Case D conditions (outrigger IDs are shown in Fig. 4–3).

Outrigger ID	Bfr. Imp.	Aftr. Imp.	10 min	20 min	30 min	40 min	40* min	40** min	43 min
West									
A	0.23	0.61	0.61	0.64	0.66	0.63	0.63	0.38	0.25
B	0.19	0.30	0.30	0.32	0.33	0.31	0.31	0.25	-0.03***
C	0.19	0.27	0.27	0.28	0.30	0.27	0.28	0.22	-0.07
D	0.21	0.18	0.18	0.19	0.21	0.18	0.20	0.19	-0.29
North									
E	0.29	0.11	0.10	0.10	0.13	0.14	0.17	0.09	-0.01
F	0.21	0.10	0.08	0.08	0.10	0.12	0.13	0.11	0.08
G	0.20	0.11	0.08	0.08	0.11	0.13	0.14	0.13	0.10
H	0.30	0.21	0.16	0.18	0.19	0.18	0.19	0.24	0.24
East									
I	0.22	0.39	0.35	0.34	0.45	0.43	0.42	0.41	-0.18
J	0.18	0.56	0.52	0.53	0.66	0.65	0.61	0.71	0.02
K	0.18	0.62	0.58	0.59	0.72	0.72	0.66	0.79	0.09
L	0.22	1.12	1.09	1.12	1.24	1.30	1.11	0.00	0.72
South									
M	0.30	0.68	0.64	0.64	0.70	0.75	0.52	0.72	0.87
N	0.22	0.34	0.32	0.33	0.36	0.38	0.28	0.34	0.40
O	0.22	0.30	0.28	0.30	0.32	0.33	0.27	0.31	0.33
P	0.31	0.51	0.50	0.52	0.53	0.53	0.50	0.57	0.49

* After load redistribution due to core column splice failures.

** After Outrigger L was removed.

*** Negative value indicates tension

Table 4–33. Demand to capacity ratios for columns supporting outriggers at Floor 107 of WTC 2 for Case D conditions.

Column ID	Bfr. Imp.	Aftr. Imp.	10 min	20 min	30 min	40 min	43 min
West							
110	0.26	0.46	0.46	0.47	0.48	0.47	0.28
111	0.26	0.39	0.39	0.40	0.41	0.40	0.26
129	0.27	0.37	0.37	0.38	0.40	0.37	0.06
130	0.31	0.39	0.39	0.40	0.41	0.39	0.09
131	0.27	0.35	0.34	0.36	0.37	0.35	0.05
149	0.25	0.24	0.24	0.25	0.25	0.24	0.08
150	0.25	0.23	0.23	0.23	0.24	0.23	0.00
North							
217	0.17	0.11	0.11	0.11	0.12	0.12	0.07
218	0.23	0.12	0.11	0.11	0.13	0.14	0.05
228	0.27	0.17	0.15	0.15	0.17	0.19	0.15
229	0.22	0.14	0.12	0.12	0.14	0.16	0.13
231	0.26	0.18	0.15	0.15	0.18	0.19	0.17
232	0.26	0.18	0.15	0.15	0.18	0.20	0.18
242	0.20	0.15	0.12	0.13	0.14	0.14	0.17
243	0.19	0.16	0.14	0.14	0.15	0.14	0.17
East							
310	0.25	0.34	0.32	0.31	0.36	0.36	0.05
311	0.27	0.33	0.32	0.31	0.35	0.35	0.13
329	0.26	0.61	0.57	0.58	0.69	0.69	0.12
330	0.31	0.68	0.65	0.66	0.77	0.77	0.19
331	0.27	0.63	0.60	0.61	0.72	0.72	0.16
349	0.26	0.56	0.55	0.56	0.60	0.62	0.42
350	0.26	0.71	0.69	0.71	0.77	0.81	0.51
South							
417	0.18	0.30	0.29	0.29	0.31	0.33	0.37
418	0.24	0.46	0.43	0.44	0.47	0.50	0.57
428	0.28	0.38	0.36	0.37	0.39	0.41	0.43
429	0.23	0.30	0.29	0.30	0.32	0.33	0.34
431	0.26	0.33	0.31	0.32	0.34	0.36	0.36
432	0.27	0.35	0.34	0.35	0.37	0.38	0.38
442	0.21	0.32	0.31	0.32	0.33	0.33	0.31
443	0.20	0.28	0.28	0.28	0.29	0.29	0.27

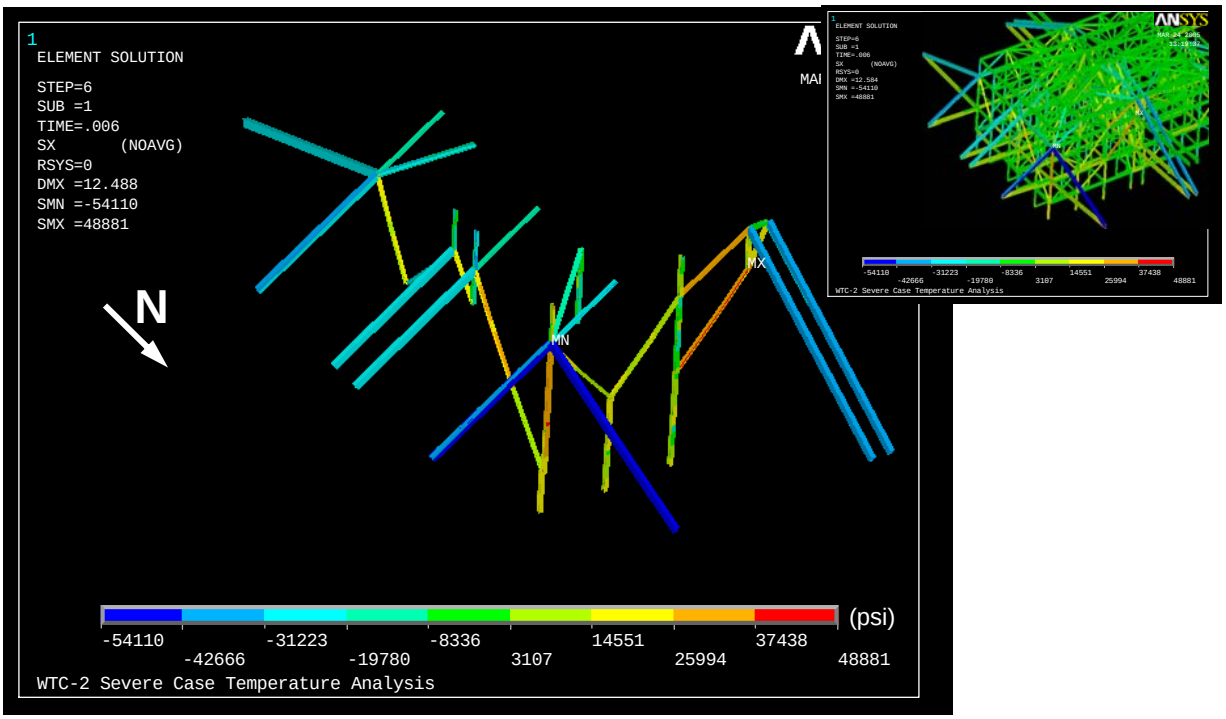

Figure 4–132. Primary load path within the hat truss of WTC 2.

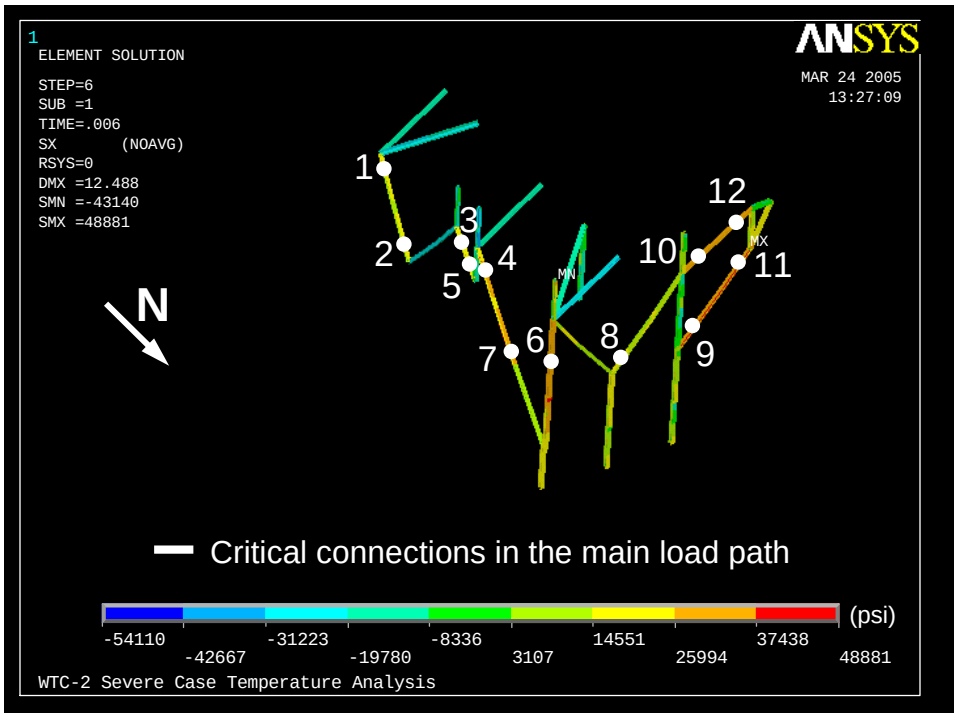

Figure 4–133. Location of hat truss connections that were in the primary load path.

Table 4–34. Demand and capacity of the hat truss connections (kip) in the primary load path at 40 min (connection IDs are shown in Fig. 4–133).

Con.	Location		Tension Capacity		Demand Force (tension)		Status	
ID	Floor	Column	Yield	Ultimate	Before Redist.	After Redist.	Before Redist.	After Redist.
1	110	501	840	1,100	567	512	Safe	Safe
2	108	601	840	1,100	567	512	Safe	Safe
3	110	701	630	870	575	370	Safe	Safe
4	110	801	840	1,100	950	510	Yielded	Safe
5	109	801	630	870	575	370	Safe	Safe
6	110	1001	760	870	1,370	760	Failed	Safe
7	108	901	840	1,100	950	510	Yielded	Safe
8	108	1002	1,250	1,250	440	110	Safe	Safe
9	108	1003	1,470	1,470	1,000	700	Safe	Safe
10	110	1003	1,250	1,250	750	550	Safe	Safe
11	110	1004	1,470	1,470	1,000	700	Safe	Safe
12	111	1004	1,250	1,250	750	550	Safe	Safe

Table 4–35. Total column loads at Floor 83 of WTC 2 for Case D conditions.

Row	Analysis Step	West	East	North	South	Core	Sum
(1)	Before Impact	18,065	18,114	13,567	13,284	61,828	124,857
(2)	After Impact	18,670	22,481	12,193	13,511	57,821	124,676
(3)	10 min	18,728	22,226	11,896	13,358	58,413	124,621
(4)	20 min	18,914	22,208	12,052	13,318	58,124	124,616
(5)	30 min	18,876	23,681	11,770	13,365	56,967	124,659
(6)	40 min	18,531	23,682	11,906	13,473	56,825	124,418
(7)	43 min	15,667	15,143	14,215	16,292	62,422	123,738
(8)	(2)-(1)	604	4,368	-1,374	227	-4,007	-181
(9)	(3)-(1)	662	4,112	-1,670	74	-3,415	-236
(10)	(4)-(1)	849	4,094	-1,515	35	-3,704	-241
(11)	(5)-(1)	811	5,567	-1,797	81	-4,861	-199
(12)	(6)-(1)	466	5,568	-1,661	190	-5,003	-439
(13)	(7)-(1)	-2,398	-2,971	648	3,009	594	-1,119

Note: Compression is positive. Units are in kip.

Table 4–36. Total column loads at Floor 105 of WTC 2 for Case D conditions.

Row	Analysis Step	West	East	North	South	Core	Sum
(1)	Before Impact	8,497	8,572	7,382	7,169	17,123	48,742
(2)	After Impact	9,170	11,272	6,487	8,432	13,382	48,742
(3)	10 min	9,182	11,061	6,250	8,275	13,975	48,742
(4)	20 min	9,279	11,120	6,311	8,351	13,682	48,742
(5)	30 min	9,370	11,859	6,416	8,553	12,544	48,742
(6)	40 min	9,198	11,927	6,524	8,691	12,402	48,742
(7)	43 min	7,086	8,026	6,546	9,169	17,915	48,742
(8)	(2)-(1)	674	2,699	-895	1,263	-3,741	0
(9)	(3)-(1)	685	2,489	-1,132	1,106	-3,148	0
(10)	(4)-(1)	783	2,547	-1,071	1,182	-3,441	0
(11)	(5)-(1)	873	3,287	-965	1,384	-4,579	0
(12)	(6)-(1)	702	3,355	-858	1,522	-4,721	0
(13)	(7)-(1)	-1,411	-547	-835	2,000	792	0

Note: Compression is positive. Units are in kip.

Table 4–37. Change in total column loads before and after aircraft impact. (Loads After Impact) – (Loads Before Impact)

Row	Floor	West	East	North	South	Core
(1)	83	604	4,368	-1,374	227	-4,007
(2)	105	674	2,699	-895	1,263	-3,741
(3)	(2) - (1)	69	-1,668	479	1,035	266

Note: Increase in compression is shown as positive. Units are in kip.

Table 4–38. Change in total column loads between 40 min and 43 min. (Loads at 43 min) – (Loads at 40 min)

Row	Floor	West	East	North	South	Core
(1)	83	-2,864	-8,539	2,309	2,819	5,596
(2)	105	-2,112	-3,901	23	479	5,513
(3)	(2) - (1)	752	4,637	-2,286	-2,340	-84

Note: Increase in compression is shown as positive. Units are in kip.

Table 4–39. Total column loads over the height for the east wall of WTC 2 for Case D conditions.

Step	Before Impact	After Impact	10 min	20 min	30 min	40 min	43 min	(2)-(1)	(3)-(1)	(4)-(1)	(5)-(1)	(6)-(1)	(7)-(1)
Floor/Col	(1)	(2)	(3)	(4)	(5)	(6)	(7)	(8)	(9)	(10)	(11)	(12)	(13)
105	8,572	11,272	11,061	11,120	11,859	11,927	8,026	2,699	2,489	2,547	3,287	3,355	-547
104	8,939	11,668	11,457	11,514	12,273	12,342	8,291	2,729	2,519	2,575	3,335	3,403	-648
103	9,419	12,256	12,048	12,102	12,890	12,968	8,735	2,837	2,628	2,683	3,470	3,549	-684
102	9,752	12,609	12,400	12,454	13,262	13,338	8,927	2,857	2,648	2,702	3,510	3,586	-825
101	10,254	13,235	13,029	13,079	13,917	14,007	9,427	2,981	2,774	2,824	3,663	3,752	-827
100	10,570	13,556	13,349	13,399	14,259	14,342	9,562	2,987	2,780	2,829	3,689	3,773	-1,008
99	11,089	14,217	14,013	14,058	14,950	15,051	10,114	3,128	2,924	2,969	3,861	3,962	-974
98	11,399	14,517	14,312	14,358	15,271	15,363	10,201	3,119	2,913	2,959	3,872	3,965	-1,198
97	11,944	15,223	15,021	15,060	16,009	16,123	10,819	3,279	3,077	3,116	4,065	4,179	-1,125
96	12,240	15,494	15,290	15,332	16,301	16,403	10,844	3,253	3,050	3,092	4,061	4,163	-1,396
95	12,804	16,234	16,035	16,069	17,076	17,204	11,524	3,430	3,232	3,265	4,272	4,400	-1,280
94	13,094	16,484	16,282	16,321	17,348	17,461	11,487	3,390	3,188	3,227	4,255	4,368	-1,607
93	13,673	17,256	17,061	17,088	18,156	18,300	12,235	3,583	3,388	3,415	4,483	4,626	-1,439
92	13,958	17,483	17,284	17,319	18,408	18,533	12,118	3,525	3,326	3,361	4,450	4,575	-1,840
91	14,553	18,287	18,098	18,117	19,250	19,410	12,953	3,734	3,544	3,564	4,697	4,857	-1,600
90	14,830	18,487	18,291	18,323	19,475	19,613	12,724	3,657	3,461	3,494	4,646	4,783	-2,105
89	15,443	19,328	19,147	19,158	20,359	20,538	13,677	3,886	3,704	3,715	4,916	5,095	-1,766
88	15,710	19,500	19,308	19,340	20,559	20,709	13,283	3,790	3,598	3,630	4,849	5,000	-2,426
87	16,341	20,381	20,213	20,211	21,489	21,690	14,400	4,039	3,872	3,870	5,147	5,348	-1,941
86	16,599	20,533	20,347	20,375	21,658	21,819	13,781	3,935	3,749	3,776	5,059	5,220	-2,818
85	17,220	21,438	21,292	21,270	22,636	22,867	15,117	4,218	4,072	4,050	5,416	5,647	-2,103
84	17,466	21,524	21,331	21,379	22,745	22,936	14,151	4,058	3,864	3,913	5,279	5,469	-3,316
83	18,114	22,481	22,226	22,208	23,681	23,682	15,143	4,368	4,112	4,094	5,567	5,568	-2,971
82	18,353	22,540	22,373	22,279	23,713	23,826	14,310	4,187	4,021	3,926	5,360	5,473	-4,043
81	19,036	23,540	23,007	23,275	24,784	24,942	16,763	4,504	3,970	4,239	5,747	5,906	-2,274
80	19,257	23,569	23,570	23,325	24,755	24,924	15,643	4,311	4,313	4,067	5,498	5,667	-3,615
79	19,970	24,634	24,431	24,381	25,821	26,023	17,571	4,665	4,461	4,411	5,851	6,053	-2,398
78	20,169	24,581	24,362	24,299	25,666	25,778	16,729	4,412	4,193	4,130	5,497	5,609	-3,440

Note: Compression is positive. Units are in kip.

Table 4–40. Total column loads over the height for the south wall of WTC 2 for Case D conditions.

Step	Before Impact	After Impact	10 min	20 min	30 min	40 min	43 min	(2)-(1)	(3)-(1)	(4)-(1)	(5)-(1)	(6)-(1)	(7)-(1)
Floor/Col	**(1)**	**(2)**	**(3)**	**(4)**	**(5)**	**(6)**	**(7)**	**(8)**	**(9)**	**(10)**	**(11)**	**(12)**	**(13)**
105	7,169	8,432	8,275	8,351	8,553	8,691	9,169	1,263	1,106	1,182	1,384	1,522	2,000
104	7,517	8,765	8,606	8,679	8,878	9,019	9,587	1,248	1,089	1,162	1,362	1,502	2,070
103	7,744	8,904	8,743	8,811	9,001	9,136	9,819	1,160	999	1,067	1,257	1,391	2,075
102	8,110	9,266	9,104	9,167	9,354	9,495	10,294	1,156	993	1,057	1,243	1,385	2,183
101	8,308	9,364	9,197	9,258	9,433	9,566	10,462	1,056	889	950	1,125	1,258	2,154
100	8,692	9,758	9,591	9,646	9,819	9,961	10,995	1,067	900	954	1,127	1,270	2,304
99	8,863	9,816	9,644	9,697	9,858	9,988	11,103	953	781	834	995	1,125	2,240
98	9,267	10,247	10,075	10,120	10,280	10,423	11,701	980	808	853	1,013	1,156	2,434
97	9,426	10,277	10,099	10,144	10,291	10,418	11,758	850	673	718	865	992	2,332
96	9,836	10,731	10,554	10,589	10,736	10,879	12,412	895	718	753	900	1,043	2,577
95	9,981	10,732	10,548	10,585	10,718	10,842	12,412	752	568	604	737	861	2,432
94	10,400	11,212	11,030	11,054	11,188	11,332	13,136	812	630	654	789	932	2,737
93	10,532	11,189	10,998	11,026	11,144	11,265	13,072	658	466	495	613	734	2,540
92	10,960	11,697	11,509	11,522	11,643	11,787	13,885	737	549	562	683	827	2,925
91	11,080	11,648	11,449	11,469	11,572	11,689	13,736	569	369	390	493	610	2,657
90	11,521	12,189	11,997	11,996	12,104	12,250	14,673	668	476	476	584	729	3,152
89	11,627	12,110	11,900	11,914	12,001	12,113	14,411	483	273	287	373	486	2,784
88	12,083	12,685	12,490	12,473	12,569	12,717	15,525	603	407	390	486	634	3,442
87	12,176	12,578	12,355	12,362	12,431	12,538	15,099	402	179	187	256	363	2,924
86	12,641	13,182	12,987	12,954	13,043	13,196	16,464	541	346	313	403	555	3,823
85	12,738	13,035	12,795	12,801	12,848	12,948	15,743	297	58	63	111	210	3,005
84	13,224	13,705	13,540	13,459	13,545	13,703	17,525	481	317	236	321	479	4,302
83	13,284	13,511	13,358	13,318	13,365	13,473	16,292	227	74	35	81	190	3,009
82	13,789	14,201	13,851	14,027	14,114	14,280	18,208	413	62	238	325	492	4,419
81	13,851	13,949	13,700	13,722	13,745	13,862	17,024	98	-151	-129	-105	12	3,173
80	14,379	14,645	14,257	14,447	14,522	14,695	18,830	266	-122	68	143	316	4,452
79	14,424	14,325	14,095	14,115	14,143	14,265	17,516	-99	-330	-309	-281	-159	3,092
78	15,000	15,110	14,866	14,916	14,982	15,178	19,109	110	-134	-84	-18	178	4,108

Note: Compression is positive. Units are in kip.

Table 4–41. Total column loads over the height for the north wall of WTC 2 for Case D conditions.

Step	Before Impact	After Impact	10 min	20 min	30 min	40 min	43 min	(2)-(1)	(3)-(1)	(4)-(1)	(5)-(1)	(6)-(1)	(7)-(1)
Floor/Col	**(1)**	**(2)**	**(3)**	**(4)**	**(5)**	**(6)**	**(7)**	**(8)**	**(9)**	**(10)**	**(11)**	**(12)**	**(13)**
105	7,382	6,487	6,250	6,311	6,416	6,524	6,546	-895	-1,132	-1,071	-965	-858	-835
104	7,738	6,822	6,583	6,648	6,742	6,850	6,946	-916	-1,155	-1,090	-997	-888	-793
103	7,963	7,030	6,790	6,859	6,939	7,052	7,257	-933	-1,173	-1,104	-1,024	-911	-706
102	8,337	7,381	7,139	7,211	7,280	7,395	7,669	-956	-1,198	-1,125	-1,057	-942	-667
101	8,533	7,560	7,316	7,393	7,447	7,565	7,960	-973	-1,217	-1,140	-1,086	-968	-573
100	8,924	7,925	7,680	7,760	7,802	7,923	8,382	-999	-1,245	-1,164	-1,123	-1,002	-542
99	9,096	8,081	7,833	7,919	7,944	8,068	8,659	-1,015	-1,263	-1,176	-1,152	-1,028	-437
98	9,506	8,461	8,212	8,302	8,314	8,440	9,089	-1,044	-1,294	-1,204	-1,192	-1,065	-416
97	9,665	8,608	8,356	8,452	8,446	8,575	9,366	-1,058	-1,309	-1,214	-1,219	-1,090	-299
96	10,081	8,991	8,738	8,837	8,818	8,949	9,793	-1,090	-1,344	-1,245	-1,263	-1,132	-289
95	10,227	9,125	8,869	8,975	8,938	9,071	10,066	-1,101	-1,357	-1,252	-1,289	-1,156	-161
94	10,652	9,514	9,257	9,366	9,315	9,450	10,491	-1,138	-1,395	-1,287	-1,338	-1,202	-161
93	10,785	9,638	9,378	9,494	9,424	9,561	10,763	-1,146	-1,407	-1,291	-1,361	-1,224	-22
92	11,220	10,031	9,769	9,887	9,802	9,941	11,182	-1,189	-1,451	-1,333	-1,418	-1,278	-37
91	11,340	10,148	9,882	10,009	9,904	10,044	11,457	-1,192	-1,458	-1,331	-1,436	-1,296	117
90	11,788	10,546	10,279	10,407	10,286	10,428	11,869	-1,241	-1,509	-1,381	-1,502	-1,359	82
89	11,895	10,658	10,385	10,523	10,381	10,524	12,149	-1,237	-1,510	-1,372	-1,514	-1,371	254
88	12,357	11,061	10,786	10,925	10,764	10,910	12,556	-1,296	-1,571	-1,433	-1,593	-1,448	199
87	12,451	11,166	10,884	11,035	10,851	10,996	12,847	-1,286	-1,568	-1,416	-1,600	-1,455	396
86	12,923	11,571	11,287	11,435	11,232	11,380	13,228	-1,352	-1,637	-1,489	-1,691	-1,543	304
85	13,014	11,686	11,393	11,559	11,327	11,470	13,573	-1,328	-1,620	-1,455	-1,687	-1,544	560
84	13,506	12,101	11,818	11,960	11,693	11,830	13,899	-1,406	-1,688	-1,547	-1,813	-1,676	393
83	13,567	12,193	11,896	12,052	11,770	11,906	14,215	-1,374	-1,670	-1,515	-1,797	-1,661	648
82	14,078	12,616	12,140	12,428	12,134	12,310	14,546	-1,462	-1,937	-1,650	-1,944	-1,768	468
81	14,141	12,725	12,380	12,512	12,121	12,367	14,824	-1,416	-1,761	-1,629	-2,020	-1,774	683
80	14,675	13,157	12,838	13,052	12,756	12,915	15,221	-1,518	-1,837	-1,624	-1,919	-1,761	546
79	14,723	13,259	12,998	13,137	12,873	13,044	15,519	-1,464	-1,724	-1,585	-1,849	-1,679	797
78	15,304	13,767	13,495	13,671	13,441	13,625	15,921	-1,537	-1,809	-1,633	-1,863	-1,679	617

Note: Compression is positive. Units are in kip.

Table 4–42. Total column loads over the height for the west wall of WTC 2 for Case D conditions.

Step	Before Impact	After Impact	10 min	20 min	30 min	40 min	43 min	(2)-(1)	(3)-(1)	(4)-(1)	(5)-(1)	(6)-(1)	(7)-(1)
Floor/Col	**(1)**	**(2)**	**(3)**	**(4)**	**(5)**	**(6)**	**(7)**	**(8)**	**(9)**	**(10)**	**(11)**	**(12)**	**(13)**
105	8,497	9,170	9,182	9,279	9,370	9,198	7,086	674	685	783	873	702	-1,411
104	8,861	9,544	9,557	9,657	9,743	9,567	7,439	683	696	796	882	706	-1,422
103	9,347	10,028	10,045	10,147	10,229	10,045	7,871	681	698	799	882	697	-1,476
102	9,678	10,370	10,388	10,493	10,570	10,380	8,195	691	710	814	892	701	-1,484
101	10,185	10,873	10,895	11,001	11,075	10,877	8,638	688	710	816	889	691	-1,547
100	10,500	11,199	11,224	11,333	11,401	11,196	8,952	700	724	833	901	696	-1,547
99	11,023	11,714	11,742	11,853	11,917	11,704	9,401	691	719	830	894	681	-1,622
98	11,331	12,038	12,068	12,182	12,240	12,020	9,717	707	737	851	908	689	-1,614
97	11,881	12,573	12,607	12,723	12,776	12,549	10,179	693	727	842	896	668	-1,701
96	12,176	12,886	12,922	13,041	13,088	12,853	10,490	710	746	865	912	678	-1,686
95	12,743	13,433	13,474	13,594	13,636	13,394	10,958	691	731	851	894	651	-1,785
94	13,032	13,742	13,784	13,909	13,944	13,694	11,269	710	753	877	913	662	-1,763
93	13,615	14,299	14,347	14,471	14,502	14,243	11,740	684	732	857	887	628	-1,875
92	13,897	14,606	14,655	14,785	14,808	14,542	12,055	709	758	888	911	644	-1,842
91	14,497	15,171	15,226	15,356	15,373	15,098	12,528	675	729	859	877	601	-1,969
90	14,771	15,476	15,531	15,668	15,678	15,394	12,847	705	760	896	907	623	-1,924
89	15,388	16,050	16,112	16,247	16,251	15,958	13,320	662	724	859	862	570	-2,068
88	15,653	16,352	16,412	16,557	16,553	16,251	13,641	699	760	904	900	598	-2,012
87	16,289	16,933	17,003	17,143	17,132	16,821	14,113	644	714	855	843	533	-2,176
86	16,554	17,233	17,297	17,451	17,433	17,115	14,446	679	743	897	880	561	-2,108
85	17,171	17,801	17,877	18,025	17,996	17,665	14,877	630	706	854	825	494	-2,294
84	17,414	18,100	18,153	18,336	18,300	17,958	15,214	686	739	922	886	544	-2,200
83	18,065	18,670	18,728	18,914	18,876	18,531	15,667	604	662	849	811	466	-2,398
82	18,301	18,970	19,060	19,204	19,155	18,795	15,989	668	758	903	854	494	-2,312
81	18,989	19,559	19,615	19,813	19,764	19,407	16,473	570	626	824	775	418	-2,516
80	19,207	19,846	19,939	20,076	20,019	19,650	16,788	639	733	870	812	443	-2,418
79	19,923	20,461	20,542	20,723	20,672	20,304	17,309	538	619	800	749	381	-2,614
78	20,119	20,723	20,828	20,968	20,912	20,542	17,637	605	710	850	793	423	-2,482

Note: Compression is positive. Units are in kip.

Table 4–43. Total column loads over the height for the core of WTC 2 for Case D conditions.

Step	Before Impact	After Impact	10 min	20 min	30 min	40 min	43 min	(2)-(1)	(3)-(1)	(4)-(1)	(5)-(1)	(6)-(1)	(7)-(1)
Floor/Col	**(1)**	**(2)**	**(3)**	**(4)**	**(5)**	**(6)**	**(7)**	**(8)**	**(9)**	**(10)**	**(11)**	**(12)**	**(13)**
105	17,123	13,382	13,975	13,682	12,544	12,402	17,915	-3,741	-3,148	-3,441	-4,579	-4,721	792
104	19,100	15,357	15,950	15,657	14,518	14,376	19,892	-3,743	-3,149	-3,443	-4,582	-4,724	792
103	21,069	17,323	17,917	17,624	16,484	16,342	21,862	-3,746	-3,152	-3,445	-4,585	-4,727	793
102	23,022	19,274	19,869	19,575	18,434	18,293	23,815	-3,748	-3,154	-3,448	-4,588	-4,730	793
101	24,980	21,228	21,824	21,529	20,388	20,247	25,773	-3,751	-3,156	-3,450	-4,591	-4,733	793
100	26,927	23,172	23,768	23,473	22,332	22,190	27,720	-3,754	-3,159	-3,453	-4,595	-4,737	793
99	28,873	25,116	25,712	25,417	24,275	24,133	29,667	-3,758	-3,161	-3,456	-4,599	-4,740	794
98	30,816	27,055	27,652	27,357	26,214	26,072	31,610	-3,761	-3,164	-3,459	-4,602	-4,744	794
97	33,524	29,760	30,357	30,062	28,918	28,776	34,318	-3,764	-3,167	-3,462	-4,606	-4,748	794
96	36,232	32,465	33,062	32,767	31,622	31,480	37,026	-3,768	-3,170	-3,465	-4,610	-4,752	794
95	38,203	34,432	35,030	34,734	33,589	33,447	38,997	-3,771	-3,173	-3,469	-4,614	-4,756	794
94	40,190	36,415	37,014	36,718	35,572	35,430	40,985	-3,775	-3,176	-3,472	-4,618	-4,760	794
93	42,144	38,365	38,965	38,668	37,522	37,379	42,938	-3,778	-3,179	-3,475	-4,622	-4,764	795
92	44,098	40,317	40,916	40,620	39,472	39,330	44,894	-3,782	-3,182	-3,479	-4,626	-4,768	795
91	46,071	42,286	42,886	42,589	41,441	41,299	46,867	-3,785	-3,185	-3,482	-4,630	-4,772	796
90	48,045	44,256	44,857	44,560	43,411	43,269	48,841	-3,789	-3,188	-3,485	-4,634	-4,776	796
89	50,020	46,227	46,829	46,531	45,382	45,239	50,816	-3,792	-3,191	-3,488	-4,638	-4,780	797
88	52,014	48,218	48,820	48,522	47,372	47,229	52,811	-3,796	-3,194	-3,492	-4,642	-4,785	797
87	54,008	50,209	50,811	50,513	49,362	49,220	54,806	-3,800	-3,197	-3,495	-4,646	-4,789	798
86	55,974	52,171	52,774	52,475	51,323	51,181	56,772	-3,803	-3,200	-3,499	-4,650	-4,793	798
85	57,967	54,106	54,742	54,460	53,308	53,165	58,648	-3,861	-3,225	-3,507	-4,659	-4,802	681
84	59,946	56,081	56,706	56,425	55,281	55,139	60,637	-3,865	-3,240	-3,521	-4,664	-4,807	691
83	61,828	57,821	58,413	58,124	56,967	56,825	62,422	-4,007	-3,415	-3,704	-4,861	-5,003	594
82	63,815	59,504	60,109	59,798	58,610	58,503	64,091	-4,311	-3,706	-4,017	-5,205	-5,312	276
81	65,866	61,218	61,823	61,382	59,979	60,205	65,813	-4,648	-4,043	-4,484	-5,886	-5,661	-53
80	68,206	63,079	63,687	63,387	62,203	62,100	67,662	-5,127	-4,519	-4,818	-6,003	-6,106	-544
79	70,246	64,597	65,201	64,907	63,760	63,626	69,179	-5,648	-5,045	-5,339	-6,485	-6,620	-1,067
78	72,156	66,093	66,719	66,432	65,277	65,141	70,691	-6,063	-5,437	-5,724	-6,879	-7,015	-1,465

Note: Compression is positive. Units are in kip.

Chapter 5
COLLAPSE SEQUENCE

5.1 INTRODUCTION

This chapter summarizes the sequences of collapse of WTC 1 and WTC 2 from the analyses of global models with creep. The basis of the conclusions derived here are as follows:

- Analyses of subcomponents, such as connections (truss seats and knuckles), components (trusses and columns), subsystems (full floors and exterior walls), preliminary global models, and isolated parts of the final global models (core and exterior wall) subjected to temperature loads from fire, were performed to identify failure modes and failure loads. These models included large deflection effects and temperature-dependent material nonlinearities due to plasticity and creep. *Break elements* were developed to capture various failure modes such as truss seat failure and web diagonal buckling (NIST NCSTAR 1-6C). As they became larger, the models were gradually reduced in complexity to enhance computational efficiency, while ensuring that key failure modes and failure sequences were captured.

- The final global models included large deflection, and temperature-dependent plasticity and creep.

- The final global models were developed based on the following assumptions:

  – Floors were modeled by plate elements with elastic properties without the ability to simulate sagging and its effect on the development of pull-in forces at floor/wall disconnections. Full floor analyses found that floors initially expanded outward but then pulled inward as the floor sag increased. Pull-in forces resulting from floor sagging and floor/wall disconnections were determined based on the results of full floor models and isolated wall models and were modified by visual observations. They were input in the global model analyses at different times as fire-induced damage.

  – Spandrels were modeled by beam elements. The axial degree of freedom of the beam elements was released to enhance numerical efficiency and avoid thermally-induced buckling; spandrel elements continued to transfer shear and bending moments. The exterior wall subsystem analysis showed that large deformations and buckling of spandrels would not affect the stability of exterior columns significantly.

  – Columns were modeled to capture inelastic buckling, but not the kink-type buckling that is initiated by the local buckling of plates and results in significant distortion of the cross section. The analysis of columns showed that when buckling occurred in a column that spanned several floors and was at high temperatures, inelastic buckling, rather than kink-type buckling, governed its load deformation characteristic.

- The building sections below the impact zones were removed, and the vertical stiffness of the removed sections was replaced with equivalent vertical springs. Preliminary analyses of the global models showed that building sections below the impact zone did not contribute much to the overall behavior of the towers.

- Construction sequence was not considered to enhance computational efficiency. A comparative study showed that the total column load on each face of the exterior wall increased by 7 percent to 15 percent and the total column load on the core decreased by about 10 percent when the construction sequence was not included.

- Structural members that were severed or heavily damaged by aircraft impact were removed from the final global models before gravity loads were applied.

- Break elements were not used in the final global models to represent component failures such as failure of column splices. However, the results of the global model analyses were examined to determine whether any component failure occurred and to what extent its failure impacted the collapse sequence.

The key structural events common to both towers are discussed below.

- Floor sagging sufficient to cause the observed inward bowing of the exterior wall was caused by the elevated steel temperatures resulting from loss of thermal insulation. The elevated temperature caused buckling of the truss web diagonals, as shown in Fig. 5–1 (NIST NCSTAR 1-6C), which caused the floor sag to increase significantly and to approach a catenary shape. The catenary action in this study refers to the combined action that results when the bending capacity of the truss is exceeded and additional load is carried by the floor system acting as a tensile structure (Fig. 5–2). Note that in Fig. 5–2, *M* refers to the residual moment capacity in the floor with highly deformed truss. Sagging of the floor resulted in pull-in forces at floor/exterior wall connections, and led to inward bowing of the exterior wall

- Bowing and buckling of the entire exterior wall of a tower occurred under the combined effects of temperature, redistributed gravity load, pull-in force from sagging floors, and loss of lateral support due to sagging or floor/wall disconnections. Floors with large sag did not restrain the exterior wall columns from buckling.

- Downward displacement of the core was due to severed core columns from the aircraft impact and redistributing column loads to non-severed core columns and due to shortening of the core columns caused by buckling, plasticity, and creep of core columns at elevated temperatures.

- Redistribution of gravity loads among exterior and interior columns resulted from aircraft impact damage, restrained thermal expansion, shortening of core columns, tilting of the tower above the impact area, and bowing and buckling of exterior walls. Gravity loads were redistributed from columns with aircraft impact or fire-induced damage, both in the core and exterior walls, primarily to neighboring columns. Loads were redistributed from the core to the exterior walls and from the exterior walls to the core primarily through the hat truss. Loads were redistributed between adjacent exterior walls primarily through the spandrels, and to a lesser extent through the hat truss. Major load redistribution mechanisms were as follows:

– Aircraft impact reduced the load on the impacted wall and on the opposite wall through the hat truss and redistributed the load to the side walls.

– Restrained thermal expansion caused increased loads in the heated elements.

– Shortening of the core columns caused a redistribution of the load from the core to the exterior walls.

– Tilting of the tower redistributed the load among the exterior walls, resulting in increased load on the compressed part of the exterior walls.

The collapse sequence of each tower is presented in detail below.

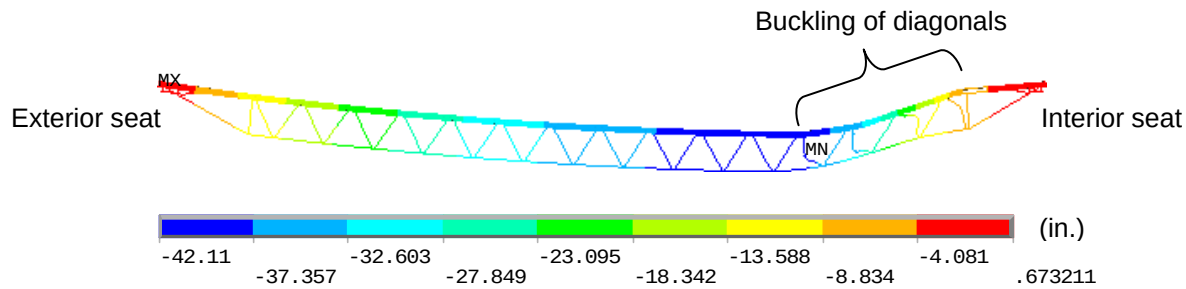

Figure 5–1. Vertical displacement of the truss model under thermal loading.

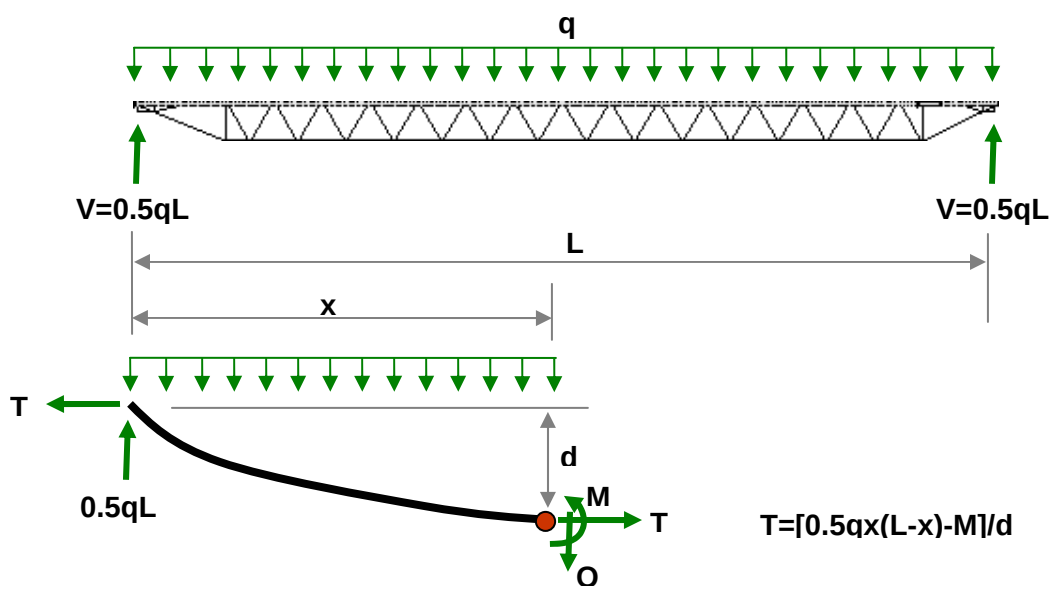

Figure 5–2. Catenary action in the floor system.

5.2 WTC 1 COLLAPSE SEQUENCE

The aircraft impacted the north wall of WTC 1 at 8:46 a.m. The aircraft severed exterior columns and floors on the north side of the tower and core columns and floor members between Floor 93 and Floor 98. The subsequent fires weakened structural subsystems, including the core columns, floors, and exterior walls. The core displaced downward, the floors sagged, and the south exterior wall bowed inward. At 10:28 a.m., about 102 min after the aircraft impact, WTC 1 began to collapse.

The sequence of main structural events that led to the collapse of WTC 1, starting from aircraft impact, and the causes and effects of these structural events along with key observations, are discussed below.

The WTC 1 collapse sequence consists of five main events, listed in Table 5–1, which are discussed below. Actual observations are summarized in Table 5–2, which are based on NIST's examination of photos and videos (NIST NCSTAR 1-6).

Table 5–1. Summary of main events that led to the collapse of WTC 1.

Event Number	Event
1	Aircraft impact
2	Unloading of core
3	Sagging of floors and floor/wall disconnections
4	Bowing of south wall
5	Buckling of south wall and collapse initiation

Table 5–2. Observations on WTC 1 provided by NIST.

Time	Time from Impact (min)	Observation
8:46:26	0	Aircraft impact on the north wall of WTC 1 between Floor 93 and Floor 99 and Columns 112 and 151.
9:25:28	39	Fire on west side of south wall.
9:40	54	No bowing of columns was observed between Columns 301 and 323 on the east side of south wall.
10:18:43	92	Smoke suddenly expelled on Floor 92 north wall, Floor 94 east side of north wall, Floor 95 to Floor 98 on west side of north wall, Floor 95 and Floor 98 on north side of west wall, lower floor on south side.
10:22:59	97	Inward bowing from Floor 95 to about Floor 99 between Columns 308 and 326 (maybe to 340) on the south wall, maximum amplitude approximately 55 in. at Floor 97.
10:28:18	102	Smoke puff out of north edge and center of west wall; smoke and debris clouds out of the north, east, and west walls on Floor 98. Fire out of windows on the north, east, west, and south walls between Floor 92 and Floor 98, and on Floor 104.
10:28:20	102	WTC 1 began to collapse. First exterior sign of collapse was at Floor 98. Rotation of at least 8 degrees to the south occurred before the building section began to fall vertically under gravity.

Aircraft Impact

The aircraft impacted WTC 1 at the north wall. The aircraft severed or heavily damaged Columns 112 to 151 between Floors 94 and 98 on the north wall. After breaching the building's perimeter, the aircraft continued to penetrate into the building. The north office area floor system sustained severe structural damage between Columns 112 and 145 at Floors 94 to 98. Core Columns 503, 504, 505, 506, 604, 704, 706, 805, and 904 were severed or heavily damaged between Floor 92 and Floor 97. The aircraft also severed a single exterior panel at the center of the south wall from Columns 329 to 331 between Floor 93 and Floor 96. In summary, 38 of 59 columns of the north wall, three of 59 columns of the south wall, and nine of 47 core columns were severed or heavily damaged. In addition, thermal insulation on floor framing and columns was also damaged from the impact area to the south perimeter wall, primarily through the center of WTC 1 and over one-third to one-half of the core width. Figures 2–2, 2–14, and 2–18 summarize aircraft impact damage to exterior and core columns and floors of WTC 1.

Gravity loads in the columns that were severed were redistributed, mostly to the neighboring columns. Due to the severe impact damage to the north wall, the wall section above the impact zone moved downward as shown in Figs. 4–9 and 4–13. The hat truss resisted the downward movement of the north wall and rotated about its east-west axis, which reduced the load on the south wall. As a result, the north and south walls each carried about 7 percent less gravity loads at Floor 98 after impact, the east and west walls each carried about 7 percent more loads, and the core carried about 1 percent more gravity loads at Floor 98 after impact (Table 5–3). Column 705 buckled, and Columns 605 and 804 showed minor buckling.

Unloading of Core

Temperatures in the core area rose quickly, and thermal expansion of the core was greater than the thermal expansion of the exterior walls in early stages of the fire. This increased the gravity loads in the core columns until 10 min after impact (Table 5–3). The additional gravity loads from adjacent severed columns and high temperatures caused high plastic and creep strains to develop in the core columns in early stages of the fire. More columns buckled inelastically due to high temperatures. Creep strain continued to increase to the point of collapse (see Fig. 4–81). By 30 min, the plastic-plus-creep strains exceeded thermal expansion strains. Due to high plastic and creep strains and inelastic buckling of core columns, the core columns shortened, and the core displaced downward. At 100 min, the downward displacement of the core at Floor 99 became 2.0 in. on the average, as shown in Fig. 4–37.

The shortening of core columns was resisted by the hat truss, which unloaded the core over time and redistributed the gravity loads from the core to the exterior walls, as can be seen in Table 5–3. As a result, the north, east, south, and west walls at Floor 98 carried about 12 percent, 27 percent, 10 percent, and 22 percent more gravity loads, respectively, at 80 min than the state after the impact, and the core carried about 20 percent less loads as shown in Table 5–3. The net increase in the total column load on the south wall, where exterior wall failure initiated, was only about 10 percent due to the downward displacement of the core (see Fig. 5–3). At 80 min, the total core column loads reached their maximum. As the floor pulled in starting at 80 min on in the south side, the south exterior wall began to shed load to adjacent walls and the core.

Sagging of Floors and Floor/Wall Disconnections

The long-span trusses of Floor 95 through Floor 99 sagged due to high temperatures. While the fires were on the north side and the floors on the north side sagged first, the fires later reached the south side, and the floors on the south side sagged. Figure 5–4 shows vertical displacements of Floors 95 through 98 determined by the full floor models at 100 min. Full floor models underestimated the extent of sagging because cracking and spalling of concrete and creep in steel under high temperatures were not included in the floor models, and because the extent of insulation damage was conservatively estimated. The sagging floors pulled in the south wall columns over Floors 95 to 99. In addition, the exterior seats on the south wall in the hot zone of Floors 97 and 98 began to fail due to their reduced vertical shear capacity at around 80 min, and by 100 min about 20 percent of the exterior seats on the south wall of Floors 97 and 98 failed, as shown in Figs. 5–4 and 5–5. Partial collapse of the floor may have occurred at Floors 97 and 98, resulting from the exterior seat failures, as indicated by the observed smoke puff at 92 min (10:19 a.m.) in Table 5–2, but this phenomenon was not modeled.

Bowing of South Wall

The exterior columns on the south wall bowed inward as they were subjected to high temperatures, pull-in forces from the floors beginning at 80 min, and additional gravity loads redistributed from the core. Figure 5–6 shows the observed and the estimated inward bowing of the south wall at 97 min after impact (10:23 a.m.). Since no bowing was observed on the south wall at 69 min (9:55 a.m.), as shown in Table 5–2, it is estimated that the south wall began to bow inward at around 80 min when the floors on the south side began to substantially sag. The inward bowing of the south wall increased with time due to continuing floor sagging and increased temperatures on the south wall as shown in Figs. 4–42 and 5–7. At 97 min (10:23 a.m.), the maximum bowing observed was about 55 in. (see Fig. 5–6).

Buckling of South Wall and Collapse Initiation

With continuously increased bowing, as more columns buckled, the entire width of the south wall buckled inward. Instability started at the center of the south wall and rapidly progressed horizontally toward the sides. As a result of the buckling of the south wall, the south wall significantly unloaded (Fig. 5–3), redistributing its load to the softened core through the hat truss and to the south side of the east and west walls through the spandrels. The onset of this load redistribution can be found in the total column loads in the WTC 1 global model at 100 min in the bottom line of Table 5–3. At 100 min, the north, east, and west walls at Floor 98 carried about 7 percent, 35 percent, and 30 percent more gravity loads than the state after impact, and the south wall and the core carried about 7 percent and 20 percent less loads, respectively. The section of the building above the impact zone tilted to the south (observed at about 8˚, Table 5–2) as column instability progressed rapidly from the south wall to the adjacent east and west walls (see Fig. 5–8), resulting in increased gravity load on the core columns. The release of potential energy due to downward movement of building mass above the buckled columns exceeded the strain energy that could be absorbed by the structure. Global collapse ensued.

Table 5–3. Total column loads at Floor 98 and Floor 105 of WTC 1 global model for Case B conditions.

Row	Analysis Step	North Wall		East Wall		South Wall		West Wall		Core	
		Floor 98	Floor 105	Floor 98	Floor 105	Floor 98	Floor 105	Floor 98	Floor 105	Floor 98	Floor 105
(1)	Before Impact	10,974	8,026	8,545	6,562	11,025	8,092	8,572	6,604	34,029	20,361
(2)	After Impact	10,137	7,294	9,071	7,028	10,356	7,488	9,146	7,076	34,429	20,761
(3)	10 min	9,796	6,944	8,490	6,461	9,848	6,981	8,536	6,469	36,473	22,790
(4)	20 min	10,437	7,551	9,108	7,075	9,900	7,057	9,202	7,158	34,495	20,806
(5)	30 min	10,913	8,020	10,034	7,998	10,420	7,569	9,715	7,685	32,060	18,377
(6)	40 min	11,068	8,193	10,599	8,571	11,004	8,129	10,178	8,147	30,294	16,608
(7)	50 min	11,149	8,285	10,908	8,878	11,192	8,315	10,458	8,428	29,435	15,743
(8)	60 min	11,205	8,351	11,168	9,130	11,285	8,414	10,716	8,687	28,766	15,069
(9)	70 min	11,286	8,435	11,366	9,319	11,343	8,481	10,939	8,914	28,205	14,502
(10)	80 min	11,376	8,528	11,555	9,497	11,409	8,551	11,119	9,097	27,681	13,978
(11)	90 min	10,916	8,096	11,991	9,847	9,949	7,327	11,657	9,506	28,587	14,876
(12)	100 min	10,828	8,023	12,249	10,076	9,638	7,066	11,905	9,720	28,478	14,767
(13)	(2) - (1)	-837	-732	526	466	-668	-604	574	472	400	400
(14)	(10) - (2)	1,239	1,234	2,484	2,470	1,052	1,063	1,973	2,021	-6,748	-6,783
(15)	(12) - (2)	692	730	3,178	3,048	-719	-422	2,759	2,644	-5,951	-5,993
(16)	(12) - (10)	-548	-504	694	579	-1,771	-1,485	786	623	797	790

Note : Compression is positive. Units are in kip.

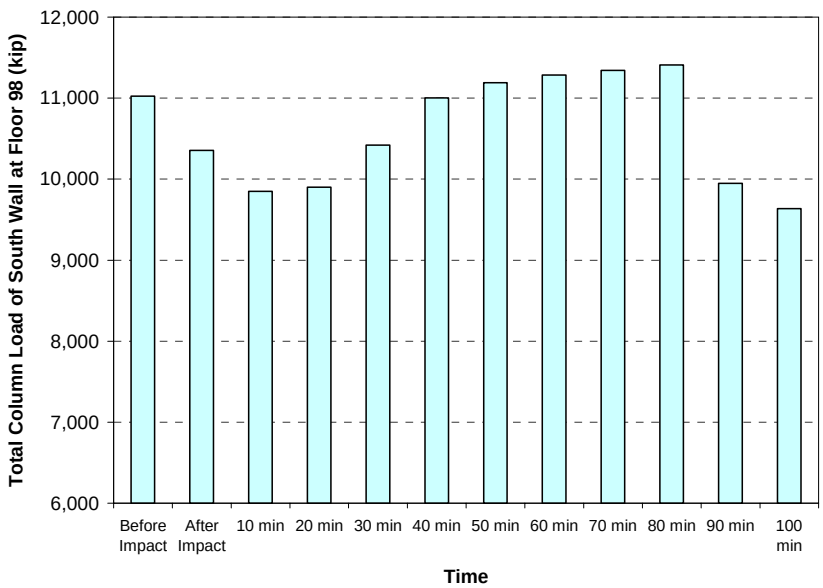

Figure 5–3. Total column loads at Floor 98 of the south wall of WTC 2 global model for Case B conditions (compression is positive).

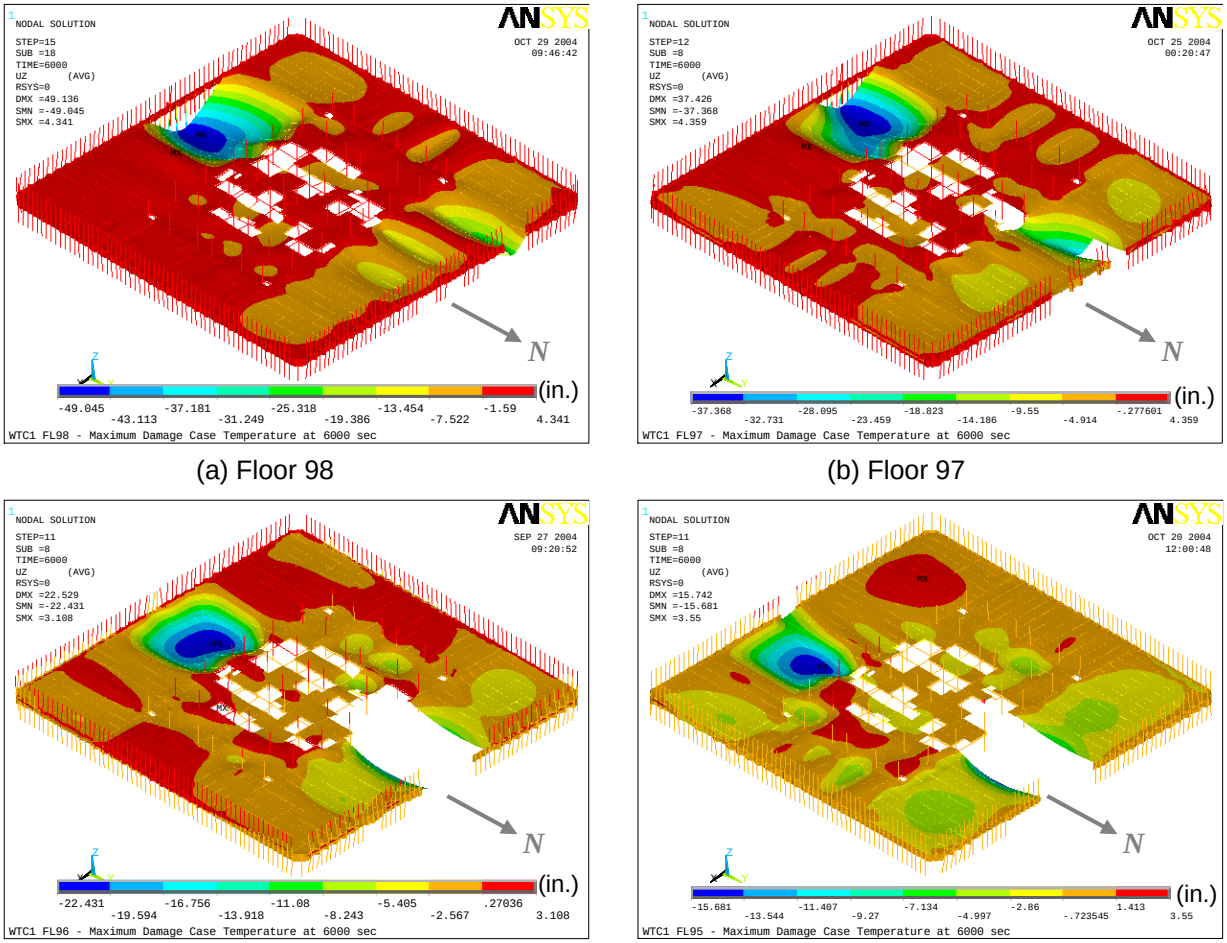

(a) Floor 98 (b) Floor 97

(c) Floor 96 (d) Floor 95

Figure 5–4. Vertical displacements of full floor models of WTC 1 for Case B_i temperature condition at 100 min (downward displacement is negative).

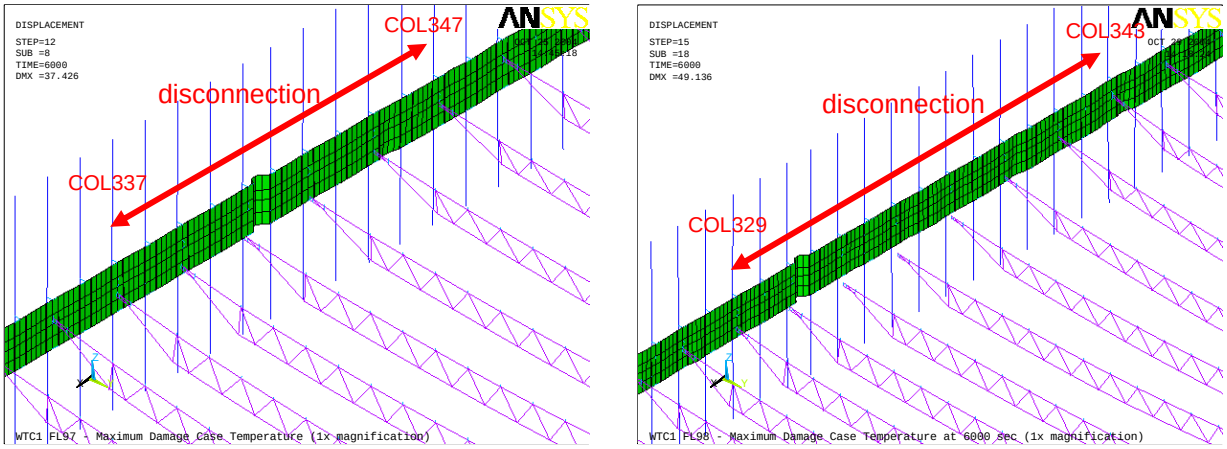

(a) Floor 97 (b) Floor 98

Figure 5–5. Loss of vertical supports obtained in Floor 97 and Floor 98 full floor models of WTC 1 for Case B_i temperature condition at 100 min (1x displacement magnification).

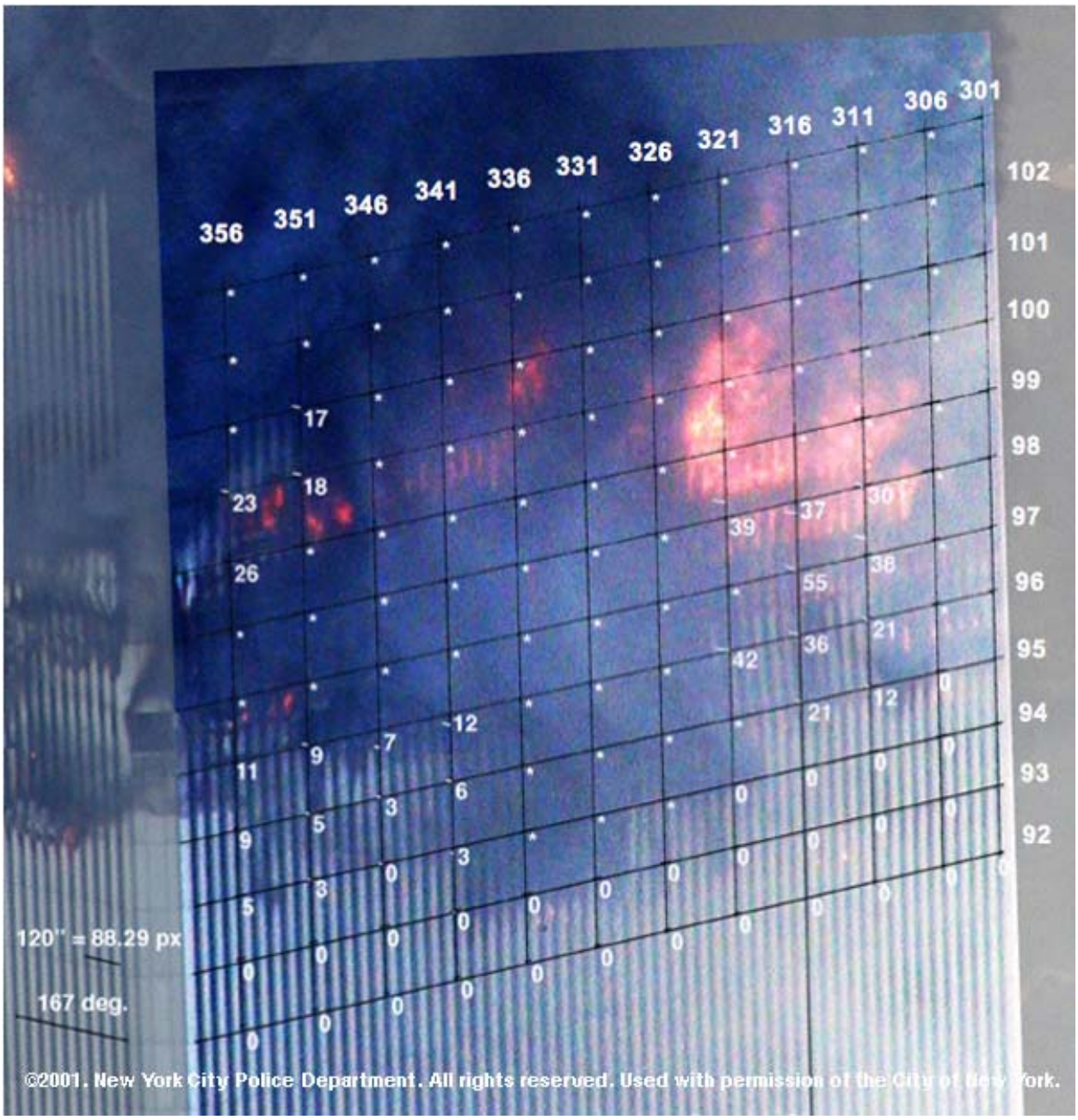

Figure 5–6. Inward bowing of exterior columns of the South wall of WTC 1 at 10:23 a.m. (97 min after impact). Displacements were estimated by NIST from the analysis of this photograph.

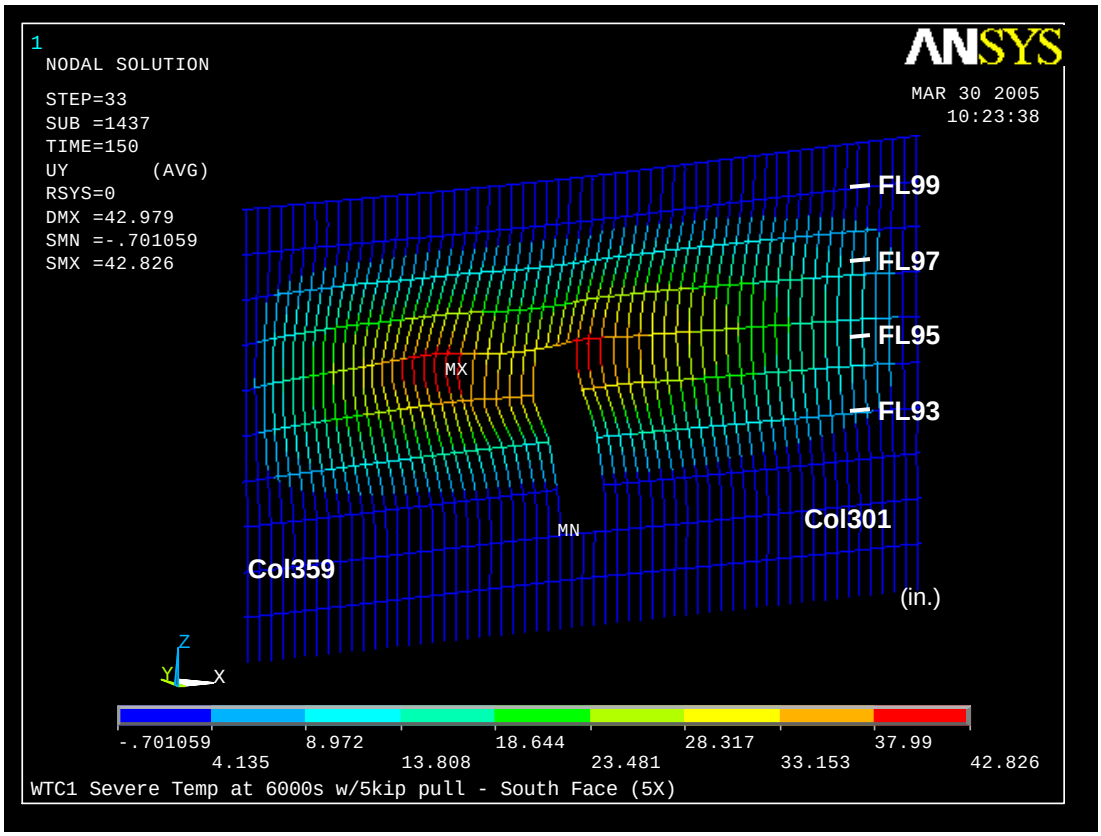

Figure 5–7. Inward bowing of south wall of WTC 1 global model with creep at 100 min for Case B conditions with 5 kip pull-in forces (5x displacement magnification).

Figure 5–8. Collapse initiation and tilting of WTC 1 (view from the northeast).

5.3 WTC 2 COLLAPSE SEQUENCE

The aircraft traveling in a north-northeast direction impacted the south wall of WTC 2 at 9:03 a.m. The aircraft mostly severed columns and floors that were on the east side of the building between Floor 78 and Floor 84. The subsequent fires were also on the east side of the building. At 9:59 a.m., about 56 min after the aircraft impact, the building started to collapse with the east wall buckling inward, followed by tilting of the building above Floor 82 to the east and south.

The section below discusses the sequence of main structural events that led to the collapse of WTC 2, and the causes and effects of these structural events along with key observations, starting from aircraft impact.

The WTC 2 collapse sequence consisted of five main structural events. These events are chronologically listed in Table 5–4 and discussed below. Actual observations for WTC 2 are summarized in Table 5–5, which are based on NIST's examination of photos and videos (NIST NCSTAR 1-6).

Table 5–4. Summary of main events that led to the collapse of WTC 2

Event number	Event
1	Aircraft impact
2	Sagging of floors and floor/wall disconnections
3	Bowing of east wall
4	Unloading and leaning of core
5	Buckling of east wall and collapse initiation

Table 5–5. Observations on WTC 2 provided by NIST.

Time	Time from Impact (min)	Observation
9:03	0	Aircraft impact on the south wall of WTC 2 between Floors 77 and 85, Columns 404 to 443.
9:21	18	Columns of the east wall bowed inward over the entire width of Floors 78 to 83; maximum of 7–9 in. at Floor 80.
9:38	35	Floor 83 disconnections on the east wall appeared to extend.
9:54	51	Columns of the east wall bowed inward between Floor 78 and Floor 84, 12 – 20 in. at Floor 80. East side of Floor 83 draped between Columns 310 to 342.
9:59	56	WTC 2 began to collapse. Column splices failed at every third panel and columns sprung back from inward bowing as collapse initiated on the east wall near the northeast corner Smoke and debris clouds were expelled from Floor 81 on the east, north, and west walls of the building. WTC 2 appeared to tilt around the base of Floor 82 and initial downward motion was visible at the same location. Tilt of approximately 3 to 4 degrees to the south and 7 to 8 degrees to the east occurred before building section fell. Kink (change in slope) on the southeast corner near Floor 94 (halfway along building section above failure). Kink (change in slope) and offset about at the Floor 106.

Aircraft Impact

The aircraft impacted the south wall of WTC 2, severing a number of exterior columns on the south wall from Floor 78 to Floor 84. The south office area floor system sustained severe structural damage between Columns 410 and 436 from Floor 79 to Floor 83. Core columns 701, 702, 801, 802, 803, 901, 903, 1001, 1002, 1003, and 1004 were severed or heavily damaged between Floor 77 and Floor 84. The aircraft also severed Column 253 of the north wall. The aircraft damaged the floor framing and core columns at the

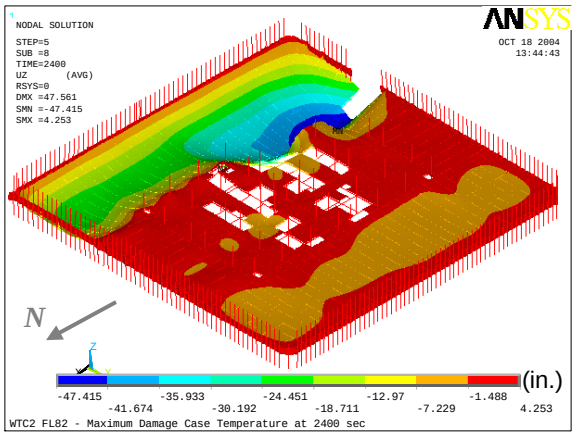

(a) Floor 82

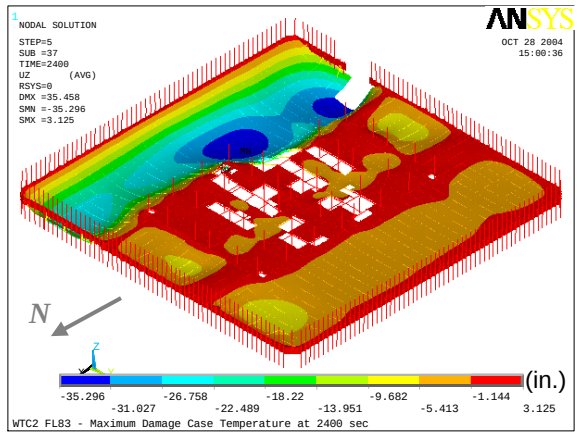

(b) Floor 83

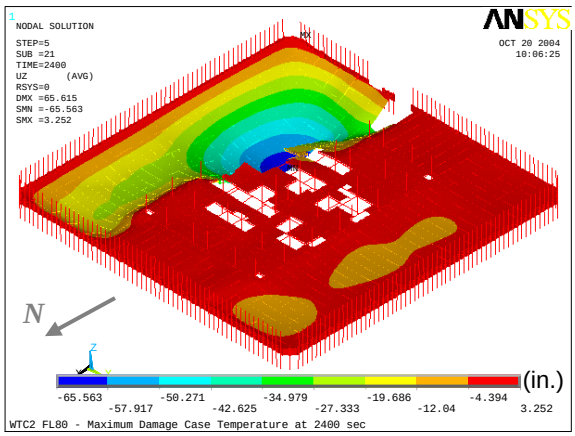

(c) Floor 80

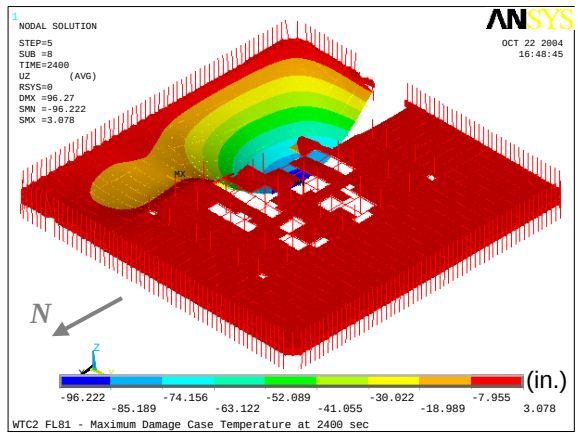

(d) Floor 81

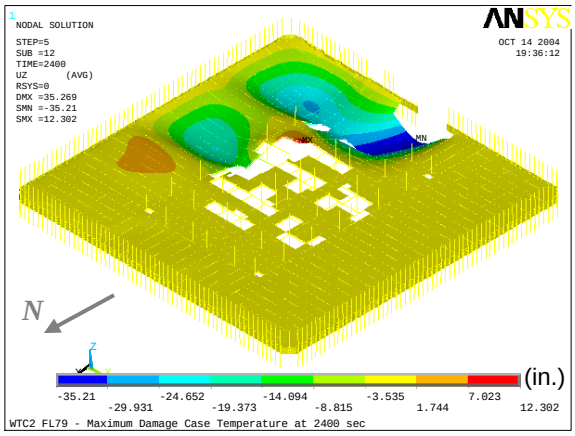

(e) Floor 79

Figure 5–9. Vertical displacements of full floor models of WTC 2 for Case D_i temperature condition at 40 min (downward displacement is negative).

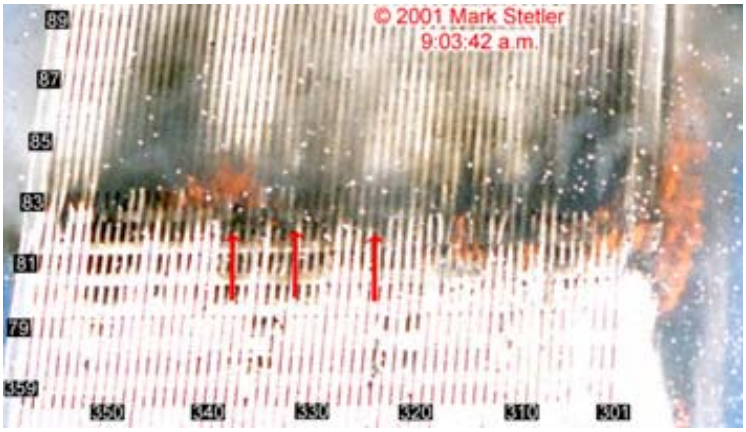

(a) After impact damage

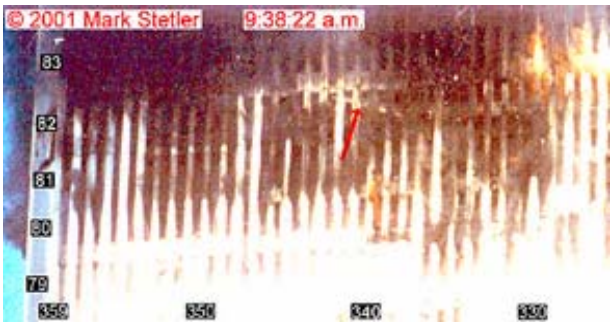

(b) South side at 9:38 a.m.
(35 min after impact)

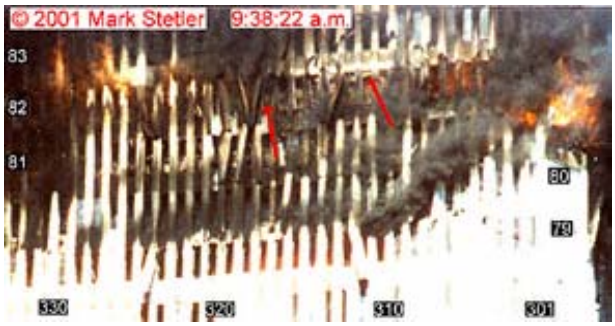

(c) North side at 9:38 a.m.
(35 min after impact)

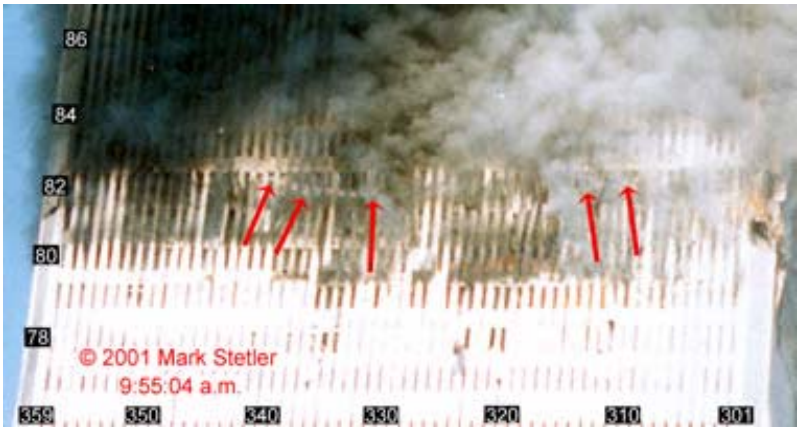

(d) At 9:54 a.m.
(51 min after impact)

Figure 5–10. Floor sagging observed on the east wall of WTC 2 at different times.

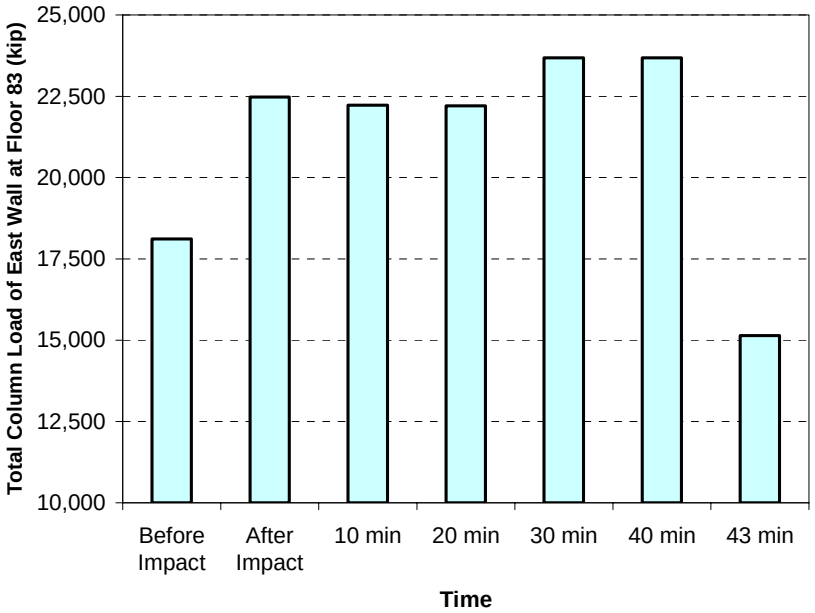

Figure 5–11. Total column loads at Floor 83 of the east wall of WTC 2 global model for Case D conditions (compression is positive).

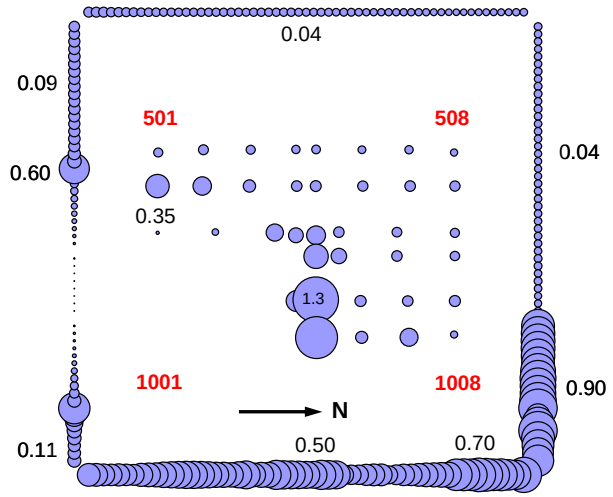

(a) At 20 min

At 30 min

(c) At 40 min

Figure 5–12. Maximum elastic + plasti[illegible] magnitu[illegible] for columns between Floor 78 and Floor 83 of WTC 2 globa[illegible] Case D condi[illegible]ns at 20 min, 30 min, and 40 min (compressive st[illegible]tive; strain val[illegible]s are in percent).

Figure 5–13. Inward bowing of the east wall of WTC 2 global model for Case D conditions at 43 min at the instant of collapse initiation (deformed shape scaled four times).

Figure 5–14. Inward bowing of exterior columns of the west wall of WTC 2 just before collapse.

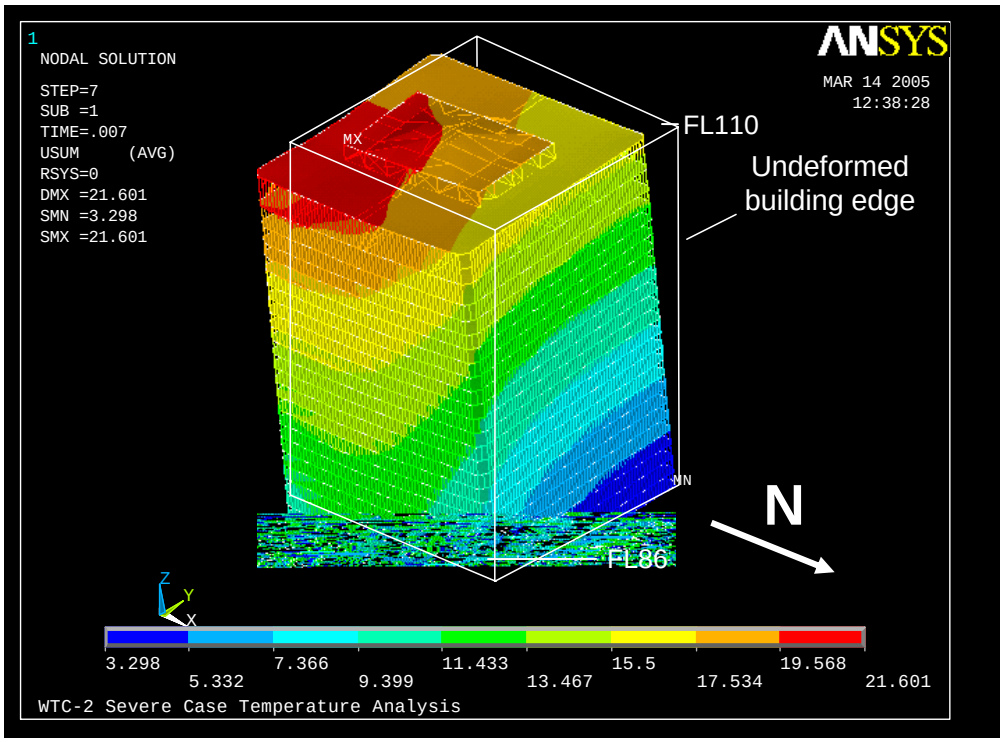

Figure 5–15. Total displacements of WTC 2 global model above Floor 86 for Case D conditions at 43 min at collapse initiation (note the tilt toward east and south; deformed shape magnified 20 times).

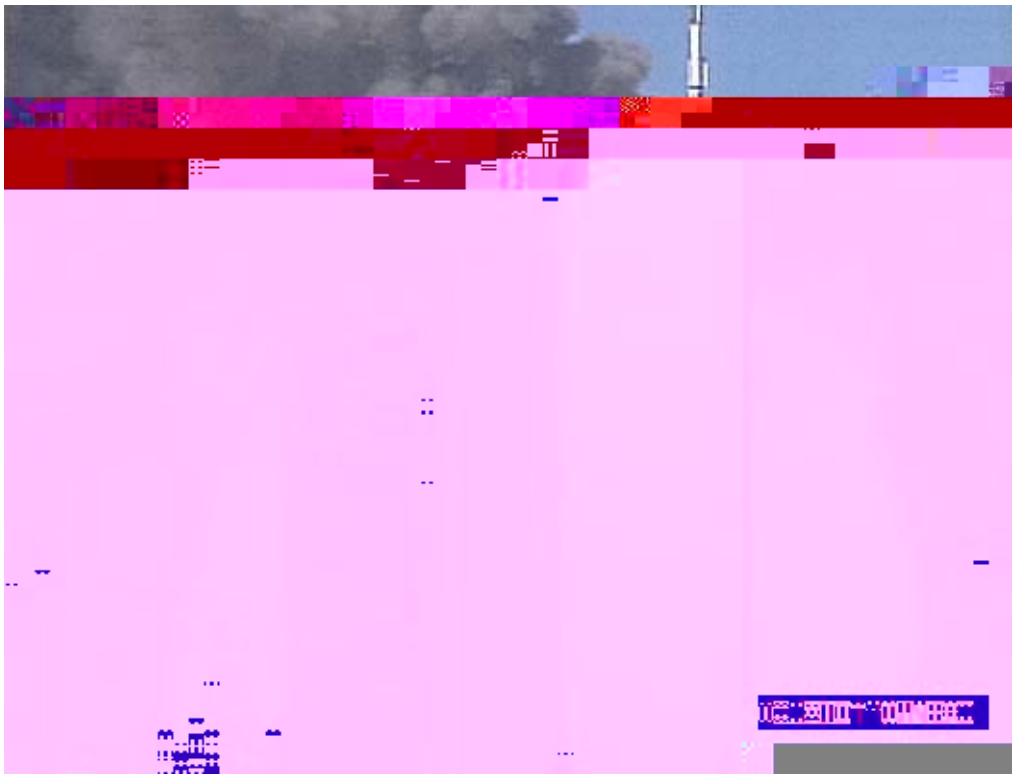

Figure 5–16. Initiation of Collapse of WTC 2. Note the tilt toward east and south.

5.4 DISCUSSION

The structural analyses of this study on components, subsystems, isolated exterior walls and cores, and global models of WTC 1 and WTC 2, as well as observations from photos and videos taken during the event, showed that the tower collapses were caused by the combined effects of the structural and thermal insulation damage from aircraft impact and the subsequent intense fires.

The structural impact damage alone did not cause the collapse of the towers, as they stood for periods of time, and collapsed after fire-induced weakening of the cores, floor systems and exterior walls. In the absence of impact damage, there would have been no insulation damage, and the likelihood of collapse of towers under the intense fires would have been very small.

The damage to insulation was a result of direct impact by debris from the aircraft impact, which knocked down walls and partitions and removed the insulation (NIST NCSTAR 1-6). Insulation is a key fire protection system for steel structural members. Without insulation, steel members may be heated during the "effective duration" of the fires to an extent that causes significant stiffness and strength reduction. According to the results of fire dynamics simulations by NIST (NIST NCSTAR 1-5), fire moved from location to location, and the "effective duration" of the fire at any one location was roughly about 20 minutes, which was much shorter than the time to collapse. It was found in the results of the thermal analysis conducted by NIST that temperatures of floor trusses and columns with insulation were lower than 400 ˚C during the Case B fire (100 min long) for WTC 1. On the other hand, temperatures of steel members that lost insulation were found to be higher than 600 ˚C and even higher than 800 ˚C. Reductions in modulus of elasticity, yield strength, and ultimate tensile strength of steel in the WTC towers were found to be 13 percent, 20 percent, and 10 percent at 400 ˚C, and 35 percent, 92 percent, and 80 percent at 700 ˚C. In addition, creep in steel may become more significant than plastic strain when the steel is exposed to temperatures higher than 500 ˚C under high stress.

The temperatures in the steel members without insulation damage were lower than those with insulation damage for the same fire (see Fig. 5–17 (c)), and the lower temperatures resulted in much reduced creep, plasticity, and buckling. Without insulation damage, floor sag would have been significantly reduced (see Figs. 5–17 (d) and (e)), and consequently the floors could not and would not have pulled inward on the exterior wall. Without insulation damage, the core columns and the exterior wall would not be significantly weakened, and the likelihood of the exterior wall buckling would be negligibly small. Without insulation damage, the likelihood of collapse of the towers would have been very small.

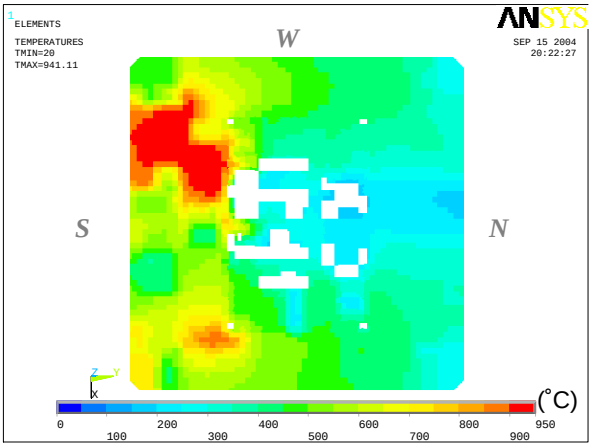

(a) Temperatures on the top surface of the slab

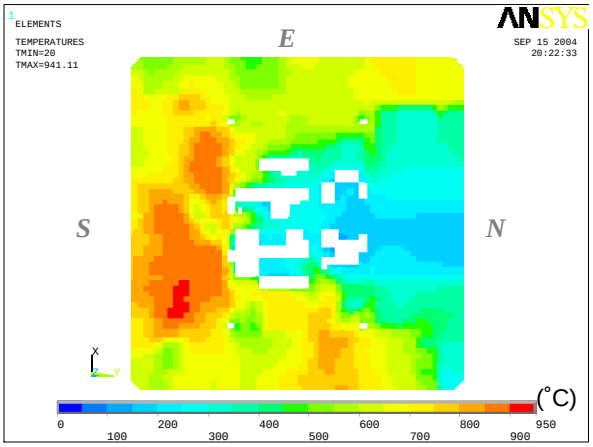

(b) Temperatures on the bottom surface of the slab

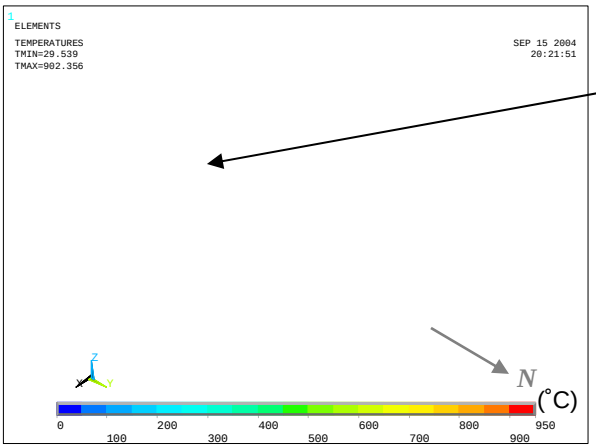

Area of insulation damage

Note: Structural members that were severed by aircraft impact are also shown in temperature plots (a), (b), and (c)

(c) Temperatures of steel members

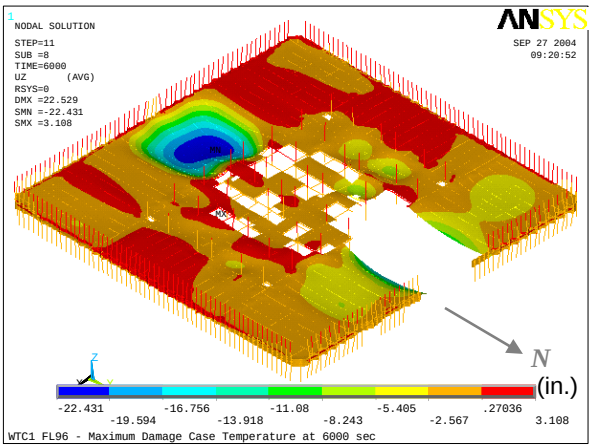

(d) Vertical displacement (entire model)

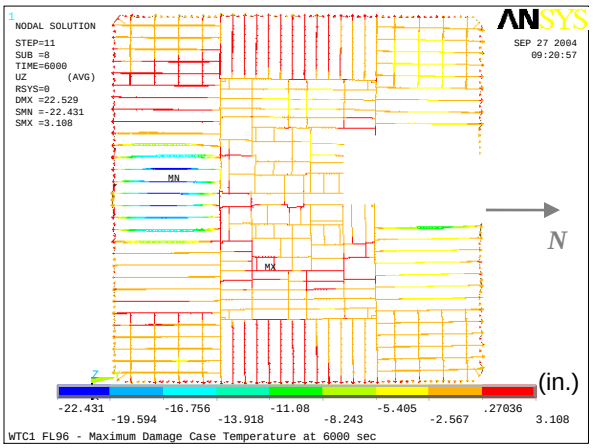

(e) Vertical displacement (top view without slab)

Figure 5–17. Full floor model of Floor 96 of WTC 1 for Case B_i temperature condition at 100 min.

Appendix A
FEA OF FLOORS

A.1 MODEL DESCRIPTION

A full floor model includes 1) both exterior and core columns extending from one floor below to one floor above, 2) spandrels of the floor of interest, 3) floor slab, 4) floor trusses including primary and bridging trusses, 5) strap anchors, 6) core beams, 7) deck support angles, and 8) break elements to capture failure modes including truss web diagonal buckling and weld failure, exterior and interior seat failure, stud failure, strap anchor weld failure, connection failure between primary and bridging trusses, and connection failure between long-span and transfer trusses. A full floor model without impact damage is shown in Fig. A–1.

The members listed below were found to fail in the early stage of thermal loading and cause large nonlinearities in the subsequent stages; therefore, they were removed from the model to enhance computational efficiency. Figure A–2 shows the full floor model with these members removed. Deck support angles and bridging trusses buckled due to their thermal expansion in the one-way area. Shear studs and welds between strap anchors and truss top chords failed due to shear force caused by the difference in thermal expansion between the floor and the exterior wall in the direction transverse to the primary trusses. Although these members did not exist in the floor model, they were not expected to control the stability and ultimate failure mode of the full floor system under fire. Analyses performed after removal of the following members showed no premature failure mode such as torsional buckling of primary trusses:

- Deck support angles
- Bridging trusses except in the two-way zone
- Shear studs connecting the slab and the spandrel
- Strap anchors

The visco-elastic dampers that connected the truss bottom chords to the spandrels were not included in the full floor model because dampers were expected to be soft when subjected to slow loading rates.

Truss members (top and bottom chords and web diagonals) were modeled by BEAM188 elements. Columns were modeled by BEAM189 elements. Spandrels were modeled by SHELL181 elements. The concrete slab was modeled by SHELL181 elements with four layers through the thickness. Each layer of the shell element for the slab had one integration point.

Nonlinear steel material properties were assigned to each structural member according to the drawings. A bilinear model with a yield point at its compressive strength was used for the concrete slab, where the yield strength was the same in both tension and compression. Creep in the steel was not included in any of the full floor analyses. It was found that creep in BEAM188/189 elements would cause severe convergence problems when those elements experience thermally-induced buckling.

Both core and exterior columns were fixed in the vertical direction at the bottom. Core columns were free in horizontal directions and fixed in all rotations at the top and bottom. Exterior columns were fixed in translation perpendicular to the face of building and in rotation about the axis parallel to the face of the building at the top and bottom. They were also fixed in torsion at the top and bottom.

Elements corresponding to severed members due to impact were removed from the model in the beginning of the analysis based on the results of the aircraft impact analysis (NIST NCSTAR 1-2 and Chapter 5 of NCSTAR 1-6).

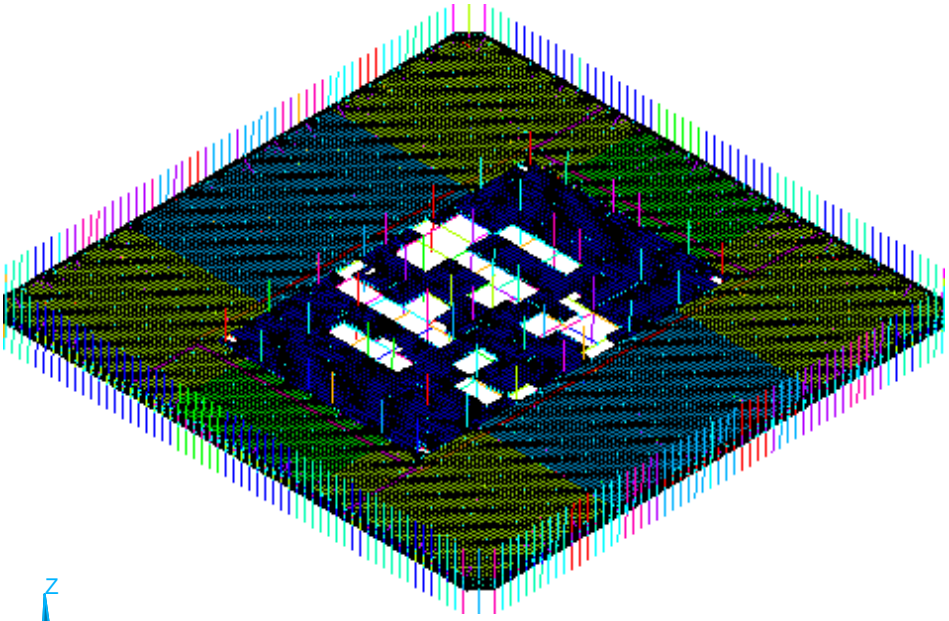

(a) Top view

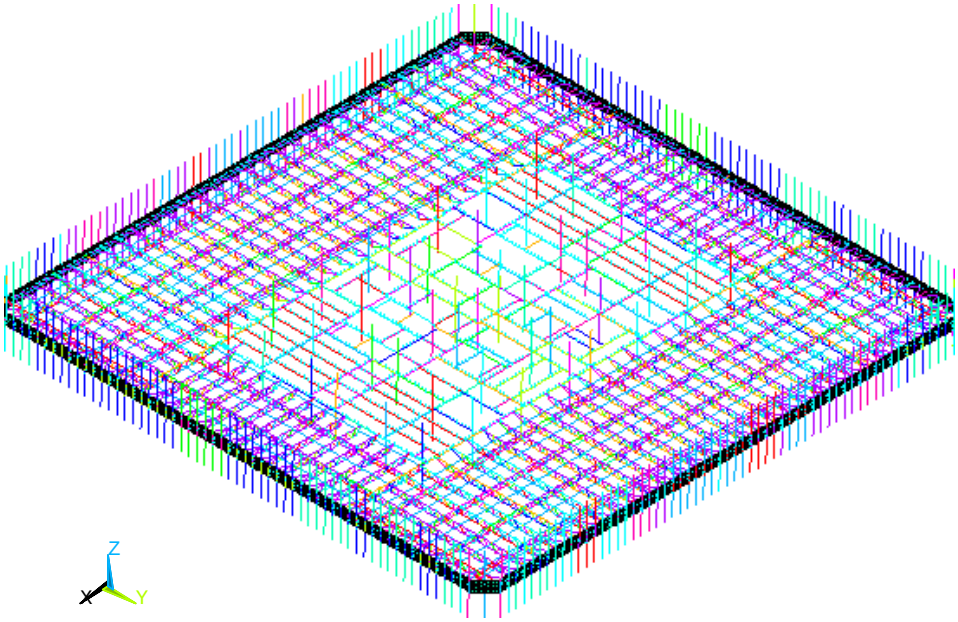

(b) Top view without concrete slab

Figure A–1. Full floor model without impact damage.

The full floor model was first analyzed for dead and live loads, and then thermal loads were applied to simulate the path-dependent nonlinear response. Dead and live loads consisted of self-weight, 8 psf superimposed dead load, and 25 percent of design live loads. Design live loads varied from 55 psf to 85 psf in the model. Vertical loads were not applied to columns. For thermal loads, NIST provided two sets of temperature time histories for each building. These temperature cases were designated as "Case A_i temperature condition" and "Case B_i temperature condition" for WTC 1, and "Case C_i temperature condition" and "Case D_i temperature condition" for WTC 2. NIST later refined these temperatures, and refined cases were referred to as "Case A temperature condition" and "Case B temperature condition" for WTC 1, and "Case C temperature condition" and "Case D temperature condition" for WTC 2. Since the largest change in thermal insulation damage and temperatures occurred for WTC 1 Floor 97, Case A_i and Case A temperature conditions were used to analyze the difference in the floor behavior for the two cases. Since results from the WTC 1 Floor 97 analysis under Case A temperature condition was very similar to those from the analysis with Case A_i condition, it was concluded that the refined temperature cases would not change the floor behavior significantly. Therefore, analysis of other floors were not conducted with the refined temperature conditions.

Temperature data sets were provided for every structural node at 10 min intervals up to 100 min for WTC 1 and up to 60 min for WTC 2 for each temperature case. In the first step of the thermal loading, temperature was linearly ramped up from room temperature to the temperature specified at 10 min. After the first step, the temperature was linearly interpolated between two data sets. Figures A–3 to A–8 show NIST temperature distributions for WTC 1 Floor 97 for Case A_i temperature condition, Case A temperature condition, and Case B_i temperature condition. For each case, temperatures were plotted at only 10 min, 50 min, and 100 min. Figures A–9 to A–12 show NIST temperature distributions for WTC 2 Floor 82 for Case C_i and Case D_i temperature conditions. In the figures, severed members were also shown; however, the severed members were removed from the floor models and did not exist in the analysis.

Temperatures for truss members and spandrels were assigned at node locations and did not change within the cross section. Temperatures for columns were assigned at node locations and had a gradient within the cross section. Temperatures for the slab were assigned at node locations, and there were five points to define the temperature distribution through the thickness at each node location.

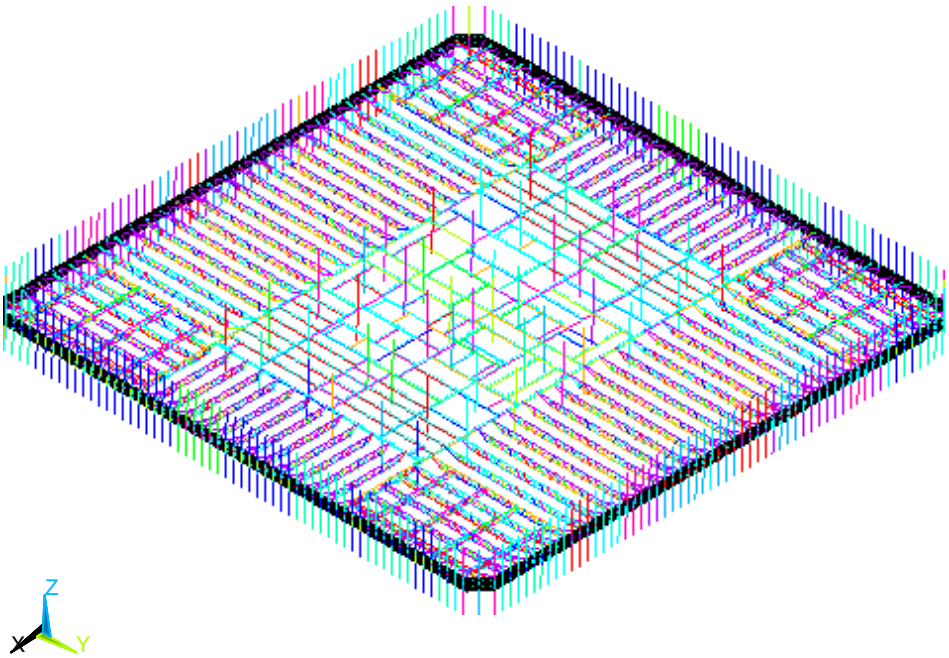

Figure A–2. Full floor model after removal of deck support angles, spandrel studs, bridging trusses outside of two-way zones, and strap anchors.

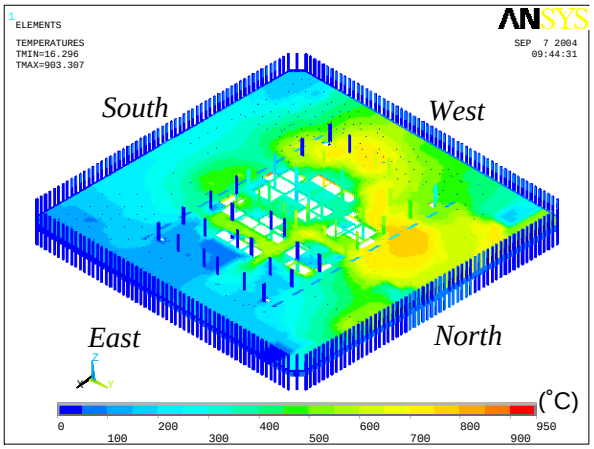

(a) Top view at 10 min

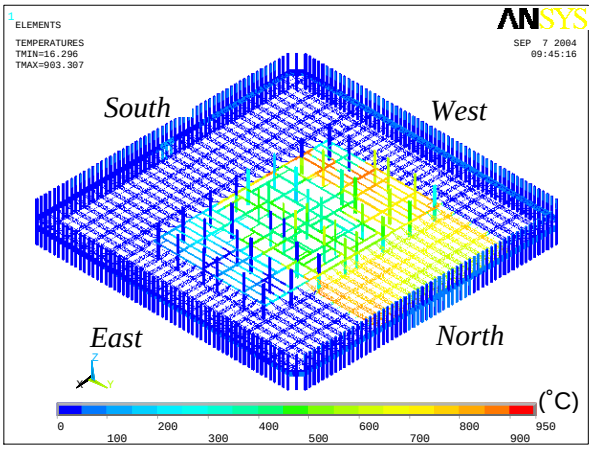

(b) Top view without concrete slab at 10 min

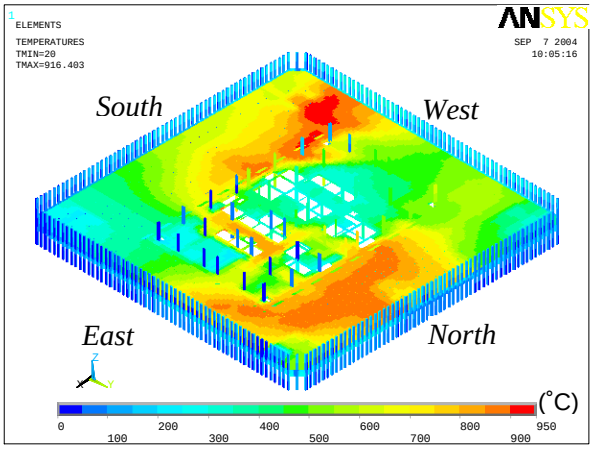

(c) Top view at 50 min

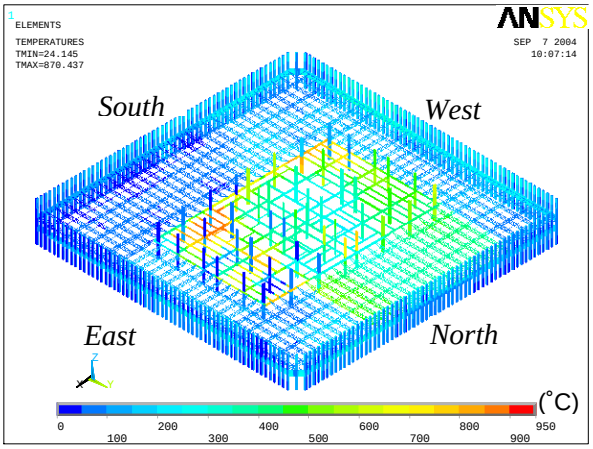

(d) Top view without concrete slab at 50 min

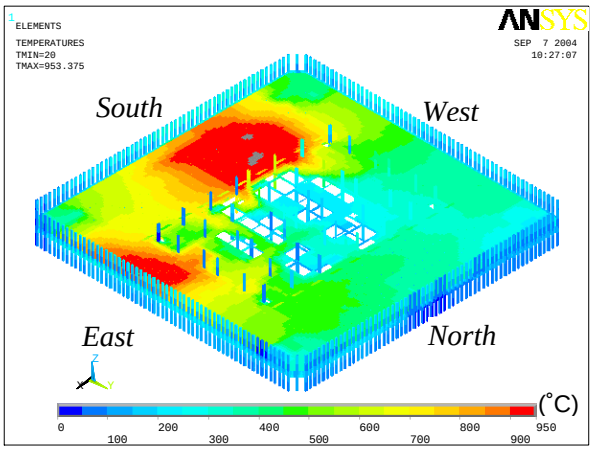

(e) Top view at 100 min

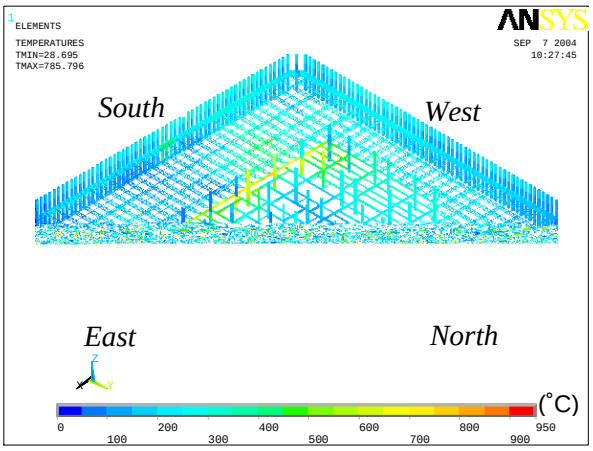

(f) Top view without concrete slab at 100 min

Figure A–3. Case A_i temperature distribution for Floor 97 of WTC 1.

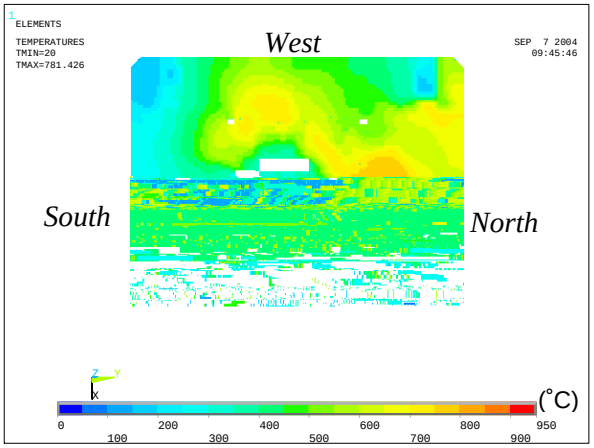

(a) Top surface at 10 min

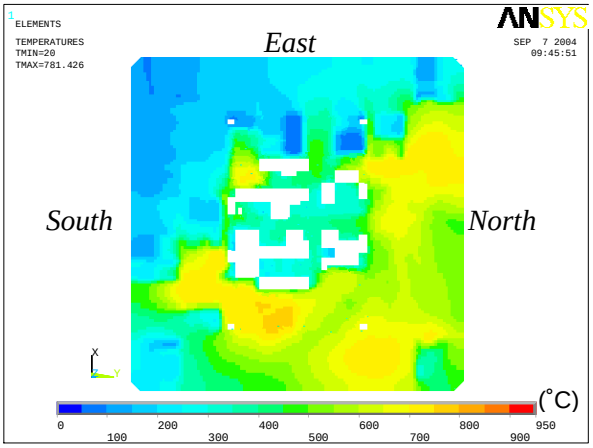

(b) Bottom surface at 10 min

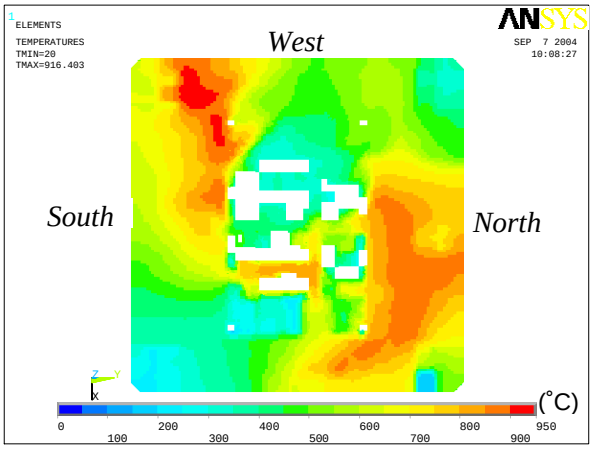

(c) Top surface at 50 min

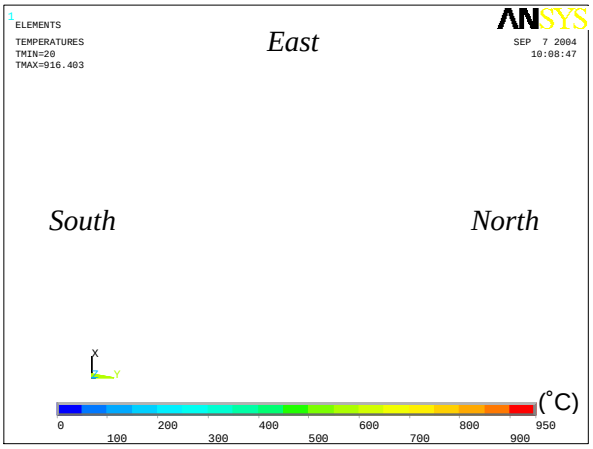

(d) Bottom surface at 50 min

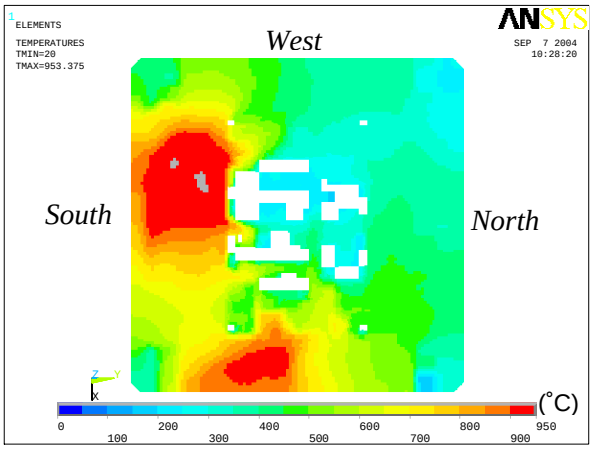

(e) Top surface at 100 min

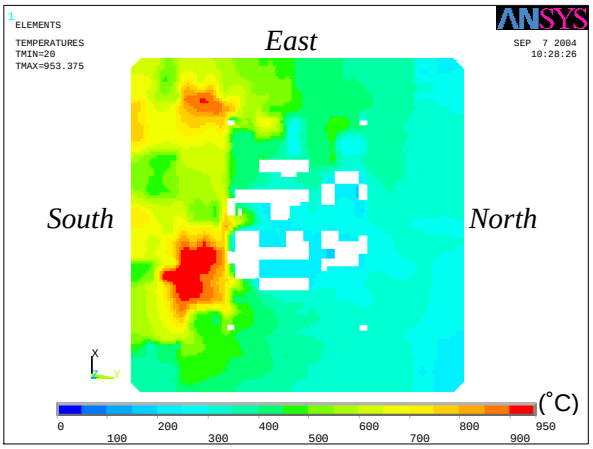

(f) Bottom surface at 100 min

Figure A–4. Case A_i temperature distribution in the slab for Floor 97 of WTC 1.

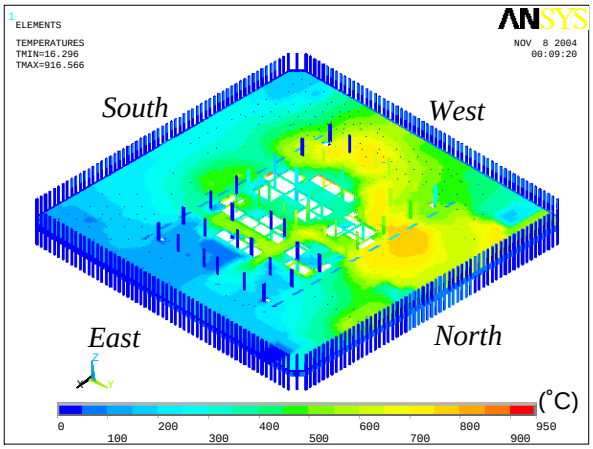

(a) Top view at 10 min

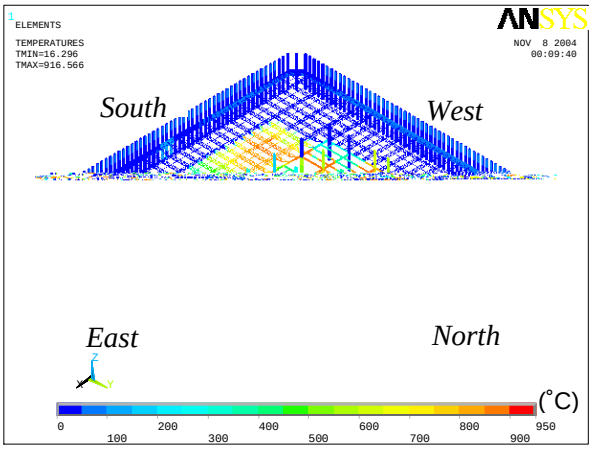

(b) Top view without concrete slab at 10 min

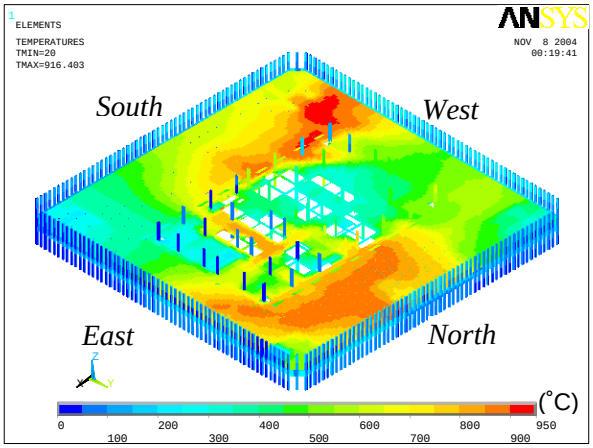

(c) Top view at 50 min

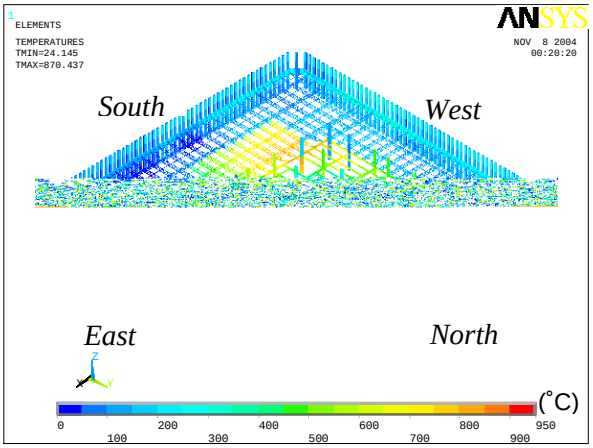

(d) Top view without concrete slab at 50 min

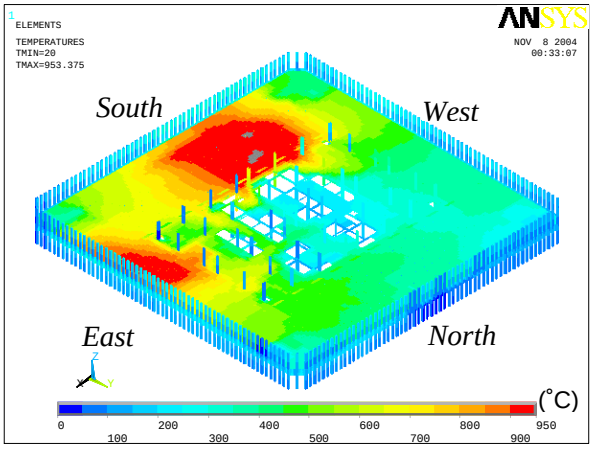

(e) Top view at 100 min

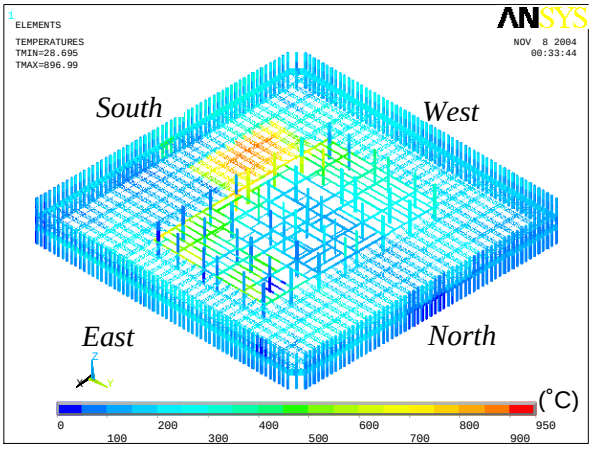

(f) Top view without concrete slab at 100 min

Figure A–5. Case A temperature distribution for Floor 97 of WTC 1.

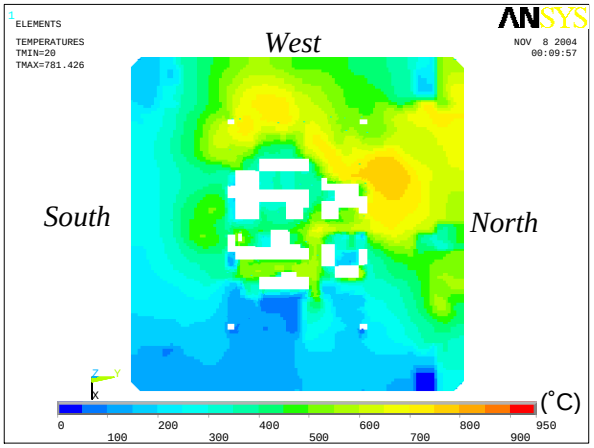

(a) Top surface at 10 min

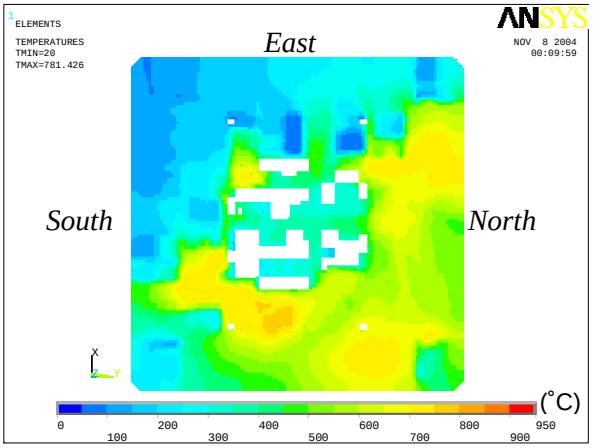

(b) Bottom surface at 10 min

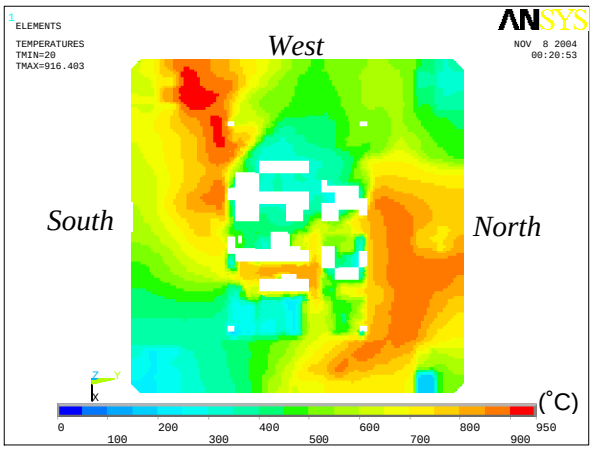

(c) Top surface at 50 min

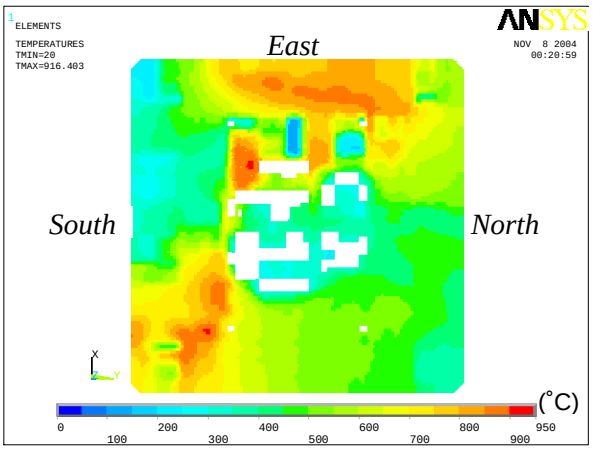

(d) Bottom surface at 50 min

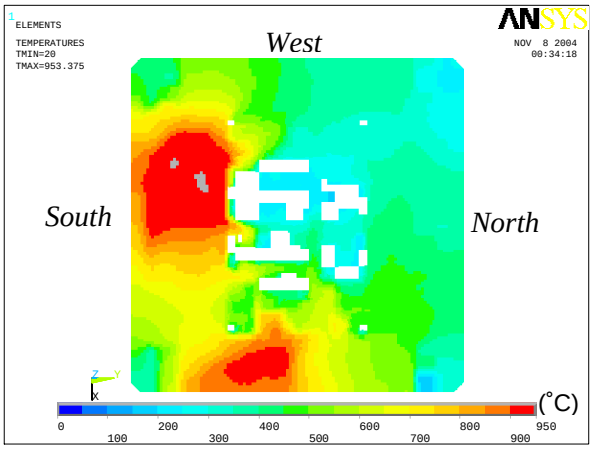

(e) Top surface at 100 min

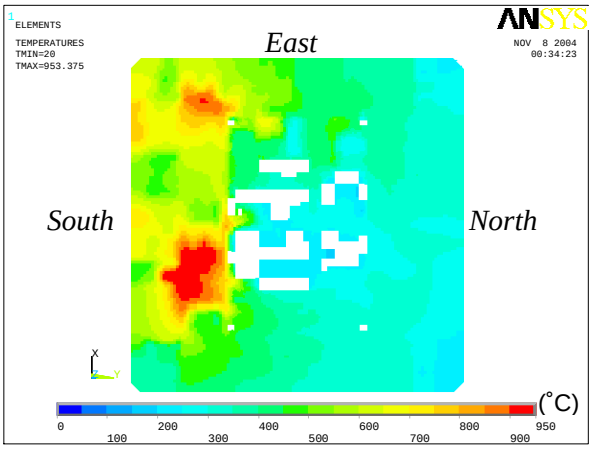

(f) Bottom surface at 100 min

Figure A–6. Case A temperature distribution in the slab for Floor 97 of WTC 1.

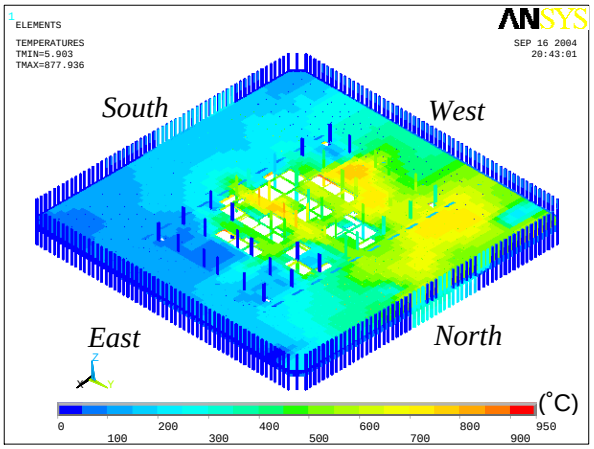

(a) Top view at 10 min

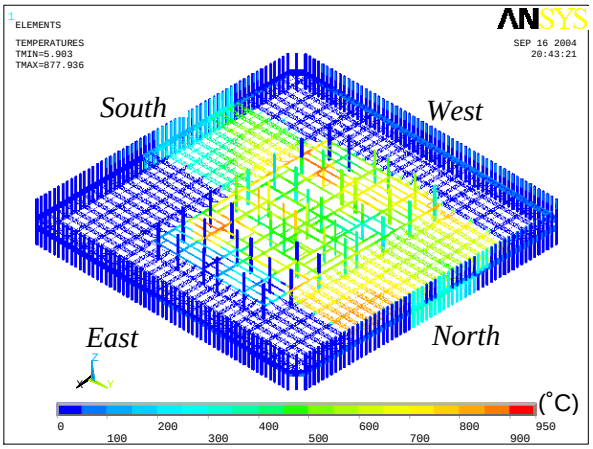

(b) Top view without concrete slab at 10 min

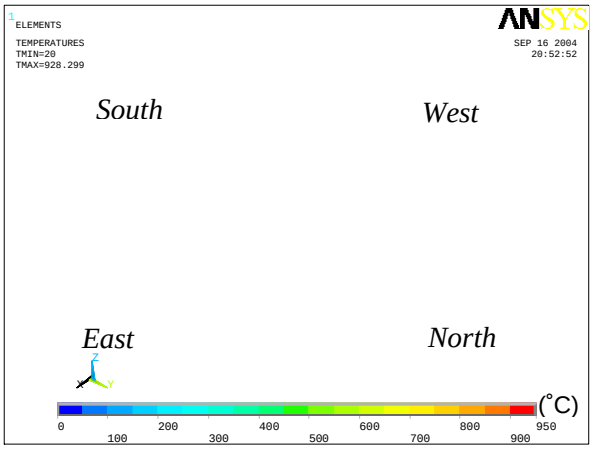

(c) Top view at 50 min

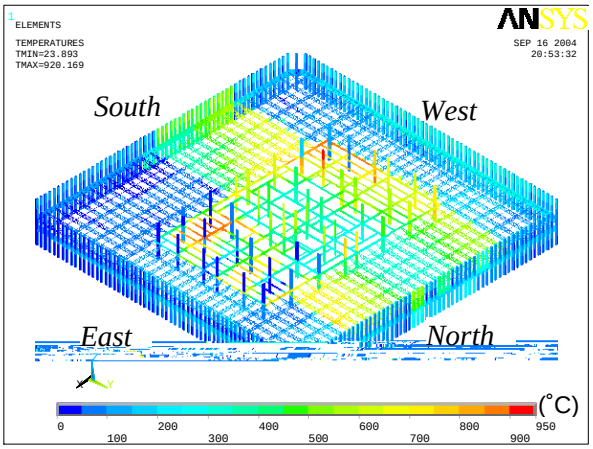

(d) Top view without concrete slab at 50 min

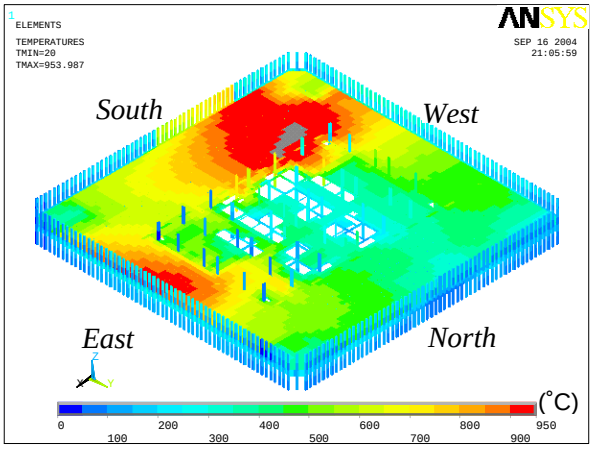

(e) Top view at 100 min

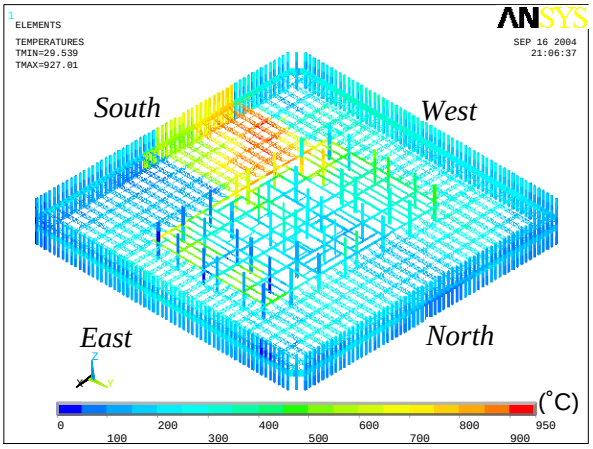

(f) Top view without concrete slab at 100 min

Figure A–7. Case B_i temperature distribution for Floor 97 of WTC 1.

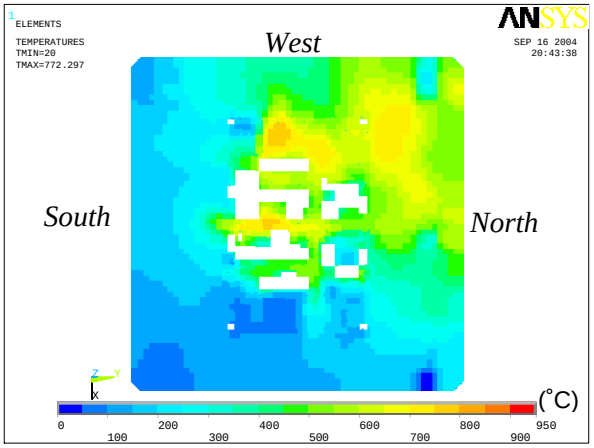

(a) Top surface at 10 min

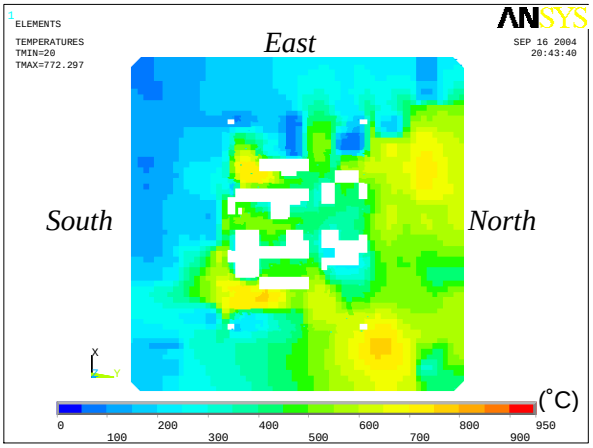

(b) Bottom surface at 10 min

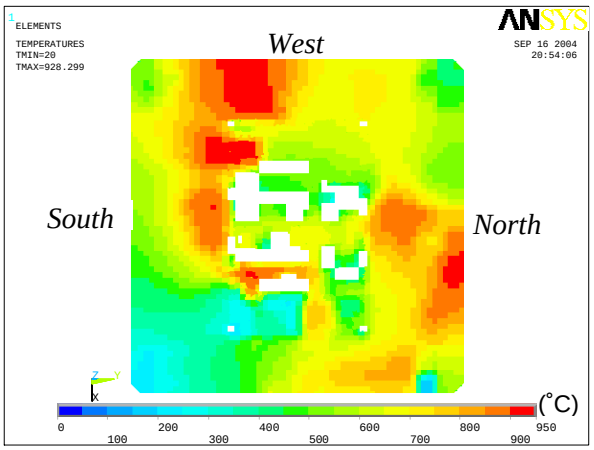

(c) Top surface at 50 min

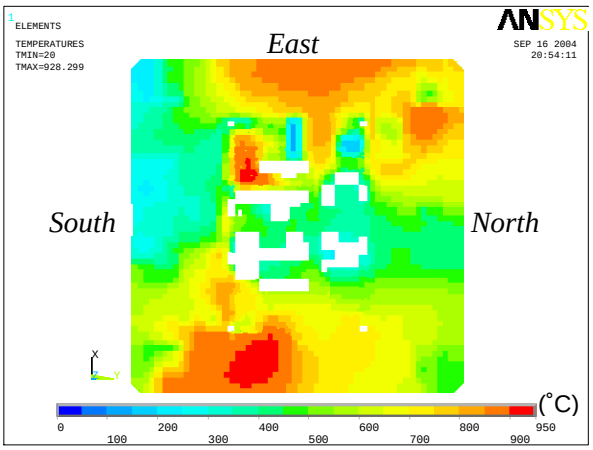

(d) Bottom surface at 50 min

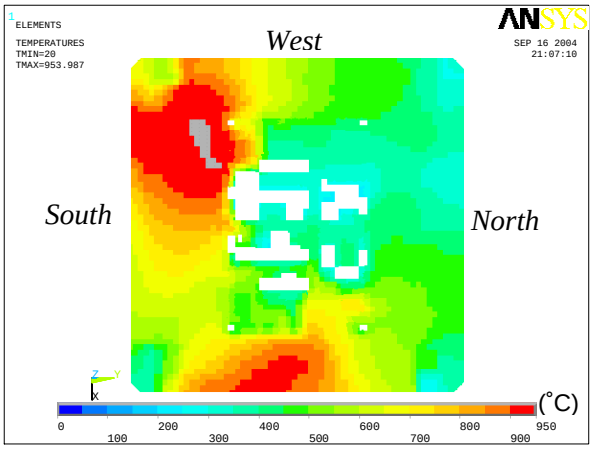

(e) Top surface at 100 min

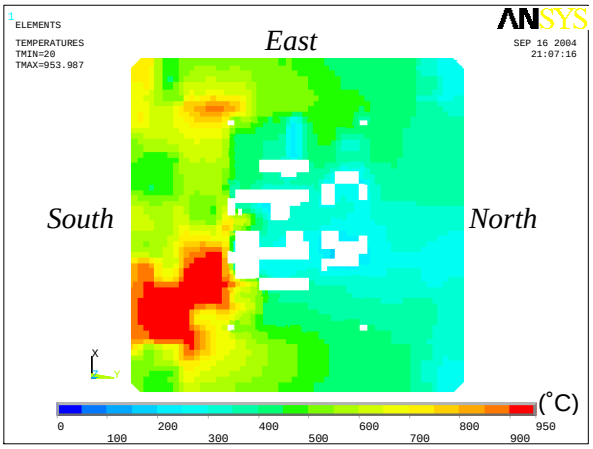

(f) Bottom surface at 100 min

Figure A–8. Case B_i temperature distribution in the slab for Floor 97 of WTC 1.

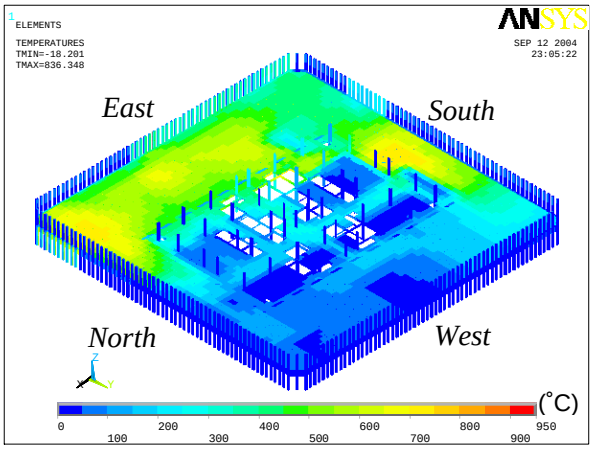

(a) Top view at 10 min

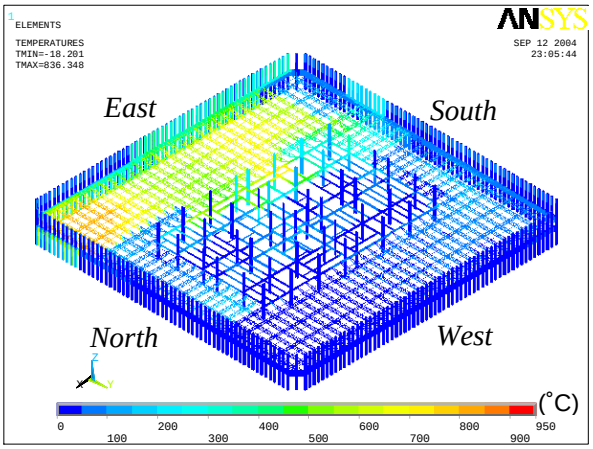

(b) Top view without concrete slab at 10 min

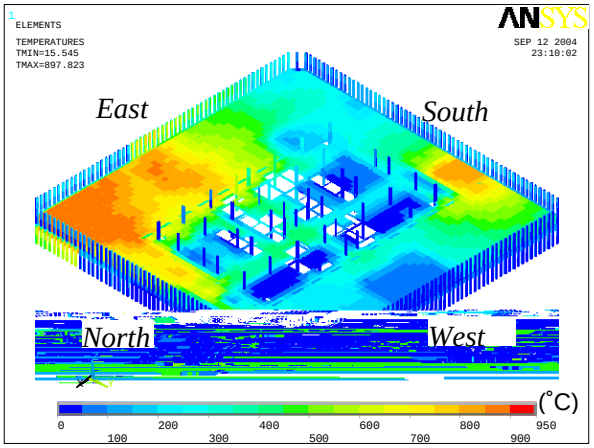

(c) Top view at 30 min

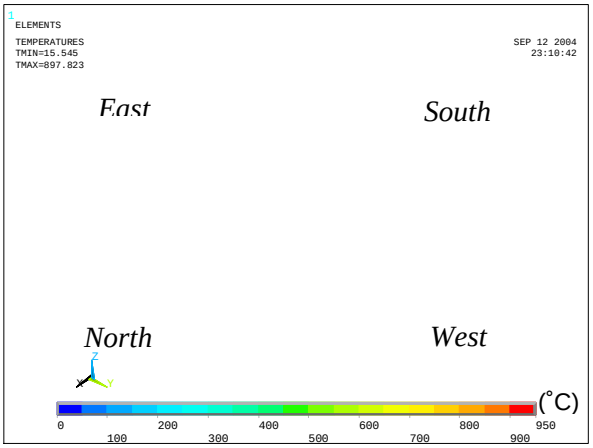

(d) Top view without concrete slab at 30 min

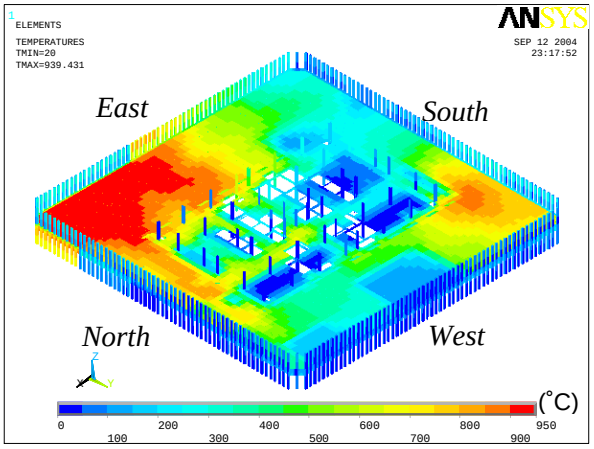

(e) Top view at 60 min

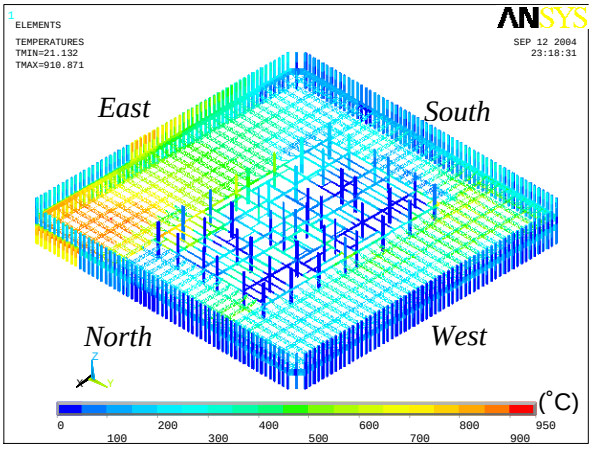

(f) Top view without concrete slab at 60 min

Figure A–9. Case C_i temperature distribution for Floor 82 of WTC 2.

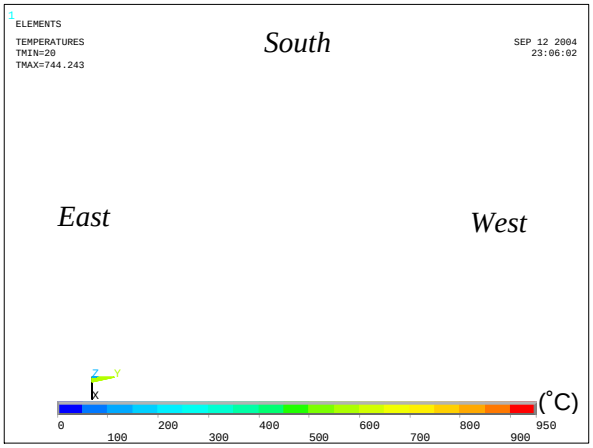

(a) Top surface at 10 min

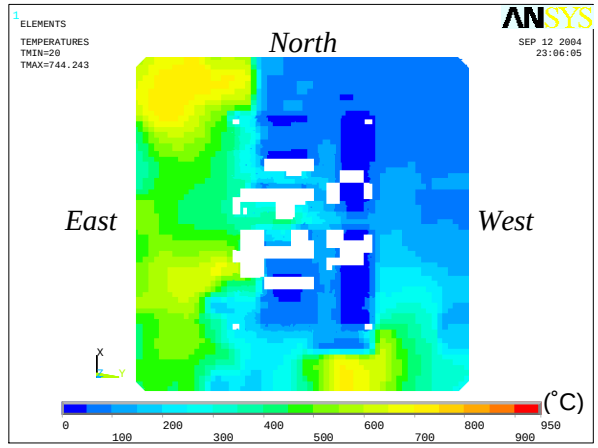

(b) Bottom surface at 10 min

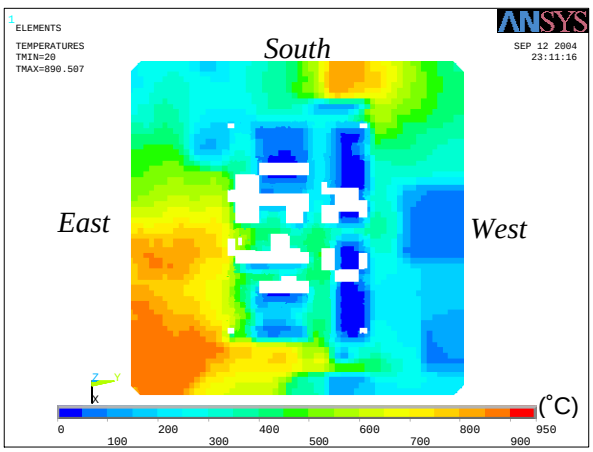

(c) Top surface at 30 min

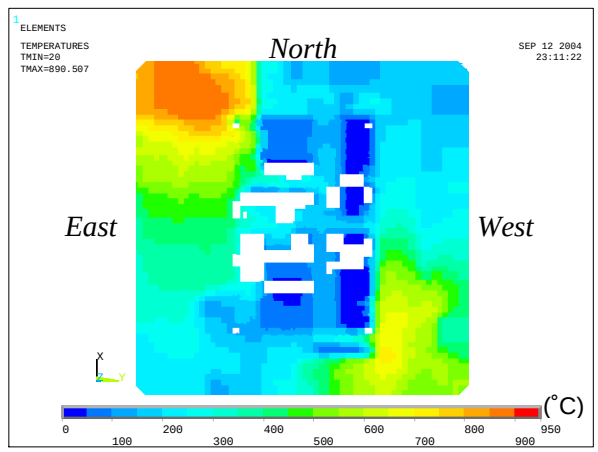

(d) Bottom surface at 30 min

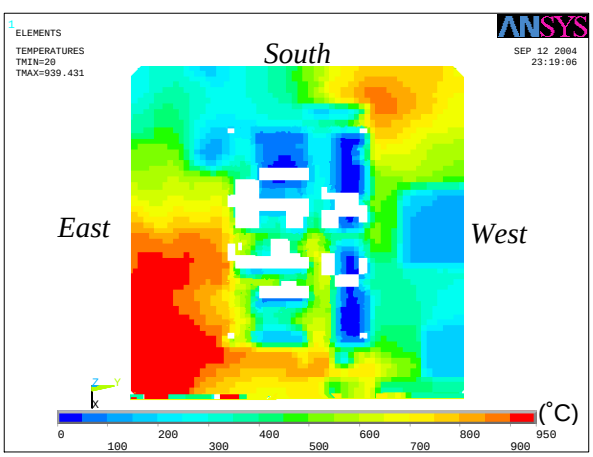

(e) Top surface at 60 min

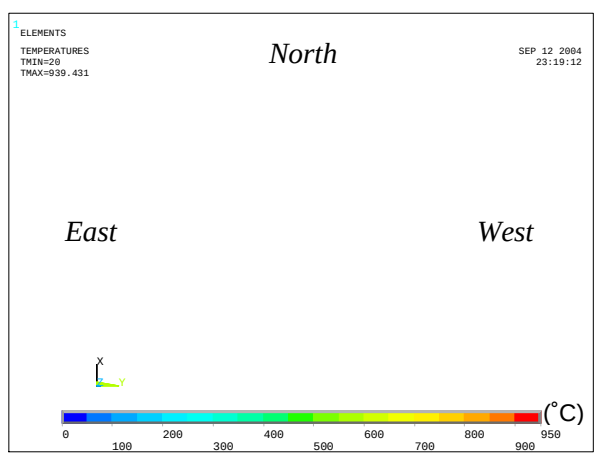

(f) Bottom surface at 60 min

Figure A–10. Case C_i temperature distribution in the slab for Floor 82 of WTC 2.

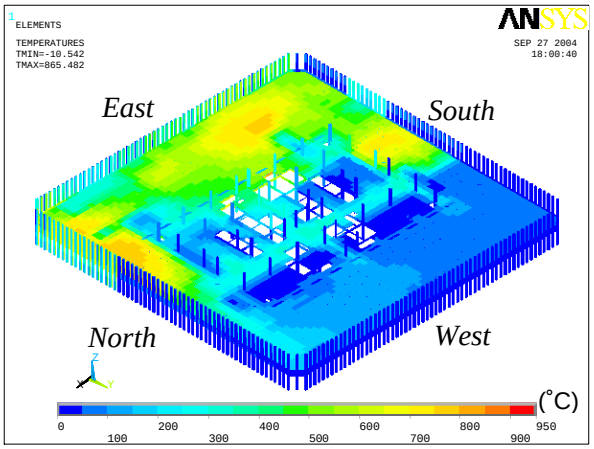

(a) Top view at 10 min

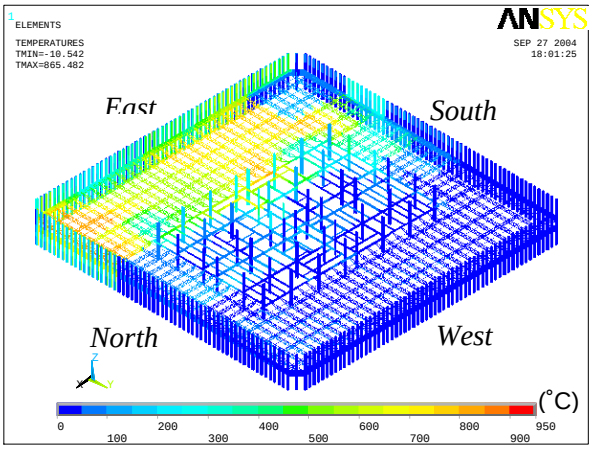

(b) Top view without concrete slab at 10 min

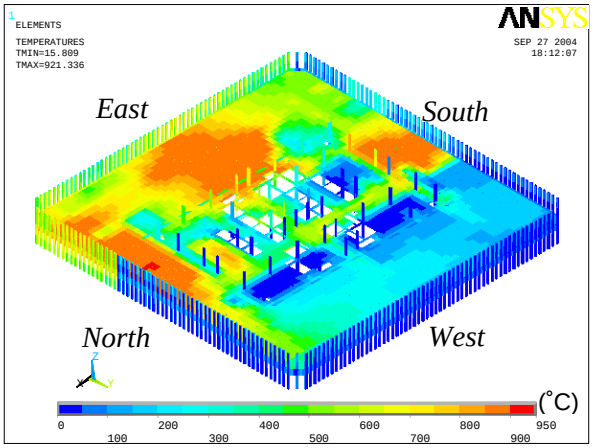

(c) Top view at 30 min

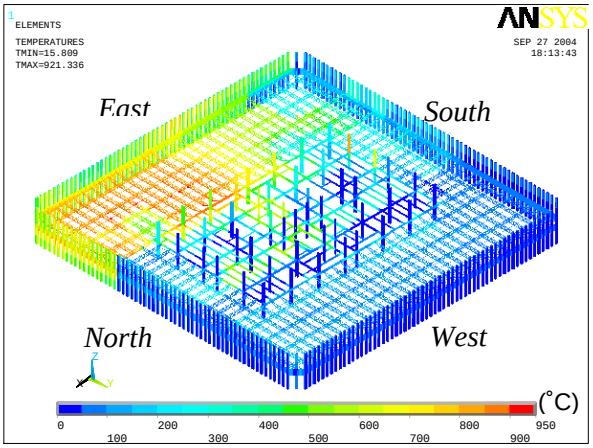

(d) Top view without concrete slab at 30 min

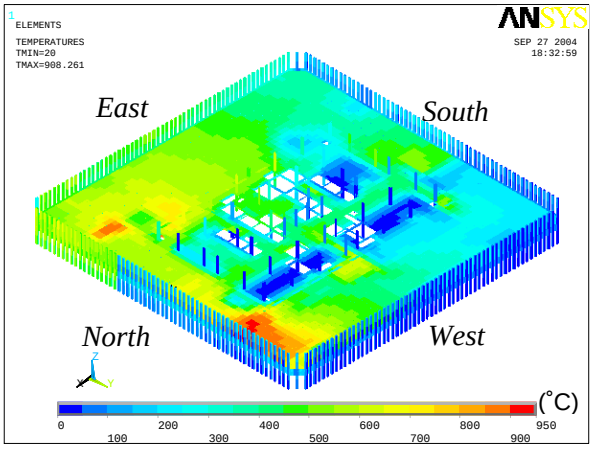

(e) Top view at 60 min

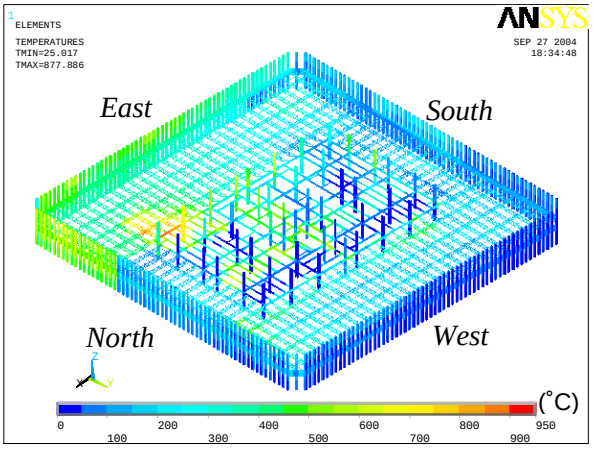

(f) Top view without concrete slab at 60 min

Figure A–11. Case D_i temperature distribution for Floor 82 of WTC 2.

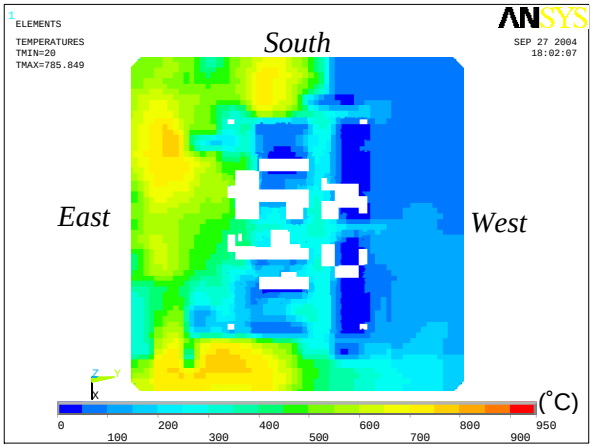

(a) Top surface at 10 min

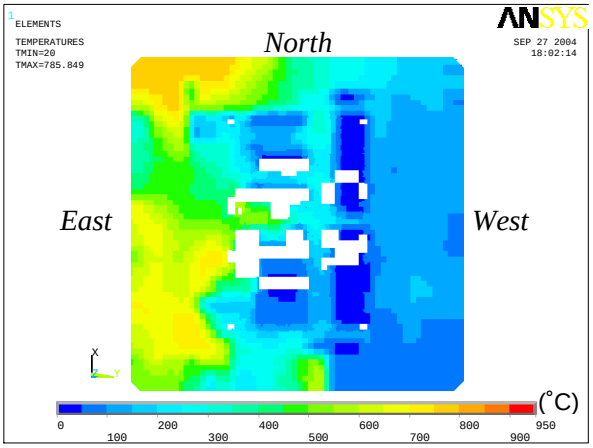

(b) Bottom surface at 10 min

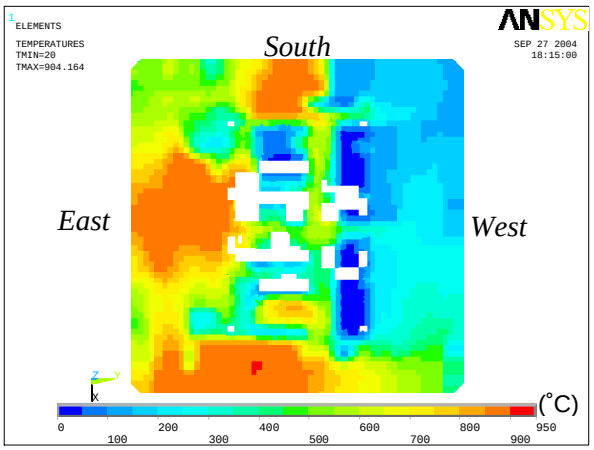

(c) Top surface at 30 min

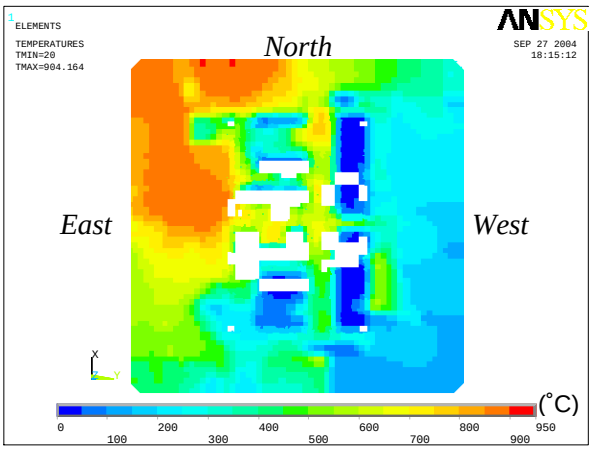

(d) Bottom surface at 30 min

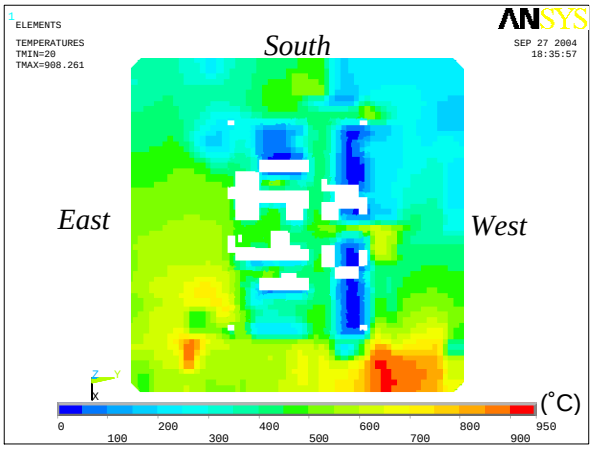

(e) Top surface at 60 min

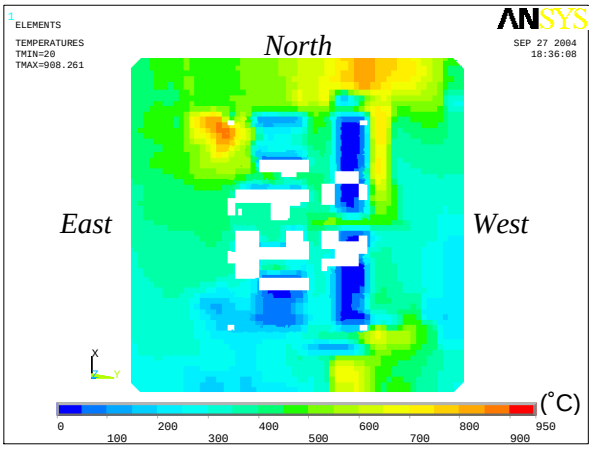

(f) Bottom surface at 60 min

Figure A–12. Case D_i temperature distribution in the slab for Floor 82 of WTC 2.

A.2 WTC 1 FLOORS

A.2.1 Case A_i Temperature Condition

Table A–1 gives the maximum vertical displacement of WTC 1 floors, and Figs. A–13 to A–19 show the vertical displacements of the floors when the maximum displacement was obtained. Floor 95 to Floor 98 showed a significant vertical displacement in the north office area near the impact damage. The maximum vertical displacement of all floors was 32 in. for Floor 97 at 60 min. The vertical displacement in the south office area was found to be insignificant on all the floors throughout the thermal loading. Figure A–20 shows the average total thermal expansion of floors over the entire width of the building at 100 min in two orthogonal directions. The total floor expansion ranged from 4 in. to 8 in. Many web diagonals of Floor 95 to Floor 98 buckled in the hot zones of the north office area. Although gusset plates fractured at several locations, a complete disconnection of the floor from the exterior wall was not observed. Figure A–21 shows horizontal reaction force at individual columns of the north and south faces of Floor 97. A positive reaction force in the figure means that the column is pulled inward by the floor, and a negative reactions force means that the column is pushed out by the floor. Since columns that were not at floor trusses were not connected to the floor in the model because of the removal of strap anchors and studs, reaction forces at those columns were small, and the plots became jagged. As can be seen in the figure, almost all the columns were pushed out by the floor. This was also the case for other floors.

Table A–1. Maximum vertical displacement of WTC 1 floors for Case A_i temperature condition.

Floor	Max. Displacement (in.)	Time at the Maximum (min)
93	5.4	30
94	13.5	100
95	30.9	10
96	23.3	10
97	31.5	60
98	26.4	30
99	7.0	50

Note: Downward displacement is positive.

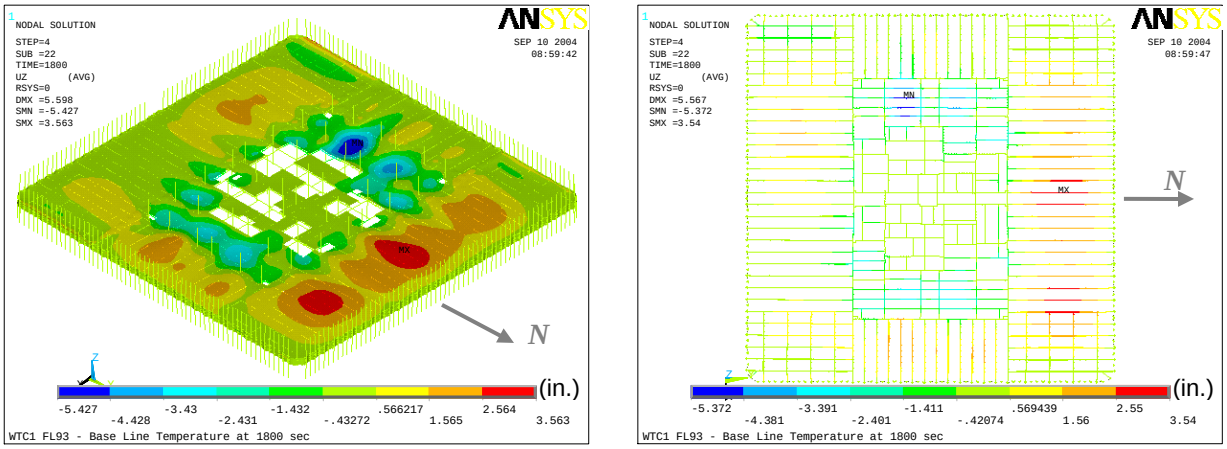

(a) Entire model (b) Top view without slab

Figure A–13. Vertical displacement of WTC 1 Floor 93 for Case A_i temperature condition at 30 min (downward displacement is negative; 5x displacement magnification).

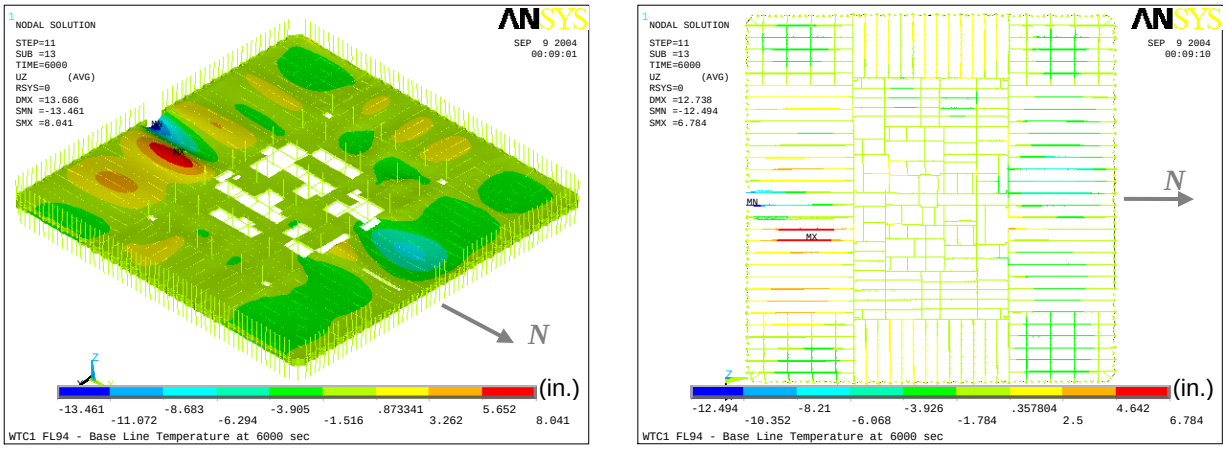

(a) Entire model (b) Top view without slab

Figure A–14. Vertical displacement of WTC 1 Floor 94 for Case A_i temperature condition at 100 min (downward displacement is negative; 5x displacement magnification).

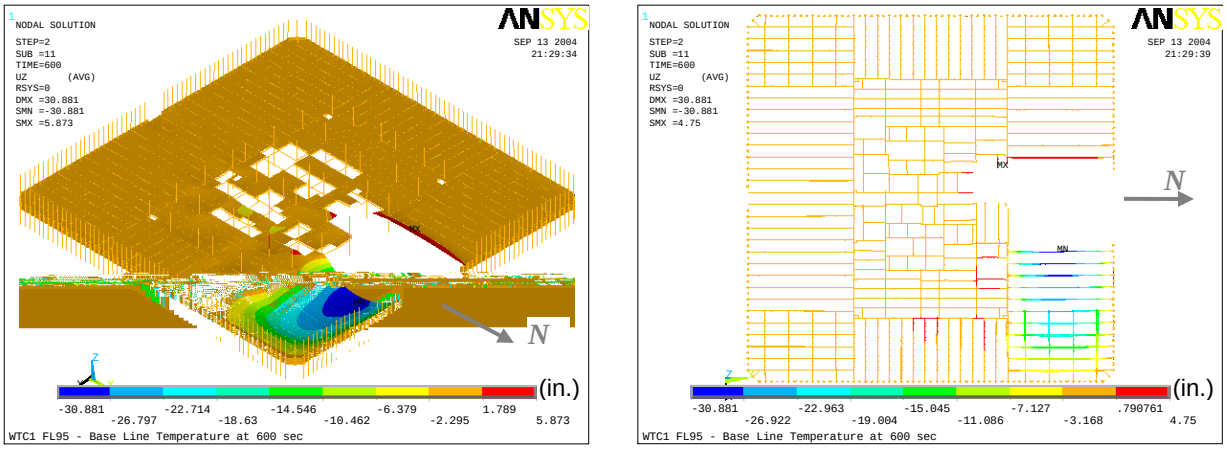

(a) Entire model (b) Top view without slab

Figure A–15. Vertical displacement of WTC 1 Floor 95 for Case A_i temperature condition at 10 min (downward displacement is negative; 5x displacement magnification).

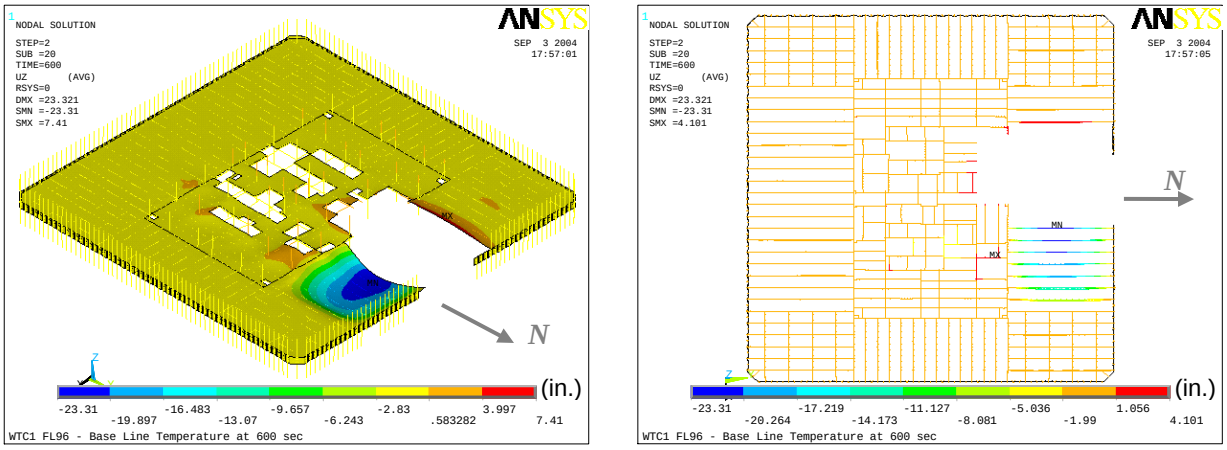

(a) Entire model (b) Top view without slab

Figure A–16. Vertical displacement of WTC 1 Floor 96 for Case A_i temperature condition at 10 min (downward displacement is negative; 5x displacement magnification).

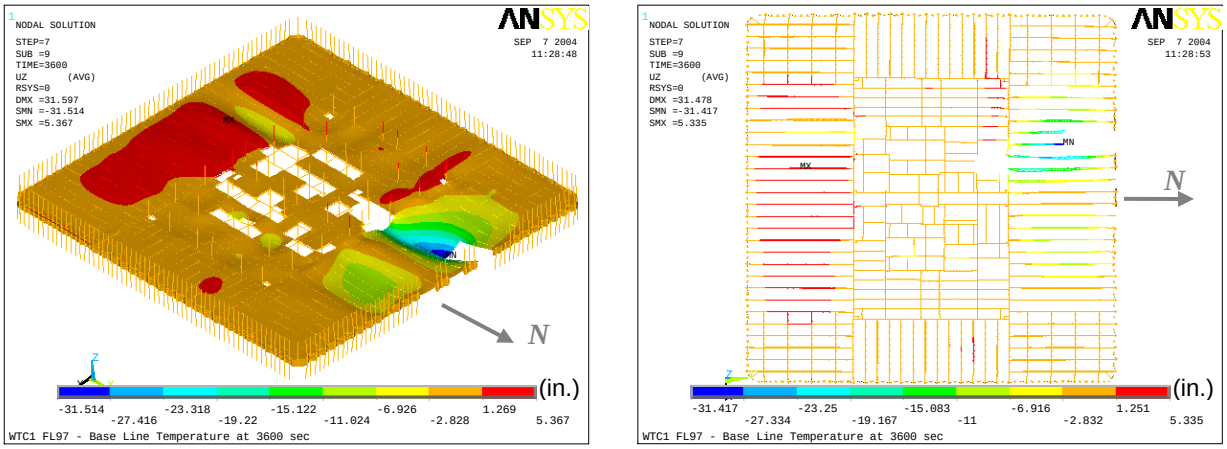

(a) Entire model (b) Top view without slab

Figure A–17. Vertical displacement of WTC 1 Floor 97 for Case A_i temperature condition at 60 min (downward displacement is negative; 5x displacement magnification).

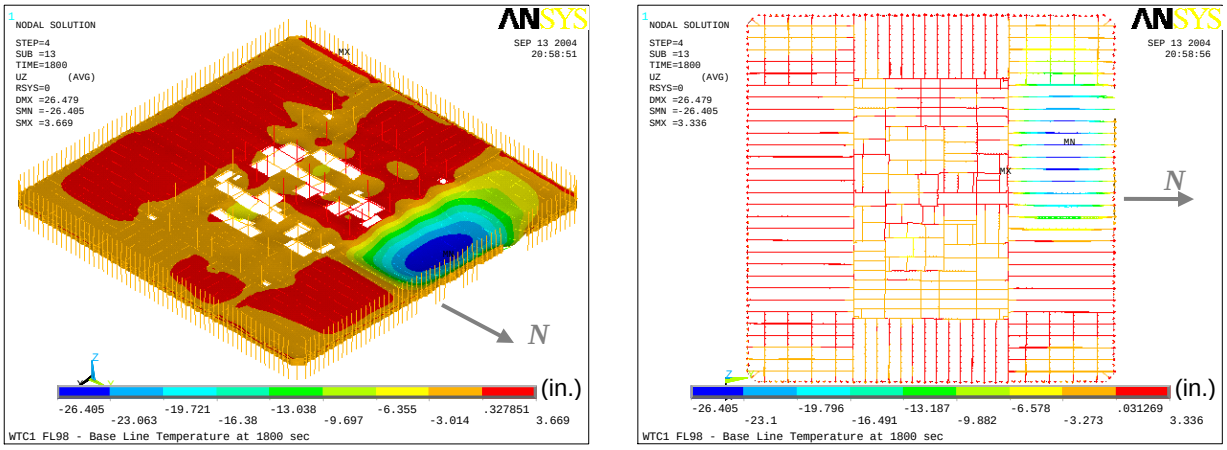

(a) Entire model (b) Top view without slab

Figure A–18. Vertical displacement of WTC 1 Floor 98 for Case A_i temperature condition at 30 min (downward displacement is negative; 5x displacement magnification).

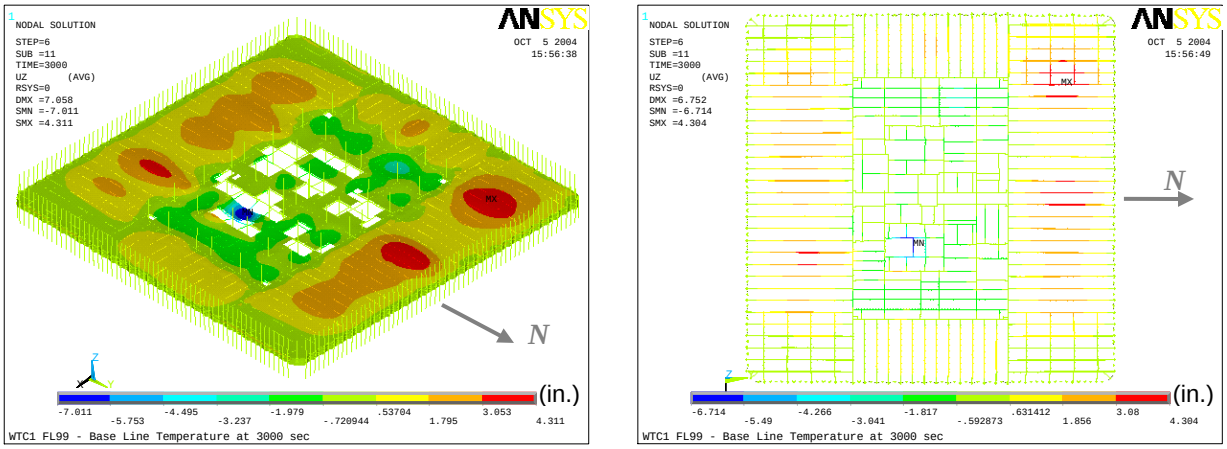

(a) Entire model (b) Top view without slab

Figure A–19. Vertical displacement of WTC 1 Floor 99 for Case A_i temperature condition at 50 min (downward displacement is negative; 5x displacement magnification).

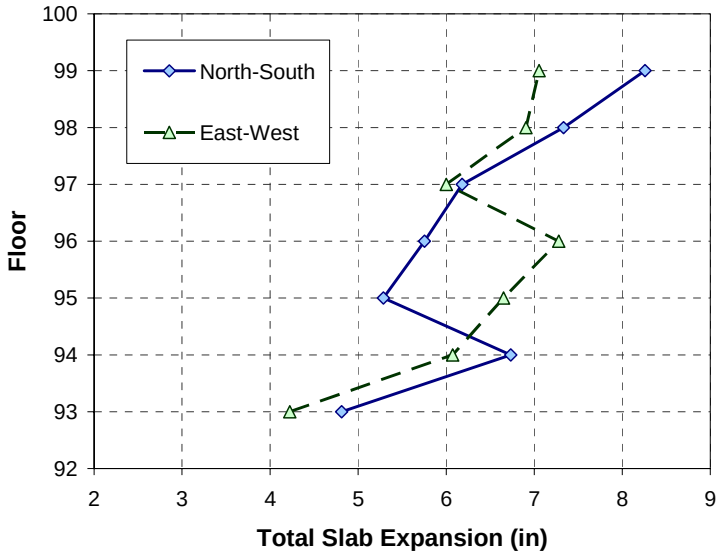

Figure A–20. Thermal expansion of floors of WTC 1 for Case A_i temperature condition at 100 min.

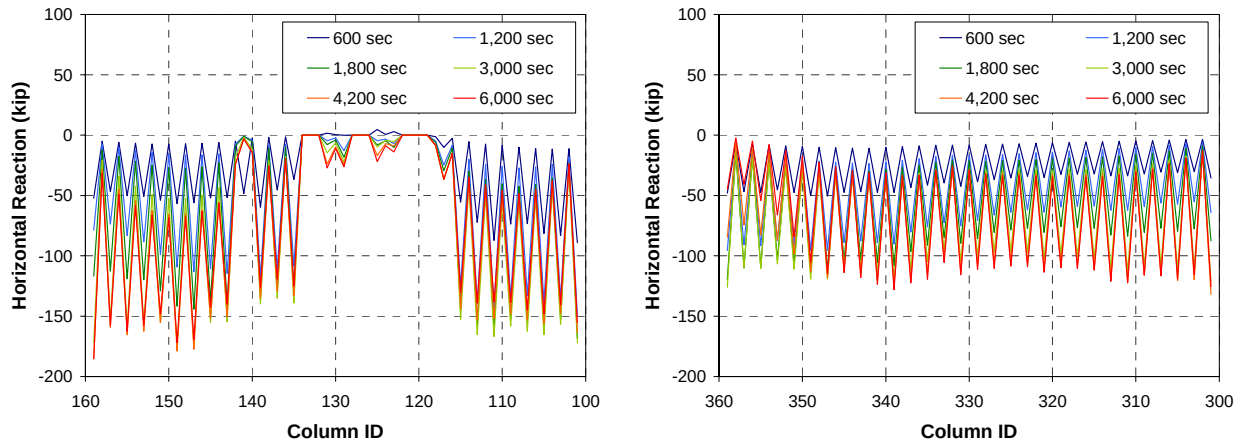

(a) North face (b) South face

Figure A–21. Horizontal reaction force per column of WTC 1 Floor 97 for Case A_i temperature condition.

A.2.2 Case B_i Temperature Condition

Table A–2 gives the maximum vertical displacement of WTC 1 floors for Case B_i temperature condition, and Figs. A–22 to A–28 show the vertical displacements when the maximum displacement was obtained. The maximum vertical displacement of Floor 95 to Floor 98 increased due to higher temperature when compared to Case A_i temperature condition. Especially, the vertical displacement in the south office area of those floors became significant. The maximum among the floors was 49 in. in the south office area of Floor 98 as shown in Fig. A–27. The large displacement on the south side of Floor 98 was caused by the exterior seat failure between Column 329 and Column 343 that started at 90 min (see Fig. A–29). Exterior seats between Column 337 and Column 347 of Floor 97 also failed, which caused a vertical displacement of 37 in. in the south office area (see Fig. A–29). These exterior seats failed due to loss of vertical shear strength under the extreme temperatures encountered. Figure A–30 shows the average total thermal expansion of floors over the entire width of the building at 100 min of Case B_i temperature condition. The total floor expansion ranged from 5 in. to 8.5 in. Figure A–31 shows horizontal reaction force at individual columns of the north and south faces of Floor 98. It can be seen in the figure that reaction forces of columns between Column 329 and Column 343 became close to zero after the trusses attached to these column lost their vertical support at the exterior seats. Almost all the columns were found to be pushed out by the floor. This was also the case for other floors.

Table A–2. Maximum vertical displacement of WTC 1 floors for Case B_i temperature condition.

Floor	Max. Displacement (in.)	Time at the Maximum (min)
93	-5.8	100
94	12.7	100
95	29.2	10
96	28.6	10
97	37.4	100
98	49.0	100
99	6.8	100

Note: Downward displacement is positive.

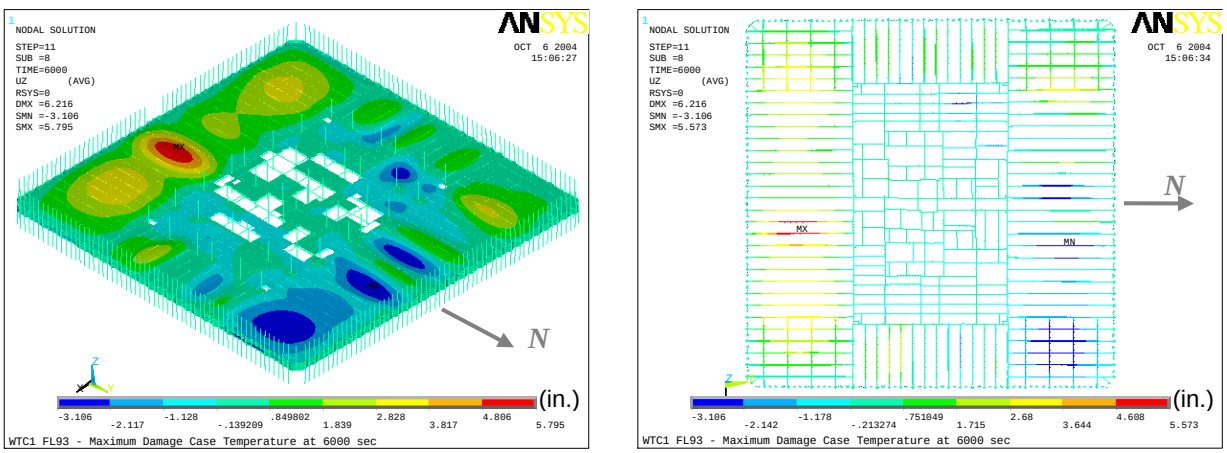

(a) Entire model (b) Top view without slab

Figure A–22. Vertical displacement of WTC 1 Floor 93 for Case B_i temperature condition at 100 min (downward displacement is negative; 5x displacement magnification).

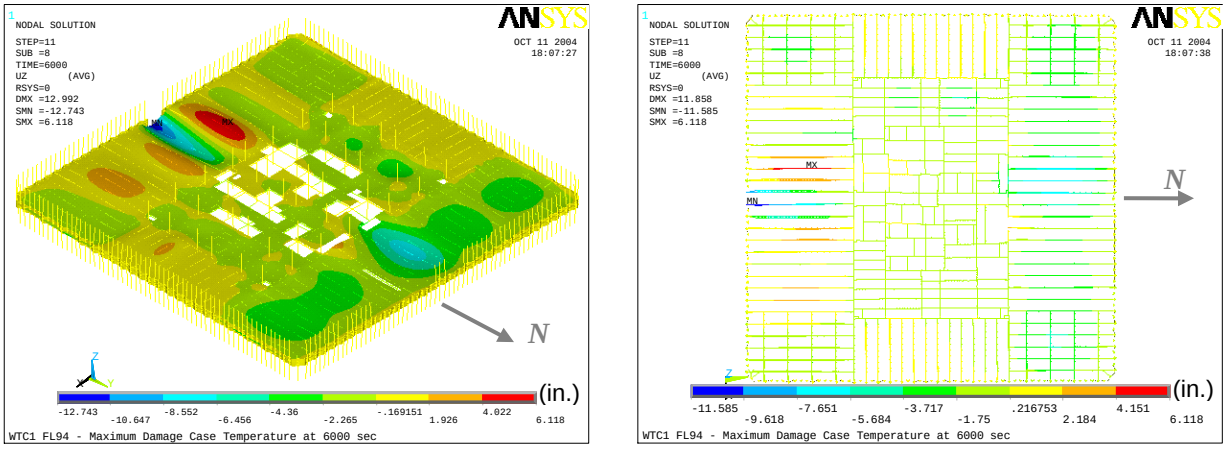

(a) Entire model (b) Top view without slab

Figure A–23. Vertical displacement of WTC 1 Floor 94 for Case B_i temperature condition at 100 min (downward displacement is negative; 5x displacement magnification).

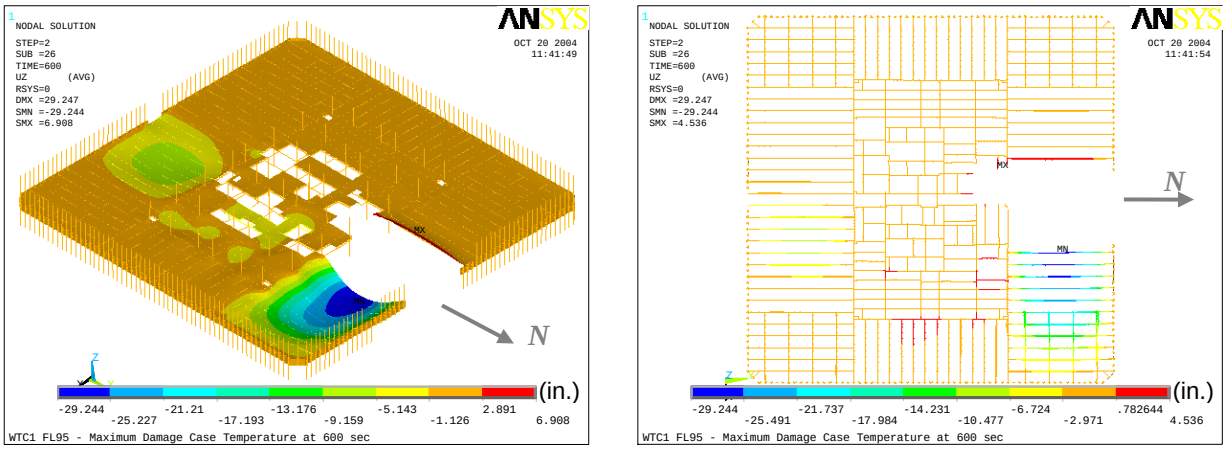

(a) Entire model (b) Top view without slab

Figure A–24. Vertical displacement of WTC 1 Floor 95 for Case B_i temperature condition at 10 min (downward displacement is negative; 5x displacement magnification).

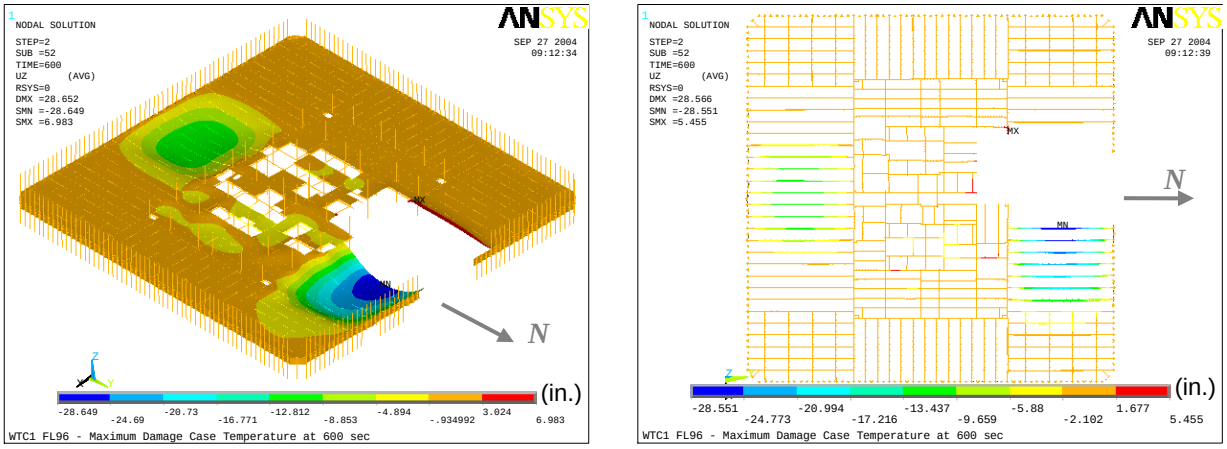

(a) Entire model (b) Top view without slab

Figure A–25. Vertical displacement of WTC 1 Floor 96 for Case B_i temperature condition at 10 min (downward displacement is negative; 5x displacement magnification).

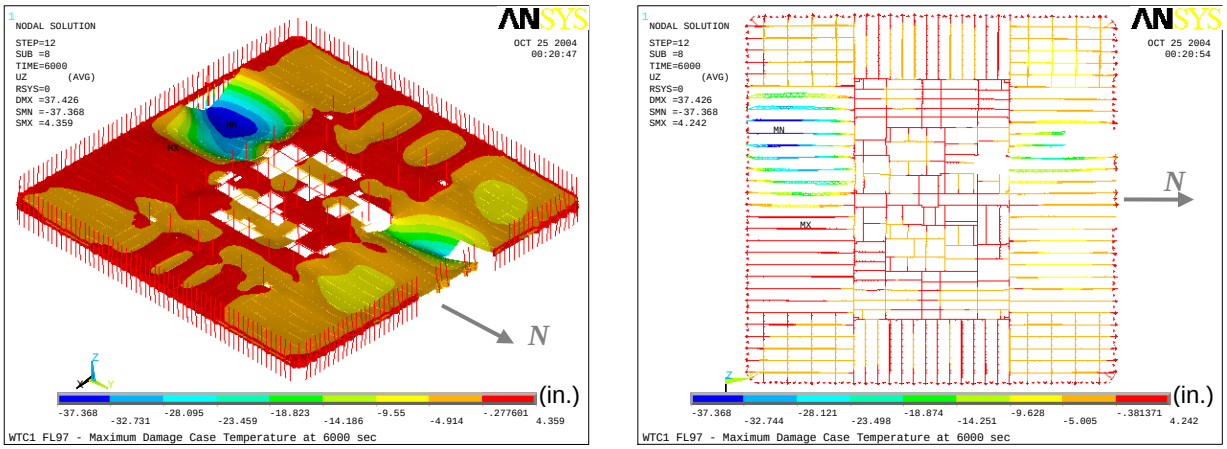

(a) Entire model (b) Top view without slab

Figure A–26. Vertical displacement of WTC 1 Floor 97 for Case B_i temperature condition at 100 min (downward displacement is negative; 5x displacement magnification).

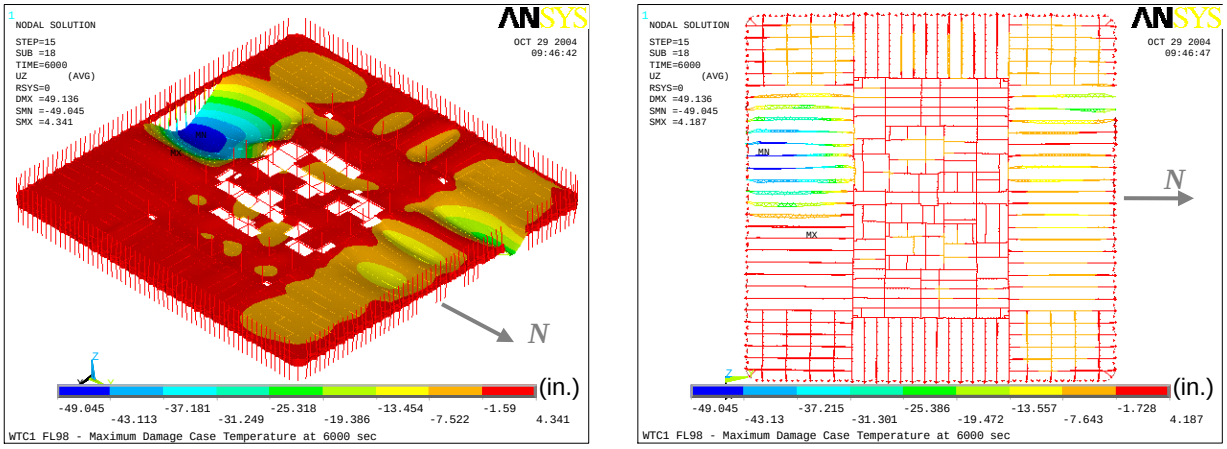

(a) Entire model (b) Top view without slab

Figure A–27. Vertical displacement of WTC 1 Floor 98 for Case B_i temperature condition at 100 min (downward displacement is negative; 5x displacement magnification).

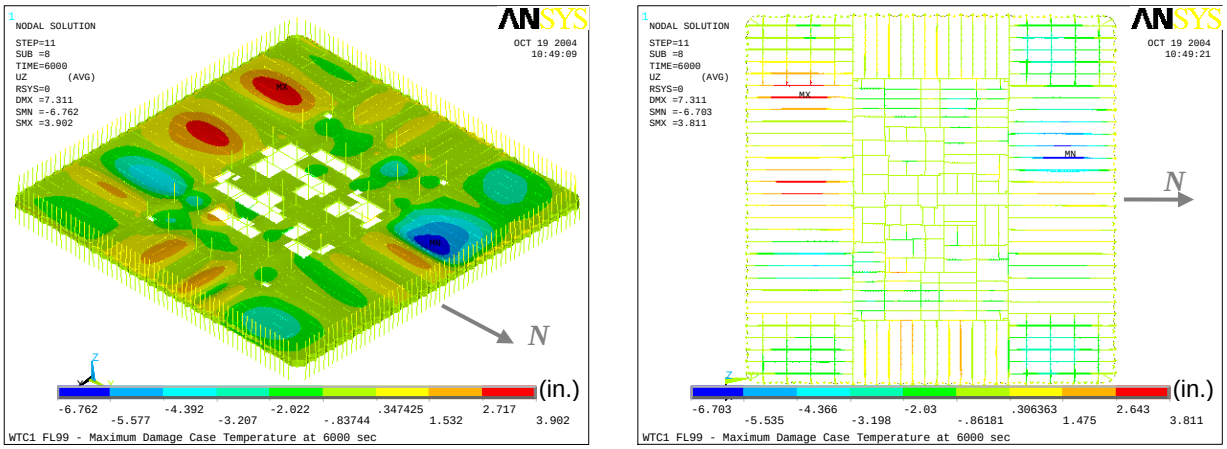

(a) Entire model (b) Top view without slab

Figure A–28. Vertical displacement of WTC 1 Floor 99 for Case B_i temperature condition at 100 min (downward displacement is negative; 5x displacement magnification).

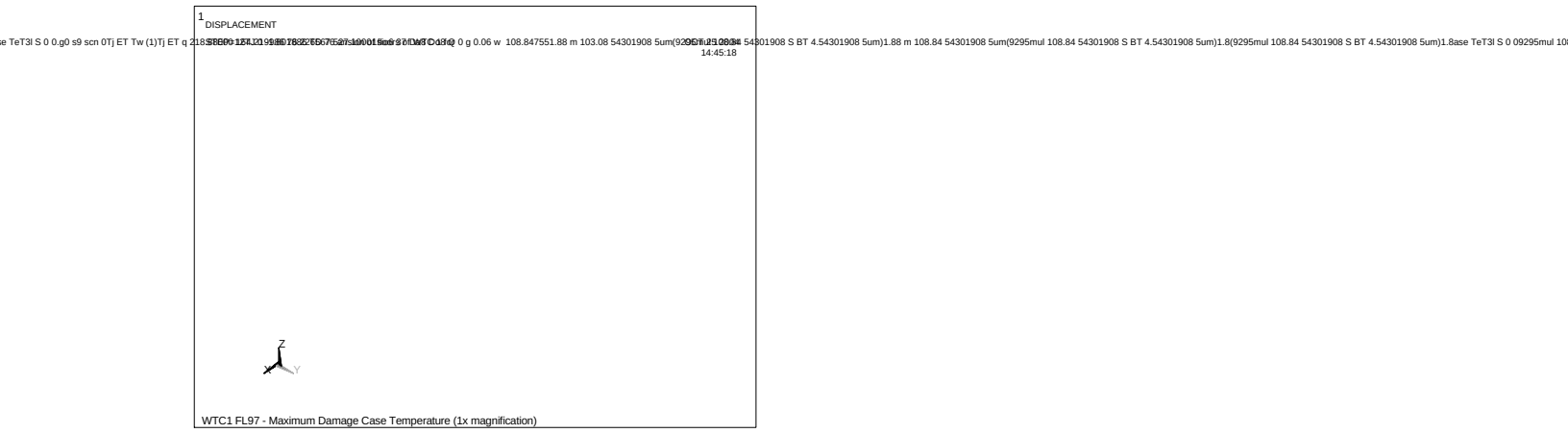

Figure A–29. Loss of vertical supports in WTC 1 Floor 97 and Floor 98 for Case B temperature condition at 100 min (1x displacement magnification).

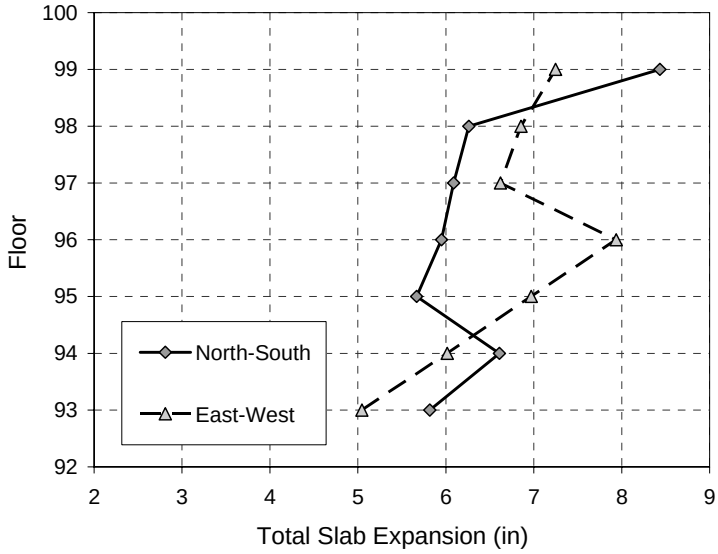

Figure A–30. Thermal expansion of floors of WTC 1 for Case B temperature condition at 100 min.

Figure A–31. Horizontal reaction force per column of WTC 1 Floor 98 for Case B_i temperature condition.

A.3 WTC 2 FLOORS

A.3.1 Case C_i Temperature Condition

Table A–3 gives the maximum vertical displacement of WTC 2 floors for Case C_i temperature condition, and Figs. A–32 to A–36 show the vertical displaceme

Table A–3. Maximum vertical displacement of WTC 2 floors for Case C_i temperature condition.

Floor	Max. Displacement (in.)	Time at the Maximum (min)
79	19.0	60
80	30.1	60
81	31.0	60
82	45.2	60
83	38.9	60

Note: Downward displacement is positive.

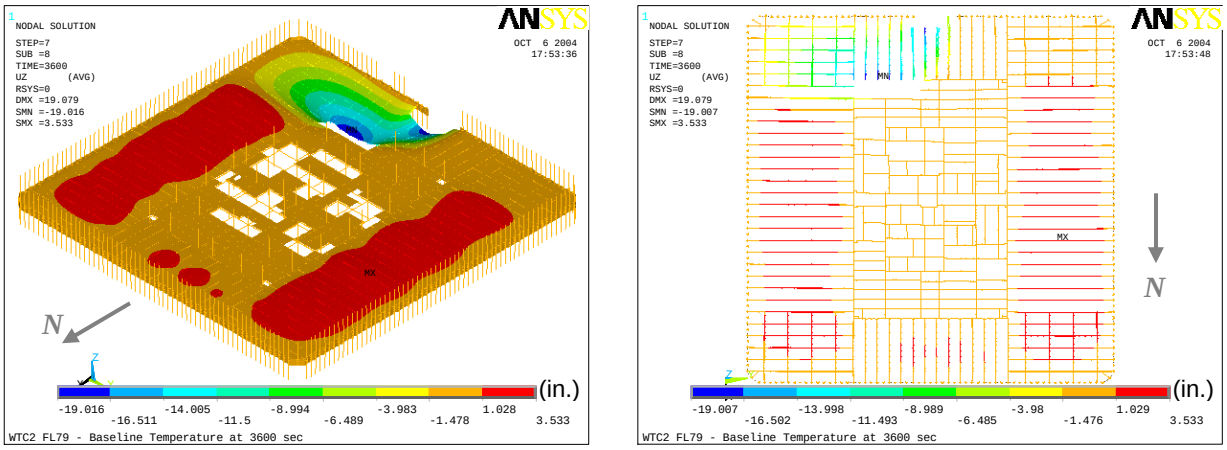

(a) Entire model (b) Top view without slab

Figure A–32. Vertical displacement of WTC 2 Floor 79 for Case C_i temperature condition at 60 min (downward displacement is negative; 5x displacement magnification).

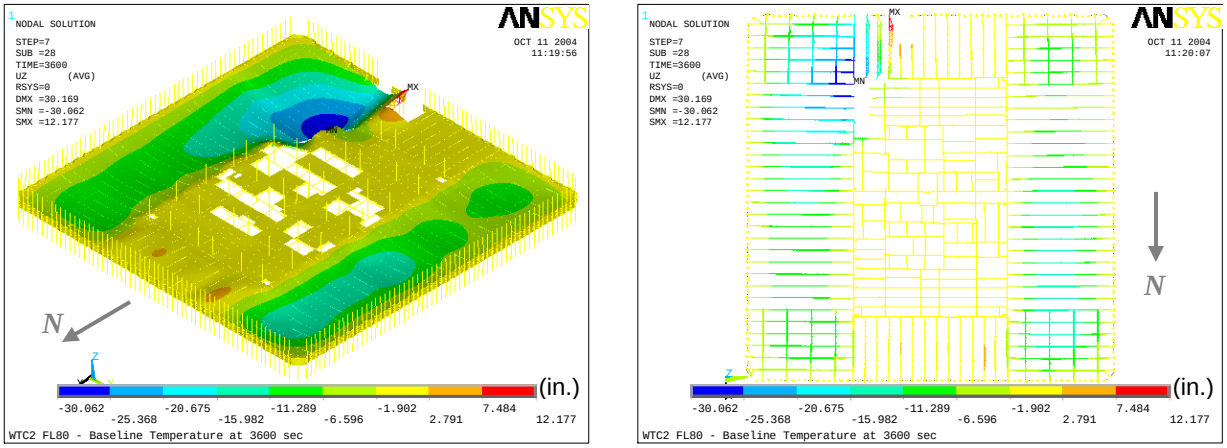

(a) Entire model (b) Top view without slab

Figure A–33. Vertical displacement of WTC 2 Floor 80 for Case C_i temperature condition at 60 min (downward displacement is negative; 5x displacement magnification).

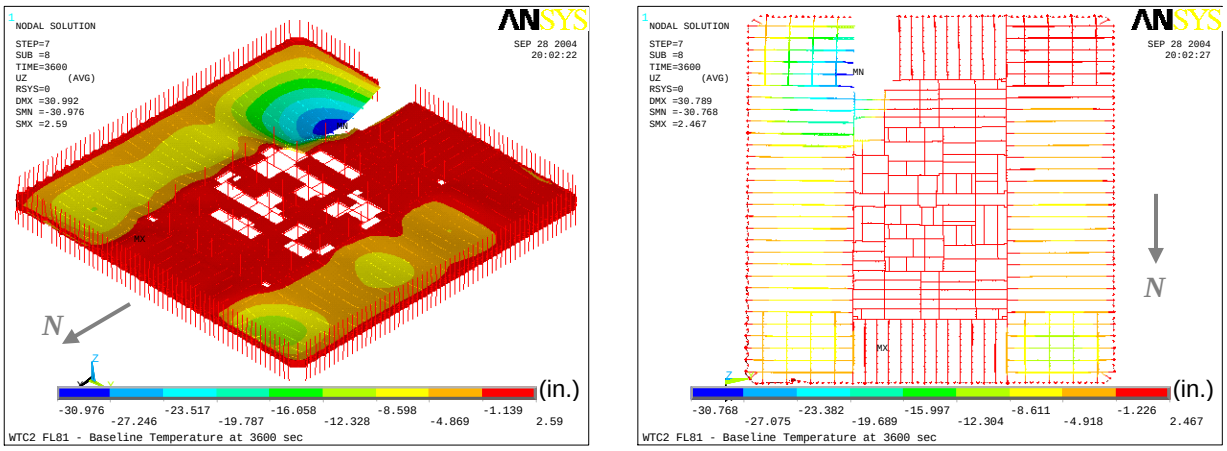

(a) Entire model (b) Top view without slab

Figure A–34. Vertical displacement of WTC 2 Floor 81 for Case C_i temperature condition at 60 min (downward displacement is negative; 5x displacement magnification).

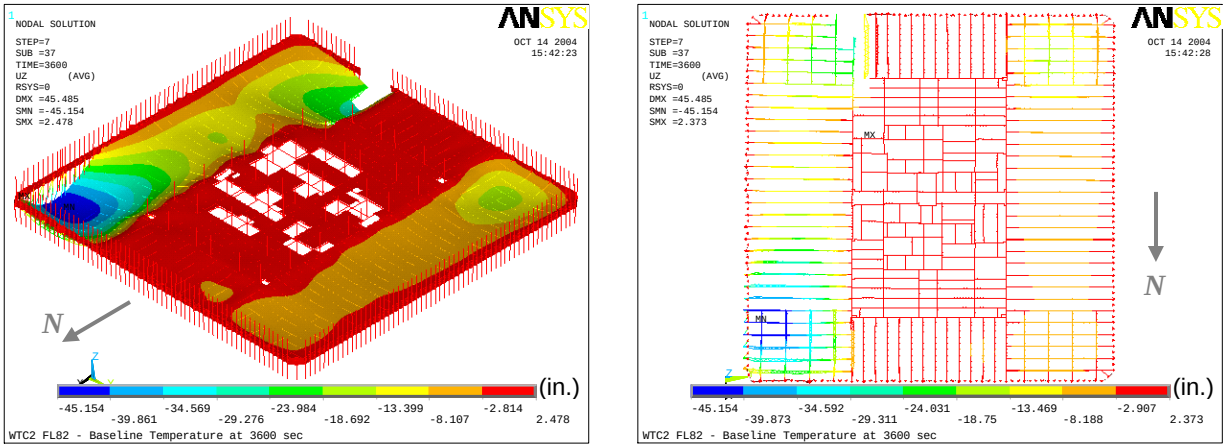

(a) Entire model (b) Top view without slab

Figure A–35. Vertical displacement of WTC 2 Floor 82 for Case C_i temperature condition at 60 min (downward displacement is negative; 5x displacement magnification).

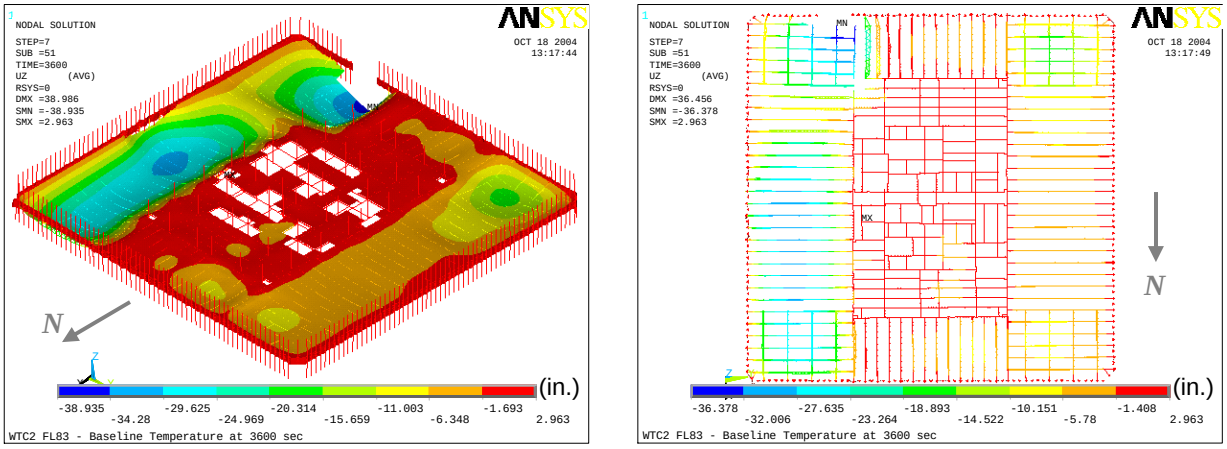

(a) Entire model (b) Top view without slab

Figure A–36. Vertical displacement of WTC 2 Floor 83 for Case C_i temperature condition at 60 min (downward displacement is negative; 5x displacement magnification).

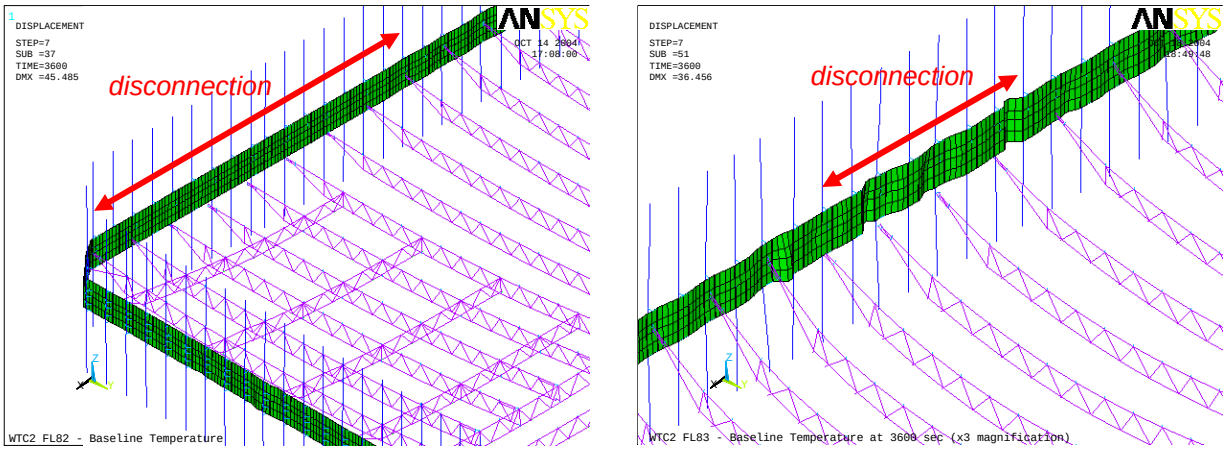

(a) Floor 82
(1X displacement magnification)

(b) Floor 83
(3X displacement magnification)

Figure A–37. Loss of vertical supports in WTC 2 Floor 82 and Floor 83 for Case C_i temperature condition at 60 min.

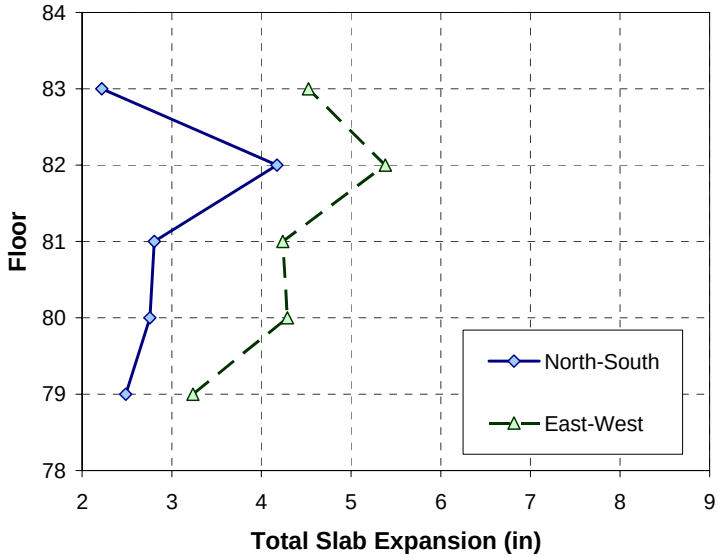

Figure A–38. Thermal expansion of floors of WTC 2 for Case C_i temperature condition at 60 min.

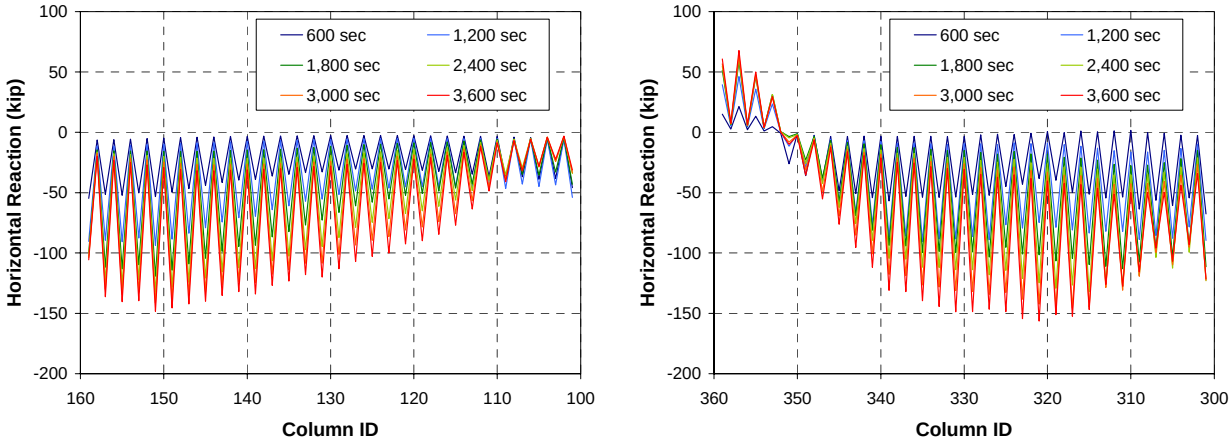

(a) West face (b) East face

Figure A–39. Horizontal reaction force per column of WTC 2 Floor 81 for Case C_i temperature condition.

A.3.2 Case D_i Temperature Condition

Table A–4 gives the maximum vertical displacement of WTC 2 floors for Case D_i temperature condition, and Figs. A–40 to A–44 show the vertical displacements when the maximum displacement was obtained. Due to more impact damage and different temperature histories than Case C_i temperature condition, all floors had larger vertical displacement. Floor 80 and Floor 81 suffered damage to many interior seats in the east office area due to the aircraft impact. Bridging trusses that had been removed in Case C_i temperature condition were replaced in these two floors in order to support primary trusses of the east

office area after the impact. The maximum vertical displacement of 97 in. was calculated at Floor 81 near the impact damage at 50 min as shown in Fig. A–42. Significant sagging of the floor was observed at Floor 79 to Floor 83. Gusset plates and bolts at more than 75 percent of all the exterior seats of the east face of Floor 82 and Floor 83 failed due to horizontal shear force that was caused by the difference in the thermal expansion between the floor and the exterior wall in the direction transverse to the primary trusses. The truss at Column 357 of Floor 81 was the only truss that lost its vertical support at the exterior seat among all the floors. This truss walked off the truss seat. Figure A–45 shows the average total thermal expansion of floors over the entire width of the building at 60 min of Case D_i temperature condition. The total floor expansion ranged from 1 in. to 5 in. Figures A–46 and A–47 show horizontal reaction force at individual columns of the north and south faces of Floor 80 and Floor 82, respectively. Column 101 to Column 111 on the west face and Column 347 to Column 359 on the east face were pulled in by the floor at 60 min on Floor 80 because of the floor sagging occurring in the southeast area. Since core columns were not restrained in the horizontal directions, when the floor pulled in one face of exterior wall, the opposite face of the exterior wall would also be pulled in. Columns at the southeast corner were pulled in by the floor at Floor 79 and Floor 81. Many columns of the west face of Floor 82 were pulled inward, while reaction forces at many columns of the east face were close to zero. As described above, gusset plates and seat bolts failed at a number trusses on the east face of Floor 82. Because columns at these locations were not supported in the horizontal direction by the floor, the reaction force became close to zero at these columns.

Table A–4. Maximum vertical displacement of WTC 2 floors for Case D_i temperature condition.

Floor	Max. Displacement (in.)	Time at the Maximum (min)
79	35.8	60
80	65.6	40
81	96.7	50
82	49.4	60
83	44.6	60

Note: Downward displacement is positive.

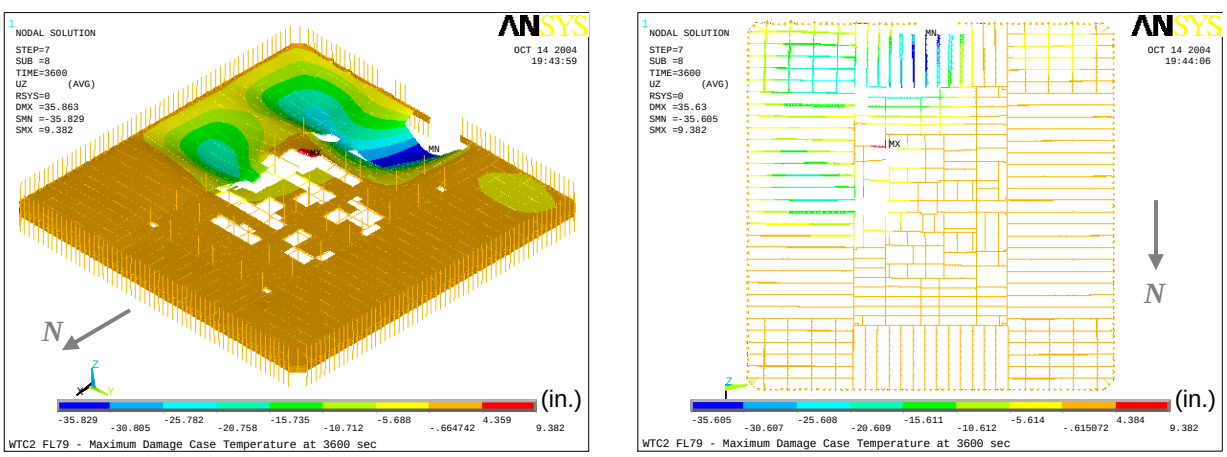

(a) Entire model (b) Top view without slab

Figure A–40. Vertical displacement of WTC 2 Floor 79 for Case D_i temperature condition at 60 min (downward displacement is negative; 5x displacement magnification).

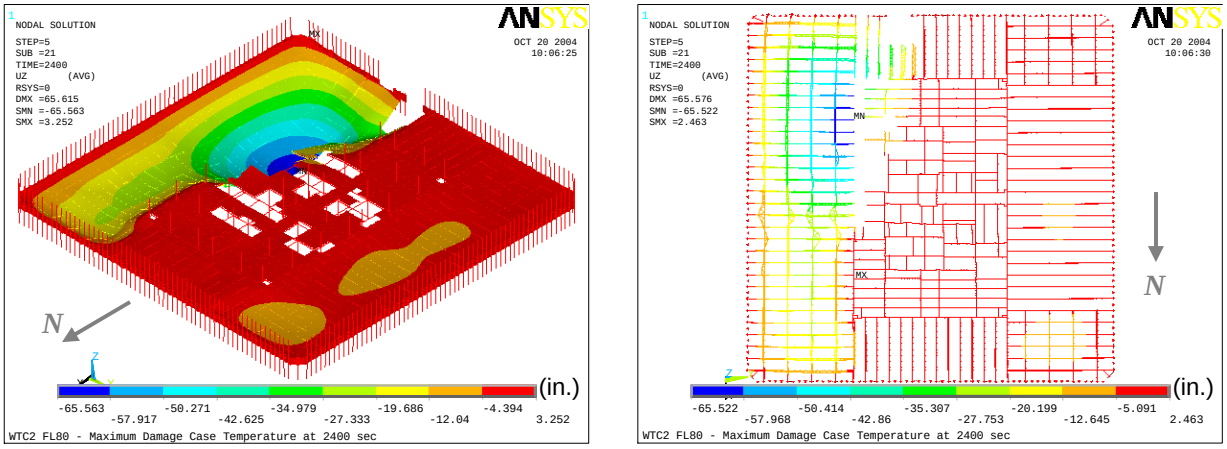

(a) Entire model (b) Top view without slab

Figure A–41. Vertical displacement of WTC 2 Floor 80 for Case D_i temperature condition at 40 min (downward displacement is negative; 5x displacement magnification).

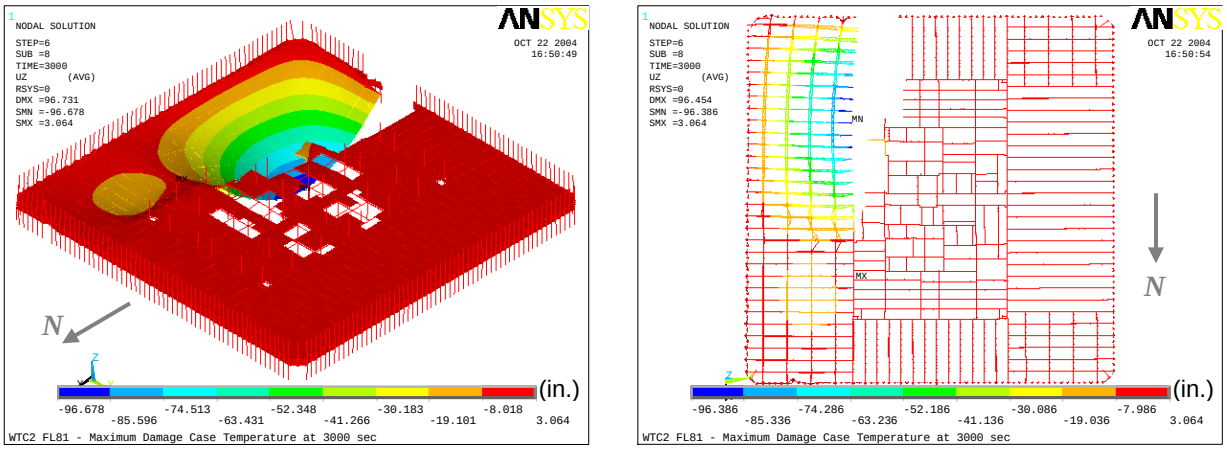

(a) Entire model (b) Top view without slab

Figure A–42. Vertical displacement of WTC 2 Floor 81 for Case D_i temperature condition at 50 min (downward displacement is negative; 5x displacement magnification).

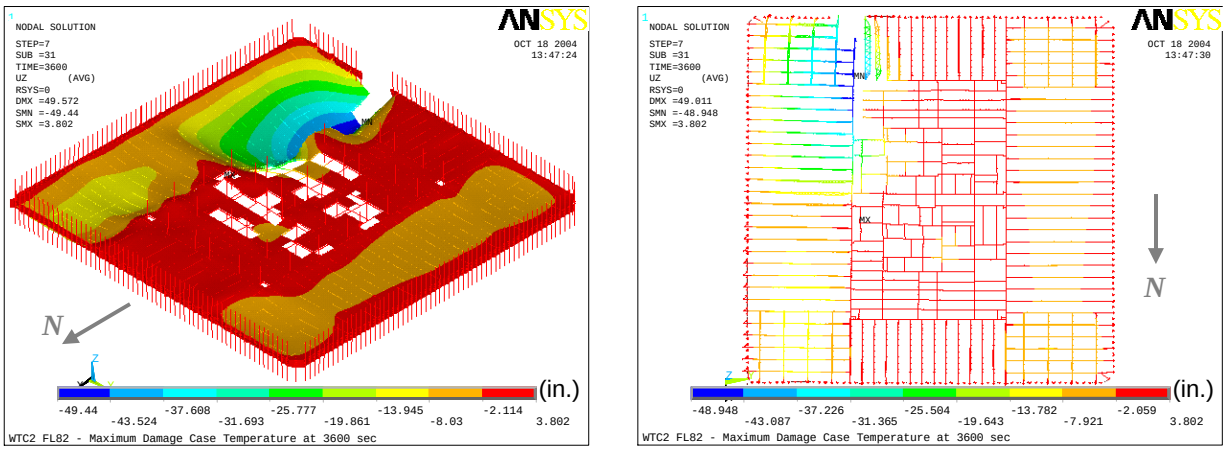

(a) Entire model (b) Top view without slab

Figure A–43. Vertical displacement of WTC 2 Floor 82 for Case D_i temperature condition at 60 min (downward displacement is negative; 5x displacement magnification).

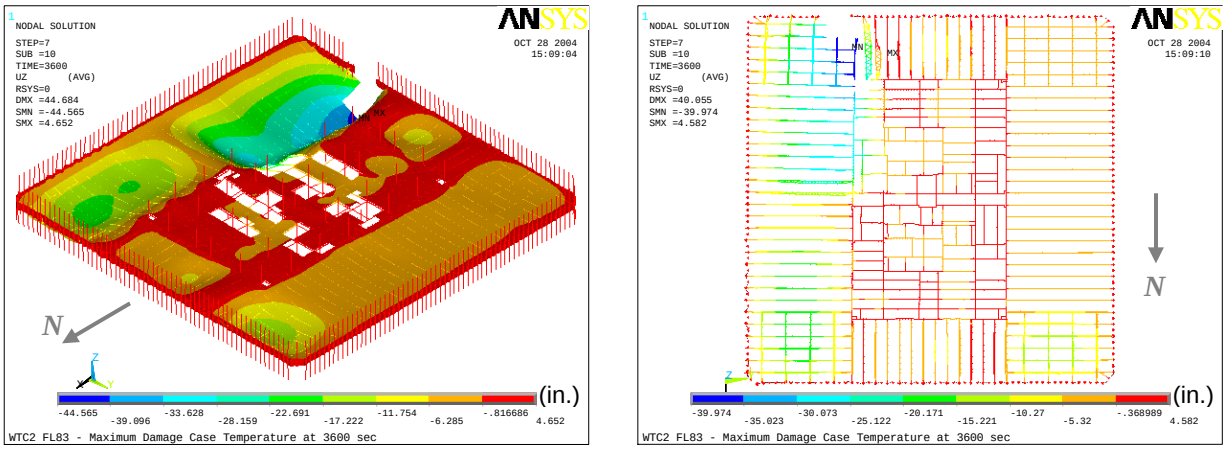

(a) Entire model (b) Top view without slab

Figure A–44. Vertical displacement of WTC 2 Floor 83 for Case D_i temperature condition at 60 min (downward displacement is negative; 5x displacement magnification).

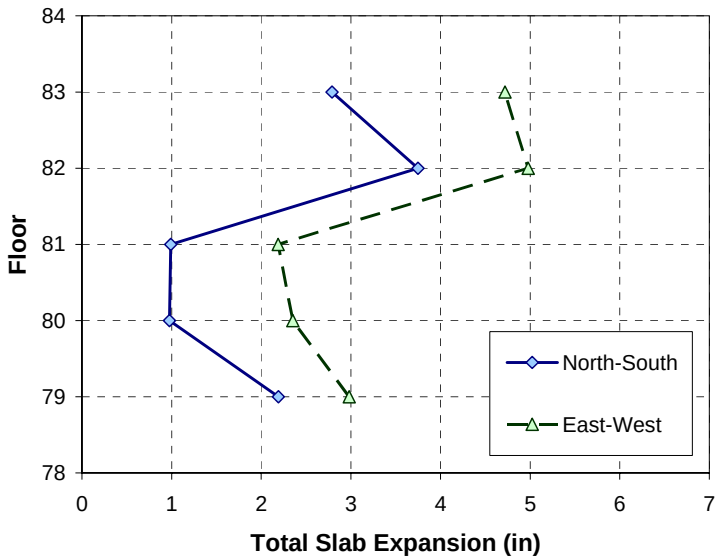

Figure A–45. Thermal expansion of floors of WTC 2 for Case D_i temperature condition at 60 min.

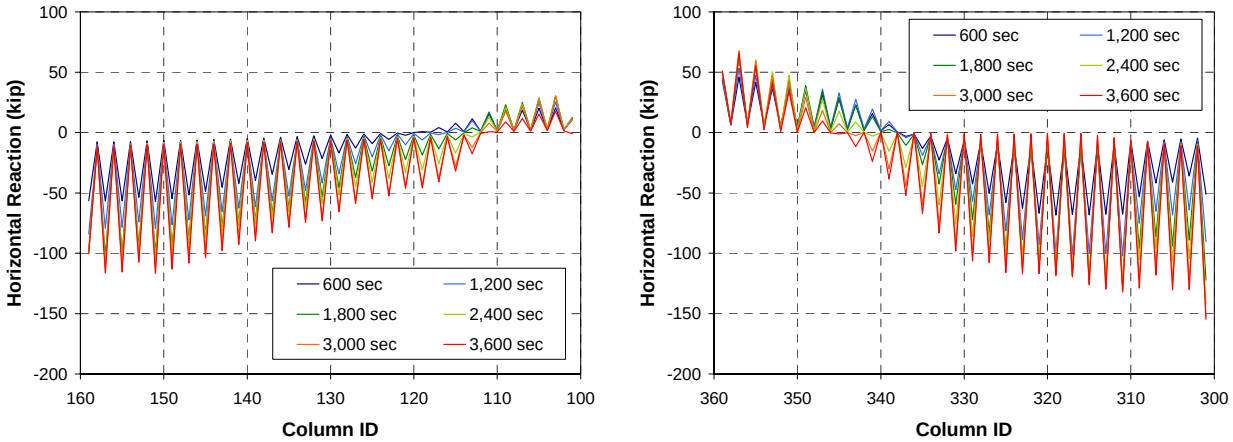

(a) West face (b) East face

Figure A–46. Horizontal reaction force per column of WTC 2 Floor 80 for Case D_i temperature condition.

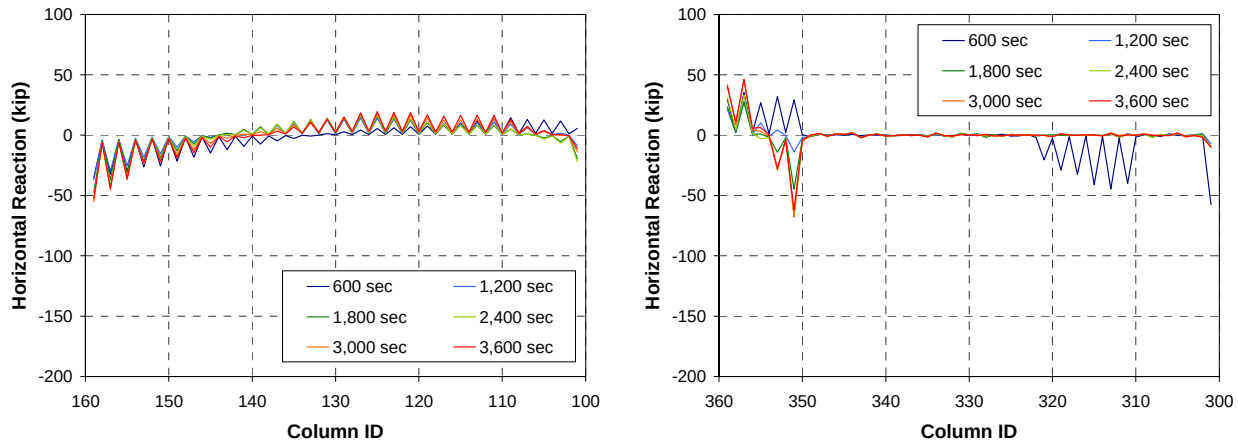

(a) West face (b) East face

Figure A–47. Horizontal reaction force per column of WTC 2 Floor 82 for Case D_i temperature condition.

A.4 SUMMARY OF RESULTS

Figures A–48 and A–49 show conditions of the connections between the exterior wall and the floors predicted by the WTC 1 floor models at 100 min for Case A_i and Case B_i temperature conditions, and Figs. A–50 and A–51 show conditions of the connections between the exterior wall and the floors predicted by the WTC 2 floor models at 60 min for Case C_i and Case D_i temperature conditions. The figures show the following conditions:

- Condition 1: gusset plate failure + seat failure due to vertical shear (loss of vertical support)
- Condition 2: gusset plate failure + bolt shear-off + truss walk-off (loss of vertical support)
- Condition 3: gusset plate failure + bolt shear-off + significant displacement (>25 in.) of the floor in that area (floor remains vertically supported)
- Condition 4: tensile force between the exterior wall and the floor system (floor remains vertically connected, but exerts pull-in force on the exterior wall)

Conditions 1 and 2 were treated as the case of floor/wall disconnections. Conditions 3 and 4 were treated as the case where the floor pulled in the exterior wall.

The behaviors of the floor system found in the full floor models subjected to impact damage and elevated temperatures from the fires can be summarized as follows:

- Bridging trusses subjected to elevated temperatures buckled between primary trusses.
- When significant differences in thermal expansion of floors and exterior walls in the direction transverse to the axes of primary trusses occurred near the corners, studs, diagonal strap anchors, gusset plates, and seat bolts at exterior truss seats failed due to the lateral shear.
- Web diagonals of floor trusses with damaged thermal insulation buckled.

- Floors sagged into catenary forms.
- Truss seats disconnected from the exterior walls.

Pull-in forces were expected to develop whenever the floor sagged. Although the floor sagging was captured by the floor models in the heated area, the pull-in force on the exterior columns was not captured in most of the full floor model analyses. To accurately calculate pull-in forces between the floor and the exterior columns in the full floor model, much more detailed modeling would be required. Such modeling includes accurate boundary conditions on columns, creep in steel, friction at the truss seats, accurate evaluation of failure of strap anchors and studs, and concrete cracking and spalling. In addition, temperature time histories that were used in the full floor model analyses may be different if improved estimates of impact damage to insulation were obtained. Further discussion on the pull-in force can be found in Section 2.5.2 of this report.

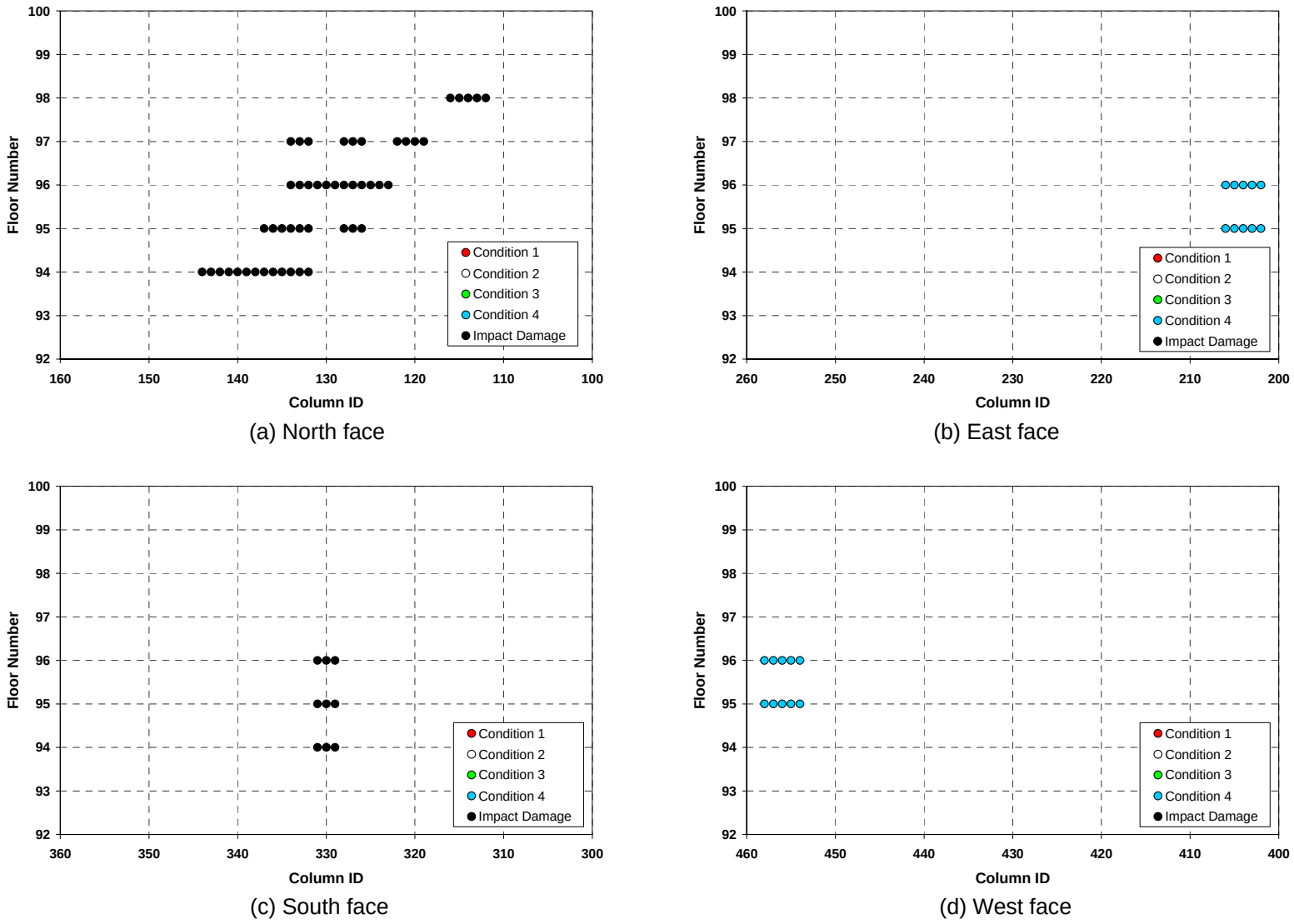

Figure A–48. Conditions of connections between the exterior wall and the floors of WTC 1 predicted for Case A_i temperature condition at 100 min.

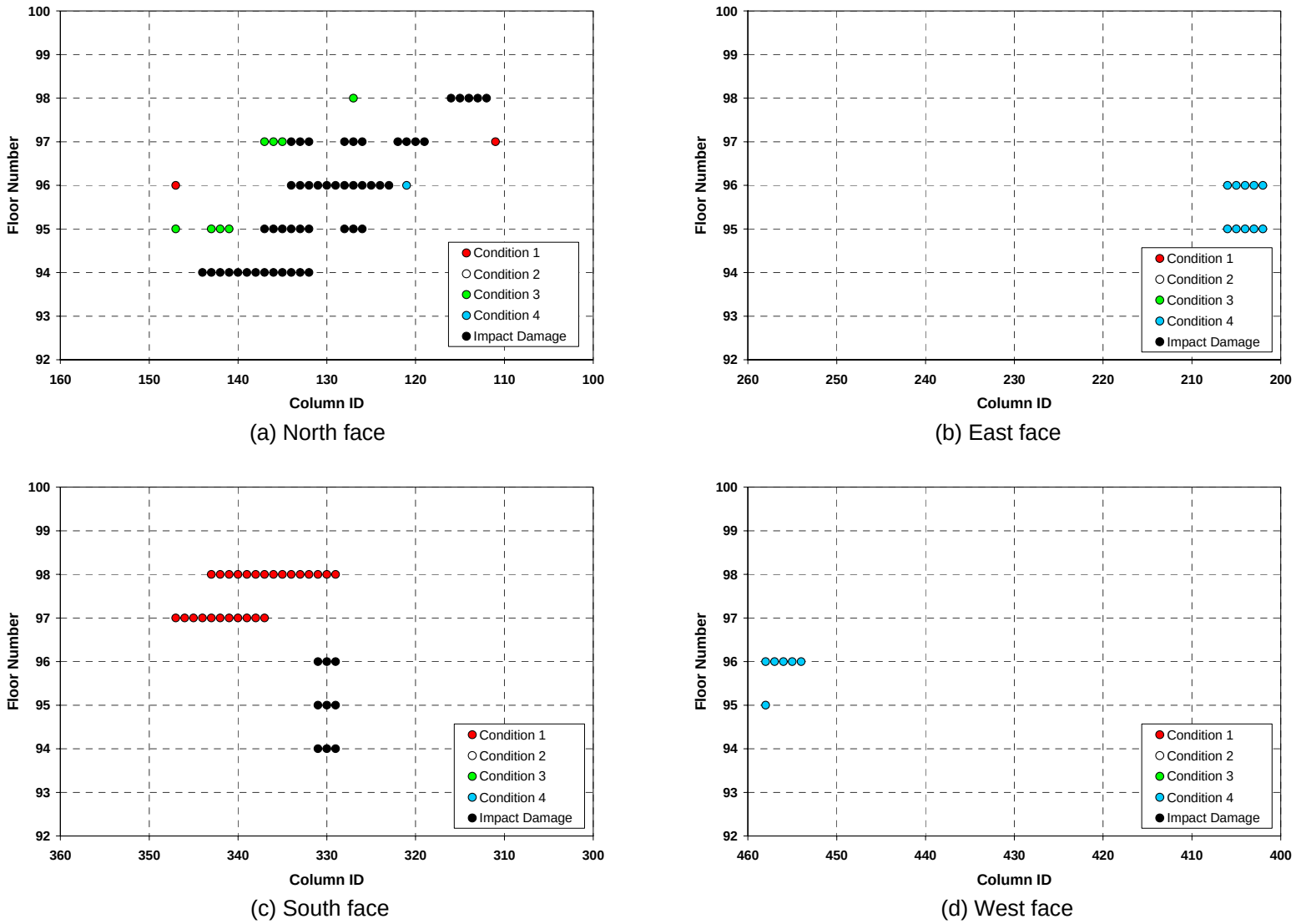

Figure A–49. Conditions of connections between the exterior wall and the floors of WTC 1 predicted for Case B_i temperature condition at 100 min.

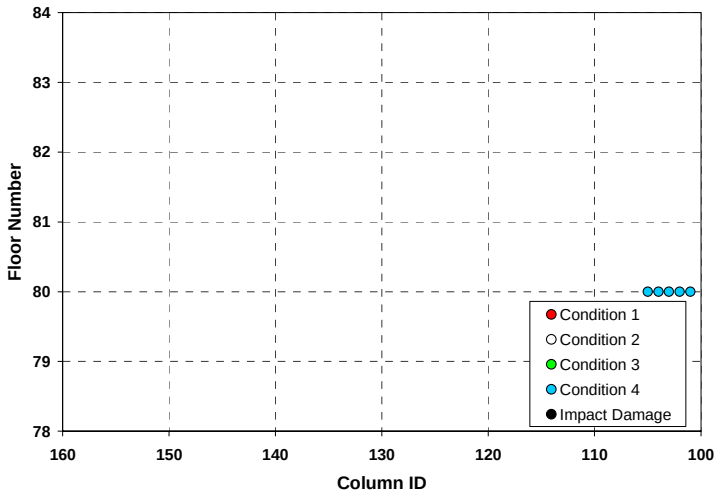

(a) West face

(b) North face

(c) East face

(d) South face

Figure A–50. Conditions of connections between the exterior wall and the floors of WTC 2 predicted for Case C_i temperature condition at 60 min.

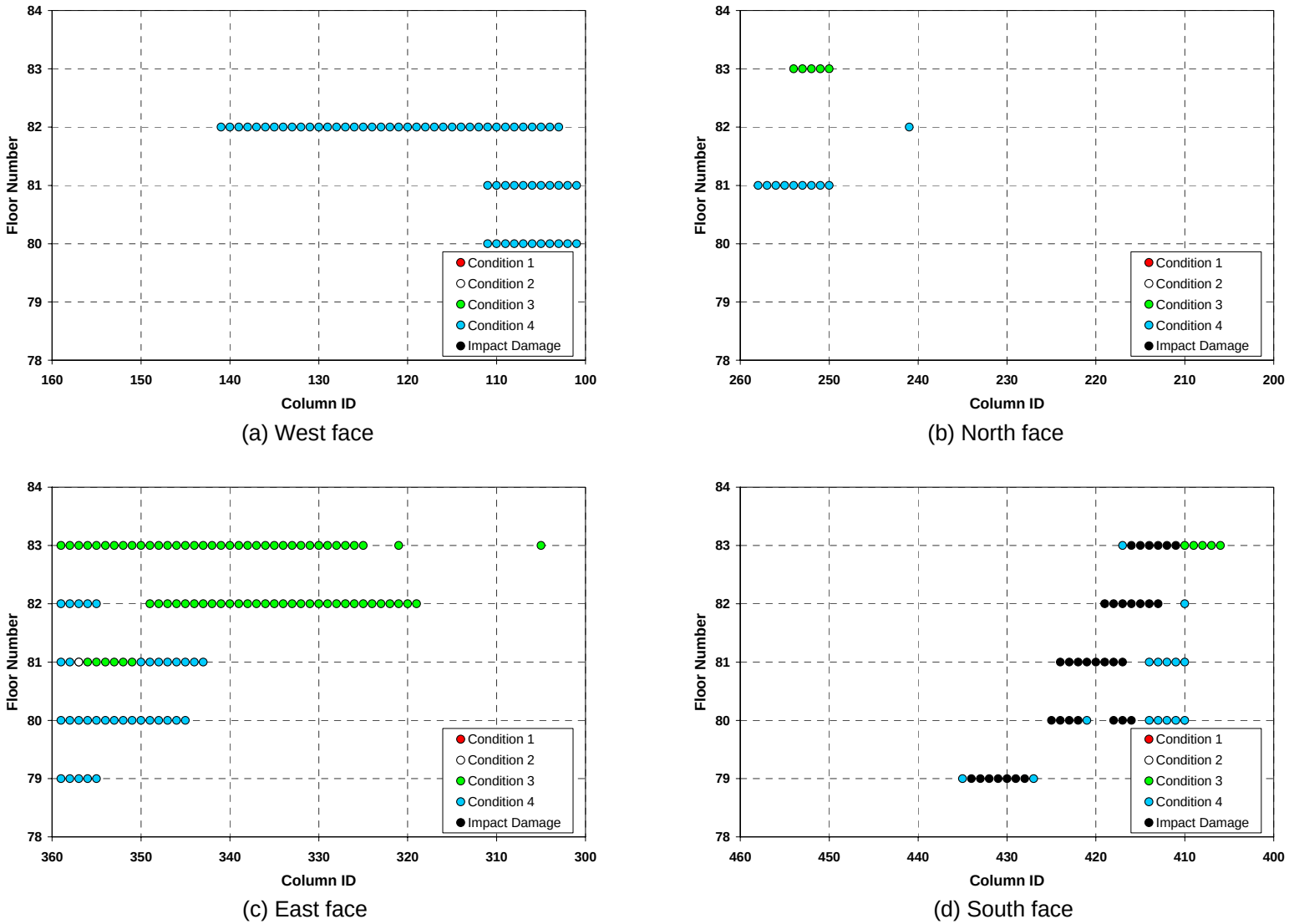

Figure A–51. Conditions of connections between the exterior wall and the floors of WTC 2 predicted for Case D_i temperature condition at 60 min.

This page intentionally left blank.

Appendix B
FLOOR TRUSS DYNAMIC RESPONSE DUE TO IMPACT OF DROPPING FLOOR

B.1 IMPACT OF DROPPING FLOOR

The failure of dropping floor may occur due to the self and/or additional debris weight on the truss, and/or as a result of the aircraft impact. A floor truss or a group of floor trusses could lose support at both the exterior and interior supporting ends and drop to the floor below. This failure mode, which is shown in Fig. B–1, will be referred to as *full truss drop*. Alternatively, a floor truss or a group of floor trusses could lose support on one side and drop down to impact the target floor below. This failure mode, which is also shown in Fig. B–1, will be referred to as *partial truss drop*.

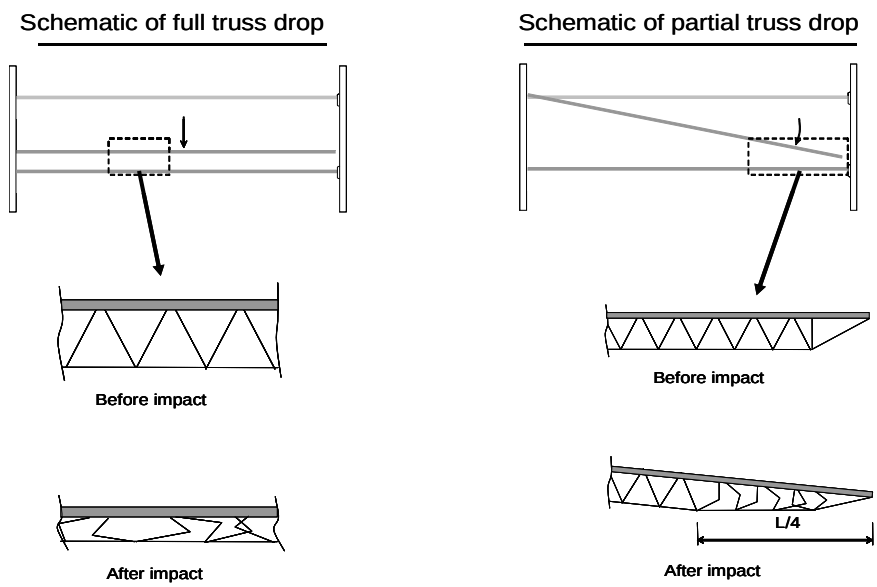

Figure B–1. Schematic of full truss or partial truss drop and web diagonal crushing at impact.

B.2 PURPOSE AND SCOPE

The purpose of this study is to determine the dynamic response of the target truss from the impact of full and partial truss drop, to determine whether the target trusses can resist such an impact load, and to determine whether the target truss will lose its compaction, sag significantly, and consequently fail to restrain the exterior column to which it is connected against instability.

B.3 METHOD OF ANALYSIS

The simulation of a floor drop is idealized with a truss drop. This has inherent assumptions that all seats for the floor fail simultaneously to cause a full or partial drop. The dynamic response of the target truss from the impact of a dropping truss is calculated using conservation of energy principle. The potential energy of the truss just before drop, which is a function of drop height, converts to the kinetic energy of the truss just before impact. As the dropping truss starts to impact the target truss, the web diagonal members of the dropping truss are assumed to deform plastically to absorb some of the kinetic energy. The energy absorption due to crushing of the furniture and partitions are neglected in this study. The energy absorption due to web diagonal member crushing reduces the kinetic energy available at impact to deform the target truss. All the web diagonal members are assumed to deform plastically for the full truss drop case, while only one quarter of the web diagonal members are assumed to deform plastically for partial truss drop, representing one quarter of the length of the truss that may come in contact at impact with the floor below. The kinetic energy loss at the time of impact of the dropping truss and the target truss is calculated based on conservation of momentum. The two trusses are assumed to travel together after the impact, at one-half of the velocity of the dropping floor before impact.

The dynamic load due to the impact of the dropping truss onto the target truss will cause the target truss to deform plastically beyond the static load due to the weight of the two trusses. The maximum dynamic deformation of the trusses is calculated by conservation of energy principle assuming that the resistance of the truss is a bilinear function of displacement. This assumption is based on fitting the acceleration-deflection relationship of target truss, calculated with finite element analysis, as shown in Fig. B–2.

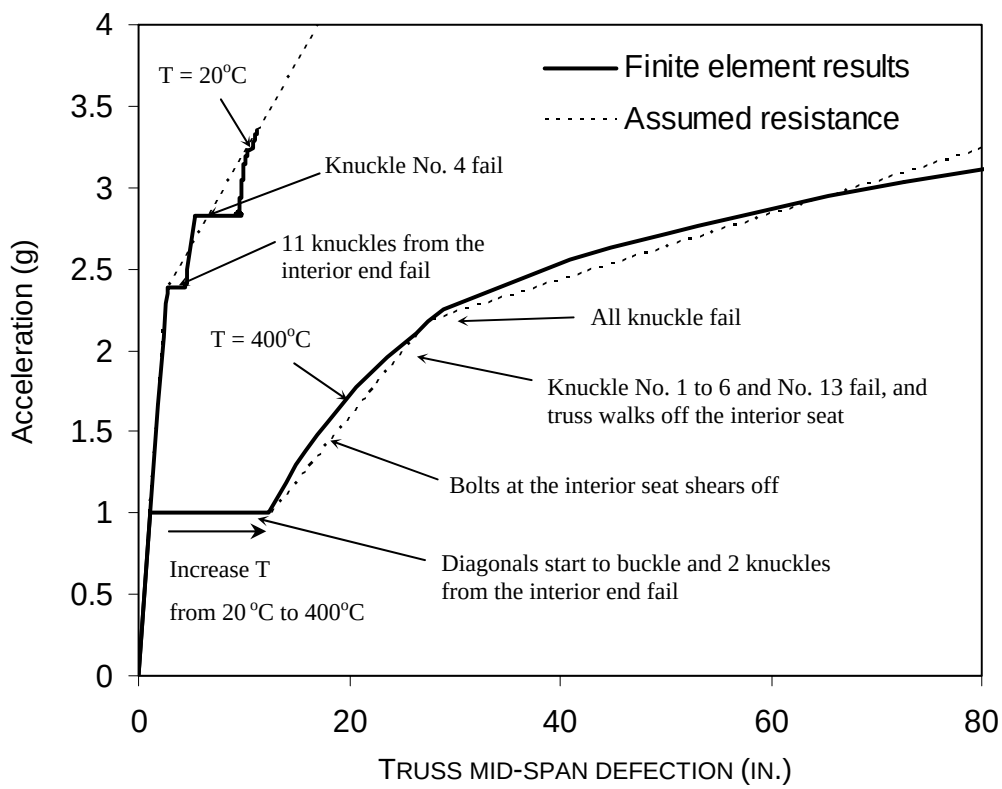

Figure B–2. Target truss resistance against increasing acceleration.

B.4 RESULTS

The ratios of demand-to-seat capacity for the gravity loads of the dropped and impacted trusses moving together for temperatures of 20 ^{o}C, 400 ^{o}C, 600 ^{o}C, and 700 ^{o}C, and the gravity plus dynamic impact loads for temperatures of 20 ^{o}C and 400 ^{o}C, are calculated. A demand-to-capacity ratio of less than one shows that the truss seat has sufficient capacity to resist the load, and a demand-to-capacity ratio of larger than one implies that the seat could fail. The range of the demand-to-capacity ratios is due to the different assumptions for the amount of energy loss due to crushing of the web diagonal members of the dropped truss.

The demand-to-capacity ratio of the long-span truss for gravity loads is shown in Table B–1 and for gravity plus impact loads is shown in Table B–2. The result for gravity loads alone shows the both the exterior and interior truss seats have sufficient capacity to support the weight of two floors for all temperatures considered. The result for gravity plus impact loads shows that at temperatures below 400 ^{o}C neither the exterior nor interior truss seats is expected to fail. Peak deflection response due to gravity and the dynamic impact of the dropping truss is given in Table B–3. The results show that at room temperature, and more so at 400 ^{o}C, the impacted truss will deflect to an extent that it loses composite action and becomes a catenary. At 400 ^{o}C the truss walks off the interior seat. Obviously, a catenary truss is not able to restrain the exterior column against transverse movement and cannot restrain it from instability. Although a truss response to increasing acceleration at 700 ^{o}C was not developed, the strength reduction of the truss seats clearly indicates that the failure of truss seats will occur.

Table B–1. Demand-to-capacity ratio of long-span truss for static gravity load.

Temp. (^{o}C)	Demand (kip)	Capacity (kip)		Demand/Capacity	
		Int. Seat	Ext. Seat	Int. Seat	Ext. Seat
20	26.4	187.3	140.0	0.14	0.19
400	26.4	166.9	125.7	0.16	0.21
600	26.4	81.6	77.8	0.32	0.34
700	26.4	37.2	35.5	0.71	0.74

Table B–2. Demand-to-capacity ratio of long-span truss for dynamic impact load from full truss drop.

Temp. (^{o}C)	Demand (kip)			Capacity (kip)		Demand / Capacity					
				Int. Seat	Ext. Seat	Int. Seat			Ext. Seat		
20	38.6	-	65.3	187.3	140.0	0.21	-	0.35	0.28	-	0.47
400	39.1	-	45.2	166.9	125.7	0.23	-	0.27	0.31	-	0.36

Table B–3. Peak deflection response due to static gravity and dynamic impact.

Temp. (^{o}C)	Static Deflection (in.)	Dynamic Deflection (in.)		
20	2.3	7.6	-	25.4
400	24.2	66.4	-	89.6

B.5 CONCLUSIONS

At room temperature, the impact of a dropping truss will not cause failure of truss seats, but will cause the impacted truss to deform into a catenary. At 400 ^{o}C, the impacted truss will walk off the interior seat. In either case the impacted floor will not restrain the exterior column against transverse movement and instability. The impact of a dropping truss at 700 ^{o}C will cause failure of truss seats.

Appendix C
GLOBAL ANALYSIS WITHOUT CREEP

The analysis results presented in this Appendix were obtained from the preliminary global analyses that were performed neglecting the effects of creep and inelastic buckling of columns. These analyses were primarily used to study the interaction between various structural components in the overall global response of the towers. Because of the significant role that creep played in the collapse process, the results from these analyses are presented without making any conclusive remarks about the collapse sequence of the towers.

C.1 WTC 1 GLOBAL ANALYSIS WITHOUT CREEP

The WTC 1 ANSYS model without creep was analyzed with Case A_i structural damage condition and subjected to Case A_i temperature time histories. Temperature-dependent plasticity and the nonlinear geometry were the major sources of nonlinearity in the model. Table C–1 summarizes the sequence of analyses that were conducted with the WTC 1 ANSYS model with Case A_i conditions (see Section 2.2 for Case A_i structural damage condition). The results of each analysis step were used as the initial conditions for the next. Case B_i was not considered for preliminary global analysis, as the lack of creep and inelastic buckling behaviors limited the usefulness of repeating this analysis.

Table C–1. Analysis Steps of WTC 1 ANSYS global model for Case A_i conditions.

Analysis Step	Description
1	WTC 1 model below Floor 106 was analyzed under its own self-weight.
2	Structures above Floor 106 were added in a stress-free state, and the model was analyzed for dead load including those above Floor 106.
3	Superimposed dead load and 25 percent of the design live loads were superimposed on the model.
4	Columns, spandrels, and floor elements that were severed during aircraft impact were removed, and the model was analyzed.
5	Column and spandrel temperatures were ramped up linearly to temperatures at 10 min.
6	Column and spandrel temperatures were changed linearly from temperatures at 10 min to 20 min.
7	Column and spandrel temperatures were changed linearly from temperatures at 20 min to 30 min.
8	Column and spandrel temperatures were changed linearly from temperatures at 30 min to 50 min.
9	Column and spandrel temperatures were changed linearly from temperatures at 50 min to 100 min.

The model was first analyzed to capture the effects of the construction sequence (analysis steps 1, 2, and 3). The results of analysis for Step 3 represent the state before the aircraft impact. In analysis step 4, the columns, spandrels, and floor elements that were severed during the aircraft impact were removed from the model, and the building was reanalyzed to redistribute the load to the non-severed members. The results of this analysis represent the state of the building after the aircraft impact. After load redistribution, the column and spandrel temperatures provided by NIST at 10 min intervals were applied to the model (analysis steps 5 through 9). Temperatures were calculated by linear interpolation for times in between 10 min intervals. In order to reduce computation time, the temperature data sets for which

temperatures remained approximately linear with time during the interval from the previous and the following temperature data sets were eliminated from the analyses. Based on this elimination, temperature analyses were performed at 10 min, 20 min, 30 min, 50 min, and 100 min. Temperatures were not applied to the floor elements to prevent unrealistic buckling of floors. As discussed earlier, the floors in the global models did not include the floor trusses and were modeled by plate elements to match their membrane stiffness; the bending stiffness of the floors was not modeled accurately.

The results of the WTC 1 global model analyses for Case A_i conditions are summarized in Figs. C–1 through C–9.

Figure C–1 shows the total displacement at different analysis steps. The maximum displacement was obtained right after aircraft impact and was equal to 4.9 in. This displacement was gradually reduced to 4.1 in. at the end of 100 min due to thermal expansion of core and exterior columns between Floor 93 and Floor 98. Figures C–2 and C–3 show the total displacements for north, south, and east exterior walls before and after aircraft impact and at 50 min and 100 min. The total displacements for the west exterior wall are not shown as they were similar to the east exterior wall. The displacements were typically at their maximum right after aircraft impact around the hat truss and gradually decreased with time, reaching their minimum value at 50 min to 100 min in the aircraft damage zone.

Figures C–4 and C–5 show the axial load variations over north, south, and east exterior wall columns and spandrels before and after aircraft impact and at 50 min and 100 min. After the aircraft impact, the loads carried by the severed columns of the north wall were primarily redistributed to the remaining columns of the north wall and also to the core and other exterior walls. As a result of this redistribution, the maximum column load increased from 265 kip to 1,200 kip on the north exterior wall and from 268 kip to 380 kip on the south exterior wall. The 1,200 kip load occurred in a column adjacent to the impact damage area. The column loads on the east and west walls slightly increased in the south side of the walls. With increasing time, the maximum column load in the south wall increased from 380 kip after aircraft impact to 670 kip at the end of 100 min. This increase was primarily due to the steady increase of column temperatures on the south wall.

Figure C–6 shows the total column loads in the core columns and the north, south, east, and west exterior walls for several floors at the end of each analysis step. Due to the removal of severed columns, spandrels, and floor elements, the total column loads below Floor 98 after aircraft impact did not equal the total column loads before the aircraft impact.

After the aircraft impact, the total load in core columns increased about 1,000 kip, in the east exterior wall columns about 200 kip, and in the west exterior wall columns about 150 kip, whereas the total load decreased in the north wall columns about 1,150 kip and in the south wall columns about 200 kip. With increasing time, the temperatures in the core and the south exterior wall columns increased more than the other exterior wall columns, causing relative thermal expansion. Relative thermal expansion caused the core and the south exterior wall columns to attract more load, and the exterior walls on the north, east, and west sides to unload. The increase in loads due to thermal expansion of the core columns increased the plastic strains with time and the resulting shortening caused the unloading of the core columns at 30 min. As time approaches 100 min, the temperatures of all columns dropped down, and the effects of thermal expansion decreased. This can be seen in the loads at 100 min, where core columns unloaded and redistributed load to each exterior wall (about 3,500 kip). About 32 percent of the redistributed load was

transferred to each of the east and west exterior wall columns, and 18 percent to each of the north and south exterior wall columns.

Figures C–7, C–8, and C–9 show the ratio of elastic-plus-plastic strain to the temperature-dependent yield strain of the core columns between Floor 96 and Floor 97 before and after aircraft impact and at 10 min, 20 min, 50 min, and 100 min. As can be noticed, the elastic-plus-plastic strain in the core columns before aircraft impact was typically 50 percent to 60 percent less than the yield strains at room temperature. After the aircraft impact, except for Column 504, the maximum strain ratio did not get beyond 1.0, indicating that almost all core columns remained in the elastic range. With increasing time and temperatures, the strain ratios started to increase, especially in the west and the south sides of the core. Strain ratios reached their maximum at the end of 50 min and remained almost constant till the end at about 100 min. Higher strain ratios were clustered around west and south side core columns, indicating a tendency to tilt toward the south and west.

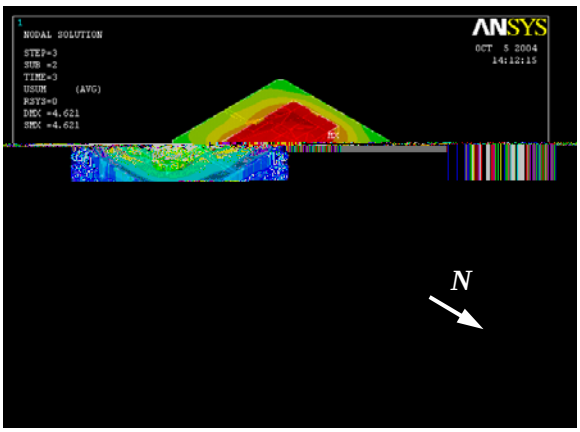

(a) Before impact

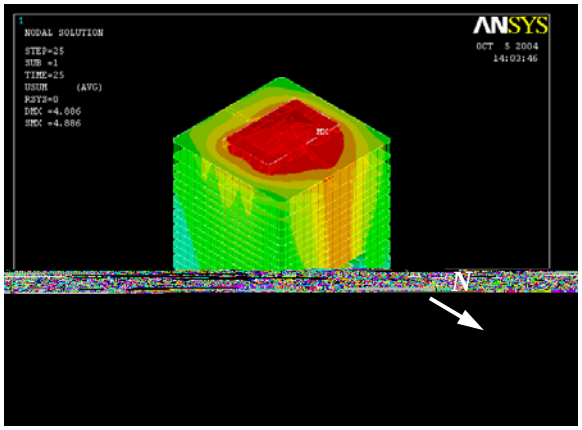

(b) After impact

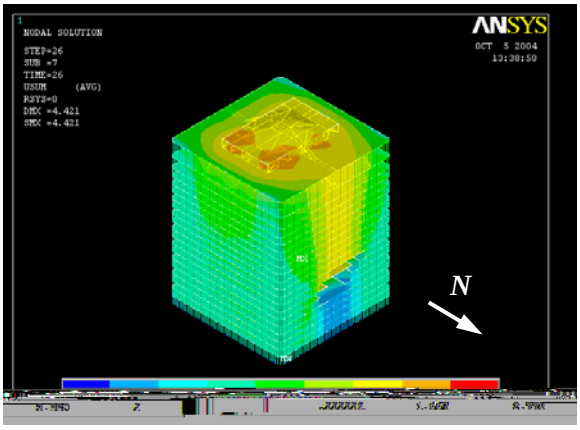

(c) At 10 min

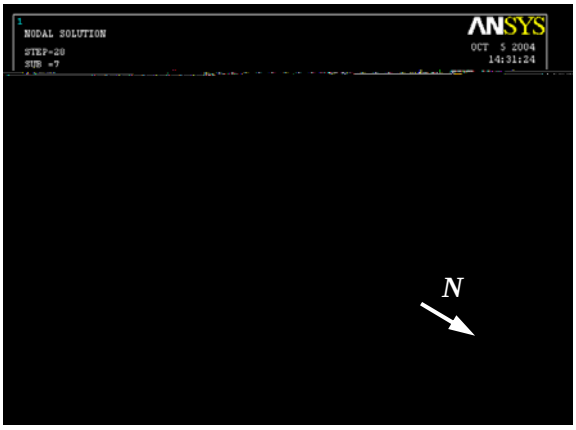

(d) At 30 min

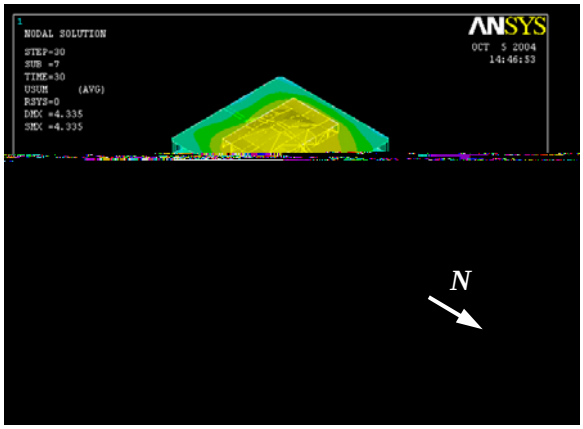

(e) At 50 min

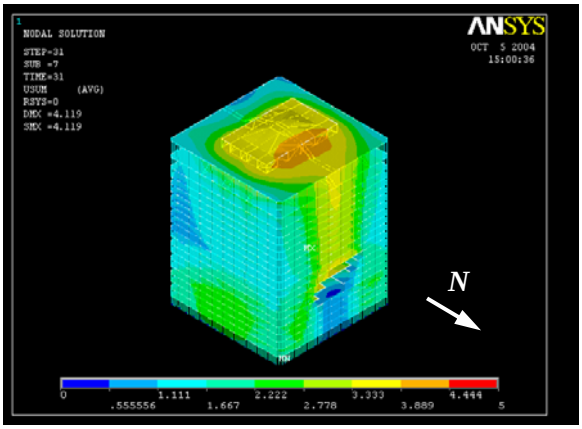

(f) At 100 min

Figure C–1. Total displacement at different stages of WTC 1 for Case A_i conditions.

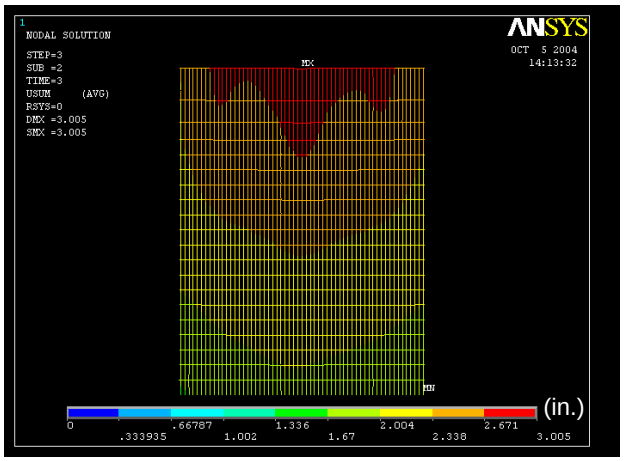

(a) North wall before impact

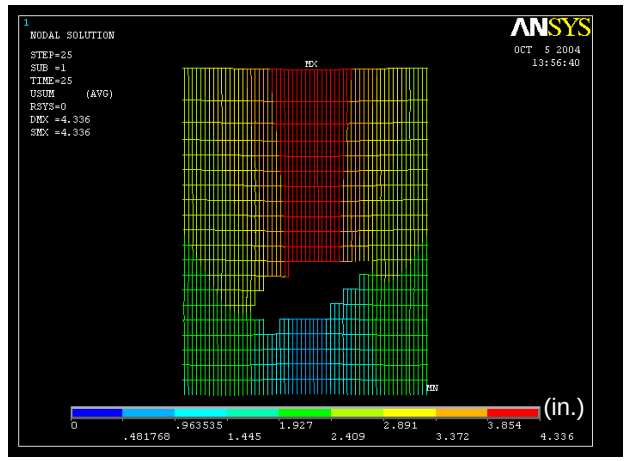

(b) North wall after impact

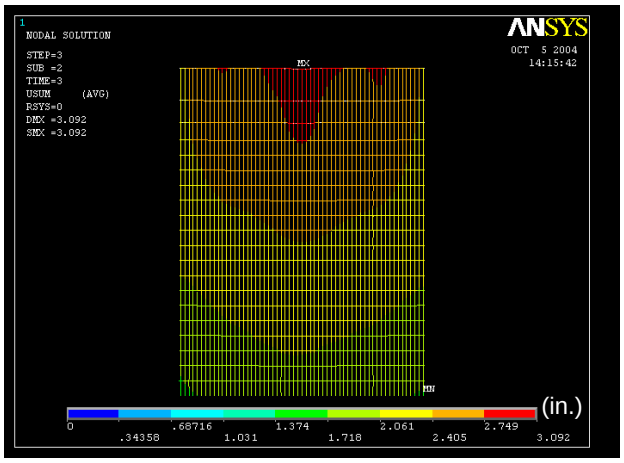

(c) South wall before impact

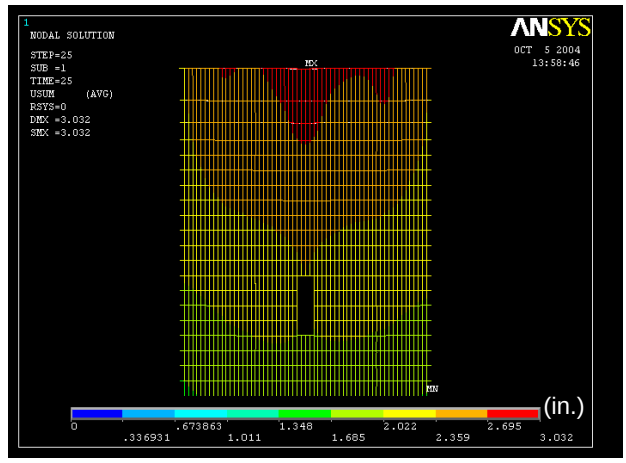

(d) South wall after impact

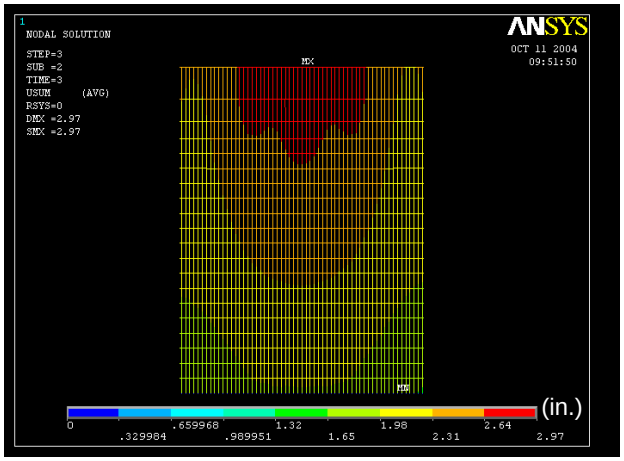

(e) East wall before impact

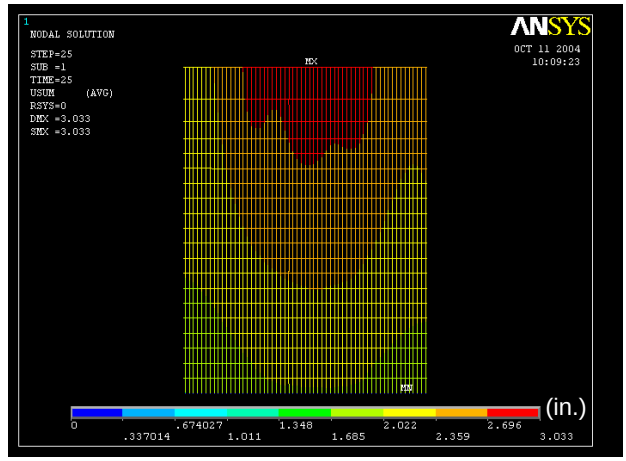

(f) East wall after impact

Figure C–2. Total displacement on the north, south, and east faces of the WTC 1 before and after aircraft impact (looking from outside).

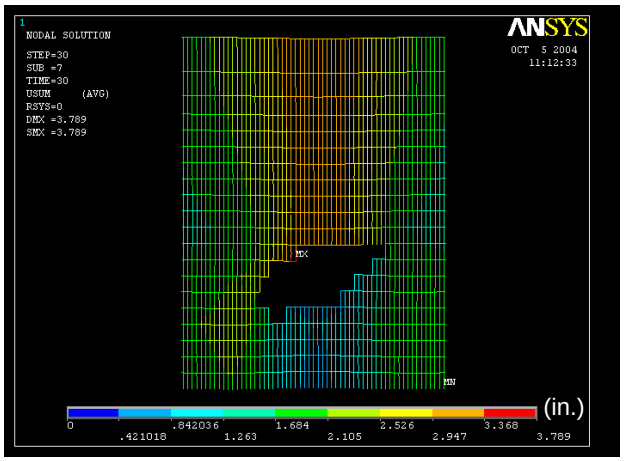

(a) North wall at 50 min

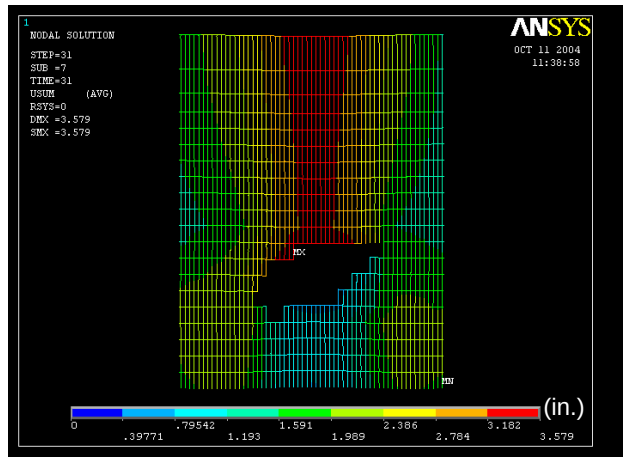

(b) North wall at 100 min

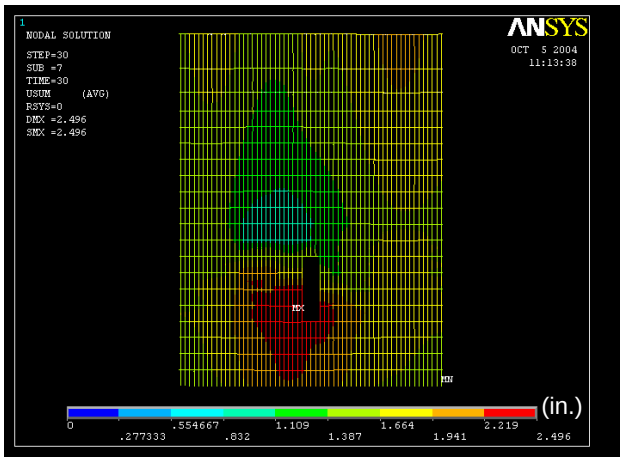

(c) South wall at 50 min

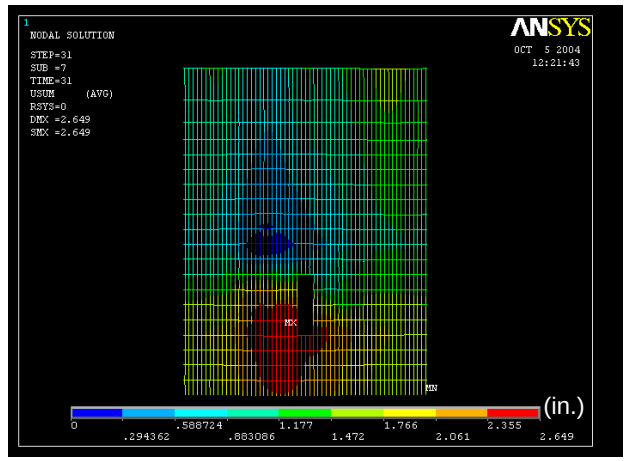

(d) South wall at 100 min

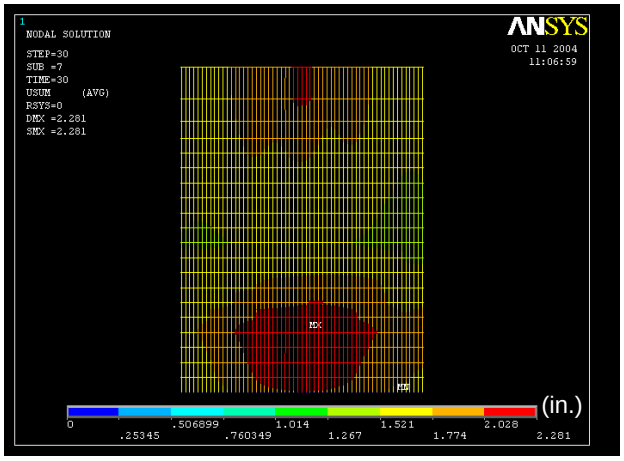

(e) East wall at 50 min

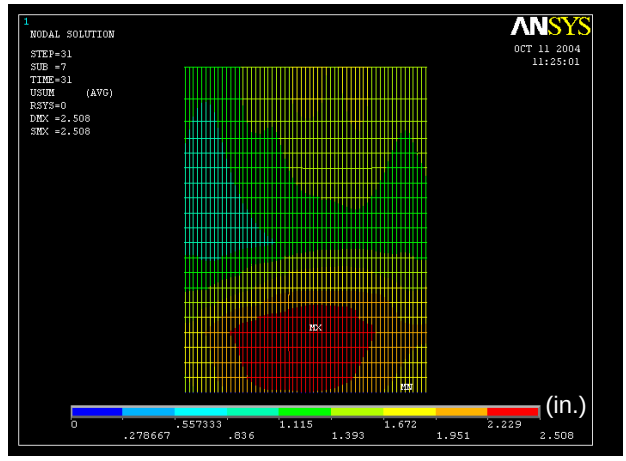

(f) East wall at 100 min

Figure C–3. Total displacement on the north, south, and east faces of the WTC 1 at 50 min and 100 min of Case A_i conditions (looking from outside).

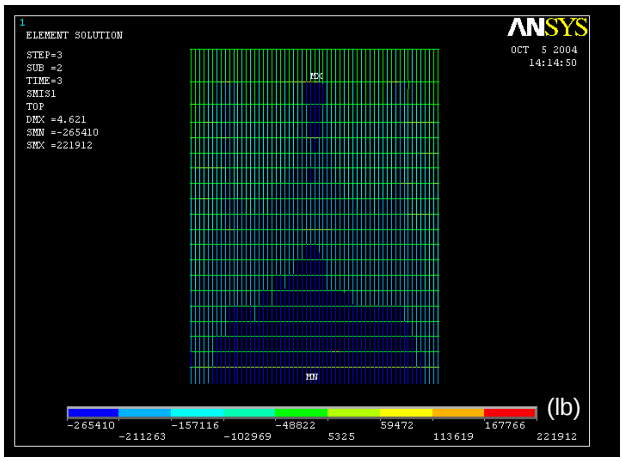

(a) North wall before impact

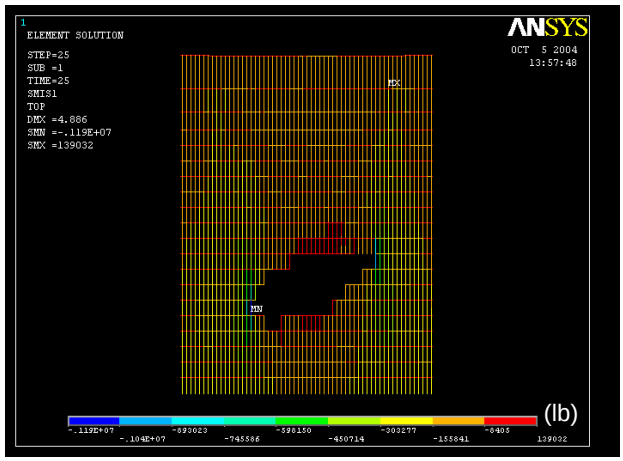

(b) North wall after impact

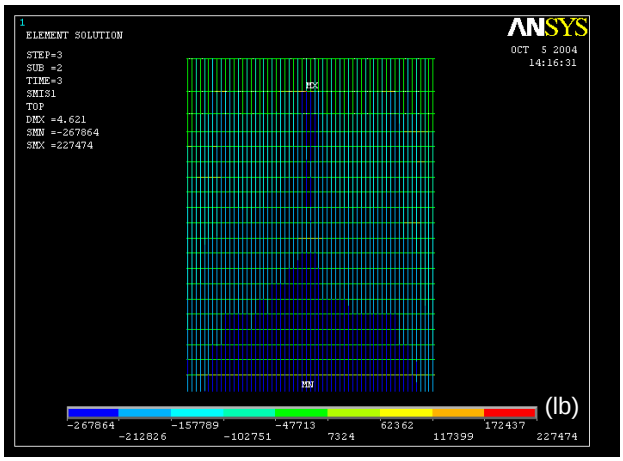

(c) South wall before impact

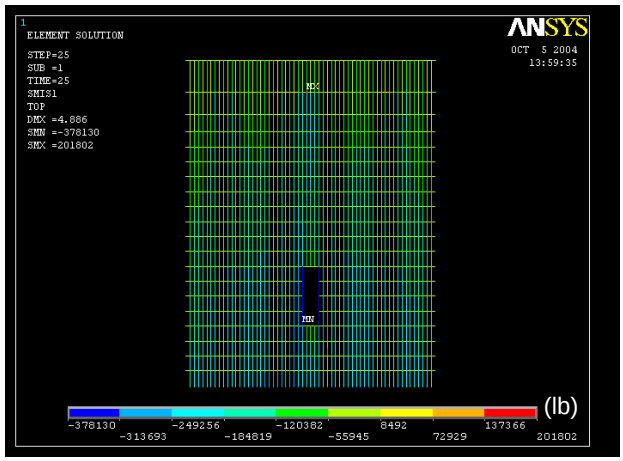

(d) South wall after impact

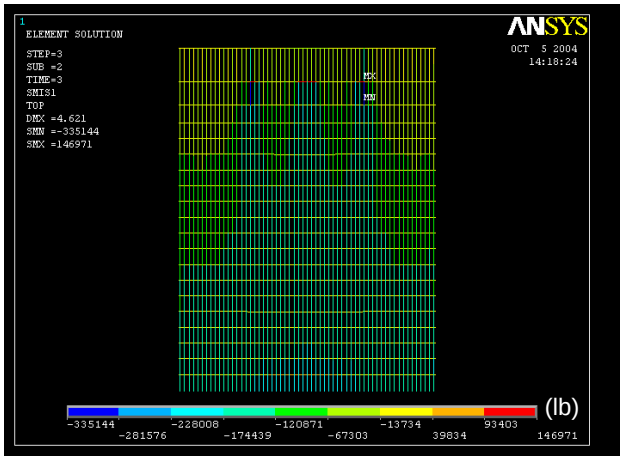

(e) East wall before impact

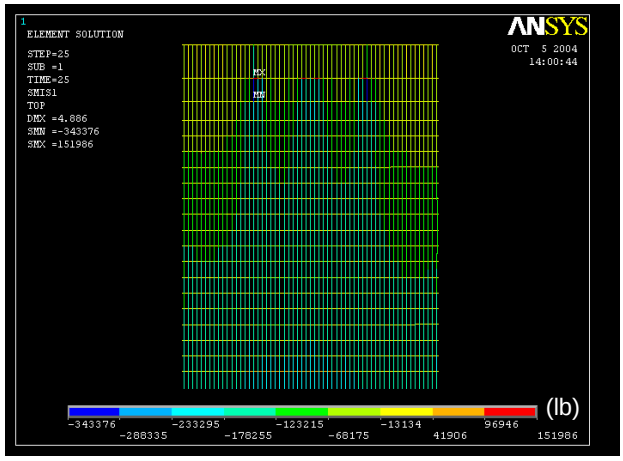

(f) East wall after impact

Figure C–4. Axial load variation on the north, south, and east faces of the WTC 1 before and after aircraft impact (looking from outside; compression is negative).

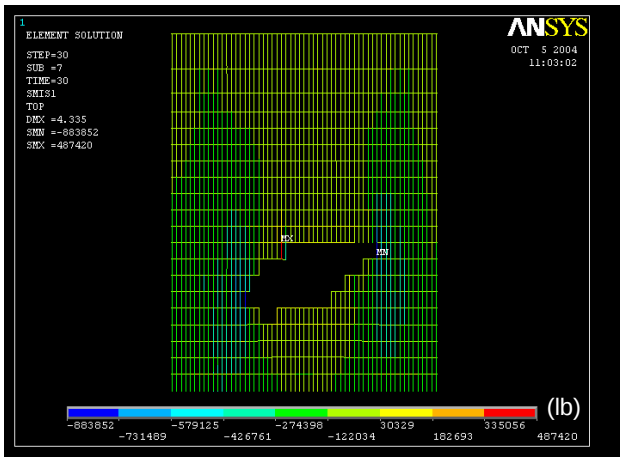

(a) North wall at 50 min

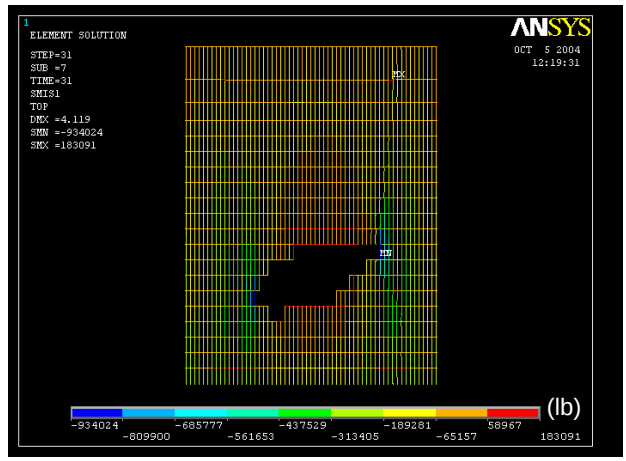

(b) North wall at 100 min

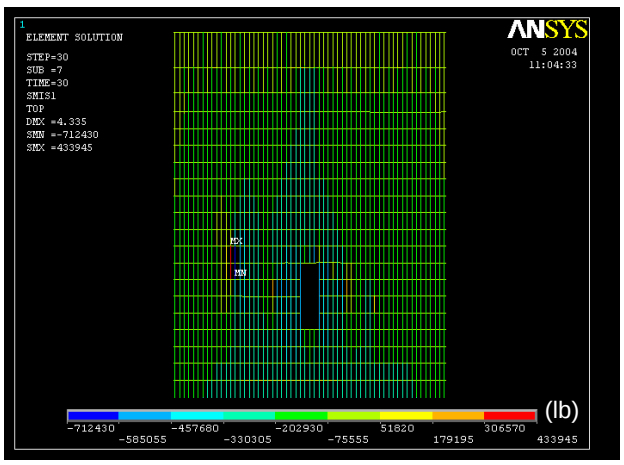

(c) South wall at 50 min

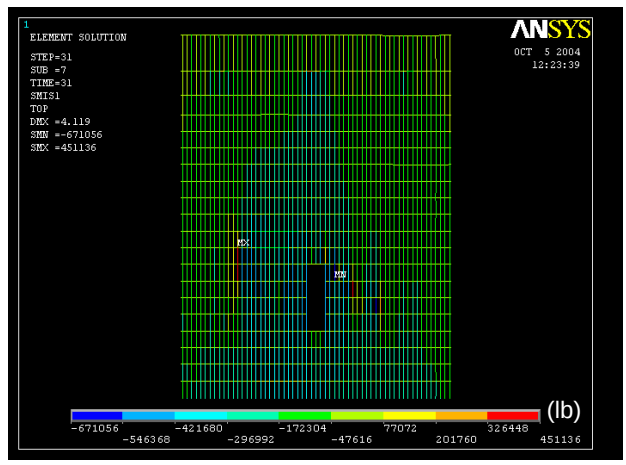

(d) South wall at 100 min

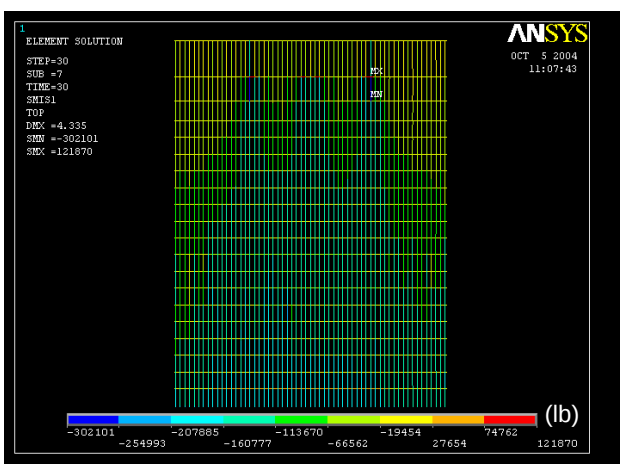

(e) East wall at 50 min

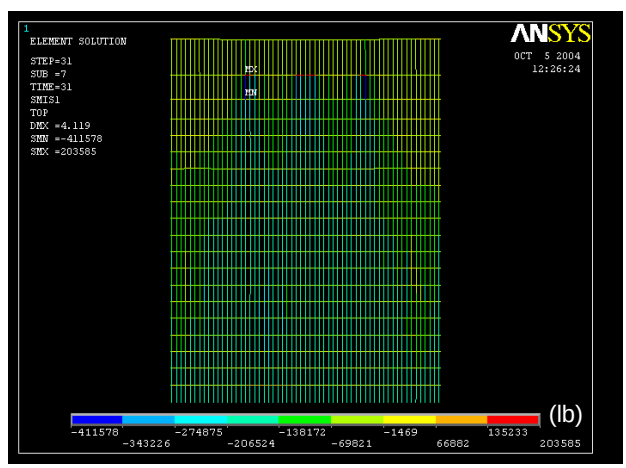

(f) East wall at 100 min

Figure C–5. Axial load variation on the north, south, and east faces of the WTC 1 at 50 min and 100 min of Case A_i conditions (looking from outside; compression is negative).

Row	Analysis Stage	North	South	East	West	Core	Sum
(1)	Before Impact	12375	12459	9006	9045	47101	89986
(2)	After Impact	10330	12151	9222	9242	47812	88757
(3)	10 min	9649	11714	8429	8142	50762	88696
(4)	20 min	9528	11761	8260	8023	51185	88757
(5)	30 min	9564	11931	8421	8060	50781	88757
(6)	50 min	9852	12228	9065	8714	48898	88757
(7)	100 min	10492	12880	10067	9880	45438	88757

(a) Above Floor 93

Row	Analysis Stage	North	South	East	West	Core	Sum
(1)	Before Impact	11119	11204	8126	8170	41216	79835
(2)	After Impact	9598	11004	8328	8339	42174	79443
(3)	10 min	8898	10573	7546	7237	45137	79391
(4)	20 min	8757	10620	7387	7128	45552	79444
(5)	30 min	8795	10780	7545	7176	45148	79444
(6)	50 min	9094	11068	8179	7840	43263	79444
(7)	100 min	9771	11668	9192	9014	39799	79444

(b) Above Floor 96

Row	Analysis Stage	North	South	East	West	Core	Sum
(1)	Before Impact	10264	10352	7564	7611	37299	73090
(2)	After Impact	9090	10171	7761	7770	38295	73087
(3)	10 min	8397	9739	6983	6661	41262	73042
(4)	20 min	8261	9783	6828	6546	41669	73087
(5)	30 min	8299	9938	6990	6594	41266	73087
(6)	50 min	8588	10223	7625	7270	39381	73087
(7)	100 min	9250	10824	8628	8466	35919	73087

(c) Above Floor 98

Figure C–6. Total column loads in the core and exterior walls of WTC 1 at different floors and at different times (compression is positive).

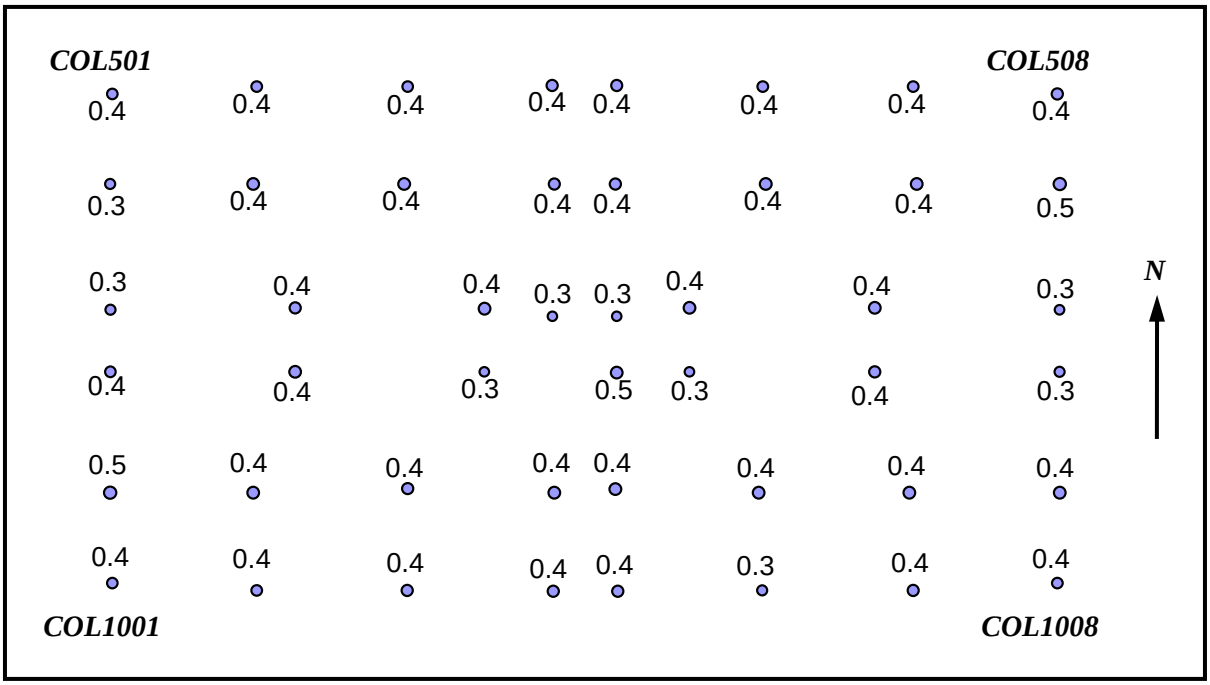

(a) Before impact

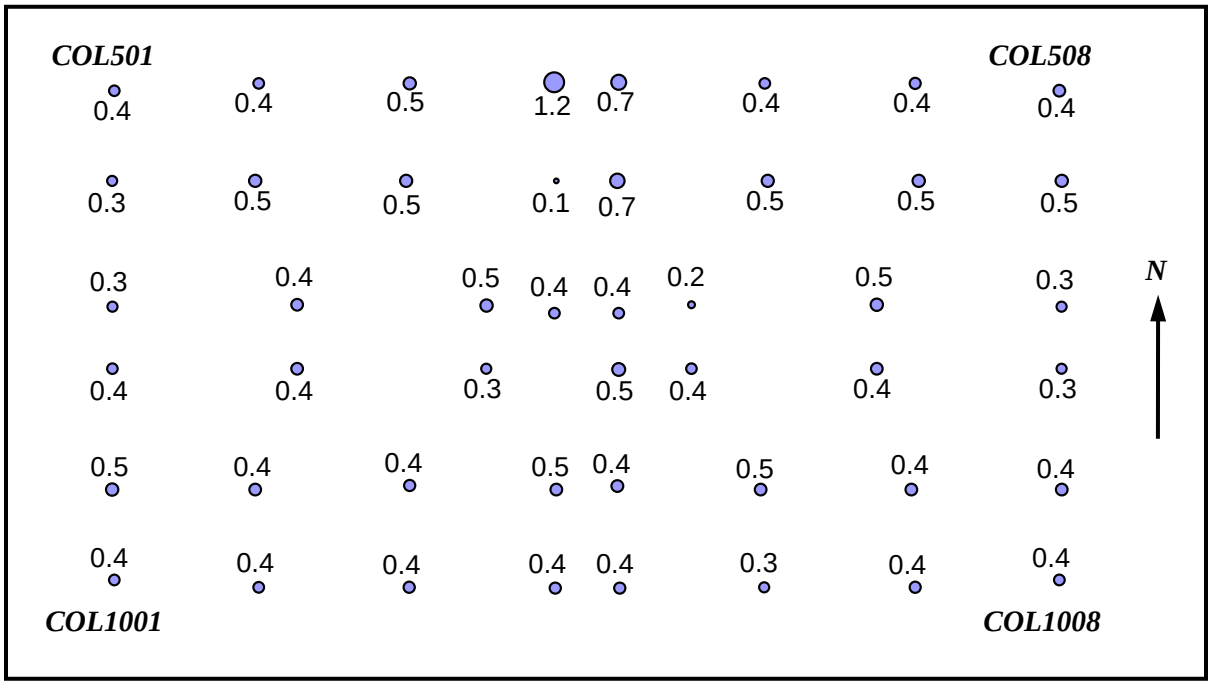

(b) After impact

Figure C–7. Ratios of axial elastic-plus-plastic strain to temperature-dependent yield strain for the core columns at Floor 96 of WTC 1 before and after aircraft impact.

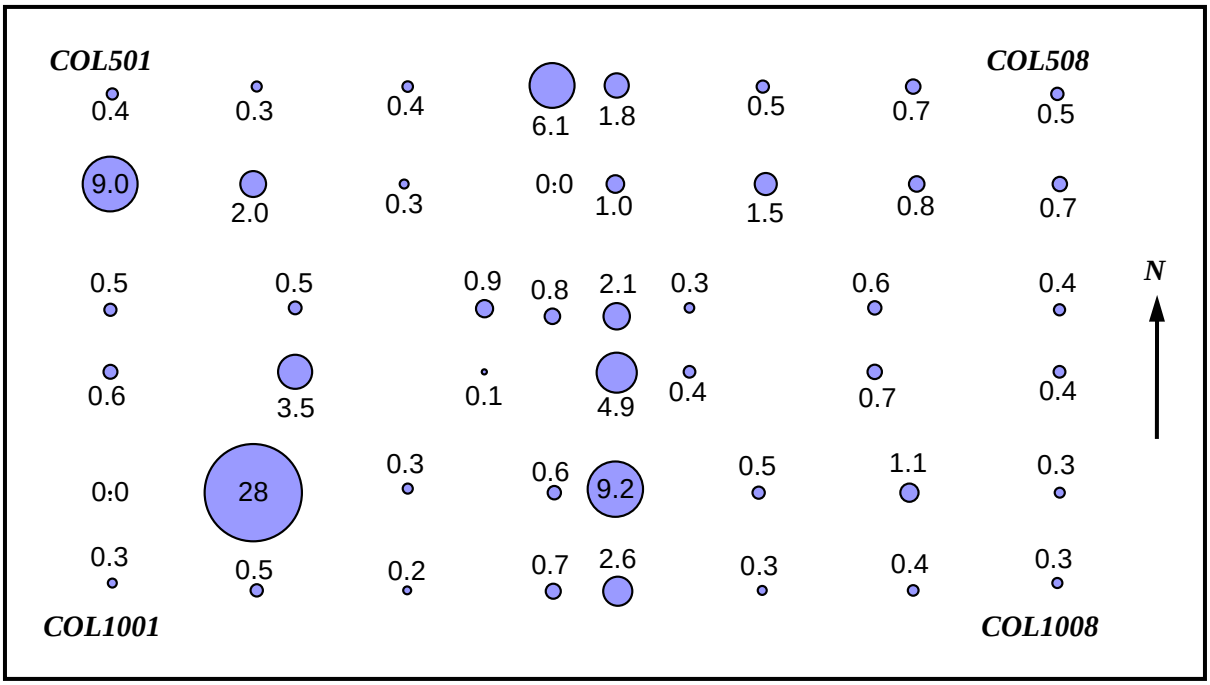

(a) At 10 min

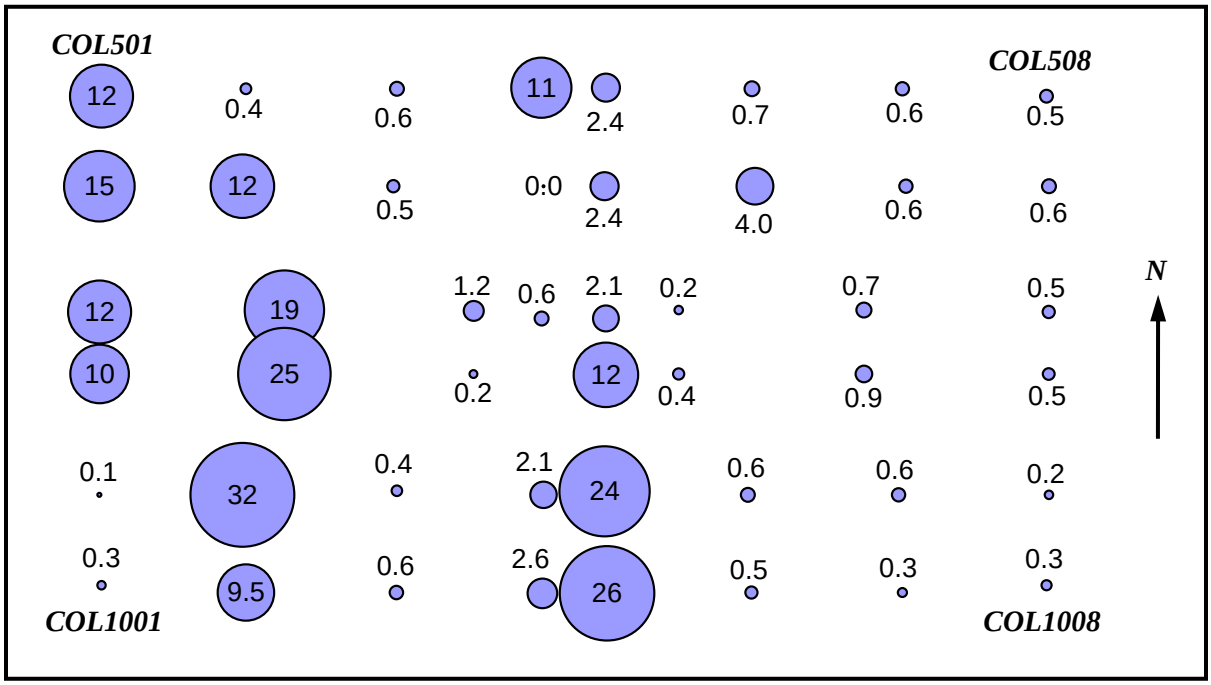

(b) At 20 min

Figure C–8. Ratios of axial elastic-plus-plastic strain to temperature-dependent yield strain for the core columns at Floor 96 of WTC 1 at 10 min and 20 min for Case A_i conditions.

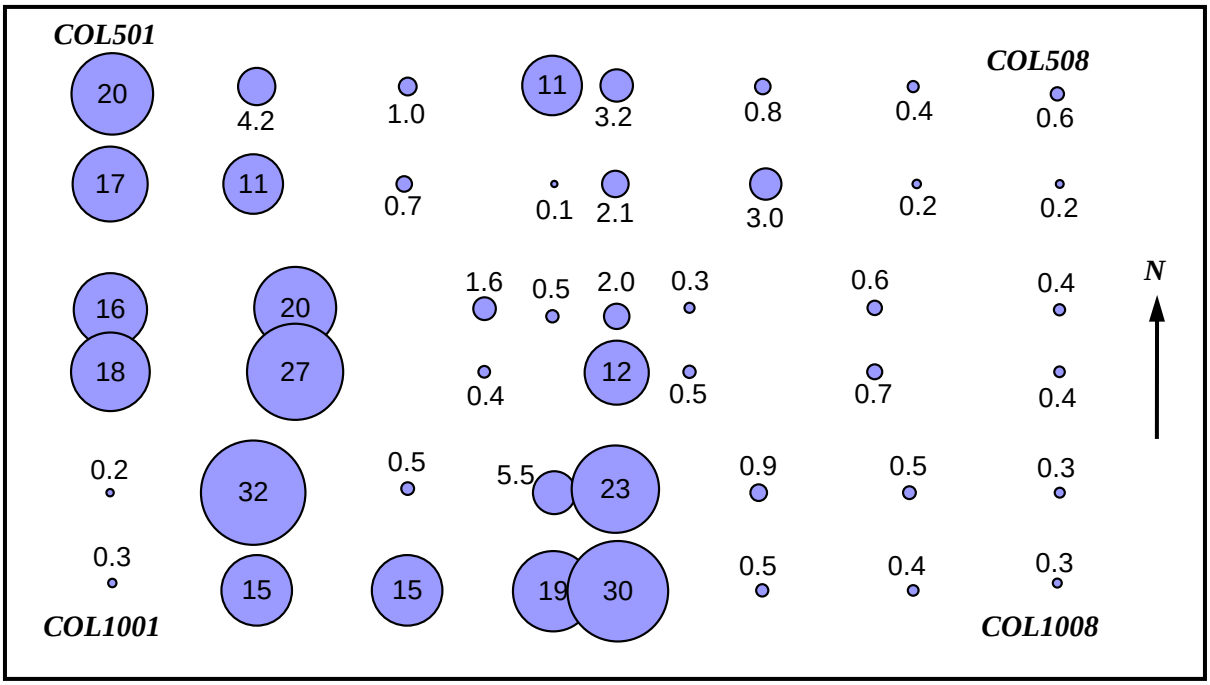

(a) At 50 min

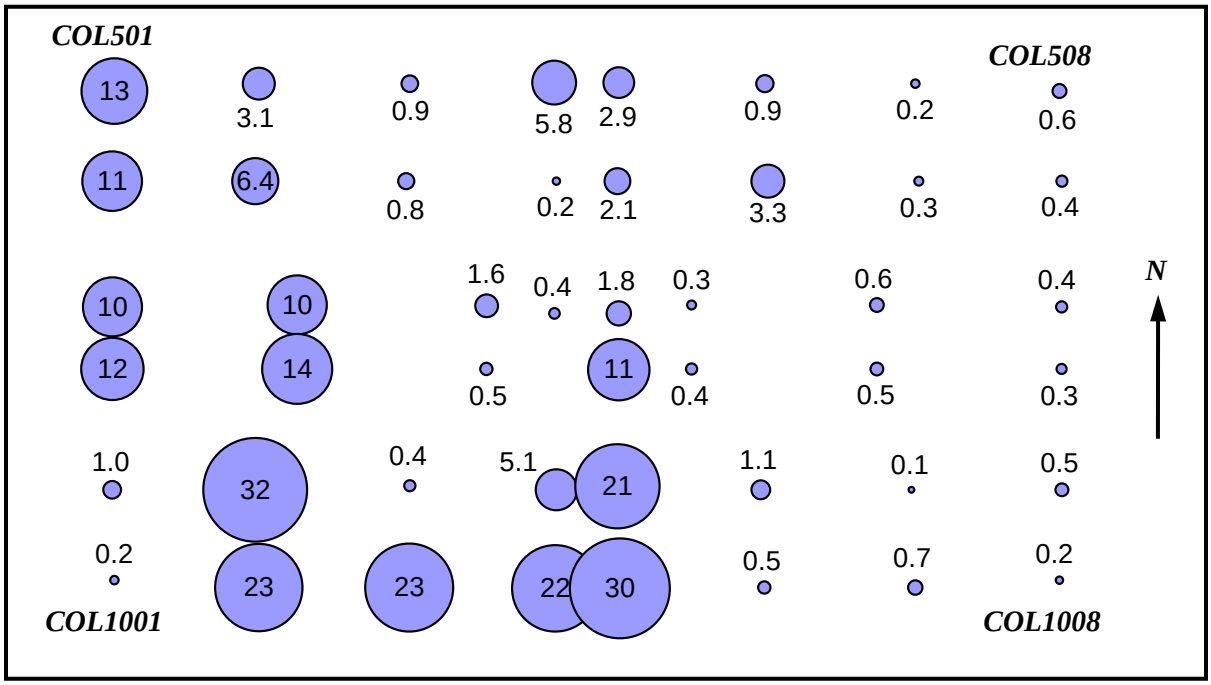

(b) At 100 min

Figure C–9. Ratios of axial elastic-plus-plastic strain to temperature-dependent yield strain for the core columns at Floor 96 of WTC 1 at 50 min and 100 min for Case A_i conditions.

C.2 WTC 2 GLOBAL ANALYSIS WITHOUT CREEP

The WTC 2 ANSYS model with no creep and no inelastic buckling of columns was analyzed with Case C_i and revised Case C_i structural damage condition and subjected to Case C_i and Case D_i temperature conditions. Temperature-dependent plasticity and the nonlinear geometry were the sources of nonlinearity in the model.

Case D_i temperature histories were analyzed with revised Case C_i structural damage as there was little structural response to Case C_i temperature histories, particularly in the core. The application of structural damage to the global model was a lengthy process, hence, only a different temperature history was considered for preliminary analysis purposes.

C.2.1 Case C_i Structural Damage and Temperature Conditions

Table C–2 summarizes the sequence of analyses that were performed with the WTC 2 ANSYS global model with Case C_i conditions (see Section 2.2 for Case C_i structural damage condition). The revised Case C_i structural damage condition was provided by NIST in the middle of the analysis for the thermal loading. Additional core columns were removed in analysis step 6 as shown in Table C–2. The results of each analysis step were used as initial conditions for the next analysis step.

Table C–2. Analysis Steps of WTC 2 ANSYS global model with Case C_i conditions.

Analysis Step	Description
1	WTC 2 model below Floor 106 was analyzed under its own self-weight.
2	Structures above Floor 106 were added in a stress-free state, and the model was analyzed for dead load including those above Floor 106.
3	Superimposed dead load and 25 percent of the design live loads were superimposed on the model.
4	Columns, spandrels, and floor elements severed during aircraft impact were removed, and the model was analyzed.
5	Column and spandrel temperatures were linearly ramped up to temperatures at 10 min.
6	Core Columns 1003 at Floor 80 and 903 between Floors 77 and 84 were removed from the model to represent the additional severed columns that were identified by NIST at later stages of the investigation (see Section 2.2 for the revised Case C_i structural damage condition).
7	Column and spandrel temperatures were changed linearly from temperatures at 10 min to 20 min.
8	Column and spandrel temperatures were changed linearly from temperatures at 20 min to 30 min.
9	Column and spandrel temperatures were changed linearly from temperatures at 30 min to 40 min.
10	Column and spandrel temperatures were changed linearly from temperatures at 40 min to 50 min.
11	Column and spandrel temperatures were changed linearly from temperatures at 50 min to 60 min.

The model was first analyzed to capture the effects of the construction sequence (analysis steps 1, 2, and 3). The results of analysis step 3 represented the structure state before the aircraft impact. In analysis step 4, the columns, spandrels, and floor elements that were severed during the aircraft impact were removed from the model, and the building was reanalyzed to redistribute the load to the non-severed members. This analysis represents the state of the building after the aircraft impact. After load redistribution, the column and spandrel temperatures were applied to the model (analysis steps 5, 7, 8, 9, 10, and 11). The column and spandrel temperatures were provided by NIST at 10 min intervals. For times between these time intervals, temperatures were calculated by linear interpolation. Analyses were

conducted at every 10 min up to 60 min. In Analysis Step 6, after the analysis of 10 min temperatures, two more core columns that were identified as severed during the aircraft impact were removed from the model. Temperatures were not applied to the floors in the global model to prevent floor buckling, as discussed for the WTC 1 global model without creep.

The results of the WTC 2 global model analyses with Case C_i structural damage and temperature conditions are summarized in Figs. C–10 through C–20.

Figure C–10 shows the vertical displacement at different analysis stages. The maximum displacement after the removal of additional severed core columns at analysis step 6 was equal to 7.2 in. This displacement gradually decreased to 7.0 in. at the end of 50 min. This reduction was due to thermal expansion of the core and the exterior wall columns between Floor 79 and Floor 83. Figures C–11 and C–12 show the vertical displacements for south and east exterior walls before and after aircraft impact and at 30 min and 60 min. The displacements were typically at their maximum near the hat truss at analysis step 6, after all severed members were removed, and gradually decreased to their minimum near Floor 77 through Floor 81 at 60 min. Figure C–11 shows that the displacement on the east wall, which was symmetric before the aircraft impact, became greater on the south side of this wall after the aircraft impact. This was due to the load redistribution to the south side of the east wall as a result of the removal of the severed columns on the south wall and in the southeast corner of the core. This was the first sign of tilting of WTC 2 toward the southeast.

Figures C–13, C–14, C–15, and C–16 show the axial loads before and after aircraft impact and at 30 min and 60 min over the south, east, and north exterior wall columns and spandrels and in the 800, 900, and 1000 core column series. After the aircraft impact, the load carried by the severed columns of the south exterior wall was primarily redistributed to the remaining columns on the same face and also to the core and other exterior wall columns. As a result of this redistribution, the maximum column load increased from 334 kip to 1,410 kip on the south exterior wall and from 451 kip to 485 kip on the east exterior wall. Similar to displacement, the axial load on the east wall, which was symmetric before the aircraft impact, became greater on the south side of this wall after the aircraft impact. This was due to the load redistribution to the south side of the east wall as a result of the removal of the severed columns on the south wall and in the southeast corner of the core. The axial load in core columns also was significantly affected by the aircraft impact and fire-induced temperatures. The maximum column load increased from 4,930 kip to 5,120 kip in the 1000 core-column series, from 1,600 kip to 2,250 kip in the 900 core column series, and from 1,740 kip to 2,630 kip in the 800 core-column series. After the removal of 1003 and 903 core columns, the column loads increased on the east and south side core columns.

With increasing time, the maximum column load on the east exterior wall columns increased from 485 kip after aircraft impact to 630 kip at the end of 60 min. This increase was primarily due to the steady increase of column temperatures on the east wall as a result of the continuous fires. Similarly, the axial loads in the 1000 core column series steadily increased due to continuous fires on the east side of the core.

Figure C–17 shows the total column loads over the entire core and north, south, east, and west exterior walls for different floors. Due to the removal of severed columns, spandrels, and floor elements, the total column loads below Floor 83 after aircraft impact are not equal to those before the aircraft impact. Referring to the total column loads above Floor 83 in Fig. C–17, after the aircraft impact (including the effects of additionally removed Column 903 and Column 1003 in the core), the total column load in the

east exterior wall columns increased about 2,600 kip, whereas the total column load decreased in the core by about 1,200 kip, in the north exterior wall by about 750 kip, in the west exterior wall by about 50 kip, and in the south exterior wall by about 600 kip. With increasing time, the temperatures in the east, the north, and the south exterior wall columns increased more than those in the west exterior wall and core columns. The higher temperatures resulted in higher thermal expansions and greater axial loads in the exterior wall columns. In Floor 83, the temperature effect alone resulted in unloading of the core by 1,820 kip and increased the total column loads by 140 kip on the south exterior wall, by 700 kip on the west exterior wall, by 600 kip on the north exterior wall, and by 380 kip on the east exterior wall.

Figures C–18, C–19, and C–20 show the ratio of elastic-plus-plastic strain to the temperature-dependent yield strain of the core columns between Floor 82 and Floor 83 before and after aircraft impact and at 10 min (analysis step 6), 30 min, 40 min, and 60 min. As can be noticed, the elastic-plus-plastic strain in the core columns before aircraft impact was typically 60 to 70 percent less than the yield strains at room temperature. After the aircraft impact, the maximum strain ratio reached 0.6, indicating that all remaining core columns were in their elastic range. After the removal of Core Columns 1003 and 903, Core Columns 1004 and 1005 started to show strain ratios greater than 1.0 (indicating plasticity) with 10 min temperatures. Strain ratios in Core Columns 1004 and 1005 continued to increase with increasing time and temperatures, reaching their maximum at the end of 60 min. High strains were clustered around the east side core columns, demonstrating possible tilting of the core.

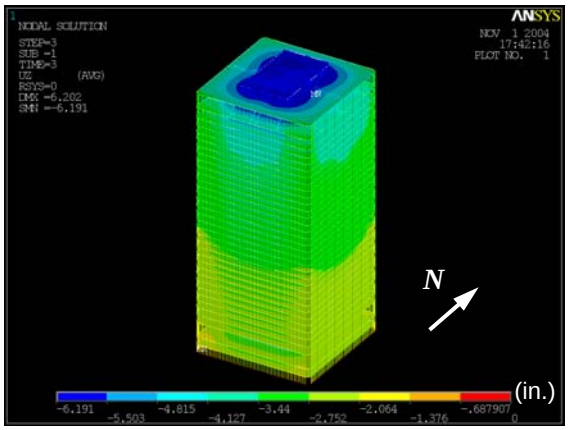

(a) Before impact

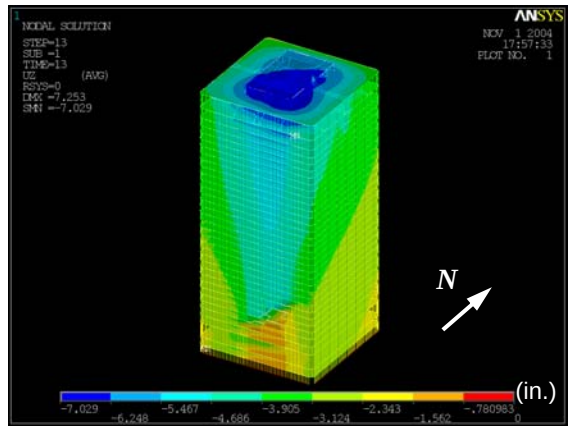

(b) After impact

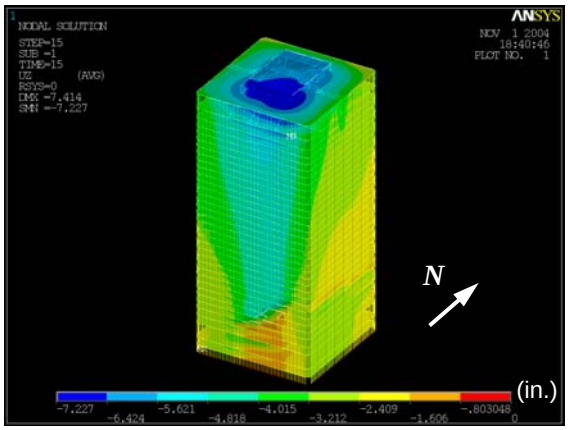

(c) At 10 min (Analysis step 6)

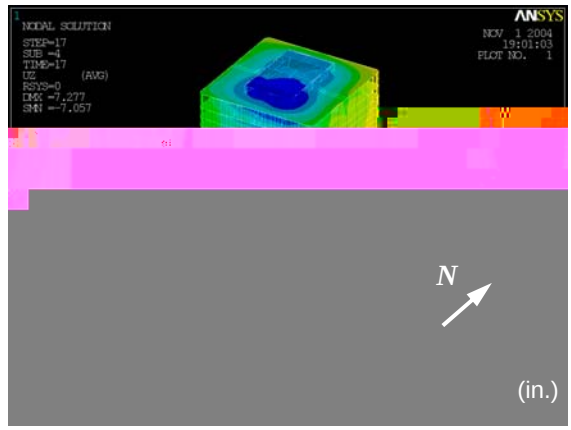

(d) At 30 min

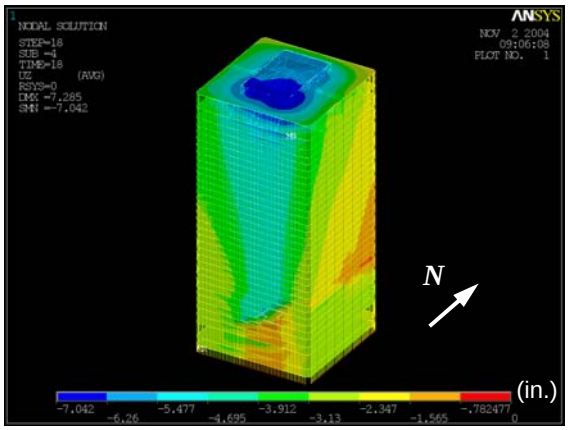

(e) At 40 min

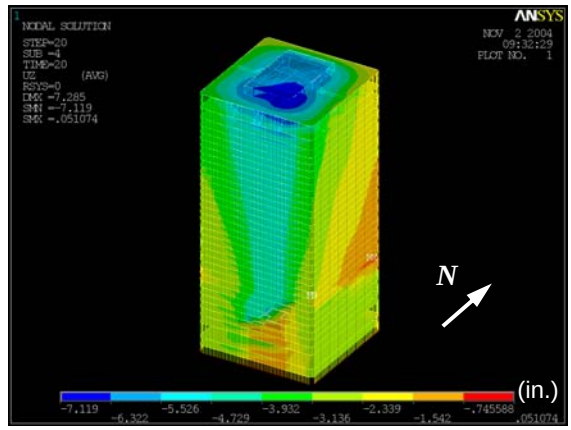

(f) At 60 min

Figure C–10. Vertical displacement at different stages of WTC 2 for Case C_i conditions.

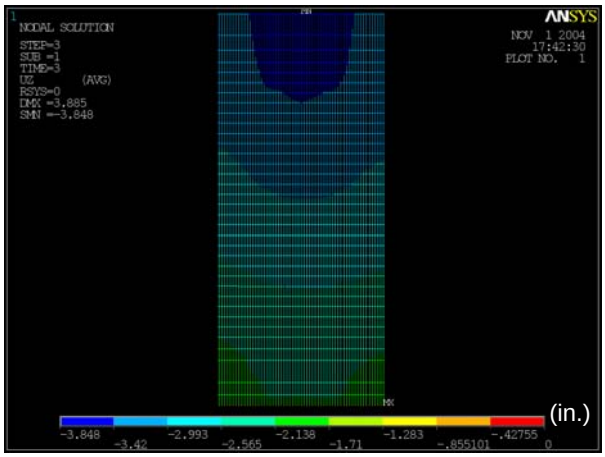

(a) South wall before impact

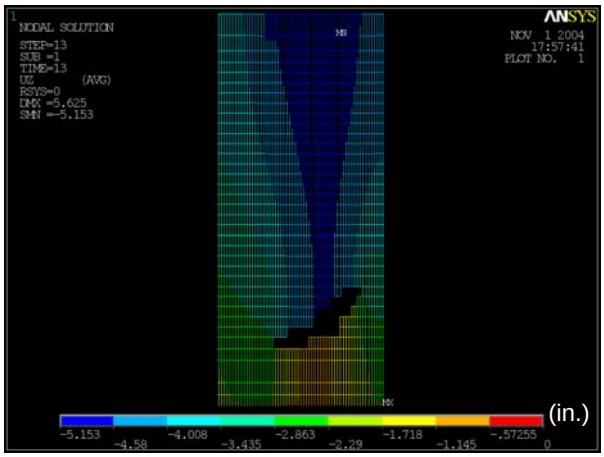

(b) South wall after impact

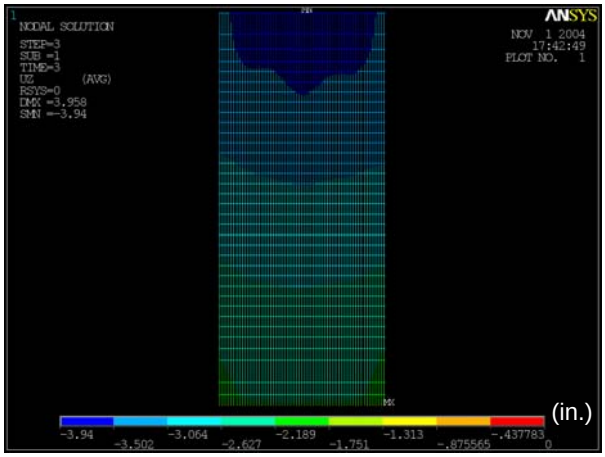

(c) East wall before impact

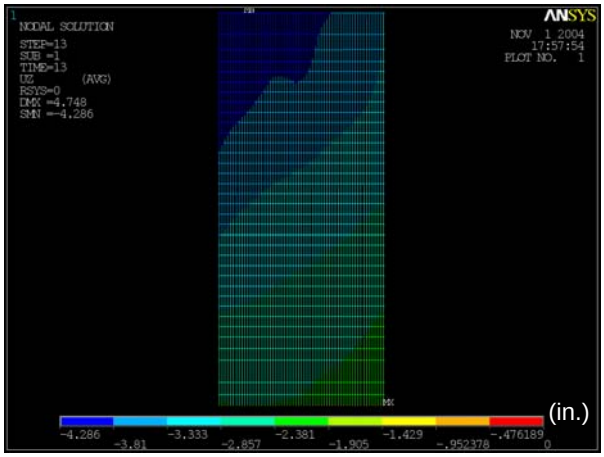

(d) East wall after impact

Figure C–11. Vertical displacement on the south and east faces of WTC 2 before and after aircraft impact (looking from outside; downward displacement is negative).

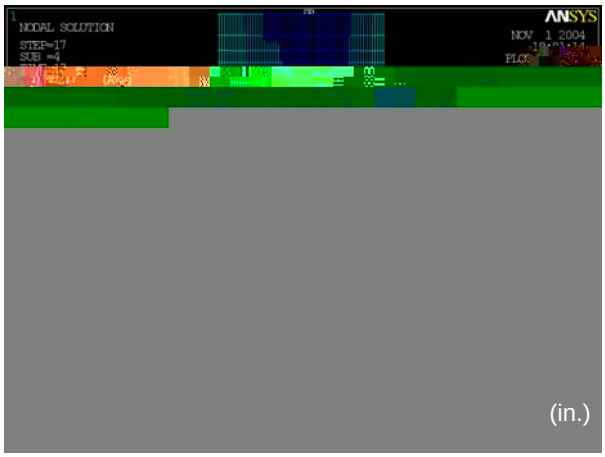

(a) South wall at 30 min

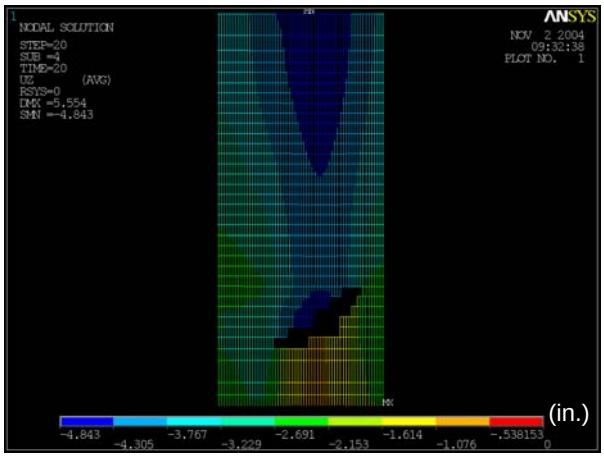

(b) South wall at 30 min

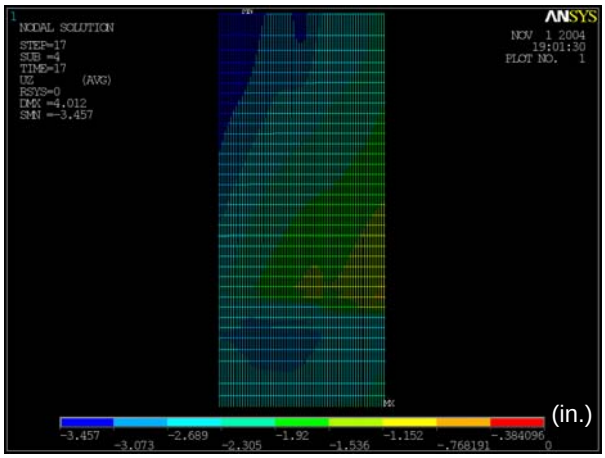

(c) East wall at 30 min

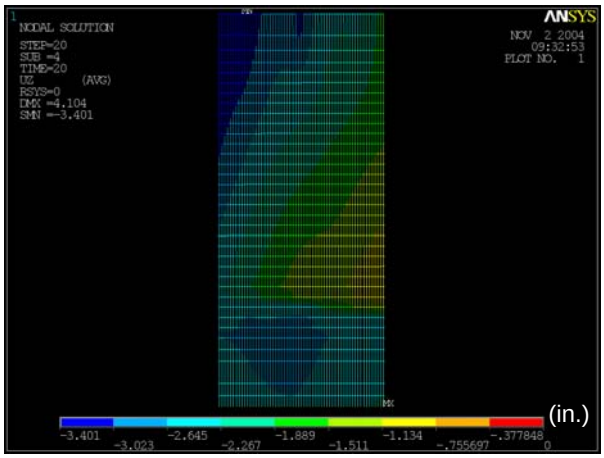

(d) East wall at 30 min

Figure C–12. Vertical displacement on the south and east faces of WTC 2 at 30 min and at 60 min of Case C_i conditions (looking from outside; downward displacement is negative).

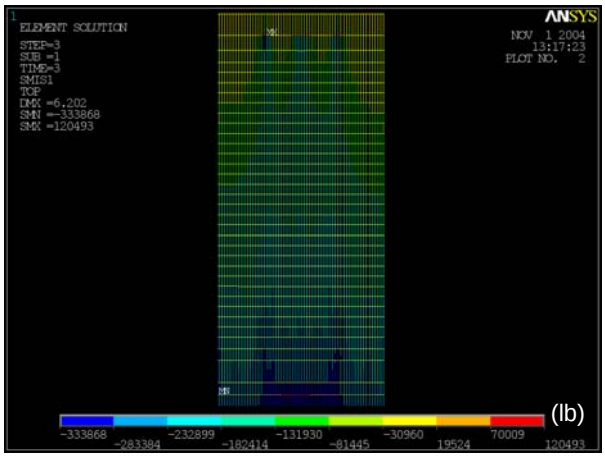

(a) South wall before impact

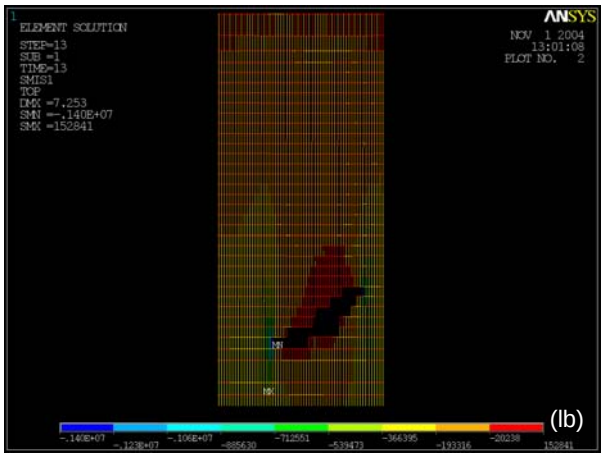

(b) South wall after impact

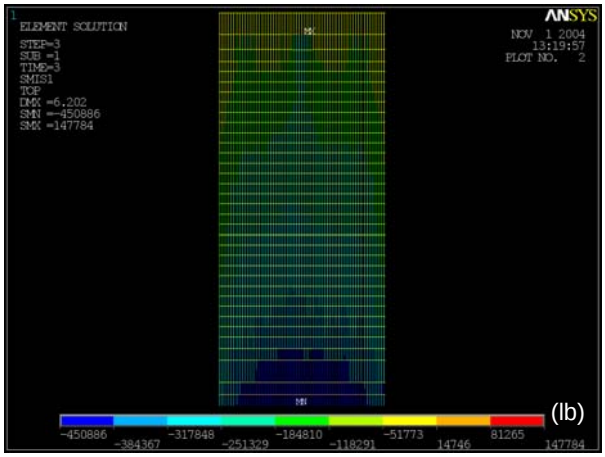

(c) East wall before impact

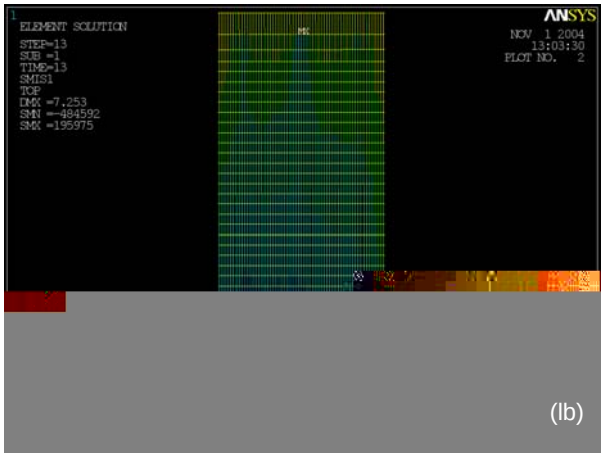

(d) East wall after impact

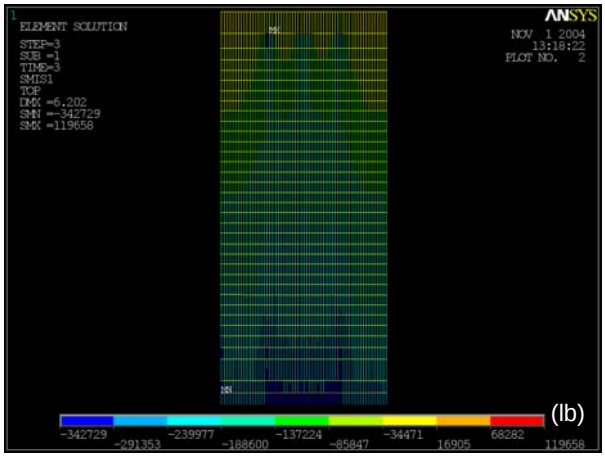

(e) North wall before impact

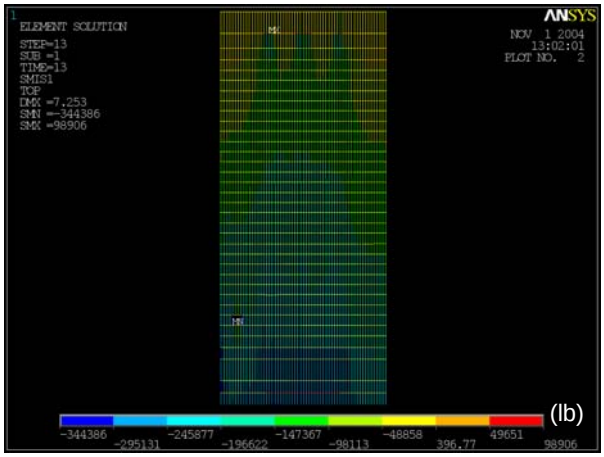

(f) North wall after impact

Figure C–13. Axial force variation on the south, east, and north faces of WTC 2 before and after aircraft impact (looking from outside; compression is negative).

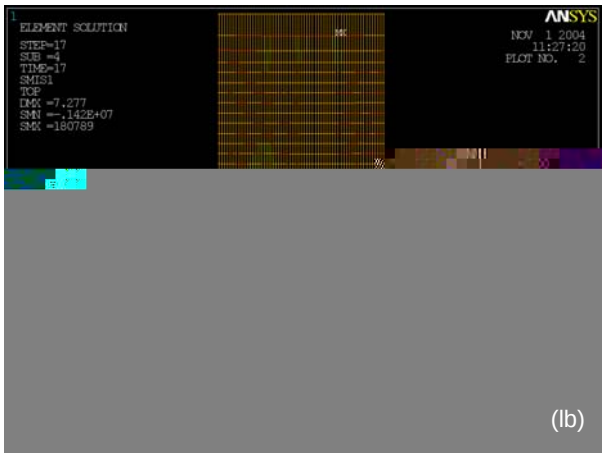

(a) South wall at 30 min

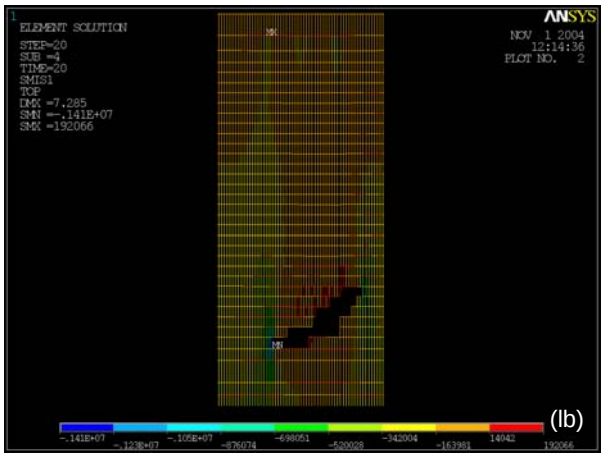

(b) South wall at 60 min

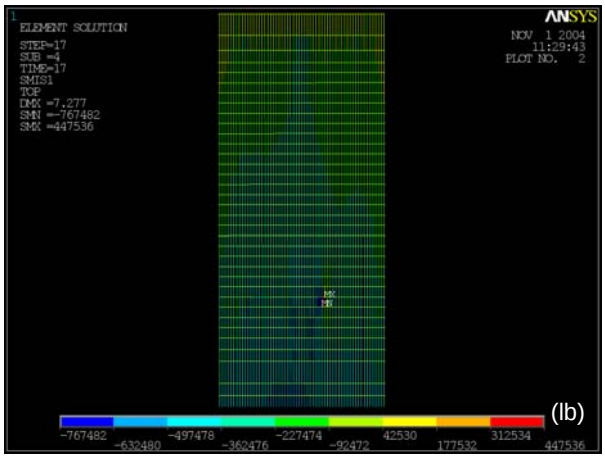

(c) East wall at 30 min

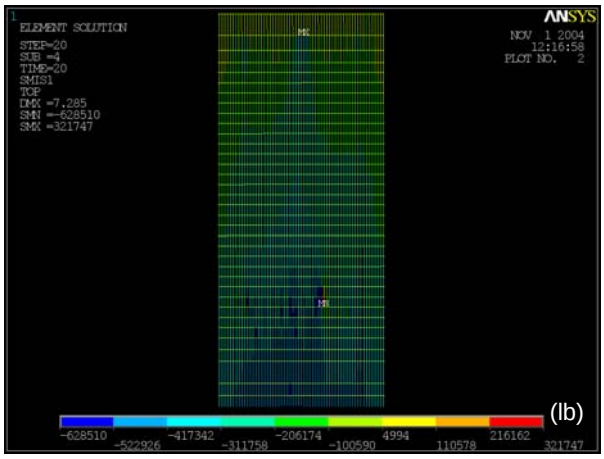

(d) East wall at 60 min

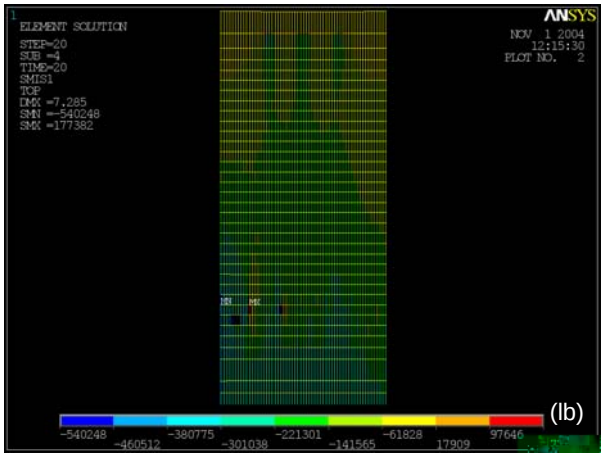

(e) North wall at 30 min

(f) North wall at 60 min

Figure C–14. Axial force variation on the south, east, and north faces of WTC 2 at 30 min and 60 min of Case C_i conditions (looking from outside; compression is negative).

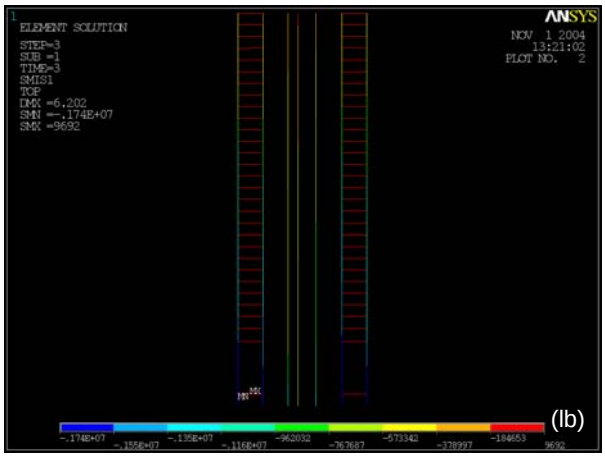

(a) 800 series columns before impact

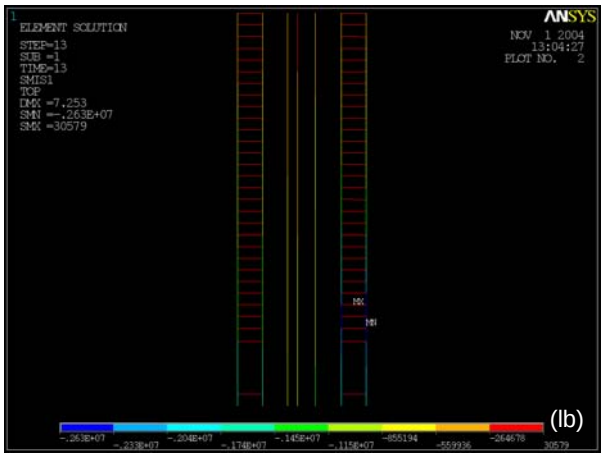

(b) 800 series columns after impact

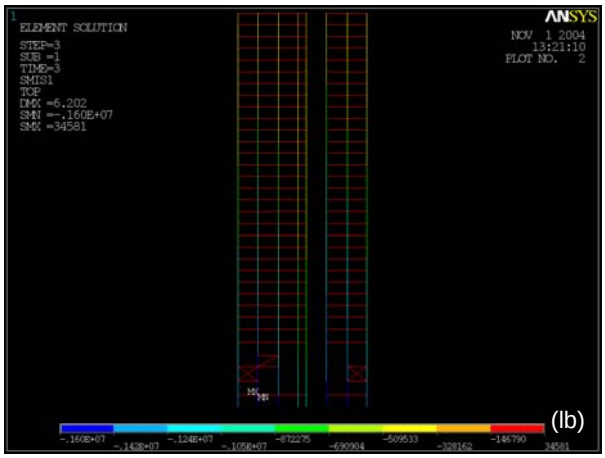

(c) 900 series columns before impact

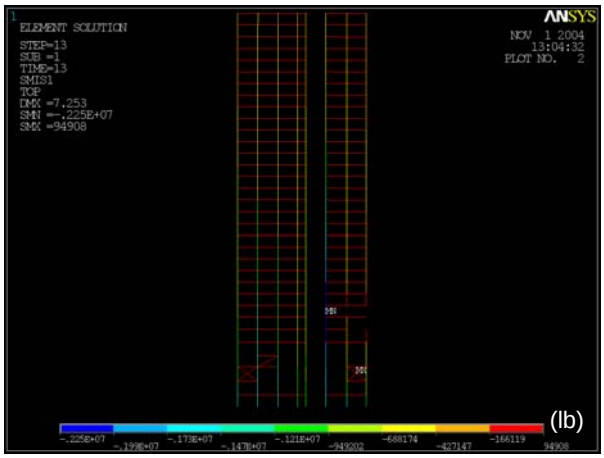

(d) 900 series columns after impact

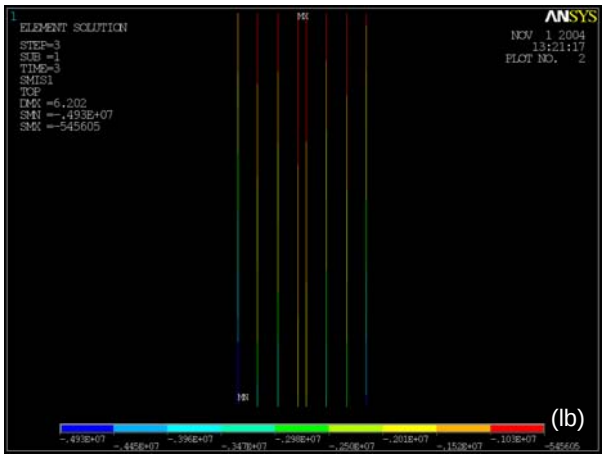

(e) 1000 series columns before impact

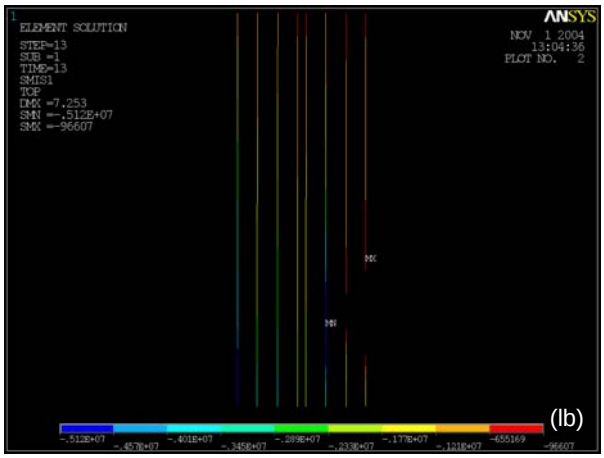

(f) 1000 series columns after impact

Figure C–15. Axial force variation on the 800, 900, and 1000 series core columns of WTC 2 before and after aircraft impact (looking from west; compression is negative).

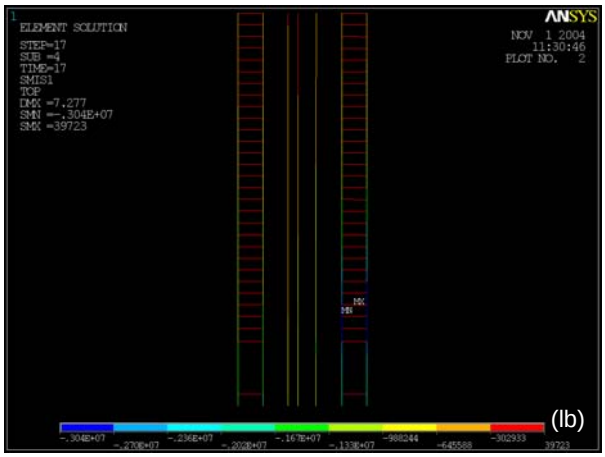

(a) 800 series columns at 30 min

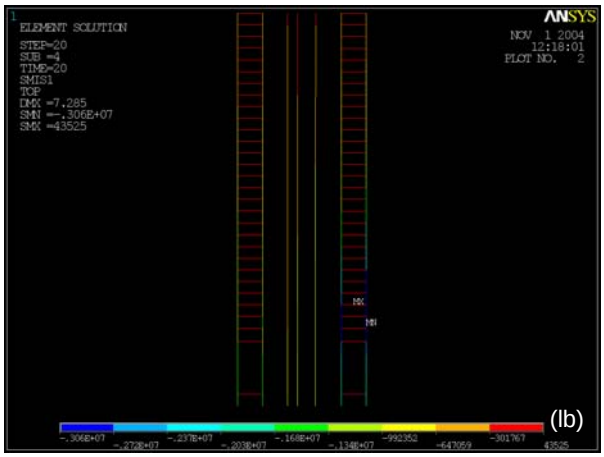

(b) 800 series columns at 60 min

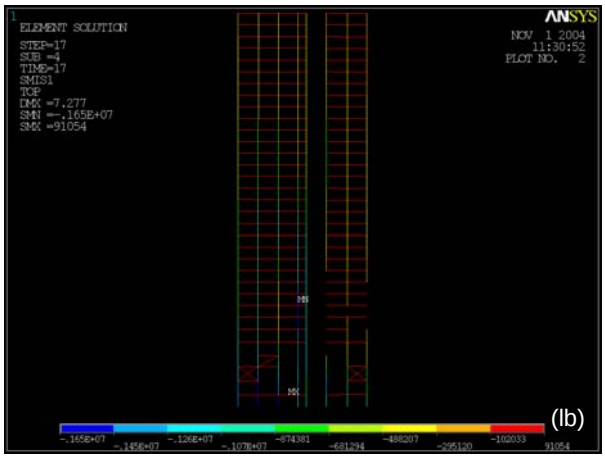

(c) 900 series columns at 30 min

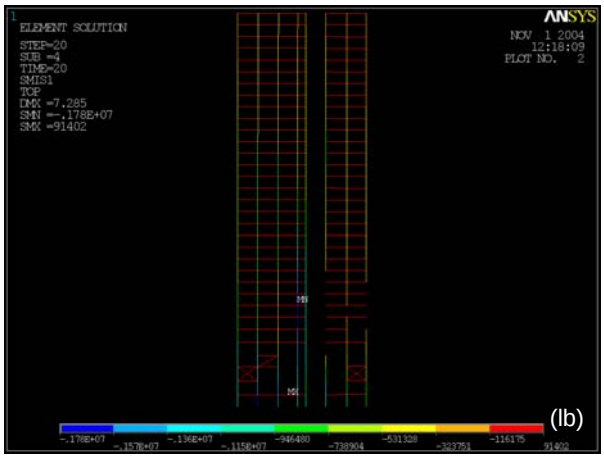

(d) 900 series columns at 60 min

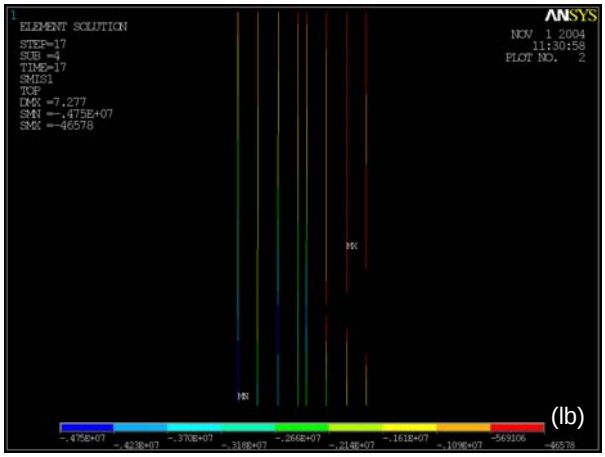

(e) 1000 series columns at 30 min

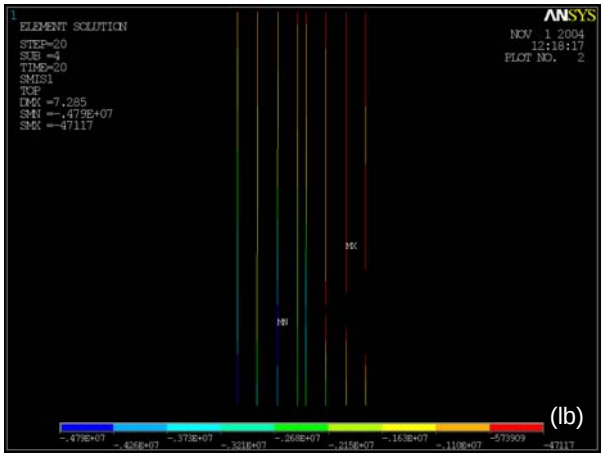

(f) 1000 series columns at 60 min

Figure C–16. Axial force variation on the 800, 900, and 1000 series core columns of WTC 2 at 30 min and 60 min of Case C_i conditions (looking from west; compression is negative).

Row	Analysis Stage	West	East	North	South	Core	Sum
(1)	Before Impact	18779	18837	13714	13529	77563	142423
(2)	After Impact	18951	20394	12892	11880	76831	140949
(3)	After Impact*	18774	21384	12800	12528	75166	140652
(4)	10 min	19499	20616	12997	11333	76504	140949
(5)	10 min (b)	19322	21606	12905	11981	74839	140652
(6)	20 min	19471	21616	12978	12130	74458	140652
(7)	30 min	19469	21637	13138	12309	74099	140653
(8)	40 min	19462	21692	13246	12427	73826	140653
(9)	50 min	19472	21795	13305	12506	73574	140653
(10)	60 min	19500	21887	13388	12538	73341	140653

* Including the effects of additionally removed Columns 903 and 1003 in the core (= (2) - (4) + (5)).

(a) Above Floor 78

Row	Analysis Stage	West	East	North	South	Core	Sum
(1)	Before Impact	17642	17697	12558	12393	71319	131609
(2)	After Impact	17755	19295	11818	10982	71249	131099
(3)	After Impact*	17557	20305	11756	11599	69754	130972
(4)	10 min	18310	19529	11942	10396	70924	131101
(5)	10 min (b)	18111	20539	11881	11014	69429	130974
(6)	20 min	18258	20479	11960	11230	69048	130974
(7)	30 min	18251	20462	12137	11435	68688	130973
(8)	40 min	18241	20502	12245	11570	68414	130972
(9)	50 min	18238	20603	12309	11660	68162	130972
(10)	60 min	18239	20690	12414	11700	67928	130972

* Including the effects of additionally removed Columns 903 and 1003 in the core (= (2) - (4) + (5)).

(b) Above Floor 81

Row	Analysis Stage	West	East	North	South	Core	Sum
(1)	Before Impact	16728	16782	11972	11820	67309	124611
(2)	After Impact	16853	18337	11241	10561	67499	124490
(3)	After Impact*	16664	19328	11184	11183	66115	124474
(4)	10 min	17398	18604	11346	9970	67172	124489
(5)	10 min (b)	17209	19595	11288	10592	65788	124473
(6)	20 min	17356	19511	11365	10833	65409	124473
(7)	30 min	17351	19482	11537	11054	65048	124473
(8)	40 min	17344	19521	11644	11191	64773	124473
(9)	50 min	17350	19619	11702	11280	64521	124473
(10)	60 min	17370	19709	11787	11320	64287	124473

* Including the effects of additionally removed Columns 903 and 1003 in the core (= (2) - (4) + (5)).

(c) Above Floor 83

Figure C–17. Total column loads in the core and exterior walls of WTC 2 at different floors and at different times for Case C_i conditions (compression is positive).

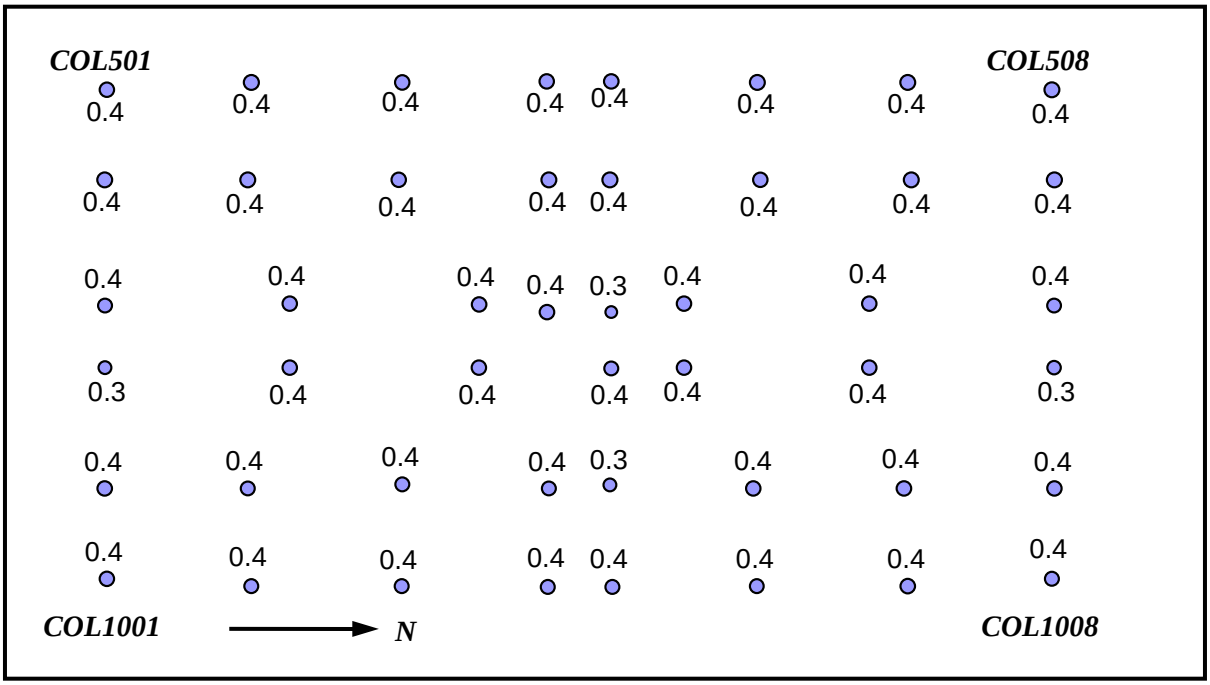

(a) Before impact

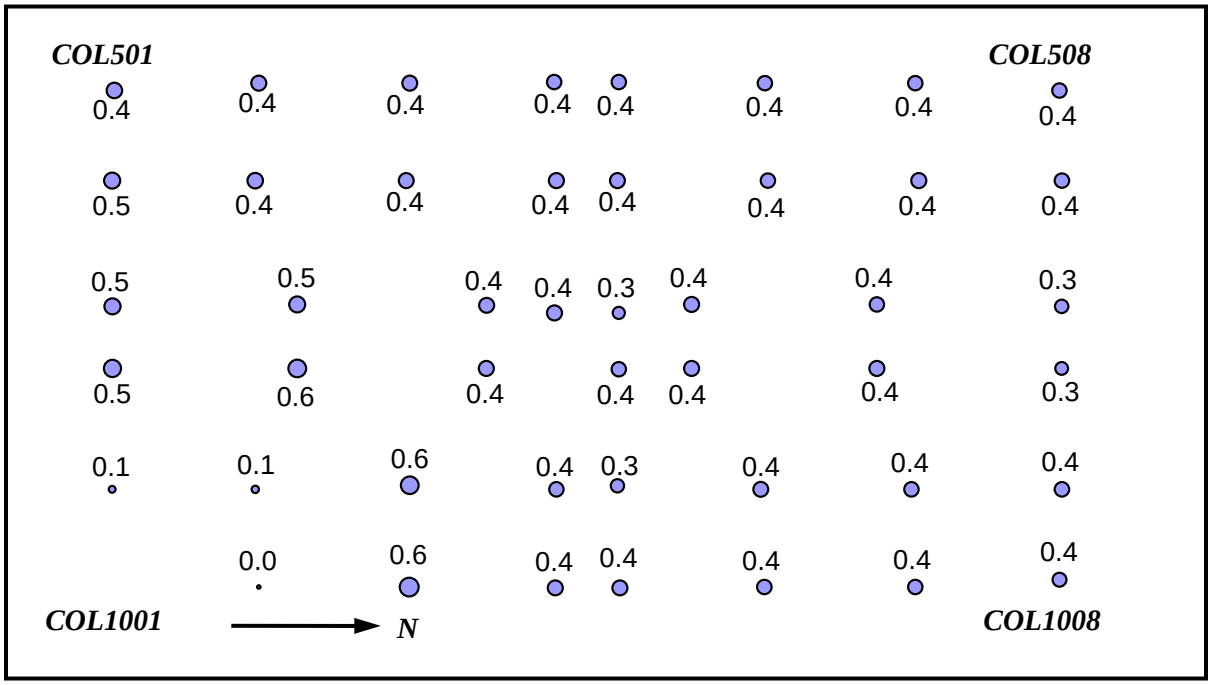

(b) After impact

Figure C–18. Ratios of axial elastic-plus-plastic strain to temperature-dependent yield strain for the core columns at Floor 82 of WTC 2 before and after aircraft impact.

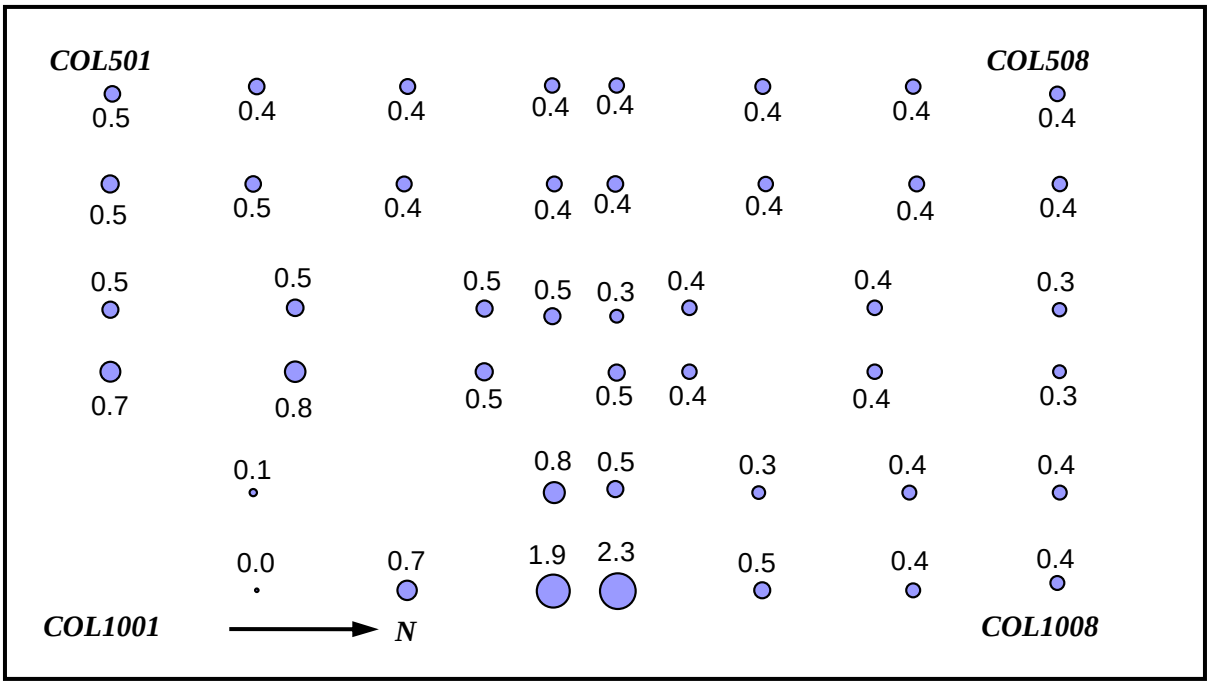

(a) At 10 min (b)

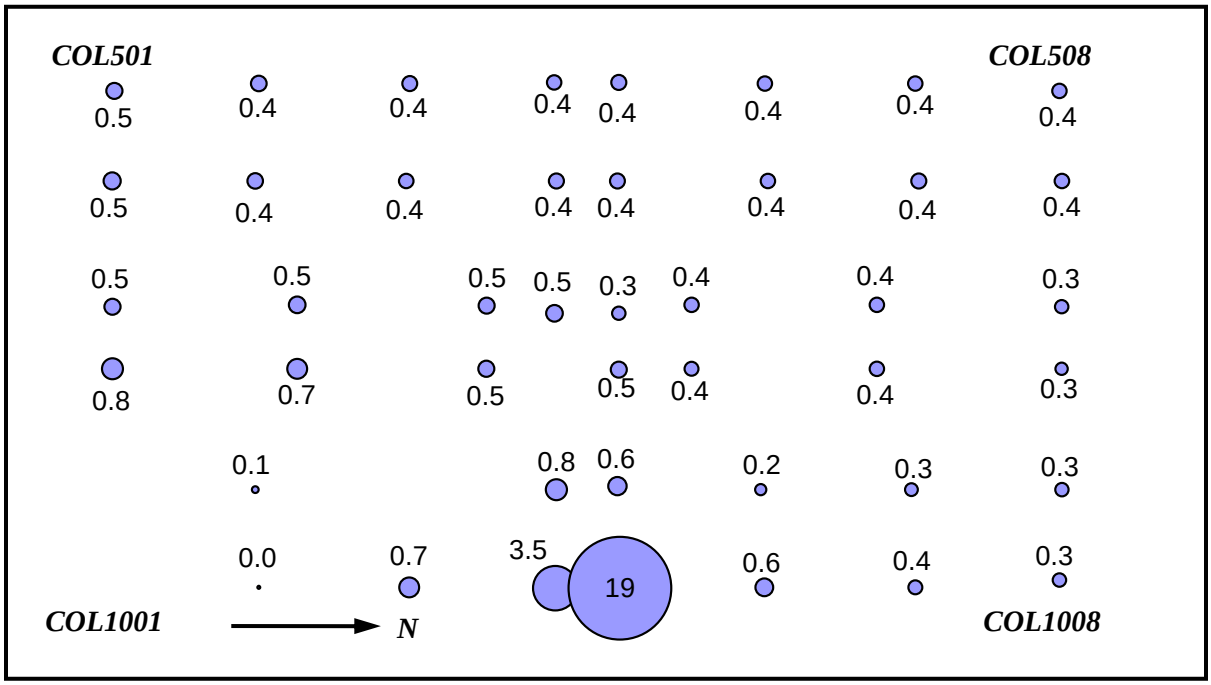

(b) At 30 min

Figure C–19. Ratios of axial elastic-plus-plastic strain to temperature-dependent yield strain for the core columns at Floor 82 of WTC 2 at 10 min and 30 min of Case C_i conditions.

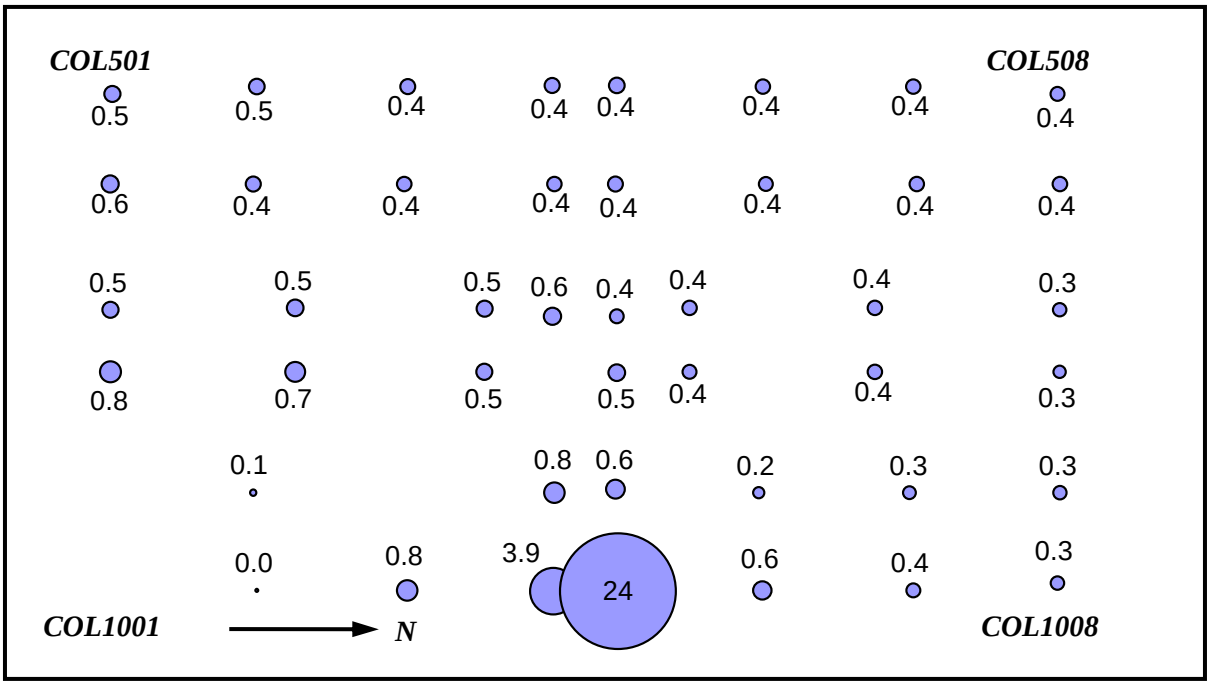

(a) At 40 min

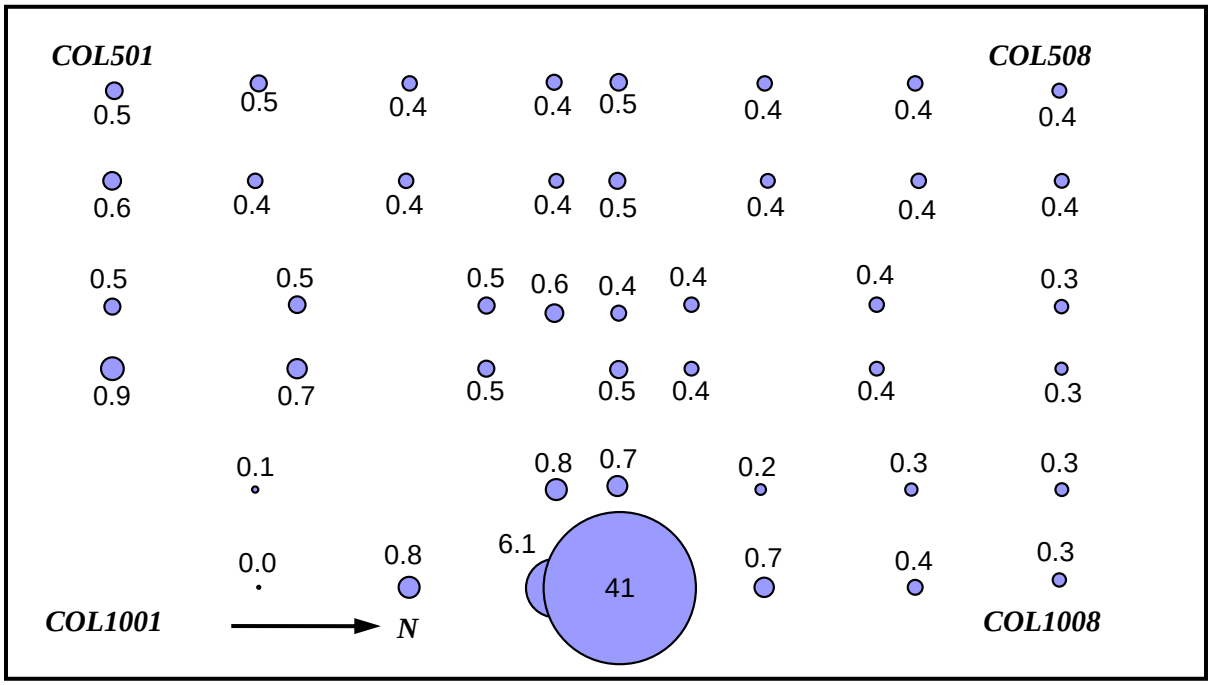

(b) At 60 min

Figure C–20. Ratios of axial elastic-plus-plastic strain to temperature-dependent yield strain for the core columns at Floor 82 of WTC 2 at 40 min and 60 min of Case C_i conditions.

C.2.2 Case D_i Temperature Condition and Case C_i Structural Damage Condition

Table C–3 summarizes the sequence of analyses that were performed with the WTC 2 ANSYS global model with the revised Case C_i structural damage condition from Step 4, and Case D_i temperature condition. Revised Case C_i structural damage refers to the removal of core columns 903 and 1003 in addition to the other core columns that were severed after the aircraft impact as shown in Section 2.2. Case D_i structural damage condition was not used as this structural damage condition was not available at the time of analyses.

Table C–3. Analysis Steps of WTC 2 ANSYS global model with Case D_i temperature condition and Case C_i structural damage condition.

Analysis Step	Description
1	WTC 2 model below Floor 106 was analyzed under its own self-weight.
2	Structures above Floor 106 were added in a stress-free state, and the model was analyzed for dead load including those above Floor 106.
3	Superimposed dead load plus 25 percent of the design live loads were superimposed on the model.
4	Columns (including the 1003 and 903 core columns), spandrels, and floor elements that were severed during aircraft impact were removed, and the model was analyzed (see Section 2.2 for the revised Case C_i structural damage condition).
5	Column and spandrel temperatures were ramped linearly up to temperatures at 10 min.
6	Column and spandrel temperatures were changed linearly from temperatures at 10 min to 20 min.
7	Column and spandrel temperatures were changed linearly from temperatures at 20 min to 30 min.
8	Column and spandrel temperatures were changed linearly from temperatures at 30 min to 40 min.
9	Column and spandrel temperatures were changed linearly from temperatures at 40 min to 50 min.
10	Column and spandrel temperatures were changed linearly from temperatures at 50 min to 60 min.

The model was first analyzed for the effects of the construction sequence (analysis steps 1, 2, and 3). The results of analysis step 3 represent the state of the structure before the aircraft impact. In analysis step 4, the columns, spandrels, and floor elements that were severed during the aircraft impact were removed, and the structure was reanalyzed to redistribute the loads to other members. This analysis represented the structure state after the aircraft impact. The column and spandrel temperatures were applied to the model (analysis steps 5 through 10). The column and spandrel temperatures were provided by NIST at 10 min intervals. Temperatures were calculated by linear interpolation for times in between 10 min intervals. Temperature analyses were performed at every 10 min up to 60 min. Temperatures were not applied to the floor elements, as discussed earlier.

The results of the WTC 2 global model analyses with Case D_i temperature condition and the revised Case C_i structural damage condition are summarized in Figs. C–21 through C–32.

Figure C–21 shows the vertical displacement at different analysis steps. The maximum vertical displacement after the aircraft impact increased from 7.0 in. to 7.7 in. with the inclusion of the additional severed core columns (1003 and 903). The 7.7 in. maximum vertical displacement after aircraft impact gradually increased to 9.2 in. at the end of the 60 min temperature analysis. The exterior columns between Floor 79 and Floor 83 thermally expanded with temperature; however, the core columns shortened due to plastic deformation, and the plastic strains in 1000 series core columns were greater than the thermal expansion strains. Figures C–22 and C–23 show the vertical displacements for the south and east exterior walls after aircraft impact, and at 30 min, 50 min, and 60 min. The displacements of these

exterior walls were typically at their maximum after aircraft impact and gradually decreased to their minimum value with time up to 50 min and then increased slightly beyond 50 min up to 60 min, as temperatures reduced.

Figures C–24, C–25, and C–26 show the axial load variation over the south, east, and north exterior wall columns and spandrels after impact and at 10 min, 20 min, 30 min, 50 min, and 60 min. The maximum column load on the east exterior wall columns increased from 485 kip after aircraft impact to about 880 kip at the end of 30 min and then dropped down to 800 kip at the end of 60 min. The increase in column forces was mostly concentrated at the center portion of the east wall. The maximum column load on the north exterior wall columns increased from 355 kip after aircraft impact to about 550 kip at the end of 30 min and then dropped down to 440 kip at 50 min; it then increased again to 700 kip at the end of 60 min.

Figures C–27, C–28 and C–29 show the axial load variations over the 800, 900, and 1000 core column series after aircraft impact and at 10 min, 20 min, 30 min, 50 min, and 60 min. Over the duration of the fires, the maximum column load after impact increased from 5,200 kip to 6,250 kip in the 1000 core column series and from 1,700 kip to 2,500 kip in the 900 core column series, and decreased slightly from 3,400 kip to 3,200 kip in the 800 core column series.

Figure C–30 shows the total column loads in the core and the north, south, east, and west exterior walls for different floors. Total column loads below Floor 83 after aircraft impact did not add up to the total column loads before the aircraft impact. This difference is equal to the self-weight of severed members and floor loads applied to severed columns.

In Floor 83, the temperature effect alone resulted in an unloading of the core columns by 2,000 kip and increased the total load by 630 kip on the south exterior wall, by 300 kip on the west exterior wall, by 540 kip on the north exterior wall, and by 530 kip on the east exterior wall.

Figures C–31 and C–32 show the ratio of elastic-plus-plastic strain to the temperature-dependent yield strain of the core columns between Floor 82 and Floor 83 at 10 min, 20 min, 50 min, and 60 min. After 10 min, except for Core Columns 801, 1004, and 1005, the strain ratios in the core columns were all less than 1.0. With increasing time, more columns from east side and center region of the core area started to show strain ratios greater than 1.0, indicating the onset of plasticity. A maximum strain ratio of 41 was reached between 40 min and 60 min at Column 1005. Higher strain ratios were clustered around the east side of the core, indicating a tendency of the core to tilt toward east.

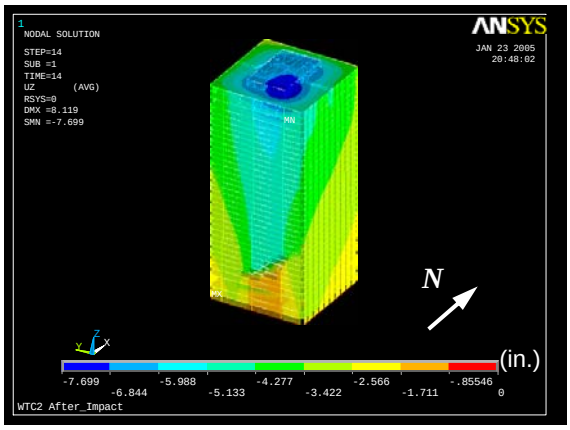

(a) After impact

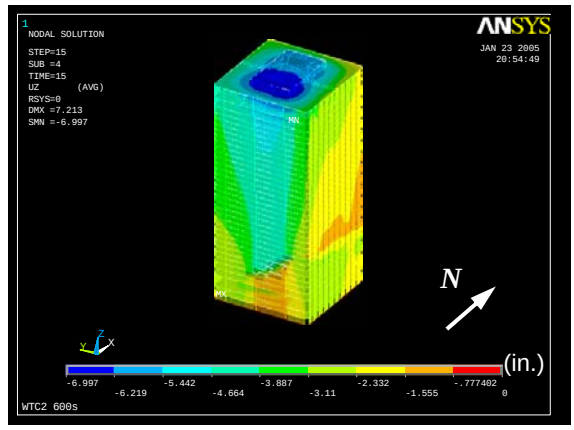

(b) At 10 min

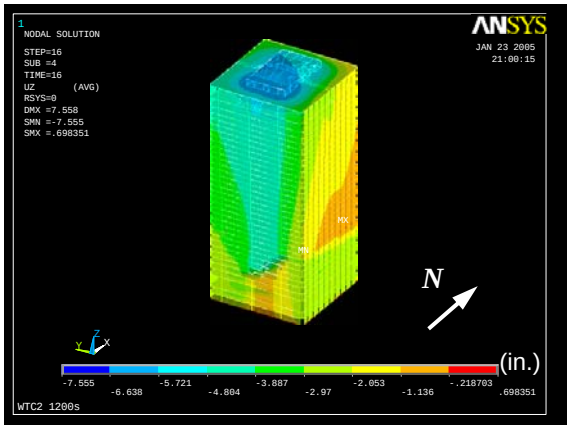

(c) At 20 min

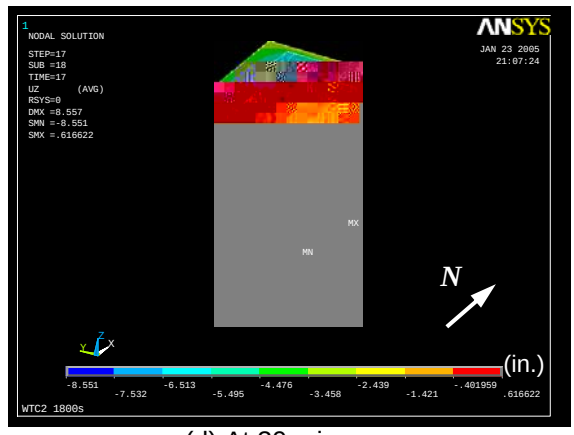

(d) At 30 min

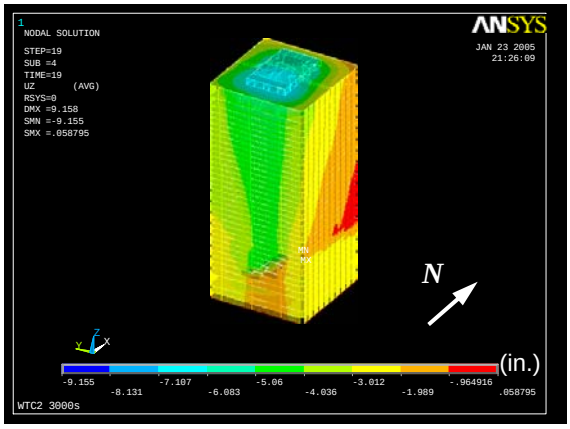

(e) At 50 min

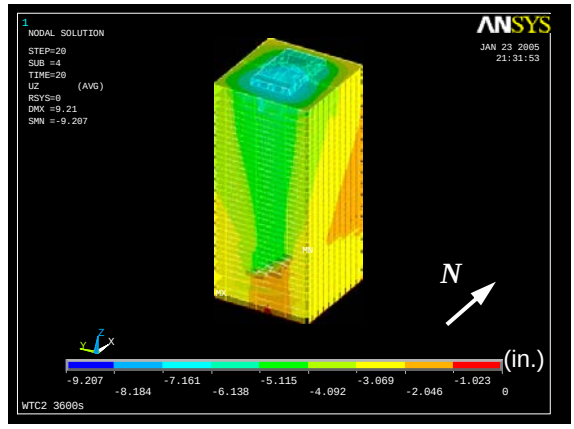

(f) At 60 min

Figure C–21. Vertical displacement at different stages of WTC 2 for Case D_i temperature condition and the revised Case C_i structural damage condition (downward displacement is negative).

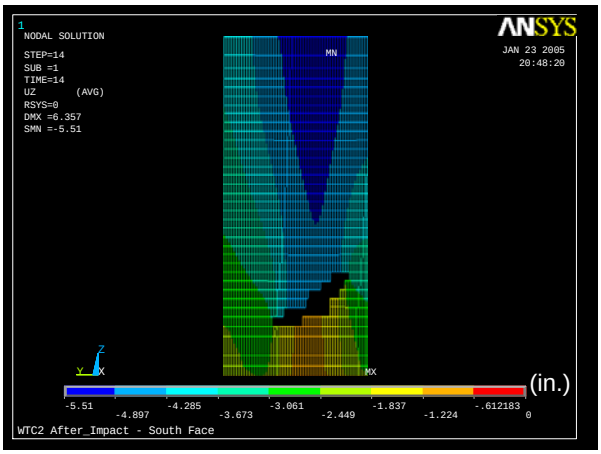

(a) South wall after impact

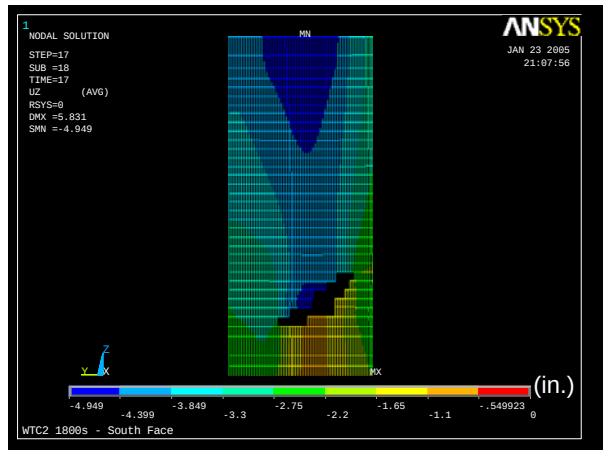

(b) South wall at 30 min

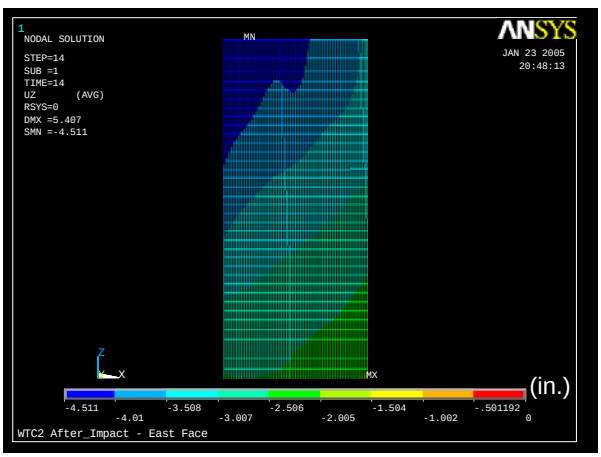

(c) East wall after impact

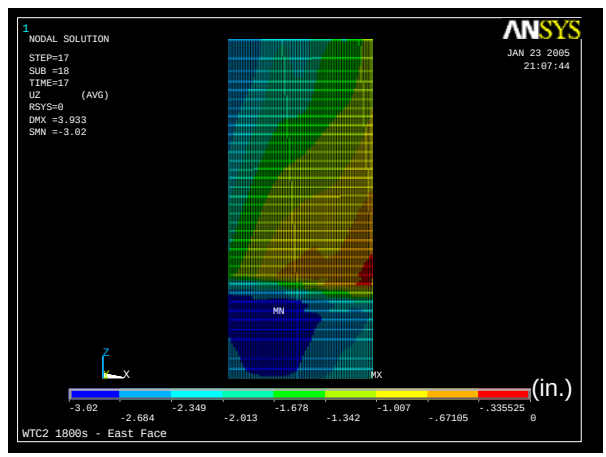

(d) East wall at 30 min

Figure C–22. Vertical displacement on the south and east faces of WTC 2 after aircraft impact and at 30 min of Case D_i temperature condition and the revised Case C_i structural damage condition (looking from outside; downward displacement is negative).

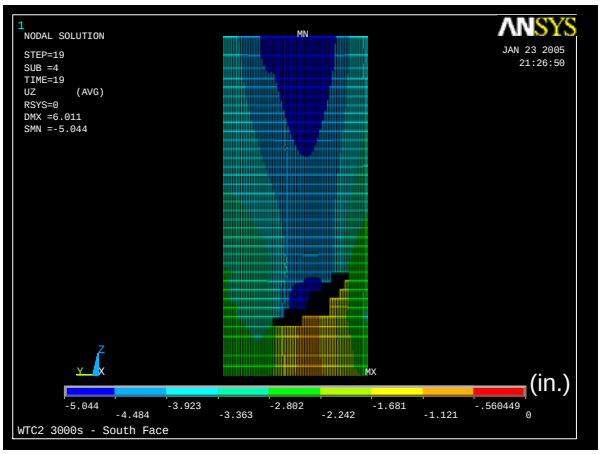

(a) South wall at 50 min

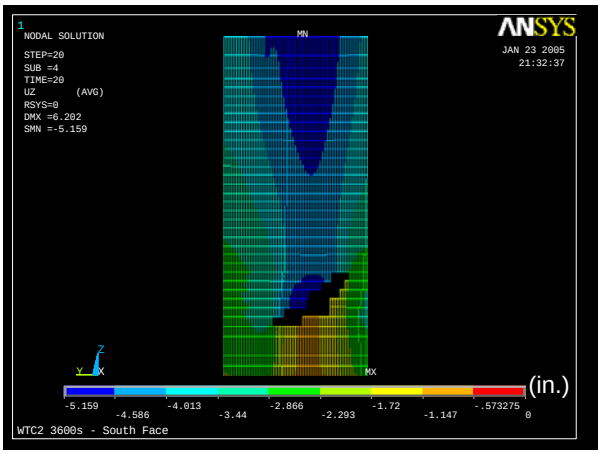

(b) South wall at 60 min

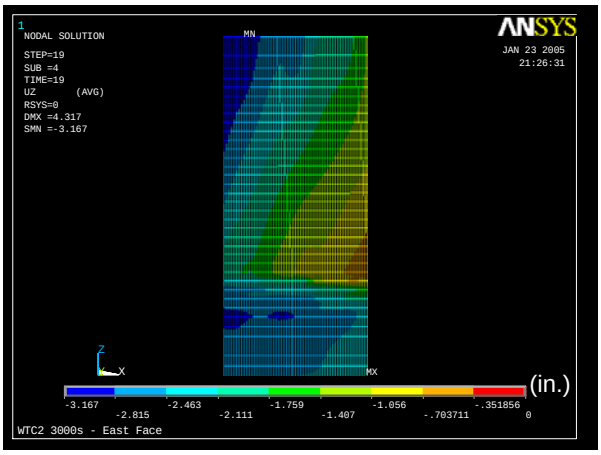

(c) East wall at 50 min

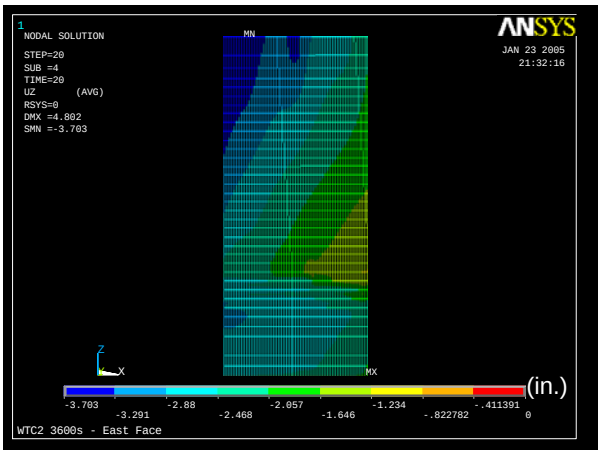

(d) East wall at 60 min

Figure C–23. Vertical displacement on the south and east faces of WTC 2 at 50 min and at 60 min of Case D_i temperature condition and the revised Case C_i structural damage condition (looking from outside; downward displacement is negative).

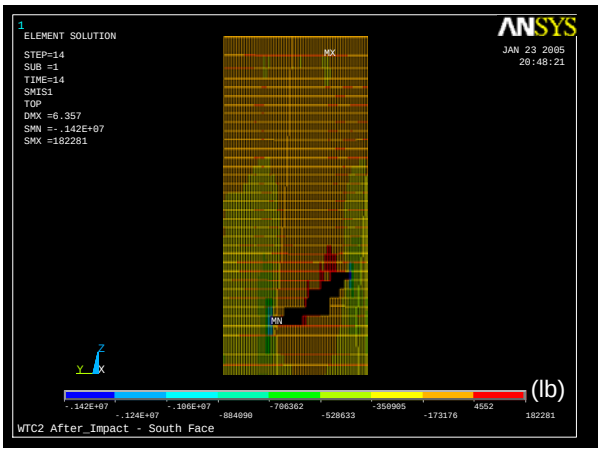

(a) South wall after impact

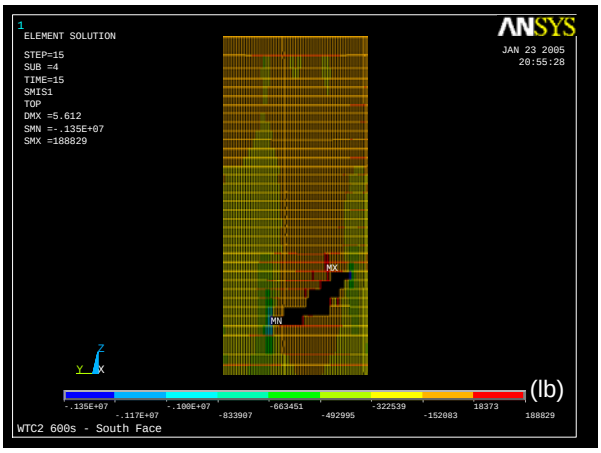

(b) South wall at 10 min

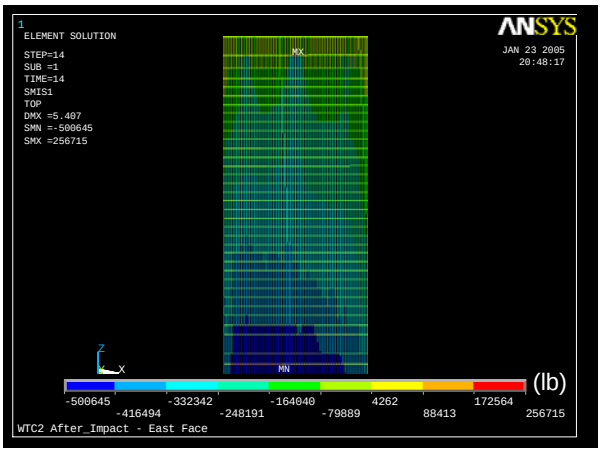

(c) East wall after impact

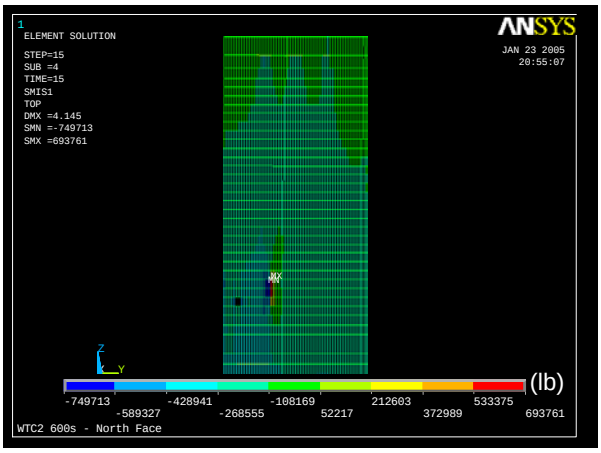

(d) East wall at 10 min

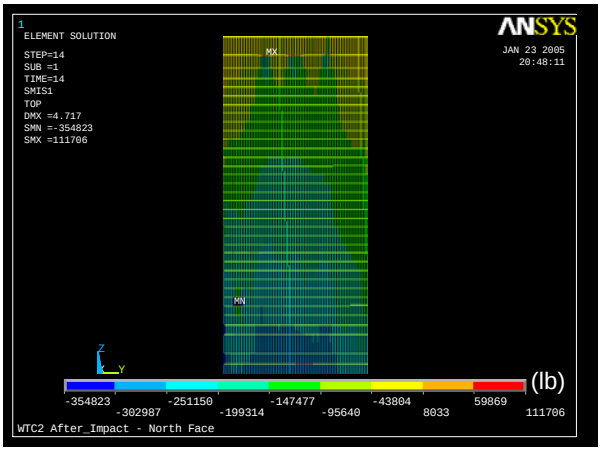

(e) North wall after impact

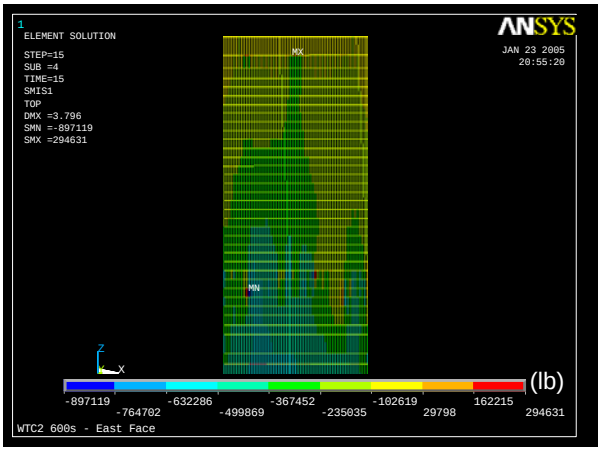

(f) North wall at 10 min

Figure C–24. Axial force variation on the south, east, and north faces of WTC 2 after impact and at 10 min of Case D_i temperature condition and the revised Case C_i structural damage condition (looking from outside; compression is negative).

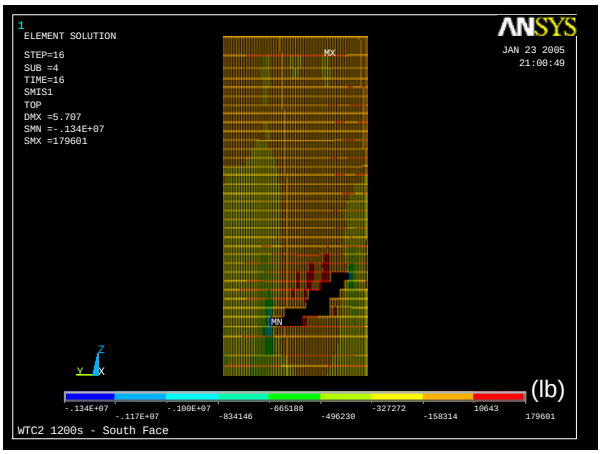

(a) South wall at 20 min

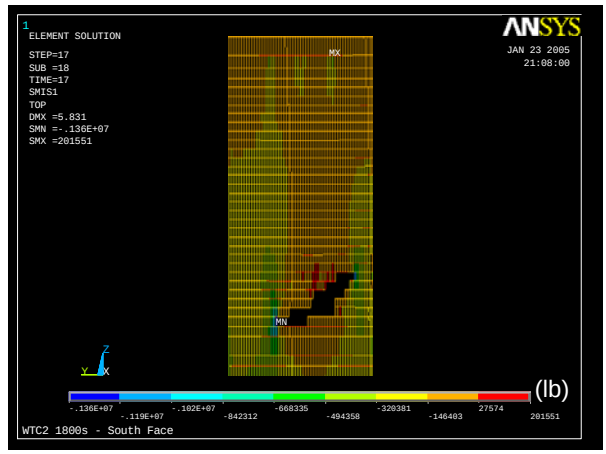

(b) South wall at 30 min

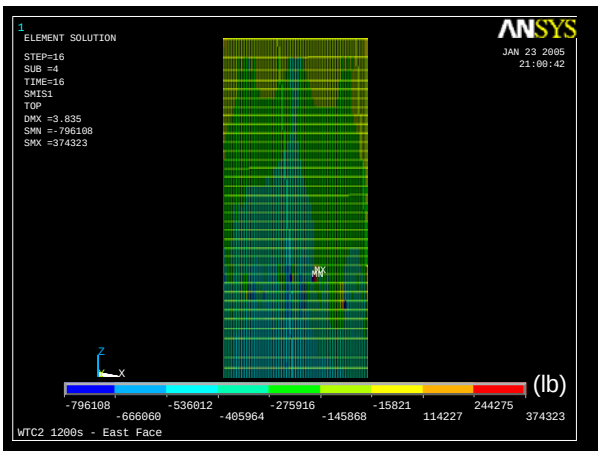

(c) East wall at 20 min

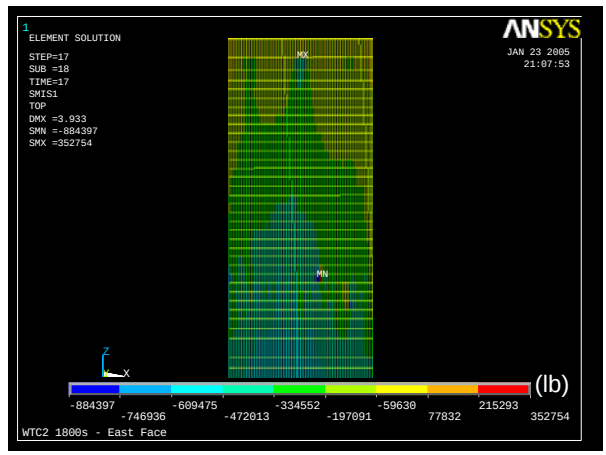

(d) East wall at 20 min

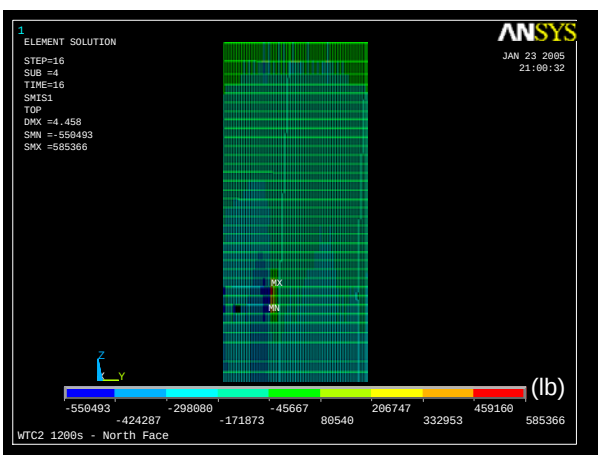

(e) North wall at 20 min

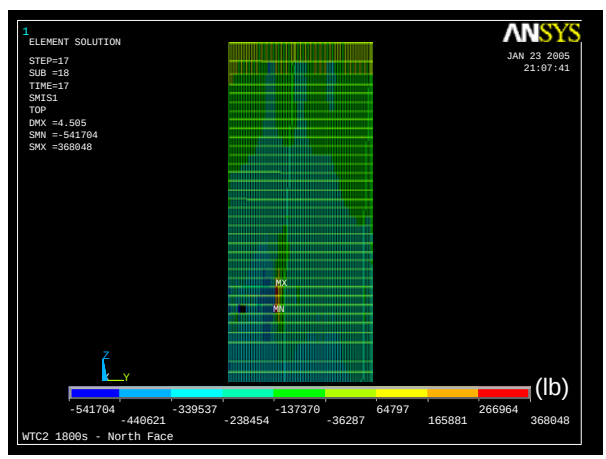

(f) North wall at 30 min

Figure C–25. Axial force variation on the south, east, and north faces of WTC 2 at 20 min and at 30 min of Case D_i temperature condition and the revised Case C_i structural damage condition (looking from outside; compression is negative).

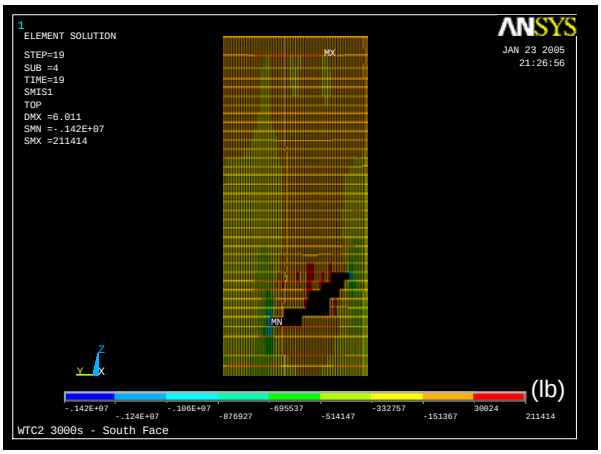

(a) South wall at 50 min

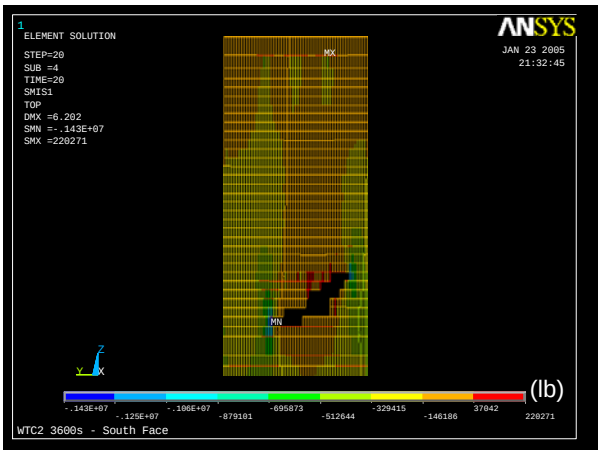

(b) South wall at 50 min

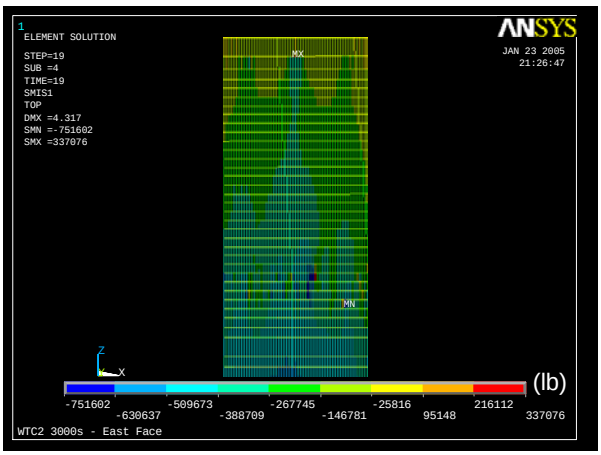

(c) East wall at 50 min

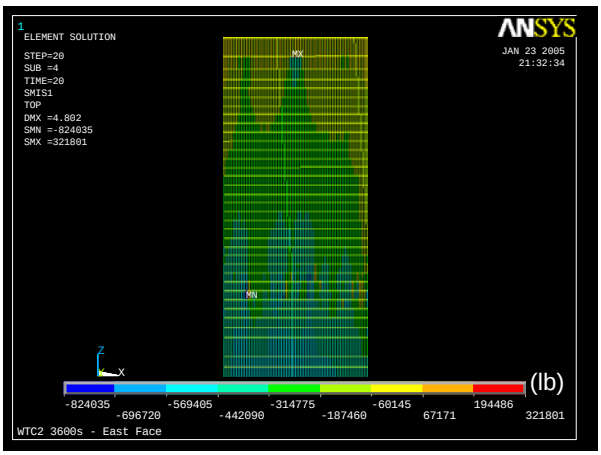

(d) East wall at 50 min

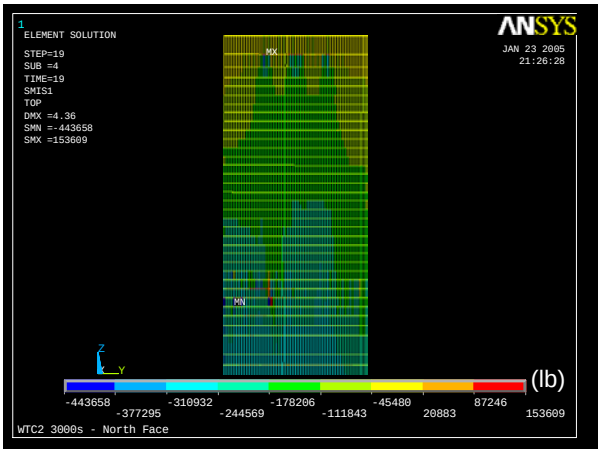

(e) North wall at 50 min

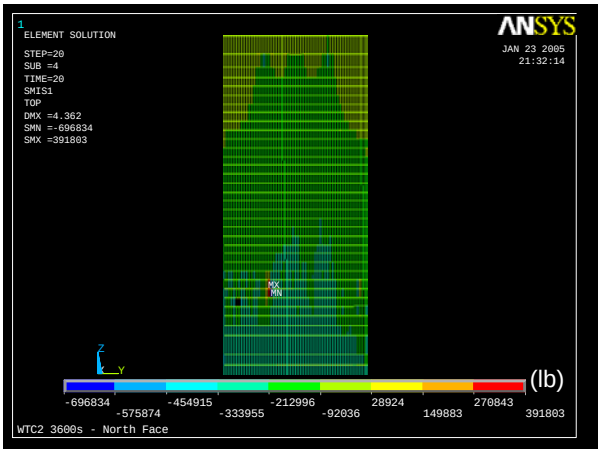

(f) North wall at 50 min

Figure C–26. Axial force variation on the south, east, and north faces of WTC 2 at 50 min and at 60 min of Case D_i temperature condition and the revised Case C_i structural damage condition (looking from outside; compression is negative).

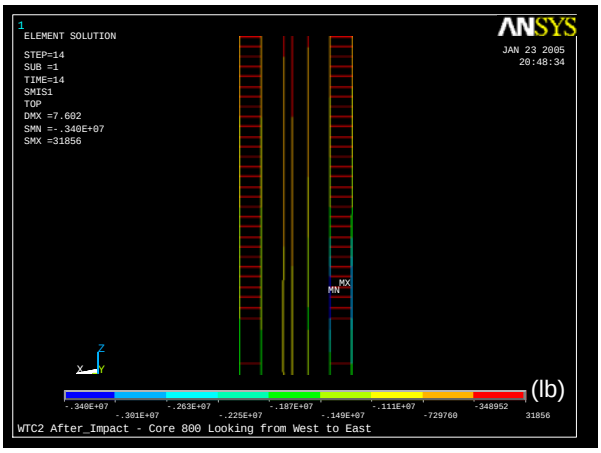

(a) 800 series columns after impact

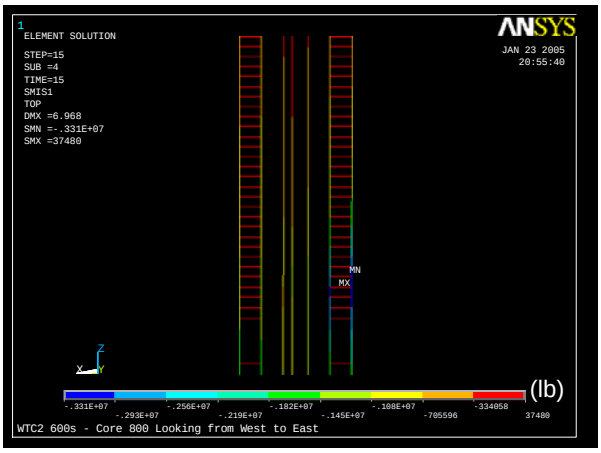

(b) 800 series columns at 10 min

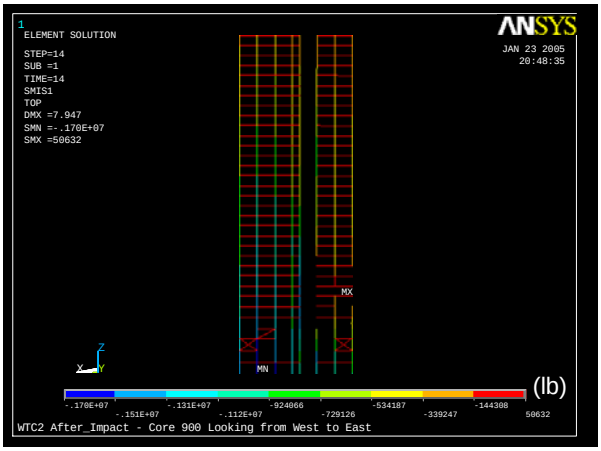

(c) 900 series columns after impact

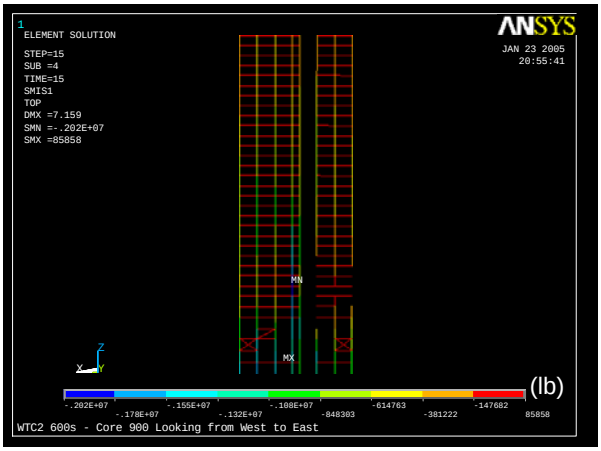

(d) 900 series columns at 10 min

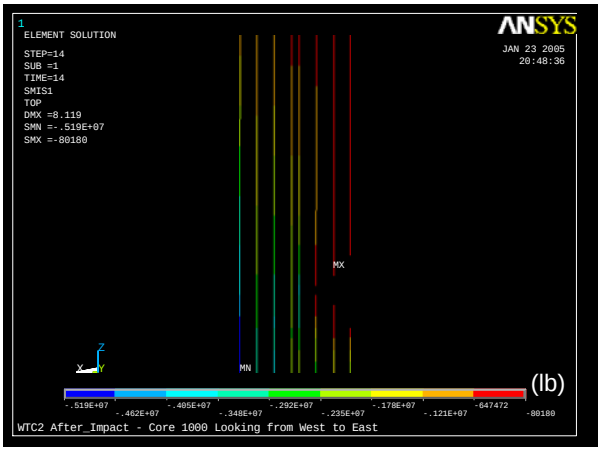

(e) 1000 series columns after impact

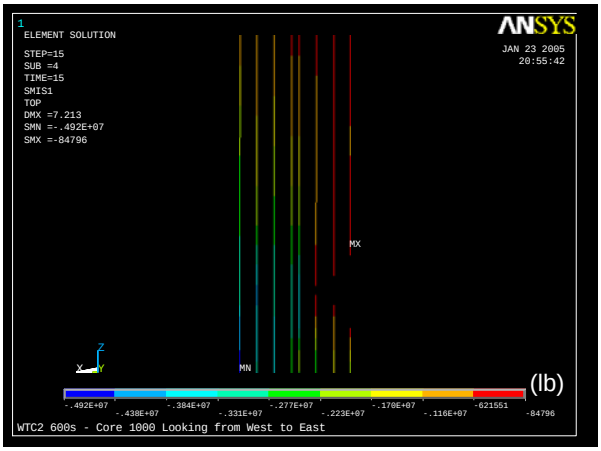

(f) 1000 series columns at 10 min

Figure C–27. Axial force variation on the 800, 900, and 1000 series core columns of WTC 2 after impact and at 10 min of Case D_i temperature condition and the revised Case C_i structural damage condition (looking from west; compression is negative).

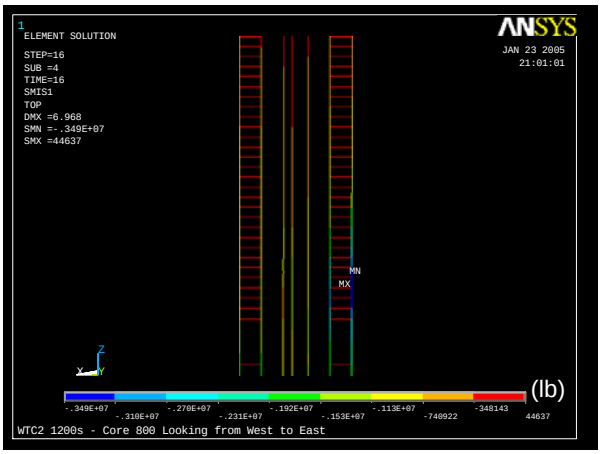

(a) 800 series columns at 20 min

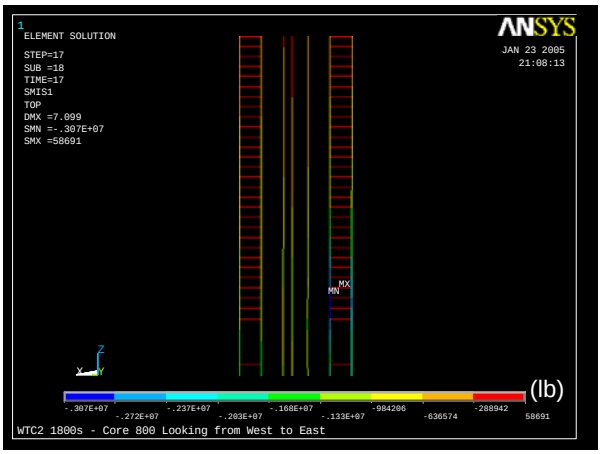

(b) 800 series columns at 30 min

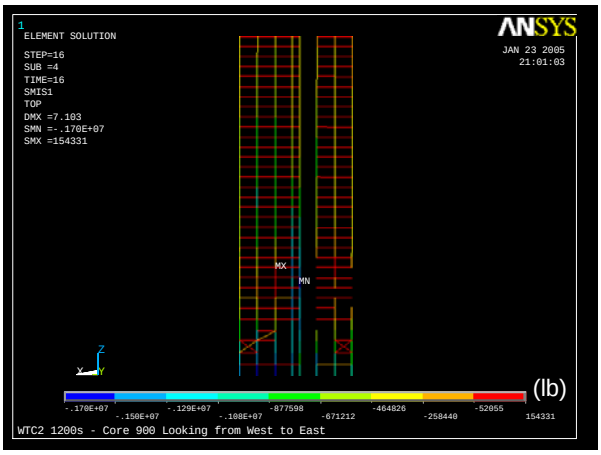

(c) 900 series columns at 20 min

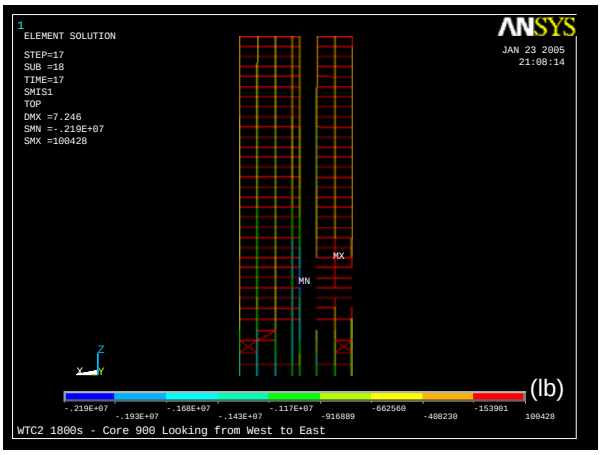

(d) 900 series columns at 30 min

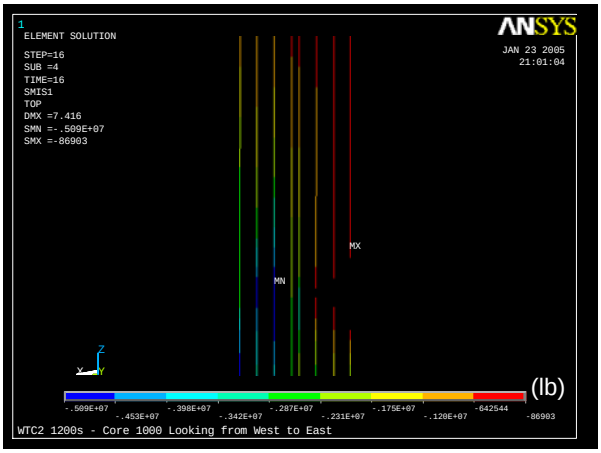

(e) 1000 series columns at 20 min

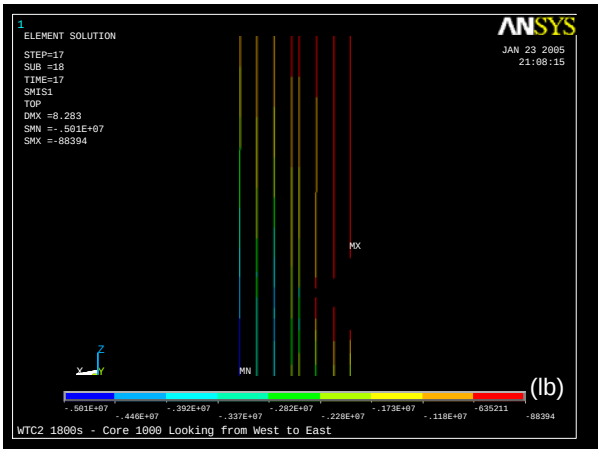

(f) 1000 series columns at 30 min

Figure C–28. Axial force variation on the 800, 900, and 1000 series core columns of WTC 2 at 20 min and at 30 min of Case D_i temperature condition and the revised Case C_i structural damage condition (looking from west; compression is negative).

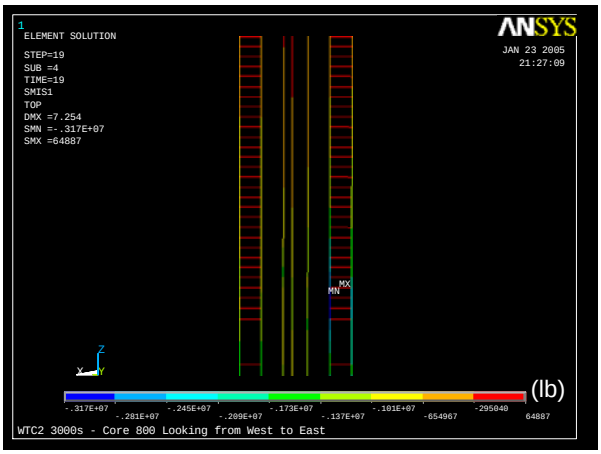

(a) 800 series columns at 50 min

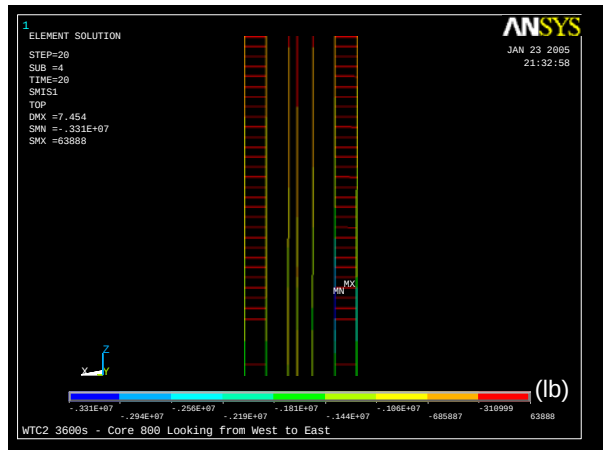

(b) 800 series columns at 60 min

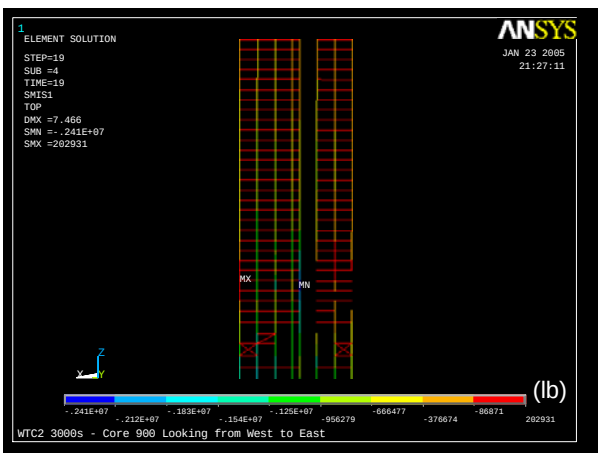

(c) 900 series columns at 50 min

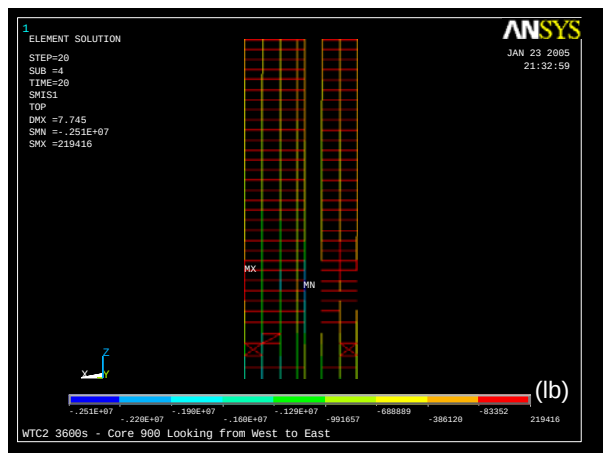

(d) 900 series columns at 60 min

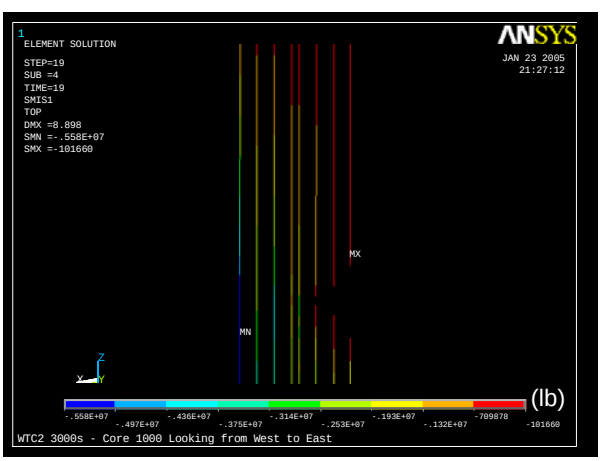

(e) 1000 series columns at 50 min

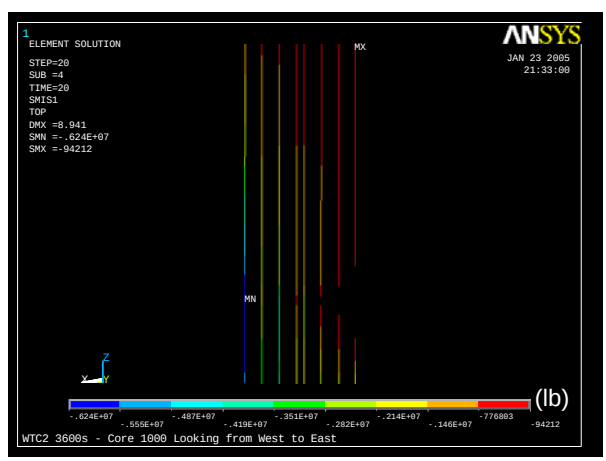

(f) 1000 series columns at 60 min

Figure C–29. Axial force variation on the 800, 900, and 1000 series core columns of WTC 2 at 50 min and at 60 min of Case D_i temperature condition and the revised Case C_i structural damage condition (looking from west; compression is negative).

Row	Analysis Stage	West	East	North	South	Core	Sum
(1)	Before Impact	18779	18837	13714	13529	77563	142423
(2)	After Impact	18824	21170	12812	12396	75450	140652
(3)	10 min	19668	21636	13148	11694	74506	140652
(4)	20 min	19984	21951	13004	11661	74053	140653
(5)	30 min	20005	22426	13129	11899	73195	140653
(6)	40 min	19980	22260	13252	12156	73005	140653
(7)	50 min	19617	22048	13211	12609	73168	140653
(8)	60 min	19161	21803	13294	12959	73436	140653

(a) Above Floor 78

Row	Analysis Stage	West	East	North	South	Core	Sum
(1)	Before Impact	17642	17697	12558	12393	71319	131609
(2)	After Impact	17613	20084	11761	11475	70039	130972
(3)	10 min	18453	20602	12152	10672	69094	130973
(4)	20 min	18759	20889	12005	10680	68640	130973
(5)	30 min	18755	21379	12146	10910	67782	130972
(6)	40 min	18718	21202	12290	11170	67593	130972
(7)	50 min	18340	20983	12237	11655	67756	130971
(8)	60 min	17876	20724	12316	12034	68022	130972

(b) Above Floor 81

Row	Analysis Stage	West	East	North	South	Core	Sum
(1)	Before Impact	16728	16782	11972	11820	67309	124611
(2)	After Impact	16717	19111	11188	11058	66400	124474
(3)	10 min	17551	19473	11596	10404	65449	124473
(4)	20 min	17864	19739	11443	10431	64996	124472
(5)	30 min	17875	20198	11573	10687	64138	124471
(6)	40 min	17847	20006	11709	10960	63950	124471
(7)	50 min	17482	19841	11651	11384	64113	124472
(8)	60 min	17025	19637	11734	11691	64384	124471

(c) Above Floor 83

Figure C–30. Total column loads in the core and exterior walls of WTC 2 at different floors and at different times for Case D_i temperature condition and the revised Case C_i structural damage condition (compression is positive).

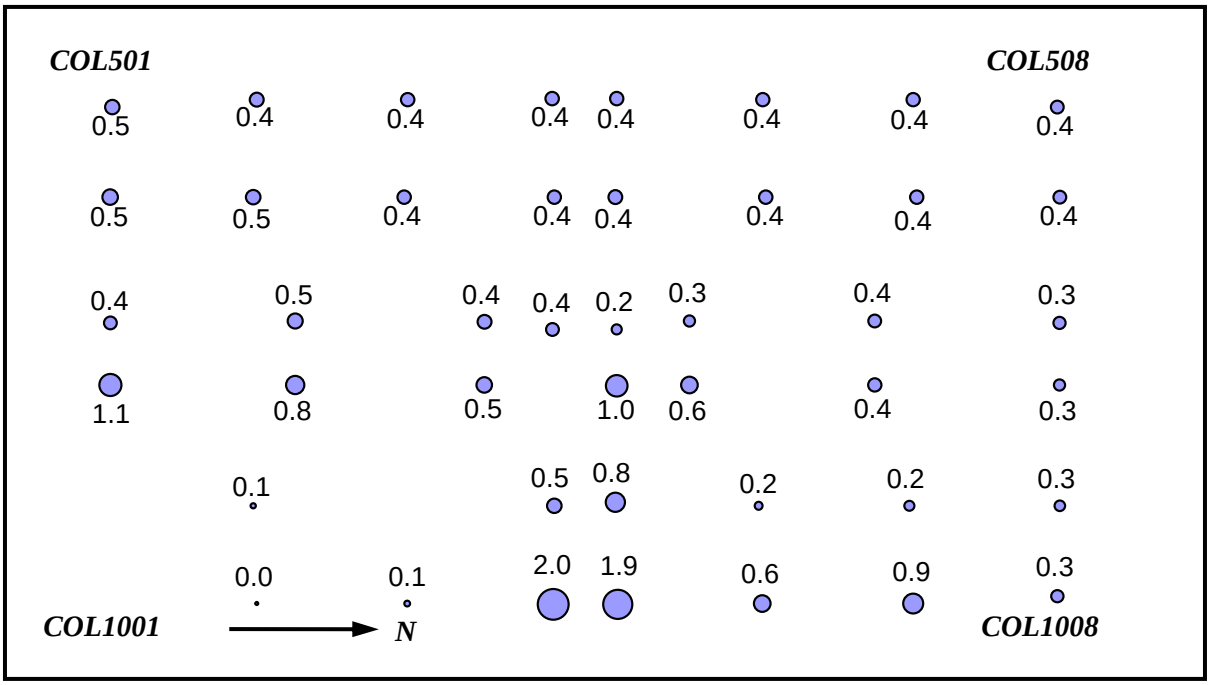

(a) At 10 min

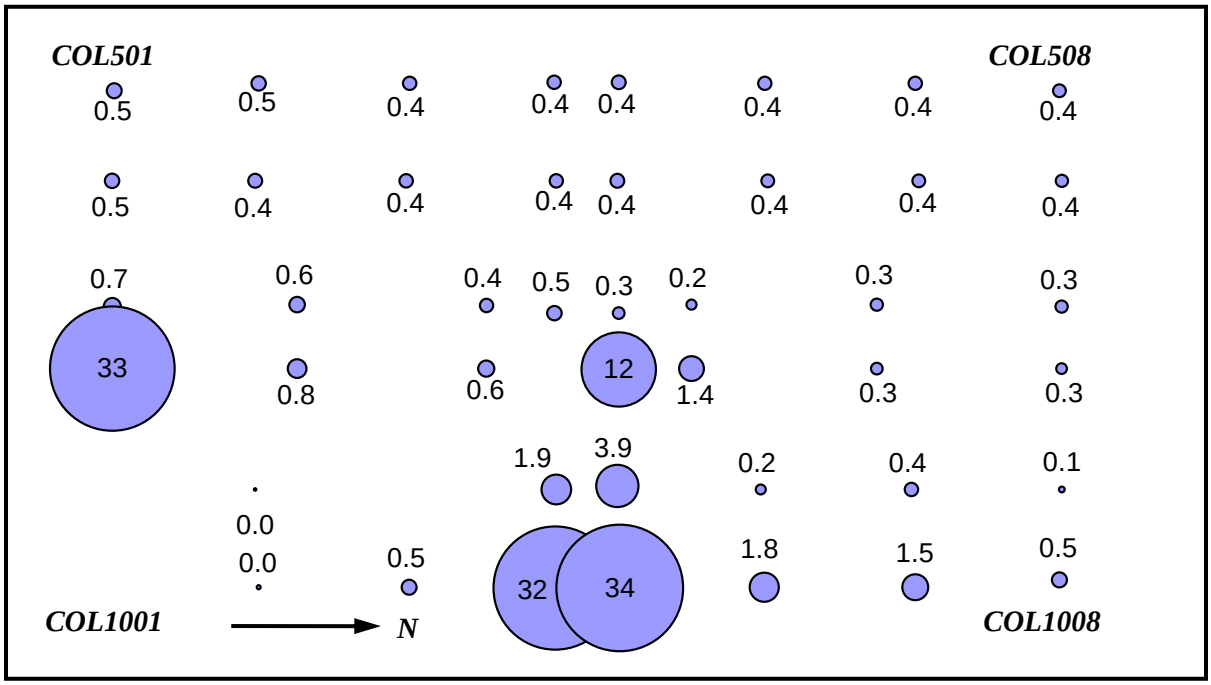

(b) At 30 min

Figure C–31. Ratios of axial elastic-plus-plastic strain to temperature-dependent yield strain for the core columns at Floor 82 of WTC 2 at 10 min and at 30 min of Case D_i temperature condition and the revised Case C_i structural damage condition.

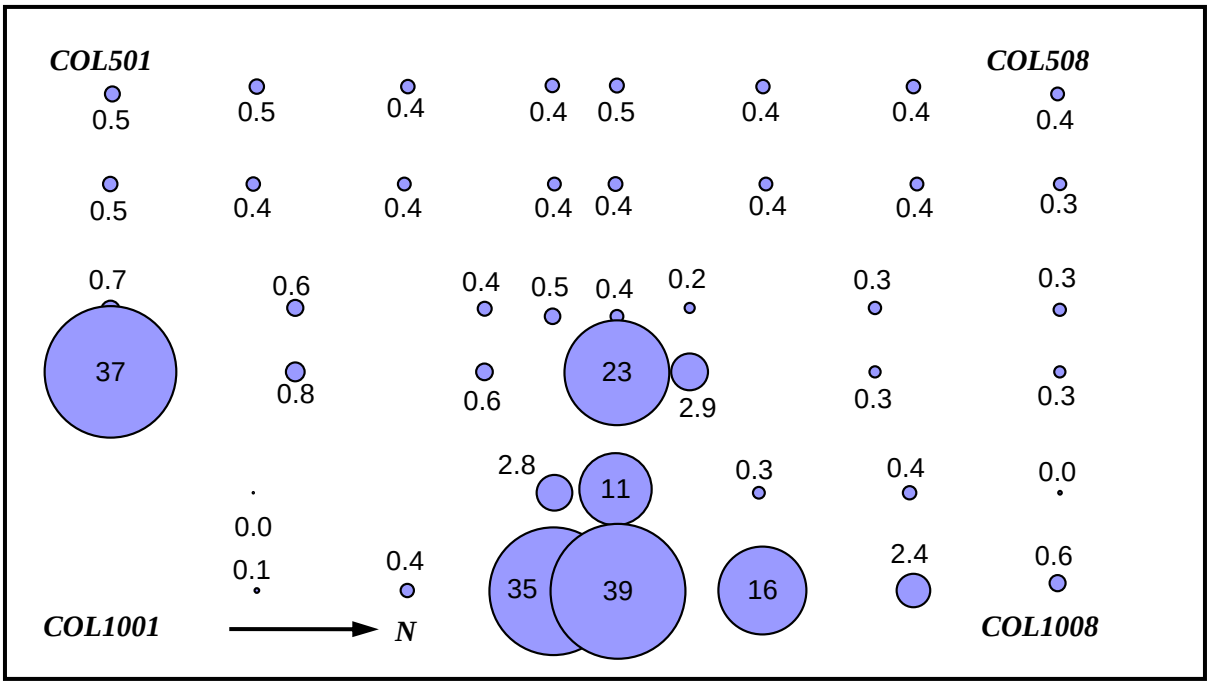

(a) At 40 min

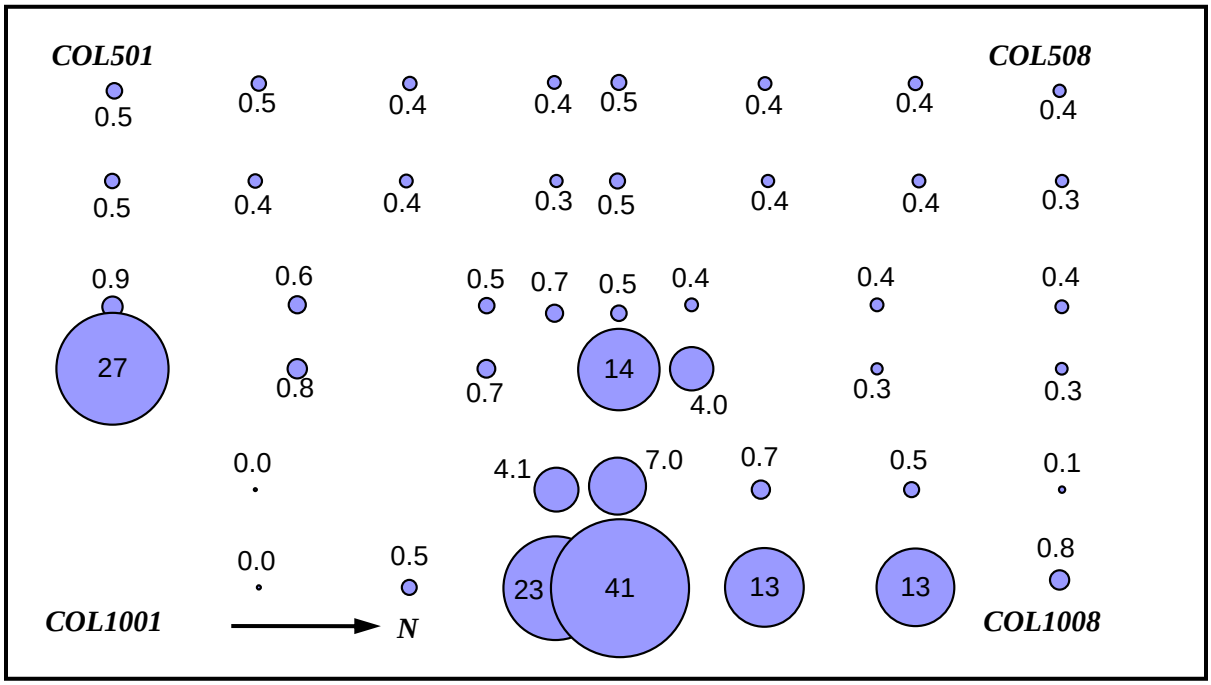

(b) At 60 min

Figure C–32. Ratios of axial elastic-plus-plastic strain to temperature-dependent yield strain for the core columns at Floor 82 of WTC 2 at 40 min and at 60 min of Case D_i temperature condition and the revised Case C_i structural damage condition.